

Volume 13 Issue 6

June 2022



ISSN 2156-5570(Online)

ISSN 2158-107X(Print)



Editorial Preface

From the Desk of Managing Editor...

It may be difficult to imagine that almost half a century ago we used computers far less sophisticated than current home desktop computers to put a man on the moon. In that 50 year span, the field of computer science has exploded.

Computer science has opened new avenues for thought and experimentation. What began as a way to simplify the calculation process has given birth to technology once only imagined by the human mind. The ability to communicate and share ideas even though collaborators are half a world away and exploration of not just the stars above but the internal workings of the human genome are some of the ways that this field has moved at an exponential pace.

At the International Journal of Advanced Computer Science and Applications it is our mission to provide an outlet for quality research. We want to promote universal access and opportunities for the international scientific community to share and disseminate scientific and technical information.

We believe in spreading knowledge of computer science and its applications to all classes of audiences. That is why we deliver up-to-date, authoritative coverage and offer open access of all our articles. Our archives have served as a place to provoke philosophical, theoretical, and empirical ideas from some of the finest minds in the field.

We utilize the talents and experience of editor and reviewers working at Universities and Institutions from around the world. We would like to express our gratitude to all authors, whose research results have been published in our journal, as well as our referees for their in-depth evaluations. Our high standards are maintained through a double blind review process.

We hope that this edition of IJACSA inspires and entices you to submit your own contributions in upcoming issues. Thank you for sharing wisdom.

Thank you for Sharing Wisdom!

Kohei Arai
Editor-in-Chief
IJACSA
Volume 13 Issue 6 June 2022
ISSN 2156-5570 (Online)
ISSN 2158-107X (Print)

Editorial Board

Editor-in-Chief

Dr. Kohei Arai - Saga University

Domains of Research: Technology Trends, Computer Vision, Decision Making, Information Retrieval, Networking, Simulation

Associate Editors

Alaa Sheta

Southern Connecticut State University

Domain of Research: Artificial Neural Networks, Computer Vision, Image Processing, Neural Networks, Neuro-Fuzzy Systems

Domenico Ciunzo

University of Naples, Federico II, Italy

Domain of Research: Artificial Intelligence, Communication, Security, Big Data, Cloud Computing, Computer Networks, Internet of Things

Dorota Kaminska

Lodz University of Technology

Domain of Research: Artificial Intelligence, Virtual Reality

Elena Scutelnicu

"Dunarea de Jos" University of Galati

Domain of Research: e-Learning, e-Learning Tools, Simulation

In Soo Lee

Kyungpook National University

Domain of Research: Intelligent Systems, Artificial Neural Networks, Computational Intelligence, Neural Networks, Perception and Learning

Krassen Stefanov

Professor at Sofia University St. Kliment Ohridski

Domain of Research: e-Learning, Agents and Multi-agent Systems, Artificial Intelligence, e-Learning Tools, Educational Systems Design

Renato De Leone

Università di Camerino

Domain of Research: Mathematical Programming, Large-Scale Parallel Optimization, Transportation problems, Classification problems, Linear and Integer Programming

Xiao-Zhi Gao

University of Eastern Finland

Domain of Research: Artificial Intelligence, Genetic Algorithms

Arun D Kulkarni

University of Texas at Tyler

Domain of Research: Machine Vision, Artificial Intelligence, Computer Vision, Data Mining, Image Processing, Machine Learning, Machine Vision, Neural Networks, Neuro-Fuzzy Systems

CONTENTS

Paper 1: Solutions to the Endless Addition of Transaction Volume in Blockchain

Authors: Hongping Cao, Hongxing Cao

PAGE 1 – 9

Paper 2: Blockchain Privacy Data Access Control Method Based on Cloud Platform Data

Authors: Biying Sun, Qian Dang, Yu Qiu, Lei Yan, Chunhui Du, Xiaoqin Liu

PAGE 10 – 17

Paper 3: Deep Convolution Neural Networks for Image Classification

Authors: Arun D. Kulkarni

PAGE 18 – 23

Paper 4: An Improved Genetic Algorithm for the Multi-temperature Food Distribution with Multi-Station

Authors: Bo Wang, Jiangpo Wei, Bin Lv, Ying Song

PAGE 24 – 29

Paper 5: An Efficient System for Real-time Mobile Smart Device-based Insect Detection

Authors: Thanh-Nghi Doan

PAGE 30 – 36

Paper 6: Novel Framework for Enhanced Learning-based Classification of Lesion in Diabetic Retinopathy

Authors: Prakruthi M K, Komarasamy G

PAGE 37 – 45

Paper 7: Hybrid Pelican Komodo Algorithm

Authors: Purba Daru Kusuma, Ashri Dinimaharawati

PAGE 46 – 55

Paper 8: Users' Acceptance and Sense of Presence towards VR Application with Stimulus Effectors on a Stationary Bicycle for Physical Training

Authors: Imran Bin Mahalil, Azmi Bin Mohd Yusof, Nazrita Binti Ibrahim, Eze Manzura Binti Mohd Mahidin, Ng Hui Hwa

PAGE 56 – 64

Paper 9: Fast and Robust Fuzzy-based Hybrid Data-level Method to Handle Class Imbalance

Authors: Kamlesh Upadhyay, Prabhjot Kaur, Ritu Sachdeva

PAGE 65 – 74

Paper 10: Proctoring and Non-proctoring Systems

Authors: Yusring Sanusi Baso

PAGE 75 – 82

Paper 11: Groundnuts Leaf Disease Recognition using Neural Network with Progressive Resizing

Authors: Rajnish M. Rakholia, Jinal H. Tailor, Jatinderkumar R. Saini, Jasleen Kaur, Hardik Pahuja

PAGE 83 – 88

Paper 12: A Proposed Architecture for Smart Home Systems Based on IoT, Context-awareness and Cloud Computing

Authors: Samah A. Z. Hassan, Ahmed M. Eassa

PAGE 89 – 96

Paper 13: Shallow Net for COVID-19 Classification Based on Biomarkers

Authors: Mahmoud B. Rokaya

PAGE 97 – 103

Paper 14: Advanced Medicinal Plant Classification and Bioactivity Identification Based on Dense Net Architecture

Authors: Banita Pukhrambam, Arun Sahayadhas

PAGE 104 – 109

Paper 15: Short Words Signature Verification using Markov Chain and Fisher Linear Discriminant Approach

Authors: M. Nazir, Surendra Singh Choudhary, Danish Ather, Latika Kharb

PAGE 110 – 116

Paper 16: Face Mask Wear Detection by using Facial Recognition System for Entrance Authorization

Authors: Munirah Ahmad Azraai, Ridhwan Rani, Raja Mariatul Qibtiah, Hidayah Samian

PAGE 117 – 123

Paper 17: A Novel Approach to Video Compression using Region of Interest (ROI) Method on Video Surveillance Systems

Authors: DewiAnggraini Puspa Hapsari, Sarifuddin Madenda, Muhammad Subali, Aini Suri Talita

PAGE 124 – 130

Paper 18: Data Augmentation Techniques on Chilly Plants to Classify Healthy and Bacterial Blight Disease Leaves

Authors: Sudeepthi Govathoti, A Mallikarjuna Reddy, Deepthi Kamidi, G BalaKrishna, Sri Silpa Padmanabhuni, Pradeepini Gera

PAGE 131 – 139

Paper 19: Towards the Smart Industry for the Sustainability through Open Innovation based on ITSM (Information Technology Service Management)

Authors: Asti Amalia Nur Fajrillah, Muharman Lubis, Arariko Rezeki Pasa

PAGE 140 – 152

Paper 20: Application of Machine Learning Algorithms in Coronary Heart Disease: A Systematic Literature Review and Meta-Analysis

Authors: Solomon Kutiname, Richard Millham, Adebayor Felix Adekoya, Mark Tettey, Benjamin Asubam Weyori, Peter Appiahene

PAGE 153 – 164

Paper 21: Vision based Human Activity Recognition using Deep Neural Network Framework

Authors: Jitha Janardhanan, S. Umamaheswari

PAGE 165 – 171

Paper 22: Internal Works Quality Assessment for Wall Evenness using Vision-based Sensor on a Mecanum-Wheeled Mobile Robot

Authors: Ahmad Zaki Shukor, Muhammad Herman bin Jamaluddin, Mohd Zulkifli bin Ramli, Ghazali bin Omar, Syed Hazni Abd Ghani

PAGE 172 – 179

- Paper 23: The 4W Framework of the Online Social Community Model for Satisfying the Unmet Needs of Older Adults
Authors: Farhat Mahmoud Embarak, Nor Azman Ismail, Alhuseen Omar Alsayed, Mohamed Bashir Buhalfaya, Abdurrahman Abdulla Younes, Blha Hassan Naser
PAGE 180 – 186
- Paper 24: Bayesian Network Modelling for Improved Knowledge Management of the Expert Model in the Intelligent Tutoring System
Authors: Fatima-Zohra Hibbi, Otman Abdoun, El Khatir Haimoudi
PAGE 187 – 192
- Paper 25: Digital Storytelling Framework to Assist Young Children in Understanding Dementia
Authors: Noreena Yi-Chin Liu, Nooralisa M Tuah, Kevin Chi-Jen Miao
PAGE 193 – 203
- Paper 26: Optimization of Small Sized File Access Efficiency in Hadoop Distributed File System by Integrating Virtual File System Layer
Authors: Neeta Alange, Anjali Mathur
PAGE 204 – 210
- Paper 27: Survey on Highly Imbalanced Multi-class Data
Authors: Mohd Hakim Abdul Hamid, Marina Yusoff, Azlinah Mohamed
PAGE 211 – 229
- Paper 28: Synthetic Data Augmentation of Tomato Plant Leaf using Meta Intelligent Generative Adversarial Network: Milgan
Authors: Sri Silpa Padmanabhuni, Pradeepini Gera
PAGE 230 – 238
- Paper 29: Comparison of Path Planning between Improved Informed and Uninformed Algorithms for Mobile Robot
Authors: Mohamed Amr, Ahmed Bahgat, Hassan Rashad, Azza Ibrahim
PAGE 239 – 248
- Paper 30: Modified Gradient Algorithm based Noise Subspace Estimation with Full Rank Update for Blind CSI Estimator in OFDM Systems
Authors: Saravanan Subramanian, Govind R. Kadambi
PAGE 249 – 257
- Paper 31: COVID-19: Challenges and Opportunities in the Online University Education
Authors: Irena Valova, Tsvetelina Mladenova
PAGE 258 – 263
- Paper 32: Multi-modal Brain MR Image Registration using A Novel Local Binary Descriptor based on Statistical Approach
Authors: Thuvanan Borvornvittholkarn
PAGE 264 – 269
- Paper 33: Core Elements Impacting Cloud Adoption in the Government of Saudi Arabia
Authors: Norah Alrebdi, Nabeel Khan
PAGE 270 – 273

Paper 34: Decentralized Tribrid Adaptive Control Strategy for Simultaneous Formation and Flocking Configurations of Multi-agent System

Authors: B. K. Swathi Prasad, Hariharan Ramasangu, Govind R. Kadambi

PAGE 274 – 282

Paper 35: Merged Dataset Creation Method Between Thermal Infrared and Microwave Radiometers Onboard Satellites

Authors: Kohei Arai

PAGE 283 – 288

Paper 36: A Hybrid RNN based Deep Learning Approach for Text Classification

Authors: Pramod Sunagar, Anita Kanavalli

PAGE 289 – 295

Paper 37: Deep Learning Approach for Masked Face Identification

Authors: Maad Shatnawi, Nahla Almenhali, Mitha Alhammadi, Khawla Alhanaee

PAGE 296 – 305

Paper 38: MSA-SFO-based Secure and Optimal Energy Routing Protocol for MANET

Authors: D. Naga Tej, K V Ramana

PAGE 306 – 313

Paper 39: An Efficient and Optimal Deep Learning Architecture using Custom U-Net and Mask R-CNN Models for Kidney Tumor Semantic Segmentation

Authors: Sitanaboina S L Parvathi, Harikiran Jonnadula

PAGE 314 – 320

Paper 40: GonioPi: Towards Developing a Scalable, Versatile, Reliable and Accurate Handheld-Wearable Digital Goniometer

Authors: Thomas Jonathan R. Garcia, Dhong Fhel K. Gom-os

PAGE 321 – 330

Paper 41: Computational Approach to Identify Regulatory Biomarkers in the Pathogenesis of Breast Carcinoma

Authors: Ghazala Sultan, Swaleha Zubair, Inamul Hasan Madar, Harishchander Anandaram

PAGE 331 – 336

Paper 42: Discourse-based Opinion Mining of Customer Responses to Telecommunications Services in Saudi Arabia during the COVID-19 Crisis

Authors: Abdulfattah Omar

PAGE 337 – 345

Paper 43: Building Footprint Extraction in Dense Area from LiDAR Data using Mask R-CNN

Authors: Sayed A. Mohamed, Amira S. Mahmoud, Marwa S. Moustafa, Ashraf K. Helmy, Ayman H. Nasr

PAGE 346 – 353

Paper 44: Cricket Event Recognition and Classification from Umpire Action Gestures using Convolutional Neural Network

Authors: Suvarna Nandyal, Suvarna Laxmikant Kattimani

PAGE 354 – 360

Paper 45: Optimization Performance Analysis for Adaptive Genetic Algorithm with Nonlinear Probabilities

Authors: Wenjuan Sun, Qiaoping Su, Hongli Yuan, Yan Chen

PAGE 361 – 366

Paper 46: Improved Particle Swarm Approach for Dynamic Automated Guided Vehicles Dispatching

Authors: Radhia Zaghdoud, Marwa Amara, Khaled Ghedira

PAGE 367 – 376

Paper 47: A New Approach for Detecting and Mitigating Address Resolution Protocol (ARP) Poisoning

Authors: Ahmed A. Galal, Atef Z. Ghalwash, Mona Nasr

PAGE 377 – 382

Paper 48: Cross-Layer based TCP Performance Enhancement in IoT Networks

Authors: Sultana Parween, Syed Zeeshan Hussain

PAGE 383 – 396

Paper 49: Sena TLS-Parser: A Software Testing Tool for Generating Test Cases

Authors: Rosziati Ibrahim, Samah W. G. AbuSalim, Sapiee Jamel, Jahari Abdul Wahab

PAGE 397 – 403

Paper 50: Deep Sentiment Extraction using Fuzzy-Rule Based Deep Sentiment Analysis

Authors: SIREESHA JASTI, G. V. S. RAJ KUMAR

PAGE 404 – 412

Paper 51: RS Invariant Image Classification and Retrieval with Pretrained Deep Learning Models

Authors: D. N. Hire, A. V. Patil

PAGE 413 – 417

Paper 52: Accuracy Enhancement of Prediction Method using SMOTE for Early Prediction Student's Graduation in XYZ University

Authors: Ainul Yaqin, Majid Rahardi, Ferian Fauzi Abdulloh

PAGE 418 – 424

Paper 53: Research on the Classification Modeling for the Natural Language Texts with Subjectivity Characteristic

Authors: Chen Xiao Yu, Gao Feng, Song Ying, Zhang Xiao Min

PAGE 425 – 432

Paper 54: Multi-layer Stacking-based Emotion Recognition using Data Fusion Strategy

Authors: Saba Tahseen, Ajit Danti

PAGE 433 – 442

Paper 55: The Implementation of a Solution for Low-Power Wide-Area Network using LoRaWAN

Authors: Nicoleta Cristina GAITAN, Floarea PITU

PAGE 443 – 448

Paper 56: Chaos Detection and Mitigation in Swarm of Drones Using Machine Learning Techniques and Chaotic Attractors

Authors: Emmanuel NEBE, Mistura Laide SANNI, Rasheed Ayodeji ADETONA, Bodunde Odunola AKINYEMI, Sururah Apinke BELLO, Ganiyu Adesola ADEROUNMU

PAGE 449 – 460

Paper 57: Integrating Big Data Analytics into Business Process Modelling: Possible Contributions and Challenges

Authors: Zaeem AL-MAdhrah, Dalbir Singh, Elaheh Yadegaridehkordi

PAGE 461 – 468

Paper 58: K-Means Customers Clustering by their RFMT and Score Satisfaction Analysis

Authors: Doae Mensouri, Abdellah Azmani, Monir Azmani

PAGE 469 – 476

Paper 59: Indoor Positioning System: A Review

Authors: N. Syazwani C. J, Nur Haliza Abdul Wahab, Noorhazirah Sunar, Sharifah H. S. Ariffin, Keng Yinn Wong, Yichief Aun

PAGE 477 – 490

Paper 60: A Lightweight ECC-based Three-Factor Mutual Authentication and Key Agreement Protocol for WSNs in IoT

Authors: Meriam Fariss, Hassan El Gafif, Ahmed Toumanari

PAGE 491 – 501

Paper 61: Threshold Segmentation of Magnetic Column Defect Image based on Artificial Fish Swarm Algorithm

Authors: Wang Jun, Hou Mengjie, Zhang Ruiran, Xiao Jingjing

PAGE 502 – 508

Paper 62: Deep Separable Convolution Network for Prediction of Lung Diseases from X-rays

Authors: Geetha. N, S. J. Sathish Aaron Joseph S. J

PAGE 509 – 518

Paper 63: Face Recognition System Design and Implementation using Neural Networks

Authors: Jamil Abedalrahim Jamil Alsyayadeh, Irianto, Azwan Aziz, Chang Kai Xin, A. K. M. Zakir Hossain, Safarudin Gazali Herawan

PAGE 519 – 526

Paper 64: Sparse Feature Aware Noise Removal Technique for Brain Multiple Sclerosis Lesions using Magnetic Resonance Imaging

Authors: Swetha M D, Aditya C R

PAGE 527 – 533

Paper 65: Sentiment Analysis of Covid-19 Vaccination using Support Vector Machine in Indonesia

Authors: Majid Rahardi, Afrig Aminuddin, Ferian Fauzi Abdulloh, Rizky Adhi Nugroho

PAGE 534 – 539

Paper 66: Application of Optimized SVM in Sample Classification

Authors: Xuemei Yao

PAGE 540 – 547

Paper 67: A Distributed Intrusion Detection System using Machine Learning for IoT based on ToN-IoT Dataset

Authors: Abdallah R. Gad, Mohamed Haggag, Ahmed A. Nashaf, Tamer M. Barakat

PAGE 548 – 563

Paper 68: COVID-19 Detection on X-Ray Images using a Combining Mechanism of Pre-trained CNNs

Authors: Oussama El Gannour, Soufiane Hamida, Shawki Saleh, Yasser Lamalem, Bouchaib Cherradi, Abdelhadi Raihani

PAGE 564 – 570

Paper 69: Sentiment Analysis of Tweets using Unsupervised Learning Techniques and the K-Means Algorithm

Authors: Orlando Iparaguirre-Villanueva, Victor Guevara-Ponce, Fernando Sierra-Linan, Saul Beltozar-Clemente, Michael Cabanillas-Carbonell

PAGE 571 – 578

Paper 70: Registration Methods for Thermal Images of Diabetic Foot Monitoring: A Comparative Study

Authors: Doha Bouallal, Hassan Douzi, Rachid Harba

PAGE 579 – 587

Paper 71: Op-RMSprop (Optimized-Root Mean Square Propagation) Classification for Prediction of Polycystic Ovary Syndrome (PCOS) using Hybrid Machine Learning Technique

Authors: Rakshitha Kiran P, Naveen N. C

PAGE 588 – 596

Paper 72: Influence of Management Automation on Managerial Decision-making in the Agro-Industrial Complex

Authors: Sergey Dokholyan, Evgeniya Olegovna Ermolaeva, Alexander Sergeevich Verkhovod, Elena Vladimirovna Dupliy, Anna Evgenievna Gorokhova, Vyacheslav Aleksandrovich Ivanov, Vladimir Dmitrievich Sekerin

PAGE 597 – 603

Paper 73: Enhancing the Security of Data Stored in the Cloud using customized Data Visualization Patterns

Authors: Archana M, Gururaj Murtugudde

PAGE 604 – 610

Paper 74: Incremental Learning based Optimized Sentiment Classification using Hybrid Two-Stage LSTM-SVM Classifier

Authors: Alka Londhe, P. V. R. D. Prasada Rao

PAGE 611 – 619

Paper 75: Data Recovery Approach with Optimized Cauchy Coding in Distributed Storage System

Authors: Snehalata Funde, Gandharba Swain

PAGE 620 – 629

Paper 76: Impact of COVID-19 Pandemic Measures and Restrictions on Cellular Network Traffic in Malaysia

Authors: Sallar Salam Murad, Salman Yussof, Rozin Badeel, Reham A. Ahmed

PAGE 630 – 645

Paper 77: A Deep Learning Classification Approach using Feature Fusion Model for Heart Disease Diagnosis

Authors: Bhandare Trupti Vasantrao, Selvarani Rangasamy, Chetan J. Shelke

PAGE 646 – 654

Paper 78: An Effective Demand based Optimal Route Generation in Transport System using DFCM and ABSO Approaches

Authors: Archana M. Nayak, Nirbhay Chaubey

PAGE 655 – 667

Paper 79: Implementation of Electronic Health Record and Health Insurance Management System using Blockchain Technology

Authors: Lincy Golda Careline S, T. Godhavari

PAGE 668 – 673

Paper 80: Predicting Blocking Bugs with Machine Learning Techniques: A Systematic Review

Authors: Selasie Aformaley Brown, Benjamin Asubam Weyori, Adebayo Felix Adekoya, Patrick Kwaku Kudjo, Solomon Mensah

PAGE 674 – 683

Paper 81: Trace Learners Clustering to Improve Learning Object Recommendation in Online Education Platforms

Authors: Zriaa Rajae, Amali Said, El Faddouli Nour-eddine

PAGE 684 – 693

Paper 82: DDoS Intrusion Detection Model for IoT Networks using Backpropagation Neural Network

Authors: Jasem Almotiri

PAGE 694 – 704

Paper 83: Analysis and Evaluation of Two Feature Selection Algorithms in Improving the Performance of the Sentiment Analysis Model of Arabic Tweets

Authors: Maria Yousef, Abdulla ALali

PAGE 705 – 711

Paper 84: Domain Human Recognition Techniques using Deep Learning

Authors: Seshaiyah Merikapudi, Murthy SVN, Manjunatha. S, R. V. Gandhi

PAGE 712 – 716

Paper 85: Tourist Reviews Sentiment Classification using Deep Learning Techniques: A Case Study in Saudi Arabia

Authors: Banan A.Alharbi, Mohammad A. Mezher, Abdullah M. Barakeh

PAGE 717 – 726

Paper 86: An Outlier Detection and Feature Ranking based Ensemble Learning for ECG Analysis

Authors: Venkata Anuhya Ardeti, Venkata Ratnam Kolluru, George Tom Varghese, Rajesh Kumar Patjoshi

PAGE 727 – 737

Paper 87: Improved Data Segmentation Architecture for Early Size Estimation using Machine Learning

Authors: Manisha, Rahul Rishi, Sonia Sharma

PAGE 738 – 747

Paper 88: Use of Information and Computer-based Distance Learning Technologies during COVID-19 Active Restrictions

Authors: Irina Petrovna Gladilina, Lyudmila Nikolaevna Pankova, Svetlana Alexandrovna Sergeeva, Vladimir Kolesnik, Alexey Vorontsov

PAGE 748 – 753

Paper 89: Detection of COVID-19 from Chest X-Ray Images using CNN and ANN Approach

Authors: Micheal Olaolu Arowolo, Marion Olubunmi Adebisi, Eniola Precious Michael, Happiness Eric Aigbogun, Sulaiman Olaniyi Abdulsalam, Ayodele Ariyo Adebisi

PAGE 754 – 759

Paper 90: A Novel Region Growing Algorithm using Wavelet Coefficient Feature Combination of Image Dynamics

Authors: Tamanna Sahoo, Bibhuprasad Mohanty

PAGE 760 – 768

Paper 91: Driver Drowsiness Detection and Monitoring System (DDDMS)

Authors: Raz Amzar Fahimi Rozali, Suzi Iryanti Fadilah, Azizul Rahman Mohd Shariff, Khuzairi Mohd Zaini, Fatima Karim, Mohd Helmy Abd Wahab, Rajan Thangaveloo, Abdul Samad Bin Shibghatullah

PAGE 769 – 775

Paper 92: BiDLNet: An Integrated Deep Learning Model for ECG-based Heart Disease Diagnosis

Authors: S. Kusuma, Jothi. K. R

PAGE 776 – 781

Paper 93: Deep-Learning Approach for Efficient Eye-blink Detection with Hybrid Optimization Concept

Authors: Rupali Gawande, Sumit Badotra

PAGE 782 – 795

Paper 94: A Hybrid Quartile Deviation-based Support Vector Regression Model for Software Reliability Datasets

Authors: Y. Geetha Reddy, Y Prasanth

PAGE 796 – 801

Paper 95: EAGL: Enhancement Algorithm based on Gamma Correction for Low Visibility Images

Authors: Navleen S Rekhi, Jagroop S Sidhu

PAGE 802 – 811

Paper 96: Approval Rating of Peruvian Politicians and Policies using Sentiment Analysis on Twitter

Authors: Jose Yauri, Luis Solis, Efrain Porras, Manuel Lagos, Enrique Tinoco

PAGE 812 – 818

Paper 97: Construction of a Repeatable Framework for Prostate Cancer Lesion Binary Semantic Segmentation using Convolutional Neural Networks

Authors: Ian Vincent O. Mirasol, Patricia Angela R. Abu, Rosula S. J. Reyes

PAGE 819 – 823

Paper 98: Methods and Directions of Contact Tracing in Epidemic Discovery

Authors: Mohammed Abdalla, Amr M. AbdelAziz, Louai Alarabi, Saleh Basalamah, Abdeltawab Hendawi

PAGE 824 – 833

Paper 99: Emergency Decision Model by Combining Preference Relations with Trapezoidal Pythagorean Fuzzy Probabilistic Linguistic Priority Weighted Averaging PROMETHEE Approach

Authors: Xiao Yue, Li jianhui

PAGE 834 – 845

Paper 100: Analysis of the Influence of De-hazing Methods on Vehicle Detection in Aerial Images

Authors: Khang Nguyen, Phuc Nguyen, Doanh C. Bui, Minh Tran, Nguyen D. Vo

PAGE 846 – 856

Paper 101: Designing a Mobile Application using Augmented Reality: The Case of Children with Learning Disabilities

Authors: Misael Lazo-Amado, Leoncio Cueva-Ruiz, Laberiano Andrade-Arenas

PAGE 857 – 864

Paper 102: Implementation of a Web System: Prevent Fraud Cases in Electronic Transactions

Authors: Edwin Kcomf Ponce, Katherine Escobedo Sanchez, Laberiano Andrade-Arenas

PAGE 865 – 876

Paper 103: Benchmarking of Motion Planning Algorithms with Real-time 3D Occupancy Grid Map for an Agricultural Robotic Manipulator

Authors: Seyed Abdollah Vaghefi, Mohd Faisal Ibrahim, Mohd Hairi Mohd Zaman

PAGE 877 – 882

Paper 104: Unsupervised Domain Adaptation using Maximum Mean Covariance Discrepancy and Variational Autoencoder

Authors: Fabian Barreto, Jignesh Sarvaiya, Sushilkumar Yadav, Suprava Patnaik

PAGE 883 – 891

Paper 105: Prediction of Quality of Water According to a Random Forest Classifier

Authors: Shahd Maadi Alomani, Najd Ibrahim Alhawiti, A'aeshah Alhakamy

PAGE 892 – 899

Paper 106: Virtual Reality Platform for Sustainable Road Education among Users of Urban Mobility in Cuenca, Ecuador
Authors: Gabriel A. Leon-Paredes, Omar G. Bravo-Quezada, Erwin J. Sacoto-Cabrera, Wilson F. Calle-Siavichay, Ledys L. Jimenez-Gonzalez, Juan Aguirre-Benalcazar

PAGE 900 – 909

Paper 107: An E2ED-based Approach to Custom Robot Navigation and Localization

Authors: Andres Moreno, Daniel Paez, Fredy Martinez

PAGE 910 – 916

Paper 108: Identifying Community-Supported Technologies and Software Developments Concepts by K-means Clustering

Authors: Farag Almansoury, Segla Kpodjedo, Ghizlane El Boussaidi

PAGE 917 – 926

Paper 109: On the Role of Text Preprocessing in BERT Embedding-based DNNs for Classifying Informal Texts

Authors: Aliyah Kurniasih, Lindung Parningotan Manik

PAGE 927 – 934

Paper 110: VIHS with ROTR Technique for Enhanced Light-Weighted Cryptographic System

Authors: Sanjeev Kumar A N, Ramesh Naik B

PAGE 935 – 942

Paper 111: Classification of Palm Trees Diseases using Convolution Neural Network

Authors: Marwan Abu-zanona, Said Elaiwat, Shayma'a Younis, Nisreen Innab, M. M. Kamruzzaman

PAGE 943 – 949

Paper 112: Dynamic Spatial-Temporal Graph Model for Disease Prediction

Authors: Ashwin Senthilkumar, Mihir Gupte, Shridevi S

PAGE 950 – 957

Paper 113: Password Systems: Problems and Solutions

Authors: Lanfranco Lopriore

PAGE 958 – 964

Solutions to the Endless Addition of Transaction Volume in Blockchain

Hongping Cao¹

School of Data Science
Guangzhou Huashang College
Guangzhou, China

Hongxing Cao²

School of Electrical and Computer Engineering
Guangzhou Nanfang College
Guangzhou, China

Abstract—In blockchain system, the problem of endless addition of transaction volume results in larger space occupation, heavier network transmission burden and the like. But the way of abandoning historical data is hindered by the characteristic of blockchain-tamper-proof. To solve this problem, this dissertation takes bitcoin system as an example, and gives a definition of expired transaction. By abandoning expired transactions and packing the rest transactions in several blocks into a new substitute block to replace old blocks, help to overcome the difficulty in clearing historical data. However, this solution fails to clear ineffective intermediate transactions. Thus, a follow-up solution is proposed, abandon the transactions whose outputs have been run out and retain the transactions where not all the outputs have been spent. Additionally, include records of the spending details of each transaction output, which allows us to clear ineffective intermediate transactions. In the end, an experiment is conducted to confirm the effectiveness of the two solutions as to clearing transactions.

Keywords—Blockchain; endless addition; expired transactions; substitute; storage problem; consensus algorithm

I. INTRODUCTION

Blockchain [1] technology has become a new data storage technology with its decentralization, anti-tampering, and traceability. In addition to the field of digital cryptocurrency [2], it also enjoys promising prospects for application in the fields of data notarization [3], resource sharing [4] and supply chain traceability [5]. It is estimated that by 2027, 10% of global GDP will be stored through blockchain technology [6].

To realize decentralization and traceability, blockchain technology uses chain storage structure [7] and multiple complete nodes to save data copies in full. However, such a storage method inevitably causes endless addition of data, and its anti-tampering feature means once the data (even the wrong data) is uploaded, it cannot be modified or deleted. As time goes on, fast-growing data of block chain leads to space occupation, which has become a problem that blockchain technology has to face. In addition, when a new complete node joins the system, the full amount of data must be synchronized, resulting in an increase in the network load of other nodes. Currently, it takes several days for Bitcoin nodes to synchronize the full amount of data every time, and every node needs to verify the correctness of the transaction when it receives a synchronization block, which will consume massive CPU computing power.

In the following sections, an overview of solutions in bitcoin system and research field, is given firstly, and find that these ideas merely mediate the effects of the problem instead of solving it. Then we define the expired transactions, based on which gives a solution of re-packing to generate substitute block to replace old blocks safely and thus abandon historical data. But this solution can only clean about 20% transactions. To clean more middle expired transactions, give a follow-up solution by recording signals of unspent transaction outputs. Finally, we verify the correctness and effectiveness of two solutions by experiments to find the second solution can clean about 80% expired transactions. With comparison to traditional solutions, reusing consensus algorithm (Power of Work) to generate substitute block to replace old blocks safely, is a brand-new and effective idea in this field.

II. SOLUTIONS IN BITCOIN

The most typical application of blockchain technology is Bitcoin. To make things easier, Bitcoin will be taken as an example. Bitcoin has been in operation for 12 years since 2019. As of February 14, 2021, there were 670,540 blocks and 18,628,343 bitcoins, with a total transaction volume of 1,232,212,522, a total data capacity of about 306 GB, a total number of 786,328,292 authentication addresses, and a market capitalization of 905.9 billion dollars [8]. According to statistics from BitNodes [9], there are currently about 10,000 complete nodes online at the same time in the entire network, and the disk space required by a single complete node is about 306 GB. Each complete node stores one copy of data, so the data capacity required by the whole system is about 3.1 PB. At present, it is growing rapidly at the rate of about 330,000 transactions per day [10]. With such high-speed transaction growth, the storage space occupation of Bitcoin has become an increasingly obvious problem.

Satoshi Nakamoto, the author of Bitcoin, once proposed a solution to the storage problem-space recycling. He believes that if the recent transaction has been included in enough blocks, the data before the transaction can be discarded to recover the hard disk space [1]. He pruned the expired transaction data, yet kept their Hash values to ensure that the Merkle root of the block is a verifiable value, as is shown in Fig. 1:

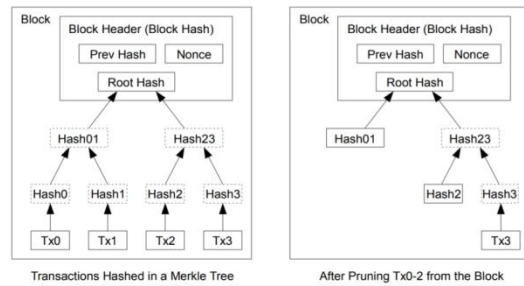


Fig. 1. Before and after Pruning Tx0-2 from Block [1].

The data before the transaction mentioned by Satoshi Nakamoto in that article can be described as follows: For example, Coinbase transaction is transferred from A to B, and then B transfers to C. If the two transactions are included in the block chain and are confirmed by sufficient subsequent blocks (more than six), the legality of the transaction can be confirmed. When the transaction from B to C is confirmed, the transaction from A to B, which is regarded as a transaction before the transaction from B to C, is no longer valuable in verifying the transaction. It only has retrospective value as an expired transaction.

Whether the pruning is correct or not, the block verification is unfaillingly correct so long as the hash algorithm is not destroyed. In this regard, verifying the correctness of the pruning result will be a problem. In practice, Bitcoin does not use the above pruning strategies when solving this problem. Instead, it uses the following strategies:

1) *Use prune parameters.* Prune parameter is used to reduce the usage of local hard disk. When launching Bitcoin core for the first time, the software will require the user to select the folder location where the blockchain is stored. All users need to do is to create a setup document named "bitcoin.conf" under the root directory of this folder, and write the code $prune=N$, where the unit of n is MB. Among them, N is the blockchain size stored locally, and $N=0$ means no limitation and complete download; If a limitation is required, the minimum value is 550 (that is, 550MB). It should be noted that even if the -prune mode is started, the node will still need to download the data of the entire blockchain network, but instead of storing all the data, it will simply delete the old blocks after building the UTXO library. In addition, if the prune mode is started, data on the entire blockchain network will have to be downloaded again during re-scanning, and the client usage will be greatly affected.

2) *Provide SPV (Simplified Payment Verification) lightweight client.* In the SPV method, SPV nodes only store the header information of the block, not the complete data. Therefore, when a transaction occurs and the validity of the transaction needs to be verified, it downloads the latest block from the complete node. When it is verified that the transaction is packed into the block and the number of blocks generated after the block is greater than six, the transaction is thus verified. However, SPV nodes completely depend on complete

nodes, and verify transactions by using simple payment verification method, so they are highly vulnerable to service denial attacks [11], witch attacks [12] and other attacks. In addition, it reduces the number of complete nodes, which will lead to a more centralized system.

3) *Use SegWit technology.* SegWit technology was officially activated on August 24th, 2017, with a block height of 481,824 [7]. SegWit thinks that the witness data (scriptSig) in the transaction input is the main contributor to the total transaction size. By migrating the witness data out of the transaction, the Bitcoin node can remove the witness data after verifying the signature, and the witness data does not need to be stored in the hard disk by all nodes, thus saving the storage space of a single node.

4) *Lightning network and SegWit technology in research and development stage.* Lightning Network [7] establishes a payment channel between the two parties in day trading, and pre-store part of the funds in the channel. The fund allocation plan after each transaction will be jointly confirmed while signing to declare invalid of the old version. When settlement is required, the final transaction result is written in the blockchain network for final confirmation. Since transactions only need to go through the blockchain when they are settled, the number of transactions submitted to the blockchain is greatly reduced.

The above solutions can optimize blockchain storage by being user-friendly and reducing the size and quantity of transactions submitted to the blockchain. However, they can neither clean out expired transaction nor address the root of the problem: endless addition of blockchain data. Therefore, they cannot solve the problem of increasing storage space essentially.

III. SOLUTIONS IN RESEARCH FIELD

A great number of researches have so far been done on storage problems in the research field, and the solutions in the research can be divided into the following categories:

1) *Sharding strategy [13-15].* In this strategy, a complete block is divided into K blocks, each block is stored in a certain proportion of nodes, and the storage conditions of nodes are recorded. When a block is needed, data is obtained from these nodes to restore the block. This strategy reduces the storage space required by a single node. But if several nodes stored in a certain block are inaccessible, the block cannot be accessed. This is a chain storage strategy, according to which, all data are stored on block chain.

2) *Distributed storage strategy [16-17].* With the latest distributed storage technology, this kind of system distributes and stores blocks in RAID (Redundant Array of Independent Disks), Clouds, P2P [16] (Peer to Peer) or Elastic Chain [17], etc. Data can be accessed from these systems when needed. These systems can effectively guarantee the storage security and access efficiency of large-scale data. This is an off-chain storage method, which moves the data in the block to the off-chain, and only keeps the Hash of the data in the block for easy

searching and tamper-proofing. In the decentralized network, the problems of data centralization and the selection of the data remains storage.

3) *Editing [18] or deleting strategy [19]*. The editing strategy uses secret sharing strategy to manage trap door keys, which enables multiple verifiers cooperate to manage the modification rights of data on the chain, and avoid a single or a small number of malicious verifiers to tamper with the data at will after getting the trap door, thus improving the security and credibility of blockchain data [18]. The deleting strategy adopts some consensus mechanisms. For instance, PoSpace (proof of space), based on the consensus mechanism of space proof, deletes the expired data after being agreed and signed by most users, and the structure of the blockchain remain unchanged [19]. The above two strategies can only modify or delete at the block level, that is, the whole block must be completely replaced, so the operation granularity is too large [18].

4) *Abandon strategy*. *Bitcoin-Core* [20] proposes a method to save storage space by deleting all blocks after UTXO (Unspent Transaction Output) library is built. In fact, some full nodes use UTXO library to speed up data verification. The prune parameter mentioned above also adopts this storage scheme. However, in this way, the UTXO library will be at the risk of being tampered with, and the node cannot provide block sharing services, which will further aggravate the centralization.

5) *Lightweight client strategy*. In addition to full nodes, different blockchain systems also define their own lightweight clients. These lightweight clients including SPV node in Bitcoin, Jaxx, Status and Trust Wallet in Ethereum do not store all data but only recent blocks. So, data verification completely depends on full nodes. They are not only vulnerable to attacks but will also exacerbate centralization. Therefore, this strategy, which is merely a scheme to improve the user experience, is not enough to tackle the increasingly growing data volume.

IV. SOLUTION

Whatever in practice research, traditional solutions to blockchain storage space can neither clean out previous transactions nor stop new transaction data from adding. That means these solutions fail to solve the problem of increasing blockchain data. Obviously, the addition of new transaction data is unavoidable, so it's necessary to clean out expired previous transaction. To be exaggerated, in order to ensure the traceability of data, should expired transactions 10,000 years ago continue to be kept in the blockchain? The answer is definitely "no". However, cleaning out expired transactions can affect the traceability of previous data. So, need to clean out expired transaction data and meanwhile ensure the correctness of the blockchain traceability, which is the root of the problem. Next, describe how to identify an expired transaction, rise a corresponding solution and then elaborate on the design of the substitute block and substitute chain of the scheme.

A. Expired Transactions

In Bitcoin system, transactions fall into two categories: Coinbase transaction and ordinary transaction (non-Coinbase). I will illustrate how they two can be deemed to be expired transactions according to different situations.

1) *Coinbase transaction*. Suppose the Coinbase transaction is transferred from A to B, and B transferred it to C. If the two transactions are included in blockchain and confirmed by a substantial number of subsequent blocks (more than 6), then the legality of the transactions is confirmed. When the transfer from B to C is confirmed, then that from A to B becomes an expired transaction since it no longer has the value of verifying a transaction but only had the value of tracing.

2) *Ordinary transaction*. The standard to judge whether an ordinary transaction is expired are as follows.

a) All the inputs of ordinary transactions are from expired transactions. As clean out expired transactions in advance, ensure all the ordinary transactions are from expired transactions by not finding such ordinary transactions in the unexpired transaction list.

b) All the outputs of ordinary transactions are spent before the expiration date.

What is expiration date? It should be noted that testing whether a transaction is expired or not at different time cut-off points (blocks) produces different results. For example, A transferred to B on February 5th, 2019, B transferred to C on March 5th, 2019, and C transferred to D on April 5th, 2019. If the deadline is March 8th, 2019, the transfer from A to B will be overdue. If the deadline is April 8th, 2019, both the transfer from A to B and the transfer from B to C are overdue.

What's worth mentioning is that to ensure the data are unalterable and traceable, many intermediate transactions cannot be defined as expired transactions. For example, a Coinbase transaction is transferred from A to B, and then B transfers to E, and E transfers to F. In order to make sure that the transfer from B to C is not miscalculated, the ordinary transaction from B to E (non-Coinbase transaction) is not defined as an expired transaction.

B. Solution

This paper proposes a solution to the problem of blockchain storage. That is re-blocking. In this solution, a certain block is taken as the cut-off block. After calculation, the unexpired transactions of several old blocks before the cut-off block (until the cut-off block) are extracted, repackaged into blocks, and these old blocks are replaced with new blocks. Thus, a substitute chain comes into being. In this way, not only can the expired transactions be cleared, but also the unexpired transactions can be kept. While replacing blocks, if the replaced block converges the cut-off block, new cut-off blocks can be re-selected to produce a new generation of substitute blockchain, as is shown in Fig. 2.

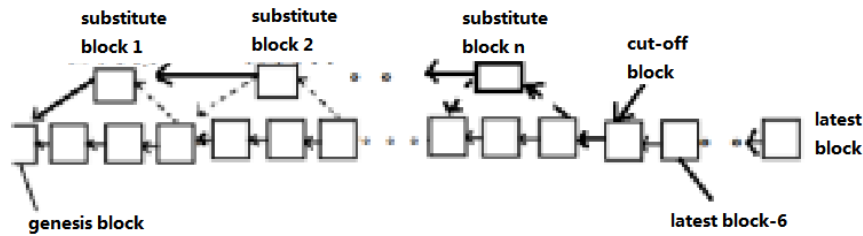


Fig. 2. Alternatives for Old Blocks.

To ensure that the data are correct, only if the latest block accepts more than six subsequent blocks can it serve as the cut-off block, which can be defined as required. A suggested figure is 3 months, because accounts in recent three months are usually included in the bank's billing system, while those three months ago are regarded as old accounts.

Bitcoin system makes miners willing to dig through reward mechanism. But substitute blocks will not generate new bitcoin rewards. If there is no reward then who will produce the substitute blocks? Rewards generate incentives, so do punishments. If a malicious node takes the opportunity to clear unexpired transactions, it will cause asset losses. If someone wants to protect its' own assets then participates in the generation of substitute blocks. The participation of plenty of nodes will generate computing power, thus safeguarding the correctness of data.

C. Design of Substitute Blocks

In Bitcoin system, one block is composed of a block header and a block body. Coinbase transaction must be the first transaction in the block body, followed by other ordinary transactions. Except for the structure of Coinbase transaction in the block head and the block body, the rest of the substitute block is consistent with the general blocks. Next, this paper will provide explanation for the block header and Coinbase transaction structure in substitute blocks.

1) Adjustment of the block header. In order to construct the block header, the mining node needs to fill in six fields: version number, timestamp, extra nonce, Hash value of the previous block, Hash of the Merkel root and difficulty coefficient. The first version number of the substitute blocks is set as to 0XFFFF, and the version number of each version upgrade will be reduced by 1 every time it upgrades. The Hash of the previous block is the Hash of the previous substitute block or the Hash of the genesis block. In order to stay consistent with the original block as much as possible, other parameters of block header are the same as those of ordinary blocks.

2) Structural adjustment of Coinbase transactions. In bitcoin system, the result of double SHA256 operation on the block header is the Hash of the block, which needs to meet the requirement of difficulty coefficient. The Hash of the block header adjusts as the variable nonce changes until the block Hash meets the requirement of the difficulty coefficient. That's when the nonce is obtained. However, the mining capacity continues to improve. When the computing power of mining nodes reaches 4GH/s, the variations of nonce in the block

header will be exhausted within one second [7], and if the block Hash meeting the requirements is not found till now, the block cannot be generated. In order to solve the problem, introduce the Coinbase in the block body.

Like ordinary transactions, Coinbase transactions are divided into two parts: input and output. However, the input of the Coinbase is empty, and only the output is used to record the reward given by the mining node. Therefore, the empty input is used to fill in extra nonce. As the miners change the input of Coinbase, the Merkel root Hash in the block header changes accordingly so that it can meet the requirements of the difficulty coefficient.

Although part of the input of Coinbase is used to fill in extra nonce, the rest remains unused. Besides, the Coinbase transaction in substitute block does not produce an output, which means that the output is also idle. As a result, these idle spaces can be utilized to record all kinds of data that need to be recorded in the substitute block.

In Coinbase transaction, it's required to record the information of several merged blocks in block chain. To safeguard the correctness of data, add another two parameters intentionally: the Hash of the previous and next block of the original chain. These two parameters make it possible to have a two-way chain structure in the substitute chain, which helps the substitute chain to be attached to the original chain. This will be elaborated in the subsequent part about the design of substitute chain.

What needs to be recorded about Coinbase transaction in the substitute blocks are as follows:

- 1) Hash and time stamp of the cut-off block.
- 2) Block height of the final merged block in the original chain and the block height of the present block in the substitute chain.
- 3) The substitute block needs to connect blocks before and after it when replacing the original block, so need to record the total number of merged blocks in the original chain, the Hash of the first and the final merged block in the original chain as well as the Hash of the precious and the next block in the original chain.
- 4) Information about all the merged blocks, including the time stamp, version number, the number of unexpired transactions of the blocks on the original chain, details of which are in Table III.
- 5) Extra nonce is used to control the difficulty coefficient in Coinbase transaction.

Detailed information about the substitute blocks is shown in Fig. 3:

Next, solve the problem of how to record parameters mentioned above into the Coinbase transaction. The original input structure of Coinbase transaction is shown in Table I:

The input structure of Coinbase transaction of the substitute block in substitute chain is shown in Table II. Through

Coinbase transaction, input an idle Hash and time stamp of the input transaction and stored the Hash and time stamp of the cut-off block. Store majority of information of the original chain and part of the information of the substitute chain into the addible transaction data.

Table III shows the original and substitute output structure of Coinbase transaction.

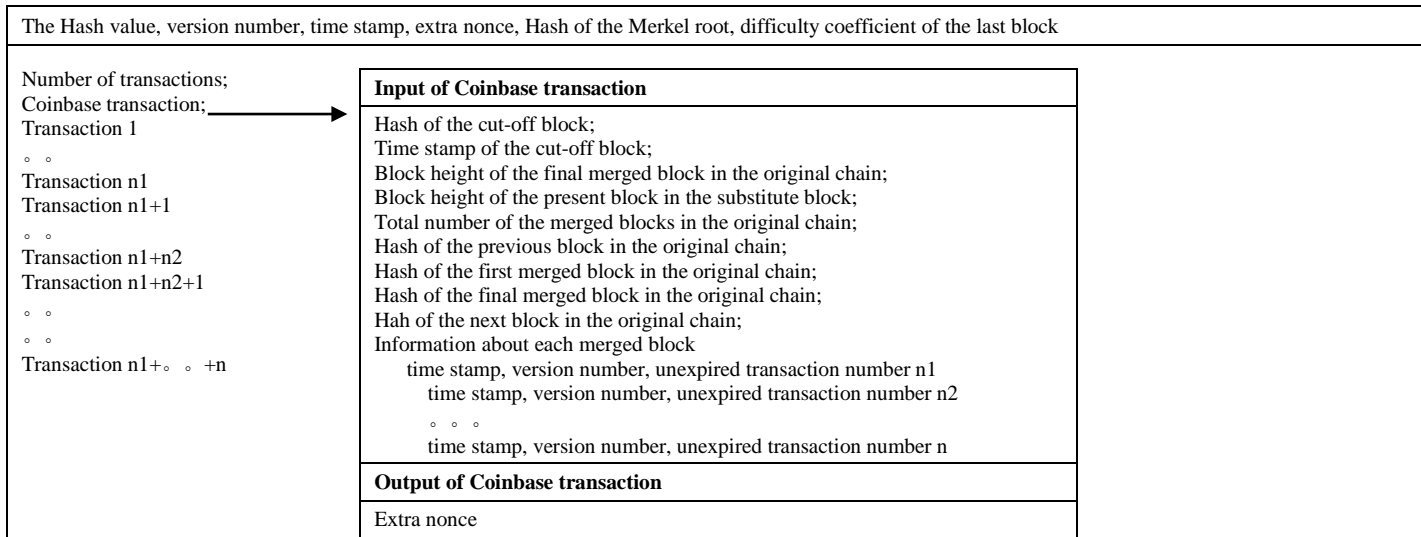


Fig. 3. Design of Substitute Block.

TABLE I. ORIGINAL COINBASE INPUT STRUCTURE

Size	Field	Description
32 bytes	Transaction Hash	Hash of transaction set to 0. No transaction is quoted.
4 bytes	Output Index	The index number of the UTXO to be spent, set to 0xFFFFFFFF
1-9 bytes	Coinbase Data Size	Coinbase Data length ranging from 2 to 100 bytes(VarInt)
Variable	Coinbase Data	Coinbase Data
4 bytes	Sequence Number	Sequence Number, currently-disabled Tx-replacement feature, set to 0xFFFFFFFF

TABLE II. SUBSTITUTE COINBASE INPUT STRUCTURE

Size	Field	Description			
32 bytes	Cut-off Block Hash	Hash of the cut-off Block			
4 bytes	Cut-off Block Time stamp	Time stamp of the cut-off Block			
3-9bytes	Coinbase Data Size	Coinbase data length (VarInt)			
Variable	Coinbase Data	Coinbase Data contains the size of original block height (1 byte), original block height, the size of substitute block height (1 byte), alternative block height, the total number of merged blocks (4 bytes), the Hash of the previous block in the original chain (32 bytes), the Hash of the first merged block in the original chain (32 bytes), the Hash of the final merged block in the original chain (32 bytes), the Hash of the next block in the original chain (32 bytes), information of each merged block in the original chain as below:			
			Size	Field	Description
			2bytes	Non-expire Transaction Number Size	The size of non-expire transaction number
			Variable	Non-expire Transaction Number	Non-expire transaction number
			4bytes	Version	Version
4bytes	Timestamp	Timestamp			
4 bytes	Sequence Number	Sequence Number, currently-disabled Tx-replacement feature set to 0xFFFFFFFF			

TABLE III. COINBASE OUTPUT STRUCTURE

Size	Field	Description in Original Coinbase	Description in Substitute Coinbase
8 bytes	Amount	Bitcoin value in Satoshis	Bitcoin value in Satoshis, set to 0
1-9 bytes (VarInt)	Locking-script Size	Locking-Script length in bytes	Data length, between 2 and 100 (length of extra nonce)
variables	Locking-script	Locking-script	Extra nonce

D. Design of Substitute Chain

Connecting the above substitute blocks one by one gets a substitute chain. But there are two special blocks that cannot be merged into the substitute chain: the genesis block (stored by clients) and cut-off block (destination of the substitute chain).

Next, questions arise: how to deal with bifurcation, how to use consensus mechanism and what kind of driving mechanism to use, how to ensure data security, how to link to the original chain, how to reach consensus on the period duration, etc.

1) *Bifurcation*: If there is bifurcation in the original chain, choose the bifurcating block as the cut-off block. After substitution is finished, no new substitute chain produced until the problem of bifurcation is solved.

If there is bifurcation in the substitute chain, employ the principle of “short chain first”. Then what if bifurcating chains are of equal length? The answer is, prevent such equally long bifurcating chains from existing. According to the design principle of POW (Proof of Work) consensus algorithm, the longer it last, the less likely that conflicts will arise; thus, prevent bifurcation from existing by extending the time of blocking of the substitute chain. It is unnecessary to produce substitute blocks at the same rate as new blocks; instead, produce substitute blocks twice as fast as the default speed. When a new generation of substitute chains is being produced and meeting bifurcation, such bifurcation can be ignored and thus wiped out.

2) *Consensus mechanism*: Although choosing POW consensus algorithm, yet, re-blocking bases on any safety consensus. POW algorithm can safeguard data security but that’s through sacrificing the inefficiency of performance. If use other consensus algorithms, consider how to protect data security.

3) *Driving mechanism*: The driving mechanism of producing substitute chain is based on punishment rather than reward, as is mention above.

4) *Data security*: There are two kinds of nodes in the bitcoin system: lightweight nodes and full nodes. Main functions of full nodes include data storage, data verification and data sharing. Most full nodes are produced for the sake of mining.

Lightweight nodes are not plagued by the problem of space recycling. There are two kinds of full nodes: existing full nodes and newly added full nodes.

Existing full nodes in the bitcoin system have already been loaded with all the data, so when they receive substitute block, so long as the latter passes verification, the latter could be accepted; otherwise, the latter will be abandoned.

Talking about newly added full nodes, as expired transactions in old blocks have been cleaned out and the old blocks have been replaced with substitute blocks, some transactions cannot be confirmed. In this case, use the data confirmation strategy of lightweight nodes (based on POW consensus algorithm) to safeguard the correctness of data. If more than 6 subsequent substitute blocks are accepted, rest assured that the degree of data security of this substitute block is acceptable. But how about the ultimate 6 substitute blocks in the substitute chain? They do not have enough subsequent blocks (over six) to ensure the security of data; therefore, they cannot be linked to the original chain as substitute blocks. But set them aside for other nodes to use.

5) *Linking mechanism*: For the sake of data security, only blocks before the ultimate seven ones in the substitute chain can be linked to the original chain. The principles of linking are as follows.

According to the Hash of the next block of the original chain recorded in the last but seven blocks, corresponding block could be found in the original chain.

Make sure whether the Hash of the previous block (recorded in the original chain block) equals the Hash of the ultimate merged block listed in the last but seven substitute blocks.

Link substitute chain to the original chain after the blocks of both the chains has confirmed each other.

This means that any substitute block in the substitute chain can be linked to the original chain. So long as the substitute blocks at the linking area are confirmed by six subsequent blocks, such practice of linking is secure.

6) *A new generation of substitute chain*: A new generation of substitute chain can be reproduced in accordance with the predefined period rules only after the ultimate substitute block comes into being. Once one substitute chain fails to go through the whole substitute process, a new generation of substitute chain cannot be produced; otherwise, the substitute chain would be in disorder.

If there is bifurcation in the original chain which is not wiped out yet, the cut-off block can only converge the bifurcation area, failing to move further until the problem of bifurcation in the original chain is solved.

Besides, as is mentioned before, the substitute chain bifurcation can be ignored and wiped out when a new generation of substitute chain is being produced.

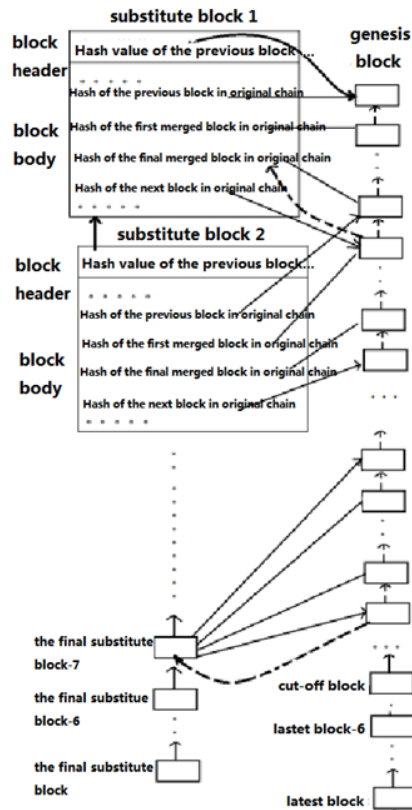


Fig. 4. Design of Substitute Blockchain.

Fig. 4 shows how a substitute chain can be linked to the original chain. The linking between the original chain and substitute chain is shown in dotted lines. This is because the two chains are linked together according to the association of block Hash, but they do not have real directivity association with each other.

V. FOLLOW-UP SOLUTION

As is mentioned in the previous chapter, to make sure the temper-proof and traceability of data, some intermediate transactions cannot be cleaned out. For example, a Coinbase transaction is transferred from A to B and C, B transfers to E, and E transfers to F. If the transfer from B to E is cleaned out while that from A to B and C is retained, the bitcoin system would take it for granted that the bitcoins transferred to B by A are not spent. Because of this, ordinary (non-Coinbase) transactions from B to E cannot be cleaned out.

If record the fact that the bitcoins transferred from A to B have already been spent, B to E could be cleaned out. Such as retaining A to B and C transaction, and label the output of the transaction (for example, 1 means the output has been spent while 0 means the output hasn't been spent), as 10, which means the first output A to B has been spent but the second one A to C hasn't.

Since the information of merged blocks in the substitute blocks would be recorded, use the same way to retain the transactions were not all the outputs are spent and include the marks of these transactions' outputs. In this way, many

intermediate transactions can be cleaned out while data security is still assured. This is in fact the way used in UTXO (unspent transaction outputs) library.

Based on the follow-up solution, the principles as to how to deal with transactions have changed as follows:

If all the transaction outputs are spent, clean out this transaction.

If part of the transaction outputs is spent, retain this transaction, and record the spending details of the transaction output.

To record how each transaction output is used, use 1 byte to mark the spending details (0 or 1) of 8 transaction outputs, then calculate how many bytes are there in total through calculation. Suppose use 1 bit to mark one output. And there are 36 outputs that need marking, since 1 byte equals 8 bits, use 5 bytes to mark 40 outputs. Then 2 bytes are needed to store that data 5, the follow-up 5 bytes to record spending details (0 or 1) of 36 transaction outputs, the surplus 4 bits being filled in with the Fig. 1.

As the solution changes, the information of each merged blocks recorded in the substitute block should also change, i.e., the information of each merged blocks in the original chain should change, including the time stamp, version number, the number of unexpired transactions (n), the size needed to store the transaction outputs (2n bytes), the spending details of each transaction output recorded by subsequent bytes. The design is shown in Table IV.

TABLE IV. INFORMATION OF ONE MERGED BLOCK

Size	Field	Description
4 bytes	Version	Version number
4 bytes	Timestamp	Time stamp
2 bytes	Non-expire Transaction Number Size	Size of the number of unexpired transactions
Variable	Non-expire Transaction Number	The number of unexpired transactions n
Variable	Non-expire Transaction Output Flags Byte Number Per 2 Bytes	2*n bytes, the number stored by every two bytes refers to the number of bytes used to record the spending details of each transaction output
Variable	Non-expire Transaction Output Flags	Record the output spending details one by one according to the bytes needed to record a transaction as stipulated before. If it takes less than 1 bytes, it is still regard as 1.

Except the above changes, others are the same as before. But in this way, Coinbase transaction may become huge, which is a problem worth consideration.

VI. EXPERIMENTAL ANALYSIS

Illustrate the correctness and effectiveness of the solutions mentioned above. The solutions are based on consensus mechanism. And since the correctness of POW consensus mechanism has been confirmed by bitcoin and many other decentralized systems, rest assured that the solutions are correct. Next, prove the effectiveness of the solution through an experiment.

How much space can the solutions in Sections III and IV save, respectively? According to the design of the algorithm, let's take the No.697546 block which get at the test time 2021-08-26 00:00 as the cut-off block and collect the data of each transaction from No.1 block to No.105,000 block along the block chain. In the solution mentioned in Chapter 3, if all the inputs of the transactions are from the outputs of expired transactions, and all the outputs have been used, then label such transactions as "expired transaction 1", otherwise as "unexpired transaction 1". In the design in Chapter 4, let's label unexpired transaction 1 whose transactions have been run out as "expired transaction 2", otherwise as "unexpired transaction 2".

Fig. 5 shows the data collected, including the number of expired transactions 1, the number of unexpired transactions 1 and additional expired transactions 2.

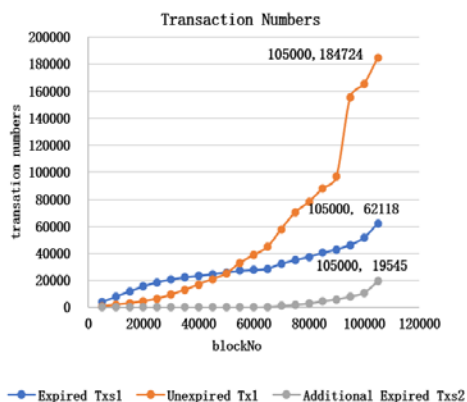


Fig. 5. Total Expired and Unexpired Transaction Number.

Applying the third solution, in bitcoin system, expired transactions account for 74.8% of the total transactions at the No. 105,000 block, and account for 77% (the peak) at the No. 95,000 block. In contrast, applying the fourth solution, more expired transactions would be cleaned out. Statistics show that cleaning out expired transactions can effectively reduce storage space occupation, which means this solution is effective. The ratio of expired transaction 1 as well as the ratio of expired transaction 2 is shown as follows in Fig. 6.

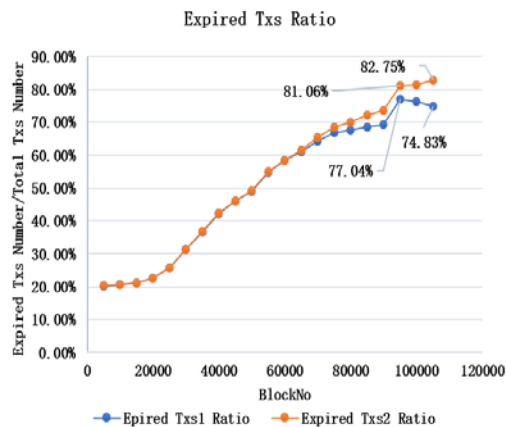


Fig. 6. Expired Transaction Ratio.

The above statistics only cover the data of the first 105,000 blocks. And how much space is unleashed? According to the solution mentioned in Section III, the expired transaction ratio will decrease after reaching the peak of 77%. And according to the solution mentioned in Chapter 4, the data of the change in size of the UTXO library would be gotten eventually. Due to the statistics of Bitaps [20], as of March, 21st, 2022 when this thesis is finished, there were 719,197,481 transactions, and 130,561,354 unspent transaction outputs in UTXO, and a total storage volume of 369.42 GB. Among them, the percentage of spent transactions is the same as that of the cleaned transactions. Roughly, the ratio of spent transactions to total transactions $[(719\ 197\ 481-130\ 561\ 354)/719\ 197\ 481]$ reached 81.8%. Although the fourth solution does not make a big difference for the first 105,000 blocks, it will play an increasingly significant role in the recycling of subsequent blocks after the 105,000th block. So, the fourth solution is also an effective one.

VII. CONCLUSION

The increasing popularity of blockchains reveals all the possibilities a decentralized ledger can offer. Nonetheless, blockchains also have their limits: the fast-growing data cause single full nodes to occupy larger storage space, which will bring increasingly heavy burdens to online transmission, CPU computing power and storage space.

Base on analyzing transactions in blockchain, propose a new solution: re-blocking. In this solution, pack unexpired transactions in old blocks into a new alternative block which constantly replaces old blocks. In this way, a substitute chain comes into being, which helps to clean out expired transactions in the bitcoin system and thus solve the problem of increasing data. We also prove the effectiveness of the solution by conducting an experiment in bitcoin system. Believe that this system would highly beneficial to blockchain applications.

Further researches:

- 1) Realize this idea to verify whether it works well in reality.
- 2) Whether split one chain into two chains, for storing expired transactions and unexpired transactions to retain historical information, and merge them two to one when necessary.
- 3) We only give experiments for the bitcoin system. In other systems like electronic medical record system and produce tracing system, further analysis is needed to define and clean expired transactions.
- 4) In this system, POW consensus algorithm is used to protect date safety. Although highly probable, it is to be confirmed: algorithms can reach a consensus is ok.
- 5) Once long bifurcation chains arise like in Ethereum, how can the solution work well.
- 6) The second solution would change the traditional system mechanisms greatly, not only to realization, but also to usage. And the Coinbase transaction will become very large. It should be considered.

ACKNOWLEDGMENT

The study was supported by “Innovation Team Project of Humanities and Social Sciences in Colleges and Universities of Guangdong Province (No. 2020WCXTD008)”.

DECLARATION

The authors declare that there are no conflicts of interest regarding the publication of this paper.

REFERENCES

- [1] NAKAMOTO S. Bitcoin: a peer-to-peer electronic cash system[R]. Bitcoin, 2009.
- [2] GUO Shang-tong, WANG Rui-jin, ZHANG Feng-li. Summary of Principle and Application of Blockchain[J]. Computer Science, 2021, 48(02):271-281.
- [3] KORPELA K, HALLIKAS J, DAHLBERG T. Digital supply chain transformation toward blockchain integration[EB/OL]. <https://scholarspace.manoa.hawaii.edu/bitstream/10125/41666/1/paper0517.pdf>.
- [4] TURKANOVIC M, HÖLBL M, KOŠIČ K, et al. EduCTX: a blockchain-based higher education credit platform[J]. IEEE Access, 2018, 6:5112-5127.
- [5] CHOWDHURY M J M, COLMAN A, KABIR M A, et al. Blockchain as a notarization service for data sharing with personal data store[C]//Proceedings of the 17th IEEE International Conference on Trust, Security and Privacy in Computing and Communications/12th IEEE International Conference on Big Data Science and Engineering. Piscataway: IEEE, 2018:1330-1335.
- [6] World economic forum. World economic forum survey [EB/OL]. <http://www.coinfox.info/news/3184-world-economic-forum-survey-10-of-global-gdp-maybe-stored-with-blockchain-technology-by-2027>.
- [7] Andreas M. Antonopoulos. Mastering Bitcoin: Programming the Open Blockchain[M]. O'Reilly Media, Inc, 2017:180.
- [8] CoinMarketCap Website. CoinMarketCap's Statistics of Bitcoin [EB/OL]. <https://coinmarketcap.com/zh/currencies/bitcoin/>.
- [9] Bitnodes Website. 730 days nodes statistics of Bitcoin[EB/OL]. [https://bitnodes.earn.com/dashboard/?days=730\(#nodes.\)](https://bitnodes.earn.com/dashboard/?days=730(#nodes.)).
- [10] Blockchair Website. Blockchair' statistics of Bitcoin[EB/OL]. <https://blockchair.com/bitcoin>.
- [11] LAU F, RUBIN S H, SMITH M H, et al. Distributed denial of service attacks[C]//Proceedings of the 2000 IEEE International Conference on Systems, Man and Cybernetics. Piscataway: IEEE, 2000:2275-2280.
- [12] DING Qian. Research on Data Storage and Sharing Algorithm Based on Blockchain[D]. China University of Mining and Technology, 2020.
- [13] Jia Dayu, XIN Junchang, WANG Zhiqiong, et al. Storage Capacity Scalable Model for Blockchain[J]. Journal of Frontiers of Computer Science and Technology, 2018(04):525-535.
- [14] SUN Zhixin, ZHANG Xin, XIANG Feng, et al. Survey of Storage Scalability on Blockchain[J]. Journal of Software, 2021, 32(01):1-20.
- [15] CAI Zhenhua, LIN Jiayun, Liu Fang. Blockchain storage: technologies and challenge[J]. Chinese Journal of Network and Information Security, 2020, 6(5):11-20.
- [16] JIA Da-Yu1, XIN Jun-Chang, WANG Zhi-Qiong, et al. Efficient Query Model for Storage Capacity Scalable Blockchain System[J]. Journal of Software, 2019, 30(09):2655-2670.
- [17] YUAN Yong, WANG Fei-Yue. Editable Blockchain: Models, Techniques and Methods[J]. ACTA AUTOMATICA SINICA, 2020, 46(05):831-846.
- [18] REN Yanli, XU Danting, ZHANG Xinpeng, et al. Deletable blockchain based on threshold ring signature[J]. Journal on Communications, 2019, 40(04):71-82.
- [19] Github website. Bitcoin source code[EB/OL]. <https://github.com/bitcoin/bitcoin/blob/v0.21.0/doc/release-notes.md>.
- [20] Bitaps websit. Bitaps' statistic data of bitcoin[EB/OL]. <https://btc.bitaps.com/>.

Blockchain Privacy Data Access Control Method Based on Cloud Platform Data

Biying Sun, Qian Dang, Yu Qiu, Lei Yan, Chunhui Du, Xiaoqin Liu
State Grid Gansu Electric Power Company Internet Division, Lanzhou, China

Abstract—With the improvement of digital informatization and openness of the smart grid, the security of all kinds of sensitive and private data in the power grid is inevitably facing severe threats and challenges. In this paper, we propose a privacy protection scheme for multidimensional data aggregation and access control in the cloud Internet of Things for smart grid. The scalable access control based on attribute encryption is used to determine the data security of power user data in the process of data information sharing in the blockchain under the large data traffic of the cloud platform, which is to achieve privacy protection and fine-grained access control for demand-side multidimensional data. By using the EBGN homomorphic encryption algorithm, the multidimensional data is encrypted, and each dimension can be decrypted separately using the corresponding private key. The multidimensional data aggregation at the gateway can aggregate the multidimensional data into cipher-text, and the control center does not need to decrypt the cipher-text data of each dimension, thereby simplifying the operation of the gateway and the control center and improving the security and privacy of the data. By encrypting the EBGN private key of each dimension through the cipher-text policy attribute encryption algorithm, the fine-grained access control at the dimension level is realized. The experimental results show that the proposed method can effectively improve the security of private data in the aspect of multidimensional data privacy protection, thus reducing the security risk of multidimensional data being illegally accessed. The research in this paper can effectively reduce the communication overhead and computational complexity, reduce the computational cost, and is suitable for data security and privacy protection of smart grid cloud Internet of Things.

Keywords—Cloud platform; blockchain; private data; data encryption; access control

I. INTRODUCTION

The combination of smart grid and the Internet of Things promote the wide application of various network information sharing technologies in the power system, which greatly changes the way of life and work, but also brings a series of hidden dangers, among which the hidden danger of information security is the core. Due to the bidirectionality of smart grid information flow, and in order to reduce communication bandwidth and achieve flexible fine-grained analysis, multidimensional aggregation and access of smart grid data are needed [1]. Each data dimension contains sensitive and private information, which may be analyzed and utilized by different research organizations. For example, in data transmission, the leakage and tampering of data information such as power information and privacy information may cause security and privacy threats to power supply companies and customers and

even serious economic losses. Therefore, the privacy protection and access control of blockchain is particularly important [2].

So far, many scholars have conducted extensive research on smart grid privacy protection based on data aggregation and access control. The schematic diagram of smart grid data aggregation and access architecture is shown in Fig. 1.

Terminal devices distributed in multiple links such as power generation, transmission, distribution, and power consumption are used for blockchain collection. The gateway aggregates the blockchain into data cipher-text for data transmission and instruction transmission with the control center [3]. The control center stores the collected data in the cloud server and can decrypt the data cipher-text of the corresponding dimension to determine the power supply strategy according to the total demand. The access authority can access the data information of the authorized dimension [4].

Due to the advantages of homomorphic encryption in data confidentiality and privacy protection, the cipher-text can be directly operated without decrypting the cipher-text. J. W. et al. [5] proposed a track protection method based on privacy clustering, which is used to resist continuous query attacks by adding Laplace noise to the track position count in the cluster. The radius-limited Laplacian noise is added to the trajectory data in the cluster to avoid affecting the clustering effect, and the noise cluster center is obtained according to the noise position data and the noise position count. J. Zhang et al. [6] proposed an algorithm to protect access to sensitive sites in privacy-preserving trajectory data release, which generalizes sensitive sites with sensitive regions and distorts sub-trajectories within sensitive regions based on privacy. K. Xue et al. [7] proposed a method to protect the release of road network trajectory traffic by using privacy technology. After counting the traffic value of the trajectory data of each road section, the method adds random noise satisfying differential privacy to the traffic value and then proposes a post-adjustment algorithm to solve the consistency characteristics of the traffic map. The complexity of smart grid architecture based on cloud Internet of Things not only makes the whole power system more intelligent but also brings a large amount of information data, which may contain a large number of sensitive information (such as security risks of nodes, voltage data of a certain place, etc.) and very important privacy information (such as user identity information, location information, etc.) [8]. The research on data access control is helpful to improve the user's access speed to the encrypted data, reduce the waiting time for users to access the encrypted data. At the same time, it is also of great significance to the network data security.

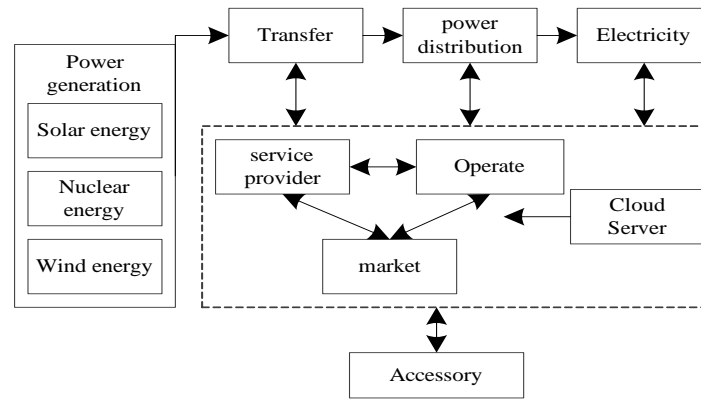


Fig. 1. System Architecture.

In the face of the large-scale and complex system of smart grid cloud Internet of Things, the above scheme is difficult to meet the security requirements of the system for data. In the smart grid cloud Internet of Things system, it also faces the problem of visitor access rights, which need to be revoked or updated in time.

In this paper, based on the attribute access control method and the data privacy protection requirements of the cloud Internet of Things on the demand side of the smart grid, a demand-side cloud Internet of Things blockchain aggregation and access control scheme is proposed, which completes the aggregation work of the blockchain and the fine-grained access control of privacy data. In the aggregation phase, Boneh-Goh-Nissim (EBGN) homomorphic encryption extended by wireless sensor networks is used to aggregate the blockchain into cipher-text, and CP-ABE encryption is used to perform fine-grained access control at the dimension level. Then, the implementation of the algorithm is introduced and the security of the scheme is proved, and a detailed comparison with other existing schemes is made in terms of functionality computation and communication overhead.

II. RELATED WORK

A. Data Aggregation

The establishment of secure information communication is the task of building the information security of smart grid cloud Internet of Things, and it is also the basis of achieving efficient communication and reducing communication overhead. Smart grid privacy protection schemes using data aggregation techniques during communication have been proposed in many studies [9]. The basic idea of these techniques is based on the use of an aggregator and a trusted authority connected to the user, as shown in Fig. 2.

In the smart grid, the analysis of all kinds of power data can not only be applied to the formulation of real-time pricing and power dispatching strategies but also may produce other commercial values. In order to carry out fine-grained analysis, it is necessary to collect the blockchain of each link of the smart grid. Taking the user side as an example, by analyzing the power consumption of air conditioning equipment at the user side in hot weather in summer, the power station can prepare enough power in similar hot weather later [10].

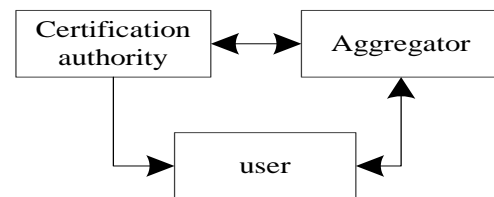


Fig. 2. Data Aggregation System Model.

B. EBGN Homomorphic Encryption Algorithm

EBGN homomorphic encryption is an extension of the BGN homomorphic encryption scheme proposed by Boneh, Goh, and Nissim. It makes up for the limitation that BGN encryption cannot support blockchain encryption. Both BGN and EBGN support addition and multiplication homomorphisms, that is, the results of addition and multiplication operations performed on cipher-text match the results of the corresponding operations performed on plaintext [11]. Because multiplication homomorphisms are computationally expensive, only additive homomorphisms are considered in this paper. EBGN consists of the following computational structure.

Let G be a group of prime order P . Let the generator of G be g , and let $e: G \times G \rightarrow G_T$ be the bilinear pairing operation. DBDH assumes that a security parameter κ is set if a quadruple $(g^a, g^b, g^c, e(g, g)^{abc})$ and a quadruple $(g^a, g^b, g^c, e(g, g)^z)$ cannot be distinguished by a non-negligible advantage by an attacker A in polynomial time, where $g^a, g^b, g^c \in G$, $a, b, c, z \in \mathbb{Z}_P$. Then the advantage $ADV_A^{DBDH}(\kappa)$ of the attacker A is defined as:

$$ADV_A^{DBDH}(\kappa) = \left| \Pr[A(g^a, g^b, g^c, e(g, g)^{abc}) = 1] - \Pr[A(g^a, g^b, g^c, e(g, g)^z) = 1] \right| \quad (1)$$

1) *EBGN.KeyGen*(l, k): Generate $k+1$ primes Q_1, Q_2, \dots, Q_{k+1} , where $|Q_i| = l, i \in \{1, 2, \dots, k+1\}$. Then, generate an elliptic curve e of order $N = \prod_{i=1}^{k+1} Q_i$ and a group g of points on its elliptic curve and have $ord(g) = N$,

where $ord(g)$ denotes the order of g . Next, randomly choose $k+1$ generators of g , namely: g_1, g_2, \dots, g_{k+1} , such that $ord(g_i) = N, i \in \{1, 2, \dots, k+1\}$. Finally, calculate $P_i = (N / Q_i) \cdot g_i, i \in \{1, 2, \dots, k+1\}$ and $R = (N / Q_{k+1}) \cdot g_{k+1}$ through $ord(P_i) = Q_i$ and $ord(R) = Q_{k+1}$. The public key $PK_{EBGN} = (N, e, \{P_1, P_2, \dots, P_k\}, R)$ and the secret key $SK_{EBGN} = (Q_1, Q_2, \dots, Q_k)$ can be obtained.

2) $EBGN.Enc(M_{S_i}, PK_{EBGN})$: For the k -dimensional data $M_{S_i} = \{M_{i,1}, M_{i,2}, \dots, M_{i,k}\}$ collected from the intelligent terminal $S_i, 0 \leq \mathfrak{R}_i \leq N$ is randomly selected. The following calculations are made:

$$C_i = \sum_{j=1}^k (M_{i,j} \cdot P_j) + \mathfrak{R}_i \cdot R \tag{2}$$

3) $EBGN.Add(C_1, C_2, \dots, C_n)$: Cipher-text aggregation is calculated as follows:

$$C = C_1 + C_2 + \dots + C_n \\ = \sum_{j=1}^k (\sum_{i=1}^n M_{i,j} \cdot P_j) + \sum_{i=1}^n \mathfrak{R}_i \cdot R \tag{3}$$

4) $EBGN.Dec(Q_j, P_j, C)$: In the decryption process, in order to understand the j th dimension data in the dense aggregate data, the method λ and Baby-step and Giant-step algorithms are required to calculate the discrete logarithm in the decryption algorithm, as shown below:

$$M_{d_j} = \sum_{i=1}^n M_{i,j} \\ = \log_{g_j}((N / Q_j) \cdot C) \tag{4}$$

Where,

$$g_j' = \prod_{i=1, i \neq j}^{k+1} Q_i \cdot P_j = N / Q_j \cdot P_j.$$

III. DEMAND SIDE BLOCKCHAIN AGGREGATION AND ACCESS CONTROL ARCHITECTURE

This paper first presents a demand-side data aggregation and access control framework, as shown in Fig. 3.

The smart meter installed on the user side can collect various privacy information, such as the user's basic identity information and the user's electricity consumption data, as shown in Table I.

Secondly, smart meters or smart terminals can collect information data such as power information and power environment. A collector, a concentrator, and gateways at all levels are adopted through a Home Area Network, BAN (Building Area Network), and NAN (Neighborhood Area Network), which is uploaded to the control center and cloud server [12]. The collected blockchain is encrypted using EBGH homomorphic encryption in the in-home network HAN, and the blockchain is aggregated at the building area network BAN gateway. The control center can decrypt and access the fine-grained data of the corresponding dimension, that is, the total power consumption data in the region, and share the data with the access authority [13]. At the same time, the access organization can access the fine-grained data of its authorized dimension to analyze the related work.

Based on the above framework, Fig. 4 shows the demand-side blockchain aggregation and access control model in this paper, which includes five parts, namely, trust authority, smart meter, gateway, control center, and access authority.

TABLE I. DATA INFORMATION MAY BE PROVIDED ON THE DEMAND SIDE

Data element	Description
Name	Account responsible party
Address	Place of service
Account	A representation unique to the account
Electricity information	Kilowatt-hour consumption recorded for the current billing period
Other information	Environmental monitoring, equipment load, fault, power quality, distribution transformer status, etc.

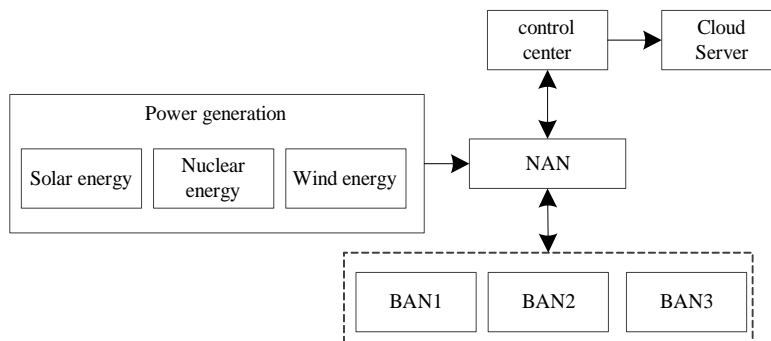


Fig. 3. Data Aggregation and Access Control Structure Block Diagram of Demand Side.

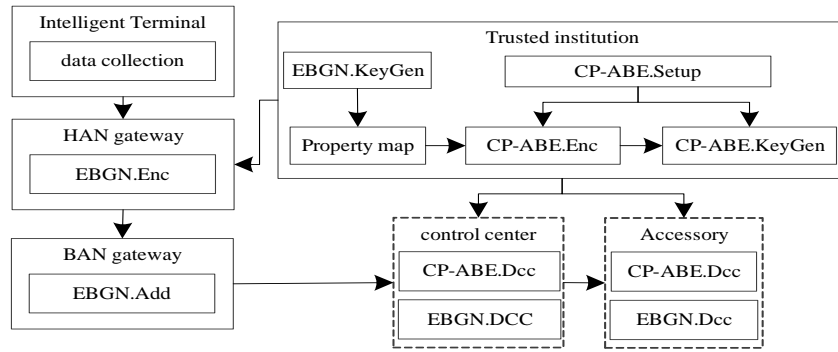


Fig. 4. Demand Side Blockchain Aggregation and Access Control Model.

The system model includes the following four operations: system initialization, blockchain encryption and aggregation, data access, and access permission update.

System initialization: The trusted authority performs the system initialization operation. First, the trusted authority generates the system parameters for EBGN and CP-ABE [14]. According to the access control policy of the control center and the access authority, the trusted authority generates the key of the CP-ABE and sends it to them. Next, it generates a mapping table indicating the mapping relationship between the public keys of the attribute set EBGN of the data. Finally, the trusted authority encrypts the EBGN key using the CP-ABE with the corresponding attribute set.

Blockchain encryption and aggregation: perform blockchain aggregation and encryption at the gateway. First, the data is categorized into multiple dimensions based on its attributes. Next, the gateway selects the corresponding EBGN public key from the mapping table and encrypts the blockchain. Finally, the cipher-text is sent to the superior gateway, and each gateway is responsible for aggregating all blockchains into one cipher-text [15].

Data access: In the data sharing process of blockchain, by using the CP-ABE key obtained from the trusted authority, the control center and each visitor can obtain the authorized data information of the corresponding dimension [16].

Access renewal: For key renewal of EBGN and CP-ABE, to revoke an accessor's access, the trusted authority first regenerates the EBGN's public and secret keys for the affected dimension. The trusted authority then re-encrypts the EBGN key and revokes the visitor's access to the corresponding attribute [17].

IV. IMPLEMENTATION OF BLOCKCHAIN DATA CONTROL SCHEME IN CLOUD PLATFORM AREA

A. Initial System Establishment

Given public parameters l and k . A security parameter k is set if, in any probabilistic polynomial time, it cannot be successfully computed by attacker A with a non-negligible advantage. The security parameter l is sent to the attribute authority, and the attribute authority calculates its own master key. The trusted authority runs $EBGN.KeyGen(l,k)$ and $ABE.Setup()$ functions to generate system public parameters:

$$\begin{cases} PK_{EBGN} = (N, e, \{P_1, P_2, \dots, P_k\}, R) \\ SK_{EBGN} = (Q_1, Q_2, \dots, Q_k) \\ PK_{CP-ABE} = (G, g^{\sum GID}, U_{GID}) \\ MK_{CP-ABE} = (\alpha, \chi) \end{cases} \quad (5)$$

The first dimension is set as the total power consumption of the user. The corresponding EBGN public key is P_1 , and the control center is granted access rights. If the key Q of EBGN is used as the plaintext data encrypted by CP-ABE, the ciphertext encrypted by CP-ABE and the CP-ABE key generated for the control center and the visitor are as follows.

$$CT_i = CP-ABE.Enc(Q_i, \tau_i, PK_{CP-ABE}), i \in \{1, 2, \dots, k\} \quad (6)$$

$$SK_{uj} = CP-ABE.KeyGen(S_{uj}, MK_{CP-ABE}, GID), j \in \{1, 2, \dots, m\} \quad (7)$$

Where S_{uj} represents the attribute set. MK_{CP-ABE} represents the master key, and GID represents the visitor identity. Let SK_{u1} denote the key of the control center and m denote the total number of visitors. The EBGN key Q_i is encrypted according to the access structure τ_i . Finally, the private data and the visitor are encrypted and accessed according to the attribute mapping table, and the key SK_{uj} is sent to the visitor uj (such as a control center) through secure communication [18].

B. Blockchain Encryption and Aggregation

A terminal S_i in an area collects k types of data information according to different attribute sets, which is represented as $M_{S_i} = (M_{i,1}, M_{i,2}, \dots, M_{i,k})$. The cipher-text after the value of $M_{i,j}$ of each dimension does not exceed the constant B and the data information C_i is encrypted by EBGN, which is shown below.

$$C_i = EBGN.Enc(M_{S_i}, PK_{EBGN}) \quad (8)$$

After receiving all the cipher-text information C_i , the gateway performs data aggregation on the cipher-text information in the following manner.

$$C = EBGN.Add(C_1, C_2, \dots, C_n) \quad (9)$$

The gateway then sends the encrypted and aggregated data to the control center.

Taking the j th dimensional data $M_{i,j}$ in the data collected by the terminal S_i as an example, the following calculation can be performed.

$$M_{i,j} = \sum_{l=0}^{|M_{i,j}|} 2^l \cdot M_{i,j,l} \quad (10)$$

$$P_{j,l} = 2^l \cdot P_j, \quad 1 \leq l \leq |B| \quad (11)$$

$$R_l = 2^l \cdot R, \quad 1 \leq l \leq |R| \quad (12)$$

The encrypted cipher-text is shown in the following calculation.

$$\begin{aligned} C_i &= \left(\sum_{j=1}^k \sum_{l=0}^{|M_{i,j}|} M_{i,j,l} \cdot P_{j,l} \right) + \sum_{l=0}^{|\mathfrak{R}_i|} \mathfrak{R}_{i,l} \cdot R_l \\ &= \left(\sum_{j=1}^k \sum_{M_{i,j,l}} P_{j,l} \right) + \sum_{l=0, \mathfrak{R}_{i,l}} R_l \end{aligned} \quad (13)$$

Where $M_{i,j,l}$ denotes the l th bit of $M_{i,j}$ and $\mathfrak{R}_{i,l}$ denotes the l th bit of \mathfrak{R}_i .

C. Data Access

For example, the first dimension is the total power consumption data. If the control center needs the total power consumption data C_1 in the access area, the control center first needs to download the cipher-text data of the EBGN key Q_1 from the trusted institution and perform CP-ABE decryption to obtain the EBGN key as shown below.

$$Q_1 = CP - ABE.Dec(C_{T_1}, SK_{u_1}, \tau, GID) \quad (14)$$

According to the key Q_1 and the aggregate cipher-text C , the control center may obtain the data information of the first dimension through the following calculation.

$$M_{d_1} = EBGN.Dec(Q_1, P_1, C) \quad (15)$$

Therefore, the control center can obtain the data information of the first dimension, that is, the total power consumption demand in the region. The control center sends the aggregate cipher-text C to the visitor in order to share the power data to the access mechanism. Similar to the control center, each visitor DA_{u_i} first needs to download the data

cipher-text C_j satisfying his access policy [19]. Then, the EBGN key Q_j of the j th dimension is obtained by decrypting C_j as follows.

$$Q_j = CP - ABE.Dec(C_j, SK_{u_i}, \tau, GID) \quad (16)$$

Next, the visitor can obtain the specific data information of the j th dimension through the EBGN decryption algorithm, as shown below.

$$M_{d_j} = EBGN.Dec(Q_j, P_j, C) \quad (17)$$

In this process, in addition to updating access rights, only the control center and each visitor need to perform CP-ABE decryption. In addition, the control center cannot obtain the data information of all dimensions, so there is no need to decrypt and re-encrypt the data information of all dimensions.

V. EXPERIMENTAL ANALYSIS

In this paper, the performance of the proposed scheme is analyzed in terms of computational cost and communication overhead. Although system initialization also incurs computational costs, it only needs to be deployed once, which has a negligible impact on smart grid performance. Therefore, only the efficiency of encryption, aggregation, and decryption is tested here in experiments.

In the experiment, we first compare the encryption efficiency of the proposed scheme with that of scheme 2 in [20] and scheme 3 in [21]. Scheme 2 uses super-increasing sequence and Paillier homomorphic encryption to achieve the privacy protection of blockchain aggregation. Reference [21] constructs a Scheme 3 scheme based on Paillier and ABE, which integrates data aggregation and access control.

Experiments were conducted using the LiDIA library and the MIRALC environment by running on a PC with a 4.6 GHz processor and 16 GB of memory. The length of the key is chosen to be $l = 256$ bits, and the length of the random number is chosen to be $|R| = 70$ bits so that the present security can be ensured. For Scenario 2, the blockchain is merged into one plain text before encryption, which is the simplest and most efficient super-incremental sequence. Scenario 2 and Scenario 3 are set the same, using the Paillier public key with a length of 1024 bits.

A. Cost Calculation

For data aggregation, the experiment takes 10 milliseconds to perform 100 aggregations in the scheme in this paper. In that data access phase, only the CP-ABE is executed to decrypt the EBGN key of the authorized single dimension, and the key of all dimensions does not need to be decrypted, so the influence on the efficiency of data share is small. Since Scenario 2 and Scenario 3 need to perform more operations on the gateway and the control center, such as decrypting and re-encrypting the aggregated data on the control center.

The experimental results are shown in Fig. 5.

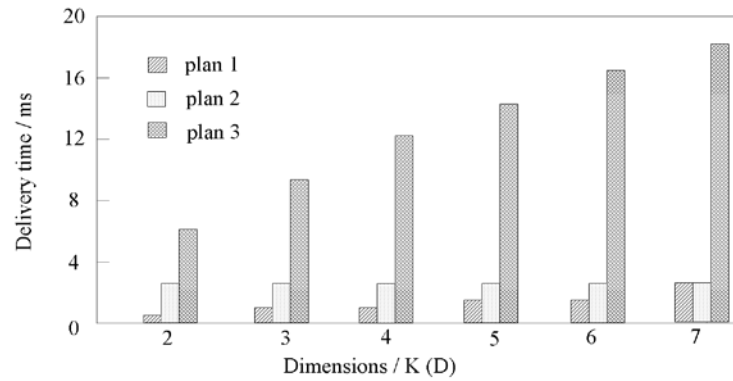


Fig. 5. Encryption Overhead in different Dimensions.

Since Scheme 2 always requires random numbers to be subjected to modular exponentiation, the encryption time of the blockchain does not increase with the number of dimensions. Moreover, Scheme 3 needs to generate multiple cipher-texts for the blockchain, and its encryption time increases linearly with the dimension. It can be concluded that the encryption time of the scheme in this paper is less than that of the scheme 2 when the dimension is $k < 7$. When $k = 7$, the efficiency of the scheme in this paper is similar to that of scheme 2.

B. Communication Overhead

The communication overhead of the data information, i.e., the cipher-text of the EBGN in the scheme in this paper, is considered. According to the encryption algorithm, the length of the power data cipher-text is $2 \cdot (k + 1) \cdot l$ bits. When we choose the length of the key to be $l = 256$ bits and set $k = 7$, the length of the power data cipher-text is 4096 bits.

For Scheme 2, the cipher-text length of the blockchain is 2048 bits, which is the same as the cipher-text of one dimension in Scheme 3. The communication comparison between the scheme in this paper and the schemes 2 and 3 is shown in Fig. 6.

When $k = 7$ and $l = 256$ bits, the length of the power data cipher-text is 4096 bits in the scheme of this paper, which is twice of the cipher-text in the scheme 2. However, it is much smaller than the cipher-text 14336 bits in Scheme 3. The transmission of the cipher-text can be done immediately according to a common communication standard between the user and the building gateway. Compared with the encryption

time, the impact of communication on the timeliness of smart grid is basically negligible.

Compared with other schemes in terms of computation cost and communication overhead, the scheme proposed in this paper is more effective in the case of low dimensionality, which is suitable for the encryption efficiency requirements of smart grid, and can achieve flexible and fine-grained access control and permission update at the dimensionality level, so the scheme proposed in this paper is more flexible and practical.

C. Privacy Protection Strength

The algorithm, PTM mechanism and GIPL mechanism are tested with different data sets. Firstly, the trajectory data is processed and then different random noises are added to the data. Then, the DTW value is calculated to represent the trajectory distortion, and the privacy protection performance of the trajectory data is analyzed. According to different distance thresholds, the experiment was divided into five groups, and the distance thresholds of each group were 100m, 300m and 500m, respectively. Each group of experiments was performed 100 times, and the final result was the average of the results of 100 times.

In a stationary user scenario, simulated data is used for experimental validation. In this scenario, because the user is in a static state, a trajectory sequence with all the same position points are simulated. There are 1000 identical position points in the trajectory sequence, so there is no need to set different distance thresholds, as shown in Fig. 7.

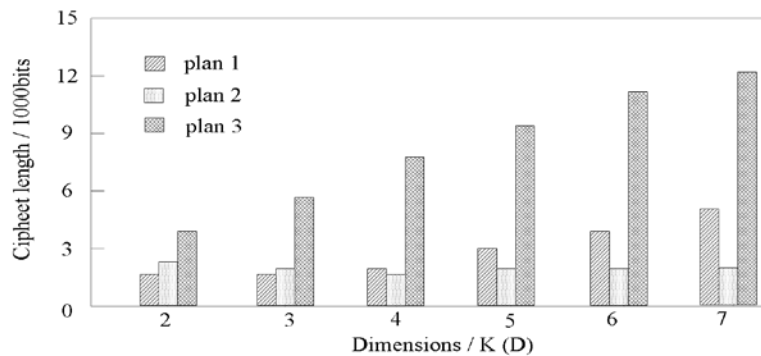


Fig. 6. Cipher-text Length in different Dimensions.

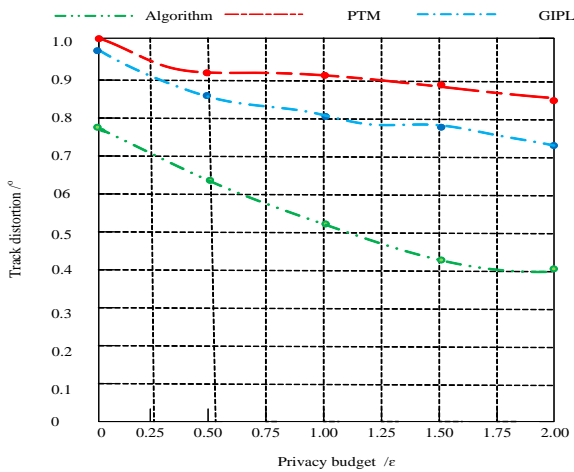


Fig. 7. Trajectory Distortion under different Privacy Budgets.

In Fig. 7, with the increase of privacy budget, the trajectory distortion of the algorithm, PTM mechanism and GIPL

mechanism in this paper are decreasing, and the degree of privacy protection is also decreasing. However, no matter how the privacy budget changes, the trajectory distortion of the proposed algorithm is always smaller than that of PTM and GIPL.

The Geolife dataset is used for experimental validation in the low-speed running user scenario as shown in Fig. 8.

In Fig. 8, in the case of the same distance threshold, the trajectory distortion of the method proposed in this paper decreases with the increase of privacy budget, that is to say, in the case of the same distance threshold, as the privacy budget continues to increase, the closer the protected trajectory is to the original trajectory, the lower the degree of privacy protection is. Moreover, under the same privacy budget, the trajectory distortion of the proposed algorithm is always lower than that of PTM and GIPL.

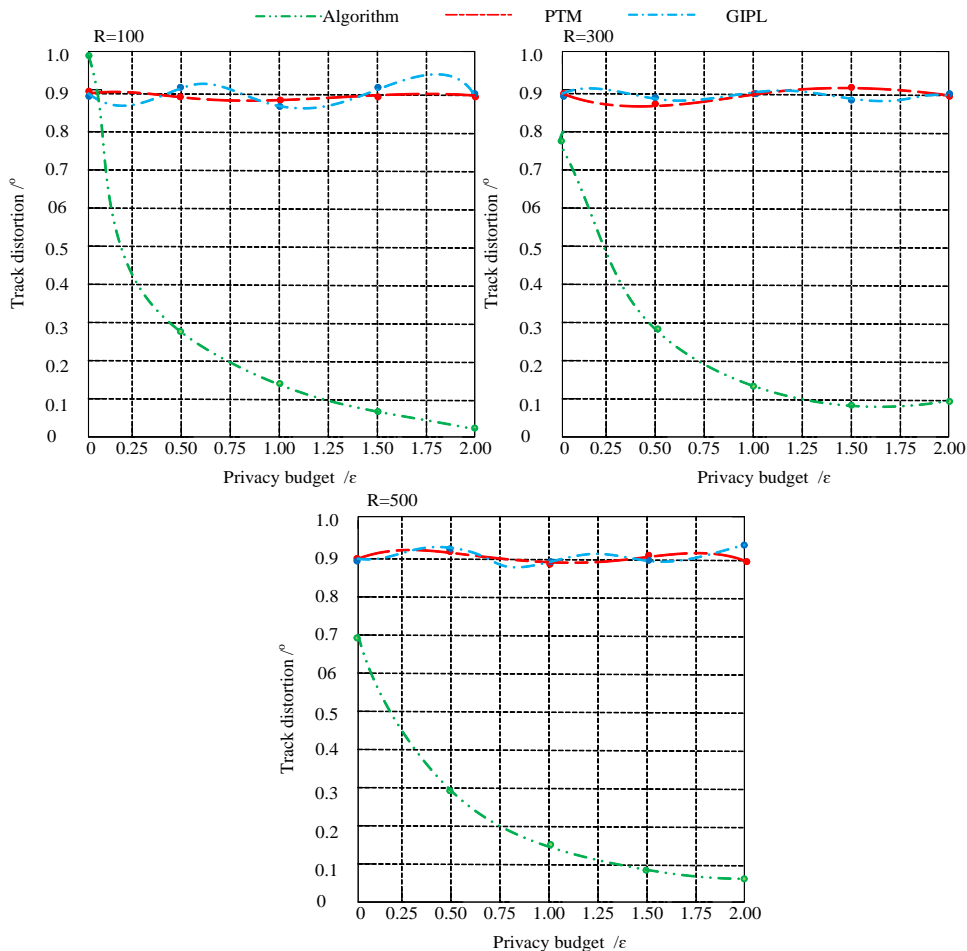


Fig. 8. Trajectory Distortion of Geolife Data Set under different Privacy Budgets.

VI. CONCLUSION

This paper explores the aggregation and access control of cloud Internet of Things blockchain on the demand side of the smart grid.

1) The related knowledge of smart grid data aggregation is studied, and the cloud Internet of Things data aggregation and access control privacy protection architecture on the demand side is proposed.

2) Based on this architecture, a blockchain aggregation and access control model is established. Encryption via EBGN preserves the priority of the blockchain and can decrypt each dimension separately using the corresponding key. By encrypting the EBGN key with a cipher-text policy attribute encryption algorithm, the scheme can achieve fine-grained access control.

3) The access rights can be updated flexibly and safely by regenerating the relevant parameters of EBGN and CP-ABE. Secondly, the security of privacy protection, access control, and access permission update of blockchain in this paper are analyzed and proved.

4) Through the performance analysis and comparison of the proposed scheme and similar schemes in terms of computing cost and communication overhead, it is shown that the proposed scheme has significant advantages in terms of computing cost and flexible fine-grained access control of blockchain in the face of a large number of smart grid demand-side terminals, large amount and variety of data, and the need for classification.

The research method in this paper realizes the encryption and aggregation of multi-dimensional data in the cloud Internet of Things. Each dimension can be encrypted with different public keys, and the multi-dimensional data is fused into a cipher-text. The EBGN private key of each dimension is encrypted by the cipher-text policy attribute encryption algorithm. The visitor is authorized to access the fine-grained data of the corresponding dimension, thus realizing the fine-grained access control of the multi-dimensional data.

In the privacy protection of the smart grid, this paper considers the privacy protection scheme on the demand side under the data aggregation model. It does not consider the smart grid marketing architecture, the home gateway smart community, and the privacy protection scheme under the vehicle networking model. In the future, the research on privacy protection schemes can be carried out under the multi-model of smart grid.

REFERENCES

- [1] A. Abdallah, X. S. Shen. Lightweight Authentication and Privacy-Preserving Scheme for V2G Connections. *IEEE Transactions on Vehicular Technology*, 2017, 66(3):2615-2629.
- [2] E. Mengelkamp, J. Gärtner, and K. Rock. Designing microgrid energy markets A case study: The Brooklyn Microgrid. *Applied Energy*, 2018, 210:870-880.
- [3] J. Hao, C. Huang, J. Ni, H. Rong, M. Xian, X. Shen. Fine-grained data access control with attribute-hiding policy for cloud-based IoT. *Computer Networks*, 2019, 153:1-10.
- [4] J. Huang, C. Lin, H. Zhou, Z. Xu, and C. Lin. Research on key technologies of deduction of multinational power trading in the context of Global Energy Interconnection. *Global Energy Interconnection*, 2019, 2(6):560-566.
- [5] J. W. Bos, W. Castryck, I. Iliashenko, F. Vercauteren. Privacy-Friendly Forecasting for the Smart Grid Using Homomorphic Encryption and the Group Method of Data Handling. *International Conference on Cryptology in Africa*, 2017, 18201.
- [6] J. Zhang, et al. Design scheme for fast charging station for electric vehicles with distributed photovoltaic power generation. *Global Energy Interconnection*, 2019, 2(2):150-159.
- [7] K. Xue, W. Chen, W. Li, J. Hong, P. Hong. Combining Data Owner-Side and Cloud-Side Access Control for Encrypted Cloud Storage. *IEEE Transactions on Information Forensics and Security*, 2018, 13(8):2062-2074.
- [8] K. Xue, Y. Xue, J. Hong, W. Li, H. Yue, D. S. L. Wei, P. Hong. RAAC: Robust and Auditable Access Control With Multiple Attribute Authorities for Public Cloud Storage. *IEEE Transactions on Information Forensics and Security*, 2017, 12(4):953-967.
- [9] K. Xue, Y. Xue, J. Hong, W. Li, H. Yue, D. S. L. Wei, P. Hong. RAAC: Robust and Auditable Access Control With Multiple Attribute Authorities for Public Cloud Storage. *IEEE Transactions on Information Forensics and Security*, 2017, 12(4):953-967.
- [10] M. A. Ferrag, L. Maglaras, A. Ahmim. Privacy-Preserving Schemes for Ad Hoc Social Networks: A Survey. *IEEE Communications Surveys & Tutorials*, 2017, 19(4):3015-3045.
- [11] M. Kim, et al. A secure charging system for electric vehicles based on blockchain. *Sensors (Switzerland)*, 2019, 19(13):1-22.
- [12] M. S. Rahman, A. Basu, S. Kiyomoto, M. Z. A. Bhuiyan. Privacy-friendly secure bidding for smart grid demand-response. *Information Sciences*, 2017, 379:229-240.
- [13] N. Saxena, B. J. Choi. Authentication Scheme for Flexible Charging and Discharging of Mobile Vehicles in the V2G Networks. *IEEE Transactions on Information Forensics & Security*, 2017, 11(7):1438-1452.
- [14] P. Liu, W. Jiang, X. Wang, H. Li, and H. Sun. Research and application of artificial intelligence service platform for the power field. *Global Energy Interconnection*, 2020, 3(2):175-185.
- [15] T. Alladi, V. Chamola, J. J. P. C. Rodrigues, and S. A. Kozlov. blockchain in smart grids: A review on different use cases. *Sensors (Switzerland)*, 2019, 19(22):1-25.
- [16] Xu Zhuxia, Zhang Chunyan, Xu Juan. Design of Storage and Service System of Meteorological Big Data Cloud Platform in Gansu Province. *Information Technology and Informatization*, 2022(02):53-57.
- [17] Y. Jiang, W. Susilo, Y. Mu, F. Guo. cipher-text-policy attribute-based encryption against key-delegation abuse in fog computing. *Future Generation Computer Systems*, 2018, 78:720-729.
- [18] Y. Xia, W. Chen, X. Liu, L. Zhang, X. Li, Y. Xiang. Adaptive Multimedia Data Forwarding for Privacy Preservation in Vehicular Ad-Hoc Networks. *IEEE Transactions on Intelligent Transportation Systems*, 2017, 18(10):2629-2641.
- [19] Y. Jiang, C. Wang, Y. Wang, and L. Gao. A cross-chain solution to integrating multiple blockchains for IoT data management. *Sensors (Switzerland)*, 2019, 19(9):1-18.
- [20] Z. Ji, X. Wang, C. Cai, and H. Sun. Power entity recognition based on bidirectional long short-term memory and conditional random fields. *Global Energy Interconnection*, 2020, 3(2):186-192.
- [21] Zhang Lu. Based on Research on data security of network service cloud platform based on OSI model. *Modern electronic technology*, 2020, 43(05):74-77+81.

Deep Convolution Neural Networks for Image Classification

Arun D. Kulkarni

Computer Science Department
The University of Texas at Tyler
Tyler, TX 75799, USA

Abstract—Deep learning is a highly active area of research in machine learning community. Deep Convolutional Neural Networks (DCNNs) present a machine learning tool that enables the computer to learn from image samples and extract internal representations or properties underlying grouping or categories of the images. DCNNs have been used successfully for image classification, object recognition, image segmentation, and image retrieval tasks. DCNN models such as Alex Net, VGG Net, and Google Net have been used to classify large dataset having millions of images into thousand classes. In this paper, we present a brief review of DCNNs and results of our experiment. We have implemented Alex Net on Dell Pentium processor using MATLAB deep learning toolbox. We have classified three image datasets. The first dataset contains four hundred images of two types of animals that was classified with 99.1 percent accuracy. The second dataset contains four thousand images of five types of flowers that was classified with 86.64 percent accuracy. In the first and second dataset seventy percent randomly chosen samples from each class were used for training. The third dataset contains forty images of stained pleura tissues from rat-lungs are classified into two classes with 75 percent accuracy. In this data set eighty percent randomly chosen samples were used in training the model.

Keywords—Deep learning; convolutional neural networks; image classification; machine learning; object recognition

I. INTRODUCTION

Image classification can be defined as categorizing images into predefined classes. Traditionally, image classification is conducted in two stages- low-level processing and high-level processing or recognition. Low level processing deals with image enhancement, filtering, detecting regions of interest, and extracting feature descriptors. High-level processing deals with classification, where feature descriptors are used to train the classifier into predefined categories. The two stages are often implemented sequentially. First, feature descriptors are obtained and subsequently are classified. The main disadvantage of this approach is that accuracy of the classifier is dependent on the design of the feature extraction stage. Many machine learning algorithms such as decision trees, Support Vector Machine (SVM), neural networks have been used to classify feature vectors obtained from images. Machine learning algorithms are known to learn the underlying relationship in data and make decisions. Deep Convolution Neural Networks (DCNNs) are one of the best learning algorithms for understanding image content and have shown exemplary performance in image segmentation, detection, and

retrieval tasks [1]. In the recent years DCNNs are preferred for image classification. DCNNs use multiple layers consisting of nonlinear information processing units for low-level as well as high-level processing. DCNNs are feedforward networks. In general, DCNNs consist of convolution and pooling layers that are grouped into modules followed by one or more fully connected layers. Convolutional layers are used for extracting features from the input image. In a convolution layer, inputs are convolved with a weighted kernel and the output is sent via a nonlinear activation function to the next layer. The purpose of pooling layers is to reduce spatial resolution of the features maps and achieve spatial invariance to input distortions and translations [2]. In earlier days, the average pooling was used, but recently the max pooling has become a common practice. Several convolution and pooling layers are stacked together. The fully connected layers are used for classification. DCNNs were successfully used to classify images in the ImageNet Large Scale Visual Recognition Challenge [3]. Recent developments in DCNNs were possible because of two main factors a) availability of faster computing resources such as Graphical Processing Units (GPUs) and b) availability of large, labeled image datasets Also, there were algorithmic improvements in Deep Neural Networks (DNNs). DCNNs commonly use the gradient decent backpropagation algorithm. There are some drawbacks with DCNNs. The first drawback is the use of Sigmoid activation functions that leads to saturation resulting into slow convergence of gradient descent. The problem becomes more severe as we move away from the output layer to hidden layers. The compounded effect of saturation at multiple layers is known as vanishing gradient [4]. In the backpropagation algorithm the mean squared error at the output layer is propagated backwards to the hidden layers to calculate the change in weights. To avoid the vanishing gradient problem, recent DCNNs use the entropy loss function with Rectified Linear Units (ReLU) in the output layer. The second drawback with DCNNs is overfitting that occurs due to the substantial number of parameters that are updated in learning. Overfitting usually occurs when the dataset is of the small size. Various regularization techniques such as the dropout or bagging are used to overcome this problem. The third drawback is due to the non-convex shape of the error function. The backpropagation algorithm is sensitive to the randomly chosen initial values of weights. The gradient descent algorithm may get stuck at a local minimum. To avoid this problem the model is initially trained with a few parameters and then more parameters can be added during the training. DCNN models trained with a large dataset and can

classify images with high accuracy. Many architectures for DCNN models have been used for image classification. In this paper we implement Alex Net using MATLAB deep learning toolbox. We use the model to classify three image datasets a) animal b) flower, and c) stained pleura tissue images. The outline of the paper is as follows. Section II describes related work. Section III deals with implementation Alex Net and results, and Section IV provides conclusions.

II. RELATED WORK

Neural networks (NN) are biologically inspired and are used for object recognition, image classification. Neural networks have been used as associative memory to store and retrieve information. Associative memories function as content addressable memories. Neural networks learn from training samples and have been used for pattern recognition since the 1950s [5]. Feedforward networks with a backpropagation learning algorithm have been used as supervised classifiers [6]. Today several well-developed learning algorithms for multi-layer neural network models are available. These include a multi-layer Perceptron, feedforward networks with back-propagation learning, Boltzman machines, Hamming net, Hopfield net, neocognitron models [7, 8, 9, 10, 11] Huang and Lippmann [12] provide a comparative study of neural networks and conventional classifiers. Neural networks have been used to implement expert systems or knowledge-based system. The success of neural networks has led to deep neural networks (DNNs). Deep learning algorithms were available since late 1980s, However, DNNs were computationally expensive. Chellapilla [13] suggested using Graphical Processing Units (GPUs) to implement deep learning algorithms faster. Deep learning is a form of machine learning that enables computers to learn from experience and understand the world in terms of hierarchy of concepts [14]. DNNs are neural networks with multiple hidden layers. The multiple hidden processing layers has dramatically improved the state-of-the art visual object recognition. DNNs discover intricate structures in large datasets by using the backpropagation algorithm [15]. Convolutional neural networks (CNN) are special type of neural networks for processing data that have a known grid-like structure [16]. Various stages of a DCNN show topology resemblance to primate's ventral pathway of visual cortex [17]. DCNNs can learn internal representations from raw pixels. DCNNs are hierarchical learning models and can extract features [18,19,20]. Rawat and Wang [21] present a comprehensive review of DCNNs. DCNNs consist of a stack of convolution and pooling layers followed by fully connected layers. Convolution and pooling layers are used for features extraction. The max-pooling method is a widely accepted method in recent DCNNs. Scherer et al [22] have shown that the max-pooling method can capture the invariance and is effective in reducing the computational time. DCNNs have been used in many computer applications that include image and object classification, face detection, image segmentation, and gesture recognition. Recent DCNNs have ten layers of ReLU, hundreds of millions of weights, and billions of connections between units [15]. Machine learning community's interest in DCNNs grew after Image Net compaction in 2012, where Alex Net achieved record breaking

results in classifying images from ILSVRC data set consisting of more than 1.2 million images in to one thousand classes. This was a landmark achievement that has revolutionized the computer vision field. Significant achievements in DCNNs are a) LeCun et al. [2] used a DCNN to classify 70,000 handwritten images of digits in to ten classes. b) Fei-Fei et al. [23] used a DCNN to classify 9,146 color images from CALTECH-101 data set in to 101 classes. c) Krizhevsky [24] classified 60,000 images in CIFAR-100 data set into one hundred classes. d) Russakovsky et al [25] classified more than 1.2 million images from ILSVRC dataset into one thousand classes. LeNet was proposed by LeCun et al. [26]. Alex Net proposed by Krizevsky et al [3] was based on principles used in LeNet Simonyan et al. [27] proposed a DCNN model VGG Net that was made nineteen layers deep and used 3x3 filters. The use of small size filters could induce the effect of large size filters and provided computational simplicity by reducing the number of parameters. Nowadays, most new DCNN architectures are built upon the principle of simple and homogenous topology as introduced in VGG Net. Zhang et al, [28] provide the taxonomy of CNNs. Khan et al. [29] discuss intrinsic taxonomy present in the recent and prominent DCNN architectures reported from 2012-2020. They have classified DCNN architectures into seven categories, namely, spatial exploitation, depth, multi-path, width, feature-map exploitation, channel boosting, and attention-based. Stacking of multiple transformations deep and in parallel fashion showed good learning for complex problems [30, 31]. Google Net was the winner of the 2014-ILSVRC competition [32]. Google Net introduced the concept of inception block, which incorporates multi-scale convolutional transforms using split, transform, and merge idea. The textbook by Szelinski [33] describes deep learning techniques including deep feedforward networks, regularization, optimization algorithms, convolutional neural networks. We have implemented Alex Net using MATLAB deep learning toolbox and have analyzed three datasets.

III. IMPLEMENTATION AND RESULTS

The simplified architecture of Alex Net is shown in Fig. 1. It contains eight layers: five convolution and three fully connected layers. Convolution layers serve as feature extractors. Inputs are convolved with learned weights to compute feature maps and results are sent through a nonlinear activation function. The output of the k th feature map Y_k is given by (1).

$$Y_k = f(W_k * x) \quad (1)$$

Where x denotes the input image, W_k is the convolution filter. The "*" sign refers to the 2D convolution operator. The purpose of the pooling layer is to reduce the spatial resolution and extract invariant features [21]. The output of a pooling layer is given by (2).

$$Y_{kij} = \max_{(p,q) \in R_{ij}} (x_{kpq}) \quad (2)$$

Where X_{kpq} denotes elements at location (p, q) contained by the pooling region R_{ij} .

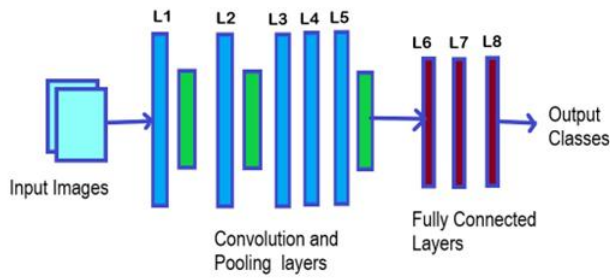


Fig. 1. Alex Net Architecture.

Fig. 2. Illustrates the max pooling operation. Inputs are mapped from a convolution layer to the pooling layer. With a 4x4 mask, the maximum value in each 2x2 sub-area is mapped. The fully connected layers follow the convolution layers that interpret extracted features and perform high level reasoning. DCNNs use learning algorithms to adjust the free parameters in the network to obtain the desired output. The most common algorithm is the backpropagation learning algorithm. The commonly experienced problem with DCNNs is overfitting. This is due to the substantial number of free parameters that are adjusted during learning. The layers in the Alex Net are shown in Table I.

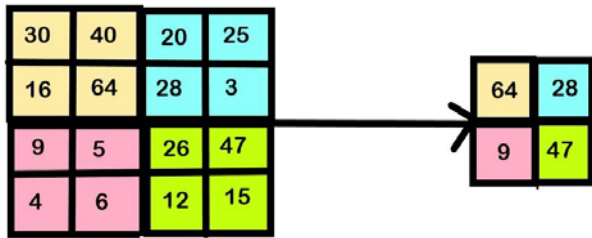


Fig. 2. Max Pooling.

TABLE I. LAYERS OF ALEX NET

Layer	Description	Parameters
	Input image	224x224x3 (Channels)
L1	Convolution Layer with a Pooling Layer	96 kernels of size 11x11x3
L2	Convolution Layer with a Pooling Layer	256 kernels of size 5x5x48
L3	Convolution Layer	384 kernels of size 3x3x256
L4	Convolution Layer	384 kernels of size 3x3x192
L5	Convolution Layer with a Pooling Layer	256 kernels of size 3x3x192
L6	Fully Connected Layer	4096 neurons
L7	Fully Connected Layer	4096 neurons
L8	Fully Connected Layer	4096 neurons

We implemented Alex Net using MATLAB deep learning toolbox. We analyzed three datasets. There are described below:

Example 1: In this example we have considered the subset of animal dataset [34]. The original dataset has 37 categories with 200 samples in each category. For this example, we have selected only two categories. The dataset consists of four hundred images of cats and dogs that are obtained with distinct

backgrounds and with a variety of sizes and positions of these animals. We used seventy percent of randomly picked samples from each class to train Alex Net and thirty percent of samples were used for validation. Fig. 3 shows some randomly picked images from the dataset. Images in the dataset we resized to 224 rows x 224 columns. There were two units in the fully connected output layer. The DCNN was able to classify the dataset with 99.9 percent accuracy. Fig. 4 shows the graph for the accuracy and the loss function with iterations. Fig. 5 shows a few classified randomly chosen images with labels.



Fig. 3. Sample Images from Animal Dataset.

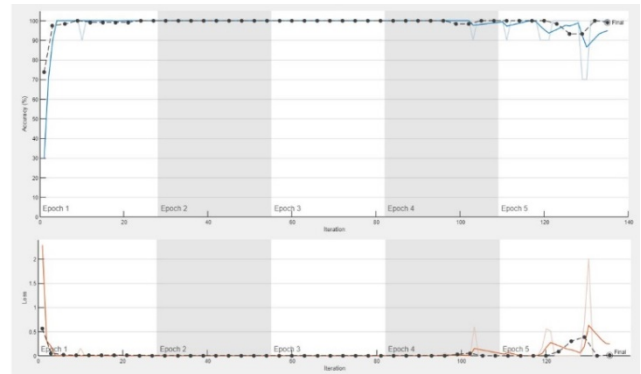


Fig. 4. Accuracy and Loss Function for Animal Dataset.



Fig. 5. Classified Sample Images with Class Labels.

Example 2: In this example we have considered a subset of the flower dataset [35]. The subset consists of four thousand images of five types of flowers: daisy, rose, dandelion, sunflower, and tulip. The dataset contains images that are obtained with distinct color background and with a variety of sizes and colors of flowers. We used seventy percent of randomly picked samples from each class to train Alex Net and thirty percent of samples were used for validation. Fig. 6 shows some randomly picked images from the dataset. Images in the dataset were resized to 224 rows x 224 columns. There were five units in the fully connected output layer. The network took 256 minutes for training on Dell Pentium processor. The DCNN was able to classify the dataset with 86.6 percent accuracy. Fig. 7 shows the graph for the accuracy and the loss function with iterations. Fig. 8 shows a few classified images with labels.

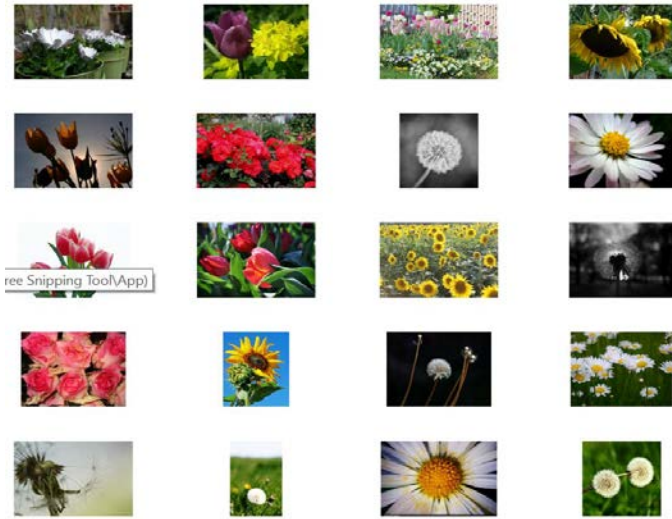


Fig. 6. Sample Images from Flower Dataset.

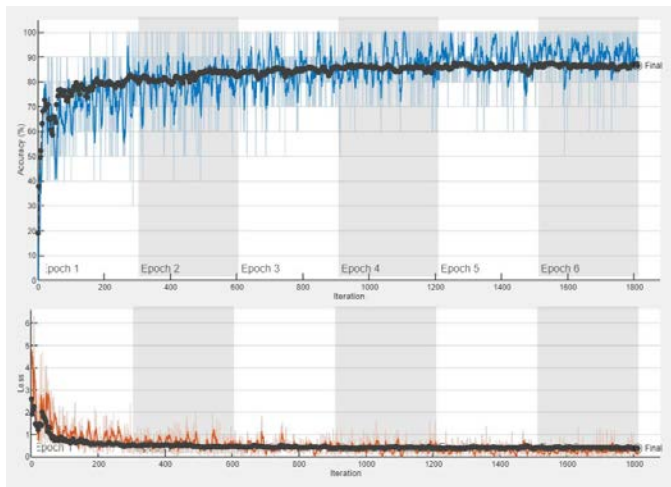


Fig. 7. Accuracy and Loss Functions for Flower Dataset.



Fig. 8. Classified Output with Class Labels.

Example 3: In this example we have considered the stained pleura images of rat-lungs. These are pathological images representing positive and negative cancer cases. The dataset consists of forty images, twenty images in each class. We used eighty percent of randomly picked samples from each class to train Alex Net and twenty percent of samples were used for validation. Fig. 9 shows some randomly picked images from the dataset. Images in the dataset we resized to 224 rows x 224 columns. There were two units in the fully connected output layer. The DCNN was able to classify the dataset with 75 percent accuracy. Fig. 10 shows the graph for the accuracy and the loss function with iterations. Fig. 11 shows a few classified images with labels.

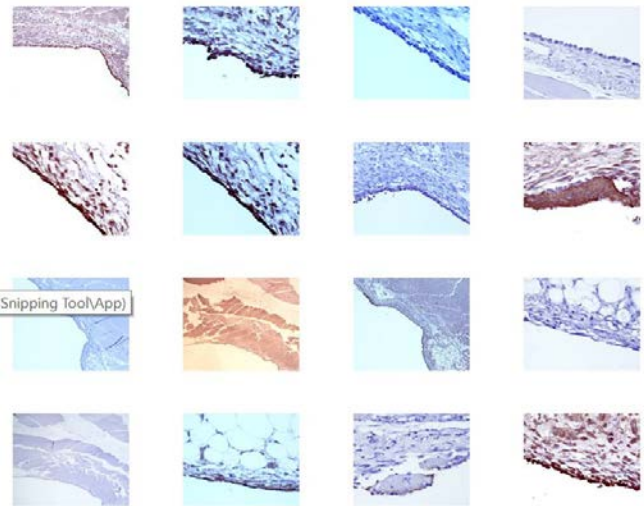


Fig. 9. Sample Images Pleura Dataset.

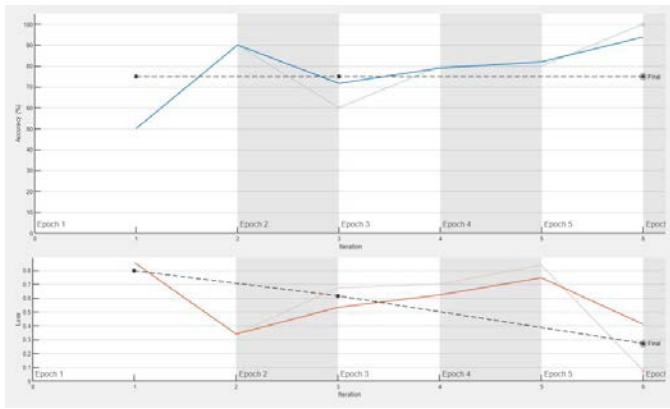


Fig. 10. Accuracy and Loss Functions Pleura Dataset.

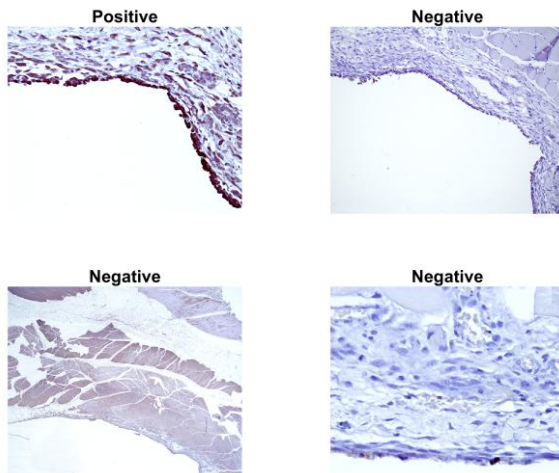


Fig. 11. Classified Output with Labels -Pleura Dataset.

IV. CONCLUSION

In this research work, we have implemented Alex Net using MATLAB deep learning toolbox and have analyzed three datasets. The classification accuracy for the animal dataset was 99.01 percent. The classification accuracy for the flower dataset was 86.64 percent. Images of several types of flowers were obtained with various backgrounds, sizes, colors. In the flower dataset, many images in two categories sunflower and dandelion are similar. It is hard to distinguish between the two classes as these classes could be non-separable or overlapping classes in the feature space. In the case of pleura image classification, we obtained the classification accuracy of 75 percent. This because the sample size for the dataset was too small. The dataset contained only forty images, out of which 80 percent were used for training. Due to the substantial number of free parameters in the model and the small sample size of the training set, there is possibility of model overfitting. This may result in less accuracy. Also, training and testing images were selected randomly and sometimes we got 100 percent accuracy. We need a large dataset to evaluate this application. The DCNN presented in the paper can be used for other practical applications such as object recognition, military reconnaissance, medical image diagnosis, etc.

Many DCNN models are proposed in the literature. These models vary in the depth, width, activation functions, kernel

size, and hardware implementation. It is possible to add layers to a DCNN to extract transformed domain features with the ring- and wedge-shaped filters to extract texture as well as scale and rotation invariant features. Also, it is not yet clear how image features or properties of image categories are represented in the DCNN models. In the case of neural networks, researchers have been able to extract knowledge in term of classification rules by tracing links in the neural net. However, in the case of DCNNs, due to the large number of free parameters, researchers have not been yet able to decode the DCNN models or extract the knowledge as how DCNNs make decision. It is an open area for the future research.

ACKNOWLEDGMENT

The author is thankful to UT Health North, Tyler, TX for providing pleura image dataset.

REFERENCES

- [1] D. Cireşan, U. Meier, J. Schmidhuber, "Multi-column Deep Neural Networks for Image Classification". Computer Vision and Pattern Recognition, 2012, pp. 3642-3649 <https://doi.org/10.48550/arXiv.1202.2745>.
- [2] Y. LeCun, L. Bottou, Y. Bengio, and P. Haffner "Gradient-based learning applied to document recognition". Proceedings of the IEEE, 1998, vol. 86, no. 11, pp. 2278–2324.
- [3] A. Krizhevsky, I. Sutskever, G. Hinton, "ImageNet classification with deep convolutional neural networks". Adv Neural Inf Process Syst. 2012 [https://doi.org/10.1061/\(ASCE\)GT.1943-5606.0001284](https://doi.org/10.1061/(ASCE)GT.1943-5606.0001284).
- [4] M. Tan and Q. V. Le, "Efficient Net: Rethinking Model Scaling for Convolutional Neural Networks," Proceedings of the 36 th International Conference on Machine Learning, Long Beach, California, PMLR 97, 2019.
- [5] F. Rosenblatt, F, "The Perceptron: a probabilistic model for information storage and organization in brain," Psychology Review, 1958, vol. 65, pp386-408. G. Eason, B. Noble, and I. N. Sneddon, "On certain integrals of Lipschitz-Hankel type involving products of Bessel functions," Phil. Trans. Roy. Soc. London, vol. A247, pp. 529–551, April 1955. (references).
- [6] A. D. Kulkarni, Computer vision and fuzzy-neural systems. Prentice Hall PTR, Upper Saddle River, NJ, 2001.
- [7] J. J. Hopfield, "Neurons with graded response have collective computational properties like those of two state neurons," Proceedings of the National Academy of Sciences, 1984, vol 81, pp. 3088-3092.
- [8] D. E. Rumelhart, J. L. McClelland, and the PDP Group, Parallel Distributed Processing, vol I. MIT Press, Cambridge, MA, 1986.
- [9] R. P. Lippmann, "An introduction to computing with neural nets," IEEE Transactions on Acoustics, Speech, and Signal Processing, 1987, vol. 32, pp. 4-22.
- [10] K. Fukushima, "Neural networks for visual pattern recognition," Computer, March 1988, pp. 65-74.
- [11] R. Hecht-Nielsen, Neurocomputing. Addison-Wesley, Reading, MA, 1990.
- [12] W. Y. Huang and R. P. Lippmann, R. P, "Comparison between neural net and conventional classifiers," Proceedings of Joint International Conference on Neural Networks, San Diego, 1988, vol. IV, pp. 485-493.
- [13] K. Chellapilla, S. Puri, and P. Simard, "High performance convolutional neural networks for document processing," In Tenth international workshop on frontiers in handwriting recognition. Suvisoft. October 2006, pp. 1-6.
- [14] K. G. Kim, "Deep Learning Book Review", Healthcare Information Research, 2016, vol. 22, no. 4. pp 351-354. <http://doi.org/10.4258/hir.2016.22.4.351>.
- [15] Y. LeCun, Y. Bengin, and G. Hinton, "Deep learning", Nature, 2015, vol. 521, pp. 436-444.
- [16] I. Goodfellow, Y. Bengin, and A. Courville, Deep Learning. The MIT Press, Cambridge, MA, USA, 2016.

- [17] M. Laskar, L. Giraldo, O. Schwartz, Correspondence of deep neural networks and the brain for visual textures, 2018, pp. 1–17.
- [18] Q. Abbas, M. Ibrahim, M. Jaffar (2019) A comprehensive review of recent advances on deep vision systems. *Artif Intell Rev*, 2019, vol. 52, pp 39–76. <https://doi.org/10.1007/s10462-018-9633-3>.
- [19] Y. Guo, Y. Liu, A. Oerlemans, S. Lao, S. Wu, and M. S. Lew, “Deep learning for visual understanding: A review”, *Neurocomputing*, 2016, vol. 187, pp. 27–48.
- [20] W. Liu, Z. Wang, X. Liu, N. Zeng, Y. Liu, and F. F. Alsaadi, “A survey of deep neural network architectures and their applications”, *Neurocomputing*, 2017, vol. 234, pp.11-26.
- [21] W. Rawat, and Z. Wang, “Deep Convolutional Neural Networks for Image Classification: A Comprehensive Review”, *Neural Computation*, 2017, vol. 29, pp. 2352–2449, 2017.
- [22] D. Scherer, A. Müller, S. Behnke, “Evaluation of pooling operations in convolutional architectures for object recognition”, In: *Artificial Neural Networks-ICANN 2010*. Springer, pp. 92–101.
- [23] L. Fei-Fei, “Knowledge transfer in learning to recognize visual objects classes”, In *Proceedings of the 4th International Conference on Development and Learning*, 2006, pp 11-17.
- [24] A. Krizhevsky, I. Sutskevee, and G. Hinton, “ImageNet classification with deep convolutional neural networks”, *Communications of the ACM* 2017, vol. 60, no. 6, pp. 84-90. Doi 10.1145/3065386.
- [25] O. Russakovsky ”. *Int J Comput Vis*. <https://doi.org/10.1007/s11263-015-0816-y> J. Deng, H. Su (2015) “ImageNet large scale visual recognition challenge.
- [26] Y. LeCun, B. Boser, J. S. Denker, D. Henderson, R. E. Howard, W. Hubbard, W., and L. D. Jackel. “Handwritten digit recognition with a back-propagation network”. In D. S. Touretzky (Ed.), *Advances in neural information processing systems*, 1989, vol. 2, pp. 396–404, Cambridge, MA: MIT Press.
- [27] K. Simonyan, A. Zisserman, “Very deep convolutional networks for large-scale image recognition”, *ICLR 2015*, vol. 75, pp. 398–406. <https://doi.org/10.2146/ajhp170251>.
- [28] S. Zhang, L. Yaq, A. Sun, Y. Tay, “Deep Learning based Recommender System: A Survey and New Perspectives”, *ACM Computing Surveys*, 2018, vol. 1, no. 1, pp. 1-35.
- [29] A. Khan, A. Sohail, U. Zahoor, A. S. Qureshi, “A Survey of the Recent Architectures of Deep Convolutional Neural Networks”, *Artificial Intelligence Review*, 2020, vol. 53, pp. 5455–5516. DOI: <https://doi.org/10.1007/s10462-020-09825-6>.
- [30] D. Han, and J. Kim, “Deep pyramidal residual networks”, In: *2017 IEEE conference on computer vision and pattern recognition (CVPR)*, pp. 6307–6315.
- [31] S. Zagoruyko and N. Komodakis, “Wide Residual Networks”, In Richard C. Wilson, Edwin R. Hancock and William A. P. Smith, editors, *Proceedings of the British Machine Vision Conference (BMVC)*, pp.1-87.12. BMVA Press, September 2016.
- [32] C. Szegedy, W. Liu, Y. Jia, “Going deeper with convolutions”. In: *2015 IEEE conference on computer vision and pattern recognition (CVPR)*. Pp. 1–9.
- [33] R. Szeliski, R., *Computer Vision: Algorithms and Applications*. Springer, 2021.
- [34] O. M. Parkhi, A. Vedaldi, A. Zisserman, C. V. Jawahar, “Cats and Dogs”. *IEEE Conference on Computer Vision and Pattern Recognition*, 2012.
- [35] Kaggle: <https://www.kaggle.com/datasets/alexamamaev/flowers-recognition>

An Improved Genetic Algorithm for the Multi-temperature Food Distribution with Multi-Station

Bo Wang¹, Jiangpo Wei², Bin Lv³, and Ying Song⁴

Software Engineering College, Zhengzhou University of Light Industry, Zhengzhou, China, 450001^{1,2}

Linyi Branch of China Mobile Communications Group Shandong Co., Ltd, Linyi, China, 277799³

Beijing Advanced Innovation Center for Materials Genome Engineering

Beijing Information Science and Technology University, Beijing, China, 100101⁴

Beijing Key Laboratory of Internet Culture and Digital Dissemination,

Beijing Information Science and Technology University, Beijing, China, 100101⁴

Abstract—This paper studies on the food distribution route planning problem for improving the customer satisfaction and the operator cost of food providers. In the first, the problem is formulated to a combinatorial optimization which is hard to be solved. Thus, a polynomial time algorithm is proposed to solve the problem, combining genetic algorithm and neighbourhood search, to increase the total amount of distributed food and reduce the distribution cost. The proposed algorithm employs the genetic algorithm with integer coding to decide the assignment of customers to distribution vehicles, and integrates the neighbourhood search strategy into the genetic algorithm to improve its performance. Experiment results show that the proposed method improved the distribution performance up-to 111.09%, 73.10% and 70.21%, respectively, in the distributed food amount, the cost efficiency, and the customer satisfaction.

Keywords—Logistics; genetic algorithm; neighbourhood search; food distribution

I. INTRODUCTION

As the development of economy and society in the global, the requirement for the food quality is increasing continuously in most countries. In 2021, the cumulative retail value of grain, oil and food commodities reaches 1675.91 billion yuan, with an increase of 10.8% from 2020, in China [1]. Modern logistics and e-commerce promote the demand growth of food logistics. The main mode of food shopping is becoming from going to retailer to on-line ordering on Internet. Recently, the scale of e-commerce market for fresh food products is increasingly growth. For example, Chinese e-commerce market for fresh food products is increased with a compound annual growth rate at 25%, from 2016 to 2019, and its growth rate has greatly increased during the COVID-19 pandemic [2].

For food suppliers, especially for fresh food suppliers, an unreasonable distribution route strategy can decrease the user satisfaction [3] and increase the distribution cost [4]. Food logistics distribution planning method is an efficient way to address this issue [5]. Unfortunately, the distribution route problem is NP-hard [6], and thus cannot be solved exactly when it is large in the scale. Two kinds of approximate methods can be applied for solving large-scale route problems, heuristics and meta-heuristics. In general, heuristic-based methods can provide a local optimization solution fast. But they usually

have a limited performance in problem solving due to their local search strategies. Meta-heuristics can achieve a better performance than heuristics, benefiting from their global search abilities inspired by natural phenomena and laws [7].

Therefore, several existing works exploited various meta-heuristic algorithms to solve the food distribution route problem, for improving the distribution cost or time. But these existing works have some issues which restrict their practices. Some works focused on the single-station distribution problem. A part of works concerned food distribution in only one temperature range. Few works considered to exploit multiple temperature zone refrigerated vehicle for simultaneously distributing foods with different temperature requirements by one vehicle, to improve the usage efficiency of distribution vehicles. Therefore, in this paper, to improve the efficiency of multi-temperature food distribution, a router algorithm is proposed by integrating the neighbourhood search strategy into the genetic algorithm, with objectives of optimizing the amount of distributed foods and the cost for the food distribution. And extensive experiment results verify the performance superiority of our proposed algorithm.

The rest of this paper is organized as follows. Section II illustrates published works aiming at solving food distribution route problems. Section III routes the route problem concerned in this paper. Section IV presents our proposed distribution planning method. Section V evaluates our proposed method by simulated experiments. And finally, Section VI concludes the paper.

II. RELATED WORK

Wang et al. [8] proposed a parthenogenetic algorithm-based method to address the route problem for flesh foods with a same temperature requirement, to optimize the customer value and satisfaction. Zhu and Wang [9] exploited ant colony algorithm to solve the distribution route problem for pharmaceutical cold chain logistics, aiming at completing a distribution task with minimal cost. Based on ant colony algorithm, Fang et al. [10] presented a distribution planning method to improve the operating cost and the green cost. Their method used A* algorithm to improve the slow convergence speed problem due to the insufficient pheromone in the initial

stage of ant colony algorithm. For optimizing the total cost of food distribution, Ren et al, [11] designed a knowledge based ant colony algorithm by integrating the elitist tabu search and the knowledge model of dynamic probability selection into ant colony algorithm. By integrating the mutation operator of simulated annealing into genetic algorithm, Li et al. [12] designed a distribution planning method for green fresh foods. These above works focused on the food distribution route problem for single-station, which limits their application scopes.

To address the multi-station problem, Prajapati et al. [13] proposed a heuristic method based on clustering algorithm, to optimize the transport distance and utilization of distribution vehicles. The proposed method first clustered customers, and then iteratively serviced a class of customers with minimal traveller's distance. This work didn't concern the temperature requirements of foods. Wang et al. [14] presented a hybrid heuristic method to optimize the distribution cost and the number of used refrigerator vehicles for fresh foods. This hybrid heuristic method first clustered customers according to their locations and requirements, and then, combine Tabu search and NSGA-II to solve the route problem, with the heuristic idea of using a vehicle to service customers with similar locations and requirements. Tsang et al. [15] exploited multi-objective genetic algorithm based on linear weighting method to improve the number of used refrigerator vehicles, customers' satisfactions and the transport time. These methods assumed there are sufficient refrigerator vehicles for satisfying all customer requirements by only one trip. These assumptions narrow down their application ranges.

Liu et al. [16] employed simulated annealing algorithm for optimizing the transport cost of cold-chain product distributions. This work assumed vehicles didn't return after finishing their distribution tasks, which results in an underestimation of the transport cost. Stellingwerf et al. [17] studied on the cold-chain distribution router problem to optimize the transport cost and the food quality. They modelled the problem into a mixed integer linear programming, and proposed to solve it by existing solvers for small-scale problems. This isn't applicable for solving large-scale problems. Ding [18] used the linear weighting method to transform three optimization objectives into one, for minimizing the distribution cost, the distribution time and the distribution risk, and applied ant colony algorithm with quantum bits to solve the distribution problem. All of these above works assumed each vehicle can transport only one kind of fresh foods. And thus they didn't consider to exploited the multiple temperature zone refrigerated vehicle [19], [20], which can distribute frozen, refrigerated and ambient foods by one vehicle at once. This can lead to a low usage efficiency of distribution vehicles by increasing the number of used vehicles, and thus increase the distribution cost.

Different from existing works, this paper focuses on the distribution router problem in multiple temperature ranges for the scenario of multi-station. This paper try to optimize the distribution efficiency by increasing the total amount of distributed foods and decreasing the total distribution cost, with limited distribution vehicles.

III. PROBLEM STATEMENT

This paper focuses on the router problem for multi-temperature foods distributed by multi-station. Each distri-

bution station is equipped with several distribution vehicles for its food distribution. There are three kinds of foods to be distributed, ambient, refrigerated, and frozen foods. Each vehicle has ability for distributing one or more kinds of foods, considering the refrigerated vehicle with multiple temperature zones. The food supplier need to decide a router strategy to distribute foods to customers of various places from its food distribution stations. The aim of this paper is to provide a router strategy, which is deciding which vehicle is used to distribute foods for each customer, and deciding the distribution router of each vehicle, for optimizing the distributed food amount and the distribution cost. In this paper, each vehicle is assumed to be used once at most for the food distribution. When some customers' requirements cannot satisfied, the food supplier executes our method more times to distribute foods ordered by these customers. Each vehicle is return its original station for subsequent distribution tasks.

Assuming there are S distribution stations, $s_k, 1 \leq k \leq S$. The location of station s_k is (x_k^s, y_k^s) , where these two dimensions can represent respectively the latitude and longitude. There are V vehicles, $v_i, 1 \leq i \leq V$. The loading capacities of vehicle v_i for distributing ambient, refrigerated, and frozen foods are respectively q_i^a, q_i^r , and q_i^f . If v_i cannot distribute refrigerated (frozen) foods, q_i^r (q_i^f) is 0. Binary constants $a_{i,k}$ are used to represent whether v_i is equipped in s_k . If v_i is equipped in s_k , $a_{i,k}$ is 1, and otherwise, $a_{i,k} = 0$. There are U customers, $u_j, 1 \leq j \leq U$, ordering various foods needed to be distributed. The amount of ambient, refrigerated, and frozen foods ordered by customer u_j are respectively qa_j, qr_j , and qf_j . The location of u_j is (x_j^u, y_j^u) . The distances between a station and a customer and between two customers can be calculated according to their locations, respectively.

Binary variables $z_{i,j}, 1 \leq i \leq V, 1 \leq j \leq U$, are used to represent whether the foods required by a customer is distributed by a vehicle. If u_j 's required foods are distributed by v_i , then $z_{i,j} = 1$, and otherwise, $z_{i,j} = 0$. To reduce the time of inspecting and tallying foods for customers for avoiding the decreasing of the customer satisfaction, all foods required by a customer are assumed to be distributed by only one vehicle, i.e.,

$$\sum_{i=1}^V z_{i,j} \leq 1, 1 \leq j \leq U. \quad (1)$$

A complete router strategy includes not only deciding the vehicle that distributes foods for each customer, but also deciding the distribution order for each vehicle when it serves multiple customers. Integer variables $o_j \in [1, U], j = 1, 2, \dots, U$, are used to represent the decision of the distribution order. For a vehicle serving multiple customers, foods required by u_{j1} are distributed before u_{j2} if and only if $o_{j1} < o_{j2}$. As the distribution orders for any two customers are not identical when they are served by one vehicle,

$$\sum_{\substack{1 \leq i \leq V \wedge \\ j1 \neq j2 \wedge \\ z_{i,j1} \cdot z_{i,j2} = 1}} (o_{j1} - o_{j2}) \leq 0, 1 \leq j1, j2 \leq U. \quad (2)$$

For each vehicle, the accumulated amount of foods distributed is not exceeding its capacity, then the following

inequation hold.

$$\sum_{j=1}^U z_{i,j} \cdot qa_j \leq q_j^a, 1 \leq i \leq V, \quad (3)$$

$$\sum_{j=1}^U z_{i,j} \cdot qr_j \leq q_j^r, 1 \leq i \leq V, \quad (4)$$

$$\sum_{j=1}^U z_{i,j} \cdot qf_j \leq q_j^f, 1 \leq i \leq V. \quad (5)$$

For a vehicle, there is a cost to use it for food distribution, which is constituted of the startup and transport costs. The commonly linear model is used for evaluating the cost of a vehicle usage,

$$C_i = e_i + \int_l (c_i^{idle} + (c_i^{full} - c_i^{idle}) \cdot \frac{w_i}{q_i^a + q_i^r + q_i^f}) dl. \quad (6)$$

Where e_i is the startup cost of v_i , which includes the driver wage, etc., and is usually considered as a constant. l represents the transport route of the vehicle. c_i^{full} and c_i^{idle} are the costs per unit of transport distance respectively when v_i is empty and full loaded. w_i is the load varied with the transport route, for v_i . $\frac{w_i}{q_i^a + q_i^r + q_i^f}$ represents the utilization of v_i .

The food distribution can be see as three stages for each vehicle, food distribution from the station to the first customer, food distributions from a customer to another customer repeatedly, and return station from the last customer. In the first stage, their is an increased cost ($P1_i$) for distributing foods to the first customer, and the load of v_i is the accumulated amount of foods required by all customers that the vehicle serves, $\sum_{j=1}^U (z_{i,j} \cdot (qa_j + qr_j + qf_j))$. $d_{i,j}^{su}$ is used to represent the distance between u_j and the station equipped with v_i , which can be easily calculated by the locations of the user and the station. Then,

$$P1_i = \sum_{\substack{1 \leq j \leq U \wedge \\ z_{i,j} \cdot o_j = 1}} (d_{i,j}^{su} \cdot (c_i^{idle} + (c_i^{full} - c_i^{idle}) \cdot \frac{\sum_{j=1}^U (z_{i,j} \cdot (qa_j + qr_j + qf_j))}{q_i^a + q_i^r + q_i^f}))). \quad (7)$$

In the second stage, their is a distribution cost for each transport from one customer to another customer, where the transport distance is the distance between these two customers, and the load is the accumulated amount of foods needed to be distributed to customers that have not been served. $d_{j,j}^{uu}$ is used to represent the distance between customer u_{jj} and customer u_j . Then the cost in the second stage can be calculated by

$$P2_i = \sum_{\substack{1 \leq j \leq U \wedge \\ z_{i,j} \cdot o_j > 1}} ((\sum_{\substack{1 \leq jj \leq U \wedge \\ z_{i,jj} \cdot o_{jj} = o_j - 1}} d_{j,j}^{uu}) \cdot (c_i^{idle} + (c_i^{full} - c_i^{idle}) \cdot \frac{\sum_{\substack{1 \leq jj \leq U \wedge \\ z_{i,jj} \cdot o_{jj} > o_j}} (z_{i,jj} \cdot (qa_{jj} + qr_{jj} + qf_{jj}))}{q_i^a + q_i^r + q_i^f}))), \quad (8)$$

where $\sum_{\substack{1 \leq jj \leq U \wedge \\ z_{i,jj} \cdot o_{jj} = o_j - 1}} d_{j,j}^{uu}$ is the transport distance from customer u_j to its next customer u_{jj} ($o_{jj} = o_j - 1$).

$\sum_{\substack{1 \leq jj \leq U \wedge \\ z_{i,jj} \cdot o_{jj} > o_j}} (z_{i,jj} \cdot (qa_{jj} + qr_{jj} + qf_{jj}))$ is the accumulated amount of foods required by customers with service orders after u_j .

After all customers have been served, in the last stage, the vehicle will return the station that is equipped with it, with idle load. The transport distance is the distance between the station and the last customer served, which is $\sum_{\arg\max_j \{z_{i,j} \cdot o_j\}} (z_{i,j} \cdot d_{i,j}^{su})$ for v_i . Therefore, the cost in the third stage for v_i is

$$P3_i = c_i^{idle} \cdot \sum_{\arg\max_j \{z_{i,j} \cdot o_j\}} (z_{i,j} \cdot d_{i,j}^{su}). \quad (9)$$

Combining all of above costs, the total distribution cost for each vehicle can be calculated by Eq. (10).

$$C_i = e_i + P1_i + P2_i + P3_i, 1 \leq i \leq V. \quad (10)$$

Then, the multi-temperature food distribution router problem can be formulated by the following optimization problem:

$$\text{Maximizing} \{ \sum_{i=1}^V \sum_{j=1}^U (z_{i,j} \cdot (qa_j + qr_j + qf_j)) - \sum_{i=1}^V C_i \} \quad (11)$$

Subjective to:

$$Eq. (1) - Eq. (10), \quad (12)$$

$$z_{i,j} \in \{0, 1\}, 1 \leq i \leq V, 1 \leq j \leq U, \quad (13)$$

$$o_j \in [1, U], 1 \leq j \leq U. \quad (14)$$

The optimization objective is maximizing the accumulated amount of distributed foods and minimizing the total distribution cost. In practice, the maximization of the distributed food amount is considered as the major optimization objective, as it directly affects the customer satisfaction, and the cost minimization as the minor one. This can be implemented by weighting foods in kilograms (kg) and counting the cost in hundred-dollar units, because a vehicle has thousands of kilograms in loading capacity and it costs hundreds of dollars to distributed foods by the vehicle at a time, in real world. Eq. (refeq:z) and (14) define the value ranges of discrete decision variables. This problem is a combinatory optimization problem, which can be solved by some existing tools, e.g., Gurobi Optimizer [21] and Ipsolve [22]. But the time exhausted by these tools are exponentially increased with the problem scale in general, which makes them not suitable for solving large scale problems. Therefore, in the next section, a food distribution router planning method is proposed based on genetic algorithm to provide a router solution in polynomial time.

IV. IMPROVED GENETIC ALGORITHM-BASED FOOD DISTRIBUTION

This section proposes a food distribution router planning method based on genetic algorithm (GA). To improve the performance of GA, the neighbourhood search (NS) strategy is integrated into GA, which helps to increase the diversity of populations. The proposed method, GANS, is outlined in Algorithm 1. As shown in the algorithm, at first, GANS initializes chromosomes by randomly setting the value of

Algorithm 1 GANS: The improved GA with NS for Food Distribution

Input: The information of distribution stations, vehicles, customers and their requirements;

Output: A food distribution router strategy;

```
1: Initializing chromosomes randomly;
2: while the terminal condition is not reached do
3:   Calculating fitness value for each chromosome by Algorithm 2;
4:   Updating the best fitness and the best chromosome;
5:   Executing crossover operator for randomly selected two chromosomes with a certain probability;
6:   Conducting mutation operator on each chromosome with a certain probability;
7:   For each chromosome, swapping two genes randomly, to produce a new chromosome;
8:   Using tournament selection operator to select chromosomes for the next evolution;
9: end while
10: return the distribution router strategy decoded from the best chromosome by Algorithm 2;
```

each gene (line 1 in Algorithm 1), where each chromosome represents an assignment of customers to vehicles. In each chromosome, There is a corresponding relationship between genes and customers, and thus its length is the number of customers. The value of a gene represent the vehicle allocated to the corresponding customer for its food distribution. After the chromosome initialization, GANS repeats the chromosome evolution by crossover and mutation crossovers as well as NS strategy (lines 2–9 in Algorithm 1).

In the stage of the chromosome evolution, a fitness function must be designed for evaluating the quality of each chromosome. In this paper, the fitness function is defined as the optimization objective (11), i.e.,

$$fitness = W - C, \quad (15)$$

where W is the total amount of distributed foods, which is $\sum_{i=1}^V \sum_{j=1}^U (z_{i,j} \cdot (qa_j + qr_j + qf_j))$. C is the total cost for food distribution, which is $\sum_{i=1}^V C_i$.

Given a chromosome, its fitness value can be calculated as following, shown in Algorithm 2. First, the chromosome is decoded into the assignment of customers to vehicles (line 1 in Algorithm 2). Then for each vehicle (line 2 in Algorithm 2), first fit heuristic method is applied for loading foods of customers assigned to the vehicle (line 3–11 in Algorithm 2). When foods required by a customer are loaded, their weights are accumulated to W (line 7 in Algorithm 2). After food loading for a vehicle, its cost can be calculated by Eq. (10), and the cost is accumulated to C (line 9 in Algorithm 2). In the end of Algorithm 2, the fitness value is achieved by $W - C$ (line 12 in Algorithm 2).

In each chromosome evolution, GANS first evaluates the fitness for every chromosome using Algorithm 2 (line 3 in Algorithm 1), and find the best fitness (new one). Then, if the best fitness is better than the current one achieved in preceding evolutions, GANS updates the current best fitness and the current best chromosome to the new best fitness and its corresponding chromosome, respectively (line 4 in Algorithm 1). After this, GANS evolves chromosomes by

Algorithm 2 Calculating the Fitness Value for a Chromosome

Input: A chromosome;

Output: The fitness value of the chromosome;

```
1: Decoding the chromosome into the customer assignment to vehicles;
2: for Each vehicle do
3:   for Each customer assigned to the vehicle do
4:     if The vehicle satisfy the customer's requirements then
5:       Loading foods required by the customer to the vehicle;
6:       Updating the residual capacity of the vehicle;
7:       Accumulating the amount of distributed foods ( $W$ );
8:     end if
9:   Calculating the distribution cost of the vehicle by Eq. (10), and accumulating it ( $C$ ).
10: end for
11: end for
12: return  $W - C$ ;
```

crossover, mutation, and NS to generate offspring, and the selection operator to produce a new generation (lines 5–8 in Algorithm 1), as detailed following:

Crossover: For the crossover operation, each chromosome is picked with a certain probability, and the one-point crossover operator is performed for every two picked chromosomes to create two new chromosomes (offspring) (line 5 in Algorithm 1).

Mutation: For each chromosome, it has a certain probability to be mutated to produce a new offspring (line 6 in Algorithm 1). In this paper, the uniform mutation is chose due to its effectiveness for large-scale problems.

Neighbourhood Search (NS): To increase the diversity of chromosomes for improving the global search ability of GA, we propose to integrate NS strategy into GA (line 7 in Algorithm 1). Specifically, for each chromosome, GANS randomly generates two points, and swaps genes in these two points, which generates a new offspring.

Selection: To realize the evolution, a selection operator must be performed for the population consisted of chromosomes in the current generation and new offspring produced by above operators, to produce a new generation (line 8 in Algorithm 1). GANS employs the tournament selection which retain the best chromosomes to the next generation.

After the generation evolution, GANS has the best chromosome with the best fitness. Then, by Algorithm 2, a distribution router strategy is provided from the best chromosome.

V. PERFORMANCE EVALUATION

To evaluate the performance of our proposed method, a simulated experiment environment is generated. In the simulated environment, as shown in Fig. 1, the distribution coverage is a square area from (-100, -100) to (100, 100) in km. Four distribution stations are respectively deployed on the points of (50, 50), (-50, 50), (-50, -50), and (50, -50). There are total 10 delivery vehicles. The probabilities of every vehicle having the abilities of distributing refrigerate foods and frozen foods are both 50%. The loading capacity of each vehicle is randomly set in the range [100, 1000] kg for each kind of foods. The startup cost is set as [1, 10] thousand dollars, randomly. The

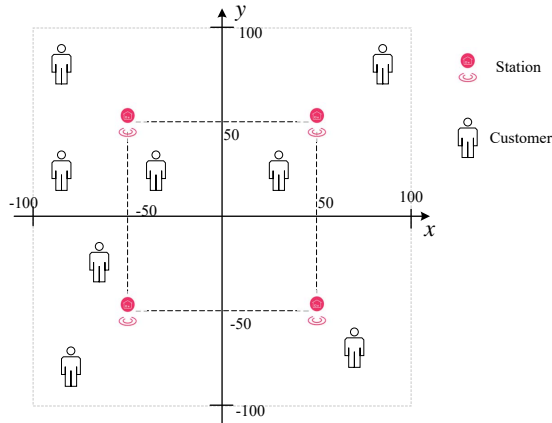


Fig. 1. The Simulated Food Distribution Environment

transport costs of every vehicle are 0.5–1 and 5–10 dollars per kilometre respectively when the vehicle is empty and full-load. There are 100 customers randomly distributed in the service area. The probabilities of each customer requiring refrigerate and frozen foods are both 50%. The amount of foods required by every customer is randomly set in the range of [10, 100] kg.

GANS is compared with the following food distribution router planning methods:

- *Random method* randomly generates a customer assignment solution to vehicles, and uses Algorithm 2 to provide a router solution.
- *Greedy method* assigned every customer to the vehicle that can satisfy its requirements and is closest to it.
- *Particle Swarm Optimization-based method (PSO)* exploits PSO algorithm using Algorithm 2 for evaluating the fitness of particle positions.
- *Genetic algorithm-based method (GA)* is same to GANS except that GA doesn't use NS for its evolution.

The performance of each method is evaluated from the following three aspects. The amount of distributed foods, the cost efficiency, and the customer satisfaction. The first one metric is the major optimization objectives this paper focused on. The second one is the distributed food amount per dollar, which is the ratio of the distributed food amount to the total cost for the food distribution. For the customer satisfaction, the ratio between numbers of served customers and all customers is used to quantify it. The experiment is repeated 20 times, and the results are given in Table I, II, and III. For each time, the environment is identical for all methods' evaluation.

As shown in these results, GANS achieves 15.82%–46.70% more distributed food amount, 17.23%–71.53% higher cost efficiency, and 9.90%–47.18% better customer satisfaction, on average, compared with other methods. This indicates that GANS performs good in all of three aspects. This is benefited from the global search ability of GA and the improvement of NS strategy.

TABLE I. THE DISTRIBUTED FOOD WEIGHTS ACHIEVED BY VARIOUS ROUTER PLANNING METHODS.

	Number	Random	Greedy	PSO	GA	GANS
Original experiment data	1	5365.95	6386.47	6462.48	6572.11	8120.50
	2	4716.03	6296.85	6719.02	6323.99	7905.31
	3	3778.02	4910.95	6112.24	6050.47	7120.83
	4	4219.83	4524.88	5855.58	5316.13	6725.65
	5	4507.84	5434.98	6443.13	5975.87	7054.76
	6	1852.15	2915.05	3146.72	3211.99	3604.26
	7	2981.32	4569.87	4287.65	4600.00	5694.37
	8	4602.64	7642.32	7797.57	7526.78	8663.24
	9	5137.87	6687.71	6014.42	6285.05	7677.78
	10	4974.85	5978.76	6971.77	6690.13	7758.95
	11	3411.31	4049.31	4098.26	4109.53	5053.88
	12	3227.71	3750.55	4643.57	4748.73	5504.71
	13	3321.59	4302.72	5025.42	4520.84	5692.75
	14	3105.22	4183.98	4341.57	3834.90	4871.31
	15	4084.14	5416.45	6112.63	5759.28	6949.34
	16	3351.64	5971.50	6164.76	5626.11	7074.99
	17	3912.65	5844.40	6086.42	5802.96	7167.40
	18	5033.22	6635.64	6930.95	6995.47	8079.62
	19	5157.40	7005.69	7326.74	7018.82	8696.81
	20	3506.32	5653.80	5759.91	5153.69	6577.58
Statistics of improved performance of GANS	Maximum	111.09%	48.64%	32.81%	27.63%	
	Average	71.53%	26.71%	17.23%	21.44%	
	Minimum	48.15%	13.36%	9.49%	12.21%	

TABLE II. THE COST EFFICIENCY ACHIEVED BY VARIOUS ROUTER PLANNING METHODS.

	Number	Random	Greedy	PSO	GA	GANS
Original experiment data	1	88.37	100.54	98.05	103.02	115.94
	2	75.40	98.10	98.80	89.24	103.41
	3	63.63	79.75	87.83	91.14	98.38
	4	55.25	60.84	73.02	68.35	78.90
	5	70.90	87.39	94.74	89.68	98.81
	6	28.39	46.11	46.19	44.83	49.05
	7	43.46	63.06	58.16	61.41	70.19
	8	66.56	105.76	99.13	96.69	108.18
	9	64.81	79.85	73.24	75.82	85.20
	10	72.63	88.33	91.34	87.45	98.78
	11	65.97	80.35	78.22	73.18	89.18
	12	59.40	69.72	79.26	78.16	88.53
	13	58.23	74.46	80.53	73.94	85.39
	14	53.52	72.41	71.62	62.26	75.25
	15	59.01	76.63	82.89	78.40	88.73
	16	54.50	88.39	86.06	80.93	94.34
	17	64.89	88.22	85.49	83.19	95.64
	18	84.97	102.74	106.33	104.36	112.65
	19	77.97	102.28	98.68	95.77	112.41
	20	63.36	92.57	93.54	86.72	98.29
Statistics of improved performance of GANS	Maximum	73.10%	29.68%	20.68%	21.87%	
	Average	47.18%	11.93%	9.90%	13.89%	
	Minimum	31.21%	2.29%	4.29%	7.95%	

Compared with GA, GANS achieves 11.29%–30.61% more distributed food amount, 12.21%–27.63% higher cost efficiency, and 7.95%–21.87% better customer satisfaction. This verifies the effectiveness of integrating NS strategy into GA for the performance improvement.

VI. CONCLUSION

This paper studies on the router planning problem for food product suppliers to efficiently distribute multi-temperature foods with several stations. First, the problem is formulated into a combinatory optimization problem. Then, a router planning method is designed based on genetic algorithm, and its performance is improved by integrating a neighbourhood

TABLE III. THE CUSTOMER SATISFACTIONS ACHIEVED BY VARIOUS ROUTER PLANNING METHODS.

	Number	Random	Greedy	PSO	GA	GANS
Original experiment data	1	55	67	61	64	77
	2	53	70	67	67	78
	3	44	53	60	58	68
	4	47	50	61	52	66
	5	49	55	55	56	66
	6	30	42	39	41	46
	7	41	55	50	57	65
	8	55	77	70	73	82
	9	49	66	55	59	72
	10	55	63	71	69	78
	11	43	50	43	48	55
	12	41	39	46	48	54
	13	44	54	54	51	64
	14	44	50	51	47	58
	15	37	57	51	54	63
	16	44	64	58	58	71
	17	45	62	60	62	69
	18	58	72	69	69	77
	19	54	70	68	68	78
	20	38	59	55	49	64
Statistics of improved performance of GANS	Maximum	70.27%	38.46%	30.91%	30.61%	
	Average	46.70%	15.82%	18.56%	17.78%	
	Minimum	27.91%	6.49%	8.20%	11.29%	

search strategy into the genetic algorithm. Experiment results prove that our method can obtain good performance in various aspects.

There are numerous crossover, mutation, NS, and selection operators that can be applied for GANS. The influences of these operators on the performance of GANS should be studied to implement algorithm instances with better performance for various food distribution scenarios. This is one of our future works.

ACKNOWLEDGMENT

The authors would like to thank the anonymous reviewers for their valuable comments and suggestions. The research was supported by the National Natural Science Foundation of China (Grant No. 61872043, 61975187, 62072414), the key scientific and technological projects of Henan Province (Grant No. 202102210149, 212102210096), the Key Scientific Research Projects of Henan Higher School (Grant No. 21A520050), Qin Xin Talents Cultivation Program, Beijing Information Science & Technology University (No. QXTCP B201904), and the fund of the Beijing Key Laboratory of Internet Culture and Digital Dissemination Research (Grant No.ICDDXN004).

REFERENCES

- [1] M. of Industry and I. T. of the PRC, "Production and marketing of food industry from january to december 2021 (in chinese)," https://www.miit.gov.cn/gyhxxhb/jgsj/xfpgys/gzdt/art/2022/art_3d9653b1e27b4a8caed9aa850494a5e2.html, March 2022.
- [2] iiMedia Research, "Data analysis of e-commerce industry: the scale of chinese e-commerce market for fresh foods will reach 311.74 billion yuan in 2021 (in chinese)," <https://www.iimedia.cn/c1061/75806.html>, December 2020.
- [3] S. Chen, Y. Wang, S. Han, and M. K. Lim, "Evaluation of fresh food logistics service quality using online customer reviews," *International Journal of Logistics Research and Applications (In Press)*, vol. 0, no. 0, pp. 1–17, 2021.
- [4] N. Paech, C. Sperling, and M. Rommel, "Cost effects of local food enterprises: Supply chains, transaction costs and social diffusion," in *Food System Transformations*. Taylor & Francis, 2021.
- [5] S. Jagtap, F. Bader, G. Garcia-Garcia, H. Trollman, T. Fadji, and K. Salonitis, "Food logistics 4.0: Opportunities and challenges," *Logistics*, vol. 5, no. 1, p. 2, 2020.
- [6] S. Pratap, S. K. Jauhar, S. K. Paul, and F. Zhou, "Stochastic optimization approach for green routing and planning in perishable food production," *Journal of Cleaner Production*, vol. 333, p. 130063, 2022.
- [7] S. Faramarzi-Oghani, P. D. Neghabadi, E.-G. Talbi, and R. Tavakkoli-Moghaddam, "Meta-heuristics for sustainable supply chain management: a review," *International Journal of Production Research (In Press)*, vol. 0, no. 0, pp. 1–31, 2022.
- [8] N. Wang, D. Hu, J. Xu, and J. Zhao, "Time-dependent vehicle routing of urban cold-chain logistics based on customer value and satisfaction," *China Journal of Highway and Transport*, vol. 34, no. 9, pp. 297–308, 1 2021.
- [9] X. Zhu and Y. Wang, "Optimization of pharmaceutical cold chain logistics distribution route based on traffic conditions," *Science Technology and Engineering*, vol. 21, no. 4, pp. 1548–1554, 2 2021.
- [10] W. Fang, S. Ai, Q. Wang, and J. Fan, "Research on cold chain logistics distribution path optimization based on hybrid ant colony algorithm," *Chinese Journal of Management Science*, vol. 27, no. 11, pp. 107–115, 1 2019.
- [11] T. Ren, T. Luo, Z. Li, S. Xiang, H. Xiao, and L. Xing, "Knowledge based ant colony algorithm for cold chain logistics distribution path optimization," *Control and Decision*, vol. 37, no. 3, pp. 545–554, 3 2022.
- [12] D. Li, Q. Cao, M. Zuo, and F. Xu, "Optimization of green fresh food logistics with heterogeneous fleet vehicle route problem by improved genetic algorithm," *Sustainability*, vol. 12, no. 5, p. 1946, 2020.
- [13] D. Prajapati, A. R. Harish, Y. Daultani, H. Singh, and S. Pratap, "A clustering based routing heuristic for last-mile logistics in fresh food e-commerce," *Global Business Review (In Press)*, vol. 0, no. 0, pp. 1–14, 2020.
- [14] Y. Wang, J. Zhang, X. Guan, M. Xu, Z. Wang, and H. Wang, "Collaborative multiple centers fresh logistics distribution network optimization with resource sharing and temperature control constraints," *Expert Systems with Applications*, vol. 165, p. 113838, 2021.
- [15] Y. P. Tsang, C. H. Wu, H. Y. Lam, K. L. Choy, and G. T. S. Ho, "Integrating internet of things and multi-temperature delivery planning for perishable food e-commerce logistics: a model and application," *International Journal of Production Research*, vol. 59, no. 5, pp. 1534–1556, 2021.
- [16] G. Liu, J. Hu, Y. Yang, S. Xia, and M. K. Lim, "Vehicle routing problem in cold chain logistics: A joint distribution model with carbon trading mechanisms," *Resources, Conservation and Recycling*, vol. 156, p. 104715, 2020.
- [17] H. M. Stellingwerf, L. H. Groeneveld, G. Laporte, A. Kanellopoulos, J. M. Bloemhof, and B. Behdani, "The quality-driven vehicle routing problem: Model and application to a case of cooperative logistics," *International Journal of Production Economics*, vol. 231, p. 107849, 2021.
- [18] Y. Ding, "Simulation of vehicle distribution path optimization for multi-temperature co-distribution cold chain logistics," *Journal of Shenyang University of Technology*, vol. 43, no. 3, pp. 311–316, 1 2021.
- [19] Y. Zhao, G. Tang, and S. Zhu, "Research of air distribution characteristic for single evaporator multiple temperature zones refrigerated truck," *Food & Machinery*, vol. 33, no. 1, pp. 119–121, January 2017.
- [20] X. Xiaofeng and Z. Xuelai, "Simulation and experimental investigation of a multi-temperature insulation box with phase change materials for cold storage," *Journal of Food Engineering*, vol. 292, p. 110286, 2021.
- [21] L. Gurobi Optimization, "Gurobi - the fastest solver," <https://www.gurobi.com/>, 2022.
- [22] K. Eikland and P. Notebaert, "Lpsolve: Mixed integer linear programming (milp) solver," <https://sourceforge.net/projects/lpsolve/>, January 2021.

An Efficient System for Real-time Mobile Smart Device-based Insect Detection

Thanh-Nghi Doan

Faculty of Information Technology, An Giang University
Vietnam National University Ho Chi Minh City, An Giang, Vietnam

Abstract—In recent years, the rapid development of many pests and diseases has caused heavy damage to the agricultural production of many countries. However, it is difficult for farmers to accurately identify each type of insect pest, and yet they have used a large number of pesticides indiscriminately, causing serious environmental pollution. Meanwhile, spraying pesticides is very expensive, and thus developing a system to identify crop-damaging pests early will help farmers save a lot of money while also contributing to the development of sustainable agriculture. This paper presents a new efficient deep learning system for real-time insect image recognition on mobile devices. Our system achieved an accuracy of $mAP@0.5$ with the YOLOv5-S model of 70.5% on the 10 insect dataset and 42.9% on the IP102 large-scale insect dataset. In addition, our system can provide more information to farmers about insects such as biological characteristics, distribution, morphology, and pest control measures. From there, farmers can take appropriate measures to prevent pests and diseases, helping reduce production costs and protecting the environment.

Keywords—Deep learning; real-time insect pest detection; YOLOv5; mobile devices

I. INTRODUCTION

Climate change has caused pests to multiply, grow quickly, and cause significant damage to the world's agricultural economy [1]. Pests are estimated to cost up to 40% of worldwide agricultural output each year, according to the Food and Agriculture Organization. At present, plant diseases cost the global economy almost \$220 billion each year, while invading insects cost at least \$70 billion [2]. Therefore, farmers in many countries have used a large number of different pesticides to protect crops and ensure the quality of agricultural products. However, due to a lack of specialized knowledge, many farmers have difficulty detecting and correctly identifying pests and diseases that cause crop damage. As a result, most farmers did not have reasonable pest control measures, including the indiscriminate and improper use of a large number of pesticides on a large scale. This not only increases production costs but also seriously pollutes the environment, destroys beneficial insects, disrupts ecosystem balance, and damages the health and living environment of humans and many other species. As a result, it is critical to research information technology systems in order to accurately, efficiently, quickly, and conveniently identify pests and diseases that harm crops. This system will aid in the resolution of the aforementioned issues, thereby contributing significantly to long-term agricultural development. Such a system must be designed for real-time identification, be simple to install and

use, and be appropriate for farmers' level of knowledge and actual working conditions, where each farmer typically has a smartphone with a basic configuration. Therefore, an automatic system to identify pests on plants using inexpensive smart phones must be developed and deployed. The primary goal is to efficiently detect insects in real-time manner, providing farmers with greater convenience and mobility in early pest treatment. Although smartphones have penetrated a variety of industries, including manufacturing, medicine, and health care, use of mobile devices in agriculture has been slower. Farmers understand the need for mobile agriculture as technology advances, which not only allow farmers to execute agricultural activities more effectively using their phones, but also transform arable farming into smart agriculture. In this research, a real-time insect object detection system is built in the context of large-scale insect pest datasets. Our system is based on the YOLOv5-S model and has been integrated onto mobile devices with limited hardware configurations, making it ideal for farmers in the field.

II. BACKGROUND STUDY

Much of the prior research has presented real-time image-based recognition systems for mobile devices based on various CNN architectures. To recognize leaves from images, the authors of [3] have developed a novel extraction and classification technique. The insect population and illness regions in the segmented images are then calculated using a region-labeling technique. A mathematical morphological algorithm is utilized to separate the items in the zones of adhesion. The proposed solution is tested in the field and deployed on mobile smart devices. The experimental findings reveal that the suggested technique has high efficiency and strong recognition performance. The authors of [4] have created a pest infestation early warning system for paddy farming that includes an Android application and a web-based application. The Agriculture Department will use the technology to identify insect infestations, locate them, and alert the early warning system. The technology will be able to enter the farmers' infestation data into databases. The data will be utilized by the agronomist to assess the paddy plot's risk in four stages. The number of pests, kind of pest, location, and present circumstances will be used to classify each stage. After the agronomist has completed their review, the system will send an email to the farmers informing them of the quality of their current paddy plot. The researchers from [5] suggested an image processing technique and a smartphone application to recognize and count insects. The nonuniform brightness of insect images obtained with mobile phones is released using a

sliding window-based binarization, and then connected domain-based histogram statistics are utilized to identify and count the insects in stored grain. Finally, testing using an Android application shows that the proposed technique can count random bug photographs from mobile phones with 95% accuracy, which is superior to the previous method. In [6], MAESTRO, a novel grasshopper identification framework that employs deep learning to recognize insects in RGB pictures, is demonstrated. MAESTRO uses a state-of-the-art two-stage deep learning training approach. The framework may be used on cellphones as well as desktop PCs. The authors of [7] offer an AI-based pest detection system that addresses the challenge of identifying scale pests using photos. Scale pests are detected and localized in the image using deep-learning-based object identification models such as faster region-based convolutional networks, single-shot multibox detectors, and YOLOv4. Among the algorithms, YOLOv4 had the highest classification accuracy, with 100% in mealybugs, 89% in Coccidae, and 97% in Diaspididae. A smartphone application based on the trained scale insect detection model has been developed to assist farmers in identifying pests and administering appropriate pesticides to reduce crop losses. The researchers at [8] have studied the best machine learning approach for developing a pest detection model for mobile information systems. The article [9] proposed a novel smartphone application that uses a deep-learning method to automatically categorize pests for the benefit of professionals and farmers. Faster R-CNN is used in the created application to do insect pest recognition using cloud computing. To assist farmers, a database of suggested pesticides is linked to the reported crop pests. This research has been validated for five distinct pest species. The suggested Faster R-CNN had the greatest accuracy in identification rate of 99% for all pest images analyzed. The study [10] provided a novel method for establishing the use of hand-held image capture of insect traps for pest detection in vineyards by embedding artificial intelligence into mobile devices. Their solution integrates many computer vision technologies to enhance numerous areas of picture quality and appropriateness. The extensive review [11] examines deep learning framework methodologies and applications in smart pest monitoring, with a focus on insect pest categorization and detection using field photos. The methodology and technical information created in insect pest classification and detection using deep learning are consolidated and distilled during multiple processing stages: picture collection, data preprocessing, and modeling strategies. Finally, a generic framework for smart insect monitoring is proposed, and future challenges and trends are discussed. In AlertTrap [12], SSD architecture implementation with different cutting-edge backbone feature extractors, such as MobileNetV1 and MobileNetV2, appears to be a viable solution to the real-time detection problem. SSD-MobileNetV1 and SSD-MobileNetV2 work well, with AP@0.5 rates of 0.957 and 1.0, respectively. YOLOv4-tiny surpasses the SSD family in AP@0.5 with 1.0; nevertheless, its throughput velocity is significantly slower, indicating that SSD models are better candidates for real-time implementation. They also ran the models via synthetic test sets that simulated predicted environmental disruptions. The YOLOv4-tiny tolerated these disruptions better than the SSD variants. By combining EfficientNet [13] and Power mean

SVM [14], the authors of the research [15] published the state of the art on insect image classification on the large-scale IP102 dataset with an accuracy of up to 71.84%. However, the abovementioned systems still have some limitations, such as the small number of pest identifications; the accuracy is not high; the equipment configuration requirements are high; and it is difficult to deploy in practice. They lack aspects such as geolocation recoding of recognized harmful pests, information about identified dangerous pests, and robust distributed mobile information frameworks. Currently, there is no real-time existing identification system for mobile devices. Therefore, this paper proposes a new real-time insect identification system with reasonable cost, efficiency, easy installation, and practical deployment on mobile devices with limited hardware configuration. Furthermore, this study also looks at lightweight network models and embedded terminal realizations, both of which are increasingly relevant and promising. The paper's main contributions are as follows:

- A novel real-time insect identification system that is ideal for mobile devices with restricted hardware configuration, easy to install, inexpensive, and user-friendly.
- The most current identification results using YOLOv5-S from the large-scale dataset IP102 are presented.
- A new system captures images and uses GPS to determine the distribution of insects in the field. This contributes to the development of a large insect database and insect distribution maps.

The rest of the article is arranged as follows. Section III describes the materials and methods used to evaluate our approach, including an overview of our system, the YOLOv5 model, and the pest insect image datasets. The experimental results and discussion are reported in Section IV. Section V presents the conclusions, limitations, and recommendations for future research.

III. MATERIALS AND METHODS

A. Overview of our System

An overview of our real-time insect identification system is shown in Fig. 1. Users can first use their mobile phones to photograph insects in a real-time manner, or they can use insect photographs found on the internet or images captured by bug traps. The YOLOv5-S model, which is already embedded into the mobile application, then identifies the insect image in real time, resulting in a very quick insect identification time. When an insect image is properly identified, the system will provide the user with detailed information on the insect, such as its name, biological characteristics, distribution, morphology, and control strategies. Our new insect recognition system can work in both online and offline mode. In the online mode, the insect identification information is sent to the Web server, which then processes and returns detailed insect information in JSON format [16]. Insect information can be viewed alongside similar images in the data warehouse. The user can also see a list of all insects, complete with detailed information and images. Users can upload insect images and shooting locations to update the data warehouse at the same time in this mode.

The entire database will be stored on the server in the online mode, making it suitable for mobile devices with limited hardware configuration and ensuring that information is always up-to-date. The application's speed, however, is determined by the available network bandwidth. In the offline mode, SQLite [17], a C-language package that creates a compact, fast, self-contained, high-reliability, full-featured SQL database engine, is used for storing insect information data on mobile devices. This mode will be very useful in cases where farmers' working environments do not have internet, such as in the fields far from urban areas, where internet, 4G, and 5G coverage are not yet available. However, in this mode, some application functions will be restricted.

B. YOLOV5

YOLOv5 [18] is a single-stage object detection system. In one-stage object identification approaches, object detection is considered as a regression issue. It estimates the class probability and the coordinates of the bounding box that will contain the object in a single step on the input picture. The backbone, neck, and head are the three main components. YOLO is another name for the head layer. The model backbone's duty is to draw attention to the image's unique features. In YOLOv5, the model backbone is a CSPNet [19] structure. The CSPNet approach divides the feature map in the base layer into two parts; some reach the transition layer through the dense block, while the other half is directly integrated with the transition layer. This not only reduces model size but also increases inference speed [20]. In this study, the YOLOv5-S model is used to develop applications on mobile devices due to its small size and model parameters, GFLOPs calculation speed and high accuracy, and lack of requirement for high hardware configuration when compared to other YOLO models such as YOLOv4 [21], YOLOX [22]. As shown in Table I, the YOLOv5-S model is relatively small in size, with a network parameter of 7.3M and a disk size of 14.2 MB, making it suitable for mobile devices with limited hardware configuration. With a GFLOPs index of 17.1, the calculating speed of the YOLOv5-S is adequate. Furthermore,

when compared to other YOLO models, the indicators of $mAP^{val}@0.5$ and the speed of the YOLOv5-S model in Table IV and Table V are quite excellent.

TABLE I. NETWORK PARAMETERS OF YOLO MODELS

Models	Params (M)	Size on disk (MB)	GFLOPs
YOLOv4	27.6	245.0	59.6
YOLOv4-tiny	5.88	23.1	6.8
YOLOv5-S	7.2	14.2	17.1
YOLOv5-M	21.2	40.8	51.4
YOLOv5-L	46.5	89.3	115.6
YOLOv5-X	86.7	167.1	219.0
YOLOX-S	9.0	68.5	26.8
YOLOX-M	25.3	193.0	73.8
YOLOX-L	54.2	413.0	155.6
YOLOX-X	99.1	757.0	281.9

C. Datasets

To create the insect pest database for machine learning models, 2,335 photos of 10 distinct pest kinds were collected from internet data sources, as shown in Fig. 2. The dataset was then split into the following proportions: 70% of the samples were utilized for training, 20% for model evaluation, and the remainder for testing. As a consequence, the result dataset has 1634 images for training, 467 images for validation, and 234 images for testing, as shown in Table II. The Labelling program [23] is utilized to manually label the insect objects and generate the .xml file containing object position information, which is then transformed into the .txt file that YOLOv5 can read. Because the IP102 data set has some constraints, such as the same class with numerous different insect stages such as larvae, caterpillars, and moths, achieving high identification efficiency is challenging. Therefore, the YOLOv5-S model was tested with 10 insect classes that were gathered by the agriculture expert volunteers.

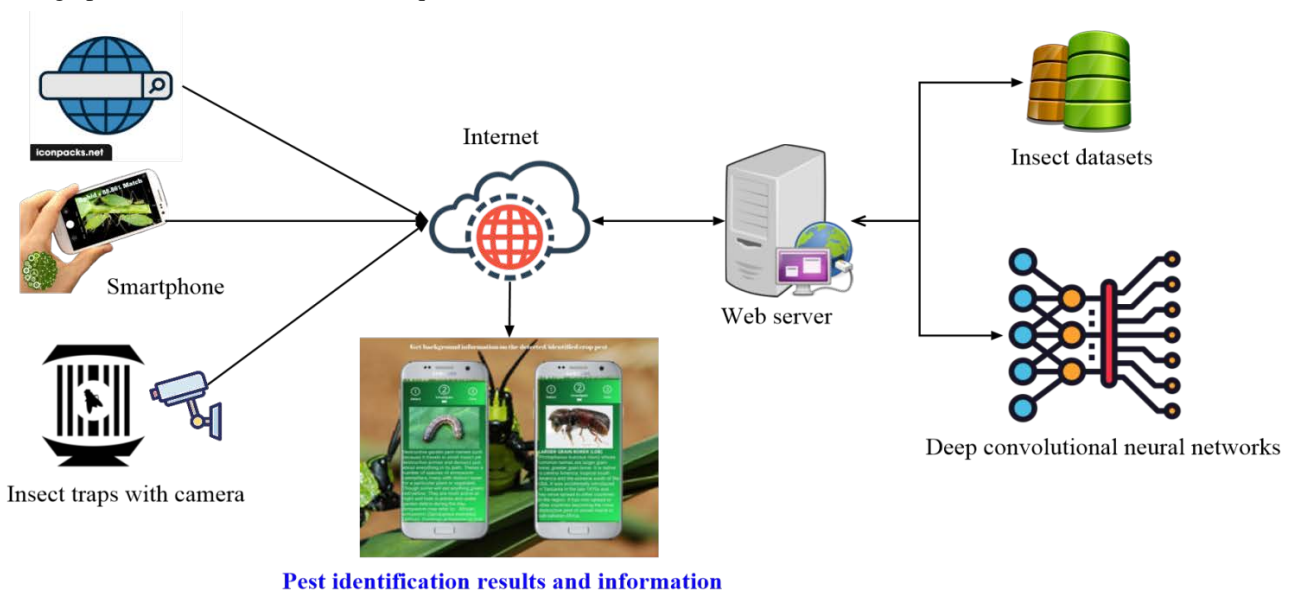


Fig. 1. Overview of our Real-time Insect Image Recognition System by Mobile Devices.



Fig. 2. Some Images of Insect Samples in the Insect10 Dataset.

TABLE II. THE NUMBER OF IMAGES IN THE INSECT10 DATASETS WITH 10 INSECT SPECIES

No	Insect name	Train	Validation	Test
1	Acalymma_vittatum	116	33	17
2	Achatina_fulica	258	74	37
3	Alticini	193	55	28
4	Asparagus_beetles	89	25	13
5	Aulacophora_similis	113	32	16
6	Cerotoma_trifurcata	86	25	12
7	Dermaptera	111	32	16
8	Leptinotarsa_decemlineata	234	67	33
9	Mantodea	185	53	26
10	Squash_bug	249	71	36
	Total	1634	467	234

In this paper, the new system was also evaluated on large-scale insect image datasets. However, collecting a large-scale insect pest image dataset is difficult due to the fact that, depending on the species and kind of insect pest, all insect pests go through several phases during their lifecycle. As a result, the insect pest pictures from the publicly available IP102 dataset [24] are used for evaluating the system. It comprises almost 75,000 photos from 102 agricultural insect pest categories. The IP102 collection includes 75,222 photos and 102 insect pest classifications, while the smallest category comprises just 71 samples. There are 18,983 annotated photos for the job of object detection. As in [24], the images with bounding box annotations were divided into training and testing sets of 15,178 and 3,798 images, respectively. Some sample images of the IP102 dataset are shown in Fig. 3.



Fig. 3. Some Images of Insect Samples in the IP102 Dataset.

IV. RESULT AND DISCUSSION

A. Experimental Setup and Training

All YOLO model training experiments were carried out on Google Colab using a Tesla K80 24 GB GPU. Algorithms are written in the Python and Keras programming languages. To train the models, the experimental setup is as follows: a learning rate of 0.01, an image size of 640 pixels, a batch size of 16, and 150 epochs for YOLOv5, YOLOX, and 2,000 epochs for YOLOv4. The Stochastic Gradient Descent [25] is used as the optimization algorithm. Devices with low configuration are utilized to conduct tests on mobile devices, as indicated in Table III.

TABLE III. SMARTPHONE DEVICE CONFIGURATION AND APPLICATION DEVELOPMENT ENVIRONMENT

Smartphone hardware configuration	The Samsung Galaxy A30 is powered by a Samsung Exynos 7 Octa 7904 processor with MHz and 8 cores. The powerful processor and 3000.0 MB of RAM give incredible performance, ensuring trouble-free operation of even the most complex program or game. The Samsung Galaxy A30 uses a microSDXC memory card. The phone carries over the 15.93-megapixel rear camera sensor at the back of the device. The front camera of the Samsung has 15.93. It gives us very high quality photos and videos with a great camera interface. The device has a 6.4-inch SUPER AMOLED display. It gives a decent display quality and a great gradation between warm and cold colors. The OS is Android 10.
Programinng language to build applications	Programing language: Java, Development Environment: Android Studio
The light	Normal luster intensity

B. Evaluation Metrics

Mean Average Precision (mAP) is a popular metric for assessing the performance of object detecting systems. The mAP computes a score by comparing the ground-truth bounding box to the detected box. The higher the score, the more precise is the model's detections. The mAP formula is based on the following sub metrics: Confusion Matrix, Intersection over Union (IoU), Recall, Precision. To create a confusion matrix, the experiments present four attributes: True Positives (TP): The model predicted a label and matched it correctly as per ground truth. True Negatives (TN): The model does not predict the label and is not a part of the ground truth. False Positives (FP): The model predicted a label, but it is not a part of the ground truth. False Negatives (FN): The model does not predict a label, but it is part of the ground truth.

In Equation (1), IoU denotes the overlap of anticipated bounding box coordinates with ground truth box coordinates. It explains how an object identification algorithm creates prediction scores. The definition of IoU is described in Fig. 4. Higher IoU implies that the anticipated bounding box coordinates are similar to the ground truth box coordinates.

$$IoU = \frac{\text{area of overlap}}{\text{area of union}} = \frac{\text{area of intersection}}{\text{area of union}} \quad (1)$$

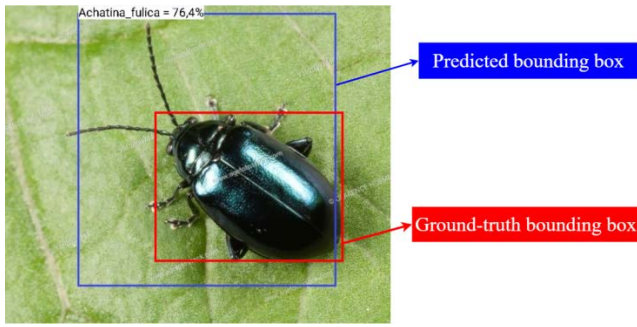


Fig. 4. IoU Definition.

In Equation (2), Precision refers to how successfully you can identify true positives (TP) from all positive predictions. In Equation (3), Recall measures how well you can find true positives (TP) out of all predictions (TP+FN).

$$Precision = \frac{TP}{TP+FP} \quad (2)$$

$$Recall = \frac{TP}{TP+FN} \quad (3)$$

In Equation (4), Average Precision is calculated as the weighted mean of precision at each threshold; the weight is the increase in recall from the prior threshold. In Equation (5), Mean Average Precision is the average of the AP of each class. However, the interpretation of AP and mAP varies in different contexts. On the validation datasets, the $mAP^{val}@0.5$ means the average mAP with IoU thresholds over 0.5. The $mAP^{val}@0.5:0.95$ means average mAP over different IoU thresholds, from 0.5 to 0.95, step 0.05.

$$AP = \sum_{k=0}^{k=n-1} [Recall(k) - Recall(k+1)] * Precision(k) \quad (4)$$

$n = \text{number of thresholds}$

$$mAP = \frac{1}{n} \sum_{k=1}^{k=n} AP_k \quad (2)$$

$AP_k = \text{the AP of class } k, \text{ and } n = \text{the number of classes}$

C. Experimental Results and Discussion

The experiment was conducted to analyze the backbone of models, input image size, $mAP@IoU:0.5$ and $mAP@IoU:0.5:0.95$ metrics as a result of the training. Table IV and Fig. 5 show the results of four different model variations on the Insect10 dataset. On the Insect10 dataset, the numerical results in Fig. 5 demonstrate that the new mobile application has a relatively high success rate in precision, recall and mAP for pest object recognition. For instance, the detection performance of the Alcalymma insect has the lowest $mAP@IoU:0.5$ identification accuracy of 0.45, while the detection performance of Leptinotarsa has the highest at 0.979. Our application is based on the YOLOv5-S model, which was trained on Insect10 datasets with 10 different insect species. The actual results show that, when compared to other object detection methods, YOLO has a faster recognition speed and can almost identify objects in real-time manner. Fig. 7 shows some examples of successful insect recognition on mobile devices using the Insect10 datasets.

Our approach has also been evaluated on the large-scale dataset IP102 [24] to see how well it scales on these datasets.

As shown in Table V and Fig. 6, our system has achieved a promising performance of $mAP^{val}@0.5$ accuracy of 42.9% with the YOLOv5-S model. This result shows that the new approach outperforms several previous approaches that were reported in [24]. However, insect object detection was still more challenging using the IP102 dataset. The reason is that the insect pests in the image are difficult to detect due to their color appearance and the image backgrounds are very similar. In addition, the morphology of an insect pest issue, such as a moth, can vary substantially as it develops. Fig. 8 depicts some images of successful insect recognition using the IP102 dataset on a mobile device. This indicates that our approach offers several benefits over existing methods, including the ability to handle massive data sets with excellent accuracy. Moreover, this new system may also be implemented on low-cost mobile devices with minimal hardware configuration. In addition, as illustrated in Fig. 9, the usage of matching pesticides is integrated with the pest categorization findings to advise professionals and farmers. In the near future, this system will be implemented on new devices like the NVIDIA Jetson Nano Developer Kit [26], which have a higher hardware configuration, a lower cost, a smaller footprint, and a better level of durability.

TABLE IV. SIMULATION RESULTS OF YOLOV4, YOLOV5, AND YOLOX MODELS ON THE INSECT10 DATASET

Models	Backbone	$mAP^{val}@0.5$	$mAP^{val}@0.5:0.95$
YOLOv4	CSPDarknet53	84.9	63.2
YOLOv4-tiny	CSPDarknet53	64.4	48.3
YOLOv5-S	Darknet-53	70.5	35.9
YOLOv5-M	Modified CSP v5	76.6	42.7
YOLOv5-L	Modified CSP v5	78.9	46.8
YOLOv5-X	Modified CSP v5	73.0	40.9
YOLOX-S	Darknet-53	84.8	58.5
YOLOX-M	Modified CSP v5	82.3	61.9
YOLOX-L	Modified CSP v5	84.0	65.0
YOLOX-X	Modified CSP v5	83.0	64.0

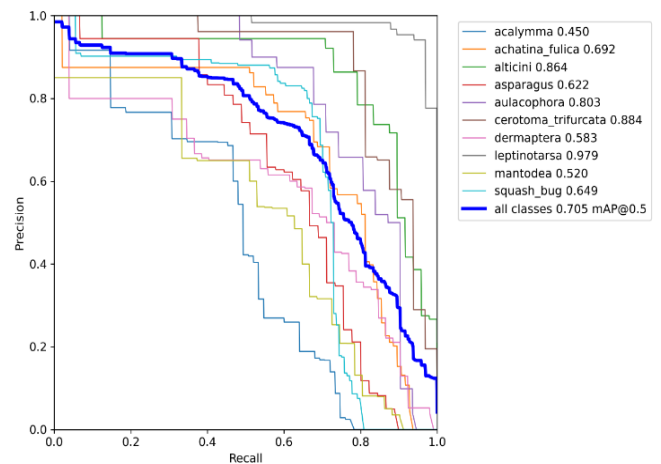


Fig. 5. Precision and Recall of Insect Recognition Results on the Insect10 Dataset using the YOLOv5-S Model.

TABLE V. SIMULATION RESULTS OF YOLOV4, YOLOV5, AND YOLOX MODELS ON THE IP102 DATASETS

Models	Backbone	mAP ^{val} @0.5	mAP ^{val} @0.5:0.95
YOLOv4	CSPDarknet53	39.2	20.1
YOLOv4-tiny	CSPDarknet53	36.1	19.0
YOLOv5-S	Darknet-53	42.9	24.0
YOLOv5-M	Modified CSP v5	47.4	27.9
YOLOv5-L	Modified CSP v5	50.1	29.9
YOLOv5-X	Modified CSP v5	54.0	32.5
YOLOX-S	Darknet-53	52.3	34.1
YOLOX-M	Modified CSP v5	54.2	35.1
YOLOX-L	Modified CSP v5	53.9	34.7
YOLOX-X	Modified CSP v5	54.1	34.9

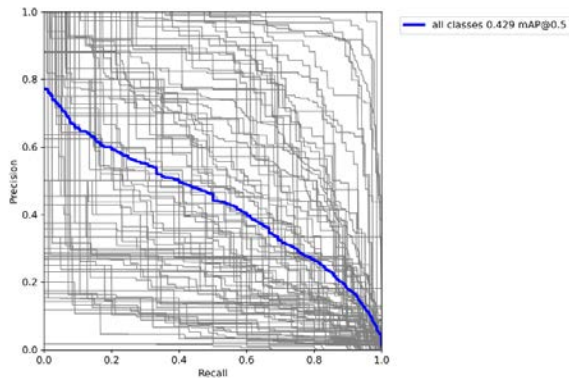


Fig. 6. Precision and Recall of Insect Recognition Results on the IP102 Dataset using the YOLOv5-S Model.



Fig. 7. Some Images were Successfully Detected on Mobile Devices using the Insect10 Dataset.



Fig. 8. Some Images were Successfully Detected on Mobile Devices using the IP102 Dataset.

The information on insect GPS location and density will be extremely useful for several Integrated Pest Management systems. Therefore, our systems are designed to allow users to automatically record this information. Then, a real-time insect distribution density map is created using this data, as illustrated in Fig. 10. This map will assist expert users in tracking and forecasting the density and evolution of insect infections over large areas. At the same time, it is possible to evaluate the potential effects of insect pests on agriculture and ecosystem production.

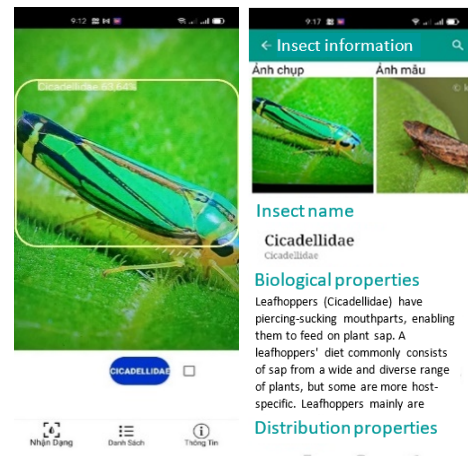


Fig. 9. The user Interface Screen shows the Successful Insect Recognition and Detailed Insect Information on a Mobile Device.



Fig. 10. The Insect Distribution Map was constructed based on GPS Location Information from the user's Insect Photos.

V. CONCLUSION AND FUTURE RESEARCH WORK

This paper presents an efficient system for real-time mobile smart device-based insect detection. Our system was developed based on the YOLOv5-S model because of its lightweight convolutional neural network and is thus suitable for mobile devices with limited hardware configuration. Moreover, insect pest detection and classification may be incorporated into hardware that farmers can utilize across a wide range of situations to safeguard their farms from pests. Therefore, our method has numerous advantages in terms of real-time insect identification, low cost, simple implementation, and practical implementation. The numerical results showed that the new system achieved 70.5% classification accuracy with mAP@0.5 on the Insect10 dataset and 42.9% accuracy with the large dataset IP102. This is the best insect pest detection result with YOLOv5-S ever reported from the largest insect dataset, IP102. However, these mAP accuracy results are still low when compared to the accuracy required for actual insect detection for agricultural production. Consequently, the next task will be to investigate more efficient recognition models in order to improve the accuracy and number of insects. Simultaneously, this work will be continued to study on better mobile devices, such as the NVIDIA Jetson Nano Developer Kit, which has a central processing unit, a graphical processing unit, a web camera, and currently only a low charge, allowing larger convolutional neural network models to be installed.

ACKNOWLEDGMENT

This study was funded by the National Geographic Society Exploration Grants (NGS-KOR-59552T-19), Microsoft AI for Earth, and the support of agriculture experts from An Giang University and Vietnam National University in Ho Chi Minh City, Vietnam.

REFERENCES

- [1] S. Skendžić, M. Zovko, I. P. Živković, V. Lešić, and D. Lemić, "The impact of climate change on agricultural insect pests," vol. 12, no. 5, 2021.
- [2] "New standards to curb the global spread of plant pests and diseases." Food and Agriculture Organization of the United Nations (FAO), 2020, [Online]. Available: <http://www.fao.org/news/story/en/item/1187738/icode/>. [Last Access: 1-07-2020].
- [3] K. Wang, Z. Shuifa, Z. Wang, Z. Liu, and F. Yang, "Mobile smart device-based vegetable disease and insect pest recognition method," *Intell. Autom. Soft Comput.*, vol. 19, 2013, doi: 10.1080/10798587.2013.823783.
- [4] H. Nasir, A. N. Aris, A. Lajis, K. Kadir, and S. I. Safie, "Development of Android Application for Pest Infestation Early Warning System," in 2018 IEEE 5th International Conference on Smart Instrumentation, Measurement and Application (ICSIMA), 2018, pp. 1–5, doi: 10.1109/ICSIMA.2018.8688774.
- [5] C. Zhu, J. Wang, H. Liu, and H. Mi, "Insect Identification and Counting in Stored Grain: Image Processing Approach and Application Embedded in Smartphones," *Mob. Inf. Syst.*, vol. 2018, no. ii, 2018, doi: 10.1155/2018/5491706.
- [6] P. Chudzik et al., "Mobile Real-Time Grasshopper Detection and Data Aggregation Framework," *Sci. Rep.*, vol. 10, no. 1, p. 1150, 2020, doi: 10.1038/s41598-020-57674-8.
- [7] J. W. Chen, W. J. Lin, H. J. Cheng, C. L. Hung, C. Y. Lin, and S. P. Chen, "A smartphone-based application for scale pest detection using multiple-object detection methods," *Electron.*, vol. 10, no. 4, pp. 1–14, 2021, doi: 10.3390/electronics10040372.
- [8] S. A. Lakmal Perera, "Pest Detecting Mobile Information System," 2021.
- [9] M. E. Karar, F. Alsunaydi, S. Albusaymi, and S. Alotaibi, "A new mobile application of agricultural pests recognition using deep learning in cloud computing system," *Alexandria Eng. J.*, vol. 60, no. 5, pp. 4423–4432, 2021, doi: 10.1016/j.aej.2021.03.009.
- [10] P. Faria, T. Nogueira, A. Ferreira, C. Carlos, and L. Rosado, "AI-Powered Mobile Image Acquisition of Vineyard Insect Traps with Automatic Quality and Adequacy Assessment," *Agronomy*, vol. 11, no. 4, 2021, doi: 10.3390/agronomy11040731.
- [11] W. Li, T. Zheng, Z. Yang, M. Li, C. Sun, and X. Yang, "Classification and detection of insects from field images using deep learning for smart pest management: A systematic review," *Ecol. Inform.*, vol. 66, p. 101460, 2021, doi: 10.1016/j.ecoinf.2021.101460.
- [12] A. D. Le, D. A. Pham, D. T. Pham, and H. B. Vo, "AlertTrap: {A} study on object detection in remote insects trap monitoring system using on-the-edge deep learning platform," *CoRR*, vol. abs/2112.1, 2021, [Online]. Available: <https://arxiv.org/abs/2112.13341>.
- [13] M. Tan and Q. V. Le, "EfficientNet: Rethinking model scaling for convolutional neural networks," 36th Int. Conf. Mach. Learn. ICML 2019, vol. 2019-June, pp. 10691–10700, 2019.
- [14] J. Wu, "Power mean SVM for large scale visual classification," *Proc. IEEE Comput. Soc. Conf. Comput. Vis. Pattern Recognit.*, pp. 2344–2351, 2012, doi: 10.1109/CVPR.2012.6247946.
- [15] D. T. Nghi, "Pest insect classification using efficientnet and power mean svm," 2021, doi: 10.15625/vap.2021.0050.
- [16] F. Pezoa, J. L. Reutter, F. Suarez, M. Ugarte, and D. Vrgoč, "Foundations of JSON schema," in Proceedings of the 25th International Conference on World Wide Web, 2016, pp. 263–273.
- [17] R. D. Hipp, "SQLite." 2020, [Online]. Available: <https://www.sqlite.org/index.html>.
- [18] G. Jocher, "YOLOv5." Zenodo, 2020, doi: 10.5281/zenodo.4154370.
- [19] C. Y. Wang, H. Y. Mark Liao, Y. H. Wu, P. Y. Chen, J. W. Hsieh, and I. H. Yeh, "CSPNet: A new backbone that can enhance learning capability of CNN," *IEEE Comput. Soc. Conf. Comput. Vis. Pattern Recognit. Work.*, vol. 2020-June, pp. 1571–1580, 2020, doi: 10.1109/CVPRW50498.2020.00203.
- [20] R. Xu, H. Lin, K. Lu, L. Cao, and Y. Liu, "A forest fire detection system based on ensemble learning," *Forests*, vol. 12, no. 2, pp. 1–17, 2021, doi: 10.3390/f12020217.
- [21] A. Bochkovskiy, C.-Y. Wang, and H.-Y. M. Liao, "YOLOv4: Optimal Speed and Accuracy of Object Detection," 2020, [Online]. Available: <http://arxiv.org/abs/2004.10934>.
- [22] Z. Ge, S. Liu, F. Wang, Z. Li, and J. Sun, "{YOLOX:} Exceeding {YOLO} Series in 2021," *CoRR*, vol. abs/2107.0, 2021, [Online]. Available: <https://arxiv.org/abs/2107.08430>.
- [23] Tzutalin, "LabelImg." 2015, [Online]. Available: <https://github.com/tzutalin/labelImg>.
- [24] X. Wu, C. Zhan, Y. K. Lai, M. M. Cheng, and J. Yang, "IP102: A large-scale benchmark dataset for insect pest recognition," *Proc. IEEE Comput. Soc. Conf. Comput. Vis. Pattern Recognit.*, vol. 2019-June, pp. 8779–8788, 2019, doi: 10.1109/CVPR.2019.00899.
- [25] S. Ruder, "An overview of gradient descent optimization algorithms," *arXiv Prepr. arXiv1609.04747*, 2016.
- [26] NVIDIA, "Jetson Nano Developer Kit User Guide." 2021, [Online]. Available: https://developer.download.nvidia.com/embedded/L4T/r32-3-1_Release_v1.0/Jetson_Nano_Developer_Kit_User_Guide.pdf.

Novel Framework for Enhanced Learning-based Classification of Lesion in Diabetic Retinopathy

Prakruthi M K¹

Department of Computer Science and Engineering, Jain
(Deemed to be University), Bengaluru, India

Komarasamy G²

School of Computing Science and Engineering, VIT Bhopal
University, Bhopal, Sehore, India

Abstract—Diabetic retinopathy is an adverse medical condition resulting from a high level of blood sugar potentially affecting the retina and leading to permanent vision loss in its advanced stage of progression. A literature review is conducted to assess the effectiveness of existing approaches to find that Convolution Neural Network (CNN) has been frequently adopted for analyzing the fundus retinal image for detection and classification. However, existing scientific methods are mainly inclined towards achieving accuracy in their learning techniques without much deeper investigation of possibilities to improve the methodology of type using CNN. Therefore, the proposed scheme introduces a computational framework where a simplified feature enhancement operation is carried out, resulting in artifact-free images with better features. The enhanced image is then subjected to CNN to perform multiclass categorization of potential stages of diabetic retinopathy to see if it outperforms existing schemes.

Keywords—Diabetic retinopathy; convolution neural network; classification; fundus retinal image; multi-class categorization

I. INTRODUCTION

The proposed study presents an analysis of the critical problem of diabetes called diabetic retinopathy (DR) that adversely affect the retina's blood vessels. The primary cause of this medical condition is a high blood sugar level which finally results in the leaking of blood vessels and causes swelling [1]. A person suffering from an advanced stage of diabetic retinopathy could also permanently lose their vision [2]. Hence, it is mandatory to undertake periodic retina assessments for diabetic patients to identify the early stages of diabetic retinopathy. The target of diagnosis and treatment of this condition is mainly to understand the specific state to resist the prominent threat of permanent blindness. This condition also results in lesions which are spots created by leaking fluids and blood in the area of the fundus retina [3]. Conceptually, there are two forms of lesions in diabetic retinopathy, i.e., bright lesion and red lesion, where hard and soft exudates characterize the former.

In contrast, the latter is characterized by hemorrhage and microaneurysm [4]. From the retinal image screening, microaneurysm can be found in red dots of darker origin while haemorrhage can be identified in more prominent spots. Apart from this, the yellow areas in the fundus retinal image represent hard exudates, while soft exudates are represented as fluffy white and yellowish spots. It is not feasible to manually evaluate diabetic retinopathy by an ophthalmologist as there are higher probabilities of outliers in its outcome and could

involve significant effort and time. Hence, such form of complications in the diagnosis of diabetic retinopathy is handled by computer-aided diagnosis, which can control effort, time, and cost during the complete diagnosis process [5]-[7]. To understand the stages of progression of diabetic retinopathy, there are five standard stage indicators of the retinal image as follows [8] [9]:

- No DR: Absence of any form of lesions in the retinal image.
- Mild DR: The retinal image is found with microaneurysm only.
- Moderate DR: The overall characteristic of the retinal image is more than the microaneurysm situation and less severe DR.
- Severe DR: There are multiple features of it. When there are significant intraretinal abnormalities within microvascular are in 1+ quadrant. There is the absence of any prominent sign of proliferative DR; this state is equivalent to severe DR. Apart from this if there are particular beading of veins in 2+ quadrant or there are more cases of 20 hemorrhage (intraretinal) in each of 4 quadrants, then this stage also represent severe DR.
- Proliferative DR: If the retinal image is witnessed with pre-retinal hemorrhage or neovascularization, it will represent this stage.

In the medical image-based diagnosis of diabetic retinopathy, there is a significant contribution of deep learning found in existing literature [10] [11]. Deep learning techniques can smartly identify the essential features from the input data subjected to either segmentation or classification tasks [12] [13]. It was also noted that diagnostical approaches using deep learning have majorly performed better in contrast to conventional techniques. One significant advantage of the deep learning technique is the independence from extracting or computing features from the medical image in the form of input. On the other hand, there is a need to carry out training that demands extensive data. It will imply that a higher quantity of trained data will assure better accuracy during the classification process.

On the other hand, there is a dependency on extracting features from the machine learning technique; however, they do not depend on massive trained data like deep learning techniques. In the case of diabetic retinopathy, the machine learning approaches are required to obtain the blood vessel

information, primarily followed by extraction of information related to the region of lesions in the form of features. These features will be used for classification. Various forms of operation carried out in the deep learning process are registration and detection of images along with retrieval, classification, and segmentation task. In this perspective, Convolution Neural Network (CNN), being one of the prominent deep learning techniques, is reported to be frequently used for classification as well as analysis of medical images [14]-[17]. Hence, these facts act as a motivation factor for undertaking CNN in the proposed study.

Currently, various research approaches are being carried out to classify diabetic retinopathy, where deep learning has played a significant role [18]-[20]. This diagnosis outcome is meant to assist the ophthalmologist in performing an early diagnosis of diabetic retinopathy concerning its various stages. Unfortunately, most of the existing approaches emphasize identifying the condition of diabetic retinopathy instead of exploring the appropriate stages of this critical medical condition. Another research problem studied from the trends of existing systems is the restricted and standard computational Framework for appropriately localizing the lesion region. Identifying the proper location of the lesion is essential to understanding the severity of diabetic retinopathy. Further, a significant research gap is found in the existing scheme where not enough emphasis is given towards feature enhancement of the fundus retinal images before subjecting it to deep learning techniques. Therefore, the proposed scheme addresses this problem with the following contribution:

- A simplified feature operation is carried out to the fundus retinal image using Gaussian blurring, while preliminary features are extracted using the Sobel Edge operator.
- An adaptive filter is applied using the fuzzy approach to ascertain the specific location in the fundus retinal image, generating different artifact-free and feature-enhanced images.
- The feature-enhanced image is then subjected to deep CNN with multiple convolution layers to analyze the fundus and classify DR stages.

All the above objectives are met to perform multiclass classification of DR with a particular emphasis on feature enhancement and its representation in the learning model. The paper's organization is as follows: Section II discusses various existing techniques for analyzing diabetic retinopathy, and Section III highlights the research gap. In contrast, Section IV introduces the research methodology being adopted followed by an elaborated discussion of algorithm implementation Section V. Section VI discusses the result analysis. In contrast, a discussion of the result is carried out in Section VII. Finally, Section VIII summarizes the proposed study contribution.

II. RELATED WORK

Currently, various approaches are being evolved for classifying diabetic retinopathy stages. From this perspective, it is seen that machine learning has always played a dominant

role. This can be seen in the review presented by Atwany et al. [12]. According to this study, deep learning offers a significant advantage in classification, but there is still a broad scope to improve the system's computational efficiency. The recent work of Abdelsalam and Zahran [21] used a Support Vector Machine using multifractal-based geometry system to diagnose and classify. The method has also used lacunarity parameters for accomplishing singular decisions. Another work carried out by Li et al. [22] has used an attention network with a unique grading system to identify the condition of macular edema. This paper aims to learn features based on disease-specific and disease-dependent attributes selectively. The feature maps were constructed using Convolution Neural Network (CNN) with different resolutions.

Study towards quantification in diabetic retinopathy is carried out by Okuwobi et al. [23], where region-of-interest is used, followed by estimation of hyperreflective foci to obtain better segmentation. Adoption of deep learning is also reported in work carried out by Qiao et al. [24] have used CNN for carrying out semantic segmentation for identifying microaneurysms. The technique has also detected lesions using a matching filter response. Further adoption of deep learning was witnessed in the work by Wang et al. [25], which has addressed the non-interpretability issues in its outcome. The model used the Kappa coefficient to assess the features of diabetic retinopathy. The idea is also to determine the severity score and build a relationship between severity scores and their corresponding features. The adoption of the neural network is seen in Zang et al. [26], where a rate dropout is designed to suppress the overfitting problem during classification. The recent work carried out by Zhou et al. [27] has emphasized improving transfer learning function to improve outcomes of classifying segmented lesions. Bilal et al. [28] emphasize detection techniques for classification. This model has presented the extraction of features as preprocessing to address the presence of abnormalities and support an effective segmentation technique.

Further the work implemented by Gayathri et al. [29] has presented a unique multiclass classification with the automated binary system. The study has used multiresolution features and different ranges of classifier e.g. J48, random trees, random forest, support vector machine, etc., over multiple datasets. The idea is to present a unique feature extraction model for assisting binary classification of retinal fundus images. Prakurthi et al. [30] proposed an on-demand preprocessing Framework capable of yielding different forms of high-quality images that could offer better clinical inference.

Hence, it can be seen that there have been various attempts in recent times to use machine learning in diagnosing diabetic retinopathy. Table I highlights the compact discussion of the studied literatures with respect to problems being identified by the researchers, adopted techniques to address the identified research problem, advantages, and limitation being identified from the adopted methodology. However, based on the summarized observation in Table I, it can be seen that irrespective of beneficial features, they are potentially associated with loopholes.

TABLE I. SUMMARY OF RECENT CLASSIFICATION OF DIABETIC RETINOPATHY

Authors	Problems	Technique	Advantage	Limitation
Abdelsalam and Zahran [21]	Early detection	Support Vector Machine, Multifractal Geometry	98.5% of accuracy, extensive classifying performance	Not applicable for higher dataset
Li et al. [22]	Grading of macular edema	CNN, attention network	Enhanced grading performance	Highly iterative process
Okuwobi et al. [23]	Hyperreflective foci	Generation of region-of-interest	Effective segmentation performance	Not benchmarked
Qiao et al. [24]	Microaneurysm	CNN, segmentation	Better classification accuracy	It doesn't emphasize signal quality
Wang et al. [25]	Non-interpretability of deep learning	Kappa coefficient, deep learning	Simplification in image grading	It doesn't consider improving feature quality
Zang et al. [26]	Overfitting during classification	CNN, adaptive rate dropout	95.7% of classification accuracy	Outcomes not benchmarked
Zhou et al. [27]	Overfitting during classification	Transfer learning function	The benchmarked model supports multi-disease identification	It doesn't emphasize preprocessing
Bilal et al. [28]	Early detection	Binary trees, K-nearest neighbor, support vector machine	Accuracy of 98.06%	The highly computational intensive process
Gayathri et al. [29]	Automated classification	Complex wavelets, multi-model classifiers	Accuracy of 99.7%	Demands higher computational resources

Apart from the above-mentioned recent studies, there are also some notable contributions in the same area to prove the effectiveness of deploying machine learning techniques in classifying diabetic retinopathy. An important work carried out by Acharya et al. [31] has used a Support Vector Machine to carry out multiclass classification of various stages of diabetic retinopathy. The model carries out training over 300 stages of disease condition where the study outcome is witnessed with approximately 82% accuracy. The Support Vector Machine has been used to classify various consequential stages of diabetic retinopathy [32]. This study has accomplished a classification accuracy more than that achieved in [31]. Nayak et al. [33] have developed and constructed a framework using CNN where strategies of morphological processing are carried out along with an assessment of texture-based features. The core idea is to find the critical regions of the lesions associated with blood vessels and exudates where the study outcome has reported a more than 90% accuracy score. Another significant modeling is carried out by Pratt et al. [34], where CNN has been deployed for analyzing the data to look for multiple consequences of diabetic retinopathy with a capability to determine various levels of a medical condition. The modeling has been implemented over the Kaggle dataset, which has large fundus images where the outcome shows better accuracy. Adoption of CNN was also reported in Shaban et al. [35], where multiclass classification of diabetic retinopathy is carried out for four different stages.

Further, the modeling implemented by Dekhil et al. [37] has presented a study, especially on the Kaggle dataset [37]. The work presented by Gao et al. [38] has constructed an image dataset consisting of images of the fundus retina. At the same time, the study mainly discusses the informative utilization of such a dataset for identifying multiple severity stages in diabetic retinopathy. Therefore, it is noted that various research is being carried out towards analyzing fundus retinal images to identify different stages of diabetic retinopathy. The majority of them have reportedly used CNN owing to the advantage of its independence from feature

engineering. However, after the adoption of CNN, there is still no significant improvement in the accuracy score of the studies [30]-[38], which demands further insights into addressing issues.

The following section briefs about the research gap explored from the existing research models.

III. RESEARCH GAP

The primary research gap identified from the existing techniques is that simplified preprocessing operation has received little emphasis in increasing classification accuracy demands. Without simplifying preprocessing from the perspective of precise feature modeling, the majority of the computational load towards classification accuracy is borne by the classifier algorithm. The secondary research gap identified is that frequent usage of CNN in the classification process of diabetic retinopathy has not addressed the prominent dependency on large data size. Apart from this, CNN doesn't encode the respective position and orientation of an object, which may lead to less accuracy. Therefore, the quality constraints of the fundus image need to be taken care of during system modeling. The tertiary research gap of the current study is that the adoption of frequently used machine learning models is relatively slower owing to the inclusion of iterative operation and extensive training process. Although preprocessing can reduce this, such an approach is significantly missing in the existing scheme. The following section outlines the solution to address this research gap.

IV. RESEARCH METHODOLOGY

The primary aim of the proposed system is to design and develop a novel classification framework that could effectively balance accuracy score and computational efficiency. However, for better standardization of an outcome, the proposed model is assessed with a standard dataset consisting of the fundus retinal images in diabetic retinopathy. The core aim of the present implementation model is to address the research gap identified in the prior section by improving upon

the methodology of implying frequently adopted machine learning for classifying multiclass stages of diabetic retinopathy with an approach of feature enhancement.

Fig. 1 highlights the adopted methodology of the proposed study, which uses an analytical research methodology scheme. The input of the retinal fundus image is subjected to precise feature modeling and representation using Gaussian blurring, which is then subjected to edge detection using the Sobel operator. The proposed system chooses to use Gaussian blurring as it is one of the simplified technique towards minimizing the noise as well as details present within an image. The prime parameters used for this purpose is the output image, size of Gaussian kernel, and standard deviation of kernel. Further, the scheme makes use of Sobel edge detection technique due to its simplicity in implementation process. One of the unique advantages of it is to offer a gradient magnitude with proper approximation. It is not only capable of identifying edges but also various perspective of orientation involved in it. Further, an integrated method of color compression and enhancement of blood vessels is used, resulting in a feature-enhanced image. This technique adoption significantly obtains an enriched set of distinct features without using many complicated and iterative steps, reducing the operational burden on the adopted CNN technique in machine learning. The classification results in five different DR states no-DR, mild, moderate DR, severe DR, and proliferative. The extensive analysis will be carried out further to justify the proposed methodology's scope that has effectively overcome the research gap. The following section illustrates the algorithm implemented to carry out the proposed classification.

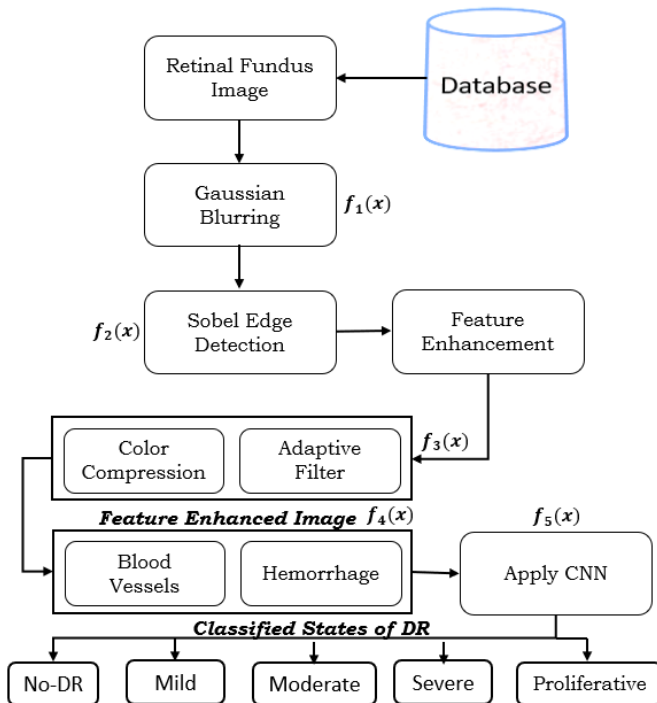


Fig. 1. Adopted Methodology of Classification.

V. SYSTEM DESIGN

From the prior section, it is now known that the proposed system targets mainly the precise classification and identification of different states of DR for a given image of the retinal fundus. In the present study, the prime emphasis is given to extracting and representing the core features of the CNN model instead of performing any general preprocessing and recognition of the disease. The justification behind this is that there are currently various existing studies (as seen in Section II) that mainly deal with classification using multiple techniques. However, the classification process can be further improved if more appropriate features are extracted in due processing and analysis steps. The proposed scheme has adopted the Kaggle eye dataset [35], which consists of a higher number of fundus retinal images characterized by higher resolution. The presented method of classification makes use of CNN to perform the determination of variable states of diabetic retinopathy. Unlike conventional mechanisms, the proposed scheme chooses to upgrade the methodology of applying CNN. This upgrading scheme involves adopting an appropriate feature enhancement action toward the fundus retinal image. The prime hypothesis behind this adoption scheme is that if the features are improved, it will benefit the classification operation without much computational burden on the CNN module. It should also be noted that the proposed scheme also offers enhancement of contrast and other factors using the prior model [30]. Therefore, the core contribution of the proposed scheme is to introduce a simplified feature enhancement mechanism that cloud further enhances the learning algorithm's performance. The algorithmic steps of the proposed system methodology are as follows:

Algorithm-1 DR States Classification

Input: i (retinal fundus image)

Output: i_{cl} (classified image)

Start

1. Load $i \leftarrow data.read(file_path, id_code)$
2. **for** each $i = 1: px$ **do**
3. $i_{gs} = f_1(i)^\sigma$ // gaussian smoothing
4. $i_{ed} = f_2(i_{gs})$ // edge detection
5. $i_{fr} = f_3(i_{ed})$ // feature representation
6. **for** each i_{fr} **do**
7. $i_c \leftarrow apply\ r2g(i_{fr})$ // color compression
8. $i_{fe} = f_4(i_c)$ // feature enhancement
9. **end for**
10. $i_{cl} = f_5(i_{fe})$ // DR State Classification
11. **end for**

End

The discussion of the above algorithmic steps of the proposed scheme is discussed concerning the following operational blocks:

A. Feature Enhancing and Representation

This algorithm's primary step (line-1) is to load all fundus images (i) from the local database. Further, the algorithm considers all the pixels p_x of an input image i (Line-2) to find that there are fair possibilities of the presence of certain features and noise that must be eliminated. For this purpose, the proposed scheme adopts the process of image blurring. The proposed method adopts a Gaussian smoothing scheme to perform feature extraction. The blurring mechanism is carried out using function $f_1(x)$ applied on input image i to obtain a smoothed image i_{gs} as an outcome (Line-3). Here, the function $f_1(x)$ represents one-dimensional Gaussian operation $G(x)$ numerically expressed as follows.

$$G(x) = \frac{1}{\sqrt{2\pi\sigma^2}} e^{-\frac{x^2}{2\sigma^2}} \quad (1)$$

While processing the input image, the mathematical expression in (1) is required to be expanded to form a two-dimension matrix. Therefore, the amended version of expression (1) can be now represented in the form of a two-dimensional matrix $G(x, y)$ as follows:

$$G(x, y) = \frac{1}{\sqrt{2\pi\sigma^2}} e^{-\frac{x^2+y^2}{2\sigma^2}} \quad (2)$$

In the above expression (2) for image blurring of $f_1(x)$, the window size is assigned to simplify computation represented by a variable σ . The presented study considers $\sigma=3$ while it is noted that this is applied to all the pixels present in an image and is not carried out selectively. The potential amount of noise in the input image is eliminated after using the Gaussian smoothing operation. After the convention of three entities of color (R, G, B), the presented algorithm is further applied to carry out this conversion. After the blurred image is obtained, the next part of the processing of an algorithm consists of getting edge-related feature information. A function $f_2(x)$ is constructed for this purpose which takes the input of smoothed image i_{gs} and applies the Sobel operator to extract edge information of an image, i.e., i_{ed} (Line-4). The next part of the implementation is associated with further performing a feature representation operation using a function $f_3(x)$ considering the input argument of edge information of an image, i.e., i_{ed} (Line-5). The operation carried out by function $f_3(x)$ is multifold. Firstly, the color compression operation is initially carried out to reduce the complexity surface in feature enhancement and model learning. In this process, the recently obtained image (i_{ed}) is compressed to a lower dimension by removing the hue and saturation component of an image while retaining the luminance (Line-7). This process leads to the generation of lower dimension images without losing their clinical attributes and diagnostic properties.

On the other hand, the proposed system constructs an adaptive filter to enhance retinal image features such as hemorrhage and blood vessel, which are very specific to DR identification. The mechanism of the adaptive filter is applied using function $f_4(x)$, which is designed based on the soft computing approach of fuzzy logic. The function $f_4(x)$ takes an input argument of the color-compressed image, i.e., i_c . After processing it, the algorithm provides an enhanced image (i_{fe}) in the form of a precise feature representation of blood vessels

and hemorrhage. The mechanism of function $f_4(x)$ is discussed in algorithm-2.

Algorithm-2 Adaptive Filter

Input: i_c (color compressed image)

Output: i_{fe} (enhanced feature representation)

Start

1. Initialize threshold $T=101$
2. $K = \text{create_kernel}(T, 2)$
3. Init $SSIM = 0$
4. Set $SSIM_thresh = 0.8$
5. While $SSIM < SSIM_thresh$
6. $i_{fe} = \text{apply_filter}(K)$
7. $U_x = \text{average}(i_c)$
8. $U_y = \text{average}(i_{fe})$
9. $S_x = \text{variance}(i_c)$
10. $S_y = \text{variance}(i_{fe})$
11. $L = \frac{2 \cdot U_x \cdot U_y}{U_x^2 + U_y^2}$
12. $C = \frac{2 \cdot S_x \cdot S_y}{S_x^2 + S_y^2}$
13. $SSIM = L \times C$
14. Optimize K with SGD

End

The above-mentioned algorithmic steps describe the procedure of adaptive filter, which adopted design characteristics of the fuzzy soft-computing approach. In the first step, the algorithm initializes an initial threshold value T for transforming each input image pixel according to whether it is inside or outside an acceptable range (Line-1). In the later process, the value of T is set automatically by stochastic gradient descent (SGD) to control the relative image intensity during the filtering operation. In the next step, the algorithm constructs a kernel K using argument T and filter size (2×2), which returns a binary image after processing the input image (Line-2). Initially, kernel k is assigned with random values, and its operation will be optimized via SGD by computing the structural similarity index (SSIM). Therefore, the algorithm initializes SSIM equal to 0 and sets a threshold equal to 0.8 because the input and out images will carry no SSIM in the initial stage (Line-3&4). The SSIM is calculated in every iteration (Line-5) as well as it is checked if it is below the threshold, the algorithm applies a filtering operation that generates a binarized image, i.e., i_{fe} (Line-6). In the subsequent steps, the algorithm computes a mean or average U_x and U_y of both input images, i.e., i_c and obtained binarized image i_{fe} , respectively (Line-7&8). Similarly, the algorithm then computes variance S_x and S_y , respectively, for both i_c and i_{fe} (Line-9&10). The computation of average and variance values is done to determine the comparison factor such as luminance (L) and contrast (C) tone (Line-11&12) and based on which the SSIM is determined (Line-13). In this way, for each iteration, SSIM is computed, and accordingly, the kernel is optimized with the help of the SGD algorithm. Here, the adaptive filter uses thresholding to convert the image into a binary image. Finally, this is used for comparing with the original image to get SSIM. When the processed and

unprocessed images are similar, the while loop ends, and the image is returned.

B. CNN Based DR State Classification

As known, CNN has the potential to resemble the conventional architecture of artificial neural networks. The prime target is learning variable forms of features associated with input images without any involvement of human intervention in the classification process. The proposed scheme implements CNN; the modeling details are highlighted as it can identify essential features without any dependencies from any user-based interaction. At the same time, there are few dependencies on carrying out preprocessing in CNN, making it a simplifier and speedy classification process. However, it cannot be denied that the application of CNN also introduces sophisticated calculations, a higher cost of memory, and uncertainty in performance. So, an improvement is required to revise the performance of CNN owing to the sensitive usage of medical images, where both accuracy and computational efficiency are demanded simultaneously. CNN architecture has various layers, ranging from convolution to polling and completely interconnected layers. A feature map is generated from this outcome of each layer that the other plays as an input argument for its successive layer. The input images associated with the activation map are subjected to a set of linear filters in the convolution layer. The purpose is mainly to obtain a variable number of features corresponding to the clinical state of diabetic retinopathy, e.g., blood vessels, curves, edges, etc. Hence, the proposed system defines its convolution layer $y(l, m, n)$ concerning the 3x3 dimension empirically represented as:

$$y(l, m, n) = \sum_{k=1}^3 \sum_{i=1}^3 \sum_{j=1}^3 H_1 + H_2 \quad (3)$$

In the above expression (3), the first component H_1 is equivalent to $w(l, i, j, k).x(i+m-1, j+n-1, k)$ while the second component H_2 is equivalent to $b(l)$. Table II highlights the configuration being used towards the development of CNN model.

TABLE II. CONFIGURATION DETAILS OF IMPLEMENTED CNN MODE

Layer	Shape	Param
Convolution Layer-1 (2D)	(598, 598, 32)	320
Maxpooling (2D)	(299,299,32)	0
Convolution Layer-2 (2D)	(297,297,64)	18496
Maxpooling (2D)	(148,148,64)	0
Convolution Layer-3 (2D)	(146,146,64)	36928
Maxpooling (2D)	(73,73,64)	0
Convolution Layer-4 (2D)	(71,71,64)	36928
Maxpooling (2D)	(35,35,64)	0
Convolution Layer-5 (2D)	(33,33,64)	73856
Maxpooling (2D)	(16,16,64)	0
Convolution Layer-6 (2D)	(14,14,64)	73792
Maxpooling (2D)	(7,7,64)	0
Convolution Layer-7 (2D)	(5,5,64)	36928
Maxpooling (2D)	(2,2,64)	0
Flatten	256	0
Dense 1	64	16448
Dense 2	5	325

The gray level of an input image is represented by the variable $x(i, j, k)$, while the weight of this is represented by $w(l, i, j, k)$. The system also uses biases represented by $b(l)$ associated with the convolution layer. The system still consists of many preferences and weights, increasing the number of parameters. This challenge is mitigated by using a pooling layer where the activation map is subjected to subsampling which significantly enhances the robustness of the features that have been extracted. A set of linear filters can be further deployed to realize the pooling layer in the proposed CNN architecture capable of computing the mean pixel values retained within the masked area of the given feature map. The system can also choose to use a non-linear filter to realize the pooling layer capable of sorting all the values of pixels retained within a specific region of the input feature map, and thereby, max pooling is accomplished.

VI. RESULT ANALYSIS

The results obtained after implementing the proposed algorithm concept discussed in the previous section are discussed in this current section. The proposed system chooses to perform five stages of classification of diabetic retinopathy, i.e., i) normal (no DR) image which doesn't have any trace of disease, ii) mild, iii) moderate, iv) severe, and v) proliferative stage of diabetic retinopathy. The proposed scheme deploys a simplified feature enhancement scheme to represent a specific feature of fundus images to the CNN model to get reliable classified states of DR. The evaluation of the proposed system is carried out on the standard dataset, namely APTOS 2019 blindness detection retrieved from Kaggle website. The dataset consists of 5590 fundus images, including both regular and DR with their ground truth in .csv file format. Among 5590, 3662 images are subjected to training CNN model, and 1928 images are considered for model testing. The experiment is performed on a standard 64-bit Windows environment with NVIDIA GEFORCE GTX graphics card, Intel(R) Core(TM) i5-9300H CPU @ 2.40GHz 2.40 GHz, and 16 GB RAM size. As shown in Fig. 2, the proposed scheme deploys seven convolution layers using the input of feature enhanced fundus image. The performance assessment of the presented system is carried out concerning precision, recall, and F1-score. The study also performs a comparative analysis where the proposed method is compared with the trained CNN, which does not include any feature enhancement module.

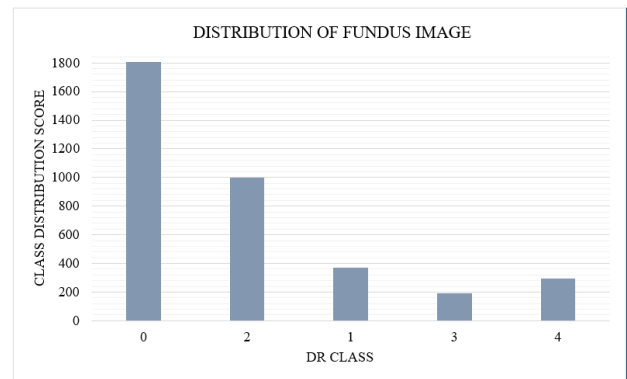


Fig. 2. Class Distribution of Fundus Image in Training Set.

Fig. 2 exhibits the class distribution of the fundus images belonging to the training set. The DR label and its description are given in Table III. There is 1805 fundus image with DR state normal, 999 images with DR state mild, 370 images are subjected moderate DR state, 193 images are related to severe DR state, and the remaining 295 fundus images are subjected to Proliferative DR. Table III highlights the labels being used with respect to the different names of classes towards fundus image.

TABLE III. LABELS OF FUNDUS IMAGE

Label	Class Name
0	No DR
1	Mild DR
2	Moderate DR
3	Severe DR
4	Proliferative DR

Fig. 3 highlights the visual outcome of the enhancing operation where Fig. 3(a) showcases the original input image while Fig. 3(b) shows the edge detected enhanced image.

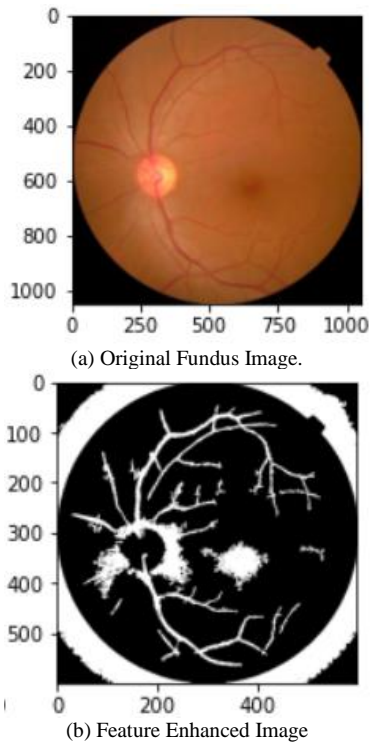


Fig. 3. Visuals of Feature Representation Operation.

From Fig. 3, it can be seen that there is an evident visual outcomes of the enhanced features, while Fig. 4 highlights various stages of processing being carried out towards the sample of normal fundus images. Adopting the proposed scheme towards the involuntary classification method by CNN offers multiple beneficial perspectives. The primary beneficial perspective, as seen from the visual outcome of Fig. 4, is that such a classification system supports any telemedicine-related application for assessing stages of diabetic retinopathy. The secondary beneficial aspect of this scheme is that its accuracy

score is highly reliable as preprocessing and feature extraction operation is carried out well before subjecting it to the learning scheme. Hence, the inference of the outcome by any ophthalmologist has become quite a simplified process. The effectiveness of the proposed feature enhancement-based CNN is assessed by comparing it with CNN implemented without any feature enhancement or preprocessing approach. Table IV and Table V highlights the quantified outcomes for proposed system and existing CNN model, respectively towards assessing accuracy as performance parameters.

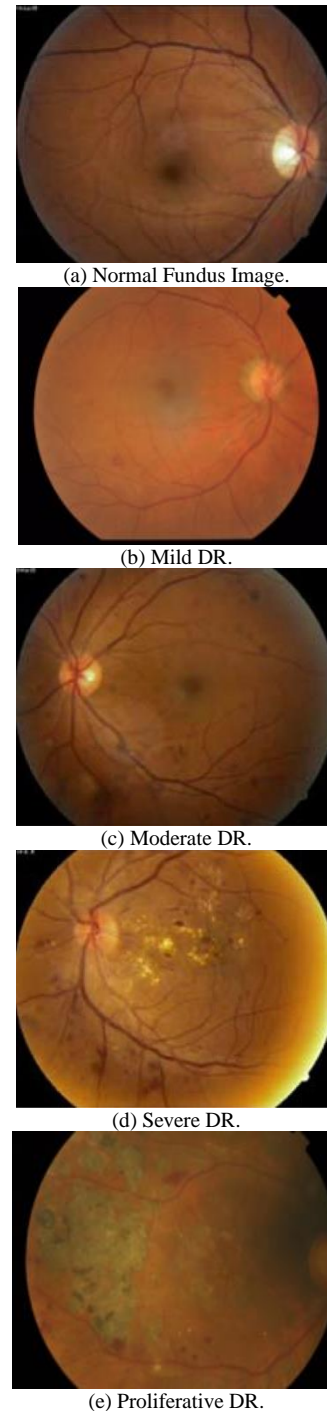


Fig. 4. Visual Outcomes of Classification.

TABLE IV. QUANTIFIED OUTCOME OF THE PROPOSED SYSTEM

CNN With Feature Enhancement			
Label	Precision	Recall	F1
0	98.60%	95.41%	96.98%
1	89.06%	91.93%	90.47%
2	97.34%	95.31%	96.31%
3	82.45%	100%	90.38%
4	89.23%	95.08%	92.06%

TABLE V. QUANTIFIED OUTCOME OF THE STANDARD CNN MODEL

CNN Without Feature Enhancement			
Label	Precision	Recall	F1
0	95.07%	88.40%	91.62%
1	68.23%	93.54%	78.91%
2	93.02%	83.33%	87.91%
3	74.54%	87.23%	80.39%
4	69.73%	86.88%	77.37%

For an effective analysis, the proposed system is also compared with the existing works done in a similar interest research area by Sikder et al. [39] and Pratt et al. [34] as shown in Table VI.

TABLE VI. NUMERICAL OUTCOMES OF COMPARATIVE ANALYSIS

Parameters	Proposed	Sikder et al. [30]	Pratt et al. [33]
Precision	95.65%	90.4%	82.3%
Recall	95.36%	89.54 %	86%
F1 score	95.42	89.97 %	83.95%

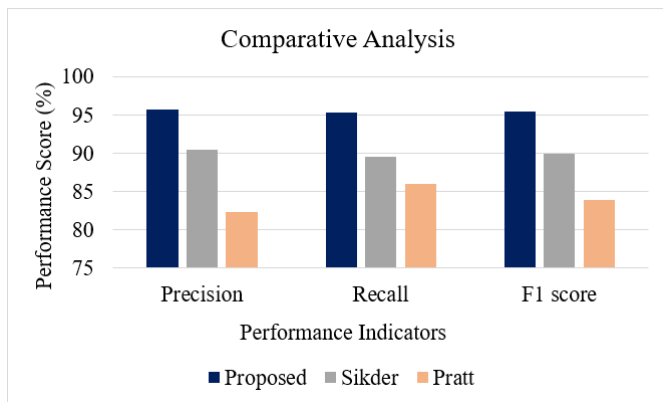


Fig. 5. Comparative Performance Metrics.

Based on the entire analysis, it can be seen that the proposed system exhibits significant enhancement in its classification performance in comparison to normal CNN and existing studies concerning the precision, recall, and F1 score (Fig. 5). The prime reason behind this outcome is as follows: The work of Sikder et al. [30] involves using conventional feature extraction techniques and an applied ensemble learning approach. Although the ensemble learning technique has its advantage in the suitable decision-making process in the

classification task, the conventional feature extraction and image enhancement approach are not appropriate for applying to massive fundus images subjected to a higher degree of artifacts and impreciseness in feature generalization, unlike proposed scheme. At the same time, the work of Pratt et al. [33] has used a different approach unlike Sikder et al. [30]; however, they are more inclined towards classification without considering the need to enhance the primary input image first. Hence, the proposed system offers a better analysis of fundus images with classified states of DR and exhibits higher performance in different assessment cases. The proposed method identifies DR in an early stage and monitors its progression.

VII. CONCLUSION

This paper has presented a simplified and unique computational modeling to carry out multiclass classification of the stages of diabetic retinopathy from a given fundus retinal image. The achievement of the proposed scheme is that unlike existing literature on classification techniques, the proposed scheme performs a sequential image feature enhancement and representation extraction prior to classification, making the accuracy score much more reliable and improving the computational burden of training by CNN and adopting two-dimensional Gaussian blurring with specific size of window assists in the simplified feature extraction process. Further feature extraction via Sobel edge detection, color compression, and enhancing the image concerning blood vessel and haemorrhage assists in better analysis of lesion in fundus retinal image. Another significant achievement is towards its potential for categorizing different DR states based on their criticality. The CNN was used with seven convolution layers with a Maxpooling layer. The quantified achievement of study is that the study outcome shows that the proposed scheme offers approximately 6% improvement over existing work and approximately 12% over another existing scheme. The feature enhancement's introduction increases the CNN classification performance and reduces the surface of computational complexity by representing specific features in the training and pattern generalization phase. In future work, the proposed system can be extended toward analyzing failed test cases due to the poor visual quality of images, which can be addressed by integrating it with our on-demand preprocessing Framework. Also, further optimization will be carried out over CNN and customization will be applied to the feature enhancement technique.

REFERENCES

- [1] Ayman S. El-Baz, Jasjit S. Suri, Diabetes and Retinopathy, Elsevier Science, ISBN: 9780128174395, 0128174390, 2020.
- [2] A. Catala, G. L. Giudice, Visual Impairment and Blindness-What We Know and What We Have to Know, IntechOpen, ISBN: 9781838802578, 1838802576, 2020.
- [3] A. S. El-Baz, J. S. Suri, Diabetes and Fundus OCT, Elsevier Science, ISBN: 9780128174401, 0128174404, 2020.
- [4] P. M. Dodson, R. R. Sivaraj, Diabetic Retinopathy: Screening to Treatment 2E (ODL), Oxford University Press, ISBN: 9780198834458, 0198834454, 2020.
- [5] F. Tecilazich, Microvascular Disease in Diabetes, Wiley, ISBN: 9781119309611, 1119309611, 2020.
- [6] C. Sabanayagam, T.Y. Wong, Diabetic Retinopathy and Cardiovascular Disease, S. Karger AG, ISBN: 9783318065077, 3318065072, 2019.

- [7] E. Trucco, T. MacGillivray, Y. Xu, Computational Retinal Image Analysis-Tools, Applications and Perspectives, Elsevier Science, ISBN: 9780081028179, 0081028172, 2019.
- [8] F. Bandello, I. Zucchiatti, M.A. Zarbin, R. Lattanzio, Management of Diabetic Retinopathy, S. Karger AG, ISBN: 9783318060423, 3318060429, 2017.
- [9] M. Porta, V. Jörgens, Unveiling Diabetes - Historical Milestones in Diabetology, S. Karger AG, ISBN: 9783318067347, 3318067342, 2020.
- [10] R. F. Mansour, "Evolutionary Computing Enriched Computer-Aided Diagnosis System for Diabetic Retinopathy: A Survey," in IEEE Reviews in Biomedical Engineering, vol. 10, pp. 334-349, 2017, doi: 10.1109/RBME.2017.2705064.
- [11] M. C. V. Stella Mary, E. B. Rajsingh and G. R. Naik, "Retinal Fundus Image Analysis for Diagnosis of Glaucoma: A Comprehensive Survey," in IEEE Access, vol. 4, pp. 4327-4354, 2016, doi: 10.1109/ACCESS.2016.2596761.
- [12] M. Z. Atwany, A. H. Sahyoun and M. Yaqub, "Deep Learning Techniques for Diabetic Retinopathy Classification: A Survey," in IEEE Access, vol. 10, pp. 28642-28655, 2022, doi: 10.1109/ACCESS.2022.3157632.
- [13] R. Sarki, K. Ahmed, H. Wang and Y. Zhang, "Automatic Detection of Diabetic Eye Disease Through Deep Learning Using Fundus Images: A Survey," in IEEE Access, vol. 8, pp. 151133-151149, 2020, doi: 10.1109/ACCESS.2020.3015258.
- [14] W. Chen, B. Yang, J. Li and J. Wang, "An Approach to Detecting Diabetic Retinopathy Based on Integrated Shallow Convolutional Neural Networks," in IEEE Access, vol. 8, pp. 178552-178562, 2020, doi: 10.1109/ACCESS.2020.3027794.
- [15] F. Saeed, M. Hussain and H. A. Aboalsamh, "Automatic Diabetic Retinopathy Diagnosis Using Adaptive Fine-Tuned Convolutional Neural Network," in IEEE Access, vol. 9, pp. 41344-41359, 2021, doi: 10.1109/ACCESS.2021.3065273.
- [16] M. Nahiduzzaman, M. R. Islam, S. M. R. Islam, M. O. F. Goni, M. S. Anower and K. -S. Kwak, "Hybrid CNN-SVD Based Prominent Feature Extraction and Selection for Grading Diabetic Retinopathy Using Extreme Learning Machine Algorithm," in IEEE Access, vol. 9, pp. 152261-152274, 2021, doi: 10.1109/ACCESS.2021.3125791.
- [17] Y. Sun, "The Neural Network of One-Dimensional Convolution-An Example of the Diagnosis of Diabetic Retinopathy," in IEEE Access, vol. 7, pp. 69657-69666, 2019, doi: 10.1109/ACCESS.2019.2916922.
- [18] S. Majumder and N. Kehtarnavaz, "Multitasking Deep Learning Model for Detection of Five Stages of Diabetic Retinopathy," in IEEE Access, vol. 9, pp. 123220-123230, 2021, doi: 10.1109/ACCESS.2021.3109240.
- [19] H. Kaushik, D. Singh, M. Kaur, H. Alshazly, A. Zaguia and H. Hamam, "Diabetic Retinopathy Diagnosis From Fundus Images Using Stacked Generalization of Deep Models," in IEEE Access, vol. 9, pp. 108276-108292, 2021, doi: 10.1109/ACCESS.2021.3101142.
- [20] X. Wang et al., "UD-MIL: Uncertainty-Driven Deep Multiple Instance Learning for OCT Image Classification," in IEEE Journal of Biomedical and Health Informatics, vol. 24, no. 12, pp. 3431-3442, Dec. 2020, doi: 10.1109/JBHI.2020.2983730.
- [21] M. M. Abdelsalam and M. A. Zahran, "A Novel Approach of Diabetic Retinopathy Early Detection Based on Multifractal Geometry Analysis for OCTA Macular Images Using Support Vector Machine," in IEEE Access, vol. 9, pp. 22844-22858, 2021, doi: 10.1109/ACCESS.2021.3054743.
- [22] X. Li, X. Hu, L. Yu, L. Zhu, C. -W. Fu and P. -A. Heng, "CANet: Cross-Disease Attention Network for Joint Diabetic Retinopathy and Diabetic Macular Edema Grading," in IEEE Transactions on Medical Imaging, vol. 39, no. 5, pp. 1483-1493, May 2020, doi: 10.1109/TMI.2019.2951844.
- [23] I. P. Okuwobi, Z. Ji, W. Fan, S. Yuan, L. Bekalo and Q. Chen, "Automated Quantification of Hyperreflective Foci in SD-OCT With Diabetic Retinopathy," in IEEE Journal of Biomedical and Health Informatics, vol. 24, no. 4, pp. 1125-1136, April 2020, doi: 10.1109/JBHI.2019.2929842.
- [24] L. Qiao, Y. Zhu and H. Zhou, "Diabetic Retinopathy Detection Using Prognosis of Microaneurysm and Early Diagnosis System for Non-Proliferative Diabetic Retinopathy Based on Deep Learning Algorithms," in IEEE Access, vol. 8, pp. 104292-104302, 2020, doi: 10.1109/ACCESS.2020.2993937.
- [25] J. Wang, Y. Bai and B. Xia, "Simultaneous Diagnosis of Severity and Features of Diabetic Retinopathy in Fundus Photography Using Deep Learning," in IEEE Journal of Biomedical and Health Informatics, vol. 24, no. 12, pp. 3397-3407, Dec. 2020, doi: 10.1109/JBHI.2020.3012547.
- [26] P. Zang et al., "DcardNet: Diabetic Retinopathy Classification at Multiple Levels Based on Structural and Angiographic Optical Coherence Tomography," in IEEE Transactions on Biomedical Engineering, vol. 68, no. 6, pp. 1859-1870, June 2021, doi: 10.1109/TBME.2020.3027231.
- [27] Y. Zhou, B. Wang, L. Huang, S. Cui and L. Shao, "A Benchmark for Studying Diabetic Retinopathy: Segmentation, Grading, and Transferability," in IEEE Transactions on Medical Imaging, vol. 40, no. 3, pp. 818-828, March 2021, doi: 10.1109/TMI.2020.3037771.
- [28] A. Bilal, G. Sun, Y. Li, S. Mazhar and A. Q. Khan, "Diabetic Retinopathy Detection and Classification Using Mixed Models for a Disease Grading Database," in IEEE Access, vol. 9, pp. 23544-23553, 2021, doi: 10.1109/ACCESS.2021.3056186.
- [29] S. Gayathri, A. K. Krishna, V. P. Gopi and P. Palanisamy, "Automated Binary and Multiclass Classification of Diabetic Retinopathy Using Haralick and Multiresolution Features," in IEEE Access, vol. 8, pp. 57497-57504, 2020, doi: 10.1109/ACCESS.2020.2979753.
- [30] M.K. Prakruthi, G. Komarasamy, "Modelling On-Demand Preprocessing Framework Towards Practical Approach in Clinical Analysis of Diabetic Retinopathy", International Journal of Electrical and Computer Engineering (IJECE), Vol. 12, No. 1, pp. 585-595, February 2022.
- [31] Acharya U., Chua C., Ng E., Yu W., Chee C., Application of Higher Order Spectra for the Identification of Diabetes Retinopathy Stages, Journal of Medical Systems, vol. 32, no. 6, pp. 481-488, 2008. <https://doi.org/10.1007/s10916-008-9154-8> PMID: 19058652.
- [32] Acharya U., Lim C., Ng E., Chee C. and Tamura T., Computer-Based Detection of Diabetes Retinopathy Stages using Digital Fundus Images, Proceedings of the Institution of Mechanical Engineers, vol. 223, no. 5, pp. 545-553, 2009. <https://doi.org/10.1243/09544119JMEIM486> PMID: 19623908.
- [33] Nayak J., Bhat P., Acharya R., Lim C. and Kagathi M., Automated Identification of Diabetic Retinopathy Stages using Digital Fundus Images, Journal of Medical Systems, vol. 32, no. 2, pp. 107-115, 2008. <https://doi.org/10.1007/s10916-007-9113-9> PMID: 18461814.
- [34] H. Pratt, F. Coenen, D. Broadbent, S. Harding, Y. Zheng, "Convolutional Neural Networks for Diabetic Retinopathy", International Conference on Medical Imaging Understanding and Analysis, Loughborough, UK, July 2016.
- [35] M. Shaban, Z. Ogur, A. Shalaby, A. Mahmoud, M. Ghazal, H. Sandhu, et al., "Automated Staging of Diabetic Retinopathy Using a 2D Convolutional Neural Network", IEEE International Symposium on Signal Processing and Information Technology, Louisville, Kentucky, USA, December 2018.
- [36] Asia Pacific Tele-Ophthalmology Society, "APTOS 2019 blindness detection," Kaggle, <https://www.kaggle.com/c/aptos2019-blindness-detection/data>, 2019, [Dataset].
- [37] Omar Dekhil, Ahmed Naglah, Mohamed Shaban, Ahmed Shalaby, Ayman El-Baz, "Deep-Learning Based Method for Computer Aided Diagnosis of Diabetic Retinopathy", IEEE International Conference on Imaging Systems & Techniques, Abu Dhabi, United Arab Emirates, December 2019.
- [38] Gao Z., Li J., Guo J., Chen Y., Yi Z., and Zhong J., Diagnosis of Diabetic Retinopathy using Deep Neural Networks, IEEE Access Journal, vol. 7, pp. 3360-3370, 2018.
- [39] Sikder, Niloy, Md Sanullah Chowdhury, Abu Shamim Mohammad Arif, and Abdullah-Al Nahid. "Early blindness detection based on retinal images using ensemble learning." In 2019 22nd International Conference on Computer and Information Technology (ICCIT), pp. 1-6. IEEE, 2019.

Hybrid Pelican Komodo Algorithm

Purba Daru Kusuma, Ashri Dinimaharawati

Computer Engineering, Telkom University, Bandung, Indonesia

Abstract—In this work, a new metaheuristic algorithm, namely the hybrid pelican Komodo algorithm (HPKA), has been proposed. This algorithm is developed by hybridizing two shortcoming metaheuristic algorithms: the Pelican Optimization Algorithm (POA) and Komodo Mlipir Algorithm (KMA). Through hybridization, the proposed algorithm is designed to adapt the advantages of both POA and KMA. Several improvisations regarding this proposed algorithm are as follows. First, this proposed algorithm replaces the randomized target with the preferred target in the first phase. Second, four possible movements are selected stochastically in the first phase. Third, in the second phase, the proposed algorithm replaces the agent's current location with the problem space width to control the local problem space. This proposed algorithm is then challenged to tackle theoretical and real-world optimization problems. The result shows that the proposed algorithm is better than grey wolf optimizer (GWO), marine predator algorithm (MPA), KMA, and POA in solving 14, 12, 14, and 18 functions. Meanwhile, the proposed algorithm creates 109%, 46%, 47%, and 1% better total capital gain rather than GWO, MPA, KMA, and POA, respectively in solving the portfolio optimization problem.

Keywords—Metaheuristic; Pelican Optimization Algorithm; Komodo Mlipir Algorithm; portfolio optimization algorithm; LQ45 index

I. INTRODUCTION

Optimization is a prevalent work that has been implemented in many areas. Optimization is essential because it aims to maximize results or minimize cost or effort. Optimization is also important because in any human process, whether the scope is individual or institution, it has a specific goal or objective. Contrary, the resources needed to execute this work are limited. The term cost can be translated in many ways, such as travel distance, consumed energy, production cost, penalty, unserved requests, and so on. On the other hand, the term result can also be translated into many ways, such as sales, profit, served customers, accuracy, and so on. In the production process, optimization is widely used, such as in the flow-shop scheduling [1], batch-shop scheduling [2], assembly line balancing [3], procurement [4], and so on. In transportation and logistics, optimization is implemented in route planning [5], storage management [6], and so on. Optimization is also implemented in finance, such as in portfolio optimization [7], option pricing [8], credit risk assessment [9], bankruptcy mitigation [10], etc.

Metaheuristic algorithm is a popular method used in many studies conducting the optimization problem. This popularity comes from its flexibility in facing the limited computation resources. Moreover, the metaheuristic algorithm is flexible enough to tackle various objective functions, from simple to complicated ones. This advantage cannot be obtained from the

exact method that needs an excessive computational resource, especially in solving a complicated problem with high dimension space [11]. However, as an approximate method, a metaheuristic algorithm does not guarantee the true optimal solution but only the acceptable or near optimal one [11]. In many metaheuristic algorithms, several parameters also must be adjusted. Proper adjustment can improve its performance, while misjudgment can worsen its performance.

Many metaheuristic algorithms are inspired by nature or behavior, especially the animal behavior during mating and foraging. This circumstance occurs due to the similarity between these behaviors and the metaheuristic algorithm. An animal has a certain degree of uncertainty during mating and foraging. In foraging, even if it is searching for a food source or hunting prey, the animal still does not know the actual location of the food source or prey. Based on it, a random search with a certain degree of certainty is conducted. Although animals have a certain degree of similarity during foraging, there is a specific strategy conducted by every animal. On the other hand, the mating process can generate new descendants from the selected parents. These descendants inherit the characteristics of their parents. Some descendants are better than their parents while the others are worse. Several metaheuristic algorithms adopt this circumstance. In several algorithms, the improvement is created by mating a selected solution with the best solution. Several algorithms that adopt foraging behavior are particle swarm optimization (PSO) [12], ant colony optimization (ACO) [13], grey wolf optimization (GWO) [14], marine predator algorithm (MPA) [15], artificial bee colony algorithm (ABC) [16], Etc. Meanwhile, several algorithms that adopt the mating process are genetic algorithm (GA) [17], evolutionary algorithm (EA) [18], Etc. Several algorithms, such as the red deer algorithm (RDA), combine mating and foraging [19].

Among many shortcoming metaheuristic algorithms, there are two brand-new algorithms that is firstly introduced in 2022. The first is Komodo Mlipir Algorithm (KMA), and the second is the Pelican Optimization Algorithm (POA). The animal's behavior inspires both algorithms. The behavior of Komodo dragon during foraging and mating inspires KMA [20]. Meanwhile, POA is inspired by the behavior of pelicans during foraging [21]. In their first appearance, both algorithms beat several algorithms. POA outperformed genetic algorithm (GA), particle swarm optimization (PSO), teaching-learning based optimization (TLBO), grey wolf optimizer (GWO), whale optimization algorithm (WOA), gravitational search algorithm (GSA), tunicate swarm algorithm (TSA), and marine predator algorithm (MPA) [21]. On the other hand, KMA outperformed six algorithms: GA, success-history based parameter adaptation differential evolution (SHADE), linear population size reduction SHADE with ensemble sinusoidal differential

covariance matrix adaptation with Euclidean neighborhood (LSHADE-CnEpSIn), equilibrium Optimizer (EO), MPA, and slime mold algorithm (SMA) [20].

Despite their outstanding performance, these algorithms are still not popular as brand-new algorithms. Studies conducting these algorithms to solve optimization problems are still hard to find. Based on this, it is challenging to explore these algorithms further. Moreover, as brand-new algorithms, the opportunity to improve and modify these algorithms is widely open.

The objective and scope of this work are as follows. This work proposes a new metaheuristic algorithm that hybridizes both shortcoming algorithms: POA and KMA. Through hybridization, the proposed algorithm is hoped to combine the strength of both algorithms and, on the other hand, tackle the weakness of both algorithms too. Based on this objective, the scope of this work is to develop new algorithms that hybridize both POA and KMA and then evaluating this proposed algorithm through simulation.

The methodology conducted to this work is as follows. First, the mechanics and strategy in both KMA and POA are explored and reviewed. This exploration is needed to analyze their strength and weakness. Then, the proposed algorithm is developed by hybridizing both algorithms. After that, this proposed algorithm is challenged to solve the theoretical and real-world optimization problems so that its performance can be evaluated. The proposed algorithm is implemented to solve the 23 benchmark functions. These functions represent the theoretical optimization problem. These functions are popular in many studies that propose a new metaheuristic algorithm. Meanwhile, the portfolio optimization problem is chosen as the real-world optimization problem. In this simulation, the proposed algorithm is compared with four shortcoming metaheuristic algorithms: GWO, MPA, KMA, and POA. GWO and MPA represent algorithms that have been implemented and modified in many studies. Meanwhile, KMA and POA are chosen because this proposed algorithm is the improved version of these algorithms. Several findings regarding the simulation result are then analyzed deeper.

There are several contributions regarding this work. These contributions are as follows.

- 1) This work proposes a new algorithm that hybridizes two brand-new algorithms: POA and KMA.
- 2) This work modifies the swarm movement in the first phase of POA by replacing the randomized target with a more deterministic target.
- 3) This work adopts the behavior of three types of Komodo in KMA to be implemented in the swarm movement in the first phase with several modifications.
- 4) This work modifies the second phase by replacing the agent's current location with the problem space to control the local problem space.

The remainder of this paper is structured as follows. The mechanics of POA and KMA are reviewed in the second section to analyze their strengths and weaknesses. Based on this review, the proposed algorithm's model is presented in the

third section. The simulation regarding the proposed algorithm is explained in the fourth section. The more profound analysis regarding the simulation result and the findings are discussed in the fifth section. In the end, the conclusion and future research potential regarding this work are summarized in the sixth section.

II. RELATED WORK

Komodo Mlipir Algorithm (KMA) is a brand-new algorithm that adopts the behavior of the Komodo dragon during mating and foraging. This algorithm is a population-based algorithm consisting of several autonomous agents. Each agent represents the solution. These agents are classified into three groups based on their quality: big male, female, and small male [20]. Each type of agent has a specific role and mechanics. The big males are agents whose qualities are better. The females are agents whose quality is mediocre. In the end, the petite males are agents whose quality is worse. The proportion of these groups is fixed and set manually before the process begins. The rank to determine the group's members is updated in every iteration.

The big male adopts foraging behavior by searching for prey [20]. The big male moves based on its current location and other big males. The big male moves toward the better big males and moves away from the worse big males. The big male does not take account of the female and small male.

The female conducts the mating process. There are two possible mating strategies for every female: sexual reproduction or asexual reproduction (parthenogenesis) [20]. Sexual reproduction is achieved by mating the female with the highest quality big male. Each female produces two descendants. The first descendant is close to the female, while the second descendant is close to the highest quality big male. Then, the best descendant between them will replace the female current's location. In parthenogenesis, a female creates a descendant randomly within the problem space.

Like a big male, the small male implements foraging [20]. The small male moves toward the cumulative of big males. As a worse solution, the small male should get closer to the better solutions (big males) to improve its quality.

Meanwhile, the Pelican Optimization Algorithm is a brand-new algorithm that adopts the pelican behavior during foraging. POA is a swarm-based intelligence. This algorithm consists of a certain number of agents (pelicans). As a swarm intelligence, collective intelligence is used or shared among the pelicans [22]. In this algorithm, the randomized target represents collective intelligence. POA consists of two steps that are executed sequentially in every iteration.

There is a global target in the first phase where all pelicans will move based on this target [21]. This global target is selected randomly within the problem space at the beginning of every iteration. The pelican can choose two possible movements. If this target is better than the pelican's current location, the pelican will move toward this target. Otherwise, the pelican will move away from this target. In POA, an acceptance-rejection strategy is adopted. The pelican will move to this new location only if this new location is better than its current location.

In the second phase, the pelican flies around its current location [21]. Although this term is not relevant in some circumstances, it can be seen as a local or neighborhood search. In this phase, a new location is selected randomly within the pelican's local problem space. The width of this local problem space declines gradually due to the increase of the iteration. It means that the local problem space is wide enough in the beginning, and it can be seen as an exploration. On the other hand, this investigation moves to exploitation as the iteration goes. Besides iteration, the local problem space is also determined by the agent's current location. Near zero current location makes the width of the local problem space narrow, although in the early iteration. Like in the first phase, in this phase, the pelican moves toward the new location only if this new location is better than the pelican's current location.

Based on the detailed description of KMA and POA, the comprehensive comparison between these algorithms is as follows. KMA splits the population into three groups. Each group represents a distinct strategy. But each agent conducts only a single procedure in every iteration. On the other hand, in POA, there is not any population split. Every agent is treated equal and conducts the same strategy. Each agent acts these two actions in every iteration.

The swarm movement toward a better solution and away from the worse solution is also conducted in both algorithms. In KMA, the big males move toward better big males and move away from the resultant of worse big males. Moreover, petite males move toward the resultant of big males. On the other hand, each pelican moves toward a randomized target if this target is better than the pelican's current location and avoids this randomized target if this target is worse than the pelican's current location. This strategy can be seen as improving the current solution based on the guidance of the better solution or avoiding the possible worse solution. Both algorithms choose a different method in determining the target in the swarm movement. POA selects the target randomly within the problem space. On the other hand, in KMA, only big males can become the target.

Random search is also conducted in both algorithms but in a different way. In POA, this strategy is undertaken in the second phase so that all agents work this strategy in every iteration. In KMA, the random search is implemented only by the female when it chooses parthenogenesis. It means that with the same population size, the probability of conducting the random search in POA is higher than in KMA.

There is a difference between KMA and POA regarding the local problem space in the local search strategy. In KMA, the local problem space width is fixed based on the problem space. In POA, the local problem space is reduced gradually as the iteration increases. Reducing the local problem space during the iteration can make the system focus on the exploration in the early iteration and then transform to the exploitation. At the end of the iteration, the system focuses on exploitation. The advantage of this strategy is that the system can concentrate on exploring any space within the problem space to find the region where the optimal global solution exists. After that, the system will improve the solution within this region. Moreover, the agent will not be thrown away to any areas within the

iteration in the later iteration, so it should start the searching. Contrary, fixed local problem space width is essential when the system still fails to find the region where the optimal global solution exists. The system can escape from the optimal local trap, although the iteration is not in the early phase.

Acceptance-rejection strategy is conducted only in POA. Meanwhile, KMA does not adopt this strategy. Acceptance-rejection has strengths and weaknesses, so not all algorithms adopt this strategy. By implementing this strategy, the agent moves to a new solution only if the new solution is better than its current solution. There is no probability of a worsening situation. But the system may be stuck in a case, such as the local optimal, when it fails to improve the current solution. On the other hand, without accepting this strategy, the system may go to a worse situation. Some algorithms, such as MPA, partially adopt this strategy. In MPA, the prey may move toward the worse solution. Contrary, the predator moves to a new location, only this new location is better than the predator's current location.

This review shows that both KMA and POA have several strengths and weaknesses. Based on this circumstance, there is the possibility of improvement by hybridizing these algorithms. Several parts that can be modified are as follows. First, modification can be conducted in the swarm movement. Second, change also can be shown in the random search.

III. PROPOSED MODEL

This section will present the detailed model of the proposed algorithm. This model consists of the conceptual model, pseudocode, and mathematical model. The conceptual model explains the framework and general mechanics of the algorithm. The pseudocode formalizes the structure of the proposed algorithm. In the end, the mathematical model describes the detailed formulation of processes and methods within the algorithm.

The conceptual model of the proposed algorithm is as follows. This proposed algorithm uses POA as its main framework. The proposed algorithm consists of two phases. The first phase is the swarm movement toward the target. The second phase is the randomized movement within the local problem space. Like in POA, these phases are conducted sequentially in every iteration.

In the first phase, four possible movements can be chosen by every agent. The first movement is the movement toward the global best solution. The second movement moves to the middle between the current location and the international best solution. The third movement is the movement related to the randomly selected agent. The fourth movement is jumping across the global best solution. KMA inspires the first, second, and third movements. The first movement is the modification of the minor male movement. The second movement is the modification of the mating process of the female with the best quality big male. The third movement is the modification of the significant male movement. MPA inspires the fourth movement. In the fourth movement, the agent's new location is obtained based on the current global best solution movement away from the related agent. The main objective of the fourth movement is to improve the global best solution. In this first

phase, the agent will move to the new location, whether this new location is better or worse. It is different from POA, where the pelican will move to the new location only if this new location is better than the pelican's current location.

In the second phase, every agent searches for a new location within its local problem space. This method also occurs in POA. In this phase, the similarity between the proposed algorithm and POA is that the local problem space is reduced gradually due to the increase of the iteration. The exploration to exploitation strategy is also adopted in the proposed algorithm. Meanwhile, there is a difference between the proposed algorithm and POA. In this proposed algorithm, the local problem space width also depends on the problem space width. It is different from POA, where the agent's current location affects its local problem space width. Like in POA, in this phase, the agent moves to the new location only if it is better than the current location.

Like many metaheuristic algorithms, this proposed algorithm consists of two steps. The first step is initialization. The second step is iteration. The agent's initial location is randomized within the problem space during the initialization. It follows uniform distribution so that the opportunity of every place is equal. The improvement is conducted during the iteration. Each time an agent moves to a new location, the global best solution will be updated in every process. The global best solution is an entity that stores the best answer so far. This best solution is applied among all agents. This international best solution is updated to its new value only if this new solution is better than the current global best solution. The global best solution becomes the final solution at the end of an iteration.

This framework is then transformed into the pseudocode and the mathematical model. The pseudocode of the proposed algorithm is shown in Algorithm 1. There are several annotations used in the pseudocode and mathematical model. These annotations are as follows.

b_l	lower bound
b_u	upper bound
d	space divider
f	objective function
r	generated random number
s	step size
x	agent
X	set of agents
x_c	candidate
x_{tar}	target
x_{sel}	selected agent
x_{best}	global best solution
t	iteration
t_{max}	maximum iteration
T_1	first threshold
T_2	second threshold
T_3	third threshold
U	uniform distribution

Algorithm 1: HPKA Algorithm

```
1  output:  $x_{best}$ 
2  begin
3  //initialization
4  for all  $X$  do
5    initialize  $x$  using (1)
6  end for
7  //iteration
8  for  $t=1$  to  $t_{max}$  do
9    for all  $X$  do
10   //first phase
11   generate  $r$  using (2)
12   if  $r < T_1$  then
13     first movement using (3)
14   else if  $T_1 \leq r < T_2$  then
15     second movement using (4)
16   else if  $T_2 \leq r < T_3$  then
17     third movement using (5) and (6)
18   else
19     fourth movement using (7)
20   end if
21   update  $x_{best}$  using (8)
22   //second phase
23   search within local problem space using (9) and (10)
24   update  $x_{best}$  using (8)
25   end for
26 end
```

All agents' initial location is determined randomly within the problem space in the initialization. This process is formalized using (1). Equation (1) shows that the lower and upper bound to become the boundaries of the problem space. These boundaries represent the single dimension problem space. Each dimension has its limits in the multiple dimension problem space, and (1) is applied in all dimensions.

$$x = U(b_l, b_u) \quad (1)$$

In the first phase, the movement is selected randomly based on the value of a generated random number. The distribution of this random number follows a uniform distribution. This random number is formalized by using (2). Then, the movement is selected based on the location of this random number related to the thresholds.

$$r = U(0,1) \quad (2)$$

In the first movement, the agent moves toward the global best solution. This first movement is chosen if the generated random number is less than the first threshold. This process is formalized by using (3). Equation (3) shows that the movement length is uniformly randomized. It also depends on the step size. A bigger step size makes the agent moves closer to the global best solution. On the other hand, a smaller step size makes the agent moves closer to its current location.

$$x' = x + s \cdot U(0,1) \cdot (x_{best} - x) \quad (3)$$

In the second movement, the agent moves to the middle between its current location and the global best solution. This movement is chosen if the generated random number is between the first and second threshold. This movement represents the deterministic version of the first movement. This movement is formalized using (4).

$$x' = \frac{x_{best} + x}{2} \quad (4)$$

In the third movement, the agent moves related to the selected agent. This agent is chosen randomly among the set of agents. This movement is selected if the generated random number is between the second and third threshold. If this agent chosen is better than the agent's current location, then this agent will move toward the selected agent. Else, this agent will move away from the designated agent. This process is formalized by using (5) and (6). Equation (5) formalizes the agent selection. Equation (6) formalized the movement related to the selected agent.

$$x_{sel} = U(X) \quad (5)$$

$$x' = \begin{cases} x + s \cdot U(0,1) \cdot (x_{sel} - x), & f(x_{sel}) < f(x) \\ x + s \cdot U(0,1) \cdot (x - x_{sel}), & else \end{cases} \quad (6)$$

In the fourth movement, the agent's new location is obtained from the direction of the global best away from the agent's current location. This movement is chosen if the generated random number is higher than the third threshold. This process is formalized by using (7). This movement is conducted to exploit the location near the global best.

$$x' = x_{best} + s \cdot U(0,1) \cdot (x_{best} - x) \quad (7)$$

This agent's new location is then used to update the global best. As mentioned in the conceptual model, the new solution will replace the global best current solution only if this new solution is better than the global best solution. This process is formalized by using (8).

$$x'_{best} = \begin{cases} x, & f(x) < f(x_{best}) \\ x_{best}, & else \end{cases} \quad (8)$$

The agent searches for a new location within its local problem space in the second phase. This process is formalized by using (9) and (10). Equation (9) formalizes the candidate for the new location. Equation (10) states that this candidate will only replace the agent's current location if it is better than its current location.

$$x_c = x + \left(1 - \frac{t}{t_{max}}\right) (2U - 1) \left(\frac{b_u - b_l}{d}\right) \quad (9)$$

$$x' = \begin{cases} x_c, & f(x_c) < f(x) \\ x, & else \end{cases} \quad (10)$$

Based on this explanation, the complexity of the proposed algorithm can be presented in the Big O notation as $O(2t_{max} \cdot n(X))$. Based on this notation, it is shown that the complexity of the proposed algorithm is linearly proportional to the maximum iteration or the population size. The number 2 represents the two phases that are conducted in every iteration.

IV. SIMULATION AND RESULT

Four simulations are conducted to evaluate the proposed algorithm's performance in this work. The first simulation is conducted to evaluate the proposed algorithm's performance in solving the theoretical mathematic optimization problem. The second simulation is conducted to assess the sensitivity of the algorithm, related to its performance. The third simulation is conducted to evaluate the proposed algorithm's performance in solving the real-world optimization problem. The fourth

simulation is conducted to evaluate the convergence of the algorithm in solving the real-world optimization problem.

In the first simulation, the proposed algorithm is challenged to solve the 23 benchmark functions representing the theoretical optimization problem. These functions are commonly used in many studies that suggest new metaheuristic algorithms, such as darts game optimizer (DGO) [23], hide objects game optimizer (HOGO) [24], KMA [20], RDA [19], POA [21], and so on. The list of these functions can be seen in Table I. These functions can be clustered into three groups based on their similar characteristics. The first group represents the high dimension unimodal functions. This group consists of function one to function seven. The second group represents the high dimension multimodal functions. This group consists of function eight to function thirteen. The third group represents the fixed dimension multimodal functions. This group consists of function 14 to function 23.

TABLE I. BENCHMARK FUNCTIONS

No	Function	Dim	Problem Space	Target
1	Sphere	10	[-100, 100]	0
2	Schwefel 2.22	10	[-100, 100]	0
3	Schwefel 1.2	10	[-100, 100]	0
4	Schwefel 2.21	10	[-100, 100]	0
5	Rosenbrock	10	[-30, 30]	0
6	Step	10	[-100, 100]	0
7	Quartic	10	[-1.28, 1.28]	0
8	Schwefel	10	[-500, 500]	-4189.8
9	Rastrigin	10	[-5.12, 5.12]	0
10	Ackley	10	[-32, 32]	0
11	Griewank	10	[-600, 600]	0
12	Penalized	10	[-50, 50]	0
13	Penalized 2	10	[-50, 50]	0
14	Shekel Foxholes	2	[-65, 65]	1
15	Kowalik	4	[-5, 5]	0.0003
16	Six Hump Camel	2	[-5, 5]	-1.0316
17	Branin	2	[-5, 5]	0.398
18	Goldstein-Price	2	[-2, 2]	3
19	Hartman 3	3	[1, 3]	-3.86
20	Hartman 6	6	[0, 1]	-3.32
21	Shekel 5	4	[0, 10]	-10.1532
22	Shekel 7	4	[0, 10]	-10.4028
23	Shekel 10	4	[0, 10]	-10.5363

The more detailed explanation related to the characteristic of these functions is as follows. The unimodal function is a function that has only one optimal solution [25], which is the optimal global solution. There is not any optimal local solution in this function. Contrary, the multimodal function is a function that has multiple optimal solutions [25]. One optimal is the optimal global solution that becomes the target of the optimization. The other optimal solutions are the local optimal.

In this function, the algorithm can be trapped in the local optimal so that the global optimal cannot be found until the iteration ends [25]. The high dimension function represents the function that has a flexible number of adjusted parameters that construct the solution. The dimension can be one and up to unlimited (hundreds or thousands). A higher dimension makes the problem more challenging to optimize. It means that more iteration or population size is needed. The fixed dimension function represents the function that its measurement is static or final. Although the dimension is static and usually low, it does not mean that this function is easy to solve.

These 23 benchmark functions also represent optimization problems with various problem space. The problem space ranges from very narrow, such as in Quartic and Hartman 6, to the very large, such as in Schwefel and Griewank. Most of these functions are centralized at 0. Meanwhile, in several functions, such as Shekel 5 and Hartman 3, the problem space central is not at 0.

In this simulation, the proposed algorithm is compared with four other algorithms: GWO, MPA, KMA, and POA. In general, these four algorithms are new. All these algorithms adopt the foraging mechanism of the animal. Meanwhile, these four algorithms have their distinct mechanics. GWO represents algorithms that every agent moves toward certain (three) best solutions or three global best solutions. MPA represents the movement of several couples of predators and preys where the predator represents the local best solution for its prey. KMA represents algorithm that combines the foraging and mating. POA represents the algorithm that all agents move toward the randomized global target. GWO and MPA also represent the shortcoming algorithms that have been widely studied, improved, and implemented. Meanwhile, KMA and POA represent brand new algorithms that are not popular yet.

The setup of all these five algorithms is as follows. The maximum iteration is set 200 that represent low iteration. The population size is set 20. In MPA, the fishing aggregate devices are set 0.5. The reason is to make balance strategy between finding the alternative randomly within the local problem space and the two randomly selected predators. In KMA, the proportion of the big males is 40%. The reason of this proportion is to make almost balance population between the big males and the small males. Meanwhile, the only one female configuration is chosen based on the recommendation in the first appearance of KMA. There is only one female. The rest population are the small males. The mlipir rate is set 0.5. This rate is chosen to speed up the movement of the small males. Meanwhile, there is not any parameter setting in GWO and POA because these algorithms do not have any adjusted parameter. In the proposed algorithm (HPKA), the proportion is equal, and the step size is set 2. This step size is chosen to so that the local problem space width is wide enough but not too wide. This parameter setting is also can be seen in Table II. Meanwhile, the first, second, and third thresholds are set to make balance proportion between among the movements. The simulation result is shown in Table III. The best result is written in bold font.

The result shows that the proposed algorithm is a good metaheuristic algorithm. It can find the acceptable optimal solution in all 23 benchmark functions. It means that the proposed algorithm is good in solving both unimodal functions and multimodal functions. Moreover, the proposed algorithm also can find the true optimal solution in solving the Six Hump Camel.

Table III also shows that the proposed algorithm is competitive enough compared with other sparing algorithms. It performs the best in solving five functions: Step, Penalized 2, Six Hump Camel, Branin, and Hartman 6. One function is the high dimension unimodal function while the other four functions are the fixed dimension multimodal functions. Compared with other four algorithms, the proposed algorithm is better than GWO, MPA, KMA, and POA in solving 14, 12, 14, and 18 functions respectively. It is also shown the GWO is very powerful in solving the high dimension unimodal functions but weak in solving the fixed dimension multimodal functions. Contrary, KMA is very powerful in solving the Shekel 5, Shekel 7, and Shekel 10.

The second simulation is conducted to evaluate the algorithm sensitivity. In this work, the sensitivity analysis is focused on the formation of the agents due to four possibilities of action chosen by every agent. Like in the first simulation, in this simulation, the proposed algorithm is implemented to solve the 23 benchmark functions. Meanwhile, the maximum iteration and the population size are not chosen to be explored deeper. It is because based on the general model of metaheuristic algorithm, where the quality of the algorithm can be improved by increasing the maximum iteration or the population size theoretically but with the expense of the computational resource and time. On the other hand, the formation does not affect to the complexity or computational consumption. In Table IV, the proportion is presented in a set that contains the proportion of the first, second, third and fourth options consecutively. The first scenario represents the first movement dominant strategy. The second scenario represents the second movement dominant strategy. The third scenario represents the third movement dominant strategy. The fourth scenario represents the fourth movement dominant strategy. The result can be seen in Table IV. The best result is written in bold font.

TABLE II. PARAMETER SETTING

Parameter	Value
$n(X)$	20
t_{max}	200
s	2
T_1	0.25
T_2	0.5
T_3	0.75

TABLE III. SIMULATION RESULT (MEANS)

Function	GWO	MPA	KMA	POA	HPKA	Better Than
1	1.326x10⁻¹⁰	4.467x10 ¹	4.047x10 ²	3.030x10 ³	1.098x10 ⁻⁹	MPA, KMA, POA
2	0	0	2.505	0	1.044x10 ⁻¹⁹	KMA
3	7.583x10⁻¹⁶	1.003x10 ²	1.704x10 ³	4.085x10 ³	4.757x10 ⁻¹	MPA, KMA, POA
4	2.804x10⁻⁹	2.764x10 ⁻¹	1.226x10 ¹	3.057x10 ¹	4.254x10 ⁻¹	KMA, POA
5	9.000	1.004x10 ¹	1.320x10 ⁴	8.090x10 ⁵	9.073x10 ¹	KMA, POA
6	2.25	3.698x10 ¹	3.291x10 ²	1.998x10 ³	6.243x10⁻¹¹	GWO, MPA, KMA, POA
7	3.971x10 ⁻²	1.546x10⁻²	4.244x10 ⁻¹	5.733x10 ⁻¹	8.457x10 ⁻²	KMA, POA
8	1.244x10 ⁻¹³	-1.922x10 ³	-3.240x10³	-2.166x10 ³	-2.786x10 ³	GWO, MPA, POA
9	0	2.174x10 ¹	3.364x10 ¹	6.631x10 ¹	4.004x10 ¹	POA
10	6.534x10⁻¹⁵	4.019	8.343	1.506x10 ¹	6.035	POA
11	0	1.425	4.176	2.446x10 ¹	4.471x10 ⁻¹	MPA, KMA, POA
12	2.639	2.182	2.184x10 ²	3.030x10 ³	2.540	GWO, KMA, POA
13	3.139	9.062	8.641x10 ³	3.119x10 ⁶	1.167	GWO, MPA, KMA, POA
14	1.267x10 ¹	3.002	4.152	1.364	6.768	GWO
15	1.484x10 ⁻¹	2.947x10⁻³	1.954x10 ⁻²	2.959x10 ⁻³	4.002x10 ⁻³	GWO, KMA
16	-1.326x10 ⁻¹⁸	-1.029	-1.031	-1.030	-1.032	GWO, MPA, KMA, POA
17	5.560x10 ¹	5.676x10 ⁻¹	4.455x10 ⁻¹	3.992x10 ⁻¹	3.981x10⁻¹	GWO, MPA, KMA, POA
18	6.000x10 ²	3.399	4.338	3.019	8.143	GWO
19	-1.936x10 ⁻³	-3.875	-5.637x10 ⁻¹	-4.954x10 ⁻²	-4.954x10 ⁻²	GWO
20	-5.089x10 ⁻³	-2.151	-3.015	-3.030	-3.150	GWO, MPA, KMA, POA
21	-0.273	-2.452	-7.943	-4.657	-4.894	GWO, MPA, POA
22	-0.294	-2.474	-8.979	-4.279	-5.817	GWO, MPA, POA
23	-0.322	-2.219	-6.590	-4.214	-5.843	GWO, MPA, POA

TABLE IV. RELATION BETWEEN FORMATION AND THE FITNESS SCORE

Function	Fitness Score			
	0.4:0.2:0.2:0.2	0.2:0.4:0.2:0.2	0.2:0.2:0.4:0.2	0.2:0.2:0.2:0.4
1	3.534x10⁻¹¹	1.977x10 ⁻¹⁰	1.359x10 ⁻²	6.729x10 ⁻⁹
2	0	4.532x10 ⁻³⁰	0	4.802x10 ⁻¹³
3	4.448x10 ²	4.857	4.302x10 ²	1.528x10 ³
4	3.038x10⁻¹	1.267	8.684x10 ⁻¹	6.504x10 ⁻¹
5	2.597x10 ²	4.506x10 ¹	1.344x10 ²	3.151x10¹
6	3.928x10⁻¹⁵	3.278x10 ⁻⁹	9.676x10 ⁻³	1.806x10 ⁻⁹
7	1.572x10 ⁻¹	1.337x10 ⁻¹	2.893x10⁻²	1.075x10 ⁻¹
8	-2.643x10 ³	-2.888x10 ³	-2.974x10³	-2.971x10 ³
9	4.399x10 ¹	2.907x10¹	2.946x10 ¹	3.787x10 ¹
10	8.203	7.871	4.262	7.120
11	6.029x10 ⁻¹	3.370x10 ⁻¹	2.377x10 ⁻¹	2.053x10⁻¹
12	1.726	2.846	5.808x10⁻¹	7.402x10 ⁻¹
13	2.145	4.561	9.026x10⁻²	1.211
14	1.086x10 ¹	9.169	1.510	6.208
15	2.225x10⁻³	3.593x10 ⁻³	5.864x10 ⁻³	4.831x10 ⁻³
16	-1.032	-1.032	-1.032	-1.032
17	3.981x10⁻¹	3.981x10⁻¹	3.981x10⁻¹	3.981x10⁻¹
18	1.040x10 ¹	1.200x10 ¹	3.000	6.857
19	-4.954x10⁻²	-4.954x10⁻²	-4.954x10⁻²	-4.585x10⁻²
20	-3.269	-3.268	-3.131	-3.227
21	-4.232	-3.965	-5.858	-4.206
22	-4.189	-5.505	-5.324	-5.601
23	-4.657	-4.207	-4.309	-4.104

Table IV shows that the relation between the proportion of the options and the algorithm's performance is various; depends on the problem (function) to be solved. There is not any proportion that is the best among other proportions. In some functions, a proportion may be better. But in other function, other proportion is better. Meanwhile, the different proportion affects significantly, especially in solving the unimodal functions. A proportion produces much better result rather than other proportions. Meanwhile, the different proportion affects less significantly in solving multimodal functions. Moreover, the proportion does not affect the result in solving the Six Hump Camel, Branin, and Hartman 3 functions.

The third simulation is conducted to evaluate the proposed algorithm in solving the real-world problem. In this work, the proposed algorithm is challenged to tackle the portfolio optimization problem. A portfolio is a set of valuable and productive assets that is owned by individual or institutions [26]. This asset can be property, stock, bond, gold, and so on. Portfolio represents the wealth of the entity. As a portfolio, an individual or institution should distribute its asset into several options [26]. The objective of this arrangement is to protect its value in the context of maximizing the profit and avoiding the lost. The profit may come from the revenue that is generated from the utilization of the asset or the increasing value of the asset in certain timespan. On the other side, lost may come from the value depreciation or reduction of the asset. Based on it, the portfolio optimization problem can be defined the arrangement of assets in the most optimal way in facing its objective.

In this work, the portfolio optimization problem focuses on the stock. The stock represents the ownership of a proportion of a company. The profit of stock comes in two ways: capital gain and dividend. Capital gain is the increasing value of a share at the end of a certain timespan. The common timespan can be daily, monthly, year-to-date (YTD), year-on-year (YOY), and five years. The dividend is a portion of net profit distributed to the company's owner or stockholder. The stock price represents the market value of a share of a company.

The selected stocks are the ten best companies listed in the LQ45 index. LQ45 index is a list that consists of 45 companies whose share is traded on the Indonesian Stock Exchange (IDX) [27]. These companies are selected because their market capitalization is the biggest, and they are very liquid [27]. These ten companies come from several industrial sectors, such as oil and gas, mining, and banking. The list of these companies is shown in Table V. Table V contains three information: the company's code, current price, and year-to-date capital gain. The current price and capital gain are presented in rupiah per share. The data is obtained from Google, which refers to the Indonesian Stock Exchange.

The stock optimization problem scenario in this work is as follows. The objective is maximizing the total capital gain. The total capital gain is obtained by accumulating the capital gain earned from all held shares. The capital gain refers to the year-to-date capital gain in Table IV. On the other side, there are several constraints used in this optimization. The allocated investment is one billion rupiahs. It means that the bought stocks cannot surpass the total investment. All stocks in

Table IV must be represented in the investment portfolio. The purchasing price refers to the current price in Table IV. The purchasing unit for every stock is presented in the lot. A lot refers to 100 shares. The investment ranges from 50 to 200 lots in every stock. Based on this scenario, this portfolio optimization problem can be seen as a high dimensional problem. The number of dimensions is 10. The problem space for every dimension is between 50 and 200.

The simulation scenario related to this portfolio optimization problem is as follows. The population size is set at 20. The maximum iteration is set at 200. The proportion among possible actions is equal. Like in the first simulation, this proposed algorithm is benchmarked with four algorithms: GWO, MPA, KMA, and POA. The result is shown in Table VI.

Table VI shows that the proposed HPKA algorithm is very competitive among algorithms in solving the portfolio optimization problem. Its total capital gain is the highest among GWO, MPA, KMA, and POA. The total capital gain created by the proposed algorithm is 109%, 46%, 47%, and 1% better than the GWO, MPA, KMA, and POA respectively.

Based on the statistic comparison, it is shown that the proposed algorithm is more stable than POA due to its lower standard deviation. Meanwhile, MPA performs as the most stable algorithm due to its lowest standard deviation. Besides, the stability of KMA is also low and it is close to MPA. Ironically, GWO becomes the most unstable algorithm.

The fourth simulation is conducted to observe the convergence of the proposed algorithm in solving the portfolio optimization problem. In this simulation, there are three values of the maximum iteration: 50, 100, and 150. In this simulation, the proposed algorithm is still compared with these fourth algorithms. The result is shown in Table VII.

TABLE V. TEN BEST COMPANIES IN LQ45 INDEX

No	Code	Current Price	YTD Capital Gain
1	MEDC	545	83
2	ITMG	29,975	10,350
3	ADRO	3,180	810
4	INCO	6,850	2,090
5	PTBA	3,710	1,040
6	UNTR	29,775	7,950
7	MDKA	4,610	570
8	ANTM	2,340	0
9	BBNI	8,450	1,725
10	HRUM	10,125	-375

TABLE VI. PORTFOLIO OPTIMIZATION PROBLEM SIMULATION RESULT

No	Algorithm	Total Capital Gain	
		Average	Standard Deviation
1	GWO	191,827,306	48,601,823
2	MPA	274,425,133	5,323,910
3	KMA	273,280,387	7,949,071
4	POA	398,494,240	20,245,548
5	HPKA	401,824,087	16,252,005

TABLE VII. SIMULATION FOR CONVERGENCE ANALYSIS

No	Algorithm	Total Capital Gain		
		$t_{max} = 50$	$t_{max} = 100$	$t_{max} = 150$
1	GWO	208,336,875	189,973,268	192,619,037
2	MPA	272,722,150	273,976,306	276,707,756
3	KMA	259,277,675	268,501,294	268,033,687
4	POA	402,265,771	416,313,431	408,763,771
5	HPKA	416,847,431	404,039,878	406,785,637

Result in Table VII shows that all five algorithms achieve their convergence in the low maximum iteration. It means that these five algorithms do not need high maximum iteration to find the near optimal solution or acceptable solution. Comparing between POA and HPKA, the gap between these two algorithms is narrow.

V. DISCUSSION

In general, the result proves that the proposed algorithm is a good and competitive metaheuristic algorithm. It is very competitive in solving theoretical optimization problem and real-world optimization problem. Its performance is better than KMA and POA in solving most of benchmark functions and the portfolio optimization problem. It means that this hybrid version is better than its origins, whether it is POA or KMA. More profound analysis regarding the findings will be discussed in the following paragraphs.

Table II shows that the proposed algorithm is better than the basic POA. This circumstance happens in most functions in all three groups: high dimension unimodal, high dimension multimodal, and fixed dimension multimodal functions. This result proves that selecting the best solution for the target is better than the randomized target for the swarm movement. Through guided movement toward the global best solution, the probability of the improvement will be higher than the randomized movement, whether it is the randomized jump as conducted in the first option or the half jump as conducted in the second option.

Table II also shows that the proposed algorithm is better than the KMA. This circumstance also occurs in most benchmark functions, exceptionally high dimension unimodal and high dimension multimodal functions. The proposed algorithm is less competitive than the KMA in solving fixed dimension multimodal functions. This circumstance shows that the mechanics of the proposed algorithm consists of four optional movements and the iteration-controlled exploration-exploitation strategy is better than the three fixed movements in KMA.

The result also strengthens the no free lunch theory. As stated in this theory, developing a general-purpose algorithm better for solving all problems is almost impossible [28]. The proposed algorithm may be less competitive than GWO in solving the high dimension unimodal functions where GWO is superior in these functions. On the other hand, GWO loses its superiority in most multimodal operations, whether they are high dimension or fixed dimension. The proposed algorithm is also significantly superior to GWO in solving the portfolio

optimization problem. On the other hand, the proposed algorithm is slightly better than the POA in solving a portfolio optimization problem. However, the proposed algorithm is significantly superior to POA in solving theoretical optimization problems.

The simulation result shows that the effectiveness of specific algorithms should not be measured by challenging them to solve only the theoretical optimization problem. In the end, any optimization algorithm must be challenged to solve the real-world optimization problem. On the other hand, the circumstance in real-world problems is various. Many problems, especially in the operational research or finance, are simpler to be presented using integer or mixed-integer programming. The problem space is often integer, such as the number of production units, vehicles, assigned employees, shares, and so on. Moreover, the objective function is also simple, such as maximizing the total sales or profit. This objective can be presented by accumulating the weighted parameters. As an integer problem, precision is not needed. It is difficult to achieve a much better result in the integer-based optimization problem. This circumstance also becomes the reason why many well-known old-fashioned algorithms, such as genetic algorithms, are still used widely in many studies in operational research and finance. It is different from the engineering optimization problem, where many parameters are presented in floating-point numbers. In this case, the high precision algorithm becomes more relevant.

The simulation result also shows that the effectiveness of the metaheuristic algorithm also depends on the tuning mechanism of its adjusted parameters. Many metaheuristic algorithms are equipped with several adjusted parameters. The algorithm will perform well when these parameters are adjusted properly. On the other hand, the algorithm will perform poorly when these parameters are not adjusted properly. This circumstance becomes the nature of metaheuristic algorithms so that they can tackle many optimization problems in flexible ways. Based on this circumstance, it is not wise to judge some algorithms are better than others. However, the phenomenon of beating the elder algorithms is common in many shortcoming studies that propose new metaheuristic algorithms. Although the old-fashioned algorithms, such as genetic algorithm, simulated annealing, tabu search, and PSO, have been beaten many times, their popularity is still high because they are simple and flexible to modify. Commonly, the effectiveness of an algorithm can be improved simply by increasing the iteration or enlarging the population size.

There are several challenges and questions regarding this circumstance. Many metaheuristic algorithms are designed based on fixed adjusted parameters. It means that these adjusted parameters can be changed manually. It will be challenging in the future to propose an adaptive algorithm where the parameters can be tuned automatically during the iteration. It means there is logic in this future algorithm that can learn the behavior of the optimization environment (objective and problem space), and then it reacts based on its knowledge.

VI. CONCLUSION

The proposed algorithm, namely the hybrid pelican Komodo algorithm, has been proposed in this work. This algorithm is developed by hybridizing the pelican optimization and Komodo Mlipir Algorithms. The work has demonstrated the outstanding performance of the proposed algorithm as a metaheuristic algorithm. It can tackle the two main objectives: finding near-optimal (acceptable) solutions and avoiding local optimal. Through simulation, the proposed algorithm is successful in solving the theoretical optimization problem and real-world optimization problem. It best solves five functions: Step, Penalized 2, Six Hump Camel, Branin, and Hartman 6. The proposed algorithm is better than GWO, MPA, KMA, and POA in solving 14, 12, 14, and 18 functions, respectively. In solving the portfolio optimization problem, the proposed algorithm creates 109%, 46%, 47%, and 1% better total capital gain than the GWO, MPA, KMA, and POA, respectively. Based on its positive result, this work shows that improving the current algorithms through modification or hybridization is as important as proposing a new algorithm with a new name.

There are several future research potentials regarding this work. This work is just one modification of the existing algorithms (KMA and POA). There are many other ways to modify and improve these two shortcoming algorithms. These algorithms can be hybridized with other battle proven algorithms. Besides, it will be challenging to implement these two algorithms to solve many other optimization problems so that the effectiveness of these two algorithms can be observed better to make the ground base for further development.

ACKNOWLEDGMENT

This work was financially supported by Telkom University, Indonesia.

REFERENCES

- [1] C. -L. Hsu, W. C. Lin, L. Duan, J. R. Liao, C. C. Wu, and J. H. Chen, "A robust two-machine flow-shop scheduling model with scenario-dependent processing times", *Discrete Dynamics in Nature and Society*, ID: 3530701, pp. 1-16, 2020.
- [2] J. W. Fowler and L. Monch, "A survey of scheduling with parallel batch (p-batch) processing", *European Journal of Operational Research*, vol. 298, no. 1, pp. 1-24, 2022.
- [3] F. Pilati, E. Ferrari, M. Gamberi, and S. Margelli, "Multi-manned assembly line balancing: workforce synchronization for big data sets through simulated annealing", *Applied Sciences*, vol. 11, ID: 2523, 2021.
- [4] D. M. Utama, I. Santoso, Y. Hendrawan, and W. A. P. Dania, "Integrated procurement-production inventory model in supply chain: a systematic review", *Operations Research Perspectives*, vol. 9, ID: 200221, pp. 1-21, 2022.
- [5] P. D. Kusuma and M. Kallista, "Pickup and delivery problem in the collaborative city courier service by using genetic algorithm and nearest distance", *Bulletin of Electrical Engineering and Informatics*, vol. 11, no. 2, pp. 1026-1036, 2022.
- [6] S. Zhang, L. Fu, R. Wang, and R. Chen, "The optimization of the location of the cargo in three-dimension shelf: employing the FP-tree and the artificial fish swarm algorithms", *Journal of Control Science Engineering*, vol. 2020, ID: 8832691, pp. 1-15, 2020.
- [7] W. Bakry, A. Rashid, S. Al-Mohamad, N. El-Kanj, "Bitcoin and portfolio diversification: a portfolio optimization approach", *Journal of Risk and Financial Management*, vol. 14, no. 7, ID: 282, pp. 1-24, 2021.
- [8] C. Bayer, R. Tempone, and S. Wolfers, "Pricing American options by exercise rate optimization", *Quantitative Finance*, vol. 20, no. 11, pp. 1749-1760, 2020.
- [9] X. Wang, "Analysis of bank credit risk evaluation model based on BP neural network", *Computational Intelligence and Neuroscience*, vol. 2022, ID: 2724842, pp. 1-11, 2022.
- [10] A. Ansari, I. S. Ahmad, A. A. Bakar, and M. R. Yaakub, "A hybrid metaheuristic method in training artificial neural network for bankruptcy prediction", *IEEE Access*, vol. 8, pp. 176640-176650, 2020.
- [11] H. R. Moshtaghi, A. T. Eshlagy, and M. R. Motadel, "A comprehensive review on meta-heuristic algorithms and their classification with novel approach", *Journal of Applied Research on Industrial Engineering*, vol. 8, no. 1, pp. 63-69, 2021.
- [12] D. Freitas, L. G. Lopes, and F. Morgado-Dias, "Particle swarm optimization: a historical review up to the current developments", *Entropy*, vol. 22, pp. 1-36, 2020.
- [13] S. Liang, T. Jiao, W. Du, and S. Qu, "An improved ant colony optimization algorithm based on context for tourism route planning", *PLoS ONE*, vol. 16, no. 9, ID: e0257317, pp. 1-16, 2021.
- [14] Y. Hou, H. Gao, Z. Wang, and C. Du, "Improved grey wolf optimization algorithm and application", *Sensors*, vol. 22, ID: 3810, pp. 1-19, 2022.
- [15] A. Faramarzi, M. Heidarinejad, S. Mirjalili, and A. H. Gandomi, "Marine predators algorithm: a nature-inspired metaheuristic", *Expert System with Applications*, vol. 152, ID: 113377, 2020.
- [16] S. Xiao, W. Wang, H. Wang, and Z. Huang, "A new multi-objective artificial bee colony algorithm based on reference point and opposition", *International Journal of Bio-inspired Computation*, vol. 19, no. 1, pp. 18-28, 2022.
- [17] X. Ding, M. Zheng, and X. Zheng, "The application of genetic algorithm in land use optimization research: a review", *Land*, vol. 10, ID: 526, pp. 1-21, 2021.
- [18] A. Slowik and H. Kwasnicka, "Evolutionary algorithms and their applications to engineering problems", *Neural Computing and Applications*, vol. 32, pp. 12363-12379, 2020.
- [19] A. M. Fathollahi-Fard, M. Hajiaghahi-Keshteli, and R. Tavakkoli-Moghaddam, "Red deer algorithm (RDA): a new nature-inspired metaheuristic", *Soft Computing*, vol. 19, pp. 14638-14665, 2020.
- [20] Suyanto, A. A. Ariyanto, and A. F. Ariyanto, "Komodo mlipir algorithm", *Applied Soft Computing*, vol. 114, ID: 108043, 2022.
- [21] P. Trojovský and M. Dehghani, "Pelican optimization algorithm: a novel nature-inspired algorithm for engineering applications", *Sensors*, vol. 22, ID: 855, pp. 1-34, 2022.
- [22] Y. Qawqzeh, M. T. Alharbi, A. Jaradat, and K. N. A. Sattar, "A review of swarm intelligence algorithms deployment for scheduling and optimization in cloud computing environments", *PeerJ Computer Science*, vol. 7, pp. 1-17, 2021.
- [23] M. Dehghani, Z. Montazeri, H. Givi, J. M. Guerrero, and G. Dhiman, "Darts game optimizer", *International Journal of Intelligent Engineering & Systems*, vol. 13, no. 5, pp. 286-294, 2020.
- [24] M. Dehghani, Z. Montazeri, S. Saremi, A. Dehghani, O. P. Malik, K. Al-Haddad, and J. M. Guerrero, "HOGO: hide objects game optimization", *International Journal of Intelligent Engineering & Systems*, vol. 13, no. 4, pp. 216-225, 2020.
- [25] K. Hussain, M. N. M. Salleh, S. Cheng, and R. Naseem, "Common benchmark functions for metaheuristic evaluation: a review", *International Journal on Informatic Visualization*, vol. 1, no. 4-2, pp. 218-223, 2017.
- [26] L. Chin, E. Chendra, and A. Sukmana, "Analysis of portfolio optimization with lot of stocks amount constraint: case study Index LQ45", *IOP Conference Series: Materials Science and Engineering*, vol. 300, pp. 1-6, 2018.
- [27] A. Santi Samasta, S. P. Lestari, and T. D. Arsanda, "The analyze of LQ45 companies stock price in 2018-2020", *Journal of Managerial and Digital Business*, vol. 1, no. 2, pp. 64-72, 2021.
- [28] W. G. Macready, "No free lunch theorems for optimization", *IEEE Transactions on Evolutionary Computation*, vol. 1, no. 1, pp. 67-82, 1997.

Users' Acceptance and Sense of Presence towards VR Application with Stimulus Effectors on a Stationary Bicycle for Physical Training

Imran Bin Mahalil¹, Azmi Bin Mohd Yusof², Nazrita Binti Ibrahim³
Eze Manzura Binti Mohd Mahidin⁴, Ng Hui Hwa⁵

College of Computing and Informatics, Universiti Tenaga Nasional^{1, 2, 3, 4}
National Sport Institute of Malaysia, Kuala Lumpur, Malaysia⁵
Putrajaya Campus, Jalan IKRAM-UNITEN, 43000 Kajang, Selangor, Malaysia

Abstract—This research's objective is to identify lacking elements in various effectors utilized in current physical training for cyclists. This encompasses both virtual reality-based system and indoor conventional training. Another objective is to identify user's acceptance from the use of vProCycle; which acts as the primary instrument of this study. Virtual Reality (VR) technology is a computer-generated simulation experience where immersive surroundings replicate lifelike environments – and is used for cyclists' physical training. Distinctive combinations of stimulus effectors (such as altitude, wind-effect, visuals, audio etcetera) have been applied to simulate actual world training environment. This is in order to increase the fidelity of presence for the participants involved, with emphasis on the five human senses. However, in this research the focus is only on hearing, sight, and interaction. The methodology of this mixed-mode pilot study is inclusive of 2 cyclists as participants and a 30 minute training session inside the hypoxic chamber room, whereby they have experienced a VR visual route replica of L'Étape du Tour, France. Variables composed of distinctive stimulus effectors are employed during the training, and survey interviews are utilized to gain users' insight. Results from this pilot study on the presence level indicate that the cyclists' have given high scores. This high score means that the cyclists were immersed while using the vProCycle system. In addition, the cyclists' also gave a high score on the level of technology acceptance towards using vProCycle. The main contribution from this study is to understand how various combinations of stimulus effectors can be applied in a VR-based training system.

Keywords—Virtual reality; sense of presence; technology acceptance; stimulus effectors

I. INTRODUCTION

This research focuses on Virtual Reality (VR) physical cycling training that highlights several preferred stimulus effectors. Subsequently, this study proposes a new indoor cycling setup that includes the identified effectors. In the sports field, VR-based applications have been employed in several distinctive sports such as boxing, soccer, tennis, cycling, etc. VR has been in sports since the year 1990. In most VR applications, it requires a high-end computer in order to run [1]. Other than sports, VR can also be applied for exercising purposes. In addition to that, VR technological applications are also used to visualize realistic 3D modeling, interaction, data acquisition, analysis, product design,

education, and even for medical practices. In terms of cyclists' physical training aims, VR-based applications have been found to gain its popularity [1,2,3]. An advantage of VR is that VR can induce a sense of being mentally or physically present in another place because VR allows individuals to interact with the environment [2]. Further advantages of VR are also noted by Sherman et al. [2], where he has stated that the VR environment can be manipulated in specific and reproducible measures. Sherman et al. [2] used these advantages to train participants to use a rowing and paddling pace strategy for a cycling race. Sherman et al. [2] also mentions that the VR exercising environment does not need to be limited to only a single person. Other individuals such as a coach, teammates, or opposing competitors, may be present even if they are physically located in another place.

In the context of cycling sports, interaction will occur based on how much physical effort from the body is applied to a machine (i.e. Kinetic Road Machine), and this interaction process is known as exertion interface noted by Alhadad et al. [1]. Kinetic Road Machine is one of the most well-known smart trainers available in the current market. A smart trainer is a machine which allows the cyclists to mount their bicycle back wheel, as shown in Fig. 1. Smart trainers are mounted onto the back wheel which have a feature to create a resistance effect. Meanwhile, ergometer is used to detect the motion speed that interactively changes the view in real-time.

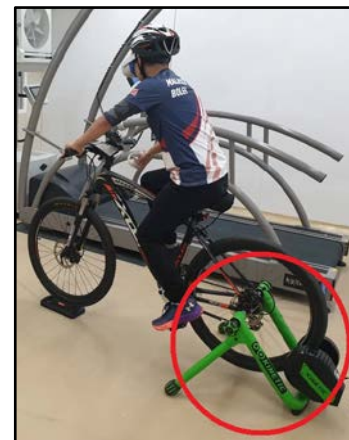


Fig. 1. Smart Trainer Machine (in Red Circle).

In a more advanced VR-based cycling application, devices such as motion capture video systems, infrared beams, and wearable sensors can be used to generate haptic effects; which then translate physical actions into virtual activity. Thus, in general, a VR computer-based sport can be an alternative for an athlete to interact with the virtual environment.

II. LITERATURE REVIEW

In this research, several literatures were reviewed to identify the current status of effectors integrated into a VR-based physical training. According to the Oxford dictionary (2021), the meaning of effectors refer to a substance that carries out a response to the stimulus. This definition is also similar in physiological terms. Meanwhile, a stimulus refers to a substance or event which evokes a specific functional reaction from the human body. From the literature review it is found that stimulus-effectors such as snow, water, wind-effect, and many others can be applied in particular events to trigger a specific body reaction. In a VR-based training, several stimulus-effectors can be applied as replication of an actual life experience.

According to Lim et al. [3], "VR technology creates a stimulation across arrays of effectors and is attached to devices to create an immersive virtual reality system". Until now, the commonly used VR effectors among cyclists comprise of visual, audio, and interaction. It is suggested by a few researchers that adding more effectors on top of the regular ones (i.e. audio, visual and interaction) will generate a significantly more immersive experience. In the area of sports, researchers have used various combination effectors to improve athletes' physical condition [3].

In various studies, different sets of combination effectors are applied to achieve specific objectives such as to increase performance, check physical fitness level, and improve body endurance [4,5,6,7]. In relation to cyclist physical training, it is suggested by the researchers that the following six main effectors; altitude, uphill elevation climb, wind-effect, visuals and audio, interaction and temperature are utilized. The strength and weakness of the effectors' piled as a combination are also identified based on the literature review.

The first stimulus-effector in this research called altitude and temperature. Altitude is referred to as the height of an object or point in relation to sea level or ground level [4]. There are two primary types of altitude training, and they are known as acclimatization and acclimation. Acclimatization is the natural outdoors and acclimation involves indoor training. In acclimatization the actual outdoor oxygen level is used during the training, while for acclimation oxygen level is generated. During a VR-based physical training, cyclists often conduct their training at a simulated high altitude with the aim to train their lungs to perform less oxygen intake [4, 5, 6].

During altitude and temperature training, three main factors may impact the cyclists' body and they are; atmospheric pressure, reduction of oxygen molecules in the air, and colder temperatures as the altitude gets higher from sea level [8]. The first factor which is atmospheric pressure, affects the cyclist as the altitude gets higher. Changes to atmospheric pressure may lead to a situation where there is

less oxygen in the cyclists' blood to carry to their muscles [9]. When cyclists train with less oxygen intake, their muscles may adapt accordingly, which means that the cyclist does not need to breathe harder or more when they are at sea level altitude. Most of the Olympic cyclists are trained at 1000 meters above sea level. At that level, the body will take in at least 20 percent lesser oxygen. This is caused by a reduction of oxygen in the atmosphere compared to sea level. Generally, higher altitudes of 5000 and above are considered dangerous due to the amount of oxygen molecules being below 17% in the air [8,9].

In a paper by Lei et al [5], they have mentioned that there is a significant impact when integrating altitude and temperature within VR-based applications. In Lei's [5] research, a setup involving a special room replicated the environment's altitude of 1000 meters above sea level; whereby the users were required to wear a HMD. The amount of oxygen was based on that height. It is to be noted that his experiment was conducted in multiple sessions. The findings from her research show that the cycling speed has improved where the difference between the first and the final sessions was greatly significant. Furthermore, Lei [5] also studied the effects of physical sport equipment such as a ball. Lei's [5] findings show a positive outcome where athletes have improved their accuracy as the participants were able to aim and kick the ball directly into the goal post.

Another essential research conducted by Mujika et al. [6] highlighted the measurement of altitude using the Meters Above Sea Level (m.a.s.l) technique. In his research, the user is also required to wear a HMD. Altitudes can be controlled indoors for training by using a chamber room. This chamber room can simulate any hypoxic environment by both latitude and longitude. Latitude is the angular distance of a place north or south of the earth's equator. On the other hand, longitude is the angular distance of a place east or west of the Greenwich meridian. As the latitude is higher above sea-level, fewer oxygen molecules are in the air and this consequently makes temperature to get colder. The longitude of a location can also determine the temperature on Earth. For example, the equator has different temperatures near the south and north poles. During the experiment, three different levels of altitudes were tested: low, medium, and high. Low altitudes represent the sea level where, at this altitude, the percentage of oxygen molecules is 20.9. This is the standard level of oxygen required by the human body to breathe normally. Meanwhile, at medium altitude (between 3000 and 4000 feet), the percentage of oxygen molecules is between 18.6% and 17%. Next at 5000 feet is considered as high altitude, whereby the oxygen may reach below 17% in the air.

Mujika's et al. [6] experiment involved the usage of a hypoxic dose, a timer, and confounding factors. Hypoxic dose is a medication given to the participating cyclists at an early stage. It helps cyclists to adapt themselves during altitude training. Meanwhile, a timer refers to a load periodization where it involves progressive cycling of various aspects in a training program during a specific period. Lastly, confounding factors used by Mujika [6] involved the use of simulated altitude, such as Meters Above Sea Level (m.a.s.l) and oxygen intake. Simulated altitude refers to the pressure and oxygen molecules available to the users while using a VR-based

system similar to that of a real-life situation. This training was conducted over multiple sessions. The impact of the training depicts that VR-based training enhances athletes' muscle buffering capacity which subsequently improves athletic physical fitness. This study also suggested that simulated altitude is incredibly effective to train athletes' endurance.

The only difference between Mujika's [6] and Lei's [5] study is that in Lei's [5] study, she did not include multiple high altitude studies.

The second effector preferred by many cyclists for training purposes is called an uphill elevation climb. Uphill elevation climb is a stationary cycling training simulated by the resistance effect on the back wheel. This resistance effect gives the cyclist the sensation of cycling uphill as they would in the real world. A back-wheel resistance machine is a piece of hardware that makes it possible to ride a bicycle with an uphill climb effect. This machine consists of a frame, a clamp, a roller on the back-wheel, and a motor which provides resistance [8, 9]. However, Yap et al. [7] has stated in his paper that the combination of back wheel resistance together with the common effectors (visual, audio and interaction) is not realistic enough to imitate an actual real life event. Many researchers have also suggested adding more varieties of different effectors to the current stationary training method.

In relation to the back-wheel resistance, Farrow et al. [8] have used HMD and uphill elevation climb to study a haptic effect. In his study, he highlighted that enjoyment levels and the force needed to paddle increases when haptic effects are experienced. Back-wheel resistance machines can be equipped with sensors that monitor the cyclists' physical fitness. Physical characteristics such as power output, cadence, virtual speed and heart rate are among the metrics that can be transmitted electronically [8]. Analyzing these physical outputs can help to fine-tune the athlete's training sessions. These sensors can also monitor data such as speed, distance traveled and time duration [8,9].

The effector of the uphill elevation climbing effect using bicycle was created using many different methods such as rollers on the back-wheel, attaching machines directly on to the bicycle wheels with the utilization of a 3D platform. One of the most popular methods in virtual reality to create the simulation of an uphill climb is by using a machine attached to the back wheel. The machine would cause resistance on the back wheel depending on the virtual environment as seen by the cyclist. In Farrow's [8] experiment, athletes' force and enjoyment levels were tested using HMD. The effector uses haptic effect from having the athletes paddle on the bicycle with resistance based on the VR system. In the study conducted by Farrow [8], he stated that with exercise enjoyment, athletes were still able to improve physical fitness using VR to train. In his findings, his results demonstrated that VR-exercise is an effective intervention as well as being credible to increase enjoyment while training [8,9]. It was calculated that 20 participants 222 were needed to identify a statistically significant gap in mean power output between 223 tracks and conditions (effect size = 0.67), with a power of 0.8 and alpha set at 0.05.

In Farrow [8] research, they developed a stationary bike reality simulation training with a back-wheel resistance device. The research was conducted using a back wheel road machine, which creates a virtual environment simulating an uphill climb. In his research, the users select the cycle path using a human-machine interface [9,10]. The stationary bicycle is used as an assisting training device that was proposed to help riders undertake simulation-based training before cycling on a real cycle path. The result of this research calculated the riding speed and accumulated the mileage as well as time-trial. Each riding session recorded distinctive elements such as mileage, time duration, average speed, and the route chosen. The results of his study using the Kinetic road machine shows that it had improved the cyclist's average speed when riding.

The third effector preferred by the cyclists during physical training is called wind-effect. Wind-effects can be used to enhance the experience and improve cyclists by exposing them to a more naturally aesthetic environment. This wind is created by using a fan. In order to simulate the wind-effect during cycling and enhance the cycling experience, a real time wind speed is needed to be generated [9, 11].

The wind speed can be measured in kilometers per hour. Integrating wind-effects for cycling training is used for endurance training focused on adaptive hypoxic training. Coaches train their athletes in a condition where the cyclist is required to paddle at maximal speed at a setup with high wind speed [9, 10]. The effect of the wind physical training is measured by the cyclist's speed together with the amount of wind speed in kilometers per hour. When used for training purposes, cycling in the wind can potentially cut one's speed in half with the same effort expended as when there is no wind. This means that the cyclist has to work twice as hard to generate the same output. The measurement from wind-effect training can be seen by the cyclist's energy output, and distance traveled in a specified time trial as in Petri et al. [9].

Research conducted by Schwind [10] found that the usage of HMD in VR sports has widely changed the way simulated sports are practiced. However, he claimed that experts still understand only a little about the use of antecedents for cyclists' sports applications. He examined attitudinal and norm-based factors that influence users' continuous intention towards sport applications usage. His research consisted of 362 sport practitioners where basic realism fidelity was integrated into the system. The results indicated that all attitudinal factors and norm-based factors have optimistically affected users' acceptance towards the inclusion of sport applications. His findings portrayed a promising acceptance level to all stimulus effectors of uphill elevation climb and wind-effect.

The last two effectors; visual and audio, are often integrated into cycling physical training aiming to produce highest fidelity of realism. A Virtual reality system renders visuals for the users to experience in a controlled virtual environment. The environment visuals are usually based on the user's bodily interactions, such as while the user rotates their head during HMD utilization, and the visuals are viewed according to the orientation of the head. Also, while using

virtual reality force feedback on bodily interactive motion, the visuals can move the 3D user's avatar in the virtual environment. This force feedback bodily interaction is what makes the VR sports exercise experience more pleasurable. Another effector is sound-effect that the user can auditorily hear while they are immersed in the virtual environment. Sound-effects in the virtual environment are 3D-surrounding. In VR, the 3D-surround sound effect uses multiple audio cue channels to stimulate the effect of an object's sound from the distance; the sound is sighted from 3D-surround sounds that come together with visuals as the two effectors complement one another for a realistic experience.

In a research conducted by Yap et al [7], a HMD with a fully immersive 360 degree view and 3D audio was used. Inside the HMD, one view is for the user's right eye and the other view is for the left eye. These two stereo views were fused by the viewer's perceptual system in the same way as humanistic right and left eye views of natural scenes [7]. The HMD system must also compute the synthetic views, track the viewer's location, and viewing orientation in the virtual world to create the correct right and left eye views. The latest VR technologies allow the development of better and cost-effective spatially immersive visualization and audio systems. His findings showed that 38 out of 50 preferred to display the simulation in HMD in comparison to non-VR-based displays such as on projectors and monitor screens.

In another research conducted by Koivisto et al. [11], he identified that users' characteristics may influence the quality of the VR experience. He also stated that users' characteristics may be influenced by the quality of the VR system. For example, the quality between visualizing through a monitor screen and using a HMD will give different impacts on the users' immersion level. It involves progressive cycling of various aspects of a training program during a specific period. Koivisto et al. [11,12] used a questionnaire method called the International Physical Activity Questionnaire (IPAQ). By using IPAQ, he found significant improvements compared to VR and non-VR visuals as well as audio.

The study conducted by Ng [13] shows that motivated cyclists using VR virtualization can contribute greatly to achieve training purposes. Ng identified research gaps in the areas of virtual reality (VR) sport applications from a systematic literature review of VR sport applications research. It showed that different physiological and psychological factors have been investigated by conducting experiments on the use of these applications in the study by Alhadad et al [1], Neumann et al. [14]. However, in Ng's study, different task purposes, like training, competition or socializing, do influence the perceived benefits which have not yet been examined. Moreover, it is unclear whether perceived benefits and risks affect actual behaviour outside laboratory environments. His study showed a significant difference in the risk assessment perceived by the cyclists.

Based on the seven papers as discussed above, six effectors have been identified. Those effectors are altitude effect, uphill elevation climb effect, realistic audio and visuals, wind-effect, realistic interaction and temperature. The

details of each of these stimuli are further explained in the following subtopics.

Through the seven main effectors as mentioned, it is noticed that many researchers have used effectors. However, the combination of implementing all stimulus effectors together into one complete system has not yet been established.

III. FINDINGS RESULTS FROM AUTHOR'S PREVIOUS STUDY

This paper is a continuation from the authors' previous research as published in "A literature review on the usage of Technology Acceptance Model for analyzing a virtual reality's cycling sport applications with enhanced realism fidelity." [15,16] and "A literature review on the effects of 6-Dimensional virtual reality's sport applications toward higher presence." [16]. During the author's previous research, several selected stimulus effectors were identified. These findings were done by conducting a questionnaire interview session and feedback gathered from recreational cyclists who have undergone current stationary indoor training in professional gyms. In the last two papers, the number of interviewees was 30 in quantity, whereby all were conducted at a professional gym.

In the Table I, it shows the list of stimulus effectors used in the current setup for a conventional indoor cycling training.

TABLE I. CYCLING TRAINING STIMULUS EFFECTORS SETUP REQUIREMENTS

Stimulus effectors	Current setup (Available Y/N)	No. of cyclists have experienced the simulator	No. of cyclists that recommend the stimulus effectors
Uphill elevation climb	Yes	30	30
Altitude	No	Nil	28
Wind-effect	Yes	25	28
Visual and sound	Yes	28	28
Interaction	Yes	30	30
Temperature	No	Nil	28

Table I shows the usage of stimulus effectors for cycling training. The data is gathered from the interview conducted with 30 recreational cyclists between the ages of 18 years and 50. Out of the 30 cyclists, 20 were male and the latter 10 were female. Column one of Table I shows the six stimulus effectors identified from the interview as discussed in the previous paper [15,16]. In the "current" setup, it is found that altitude and temperature stimulus effectors are not being integrated. It is also identified as shown in the table that all participants were trained with uphill elevation climb and interaction. As for visual and sound, only 28 participants used a device to display their physical or other visual activities during a training session. While cycling in the gym, the standard setup includes a big screen in front of the cyclist. However, some cyclists often watch or listen to other

technological sources such as mobile phones and tablets. This action of extra displays can cause distraction while they undergo a training session. As for wind-effect utilization while training, every stationary bicycle comes with a built-in fan. Despite the availability of the fan feature, only 25 cyclists out of 30 actually employed it during training. Table I also portrays the number of cyclists who felt that using stimulus effectors while training is of great importance. A majority of the cyclists perceived all six stimulus effectors as necessary for the purpose of cycling training.

From the findings listed in Table I, it has been identified that the six stimulus effectors are important towards creating a highly effective training platform among cyclists. The combination of two or three stimulus effectors have already been experimented by other researchers as discussed in the literature above. In this paper, the combination of all six stimulus effectors is proposed, which deem it as distinctive from other researchers as cited in the literature review section. In the following sections (4.0), the implementation of the proposed VR setup with the combination of stimulus effectors to meet the requirement of a current cycling training system will be explained in detail.

IV. HARDWARE AND TECHNOLOGY REQUIREMENT

Table II shows the list of technology providers that fulfill the requirements for a cycling training system. The six effectors are matched to a specific technology to provide a distinguished experience for the user.

Table II shows a list of effectors and their technology providers integrated into the vProCycle system. The effectors employed are audio and visuals, altitude, uphill elevation climb, temperature, wind-effect, as well as paddling interaction.

From the literature, it was found that with distinctive stimulus effectors, the cyclist had experienced a higher level of immersion and presence. This situation is similar to the experience gained by the cyclist during their training in the real world.

Many literature encourages the use of more distinctive stimulus effectors for a better VR application out-put. The individual stimulus effectors have already been investigated. However a comprehensive study on a VR application that consists of several stimulus effectors have not been maximized.

TABLE II. LIST OF EFFECTORS AND TECHNOLOGY PROVIDER

List of effectors and technology provider		
No.	Effectors	Technology provider
1.	Audio and visuals	HMD
2.	Altitude	Altitude chamber room
3.	Uphill elevation climb	Backwheel resistance machine
4.	Temperature	Altitude chamber room
5.	Wind-effect	Fan
6.	Realistic paddling interaction	Blue-tooth device

V. IMPLEMENTATION OF VR-BASED SYSTEM WITH STIMULUS EFFECTORS

From the findings where the providers and effectors have been matched, the following setup design inclusive of all the six stimulus effectors was generated. Before discussing in detail about the proposed setup, a few current cycling training systems are discussed here.

As shown in Fig. 2(a), (b) and (c), the cyclists are conducting their training using a conventional setup where they are not complementing the training with VR technology visual and audio. In Fig. 2(a), the cyclist is interactively viewing the cycling track based on the paddling speed. However, there is no interactive resistance applied while cycling as viewed when climbing uphill. Fig. 2(b) shows a combination of both external visuals (i.e. big screen TV) and a backwheel resistance that simulates the effect of cycling uphill. Fig. 2(c) shows the training setup done inside a chamber room where no VR is applied. However, the cyclist gets the effects from temperature, humidity and latitude control. VR is also applied as mentioned in the LR, however with a limited combination of stimulus effectors. Based on all the existing setups as discussed above, it is found that there is no setup that exists yet that integrates all the components comprehensively. As a result, a new setup is then proposed.



Fig. 2. Traditional Training without VR (a), (b), (c).

Fig. 2 shows a traditional training without VR and with back wheel resistance (a). Fig. 2(b) shows a traditional training without VR with big screen and backwheel resistance to stimulate uphill climb. Fig. 2(c) shows a cycling training without VR in an altitude chamber room. From the findings as discussed above, the following design setup involves all the six stimulus effectors.

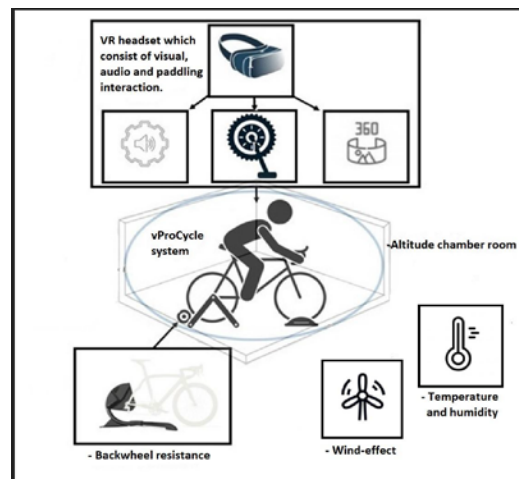


Fig. 3. Proposed Setup of VR Cycling Training System.

Fig. 3 shows the proposed setup of the VR cycling training system with the combination of various effectors. As previously stated, the elements encompass uphill elevation climb, altitude, temperature, wind-effect, interaction, visual, and audio. This proposed VR cycling training system is named as the “vProCycle system”.

The selected effectors and technology providers must match the requirements of the current cycling system, hence the methodology is justified in the next section.

VI. EXPERIMENTAL METHODOLOGY AND RESULTS

In this section, the generated vProCycle is used for the experiment and will be discussed in detail. Through this vProCycle cycling training system, the sense of presence and users’ immersion rate in the virtual environment are both evaluated. In addition, the technology acceptance of the cyclist is also to be determined. The first stage of the experiment involved a pilot study by two well- trained cyclists. After the data is collected from the pilot study, the vProCycle system is then further tested in experiment 1.

VII. PILOT STUDY AND OBJECTIVES

The objective of the pilot study is to evaluate whether the designated reaches a high fidelity of VR presence level from using the vProCycle system. Another objective is to evaluate their acceptance or outlook towards the technology when using vProcycle.

VIII. PILOT STUDY SETUP REQUIREMENTS AND DESIGN MATERIALS

In this subsection, the cyclists' setup requirements and design materials used to conduct the pilot study are identified. The figure shows a visual of the setup requirement and design materials utilized throughout the pilot study.

Fig. 4 shows the setup requirements and design materials during the pilot testing. This pilot test is conducted at Institut Sukan Negara (ISN). ISN is a Malaysian government agency - and it is established to provide sports science services, conduct research and development in the sports spectrum. Specifically, the study was conducted inside a hypoxic chamber. A stationary bicycle was used in the experiment whereby it was mounted on a back wheel machine. The machine is used to create an effect of resistance to the back wheel of the bicycle to simulate an uphill elevation climb. The paddles were also equipped with a Bluetooth sensor that sends signals to the HMD. This indicates that the bicycle is being paddled for it to move in the virtual environment. When the cyclist paddles forward, the visuals in the HMD change accordingly to the motion speed of the paddles. The HMD provides a complete 360° audio of the virtual environment sound to the cyclist participating. The visuals used in this study was a 360° view of L'Étape du Tour, France, as recorded by a 360 camera.

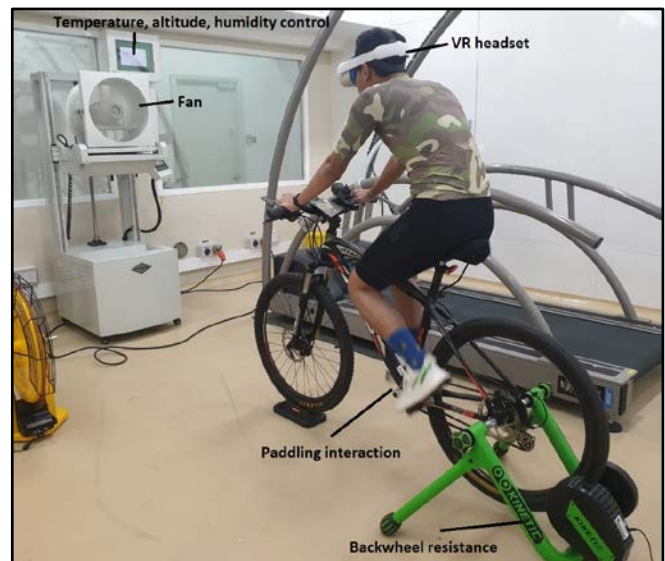


Fig. 4. Pilot Study Setup.



Fig. 5. A Sample Visual of L'Étape du Tour, France.

Fig. 5 shows a sample visual of the cyclist’s view in the HMD while undergoing the pilot study. As mentioned earlier, another effector applied in the system is wind-effect. The wind-effect is generated by a fan placed at one and a half meters in front of the cyclist. The overall listed requirements and design materials are placed in a hypoxic chamber room; which controls the altitude, temperature, and humidity in the designated area. During the pilot study, a 1x9 MTB gear setup mountain bicycle was mounted onto the back wheel machine. This bicycle was selected to test the detected changes on the back wheel elevation climb-effect. This climb-effect is computer generated and controlled by the virtual reality program, which means that it adjusts the resistance of the wheel. This is executed by gripping or releasing of the rotation wheel as the virtual landscape changes. The session of this experiment was conducted for 30 minutes.

IX. PILOT STUDY CYCLISTS' REQUIREMENT

The pilot study involved identifying the basic requirement of the cyclist participating. The first requirement is that the cyclist must be above 18 years old. The second is that the cyclist must have the experience of participating in a cycling state event and have completed the flag-off time limit.

X. PILOT STUDY TOOLS SETTINGS

The pilot study tool settings were that both cyclists are required to cycle at least 30 minutes in a virtual environment based on the Google map view of L'Étape du Tour, France. L'Étape du Tour map view is an official, professional cyclist training route. This route is 13 kilometers in length, with an altitude of 1,800 to 2,000 meters above sea level. The temperature level at this location is between 18°C to 26.5°C and at this altitude, the oxygen molecules in the air is about 20 percent lesser than at sea level. On this route, there are a lot of uphill elevations in narrow turns, which indefinitely creates a physical challenge when cyclists train at that exact location.

XI. PILOT STUDY RESULT

In this study, two participants were involved, one male and one female. The data collected were divided into two categories: (1) sense of presence level and (2) technology acceptance. Presence is measured using a questionnaire based on the Witmer and Singer Presence Questionnaire [3], which uses a Likert scale from 1 to 7. The indicator of the Likert scale is the lowest of 1 being not immersive and 7 being highly immersed. An example of the questions used are "When you bicycle forward, did the feeling of moving forward in the virtual world seem realistic?" and "When you paddled the bicycle, did you feel the movement speed as realistic according to the change of view?" The two participants were required to answer a series of questions addressing each effector. The presence questionnaire was given after the cyclists had undergone a training session using vProCycle.

XII. PILOT STUDY RESULT: SENSE OF PRESENCE

Results of the cyclists' sense of presence data can be used to determine whether the vProCycle system is credible in creating the sense of realism as though they were cycling in L'Étape du Tour, France. The table shows the results of the cyclists' sense of presence using vProCycle system.

The number of questions asked in relation to the effectors listed in Table III were: 14 questions related to visuals, 5 questions on audio, 6 questions on altitude, 6 questions on the uphill elevation climb, 3 questions on temperature, 3 questions on wind-effect and lastly, 7 questions on interaction. Table III shows the cyclists' sense of presence using the vProCycle system. The first effector listed is "visual". The score given by the male cyclist is 4.1 out of 7, which indicates that the visuals are moderate for him. On the other hand, the female cyclist rated the "visual" with a score of 5.1 out of 7, which is considered upper-moderate. Secondly is audio effects, whereby the male cyclist gives it a score of 5.2 and simultaneously, a score of 5.6 by the female cyclist, which indicates that both cyclists give the audio presence level an upper-moderate score. Thirdly, in regard to the altitude-effect,

the male gives it a score of 5.4 out of 7 while the female gives it a score of 5.7. Both rated the altitude-effect score as highly immersive, an almost exact replica of being at the high altitude of the L'Étape du mountain. Fourth is on the uphill elevation climb, where the male gives it a score of 2.6 out of 7 and the female gives it a score of 4.5 out of 7. This signifies that the uphill elevation climb has the lowest score out of all the other effectors. An open-ended interview session gained insight on why the male cyclist gave the very low score on the uphill elevation climb. It was mentioned that the maximal 10 degrees angle uphill inclination that the VR back wheel machine produced does not feel immersive. This is in liaison as the visuals appeared to look like more than a 10 degrees angle slope. Fifth is regarding the temperature, whereby both participants scored a 5.3 out of 7. This indicates that the temperature simulation within the VR immersion experience was very realistic. Sixth is on the wind-effect, the male gives it a score of 5.3 out of 7 while the female gives it a score of 5.66. This indicates that both cyclists found the wind-effect to be quite similar to lifelike surroundings. Lastly is the paddling interaction, whereby the male cyclist gives it a 4.5 and the female cyclist gives it a 4.6. Both cyclists gave the paddling interaction a reasonably decent, high score. All the scores from the questionnaire were added, then averaged based on the effectors.

TABLE III. PILOT STUDY OF THE CYCLIST SENSE OF PRESENCE

The cyclists sense of Presence using vProCycle system			
No.	Effectors	Male cyclist (Average)	Female cyclist (Average)
1.	Visuals	58/98 = 4.1	72/98 = 5.1
2.	3D Audio	26/35 = 5.2	28/35 = 5.6
3.	Altitude	27/35 = 5.4	27/35 = 5.4
4.	Uphill elevation	16/42 = 2.6	32/42 = 4.5
5.	Temperature	16/21 = 5.3	16/21 = 5.3
6.	Wind-effect	16/21 = 5.3	17/21 = 5.66
7.	Paddling interaction	32/42 = 4.5	33/42 = 4.7

XIII. PILOT STUDY RESULT: TECHNOLOGY ACCEPTANCE

This section explains both cyclists' technology acceptance using vProCycle system during the pilot study. All the scores from the questionnaire were added then later averaged based on the independent variables of TAM. The number of questions asked in relation to the independent variable listed in Table III are composed of 8 questions related to perceived usefulness, 7 questions on ease of use, 4 questions on behavioural intention to use, and 5 questions on attitude towards usage.

Table IV shows five independent variables of TAM. Those variables are: perceived usefulness, perceived ease of use, attitude towards using, behavioural intention to use, and actual use. The first independent variable is "perceived usefulness", the male cyclist rated it a 7 while the latter gave it a 5.5. This shows that both cyclists found it quite useful; using vProCycle as a hypoxic cycling training. The second variable is "perceived ease of use"; the male ranked a score of 5.7 while

the female gave it a score of 6.2. This implies that the vProCycle system was very easy to use by both cyclists. The third variable is “attitude towards using vProCycle”, where the male rated 5.6 while the female gave a 5.6. This signifies that the cyclists' attitude towards using vProCycle is incredibly positive. The fourth independent variable is on the “behavioural intention to use”, the male puts a value of 6 while the latter gives it a score of 6.75. This indicates that both cyclists would have the intention to continually use vProCycle. The last variable is called “actual use”, with the male giving a score of 7 and the female cyclist a score of 6. Both cyclists highly recommended vProCycle to be used for hypoxic training.

TABLE IV. PILOT STUDY OF THE CYCLISTS' TECHNOLOGY ACCEPTANCE TOWARDS USING vPROCYCLE

The cyclists' technology acceptance towards using vProCycle			
No.	Independent variables of TAM	Male cyclist	Female cyclist
1.	Perceived Usefulness	49/56 = 6.18	44/56 = 5.5
2.	Perceived Ease of use	40/49 = 5.7	44/49 = 6.2
3.	Attitude towards using	28/35 = 5.6	28/35 = 5.6
4.	Behavioural intention to use	24/28 = 6	27/35 = 6.75
5.	Actual use	21/21 = 7	18/21 = 6

XIV. PILOT STUDY AND ISSUES

It was advised by ISN that some cyclists may encounter hypoxemia which may lead to nausea, headache, dizziness or even vomiting. Fortunately, none of the participants encountered any of the symptoms of hypoxemia during this study.

Another issue was related to the uphill elevation climb. This is when the cyclist sees an incline of greater than 10 degrees steepness slope angle; while the back wheel machine can only create a maximum of 10 degrees. Some cyclists may expect to get greater resistance when encountering a stiff uphill climb as the hill has a steepness of 60 degrees. However, there is a device that can go up to 60% but is not currently available in VR. From the open interview in relation to the uphill elevation climb, the middle score is given only in relation to the back wheel resistance compared to the elevation climb that is visible in the HMD. There is a solution available that gives a better uphill climb using other devices. However, that device will not be used in the VR environment.

XV. PILOT STUDY CONCLUSION

From the pilot study, it was highlighted that both the sense of presence in the VR cycling stimulation and technology acceptance of vProCycle were given high scores as well as positive feedback. This suggests that further testing can be conducted for professional cyclists. The test conducted in experiment 1 will be explained in detail below. In experiment 1, additional data from a heartbeat reader will be collected on top of other data similar to the pilot study executed.

XVI. CONCLUSION

In conclusion, this paper shows how vProCycle offers new possibilities to understand and experience VR potential to be used for cycling training; when combined with a combination of stimulus effectors. It is to be highlighted that distinctive stimulus effectors do greatly influence the presence level of participating cyclists. This presence level is experienced by a realistic simulation integrated with the system. This simulation creates an experience as though the cyclist is cycling in the distinctive actual real environment. This high level of presence thus generates a positive outlook in terms of the users' acceptance towards the generated VR-based system.

However, there were also a few research limitations in this study, inclusive of the possibility that the participants may encounter hypoxemia which may lead to nausea, headache, dizziness or vomiting. In this pilot study, the cyclists who had undergone training using vProCycle did not encounter any hypoxemia experience. In addition, the availability of the hypoxic chamber room is limited and costly. As a result, conducting an experiment is limited by the financial and chamber room availability. Some recommendations for future studies may include the usage of backwheel resistance machine that can increase the elevation uphill climb resistance more accurately. In this pilot study the Kinetic machine used to stimulate resistance on the backwheel can only create a resistance equivalent to 10 degrees uphill slope. This specific machine was selected due to the ability to connect to the virtual reality devices. Other backwheel machines currently do not have the features to connect to the virtual reality devices. The cyclists during an open interview did mention they would like to have a higher resistance to the back wheel when climbing steep slopes as viewed in the HMD.

In addition, the 360 degree visuals provided by Google viewed inside the HMD were picture to picture based. In the future, a fully recorded video moving forward based on the cyclist paddling should be used if it is available.

Moreover, the wind-effect simulation speed generated by the fan is constant at all times. It is recommended that future researchers integrate the bicycle with a wind speed-based technology to simulate a realistic effect while inside the virtual environment.

Also, a stationary bicycle with tilting slope effect machine can be used for the cyclist to experience how to tilt their bicycle according to the virtual environment. This tilting slope effect can be achieved by using a motion platform that can tilt according to the body movement of the cyclists'.

This paper focuses on TAM analysis and the perception of presence using vProCycle. Based on cyclist's feedback to the TAM questionnaire, cyclists have given a high acceptability level towards using vProCycle. A positive correlation between TAM and also perception of presence shows that this combination may produce a positive outlook.

The contribution and innovation of this research includes the setup of the vProCycle system with a more comprehensive stimulus effectors. These combinations consist of an uphill

elevation climb, altitude, temperature, wind-effect, interaction, visual, and audio. For future research, researchers may integrate more stimulus effectors such as weather effect, road surface and light visibility.

ACKNOWLEDGMENT

This work is supported by the Universiti Tenaga Nasional BOLD research grant.

REFERENCES

- [1] Alhadad SA, Abood OG. Application of virtual reality technology in sport skill. *International Journal of Academic Management Science Research*. 2018;2(12):31-40.
- [2] Sherman WR, Craig AB. *Understanding virtual reality: Interface, application, and design*. Morgan Kaufmann; 2018 Nov 8.
- [3] Lim JS, Hwang Y, Kim S, Biocca FA. How social media engagement leads to sports channel loyalty: Mediating roles of social presence and channel commitment. *Computers in Human Behavior*. 2015 May 1;46:158-67.
- [4] Czuba M, Waskiewicz Z, Zajac A, Poprzecki S, Cholewa J, Roczniok R. The effects of intermittent hypoxic training on aerobic capacity and endurance performance in cyclists. *Journal of sports science & medicine*. 2011 Mar;10(1):175.
- [5] Lei MK, Cheng KB, Lee YC. The Validity of using Virtual Reality Head-Mounted Display for Agility Training. *ISBS Proceedings Archive*. 2018;36(1):122.
- [6] Mujika I, Sharma AP, Stellingwerff T. Contemporary periodization of altitude training for elite endurance athletes: a narrative review. *Sports Medicine*. 2019 Nov;49(11):1651-69.
- [7] Yap HJ, Hau TC, Taha Z, Wee CS, Sekaran SC, Lim WW. Design and development of a spatial immersive track cycling simulator. *Malaysian Journal of Movement, Health & Exercise*. 2018 Jul 1;7(2):39-52.
- [8] Farrow M, Lutteroth C, Rouse PC, Bilzon JL. Virtual-reality exergaming improves performance during high-intensity interval training. *European journal of sport science*. 2019 Jul 3;19(6):719-27.
- [9] Petri K, Feuerstein K, Folster S, Bariszlovich F, Witte K. Effects of Age, Gender, Familiarity with the Content, and Exposure Time on Cybersickness in Immersive Head-mounted Display Based Virtual Reality. *American Journal of Biomedical Sciences*. 2020 Apr 1;12(2).
- [10] Schwind V, Knierim P, Haas N, Henze N. Using presence questionnaires in virtual reality. In *Proceedings of the 2019 CHI conference on human factors in computing systems 2019* May 2 (pp. 1-12).
- [11] Koivisto J, Hamari J. The rise of motivational information systems: A review of gamification research. *International Journal of Information Management*. 2019 Apr 1;45:191-210.
- [12] Petri K, Ohl CD, Danneberg M, Emmermacher P, Masik S, Witte K. Towards the usage of virtual reality for training in sports. *Biomedical Journal of Scientific & Technical Research*. 2018;7(1):1-3.
- [13] Ng YL, Ma F, Ho FK, Ip P, Fu KW. Effectiveness of virtual and augmented reality-enhanced exercise on physical activity, psychological outcomes, and physical performance: A systematic review and meta-analysis of randomized controlled trials. *Computers in Human Behavior*. 2019 Oct 1;99:278-91.
- [14] Neumann DL, Moffitt RL, Thomas PR, Loveday K, Watling DP, Lombard CL, Antonova S, Tremeer MA. A systematic review of the application of interactive virtual reality to sport. *Virtual Reality*. 2018 Sep;22(3):183-98.
- [15] Mahalil I, Yusof AM, Ibrahim N. A literature review on the usage of Technology Acceptance Model for analysing a virtual reality's cycling sport applications with enhanced realism fidelity. In *2020 8th International Conference on Information Technology and Multimedia (ICIMU) 2020* Aug 24 (pp. 237-242). IEEE.
- [16] Mahalil I, Yusof AM, Ibrahim N. A literature review on the effects of 6-Dimensional virtual reality's sport applications toward higher presence. In *2020 8th International Conference on Information Technology and Multimedia (ICIMU) 2020* Aug 24 (pp. 277-282). IEEE.

Fast and Robust Fuzzy-based Hybrid Data-level Method to Handle Class Imbalance

Kamlesh Upadhyay¹, Prabhjot Kaur², Ritu Sachdeva³

Research Scholar, Lingayas Vidyapeeth, Faridabad, New Delhi, India¹

Department of Information Technology, Maharaja Surajmal Institute of Technology²
GGSIIP University, New Delhi, India²

Professor, Lingayas Vidyapeeth, Faridabad, UP, India³

Abstract—Conventional classification algorithms do not provide accurate results when the data distribution (class sizes) is unequal or data is corrupted with noise because the results are biased towards the bigger class. In many real life cases, there is a requirement to uncover unusual/smaller classes. There are a bundle of examples where importance of smaller/rare class is much-much higher than the bigger class for example- brain tumor detection, credit card fraud or anomaly detection and many more. This is usually called as problem of imbalance classes. The situation becomes worst when the data is corrupted with extra impurities like noise in data or overlapping of class or any other glitch in data because in this scenario traditional methods produce more poor results. This paper proposed a fast, simple and effective data level hybrid technique based on fuzzy concept to overcome the class imbalance problem in noisy condition. To appraise the classification performance of the offered technique it is tested with 40 UCI real imbalanced data sets having imbalance ratio ranges from 1.82 to 129.44 and compared with 12 other approaches. The outcome specifies that the presented hybrid data level technique performed better and in a fast manner when compared to other approaches.

Keywords—Data level approaches; undersampling; oversampling; fuzzy concept; imbalanced data-sets; classification

I. INTRODUCTION

Classification methods are very useful in solving many real life problems. In the research literature, so many classification techniques are proposed like Decision Tree, SVM, Neural networks etc. These classification techniques work efficiently in classifying the balanced data-sets wherein the number of instances in the classes are approximately equal. Their internal design favors the balanced data-sets. These techniques fail to detect classes when used with imbalanced data-set, because as per their internal design the results in case of unequal size of classes deviate towards the bigger class. These algorithms ignore the smaller class as noise.

In real life situations, sometimes there is a need to detect exceptional cases e.g. credit card frauds, tumor detection, fraudulent telephone calls, shuttle system failure, text classification, oil spill detection, web spam detection, risk management, information retrieval, intrusion detection, earthquake and nuclear explosion, helicopter gear-box fault monitoring [1-4], etc. In such cases, Traditional Classification Algorithms do not work well. This problem is identified as Class Imbalance Problem (CIP). Class Imbalance problem is the classification problem wherein we are using traditional

classification algorithms to classify data with unequal size classes and our objective is to identify smaller class from the data. Researchers have addressed this problem in various diversified ways and a new field of research has emerged under the name Class Imbalance Learning (CIL) and it is evolving day by day. In many papers it is referred to as dealing with IDS (Imbalanced data sets) or with rare cases or dealing with skewed data sets (SDS) or skewed distributions. The smaller class in CIL is known as minority class and bigger class is known as majority class.

Class Imbalance Problem does not exist if the purpose is to identify majority class, it actually exists because the purpose is to identify minority class. The ratio of the number of majority to minority class data instances is called imbalance ratio. The problem becomes more risky as this ratio increases i.e. when data-set is highly imbalanced. The techniques proposed by researchers to solve the Class Imbalance Problem are majorly classified into data-level approaches (Pre-processing techniques), algorithm level approaches and their hybrid forms [5-6]. In data-level approach, the researchers have tried to balance the data-sets before applying traditional classification algorithms so that results may not be overwhelmed by the majority class [7-15]. In algorithm level approaches, the researchers have worked upon the internal algorithm structure and tried to work upon the sensitivity of algorithm towards the majority class. These algorithms come under the category of cost sensitive algorithms [16-35]. Third approach is the hybrid form, which is the combination of data-level and algorithm level approaches. The advantage of data level approaches is that, the researcher will work at the data level and balance the data before classification and hence same classification algorithms can be used. This paper proposed a fast and robust hybrid data level approach based upon fuzzy logic. The proposed method can work with any level of imbalance data. It is tested with 40 UCI real world imbalanced data sets and its performance is compared with 12 other methods. It is observed that performance of proposed method is best compared to other methods. Rest of the paper is organized as follows. Section II explains the background information required to develop the method. Section III describes the proposed approach followed by conclusion in Section IV.

II. BACKGROUND INFORMATION

This section explains various techniques and terms, which are required to develop the proposed approach.

A. Density Oriented Fuzzy C means (DOFCM)

Density oriented FCM is a robust clustering approach, which identifies and removes noise from the data based upon the density of the data [36, 37]. It uses density factor (neighborhood membership) to remove the outliers from the data. Density factor of DOFCM is defined as:

$$DensityFactor(D) = \frac{\eta_{neighborhood}^i}{\eta_{max}} \quad \forall i \text{ in } D \quad (1)$$

Where $\eta_{neighborhood}^i$ is the total number of points around i

η_{max} is the maximum number of points around any point in the whole D. D is the complete data-set.

DOFCM clusters the data into clusters using the following Objective function:

$$DOFCM_{Obj_fun} = \sum_{l=1}^{c+1} \sum_{m=1}^n u_{lm}^{\zeta} d_{lm}^2 \quad (2)$$

Where d_{lm} is the distance between center of a cluster ' l ' and a point ' m ' in the data-set. u_{lm} is the fuzzy membership between ' l ' and ' m '. ζ is the fuzziness index. The membership equation for DOFCM is as below:

$$u_{lm} = \begin{cases} \frac{1}{\sum_{j=1}^c \left(\frac{d_{lm}}{d_{jm}}\right)^{\frac{2}{\zeta-1}}} & \forall l,m \text{ if } densityfactor \geq Threshold \\ 0 & \text{if } densityfactor < Threshold \end{cases} \quad (3)$$

B. Modified SMOTE

Chawla et al. in 2002 proposed Synthetic Minority Oversampling approach (SMOTE) [7]. This approach randomly selects candidate points and uses interpolation method to generate synthetic points in between the selected candidate points. Although the method is very simple but the limitation of existing SMOTE is that, it is not effective in case the data-set is corrupted with noise. In that situation, SMOTE method may select noise points as the candidate points (Fig. 1) and generate synthetic data within the candidate points. This situation may end up by generating more noise points within the data-set.

In the proposed approach, authors have used the variation of existing SMOTE method in order to avoid the limitation. The proposed method doesn't use random approach to select candidate points. It uses those points as candidate points which have large fuzzy membership values, which means the selected points will be close to the center of the minority class. It then uses interpolation method to generate the synthetic data between selected candidate points and the center of the minority cluster. Fig. 2 shows the process of synthetic data generation in case of modified SMOTE. In the figure, 'c' is the center of cluster, 'r' is the selected candidate point and 'n' is the synthetic point generated through interpolation. This approach intelligently generates the synthetic points by selecting only those points as candidate points, which are close to the center point; hence works on the limitation of existing SMOTE.

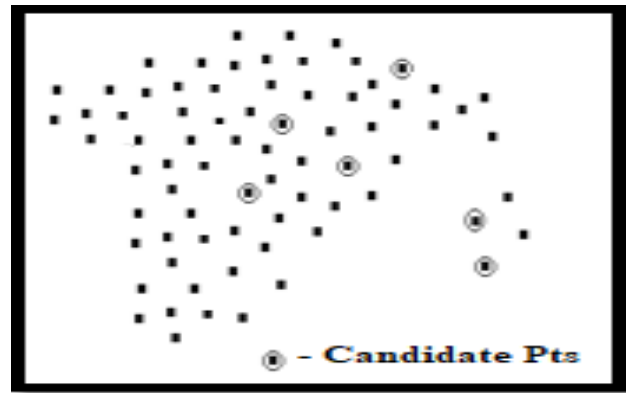


Fig. 1. Limitation of SMOTE

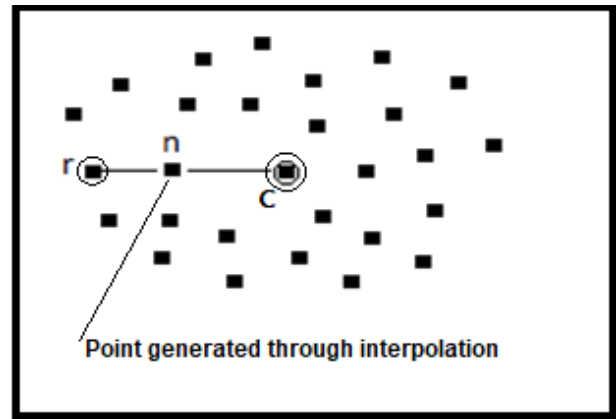


Fig. 2. Modified SMOTE.

C. Performance Criteria

Proposed approach used AUC (Area under the curve), F-measure and G-mean (Geometric mean) performance criteria's, which are majorly used by researchers in case of imbalanced data-sets, to compare the performance of proposed approach with their counterparts. As the focus of imbalance data sets is majorly to identify minority class so author considered minority class as the positive class in the confusion matrix (Table I) as mentioned.

AUC is a plot of false-positive rate on x-axis and true positive rate on y-axis. It is the best method to compare the performance of multiple classifiers. It is represented quantitatively by ROC and is calculated as the arithmetic mean of True Positive rate and True Negative rate.

$$AUC = \frac{TruePosRate + TrueNegRate}{2} \quad (4)$$

Where $TruePosRate$ represents the amount of positive data categorized as positive and $TrueNegRate$ represents negative data, which is correctly identified as negative.

TABLE I. CONFUSION MATRIX

	Minority (Positive)	Majority (Negative)
True	TP (True Positive)	TN (True Negative)
False	FP (False Positive)	FN (False Negative)

F-measure is the harmonic mean of precision and recall. Recall is the rate of total positive data, which is correctly identified as positive and Precision is the rate of correctly identified positive data out of total identified positive data. Recall is also known with the name as Sensitivity or True positive rate.

$$F - measure = \frac{(1+\gamma^2).Recall.Precision}{\gamma^2.Recall+Precision} \quad (5)$$

Where

$$Recall = \frac{TruePos}{TruePos+FalseNeg} \quad (6)$$

$$Precision = \frac{TruePos}{TruePos+FalsePos} \quad (7)$$

' γ ' parameter is used to set the importance of recall or precision.

Geometric mean represents the accuracy of every class. It is the geometric mean of True positive rate and True negative rate. It considers the performance of both the classes.

$$G - Mean = \sqrt{TruePos_{rate}.TrueNeg_{rate}} \quad (8)$$

III. PROPOSED METHOD

A. Description of the Proposed Method

This paper proposed fast, robust and effective hybrid data level approach based upon fuzzy concept to handle the imbalanced data. It is called fast and robust because it can handle any amount of noise in the data-set and has least time complexity compared to other methods. It is the most effective approach in case of real time datasets because of its noise resistant nature. It can work with any level of imbalance situation. (Refer to Section III-B). Fig. 3 and Fig. 4 show the algorithm and model of the proposed approach.

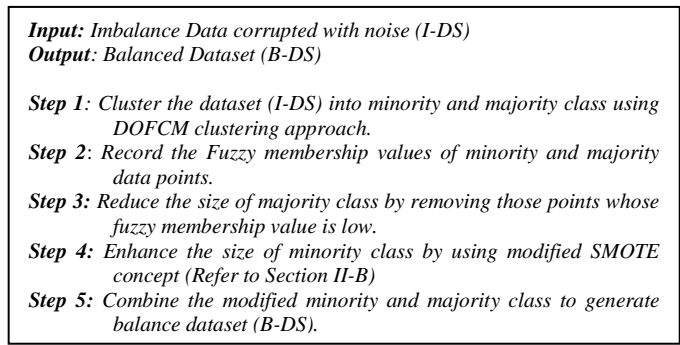


Fig. 3. Algorithm of Proposed Method.

B. Results and Simulations

To assess the performance of proposed approach, it is tested with 40 UCI real time imbalanced datasets [38] having an imbalance ratio ranging from 1.82 to 129.42. The properties of 40 UCI data sets are listed in Table VI (Appendix A). MATLAB R2018A [39] and Python framework are used to do the simulations. Its performance is compared with 12 other approaches namely RUSBoost [40], SMT-ENN [43], BalanceRandomForest (BRForest)[42], One Sided Selection (OSS) [43], ADASYN [44], SVMSMOTE [45], SMOTETomek (SMT-TL)[46][41], BorderLineSMOTE (B-

SMT) [45], Edited Nearest Neighbor (ENN) [47], Condensed Nearest Neighbor (CNN) [48], Neighborhood Cleaning Rule (NCR) [49] and GradientBoosting (GBoosting)[50]. In these simulations, authors have used Decision Tree method (C4.5) as the base classifier because in most of the research papers, C4.5 is widely used by the researchers to compare the methods in imbalance domains [51, 52]. Table II, Table III and Table IV list the AUC, G-mean and F-measure values of all the methods corresponding to 40 UCI real time imbalanced data-sets. Table V lists the average execution time against every method. As it is not possible to plot all the values hence authors plotted the average values of AUC, G-mean and F-measure in Fig. 5, Fig. 6 and Fig. 7. Average execution time in seconds is shown in Fig. 8.

C. Visual Interpretations and Discussions

It is observed from the Table II, Table III, Table IV and Fig. 5, Fig. 6, Fig. 7 that the performance of proposed data level hybrid method is best and consistent compared to all other methods irrespective of any imbalance ratio. It is seen that CNN performed worst in every case. The performance of RUSboost, GBoosting, ENN, OSS, NCR varies with the variation in imbalance ratio. Their performance degrades with the highly imbalance data-sets (abalone-19). Performance of SMT-TL, SMYSVM, ADASYN, B_SMT and SMT-ENN is almost similar in case of every data-set.

In case of execution time (Table V, Fig. 8), it is reported that the execution time in case of proposed method is least compared to other methods. Other methods are also taking less than one second in execution except CNN, which took the maximum time (up to three seconds).

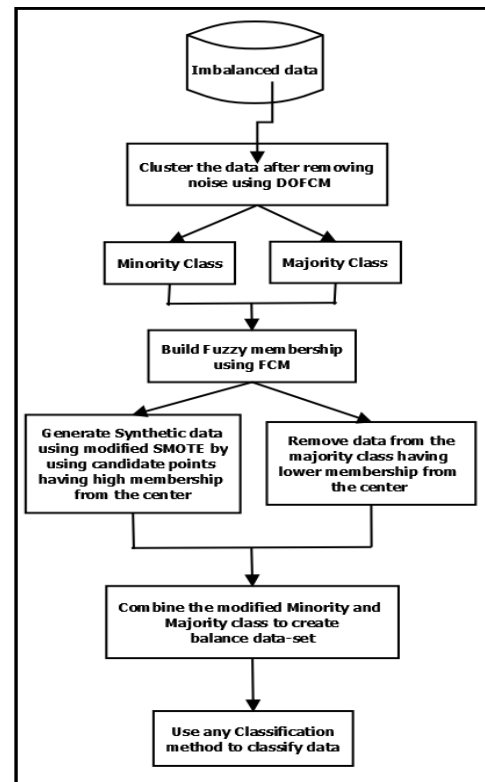


Fig. 4. Model of Proposed Method.

TABLE II. AUC VALUES OF 13 APPROACHES

Data Set	Proposed method	RUSBoost	BRForest	SMT-ENN	SMT-TL	GBoosting	SMTSV M	ADASYN	B-SMT	ENN	CNN	OSS	NCR
abalone19_b	1	0.57	0.72	0.98	0.96	0.5	0.98	0.97	0.99	0.49	0.4	0.5	0.49
abalone9_18	1	0.67	0.73	0.92	0.92	0.64	0.93	0.91	0.93	0.61	0.6	0.59	0.71
ecoli0137_vs_26	1	0.98	0.98	0.99	0.99	0.98	0.96	0.95	0.97	0.95	0.88	0.96	0.98
ecoli0_vs_1	1	0.98	0.98	1	1	0.98	0.96	0.95	0.97	0.95	0.88	0.96	0.98
ecoli1	1	0.85	0.9	0.97	0.92	0.86	0.92	0.87	0.9	0.63	0.9	0.92	0.97
ecoli2	1	0.85	0.9	0.97	0.92	0.86	0.92	0.87	0.9	0.63	0.9	0.92	0.97
ecoli3	1	0.85	0.9	0.97	0.92	0.86	0.92	0.87	0.9	0.63	0.9	0.92	0.97
ecoli4	1	0.85	0.9	0.97	0.92	0.86	0.92	0.87	0.9	0.63	0.9	0.92	0.97
glass_016_vs_2	1	0.67	0.83	0.92	0.95	0.58	0.92	0.92	0.92	0.42	0.42	0.54	0.44
glass_0123_vs_456	1	0.93	0.98	1	0.98	0.89	0.92	0.95	0.95	0.85	0.66	0.77	0.97
glass0	1	0.93	0.98	0.97	0.98	0.89	0.92	0.95	0.95	0.85	0.66	0.77	0.97
glass1	1	0.93	0.98	1	0.98	0.89	0.92	0.95	0.95	0.85	0.66	0.77	0.97
glass2	1	0.93	0.98	0.97	0.98	0.89	0.92	0.95	0.95	0.85	0.66	0.77	0.97
glass4	1	0.93	0.98	0.98	0.98	0.89	0.92	0.95	0.95	0.85	0.66	0.77	0.97
glass6	1	0.93	0.98	1	0.98	0.89	0.92	0.95	0.95	0.85	0.66	0.77	0.97
haberman	1	0.55	0.79	0.85	0.73	0.61	0.76	0.73	0.78	0.66	0.48	0.67	0.71
new_thyroid1	0.99	0.98	0.97	0.99	0.96	0.91	0.94	0.97	0.98	0.93	0.75	0.92	0.96
new_thyroid2	0.99	0.98	0.97	0.99	0.96	0.91	0.94	0.97	0.98	0.93	0.75	0.92	0.96
pima	1	0.69	0.75	0.88	0.76	0.73	0.72	0.7	0.7	0.84	0.59	0.67	0.8
segment0	1	1	1	1	0.99	0.99	0.99	1	0.99	0.99	0.91	0.99	0.98
shuttle_c2_vs_c4	1	1	1	1	0.99	0.99	0.99	1	0.99	0.99	0.91	0.99	0.98
shuttlec0_vs_c4	1	1	1	1	1	1	1	1	1	1	0.49	1	1
vehicle1	1	0.61	0.8	0.89	0.84	0.65	0.8	0.84	0.83	0.78	0.57	0.71	0.74
vehicle2	1	0.61	0.8	0.89	0.84	0.65	0.8	0.84	0.83	0.78	0.57	0.71	0.74
vehicle3	1	0.61	0.8	0.89	0.84	0.65	0.8	0.84	0.83	0.78	0.57	0.71	0.74
vowel0	0.99	0.98	0.97	0.98	0.99	0.88	0.99	0.99	0.99	0.96	0.64	0.93	0.98
wisconsin	1	0.92	0.99	0.97	0.97	0.96	0.97	0.98	0.93	0.94	0.6	0.74	0.93
yeast_05679_vs_4	0.99	0.66	0.82	0.94	0.89	0.72	0.94	0.91	0.9	0.73	0.6	0.8	0.77
yeast1	0.99	0.67	0.74	0.91	0.79	0.69	0.78	0.76	0.78	0.65	0.56	0.68	0.79
yeast1v6	0.99	0.67	0.74	0.91	0.79	0.69	0.78	0.76	0.78	0.65	0.56	0.68	0.79
yeast1v7	0.99	0.65	0.76	0.93	0.91	0.67	0.93	0.91	0.93	0.76	0.48	0.8	0.65
yeast2_vs_4	0.99	0.92	0.92	0.98	0.98	0.9	0.95	0.94	0.95	0.79	0.59	0.86	0.94
yeast2_vs_8	0.99	0.56	0.7	0.98	0.95	0.67	0.95	0.94	0.93	0.75	0.89	0.75	0.68
yeast3	0.99	0.87	0.93	0.94	0.94	0.86	0.96	0.94	0.94	0.87	0.78	0.87	0.93
yeast4	0.99	0.87	0.93	0.94	0.94	0.86	0.96	0.94	0.94	0.87	0.78	0.87	0.93
yeast4_u	0.99	0.87	0.93	0.94	0.94	0.86	0.96	0.94	0.94	0.87	0.78	0.87	0.93
yeast5	0.99	0.87	0.93	0.94	0.94	0.86	0.96	0.94	0.94	0.87	0.78	0.87	0.93
yeast6	0.99	0.87	0.93	0.94	0.94	0.86	0.96	0.94	0.94	0.87	0.78	0.87	0.93
yeast1289_vs_7	0.99	0.67	0.78	0.94	0.93	0.55	0.93	0.96	0.95	0.69	0.5	0.63	0.62
yeast1458_vs_7	0.99	0.64	0.69	0.94	0.92	0.55	0.9	0.9	0.93	0.58	0.47	0.53	0.52
Average	0.996	0.81425	0.884	0.952	0.92775	0.80325	0.91525	0.913	0.919	0.78925	0.678	0.79725	0.85575

TABLE III. G-MEAN VALUES OF 13 APPROACHES

Data Set	Proposed Method	RUSBoost	BRForest	SMT-ENN	SMT-TL	GBoosting	SMTS VM	ADASYN	B-SMT	ENN	CNN	OSS	NCR
abalone19_b	0.996	0.437	0.755	0.975	0.959	0	0.984	0.967	0.991	0	0	0	0
abalone9_18	0.995	0.585	0.757	0.916	0.92	0.541	0.93	0.908	0.93	0.519	0.55	0.457	0.657
ecoli0137_vs_26	0.995	0.985	0.757	0.981	0.973	0.541	0.977	0.968	0.968	0.994	0	0	0
ecoli0_vs_1	1	0.982	0.969	1	1	0.982	0.963	0.953	0.973	0.951	0.866	0.96	0.981
ecoli1	0.987	0.875	0.914	0.97	0.882	0.87	0.916	0.867	0.896	0.903	0.606	0.92	0.971
ecoli2	0.987	0.875	0.914	0.97	0.882	0.87	0.916	0.867	0.896	0.903	0.606	0.92	0.971
ecoli3	0.987	0.875	0.914	0.97	0.882	0.87	0.916	0.867	0.896	0.903	0.606	0.92	0.971
ecoli4	1	0.875	0.914	0.97	0.882	0.87	0.916	0.867	0.896	0.903	0.606	0.92	0.971
glass_016_vs_2	1	0.665	0.784	0.921	0.952	0.408	0.917	0.961	0.924	0.429	0.382	0.496	0
glass_0123_vs_456	1	0.944	0.981	1	0.977	0.887	0.92	0.95	0.947	0.838	0.658	0.754	0.966
glass0	1	0.944	0.981	1	0.977	0.887	0.92	0.95	0.947	0.838	0.658	0.754	0.966
glass1	1	0.944	0.981	1	0.977	0.887	0.92	0.95	0.947	0.838	0.658	0.754	0.966
glass2	1	0.944	0.981	1	0.977	0.887	0.92	0.95	0.947	0.838	0.658	0.754	0.966
glass4	1	0.944	0.981	0.98	0.977	0.887	0.92	0.95	0.947	0.838	0.658	0.754	0.966
glass6	1	0.944	0.981	0.98	0.977	0.887	0.92	0.95	0.947	0.838	0.658	0.754	0.966
haberman	1	0.646	0.746	0.842	0.718	0.535	0.756	0.725	0.777	0.651	0.482	0.667	0.711
new_thyroid1	0.995	0.96	0.98	0.98	0.956	0.907	0.942	0.974	0.983	0.936	0.707	0.92	0.961
new_thyroi2	0.995	0.96	0.98	0.98	0.956	0.907	0.942	0.974	0.983	0.936	0.707	0.92	0.961
pima	1	0.709	0.728	0.884	0.758	0.718	0.712	0.702	0.704	0.833	0.592	0.67	0.802
segment0	1	1	0.998	0.997	0.995	0.995	0.994	0.997	0.994	0.99	0.908	0.987	0.983
shuttle_c2_vs_c4	1	1	0.998	0.997	0.995	0.995	0.994	0.997	0.994	0.99	0.908	0.987	0.983
shuttlec0_vs_c4	1	1	1	1	1	1	1	1	1	1	0	1	1
vehicle1	1	0.689	0.799	0.885	0.84	0.587	0.804	0.836	0.83	0.784	0.571	0.697	0.733
vehicle2	1	0.689	0.799	0.885	0.84	0.587	0.804	0.836	0.83	0.784	0.571	0.697	0.733
vehicle3	1	0.689	0.799	0.885	0.84	0.587	0.804	0.836	0.83	0.784	0.571	0.697	0.733
vowel0	0.989	0.936	0.968	0.981	0.993	0.874	0.991	0.991	0.992	0.962	0.593	0.926	0.978
wisconsin	1	0.95	0.99	0.968	0.966	0.964	0.966	0.985	0.928	0.935	0.468	0.715	0.927
yeast_05679_vs_4	0.989	0.32	0.795	0.972	0.891	0.637	0.943	0.907	0.896	0.706	0.544	0.787	0.742
yeast1	0.963	0.663	0.729	0.913	0.785	0.649	0.779	0.756	0.783	0.636	0.557	0.675	0.789
yeast1v6	0.963	0.663	0.729	0.913	0.785	0.649	0.779	0.756	0.783	0.636	0.557	0.675	0.789
yeast1v7	0.933	0.573	0.752	0.925	0.909	0.603	0.933	0.914	0.934	0.734	0.377	0.783	0.589
yeast2_vs_4	0.984	0.919	0.926	0.981	0.979	0.897	0.95	0.936	0.95	0.769	0.566	0.849	0.963
yeast2_vs_8	0.993	0.562	0.709	0.984	0.948	0.577	0.946	0.936	0.928	0.707	0.889	0.707	0.621
yeast3	0.993	0.847	0.941	0.985	0.944	0.853	0.956	0.944	0.943	0.865	0.777	0.86	0.933
yeast4	0.993	0.847	0.941	0.985	0.944	0.853	0.956	0.944	0.943	0.865	0.777	0.86	0.933
yeast4_u	0.993	0.847	0.941	0.985	0.944	0.853	0.956	0.944	0.943	0.865	0.777	0.86	0.933
yeast5	0.993	0.847	0.941	0.985	0.944	0.853	0.956	0.944	0.943	0.865	0.777	0.86	0.933
yeast6	0.993	0.847	0.941	0.985	0.944	0.853	0.956	0.944	0.943	0.865	0.777	0.86	0.933
yeast1289_vs_7	0.993	0.659	0.782	0.948	0.929	0.332	0.929	0.958	0.953	0.647	0.413	0.558	0.495
yeast1458_vs_7	0.993	0.574	0.566	0.925	0.922	0.946	0.905	0.904	0.929	0.439	0.387	0.309	0.293
Average	0.992	0.80535	0.87605	0.960	0.922975	0.762125	0.9152	0.914125	0.9192	0.792925	0.585575	0.741075	0.794225

TABLE IV. F-MEASURE VALUES OF 13 APPROACHES

Data Set	Proposed Method	RUSBoost	BRForest	SMT-ENN	SMT-TL	GBoosting	SMTS VM	ADAS YN	B-SMT	ENN	CNN	OSS	NCR
abalone19_b	0.996	0.06	0.043	0.977	0.96	0	0.979	0.968	0.991	0	0	0	0
abalone9_18	0.996	0.41	0.358	0.918	0.919	0.435	0.908	0.909	0.93	0.267	0.4	0.273	0.421
ecoli0137_vs_26	0.996	0.41	0.358	0.981	0.978	0.435	0.968	0.972	0.972	0.667	0	0	0
ecoli0_vs_1	1	0.98	0.964	1	1	0.982	0.969	0.959	0.98	0.923	0.979	0.957	0.98
ecoli1	0.987	0.76	0.772	0.97	0.883	0.783	0.918	0.868	0.9	0.852	0.792	0.857	0.913
ecoli2	0.987	0.76	0.772	0.97	0.883	0.783	0.918	0.868	0.9	0.852	0.792	0.857	0.913
ecoli3	0.987	0.76	0.772	0.97	0.883	0.783	0.918	0.868	0.9	0.852	0.792	0.857	0.913
ecoli4	0.987	0.76	0.772	0.97	0.883	0.783	0.918	0.868	0.9	0.852	0.792	0.857	0.913
glass_016_vs_2	1	0.4	0.375	0.921	0.948	0.286	0.909	0.959	0.923	0.2	0.2	0.125	0
glass_0123_vs_456	1	0.91	0.917	1	0.977	0.818	0.911	0.941	0.943	0.786	0.72	0.692	0.966
glass0	1	0.91	0.917	1	0.977	0.818	0.911	0.941	0.943	0.786	0.72	0.692	0.966
glass1	1	0.91	0.917	1	0.977	0.818	0.911	0.941	0.943	0.786	0.72	0.692	0.966
glass2	1	0.91	0.917	1	0.977	0.818	0.911	0.941	0.943	0.786	0.72	0.692	0.966
glass4	1	0.91	0.917	1	0.977	0.818	0.911	0.941	0.943	0.786	0.72	0.692	0.966
glass6	1	0.91	0.917	1	0.977	0.818	0.911	0.941	0.943	0.786	0.72	0.692	0.966
haberman	1	0.5	0.613	0.873	0.769	0.4	0.752	0.732	0.766	0.49	0.48	0.5	0.612
new_thyroid1	0.991	0.88	0.933	0.984	0.95	0.857	0.938	0.97	0.98	0.833	0.96	0.88	0.96
new_thyroi2	0.991	0.88	0.933	0.984	0.95	0.857	0.938	0.97	0.98	0.833	0.96	0.88	0.96
pima	1	0.64	0.667	0.89	0.764	0.654	0.707	0.684	0.716	0.8	0.646	0.6	0.798
segment0	1	1	0.989	0.997	0.995	0.995	0.994	0.997	0.994	0.99	0.965	0.973	0.951
shuttle_c2_vs_c4	1	1	0.989	0.997	0.995	0.995	0.994	0.997	0.994	0.99	0.965	0.973	0.951
shuttlec0_vs_c4	1	1	1	0.91	1	1	1	1	1	1	0.974	1	1
vehicle1	1	0.57	0.693	0.915	0.856	0.475	0.811	0.834	0.838	0.662	0.557	0.574	0.646
vehicle2	1	0.57	0.693	0.915	0.856	0.475	0.811	0.834	0.838	0.662	0.557	0.574	0.646
vehicle3	1	0.57	0.693	0.915	0.856	0.475	0.811	0.834	0.838	0.662	0.557	0.574	0.646
vowel0	1	0.84	0.779	0.982	0.992	0.852	0.99	0.99	0.992	0.962	0.83	0.897	0.947
wisconsin	1	0.95	0.987	0.968	0.966	0.961	0.966	0.984	0.925	0.929	0.946	0.932	0.919
yeast_05679_vs_4	0.972	0.16	0.528	0.955	0.895	0.5001	0.945	0.914	0.905	0.5	0.444	0.667	0.593
yeast1	0.966	0.54	0.609	0.922	0.787	0.564	0.78	0.769	0.793	0.5	0.635	0.558	0.731
yeast1v6	0.966	0.54	0.609	0.922	0.787	0.564	0.78	0.769	0.793	0.5	0.635	0.558	0.731
yeast1v7	0.942	0.22	0.261	0.936	0.906	0.4	0.929	0.912	0.931	0.552	0.222	0.643	0.3

yeast2_vs_4	0.983	0.65	0.686	0.962	0.978	0.71	0.949	0.934	0.949	0.692	0.629	0.774	0.759
yeast2_vs_8	0.983	0.32	0.37	0.945	0.947	0.5	0.945	0.932	0.925	0.667	0.5	0.667	0.421
yeast3	0.988	0.68	0.748	0.936	0.946	0.776	0.957	0.945	0.944	0.771	0.804	0.731	0.848
yeast4	0.988	0.68	0.748	0.936	0.946	0.776	0.957	0.945	0.944	0.771	0.804	0.731	0.848
yeast4_u	0.988	0.68	0.748	0.936	0.946	0.776	0.957	0.945	0.944	0.771	0.804	0.731	0.848
yeast5	0.988	0.68	0.748	0.936	0.946	0.776	0.957	0.945	0.944	0.771	0.804	0.731	0.848
yeast6	0.988	0.68	0.748	0.936	0.946	0.776	0.957	0.945	0.944	0.771	0.804	0.731	0.848
yeast1289_vs_7	0.96	0.14	0.155	0.953	0.93	0.167	0.908	0.958	0.953	0.276	0.2	0.214	0.3
yeast1458_vs_7	0.96	0.16	0.116	0.933	0.922	0.182	0.871	0.905	0.932	0.211	0.19	0.1	0.087
Average	0.989	0.66	0.693275	0.955	0.92575	0.666028	0.911875	0.913225	0.9204	0.693675	0.648475	0.6532	0.726175

TABLE V. AVERAGE EXECUTION TIME (SECONDS)

Algorithms	Proposed	RUSBoost	BRForest	SMT-ENN	SMT-TL	GBoosting	SMT-SVM	ADASYN	B-SMT	ENN	CNN	OSS	NCR
Average Time (Sec.)	0.004	0.513	0.330	0.079	0.054	0.156	0.045	0.019	0.021	0.046	3.506	0.048	0.050

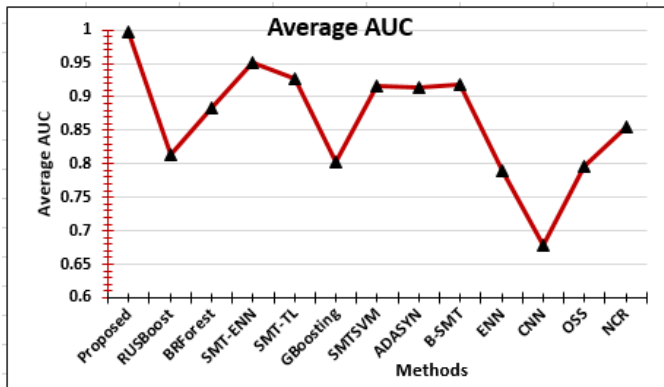


Fig. 5. Average AUC Results of 13 Methods.

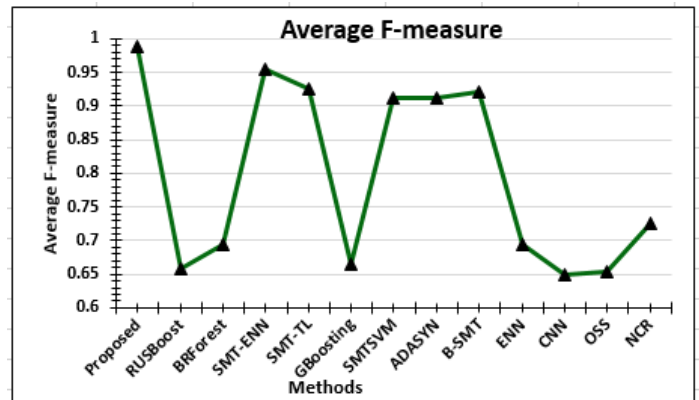


Fig. 7. Average F-measure Results of 13 Methods.

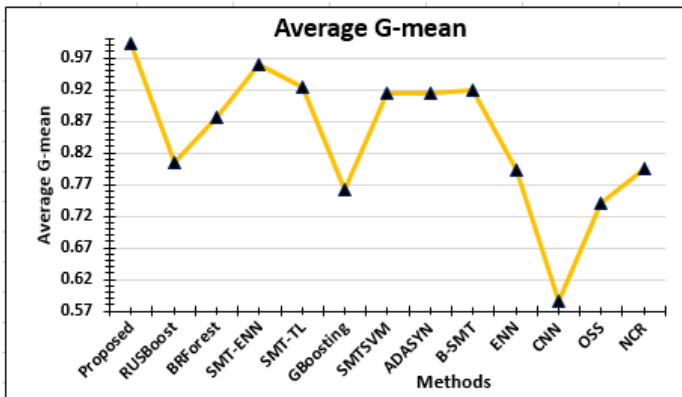


Fig. 6. Average G-mean Results of 13 Methods.

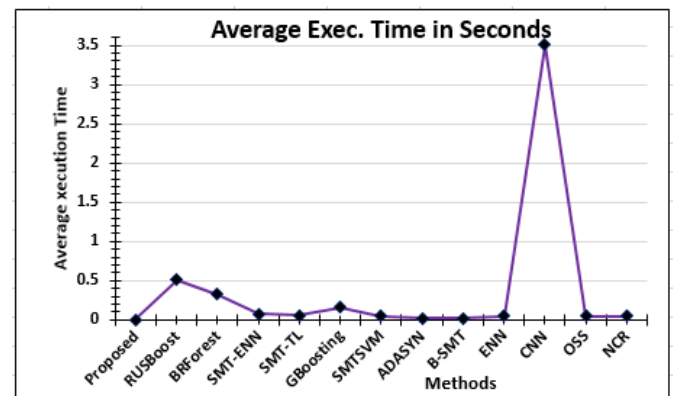


Fig. 8. Average Execution Time (Seconds) of 13 Methods.

From the simulations and observations, it is concluded that proposed method is a robust and fast approach to balance the data because it works consistently for any kind of data set within least time.

IV. CONCLUSION

In this paper, authors proposed fuzzy based fast and robust hybrid data level approach to balance the data. Its performance is tested with 40 UCI real time data-sets (Imbalance ratio- 1.82 to 129.44) and is compared with 12 other methods. After conducting the simulations, it is observed that proposed method can perform consistently with any level of imbalanced data compared to others and converge with the least execution time.

REFERENCES

- [1] Yang Yong, "The Research of Imbalanced data-set of sample sampling method based on K-means cluster and Genetic algorithm", Energy Procedia, Vol. 17, pp 164-170, 2012 Sciverse ScienceDirect.
- [2] V. Garcia et al., "The class imbalance problem in pattern classification and learning", Pattern analysis and learning group, Congreso Espanol de Informatica; pp 283-291, 2007.
- [3] Sofia Visa, and Anca Ralescu, "Issues in Mining Imbalance data-sets – A Review paper", Proceedings of the Sixteen Midwest Artificial Intelligence and Cognitive Science Conference, pp. 67-73, 2005.
- [4] Guo Hongyu and Herna L. Viktor, "Learning from imbalanced data sets with boosting and data generation: the databoost-im approach.", ACM Sigkdd Explorations Newsletter, Vol. 6, No.1, pp. 30-39, 2004.
- [5] Napierała Krystyna, Jerzy Stefanowski and Szymon Wilk, "Learning from imbalanced data in presence of noisy and borderline examples." In Proceedings of International Conference on Rough Sets and Current Trends in Computing, Springer, Berlin, Heidelberg, 2010, pp. 158-167.
- [6] K. P. N. V. Satyashree and J. V. R. Murthy, "An Exhaustive Literature Review on Class Imbalance Problem", Int. Journal of Emerging Trends and Technology in Computer Science, Vol. 2, No.3, pp. 109-118, May 2013.
- [7] N. V. Chawla et al., "SMOTE: Synthetic Minority Over-sampling Technique", Journal of artificial Intelligence Research, Vol. 16, pp. 321-357, 2002.
- [8] Bunkhumpornpat Chumphol, Krung Sinapiromsaran and Chidchanok Lursinsap, "Safe-level-smote: Safe-level-synthetic minority over-sampling technique for handling the class imbalanced problem", In Proceedings of Pacific-Asia conference on knowledge discovery and data mining, Springer, Berlin, Heidelberg, 2009.
- [9] Han Hui, Wen-Yuan Wang and Bing-Huan Mao, "Borderline-SMOTE: a new over-sampling method in imbalanced data sets learning", In Proceedings of International Conference on Intelligent Computing, Springer, Berlin, Heidelberg, 2005.
- [10] S. Hu et al., "MSMOTE: Improving classification performance when training data is imbalanced", In proceedings of 2nd Int. Workshop Computer Sci. Eng., Vol. 2, pp. 13-17, 2009.
- [11] Nakamura Munehiro et al., "Lvq-smote-learning vector quantization based synthetic minority over-sampling technique for biomedical data", BioData Mining, Vol. 6, No. 1, pp. 16, 2013.
- [12] García Salvador and Francisco Herrera, "Evolutionary undersampling for classification with imbalanced datasets: Proposals and taxonomy", Evolutionary computation, Vol. 17, No.3, pp. 275-306, 2009.
- [13] Barua Sukarna et al., "MWMOTE--majority weighted minority oversampling technique for imbalanced data set learning," IEEE Transactions on Knowledge and Data Engineering, Vol. 26, No.2, pp. 405-425, 2014.
- [14] Rahman, M. Mostafizur and D. Davis, "Cluster based under-sampling for unbalanced cardiovascular data", In Proceedings of the World Congress on Engineering, 2013, Vol. 3.
- [15] Ying Mi, "Imbalanced classification based on Active Learning SMOTE", Research Journal of Applied Sciences, Engg. And Tech., Vol. 5, issue 3, pp. 944-949, 2013.
- [16] R. Akbani, S. Kwek and N. Japkowicz, "Applying Support Vector Machines to Imbalanced Datasets", In Proceedings of ECML 2004, LNAI 3201, pp. 39-50, 2004. Springer-Verlag Berlin Heidelberg.
- [17] Fernández Alberto et al., "A study of the behaviour of linguistic fuzzy rule based classification systems in the framework of imbalanced data-sets", Fuzzy Sets and Systems, Vol. 159, No. 18, pp. 2378-2398, 2008.
- [18] R. Batuwita and V. Palade, "FSVM-CIL: Fuzzy Support vector machine for class imbalanced learning", IEEE Transactions on Fuzzy Systems, Vol. 18, No. 3, pp. 558-571, 2010.
- [19] H-L. Dai, "Class Imbalance Learning via a Fuzzy Total Margin based Support Vector Machine", Applied Soft Computing, Vol. 31, pp.172-184, 2015.
- [20] A. Fernandez et al., "A study of the behaviour of linguistic fuzzy rule base classification systems in the framework of imbalanced data-sets", Fuzzy Sets and Systems, Vol. 159, issue 18, pp. 2378-2398, 2008.
- [21] Galar, M., et al. (2013) 'Dynamic classifier selection for One-vs-One strategy: Avoiding non-competent classifiers', Pattern Recognition, Vol. 46, pp. 3412-3424.
- [22] Gu, X., et al. (2014) 'New Fuzzy Support Vector machine for the Class Imbalance Problem in Medical data-sets Classification', The Scientific World Journal. Vol. 2014, pp. 1-12, Hindawi Publishing Corporation.
- [23] He Haibo et al., "ADASYN: Adaptive synthetic sampling approach for imbalanced learning", In Proceedings of IEEE International Joint Conference on Neural Network, 2008, IEEE.
- [24] T. Iman, K. Ting and J. Kamruzzaman, "z-SVM: An SVM for improved classification of imbalanced data", In proceedings of the 19th Australian joint conference on Artificial Intelligence, springer-verlag, 2006, pp. 264-273.
- [25] Y. Tang, B. Jin and Y. Q. Zhang, "Granular support vector machines with association rules mining for protein homology prediction", Artificial Intelligence in Medicine, Vol. 35, No.1-2, pp. 121-134, 2005.
- [26] Y. Tang, B. Jin, Y. Q. Zhang, H. Fang, B. Wang, "Granular support vector machines using linear decision hyperplanes for fast medical binary classification", In Proceedings of FUZZ'05, The 14th IEEE International Conference on Fuzzy Systems, 2005, May 25, pp. 138-142.
- [27] Y. C. Tang, Y.Q. Zhang, Z. Huang, Hu XT and Y. Zhao, "Granular SVM-RFE feature selection algorithm for reliable cancer-related gene subsets extraction on microarray gene expression data", In Proceedings of IEEE Symp. Bioinformatics and Bioeng, 2005, pp. 290-293.
- [28] Fan Wei et al., "AdaCost: misclassification cost-sensitive boosting", In Proceedings of Icml, Vol. 99, 1999.
- [29] S. Wu and S. Amari, "Conformal Transformation of kernel functions: A data-dependent way to improve the performance of support vector machine classifier", Neural Networks Letter, Vol. 15, 2002.
- [30] G. Wu and E. Chang, "Kba: Kernel Boundary alignment considering imbalanced dataset distribution", IEEE Transactions on Knowledge and Data Engineering, Vol. 17, No. 6, pp. 786-795, 2005.
- [31] Fernández Alberto, María José del Jesus and Francisco Herrera, "Hierarchical fuzzy rule based classification systems with genetic rule selection for imbalanced data-sets", International Journal of Approximate Reasoning, Vol. 50, No. 3, pp. 561-577, 2009.
- [32] Z. Chi, H. Yan and T. Pam, "Fuzzy algorithms with application to image processing and pattern recognition", Vol. 10, World Scientific, Singapore, 1996.
- [33] H. Ishibuchi and T. Yamamoto, "Fuzzy rule selection by multi-objective genetic local search algorithms and rule evaluation measures in Data mining", Fuzzy Sets and Systems, Vol. 141, No.1, pp. 59-88, 2004.
- [34] H. Ishibuchi and T. Yamamoto, "Comparison of Heuristic criteria for fuzzy rule selection in classification problems", Fuzzy Optim. Decision making, Vol. 3, No. 2, pp. 119-139, 2004.
- [35] H. Ishibuchi, and T. Yamamoto, "Rule weight specification in fuzzy rule based classification systems", IEEE Trans. Fuzzy Systems, Vol. 13, pp. 428-435, 2005.
- [36] Prabhjot, Kaur, I. M. S. Lamba, and Gosain Anjana. "DOFCM: a robust clustering technique based upon density." International Journal of Engineering and Technology 3.3 (2011): 297.

- [37] Kaur, Prabhjot, and Anjana Gosain, "Density-oriented approach to identify outliers and get noiseless clusters in Fuzzy C—Means." International Conference on Fuzzy Systems. IEEE, 2010.
- [38] Alcalá-Fdez Jesús et al., "Keel data-mining software tool: data set repository, integration of algorithms and experimental analysis framework", Journal of Multiple-Valued Logic & Soft Computing, Vol. 17, 2011.
- [39] Natick, Massachusetts MATLAB version 8.1 (2013): The MathWorks Inc., 2013.
- [40] C. Seiffert et al., "RUSBoost: A Hybrid Approach to Alleviating Class Imbalance", IEEE Trans. on Sys. Man and Cyber.-Part A, Vol. 40, No. 1, pp. 185-197, 2010.
- [41] Gustavo EAPA Batista, Ana LC Bazzan, and Maria Carolina Monard, "Balancing training data for automated annotation of keywords: a case study", In WOB, 10–18. 2003.
- [42] Chen, Chao, Andy Liaw, and Leo Breiman. "Using random forest to learn imbalanced data." University of California, Berkeley 110 (2004): 1-12.
- [43] M. Kubat, S. Matwin, "Addressing the curse of imbalanced training sets: one-sided selection," In ICML, vol. 97, pp. 179-186, 1997.
- [44] He, Haibo, Yang Bai, Eduardo A. Garcia, and Shutao Li. "ADASYN: Adaptive synthetic sampling approach for imbalanced learning," In IEEE International Joint Conference on Neural Networks (IEEE World Congress on Computational Intelligence), pp. 1322-1328, 2008.
- [45] H. M. Nguyen, E. W. Cooper, K. Kamei, "Borderline over-sampling for imbalanced data classification," International Journal of Knowledge Engineering and Soft Data Paradigms, 3(1), pp.4-21, 2009.
- [46] G. Batista, B. Bazzan, M. Monard, "Balancing Training Data for Automated Annotation of Keywords: a Case Study," In WOB, 10-18, 2003.
- [47] D. Wilson, Asymptotic, "Properties of Nearest Neighbor Rules Using Edited Data," In IEEE Transactions on Systems, Man, and Cybernetics, vol. 2 (3), pp. 408-421, 1972.
- [48] P. Hart, "The condensed nearest neighbor rule," In Information Theory, IEEE Transactions on, vol. 14(3), pp. 515-516, 1968.
- [49] J. Laurikkala, "Improving identification of difficult small classes by balancing class distribution," Springer Berlin Heidelberg, 2001.
- [50] Basha, S.; Vellore Institute of Technology University; Rajput, D.; Vandhan, V, "Impact of Gradient Ascent and Boosting Algorithm in Classification" Int. J. Intell. Eng. Syst. 2018, 11, 41–49.
- [51] J. Demšar, "Statistical comparisons of classifiers over multiple datasets", Journal of Machine Learning Research, Vol. 7, pp. 1–30, 2006.
- [52] S. García and F. Herrera, "An extension on statistical comparisons of classifiers over multiple datasets for all pairwise comparisons", Journal of Machine Learning Research, Vol. 9, pp. 2677–2694, 2008.

APPENDIX A

TABLE VI. PROPERTIES OF DATA SETS

Sr. No	Data Sets (Imbalance Ratio)	Dimensions	Total Size
1	glass1(1.82)	9	214
2	ecoli-0_vs_1(1.86)	7	220
3	wisconsin(1.86)	9	683
4	pima(1.87)	8	768
5	iris0(2.00)	4	150
6	glass0(2.06)	9	214
7	yeast1(2.46)	8	1484
8	haberman(2.78)	3	306
9	vehicle2(2.88)	18	846
10	vehicle1(2.90)	18	846
11	vehicle3(2.99)	18	846
12	glass-0-1-2-3_vs_4-5-6(3.20)	9	214
13	ecoli1(3.36)	7	336
14	new-thyroid2(5.14)	5	215
15	new-thyroid1(5.14)	5	215
16	ecoli2(5.46)	7	336
17	segment0(6.02)	19	2308
18	glass6(6.38)	9	214
19	yeast3(8.10)	8	1484
20	ecoli3(8.60)	7	336
21	yeast-2_vs_4 (9.08)	8	514
22	yeast-0-5-6-7-9_vs_4 (9.35)	8	528
23	vowel0 (9.98)	13	988
24	glass-0-1-6_vs_2 (10.29)	9	192
25	glass2 (11.59)	9	214

26	shuttle-c0-vs-c4 (13.87)	9	1829
27	yeast-1_vs_7 (14.30)	8	459
28	glass4 (15.46)	9	214
29	ecoli4 (15.80)	7	336
30	abalone9-18 (16.40)	8	731
31	glass-0-1-6_vs_5 (19.44)	9	184
32	shuttle-c2-vs-c4 (20.50)	9	129
33	yeast-1-4-5-8_vs_7 (22.10)	8	693
34	yeast-2_vs_8 (23.10)	8	482
35	yeast4 (25.08)	8	1484
36	yeast-1-2-8-9_vs_7 (30.57)	8	947
37	yeast5 (32.78)	8	1484
38	ecoli-0-1-3-7_vs_2-6 (39.14)	7	281
39	yeast6 (41.40)	8	1484
40	abalone19 (129.44)	8	4174

Proctoring and Non-proctoring Systems

A Comparative Study of Online Exam Scores for an Arabic Translating Course

Yusring Sanusi Baso

Department of Arabic Studies, Faculty of Cultural Science
Hasanuddin University, Makassar, Indonesia 90245

Abstract—This research describes learning achievement assessment technology, especially proctor technology. This study compares and contrasts proctoring and non-proctoring procedures used for online exams. The sample case used was the test scores of students enrolled in Hasanuddin University's Indonesian Arabic translation course. The research method used was a non-experimental quantitative method that compared students' online test results using proctoring and non-proctoring systems during online exams. The test scores of 101 students (40 male and 61 female students) from two different classes were sampled. The results of the tests for both classes were collected six times: three times using the proctoring method and three times using the non-proctoring system. A trend analysis was performed on the data. SPSS 26 was used to analyze the data via the two-way ANOVA procedure. The results indicate that the online proctoring system resulted in lower test scores than the online non-proctoring system, while the variables of class and gender did not affect the learning results.

Keywords—Proctoring system; comparative study; Arabic translating course; online exam

I. INTRODUCTION

Academic dishonesty has long been a concern of academicians. As the number of online courses offered by universities has increased dramatically, so too has academic dishonesty; due to the inherent chances for academic dishonesty that online courses present students. This includes students collaborating on individual assessments and students using sources during tests that are prohibited—e.g., using notes and/or the textbook during a closed-book exam. Internet plagiarism is also on the increase as a form of academic dishonesty [1]. Academic dishonesty is a global problem that affects universities in many places. Moreover, multiple studies have shown an increase in cheating and plagiarism over the last few decades, with various explanations and ideas. The rising market for online education is a relatively new element of both higher education and academic dishonesty. Online education has established a permanent presence in global education marketplaces over the last decade and is considered to present new chances and problems regarding academic dishonesty [2].

As online college courses grow more widespread, concerns about academic integrity continue to arise. The prevention of cheating during unproctored online exams has gained significant attention [3]. Academic dishonesty is unethical, and exam cheating is more dangerous than other forms [2], [4]–[8], [9]. Online education will continue to expand, posing new obstacles. One major issue in this is the validity of online

assessments. Questions concerning cheating arise, such as whether the individual taking the examinations is a registered student. Student self-reporting has been used to assess online assessment cheating. In a previous study, unproctored online students' exam results were found to be identical to other groups' scores, but their time spent on the exams was much more than that spent by the other groups. Due to the extra time spent by unproctored students, it is likely that they looked up answers during tests [10].

Integrity and adaptability are two of the most fundamental issues of real-time online examination monitoring systems. Several studies have been conducted to examine how dishonest students behave during remote assessments and possible safeguards against this. Reports and online submissions can help reduce academic dishonesty, according to Guangul and colleagues 2020 [6]. An optimization-based anti-collusion technique for distant online testing was developed by Li et al. [11] to minimize the benefits of collusion. A review published by Pettit and colleagues [12]–[14] provides advice on how to improve candidate authentication and prevent cheating.

Many methods exist to ensure the validity and reliability of online tests, such as deploying an on-site proctor or a real-time supervisor system [1], [15]–[22], [18]. One of these real-time online supervisor systems is Sikoola [23], which delivers real-time online monitoring services that take advantage of laptop webcams that students use in online exams. Sikoola, an online exam app that takes students through the exam procedure and monitors their progress, is used to connect students to the exam. Students are asked to log in according to the identity sent to their respective emails, usually one day ahead. After logging in, students must check the network to find out whether their internet access is good or not. If the student does not check the network, then the student cannot continue to the next stage. Next, students must check the laptop or PC webcam used for the exam. This webcam will record all the behavior of the examinees. If the webcam of the laptop or PC does not work, then the student cannot enter the online exam page. Students are expected to read all the rules of this online exam to avoid recordings that are considered dishonest in the exam.

The primary goal of this study is to compare the results of two different models of skills exams for translating Indonesian scripts into Arabic, namely, online exams using Sikoola, which utilizes an examinee dishonesty monitoring feature, and online exams using a Chamilo-based learning management system that is not equipped with a dishonesty surveillance feature.

To summarize the methods of this study, two websites, <https://ujian.sikoola.com> and <https://sikola.unhas.ac.id>, were employed in the investigation. The Sikoola tests utilize video surveillance tools and other features to detect and record dishonesty during online exams. While the URL sikola.unhas.ac.id gives the exam questions, it does not include a function that tracks whether a student has been dishonest during the exam

Based on this explanation, the researcher wants to address the following research questions:

- 1) Is there a difference in test scores between students who use Sikoola and Sikola in translation courses?
- 2) Is there a difference in the mean of the two classes sampled in this study?
- 3) Is there a difference in the mean of the scores acquired by female and male students utilizing the two systems?

II. MATERIALS AND METHODS

The research method used herein is a non-experimental quantitative method that compares students' online test results using proctoring and non-proctoring systems during online exams in Arabic Translation Skill.

A. Population and Sample

The experiment was carried out within Hasanuddin University's Arabic Language Study Program, part of the Faculty of Cultural Sciences. The participants were second-year students. In this inquiry, two different classes of academic levels are portrayed. These students were responsible for programming the Indonesian–Arabic Translation course in the last semester of the 2021/2022 academic year. At the time of the experiment, they were all between the ages of 19 and 21. The first class had a total of 52 students, with 20 men and 32 women in attendance. The second class was limited to 20 men and 29 women, with a total of 49 students.

Exams were held six times over the course of three successive weeks. Tests were administered every week following the lecture schedule. The supervised test was administered at the beginning of the lecture, and the unsupervised test was administered at the end of the session. Thus, students were required to take a test twice a week on the two different systems.

The initial test materials included the criteria for translating complete sentences in Arabic, known as *al-mubtada wal khabar* in Arabic. The second piece of exam content focused on the Arabic *ash-shifah wal maushuf*, which translates as "the adjective phrases." The third and final test's material was a sentence that contains the Arabic term for possessive phrases, *al-mudhaf wa mudhaf ilaih*, which is referred to herein as the third test material

B. Study Design

Tests were administered six times. Each class was tested three times on the website <https://ujian.sikoola.com>, which contains the camera surveillance function and other elements that record dishonesty during the exam, and three times on the website <https://sikola.unhas.ac.id>, which does not utilize

dishonesty recorders. There were 10 questions for each exam and a maximum score of 100. Ten points were given to each item. It should be noted that this exam was conducted online. Students were permitted to take the exam from any location with an adequate internet connection.

Even though these students were already aware of the two websites used in this research, they were reminded to adhere to exam procedures. The lecturer repeatedly encouraged students to check their network connections throughout the online exam before starting the exam. Additionally, students were required to utilize a laptop/PC equipped with a camera. If a student's laptop/PC camera was not functional, they would be unable to take the online exam.

Students must check the network and camera function on the website equipped with a dishonesty recording feature before the exam. If the internet network is not good, students cannot continue to check the camera. Checking the internet network is an absolute requirement in online exams to reduce complaints from examinees. Some examinees or students sometimes do not realize that their internet network connection is poor. Students or examinees should find an excellent place to access the internet with the internet network checking feature.

In the screenshot of Fig. 1, the instruction language used is still in Indonesian. The use of Indonesian is prioritized considering that students are not familiar with English and it is not the official language.

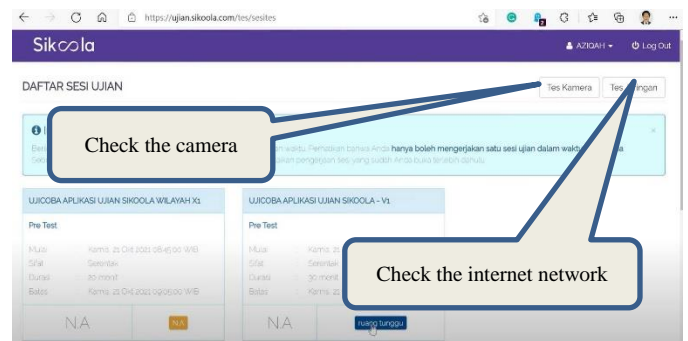


Fig. 1. A Screenshot of What Students See when they enter the Exam Question Room.

Examinees who have verified their network and camera will be taken directly to the exam page. This page contains critical information, including questions, question numbers, cameras, and remaining time information, as shown in Fig. 2.

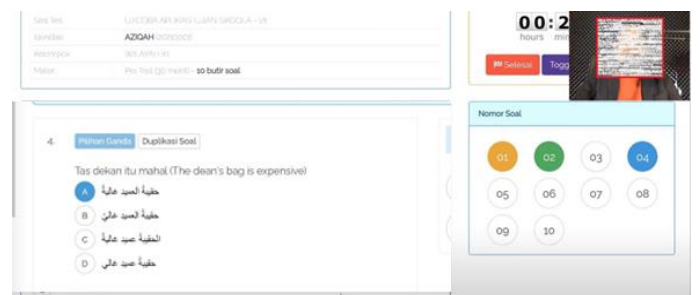


Fig. 2. An Image of the Questions on the Exam.

On the right, each question number has a color. The blue color shows the number of the question being worked on. The yellow color means that the question has been answered, but the examinee is still unsure of their answer. Therefore, examinees can reread the questions and revise their answers. The green color means that the question has been answered, and the examinee is sure that their chosen answer is correct. The white color represents a question that has not been answered. The Sikoola application allows examinees to work on questions in any order. Examinees can work on the questions they think are easy first and then answer the remaining questions. The color on the number is beneficial for examinees in solving each of these exam questions.

The above Fig. 2 also shows the Arabic exam questions and the number of each question. The exam questions were almost the same, but the words that made up the sentences were different only in alif-lam (mainly like “the” in English) and harakat (marking). Many things can change the meaning of a word, like where alif-lam is and how each last letter is marked. Therefore, students need to pay close attention to each word to find the best translation.

A camera view is displayed at the top right of the examinee's monitor screen. This live recording is transmitted to the online exam supervisor for review as can be seen in the following Fig. 3. The Sikoola application takes screenshots of events every five seconds. Sikoola saves the screenshots to its server.

If an examinee opens another browser or taps on a page other than the exam page during the exam, the Sikoola system will deliver a warning. This warning will occur after 20, 30, or even more seconds, depending on the test parameters. As long as a notification appears on the screen, the examinee's mouse and keyboard are rendered inoperable. After the warning period has expired, the OK button will become active. If the examinee hits the OK button, the warning will be removed.

Online exam designs with dishonesty recording features are likely to be a helpful tool for monitoring online exams, especially when the exam participants number in the hundreds.

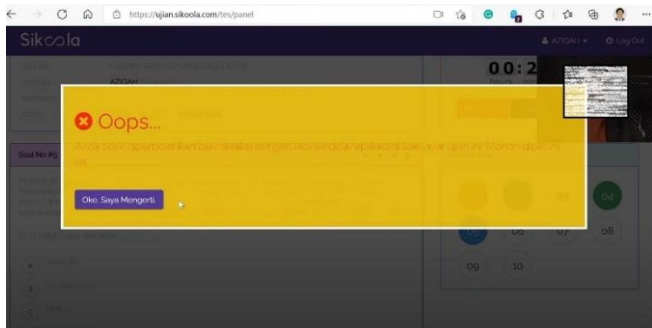


Fig. 3. An Example of a Warning from the Sikoola System when a Student Opens another Browser or uses the Keyboard to Copy–Paste.

C. Statistical Analysis

SPSS 26 was used for statistical analysis. The Wilson score interval method was used to obtain the 95 percent confidence intervals for prevalence estimations. Pearson's Chi-squared test was used to compare categorical factors. The Shapiro–Wilk test for normality and Levene's test for homogeneity were employed to determine whether there was a statistically significant difference in the variances of the two systems. To evaluate the variations in scores, a General Linear Model was used. The variables analyzed were the exam system, the student's gender, and their interactions. The mean and standard deviation were used to express the data (SD). A p-value of 0.05 was used to indicate statistical significance.

III. RESULT

The researcher conducted this analysis via the two-way ANOVA test using SPSS 26. As a result, the researcher first determined the normality and homogeneity of the data. As shown in the Table I, the value of Sig. 0.164 > 0.05 indicates that the standardized residual was normal. The findings indicate that the data are normally distributed, as illustrated in Table I.

TABLE I. TEST OF NORMALITY

	Kolmogorov-Smirnova			Shapiro-Wilk		
	Statistic	df	Sig.	Statistic	df	Sig.
Standardized Residual for SCORE	0,05	202	,200*	0,99	202	0,164
* This is a lower bound of the true significance.						
a Lilliefors Significance Correction						

Concerning the variance of the examined variables, it should be noted that Sig 0,103 > 0.05 indicates that the variance is homogeneous, as referred in the Table II.

Additionally, as evidenced by the data in the Table III, there are two system variables, two class variables, and two gender variables.

TABLE II. LEVENE'S TEST OF EQUALITY OF ERROR VARIANCES A,B

		Levene Statistic	df1	df2	Sig.
SCORE	Based on Mean	1,734	7	194	0,103
	Based on Median	1,619	7	194	0,132
	Based on Median and with adjusted df	1,619	7	164,944	0,133
	Based on trimmed mean	1,78	7	194	0,093
Tests the null hypothesis that the error variance of the dependent variable is equal across groups.					
a Dependent variable: SCORE					
b Design: Intercept + MEDIA + CLASS + GENDER + MEDIA * CLASS + MEDIA * GENDER + CLASS * GENDER + MEDIA * CLASS * GENDER					

TABLE III. BETWEEN-SUBJECT FACTORS

		Value Label	N
MEDIA	1	SIKOOLA	101
	2	SIKOLA	101
CLASS	1	CLASS A	104
	2	CLASS B	98
GENDER	1	Male	80
	2	Femle	122

Also, descriptive statistics are presented in Table IV.

TABLE IV. DESCRIPTIVE STATISTICS

MEDIA			Mean	Std. Deviation	N
SIKOOLA	CLASS A	Male	78,90	3,216	20
		Femle	79,69	3,423	32
		Total	79,38	3,335	52
	CLASS B	Male	78,07	4,569	20
		Femle	78,50	3,181	29
		Total	78,33	3,770	49
	Total	Male	78,48	3,923	40
		Femle	79,12	3,336	61
		Total	78,87	3,575	101
SIKOLA	CLASS A	Male	89,45	2,934	20
		Femle	89,54	2,751	32
		Total	89,51	2,795	52
	CLASS B	Male	92,28	2,561	20
		Femle	93,17	2,858	29
		Total	92,81	2,749	49
	Total	Male	90,87	3,074	40
		Femle	91,27	3,327	61
		Total	91,11	3,219	101
Total	CLASS A	Male	84,17	6,146	40
		Femle	84,61	5,844	64
		Total	84,44	5,936	104
	CLASS B	Male	85,18	8,073	40
		Femle	85,84	7,982	58
		Total	85,57	7,985	98
	Total	Male	84,68	7,147	80
		Femle	85,20	6,941	122
		Total	84,99	7,010	202

To address the research questions, the Table V summarizes the findings of the two-way ANOVA statistical test:

1) Sig 0.000 < 0.05 means that there were significant differences in the test output results based on the SYSTEM variable used in this study. In other words, there were differences in student test scores in the exam when using the

system <https://ujian.sikoola.com> as a proctoring system or the system <https://sikola.unhas.ac.id> as a non-proctoring system;

2) As evidenced by the value of Sig 0.071 > 0.05, there was no variation in student test scores based on class variables;

3) Similarly, there was no difference in scores between male and female students, as evidenced by Sig 0.234 > 0.05.

TABLE V. TESTS OF BETWEEN-SUBJECT EFFECTS

Dependent Variable: SCORE					
Source	Type III Sum of Squares	df	Mean Square	F	Sig.
Corrected Model	7885,882a	7	1126,555	109,76	0
Intercept	1393397,684	1	1393397,684	135758,527	0
MEDIA	7328,828	1	7328,828	714,047	0
CLASS	59,802	1	59,802	5,827	0,071
GENDER	14,658	1	14,658	1,428	0,234
MEDIA * CLASS	216,881	1	216,881	21,131	0
MEDIA * GENDER	0,179	1	0,179	0,017	0,895
CLASS * GENDER	0,603	1	0,603	0,059	0,809
MEDIA * CLASS * GENDER	3,974	1	3,974	0,387	0,535
Error	1991,176	194	10,264		
Total	1468975,179	202			
Corrected Total	9877,058	201			

a R Squared = ,798 (Adjusted R Squared = ,791)

Some examinees' attempts to unfocus or engage in academic dishonesty are revealed via proctored online examinations. Unethical conduct includes opening the website and hitting the keyboard, which is deemed an attempt to access another application besides the opened exam page, as seen in Table VI.

TABLE VI. ACADEMIC DISHONESTY

Classes	Gender	Unfocus	Efforts
CLASS A	Male	16	18
	Female	17	18
CLASS B	Male	17	18
	Female	15	19

IV. DISCUSSION

The COVID-19 pandemic has compelled teachers and students to alter their academic activities, one of which is assessing a student's acquired knowledge. According to certain studies, the acceptability of new approaches has been consistent across countries [24]–[26]. The primary reasons for

student opposition (to the online format) varied in various studies but included the risk of cheating or even receiving lower grades due to a lack of concentration [27], [28]. The former of these is easily overcome by employing a proctoring system during the remote electronic examination (like Sikoola, as was used in this study).

Sikola [29] is the website used to administer online exams without proctoring features in this study. This webpage is based on Chamilo [30]. Similar to other Learning Management systems (LMS), the LMS Chamilo application has an exercise menu. This menu has a variety of questions ranging from conventional types like multiple-choice questions to multiple-choice questions that force examinees to think more carefully in deciding their responses, such as multiple-choice questions with a degree of certainty.

The proctored website for online examinations is Sikoola. Sikoola is a program built exclusively for tests. The website Sikola's online exam elements are likewise owned by Sikoola. The only difference between the two is the proctoring system capabilities in terms of online examinations.

The statistics in this study demonstrate that student test scores were lower when distant electronic examinations were proctored. The proctoring system's documentation of the online exam process revealed that some students were flagged as dishonest throughout the exam. The information gathered was the appearance of notifications from examinees who wished to access a website other than the exam page. Another piece of information supplied by the system is the copy-paste usage of the keyboard. It is natural for the test taker's score to be lower when the exam is proctored. Additionally, the research indicated no difference in test scores when considering the class and gender variables.

The employment of a proctoring system during remote electronic examinations does assist institutions in educating students to always be truthful throughout exams. However, examinees complained that the employment of a proctoring system during the remote electronic examination drained a significant amount of credit from them; however, this assertion was not backed up by reliable statistics. Another student complaint apart from credit is the internet network. Some students who live outside the city frequently express dissatisfaction with the city's internet network. Students report having difficulty taking online tests due to insufficient internet availability. Students who experience this difficulty frequently want a policy requiring them to take a follow-up exam.

Therefore, under these conditions, the researcher took the initiative to prepare an online exam model for Arabic translating skills by utilizing an application to monitor student's behavior during online exams. The internet access check tool, the PC/laptop camera, and keyboard usage monitoring are just a few of the features required to monitor the translation skills test from the application. This program is anticipated to determine the strength of a student's internet connection. This feature's purpose is to educate students about the status of their internet access. Thus, if internet access is inadequate, the instructor is no longer held responsible for slow loading of the substance of the questions being worked

on. The difficulty, however, returns to students who are unprepared for online exams.

Another must-have feature is a surveillance camera. Every modern laptop, by and large, is equipped with a camera. This camera can be used when the owner is taking an online exam; for example, the camera can be compelled to turn on to capture the laptop's owner sitting in front of the screen. This online exam application system can periodically record the behavior of the laptop owner.

Additionally, an application that can monitor students' laptop keyboard usage is considered necessary for online tests. This cheating tracking tool instantly tells the laptop/PC owner if someone attempts to use the keyboard during an online exam. Thus, if students try to open another browser (new window) to search or copy and paste, the proctoring system will block the examinee's screen. As a result, students who attempt to cheat on online tests will be identified and may face disciplinary action.

The following Table VII summarizes the elements of Sikoola that enable it to monitor and record dishonesty during online exams.

TABLE VII. LECTURERS CAN SELECT FROM THESE VARIOUS FEATURES WHEN PRAPARING FOR ONLINE EXAMS

FEATURE	CHOICES		DESCRIPTION
Is time flexible?	No	Yes	A flexible period can be set if the participants do not begin the exam simultaneously. Participants can begin the exam within the chosen time range using flexible mode.
Minimum completeness criteria	Filled with a minimum passing grade		Minimum requirements for completion are used to determine whether or not a participant passes the exam. If the lecturer is going to do remedial work, only examinees who do not meet the passing grade are permitted to take it.
Stop the timer when offline?	No	Yes	When the examinee cannot connect to the server, for example, during a power outage, the countdown timer can be paused to ensure that processing time is not shortened when the participant reconnects.
Activate test tokens?	No	Yes	The organizer may need activation of the test token. Participants who do not know their exam token are unable to begin the examination. The institution's supervisor/admin can view the exam token. Every 30 minutes, the exam token will change.
Require camera?	No	Yes	If you select YES, all participants must consent to camera access. If this is NOT permitted, the participant will be unable to continue the examination. Ascertain that all examinees comprehend how to use the browser's camera.

Enable network checker?	No	Yes	If you select YES, all participants will be required to click the network check button. If NO, the individual is unable to proceed with the examination.	Limit participant browser?	No	Yes	This restriction only allows specific browsers to be used. Specify the allowed browsers, e.g., Edge, Chrome, Safari, etc.
Enable snapshots?	No	Yes	If this option is enabled, when the examinee's webcam is recognized as being out of focus in front of the exam screen, a snapshot from the examinee's webcam is saved and can be downloaded in .zip format once the test concludes (up to 7 days after the exam, after which the system will delete it). Please keep in mind that this option is only effective if your examinee is obliged to stare at the exam screen constantly. If your examinee needs to draw on paper, keeping their face down, this option should not be activated.	Limit internet provider	Specify the allowed internet provider		If the test is not being run in a dedicated room or no IP address limitations are required, leave the room selection blank.
Enable Live Score?	No	Yes	By enabling Live Score, institutions can track test taker acquisition in real time via the session administration menu. Please utilize this function only when necessary. If it is not critical to the institution, we recommend that it is disabled. Important! For the time being, the maximum number of participants in a session that can activate this function is 500, and the sessions must be concurrent.	Show final result?	No	Yes	If desired, the outcome (points gained) will be shown to participants. Additionally, improper problem solutions will be revealed if this option is enabled. These displays are offered to participants only after completing their work on the questions.
Screen block duration	No	Yes	When participants engage with other tabs/windows/applications outside the test screen display, their screen may be blocked (they will be unable to answer/change questions). Enter the duration in seconds during which the participant will be blocked. If it is set to 0, no screen blocking occurs. Take note that this approach of screen blocking is relatively basic but quite successful for participants in general.	Show rank?	No	Yes	This feature will display the ranking order of participants.
Check screen ratio?	No	Yes	If the screen ratio check is performed, the system will verify the participant's browser size every three seconds. If the screen size is deemed unsuitable, the test page will be blocked briefly. Before participants can proceed with the exam, they must alter the screen size. This method is intended to minimize the likelihood of participants exploiting the split-screen feature to launch additional windows/applications.	Show errors?	No	Yes	This feature will indicate whether the participant's response was incorrect. Caution should be exercised when activating this function, as it may create stress for individuals.
Allowed devices	PC/ laptop	Mobiles or tablets	The type of gadget that participants may use to work on this session is entirely up to them. Leave it as-is for unlimited access from any device.	Show discussion?	No	Yes	This setting is only available if displaying errors is also enabled. After the test/test period is declared complete by the system, incorrect answers will be revealed along with the answer key and discussion (if applicable).
				Show Done button?	No	Yes	This button allows the participant to exit the exam/test even if there is still time remaining.
				Thorough discussion?	No	Yes	When the complete discussion option is enabled, all answers are shown to participants at the conclusion of the test, regardless of whether they were answered correctly or wrongly.
				Engaged teachers	Fill in the teacher's name		This field is optional. The test session outcome report is accessible solely to the specified teacher when completed. However, if it is left blank, no teacher will be able to view the test results.
				Supervisors involved	Filled with the supervisor's name		This field is optional. Supervisors may be assigned only to monitor the exam's progress.
				Report model	Selected from the provided options, including standard reports, sorting, personality		If you are unsure, use the Standard report model. Specific report models require the development of a question package to meet specific criteria; please consult us if your institution requires this.
				Additional information	Filled with additional information		Fill in the required information that has not been provided in the online exam system.
				Show feedback form?	No	Yes	This feature will display feedback from the answers given by the examinees.

Based on the facts, it was discovered that students were murmuring while taking online tests. This behavior is regarded abnormal, and as a result, the lecturer talks with the mumbling examinee by asking about his or her mouth. Evidently, the response to the inquiry was unexpected; hence, he had to read with his mouth jumbled to comprehend what he was reading. Obviously, this is an entirely different explanation from the lecturer's opinion that the student was muttering because he was reading the exam questions to his colleague standing in front of him, even though the PC/laptop used for the exam was not recorded. This fact also demonstrates that Sikoola's proctoring method must be improved, particularly in capturing students' voices during online exams.

V. CONCLUSION

A proctoring system is a web-based program that assists instructors and students with online exams. In the case of Arabic translation examinations, the test scores of students who utilized the proctoring system were lower than the test scores of students who took the exam without using the proctoring system. Additionally, this study established that class and gender variables did not affect test scores. The online exam system variable—more precisely, the proctoring method used during the online exam—impacted the test score. A proctoring system in online exams can keep the examinees from engaging in dishonest behavior. Further improvements can be made to the proctoring system program to enhance its capabilities to record and track dishonesty during online exams.

According to recent findings, academic dishonesty appears prevalent among students enrolled in Arabic Translation courses. It is believed that, with the implementation of the proctored system, this unethical behavior among students would be eliminated in the future. One of the functions of higher education is to instill values in students, instilling the belief that academic dishonesty is unethical and should be avoided at all costs.

ACKNOWLEDGMENT

Although this study got no external support, I must thank the two teams, namely the Sikola and the Sikoola teams, for their assistance in presenting diverse online questions. I would also like to thank the students that were involved and eager to participate in this research. I extend the same appreciation to the team of instructors in the Arabic study program who provided suggestions for improving the layout of Arabic translation problems.

REFERENCES

- [1] T. H. Reisenwitz, "Examining the necessity of proctoring online exams," *J. High. Educ. Theory Pract.*, vol. 20, no. 1, pp. 118–124, 2020.
- [2] K. Adzima, "Examining online cheating in higher education using traditional classroom cheating as a guide," *Electron. J. e-Learning*, vol. 18, no. 6, pp. 476–493, 2020.
- [3] J. Pleasants, J. M. Pleasants, and B. P. Pleasants, "Cheating on Unproctored Online Exams: Prevalence, Mitigation Measures, and Effects on Exam Performance," *Online Learn. J.*, vol. 26, no. 1, pp. 268–284, 2022.
- [4] K. A. D'Souza and D. V. Siegfeldt, "A Conceptual Framework for Detecting Cheating in Online and Take-Home Exams," *Decis. Sci. J. Innov. Educ.*, vol. 15, no. 4, pp. 370–391, 2017.
- [5] M. Castaño, C. Noeller, and R. Sharma, "Implementing remotely proctored testing in nursing education," *Teach. Learn. Nurs.*, vol. 16, no. 2, pp. 156–161, 2021.
- [6] F. M. Guangul, A. H. Suhail, M. I. Khalit, and B. A. Khidir, "Challenges of remote assessment in higher education in the context of COVID-19: a case study of Middle East College," *Educ. Assessment, Eval. Account.*, vol. 32, no. 4, pp. 519–535, 2020.
- [7] E. Siniver, "Cheating on Exams: the Case of Israeli Students," *Coll. Stud. J.*, vol. 47, no. 4, pp. 593–604, 2013.
- [8] E. R. Cavalcanti, C. E. Pires, E. P. Cavalcanti, and V. F. Pires, "Detection and evaluation of cheating on college exams using supervised classification," *Informatics Educ.*, vol. 11, no. 2, pp. 169–190, 2012.
- [9] L. Nath and M. Lovaglia, "Cheating on Multiplechoice Exams: Monitoring, Assessment, and an Optional Assignment," *Coll. Teach.*, vol. 57, no. 1, pp. 3–8, 2009.
- [10] D. Howard, "Comparison of exam scores and time taken on exams between proctored on-campus and unproctored online students," *Online Learn. J.*, vol. 24, no. 4, pp. 204–228, 2020.
- [11] M. Li, "Optimized collusion prevention for online exams during social distancing," *npj Sci. Learn.*, vol. 6, no. 1, 2021.
- [12] P. J. Marín García, A. Arnau, and L. Llobat, "Preferences and scores of different types of exams during COVID-19 pandemic in faculty of veterinary medicine in Spain: A cross-sectional study of paper and E-exams," *Educ. Sci.*, vol. 11, no. 8, pp. 0–5, 2021.
- [13] M. Valizadeh, "Cheating in online learning programs: Learners' perceptions and solutions," *Turkish Online J. Distance Educ.*, vol. 23, no. 1, pp. 195–209, 2022.
- [14] M. Pettit, S. Shukla, J. Zhang, K. H. Sunil Kumar, and V. Khanduja, "Virtual exams: has COVID-19 provided the impetus to change assessment methods in medicine?," *Bone Jt. Open*, vol. 2, no. 2, pp. 111–118, 2021.
- [15] A. A. Turani, "Students Online Exam Proctoring: A Case Study Using 360 Degree Security Cameras," *ETCCE 2020 - International Conference on Emerging Technology in Computing, Communication and Electronics*. 2020.
- [16] N. Chotikakamthorn, "Affordable Proctoring Method for Ad-hoc Off-campus Exams," *SIGITE 2020 - Proceedings of the 21st Annual Conference on Information Technology Education*. pp. 266–272, 2020.
- [17] N. Selwyn, "A necessary evil? The rise of online exam proctoring in Australian universities," *Media Int. Aust.*, 2021.
- [18] F. F. Kharbat, "E-proctored exams during the COVID-19 pandemic: A close understanding," *Education and Information Technologies*, vol. 26, no. 6, pp. 6589–6605, 2021.
- [19] A. A. Turani, J. H. Alkhateeb, and A. R. A. Alsewari, "Students Online Exam Proctoring: A Case Study Using 360 Degree Security Cameras," *ETCCE 2020 - Int. Conf. Emerg. Technol. Comput. Commun. Electron.*, no. January, 2020.
- [20] H. Li, "A visual analytics approach to facilitate the proctoring of online exams," *Conference on Human Factors in Computing Systems - Proceedings*. 2021.
- [21] S. Draaijer, "Online proctoring for remote examination: A state of play in higher education in the EU," *Communications in Computer and Information Science*, vol. 829, pp. 96–108, 2018.
- [22] K. P. Kamble, "Video Interpretation for Cost-Effective Remote Proctoring to Prevent Cheating," *Lecture Notes in Networks and Systems*, vol. 169, pp. 259–269, 2021.
- [23] Sikoola, "Advanced Analytical and Artificial Intelligence Based Platform, E-Learning & AI Online CBT," *PT Sikoola Teknologi Indonesia*, 2020. [Online]. Available: <https://ujian.sikoola.com/>.
- [24] H. Meishar-Tal and A. Levenberg, "In times of trouble: Higher education lecturers' emotional reaction to online instruction during COVID-19 outbreak," *Educ. Inf. Technol.*, vol. 26, no. 6, pp. 7145–7161, 2021.

- [25] A. Sangwan, A. Sangwan, and P. Punia, "Development and Validation of an Attitude Scale towards Online Teaching and Learning for Higher Education Teachers," *TechTrends*, vol. 65, no. 2, pp. 187–195, 2021.
- [26] A. Sharma and I. Alvi, "Evaluating pre and post COVID 19 learning: An empirical study of learners' perception in higher education," *Educ. Inf. Technol.*, vol. 26, no. 6, pp. 7015–7032, 2021.
- [27] L. Elsalem, "Remote E-exams during Covid-19 pandemic: A cross-sectional study of students' preferences and academic dishonesty in faculties of medical sciences," *Ann. Med. Surg.*, vol. 62, pp. 326–333, 2021.
- [28] A. Hochlehnert, K. Brass, A. Moeltner, and J. Juenger, "Does Medical Students' Preference of Test Format (Computer-based vs. Paper-based) have an Influence on Performance?," *BMC Med. Educ.*, vol. 11, no. 1, pp. 1–6, 2011.
- [29] Sikola, "SIKOLA UNIVERSITAS HASANUDDIN," Hasanuddin University, 2009. [Online]. Available: <https://sikola.unhas.ac.id/index.php>.
- [30] The Chamilo Association, "Chamilo," Chamilo, 2010. [Online]. Available: <https://chamilo.org/en/>.

Groundnuts Leaf Disease Recognition using Neural Network with Progressive Resizing

Rajnish M. Rakholia¹, Jinal H. Tailor², Jatinderkumar R. Saini^{3*}, Jasleen Kaur⁴, Hardik Pahuja⁵

S. S. Agrawal Institute of Management & Technology, Navsari, India¹

S. S. Agrawal Institute of Management & Technology, Navsari, India²

Symbiosis Institute of Computer Studies and Research³

Symbiosis International (Deemed University), Pune, India³

School of Engineering, P P Savani University, Surat, India⁴

Yardi Systems Inc., Pune, India⁵

Abstract—Groundnut is an important oilseed crop in the world, and India is the second-largest producer of groundnuts. This crop is prone to attack by numerous diseases which is one of the most important factors contributing to the loss of productivity and degradation in the quality; both of these finally result in a low agricultural economy. Therefore, it is necessary to find better and more reliable automation solutions to recognize groundnut leaf diseases. In this paper, a deep learning based model with progressive resizing is proposed for groundnut leaf disease recognition and classification tasks. Five major categories of groundnut leaf diseases namely leaf spot, armyworms effect, wilts, yellow leaf, and healthy leaf are considered. The proposed model was trained with and without progressive resizing while it was validated using cross-entropy loss. The first of its kind dataset used for training and validation purposes was manually created from the Saurashtra region of Gujarat state of India. The created dataset was imbalanced in terms of a different number of samples for each category. To handle the imbalanced dataset problem, the extended focal loss function was used. To evaluate the performance of the proposed model, different performance measures including precision, sensitivity, F1-score, and accuracy were applied. The proposed model achieved state-of-the-art accuracy of 96.12%. The model with progressive resizing performed better than the traditional core neural network-based model built on cross-entropy loss.

Keywords—Groundnut leaf disease recognition; progressive resizing; deep learning; neural network

I. INTRODUCTION

The groundnut crop plays an important role in the agricultural export commodity and edible oilseed economy of India. In the year 2019 alone, total groundnut acreage and production in India were 3.931 million hectares and 6.862 million MT respectively (IOPEPC, 2019)[1], but still, the average yield is low. Disease attack is a major factor contributing to the loss of productivity, quality, and early death of the leaves (Konate et al., 2020)[2]. Therefore, it is necessary to take steps toward developing a fast and accurate groundnut leaf disease recognition methodology to increase productivity sustainably. This will be of great significance to the various stakeholders. Till now almost no commercial tools are available for accurate recognition of groundnut leaf disease and very less quality research articles are published for the same. One of the key reasons behind this might be a lack of

benchmark datasets available for groundnut leaf disease recognition research and experiments.

In this research, the groundnut leaf dataset was created manually from the Saurashtra regions of Gujarat. Initially, all images were captured in fixed background squared format with the size of 3000x3000 pixel (3 color channels), and then final datasets were prepared in different sizes of images including 32x32, 64x64, 128x128, and 256x256. Based on the thorough review of the literature and a comprehensive review carried out by (Ngugi et al., 2020; Chouhan et al., 2020; Kaur et al., 2019) [3-5] on methods used in leaf disease recognition using image processing, machine learning, and deep learning techniques, it was derived for the current research work that very few researchers have worked on groundnut leaf disease recognition. Chen et al. (2019) [6] used spectral index and disease index based on their correlation in leaf spectrum range between 325nm to 1075nm. Their results showed that near-infrared regions' canopy spectral reflectance decreased as the disease index increased. In the regression model, normalized difference spectral indexes were R938, R761 with the value of R2 up to 0.68 for peanut leaf spot disease detection. Based on the index model high fit between estimated and observed values, they concluded that the model could be used for peanut leaf spot disease detection. For groundnut disease classification (Chaudhary et al., 2016)[7] proposed an improved Random Forest Classifier using instance Filter-Resample and attribute evaluator methods for balancing the class distributions of the multi-class dataset. The proposed method was also applied on five different datasets such as Diabetes, Soybean, Audiology, Vote, and Breast Cancer, and obtained the value of the F1-measure in the range between 0.89 and 0.97. They advocated that the result of their method was effective when the dataset is unbalanced in terms of the number of samples varying among different classes. Ramakrishnan and Sahaya (2015) [8] applied a backpropagation algorithm for groundnut leaf disease detection and classification. Initially, RGB was converted into HSV and then plane separation and color features extraction steps were carried out. Dong et al. (2019)[9] applied a capsule network for peanut leaf disease recognition with the use of dynamic routing to overcome the problem of rotational invariance and spatial relationships. Their empirical observations showed that the recognition accuracy of the capsule network is 82.17% which is better than the

*Corresponding Author.

corresponding value of 81.14% of the convolutional neural network. It is notable to mention here that the capsule network was originally proposed by Sabour et al. (2017) [10]. Vaishnave et al. (2020)[11] used a convolutional network for groundnut disease classification and claimed higher accuracy for training and testing on the PlantVillage dataset, but the fact is, till now no benchmark image dataset for groundnut diseases is released or published by PlantVillage (PlantVillage, 2020) [12].

Since the introduction of Deep learning, many state-of-the-art benchmark architectures such as DenseNet (Huang et al., 2017) [13], Deep residual learning (He et al., 2016) [14], Inception-v4 (Szegedy et al., 2017) [15], GoogLeNet (Szegedy et al., 2015) [16], VGG (Simonyan and Zisserman, 2014) [17] and AlexNet (Krizhevsky et al., 2012) [18] have been found to give an incredible performance for object detection and various computer vision tasks. Many researchers have also used these architectures for transfer learning for plant disease recognition e.g. (Fuentes et al., 2018) [19] have used R-CNN, AlexNet, GoogLeNet for the identification of tomato leaf disease, (Liu et al., 2018)[20] have used AlexNet for apple leaf disease detection, (Kaya et al., 2019; Barbedo 2019; Brahimi et al., 2018; Mohanty et al., 2016)[21-24] have used multiple benchmark architectures for multiple plant disease recognition.

In recent times, convolutional neural network-based methods are great in demand for plant leaf disease recognition due to automatic deep feature extraction. For corn leaf disease recognition and classification (Waheed et al., 2020) [25] proposed an optimized dense convolutional neural network model. Ji et al. (2020) [26] proposed a Convolutional Neural Network-based architecture for multi-label learning for crop leaf diseases recognition and severity estimation. To overcome the problem of the unbalanced dataset (Zhong and Zhao, 2020) [27] have proposed DenseNet-121 as the backbone network and used three methods regression, multi-label classification, and focus on loss function to identify apple life disease and obtained test accuracy of 93.51%, 93.31% and 93.71% respectively which was better than the accuracy of 92.29% obtained by traditional multi-classification method with a cross-entropy loss function. Sethy et al. (2020) [28] used different CNN architectures based on deep features using a support vector machine to identify rice leaf disease.

Self-attention CNN-based architecture was proposed by (Zeng and Li, 2020) [29] for crop leaf disease recognition. Zhang et al. (2019) [30] have used global pooling dilated convolutional neural network for cucumber leaf disease identification. Karlekar and Seal (2020) [31] proposed CNN-based SoyaNet for soybean leaf disease classification. Their proposed network obtained higher precision, recall, and f1-score value compared to the other nine state-of-the-art models.

Almost all the existing CNN-based architectures designed for leaf disease recognition and classification perform well at some level in terms of precision, recall, f1-score, and accuracy. However, the time complexity and model generalization are major problems when CNN-based architecture is trained and

optimized on the high volume of small and large images or in a real-time environment due to the range of features and number of layers in the architecture. In this paper, a CNN-based architecture with progressive resizing for model generalization, optimization, and performance improvement is proposed.

II. MATERIALS AND METHODS

A. Dataset

Based on the best knowledge of related literature, almost no benchmark dataset of groundnut leaf disease is publicly available for research. The dataset for the current research was created manually and comprised of five major groundnut leaf classes, viz. leaf spot, armyworm effects, wilts, yellow leaf, and healthy leaf. All major types of symptomatic leaves were plucked manually from the plants and put onto the fixed background to capture the images. Initially, all the images are captured in squared format with the size of 3000x3000 (3 color channels), and then later all the captured images are resized in different sizes of 32x32, 64x64, 128x128, and 256x256 for model development using progressive resizing. The created dataset was divided into a ratio of 80:20 for training and testing. All the classes and corresponding labels considered for this research are shown in Table I.

The distribution of training and testing datasets is depicted in Fig. 1 which also indicates that the dataset is imbalanced as the distribution is not in equal proportion for each class. This was solved using the Focal loss function and is discussed in section 2.4 in detail. According to the data presented in Fig. 1, the most commonly occurring leaf disease in the groundnut crop is Leaf Spot which contributes the largest proportion, except healthy leaf, in the dataset. Similarly, the least proportion in the dataset is comprised of groundnut wilts. Notably, it is also a more harmful disease.

B. Proposed Network Architecture

The well-known terminologies used in CNN such as a convolutional layer, pooling layer, filters, fully connected layer, etc., are not addressed here to rule out redundancy.

Model built on the standard convolutional neural network works well when input images are fixed in size. The model gives good accuracy when feeding larger images but it takes a long time and uses more computation power during the training phase. Scale-up and scale-down are required during training when input images are very small and large, respectively.

TABLE I. GROUNDNUT LEAF DISEASE CLASSES AND CORRESPONDING LABEL

Class Name	Class Label
Groundnut Yellow Leaf	0
Groundnut Wilts	1
Groundnut Leaf Spot	2
Groundnut Healthy Leaf	3
Groundnuts ArmywormsEffect	4

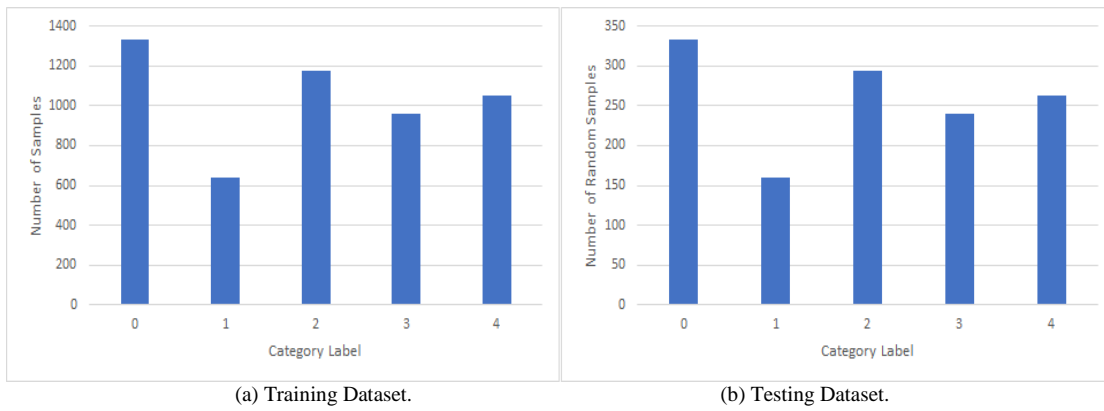


Fig. 1. Data Distribution for Training and Testing.

In this research, we have considered progressive-resizing methodology (originally proposed by Jeremy Howard, 2018) [32] for training a model to improve the recognition rate and for the model generalization. The workflow of progressive resizing for the proposed work is as follows:

Phase-1: The first model was trained on small images with the size of 32x32 with 3 color channels.

Phase-2: The next model was trained on upscaled images with the size of 64x64. Here, the layers and weights used in the previous smaller scale model were incorporated during training.

Phase-3: The third model was trained on 128x128 images; the output of phase-2 was fed as the input of phase-3. Each model is responsible to find some new features and patterns which were hidden in a previous smaller-scale model.

Phase-4: The final architecture was built and trained using the size of 256x256 images. Each larger scale model incorporates the previous smaller scale model in its architecture.

The proposed model was started to be built on 32x32 sizes and then scaled up to 4X, where X was the initial size of input images. Each phase of the proposed network was trained on the specific size of images and extracted some features. The trained model was saved with their weights and the weight was not changed in further training. Each subsequent phase was

responsible to extract additional findable features which were hidden and not found in the previous phase of the network. Models built on small-size images generalize well to larger input sizes and they take less time in processing (Howard, 2018) [33]. The proposed combined architecture is depicted in Fig. 2.

In order to introduce nonlinearity into the model, Rectified Linear Unit (ReLU) was used in each convolution operation. The ReLU function, $F(x) = \max(0, x)$, returns x for all values of $x > 0$, and returns 0 for all values of $x \leq 0$.

C. SoftmaxLoss

Here, the Softmax loss is categorical cross-entropy loss which is computed based on class probability generated by Softmax activation and using cross-entropy loss function. It has been referred to as $f(s_i)$ and defined as follows:

$$f(s)_i = \frac{e^{s_i}}{\sum_j^C e^{s_j}}$$

Where s_i , is a network score of each class i in C .

In this research specifically disease classification, labels are considered as one-hot, which means only positive class C_p were considered in cross-entropy loss which can be defined as follows:

$$\text{Cross-Entropy} = - \sum_i^C t_i \log(f(s)_i)$$

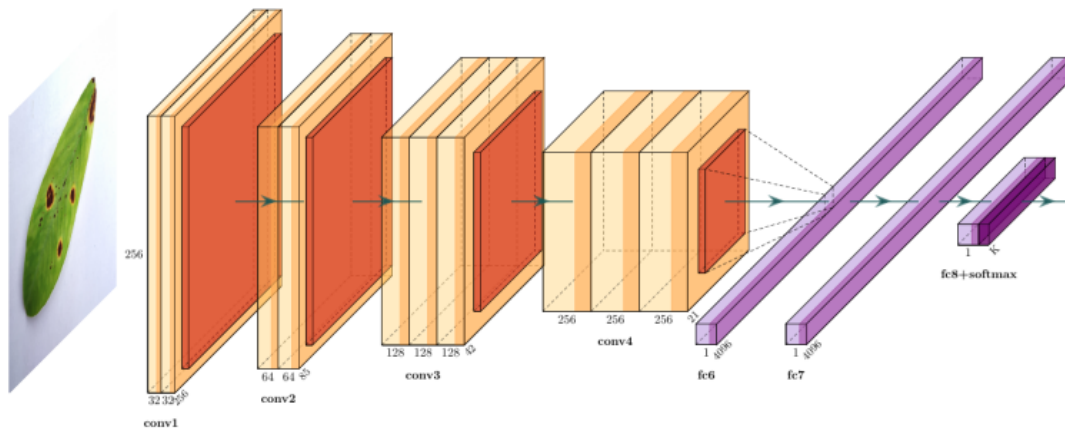


Fig. 2. Proposed CNN based Architecture [Image by Author].

Target vector t only contained non-zero elements. We can write the following equation for cross-entropy loss after discarding the elements of summation which are zero because of target labels, so $t_i=t_p$.

$$\text{Cross-entropy} = -\log\left(\frac{e^{s_p}}{\sum_j^c e^{s_j}}\right)$$

Where s_p is a score of positive class in CNN.

D. Focal Loss

The proposed classification also involved the problem of the imbalanced dataset. Some classes have a very small number of samples whereas some other classes contained almost double the number of samples. The network trained using an imbalanced dataset makes the network biased towards learning in favor of the classes having a higher number of samples while the remaining classes go under-looked. To tackle the class imbalance problem, a focal loss function with the multiplication of cross-entropy loss function with modulating factors was used. The Focal Local loss function is an improved version of cross-entropy loss which is made by adding focusing and balancing parameters in the cross-entropy loss function. This enhances the efficiency of the network and improves the results of misclassified observations. The focal loss function was originally proposed by Facebook AI Research (Lin et. al., 2017) [33] for binary classification in the object detection task. We have extended the concept of focal loss for multi-class classification. The general form of the focal loss function is:

$$\text{Focal Loss} = -(1 - p_t)^\gamma \log(p_t)$$

The focal loss for multi-class classification can be derived as follows:

$$\text{Focal Loss} = -(1 - f(s)_i)^\gamma \log(f(s)_i)$$

Where gamma (γ) is focusing parameter and $f(s)_i$ is softmax used for multi-class classification in cross-entropy. If $\gamma = 0$, then this equation is equivalent the equation of cross-entropy loss. Tunable focusing parameter γ should be ≥ 0 . Gamma (γ) controls the shape of the curve. The higher value of gamma (γ) reduces the loss of well-classified observations at some level. In this equation $(1 - f(s)_i)^\gamma$ is considered as modulating factor.

Finally, focal loss function can be defined with balancing parameter for imbalanced data as follows:

$$\text{Focal Loss} = -\alpha(1 - f(s)_i)^\gamma \log(f(s)_i)$$

Where, alpha (α) is a balancing parameter. In this case, alpha refers to the weights used in the network, and small weights were assigned to dominating class while higher weights were assigned to the rare class.

III. RESULT AND DISCUSSION

The training parameters used for the proposed model are shown in Table II. The model was trained on different sizes of images starting from 32x32x3 and the final model was trained on 256x256x3 images. After doing many experiments, the final batch size and learning rate were set to 32 and 1e-3 respectively. Optimizer Adam was used with the decay of 1e-5.

TABLE II. TRAINING PARAMETERS

Parameter	Settings
Final Input size	(256,256,3)
Batch size	32
Learning Rate	1e-3
Optimizer	Adam with decay of 1e-5

The distribution of testing data for each category is shown in Table III.

TABLE III. DISTRIBUTION OF TEST DATASET

Class	Number of Samples
Groundnuts Healthy Leaf	333
Groundnuts Armyworms Effect	263
Groundnuts Wilts	160
Groundnuts Leaf Spot	293
Groundnut Yellow Leaf	240

The core CNN-based model without progressive resizing was evaluated using cross-entropy loss with different statistical measures, as shown in Table IV. The maximum and minimum F1 scores obtained were 0.934773 and 0.853771 for leaf spot and Wilts categories respectively. The average accuracy was reported to be 0.918823. The evaluation of the proposed model with progressive resizing and cross-entropy loss is shown in Table V. The result shows that the accuracy of 0.949381 obtained in progressive resizing is better than the accuracy of 0.918823 obtained with the core CNN model.

TABLE IV. CROSS ENTROPY LOSS WITHOUT PROGRESSIVE RESIZING

	Precision (%)	Sensitivity (%)	F1 score (%)
Groundnuts Healthy Leaf	0.929509	0.919712	0.924585
Groundnuts Armyworms Effect	0.929019	0.937031	0.933008
Groundnuts Wilts	0.857722	0.849856	0.853771
Groundnuts Leaf Spot	0.938732	0.930847	0.934773
Groundnut Yellow Leaf	0.919686	0.928934	0.924287
Weighted avg	0.920766	0.918823	0.919774

TABLE V. CROSS ENTROPY LOSS WITH PROGRESSIVE RESIZING

	Precision (%)	Sensitivity (%)	F1 score (%)
Groundnuts Healthy Leaf	0.963758	0.958712	0.961228
Groundnuts Armyworms Effect	0.961034	0.960001	0.960517
Groundnuts Wilts	0.913827	0.901834	0.907791
Groundnuts Leaf Spot	0.962093	0.959823	0.960957
Groundnut Yellow Leaf	0.942003	0.943748	0.942875
Weighted avg	0.952575	0.949381	0.950971

The results of the proposed model without progressive resizing using focal loss ($\gamma=2$) is shown in Table VI. The average accuracy of 0.930404 was reported which is better

than the accuracy of 0.918823 achieved in cross-entropy loss. The training-validation accuracy and training validation loss using the focal loss function are depicted in Fig. 3(a) and Fig. 3(b) respectively. Here, focal loss down-weighted the easy observations and focused training on hard observations of imbalanced classes.

The evaluation results of the proposed CNN-based model with progressive resizing using focal loss function is shown in Table VII. The obtained average accuracy was 0.961229 which is better than the accuracy obtained in all other cases. Basically, setting the value of $\gamma > 0$ reduces the relative loss for well-classified observations, for the proposed model we obtained a higher accuracy when $\gamma=2$ set. The minimum F1 score was reported for the Groundnuts Wilts class and the maximum F1 score was reported for the Groundnuts Armyworms Effect class. The training and validation accuracy and loss for CNN-based model with progressive resizing using focal loss function is depicted in Fig. 4(a) and 4(b), respectively.

TABLE VI. FOCAL LOSS ($\Gamma=2$) WITHOUT PROGRESSIVE RESIZING

Categories	Precision (%)	Sensitivity (%)	F1 score (%)
Groundnuts Healthy Leaf	0.937483	0.929594	0.933522
Groundnuts Armyworms Effect	0.932743	0.942032	0.937364
Groundnuts Wilts	0.896029	0.88	0.887942
Groundnuts Leaf Spot	0.9488	0.948921	0.948860
Groundnut Yellow Leaf	0.926023	0.929782	0.927899
Weighted avg	0.931809	0.930404	0.931088

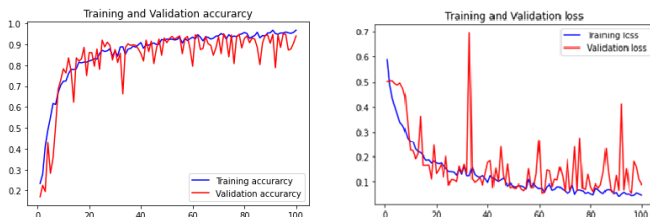


Fig. 3. Training and Validation of Core CNN Model with Focal Loss.

TABLE VII. FOCAL LOSS ($\Gamma=2$) WITH PROGRESSIVE RESIZING

Categories	Precision (%)	Sensitivity (%)	F1 score (%)
Groundnuts Healthy Leaf	0.978302	0.9702	0.974234
Groundnuts Armyworms Effect	0.972003	0.98	0.975985
Groundnuts Wilts	0.92904	0.92893	0.928985
Groundnuts Leaf Spot	0.97	0.9610212	0.965490
Groundnut Yellow Leaf	0.958003	0.95	0.953985
Weighted avg	0.965235	0.961229	0.963217

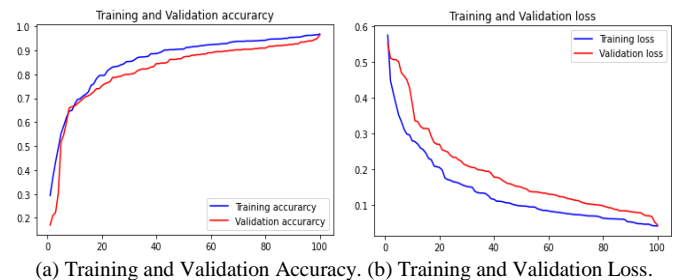


Fig. 4. Training and Validation with Progressive Resizing and Focal Loss.

IV. CONCLUSION

CNN-based architecture with progressive resizing was proposed to classify groundnut leaves into classes, namely, healthy leaf, armyworm effect, groundnut wilts, yellow leaf, and leaf spot which happen to be the most occurring disease in groundnut leaves. The proposed architecture with and without progressive resizing was evaluated using cross-entropy loss and focal loss functions. The obtained results of the proposed model without progressive resizing were 91.88% and 93.04% using cross-entropy loss and focal loss respectively while the average accuracy of the proposed model with progressive resizing using focal loss was 96.12%. Based on the empirical results, it is concluded that the progressive resizing-based model is a more generalized model and it was trained on different scales starting from the small-scale images of 32x32 size while the final model was built using 256x256 size images. The results obtained on different scenarios show that the CNN-based model with progressive resizing outperforms the core CNN-based architecture while the focal loss function helped out to deal with the imbalanced dataset problem. In the future, we plan to implement the proposed concept to recognition of diseases in real-time farm fields by combining computer vision technologies.

REFERENCES

- [1] Indian Oilseed and Produce Export Promotion Council (IOPEPC, 2019), Kharif-2019 Groundnut Crop Survey, retrieved on Feb 4, 2021, from http://www.iopec.org/misc/2019_20/Kharif%202019%20Groundnut%20Crop%20Survey.pdf.
- [2] Konate, M., Sanou, J., Miningou, A., Okello, D. K., Desmae, H., Janila, P., & Mumm, R. H. (2020). Past, present and future perspectives on groundnut breeding in Burkina Faso. *Agronomy*, 10(5), 704.
- [3] Ngugi, L. C., Abelwahab, M., & Abo-Zahhad, M. (2020). Recent advances in image processing techniques for automated leaf pest and disease recognition-a review. *Information Processing in Agriculture*.
- [4] Chouhan, S. S., Singh, U. P., & Jain, S. (2020). Applications of computer vision in plant pathology: a survey. *Archives of computational methods in engineering*, 27(2), 611-632.
- [5] Kaur, S., Pandey, S., & Goel, S. (2019). Plants disease identification and classification through leaf images: A survey. *Archives of Computational Methods in Engineering*, 26(2), 507-530.
- [6] Chen, T., Zhang, J., Chen, Y., Wan, S., & Zhang, L. (2019). Detection of peanut leaf spots disease using canopy hyperspectral reflectance. *Computers and electronics in agriculture*, 156, 677-683.
- [7] Chaudhary, A., Kolhe, S., & Kamal, R. (2016). An improved random forest classifier for multi-class classification. *Information Processing in Agriculture*, 3(4), 215-222.

- [8] Ramakrishnan, M. (2015, April). Groundnut leaf disease detection and classification by using back propagation algorithm. In 2015 International Conference on Communications and Signal Processing (ICCSP) (pp. 0964-0968). IEEE.
- [9] Dong, M., Mu, S., Su, T., & Sun, W. (2019, August). Image Recognition of Peanut Leaf Diseases Based on Capsule Networks. In International CCF Conference on Artificial Intelligence (pp. 43-52). Springer, Singapore.
- [10] Sabour, S., Frosst, N., & Hinton, G. E. (2017). Dynamic routing between capsules. In Advances in neural information processing systems (pp. 3856-3866).
- [11] Vaishnav, M. P., Devi, K. S., & Ganeshkumar, P. (2020). Automatic method for classification of groundnut diseases using deep convolutional neural network. SOFT COMPUTING.
- [12] Plantvillage (2020), Topics, retrieved on August 08, 2020, from <https://plantvillage.psu.edu/topics>.
- [13] Huang, G., Liu, Z., Van Der Maaten, L., & Weinberger, K. Q. (2017). Densely connected convolutional networks. In Proceedings of the IEEE conference on computer vision and pattern recognition (pp. 4700-4708).
- [14] He, K., Zhang, X., Ren, S., & Sun, J. (2016). Deep residual learning for image recognition. In Proceedings of the IEEE conference on computer vision and pattern recognition (pp. 770-778).
- [15] Szegedy, C., Ioffe, S., Vanhoucke, V., & Alemi, A. (2017, February). Inception-v4, inception-resnet and the impact of residual connections on learning. In Proceedings of the AAAI Conference on Artificial Intelligence (Vol. 31, No. 1).
- [16] Szegedy, C., Liu, W., Jia, Y., Sermanet, P., Reed, S., Anguelov, D., ... & Rabinovich, A. (2015). Going deeper with convolutions. In Proceedings of the IEEE conference on computer vision and pattern recognition (pp. 1-9).
- [17] Simonyan, K., & Zisserman, A. (2014). Very deep convolutional networks for large-scale image recognition. arXiv preprint arXiv:1409.1556.
- [18] Krizhevsky, A., Sutskever, I., & Hinton, G. E. (2012). Imagenet classification with deep convolutional neural networks. Advances in neural information processing systems, 25, 1097-1105.
- [19] Fuentes, A. F., Yoon, S., Lee, J., & Park, D. S. (2018). High-performance deep neural network-based tomato plant diseases and pests diagnosis system with refinement filter bank. Frontiers in plant science, 9, 1162.
- [20] Liu, B., Zhang, Y., He, D., & Li, Y. (2018). Identification of apple leaf diseases based on deep convolutional neural networks. Symmetry, 10(1), 11.
- [21] Kaya, A., Keceli, A. S., Catal, C., Yalic, H. Y., Temucin, H., & Tekinerdogan, B. (2019). Analysis of transfer learning for deep neural network based plant classification models. Computers and electronics in agriculture, 158, 20-29.
- [22] Barbedo, J. G. A. (2016). A review on the main challenges in automatic plant disease identification based on visible range images. Biosystems engineering, 144, 52-60.
- [23] Brahimi, M., Arsenovic, M., Laraba, S., Sladojevic, S., Boukhalfa, K., & Moussaoui, A. (2018). Deep learning for plant diseases: detection and saliency map visualisation. In Human and machine learning (pp. 93-117). Springer, Cham.
- [24] Mohanty, S. P., Hughes, D. P., & Salathé, M. (2016). Using deep learning for image-based plant disease detection. Frontiers in plant science, 7, 1419.
- [25] Waheed, A., Goyal, M., Gupta, D., Khanna, A., Hassani, A. E., & Pandey, H. M. (2020). An optimized dense convolutional neural network model for disease recognition and classification in corn leaf. Computers and Electronics in Agriculture, 175, 105456.
- [26] Ji, M., Zhang, K., Wu, Q., & Deng, Z. (2020). Multi-label learning for crop leaf diseases recognition and severity estimation based on convolutional neural networks. Soft Computing, 24(20), 15327-15340.
- [27] Zhong, Y., & Zhao, M. (2020). Research on deep learning in apple leaf disease recognition. Computers and Electronics in Agriculture, 168, 105146.
- [28] Sethy, P. K., Barpanda, N. K., Rath, A. K., & Behera, S. K. (2020). Deep feature based rice leaf disease identification using support vector machine. Computers and Electronics in Agriculture, 175, 105527.
- [29] Zeng, W., & Li, M. (2020). Crop leaf disease recognition based on Self-Attention convolutional neural network. Computers and Electronics in Agriculture, 172, 105341.
- [30] Zhang, S., Zhang, S., Zhang, C., Wang, X., & Shi, Y. (2019). Cucumber leaf disease identification with global pooling dilated convolutional neural network. Computers and Electronics in Agriculture, 162, 422-430.
- [31] Karlekar, A., & Seal, A. (2020). SoyNet: Soybean leaf diseases classification. Computers and Electronics in Agriculture, 172, 105342.
- [32] Jeremy Howard (2018), Now anyone can train Imagenet in 18 minutes, retrieved on Jan 1, 2021, from <https://www.fast.ai/2018/08/10/fastai-diu-imagenet/>.
- [33] Lin, T. Y., Goyal, P., Girshick, R., He, K., & Dollár, P. (2017). Focal loss for dense object detection. In Proceedings of the IEEE international conference on computer vision (pp. 2980-2988).

A Proposed Architecture for Smart Home Systems Based on IoT, Context-awareness and Cloud Computing

Samah A. Z. Hassan¹

Information Systems Department, Faculty of Computers &
Information, Suez University, Suez, Egypt

Ahmed M. Eassa²

MIS Department, Faculty of Management
MTI University, Cairo, Egypt

Abstract—The main objective of this paper is to propose a simple, low cost, reliable and scalable architecture for building Smart Home Systems (SHSs) that can be used to remotely automate and control home appliances, using microcontroller. The proposed architecture aims to take advantage of emerging technologies to make it easier to develop Smart Home systems and to provide more management by expanding its capabilities suitably. The suggested design intends to make it easier and more convenient for many applications to access context data, as well as providing a new schematic guide for creating as complete and comprehensive Smart Home Systems and data processing as possible. Related topics like smart homes and their intelligent systems will be addressed by examining prior work and proposing the authors' opinions in order to suggest the new architecture. The proposed advanced architecture's building blocks include Classic Smart Homes, Internet of Things (IoT), Context-awareness (CA), Cloud Computing (CC), and Rule-based Event Processing Systems (RbEPS). Finally, the proposed architecture is validated and evaluated by constructing a smart home system.

Keywords—Smart Home Systems (SHS); Internet of Things (IoT); Context-awareness (CA); Cloud Computing (CC); Rule-based Event Processing Systems (RbEPS); Smart Home System architecture

I. INTRODUCTION

Time, money, and energy are very valuable things. Smart Home Systems (SHSs) save time and reduce their owners' stress by ensuring homes are secured even when they are far away. Also, they save money and reduce the amount of effort put every day into running household helping owners having a better life [1], as they alert them of any change, allow users to control their homes when they are out, add safety through appliance, secure home through automated door locks [2], and increase peace of mind and convenience through temperature adjustment and lighting control [3, 4].

The proposed architecture is based on work done by [5], Internet of Things (IoT), Context-awareness (CA), Cloud Computing (CC) and Rule-based Event Processing Systems (RbEPS). Researchers frequently classify the problem of control as one of end-user programming, which causes them to think about research and assessment in terms of device control. End-user programming, on the other hand, gives the user some power over reprogrammed or learning-only systems [6]. The proposed architecture composition incorporates essential traits

and technologies from each of the four main paradigms. In the construction of smart homes, the Internet of Things (IoT) plays a significant role. IoT allows for remote management of mobile users/devices/sensors by utilizing an internet connection [5,7,8]. Practically anything in a home might be associated with the Internet via IoT, allowing for remote monitoring and control of all connected objects regardless of time or location [9,10]. Smart homes need to detect, expect and react to home activities to improve families' lives through socially appropriate and timely assistance [11]. In CA, Sensors can be attached to residential systems like air conditioning, lights, and other environmental devices. Computer intelligence is embedded into home devices by attaching sensors to them in order to monitor/control home appliances' functionalities and detect/measure home conditions/context. CC provides scalable infrastructures and platforms for accessing home devices and developing, managing, and executing home services anywhere at any time, in terms of processing power and/or storage space. The RbEPS allows building and controlling a full advanced smart home [5]. Scaling system capabilities, interestingly, might easily transcend some unseen threshold, leaving families feeling at the mercy of, rather than in charge of, technology [6].

There are four specific problems which are addressed for this kind of computing environments, which are: (1) How to combine and integrate the building blocks. (2) How to acquire, distribute, and store context data. (3) How to create means for Smart Home service discovery; for example, how sensors can discover resources in the nearby. (4) Because there is no universal standard for IoT interoperability, it is difficult for devices from various manufacturers to connect with one another.

The following section, the Related Work section, states the main four paradigms' definitions and descriptions. Secondly, the paper presents the proposed architecture which contains new milestones based on previous work to integrate and link the main four paradigms. Thirdly, the proposed architecture is examined by building an intelligent Smart Home System (SHS). Then, the paper is concluded in section four and finally, the future work is stated.

II. RELATED WORK

A Smart Home can make things easier as it provides great convenience for users by remotely controlled via Internet. It appears smart and intelligent because its computer systems are

capable of monitoring a wide range of activities. For example, the lights will automatically turn off as soon as the sun rises [3]. In addition, such systems also provide security and safety for their users [1]. Developing such kind of systems are made easier with the rise of services provided by IoT, CA, CC, and RbEPS, which are discussed in the following subsection.

A. Related Paradigms

A Smart Home has advanced automatic systems for monitoring, controlling, and automating home capacities with electronic devices throughout the house [12]. It is a central system that can control and create communication between nearly all aspects of the house, which includes lighting, heating and air conditioning, security systems, gas and electric fireplaces, irrigation systems, doors, appliances, and more coming all of the time [13]. A Smart Home may be described as a residence which is equipped with modern technology sensors, appliances and devices that can be controlled, accessed, and monitored remotely in order to deliver services to the home's residents [14]. Smart Homes provide unlimited number of services, as [5]: (1) Measuring Home Conditions, (2) Managing Home Appliances, and (3) Controlling Home Access.

Smart home systems use services provided by Internet of Things (IoT). Academicians, researchers, practitioners, scientists, professionals, innovators, developers, pioneers, and corporate leaders have all come up with their own definitions for the Internet of Things. The initial version of the Internet, according to all definitions, was about data created by people, while the following iteration is about data created by things/objects [15]. The Internet of Things' purpose is to allow things to connect with anything and anybody at anytime, anywhere, and utilizing any path/network and service [16]. According to [16], IoT is classified into three categories interacting through internet, which are: (1). Things/machine to things/machine, (2) People to machine/things, and (3) People to people. The author in [17] defined IoT as "group of infrastructures interconnecting connected objects and allowing their management, data mining and the access to the data they generate." While [18] defined it as "an open and comprehensive network of intelligent objects that have the capacity to auto-organize, share information, data and resources, reacting and acting in face of situations and changes in the environment".

Context-aware computing is used to enhance Smart Home Systems. It is concerned with computer systems' ability to collect contextual knowledge to provide better services. Rather than considering mobility as a problem to be solved, context-aware computing attempts to take advantage of its inherent characteristics. A new breed of applications has emerged that increase user-app interaction by seeing/detecting the surrounding environment. Context-aware applications consider both explicit and implicit input. This contextual data is inferred from the application's surroundings. Context-aware applications are defined in terms of their flexibility, adaptability, reactivity, responsiveness, and sensitivity to context. The most prominent definition is defined by Dey et al. In [19], "Context is any information that can be used to

characterize the situation of an entity. An entity is a person, place, or object that is considered relevant to the interaction between a user and an application, including the user and applications themselves". Also [20] defined context as "any continuous/discrete, dynamic/static, fixed/mobile, self-initiated/non-self-initiated, synchronous/asynchronous and volatile/nonvolatile available data that describe or characterize a principal entity. A principal entity may be a person or an object. Each principal entity has a set of elementary, mandatory and unique attributes. A principal entity has an associated one termed complementary entity. A complementary entity describes the principle one and contains any selective, secondary, inferred or profiling attributes. Its aim is to give more insight and details about the principal entity according to the application requirements. This data when captured, triggers specific events or enables interaction/querying with an application at certain time and responds depending on the current context at the time of service/output delivery".

As systems based on IoT need a huge amount of data to be stored, Cloud Computing paradigm is used. There have been many definitions of Cloud Computing by different researchers since it can and does mean different things to different people. The National Institute of Standards and Technology (NIST) defined cloud computing informally as [21]: "a model for enabling ubiquitous, convenient, on-demand network access to a shared pool of configurable computing resources (e.g., networks, servers, storage, applications, and services) that can be rapidly provisioned and released with minimal management effort or service provider interaction" while [22] defined cloud computing as "a paradigm which enables unlearned users as well as well-educated developers to create, develop, customize, migrate, deploy, and/or manage legacy, custom, and/or new applications over the Clouds' infrastructure by providing ease of use tools, programming languages, services and/or hardware resources on the basis of a predefined Service Level Agreement (SLA) with the possibility to reconfigure/change application features explicitly by users or implicitly/dynamically by Cloud providers such as scaling, deployment and/or resource allocation".

Event processing systems react to events in the system's environment or user interface and able to perform operations on events, such as: reading, creating, transforming, and deleting events. These systems examine events or streams of events before taking automated actions. Anything that occurs at a given moment and can be documented is referred to as an event. Pre-defined decision tables or more powerful machine learning algorithms can be used to analyze data, and there are a variety of actions that can be taken, from generating a new event to modifying a customer's experience to scaling cloud resources up or down. The key characteristic of event processing systems is that the circumstance of events is unpredictable and the system must be able to deal with these events when they occur [23]. While event processing is concerned with detecting events from large event clouds or streams in almost real-time, reaction rules are concerned with the invocation of actions in response to events and actionable situations [24].

TABLE I. A COMPARISON OF RELATED SMART HOME SYSTEM ARCHITECTURES AND THE PROPOSED ARCHITECTURE

Paper	Purpose	Technologies	Layers / Components
[5, 2019]	An architecture for integrating classic smart home, IoT, and cloud computing.	IoT, Cloud Computing, and rule-based event processing.	(1) Sensors: not IoT sensors, used to collect internal and external data which transferred via the local network to server. (2) Processors: used to process sensors' data and perform local and integrated actions. (3) APIs: A collection of external software components used to process sensors data or manage actions. (4) Actuators: used to execute commands in the server or other control devices. (5) Database: used to store, analyze, present, and visualize the processed data.
[25, 2019]	An architecture for big data-driven processing and management.	IoT and Cloud Computing.	(1) Physical Layer: includes three types of sensing technologies and devices for health, energy, and security and safety. (2) Fog-computing Layer: includes sensor hubs for simple data processing and computing. (3) Network Layer: includes gateway and communication protocols. (4) Cloud-computing Layer: It is used for extensive processing, computing and for data communication. It includes Data Stream Management System (DSMS), Data Lake, Real-time processing system, and Batch processing system. (5) Service Layer: includes two main types of data views for operational and analytical data. (6) Session Layer: provide standards and APIs to exchange data between services and application layers. The RESTFUL APIs and URL-based communication are used in this layer. (7) Application Layer: includes all the applications which are subscribed to use or exchange data-driven services with such as domestic applications and/or third-parties.
[26, 2019]	An architecture for managing heterogeneous data from third parties.	IoT and Cloud Computing.	(1) Device Layer: includes connected IoT devices such as sensors, actuators, and/or appliances. (2) Gateway Layer: provides the ability to communicate with different smart devices. It also interacts with databases for data storage. (3) Application and Service Layer: provides the main services related to health and energy.
[27, 2021]	An architecture for discovery of resident behavior patterns.	IoT and Machin Learning.	(1) Presentation Layer: provides an interface for users to get access to the system. (2) Security Layer: provides modules; such as authentication module, to ensure secure access to the platform's functions. (3) Control Layer: includes necessary methods/modules; such as user control and automatic control modules, to access connected device's functions. (4) Communication Layer: provides communication between different modules and elements through APIs such as REST. (5) Data Layer: provides data of interest and/or information needed for other modules. It consists of device data, device history, user data, house data, and configuration rules. (6) Devices Layer: includes the communication technology necessary to control and monitor devices such as sensors and IoT devices.
[28, 2021]	An architecture for home integration and automation with security services	IoT	(1) Application Layer: provides services such as health care, security, video monitoring, entertainment, etc. (2) Network Layer: uses internet to transmit information to application level. (3) Sensing Layer: guarantees that data from all connected devices/sensors are transferred to the network layer after processing.
[29, 2021]	An architecture for providing secure and safe environment and reducing energy consumption.	IoT, Cloud Computing, and Edge Computing.	(1) Device Layer: used to integrate sensors into the system to collect data. (2) Broker Layer: used to transmit data and commands from different sensors to the service layer. (3) Service Layer: used to receive data from the broker layer to make one or more of the following features; data management, software management, personal cloud, and data aggregation. (4) Application Layer: used to implement a user-friendly dashboard to manage and control IoT devices. (5) Cloud Layer: used to store home data as a long-term storage for future analysis.
The proposed architecture.	For controlling smart home systems based on context awareness.	IoT, Cloud Computing and Context-awareness.	(1) Data Collection Layer (DCL): used to sense and collect data from various devices. (2) Data Management Layer (DML): used to manage the collected data. (3) Context Formulation Layer (CFL): used to formulate a context based on the collected data, while the fourth one. (4) Service Inference Layer (SIL): used to infer specific activities and tasks according to the formulated context. (5) Service Management Layer (SML): used to save/manage all this data, information, and/or context.

B. Related Architectures

Table I compares among some related Smart Home System architectures done by [5,25,26,27,28,29] and the proposed architecture in terms of purpose, used technologies and consisted layers/components.

III. CONTRIBUTION

A. The Proposed Architecture

As stated in Table I, the proposed architecture composed of five phases achieved by five layers as shown in Fig. 1. The

proposed architecture adds a context-awareness layer; data formulation layer, to formulate meaningful data from small pieces of data collected by sensors/actuators.

The first and second layers belong to IoT, the third layer belongs to context-awareness, while the fourth layer is for Rule-based Event Processing Systems, and the fifth one belongs to Cloud Computing in addition to IoT and context-awareness. All of the architecture layers are discussed as follows:

- **Data Collection Layer (DCL):** This layer is responsible of collecting data from various user devices, sensors, actuators and/or databases (DBs). Smart actuators are devices, such as valves and switches that conduct activities such as turning items. Sensors collect internal and external home data, which is used to measure home conditions and recognize its context. Sensors are linked to both the home and the devices that are connected to it. Users can control the output of smart actuators related with household appliances (Smart Remote), such as lighting and doors, using User Devices (APIs).
- **Data Management Layer (DML):** The main job of this layer is to provide required data to the Context Formulation Layer (CFL) through the Data Acquisition component. All data collected in the DCL is sent across the local network to the smart home server (Data Storage), which stores the processed data collected from sensors and/or cloud services. It will be used for data analysis, data visualization, and data presentation. For future usage, the processed data is saved in the associated database. The Monitor is specifically designed to collect data; context attributes, in the environment by collaborating with some type of sensor equipment, and properly associate it with a context, whilst Listeners allow users to subscribe to changes to specific data.
- **Context Formulation Layer (CFL):** A single sensor, in most circumstances, only gives a fraction of contextual data diversity and is susceptible to several constraints. In order to fully understand and increase benefits of captured data, it must be refined by aggregation, transformation, interpretation, filtering, and splitting. These refinements bridge the gap between the raw sensor output and the level of abstraction required by applications through one of the following operations. Although there is enormous amount of low-level context data, it is suggested to store it for better monitoring and auditing as well as expanding context usage. Context Storage provides a data pool with a history of all contextual data obtained. This history can be used to access entities' prior contexts, deduce their activities, make conclusions about their requests, anticipate future situations, and analyze sensor performance. Based on [11], context main operations and their usage are described in Table II.
- **Service Inference Layer (SIL):** The Service Inference Layer's (SIL) responsibility is to infer appropriate context services which are related to the formulated context given by previous layer and/or any acquired/reasoned context. The inference process is based on Access Control for security reasons. Context Services are controlled by the Access Control component, which ensures that client requests are authenticated correctly. The access control list, which specifies what the requesting clients can access, and the means for authenticating the client, are the two main aspects of this component.

- **Service Management Layer (SML):** The management of any component included in this architecture is done by this layer. The Data/Context/Service Management is for managing any process related to data, context, and/or services such as context formulation/acquisition, service inference and/or storing data/context while the Device/Sensor Management responsibility is to manage devices/sensors such as attach/reattach them to the Smart Home System. The Communication management component is responsible of managing protocols, technologies, and/or tools needed for the communication process. Also, this layer is responsible of the management of Data/Context Storage, Context Services and/or the Cloud.

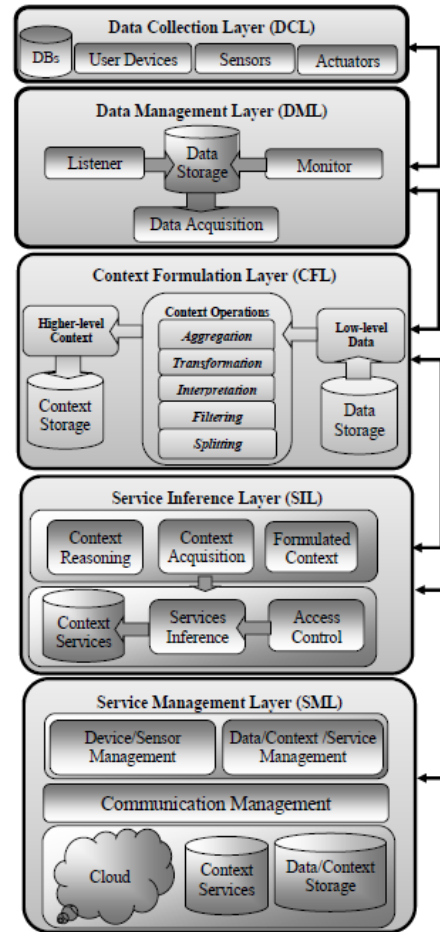


Fig. 1. The Proposed Architecture.

TABLE II. CONTEXT OPERATIONS

Operation	Usage
Aggregation	To construct a higher-level context from a variety of logically connected context data collected from various sensors.
Transformation	To convert context data into an appropriate format.
Interpretation	For reusability, the same attributes may be interpreted differently in different contexts.
Filtering	To select an appropriate context by filtering in different context data values.
Splitting	To extract the sensed attribute according to the needed data/format. E.g., extract hours from timestamp.

B. Mapping the Proposed Architecture

In this section, an implemented Smart Home system (SHS) is build based on the proposed architecture, as shown in Fig. 2, SHS consists of eight main components which are described in the following Table III.

C. Applying the Proposed Architecture

The proposed architecture was applied to implement a Smart Home System using the following hardware: (1) Arduino Uno microcontroller board, (2) ESP32 chip microcontroller with integrated Wi-Fi and dual-mode Bluetooth, and (3) Sensors & Actuators such as: (Solenoid Valve, 4x4 keypad, R305 Optical Fingerprint Scanner Sensor, FC-28 Soil moisture Sensor, rain sensor, photoresistor sensor, PIR sensor, DHT11 Sensor, and MQ2 gas sensor), while the software needed for implementation is as the following: (1) Arduino Integrated Development Environment (IDE). Code is written in C++ with an addition of special methods and functions. (2) IFTTT Driver, which is a software platform that links multiple developers' applications, devices, and services in order to trigger one or more automations involving those applications, devices, and services. (3) MQTT, which is an "IoT" connectivity protocol. It was created to be a very light weight publish/subscribe messaging service. (4) an account on the Ubidots cloud by which events are sent, triggered, and brought via Email, SMS, Telegrams, or Voice Call based on a customized design rule created in the application.

A SHS complete scenario may be detailed as: (1) The owner enters the smart home by inputting his/her password on

the keypad or finger on the fingerprint sensor. The door will open in case of a known owner, otherwise an alarm will be fired, and a message will be sent to the owner if three tries to open the door are failed. (2) When the owner enters the house, his/her motion will be detected by the motion detection sensor. The light will be automatically turned on. It will be opened and closed using Google assistant or Ubidots cloud. In the night, lights out-of-doors will be turned on based on signals got from the photoresistor sensor. (3) If the temperature sensor detects temperature increase to a certain degree and the motion detection sensor detects that there is a movement in the room, the air conditioner will be opened and a message to inform the owner will be sent. (4) When the soil sensor detects that the quantity of water in soil decreases, the solenoid valve of water will be opened until the value of sensor will be increasing and a message will be sent to owner to monitor the condition of soil through the cloud. (5) When the rain sensor detects that it's raining, a message will be sent to the owner that rains fall outside. (6) If the gas sensor detects a gas leak, an alarm will be fired, and a message will be sent to the owner. (7) If someone asked to open the garage door, the Infrared obstacle avoidance sensor module detects there is a car inside the garage or not. The door will be opened using Google assistant if there is no car inside.

When any specific activity occurs, SHS gets to work. Table IV, shows some defined activities and related actions inferred according to those activities.

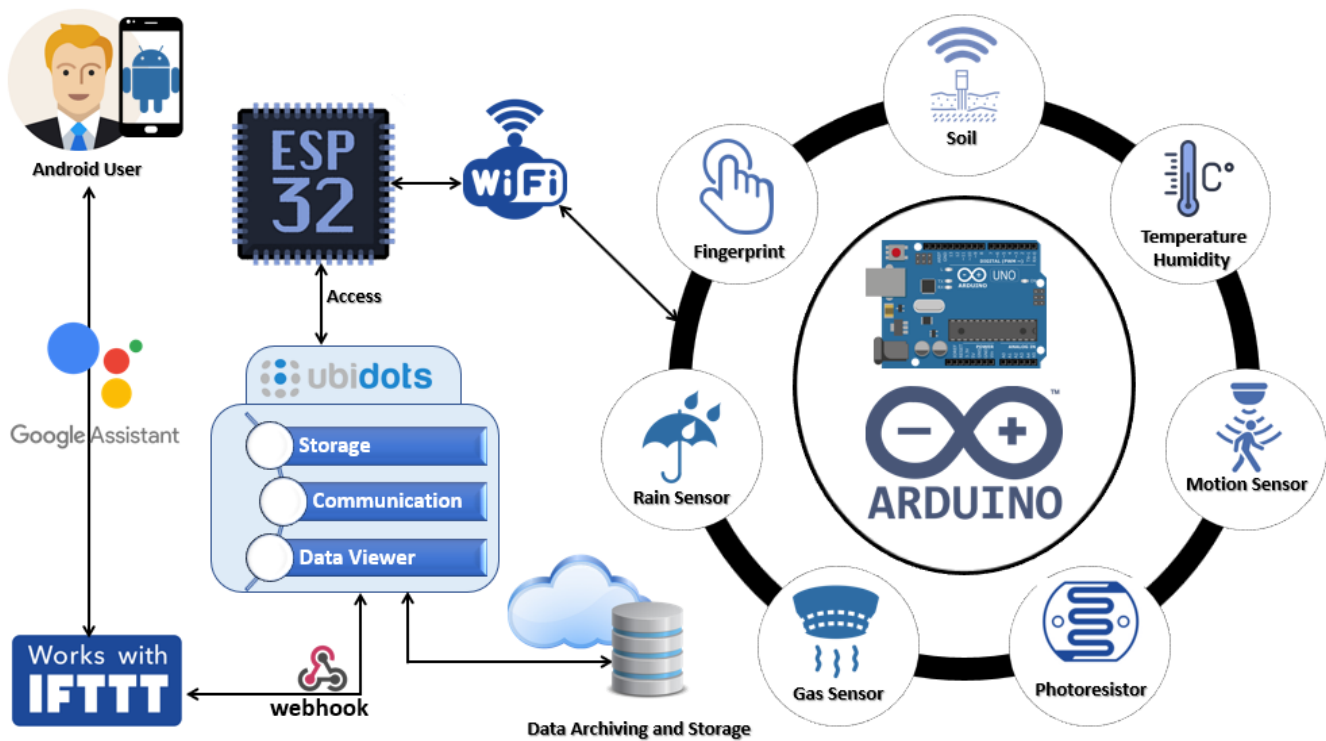


Fig. 2. The Implemented Smart Home System (SHS).

TABLE III. THE PROPOSED ARCHITECTURE MAIN COMPONENTS

Component	Description	Usage
User Device	Allows users to regulate the outputs of smart actuators connected to home appliances (Smart Remote) mobile phone.	Control the connected home devices from smart home app (IFTTT).
Home/Residential Gateway	Permits a small network, known as a Local Area Network (LAN), to be connected to a larger network, known as a Wide Area Network (WAN).	It connects home elements with the Internet via Wi-Fi.
ESP32	The ESP32 is a family of low-cost, low-power system-on-a-chip microcontroller that incorporate implicit Wi-Fi and dual-mode Bluetooth.	The principal usage of this board is dealing with all communication, sensor readings, and outputs.
Ubidots	Ubidots is an Internet of Things (IoT) data analytics and visualization company. It keeps dots from devices into variables, and these dots have timestamps associated with them. A "dot" or a data-point is framed each time a gadget refreshes a sensor esteem in a variable. The following items are found in each dot: - Value: A numerical value. Ubidots takes values of up to 16 floating-point in length. - Timestamp: Unix Epoch time, in milliseconds. If not determined, then servers will assign one upon reception. - Context: A set of unlimited arrangement key-value pairs with no restrictions. Latitude and longitude coordinates of GPS devices.	It is the cloud by which the computing and storage takes place on servers in a data center, instead of locally on the user device. It enables users to access files and applications from almost any device. So, users can control their home anywhere. Sensor data is transformed into useful information for corporate choices, machine-to-machine interactions, educational research, and increased global resource economization.
IFTTT	Stands for "If This Then That", known as IFTTT is a freeware web-based service that builds applets, which are chains of basic conditional statements.	IFTTT helps connecting different applications and devices, manage them from Google assistant in phone.
Database	A repository for storing data collected from sensors and/or cloud services that has been processed.	Utilized for data processing, data visualization, and data display for future usage.
Google Assistant	This service works with Google Home or Pixel devices. It's incredibly flexible.	Used to create custom voice commands for home control, send updates, and more.
Webhooks	Webhooks are the way by which apps can send automated messages or information to other apps when something happens.	Used for speaking between online accounts and receiving automatic notifications when something new occurs. It is used to send data from one application to another automatically.
Sensors / Actuators	Collect data from both inside and outside the home. They are connected to the home and to the gadgets that are connected to the home	Used to capture data and send it to the smart home server on a regular basis across the local network.
- Fingerprint	It is one of the most secure methods for detecting and identifying authorized persons.	Used to make pretty sure about security needs.
- Soil Sensor	Determine the volumetric water content in soil.	It aids home owners Knowing their gardens' specific soil moisture conditions for helping them better managing their irrigation systems.
- Temperature/humidity	Measures the temperature/humidity and converts input data into electronic format for recording/monitoring.	This sensor may simply be connected to any microcontroller, such as an Arduino or a Raspberry Pi, to measure temperature and humidity in real time.
- Motion	Designed to detect and measure movement.	Used to detect the movement of home owners to perform highly specific functions.
- Photoresistor	Light sensitive resistors most often used to indicate the presence or absence of light, or to measure the light intensity.	Utilized when it is required to detect the presence and absence of light or measure the light intensity.
- Gas Sensor	The gas sensor is an electrical device that detects the presence of gas in the atmosphere.	Utilized to detect the presence of gases such as LPG, propane, methane, hydrogen, alcohol, smoke, and carbon monoxide in the air.
- Keypad	A keypad is a set of buttons arranged in a block or "pad" which bear digits, symbols, or alphabetical letters. Pads mainly include numbers are called a numeric keypad.	Used for the entry of PINs including Point of Sale payment devices, ATMs, vending machines, combination locks and digital door locks.
- Rain sensor	The rain sensor module is a simple tool for detecting rain. It is a rain-activated switching gadget.	When a raindrop falls through the rainy board, it can be used as a switch, as well as for gauging rainfall intensity. Rain sensors have two primary applications: (1) is a water-saving device that is attached to an automatic irrigation system and causes the system to shut down if it rains. (2) is a device that protects the interior of a car from rain and allows windscreen wipers to operate in automated mode.

TABLE IV SHS MAIN ACTIVITIES AND ACTIONS

Service	Activity	Initialization	Sensor/Device	Input	Processing	Output/Action	
Smart Lighting system	Inside home.	Owner enters the home.	Owner movement.	A passive infrared sensor (PIR).	Signal from the motion detection sensor.	The system detects there is a movement.	The light automatically turns on. It will be opened and closed using Google assistant or Ubidots cloud.
	Outside home.		Sun set.	Photoresistor sensor.	Signal from the photoresistor sensor.	The system detects that it is night.	Lights out-of-doors will be turned on only in the night.
Smart Security system	Fingerprint	A person puts his/her finger on the fingerprint sensor.	Detecting finger on fingerprint sensor.	Fingerprint sensor.	Person fingerprint.	The system compares between this fingerprint and enrolled fingerprints; then sends a signal to door lock and alarm.	1) If the fingerprint/password is known: the door will open. 2) If a wrong fingerprint/password was entered three times: turn alarm on and send owner a message that there was an attack.
	Keypad	A person enters his/her password.	Entered password in the keypad.	keypad 4*4 standard device.	The entered password.	The system compares between the entered password and saved ones, then sends a signal to door lock and alarm.	
Smart watering system.	No or less water in soil.	The quantity of water soil decreases.	FC-28 Soil moisture sensor.	The value of soil sensor.	Solenoid valve of water opens.	The solenoid valve of water will be opened until the value of sensor increases. A message to owner will be sent to monitor the conditions of soil through the cloud.	
Smart Rain system	Rain drops fall on the sensor.	The rain drop fall.	Rain sensor.	The value of the rain sensor.	The sensor detects that it's raining.	A message will be sent to the owner that it's raining. Store that in the database weather session.	
Smart Temperature	A certain temperature degree has reached and there is a movement.	The temperature degree increases	DHT11 Precision humidity & temperature.	Temperature degree and movement in the room.	Temperature will adjust by opening air conditioner.	Temperature will adjust by opening air conditioner and a message was sent to inform the owner.	
Smart Gas system	A gas leak is detected by the gas sensor.	There is a gas leak in the home.	MQ2 smoke, gas, liquid-field module.	The gas sensor's value.	The gas sensor detects the leak and alerts the alarm system.	The owner will receive an alert message, and the alarm is fired. Data is stored in the database.	
Smart Garage door	Detecting car in the garage.	A person asked to open the garage door.	Infrared obstacle avoidance sensor module.	Number of cars inside.	Detect if there is car inside or not and send a signal to door lock.	Unlock the garage door if there's no care inside using Google assistant.	

IV. CONCLUSION

Smart homes are large systems that comprise a variety of technologies and applications that can be utilized to provide home protection and control. They have wireless communications, sensors, monitors, and tracking connections.

An efficient technique for smart home systems was presented and implemented in this paper. The proposed architecture shows how to combine benefit features from IoT, Context-Awareness, Cloud Computing and Rule-based event processing systems paradigms to facilitate the building of Smart Home systems in a more systematic manner.

The implemented system has been subjected to a range of tests and experiments. These experiments demonstrate the concept of employing ultrasonic sensors to create a house navigator that can measure and control temperature in all rooms, detect any fires, water leaks, smoke, and/or detect any motion in the home. Furthermore, these experiments demonstrate how to observe and track the home by sending

messages to the owner about actions that have occurred, as well as how to secure it using an access code.

Three microcontroller system designs were used to create a central control system for the entire house. These designs were for home access control, temperature validation, and a control board system that would connect all of the security and control circuits.

V. FUTURE WORK

Regarding the proof-of-concept system developed by this work, it is understood that it provides a subset of a fully functional smart home system. Therefore, the first recommendation would be to develop and implement other areas. Additionally, future work should also include the implementation of the core as a web service and the development of a web-based user interface to accommodate heterogeneous web-based clients.

There are several improvements that might be made to the existing system to improve sensing and detection accuracy. There are also a variety of different sensors that can be utilized to improve the security and control of the home.

REFERENCES

- [1] Angel Gabriel Meela, "Design Of An Energy Efficient System For Smart Home", Msc. In IoT, College of Science and Technology, Rawanda university, REF.NO: 219011247, 2020.
- [2] Yordan Hasan, Abdurrahman, Yudi Wijanarko, Selamat Muslimin, and Renny Maulidda, "The Automatic Door Lock to Enhance Security in RFID System", Journal of Physics: Conference Series. 1500, 2020.
- [3] Dimas Budianto, Siti Nurmaini, Bambang Tutuko, and Sarifah Raflesia, "Real-Time Lighting Control System for Smart Home Applications", Computer Engineering and Applications Journal, Volume 7, 2018.
- [4] Benjamin K. Sovacool and Dylan D. Furszyfer Del Rio, "Smart home technologies in Europe: A critical review of concepts, benefits, risks and policies", Renewable and Sustainable Energy Reviews, Volume 148, 2021.
- [5] Menachem Domb, "Smart Home Systems Based on Internet of Things". Internet of Things (IoT) for Automated and Smart Applications, IntechOpen, 2019.
- [6] Scott Davidoff, Min Kyung Lee, Charles Yiu, John Zimmerman, and Anind K. Dey, "Principles of Smart Home Control", 8th International Conference, UbiComp, pp 19-34, 2006.
- [7] Bata K. Tripathy, Swagat K. Jena, Vineeth Reddy, Satyabrata Das, and Sanjaya K. Panda, "A novel communication framework between MANET and WSN in IoT based smart environment", International Journal of Information Technology, 13, pp. 921-931, 2021.
- [8] Azeddine Khiat, Ayoub Bahnasse, Jamila Bakkoury, Mohamed El Khaïli, and Fatima Ezzahraa Louhab, "New approach based internet of things for a clean atmosphere", International Journal of Information Technology, 11, pp. 89-95, 2019.
- [9] Timothy Malche and Priti Maheshwary, "Internet of Things (IoT) for building Smart Home Systems", International conference on I-SMAC (IoT in Social, Mobile, Analytics and Cloud), 2017.
- [10] Ahmed S. Salama and Ahmed M. Eassa, "IoT and Cloud based Blockchain Model for Covid-19 Infection Spread Control", Journal of Theoretical and Applied Information Technology, Little Lion Scientific, Volume 100, pp. 113-126, 2022.
- [11] Bin Guo, "An Ontology-based Programming Platform for Smart Artifact Systems", Ph.D dissertation, Keio University, 2009.
- [12] N. A. Ali, A.R. Syafeeza, A. S. Ja'afar, Norihan Abdul Hamid, and Ts Saleha binti Mohamad Saleh, "Home automation monitoring system based on Internet-of-Things application", Journal of Physics: Conference Series, International Conference on Telecommunication, Electronic and Computer Engineering, Volume 1502, 2020.
- [13] Péter Zsolt and Dániel Orosz, "Characteristics of Smart Home Systems, Directions and Development of the Domestic and International Markets", Miskolc university, 2018.
- [14] Aleksandar Georgiev and Stephan Schlögl, "Smart Home Technology: An Exploration of End User Perceptions", Smarter Lives, pp. 64-78, 2018.
- [15] A.Pavithra, C.Anandhakumar, and V.Nithin Meenashisundharam, "Internet of Things with BIG DATA Analytics – A Survey", International Journal of Scientific Research in Computer Science Applications and Management Studies, Volume 8, Issue 1, ISSN 2319 – 1953, 2019.
- [16] Keyur K Patel and Sunil M Patel, "Internet of Things-IOT: Definition, Characteristics, Architecture, Enabling Technologies, Application & Future Challenges", International Journal of Engineering Science and Computing (IJESC), Volume 6 Issue No. 5, 2016.
- [17] B. Dorsemaine, J. Gaulier, J. Wary, N. Kheir, and P. Urien, "Internet of Things: a definition & taxonomy", 9th International Conference on Next Generation Mobile Applications, Services and Technologies, pp. 72-77, 2015.
- [18] Somayya Madakam, R. Ramaswamy, and Siddharth Tripathi, "Internet of Things (IoT): A Literature Review, Journal of Computers and Communications, 3, pp. 164-173, 2015.
- [19] Gregory D. Abowd, Anind K. Dey, Peter J. Brown, Nigel Davies, Mark Smith, and Pete Steggles, "Towards a Better Understanding of Context and Context-Awareness", Georgia Institute of Technology, Atlanta, GA, USA 30332-0280, 1999.
- [20] Yehua Helmy, Maha Attia Hana, and Samah Zaki, "A Roadmap Towards Context Aware Applications", International journal of Intelligent Computing and information science (IJICIS), Volume 9, No.2, 2009.
- [21] Peter M. Mell and Timothy Grance, "The NIST Definition of Cloud Computing", National Institute of Standards and Technology Special Publication (NIST), Special Publication 800-145, Gaithersburg, MD 20899-8930, 2011.
- [22] Samah Ahmed Zaki Hassan, "SONA: A Service Oriented Nodes Architecture For Developing Cloud Computing Applications", International Conference on Advanced Computing and Communication Systems (ICACCS -2013), Coimbatore, India, pp. 1-6, 2013.
- [23] Opher Etzion and Peter Niblett, "Event Processing in Action", ISBN: 9781935182214, 2011.
- [24] Adrian Paschke and Alexander Kozlenkov, "Rule-based Event Processing and Reaction Rules", Springer-Verlag Berlin, Heidelberg, pp.53-66, 2009.
- [25] Ghassem Mokhtari, Amjad Anvari-Moghaddam, and Qing Zhang, "A New Layered Architecture for Future Big Data-driven Smart Homes", IEEE Access, Volume 7, pp.19002-19012, 2019.
- [26] Saad EL Jaouhari, Emilio Jose Palacios-Garcia, Amjad Anvari-Moghaddam, and Ahmed Bouabdallah, "Integrated Management of Energy, Wellbeing and Health in the Next Generation of Smart Homes", Sensors (Basel), Volume 19, 2019.
- [27] Josimar Reyes-Campos, Giner Alor-Hernández, Isaac Machorro-Cano, José Oscar Olmedo-Aguirre, José Luis Sánchez-Cervantes and Lisbeth Rodríguez-Mazahua, "Discovery of Resident Behavior Patterns Using Machine Learning Techniques and IoT Paradigm", Mathematics, Volume 9, Issue 3, 2021.
- [28] J. Deepika and J. Gokulraj, "Internet of Things Device Enabled Smart Home Integrated Architecture with Security Services", Turkish Journal of Computer and Mathematics Education, Volume 12, No.6, pp.2614-2623, 2021.
- [29] Hikmat Yar, Ali Shariq Imran, Zulfiqar Ahmad Khan, Muhammad Sajjad, and Zenun Kastrati, "Towards Smart Home Automation Using IoT-Enabled Edge-Computing Paradigm", Sensors (Basel), Volume 21, 2021.

Shallow Net for COVID-19 Classification based on Biomarkers

Mahmoud B. Rokaya

Department of Information Technology, Taif University, Taif, Saudi Arabia
Department of Mathematics, Faculty of Science, Tanta University, Tanta, Egypt

Abstract—In many cases, especially at the beginning of epidemic disaster, it is very important to be able to determine the severity of illness of a given patient. Picking up the severe status will help in directing the effort in a proper way. At the beginning, the number of classified status and the available data are limited, so, in such situation, one needs a system that can be trained based on limited data to give a trusted result. The current work focuses on the importance of the bioscience in differentiation between recovered patients and mortalities. Even with limited data, the decision trees (DT) was able to distinguish between recovered patients and mortalities with accuracy of 94%. Shallow dense network achieved accuracy of 75%. However, when a 10-fold technique was followed with the same data, the net achieved 99% of accuracy. The used data in this work was collected from King Faisal hospital in Taif city under a formal permission from the health ministry. PCA analysis confirmed that there are two parameters that have the greatest ability to differentiate between recovered patients and mortalities. ROC curve reveals that the parameters that can differentiate between recovered patients and mortalities are calcium and hemoglobin. The shallow net gives an accuracy of 92% when trained using calcium and hemoglobin only. This paper shows that with a suitable choosing of the parameters a small decision tree or shallow net can be trained quickly to decide which patient needs more attention so as to use the hospitals resources in a more reasonable way during the pandemic. All codes and data can be accessed from the following link “codes and data”.

Keywords—COVID-19; pandemic; shallow net; deep learning; decision trees; ROC curve; PCA analysis; biomarkers

I. INTRODUCTION

During the early days of any pandemic, it is very important to provide a quick and cheap tool to detect infected people [1]. Also, it is very important to provide a tool to differentiate between the degrees of infection [2]. Moderate infections can be treated at home [4] but severe cases need to be under intensive care [3]. Intensive care needs huge resources that might not be available especially in areas that suffer from the low quality of health services [5]. Also, providing a service to differentiate between moderate cases and intensive cases should be with low cost for developing and especially for use [6].

This work will explore developing a cheap tool based on few data that can be collected at the early days of the pandemic. COVID-19 is an example of pandemic related to respiratory system but affects all body systems [7].

Many studies concentrated on detecting and clustering the cases based on images of lungs [8, 9, 10, 11]. Few papers give

some interest to the levels of essential body parameters like hemoglobin, vitamins, and mineral levels as a tool to differentiate between categories of severe and light infections [2, 12, 13]. Most of these papers consider only one aspect to analyze and use as a tool of detection. Few papers discussed or proposed an intelligent tool to classify the infection degree [2, 14, 15]. No work discussed the computation cost of such tools and its validity to be applied in poor areas where health services might not be available.

In this work, the proposed solution can be applied based on the available resources, (Resources here means the availability of data and the availability of computing resources). Decision trees can be used in the case of availability of few cases with a good number of parameters, but it needs a suitable computing resource to be distributed over cloud or edge environments [16]. Another alternative is the shallow nets. Shallow nets do not need a big number of parameters and in many cases, it can achieve an accepted accuracy [17]. Based on experienced works in the pandemic domain, a suitable and limited number of parameters can be proposed to be used as the classification parameters. Providing such limited number of parameters might be expensive and cannot be provided in a suitable time [18]. So, getting a good sample of complete data to be analyzed using “reduction dimensionality tools” will help to reduce the number of parameters [19].

In this work, PCA and ROC curves will be used to determine the most important parameters. Also, the work will check the validity of training a shallow net on these limited set of parameters. The results ensure that training a shallow net on carefully reduced set of parameters will produce a light model that can differentiate between the patients’ classes with a high suitable accuracy.

The remaining of this paper will continue as follows. Section II provides information regarding related works. The methods are explored in Section III. Detailed experiments and results are explored in Section IV. Finally, the whole paper is concluded in Section V.

II. RELATED WORK

This part will explore studies made to detect COVID-19 using AI approaches and different studies based on the type of data. Some studies depended on X-Ray images, then studies that use a mix of X-Rays and other symptoms. Also, it will explore studies that either used an AI for purpose different from detecting COVID-19 or used a different type of data.

Finally, studies that tried to review works related to AI and COVID-19 will be reviewed.

Based on images for X-Rays, some papers proposed a method to predict and detect COVID-19. For example, Qayyum et al. proposed a new depth-wise dense network to compete the ordinary convolutional layers in detecting COVID-19 based on analyzing image of lungs x-rays for suspected cases [7]. Sharma et al. proposed a deep learning model for quick identification of COVID-19 infected patients based on chest X-ray images. They implemented a variety of methods for data augmentations [8]. Jin et al. proposed a deep convolutional neural network for quick COVID-19 detection [9]. Vaid et al. developed a deep learning model that consists mainly of convolutional neural networks to improve the accuracy of detecting and predicting COVID-19 cases based on chest X-ray scans [10]. Based on Chest CT, Harmon et al. applied a series of deep learning algorithms to classify patients with COVID-19 [11].

Since the X-Rays images do not provide a quick tool to detect COVID-19 early enough, some works tried to combine X-Rays images with additional data in one model for more efficient system. For example, Ming et al. developed a method to separate between patients with COVID-19 and healthy individuals depending on clinical and laboratory testing data and imagining data. They developed a deep learning model for feature extraction then fed these data to three machine learning models for the classification process [2]. Attaullah et al. proposed a method that depends on X-Rays images and labeled patients' symptoms for early detection of COVID-19. All features are fed to a deep learning model that can benefit from the characteristics of patients' symptoms in early detection of COVID-19 and X-rays images that can define the type of infection [12]. Depending on a combination of chest CT and clinical symptoms, exposure history and laboratory testing, Mei et al proposed an AI algorithm for quick and accurate diagnosis of cases with COVID-19.[13]. Mario et al. proposed a machine learning method to detect risk COVID-19. They used historical data that include medical history, demographic data, as well as COVID-19-related information. The aim of their work is to differentiate between recovered patients and mortalities [14].

Some works tried to explore problems other than detecting or classifying COVID-19 patients. Also, some works implemented non-ordinary data for classifying or detecting COVID-19 patients. For example, JAMSHIDI et al. proposed intelligent framework to help physicians and researchers in detecting and treating COVID-19. The framework depends on unstructured and structured data that are fed to three types of deep learning net to implement each different data type [20]. Laguarda et al. proposed a method that depends on Cough Recordings only. Based on cough recordings of biomarkers can be extracted and used to monitor the patient in real time mode to detect COVID-19 in low cost [21]. Nawaz et al. used artificial intelligence methods to analyze hidden pattern in COVID-19 genome and then used these patterns to evaluate the ability of predicting nucleotide base(s) from historical data. Also, they used AI to analyze the mutation possibilities in the structure of COVID-19 genome [22]. Based on patients' self-reported symptoms, Obeid et al. proposed convolutional neural

network for predicting COVID-19. The algorithm was fed by unstructured patient data collected through telehealth visits to predict COVID-19 possible infection [23].

Since there are a plenty of works related to AI and COVID-19, many works presented a review for these works to define the main trends in these works and try to define the main factors that direct these studies and affect their results. For example, Ahmad et al. compared between methods for predication COVID-19 depending on decision tree properties, the method can predict COVID-19 cases although there is imbalance in data availability [24]. Vaishya et al. reviewed possible application of AI in COVID-19. The study aimed to define the important application and their possible usages in the future to deal with pandemic like COVID-19 more effectively. The study results show that there is a proper application for screening, analyzing, prediction and tracking of current patients and future patients [25]. Shi et al. focused on reviewing works done during COVID-19 pandemic focusing on the integration of AI with X-ray and CT. They reported COVID-19 research works in enhancing the available technologies in the field of image acquisition scanning and image protection methods. Some works provide means to increase the accuracy of segmentation diagnosis, and follow-up methods [26]. Swapnarekha et al. reviewed methods proposed on decision trees, SVM and neural networks as well as statistical and mathematical models for COVID-19 detection. The work analyzed the factors that affect the efficiency of the classification method like the classification method and the impact of COVID-19 on the nature of data. Also, they discussed important research directions on COVID-19 research [27]. Ilyas et al reviewed many works that tried to classify patients with COVID-19 based on chest x-rays. Basically, all studies tried to develop a method for automatic detection of COVID-19. Varieties of deep learning models were built to overcome the difficulty to decide if the pneumonia was caused by COVID-19 or another cause [28]. Albahri et al. performed a study to review the proper AI studies in the field of detecting and predicting COVID-19 infections. The study tried to propose a systematic model to evaluate AI techniques for COVID-19. The work revealed the importance of combining between multi approach in the classification process [29]. Murphy et al. evaluated AI system for detection of COVID-19 based on chest X-Raya images. Six experts evaluated each testing image and their evaluation compared to the results of the AI system. AI system could outperform the experts and achieved an area 0.8 under ROC curve [30]. Piccialli et al. discussed the role of AI in facing COVID-19 pandemic. The work shows that AI alone cannot be enough without human clinical skills to detect or predict COVID-19. However, AI approved that it could play a significant role in health emergency and complex scenario of such pandemic. [31].

Recently, algorithms based on the intelligent behavior of animals and insects have been adopted in research and classification methods, such as the behavior of bees in swarm optimization techniques for medical diseases detection [32, 33], which aims to predict and classify diseases.

Also, depending on the characteristics of cooperative birds, hawks, methods for searching for preys by field detection have been developed [34]. The bat's radar feature was also relied

upon to develop research methods that depend on the concept of echo as a basis for the research process [35].

Despite huge amount of works presented to tackle the COVID-19 pandemic, few works concentrated on studying the importance of reasonable use of resources in hospitals especially in poor areas in the world. This work presents a cheap and quick approach that can be built quickly on a well-chosen data set to develop a light model that consumes a little computation power and less data to differentiate between severe and light cases during pandemic. The proposed model enables the decision-maker stationed in the place of receiving infected cases to identify severely infected cases that need intensive care inside the hospital from those that can be sent home to complete treatment safely.

III. METHOD

Fig. 1 explains the steps followed in this work. A shallow net consists of three dense layers was used to classify a number of samples. Also, a decision tree was built for the same purpose. The results reflect a huge gap between the accuracy of decision tree and shallow net. A cleaning and investigation process based on PCA and ROC curve determine which parameters have the main role in discrimination between recovered patients and mortalities. The shallow net was retrained using the principal components to show that a shallow net with suitable and carefully chosen parameters can

help effectively to separate early between patients who have light conditions and can easily recover with normal care and the severe patients' instances who need a special care.

A sample of 1000 recovered patients and 900 mortalities during 2020 from the records of patients in King Faisal hospital was retrieved to distill the data related to COVID-19. 53 parameters were collected according to data availability and doctors' recommendation for analysis. These data include information related to age, nationality, gender, blood analysis, minerals and vitamins levels. The main hypothesis in this study is to be able to differentiate between recover patients and mortalities based on a few numbers of samples. Also, with the aid of principal component analysis (PCA) and Receiver Operating Characteristic (ROC) curve a simple weak learner can be built to differentiate between recovered patients and mortalities. To this end a shallow net was designed as appears in Fig. 1. Also, a decision tree was built to support the shallow net. The decision tree was trained using only 10% of data to explore the validity of the data to be used in the case of availability of few samples especially in the beginning of the pandemic and the number of levels was tuned to be three.

All codes were written using python 3.10; however, ROC curve was implemented using SPSS. A specific code was written for the decision tree, PCA and the shallow net. All codes were run on a machine "11th Gen Intel(R) Core (TM) i7-1165G7 @ 2.80GHz 2.80 GHz" and 16.0 GB for RAM.

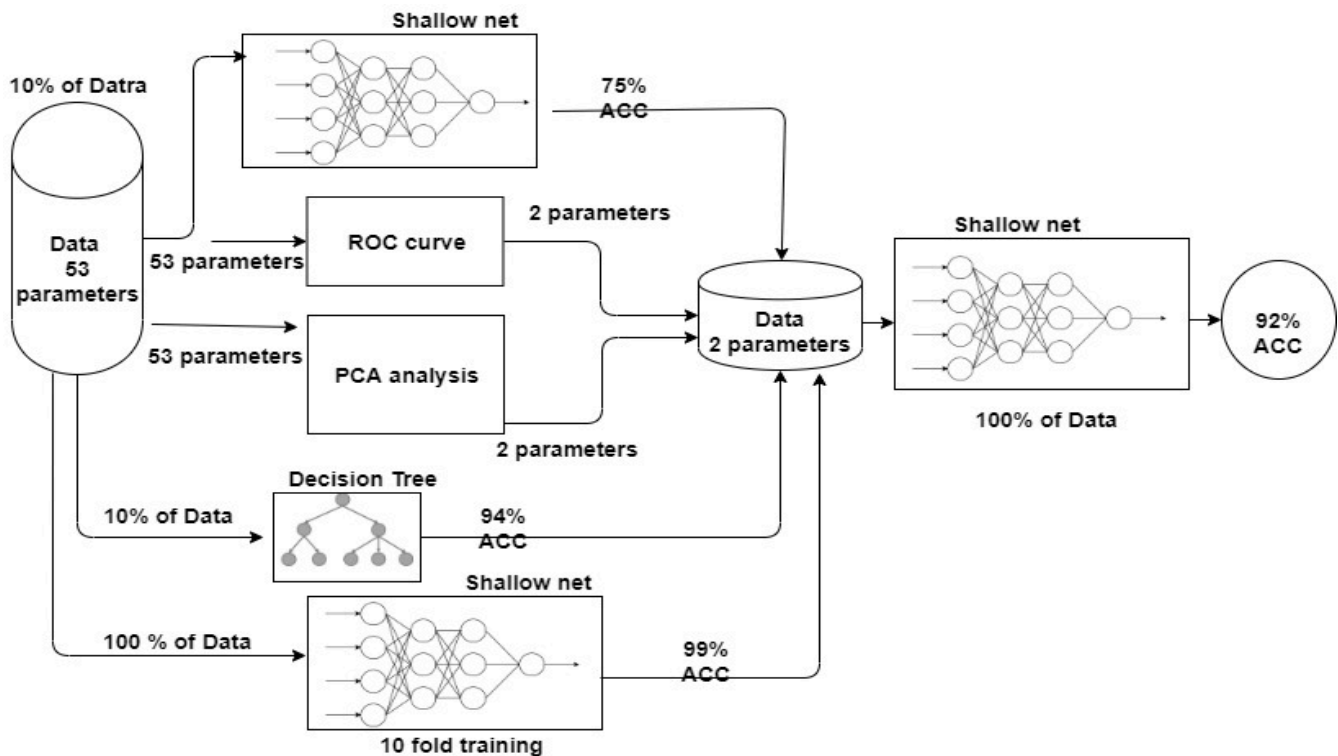


Fig. 1. Method Steps and Stages.

IV. RESULT AND DISCUSSION

The 53 parameters are divided into sets. Demographic parameters include (sex, age and nationality), vitamin sets, minerals set, extra. ROC curve was produced for each group and any parameter with area curve under the reference line was excluded. This gradual process leads to filter all the 53 parameters into two parameters, namely, calcium and hemoglobin (HEMO).

Table I says that hemoglobin and Calcium has at least one tie between the positive actual state group and the negative actual state group. Also, the area under the curve of calcium is 0.963 and the area under the curve of hemoglobin is 0.938. This means that both calcium and hemoglobin have a high ability to discriminate between recovered patients and mortalities with Bayes to the calcium ability.

Fig. 2 shows the structure of the used shallow nets used in the experiments. The first net used the whole 53 parameters as inputs while the next net used only two parameters. Fig. 3 represents final ROC curve. ROC curve expects that based on only two parameters; the shallow net can achieve a complete performance using the whole parameters. This assumption has been proved in the following sections.

A piece of code was written using python 3.10 to perform the PCA analysis to explore the nature of the data classes and determine the number of principal components. Fig. 4 gives the simulated graph of PCA results. The results ensure that there is a separable two classes and the fact that there are two principal components. This ensures the conclusion that was expected in Fig. 2 through gradual manual reduction of parameters using ROC curve. A 10% of the shuffled data using NumPy shuffle function was kept for training a decision tree and a shallow dense net. The decision was tuned to three levels. The final accuracy of the decision tree is 94% on test data. This result was expected since it is known that decision tree gives the optimal results if it is used with separable classes as given based on the PCA analysis. The shallow dense net failed to give a near result. Fig. 5 gives a comparison between the decision tree and the shallow dense net based on 10% of Data.

Shallow net using 53 parameters			Shallow net using 2 parameters		
Layer (type)	Output Shape	Param #	Layer (type)	Output Shape	Param #
dense_15 (Dense)	(None, 16)	864	dense_3 (Dense)	(None, 16)	160
dense_16 (Dense)	(None, 16)	272	dense_4 (Dense)	(None, 16)	272
dense_17 (Dense)	(None, 1)	17	dense_5 (Dense)	(None, 1)	17
Total params: 1,153			Total params: 449		
Trainable params: 1,153			Trainable params: 449		
Non-trainable params: 0			Non-trainable params: 0		

Fig. 2. Shallow Net Model in the Case of 53 and 2 Parameters.

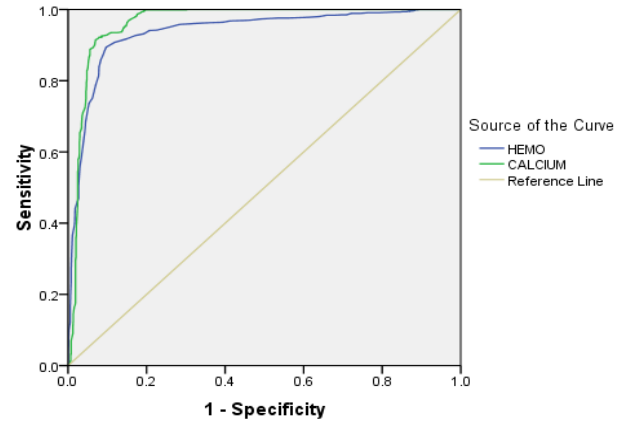


Fig. 3. Final ROC Curve.

TABLE I. AREA UNDER THE CURVE FOR HEMO, CALCIUM

Test Result Variable(s)	Area	Std. Error ^a	Asymptotic Sig. ^b	Asymptotic 95% Confidence Interval	
				Lower Bound	Upper Bound
HEMO	.938	.006	.000	.927	.949
CALCIUM	.963	.005	.000	.953	.972

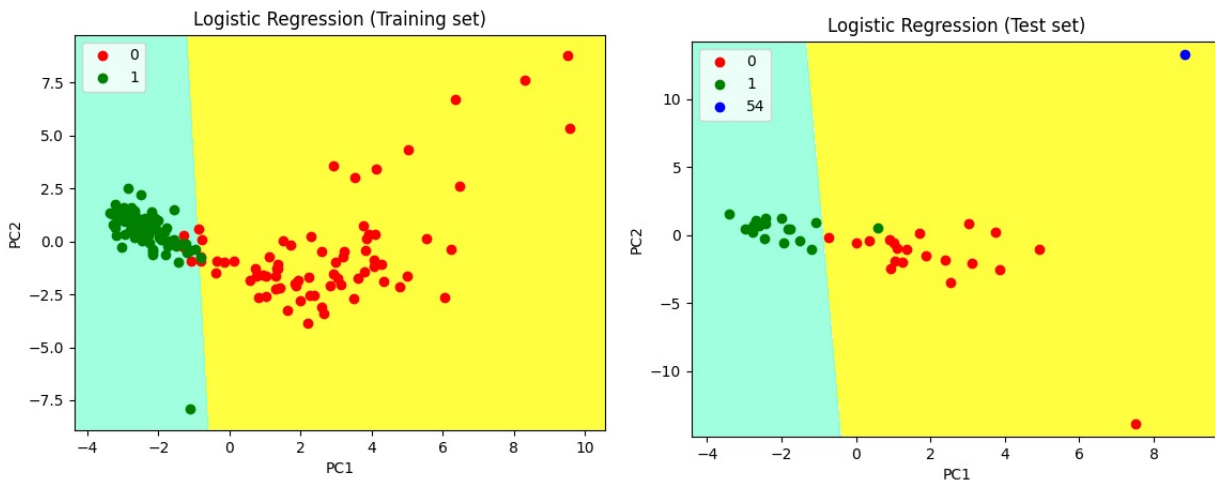


Fig. 4. PCA Results.

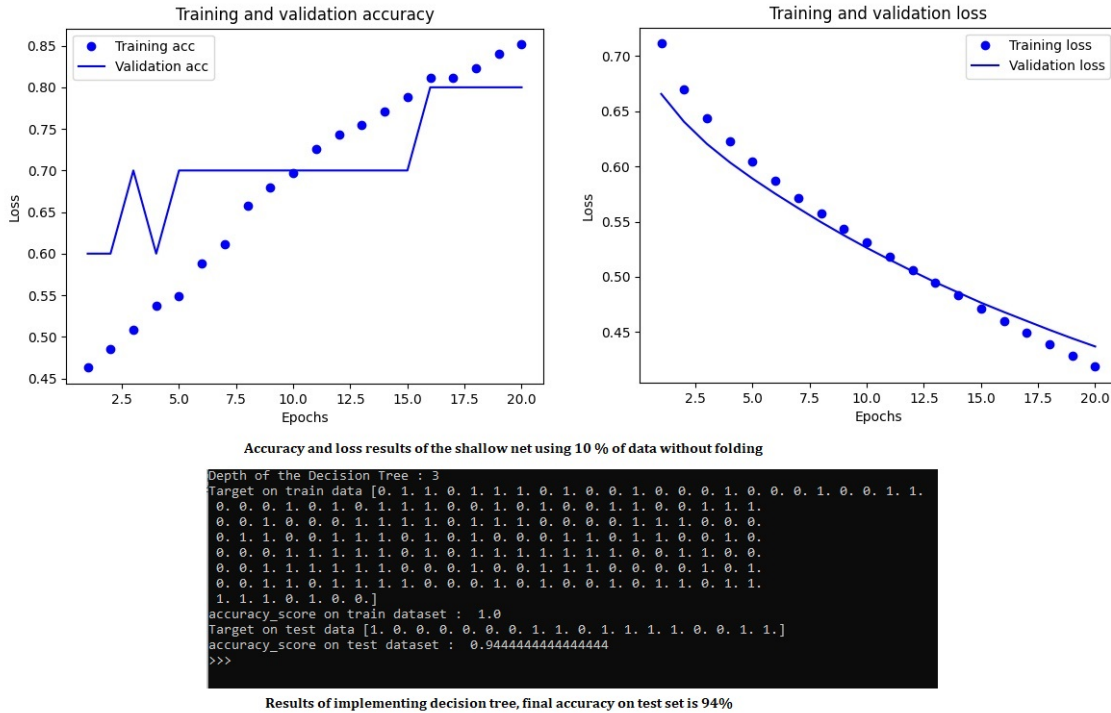


Fig. 5. Implementation of Decision Tree and Shallow Net using 10% of Data.

The whole data was divided into 10 % for final testing and 90% for training. Using 90% of the data, a 10-fold training for the shallow net was done. In each fold the training data were divided into 10 % for validating and 90 % for training as appear in Fig. 6. Then re-trained the resulting model using the whole training data (90 % of the whole data). Following this technique, a 99% of accuracy was achieved. Fig. 7 shows the loss and accuracy when applying 10-fold method. Usually during the early pandemic days, it is not easy to provide such

huge number of parameters to be tested. The results show that we can get a close result under suitable choosing of the parameters (two parameters in the case under consideration), which might be done based on the advice of doctors responsible for monitoring the pandemic and will lead to optimal trained model or under quick analysis of carefully selected sample data. Fig. 8 shows the ‘accuracy and loss of the resulting model using only two parameters.

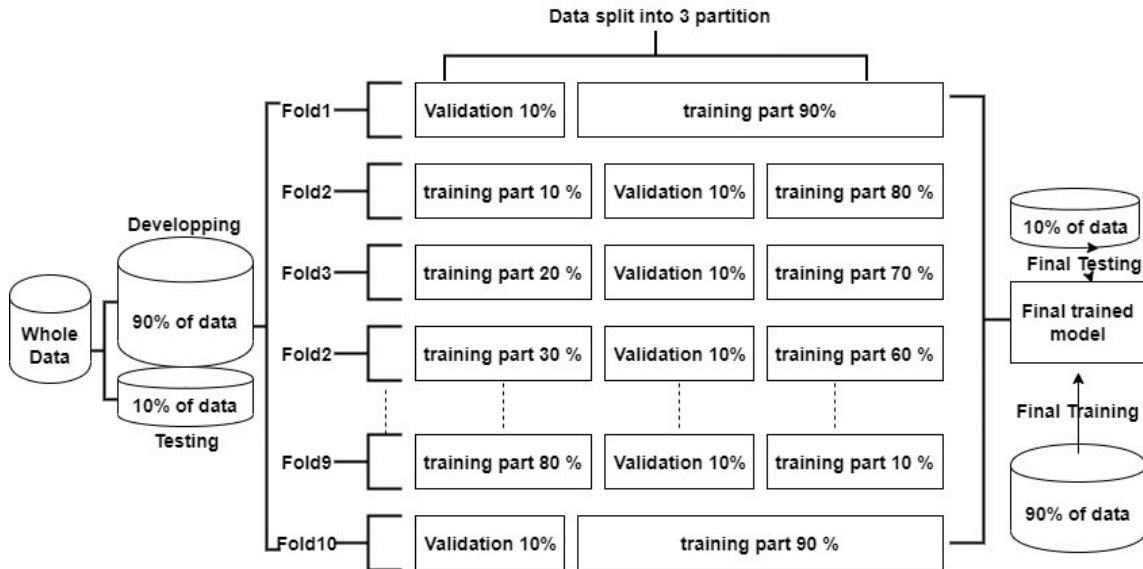


Fig. 6. 10-fold Training Data for the Shallow Net.

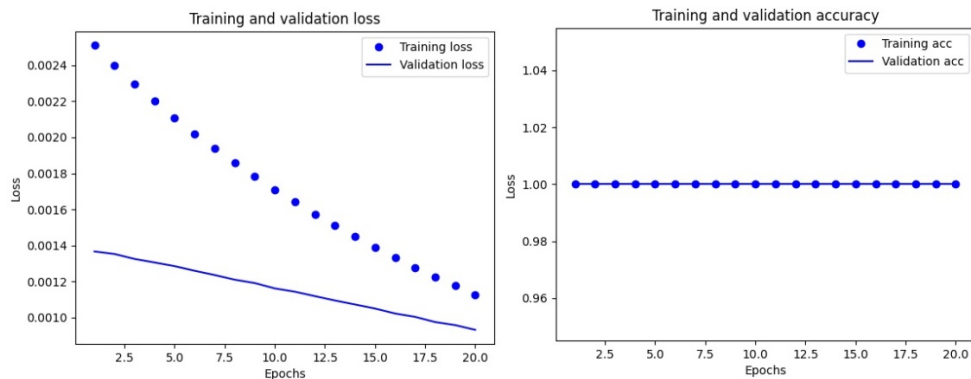


Fig. 7. Loss and Accuracy of Final 10-fold Model.

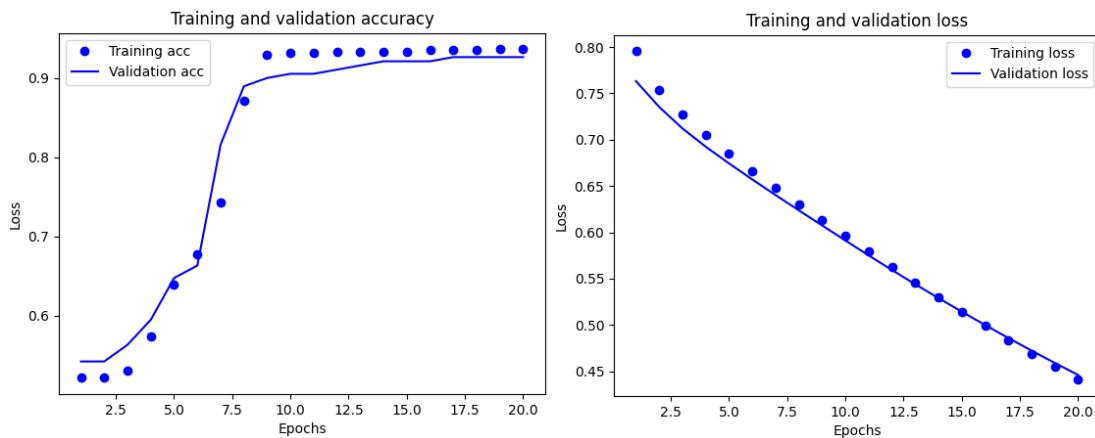


Fig. 8. Loss and Accuracy Training Results of Shallow Net using 2 Parameters.

V. CONCLUSION

This paper addressed the need of a light model with fewer data to differentiate between moderate patients and severe cases so as to use the hospitals resources more reasonably. The work begins using a real, officially collected and reviewed data under the supervision of expert doctors to determine which are the most suitable set of parameters that can be used to differentiate between recovered patients and mortalities. The number of parameters were 53. This number is not huge for ordinary computation available on any prepared machine for deep learning training and the results that achieved using decision trees (94% of accuracy) or 10-fold training (99% of accuracy) ensures that the used parameters can effectively differentiate between recovered patients and mortalities. However, it is better to get a light model with very few parameters (two parameters in this work) and achieve a reasonable result. Using the results of ROC and PCA analysis, the shallow net trained using two parameters achieved 92% accuracy on testing data. So, using a few carefully chosen parameters and a light architecture of shallow net, a light model that needs a very limited computation resources can be built to differentiate between moderate and sever patients during the early days of pandemic like COVID-19.

ACKNOWLEDGMENT

The author would like to thank Professor Dalia I. Hemdan, Taif University, for providing the official data that had been used in this work.

REFERENCES

- [1] B. Udagama, P. Kadhiresan, H. N. Kozlowski, A. Malekjahani, M. Osborne, V. Y. C. Li, H. Chen, S. Mubareka, J. B. Gubbay, and W. C. W. Cha, "Diagnosing COVID-19: The Disease and Tools for Detection, ACS", *Nano*, Vol. 14, Issue 4, 2020, pp. 3822–3835. doi.org/10.1021/acsnano.0c02624.
- [2] M. Xu, L. Ouyang, L. Han, K. Sun, T. Yu, Q. Li, H. Tian, L. Safarnejad, H. Zhang, Y. Gao, F. Bao, Y. Chen, P. Robinson, Y. Ge, B. Zhu, J. Liu and S. Chen, "Accurately Differentiating Between Patients With COVID-19, Patients With Other Viral Infections, and Healthy Individuals: Multimodal Late Fusion Learning Approach" *J Med Internet Res*. Vol. 23 Issue 1, 2021, doi: 10.2196/25535. PMID: 33404516; PMCID: PMC7790733.
- [3] R. Gandhi, J. Lynch, V. D. Rio, "Mild or Moderate Covid-19", *The new england journal of medicine*, Vol. 383 Issue 1, pp. 1757-1766, 2020, Doi: 10.1056/NEJMc2009249.
- [4] L.A. Hajjar, I. B. S. Costa, S.I. Rizk, et al. "Intensive care management of patients with COVID-19: a practical approach" *Ann. Intensive Care*, Vol. 11 Issue 36, pp. 1-17 (2021). <https://doi.org/10.1186/s13613-021-00820-w>.
- [5] S. R. DeWan, "Health system quality in the time of COVID-19" *The Lancet Global Health*, Vol. 8, Issue 6, pp. E738-E739, 2020, [https://doi.org/10.1016/S2214-109X\(20\)30223-0](https://doi.org/10.1016/S2214-109X(20)30223-0).
- [6] J. Uday, "Effect of COVID-19 on the Organs." *Cureus* vol. 12, Issue 8, pp. 1-8 e9540. 3 Aug. 2020, doi:10.7759/cureus.9540.
- [7] A. Qayyum, I. Razzak, M. Tanveer, et al. "Depth-wise dense neural network for automatic COVID19 infection detection and diagnosis". *Ann Oper Res*, 2021, <https://doi.org/10.1007/s10479-021-04154-5>.
- [8] A. Sharma, S. Rani, D. Gupta "Artificial Intelligence-Based Classification of Chest X-Ray Images into COVID-19 and Other Infectious Diseases" *International Journal of Biomedical Imaging*, Vol.

- 2020, Article ID 8889023, 10 pages, 2020. <https://doi.org/10.1155/2020/8889023>.
- [9] C. Jin, W. Chen, Y. Cao, et al. "Development and evaluation of an artificial intelligence system for COVID-19 diagnosis" *Nat Commun*, Vol 11, 5088, 2020. <https://doi.org/10.1038/s41467-020-18685-1>.
- [10] S. Vaid, R. Kalantar, and M. Bhandari, "Deep learning COVID-19 detection bias: accuracy through artificial intelligence" *International Orthopaedics* Vol 44, pp. 1539–1542, 2020, <https://doi.org/10.1007/s00264-020-04609-7>.
- [11] S.A. Harmon, T.H. Sanford, S. Xu, et al. "Artificial intelligence for the detection of COVID-19 pneumonia on chest CT using multinational datasets" *Nat Commun*, Vol. 11, 4080, 2020), <https://doi.org/10.1038/s41467-020-17971-2>.
- [12] M. Attaullah, M. Ali, M. F. Almufareh, M. Ahmad, L. Hussaind, "Initial Stage COVID-19 Detection System Based on Patients' Symptoms and Chest X-Ray Images" *Applied Artificial Intelligence*, 2022, <https://doi.org/10.1080/08839514.2022.2055398>.
- [13] X. Mei, H. Lee, K. Diao, et al. "Artificial intelligence-enabled rapid diagnosis of patients with COVID-19. *Nat Med*" Vol. 26, pp. 1224–1228, 2020, <https://doi.org/10.1038/s41591-020-0931-3>.
- [14] M. Q. Jua rez, T. Go´mez, H. Ulloa, L. Montiel, "Identification of high-risk COVID-19 patients using machine learning" *PLoS ONE*, Vol. 16. Issue 9, 2021, e0257234. <https://doi.org/10.1371/journal.pone.0257234>.
- [15] K. B. Son, T. J. Lee, S. S. Hwang "Disease severity classification and COVID-19 outcomes, Republic of Korea" *Bull World Health Organ*, Vol. 99, Issue 1, 2021, pp. 62-66, doi:10.2471/BLT.20.257758.
- [16] J. R. Quinlan, "Simplifying decision trees". *International Journal of Man-Machine Studies*, Vol. 27, Issue 3, pp. 221–234. 1987, CiteSeerX 10.1.1.18.4267. doi:10.1016/S0020-7373(87)80053-6.
- [17] K. Daniel and G. Mikhail "Comparison of shallow and deep neural networks for network intrusion detection" *IEEE 8th Annual Computing and Communication Workshop and Conference (CCWC)*, pp. 204-208, 2018. 10.1109/CCWC.2018.8301755.
- [18] L. Changjie, L. Chun-Te, Q. Hailu and L. Meili. (2021). Compare Shallow Neural Network and Conventional Machine Learning in Predicting Money Laundering Crimes, 2021 <https://www.researchgate.net/publication/348751150>.
- [19] M. Sugiyama, Dimensionality Reduction of Multimodal Labeled Data by Local Fisher Discriminant Analysis, *Journal of Machine Learning*, Vol. 8, Issue 37, pp. 1027–1061, 2007. <https://www.jmlr.org/papers/volume8/sugiyama07b/sugiyama07b.pdf>.
- [20] M. Jamshidi et al., "Artificial Intelligence and COVID-19: Deep Learning Approaches for Diagnosis and Treatment," *IEEE Access*, vol. 8, pp. 109581-109595, 2020, doi: 10.1109/ACCESS.2020.3001973.
- [21] J. Laguarda, F. Hueto and B. Subirana, "COVID-19 Artificial Intelligence Diagnosis Using Only Cough Recordings," *IEEE Open Journal of Engineering in Medicine and Biology*, vol. 1, pp. 275-281, 2020, doi: 10.1109/OJEMB.2020.3026928.
- [22] M. S. Nawaz, P. F. Viger, A. Shojae, A. et al. "Using artificial intelligence techniques for COVID-19 genome analysis" *Appl Intell*, Vol. 51, pp. 3086–3103, 2021. <https://doi.org/10.1007/s10489-021-02193-w>.
- [23] J. S. Obeid, M. Davis, M. Turner, S. M. Meystre, P. M. Heider, E. C O'Bryan, L. A. Lenert, "An artificial intelligence approach to COVID-19 infection risk assessment in virtual visits: A case report", *Journal of the American Medical Informatics Association*, Vol. 27, Issue 8, pp. 1321–1325, August 2020, , <https://doi.org/10.1093/jamia/ocaa105>.
- [24] A. Ahmad, O. Safi, S. Malebary, S. Alesawi, and E. Alkayal "Decision Tree Ensembles to Predict Coronavirus Disease 2019 Infection: A Comparative Study" *Complexity*, Vol. 2021, 2021, |Article ID 5550344 | <https://doi.org/10.1155/2021/5550344>.
- [25] R. Vaishya, M. Javaid, I. Khan, A. Haleem "Artificial Intelligence (AI) applications for COVID-19 pandemic". *Diabetes Metab Syndr*, Vol. 14, Issue4, pp. 337-339, 2020. doi:10.1016/j.dsx.2020.04.012.
- [26] F. Shi et al., "Review of Artificial Intelligence Techniques in Imaging Data Acquisition, Segmentation, and Diagnosis for COVID-19," *IEEE Reviews in Biomedical Engineering*, Vol. 14, pp. 4-15, 2021, doi: 10.1109/RBME.2020.2987975.
- [27] H. Swapnarekha, H. Behera, J. Nayak, B. Naik "Role of intelligent computing in COVID-19 prognosis: A state-of-the-art review" *Chaos, Solitons & Fractals*, Vol. 138, 2020, doi:10.1016/j.chaos.2020.109947.
- [28] I. Muhammad, R. Hina and N. Amine "Detection of Covid-19 From Chest X-ray Images Using Artificial Intelligence: An Early Review" *arXiv*, 2020. <https://doi.org/10.48550/arxiv.2004.05436>, doi = 10.48550/ARXIV.2004.05436, 2020.
- [29] O. S. Albahri, A. A. Zaidan, A. S. Albahri, B. B. Zaidan, K. H. Abdulkareem, Z. T. Al-qaysi, A. H. Alamoody, A. M. Aleesa, M. A. Chyad, R. M. Alesa, L. C. Kem, M. M. Lakulu, A. B. Ibrahim, N. A. Rashid "Systematic review of artificial intelligence techniques in the detection and classification of COVID-19 medical images in terms of evaluation and benchmarking: Taxonomy analysis, challenges, future solutions and methodological aspects" *Journal of Infection and Public Health*, Vol 13, Issue 10, pp. 1381-1396, 2020, ISSN 1876-0341, <https://doi.org/10.1016/j.jiph.2020.06.028>.
- [30] K. Murphy, H. Smits, J. G. Arnaud , M. Korst, T. Samson, E. T. Scholten, S. Schalekamp, C. M. Schaefer-Prokop, R. M. Philipsen, A. Meijers, J. Melendez, B. Ginneken, M. Rutten "COVID-19 on Chest Radiographs: A Multireader Evaluation of an Artificial Intelligence System" *Radiology*, Vol. 296, pp. E166–172, 2020, <https://doi.org/10.1148/radiol.2020201874>.
- [31] F. Piccialli, V. di Cola, F. Giampaolo, et al."The Role of Artificial Intelligence in Fighting the COVID-19" *Pandemic. Inf Syst Front*, Vol. 23, pp. 1467–1497, 2021. <https://doi.org/10.1007/s10796-021-10131-x>.
- [32] A. Shakeel, P. Sobia, U. Zia, B. Haider, G. Liang, A. Jamil, "A Systematic Literature Review on Particle Swarm Optimization Techniques for Medical Diseases Detection", *Computational and Mathematical Methods in Medicine*, Volume 2021, pp. 1-10, 2021. <https://doi.org/10.1155/2021/5990999>.
- [33] D. António, B. Haider, H. Abdul, W. Alosaimi, H. Alyami, "A New Initialization Approach in Particle Swarm Optimization for Global Optimization Problems", *Computational Intelligence and Neuroscience*, Vol. 2021, 2021. <https://doi.org/10.1155/2021/6628889>.
- [34] H. Turabieh, S. Azwari, M. Rokaya et al, "Enhanced Harris Hawks optimization as a feature selection for the prediction of student performance", *Computing* Vol. 103, pp. 1417–1438, 2021. <https://doi.org/10.1007/s00607-020-00894-7>.
- [35] W. Bangyal, A. Hameed, J. Ahmad, K. Nisar, M. Haque, et al., "New Modified Controlled Bat Algorithm for Numerical Optimization Problem", *Computers, Materials & Continua*, Vol. 70, PP. 2241--2259, 2022. <http://www.techscience.com/cmc/v70n2/44613>.

Advanced Medicinal Plant Classification and Bioactivity Identification based on Dense Net Architecture

Banita Pukhrambam, Dr. Arun Sahayadhas

Department of Computer Science and Engineering

Vels Institute of Science, Technology and Advanced Studies, Pallavaram, Chennai, 600117, India.

Abstract—Plant species identification helps a wide range of stakeholders, including forestry services, botanists, taxonomists, physicians and pharmaceutical laboratories, endangered species organizations, the government, and the general public. As a result, there has been a spike in interest in developing automated plant species recognition systems. Using computer vision and deep learning approaches, this work proposes a fully automated system for finding medical plants. As a result, work is being done to classify the correct therapeutic plants based on their images. A training data set contains image data; this work uses the Indian Medicinal Plants, Photochemistry, and Therapeutics (IMPPAT) benchmark dataset. Convolutional Neural Network (CNN) with DenseNet algorithm is a classification system for medicinal plants that explains how they work and what they're efficient. This study also suggests a standard dataset for medicinal plants that can be found in various parts of Manipur, India's northwest coast state. On the IMPPAT dataset, the suggested DenseNet model has a recognition rate of 99.56% and on the Manipuri dataset; it has a recognition rate of 98.51%, suggesting that the DenseNet method is a promising technique for smart forestry.

Keywords—Indian medicinal plants; convolutional neural network; DenseNet; IMPPAT dataset

I. INTRODUCTION

In Siddha, Unani, Ayurveda, and homeopathic medicines, there are around 8,000 herbal cures. Herbal plants are used for medical purposes by nearly 75% of the migrant population, according to survey results [1]. Drugs are used to make herbal medicines in both developed and developing countries, and India's economic importance is taken into account. For accurate plant categorization, more taxonomic traits of a plant are collected from the images.

The most prevalent approach for classifying medicinal plants is by manual identification. To begin, people use their eyes, noses, hands, or other human organs to obtain information about the full plant or specific sections (leaf, flower, fruit, or bark) [2, 3]. They will identify therapeutic plant species based on either references or personal experience. However, the practice has shown that such an identification approach is time-consuming, inefficient, and strongly reliant on people's knowledge and subjective experience.

Computer-based automated image identification is now widely employed in practice, thanks to advancements in image

processing and pattern recognition technologies. Because plant leaves are simple to gather, recognize, and catch, they are frequently employed as the primary foundation for identifying medicinal plants. To categorize medicinal plants and transmit their distinct medicinal purposes, this study employs a Convolutional Neural Network (CNN) with the DenseNet method.

II. LITERATURE SURVEY

This section discusses the method of systematic literature review for research published in Automated Medicinal Plant Taxonomy. Researchers have explored a variety of methods to extract traits and automatically identify plant species. Many characteristics, such as color, form, texture aspects, and so on, are combined in most of these approaches [4-6]. To acquire the optimum discriminant characteristics for recognizing unique plant species, the Hybrid Feature Selection (HFS) technique is applied [7,8]. To classify the leaves, the system in [9] employs to train the dataset, use decision trees, and variables such as lengths, breadth, aspect ratio, dimension, leaf boundary, and form of property are extracted from the leaves.

They introduced a new approach for categorizing plant leaves in [10, 11], which uses the Maximum Margin Criterion (MMC) to reduce the dimensionality and the Radial Base as new form storage. In [12-14], the researcher combined shape and textural features from leaf images to classify the medical plants. Researchers from India's Western Ghats reported on a computer vision approach for recognizing Ayurveda medicinal plant species in [15, 16]. Using the K-NN classification approach [17], a collection of SURF and HOG features were extracted from leaf pictures for identification.

Researchers [18-20] devised a CNN-based plant identification tool called CNN codes to collect bottleneck features. Finally, SVM was used to train these CNN codes for classification. D-Leaf, fine-tuned Alex Net, and pre-trained Alex Net are three different Convolutional Neural Network (CNN) approaches used to pre-process the leaf images and extract the properties [21, 22]. According to the analysis, identifying several traits such as form, vein, color, and texture would also have a substantial impact on the classifier's accuracy. Higher accuracy may affect the development of medicinal plant use in medicine, as well as the automatic detection identification number, which would have a significant impact on environmental conservation and

preservation. Therefore, this work uses Convolutional Neural Network (CNN) with DenseNet algorithm to classify the medicinal plants and convey their respective medicinal uses [23-24].

III. PROPOSED METHODOLOGY

The proposed DenseNet Classifier-based medicinal plant classification system is discussed in this section. The suggested system's block diagram is shown in Fig. 1. For classifying medicinal plants, the suggested system has four stages: image acquisition, image pre-processing, segmentation, and classification.

A. Preprocessing Adaptive Vector Median Filter

This research work used a combination of an Adaptive Vector Median Filter and an average detection filter to reduce high-density impulse noise from feature extraction. A windscreen is used to process a W (5×5) image that has been influenced by noise sources. Using the non-causal region, the non-causal linear forecasting error for the pixel in question will be computed initially. Let I_x be the pixel undergoing operation, y be the related non-causal area, and W (5×5) be the non-causal region. The pixel window of W (5×5) is calculated using equation (1).

$$W_{(5 \times 5)} = P(a, b), x - 2 \leq a \leq x + 2, y - 2 \leq b \leq y + 2 \quad (1)$$

Where $I(a, b)$ = Processing region of inside pixel.

$$I(a, b) = [I(a, b) R, I(a, b)G, I(a, b) B] \quad (2)$$

The R, G, and B channels make up each pixel in a color image. A substantial correlation exists between pixels in the two-dimensional surroundings. The current pixel value is calculated using this method as a weighted linear combination of the adjacent noise clean pixels. As an outcome, the particles' unity may be lost when aggressive input affects an image. The workflow for preprocessing is shown in Fig. 2.

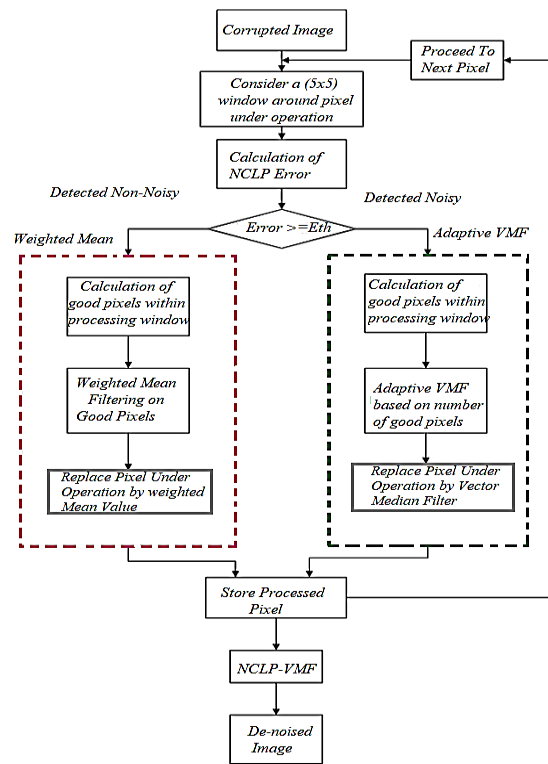


Fig. 2. Flow Chart of Pre-Processing.

B. Segmentation –Fuzzy C Means Clustering

In image processing, fuzzy C – Means clustering has proven to be a very useful strategy for segmenting elements in an image. Unlike other clustering techniques such as k-means segmentation that requires particles to belong to only one classification, FCM permits pixels to belong to several clusters with various class labels. The Fuzzy C - Means (FCM) algorithm is a widely used fuzzy inference approach. It's based on Ruspini's fuzzy partitioning technique; therefore fuzzy c- space for X is discussed below.

For clustering, the Fuzzy C-Means (FCM) algorithm is commonly used. The FCM algorithm's performance is determined by the initial centroids and/or the initial membership value. If a better initial pinpoint the exact that is close to the actual final data point can be found, the FCM algorithm will converge very quickly, reducing processing time significantly. K-means is one of the most basic unsupervised learning algorithms for dealing with the well-known clustering problem. The procedure follows a simple and easy method for classifying a given data set using a fixed number of clusters (assume k clusters). The central concept is to define k centroids, one for each cluster. These centroids should be housed cleverly.

$$M_{fcm} = \{U \in U_{cn} : u_k \in [0,1]\} \quad (3)$$

$$\sum_{i=1}^E u_{ik} = 1, 0 < \sum_{k=1}^n u_{ik} < n \quad (4)$$

Where

U_{cn} = real $c \times n$ matrices c = integer Value with the range of $2 < c < n$.

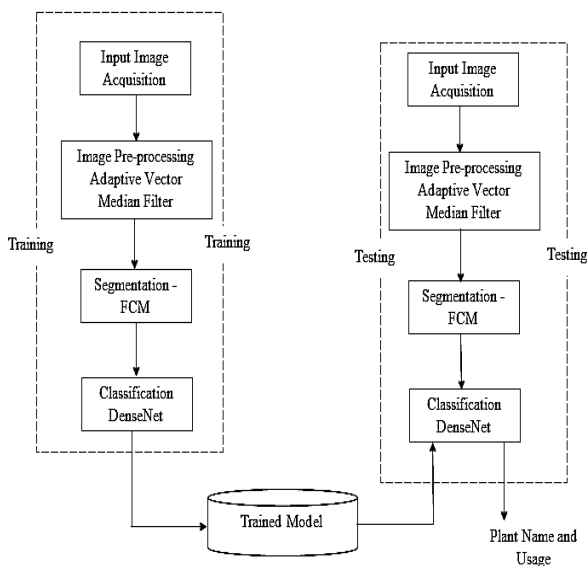


Fig. 1. Block Diagram of Proposed System.

$x_k(k=1, \dots, n) =$ vector in R^P , u_{ik} = membership value for k in cluster $i(i = 1, \dots, c)$

The primary purpose of FCM analysis is to find the best fuzzy c -partition and prototype while keeping the feature subset to a minimum.

$$J_m(U, V; X) = \sum_{k=1}^n \sum_{i=1}^c (u_{ik})^m |X_k - V_i|^2 \quad (5)$$

Where

$V =$ cluster center (v_1, v_2, \dots, v_c) $V_i \in R^P, || \cdot || =$ Norm of Euclidean

$m =$ Exponent of weighting $[1, \infty)$.

The FCM algorithm is a fuzzy constraint minimization technique that uses alternating minimization to minimize the criterion J_m . Choose a value for c , m , and a tiny positive variable; use a clustering U_0 with $t=0$ as the iteration number in random design. The FCM algorithm is a fuzzy constraint minimization approach that minimizes the criteria J_m using minimization that alternates. Choose a value for c , m , and a tiny positive variable, then construct a clustering U_0 at random using $t=0$ as the number of iterations. It's a two-step incremental method; approach is illustrated in the diagram below. The $U^{(i)}$ ($i=1, c$) method is used to determine the membership values.

$$V_i^{(t)} = \frac{\sum_{k=1}^n (u_{ik}^{(t)})^m X_k}{\sum_{k=1}^n (u_{ik}^{(t)})^m} \quad (6)$$

Given the new cluster centers $V_i^{(t)}$ update membership values $u_{ik}^{(t)}$

$$u_{it}^{(t+1)} = \left[\sum_{j=1}^c \frac{|x_k - v_j^{(t)}|^2}{|x_k - v_i^{(t)}|^2} \right]^{-\frac{1}{m-1}} \quad (7)$$

The $|U^{(t+1)} - U^{(t)}|$ is the difference of Gaussians Pyramid. By deleting a low pass filtered copy first, the image's pixel-to-pixel correlation is decreased. The variance and entropy of the difference or error image are low, and the low pass filtered image can be described with a lower sample density. When you cycle the procedure at large enough scales, you have a pyramid data structure. Assume that I represent the original image and J represents the applied low pass filter. The method ends when the specified number of repeats is reached. The term "Laplacian Pyramid" is misleading because each level (i.e., image) is created by smoothing with two Gaussians of different sizes, then deleting and subsampling.

C. Convolutional Neural Network with DenseNet Classifier

Deep Learning (DL) is proposed because approaches can learn substantial characteristics from input images at multiple convolutional levels, which is comparable to how the real brains functions, this is the most prevalent architecture. DL can tackle complex issues successfully and quickly, thanks to its high classification accuracy and low error rate. The composed view of DenseNet architecture is shown in Fig. 3.

The convolutional layer, pooling layer, fully connected layer and activation functions are the essential components in the DL model. In this study, CNN was combined with the DenseNet Classification approach to acknowledge plants. The

vanishing gradient problem induced by network depth is likewise addressed by this network. The connection designs of all layers are employed to ensure that the maximum amount of information may travel across levels. Each layer gets input from the layers above it and communicates its feature maps to the layers below it in this configuration. By concatenating the local characteristics at each layer, information is transmitted from one level to the next. This network architecture minimizes the need to remember redundant data, reducing the number of parameters to learn significantly (i.e., parameter efficiency).

DenseNet121 does not suffer from generalizing and performed admirably for categories with a little training data set. In this work, Dense Net was used, and Fig. 4 shows a compressed version of it. DenseNet alternates dense and transition blocks with fully-connected layers and a nonlinear activation classifier. So based on this BN layer, Convolutional Layer (Conv) and leaking rectified linear unit layers are merged with the cascaded format in a dense block such as BN-Conv-LReLU.

The first BN-Conv-LReLU is generating $4r$ output features using 1×1 kernels, where r is a pre-defined value of 32 in this work. The dense block increases the number of maps by connecting output feature maps to the ability to segment. During the transition, a convolutional unit is used, followed by average max pooling with a pool size of 2×2 . The transition construction's goal is to find the best combination of extracted characteristics produced by a large number of convolutional layers while saving time and money. The number of output feature maps in the transition block in this exercise is equal to the number of input nodes.

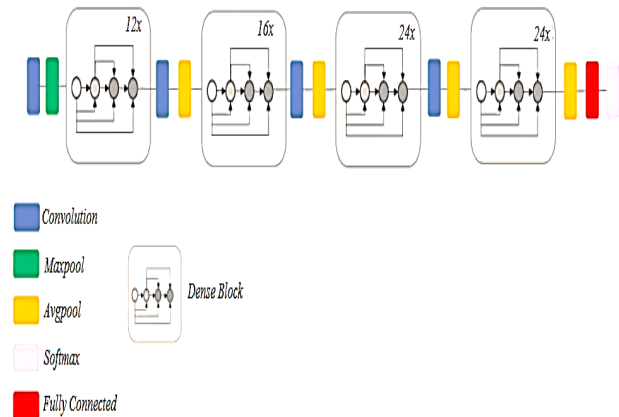


Fig. 3. Composed View of Dense Net Architecture.

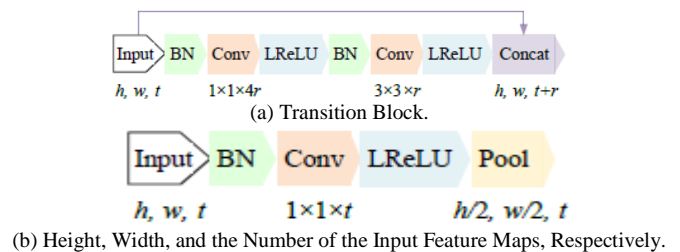


Fig. 4. Details of Dense Block

TABLE I. DENSE NET STRUCTURE AND OUTPUT

Module	Detail	Output
Convolution	1 x 1 x64 conv	128 x 128x 64
Max-pooling	2 x2 pool	64 x 64 x 64
Dense block 1	1 x 1 x 128 conv ,3 x 3 x 32 conv	x 2 64 x 64 x 128
Transition block 1	1 x 1 x 128 conv, 2 x 2 pool	32 x 32 x 128
Dense block 2	1 x 1 x 128 conv, 3 x 3 x 32 conv	x 3 32 x 32 x 224
Transition block 2	1 x 1 x 224 conv, 2 x 2 pool	16 x 16 x 224
Dense block 3	1 x 1 x 128 conv,3 x 3 x 32 conv	x 4 16 x 16 x 352
Transition block 3	1 x 1 x 352 conv,2 x 2 pool	8 x 8 x 352
Dense block 4	1 x 1 x 128 conv,3 x 3 x 32 conv	x 2 8 x 8 x 416
Global average pooling		1 x 1 x 416
Full-connection	416 x θ full-connection	θ
Softmax	softmax classifier	θ

Table I shows the DenseNet structure and output, assuming that the input images are 128x128 and the input image size is 128x128, respectively. The algorithm uses the Indian Medicinal Plants, Phytochemistry, and Therapeutics (IMPPAT) benchmark dataset to classify medicinal plants, and it also has a dataset from the Manipuri district.

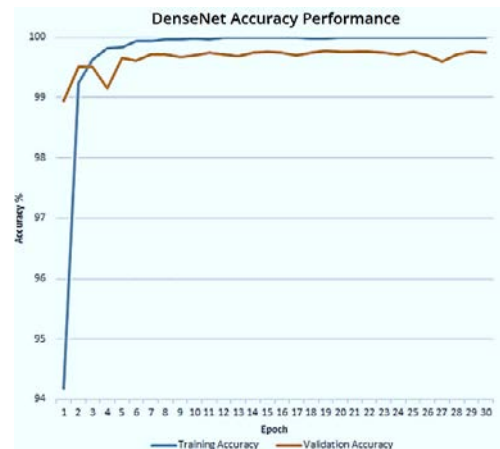
IV. RESULT AND DISCUSSION

The proposed medicinal plant classification system's implementation results and performance analysis are discussed in this section. Table II contains information about the dataset utilized in this study.

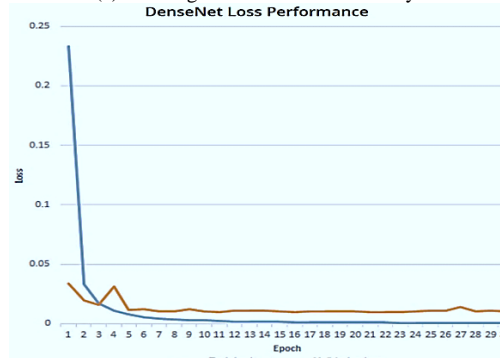
The simulation result of training and validation accuracy and Training and Validation Loss of proposed CNN with DenseNet classifier is shown in Fig. 5 and Fig. 6. By using CNN DenseNet the training and validation accuracy is 99.45% and 99.26% against IMPPAT Dataset. By using CNN DenseNet with IMPPAT dataset the training and validation loss is 0.05MSE and 0.065MSE. By using CNN DenseNet the training and validation accuracy is 99.68% and 99.41% against own dataset. By using CNN DenseNet with its own dataset the training and validation loss is 0.041MSE and 0.052MSE.

TABLE II. DATASET DETAILS

Dataset Name	IMPPAT database	Own database
Number of Images	1742	200
Training Images	1404	160
Testing Image	338	40
Software Used	Python	Python

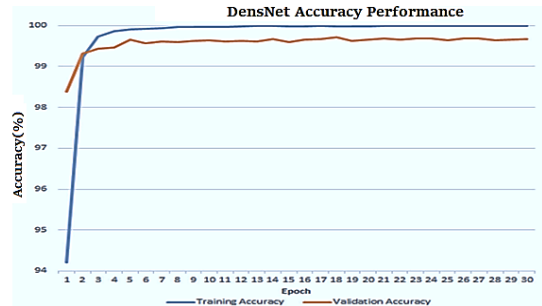


(a) Training and Validation Accuracy.

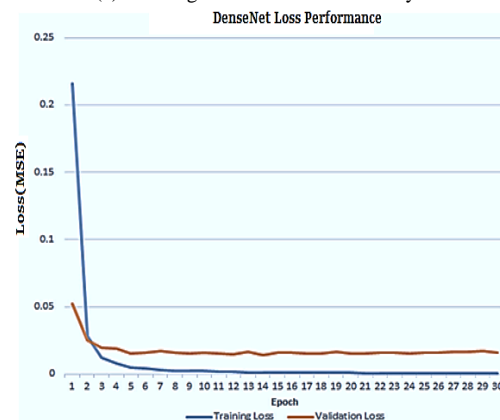


(b) Training and Validation Loss.

Fig. 5. Accuracy and Validation Loss of Impact Dataset.



(a) Training and Validation Accuracy.



(b) Training and Validation Loss.

Fig. 6. Accuracy and Validation Loss of Own Dataset.

A. Performance Analysis

The classifier's performance is assessed by different statistical measurements, such as sensitivity, specificity, accuracy and F1-score. Table III shows the comparing the suggested CNN-DenseNet Classifier-based medical plant classification with existing approaches in terms of total classification ratio analysis. CNN-DenseNet gives good results compared with conventional methods. The sensitivity, specificity, accuracy, and F1-score of CNN-DenseNet against the IMPPAT dataset are 99.25%, 99.56%, 99.78%, and 0.61. The sensitivity, specificity, accuracy, and F1-score of CNN-DenseNet against own dataset is 98.12%, 97.56%, 98.01%, and 1.25.

TABLE III. PERFORMANCE ANALYSIS OF CLASSIFICATION

Methods	Classification Sensitivity (%)	Classification Specificity (%)	Classification Accuracy (%)	F-Measure (%)	
SVM	89.46	91.23	89.49	15.03	
SVM-PCA	90.06	91.56	89.11	12.06	
SVM-GA	92.13	93.20	90.27	10.23	
AUSP	97.29	97.41	97.73	5.01	
CNN-Google Net	98.16	98.08	98.26	2.65	
CNN-DenseNet	IMPPAT Dataset	99.25	99.56	99.78	0.61
	Own Dataset	98.12	97.56	98.01	1.25

B. Real Time Experimental Evaluation

This section discusses the working function of real time medical plant recognition using Mat-lab with webcam of proposed CNN-DenseNet Method.

The Real Time Experimental Evaluation of the proposed CNN-DenseNet Method-based medical leaf identification system is shown in Fig. 7. By using the CNN-DenseNet Method, the medical plants are identified and also suggest the bioactivity of that particular plant. In Fig. 7 the identified leaf name is a Gale of Wind and it's widely used to clear jaundice.

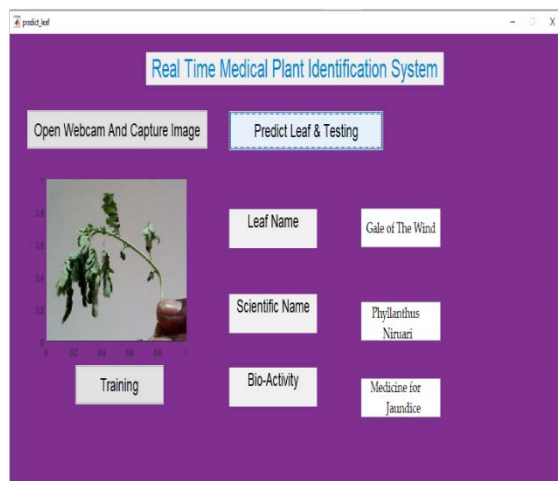


Fig. 7. Real Time Experimental Evaluation.

V. CONCLUSION

A unique deep learning-based technique for automatically identifying and detecting medicinal plants and their applications was examined in this study. The Indian Medicinal Plants, Phytochemistry, and Therapeutics (IMPPAT) benchmark dataset were used in this study and used its dataset, which is common in Manipuri, a state on India's northeastern coast. From gathering the images required for training and validation to data preprocessing and segmentation, and eventually training and perfectly alright the deep CNN-DenseNet, the entire method was covered. The performance of the newly designed model was evaluated through a series of experiments. CNN-DenseNet has 99.25% sensitivity, 99.56% specificity, 99.78% accuracy, and 0.61 percent F1-score against the IMPPAT dataset. CNN-DenseNet's sensitivity, specificity, accuracy and F1-score against the own dataset are 98.12%, 97.56%, 98.01%, and 1.25%, respectively. The challenge of recognizing medicinal plant species was also solved in this study by analyzing leaf photos taken straight from their habitat, regardless of lighting conditions. We intend to build and develop a system that automatically recognizes plant species by analyzing not just leaf photos but also images of other sections of the plant taken directly in their environment, regardless of complicated backdrops or lighting conditions.

VI. FUTURE WORK

A deep learning based detection approach is proposed in future work to recognize and classify the different types of plant actions. Future capturing the abnormal leaf image that contains activation of different leaf and finding specific part of area with more improved efficiency (per-packet classifications) and accuracy of these detections.

REFERENCES

- [1] S. Talwar, S. Sood, J. Kumar, "Ayurveda and allopathic therapeutic strategies in coronavirus pandemic treatment", Current Pharmacol Reports, pp. 354–363, 2020.
- [2] K. Mohanraj, B. S. Karthikeyan, Vivek-Ananth, "IMPPAT: A curated database of Indian medicinal plants, Phyto chemistry and Therapeutics", 2018.
- [3] M. Fitzgerald, M. Heinrich, A. Booker, "Medicinal plant analysis: a historical and regional discussion of emergent complex techniques", Front Pharmacol, Published, 2020.
- [4] Swu, Vikaho Bora, Dibya, "Identification of different plants through image processing using different machine learning algorithms", pp. 172-179, 2020.
- [5] Y. H. Lin, L. Luo and L. Lin, "A biosensor for simazine herbicides detection using sub-cellular plant photosystems", 1st IEEE International Conference on Nano-Micro Engineered and Molecular Systems, pp. 1354-1357, 2006.
- [6] M. Fathi Kazerouni, M. Mohammed Saeed, N.T. Kuhnert, "Fully-automatic natural plant recognition system using deep neural network for dynamic outdoor environments", SN Applied Science, 2019.
- [7] Tomar, Divya Agarwal, Sonali, "Leaf recognition for plant classification using direct acyclic graph based multi-class least squares twin support vector machine", International Journal of Image and Graphics, 2019.
- [8] Tomar, Divya and Agarwal, Sonali, "A comparison on multi-class classification methods based on least squares twin support vector machine", Knowledge-Based Systems, 2015.
- [9] Mr. Shailesh Sangle, Mrs. Kavita Shirsat, Mrs. Varsha Bhosle, "Shape-based plant leaf classification system using android", International journal of engineering research and technology (IJERT), Volume 02, Issue 08, 2013.

- [10] H. A. Gabbar, "Intelligent topology analyzer for improved plant operation", SICE-ICASE International Joint Conference, pp. 5737-5742, 2006.
- [11] Islam, Mohammad Billah, Mustagis Yousuf, Md. "Automatic plant detection using hog and LBP features with SVM", International Journal of Computer (IJC), 33, 26-38, 2019.
- [12] Olsen, Alex Han, Sunghyu Calvert, Brendan Ridd, Peter Kenny, O.P, "In situ leaf classification using histograms of oriented gradients, pp. 1-8, 2015.
- [13] Bao, Truong Truong, Quoc-Dinh Huynh, Hiep, "Plant species identification from leaf patterns using histogram of oriented gradients features space and convolution neural networks", Journal of information and telecommunication, Pp. 1-11, 2019.
- [14] H. A. Gabbar, K. Nishiyama, S. Ikeda, T. Ooto and K. Suzuki, "Virtual Plant Design for Future Production Management", SICE-ICASE International Joint Conference, pp. 1866-1870, 2006.
- [15] Ibrahim, Zaidah Sabri, Nurbaity Abu Mangshor, Nur Nabilah, "Leaf recognition using texture features for herbal plant identification", Indonesian journal of electrical engineering and computer science. Pp.152-156, 2006.
- [16] H. Fujii, A. Gofuku and T. Ago, "Operation support in anomalous plant conditions using PKY knowledge", SICE Annual Conference, pp. 293-296, 2008.
- [17] Rahaman, Mohammad Hossain, Eftekhari Hossain, Md. "A color and texture based approach for the detection and classification of plant leaf disease using KNN classifier", 1-9, 2019.
- [18] Lee, Sue Han and Chan, Chee Seng Wilkin, Paul Remagnino, Paolo, "Deep-plant: Plant identification with convolutional neural networks", 452-456, 2015.
- [19] Bisen, Dhananjay, "Deep convolutional neural network based plant species recognition through features of leaf". Multimedia Tools and Applications, pp. 1-14, 2021.
- [20] M. Paolone, "A research on plants for in-situ verification of contaminated soils", IEEE bologna power tech conference proceedings, pp. 5, Vol.4, 2003.
- [21] Mehdipour Ghazi, Mostafa Yanikoglu, Berrin Aptoula, Erchan, "Plant identification using deep neural networks via optimization of transfer learning parameters", Neuro computing, 2017.
- [22] Ahmed, Nisar Khan, Muhammad Usman Asif, Shahzad, "An automatic leaf-based plant identification system", Science International-Lahore, pp. 427-430, 2016.
- [23] Singh, Kh Bora, Prabin, "Switching vector median filters based on non-causal linear prediction for detection of impulse noise", The Imaging Science Journal, 2014.
- [24] Roy, Amarjit Singha, Joyeeta Manam, Lalit Laskar, Rabul, "Combination of adaptive vector median filter and weighted mean filter for removal of high-density impulse noise from color images", IET Image Processing, 2014.

Short Words Signature Verification using Markov Chain and Fisher Linear Discriminant Approach

M.Nazir¹

Department of Basic Sciences
Deanship of Common First Year
Majmaah University, Majmaah, 11952
Saudi Arabia

Danish Ather³

Department of Computer Science and Engineering
School of Engineering and Technology
Sharda University, Greater Noida-201310, India

Surendra Singh Choudhary²

Department of CSE
Sri BalaJi College of Engineering and Technology
Jaipur- 302012, India

Latika Kharb⁴

Department of Information Technology
Jagan Institute of Management Studies (JIMS)
Delhi-110085, India

Abstract—Writer identification is the domain of documents image analysis which is popularly sound in many applications like banking, academic professional in Optical Character Recognition (OCR) Signature verification remains one of the most important entities to authenticate document in these applications. In view of technical breakthrough, we have focused on short words signatures which are very hard to verify as they raise issues of ambiguities. From the geometrical studies of signature-based images, it is stated that the morphology of directional transformations (MDT) is right to extract the suitable features in case of short words for writer identification. MDT takes the data in the form of Structure Element (SE). The directional morphological structures (DMS) of SE are used as a key factor for performing morphological operations on the signature images. We have adopted Markov chains and Fisher Linear Discriminant (FLD) for computing the gradients from line features corresponding to the word. Neural network is used to evaluate the proposed model. In case of training and testing of the signature, images of short words leave-one-out are followed. Our purposed model is tested on NIST database for extracting the words length with three letters. It is observed that a very simple architecture of neural network achieved 100% satisfactory results using short words.

Keywords—Human signature verification; morphological directional transformations; structuring element; optical character recognition; fisher linear discriminant

I. INTRODUCTION

The document in digital world can be authenticated from unique and confidential mark referred as signature. For developing an automated hand signature based authentication system, the researchers have supported at large scale to several real life applications used in banking, academic and defense. Their main objective is that the documents are kept safe from illegal access and forgery. From a decade, it is observed that many cases of forensic and legal research paid serious attention to develop an automated signature verification system. The research of hand written signature matches with the problem of Optical Character Recognition (OCR), which is a broad area of computer vision and image processing domains. In OCR, the

algorithms used for signature verifications follow the segmentation of signatures into characters, then by formatting the characters, it finds the word with highest matching score. For the developing system of writer verification, both signatures and handwritten text are used as complimentary components. From the mechanism of the information collected from the users, the verification system can be categorized as static and dynamic. When, text used for authentication is extracted from any document, it is referred to as static signature verification whereas, in dynamic verification the users' information is collected with help of electronic devices like sensing tip-pressure, pen-based computer screening etc. Dynamic signature verification requires more processing efforts as compared to static signature verification. Dynamic verification considers the complex information like neurological health and real-time circumstances when signature is collected. Chaabouni et al. (2011) also observed that more reliability and robustness can be added in signature verification with dynamic approach [1].

The research of writer identification is the main motive behind the task of signature verification. In image processing literature, every object may have important pattern to characterize the feature of the objects. The pattern recognition recommended several sets of algorithms which can support to avoid the complex process of dynamic verification. But reliability remains a challenging issue with all pattern recognition based static approaches since document is generally affected due to its chemical dating process which badly impacts the static signature verification system. Lorigo et al. (2006) [2] also mentioned important significances by designing various pattern recognition based verification systems. All the approaches focused on the basics presented in [11] for developing a better pattern recognition system. Further, Wu et al. (2014) [3] performed experiments in offline mode with text-independent approach. They experimented three major languages, English, Arabic and Chinese. Another approach presented by Newell et al. (2014) [4] utilized basic image features which are referred to Oriented Basic Image

Feature Columns (OBIF) for developing a writer identification system.

The remaining structure of the papers is as follows: Section II illustrates the descriptive analysis of recent state-of-the-art on signature verification. Section III represents the proposed mythology of short signature verification model. The dataset along with experimental settings is presented in Section IV. After giving a detailed insight on result and discussion, the Section IV concludes the signature verification system with the future recommendation.

II. RELATED WORK

Signature verification can be considered as a collective project of different schemes of optical character recognition. Every character in a particular signature preserves the unique identity of the users. Detecting such a unique identity of every individual user for the authentication of a digital verification system is quite a tedious task. For the sake of convenience, the morphological studies of short signature can be utilized to verify the user. Kumar et al. (2014) [5] proposed a writer authentication system referred as graphemes which extracts the documents' features using wavelet and Fourier descriptors. Taking the advantages of morphological features, Zois et al. (2000) [7] derived the feature vector from the horizontal profile of the projection from the given signature images. The developed projection function can easily match the signature image verification. Online text-independent scheme for signature verification ensured more advantages against offline system. Zhang et al. (2016) [8] proposed an end-to-end framework which verifies the users in text-independent online mode. They used recurrent neural network (RNN) for matching the short words in signature image. Looking towards avoiding the overhead in online mode, Wu et al. (2014) [9] followed offline text-independent scheme for writer verification. They mainly focused on handcrafted Scale Invariant Feature Transform (SIFT) and final outcome goes through training, registration and identification of signature images. In both the cases, offline and online schemes, neural network and machine learning algorithms play a very important role. Kumar et al. (2019) [12] presented a detailed state-of-the-art neural networks with deep learning methodology. According to Lippmann et al. [13], the author discussed the significance of optimal transformations and emphasized on the consideration for the advancement of control structure of data items which reduce the signature image quite hard to process.

In the early stage of authentication system, offline signature verification has been quite popular in several departments of academic and administration [17]. At that time, classical feature extraction methods have produced satisfactory results [18, 15]. But for matching the recently raised issues, automated feature learning is incorporated with deep network architectures [6]. Among all, deep network, the convolution neural network (CNN) remains a buzz technology. In [19], Day et al. developed a loosed Siamese Convolution Network (SCN) which follows the contraction of signature images for user verification. Following deep learning as an agent of higher performance, Shariatmadari et al. [20] proposed a hierarchical CNN easily capable to extract the signature patches from the given images. In same direction of research, hybrid CNN with

two-channel is presented in [21] which produced satisfactory performance in offline signature verification. Image surface-based deep learning methods are referred to as region based signature verification algorithms [22]. For real-time signature verification system, a human neurology based motor signature model is developed [23]. The motor signature CBCapsNet model works on capsule based CNN for offline signature verification [24]. Another Graph based CNN (GCNN) improved the task coevolution kernel for signature verification [25].

The concept of short length words with machine learning addressed the issues discussed in the literature. In our proposed writer verification system, the feature elements are the transition matrix of Markov chains. These features mark the alternation of the morphological directional transformation (MDT) from the line features and accordingly the gradient updates along with the image of the word. The neural structure of signature images helps in accessing the separability of the clusters which are designed on high dimensional space. In case of deciding the regions formation, a theoretical insight is presented based on the limitation of perceptron. The input layers of perceptron draw the linear (N-1)-D subspaces from the feature space of N-D dimension. In the base work presented by Stanley et al. (2007) [14] NIST Special Database is used for 19 features components. The noticed gap of the research is highlighted in extracting few short words like "the" or "end" for test training a very simple neural network. Another side, for developing a digital signature verification system security issues can motivate the researchers extend at higher state-of-the-art [16].

III. PROPOSED METHODOLOGY

The proposed writer verification system follows the short signature images. In testing the proposed model NIST database is used for extracting these words where total ten writers are allocated as source of data collection. In this dataset, the signature of unknown person is also considered and classified according to the person belonging to the group of signatures. The methodology is slightly irrelevant of the literature used and followed in baseline of research. The following steps are considered while designing and developing the proposed signature verification model: 1) Preprocess steps of the signature images of the short word capture from unknown person, 2) The step of thresholding to isolate the short words from the background, 3) Extract the orientation features by means of MDT. The descriptive short words signature verification algorithm can be pointed as follows-

- Develop a feature descriptor by updating orientation with Markov chain. The feature vector is generated from the components used in transition matrix. Fisher Linear Discriminant (FLD) approach encourages reducing the dimension of signature image.
- The capability of cluster separability is enhanced by simplest neural architecture in the predetermined feature space. The performance is enhanced when morphological transformation is applied at different lengths of line segments.

- The feature space is characterized to the clusters separability with architecture of neural network.

A. NIST Database-19(SD-19)

The NIST database is generated from the thousands of writers with repeating single text only once. SD19 is the updated web released NIST special dataset. SD19 consists of binary images of 3669 (ref. Fig. 1) samples of handwriting forms (HSF). The text page consists of the hand printed digits and alphanumeric characters. The detailed information of text is explained for characteristic of signature images by Stanley et al. (2007) [14]. HSF from NIST-SD-19, special database provide an opportunity to discriminate the text with short length coming very frequently from the different writers. This helps in generating cluster of the words appearing many times from each writer.

Specially noted from Fig. 1, the text word 'the' is repeated six times and the text word 'and' is repeated three times. In case large number of writers, the verification with short words is expected suitable to develop a robust system.

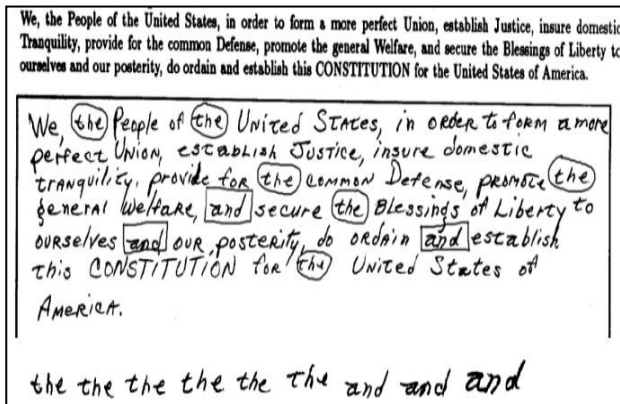


Fig. 1. Six Replicas of the Word "the" and Three for the Word "and" have been Extracted to Uniquely Represent the Specific Writer.

B. Directional Morphological Transformations

The task of preprocessing targets the isolation of the text word taken from HSF form. For preserving the important information, the background image of text and directional features are transformed into thin line. The results of preprocessing steps performed on short word are shown in Fig. 2.



Fig. 2. The Thresholding of Word Image after Applying the Negative and Line-thinning Operations.

The approach of applying MDT on processed short word included generating the negative of the word image. On the black background of word image, the thinning operation is performed using morphological operations. This helps in maintaining the strong line features of the word. Fig. 2 refers to the thinned image after applying MDT with structure element

(SE). In this way, the feature localization of dominating directionality is achieved to perform easiest clustering. Fig. 3 shows the directional structure elements of length three. The fitting of SEs on any part of the line image indicates that the image is oriented towards the SE. The measures of fitness function of SE on line image are determined by morphological operation called opening [6]. During the process of opening, fitting of SE on line image also measures the originality of the line image. Fig. 4 demonstrates the impact of fitting SE with length three on vertical line image, contains the text letter 'h'.

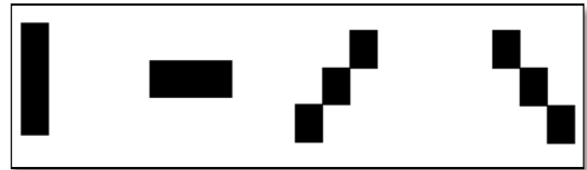


Fig. 3. Directional Morphological Structuring Elements with Length 3 Pixels, from Left to Right: Vertical, Horizontal, 45 Degrees, and 135 Degrees.

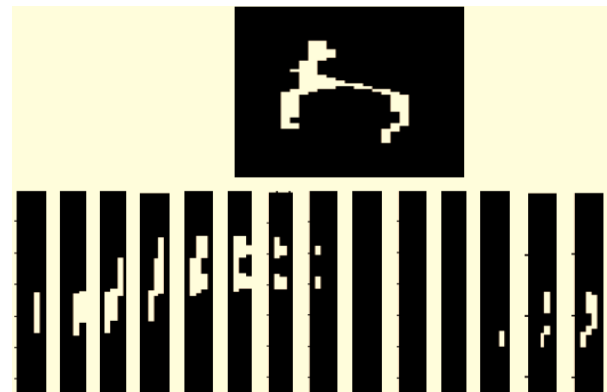


Fig. 4. Processing of the Letter 'h' in the Word 'the' with Morphological Opening using a Vertical Directional Structuring Element of Length 3.

In detail, morphological operation 'opening' is responsible for the directionality of line image in each location the specific word. Here in our experiment the word 'the' is chosen from HSF form. Fig. 4 shows the pixel by pixel scanning from left to right. As shown in Fig. 3, each strip follows the opening operation separately with each of the four given directional SEs. The operation of opening is adopted as a margin by adding the one line of pixels around the strip. The selection of best SEs is determined by the strip which remains unaffected after applying operation with majority of pixels on word image. The set of SEs determines the specific strip responsible for signature verification. The best fit of SEs can be determined in alternation from the stochastic process of Markov model. In this way, Markov model enables the selection of SEs and strips for better designing for signature verification.

Fig. 3 represents the sequence of 4 best fitting SEs on line image. The sequence of four SEs adopts morphological operation on word image 'the'. Fig. 5 presents the line image of word 'the' along with its best sequence of the fitting with directional SEs. Each number of the sequence corresponds to structuring elements, e.g., zero corresponds to the blank space.

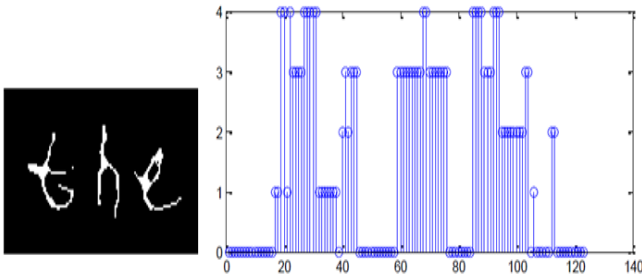


Fig. 5. The Word ‘the’ in the Image ‘f0000_1_1.tif’ from the NIST SD-19 and the Related Sequence Directed SEs of Figure 3, which fits along the Word.

First order Markov Chain models (FMCs) are used to generate feature vector for writer identification. The various orientations of SEs are governed by alternation with FMCs to the best fit of specific location of word in line image. The different states in Markov chain map the oriented SEs following the property of probabilistic states. That means (ref. Equation-1), every previous strip determines state of SEs in the following strips.

$$Pr(r_j(k)|r_j(k-1), r_m(k-2), \dots, r_n(1)) = Pr(r_i(k)|r_j(k-1)) = t \left(\frac{i}{j} \right) \quad (1)$$

Where the subscript r_n stands for the various oriented states of the SEs. In this work, the oriented states take five values from 0 to 4 and k is spatial variable corresponding to the movement performed around the word image. State 0 refers to blank space or SE does not present in that state. Fig. 5 shows all possible sequence the oriented SEs of word image ‘the’ from SD19 database. It is informative to note that absences of SEs indicate the blank which means the gap is between the two words. As represented by Equation-2, the matrix T allocates the all possible probabilities $t(i/j)$ making a square matrix referred as the transition matrix T . The i^{th} row of the transition matrix T assigns each of the previous states to j^{th} column of the next state. The specific probability value in transition matrix T verifies the signatures.

The transition T allocates the second order statistics of oriented SEs. From the experiments performed, it is observed that the feature vector writer identification follows Equation-3, which transforms the transition matrix into one Dimensional vector v of length 25.

$$T = \begin{pmatrix} t_{11} & \dots & t_{51} \\ \vdots & \ddots & \vdots \\ t_{51} & \dots & t_{55} \end{pmatrix} \xrightarrow{rd} \begin{pmatrix} t_{11} \\ t_{12} \\ \vdots \\ t_{15} \\ t_{51} \\ \vdots \\ t_{55} \end{pmatrix} \xrightarrow{rd} \vec{v} = \begin{pmatrix} v_1 \\ \vdots \\ v_{25} \end{pmatrix} \quad (2)$$

The dimensionality reduction is achieved by performing a linear transformation W . Here we used Fisher Linear Discriminant (FLD) transformation for accomplishing the task of dimensionality reduction. The vector space generated w_i vectors generate a new spaces in which every vector 25-dimensional.

$$Y_i = W^t v_i \quad (3)$$

Where each vector y_i is transformed into v_i . The transformed function $J(w)$ (ref. Equation-4) is maximized with the concept presented in [10] which helps for separating all the clusters.

$$J(w) = \frac{w^t S_B w}{w^t S_W w} \quad (4)$$

The Eigen vales solution of transformed vector spaces of W follows Equation-5.

$$S_B W_i = \lambda_i S_W W_i \quad (5)$$

where, S_W is referred as the Within-Scatter-Matrix(WSM) and S_B the Between-Scatter-Matrix(BSM). From the solutions of Eigen value problems, the most important concept is the significance of the largest eigenvalue. It means the sum of the first two largest eigenvalues can indicates the cluster separability among the reduced 2-D feature matrix. Therefore, the capabilities of clustering of the directional SEs with length three and five are useful to demonstrate short words ‘the’ and ‘and’ in SD19 dataset. The combination of these SEs gives a 50-D feature vector correspondence to the largest eigenvalue. For the word ‘the’ Table I show sequences of Eigen values.

The information of separability of words gives the square root of the relevant eigenvalue. It is observed that approximately, 65% of the information for cluster separability is determined by three directions related to the first three largest eigenvalues. Fig. 6 presents the difference among the clusters generated against ten writers. It is clearly noticed that all the clusters are separable. But we target to three largest eigenvalues. The remaining Eigen values can be utilized to support the separability. Fig. 6(a) and Fig. 6(b) demonstrate the objectives of ten clusters summarized in three most suitable directions. All the available inputs of separability information to the neural network enhance the higher separability performance with short words.

TABLE I. TEN LARGEST EIGEN VALUES CORRESPONDING TO MOST PROMINENT DIRECTIONS OF CLUSTER SUPERAGILITY IN 5-D FEATURE SPACE FOR THE WORD PERCEPTONS

λ	363	121	47	32	14	11	7	5	4	1
Sqrt(λ)	19	11	6.8	5.6	3.7	3.3	2.6	2.2	2	1

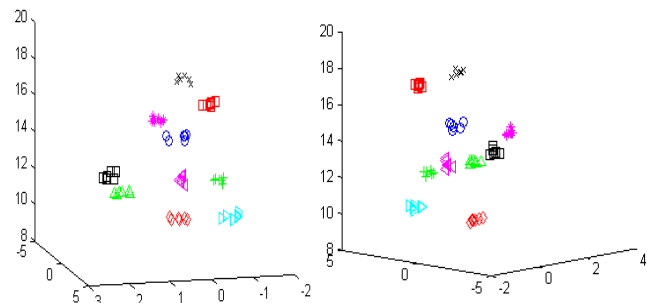


Fig. 6. Two different Aspects of the same 3-D Feature Space are given in (a) and (b).

C. Space Separability

The limitation of classical multilayer Neural Networks (NNs) has been addressed by Lipmann et al. [11]. In their work, the following things can be summarized as key points:

- The first layer of perceptron considers the linear subspaces of (N-1)D dimensional from that of N-D dimensional feature space.
- The upper layers second and third target to create convex and non-convex decision regions from the original surface by combining all the linear subspace of the above layers.

The simplest neural structure is supposed to be more suitable to separate the feature space by separating the populations of clusters. The same concept is explained in Fig. 6. More clearly to understand this concept of separability, the subfigure of Fig. 7 gives a suitable example. Fig. 7(a) shows the requirement of one linear subspace while two different populations are separated, whereas four populations require two subspaces (ref. Fig. 7(b)). In Fig. 7(c), it is shown that these subspaces divide the 2D feature space into seven regions.

From this study, it is a very basic question to ask how many separable regions can be generated from a given n-dimensional feature space. It can be answered that by considering a region A with n dimensions in which m hyperplanes with n-1 dimensions can occupy the normal position. Then the separated regions r(A) can be determined accordingly the Equation-6.

$$r(A) = 1 + \binom{m}{1} + \binom{m}{2} + \dots + \binom{m}{k} + \dots + \binom{m}{n} \quad (6)$$

For understanding the concept of separability of region, it is clear that (n-1)-D subspaces are needed to separate ten populations. According to this inference, Fig. 6 should have more than three subspaces for generating ten separated regions. But, this is not a valid inference in case the structure combines the (n-1) D linear subspaces which are generated from the first layer of the perceptron.

The same concept is presented in Fig. 6 that the clusters having best separability in 2D space follow Fisher Linear Discriminant as given in Equation 5. The Fig. 8 shows the position of cluster which are separated by two dimensional subspace. The population is separated by utilizing only two layers in which three and four perceptron are used (ref. Fig. 9). It is clear that shape of the clusters reduce the linear subspace into curved shape for separating the population. The writer separability is nicely visualized in Fig. 8.

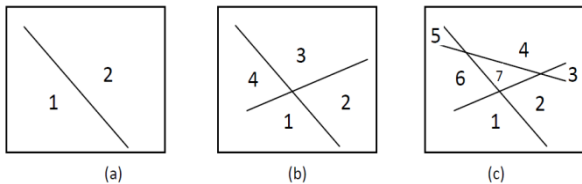


Fig. 7. Maximum Number of Separable Regions in a 2-D Feature Space. (a) Two Regions are Defined with One Linear Subspace. (b) Four Regions are Defined with Two Linear Subspaces. (c) Seven Regions are Defined with Three Subspaces in General Position.

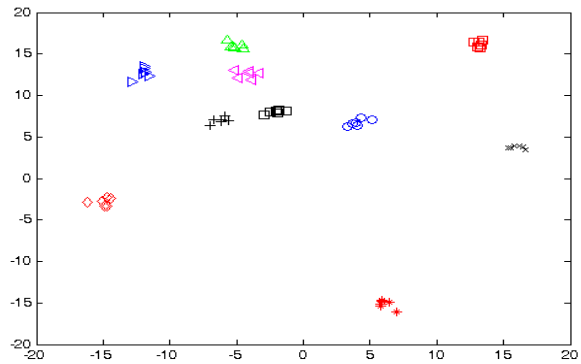


Fig. 8. The 2-D Space Representation with Maximum Separability Received by Applying FLD.

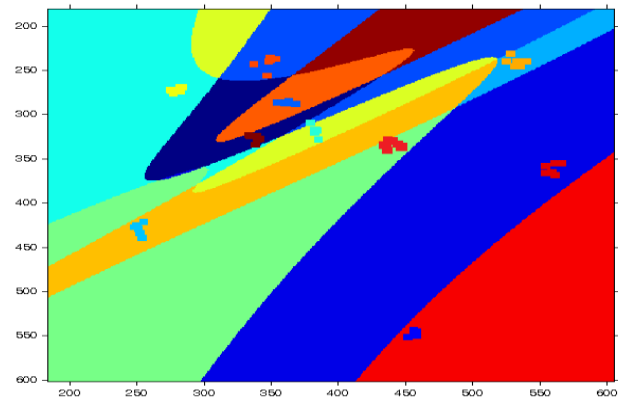


Fig. 9. The Separated Feature of Fig. 8, after Applying Simple Neural Network Architecture with Two-layer Containing 3 and 4 Perceptrons.

IV. RESULT AND DISCUSSION

In our experimental set up, the classification of the signature verification is performed with very simple neural networks. Two words ‘and’ and ‘the’ with the three unit length of SE from NIST DB19 database are considered for the experiments of signature verification. Another set of experiments are performed on the word ‘the’ with joint of SEs with length of three and five units. Following data statistics were used for performing the experiments to discriminate the writers based on short signature.

- Total ten writers are selected from NIST DB19 database. Each of writers generates the words ‘and’ and ‘the’ three and five times separately.
- DMT is applied on SEs of length of three and five units to generate a 25-D feature word vector. It helps to test classification separability.
- The vector generated the SEs length of three and five units which are merged to perform writer identification only with one 50-dimensional vector.
- The generalization and clarification capabilities are tested using classical neural network by training from 50-D vectors with leave-one-out method.

1) *Classification with word 'and'*: In case of simple classification with word 'and', total ten clusters are generated in which each vector is 25-D belonging to feature space. According to the appearance of the word 'the' in NIST database, the strength of cluster is decided. In our experiments, 'the' appears six times so, each cluster contains six members. The training of neural network follows the complicated neural architecture of the perceptions. We extend the set of experiments by adding more layers and neurons in each layer. The selecting strategy of the clusters out of ten members depends on the training of neural network. Therefore, 5five members from the clusters are used for training. In second and third layers, 3-4 neurons are considered suitable to separate the ten clusters. From the training and testing results, it is observed that clusters correctly classified are excluded from this network. It excluded the specific members from the clusters with random frames.

2) *Classification with word 'the' and SEL-3*: In case of classification of the word 'the', proposed model produced similar results to discriminate the writers. Accordingly three times appearance of the word 'and', each of ten clusters maintains the word 'and' 3 times. The structure of this network also follows two-layer architecture with three and four neurons respectively. All the excluded clusters are classified with leave-one-out method from the trained neural structure.

3) *Classification with word 'the' and SEL-5*: In this network model, each of the ten clusters is generated with six members with the word 'the'. Each of the word is dynamically replaced since the new information is added using DMT on SEs with 5 unit length. Ten writers corresponding to 10 clusters are separated by using two-layer architecture of three and four neurons respectively. In this case also, the satisfactory performance is achieved by leave-one-out method.

V. CONCLUSION AND FUTURE RECOMMENDATIONS

The research problem of signature verification requires developing an authentication system for making digital media safe and secured. In this paper, we proposed the solution of signature verification based on the information contained in short text of signature. More specifically, the concept of short signature is attributed to that particular person for asking simply key letter of the signature. Proper matching of lowest features extracted from the short signature suits better to train with simple architecture of neural network. Before the classification process, morphological transformation is applied on the lines of the short word. Markov chain model is adopted for the alternation of the directional information of short signature. Fitting all the directional structuring elements provide normalized information to analyze the performance of signature verification. The feature space generated from the elements of transition matrices of Markov model is the outcome of fitting directional structuring elements. For resolving the issue with high dimensionality features Fisher Linear Discriminant is ensured to provide suitable insights in reducing the dimension. It results in better separability of short words verification.

We also achieved the significant improvement on the separated writers' clusters. This proposed network of ten user writers is very simple with two layers consisting of three and four perceptrons for developing signature verification system. Dimensionality issues can be entertained as sounding future recommendation to deal with the problem of large samples collected from the users of different ethnicity. There is another side open for tackling the problem of neurological conditions in dynamic signature verification.

ACKNOWLEDGMENT

Muhammad Nazir would like to thank the Deanship of Scientific Research at Majmaah University for supporting this work under Project No. R-2022-158.

REFERENCES

- [1] Chaabouni A, Boubaker H, Kherallah M, Alimi AM, El Abed H (2011) Combining of Off-line and On-line Feature Extraction Approaches for Writer Identification. IEEE International Conference on Document Analysis and Recognition, 18-21.
- [2] Lorigo, L. M., & Govindaraju, V. (2006). Offline Arabic handwriting recognition: a survey. IEEE transactions on pattern analysis and machine intelligence, 28(5), 712-724.
- [3] Wu, X., Tang, Y., & Bu, W. (2014). Offline text-independent writer identification based on scale invariant feature transform. IEEE Transactions on Information Forensics and Security, 9(3), 526-536.
- [4] Newell, A. J., & Griffin, L. D. (2014). Writer identification using oriented basic image features and the delta encoding. Pattern Recognition, 47(6), 2255-2265.
- [5] Kumar R, Chanda B, Sharma JD (2014) A novel sparse model based forensic writer identification. Pattern Recognition Letters, 35(1), 105-112.
- [6] Kumar, N. (2019). Human activity recognition from histogram of spatiotemporal depth features. International Journal of Computational Intelligence Studies, 8(4), 309-329.
- [7] Zois EN, Anastassopoulos V (2000) Morphological waveform coding for writer identification. Pattern Recognition, 33(3), 385-398.
- [8] Zhang XY, Xie GS, Liu CL, Bengio Y (2016) End-to-End Online Writer Identification With Recurrent Neural Network. IEEE Transactions on Human-Machine Systems, 99, 1-9.
- [9] Wu X, Tang YY, Bu W (2014) Offline Text-Independent Writer Identification Based on Scale Invariant Feature Transform. IEEE Transactions on Information Forensics and Security, 9(3), 526-536.
- [10] Grother P, Hanaoka K (2019) NIST Special Database 19 (SD19), Handprinted Forms and Characters. 2nd Edition, Information Access Division, Information Technology Laboratory, NIST, National Institute of Standards and Technology, U.S. Department of Commerce.
- [11] Duda R, Hart P, Stork D (2001) Pattern Classification. 2nd Edn., Wiley & Sons, New York.
- [12] Kumar, N., & Sukavanam, N. (2017). Deep Network Architecture for Large Scale Visual Detection and Recognition Issues. Journal of Information Assurance & Security, 12(6).
- [13] Lippmann R (1987) An Introduction to computing with neural nets. IEEE ASSP Magazine, Volume 4, No. 2, pp. 4-22.
- [14] Stanley RP (2007) An Introduction to Hyperplane Arrangements (Chapter). Geometric Combinatorics, IAS/Park City Mathematics Series, Volume 13.
- [15] Goyal, V., Mishra, P., Shukla, A., Deolia, V. K., & Varshney, A. (2019). A fractional order parallel control structure tuned with meta-heuristic optimization algorithms for enhanced robustness. Journal of Electrical Engineering, 70(1), 16-24.
- [16] Sonowal, G., Sharma, A., & Kharb, L. (2021). Spear-Phishing Emails Verification Method based on Verifiable Secret Sharing Scheme. Journal of Information Assurance & Security, 16(3).

- [17] Kaur, H., & Kumar, M. (2021). Signature identification and verification techniques: state-of-the-art work. *Journal of Ambient Intelligence and Humanized Computing*, 1-19.
- [18] Alaei, A., Pal, S., Pal, U., & Blumenstein, M. (2017). An efficient signature verification method based on an interval symbolic representation and a fuzzy similarity measure. *IEEE Transactions on Information Forensics and Security*, 12(10), 2360-2372.
- [19] Dey, S., Dutta, A., Toledo, J. I., Ghosh, S. K., Lladós, J., & Pal, U. (2017). Signet: Convolutional siamese network for writer independent offline signature verification. *arXiv preprint arXiv:1707.02131*.
- [20] Shariatmadari, S., Emadi, S., & Akbari, Y. (2019). Patch-based offline signature verification using one-class hierarchical deep learning. *International Journal on Document Analysis and Recognition (IJDAR)*, 22(4), 375-385.
- [21] Berkay Yilmaz, M., & Ozturk, K. (2018). Hybrid user-independent and user-dependent offline signature verification with a two-channel CNN. In *Proceedings of the IEEE Conference on Computer Vision and Pattern Recognition Workshops* (pp. 526-534).
- [22] Liu, L., Huang, L., Yin, F., & Chen, Y. (2021). Offline signature verification using a region based deep metric learning network. *Pattern Recognition*, 118, 108009.
- [23] Diaz, M., Ferrer, M. A., & Sabourin, R. (2016, December). Approaching the intra-class variability in multi-script static signature evaluation. In *2016 23rd international conference on pattern recognition (ICPR)* (pp. 1147-1152). IEEE.
- [24] Parcham, E., Ilbeygi, M., & Amini, M. (2021). CBCapsNet: A novel writer-independent offline signature verification model using a CNN-based architecture and capsule neural networks. *Expert Systems with Applications*, 185, 115649.
- [25] Nguyen, B. X., Nguyen, B. D., Do, T., Tjiputra, E., Tran, Q. D., & Nguyen, A. (2021). Graph-based person signature for person re-identifications. In *Proceedings of the IEEE/CVF conference on computer vision and pattern recognition* (pp. 3492-3501).

Face Mask Wear Detection by using Facial Recognition System for Entrance Authorization

Munirah Ahmad Azraai¹, Ridhwan Rani², Raja Mariatul Qibtiah³, Hidayah Samian⁴
Faculty of Technical and Vocational Education, Universiti Tun Hussein Onn, Parit Raja, Johor, Malaysia^{1,2,4}
Department of Electric and Electronic, German Malaysian Institute, Kajang Selangor, Malaysia³

Abstract—A Face Mask Wear Detection Device for Entrance Authorization is designed to ensure that everyone wears a face mask at all times in a confined space. It is one of the easiest methods to lower the rate of coronavirus infection and hence save lives. Asthma, high blood pressure, heart failure, and many other chronic conditions can be fatal to those who are infected by the novel Coronavirus (nCoV-21). Consequently, the goal of this research is for face mask wear detection devices that help to reduce the rate of Novel Coronavirus infection on-premises or in public places by ensuring that customers comply with Standard Handling Procedures (SOP) set by the Ministry of Malaysian Health (MOH). Customers' faces are recognized by this device whether or not they are covered by a face mask upon entry into a facility. Additionally, the use of this device can contribute to ensuring compliance with the maximum number of customers allowed on the premises. A facial recognition system is the goal of this study that uses technology designed as an individual disciplinary aid and follows the safety procedure at this critical time. This research was developed using the engineering design process development model which has four phases namely; identifying the problem, making possible solutions, prototype development and testing and evaluating the solution. Results indicate that the developed product can function effectively. Experts have discovered that using this product helps people stick to their face mask routines. The design of this product has improved, which means that the overall quality of the product is elevated to be capable of performing as intended in terms of intelligent technologies.

Keywords—Face recognition; face detection; face mask; coronavirus; intelligent system

I. INTRODUCTION

COVID-19 is the group of viruses that infect humans through inhalation and contact to the point of death which is transmitted by the SARS-CoV-2 virus, which is a new type of virus from Novel Coronavirus (2021-nCoV). This can lead to lung injury (ALI) and respiratory distress syndrome (ARDS) which affects lung failure and results in death [1]. The current COVID-19 pandemic caused by the novel SARS-CoV-2 Coronavirus (2021-nCoV), first detected in late 2019 in Wuhan province, China, has spread rapidly worldwide and has infected more than 10 million individuals on 29 Jun 2020 [2].

Standard Operating Procedures (SOP) are work instructions and detailed guidelines for work that are documented in writing by the responsible party. SOPs detail the repetitive work processes that will be carried out or followed in the

organization. They keep a record of how activities are carried out to support and facilitate quality data as well as consistent compliance with technical and quality device requirements [3]. The development and application of SOPs are an essential part of a successful quality device since it provides information to individuals performing tasks effectively, and facilitates consistency in the quality and integrity of the product or result.

Face masks are made of fabric that works to prevent germs from entering the human body through respiration. Face masks are respiratory protection used as a way to protect individuals from inhaling harmful substances or contaminants in the air. Respiratory protection or face masks are not intended to replace the preferred method of eliminating disease but are used to adequately protect the wearer [4]. However, hygiene is a widely accepted method of preventing the spread of disease infection. Washing hands with soap have been recommended as a primary and cost-effective preventative measure to prevent bacterial infections that cause influenza-related respiratory illnesses [5].

The National Health Council (NSC) issued Standard Operating Procedures (SOP) to ensure the reduction of Novel Coronavirus (2021-nCoV) infections among Malaysians are still not fully complied with. The National Security Council (NSC) in Malaysia still has a few citizens who don't abide by the NSC's SOPs. It is necessary to conduct surveillance at all building entrances to address this issue. However, a large number of people will be affected by this change. The current staff is unable to monitor and care for all of the areas that the public uses.

Consequently, this study is intended for customers who enter a business. The purposes of this study, which focus on three key areas, are as follows:

- Design a face mask wear detection device.
- Develop a face mask wear detection device.
- Test the functionality of this device designed to detect faces and to determine whether the customer is wearing a face mask properly or not.

Artificial Intelligence (AI) must be utilized to simplify efforts to halt the spread of the COVID-19 virus and find solutions to all of the challenging detection issues outlined above.

II. RELATED WORK

Facial recognition is a technology that is becoming increasingly prevalent today. Images taken with this technology can be compared to a database of reference images. In addition, pattern recognition is an important aspect of the field. Automatic Teller Machines (ATMs), e-banking systems like Maybank2u and CIMB Click, and computer logins for security gates and computer networks are just a few instances of security systems that rely solely on pass numbers. Unauthorized individuals who come into possession of this route number will be able to use it in place of the original owner. However, one's face is inalienable as one's own. In this way, the current security system can be enhanced by utilizing facial recognition technology. As stated by Lee, H.S et al., if the facial image recognition path number is compromised, it will constitute the best security feature [6].

According to Yaaseen, M. S. et.al, facial recognition is the most difficult aspect of picture analysis since it involves the human body [7]. Facial recognition is a problem of pattern recognition, and its primary goal is to identify reasoning from facial expressions that are not fixed. Since the 1980s, facial recognition has been a widely discussed topic aimed at solving several practical problems. Face recognition uses biometric methods, which is a distinguishable and quantifiable characteristic that is used to label and describe specific individuals to identify personalities primarily by their faces.

It is shown in Fig. 1, how the basic structure of face recognition works in its simplest form. The facial features are captured and stored in a database during the first stage. It is performed in the extraction stage to find or remove specific facial features. The database will be evaluated by comparing it to previously captured facial features for reference. A comparison is made between the features that were captured and the features that were registered in the database based on the extraction and process reference [8]. According to previous studies, several conclude that there are numerous facial recognition techniques, including:

A. Holistic Matching Method

Sreen et al. [9] used this method to make a match when the captured facial features are crooked or the facial expressions don't match the database system. This method has unique characteristics, such as pattern points. The difference between the distances between the two eyes will aid in distinguishing the various facial angles of each individual. This method makes use of 2D technology to aid the expertise.

B. Feature-Based Method

Shen Li et al. [10] discussed this type of feature-based recognition which is an improvement on previous methods of recognition technology. Features detected on 2D images use geometric classification and facial structure in terms of points, lines or areas. The data obtained from those features are converted to mathematical data.



Fig. 1. Basic Structure of Face Recognition.

C. Hybrid Method

HiviIsmat Dino et al. [11] designed a system using the holistic matching method and the feature-based method, this hybrid method employs 3D technology. The hybrid model is the result of the advancement of the previous two methods, with the exception that it uses more accurate and sophisticated recognition. This type of hybrid recognizes more features on the face known as facial node points and identifies the face more deeply.

D. Skin Texture Analysis Method

Shepley developed a Skin Texture System Analysis using facial recognition technique by converting unique lines, patterns, and spots visible on an individual's skin translated into mathematical space. Therefore, skin texture analysis is more sophisticated compared to the Hybrid type [12].

E. Thermal Cameras Method

Arthur et al. [13] proposed thermal face verification to recognize faces using thermal cameras, which is a more advanced face recognition method. As shown in Fig. 2, this technique measures the rate at which heat is emitted from individuals or other sources of heat. The object's heat output determines the image that is produced.



Fig. 2. Camera Thermal.

A number of previous studies employing various face recognition-related technologies have been identified in the Table I. Nonetheless, the study has provided suggestions for improving this system. Among previous research are shown in the following tables [14]-[16].

Table II depicts the commercially available products that are relevant to this study. An overview and theoretical description of the face mask wear detection device for determining whether a person can enter a building has been presented in this review. The researcher can use this literature review to identify the hardware, equipment, and software required to continue the study.

TABLE I. REFERENCES LIST PREVIOUS RESEARCH

No	Innovation System		
	Author	Product Name	Description
1	Hung-Che June 30, 2020	Facemask ATM and Reminder	<ul style="list-style-type: none"> The ATM and Reminder Facemask was developed to discipline each individual to wear a face mask when leaving the house and premises. The method used is Motion Sensor and Piezo Buzzer, it works to detect the user's movement when crossing the device while the Piezo Buzzer will buzz very loudly. The ultrasonic sensor works to calculate the number of face masks in the device. Furthermore, the LCD serves to display the number of face masks. Finally, it uses the Arduino Uno in this research.
2	Julian-grodzicky Dec 1, 2018	Face Tracking and Recognition using Matlab	<ul style="list-style-type: none"> Face Tracking and Recognition using Matlab and Arduino is a study of various image preparation procedures to better extract half of the face and upgrade RGB images to GRAY. Customization of channel combinations for Find Neighbor extraction via a pre-adjusted interface. With this technique, the use of these coordinated channels can be analyzed and thus guarantee facial recognition
3	Khanday & Bashir, 2018	Face Recognition Techniques: Critical Review	<ul style="list-style-type: none"> This article discusses the study of the types of face recognition and the challenges of how to improve the efficiency and rate of recognition for face identification in large databases. Then, it is compared with the accuracy or rate of recognition. This study stated The advantage of using the biometric artificial intelligence (AI) method is easier when compared to the biometric method which requires special help from people for authentication. This biometric artificial intelligence (AI) has challenges in recognizing faces in moving face conditions, twin poses variations and good lighting conditions for face recognition to be made.

TABLE II. CURRENT PRODUCT IN THE MARKET

No	In-Market		
	Product Image	Product Name	Description of product
1		Barth People Counter PC-10	-The maximum limit of people can be set easily via Touch Display -High-quality aluminium stele with stainless steel base -Fast and easy setup in less than 5 minutes shortcomings: <ul style="list-style-type: none"> Need large and heavy space Affordable cost (~RM 7,497.95)
2		Face recognition system	-Supports face mask detection -Record staff entry and exit times -Record both staff and visitor records -Supports door/door access control protocol shortcomings: <ul style="list-style-type: none"> Cannot limit the number of customers Cost is quite expensive (~RM3,500.00)
3		Automatic infrared heat scanner	-Shorter filtering period shortcomings: <ul style="list-style-type: none"> Cannot limit the number of customers. No automatic doors. Price in the range of RM8,000.00

III. METHODOLOGY

The methodology section describes all the necessary information that is required to obtain the results of the study. Six work steps need to be done by the researcher to develop a Face Mask Wear detection Device. There are four phases underway to develop a face mask wear detection device for entry into the premises. Phase 1: Determining the Problem and Background of the research, Phase 2: Making Solutions Possible, Phase 3: Prototype Development and Phase 4: Test and evaluate the solution.

A. Research Design

Problem analysis is the initial phase of the study conducted to identify problems that arise and set the direction of product development as well as identify the function of the product to be developed. At this stage, the objectives and goals of the study are determined based on the problem factors that exist. This determination is made to ensure that the development process is carried out following the objectives and purposes of the study and is used as a guide throughout the development period.

Furthermore, suggest solutions to problems encountered. Problem-solving in the study conducted is a step taken to propose appropriate solutions and methods to be applied throughout the development process done by developing or proposing some solutions that are capable of overcoming the problems encountered.

Data collection has been done for customers that follow SOPs when entering premises. Based on the data, most of the customers failed to wear mask properly when entering a premise. This also violates the limit of customers on a premise. Thus, the customer's failure to comply with SOPs during the endemic is the problem statement for this research.

The selection of this problem-solving method consists of several factors that influence the development process of the Face Mask Wear Detection Device by using the Facial Recognition System for Entrance Authorization which consists of the design method, material to be used, required functionality and complexity of the development method. Lastly, create a form of control model capable of solving the problems encountered by developing a prototype.

B. Development Procedure

Engineering Design Process (EDP) is a process for solving problem statements that occur and can be used in almost any situation [17]. The use of this model helps to study and understand the problem and its possible solutions at each step or phase of the research process. EDP is a process that includes steps that can be repeated, although not always in the same sequence but still guided by the objectives of the study. Furthermore, several steps cover several aspects such as planning, designing, testing, and refining the design. This process is often initiated based on clear research objectives and goals and is a journey process aimed at solving problems (National Academy of Engineering, 2020). Based on Fig. 3, six work steps need to be done by the researcher to develop a Face Mask Wear Detection System for Premises Entry Permission. There are four phases carried out to develop the system [18].

The stages of product development that have been completed in the creation of the face mask wear detection system. By adhering to this methodology, the success of product development is made more systematic [19]-[21].

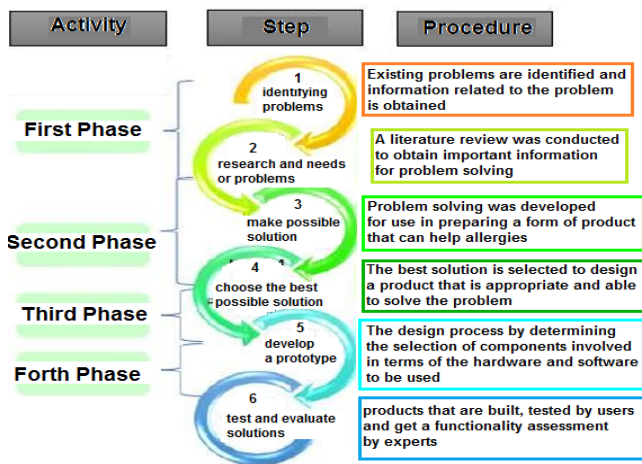


Fig. 3. Phases in Product Development.

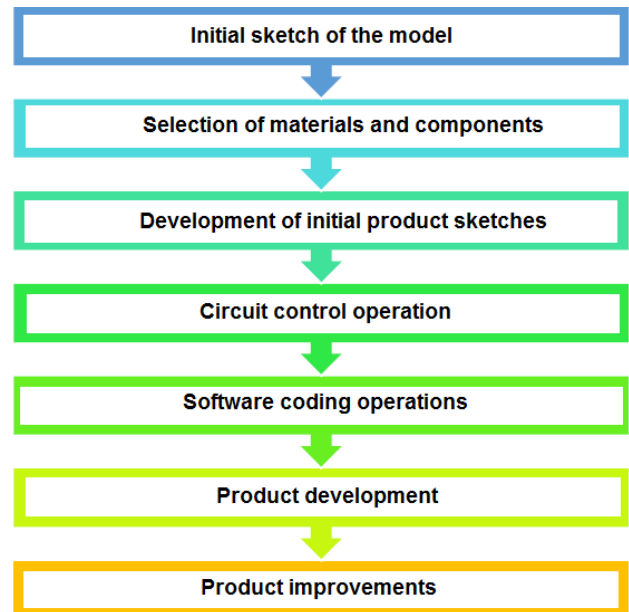


Fig. 4. Product Development Process.

Fig. 4 illustrates the stages of the product development process of the SOP Compliance Testing Device and the Application of Face Mask.

C. Model Development

The model development is influenced by suitability and user-friendliness. It is always used according to the objectives of the study. The design produced must be durable, easy to move, lightweight, affordable and easy to work with users. Therefore, the researcher proposed a model for the use of face mask detection device for entry into the premises based on the suitability and needs of users. Fig. 5 shows a model sketch of a face mask wear detection device for entrance authorization.

D. FaceMack Detection Method

The system will start by tracking the physical distance with the device using an IR sensor. Then proceed with the recognition of the physical face by using the ESP32-CAM module. The client image is detected and matched with the image that is in the user database but if, the distance setting is not reached by the IR sensor, the ESP32-CAM Module is inactive and the LCD will display “Take a step back to re-scan”.

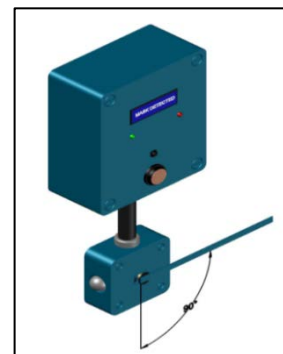


Fig. 5. Model Sketch of A Face Mask Wear Detection Device for Entrance Authorization.

On activation of ESP32 - CAM, it will detect the physical face whether the customer is wearing a face mask or not. The calculation of the percentage of customer face recognition implemented by the ESP32-CAM will be sent to the Arduino Uno for further decision.

If, the percentage is equal to or greater than 99%, the LCD will display “Mask: (percentage)” and “ENTER ALLOWED” and the Servo will rotate 90 degrees clockwise and it will rotate 90 degrees counterclockwise after a few seconds delay. While the percentage is less than 99%, the LCD will display “Mask: (percentage)” and “PLEASE WEAR MASK” as well as the Servo will not rotate. The process is illustrated in Fig. 6.

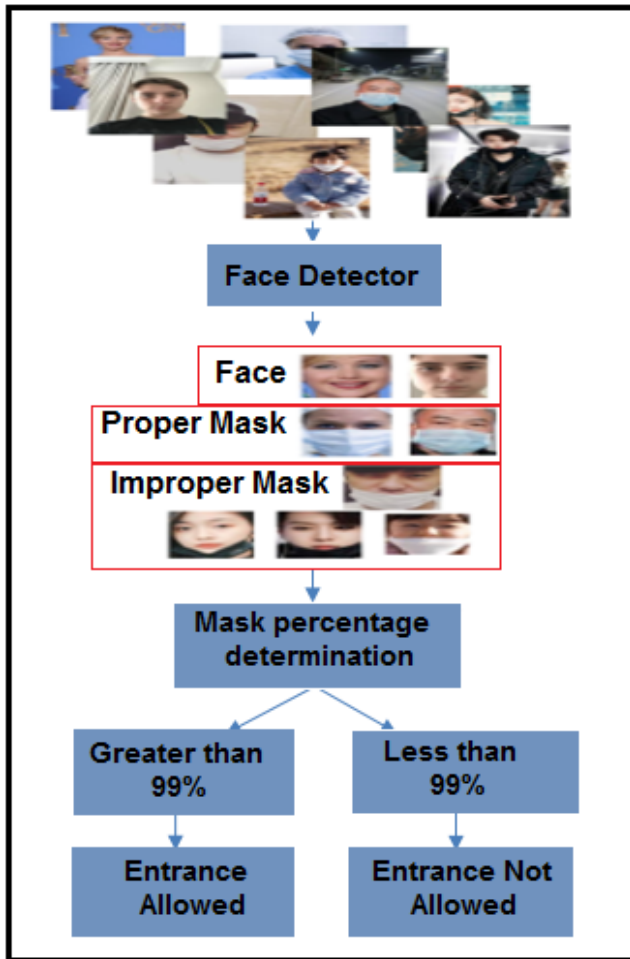


Fig. 6. A Flowchart for Methods Aiming to Identify Wearing Mask Conditions.

IV. RESULT AND DISCUSSION

The face mask wear detection device for entry into the premises has several key components required to complete the entire system and be able to operate properly and effectively. This main component has been conducted a functionality test so that researchers can identify whether it can operate well and under the requirements of the operation.

A. Facial Recognition Functionality Analysis (ESP32-CAM)

In the development of this product, facial recognition technology is utilized to compare database images with

captured images. The researcher has devised a testing method that involves measuring the distance between the prototype and the human face to determine the functionality and effectiveness of facial recognition. Setting the test distance scale from 0 cm to 100 cm and measuring the recognition time required to detect the face yielded data from three different angle view which is left, front and right angle view. The data collected was recorded for the front angle view, left angle view and right angle view of the facial recognition effectiveness test in Table III, Table IV, and Table V, respectively.

Based on the collected analytical data, the researcher can identify the distance that must be determined for the system to initiate facial recognition. This is to ensure that face recognition is performed by a single person at a distance from the customer in front of the device. The researcher used an IR sensor to support the system by setting the distance between the customer's face recognition and the distance set by the customer. Fig. 7 shows the IR sensor's detection distance for initiating facial affirmation in the following way.

TABLE III. LEFT ANGLE VIEW OF FACIAL RECOGNITION EFFECTIVENESS TEST

No	Left Angle View		
	Distance (cm)	Detected	Time to detect(s)
1	0	No	-
2	10	No	-
3	20	No	-
4	30	No	-
5	40	Yes	4.0
6	50	Yes	4.5
7	60	Yes	4.3
8	70	Yes	4.0
9	80	No	-
10	90	No	-
11	100	No	-

TABLE IV. FRONT VIEW OF FACIAL RECOGNITION EFFECTIVENESS TEST

No	Front View		
	Distance (cm)	Detected	Time to detect(s)
1	0	No	-
2	10	No	-
3	20	Yes	4.2
4	30	Yes	4.0
5	40	Yes	4.1
6	50	Yes	3.6
7	60	Yes	3.6
8	70	Yes	5.4
9	80	No	-
10	90	No	-
11	100	No	-

TABLE V. RIGHT ANGLE VIEW OF FACIAL RECOGNITION EFFECTIVENESS TEST

No	Right Angle View		
	Distance (cm)	Detected	Time to detect(s)
1	0	No	-
2	10	No	-
3	20	No	-
4	30	No	-
5	40	Yes	4.3
6	50	Yes	4.5
7	60	Yes	4.2
8	70	Yes	4.1
9	80	No	-
10	90	No	-
11	100	No	-

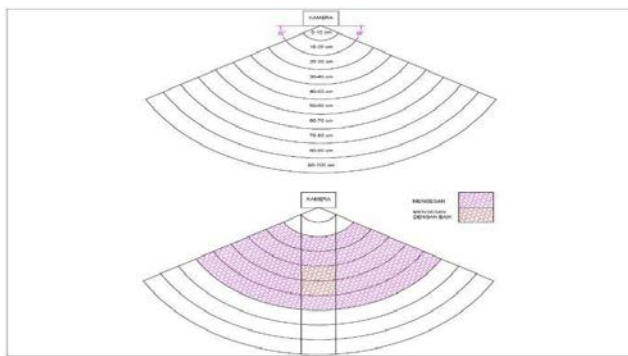


Fig. 7. Operating Face Recognition Area.

Another aspect of facial recognition that requires investigation is the rate of recognition. This is since researchers must examine the percentage of faces detected in clients who wear face masks in a variety of ways. As a result, the researchers created various face mask wear variations and tested the detected face rate to reduce the device's error rate in determining which customers were correctly wearing face masks.

Fig. 8 presents the fact that the consumer is not concealing their face resulting in 80% of displays on the LCD.



Fig. 8. The Device Displays "Please Wear the Mask".



Fig. 9. The Device Displays "Enter Allowed".

Since the customer is concealing their identity with a face mask, the LCD has a display rate of 100% as shown in Fig. 9.



Fig. 10. Side View of Customer's Face.

Since the customer is not wearing a face mask, 60% of the displays on the LCD are visible even inside view as shown in Fig. 10. Data analysis is to determine the percentage value of wearing the mask for the proper way of wearing the mask. The images recorded by ESP32-CAM were compared to face shapes in the database and made face detection results. The percentage value of wearing the mask for the prototype to allow the customer to enter the premises is above 98%. The gate was controlled by a servo motor the rotation is 90°.

Arduino Uno programming is carried out using an Arduino IDE where the Arduino Uno circuit is connected to a face mask wear detector device for premise entry permission and connected to the laptop port using a Universal Serial Port (USB) cable. In this product two components need coding namely ESP32-CAM and also Arduino Uno it is written in C++ language through the Arduino IDE platform. ESP 32 CAM needs to use CH340G USB to TTL Serial Converter to send code from PC into ESP32-CAM while Arduino Uno only uses USB Printer Cable B Type for Arduino Printing to transfer code from PC to Arduino Uno.

V. CONCLUSION AND FUTURE WORK

The purpose of the face mask wear detection by using a facial recognition system for premise entry permission is to assist customers in determining whether they are wearing a face mask or not. The overall functionality of this system, which is designed to detect this face, has been thoroughly tested so that it can perform as expected. The percentage of

customer face recognition achieved using the codes (coding) set in the ESP32-CAM will be sent to the Arduino Uno for further consideration. If a percentage equal to or greater than 99% is calculated, the bar will be raised to allow entry into the premises. While calculations with a percentage less than 99% are not permitted.

The development of a product necessitates careful and systematic planning to be successfully implemented.

The researcher can learn about the benefits and drawbacks of the product development process based on this discussion. As a result, the study contributes to create a face mask wear detection device and follow SOPs to self-discipline to properly wear face masks. The study produces a face mask wear detection device to improve the efficiency and ease of use of Covid-19 transmission. The system's functionality is being tested to detect faces and determine whether or not the customer is wearing a face mask. Ensure that the number of customers does not exceed the limits set by the premises' owner by reducing the labour cost. Another contributions that can be highlighted in this manuscript is the use of real data obtained by testing the level of effectiveness face-to-face and the provision of accurate results. Furthermore, the two levels emphasised which are proper and improper, are to form a system that will be used to assist researchers in taking into account the mask's position factor.

Since there is currently a limit to how far a sensor can detect, the results may be skewed if we don't make the above-mentioned improvements. However, without the above-mentioned body temperature monitoring system, the objective and interpretation of the results will not be affected because the scope of analysis will be different. It is only beneficial to enhance the functionality of the system.

In the future, some improvements and refinements to this existing system have been proposed by researchers as opportunities for others to participate. The following suggestions can be implemented such as combining this facial recognition technology with a body temperature monitoring system for online health monitoring and; it is advised to include a product efficiency analysis by calculating the average error rate of face detection at a distance.

ACKNOWLEDGMENT

Communication of this research is made possible through monetary assistance by Universiti Tun Hussein Onn Malaysia and the UTHM Publisher's Office via Publication Fund E15216".

REFERENCES

- [1] Shereen, M. A. Khan, S. Kazmi, A. Bashir, N and Siddique, R. "COVID-19 infection: Emergence, transmission, and characteristics of human Novel Coronavirus (2021-nCoV)," *Journal of Advanced Research*, vol. 24, no. 11, pp. 91-98, 2020.
- [2] Buck, M. D, Poirier, E. Z, Cardoso, A, Frederico, B, Canton, J and Barrell, S. "SARS-CoV-2 detection by a clinical diagnostic RT-LAMP assay," *Wellcome Open Research*, vol. 6, no. 9, 2021.
- [3] Garcés Gómez, M. P, "Tradición y modernidad en la organización del discurso en español en el siglo XVIII," *Verba: Anuario Galego de Filoloxía*, vol. 46, pp. 403-409, 2019.
- [4] E.S. Han, A. Goleman, daniel, boyatzis and Richard, "Genetic variations determine susceptibility to organophosphate effects," *Journal Chemical Information Model*, vol. 53, pp. 1689-1699, 2019.
- [5] Saunders-Hastings, P, Crispo, J. A, Sikora, L and Krewski, D, "Effectiveness of personal protective measures in reducing pandemic influenza transmission: A systematic review and meta-analysis," *Epidemics*, vol. 20, pp. 1-20, 2017.
- [6] Lee, H. S and Kim, D, "Expression-invariant face recognition by facial expression transformations," *Pattern Recognition Letters*, vol. 29, no. 13, pp. 1797-1805, 2008.
- [7] Yaaseen Muhammad Saib and Sameerchand Pudaruth, "Is Face Recognition with Masks Possible?," *International Journal of Advanced Computer Science and Applications*, vol. 12, no. 7, pp. 43-50, 2021.
- [8] Dubey A. K and Jain, V, "A review of face recognition methods using deep learning network," *Journal of Information and Optimization Sciences*, vol. 40, no. 7, pp. 547-558, 2019.
- [9] Sereen Alkhazali and Mohammad El-Bashir, "Local Binary Pattern Method (LBP) and Principal Component Analysis (PCA) for Periocular Recognition," *International Journal of Advanced Computer Science and Applications*, vol. 11, no. 8, pp. 70-76, 2020.
- [10] Shen Li, Yang Cheng, Peter Jin, Fan Ding, Qing li and Bin Ran, "A Feature-Based Approach to Large-Scale Freeway Congestion Detection Using Full Cellular Activity Data," *IEEE Transactions on Intelligent Transportation Systems*, vol. 23, no. 2, pp. 1323 - 1331, Feb 2022.
- [11] Hivlsmat Dino, Maiwan Bahjat Abdulrazzaq, Subhi R. M. Zeebaree, Amira B. Sallow, Rizgar R. Zebari, Hanan M. Shukur and Lailan M. Haji, "Facial Expression Recognition Based on Hybrid Feature Extraction Techniques with Different Classifiers," *Journal of Engineering and Management (TEST)*, vol. 83, no. 6, pp. 22319-22329, 2020.
- [12] Assyakirin M H, Shafriza Nisha B, Haniza Y, Fathinul Syahir A S and Muhammad Juhairi A S, "Modelling of Facial Images for Analysis of Recognition," in *International Conference on Man-Machine Systems (ICoMMS 2021)*, Arau, Perlis, 2021.
- [13] Artur Grudzien, Marcin Kowalski and Norbert Pałka, "Thermal Face Verification through Identification," *sensors*, vol. 21, no. 3301, pp. 1-15, 2021.
- [14] Kaur G, Sinha R, Tiwari PK, Yadav SK, Pandey P, Raj R, et al. Face mask recognition system using CNN model. *Neurosci Inform.* (2021).
- [15] Rosebrock A. COVID-19: Face mask detector with OpenCV, Keras/TensorFlow, and Deep Learning. PyImageSearch. (2020).
- [16] Chiang D. Detecting Faces and Determine Whether People Are Wearing Mask. (2020).
- [17] Mata BU, Bhavya S2, Ashitha S3. Face mask detection using convolutional neural network. *J Nat Rem.* (2021).
- [18] Le DN, Parvathy VS, Gupta D, Khanna A, Rodrigues JJ, Shankar K, et al. IoT enabled depthwise separable convolution neural network with deep support vector machine for COVID-19 diagnosis and classification. *Inter J Mac Learn Cybernet.* (2021).
- [19] Roy B, Nandy S, Ghosh D, Dutta D, Biswas P, Das T, et al. Moxa: a deep learning based unmanned approach for real-time monitoring of people wearing medical masks. *Trans Indian National AcademyEng.* (2020).
- [20] Deb C. Face-Mask-Detection: Face Mask Detection system based on computer vision and deep learning using OpenCV and Tensorflow/Keras. (2020).
- [21] J. Deng, J. Guo, X. An, Z. Zhu, and S. Zafeiriou, "Masked face recognition challenge: The insightface track report," arXiv preprint arXiv:2108.08191, 2021.

A Novel Approach to Video Compression using Region of Interest (ROI) Method on Video Surveillance Systems

DewiAnggraini Puspa Hapsari¹, Sarifuddin Madenda², Muhammad Subali³, Aini Suri Talita⁴
Faculty of Computer Science and Information Technology, Gunadarma University, Jakarta, Indonesia^{1,2,4}
Faculty Information Technology, Universitas Cendekia Abditama, Tangerang, Indonesia³

Abstract—With the increasing of criminal actions, people use various surveillance techniques to create a sense of security. One of the most widely used surveillance technique is installing CCTV cameras at various locations. On the surveillance systems, there are other supporting devices apart from CCTV cameras. One of such supporting devices is a hard disk to save the recorded data. The recording on CCTV has two modes: motion detection mode and continuous mode. The continuous mode will record continuously, which affects the amount of hard disk space used. Motion detection mode records one event only, not all recordings, saving hard disk space, however, it may miss some events. Based on these two modes, compression technology is required. The current compression technology applies the ROI method. A ROI (Region of Interest) is the part of the image that wants to filter to form some operations against it. ROI allows coding differently in certain areas of the digital image to have a higher quality than the surrounding area (background). This paper offers a novel approach to saving the foreground frame generated from the ROI method and compressing it. The novel approach will be applied to the AVI, MJPEG 2000, and MPEG-4 video formats. The decompression process is used to restore the original video data to measure the method's performance. To measure the proposed method's performance, it will compare the compression ratio and Peak Signal-to-Noise Ratio (PSNR) with the traditional method without implementing the ROI-based method. The PSNR value in this paper, that measures the quality of the compression results, are above 40 dB. It indicates that the resulting video is similar to the original video. The ROI-based compression method can increase the compression ratio 5-7 times higher than the existing method for lossy AVI format video. While on MJPEG-2000 and MPEG-4 format video, it increases the compression ratio 7-15 times and 1-3 times, respectively. The PSNR value for the proposed method is above 40 dB, which indicates that the reconstructed video is similar to the original video, even though the pixel values have changed slightly.

Keywords—Compression; decompression; foreground; region of interest; video surveillance systems

I. INTRODUCTION

The increasing criminal actions result in people using various surveillance techniques to ensure security and manage communities to create a sense of security [1, 2]. One commonly used surveillance technique is to use video surveillance cameras installed in several places [3]. The development of the internet also supports the increase in surveillance cameras to analyze the recordings [4]. Video surveillance is currently an active field of research that aims to

analyze video captured by cameras. This functionality makes it suitable for security applications, object identification and tracking, gender classification, et al. [5].

Nowadays, CCTV is facilitated by remote location monitoring with mobile phones. CCTV does not stand alone but has other supporting devices [6]. These supporting devices are used to monitor and record image objects seen by CCTV cameras [7]. CCTV cameras that produce a low-quality video which is generally recorded at a resolution of 352x240 and have a frame rate of 30 fps, occupy 10 GB of storage in one day [8].

The footage on CCTV is mainly stored on secondary storage devices. CCTV recording equipment has two modes, continuous and motion detection [9]. In continuous mode, CCTV will record continuously so that the hard disk capacity runs out quickly because it stores all the information captured by the camera without choosing whether the data is needed or not. In motion detection mode, also called event recording mode, CCTV only records when specific events occur. Because it only saves when an event occurs, the hard disk capacity does not run out quickly. Its limitation is that not all events are held because CCTV only stores when an object is moving, so some information is lost [10]. A video compression technique is needed that can combine the two modes' advantages.

Several types of video compression used in CCTV are Motion JPEG (MJPEG), Motion JPEG 2000 (MJPEG 2000), MPEG-4, and H.264 [11, 12]. MPEG-4 can be three times more efficient in compression than MJPEG. When the number of frame rates is less than 5-6 frames per second, then MPEG-4 will be less favorable. MPEG-4 uses H-264 video compression and will be efficient when bandwidth conditions are limited and stable. MJPEG uses the Discrete Continuous Transform (DCT) algorithm, while MJPEG 2000 uses the Discrete Wavelet Transform (DWT) algorithm to produce better image quality at higher compression levels. On MJPEG 2000 it is possible to perform a decompression process with a lower resolution representation than the original image, so it is suitable for motion detection algorithms [12].

Video contains data redundancy by which the differences can be recorded within frames or between frames. There are two types of video compression, based on the structure's color component (spatial redundancy) and based on changes between frames (temporal redundancy). The first type is based on the

fact that the human eye cannot distinguish colors well enough because it is affected by the object's brightness. While the other type only encodes the changing frames and directly stored the rest data [13].

The frame changes because there is movement in the object (foreground) captured in the video. Each frame in video data generally contains objects (foreground) and background. The foreground and background detection processes are based on Region of Interest (ROI) that was chosen. It allows different encoding in some regions of the digital image to have a better quality than the surrounding area (background) [14]. ROI is a part of the image that you want to filter to perform some operations.

The application of ROI uses the Max-shift method. In [15], the Max-shift method is used to choose the ROI on an image. The Max-shift method works by shifting the bit-plane from the selected ROI so that it occupies a higher position than the surrounding bit-plane (background), where the shift is conducted to the maximum extent resulting in the maximum quality on foreground compared to the surrounding area. ROI can also reduce the size of the data volume.

Based on these descriptions, this research offers a compression and decompression technique for video surveillance systems by applying a modified ROI method. Modifications are made by using a cropping process to the foreground by implementing the ROI method. And then compress the foreground frame so that the background does not change. The proposed method is implemented on three types of video compression format, lossy video compression in AVI, MJPEG 2000, and MPEG-4.

The rest of this article is as follows; Section II describes the related works of the proposed method. Section III describes the dataset and explains the detail of the proposed method. Section IV describes the results and discussion. The paper is concluded in Section V.

II. RELATED WORK

In a technical review paper conducted by Seagate in 2012 showed that the compression techniques, used to store CCTV footage, can result in a decrease in quality and have little effect on video size [8]. Seagate conducted the review using a very large variation in hard drive recording capacity based on 24x7 video streaming resolutions. With many security applications requiring dozens of cameras and streaming 24x7 video, this can result in storage volumes reaching hundreds of gigabytes.

Cisco estimates that bandwidth usage for data globally will grow 71% in 2017 and forecasts an annual growth rate of 46% from 2017 to 2022 [16]. A CCTV camera connected to the internet with a stable video stream to the cloud will share a usage share of 2% and will grow seven times to increase to 3% by 2022 [17]. Based on the growth of data usage from 2019 to 2020, it is predicted in [18] that video data usage will continue to increase until 2025. It is due to the size of the recorded storage capacity depending on the hard disk installed (typically 160 GB, but some are up to 1 TB), whereas many security applications require dozens of cameras and 24x7 video streams and result in storage volumes running up to hundreds of Gigabytes.

Recordings are mostly stored on secondary storage devices such as hard disks. So, to reduce storage space, a compression technique is applied. In some research, it is recommended to use cloud storage for CCTV footage using IP Camera and storage using NVR (Network Video Recorder) [16, 19]. The limitations are that it requires a fast internet connection on each CCTV camera and requires a large bandwidth when transmitting. So, the storage method using DVR is still being used.

Research on compression to reduce data volume has been conducted by developing motion detection recording modes [20]. In [21], other providing motion detection information, the CCTV video processing also provides two other output that is face detection information and identification information. ROI based method to classify and detecting vehicles was given in [22].

In [23], the author designs a lossy and lossless algorithm by applying ROI to video compression. This algorithm design applies lossy and lossless video compression to raw video. Raw video in the form of cif or qcif is an uncompressed image file. The proposed approach is in which the selected ROI area is based on the human face (face detection). The limitation of this study is that it does not show any effect on data volume.

III. MATERIAL AND PROPOSED METHOD

Fig. 1 is describing the research framework. There are two stages in this research, the compression stage, and the decompression stage. This stage is generating a modified algorithm design from the proposed research topic. The result of this algorithm design will be implemented in MATLAB software.

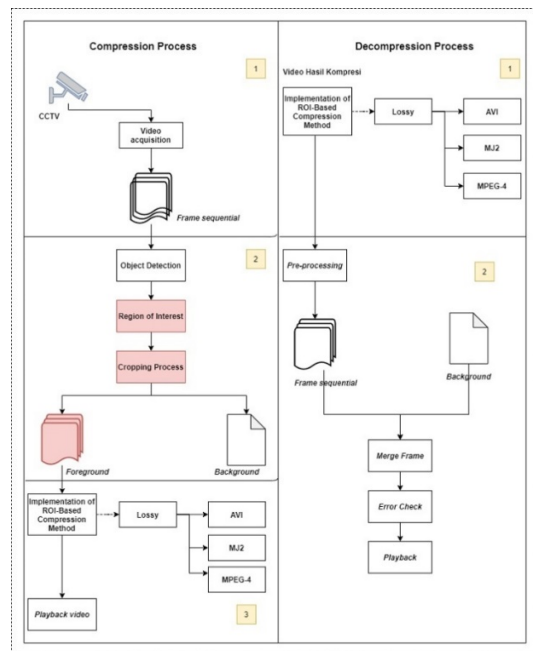


Fig. 1. The Research Framework.

The research phase begins with video acquisition. Video acquisition here is intended to collect video data used in this research. The next stage is to separate the video into some

consecutive frames (sequential frames). Frames (digital images) are collection of pixels such as RGB or YCbCr. It is continued by video compression process. The difference between this proposed method and the common traditional compression method by AVI, MJPEG 2000 and MPEG-4 is that on this research the compression was implemented on the cropped frame. Based on the ROI method, the cropping process was held on the foreground frame that separates it from the background. At the compression stage, there are three stages: object detection by applying the background subtraction algorithm, followed by determining the ROI area to be separated between background and foreground, and third one is cropping process. The DCT algorithm will compress the foreground cropping results for AVI and MPEG-4 video formats and the DWT algorithm for MJPEG 2000 video format.

The decompression stage consists of three stages, namely, reading the compressed video, merging the foreground and background of each sequential frame, and generating the reconstructed video. The merging of the foreground and background of each sequential frame begins with the pre-processing stage. The pre-processing process is performed by reading the length of the video, determining the minimum and maximum of the width and height of each sequential frame. Next, separate the video data into sequential frames. After getting the sequential frames, read the background frame and combine it with the sequential frames based on its maximum width and height. Perform an error check on the mixed results to see whether each frame can be merged correctly.

A. Video Acquisition

Video acquisition is the process of capturing or scanning video so that digital video will be obtained [24]. In the video acquisition process, several factors need to be the main concern in the process. These factors are the types of acquisition tool, camera resolution, lighting techniques, zooming techniques (enlarge and reduce the camera) and the angle of data collection [25].

Each type of camera has its characteristics. Therefore, this research uses some different cameras. It consists of 1 CCTV camera and two non-CCTV cameras with different camera resolutions, i.e., 1.3 MP for CCTV cameras and 5 MP and 13 MP for Non-CCTV cameras. The video capture process is conducted simultaneously. The three cameras are placed at the height of one meter from the ground and distances two meters from the observed object. The dataset at the research location was taken at night, requiring additional artificial light. The object of this research focuses on the coordinated movement of objects that move at a certain speed that can be captured by the camera and it consists of an object only, a remote-controlled toy car.

B. Sequential Frames

Video is a collection of images that are recorded sequentially, and their movements are according to a function of time. After the video acquisition process, frames from the video will be separated [26]. The frame splitting stage begins by reading the length of the image on the video to find out how many frames the video has. Next will be determined the size of the image that is the width and height of the image.

C. Object Detection using Background Subtraction Method

After sequential frame stage, next is detecting the object. Video acquisition in this research uses a static camera so that it does not move and the point of view of taking the objects is fixed. The resulting background remains same from the beginning of the video to the end. It makes the research direction focuses on the movement of objects, so the algorithm used for object detection is the background subtraction algorithm [26].

The initial step to be conducted is to read the first frame of the video data. This initial frame will be used as the background frame. The next step is to apply edge detection using the background subtraction method to produce a foreground mask. This foreground mask will be used as a reference for the next stage. The background image is the frame that will be compared with the next frame (second frame, third frame, etc.), and then the result is reduced to get the difference. The difference will be used to detect the movement of the object. The result of image reduction is converted into a greyscale image. If there is a change in the value of a particular pixel, assign value 1 (marked in white). If there is no change in the pixel value, give the value 0 (marked in black). The difference from this greyscale image will produce a foreground mask.

D. Region of Interest

After getting the foreground mask by applying background subtraction algorithm, it will use the foreground mask as the area of interest for ROI. ROI area is marked by a bounding box, which is a box with x and y coordinates representing the width and length of the detected object [27]. Building the bounding box requires a background image, foreground image, and foreground mask. In making a bounding box, start by measuring the size in the region of the image. Then read the foreground mask generated by the background subtraction algorithm. Continue with displaying the box from the bounding box so that it will visually illustrate the separation.

E. Cropping Process

At this stage, a cropping process is conducted from the ROI results. The input image from the previous stage will be read and then cropped to get a new image. Image cropping in general, can be done based on the coordinates, the number of pixels or the results of zooming a certain area.

This research uses the foreground's width and height information to calculate the intersection point's coordinates after reading the bounding box image. The image cropping process is conducted based on the intersection point coordinates. The result of this stage is a sequential frame containing only objects and a background frame. Sequential frames have objects (foreground) that will be used as input for the compression stage, while the background frame will be saved for the decompression stage. It will merge the foreground and background later in the decompression stage.

F. Implementation of ROI-based Compression Method

This stage implements a lossy compression method in AVI, MJPEG 2000 and MPEG-4 video compression formats on the cropped foreground frame. The lossy compression method is a

compression method that removes some information from the original data during the compression process, such as reducing the pixel value but does not significantly cross the limits of the visual perception of the human eye.

The AVI and MPEG-4 video formats use the DCT transformation algorithm, while the MJPEG 2000 video format uses the DWT transformation algorithm [28]. A quantization process will be applied to each video format to reduce the amount of information needed to represent the frequency so that unnecessary information can be eliminated. The entropy coding process is conducted after the quantization process is complete. The result of this process is a compressed image where for the AVI video format, it will be saved using a bitmap (.bmp) file, while for the MJPEG 2000 it will be saved using a JPEG 2000 file (.jp2) and for the MPEG-4, it will be saved using a JPEG (.jpg) file. The last step is to combine all compressed foreground frames into a video file for each video formats.

G. Implementation of ROI-based Decompression Method

The decompression process aims to restore the compressed image into an image representation like the original image [29]. It begins by reading the compressed video for three formats and then saving the information about the length of the video, minimum and maximum value of the width and height of each sequential frame. After separating, the video into a sequence of frames, combine the background and foreground for each frame. It turns the frame sequence into a video representation.

H. Cropping Process

The proposed method performance evaluation measures include compression ratio and Peak Signal-to-Noise Ratio (PSNR). The performance of a data compression algorithm can be measured by calculating the compression ratio. It measures the physical substance, how much capacity the original compressed file has. The compression ratio (CR) is defined as the ratio of the size of the original data (uncompressed) and the size of the compressed data, which is expressed by (1) [13].

$$CR = \frac{x}{x'} \quad (1)$$

where x = the size of the original data (bytes), and x' = the size of the compressed data (bytes). The compression ratio is closely related to how much memory space can be saved.

Calculating the quality of the decompressed image can be done by calculating the PSNR value. To calculate PSNR, it takes the Mean-Square Error (MSE) value given by (2) [13]:

$$MSE = \frac{1}{CM.N} \sum_{i=0}^{M-1} \sum_{j=0}^{N-1} [|I(i,j) - R(i,j)|]^2 \quad (2)$$

where, $I(i, j)$ represent the original image before compression, while $R(i, j)$ represents the compressed image, C represents the color component of the image where $C=1$ for binary images or grey level, $C=3$ for color images and the size

of the image is $N \times M$. A significant MSE value indicates that the deviation or difference between the reconstructed and original images is quite significant. Meanwhile, for calculating the PSNR value we can use (3) [13]:

$$PSNR = 10 \log_{10} \left(\frac{\max_1^2}{MSE} \right) = 20 \log_{10} \left(\frac{\max_1}{\sqrt{MSE}} \right) \quad (3)$$

where, \max_1 is the maximum value of a pixel in the original image I . The smaller the MSE noise value, the higher the PSNR value, the higher the image quality. On the other hand, the higher the MSE noise value, the smaller the PSNR value, the lower the image quality. Typical values for PSNR in the lossy image and video compression are between 30 dB and 50 dB, where higher is better [30, 31]. Values above 40 dB are usually considered very well, and values below 20 dB are usually unacceptable [31, 32]. When the two images are identical, the MSE value will be zero, which will result in infinite PSNR [31].

IV. RESULTS AND DISCUSSION

A. Result of Video Acquisition

Table I shows the specifications of the video used. Data was taken with three cameras, one CCTV camera and two non-CCTV cameras, with different specifications to produce three video data. The video acquisition is held at night, so it requires additional lighting, which is placed in front of the object.

TABLE I. SPECIFICATIONS OF THE VIDEO USED

Video Name	Number of frames	Video file sizes
Car1	157 frames	138.87 MB
Car2	294 frames	290.70 MB
Car3	175 frames	461.43 MB

B. Result of Sequential Frames

On this stage, the results of sequence frames are saved in BMP format. For video Car1, the data size of each frame is 676 KB with the time required for sequential frame processing is 6.765 seconds. While for video Car2, the data size of each frame is 1 MB with the time required for sequential frame processing is 12.607 seconds. For the third video, the data size of each frame is 2.7 MB with the time required for sequential frame processing is 9.095 seconds. Fig. 2 gives examples of frame sequential results from three video data.

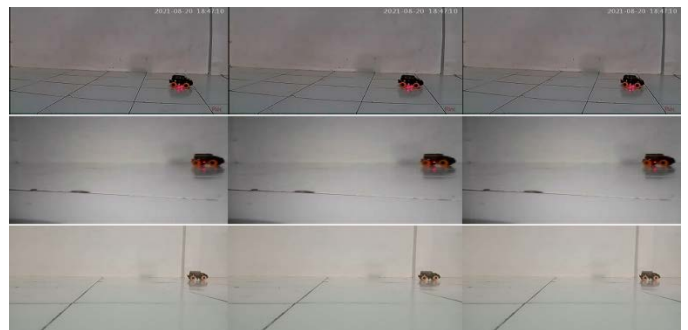


Fig. 2. Example of Frame Sequential Results.

C. Result of Object Detection using Background Subtraction Method

The background subtraction method takes the difference from the frame value by calculating it based on subtracting the current frame from the predefined background frame. Video input in sequential frames will be separated from the first frame by the next frame. The resulting image will be converted into a grey-level image. The grey-level image will be filtered and binarized to determine the foreground and background edges threshold.

Fig. 3 gives examples of object detection resulting from three video data, which shows the difference between foreground and background. The foreground is marked in white, while the background is marked in black. The time required for the object detection process in the first video is 6.763 seconds. While the time required for the object detection process in the second and third video is 13.140 seconds and 9.348 seconds, respectively.

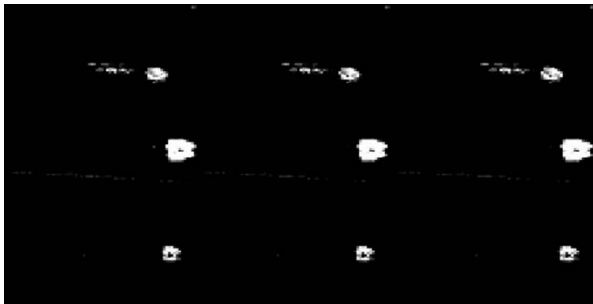


Fig. 3. Example of Object Detection Results.

D. Result of Region of Interest

Fig. 4 gives examples of the result of applying the ROI method on three video data. The yellow box can be seen visually as a separation sign of the foreground and inside the yellow box, while the background area is outside the yellow box.

E. Result of Cropping Process

The result of the bounding box process will be the input image for the cropping process. This cropped image contains information about the object of interest from each sequential frame. The cropping process will only keep the foreground from the sequential frame to produce a new image. The new image that contains information about the object will later become the input image of the compression process.

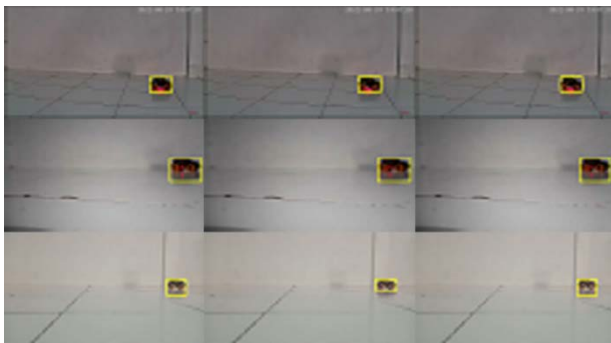


Fig. 4. Example of ROI Results.

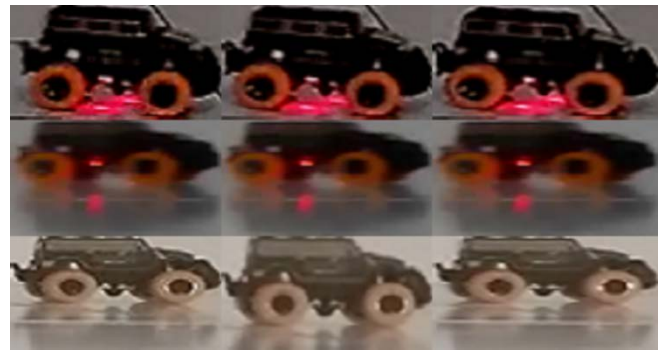


Fig. 5. Example of Cropping Process.

Fig. 5 gives examples of the cropped images from three video data. The sizes of the resulting frames have a different size according to the size of each bounding box.

F. Result of Implementation of ROI-based Compression Method

Table II shows video compression results and the time required to perform the compression process based on this proposed method. It can be seen in Table II that the sizes of compressed data with the ROI-based compression method are smaller than the size of the original data. For example, on the first video, Car1 with AVI format, the compressed data size is 1.50 MB, much smaller than the original video size of 138.87 MB (Table I).

G. Processing Time for Implementation of ROI-based Decompression Method

Table III shows the time that it takes to process the decompression stage. All sequential frames result from combining background and foreground frames, will then be saved in AVI, MJPEG 2000 and MPEG-4 video formats. For each video playback process, the processing time will be calculated. The reconstructed video from decompression method will be used later to count PSNR.

H. Compression Ratio and PSNR Values

Compression ratio that is calculated by (1) is defined as the ratio of the size of the original data (uncompressed) and the size of the compressed data. Table IV gives the comparison of compression ratio between the result by proposed method (with ROI) and existing method (without ROI).

TABLE II. THE RESULTS OF VIDEO COMPRESSION USING THE ROI-BASED COMPRESSION METHOD FROM THE DATA CIDEO

	Video compression format	Size of compressed data with ROI's	Processing time (seconds)
Car1	AVI	1.50 MB	0.904519
	MJPEG 2000	0.61 MB	0.978303
	MPEG-4	0.11 MB	0.981535
Car2	AVI	2.12 MB	1.837451
	MJPEG 2000	1.12 MB	1.790168
	MPEG-4	0.15 MB	1.772530
Car3	AVI	1.45 MB	3.526940
	MJPEG 2000	0.61 MB	3.324557
	MPEG-4	0.19 MB	3.473233

TABLE III. PROCESSING TIME FOR VIDEO DECOMPRESSION USING THE ROI-BASED COMPRESSION METHOD

	Processing time for AVI format videos (second)	Processing time for MJPEG 2000 format videos (second)	Processing time for MPEG-4 format videos (second)
Car1	0.321361	0.314064	0.215553
Car2	0.208899	0.193403	0.153938
Car3	0.180601	0.192206	0.112877

In Table IV, the compression ratio of the proposed method (with ROI) in all cases is higher than the compression ratio of the existing method (without ROI). So, it can claim that this proposed method works better in compressing the video data than the current method if it uses a compression ratio to measure the performance.

Table V gives the result of PSNR calculation using ROI-based compression method from three video file formats. The higher PSNR value means the higher reconstructed video quality (result of decompression process). On the other hand, the smaller the PSNR value, the lower the video quality.

TABLE IV. PERFORMANCE COMPARISON OF THE COMPRESSION RATIO FOR THE PROPOSED METHOD (WITH ROI) AND WITHOUT ROI ON VARIOUS VIDEO

	Video compression format	Original size data (a)	Size compressed data without ROI (b)	Size Compressed data with ROI (c)	Compression ratio without ROI (a/b)	Compression ratio with ROI (a/c)	Improved compression ratio (b/c)
Car1	AVI	138.87 MB	10.3 MB	1.50 MB	13.4825	92.58	6.8667
	MJPEG 2000		7.05 MB	0.61 MB	19.6979	227.6557	11.5574
	MPEG-4		0.21 MB	0.11 MB	670.7683	1262.4545	1.9091
Car2	AVI	290.70 MB	15.7 MB	2.12 MB	18.516	137.1226	7.4057
	MJPEG 2000		8.27 MB	1.12 MB	35.1511	259.5536	7.3839
	MPEG-4		0.61 MB	0.19 MB	476.5574	1530	3.2105
Car3	AVI	461.43 MB	7.71 MB	1.45 MB	59.8482	318.2276	5.3172
	MJPEG 2000		9.61 MB	0.61 MB	48.0156	756.4423	15.7541
	MPEG-4		0.53 MB	0.19 MB	870.6226	2428.5789s	2.789

TABLE V. PERFORMANCE OF THE PROPOSED METHOD BY PSNR

	PSNR for AVI format videos with ROI (dB)	PSNR for MJPEG 2000 format videos with ROI (dB)	PSNR for MPEG-4 format videos with ROI (dB)
Car1	56.9328	52.3866	64.2107
Car2	62.7869	57.8663	63.1144
Car3	51.0671	46.9997	46.8808

In Table V, all PSNR values are above 40 dB, indicating that the reconstructed video resulting from decompression is similar to the original video.

V. CONCLUSION AND FUTURE WORK

This paper proposes an ROI-based compression-decompression method that separates foreground and background on each sequential frame by the background subtraction method. Based on experiment results, for all videos that were acquired, this proposed method gives better results in compression ratio and PSNR values compared with existing methods (without ROI). That is, it increases the compression ratio and PSNR values.

The results of increasing the compression ratio for the video compression method with ROI on the AVI compression video format are 6.8667, 7.4057, and 5.3172. The results of increasing the compression ratio for the video compression method with ROI on the MJPEG 2000 compression video format are 11.5574, 7.3839, and 15.7541. At the same time, the results of increasing the compression ratio for the video compression method with ROI on the MPEG 4 compression video format are 1.9091, 3.2105, and 2.789. The ROI-based compression method can increase the compression ratio 5-7 times higher than the existing method for lossy AVI format video. While on lossy MJPEG-2000 and MPEG-4, it increases the compression ratio 7-15 times and 1-3 times, respectively.

The results of the PSNR value for the video compression method in the AVI compression video format are 56.9328, 62.7869, and 51.0671. The PSNR values for the video compression method in the MJPEG 2000 compression video format are 52.3866, 57.8663, and 46.9997. And the results of the PSNR value for the video compression method in the MPEG-4 video compression format are 64.2107, 63.1144, and 46.8808. The PSNR value for the proposed method is above 40 dB [31, 32], which indicates that the reconstructed video is similar to the original video, even though the pixel values have changed slightly.

This study only uses one object, while there can be more than one object in the field (crowd people). The camera used in this study is still, while the camera used in CCTV may be a camera that moves which results in changes in the background. So further research can be conducted to detect more than one object, moving cameras, or changes in the camera's background.

ACKNOWLEDGMENT

This work was supported by Research Program supported by the Kemendikbudristek Indonesia in Hibah Penelitian Disertasi Contract Number: 064/E4.1/AK.04.PT/2021 dated July 12, 2021, and Yayasan Pendidikan Gunadarma Jakarta Indonesia, Contract Number: 09.25/LP/UG/VII/2021 dated July 13, 2021.

REFERENCES

- [1] Cumming D, Johan S. Cameras tracking shoppers: the economics of retail video surveillance. Eurasian Business Review 2015; 1 (2): 235-257.
- [2] Tang Y, Ma B, Yan H. Intelligent video surveillance system for elderly people living alone based on ODVS. Scientific Research Publishing 2013.

- [3] Porikli F, Bremond F, Dockstader SL, Ferryman J, Hoogs A, Lovell BC, Pankanti S, Rinner B, Tu P, Venetianer PL. Video surveillance: past, present, and now the future [DSP Forum]. *IEEE Signal Processing Magazine* 2013; 30 (3): 190–198.
- [4] Such JM, Espinosa A, Garc'ia-Fornes A. A survey of privacy in multi-agent systems. *The Knowledge Engineering Review* 2014; 29 (3): 314–344.
- [5] Ye Y, Ci S, Katsaggelos A, Liu Y, Qian Y. Wireless video surveillance: a survey. *IEEE Access* 2013; 1: 646–660.
- [6] Elharrouss A, Al-Maadeed. A combined multiple action recognition and summarization for surveillance video sequences. *Applied Intelligence* 2021; 51 (2): 690–712.
- [7] Kruegle H. *CCTV Surveillance: Video Practices and Technology*. Great Britain, England: Elsevier Butterworth Heinemann, 2011.
- [8] Suganya D, Shyla R, Jayasudha V, Marirajan S. Storage optimization of video surveillance from CCTV camera. *International Research Journal of Engineering and Technology (IRJET)* 2018; 5 (3): 1356–1359.
- [9] Liu H, Chen S, Kubota N. Intelligent video systems and analytics: a survey. *IEEE Transactions on Industrial Informatics* 2013; 9 (3): 1222–1233.
- [10] Han J, Jeong D, Lee S. Analysis of the HIKVISION DVR file system. In: *International Conference on Digital 18 Forensics and Cyber Crime*; Seoul, South Korea; 2015. pp. 189–199.
- [11] Damjanovski V. *CCTV: Networking and Digital Technology*. Great Britain, England: Elsevier Butterworth Heine-mann, 2005.
- [12] Nihal KNAK, Shanavas ARM. A novel approach for compressing surveillance system videos. *International Journal of Advanced Engineering, Management and Science* 2016; 2 (2): 239374.
- [13] Sarifuddin M. *Pengolahan Citra dan Vidio Digital*. Jakarta, Indonesia: Erlangga, 2015 (in Bahasa).
- [14] Acharya T, Tsai P. *JPEG2000 Standard for Image Compression: Concepts, Algorithms and VLSI Architectures*. Hoboken, NJ, USA: John Wiley & Sons, 2005.
- [15] Tahoces P, Varela R, Lado M, Sauto M. Image compression: maxshift ROI encoding options in JPEG2000. *Computer Vision and Image Understanding* 2008; 109 (2): 139–145.
- [16] Shin H, Jung J, Koo Y. Forecasting the video data traffic of 5G services in South Korea. *Technological Forecasting and Social Change* 2020; 153: 119948.
- [17] Index, Cisco Visual Networking. *Global Mobile Data Traffic Forecast Update, 2017–2022*. USA: Cisco White Paper, 2019.
- [18] Khan PW, Byun Y, Park N. A data verification system for CCTV surveillance cameras using blockchain technology in smart cities. *Electronics, Multidisciplinary Digital Publishing Institute* 2020; 9 (3): 484.
- [19] Shidik GF, Noersasongko E, Nugraha A, Andono PN, Jumanto, Kusuma EJ. A systematic review of intelligence video surveillance: trends, techniques, frameworks, and datasets. *IEEE Access* 2019; 7: 170457–170473.
- [20] Sagala JP, Candradewi I, Harjoko A. Penggunaan deteksi gerak untuk pengurangan ukuran data rekaman video kamera CCTV. *IJEIS (Indonesian Journal of Electronics and Instrumentation Systems)* 2020; 10 (1): 99–108 (in Bahasa).
- [21] Nurhopiah A, Harjoko A. Motion detection and face recognition for CCTV surveillance system. *IJCCS (Indonesian 40 Journal of Computing and Cybernetics Systems)* 2018; 12 (2): 107–118.
- [22] Pratomo AH, Kaswidjanti W, Mu'arifah S. Implementasi algoritma region of interest (ROI) untuk meningkatkan performa algoritma deteksi dan klasifikasi kendaraan. *Jurnal Teknologi Informatika dan Ilmu Komputer* 2020; 7(1): 155–162 (In Bahasa with an abstract in English).
- [23] Ramadoss, M. (2019). Design of Lossy and Lossless Algorithms for ROI-based Video Compression.
- [24] Camastra F, Vinciarelli A. *Machine Learning for Audio, Image, and Video Analysis*. London: Springer, 2015.
- [25] Tjin E. *Kamera DSLR Itu Mudah*. Jakarta, Indonesia: Bukune, 2011 (in Bahasa).
- [26] Das K, Bhowmik MK, De BK, Bhattacharjee D. Background subtraction algorithm for moving object detection using SAMEER-TU dataset. In: *Proceedings of Fourth International Conference on Soft Computing for Problem Solving*; India; 2015. pp. 279–291.
- [27] Fauzi A, Madenda S, Ernastuti, Wibowo EP, Masruriyah AFN. The importance of bounding box in motion detection. In: *2020 Fifth International Conference on Informatics and Computing (ICIC)*; Indonesia; 2020. pp. 1–5.
- [28] Furht B, Greenberg J, Westwater R. *Motion Estimation Algorithms for Video Compression*. Berlin/Heidelberg, Germany: Springer Science & Business Media, 2012.
- [29] Putra D. *Pengolahan Citra Digital*. Yogyakarta, Indonesia: Penerbit Andi, 2010 (in Bahasa).
- [30] Murpratiwi SI, Widyantara, IMO. Pemilihan algoritma kompresi optimal untuk citra digital bitmap. *Majalah Ilmiah Teknologi Elektro* 2018; 17 (1): pp. 94-101 (in Bahasa).
- [31] Bul DR. Digital picture format and representations. *Communicating pictures* 2014. pp. 99-132.
- [32] Susanto A, Mulyono IUW, Fajar MR, Febrian GAR. A combination of hill cipher and LSB for image security. *Scientific Journal of Informatics* 2019; 6 (1): pp. 241-248.

Data Augmentation Techniques on Chilly Plants to Classify Healthy and Bacterial Blight Disease Leaves⁶

Sudeepthi Govathoti¹

Department of Computer Science and Engineering
SoT, Gitam University, Hyderabad Campus-502329
Hyderabad, India

A Mallikarjuna Reddy², G BalaKrishna⁴

Department of Computer Science and Engineering
Anurag University
Hyderabad, India

Deepthi Kamidi³

Department of Computer Science and Engineering
Vignan Institute of Technology and Sciences
Hyderabad, India

Sri Silpa Padmanabhuni⁵, Pradeepini Gera⁶

Department of Computer Science and Engineering
Koneru Lakshmaiah Education Foundation, Vaddeswaram
AP, India

Abstract—Designing an automation system for the agriculture sector is difficult using machine learning approach. So many researchers proposed deep learning system which requires huge amount of data for training the system. The proposed system suggests that geometric transformations on the original dataset help the system to generate more images that can replicate the physical circumstances. This process is known as “Image Augmentation”. This enhancement of data helps the system to produce more accurate systems in terms of all metrics. In olden days when researchers work with machine learning techniques they used to implement traditional approaches which are a time consuming and expensive process. In deep learning, most of the operations are automatically taken care by the system. So, the proposed system applies neural style and to classify the images it uses the concept of transfer learning. The system utilizes the images available in the open source repository known as “Kaggle”, this majorly consists of images related to chilly, tomato and potato. But this system majorly focuses on chilly plants because it is most productive plant in the South Indian regions. Image augmentation creates new images in different scenarios using the existing images and by applying popular deep learning techniques. The model has chosen ResNet-50, which is a pre-trained model for transfer learning. The advantage of using pre-trained model lies in not to develop the model from scratch. This pre-trained model gives more accuracy with less number of epochs. The model has achieved an accuracy of “100%”.

Keywords—Image augmentation; geometric transformations; transfer learning; neural style learning; residual network

I. INTRODUCTION

The main goal of the data augmentation technique is to develop the model which is capable of handling the input that is unknown to the system and to develop a generalized training model. The proposed system focused on chilly plants but there is a situation where it can get similar leaf images of chilly but it is really chilly. So the proposed system uses the neural style learning to combine images of different plants and produce a new synthetic image. The image augmentation acts as a pre-processing step in the deep learning area to train the model. The proposed paper discusses the basic image manipulation operations, deep learning[5] and meta-learning

techniques that can be performed on the image. The image augmentation operation is classified into two ways as shown in Fig. 1.

Offline mode stores the different augmented images in the hard disk, which requires high configuration of processor and RAM to run the program. Online mode utilizes the cloud services to store the image and it uses GPU’s to run the program [19]. Google CoLab is an open source tool that run huge amount of images at a faster rate. Among the two types augmentations namely offline and online modes, this paper considers the online augmentation techniques since all the operations are performed in cloud using GPUs due to which waste of disk space is reduced. The offline data augmentation is preferred for the smaller datasets; the newly created images will be stored in the disk. This offline process is time-consuming and is expensive whereas in online or real data augmentation the transformation images occur randomly on different batches and the model is trained with more cases in each epoch in this method [8]. There three ways to generate augmented images as shown in Fig. 2.

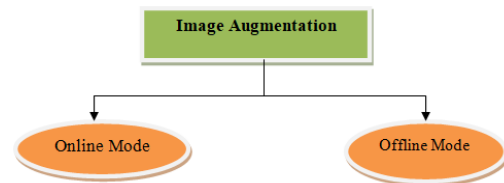


Fig. 1. Modes of Image Augmentation.

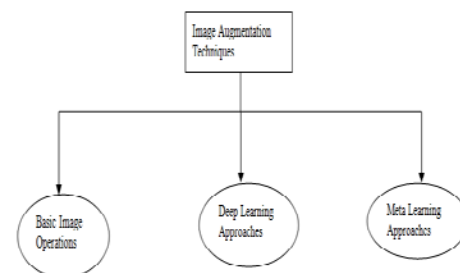


Fig. 2. Different Ways of Image Augmentation Techniques.

1) *Basic image operations*: The basic image operations include geometric transformations, which is a sequence of steps consisting of rotations, flip, resize, shift, zoom, crop, and adding of noise operations [9]. It also includes color space transformations; in general, images are composed of RGB color convention but for efficient processing of the data the image has to be transformed into gray-scale or other color saturation values. The basic operation also includes kernel filter, using convolution neural networks, the region of interest is extracted from the image. The image is stored as a two-dimensional matrix and the filter performs a dot product between the input and filter layers and the values are added to get a single value in each position. Kernel filtering helps in edge detection, image sharpening, and blurring operations [10]. The latest improvement has included random erasing techniques to erase the pixels in the image by selecting a rectangular region, an area is selected based on the probability which is calculated with help of aspect ratio and area ratio. It plays a vital role in image classification, object detection, and person re-identification. It can be easily integrated with the neural networks and it can use on pre-trained models. The basic image operations categories are presented in Fig. 3.

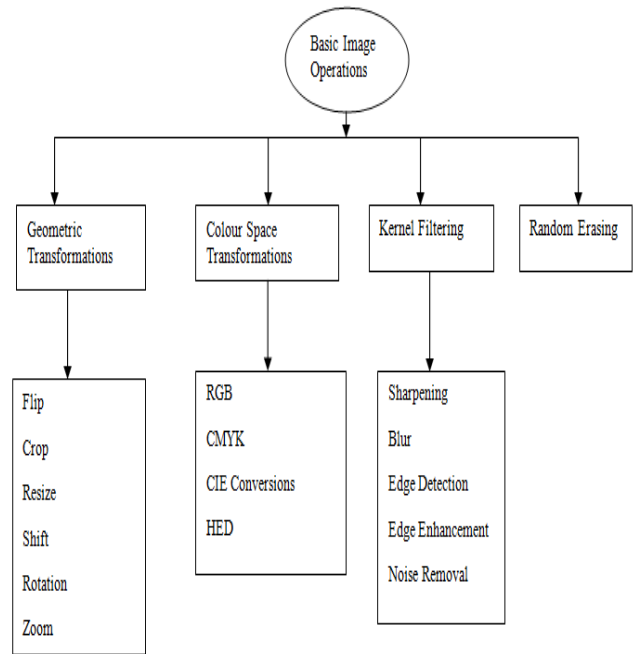


Fig. 3. Summary of Basic Image Operations.

2) *Deep learning approaches*: These approaches consist of adversarial training, this type of approach is highly needed in the models where Gaussian noise is injected and images are transformed with worst-case perturbations, this results in incorrect answer with high confidence values [11]. Deep learning also involves neural style transferring technique which helps to create new images by blending images especially when the model has content or style reference images. It uses two different distance functions, one is used to identify the differences in terms of content, and the other is used to identify the differences in terms of style. The third and important approach is the usage of GAN models, an unsupervised technique that can generate new images by learning from the patterns that exist in between the input image. GAN's consists of two components: generator to create new images by training the model and discriminator for classification purpose [12, 13]. In GAN's, the generator takes input as a fixed-length vector, which is known as "Noise Vector" for producing the salt and pepper noise images because most of the plants have smoked layer above them. Generator produces outputs samples that belong to the domain of leaves but with different styles. Discriminator takes the input from the domain and outputs a binary value based on the prediction performed. The task of this component is predict whether the scanned image is a real or augmented image. Higher the misclassification produced by this component higher will be accuracy of system because more number of augmented images has passed the test. So in designing the GAN, the major focus should be on layers of the generator. The general architecture of GAN is presented in the Fig. 4.

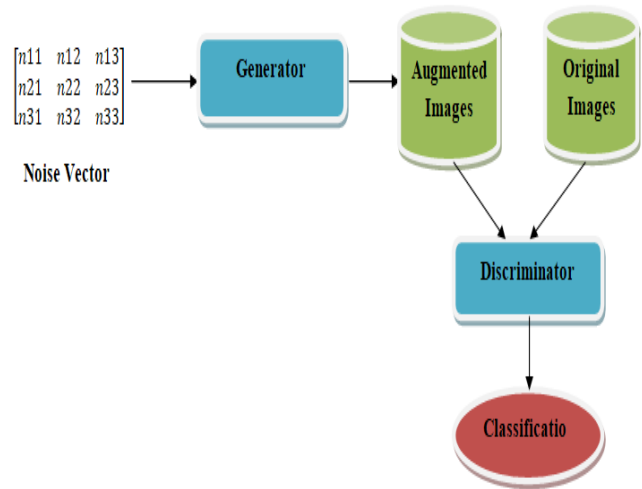


Fig. 4. GAN Architecture.

3) *Meta-Learning approaches*: These approaches are used to balance the data between the real world and the simulated world. Recently Google has designed a novel method known as "AutoAugment", it is a policy-based approach to identify the best augmentation suited for the dataset. The search space of the AutoAugment has 5 sub-policies with 2 operations each. This process of AutoAugment will save us a lot of time in checking and applying all the possible combinations of operations that can be performed to increase our dataset size. The selection of operation to be performed is based on the dataset system supply, this automatic selection of operation is acquired from the reinforcement learning. Fig. 5 illustrates the process of Auto Augmentation using the optimizers.

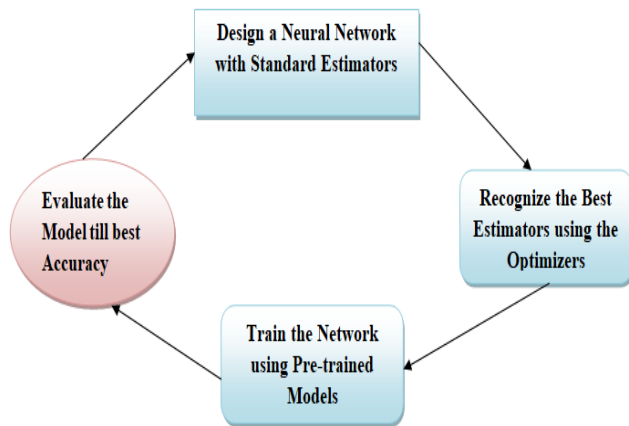


Fig. 5. Auto Augmentation Process.

The design considerations for augmentation involve train-time data augmentation to reduce the generalization error and test-time data augmentation to improve predictive performance. The most important operation that should be performed is resizing operation that all the images should be of the same size and some pixel scaling and normalization operations should be performed.

The paper first presented introduction section, which describes about different augmented images generation techniques in online mode. The second section literature analyzes the previous works to identify the gaps in the research. The proposed model section discusses about the basic image operations along with the ResNet-50 CNN for classification [15]. The results section discusses about both proposed results along with the compared results of previous works in terms of every metric. The last section i.e., conclusion presents the advantages of pre-trained model then it extends the section by coining the limitations of the present work.

II. LITERATURE REVIEW

Many Research Scholars and Scientists are continuously working on various plant diseases to improve the quality of production using machine learning and deep learning techniques. All these researchers have considered the controlled conditions and obtained the plant images from PlantVillage dataset. The application of computer vision and deep learning techniques has given good accuracy systems for automatic detection of diseases in plants.

Quan Huu Cap[1] developed a Generative Adversarial Networks known as “LeafGAN”, which act as a data

augmentation tool by creating new diseased images from the healthy images. This system preserves the background of the image as well as generates the images of high quality. The core component of this model is LFLSeg, which is a label-free and weakly supervised segmentation module. In this model, it uses feature maps to extract the segmentation information[6], and this in return helps the model to learn about dense and interior regions of the leaf images implicitly. The output of the segmented image is projected as a heat map so that it calculates the probability of each pixel in the final decision. Finally, this model has boosted the diagnosis system and it solved the problems that arise due to the overfitting of the data.

Haseeb Nazki[2] proposed Pipelined Generative Adversarial Networks for plant disease detection to address the problem of imbalanced data shifting. The working of this model consists of two major components. The first component is AR-GAN, which is used for generating the data augmentation synthetically by translating an image from one domain into another domain. A parameter known as discriminator decides whether an image belongs to a particular domain or not. Based on the dataflows and loss functions, the image is reconstructed so that its performance is improved over cycle GAN. AR-GAN has a network that has an activation reconstruction for feature extraction. The second component is RESNET-50 CNN for disease detection with the same configuration as the baseline with RELU as activation functions [16]. The network is fine-tuned by using ImageNet pre-trained weights.

Daniel Ho[3] suggested a population-based augmentation algorithm, which uses a dynamic strategy. The main goal of this algorithm is to optimize the hyperparameter by using schedule learning policies. The PBA first runs a gradient descent algorithm on each epoch and then it does the evaluation on the validation data. Truncation selection is applied to the bottom 25% of the data based on the weights and top25% of the data based on the hyperparameters.

Sungbin Lim [4] proposed the Fast AutoAugment Algorithm based on density matching. The model constructs a search space for the images and defines two efficient operations known as calling probability and the magnitude. The search strategy uses the probability distribution on a pair of training datasets, the values are parameterized and evaluated the accuracy and loss values. The performance is measured by comparing the amount of the data that is similar in both datasets and it uses K-fold stratified shuffling. At last, the policy is explored by using Bayesian Optimization by employing a kernel density estimator. Table I illustrates the advantages and disadvantages of the previous works.

TABLE I. COMPARATIVE ANALYSIS

S.No	Author Name	Algorithm Name	Merits	Demerits
1	Quan	LeafGAN	The classification process by taking the segmented images is easy for the GAN	The model has used traditional segmentation approach for feature extraction. The annotation process is difficult
2	Haseeb	ARGAN	The residual component used tries to minimize the loss function at every iteration	The usage of ImageNet which less number of leaf images for knowing the weights of the layer has reduced the accuracy of the model.
3	Daniel	PBA	During the process of distribution of data the model has wisely chosen mixture of top and bottom layers of data for validation purpose	The learning policy implemented by the population is difficult since all the combinations of learning policies are to be computed
4	Sungbin	Fast Auto Augment	The model uses the probability to construct the search space. This helps the model to have very small search area to recognize the desired regions	The density parameters are found using the optimization technique based on bayes theorem. But since it is applied for K-fold, it is very expensive process

III. PROPOSED MODEL

The aim of the proposed model is to develop basic online augmentation techniques along with convolutional neural networks[7] and calculate the accuracy for the identification of bacterial blight disease in chilly plants.

A. Basic Image Augmentation Operations

The main advantage of these geometric operations is that even though various operations are performed on these images, the features of the image remain the same. All these operations are performed with the help of ImageDataGenerator class of the Tensorflow library and all the images captured will have different dimensions so to maintain all the images with the same dimensions the common operation of resizing is applied to all the images [18].

1) *Rotation*: The basic operation that can be applied to any image to change the orientation of the image is rotated. The rotation angle is specified in terms of degrees which can accept the values from 0 to 360 in the clockwise direction. [14].

2) *Flipping*: It is an extension of rotation operation. Flipping operation is used to perform the transposition of a row and column pixels. Here, two types of flipping operations can be performed. Depending on the nature of the images, either of the horizontal or vertical flips can be applied.

3) *Shearing*: The process in which the pixels can be shifted from one position to another position either horizontally or vertically is known as “Shearing”. Here, the dimensions of the image remain the same i.e., few pixels will be clipped off.

4) *Cropping*: In general, the images contain a region of interest at various locations. To find that location the best operation that one can use is cropping the image at the required place. Since the proposed system is a classification model, the output generated by the model should be the subset of the whole image.

5) *Zooming*: Zoom operation either adds new pixel values or interpolates pixel values. Let us consider the value specified is x then zoom performs $1+x$ and $1-x$ operations around the pixels of the image. It helps in the uniform sampling of the image.

6) *Brightness or contrast*: This operation is used to perform either to darken or brighten the image. This operation mainly helps the model to train the system under various lighting conditions. Here, we can specify the minimum and maximum value as a percentage. A value of less than 1.0 darkens the image and a value greater than 1.0 brightens the image. All the sub sections of Fig. 6 show the output of different image operations on the chilly leaves. The order of selection for these operations doesn't have any impact on the augmentation and classification process [20]. There are many image manipulation operations but the proposed system implements only five of the important operations so that the burden on the neural network gets reduced.

B. Basic Geometric Image Operations Algorithm

Step 1: All the images should be of the same size. To do this, we apply to rescale the images to $1/255$, because the minimax pixel value is 255.

Step 2: Image is rotated to 40° to make the image out of the frame and used nearest neighbor fill interpolation.

Step 3: Apply both horizontal shift and vertical shift with 20%.

Step 4: Apply the sheer range and zoom range of 20%.

Step 5: Apply horizontal flip.

The algorithm will give the augmented images as follows. A sample screenshot is shown in Fig. 7.

C. Applying Convolution Neural Networks

2D convolution takes an image as input and passes it through a kernel filter to calculate the dot product. The weighted matrix is converted into a feature matrix. These features are important to find the nearest weights to identify the region of interest. This helps to reduce the number of pixel operations to perform. In the proposed paper, the model uses padding with value as the same, which determines the amount of the pixels to be added to the image and add layers with pixel value as zeros. In general, the pixels stored in the center are used more than corners and edges. So to preserve the edge's information, padding helps a lot. The same value for the attribute padding is illustrated as follows:

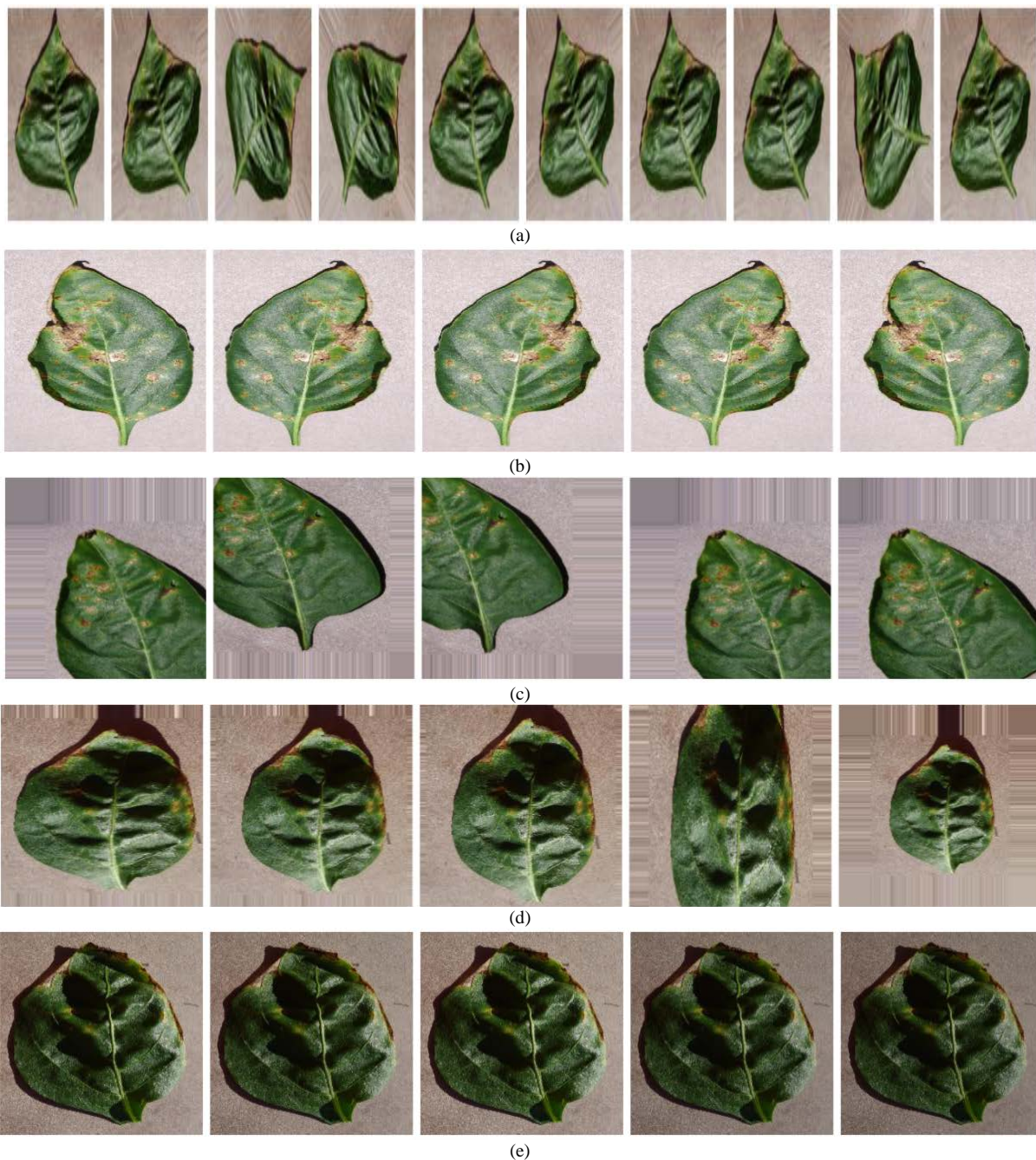


Fig. 6. (a) Output of Images Generated Randomly at the Angle of 95 Degrees, (b) Output Images Generated by Performing Horizontal Flip, (c) Output Images Generated by Performing Shearing Operation with Both width and Height, (d) Output Images Generated by Performing Zoom, (e) Output Images Generated by Performing Brightness.



Fig. 7. Screenshot of Augment Images Created using the Online Data Augmentation Process.

Let, the number of layers to be added be as the border of an image be $(w \times w)$ and the image size be $(m \times m)$. After padding the image, the size of the image becomes as $(m+2w)$. Let the kernel filter size be $(y \times y)$, then after applying the kernel filter, the output image size is $(m+2w-y+1)$. The padding maintains the same size as of input image by using the notation shown in equation (1).

$$\text{length_padding} = \frac{[(m+2*w)*(m+2*w)]*y^2}{m*m} \quad (1)$$

The transfer function or activation function determines the output of the node in the neural network. This converts the corresponding output into binary values. The proposed paper uses ReLU, a nonlinear transfer function, which gives the output as the maximum value of the input. It is a widely used transfer function because it implements backpropagation and as well as it doesn't activate all the values simultaneously [17]. The equation of the function is shown in (2).

$$f(\text{input_feature}) = 0, \text{ if } \text{input_feature} < 0 \\ = 1, \text{ if } \text{input_feature} \geq 0 \quad (2)$$

The proposed system uses the CIFAR-100 predefined dataset with 100 class labels using the ResNet-50 to get the proper weights for training the network. After training the model, the augmentation techniques can create different feature maps and sometimes lower resolution pixels may contain important structural elements. So, these issues can be solved by designing pooling layers. The pooling layers create a subset of feature maps for each operation separately. It

detects the features irrespective of augmentation and noises contained in the image. In the proposed paper, the model used the max-pooling layer. It takes the maximum value that occurs in the filter applied. The main advantage of pooling in smaller datasets is it can avoid the overfitting problem by implementing the dropout regularization mechanism. For having a good performance, the dropout value for the hidden layers can be between 0.5 and 0.8.

Now the pooled feature map should be transferred into the column, because the neural network can accept only the long vector of inputs. Then, a dense layer is applied to the neural network, which calculates the dot product of the input image and weighted data i.e., kernel, and added to the bias value with the usage of activation function to optimize the model. Finally, the model is compiled with the help of Adam optimizer, it updates the network weights iteratively based on the training data. It is popular for its fastness by updating velocity and momentum parameters as shown in equations (3) & (4).

$$\text{Momentum}_i = \beta * \text{Momentum}_{i-1} + (1 - \beta) * \text{gradientvalue} \quad (3)$$

$$\text{Velocity}_t = \alpha * \text{velocity}_{t-1} + (1 - \alpha) * \text{momentum}_i \quad (4)$$

The extracted features from the chilly plants after training the model are presented in Fig. 8. This figure shows the layer by layer output of CNN for better visualization of essential features.

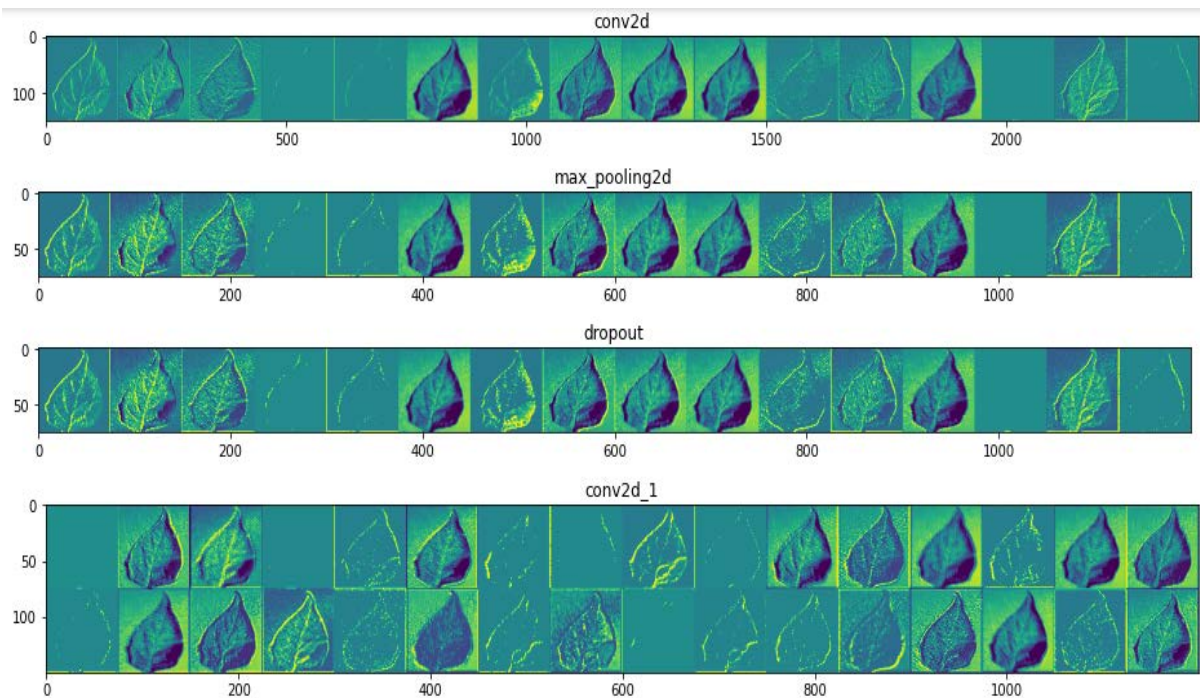


Fig. 8. Screenshot of Feature Maps after Every Layer in CNN.

IV. EXPERIMENTAL RESULTS

Since the model uses the pre-trained model ResNet-50, the number of trainable parameters get reduced from 1,67,300 to 10,400. So the model can claim that it has good dimensionality reduction. The system to overcome the drawbacks of the machine learning models it stacks layers of network to learn the complex features with efficient learning

rate. The proposed system uses that stacked layer architecture which consists of a pile of conv2d, activation and batch normalization layer. The major advantage of this network lies in reducing the dimensions drastically at every step of training. The model also uses the best estimators like using Adam optimizer, learning rate as 0.5 and others. The systems presents a sample summary of the training model in the Fig. 9 to understand the underlying parameters.

Model: "model"

Layer (type)	Output Shape	Param #	Connected to
input_1 (InputLayer)	[(None, 32, 32, 3)]	0	
conv2d (Conv2D)	(None, 32, 32, 16)	448	input_1[0][0]
batch_normalization (BatchNorma)	(None, 32, 32, 16)	64	conv2d[0][0]
activation (Activation)	(None, 32, 32, 16)	0	batch_normalization[0][0]
conv2d_1 (Conv2D)	(None, 32, 32, 16)	272	activation[0][0]
batch_normalization_1 (BatchNor)	(None, 32, 32, 16)	64	conv2d_1[0][0]
activation_1 (Activation)	(None, 32, 32, 16)	0	batch_normalization_1[0][0]
conv2d_2 (Conv2D)	(None, 32, 32, 16)	2320	activation_1[0][0]
batch_normalization_2 (BatchNor)	(None, 32, 32, 16)	64	conv2d_2[0][0]
activation_2 (Activation)	(None, 32, 32, 16)	0	batch_normalization_2[0][0]

Fig. 9. First 2 Layers Summary in the ResNet-50.

```

Epoch 1/15
49/49 [=====] - 36s 733ms/step - loss: 0.2839 - accuracy: 0.9122 - val_loss: 0.7233 - val_accuracy: 0.4000
Epoch 2/15
49/49 [=====] - 26s 527ms/step - loss: 0.1507 - accuracy: 0.9183 - val_loss: 0.9869 - val_accuracy: 0.3900
Epoch 3/15
49/49 [=====] - 25s 502ms/step - loss: 0.1114 - accuracy: 0.9524 - val_loss: 0.3323 - val_accuracy: 0.8400
Epoch 4/15
49/49 [=====] - 25s 502ms/step - loss: 0.0494 - accuracy: 0.9835 - val_loss: 0.3017 - val_accuracy: 0.8500
Epoch 5/15
49/49 [=====] - 25s 502ms/step - loss: 0.0485 - accuracy: 0.9886 - val_loss: 0.2070 - val_accuracy: 0.9200
Epoch 6/15
49/49 [=====] - 24s 499ms/step - loss: 0.1324 - accuracy: 0.9462 - val_loss: 0.7213 - val_accuracy: 0.5300
Epoch 7/15
49/49 [=====] - 24s 498ms/step - loss: 0.0929 - accuracy: 0.9659 - val_loss: 0.3181 - val_accuracy: 0.7900
Epoch 8/15
49/49 [=====] - 25s 500ms/step - loss: 0.0611 - accuracy: 0.9741 - val_loss: 0.4429 - val_accuracy: 0.7900
Epoch 9/15
49/49 [=====] - 25s 502ms/step - loss: 0.0557 - accuracy: 0.9659 - val_loss: 0.6358 - val_accuracy: 0.5800
Epoch 10/15
49/49 [=====] - 25s 502ms/step - loss: 0.0165 - accuracy: 0.9928 - val_loss: 0.1411 - val_accuracy: 0.9200
Epoch 11/15
49/49 [=====] - 25s 502ms/step - loss: 0.0040 - accuracy: 0.9990 - val_loss: 0.0612 - val_accuracy: 0.9700
Epoch 12/15
49/49 [=====] - 25s 503ms/step - loss: 0.0061 - accuracy: 0.9990 - val_loss: 0.2557 - val_accuracy: 0.9100
Epoch 13/15
49/49 [=====] - 25s 503ms/step - loss: 7.3316e-04 - accuracy: 1.0000 - val_loss: 0.3898 - val_accuracy: 0.9000
Epoch 14/15
49/49 [=====] - 25s 507ms/step - loss: 2.6175e-04 - accuracy: 1.0000 - val_loss: 0.2725 - val_accuracy: 0.9100
    
```

Fig. 10. Evaluation Metrics in all Epochs.

Fig. 10 shows the accuracy for every iteration by setting the epoch value to 15. It computes accuracy and loss of training data and it also computes the accuracy and loss of validation data. From the figure, it is evident that the model has started with good accuracy of “91.22” and slowly it has reached to 100% accuracy.

The evaluation of deep learning algorithms is measured using the both training and testing data. Fig. 11 visualizes the metrics obtained in the Fig. 10 as a graph for the users to understand the nature of the system. Fortunately, in case of training data, the model performed stable by getting more

accuracy for training than testing data and more over it has increased gradually. In the loss graph, it is clearly evident that the loss is also decreasing gradually. The loss rate is also very less.

The below section compares the output of the proposed model with the previous works studied in the literature section to prove the efficiency of the model. Fig. 12 visualizes the graphs obtained by the algorithms in terms of different metrics. X-axis represents methodology and Y-axis represents the measuring scale.

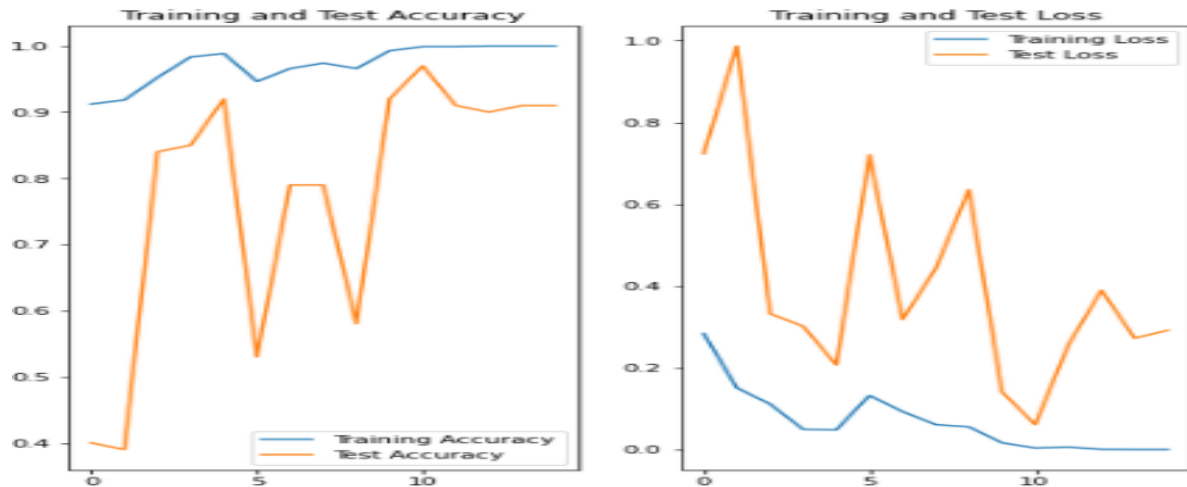


Fig. 11. Screenshot of Training, Test Accuracy.

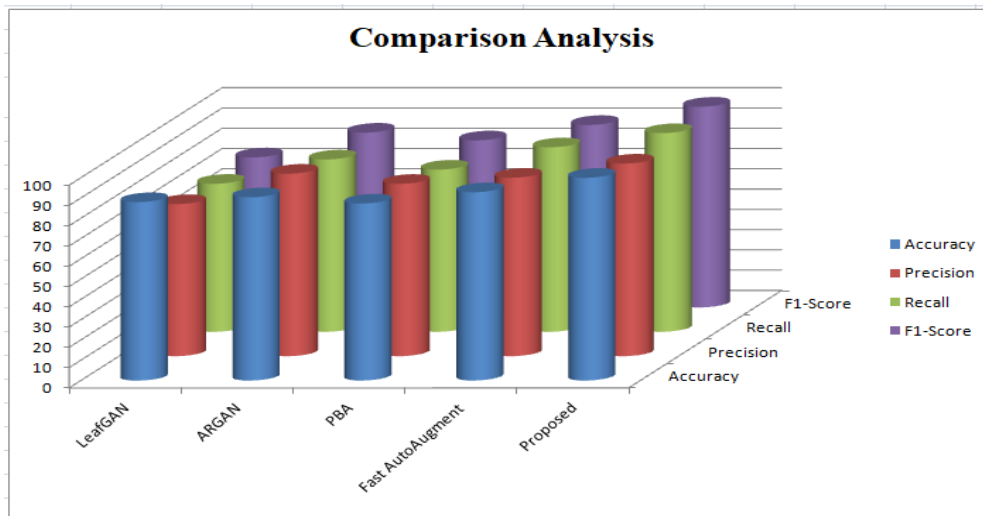


Fig. 12. Comparison Analysis over Metrics.

V. CONCLUSION

In a real-time environment the conditions are uncontrolled and the system may face problems like labeling of disease dataset, and addressing the data imbalance problems. The size of dataset is smaller in size in the real-time environment so they cannot work properly. The traditional systems take a lot of computations to select and apply all the possible geometric transformations. So, the proposed system by designing a good policy schema like using pre-trained model to get the weights

of neural networks and applying five basic transformations to create augmented images helps the model to design an accurate system. In future, the model can be transformed to use GAN approaches to create images because the model has achieved 100% accuracy whose state is claimed as “Overfitting”.

REFERENCES

[1] Saikawa, Takumi & Cap, Quan & Kagiwada, Satoshi & Uga, Hiroyuki & Iyatomi, Hitoshi. (2019). AOP: An Anti-overfitting Pretreatment for

- Practical Image-based Plant Diagnosis. 5177-5182. 10.1109/BigData47090.2019.9006567.
- [2] Nazki, Haseeb. (2018). Synthetic Data Augmentation for Plant Disease Image Generation using GAN.
- [3] Ho, Daniel & Liang, Eric & Stoica, Ion & Abbeel, Pieter & Chen, Xi. (2019). Population Based Augmentation: Efficient Learning of Augmentation Policy Schedules.
- [4] Lim, Sungbin & Kim, Ildoo & Kim, Taesup & Kim, Chiheon & Kim, Sungwoong. (2019). Fast AutoAugment.
- [5] Ayaluri MR, K. SR, Konda SR, Chidirala SR. 2021. Efficient steganalysis using convolutional auto encoder network to ensure original image quality. PeerJ Computer Science 7:e356 <https://doi.org/10.7717/peerj-cs.356>.
- [6] BANGARE, S.L., PRADEEPINI, G. and PATIL, S.T., 2018. Regenerative pixel mode and tumour locus algorithm development for brain tumour analysis: A new computational technique for precise medical imaging. *International Journal of Biomedical Engineering and Technology*, 27(1-2), pp. 76-85.
- [7] Grandhe, Padmaja. (2020). A Novel Method for Content based 3D Medical Image Retrieval System Using Dual Tree M-Band Wavelets Transform and Multiclass Support Vector Machine. *Journal of Advanced Research in Dynamical and Control Systems*. 12. 279-286. 10.5373/JARDCS/V12I3/20201192.
- [8] Ilaiah Kavati, A. Mallikarjuna Reddy, E. Suresh Babu, K. Sudheer Reddy, Ramalinga Swamy Cheruku, Design of a fingerprint template protection scheme using elliptical structures, *ICT Express*, Volume 7, Issue 4, 2021, Pages 497-500, ISSN 2405-9595, <https://doi.org/10.1016/j.icte.2021.04.001>.
- [9] Sahu, A.K., & Swain, G. (2018). A Novel n-Rightmost Bit Replacement Image Steganography Technique. *3D Research*, 10, 1-18.
- [10] Padmanabhuni, Ms. S. S. (2020). An Extensive Study on Classification-based Plant Disease Detection Systems. *Journal of Mechanics of Continua and Mathematical Sciences*, 15(5). <https://doi.org/10.26782/jmcms.2020.05.00002>.
- [11] A Mallikarjuna Reddy, Vakulabharanam Venkata Krishna, Lingamgunta Sumalatha and Avuku Obulesh, "Age Classification Using Motif and Statistical Features Derived On Gradient Facial Images", *Recent Advances in Computer Science and Communications (2020)* 13: 965. <https://doi.org/10.2174/2213275912666190417151247>.
- [12] KUMAR, P., PRADEEPINI, G. and KAMAKSHI, P., 2019. Feature selection effects on gradient descent logistic regression for medical data classification. *International Journal of Intelligent Engineering and Systems*, 12(5), pp. 278-286.
- [13] Divya, T. V., & Banik, B. G. (2021). Detecting Fake News Over Job Posts via Bi-Directional Long Short-Term Memory (BIDLSTM). In *International Journal of Web-Based Learning and Teaching Technologies* (Vol. 16, Issue 6, pp. 1-18). IGI Global. <https://doi.org/10.4018/ijwlut.287096>.
- [14] Kishore, P.V.V., Kumar, K.V.V., Kiran Kumar, E., Sastry, A.S.C.S., Teja Kiran, M., Anil Kumar, D. & Prasad, M.V.D. 2018, "Indian Classical Dance Action Identification and Classification with Convolutional Neural Networks", *Advances in Multimedia*, vol. 2018.
- [15] C. R. T, G. Sirisha and A. M. Reddy, "Smart Healthcare Analysis and Therapy for Voice Disorder using Cloud and Edge Computing," *2018 4th International Conference on Applied and Theoretical Computing and Communication Technology (iCATccT)*, Mangalore, India, 2018, pp. 103-106, doi: 10.1109/iCATccT44854.2018.9001280.
- [16] Soumya Ranjan Nayak, Jibitesh Mishra, G. Palai, A modified approach to estimate fractal dimension of gray scale images. *Optik*, Volume 161, 2018, Pages 136-145, ISSN 0030-4026, <https://doi.org/10.1016/j.ijleo.2018.02.024>.
- [17] A. M. Reddy, K. SubbaReddy and V. V. Krishna, "Classification of child and adulthood using GLCM based on diagonal LBP," *2015 International Conference on Applied and Theoretical Computing and Communication Technology (iCATccT)*, Davangere, 2015, pp. 857-861, doi: 10.1109/ICATccT.2015.7457003.
- [18] Akbar, S., & Midhunchakkaravarthy, D. (2020). A Novel Filtered Segmentation-Based Bayesian Deep Neural Network Framework on Large Diabetic Retinopathy Databases. In *Revue d'Intelligence Artificielle* (Vol. 34, Issue 6, pp. 683-692). International Information and Engineering Technology Association. <https://doi.org/10.18280/ria.340602>.
- [19] Swarajya Lakshmi V Papineni, Snigdha Yarlagadda, Harita Akkineni, A. Mallikarjuna Reddy. Big Data Analytics Applying the Fusion Approach of Multicriteria Decision Making with Deep Learning Algorithms *International Journal of Engineering Trends and Technology*, 69(1), 24-28, doi: 10.14445/22315381/IJETT-V69I1P204.
- [20] A. M. Reddy, V. V. Krishna, L. Sumalatha and S. K. Niranjana, "Facial recognition based on straight angle fuzzy texture unit matrix," *2017 International Conference on Big Data Analytics and Computational Intelligence (ICBDAC)*, Chirala, 2017, pp. 366-372, doi: 10.1109/ICBDACI.2017.8070865.

Towards the Smart Industry for the Sustainability through Open Innovation based on ITSM (Information Technology Service Management)

Asti Amalia Nur Fajrillah, Muharman Lubis, Arariko Rezeki Pasa
Department of Information System, Telkom University, Bandung, Indonesia

Abstract—The Indonesian coffee industry has become a trend that has a strategic role and potential for the livelihoods of the business people in it, as well as Indonesia's economic growth. One of the trends that stole attention is the concept of smart industry, the concept of a digital-based industry that is highly relevant to technological developments in this era. When companies want to implement a smart industry, companies need a strategy to implement IT (Information Technology) so that the investment spent is right to build the company's targets. This study aims to design a systematic IS/IT strategy to realize the concept of smart industries that are effective. The analysis and design method used is the Ward & Peppard framework which consists of two phases, namely the input and output phases. The input phase consists of internal business analysis, external business, IT internal and external. The output stage includes the design of IT management strategies, business information systems and IT strategies. The results of this study are in the form of a portfolio of IT designs at the Margamulya Coffee Producers Cooperative consisting of business strategy designs and IT management.

Keywords—Smart industry; Ward and Peppard; IS/IT strategy

I. INTRODUCTION

Industry 4.0 requires many companies to use these technologies to move to a digitally connected industrial environment, providing regulatory and legal flexibility for additional ubiquitous, cloud-based production. It is management and can provide hands-on training and innovative education [1]. After a successful implementation, some potential benefits can be recognized, but the resulting effects are not always obvious. In addition, the impact of making changes to the current production environment, and therefore the risks, is difficult to predict. If you know the consequences of your changes, you can always look forward to them in multiple steps and can easily modernize and change your manufacturing company [2]. Coffee is the third largest contributor to foreign exchange for plantations for Indonesia with a total plantation area of 1,227,787 ha. The level of coffee production in Indonesia reached 11,491,000 tons in the period 2016-2017 while occupying the position of the 4th largest coffee producer and exporter in the world. Based on company status, the Indonesian coffee industry is divided into three categories, namely smallholders, government, and private.

Smallholders are plantations owned by households and are not a legal business entity. In general smallholder farmers form

a legal community called the Cooperative. Meanwhile, with a land area of 96.19%, smallholder farmers are the largest contributor of all types of coffee producers, both private and government. With this strategic role and potential, Indonesian coffee smallholders are expected to continue to grow amid global competition. However, Indonesian coffee smallholders have complex problems, namely low-quality control, inadequate infrastructure, climate change, socio-economic conditions and technological limitations. In the end, these problems have caused various losses in the Indonesian coffee industry such as vulnerability to price fluctuations, crop failure and low productivity. The benefits of smart industry for organizations is that product development can be faster, save resources, improve productivity, increase the need for skilled labour, increase investment, make optimal decision making, engineering. Business processes become dynamic, and can give birth to new business models and new ways to create added value. However, in Indonesia, technological issues are included as one of the main problems that hinder the development of the industrial sector, especially in the type of Small Medium Enterprises (SMEs).

The method used to design information system in the KPKM is the Ward & Peppard framework. The strengths of Ward & Peppard's framework are, in the business analysis phase that can design business strategies before entering the IT strategy design phase, the classification between the definitions of IS and IT is structured to facilitate the strategy to be understood, the existence of external analysis that can take into account factors outside the company that affects the company's business processes, and the steps taken do not have to be sequential so that they can prioritize which steps are most likely to be done. This framework is divided into 2 stages, namely the input and output stages. The input phase includes analysis of internal business, external business, IT internal and external. At the output stage consists of designing business strategies, IS, IT and IT management that will produce a portfolio of what Information Systems will be needed to support the company's business processes. The output produced in this study is in the form of a portfolio of strategy designs. It is hoped that this strategy can help coffee cooperatives in realizing the application of smart industries to increase the competitive advantage and productivity of cooperatives and can be a solution to smallholder problems in general and specifically on the object of study.

II. LITERATURE REVIEW

A. Digital Transformation

A coffee shop lifestyle as a trend in modern society can be a good business opportunity as competition intensifies among entrepreneurs. The growth of coffee shop consumers is accompanied by the growth of entrepreneurs, who are now very popular with the youth. The most important thing about having a coffee shop is promoting on social media. Using filters on social media or application in the phone is a very valuable way for someone or a product to convey expectations to consumers [3]. One such potential tool for coffee farmers is to foster a strong awareness of profitability across their geographic regions given the importance of scenario planning in the coffee production cycle. Understanding the spatial characteristics of profitable producers can provide better decision-making insights into production and management decisions in the coffee industry, even across the globe [4]. This digital transformation has become one of the pillars of industrial strategy that has completely changed the job patterns of the majority of industrial applications, and companies need their employees to understand and use the new developed business models. Therefore, interests of this transformation are characterized by mastering the process of digitization of operations, redefining of business lines, good data analysis, and rapid integration within the organization [5], which collaboration and data sharing become the key consideration.

The adoption of smart industry concepts, including operating procedures, technologies and systems, is dependent on human factors. Training, professional function, well-being, human performance, and physical and mental health are factors that influence the decisions and behaviors of one or more productive organizations. Human workers want to enter the market, stay in the market, building their careers, earned fair wages, stability, intellectual growth, learning, and / or professional achievement. On the other hand, companies generally want the best possible human performance to improve productivity [6]. The limitations and requirements placed on the devices and systems used depend heavily on the application chosen and the layers considered [7]. In addition, ensuring adequate production of coffee plantations requires government support for additional investments in construction that have a negative impact on the ecosystem [8]. Despite the apparent efforts of the scientific community to articulate the vision of strategic alignment of IT and business, IT and business are inevitably dynamic so that organizations can be applied to the real world. Contributions to this topic grow very rapidly, but the relationship between assumptions and conclusions is inconsistent and inconsistent. The main reason is that the proposed model is highly conceptual and detached from the actual reality of the organization [9], [10].

B. Profit Optimization

The main goal of the transition to the smart industry is to enable organizations to monitor machines and equipment directly in real time by implementing smart operations using machines that can analyze their data and predict when maintenance will take place. It also improves supply chain management through product tracking, logistics tracking, inventory management, and scanning real factory process cases

to clear processes in use and verify compliance with designed business processes [5]. Interestingly, at certain countries, the number of profit was earned from coffee industry has the power in economic to strengthen the national currency through hexport import trading [11]. Of course, critical factors can be linked to the support from government regulation related to the tariff barriers [12]. Therefore, ultimate developments, especially post-harvest processing, can add value to coffee products, open up business and employment opportunities, and can lead to a wider multiplier effect [13].

In the coffee industry, some by-products are produced during the production and consumption of coffee, which makes them an important waste from an environmental point of view, preventing the worst in the future, and detrimental to long-term operations [14]. One way to increase quality awareness is to emphasize brand personality. When communicated properly, there are personal characteristics that are preserved to create value for potential customers in increasing the quality of the brand itself [15]. The upgrade process with appropriate technology allows company to better respond to competitors in the globalized market through high added value activities, achieving a better positioning process in the international market and help promote it. It may have a positive impact on the sector or industry by improving value chain practices to improve performance, increase return on investment, and ultimately improve profits [16].

C. Innovation Ecosystem

Rapidly changing topics are underway for a future where less has and more is shared. Home appliances are connected via the Internet of Things (IoT), and homes are powered by renewable energy. New entrepreneurs take inspiration from the success of the founder's last wave, in which several web services are available to facilitate entrepreneurship and improve access to capital. Industry 4.0 is an industry approach that addresses all aspects of the industrial operating model, including culture, management responsibility, and interaction with regulators that require companies to consider new models in the ecosystem [17]. Most industries began with some kind of invention, such as telephones, light bulbs, radios, and television. Credits for the invention are awarded to the inventor, while credits for establishing the industry are awarded to entrepreneurs who establish new companies. There is the required question on the exact definition on what happens before industry, and not just how it emerged or who the perpetrator is involved but when they participate and how they participate [18]. In the technology-intensive industries, the teamwork process is often complicated by dispersed interests among industry participants. Such competition can hinder teamwork, as industry participants fail to advance their own interests and the interests of the industry as a whole to gain legitimacy.

Like the history of the Industrial Revolution, innovation also has evolved in several stages. In the beginning, it can be defined as a closed or regulatory binding innovation, in which the most of new ideas are the result of the organization's in-house research and development to develop its own core competencies such as Bell Labs and NASA. The second stage is collaborative innovation in which the organization collaborates with outside sources or partners for value chain

innovations such as Apple, Dell, Zara, and Boeing. Therefore, the third stage is open innovation, as organizations search for new sources of innovation internally and externally. This is very similar to the crowdsourcing innovation that the most famous ones are NineSigma, InnoCentive, and YourEncore. Then, the trend is shifting to Innovation 4.0 or co-innovation where the organizations develop an innovation ecosystem to evaluate and approximate the ideas generated through all useful sources, including in-house research and development, collaboration, open sourcing and co-creation with clients and partners to create an implementation plan [19].

The future of the ecosystem should be seen as a new paradigm as a set of cutting-edge technologies that support effective and accurate engineering decisions in real time by introducing various ICT technologies and integrating existing technologies [20]. The innovation ecosystem concept put more emphasis on value creation and collaboration where the companies co-evolve capabilities around a new engagement method or mechanism to support new product, satisfy customer need and incorporate to the advancement process competitively [21]; the question of who belongs in an ecosystem and who does not cause the natural and natural problems of the ecosystem structure. The diversity in the types of participants, their roles, and their interconnectedness means that issues are not distributed evenly among the participants. The interconnectedness of ecosystem participants also raises the issue of how ecosystems are coordinated and managed. In many cases, there are central companies that coordinate services for the system. These firms may control the technology or brand architecture that drives the value of the ecosystem, and coordination may depend on the management of the architecture in regards to organizing access to specific common platforms. Indeed, a large subset of the literature proposes platforms as tuning artifacts used by pivotal firms, services, tools, and technologies that other members of the ecosystem can use to enhance their unique performance characteristics [22].

III. METHODOLOGY

The smart future should help innovate and develop smart solutions to complex problems and ensure a human environment with dynamic change. This is due to natural phenomenon, the deliberate design of human ingenuity, or the cooperation of individuals and can be classified as incremental (exploitative), radical (exploratory), ambidextrous (responsive) and disruptive (destructive) [19]. In this case, Ward & Peppard framework was adopted. By using the business and IS/IT environment analysis as an input, the output of this framework consists of business/IS strategy, IS/IT strategy, and IT strategy. There are several analyses used to generate business/IS strategy, the step by step shown in the following Fig. 1, Business Environment Analysis, which started from business environment analysis on both internal and external side.

This business environment analysis aims to assess the strength-weakness factors from the internal environment and the opportunities-threat factors from the external environment. These strength and weakness factors are internal factors that are generated from the business processes that occur within Margamulya coffee producer called KPKM. While the

opportunity and threat factors are external factors that explain things that can affect the business processes within the organization, both direct and indirect.

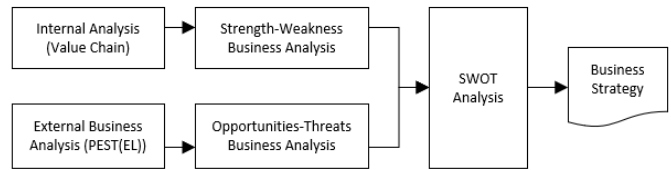


Fig. 1. Business Environment Analysis.

The next step is to align the business strategy generated from previous analysis into IS/IT strategy needed by KPKM. Critical Success Factor Analysis (CSF) used to map the main factors considered in achieving the organization's vision and mission. Based on the results of CSF, an information system (IS) to be developed was formed, which indirectly support the KPKM business strategy. Those information systems are mapped using McFarlan quadrant.

The last step in Ward & Peppard framework is generate the IT strategy and infrastructure to support the IS strategy. IT requirements are carried out by mapping IS/IT strategic principles with IS requirements.

IV. RESULT AND ANALYSIS

A. Internal Analysis

In the formulation of the IS strategy at KPKM, the first step taken is a business analysis from both internal and external sides. Analysis of the business environment aims to see and assess the strength - weakness factors of the internal environment and the opportunities - threat factors of the external environment. These strengths and weaknesses are internal factors that are compiled from the business process that occurs so that the advantages and disadvantages of KPKM are obtained. On the business process, the opportunity and threat factors are external factors that explain things that can affect the running of an organization's business processes, both direct and indirect. Many manufacturers are already leveraging smart plant components in areas such as advanced planning and scheduling with real-time production and inventory data, or augmented reality for maintenance. But a true smart factory is a more inclusive effort, going beyond the manufacturing floor to impact businesses and the wider ecosystem. Smart factories are essential to a wider digital supply network and have multiple aspects that manufacturers can leverage to better adapt to changing markets. On the one hand, industrial policy is designed to encourage exporters by offering special treatment to preferential sectors, such as tax exempt periods, large investors' access to land, and special credit terms [23].

Many manufacturers are already leveraging smart plant components in areas such as advanced planning and scheduling with real-time production and inventory data, or augmented reality for maintenance. But a true smart factory is a more comprehensive effort that goes beyond the manufacturing floor and impacts businesses and the wider ecosystem. Smart factories are essential to a wider digital supply network and have multiple aspects that manufacturers can leverage to better

adapt to changing markets. Based on activity internal to the analysis value chain, subsequently carried out the analysis by doing the identification of the factor of strength and weakness of the activities of internal compiled from the business to get things that become advantages and weaknesses of KPKM in the business, which is based on SWOT analysis in Table I, Internal Analysis.

TABLE I. INTERNAL ANALYSIS

S /W	Internal Condition Indicator	Internal Activities
Strength	Has a unique coffee taste characteristic	Cultivation
	A good brand image with the various champions that have been achieved	Marketing and cultivation
	reliable, has various certificates both national and international	Audit
	Has relationships with various business sectors	<i>Public Relations</i>
Weakness	Low accountability	Production, Finance and secretary
	A less transparent financial system	Finance
	Low Documentation	Finance and marketing
	The capital system still depends on the bank	Finance

B. Root Cause Analysis

Root Cause analysis is used to identify the root of the problem which becomes weakness KPKM with the results of this analysis will be processed into input as can be seen in Table II, Root Cause Analysis, that later on use as the requirements needed to produce reference solutions. Most organizations cannot focus on just one type of innovation, exploitative or exploratory. Many organizations have specific core competencies that are built over time, which can continually improve these capabilities to increase your productivity to generate additional financial benefits. However, in a volatile and rapidly changing market environment, we cannot focus on improving our existing core competencies. Therefore, exploratory innovation is essential. An important strategic issue for enterprises is to balance exploitative and exploratory innovations, making use of their existing core competencies, while striving to develop new competitive advantages through exploratory innovations. When workplace problems occur, the immediate symptoms are hard to overcome. In other words, the root cause has not been addressed and needs to be fixed multiple times. Organizations that can strike the right balance between the two types of innovation can not only alleviate the tension between two major pathways to innovation, but they can also pursue the synergies between their strengths. In this way, an eye-catching innovation is a rapidly changing market setting where organizational strategies are global, technological advances, dynamic changes, global urbanization trends, and environmental sustainability initiatives to create competitive advantage [19]. To commercialize new technologies, licensing is often used to existing companies rather than by step-by-step, which is the traditional method of technology transfer.

TABLE II. ROOT CAUSE ANALYSIS

Problem (Effect)	Cause (Cause)
Low Accountability	There is no recording process
Financial System Lack of Transparency	Financial accountability systems are less informative
Low Documentation	Document storage is still paper based
	Document storage is not organized and centralized.
The financial system is not yet independent	The financial capacity of cooperative members is inadequate

C. Requirement Analysis

Requirement analysis is the process of determining user expectations for an application that has been created or modified. In short, it includes every task that is performed to identify the needs of different stakeholders within the organization environment, at certain extent may relate to the culture. Therefore, it means analyzing, documenting, validating and managing software or system requirements that are high-quality documented, workable, measurable, testable and traceable requirements that help identify business opportunities and systems. It is defined to facilitate design. An entrepreneurial process can take place in any enterprise or organization and hence even the government can host such a process. The government's role in entrepreneurship is particularly wide-ranging, given that the decisions and policies adopted can contribute directly to the development of entrepreneurial activity in the sector by both private and public companies [23]. The coffee industry is attracting attention as a product that a large proportion of consumers around the world buy frequently daily at social events, as well as the interest of non-governmental, governmental, multilateral and development professionals with early adoption of certain standard in developing the strategy. Therefore, it is not surprising that coffee remains at the forefront of sustainability initiatives going beyond other agro-industries in response to the growing interest in sustainability [24].

Typically, IT management stakeholders use the integration of enterprise applications strategically from the top down rather than technically from the bottom up. Initially, through the systematic integration of BPM technology, knowledge management technology and social software, supporting the value-added processes of modern enterprises would be an entirely new IT quality. In a good organization, all value-added processes, whether formal or tightly organized and informal, and social processes are subject to management and IT support [26], [27]. The Table III, Requirement Analysis shows the requirement analysis by aligning internal activity and objective of the organization based on internal activity identified in the organization.

D. External Analysis

External analysis means investigating the company's industry environment, including factors such as competitive structure, competitiveness, dynamics, and history. At the macro level, external analysis includes macroeconomic analysis, global, political, social, demographic and technical analysis. The primary purpose of external analyzes is to identify opportunities and threats in an industry or any sector that drives

profitability, growth and volatility. Firms make decisions on sustainability issues based on available information and management is responsible for considering the best information. In the case of sustainability, decision makers often face complex and ambiguous scenarios, and as a result, they do not make fundamental changes to enhance the company's sustainability. It is also true that companies are becoming more interested in developing environmentally friendly and healthy products, so they should prioritize profits in decision-making and not use them as an excuse to not take any action [24]. It is possible to increase profits while protecting the environment by reducing waste or emissions, in which most occasion, societies still ask more due to the expectation of the industry to take active role in the issues of environmental and ecological.

To complete and support the external analysis, companies need to conduct a survey of the political, economic, social and technical situation of the industry, which is also known as PEST analysis as can be seen in Table IV, PESTEL Analysis. In politics, the analysis on issues such as international trade barriers and changes in the regulatory environment consists of several issues in the economy, such as interest rates, exchange rates and inflation. On the other hand, social demography raises the issue of changing populations and age groups, while technical issues represent scientific progress, research and development investments, and emerging technologies. The main purpose of PEST analysis is to use business plans to test major external shifts in the industry, and strategies must be updated to align with common industry trends. In fact, this data helps organizations get to know their customers better, and suggests increasing sales, especially in the form of differentiating marketing strategies and creating targeted marketing. Companies can also change their supply chain and adapt to obtain more accurate data from their partners [28].

TABLE III. REQUIREMENT ANALYSIS

Internal Activity	Objective	Requirements
Production, Secretary & Finance	Increase accountability	There is periodic reporting of information from each division to the central management
		The existence of a clear and efficient format and recording procedure.
Secretary & Finance	Increase the role of information documentation	The documentation process is digitized
		All cross-sectional documents are integrated and can be managed centrally. Cooperative documents can be stored safely and can be accessed easily by those who need them
Finance	Increase Financial Transparency	The existence of regular reporting in a shorter period of time (per week to per month)
		Financial statement information consists of a complete and accountable collection of data elements
	Has an independent financial system	There is access or media that makes it easy for each member to find out the results of cooperative financial reports Increase the income and welfare of members

TABLE IV. PESTEL ANALYSIS

PEST (EL)	External Environment	Impact on Organization
Political	The West Java Provincial Government is specifically paying attention to the coffee industry with the campaign "World Quality Java Preanger, Towards the World Market"	O-1 Create opportunities to massively market products and receive assistance in various forms (subsidized tools, seeds and training)
	Jokowi, as the president, will issue a policy on forest land use under a 30-year contract	O-2 Cooperatives will find it easier to collaborate with borrowers and sponsors.
Economy	Trends in world coffee consumption and foreign currency fluctuations greatly affect the selling price of coffee	O-3 The selling price of Gunung Tilu coffee can be high T- 1 The selling price of Gunung Tilu coffee could be lower
	Vulnerability of IJON practice	T- 2 Causes farmers to sell coffee at a lower price and not distribute it to the cooperative
Social	The number of coffee industry players in the Bandung Regency environment in particular.	O-4 Must have relations among themselves because of the need for imports which must have a certain quota
		O-5 In terms of marketing, in general, between them can complement each other's customer demands.
	participation of the international community through certification	T- 3 When the demand for Preanger (West Java) is low, a similar coffee industry can become a competitor O-6 Can guarantee the welfare of farmers
Technology	The role of ICT in the industrial world has developed rapidly, therefore adequate infrastructure is needed by cooperatives	O-7 Can provide competitive advantage, efficiency and various other advantages if implemented properly
		T- 4 If it cannot adapt to developmental conditions, it will be difficult for the competitiveness of KPKM to increase. In the end, it was difficult for KPKM to advance to the level of an independent exporter.
Environment	Unpredictable climate change	T- 5 The emergence of various diseases in plants, ahm appears and has the potential for crop failure
Regulation	The Indonesian government regulates the operation of cooperatives Law 25 of 1992 where the Law requires cooperatives to regulate several principles, capital, business processes and organizational structures that must exist in cooperatives	O-8 Facilitates cooperatives in shaping their organizational principles and forms.
	Law 19 of 2013 regulates agricultural cooperatives in importing, extension services, and land empowerment	O-9 Make it easy for cooperatives to import and minimize the potential for fraud by competitors

After defining the strengths, weaknesses, opportunities and threats of the organization, a business strategy is mapped based on a matrix of strengths-opportunities (SO), weaknesses-opportunities (WO), weaknesses-threats (WT) and weaknesses-opportunities (WO) as shown in the following Table V, SWOT analysis.

Based on the SWOT analysis, a business strategy is generated as shown in Table VI, Mapping Business Analysis. Then the new business strategy is then being compared with the old business strategy as depicted in Table VII, Comparison Analysis.

TABLE V. SWOT ANALYSIS

	Strength (4 factors)	Weakness (4 factors)
Opportunities (8 factors)	Strengthen the role of <i>branding</i> and marketing functions. [1]	Following international coffee certification. [2] Technology optimization to improve internal / external transparency, customer service quality and data utilization. [3]
Threats (6 factors)	Carry out research and development efforts [4] Collaborate with organizations that specialize in agriculture and / or meteorology [5]	Implementing an integrated SI, especially in the production, membership (HR), finance and reporting business processes [6] Improvement of education methods and capital systems [7]

TABLE VI. MAPPING BUSINESS ANALYSIS

Internal Business	External Business	Business strategy
S-1 Has a unique coffee flavour characteristic	O-1 Opportunities are created to market massively products and receive assistance in various forms (subsidized tools, seeds and training)	Strengthen the role of <i>branding</i> and marketing functions
W-5 The capital system still depends on the bank	O-5 International Community Can guarantee the welfare of farmers	Following international coffee certification
W-1 Low accountability W-2 A less transparent financial system	O-6 Can provide competitive advantage, efficiency and various other advantages if implemented properly	Technology optimization to improve internal / external transparency , customer service quality and data utilization
S-1 Has a unique coffee flavour characteristic	T-2 The selling price of Gunung Tilu coffee could be lower	Conduct research and development efforts
S-4 Has collaborated with various business sectors	T-6 Bad weather causes crop disease and crop failure	Cooperate with organizations that specialize in agriculture and / or meteorology
W-1 Low accountability W-2 A less transparent financial system	T-5 If it cannot adapt to developmental conditions, it will be difficult for the competitiveness of KPKM to increase	Implementing an integrated SI, especially in the production, membership (HR), finance and reporting

		business processes
W-5 The capital system still depends on the bank	T-3 Causes farmers to sell coffee at a lower price and not distribute it to the cooperative	Improving education methods and capital systems

E. IT Business Alignment Strategy

The points to be considered in the preservation of the coffee industry relate to the role of the natural environment and characteristics of the ecosystem, the existing traditional agricultural knowledge and local farming practices, and the socio-economic conditions of the agricultural community [25]. Consider the development of same concept of smart but different field, the input-output development model, which considers a diverse set of smart city domains, characterizes the externalities of resources, productivity, applications, and establishment processes. “Resources” relates to human resources, knowledge, creativity, ICT infrastructure, and financial assets. Productivity is categorized as “dynamic productivity” and “management and leadership capacity” that adds value to resources and turns them into intended outputs. “Applications” are related to outputs, and “externalities” are management and regulation, technology, governance, policy contexts, people, economic infrastructure, and environmental conditions [29], [30]. Undoubtedly, there is also widespread criticism of the concept of intelligence in relation to an important and important issue that is the fairness of one of the beneficiaries of the smart industry strategy and do local citizens benefit from their investments more than economic and political actors [31].

Increased social distancing affects the number of interactions, the potential for knowledge and creativity sharing, and trust in society. Digital or technological disparities are specific issues that some smart action can address by providing all citizens with access to technology or specific knowledge. While the technology itself opens the gaps, it is taken for granted that smart concepts have a promise to bring them to an end. This has to be anticipated and planned for both cases as there has to be a balance between efficiency and equity that is of course required the support from the government such as the regulatory and tax incentive [32], [33]. In aligning the cooperative business strategy into the KPKM strategy where the information on the analysis process is needed to identify the needs that are in line with the business strategy, which in this case using the Critical Success Factor (CSF) analysis which is used to map the main factors that concern the organization in achieving the organization's vision and mission. Based on the results of observations and interviews, a CSF was obtained for each of the KPKM Business Plans as in Table VIII, Business Plan below. Further based on CSF, the information system is mapped using McFarlan quadrant which divided into four (4) types namely Strategic (St), High Potential (HP), Key Operational (KO), and Support (Sup). The result of mapping analysis can be seen in Table IX, Mapping Using McFarlan Quadrant.

TABLE VII. COMPARISON ANALYSIS

No.	Old Business Strategy	New Business Strategies
1	Improve member welfare	Improve member welfare
2	Expanding the types of products / services	Expanding the types of products / services
3	Build credibility of cooperatives to stakeholders who have the potential to prosper farmers.	Build credibility of cooperatives to stakeholders who have the potential to prosper farmers.
4	-	Increase member loyalty and trust
5	-	Improve product quality
6	-	Maintain the continuity of the organization
7	-	Improve service quality
8	-	Increase market segmentation and penetration
9	-	Developing an independent capital system

TABLE VIII. BUSINESS PLAN

Strategic theme	Strategy Explanation	CSF	Information Needs	SI Strategies and SI Needs
Increased member income	Maximizing the income of each member	Good knowledge and skill	<ul style="list-style-type: none"> Knowledge level of member Member profile Member needs Types of training and development 	<p>Create a system that can measure and provide information related to member performance and training information.</p> <ul style="list-style-type: none"> IS (Information System) training and member profiles integrated into HRIS. Features measuring the level of knowledge of members integrated in HRIS.
Build company credibility towards stakeholders who have the potential to prosper farmers.	Increase trust in consumers, potential consumers as well as partners and prospective partners	Participation in national and international certifications	<ul style="list-style-type: none"> Level of certification readiness Audit report 	<ul style="list-style-type: none"> Creating a special system related to certification including the specifications for the audit report and documentation requirements. Creating a reporting system for each part of the cooperative that is centralized to the core board. Determine the format and recording procedure. Create an IS Audit
Increase member loyalty and trust	Accountability and transparency of assets.	There is informative data on assets and finance	<ul style="list-style-type: none"> Subsidies and external assistance Cooperative finance Asset and borrowing records 	<ul style="list-style-type: none"> Realizing the financial reporting mechanism consisting of complete and accountable data elements. Make it easy for members to access and find out the results of financial reports. Become a media for routine cooperative financial reporting. IS Finance Create IS that can record and notify members regarding old and new assets IS Asset Management system
Expanding the types of products / services	Have product / service innovations in accordance with market needs	Marketing effectiveness The quality of the type of product / service	<ul style="list-style-type: none"> Criteria for segmenting prospective customers Position of organization among competitors Detailed product / service innovation research 	<p>Making IS that can help make organizational decisions in terms of marketing and product / service development.</p> <ul style="list-style-type: none"> Customer Relationship Management IS Marketing Business Intellegent
Improve product quality	Have good product development and production management	<ul style="list-style-type: none"> Can consistently maintain product quality Possess innovative and efficient cultivation and processing techniques 	<ul style="list-style-type: none"> Product specifications Type of product processing Recommendations for cultivation and / or processing innovations 	<ul style="list-style-type: none"> Build IS that can record and analyze the production process, and can provide suggestions related to improving the quality of cultivation and production. IS Cultivation and Production
Organizational sustainability	Guarantee the regeneration of cooperative	<ul style="list-style-type: none"> Have authentic documentation both on the 	<ul style="list-style-type: none"> Annual Meeting result Company Profile Documents of each section 	<ul style="list-style-type: none"> Creating a reporting system for each part of the cooperative that is centralized to the core board.

	management	management and function side of each division of the cooperative. • Cooperatives are able to compete with competitors	of the cooperative	<ul style="list-style-type: none"> • Determine the format and recording procedure. • Making IS that can digitize the cooperative strategy record (Annual Meeting) and the work of each section. • Keep cooperative documents safely and easily accessible to those who need them . • Making cross-sectional documents can be integrated at the same time can be managed centrally. - Archive feature in IS Asset Management - Profile feature on cooperative websites
Improve service quality	Improve the quality of service to customers and potential customers	Have services and provide information that can be accessed at any time by customers or prospective customers and can accommodate suggestions or criticism	<ul style="list-style-type: none"> • Information on services and product variants • Cooperative location and contact information • Payment information 	Create various e-banking or fintech features and handle purchasing services - Multi paymnet purchase system - Feature services are contained in the Website
Has an independent capital system	Transfer of capital originating from the bank to members and sponsors	Each member is able to contribute a large amount of capital	<ul style="list-style-type: none"> • Member profile • Member financial level 	Provide information on the financial capacity and condition of members (health, children's education, etc.) - Financial data of members in HRIS

TABLE IX. MAPPING USING MCFARLAN QUADRANT

Information Systems (IS)	Function	Type	Explanation
Human Resource IS	A system for monitoring the welfare conditions and performance of cooperative members	Sup	This system is only used to support the performance of KPKM members
IS Audit	A system for conducting audits and measuring certification readiness.	St	This system can increase the trust of stakeholders who have and will collaborate with KPKM.
IS Finance	A system for calculating, recording and managing cooperative finances in detail, accurately and transparently	Sup	This system supports the performance of the KPKM in terms of financial management
Asset Management	A system that records and manages asset data. Starting from procurement, repair to borrowing assets.	Sup	This system supports the performance of the KPKM in terms of asset management
Customer Relation Management	A system that analyzes and predicts customer behavior as a decision support tool 3	St	This system is used to support the performance of the KPKM in identifying customer needs
IS Marketing	A system that manages all product marketing activities carried out by the marketing department from measuring the performance of the marketing team, achieving sales targets to designing marketing strategies.	HP	With this system, it is hoped that KPKM can improve the performance of marketing activities
BI	System To provide information on policy indicators quickly and accurately to cooperative administrators in setting policies.	St	If this system does not exist, the cooperative management will not have accurate information
IS Cultivation & Production	A system that helps monitor, manage and make decisions regarding cultivation and production activities	KO	This system helps and provides accurate data about the efficiency, effectiveness and development of cultivation and production processes.
Official Website	Help market cooperative products and services, display cooperative profile information, and become a medium for customer service.	HP	With this system, KPKM can facilitate promotional activities and services to customers
Multi paymnet purchase system	Providing an electronic transaction system through various types of payment methods that make it easier for customers to make transactions. The methods referred to are ATM, Internet banking, Mobile Banking, and E Money	KO	The absence of this system will make it difficult for KPKM transactions with customers who are familiar with using online-based payments

Information:

*) Types of Information Systems are classified based on the McFarlan quadrant which is divided into 4 types: Strategic (St), High Potential (HP), Key Operational (KO), and Support (Sup).

From the results of the identification of the information system using the CSF method, the results of the needs for the JPIC information system were obtained. The requirements for the JPIC information system can be mapped into the SI strategy portfolio using the McFarlan matrix. Starting with the situation in which all production activities are traditional, industrial cavitation can be considered as a situation in which

companies in one country switch to more modern technology and the industrial sector in another country cannot participate in this movement. But in some industries, there are huge multitudes: access to cloud technology, predictive analytics, and IaaS services for both virtual data centers and storage systems, and the use of Monitoring Surveillance and Data Acquisition (SCADA) [34], [35], [36]. KPKM does not yet

have an existing technology-based information system, so the GAP between the existing IS & IT portfolio and the targeting business process is entirely new with the matrix for the SI-KPKM strategy can be seen in Table X, Matrix Strategy. The service operation manages the services the company is currently using, focuses on service management practices.

TABLE X. MATRIX STRATEGY

Strategic -IS Audit -CRM -BI	High Potential - Official Website -IS Marketing
Support -Human Resource (HRIS) -IS Asset Management -IS Finance	Key Operational -IS Cultivation and Production - Multi payment purchase system

One of the most important technologies is blockchain technology. In theory this is a clever industry concept that can provide many features such as replacing slow manual steps with fast automation, tracing the origin and characteristics of goods, including raw materials, semi-finished products and finished products. Information that includes passengers, timely payments, insurance and customs payments, and information to regulators about cargo and passengers includes participants such as exporters, importers, and carriers [37]. There are other technologies that are important components of a smart industry, which is the Internet of Things (IoT) provides convenience for continuous spatial analysis over a relatively large coverage area by optimizing between remote sensing and GIS to develop an ecosystem for digital innovation [38]. The growth of new digital industrial technology, also known as Industry Revolution 4.0, is an innovation that allows data to be aggregated and analyzed between machines, with faster and more efficient operations of high-quality products at a lower cost [39]. Other technologies, such as autonomous robotics, cloud computing and augmented reality, can also be seen as supporting the smart industry. Unfortunately, there are certain deficiencies related to the presence of a deteriorated educational system with low training of engineers where a lot of technology transfer but a low absorption capacity due to the small investment of local companies in research and development together with weak infrastructure to support smart industry concept with significance delay and no emphasis on the development of electronic product and weak articulation [40]. To understand the IS strategy in Table X, Matrix Strategy, we describe the application architecture layers consisting of the front office, middle office, and back office as shown in the Fig. 2, Layers of Propose KPKM Application Architecture.

Once the IS strategy has been defined, the IT and infrastructure are generated to support the information system. IT requirements are generated by mapping IS/IT strategic principles and IS requirements. The IT strategy can be seen in Table XI, IT Strategy.

Innovation is a tool to promote the sustainable development of education and attract the attention of teachers, educators and researchers around the world. The introduction of new

concepts and technologies into the curriculum and the removal of old concepts and techniques is sometimes referred to as curriculum innovation [41]. The increasing social role of the coexistence of robots, humans, and technology is a precursor to unknown and possibly fundamental changes, but there is no single human perspective to this change [42]. Shifting product development to concurrent engineering mode requires industrial engineers to be actively involved from the initial concept design stage. Therefore, it increases product safety and participation in environmental issues, affecting individual workplaces and society as a whole. Code of Ethics is discussed in [43], [44]. Interestingly, the leading position of such new technological systems that support smart concepts is believed to be of great benefit to the economic catch-up and long-term competitiveness of developing countries [45].

F. Smart Industry based on Innovation Ecosystem

In terms of innovation, the position and support for employing research and development in the private sector has the strongest impact on patents for all sources of knowledge. In short, the quality of research in the university is very important to contribute to the smart industry [46]. Innovative companies are not isolated, self-sufficient entities, but are very environmentally friendly. This inclusion can have a significant impact on the innovation process, and it is not too far to assume that not all types of environments are equally suitable for a particular type of R&D activity [47]. The production elasticity of spending on R&D can be interpreted as an indicator of the productivity of inputs in the innovation process, and hence the efficiency of the innovation system in a given region. In particular, good availability of inputs for this kind of process, extensive division of innovative work, and superb knowledge among local stakeholders, either in the public research institute or in the private sector brings the flexibility to be relatively high if the site is spread out within company [48]. However, the smallholder coffee sector continues to suffer from a lack of efficient and effective support services such as publishing, credit and input supply. In particular, there is no for-profit company engaged in the growth and dissemination of improved coffee beans [49].

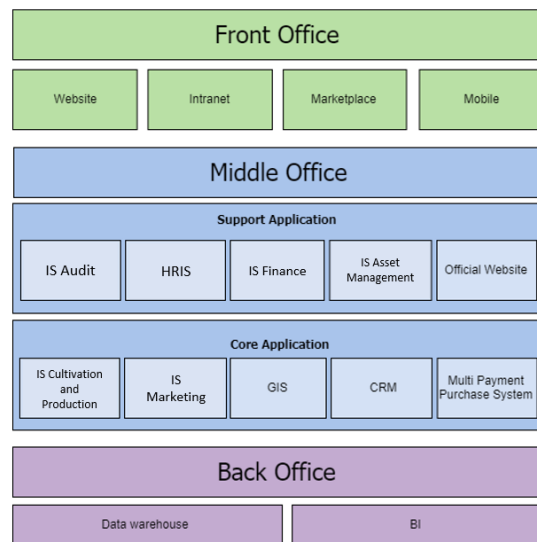


Fig. 2. Layers of Propose KPKM Application Architecture.

TABLE XI. IT STRATEGY

IS/IT strategy based on Int & Ext analysis	Information System (IS)	Information Technology (IT)	Information
The development of IS / IT integration is in line with the business strategy	IS Marketing and Strategy Archive system Multi payment purchase system; BI; CRM	Web Server (APACHE); Database Server (MySQL); Platform (PHP); Multipayment Purchase System; BI; CRM	CRM software is recommended to use a third party, namely "FarmLogics". On the other hand, the ATM, Mobile Banking, E-Wallet applications will be connected via the server.
Appropriate IT security infrastructure (not under / over protective)		Unified Threat Management (UTM); Intrusion Detection System (IDS)	UTM and IDS are needed to deter and detect attacks from external parties
IS / IT development in managing and utilizing data	IS Finance; IS Asset Management	DSS; Intranet; Web Server (APACHE); Database Server (MySQL)	The DSS application on IS Finance will be integrated with SI Cultivation and Production to conclude a series of decisions. On the other hand, IS Asset Management will actively record internal borrowing transactions.
Development of a data exchange system with the government and certificate providers	IS Audit and Certification	Web Server (APACHE); Database Server (MySQL); Intranet	Data and information exchange system with internal and external auditors.
The development of IS / IT supports the level of production and quality of plantation products	IS Cultivation and Production	GIS; Web Server (APACHE); Database Server (MySQL); Android SDK (Java); Intranet	IS Production involves many technologies where GIS will generate geographic plantation information, while SDK will generate technical information (such as seed moisture, moisture content, etc.)
Increasing the number and competence of human resources who are experts in the IS / IT field	HRIS	Android SDK (Java); Web Server (APACHE); Database Server (MySQL); Intranet	HRIS uses an integrated and centralized application and website platform on the web server.
Adjustment of infrastructure capacity (network , server , storage) that supports integrated IS / IT		LAN network between offices, cafes and warehouses; Core Switch	LAN networks are needed for the acceleration and security of the internal information exchange process.

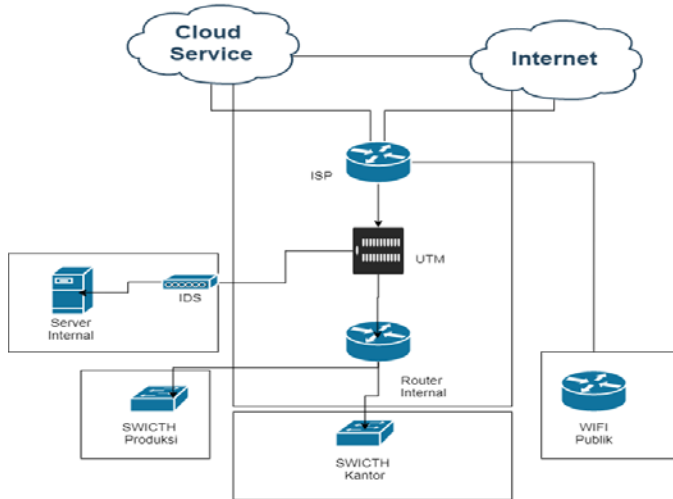


Fig. 3. New Network Topology.

To better understand the proposed infrastructure topology can be seen in Fig. 3, New Network Topology.

Due to the factors and their influence on the adoption of improved coffee production technology, access to credit, availability of non-farm income, level of education, availability of manpower and access to extension services, it is assumed that it has become evident to have a major influence on the adoption of scale. The gender and age of farmers do not have a significant influence on adoption, suggesting that the improved coffee technology is primarily size, gender and age

neutral. On the other hand, the decision to adopt agricultural technology for coffee households depends on their economic situation, farm characteristics, and institutional effectiveness [50]. On the other hand, other descriptive results show that there is a significant difference between employers and non-employees in terms of number of livestock ownership, spades or shovels belongings and model farming. This indicates that the ownership number is a typical farmer in which adult education and the possession of pruning shears have been found to have a positive effect on the adoption of coffee technology. On the other hand, family marriage and radio ownership negatively affected coffee technology adoption. Educating farmers through formal or informal programs, increasing production skills to strengthen and increase the number of exemplary farmers, providing pruning shears and improving the livestock sector focused are good policy recommendations where the presence has been disclosed [51]. On the other hand, the results of the multivariate model showed that the adoption was positively associated with improved recruitment of corn strains and the abandoned cows, which will enhance the adoption of other agricultural technologies. The land area, television, and radio ownership also have positively and significantly influenced the adoption of the improved coffee varieties while the distance to all-weather roads has a negative in decreasing the adoption of coffee varieties due to the remoteness of farmers from roads in all weather conditions. The size of the land and the education of the household heads also have a positive and significant impact on the adoption of improved varieties of maize but the distance between TLU and city area has a big negative effect [52].

TABLE XII. IS/IT MANAGEMENT STRATEGY

No.	IS / IT Management	Classification	Description
1	Making good IS / IT governance based on <i>best practices</i>	Regulation and governance	Design and use IS / IT governance that refers to <i>best practices</i> in the JPIC environment
2	Procurement and improvement of HR competencies in the IS / IT domain	HR	Recruit human resources in accordance with the needs of the cooperative as well as conduct training and briefings.
3	Addition of IS / IT division	Organizational Structure	Creating a special section that handles Cooperative IS / IT issues

Aside from infrastructure topology, following in Table XII is the proposed IS/IT Management Strategy for KPKM.

Specialty coffee is standardized throughout the coffee processing cycle, from selecting the criteria for growing coffee to brewing coffee for customers, with an emphasis on fruity, floral and citrus flavors. The coffee is rated higher organoleptic, which in fact that the coffee grounds must be able to pass the side or elementary grading and cupping tests [53]. The economic value of the coffee beans depends on the quality of the flavor, but the quality and quality of cupping for the three types of coffee varies greatly depending on the type and amount of compounds present in the esteemed beans [54]. Unfortunately, in many cases, all used warehouses can be classified as substandard, a condition that accelerates quality deterioration due to moisture loss, coffee weight loss and compensation between management and store managers [55]. After all, coffee has been cultivated, processed, roasted and brewed for many years, and coffee beans make up about 50% of coffee cherries, and it produces a large amount of by-products. In fact, coffee is the second largest commodity after oil and the second most popular beverage after water, and most coffee product manufacturers face high prices for imported raw materials and energy, which is a major factor [56]. Production processes such as extraction and drying are both energy intensity and environmental issues from many studies that have been identified to improve the quality of the flavor and other attribute within the coffee [57], [58].

In order to find out how significant the contribution of the proposed IS/IT strategy in optimization of the smart industry concept, measurements are conducted using the smart industry readiness index. The following Table XIII is the result of smart industry measurement.

TABLE XIII. SMART INDUSTRY MEASUREMENT

Dimension	Index					Information		
	0	1	2	3	4	5	Existing	Targeting
Vertical Integration							Undefined	Intelligent
Horizontal Integration							Undefined	Intelligent
Integrated Product Lifecycle							Undefined	Intelligent
Shop Floor Automation							Basic	Basic

Enterprise Automation							None	Flexible
Facility Automation							None	Basic
Shop Floor Connectivity							None	Interoperable and Secure
Enterprise Connectivity							None	Interoperable and Secure
Facility Connectivity							None	Interoperable and Secure
Shop Floor Intelligence							None	Computerized
Enterprise Intelligence							Computerized	Predictive
Facility Intelligence							None	Computerized
Workforce Learning & Development							Structured	Structured
Leadership Competency							Structured	Structured
Inter- and Intra-Company Collaboration							Structured	Structured
Strategy & Governance							Structured	Structured

Information:

*) As Is Index

To Be Index

V. CONCLUSION

In short, smart industry refers to a more responsive organization or company that allows all components in the supply chain to be shared in the form of an innovation ecosystem and uses smart technology to work with a variety of partners. The alignment IT and business strategy can guarantees the most effective transparency and collaboration, which is expected to eliminate the complexity of the existing problems with the development. Organizations manage relationships with different stakeholders, balance the three aspects of social, economic and environmental sustainability, to support green initiatives and plan using information and communications technology. It needs to link the systems and coordinate smart industry integration. It governs with a focus on the needs of customer-driven enterprises, especially using information and communication technology to make decisions, involve multiple stakeholders, and use collaborative methods with internal control and external cooperation.

Further research can describe more specific on the business strategy side. As for IS/IT strategy, further research can provide additional parameters such as financial by adding a Break Event Point to the technology investment list, in order to measure the readiness of cooperative organizations in implementing smart industry.

REFERENCES

- [1] Md. Khan, "Implementation of Industry 4.0 Smart Manufacturing," The Platform for the Future of Smart Manufacturing, March 2019.
- [2] R. Damgrave and E. Lutters, "Smart Industry Testbed," Procedia CIRP 84, pp. 387-392, 2019.

- [3] S.M. Setiana and A. Khaerani, "Information Technology for Coffee Industry," IOP Conference Series: Materials Science and Engineering Vol. 879, No. 1, p. 012129, 2020.
- [4] M. Mighty and G. Granco, "Modeling Profitability in the Jamaican Coffee Industry," Agriculture 11(2), pp. 121, 2021.
- [5] M. Tabaa, F. Monteiro, H. Bensag and A. Dandache, "Green Industrial Internet of Things from a Smart Industry Perspectives," Energy Reports vol. 6(6), pp. 430-446, 2020.
- [6] V.L. da Silva, J. Kovaleski, R.N. Pagani, A. Corsi and M. Gomes, "Human Factor in Smart Industry: A Literature Review," Future Studies Research Journal Trends and Strategies vol. 12(1), pp. 87-111, 2019.
- [7] S. Aleksic, "A Survey on Optical Technologies for IOT, Smart Industry and Smart Infrastructures," Journal of Sensor and Actuator Networks, vol. 8(47), pp. 1-18, 2019.
- [8] H.A.T. Nguyen and T.H.T. Vo, "The Role of the Coffee Industry in Sustainable Economic Development in Vietnam," Accounting vol. 7, pp. 683-690, 2021.
- [9] M. Henriques, J.B. de Vasconcelos, G. Pestana and A. Rocha, "Strategic Alignment IT-Business: Towards a Proactive e-Public Sector," J. of Information Systems Engineering & Management 4(2), 2019.
- [10] M. Henriques, J.B. de Vasconcelos, G. Pestana and A. Rocha, "IT-Business Strategic Alignment in Social era," 14th Iberian Conf. on Information Systems and Technologies, pp. 1-6, IEEE 2019.
- [11] H.W. Ibrahim and S. Zailani, "A Review on the Competitiveness of Global Supply Chain in a Coffee Industry in Indonesia," International Business Management vol 4(3), pp. 105-115, 2010.
- [12] K. Mendes and A.A. Luchine, "Non-tariff Barriers Removal in the Brazilian Coffee Industry," J. of International Trade Law and Policy vol. 19(3), 2020.
- [13] K.J. Kamuri, R.P. Fanggidae and R.E. Fanggidae, "Productivity Factor Analysis of Timor Coffee in Coffee Industry," Int. Conf. on Tourism, Economics, Accounting and Management, pp. 87-90, 2018.
- [14] M.A. Golezalez-Moreno, B.G. Gracianteparaluceta, S. Marcelino-Sadaba, J.Z. Urdin, E. Robles, M.A.P. Ezcurdia and A.S. Meneses, "Feasibility of Bermiocomposting of Spent Coffee Grounds and Silverskin from Coffee Industries: A Laboratory Study," Agronomy vol. 10(8), 2020.
- [15] A. Prakosa, "Brand Personality and Brand Quality Rating in the Coffee Industry," Int. Conf. on Technology, Education and Science 2019.
- [16] A. Parente, "Value Chain and Economic Development: The Case of the Colombian Coffee Industry," Organizations and Markets in Emerging Economies vol. 11(1), 2020.
- [17] I.C. Reinhardt, J.C. Oliveira and D. Ring, "Industry 4.0 and the Future of the Pharmaceutical Industry," Pharmaceutical Engineering vol 41(2): Online Exclusive 2021.
- [18] C. Lechner and A. Pervaiz, "From Invention to Industry from a Social Movement Perspective: The Emergence of the 3D Printing Industry," J. of Innovation and Entrepreneurship vol. 9(1), 2020.
- [19] S.M. Lee and S. Trimi, "Innovation for Creating a Smart Future," J. of Innovation & Knowledge, vol. 3(1), 2018.
- [20] H.S. Kang, J.Y. Lee, S. Choi, H. Kim, J.H. Park, J.Y. Son, B.H. Kim and S.D. Noh, "Smart Manufacturing: Past Research, Present Findings, and Future Directions," Int. J. of Precision Engineering and Manufacturing-Green Technology vol. 3, pp. 111-128, 2016.
- [21] O. Granstrand and M. Holgersson, "Innovation Ecosystems: A Conceptual Review and a New Definition," Technovation 102098, 2020.
- [22] E. Autio and L.D.W. Thomas, "Innovation Ecosystems: Implication for Innovation Management," in Book: The Oxford Handbook of Innovation Management, ed. 1, Chapter 11. Oxford University, 2014.
- [23] T. Curtis and R. Nalbandian, "Institutional Entrepreneurship in the Ethiopian Coffee Industry," Int. J. of Social Entrepreneurship and Innovation vol. 1(3), pp. 281-294, 2012.
- [24] L.F. Samper and X.F. Quinones-Ruiz, "Towards a Balanced Sustainability Vision for the Coffee Industry," Resources vol. 6(2), 2017.
- [25] N. Munguia, A. Varela, J. Esquer and L. Velazquez, "Fostering Corporate Sustainability in the Mexican Coffee Industry," PSU Research Review vol. 1(1), pp. 51-62, 2017.
- [26] D. Draheim, "Smart Business Process Management," in book: Social Software – BPM and Workflow Handbook, Digital Edition, Chapter: Smart Business Process Management. Future Stategies, Workflow Management Coalition, 2021.
- [27] L-F. Pau, "Smart Business Networks: Their Evolution," SSRN Electronic Journal, 2017.
- [28] M. Hudik, G. Koman, J.J. Impolla and J. Vodak, "Use of the Internet of Things in the Business Environment to Smart Business," LOGI – Scientific Journal on Transport and Logistics vol. 10(2), pp. 42-50, 2019.
- [29] N. Noori, T. Hoppe and W.M. de Jong, "Classifying Pathways for Smart City Development: Comparing Design, Governance and Implementation in Amsterdam, Barcelona, Dubai and Abu Dhabi," Sustainability vol. 12(10), 2020.
- [30] N. Noori, W.M. de Jong, M. Janssen, D. Schraven and T. Hoppe, "Input-Output Modeling for Smart City Development Input-Output Modeling for Smart City Development," J. of Urban Tech. vol. 27(3), pp. 1-22, 2020.
- [31] M. Csukas and R.Z. Szabo, "The Many Faces of the Smart City: Differing Value Proposition in the Activity Portfolios of Nine Cities," Cities vol. 112: 103116, 2021.
- [32] G. Masik, I. Sagan and J. Scott, "Smart City Strategies and New Urban Development Policies in the Polish Context," Cities vol. 108:102970, 2021
- [33] L.S. de Azambuja, G.V. Pereira and R. Krimmer, "Clearing the Existing Fog over the Smart Sustainable City Concept: Highlighting the Importance of Governance," Int. Conference on Theory and Practice of Electronic Governance 2020.
- [34] M.Y. Uchirova, S.B. Baurina, S. Khudyakov, "Industrial Technologies in the Context of Digital Transformation," In book: Modern Global Economic System: Evolutional Development vs. Revolutionary Leap, 2021.
- [35] S.B. Baurina, "Smart Industry: Technology for the Future," Int. Multi-Conference on Industrial Engineering and Modern Technologies 2020.
- [36] A.J.G. Pires and J.P. Pontes, "(De)Industrialization, Technology and Transportation," Open Economic Review 2020.
- [37] A.A. Bilyalova, I. Vaslavskaya and R. Gaifutdinova, "Digitalization of the Transport Industry: Technology of Blockchain," 2nd International Scientific and Practical Conference 2020.
- [38] R. Yusianto, M. Marimin, S. Suprihatin and H.J. Hardjomidjojo, "IOT based Smart Agro-Industrial Technology with Spatial Analysis," Jurnal Teknologi Industri Pertanian vol. 30(3), pp. 319-328, 2021.
- [39] S. Shanker and S. Bhushan, "Acceptance of Industry 4.0 in Digital Industrial Technology and Rediscovering Growth," Int. Research J. of Engineering and Technology vol. 7(8) 2020.
- [40] M.G. Rodrigues and F.J.P. da Costa, "Industry, Technological Progress and Development: The Case of Southeast Asia," Int. J. of Advances in Management and Economics vol. 9(6), 2020.
- [41] B. Jimoh, H.O. Omeje, S. Ariyo, S.I. Nwaodo, O.P. Ijeoma, O.J. Ogunmilade and O.A. Olaoye, "Innovations into Industrial-Technology Programmes of Nigerian Universities for Quality Assurance," Indonesian Journal of Electrical Engineering and Com. Science vol. 20(3), pp. 1315-1324, 2020.
- [42] R. Firth and A. Robinson, "Robotopias: Mapping Utopian Perspectives on New Industrial Technology," Int. Journal of Sociology and Social Policy 2020.
- [43] V.S. Toropov and E.S. Toropov, "System Approach to Modeling of Industrial Technologies," IOP Conference Series Materials Science and Engineering 327(4):042109, 2018.
- [44] K.A. Rosentrater and R. Balamuralikrishna, "Ethics for Industrial Technology," The Journal of Technology Studies 31(1), 2005.
- [45] L. Wang and Zexia Li, "Knowledge Flows from Public Science to Industrial Technologies," The Journal of Technology Transfer 2019.
- [46] M. Fritsch and V. Slavtchev, "The Role of Regional Knowledge for Innovation," 45th ERSA Conference 2005.
- [47] M. Fritsch and V. Slavtchev, "Industry Specialization, Diversity and the Efficiency of Regional Innovation Systems," SSRN Electronic Journal, Jena Economic Research Papers 016, 2007.

- [48] M. Fritsch and G. Franke, "Innovation, Regional Knowledge Spillovers and R&D Cooperation," *Research Policy* vol. 33(4), pp. 245-255, 2004.
- [49] N. Efa, D. Teshome, B. Megersa and G. Weldemichael, "Research Center-based Extension Interventions on Improved Coffee Technologies," *Coffee Diversity and Knowledge Conference* 2021.
- [50] H. Luzinda, "Factors Influencing Adoption of Improved Robusta Coffee Technologies in Uganda," *Uganda Journal of Agricultural Science*, vol 18(1), pp. 33-41, 2018.
- [51] D. Teshale, "Analysis and Adoption of Coffee Technologies in Major Coffee Growing Areas: The Case of Wombera District, Metekel Zone, Ethiopia," *Int. J. of Scientific and Engineering Research* vol. 10(5), pp. 592-600, 2019.
- [52] S. Diro, A. Tesfaye, B. Erko and T. Girma, "The Role of Improved Coffee Variety Use on the Adoption of Key Agricultural Technologies in the Coffee-based Farming System of Ethiopia," *East African Scholars Journal of Economics, Business and Management* vol. 4(1), 2021.
- [53] M. Bolka and S.A. Emire, "Effects of Coffee Roasting Technologies on Cupt Quality and Bioactive Compounds of Specialty Coffee Beans," *Food Science & Nutrition* vol. 8(10), 2020.
- [54] S. Salengke, A. Hasizah, R. Reta and A.A. Mochtar, "Technology Innovation for Production of Specialty Coffee," *IOP Conference Series Earth and Environmental Science* 355:012105, 2019.
- [55] F.B. Georgise and A.T. Mindaye, "Technology for Storage & Warehouse Management of Coffee Beans in ehtiopia," *Technology Reports of Kansai University* vol. 62(9), pp. 5375-5393, 2020.
- [56] A. Hejna, "Potential Applications of by-products from the Coffee Industry in Polymer Technology – Current State and Perspectives," *Waste Management* vol. 121(3): 296-330, 2021.
- [57] A. Zykov, O. Burdo, A. Gavrilov, I. Mazurenko and I. Bezbakh, "Development of Power Efficient and Environmentally Safe Coffee Product Technologies," *Eastern-European journal of Enterprise Technologies* vol. 1/11 (103), 2020.
- [58] R. Kwok, K.L.W. Ting, S. Schwarz, L. Claaßen and D.W. Lachenmeier, "Current Challenges of Cold Brew Coffee – Roasting, Extraction, Flavor Profile, Contamination and Food Safety," *Challenges* vol. 11(2), 2020.

Application of Machine Learning Algorithms in Coronary Heart Disease: A Systematic Literature Review and Meta-Analysis

Solomon Kutiname¹, Richard Millham², Adebayor Felix Adekoya³
Mark Tetley⁴, Benjamin Asubam Weyori⁵, Peter Appiahene⁶

University of Energy and Natural Resources, Ghana¹

Durban University of Technology, South Africa²

National Cardiothoracic Center, Korle Bu Teaching Hospital, Accra – Ghana⁴

University of Energy and Natural Resources, Ghana^{3,5,6}

Abstract—This systematic review relied on the Preferred Reporting Items for Systematic reviews and Meta-Analysis (PRISMA) statement and 37 relevant studies. The literature search used search engines including PubMed, Hindawi, SCOPUS, IEEE Xplore, Web of Science, Google Scholar, Wiley Online, Jstor, Taylor and Francis, Ebscohost, and ScienceDirect. This study focused on four aspects: Machine Learning Algorithms, datasets, best-performing algorithms, and software used in coronary heart disease (CHD) predictions. The empirical articles never mentioned 'Reinforcement Learning,' a promising aspect of Machine Learning. Ensemble algorithms showed reasonable accuracy rates but were not common, whereas deep neural networks were poorly represented. Only a few papers applied primary datasets (4 of 37). Logistic Regression (LR), Deep Neural Network (DNN), K-Means, K-Nearest Neighbors (KNN), Support Vector Machine (SVM), and boosting algorithms were the best performing algorithms. This systematic review will be valuable for researchers predicting coronary heart disease using machine learning techniques.

Keywords—Coronary heart diseases; algorithms; datasets; ensembling algorithms; machine learning; artificial intelligence

I. INTRODUCTION

The rate at which people are losing their lives due to cardiovascular disease (CVD) is devastating, with the World Health Organization (WHO) estimating annually 17.9 million deaths globally. The heart and blood vessels [1] are the centers of CVD. There are several types of CVDs, such as coronary heart disease (CHD), abnormal heart rhythms (arrhythmias), and heart muscle disease (cardiomyopathy) with CHD being the primary type of CVD [2], contributing to approximately 64% of all CVDs [3]. Men are mainly affected by CHD compared to women.

In most cases, CHD begins in the fourth decade of life and progresses with age [4]. Recent statistics indicate that continentally, for CVD and CHD, Europe has (44%, 24%), North America (32%, 19%), Latin America and Caribbean (27%, 14%), Asia (35%, 16%), Africa (18%, 9%), and Australia (31%, 16%) respectively making a global percentage of 33% of deaths due to cardiovascular disease in general and 16% of deaths due to coronary heart disease [5]. The most precise method for diagnosing CHD is angiography, but it is

invasive and expensive [6]. CVD is a global problem and a leading cause of death in Ghana [7]. Early detection and prognosis are critical for reducing the disease burden. Artificial Intelligence (AI) assists in identifying critical indicators of cardiac disease. AI helps determine disease history and supplies appropriate treatment [8]. AI has several benefits as identified in the literature. These include timely decision-making, helping surgeons perform complex surgeries and tasks, providing accurate cardiovascular imaging, reducing the risks of complex treatments, enhancing cardiology knowledge about patient behavior, and improving computer-aided diagnosis [8]. Artificial Intelligence and Machine Learning Algorithmic research focus on inexpensive, rapid, and non-invasive methods to accurately diagnose all CHD using high-level performance metrics, including Accuracy, precision, specificity, and sensitivity.

AI and machine learning allow computers to find, quantify, and interpret correlations between variables to improve patient care by algorithmically learning optimal data representations[9]. Machine-learning algorithms can sift through considerable amounts of cardiovascular data, making it easier to uncover predictive, diagnostic, and therapeutic options for various cardiovascular diseases. There are three types of machine learning algorithms: unsupervised, supervised, and reinforcement learning [10]. Supervised learning is a robust approach that uses machine language to classify and interpret labelled cardiovascular data [11]. For instance, in supervised learning, a physicist may seek to determine whether a particular electrocardiogram represents sinus rhythm or coronary artery, or ventricular fibrillation? Thus, supervised learning requires a dataset with predictor variables, also known as features in machine learning terminology, and labelled outcomes [9]. Unsupervised learning attempts to uncover the underlying structure or correlations between variables in a dataset [12]. This dataset was trained without explicit labels, and the algorithm clustered the data to identify the underlying patterns. Based on behavioural psychology, reinforcement learning employs a different strategy in which a software program operates in a pre-determined environment to maximise a reward. The main objective of this systematic literature review was to determine which supervised machine learning algorithms exhibit the best

results for coronary heart disease prediction. In this systematic review: 1) the authors identified studies that employed machine learning techniques to diagnose coronary heart diseases in this systematic review; 2) to determine the most utilized supervised machine learning algorithms for coronary heart disease prediction; 3) to evaluate the performance of supervised machine learning algorithms relative to selected features such as Accuracy, specificity, sensitivity, and precision; and 4) to analyze the data sources for predicting coronary heart disease. The outcomes of this review will contribute to policy directions, practice, and further research on cardiovascular diseases, mainly coronary heart disease. The following sections are as follows: Section II, Materials and Methods, Section III, Literature Review, Section IV, Discussion, and the final part is Conclusion and future work.

II. MATERIALS AND METHODS

This systematic review adopted the Preferred Reporting Items for Systematic reviews and Meta-Analysis (PRISMA) statement. PRISMA is a collection of elements used to report systematic reviews and meta-analyses [13]. This approach is intended to help report reviews and assess randomized trials [14], but may also be used as a foundation for reporting systematic reviews [15]. Following the PRISMA approach, this study considered research questions guiding the review, literature search criteria, and selection criteria.

A. Literature Search Criteria

Our selection criteria identified relevant published research and review papers by using keywords such as cardiology, cardiovascular disease, coronary heart disease, ischemic heart disease, coronary artery disease, machine learning algorithms, machine learning techniques, data mining, and artificial intelligence in cardiovascular disease. This study adopted composite literature search criteria which combine keywords using Boolean operators such as AND, --, ",", ~, and OR. The search engines used included PubMed, Hindawi, SCOPUS, IEEE Xplore, Web of Science, Google Scholar, Wiley Online, Jstor, Taylor and Francis, Ebscohost, and ScienceDirect. Furthermore, the search outcome produced over 563 papers, of which 37 were deemed appropriate based on the selection criteria of this study.

B. Selection Criteria

The study utilized peer-reviewed papers published in the English language only. Table I lists the exclusion and inclusion criteria used in this study. These peer-reviewed papers focused on the application of Machine Learning Techniques in investigating CHD. The selection criteria excluded non-peer-reviewed articles such as Dissertation, theses, books, chapters, etc. were excluded from the review.

TABLE I. ARTICLE SELECTION CRITERIA

Features	Inclusion Criteria	Exclusion Criteria
Language of Publication	English language	Not in the English Language
Research Type	Peer-reviewed	Thesis/Dissertation, case studies, books, reports, and magazines.
Research Focus	Related to ML techniques in CHD.	Not related to ML and CHD
Context	Global	Not Applicable (N/A)

III. RESULTS

A literature search of the above databases identified 563 publications (Fig. 1). Screening by title indicated that 374 papers did not meet the selection criteria for this review. Additional screening by abstract revealed that 75 studies did not match the focus of the review. In contrast, full-text screening of the remaining papers revealed that 108 articles were related and did not apply machine learning techniques to CHD. Therefore, these papers were excluded from the final list. Finally, 37 articles on the implementation of ML algorithms in CHDs were included in this review.

The reference lists of the 37 studies used in this review are listed in Table II. In the literature, it was found that these papers focused on three major areas: 1) CHD Prediction, 2) CHD detection, and 3) CHD diagnosis using ML techniques. A significant proportion of the studies aimed at predicting CHD were based on risk factors and classification methods. The retrieved papers covered 2014, 2016, 2017, 2018, 2019, 2020, and 2021. Fig. 2 depicts the rate of the collected publications on the phenomenon over the periods. The number of publications varied slowly over time except from 2018 to 2019, which saw a significant increase (from 3 to 12 papers). Our search results revealed no studies on CHD prediction using ML methods in 2015 and before 2014. This may be explained by the limited access to open datasets and the arguably emerging nature of ML methods before 2014. The focused nature of the topic and its accompanying paper selection process can also be attributed to the absence of studies in 2015. The number of publications on this phenomenon decreased from 12 in 2019 to 7 in 2020.

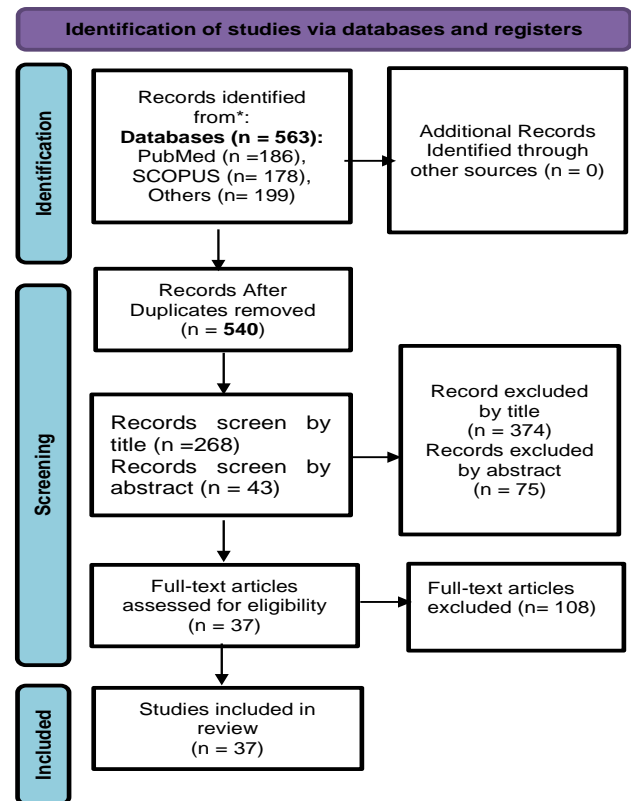


Fig. 1. PRISMA Flow Diagram.

TABLE II. THE LIST OF SELECTED STUDIES FOR THIS SYSTEMATIC LITERATURE REVIEW WITH THEIR FOCUS AREAS

#	Studies	Focus	#	Studies	Focus
1	[18]	Detection of CAD	20	[19]	detection and diagnosis of CHD
2	[20]	Improve the prediction CHD	21	[21]	CAD classification
3	[22]	CAD presence prediction	22	[23]	CHD Prediction
4	[24]	CAD presence prediction	23	[25]	Heart disease prediction
5	[26]	Coronary heart disease prediction	24	[27]	Heart disease prediction
6	[28]	CHD detection	25	[29]	CHD prediction
7	[30]	CAD prediction	26	[31]	CHD prediction
8	[32]	predict coronary heart disease	27	[33]	prediction of CHD
9	[16]	CHD Prediction based on risk factors	28	[34]	classification of coronary artery disease medical data sets
10	[1]	Accuracy of ML algorithms for predicting clinical events	29	[35]	Prediction of CHD
11	[17]	methodology of predicting CHD	30	[36]	CAD detection
12	[37]	CAD detection	31	[2]	CHD Prediction
13	[38]	prediction of heart diseases	32	[39]	Heart Disease Diagnosis
14	[40]	prediction of heart diseases	33	[41]	CHD prediction
15	[42]	CAD diagnosis	34	[43]	CHD prediction
16	[44]	Prediction of CHD	35	[45]	NN-based prediction of CHD
17	[46]	Diagnosing CHD	36	[47]	Prediction of CHD
18	[48]	prediction of heart disease	37	[49]	Prediction of CHD
19	[50]	CHD Diagnosis			

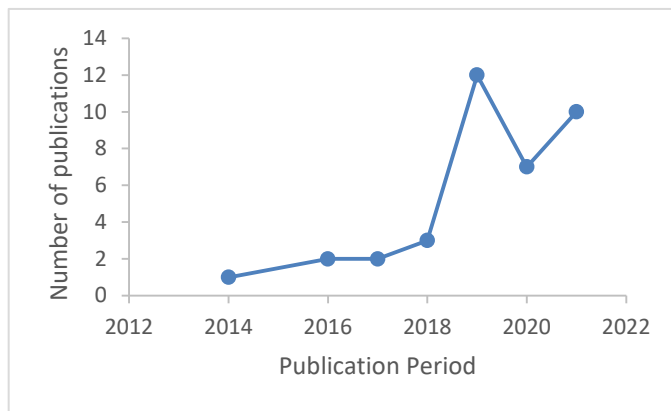


Fig. 2. Number of Publications on CHD using ML Techniques between 2014 and 2021.

A. Algorithm

This review considers all reported algorithms applied in previous studies. Table III and Fig. 3 show a group of algorithms applied in the 37 papers and the number of papers that adopted these methods. The review revealed that the most frequently used machine learning algorithms was Decision Tree (n=26, 24%), followed by support vector machines

(n=24, 22%), Naïve Bayes (n=23, 21%), K-Nearest Neighbors (n= 19, 17%) and random forests (n=18, 16%). All studies employed multiple algorithms. Few employed five (5) (DT, KNN, SVM, RF, and NN) supervised learning ML algorithms and compared their predictive performance [18]. More than 95% of the studies employed supervised classification algorithms to process features. From Fig. 3, it can be observed that SVM, DT, and KNN retained their popularity. DT has attracted more attention in this field than the other algorithms. Over the periods (2014, 2016, 2017, 2018, 2019, 2020, and 2021), at least one article has been published using DT. SVM and Naïve Bayes have almost the same usage frequencies as DT. Another frequently used method is Logistic regression. Although Deep Neural Networks have demonstrated high predictive power, they have recorded few applications in the field of CHDs. 2017, 2019, and 2021 recorded an increasing usage of boosting and assembling techniques from 2 to 9 publications and a slight decrease to 7 in 2021. From Table II, it is noticeable that XGBoost, Adaboost, Boosted DT, and other ensemble techniques were applied. In addition, while no paper reported the application of reinforcement methods, only one article used an unsupervised algorithm (K-Means) to predict CHDs, although the algorithm performed well. Computational-intelligence-based methods, such as neural networks, have recorded the lowest number of applications.

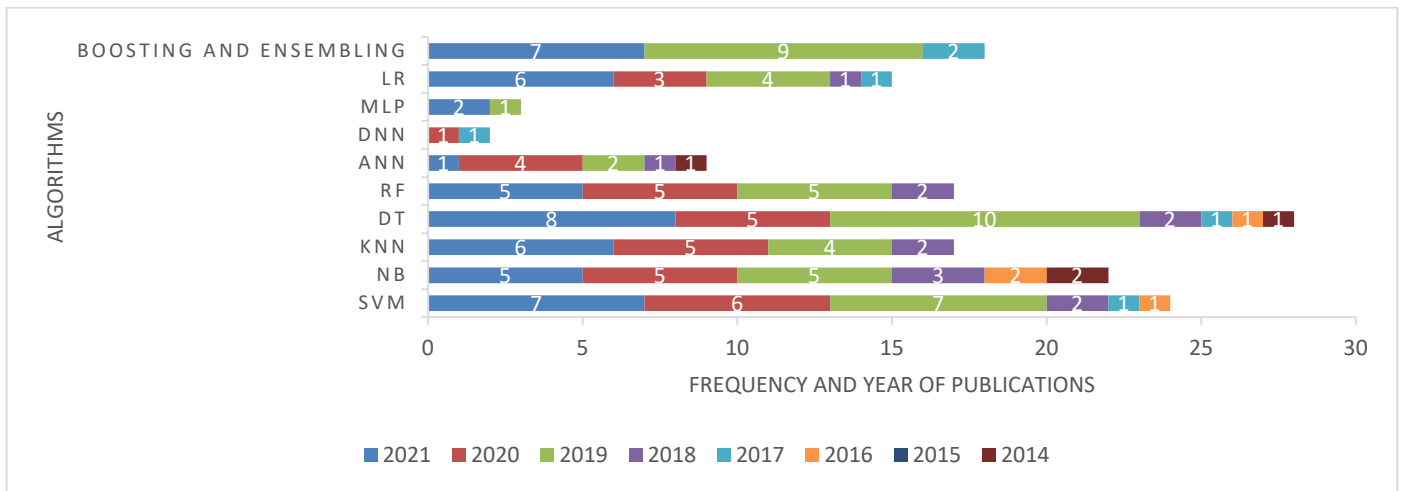


Fig. 3. Shows the Yearly usage Frequencies of Popular ML Methods for CHD Prediction.

TABLE III. ML ALGORITHMS APPLIED IN OBSERVED WORKS

Algorithms	No. of Papers
Support Vector Machine	24
Naïve Bayes	23
K-Nearest Neighbors	19
Decision Tree	26
Random Forest	18
Neural Network	14
Regression	17
Boosting & Ensembles	19

B. Algorithm Performance Metrics

One of the most crucial processes in the machine learning prediction process is model evaluation. A model’s performance can be assessed using a variety of metrics. During the training process, measurements are frequently performed on unseen samples. The model performance measurement metrics used in the included studies were Accuracy, Precision, Recall/Sensitivity, Specificity, and F1 Score. The review revealed that the most used evaluation metrics in CHD prediction are Accuracy, followed by Recall/Sensitivity, F1 Score, Precision, and Specificity. Table IV shows that out of the 37 papers included, 36 reported the accuracy scores of the models used for the prediction. Supplementary Fig. 4 shows the usage percentages of the metrics in the investigated articles. This analysis focused on examining the performance of the algorithms applied in previous studies. However, because it is not advisable to “directly compare the efficiency of two algorithms or systems if they were evaluated on different datasets” [13], the evaluation of the best-performing algorithms is based on the datasets used. Drawing on the most used evaluation method (i.e. Accuracy), the best performing algorithms were determined based on the mean values of the accuracy scores of the models obtained from the 37 papers. As clinical data and study scope differ greatly among disease prediction studies, a comparison can only be made after a consistent benchmark on the dataset and scope are established. Therefore, only studies

that implemented multiple machine learning methods were selected to compare the same data and disease prediction. The authors determined the best-performing algorithm for the phenomenon by comparing the mean accuracy scores of the models that utilized the same datasets. Table V lists the algorithms used on the different datasets and the computed mean scores in terms of specificity, Recall/sensitivity, precision, F1 score, and Accuracy. The current study draws on the computed average scores of the 36 studies to rank the most performing algorithms.

Thus, the higher the accuracy of an algorithm, the higher is the chance of making an accurate prediction. Fig. 5 indicates that among the common algorithms applied on the Z-Alizadeh Sani Heart Disease Dataset, LR (87.51%) had a higher predictive accuracy rate, followed by RF (86.07%), NN (85.74%), SVM (85.55%), KNN (75.72%), NB (68.34%), and DT (68.95%). For the Statlog Heart Disease Dataset, the DNN (98.15%) algorithm obtained the highest predictive accuracy score, as shown in Fig. 6. On this dataset, SVM, LR, NB, NN, and KNN obtained accuracy scores greater than 90%, indicating that these algorithms make significant contributions to disease predictions. Only four algorithms (DNN, DT, KNN, and SVM) have been applied to the long beach dataset so far per the findings of this review. In terms of the best performance, Fig. 7 shows that the DNN has a higher predictive accuracy score compared to the remaining algorithms for the long beach dataset. Fig. 8 and 11 show that the MLP-NN algorithm obtained the highest accuracy rates on the Framingham (73.4%) and South African Heart Disease datasets (73.4%).

TABLE IV. ALGORITHM PERFORMANCE METRICS APPLIED IN THE OBSERVED STUDIES

Metric	Number of studies
Accuracy	36
F1 Score	15
Precision	13
Recall/Sensitivity	20
Specificity	10

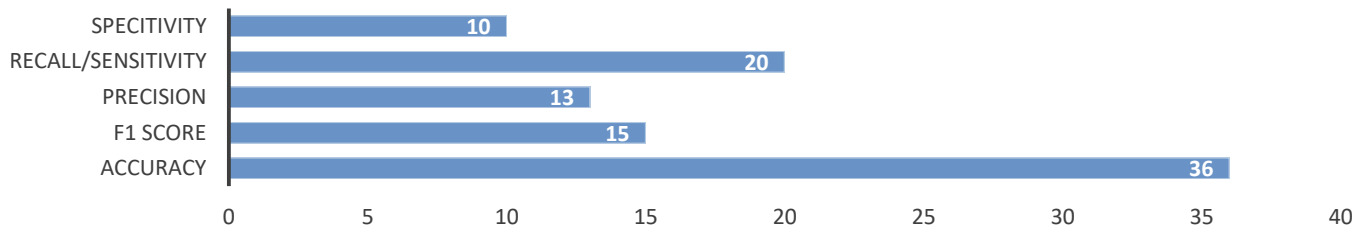


Fig. 4. Number of Algorithm Performance Metrics Applied in Observed Studies.

TABLE V. ALGORITHM PERFORMANCE BASED ON EVALUATION METRICS AND DATASETS

Dataset	Sample Size	Algorithms	ACC	F1	Recall/Sensitivity	Specificity
Z-Alizadeh Sani Heart Disease	303	DT	68.95	85.31	90.77	-
		SVM	85.55	88.85	86.23	88
		RF	86.07	92.80	93.85	-
		LR*	87.51	93.00	89.23	-
		NB	68.34	73.18	94.00	41
		NN	85.74	85.94	84.62	-
		KNN	75.72	90.76	90.77	-
Cleveland Dataset	303	DT	81.75	83.35	78.16	85.51
		SVM	84.72	82.65	81.69	84.15
		RF	83.02	85.33	88.84	91.32
		LR	85.24	81.28	77.58	81.17
		NB	82.74	77.73	81.82	84.34
		NN	83.03	89.84	76.9	82.04
		KNN	81.71	79.99	76.36	78.56
		SSA-N	86.7	-	60	100
		BO-SVM	93.3	-	80	100
		Adaboost	82.12	80.43	79.85	81.02
		DT+RF	88	-	---	-
		DT(SVC)	72.2	69.1	72.2	76.70
		DT(J48)	73	69.8	63.3	77.80
		MLP	-	72	73.9	73.90
GB	-	92	92.84	90.32		
K-Means	94.06	-	-	-		
Statlog Disease Dataset	270	DT	88.1	87.85	84.96	91.15
		SVM	91.97	91.26	87.46	94.64
		RF	89.05	91.93	86.50	90.42
		LR	91.97	91.93	89.34	91.41
		NB	91.38	92	90.86	90.71
		NN	93.03	89.60	93.8	
		KNN	90.35	89.60	86.02	93.42
		DNN	98.15	98	98	91.76
Framingham Heart Study" dataset	4240	DT	82.4	91.47	52.40	81.60
		SVM	68	-	68	68
		RF	83.68	96.61	84.74	80
		LR	66.83	-	67	66.5
		NB	60	-	31	
		NN	69.5	-	69.5	69.5
		KNN	85.45	90.76	86.21	98.67
		Boosted DT	73	-	36	73

		Adaboost	66.60	-	67	-
South African Heart Disease dataset	462	DT	70.07		50	
		SVM	72.75	55	50	88.4
		LR	72.7	56.3		84.44
		NB	71.6		62	
		KNN	73.2	50.4		91.1
		MLP-NN	73.4	55.3		87.1
Long Beach data set	200	DT	68.4			
		KNN	81.1			
		SVM	83.4			
		DNN	84			
the Korea National Health and Nutrition Examination Survey (KNHANES) 2007-2016	4146	LR	85.61		51.44	91.15
		SVM	77.87		77.40	77.81
		RF	76.06		76.44	76.06
		AdaBoost	90.12		52.88	90.36
		MLP	78.8		66.34	78.88
		NN-FRS	81.09			
		NN-FCA	23.87			

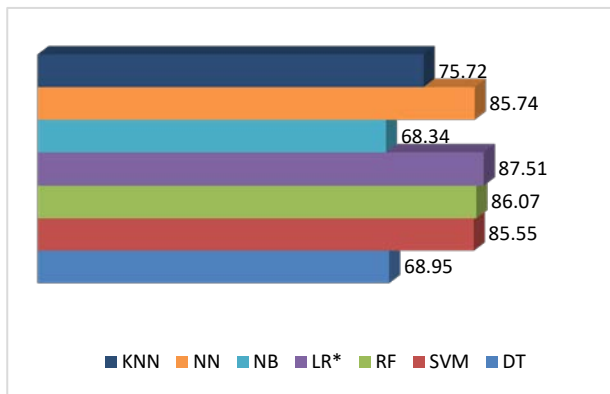


Fig. 5. Best Performing Algorithm - Z-Alizadeh Sani Heart Disease Dataset.

In the KHANNES and Cleveland heart disease dataset, it was found that the ensemble algorithms performed better than single algorithms. This is evident from Fig 7, Fig. 9, Fig 10, and Fig. 11, respectively. In Table VI, the primary dataset names and metrics and the corresponding machine learning algorithms used to predict them are discussed. This table also

describes the best-performing algorithm for each model. From the clinical data obtained from primary sources, it was observed that the SVM algorithm is applied most frequently (in all four datasets), followed by the NB algorithm (in 3 datasets). Although AdaBoost has been considered the second least number of times, it showed the highest percentage (i.e. 90.12%) in revealing superior Accuracy followed by SVM.

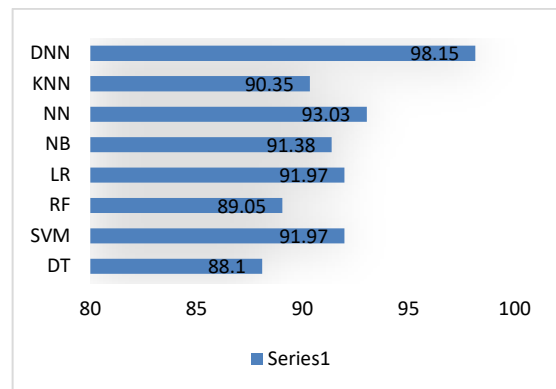


Fig. 6. Best Performing Algorithm - Statlog Heart Disease Dataset.

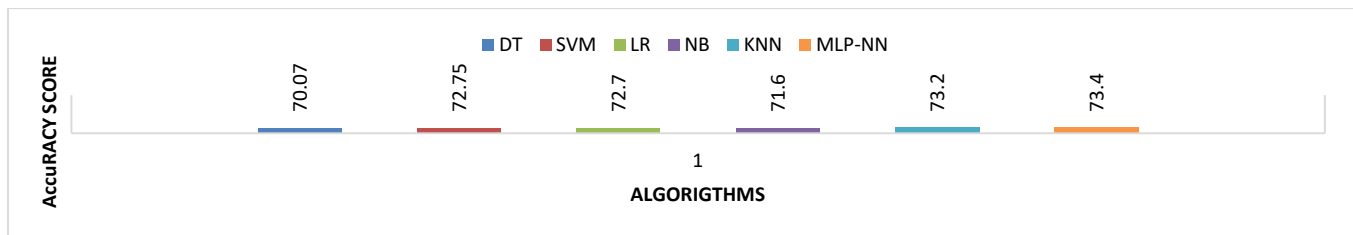


Fig. 7. Best Performing Algorithm - Framingham Heart Study Dataset.

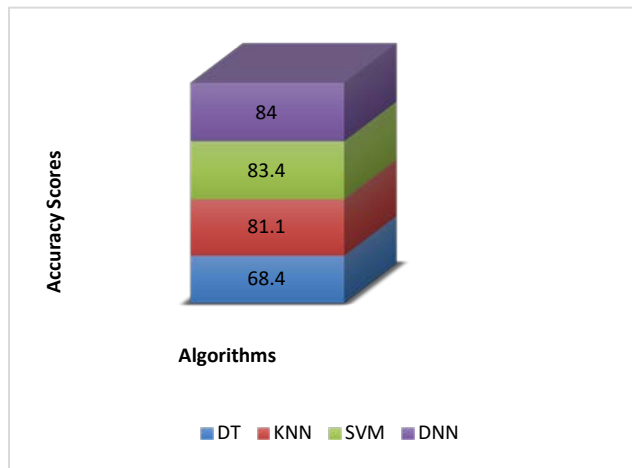


Fig. 8. Best Performing Algorithm – Long Beach Dataset.

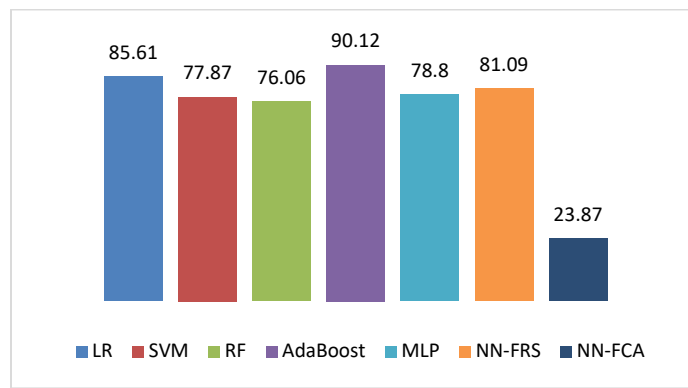


Fig. 9. Best Performing Algorithm – KIHANES Dataset.

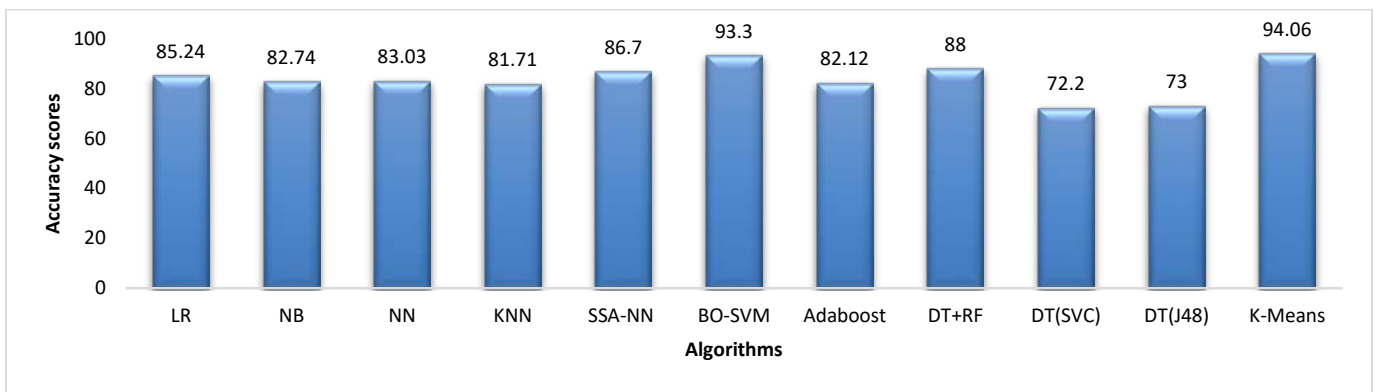


Fig. 10. Best Performing Algorithm: Cleveland Heart Disease Dataset.

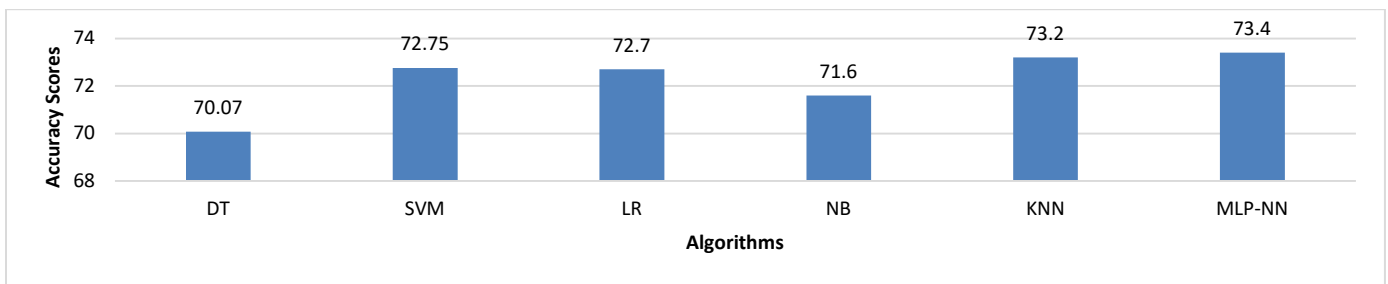


Fig. 11. Best Performing Algorithm: South African Heart Disease Dataset.

TABLE VI. PERFORMANCE METRICS FOR UNPUBLISHED PRIMARY DATASETS

Dataset	Sample Size	Algorithms	Accuracy Score	F1	Recall/ Sensitivity	Specificity
The sample was the medical records of the patients with coronary artery disease who were hospitalized in three hospitals affiliated with AJA University of Medical Sciences between March 2016 and March 2017	1324	ANN	87.52	70.6	88.01	73.64
		SVM	88.91	87.1	92.23	74.42
data from the Sylhet region of Bangladesh by physically going to door-to-door hospitals and healthcare industries	564	DT	82.45			
		SVM	86.03			
		LR	83.12			
		NB	83.14			
medical records data collected from Harapan Kita Hospital	450	DT	84.44	56		88
		SVM	75.5	75		88
		LR	73.3	60		92
		NB	76.6	38		86
		KNN	72.2	72.2		95
A dataset of 299 heart failure patients. Faisalabad Inst. Of cardiology and the Allied Hospital in Faisalabad.	299	DT	82.4	91.47	52.40	81.60
		SVM	68	-	68	68
		RF	83.68	96.61	84.74	80
		LR	66.83	-	67	66.5
		NB	60	-	31	
		NN	69.5	-	69.5	69.5
		KNN	85.45	90.76	86.21	98.67
		MLP-NN	73.4	55.3		87.1
		SVM	77.87		77.40	77.81
		RF	76.06		76.44	76.06
		AdaBoost	90.12		52.88	90.36
		MLP	78.8		66.34	78.88
		NN-FRS	81.09			
NN-FCA	23.87					

C. Datasets and Data Source

In machine learning, datasets must be trained to test models for accurate predictions. In the studies reviewed in our research, two primary data sources were observed: (1) open access; and (2) unpublished primary datasets (Fig. 13). The open-access datasets employed in these studies include the Z-Alizadeh Sani, Cleveland, Statlog, Framingham Heart Study, South African Heart Disease, Long Beach, and KNHANES datasets. These datasets can be accessed from the UCI machine learning data repository. The open-access group comprises thirty-six studies and five databases (Table VII), but some datasets were used in more than one study. For example, [32][30] used the Cleveland Heart disease dataset obtained from the UCI database. The dataset contained 303 patients with heart diseases. According to the homepage of the dataset, most researchers allude to utilizing a subset of 14 of the 76 features. The subset includes sex, age, maximum heart rate achieved, chest pain type, serum cholesterol in mg/dl, fasting blood sugar, resting blood pressure, resting

electrocardiographic results, exercise-induced angina, ST depression, number of major vessels and diagnosis of heart disease (the predictable attribute), and the slope of the peak exercise ST segment. Out of the 37 papers used in this study, ten (10) articles used the dataset to study the prediction of CHDs. The second most popular dataset used in previous CHD prediction studies was the Z-Alizadeh Sani heart disease dataset. The dataset contains features arranged into four groups: demographic, symptom and examination, ECG, and laboratory and echo features. It categorizes patients into CAD or Normal if their diameter narrowing is greater than or equal to 50%, and otherwise as Normal. The dataset was employed in six studies and is accessible from the UCI Repository. The Statlog heart disease database has 13 attributes that include age, sex, chest pain type (4 values), resting blood pressure, serum cholesterol in mg/dl, fasting blood sugar > 120 mg/dl, resting electrocardiographic results (values 0,1,2), maximum heart rate achieved, exercise-induced angina, old peak = ST depression induced by exercise relative to rest, the slope of the peak exercise ST segment, number of major vessels (0-3)

colored by fluoroscopy, and thal. Two researches used the Framingham dataset, which is openly accessible on Kaggle.com. The data is from an active cardiac study on Massachusetts and Framingham residents. The classification objective was to determine the patient's 10-year risk of CHD. The dataset contains more than 4,000 patient information and 15 features. Every feature is a prospective risk indicator. The risk indicators include behavioral, medical, and demographic factors. One study used a Dataset obtained from the Korean National Health and Nutrition Examination Survey VI (KNHANES-VI) to develop a CHD prediction model. These studies reported 25,340 records without previous myocardial infarction or angina from the KNHANES dataset.

D. Software/Tools used for the CHD Prediction

Machine learning-based approaches are commonly used to predict CHD. Several tools and programming techniques are used for developing the models for the predictions. The reviewed studies utilized different software for the analyses. These software/tools were categorized into programming and

data mining software (Fig. 12). The programming software for machine learning data analysis reported by the studies includes Python programming environments such as Jupyter Notebook and the R programming environment RStudio. WEKA, MATLAB, and Rapid Miner are the commonly used data mining software for CHD prediction in these studies. Of the 27 papers reviewed, 63% (17 articles) reported on the software used. Out of these, 65% used data mining tools, while the remaining 35% used programming technologies. A comparison and evaluation of the different algorithms showed the highest prediction accuracy with the programming tools. Several algorithms, such as DT, RF, SVM, NN, and LR, have been tested on the Framingham Heart Disease dataset, for example, using Rapid Miner and R. The results showed that DT, RF, SVM, NN, and LR achieved accuracy rates of 84%, 78%, 68%, 71%, and 66% with R. Accuracy values obtained with Rapid Miner were as follows; DT (62%), RF (63%), SVM (68%), NN (68%), and LR (67%). The evaluation results show that the accuracy, specificity, and recall values of the various algorithms improved with R.

TABLE VII. SOFTWARE USED FOR ML DATA ANALYSES

Study	Software/Tool	Algorithm	Accuracy
[41]	WEKA	J48, BF Tree, REP Tree, NB Tree	55.77, 62.04, 60.06, 60.06
[18]	R	LR, DT, RF, SVM, NN, KNN	87.64, 79.78, 87.64, 86.52, 93.03, 84.27
[45]	R	SVM, ANN	NR
[49]	R	DT, Boosted DT, RF, SVM, NN, LR	84, 84, 78, 68, 71, 66
[49]	Rapid Miner	DT, Boosted DT, RF, SVM, NN, LR	62, 62, 63, 68, 68, 67
[22]	Python	DT, LR, KNN, NB, SVM	82.45, 83.12, 81.12, 83.14, 86.03
[19]	WEKA	DT, NB, SVM	70.70, 71.60, 71.00
[26]	WEKA	SVM, MLP NN, KNN, LR	73.80, 73.40, 73.20, 72.70
[21]	WEKA	RF, DT, KNN	96.71, 92.1, 91.49
[39]	WEKA	NB, DT, ANN	86.53, 89, 85.53
[42]	WEKA	KNN, DT, GB, RF, SVM, NB LR, ANN	85.55, 86.82, 91.34, 89.45 84.28, 82.33, 84.08, 85.07
[33]	WEKA	SVM, NB, KNN	0.83, 0.84, 0.80
[25]	WEKA	NB, DT, RF	78.56, 82.43, 85.78
[28]	MATLAB	KNN, NB, NN, SSA-NN, SVM, BO-SVM	80, 86.7, 80, 86.7, 80, 93.3
[32]	Python	DT, RF, (DT+RF)	79, 81, 88
[16]	Python	LR, KNN, DT(J48), DT (SVC), NB, NN (MLP)	71.4, 71.6, 73.0, 72.2, 71.4, 73.9
[27]	WEKA	RF, KNN, MLP, Bagging, C4.5, LR, NB, AdaBoost SVM	78.0%, 71.6%, 63.8%, 63.1%, 62.9%, 62.4%, 60.5%, 50.4%, 46%

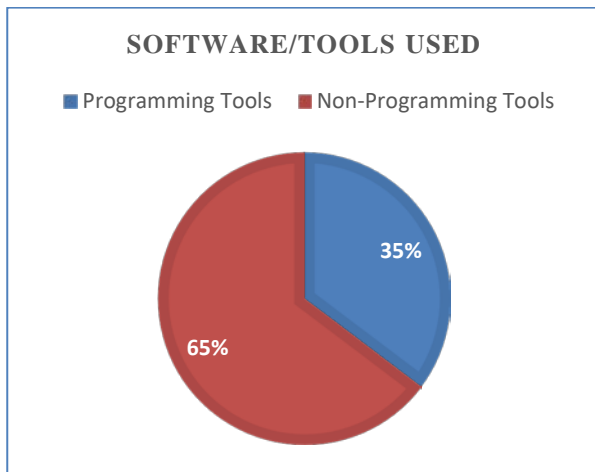


Fig. 12. Distribution of Analysis Tools.

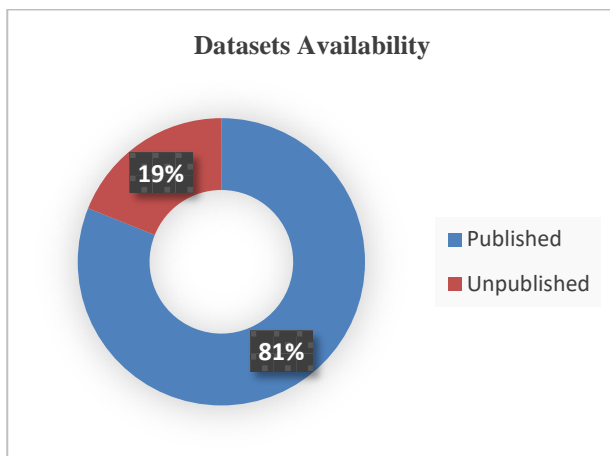


Fig. 13. Distribution of Dataset Types used.

IV. DISCUSSION

This study systematically reviewed 37 studies that utilized machine learning algorithms for CHD prediction. Following the review questions, the study sought to identify the ML algorithms used for CHD predictions, evaluation techniques used and best-performing algorithms, the dataset used, and the software used for the analysis. The outcome of this review highlights the state-of-the-art ML Algorithms applied in predicting CHDs, their performance, and gaps future studies should pay attention to. The results show that previous studies have focused on supervised machine learning classification-based algorithms for observed algorithms. The review indicated that Decision trees, support vector machines, naïve Bayes, and K-Nearest Neighbors were the most utilized algorithms in CHD prediction studies, followed by Random Forest, Logistic Regression, Neural Network, and Bagging and Ensemble algorithms. There is insufficient application of innovative and sophisticated ensemble algorithms such as XGBoost despite gaining popularity as “an ensemble method that has empirically proven to be a highly effective approach by gaining the best results in numerous machine learning competitions” [13]. For CHD prediction using ML, only one study [20] implemented XGBoost. Adaboost, Boosted Decision Tree, and Bagging have received minimal attention

despite their promising performance. Moreover, only one study employed the K-Means clustering algorithm. ML approaches can solve regression and clusterization problems, but such works were not observed in the reviewed articles. Many predictions were performed through binary options selection only. The review also revealed that in all the experimental works, single studies applied and compared multiple algorithms (e.g., five to ten algorithms in a single paper). This variety is considered to be more appropriate than a single algorithm for CHD prediction. Similarly, no study has reported on the use of the RL method. This could be due to the complexity of the RL algorithms, and the lack of relevant data, as pointed out by [13]. Nonetheless, the application of RL in medicine is rapidly gaining attention and requires a closer examination in CHD. State-of-the-art algorithms remain outside existing studies. Thus, the application of cutting-edge ML algorithms in CHD remains immature.

This systematic review also focused on investigating the most performing ML algorithms for CHD prediction based on reported evaluation techniques. The study identified five (5) performance measurement metrics for model evaluation. These are as follows precision, F1 Score, Accuracy, specificity, and recall/sensitivity. This number is considered sizeable for comparing and understanding the research results. Including other metrics such as AUC in future studies is imperative. AUC is regarded as a better measure of classifiers than Accuracy due to its unbiased nature on the test data. In terms of best-performing algorithms, the findings showed that boosting algorithms perform better than single algorithms for CHD prediction in terms of Accuracy comparison. This result contradicts the findings of [51] because the authors measured the performance of the algorithms using the AUC evaluation metric. In general, the overall analyses show that the Accuracy of ML algorithms are mostly between 0.8 and 0.9+ in CHD prediction. This indicates that the predictive ability of ML algorithms in CHD is promising, particularly with LR, DNN, K-Means, KNN, SVM, and boosting algorithms. However, there may be methodological barriers to matching clinician-level Accuracy. For example, there are insufficient cases for model training and testing. Therefore, further studies comparing ML models and human expertise are required. In addition, the optimal cut-off for Accuracy remains unclear in the examined studies. For instance, an AUC score of 0.95 or more is recommended, but this is not clear with Accuracy.

The review also indicated that out of the 37 studies, only five (5) employed primary clinical datasets. It is suggested that such data be used in future studies to increase the commitment to predicting real-life CHDs in local environments. This allows for comparing the results and seeing the real advantages or disadvantages of the proposed algorithms. The study also suggests that the publication of primary clinical datasets and research papers will positively impact future developments. The review found no standard guidelines for data partitioning. Most studies used a 10-fold cross-validation technique and a 70/30 or 80/20 splitting method for the training and validation sets. In addition, because the sample size of most datasets was relatively small, the pooled results could be biased. This systematic review shows that most studies employed data mining tools more than programming

software, including R, Python (Jupyter Notebook, Google Collab, etc.). In general, the predictive performances in terms of the accuracy scores of the algorithms (i.e., SVM, DT, NN, RF, LR, and Boosted DT) obtained with the data mining software improved with R and Python on the same dataset. However, the runtime of a given algorithm is also crucial because if such a system is to be employed in intensive care units, a speedy decision needs to be made.

A. Gaps and Future Research Directions

This novel work represents the first systematic review of machine learning predictions in CHDs. Given that predicting diseases can help draw attention to avoidable interventions, it is imperative to know the state-of-the-art predictive models, their predictive performance, the nature of datasets, and the technologies for analysis. This review is important because it offers an opportunity to improve these models. Based on the findings of this study, future researchers should consider the following gaps:

- 1) A lot more studies employing XGBoost, deep neural networks are anticipated.
- 2) Limited studies focused on clustering and RL algorithms.
- 3) More studies employing ensemble algorithms, such as the ensemble of Logistic Regression (LR) and Support Vector Machine are suggested for improved prediction.
- 4) Nearly half of the included studies were conducted in the USA or China. Studies from Oceania, Africa, and the Americas (outside the USA) were limited. This may be partly due to the limited availability of traditional structured health data. Further studies from the perspective of developing countries are required.
- 5) A dominant reliance on small sample-sized datasets in the included studies. Considering that this may impact the performance of machine learning algorithms, studies with higher data sample sizes are required.
- 6) Included studies rarely assessed predictive performance in terms of AUC, which is posited to be the best accuracy measurement metric for classifiers. Future studies may focus on having AUC as a model performance metric measure.

V. CONCLUSION

Although CHD predictions using machine learning applications are being widely researched, many issues remain unaddressed. This study employed a systematic literature review technique to investigate the state-of-the-art ML algorithms used for CHD predictions, evaluation techniques used and best-performing algorithms, the dataset used, and software used for the analyses. The study revealed that a variety of algorithms can be applied to CHD predictions. However, all approaches belong to a class of supervised learning classification methods; most studies utilize published data, whereas fewer studies use primary clinical data. LR, DNN, K-Means, KNN, SVM, and boosting algorithms were found to be the best performing algorithms for CHD prediction; and programming data analysis techniques such as R, and Python were found to produce higher predictive scores than data mining tools such as Rapid miner, WEKA, and

MATLAB. This study has some limitations. For instance, only papers from multidisciplinary peer-reviewed databases were, but we did not include articles found in the gray literature. Theses and book chapters are excluded. Considering that CHD is the third cause of total global deaths, understanding the most performing algorithms and software environment for predicting or diagnosing the disease will guide health practitioners and researchers in making proactive decisions to reduce the dangers. The study discovered that the DT algorithm was used the most (in 28 studies), followed by the SVM method (in 24 studies). However, the LR, DNN, K-Means, KNN, and SVM algorithms performed better in comparison. LR demonstrated the highest accuracy, 52 percent, in 8 of the 37 investigations where it was used. This was followed by DNN, which came out on top in 41% of the experiments analyzed.

REFERENCES

- [1] M. Al Mehedi Hasan, J. Shin, U. Das, and A. Yakin Srizon, "Identifying Prognostic Features for Predicting Heart Failure by Using Machine Learning Algorithm," pp. 40–46, 2021, doi: 10.1145/3460238.3460245.
- [2] R. Alizadehsani et al., "Coronary artery disease detection using computational intelligence methods," *Knowledge-Based Syst.*, vol. 109, pp. 187–197, 2016, doi: 10.1016/j.knosys.2016.07.004.
- [3] J. C. Tardif, "Coronary artery disease in 2010," *Eur. Hear. Journal, Suppl.*, vol. 12, no. SUPPL. C, pp. 2–10, 2010, doi: 10.1093/eurheartj/suq014.
- [4] M. A. Khan et al., "Global Epidemiology of Ischemic Heart Disease: Results from the Global Burden of Disease Study," *Cureus*, vol. 12, no. 7, 2020, doi: 10.7759/cureus.9349.
- [5] Statista, "Small business statistics 'scary,'" *Finweek*, 2020. <https://www.statista.com/statistics/880155/number-of-smes-in-united-kingdom-uk/>.
- [6] N. Kumar and D. Kumar, "Machine Learning based Heart Disease Diagnosis using Non-Invasive Methods: A Review," *J. Phys. Conf. Ser.*, vol. 1950, no. 1, 2021, doi: 10.1088/1742-6596/1950/1/012081.
- [7] P. K. A. Abanilla et al., "Cardiovascular disease prevention in Ghana: Feasibility of a faith-based organizational approach," *Bull. World Health Organ.*, vol. 89, no. 9, pp. 648–656, 2011, doi: 10.2471/BLT.11.086777.
- [8] A. Haleem, M. Javaid, R. P. Singh, and R. Suman, "Applications of Artificial Intelligence (AI) for cardiology during COVID-19 pandemic," *Sustain. Oper. Comput.*, vol. 2, no. February, pp. 71–78, 2021, doi: 10.1016/j.susoc.2021.04.003.
- [9] K. W. Johnson et al., "Artificial Intelligence in Cardiology," *J. Am. Coll. Cardiol.*, vol. 71, no. 23, pp. 2668–2679, 2018, doi: 10.1016/j.jacc.2018.03.521.
- [10] P. Constantinides and D. A. Fitzmaurice, "Artificial intelligence in cardiology: Applications, benefits and challenges," *Br. J. Cardiol.*, vol. 25, no. 3, pp. 86–87, 2018, doi: 10.5837/bjc.2018.024.
- [11] M. R. M. Talabis, R. McPherson, I. Miyamoto, J. L. Martin, and D. Kaye, "Analytics Defined," *Inf. Secur. Anal.*, pp. 1–12, 2015, doi: 10.1016/b978-0-12-800207-0.00001-0.
- [12] P. Sardar, J. D. Abbott, A. Kundu, H. D. Aronow, J. F. Granada, and J. Giri, "Impact of Artificial Intelligence on Interventional Cardiology: From Decision-Making Aid to Advanced Interventional Procedure Assistance," *JACC Cardiovasc. Interv.*, vol. 12, no. 14, pp. 1293–1303, 2019, doi: 10.1016/j.jcin.2019.04.048.
- [13] A. Dudchenko, M. Ganzinger, and G. Kopanitsa, "Machine Learning Algorithms in Cardiology Domain: A Systematic Review," *Open Bioinform. J.*, vol. 13, no. 1, pp. 25–40, 2020, doi: 10.2174/1875036202013010025.
- [14] D. Moher et al., "Preferred reporting items for systematic reviews and meta-analyses: The PRISMA statement," *PLoS Med.*, vol. 6, no. 7, 2009, doi: 10.1371/journal.pmed.1000097.

- [15] D. Moher et al., "Preferred reporting items for systematic review and meta-analysis protocols (PRISMA-P) 2015 statement," *Syst. Rev.*, vol. 4, no. 1, pp. 1–9, 2015, doi: 10.1177/1755738018823800.
- [16] V. Shorewala, "Early detection of coronary heart disease using ensemble techniques," *Informatics Med. Unlocked*, p. 100655, 2021, doi: 10.1016/j.imu.2021.100655.
- [17] A. Akella and V. Kaushik, "Machine learning algorithms for predicting Coronary Artery Disease: Efforts toward an open source solution," *bioRxiv*, 2020, doi: 10.1101/2020.02.13.948414.
- [18] A. Akella and S. Akella, "Machine learning algorithms for predicting coronary artery disease: Efforts toward an open source solution," *Futur. Sci. OA*, vol. 7, no. 6, 2021, doi: 10.2144/fsoa-2020-0206.
- [19] A. H. Gonsalves, F. Thabtah, R. M. A. Mohammad, and G. Singh, "Prediction of coronary heart disease using machine learning: An experimental analysis," in *ACM International Conference Proceeding Series*, 2019, no. July, pp. 51–56, doi: 10.1145/3342999.3343015.
- [20] L. Ashish, S. K. V, and S. Yeligeti, "Materials Today: Proceedings Ischemic heart disease detection using support vector Machine and extreme gradient boosting method," *Mater. Today Proc.*, no. xxxx, pp. 1–5, 2021, doi: 10.1016/j.matpr.2021.01.715.
- [21] D. Krishnani, A. Kumari, A. Dewangan, A. Singh, and N. S. Naik, "Prediction of Coronary Heart Disease using Supervised Machine Learning Algorithms," *TENCON 2019 - 2019 IEEE Reg. 10 Conf.*, pp. 367–372, 2019.
- [22] M. Nowshad, R. Chowdhury, E. Ahmed, A. D. Siddik, and A. U. Zaman, "Heart Disease Prognosis Using Machine Learning Classification Techniques," pp. 1–6, 2021.
- [23] N. Louridi, M. Amar, and B. El Ouahidi, "Identification of Cardiovascular Diseases Using Machine Learning," *7th Mediterr. Congr. Telecommun. 2019, C. 2019*, pp. 1–6, 2019, doi: 10.1109/CMT.2019.8931411.
- [24] D. Hemalatha and S. Poorani, "Machine learning techniques for heart disease prediction," *J. Cardiovasc. Dis. Res.*, vol. 12, no. 1, pp. 93–96, 2021, doi: 10.31838/jcdr.2021.12.01.05.
- [25] A. K. Pal, P. Rawal, R. Ruwala, and V. Patel, "Generic Disease Prediction using Symptoms with Supervised Machine Learning," *Int. J. Sci. Res. Comput. Sci. Eng. Inf. Technol.*, pp. 1082–1086, 2019, doi: 10.32628/cseit1952297.
- [26] H. Khdaif and N. M. Dasari, "Exploring Machine Learning Techniques for Coronary Heart Disease Prediction," vol. 12, no. 5, 2021.
- [27] I. K. A. Enrico, "Comparative study of heart disease diagnosis using top ten data mining classification algorithms," *ACM Int. Conf. Proceeding Ser.*, pp. 159–164, 2019, doi: 10.1145/3338188.3338220.
- [28] S. P. Patro, G. S. Nayak, and N. Padhy, "Heart disease prediction by using novel optimization algorithm: A supervised learning prospective," *Informatics Med. Unlocked*, vol. 26, p. 100696, 2021, doi: 10.1016/j.imu.2021.100696.
- [29] S. Dhar, K. Roy, T. Dey, P. Datta, and A. Biswas, "A hybrid machine learning approach for prediction of heart diseases," *2018 4th Int. Conf. Comput. Commun. Autom. ICCCA 2018*, pp. 1–6, 2018, doi: 10.1109/CCAA.2018.8777531.
- [30] P. Rani, R. Kumar, N. M. O. Sid, and A. Anurag, "A decision support system for heart disease prediction based upon machine learning," *J. Reliab. Intell. Environ.*, no. 0123456789, 2021, doi: 10.1007/s40860-021-00133-6.
- [31] A. U. Haq, J. P. Li, M. H. Memon, S. Nazir, and R. Sun, "A Hybrid Intelligent System Framework for the Prediction of Heart Disease Using Machine Learning Algorithms," vol. 2018, 2018.
- [32] G. Renugadevi, G. Asha Priya, B. Dhivyaa Sankari, and R. Gowthamani, "Predicting heart disease using hybrid machine learning model," *J. Phys. Conf. Ser.*, vol. 1916, no. 1, 2021, doi: 10.1088/1742-6596/1916/1/012208.
- [33] A. B. Nassif, O. Mahdi, Q. Nasir, M. A. Talib, and M. Azzeh, "Machine Learning Classifications of Coronary Artery Disease," *2018 Int. Jt. Symp. Artif. Intell. Nat. Lang. Process. iSAI-NLP 2018 - Proc.*, pp. 1–6, 2018, doi: 10.1109/iSAI-NLP.2018.8692942.
- [34] J. K. Kim and S. Kang, "Neural Network-Based Coronary Heart Disease Risk Prediction Using Feature Correlation Analysis," vol. 2017, 2017.
- [35] A. Caliskan and M. E. Yuksel, "Classification of coronary artery disease data sets by using a deep neural network," vol. 1, no. 4, pp. 271–277, 2017, doi: 10.24190/ISSN2564-615X/2017/04.03.
- [36] K. Miao, J. Miao, and G. Miao, "Diagnosing Coronary Heart Disease using Ensemble Machine Learning," *Int. J. Adv. Comput. Sci. Appl.*, vol. 7, no. 10, pp. 30–39, 2016, doi: 10.14569/ijacsa.2016.071004.
- [37] S. I. Ayon, M. M. Islam, and M. R. Hossain, "Coronary Artery Heart Disease Prediction: A Comparative Study of Computational Intelligence Techniques," *IETE J. Res.*, vol. 0, no. 0, pp. 1–20, 2020, doi: 10.1080/03772063.2020.1713916.
- [38] U. Das, A. Y. Srizon, and M. A. M. Hasan, "Accurate Recognition of Coronary Artery Disease by Applying Machine Learning Classifiers," *ICCIT 2020 - 23rd Int. Conf. Comput. Inf. Technol. Proc.*, pp. 19–21, 2020, doi: 10.1109/ICCIT51783.2020.9392732.
- [39] M. E. Elizabeth, B. Rickner, and A. L. Ange, "C ONGENITAL H EART D ISEASE IN A DULTS First of Two Parts," *Rev. Artic. Med. Prog.*, vol. 256, pp. 53–59, 2014.
- [40] M. M. Ghiasi, S. Zendeheboudi, and A. A. Mohsenipour, "Decision tree-based diagnosis of coronary artery disease: CART model," *Comput. Methods Programs Biomed.*, vol. 192, p. 105400, 2020, doi: 10.1016/j.cmpb.2020.105400.
- [41] M. Abdar, E. Nasarian, X. Zhou, G. Bargshady, V. N. Wijayaningrum, and S. Hussain, "Performance improvement of decision trees for diagnosis of coronary artery disease using multi filtering approach," *2019 IEEE 4th Int. Conf. Comput. Commun. Syst. ICCCS 2019, no. Dm*, pp. 26–30, 2019, doi: 10.1109/CCOMS.2019.8821633.
- [42] M. Yaqoob, F. Iqbal, and S. Zahir, "Comparing predictive performance of k-nearest neighbors and support vector machine for predicting ischemic heart disease," vol. 1, no. 2, pp. 49–60, 2020.
- [43] R. Alizadehsani et al., "Machine learning-based coronary artery disease diagnosis: A comprehensive review," *Comput. Biol. Med.*, vol. 111, p. 103346, 2019, doi: 10.1016/j.combiomed.2019.103346.
- [44] V. Sharma, S. Yadav, and M. Gupta, "Heart Disease Prediction using Machine Learning Techniques," *Proc. - IEEE 2020 2nd Int. Conf. Adv. Comput. Commun. Control Networking, ICACCCN 2020*, vol. 1, no. 6, pp. 177–181, 2020, doi: 10.1109/ICACCCN51052.2020.9362842.
- [45] H. Ayatollahi and L. Gholamhosseini, "Predicting coronary artery disease : a comparison between two data mining algorithms," pp. 1–9, 2019.
- [46] M. T. Islam, S. R. Rafa, and M. G. Kibria, "Early Prediction of Heart Disease Using PCA and Hybrid Genetic Algorithm with k-Means," *ICCIT 2020 - 23rd Int. Conf. Comput. Inf. Technol. Proc.*, 2020, doi: 10.1109/ICCIT51783.2020.9392655.
- [47] N. Basha, S. P. Ashok Kumar, C. Gopal Krishna, and P. Venkatesh, "Early Detection of Heart Syndrome Using Machine Learning Technique," *4th Int. Conf. Electr. Electron. Commun. Comput. Technol. Optim. Tech. ICEECOT 2019*, vol. 90, pp. 387–391, 2019, doi: 10.1109/ICEECOT46775.2019.9114651.
- [48] O. Terrada, S. Hamida, B. Cherradi, A. Raihani, and O. Bouattane, "Supervised machine learning based medical diagnosis support system for prediction of patients with heart disease," *Adv. Sci. Technol. Eng. Syst.*, vol. 5, no. 5, pp. 269–277, 2020, doi: 10.25046/AJ050533.
- [49] J. Beunza et al., "Comparison of machine learning algorithms for clinical event prediction (risk of coronary heart disease)," *J. Biomed. Inform.*, p. 103257, 2019, doi: 10.1016/j.jbi.2019.103257.
- [50] A. Dutta, T. Batabyal, M. Basu, and S. T. Acton, "An Efficient Convolutional Neural Network for Coronary Heart Disease Prediction."

Vision based Human Activity Recognition using Deep Neural Network Framework

Jitha Janardhanan^{1*}

Research Scholar, Department of Computer Science
Dr.G.R. D College of Science
Coimbatore, Tamil Nadu, India

Dr.S.Umamaheswari²

Associate Professor, Department of Computer Science
Dr.G.R. D College of Science
Coimbatore, TamilNadu, India

Abstract—Human Activity Recognition (HAR) has become a well-liked subject in study as of its broad application. With the growth of deep learning, novel thoughts have emerged to tackle HAR issues. One example is recognizing human behaviors without exposing a person's identify. Advanced computer vision approaches, on the other hand, are still thought to be potential development directions for constructing a human activity classification approach from a series of video frames. To solve this issue, a deep learning neural network technique using Depthwise Separable Convolution (DSC) with Bidirectional Long Short-Term Memory (DSC-BLSTM) is proposed here. The redeeming features of the proposed network system comprises a DSC convolution that helps to reduce not only the number of learnable parameters but also computational cost in together training and testing method The bidirectional LSTM process can combine the positive and the negative time direction. The proposed method comprises of three phases, which includes Video data preparation, Feature Extraction using Depthwise Separable Convolution Neural Network algorithm and DSC-BLSTM algorithm. The proposed DSC-BLSTM method obtains high accuracy, F1-score when compared to other HAR algorithms like MC-HF-SVM, Baseline LSTM Bidir-LSTM algorithms.

Keywords—Activity recognition; long short-term memory (LSTM); deep learning; feature extraction

I. INTRODUCTION

The Human Activity Recognition (HAR) system, a broadly used pattern recognition system discussed by [1], can be separated into numerous parts such as feature extraction, sensing segmentation, post-processing and classification ([11], [15]–[19]). HAR systems can be classified into two categories acceleration-based and time-based. Acceleration-based techniques need several accelerometers to be used for data gathering, but time-based techniques normally require the use of additional cameras to gather data. The drawback of the acceleration technique is that it can cause discomfort to the human body when performing behavior such as running, lying down and walking.

The different human activities to be observed in this paper include hand washing, punching, kicking, yoga, riding a bike, curling hair, ice skating etc. The benefit of a vision-based system is that the sensor works without attaching to the body.

The detection of performance depends on illumination surroundings, screening angle, and extra factors. The paper proposed a system that uses a kinetics data set [3] and a MobileNetV2 structure with Bidirectional Long Short-Term Memory (Bidir-LSTM) classification ([4], [25]) to solve this problem. This can decrease the actions of the handcraft procedure and boost the accuracy [20].

Human activity recognition is the problem of recognizing and classifying specific human actions executed in video frames. An instance of such a human action could be kicking or pull-ups. A classification can be trained on specific instances of an activity (training set) and then tested on a specific instance of an activity (test set). The aim of the system is to recognize the proper class of action to which a video frame belongs, or further generally, to recognize and appreciate what the human is doing in the video frames [13].

MobileNetV2 is 2D resource efficient architecture. It implements of MobileNetV1 using depth-wise separable convolutions. It establishes 2 novel sections: 1) linear bottlenecks among the layers, and 2) shortcut connections among the bottlenecks. The design is following the dimension that reduces amount of channels and extracts as much as information by depth-wise convolution after decompressing the data. This convolutional module permits reducing memory usage during inference ([21], [23]).

The objective of this Human activity recognition is to extend the deep learning approaches currently being developed, specifically targeting classification and potentially training/retraining on constrained computing environments. However, an integration of Depthwise Separable Convolution with LSTMs incurs significant computational expenses and prevents the network from running in real-time. To solve this problem, this paper introduced a Depthwise Separable Convolution with Bidirectional-LSTM (DSC-BLSTM) principles to reduce computational costs.

The rest of the paper is organized as follows: Related work is detailed in Section 2. In Section 3, proposed methodology of video frame extraction and Depthwise Separable Convolution with Bidirectional-LSTM (DSC-BLSTM) are described. In Section 4, experimental results and discussion are described finally conclusion portion is in Section 5.

*Corresponding Author.

Paper Submission Date: May 11, 2022

Acceptance Date: June 13, 2022

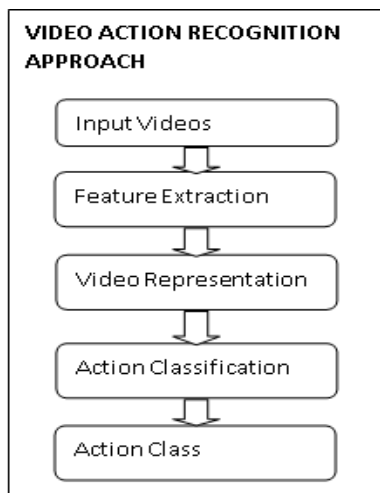


Fig. 1. Overview of Typical Video Action Recognition Approach.

II. RELATED WORK

Das and Chakrabarty [5] have presented human gender detection system approach. The Silhouettes from Center for Biometrics and Security Research (CASIA) step are portioned to recognize main body locations and to produce equivalent point-light demonstrate. The attributes such as two dimensional coordinates of main body locations and combined positions are mined from the point-light present. The attributes are categorized using Support Vector Machines (SVM) and Hidden Markov Model (HMM). The revision performs a detection rate of 76.79 percent and 69.18 percent with 100 subject data using SVM and HMM correspondingly.

Hammerla et al., [6] authors use sensor data that contains different motions, explored deep, convolution and recurrent approaches on these datasets. A new proposal has been put forth for regularization of recurrent networks. They have concluded that discovered recurrent networks outstripped the state-of-art and illustrated sample by sample prediction of physical activity.

Munzner et al [7], has evaluated PAMP2 and RBK dataset with convolutional neural network. The article illustrates the outperformance of early fusion technique over late -hybrid fusion by improvising F1 -score on RBK dataset.

M. Panwar et al., [8], discussed various developments that had taken place in human activity recognition using different machine learning approaches. Though, feature engineering has conquered conventional techniques connecting the complicated procedure of best feature selection. This difficulty has been mitigated by using a new method based on deep learning framework which automatically mines the positive features and decrease the processing cost.

A. Jain and V. Kanhangad [9] proposed a descriptor-based approach for action prediction using built-in sensors of smart-phones. Gyroscope and accelerometer sensor signals are obtained to recognize the behaviors achieved by the client. The authors described a histogram of gradient and centroid signature-based Fourier descriptor that are utilized to mine feature or attribute sets from these signals. Attribute and gain level synthesis are discovered for in order fusion.

A. Ignatov [10] presented a user-independent deep learning-based approach for online human activity classification. The authors proposed Convolutional Neural Networks for local attribute extraction jointly with plain arithmetical attributes that conserve information regarding the large-scale form of time series. Moreover, they investigated the crash of time series length on the identification accuracy and boundary it up to one second that builds potential and permanent real-time action prediction.

III. PROPOSED METHODOLOGY

The proposed Depthwise Separable Convolution with Bidirectional-LSTM (DSC-BLSTM) technique performs to test the experimentations that were accomplished with kinetics-400 dataset [3]. The DSC-BLSTM algorithm successfully detects the human activity in video frames and is grouped into different activity classes. The overall DSC-BLSTM workflow is illustrated in Fig. 2.

A. Video Frame Extraction

Video frame extraction is executed with Kinetics 400 action recognition dataset of action videos, accumulated from YouTube. With 306,245 short trimmed videos from 400 action categories. It is one of the largest and most widely used dataset in the research community for benchmarking state-of-the-art video action recognition models [24], described in Fig. 1. Since some YouTube links are expired, so could only download 234,584 of the original datasets, thus missing 11,951 videos from the training set, which are about 5%. This leads to a slight drop in performance of about 0.5%. The example video frame extraction result of riding camel video illustrated in Fig. 3.

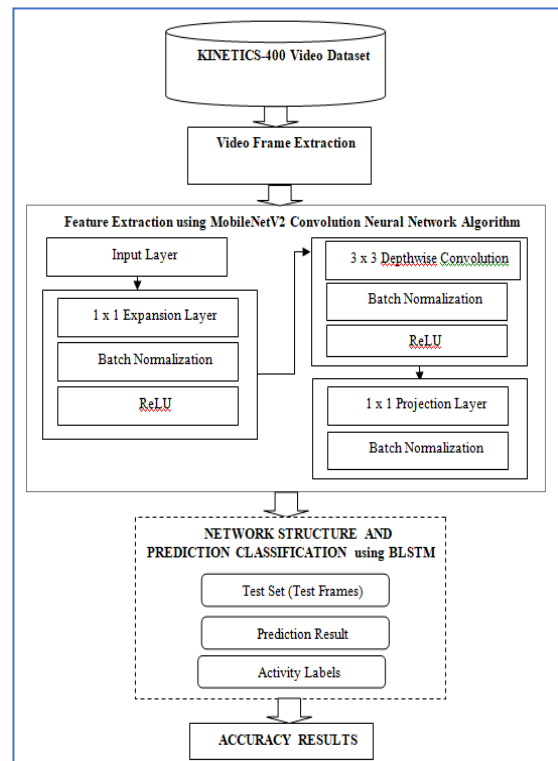


Fig. 2. Proposed DSC-BLSTM Algorithm Flow Diagram.

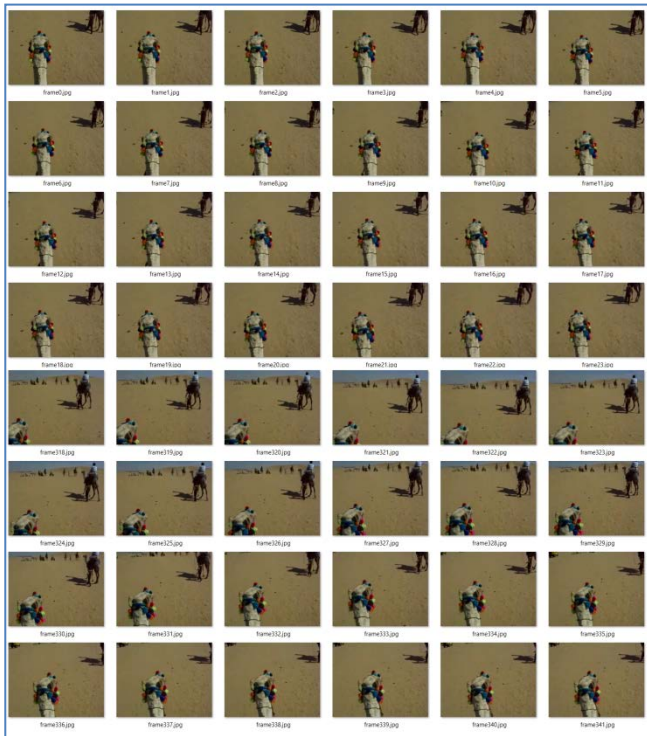


Fig. 3. Video Frame Extraction Result.

B. Feature Extraction using Depthwise Separable Convolution Neural Network Algorithm

The Feature extraction using MobileNetV2 convolution network using DSC is a factorized form of the standard convolution. The initial feature extraction layer is a 1 x 1 expansion layer. It increases the data (enhancing the number of channels) that flows through it. It does the opposite of the projection layer. The each video frame gets expanded based on the expansion factor [22]. This is a hyper parameter to be found from different architecture trade-offs. The default expansion factor is 6. A normal convolution is separated into a DC and a 1 x 1 PC. Instead of applying each filter to all the channels of the input like the standard convolution, the DC layer applies one filter to one input channel, then a 1x1 PC is employed to combine the outputs of the DC. DSC helps to reduce not only the number of learnable parameters but also the computational cost in both training and testing process. The flow diagram of DSC is described in Fig. 4.

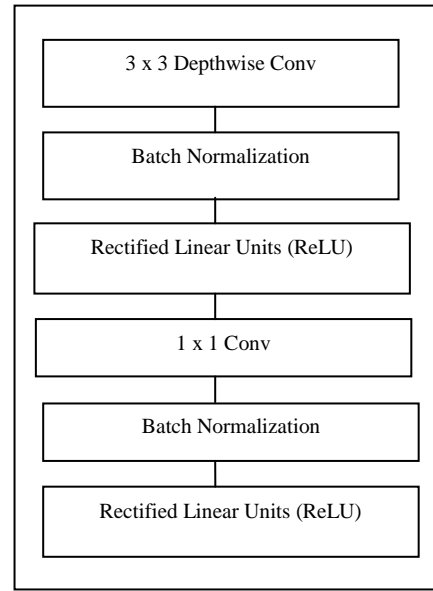


Fig. 4. Flow Diagram of DSC.

The proposed system of DSC is performed by 2 layers: 1) Depthwise Convolutions (DC) and 2) Point wise Convolutions (PC). The every input (contribution) channel (contribution depth) is applied by a filter with DC PC is a simple 1 x 1 convolution, is used to build linear permutation of the result of DC layer. MobileNets utilize equally batchnorm and ReLU nonlinearities layers. DC with single filter for each contribution channel can be written as:

$$Fmap_{k,m,n} = \sum_{a,b} Dw_{i,j,n} \cdot F_{k+i-1,m+j-1,n} eqn. \quad (1)$$

where Dw is the DC kernel size $Dw_k * Dw_k * N$ where n^{th} filter in Dw is functional to the n^{th} channel in F to create n^{th} channel filtered result of feature map Fmap.

DC cost is defined by,

$$Dw_k \cdot Dw_k \cdot N \cdot D_F \cdot D_F eqn. \quad (2)$$

The grouping of DC and 1 x 1 PC is called DSC which was formerly introduced by [11].

DSC cost is defined by equation 3,

$$Dw_k \cdot Dw_k \cdot N \cdot D_F \cdot D_F + N \cdot M \cdot D_F \cdot D_F eqn. \quad (3)$$

By stating convolution as a two-step procedure of filtering and combining to obtain decrease in calculation is,

$$\frac{Dw_k \cdot Dw_k \cdot N \cdot D_F \cdot D_F + N \cdot M \cdot D_F \cdot D_F}{Dw_k \cdot Dw_k \cdot N \cdot D_F \cdot D_F} = \frac{1}{N} + \frac{1}{Dw_k^2} eqn \quad (4)$$

Layer (Type)	Output Shape	Param #	Connected to
Input_1 (InputLayer)	(None, 224, 224, 3)	0	
conv1 (Conv2D)	(None, 112, 112, 32)	864	Input_1[0][0]
conv1_bn (BatchNormalization)	(None, 112, 112, 32)	128	conv1[0][0]
conv1_relu (Activation)	(None, 112, 112, 32)	0	conv1_bn[0][0]
conv_dw_1 (DepthwiseConv2D)	(None, 112, 112, 32)	288	conv1_relu[0][0]
conv_dw_1_bn (BatchNormalization)	(None, 112, 112, 32)	128	conv_dw_1[0][0]
conv_dw_1_relu (Activation)	(None, 112, 112, 32)	0	conv_dw_1_bn[0][0]
conv_pw_1 (Conv2D)	(None, 112, 112, 16)	432	conv_dw_1_relu[0][0]
conv_pw_1_bn (BatchNormalization)	(None, 112, 112, 16)	64	conv_pw_1[0][0]
conv_expand_1 (Conv2D)	(None, 112, 112, 96)	1536	conv_pw_1_bn[0][0]
conv_expand_1_bn (BatchNormalization)	(None, 112, 112, 96)	384	conv_expand_1[0][0]
conv_expand_1_relu (Activation)	(None, 112, 112, 96)	0	conv_expand_1_bn[0][0]
conv_dw_2 (DepthwiseConv2D)	(None, 56, 56, 96)	864	conv_expand_1_relu[0][0]
conv_dw_2_bn (BatchNormalization)	(None, 56, 56, 96)	384	conv_dw_2[0][0]
conv_dw_2_relu (Activation)	(None, 56, 56, 96)	0	conv_dw_2_bn[0][0]
conv_dw_2 (Conv2D)	(None, 56, 56, 24)	2304	conv_dw_2_relu[0][0]
conv_dw_2_bn (BatchNormalization)	(None, 56, 56, 24)	96	conv_dw_2[0][0]
conv_expand_2 (Conv2D)	(None, 56, 56, 144)	1456	conv_dw_2_bn[0][0]
conv_expand_2_bn (BatchNormalization)	(None, 56, 56, 144)	576	conv_expand_2[0][0]
conv_expand_2_relu (Activation)	(None, 56, 56, 144)	0	conv_expand_2_bn[0][0]
conv_dw_3 (DepthwiseConv2D)	(None, 56, 56, 144)	1296	conv_expand_2_relu[0][0]
conv_dw_3_bn (BatchNormalization)	(None, 56, 56, 144)	576	conv_dw_3[0][0]
conv_dw_3_relu (Activation)	(None, 56, 56, 144)	0	conv_dw_3_bn[0][0]
conv_pw_3 (Conv2D)	(None, 56, 56, 24)	1456	conv_dw_3_relu[0][0]

Total params:	2,257,984		
Trainable params:	2,223,872		
Non-trainable params:	34,112		

Fig. 5. Depthwise Separable Convolutions base Model Result.

MobileNetV2 uses 3 x 3 DSC take on among eight to nine times less computation than normal convolutions having less accuracy. By exploring the network in simple terms that are proficient to simply explore network topologies to discover an excellent network. The proposed training model is defined in Fig. 5. The entire layers are trailed by batchnorm and ReLU nonlinearity with the exclusion of the last completely connected layer which has no nonlinearity and brought into a SoftMax layer for classification.

C. Depthwise Separable Convolution with Bidirectional-LSTM (DSC-BLSTM)

According to [2], [12], authors described LSTM as an expansion of recurrent neural networks. Appropriate to unique architecture, which conflicts the disappearance and ignition gradient issues, it is fine at managing time series issues up to a positive depth. LSTM conserve information from inputs that has previously passed through it via the hidden state. Unidirectional LSTM only conserve information of the precedent because of the simple inputs it has observed from the past. The bidirectional LSTM will process the inputs with one from past to future and one from future to past and what varies this approach from unidirectional is that in the LSTM processes backwards to protect information from the future and using the two hidden states that are combined in some point to protect information from together past and future. Bidirectional LSTM (see Fig. 6) comprises of 2 LSTM cells, and the result is resolute. The bidirectional LSTM presented result is not only associated to prior information but also connected to consequent information. The overall DSC-BLSTM flow diagram is illustrated in Fig. 7.

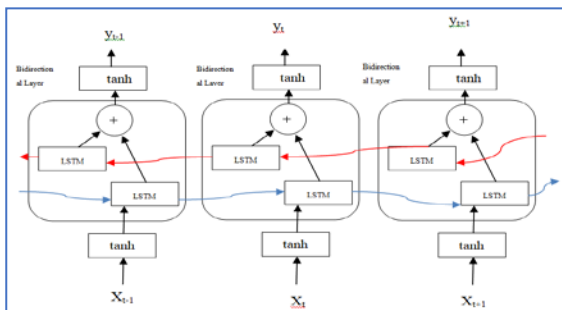


Fig. 6. Bidirectional LSTM Construction.

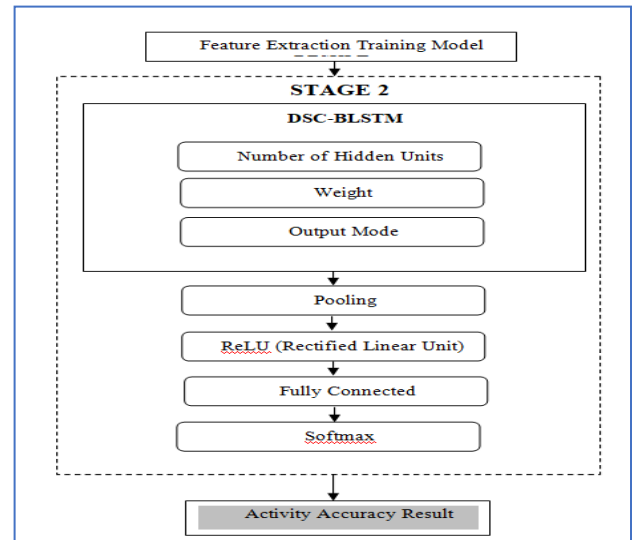


Fig. 7. DSC-BLSTM Flow Diagram.

Algorithm: DSC-BLSTM Pseudo code

Input: Continuous Video Frames f , Class Labels C
Output: Predicted activity class with accuracy score

Preparation:

1. Video Data Preparation
2. Feature Extraction using Depthwise Separable Convolution Neural Network (DSC)
3. Depthwise Separable Convolution with Bidirectional-LSTM (DSC-BLSTM)

Steps:

While (video frame)

1. Frame $f \leftarrow$ Extract frames from videos

//Fix sample duration (i.e., frames taken per loop/iteration) = 16 frames per iteration and sample size (i.e., Frame width size) = 112pixels wide

2. $M \leftarrow$ Create trained model using DSC method

End While

3. **for** $t = 1$ to n **do** // where n represents number of video frames
 - a. frame $f(t) \leftarrow$ Read the test video frame.
 - b. Apply $f(t)$ to DSC Model // Calculate Similarity matrix value of test frame $f(t)$ with trained model
 - c. Predict activity Class label with frame $f(t)$ using (DSC-BLSTM)
4. Label Predicted activity \leftarrow Result class label
5. Display predicted activity class with accuracy score

End for

The DSC-BLSTM algorithm takes these three inputs Model M , classes C and test video frames f . Initially, load the trained human activity recognition DSC model M and contents of the class labels C file. After that, test frames are grouped and resized with defined sample duration (i.e., number of frames for classification) and test size (i.e., the spatial dimensions of the frame). Next, test input video frames are looped over the amount of essential test frames (i.e., duration of 16 frames per loop) and read a test frame from the video stream. The test frame streams are forwarded to the network model for checking the distance matrix (i.e., similarity) between train model M and test frame f model outputs. The outputs matrix is passed through Bidirectional LSTM process to get the activity label. Finally, the maximum classes of label are the predicted activity for the processed frame. The Table I shows the parameters, symbol with the corresponding value of the proposed system implementation.

TABLE I. PARAMETERS DESCRIPTION

Parameter Name	Symbol	Value
Total Classes	C	400 action classes
Frame Duration	Sample_duration	16 frames per iteration
Sample window Size	Sample_size	112 pixel wide
Training Model	M	2000 Videos model
Test video frame	f	-
Total Number of Frames	n	Total no of frames in a video

IV. EXPERIMENTAL RESULTS AND DISCUSSION

A. Experimental Environment

The results have been estimated with the proposed DSC-BLSTM algorithm. The results are implemented with Intel I5-6500U series 2.71 GHz, x64-based processor, 8GB main memory, and run on the Windows 10 operating system using python 3.8 simulations. This paper is implemented with Kinetics 400 action recognition dataset which consists of 2000 videos as training dataset with 21 classes that includes massage, Ice Skating, Yoga, Playing, Pull ups, Pushing, Reading, Tasting, Skating, Side Kick, Filling, Crawling, Waiting, Washing, Making Pizza, Kicking, Jumping, Curling, Dancing, Massage, Shaving and Shooting. The resulting parameters of Ice-Skating activity are described in Fig. 8 to Fig. 10.

B. Discussion

This section presents a detailed analysis of experimental outcomes through the proposed method on the basis of accuracy measures such as precision, recall, accuracy, and F1-score. The proposed algorithm consists of three main stages. These three main stages include the video frame extraction which is performed first in which datasets are normalized to get better results. The accurate results will give more accuracy. In the second step, feature extraction is implemented using Depthwise Separable Convolution Neural Network algorithm. In this step, features is implemented separately based on DSC to get the best features are stored in trained dataset. In the third step, features are fused, while in the final stage, results are taken through the classification learner. In video frame

extraction, all individual frames are stored as images to detect the activity from the image. After the frame extraction, MobileNetV2 convolution network using DSC method to create a feature model from extracted images. Finally, Depthwise Separable Convolution with Bidirectional-LSTM (DSC-BLSTM) classifier to discover the similarity matrix value of test frame with trained model to attain the prediction activity result. Combining DSC-BLSTM have achieved higher accuracy than the other classification learners on the “MC-HF-SVM, Baseline LSTM and Bidir-LLSTM algorithms”, respectively.



Fig. 8. HAR Result of Ice Skating with Accuracy.

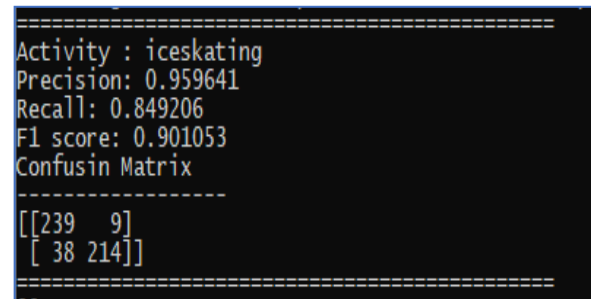


Fig. 9. HAR Result of Ice Skating Performance Measure of Precision, Recall, F1 Score and Confusion Matrix.

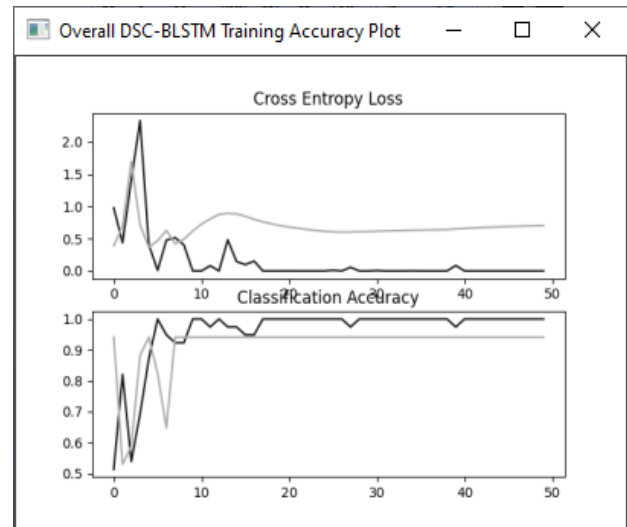


Fig. 10. Overall DSC-BLSTM Training Loss and Accuracy Plot Result.

C. Evaluation Index

To evaluate the performance of the proposed model for HAR, the followed metrics [26] were used for evaluation generally.

$$Accuracy = \frac{tp+tn}{tp+fn+fp+tn} \tag{5}$$

$$Precision = \frac{tp}{tp+fp} \tag{6}$$

$$Recall = \frac{tp}{tp+fn} \tag{7}$$

$$F1 - score = \frac{2 \times Precision \times Recall}{Precision + Recall} \tag{8}$$

The proposed DSC-BLSTM method substantiates with high Accuracy and F1-score ratio when compared to other HAR algorithms like Multiclass Hardware-Friendly Support Vector Machine (MC-HF-SVM) [7], Baseline LSTM [14], Bidirectional Long Short Term Memory (Bidir-LSTM) [4] algorithm. As a result of the improved human activity recognition presentation, there is a higher accuracy. The proposed DSC-BLSTM method proves high Accuracy and F1-score ratio when compared to other HAR algorithms like Multiclass Hardware-Friendly Support Vector Machine (MC-HF-SVM) [7], Baseline LSTM [14], Bidirectional Long Short Term Memory (Bidir-LSTM) [4] algorithm are described in Table II and Fig. 11 shows the comparison chart.

In Table III shows the comparison of precision, recall, accuracy and F1 score with kinetics 400 dataset of test videos prediction activity measures and Fig. 12 shows the comparison chart.

TABLE II. COMPARISON OF ACCURACY AND F1 SCORE WITH EXISTING AND PROPOSED DSC-BLSTM ALGORITHM OF KINETICS 400 DATASET

Methods	MC-HF-SVM	Baseline LSTM	Bidir-LSTM	DSC-BLSTM
Accuracy	89.3	90.8	91.1	93.8
F1-Score	89.0	90.8	91.1	92.637

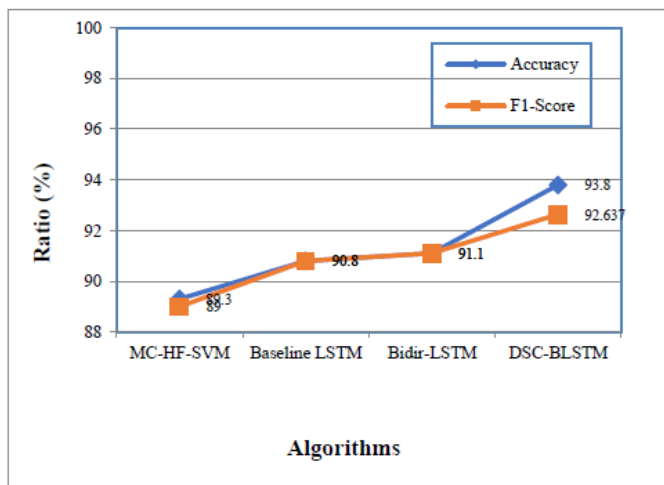


Fig. 11. Comparison Measures of Accuracy and F1 Score Chart.

TABLE III. COMPARISON OF TEST VIDEOS PREDICTION ACTIVITY MEASURES OF PROPOSED DSC-BLSTM ALGORITHM OF PRECISION, RECALL, ACCURACY AND F1 SCORE WITH KINETICS 400 DATASET

Prediction Activity	Precision	Recall	Accuracy	F1-Score
Ice Skating	96.25	91.66	94	93.90
Yoga	94.23	90.87	92.60	92.52
Playing	91.56	90.47	91	91.01
Pull ups	95	90.47	92.80	92.68
Pushing	95.08	92.06	93.60	93.54
Reading	91.49	89.68	90.60	90.58
Tasting	92.68	90.47	91.60	91.56
Skating	93.56	86.50	90.20	89.89
Side Kick	94.34	86.11	90.40	90.04
Filling	95.08	84.52	90.00	89.49
Crawling	96.39	84.92	90.80	90.29
Waiting	89.23	92.06	90.40	90.62
Washing	97.83	89.68	93.80	93.58
Making	94.97	90.07	92.60	92.46
Kicking	91.76	92.85	92.20	92.30
Jumping	95.79	90.47	93.20	93.06
Curling	93.00	89.68	91.40	91.31
Dancing	91.20	90.47	90.80	90.83
Massage	90.38	93.25	91.60	91.79
Shaving	91.39	88.49	90	89.91
Shooting	94.44	89.69	91.20	90.94



Fig. 12. Comparison of Test Video Class Prediction Activities of Performance Measures of Kinetics 400 Dataset.

V. CONCLUSION

This paper analyzed the advancement of Human Activity Recognition (HAR) concepts in the field of deep neural network technique. The proposed work presents a Depthwise Separable Convolution with Bidirectional long short-term

memory (DSC-BLSTM) algorithm adapted to the HAR task. This system seeks to improve the accuracy of activity recognition by leveraging the robustness in feature extraction and classification model. The results were impressive and worked well after we used the DSC-BLSTM method in the HAR system. The result is shown as 93.8%, and is more recognizable than the other HAR algorithms like MC-HF-SVM, Baseline LSTM, Bidir-LSTM algorithms.

VI. CONFLICT OF INTEREST

The authors declare no conflict of interest

REFERENCES

- [1] J. Schmidhuber, "Deep Learning In Neural Networks: An Overview", *Neural Networks*, vol. 61, pp. 85-117, 2015.
- [2] D. C. Ciresan, U. Meier U, and L. M. Gambardella, "Deep, Big, Simple Neural Nets For Handwritten Digit Recognition", *Neural computation*, vol. 22, no. 12, pp. 3207-3220, 2010.
- [3] Kay W, Carreira J, Simonyan K, Zhang B, Hillier C, Vijayanarasimhan S, Viola F, Green T, Back T, Natsev P, "The Kinetics Human Action Video Dataset", 2017.
- [4] Yu Zhao, Rennong Yang, Guillaume Chevalier, Ximeng Xu, and Zhenxing Zhang, "Deep Residual Bidir-LSTM for Human Activity Recognition Using Wearable Sensors," *Mathematical Problems in Engineering*, Volume 2018.
- [5] D. Das and A. Chakrabarty, "Human Gait-Based Gender Identification System Using Hidden Markov Model And Support Vector Machines," in *Conf. Comput. Commun. Autom. ICCA 2015*, pp. 268–272, 2015.
- [6] N. Y. Hammerla, S. Halloran, and T. Ploetz, "Deep, Convolutional, And Recurrent Models For Human Activity Recognition Using Wearables," *arXiv preprint arXiv:1604.08880*, 2016.
- [7] S. M'uzner, P. Schmidt, A. Reiss, M. Hanselmann, R. Stiefelhagen, and R. D'urichen, "Cnn-Based Sensor Fusion Techniques For Multimodal Human Activity Recognition," in *Proceedings of the 2017ACM International Symposium on Wearable Computers*, ser. *ISWC '17*. New York, NY, USA: ACM, 2017, pp. 158–165.
- [8] M. Panwar et al., "CNN Based Approach For Activity Recognition Using A Wrist-Worn Accelerometer," in *Proc. Annu. Int.Conf. IEEE Eng. Med. Biol. Soc. EMBS*, no. July, pp. 2438–2441, 2017.
- [9] A. Jain and V. Kanhangad, "Human Activity Classification in Smartphone's Using Accelerometer and Gyroscope Sensors," *IEEE Sensors Journal*, vol. 18, no. 3, pp. 1169-1177, 1 Feb.1, 2018.
- [10] A. Ignatov, "Real-Time Human Activity Recognition From Accelerometer Data Using Convolutional Neural Networks," *Appl. Soft Comput. J.*, vol. 62, pp. 915–922, 2018.
- [11] L. Sifre, "Rigid-motion Scattering for Image Classification," PhD thesis, Department of Informatics, CMP Ecole Polytechnic, France., 2014.
- [12] A. Krizhevsky, I. Sutskever, and G. E.Hinton, "Imagenet Classification With Deep Convolutional Neural Networks," in *Proceedings of the 26th Annual Conference on Neural Information Processing Systems (NIPS '12)*, pp. 1097–1105, Lake Tahoe, Nev, USA, December 2012.
- [13] D. Anguita, A. Ghio, L. Oneto, X. Parra, and J. L. Reyes-Ortiz, "Energy Efficient Smartphone-Based Activity Recognition Using Fixed-Point Arithmetic," *Journal of Universal Computer Science*, vol. 19, no. 9, pp. 1295–1314, 2013.
- [14] N Srivastava, E Mansimov, R Salakhudinov, "Unsupervised Learning Of Video Representation Using LSTM", *International conference on machine learning*, pp 843–852, 2015.
- [15] M. Baccouche, F. Mamalet, C. Wolf, C. Garcia, and A. Baskurt, "Action Classification In Soccer Videos With Long Short Term Memory Recurrent Neural Networks", in *Proceedings of ICANN*, 2010.
- [16] M. Baccouche, F. Mamalet, C. Wolf, C. Garcia, and A. Baskurt. *Sequential Deep Learning For Human Action Recognition*, "Human Behavior Understanding, 2011.
- [17] Jeffrey Donahue, Lisa Anne Hendricks, Sergio Guadarrama, Marcus Rohrbach, Subhashini Venugopalan, Kate Saenko, and Trevor Darrell., "Long-Term Recurrent Convolutional Networks For Visual Recognition And Description". In *Proceedings of the IEEE Conference on Computer Vision and Pattern Recognition*, pages 2625–2634, 2015.
- [18] A. Karpathy, G. Goderici, S. Shetty, T. Leung, R. Sukthankar, and F. F. Li., "Large-Scale Video Classification With Convolutional Neural Networks," In *Proceedings of CVPR*, 2014.
- [19] K. Simonyan and A. Zisserman, "Two-Stream Convolutional Networks For Action Recognition In Video." In *arXiv preprint arxiv:1406.2199*, 2014.
- [20] M. Sandler, A. Howard, M. Zhu, A. Zhmoginov, and L.-C. Chen., "Mobilenetv2: Inverted Residuals And Linear bottlenecks." In *2018 IEEE/CVF Conference on Computer Vision and Pattern Recognition*, pp 4510–4520. IEEE, 2018.
- [21] P. Molchanov, S. Tyree, T. Karras, T. Aila, and J. Kautz, "Pruning convolutional neural networks for resource efficient inference," *arXiv preprint arXiv:1611.06440*, 2016.
- [22] D. Tran, J. Ray, Z. Shou, S.-F. Chang, and M. Paluri, "Convnet Architecture Search for Spatiotemporal Feature Learning," *arXiv preprint arXiv:1708.05038*, 2017.
- [23] G. Huang, Z. Liu, L. Van Der Maaten, and K. Q. Weinberger. "Densely Connected Convolutional Networks," in *Proceedings of the IEEE conference on computer vision and pattern recognition*, pp 4700–4708, 2017.
- [24] Heng Wang and Cordelia Schmid. "Action recognition with improved trajectories", in *Computer Vision (ICCV)*, 2013 IEEE International Conference on, pp 3551–3558. IEEE, 2013.
- [25] F. J. Ordonez and D. Roggen, "Deep Convolutional and LSTM Recurrent Neural Networks for Multimodal Wearable Activity Recognition," *Sensors*, vol. 16, no. 1, pp. 115–140, 2016.
- [26] Yang, D.; Huang, J.; Tu, X.; Ding, G.; Shen, T.; Xiao, X, "A Wearable Activity Recognition Device Using Air-Pressure and IMUSensors," *IEEE Access* 2019,7, 6611–6621.

Internal Works Quality Assessment for Wall Evenness using Vision-based Sensor on a Mecanum-Wheeled Mobile Robot

Ahmad Zaki Shukor¹, Muhammad Herman bin Jamaluddin²

Mohd Zulkifli bin Ramli³, Ghazali bin Omar⁴, Syed Hazni Abd Ghani⁵

Faculty of Electrical Engineering, Universiti Teknikal Malaysia Melaka, Malaysia^{1,2,3}

Advanced Manufacturing Centre, Universiti Teknikal Malaysia Melaka, Malaysia⁴

Construction Quality Assessment Centre (CASC), Construction Research Institute of Malaysia (CREAM), Malaysia⁵

Abstract—Robotics in the construction industry has been used for a few decades up to this present time. There are various advanced robotics mechanisms or technologies developed for specific construction task to assist construction. However, not many researches have been found on the quality assessment of the finished structures. This research proposes a quality assessment robot that will assist in performing the assessment of the internal works of a building by assessing a quality assessment criterion in the Malaysian Construction Industry Standards. There are various assessment criteria such as hollowness, cracks and damages, finishing and jointing. This paper will focus on the wall evenness using a camera mounted on a mobile robot with a Mecanum wheel design. The wall evenness assessment was done via projecting a laser leveler on the wall and capturing the images by using a camera, which is later processed by a central controller. Results show that the deviation calculation method can be used to differentiate between even and uneven walls. Pixel deviations for even walls show values of less than 15 while uneven walls show values of more than 20 pixels.

Keywords—Construction industry standards; internal works quality assessment; vision; Mecanum wheels

I. INTRODUCTION

In this era of Industrial Revolution 4.0, many technologies are being used in various application areas. Internet-of-Things, virtual reality, data analytics, additive manufacturing and robotics are some of the interesting technologies that have accelerated various manufacturing sectors throughout the current years. In the construction industry, robotics has been applied since the early 1980's. In the Japan visit, Dr. James S. Albus from National Bureau of Standards [1] and six construction companies (Taisei Corporation, Takenaka, Hazama Gumi Ltd, Shimizu Construction, Kumagai Gumi Company and Toshiba Nuclear Group) had large research on budgets for construction robotics. There are many related researches of cooperative or multi-robots that were proposed in construction environment, such as multi-robot teleoperation using humanoid and legged robots [2], multi-robot material deposition using autonomous mobile robot extruder platform [3], human-robot collaboration for interior finishing [4] and distributed climbing strut robots that was used for guiding construction [5]. There were also studies on simulating robots in construction via haptic control for drywall installation, painting, welding, bolting and concrete pouring [6]. In another

research, a robot was proposed for monitoring the work progress in a building construction site [7] and a façade cleaning robot was proposed in [8].

However, not many researches have been focused on the automated internal or external works of finished building or construction sites. At present, the quality assessment is performed by manual inspection by a human assessor or a panel of assessors. This is tedious and tiring work because assessors usually complete a substantial amount of sample houses or buildings within a few days. The research of a custom-built quality assessment robot could reduce the burden of human inspectors by carrying out assessment of some criteria of the structure quality. A bridge statics assessment robot for flood evacuation planning was designed by Maik Benndorf et al. in [9]. This is an example of an external structure assessment that uses vibration measurement sensors mounted on an Unmanned Ground Vehicle equipped with a robotic manipulator. For internal works, a custom-designed quality assessment robot was proposed by Rui-Jun Yan et al. [10]. In assessing the different criteria, Rui-Jun Yan attached several devices for the quality assessment robot, Quicabot. A thermal camera was used to assess the hollowness of the ground and walls, an RGB camera to detect cracks on the ground and walls, a laser scanner to measure the evenness of the ground and walls and alignment of two connected walls while an inclinometer to measure the inclination of the ground.

The use of laser projection and vision sensors were seen in other applications. Andrzej Sioma used laser and a camera to measure the surface defect of a ceramic tile [11]. The longitudinal rip of conveyor belt detection was performed by Xianguo Li et al. using laser-based machine vision in [12] because of the use of such belt mechanisms to transfer materials or products. Other than that, bubble defects on tire surface were also detected by Hualin Yang et al. in [13] by using laser and machine vision. Daniel Lopez-Escogido et al. [14], detected small defects in PCB using 2-D high precision laser sensors, which investigated high errors of units of micrometers due to the small outline of Surface-Mount-Devices (SMD).

Jorge Rodríguez-Araújo and Antón García-Díaz [15] investigated in-line Defect Classification and localization in Solar Cells for Laser-Based Repair. This is because the faulty

cells need to be identified to be repaired. In [16], Dong-Gi Woo et al. used multi-lasers to perform the inspection of the surface of a car door chassis by using a robot arm manipulator projecting the lasers in different poses, which could be used as a 3D measurement system. Other than that, Ting Lei et al. [17] used laser vision to identify thermal deformation of tube sheet welding by using a Cartesian robot, CCD camera, hoop assembly, laser sensors and single-line lasers. A combination of line scan camera and frame camera was used to detect product surface defects by applying the ideas of both surface grayscale image and depth image simultaneously [18] in which Zhen Liu et al. claim the accuracy of 0.13mm within a measurement of 500x300x200 mm³. In [19] Simone Pasineet et al. investigated in-line monitoring of laser welding using vision system, which applied thresholding, binarization and blob-counting to robustly detect joint and obtain optimal acquisition of the melt pool during welding.

The weld seam detection and feature extraction of butt-welding was investigated by Wang Xiuping et al. [20] in which the laser stripe edges were detected. The welding was performed by a welding robot arm manipulator. Feature extraction of butt-joint was also investigated by Yuanyuan Zou et al. [21] which used three-line stripe laser vision sensor. The algorithm uses Laws texture energy filter, Canny operator, thresholding and textural feature; laser stripes were used as its feature points.

Although there is not much research or references in the area of building quality assessment using robots, the idea of using laser projection and image acquisition and processing has been used in some applications mentioned previously, i.e. weld seam identification, and defect detection of tiles or panels.

For this paper, our objective is to explore and propose quality assessment of a criterion in the Construction Industry Standards for internal works, which is the wall evenness assessment. We propose the use of laser projection and image processing for the assessment. A custom-made mobile robot was designed and developed for the assessment, which can be further upgraded to include assessment of other criteria such as hollowness, cracks and damages, wall alignment and others. The advantage of our method is the use of cost-effective devices such as laser leveler and standard High Definition (HD) USB cameras.

II. THE CONSTRUCTION QUALITY ASSESSMENT ROBOT

The robot for the quality assessment of internal works was custom-built as shown in Fig. 1. Fig. 1(a) shows the 3D drawing of the robot and Fig. 1(b) shows the actual robot. It is a mobile robot equipped with the sensors used for assessment. The base of the robot which is mostly rectangular is driven by four planetary geared motors connected to couplings of the Mecanum wheels to enable multi-direction motion of the mobile robot. The details of the components are shown in Table I.

As described in Table I, there are several parts that are required for the robot to function. It includes the robot base, power supply, controllers, sensors and tapping rod mechanism. The robot structure is custom-built using the frames consisting

of 20 x 20 aluminum profiles with a square base of 300 x 300 mm² size.

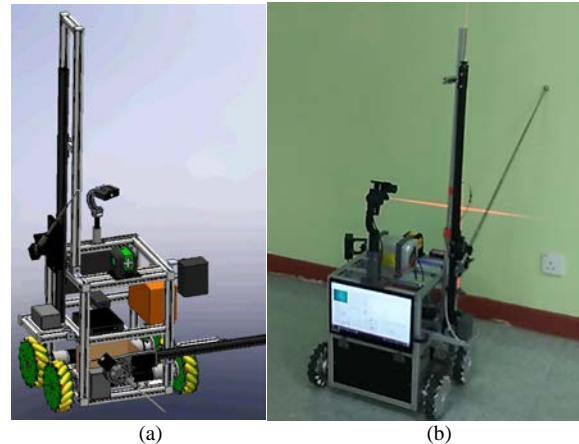


Fig. 1. 3D Drawing of the Assessment Robot, (b) Actual Robot.

TABLE I. QUALITY ASSESSMENT ROBOT COMPONENTS

Main Part	Sub-component	Details
Robot base	Planetary-gear DC motors (4)	24V 148RPM 18kgfcm 45mm
	Coupling (4)	10mm Key Hub for 152mm Mecanum Wheel
	Mecanum wheel (4)	152mm
	Structure	Aluminum Profile 2020, 300mm length each
Power supply	Motor Drivers (2)	10Amp 5V-30V DC Motor Driver (2 Channels)
	36 V DC Batteries	Rechargeable Lithium Ion 36V Batteries with BMS
	DC-DC converters	24V, 9V
Controller	Mobile Robot Controller	Arduino Pro-Mega
	Data acquisition and Processing	Intel BOXNUC8i6BEH3 (Intel i5)
	Display	13.3 inch USB-C Monitor
Sensors	Ranging sensors (8)	Time of Flight (TOF) VL 53L0X
	Corner alignment sensor	Time of Flight (TOF) VL 53L0X
	Camera (4)	2MP Webcam
	Laser leveler Gimbal	1-axis, mounted with camera
Tapping Rod	Slider	V-Slot Y-axis slider with Belt Buckle
	Servo Motor	4.5 – 6.0V RC Servo Motor
	Aluminum	V-Slot Aluminum Profile (Black Anodized) 2020
	Tensioner	Timing Belt Tensioner 2020

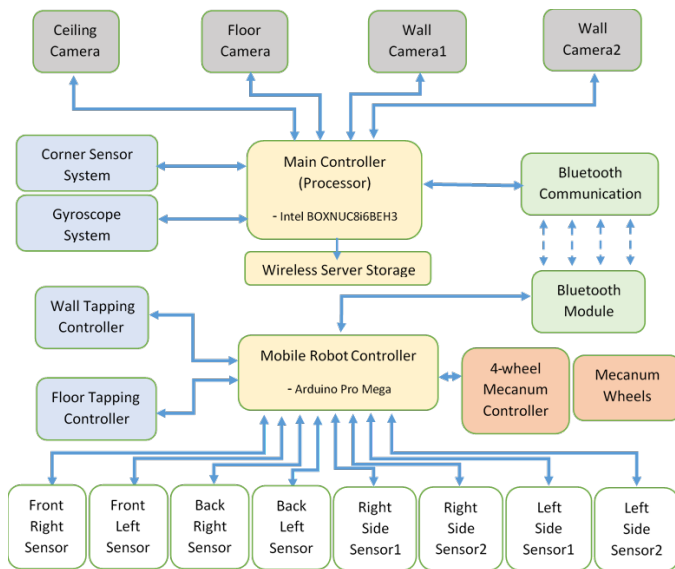


Fig. 2. Overall Block Diagram of the Quality Assessment Mobile Robot.

The overall block diagram of the Quality Assessment Robot is shown in Fig. 2. It consists of two main parts/controllers, which are the Main Processor and the Mobile Robot Controller. The main controller parts consist of the Central Processing Unit (CPU), four High Definition (HD) cameras, the corner sensor system and the gyroscope sensor system. The Mobile Robot Controller controls the four motors which are connected to the Mecanum wheels, the two tapping rod mechanisms which actuate the tapping rod motion and the interface with the eight (8) proximity sensors (Time-Of-Flight sensors).

The reason for using four cameras simultaneously is to enable four snapshots that can be taken which cover two walls (lower and upper), floor and ceiling view. This method can save time because it captures images at the same time, rather than moving a camera in different angles to capture the four images. The mechanical motion is only for the navigation of the mobile robot base. For the purpose of quality assessment, the obstacle detected using the proximity sensors is the wall it faces. Two sensors are placed at each side of the robot for the robot to navigate around its surroundings. The front side has two sensors to sense the wall facing the robot, the right side has two sensors to sense the right wall, the left side has two sensors to sense the left wall and the rear side has two sensors to sense the wall facing the robot's rear.

The mobile robot controller actuates the tapping rod movement, which is the wall tapping rod mechanism and the floor tapping rod mechanism. The wall tapping rod mechanism is located at the right side of the robot while the floor tapping rod mechanism is placed at the front side of the robot, as shown in Fig. 3. This tapping mechanism which consists of a tapping rod, a microphone and sliding mechanism, is used to assess the hollowness of the wall and floor by acquiring the sound waves recorded by the microphone attached to the tapping mechanism. However the tapping mechanism is not the focus in this paper.

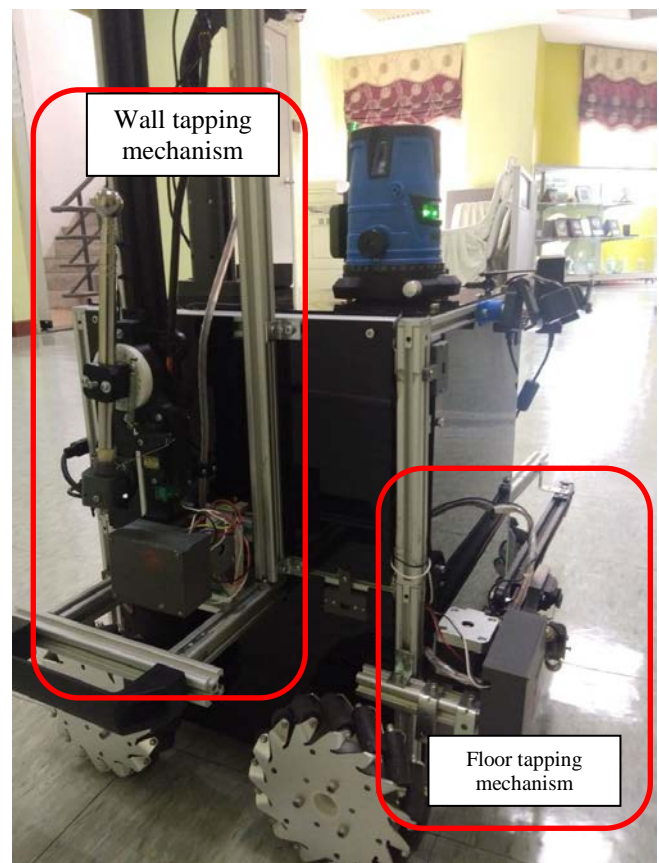


Fig. 3. The Wall-tapping Mechanism and Floor-tapping Mechanism.

The main processor controls the overall data acquisition of the mobile robot, such as image acquisition and processing, corner sensor data acquisition and evenness data acquisition. The pictures of the main processor-connected components are shown in Fig. 4.

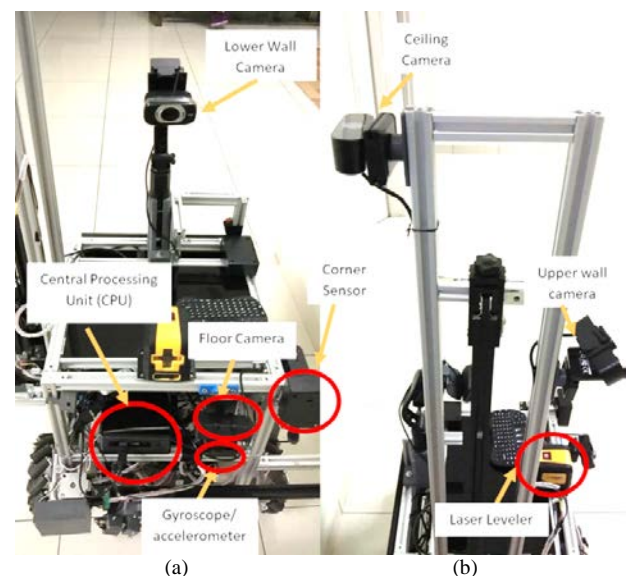


Fig. 4. (a) The Floor Camera and Lower Wall Camera Connected to the CPU, (b) The Laser Leveler, Upper Wall Camera and Ceiling Camera.

The four cameras consist of a camera for the floor image capture, a camera for the ceiling image capture, a lower wall camera for capturing the image with the laser leveler projected lines and an upper wall camera to capture the upper wall area. These cameras are connected to the CPU and controlled by a custom-developed software. The laser leveler is attached on the upper frame of the robot, at a suitable height for the lower wall camera to capture the image. The other two cameras are located on the tapping rod holding frame, which is the upper wall camera and the ceiling camera.

There are two external sensor systems connected to the CPU; the corner detection sensor system and the gyroscope/accelerometer sensor system. These two sensors will record data and send it to the CPU for storage and processing. The data collected by the CPU (images, accelerometer readings, corner sensor readings) are stored in the wireless server data storage provided. The wireless server is accessed via the Wi-Fi network established between the CPU and the server. For the robot to move, the main controller will send commands to the mobile robot controller, which is connected to the CPU using Bluetooth Serial Port connection.

The simultaneous multi-assessment capability of the mobile robot is the clear advantage, acquiring different data for different criteria in the Quality Assessment System in Construction (QLASSIC) Construction Industry Standards. Its purpose at this time is not to replace the human assessor completely, but to assess some criteria. Hence it will lessen the burden of the human assessor and save time to complete a full assessment.

III. THE WALL EVENNESS ASSESSMENT USING VISION-BASED APPROACH

For this paper, we will focus on the wall evenness assessment using vision-based approach. The intention of applying the mobile robot into the construction assessment is to assist in assessing compliance with the Malaysian Construction Industry Standards (CIS). In the Standards, the wall surface evenness is considered “comply” if the deviation of wall surface is within 3mm, measured by 1.2m spirit level and steel wedge held by a human assessor. When the spirit level is placed on the wall, the steel wedge will be inserted in areas where there is space between the spirit level and the wall. This space should be within 3mm. This method using human assessment will depend on the consistency of human assessor evaluation. While some assessors take large samples of the wall in a room, others may only take samples of wall that he/she sees as a probable defect. This is due to the large number of rooms that the assessor is assigned to evaluate. This inconsistency is due to the human factor.

Thus, to assist the assessment, the mobile robot will help in acquiring images and later processing the images to determine wall evenness. By using a mobile robot, the image acquired will be at consistent distances set in the mobile robot controller program. The arrangement or setup of the mobile robot to acquire the images is illustrated as shown in Fig. 5.

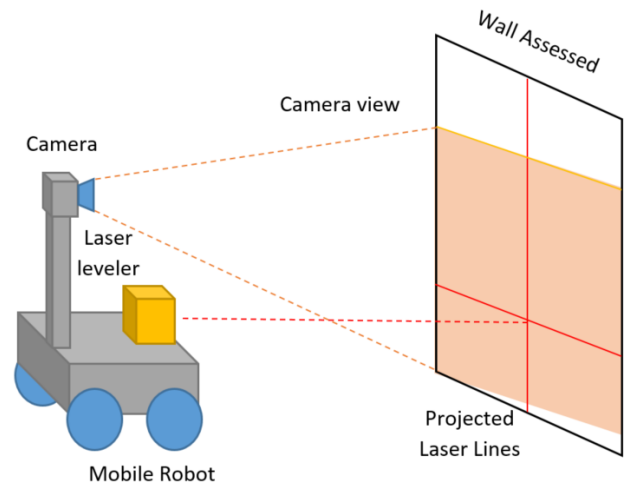


Fig. 5. Illustration of Image Capture of Wall for Surface Evenness Assessment.

The idea is to project the laser lines from the laser leveler to the wall facing the robot. At the same time, the camera mounted on the mobile robot will be able to view the laser lines on the surface of the wall. Then the image will be captured by the camera that contains the picture of the wall with the projected laser lines. The lines will not be deflected/deviated if the surface of the wall is even. If the lines are broken or deviated, it is an indication of non-compliance to the surface wall evenness criteria.

When measuring the wall, the robot navigates around by using the proximity sensors to slide left to be while maintaining its front to be parallel with the wall. This sliding motion is only possible by using the Mecanum wheels arrangement using the four DC motors driving the wheels. The sliding motion is shown in Fig. 6 and the motion of the robot inside a rectangular-shaped room is shown in Fig. 7. The robot in Fig. 7 is facing the wall on the right side. In short, the robot will automatically navigate around a rectangular-shaped room and stop evaluation once it reaches the fourth corner (start position).

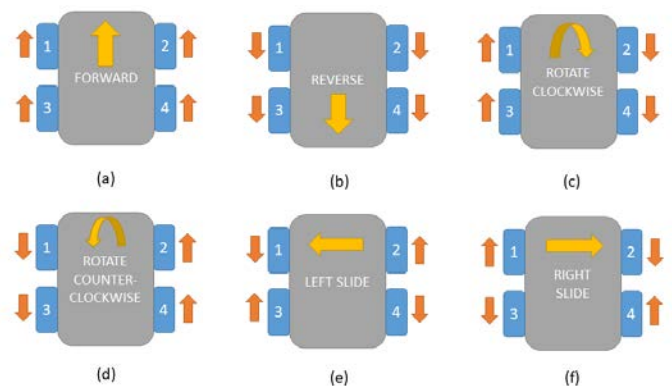


Fig. 6. Illustration of Mecanum Wheel Motions.

The Mecanum wheel motions (top view) in Fig. 6 shows the six different motions used for the mobile robot. The wheels are labeled as 1, 2, 3 and 4. With the right combination, different motions can be realized. The basic motions labeled as (a), (b), (c) and (d) shows the forward, reverse, rotate clockwise and rotate counter-clockwise motions of the mobile robot base. The other two motions, (e) and (f) are the sliding motions, in which (e) is left-slide motion while (f) is right-slide motion. Although the Mecanum wheels allow a lot more motions such as diagonal motions, the six motions in Fig. 6 is sufficient for the quality assessment mobile robot.

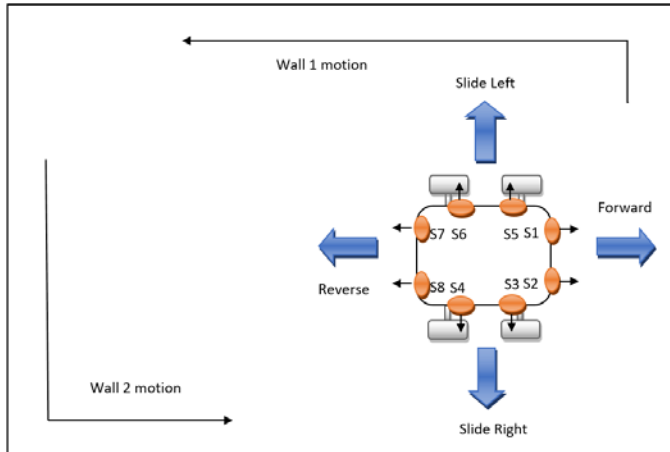


Fig. 7. Illustration of Sliding Motion during Wall Assessment.

The motion of the robot in the rectangular shaped room in Fig. 7, is performed by using the proximity sensors, for example, for the sliding left motion, sensors S1 and S2 will be used to follow the wall, while sensors S5 and S6 will be used to detect the first corner (top right in Fig. 7). After arriving at the corner, the robot will rotate itself counter-clockwise until it sensors the wall by using sensors S1 and S2. After that, it will perform the sliding left motion until it reaches the wall corner, completing the Wall 1 motion in Fig. 7. Similarly, Wall 2 motion will be performed after Wall 1 motion. During the sliding motion, the robot will stop momentarily, to acquire the images of the wall to be processed later. This is because if the robot acquires images while moving, the image might be blurred and causes difficulty for image processing. For a wall motion, there could be several images acquired, depending on the length of the wall. The distance between the robot and the wall is set at 60cm. If the distance is too short, the images captured will not cover enough area of the lower wall.

The image processing that needs to be done on the captured camera image, is HSL color filtering, Grayscale Conversion, Thresholding. By defining the range of acceptable color for the Red Laser line using HSL, the processing of the image will produce a black and white image. The white connected dots in the image will show the laser lines while the other colors will be turned to black.

Next, further image processing can be done, such as convex hull identification from blob, which will produce coordinates of the edges of the hull covering the vertical and horizontal laser line. The next step is to draw a red line from

the top edge to the bottom edge to compare with the white lines of the laser leveler. The details of all these processes will be explained and shown in Section IV.

IV. RESULTS AND ANALYSIS

For the site-testing of the mobile robot, the images are acquired from a finished housing area in Pulau Sebang, Melaka in September 2021. Additionally, the Skyworld Quality Center was also visited for another site-test for the mobile robot, in October 2021. The process for the image processing on the acquired images is shown in Fig. 8.

The results of image acquisition and processing are shown in Fig. 9.

The image in Fig. 9(a) shows a clear red-line projected image captured by the camera on a white-colored wall surface at the first site test, a house in a residential area in Pulau Sebang. The images acquired from the second site test at Skyworld Quality Centre are shown next in Fig. 9(d). This time the color of the wall is not white, but light yellow and the wall is uneven. Nevertheless, the red lines are still seen in the images. The sample image in Fig. 9(d) shows a slightly deflected vertical line.

The images in Fig. 9(a) are then color-filtered using Hue, Saturation, and Luminance (HSL) filtering from AForge library in Visual Studio (C #Net). The values used for HSL is 320 – 50 for Hue, 40%-100% for saturation and 40%-100% for luminance. These values are suitable for the red lines from the laser leveler. The results of the HSL filtering are shown in Fig. 9(b). For the image in Fig. 9(d), the same process is applied and the result image is shown in Fig. 9(e).

It can be seen in Fig. 9(b) and Fig. 9(e), the red lines were successfully seen and other backgrounds were eliminated. The next process is the Grayscale filtering and the Thresholding to ensure the image consists of only black and white colors for the next process to take place. For grayscale filter, the parameters are the values suggested from the AForge Grayscale filter library (0.2125, 0.7154, 0.0721). Grayscale filtering results are shown in Fig. 9(c) and Fig. 9(f).

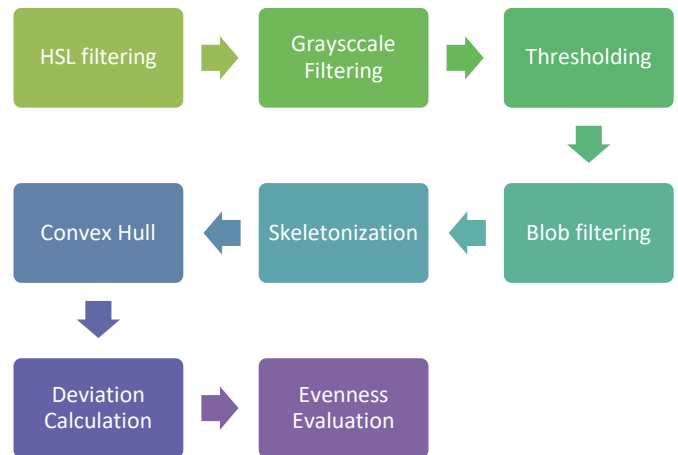


Fig. 8. Image Processing Method for the Wall Evenness Quality Assessment.

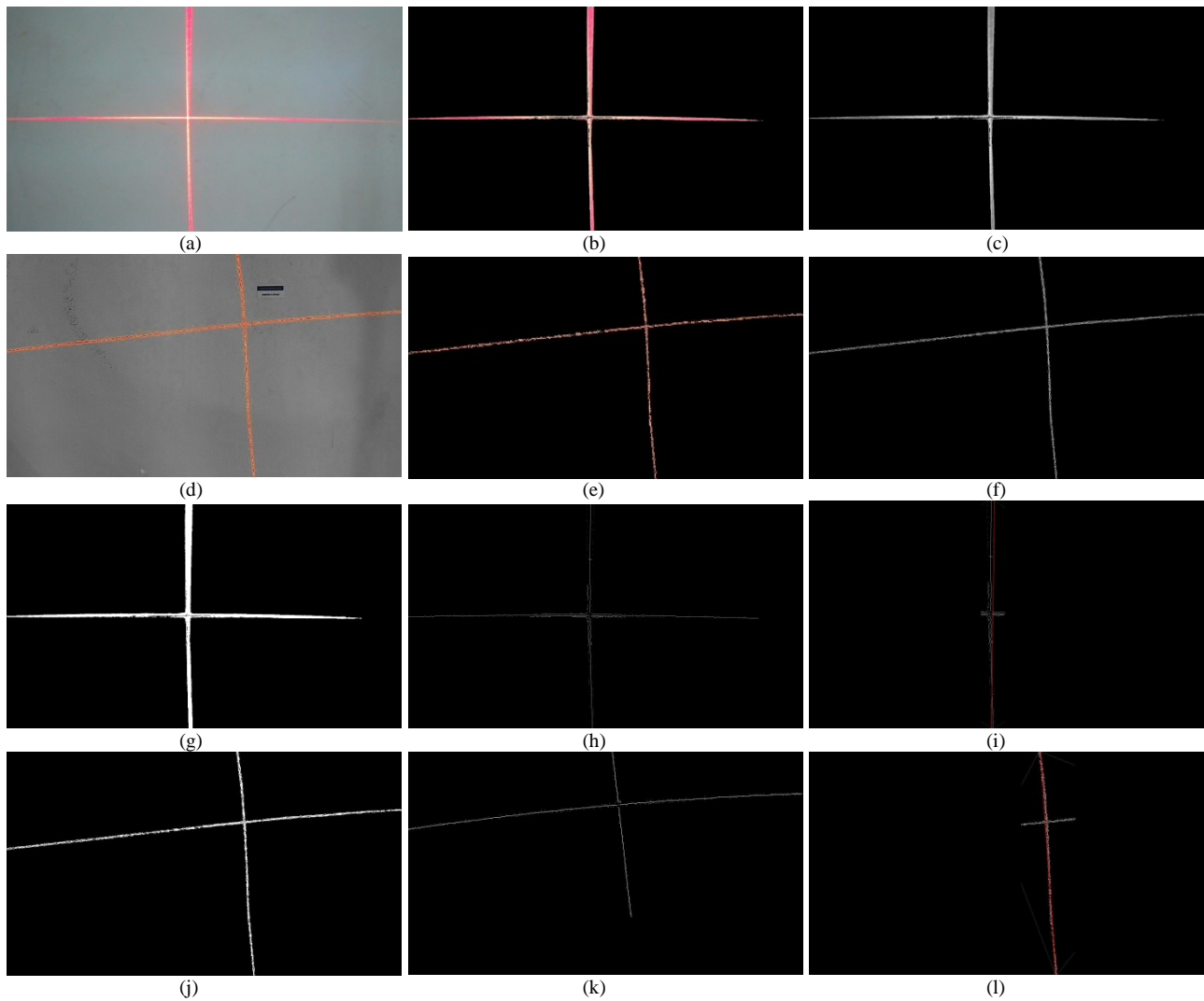


Fig. 9. Image Processing Results; (a) Image Acquired for Even Wall, (b) HSL Filtering on Even Wall, (c) Grayscale Filtering on Even Wall, (d) Image Acquired for Uneven Wall, (e) HSL Filtering on Uneven Wall, (f) Grayscale Filtering on Uneven Wall, (g) Thresholding Result on Even Wall, (h) Convex Hull of Even Wall, (i) Connected Edge Lines for Pixel Deviation of Even Wall, (j) Thresholding Result on Uneven Wall, (k) Convex Hull of Uneven Wall, (l) Connected Edge Lines for Pixel Deviation of Uneven Wall.

The next process after grayscale filtering is thresholding. For thresholding, the value set to allow the line to be converted to white color is 80. Values of grayscale below 80 will be turned to black color. This is to ensure that the Blob filtering process can take place, as it only receives black and white images. Thresholding results are shown in Fig. 9(g) and Fig. 9(j).

After thresholding, blob filtering is then applied, and then skeletonization. This is because blob filtering will extract blob sizes which are more than a certain width and height, in this case it is set at a width of 70 and height of 70. Any blobs smaller than this size will be neglected because it may consist of small errors which are not from the red line processed. Skeletonization is later applied to ensure that the line is thin for the next process.

Once skeletonization has been completed, the convex hull determination is performed to detect the top, bottom, most-left and most-right points that cover the blob. This is to ensure that

the lines are all in one blob. The convex hull results are shown in Fig. 9(h) and Fig. 9(k). It can be seen that in convex hull draws the limits of the up, bottom, left and right edges of the lines. These edge points can be used as reference for the deviation of the line to determine evenness.

The next process is to draw a reference line from the top-most and bottom-most points of the convex hull. This is done by using a different color, to differentiate between the projected laser line (processed) and the reference line. The reference line is drawn in red color, while the processed lines are in white. The results are shown in Fig. 9(i) and Fig. 9(l).

After drawing the red line, it can be seen that the uneven wall from Fig. 9(l) has (white) lines deviating from the reference line. From Fig. 9(i) and Fig. 9(l), the deviation from the drawn red reference line can be calculated by using (1);

$$D_{wr} = \frac{\sum(P_{wi} - P_{ri})}{i_{wr}} \quad (1)$$

Where D_{wr} represents the indicator value for deflection between white and red dots, P_w represents the coordinates of the white dot, P_r represents the coordinates of the red dot and i_{wr} represents the number of white and red dots used in the process. If this indicator value is large, then it means that there are a lot of deflections of the white red with the red line. This can be used to classify that the wall is uneven. The distance between the camera and the wall set is 800mm. The resolution of the image captured is 1920 x 1080. The results of the tests for the uneven and even wall images are shown in Table II. The values are the average deviation of pixels from the reference line. The results obtained for six images, and three images are uneven walls.

TABLE II. AVERAGE PIXEL DEVIATION FOR EVEN AND UNEVEN WALL

Criteria	Image	Even Wall Image	Uneven Wall Image
Deviation (pixel)	1	13.39	53.18
	2	10.99	25.98
	3	11.36	30.57

Based on the results in Table II, the Even wall results shows that pixel deviation is lower than 15. The uneven wall has higher values of more than 20 for the images captured. The proposed method has shown that the deviation of the line is quantifiable and can be used to differentiate between even wall and uneven wall surface. At present, the deviations are measured for the vertical lines, but could be extended to horizontal lines in the future.

V. CONCLUSION

This research proposed a new method of assessing the wall surface evenness for quality assessment of internal building works. This approach uses vision-based method by capturing the images of the wall with the projected laser lines. The robot captures images of the wall in front while sliding to the left and pausing during capturing images to ensure the images are stable. The motion was implemented using four Mecanum wheels. Results show that the pixel deviation values can be used as an indicator to distinguish between even wall and uneven wall surface. The uniqueness of the proposed method is the use of fast image processing technique that does not use training data sets and the use of cost-effective devices such as laser-leveler and standard High Definition USB cameras available in the market instead of high cost sensors [10].

At present, the results shown are from concrete walls with a single color. Future work includes the testing of mixed wall colors and different wall surface types such as wood, foam or other types of materials. Other criteria should also be investigated, such as wall hollowness, cracks and damages.

ACKNOWLEDGMENT

Authors would like to acknowledge Construction Research Institute of Malaysia (CREAM) and Universiti Teknikal Malaysia Melaka for this collaborative research project.

REFERENCES

[1] J. S. Albus, "Trip Report: Japanese Progress in Robotics for Construction" Elsevier Science Publishers, B.V (North-Holland), 1986.

[2] D. Wallace, Y. H. He, J. Chagas Vaz, L. Georgescu and P. Y. Oh, "Multimodal Teleoperation of Heterogeneous Robots within a Construction Environment," 2020 IEEE/RSJ International Conference on Intelligent Robots and Systems (IROS), 2020, pp. 2698-2705, doi: 10.1109/IROS45743.2020.9340688.

[3] J. Sustarevas, K. X. Benjamin Tan, D. Gerber, R. Stuart-Smith and V. M. Pawar, "YouWasps: Towards Autonomous Multi-Robot Mobile Deposition for Construction," 2019 IEEE/RSJ International Conference on Intelligent Robots and Systems (IROS), 2019, pp. 2320-2327, doi: 10.1109/IROS40897.2019.8967766.

[4] E. Asadi, B. Li and I. Chen, "Pictobot: A Cooperative Painting Robot for Interior Finishing of Industrial Developments," in IEEE Robotics & Automation Magazine, vol. 25, no. 2, pp. 82-94, June 2018, doi: 10.1109/MRA.2018.2816972.

[5] N. Melenbrink, P. Michalatos, P. Kassabian and J. Werfel, "Using local force measurements to guide construction by distributed climbing robots," 2017 IEEE/RSJ International Conference on Intelligent Robots and Systems (IROS), 2017, pp. 4333-4340, doi: 10.1109/IROS.2017.8206298.

[6] C. Brosque, E. Galbally, O. Khatib and M. Fischer, "Human-Robot Collaboration in Construction: Opportunities and Challenges," 2020 International Congress on Human-Computer Interaction, Optimization and Robotic Applications (HORA), 2020, pp. 1-8, doi: 10.1109/HORA49412.2020.9152888.

[7] J. H. Lee, J. Park and B. Jang, "Design of Robot based Work Progress Monitoring System for the Building Construction Site," 2018 International Conference on Information and Communication Technology Convergence (ICTC), 2018, pp. 1420-1422, doi: 10.1109/ICTC.2018.8539444.

[8] M. A. V. J. Muthugala, M. Vega-Heredia, A. Vengadesh, G. Sriharsha and M. R. Elara, "Design of an Adhesion-Aware Façade Cleaning Robot," 2019 IEEE/RSJ International Conference on Intelligent Robots and Systems (IROS), 2019, pp. 1441-1447, doi: 10.1109/IROS40897.2019.8967978.

[9] M. Benndorf, T. Haenselmann, M. Garsch, N. Gebbeken, C.A. Mueller, T. Fromm, T. Luczynski, A. Birk, "Robotic Bridge Statics Assessment Within Strategic Flood Evacuation Planning using Low-Cost Sensors," 2017 IEEE International Symposium on Safety, Security and Rescue Robotics (SSRR), Shanghai, China, 2017.

[10] R.J. Yan, E. Kayacan, I.M. Chen, K.T. Lee "QuicaBot: Quality Inspection and Assessment Robot," IEEE Trans. on Automation Science and Engineering, vol. 16, no. 2, pp. 506-517, 2019.

[11] A. Sioma, "Automated Control of Surface Defects on Ceramic Tiles Using 3D Image Analysis", MDPI Journals - Materials, Vol. 13, No. 1250, pp. 1-13, 2020.

[12] X. Li, L. Shen, Z. Ming, C. Zhang, H. Jiang, "Laser-based on-line machine vision detection for longitudinal rip of conveyor belt", Optics, Elsevier, pp.360-369, 2018.

[13] H. Yang, Y. Jiang, F. Deng, Y. Mu, Y. Zhong, D. Jiao, "Detection of Bubble Defects on Tire Surface Based on Line Laser and Machine Vision", MDPI Journals - Processes, Vol 10. No. 2, pp. 1-14, 2022.

[14] D.L. Escogido, A.D. Luca, "2-D High Precision Laser Sensor for Detecting Small Defects in PCBs", 2012 9th International Conference on Electrical Engineering, Computing Science and Automatic Control (CCE), 2012.

[15] J.R.Araújo, A.G. Díaz, "Automated in-Line Defect Classification and Localization in Solar Cells for Laser-Based Repair", -2014 IEEE 23rd International Symposium on Industrial Electronics (ISIE), 2014.

[16] D.G. Woo, J.K. Oh, C.H. Lee, S.H. Lee, S.H. Jung, "Development of a Multi-Line Laser Sensor Based Robotic 3D Measurement System", 2011 11th International Conference on Control, Automation and Systems, pp. 1777-1782, 2011.

[17] T. Lei, H. Wang, P.Xiong, Y. Huang, H.Liu, "Laser Vision Detection Method for the Thermal Deformation of Tubesheet Welding", 2019 4th International Conference on Robotics and Automation Engineering, pp. 116-119, 2019.

[18] Z. Liu , S.Wu, Q. Wu, C. Quan, and Y. Ren," A Novel Stereo Vision Measurement System Using Both Line Scan Camera and Frame

- Camera”, IEEE Transactions on Instrumentation and Measurement, Vol. 68, No. 10, pp. 3563-3575, 2019.
- [19] S. Pasinetti, G.Sansoni, F. Docchio, “In-line monitoring of laser welding using a smart vision system”, 2018 Workshop on Metrology for Industry 4.0 and IoT, 2018, doi: 10.1109/METROI4.2018.8428332.
- [20] W. Xiuping, B. Ruilin, L. Ziteng, “Weld Seam Detection and Feature Extraction Based on Laser Vision,” Proceedings of the 33rd Chinese Control Conference, pp. 8249-8252, Nanjing, 2014, doi: 10.1109/ChiCC.2014.6896382.
- [21] Yuanyuan Zo, Shang Cai, Pengfei Li, Kezhu Zuo, “Features Extraction of Butt Joint for Tailored Blank Laser Welding Based on Three-line Stripe Laser Vision Sensor,” 2017 29th Chinese Control And Decision Conference (CCDC), pp. 7736-7739, Chongqing, China, 2017, doi: 10.1109/CCDC.2017.7978594.

The 4W Framework of the Online Social Community Model for Satisfying the Unmet Needs of Older Adults

Farhat Mahmoud Embarak¹, Nor Azman Ismail², Alhuseen Omar Alsayed³
Mohamed Bashir Buhalfaya⁴, Abdurrahman Abdulla Younes⁵, Blha Hassan Naser⁶
School of Computing, Faculty of Engineering, University Teknologi Malaysia (UTM), Johor Bahru, Malaysia^{1,2}
Deanship of Scientific Research, King Abdulaziz University, Jeddah 21589, Saudi Arabia³
Faculty of Information and Technology University of Ajdabiya, Ajdabiya, Libya^{1,4,5,6}

Abstract—Human's cherished and respectable desires could be fulfilled by social integration through interaction with their friends and families. These kinds of interactions are critical for the elderly, particularly for someone who has retired. Online social communities could assist them and offer a beneficial impact on the elderly. However, because the elderly people are hesitant to use new technology, researchers have attempted to integrate specially built social networking applications into simple user-interface gadgets for the elderly through the context aware systems. A proper understanding amongst the aged and the supporting community people is needed for optimal execution of the platform. The study presents a 4W framework (Who, What, Where, When) to effectively comprehend and portray the online social interaction community model's application in assisting the elderly in satisfying their unmet needs, as well as to improve the system's efficiency in addressing the elderly's unfulfilled demands. It is essential to discover what the users are keen on and provide a chance for the community group to take good decisions by utilizing the insights gained from these events.

Keywords—Online social community; elderly's unmet needs; 4w framework; elderly's requirements

I. INTRODUCTION

Nowadays, digital media has grown ubiquitous and are easier to utilise through tablets, internet as well as the smartphones. As so much information, services, goods, and people are most often exclusively available on the internet, staying online has now become more attractive [1]. Furthermore, an age group is not a fixed category. Several elder people have grown up with digital media and they do not need to stop even when they reach the age of 65 [2]. Since they might lose some links with their co-workers when they retire, they gain more free time to spend with their families and friends. However, when it comes to their digital media requirements and preferences, elderly people are the least studied age groups, and researchers know only little about the differences in their use [3]. Through online support platforms and other means, the resources streaming through social media could assist both the younger and older persons.

People become much more sensitive when they grow old and feel socially isolated. This is primarily because of various factors like residing alone or in rural areas, as well as health factors such as health issues, mobility issues, and so on [4]. Elderly people suffer both physically and mentally when they are left alone. It is also vital to maintain the elderly as active and make them participate in society, both cognitively and

physically. Social networks could provide emotional support to elderly individuals, which is important since social integration is necessary to meet basic human requirements like being connected and loved [5]. Communication and interchange with friends and other senior people especially family members could aid in the development of social connectivity feelings and the expansion of social relationships.

The digital interactions with their family and friends provide a lot of social support that are observed to be especially essential for older persons with mobility issues [6]. This was also evident in their daily actions, like finding quicker ways to maintain their residences and preparing healthier dishes [7]. Despite the challenges of a complicated user interface and an abundance of data, social media platforms such as Twitter, Facebook, Pinterest, Google Hangouts, and Instagram have recently seen greater adoption rates amongst the elderly [8]. Online Social Networks have expanded options for social interaction and collaboration, allowing users to communicate and collaborate with others as part of a continuous social dialogue. Computerized systems must have a better knowledge of the situations in which they offer services or activities, and they must be able to adjust correspondingly. It could be accomplished through context awareness.

In this paper, a 4W framework that offers a general view of the online supporting community model is presented. The framework gives a comprehensive overview of the concepts in the elderly supporting community and serves as a foundation for defining the elderly's needs. The 4Ws mapping data could be used to develop national emergency response plans, as well as to detect discrepancies in supply, human resources, geographic and target group coverage, and technical competence. Participating groups can also utilize it to manage their fund raising and programming efforts. This framework enables us to observe the model's fundamental requirements, review existing ways towards geriatric support, and identify emerging research topics in this sector. It may be applied onto any project under this area and is used for analysis.

The rest of the sections are summarized as follows. Section II explains the recent literature works of supporting frameworks for the elderly people, Section III illustrates the proposed online social community module with components and the tasks performed by each components. Section IV illustrates the application of 4W framework on the proposed online social community model. Section V provides the evaluation of the proposed model through User journey map

followed by its results and finally, section VI concludes the paper.

II. RELATED WORK

This section gives a background review in the field of using 4W in the social media. Related issues and problems that have been solved in previous works are reported. A context aware system for business-to-government (B2G) information exchange in the container shipping domain was developed in [9] for identifying what environmental components are the significant context, what are the required elements to recognize and adjust to context, and what are the rules for the adapting the system under various circumstances. The highly organized manner in which the elements and criteria are formed from insight into context gives a technique for dealing with the tremendous complexity of the context in this approach along with ambiguity elimination.

Another model of a context aware approach was presented by Hossain et al. [10] for supporting the elderly for entertainment. It covers the entertainment demands of the aged people and allows multiple residents (e.g., caregivers and old adults) to connect multiple media sources in either a formal and informal manner so as to improve the quality of their experience of life in diverse circumstances. The model aids in the development of entertainment systems and services for the aged people, allowing them to more effectively address the issues that arise from their ability to live independently, happily, and actively.

For a persistent Elderly Homecare, Pung et al. [11] developed a Context-Aware Middleware framework for supporting the elderly. It assists through designing and implementing a variety of geriatric home healthcare activities, including location-based emergency response, patient monitoring, unusual daily task detection, persistent accessing of health data, and social networking. This approach has a high level of context query processing efficiency and activity recognition accuracy. However, it confronts challenges in dealing with enormous amounts of data from various sources.

Another platform presented in context aware filed called the OCare Platform to support for caring the persons in independent living facilities. This conceptual, data-driven,

cloud-based back-end platform supports people to live independently through providing residents and their informal caretakers with information and knowledge-based services. This system has the potential to offer a realistic working environment and adapt considerably and more quickly [12].

III. ONLINE SOCIAL COMMUNITY MODEL

In this stage, model components were designed according to the requirement of users. The proposed architecture consists of six core components based on requirements analysis [13]. More detailed description on these components is given in Section 4B. However, the complete system architecture of the proposed model which includes the online social interaction, unmet needs interaction, profile management, recommendation component and unmet needs plan is represented in Fig. 1.

A. The Concept Groups

The suggested framework's core assumption is an online social community model for elderly Libyans assistance. The broad perspective of the 4W framework is formed by the concept groupings Who, Where, What, and When. The methods that follow to build this framework is similar to that used to build Zachman architecture [14] and Angelov and Geffen models [15]. However, according to Abowd et al. [16], the definition of context is given as, "Any information that can be used to characterize the situation of an entity", where "an entity can be a person, place, or object that is considered relevant to the interaction between a user and an application, including the user and applications themselves".

This definition outlines four distinct kinds of elderly supporting concepts that could be modeled. They are: Where concept (location context); Who concept (Identity context); What concept (Activity context); and When concept (Time context). Similarly, the definition of the online community by Rheingold (1993) which is "[online] Communities are social aggregations that emerge from the Net when enough people carry on those public discussions long enough, with sufficient human feeling, to form Webs of personal relationships in cyberspace" is used to build the 4W framework of the online social community process for elderly Libyans. The next section details how these four concepts can be represented by the process of model components.

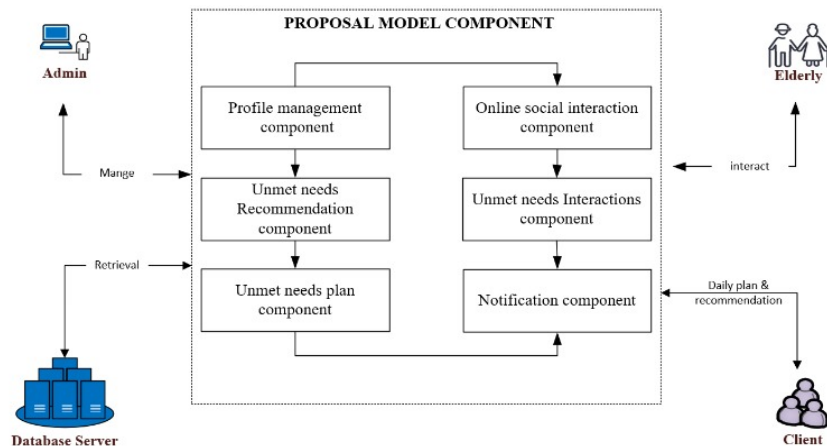


Fig. 1. The Online Social Community Model of Elderly Libyans.

TABLE I. THE TASKS THAT RELATED TO EACH COMPONENTS' FUNCTION

Code	Task	Descriptions	Component
Task 1:	Build your private network community with name (your name care community)	Registering in the community, creating community groups under the name "your name care community" and inviting your family members or friends to this community	Online Social interaction
Task 2:	Provide a comprehensive assessment of the ability to perform activities of daily living and health status	Evaluating your ability to perform activities of daily living and health status.	Profile Management
Task 3:	Fulfill your daily unmet need "looking after your home"	Interacting your need "looking after home" with social group network to share interaction requests.	Interaction Unmet Needs
Task 4:	Generate a plan of your frequently unmet daily needs for this week.	Creating plan of list of your unmet needs for the current week with an optimal balance of work and care duties of your community members.	Unmet needs Plan
Task 5:	Find a way to get emergency support from group members	Sending an emergency post to a social group members or to a specific recommended member.	Online Social
Task 6:	Accept any recommendations about your unmet daily need "looking after your home" sent by community group members.	Posting an acceptance on the advice or suggestions about your unmet daily need "looking after your home".	Unmet needs recommendation
Task 7:	Track your unmet need "looking after your home" and look up activated members who will accept.	Tracking your unmet need "looking after your home" requests and the state of activate group members.	Interaction Unmet Needs

B. Corresponding Model Components

The 4W Framework process in the online social community is modelled by representing the model components and applying a set of tasks related to each components' function. However, the tasks represent the components that frame the model as shown in Table I.

IV. THE 4W ONLINE SOCIAL COMMUNITY FRAMEWORK PROCESS

The 4W online social community framework process is shown in Fig. 2. Each concept is associated with their corresponding components which is represented by the task. The 'what' and 'who' concepts corresponds to all of the seven tasks. The 'What' concept represents the activity contexts that responses the question what is happening in the circumstances;

in the case of model, it represents the activity that is going to be done by elderlies. The 'Who' concept illustrates the identity contexts that responses the question who is the individual, which is elderly Libyans or their community members. The 'Where' concept corresponds the location contexts that responses the question of where the elderly is located or where the task is going to be completed. For instance, tasks such as fulfilling their unmet needs, generating the daily unmet need plans, sending the emergency report and tracking the request with where concept will represent the place that the task starts or completest in it. 'When' concept corresponds to tasks such as building the private network, fulfilling the unmet needs request and tracking the request (represents the time contexts that responses the question when the task defining the circumstances is occurring to record when the task was).

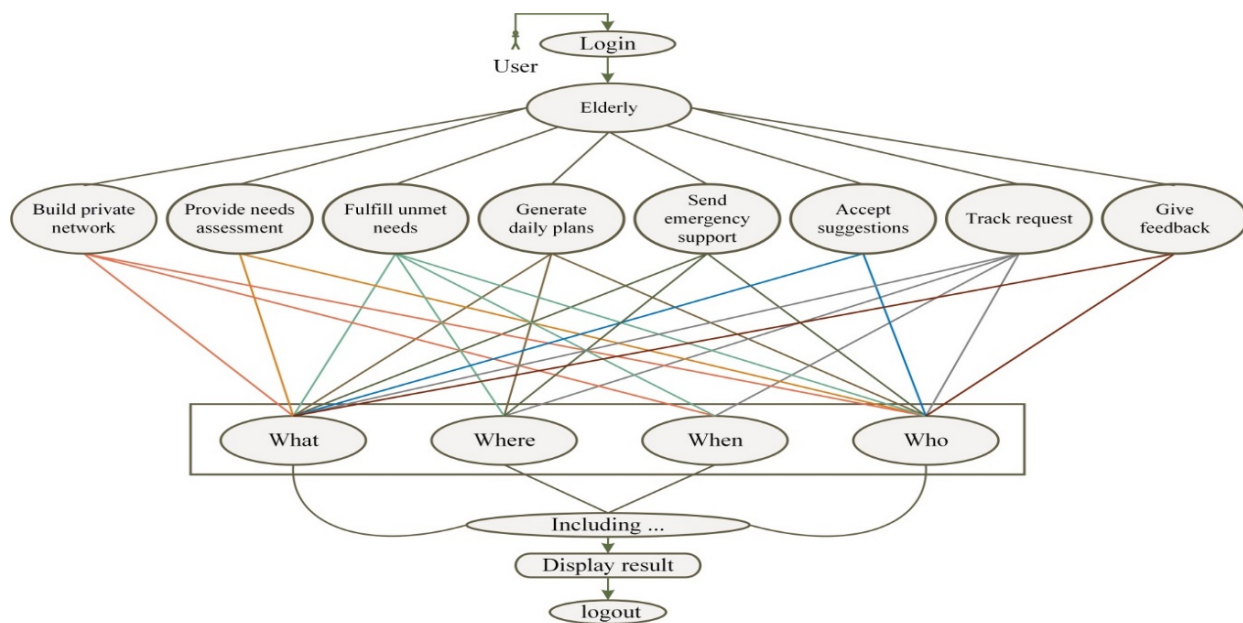


Fig. 2. The 4W Online Social Community Framework Process.

The online social interaction component is related to the task one and task five. It creates the confidential social network community set up for the elderly as well as the service expert volunteers for helping the elderly Libyans. It also sends an emergency post to social group members or to a specific recommended member in case of seeking emergency support. The profile management component is related to task two. It provides a comprehensive assessment of their ability to perform activities of daily living and their health status. It maintains the elderly's as well as the caretaker's profile, and thereby it regulates and keeps the elderly profile updated. The unmet needs interaction component is related to task three and task seven. It develops a brief layout of the list of unmet needs and frequent sending of daily need requests, it also keeps trace of the status of the recent unmet needs and the existence of currently active supporting community members, and promotes responding to the elderly's request. The unmet needs plan component is related to task four. It creates a plan of list of unmet needs under every time slot with an optimal balance of work and care duties of the community members. The unmet needs recommendation component is related to task six. It corresponds to the elderly requirements towards the supporting services. It also endorses a suitable group or an individual to assist the elders in satisfying their unmet requirements. It posts an acceptance on the advice or suggestions about elderly Libyans' unmet daily needs.

In this section, the process of 4W online social community framework is elaborated in a detailed manner. The four groups of concepts which are who concept, where concept, what concept and when concept describe with the online social community component representation.

A. The Who Group of Concepts

The 'Who' concepts describe the actors who participate in a community framework for supporting the elderly people towards fulfilling their unmet needs as it can be seen in Fig. 3. The members in 'who' concept would be a family member, relatives, neighbours, or social supporting community members.

In 4W online social community framework, the 'Who' concept represents many entities based on the task which is performed. In case of building the private network, the 'Who' concept represents the elderly who request for the unmet needs and the private network members who are going to satisfy these needs. Only the group community members who accept to fulfil the elderly needs will represent 'Who' concept. It also represents the member who accepts the elderly person's daily needs plan to satisfy their unmet need request, the member who supports the elderly people when they seek any emergency support. Fig. 3 shows all actors who represent the 'Who' concept in the 4W online social community framework.

B. The Where Group of Concepts

The 'Where' group of concepts describe the place or location from where the requests arise as shown in Fig. 4. The place could be either from their residence, in private or public place, schools, or markets. It focusses on the location from where the unmet need request arises, the location of the elderly

and the location of their activity in order to generate the unmet needs plan, elderly coordinates to support the elderly in requirement of emergency support. Fig. 4 describes the details of 'Where' concept in the 4W online social community framework.

C. The What Group of Concepts

The 'What' group of concepts describes what the elderly's request about, what the elderly people exactly need in their request or what are the contents of the daily unmet needs required to be fulfilled. The unmet needs of elderly Libyans come from the geriatric Assessment or the group community member's suggestions based on comprehensive assessment. The nature of those needs is what represents the 'What' concept which includes building community group, needs assessment and unmet needs request, daily plan generation, emergency support, and accepting suggestions. Fig. 5 details the description of 'What' concept in 4W online social community framework.

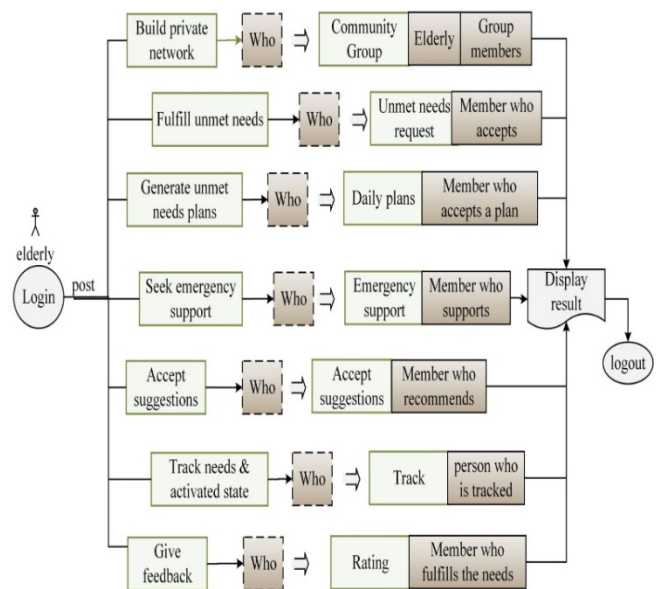


Fig. 3. Detailed Who Concept.

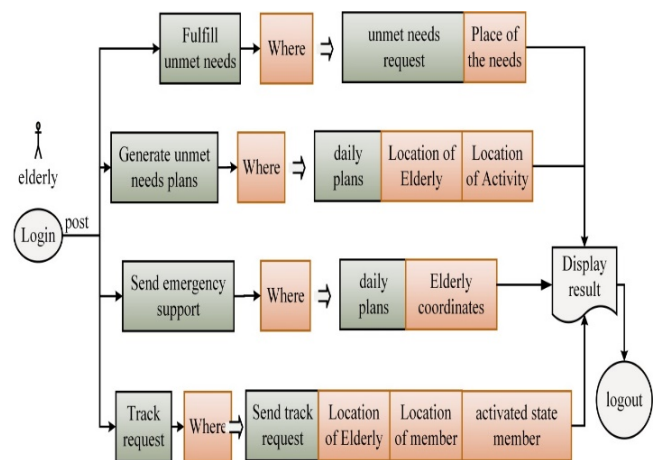


Fig. 4. Detailed Where Concept.

V. EVALUATION USING USER JOURNEY MAP

In order to visualize the user’s experience towards the developed model, the user journey map is developed. User journey mapping was chosen as a method for this analytical study as it gives the understanding of the positive and negative feelings that the user was experiencing while completing their journey. In this section, one user journey map for multiuser was created to understand how users would interact with the prototype. It also reflects the interaction between the user and the interface. This allows for further improvement of the prototype and makes the design better suit the elderly Libyans. The journey maps defined in this section includes four categories as “Pain point”, “Action”, “Touchpoint”, and “Emotion”. “Pain points” refers to burdens and obstacles which prevent a user from using a feature. “Action” is how the user interacts with the channel and what actions they undertake. “Touchpoint” refers to places that customers can interact within the channel. “Emotion” refers to how customers feel during each phase of the journey. Table I shows the tasks were assigned for each user when they drew their journey map. However, to empathize with the user experience and understand the issues they are facing, only four personas were considered in this study to draw one journey map.

A. User Journey Map Results

The results of applying a journey map based on participants’ emotions and actions while they were accomplishing their tasks are discussed below. This highlights the importance of graphic design, attitudinal behaviour, and control and emotional issues in the interface design process for elderly people. Fig. 7 depicts the outcome of the journey map of four elderly people with eight steps based on their tasks. It displays their emotions through each step.

The Four personas are created based on randomly chosen but with made-up identity information such as names, ages, gender, and what they like or dislike with different perspectives. Creating personas allows the researcher to understand user emotions with the interface. Therefore, the final interface would be more efficient and user-friendly.

In general, elderly Libyans in most cases felt comfortable and confident while using the prototype interface because of the overall design and the information layout. Also, they feel more comfortable when the map window is kept at the centre of the user. In contrast, they were disappointed in waiting for group members’ acceptance which led to providing some clues to make improvements in the design interface, for instance, notifying the users that they are in a waiting status.

From the user journey map, it is observed that the users feel comfortable and satisfied with the social interaction component of the model as it simplifies the process of interaction and login into the account and inviting their relatives and friends to become members of their group community for fulfilling their unmet needs.

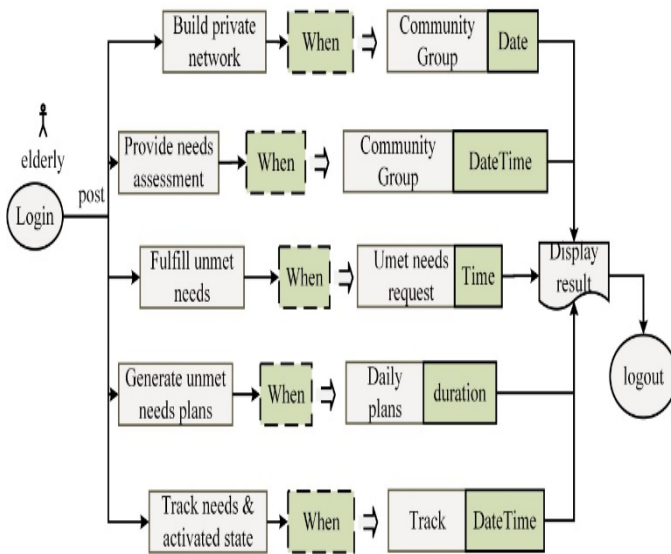


Fig. 5. Detailed When Concept.

D. The When Group of Concepts

The ‘when’ group of concepts represents the time context that responses the question when the event defining the circumstances is occurring. In 4W online social community framework, the ‘when’ group represents the duration of the daily needs plan, at which time and date the elderly information are traced, when to generate the unmet daily needs plan. It also focuses on at which time the unmet daily needs are fulfilled and when to provide the comprehensive assessment of the needs. Fig. 6 shows detailed process of ‘When’ concept in 4W online social community framework.

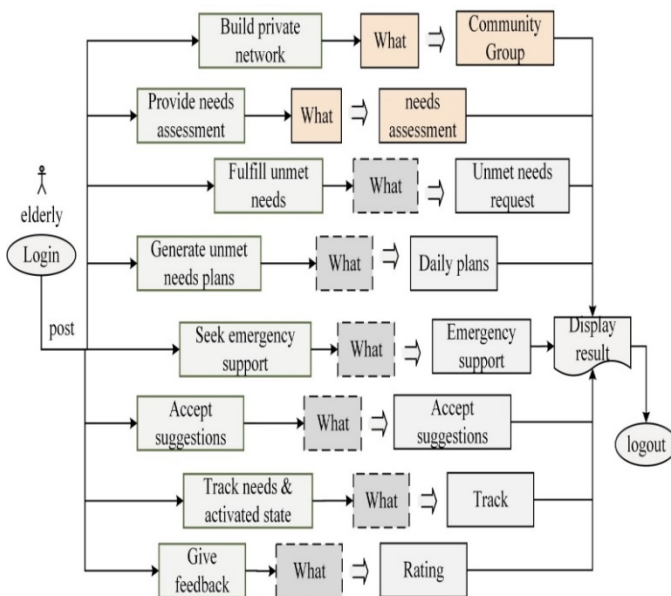


Fig. 6. Detailed What Concept.

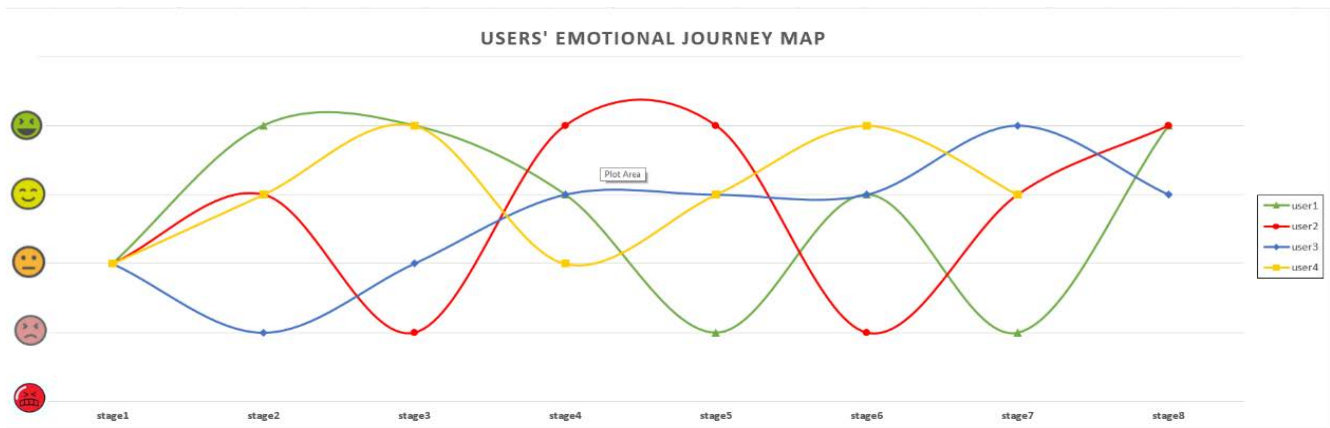


Fig. 7. User Journey Map Outcome.

Researcher: "Are you able to send invitations?"

User: "Yes, I'm trying. I'm attempting to click on the image but I am unable to do so. It's lame. It would be good if it was a button for me because I am a visual person. But for me it is ok, it's clear I can overcome it."

According to the findings, the interface designing should be carefully developed to address consumers' concerns. It's critical to provide a "home" section for elderlies to return to when they feel insecure or misplaced in order to promote a sense of confidence. This establishes the user satisfaction toward the interface of prototype.

Researcher: "So, which one do you prefer?"

User: "I prefer a simple navigation system. I'd go home because everything is there".

Returning to the home page during doing the tasks gives the elderly a sense of safety and security, reassuring them that they are in the correct place. When elderlies couldn't locate what they were doing or searching for, they all opted to return to the main page. It was comfortable for users to return "home."

One of the participants said, "I'd probably go to the main page because it's crucial."

The participants feel very comfortable when they discover what they're accomplishing of tasks on the platform. They wish to use a single working window with lists in order to control window proliferation. It would be more helpful for them if the tool tip pop-ups are provided while the elderly move the pointer towards the key elements of the graphical user interface. Hence, they could get easy access to the task elements of the interface design.

Researcher: "How do you feel mentally, say do the icons of choices in front of you (in the header bar region) make you feel comfortable?"

User: "I feel better instead of searching; I can access many options with this bar."

Researcher: "Where can you usually obtain a list of all available members?"

User: "So maybe back to Home... in the profile of members or friends. I will go to the profile. No... No..., Here... in the member icon on the home page. Why there is no direct link get me here?"

In some cases, the elderly feel quietly disappointed in waiting for group members' acceptance to join and they feel difficulty in inviting the community members to their group. Once they get the response, they feel much happy and excited for the attendance of the supporting community member.

Researcher: "Why are you looking not comfortable?"

User: "Ummm... they have to do something to show we're in a waiting status." Moreover, while creating the list of unmet needs plan, they feel confused of where to slide.

Researcher: "So, what prompted you to return home?"

User: "I have no idea... I just felt it should be a separate part; however, it would've been preferable to keep with unmet demands down the bottom and see if it generates any plans."

Researcher: "How are you feeling right now?"

User: "A little sad."

Researcher: "So, you start from the Home page. Isn't it?"

User: "I'm not sure what they're saying, but there's something."

Also, participants felt unsatisfied to read long text rather visual images. Elderly Libyans respond more quickly to images. One of them expressed the following: "It appears to be in good working order. However, I'm sure there would be more information available on this. I love to work with pictures just because I am a visual person." Besides that, there was no quick access heading bar that allows users to quickly navigate between module components without getting lost.

VI. DISCUSSION

This designed model includes the reorganization of tasks, a reorganization of data entry windows, and a reorganization of asset groups. The user could also perform the real task of creating the 4W grid using this prototype. The design prototype contains two side panes, left and right pane. The left pane contains the group details and the right pane contains the

details regarding the group members as well as the group recommendations. And, the task pane is available at the centre of the window that switches among the various tabs like recommendations and unmet need plans.

The created website model matched the users' desires and functionality, as per the user task analysis. Users had easy access to the web page and navigation. The majority of users were delighted with the webpage usability characteristics, such as navigation, accessibility, attractiveness and design consistency. The findings demonstrate that the proposed design process efficiently fulfils the webpage accessibility and functionality objectives.

VII. CONCLUSION

In this paper, the 4W framework of online supporting community model for supporting the elderly towards satisfying their unmet needs is presented. It assists in determining what characteristics of model elements could be upgraded and what new opportunities could be introduced to the supporting community model. From the current design, the participants found that most of the tasks are easy to access and apply. The created platform model matched the users' desires and functionality, as per the user task analysis. Elderlies had easy access to the web page and navigation. The majority of elderly users were delighted with the webpage usability characteristics, such as navigation, accessibility, attractiveness and design consistency. The findings demonstrate that the proposed design process efficiently fulfils the webpage accessibility and functionality objectives of the user.

REFERENCES

- [1] Liberatore, E. Bowkett, C. J. MacLeod, E. Spurr, and N. Longnecker, "Social media as a platform for a citizen science community of practice," *Citizen Science: Theory and Practice*, vol. 3, no. 1, 2018.
- [2] A. Quan-Haase, G. Y. Mo, and B. Wellman, "Connected seniors: How older adults in East York exchange social support online and offline," *Information, Communication & Society*, vol. 20, no. 7, pp. 967–983, 2017.
- [3] S. J. Czaja, "Long-term care services and support systems for older adults: The role of technology", *American Psychologist*, vol. 71, no. 4, p. 294, 2016.
- [4] F. Embarak, N. A. Ismail, and S. Othman, "A systematic literature review: the role of assistive technology in supporting elderly social interaction with their online community," *Journal of Ambient Intelligence and Humanized Computing*, vol. 12, no. 7, pp. 7427–7440, 2021.
- [5] F. Boll and P. Brune, "Online support for the elderly—why service and social network platforms should be integrated," *Procedia Computer Science*, vol. 98, pp. 395–400, 2016.
- [6] S. Willard, G. Cremers, Y. P. Man, E. van Rossum, M. Spreeuwenberg, and L. de Witte, "Development and testing of an online community care platform for frail older adults in the Netherlands: a user-centred design," *BMC geriatrics*, vol. 18, no. 1, pp. 1–9, 2018.
- [7] S. Wongpun and S. Guha, "Elderly care recommendation system for informal caregivers using case-based reasoning," in *2017 IEEE 2nd Advanced Information Technology, Electronic and Automation Control Conference (IAEAC)*, 2017, pp. 548–552.
- [8] P. Spagnoletti, A. Resca, and G. Lee, "A design theory for digital platforms supporting online communities: a multiple case study," *Journal of Information technology*, vol. 30, no. 4, pp. 364–380, 2015.
- [9] S. van Engelenburg, M. Janssen, and B. Klievink, "Designing context-aware systems: a method for understanding and analysing context in practice," *Journal of logical and algebraic methods in programming*, vol. 103, pp. 79–104, 2019.
- [10] M. A. Hossain, A. Alamri, A. S. Almogren, S. A. Hossain, and J. Parra, "A framework for a context-aware elderly entertainment support system," *Sensors*, vol. 14, no. 6, pp. 10538–10561, 2014.
- [11] H. K. Pung et al., "Context-aware middleware for pervasive elderly homecare," *IEEE Journal on Selected Areas in communications*, vol. 27, no. 4, pp. 510–524, 2009.
- [12] E. Backer and B. W. Ritchie, "VFR travel: A viable market for tourism crisis and disaster recovery?," *International Journal of Tourism Research*, vol. 19, no. 4, pp. 400–411, 2017.
- [13] F. Embarak, Nor. Azman Ismail, Osama. R. Shahin, and Raed. N. Alabdali, "Design of autonomous online social community architecture for older adults," *Computers and Electrical Engineering*, vol. 100, p. 107900, May 2022, doi: 10.1016/J.COMPELECENG.2022.107900.
- [14] J. A. Zachman, "The zachman framework for enterprise architecture," *Primer for Enterprise Engineering and Manufacturing.[s.l]: Zachman International*, 2003.
- [15] S. Angelov and P. Grefen, "The 4W framework for B2B e-contracting," *International journal of networking and virtual organisations*, vol. 2, pp. 78–97, 2003.
- [16] G. D. Abowd, A. K. Dey, P. J. Brown, N. Davies, M. Smith, and P. Steggle, "Towards a better understanding of context and context-awareness," in *International symposium on handheld and ubiquitous computing*, 1999, pp. 304–307.

Bayesian Network Modelling for Improved Knowledge Management of the Expert Model in the Intelligent Tutoring System

Fatima-Zohra Hibbi, Otman Abdoun, El Khatir Haimoudi

Computer Science Department, Advanced Science and Technologies Laboratory
Polydisciplinary Faculty, Abdelmalek Essaadi University, Larache, Morocco

Abstract—The expert module is an essential part of the intelligent tutoring system. This module uses only declarative knowledge, excluding other types of domain knowledge: procedural and conditional. This elimination makes the expert module very delicate. To solve this issue, the authors propose to embed knowledge processing into the expert model. The contribution aims to empower the expert model via the fragmentation of the knowledge process into four categories: Analyzation, Application, Conceptualization, and Experimentation using the Bayesian Network method as an instrument for modelling expert systems in uncertain areas. According to the management of the expert system through a list of criteria, the expert module can suggest the correct type of knowledge and their following status.

Keywords—Smart tutoring system; expert model; knowledge processing; Bayesian network

I. INTRODUCTION

The accompaniment of students is a very important function in a learning situation, and its guarantee promotes motivation, attendance and the smooth running of all learning activities. For this purpose, the researchers tried to integrate techniques of Artificial Intelligence to propose accompanying mechanisms to guarantee the users' assiduity. Several contributions have focused on improving the intelligent tutoring system to make it more efficient, such as the integration of the two tutors: implicit and explicit, or each tutor uses his strategies and toolbox. The choice of one of the tutors is based on the following criteria: learner profile, effective feedback and learning progress data [1]; the latter needs Learning Analytics to collect the traces that learners leave behind and the uses these traces to improve learning [2].

The tutoring system is based during their interventions on the interconnection of these different models and especially the expert model. The knowledge representation in the expert module explores a set of strategies such as schemes, conditions, etc. The orientation of the system is based on the use of the knowledge of the expert module. Some systems use many techniques to formalize the expert module.

The CREAM system is one of the creation devices that offer the user to write specific objectives independently of the subjects. Thus, it uses various terminologies for the acquired skills [17].

However, the classical expert model in the previous intelligent tutoring system handles just declarative knowledge, which means the tutor intervenes in the activities in which the learner needs only definition and examples. This implies a lack of the taxonomy of the knowledge domain. To enhance the learner evaluation the authors [3] proposed a pedagogical solution based on the combination of three bits of knowledge: Declarative, procedural and conditional according to their status.

To enlighten the purpose of this work it would be noteworthy that the work presented in this paper is related to our previous work named: "Knowledge Management in the Expert Model of the Smart Tutoring System". In other words, the objective of the previous work was the management of the knowledge and subdivided into three categories: declarative, procedural and conditional knowledge in the expert model. To confirm this assumption, they investigate the efficiency of the proposed solution presented in the paper above. This article presents the experiments and results of knowledge processing using a Bayesian network technique and shows how the proposed approach can be applied and enhance the learner evaluation. To measure the performance of knowledge processing; they will use metrics, that evaluate the efficiency of each node dynamically in real-time.

The article is organized as follow: the second section describes the problem of the expert model in the smart tutoring system and clarifies the proposed solution; after that, the authors illustrate the construction of the Bayesian network for our model; then, section four details the conditional probability table. Last but not least, the implementation phase is subdivided into three subsections presented as bellow: the Bayesian network program, the results and the evaluation part. Finally, this article will be ended with a conclusion and future works.

II. RELATED WORKS

A. The Expert Model of Smart Tutoring System

An intelligent tutoring system (ITS) is a system that provides feedback and helps learners in their learning process such as remediation in a specific field like mathematics [4], or facilitating computer theory [5]. ITS contains four components; the first one is the interface model which can help the learner in a task via a learning environment; the second one is the learner model that has the personal information of the learner, their

preferences and characteristics; then, the instructional model which makes a decision about teaching method via a diagnostic process of the learner model; the last one is the expert model which has the representation of the declarative knowledge [3].

The expert module allows referencing an expert or a domain model. It provides a description of the knowledge or behaviours that represent the expertise in the domain [6]. It is a module where the main information is unrolled and will be taught. The best expert module is the most designed and appropriate [7]. This system must be performed in accordance with the knowledge that is available in the Learner module [8]. The expert module has two main functions [9], [10], [7] to elaborate questions, answers and explanations, and to act as a reference.

Several systems use different tools to model the expert module; among those techniques: the fuzzy cognitive map [11]. Another tool that uses thematic maps is the EON tool, which allows the creation of intelligent tutors oriented towards pedagogy [12] etc. The majority of these tools have a feature of authoring instructional objectives and the lack of the taxonomy of learning inside the expert modules. For that reason, in our previous work, the authors proposed to integrate the implicit and explicit intervention to ITS [2]. This tutor will select the appropriate strategy according to three criteria. This modification is concerned with the instructional model; this later has bidirectional communication with the expert model; this module is a computer representation of declarative knowledge, this knowledge allows the ITS to compare the learner's actions and choices with those of an expert in order to evaluate what he understands and what he does not understand [13], [14]. This module encounters a lot of issues, for that reason the authors propose the solution illustrated in Fig. 1.

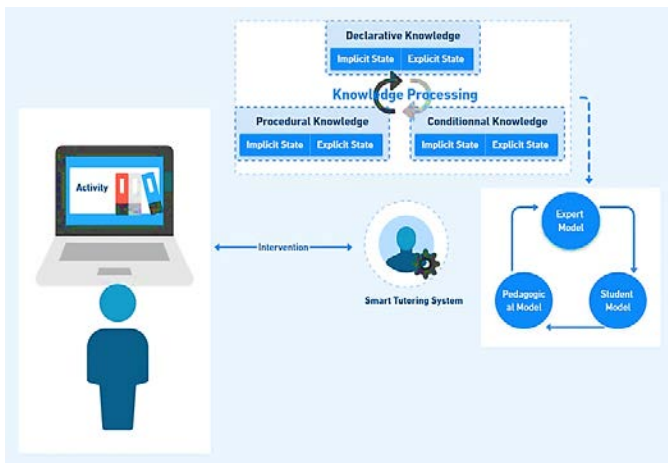


Fig. 1. Knowledge Processing in the Expert Model [3].

This solution combined the three categories of knowledge in the expert model. Declarative: definition of the concepts, procedural: problem-solving ability and conditional knowledge may have an implicit or explicit status, maybe both; and a type of assessment (memorization, administration, Expertise). The modelization of these large numbers of states that have a dispersed representation required the Bayesian network modelling. The choice of Bayesian Network is not arbitrary. This type of network is versatile: they can use the same model

to evaluate, predict, diagnose, or optimize decisions, which helps to make the effort of building the Bayesian network profitable.

Therefore, the graphical representation of a Bayesian network is explicit, intuitive and understandable by a non-specialist, which facilitates both the validation of the model, its eventual evolutions and especially their uses.

B. The Development of Bayesian Network

Bayesian networks (BNs) are a tool for representing uncertainty using probabilities and robust mathematical foundations. BNs correspond to the probability distributions that can be generated by products of conditional probability distributions [3]. Several models are created based on knowledge representation and reasoning. Probabilistic graphical models, especially the Bayesian networks initiated by Pearl [15], have appeared as tools to describe uncertain knowledge and thoughts based on limited information.

Bayesian networks have been proven successful in modelling any kind of knowledge problem. Thus, Bayesian networks have been applied in numerous diverse fields, including medical diagnostics, information retrieval, and marketing. There are a lot of tools to create efficient Bayesian networks in an easy way like GeNIe [18] and SMILE [19]. Based on the literature, Bayesian Networks have been a positive effect in the student model of the ITS. ANDES is an example of an intelligent tutoring system which used Bayesian networks to conduct a long-term knowledge evaluation, and prediction of learners' behaviors while problem solving [20].

A Bayesian network $BN = (G, N)$ is characterized by

$G = (Y, E)$ directed acyclic graph with a set of vertices associated and random parameters, which is expressed by the following formula:

$$N = P(Y_i - Pa(Y_i)) \tag{1}$$

With $Y = (Y_1, \dots, Y_n)$

In a real-world application, the modelization of a large number of states that have a dispersed representation is indispensable. For that reason, to generate a classification with a representation that allows modelling with many variables a Bayesian network method is required [16]. The graphical representation of the BN describes the conditional independencies between variables which is easy to figure the joint probability. The Fig. 2 presents the Bayesian Network schema:

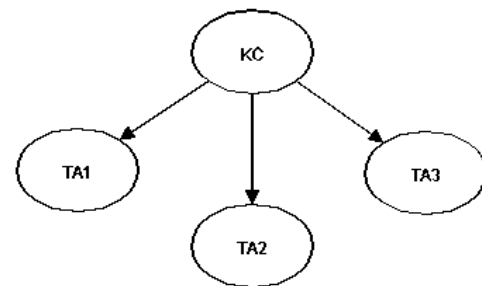


Fig. 2. Bayesian Network Schema.

To construct the Bayesian network model for our issue, two essential steps are required: specification of the structure model and specification of variable values.

1) *The specification of the structure model:* To describe the development of the Bayesian network, the authors start by defining the nodes of our model; the model involves an initial node “knowledge category”, which is composed of several parent nodes presented as bellow: typeActivity1, typeActivity2 and typeActivity3. Each of these nodes contain child nodes. The links to these nodes are prerequisite relationships:

a) *TypeActivity 1:* The activity is based on a declarative knowledge; this type contains two nodes: Memorization: this activity uses a definition or examples of the concept and status; this is a type of evaluation, it reflects the learner’s knowledge; the states of knowledge can be: Implicit: the learner knows what this is meaning, or explicit: the learner knows how to describe it. Fig. 3 presents the node “TypeActivity1” and their child.

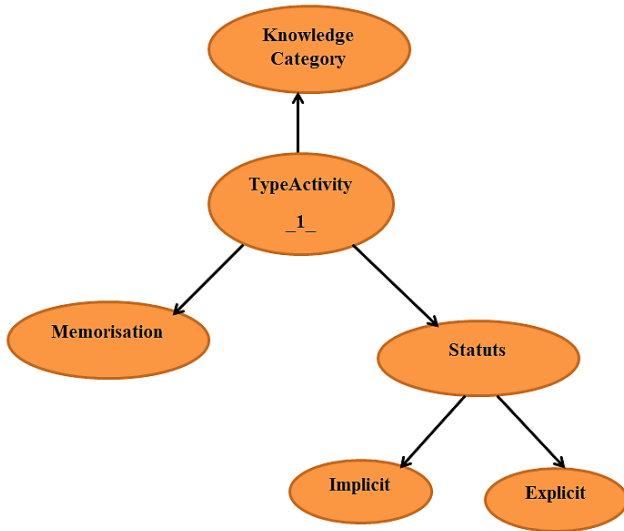


Fig. 3. The Node “TypeActivity1” and the Descendant.

b) *TypeActivity 2:* The activity is based on a procedural knowledge; it is composed of Administration: the activity applies case studies; and the learner tries to figure out how to do the exercise (Explicit status) and how can do it (implicit status). Fig. 4 describes the node “TypeActivity2” and their child: Administration and status (implicit and explicit).

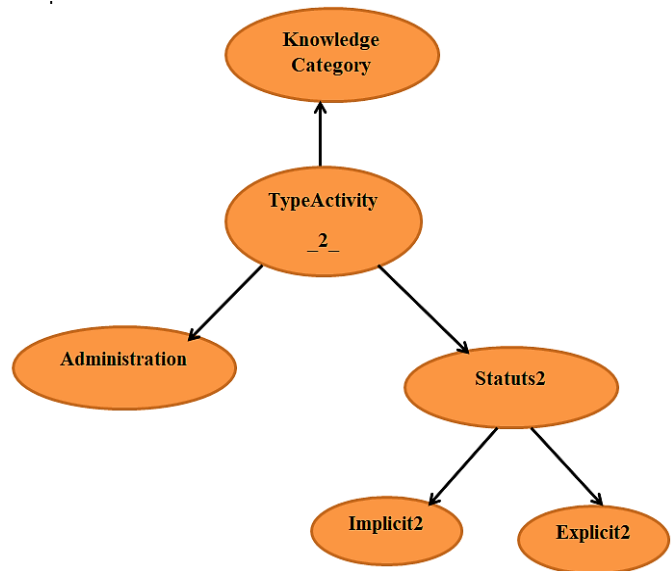


Fig. 4. The Node “TypeActivity2” and their Child.

c) *TypeActivity 3:* This type of activity is based on conditional knowledge; it comprises: Expertise exercises. The activity develops the ability to realize a project based on both activities described above: TypeActivity1 and TypeActivity2; and the states of knowledge. The Fig. 5 illustrates the Bayesian network of the “TypeActivity3” as a node and their child.

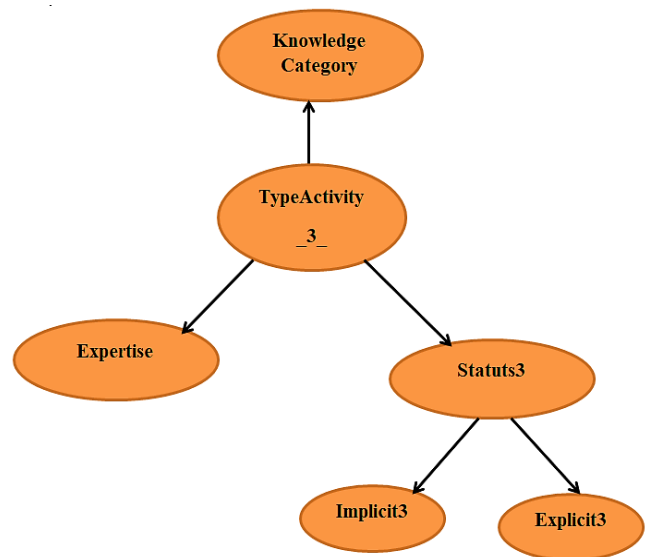


Fig. 5. The Node “TypeActivity3” and their Descendants.

relationship. The initial node Knowledge Category (KC) comprises three parents: typeActivity1 (TA1), typeActivity2 (TA2) and typeActivity3 (TA3) which are corresponding to three weight: w1=0.2, w2=0.3 and w3=0.5. The conditional probability of KC is calculated using the formula bellow:

$$P(KC|TA1, TA2, TA3) = w1 * h1 + w2 * h2 + w3 * h3 \quad (2)$$

With:

$$h1 = \begin{cases} 1 & \text{if } TA1 = KC \\ 0 & \text{Otherwise} \end{cases}$$

$$h2 = \begin{cases} 1 & \text{if } TA2 = KC \\ 0 & \text{Otherwise} \end{cases}$$

$$h3 = \begin{cases} 1 & \text{if } TA3 = KC \\ 0 & \text{Otherwise} \end{cases}$$

2) *The specification of variable values:* After presenting the network model, the authors will define the values of the variable. In the construction of Bayesian network, the authors observe that the knowledge category depends of the type of activity. Which make us deduce that is the diagnostic

The authors mention that {KC, AT1, AT2, AT3} is a complete set of mutually exclusive variables, whose variable is also random and binary. As a generalization on the formula presented in (3) and (4), it can be said that:

$$P(X=1|Y1, Y2, \dots Yn) = w_i * h_i, \{i=1, \dots, n\} \tag{3}$$

$$P(\text{not } X|Y1, Y2 \dots Yn) = 1 - P(X=1|Y1, Y2, \dots Yn) \tag{4}$$

The Table I presents the conditional probability of the node “knowledge category”.

TABLE I. THE CONDITIONAL PROBABILITY TABLE OF THE NODE “KNOWLEDGE CATEGORY”

TA1	TA2	TA3	P(X=1)	P(X=0)=1-P(X=1)
0	0	0	0,0	1,0
0	0	1	0,5	0,5
0	1	0	0,3	0,7
0	1	1	0,8	0,2
1	0	0	0,2	0,8
1	0	1	0,7	0,3
1	1	0	0,5	0,5
1	1	1	1,0	0,0

III. IMPLEMENTATION PHASE

In this section, the authors will describe the environments, present the results and evaluate the efficiency of the proposed solution:

A. Environments

After the construction of our Bayesian network model, the authors validate the proposed solution using the ANACONDA navigator. Spyder 3.3.6 is a scientific Python development environment and they work with python 3.7 as a programming language. In the phase of coding, they apply the POMEGRANATE package for building probabilistic models. Based on the conditional probability table that they built in the previous section, they initialized the status and activity using Univariate distribution (), which made up of characters and their probabilities. The sum of the probability will be 1.0. The Fig. 6 presents the Parameters of the development environment:

B. The Results

Fig. 7 illustrates the probability of activity containing conditional knowledge; the result shows us that this activity should have an expertise activity, including the implicit and explicit status.

The probability of an activity containing declarative knowledge is that it should have a memorization activity, including the implicit and explicit status. The results are described in the Fig. 8.

The Fig. 9 presents the probability of activity containing procedural knowledge; the result shows us this activity should have an administration activity including the implicit and explicit status:

```

1 # -*- coding: utf-8 -*-
2 """
3 Spyder Editor
4
5 This is a temporary script file.
6 """
7 import math
8 from pomegranate import *
9
10 status = DiscreteDistribution( { 'im': 1./2, 'ex': 1./2 } )
11 Activity = DiscreteDistribution( { 'memo': 0.2, 'admin': 0.3, 'expert': 0.5 } )
12 knowledge = ConditionalProbabilityTable(
13 [[ 'memo', 'ex', 'declarative', 0.10 ],
14 [ 'memo', 'im', 'declarative', 0.10 ],
15 [ 'admin', 'ex', 'procedural', 0.15 ],
16 [ 'admin', 'im', 'procedural', 0.15 ],
17 [ 'expert', 'ex', 'conditional', 1.0 ],
18 [ 'expert', 'im', 'conditional', 1.0 ],
19 [ 'memo', 'ex', 'procedural', 0.0 ],
20 [ 'memo', 'im', 'procedural', 0.0 ],
21 [ 'memo', 'ex', 'conditional', 0.0 ],
22 [ 'memo', 'im', 'conditional', 0.0 ],
23 [ 'admin', 'ex', 'declarative', 0.0 ],
24 [ 'admin', 'im', 'declarative', 0.0 ],
25 [ 'expert', 'ex', 'declarative', 0.0 ],
26 [ 'expert', 'im', 'declarative', 0.0 ],
27 [ 'expert', 'ex', 'procedural', 0.0 ],
28 [ 'expert', 'im', 'procedural', 0.0 ],
29 [ 'admin', 'ex', 'conditional', 0.0 ],
30 [ 'admin', 'im', 'conditional', 0.0 ]], [Activity, status] )
    
```

Fig. 6. Parameters of the Development Environment.

```

In [1]: runfile('C:/Users/lenovo/.spyder-py3/temp.py', wdir='C:/Users/lenovo/.spyder-py3')
statust{
  "class": "Distribution",
  "dtype": "str",
  "name": "DiscreteDistribution",
  "parameters": [
    {
      "im": 0.5,
      "ex": 0.5
    }
  ],
  "frozen": false
}nActivityt{
  "class": "Distribution",
  "dtype": "str",
  "name": "DiscreteDistribution",
  "parameters": [
    {
      "memo": 0.0,
      "admin": 0.0,
      "expert": 1.0
    }
  ],
  "frozen": false
}nknowledgegetconditional
    
```

Fig. 7. The Probability to have a Conditional Knowledge.

```

Python 3.7.4 (default, Aug 9 2019, 18:34:13) [MSC v.1915 64 bit (AMD64)]
Type "copyright", "credits" or "license" for more information.

IPython 7.8.0 -- An enhanced Interactive Python.

In [1]: runfile('C:/Users/lenovo/.spyder-py3/temp.py', wdir='C:/Users/lenovo/.spyder-py3')
statust{
  "class": "Distribution",
  "dtype": "str",
  "name": "DiscreteDistribution",
  "parameters": [
    {
      "im": 0.5,
      "ex": 0.5
    }
  ],
  "frozen": false
}nActivityt{
  "class": "Distribution",
  "dtype": "str",
  "name": "DiscreteDistribution",
  "parameters": [
    {
      "memo": 1.0,
      "admin": 0.0,
      "expert": 0.0
    }
  ],
  "frozen": false
}nknowledgegetdeclarative
    
```

Fig. 8. The Probability to have a Declarative Knowledge.

```
In [2]: runfile('C:/Users/lenovo/.spyder-py3/temp.py', wdir='C:/Users/lenovo/.spyder-py3')
statust{
  "class": "Distribution",
  "dtype": "str",
  "name": "DiscreteDistribution",
  "parameters": [
    {
      "im": 0.5,
      "ex": 0.5
    }
  ],
  "frozen": false
}
}nActivity{
  "class": "Distribution",
  "dtype": "str",
  "name": "DiscreteDistribution",
  "parameters": [
    {
      "memo": 0.0,
      "admin": 1.0,
      "expert": 0.0
    }
  ],
  "frozen": false
}
}nknowledgeprocedural
```

Fig. 9. The Probability to have a Procedural Knowledge.

To summarize the results illustrated in the figures above, the authors can conclude the following points:

To create an activity that can attend the conditional knowledge; a pedagogical sequence must contain an expertise exercise, such as the ability to choose the appropriate method to solve a problem in a case study.

To achieve the declarative knowledge, the activity should have a memorization exercise like the recognition, categorization and differentiation between different objects (implicit status) and schematization, graphic, symbolic, linguistic (Explicit status).

A pedagogical sequence based on procedural knowledge should contain administration exercises in such a way that the learner tries to figure out how to do the exercise (Explicit status) and he can do it (Implicit status).

C. Evaluation and Discussion

To measure the performance of knowledge processing, the authors used a lot of metrics; the first one is the calculation of the target node and all the evidences using the global confusion matrix (GCM); the obtained results from the GCM helps to know the probability of the correct classification (PCC), after that, they calculated the marginal probability of the correct classification (MPCC), and finally they obtained the marginal improvement (MI), individual PCC (IPCC) and the cost rate.

To evaluate the performance of the Bayesian network, validation of each node is necessary. The Fig. 10 illustrates the node evaluation "Type Activity1" as a target and their two fragments of evidence: "Memorization" and "Status": implicit and explicit.

From the results, the authors find that by adding the evidence nodes in the evaluation of the target node, the percentage probability of correct classifications is rising. By measuring the probability of each node's correct classification, they see how each node contributes separately to the classification. In this evaluation, the "Memorization" node is the biggest contributor. In this evaluation, they find the influence of the node "Memorization" to the target node.

The results reflect the choice of the TypeActivity1 which means that the expert model will concentrate the knowledge on the declarative one; for example: definition and explanation

with the uses of (58, 70%) as an explicit knowledge likes the graphs and schemas; and, (56, 90%) as an implicit knowledge which contains a recognition exercises.

According to the results and the validation of each node of the Bayesian network, the authors were able to handle globally the functioning of the network. According to the management of the expert system through a list of criteria that contains the type of knowledge as well as their status; the expert model can suggest knowledge in the right type as well as the appropriate status. If, for example, the expert system chooses the type of activity1, then suggestions can be demonstrated based on declarative knowledge (memorization) and appropriate status (implicit/explicit).

The Bayesian network modelling helps us to modelize the large number of states that have a dispersed representation. This modelization helps to make a prediction and evaluation of the three categories of knowledge and their child: type of assessment and status.

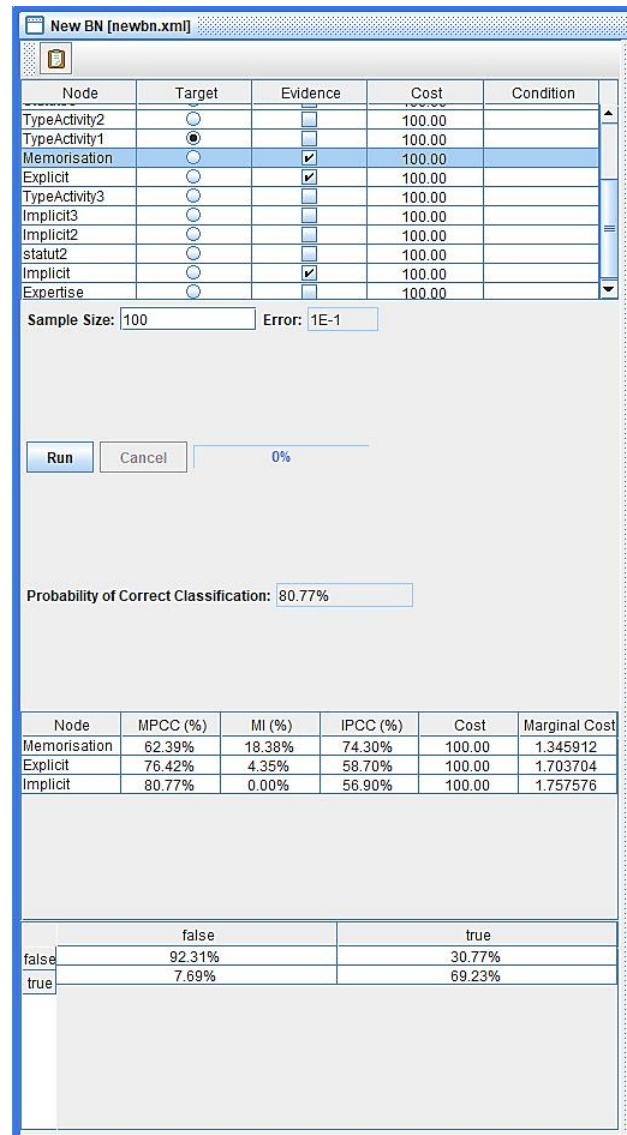


Fig. 10. The Node Evaluation "Type Activity1".

IV. CONCLUSION

The evaluation part is an essential step in the learning process. To enhance this step in the expert model of intelligent tutoring system, knowledge processing is required. In this paper, the authors have presented the problem of the expert model; after that, they illustrate the construction of the Bayesian network; then, they evaluate the efficiency of the proposed process and the results in the implementation phase. This paper aims to investigate the efficiency of the pedagogical solution presented in their previous research paper via the Bayesian network model. This study analyses the knowledge processing according to the type of activity; this later depends on the knowledge and the status. In future work, we aim to study the process of the selected knowledge, and we will integrate the intelligent tutoring system into the FPL E-learning platform and the different contributions in one solution.

REFERENCES

- [1] F.-Z. Hibbi, O. Abdoun, en H. El Khatir, "Extract tacit knowledge in the learner model of the smart tutoring system", *Int. J. Emerg. Technol. Learn.*, vol 15, no 04, bl 235, Feb 2020.
- [2] F.-Z. Hibbi, O. Abdoun, en E. L. K. Haimoudi, "Exploration of Analytical Mechanisms in the Feedback model", *Procedia Comput. Sci.*, vol 148, bl 201–207, 2019.
- [3] F.-Z. Hibbi, O. Abdoun, en E. K. Haimoudi, "Knowledge management in the expert model of the smart tutoring system", in *Proceedings of the 3rd International Conference on Networking, Information Systems and Security, Marrakech Morocco, 2020*.
- [4] M. Mohammed A en S. S. Al-Nakhal, *Adaptive Intelligent Tutoring System for Learning Computer Theory*. 2017.
- [5] R. Nkambou en C. Frasson, "A New Approach to IT Scurriculum and Course Authoring: The Authoring Environment, Elsevier Science Ltd", *Pergamon Computers Educ, great Britian*, vol 31, bl 105–130, 1998.
- [6] M. A. Mark en J. E. Greer, "Evaluation Methodologies for Intelligent Tutoring Systems", *Journal of Artificial Intelligence in Education*, 1999.
- [7] M. Grandbastien, *Teaching Expertise is at the Core of ITS Research*, *International journal of Artificial Intelligence in Education*. 1999.
- [8] R. McNally en J. Shute, "Intelligent Tutoring Systems: Past, Present and Future", in *Communications and Technology*, D. Jonassen, Red Macmillan, 1996.
- [9] J. A. Self, "The Distinctive Characteristics of Intelligent tutoring Systems Re-search: ITSs Care, Precisely", *International Journal of Artificial Intelligence in Edu-cations*, 1999.
- [10] T. Murray, "Authoring knowledge-based tutors: Tools for content, instructional strategy, student model, and interface design", *J. Learn. Sci.*, vol 7, no 1, bl 5–64, Jan 1998.
- [11] J. Pearl, *Probabilistic reasoning in intelligent systems*. London, England: Morgan Kaufmann, 2014.
- [12] J. Pearl, *Probabilistic Reasoning in Intelligent Systems*. Elsevier Science, 2014.
- [13] H. E. Kyburg, "Probabilistic reasoning in intelligent systems: Networks of plausible inference", *J. Philos.*, vol 88, no 8, bl 434, Aug 1991.
- [14] Pipatsarun Phobun and Jiracha Vicheanpanya, "Adaptive intelligent tutoring system for e-learning systems", ELSEVIER. 2010.
- [15] E. Castillo, J. M. Gutierrez, en A. S. Hadi, *Expert Systems and Probabilistic Network Models*. Springer, 1997.
- [16] R. Nkambou, R. Gauthier, en M. C. Frasson, "CREAM-Tools: an authoring environment for curriculum and course building in an ITS", in *Proceedings of the Third International Conference on Computer Aided Learning and Instructional Science and Engineering*, New York: Springer Verlag, 1996.
- [17] N. Jongsawat, Anunucha, en Wichian, "Dynamic data feed to Bayesian network model and SMILE web application", in *Bayesian Network, Sciyo*, 2010.
- [18] N. Jongsawat, P. Poompuang, en W. Premchaiswadi, "Dynamic data feed to Bayesian network model and SMILE web application", in *2008 N Ninth ACIS International Conference on Software Engineering, Artificial Intelligence, Networking, and Parallel/Distributed Computing*, Phuket, Thailand, 2008.
- [19] M. J. Smile, "Structural modeling, inference, and learning engine and genie: A development environment for graphical decision-theoretic models", in *Proceedings of the Sixteenth National Conference on Artificial Intelligence (AAAI-99)*, 1999, bl 18–22.
- [20] E. Millan en J. L. P ´erez-De-La-Cruz, "A Bayesian diagnostic algorithm for student modeling and its evaluation", *User Modeling and UserAdapted Interaction*, vol 12, no 2–3, bl 281–330, 2002.

Digital Storytelling Framework to Assist Young Children in Understanding Dementia

Noreena Yi-Chin Liu¹

Faculty of Arts and Social Sciences
Universiti Brunei Darussalam
Brunei Darussalam

Nooralisa M Tuah²

Faculty of Computing and
Informatics
Universiti Malaysia Sabah
Malaysia

Kevin Chi-Jen Miao³

Faculty of Design and Creative
Technologies
Auckland University of Technology
& Blossom Lab
Taiwan

Abstract—A digital storytelling tool is one of the interactive technologies that can help youngsters better comprehend Dementia. Dementia makes it difficult for older people to maintain their daily routines. They have difficulties in effectively communicating with those around them. Similarly, children whose grandparents have Dementia will struggle to understand their grandparents' situation. It will also negatively influence children's relationships with their grandparents. Learning through interactive digital storytelling will affect younger people's entertainment experiences, which may help them better comprehend Dementia. As a result, the children's relationships with their grandparents may be strengthened. This study aims to present the framework of digital storytelling in helping young children understand more about Dementia. The framework was developed in a step-by-step procedure that included analyzing and synthesizing current applications and relevant research, constructing the framework, and having it confirmed by experts. Researchers and developers may use the framework as a guideline to build meaningful digital storytelling features.

Keywords—Digital storytelling; Dementia; interactive learning; entertainment experience

I. INTRODUCTION

Dementia is one of the most common public health concerns among the elderly. Most of the research on Dementia treatments focuses on mental health assistance. When a patient is diagnosed with Dementia, it usually affects their family [1]. Children are particularly vulnerable because they lack the necessary information to understand Dementia. Maintaining a relationship with grandparents is difficult for youngsters since they don't know what to say or how to act [2].

Dementia technology intervention has been widely used. Healthcare tracking devices [3], brain training [4] and rehabilitation platforms [5], and predictive analytics and diagnosis [6] are all examples of its applications. Fitbit, Apple Watch, and other personal GPS trackers for the elderly are among the most popular interventions on the market for health tracking gadgets that could be utilized for Dementia treatment. Fitbit is a wearable device that tracks activity, exercise, diet, weight, and sleep to help individuals stay motivated and improve their health. Meanwhile, *BoundaryCare* is a location and health tracking software for Apple's iWatch and iPhone. The apps were created with Dementia in mind, but the apps also may be used to track other cognitive issues, including

Down syndrome and Parkinson's disease. Various devices can be used as personal GPS trackers for the elderly in addition to these. *Mindmate* and *Lumosity* are two other Dementia interventions that can be further considered. These apps are among the various brain training and rehabilitation platforms accessible.

Brain training is one of the most significant parts of improving Dementia symptoms [7]. According to this perspective, the applications are intended to prevent Dementia by training in cognitive processes such as speed, memory, attention, problem-solving, and others. Furthermore, numerous studies in the literature focus on having a mobile application to reduce cognitive impairment among patients [8]. This technological solution aims to improve a person's Dementia status by providing improved treatment support.

Within these five years, the United Kingdom's government, organizations, and communities began an educational information campaign regarding Dementia for the public, focusing on Dementia in family members, for example, the Dementia Friend, the Alzheimer's Association, and the Alzheimer's Disease International. However, the available resources for children are fairly restricted since, at times, children may find it difficult to understand owing to a language barrier that prevents them from grasping the situation. As a result, a more targeted intervention or programme to assist youngsters in understanding Dementia and how to care for their grandparents with Dementia is required. Furthermore, this arrangement will help the children maintain their bond with their grandparents.

It has been discussed who, when, and how to inform children and young people about Dementia. Dementia Friends proposed five key messages about Dementia to help them understand what Dementia is and what a diagnosis means for their relationship: 1) Dementia is not a natural part of ageing, 2) Dementia is caused by diseases of the brain, 3) Dementia is not just about losing your memory, 4) It is possible to live well with Dementia, and 5) There is more to the person than the Dementia. These five stages are the first to learn about Dementia, and an interactive version may also be utilized for youngsters.

Children today are exposed to technology and digital information from an early age. As a result of their early

exposure, they are more comfortable spending time interacting with digital information. The interaction is either for education, entertainment, or a change of lifestyle. Online learning has become the new standard for encouraging self-learning in schools. One of the online learning methodologies, digital storytelling, is regarded as helpful in raising children's motivation [9]. Furthermore, learning using interactive methods such as digital storytelling can aid in developing children's brains [9].

Education and computer application research is now generating a lot of interest in enhancing teaching and learning activities and raising children's productivity. Digital storytelling for Dementia may help youngsters comprehend the situation better [10]. In general, digital storytelling is a narrative style that combines digital pictures, texts, sounds, and other interactive components [11]. Digital tales are typically two to 10 minutes long. They are often saved in digital form and posted to internet sites where they may be viewed with web browsers [12].

Digital storytelling is also defined as short personal stories created with computer software and shared with others to transmit ideas, facts, and views on a wide range of subjects and themes [13]. They're also referred to as picture books [14] and are made up of various digital stories. According to Robin [13], the applications of digital storytelling may be divided into three categories: 1) personal narratives: stories about significant events in one's life; 2) historical documentaries: stories about critical events that help us understand history; and 3) stories that enlighten or instruct the viewer on a particular subject or practise. The application of Dementia to these domains might fall into one of three categories.

As children became more involved in and influenced by digital storytelling material, it is imperative to examine a relevant framework that can guide designers and developers on the appropriate design and development of digital storytelling [13]. Although many academics investigate the design and development of digital stories and picture books, they are mainly focused on specific issues and traits, particularly when developing an interactive tool. There has been minimal research on the appropriate content and design of stories for young children, especially when it comes to Dementia prevention via a digital picture book. There is presently no comprehensive framework that researchers and developers may use as a guide to compare and select relevant parts for digital storybooks. As a result, a comprehensive digital storytelling framework must be developed to create practical guidelines in the future. Therefore, to develop the framework, this paper will address the following:

- To analyze the current implementation of digital storytelling for young children in an online learning environment.
- To identify the essential elements of storytelling to motivate young children's engagement in online learning environments.
- To develop a suitable framework of digital storytelling for young children that can guide designers and

developers on the appropriate design and development of digital storytelling tools.

This paper is organized as follows. The research underpinning interactive learning in digital storytelling is presented in Section 2. In addition, the experiences of involvement and amusement in digital storytelling are described. The many tools for implementing digital storytelling are outlined as well. The discussion of approaches to adopting digital storytelling in education is also presented in Section 2. Section 3 offers the development of the framework. The framework validation research is discussed in Section 4, and Section 5 discuss the result obtained from a focus group discussion with experts in the field. Finally, Section 6 concludes with some remarks on the study's significance.

II. RESEARCH BACKGROUND

A. Digital Storytelling and Interactive Learning

Digital storytelling is a method widely applied for interactive learning in which it could help to increase students' motivation to learn [13],[15], and it could evoke a sense of entertainment in learning [13]. Digital storytelling can also be viewed as an interactive platform that leverages information visualization to provide fun learning. Interactive learning is a merging technology in traditional education. It provides students with a platform to interact with the content in the learning process. The digital story also plays as a communication tool that conveys information between a teacher and their student based on the interactive story. In this environment, the student's role in the course changes from a passive receiver into an active participant. Interactive learning usually involves social networking. Community on social networks allows students to easily and effortlessly access the learning material, and learn from teachers and other students.

When digital storytelling is used for educational purposes or used for conveying knowledge and ideas, the environment becomes part of an interactive learning platform. Digital storytelling typically transmits stories in the form of a video as it can be readily shared to reach a larger audience [16],[17]. Students and teachers can easily access and share content using social media sites like Facebook and Twitter. Furthermore, students can respond to these digital stories by leaving comments and sharing them. To some extent, they could be able to interact with others when utilizing the provided content. It is believed that the determination to get attention on social media is the kind of reason for the students to get engaged with the digital storybook. Having a good internet connection and tools, on the other hand, is regarded as critical in interactive learning since it determines the ease with which students may gain knowledge both online and outside of class. These technologies function as interactive learning components, substantially altering the engagement between teacher and student.

Apart from that, one of the advantages of digital storytelling is that it can be generated using various media, including video, photos, audio, and music, to build a rich content project. Such inventions may provide viewers with a more profound sense of amusement and excitement when

viewing. As a result, digital storytelling has been applied to various disciplines to reach a wider audience or provide more profound knowledge. Digital storytelling, for example, is used in education to stimulate students' interest in learning and museum tours to enhance the tour experience.

B. Digital Storytelling in Different Fields

Digital storytelling approaches have become increasingly popular in recent years as the barrier to entry has lowered. Teachers have used it at many school levels to improve students' learning experiences and increase their interest and motivation in the course [18]. Digital storytelling is also used in various domains, such as health care, ageing, and social issues [19].

1) *Digital storytelling in school*: Teachers worldwide have incorporated digital storytelling into their classes to aid in teaching and improve their students' learning experience. Digital storytelling has the potential to stimulate students' interest in learning and boost their drive to learn [15]. Students will benefit from the process of producing a digital story because the goal of a digital story is usually to deliver a message. Students would need to improve their communication abilities to create a digital story. In this way, they learn to arrange their thoughts and create narratives [12]. Creating a digital story might encourage kids to think creatively while improving their cultural literacy [20].

2) *Digital storytelling in museum*: Digital storytelling, as a form of multimedia that combines audio and video, may be more appealing and exciting than traditional oral communication. For example, digital storytelling in a museum tour guide's tour could enhance the tour experience and narrative for guests. Digital stories developed for the museum could serve various functions, like offering advanced information about the exhibition's showpieces or answering visitor queries [21]. For a more engaging and personal tour experience, museums merge digital tales with modern technologies such as smartphone applications, augmented reality, virtual reality, and more.

3) *Digital storytelling in community and non-profit organization*: On the social networking site, digital stories are straightforward and easy to share. As a result, communities and non-profit organizations frequently use it to spread their messages and raise public awareness. For example, a local government-sponsored awareness campaign might simply use and share the stories on social media sites like Facebook, Twitter, and Instagram. Furthermore, digital storytelling can make a complex or abstract subject more understandable for individuals. As a result, it has the potential to attract a more extensive range of people's attention [22].

4) *Digital storytelling in healthcare*: In health care, digital storytelling could be used as an educational tool to assist patients, their families, and caregivers understand their condition. Patients or their families who have gone through a challenging time, difficulties, or trauma due to illness could share their stories and offer advice. This information can be presented as a digital tale. Patients and their families may find

that sharing their tales is a powerful and emotional tool that can help them cope with the pain and challenges they may encounter in the future. It arouses a sense of empathy among caregivers toward their patients indirectly [23]. Hardy & Sumner [10] advocate for patients, family members, and caregivers to create digital tales based on their experiences with physical and mental disorders such as arthritis and Dementia. People who have lived through or experienced a similar event benefited from the digitization of stories.

C. Engagement and Digital Storytelling

Children are exposed to various stories as they grow up, influencing their behaviour and acceptance of their surroundings. Children appear to be able to process and grasp complex information through narrative and apply it wherever possible [9]. Digital storytelling, enabling youngsters to learn something, has been proved to be an effective strategy in studies [9],[13]. This is because visual signals may assist children in focusing and thus become more engaged with the content. As a result, engagement, engrossment, and absolute immersion have been proposed as three levels of immersion [24].

- **Engagement**: The term "engagement" refers to both cognitive and emotional states [25],[26]. The interaction encourages the user to use the platform, or at the very least be aware of its existence, and piques the user's interest in digital technology, particularly game theory. Forcing anyone to use the platform, especially young children, is unconstitutional. Rather than forcing them to utilize any digital technology, they should be encouraged to do so. It will have a negative influence, and its monetary value will be lost. Engagement aims to provide a personalized experience through a platform that will attract and spark people's interest [25].
- **Engrossment**: The user may become highly absorbed and engrossed due to the involvement [24]. A game-created environment can be entered, explored, enjoyed, and defended by users. The player becomes an integral part of the game, and the game immediately impacts their emotions. At this point, players want to keep playing, which allows them to achieve complete immersion [27].
- **Total Immersion**: The final immersion stage is total immersion [24], which occurs when the user is fully immersed. The most important aspect of total immersion is paying attention. In video games, there are three types of attention: visual, aural, and mental. Combine visual and auditory elements to create an ambience that directs the user's experience [27]. Users must pay close attention to sound and vision, which requires extra effort. Consumers become more engrossed as a result of increased attention and effort.

D. Digital Storytelling Tools

There are three different types of tools for generating digital stories. 1) Computer-based software programmes.

2) Tools that can be accessed via a web browser. 3) Apps for mobile devices such as smartphones and tablets [12].

- **Computer-based Tools:** Computer-based tools are software programmes that run on Windows or Mac OS X. They're most commonly used for non-linear editing. The basic functionality of free tools like Windows Movie Maker or iMovie for Mac is necessary to make digital stories. For the construction of digital storytelling, video and audio editing are sufficient. Paid editing applications with greater functionality, such as Adobe Premiere and Final Cut Pro, include transitions, filters, special effects, and more. Globally, computer-based tools have the most users. As a result, many online resources, such as articles, video tutorials, and online courses, explain how to utilize and create.
- **Web-based Tools:** Web browsers are used to generate these tools. As a result, it is useful for users whose operating systems are continually changing. The utilities are compatible with various operating systems, including Windows, Mac OS X, and Linux. After logging in with a web browser, the data will be synthesized for further processing. WeVideo is the most widely used of these tools. WeVideo, launched in 2011, offers the most functions and is similar to computer-based technologies.
- **Applications for iOS or Android:** In recent years, many people have switched from PCs to mobile devices as their primary means of work. As a result, professional editing apps for smartphones and tablets are now available. Some, including Adobe Premiere Rush (for iOS and Android) and iMovie for iOS, have grown from computer-based software. These apps are designed for users who are already comfortable with smartphones or tablets and are great for producing digital stories with limited content.

E. Digital Storytelling as Entertainment Approach

Digital storytelling is an approach to telling stories through digital technologies. It is considered a fun and entertaining approach when involved with technology. The story will be digitalized and designed with sound, video, or some interactive activities. Also, some are installed with external devices for enhanced learning. Following Hardy & Sumner [10], the storytelling is digitalized in six steps: writing, script, the storyboard, locating multimedia, creating the digital story, and sharing.

The first step is about writing activity. The purpose of this step is to introduce a personal narrative and the main idea for the storytelling. Scripting comes next in step two. It has been refined, and the elements of the narrative story have been defined. Step three is the creation of a storyboard. The storyline for each scene in the storybook will focus on this step. Through a succession of visuals, the storyboard will define the specific aspect and segment of the plot. The next stage is to locate Multimedia, which is the fourth phase. Step four is collecting the materials, which comprise sounds, films, music, graphics, pictures, and images, among other things. Then, in step five, create the digital story. Users will create

their stories using technology or software at this level. Step six is the final step, which is to share. It is critical to share user tales and solicit audience feedback. The digitalizing phases illustrate that when creating a digital tale, the storyline, the fun component, and the entertainment effect were all considered to make the story appealing and impactful to its intended audience.

Learning through entertainment is a valuable method for children because it helps draw their attention and imitate their experiences while learning. Learning and enjoyment are combined in one platform with digital storytelling. Whether digital storytelling is about pleasure, emotion, or suspense, it will interest its readers passively, actively, or enormously [28],[29]. Games, immersive technologies, and artificial intelligence technology can all be used to understand this type of involvement.

- **Digital Storytelling in Games:** In recent years, many people have switched from PCs to mobile devices as their primary means of work. As a result, professional editing apps for smartphones and tablets have been developed. Some, like Adobe Premiere Rush (for iOS and Android) and iMovie for iOS, arose from computer-based applications. These apps are designed for users who are already comfortable with smartphones or tablets, and they are great for producing digital stories with limited content.
- **Digital Storytelling with Immersive Technology:** Augmented reality (AR), virtual reality (VR), and mixed reality are examples of immersive technologies (MR). These techniques create a more immersive interaction experience [30], opening more possibilities in content creation, including digital storytelling. Virtual reality (VR) applications for digital storytelling with immersive technologies are the most common. VR is presented via a head-mounted display, allowing users to experience a fully simulated virtual environment. Some forms of digital storytelling will enable the audience to participate. The audience, on the other hand, is primarily passive and consumes the author's substance. In digital storytelling, VR could allow the audience to participate in the environment and provide a direct response to the event [31]. The audience can participate in digital storytelling made in VR. "In the future, you will be the character. The story will happen to you," said Chris Milk, an immersive artist. [32].
- **Artificial Intelligence Techniques in Interactive Digital Storytelling:** Artificial intelligence (AI) has traditionally been used in video games to enhance digital storytelling. These games give players various options for what the main character does, giving them the feeling of being the story's protagonist. AI would then shape the tale based on the player's decisions. Among the AI approaches are case-based, FSM, genetic algorithms, goal net and fuzzy cognitive mapping, natural language processing, and search algorithms [33].

III. DEVELOPMENT OF THE PROPOSED CONCEPTUAL FRAMEWORK

A. The Framework Development Process

The conceptual framework was developed according to the previous literature review. The research field includes digital storytelling, learning cycle, technology intervention and user engagement. Fig. 1 depicts the four processes involved in developing a framework. The initial stage is to summarise and list the aspects and define the main elements based on the existing literature. According to theories in serious games, interactive technologies, and learning cycles, the second stage is to group the pieces into interactive learning. In this study, the third phase is to build up the elements of digital storytelling. Discussions about technology theories relate to the digital storytelling platform at this point. The framework is built at the last stage.

B. List of Elements

Interactive learning and digital storytelling are the two elements of the framework. This section separates the satisfaction of needs in interactive learning and the satisfaction of requirements in digital narrative design. The concept of interactive learning is derived from the theoretical learning cycle and serious gaming, as shown in Table I. Education, engagement, and amusement are three components of interactive learning that are relevant to the primary goal of the research. Each component contains three elements. The first component, education, has three components: empowered learning, problem-based learning, and deep knowledge. The second component is engagement, which has three levels: engagement, engrossment, and ultimate immersion. The third component is entertainment, including passive, active, and immersive forms.

Table II depicts Lambert's digital storytelling concept [12], which includes the seven components of digital storytelling and the establishment of the San Francisco Center for Digital Storytelling. However, the consumers in this study are children who are not suited to complex design. As a result, the five critical factors for launching digital storytelling pique children's interest while also providing an easy-to-use platform in Table II.

C. Group Elements of Interactive Learning

Education, engagement, and entertainment are the three components of interactive learning. Educational components are concerned with the learning process; engagement components are concerned with the amount of engagement; and entertainment components are involved with the entertainment experience. The proposed components are based on game theory, learning cycles, and the realm of immersion technologies.



Fig. 1. Framework Development Process

TABLE I. ELEMENT OF INTERACTIVE LEARNING

Components	Elements	Description
Education	Empowered Learning	To help the user's motivated to complete tasks.
	Problem-Based Learning	It develops problem-solving skills and critical thinking skills.
	Deep Understanding	Every decision and action have a meaning, also called meaning as action.
Engagement	Engagement	Invite the user to use or know the platform exists and bring the user's interest.
	Engrossment	The user becomes deeply involved and becomes engrossed. So, the user's emotions will be affected.
	Total Immersion	The Final stage of immersion is total immersion, when the user is fully engaged.
Entertainment	Passive Entertainment	It lacks the interaction of the user or viewer.
	Active Entertainment	Increases the user's participation and expectations that they have different reactions to respond to different situations.
	Immersive Entertainment	Immersive entertainment comes with immersive technology such as Virtual reality (VR) and Augmented Reality (AR).

TABLE II. LEARNING ELEMENTS OF DIGITAL STORYTELLING

Elements	Literature
Setting	It refers to the physical location, including time, action, place, etc.
Characters	The most often-used cartoon or animals as characters. It also can affect the story
Plot	It is related to the storyline.
Conflict	It brings the challenge of problems that affect the action of the story.
Resolution	It is the underlying insight which is the message of the story.

- Education-Learning Process: Kolb's learning cycle [34] and Gee's ideas for learning games [24] were used to guiding the learning process. These theories look at the deep learning cycle from a user's perspective, allowing them to apply their knowledge to new areas or solve challenging problems. Empowered Learning, Problem-Based Learning, and Deep Learning are the three stages. Empowered Learning, Stage 1: Empowered Learning is the first stage in motivating or encouraging people to use the platform. It is vital at this stage to pique users' interests to finish the work, and as a result, users will continue to use the platform. Stage 2: Problem-Based Learning: During this stage, the user will get experience in solving problems. Stage 3: Deep Understanding: Users must comprehend the meaning of each decision and action to attain deep understanding.

- **Education-Engagement Level:** The purpose of the engagement level is to assist the user in becoming more engaged. It has been debated in serious game theories as to how to create higher-quality serious games. Gee [24] hypothesized three immersion levels: engagement, engrossment, and ultimate absorption. Stage 1 Engagement: This is the stage in which the user is invited to utilize or become aware of the platform and pique their curiosity. The user begins to devote time, effort, and focus. Stage 2 Engrossment: Following the previous stage, the user becomes more immersed and captivated, which has a direct impact on the user's emotions. Total immersion is the third stage, which describes the circumstance in which the user is completely immersed. Total immersion is the final immersion stage and impacts the user's ideas and feelings. Aside from that, one of the most significant aspects of immersion is paying attention.
- **Entertainment – Entertainment Experience:** Entertainment Experience has been considered across various platforms, including video, games, and film [29]. Oliver & Bartsch [35] stated that theories on the entertainment experience are divided into three categories: Suspense, Appreciation, and Fun [28],[29]. According to Hall [36], suspense is related to the tension and excitement experiment. Whereby fun refers to enjoyment, appreciation relates to user experience, and suspense refers to the anticipation and excitement experiment. It resembles three cinematic elements: light, serious, and action-oriented [29],[35]. These theories are also similar to the "engagement Level", which has been discussed in the previous section. However, the conceptual framework proposed in this study is for digital interactive learning. Thus, the entertainment experience has been refined within three stages: Passive Entertainment, Active Entertainment and Immersive Entertainment.

1) *Stage 1 passive entertainment:* Passive entertainment lacks the user's or viewer's interaction. It is a type of entertainment produced by others and distributed to others, such as viewing movies or reading a book.

2) *Stage 2 active entertainment:* As the name implies, active entertainment places a premium on your participation and requires you to react and respond to various scenarios. Active entertainment, such as decision-making or character control in video games or interactive digital storytelling, will involve your participation rather than passive entertainment.

3) *Stage 3 immersive entertainment:* Immersive entertainment is a brand-new idea that has emerged as a result of the advent of immersive technology. Virtual reality (VR), which requires the user to interact with a VR headset and VR controller for an immersive experience, is an example of active entertainment with a higher interactive level and immersive simulation.

D. Relationship between Components

This section discussed the relationship between interactive learning components: 1) Interest links education and

entertainment, 2) Immersion links engagement and entertainment, and 3) Interactivity connects education and engagement. We illustrate the interrelationship of these three components in Fig. 2.

1) *Education – entertainment (interest):* It is already termed in serious games called "Edutainment". However, the best association is "Interest". The more entertained they are by the APP (Games), the more interested the users will be in the learning content conveyed.

2) *Engagement – entertainment (immersion):* The similarity between "Engagement" and "Entertainment" is in trying to approach the immersion stage, which brings the user totally involved with the platform.

3) *Education – engagement (interactivity):* Interactivity increases engagement and brings users' attention. Thus, "Interactivity" enhances the learning process to provide an in-depth education system.

E. A Set of Elements for Digital Storytelling

Digital Storytelling has five elements: Setting, Characters, Plot, Conflict, and resolution. The detail of each component is described in the following Table III.

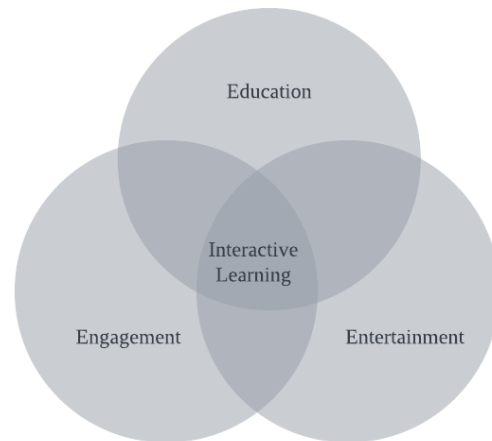


Fig. 2. Framework Development Process.

TABLE III. ELEMENTS FOR DIGITAL STORYTELLING

Elements	Description
Setting	A story's setting refers to the physical location and includes the time, action, place etc. For example, historical stories.
Character	It depends on the story. People or animals are most often used as characters. Characters can also affect the story, such as some characters are set up as heroes who have a sense of fair play.
Plot	It is related to the storyline. The plot usually begins with a problem and resolves it at the end of the story.
Conflict	Most of the story requires conflict, which brings the challenge of problems that affect the action of the story.
Resolution	Resolution refers to the underlying insight to find out the "message" of the story.

F. Constructing the Framework

The framework's construction follows the previous part and is divided into three stages, as follows:

Stage 1: The framework is established based on the understanding of interactive learning elements and the components of digital storytelling in constructing a digital storytelling application for promoting Dementia among young children. The framework is established into two sections: interactive learning and digital storytelling.

Stages 2: After establishing the essential component of the framework, the following step is to identify the sub-components for each of the components established for interactive learning – education, engagement, and entertainment. Following the discussion of the education component in Section III(C), the sub-components of the learning process comprise empowered learning, problem-based learning, and deep learning. The sub-components of engagement also discussed in Section III(C) include engagement, engrossment, and total immersion. For the entertainment component, the sub-components contained the entertainment experience, passive entertainment, active entertainment, and immersive entertainment. The relationship between these components was also mentioned in Section III(D). We illustrate this relationship in Fig. 3.

Stage 3: Establishing the connectivity of interactive learning and its requirement for digital storytelling. This study

aims to learn more about how this connectivity has a significant impact on the promotion of Dementia in young children. The digital storytelling element mentioned in Section III(E) is related to technological advancement. The framework of this study is formed by combining the theoretical aspect of interactive learning and the technical part of digital storytelling in Fig. 4.

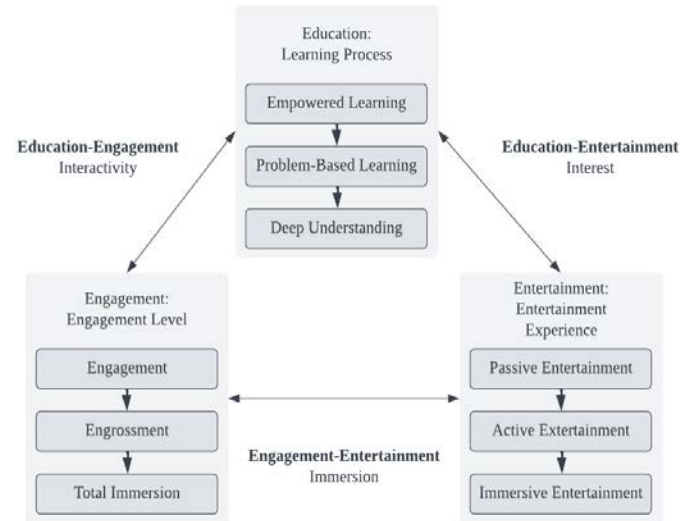


Fig. 3. Component and Sub-Components Relationship Establishment.

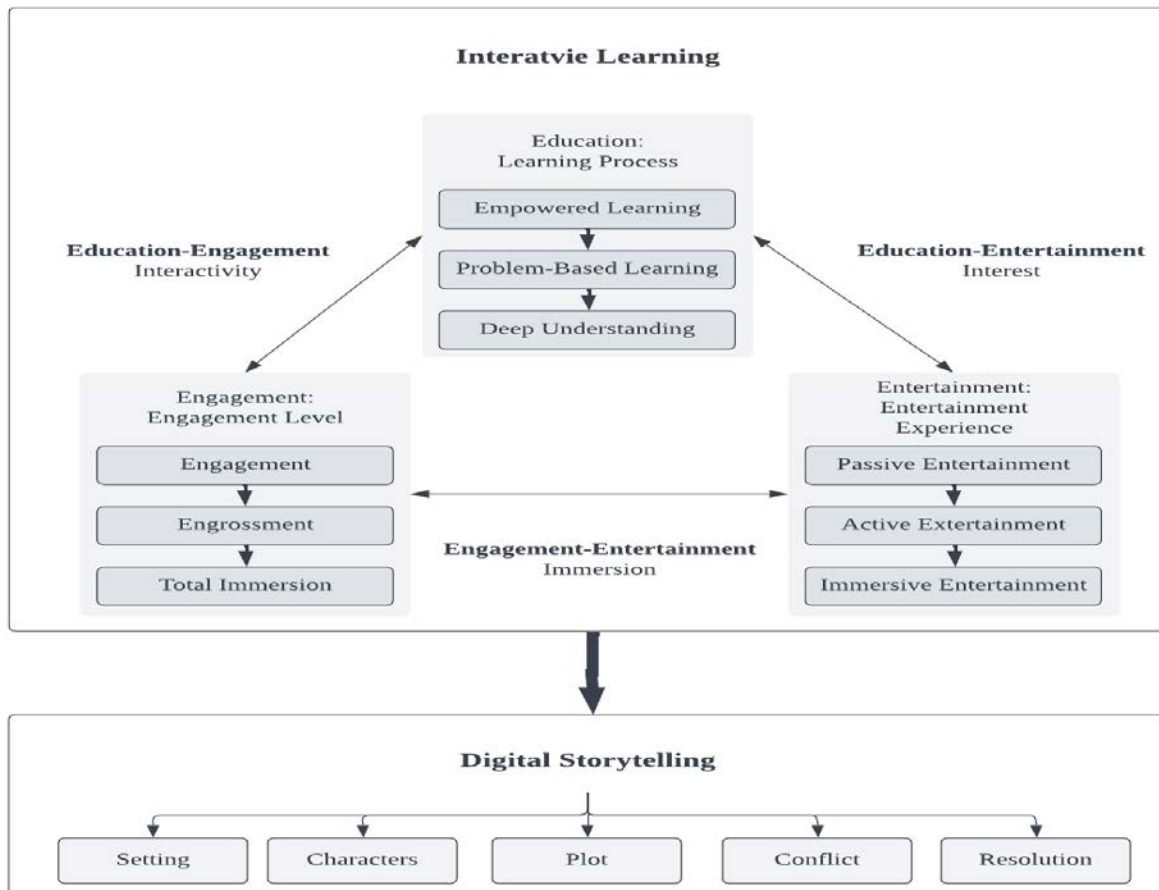


Fig. 4. Digital Storytelling Conceptual Framework.

IV. FRAMEWORK VALIDATION

Research methods are procedures for collecting and analyzing data. There are various research methods for different types of research. The methodologies used will generally be determined by the research paradigm or how the researcher perceives things related to the study context. In this study, the research method used to validate the framework is through expert review studies. We assumed a framework validation should be conducted in looking into the need to explore and further comprehend the developed conceptual framework. It will uncover the framework limitations or ambiguities that the literature study does not comprehend [37].

A. Validation Study with Expert Review

The validation study was conducted in the form of an online focus group discussion. The focus group discussion is designed to get collective feedback on the developed framework and plan the future work for developing the AR application. We introduced the framework by explaining the background of the framework, its purpose, the development process, the components, and their relationship at the beginning of the discussion. Then, during the discussion, we asked four questions. The questions are:

- Do you think the framework is comprehensive?
- Do you agree with all the components in the framework?
- Do you find any confusing components in the framework?
- Do you have any comments to improve the framework?

B. The Participants and Discussion Design

The focus group discussion was participated by six experts. The six experts have decided to follow the minimum of five experts suggested in the heuristics study's guideline for finding average problems [38]. The experts were identified based on their research work and activities as well as their years of experience in user experiences, serious games, and persuasive computing. The demographic of the experts is presented in Table IV. These experts had agreed to participate in the study.

The discussion session was conducted via online meeting. These six experts were first invited via email, asking for their participation and valuable input in the study. When all invited participants consented to participate, all meeting information and survey materials were forwarded to the participants. During the discussion session, experts were briefed beforehand. After the briefing, the session starts with the framework explanation, followed by the question-and-answer session. In the question-and-answer session, the moderator will ask a question, and participants will take turns giving their valuable insight. The online meeting was recorded, lasting about one and a half hours.

TABLE IV. PARTICIPANT DEMOGRAPHIC

Demographic	No
Gender	
Female	4
Male	2
Age	
30 - 34	1
35 - 40	1
41 - 45	4
Employment Status	
Academician	4
Researcher	2
Field of Expertise	
User experiences	2
Serious games	3
Persuasive Computing	1
Years of experience in the field	
5 - 9	3
Ten and Above	3

V. DISCUSSION

A. Result and Findings

Based on the discussion, we present the results and analyze them based on the questions during the discussion. The first question gauged the comprehensiveness of the proposed framework. The experts agreed that the components related to interactive learning have a direct effect on the digital storytelling application. Although, some comments are worth to be considered for further improvement. The synchronization of component plot and characters is a noteworthy point. When designing digital storytelling, it is important to ensure that the character's design and implementation are suitable to the story's context. As a result, the impact on interactive learning may be observed more clearly. Two experts discovered that the settings component has little effect on the digital storytelling parts. However, the other experts contended the setting is needed to differentiate the stories and their environment. Thus, the setting component remains in the framework.

The discussion also revolved around the issues of improving the learning outcome. However, it was explained that the issue is not the main objective of the framework. It is part of the learning process that should be considered in future work. Therefore, all experts mutually agreed that based on the given input, the scope of the study, and their expertise in the field, the framework and its constituents are likely to be deemed comprehensive.

The second question concerns consensus on the framework's components. This question was posed as a follow-up to the previous one. The purpose of this question was to ensure that the components were well-considered. After the discussion, the experts generally agreed on all the components. In response to the third question, none of the experts mentioned any concerns that would suggest a problem

with the components. After further explanation, the experts remark on their understanding of the study context.

The discussion for the final topic revolves around remarks and suggestions for further improvement. Apart from what has already been stated, the experts are more interested in the framework's implementation, notably the application design and evaluation strategy. It would be beneficial if the findings were presented in separate sessions.

B. Refind Framework

According to the expert interviews, the framework was devoid of Dementia-related features. As a result, the Dementia parts were included in the framework as shown in Fig. 5. To make each session more pronounced, the title will be included. Furthermore, significant sections between each framework session may be tightly associated.

Based on the expert interview comments, the following adjustments were made to the proposed model:

- Add framework sections- Information: The five key messages of Dementia friends which involved with 1) Dementia is not a natural part of ageing, 2) Dementia is caused by diseases of the brain, 3) Dementia is not just about losing your memory, 4) It is

possible to live well with Dementia, 5) There is more to the person than the Dementia.

These five fundamental messages are a starting point for understanding Dementia [39]. It is a critical step toward understanding Dementia. The five significant messages were reviewed and turned into a game called Teatime. The game's intended audience is the family of patients in the early stages of Dementia. The game symbolizes a possible Dementia symptom. However, another interactive platform to comprehend Dementia for youngsters will need to be created [39].

- Add a title to each section;
- System: Interactive Learning Setting Platform
- Platform: Digital storytelling Delivery Information: The key message of Dementia friends.
- Links were added to each session;
- System Applied Platform. Use the interactive learning system to apply to the digital storytelling platform.
- Platform Deliver Information. For the user to receive the information to increase their knowledge.

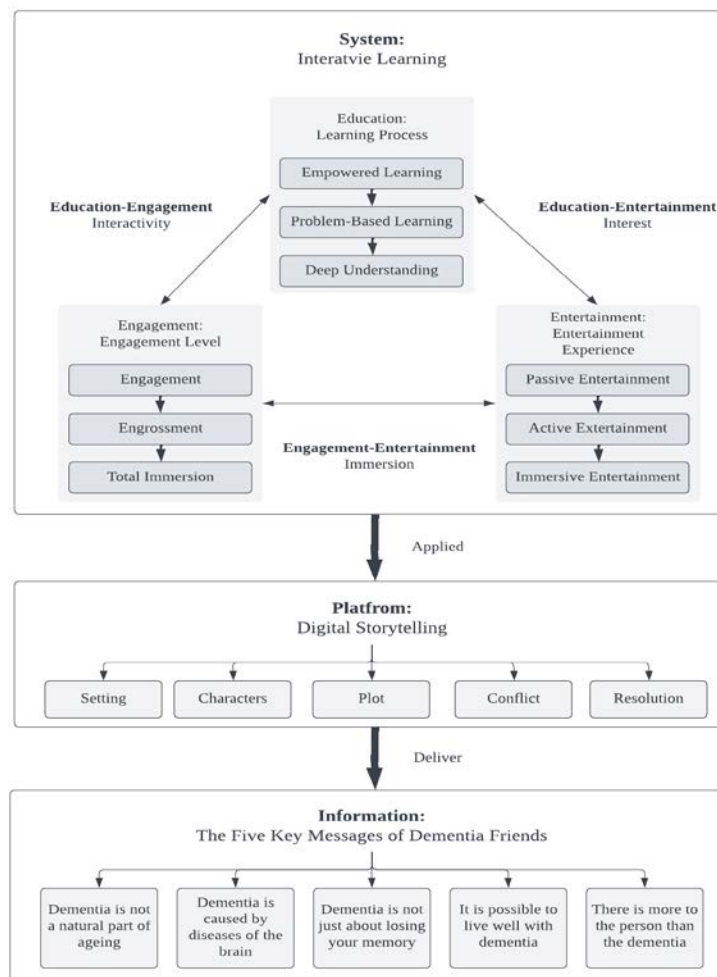


Fig. 5. Refined Conceptual Framework.

VI. CONCLUSION

In general, having a digital storybook can help young children interact with and sustain relationships with their grandparents. This study proposes a framework for a Dementia digital storybook for young children to assist them in comprehending their grandparents' condition. The framework was developed after an examination of applications and a review of the literature. The system featured two key interconnected components: an interactive learning environment and digital storybook elements. The framework's relevant components have been synthesized, and an expert review study has verified it. As a result, while considering the specific application for a Dementia digital storybook, these elements are seen as critical. This study contributes a new guideline for the designer and developer of a Dementia-related application to increase children's comprehension.

A prototype of a Dementia digital storybook for youngsters will be built for future development. This prototype will be evaluated with a range of users, including youngsters and family members with Dementia. The testing findings will eventually be used to prove the framework's validity. Overall, this approach is a useful resource for creating interactive learning aids to understand Dementia better. As part of the current study, children may learn about many long-term diseases (such as [16]) using a digital narrative framework.

The conceptual framework may be expanded with extensive knowledge about Dementia or substituted for various issues, particularly during an informative session. As a result, this research may be broadened to analyze how individuals become more aware of social concerns such as human rights, gender equality, and global warming.

REFERENCES

- [1] Hughes, J. C., Hope, T., Savulescu, J., & Ziebland, S. "Carers, ethics and Dementia: a survey and review of the literature", *International Journal of Geriatric Psychiatry*, vol. 17, no. 1, pp.35–40, 2002.
- [2] Miron, A. M., Thompson, A. E., McFadden, S. H., & Ebert, A. R. "Young Adults' Concerns and Coping Strategies Related to their Interactions with their Grandparents and Great-Grandparents with Dementia", *Dementia*, vol. 18, pp. 1025–1041, 2019.
- [3] Sun, Y., Wang, Y., Kim, H. M., Kwong, J., Xu, Y., Kim, S., McLaughlin, M. "GPS tracking in Dementia caregiving: Social norm, perceived usefulness, and behavioral intent to use technology", *Proceedings of the Annual Hawaii International Conference on System Sciences*, vol. 2020-January, pp. 3804–3817, 2021. <http://doi.org/10.24251/hicss.2021.461>.
- [4] Vallejo, D., Schez-Sobrino, S., Albusac, J., Castro-Schez, J. J., & Glez-Morcillo, C. "An agent-based approach to physical rehabilitation of patients affected by neurological diseases", *Procedia Computer Science*, vol. 160, pp. 346–353, 2019. <http://doi.org/10.1016/j.procs.2019.11.081>.
- [5] Thorpe, J., Forchhammer, B. H., Maier, A. M., Ortiz-Barrios, M., Nugent, C., Cleland, I., McLaughlin, M. "Brain Training Games Enhance Cognitive Function in Healthy Subjects", *Proceedings of the 54th Hawaii International Conference on System Sciences*, vol. 38, no. 1, pp. 1260–1262, 2020. <http://doi.org/10.21462/ijefl.v4i1.94>.
- [6] Ortiz-Barrios, M., Nugent, C., Cleland, I., Donnelly, M., & Verikas, A. "Selecting the most suitable classification algorithm for supporting assistive technology adoption for people with Dementia: A multicriteria framework", *Journal of Multi-Criteria Decision Analysis*, vol. 27, no. 1–2, pp. 20–38, 2020.
- [7] Al-Thaqib, A., Al-Sultan, F., Al-Zahrani, A., Al-Kahtani, F., Al-Regaiey, K., Iqbal, M., & Bashir, S. "Brain Training Games Enhance Cognitive Function in Healthy Subjects", *Medical Science Monitor Basic Research*, vol. 24, pp. 63–69, 2018.
- [8] Mohd Hassan, N. A., Baharum, A., Abdullah Sani, Z. H., Chau, K., & Mat Noor, N. A. (2021). "Reducing Cognitive Impairment Among Dementia Users Through Mobile Application". *Pertanika Journal of Science & Technology*, 29(2).
- [9] Wang, L., Lee, H., & Ju, D. Y. "Impact of digital content on young children's reading interest and concentration for book", *Behaviour & Information Technology*, vol. 38, no. 1, pp. 1–8, 2019.
- [10] Hardy, P., & Sumner, T. "Cultivating Compassion: How Digital Storytelling is Transforming Healthcare (Second Edi)", Palgrave Macmillan, 2018.
- [11] Chan, C., & Sage, M. "A narrative review of digital storytelling for social work practice", *Journal of Social Work Practice*, vol. 35, no. 1, pp. 63–77, 2021.
- [12] Yuksel-Arslan, P., Yildirim, S., & Robin, B. R. "A phenomenological study: teachers' experiences of using digital storytelling in early childhood education", *Educational Studies*, vol. 42, no. 5, pp. 427–445, 2016.
- [13] Robin, B. R. "The power of digital storytelling to support teaching and learning", *Digital Education Review*, 30(30), 17–29, 2016.
- [14] Zapata, A., & Van Horn, S. "Because I'm smooth": Material intra-action and text productions among young Latino picture book makers", *Research in the Teaching of English*, vol. 51, no. 5, pp. 290–315, 2017.
- [15] Rossiter, M. Gracia, P. A. "Digital storytelling: A new player on the narrative field", *New Directions for Adult and Continuing Education*, pp. 37–48, 2010.
- [16] Laing, C. M., Moules, N. J., Estefan, A., & Lang, M. "Stories That Heal: Understanding the Effects of Creating Digital Stories With Pediatric and Adolescent/Young Adult Oncology Patients", *Journal of Pediatric Oncology Nursing*, vol. 34, no. 4, pp. 272–282, 2017.
- [17] Qian, M., & Clark, K. R. "Game-based Learning and 21st century skills: A review of recent research", *Computers in Human Behavior*, vol. 63, pp. 50–58, 2016. <http://doi.org/10.1016/j.chb.2016.05.023>.
- [18] Robin, B. "The Educational Uses of Digital Storytelling", In C. Crawford, C. R. Carlsen, K. McFerrin, J. Price, R. Weber, & Willis, D. (Eds.), *Proceedings of SITE 2006--Society for Information Technology & Teacher Education International Conference*, pp. 709–716, 2006. Orlando, Florida, USA: Association for the Advancement of Computing in Education (AACE).
- [19] Yuksel, P., Robin, B., & McNeil, S. "Educational Uses of Digital Storytelling all around the World", In M. Koehler & P. Mishra (Eds.), *Proceedings of SITE 2011--Society for Information Technology & Teacher Education International Conference*, pp. 1264–1271, 2011. Nashville, Tennessee, USA: Association for the Advancement of Computing in Education (AACE).
- [20] Ali Ismail, H. A. "Integrate Digital Storytelling in Education", *Journal of Education and Practice*, vol. 6, no. 9, pp. 126–129, 2015.
- [21] Benmayor, R. "Digital Storytelling as a Signature Pedagogy for the New Humanities", *Arts and Humanities in Higher Education*, vol. 7, no. 2, pp. 188–204, 2008.
- [22] Ioannidis, Y., Raheb, K. E., Toli, E., Katifori, A., Boile, M., & Mazura. "One object many stories: Introducing ICT in museums and collections through digital storytelling", In *Digital Heritage 2013 - International Congress (DigitalHeritage)*, pp. 421–424, 2013.
- [23] Geneske, J. (2014). "Digital Storytelling For Social Impact", the Rockefeller Foundation, Accessed on: Oct 13, 2021. [Online]. Available: <https://www.rockefellerfoundation.org/blog/digital-storytelling-social-impact/>
- [24] Gee, J. P. "Video Games, Design, and Aesthetic Experience", *Rivista Di Estetica*, vol. 63, no. 63, pp. 149–160, 2016.
- [25] Rungsrirawat, S., & Chankoson, T. "Engagement With Online Media", *Journal of Security and Sustainability Issues*, vol. 9, no. 4, pp. 1379–1391, 2020.

- [26] Smith, B. G., & Gallicano, T. D. "Terms of engagement: Analyzing public engagement with organizations through social media", *Computers in Human Behavior*, vol. 53, pp. 82–90, 2015.
- [27] Galloway, A. T., Fiorito, L. M., Francis, L. A., & Birch, L. L. 'Finish your soup': Counterproductive effects of pressuring children to eat on intake and affect", *Appetite*, vol. 46, no. 3, pp. 318–323, 2006.
- [28] Bartsch, A., & Hartmann, T. "The Role of Cognitive and Affective Challenge in Entertainment Experience", *Communication Research*, vol. 44, no. 1, pp. 29–53, 2017.
- [29] Brown, E., & Cairns, P. "A grounded investigation of game immersion", In ACM (Ed.), *CHI '04 Extended Abstracts on Human Factors in Computing Systems (CHI EA' 04)*, pp. 1297–3000, 2004, New York, NY, USA.
- [30] Jantakoon, T., Wannapiroon, P., & Nilsook, P. "Synthesis of Framework of Virtual Immersive Learning Environments (VILEs) Based on Digital Storytelling to Enhance Deeper Learning for Undergraduate Students". *International Education Studies*, vol. 12, no. 4, pp.198–207, 2020.
- [31] Pereira, M. F., Prahm, C., Kolbensschlag, J., Oliveira, E., & Rodrigues, N. F. "Application of AR and VR in hand rehabilitation: A systematic review", *Journal of Biomedical Informatics*, vol. 111, no. 103584, 2020.
- [32] Milk, C. (2016). Chris Milk: The birth of virtual reality as an art. Accessed on: Oct 15, 2021. [Online]. Available: https://www.ted.com/talks/chris_milk_the_birth_of_.
- [33] Molnar, A., & Kostkova, P. "Edu-interact: An authoring tool for interactive digital storytelling-based games", *Bulletin of the Technical Committee on Learning Technology*, vol. 1, no. 2–3, pp. 10–13, 2016.
- [34] Kolb, D. A. *Experiential learning: Experience as the source of learning and development* (Second Edi). Upper Saddle River, New Jersey: Pearson FT Press. 2015.
- [35] Oliver, M. B., & Bartsch, A. "Appreciation as audience response: Exploring entertainment gratifications beyond hedonism", *Human Communication Research*, vol. 36, no. 1, pp. 53–81. 2010.
- [36] Hall, A. "Personality and the use and selection of media materials", *Media Psychology*, vol. 7, pp. 377–398, 2005.
- [37] Tuah, N. M., Nizam, D. @ N. M., & Sani, Z. H. A. "Modelling the Player and Avatar Attachment based on Student's Engagement and Attention in Educational Games", *International Journal of Advanced Computer Science and Applications(IJACSA)*, vol. 12, no. 7, 2021.
- [38] Nielsen, J. "Estimating the number of subjects needed for a thinking aloud test", *International Journal of Human-Computer Studies*, vol. 41, no. 3, pp. 385–397, 1994. <http://doi.org/10.1006/ijhc.1994.1065>.
- [39] Liu, N. Y. C., Wills, G., & Ranchhod, A. "Game for supporting Dementia carers". In *2018 IEEE Games, Entertainment, Media Conference (GEM)*, pp. 1-8, August 2018, Galway, Ireland, IEEE.

Optimization of Small Sized File Access Efficiency in Hadoop Distributed File System by Integrating Virtual File System Layer

Neeta Alange¹

Research Scholar

Department of Computer Science and Engineering
Koneru Lakshmaiah Education Foundation
KL Deemed to be University, Vaddeswaram, AP, India

Anjali Mathur²

Associate Professor

Department of Computer Science and Engineering
Koneru Lakshmaiah Education Foundation
KL Deemed to be University, Vaddeswaram, AP, India

Abstract—Storage for large datasets, handling data in different formats and data getting generated with high speed are the major highlights of the Hadoop because of which the Hadoop got invented. Hadoop is the solution for the big data problems as discussed above. In order to give the improved solution (in terms of access efficiency and time) for small sized files, this solution is proposed. A novel approach called VFS-HDFS architecture is designed in which the focus is on optimization of small sized files access problems with significant development compared with the existing solutions i.e. HDFS sequence files, HAR, NHAR. In the proposed work a Virtual file system layer has been added as a wrapper over the top of existing HDFS architecture. However, the research work is carried out without altering the existing HDFS architecture. In this paper drawbacks of existing techniques i.e. Flat File Technique and Table Chain Technique which are implemented in HDFS HAR, NHAR, sequence file is overcome by using Bucket Chain Technique. The files to merge in a single bucket are selected using ensemble classifier which is a combination of different classifiers. Combination of multiple classifiers gives the better accurate results. Using this proposed system, better results are obtained compared with the existing system in terms of access efficiency of small sized files in HDFS.

Keywords—HDFS; Small sizes files; virtual file system; bucket chain; ensemble classifiers; text classification

I. INTRODUCTION

This Hadoop Distributed File System (HDFS) is a core component of Hadoop which works at storage layer of Hadoop. Advantages of HDFS includes varied data sources, availability, scalable, cost effective, low network traffic, ease of use, performance, high throughput, compatibility, fault-tolerant, open source and multiple language support etc. Apart from these multiple advantages, HDFS have limitations too such as handling small files, slow processing speed, support for batch processing, no real time data processing, no Delta Iteration, latency, not easy to use, security etc. Storing and processing of large number of small sized files in HDFS is a major problem. Hadoop Archives provides an efficient way to handle with small files [20].

Hadoop working is best with respect to big data files; small sized files are handled inefficiently in HDFS. NameNode carries the metadata information in memory for the files which are stored in HDFS. Consider a file which is stored in HDFS

having size as 1 GB and the NameNode is responsible for storing the information such as filename, offset, length etc. which are split into 1000 fragments and stored all 1000 small files in HDFS. It is mandatory for the NameNode to store metadata information of 1000 small files in memory. This is not efficient way; first it takes up a lot of memory and second soon NameNode will become a bottleneck as it is trying to manage a lot of data [30].

Due to the outbreak of a COVID-19 pandemic, the entire world is now working in online mode. As a result, a massive volume of data has been generated, making it extremely complex to store, analyze and handle. The term big data generally used for this. The generated large volume of data which is in the form of structured or unstructured format. There is an immense need of analyzing and classifying this data in terms of size. HDFS gives the solution for this, which is responsible for handling large files in GBs or TBs in size of unlimited storage. HDFS works closely with the small number of large files. It is inefficient for handling large number of small files. Large number of small sized files consume more memory on the NameNode of the HDFS. Access mechanism of small sized files concept is a major problem in HDFS[8],[9],[10].

1) *Paper organization:* The rest of the paper is organized as follows: Section II gives the related surveys present in the existing literature. Section III provides the discussion on existing solutions on the given problem statement. Section IV describes the proposed work. Section V focusses on experimental set up and results produced. Section VI finally concludes the article.

II. LITERATURE REVIEW

Xiong et al [1] employed a small file usage pattern to identify candidate files for merging into a single container. Identified gap in this article as and when the HDFS user request pattern changes there is a chance of cache missing.

Zhipeng et. al [4] discussed about merge strategy based hierarchy for improving the small file problem in HDFS, Bing et.al [5] created a novel approach HDFS:TLB MapFile for efficient accessing of small files, Sachin et al [6] discussed about different techniques of dealing with a small files

problem. Authors discussed about Hadoop Archive i.e. achieving technique which binds number of small files into HDFS blocks. Another technique improved HDFS model is index-based i.e. index is built for each small file to reduce the waste caused by them which reduces the burden on the NameNode. EHDFS gives an improved indexing mechanism and prefetching of index information. Lion Jude Tchaye-Kondi et al. [13] encouraged using hash functions to create a perfect file. To get the metadata of a specific file, this approach removes the requirement of parsing the index file. Xun Cai et al. [14] improved the access and storage efficiency of small files. Yanfeng Lyu et al. [15] proposed an efficient merging method that substantially reduces the access time for small files by using caching and prefetching methods. X. Fu et al. [16] proposed a block replica placement technique for effectively processing small files where files are merged as per the pre-determined parameters. Qi Mu et al. [17] advised a method for dealing with small files that is both efficient and effective. T. Wang et al. [18] suggested a method based on the behavior of small files access to build association between the small files. In this article, the concept focusses exclusively on file size. The gap identified in this, file contents have not been checked. If there is a mismatch in the file sizes, then cache will be missed.

III. EXISTING METHODS

A. HAR (Hadoop Archives)

HAR files were created to reduce the problem among several files putting a pressure on the memory of name nodes. On the HDFS, a layered system has been installed. The Hadoop archive command is used to create HAR files. It is not more efficient to read through files in a HAR than it is to read across files in Hadoop. Each HAR file access needs the reading of two index files in addition to the data file, which slows down the process [2],[7],[19],[20]. The flat table technique is used to implement the HAR.

Limitations of HAR files:

- Hadoop archive file once created is not updatable i.e. to adding or removing of the file is not possible.
- This archive file will contain a replica of all the original files when ‘.har’ is created and it will take more space as the original files.

B. NHAR (New HAR)

For NameNode, processing a large number of small files takes more time. In fact, the amount of time it takes to access such data should be minimized. NHAR [2],[7],[11],[12] is a novel solution that relies on Apache Hadoop’s HAR. The table chain technique is used to implement NHAR.

C. Spatiotemporal Small File Merging Strategy

In previous work, Lion Xiong et al. [1] employed a small file usage pattern to identify candidate files for merging into a single container. They employed file access time stamps to analyze usage patterns, then grouped files with sequential time stamps and generated support files for each file group. A single container is used to store a file group with a high support value.

IV. PROPOSED SYSTEM

In this paper, the proposed technique is implemented by creating a wrapper over existing HDFS architecture without altering the HDFS architecture[5]. The Wrapper contains the Virtual file table which maintains the records of every file category wise like offset, length etc. Using large number of small files with different sizes analyzed the experimental results. Ultimately the time required for accessing files in HDFS is improved.

A. Bucket Chain Technique

Working methodology of the proposed system is shown in Fig. 1. The root file table contains the list of files category wise, in which the information is gained about the existence of file category. The Bucket or child per category file table contains the metadata of the per category container which holds the metadata as Name, Offset and length of the category. Every child per category file table gives the metadata of the per category container file where the actual contents of the file can receive. Then it can directly access the contents of the actual file as that of reading or getting a file which is working with HDFS.

The advantages of the technique are if a user tries to access the same file repeatedly, the cache only gives the information quickly about the file location reducing the multiple searching and reading overheads.

B. Methodology

In this method all file’s metadata is stored in a single file, this file is called File Table. This file contains linked list of tables, forming a table chain. Another file is used to store actual contents of files; this file is called Container File. One container file is used for each category. All these files are stored on HDFS. File table contains metadata of a file such as filename, offset, and length.

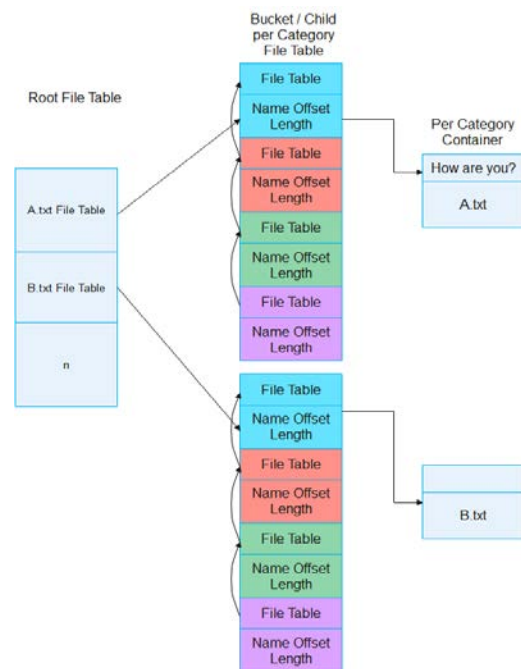


Fig. 1. Bucket Chain Technique for Proposed System (VFS-HDFS).

Before storing every file, it is classified using ensemble classifier to get its category. That file is then stored in container of that category and corresponding file table is also updated.

On startup, the file table for each category is loaded in memory. First the latest file table is located in file table and its contents are added to in-memory file table, then previous file table is located and the process continues until first file table is reached. While doing this, a file's metadata is already found in in-memory file table, then that entry is discarded (as it has become old due to updating or deletion of file).

In every run, a new in-memory file table for each category is created to track new or updated files in that category. At runtime all metadata is created and updated operations are performed on this in-memory file table. Actual contents of the files are appended in container file. On shutdown, the contents of in-memory file tables are appended to file table in HDFS. This creates a chain of buckets, each bucket stores list of file tables which makes it possible to update and delete files.

For reclaiming space used by deleted or updated files, the technique of pruning is used. In this technique new copies of file tables are creating while skipping the deleted or updated entries. This will reduce space required for file tables and containers.

Caching is used to reduce time required for reading files in already retrieved blocks. Each cache entry stores tuple of category, file, position, length and its complete block content. This will reduce time at the cost of increased memory requirement.

C. Algorithm: Bucket Chain

```
globals:
    filenametable
    indexfilemap
    containerfilemap
    filetablemap
    newfiletablemap
    classification_model
    categorylist
function initialize()
    filenamemap=load_filenamemap()
    for cat ∈ categorylist
        indexfile=indexfilemap[cat]
        containerfile=containerfilemap[cat]
        filetable=filetablemap[cat]
        file_index_location=get_last_index(indexfile)
        while file_index_location != NULL
            indices=read_index(file_index_location)
            filetable = filetable ∪ (indices - (filetable ∩ indices))
        file_index_location=get_prev_index(file_index_location)
```

```
function add_file(filename, content)
    cat = classify(classification_model, content)
    location=append_content(containerfilemap[cat], content)
    add_file_entry(newfiletablemap[cat], filename, location, len(content))
    add_filenametable(filenametable, filename, cat)
function get_file(filename)
    cat = get_category(filenametable, filename)
    location, length = find_file(newfiletablemap[cat], filetable[cat], filename)
    data = read_content(containerfilemap[cat], location, length)
    return data
function close()
    for cat ∈ categorylist
        last_index=get_last_index(indexfilemap[cat])
        append_entry_table(indexfilemap[cat], newfiletable[cat])
        append_prev_index(last_index)
    update_filenametable(filenametable)
```

D. Advantages of Bucket Chain Technique

- 1) It has separate category wise containers.
- 2) It contains cache memory.
- 3) Pruning is applied to remove unused files in containers to reduce the memory wastage.
- 4) Optimal File Table Size.
- 5) Access time efficiency improved.

E. Text Classification

It is used to classify the text documents automatically into one or multiple defined categories (Fig. 2). Category of news article from Reuters-21578 Text Categorization dataset [21] is taken into consideration for text classification Text classification consists of main components [23].

- 1) Dataset Preparation.
- 2) Feature Engineering.
- 3) Model Training.
- 4) Improve Performance of text classifier.

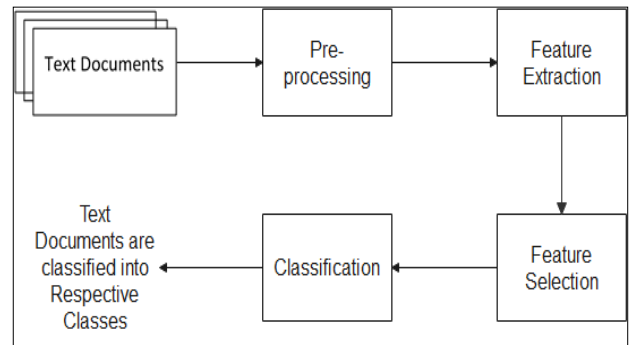


Fig. 2. Text Classification Task.

F. Datasets Used

Experimentation is done on the Reut2-000.sgm & Reut2-002.sgm files. of Reuters dataset.

Table I gives information about the datasets used.

TABLE I. DESCRIPTION OF DATASET

Name of Dataset	Data Types	Default Task	Attribute Type	No. of Instances	No. of Classes	Year
Reuters-21578 Text Categorization Collection	Text	Classification	Categorical	1000	70	1997

G. TF-IDF

The technique stands for Term Frequency- Inverse Document Frequency which is used to quantify words from documents; a weight has been assigned to each word which states the significance of each word in the document and its collection. TF-IDF score signifies the relative importance of a keyword or a term in the document and the entire corpus. It is calculated as the logarithm of the number of the documents in the corpus divided by the number of documents where the definite term appears [23].

Formula: $idf(t) = \log(N/df)$

The tf-idf metric is calculated by considering the total number of documents, dividing it by the number of documents that which contain a word and calculating the logarithm.

$tfidf(t) = tf(t) * idf(t)$

H. Classifiers used for Experimentation:

1) *J48 classifiers*: It deals with issues such as numeric attributes, missing values, pruning, predicting error rates, decision tree induction complexity etc[3].

2) *Random forest*: It determines the outcome based on decision tree predictions. It estimates an average of the output of various trees [24].

3) *Naive bayes classifiers*: It is capable of dealing with both discrete and continuous data. It can handle a large number of predictions and data sets [25].

4) *Ensemble classifiers*: For classification purpose the ensemble learning method is used. Fig. 3 describes the architecture of ensemble classifier. These ensembles combine multiple hypotheses to form a better hypothesis. Ensemble learning supports to improve machine learning results as compared to a single model by combining several models. Basic idea is to learn a set of classifiers and to allow them for vote. Combination of Random Forest, Naïve Bayes and J48 classifiers are used for experimentation [26].

Advantages: Motivation behind to use ensemble classifier is to improve the predictive accuracy.

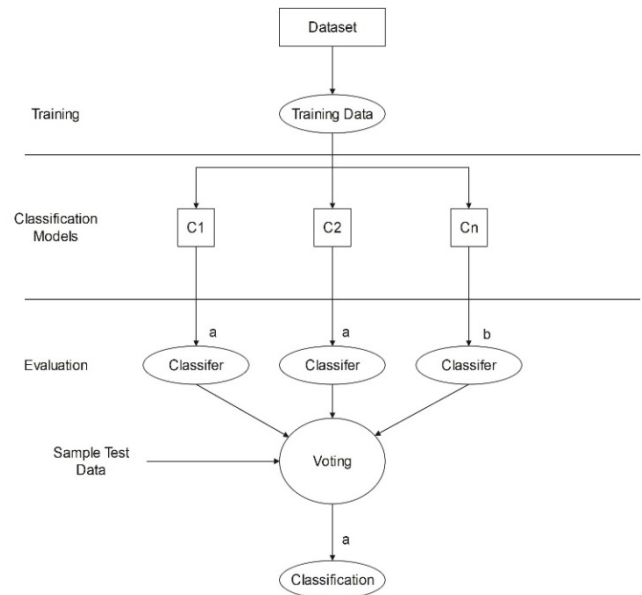


Fig. 3. Architecture of Ensemble Classifier.

V. EXPERIMENTAL SETUP, RESULTS AND ANALYSIS

The proposed system is implemented on top of existing HDFS architecture. The proposed algorithm is experimented on Fedora 32.0 Operating System, Hadoop 3.2.0 and Java 1.8.0 Version. It contains 16 GB of RAM and 500 GB of Hard Disk with i5-5500U CPU @ 2.20GHz processor. Reuters-21578 Text Categorization Collection dataset is used to test the proposed system.

Table II shows the experimental set up used to execute the proposed work.

Table III shows how much memory and time is required to access small sized files in bucket chain algorithm.

TABLE II. EXPERIMENTAL SETUP

Sr. No.	Parameters	Description
1	No. of Nodes	Single Node (Acts as both Master & Slave)
2	Node Configuration	Intel(R) Core(TM) i5-5500U CPU @ 2.20GHz
3	RAM	16 GB
4	Hard Disk	500GB
5	Operating System	Fedora 32.0
6	Execution Platform	JDK 1.8.0
7	Hadoop Version	3.2.0
8	Development Tool	Net Beans 12.0
9	Dataset	Reuters containing TEXT files
10	Number of Files considered	2138
11	File Size Range	Average From 1 KB to 100 KB
12	No. of Iterations	1000
13	No. of Classes	70

TABLE III. MEMORY AND TIME REQUIREMENT FOR PROPOSED SYSTEM (VFS-HDFS I.E. BUCKET CHAIN TECHNIQUE)

Memory & Time Requirement for Proposed Technique (VFS-HDFS i.e. Bucket Chain Algorithm) for 1000 Iterations		
Average File Size	Memory (in MB)	Time (in Seconds)
1K	30.7	39
5K	31	39
10K	35.2	41
50K	40.5	46
100K	55.2	55

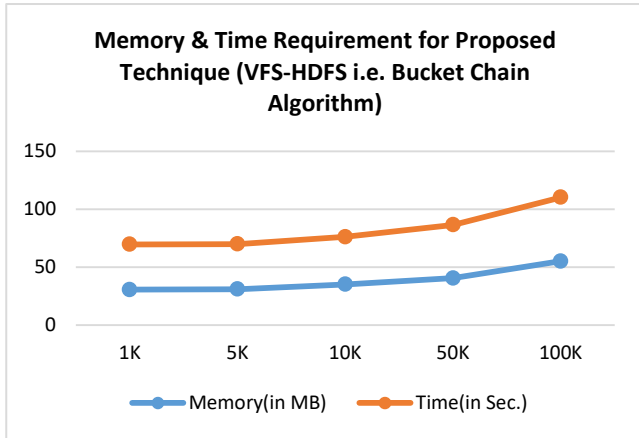


Fig. 4. Performance with respect to Time and Memory for Proposed Technique (VFS-HDFS, using Bucket Chain Algorithm).

The above graph in Fig. 4 indicates the performance of the proposed technique in terms of time and memory.

Table IV shows the comparative chart of Experimental results of existing technique and proposed Technique VFS-HDFS using Bucket chain algorithm. where the memory requirement is increased due to the cache.

The graph in Fig. 5 shows the comparative chart of experimental results of existing and proposed technique VFS-HDFS using Bucket chain algorithm.

Table V shows the comparative chart of Experimental results of existing technique and proposed technique-VFS-HDFS using Bucket chain algorithm; where small files access time efficiency is increased.

TABLE IV. COMPARATIVE CHART FOR MEMORY REQUIREMENT FOR EXISTING (HAR & NHAR) AND PROPOSED TECHNIQUE (VFS-HDFS USING BUCKET CHAIN ALGORITHM)

Memory Requirement for 1000 Iterations			
Average File Size	HAR (in MB)	NHAR (in MB)	VFS-HDFS (in MB)
1K	16.2	19	30.7
5K	16.5	19.1	31
10K	17.1	21.2	35.2
50K	19.3	23.1	40.5
100K	27.4	35.8	55.2

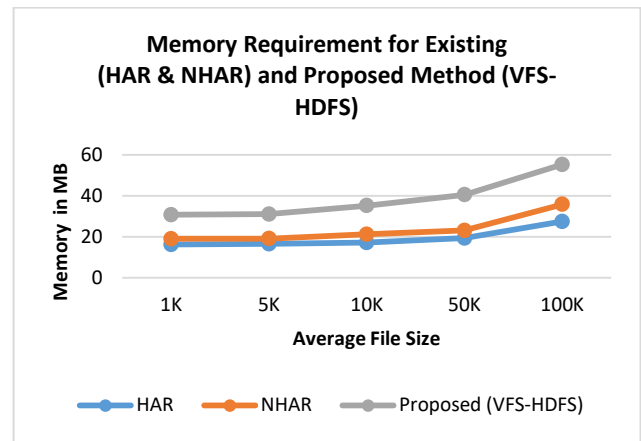


Fig. 5. Memory Requirement Existing and Proposed Technique VFS-HDFS using Bucket Chain Algorithm.

TABLE V. COMPARATIVE CHART FOR TIME REQUIREMENT FOR EXISTING AND PROPOSED TECHNIQUES USING BUCKET CHAIN ALGORITHM

Time Requirement for 1000 Iterations			
Average File Size	HAR (in Seconds)	NHAR (in Seconds)	VFS-HDFS (in Seconds)
1K	56	45	39
5K	58	45	39
10K	64	48	41
50K	71	57	46
100K	97	70	55

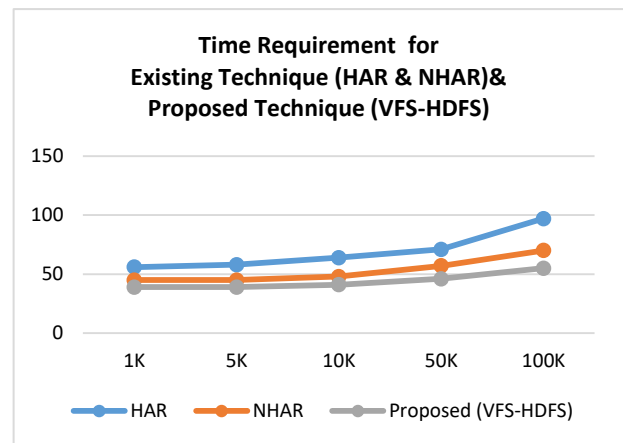


Fig. 6. Time Requirement for Existing and Proposed Technique VFS-HDFS using Bucket Chain Algorithm.

Fig. 6. shows the comparative chart of Experimental results of existing technique and proposed Technique-VFS-HDFS in terms of time using Bucket chain algorithm.

Classifier Metrics:

Table VI gives the information about different classifiers used and the corresponding experimental results.

Confusion Matrix for a single class:

Confusion matrix is created for class “earn” from ret2-002.sgm file.

TABLE VI. DIFFERENT CLASSIFIER METRICS ALONG WITH ENSEMBLES

Parameters	Naïve Bayes	J48	Random Forest	Ensemble (Naïve Bayes+J48+Random Forest)
Total Instances	962	962	962	962
Correctly Classifies Instances	684	738	899	922
Incorrectly Classified Instances	278	224	63	40
Accuracy	71%	77%	93%	96%

TABLE VII. CONFUSION MATRIX

Total Instances N=962	Actually Positive	Actually Negative
Predicted Positive	131	40
Predicted Negative	0	791

Table VII shows the confusion matrix [22] of the instances of the earn class.

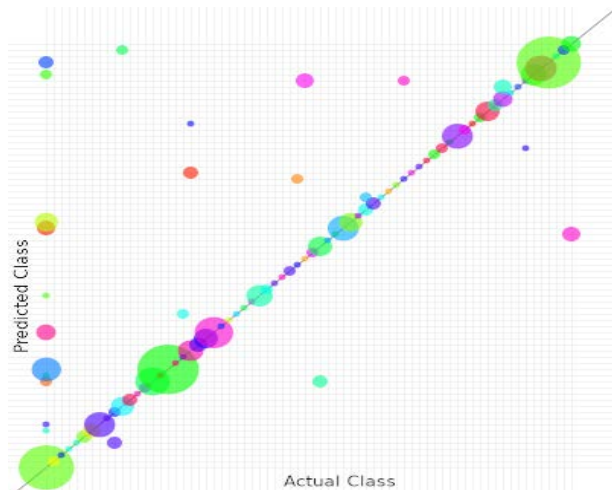


Fig. 7. Accuracy of Classification and Predictions.

The above graph in Fig. 7 shows the bubble chart of accuracy of classification and predictions of total 70 classes. X-axis indicates the actual class. Y-axis indicates the predicted class. Instances on 45-degree line are correctly classified instances. Incorrectly identified instances are randomly shown in random positions. Size of bubble indicates number of instances in that position.

VI. CONCLUSION

In this paper, a novel approach called *VFS-HDFS* architecture is proposed in which exclusive focus is on optimization of the access efficiency of small sized files in HDFS with a significant improvements compared with the existing techniques i.e. flat table (HAR) and table chain (NHAR) technique. A new algorithm is proposed called bucket chain algorithm and the entire work is executed using this algorithm where memory requirement is increased to store the files in cache and time required to access the files from the cache is reduced. The proposed work uses the ensemble classifiers to classify the data sets. It helps to group the similar files in same container. Comparison is made between the

experimental results of existing approach-i.e. flat table and table chain techniques and the proposed technique-bucket chain technique. In the proposed system it is observed that time required to access the files is reduced at the cost of memory required to store the files.

REFERENCES

- [1] Lian Xiong et al. "A Small File Merging Strategy for Spatiotemporal Data in Smart Health", IEEEAccess Special Section on Advanced Information Sensing and Learning Technologies for Data-Centric Smart Health Applications, Volume 7, 2019.
- [2] Neeta Alange, Anjali Mathur, "Access efficiency of small sized files in Big data using various techniques on Hadoop Distributed File System Platform", International Journal of Computer Science and Network Security Volume.21, No.7, July 2021.
- [3] N. Saravanan et. al "Performance and Classification Evaluation of J48 Algorithm and Kendall's Based J48 Algorithm (KNJ48)" International Journal of Computational Intelligence and Informatics, Vol.7:No.4, March 2018.
- [4] Zhipeng et al "An Effective Merge Strategy Based Hierarchy for Improving Small File Problem on HDFS" IEEE Proceedings of CCIS 2016, pp. 327-331.
- [5] Alam et al. "Hadoop Architecture and its issues." International Conference on Computational Science and Computational Intelligence (CSCI), 2014 Vol. 2. IEEE, 2014.
- [6] Sachin et al "Dealing with small files problem in hadoop distributed file system", Procedia Computer Science Volume 79, 2016.
- [7] Ankita et al "A Novel Approach for Efficient Handling of Small Files in HDFS", IEEE International Advance Computing Conference (IACC, 2015), pp.1258-1262.
- [8] Nivedita et. al "Optimization of Hadoop Small File Storage using Priority Model", 2nd IEEE International Conference On Recent Trends in Electronics Information & Communication Technology (RTEICT), pp. 1785-1789, May 2017.
- [9] Awais et al "Performance Efficiency in Hadoop for Storing and Accessing Small Files" 7th International Conference on Innovative Computing Technology (INTECH 2017), pp.211-216.
- [10] Neeta Alange, Anjali Mathur, "Small Sized File Storage Problems in Hadoop Distributed File System", 2nd International conference on Smart Systems and Inventive Technology (ICSSIT 2019) vol. pp. 1198-1202, November 2019 proceedings published in IEEE Digital Xplore.
- [11] Shubham et. al "An approach to solve a Small File problem in Hadoop by using Dynamic Merging and Indexing Scheme", International Journal on Recent and Innovation Trends in Computing and Communication [IJRITCC], November 2016, Volume: 4, Issue:11.
- [12] Priyanka et al "An Innovative Strategy for Improved Processing of Small Files in Hadoop", International Journal of Application or Innovation in Engineering & Management (IJAIEM), Volume 3, Issue 7, July 2014, pp. 278-280, ISSN 2319 – 4847.
- [13] J. Tchaye-Kondi, Y Zhai et al. "Hadoop Perfect File: A fast access container for small files with direct in disc metadata access", 2019, arXiv:1903.05838.
- [14] X. Cai, C. Chen et al. "An optimization strategy of massive small files storage based on HDFS", in Proc. JIAET, 2018, PP. 225-230.
- [15] Y. Lyu, X. Fan, and K. Liu, "An optimized strategy for small _les storing and accessing in HDFS," in Proc. IEEE Int. Conf. CSE, IEEE Int. Conf. EUC, Jul. 2017, pp. 611_614.
- [16] X. Fu,W. Liu, Y. Cang, X. Gong, and S. Deng, "Optimized data replication for small _les in cloud storage systems," Math. Problems Eng., vol. 2016, pp. 1_8, Dec. 2016.
- [17] Q. Mu,Y. Jia, and B. Luo, "The optimization scheme research of small _les storage based on HDFS," in Proc. 8th Int. Symp. Comput. Intell. Design, Dec. 2015, pp. 431_434.
- [18] T. Wang, S. Yao, Z. Xu, L. Xiong, X. Gu, and X. Yang, "An effective strategy for improving small _le problem in distributed _le system," in Proc. 2nd Int. Conf. Inf. Sci. Control Eng., Apr. 2015, pp. 122_126.
- [19] Online Reference Apache Hadoop, <http://hadoop.apache.org/>.

- [20] Online Reference <https://blog.cloudera.com/blog/2009/02/the-small-files-problem/>.
- [21] Dua, D. and Graff, C. "UCI Machine Learning Repository Dataset" [<http://archive.ics.uci.edu/ml>]. Irvine, CA: University of California, School of Information and Computer Science, 2019.
- [22] Online Reference <https://www.dataschool.io/simple-guide-to-confusion-matrix-terminology/>.
- [23] Online Reference <https://www.analyticsvidhya.com/blog/2018/04/a-comprehensive-guide-to-understand-and-implement-text-classification-in-python/>.
- [24] Online Reference <https://www.section.io/engineering-education/introduction-to-random-forest-in-machine-learning/> random forest classifier.
- [25] Wikipedia contributors. Naive Bayes classifier. In Wikipedia, the Free Encyclopedia. Retrieved 14:24, September 30, 2021, from https://en.wikipedia.org/w/index.php?title=Naive_Bayes_classifier&oldid=1039393803.
- [26] Online Reference <https://subscription.packtpub.com/book/data/9781789955750/7/ch07lv1sec45/bagging-building-an-ensemble-of-classifiers-from-bootstrap-samples>.

Survey on Highly Imbalanced Multi-class Data

Mohd Hakim Abdul Hamid¹

INSFORNET, C-ACT and Fakulti Teknologi Maklumat dan
Komunikasi (FTMK), Universiti Teknikal Malaysia Melaka
(UTeM), Hang Tuah Jaya, Melaka, Malaysia

Marina Yusoff², Azlinah Mohamed³

Institute for Big Data Analytics and Artificial Intelligence
Universiti Teknologi MARA (UiTM)
Shah Alam, Selangor, Malaysia

Abstract—Machine learning technology has a massive impact on society because it offers solutions to solve many complicated problems like classification, clustering analysis, and predictions, especially during the COVID-19 pandemic. Data distribution in machine learning has been an essential aspect in providing unbiased solutions. From the earliest literatures published on highly imbalanced data until recently, machine learning research has focused mostly on binary classification data problems. Research on highly imbalanced multi-class data is still greatly unexplored when the need for better analysis and predictions in handling Big Data is required. This study focuses on reviews related to the models or techniques in handling highly imbalanced multi-class data, along with their strengths and weaknesses and related domains. Furthermore, the paper uses the statistical method to explore a case study with a severely imbalanced dataset. This article aims to (1) understand the trend of highly imbalanced multi-class data through analysis of related literatures; (2) analyze the previous and current methods of handling highly imbalanced multi-class data; (3) construct a framework of highly imbalanced multi-class data. The chosen highly imbalanced multi-class dataset analysis will also be performed and adapted to the current methods or techniques in machine learning, followed by discussions on open challenges and the future direction of highly imbalanced multi-class data. Finally, for highly imbalanced multi-class data, this paper presents a novel framework. We hope this research can provide insights on the potential development of better methods or techniques to handle and manipulate highly imbalanced multi-class data.

Keywords—Imbalanced data; highly imbalanced data; highly imbalanced multi-class; data strategies

I. INTRODUCTION

Every single piece of information in this world is data. The nature of data is that it is not absolutely balanced [1], [2]. It is either slightly imbalanced or highly imbalanced. Highly imbalanced is a situation where the ratio among classes is elevated. For example, 80:20 or 90:10 or 95:5 (majority: minority). While the example of slightly imbalanced is 60:40 or 55:45 or 70:30 (majority: minority). According to Bellinger et al., the imbalance ratio (IR) for highly imbalanced is 1000:1 (majority: minority) [3]. A well-balanced dataset is only possible in a controlled environment in which variables are preset, and data undergoes proper preprocessing.

The advancement of machine learning (ML) facilitates and alleviates problems in data analysis. The Internet of Things (IoT) and big data technology have accelerated the utilization of big data. During the Covid-19 pandemic, ML analysis helps in many ways like in vaccine development in which the cure is

required to restrain the virus spread concisely. With advanced computers, machine learning algorithms can process trillions of data within a short period of time and make accurate predictions, or classification of the problem.

To solve imbalanced data problems, researchers employ three strategies: 1) Data Level or DL 2) Algorithm Level or AL, and 3) Combination Level or CL. DL strategy involves data manipulation activities during the pre-processing phase. Most of the DL strategies involve approaches on data before it enters classifiers. Examples of such methods are undersampling and oversampling and their variants. AL strategy involves classifier-related activities. The main objective of the AL strategy is to apply algorithms or classifiers to manage dataset and handle imbalanced data problems. There are a lot of examples for AL such as Deep Learning variants, and Support Vector Machine (SVM) and their variants. CL strategy is a combination of both DL and AL strategy. This strategy applies to both hybrid and ensemble methods, even though ensemble can also work alone in AL. Ensemble is listed under CL because in most literatures about highly imbalanced data, the ensemble algorithm is combined with some other method(s) to achieve better performance. Some literatures only mention hybrid level, without the ensemble method as part of CL strategy [4], [5]. In some other literature, the ensemble method is mentioned along with DL and AL without the hybrid method [6].

The ensemble method is an interesting area of research. Ensemble algorithms can apply ensemble algorithm to other algorithms, either supervised, semi-supervised or unsupervised (or combination of all) to produce a better algorithm. The hybrid method is also a very interesting method in ML. It combines any method in DL with AL, combines DL method with another DL algorithm(s), or combines AL with another AL method(s). Therefore, this study proposes a new term “Combination Level” for both the hybrid and ensemble methods in highly imbalanced multi-class (HIMC) data. This article then will propose a novel framework for highly imbalanced multi-class data (HIMC). This is crucial so that the structure of the framework and the relevance to future of ML can be explored. It is hoped that this research will pave the road for other researchers to excavate deeper into the nature of HIMC data and various ways to handle it.

This paper is organized into several sections. Section I presents the definition of imbalanced data, highly imbalanced data, multi-class data and highly imbalanced multi-class data. Section II provides the explanations on the research gap, research questions and research objectives. Section III presents the descriptions on the current and previous solutions in

handling imbalanced data, previous solutions in handling multi-class data and previous solutions in handling HIMC data. Section IV provides the descriptions on the prominent validation metrics for HIMC data, data type and dataset behavior along with discussion on the case study dataset. Finally, Section V presents the explanations on the proposed and refined framework of HIMC data and will be followed by Section VI, discussions on open issues. Finally, Section VII provides the conclusion.

A. Imbalanced Data

Imbalanced data is currently a prominent research topic and acts as a relatively new research interest in machine learning [1], [7]. A circumstance in which the total number of the majority class is significantly greater than the data of the minority class is known as data imbalanced [8]. Most classifiers are designed to work with a balanced dataset in which the majority class is comparable to or equal to the minority class, or the ratio between the two classes is 50:50. A balanced environment is essential to make sure the classifier can perform at the best level of accuracy. Therefore, when unequal data exists, an imbalance data problem transpires [9], [10]. Imbalanced data also occurs because of the existence of minority classes that are lowly represented [11]. It also can happen when the dataset is skewed [12]. Most classifiers in a balanced class are biased toward the majority class [13], [14], [15]. In real life, all real-world data is imbalanced [16], [17]. Real-world data can have a high chance to fall in the category of highly imbalanced data [18]–[20] or slightly imbalanced data [21].

Imbalanced data exists in numerous disciplines for example, wind turbine fault prediction [11], network diagnosis, wireless sensor application [22], acid amino detection [23], medical diagnosis [24], Internet of Things [25], fraud detection [26], and other domains. Many approaches to overcoming the problem have been offered with regard to data imbalanced problem using different solutions from DL to AL and CL strategy, such as those found in [5], [8], [11], [26]–[29].

B. Highly Imbalanced Data

To deal with the problem of data imbalance, a variety of approaches and methodologies have been proposed. DL and AL strategies focus on ways to reduce biases of classes in a dataset. CL strategy involves an ensemble or a hybrid of several algorithms to achieve the best results. Nevertheless, the problem with imbalance data is far from settled, especially in highly imbalanced data scenarios. The problem with highly imbalanced data is that the ratio is extremely high. The solution that works in slightly imbalanced data might not work in highly imbalanced data. Therefore, highly imbalanced data needs more consideration and investigation. Normal graph distribution does not present in highly imbalanced data as the graph is highly skewed.

In a slightly imbalanced data environment, a conventional method such as Synthetic Minority Over Sampling Technique (SMOTE) can help solve the problem of imbalanced data. Unfortunately, DL method like SMOTE can worsen the classification performance in highly imbalanced data environment. Using randomized methods like Random Undersampling (RUS) is also not effective due to a high

variance created in the IR. To overcome the problem of noisy data and overlapping classes, a new approach for data preprocessing is needed to boost classifiers' performance. A new approach to handle detection and filtering noisy data is needed in the scenario of relabeling classes. The problem can increase the imbalance among classes. It could result in the classifier rebalancing the wrong classes.

A highly imbalanced data problem arises when the IR is too high compared to slightly imbalanced data. For example, the ratio of minority to majority less than 50:1 can be considered slightly imbalanced while imbalance ratio (IR) more than 50:1 can be considered highly imbalanced. According to Triguero et al., IR for highly imbalanced data is 50:1 (majority: minority) [30], [31]. Another well-known IR is 100:1 up to 10000:1 [32]. The same IR (100:1) was suggested by Sharma et al. [33]. Sharma et al. suggest 100:1 as highly imbalanced while 1000:1 was categorized as extreme imbalance [33]. Table I shows benchmark of IR.

TABLE I. BENCHMARK OF IR

No.	Reference	IR	Year
1.	He & Garcia	100: 1 up 10,000:1	2009
2.	Triguero et al., Leevy et al.	50:1	2015, 2018
3.	Sharma et al.	>1000:1	2018
4.	Bellinger et al.	1000:1	2019

More practical IR was found among bioinformatics and biotechnology domains, and it was 50:1 [30], [31]. In other literatures, highly imbalanced are also known as rare events in which researchers and scholars stated that the minority data that was from 0.1% to less than 10% , can be considered as rare events [34], [35]. In the real-world, IR ranging from 1000:1 up to 5000:1 is possible in fraud detection and medical science [4], [36], [37].

This research has chosen the latest literatures as the benchmark for highly imbalanced data ratio. The latest found in literatures on IR is suggested by Bellinger et al. which is 1000:1 [3]. Therefore, for the purpose of this research, the IR stated by Bellinger et al. will be used. The ratio from Bellinger et al. has also been chosen because the dataset used in this research matches with the stated IR.

C. Highly Imbalanced Multi-Class (HIMC) Data

Problems in highly imbalanced data originate from problems in slightly imbalanced data, which are alleviated due to the nature of severe IR [3], [33]. Thus, problems in imbalanced multi-class data and highly imbalanced multi-class data can be considered similar in nature, with the difference laying in the IR.

To overcome the HIMC data issue, a new approach for data pre-processing is needed to boost classifiers' performance in HIMC data. Another solution to overcome the problem is by creating synthetic data to move overlapping data to new spaces [38]. Another method is to remove excessive samples and maintain the quality of the data [2], [6] [1], [6].

Relationship among classes is an issue in multi-class data. It is a complicated situation as each group of classes presents

different problems to the data [1], [2], [4], [38], [39]. This problem is elevated in HIMC data, and affects classifiers' performance [40], [41]. Leevy et al. and Rendon et al. suggest that more flexible methods such like the heuristic-based method should be explored to solve multi-class data problems [31], [42]. The HIMC data has multiple skewed classes which reduce classifiers' performance as it is challenging to normalize skewness [31], [43], [44], [45]. Due to skewness, it is also difficult to define borders of the overlap classes [4], [46], [47].

D. HIMC Data Research Gap

Among the major challenges with highly unbalanced data are the accuracy of classifying highly imbalanced multi-class data, training efficiency for large data, and sensitivity to high imbalance ratio (IR) [48]. In highly imbalanced data, classifiers are prone to a strong bias toward the majority class, which cannot accurately represent the true problem or convey essential information. The minority class were treated as noisy data at the pre-processed level and will cause the loss of crucial information [1], [21]. This creates new challenges to data level strategy in handling biasness [49], [43], [45].

A dataset with multiple target classes is skewed in distribution in imbalanced multi-class data, and this has a substantial effect on classifier performance [38]. HIMC data has multiple skewed classes which significantly reduce classifiers' performance as it is difficult to normalize skewness [31], [43], [44] due to the difficulty to define borders of the overlap classes [4], [47].

At algorithms level, existing classifiers are modified to remove the biases toward the majority classes. One of the methods is the cost-sensitive method. The cost of misclassification for minority samples is higher than for majority samples in the cost-sensitive method. Determining the cost values of trained data is complex since they are dependent on multiple aspects that have trade-off relationships, such as high-dimension, high noise, small sample size, and others [1], [21]. In financial data, biasness causes highly imbalanced distribution [50].

Therefore, based on arguments regarding HIMC data, this research addresses three research questions and three research objectives.

The developed research questions for this study are:

- 1) What is the current trend in handling highly imbalanced multi-class data?
- 2) How to handle highly imbalanced multi-class data?
- 3) How to develop a framework of highly imbalanced multi-class data?

The following objectives are developed based on the research problem:

- 1) To understand the trend of highly imbalanced multi-class data through analysis of all related literatures.
- 2) To analyze the previous and current method of handling highly imbalanced multi-class data.
- 3) To construct a framework handling highly imbalanced multi-class data through research and literature study.

II. STRATEGIES IN HANDLING IMBALANCED DATA

Based on previous studies on HIMC data, it is imperative to understand these related sub-topics: (1) Strategies in handling imbalanced data; (2) Previous solutions in handling imbalanced data, imbalanced multi-class data and HIMC data; (3) Related method or technique used in solving HIMC data problems.

The same three strategies in handling slightly imbalanced data can be used in handling highly imbalanced multi-class data. The details of these strategies and their methods are put under Appendix 1. There are three types of DL strategies which are oversampling, undersampling and hybrid strategy. AL strategy can be divided further into four methods which are cost-sensitive learning, skewed learning function, sampling-based and other methods. The CL strategy can be divided into two main methods: hybrid and ensemble. The Hybrid method can be divided further into MTD-based, SVM-variants and other hybrid methods. While ensemble method can be divided further into four methods which are integration with data level, integration with cost-sensitive, bagging variants and boost variants.

DL strategy involves data manipulation activities during the pre-processing phase in machine learning. An example of oversampling-related method is Synthetic Minority Oversampling Technique (SMOTE) [51], while an example of undersampling related method is Random Under sampling (RUS) [52]. From the literature review conducted, several literatures related to HIMC data have been found. However, the strategy or method proposed at DL in HIMC data is hardly mentioned. Therefore, this can be a promising area for future research in HIMC data.

AL strategy involves classifier related activities such as Support Vector Machine (SVM) [53], Deep Learning method using Convolutional Neural Network model (CNN) [54], and K-Nearest Neighbor [55]. Convolutional Neural Network (CNN) model was used to predict Chlorophyll-A concentration in Algal Bloom in managing data imbalance and skewness [56], and a Deep Self-Organizing Map (DSOM) was proposed to detect a well-known pre-miRNA protein as compared to a genome's hundreds of thousands of potential sequences [18].

The CL strategy is a combination of both DL and AL strategies, or combination of DL strategy with another DL, and a combination of AL with another AL strategy. In addition, it can also be a combination of ensemble method with AL strategy, or combination of ensemble method with DL strategy, or it can be a combination of both hybrid and ensemble methods [57], [58]–[60]. For example, based on a combination of data rebalancing and Extreme Gradient Boosting (XGBoost), a unique form of malicious synchrophasors detector is developed [61].

Oversampling and under sampling were combined with SVM in solar flare prediction [7]. Fujiwara et al. proposed a heuristic undersampling and distribution-based sampling with boosting method (HUSDOS-Boost) in handling data problems in health record analysis [44]. The strategies and methods used in handling imbalance data are shown in Fig. 1.

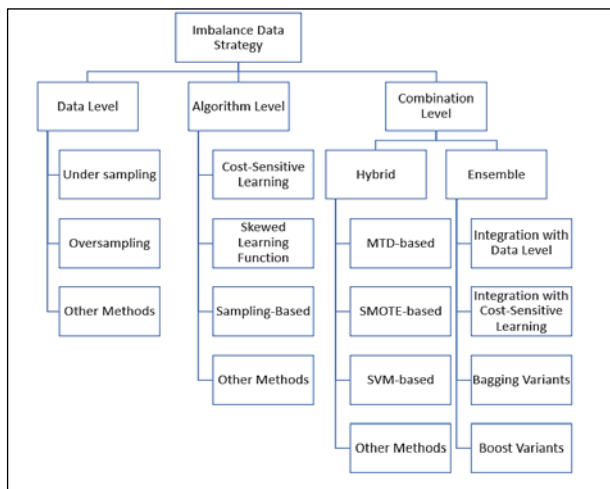


Fig. 1. List of Strategies in Handling Imbalanced Data.

Fig. 1 shows a list of strategies in handling imbalanced data. Imbalanced data can be divided into three strategies namely DL, AL, and CL strategy. Literatures related to DL and AL can be found in many studies while CL concept is still fresh. In literatures such as Kaur et al. and Johnson and Koshgoftaar, DL and AL have been mentioned along with Hybrid Method (HM). The logic behind this concept is that HM is a combination of both DL and AL [29], [42]. In other literatures such as in Sleeman & Krawczyk, DL and AL have been mentioned along with Ensemble Method (EM), while HM has not been specifically mentioned as their work was more focused on EM [6]. Some might argue on the reason to categorize EM into CL, as EM might also fall into AL strategy.

It is imperative to understand that in recent highly imbalanced data research, EM is usually not working alone and is combined with another method except for performance comparison or proposal of a new framework [62], [63]. In highly imbalanced classification, research of supervised and unsupervised fuzzy measure approaches was conducted by Uriz et al. The authors integrated EM with fuzzy integrals and their synergy with various fuzzy measures [64]. Another study was by Liu et al. where they established a unique framework for imbalance classification that was intended at building a strong ensemble by self-paced harmonizing data hardness by under-sampling, in which a classifier was combined with self-paced EM. [15].

Ghorbani et al. proposed a new hybrid model based on a highly imbalanced dataset to predict early mortality risk in intensive care units (ICU). The authors developed an SVM and SMOTE hybrid strategy (SVM-SMOTE) that included several methods, including a Genetic Algorithm (GA) for feature selection (FS) and Stacking and Boosting (EM) for prediction. SVM-SMOTE was used to tackle imbalanced data problems [65]. Using clustering, weighted scoring, SVM, and EM, Ksieniewicz et al. suggested a hybrid method for managing severely imbalanced data categorization in geometric space [66]. Using a combination of data rebalancing, bagging-based ensemble learning, and the Extreme Gradient Boosting (XGBoost) algorithm, a unique form of malicious synchrophasors detector was developed to address the highly imbalanced data problem. Even if malicious synchrophasors

occur seldom in practice, a detector trained on a highly imbalanced dataset drawn straight from previous operational data is biased toward the majority class. [61]. Tran et al. proposed a combination of K-Segments, under sampling and bagging EM as experimental research to approach extreme imbalanced data classification [64]. From the examples mentioned in this study, EM was combined with other methods to achieve better performance. Appendix 1 until Appendix 4 will entail strategies and methods involved in handling imbalanced data.

III. PREVIOUS SOLUTIONS IN HANDLING HIGHLY IMBALANCED MULTI-CLASS DATA

Ahmadzadeh et al. is one of the most current approaches for extremely unbalanced data that has been proposed [7]. The reviewed literatures discussed solar flare forecasts using under-sampling, over-sampling, and Support Vector Machine (SVM) to handle highly or extremely imbalanced solar flare data. For future development, these works suggested exploring hyperparameter tuning of the proposed method to enhance the model. A multi-class dataset was initially used but then it was converted to binary classification data to make predictions.

Fujiwara et al. published an article in the medical field. In this research, oversampling and undersampling methodologies for highly imbalanced data in health records analysis were presented. When minority samples are too tiny, undersampling and oversampling, or a mix of the two via hybrid and ensemble, did not give satisfactory results. The authors developed HUSDOS-Boost, which stands for Heuristic Under-sampling and Distribution Based Sampling paired with a Boosting ensemble, to cope with the extreme imbalanced and small minority (EISM) problem. When compared to other ensemble approaches, the result was superior. The authors proposed that a hierarchical Bayes model be used to estimate the distribution parameter in future work to improve over-sampling performance [44].

Managing cyber-attacks such as in detecting malicious synchrophasors is very important especially among energy-based companies. Performance of the detectors might be deteriorated severely due to quality of extremely imbalanced data. The authors developed a malicious synchrophasors detector based on data rebalancing, ensemble learning with bagging, and Extreme Gradient Boosting (XGBoost). The proposed method can detect malicious synchrophasors even though only a minimum number of malicious instances were provided [61]. There are several other methods or solutions proposed by different researchers involving different kinds of algorithms or solutions in different kinds of extreme imbalance dataset. Despite all the proposed methods, an extreme or highly imbalance dataset is still a challenging area to explore [44].

A. Related Method/Technique In Handling Highly Imbalanced Multi-Class Data

This section presents the related methods or techniques that have been used by researchers to handle highly imbalanced multi-class data. In the context of this study, the methods described are ensemble, deep learning, and cost-sensitive method.

1) *Ensemble method*: Research works on highly imbalanced data using ensemble method have become more prevalent since the emergence of Big Data technology [14]. Ensemble method along with hybrid method is steadily gaining attention from researchers around the world. From 2010 to 2021, there are many literatures regarding research works on highly imbalanced data using ensemble method [15], [61], [62], [63], [64] [65], [66], [67], [68]–[74]. The ensemble technique is popular because it combines many algorithm approaches with the ensemble algorithm in machine learning to improve performance [60], [75]–[77]. Compared to a single classifier, the ensemble's total performance was improved by combining several approaches or algorithms. Ensemble modelling is a set of models that work collaboratively to provide a more efficient predictive model. Different modelling techniques, such as Decision Tree (DT) [78]–[82], Neural Networks (NN) [83]–[86], Random Forests (RF) [87], [88]–[91], Support Vector Machines (SVM) [43], [92]–[95] and others can be integrated with ensemble.

Bagging, boosting, and stacking are examples of ensemble techniques that are used to improve the performance of a model or reduce the likelihood of selecting a bad one. There are many literatures on the performance of ensemble method. Among more prevalent methods are Bagging (Bootstrap aggregation) [6], [28] [96]–[99], [100], Stacking (Stacked Generalization) [98], [101], [102], Random Forest (RF) [87], [91], [103], [13], [104]–[109] and Mixtures of Experts [8], [42], [110], [111], [112], [113].

In 1996, Bagging or Bootstrap Aggregating was established as one of the first ensemble approaches. To reduce variance error, this technique trains and picks strong classifiers on subsets of data. Robust performance on outliers, decrease of variance to minimize over-fitting, which requires minimum further parameter adjustment, and the ability to accept high nonlinear interactions are just a few of the advantages. One of the drawbacks of bootstrap aggregation is that the more complicated the model becomes, the less visible and interpretable it becomes [114]–[117].

Boosting is like bagging, but it gives weak classifiers more weight. The weaker classifiers are given additional weight in the following classification phase with each iteration of classifications, increasing their chances of being categorized properly until a stopping point is reached. This can be thought of as course-correcting by re-energizing the data weights that require it. Over-fitting, outlier influence, revision on iteration ending point, and lack of transparency owing to complexity are some of the flaws of this technique, which optimize the cost function. [96], [118]–[120], [121].

Stacking, sometimes known as the least understood ensemble technique, produces ensembles by combining a variety of powerful classifiers. When developing ensemble models, diversity is crucial because it allows stronger learners from various regions to combine their abilities to lower the chance of misclassification. Stacking employs various levels of classification training [98], [102], [122]–[124]. Tier two (2) will use the misclassified regions to adjust the behavior in the

next phase if tier one has feature spaces that are misclassified. The biggest flaw in this form of ensemble is that it lacks transparency when it comes to determining a metadata classifier that adjusts for errors to improve prediction accuracy [59], [125]–[128].

When compared to the implementation in a single classifier, the ensemble's total performance is improved by combining several approaches or algorithms. There is a lot of literature stating about the performance regarding ensemble method [1], [2], [125], [129]–[132].

An effective and popular tool for optimizing ensembles of classifiers is the genetic algorithm (GA), belonging to the family of evolutionary algorithms [133]–[135]. The inspiration to study evolutionary computation (EC) was the imitation of nature in its mechanism of natural selection, inheritance, and functioning. Evolutionary computation is used to demonstrate and unravel complex tasks, primarily for optimization. It is trained based on species, not on an entity, that extends across the lifespan of numerous generations of entities. As a result, generations that are produced progressively meet the conditions of the task, and this would improve the adjustments made to the environment.

It is also worth observing the combination of evolutionary computation with ensemble methods. Examples of such combination can be found in several areas of research like in model-based ensemble [136], micro genetic algorithm, parallel genetic algorithms [137], GA with ensemble method [138], [139], and stacking ensemble [58], [124]. The algorithms mentioned are examples of hybrid and ensemble algorithm that falls into the CL strategy.

Ensemble approaches have been widely applied across several disciplines in the domain of credit scoring and bankruptcy prediction [99], [139], [140], [141] including the latest on personal bankruptcy prediction on imbalanced dataset can be found in several literatures [79], [88], [89], [141], [142].

2) *Extreme Gradient Boosting (XGBoost)*: The consequences of noisy data and redundant features, which contributed to the unbalanced data scenario, are mitigated by feature selection methods. In boosting approaches, such as extreme gradient boosting (XGBoost), distributed learning, and multi-core computation, which fully employ the computer's capabilities to speed learning, are possible. As a result, more investigation into boosting is strongly recommended in the highly or extreme imbalanced data research. Chen and Guestrin developed XGBoost which is an advance gradient boosting (GB) [164]. It is a fast, scalable, and efficient algorithm that won Kaggle machine learning competition and was applied in many applications and is used by many corporations.

Base classifiers are known as weak learners. In boosting, models are added concurrently until there is no further change. Boosting is an additive ensemble method that combines new models with existing models to reduce errors. Boosting is a technique for integrating many base classifiers to produce classification accuracy that is considerably better than any single base classifier's performance. A boosted model will

produce a good result even if the base classifiers have a marginally better accuracy than random. XGBoost is an open-source library providing a gradient boosting platform for Python, R, C++, and Java. It employs a gradient-boosting technique to generate a prediction model in the form of an ensemble of weak prediction models, most commonly decision trees.

Gradient boosting (GB), stochastic GB, and regularized GB are the three major types of gradients boosting that XGBoost can perform. The XGBoost approach is flexible in its implementation of distributed and parallel computing and can handle sparse data [143]. It is strong enough to handle hyper parameter fine tweaking and regularization parameter addition. It's been put to the test on large-scale challenges and can handle most regression, classification, and ranking problems, as well as custom objective functions. XGBoost is also portable and compatible, allowing it to run on any operating system. It works with AWS, Azure, and GCE, as well as other distributed cloud platforms.

XGBoost is easily coupled to large-scale cloud data-flow systems like Flink and Spark, which were designed specifically for model performance and computing speed. Model tuning, computational environments, and algorithm enhancement are all available in XGBoost. The algorithm was created with the goal of reducing computation time and allocating memory resources efficiently. XGBoost improves classification accuracy and performs calculations 10 times faster than commercial software. It can prevent over-fitness and dealing with missing values. With learning, XGBoost can figure out the dividing path for the test with incomplete eigenvalues. [60].

3) *Deep learning method:* Research of deep learning in imbalanced data was overwhelming, however research of deep learning in highly imbalanced data still has much room for expansion. The length of the majority data or class is substantially longer than the length of the minority data component in highly imbalanced data settings. To put it another way, the minority data has essentially been ignored by the classifier and most of the time considered as a noisy data [4]. The net gradient, which is responsible for updating the classifier weights, is dominated by the majority data. During early iterations, this reduces the error of the dominant majority quickly, but it often raises the error of the minority group, trapping the algorithm in a slow convergence state. [5].

In the fields of image identification [144], speech recognition [145] and natural language processing [146], [147], deep learning has been widely utilized. However, there have been few studies on the use of deep learning in highly imbalanced data. As the RNN is ideal for time series analysis, one popular application is the deployment of a recurrent neural network (RNN) to investigate network intrusion detection on an imbalanced dataset [148].

Convolutional Neural Network (CNN) is another deep learning model that has been used to forecast bankruptcy. Hosaka et al. took financial statement data from Japanese publicly traded firms and converted the numerical financial ratio data into a grayscale image that was tailored to CNN's

characteristics and could be evaluated directly by CNN. To cope with bankruptcy prediction difficulties, Hosaka suggested a CNN framework, and this model beat comparable conventional solutions, including most of the established machine learning techniques [149]. Mai et al. used layers of neural networks to extract attributes from textual data from over 10000 public corporations in the United States to incorporate deep learning into the prediction of bankruptcy. [150].

It has been revealed that when textual data (e.g., news, public company reports) is combined with classical numerical data (e.g., financial ratio data), deep learning performs better in imbalanced data study using textual disclosures, improving prediction accuracy even more. These intriguing findings open up new avenues for research in the field of bankruptcy prediction on imbalanced datasets, providing new insights and ideas. [151].

4) *Cost-Sensitive learning:* When training a model, cost-sensitive learning considers the costs of prediction errors as well as any additional cost that may be necessary. It is related to classification on datasets that are imbalanced or have skewed class distribution. As a result, a variety of cost-sensitive learning approaches and strategies can be used to solve problems with imbalanced data. [50], [58], [152].

The goal of cost-sensitive learning for imbalanced classification is to assign different costs to different types of misclassification errors, then utilize specific algorithms to compensate for those costs. The concept of a cost matrix facilitates to understand the varied costs of misclassification. A confusion matrix is a list of a model's predictions on classification tasks. It is a table that lists the number of predictions made for each class, separated by the actual class [153].

It is easiest to understand using a classification issue with negative and positive classes, which are commonly labelled with 0 and 1 class labels. Although the meanings of rows and columns can be and often are interchanged with no loss of meaning, the columns in a matrix table indicate the actual class to which the instances belong, and the rows represent the anticipated class. A cell is the number of samples that fulfil the row and column's requirements, and each cell has a unique common name. A confusion matrix for a classification problem is shown in Table II.

The confusion matrix's cost matrix is a matrix that allocates a cost to each cell. The focus of the research on the unbalanced data problem, in relation to the confusion matrix, is on errors, hence 'False Positive' and 'False Negative' will be the primary focal areas. In an imbalanced classification task or a challenge with imbalanced data, the latter is more common than the former.

TABLE II. A CONFUSION MATRIX FOR A CLASSIFICATION TASK

	Actual Negative	Actual Positive
Predicted Negative	True Negative (TN)	False Negative (FN)
Predicted Positive	False Positive (FP)	True Positive (TP)

IV. PROMINENT VALIDATION METRICS FOR HIGHLY IMBALANCED MULTI-CLASS DATA

The precision metric, defined as Equation (1), measures the accurately categorized positive class samples.

$$\text{Precision} = \frac{TP}{TP+FP} \quad (1)$$

where TP and FP stand for true-positive and false-positive counts, respectively.

The fraction of accurately identified true positive samples is measured by recall, which is calculated using Equation (2):

$$\text{Recall} = \frac{TP}{TP+FN} \quad (2)$$

G-mean and AUC have been designed for class imbalanced problem-measurement. As shown in Equation (3), the F-measure or F-1 score is the harmonic mean of precision and recall:

$$f - \text{measure} = \frac{(1+\beta)^2 \times \text{recall} \times \text{precision}}{\beta \times \text{recall} + \text{precision}} = \frac{(1+\beta) \times \frac{TP}{P} \times \frac{TP}{PP}}{\frac{TP}{P} \times \beta + \frac{TP}{PP}} \quad (3)$$

The geometric mean, or G-mean, is a metric that assesses the balanced performance of a classifier, as shown in Equation (4):

$$G - \text{mean} = \sqrt{\frac{TP}{TP+FN} \times \frac{TN}{TN+FP}} \quad (4)$$

The AUC stands for Area under the ROC Curve, which is used to assess the model's performance [21] and can be used to estimate it, as demonstrated in Equation (5):

$$\text{AUC} = \left(\frac{TP}{TP+FN} + \frac{TN}{TN+FP} \right) / 2 \quad (5)$$

As a result, the performance evaluators of the classifier employed in most imbalanced data research include F-measure, G-mean, AUC, and Accuracy [1], [154]. However, in a highly imbalanced data situation, accuracy, also known as balanced accuracy, is not a feasible validation metric due to the nature of the classifier, which is bias towards the majority class and ignores the minority class [21], [63], [155].

A. Related Study on HIMC Data Framework

Before a new framework on highly imbalanced multi-class data can be proposed, related studies on both highly imbalanced binary data and highly imbalanced multi-class data must be discussed thoroughly. This section will present the descriptions and discussions on the differences between highly imbalanced binary data and highly imbalanced multi-class data in terms of literatures, technologies, and domain in real world.

Table III shows literature related to highly imbalanced binary (HIB) data and highly imbalanced multi-class (HIMC) data. Before further explanation on this table is given, a clarification on "Data Mining" domain will be given. It is known as "Data Mining" domain due to the nature of the research which uses multiple different datasets ranging from five datasets to 35 datasets. Each of the datasets are different in terms of discipline and areas of interest such as Abalone, Glasses, Cars, and Credits etc. Therefore, each dataset is a unique domain and thus it is called "Data Mining" domain.

From 2006 to 2021, there were many literatures published about highly imbalanced data. Some of the literatures were on HIB data and the rest were on HIMC data. The related HIB data was from the data mining domain, and this data was grouped based on these algorithms: SR 0-1 LOSS [15], F-BFR [156], T-BFS [157], K-SUB [64], PSU [102], C4.5N [158], DWCE [159], ECSM [72], GP-COACH [160], Fuzzy [161], [162], OSPREY [163], Chi Method, CNN [164], WL-Norm SVM [165], EAIS + Fuzzy [166], GA + Fuzzy [167], US + Ensemble (Data Hardness) [15], Clustering + WS [66], DBE-DCR [73], EUBoost [168], GA-FS-GL [169], GSVM-RU [170], GA-GL+FRBC [171], K-Means + HFS [172], REPMAC k-Means +SVM +DT [173], SwitchingNED [70], SVM-US [174], B-BFS [67].

For the HIMC data, the related domain was the data mining: FMFS [186], DM-UCML [188], WRSEW + RDL [189], aerial imaging: RF-MML [187], bioinformatics: DBNN (DEEP SOM) [18], CNN [56], cyber-attack detection: SAE [190], facial recognition: VFSG [191], fetal aneuploidies: ANN [192], medical: CRF [40], CNN [144], pathology: CNN [193], power synchropasor detection: RXGBOOST [61] and flare forecast: US + OS + SVM [7].

In HIB data, specifically in the data mining domain, there are many published literatures between 2006 and 2021. For data mining domain, several novel methods were developed. For example, Calvert et al. who focused on severely imbalanced big dataset found that C4.5N was by far the best learner in terms of Slow POST attack data. Nevertheless, C4.5 Decision Tree and Chi Algorithm were found to be less effective compared GP-COACH in highly imbalanced dataset [158]. Among the more recent literatures in HIB in data mining domain come from Bringer et al. The authors found that data labeling is difficult in highly imbalanced data environment. Therefore, the authors have proposed OSPREY which is a system to cater data labeling in highly imbalanced data. The system was developed on top of Snorkel framework [163].

The CL is the most popular strategy in HIB data. It can be seen by the number of literatures found especially in the data mining domain. For example, Fernandez et al. studied the behavior of GP-COACH algorithm in highly imbalanced data scenario [160]. Liu et al. developed a novel framework for unbalanced classification that focuses on generating a strong ensemble by self-paced harmonizing data hardness using a mix of under sampling and self-paced ensemble in CL for HIB data [15].

For HIMC data, less literatures were found from 2006 to 2021. Unlike HIB data, there is less research in data mining domains where there is only a single literature at DL [219] and few literatures at AL [18], [56], [40], [190], [144], [187], [121], [191]–[193], and some literature in CL [61], [63], [188], [189], [7].

Domains such imaging [187], bioinformatics [18], [56], cyber-attack [190], facial recognition [191], fetal aneuploidies [192], medical [40], [144] and pathology [193] concentrated on AL strategy while domains such as medical [63], power [61] and solar forecast [7] employed CL strategy. Nonetheless, the only research using DL strategy focused on data mining domain.

TABLE III. HIGHLY IMBALANCED BINARY DATA VS HIGH IMBALANCED MULTI-CLASS DATA

Class	Data Level	Domain	Algorithm Level	Domain	Combination Level	Domain
Binary class	SR 0-1 LOSS [15], F-BFR [156], T- BFS [157], K-SUB [64], PSU [102]	Data Mining	C4.5N [158], DWCE [159], ECSM [72], GP- COACH [160], Fuzzy [161], [162], OSPREY [163], Chi Method, CNN[164], WL-Norm SVM [165]	Data Mining	EAIS + Fuzzy [166], GA + Fuzzy [167], US + Ensemble (Data Hardness) [15], Clustering + WS [66], DBE-DCR [73], EUBoost [168], GA-FS-GL [169], GSVM-RU [170], GA- GL+FRBC [171], K-Means + HFS [172], REPMAC k-Means +SVM + DT [173], SwitchingNED [70], SVM-US [174], B-BFS [67]	Data Mining
	NRA [175]	Fraud Detection	BERT [19]	Malware Detection	Ensemble + RF [68]	Disease Prediction
	SSFS [176]	Phishing Detection	CNN [177], ECDL [178]	Medical Imaging	DS + ST [179]	Hospital Admission
	BPFs [180], MPRM [181]	Speech Recognition	AL [168]	Social Media	PCA + DA + CNN [145]	Imaging
			GSVM-BA [182]	Spam Detection	SMOTE-tBPSO-SVM [183]	Malware Detection
					Boosting + Sampling [184], SMOTE + RF [185]	Medical
				GA + SVM-SMOTE [65]	Mortality Prediction	
				Ensemble + SMOTE [71]	Sentiment Analysis	
Multi-class	FMFS [186]	Data Mining	RF-MML [187]	Imaging	DM-UCML [188], WRSEW + RDL [189]	Data Mining
			DBNN (DEEP SOM) [18], CNN [56]	Bioinformatics	ELF [63]	Medical
			SAE [190]	Cyber Attack	RXGBOOST [61]	Power
			UCML [121]	Data Mining	US + OS + SVM [7]	Solar Forecast
			VFSG [191]	Facial Recognition		
			ANN [192]	Fetal Aneuploidies		
			CRF [40], CNN [144]	Medical		
			CNN [193]	Pathology		

Therefore, it clear that HIB data is more prominent than HIMC data and there is more room for future research to be conducted in highly imbalanced data. HIB data alone dominates the research with 72.7% while HIMC data with only 27.3%.

Table III demonstrates highly imbalanced data categorization based on techniques used. There are four categories of technique that have been used in HIB data and HIMC data research works. They are statistical, semi-supervised, supervised, and unsupervised. This consists of 81.6% from the overall literatures in CL and almost half which is 46.3% from overall literatures in highly imbalanced data.

Combination Level (CL) dominated in terms of number of literatures in both HIB and HIMC data. Supervised type of research in HIB using ensemble were published between 2006 and 2021. In the same technique category (supervised in HIB data), hybrid method is also not less popular with quite several literatures published within the same period while several literatures for unsupervised type of research have been found in binary class data using hybrid technique. Overall, there have been quite satisfying number of literatures published on CL in term of HIB data.

For HIMC data, number of research in ensemble and hybrid was not as many as HIB data, there are only few literatures published between 2006 until 2021 which was literatures in

statistical area using hybrid, and in unsupervised area and other literatures in the area were using ensemble technique. Research in HIMC data area is still quite new.

In terms of feature selection methods in both HIB data and HIMC data, there were several techniques involved in the list of literatures. The technique used was Repetitive Feature Selection, Threshold-based Feature Selection, Binary to Multi-class Feature Selection, Program to Detect Phishing and Feature Maximization for Feature Selection.

The rise of Big Data is one of the most prominent justifications for the adoption of both ensemble and hybrid in all three data techniques (DL, AL, and CL) in both HIB and HIMC data. Big data processing, as well as hybridization and algorithm ensembles have attracted much interest in the research community. Referring to the literatures that have been analyzed, the earliest literature on highly imbalanced data was published in 2006 for HIB data and 2013 for HIMC data respectively, after the emergence of Big Data technology.

V. PROPOSED NOVEL HIMC DATA FRAMEWORK

This article presents the descriptions on the technologies used and gathered from previous studies and the domains of the literatures published between 2013 and 2021. The literatures were divided further into four categories which were Supervised, Semi-supervised, Unsupervised, and Statistical. In terms of types of algorithms, the publications were segregated based on several groups which were feature selection, artificial neural network, deep learning, case-sensitive learning, ensemble, and hybrid, including two specific algorithms developed for aerial scene imaging and facial expression recognition.

Fig. 2 illustrates the proposed framework of HIMC data. The framework has been developed based on important elements like data category, data behavior, data characteristics, data strategy, model or technique type, and algorithm or model used in HIMC data research. The HIMC data framework can be used as the underlying basis of highly imbalanced data research both binary data and multi-class data.

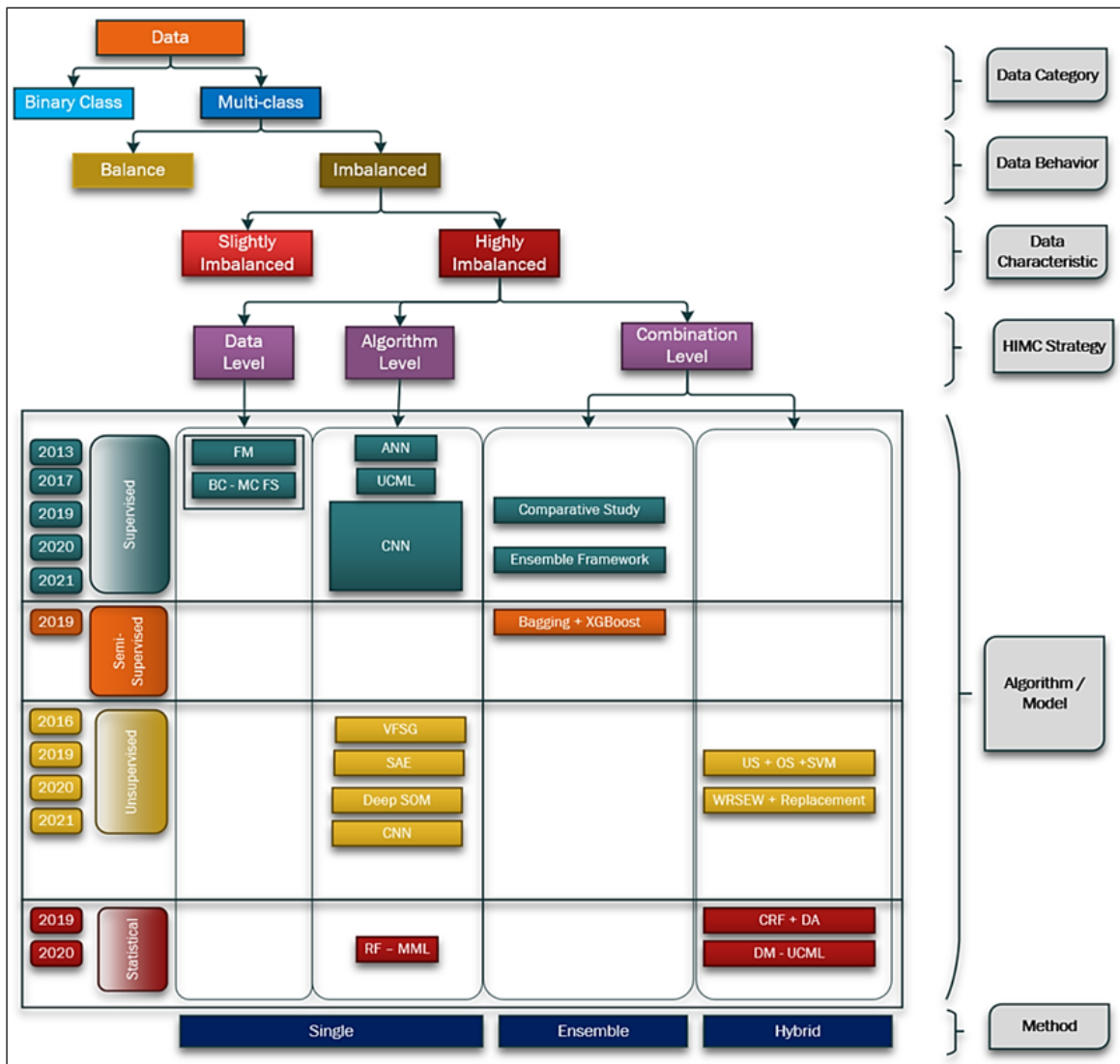


Fig. 2. HIMC Data Framework.

Based on the framework, data can be categorized into binary and multi-class. There are other categories of data such as streamed data and big data, but this research only focuses on these two categories of data. Moreover, both streamed data and big data research are higher-level research when the underlying data categories will come back to multi-class data and binary class data as the base category. Multi-class data can be further divided into balanced and imbalanced data. Balanced data is only present in controlled environment where both majority and minority classes and data are divided to 50-50 percent ratio.

Algorithms or techniques or methods can be divided into different categories which are Supervised, Semi-Supervised, Unsupervised and Statistical. In this framework, year of publication has also been added for easy referencing. Finally, there is technique or model group. It can be categorized into single method, ensemble, and hybrid group. Single method group lists only research works that use a single algorithm or technique or method. Ensemble group is a list of studies that employ ensemble method and hybrid group is a list of research that employ hybrid method. Finally, it is worth mentioning that in this framework, domains for each literature are also stated next to the method used. Multiple domains mean that the referred articles mentioned the use of many benchmarks in many disciplines.

In the framework, highly imbalanced data is further divided into DL, AL, and HM [4], [21]. Since ensemble can work independently or combined with other methods in DL or AL, HM and EM are combined to employ CL strategy. In HIMC data framework, there have been only a couple of literatures related to DL strategy. Using Feature Maximization in Feature Selection, Jean-Charles Lamirel devised a strategy for coping with severely imbalanced textual data grouped into similar classes. [194]. Another study came from Kubler et al. where FS was used to handle problem with how to extend FS from binary classification data to multi-class data [195]. Both literatures used multiple domains in their research.

There are several literatures published between 2016 and 2021 on HIMC data in AL. Domains such as in the study of fetal aneuploidies, medical, application development of facial expression recognition, cyber-attack, aerial scene imaging and bioinformatics. Several articles stated the use of supervised method [56], [144], [121], [192], [196] and others stated the use of unsupervised method [191], [18], [83], [193] and one article mentioned the use of statistical method. All research related in DL and AL employed single method and thus, they were categorized into single method group [187].

CL gained more popularity in recent times. Even though there have been only little literatures related to CL strategy, most of these articles have the best performance benchmark. Two articles mentioned the use of supervised method in medical and malware detection domains [62], [63]. One article mentioned the employment of semi-supervised in power synchrophasors detector domain [61]. Other articles mentioned the use of unsupervised method in rare event of flare forecast and multiple domains [7], [189] and finally the statistical method was used in medical imaging and multiple domains based on several articles [40], [121].

VI. DISCUSSION

Multi-class data issues are more difficult to solve compared to binary classification data [22]. Most of the articles published recently focus on handling problems in binary classes such as bankruptcy prediction (bankrupt vs. non-bankrupt), computer security (normal activity vs. malicious activity), medical (healthy vs. infected). Because multi-class data can be dissected and handled using binary class methods, many literatures focus on binary class data [21], [31].

Multi-class data have different challenges. If the output for binary classification is binary, multi-class output will be multiplied (more than two targets or results) [1]. Several examples of real-world cases involving highly imbalanced data are like hospital readmission [197], feature pattern of Thoracolumbar spine fracture [87], solar flare forecast [7], modeling of Chlorophyll concentration in Algal Bloom [56], semantic segmentation [198], [199], medical imaging [40], malware detection [19], cyber-physical strike discovery [190] and Bioinformatics [18].

In highly imbalanced multi-class data, a multiple skewed distribution is an issue which affects classifiers' performance as it is difficult to decide the boundaries in highly imbalanced multi-class data. A distance-based algorithm such as Hellinger distance has been used to handle the problem. However, there are issues on overlapping class and noisy data [21], [33], [155]. A good solution for the problem is to combine a method that can minimize overlapping class and reduce noisy data [2], [31], [200]. A promising solution that might handle both problems is by using ensemble methods. This is because this method is capable of rectifying imbalance class and improving weak classifiers [201]. However, ensembles suffer from lack of interpretability and are usually computationally expensive [26].

Problems in highly imbalanced data originate from problems in slightly imbalanced data which are alleviated due to the nature of severe imbalance ratio (IR) [3], [33]. Thus, problems in imbalanced multi-class data and highly imbalanced multi-class data can be considered similar in nature with high IR. In ML, multinomial or multi-class classification is the problem of classifying instances into one of three or more classes [21]. A multi-class classification problem is not as developed as the binary classification problem in imbalanced data [4], [21], [110].

High IR has negative impact toward the minority class and overall performance of data may result in information loss [102], [202]. In multi-class data, performance of each class needs to be focused specifically because each class is distinctive. A classifier might obtain good performance in some classes while unsatisfactory results in other classes [4], [18], [21].

Relationship among classes is another issue in multi-class data. It is a complicated situation because each group of classes presents different problems [4]. Two or more classes might overlap in some group. While other classes might have a normal borderline and considered as normal classes. This problem is elevated in highly imbalanced multi-class data, and it affects classifiers' performance [159], [40].

Leevy et al. and Rendon et al. suggest that heuristic-based and more flexible methods have been less developed to solve multi-class data problems [31], [203]. There are literatures in the analysis of relationships among classes in multi-class data that have produced satisfactory results [155]. However, there is a need to improve on highly imbalanced multi-class data domains as the same method has not produced good results in a highly imbalanced environment.

In multi-class data, class overlapping is an issue because it may happen anywhere within the dataset with different groups of overlap classes. The problem is more complicated in highly imbalanced multi-class data scenarios, as it is hard to define borders of the overlapped classes. The problem will affect the classification or prediction performance of the classifier. The data needed to be properly pre-processed and appropriate sampling procedure be applied [4], [47], [47]. The challenge is to develop solutions that consider the different features within the overlapped classes and at the same time also showing good classification or prediction performance [204].

The presence of noisy data in a dataset can increase the imbalance among classes and eventually could result in the classifier rebalancing the wrong classes [205]. To overcome the issue, a new approach for data cleaning is needed to boost classifier performance in multi-class data [46]. Another way to solve the problem is to create synthetic data, which allows overlapping data to be transferred to other locations. Another method is to remove excessive samples. New approaches should consider removing excessive samples while maintaining the quality of the data [2], [6].

In summary, in highly imbalanced multi-class data, minority classes are treated as noisy data. However, the minority data might have crucial information [1], [21]. Another issue is the misclassification cost between the majority and minority data. The cost-sensitive strategy is a well-known method for dealing with data imbalances. Minority samples, on the other hand, had a higher cost of misclassification than majority samples. [50]. Finally, a highly imbalanced multi-class data has multiple skewed classes which reduces classifier performance as it is difficult to normalize the skewness [26], [31], [44] and difficult to define borders of the overlap classes [4], [46]. Future research in highly imbalanced multi-class data should focus on these issues.

Future direction of HIMC data is clear, that is to have more research focusing on the issues presented in this article. One of the main issues of HIMC was the high IR between data classes. This was because the presence of multiple classes with high IR caused multiple skewed distribution and would affect the minority class as it was ignored by the classifiers because they tended to be biased toward the majority class. Another issue was the overlapping classes. This involved the difficulty to define borders of multiple classes. Finally, the issue on the presence of noisy data especially in big dataset. In this issue, classifiers tended to treat the minority data as noisy data due to the high IR.

VII. CONCLUSION

Data-related research has evolved as more essential, exciting, and beneficial due to the rapid rise of Big Data. In this

research, machine learning algorithms at different levels have been addressed by using different strategies which are DL, AL, and CL to properly manage highly imbalanced multi-class data problems. It has proposed a novel framework for HIMC data in the wake of issues concerning HIMC data. However, due to the dynamism and uniqueness of each dataset and the heterogeneity of data, developing a proper method or technique in handling highly imbalanced multi-class data remains a challenge. As a result, the current state-of-the-art algorithms were found and categorized in four different types in this study: supervised, semi-supervised, unsupervised, and statistical. Finally, the performance of various machine learning techniques used to handle HIMC data is compared in this research. Hence, based on the analysis performed, there is a need for a novel framework of HIMC data to be designed. Finally, open issues, challenges, and future direction of HIMC data have been discussed and presented in this article to pave the road for extended research works in HIMC data to be conducted in the future.

ACKNOWLEDGMENT

Ts. Mohd Hakim bin Abdul Hamid, a PhD candidate, would like to express his gratitude to the Information Security, Digital Forensic, and Computer Networking (INSFORNET) research group, Center for Advanced Computing Technology (C-ACT), Fakulti Teknologi Maklumat dan Komunikasi (FTMK), and Universiti Teknikal Malaysia Melaka (UTeM) for funding his PhD scholarship program. He would also want to thank his supervisor and co-supervisor, both of whom are co-authors on this study. He would like to express his gratitude to the Institute for Big Data Analytics and Artificial Intelligence (IBDAAI) and Universiti Teknologi MARA (UiTM) for providing him with the chance to pursue his Ph.D. at UiTM.

REFERENCES

- [1] J. Tanha, Y. Abdi, N. Samadi, N. Razzaghi, and M. Asadpour, "Boosting methods for multi-class imbalanced data classification: an experimental review," *J. Big Data*, vol. 7, no. 1, 2020, doi: 10.1186/s40537-020-00349-y.
- [2] D. Devi, S. K. Biswas, and B. Purkayastha, "A Review on Solution to Class Imbalance Problem: Undersampling Approaches," *2020 Int. Conf. Comput. Perform. Eval. ComPE 2020*, pp. 626–631, 2020, doi: 10.1109/ComPE49325.2020.9200087.
- [3] C. Bellinger, S. Sharma, N. Japkowicz, and O. R. Zaiane, "Framework for extreme imbalance classification: SWIM—sampling with the majority class," *Knowl. Inf. Syst.*, vol. 62, no. 3, pp. 841–866, 2020, doi: 10.1007/s10115-019-01380-z.
- [4] B. Krawczyk, "Learning from imbalanced data: open challenges and future directions," *Prog. Artif. Intell.*, vol. 5, no. 4, pp. 221–232, 2016, doi: 10.1007/s13748-016-0094-0.
- [5] J. M. Johnson and T. M. Khoshgoftaar, "Survey on deep learning with class imbalance," *J. Big Data*, vol. 6, no. 1, 2019, doi: 10.1186/s40537-019-0192-5.
- [6] W. C. Sleeman and B. Krawczyk, "Bagging Using Instance-Level Difficulty for Multi-Class Imbalanced Big Data Classification on Spark," *Proc. - 2019 IEEE Int. Conf. Big Data, Big Data 2019*, pp. 2484–2493, 2019, doi: 10.1109/BigData47090.2019.9006058.
- [7] A. Ahmadzadeh et al., "Challenges with extreme class-imbalance and temporal coherence: A study on solar flare data," *arXiv*, 2019.
- [8] B. Mirzaei, B. Nikpour, and H. Nezamabadi-pour, "CDBH: A clustering and density-based hybrid approach for imbalanced data classification," *Expert Syst. Appl.*, vol. 164, no. April 2020, p. 114035, 2021, doi: 10.1016/j.eswa.2020.114035.

- [9] J. Jedrzejowicz and P. Jedrzejowicz, "GEP-based classifier with drift detection for mining imbalanced data streams," *Procedia Comput. Sci.*, vol. 176, pp. 41–49, 2020, doi: 10.1016/j.procs.2020.08.005.
- [10] J. Jedrzejowicz and P. Jedrzejowicz, "GEP-based classifier for mining imbalanced data," *Expert Syst. Appl.*, vol. 164, no. May 2020, p. 114058, 2021, doi: 10.1016/j.eswa.2020.114058.
- [11] N. Jiang and N. Li, "A wind turbine frequent principal fault detection and localization approach with imbalanced data using an improved synthetic oversampling technique," *Int. J. Electr. Power Energy Syst.*, vol. 126, no. PA, p. 106595, 2021, doi: 10.1016/j.ijepes.2020.106595.
- [12] S. Wang and L. L. Minku, "AUC Estimation and Concept Drift Detection for Imbalanced Data Streams with Multiple Classes," *Proc. Int. Jt. Conf. Neural Networks*, vol. 2, no. Section V, 2020, doi: 10.1109/IJCNN48605.2020.9207377.
- [13] B. Mirzaei, B. Nikpour, and H. Nezamabadi-Pour, "An under-sampling technique for imbalanced data classification based on DBSCAN algorithm," pp. 21–26, 2020, doi: 10.1109/cfis49607.2020.9238718.
- [14] A. Goyal and J. Khiari, "Diversity-aware weighted majority vote classifier for imbalanced data," arXiv, 2020.
- [15] Z. Liu et al., "Self-paced ensemble for highly imbalanced massive data classification," *Proc. - Int. Conf. Data Eng.*, vol. 2020-April, pp. 841–852, 2020, doi: 10.1109/ICDE48307.2020.00078.
- [16] M. E. Khoda, "Mobile Malware Detection with Imbalanced Data using a Novel Synthetic Oversampling Strategy and Deep Learning," 2020, doi: 10.1109/WiMob50308.2020.9253433.
- [17] J. Zhao, J. Jin, S. Chen, R. Zhang, B. Yu, and Q. Liu, "A weighted hybrid ensemble method for classifying imbalanced data," *Knowledge-Based Syst.*, vol. 203, p. 106087, 2020, doi: 10.1016/j.knsys.2020.106087.
- [18] L. A. Bugnon, C. Yones, D. H. Milone, and G. Stegmayer, "Deep neural architectures for highly imbalanced data in bioinformatics," *IEEE Trans. Neural Networks Learn. Syst.*, vol. 31, no. 8, pp. 2857–2867, 2020, doi: 10.1109/TNNLS.2019.2914471.
- [19] R. Oak, M. Du, D. Yan, H. Takawale, and I. Amit, "Malware detection on highly imbalanced data through sequence modeling," *Proc. ACM Conf. Comput. Commun. Secur.*, pp. 37–48, 2019, doi: 10.1145/3338501.3357374.
- [20] R. Zhu, Y. Guo, and J. H. Xue, "Adjusting the imbalance ratio by the dimensionality of imbalanced data," *Pattern Recognit. Lett.*, vol. 133, pp. 217–223, 2020, doi: 10.1016/j.patrec.2020.03.004.
- [21] H. Ali, M. N. M. Salleh, R. Saedudin, K. Hussain, and M. F. Mushtaq, "Imbalance class problems in data mining: A review," *Indones. J. Electr. Eng. Comput. Sci.*, vol. 14, no. 3, pp. 1552–1563, 2019, doi: 10.11591/ijeecs.v14.i3.pp1552-1563.
- [22] H. Patel, D. Singh Rajput, G. Thippa Reddy, C. Iwendi, A. Kashif Bashir, and O. Jo, "A review on classification of imbalanced data for wireless sensor networks," *Int. J. Distrib. Sens. Networks*, vol. 16, no. 4, 2020, doi: 10.1177/1550147720916404.
- [23] Q. Ya-Guan et al., "EMSGD: An Improved Learning Algorithm of Neural Networks with Imbalanced Data," *IEEE Access*, vol. 8, pp. 64086–64098, 2020, doi: 10.1109/ACCESS.2020.2985097.
- [24] D. Gan, J. Shen, B. An, M. Xu, and N. Liu, "Integrating TANBN with cost sensitive classification algorithm for imbalanced data in medical diagnosis," *Comput. Ind. Eng.*, vol. 140, no. June 2019, p. 106266, 2020, doi: 10.1016/j.cie.2019.106266.
- [25] C. C. Lin, D. J. Deng, C. H. Kuo, and L. Chen, "Concept drift detection and adaption in big imbalance industrial IoT data using an ensemble learning method of offline classifiers," *IEEE Access*, vol. 7, pp. 56198–56207, 2019, doi: 10.1109/ACCESS.2019.2912631.
- [26] Z. Chen, J. Duan, L. Kang, and G. Qiu, "A hybrid data-level ensemble to enable learning from highly imbalanced dataset," *Inf. Sci. (Ny)*, vol. 554, pp. 157–176, 2021, doi: 10.1016/j.ins.2020.12.023.
- [27] B. Zhao and Q. Yuan, "Improved generative adversarial network for vibration-based fault diagnosis with imbalanced data," *Meas. J. Int. Meas. Confed.*, vol. 169, no. July 2020, p. 108522, 2021, doi: 10.1016/j.measurement.2020.108522.
- [28] P. Zyblewski, R. Sabourin, and M. Woźniak, "Preprocessed dynamic classifier ensemble selection for highly imbalanced drifted data streams," *Inf. Fusion*, vol. 66, no. June 2020, pp. 138–154, 2021, doi: 10.1016/j.inffus.2020.09.004.
- [29] H. Kaur, H. S. Pannu, and A. K. Malhi, "A systematic review on imbalanced data challenges in machine learning: Applications and solutions," *ACM Comput. Surv.*, vol. 52, no. 4, 2019, doi: 10.1145/3343440.
- [30] I. Triguero, S. Del Río, V. López, J. Bacardit, J. M. Benítez, and F. Herrera, "ROSEFW-RF: The winner algorithm for the ECBDL'14 big data competition: An extremely imbalanced big data bioinformatics problem," *Knowledge-Based Syst.*, vol. 87, pp. 69–79, 2015, doi: 10.1016/j.knsys.2015.05.027.
- [31] J. L. Leevy, T. M. Khoshgoftaar, R. A. Bauder, and N. Seliya, "A survey on addressing high-class imbalance in big data," *J. Big Data*, vol. 5, no. 1, 2018, doi: 10.1186/s40537-018-0151-6.
- [32] H. He and E. A. Garcia, *Learning from imbalanced data*, vol. 21, no. 9, 2009.
- [33] S. Sharma, C. Bellinger, B. Krawczyk, O. Zaiane, and N. Japkowicz, "Synthetic Oversampling with the Majority Class: A New Perspective on Handling Extreme Imbalance," *Proc. - IEEE Int. Conf. Data Mining, ICDM*, vol. 2018-Novem, pp. 447–456, 2018, doi: 10.1109/ICDM.2018.00060.
- [34] A. Lazarevic, J. Srivastava, and V. Kumar, "Data Mining for Analysis of Rare Events: A Case Study in Security, Financial and Medical Applications," *Pacific-Asia Conf. Knowl. Discov. Data Min.*, no. December 2014, 2004.
- [35] J. Roland, "How negative sampling provides class balance to rare event case data using a vehicular accident prediction project as a use case scenario," 2020, [Online]. Available: <https://scholar.utc.edu/theses/681/>.
- [36] F. Carcillo, Y.-A. Le Borgne, O. Caelen, Y. Kessaci, F. Oblé, and G. Bontempi, "Combining unsupervised and supervised learning in credit card fraud detection," *Inf. Sci. (Ny)*, 2019, doi: <https://doi.org/10.1016/j.ins.2019.05.042>.
- [37] W. Wei, J. Li, L. Cao, Y. Ou, and J. Chen, "Effective detection of sophisticated online banking fraud on extremely imbalanced data," *World Wide Web*, vol. 16, no. 4, pp. 449–475, 2013, doi: 10.1007/s11280-012-0178-0.
- [38] B. Krawczyk, "Cost-sensitive one-vs-one ensemble for multi-class imbalanced data," *Proc. Int. Jt. Conf. Neural Networks*, vol. 2016-Octob, pp. 2447–2452, 2016, doi: 10.1109/IJCNN.2016.7727503.
- [39] M. S. Sainin, R. Alfred, and F. Ahmad, "Ensemble Meta Classifier with Sampling and Feature Selection for Data with Multiclass Imbalance Problem," *J. Inf. Commun. Technol.*, vol. 20, no. 2, pp. 103–133, 2021, doi: 10.32890/jict2021.20.2.1.
- [40] J. Wang and S. Valaee, "From whole to parts: Medical imaging semantic segmentation with very imbalanced data," 2019 *IEEE Glob. Commun. Conf. GLOBECOM 2019 - Proc.*, pp. 1–6, 2019, doi: 10.1109/GLOBECOM38437.2019.9014112.
- [41] Y. Lu, "HKBU Institutional Repository Advances in imbalanced data learning Doctor of Philosophy," 2019.
- [42] J. M. Johnson and T. M. Khoshgoftaar, "Deep learning and thresholding with class-imbalanced big data," *Proc. - 18th IEEE Int. Conf. Mach. Learn. Appl. ICMLA 2019*, pp. 755–762, 2019, doi: 10.1109/ICMLA.2019.00134.
- [43] Z. Chen, W. Chen, and Y. Shi, "Ensemble learning with label proportions for bankruptcy prediction," *Expert Syst. Appl.*, vol. 146, p. 113155, 2020, doi: 10.1016/j.eswa.2019.113155.
- [44] K. Fujiwara et al., "Over- and Under-sampling Approach for Extremely Imbalanced and Small Minority Data Problem in Health Record Analysis," *Front. Public Heal.*, vol. 8, no. May, pp. 1–15, 2020, doi: 10.3389/fpubh.2020.00178.
- [45] X. Huang, C. Z. Zhang, and J. Yuan, "Predicting Extreme Financial Risks on Imbalanced Dataset: A Combined Kernel FCM and Kernel SMOTE Based SVM Classifier," *Comput. Econ.*, vol. 56, no. 1, pp. 187–216, 2020, doi: 10.1007/s10614-020-09975-3.
- [46] M. Koziarski, "Radial-Based Undersampling Algorithm for Classification of Breast Cancer Histopathological Images Affected by Data Imbalance," *Proc. - 2019 12th Int. Congr. Image Signal Process. Biomed. Eng. Informatics, CISP-BMEI 2019*, no. 1, pp. 2–6, 2019, doi: 10.1109/CISP-BMEI48845.2019.8966010.

- [47] M. Koziarski, B. Krawczyk, and M. Woźniak, "Radial-Based oversampling for noisy imbalanced data classification," *Neurocomputing*, vol. 343, pp. 19–33, 2019, doi: 10.1016/j.neucom.2018.04.089.
- [48] C. M. Vong and J. Du, "Accurate and efficient sequential ensemble learning for highly imbalanced multi-class data," *Neural Networks*, vol. 128, pp. 268–278, 2020, doi: 10.1016/j.neunet.2020.05.010.
- [49] J. M. Johnson and T. M. Khoshgoftaar, "Deep learning and data sampling with imbalanced big data," *Proc. - 2019 IEEE 20th Int. Conf. Inf. Reuse Integr. Data Sci. IRI 2019*, pp. 175–183, 2019, doi: 10.1109/IRI.2019.00038.
- [50] N. Ghatasheh et al., "Cost-sensitive ensemble methods for bankruptcy prediction in a highly imbalanced data distribution: a real case from the Spanish market," *Prog. Artif. Intell.*, vol. 9, no. 4, pp. 361–375, 2020, doi: 10.1007/s13748-020-00219-x.
- [51] A. D. Amiruddin, F. M. Muharam, M. H. Ismail, N. P. Tan, and M. F. Ismail, "Hyperspectral spectroscopy and imbalance data approaches for classification of oil palm's macronutrients observed from frond 9 and 17," *Comput. Electron. Agric.*, vol. 178, no. August, p. 105768, 2020, doi: 10.1016/j.compag.2020.105768.
- [52] M. Moniruzzaman, A. Bagirov, and I. Gondal, "Partial Undersampling of Imbalanced Data for Cyber Threats Detection," *ACM Int. Conf. Proceeding Ser.*, pp. 2–5, 2020, doi: 10.1145/3373017.3373026.
- [53] J. Novakovic and S. Markovic, "Performance of Support Vector Machine in Imbalanced Data Set," 2020 19th Int. Symp. INFOTEH-JAHORINA, INFOTEH 2020 - Proc., no. March, pp. 1–5, 2020, doi: 10.1109/INFOTEH48170.2020.9066276.
- [54] P. B. C. Castro, B. Krohling, A. G. C. Pacheco, and R. A. Krohling, "An app to detect melanoma using deep learning: An approach to handle imbalanced data based on evolutionary algorithms," *Proc. Int. Jt. Conf. Neural Networks*, pp. 2–7, 2020, doi: 10.1109/IJCNN48605.2020.9207552.
- [55] J. Ahammad, N. Hossain, and M. S. Alam, "Credit card fraud detection using data pre-processing on imbalanced data - Both oversampling and undersampling," *ACM Int. Conf. Proceeding Ser.*, pp. 18–21, 2020, doi: 10.1145/3377049.3377113.
- [56] J. H. Choi, J. Kim, J. Won, and O. Min, "Modelling Chlorophyll-a Concentration using Deep Neural Networks considering Extreme Data Imbalance and Skewness," *Int. Conf. Adv. Commun. Technol. ICACT*, vol. 2019-Febru, pp. 631–634, 2019, doi: 10.23919/ICACTION.2019.8702027.
- [57] K. Cheng, S. Gao, W. Dong, X. Yang, Q. Wang, and H. Yu, "Boosting label weighted extreme learning machine for classifying multi-label imbalanced data," *Neurocomputing*, vol. 403, pp. 360–370, 2020, doi: 10.1016/j.neucom.2020.04.098.
- [58] L. Loezer, F. Enembreck, J. P. Barddal, and A. De Souza Britto, "Cost-sensitive learning for imbalanced data streams," *Proc. ACM Symp. Appl. Comput.*, pp. 498–504, 2020, doi: 10.1145/3341105.3373949.
- [59] Q. Liu, W. Luo, and T. Shi, "Classification method for imbalanced data set based on EKCStacking algorithm," *ACM Int. Conf. Proceeding Ser.*, pp. 51–56, 2019, doi: 10.1145/3375998.3376002.
- [60] H. Li, Y. Cao, S. Li, J. Zhao, and Y. Sun, "XGBoost Model and Its Application to Personal Credit Evaluation," *IEEE Intell. Syst.*, vol. 35, no. 3, pp. 52–61, 2020, doi: 10.1109/MIS.2020.2972533.
- [61] J. Wang, Z. Sun, B. Bao, and D. Shi, "Malicious synchrophasor detection based on highly imbalanced historical operational data," *CSEE J. Power Energy Syst.*, vol. 5, no. 1, pp. 11–20, 2019, doi: 10.17775/cseejpes.2018.00200.
- [62] Y. Pang et al., "Finding Android Malware Trace from Highly Imbalanced Network Traffic," *Proc. - 2017 IEEE Int. Conf. Comput. Sci. Eng. IEEE/IFIP Int. Conf. Embed. Ubiquitous Comput. CSE EUC 2017*, vol. 1, pp. 588–595, 2017, doi: 10.1109/CSE-EUC.2017.108.
- [63] J. Li, B. Xin, Z. Yang, J. Xu, S. Song, and X. Wang, "Harmonization centered ensemble for small and highly imbalanced medical data classification," *Proc. - Int. Symp. Biomed. Imaging*, vol. 2021-April, pp. 1742–1745, 2021, doi: 10.1109/ISBI48211.2021.9433824.
- [64] T. Tran, L. Tran, and A. Mai, "K-Segments under Bagging approach: An experimental Study on Extremely Imbalanced Data Classification," *Proc. - 2019 19th Int. Symp. Commun. Inf. Technol. Isc. 2019*, pp. 492–495, 2019, doi: 10.1109/ISCIT.2019.8905145.
- [65] R. Ghorbani, R. Ghouisi, A. Makui, and A. Atashi, "A New Hybrid Predictive Model to Predict the Early Mortality Risk in Intensive Care Units on a Highly Imbalanced Dataset," *IEEE Access*, vol. 8, pp. 141066–141079, 2020, doi: 10.1109/ACCESS.2020.3013320.
- [66] P. Ksieniewicz and R. Burduk, "Clustering and weighted scoring in geometric space support vector machine ensemble for highly imbalanced data classification," *Lect. Notes Comput. Sci. (including Subser. Lect. Notes Artif. Intell. Lect. Notes Bioinformatics)*, vol. 12140 LNCS, pp. 128–140, 2020, doi: 10.1007/978-3-030-50423-6_10.
- [67] M. Alshawabkeh, M. Moffie, F. Azmandian, J. A. Aslam, J. Dy, and D. Kaeli, "Effective virtual machine monitor intrusion detection using feature selection on highly imbalanced data," *Proc. - 9th Int. Conf. Mach. Learn. Appl. ICMLA 2010*, pp. 823–827, 2010, doi: 10.1109/ICMLA.2010.127.
- [68] M. Khalilia, S. Chakraborty, and M. Popescu, "Predicting disease risks from highly imbalanced data using random forest," *BMC Med. Inform. Decis. Mak.*, vol. 11, no. 1, 2011, doi: 10.1186/1472-6947-11-51.
- [69] M. Galar, A. Fernández, E. Barrenechea, and F. Herrera, "EUSBoost: Enhancing ensembles for highly imbalanced data-sets by evolutionary undersampling," *Pattern Recognit.*, vol. 46, no. 12, pp. 3460–3471, 2013, doi: 10.1016/j.patcog.2013.05.006.
- [70] S. González, S. García, M. Lázaro, A. R. Figueiras-Vidal, and F. Herrera, "Class Switching according to Nearest Enemy Distance for learning from highly imbalanced data-sets," *Pattern Recognit.*, vol. 70, pp. 12–24, 2017, doi: 10.1016/j.patcog.2017.04.028.
- [71] S. Al-Azani and E. S. M. El-Alfy, "Using Word Embedding and Ensemble Learning for Highly Imbalanced Data Sentiment Analysis in Short Arabic Text," *Procedia Comput. Sci.*, vol. 109, pp. 359–366, 2017, doi: 10.1016/j.procs.2017.05.365.
- [72] P. Zybiewski, P. Ksieniewicz, and M. Woźniak, "Classifier Selection for Highly Imbalanced Data Streams with Minority Driven Ensemble," *Lect. Notes Comput. Sci. (including Subser. Lect. Notes Artif. Intell. Lect. Notes Bioinformatics)*, vol. 11508 LNAI, no. May, pp. 626–635, 2019, doi: 10.1007/978-3-030-20912-4_57.
- [73] D. Chen, X. J. Wang, C. Zhou, and B. Wang, "The Distance-Based Balancing Ensemble Method for Data With a High Imbalance Ratio," *IEEE Access*, vol. 7, pp. 68940–68956, 2019, doi: 10.1109/ACCESS.2019.2917920.
- [74] M. Abouelenien, Xiaohui Yuan, P. Duraisamy, and Xiaojing Yuan, "Improving classification performance for the minority class in highly imbalanced dataset using boosting," 2013, doi: 10.1109/icccnt.2012.6477850.
- [75] N. Liu, X. Li, E. Qi, M. Xu, L. Li, and B. Gao, "A Novel Ensemble Learning Paradigm for Medical Diagnosis With Imbalanced Data," *IEEE Access*, vol. 8, pp. 171263–171280, 2020, doi: 10.1109/access.2020.3014362.
- [76] P. Pławiak, M. Abdar, J. Pławiak, V. Makarenkov, and U. R. Acharya, "DGHNL: A new deep genetic hierarchical network of learners for prediction of credit scoring," *Inf. Sci. (Ny)*, vol. 516, no. April, pp. 401–418, 2020, doi: 10.1016/j.ins.2019.12.045.
- [77] P. Pławiak, M. Abdar, and U. Rajendra Acharya, "Application of new deep genetic cascade ensemble of SVM classifiers to predict the Australian credit scoring," *Appl. Soft Comput.*, vol. 84, p. 105740, 2019, doi: https://doi.org/10.1016/j.asoc.2019.105740.
- [78] E. I. Altman, M. Iwanicz-Drozdowska, E. K. Laitinen, and A. Suvas, "A Race for Long Horizon Bankruptcy Prediction," *Appl. Econ.*, vol. 52, no. 37, pp. 4092–4111, 2020, doi: 10.1080/00036846.2020.1730762.
- [79] M. Soui, S. Smiti, M. W. Mkaouer, and R. Ejbali, "Bankruptcy Prediction Using Stacked Auto-Encoders," *Appl. Artif. Intell.*, vol. 34, no. 1, pp. 80–100, 2020, doi: 10.1080/08839514.2019.1691849.
- [80] Q. Zhu, H. Liu, J. Wang, S. Chen, P. Wen, and S. Wang, "Research of System Fault Diagnosis Method Based on Imbalanced Data," 2019 Progn. Syst. Heal. Manag. Conf. PHM-Qingdao 2019, pp. 1–5, 2019, doi: 10.1109/PHM-Qingdao46334.2019.8943068.
- [81] E. Kaya, S. Korkmaz, M. A. Sahman, and A. C. Cinar, "DEBOHID: A differential evolution based oversampling approach for highly

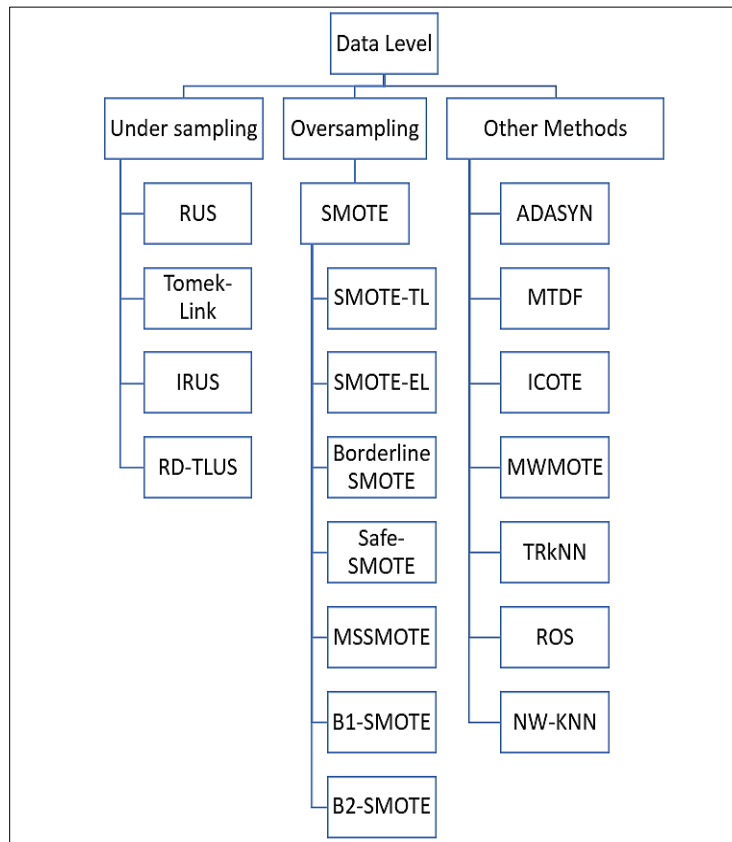
- imbalanced datasets," *Expert Syst. Appl.*, vol. 169, p. 114482, 2021, doi: 10.1016/j.eswa.2020.114482.
- [82] H. Faris et al., "Improving financial bankruptcy prediction in a highly imbalanced class distribution using oversampling and ensemble learning: a case from the Spanish market," *Prog. Artif. Intell.*, vol. 9, no. 1, pp. 31–53, 2020, doi: 10.1007/s13748-019-00197-9.
- [83] Z. Moti, S. Hashemi, and A. N. Jahromi, "A Deep Learning-based Malware Hunting Technique to Handle Imbalanced Data," pp. 48–53, 2020, doi: 10.1109/ISCISC51277.2020.9261913.
- [84] Y. Qu, P. Quan, M. Lei, and Y. Shi, "Review of bankruptcy prediction using machine learning and deep learning techniques," *Procedia Comput. Sci.*, vol. 162, no. Itqm 2019, pp. 895–899, 2019, doi: 10.1016/j.procs.2019.12.065.
- [85] M. Duan, D. Liu, X. Chen, R. Liu, Y. Tan, and L. Liang, "Self-Balancing Federated Learning with Global Imbalanced Data in Mobile Systems," *IEEE Trans. Parallel Distrib. Syst.*, vol. 32, no. 1, pp. 59–71, 2021, doi: 10.1109/TPDS.2020.3009406.
- [86] P. du Jardin, "Forecasting bankruptcy using biclustering and neural network-based ensembles," *Ann. Oper. Res.*, vol. 299, no. 1–2, pp. 531–566, 2021, doi: 10.1007/s10479-019-03283-2.
- [87] P. S. Nitu, P. Madiraju, and F. A. Pintar, "Identifying Feature Pattern for Weighted Imbalance Data: A Feature Selection Study for Thoracolumbar Spine Fractures in Crash Injury Research," *Proc. - 2020 IEEE 21st Int. Conf. Inf. Reuse Integr. Data Sci. IRI 2020*, pp. 142–147, 2020, doi: 10.1109/IRI49571.2020.00028.
- [88] U. Mahapatra, S. M. Nayak, and M. Rout, "A Systematic Approach to Enhance the Forecasting of Bankruptcy Data," *Adv. Intell. Syst. Comput.*, vol. 1119, no. January, pp. 641–650, 2020, doi: 10.1007/978-981-15-2414-1_64.
- [89] M. Zoričák, P. Gnip, P. Drotár, and V. Gazda, "Bankruptcy prediction for small- and medium-sized companies using severely imbalanced datasets," *Econ. Model.*, vol. 84, no. April, pp. 165–176, 2020, doi: 10.1016/j.econmod.2019.04.003.
- [90] T. Fitzpatrick and C. Mues, "An empirical comparison of classification algorithms for mortgage default prediction: Evidence from a distressed mortgage market," *Eur. J. Oper. Res.*, vol. 249, no. 2, pp. 427–439, 2016, doi: 10.1016/j.ejor.2015.09.014.
- [91] L. E. Boiko Ferreira, H. Murilo Gomes, A. Bifet, and L. S. Oliveira, "Adaptive Random Forests with Resampling for Imbalanced data Streams," *Proc. Int. Jt. Conf. Neural Networks*, vol. 2019-July, no. July, pp. 1–6, 2019, doi: 10.1109/IJCNN.2019.8852027.
- [92] E. I. Altman, M. Iwanicz-Drozdowska, E. K. Laitinen, and A. Suvas, "A Race for Long Horizon Bankruptcy Prediction," *Appl. Econ.*, vol. 00, no. 00, pp. 1–20, 2020, doi: 10.1080/00036846.2020.1730762.
- [93] J. Sun, H. Li, H. Fujita, B. Fu, and W. Ai, "Class-imbalanced dynamic financial distress prediction based on Adaboost-SVM ensemble combined with SMOTE and time weighting," *Inf. Fusion*, vol. 54, no. July 2019, pp. 128–144, 2020, doi: 10.1016/j.inffus.2019.07.006.
- [94] L. Yanze and O. Harutoshi, "Quasi-Linear SVM with Local Offsets for High-dimensional Imbalanced Data Classification," 2020.
- [95] Y. Chen, "A selective under-sampling based bagging SVM for imbalanced data learning in biomedical event trigger recognition," *ACM Int. Conf. Proceeding Ser.*, pp. 112–119, 2018, doi: 10.1145/3278198.3278221.
- [96] Z. Luo, X. Zeng, Z. Bao, and M. Xu, "Deep learning-based strategy for macromolecules classification with imbalanced data from cellular electron cryotomography," *arXiv*, no. July, pp. 1–8, 2019.
- [97] T. Handhika, A. Fahrurrozi, R. I. M. Zen, D. P. Lestari, I. Sari, and Murni, "Modified average of the base-level models in the hill-climbing bagged ensemble selection algorithm for credit scoring," *Procedia Comput. Sci.*, vol. 157, pp. 229–237, 2019, doi: 10.1016/j.procs.2019.08.162.
- [98] Y. Xia, C. Liu, B. Da, and F. Xie, "A novel heterogeneous ensemble credit scoring model based on bstacking approach," *Expert Syst. Appl.*, vol. 93, pp. 182–199, 2018, doi: <https://doi.org/10.1016/j.eswa.2017.10.022>.
- [99] V. García, A. I. Marqués, and J. S. Sánchez, "Exploring the synergetic effects of sample types on the performance of ensembles for credit risk and corporate bankruptcy prediction," *Inf. Fusion*, vol. 47, no. June 2018, pp. 88–101, 2019, doi: 10.1016/j.inffus.2018.07.004.
- [100] M. Schlögl, "A multivariate analysis of environmental effects on road accident occurrence using a balanced bagging approach," *Accid. Anal. Prev.*, vol. 136, no. December 2019, p. 105398, 2020, doi: 10.1016/j.aap.2019.105398.
- [101] L. Wang et al., "Classifying 2-year recurrence in patients with dbcl using clinical variables with imbalanced data and machine learning methods," *Comput. Methods Programs Biomed.*, vol. 196, p. 105567, 2020, doi: 10.1016/j.cmpb.2020.105567.
- [102] Y. S. Jeon and D. J. Lim, "PSU: Particle Stacking Undersampling Method for Highly Imbalanced Big Data," *IEEE Access*, vol. 8, pp. 131920–131927, 2020, doi: 10.1109/ACCESS.2020.3009753.
- [103] W. Wang, M. Zhang, L. Zhang, and Q. Bai, "Imbalanced Data Classification for Multi-Source Heterogenous Sensor Networks," *IEEE Access*, vol. 8, pp. 27406–27413, 2020, doi: 10.1109/ACCESS.2020.2966324.
- [104] P. Branco and L. Torgo, "A study on the impact of data characteristics in imbalanced regression tasks," *Proc. - 2019 IEEE Int. Conf. Data Sci. Adv. Anal. DSAA 2019*, pp. 193–202, 2019, doi: 10.1109/DSAA.2019.00034.
- [105] W. Feng et al., "Dynamic synthetic minority over-sampling technique-based rotation forest for the classification of imbalanced hyperspectral data," *IEEE J. Sel. Top. Appl. Earth Obs. Remote Sens.*, vol. 12, no. 7, pp. 2159–2169, 2019, doi: 10.1109/JSTARS.2019.2922297.
- [106] S. Lyra, S. Leonhardt, and C. Hoog Antink, "Early Prediction of Sepsis Using Random Forest Classification for Imbalanced Clinical Data," *2019 Comput. Cardiol. Conf.*, vol. 45, pp. 1–4, 2019, doi: 10.22489/cinc.2019.276.
- [107] M. Yahaya, X. Jiang, C. Fu, K. Bashir, and W. Fan, "Enhancing Crash Injury Severity Prediction on Imbalanced Crash Data by Sampling Technique with Variable Selection," *2019 IEEE Intell. Transp. Syst. Conf. ITSC 2019*, pp. 363–368, 2019, doi: 10.1109/ITSC.2019.8917223.
- [108] R. O'Brien and H. Ishwaran, "A random forests quantile classifier for class imbalanced data," *Pattern Recognit.*, vol. 90, pp. 232–249, 2019, doi: 10.1016/j.patcog.2019.01.036.
- [109] T. M. Shearman, J. M. Varner, S. M. Hood, C. A. Cansler, and J. K. Hierns, "Modelling post-fire tree mortality: Can random forest improve discrimination of imbalanced data?," *Ecol. Modell.*, vol. 414, no. November, p. 108855, 2019, doi: 10.1016/j.ecolmodel.2019.108855.
- [110] W. hui Hou, X. kang Wang, H. yu Zhang, J. qiang Wang, and L. Li, "A novel dynamic ensemble selection classifier for an imbalanced data set: An application for credit risk assessment," *Knowledge-Based Syst.*, vol. 208, p. 106462, 2020, doi: 10.1016/j.knsys.2020.106462.
- [111] Y. Deng, P. Dolog, J. M. Gass, and K. Denecke, "Obesity entity extraction from real outpatient records: When learning-based methods meet small imbalanced medical data sets," *Proc. - IEEE Symp. Comput. Med. Syst.*, vol. 2019-June, pp. 411–416, 2019, doi: 10.1109/CBMS.2019.00087.
- [112] J. M. Melo Neto, H. S. Bernardino, and H. J. C. Barbosa, "On the Impact of the Objective Function on Imbalanced Data using Cartesian Genetic Programming Neuroevolutionary Approaches," *2019 IEEE Congr. Evol. Comput. CEC 2019 - Proc.*, pp. 1860–1867, 2019, doi: 10.1109/CEC.2019.8789947.
- [113] G. Wang, T. Zhou, K.-S. Choi, and J. Lu, "A Deep-Ensemble-Level-Based Interpretable Takagi-Sugeno-Kang Fuzzy Classifier for Imbalanced Data," *IEEE Trans. Cybern.*, pp. 1–14, 2020, doi: 10.1109/tyb.2020.3016972.
- [114] B. Efron and R. J. Tibshirani, *An Introduction to the Bootstrap*. 1993.
- [115] L. Breiman, "Bagging predictions," *Mach. Learn.*, vol. 24, no. 2, pp. 123–140, 1996.
- [116] G. Rekha, V. K. Reddy, A. K. Tyagi, and M. M. Nair, "Distance-based Bootstrap Sampling in Bagging for Imbalanced Data-Set," *Int. Conf. Emerg. Trends Inf. Technol. Eng. ic-ETITE 2020*, pp. 1–6, 2020, doi: 10.1109/ic-ETITE47903.2020.345.
- [117] X. Wang, J. Xu, T. Zeng, and L. Jing, "Local distribution-based adaptive minority oversampling for imbalanced data classification," *Neurocomputing*, vol. 422, pp. 200–213, 2021, doi: 10.1016/j.neucom.2020.05.030.

- [118] L. G. Valiant, "A theory of the learnable," *Proc. Annu. ACM Symp. Theory Comput.*, vol. 27, no. 11, pp. 436–445, 1984, doi: 10.1145/800057.808710.
- [119] M. J. Kearns, R. E. Schapire, and L. M. Sellie, "Toward efficient agnostic learning," *Proc. Fifth Annu. ACM Work. Comput. Learn. Theory*, vol. 141, pp. 341–352, 1992, doi: 10.1007/bf00993468.
- [120] Y. Wang, L. L. Sun, and Q. Jin, "Enhanced Diagnosis of Pneumothorax with an Improved Real-time Augmentation for Imbalanced Chest X-rays Data Based on DCNN," *IEEE/ACM Trans. Comput. Biol. Bioinforma.*, vol. 14, no. 8, pp. 1–1, 2019, doi: 10.1109/tcbb.2019.2911947.
- [121] X. Y. Jing et al., "Multiset Feature Learning for Highly Imbalanced Data Classification," *IEEE Trans. Pattern Anal. Mach. Intell.*, vol. 43, no. 1, pp. 139–156, 2021, doi: 10.1109/TPAMI.2019.2929166.
- [122] D. Wolpert, "Stacked Generalization (Stacking)," *Neural Networks*, vol. 5, pp. 241–259, 1992.
- [123] H. He, W. Zhang, and S. Zhang, "A novel ensemble method for credit scoring: Adaption of different imbalance ratios," *Expert Syst. Appl.*, vol. 98, pp. 105–117, 2018, doi: <https://doi.org/10.1016/j.eswa.2018.01.012>.
- [124] S. Layeghian Javan, M. M. Sepehri, M. Layeghian Javan, and T. Khatibi, "An intelligent warning model for early prediction of cardiac arrest in sepsis patients," *Comput. Methods Programs Biomed.*, vol. 178, pp. 47–58, 2019, doi: 10.1016/j.cmpb.2019.06.010.
- [125] L. I. Kuncheva and E. Alpaydin, *Combining Pattern Classifiers: Methods and Algorithms*, vol. 18, no. 3, 2007.
- [126] M. D. Muhlbaier, A. Topalis, and R. Polikar, "Learn++ .NC: Combining ensemble of classifiers with dynamically weighted consult-and-vote for efficient incremental learning of new classes," *IEEE Trans. Neural Networks*, vol. 20, no. 1, pp. 152–168, 2009, doi: 10.1109/TNN.2008.2008326.
- [127] Garcia-Pedrajas, "Constructing Ensembles of Classifiers by Means of Weighted Instance Selection," vol. 20, no. 2, pp. 258–277, 2009.
- [128] A. Rahman and B. Verma, "Novel layered clustering-based approach for generating ensemble of classifiers," *IEEE Trans. Neural Networks*, vol. 22, no. 5, pp. 781–792, 2011, doi: 10.1109/TNN.2011.2118765.
- [129] D. Opitz and R. Maclin, "Popular Ensemble Methods: An Empirical Study," *J. Artif. Intell. Res.*, vol. 11, no. April, pp. 169–198, 1999, doi: 10.1613/jair.614.
- [130] T. G. Dietterich, "Ensemble methods in machine learning," *Lect. Notes Comput. Sci. (including Subser. Lect. Notes Artif. Intell. Lect. Notes Bioinformatics)*, vol. 1857 LNCS, pp. 1–15, 2000, doi: 10.1007/3-540-45014-9_1.
- [131] R. Polikar, "Ensemble based systems in decision making," *IEEE Circuits Syst. Mag.*, vol. 6, no. 3, pp. 21–44, 2006, doi: 10.1109/MCAS.2006.1688199.
- [132] L. Rokach, "Ensemble-based classifiers," *Artif. Intell. Rev.*, vol. 33, no. 1–2, pp. 1–39, 2010, doi: 10.1007/s10462-009-9124-7.
- [133] L. I. Kuncheva and L. C. Jain, "Designing classifier fusion systems by genetic algorithms," *IEEE Trans. Evol. Comput.*, vol. 4, no. 4, pp. 327–336, 2000, doi: 10.1109/4235.887233.
- [134] M. L. Raymer, W. F. Punch, E. D. Goodman, L. A. Kuhn, and A. K. Jain, "Dimensionality reduction using genetic algorithms," *IEEE Trans. Evol. Comput.*, vol. 4, no. 2, pp. 164–171, 2000, doi: 10.1109/4235.850656.
- [135] M. Chabbouh, S. Bechikh, C. C. Hung, and L. Ben Said, "Multi-objective evolution of oblique decision trees for imbalanced data binary classification," *Swarm Evol. Comput.*, vol. 49, no. May 2018, pp. 1–22, 2019, doi: 10.1016/j.swevo.2019.05.005.
- [136] A. Bequé and S. Lessmann, "Extreme learning machines for credit scoring: An empirical evaluation," *Expert Syst. Appl.*, vol. 86, pp. 42–53, 2017, doi: 10.1016/j.eswa.2017.05.050.
- [137] M. Abdar, W. Książek, U. R. Acharya, R. S. Tan, V. Makarenkov, and P. Pławiak, "A new machine learning technique for an accurate diagnosis of coronary artery disease," *Comput. Methods Programs Biomed.*, vol. 179, no. August, 2019, doi: 10.1016/j.cmpb.2019.104992.
- [138] Y. Liu, Y. Wang, X. Ren, H. Zhou, and X. Diao, "A Classification Method Based on Feature Selection for Imbalanced Data," *IEEE Access*, vol. 7, pp. 81794–81807, 2019, doi: 10.1109/ACCESS.2019.2923846.
- [139] W. C. Lin, Y. H. Lu, and C. F. Tsai, "Feature selection in single and ensemble learning-based bankruptcy prediction models," *Expert Syst.*, vol. 36, no. 1, pp. 1–8, 2019, doi: 10.1111/exsy.12335.
- [140] H. Faris et al., "Improving financial bankruptcy prediction in a highly imbalanced class distribution using oversampling and ensemble learning: a case from the Spanish market," *Prog. Artif. Intell.*, vol. 9, no. 1, pp. 31–53, 2020, doi: 10.1007/s13748-019-00197-9.
- [141] T. Pisula, "An Ensemble Classifier-Based Scoring Model for Predicting Bankruptcy of Polish Companies in the Podkarpackie Voivodeship," *J. Risk Financ. Manag.*, vol. 13, no. 2, p. 37, 2020, doi: 10.3390/jrfm13020037.
- [142] I. Hermadi, Y. Nurhadryani, I. Ranggadara, and R. Amin, "A Review of Contribution and Challenge in Predictive Machine Learning Model at Financial Industry," *J. Phys. Conf. Ser.*, vol. 1477, no. 3, pp. 5–9, 2020, doi: 10.1088/1742-6596/1477/3/032021.
- [143] Y. C. Chang, K. H. Chang, and G. J. Wu, "Application of eXtreme gradient boosting trees in the construction of credit risk assessment models for financial institutions," *Appl. Soft Comput. J.*, vol. 73, pp. 914–920, 2018, doi: 10.1016/j.asoc.2018.09.029.
- [144] W. Lei, R. Zhang, Y. Yang, R. Wang, and W. S. Zheng, "Class-Center Involved Triplet Loss for Skin Disease Classification on Imbalanced Data," *Proc. - Int. Symp. Biomed. Imaging*, vol. 2020-April, pp. 16–20, 2020, doi: 10.1109/ISBI45749.2020.9098718.
- [145] J. F. Ramirez Rochac, N. Zhang, L. Thompson, and T. Oladunni, "A Data Augmentation-Assisted Deep Learning Model for High Dimensional and Highly Imbalanced Hyperspectral Imaging Data," *9th Int. Conf. Inf. Sci. Technol. ICIST 2019*, pp. 362–367, 2019, doi: 10.1109/ICIST.2019.8836913.
- [146] B. Jonathan, P. H. Putra, and Y. Ruldeviyani, "Observation Imbalanced Data Text to Predict Users Selling Products on Female Daily with SMOTE, Tomek, and SMOTE-Tomek," *Proc. - 2020 IEEE Int. Conf. Ind. 4.0, Artif. Intell. Commun. Technol. IAICT 2020*, pp. 81–85, 2020, doi: 10.1109/IAICT50021.2020.9172033.
- [147] M. Z. Alom et al., "A state-of-the-art survey on deep learning theory and architectures," *Electron.*, vol. 8, no. 3, pp. 1–67, 2019, doi: 10.3390/electronics8030292.
- [148] M. Azizjon, A. Jumabek, and W. Kim, "1D CNN based network intrusion detection with normalization on imbalanced data," *2020 Int. Conf. Artif. Intell. Inf. Commun. ICAIIC 2020*, pp. 218–224, 2020, doi: 10.1109/ICAIIIC48513.2020.9064976.
- [149] T. Hosaka, "Bankruptcy prediction using imaged financial ratios and convolutional neural networks," *Expert Syst. Appl.*, vol. 117, pp. 287–299, 2019, doi: 10.1016/j.eswa.2018.09.039.
- [150] F. Mai, S. Tian, C. Lee, and L. Ma, "Deep learning models for bankruptcy prediction using textual disclosures," *Eur. J. Oper. Res.*, vol. 274, no. 2, pp. 743–758, 2019, doi: 10.1016/j.ejor.2018.10.024.
- [151] C. Clement, "Machine Learning in Bankruptcy Prediction," *J. Public Adm. Financ. Law*, no. 17, p. 20, 2020.
- [152] H. Dong, B. Zhu, and J. Zhang, "A Cost-sensitive Active Learning for Imbalance Data with Uncertainty and Diversity Combination," *ACM Int. Conf. Proceeding Ser.*, pp. 218–224, 2020, doi: 10.1145/3383972.3384002.
- [153] N. W. S. Wardhani, M. Y. Rochayani, A. Iriany, A. D. Sulistyono, and P. Lestantyo, "Cross-validation Metrics for Evaluating Classification Performance on Imbalanced Data," *2019 Int. Conf. Comput. Control. Informatics its Appl. Emerg. Trends Big Data Artif. Intell. IC3INA 2019*, pp. 14–18, 2019, doi: 10.1109/IC3INA48034.2019.8949568.
- [154] L. B. Laureano, A. M. Sison, and R. P. Medina, "Handling imbalanced data through affinity propagation and SMOTE," *ACM Int. Conf. Proceeding Ser.*, pp. 22–26, 2019, doi: 10.1145/3366650.3366665.
- [155] B. Krawczyk, M. Koziarski, and M. Wozniak, "Radial-based oversampling for multiclass imbalanced data classification," *IEEE Trans. Neural Networks Learn. Syst.*, vol. 31, no. 8, pp. 2818–2831, 2020, doi: 10.1109/TNNLS.2019.2913673.
- [156] T. M. Khoshgoftaar, K. Gao, and J. Van Hulse, "A novel feature selection technique for highly imbalanced data," *2010 IEEE Int. Conf. Inf. Reuse Integr. IRI 2010*, pp. 80–85, 2010, doi: 10.1109/IRI.2010.5558961.

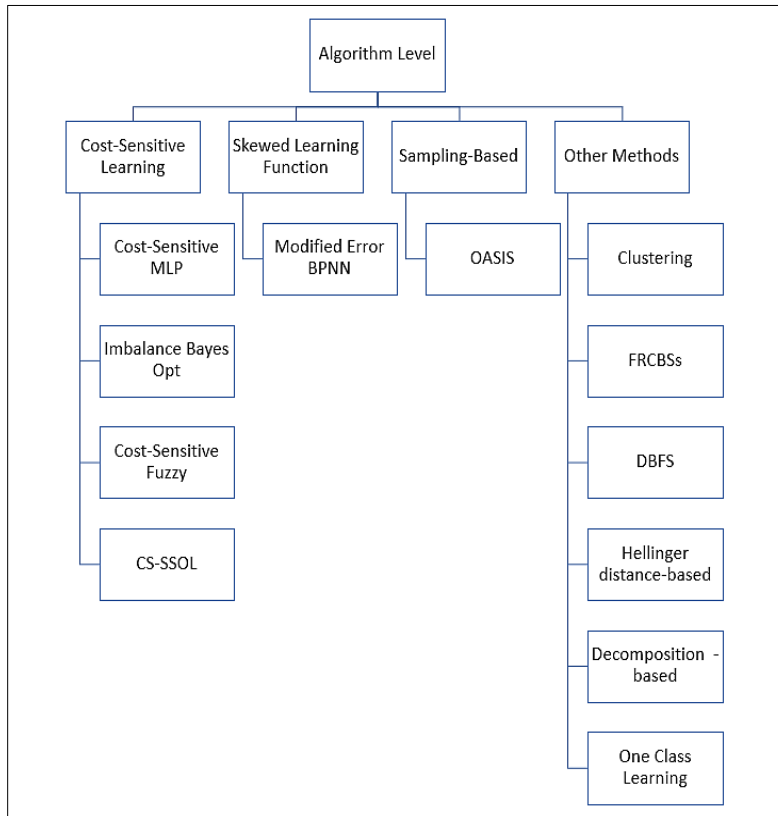
- [157] T. M. Khoshgoftaar, K. Gao, and A. Napolitano, "Exploring an iterative feature selection technique for highly imbalanced data sets," Proc. 2012 IEEE 13th Int. Conf. Inf. Reuse Integr. IRI 2012, pp. 101–108, 2012, doi: 10.1109/IRI.2012.6302997.
- [158] C. L. Calvert and T. M. Khoshgoftaar, "Threshold based optimization of performance metrics with severely imbalanced big security data," Proc. - Int. Conf. Tools with Artif. Intell. ICTAI, vol. 2019-Novem, pp. 1328–1334, 2019, doi: 10.1109/ICTAI.2019.00184.
- [159] S. Lu, F. Gao, C. Piao, and Y. Ma, "Dynamic Weighted Cross Entropy for Semantic Segmentation with Extremely Imbalanced Data," Proc. - 2019 Int. Conf. Artif. Intell. Adv. Manuf. AIAM 2019, pp. 230–233, 2019, doi: 10.1109/AIAM48774.2019.00053.
- [160] A. Fernández, F. J. Berlanga, M. J. Del Jesus, and F. Herrera, "Genetic cooperative-competitive fuzzy rule based learning method using genetic programming for highly imbalanced data-sets," 2009 Int. Fuzzy Syst. Assoc. World Congr. 2009 Eur. Soc. Fuzzy Log. Technol. Conf. IFSAEUSFLAT 2009 - Proc., pp. 42–47, 2009.
- [161] M. Uriz, D. Paternain, H. Bustince, and M. Galar, "A first approach towards the usage of classifiers' performance to create fuzzy measures for ensembles of classifiers: A case study on highly imbalanced datasets," IEEE Int. Conf. Fuzzy Syst., vol. 2018-July, pp. 1–8, 2018, doi: 10.1109/FUZZ-IEEE.2018.8491440.
- [162] M. Uriz, D. Paternain, H. Bustince, and M. Galar, "An empirical study on supervised and unsupervised fuzzy measure construction methods in highly imbalanced classification," IEEE Int. Conf. Fuzzy Syst., vol. 2020-July, pp. 1–8, 2020, doi: 10.1109/FUZZ48607.2020.9177789.
- [163] E. Bringer, A. Israeli, Y. Shoham, A. Ratner, and C. Ré, "Osprey: Weak Supervision of Imbalanced Extraction Problems without Code," Proc. ACM SIGMOD Int. Conf. Manag. Data, 2019, doi: 10.1145/3329486.3329492.
- [164] W. Ding, D. Y. Huang, Z. Chen, X. Yu, and W. Lin, "Facial action recognition using very deep networks for highly imbalanced class distribution," Proc. - 9th Asia-Pacific Signal Inf. Process. Assoc. Annu. Summit Conf. APSIPA ASC 2017, vol. 2018-Febru, no. December, pp. 1368–1372, 2018, doi: 10.1109/APSIPA.2017.8282246.
- [165] E. Kim and S. Bang, "Weighted L 1 -Norm Support Vector Machine for the," vol. 28, pp. 9–21, 2015.
- [166] A. Fernández, M. J. Del Jesus, and F. Herrera, "Improving the performance of fuzzy rule based classification systems for highly imbalanced data-sets using an evolutionary adaptive inference system," Lect. Notes Comput. Sci. (including Subser. Lect. Notes Artif. Intell. Lect. Notes Bioinformatics), vol. 5517 LNCS, no. PART 1, pp. 294–301, 2009, doi: 10.1007/978-3-642-02478-8_37.
- [167] P. Villar, A. Fernández, R. A. Carrasco, and F. Herrera, "Feature selection and granularity learning in genetic fuzzy rule-based classification systems for highly imbalanced data-sets," Int. J. Uncertainty, Fuzziness Knowledge-Based Syst., vol. 20, no. 3, pp. 369–397, 2012, doi: 10.1142/S0218488512500195.
- [168] B. Liu, M. Zhang, W. Ma, X. Li, Y. Liu, and S. Ma, "A two-step information accumulation strategy for learning from highly imbalanced data," Int. Conf. Inf. Knowl. Manag. Proc., vol. Part F1318, pp. 1289–1298, 2017, doi: 10.1145/3132847.3132940.
- [169] P. Villar, A. Fernández, and F. Herrera, "A genetic algorithm for feature selection and granularity learning in fuzzy rule-based classification systems for highly imbalanced data-sets," Commun. Comput. Inf. Sci., vol. 80 PART 1, pp. 741–750, 2010, doi: 10.1007/978-3-642-14055-6_78.
- [170] Y. Tang, Y. Q. Zhang, and N. V. Chawla, "SVMs modeling for highly imbalanced classification," IEEE Trans. Syst. Man, Cybern. Part B Cybern., vol. 39, no. 1, pp. 281–288, 2009, doi: 10.1109/TSMCB.2008.2002909.
- [171] P. Villar, A. Fernández, and F. Herrera, "A genetic learning of the fuzzy rule-based classification system granularity for highly imbalanced datasets," IEEE Int. Conf. Fuzzy Syst., pp. 1689–1694, 2009, doi: 10.1109/FUZZY.2009.5277304.
- [172] S. Sardari, M. Eftekhari, and F. Afsari, "Hesitant fuzzy decision tree approach for highly imbalanced data classification," Appl. Soft Comput. J., vol. 61, pp. 727–741, 2017, doi: 10.1016/j.asoc.2017.08.052.
- [173] H. Ahumada, G. L. Grinblat, L. C. Uzal, P. M. Granitto, and A. Ceccatto, "REPMAC: A new hybrid approach to highly imbalanced classification problems," Proc. - 8th Int. Conf. Hybrid Intell. Syst. HIS 2008, pp. 386–391, 2008, doi: 10.1109/HIS.2008.142.
- [174] A. Anand, G. Pugalenth, G. B. Fogel, and P. N. Suganthan, "An approach for classification of highly imbalanced data using weighting and undersampling," Amino Acids, vol. 39, no. 5, pp. 1385–1391, 2010, doi: 10.1007/s00726-010-0595-2.
- [175] Q. Li and Y. Xie, "A behavior-cluster based imbalanced classification method for credit card fraud detection," ACM Int. Conf. Proceeding Ser., pp. 134–139, 2019, doi: 10.1145/3352411.3352433.
- [176] B. Gyawali, T. Solorio, M. Montes-Y-Gómez, B. Wardman, and G. Warner, "Evaluating a semisupervised approach to phishing URL identification in a realistic scenario," ACM Int. Conf. Proceeding Ser., pp. 176–183, 2011, doi: 10.1145/2030376.2030397.
- [177] S. R. Hashemi, S. S. M. Salehi, D. Erdogmus, S. P. Prabhu, S. K. Warfield, and A. Gholipour, "Asymmetric Loss Functions and Deep Densely-Connected Networks for Highly-Imbalanced Medical Image Segmentation: Application to Multiple Sclerosis Lesion Detection," IEEE Access, vol. 7, pp. 1721–1735, 2019, doi: 10.1109/ACCESS.2018.2886371.
- [178] Y. Lu, J. H. Zhou, and C. Guan, "Minimizing Hybrid Dice Loss for Highly Imbalanced 3D Neuroimage Segmentation," Proc. Annu. Int. Conf. IEEE Eng. Med. Biol. Soc. EMBS, vol. 2020-July, pp. 1059–1062, 2020, doi: 10.1109/EMBC44109.2020.9176663.
- [179] P. Jain, A. Agarwal, and R. Behara, "An approach to supervised classification of highly imbalanced and high dimensionality COPD readmission data on HPCC," SysCon 2019 - 13th Annu. IEEE Int. Syst. Conf. Proc., pp. 5–9, 2019, doi: 10.1109/SYSCON.2019.8836797.
- [180] C. F. Yeh, A. Heidele, H. Y. Lee, and L. S. Lee, "Recognition of highly imbalanced code-mixed bilingual speech with frame-level language detection based on blurred posteriorgram," ICASSP, IEEE Int. Conf. Acoust. Speech Signal Process. - Proc., pp. 4873–4876, 2012, doi: 10.1109/ICASSP.2012.6289011.
- [181] C. F. Yeh and L. S. Lee, "An improved framework for recognizing highly imbalanced bilingual code-switched lectures with cross-language acoustic modeling and frame-level language identification," IEEE Trans. Audio, Speech Lang. Process., vol. 23, no. 7, pp. 1144–1159, 2015, doi: 10.1109/TASLP.2015.2425214.
- [182] Y. Tang, S. Krasser, P. Judge, and Y. Q. Zhang, "Fast and effective spam sender detection with granular SVM on highly imbalanced mail server behavior data," 2006 Int. Conf. Collab. Comput. Networking, Appl. Work. Collab., 2006, doi: 10.1109/COLCOM.2006.361856.
- [183] I. Almomani et al., "Android Ransomware Detection Based on a Hybrid Evolutionary Approach in the Context of Highly Imbalanced Data," IEEE Access, vol. 9, pp. 57674–57691, 2021, doi: 10.1109/ACCESS.2021.3071450.
- [184] M. Abouelenien, Xiaohui Yuan, P. Duraisamy, and Xiaojing Yuan, "Improving classification performance for the minority class in highly imbalanced dataset using boosting," 2012 Third Int. Conf. Comput. Commun. Netw. Technol., pp. 1–6, 2013, doi: 10.1109/iccnet.2012.6477850.
- [185] M. Bach, A. Werner, J. Zywiec, and W. Pluskiewicz, "The study of under- and over-sampling methods' utility in analysis of highly imbalanced data on osteoporosis," Inf. Sci. (Ny), vol. 384, pp. 174–190, 2017, doi: 10.1016/j.ins.2016.09.038.
- [186] J. C. Lamirel, "Dealing with highly imbalanced textual data gathered into similar classes," Proc. Int. Jt. Conf. Neural Networks, pp. 1–7, 2013, doi: 10.1109/IJCNN.2013.6707044.
- [187] J. Guan, J. Liu, J. Sun, P. Feng, T. Shuai, and W. Wang, "META METRIC LEARNING FOR HIGHLY IMBALANCED AERIAL SCENE CLASSIFICATION College of Computer Science and Technology, Harbin Engineering University, Harbin, 150001, China State Key Laboratory of Space-Ground Integrated Information Technology, Beijing,," ICASSP 2020 - 2020 IEEE Int. Conf. Acoust. Speech Signal Process., pp. 4042–4046, 2020.
- [188] F. Wu, X. Y. Jing, S. Shan, W. Zuo, and J. Y. Yang, "Multiset feature learning for highly imbalanced data classification," 31st AAAI Conf.

- Artif. Intell. AAAI 2017, vol. PP, no. c, pp. 1583–1589, 2017, doi: 10.1109/tpami.2019.2929166.
- [189] L. V. B. Beltrán, M. Coustaty, N. Journet, J. C. Caicedo, and A. Doucet, “Multi-attribute learning with highly imbalanced data,” Proc. - Int. Conf. Pattern Recognit., pp. 9219–9226, 2020, doi: 10.1109/ICPR48806.2021.9412634.
- [190] A. N. Jahromi, H. Karimpour, J. Sakhnini, and A. Dehghantanha, “A deep unsupervised representation learning approach for effective cyber-physical attack detection and identification on highly imbalanced data,” CASCON 2019 Proc. - Conf. Cent. Adv. Stud. Collab. Res. - Proc. 29th Annu. Int. Conf. Comput. Sci. Softw. Eng., pp. 14–23, 2020.
- [191] S. Li and W. Deng, “Real world expression recognition: A highly imbalanced detection problem,” 2016 Int. Conf. Biometrics, ICB 2016, pp. 1–6, 2016, doi: 10.1109/ICB.2016.7550074.
- [192] A. C. Neocleous, K. H. Nicolaides, and C. N. Schizas, “Intelligent Noninvasive Diagnosis of Aneuploidy: Raw Values and Highly Imbalanced Dataset,” IEEE J. Biomed. Heal. Informatics, vol. 21, no. 5, pp. 1271–1279, 2017, doi: 10.1109/JBHI.2016.2608859.
- [193] Y. B. Hagos et al., “Cell abundance aware deep learning for cell detection on highly imbalanced pathological data,” Proc. - Int. Symp. Biomed. Imaging, vol. 2021-April, pp. 1438–1442, 2021, doi: 10.1109/ISBI48211.2021.9433994.
- [194] J. C. Lamirel, “Dealing with highly imbalanced textual data gathered into similar classes,” Proc. Int. Jt. Conf. Neural Networks, 2013, doi: 10.1109/IJCNN.2013.6707044.
- [195] S. Kübler, C. Liu, and Z. A. Sayyed, To use or not to use: Feature selection for sentiment analysis of highly imbalanced data, vol. 24, no. 1. 2018.
- [196] N. Anantrasirichai, D. Bull, and D. Bull, “DEFECTNET: MULTI-CLASS FAULT DETECTION ON HIGHLY-IMBALANCED DATASETS N . Anantrasirichai and David Bull,” 2019 IEEE Int. Conf. Image Process., pp. 2481–2485, 2019.
- [197] P. Jain, A. Agarwal, and R. Behara, “An approach to supervised classification of highly imbalanced and high dimensionality COPD readmission data on HPCC,” SysCon 2019 - 13th Annu. IEEE Int. Syst. Conf. Proc., pp. 1–7, 2019, doi: 10.1109/SYSCON.2019.8836797.
- [198] K. Fujiwara, M. Shigeno, and U. Sumita, “A New Approach for Developing Segmentation Algorithms for Strongly Imbalanced Data,” IEEE Access, vol. 7, pp. 82970–82977, 2019, doi: 10.1109/ACCESS.2019.2923524.
- [199] Y. Lu, Y. M. Cheung, and Y. Y. Tang, “Bayes Imbalance Impact Index: A Measure of Class Imbalanced Data Set for Classification Problem,” IEEE Trans. Neural Networks Learn. Syst., vol. 31, no. 9, pp. 3525–3539, 2020, doi: 10.1109/TNNLS.2019.2944962.
- [200] E. R. Q. Fernandes, A. C. P. L. F. De Carvalho, and X. Yao, “Ensemble of classifiers based on multiobjective genetic sampling for imbalanced data,” IEEE Trans. Knowl. Data Eng., vol. 32, no. 6, pp. 1104–1115, 2020, doi: 10.1109/TKDE.2019.2898861.
- [201] K. Yang et al., “Hybrid Classifier Ensemble for Imbalanced Data,” IEEE Trans. Neural Networks Learn. Syst., vol. 31, no. 4, pp. 1387–1400, 2020, doi: 10.1109/TNNLS.2019.2920246.
- [202] G. Wang, J. Ma, L. Huang, and K. Xu, “Two credit scoring models based on dual strategy ensemble trees,” Knowledge-Based Syst., vol. 26, pp. 61–68, 2012, doi: 10.1016/j.knosys.2011.06.020.
- [203] E. Rendón, R. Alejo, C. Castorena, F. J. Isidro-Ortega, and E. E. Granda-Gutiérrez, “Data sampling methods to deal with the big data multi-class imbalance problem,” Appl. Sci., vol. 10, no. 4, 2020, doi: 10.3390/app10041276.
- [204] C. L. Liu and P. Y. Hsieh, “Model-Based Synthetic Sampling for Imbalanced Data,” IEEE Trans. Knowl. Data Eng., vol. 32, no. 8, pp. 1543–1556, 2020, doi: 10.1109/TKDE.2019.2905559.
- [205] G. Shi, C. Feng, W. Xu, L. Liao, and H. Huang, “Penalized multiple distribution selection method for imbalanced data classification,” Knowledge-Based Syst., vol. 196, p. 105833, 2020, doi: 10.1016/j.knosys.2020.105833.

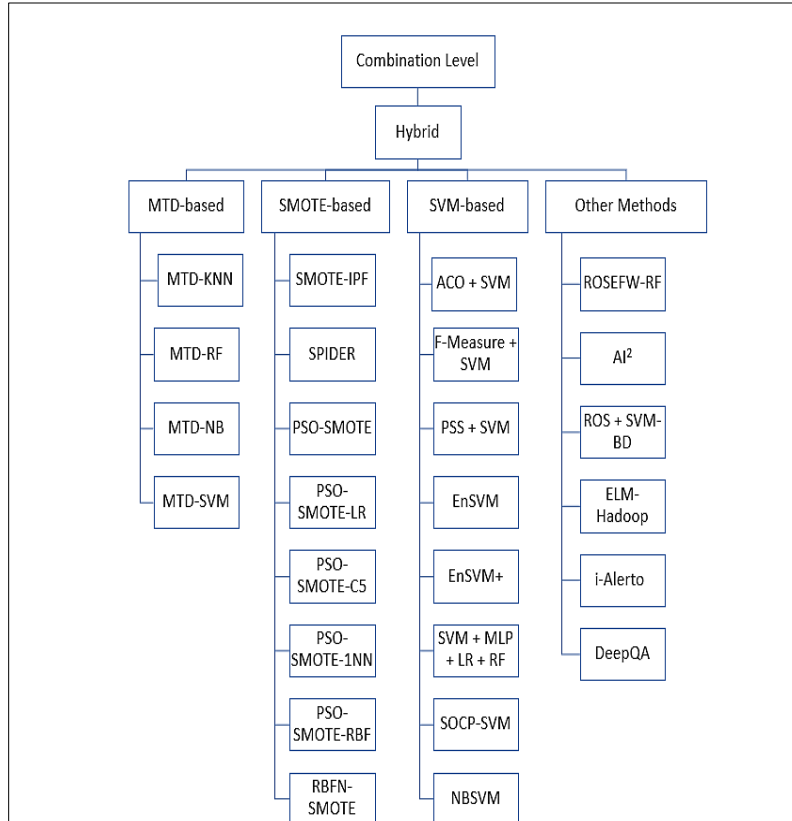
Appendix I. METHODS IN DATA LEVEL STRATEGY



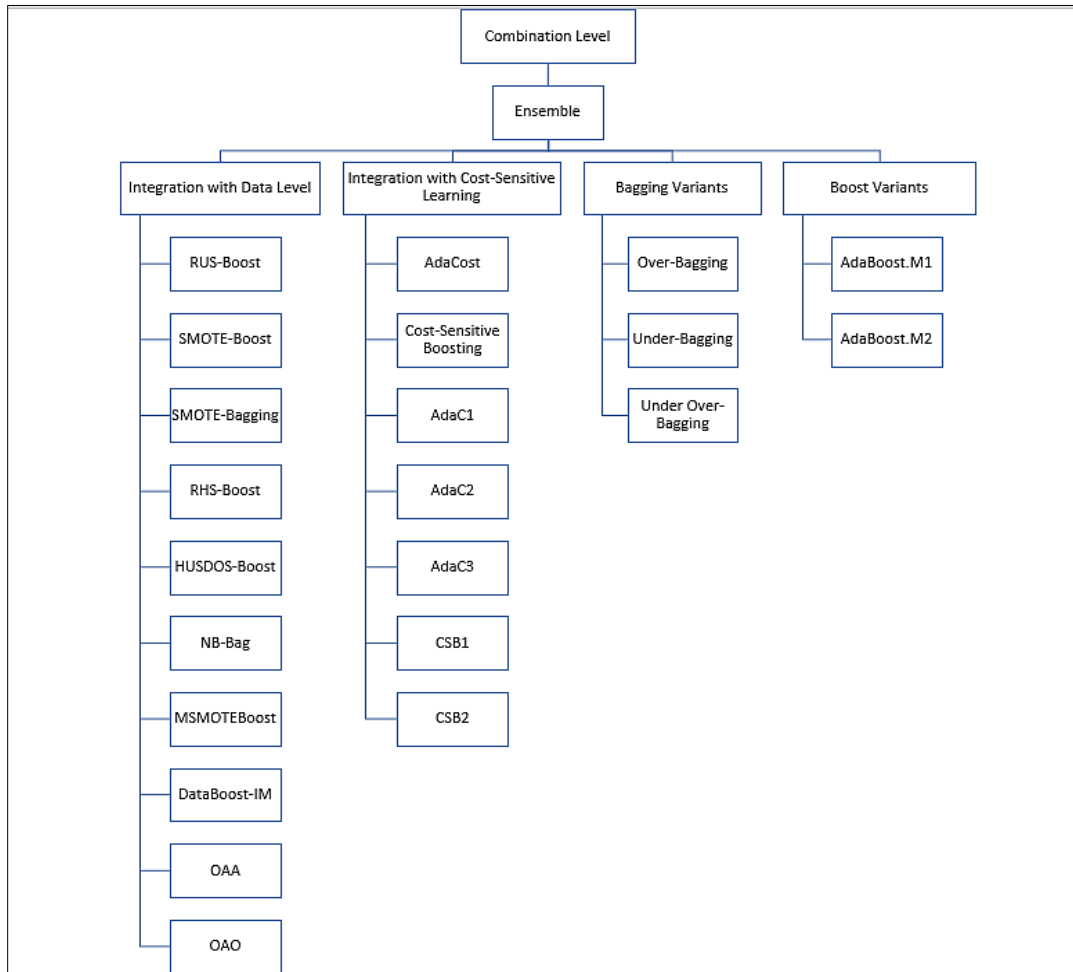
Appendix. II. METHODS IN ALGORITHM LEVEL STRATEGY



Appendix. III. METHODS IN COMBINATION LEVEL STRATEGY (HYBRID)



Appendix. IV. METHODS IN COMBINATION LEVEL STRATEGY (ENSEMBLE)



Synthetic Data Augmentation of Tomato Plant Leaf using Meta Intelligent Generative Adversarial Network: Milgan

Sri Silpa Padmanabhuni, Pradeepini Gera

Department of Computer Science and Engineering
Koneru Lakshmaiah Education Foundation, Vaddeswaram, AP, India

Abstract—Agriculture is one of the most famous case studies in deep learning. Most researchers want to detect different diseases at the early stages of cultivation to save the farmer's economy. The deep learning technique needs more data to develop an accurate system. Researchers generated more synthetic data using basic image operations in traditional approaches, but these approaches are more complicated and expensive. In deep learning and computer vision, the system's accuracy is the crucial component for deciding the system's efficiency. The model's precision is based on the image's size and quality. Getting many images from the real-world environment in medicine and agriculture is difficult. The image augmentation technique helps the system generate more images that can replicate the physical circumstances by performing various operations. It also prevents overfitting, especially when the system has fewer images than required. Few researchers experimented using CNN and simple Generative Adversarial Network (GAN), but these approaches create images with more noise. The proposed research aims to develop more data using a Meta approach. The images are processed using kernel filters. Different geometric transformations are passed as input to the enhanced GANs to reduce the noise and create more fake images using latent points, acting as weights in the neural networks. The proposed system uses random sampling techniques, passes a few processed images to the generator component of GAN, and the system uses a discriminator component to classify the synthetic data created by the Meta-Learning Approach.

Keywords—Basic image operations; meta-learning techniques; generator; discriminator; synthetic data; sampling techniques; latent points; kernel filters

I. INTRODUCTION

Deep Learning algorithms are famous for solving case studies related to medicine and agriculture. The efficiency of the deep learning model depends on the selection of neural network design. The process of defining the best estimators for a network is coined "Hyper Turning." The system needs more balanced and huge of data to estimate the proper parameters that suit the network. It is highly impossible to collect the real-time images from the farming lands using digital cameras, and the collection of satellite images covers the entire crop. However, it cannot provide individual leaf analysis [19]. So, the agriculture industry needs a system that can generate similar images covering controlled and

uncontrolled situations like blur leaf images due to heavy wind effects, half leaf images due to the distance, and others. The generation of similar images is known as "Data Augmentation," and the data is known as "Synthetic Data." The previous researchers created synthetic data using basic image manipulation techniques, GANs or Auto encoders and decoders [10]. The number of images will increase using manipulation techniques like transformation and rotation, but they cannot produce uncontrolled images. Researchers have introduced GANs and encoders over the past few years to create compressed and noisy images so they can handle uncontrolled conditions. However, due to single components of GANs, they produce more noise than required. The proposed system to reduce the number of noisy images and enhance the quality of controlled images introduced a meta-intelligent environment where the architecture is improved by increasing the components of GAN, and these components take the manipulated images rather than the original images from the GAN. The proposed research generates images using simple operations, as discussed below.

A. Basic Image Operations

Traditionally, to manipulate the images, researchers performed Geometric transformations [18], which involve rotations, flipping, resizing, shifting, zooming, cropping, and noise operations. The system can also perform color space transformations. Images are composed of RGB color conventions but must be converted into grey-scale or other color saturation values for efficient data processing. The essential operations involve a kernel filter [16], extracting the region of interest from the image using convolution neural networks. The image is saved as a two-dimensional matrix, and the filter does a dot product between the inputs and filter layers and then adds the values to get a single value in each location. Edge detection, image sharpening, and blurring operations benefit from kernel filtering. The most recent improvements are the random erasing technique to remove pixels in an image by choosing a rectangular region based on the likelihood determined by aspect and area ratios. The Random Erasing technique is essential for image recognition, object detection, and people re-identification. It can be used on pre-trained models and easily combined with neural networks [13]. The different types of image operations are shown in Fig. 1.

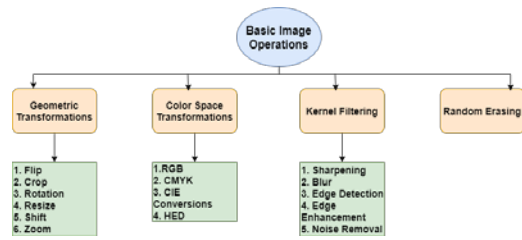


Fig. 1. Types of basic Image Operations.

1) *Rotation*: Rotation is the most straightforward operation that can be applied to any image to change its orientation. The rotation angle is expressed in degrees, ranging from 0 to 360 clockwise[21].

2) *Flipping*: It is a variation in the rotational operation. The transposition of row and column pixels is accomplished using a flipping operation. Two types of flipping operations can be carried out here. Horizontal and vertical flips may be used, depending on the quality of the images.

3) *Shearing*: Shearing is moving pixels from one location to another, either horizontally or vertically. The image's dimensions remain unchanged. Only a few pixels will be clipped off.

4) *Cropping*: The images generally have a region of interest at different locations. Cropping the image at the required area is the best operation to identify the location. Since the proposed system is a classification model, the model's output should be a subset of the entire image[17].

5) *Zooming*: When a system zooms in, the system can either add new pixel values or interpolate existing ones. If we take the value x as an example, the zoom will perform $1+x$ and $1-x$ operations on the image pixels. It aids in the image's standardized sampling.

6) *Brightness or contrast*: This operation can darken or brighten an image. This operation primarily assists the model in training the device in various conditions. The system may use percentages to specify the minimum and maximum values. The image is darkened if the value is less than 1.0 and brightened if the value is more than 1.0.

The below section presents the algorithm in which all the manipulation operations are randomly applied to the dataset's images.

Algorithm: Basic Image Operations

```

Input: Load the tomato dataset from the data repository, T_Data
Output: Retransformed Images
1. for i in len(T_Data):
    Resize_timage ← ImageGenerator(T_Data, rescale=1/255).
2.     train_img_gen ← ImageDataGenerator(rotation_range=45,
width_shift_range=0.20, height_shift_range=0.25, horizontal_flip=
True, zoom_range=0.50)
3.     img_gen ← train_img_gen.flow_from_directory(directory=path, batch
_size=32)
4. for img in img_gen:
    imshow(img)
    
```

The algorithm will give the individual operations augmented images, as shown in Fig. 2(a), and the combined basic image operations are shown in Fig. 2(b).

Fig. 2(a) represents the individual operation on each image, whereas the proposed system uses the "Data Generator" module to apply different processes on the dataset images. Fig. 2(b) represents five such figures as sample output.

B. Data Augmentation

Manually increasing the size of the image dataset is complicated. Neural networks provide different "data augmentation through GAN" [11], as shown in Fig. 3, to simplify the process. The data augmentation can be performed in either online mode or offline mode. This research implements online augmentation techniques since the offline [12] mode involves high memory usage, which is expensive and time-consuming. In online data augmentation, images are transformed randomly in different batches, and the model is trained with more cases in each epoch.

The two design considerations for augmentations are Train-time data augmentation to minimize generalization error and test-time data augmentation to increase predictive accuracy. The most critical operation to perform is resizing. Resizing ensures that all images are the same size. Specific pixel scaling and normalization operations can be carried out.

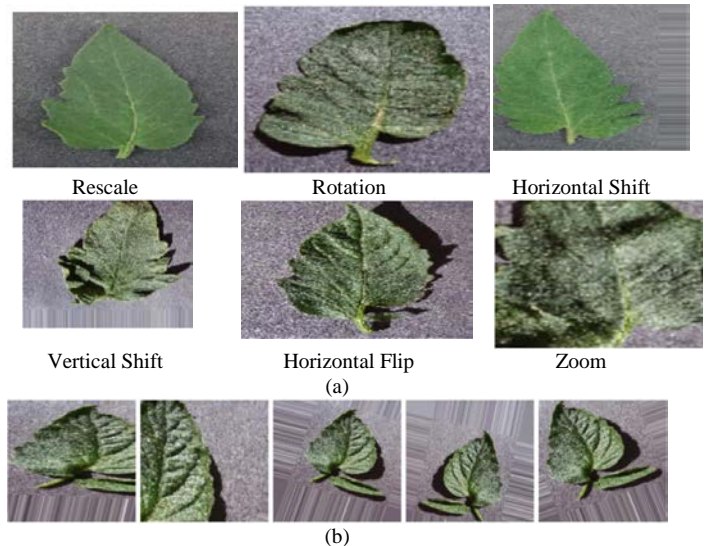


Fig. 2. (a) Individual basic Image Operations on Tomato Leaves, (b) Combined basic Image Operations using Image Data Generator.

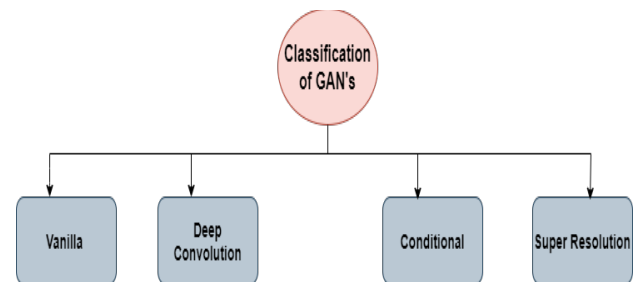


Fig. 3. GAN's Classification.

GAN technique provides adversarial preparation in critical models where Gaussian noise is injected, and images are transformed with worst-case perturbations [15], resulting in incorrect results with high confidence values. It also includes a neural style transferring technique that aids in the creation of new images by blending them, mainly when the model contains text or kinds. It employs two distinct distance roles, one for identifying text differences and the other for identifying style differences. In GANs, the generator takes a fixed-length vector as input and gives a domain-specific sample as output. Discriminator [14] takes the domain's information and generates a binary value depending on the prediction.

The entire paper organizes into five sections, where the introduction discusses the techniques related to image manipulation and data creation operations. The literature review section focuses on the previous researchers' methodologies and their merits and demerits. The literature section and also represents the gaps in the earlier works by analyzing the fallbacks associated with each method. The proposed process initially defines the architectural difference between the existing and proposed techniques. It also presents the layered architecture of the discriminator component and generator component. Finally, it describes the overall process of creating the synthetic data to enhance the size of the data. The result section describes how the accuracy of creating fake and real images in every epoch is computed. It also proves state-of-the-art compared with the other works mentioned in the literature survey. The paper in the last section concludes the piece by justifying the need for intelligent approaches to enhancing data size and presents the future to design an automated system for agriculture [21-24].

II. LITERATURE REVIEW

A. Methodologies Implemented using Researchers

[1] Ahmed Ali et al. proposed a framework in which GANs are integrated with CNN to classify mosaic virus in tomato plants. The author increased the dataset size by generating fake images stage by stage. This research's stages are healthy, early, and late infection. Random noise and each stage are passed as discriminators' inputs to generate synthetic samples. In hidden layers, global pooling is applied to create fake images almost nearer to the real images in the training dataset. It generates 512 feature vector dimensions and is passed as input to the discriminator to check its authenticity. If the accuracy rate is low, it loops the entire process for that particular image until it obtains a high accuracy rate. Finally, the model takes these augmented images as input to the neural network and performs multi-classification. CNN uses a 4-layered architecture by taking the standard activation function "ReLU" and standard optimizer "ADAM." This model balanced the dataset by producing an equal number of images in each stage.

In [2], Umit Atila et al. experimented with EfficientNet to eliminate the problems caused by the ImageNet pre-trained Model. The first step to improving efficiency is to perform the uniform scaling operation in all directions along with uniform translations and rotations. The uniform scaling factor is measured by drawing the grid relation between neighboring

pixels. The obtained values act as the constraints based on which a neural network is designed to predict the class labels approximately. This research constructed inverted bottleneck layers available in MobileV2Net to generate the images based on the expansion and contraction techniques. Transfer learning replaces the last layers of the B5 model, with 16 layers of MobileNet and four fully connected layers as a classifier. The disadvantage of this model is that it initialized the learning rate as 0.0001 but obtained an accuracy of 99.97%, which means this model cannot learn the complex relationships among the features.

In [3], Hongxia Deng et al. designed RHAC_GAN using the hidden variable mechanism to increase the dataset size because the collection of small data would not make many effects and would not get better results by using the CNN algorithm. Traditional approaches used image rotation, increased image brightness, and many other factors to solve this problem. Even these cannot help collect extensive data, which results in less accuracy. In the case of agriculture, it needs a large amount of data to identify the disease; however, due to insufficient data collected, even the best method, CNN, cannot give the best results. For the more extensive data collection, they proposed an ACGAN method that takes the generated images and divides them into parts to visualize the disease better. The hidden parameters in this model aim at low-frequency parameters in the image and show it as the disease-affected place.

In [4], Yang Wu et al. implemented an Adversarial VAE encoding mechanism for increasing the number of tomato leaf images in the dataset. Traditional VAE is extended by replacing the single scaling component with a multi-residual member for generating different scaling images in different directions. It is not easy to extract and train the parameters in the model, so the system needs a generalized learning environment and the labels associated with images. In this Model, GAN is integrated with the encoder in stage 1 to create compressed images as a dummy dataset. In stage 2 decoder is attached to reconstruct by creating latent space variables. Usage of the mean pre-processing technique helps the model enhance the dimension from 128 to 256 during the encoding process. The downsampling of neural networks helps the model create a scale block using reduced mean operation.

In [5], Amreen Abbas et al. designed conditional GAN using a transfer learning technique on nine diseases. The model uses a generator of CGAN to create augmented images using three layers. One of the three layers is implemented using an embedded pairing mechanism, consisting of a series of flatten and dropout layers. The advantage of CGAN lies in the fast creation of enhanced images by learning approximately seven lakhs of training parameters, and all the images are labeled from 0 to 9. In the next phase, the augmented images are merged with DenseNet using max pooling and average pooling layer alternately to minimize the number of features in every layer. A fine-tune layer is attached to the pre-trained network, which helps adjust weights optimally and perform the hyper tuning.

In [6], Jashraj Karnik et al. used a new way of classification called YOLOv3. KNN, K-means, and SVM did

the data classification in the olden days. However, with the help of YOLOv3, it would be better and more accessible. They had proposed four ways for the farmers to understand the problem. Pre-processing, data augmentation, classification, and intersection over union have been done. The farmers who lived far away would face a problem identifying the disease.

Moreover, with the help of deep learning and AI, they can only identify the disease in the early stage. All farmers who do not know which plant to have or not and what fertilizers to use were also present in the AI, which would help the farmers increase their growth. YOLOv3 would work in 2 ways: classifying the leaves and the disease. This way, the output would be given to the CNN, identifying the disease. In their proposed AI, they would recognize the disease and help the farmers take the next step that would help them increase their growth.

In [7], Aaditya Prasad et al had implemented a two-step machine learning model for better accuracy for low- and high-fidelity pictures. Here they used UAV images. The two data collectors were used to reduce the imbalance in the high fidelity. One was a data generator, and the other was modeling, and each of these elements had two-step for identification and classification. This model identifies the affected region and captures high-definition images for better understanding and classification. The second phase deals with the technical method for proletarian revolution: synthetic crop images in data generators.

In [8], using MATLAB, Bhattacharya developed a method based on CNN. The rapid investigation and diagnosis of plant illnesses can help manage disease development on various crops, enhancing harvest growth and yield. Apply image analysis and deep learning approaches to automatically discover acceptable features for differentiating the different types of plant disease to make the system efficient. The author introduced the method called convolution neural network architecture. This deep learning technique autonomously categorized three types of wheat leaf disease detection (fungal blight, blasting, and black mark) inside this study [25-28]. They have created a technique for recognizing normal and diseased plants from a batch of 1000 rice plants during the classification stage.

In [9], Guo et al. proposed a method based on RPN integrated with image Segmentation. This work provides a deep learning-based statistical equation for plant disease diagnosis and identification that increases the accuracy, flexibility, and training effectiveness. Its region proposal network is used to identify and locate the affected parts in the plants. So therefore, Chan–Vese (CV) method segments the image to find the illness attribute. Lastly, the separated leaves were fed into a transferring learning model, developed on a dataset containing diseased leaves inside a simplified environment. This prototype is also tested for brown rot, fungal disease, and rust disease. This analysis shows an accuracy of 83.57 percent, which is greater than the best way to minimize the disease impact on food production and promote agriculture's long-term sustainability. As a result, the deep learning methodology suggested in the research has a lot

of potential in smart agriculture, environmental regulation, and agricultural output.

B. Comparison Analysis

Table I coins all the methodologies presented in the above section with their advantages and limitations to identify the gaps associated with each methodology to solve the problems efficiently.

TABLE I. COMPARATIVE ANALYSIS OF EXISTING APPROACHES

S.No	Author Name	Algorithms Used	Merits	Demerits
1	Ahmed Ali	GANs integrated with CNN	Since the model produces images stage by stage, it can productively increase the size of the dataset.	To increase the accuracy rate for each image, it iterates in loops, which makes the system expensive.
2	Umit Atila	EfficientNet	Because of the inverted layer architecture, more similar images are generated at a low cost by reducing the generation cycles from $k*k$ to k .	It has hardware limitations because of which it can perform only binary classification. So, plants with multiple diseases cannot be predicted using this model.
3	Hongxia Deng	RAHC-GAN	Used for a large amount of data.	Have to explore more data to maintain high value and accuracy
4	Yang Wu	AVE	The architecture with complete dense layers helps the model to train the system with	The model requires a large amount of annotation data to identify the correct labels for each image
5	Amreen Abbas	CGAN using transfer learning	Usage of fine-tuned layers in DenseNet improves the multi-classification rate without overfitting.	The model needs retraining to work with compressed images efficiently.
6	Karnik	CNN	Here a pixel identification has been made	Rotational image identification is complex.
7	Aaditya Prasad	GAN	Had two steps approach for classification and identification	Had to increase the accuracy and classification model
8	Bhattacharya	CNN using MATLAB	Image-based classification has been done	Pre-trained the model based on size.
9	Guo	RPN and Image Segmentation, SVM	Here migration learning model is used to identify the diseased leaf.	Iteration calculation is significantly less when compared to other algorithms.

C. Research Gaps Identified and Solutions to Solve them

1) Most existing systems cannot produce good images using the basic operations because they are costly and cannot simulate real-world conditions.

2) Usage of CNN will complicate the model because the direct conversion of the image into a matrix will increase the training time.

3) Traditional GANs use the MNIST dataset to regenerate the images. We need to use 2-layered architecture to extract simple 28*28 images, which produce noisy images as fake images.

So, in the proposed research, instead of 3-layered architecture, the model presents a 4-layered Enhanced Cyclic GAN to extract the features from the image and reconstruct it as early as possible. To overcome the problem of the noisy image, the model initially performs pre-processing using kernel filters, and a few images are constructed using the basic image manipulations. These pre-processed and manipulated images are passed as input to Enhanced Cyclic GAN to create the synthetic data. This process is known as the "Meta-Learning Technique," as shown in Fig. 4.

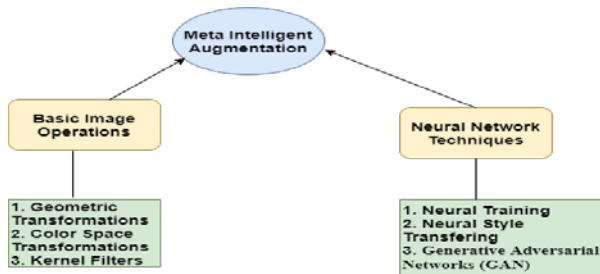


Fig. 4. Operations in Meta Intelligent Image Augmentation Process.

III. PROPOSED METHODOLOGY

Using machine learning and deep learning techniques, several Research Scholars and Scientists are constantly working on various plant diseases to improve production quality. These researchers used the PlantVillage dataset [20] to obtain plant images under controlled conditions. The use of computer vision and deep learning techniques have resulted in high-accuracy systems for detecting plant diseases automatically. The images of the dataset are presented in Fig. 5. Image augmentation creates new images in different scenarios using the existing images and applying popular deep learning techniques. The proposed paper discusses the various image augmentation techniques applied to the tomato plant's dataset from the PlantVillage open source. It also suggests the best method to use the data augmentation by comparing the performance evaluation metrics.

A. Pre-Processing

The best solution for solving the random and uneven noise is to apply filters to the images. Analyzing the dataset makes it clear that most of the images have salt and pepper noise. The proposed research used a median filter to reduce these noises and obtained the results shown in Fig. 6(b).

In Fig. 6(a), the original image contains more disturbances due to signal fluctuations. The median filter smoothens the

images by replacing each pixel with the median of neighboring pixels. The main advantage of the median filter lies in its edge preservation and removing the spikes.

B. Discriminator

GAN works as a classifier to distinguish real and fake images. Real images are positive points, and counterfeit images are negative points. The discriminator gets input from training samples and the generator component of the GAN. The working of this component is based on conditional probability; this component calculates the chance for an image authenticity. The discriminator has associated loss functions because the system has accuracy in classifiers. The GAN structure imposes a penalty for misclassification. This component reduces the penalty by adjusting the latent points through the backpropagation technique. The primary focus of the loss function is to analyze the difference between sample distribution among real and fake images. The proposed research designed the layers in the discriminator component, as shown in Fig. 7.

C. Generator

It acts as a creative tool to generate fake images to mislead the discriminator in the classification process by maximizing the penalty and taking the feedback from the above component. Creating a random sample image induces noise as input and then converts it into necessary output. In the GAN structure, the training of the generator is the most crucial part, so the noise is converted into vector space. This space should be balanced by reducing one component and increasing another component's performance. During the training process, using the cross-entropy mechanism, GANs use the min-max loss function as shown in equation (1).

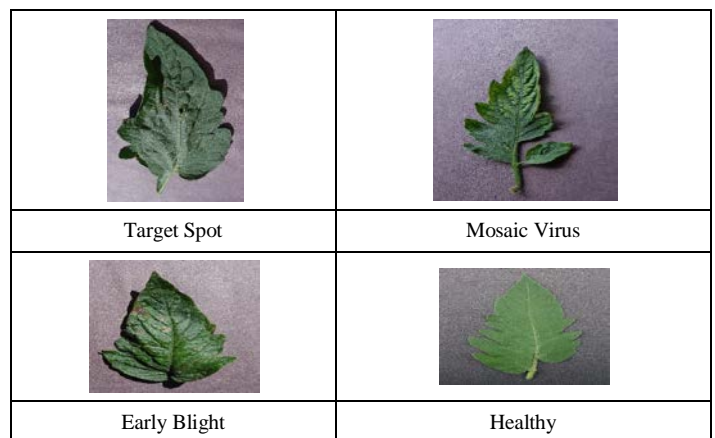


Fig. 5. Original Dataset Images of Different Diseases of Tomato.

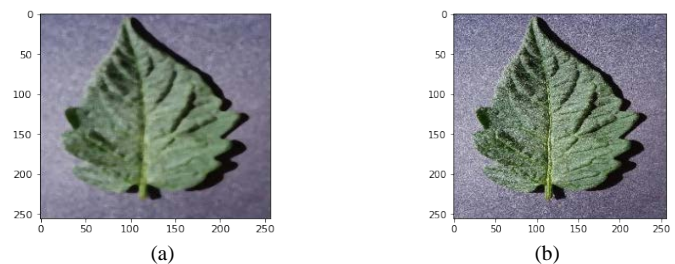


Fig. 6. (a): Original Image, (b): Filtered Image.

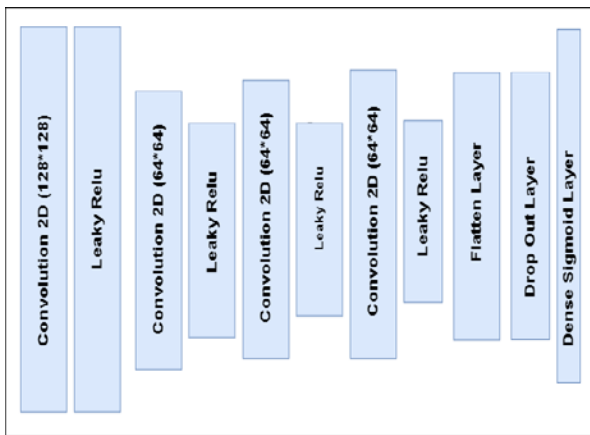


Fig. 7. Layers Design in Discriminator Module.

$$\text{MinMax_CGAN_Loss} = \text{Expected_Real}(\log(\text{Discriminator}(X))) + \text{Expected_Fake}(\log(1 - \text{Discriminator}(\text{Generator}(Y)))) - (1)$$

Where

Discriminator(X) analyzes the probability associated with the real images.

Generator(Y) analyzes the probability associated with the fake images along with the noise.

The summary evaluation of the layered architecture of the generator component is represented in Fig. 8.

```
Model: "sequential_1"
```

Layer (type)	Output Shape	Param #
dense_1 (Dense)	(None, 65536)	6619136
leaky_re_lu_4 (LeakyReLU)	(None, 65536)	0
reshape (Reshape)	(None, 16, 16, 256)	0
conv2d_transpose (Conv2DTranspose)	(None, 32, 32, 128)	524416
leaky_re_lu_5 (LeakyReLU)	(None, 32, 32, 128)	0
conv2d_transpose_1 (Conv2DTranspose)	(None, 64, 64, 128)	262272
leaky_re_lu_6 (LeakyReLU)	(None, 64, 64, 128)	0
conv2d_transpose_2 (Conv2DTranspose)	(None, 128, 128, 128)	262272
leaky_re_lu_7 (LeakyReLU)	(None, 128, 128, 128)	0
conv2d_4 (Conv2D)	(None, 128, 128, 3)	18819

=====
 Total params: 7,686,915
 Trainable params: 7,686,915
 Non-trainable params: 0

Fig. 8. Summary Evaluation Report of Generator Component.

D. Enhanced Cyclic Generative Adversarial Networks

In practice, GANs act as a tool to generate a fake image by analyzing the sample distribution of the real image. GANs should be designed with the help of two components. One is a generator to take care of modifications in the real images, and the other is a discriminator that focuses on the wrong assumptions made by the model in the identification process. The basic element needed by any GAN to generate fake images is "noise" to generate different variations in images. However, GANs can accept only random noise or probability distribution. In reality, GAN acts as a mapping function between two different dimensional spaces. Designing a good model requires the dimensionality of sample space to map with latent space. Otherwise, the model may lose all the essential properties in the classification process based on the distance. In general, to convert 1D into 2D, the traditional Vanilla GAN tries to analyze the Gaussian distribution among the random samples, but the model fails after a few training epochs. The proposed research defined the latent space dimension as 100, as the traditional GANs cannot support high dimensional conversion, and also, the dataset consists of images of multiple diseases. Hence, the model needs a GAN that can convert one domain to another, which is the basic phenomenon of the consistent cyclic GAN. CGAN consists of two generators and two discriminators, each consisting of 3 layers of CNN in each component, as shown in Fig. 9.

The proposed research modifies the existing 3-layered architecture of GANs into 4-layered architecture (shown in Fig. 10), with a single generator and discriminator, shown in Fig. 10.

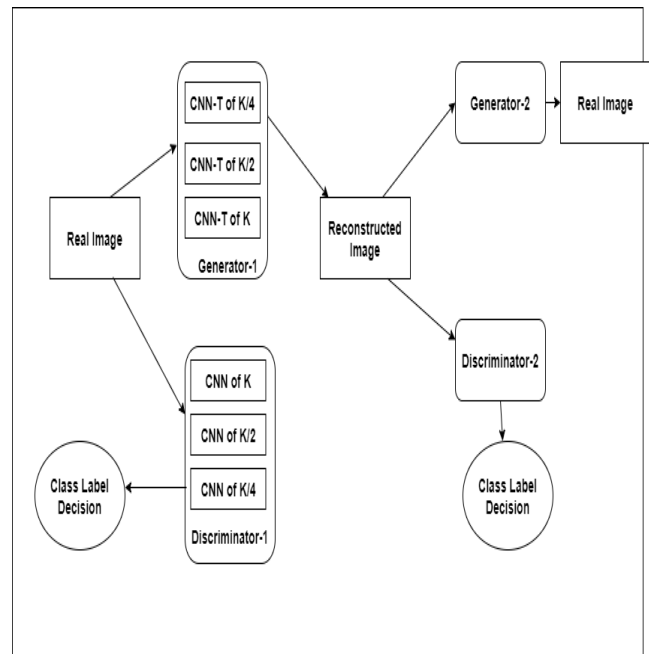


Fig. 9. Existing Architecture of Cycle GAN.

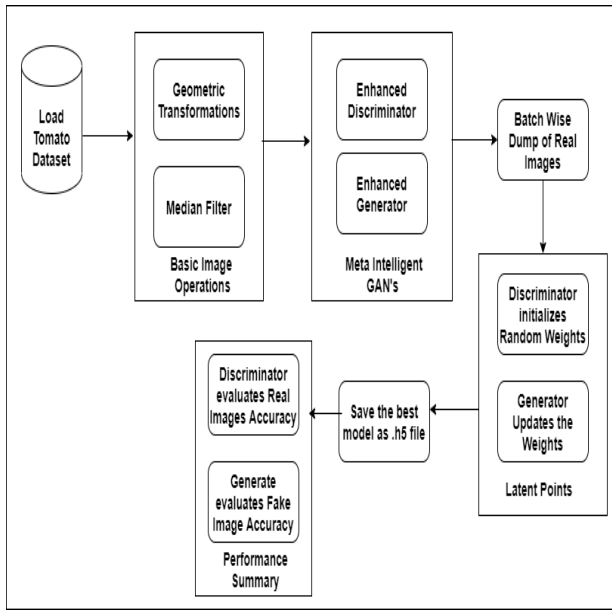


Fig. 10. Complete MI-Leaf GAN Architecture for the Synthetic Data Creation.

Algorithm for MI-Leaf GAN:

Input: T_Data ← Load the Pre-processed Images of Tomatoes from the repository
 Data: Generates more number of augmented images
 Begin:
 1. Initialize latent_dspace with 100
 2. model_discriminator ← call enhanced_discriminator()
 3. model_generator ← call enhanced_generator(latent_dspace)
 4. model_enhanced_CGAN ← call enhanced_CGAN(model_generator, model_discriminator)
 5. Call train_enhanced_model(model_generator, model_discriminator, model_enhanced_CGAN, T_Data[0], latent_dspace)
 6. decision ← call generate_latent_points()
 7. fake_img ← model.predict(decision)
 8. Plot the images
 End

Pseudocode for Enhanced Discriminator using Sequential Network:

1. Resize the input image to k (where k defines the size as 128)
 2. Define four convolution layers of size k/2
 3. Define 4 LeakyReLu layers with αn 0.2
 4. Add a Flatten layer
 5. Add dropout layer to normalize with threshold value as 0.4
 6. Add a fully connected layer with sigmoid as an activation function
 7. Compile the Model by defining the optimizer, learning rate, loss function, and accuracy

Pseudo code for Training of Enhanced Model

1. Set up number of batches in each epoch i.e., bperepoch as number of images per number of batches
 2. Initialize number_of_epochs as “35000”
 3. a. for i in number_of_epochs:
 b. for j in bperepoch:
 c. $img_real,$
 $label_real \leftarrow generate_real_images(T_Data, bperepoch/2)$

d. $img_fake,$
 $label_fake \leftarrow generate_fake_images(model_generator, latent_dspace, bperepoch/2)$
 e. $d_loss \leftarrow model_discriminator.train_on_batch(img_real, label_real, img_fake, label_fake)$
 f.
 $img_gan \leftarrow generate_latent_points(latent_dspace, batch_size)$
 g. $label_gan \leftarrow np.ones((batch_size, 1))$
 h.
 $g_loss \leftarrow model_enhanced_CGAN.train_on_batch(img_gan, label_gan)$

In binary machine learning algorithms, the class labels will be either 0 or 1, but in GANs, the class labels are assigned as -1, 0, and 1 due to Gaussian distribution. In GANs, the latent space tries to identify the region of interest by performing addition and subtraction operations, i.e., finding the compressed image of the original image by acting as the hidden layer. Each latent space is associated with latent points, which are used to assign random values initially with a discriminator's help. Later, these values are updated through the generator component.

IV. RESULTS AND DISCUSSION

The Meta Intelligent Leaf GAN designed using a single discriminator and generator with a constant number of neurons in the hidden layers produces the fake images, as shown in Fig. 11. Since the proposed research uses online data augmentation techniques, these are stored in Google drive for further access.

Fig. 12 shows the accuracy produced by the GAN structure at a different number of epochs. The number of epochs is set to 35000, and the model exhibited an output of 400 epochs as a sample. Similarly, the model can also plot the accuracy rate for the fake images.

To train the GAN structure, the model initially defines the latent space with 100 dimensionalities, and then the pre-processed images are passed as input to the GAN. The proposed model computes the loss functions for both components. Fig. 13 presents a sample output for a single iteration with the corresponding accuracy of real and fake images.



Fig. 11. Synthetic Images Created using MI-GAN.

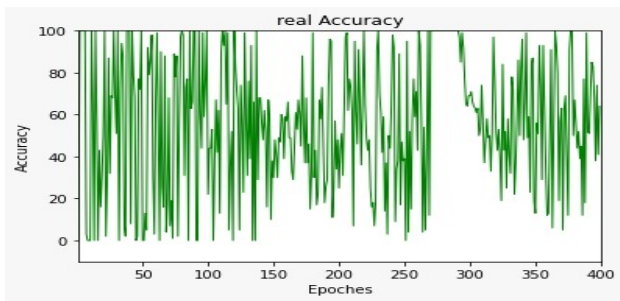


Fig. 12. Accuracy for Generating Real Images at Different Epochs.

```

Accuracy real: 100%, fake: 49%
21, 1/1, d=0.653, g=0.678
22, 1/1, d=0.624, g=0.660
23, 1/1, d=0.593, g=0.635
24, 1/1, d=0.589, g=0.611
25, 1/1, d=0.634, g=0.587
26, 1/1, d=0.714, g=0.593
27, 1/1, d=0.760, g=0.633
28, 1/1, d=0.744, g=0.684
29, 1/1, d=0.708, g=0.744
30, 1/1, d=0.671, g=0.794
    
```

Fig. 13. Loss Function Computation for GAN.

To date, many researchers worked on different GAN structures. Most of the problems faced are either due to noise or complexity of the design rather than random noise. The first traditional GAN was developed for the MNIST dataset. For 28*28 images, they have used two generators and discriminators with three layers each. Similarly, Table II represents the other mechanisms with the corresponding accuracy and proves that the proposed model has achieved good accuracy and simple architecture.

From Table II, the GAN approach has crossed approximately 90% out of the traditional CNN and GAN. So the proposed system enhanced the GAN technique using meta intelligent concept and reached 99.29%, which is approximately a 2.29% improvement from previous approaches. Accuracy alone cannot be stated as state of the art. So in Table III, the model presents other metrics of learning approaches.

TABLE II. ACCURACY ANALYSIS BETWEEN EXISTING AND PROPOSED GAN

Reference Number	Algorithm	Accuracy
[1]	CNN Integrated GAN	97
[3]	Feature Fusion	78.80
[5]	CNN	97.1
[7]	RPN for Image Segmentation and GAN	83.5
[9]	RAHC-GAN	93.28
Proposed Work	MI-GAN	99.29

TABLE III. EVALUATION METRICS

Algorithm	Accuracy	Precision	Recall	F1-Score
CNN Integrated GAN	97	90	85	87
Feature Fusion	78.8	73	76	74.5
CNN	97.1	90	85	88
RPN for Image Segmentation and GAN	83.5	80	80	80
RAHC-GAN	93.28	85.1	89	87
MI-GAN	99.29	96	98	97

The visualization graph of the Table III analysis is presented in Fig. 14, where the X-axis represents the algorithm's name and the Y-axis represents the measurement scale. The proposed system has performed accurately in all metrics. So, the state-of-the-art for the proposed system is achieved.

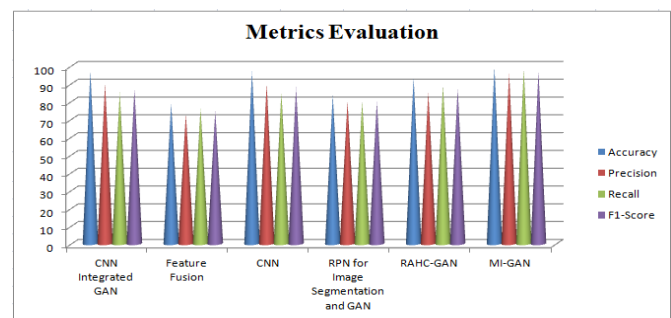


Fig. 14. Metrics Evaluation Analysis.

V. CONCLUSION

It is complicated to label every image from the live capturing. It is difficult to predict the type of disease using unsupervised algorithms like clustering. So, the model should develop a classification system where data labeling is mandatory. In a real-time environment, the conditions are uncontrolled. The method may face problems like labeling disease datasets, addressing the data imbalances, and overfitting because of the size of diagnostic clues, which are smaller than in the real-world scenario. The system also suffers from overfitting because it takes many computations to select and apply possible geometric transformations. Designing a GAN structure for high dimensionality images is challenging because the standard MNIST uses three-layered architecture for simple 28*28 size images. If the size increases, the number of layers get increased, and the model becomes complicated. So, by designing a good policy schema, like Meta Intelligent Leaf GAN, the auto augmentation process can efficiently improve the accuracy where the enhanced GAN model uses an integrated filter. The MI Leaf GAN modules generate more training data because the system addresses the overfitting problem that occurs due to basic image operations. Fig. 13 shows that accuracy is more accurate for the proposed research in generating fake images and successfully fooling the discriminator after performing more epochs. Even though the size of the images is vast, the model considered is more significant than standard GAN; it was designed only in four layers to complete the task.

REFERENCES

- [1] Ahmed, S., Hasan, M., Ahmed, T., Sony, R. K., & Kabir, M. (2021). Less is More: Lighter and Faster Deep Neural Architecture for Tomato Leaf Disease Classification. arXiv preprint arXiv:2109.02394. <https://arxiv.org/abs/2109.02394>.
- [2] Atila, Umüt & Ucar, Murat & Akyol, Kemal & Uçar, Emine. (2021). Plant leaf disease classification using EfficientNet deep learning model. *Ecological Informatics*. 61. 101182. [10.1016/j.ecoinf.2020.101182](https://doi.org/10.1016/j.ecoinf.2020.101182).
- [3] Deng, H.; Luo, D.; Chang, Z.; Li, H.; Yang, X. RAHC_GAN: A Data Augmentation Method for Tomato Leaf Disease Recognition. *Symmetry* 2021, 13, 1597. <https://doi.org/10.3390/sym13091597>. <https://www.mdpi.com/2073-8994/13/9/1597>.
- [4] Wu, Y.; Xu, L. Image Generation of Tomato Leaf Disease Identification Based on Adversarial-VAE. *Agriculture* 2021, 11, 981. <https://doi.org/10.3390/agriculture11100981>. <https://www.mdpi.com/2077-0472/11/10/981>.
- [5] Abbas, A., Jain, S., Gour, M., & Vankudothu, S. (2021). Tomato plant disease detection using transfer learning with C-GAN synthetic images. *Computers and Electronics in Agriculture*, 187, 106279. doi:10.1016/j.compag.2021.106279. <https://www.sciencedirect.com/science/article/abs/pii/S0168169921002969>.
- [6] Karnik, Jashraj and Suthar, Anil, Agricultural Plant Leaf Disease Detection Using Deep Learning Techniques (June 27, 2021). Proceedings of the 3rd International Conference on Communication & Information Processing (ICCIP) 2021, Available at SSRN: <https://ssrn.com/abstract=3917556> or <http://dx.doi.org/10.2139/ssrn.3917556>.
- [7] Aaditya prasad, Nikhil Mehta, Matthew Horak, and wan d. bae. A Two-Step Machine Learning Approach For Crop Disease Detection: An Application Of GAN and UAV Technology. (Sep 19, 2021), consideration in the International Journal on Artificial Intelligence Tools. <https://arxiv.org/abs/2109.11066>.
- [8] Bhattacharya S., Mukherjee A., Phadikar S. (2020) A Deep Learning Approach for the Classification of Rice Leaf Diseases. In: Bhattacharyya S., Mitra S., Dutta P. (eds) Intelligence Enabled Research. Advances in Intelligent Systems and Computing, vol 1109. Springer, Singapore. https://doi.org/10.1007/978-981-15-2021-1_8.
- [9] Guo, Yan; Zhang, Jin; Yin, Chengxin; Hu, Xiaonan; Zou, Yu; Xue, Zhipeng; Wang, Wei (2020). Plant Disease Identification Based on Deep Learning Algorithm in Smart Farming. *Discrete Dynamics in Nature and Society*, 2020(), 1–11. doi:10.1155/2020/2479172.
- [10] Faye Mohamed, Chen Bingcai, Kane Amath Sada; Plant Disease Detection with Deep Learning and Feature Extraction Using Plant Village, *Journal of Computer and Communications*, Vol.8 No.6, 2020; DOI: 10.4236/jcc.2020.86002.
- [11] Ayaluri MR, K. SR, Konda SR, Chidirala SR. 2021. Efficient steganalysis using convolutional auto encoder network to ensure original image quality. *PeerJ Computer Science* 7:e356 <https://doi.org/10.7717/peerj-cs.356>.
- [12] Shorten, C., Khoshgoftaar, T.M. A survey on Image Data Augmentation for Deep Learning. *J Big Data* 6, 60 (2019). <https://doi.org/10.1186/s40537-019-0197-0>.
- [13] A Mallikarjuna Reddy, Vakulabharanam Venkata Krishna, Lingamgunta Sumalatha and Avuku Obulesh, "Age Classification Using Motif and Statistical Features Derived On Gradient Facial Images", Recent Advances in Computer Science and Communications (2020) 13: 965. <https://doi.org/10.2174/2213275912666190417151247>.
- [14] Maniyar H.M., Budihal S.V. (2020) Plant Disease Detection: An Augmented Approach Using CNN and Generative Adversarial Network (GAN). In: Badica C., Liatsis P., Kharb L., Chahal D. (eds) Information, Communication, and Computing Technology. ICICCT 2020. Communications in Computer and Information Science, vol 1170. Springer, Singapore. https://doi.org/10.1007/978-981-15-9671-1_22.
- [15] Abdul Waheed, Muskan Goyal, Deepak Gupta, Ashish Khanna, Aboul Ella Hassanien, Hari Mohan Pandey, An optimized dense convolutional neural network model for disease recognition and classification in corn leaf, *Computers and Electronics in Agriculture*, Volume 175, 2020, 105456, ISSN 0168-1699, <https://doi.org/10.1016/j.compag.2020.105456>.
- [16] Ilaiah Kavati, A. Mallikarjuna Reddy, E. Suresh Babu, K. Sudheer Reddy, Ramalinga Swamy Cheruku, Design of a fingerprint template protection scheme using elliptical structures, *ICT Express*, Volume 7, Issue 4, 2021, Pages 497-500, ISSN 2405-9595, <https://doi.org/10.1016/j.icte.2021.04.001>.
- [17] Xiao, Jia-Rong; Chung, Pei-Che; Wu, Hung-Yi; Phan, Quoc-Hung; Yeh, Jer-Liang A.; Hou, Max T.-K. 2021. "Detection of Strawberry Diseases Using a Convolutional Neural Network" *Plants* 10, no. 1: 31. <https://doi.org/10.3390/plants10010031>.
- [18] C. R. T. G. Sirisha and A. M. Reddy, "Smart Healthcare Analysis and Therapy for Voice Disorder using Cloud and Edge Computing," *2018 4th International Conference on Applied and Theoretical Computing and Communication Technology (iCATccT)*, Mangalore, India, 2018, pp. 103-106, doi: 10.1109/iCATccT44854.2018.9001280.
- [19] Rakesh Chandra Joshi, Manoj Kaushik, Malay Kishore Dutta, Ashish Srivastava, Nandlal Choudhary, VirLeafNet: Automatic analysis and viral disease diagnosis using deep-learning in Vigna mungo plant, *Ecological Informatics*, Volume 61, 2021, 101197, ISSN 1574-9541, <https://doi.org/10.1016/j.ecoinf.2020.101197>.
- [20] Padmanabhuni, Ms. S. S. (2020). AN EXTENSIVE STUDY ON CLASSIFICATION-BASED PLANT DISEASE DETECTION SYSTEMS. *JOURNAL OF MECHANICS OF CONTINUA AND MATHEMATICAL SCIENCES*, 15(5). <https://doi.org/10.26782/jmcs.2020.05.00002>
- [21] Wu, Q., Chen, Y., & Meng, J. (2020). DCGAN-Based Data Augmentation for Tomato Leaf Disease Identification. *IEEE Access*, 8, 98716–98728. doi:10.1109/access.2020.2997001.
- [22] A. M. Reddy, K. SubbaReddy and V. V. Krishna, "Classification of child and adulthood using GLCM based on diagonal LBP," *2015 International Conference on Applied and Theoretical Computing and Communication Technology (iCATccT)*, Davangere, 2015, pp. 857-861, doi: 10.1109/ICATCCCT.2015.7457003.
- [23] Mohana Saranya, S., Rajalaxmi, R. R., Prabavathi, R., Suganya, T., Mohanapriya, S., & Tamilselvi, T. (2021). Deep Learning Techniques in Tomato Plant – A Review. *Journal of Physics: Conference Series*, 1767(1), 012010. doi:10.1088/1742-6596/1767/1/012010 <https://iopscience.iop.org/article/10.1088/1742-6596/1767/1/012010/meta>.
- [24] Swarajya Lakshmi V Papineni, Snigdha Yarlagadda, Harita Akkineni, A. Mallikarjuna Reddy. Big Data Analytics Applying the Fusion Approach of Multicriteria Decision Making with Deep Learning Algorithms *International Journal of Engineering Trends and Technology*, 69(1), 24-28, doi: 10.14445/22315381/IJETT-V69I1P204.
- [25] Abd El-Latif, Yasser. (2021). Early Prediction of Plant Diseases using CNN and GANs. *International Journal of Advanced Computer Science and Applications*. 12. 514-519. [10.14569/IJACSA.2021.0120563](https://doi.org/10.14569/IJACSA.2021.0120563).
- [26] PlantVillage Dataset Repository: <https://github.com/spMohanty/PlantVillage-Dataset>.
- [27] A. M. Reddy, V. V. Krishna, L. Sumalatha and S. K. Niranjan, "Facial recognition based on straight angle fuzzy texture unit matrix," *2017 International Conference on Big Data Analytics and Computational Intelligence (ICBDAC)*, Chirala, 2017, pp. 366-372, doi: 10.1109/ICBDACI.2017.8070865.
- [28] P. Jiang, Y. Chen, B. Liu, D. He, and C. Liang, "Real-Time Detection of Apple Leaf Diseases Using Deep Learning Approach Based on Improved Convolutional Neural Networks," in *IEEE Access*, vol. 7, pp. 59069-59080, 2019, DOI: 10.1109/ACCESS.2019.2914929.

Comparison of Path Planning between Improved Informed and Uninformed Algorithms for Mobile Robot

Mohamed Amr¹, Azza Ibrahim⁴
Computers and Systems Department
Electronic Research Institute
ERI, Cairo, Egypt

Ahmed Bahgat², Hassan Rashad³
Power and Machines Department
Cairo University Faculty of Engineering
CUFE, Cairo, Egypt

Abstract—This work is concerned with the Path Planning Algorithms (PPA), which hold an important place in Robotics navigation. Navigation has become indispensable to most modern inventions. Mobile robots have to move to a relevant task point in order to achieve the tasks assigned to them. The actions, which are planned in a structure, may restrict the task duration and even in some situations, the mission tends to be accomplished. This paper aims to study and compare six commonly used informed and uninformed algorithms. Three different maps have been created with gradually increasing difficulty levels related to a number of obstacles in the tested maps. The paper provides a detailed comparison between the algorithms under investigation of several parameters such as: Total steps, straight steps, rotation steps, and search time. The promised results were obtained when the proposed algorithms were applied to a case study.

Keywords—Mobile robots; informed algorithm; uninformed algorithm; path planning

I. INTRODUCTION

Mobile robots [1] are getting more important in daily life as a result of their increasing role in making human's life easier. According to this point of view, it is obvious that Mobile Robots will be an indispensable part of future life [2]. To make Mobile Robots able to perform an assigned task, they have to know their locations [3], how to navigate [4] within their environment [5] and how to comprehend what the world around them looks like in order to choose the optimal path [6] from the start to the end point in order to reach the target. The path selection depends on the selected criteria to evaluate the path (ex: travel time, number of visited nodes, etc.). The optimal route [7] can be obtained by a variety of methods like the graph theory [8], probabilistic or heuristic [9] based optimization methods [10]. At every point in the grid map representing the working area of the robot, the selected algorithm assigns a direction for the robot out of the possible four directions: Right, Left, Up, and Down. In this paper six different algorithms have been studied, categorized as Informed [11] and Uninformed types [12], a differentiation between them in characteristics is applied, how the algorithm itself works, how the steps of work are correctly applied, and finally, there were three different maps that graduate in their

difficulty related to a number of obstacles [13] to test those algorithms, testing six different types of path planning algorithms with three different maps was a challenging work that has been done successfully.

The key objectives of the research are the following:

- 1) Single mobile robot represents as one node mass.
- 2) Start and End from Fixed node. Easy, Medium, Hard Map depend on the number of obstacles.
- 3) Modified informed algorithms and adjusted all algorithms to make the Mobile Robot pass in four dimensions; now no longer in eight directions to ensure that modified algorithms move with less rotation and short pass.
- 4) Compared all algorithms with each other and get results.

This paper is organized as follows: Section II briefly views the general optimal path problems definitions and the methods, which are executed and discussed in this study. Section III presents the Simulation and the results. Section IV presents the conclusion and the future work.

II. PATH PLANNING PROBLEM AND ALGORITHMS

A. Path Planning Problem

First, the path planning is traditionally divided into two categories: local [14], and global [15]. The local is used in an unknown environment while the global is a prior knowledge of the work environment. In this classification, path or route planning [16] is defined as a problem in which an agent moves from a start to an endpoint by avoiding the obstacles in order to reach the target with minimum cost. The starting and the endpoints could be the same (loop closure) or even different. It is preferably desired to have the shortest distance [17] between the start/endpoints. However, the definition of the optimal path can be changeable in some situations. For example, if the tasks are successively assigned to the robots, the elapsed time to calculate the optimal path also matters. When the computation time is too long to obtain the optimal path, it will be difficult to provide the task continuity. According to this reason, the most suitable algorithm has to be chosen according to the desired optimal criterion.

Fig. 1 to 8 demonstrates the different types of the environments as following:

- 1) Creating a grid map environment for all experiments.
- 2) Fixed dimensions for the grid map shall be (30*40).
- 3) Making sure to start and end from a fixed node.
- 4) Categorizing different Maps depending on a number of obstacles to: Easy, Medium, and Hard Maps.
- 5) Making modifications and adjustments for the informed algorithms by making them work in four dimensions rather than eight directions.
- 6) Choosing a single mobile robot to represent only one node mass.

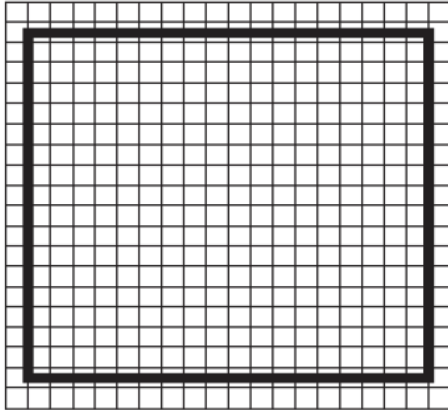


Fig. 1. Grid Map.

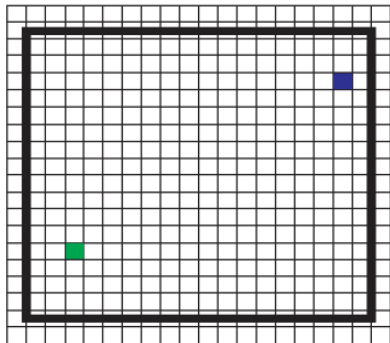


Fig. 2. Fixed Start, End Node.

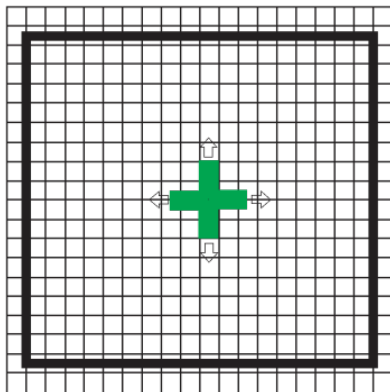


Fig. 3. Four Dimension.

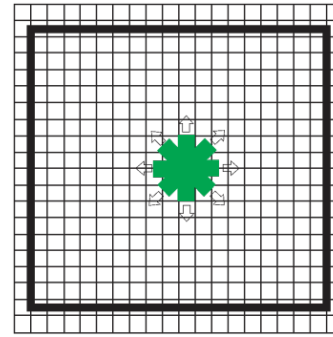


Fig. 4. Eight Direction.

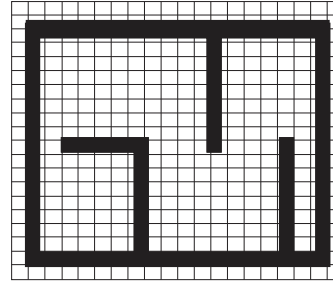


Fig. 5. Easy Map.

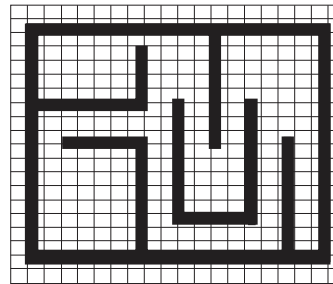


Fig. 6. Medium Map.

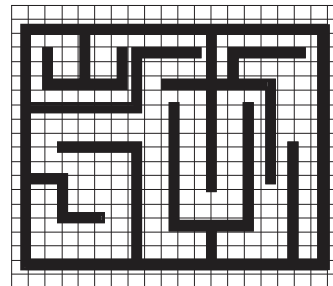


Fig. 7. Hard Map.

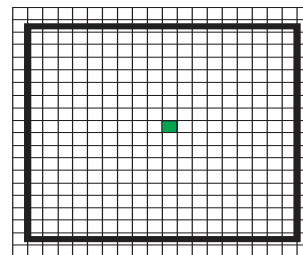


Fig. 8. Single Mobile Robot.

B. Path Planning Algorithm

Optimal path planning algorithm can be classified to informed or uninformed (blind) one. Table I summarizes the algorithms which will be discussed in this paper.

1) *Informed algorithms*: Informed Algorithms are the algorithms that can be applied if complete information about the working area is available.

TABLE I. INFORMED AND UN-INFORMED ALGORITHMS

Informed	Un-Informed
1-Dijkstra [18]	4-Best First Algorithm [19]
2-A star search [20]	5-Breadth First Search [21]
3-Bidirectional A Star [22]	6-Depth First Search [23]

Several algorithms are related to informed algorithms. In this paper, the most common algorithms were selected, which are Dijkstra, A star, and Bidirectional A star.

a) *Dijkstra's Algorithm*: Dijkstra algorithm is one of the oldest algorithms used in path planning. It was published by Dijkstra in 1959. However, it is still being widely used in several applications [24], [25] [26]. The problem which is handled by Dijkstra Algorithm is represented as follows: when given a graph and a source vertex in that graph, it's obligatory to find the shortest paths from the source to all vertices in the given graph.

The algorithm can be summarized by using the following flowchart:

<p>Algorithm 1: Dijkstra's Algorithm</p> <p>Initialization: for every vertex X in Graph: Dst[X] = infinity // initial distance from source to vertex X is set to infinite previous[X] = undefined // Previous node in optimal path from source Dst[source] := 0 // Distance from source to source D := the set of all nodes in Graph // all nodes in the graph are unoptimized - thus are in D</p> <p>Main Loop While D is not empty S = node in D with shortest distance from source Remove S from D for each neighbor X of S such that X ∈ D alt = Dst[S] + distance between (S, X) if alt < Dst[X] then Dst[X] = alt previous[X] := S End while</p>

The algorithm outputs an array indicating the best previous node (previous) for every node and another array stores the best distance from the source to every node in the graph (dist).

b) *A star search (A* or A-star or A* search)*: A search

method [27][28][29] based on a heuristic function, h (n), where n refer to a node n. Every node is associated an estimation h(n) of a route's cost from n to a goal node, while h(n) is equivalent to the actual distance (cost) from n to the goal node.

The other part of this function is g(n), that represents the cost of the path from the beginning node to node n, and f(n), which shows the estimated cost of the path that is being obtained which moves via n to reach to the goal node. f (n) is defined as the total of g (n) with h (n), as in shown Equation:

$$f(n) = g(n) + h(n) \quad (1)$$

Two lists are mentioned in following flowchart:

<p>Algorithm 2: A Star Algorithm</p> <p>Initialization: Let open list have only the starting node Let closed list empty</p> <p>Main Loop While (the destination node has not been reached): consider the node with the lowest f score in the open list If (this node is destination node): we are finished. Else If: put the current node in the closed list and look at all of its neighbors. For (each neighbor of the current node): If (neighbor has lower g value than current and is in the closed list). replace the neighbor with the new, lower, g value current node is now the neighbor's parent Else If (current g value is lower and this neighbor is in the open list). replace the neighbor with the new, lower, g value change the neighbor's parent to current node Else If this neighbor is not in both lists: add it to the open list and set its g . End while.</p>
--

The algorithm outputs an array indicating the best path related to the lowest cost 'g value' for every node and an array stores the best distance from the source to every node in the graph (closed list).

c) *Bidirectional A Star Algorithm*: The bidirectional search algorithm combines two separate searches. The search that is performed from both the origin and destination simultaneously, and when these two searches meet, then the shortest path can be obtained.

Next are the steps and pseudocode to show how bidirectional A star search works:

- Search forward from the start point.
- Search backward from the goal point.
- Using "fF", "gF", "hF" to indicate f, g, and h-costs in the forward search.
- Also using "fB", "gB", "hB" similarly in the backward search.

Algorithm 3: Bidirectional A Star Algorithm

Initialization:

Open F and Open B
store states generated in the forward and back ward directions,
Finally, $g_{min} F$, $g_{min} B$, $f_{min} F$ and $f_{min} B$

denote the minimal g - and f -values in OpenF and OpenB
 $d(x, y)$ denotes the shortest distance between x and y . **Front-to-end** algorithms use two heuristic functions. **Main Loop**

The **forward heuristic**, hF , is forward admissible

If $f hF(u) \leq d(u, goal)$

For all u in G and is forward consistent

If $f hF(u) \leq d(u, u') + hF(u')$

For all u and u' in G .

The backward heuristic, hB , is backward admissible

If $f hB(v) \leq d(start, v)$

For all v in G and is backward consistent

If $f hB(v) \leq d(v', v) + hB(v')$

For all v and v' in G .

final $f = d(start, goal)$ is the cost of an optimal solution.

End

After this implementation, some modifications in informed algorithms are needed to improve path length to make them more optimum and straight as possible.

The huge problem in informed algorithms which is related to the cost function search is that they cannot find the least rotation steps in many paths with the same path length. In this paper, informed algorithms are improved by adding the rotation cost estimation method based on a moving direction. Assuming that the node n coordinate is (x_n, y_n) , then the previous node coordinate is (x_{n-1}, y_{n-1}) , and the coordinates of the next node is (x_{n+1}, y_{n+1}) . Then the rotation evaluation function of node n is $k(n)$.

$$f(n) = g(n) + h(n) + K(n) \quad (2)$$

2) *Uninformed algorithms*: Blind search is another name for uninformed search formulas. The search algorithm generates the search tree without relying on any domain knowledge, which is a brute force in nature. Uninformed Algorithms lack background information on how to approach the goal or destination that must be reached.

Best First Algorithm "BFS" stands for Best First Search, it's an evaluation function that measures distance to the goal, the general approach of this search algorithm is that the node is selected for expansion based on an evaluation function $f(n)$.

It combines the advantages of both DFS and BFS in a single method; in DFS not all combining branches have to be expanded; on the other hand, the BFS are not trapped on dead-end paths. Combining the two to follow a single path at some time, but switching between paths whenever there is some competing path looks more promising than the current one.

a) *Best first search algorithm*: At every step of the BFS [30] search process, The most promising nodes are selected that have been generated thus far, applying some appropriate heuristic function to each of them, and then making an expansion to the chosen node by using the specified rules to generate its successors, which is known as an OR-graph, because each of its branches representing an alternative problem-solving path, and storing the nodes in the to Visit Nodes data structure using a queue.

Algorithm4: Best First Search Algorithm

Initialization:

open list containing the start state.

CLOSED list empty.

BEST =start state.

lets $s = \arg \max e(x)$.

(get the state from OPEN with the highest evaluation)

remover S from OPEN and add to CLOSED

if $e(S) > e(BEST)$,

then $BEST = S$

Main Loop

for each child t of s that is not in the OPEN or CLOSED list, evaluate and add to OPEN

if BEST changed in the last set of expansions

goto step four

Return BEST

b) *Breadth first search*: There are different ways to traverse graphs, this algorithm means by graph traversal visiting every vertex and edge exactly one time in a well-defined order, as using a certain graph algorithm, each vertex of the graph must be visited one time exactly, and the order in which the vertices are visited are so important as it may depends on the algorithm or the problem that is needed to be solved.

Next are steps and pseudo code explaining BFS methodology.

First step: move horizontally then visit all the nodes of the present layer.

Second step: Move to the following layer

Algorithm 5: Breadth First Search

Initialization

Set all nodes to "not visited";

$q = \text{new Queue}()$;

$q.\text{enqueue}(\text{initial node})$;

Main Loop

While ($q \neq \text{empty}$)

do { $x = q.\text{dequeue}()$;

If (x has not been visited)

{visited[x] = true; // Visit node x

for (every edge (x, y) // we are using all edges

If (y has not been visited)

$q.\text{enqueue}(y)$; // Use the edge (x, y)

End While

c) *Depth first search*: DFS stands for Depth First Search, it is an algorithm for traversing or searching a tree or graph data structure, it uses a stack data structure for implementation. In DFS, one starts at the root and explores as far as possible along each branch before backtracking. Next are steps and pseudocode explaining DFS methodology.

- Initializing nodes with status =1(ready data).
- Put starting node in the stack and change status to status=2(waiting state).
- Loop: repeat the next two steps until stack gets empty or algorithm reaches goal node.
- Remove front node N from stack, process them and change the status of N to status=3(processed stat).
- Add all the neighbors of N to the stack and change status to status=2(waiting status).

<p>Algorithm 6:Depth First Search</p> <p>Initialization: procedure DFS-iterative (G, v) is let S be a stack S.push (v)</p> <p>Main Loop While S is not empty do v = S.pop() If v is not labeled as discovered then label v as discovered For all edges from v to w in G.adjacent Edges (v) do S.push(w)</p> <p>End while</p>

III. SIMULATION AND RESULTS

To demonstrate the benefits of the modification for the algorithms in terms of search speed, visited nodes, number of rotations, path selection, and path length, Three separate experimental locations have been created, basic and modified algorithms are compared then comparing those algorithms with uninformed ones, The experiments aim to establish a starting point and a target point environment.

Fig. 9(a) to 11(b) shows the difference between Basic and Modified Dijkstra is in three different maps.

A. *Dijkstra Algorithm*

In this environment, it shows the search methods and gives a comparison between the two algorithms (Dijkstra algorithm and modified Dijkstra algorithm) in three environments.

Fig. 9(a) to 11(b) shows the difference between Basic and Modified Dijkstra in three different maps.

Also, Tables II to IV compare Basic and Modified Dijkstra in total steps, straight steps, rotation steps, visited nodes, and search time on three different maps.

1) *Dijkstra and modified Dijkstra algorithm in Easy Map.*

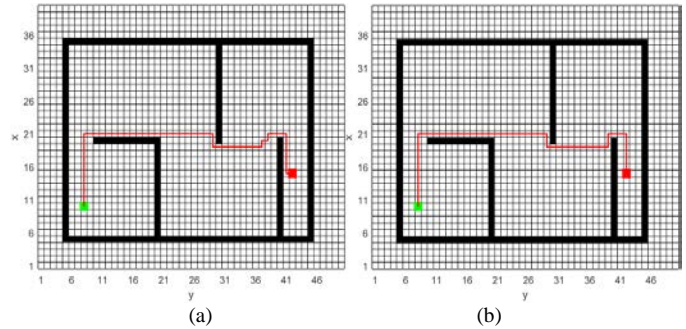


Fig. 9. (a) Modified Dijkstra for Easy Map (b) Basic for Easy Map.

TABLE II. COMPARISON BETWEEN BASIC AND MODIFIED DIJKSTRA ALGORITHM IN EASY MAP

Algorithm	Total Steps	Straight Steps	Rotation Steps	Visited nodes	Search time
Basic Dijkstra	56	47	9	986	4.9
Modified Dijkstra	56	50	6	1010	5.3

2) *Dijkstra algorithm in Medium Map*

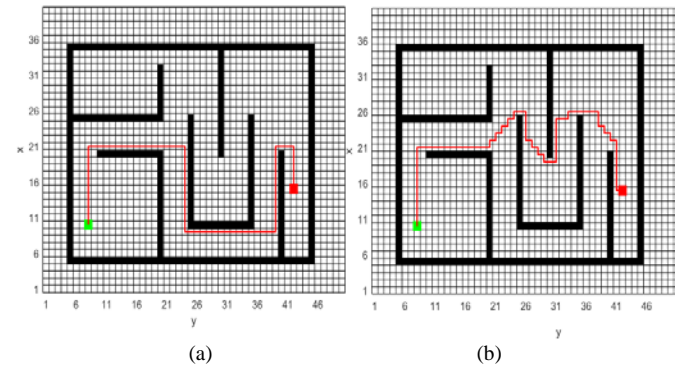


Fig. 10. (a) Modified Dijkstra for Medium Map (b) Basic Dijkstra for Medium Map.

TABLE III. COMPARISON BETWEEN BASIC AND MODIFIED DIJKSTRA ALGORITHM IN MEDIUM MAP

Algorithm	Total Steps	Straight Steps	Rotation Steps	Visited nodes	Search time
Basic Dijkstra	76	45	31	974	4.29
Modified Dijkstra	76	70	6	976	4.32

3) Dijkstra Algorithm in Hard Map.

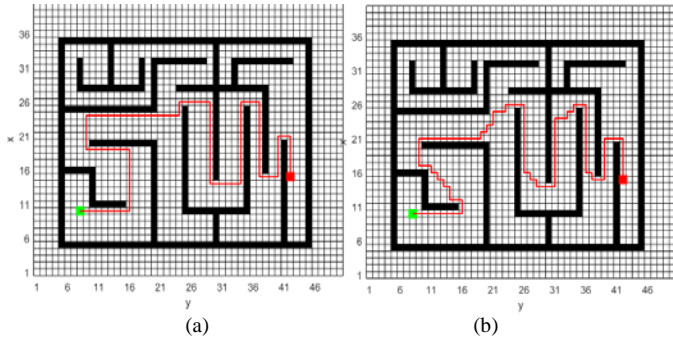


Fig. 11. (a) Modified Dijkstra for Hard Map (b) Basic Dijkstra for Hard Map.

TABLE IV. COMPARISON BETWEEN BASIC AND MODIFIED DIJKSTRA ALGORITHM IN HARD MAP

Algorithm	Total Steps	Straight Steps	Rotation Steps	Visited nodes	Search time
Basic Dijkstra	112	73	39	812	3.95
Modified Dijkstra	112	97	15	814	3.96

As shown in the Fig. 9(a) to 11(b) and Tables II to IV, both of the Dijkstra algorithm and the improved Dijkstra algorithm can search for symmetric paths of the same length, but the search path of the improved Dijkstra algorithm has more straight length, the path trajectory is different, and the number of rotation points in the paths are also different. It is obvious that the improved Dijkstra algorithm search straighter than the Dijkstra algorithm by equal to 3 steps in easy map, 25 steps in medium map and 19 steps in hard map.

B. A Star Algorithm

In this environment, Fig. 12(a) to 14(b) shows the difference between basic and modified A Star in three different maps.

In addition, Tables V to VII gives a comparison between the two algorithms in total steps, straight steps, rotation steps, visited nodes, and search time on three different maps.

1) A Star Algorithm in Easy Map

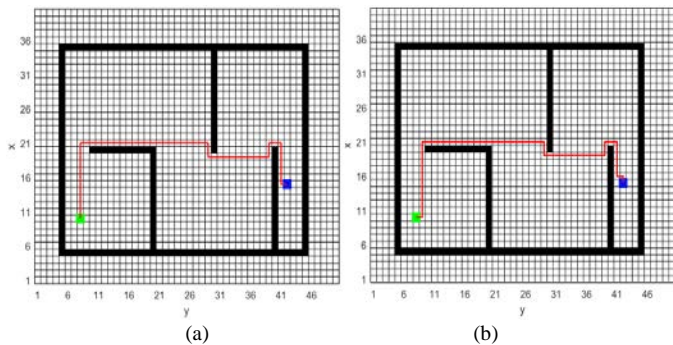


Fig. 12. (a) Modified a Star for Easy Map, (b) Basic a Star for Easy Map

TABLE V. COMPARISON BETWEEN BASIC AND MODIFIED A STAR ALGORITHM IN EASY MAP

Algorithm	Total Steps	Straight Steps	Rotation Steps	Visited nodes	Search time
Basic A Star	56	47	9	569	2.96
Modified A Star	56	49	7	726	3.15

2) A Star Algorithm in Medium Map.

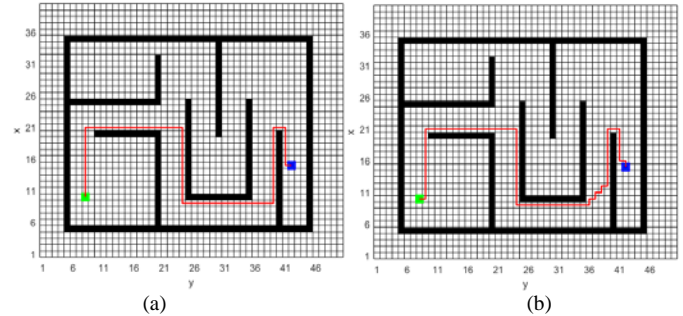


Fig. 13. (a) Modified a Star for Medium Map, (b) Basic a Star for Medium Map.

TABLE VI. COMPARISON BETWEEN BASIC AND MODIFIED A STAR ALGORITHM IN MEDIUM MAP

Algorithm	Total Steps	Straight Steps	Rotation Steps	Visited nodes	Search time
Basic A Star	76	61	15	758	3.19
Modified A Star	76	69	7	768	3.21

3) A Star Algorithm in Hard Map

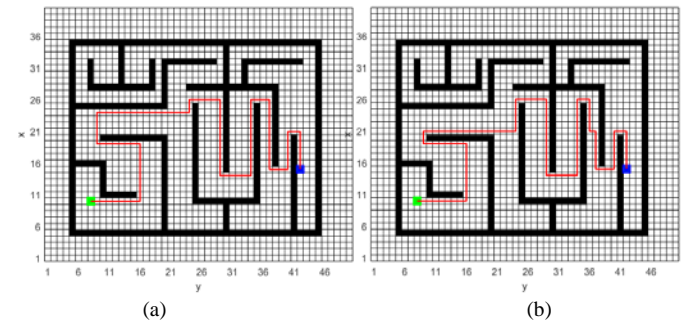


Fig. 14. (a) Modified a Star for Hard Map, (b) Basic a Star for Hard Map.

TABLE VII. COMPARISON BETWEEN BASIC AND MODIFIED A STAR ALGORITHM IN HARD MAP

Algorithm	Total Steps	Straight Steps	Rotation Steps	Visited nodes	Search time
Basic A Star	112	95	17	679	2.96
Modified A Star	112	97	15	698	2.97

As shown in above Fig. 12(a) to 14(b) and Tables V to VII, both A Star algorithm and the improved A Star algorithm can search for symmetric paths of the same length, but the search path of the improved A Star Algorithm has more straight length, the path trajectory is different, and the number of rotation points in the paths are also different. And it is obvious that the improved A Star Algorithm search straighter than A Star Algorithm by equal to 3 steps in easy map, 8 steps in medium map and 2 steps in hard map.

C. Bidirectional a Star

In this environment, Fig. 15(a) to 17(b) shows the difference between Basic and modified Bidirectional A Star in three different maps.

In addition, Tables VIII to X give a comparison between the two algorithms in total steps, straight steps, rotation steps, visited nodes, and search time on three different maps.

1) Bidirectional A Star algorithm in Easy Map:

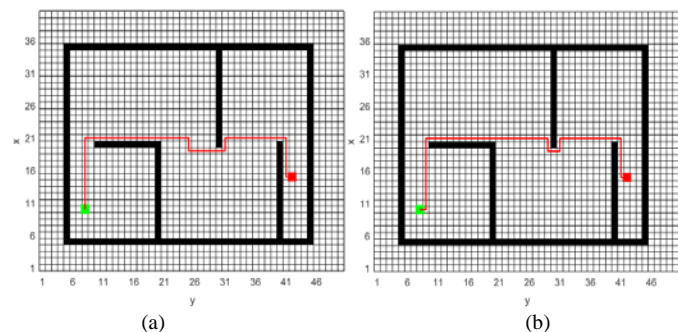


Fig. 15. (a) Modified Bidirectional a Star for Easy Map (b) Basic Bidirectional a Star for Easy Map.

TABLE VIII. COMPARISON BETWEEN BASIC AND MODIFIED BIDIRECTIONAL A STAR ALGORITHM IN EASY MAP

Algorithm	Total Steps	Straight Steps	Rotation Steps	Visited nodes	Search time
Basic Bidirectional A Star	56	48	8	437	1.32
Modified Bidirectional A Star	56	49	7	462	1.57

2) Bidirectional A Star Algorithm in Medium Map

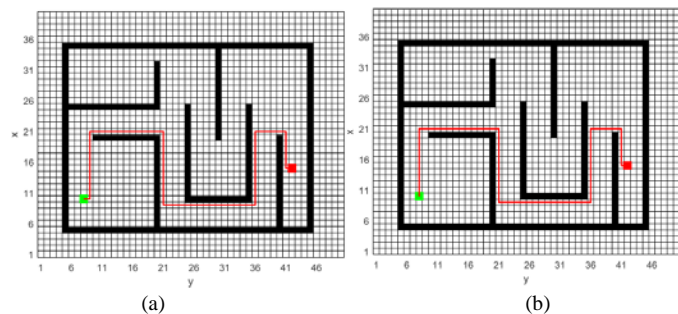


Fig. 16. (a) Modified Bidirectional a Star for Medium Map, (b) Basic Bidirectional a Star for Medium Map.

TABLE IX. COMPARISON BETWEEN BASIC AND MODIFIED BIDIRECTIONAL A STAR ALGORITHM IN MEDIUM MAP

Algorithm	Total Steps	Straight Steps	Rotation Steps	Visited nodes	Search time
Basic Bidirectional A Star	76	68	8	651	2.71
Modified Bidirectional A Star	76	69	7	659	2.73

3) Bidirectional A Star Algorithm in Hard Map.

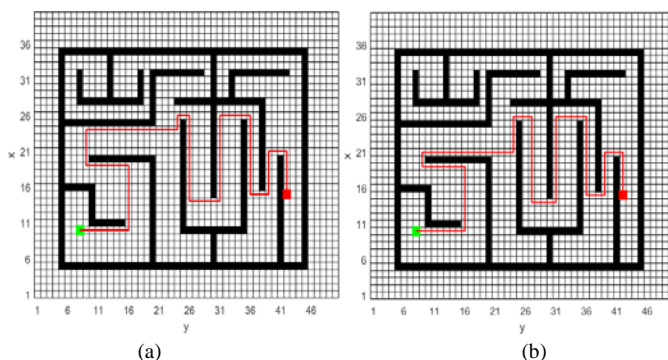


Fig. 17. (a) Modified Bidirectional a Star for Hard Map (b) Basic Bidirectional a Star for Hard Map.

TABLE X. COMPARISON BETWEEN BASIC AND MODIFIED BIDIRECTIONAL A STAR ALGORITHM IN HARD MAP

Algorithm	Total Steps	Straight Steps	Rotation Steps	Visited nodes	Search time
Basic Bidirectional A Star	112	97	15	747	3.16
Modified Bidirectional A Star	112	97	15	756	3.19

As shown in Fig. 15(a) to 17(b) and Tables VIII to X, it can be seen that both the Bidirectional A Star algorithm and the improved Bidirectional A Star algorithm can search for symmetric paths of the same length, but the search path of the improved Bidirectional A Star algorithm has more straight length, the path trajectory is different, and the number of rotation points in the paths are also different. In addition, it is obvious that the improved Bidirectional A Star algorithm search straighter than Bidirectional A Star algorithm can reach to one-step in easy map one-steps in medium map and the same steps in hard map.

D. Best First Search Algorithm

1) Best first search algorithm in easy map: The three different maps of BFS are demonstrated in three figures [Fig. 18(a) to 18(c)].

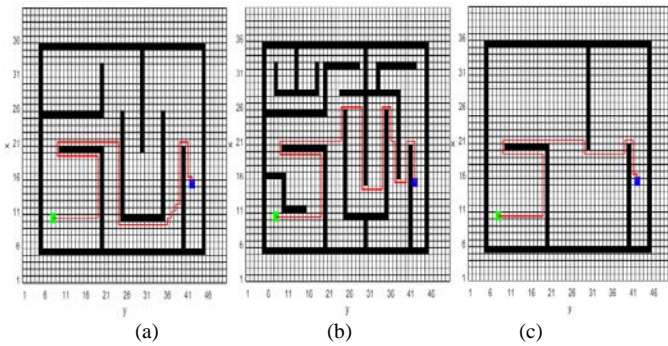


Fig. 18. (a) BFS Easy Map, (b) BFS Medium Map, (c) BFS Hard Map.

Tables XI gives the result of BFS in total steps, straight steps, rotation steps, visited nodes, and search time on three different maps.

TABLE XI. RESULTS OF BFS IN EASY, MEDIUM AND HARD MAP

Algorithm	Path Length	Straight Steps	Rotation Steps	Visited nodes	Search time
BFS Easy Map	76	65	11	462	1.54
BFS Medium Map	96	78	17	659	2.75
BFS Hard Map	118	101	17	756	3.17

E. Breadth First Search

1) *Breadth first algorithm in easy map:* The three different maps of BFS is demonstrated in three Fig. 19(a) to 19(c).

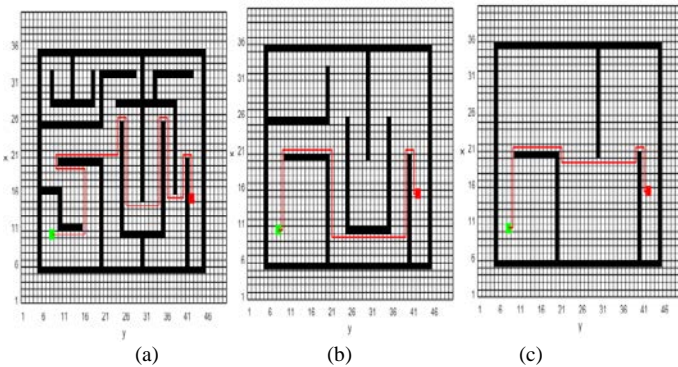


Fig. 19. (a) BFS Easy Map, (b) BFS Medium Map, (c) BFS Hard Map.

The Table XII gives the result of BRFS in total steps, straight steps, rotation steps, visited nodes, and search time on three different maps.

TABLE XII. RESULTS OF BRFS IN EASY, MEDIUM AND HARD MAP

Algorithm	Total Steps	Straight Steps	Rotation Steps	Visited nodes	Search time
BRFS Easy Map	56	48	8	678	2.95
BRFS Medium Map	76	68	8	673	2.97
BRFS Hard Map	112	97	15	805	3.81

F. Depth First Search

1) *Depth First algorithm in Easy Map:* The three different maps of DFS is demonstrated in three figures below [Fig. 20(a)-(c)].

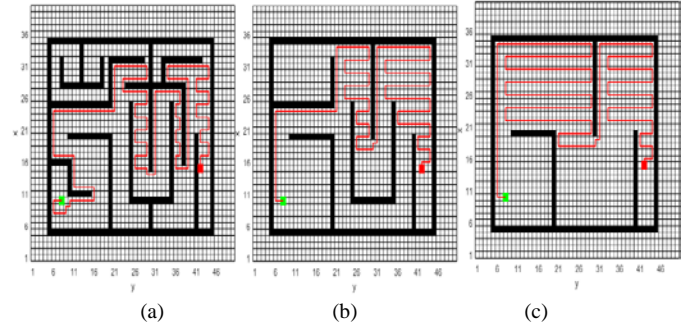


Fig. 20. (a) DFS Easy Map, (b) DFS Medium Map, (c) DFS Hard Map.

The Table XIII gives the result of DFS in total steps, straight steps, rotation steps, visited nodes, and search time on three different maps.

TABLE XIII. RESULTS OF DFS IN EASY, MEDIUM AND HARD MAP

Algorithm	Total Steps	Straight Steps	Rotation Steps	Visited nodes	Search time
DFS Easy Map	332	289	41	625	2.68
DFS Medium Map	220	177	43	526	2.61
DFS Hard Map	224	159	65	526	2.35

2) *Comparison between modified informed algorithm and informed algorithms:* In all informed and modified informed algorithms path length are equal in all maps, but trajectory path and straight length in selected path is improved as shown in Table XIV.

TABLE XIV. COMPARISON OF STRAIGHT LENGTH IN UNINFORMED ALGORITHMS

Algorithm	Easy Map straight Length	Medium Map Path Length	Hard Map Path Length
BFS	65 /76	78/96	101/118
BRFS	48/56	68/76	97/112
DFS	289/332	177/220	159/224

G. *These Experiments Show us Best Uninformed Algorithm in all Maps is BRFS*

1) *Comparison between modified informed algorithm and informed algorithms:* In Table XV all informed and modified informed algorithms path length are equal in all maps, but trajectory path and straight length in selected path is improved, in easy map path equal 56 steps, in medium map 76 steps, in hard map 112 steps.

TABLE XV. COMPARISON OF STRAIGHT LENGTH IN MODIFIED INFORMED AND INFORMED ALGORITHMS

Algorithm	Easy Map straight Length	Medium Map straight Length	Hard Map straight Length
Dijkstra	47 /56	45/76	73/112
Mod Dijkstra	50/56	70/76	97/112
A star	47/56	61/76	95/112
Mod A star	49/56	69/76	97/112
Bidirectional A star	48/56	68/76	97/112
Mod Bidirectional A star	49/56	69/76	97/112

Table XV shows us that:

- Dijkstra algorithm is improved by more than 5% in Easy Map, more than 32% in medium Map, more than 19% in Hard Map.
- A Star Algorithm is improved by more than 3% in Easy Map, more than 10% in medium Map, more than 1% in Hard Map.
- Bidirectional A Star Algorithm is improved by more than 1% in Easy Map, more than 2% in medium Map.
- Modified Dijkstra has higher effect in results more than other two algorithms.

2) *Comparison between modified informed algorithm and uninformed algorithms:* According to informed and uninformed algorithms experiment data as shown in Table XVI, the obtained path trajectories are not the same for all algorithms, which indicates that the Modified Dijkstra algorithm has Minimum straight length path in all maps, in other side modified A Star, modified Bidirectional A Star have same straight length easy and medium map, also all of three modified informed algorithms have Minimum straight length path Comparing the search time easy, medium and hard map informed and uninformed search.

TABLE XVI. COMPARISON BETWEEN MODIFIED INFORMED AND UNINFORMED ALGORITHMS

Algorithm	Visited nodes			Search time in second		
	Easy	Medium	Hard	Easy	Medium	Hard
Mod Dijkstra	1010	976	814	5.3	4.32	3.96
Mod A star	726	768	698	3.15	3.21	2.97
Mod Bidirectional A star	462	659	756	1.57	2.73	3.19
BFS	462	659	756	1.54	2.75	3.17
BRFS	678	673	805	2.95	2.97	3.81
DFS	625	526	526	2.68	2.61	2.35

IV. DISCUSSION

To demonstrate the Benefits of the modified algorithms in terms of search speed, number of rotation, path selection and

path length, three separate experimental locations have been created. The experiments establish a starting point and target point environment. Dijkstra algorithm improved by more than 5% in Easy Map, more than 32% in medium Map, more than 19% in Hard Map.

A Star Algorithm improved by more than 3% in Easy Map, more than 10% in medium Map, more than 1% in Hard Map.

Bidirectional A Star Algorithm is improved by more than 1% in Easy Map, more than 2% in medium Map.

Modified Dijkstra has better results over the other two algorithms.

V. CONCLUSION

The purpose of this paper is to modify and adjust informed search algorithms and compare pure informed algorithms and uninformed algorithms to find the shortest path between the start and the goal on designed maps of various obstacles' quality. Additionally, to enhance the identification of the shortest path for each algorithmic search with less rotation within the path and to simulate its performance in the designed maps, it can be noticed from the results that algorithms that have high visited nodes have more optimums than algorithms with low visited nodes. Search time is directly proportional to the number of visited nodes. Finally, heuristic search algorithms are more flexible than blind search algorithms.

Future work will involve the proposed algorithms that are compatible with Artificial Intelligence to make high-response and more features to keep up with the modern technology requirements.

REFERENCES

- [1] Mester, "Applications of mobile robots," 2006.
- [2] P. E. Teleweck and B. Chandrasekaran, "Path planning algorithms and their use in robotic navigation systems," in *Journal of Physics: Conference Series*, 2019, vol. 1207, no. 1, p. 12018.
- [3] C. M. Pop, G. L. Mogan, and M. Neagu, "Localization and Path Planning for an Autonomous Mobile Robot Equipped with Sonar Sensor," in *Applied Mechanics and Materials*, 2015, vol. 772, pp. 494–499.
- [4] T. T. Hoang, D. T. Hiep, P. M. Duong, N. T. T. Van, B. G. Duong, and T. Q. Vinh, "Proposal of algorithms for navigation and obstacles avoidance of autonomous mobile robot," in *2013 IEEE 8th Conference on Industrial Electronics and Applications (ICIEA)*, 2013, pp. 1308–1313.
- [5] Stentz, "Optimal and efficient path planning for partially known environments," in *Intelligent unmanned ground vehicles*, Springer, 1997, pp. 203–220.
- [6] I-H. Zhou and H-Y. Lin, "A self-localization and path planning technique for mobile robot navigation," in *2011 9th World Congress on Intelligent Control and Automation*, 2011, pp. 694–699.
- [7] G. E. Jan, K.-Y. Chang, and I. Parberry, "A new maze routing approach for path planning of a mobile robot," in *Proceedings 2003 IEEE/ASME International Conference on Advanced Intelligent Mechatronics (AIM 2003)*, 2003, vol. 1, pp. 552–557.
- [8] R. Katsuki, T. Tasaki, and T. Watanabe, "Graph Search Based Local Path Planning with Adaptive Node Sampling," in *2018 IEEE Intelligent Vehicles Symposium (IV)*, 2018, pp. 2084–2089.
- [9] C. R. Reeves, "Heuristic search methods: A review," *Oper. Res. Pap.*, pp. 122–149, 1996.
- [10] C. A. Floudas and P. M. Pardalos, *Encyclopedia of optimization*. Springer Science & Business Media, 2008.

- [11] C. Grosan and A. Abraham, "Informed (Heuristic) Search," in *Intelligent Systems*, Springer, 2011, pp. 53–81.
- [12] S. Pooja, S. Chethan, and C. V Arjun, "Analyzing uninformed search strategy algorithms in state space search," in *2016 International Conference on Global Trends in Signal Processing, Information Computing and Communication (ICGTSPICC)*, 2016, pp. 97–102.
- [13] Hassani, I. Maalej, and C. Rekik, "Robot path planning with avoiding obstacles in known environment using free segments and turning points algorithm," *Math. Probl. Eng.*, vol. 2018, 2018.
- [14] Y. Wang, X. Yu, and X. Liang, "Design and implementation of global path planning system for unmanned surface vehicle among multiple task points," *Int. J. Veh. Auton. Syst.*, vol. 14, no. 1, pp. 82–105, 2018.
- [15] N. Buniyamin, W. W. Ngah, N. Sariff, and Z. Mohamad, "A simple local path planning algorithm for autonomous mobile robots," *Int. J. Syst. Appl. Eng. Dev.*, vol. 5, no. 2, pp. 151–159, 2011.
- [16] Selamat, M. Zolfpour-Arokhlo, S. Z. Hashim, and M. H. Selamat, "A fast path planning algorithm for route guidance system," in *2011 IEEE International Conference on Systems, Man, and Cybernetics*, 2011, pp. 2773–2778.
- [17] Jiang, L. D. Seneviratne, and S. W. E. Earles, "A shortest path based path planning algorithm for nonholonomic mobile robots," *J. Intell. Robot. Syst.*, vol. 24, no. 4, pp. 347–366, 1999.
- [18] D. B. Johnson, "A note on Dijkstra's shortest path algorithm," *J. ACM*, vol. 20, no. 3, pp. 385–388, 1973.
- [19] R. Dechter and J. Pearl, "Generalized best-first search strategies and the optimality of A," *J. ACM*, vol. 32, no. 3, pp. 505–536, 1985.
- [20] X. Liu and D. Gong, "A comparative study of A-star algorithms for search and rescue in perfect maze," in *2011 International Conference on Electric Information and Control Engineering*, 2011, pp. 24–27.
- [21] F. Zhang et al., "An adaptive breadth-first search algorithm on integrated architectures," *J. Supercomput.*, vol. 74, no. 11, pp. 6135–6155, 2018.
- [22] P. Muntean, "Mobile robot navigation on partially known maps using a fast a star algorithm version," *arXiv Prepr. arXiv1604.08708*, 2016.
- [23] Kaur, P. Sharma, and A. Verma, "A appraisal paper on Breadth-first search, Depth-first search and Red black tree," *Int. J. Sci. Res. Publ.*, vol. 4, no. 3, pp. 2–4, 2014.
- [24] H. Wang, Y. Yu, and Q. Yuan, "Application of Dijkstra algorithm in robot path-planning," in *2011 second international conference on mechanic automation and control engineering*, 2011, pp. 1067–1069.
- [25] G. Qing, Z. Zheng, and X. Yue, "Path-planning of automated guided vehicle based on improved Dijkstra algorithm," in *2017 29th Chinese control and decision conference (CCDC)*, 2017, pp. 7138–7143.
- [26] P. Sari, M. F. Fahroza, M. I. Mufit, and I. F. Qathrunad, "Implementation of Dijkstra's Algorithm to Determine the Shortest Route in a City," *J. Comput. Sci. Inf. Technol. Telecommun. Eng.*, vol. 2, no. 1, pp. 134–138, 2021.
- [27] B. Wang, "Path Planning of Mobile Robot Based on A* Algorithm," in *2021 IEEE International Conference on Electronic Technology, Communication and Information (ICETCI)*, 2021, pp. 524–528.
- [28] F. Duchoň et al., "Path planning with modified a star algorithm for a mobile robot," *Procedia Eng.*, vol. 96, pp. 59–69, 2014.
- [29] T. XiangRong, Z. Yukun, and J. XinXin, "Improved A-star algorithm for robot path planning in static environment," in *Journal of Physics: Conference Series*, 2021, vol. 1792, no. 1, p. 12067.
- [30] H. K. Tripathy, S. Mishra, H. K. Thakkar, and D. Rai, "CARE: A Collision-Aware Mobile Robot Navigation in Grid Environment using Improved Breadth First Search," *Comput. Electr. Eng.*, vol. 94, p. 107327, 2021.

Modified Gradient Algorithm based Noise Subspace Estimation with Full Rank Update for Blind CSI Estimator in OFDM Systems

Saravanan Subramanian, Govind R. Kadambi

Faculty of Engineering and Technology
Ramaiah University of Applied Sciences
Bangalore, India

Abstract—This paper presents a modified Gradient-based method to directly compute the noise subspace iteratively from the received Orthogonal Frequency Division Multiplexing (OFDM) symbols to estimate Channel State Information (CSI). By invoking the matrix inversion lemma which is extensively used in Recursive Least Square (RLS) algorithms, the proposed computationally efficient method enables direct computation of noise subspace using the inverse of the autocorrelation matrix of the received OFDM symbols. In the case of a vector input, the modified Gradient algorithm uses rank one update to calculate noise subspace recursively. For an input in the matrix form, the modified Gradient algorithm uses a full rank update. The validity, efficacy, and accuracy of the proposed modified Gradient algorithm have been substantiated through a relative comparison of the results with the conventional Singular Value Decomposition (SVD) algorithm, which is in wide use in the estimation of the subspaces. The simulation results obtained through the modified Gradient algorithm show a satisfactory correlation with the results of SVD, even though the computational complexity involved in modified Gradient is relatively less. Apart from the results encompassing various power levels of the multipath channel, this paper also discusses the adaptive tracking of CSI and presents a comparative study.

Keywords—Orthogonal Frequency Division Multiplexing (OFDM); Carrier Frequency Offset (CFO); Channel State Information (CSI); Recursive Least Square (RLS); Singular Value Decomposition (SVD); Channel Impulse Response (CIR); BPSK; QPSK; QAM

I. INTRODUCTION

Radio systems based on Orthogonal Frequency Division Multiplexing (OFDM) are increasingly being adopted by many wireless communication standards [1]. With the ability of OFDM systems to effectively handle impairments of wireless channels, communication engineers and system designers can use standards for broadband digital data communication standards such as IEEE 802.11 [a, b, j, n], IEEE 802.15.3a, etc. OFDM is adopted as the waveform in IEEE 802.16 [d, e], IEEE 802.120, digital video broadcasting, digital audio broadcasting and cellular [3G, 4G]. Additionally, in high-speed wireless data communication using OFDM waveforms, the effects of multipath and the delayed spread of channels have a significant impact on data throughput. Figure 1 describes a typical OFDM transmitter and Receiver operating in a multipath wireless channel. For efficient operation and

throughput of the OFDM system, it is important to estimate the multipath wireless channel (Channel State Information) at the receiver end.

In summary, accurate estimation of Carrier Frequency Offset (CFO) and CSI is essential for ensuring the satisfactory performance of the OFDM system. The attainment of time synchronization between OFDM symbols is assumed to be present. The emphasis of this paper is on CSI which deals with the estimation of the multipath wireless channel. Instead of conventional SVD, this paper presents a computationally efficient modified gradient algorithm to estimate the noise subspace directly (Instead of signal subspace first and then through it, the noise subspace). The noise subspace is then utilized for the estimation of CSI.

This paper is structured as follows. Section II presents the review of CSI estimation techniques. Section III presents the OFDM system model. Section IV deals with the second-order statistics and the blind CSI estimation process of the subspace. Section V discusses the proposed modified Gradient based noise subspace. Section VI presents the formulation for the estimation of CSI using the proposed modified gradient algorithm. Section VII analyses the performance of modified Gradient based CSI estimator, to substantiate its efficacy and ability in improving the estimation accuracy of CSI. Section VIII presents the conclusions of the paper.

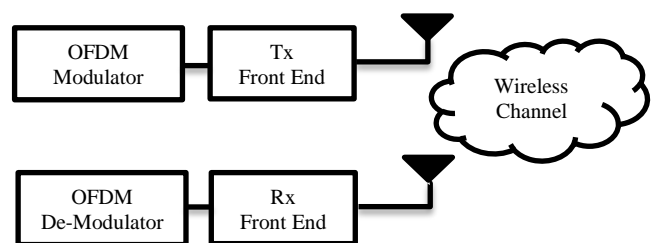


Fig. 1. OFDM System Block Diagram.

II. RELATED WORK

This section presents a comprehensive review of research studies pertaining to OFDM in general and estimation of CSI in particular.

The authors in [2] propose an Integrated OFDM (I-OFDM) system to meet the BER performance of Enhanced Long-Term Assessment (LTE-A). For the pilot-aided CSI estimation

technique, pilot arrangement of comb type as well as convolution (Channel) encoder with best-known bounds of Coding Bounds are used. "Maximum A Posteriori (MAP)" decoder for the convolution encoder is at the receiver. The evaluation of BER performance was through convolution codes of Recursive systematic and non-systematic nature. The proposed I-OFDM showed significant improvement in the system performance combining traditional IM and multiple-mode IM in [3]. To achieve the varied diversity order and spectral efficiency required next-generation wireless communication networks, CIM techniques (subcarrier-wise and subblock-wise) are presented.

To achieve higher data bandwidth in such systems, it is of greater importance to estimate the CSI, the transfer function of the wireless channel. Author in [4] addresses the clustering strategy for heterogeneous wireless sensor networks. The clustered heads are chosen based on the CSI, the nodes' residual energy, and the network's average energy. Author proposes periodic transmission of a data packet containing the information about the energy dissipation of the wireless sensor nodes using Bluetooth low energy, ZigBee, and ANT protocols for the appropriate choice for the protocol selection.

The authors in [5] propose the OFDM/OFDMA system's improved performance by introducing closed-loop rotate modulation schemes involving BPSK, QPSK, and QAM. The method utilizes the feedback of the complex-valued CSI. The rotate modulation serves the role of channel equalizer and does not need the guard interval insertion. With BPSK and QPSK, the proposed method does not degrade BER performance with feedback delay. However, with QAM, the feedback delay degrades BER performance.

The authors of [6] discuss the potential demands and challenges of the emerging 6G wireless communication network. The authors address system capacity requirements, data rate, latency, enhanced security, and the improved quality of service of 6G relative to 5G. The paper also dwells on the potential applications of mm-wave, terahertz communications, and massive MIMO systems in 6G.

This paper [7] addresses the issue of Pilot contamination in a massive MIMO system. The authors proposed a scheme for reducing pilot contamination by combining time-shifting protocol, the directional pilot scheme, and a greedy algorithm-based pilot allocation scheme for channel estimation. The simulation results show the significantly enhanced performance of a massive MIMO system with the proposed combinatorial scheme compared to the individual constituents of the combination.

The receiver improves the overall bandwidth efficiency of the system by detecting CSI accurately and efficiently. CSI acquisition is generally performed using pilot or non-pilot techniques. To estimate CSI, pilot-based techniques typically use significant bandwidth to train the channel estimator at the receiver and send the training sequence. Paper [7] addresses the issue of pilot contamination in large-scale MIMO systems. The authors proposed a scheme to reduce pilot contamination by combining a time-shift protocol, a directional pilot scheme, and a pilot allocation scheme based on a greedy channel estimation algorithm. The simulation results show that the performance of

large MIMO systems using the proposed combination scheme has improved significantly.

For non-pilot assisted methods, CSI estimation requires statistical information about the data received. In addition, non-pilot assistive techniques (often referred to as blind techniques) are more bandwidth efficient because they do not require a unique training sequence.

The authors in [8,9] proposed pilot aided technique for channel estimation. The authors investigated the performance of block type and comb type pilot insertion technique in estimation of the channel. Comb time pilot insertion scheme is found to be more appropriate to track time varying channel. The technique involves the pilot insertion on the estimation. The frequency domain interpolations are carried in case of the block type pilot insertions and time domain interpolation is carried in case of the comb type pilot insertions.

In [10], the authors presented the pilot aided technique for channel estimation in OFDM. The performance of two pilot based estimators performance is evaluated at different SNRs. Bayesian based Minimum Mean Square Estimator (MMSE) performs better at low SNR when compared to the Maximum Likelihood (ML) estimator. Both MMS and Bayesian estimators require a prior information about the channel statistics. The estimator requires more number of pilot tones as compared to the Channel Impulse Response (CIR) length.

Linear Redundancy Precoding (LRP) uses either cyclic prefixes (CPs) or zero pads (ZPs) in OFDM systems [11, 12]. LRP is one of the categories of blind techniques for estimating the CSI of OFDM systems. The estimation accuracy of the LRP technique depends on the CP / ZP length of the OFDM symbol. The second category of blinding techniques relies on the subspace of the secondary statistics of the received sample to estimate the CSI of the OFDM system. The performance of the subspace-based method depends heavily on the accuracy in estimating the autocorrelation matrix of the received sample. This paper focuses on a subspace-based approach with improved stability in CSI numerical estimation and improved channel bandwidth efficiency.

In [12] and [13], the underlying method for estimating CSI is based on the singular vector of the covariance matrix. CSI estimation requires a noise subspace of the autocorrelation matrix. Computing the required noise subspace with traditional algorithms such as SVD requires extensive computation. A zero padded OFDM system is explored in [14] for CSI estimation based on subspace.

Numerical methods for calculating noise subspaces are not as common as signal subspace estimators. In addition, most algorithms for estimation [15] that combine signal and noise subspaces are available with high complexity. The estimation algorithm exists exclusively for the signal subspace, but there seems to be no algorithm dedicated to the noise subspace.

This paper presents a Gradient [16] based method for iteratively calculating noise subspaces from received OFDM symbols. The method proposed in this paper directly calculates the noise subspace required to estimate the CSI. In the proposed method, the calculation of the noise subspace requires the inverse of the autocorrelation matrix of the

received OFDM symbols. In addition, this paper employs the matrix inversion lemma, which is very commonly used in recursive least squares algorithms (RLS) [17], to overcome the high computational cost of direct inversion of autocorrelation matrices.

Also, the noise subspace of the autocorrelation matrix is just the signal subspace of the inverse autocorrelation and is calculated using the numerically stable Gradient algorithm. In this paper, the modified Gradient refers to fitting the inverse matrix to compute the inverse of the autocorrelation matrix and using the numerically stable Gradient algorithm to estimate the noise subspace. This paper also shows two schemes of modified gradient based on whether the underlying input to the modified Gradient algorithm is a vector or a matrix. For vector inputs, the modified Gradient recursively calculates the noise subspace using rank one updates. On the other hand, modified Gradient algorithm recursively computes the noise subspace using a full-rank update if the input is in the form of a matrix. Without loss of generality, this paper assumes channel matrix to be a full-rank Hankel matrix.

The emphasis of this paper is on CSI which deals with estimation of multipath wireless channel. Instead of conventional direct SVD, this paper presents a computationally efficient modified gradient algorithm to estimate the noise subspace directly. The noise subspace is then utilized for the estimation of CSI. The application of the new algorithm has been substantiated in the estimation of CFO using MUSIC algorithm [18], which also requires the noise subspace. This paper extends the utility of the modified gradient algorithm for the estimation of CSI. It is envisaged that the modified gradient algorithm proposed by the authors [18] is new way of estimating CFO and CSI, since modified Gradient algorithm is computationally efficient compared to the conventional direct SVD[19].

III. OFDM SYSTEM MODEL

In this section, the basic OFDM symbol is formed by N carriers. The basic OFDM symbol is followed by L zeros. Where $L \geq L_H$ (length of channel impulse response). In this document, the zero-pad OFDM system eliminates ISI. Equation (1) represents the n th received OFDM symbol Y_n after full time synchronization.

$$Y_n = HF^H x_n + w_n \quad (1)$$

Y_n is n^{th} Received OFDM symbol with L zero padding of size $(N+L) \times 1$

H is channel convolution matrix of size $N+L \times N$.

F^H is the orthonormal IFFT matrix.

x_n is n^{th} i.i.d unit norm data vector of size $N \times 1$.

w_n is i.i.d additive white Gaussian noise of variance σ^2 .

$$H = \begin{bmatrix} h(0) & 0 & \dots & 0 \\ \vdots & h(0) & \ddots & \vdots \\ h(L_H) & \vdots & \ddots & 0 \\ 0 & h(L_H) & \ddots & h(0) \\ \vdots & \vdots & \ddots & \vdots \\ 0 & 0 & \dots & h(L_H) \end{bmatrix}$$

H is a full-rank non-negative Toeplitz channel convolution matrix. The element of matrix H is the normalized channel impulse response of length L_H . The channel is assumed to be time-invariant and frequency-selective over the symbol period. To overcome the effects of ISI, the length of the selected ZP will be $L \geq L_H$. The CSI estimate assumes carrier frequency offset (CFO) cancellation introduced by the Doppler or local oscillator of the received OFDM symbol Y_n .

IV. BLIND CSI ESTIMATION

The blind CSI estimation algorithm in this document uses the noise subspace calculated from the quadratic statistics of the received OFDM symbols [14]. The quadratic statistics (autocorrelation) of the received OFDM symbols contain only the information about the transmitted OFDM symbols and the convoluted channels. However, due to the orthonormal nature of the inverse Fast Fourier Transform (IFFT) and the nature of the independent identical distribution and unit norm of the transmitted data X_n , the autocorrelation matrix can be used to estimate the CSI [14].

$$R_n = E\{Y_n Y_n^H\} \quad (2)$$

$$R_n = HH^H + \sigma_{noise}^2 I_{N+L} \quad (3)$$

Where R_n is the autocorrelation matrix and E is the expected value operator. The matrix HH^H is the Hermitian positive semi-definite matrix, I_{N+L} is the identity matrix, and σ_{noise}^2 is the noise power of the channel. The size of the resulting autocorrelation matrix R_n is $N+L \times N+L$. The identity matrix can diagonalize the resulting R_n by applying the spectral theorem. SVD is used to diagonalize R_n .

$$R_n = U \Sigma V^H \quad (4)$$

$$U = [U_{signal} U_{noise}] \quad (5)$$

$$V^H = [U_{signal}^H U_{noise}^H] \quad (6)$$

$$\Sigma = \begin{bmatrix} \Delta + \sigma_{noise}^2 I_N & 0 \\ 0 & \sigma_{noise}^2 I_L \end{bmatrix} \quad (7)$$

The orthonormal matrices U and V^H contain subspace components of signal and noise subspaces. U_{signal} corresponds to the signal subspace of dimension $N+L \times N$ of the autocorrelation matrix R_n , and U_{noise} corresponds to the noise subspace of dimension $N+L \times L$. Δ is a diagonal matrix with diagonal elements representing the signal power of each N -subcarrier. Equation (1) shows that the received OFDM symbol Y_n is basically in the signal space across the channel convolution matrix H . A linear combination of the channel convolution matrix H multiplied by $F^H x_n$ yields the received OFDM symbol Y_n . The channel convolution matrix H is a Toeplitz matrix of size $N+L \times N$, so there are N non-identical columns and the rank is N . This indicates that the rank of the

main subspace (signal subspace) of this matrix H is N , and the rank of that subspace (noise subspace) is L .

$$U_{noise}^H \times U_{signal} = 0 \quad (8)$$

Equation (8) states that the U_{signal} and U_{noise} are orthogonal subspaces. Each vector in the noise space is orthogonal to the entire signal space U_{signal} . Similarly, each vector in the signal space is orthogonal to the total noise space U_{noise} . This special property is used to estimate the channel impulse response h_n . Since the columns of the channel convolution matrix H span the entire signal space, the received OFDM symbol Y_n is also in the signal space across H . Therefore, this space is also orthogonal to any vector in the noise space U_{noise} calculated from the SVD on the autocorrelation matrix R_n .

$$U_{noise}^H \times H = 0 \quad (9)$$

$$u^H = [u_1 \quad u_2 \quad \dots \quad u_{N+L}] \quad (10)$$

$$u^H \times H = 0 \quad (11)$$

if u^H in Equation (10) is a vector of length $N+L$ in the noise subspace, it is also an orthogonal complement of the channel convolution matrix H by equation (11). From Equation (11) to Equation (12) rewritten by the Toeplitz structure of the channel convolution matrix H . Where V is a Hankel matrix of size $L+1 \times N$ formed using the elements of u , which is the noise vector of the noise subspace U_{noise} . The cost function for estimating CSI includes the complex conjugate of equation (12).

$$h^H \times V = 0 \quad (12)$$

$$(h^H \times V) \times (h^H \times V)^H \quad (13)$$

$$h^H V V^H h = 0 \quad (14)$$

By using all the noise vectors in the noise subspace U_{noise} , Equation (14) is rewritten as the cost function of Equation (16) to estimate the CSI.

$$W = \sum_{i=0}^L V_i V_i^H \quad (15)$$

$$h^H W h = 0 \quad (16)$$

V_i is a Hankel matrix formed from the individual noise vector elements of the noise subspace U_{noise} . Equation (16) means that the vector h , which is a small singular vector of W , can minimize the cost function. This small normalized singular vector is an estimate of CSI with phase ambiguity. Each complex element, when scaled, is a small singular vector that is also the solution to the cost function defined in Equation (16).

V_i is the Hankel matrix formed by using the elements of the individual noise vectors of the noise subspace U_{noise} . Equation (16) implies that the vector h , a minor singular vector of W , can minimize the cost function. This minor singular vector normalized is the estimate of CSI with a phase ambiguity. Any complex element, when scaled, a minor singular vector, is also a solution to the cost function defined by Equation (16). This phase ambiguity is attributed to the above.

Considering the process of CSI estimation from the reception of OFDM symbol Y_n to the solution of equation (16), the calculation of equations (4) and (16) uses a computationally

intensive algorithm (SVD) in two steps. Analysis of the steps involved in the CSI estimation shows that noise space is more important in the CSI estimation. In fact, of the results of Equations (4) and (16), the noise vector from each calculation is used in the subsequent process of the CSI estimation method. However, the computational cost of the $O((N+L)^3)$ SVD method makes this estimation method a non-viable option for real-time implementations. In the next section, this paper proposes a new algorithm for efficiently estimating the noise vectors in Equation (4) (using rank-one updates) and equation (16) (using full-rank updates). The proposed algorithm has computational advantages over existing algorithms such as SVD.

V. MODIFIED GRADIENT ALGORITHM

Let $x(t)$ be a column vector in complex vector space C^n observed at instant t . In time domain spectral analysis, it is a vector of n consecutive samples of summation of r non coherent complex sinusoids corrupted by additive complex Gaussian noise $n(t)$ with variance σ^2 .

$$x(t) = \sum_{k=1}^r s_k a(w_k) + n(t) \quad (17)$$

$$x(t) = A s(t) + n(t) \quad (18)$$

Where $A = [a(w_1) \ a(w_2) \ \dots \ a(w_r)]$ is the deterministic matrix of size $n \times r$. $a(w_p) = [1 \ e^{jw_p} \ e^{j2w_p} \ \dots \ e^{j(n-1)w_p}]^T$ is the frequency vector and $S(t) = [s_1 \ s_2 \ \dots \ s_r]$ is the random source vector. The correlation matrix R is formed from the snapshot vector $x(t)$.

$$R = E[x(t) x^H(t)] = A C_s A^H + I \sigma^2 \quad (19)$$

Where $C_s = E[S(t) S^H(t)]$, I denotes the identity matrix and E stands for expectation. Taking Eigen decomposition of Equation (5).

$$R = U \Sigma U^H \quad (20)$$

$$U = [U_s \ U_n] \quad (21)$$

U_s contains the signal space vectors and U_n has the noise space vector. The first r vectors in U (Equation (21)) form the signal subspace vector alias column subspace vectors. The remaining $(n-r)$ vectors form the noise subspace vectors alias left Null subspace vector. Similarly, Σ (Equation (20)) is the diagonal matrix containing the Eigen values corresponding to the signal and noise subspace respectively. It is important to note that both the matrices A and U_s span the same column space alias the signal subspace. The U_s signal subspace vectors and U_n noise subspace vectors are orthogonal and they complement each other. The above-mentioned properties are exploited in high resolution spectral estimation technique using MUSIC [20] and ESPRIT algorithms [21].

It is clear that the matrices A and U_s span the same column space alias the signal subspace. This enables to build a cost function to estimate the signal subspace. Let $y(t)$ be a vector in the column space of the U_s^H . Then,

$$y(t) = U_s^H x(t) \quad (22)$$

$$x(t) = U_s y(t) \quad (23)$$

$$x(t) = U_s U_s^H x(t) \quad (24)$$

Superscript H denotes the Hermitian transpose. For convenience U_s and U_s^H are rewritten as W and W^H respectively. The scalar cost function can be arrived as

$$J(W) = E \|x(t) - WW^H x(t)\|^2 \quad (25)$$

$J(W)$ has global minimum only at when the columns of W span the signal space of A .

Global minimum of Equation (25) can be found recursively using the Gradient Descent method [16]. As a first step, the gradient of the unconstrained cost function with respect to W is derived.

$$\nabla J = [-2R + RWW^H + WW^H R]W \quad (26)$$

The update on the subspace can be written as

$$W(t) = W(t-1) + [2R(t) - R(t)W(t-1)W^H(t-1) - W(t-1)W^H(t-1)R(t)]W(t-1) \quad (27)$$

The above Equation (27) converges to the signal subspace of the correlation matrix $R(t)$. This implies that the conventional Gradient algorithm facilitates the computation of signal subspace only. One has to compute the noise subspace after computing the signal subspace. The proposed modified Gradient algorithm is aimed for the direct computation of noise subspace instead of first computing the signal subspace and then computing the noise subspace from the knowledge of auto correlation matrix. To obtain the noise subspace, $R(t)$ in Equation (27) is to be replaced with $R_{inv}(t)$, where $R_{inv}(t)$ is the inverse of correlation matrix $R(t)$. With this modification, Equation (27) can be rewritten as shown in Equation (28).

$$W(t) = W(t-1) + [2R_{inv}(t) - R_{inv}(t)W(t-1)W^H(t-1) - W(t-1)W^H(t-1)R_{inv}(t)]W(t-1) \quad (28)$$

Equation (28) is the modified Gradient Method for the noise subspace estimation. The computational complexity of Equation (28) is comparatively less when compared to the batch based SVD or EVD techniques [19] which is of the order of $O(n^3)$ operations.

VI. MODIFIED GRADIENT IN CSI ESTIMATION

This section presents a unique method for calculating the noise vector of R_n , the autocorrelation matrix by altering the current Gradient method [16]. The Gradient-based subspace estimation method is a member of the iterative power-based subspace estimation algorithm class. These categories of algorithms estimate and track signal vectors more effectively than the noise vector of the subject matrix. In addition, the iterative power-based approach predicts the greatest vector in the signal space. Typically, signal subspace vectors are computed prior to noise subspace estimation. The noise subspace created by inverting R_n , the autocorrelation matrix eliminates the need to compute the noise subspace following the signal subspace. Taking into account the inversion of the subjected R_n matrix, the same power-based technique will be more effective at directly estimating and tracking the noise space vector or minor vectors.

The inverse of the autocorrelation matrix R_n is calculated in the proposed modified Gradient, X_n , by utilizing the underlying received OFDM symbol Y_n . This is carried out in a recursive fashion. The classic matrix inversion lemma is used in the recursive least square estimation techniques, and it is utilized by the modified Gradient. The underlying matrix that will be employed in tracking the noise vectors in Equations (4) and (16) of interest for estimating the CSI will be the inverted version of X_n , which will have a dimension of $N+L \times N+L$. During the process of estimating the CSI, this modified Gradient method will be used to calculate and keep track of the noise vectors. In terms of the amount of computing power required, a technique of this iterative nature is quite effective. The comparative performance of blind CSI estimation using the proposed modified Gradient algorithm and SVD based approach will be described later in section VI with a random complex channel. The focus of this section is on the performance of blind CSI estimation using modified Gradient method.

This paper describes the procedure for computing the noise subspace vectors specified in Equation (4) and (16) using the modified Gradient approach. A pseudocode for the CSI estimation is also presented. Estimation of CSI begins with the OFDM signals that were successfully received. X_n denotes the n^{th} estimate of the inverse of the autocorrelation matrix, R_n .

A brief explanation of pseudo-code is presented here in order to estimate the noise subspace vectors making use of modified Gradient, with rank one update being performed by the underlying OFDM signal Y_n . As shown in the Equation (31), the rank-one update of the inverse autocorrelation matrix X_n is computed using Y_n , the received OFDM signal.

Initialize

$$V_{noise}(0) = [I]_{N+L \times L}$$

$$X(0) = [I]_{N+L \times N+L}$$

Where N is the number of carriers and L is the zero-padding length. $V_{noise}(0)$ is the initial noise subspace matrix of X_n^H , and $X(0)$ is the initial inverse of R_n .

For $n = 1, 2, 3, \dots$,

$$KalGain A(n) = X(n-1)Y(n) \quad (29)$$

$$Gamma A(n) = \frac{1-\lambda}{\lambda + (1-\lambda)Y^H(n)KalGainA(n)} \quad (30)$$

$X(n) =$

$$\frac{1}{\lambda} (X(n-1) - GammaA(n)KalGainA(n)KalGainA^H(n)) \quad (31)$$

$$V_{noise}(n) = V_{noise}(n-1) + [2X(n) - X(n)V_{noise}(n-1)V_{noise}^H(n-1) - V_{noise}(n-1)V_{noise}^H(n-1)X(n)]V_{noise}(n-1) \quad (32)$$

End

λ is the forgetting factor between 0 and 1.

V_{noise} , which has the noise vectors corresponding to the noise subspace vector of Equation (10). The L_{noise} vectors

from V_{noise} construct the Henkel matrix V needed to compute W , as shown in Equation (15). The smallest singular vector of W is obtained using the procedure listed below.

A summary of pseudo code for estimating the noise vectors using the modified Gradient method is presented with full-rank updating of W , which is computed from the V_{noise} as described in the Equation (15).

Initialize

$$Q(0) = \begin{bmatrix} I \\ 0 \end{bmatrix}_{N+L \times L}$$

$$W_{inv}(0) = [I]_{L \times L}$$

for $n = 1, 2, 3, \dots$

$$KalGainB(n) = W_{inv}(n-1)W(n) \quad (33)$$

$$GammaB(n) = \frac{1-\lambda}{\lambda+(1-\lambda)\det(W^H(n)KalGainB(n))} \quad (34)$$

$$W_{inv}(n) =$$

$$\frac{1}{\lambda}(W_{inv}(n-1) - GammaB(n)KalGainB(n)KalGainB^H(n)) \quad (35)$$

$$Q(n) = Q(n-1) + [2W_{inv}(n) - W_{inv}(n)Q(n-1)Q^H(n-1) - Q(n-1)Q^H(n-1)W_{inv}(n)]Q(n-1) \quad (36)$$

End

Q in Equation (36) contains noise subspace vectors of W_{inv} of Equation (35). The first singular vector is the estimate of the channel's impulse response. The impulse response estimate is normalized to get the estimate of CSI. The estimated normalized impulse response will have a phase ambiguity and is resolved with the help of a single pilot carrier.

The Gradient class of subspace estimation algorithms typically exhibit a complexity of $O((N+L)L)$ with the additional complexity of $O((N+L)^2)$ for inversion of matrix using matrix inversion lemma of Equation (31). In general, computational complexity in the estimation of noise spaces through the proposed modified Gradient scheme is $O((N+L)^2+(N+L)L)$, instead of $O((N+L)^3)$ operations of the conventional SVD based methods. This in turn implies a reduction in computational complexity of modified Gradient method. Table I presents the comparison of computational complexity between the direct SVD and modified Gradient algorithms in computing the noise subspace with rank one update. As shown in Table I, the computational complexity of modified Gradient is comparatively less than the direct SVD based algorithms for various values of N and L .

TABLE I. COMPARISON OF COMPUTATIONAL COMPLEXITY OF DIRECT SVD AND MODIFIED GRADIENT IN ESTIMATION NOISE SUBSPACE WITH RANK ONE UPDATE

SI. No	N	L	SVD	Modified Gradient
1	128	8	$O(136^3)$	$O(26.955^3)$
2	256	16	$O(272^3)$	$O(42.788^3)$
3	512	32	$O(544^3)$	$O(67.921^3)$

VII. PERFORMANCE ANALYSIS

This section presents the results of the simulation to establish the ability modified Gradient based CSI estimation algorithm using the directly computed noise subspace. The simulation model assumes the reception of the OFDM symbol with 128 carriers and zero-padded to the extent of $1/4^{\text{th}}$ of the OFDM symbol. Out of 128 carriers, one carrier is a reference carrier to resolve the issue of phase ambiguity. The simulation of the Rayleigh channel model mimicking the outdoor channel is through 16 tap FIR filter. The subcarriers of the OFDM use the modulation scheme of the QPSK constellation. The simulation is with 1500 OFDM symbols. The changes in the Rayleigh channel model are induced to occur at the time instances of 500^{th} and 1000^{th} OFDM symbols. The Channel Impulse Response, which is nothing but CSI, is estimated and is tracked using a subspace-based technique at various power levels. The estimate of CSI is compared with a response of modelled ideal Rayleigh channel. Direct SVD and proposed modified Gradient techniques are adopted to estimate the noise subspace. Noise subspace, in turn, is used to estimate the CSI. Fig. 2 to Fig. 4 present the comparative performance and analysis of CSI estimates obtained through modified Gradient, Direct SVD, and the ideal channel response.

Fig. 2 to Fig. 4 illustrate the comparative estimation performance of the modified Gradient and direct SVD-based noise subspace estimators in the estimation of CSI of the OFDM system. In the simulation studies presented in this paper, 400 OFDM symbols are utilized to reconstruct the autocorrelation matrix which is required for noise subspace estimation. The results of Fig. 2 correspond to the power level (SNR) of the wireless channel at 10 dB. The ideal Rayleigh channel shown in Fig. 2, is the reference for comparison and has been modeled through 16 tap FIR filter. Fig. 2 depicts the estimation of the Rayleigh channel state (at SNR of 10 dB) at the 400^{th} OFDM symbol. While Fig. 2(a) depicts the amplitude response of the CSI estimation, the corresponding phase response is shown in Fig. 2(b). There is an excellent agreement between the results obtained through the modified Gradient and direct SVD-based blind CSI estimators. The results of Fig. 2(b) reveal a fixed offset between the results of modified Gradient and Direct SVD relative to the ideal Rayleigh channel. The referred fixed offset in the phase of estimated CSI is attributed to the phase ambiguity (which is already explained while discussing Equation (16)). This phase ambiguity is resolved or negated using a single reference subcarrier.

Similarly, Fig. 3(a) and Fig. 3(b) depict the amplitude and the phase of the CSI estimation (SNR of 20 dB) at the 400^{th} OFDM symbol. At increased power level of the channel (SNR), the correlation between the CSI estimation by the blind CSI estimators and the ideal channel improves.

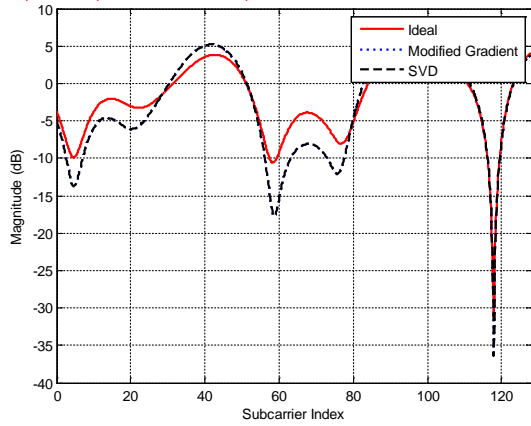
The analogous results at SNR of 30 dB are shown in Figures 4a and 4b. The results on amplitude response of CSI estimation shown in Figure 4a show perfect agreement among the blind CSI estimators and ideal channel. It is pertinent to note that modified Gradient requires relatively lesser computational effort compared to direct SVD.

Fig. 5 depicts the channel tracking performance of the proposed modified Gradient algorithm with direct SVD at SNR

of 10 dB. It also illustrates the Relative Error Norm performance of the proposed modified Gradient and direct SVD-based blind CSI estimators. Whenever there is a change in the state of the Rayleigh channel, the blind CSI estimator

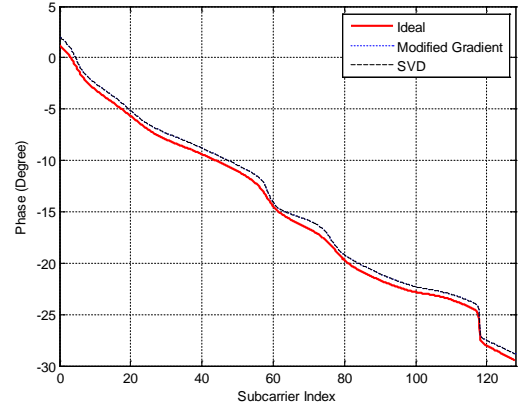
takes around 100 OFDM symbols for attaining the steady state. Post 100 symbols, the Relative Error Norm falls to around -6 dB at 1000th and 1500th OFDM symbols.

Amplitude Response of Wireless Multipath Channel at 10 dB SNR and 400th OFDM Symbol



(a)

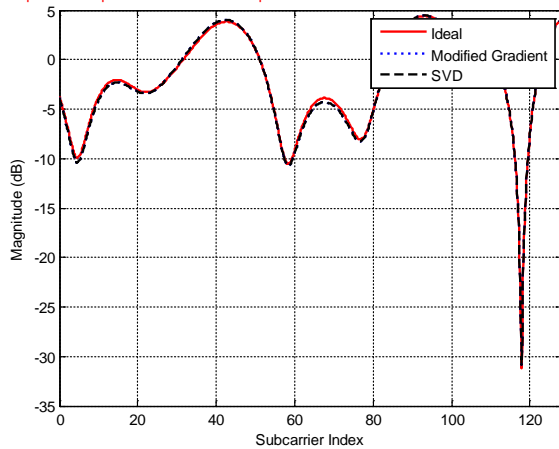
Phase Response of Wireless Multipath Channel at 10 dB SNR and 400th OFDM Symbol



(b)

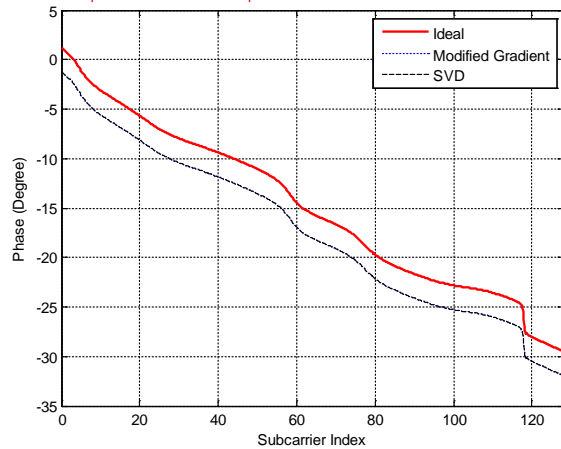
Fig. 2. (a) Amplitude Response: CSI Estimation for Rayleigh Channel at 400th OFDM Symbol (SNR of 10 dB), (b) Phase Response: CSI Estimation for Rayleigh Channel at 400th OFDM Symbol (SNR of 10 dB).

Amplitude Response of Wireless Multipath Channel at 20 dB SNR and 400th OFDM Symbol



(a)

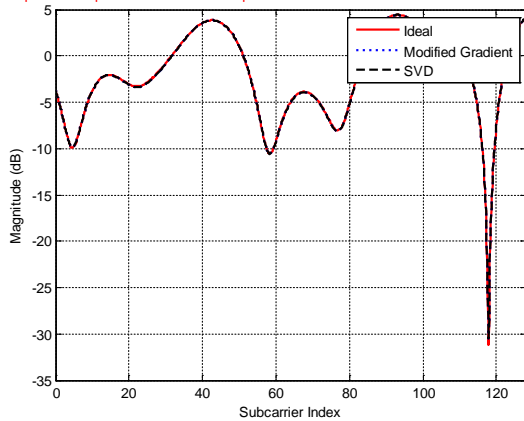
Phase Response of Wireless Multipath Channel at 20 dB SNR and 400th OFDM Symbol



(b)

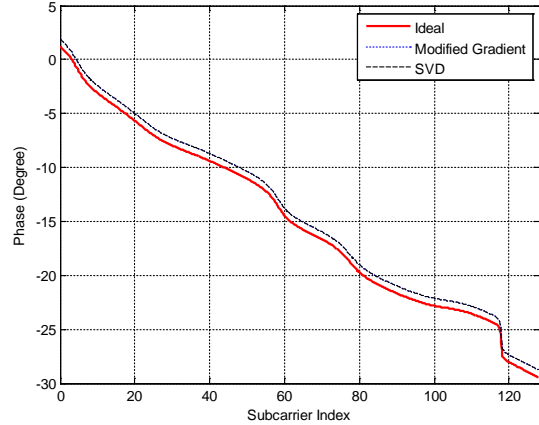
Fig. 3. (a) Amplitude Response: CSI Estimation for Rayleigh Channel at 400th OFDM Symbol (SNR of 20 dB), (b) Phase Response: CSI Estimation for Rayleigh Channel at 400th OFDM Symbol (SNR of 20 dB)

Amplitude Response of Wireless Multipath Channel at 30 dB SNR and 400th OFDM Symbol



(a)

Phase Response of Wireless Multipath Channel at 30 dB SNR and 400th OFDM Symbol



(b)

Fig. 4. (a) Amplitude Response: CSI Estimation for Rayleigh Channel at 400th OFDM Symbol (SNR of 30 dB), (b) Phase Response: CSI Estimation for Rayleigh Channel at 400th OFDM Symbol (SNR of 30 dB)

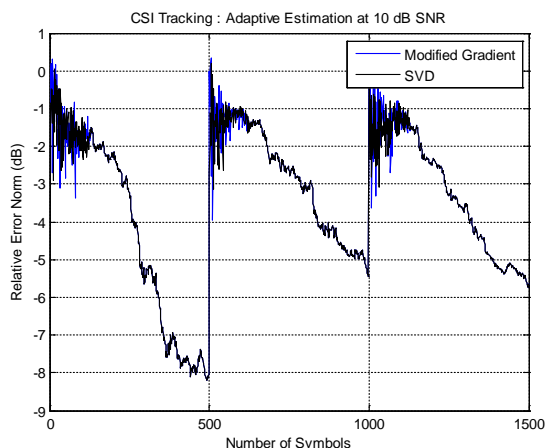


Fig. 5. CSI Tracking of Rayleigh Channel at SNR of 10 dB.

Similarly at the higher SNR value of 20 dB (Fig. 6), the Relative Error Norm shows decreasing trend (as low as -16 dB).

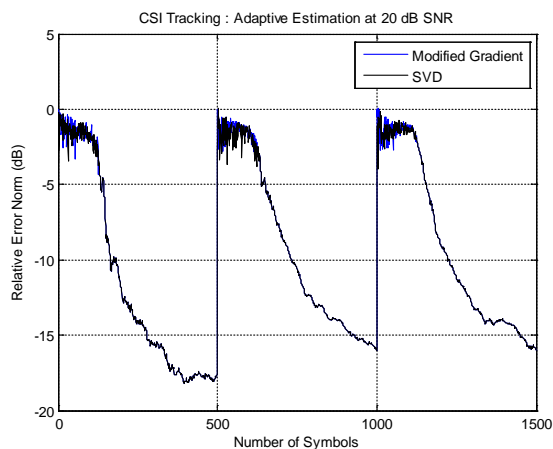


Fig. 6. CSI Tracking of Rayleigh Channel at SNR of 20 dB.

The results of Fig. 7 reveal that for a channel power level (SNR of 30 dB), the Relative Error Norm is as low as -22 dB. As the power level increases, the difference in the Relative Error Norm continuously decreases leading to very good agreement between the results of direct SVD and the modified Gradient method. This substantiates the ability of modified Gradient algorithms to accurately estimate the CSI of the wireless multipath channel at a lower computational cost.

Fig. 8 presents the comparison of the Mean Square Estimate (MSE) of CSI estimation performed through Modified Gradient algorithm and with that of Cramer Rao Lower Bound (CRLB). The subspace-based techniques which are blind in nature are formulated to perform the estimation of CSI without the knowledge of complete information. The proposed modified Gradient algorithm compares favorably with CRLB at high SNR. At SNR of about 15 dB and above, the modified Gradient algorithm requires about 2 to 3 dB additional power gain to attain the limits of CRLB. Indeed, it is

exhibiting a good performance in spite of complete blind operation.

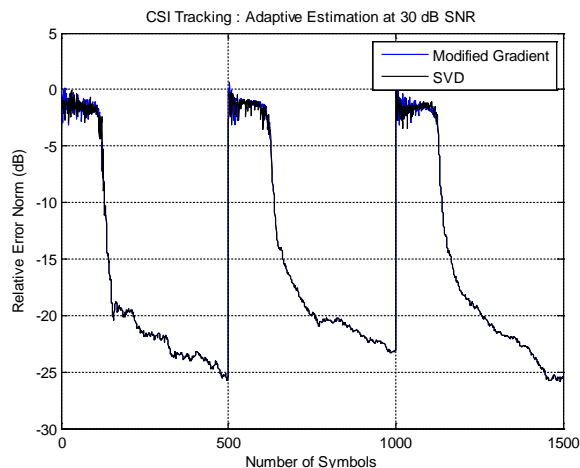


Fig. 7. CSI Tracking of Rayleigh Channel at SNR of 30 dB.

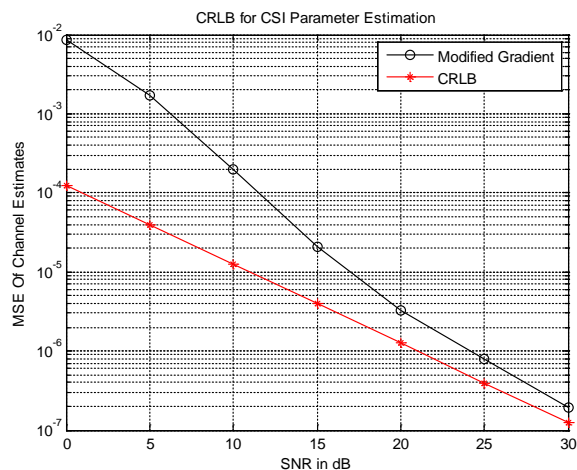


Figure 8: CRLB Comparison.

VIII. CONCLUSION

This paper presents a modified Gradient based method to directly compute the noise subspace iteratively from the received OFDM symbols to estimate CSI. The proposed method enables direct computation of noise subspace using the inverse of the autocorrelation matrix of the received OFDM symbols. This paper adopts a matrix inversion lemma to overcome the heavy computational efforts in the direct inversion of an autocorrelation matrix. This paper also introduced two schemes of modified Gradient based on whether the underlying input to the algorithm is a vector or matrix. In the case of a vector input, the modified Gradient algorithm uses rank one update to calculate noise subspace recursively. For the matrix input, modified Gradient algorithm uses full rank update. The validity, efficacy and the accuracy of the proposed modified Gradient algorithm have been substantiated through a relative comparison of the results with the conventional SVD algorithm, which is in wide use in

estimation of the subspaces. The results of performance analysis obtained through modified Gradient algorithm show satisfactory correlation with the results of SVD, even though the computational complexity involved in modified Gradient method is relatively less. This enables to adopt the noise subspace-based CSI estimation in realistic scenario of OFDM system. The reduced computation complexity in the estimation of the noise subspace estimation by the proposed modified Gradient can be of potential utility for the use of a subspace-based technique in the estimation of CSI for coherent demodulation in OFDM systems. Through simulation studies, this paper also has illustrated the ability of the blind CSI estimator in tracking the changes in the wireless channel state at various time instants.

The focus of this paper is on CSI estimation assuming the presence of perfect carrier frequency synchronization. However, the joint CSI and CFO estimation without the assumption of perfect carrier frequency synchronization will be of practical relevance from the performance perspective of the OFDM system. The joint CFO-CSI estimators based on the noise subspace technique is a topic of research interest of the authors.

REFERENCES

- [1] R. van Nee and R. Prasad. OFDM for Wireless Multimedia Communications (Artech House Publishers-2000).
- [2] Srinu Pyla, K. Padma Raju, N. Balasubrahmanyam, Performance Analysis of OFDM System Using Pilots, Coding Bounds and MAP Decoder for Next Generation Applications, (2017) International Journal on Communications Antenna and Propagation (IRECAP), 7(5), pp. 364-369.
- [3] Zeng Hu1 Jing Yang2 Pengfei Guo3 Qiang Li4, Orthogonal frequency division multiplexing with cascade index modulation, IET Commun. 2021 pp 1–14.
- [4] Raed S. M. Daraghma, A Comparative Study of Wireless Sensor Network Using Cooperative Protocol,(2020) International Journal on Communications Antenna and Propagation (IRECAP), 10(3).
- [5] Budi Prasetya, Adit Kurniawan, Iskandar Iskandar, Arfianto Fahmi,, The Effect of Feedback Delay on the Performance of Closed-Loop Rotate Modulations on OFDM/OFDMA Systems, (2020) International Journal on Communications Antenna and Propagation (IRECAP), 10(4), pp. 230-239.
- [6] Chowdhury, M.Z., Shahjalal, M., Ahmed, S., et al.: 6G wireless communication systems: applications, requirements, technologies, challenges, and research directions, (2020) IEEE Open J. Commun. Soc. 1, pp. 957–975.
- [7] Dua'a Al-Lafi, Omar Banimelhem, Mohammad Shurman, Eyad Taqieddin, Salim Alkhalwaldeh, Pilot Contamination Mitigation in Massive Multi-Input Multi-Output (MIMO) System, (2020) International Journal on Communications Antenna and Propagation (IRECAP), 10(6), pp. 377-38.
- [8] Coleri, S., Ergen, M., Puri, A., and Bahai, A., Channel Estimation Techniques Based on Pilot Arrangement in OFDM Systems, IEEE Transactions on Broadcasting, Vol. 48, Sept. 2002. pp. 223–229.
- [9] S. Coleri, M. Ergen, A. Puri, and et al, A Study of Channel Estimation in OFDM Systems, IEEE 56th Vehicular Technology Conference, Vol.2, 2002, pp. 894-898.
- [10] M. Morelli and U. Mengali, A Comparison of Pilot-Aided Channel Estimation Methods for OFDM Systems, IEEE Transactions on Signal Processing, Vol.49, No.12, 2001, pp. 3065-3073.
- [11] S. Zhou and G. B. Giannakis, "Finite-Alphabet Based Channel Estimation for OFDM and Related Multicarrier Systems," IEEE Trans. Commun., Vol.49, pp. 1402-1414, Aug. 2001.
- [12] A. P. Petropulu, R. Zhang, and R. Lin, "Blind OFDM Channel Estimation Through Simple Linear Precoding," IEEE Trans. on Wireless Communications, Vol. 3, no. 2, pp. 647-655, Mar. 2004.
- [13] C.-Y. Li and S. Roy, "Subspace Based Blind Channel Estimation for OFDM by Exploiting Virtual Carriers," IEEE Globecom 2001, San Antonio, TX, Nov. 2001.
- [14] X.G. Doukopoulos and G.V. Moustakides, "Blind Adaptive Channel Estimation in OFDM Systems," IEEE Transactions on Wireless Communications, Vol. 5, no. 7, pp. 1716-1725, July 2006.
- [15] Tuan Duong Nguyen and Isao Yamada, "A Unified Convergence Analysis of Normalized PAST Algorithms for Estimating Principal and Minor Components", Signal Processing, Vol. 93, pp. 176, 2013.
- [16] Yang, B., Projection Approximation Subspace Tracking, IEEE Trans. SP, SP-43(1), 95–107, Jan.1995.
- [17] John G. Proakis, and Dimitris G. Manolakis "Digital Signal Processing", Pearson Prentice Hall", 2007.
- [18] Saravanan Subramanian and Govind R. Kadambi, "Modified Bi-SVD and Modified Gradient Algorithms for Noise Subspace Estimation with Full Rank Update for Blind CFO Estimator in OFDM Systems" International Journal on Communications Antenna and Propagation, Accepted for Publication, (Paper ID 21862, April 2022).
- [19] G. H. Golub and C. F. , Matrix Computations. Baltimore: John Hopkins University Press. (3rd edition, 1996).
- [20] R. O. Schmid, Multiple Emitter Location and Signal Parameter Estimation, IEEE Trans. Antennas and Propagation, vol.34, pp. 276 – 280, March 1986.
- [21] R. Roy and T. Kailath, ESPRIT –Estimation of Signal Parameters via Rotation Invariance Techniques, IEEE Trans. Acoust., Speech, Signal Proc., vol. 17, no. 7, July 1989.

COVID-19: Challenges and Opportunities in the Online University Education

Irena Valova, Tsvetelina Mladenova

Department of Computer Systems and Technologies
University of Ruse, Ruse, 7017
Bulgaria

Abstract—The COVID-19 pandemic had a very severe impact on the education both in schools and in universities. In the span of several weeks, educators around the world had to transform completely the teaching method and students had to adapt to the new form of learning. The following article reviews the opinions of university students based on three different studies – one before the pandemic and the distance learning, one in the middle of it and one in the end of the distance learning. The goal is to see how students' thinking and perceptions of online learning has changed over the last three years as a result of different conditions.

Keywords—*e-Learning; online learning; students' attitude to e-learning; pandemic outbreak; COVID-19*

I. INTRODUCTION

Undoubtedly, in the last two years, the COVID-19 pandemic has been decisive in the lives of people around the world and has greatly changed their habits and daily lives. The education sector is one of the key sectors that have borne much of the burden of this pandemic. Hospitals, doctors and medical staff were invariably under the greatest strain, as they met directly with the illness. In addition, the COVID-19 pandemic had a very severe impact on education. The Government closed schools and universities to prevent the spread of the infection. This closure was not expected by anyone and was unprecedented, so both students and teachers were not at all prepared for it. Within two weeks, the teaching had to be transferred entirely to the electronic environment, online. These conditions forced the teachers to prepare their lectures and teaching materials in a completely new way. Students should look at e-learning not as a supplement to the standard learning, but as the main and only way. Since this has never happened to neither lecturers, nor students before - both sides faced many challenges and overcame many problems together.

II. STATE AND RELEVANCE OF THE PROBLEM

Before the spring of 2020, e-learning was seen as an object of research and an opportunity to complement standard education in schools and universities, but since that spring online learning was introduced as a means of ensuring continuing education. The pros and cons of online learning and the comparison of the results of standard and online learning or standard and blended learning [3, 4, 5] are mainly examined before the pandemic, while online learning is the only option after the pandemic and research is addressed mainly to its refinement or improvement [6, 7, 8]. Online learning is a convenient form of distance learning that has developed since

2000. Initially, to provide access to teaching materials and training for students who are far from the place of the school or university, for those who are professionally engaged and cannot afford to attend standard university courses. This form of learning gives access to training and materials to a wide range of people, regardless of their age and previous experience or profession [1]. In addition, education is generally expensive and offering online courses at a lower cost makes them much more accessible to a wider range of learners. Anyone who has access to the Internet and an interest in a field has access to materials from top universities and can study and develop for free or at a relatively low cost [2]. Last but not least, the advantage of online courses is that they are available at a time convenient for the learner. They can watch, listen to or read them as many times as they want.

In order for online learning to be successful, the environment or the learning management system (LMS) that will be used plays a very important role. Before 2020, most of the courses were offered on popular platforms for sharing audio and video materials, the universities themselves used LMS systems [11, 12, 13] or teachers supplemented the systems and communication with students using social networks [9, 10, 13]. After the announcement of the 2020 pandemic and the transition to full online learning, it was necessary to improve and adapt LMS systems to the new conditions very quickly. It was no longer enough for students to have access to structured materials - lectures, exercises, homework, as the LMS had to allow direct communication in real time and the opportunity for direct conversations and meetings [14, 15]. An analysis of the impact of the pandemic on the development of this type of system is described in [16]. Before the pandemic, our university used LMS, which was more of a file management system (file manager) with materials for students in various disciplines in PDF or PPT formats. Therefore, the university management had to make a choice promptly and decide to introduce another system, with more opportunities and, above all, the possibility of synchronous online learning.

III. STUDY, METHOD, PARTICIPANTS, CONDITIONS AND DURATION OF THE RESEARCH

With the help of Google Forms, we collected the opinions of the students from the department of Computer systems and technologies in the University of Ruse, Bulgaria, regarding their opinion about online learning. Three studies have been conducted - one before the pandemic [18], the second one at

the beginning of the pandemic [17] and the third one recently at the end of the distance learning. Our goal was to see how students' thinking and perceptions of online learning has changed over the last three years as a result of different conditions.

A few months before the COVID-19 pandemic, without even suspecting it, we wanted to see what the students thought about the materials provided by the lecturer. How, in what form and whether there is a need to have access to them, do they think it makes sense to combine traditional with online learning. This questionnaire was completed by 201 participants in the study. It was distributed publicly and filled not only by our current students, but also by former ones, with the idea to see different points of view.

At the beginning of the COVID-19 period (the first online semester for them), we tried to assess students' attitudes and sense of learning during the pandemic. Number of students participated were 109, average age being 22 years. For some of the participants in the survey, this was the only semester online, and for others - this is the second semester of learning and they had no real experience in normal university education.

Our latest study involved 75 students with an average age of 22, mostly men. They studied 4 semesters online, they were also online at the beginning of the current semester and have been in-person for several weeks now. Some of them have been entirely online since the beginning of their university studies and have no experience with standard academic lecturing at the university. Some of these students (about 50%) also participated in the first study.

In Bulgaria, schools were one of the first and very quick to return to normal education, starting with the youngest. Universities had the opportunity to decide what form of education to use independently and at our university we had 2 trials in 2-3 weeks for in-person lecturing and education but came back to online again. We hope that the return to the normal form of study this semester will last at least until its end, if not permanently.

After the two surveys, we wanted to see what the students thought and what their experience of those two years was after almost entirely online education.

IV. RESULTS ANALYSIS

After the experience gained in online teaching, we can say that due to the compulsory online training the various IT technologies are widely used in the teaching itself, as well as that this teaching has been the engine for active development of these technologies in the last two years.

Advantages of online learning: Students have the opportunity to study and learn the material at their own pace, thus encouraging engagement, independent thinking and working on problems. There were no problems with technology and information technologies in general, because they are studying such courses, but there were those who did not have good internet connection or suitable devices, for example.

In the meantime, lecturers and students had to face some challenges:

- They had to quickly learn to use different LMS systems with the possibility of online connection in real time with the students.
- In a short time, they had to adapt their materials so that they can be used online. And all this without any special training before that.
- It is inevitably a big challenge to face the use of new technologies and various digital devices.
- Uncertainties about students' readiness for learning, social isolation and participation in online classes.
- The need to develop materials in an attractive and appropriate form.
- Developing and using training strategies tailored to the new conditions.
- The transition from face to face to online learning is related to overcoming communication barriers for both parties.
- Measures and methods for overcoming the lack of interest in both sides of the learning process.
- Ways to organize and conduct online exams and presentation of diploma projects.

At first glance, it may be considered that when teaching is in the field of computer systems and technologies, online teaching is not so complicated. There are indeed courses that may be more appropriate and productive for online rather than standard teaching, but there are many courses that are very difficult to adapt for online use - for example, those that require specific hardware, laboratory facilities or equipment.

Before COVID-19, students said that they found classes in the form of exercises and workshops the most useful for them. They are the most difficult to conduct online if they involve any specialized equipment. For courses related to programming and using a popular, unlicensed environment, conducting it online may be even more useful for the students. In these courses, they are forced to install and configure the various software environments needed to conduct practical exercises in the learning process on their own, under the supervision and assistance of the teacher remotely. Some students said that this was one of the very useful aspects of the teaching, because if they were taught in-person, most of them do not install the used environments at all and do nothing at home. 52% of the respondents said that they had installed all the software products that were necessary for their teaching and 72% performed all the tasks set by the lecturers.

During the long period of online learning, the university improved their chosen platform and the hardware resources, while the lecturers got used to it and did not have a need for the university's LMS at all. The students themselves (73.3%) think that the platform used for online learning is the main issue during teaching (Fig. 1).

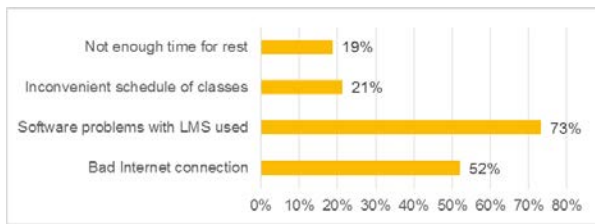


Fig. 1. What are the Main Issues during the Online Learning According to the Students.

Although 89% of students used a computer to participate in lectures and 93% to participate in exercises, there were still students using mobile phones at the end of the pandemic. This means that these students practically only attended, but did not fully participate in the classes. 40% of respondents said that they kept notes, 17.3% that they used specialized recording software (which is not regulated and allowed because teachers are not informed about it) and almost 35% did not need notes because the teachers provided the necessary materials and presentations. 52% attended all the lectures, 28% attended 75% of the lectures and unfortunately there are still students - 13.3% who attended the classes online only because the teachers said it is mandatory to attend and checked attendance. Graphic representation of the attendance of online classes for all respondents, as well as depending on the number of semesters in which they studied online, is shown in Fig. 2.

Given that the surveyed students are studying Computer Science, the use of mobile devices for classes makes virtually no sense. It is assumed that in order to actively participate in the teaching, they must use different programming environments or software products for various engineering research, which is not possible to have on their phones or tablets. Despite the presence of such students who are still using mobile devices, 52% answered that during the exercises they had software installed to perform the tasks and 72% tried to do everything assigned to them by the teacher. However, there are still those who have just joined the online classroom and did not stay in front of the device, did not listen or did not participate in the classes and 19% who have only listened and watched and done nothing. Although a small percentage, this means that about 20% of students have trained as a computer engineer for 4 semesters, but have not tried to program or solve their own tasks. They do not even participate in discussions during the classes.

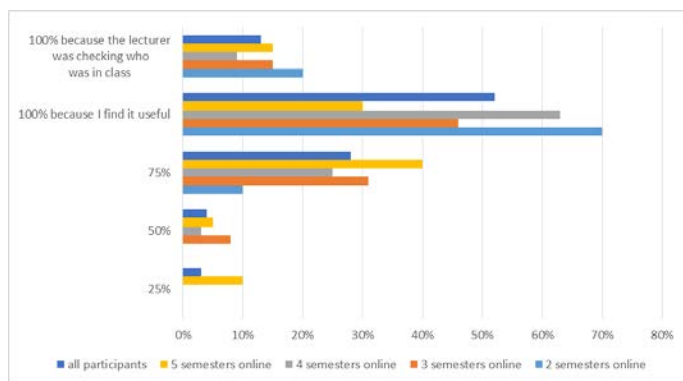


Fig. 2. Graphic Representation of the Attendance of Online Classes Depending on the Number of Semesters in which they Studied Online.

What do students think about their lecturers? Only 9.3% of students think that very few lecturers have provided materials, 40% thinks most teachers have had and have provided materials and 50.7% say that all teachers have provided their materials. The differences probably come from the different courses, as in the first 2 semesters of their education they study only basic and general courses: mathematics, physics, foreign languages, etc. which are not so suitable for providing materials and online learning. From the third semester onwards, they are taught mainly by the specialized department and the courses are more appropriate for online teaching. 56% answered that by studying online they were able to learn and understand the material better because they were provided with materials by the teacher and the teachers themselves spent more time and attention and answered additional questions and organized online consultations if necessary.

Students are almost equally divided in their assessment of workload during online learning. 53.4% of all participants think that it is not burdensome for them since 34.7% of them think that they can just start their online classroom and do other things while 18.7% definitely do not find this form of training stressful and work loading.

For the other half of the participants, this form of training was more stressful since for 33% of them it was more difficult due to the lack or limitation of social contacts with other students. For 21% the workload felt hard due to longer duration, and for 16% it was stressful because they had to work alone, while in face to face education they work in teams and they are not active during classes.

Unlike the traditional way of teaching, where students use laboratories and computer rooms with installed software environments and applications with no commitment to install and configure, online teaching requires additional commitments from the students to install and configure everything on their computers. The students themselves shared that for some of them these were the first encounters with this type of problem. Although the lecturers helped, this process was long and complicated for some students, and some did not manage to cope, mostly due to lack of interest on their part. This moment of online training was burdensome for lecturers as well, because they had to prepare a step-by-step description of the installation itself, and some of them had to find and replace their prepared materials for another environment that is free and does not require licenses. Unfortunately, we did not have opportunities for remote access to the university resources for each of the students. Despite the difficulties for both parties, this part of the learning process and the opportunity for everyone to work independently on their own computer (in traditional learning we do not provide a separate computer for each student, usually 2 students are working together on one computer) were very useful. The students were able to try to solve their tasks on their own, to share their screen with the teacher and others and to get quick and adequate answers to their questions. They saw that they could do much more on their own than they expected, and that made them more confident and more willing to work. 25.3% believe that they have learned more online than they would have learned in-person, for 54.7% this way of learning was quite acceptable given the circumstances, 9.3% cannot judge. Unfortunately,

there are those who think that they have not learned anything more and even that was a complete waste of time. For 65.3%, online learning has helped them become more confident and independent in solving various practical tasks, and 34.7% do not think that there has been an impact.

The answers to the question about the understanding of the taught material, shown in Fig. 3, are optimistic. It can be seen that for 56% of the respondents the assimilation and understanding of the material was easier, because they had materials provided by the teachers and the latter spent more time for additional explanations of the material or to discuss with students' various problems. 19% answered that they spent a lot more effort and time and thanks to this they were able to understand and learn the material. A quarter of them failed to understand and master the material taught and believe that the teachers did not devote the necessary time and effort or that the problems with LMS did not allow them to cope.

As can be seen from the graph in Fig. 4, the best part of the online teaching according to the students was that they were provided with all the materials and did not have to take notes, write or look for specific books or materials to prepare for classes or for the exam. It is impressive as well that according to 44% the good thing about online learning were the easy exams.

During the pandemic, not only teaching but also exams had to be conducted online. We had written rules of procedure for online exams, most teachers tried to adapt to the conditions and took advantage of the opportunities provided by Google to create online tests, but there were some that remained on the classic type of exams with writing on selected topics. The system used was quite limited and did not provide opportunities to conduct tests or exams online, so we had to look for other options. Students are generally satisfied with the online exams, but unfortunately admit that they have used unregulated materials to take the exam easily (have copied from their colleagues or from the Internet, used pre-prepared materials or used someone else's help, which is not allowed, according to the rules). 26.7% did not take advantage of the situation, 24% used unregulated materials for all exams, and the rest for at least one or several exams. Fig. 5 shows how many of the exams students have taken using unregulated materials, according to the number of semesters taught online (2, 3, 4 or 5).

An interesting fact is that students prefer to take exams in the form of an online test (85%). They don't like exams that involve writing on some questions and solving problems (Fig. 6).

50.7% said that during the online teaching they lacked communication with other students, 42.7% missed on the environment and conditions of study at the university, and 26.7% missed on direct communication with lecturers and professors. For communication with each other they mostly used social networks, such as Facebook - messenger and Facebook groups and Discord. It is noteworthy that information about the learning process and related messages

were received not only through their university e-mail addresses (86.7% indicated this option) but also from social networks, mainly Facebook pages (56%) and groups in various courses (82,7%).

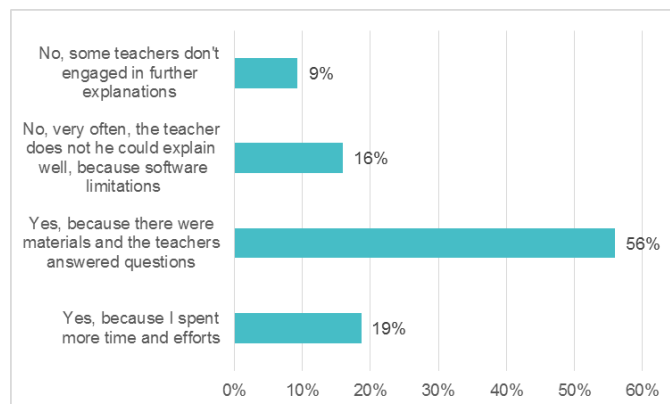


Fig. 3. Were you Able to Understand the Material Taught Better?

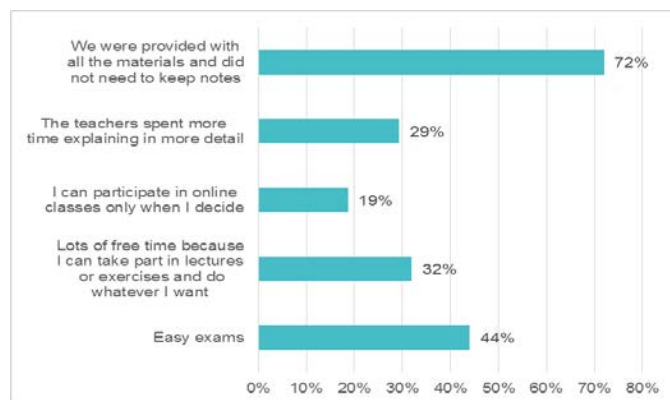


Fig. 4. What was the Best thing about Online Learning?

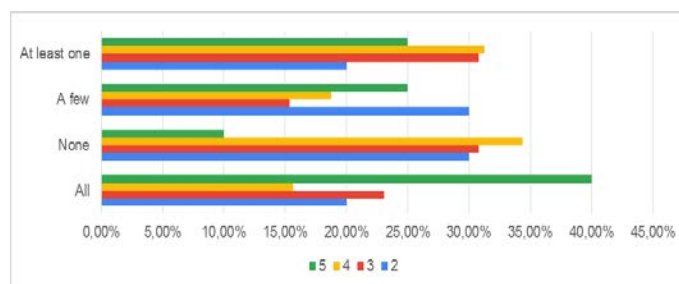


Fig. 5. How Often and Whether Students use Unregulated materials during the Online Exams.

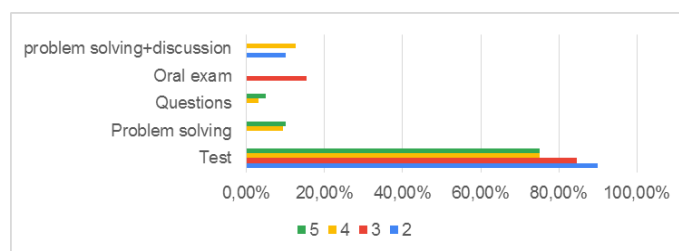


Fig. 6. Preferable Exam Type According to the Students' Answers.

During the first few months of the pandemic most lecturers were using Facebook groups to organize their online teaching. This method proved quite useful for communication with the students, instead of exchanging emails. One of the reasons for this is that in our university, we do not store information about which students are taking each course and no record of their university email address. Even now, when we have gone back to in-person teaching, the Facebook groups are still used to exchange information and for discussions.

Communication between the students has been a useful channel of information (75%), as well as communication with the lecturers (55%) (Fig. 7). It is worth noting that despite the online teaching, a positive tendency was that some students would take a leadership role and mediate the information between lecturers and students and aid the teaching process. These leaders, typically one or two, were responsible for collecting the materials and messages from the different courses, reminding and organizing their fellow students and quite often to motivate them to be more active in the teaching process.

During the COVID-19 pandemic, although isolated in their homes, students kept in touch with each other (Fig. 8). Messenger was cited as the most popular means of communication (96%), followed by Discord. Young people prefer online communications to telephone calls.

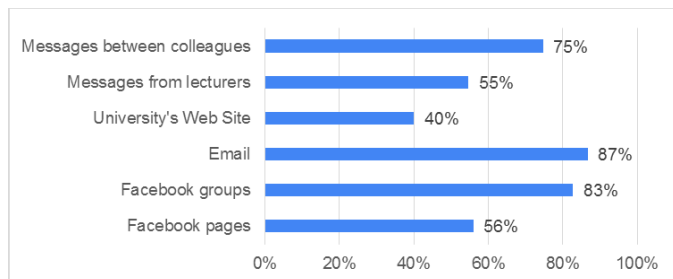


Fig. 7. How and from Where the Students Received Information about the Learning Process?

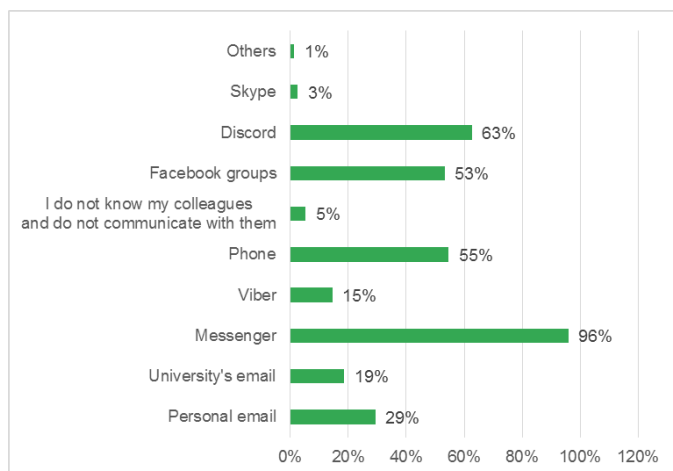


Fig. 8. How you Communicated with each other during Online Learning.

The number of students has significantly dropped in the last two years while the teaching has been almost entirely completed remotely. Each year there are 70-75 new students on average, while at the moment the students are: 1st year - 37, 2nd year - 36, 3rd year - 22 and 4th year - 34. The drop in students is most noticeable in third year and this is due to the fact that these students have only had 1 semester of in-person teaching, did not expect that the teaching would transform to online learning when they enrolled and after 1 semester in university they were not at all used to the different method of teaching compared to high school. They were the most affected by the sudden change in teaching. However, undeniably there has never been such a drop in student numbers within our department. Unfortunately, we are unable to speak directly to the students and we do not have clear information why they chose to drop out. It can only be speculated that these students were forced to go back to their hometowns and families due to the pandemic and were not interested in finishing their education. When asked if they would continue their education if the teaching was entirely online, 86.7% say they would definitely continue or would continue as part-time students. The responses are positive since only 8% would not want to continue their education online, but expect and would go back if the teaching was in-person (Fig. 9).



Fig. 9. Would you Continue your Education if you were Online Again?

V. CONCLUSIONS

Despite all the negatives of social isolation due to COVID-19 measures and restrictions, there are some positive moments from online education during the last 5 semesters.

Students have become more confident and independent, they have to and manage to solve problems and tasks of the learning process, which in normal conditions in standard education do not arise before them - installing and configuring software environments and products and working independently with them.

Teachers and professors (for the most part) have prepared and provided students with much more materials and resources in the courses they teach. They also manage to spend more time consulting and discussing with students, albeit online.

Students feel much freer to ask questions and discuss learning materials. They admit that online exams are easier, they use unregulated materials and they have even started to prefer online forms of exams. They recommended in the survey that even under normal conditions, lectures and exams should be held online.

Perhaps with a more developed online LMS than the one used by our university, it would be more convenient for lecturers to give online lectures. At the moment, this is not appropriate, because you never know who is actually in class and whether the lecturer is not "teaching to themselves". In all cases, online learning is much more stressful, time consuming and difficult for lecturers (especially for those who have not had prepared materials in an appropriate form for online learning).

REFERENCES

- [1] G. Sherron and J. Boettcher, "Distance learning: The shift to interactivity", CO:CAUSE, vol. 17, January, 1997.
- [2] C. Stöhr, C. Demazière and T. Adawi, "The polarizing effect of the online flipped classroom", *Computer&Education*, vol. 147, April, 2020
- [3] Desai, M. S., Hart, J., & Richards, T. C. (2008). E-learning: Paradigm shift in education. *Education*, 129(2).
- [4] Xu, D., & Jaggars, S. S. (2013). The impact of online learning on students' course outcomes: Evidence from a large community and technical college system. *Economics of Education Review*, 37, 46-57.
- [5] Gray, J. A., & DiLoreto, M. (2016). The effects of student engagement, student satisfaction, and perceived learning in online learning environments. *International Journal of Educational Leadership Preparation*, 11(1), n1.
- [6] Adedoyin, O. B., & Soykan, E. (2020). Covid-19 pandemic and online learning: the challenges and opportunities. *Interactive learning environments*, 1-13.
- [7] Mukhtar, K., Javed, K., Arooj, M., & Sethi, A. (2020). Advantages, Limitations and Recommendations for online learning during COVID-19 pandemic era. *Pakistan journal of medical sciences*, 36(COVID19-S4), S27.
- [8] Heng, K., & Sol, K. (2021). Online learning during COVID-19: Key challenges and suggestions to enhance effectiveness. *Cambodian Journal of Educational Research*, 1(1), 3-16.
- [9] Valova, I. (2015). Facebook or learning management system. In *International Conference on e-Learning* (Vol. 15, p. 237).
- [10] Valova, I., & Marinov, M. (2019). Facebook as a tool aiding university education-whether it is possible and useful. *tem Journal*, 8(2), 670.
- [11] Black, E. W., Beck, D., Dawson, K., Jinks, S., & DiPietro, M. (2007). Considering implementation and use in the adoption of an LMS in online and blended learning environments. *TechTrends*, 51(2), 35-53.
- [12] Zheng, Y., Wang, J., Doll, W., Deng, X., & Williams, M. (2018). The impact of organisational support, technical support, and self-efficacy on faculty perceived benefits of using learning management system. *Behaviour & Information Technology*, 37(4), 311-319.
- [13] Wang, Q., Woo, H. L., Quek, C. L., Yang, Y., & Liu, M. (2012). Using the Facebook group as a learning management system: An exploratory study. *British journal of educational technology*, 43(3), 428-438.
- [14] Mohammadi, M. K., Mohibbi, A. A., & Hedayati, M. H. (2021). Investigating the challenges and factors influencing the use of the learning management system during the Covid-19 pandemic in Afghanistan. *Education and Information Technologies*, 26(5), 5165-5198.
- [15] Raza, S. A., Qazi, W., Khan, K. A., & Salam, J. (2021). Social isolation and acceptance of the learning management system (LMS) in the time of COVID-19 pandemic: an expansion of the UTAUT model. *Journal of Educational Computing Research*, 59(2), 183-208.
- [16] Georges, J., & Magdi, D. (2022). COVID-19 Pandemic's Impact on E-learning Platforms: A Survey. In *Digital Transformation Technology* (pp. 253-264). Springer, Singapore.
- [17] Mladenova, T., Kalmukov, Y., & Valova, I. (2020). Covid 19–A major cause of digital transformation in education or just an evaluation test. *TEM journal*, 9(3), 1163.
- [18] Mladenova, T., Kalmukov, Y., & Valova, I. (2019). Research on Students' Opinion on the Method of Presenting Teaching Materials. In *2021 44th International Convention on Information, Communication and Electronic Technology (MIPRO)* (pp. 810-814). IEEE.

Multi-modal Brain MR Image Registration using A Novel Local Binary Descriptor based on Statistical Approach

Thuvanan Borvornvitchotikarn

Center for Information Technology and Communication Services
University of Phayao, Phayao, Thailand

Abstract—Medical image registration (MIR) has played an important role in medical image processing during the last decade. Its main objective is to integrate information inherent in two images, from different scanning sources, of the same object for guiding medical treatments such as diagnostic, surgery and therapy. A challenging task of MIR arises from the complex relationships of image intensities between the two images. Its performance is primarily depending on a chosen similarity measure technique. In this work, a statistical local binary descriptor (SLBD) is proposed as novel local descriptor of similarity measure, which is simple for computation and can handle Multi-modal registration more effectively. The proposed SLBD employs two statistical values, i.e., the mean and the standard deviation, of all intensities within the image patch for its computation. Finally, these experimental results have shown that SLBD outperforms other descriptors in terms of registration accuracy. In addition, SLBD has demonstrated that SLBD is robust to different modalities.

Keywords—Local binary descriptor; multi-modal image registration; statistical approach; medical image registration; similarity measure

I. INTRODUCTION

Nowadays, medical imaging techniques (MIT) have been continuously improved, and this leads to the advancement in computer-aided surgery and radiotherapy (CAS). In general, in the procedure of CAS, medical practitioners need to utilize medical images produced from different scanning protocols [1] to perform their works. The medical images from different sources can provide different kinds of information for them. For instance, an MRI image provides functional information whereas anatomical information is from an X-Ray image. Multi-modal image registration (MIR) is the process of finding an optimal amalgamation of both corresponding anatomical and/ or functional structures of the two images [2]. Therefore, MIR can help medical practitioners to perform more effective diagnosis of a disease. Basically, MIR has three main components: 1) the similarity measure used to evaluate the similarity between images that are to be registered, 2) the transformation model deforming the moving image to the fixed image, 3) the optimization method determining the optimal parameter for the transformation to achieve the best similarity [3]. Applications of MIR in medical image processing have faces more challenges due to the complex relationships of intensities between multi-modal

images. One major challenge task is how to improve the similarity measure between the two multi-modal medical images in order to achieve more accurate and efficient registration [4, 5].

In the last decade, Mutual information (MI) is an important concept relevant to several theorems of information theory and most widely studied as similarity measures. Particularly, it has been extensively and successfully used to measure the intensity relationships in image processing [6] [7]. During the last decade, many researchers have enhanced the accuracy of image registration based on MI, such as Tsallis and Renyi's entropies [8], Jensen- Renyi's entropy [9], hybrid EMPCA-Scott approach [10], and self-similarity α -MI (SeSaMI) [11]. However, the notion of MI alone still has a well-known drawback, i.e., it ignores spatial information [12]. For medical image registration, spatial information is important because it provides the medical information. Therefore, many researchers have enhanced MI to handle spatial information, such as second-order MI (SMI) [13], Regional MI (RMI) [14], PCA Regional MI (PRMI) [15], Conditional MI (CMI) [16]. However, Heinrich et al. [17] have noticed that these approaches are still difficult to find an accurate correspondence between different modality images. Therefore, they proposed a method, called MIND, based on neighbourhood information. MIND uses the sum of squared differences (SSD) to estimate the similarity of two images. It has higher accuracy than several methods. However, MIND is highly subject to the central patch. This limitation affects the noise robustness [18]. Hence, they introduced a so-called self-similarity context (SSC) to improve the noise robustness of MIND. SSC avoids the central patch and uses pairs of patches within six-neighbourhood [18].

Local binary pattern (LBP) is one of the most effective and well-known approaches used in texture classification [19]. Trichet and Bremond [20] introduced a novel pedestrian detection technique by using a 12-valued filter representation based on LBP. It can improve filtering performance, which leads to a sharper feature. Hong et al. [21] proposed the LBP-Top for facial expression recognition to reduce the demand of loops and the computational cost. Weber Local binary pattern (WLBP) was presented by Liu et al [22]. It is a combination of Weber local descriptor and LBP and is robust to many challenges. The non-local mean local binary descriptor (NLM-LBD) was presented in [23]. By taking advantage of structural information, he NLM-LBD can improve the NLM method in

terms of both computation time and quality for real-time denoising applications. DRLBP [24] was an enhancement of LBP for rotation robustness. These approaches have high computation speeds for registration, but some structural information may be lost.

Recently, Jiang et al. [25] proposed miLBP descriptor that can improve robustness to noise, intensity and non-uniformity of medical image processing. Its performance is better than recent methods such as SeSaMI [11], CoCoMI [26], and SSC [18]. In addition, Lu et al. [27] introduced a registration technique by combining local features and geometric invariants. Shen et al. [28] enhanced MI with a hybrid optimization technique based on Powell's method and cuckoo search. Yonghong et al. [29] applied an improved particle swarm optimization (PSO) to an image registration algorithm based on MI. The value of MI of the registered image is calculated and is used in the fitness function of PSO. Bai et al. [30] presented Multi-modal CT rigid MIR with regional weighted mutual information (RWMI), which is robust to large rotation and translation. However, RWMI is sensitive to registration with very small overlap and small intensity variance. Furthermore, Borvornvitchotikarn and Kurutach [31] have improved miLBP, which combines miLBP and DRLBP. This method achieves the best results for registration with rotational transformations. The other work of authors also enhanced the miLBP, which adopts the mean and standard deviation of the image patch for adaptive threshold and uses the sorting operation for sorting the pixels within image patch. Therefore, it could provide terms of robustness in modality-independent and rotation-invariant descriptor (miRID) [32]. Yang et al. [33] have proposed MIR based on image segmentation and symmetric self-similarity. This method uses BCFCM to segment multi-modal medical images and extracts target regions in medical images.

However, due to limitations of existing approaches, the spatial information may be lost from the computation of those descriptors. Hence, the key reason for the proposed SLBD approach is that it makes the multi-modal image similarity measure remain the spatial information of the regions of interest.

The contributions of this work are summarized as follows:

- This work points out and proposes a novel approach to measure the similarity or dissimilarity between the intensities of pixels in the regions of interest on multi-modal medical images. The proposed similarity measure is suitable to handle the complexity of intensity relationships between two modalities of images more effectively. In addition, it can avoid the weakness of the traditional LBD, where image artefacts within the central patch directly affect its performance. Moreover, this method still retains the structural information potentially, which can estimate a direct patch-to-patch mapping between image multi-modality. This proposed approach will be called SLBD (for statistical local binary descriptor) and will be described in detail in Section III.

- The proposed similarity measure is a complementary method to previous LBD-based methods such as miLBP and miRID.

This paper is organized as follows. Section II presents the background. Section III describes the proposed method. The experimentations and results present in Section IV. The discussions and conclusion will be discussed in Sections V and VI, respectively.

II. BACKGROUND CONCEPTS

A. Image Registration

MIR is a process of transforming a moving image to optimally align with a fixed or target image. Its goal is to maximize the similarity or minimize the dissimilarity between the two registered images. To accomplish the task, MIR needs to have three main components: a similarity metric, a transformation model, and an optimization model. The similarity metric is a measure of how well the two images match. The transformation model is used to transform the moving image to match the fixed image. The optimization model is to find a variation of parameters in the transformation model to maximize the matching criteria [34]. To formally formulate the notion, registration T' of a moving image I_m and a fixed image I_f is defined by (1),

$$T' = \arg \min_T D(I_f, T(I_m)) \quad (1)$$

where $D(I_f, T(I_m))$ is a dissimilarity measure which determines the degree of alignment between I_f and $T(I_m)$ and T denotes a deformable transformation. In (1), T' is to find the optimal transformation T that provides the minimum value of D [12].

B. Similarity Measure based on Local Binary Pattern

The standard LBP was introduced by Ojala et al. [35]. It is a simple principle of the texture classification. For the patch size of 3×3 , the binary result gives 8-bit integer codes. The LBP operator can be defined as follows:

$$LBP = \sum_{n=1}^N s(g_n - g_c) \cdot 2^{n-1}, \text{ with} \quad (2)$$

$$s(x) = \begin{cases} 1, & x \geq Th \\ 0, & x < Th \end{cases} \quad (3)$$

where n is the position of a neighbouring pixel, N denotes the number of the neighbouring pixels, g_n is the intensity of the neighbouring pixel at the position n , g_c is the intensity of the central pixel, and Th is the threshold value. In the area of medical image analysis, LBP-based similarity metrics, such as miLBP [25] and Hybrid LBP (HLBP) [36], could provide higher accuracy in registration results. HLBP can cope well with the variation of the local intensity on the 4D CT lung registration, which includes a median binary pattern and a generalised central-symmetric LBP. The miLBP is another LBP-based method which can provide the highest accuracy on the registration of CT-MR images with different modalities from Brainweb [37] and RIRE [38] datasets. Moreover, miLBP adopts the technique of the adaptive threshold using the standard deviation δ of the intensity values of the

neighbouring pixels. The miLBP is defined by (4), (5) [25]. The concept of miLBP can be illustrated in Fig. 1.

$$miLBP = \sum_{n=1}^N s(|g_n - g_c|) \cdot 2^{n-1}, \text{ with} \quad (4)$$

$$s(|g_n - g_c|) = \begin{cases} 1, & |g_n - g_c| > \delta \\ 0, & |g_n - g_c| \leq \delta \end{cases} \quad (5)$$

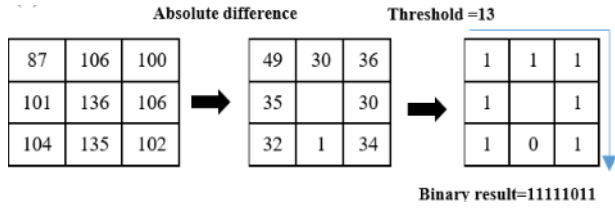


Fig. 1. Illustration of the miLBP Performed on Image Pixels (here: $\delta = 13$).

miRID [32] has the potential to increase the stability of medical image registration to rotation variations. Instead of utilizing the intensity of the center pixel, miRID uses the mean of all intensity values inside the patch to achieve this. In addition, the sorting procedure is conducted on intensity values within the patch to make miRID stable against rotational deformations. The miRID is defined by (5), (6).

$$miRID_i^P = \mathbb{I}_{i=1}^P s(\text{Sort}|g_i - M|), \text{ with} \quad (5)$$

$$s(|g_i - M|) = \begin{cases} 1, & |g_i - M| > \delta \\ 0, & |g_i - M| \leq \delta \end{cases} \quad (6)$$

where $\mathbb{I}_{i=1}^P$ represents the bitcount operation, which counts the number of bits having the value of 1. $|g_i - M|$ denotes the absolute difference of the intensity difference between g_i and M . M represents the mean of intensity of all pixels. *Sort* operation indicates the descending order operation. P denotes the number of the pixels in the patch and δ represents the standard deviation of all pixels.

III. PROPOSED METHOD

This section will present a novel local binary descriptor, which enhances the technique of LBP. This descriptor can prominently handle the complexity of intensity relationships between different modalities. Both LBP and miLBP methods estimate the similarity value based on the use of the central pixel. However, image artifacts within the central patch can affect the performance of the descriptors. Therefore, this method needs to avoid the use of the central pixel in computing the intensity relationships in a descriptor that is to register multi-modal images. To accomplish that, the proposed method adopts the mean m and the standard deviation δ of all intensity values within the patch as the threshold values instead of using the intensity of the central pixel. Evaluating the similarity between two images is formally defined by (7) - (11). The overview of the proposed SLBD is illustrated in Fig. 2.

This work will define the binary pattern $SLBD_i^P$ of the intensities within the region of interest as follows:

$$SLBD_i^P = C_{i=1}^P s(g_i), \text{ with} \quad (7)$$

$$s(g_i) = \begin{cases} 1, & \lambda_{lower} \leq g_i \leq \lambda_{upper} \\ 0, & \text{otherwise} \end{cases} \quad (8)$$

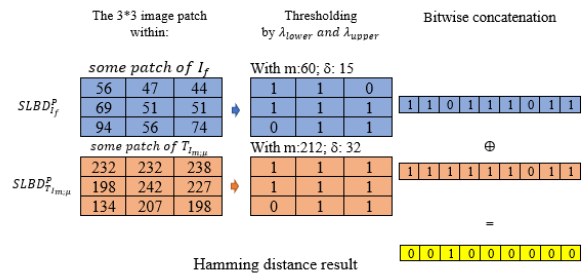


Fig. 2. Overview of the SLBD Concept.

where:

$SLBD_i^P$ is the binary pattern of pixels' intensities within the interesting region of image I .

$C_{i=1}^P$ is the bitwise concatenation operation, where:

P represents the total number of pixels within the image patch.

$i, 1 \leq i \leq P$, is a pixel location in the patch ;

$s(g_i)$ is a binary value assigned to the pixel i based upon the intensity value g_i against the boundary values $(m - \delta)$ and $(m + \delta)$;

m denotes the mean value of the intensities of all pixels within the patch, as defined in (9):

$$m = \frac{1}{P} \sum_{i=1}^P g_i \quad (9)$$

δ denotes the standard deviation of the intensity values of all pixels within the patch, as defined by (10):

$$\delta = \sqrt{\frac{1}{P-1} \sum_{i=1}^P (g_i - m)^2} \quad (10)$$

λ_{lower} and λ_{upper} are the threshold values defined as follows:

$$\lambda_{lower} = (m - \delta);$$

$$\lambda_{upper} = (m + \delta);$$

In this proposed approach, it is assumed that the moving image I_m and the fixed image I_f are of the same size G . Then, the dissimilarity measure $A_{(I_f, T_{I_m; \mu})}$ between the two images can be evaluated by (11). The value of $A_{(I_f, T_{I_m; \mu})}$ is within a range of $[0, 1]$.

$$A_{(I_f, T_{I_m; \mu})} = \frac{1}{G} \text{bitC} \left\{ C_{i=1}^G SLBD_{I_f} \oplus C_{i=1}^G SLBD_{T_{I_m; \mu}} \right\} \quad (11)$$

where:

$SLBD_{I_f}$ and $SLBD_{T_{I_m; \mu}}$ are the binary patterns of image I_m and image I_f .

\oplus denotes Hamming distance operation.

G is the image size.

$T_{I_m; \mu}$ represents a transformation with respect to transformation parameters μ .

The *bitC* function is bit count operation which counts the number of bits having the value of 1.

For solving (1), this experiment will find the optimal transformation using a gradient descent optimization method. where $\nabla A_{(I_f, T_{I_m}; \mu)}$ is derivative of the cost function $A_{(I_f, T_{I_m}; \mu)}$ with respect to the non-rigid transformation parameter μ in (12). The optimization of the cost function is shown in (13). where ϕ_{k+1} is the next position, ϕ_k denotes the current position and s_k represents the step size.

$$\nabla A_{(I_f, T_{I_m}; \mu)} = \frac{\partial A_{(I_f, T_{I_m}; \mu)}}{\partial \mu} \quad (12)$$

$$\phi_{k+1} = \phi_k - s_k \nabla A_{(I_f, T_{I_m}; \mu)} \quad (13)$$

Fig. 3 shows the block diagram illustrating the proposed registration model. Formulas for evaluating the values of some components can be found in (7) - (13). Specifically, the *SLBD* is used to represent the binary pattern of the original fixed image and the transformed moving images. The dissimilarity value between *SLBD* of I_f and *SLBD* of $T_{I_m}; \mu$ is calculated by $A_{(I_f, T_{I_m}; \mu)}$ as defined by (10). To find the optimal transformations, *SLBD* minimizes the dissimilarity values with $A_{(I_f, T_{I_m}; \mu)}$.

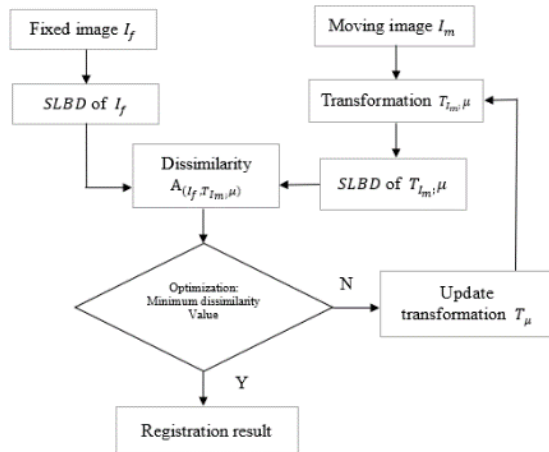


Fig. 3. Block Diagram of the Registration Model.

IV. EXPERIMENTATION AND RESULTS

The previous section has presented *SLBD* as a local similarity descriptor for measuring the dissimilarity of the image patches in MIR. Its advantages are simplicity of computation and effectiveness in dealing with different modalities. This section will investigate the performance, in terms of registration accuracy, of the proposed algorithm in comparison with other approaches: MI [38], SSC [18], miLBP [25], RWMI [30], and miRID [32]. This experiments were configured the image patch size as follows: for the MI and RWMI methods, the image patch with the size of 7 x 7 pixels and 64 bins was used. For the SSC, miLBP, miRID, and *SLBD* methods, an image patch with the size of 3 x 3 pixels was chosen. More details for parameter setting on SSC, miLBP methods can be found in their original works [18] and [25], respectively. These methods were quantitatively assessed

by the mean target registration error (mTRE) [17] and tested on a computer with an Intel® Core™ i7-7700 CPU 3.60 GHz and RAM memory 16.0 GB. *SLBD* is implemented as a local similarity descriptor into non-rigid image registration, which uses Free-form deformation (FFD) with three hierarchical levels of B-spline central point [39].

This experiment carries out registrations of T1-T2, T1-PD, and T2-PD modalities from the BrainWeb dataset [37]. The voxel values are defined at a 1mm. and an image size of 181 x 217 x 181 voxels with 3% noise and 40 % intensity non-uniformity. As the moving images, the 2D 15th slice of a T1-weighted image is shown in both Fig. 4(a) and Fig. 5(a) and the 2D 15th slice of T2-weighted image in Fig. 6(a). In the first experiment, they were rotated within the range of -20°. Fig. 4(b) shows the corresponding T2-weighted image and Fig. 5(b) and Fig. 6(b) show the corresponding PD-weighted images, as the fixed images. The checkerboard images of the registered images using *SLBD* are shown in Fig. 4(c), Fig. 5(c), and Fig. 6(c). The transformations of these registrations are shown in Fig. 4(d), Fig. 5(d), and Fig. 6(d).

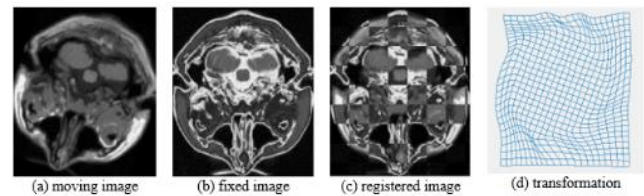


Fig. 4. T1-T2 Registration.

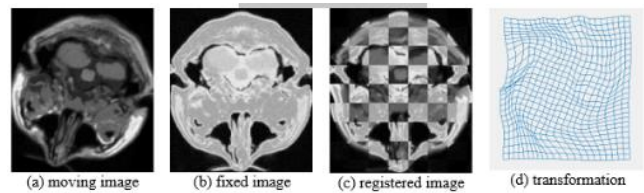


Fig. 5. T1-PD Registration.

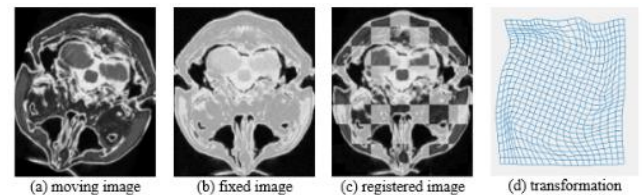


Fig. 6. T2-PD Registration.

Fig. 7(a), (b) show the expansion of the inner contour area indicated by the red circles. The proposed *SLBD* method performs better compared to the miRID method.

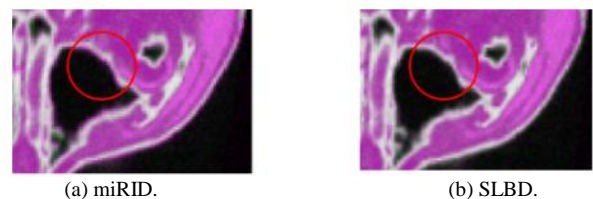


Fig. 7. (a),(b) The Expansion of the Overlapped Inner Contour Area of the Registration Results for the miRID, and *SLBD*.

TABLE I. RESULTS OF MULTI-MODAL NON-RIGID IMAGE REGISTRATION WITH BRAINWEB DATASET

Methods	Modalities			mTRE.
	T1- T2	T1-PD	T2-PD	
MI [38]	2.63	2.88	3.01	2.84
SSC [18]	2.46	2.27	2.47	2.40
miLBP [25]	2.44	2.45	2.35	2.41
RWMI [30]	2.48	2.49	2.51	2.49
miRID [32]	2.35	2.37	2.43	2.38
SLBD	2.12	2.23	2.11	2.15

Table I shows the performance evaluation of T1-T2, T1-PD, and T2-PD registrations in terms of the target registration error (TRE.). It is obvious that the registration errors of SLBD are the lowest, especially in the cases of T1-T2, and T2-PD. SLBD could achieve the best overall registration accuracy (mTRE=2.15). They are a significant improvement compared to miRID (2.38), SSC (2.40), miLBP(2.41), RWMI (2.49), and MI (2.84), respectively. To illustrate the cases, Fig. 4 to 6 show the visual results of the SLBD method experimenting on the T1, T2, and PD-weighted MR images. These resulting images estimated by SLBD are more like the fixed images.

V. DISCUSSIONS

Generally, white matter appears as a bright grey in both T1 and PD and a dark grey in T2. Cerebro-spinal fluid appears as a dark grey in T1, a light grey in T2, and a grey in PD. These are the challenges in the non-rigid image registration with different MR modalities. However, in this experimentation on the registrations of T1-T2, T1-PD, and T2-PD using various approaches, it has been found that the proposed method, SLBD, has the least errors. In comparison, the miLBP [25], RSSD [31], and miRID [32] have the high speeds of MIR and also have the robustness of modality-independent. The miRID [32] could perform the best performance in MIR both rigid and non-rigid registration. However, those descriptors may lose the structural information due to their calculation. For example, miLBP represents the 8-pixels within the image patch to the single value of 0-255 ranked by multiple 2^{n-1} and miRID uses the sorting operation for sorting the pixels in the image patch. The computation of both miLBP and miRID may be possible to lose the spatial information of the regions of interest in the computation of both miLBP and miRID. Unlike, miLBP, RSSD, and miRID, SLBD was easily represented by the pixels within the image patch by an adaptive threshold. Another advantage is that SLBD can maintain the spatial information appropriately. The binary pattern results of SLBD can be estimated by the similarity with the patch-to-patch mapping of the corresponding regions.

VI. CONCLUSION

This paper has presented a novel similarity descriptor, called SLBD, based on a simple statistical concept. It is an enhancement of the local binary descriptor for multi-modal image registration. This experimentation shows that proposed approach outperforms others in terms of accuracy of multi-modal medical image registration. In addition, the proposed method is simpler in its computation. In future work, SLBD

will implement as the loss function of deep convolutional neural networks for estimating the similarity between the ground truth and the prediction.

ACKNOWLEDGMENT

The author would like to thank the editors' and reviewers' work on this paper.

REFERENCES

- [1] Y. Ou, Development and validations of a deformable registration algorithm for medical images: Applications to brain, breast and prostate studies. University of Pennsylvania, 2012.
- [2] K. A. Bachman, "Mutual information-based registration of digitally reconstructed radiographs and electronic portal images," Master's thesis, Applied Mathematics, University of Colorado at Denver, 2005.
- [3] W. R. Crum, T. Hartkens, and D. Hill, "Non-rigid image registration: theory and practice," The British Journal of Radiology, 2014.
- [4] F. Alam, S. U. Rahman, and A. Khalil, "An investigation towards issues and challenges in medical image registration," Journal of Postgraduate Medical Institute (Peshawar-Pakistan), vol. 31, no. 3, 2017.
- [5] F. Alam, S. U. Rahman, S. Ullah, and K. Gulati, "Medical image registration in image guided surgery: Issues, challenges and research opportunities," Biocybernetics and Biomedical Engineering, vol. 38, no. 1, pp. 71-89, 2018.
- [6] A. Sotiras, C. Davatzikos, and N. Paragios, "Deformable medical image registration: A survey," Medical Imaging, IEEE Transactions on, vol. 32, no. 7, pp. 1153-1190, 2013.
- [7] F. Maes, A. Collignon, D. Vandermeulen, G. Marchal, and P. Suetens, "Multimodality image registration by maximization of mutual information," Medical Imaging, IEEE Transactions on, vol. 16, no. 2, pp. 187-198, 1997.
- [8] S. Sahoo, P. K. Nanda, and S. Samant, "Tsallis and Renyi's embedded entropy based mutual information for multimodal image registration," in Computer Vision, Pattern Recognition, Image Processing and Graphics (NCVPRIPG), 2013 Fourth National Conference on, pp. 1-4: 2013.
- [9] Y. He, A. B. Hamza, and H. Krim, "A generalized divergence measure for robust image registration," Signal Processing, IEEE Transactions on, vol. 51, no. 5, pp. 1211-1220, 2003.
- [10] T. Borvornvitchotikarn and W. Kurutach, "A hybrid EMPCA-Scott approach for estimating probability distributions in mutual information," in 2016 International Computer Science and Engineering Conference (ICSEC), pp. 1-5, 2016.
- [11] H. Rivaz, Z. Karimghaloo, and D. L. Collins, "Self-similarity weighted mutual information: A new nonrigid image registration metric," Medical image analysis, vol. 18, no. 2, pp. 343-358, 2014.
- [12] K. Kasiri, P. Fieguth, and D. A. Clausi, "Self-similarity measure for multi-modal image registration," in Image Processing (ICIP), 2016 IEEE International Conference on, pp. 4498-4502, 2016.
- [13] D. Rueckert, M. Clarkson, D. Hill, and D. J. Hawkes, "Non-rigid registration using higher-order mutual information," International Society for Optics and Photonics, pp. 438-447, 2000.
- [14] D. B. Russakoff, C. Tomasi, T. Rohlfing, and C. R. Maurer Jr, "Image similarity using mutual information of regions," in Computer Vision-ECCV 2004: Springer, pp. 596-607, 2004.
- [15] Y.-W. Chen and C.-L. Lin, "PCA based regional mutual information for robust medical image registration," in Advances in Neural Networks-ISNN 2011: Springer, pp. 355-362, 2011.
- [16] D. Loeckx, P. Slagmolen, F. Maes, D. Vandermeulen, and P. Suetens, "Nonrigid image registration using conditional mutual information," Medical Imaging, IEEE Transactions on, vol. 29, no. 1, pp. 19-29, 2010.
- [17] M. P. Heinrich et al., "MIND: Modality independent neighbourhood descriptor for multi-modal deformable registration," Medical Image Analysis, vol. 16, no. 7, pp. 1423-1435, 2012.

- [18] M. P. Heinrich, M. Jenkinson, B. W. Papiez, S. M. Brady, and J. A. Schnabel, "Towards realtime multimodal fusion for image-guided interventions using self-similarities," (in eng), Medical image computing and computer-assisted intervention : MICCAI ... International Conference on Medical Image Computing and Computer-Assisted Intervention, vol. 16, no. Pt 1, pp. 187-194, 2013.
- [19] T. Ojala, M. Pietikainen, and T. Maenpaa, "Multiresolution gray-scale and rotation invariant texture classification with local binary patterns," IEEE Transactions on pattern analysis and machine intelligence, vol. 24, no. 7, pp. 971-987, 2002.
- [20] R. Trichet and F. Bremond, "LBP Channels for Pedestrian Detection," in 2018 IEEE Winter Conference on Applications of Computer Vision (WACV), pp. 1066-1074, 2018.
- [21] X. Hong, Y. Xu, and G. Zhao, "LBP-TOP: a Tensor Unfolding Revisit," Asian Conference on Computer Vision, Springer, Cham, pp. 513-527, 2016.
- [22] F. Liu, Z. Tang, and J. Tang, "WLBP: Weber local binary pattern for local image description," Neurocomputing, vol. 120, pp. 325-335, 2013.
- [23] H. Yu and A. Li, "Real-Time Non-Local Means Image Denoising Algorithm Based on Local Binary Descriptor," KSII Transactions on Internet & Information Systems, vol. 10, no. 2, 2016.
- [24] R. Mehta and K. Egiazarian, "Dominant Rotated Local Binary Patterns (DRLBP) for texture classification," Pattern Recognition Letters, vol. 71, no. Supplement C, pp. 16-22, 2016.
- [25] D. Jiang, Y. Shi, D. Yao, M. Wang, and Z. Song, "miLBP: a robust and fast modality-independent 3D LBP for multimodal deformable registration," International Journal of Computer Assisted Radiology and Surgery, journal article vol. 11, no. 6, pp. 997-1005, 2016.
- [26] H. Rivaz, Z. Karimaghloo, V. S. Fonov, and D. L. Collins, "Nonrigid registration of ultrasound and MRI using contextual conditioned mutual information," IEEE transactions on medical imaging, vol. 33, no. 3, pp. 708-725, 2014.
- [27] Y. Lu, K. Gao, T. Zhang, and T. Xu, "A novel image registration approach via combining local features and geometric invariants," PloS one, vol. 13, no. 1, 2018.
- [28] L. Shen, X. Huang, C. Fan, and Y. Li, "Enhanced mutual information-based medical image registration using a hybrid optimisation technique," Electronics Letters, vol. 54, no. 15, pp. 926-928, 2018.
- [29] Y. Yonghong, L. Jiying, W. Qiang, and Z. Tao, "Improved Particle Swarm Optimization Image Registration Based on Mutual Information," in 2019 11th International Conference on Measuring Technology and Mechatronics Automation (ICMTMA), pp. 450-453, 2019.
- [30] L. Bai, G. Li, C. Zhu, E. Wu, and R. Ma, "Regional Weighted Mutual Information for Multimodal Rigid Registration," in 2018 11th International Congress on Image and Signal Processing, BioMedical Engineering and Informatics (CISP-BMEI), pp. 1-6, 2018.
- [31] T. Borvornvitchotikarn and W. Kurutach, "Robust Self-Similarity Descriptor for Multimodal Image Registration," in 2018 25th International Conference on Systems, Signals and Image Processing (IWSSIP), pp. 1-4, 2018.
- [32] T. Borvornvitchotikarn and W. J. S. Kurutach, "miRID: Multi-Modal Image Registration Using Modality-Independent and Rotation-Invariant Descriptor," vol. 12, no. 12, p. 2078, 2020.
- [33] Z. Yang, N. Kuang, Y. Yang, B. J. K. T. o. I. Kang, and I. Systems, "Brain MR Multimodal Medical Image Registration Based on Image Segmentation and Symmetric Self-similarity," vol. 14, no. 3, 2020.
- [34] Y. Ou, A. Sotiras, N. Paragios, and C. Davatzikos, "DRAMMS: Deformable registration via attribute matching and mutual-saliency weighting," presented at the Medical image analysis, 2011.
- [35] T. Ojala, M. Pietikäinen, and D. Harwood, "A comparative study of texture measures with classification based on featured distributions," Pattern recognition, vol. 29, no. 1, pp. 51-59, 1996.
- [36] Z. Cao, E. Dong, Q. Zheng, W. Sun, and Z. Li, "Accurate inverse-consistent symmetric optical flow for 4D CT lung registration," Biomedical Signal Processing and Control, vol. 24, pp. 25-33, 2016.
- [37] B. BrainWeb, "Simulated Brain Database," Online: <http://brainweb.bic.mni.mcgill.ca/cgi/brainweb2>, 2010.
- [38] T. M. Cover and J. A. Thomas, Elements of information theory. John Wiley & Sons, 2012.
- [39] D. Rueckert, L. I. Sonoda, C. Hayes, D. L. Hill, M. O. Leach, and D. J. Hawkes, "Nonrigid registration using free-form deformations: application to breast MR images," Medical Imaging, IEEE Transactions on, vol. 18, no. 8, pp. 712-721, 1999.

Core Elements Impacting Cloud Adoption in the Government of Saudi Arabia

Norah Alrebdi, Nabeel Khan

Department of Information Technology
College of Computer, Qassim University, Buraydah, Saudi Arabia

Abstract—The Kingdom of Saudi Arabia is taking rapid steps towards digital transformation in the field of government services. Cloud computing adoption may be the next step that supports this digital transformation to providing many features and reducing costs. Therefore, this paper will present multiple factors that may make it difficult to move to the cloud by conducting several interviews and questionnaires with government sector workers, those with technical experience, and that too to take caution and develop suitable solutions in advance. This paper also presents some recommendations and suggestions useful to consider when adopting the cloud in the public sector.

Keywords—Cloud computing; e-governance; cloud computing adoption; smart government; Saudi Arabia vision 2030

I. INTRODUCTION

Based on trends of using technology, a basis in all government transactions within the Kingdom of Saudi Arabia (KSA) and in solidarity with the 2030 vision for digital transformation, several technologies should be considered and used in several fields. Cloud computing is one of the foremost necessary technical revolutions due to the advantages it offers. Therefore, the cloud is one of the technologies that the Kingdom attached great importance during this vision [1]. The World Bank defines e-government as “the use by government agencies of information technologies (such as Wide Area Networks, the Internet, and mobile computing) that have the ability to transform relations with citizens, businesses, and other arms of government” [2]. While cloud computing is defined by the National Institute of Standards and Technology as “a model for enabling ubiquitous, convenient, on-demand network access to a shared pool of configurable computing resources (e.g., networks, servers, storage, applications, and services) that can be rapidly provisioned and released with minimal management effort or service provider interaction” [3]. The resources vary according to their type. They may be an Infrastructure, platform, or software [4]. While deployment models of cloud vary rely upon the goals. It might be a Public, Private, Hybrid, or Community cloud [5]. Cloud computing provides several features relating to performance, availability, and reducing costs [6,7]. Therefore, the government of Saudi Arabia confirmed cloud computing’s value, so it worked to develop some procedures for providing government services as a cloud service [8]. On the other hand, cloud computing in the government sector correlated with specific considerations. This research would address some factors influencing cloud computing implementation in government organizations based on prior literature review [9,10]. This research aims to assist

decision makers in implementing cloud computing in government organizations and make them aware of the essential concerns to put in place the necessary measures to protect their organizations.

II. LITERATURE REVIEW

This section will discuss related works that discussed the factors affecting cloud adoption in government institutions in Saudi Arabia. By studying the previous literature, Alanezi in [11] conducts several discussions with IT employees in different organizations in different fields, for instance, the health field, finance field, education field, etc., in Saudi Arabia. They examine some expected effect factors when embracing cloud computing in their public or private organization. These discussions covered two aspects: negative and positive factors. The study shows four negative factors: Security and privacy challenges, government rules, lack of experience, and control loss. While the positive aspects contain three factors: the low cost, enhance performance, and the potential of scalability and flexibility, as shown in Table I.

Al-Ruithe et al. in [12] put forward several risks that may prevent the government sector from moving to the cloud. These risks are related to many technical, security, legal, and other aspects. Likert scale was used to measure these factors’ effect on adopting cloud in public organizations based on 206 public sector workers’ answers. The Table II illustrates these concerns and the average measure of responses. The findings indicate that Privacy issues and Trust issues represent the biggest fear of cloud adoption.

In [8] author proposed a framework of critical security elements using the triangulation method to validate results. The triangulation method contains three steps. First, review a previous literature review to collect the elements considered as critical security elements. Second is to organize interviews with IT professionals to review the data collected in the first step, besides suggesting new elements from experts. The final step is for conducting a survey using a close-end questionnaire to assure effective operation of framework. This framework dealt with three aspects: security risk elements, Social elements, and expected security advantages, as illustrated in Table III. Security risk elements contain interface security risks, threats of sharing the same sources, steal some accounts or services, malicious insiders, violating rules and regulations, the possession of data, data protection, data Spread, and client-side encryption error. The social elements contain confidence, security, and privacy. While the expected security advantages aspect contains scalability, take benefit of the advanced

security tools in the cloud market, a system of sophisticated security, standardized security interfaces, cloud security checking, check the implementation of Service Level Agreement (SLAs), and resource concentration [13].

TABLE I. POSITIVE AND NEGATIVE FACTORS OF ADOPTING CLOUD COMPUTING

S.No	Factors Affecting Cloud Computing Adoption	
	Negative	Positive
1.	Security and Privacy	Low cost
2.	Government Rules	Enhance Performance
3.	Lack of Experience	Ability of Scalability and flexibility
4.	Loss of Control	

TABLE II. SAUDI ARABIAN PUBLIC SECTOR CONCERNS ABOUT CLOUD COMPUTING

S.No.	Risks with Statistical Ratio	
	Risk	Statistical Ratio
1.	Unsatisfactory Financial Benefit	3.47
2.	Unripe Cloud Computing	3.76
3.	Unknown Data Storage place	3.91
4.	Lack of Functionalities	3.69
5.	Lack of Performance	3.71
6.	Loss of Control	4.04
7.	Data Governance Failure	4.03
8.	Proprietary lock in	3.67
9.	Dangerous Availability	3.8
10.	Integration problems	3.7
11.	Trust problems	4.1
12.	Privacy Problems	4.15
13.	Compliance Problems	3.86
14.	Legal Problems	3.96
15.	Security Problems	4.07

TABLE III. FRAMEWORK OF CRITICAL SECURITY ELEMENTS

S.No.	Framework Elements Based on Security Aspects		
	Security Threats Elements	Social Elements	Expected Security Advantage
1.	Interface Security Risk	Security	Scalability.
2.	Threats of Sharing the Same Services	Confidence	Advanced Security tools in the cloud Market.
3.	Steal some accounts or services.	Privacy	System of Sophisticated Security.
4.	Malicious Insider		Security Interfaces Unified
5.	Violating rules and regulations.		Cloud Security Checking.
6.	Possessions of Data		Checking the Implementation of SLAs
7.	Data Incorporation and Service		Resource Concentration
8.	Data Spread		
9.	Client Side Encryption Error		

III. PROBLEM STATEMENT

With the growth of electronic services of Saudi Arabian government, it has become crucial to adopt cloud computing technology to make it robust and secured. Due to immense benefits offered by cloud computing, such as low cost and scalability, its necessary to guide ever emerging public sector. On the other hand, the implementation of cloud computing may bring some concerns and risks. Therefore, this paper aims to summarize the concerns that government institutions in the Kingdom of Saudi Arabia may face when adopting the cloud by reviewing previous literature to try controlling it and finding precautionary measures to avoid.

IV. RESULTS AND DISCUSSION

A. Research Method

This research incorporated quantitative research method to list factors that are important in Saudi Arabian public sector. It involves two steps; the first step was used by applying systematic literature review method which involved searching for the literature on this topic by using several approved search engines for papers such as Google Scholar and some popular databases such as ScienceDirect. In this research, authors used some keywords to help find papers related to the topic, such as: "cloud adoption," "public sector in Saudi Arabia," "affect factors," in addition to several other keywords. The research focused on papers published from 2017 to the present day of 2022. In the second step of this paper, we conducted a detailed review and analysis of the factors mentioned in the literature related to cloud adoption in the Saudi Arabian public sector. This paper introduces some of the concerns mentioned in previous literature to help researchers and government organization officials find solutions to overcome cloud adoption issues.

B. Results

Cloud usage in the public sector leads to the elimination of tremendous costs and adding several advantages. However, its adoption may pose some risks, making decision-makers hesitant about adopting it in their institutions. This study reviewed three research papers that discussed the factors affecting the implementation of cloud computing in the Saudi Arabian public sector. One of the papers mentioned in this research identifies factors affecting the public and private sectors. We noticed some similarities in the factors extracted, which may signify that there are common factors between the two sectors, so this research may help officials in the private sector also in the decision to adopt the cloud. Table IV shows general information on these papers. This review revealed that cloud and data security are the most important concerns affecting cloud adoption, in addition to the loss of control and data governance.

C. Recommendations

This section recommends solutions suggested by some researchers. In [14], its stated that Saudi government has expedite the process of restructuring and transforming the e governance strategy ensuring; cost reduction, improvement in services, time saving, increase in effectiveness and efficiency across all government organizations. "YASSER" platform has already been developed ensuring overall control of all

procedures, activities and all other issues related to implementation of effective e-governance. Moreover, the kingdom has recently taken a forward step to facilitate its adoption across government bodies by establishing committee to develop the necessary regulations for the cloud paradigm. Based on the findings in this research a comprehensive cloud system is recommended as shown in Fig. 1.

TABLE IV. LITERATURE REVIEW COMPARISON

Framework Elements Based on Security Aspects					
Research Reference	Approach type	Sample Size	Year	Discuss Risk factors	Discuss Benefit factors
	Quantitative Study	55 Universities	2021	Yes	Yes
[9]	Qualitative Study	32 Interviews	2018	Yes	Yes
[10]	Empirical Study (Quantitative)	206 Questionnaires	2018	Yes	No
[8]	Mixed: Qualitative and Quantitative	12 Interviews and 32 Questionnaires	2017	Yes	Yes

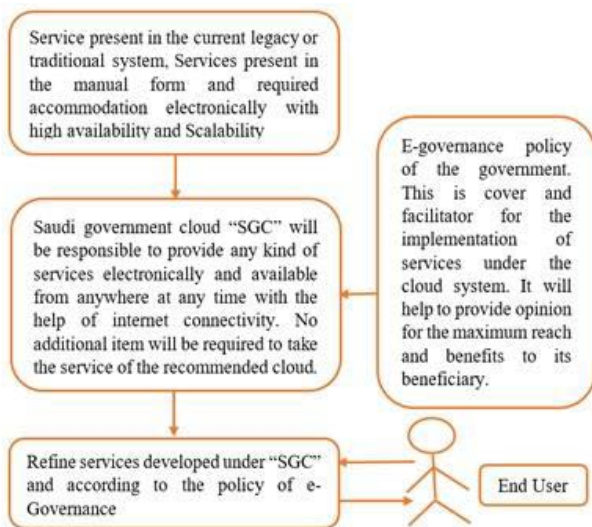


Fig. 1. Recommended Cloud System.

In this research authors proposed to plan for an umbrella Saudi Government Cloud i.e., “SGC”. A number of teams to be formed aiming to work specially in the reformation of cloud and e-governance resulting in implementation of SGC. These teams should have members from the government organizations to facilitate the process of investigating technical and financial feasibility of the system. Once the system is ready, it should be included under SGC with classification based on services and policies of e-governance.

Alansary and Hausawi in [15] proposed a solution using cloud computing in the public organizations of Saudi Arabia. This solution is to launch a national cloud center headed by a Communication and Information Technology Commission (NCC). NCC will take responsibility for the cloud services of

infrastructures and platforms. Besides the solutions and maintenance of the cloud services of software, this solution helps to decrease cost and IT resources. In contrast, SaaS’s control, rules, and management will be the prerogative of each government agency. As for solutions that will provide by NCC, they propose two methods, either by studying the solutions that agencies are currently using and converting them into SaaS solutions. While the other is developing solutions they are needed from scratch, which may reduce time and cost.

In 2019, the same authors in [16] presented the previous proposal in detail and considered all parties contributing to developing and protecting this system. They proposed to create an Intelligent Government Cloud (IGC) powered by the National Center. This cloud provides services of all types to government agencies besides accountable for maintenance and verification work. The paper proposes that Riyadh be the headquarters of the IGC, with the establishment of several physical centers throughout the Kingdom to act as backup sites. The author suggests that the centers be part of Saudi universities due to many specialists who may contribute to this work’s development. All government institutions must follow the Ministry of Finance regulations and the Ministry of Civil Service. IGC will provide any software solutions currently used in government organizations to a SaaS solution, which will contribute to reducing the costs paid by making them usable by any party separately. This proposal is consistent with the concern of the Kingdom in cybersecurity. Several organizations established interested in this field: The National Authority for Cyber-Security, the Saudi Federation for Cyber Security and Programming, the National Center for Information Security Technology, and the National Cyber-Security Center. Having these organizations may help implement the solution safely and accurately in compliance with government procedures and regulations.

In [17, 18], Al-Ruithe and Benkhelifa suggested a research paradigm focused on nine factors in the public organization of Saudi Arabia as helpful factors for the effective adoption of cloud data governance. These factors contribute to managing data, determining the requirements for data management, knowledge of the required functions of the data governance team, and align cloud data with other data in the organization. In addition to the ability to integrate cloud data governance functions with the cloud computing context adopted by the data-owning organization, development of the necessary contracts between the cloud consumer and the provider, the deployment of the system and the capacity to manage it in real-time, the attempt to sustain the data management program for a long period of time, the monitoring of the implementation method to ensure its correctness. Each factor contains some items that are defined from literature reviews and questionnaires. 28 hypotheses were brought up that fall under two types of hypotheses that are associative and causal. It was evaluated using Structural Equation Modelling (SEM). The results of hypothesis testing demonstrated that the model was adequate.

V. CONCLUSION

Due to the tremendous interest exhibited by Saudi Arabia in providing government services electronically, the next step

for Saudi's government sector should be in adopting the cloud. For this reason, this paper discusses several previous research that discussed concerns related to cloud adoption in the government sector. This research provides a thorough overview of the risks that can arise when adopting a cloud to prepare for it and create innovative solutions before it crashes into failure. This review illustrates that the security element occupies a large proportion of concerns. Besides this, loss of control and data governance is potentially severe concerns.

As future work, we look forward to making a case study for one of the government organizations that adopted the cloud and investigating the amount of reduced costs after adopting it. As well as understanding the consequences and difficulties they faced at present and how they overcome them.

ACKNOWLEDGMENT

With many thanks to College of Computing, Qassim University for dedicated support and guidance during this research and offering authors the great chance to write this research paper "Core Elements Impacting Cloud Adoption in the Government Sector of Saudi Arabia", which has really helped us to broaden our research area interests. Finally, authors would like to thank their family and friends for supporting in this research work.

REFERENCES

- [1] The Council of Economic and Development Affairs, Cloud and E-Governance Program, <https://vision2030.gov.sa/ar/node/386>, Accessed on June 24, 2022.
- [2] M. M. Alkhusaili, "The Evolution of E-government Project in GCC Countries," pp. 2001–2012, 2020.
- [3] I. Ahmed, "A brief review: Security issues in cloud computing and their solutions," *Telkomnika (Telecommunication Comput. Electron. Control.*, vol. 17, no. 6, pp. 2812–2817, 2019.
- [4] U. A. Butt, M. Mehmood, S.B. H. Shah, R. Amin, M.W. Shaukat, S.M. Raza, D.Y. Suh, M.J. Pilan, "A review of machine learning algorithms for cloud computing security," *Electron.*, vol. 9, no. 9, pp. 1–25, 2020.
- [5] A. Ullah, N. M. Nawi, and M. H. Khan, "BAT algorithm used for load balancing purpose in cloud computing: an overview," *Int. J. High Perform. Comput. Netw.*, vol. 16, no. 1, p. 43, 2020.
- [6] A. Albelaihi and N. Khan, "Top benefits and hindrances to cloud computing adoption in Saudi Arabia: A brief study," *Journal of Information Technology and Management*, 2020.
- [7] M. Hosseini Shirvani, "An iterative four-phase cloud adoption decision model for IT outsourcing based on TCO," *J. Soft Comput. Information Technology*, vol. 9, no. 1, pp. 1–13, 2019.
- [8] M. O. Alassafi, A. Alharthi, R. J. Walters, and G. B. Wills, "A framework for critical security factors that influence the decision of cloud adoption by Saudi government agencies," *Telemat. Informatics*, vol. 34, no. 7, pp. 996–1010, 2017.
- [9] N.S.Aldahwan, M.S. Ramzan; "Factors Affecting the Organizational Adoption of Secure Community Cloud in KSA"; *Security and Communication Networks*; Volume, 10 Spetember, 2021.
- [10] N.S.Aldahwan, M.S. Ramzan; "The Descriptive Data Analysis for the Adoption of Community Cloud in HEI-Based Factor Adoption"; *BioMed Research International*; Volume, 8 June, 2022.
- [11] M. A. Alanezi, "Factors influencing cloud computing adoption in Saudi Arabia's private and public organizations: A qualitative evaluation," *International Journal of Advance Computing and Science Application*, 2018.
- [12] M. Al-Ruithe, E. Benkhelifa, and K. Hameed, "Key Issues for Embracing the Cloud Computing to Adopt a Digital Transformation: A study of Saudi Public Sector," in *Procedia Computer Science*, 2018.
- [13] F. Aldosari, A. Almiman; "Investigating the Effect of Cloud Computing Adoption on Improving the Digital Competitiveness Index-An Empirical Study: Case of Kingdom of Saudi Arabia"; *International Journal of Computer Science and Network Security*, Vol 22, No.4, April, 2022.
- [14] A.Ali, D. Manzoor, A. Alouraini, "The Implementation of Government Cloud for the Services Under E-Governance in the KSA", *Science Internation (Lahore)*, Vol. 33,no.3, pp 249-257, 2021.
- [15] M. O. Alanssary and Y. M. Hausawi, "Adopting Software As a Service (Saas) in the," no. 3, pp. 124–130, 2017.
- [16] M. O. Alanssary and Y. M. Hausawi, "Adopting and implementing a government cloud in Saudi Arabia, an integral part of vision 2030," in *Proceedings of 34th International Conference on Computers and Their Applications, CATA 2019*, 2019.
- [17] M. Al-Ruithe and E. Benkhelifa, "Determining the enabling factors for implementing cloud data governance in the Saudi public sector by structural equation modelling," *Futur. Gener. Comput. Syst.*, 2020.
- [18] A. Almukhlifi, H. Deng, and B. Kam, "E-Government Adoption in Saudi Arabia: The Moderation Influence of Transparency," *Journal of Advance Information Technology.*, 2019.

Decentralized Tribrid Adaptive Control Strategy for Simultaneous Formation and Flocking Configurations of Multi-agent System

B.K. Swathi Prasad¹

Dept. of Electrical Engineering
M S Ramaiah University of Applied
Sciences, Bangalore, India

Hariharan Ramasangu²

Relecura Inc.
Bangalore
India

Govind R. Kadambi³

Dept. of Research
M S Ramaiah University of Applied
Sciences, Bangalore, India

Abstract—This paper focuses on the development of a tribrid control strategy for leader-follower flocking of multi-agents in octagonal polygonal formation. The tribrid approach encompasses Reinforcement Learning (RL), centralized and decentralized control strategies. While the RL for multi-agent polygonal formation addresses the issues of scalability, the centralized strategy maintains the inter-agent distance in the formation and the decentralized strategy reduces the consensus (in position and velocity) error. Unlike the previous studies focusing only on the predefined trajectory, this paper deals with the leader-follower scenario through a decentralized tribrid control strategy. Two cases on initial positions of multi-agents dealt in this paper include the octagonal pattern from RL and the agents randomly distributed in spatial environment. The tribrid control strategy is aimed at simultaneous formation and flocking, and its stability in a shorter response time. The convergence of flocking error to zero in 3s substantiates the validity of the proposed control strategy and is faster than previous control methods. Implicit use of centralized scheme in decentralized control strategy facilitates retention of formation structure of the initial configuration. The average position error of agents with the leader is within the position band in 3s and thus it confirms the maintenance of formation during flocking.

Keywords—Simultaneous; flocking; polygonal formation; decentralized; hybrid; adaptive; control strategy; simulation

NOMENCLATURE

r_{ox} & r_{oy}	Position of leader along x and y axes respectively
V_{ox} & V_{oy}	Velocity of leader along x and y axes respectively
A_l	System matrix of leader dynamics
r_{ix} & r_{iy}	Position of i^{th} agent along x and y axes respectively
V_{ix} & V_{iy}	Velocity of i^{th} agent along x and y axes respectively
u_{ix} & u_{iy}	Control input of i^{th} agent along x and y axes respectively
v	Vertices
E	Edges
a_{ij}	Adjacency matrix
N_i^t	Neighbours of i^{th} agent at time t
C_s	Spatial communication range
$R(\emptyset)$	Rotation transformation matrix
\emptyset	Rotation angle
d	Inter-agent distance
H, D	Observation matrices of position and velocity, respectively
a, b, c, \tilde{c}	Constants

I. INTRODUCTION

The connectivity among mobile agents imposes a challenge for coordination and communication among agents, during flocking. The multi-agents interact with each other using the communication strategy and achieve formation and flocking configuration. This communication strategy encompasses a challenge for the MAS, having both homogeneous and heterogeneous agents. The challenges include interactions with the environment, and the use of various sensors for communication between the homogeneous and heterogeneous agents [1]. For the ease of operation during flocking and formation configuration by multi-agents, either homogeneous or heterogeneous multi-agents are considered. The consideration is due to the mismatch in the communication frequency [2] and may lead to diverging behaviour. The collective operation of communication and control strategies is required to establish coordination among agents. These strategies also enable to obtain cohesion in formation and flocking configurations of MAS.

Many formation and flocking control strategies have been proposed. For example, leader-follower, behavioural and virtual structure [3] for preserving formation among agents. The formation of agents can include a specific pattern: triangle [4, 5], rectangle [6] and ellipse [7]. These patterns are achieved with agent's control reference to the virtual leader trajectory tracking configuration [8]. The agent's position changes dynamically based on the velocity at which the agents are travelling. The agent's position is controlled such that no agents collide with each other to preserve the formation and achieve the stability. The control of agents [9] depends on the dynamics of each agent and the rotational transformation matrix (to transfer the agent's position from the body reference frame to the global frame).

The cyclic pursuit control strategy [10] is suitable to achieve polygonal shape. This control strategy uses a centralized control station for controlling the angle and distance of each agent. The centroid of the polygon is referred to as the virtual leader and controls the position of each agent. If there is non-availability of the virtual leader due to some destruction in the environment, then the centralized control strategy fails. Thus, the formation and stability of the MAS will not be achieved.

The centralized control strategy is also used in trajectory tracking application to control the agents from a single control station. It is challenging with the expansion of several agents and can increase the computation time with energy consumption [1]. The distributed and decentralized control strategies will overcome the disadvantages of the centralized control strategy. However, to operate simultaneous polygon formation and leader-follower flocking of multi-agents, the solitary control strategy is not useful. In this paper, the tribrid approach of a centralized and decentralized control strategy with Reinforcement Learning (RL) is proposed to perform analysis of simultaneous polygon formation and leader-follower flocking of multi-agents.

In the proposed tribrid control strategy, the polygon obtained using RL [11] is utilized along with the transformation technique (centralized control technique) to maintain the formation. The decentralized control strategy is used along with the centralized strategy for simultaneous pattern formation and leader-follower flocking of multi-agents. The proposed tribrid control strategy maintains the initial formation configuration and achieves time-varying flocking configuration at a quicker response time. The rest of this paper is organized as follows. In Section II, the review on centralized and decentralized control strategies are discussed. In Section III, the MAS model and proposed tribrid control strategy are discussed for communication and control of multi-agents, followed by consensus topology. Section V presents the simulation results and analysis for tribrid control strategy. Section VI provides conclusions.

II. LITERATURE REVIEW

The trajectory tracking and formation of multi-agents are research topics of significant importance in MAS. The application of flocking in polygon contour is required in coverage control of multi-agent surveillance systems [12, 13]. The centralized, decentralized and distributed control strategies are used in the formation and flocking configurations of MAS [4, 14, 15]. The centralized control strategy in [9] uses a control strategy to control all agents based on the availability of information of agents as a whole. The control law is designed for decentralized or distributed control strategy based on the neighbourhood information of agents in MAS.

The decentralized control strategy is preferred over centralized control strategy (cyclic pursuit strategy) [5,10] for achieving the flexibility in changing the polygonal formation [9,14,16]. The decentralized control strategy is required to make agents in pattern follow the leader's trajectory for a multi-agent dynamical system with time-varying velocity [15,17]. The distributed control strategy is used for the agents in hexagon to flock along the pre-defined trajectory [8]. The pre-defined trajectory is addressed only for the constant velocity profile. And also, the analysis is not performed for the pattern of agents in leader-follower scenario. The bearing control approach in [18] uses positive gains to obtain formation maneuvering or flocking in a pattern. However, this decentralized bearing control approach has converged flocking

error to zero in 20s (larger settling time). The desired bearing angle between the agents is required for formation maneuvering. Any communication failure in maintaining the bearing angle can affect the MAS stability [19, 20]. The switching of formations maneuvering may not be useful for time-varying trajectory [21]. The novelty of this proposed paper is to overcome the disadvantages of bearing angle control approach and use tribrid of centralized and decentralized control strategies to achieve time-varying formation maneuvering with lesser settling time.

III. MULTI-AGENT DYNAMICS AND CONTROL

In this paper, we will consider double integrator system for leader and multi-agent dynamics. The leader dynamics depends on its own states, given by:

$$\dot{r}_{ox} = V_{ox} \quad (1)$$

$$\dot{r}_{oy} = V_{oy} \quad (2)$$

$$\dot{V}_{ox} = g_{11}V_{ox} + g_{12}V_{oy} \quad (3)$$

$$\dot{V}_{oy} = g_{21}V_{ox} + g_{22}V_{oy} \quad (4)$$

where, r_{ox} and r_{oy} represent position of leader along x and y axes respectively. V_{ox} and V_{oy} represents velocity of leader along x and y axes respectively. $A_l = \begin{bmatrix} g_{11} & g_{12} \\ g_{21} & g_{22} \end{bmatrix}$ is the system matrix of the leader.

The agent dynamics depends on its own state and control input of neighbour states, position consensus terms and velocity consensus terms, given by:

$$\dot{r}_{ix} = V_{ix}$$

$$\dot{r}_{iy} = V_{iy} \quad (5)$$

where r_{ix} and r_{iy} are x and y position vector components of the i^{th} agent. V_{ix} and V_{iy} are x and y velocity vector components of the i^{th} agent. $i = \{1,2,3,\dots,8\}$

The velocity vector components of i^{th} agent uses an additional term of control input to perform flocking in leader-follower scenario.

$$\dot{V}_{ix} = g_{11}V_{ix} + g_{12}V_{iy} + u_{ix} \quad (6)$$

$$\dot{V}_{iy} = g_{21}V_{ox} + g_{22}V_{oy} + u_{iy} \quad (7)$$

where u_{ix} and u_{iy} are x and y control input vector components of the i^{th} agent.

The distributed control and communication network consisting of eight agents is represented using undirected graph G in Fig. 1.

In the Fig. 1, A represents agent, u represents control input to the agent and C represents centralized control station. The decentralized control inputs $\{u_1, u_2, \dots, u_8\}$ to the agents $\{A_1, A_2, \dots, A_8\}$ are used for flocking in the leader-follower configuration.

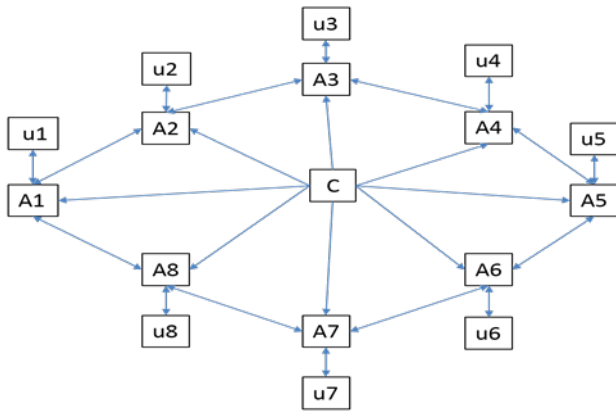


Fig. 1. Proposed Control Configuration for Agents in Octagonal Formation.

A graph, G is defined as: $G = (\nu, E)$, where ν is the set of vertices, $\nu = \{A1, A2, A3, \dots, A8\}$ and E is the edges, $E = \nu \times \nu$, i.e., a pair of vertices in a given spatial environment. Each vertex represents the identity of an agent in the graph. The connection between two agents is bi-directional, represented using the adjacency matrix. The adjacency matrix definition is given in (8).

$$a_{ij} = \begin{cases} 1 & \text{if two agents are connected} \\ 0 & \text{otherwise} \end{cases} \quad (8)$$

The neighbors of i^{th} agent are given in (9).

$$N_i^t = \{j: \|r_j(t) - r_i(t)\| \leq C_s, j \in \nu, j \neq i\} \quad (9)$$

where C_s indicates the spatial communication range, r_i is the position of i^{th} agent and r_j is the neighbour position of i^{th} agent. The neighbours of the agent are determined for the inter-agents positions lying within the spatial communication range. Apart from the communication strategy to connect the agents, control strategy is required to achieve flocking (trajectory tracking) and formation configuration of MAS.

The centralized control strategy is used in trajectory tracking application to control the agents from a single control station. It is challenging with the expansion of several agents and can increase the computation time with energy consumption [1]. The distributed and decentralized control strategies will overcome the disadvantages of the centralized control strategy. However, to operate simultaneous polygon formation and leader-follower flocking of multi-agents, the solitary control strategy is not useful. In this paper, the tribrid approach of a Reinforcement Learning (RL), centralized and decentralized control strategy is proposed to perform analysis of simultaneous polygon formation and leader-follower flocking of multi-agents.

The octagonal formation obtained using a RL technique [15] is maintained using a centralized (transformation technique) control strategy and then is integrated with a decentralized control strategy to obtain a leader-follower flocking configuration of multi-agents. In this proposed control strategy, the agent's position in the polygon is computed using RL and updated with initial position while tracing the leader's trajectory (5). The initial position of formation is computed using (10).

$$\dot{r}_i = R(\phi)(r_{i+1} - r_i)$$

where

$$R(\phi) = \begin{bmatrix} \cos \phi & \sin \phi \\ -\sin \phi & \cos \phi \end{bmatrix}$$

and ϕ is the rotation angle along z-axis, given by: $0 < \phi < \frac{\pi}{N}$, N is the number of agents.

The rotation angle, ϕ is adjusted to maintain the desired distance between positions of agents. It is given by:

$$\phi = \frac{\pi}{N} + g(100 - d)$$

Here 100 is the desired distance and $g = 0.014706$ is the value of gain obtained by trial and error to adjust inter-agent distance (d) between the agents. The distance, d between agents is calculated using,

$$d_{ij} = \|r_i - r_j\|$$

The decentralized control inputs (u_{ix} and u_{iy}) of i^{th} agent for (6) and (7) is described in (11) and (12), respectively.

$$u_{ix} = -d_{11}h_{11}(r_{ix} - r_{ox}) - d_{11}h_{12}(r_{iy} - r_{oy}) - d_{11}h_{11}(V_{ix} - V_{ox}) - d_{11}h_{12}(V_{iy} - V_{oy}) + \sum_{j \in N_i} g_{ij}(\|r_j - r_i\|) \left(a - b e^{-\frac{\|r_{ij}^2\|}{\epsilon}} \right) (r_{jx} - r_{ix}) + \sum_{j \in N_i} a_{ij}(\|r_j - r_i\|)(V_{jx} - V_{ix}) \quad (10)$$

$$u_{iy} = -d_{21}h_{11}(r_{ix} - r_{ox}) - d_{21}h_{12}(r_{iy} - r_{oy}) - d_{21}h_{11}(V_{ix} - V_{ox}) - d_{21}h_{12}(V_{iy} - V_{oy}) + \sum_{j \in N_i} a_{ij}(\|r_j - r_i\|) \left(a - b e^{-\frac{\|r_{ij}^2\|}{\epsilon}} \right) (r_{jy} - r_{iy}) + \sum_{j \in N_i} a_{ij}(\|r_j - r_i\|)(V_{jy} - V_{iy}) \quad (11)$$

where $i = 1, 2, \dots, N = 8$, r_{ix} and r_{iy} are positions of agent along x and y component respectively. V_{ix} and V_{iy} are velocities of leader along x and y axes respectively. a_{ij} is the adjacency matrix. $H = [h_{11} \ h_{12}] = [0 \ 1]$, 8 agents can observe the second (y component) position of leader. $D = [d_{21}; \ d_{22}] = [0 \ 1]$, 8 agents can observe the second (y component) velocity of leader. $a = 1, b = 20, \epsilon = 0.2$ are constants [17].

IV. CONSENSUS TOPOLOGY IN LEADER-FOLLOWER FLOCKING CONFIGURATION

The MAS consisting of N agents should ensure position and velocity consensus among the agents during flocking and formation of multi-agents. Suppose the network of multi-agents in polygon is connected, the control input (u_{ix} and u_{iy}) ensure semi-global consensus in formation and flocking. For the global consensus of multi-agents, the conditions below are required to be satisfied.

Position Consensus

- For any position of i^{th} agent in the bounded set, i.e., $r_i \in \mathbb{R}^n$, position of leader, $r_o \in \mathbb{R}^n$, there is an \mathcal{E}^* such that, for each $\mathcal{E} \in (0, \mathcal{E}^*)$,

$$\lim_{t \rightarrow \infty} \left\| \frac{1}{N} r_i(t) - r_o(t) \right\| = \mathcal{E}^*,$$

$$i = \{1, 2, 3, \dots, N; N = 19\}$$

where \mathcal{E} represents small value in r^*

- For any position of i^{th} agent in the bounded set, i.e., $r_i \in \mathbb{R}^n$, neighboring agent, $r_j \in \mathbb{R}^n$, there is an r^* such that, for each $r \in (0, r^*)$,

$$\lim_{t \rightarrow \infty} \|r_i(t) - r_j(t)\| = r^*,$$

$$i = \{1, 2, 3, \dots, N = 19\}$$

where r^* is in the band of $[0, 10] \times [0, 10]$

Velocity Consensus

The velocity of i^{th} agent is in the bounded set, i.e., $V_i \in \mathbb{R}^n$, velocity of leader, $V_o \in \mathbb{R}^n$

$$\lim_{t \rightarrow \infty} \|V_i(t) - V_o(t)\| = 0,$$

$$i = \{1, 2, 3, \dots, N; N = 19\}$$

The above position and velocity consensus terms are substantiated using simulation results of flocking behaviour of multi-agents.

V. SIMULATION ANALYSIS OF TRIBRID CONTROL STRATEGY FOR SIMULTANEOUS POLYGONAL FORMATION AND FLOCKING OF MAS

The analysis is performed for two cases of initial position of agents: polygon pattern (in Fig. 2, obtained using Reinforcement Learning (RL), [11]) and randomly distributed in the environment (in Fig. 3). The velocity is chosen randomly in the range $([0, 2] \times [0, 2])$ (in Fig. 4).

The spatial communication or interaction range is 2 and the connectivity is established among all agents with the leader. The cyclic pursuit and the adaptive control strategies are used to achieve synchronization of octagonal formation and tracing the leader's trajectory.

A. Formation Control using Cyclic Pursuit Strategy

In this paper, the cyclic pursuit strategy (centralized control strategy) is preferred over decentralized control strategy for achieving the flexibility in changing the polygonal formation [15]. The formation of a polygon is described by deviated cyclic pursuit in \mathbb{R}^2 by maintaining the desired distance between positions of agents. In a deviated cyclic pursuit strategy, the rotation angle (in (10)) is adjusted to maintain the desired distance between the agents. The inter-agent distance between the neighbours has converged to maintain a constant value of 100 and is shown in Fig. 5.

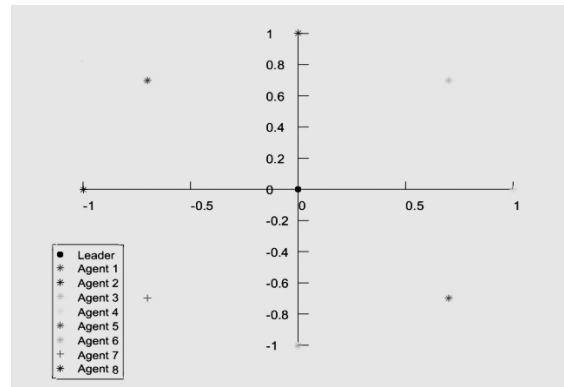


Fig. 2. Initial Position in Octagonal Formation.

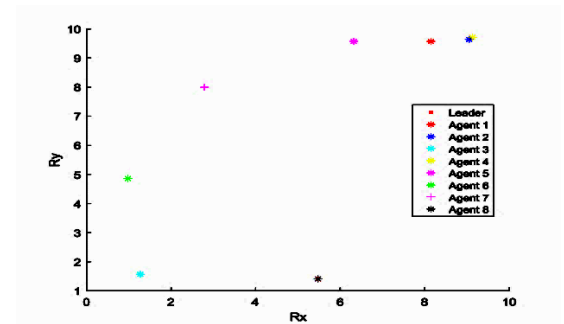


Fig. 3. Random Initial Position of Eight Agents and the Leader.

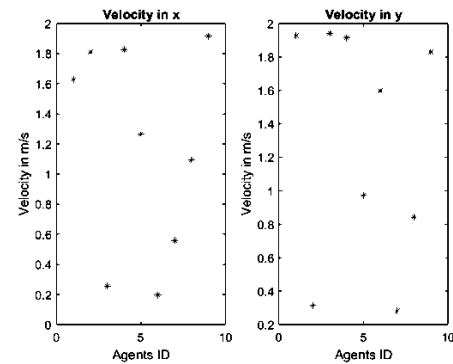


Fig. 4. Initial Velocity of Eight Agents and Leader.

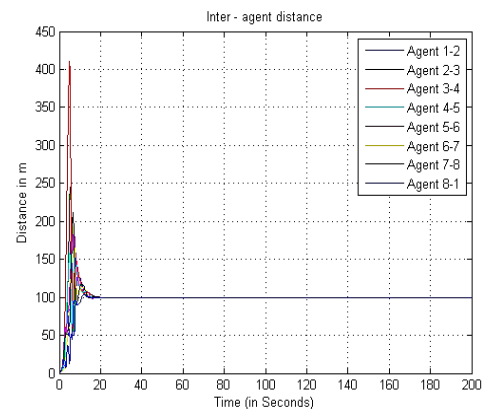


Fig. 5. Inter-agent Distance for All Agents.

The angle is increased to maintain the distance between the agents. Also, a constant multiplying gain factor is adjusted to maintain a constant inter-agent distance between the agents. In Fig. 5, it is observed that, initial transient period is around 9s to achieve the steady-state behaviour.

Apart from maintaining the distance, it is also necessary to check whether the formation is maintained. To check that the formation is maintained, all agents should agree to the same point during flocking. This agreement is captured by averaging the positions of agents in x and y axes. The simulation substantiates that all agents have agreed on the position pursuit of interest (shown in Fig. 6) in 20s. It can be observed that, all agents collectively agree on the same point, (50, -50) i.e., the pursuit point of interest. The rotation angle in (10) is adjusted to maintain the inter-agent distance and angle from the centroid of eight agents. The maintenance of inter-agent distance, angle from the centroid and consensus agreement among agents during the flocking validates the pattern in polygon.

B. Flocking of Agents in Polygon using Adaptive Strategy

The flocking behaviour is obtained by integrating the agent's dynamics with the adaptive controller. The position of agents is updated using the cyclic pursuit strategy (discussed in Section 4A.). The communication or interaction range is 2 and the connectivity is established among all agents with the leader. The cyclic pursuit and the adaptive control strategies are used to achieve synchronization of octagonal formation and tracing the leader's trajectory. The analysis of simultaneous formation and flocking is discussed in two cases:

- The octagonal formation is developed using Q-learning, where the eight agents learn independently in x and y frames. The agents are subjected to follow the leader's trajectory after the octagonal contour is formed. The initial position of the agent is the same as the vertices of the octagon pattern (in Fig. 2) and the velocity is chosen randomly in the range $[0, 2] \times [0, 2]$ (in Fig. 4).

The flocking error is analyzed to match the velocity of agents with the leader and achieve one of the flocking attributes: alignment [21]. The variation in the relative velocity of agents with the leader results in flocking error in leader-follower configuration of MAS. The relative velocity of agents with the leader is shown in Fig. 7. It is observed that the agents in polygon formation follow the leader's trajectory in 1.5s (settling time) along x and y axes [shown in Fig. 7(a) and Fig. 7(b)]. The transient time for both axes is around 1s at 0.2 amplitude. This infers that the agents are flocking quickly at less peak amplitude value. The distributed control strategy is used for the agents in hexagon to flock along the pre-defined trajectory [8]. The flocking of the hexagon pattern converges to zero at 5s using the distributed control strategy [8]. The proposed strategy is useful to achieve convergence of flocking error to zero, faster than in [8] and is suitable for any polygonal configuration. The cycle change is observed every 20s and follows the trajectory of the leader.

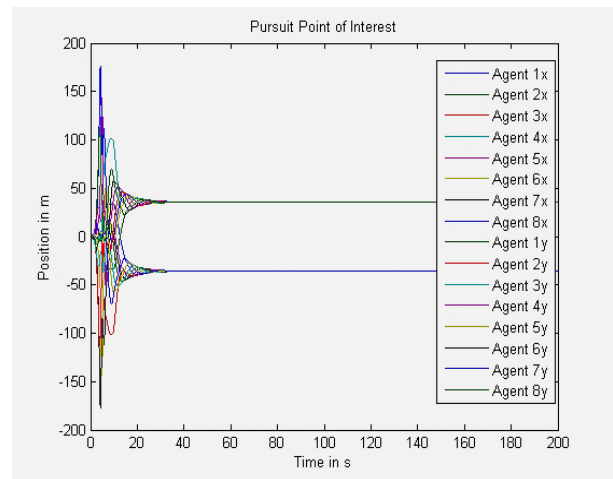
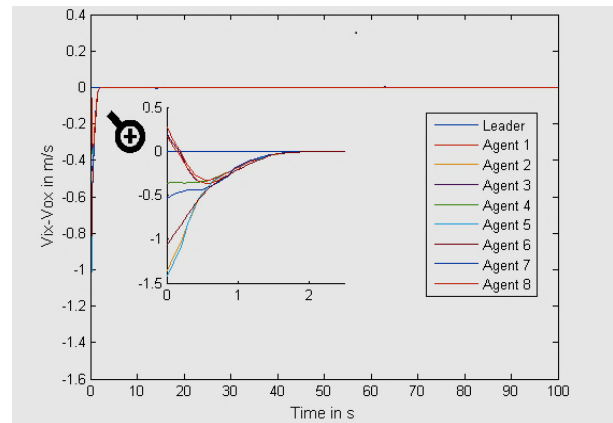
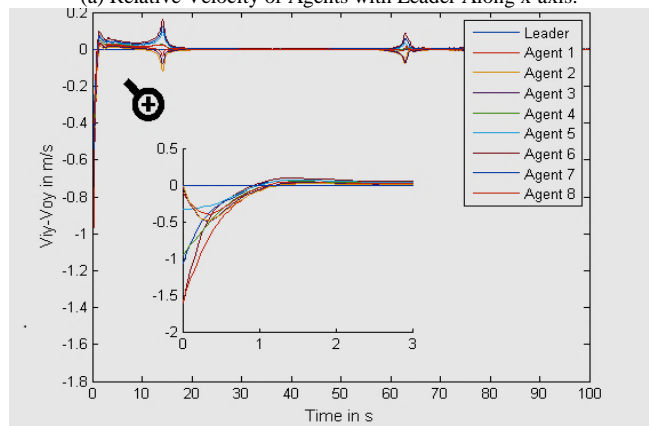


Fig. 6. Consensus Agreement for All Agents.

The robustness of MAS is achieved by maintaining average position error of agents with the leader as minimal as possible (band of $[-1,1] \times [-1,1]$). The robustness of flocking behaviour is analyzed to stay close to nearby agents and avoid the collision. The agents are informed to establish a connection with the leader after updating the position using the cyclic pursuit strategy. The connection indicates that the agents are tracing the leader's trajectory, as shown in Fig. 8.



(a) Relative Velocity of Agents with Leader Along x-axis.



(b) Relative Velocity of Agents with Leader Along y-axis.

Fig. 7. Velocity Consensus of Multi-Agents for the Case 1.

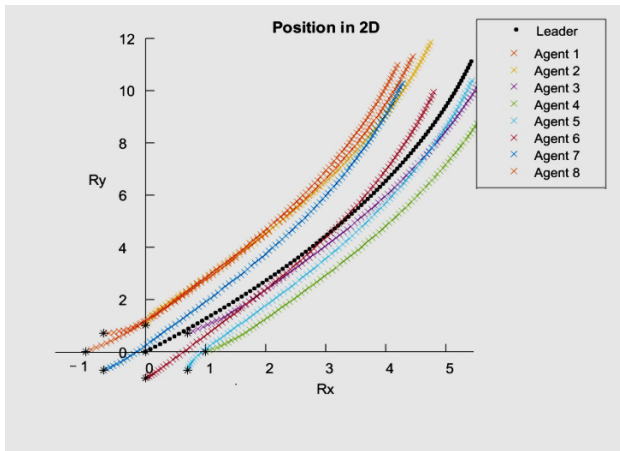
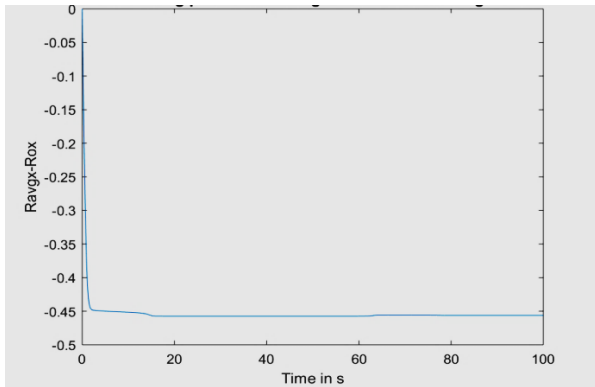


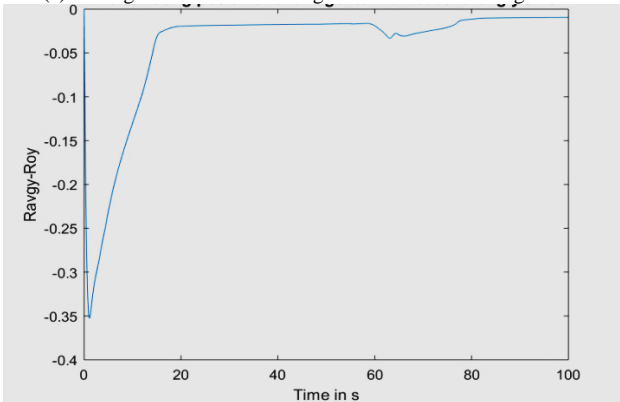
Fig. 8. Trajectory Tracking by Agents in a Closer View using Tribrid Control Strategy for the Case 1.

Because the agents are following the leader's trajectory, the relative velocity of agents with the leaders is converging to zero. Since the agent's velocity is closely observable with that of the leader, the average position error of the agents with the leader is decreased to a minimum constant value of -0.45 in x axis and -0.02 in y axis in $20s$.

The average position error in \mathcal{R}^2 , is shown in Fig. 9(a) and Fig. 9(b), respectively. The error is within the position band and the settling time is, $20s$ as the formation should also be maintained during flocking.



(a) Average Position Error of Agents with Leader Along x-axis.



(b) Average Position Error of Agents with Leader Along y-axis.

Fig. 9. Position Consensus of Multi-Agents for the Case 1.

The octagon formation should be maintained while tracking the leader's trajectory. It is analyzed by using the agent's position at various time and distance between the agents. The distance is maintained at a constant value between 0.19 and 1.18 in $20s$, as shown in Fig. 10.

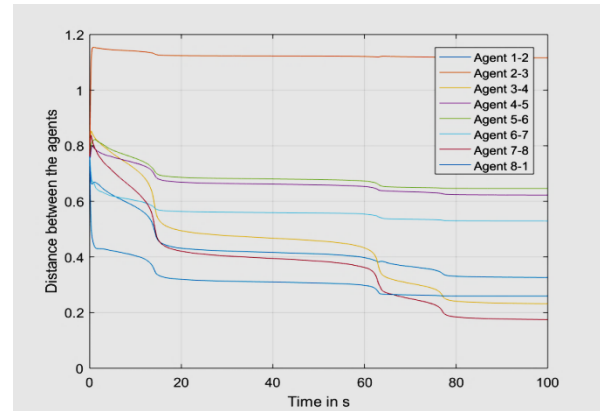


Fig. 10. Inter-agent Distance in Tribrid Strategy for the Case 1.

The structure of the formation is maintained in initial octagonal pattern as shown in Fig. 11. During flocking, the switching in position affects the initial octagonal pattern, as observed in every iteration. The octagonal pattern is achieved in $20s$ (at the iteration $t = 200$). It is observed that in every iteration, two agents are little away from the remaining six agents. It is also inferred in Fig. 11 that inter-agent distance, 2-3, 4-5 and 5-6 are high compared with the other inter-agent distances.

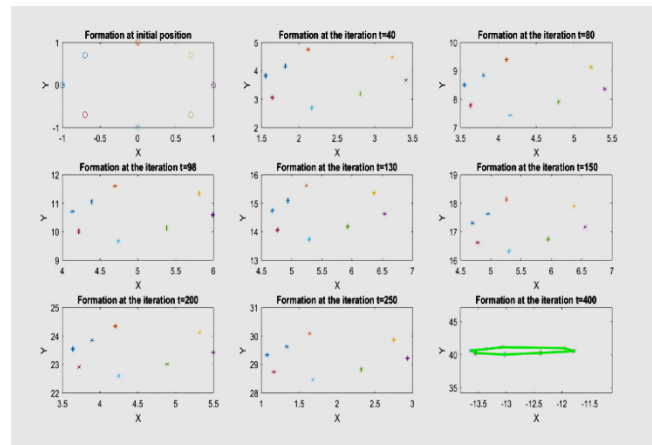


Fig. 11. Formation using Tribrid Control Strategy for the Case 1.

- The agents distributed randomly in space are subjected to follow the leader's trajectory. The initial position of the agent is distributed randomly in the space (in Fig. 3) and the velocity is chosen randomly in the range $[0, 2] \times [0, 2]$ (in Fig. 4).

The variation in the relative velocity of agents with the leader results in flocking error in leader-follower configuration of MAS. The relative velocity of agents with the leader is shown in Fig. 12(a) and Fig. 12(b). It is observed that the agents in octagonal formation follow the leader's trajectory by observing the value of the leader's velocity in $20s$. The

cycle change is observed every 60s and follows the trajectory of the leader. However, in 3s, the agents follow the trajectory of the leader with the flocking error of 0.2m/s.

The robustness of MAS is achieved by maintaining average position error of agents with the leader as minimal as possible (band of $[0,10] \times [0,10]$). The robustness of flocking behaviour is analyzed for an agent to stay close to nearby agents and avoid the collision. The agents are informed to establish a connection with the leader after updating the position using the cyclic pursuit strategy. The connection indicates that the agents are tracing the leader's trajectory, as shown in Fig. 13.

The agents' velocity is closely observable with that of the leader's velocity. Hence, the average position error of the agents with the leader has decreased to a minimum constant value of -0.065 in x axis and -0.6 in y axis in 20s. The average position error in \mathbb{R}^2 along x - and y axes is shown in Fig. 14(a) and Fig. 14(b), respectively.

The formation should be maintained while tracking the leader's trajectory. It is analyzed by using the agent's position at various time and distance between the agents. The distance is maintained at a constant value between 1.5 and 9 in 80s, as shown in Fig. 15.

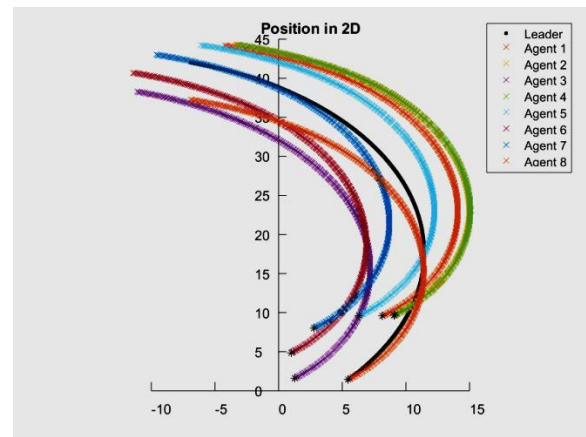
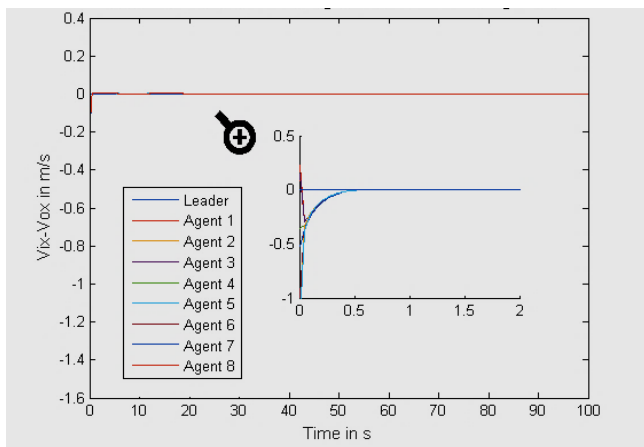
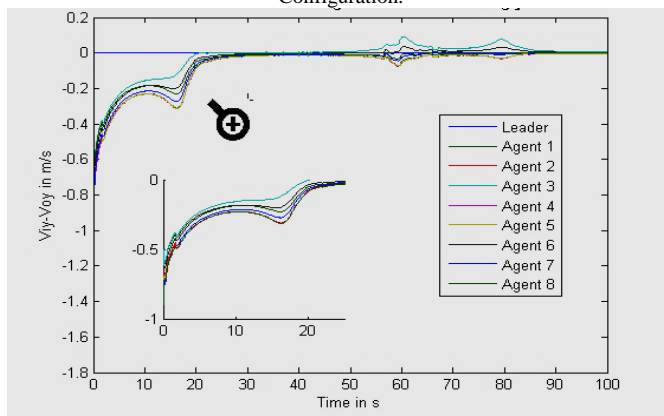


Fig. 13. Trajectory Tracking by Agents in a Closer View using Tribrid Control Strategy for the Case 2.

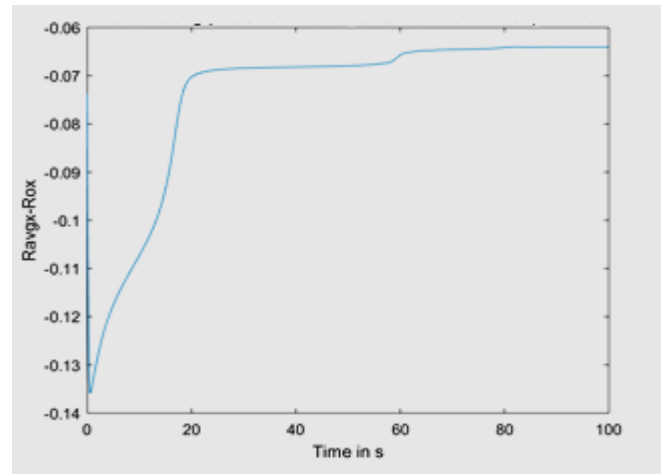


(a) Relative Velocity of Agents with Leader Along x-axis for Random Configuration.

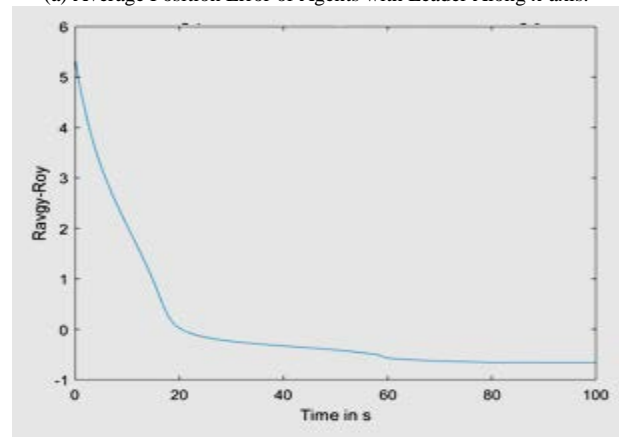


(b) Relative Velocity of Agents with Leader Along y-axis for Random Configuration.

Fig. 12. Velocity Consensus of Multi-Agents for the Case 2.



(a) Average Position Error of Agents with Leader Along x-axis.



(b) Average Position Error of Agents with Leader Along y-axis.

Fig. 14. Position Consensus of Multi-Agents for the Case 2.

The structure of the formation is maintained with the initial pattern as shown in Fig. 16. During flocking, the switching in position affects the initial pattern, as observed in every iteration. The initial pattern is achieved in 20s (at the iteration $t = 200$). It is observed that in any iteration, the configuration is the same as the initial pattern.

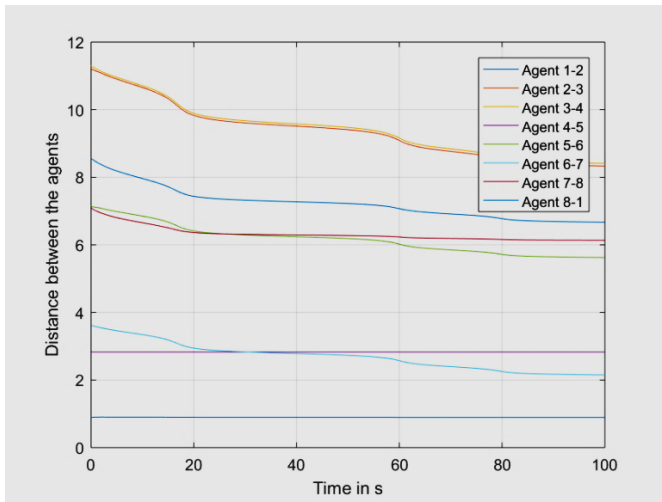


Fig. 15. Inter-agent Distance in Tribrid Strategy for the Case 2.

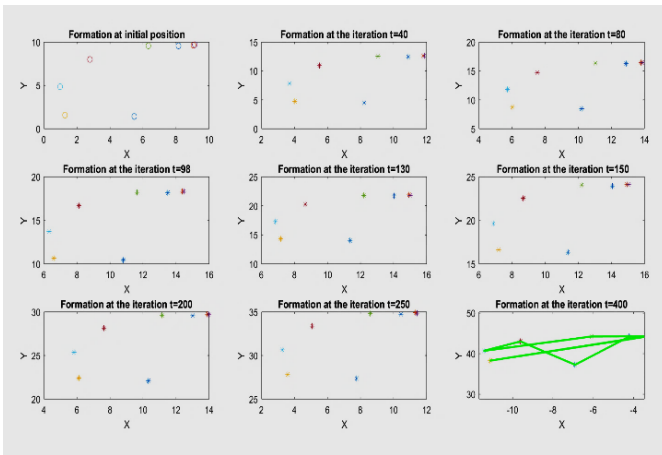


Fig. 16. Formation using Tribrid Control Strategy for the Case 2.

The distributed control strategy is used for proper communication and coordination among agents and avoids a collision while flocking in a pre-defined trajectory [8] and in the leader-follower scenario [17]. The analysis does not focus on simultaneous polygon formation and flocking in the leader-follower scenario. The proposed tribrid control strategy is discussed under two cases: the octagonal pattern from RL and agents distributed in the spatial environment are chosen as the initial position of agents. The comparative analysis for the two cases is given in Table I and Table II.

TABLE I. COMPARATIVE ANALYSIS OF FLOCKING AND FORMATION BEHAVIOUR IN TRIBRID CONTROL STRATEGY

Flocking Configuration					
Cases	Relative Velocity of Agents with the Leader in m/s		Average Position Error of Agents in m		
	Transient Time in s	Settling Time in s	x- coordinate	y- coordinate	Settling Time in s
Case 1	0.2	1.5	-0.45	-0.02	1.5
Case 2	1	20	-0.065	-0.6	20

TABLE II. COMPARITIVE ANALYSIS OF FORMATION BEHAVIOUR IN TRIBRID CONTROL STRATEGY

Formation Configuration		
Cases	Inter-agent Distance Range	Formation Structure
Case 1	0.19-1.18	Same as initial position
Case 2	1.5-9	Same as initial position

The flocking error of eight agents in the polygon pattern has converged to zero at 1.5s for the Case 1 and 20s for the Case 2. The distributed control strategy is used for the agents in hexagon pattern to flock along the pre-defined trajectory [8]. The flocking of the pattern converges to zero in 5s using the distributed control strategy [8]. Thus, the proposed strategy enables the system to converge faster. The details of comparison of various configurations of flocking at time-varying velocity are described in Table III. As can be observed in Table III, the earlier studies [8,19,22] did consider configurations which have dimensions smaller than octagon configuration to flock at time-varying velocity. In this paper which considers octagonal contour for flocking, the convergence of flocking error to zero has been achieved faster than the existing studies [8, 19, 22].

TABLE III. COMPARITIVE ANALYSIS OF VARIOUS CONTOUR CONFIGURATION FLOCKING AT TIME-VARYING VELOCITY

		Flocking Error
Sl. No.	Contour configurations flocking at time- varying velocity	Settling Time in s
1	Octagonal contour flocking at time-varying velocity (Proposed Tribrid Control Strategy for Case 1)	1.5
2	Square contour flocking at time – varying velocity [22]	5
3	Formation tracking control [19]	2
4	Hexagonal contour flocking at time – varying velocity [8]	5

The settling time is high (20s) for the Case 2, compared to Case 1. If the agents are randomly distributed in an environment, then the centroid of agents cannot be maintained with the leader's position. It results in a larger average position error, as observed in Table I. Also it results in larger inter-agent distance range, as observed in Table II. The advantage of the tribrid approach is that the formation structure will remain the same as the initial configuration.

VI. CONCLUSIONS

In this paper, the simulation model of flocking uses the tribrid control strategy for demonstration of two cases: multi-agents distributed randomly in the environment and multi-agents in polygonal formation (obtained from Reinforcement Learning (RL)). The initial positions of multi-agents are varied with the variation of gain value in the cyclic pursuit strategy to maintain the distance between the agents at a constant value. Also, the cyclic pursuit strategy is applied to the multi-agent dynamics to achieve consensus among the agents and to maintain the formation. The analysis of simultaneous formation and flocking is discussed in two cases:

- The agents form polygonal formation using Q-learning and are integrated with cyclic pursuit strategy to maintain the octagonal formation.
- The agents in a randomly distributed environment use cyclic pursuit strategy to achieve and maintain the octagonal formation.

In both the cases, the inter-agent distance and cyclic pursuit interest are achieved in 20s. The positions of agents are updated using the cyclic pursuit strategy before performing flocking. The flocking error of eight agents in the polygon pattern has converged to zero at 1.5s in first case and at 20s in the second case, with the proposed tribrid control strategy. The average position error of agents with the leader has increased by 4% for the second case, compared with the first case. In both the cases, the agents in the octagonal polygon configuration follow the leader's trajectory in 0.2s. To conclude, the proposed tribrid control strategy enables the flocking error of multi-agents to converge faster and is suitable for closed contour configuration of multi-agents. The advantage of the tribrid approach is the facilitation of the retention of formation structure of the initial configuration. The proposed approach has the assumption that all the agents are always connected during flocking and formation. The disconnection leads to diverging behavior of flocking and formation configuration of multi-agents. Hence an analysis for the scenario of loss of connectivity during simultaneous polygonal formation and leader-follower flocking of multi-agents can be of significant importance from both research and system perspectives.

REFERENCES

- [1] Z. H. Ismail, N. Sariff and E. G. Hurtado, "A survey and analysis of cooperative multi-agent robot systems: challenges and directions," in *Applications of Mobile Robots, IntechOpen*, 2018, pp. 8-14.
- [2] A. Dorri, S. S. Kanhere and R. Jurdak, "Multi-Agent Systems: A Survey," *IEEE Access*, vol. 6, pp. 28573-28593, 2018.
- [3] W. Ren, "Consensus strategies for cooperative control of vehicle formations," *IET Control Theory & Applications*, vol. 1, no. 2, pp. 505-512, 2007.
- [4] T. M. Cheng and A. V. Savkin, "Decentralized control of multi-agent systems for swarming with a given geometric pattern," *Computers & Mathematics with Applications*, vol. 61, no. 4, pp. 731-744, 2011.
- [5] Jaydev P Desai, James P Ostrowski, and Vijay Kumar, "Modeling and control of formations of nonholonomic mobile robots", *IEEE transactions on Robotics and Automation*, 17(6):905-908, 2001.
- [6] I. M. H. Sanhoury, S. H. M. Amin and A. R. Husain, "Synchronizing Multi-robots in Switching between Different Formations Tasks While Tracking a Line," in *Trends in Intelligent Robotics, Automation, and Manufacturing*, Springer, 2012, pp. 28-36.
- [7] A. Guillet, R. Lenain, B. Thuilot, and P. Martinet, "Adaptable robot formation control: Adaptive and predictive formation control of autonomous vehicles," *IEEE Robotics Automation Magazine*, 21(1):28{39, March 2014, ISSN 1070-9932. doi: 10.1109/MRA.2013.2295946.
- [8] A. Mondal, C. Bhowmick, L. Behera and M. Jamshidi, "Trajectory tracking by multiple agents in formation with collision avoidance and connectivity assurance," *IEEE Systems Journal*, vol. 12, no. 3, pp. 2449-2460, 2018.
- [9] F. Liao, R. Teo, J. L. Wang, X. Dong, F. Lin and K. Peng, "Distributed Formation and Reconfiguration Control of VTOL UAVs," *IEEE Transactions on Control Systems Technology*, vol. 25, no. 1, pp. 270-277, Jan 2017.
- [10] H. Rezaee and F. Abdollahi, "Pursuit formation of double-integrator dynamics using consensus control approach," *IEEE Transactions on Industrial Electronics*, vol. 62, no. 7, pp. 4249-4256, 2015.
- [11] B. K. S. Prasad, A. G. Manjunath and H. Ramasangu, "Multi-agent Polygon Formation using Reinforcement Learning," in *Proceedings of the 9th International Conference on Agents and Artificial Intelligence - Volume 1: ICAART*, 2017.
- [12] Junyan Hu, Parijat Bhowmick, Inmo Jang, Farshad Arvin, and Alexander Lanzon, "A decentralized cluster formation containment framework for multirobot systems," in *IEEE Transactions on Robotics*, 37(6):1936{1955, 2021a. doi: 10.1109/TRO.2021.3071615.
- [13] Junyan Hu, Parijat Bhowmick, and Alexander Lanzon, "Group coordinated control of networked mobile robots with applications to object transportation," *IEEE Transactions on Vehicular Technology*, 70(8):8269-8274, 2021b. doi: 10.1109/TVT.2021.3093157.
- [14] S. Keshmiri and S. Payandeh, "A centralized framework to multi-robots formation control: Theory and application," in *Collaborative Agents-Research and Development*, Springer, 2009, pp. 85-98.
- [15] S. Ghapani, J. Mei and W. Ren, "Flocking with a moving leader for multiple uncertain lagrange systems," in *American Control Conference (ACC)*, 2014, 2014.
- [16] G. R. Mallik, S. Daingade and A. Sinha, "Consensus based deviated cyclic pursuit for target tracking applications," in *2015 European Control Conference (ECC)*, 2015.
- [17] W. Yu, G. Chen and M. Cao, "Distributed leader-follower flocking control for multi-agent dynamical systems with time-varying velocities," *Systems & Control Letters*, vol. 59, no. 9, pp. 543-552, 2010.
- [18] S. Zhao, D. Zelazo, Translational and scaling formation maneuver control via a bearing-based approach, *IEEE Transactions on Control of Network Systems* 4 (3) (2017) 429{438. doi:10.1109/TCNS.2015.2507547.
- [19] S. Li, Q. Wang, E. Wang, Y. Chen, Bearing-only adaptive formation control using back-stepping method, *Frontiers in Control Engineering* (2021). doi:10.3389/fcteg.2021.700053.
- [20] Q. Van Tran, J. Kim, Bearing-constrained formation tracking control of nonholonomic agents without inter-agent communication, *IEEE Control Systems Letters* (2022) 2401{2406. doi:10.1109/LCSYS.2022.3159128.
- [21] C. W. Reynolds, "Flocks, herds and schools: A distributed behavioral model," in *ACM SIGGRAPH computer graphics*, 1987.
- [22] Jia Wang, Jiannong Cao, Milos Stojmenovic, Miao Zhao, Jinlin Chen, and Shan Jiang, "Pattern-rl: Multi-robot cooperative pattern formation via deep reinforcement learning", pages 210–215, 12 2019a. doi: 10.1109/ICMLA.2019.00040

Merged Dataset Creation Method Between Thermal Infrared and Microwave Radiometers Onboard Satellites

Kohei Arai

Saga University, Saga City, Japan

Abstract—Merged dataset creation method between Thermal Infrared (TIR) and Microwave Scanning Radiometer (MSR) onboard remote sensing satellites is proposed. One of the key issues here is the relation between thermal and microwave emissions from the same observation target in particular, Sea Surface Temperature (SST). An example of Tropical Rainfall Measuring Mission (TRMM) satellite based TIR and MSR, Visible Infrared Scanner (VIRS) and TRMM Microwave Imager (TMI) is shown in this paper. SST is estimated, independently, with VIRS or TMI. A method for interpolation of multi-sensor satellite images based on Multi-Resolution Analysis (MRA) is also proposed. The experimental results with TMI/SST image and VIRS/SST image show that Root Mean Square (RMS) error ranges from 0.87 to 0.91-degree C.

Keywords—Wavelets; VIRS/SST; TMI/SST; MRA; Daubechies; TRMM; TIR; MSR

I. INTRODUCTION

In order to increase observation chances of SST, both of TIR radiometer data and microwave radiometer data are desirable to use with consideration of the difference of radiative transfer processes and interactions between electronic magnetic waves and the sea surfaces. Also, a merged dataset between TIR and microwave radiometer data is also desirable together with a combined SST dataset derived from the TIR and microwave radiometer data.

In general, spatial resolution of TIR is better than that of MSR. TIR data can be acquired in a clear weather condition only. On the other hand, MSR data can be acquired in a cloudy condition as well as rainy condition. If these data can be merged, then fine resolution of microwave and thermal emission of data can be available to use. Also, it becomes possible to increase observation frequency.

Merged dataset creation method between TIR and microwave radiometers onboard remote sensing satellites is proposed. One of the key issues here is the relation between TIR and microwave emissions from the same observation target in particular, SST.

As an example of applying wavelet analysis (expansion, transformation, etc.) to the processing analysis of earth observation satellite images, a method of superimposing multiple visible images after wavelet transform [1], superimposing multiple Synthetic Aperture Radar: SAR images with different off-nadir angles [2], a method of

applying the wavelet transform to the pattern of annual fluctuation of the sea surface temperature estimated from satellite data and extracting its characteristics [3], and applying the wavelet transform to the extraction of the surface roughness of sea ice. There are methods [4], methods [5] for extracting spatial features from images extracted from soil moisture, etc. [6].

By the way, in November 1997, the TRMM (Tropical Rainfall Measuring Mission) satellite [Solar Asynchronous Orbit] was launched. The Sea Surface Temperature (SST) is estimated independently by the sensor TMI (TRMM Microwave Imager) and the sensor VIRS (Visible Infrared Scanner) mounted on the TRMM satellite [7]. In this paper, the relationship between SST (TMI / SST) estimated from TMI observation data and SST (VIRS / SST) estimated from VIRS observation data is examined using multi-resolution analysis. That is, the relationship between the actual observation satellite data questions of different types of sensors.

The proposed method considers Multi-Resolution Analysis (MRA). The Daubechies basis (orthonormal basis) is used as the mother wavelet when performing multi-resolution analysis.

The next section describes the related research works in particular SST estimation methodology then the proposed method of merged dataset is created between TIR and microwave radiometer data and theoretical background of fundamentals of wavelet analysis. After that experimental method and results are described followed by conclusion with some discussions.

II. RELATED RESEARCH WORKS

As for the SST estimation method, there are the following related research works.

SST estimation of the pixels partially contaminated with cloud is conducted [8]. A merged dataset for obtaining cloud free Infrared (IR) data and a cloud cover estimation within a pixel for SST retrieval is defined [9]. SST estimation with Advanced Earth Observing Satellite (ADEOS) / Ocean Color and Temperature Scanner (OCTS) data is conducted [10].

Cross validation of OCTS Global Area Coverage (GAC) SST with Multi-Channel SST (MCSST) is conducted [11]. On the other hand, antenna pattern correction and SST estimation algorithms for Advanced Microwave Scanning Radiometer: AMSR is made [12].

SST estimation method with linearized inversion of radiative transfer code for ADEOS/OCTS is proposed [13]. SST estimation accuracy assessment for ASTER/TIR is conducted and also an effectiveness of 8.3 μ m water vapor absorption band for SST retrieval is investigated [14].

SST estimation with microwave radiometers by means of simulated annealing based on an ocean surface model is conducted [15] together with SST retrieval with microwave radiometer data based on simulated annealing [16].

Estimation of SST, wind speed and water vapor with microwave radiometer data based on simulated annealing is attempted [17] together with estimation of SST, wind speed and water vapor with microwave radiometer data based on simulated annealing [18].

Estimation method of SST with Moderate resolution of Imaging Spectrometer: MODIS data in particular utilizing Band 29 for reducing water vapor influence on SST retrievals is proposed [19]. Nonlinear optimization-based SST estimation methods with remote sensing satellite based Microwave Scanning Radiometer: MSR data are proposed [20].

Comparative study on sea surface temperature estimation with thermal infrared radiometer data among conventional MCSST, split window and conjugate gradient-based methods is conducted [21]. Effectiveness of Noise Equivalent delta Temperature: NEdT and Band 10 (8.3 μ m) of The Advanced Spaceborne Thermal Emission and Reflection Radiometer: ASTER/ Thermal Infrared Radiometer: TIR on Skin SST: SSST estimation is estimated [22].

Band combination selection method for SST estimation with satellite data is proposed [23]. Artificial Intelligence: AI and remote sensing satellite big data analysis is overviewed [24].

On the other hand, there are the following related research works on the microwave remote sensing.

Data fusion between microwave and thermal infrared radiometer data and its application to skin sea surface temperature, wind speed and salinity retrievals are proposed [25]. Comparative study of optimization methods for estimation of Sea Surface Temperature (SST) and Ocean Wind (OW) with Microwave Radiometer data is conducted [26]. Also, method for rainfall rate estimation with satellite-based microwave radiometer data is proposed [27]. Meanwhile, ice concentration estimation method with satellite-based microwave radiometer by means of inversion theory is proposed [28].

III. PROPOSED METHOD WITH THEORETICAL BACKGROUND

A. Proposed Method

Merged dataset creation method proposed here is to utilize both of TIR and microwave radiometer data together. Therefore, the relation between TIR and microwave radiometer data is a key issue here. Moreover, missing data are another issue. TIR radiometer data does not work in a cloudy condition and rainy condition. Furthermore, spatial resolutions are different between TIR and microwave radiometers. Therefore, some treatments of the missing data as well as spatial

resolution difference are needed to use both radiometer data together. In order to take into account the missing data and spatial resolution difference, wavelet Multi-Resolution Analysis (MRA) is featured.

B. Theoretical Background on Wavelet Analysis

Multi-Resolution Analysis (MRA) needs Mother wavelet and is based on Discrete Wavelet Transform: DWT. As a mother wavelet is defined as follows:

The function ϕ that satisfies the two-scale relationship as follows:

$$\phi(x) = \sum_{k \in \mathbb{Z}} p_k \phi(2x - k) \quad (1)$$

This is called the scaling function.

The sequence $\{p_k / k \in \mathbb{Z}\}$ is called a two-scale sequence, and the scaling function ϕ is determined by the sequence $\{p_k / k \in \mathbb{Z}\}$. The mother wavelet ψ is determined by equation (2).

$$\psi(x) = \sum_{k \in \mathbb{Z}} q_k \phi(2x - k) \quad (2)$$

Also, Discrete Wavelet Transform: DWT is defined as follows:

The transformation of the discrete wavelet of the function $f(x)$ by mother wavelet $\psi(x)$ is also given by (3), and its inverse transformation is given by (4).

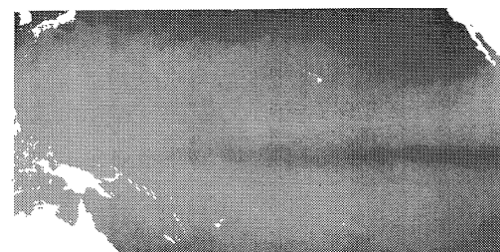
$$d_k^{(j)} = 2^j \int_{-\infty}^{\infty} \overline{\psi(2^j x - k)} f(x) dx \quad (3)$$

$$f(x) \sim \sum_j \sum_k d_k^{(j)} \psi(2^j x - k) \quad (4)$$

IV. NUMERICAL EXPERIMENT

A. Outline of Experiment

The data used this time are SST estimated images from November 1998 to September 2000 estimated by sensor TMI and sensor VIRS, respectively. Fig. 1(a) shows an example of SST (VIRS / SST) estimated from VIRS observation data, and Fig. 1(b) shows an example of SST (TMI/SST) estimated from TMI observation data.



(a) VIRS.



(b) TMI.

Fig. 1. Examples of SST Images Estimated with VIRS or TMI.

From Fig. 1, it can be seen that the spatial resolution of the VIRS observation data and the TMI observation data are different. The image size of VIRS / SST is 1024 x 512, and the image size of TMI / SST is 512 x 256. The spatial resolution of VIRS observation data is about twice the spatial resolution of TMI observation data.

In this experiment, wavelet decomposition is performed on the VIRS / SST image, and the relationship between the result (LL component) and the TMI / SST image is examined. In addition, consider the impact of differences in support length. By the way, the target VIRS / SST and TMI / SST each include missing data due to the influence of the atmosphere, sensor characteristics, satellite orbit characteristics, and the like. In this experiment, the land data is regarded as missing data. Therefore, the multi-resolution analysis is performed in consideration of the missing data. That is:

- 1) Data of points where TMI / SST is not missing.
- 2) All VIRS / SST for generating data corresponding to the points where TMI / SST is not missing by using wavelet decomposition have been observed.

Consider using data that satisfies the two conditions of the data in the region (not missing) [problem of support length during wavelet decomposition]. The above two conditions are called considerable conditions.

First, $Z(\text{sup}, i, j, t)$ def is defined as follows:

$$\vartheta(\text{sup}, i, j, t) = 1 \text{ or } 0 \tag{5}$$

1: Satisfy the conditions for consideration.

0: Does not meet the considerable conditions.

Then, evaluation is performed using the following.

$$J1(\text{sup}) = \sqrt{\frac{\sum_{t=1}^{22} \sum_{(i,j)} (\vartheta(\text{sup}, i, j, t) \varepsilon_1(i, j, t))}{N}} \tag{6}$$

$$\varepsilon_1(i, j, t) = (G(i, j, t) - H(i, j, t))^2 \tag{7}$$

However, sup represents the support length of the mother wavelet, t represents the time, [i, represents the position, and (i, j, t) represents the TMI / SST, and $\sigma(i, j, t)$]. Represents the LL component when VIRS / SST is wavelet-decomposed. Further, N represents the number of $Z(\text{sup}, i, j, t) = 1$.

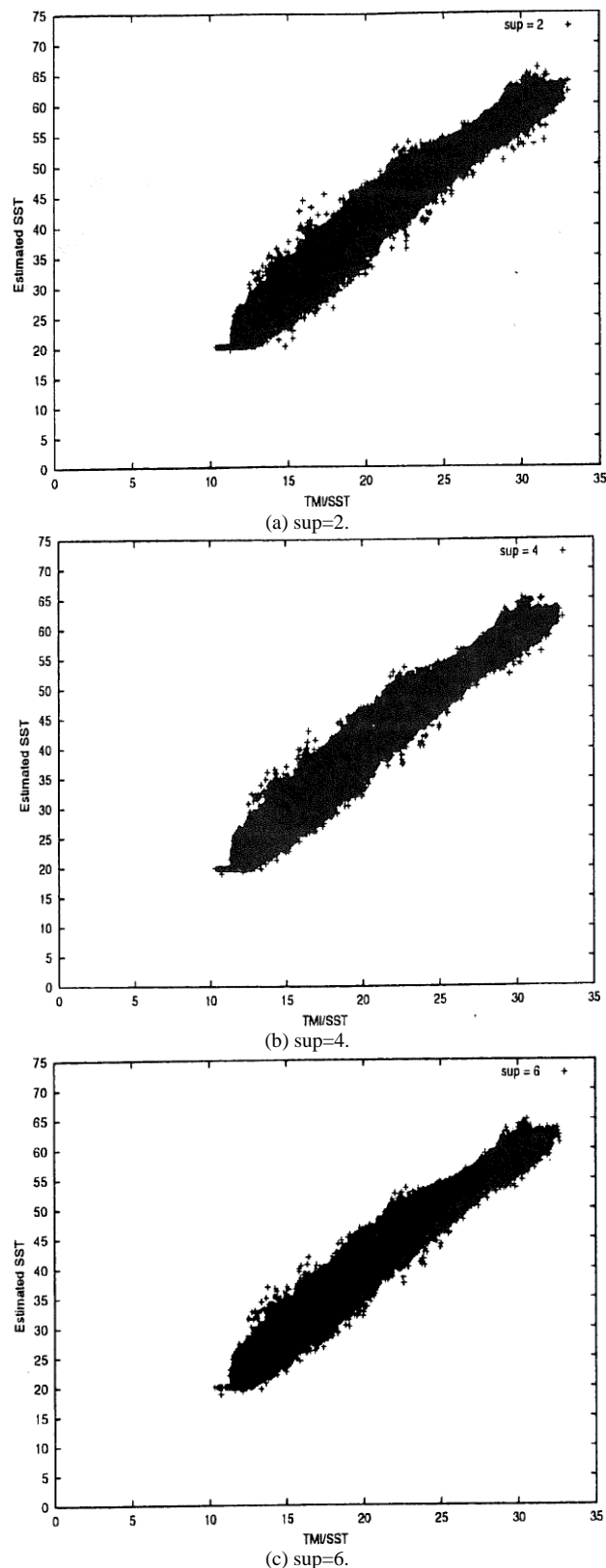
B. Experimental Results

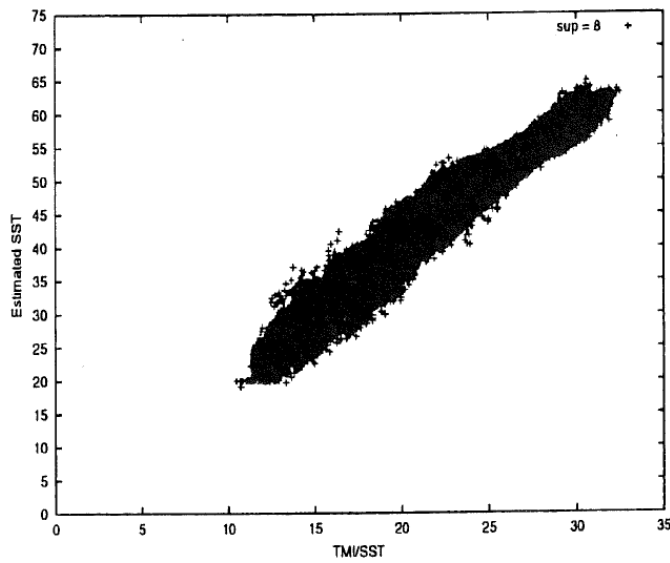
Table I shows the value of $J1(\text{sup})$ when the support length sup is changed and the number of data N that satisfies the conditions that can be considered for each support length.

TABLE I. THE ERROR $J1(\text{SUP})$ AND NUMBER OF OBSERVED DATA N FOR THE SUPPORT LENGTH SUP

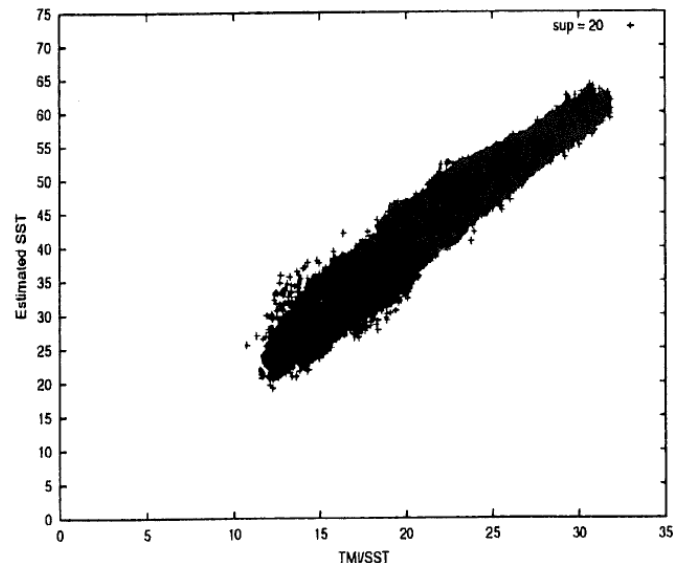
SUP	J1(SUP)	N
2	25.63	2559974
4	25.644	2537353
6	25.652	2506378
8	25.659	2471573
16	25.676	2331352
20	25.681	2264613

Fig. 2 shows the relationship between the LL component and TMI / SST when the VIRS / SST is wavelet-decomposed when the support length sup is changed [under the conditions that can be considered].





(d) sup=8.



(g) sup = 20.

Fig. 2. Relationship between TMI / SST Data and the Estimated SST through MRA.

The horizontal axis shows TMI / SST, and the vertical axis shows the LL component when VIRS / SST are wave-resolved. Also, physical properties of the ocean surface in thermal emission and microwave emission are different each other so that these effects have to be clarified. For instance, penetration depth of the ocean surface is different between thermal and microwave electric magnetic wave. The divergence shown in the Fig. 2 is caused by the different physical properties of the ocean between thermal and microwave electric magnetic wave.

Table II shows the results of regression analysis on the scatter plots at each support length in Fig. 2, that is, the unknown regression coefficient (a, b) was obtained using the following:

$$J2(sup) = \sqrt{\frac{\sum_{t=1}^{22} \sum_{(i,j)} (\theta(sup,t,j,t) \varepsilon_2(i,j,t))}{N}} \quad (8)$$

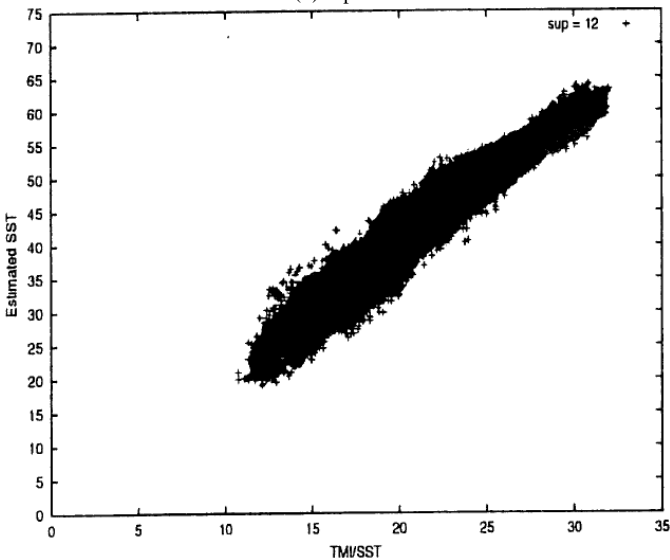
$$\varepsilon_2(i,j,t) = (G(i,j,t) - H(i,j,t))^2 \quad (9)$$

TABLE II. REGRESSION COEFFICIENTS OF SST ESTIMATION AND THE ERROR J2(SUP), FOR THE SUPPORT LENGTH SUP

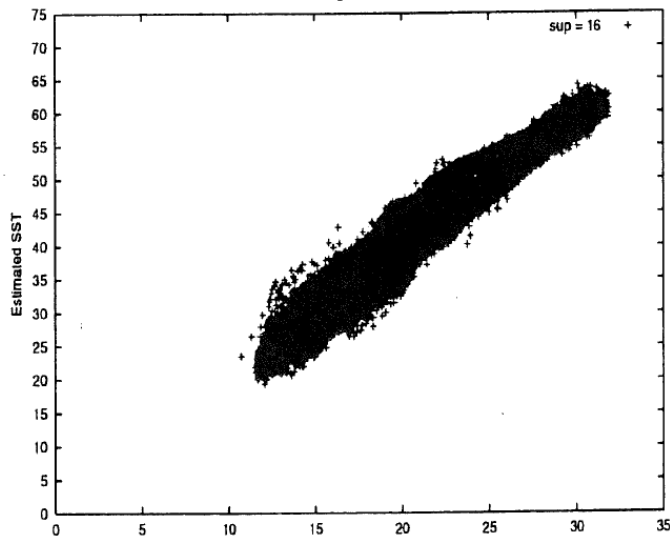
SUP	A	B	J2(SUP)	N
2	1.948	0.873	0.87	2559974
4	1.947	0.927	0.873	2537353
6	1.944	0.997	0.873	2506378
8	1.942	1.07	0.875	241573
12	1.937	1.219	0.883	2400801
16	1.932	1.363	0.895	2331352
20	1.927	1.505	0.909	2264613

V. CONCLUSION

Merged dataset creation method between Thermal Infrared (TIR) and Microwave radiometers onboard remote sensing satellites is proposed. One of the key issues here is the relation



(e) sup=12.



(f) sup=16.

between TIR and microwave emissions from the same observation target in particular, Sea Surface Temperature (SST). An example of Tropical Rainfall Measuring Mission (TRMM) satellite based TIR and microwave radiometers, Visible Infrared Scanner (VIRS) and TRMM Microwave Imager (TMI) is shown in this paper. SST is estimated, independently, with VIRS or TMI. A method for interpolation of multi-sensor satellite images based on Multi-Resolution Analysis (MRA) is also proposed.

In this paper, the relationship between the actual observation satellite data questions of different types of sensors including missing data was examined using multiple resolution analysis. From Table I, when examining the relationship between different types of sensors and data questions using multiple resolution analysis, it was confirmed that the shorter the support length, the better the error J1 (sup). From Table II, the regression error J2 (It was confirmed that sup) was 0.87 to 0.91 [C].

VI. FUTURE WORKS

In the future, the author will continue to validate of the proposed method with a variety of TIR and microwave radiometer data. Improvement of observation frequency by the proposed method is another issue. Also, physical properties of the ocean surface in thermal emission and microwave emission are different each other so that these effects have to be clarified. For instance, penetration depth of the ocean surface is different between thermal and microwave electric magnetic wave.

ACKNOWLEDGMENT

This is a report of the research results (or part of it) by the Grant-in-Aid for Scientific Research (Special Researcher Incentive). The author would like to express my gratitude to the Grant provider. The author would like to thank Dr. Kaname Seto of former student of Saga University and Dr. Leland M. Jameson of Naval Research Laboratory for their contribution of this study. The author, also, would like to thank Professor Dr. Hiroshi Okumura and Professor Dr. Osamu Fukuda for their valuable discussions.

REFERENCES

- [1] J.P. Djamdji, A. Bijaoui, and R. Maniere: "Geometrical Registration of Images: The Multiresolution Approach," *Photogrammetric Engineering & Remote Sensing*, Vol.59, No. 5, pp.645-653, (1993).
- [2] WM Moon, JS Won, V. Singhroy, and PD Lowman Jr.: "ERS-1 and CCRS CSAR data integration for look-direction bias correction using wavelet transform," *Canadian Journal of Remote Sensing*, Vol.20, No. 3, pp.280-285, (1994).
- [3] M. Mak: "Orthogonal Wavelet analysis: Interannual Variability in Sea Surface Temperature," *Bulletin of the American Meteorological Society*, Vol.76, No.11, pp.2179-2186, (1995).
- [4] R.W. Lindsay, D.B. Percival, and D.A. Rothrock: "The Discrete Wavelet Transform and the Scale Analysis of the Surface" *Properties of Sea Ice*, "IEEE Transactions on Geoscience and Remote Sensing", Vol.34, No.3, pp.771-787, (1996).
- [5] Z. Hu, Y. Chen, and S. Islam: "Multiscaling properties of soil moisture images and decomposition of large- and small-scale features using wavelet transforms," *International Journal of Remote Sensing*, Vol.19, No.13, pp.2451-2467, (1998).
- [6] Kohei Arai, Kaname Seto, LM Jameson: "Extraction of water mass features from satellite images using polar coordinate expression Wavelet," *Journal of Visualization Information Society*, Vb1.19, Suppl.No. 1, pp. 99-102, (1999).
- [7] Kohei Arai and Kaname Seto: "Extraction of change points of multi-period earth observation satellite images based on wavelet decomposition and tiling," *Journal of Visualization and Information Science*, Vol.20, Suppl. No. 1, pp. 285-288, (2000).
- [8] Kohei Arai, SST estimation of the pixels partially contaminated with cloud, *Proceedings of the Asian-Pacific ISY (International Space Year) Conference*, 1992.
- [9] Kohei Arai, A Merged Dataset for Obtaining Cloud Free IR Data and a Cloud Cover Estimation within a Pixel for SST Retrieval, *Asian-Pacific Remote Sensing Journal*, Vol.4, No.2, pp.121-127, Jan.1992.
- [10] Kohei Arai and M.Matsumoto, SST estimation with ADEOS/OCTS data, *Proceedings of the 4th Annual Japan-US Workshop on Ocean Color*, 1993.
- [11] Kohei Arai, Cross Validation of OCTS GAC SST with MCSST, *Proceedings of the 2nd ADEOS Symposium*, 905-907(1997).
- [12] Kohei Arai and K.Teramoto, Antenna Pattern Correction and SST Estimation Algorithms for AMSR *Proceedings of the AMSR Science Workshop*, (1997).
- [13] Kohei Arai and Masao Moriyama, SST Estimation Method with Linearized Inversion of Radiative Transfer Code for ADEOS/OCTS, *Proc. of the COSPAR Congress*, A0.1-0021, 1998.
- [14] Kohei Arai, Sea Surface Temperature (SST) estimation accuracy assessment for ASTER/TIR -An effectiveness of 8.3 μ m water vapor absorption band for SST retrieval-, *Canadian Journal of Remote Sensing*, Vol.26, No.6, pp.576-579, (2000).
- [15] Kohei Arai, Sea Surface Temperature (SST) estimation with microwave radiometers by means of simulated annealing based on an ocean surface model, *Proceedings of the NASA Oceanography Scientific Conference*, Florida, USA, 2001.
- [16] Kohei Arai, Sea Surface Temperature (SST) retrieval with microwave radiometer data based on simulated annealing, *Electrical Association Kyushu Branch Joint Conference*, Asian Session, 2001.
- [17] Kohei Arai and Jun Sakakibara, Estimation of SST, wind speed and water vapor with microwave radiometer data based on simulated annealing, *Abstracts of the 35th Congress of the Committee on Space Research of the ICSU*, A1.1-0130-04, (2004).
- [18] Kohei Arai and J.Sakakibara, Estimation of SST, wind speed and water vapor with microwave radiometer data based on simulated annealing, *Advances in Space Research*, 37, 12, 2202-2207, 2006.
- [19] Kohei Arai, Estimation method of Sea Surface Temperature: SST with MODIS data in particular utilizing Band 29 for reducing water vapor influence on SST retrievals, *International Journal of Research and Review on Computer Science*, 3, 5, 1808-1812, 2012.
- [20] Kohei Arai, Nonlinear Optimization Based Sea Surface Temperature: SST Estimation Methods with Remote Sensing Satellite Based Microwave Scanning Radiometer: MSR Data, *International Journal of Research and Reviews in Computer Science (IJRRCS)* Vol. 3, No. 6, 1881-1886, December 2012, ISSN: 2079-2557.
- [21] Kohei Arai, Comparative study on sea surface temperature estimation with thermal infrared radiometer data among conventional MCSST, split window and conjugate gradient based methods, *International Journal of Advanced Research in Artificial Intelligence*, 2, 8, 7-15, 2013.
- [22] Kohei Arai, Effectiveness of NEdT and Band 10 (8.3 μ m) of ASTER/TIR on SSST Estimation, *Proceedings of the FICC Conference 2018*, 744-748, .2018.
- [23] Kohei Arai, Band Combination Selection Method for SST Estimation with Satellite Data, *Proceedings of the FICC Conference*, Singapore, 1-5, 2018.
- [24] Kohei Arai, (Keynote Speech), AI and Remote Sensing Satellite Big Data Analysis, *Proceedings of the 1st Annual Advanced Technology Applied Science and Engineering Conference*, ATASEC 2019, Polytechnics State of Malang, 2019.
- [25] Kohei Arai, Data fusion between microwave and thermal infrared radiometer data and its application to skin sea surface temperature, wind speed and salinity retrievals, *International Journal of Advanced Computer Science and Applications*, 4, 2, 239-244, 2013.
- [26] Kohei Arai, Comparative Study of optimization Methods for Estimation of Sea Surface Temperature and Ocean Wind wit microwave

Radiometer data, International Journal of Advanced Research on Artificial Intelligence, 5, 1, 1-6, 2016.

- [27] Kohei Arai, Method for rainfall rate estimation with satellite based microwave radiometer data, International Journal of Advanced Computer Science and Applications IJACSA, 11, 3, 82-91, 2020.
- [28] Kohei Arai, Ice Concentration Estimation Method with Satellite based Microwave Radiometer by Means of Inversion Theory, International Journal of Advanced Computer Science and Applications, Vol. 11, No. 12, 88-95, 2020.

AUTHORS' PROFILE

Kohei Arai, He received BS, MS and PhD degrees in 1972, 1974 and 1982, respectively. He was with The Institute for Industrial Science and Technology of the University of Tokyo from April 1974 to December 1978 also was with National Space Development Agency of Japan from January, 1979 to March, 1990. During from 1985 to 1987, he was with Canada Centre

for Remote Sensing as a Post Doctoral Fellow of National Science and Engineering Research Council of Canada. He moved to Saga University as a Professor in Department of Information Science on April 1990. He was a councilor for the Aeronautics and Space related to the Technology Committee of the Ministry of Science and Technology during from 1998 to 2000. He was a councilor of Saga University for 2002 and 2003. He also was an executive councilor for the Remote Sensing Society of Japan for 2003 to 2005. He is a Science Council of Japan Special Member since 2012. He is an Adjunct Professor of University of Arizona, USA since 1998. He also is Vice Chairman of the Science Commission "A" of ICSU/COSPAR since 2008 then he is now award committee member of ICSU/COSPAR. He wrote 55 books and published 620 journal papers as well as 450 conference papers. He received 66 of awards including ICSU/COSPAR Vikram Sarabhai Medal in 2016, and Science award of Ministry of Education of Japan in 2015. He is now Editor-in-Chief of IJACSA and IJISA. <http://teagis.ip.is.saga-u.ac.jp/index.html>.

A Hybrid RNN based Deep Learning Approach for Text Classification

Pramod Sunagar, Anita Kanavalli

Department of Computer Science and Engineering
M S Ramaiah Institute of Technology (Affiliated to VTU)
Bangalore, India

Abstract—Despite the fact that text classification has grown in relevance over the last decade, there are a plethora of approaches that have been created to meet the difficulties related with text classification. To handle the complexities involved in the text classification process, the focus has shifted away from traditional machine learning methods and toward neural networks. In this work the traditional RNN model is embedded with different layers to test the accuracy of the text classification. The work involves the implementation of RNN+LSTM+GRU model. This model is compared with RCNN+LSTM and RNN+GRU. The model is trained by using the GloVe dataset. The accuracy and recall are obtained from the models is assessed. The F1 score is used to compare the performance of both models. The hybrid RNN model has three LSTM layers and two GRU layers, whereas the RCNN model contains four convolution layers and four LSTM levels, and the RNN model contains four GRU layers. The weighted average for the hybrid RNN model is found to be 0.74, RCNN+LSTM is 0.69 and RNN+GRU is 0.77. RNN+LSTM+GRU model shows moderate accuracy in the initial epochs but slowly the accuracy increases as and when the epochs are increased.

Keywords—F1 score; gated recurrent unit; GloVe; long - short term memory; precision; recall; recurrent neural network; region-based convolutional neural network; text classification

I. INTRODUCTION

Text classification has posed a necessity in the current generation, which is precisely due to the fact that the data being handled is increasing in volume at an alarming rate [1]. This can be attributed to the increase in the number of end-users, thereby necessitating effective data handling. Effective handling also involves uploading and retrieval of data at least possible time. The data being uploaded and retrieved may be in the context of many real-time applications like web applications, banking servers, scientific literature, or digital libraries of documents. Some of the applications also involve data filtering [2] and organization, where voluminous data is sorted and categorized as per the relevance [3]. Also, apart from data organization, opinion mining is an application of utmost importance. Therefore, efforts have been put-forth to extend the classified data for opinion mining [4]. Lastly, e-mail classification is also an application of great significance, where text classification is used to identify spam e-mails [5-7]. The applications, as mentioned earlier, also include challenges that are to be addressed critically and with utmost precision.

Researchers have made few significant efforts toward addressing real-world problems in the recent past [8-14]. Most

of the applications concentrate on Natural Language Processing (NLP) and text analytics, with enormous efforts to efficiently handle the data. The extension of efforts also aims at text classification more effectively and intricately. In general, post receipt of the raw data, text classification can be executed stage-wise, viz. feature extraction, reduction of dimensions of the data, selection of the classifier, and finally, the metrics that facilitate quantifying the accuracy of classification. Although many models have been implemented to improve the text classifications, still there are lot of challenges persists. The proposed model tries to improve the text classification by creating a hybrid models and utilizes the advantages of RNN, LSTM and GRU models. Transfer learning is a strategy that involves developing a model for one problem and then utilizing it to train another related problem [37]. Using transfer learning the accuracy of the text classification tasks can be improved [38].

II. RELATED WORKS

The authors have used a BBC news text categorization structure in this work and implemented ML algorithms like logistic regression, KNN algorithms [15] and random forest. These methods are evaluated using measures such as accuracy, precision, F1-score, confusion matrix, and support. The logistic regression algorithm has better accuracy than other algorithms in classifying the text in the given dataset. In this work, the authors have performed a comparative analysis of deep learning models on Arabic text for the single and multi-label text classification [16]. Authors have demonstrated that the pre-processing stage is not required when using the suggested models. The word2vec embedding method is included to enhance the accuracy of the deep learning models. In this work, the authors have projected a model which utilizes a convolutional layer, Bi-LSTM, and attention mechanism to understand the semantics and improve the text classification accuracy [17]. The authors have analyzed the traditional deep learning models and proved that the proposed model has the highest accuracy over others. The feature extraction methods and developing classifiers are significant for the text classification techniques. In this work, the authors have highlighted the improved word embeddings with machine learning models for automatic document classification jobs [18]. The authors have used the word embedding techniques such as word2vec, Glove, and fastText. The authors have used the freely available dataset and implemented algorithms such as SVM, XGBoost, and CNN to use hierarchical and flat measures. The fastText embedding technique has proved to

improve the classification accuracy of the text. The authors have investigated the hierarchical multi-label text classification task [19]. Since the documents are stored in a hierarchical structure, the classification task becomes tough. The authors have proposed a new framework called Hierarchical Attention-based Recurrent Neural Network (HARNN) for categorizing documents into the appropriate labels by integrating texts and the hierarchical category structure.

The authors examined text categorization techniques based on machine learning [20]. AG's News Topic Classification Dataset, which comprises 120000 training and 7600 testing samples, was used in this case. Support vector machine, Rocchio, bagging, boosting, naive bayes, and KNN are examples of commonly used machine learning algorithms that are implemented and assessed using accuracy, precision, F1 score, and recall. According to the authors, the SVM technique outperformed all other algorithms tested for this job. The authors classified tweets regarding Covid-19 pandemic using DL techniques [21]. They have investigated three traditional deep learning algorithms, CNN, RNN, and RCNN, and two hybrid algorithms, RNN+LSTM and RNN+Bi-LSTM with Attention. When coupled with GloVe and Word2Vec, the RNN+Bi-LSTM with Attention mechanism correctly classified tweets. The time taken to train and predict the accurate labels is more for RNN+LSTM when compared to other deep learning models.

The authors provide a different feature selection approach called Multivariate Relative Discrimination Criterion (MRDC) in this study to minimize dimensionality and feature space in order to enhance text classification performance [22]. The suggested technique focuses on reducing duplicate features by employing the notions of minimal redundancy and maximal relevancy. The suggested approach considers document frequency for each word while assessing its usefulness for that purpose. The suggested technique picks the characteristics with the highest relevance and considers the redundancy between them using a correlation metric. The authors discussed a deep learning strategy called HDLTex, which integrates various deep learning algorithms to create hierarchical classifications [23].

The authors' proposed architecture uses a mix of RNN at the top level and DNN or CNN at the bottom level to classify articles more accurately than standard SVM or Naive Bayes. The deep learning models were optimized using RMSProp and Adam to improve accuracy. The DNN has eight hidden layers. RNN was built using LSTM and GRU, and CNN with eight hidden layers. The authors have presented a comprehensive overview of the 150 classifiers introduced in recent years to accomplish this study's text categorization problems [24]. The work comprises 40 widely used datasets for text categorization. To improve the precision of text categorization, the authors proposed combining transformers and pre-trained language models with deep learning techniques. The work also establishes the grouping of 150 DL models into ten broad categories: feed-forward networks, CNN-based models, RNN-based models, Graph neural networks, hybrid models, etc.

III. METHODOLOGY

Based on earlier efforts, it is clear that every neural network architecture has shortcomings, which can be addressed by combining other architectures to compensate for the deficiencies. Therefore, embedding layers of other architectures to the existing neural network model and their contribution to the model's performance has been studied in the present work. For example, the Long Short Term Memory (LSTM) layer [25-27] (Fig. 1) has the ability to remember long-distance relations when compared to Gated Recurrent Unit (GRU) [28-29] (Fig. 2).

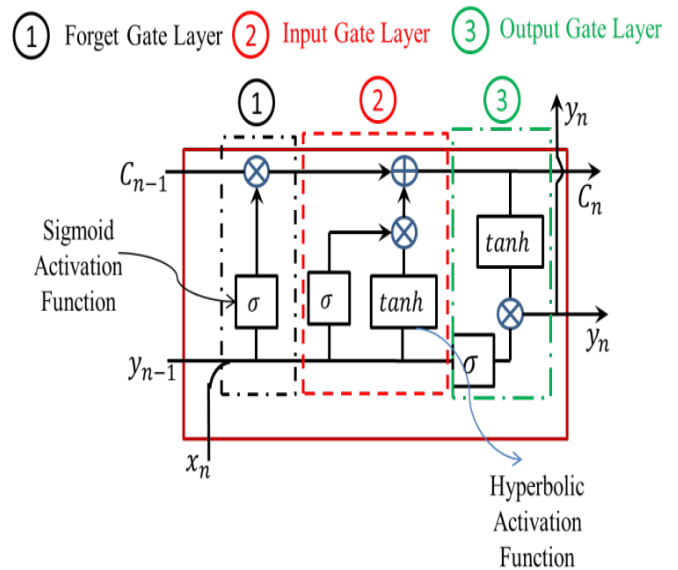


Fig. 1. Long Short Term Memory Units.

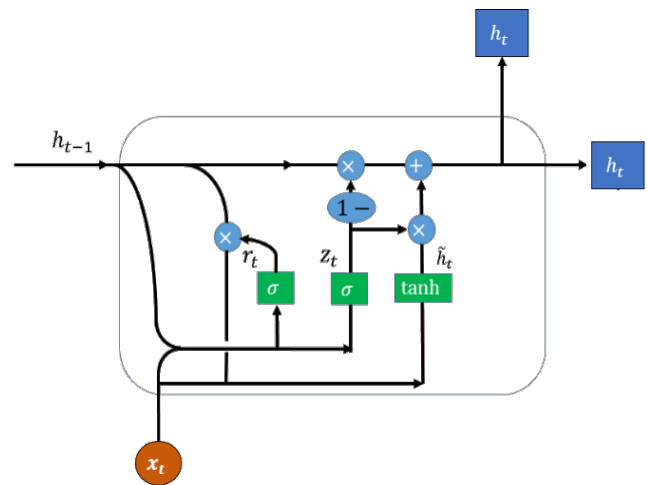


Fig. 2. Gated Recurrent Units.

The sigmoid function is used in both LSTM and GRU units, whereas the hyperbolic activation function in the output layer facilitates data retrieval even after a considerable amount of time. On the other hand, GRU is easy to train compared to LSTM, with a lesser number of data and a better performance than LSTMs. This motivates researchers to embed GRUs against LSTM when retrieval is not of great significance.

Three models are considered for the present study namely Recurrent Neural Network (RNN) [30-31] with GRU unit, RNN with LSTM as well as GRU units and Region-Based Convolutional Neural Network (RCNN) with LSTM layer. A conventional RCNN [32] model is modified by adding four LSTM layers along with the convolutional layers as indicated in Fig. 3, the performance of which is compared with two models comprising a typical RNN model with four GRU layers (Fig. 4) and RNN model with 3 LSTM layers and 2 GRU layers (Fig. 5). The LSTM layer used in RCNN and RNN architectures is a forgotten gate type and an input and output gate, as shown in Fig. 1.

The output gate layer is the most significant layer that enables long-term dependencies handling. The forget gate layer assigns a value based on the input vector of the current cell, the output vector of the previous and the previous cell state. This is also indicative that the forget layer carries out the decision of allowing the value to the input layer. The sigmoid neural function with a point-wise multiplication operator is used to generate values in the LSTM's forget gate layer. The Input gate layer is responsible for two tasks. The entering vector data is first updated using a sigmoid activation function, and the value created by the sigmoid activation function is then compared to the hyperbolic activation function. The new values obtained as a result of the comparison are combined with the prior cell state. The Output Gate Layer compares the input vector generated by the sigmoid activation function to the updated cell state generated by the hyperbolic activation function.

Whereas, irrespective of LSTM, a fully gated GRU comprises only two gates, viz. forget gate layer and an input gate. Though GRU is around half a decade old, it is preferred in specific, precise circumstances because they need a considerably smaller dataset and time for training the model. It can be observed that LSTM has a separate update gate and forget gate, rendering it more sophisticated. Therefore, the complexity of the LSTM paves the way for the usage of GRU, wherein the control on the model embedded with GRU units is better. Based on the earlier observations, three models are considered with LSTM, GRU, and LSTM-GRU units embedded, respectively, and their performances are evaluated. The training of the models is facilitated by the GloVe dataset [14], which can effectively capture syntactic and semantic representations of the words. The shortcoming of GloVe [33] is its inability to capture out-of-vocabulary words, which demands a considerable corpus to train the model, thereby eventually increasing the memory requirement. Though GloVe is similar to Word2Vec [34-35] in its operation, the weights associated with frequent word pairs will not pre-occupy the training process. The merits mentioned above support the usage of the GloVe dataset for training the models considered for the study.

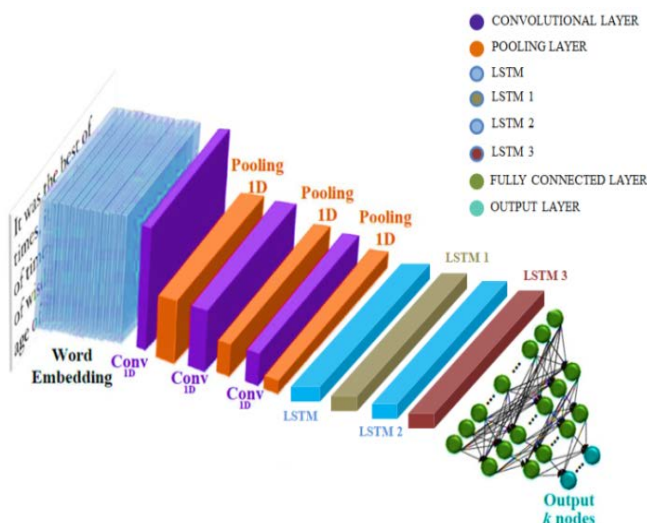


Fig. 3. RCNN Model with LSTM Layers.

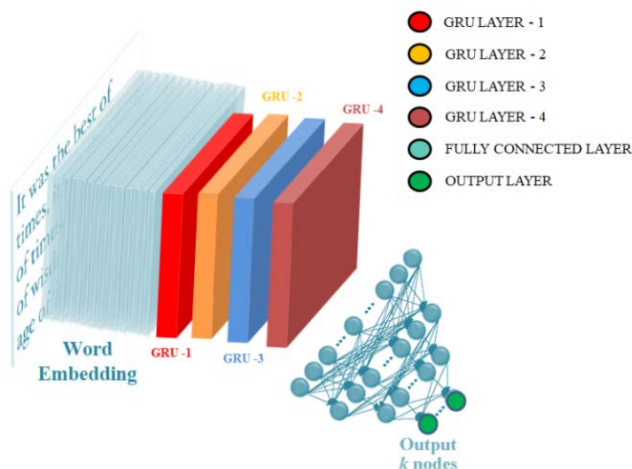


Fig. 4. RNN Model with GRU Layers.

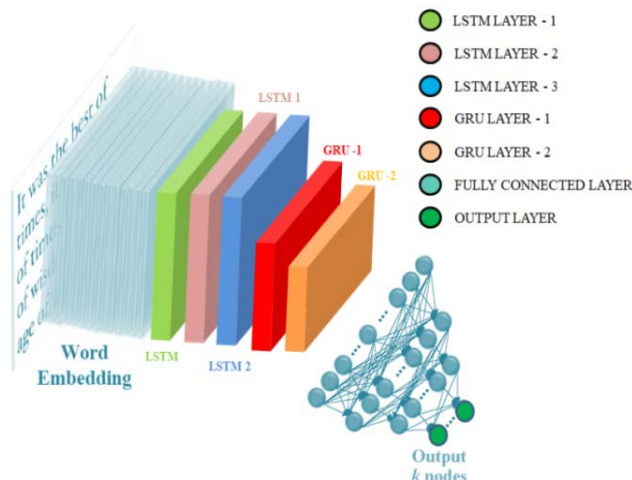


Fig. 5. RNN Model with LSTM and GRU Layers.

IV. EVALUATION

The evaluation of the models is carried out with the help of two parameters, viz. precision, and recall. Precision is the ratio of true prediction to a total number of predictions (Equation 1), while recall is the ratio of true positive to the sum of true positive and false negative. Though precision highlights the accuracy of the model, recall indicates sensitivity. An increase in precision reduces the number of false positives, increasing false negatives. Therefore increase in false negative decreases the recall value. It is undoubtedly a balance between precision and recall, which renders a valuable model for a given application as they demonstrate an inverse behavior. The cumulative effect of precision and recall are captured using the F1 score, which can be obtained by evaluating the area under the precision and recall curve plotted for both models. F1 score is the harmonic mean calculated from precision and recall values (eq. 3), which forms a significant metric to evaluate the performance of the models.

$$Precision (P) = \frac{True\ Positive}{True\ Positive + False\ Positive} \quad (1)$$

$$Recall (R) = \frac{True\ Positive}{True\ Positive + False\ Negative} \quad (2)$$

$$F_1 = 2 \left[\frac{P \times R}{P + R} \right] \quad (3)$$

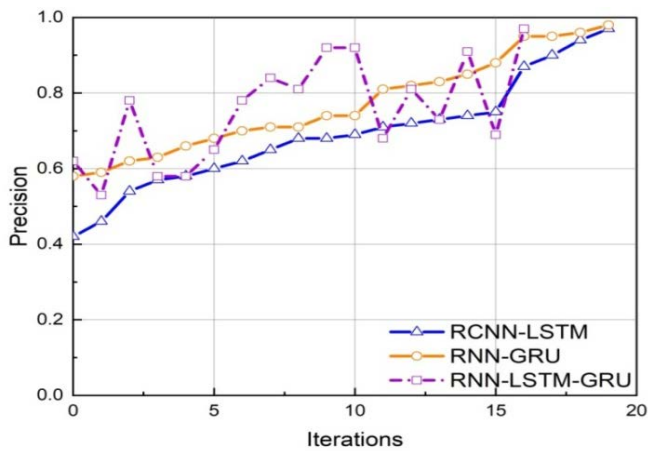


Fig. 6. Comparison of Precision for RCNN-LSTM, RNN-GRU, and RNN-LSTM-GRU Models.

The results are plotted for the precision and recall as shown in Fig. 6 and Fig. 7, respectively. It is observed that the RNN model consistently outperforms the RCNN model. After the 18th iteration, hybrid RNN and RCNN provide almost the same precision and recall values. Hybrid RNN is embedded with GRU layers that can be trained for a lesser number of data and for a lesser time to generate a greater accuracy, as indicated in Fig. 6 and Fig. 7.

The recall precision curve is of great significance for assessing the performance of the RCNN-LSTM, RNN-GRU and RNN-LSTM-GRU model as shown in the Fig. 8, 9 and 10. The results obtained are plotted, for which the polynomial curve is fitted by using the least-squares method. The area under the curve (AUC) [36] indicates the F1 score for each model, thereby depicting the optimum blend of precision and recall of the model. The RCNN-LSTM model occupies a

larger area when compared to RNN-GRU and RNN-LSTM-GRU models, indicating a more extensive range of recall-precision values.

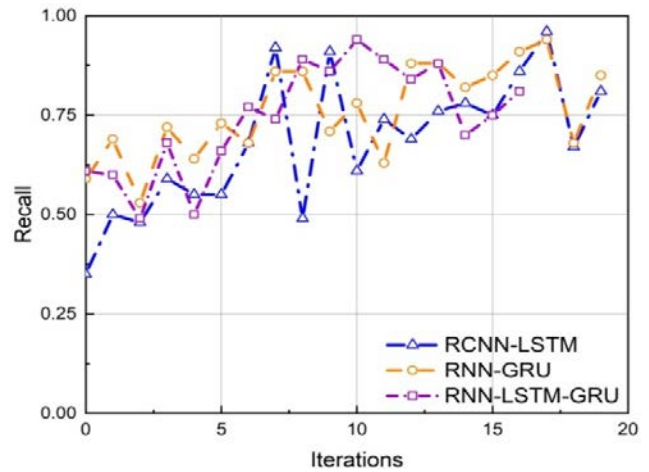


Fig. 7. Comparison of Recall for RCNN-LSTM, RNN-GRU, and RNN-LSTM-GRU Models.

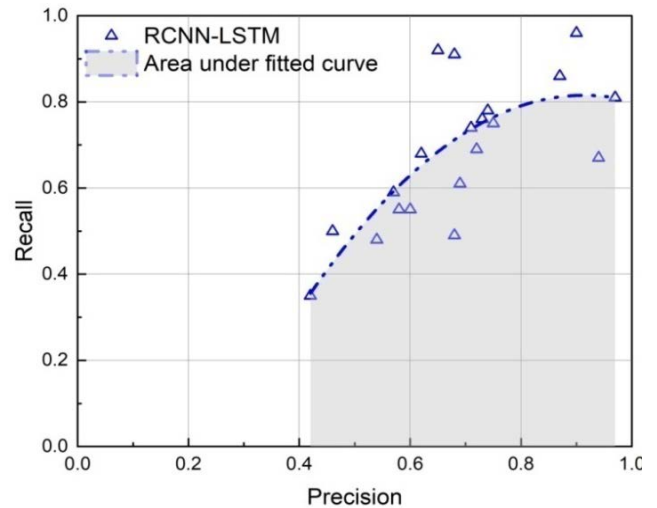


Fig. 8. Variation of Precision with Recall for RCNN-LSTM Model.

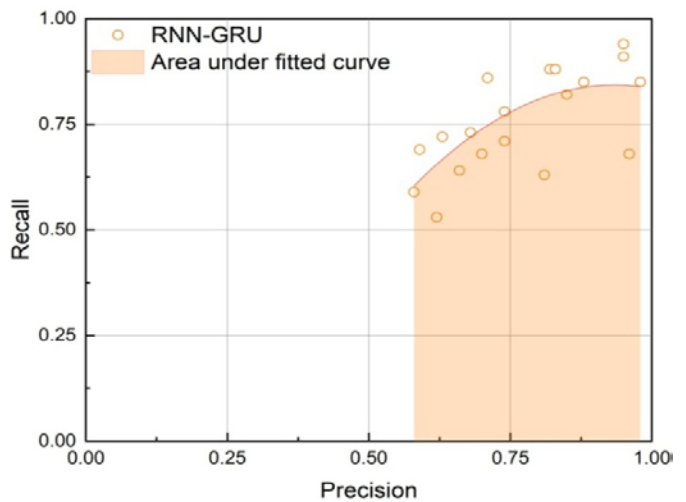


Fig. 9. Variation of Precision with Recall for RNN-GRU Model.

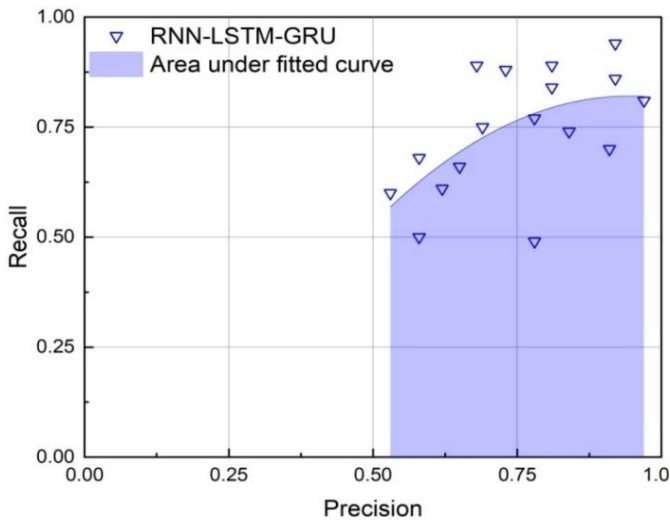


Fig. 10. Variation of Precision with Recall for RNN-LSTM-GRU Model.

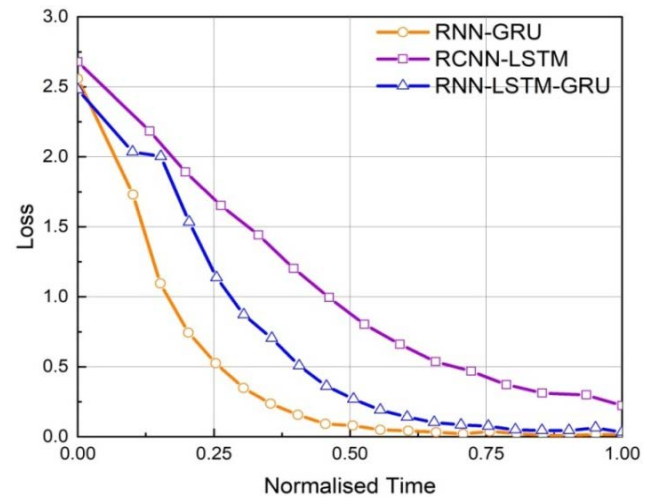


Fig. 12. Variation of Loss in values for RCNN-LSTM, RNN-GRU, and RNN-LSTM-GRU Models.

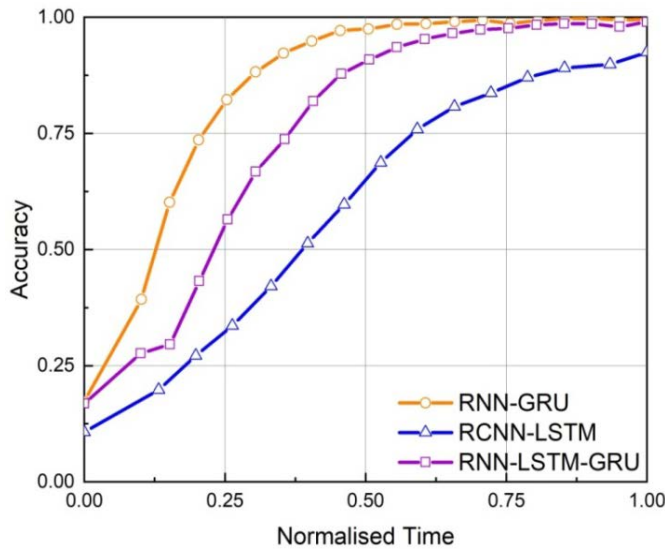


Fig. 11. Comparison of Accuracy for RCNN-LSTM, RNN-GRU, and RNN-LSTM-GRU Models.

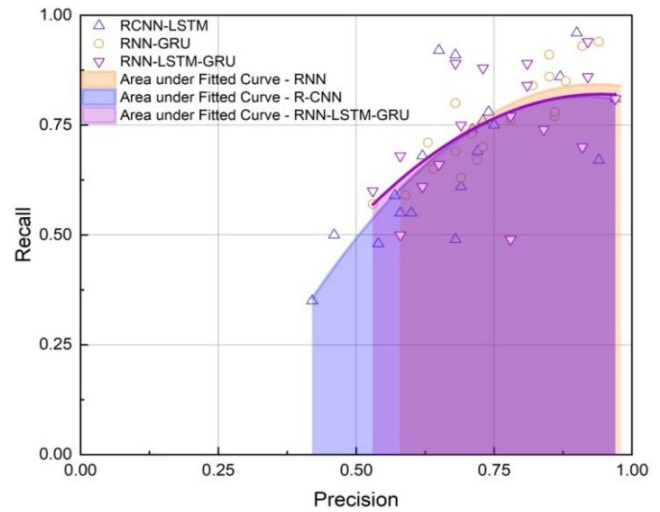


Fig. 13. Comparison of Precision-Recall for RCNN-LSTM, RNN-GRU, and RNN-LSTM-GRU Models.

The comparison can be more clearly observed in Fig. 13, and the corresponding variations in the F1 score are indicated in Fig. 14. The average F1 score for RCNN-LSTM, RNN-GRU, and RNN-LSTM-GRU models are indicated in Table I. It can be observed that the RNN-GRU model outperforms RCNN and RNN-LSTM-GRU model by a margin of 10% and 4%, respectively. Since the GRU layers embedded in the RNN model require lesser time and smaller datasets for training, the F1 curve of the RNN model consistently dominates over RCNN and RNN-LSTM-GRU models. RNN-GRU model is embedded with the GRU layer, which cannot handle long-term dependencies. When long-term dependencies are of great significance, as is the case in text classification, RNN-LSTM-GRU is preferred the most, which carries the merits of both LSTM and GRU layers. RCNN has LSTM layers, which are capable of handling long-term dependencies; they take more significant time and more extensive data to get trained, which renders RNN-LSTM-GRU more suitable for text classification.

Also, Fig. 11 and Fig. 12 indicate the variation of accuracy with the normalized time. It can be observed that the RNN-GRU model and RNN-LSTM-GRU model perform almost the same after a normalized time of 0.75s. The accuracy of both the models is nearly the same, which is indicative that the RNN-LSTM-GRU can replace the RNN-GRU model to enable the retrieval of long-term dependencies. The difference in slopes over the initial normalized time from 0 to 0.6s is because of the presence of the LSTM layer in the RNN-LSTM-GRU model, which requires more time for training, while the GRU layer compensates for the initial delay by matching the slope when trained beyond a normalized time of 0.75s.

The area under the precision-recall curve gives the F1 score (Fig. 13). The variation of the F1 score for all three models is depicted in Fig. 14. Though the fluctuation of RNN-LSTM-GRU is considerably significant compared to RNN-GRU and RCNN-LSTM, the average F1 value is more significant than RCNN-LSTM and marginally less than RNN-GRU. The values are listed in Table I.

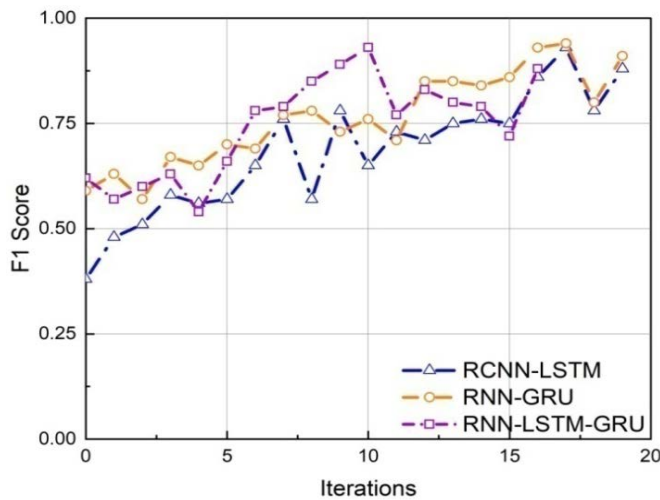


Fig. 14. Variation of F1 Score with Epoch for RCNN-LSTM, RNN-GRU, and RNN-LSTM-GRU Models.

TABLE I. COMPARISON OF PRECISION, RECALL, AND F1 SCORE

Model	Average Precision	Average Recall	F1 Score
RCNN-LSTM	0.691	0.6825	0.682
RNN-GRU	0.7695	0.7615	0.7615
RNN-LSTM-GRU	0.7395	0.7163	0.7226

V. CONCLUSION

The present comprehensive study intends to address three text classification strategies by modifying the models and evaluating the performances in connect with precision and sensitivity. It is observed that the model selection for a given application is a trade-off among the variables such as time, dataset, and handling of the long-term dependencies, which define a suitable model for the application. Hence, RCNN with more accurate when compared to RNN with an ability to remember the dependencies, whereas RNN embedded with GRU has a shorter learning time which a smaller volume of the dataset can train. The average F1 score of RNN (4 layer model) is 0.77, whereas, for RCNN (8 layer model), the average F1 score is 0.69, which is around 10% less than RNN.

ACKNOWLEDGMENT

This work was supported by M S Ramaiah Institute of Technology, Bangalore-560054, and Visvesvaraya Technological University, Jnana Sangama, Belagavi-590018.

REFERENCES

- [1] Kowsari, K., Jafari Meimandi, K., Heidarysafa, M., Mendu, S., Barnes, L., & Brown, D. (2019). Text classification algorithms: A survey. *Information*, 10(4), 150.
- [2] Lang, K. (1995). Newsweeder: Learning to filter netnews. In *Machine Learning Proceedings 1995* (pp. 331-339). Morgan Kaufmann.
- [3] Chakrabarti, S., Dom, B., Agrawal, R., & Raghavan, P. (1997, August). Using taxonomy, discriminants, and signatures for navigating in text databases. In *VLDB* (Vol. 97, pp. 446-455).
- [4] Liu, B., & Zhang, L. (2012). A survey of opinion mining and sentiment analysis. In *Mining text data* (pp. 415-463). Springer, Boston, MA.

- [5] Lewis, D. D., & Knowles, K. A. (1997). Threading electronic mail: A preliminary study. *Information processing & management*, 33(2), 209-217.
- [6] Sharma, P., & Bhardwaj, U. Machine learning based spam e-mail detection. *International Journal of Intelligent Engineering and Systems*, 11(3), 1-10, 2018.
- [7] Cohen, W. W. (1996, March). Learning rules that classify e-mail. In *AAAI spring symposium on machine learning in information access* (Vol. 18, p. 25).
- [8] Carvalho, V. R., & Cohen, W. W. (2005, August). On the collective classification of email" speech acts". In *Proceedings of the 28th annual international ACM SIGIR conference on Research and development in information retrieval* (pp. 345-352).
- [9] Jiang, M., Liang, Y., Feng, X., Fan, X., Pei, Z., Xue, Y., & Guan, R. (2018). Text classification based on deep belief network and softmax regression. *Neural Computing and Applications*, 29(1), 61-70.
- [10] Aggarwal, C. C., & Zhai, C. (2012). A survey of text classification algorithms. In *Mining text data* (pp. 163-222). Springer, Boston, MA.
- [11] Kowsari, K., Heidarysafa, M., Brown, D. E., Meimandi, K. J., & Barnes, L. E. (2018, April). Rmdl: Random multimodel deep learning for classification. In *Proceedings of the 2nd International Conference on Information System and Data Mining* (pp. 19-28).
- [12] McCallum, A., & Nigam, K. (1998, July). A comparison of event models for naive bayes text classification. In *AAAI-98 workshop on learning for text categorization* (Vol. 752, No. 1, pp. 41-48).
- [13] Heidarysafa, M., Kowsari, K., Brown, D. E., Meimandi, K. J., & Barnes, L. E. (2018). An improvement of data classification using random multimodel deep learning (rmdl). *arXiv preprint arXiv:1808.08121*.
- [14] Lai, S., Xu, L., Liu, K., & Zhao, J. (2015, February). Recurrent convolutional neural networks for text classification. In *Twenty-ninth AAAI conference on artificial intelligence*.
- [15] Altinel, B., & Ganiz, M. C. (2018). Semantic text classification: A survey of past and recent advances. *Information Processing & Management*, 54(6), 1129-1153.
- [16] Shah, K., Patel, H., Sanghvi, D., & Shah, M. (2020). A comparative analysis of logistic regression, random forest and KNN models for the text classification. *Augmented Human Research*, 5(1), 1-16.
- [17] Elnagar, A., Al-Debsi, R., & Einea, O. (2020). Arabic text classification using deep learning models. *Information Processing & Management*, 57(1), 102121.
- [18] Liu, G., & Guo, J. (2019). Bidirectional LSTM with attention mechanism and convolutional layer for text classification. *Neurocomputing*, 337, 325-338.
- [19] Stein, R. A., Jaques, P. A., & Valiati, J. F. (2019). An analysis of hierarchical text classification using word embeddings. *Information Sciences*, 471, 216-232.
- [20] Huang, W., Chen, E., Liu, Q., Chen, Y., Huang, Z., Liu, Y., ... & Wang, S. (2019, November). Hierarchical multi-label text classification: An attention-based recurrent network approach. In *Proceedings of the 28th ACM International Conference on Information and Knowledge Management* (pp. 1051-1060).
- [21] Sunagar, P., Kanavalli, A., Nayak, S. S., Mahan, S. R., Prasad, S., & Prasad, S. (2021). News Topic Classification Using Machine Learning Techniques. In *International Conference on Communication, Computing and Electronics Systems: Proceedings of ICCES 2020* (Vol. 733, p. 461). Springer Nature.
- [22] Sunagar, P., Kanavalli, A., Poornima, V., Hemanth, V. M., Sreeram, K., & Shivakumar, K. S. (2021). Classification of Covid-19 Tweets Using Deep Learning Techniques. In *Inventive Systems and Control* (pp. 123-136). Springer, Singapore.
- [23] Labani, M., Moradi, P., Ahmadizar, F., & Jalili, M. (2018). A novel multivariate filter method for feature selection in text classification problems. *Engineering Applications of Artificial Intelligence*, 70, 25-37.
- [24] Minaee, S., Kalchbrenner, N., Cambria, E., Nikzad, N., Chenaghlu, M., & Gao, J. (2021). Deep Learning-based Text Classification: A Comprehensive Review. *ACM Computing Surveys (CSUR)*, 54(3), 1-40.

- [25] Kowsari, K., Brown, D. E., Heidarysafa, M., Meimandi, K. J., Gerber, M. S., & Barnes, L. E. (2017, December). Hdtex: Hierarchical deep learning for text classification. In 2017 16th IEEE international conference on machine learning and applications (ICMLA) (pp. 364-371). IEEE.
- [26] Hochreiter, S., & Schmidhuber, J. (1997). Long short-term memory. *Neural computation*, 9(8), 1735-1780.
- [27] Graves, A., & Schmidhuber, J. (2005). Framewise phoneme classification with bidirectional LSTM and other neural network architectures. *Neural networks*, 18(5-6), 602-610.
- [28] Pascanu, R., Mikolov, T., & Bengio, Y. (2013, May). On the difficulty of training recurrent neural networks. In International conference on machine learning (pp. 1310-1318). PMLR.
- [29] Chung, J., Gulcehre, C., Cho, K., & Bengio, Y. (2014). Empirical evaluation of gated recurrent neural networks on sequence modeling. arXiv preprint arXiv:1412.3555.
- [30] Cho, K., Van Merriënboer, B., Gulcehre, C., Bahdanau, D., Bougares, F., Schwenk, H., & Bengio, Y. (2014). Learning phrase representations using RNN encoder-decoder for statistical machine translation. arXiv preprint arXiv:1406.1078.
- [31] Sutskever, I., Martens, J., & Hinton, G. E. (2011, January). Generating text with recurrent neural networks. In ICML.
- [32] Mandic, D., & Chambers, J. (2001). *Recurrent neural networks for prediction: learning algorithms, architectures and stability*. Wiley.
- [33] Wang, B., Xu, J., Li, J., Hu, C., & Pan, J. S. (2017, June). Scene text recognition algorithm based on faster RCNN. In 2017 First International Conference on Electronics Instrumentation & Information Systems (EIIS) (pp. 1-4). IEEE.
- [34] Pennington, J., Socher, R., & Manning, C. D. (2014, October). Glove: Global vectors for word representation. In Proceedings of the 2014 conference on empirical methods in natural language processing (EMNLP) (pp. 1532-1543).
- [35] Mikolov, T., Chen, K., Corrado, G., & Dean, J. (2013). Efficient estimation of word representations in vector space. arXiv preprint arXiv:1301.3781.
- [36] Pencina, M. J., D'Agostino Sr, R. B., D'Agostino Jr, R. B., & Vasan, R. S. (2008). Evaluating the added predictive ability of a new marker: from area under the ROC curve to reclassification and beyond. *Statistics in medicine*, 27(2), 157-172.
- [37] Shreyashree, S., Sunagar, P., Rajarajeswari, S., & Kanavalli, A. (2022). A Literature Review on Bidirectional Encoder Representations from Transformers. *Inventive Computation and Information Technologies*, 305-320.
- [38] Qasim, R., Bangyal, W. H., Alqarni, M. A., & Ali Almazroi, A. (2022). A fine-tuned BERT-based transfer learning approach for text classification. *Journal of healthcare engineering*, 2022.

Deep Learning Approach for Masked Face Identification

Maad Shatnawi, Nahla Almenhali, Mitha Alhammadi, Khawla Alhanaee

Department of Electrical Engineering Technology, Higher Colleges of Technology, Abu Dhabi, UAE

Abstract—Covid-19 is a global health emergency and a major concern in the industrial and residential sectors. It has the ability to spread leading to health problems or death. Wearing a mask in public locations and busy areas is the most effective COVID-19 prevention measure. Face recognition provides an accurate method that overcomes uncertainties such as false prediction, high cost, and time consumption, as it is understood that the primary identification for every human being is his face. As a result, masked face identification is required to solve the issue of recognizing individuals with masks in several applications such as door access systems and smart attendance systems. This paper offers an important and intelligent method to solve this issue. We propose deep transfer learning approach for masked face human identification. We created a dataset of masked-face images and examined six convolutional neural network (CNN) models on this dataset. All models show great performance in terms of very high face recognition accuracy and short training time.

Keywords—Masked face human identification; face recognition; deep transfer learning; convolutional neural networks

I. INTRODUCTION

Covid-19 is a global pandemic that began in the year 2020 and has triggered a global health crisis and impacted a wide range of businesses, including education, aviation, health care, tourism, luxury shopping, religion, and so on. It had a significant impact on people's daily lives as well. Wearing a face mask in public areas, according to the World Health Organization (WHO), is one of the most effective preventative measures to stop the spread of disease and save lives [1]. Furthermore, several public service providers restrict customers to utilize their services while wearing facemasks that meet specific standards. However, due to the face mask covering the majority of the crucial facial characteristics, such as the nose and mouth, conventional face recognition systems used for security have proven ineffective in the current circumstance making it exceedingly challenging to identify the person [2].

The unlocking techniques based on passwords or fingerprints are risky since the COVID-19 virus can be transmitted through contact. Without touching, face recognition makes it considerably safer, but when wearing a mask, existing face recognition technologies become unreliable. To address the current challenges, it is essential to enhance the current face recognition techniques, which primarily rely on all facial feature points, so that identity verification may still be carried out with reliability even when faces are only partially revealed. [3] These systems recognize people identities without the need to take off the mask which can be used in hospitals, offices, educational institutes,

construction sites, manufacturing plants, airports, and in many other places. Masked-face recognition can also be used in attendance systems in schools, offices, and other working places.

Extensive studies enable the establishment of new datasets or masked face recognition. These studies significantly contribute since datasets of masked faces are correspondingly few and make it difficult to train suggested algorithms. There are several machine learning and deep learning techniques used to identify a face mask, some of which are based on enhanced pre-trained and existing models that all perform effectively [4].

Machine learning is a rapidly growing field of computational intelligence that seeks to emulate human learning from their environment. Computer vision, image recognition, speech recognition, natural language processing, and bioinformatics are some domains of machine learning. It is currently a primary competence of computer scientists. It includes computationally intensive methods, and is already widely utilized in the social sciences, marketing, systems engineering, and applied sciences. The degree of complexity of these systems can vary, and they may comprise multiple phases of complex human-machine interactions and decision making, which would naturally draw machine learning algorithms to enhance and automate various procedures. Numerous systems' efficiency and safety may be increased if machine learning algorithms had the potential to generalize from their current context and learn new tasks [5].

Deep learning is a type of machine learning that mimics the human brain's data processing to detect objects, recognize speech, translate languages, and make decisions. It is learning from both labeled and unlabeled data without the need for human interaction. Deep learning's capacity to handle large amounts of information makes it extremely powerful when dealing with unstructured data [6]. Deep learning has been effectively used to handle a broad variety of issues in the fields of image identification and natural language processing. It is based on neural network architectures with several layers of processing units [7].

Transfer learning is a type of machine learning in which a model is designed for one task and then utilized as the starting point for another task to be modified. People's ability to logically use previously acquired knowledge to solve new issues more quickly or effectively is what drives the study of transfer learning. Transfer learning is particularly beneficial in science as most real-world problems involve big amount of labeled data, demanding complicated models. Transfer learning can be used by developers to combine multiple applications

into one. Developers can also train new models for difficult applications quickly. It's also a useful tool for improving the accuracy of computer vision models [8].

This paper proposes a deep transfer learning approach for masked face recognition. We trained and tuned six convolutional neural network (CNN) models based on a masked face dataset.

II. PRE-TRAINED NETWORKS

Pre-trained networks have various characteristics that are important to consider when choosing a network to perform a certain task. The most important performance measure of a network is accuracy, computational time, and memory size. Choosing a network is usually alternated between these functions. In this work, we have examined six pre-trained convolutional neural network models which are briefly explained in this section.

A. SqueezeNet

SqueezeNet is an eighteen-layer deep convolutional neural network that can classify images into 1000 different classes. The network has learned sophisticated function representations for a wide spectrum of pictures. The goal of utilizing SqueezeNet is to create a smaller neural network with fewer datasets that can be more readily integrated into computer memory and transmitted across a computer network [9]. SqueezeNet architecture is illustrated in Fig. 1.

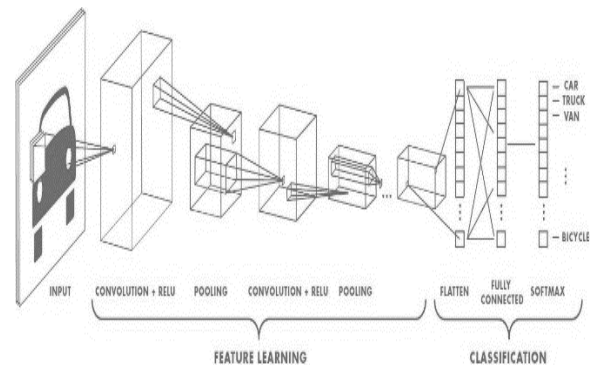


Fig. 1. SqueezeNet Architecture.

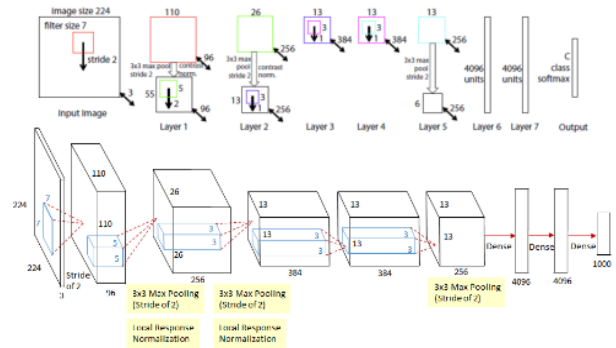


Fig. 2. GoogleNet Architecture.

B. GoogleNet

GoogleNet has twenty two layers with twenty seven levels dedicated to pooling. There are a total of nine initiation modules layered in a linear fashion. It also employs eleven convolution filters. The parallel network architecture significantly contributes to minimize computational time and memory requirements. GoogleNet architecture is illustrated in Fig. 2.

C. AlexNet

AlexNet is one of the most widely used neural network designs nowadays. It's been used to train and classify millions of object images. The network input is $227 \times 227 \times 3$ RGB images. AlexNet solves the over-fitting issue by using dropout layers. AlexNet architecture is illustrated in Fig. 3.

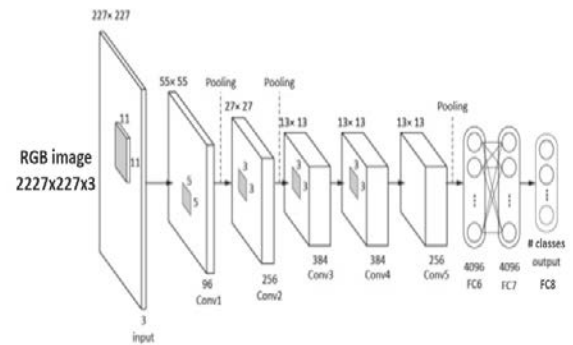


Fig. 3. AlexNet Architecture.

D. ResNet-50

ResNet-50 is a 50-layer deep convolutional neural network that has been trained on over a million of images. The network has been pre-trained to classify images into 1000 different classes. The network input is $224 \times 224 \times 3$ RGB images [10]. The network architecture is illustrated in Fig. 4.

E. VGG-16

VGG-16 is one of the very deep convolutional networks for large-scale image recognition. In ImageNet, a dataset with over 14 million pictures divided into 1000 classes, VGG-16 model achieves 92.7% classification accuracy. The network input is $224 \times 224 \times 3$ RGB images [11]. The network architecture is illustrated in Fig. 5.

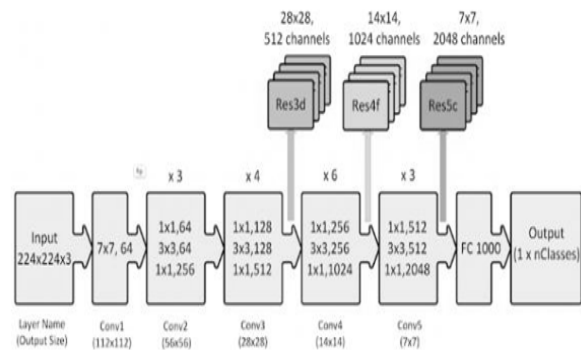


Fig. 4. ResNet-50 Architecture.

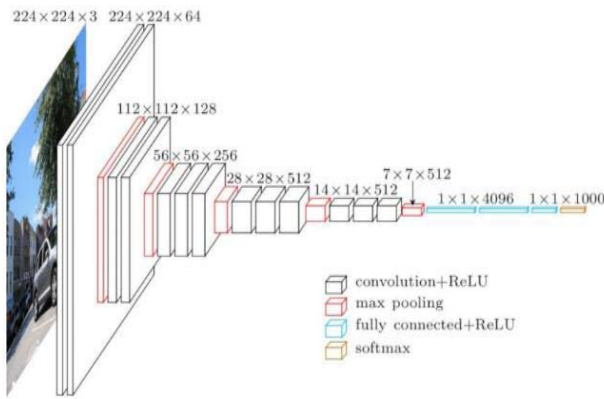


Fig. 5. VGG-16 Net Architecture.

F. MobileNet-V2

MobileNet-V2 was one of the first initiatives to create CNN architectures that could be readily implemented in mobile apps. Depth-wise separable convolutions, which are illustrated here, are one of the key advances. A separable convolution divides a single convolution kernel into two. Instead of a 3x3 kernel, we get a 3x1 and a 1x3 kernel, for example. It scales the image's input size from 224 to 128 pixels. You can train your MobileNet-V2 on 224x224 pictures and then use it on 128x128 images since it utilizes global average pooling instead of flattening [12]. The network architecture is illustrated in Fig. 6.

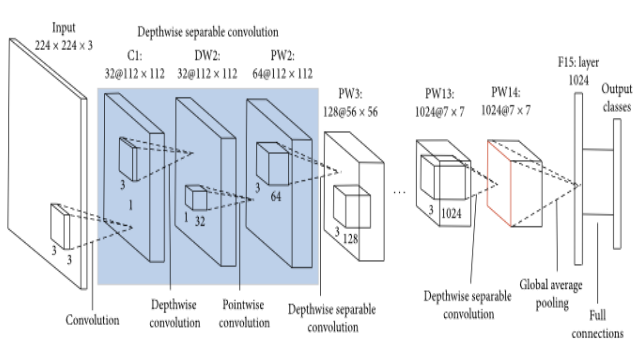


Fig. 6. MobileNet-V2 Architecture.

III. CURRENT APPROACHES

The current face mask detection approaches are summarized and discussed in this section.

Cabani et al. [13] presented a dataset of correctly and incorrectly masked face images. Each set has 49 randomly sampled images, with 70,000 high-quality images in PNG and 1024 x1024 resolution. The masked Face-Net dataset contained 139,646 images with 49% of correctly masked faces and 51% of incorrectly masked faces.

Mingjie et al. [14] proposed a Retina Face Mask method that uses transfer learning. The proposed method is a one-stage detector that combines a feature pyramid network with several feature maps to fuse high-level semantic information with a unique context attention module to focus on identifying face masks. The dataset has been split into a train, validation, and test set with 4906, 1226, and 1839 images individually; each

experiment operates 250 epochs. The Advantage of the method MobileNet-V2 backbone shows that transfer learning can increase the detection performance by 3 to 4% in face and mask detection results. Also, feature extraction ability is enhanced by utilizing pre-trained weights.

Loey et al. [15] presented a hybrid model with deep transfer learning and classical machine learning for face mask detection. The machine learning approach uses decision trees and Support Vector Machines (SVM) to classify face masks. Three face masked datasets have been selected for investigation. The decision trees classifier achieved 96% of validation accuracy. The SVM classifier achieved 98% of validation accuracy with the least time consumed in the training process.

Chavda et al. [16] presents a CNN-based architecture for detecting instances of incorrect use of face masks. The system uses transfer learning technique with three nets which are MobileNetV2, DenseNet121, and NASNet. The system classifies images into three classes: correct face mask covering, incorrect face mask covering and no face mask. The dataset is used from a pre-trained model in Kaggle for quick generalization and stable detection. The results and accuracy percentage of each net are: MobileNetV2 is 99.12%, DenseNet121 is 99.40%, NASNet is 99.13%. The advantages are high accuracy while having using less training data, the inference time is significantly shorter, and the system can be integrated with an image or video capturing device. On the other hand, the disadvantages are having a motion blur, dynamic focus and frame transition may face in video feed analysis.

Hariri [17] presents a masked face recognition technique based on occlusion removal and deep learning-based features. The system utilizes three pre-trained deep Convolutional Neural Networks (CNNs) to extract deep features from the resulting regions which are: VGG-16, AlexNet, and ResNet-50. This system is using two datasets which are, Masked Face Recognition Dataset (RMFRD), and Simulated Masked Face Recognition Dataset (SMFRD) that are from an open source [17]. The advantages are that the system obtained high accuracy compared to other face recognizers due to the best features extracted from the last convolutional layers of the pre-trained models, and the high efficiency. Recognition performance on RMFRD dataset obtained 91.3% accuracy, and SMFRD dataset is 88.9%.

Nagrath et al. [18] presented a method that uses deep learning, TensorFlow, Keras, and OpenCV to detect face masks. The SSDMNV2 method employs the Single Shot Multibox Detector as a face detector and the MobilenetV2 architecture as a framework for the classifier. The dataset used in this method is from Kaggle's Medical Mask Dataset (678 images) and the dataset available at PyImageSearch (1,376 images; wearing masks 690 pictures, and without wearing a mask, 686 pictures). The advantages are that SSDMNV2 is very lightweight and can even be used in embedded devices, it is useful method for real-time mask detection, and it achieved a high accuracy score of 92% which indicated a well-trained model.

Aswal et al. [19] presented two techniques that are used to recognize and identify masked faces. Using a single camera: A two-step process with a pre-trained one-stage feature pyramid detector network RetinaFace for localizing masked faces and VGGFace2 that generates facial feature vectors for efficient mask face verification; and (ii) a single-step pre-trained YOLO-face/trained YOLOv3 model on the set of known individuals. The dataset consists of 17 videos of individuals wearing face masks nearby. The dataset contains variations in orientation, scale, occlusions, illumination, and appearance. On their dataset, experimental results show that RetinaFace and VGGFace2 deliver state-of-the-art results in 1:1 face mask verification, with 92.7% overall performance, 98.1% face detection, and 94.5% face verification accuracy, respectively. The advantage of using transfer learning on YOLOv3 pre-trained the dataset is that the training process requires fewer images per class. And the YOLOv3 is a more advanced version of YOLO, Darknet-53, with shortcut connections for better GPU utilization, efficient evaluation, and faster performance. In comparison, the YOLO-face is to increase face detection performance at a fast detection speed.

Ding et al. [20] constructed two datasets created for masked faces recognition (MFR) for masked faces verification (MFV), which contains 400 pairs of 200 identities for verification, and masked faces identification (MFI), which contains 4,916 images of 669 identities for identification. A latent part detection (LPD) method is also developed for locating the latent facial part that is robust to mask wear. Extensive tests on the MFV, MFI and synthetic masked LFW data show that the LPD model outperforms alternative approaches. They use the LPD network, which has a level of accuracy of 94.34 %. There are two major drawbacks, when using these approaches to solve the MFR problem directly. First, the PFR techniques need the use of pre-defined partial face images as inputs, which are difficult to identify or define semantically in masked faces. Second, the PRF techniques disregard global signals such as chin contours in masked face images.

Most of the current approaches aims to detect whether an individual is wearing a face mask or not or to detect if the mask is worn in a correct way or not. There are few masked-face human identification approaches. This work proposes a deep transfer learning approach for masked face recognition that outperform existing approaches in terms of identification accuracy.

IV. METHOD

A. Dataset

We collected a dataset of 400 RGB images for ten human masked faces. Each individual class includes 30 images for the training and validation, and 10 images for the testing. Examples of the masked face data are illustrated in Fig. 7. The image sizes are in the range of 1.5 and 4 MB. We resized the images to match the required input dimensions of each of the six networks. SqueezeNet and AlexNet use 227×227 pixels, while GoogleNet, VGG16, and ResNet-50 use 224×224 pixels. However, MobileNet-V2 uses an input size of 128×224 pixels.

Data augmentation is a technique used in machine learning to expand the quantity of data by introducing slightly modified copies of available image data or newly created artificial data from real data. It functions as a preprocessing step and aids in the training of a machine learning model in order to reduce overfitting. Geometric transformation, flipping, color altering, cropping, rotation, noise injection, and random erasure are all examples of data augmentation techniques. We used data augmentation in our trained networks by acquiring many photos from various perspectives, surroundings and conditions, orientation, position, and brightness. The objective for this is to ensure that the output contains accurate predictions. We also applied several geometric transformations to the existing images to generate synthetic images. These transformations are random rotation in the range of -90° and $+90^\circ$ and random scaling in the range of 1 and 2.

B. CNN Model Training and Validation

We trained and evaluated six pre-trained CNN models which are SqueezeNet, GoogleNet, AlexNet, ResNet-50, VGG-16, and MobileNet-V2. The training was performed using a single CPU. The validation was done in a 10-iteration process to ensure that the system is trained well without overfitting.

SqueezeNet training takes 33 minutes and 46 seconds. The network achieved a validation accuracy of 97.78% as illustrated in Fig. 8. GoogleNet training takes 46 minutes and 59 seconds and achieved a validation accuracy of 100% as illustrated in Fig. 9.

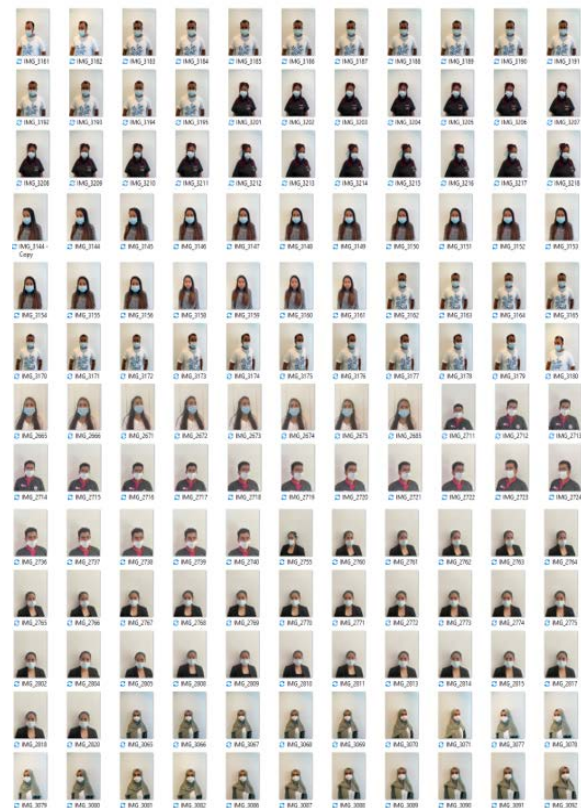


Fig. 7. Sample of Masked Face Dataset.

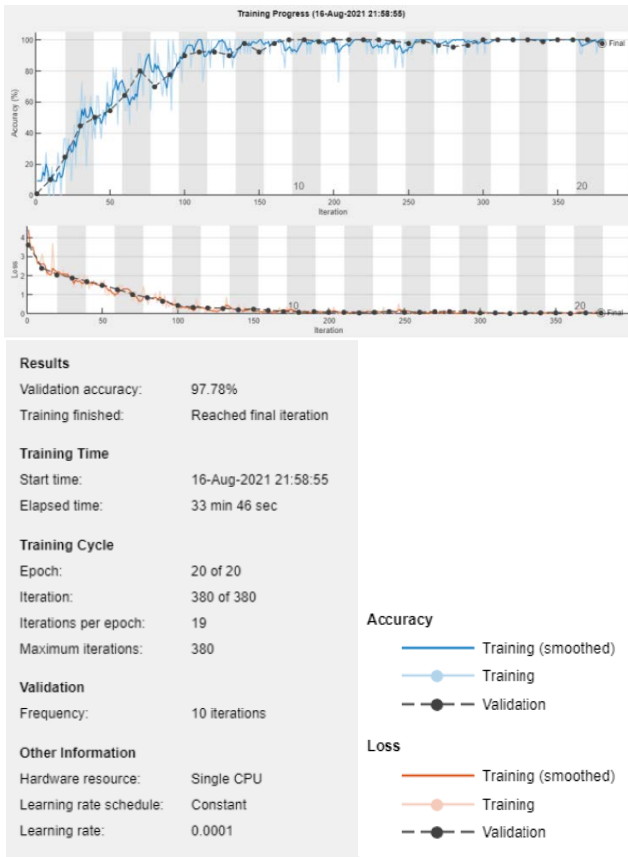


Fig. 8. SqueezeNet Training and Validation.

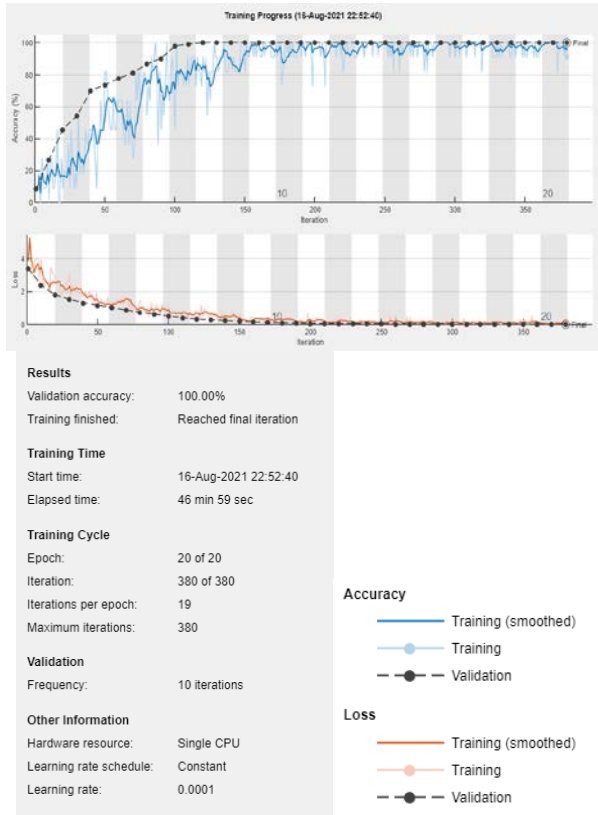


Fig. 9. GoogleNet Training and Validation.

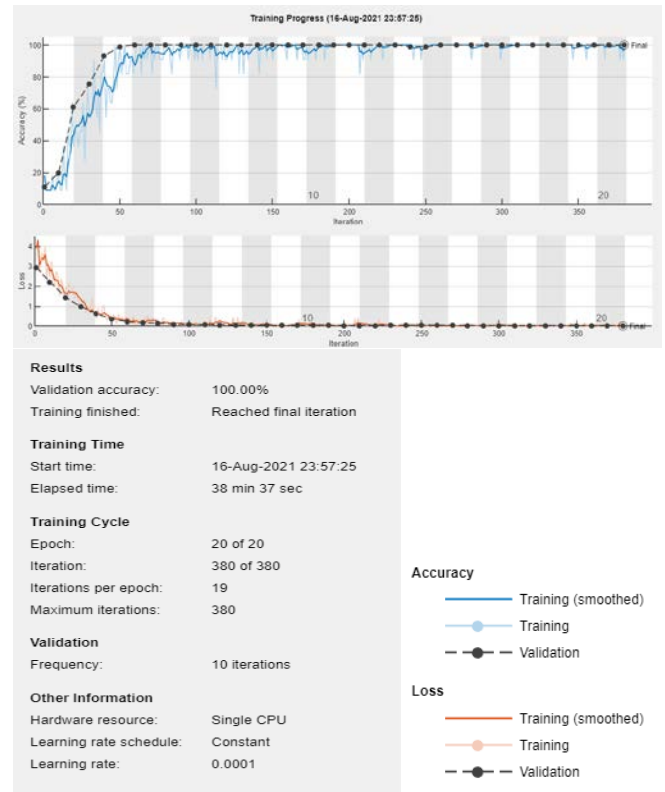


Fig. 10. AlexNet Training and Validation.

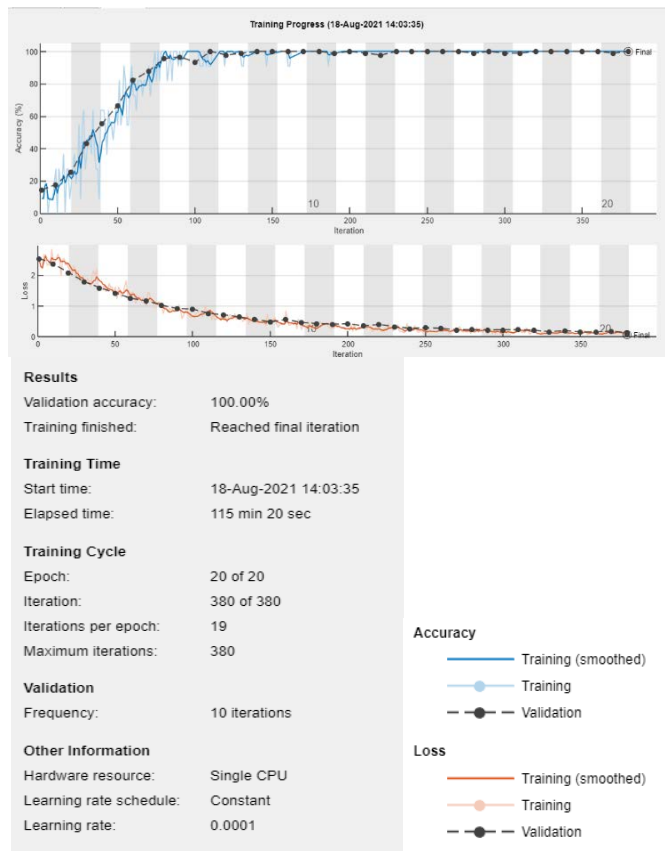


Fig. 11. ResNet-50 Training and Validation.

AlexNet training takes 38 minutes and 37 seconds and achieved a validation accuracy of 100% as illustrated in Fig. 10. Training the ResNet-50 network takes 115 minutes and 20 seconds and achieved a validation accuracy of 100% as illustrated in Fig. 11. Training the VGG-16 network takes 148 minutes and 50 seconds and achieved a validation accuracy of 100% as illustrated in Fig. 12. Training the MobileNet-V2 training takes 62 minutes and 20 seconds. The network achieved a validation accuracy of 100% as illustrated in Fig. 13.

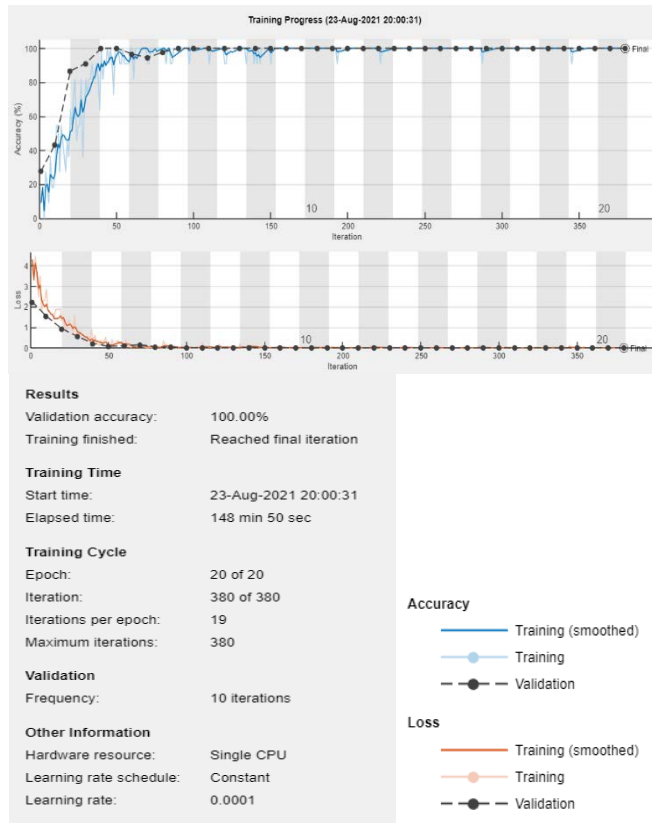


Fig. 12. VGG-16 Training and Validation.

The training performance of the six CNN is summarized in Table I. According to the results, most of the nets achieved a very high accuracy, but when the training time is considered, AlexNet has the shortest training time. GoogleNet is the second-best model which achieved an accuracy of 100% with a reasonable training time of 46 mins 59 sec. However, MobileNet-V2 is the third-best model which achieved a validation accuracy of 100% with a good training time which is 62 mins 20 sec. Moreover, the fourth-best network is ResNet-

50 as it achieved validation accuracy of 100% but in a long training time of 115 mins 20 sec. The fifth network is VGG-16 that has achieved high validation accuracy of 100% but in a very long training time. The lowest network performance was observed is in SqueezeNet because it provides the lowest validation accuracy among the six networks, but it took a very good training time, which is 33 minutes and 46 seconds.

C. CNN Model Testing

The six CNN models were tested on unseen images from each of the ten classes; we tested the system on ten images for each class, the models output the predicted label and the confidence level of each prediction. Fig. 14 illustrates samples of testing results of each of the six models on three unseen images. All the six models have successfully identified all the images correctly with very high confidence level indicating that the six models achieve 100% recognition rate. The overall testing results are summarized in Table II. In the presence of the mask, the suggested method enhances the generalization of the face recognition process.

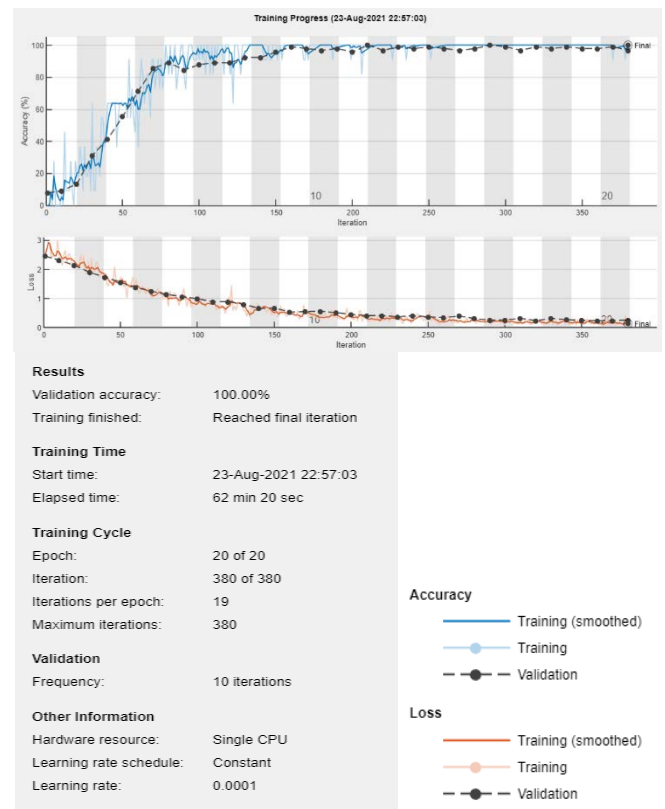


Fig. 13. MobileNet-V2 Training and Validation.

TABLE I. COMPARISON OF CNN TRAINING PERFORMANCE

Model	Learning rate	Epochs	Validation Accuracy	Elapsed Time	Hardware Resource	Max. iterations
SqueezeNet	0.0001	20	97.78%	33 mins 46 sec	Single CPU	380
GoogleNet	0.0001	20	100%	46 mins 59 sec	Single CPU	380
AlexNet	0.0001	20	100%	38 mins 37 sec	Single CPU	380
ResNet-50	0.0001	20	100%	115 mins 20 sec	Single CPU	380
VGG-16	0.0001	20	100%	148 mins 50 sec	Single CPU	380
MobileNet-V2	0.0001	20	100%	62 mins 20 sec	Single CPU	380



Fig. 14. Samples of Testing Results.

TABLE II. TESTING RESULTS

Model	Name	Results			Testing Accuracy	Percentage Confidence level		
						Max	Min	Average
SqueezeNet	Annet	100	100	100	100%	100	100	100
	Ella	96.8	98.8	99.4	100%	99.4	96.8	98.33
	Krisdna	100	99.7	97.4	100%	100	97.4	99.03
	Mouza	100	99.9	100	100%	100	99.9	99.97
	Priya	100	84.2	96.4	100%	100	84.2	93.53
	Ronalie	100	100	100	100%	100	100	100
	Saddam	99.1	100	100	100%	100	99.1	99.70
	Salah	84.8	63.3	99.2	100%	99.2	63.3	82.43
	Wafa	100	100	100	100%	100	100	100
Zeeshan	97.6	97.6	98.9	100%	98.9	97.6	98.03	
GoogleNet	Annet	99.9	93	99.7	100%	99.9	93	97.53
	Ella	66.4	94	99.4	100%	99.4	66.4	86.60
	Krisdna	80.9	99.6	98.8	100%	99.6	80.9	93.10
	Mouza	99.6	99.7	99.9	100%	99.9	99.6	99.73
	Priya	89.6	97.5	97.5	100%	97.5	89.6	94.87
	Ronalie	99.3	100	100	100%	100	99.3	99.77
	Saddam	97.2	99.7	98.4	100%	99.7	97.2	98.43
	Salah	40.9	99.8	97.9	100%	99.8	40.9	79.53
	Wafa	95.6	98	99.6	100%	99.6	95.6	97.73
Zeeshan	98.9	97	98.8	100%	98.9	97	98.23	
AlexNet	Annet	100	100	100	100%	100	100	100
	Ella	46.4	100	99.9	100%	100	46.4	82.10
	Krisdna	90.7	99.9	100	100%	100	90.7	96.87
	Mouza	100	99.5	100	100%	100	99.5	99.83
	Priya	99.7	100	42.6	100%	100	42.6	80.77
	Ronalie	99.9	100	99.9	100%	100	99.9	99.93
	Saddam	99.9	99.9	100	100%	100	99.9	99.93
	Salah	99.6	77.7	100	100%	100	77.7	92.43
	Wafa	99.8	99.7	96.8	100%	99.8	96.8	98.77
Zeeshan	63.3	98.4	99.8	100%	99.8	63.3	87.17	
ResNet-50	Annet	96.9	93.2	80.9	100%	96.9	80.9	90.33
	Ella	76	99.9	96.9	100%	99.9	76	90.93
	Krisdna	76.4	85	79	100%	85	76.4	80.13
	Mouza	91.2	98	92.4	100%	98	91.2	93.87
	Priya	78.4	81.3	95	100%	95	78.4	84.90
	Ronalie	99.3	98.8	98.6	100%	99.3	98.6	98.90
	Saddam	67.2	95.4	95.7	100%	95.7	67.2	86.10
	Salah	92.6	50.6	96	100%	96	50.6	79.73
	Wafa	96.8	92.6	93	100%	96.8	92.6	94.13
Zeeshan	49.4	63	79	100%	79	49.4	63.80	
VGG-16	Annet	100	99.8	100	100%	100	99.8	99.93
	Ella	74.3	99.8	86.5	100%	99.8	74.3	86.87
	Krisdna	99.9	100	100	100%	100	99.9	99.97

	Mouza	100	100	100	100%	100	100	100
	Priya	99.9	100	100	100%	100	99.9	99.97
	Ronalie	100	100	100	100%	100	100	100
	Saddam	100	100	100	100%	100	100	100
	Salah	42.1	100	100	100%	100	42.1	80.70
	Wafa	100	100	100	100%	100	100	100
	Zeeshan	97.9	100	100	100%	100	97.9	99.30
MobileNet-V2	Annet	95.1	97.4	96.2	100%	97.4	95.1	96.23
	Ella	56.9	99.3	85.4	100%	99.3	56.9	80.53
	Krisdna	90.9	83.3	71.6	100%	90.9	71.6	81.93
	Mouza	87.2	88.2	93.3	100%	93.3	87.2	89.57
	Priya	75.4	90.2	90.9	100%	90.9	75.4	85.50
	Ronalie	81.8	86.3	85.8	100%	86.3	81.8	84.63
	Saddam	77.9	91.7	95.5	100%	95.5	77.9	88.37
	Salah	47	86.9	72.1	100%	86.9	47	68.67
	Wafa	66	90.5	81.7	100%	90.5	66	79.40
	Zeeshan	82.7	92.8	95.2	100%	95.2	82.7	90.23

REFERENCES

V. CONCLUSION

We propose a deep transfer learning approach for masked face recognition. We were able to find an appropriate pre-trained network models and utilize them as a starting point for fine-tuning and developing a deep neural network for a new image classification job using our training masked face data. We successfully utilized transfer learning to speed up training and increase the deep learning model's performance. We examined six convolutional neural network (CNN) models on this dataset. All models show great performance in terms of very high face recognition rate and short training time. The models are SqueezeNet, GoogleNet, AlexNet, ResNet-50, VGG-16, and MobileNet-V2.

These six models achieved validation accuracy between 97.8% and 100%. When tested on unseen data, all the models were able to identify all masked faces correctly with very high confidence level indicating that the six models achieve 100% recognition rate. The proposed approach is critical because it detects a person faster than the human eye, it is more accurate, and provides complete security. In the presence of the mask, the suggested method enhances the generalization of the face recognition process. The proposed approach can be applied in smart access systems and intelligent attendance systems in schools, hospitals, and various industries. The work can be expanded by evaluating more CNN models and by including more human masked-face image data.

The research opens up exciting new areas for study. The suggested method is not restricted to mask detection only and can be incorporated into any high-resolution video surveillance systems. A face mask may be used with the model to recognize facial landmarks for biometric applications. In future work, we anticipate being able to create our own network and provide it with the tools it needs to be well-trained to suggest a more extensive work.

- [1] K. Suresh, M. Palangappa and S. Bhuvan, "Face Mask Detection by using Optimistic Convolutional Neural Network," in 2021 6th International Conference on Inventive Computation Technologies (ICICT), 2021, pp. 1084--1089.
- [2] X. Li, "Masked Face Detection and Calibration with Deep Learning," IOP Science, vol. 2196, p. 10, 2022.
- [3] Zhongyuan Wang; Guangcheng Wang; Baojin Huang; Zhangyang Xiong; Qi Hong; Hao Wu; Peng Yi; Kui Jiang., "Masked Face Recognition Dataset and Application," Arxiv , no. 2, p. 3, 2020.
- [4] R. Golwalkar and N. Mehendale, "Masked-face recognition using deep metric learning and FaceMaskNet-21," 2022. [Online]. Available: <https://doi.org/10.1007/s10489-021-03150-3>.
- [5] E. Naqa, Issam, Murphy and M. J, What is machine learning?, Springer, 2015, pp. 3--11.
- [6] M. Hargrave, "Deep Learning," Investopedia, 17 May 2021. [Online]. Available: <https://www.investopedia.com/terms/d/deep-learning.asp>.
- [7] B. Antonio, F. Boris, T. David and C. Borja, "A Systematic Review of Deep Learning Approaches to Educational Data Mining," Complexity, vol. 2019, no. 1306039, p. 22, 2019.
- [8] K. Alhaneaee, M. Alhammadi, N. Almenhali and M. Shatnawi, "Face Recognition Smart Attendance System using Deep Transfer Learning," Procedia Computer Science, vol. 192, pp. 4093--4102, 2021.
- [9] T. M. Ayyar, "A practical experiment for comparing LeNet, AlexNet, VGG and ResNet models with their advantages and disadvantages,," [Online]. Available: <https://tejasmohanayyar.medium.com/a-practical-experiment-for-comparing-lenet-alexnet-vgg-and-resnet-models-with-their-advantages-d932fb7c7d17>.
- [10] Mathworks, "ResNet-50 convolutional neural network," [Online]. Available: <https://www.mathworks.com/help/deeplearning/ref/resnet50.html>.
- [11] Neurohive, "VGG16 – Convolutional Network for Classification and Detection," [Online]. Available: <https://neurohive.io/en/popular-networks/vgg16/>.
- [12] C. Lepelaars, "The Evolution Of Mobile CNN Architectures," 2020. [Online]. Available: https://wandb.ai/carlolepelelaars/mobile_architectures/reports/The-Evolution-Of-Mobile-CNN-Architectures--VmlldzoyMDQ0ODQ.

- [13] A. Cabani, K. Hammoudi, H. Benhabiles and M. Melkemi, "MaskedFace-Net--A dataset of correctly/incorrectly masked face images in the context of COVID-19," *Smart Health*, vol. 19, no. Elsevier, p. 100144, 2021.
- [14] J. Mingjie, F. Xinqi and Y. Hong, "Retina facemask: A face mask detector," *arXiv preprint arXiv:2005.03950*, vol. 2, p. 2020.
- [15] M. Loey, G. Manogaran, M. H. N. Taha and N. E. M. Khalifa, "A hybrid deep transfer learning model with machine learning methods for face mask detection in the era of the COVID-19 pandemic," *Measurement*, vol. 167, no. Elsevier, p. 108288, 2021.
- [16] A. Chavda, J. Dsouza, S. Badgujar and A. Damani, "Multi-stage cnn architecture for face mask detection," in *2021 6th International Conference for Convergence in Technology (I2CT)*, IEEE, 2021, pp. 1–8.
- [17] W. Hariri, "Efficient masked face recognition method during the covid-19 pandemic," *rXiv preprint arXiv:2105.03026*, 2021.
- [18] P. Nagrath, R. Jain, A. Madan, R. Arora, P. Kataria and J. Hemanth, "SSDMNV2: A real time DNN-based face mask detection system using single shot multibox detector and MobileNetV2," *Sustainable cities and society*, vol. 66, p. 102692, 2021.
- [19] V. Aswal, O. Tupe, S. Shaikh and N. N. Charniya, "Single Camera Masked Face Identification," in *2020 19th IEEE International Conference on Machine Learning and Applications (ICMLA)*, IEEE, 2020, pp. 57--60.
- [20] F. Ding, P. Peng, Y. Huang, M. Geng and Y. Tian, "Masked face recognition with latent part detection," in *Proceedings of the 28th ACM International Conference on Multimedia*, 2020, pp. 2281--2289.

MSA-SFO-based Secure and Optimal Energy Routing Protocol for MANET

D.Naga Tej¹

Research Scholar, JNTUK, Kakinada
Assistant Professor, Gayatri Vidya Parishad College of
Engineering, Madhurawada, Visakhapatnam
Andhra Pradesh, India

K V Ramana²

Professor
JNTUK Kakinada
Kakinada
Andhra Pradesh, India

Abstract—Mobile Adhoc Network (MANET) is a fast deployable wireless mobile network with minimal infrastructure requirements. In these networks, autonomous nodes may function as routers. Due to the mobility of MANET nodes, the network's topology is dynamic. Recent scientific emphasis has been placed on MANET security. Few MANET attacks have been discussed in the existing literature. Wired networks provide more security choices than wireless networks. Most routing protocols fail in a MANET with a malicious node. This research focuses on S-DSR, a novel hybrid secure routing system that guarantees the delivery and performance of packets across network nodes. This protocol leverages neighbor trust information to choose the most secure route for file transfer. This protocol is used by OMNET++. It offers a higher delivery rate and lower delay than AODV, AOMDV, and other similar protocols. MANETs, or mobile ad-hoc networks, will be used in the future communication protocols of industrial wireless networks. These protocols will decentralise the connection of smart devices. Due to the unidimensional nature of digital data, it is impossible to apply encryption methods indirectly. These publications are digital. To strengthen the privacy of e-healthcare MANETs, a safe, lightweight keyframe extraction technique is required. The purpose of this project is to develop a secure protocol for MANET wireless networks. This study proposes the use of chaotic cryptography to enhance the security of MANET Wireless networks. Using Modified Self-Adaptive Sailfish Optimization (MSA-SFO), it is possible to construct vital maps in a chaotic setting. This method produces secure key pairs.

Keywords—MANET; sail fish optimization; energy; routing protocol

I. INTRODUCTION

One of the most often used kinds of independent wireless technology for communication with mobile nodes is called a MANET. Mobile ad hoc networks (MANETs) rely on mobile nodes to perform dual roles as end systems and routers for the network's packet transmissions [1]. Due to the fact that wireless communication is used, it is much simpler to reestablish the connection, and moreover, nodes might be designed to be mobile. Given the nature of the nodes, which is that they are movable, it is not required that a permanent network structure be used for communication. MANET, on the other hand, does not make use of base stations, which might be helpful in a number of different networking configurations. Due to the number of users using the MANET for diverse purposes, such as military and emergency operations, it is

crucial that the platform be safeguarded from unwanted users. This is due to the fact that the network's popularity has made it hard for illegal users to connect to it.

There are several uses for mobile ad hoc networks (MANETs), such as between special events, communications in places where radio infrastructure does not exist, catastrophes, and military surgery. MANET's flexibility and dynamic topology make it vulnerable to a variety of attacks, including eavesdropping, routing, and the modification of applications. The quality of services has been surpassed by MANET's security problems (QoS). So, the best way to ensure MANET's security is to use intrusion tracking, which modifies the system to notice any other vulnerability. Anti-intrusion detection is vital to providing safeguards and serves as an additional layer of security against unauthorized entry. In the presence and absence of a selective packet dropping attack, this solution was put to the test against the best-known practices [1].

Ad hoc network (MANET) is a grouping of nodes that communicate without the intervention of a central administrator in an infrastructure-free environment. The nodes in these networks are more dependent on each other to perform basic network activities. Secure routing is difficult to establish because of the shortage of resources. A system must be in place to deter misbehavior and preserve the network's synergy in order to assure safe routing. At each node, a partly distributed dynamic model is used to enhance the overall network's security and privacy. During route creation, additional information about network misbehavior is provided across the nodes as a precautionary step to maintain safe routing. In the real world, a node may engage in many forms of misbehavior at various points in time. To cope with nodes that show different levels of misbehavior, it offers a dynamic decision-making method. The model's ability to cope with misbehaving nodes has been shown in a series of simulations [2].

Unlike traditional networks, mobile ad-hoc networks (MANETs) are self-contained and do not rely on centralized access. MANET's rapid and flexible networking style allows it to be used in a broad range of situations. However, the network's constantly shifting architecture and open communication channels provide security risks. Active-routing authentication (AAS) was suggested in this work using the properties of active routing protocols. In order to prove the

AAS's effectiveness against selective forwarding, fake routing, byzantine, and spoofing attacks, we used BAN logic to examine the potential of hostile nodes mixing in a MANET [3][4].

The research problem and contribution of this research is to design a brand-new heuristic algorithm known as MSA-SFO by enhancing the already existing SFO algorithm's capacity for self-adaptation. This study was done with the intention of preserving users' privacy inside MANETs. This speeds up the process of convergence and decrease the likelihood of being stuck in a local minimum.

Paper organization is as follows:

The section outlines the format of this paper: The work that is connected to Optimal Energy Routing Protocol is shown in Section 2. This part also provides an explanation of the fundamental Routing Protocol for MANET techniques that were used throughout this research. The planned MSA-SFO-Modified Self Adaptive Sail Fish Optimization is described in Section 3, which reflects its current state. The analysis and discussion of the obtained data are presented in Section 4. Our results are summarised in Section 5, which also includes a discussion of the work that will be done in the future.

II. RELATED WORK

Despite extensive deployment, the AOVDV routing scheme remains vulnerable to blackhole attacks. Lu and his team developed the SAODV protocol, a secure mechanism for routing networks, to overcome this problem. Due to the nature of a blackhole assault, which requires the cooperation of two nodes, it cannot be defended against using conventional protection measures. The BP-AODV protocol was created to solve this concern. It combines the features of the original AOVDV protocol with the BP-AODV to provide a secure and efficient routing system. A study of the BP-AODV protocol found that it can effectively repel a blackhole assault, regardless of whether it is launched by a forwarding node or a malicious actor. It also shows that BP-AODV may avoid a blackhole attack even if it happens throughout the whole routing procedure.

One of the most difficult and significant routing security concerns in VANETs and self-driving and connected cars is the detection of Black Hole attacks (ACVs). Cyber-physical paths may be hacked by malicious vehicles or nodes, converting a safe route into a less secure and dependable one. To avoid a neighboring node, malevolent nodes snatch data packets that may include emergency alerts and discard them instead [5]. When using MANETs, the nodes are on the move at all times. Macro-area networks (MANETs) have unique issues due to their inherent vulnerability to several types of security assaults and their inability to maintain secure operations while protecting their resources and providing safe routing among nodes. It is critical, therefore, to provide a reliable secure routing protocol to guard against anonymous attacks on nodes. Selfishness problems may now be studied, formulated, and solved using game theory. Malicious activity in networks is seldom detected using this technique. Instead, it focuses on the nodes' strategic and logical conduct. The dynamic Bayesian signaling game was utilized to examine the strategy profile of

normal and malicious nodes in our research. In this game, specific tactics for each node were also disclosed. Combining player payoffs and tactics to achieve perfect Bayesian equilibrium (PBE) serves as a popular solution for signaling games dealing with partial knowledge. For both ordinary and malicious nodes, the use of PBE techniques is private information. In order to avoid being detected, legitimate nodes should cooperate with routing and keep their payoffs up-to-date, whereas malevolent nodes take calculated risks to avoid being detected. The reputation mechanism encourages improved collaboration between nodes by reducing the utility of malevolent nodes. [6] Bayes rule-based belief updating systems are used by regular nodes to continually assess their neighbors.

Since the beginning of the previous decade, MANET has been a major research focus. As the Internet-of-of-Things (IoT) expands into urban areas, this sort of networking paradigm is becoming more widely accepted as an essential component of the IoT's impending urban applications. Existing routing techniques in traditional MANETs cannot be used with IoT because of a considerable hurdle. The MANET-based application linked to the IoT platform may be exposed to security threats as a result of this routing mismatch. In order to enable real-time streaming applications, the mobile nodes in this study must communicate multimedia signals. Understanding the attacker's unexpected behavior is one of the most important aspects of safeguarding data. Attackers' sophistication is examined in the present research. To perform fatal assaults, they know one other's identities and collaborate, which is seldom represented in current security modeling data. This study utilizes the modeling capabilities of game theory to represent the multiple-collusion attacker situation. Modeling strategies of regular/malicious nodes as well as employing an optimization technique utilizing innovative auxiliary information to build the best strategies are some of its contributions. Malicious nodes may now be accurately predicted by each normal node, thanks to the new model's enhanced capacity to do exact computations. Game theory's baseline method is outperformed by the suggested mathematical model in MATLAB simulations [7].

Intelligent Transportation Systems may benefit from the use of Vehicular Ad-hoc Networks (VANET), which are a subset of Mobile Ad-hoc Networks (MANET) (ITS). Due to quick topological changes, high mobility, and frequent link disconnections, routing in these networks is a difficult issue. Because of this, establishing an effective routing system that meets the time constraints and minimizes the amount of overhead is a challenge. VANETs must also be capable of identifying malevolent vehicles. Using Unmanned Aerial Vehicles (UAVs) may be a useful tool in dealing with these constraints. UAVs in VANETs may be used to aid in the identification of potentially harmful vehicles by operating in ad hoc mode and collaborating with the vehicles. There are two unique modes of routing data in the VRU routing protocol: (1) sending packets of data between vehicles using UAVs, and (2) routing packets of data between UAVs. Using the NS-2.35 simulator on Linux Ubuntu 12.04, the performance of VRU routing components in an urban setting is evaluated. VANET MobiSim, a generator of mobility, and MobiSim, a UAV

motion generator, are both used in the generation of vehicle movements. Comparatively, the performance study shows that the VRU protocol may increase the delivery and detection rates by 16 and 7 per cent, respectively, over existing routing protocols. End-to-end latency and overhead are both reduced by 40% using the VRU protocol [8].

Nodes in a mobile network self-organize into mobile ad hoc networks (MANETs), which develop a dynamic network architecture to link them. Before reaching its final node, data in a MANET must travel via a series of intermediate nodes. To keep malicious nodes from gaining access to this data, we need to have some kind of protection in place. Routing security has been addressed in a variety of ways in the literature, each of which addresses a distinct component of security [9].

Multipath routing, as compared to the conventional single-path routing, is often employed in wireless networks to increase their fault tolerance. The GAHC algorithm is a mix of the Hill-Climbing and Genetic Algorithms that takes into consideration all of the variables that influence route selection. In addition, an enhanced C-means algorithm was created to apply this method [10]. A computation is conducted based on the value of the nodes that fulfill the trust threshold for a certain route. The cluster heads then route their networks through other routes. The ideal route for their applications is then determined by analyzing these routes. MSA-SFO is a multi-path routing scheme with a maximum throughput of 0.85 bits per second and a 90 percent detection rate. Additionally, its packet delivery rate is 89 percent. To evaluate its performance, selective packet dropping was used [11].

Mobile ad hoc networks are well suited for emergency communications and rural locations lacking radio infrastructure. They may also be used for emergency communications. Nonetheless, owing to the network's changeable topologies, security is its most susceptible point. Due to the nature of the MANET's security challenges, it is advised that network managers monitor and identify possible attacks on a frequent basis, prior to them becoming severe. This may prevent them from influencing the performance of the system. The ability of a mobile node to forward packets is one of the most crucial aspects that might impact its performance [12]. This research intends to build a trust-based multi-path routing algorithm for usage in MANETs. The selected cluster heads based on the suggested method are next examined to find the appropriate application path. After calculating the trust levels of the nodes, the ideal path for the applications was determined. The cluster heads then route their networks using multi-hop routing. This approach calculates the ideal path based on several performance-affecting criteria.

Multiple Sub-Silo Order (MSA-SFO) is a multi-path routing technique that greatly outperforms previous algorithms. It may also lower network energy usage by around 80 percent. Due to its adaptability and portability, the mobile ad hoc network (MANET) is gaining popularity. Although security procedures have been implemented to secure the networks, they do not protect the communication channels. To provide total security, it is necessary to create both the communication

and routing protocols. The implementation of security procedures developed for wireless and wired networks may be particularly costly on MANETs due to their restricted network resources. This research attempts to create a secure architecture that can guarantee total network security. SUPERMAN, a proposed security framework, was evaluated against three distinct security protocols: IPsec, SAODV, and SOLSR. The simulation results demonstrated that the SUPERMAN architecture is optimal for wireless communication security. Due to the nature of the mobile ad-hoc network, a significant portion of its nodes are susceptible to assault. These nodes offer access to the network by unauthorized persons and organizations. In order to preserve the network's functioning, network administrators must routinely monitor and identify possible risks. The study provides a safe approach for selecting neighbors that combines machine learning and conventional routing techniques. By combining these strategies, it may be feasible to construct safe and dependable routes to a target. By observing the behavior of the nodes at changing connection levels, this technique may be implemented [13].

Various measures, such as the packet delivery ratio and the throughput, are used while evaluating the performance of a suggested method. The research demonstrates via experimental analysis that the suggested technique can perform consistently. Due to the nature of mobile ad hoc networks, it is becoming more challenging to create and maintain end-to-end infrastructure in specific places. As a consequence, DTN networks are becoming increasingly prevalent in these regions. DTNs are appropriate for high-latency applications, but they should also be considered for maritime networks. Due to the characteristics of the maritime environment, DTN networks are also addressed while addressing security issues. In order to provide tactical signals, for instance, the article demonstrates how to employ a DTN to address perimeter security issues. This study suggests utilizing the discriminant analysis to enhance the security of DTN connections. NDN is a future Internet architecture that permits the efficient delivery of the material as opposed to the standard data carriers. With its diverse forwarding techniques, NDN-based wireless networks are able to maintain safe and dependable communication. The two primary kinds of packets that NDN networks send back and forth are INTEREST and DATA. This study examines the strategies and issues found during the implementation of NDN-based networks such as MANETs, VANETs, WSNs, and WMNs [14].

III. PROPOSED MSA-SFO-MODIFIED SELF ADAPTIVE SAIL FISH OPTIMIZATION

The mobile networks serve as the terminal service in the wireless MANET, which allows for communication between the different wireless network devices. This communication has completely transformed the digital age. Because of its widespread use across a wide variety of sectors and employees, it is essential to provide a protected setting for the communication process at all times. The computing platform at the network's edge is often targeted in MANET, which is designed for wireless networks. This has the effect of reducing the platform's popularity in crucial services.

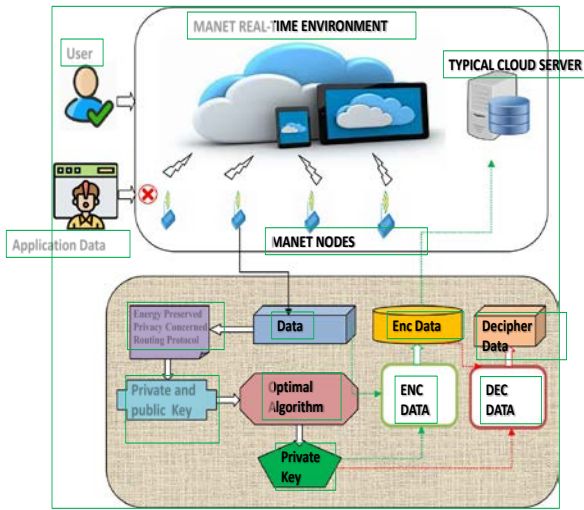


Fig. 1. Perspective on the Proposed MSA-SFO Architecture.

After the detailed analysis of the parallel and recent research outcomes, in this section of the work, the problem is formulated using the mathematical model.

In order for a network to have a long-life span, the cluster head must be replaced on a regular basis to ensure the security and the proposed architecture shown in Fig. 1.

At every moment, $T(CH)$ signifies the cluster head determining function, which yields the cluster head instance g is a collection of groups. Any cluster has a total number of nodes known as N .

For the above lemma to hold, it must be shown (Eq. 1) that a cluster of nodes (Eq. 2) exists in the complete network, where the number of non-dead or active nodes is not zero.

$$\forall g \subset G \quad (1)$$

And,

$$\emptyset(g) \neq NULL \quad (2)$$

Also,

$$\forall n \subset N \quad (3)$$

Consequently, Eq. 4 and 5 so that the newly picked cluster head may avoid being comparable to the previous one.

$$\forall n(t) \subset N' \quad (4)$$

And,

$$N \notin N' \text{ and } N' \notin N \quad (5)$$

If the $R(k)$ represents the proportion of cluster heads in the N that are still available, then (Eq. 6) represents the percentage of cluster heads in the N that are still accessible.

$$1 - R(k)[k \cdot \text{mod} \frac{1}{R(k)}] \quad (6)$$

As a result, we can write the cluster dead decision function as follows:

$$T(CH) = \frac{R(k)}{1 - R(k)[k \cdot \text{mod} \frac{1}{R(k)}]} \quad (7)$$

The energy consumption is evenly distributed throughout the cluster's many components. In Eq. 5, the rationale for avoiding repeating clusters in subsequent eras is made evident.

The suggested algorithm for the control of energy consumption in clusters is presented in the following section:

Step (1). MSA-SFO serves as the foundation for the suggested approach. Before installing the cluster, the list of active nodes is compiled.

Step (2). After choosing it from the list of active nodes, the node's energy status is calculated. The node's status will be presented in the subsequent phase.

Step (3). For the time being, the cluster head will be chosen based on the weight function, which includes the amount of available energy and the number of non-repeating nodes. Cluster heads are referred to as CH.

Step (4). This data will be stored in the routing table RTab using the settings listed below in Step 4 of the installation process.

Step (5). After that the closest neighbour node will be determined, and the process will be repeated from steps 1 through 4.

Step (6). After deciding on a route, the data is sent. If the network topology changes, go back to step 1 to 5 and repeat the process.

It may have a larger delay than other algorithms, but it will be more secure and energy-conscious than others.

Further, based on the Proposed MSA-SFO algorithm, the obtained results are discussed in the next section of the work.

A Stepwise Procedure for the Protection of Privacy When Utilizing the Modified Self-Adaptive Sailfish Optimization (MSA-SFO) Algorithm

In order to provide a concise explanation of the technique for the suggested privacy preservation in the MANET environment, the following is provided:

1) *Data collecting* the first thing that has to be done in order to complete this procedure is to acquire the necessary data set from the MANET environment. Text messages are used to carry out communication amongst the various mobile devices that are part of a MANET. These mobile devices serve as the edge platform for the MANET. These text messages include vital information, and the privacy settings ensure that it will not be disclosed to unauthorized parties. The subsequent step is to compose the basic text. The text message is generated using the cluster's acquired data. The raw data contains a number of different characters and strings. To guarantee the appropriate formatting of the text message, each character is converted into a 16-digit number.

2) If a 16-character-long text message is deemed to be covered by the privacy policy. To convert it to a simple text, each letter is converted to a binary value of 16 bits. This number is subsequently converted into the text's length. After the plain text has been generated, the ideal key must be generated. This procedure is performed to enhance privacy protection. The key is then sent to the hybrid chaotic map that processes the text. Using the suggested approach, the fundamental parameters of the map are adjusted, and the optimum key is then generated.

3) The encryption of a data file occurs immediately after the generation of the key. This phase entails utilising the binary plain text as the encryption's foundation. The result of the encryption is stored on the cloud, and only the owner has access to it. The process of producing ciphertext is referred to as the binary extension-or operation.

4) The decoding procedure is executed to extract the file's data. The key and the binary representation of the encryption are then subjected to a kind of XOR to guarantee the integrity of the original data.

IV. RESULTS AND DISCUSSIONS

The obtained results are highly satisfactory and are furnished in this section of the work.

The simulation results with 30 notes are formulated here (Table I).

TABLE I. SIMULATION WITH 30 NODES

Node Seq	Number of times Identify Disclosed (#)			
	FSR	AODV	AOMDV	Proposed MSA-SFO Algorithm
1	15	5	5	0
2	17	9	5	0
3	17	9	4	0
4	13	10	4	0
5	14	8	5	3
6	13	8	5	3
7	12	7	3	1
8	11	5	3	2
9	12	6	4	2
10	13	9	4	3
11	18	10	5	2
12	16	7	4	1
13	18	6	3	0
14	10	7	5	1
15	13	5	4	3
16	15	8	5	0
17	15	10	4	3
18	16	10	4	3
19	13	7	5	1
20	12	8	3	3
21	19	8	4	0

Node Seq	Number of times Identify Disclosed (#)			
	FSR	AODV	AOMDV	Proposed MSA-SFO Algorithm
22	13	8	4	2
23	11	8	5	1
24	10	8	4	0
25	20	6	5	2
26	10	8	5	2
27	14	8	3	0
28	20	5	3	2
29	15	8	5	0
30	16	8	4	1

The results are visualized graphically here (Fig. 2).

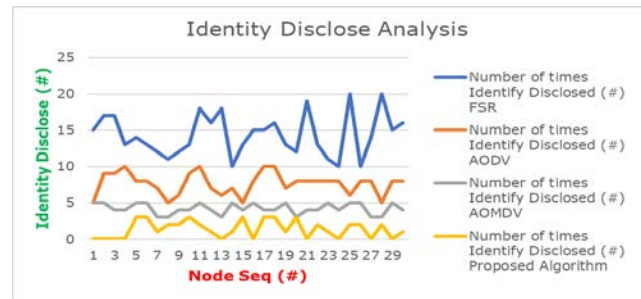


Fig. 2. Identify Disclose Analysis.

Further, in the next section of this work, the research conclusion is furnished.

The performance of the suggested MSA-SFO, as well as the performance of the comparison heuristic models is stated by the measurements. Tables II, III, IV, V, and VI exhibit the statistical performance of the suggested MSA-SFO as well as the comparing methodologies for different character lengths, including 20, 40, 60, 80, and 100 correspondingly. And the results are visualized graphically shown in Fig. 3, 4, 5, 6 and 7.

In comparison to the PSO, GWO, and SFO, the MSA-SFO framework has achieved the highest values. Additionally, it is 48 percent greater than the average performance. In terms of plot count, the proposed structure is likewise 90% better than the simple parameters. In addition, it has been 60 percent better than the GWO and 50 percent better than the WOA.

TABLE II. STATISTICAL ANALYSIS OF WITH KEY GENERATION WITH LENGTH 20

Optimization Algorithm	PSO [15]	GW O [16]	WO A [17]	SFO [18]	Pamart hi [19]	Proposed MSA-SFO
Worst	0.0129	0.0136	0.0127	0.0127	0.0144	0.01512
Best	0.0497	0.0548	0.0457	0.053	0.0767	0.080535
Mean	0.0318	0.0342	0.0302	0.0335	0.0453	0.047565
SD	0.0112	0.0122	0.0101	0.012	0.0187	0.019635

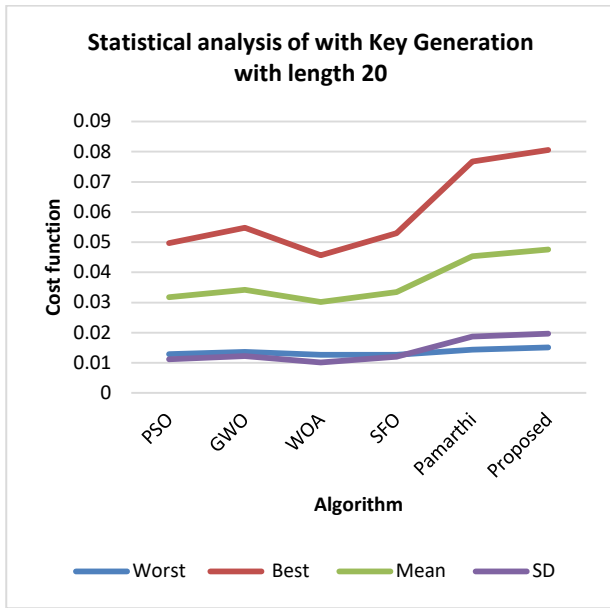


Fig. 3. Statistical Analysis of with Key Generation with Length 20.

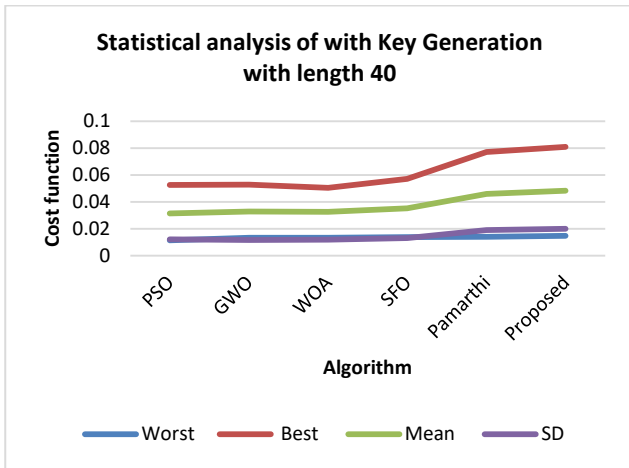


Fig. 4. Statistical Analysis of with Key Generation with Length 40.

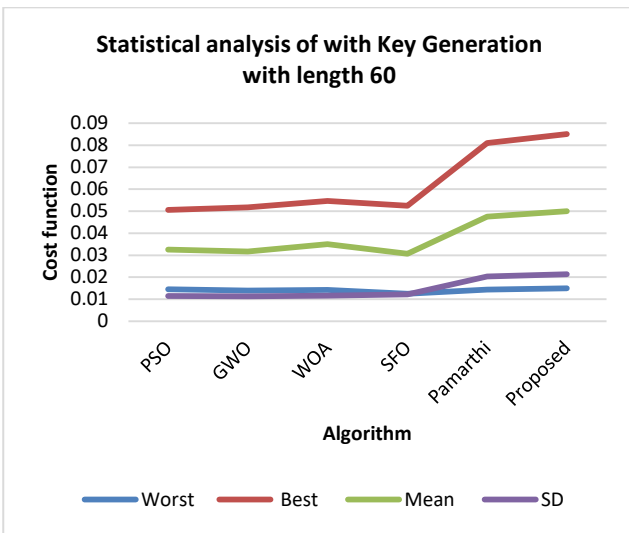


Fig. 5. Statistical Analysis of with Key Generation with Length 60.

TABLE III. STATISTICAL ANALYSIS OF WITH KEY GENERATION WITH LENGTH 40

Optimization Algorithm	PS O	GW O	WO A	SF O	Pama rthi	Proposed MSA-SFO
Worst	0.01 16	0.01 34	0.01 35	0.01 38	0.0141	0.014805
Best	0.05 26	0.05 29	0.05 05	0.05 73	0.0771	0.080955
Mean	0.03 16	0.03 29	0.03 28	0.03 53	0.046	0.0483
SD	0.01 23	0.01 18	0.01 19	0.01 33	0.0192	0.02016

TABLE IV. STATISTICAL ANALYSIS OF WITH KEY GENERATION WITH LENGTH 60

Optimization Algorithm	PS O	GW O	WO A	SF O	Pama rthi	Proposed MSA-SFO
Worst	0.01 45	0.01 39	0.01 42	0.01 25	0.0143	0.015015
Best	0.05 06	0.05 17	0.05 46	0.05 25	0.081	0.08505
Mean	0.03 26	0.03 17	0.03 5	0.03 07	0.0476	0.04998
SD	0.01 14	0.01 13	0.01 16	0.01 22	0.0203	0.021315

TABLE V. STATISTICAL ANALYSIS OF WITH KEY GENERATION WITH LENGTH 80

Optimization Algorithm	PS O	GW O	WO A	SF O	Pama rthi	Proposed MSA-SFO
Worst	0.01 43	0.01 46	0.01 33	0.01 29	0.0138	0.01449
Best	0.04 96	0.05 26	0.05 31	0.04 43	0.079	0.08295
Mean	0.03 24	0.03 4	0.03 37	0.02 85	0.046	0.0483
SD	0.01 1	0.01 2	0.01 18	0.00 93	0.0196	0.02058

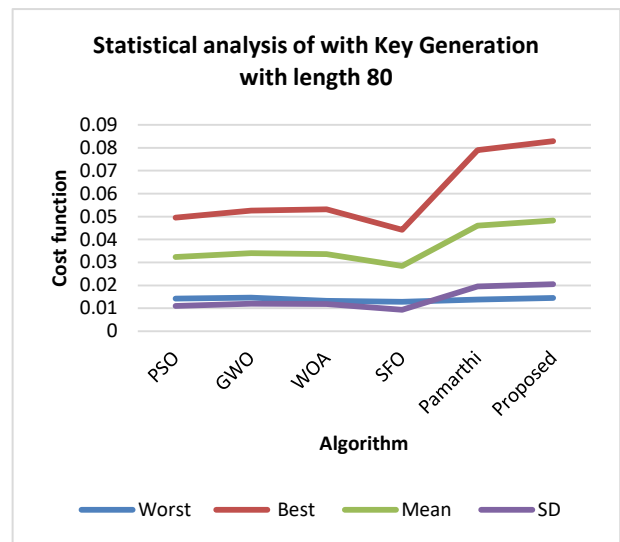


Fig. 6. Statistical Analysis of with Key Generation with Length 80.

TABLE VI. STATISTICAL ANALYSIS OF WITH KEY GENERATION WITH LENGTH 20

Optimization Algorithm	PS O	GW O	WO A	SF O	Pama rthi	Proposed MSA-SFO
Worst	0.0129	0.0136	0.0121	0.0121	0.0148	0.01554
Best	0.047	0.0526	0.053	0.0533	0.0794	0.08337
Mean	0.0296	0.0326	0.0338	0.0325	0.0466	0.04893
SD	0.0103	0.0122	0.013	0.0128	0.0196	0.02058

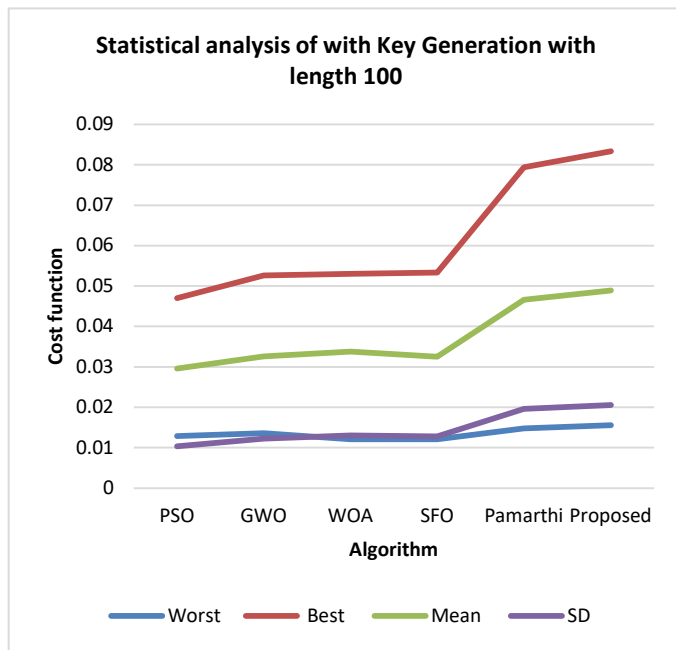


Fig. 7. Statistical Analysis of with Key Generation with Length 20.

V. CONCLUSION

MSA-SFO (Modified Self Adaptive Sail Fish Optimization) is a cluster-based routing method designed to increase the energy efficiency of current MANET routing algorithms. This research focuses on examining the different denial criteria of current algorithms. The researches compared the proposed system's performance to that of the current systems. Then, a performance study was conducted on the various systems, including the DSDV, DLSR, and FSR. It was discovered that the suggested strategy is more consistent and energy-efficient. The suggested algorithm, which has a 50 percent improvement in power awareness, serves as the foundation for a new algorithm designed to enhance the energy efficiency of current algorithms. In addition, a privacy preservation model was created to improve the security of MANET Wireless networks. The development of the suggested method has been significantly enhanced by the incorporation of the multi-state adaptive scheduling optimization approach (SFO). Utilizing this method, optimum key pairs were generated for the chaotic map. Messages were then encrypted and decrypted using the suggested technique. The development of the suggested method has been substantially enhanced by

the use of the multi-state adaptive scheduling optimization approach (SFO). Utilizing this method, optimum key pairs were generated for the chaotic map. It has also increased the degree to which text messages may be secured from prying eyes. To verify that the suggested algorithm can safeguard the privacy of sensitive data, the investigators altered the length of the text messages. The suggested method has acquired the highest performance values, which are much greater than those of the PSO, GWO, and SFO. It is also much superior than the maximum character count for text messages, which is 100. In terms of performance, the suggested method has enhanced its values by around 90 percent. According to the results, the suggested algorithm MSA-SFO provides more security for MANET Wireless networks than alternative models. It also provides a high degree of security. Implementation of the suggested technique on a large number of nodes will increase the scope of this investigation.

REFERENCES

- [1] N. Veeraiyah et al., "Trust Aware Secure Energy Efficient Hybrid Protocol for MANET," in *IEEE Access*, vol. 9, pp. 120996-121005, 2021.
- [2] A. Anand, H. Aggarwal and R. Rani, "Partially distributed dynamic model for secure and reliable routing in mobile ad hoc networks," in *Journal of Communications and Networks*, vol. 18, no. 6, pp. 938-947, Dec. 2016.
- [3] M V Narayana, Rishi Sayal, H.S. Saini, Apama Manikonda "Timestamp Based Certified Routing For Authorization And Authentication In Mobile Ad Hoc Network" *Journal of Advanced Research in Dynamical and Control Systems*, Volume-10, Issue-10, Page no.351-358, October-2018 -ISSN: 1943-023X.
- [4] A. M. El-Semary and H. Diab, "BP-AODV: Blackhole Protected AODV Routing Protocol for MANETs Based on Chaotic Map," in *IEEE Access*, vol. 7, pp. 95197-95211, 2019.
- [5] Z. Hassan, A. Mehmood, C. Maple, M. A. Khan and A. Aldegheshem, "Intelligent Detection of Black Hole Attacks for Secure Communication in Autonomous and Connected Vehicles," in *IEEE Access*, vol. 8, pp. 199618-199628, 2020.
- [6] M V Narayana, G Narsimha, SSVN Sarma, "Genetic - ZHLS Routing Protocol for Fault Tolerance and Load Balancing" *Journal of Theoretical and Applied Information Technology*, ISSN: 1992-8645 and E-ISSN: 1817-3195, 10th January 2016. Vol.83. No.1, pp. 72 – 80.
- [7] B. U. I. Khan, F. Anwar, R. F. Olanrewaju, M. L. B. M. Kiah and R. N. Mir, "Game Theory Analysis and Modeling of Sophisticated Multi-Collision Attack in MANETs," in *IEEE Access*, vol. 9, pp. 61778-61792, 2021.
- [8] H. Fatemidokht, M. K. Rafsanjani, B. B. Gupta and C. -H. Hsu, "Efficient and Secure Routing Protocol Based on Artificial Intelligence Algorithms With UAV-Assisted for Vehicular Ad Hoc Networks in Intelligent Transportation Systems," in *IEEE Transactions on Intelligent Transportation Systems*, vol. 22, no. 7, pp. 4757-4769, July 2021.
- [9] M V Narayana, Aparnarajesh Atmakuri "A-ZHLS: Adaptive ZHLS Routing Protocol for Heterogeneous Mobile Adhoc Networks" *International Journal of Engineering & Technology*, Volume 7 Issue 3(2018), PP.1626- 1630-ISSN: 2227-524X.
- [10] U. Srilakshmi, S. A. Alghamdi, V. A. Vuyuru, N. Veeraiyah and Y. Alotaibi, "A Secure Optimization Routing Algorithm for Mobile Ad Hoc Networks," in *IEEE Access*, vol. 10, pp. 14260-14269, 2022.
- [11] D. Hurley-Smith, J. Wetherall and A. Adekunle, "SUPERMAN: Security Using Pre-Existing Routing for Mobile Ad hoc Networks," in *IEEE Transactions on Mobile Computing*, vol. 16, no. 10, pp. 2927-2940, 1 Oct. 2017.
- [12] M V Narayana, G Narsimha, SSVN Sarma, "Secure- ZHLS: Secure Zone Based Hierarchical Link State Routing Protocol using Digital Signature", *International Journal of Applied Engineering Research*, ISSN 0973-4562 Volume 10, Number 9 (2015) pp. 22927-22940..

- [13] D. Falcão, R. Salles and P. Maranhão, "Performance evaluation of disruption tolerant networks on warships' tactical messages for secure transmissions," in *Journal of Communications and Networks*, vol. 23, no. 6, pp. 473-487, Dec. 2021.
- [14] A. Tariq, R. A. Rehman and B. Kim, "Forwarding Strategies in NDN-Based Wireless Networks: A Survey," in *IEEE Communications Surveys & Tutorials*, vol. 22, no. 1, pp. 68-95, Firstquarter 2020.
- [15] Challa, S., Wazid, M., Das, A. K., Kumar, N., Reddy, A. G., Yoon, E. J., & Yoo, K. Y. (2017). Secure signature-based authenticated key establishment scheme for future IoT applications. *IEEE Access*, 5, 3028-3043.
- [16] Gomes, G. F., da Cunha, S. S., Jr., & Ancelotti, A. C., Jr. (2019). A sunflower optimization (SFO) algorithm applied to damage identification on laminated composite plates. *Engineering with Computers*, 35, 619-626.
- [17] Shadravan, S., Naji, H. R., & Bardsiri, V. K. (2019). The sailfish optimizer: A novel nature-inspired metaheuristic algorithm for solving constrained engineering optimization problems. *Engineering Applications of Artificial Intelligence*, 80, 20-34.
- [18] Pedersen, M. E. H., & Chipperfield, A. J. (2010). Simplifying particle swarm optimization. *Applied Soft Computing*, 10(2), 618-628.
- [19] Pamarthi, Satyanarayana, and R. Narmadha. "Adaptive Key Management-Based Cryptographic Algorithm for Privacy Preservation in Wireless Mobile Adhoc Networks for IoT Applications." *Wireless Personal Communications* 124.1 (2022): 349-376.

An Efficient and Optimal Deep Learning Architecture using Custom U-Net and Mask R-CNN Models for Kidney Tumor Semantic Segmentation

Sitanaboina S L Parvathi¹

Research Scholar, School of Computer Science and Engineering, Vellore Institute of Technology VIT-AP University, Vijayawada, India

Harikiran Jonnadula²

Associate Professor, School of Computer Science and Engineering, Vellore Institute of Technology VIT-AP University, Vijayawada, India

Abstract—Today, kidney medical imaging has become the backbone for health professionals in diagnosing kidney disease and determining its severity. Physicians commonly use Computerized Tomography (CT) and Magnetic Resonance Imaging (MRI) scan models to obtain kidney disease information. The significance and impact of kidney tumor analysis drew researchers to semantic segmentation of kidney tumors. Traditional image processing methodologies, in general, require more computational power and manual assistance to analyze kidney medical images for tumor segmentation. Deep Learning advances are enabling less computational and automated models for kidney medical image analysis and tumor lineation. Blobs (regions of interest) detection from medical images is gaining popularity in kidney disease diagnosis and is used widely in detecting tumors, glomeruli, and cell nuclei, among other things. Kidney Tumor segmentation is challenging compared to other segmentation models due to morphological diversity, object overlapping, intensity variance, and integrated noise. In this paper, It have proposed a kidney tumor semantic segmentation model based on CU-Net and Mask R-CNN to extract kidney tumor information from abdominal MR images. Initially, It trained the Custom U-Net architecture on abdominal MR images with kidney masks for kidney image segmentation. The Mask R-CNN model is then used to lineate tumors from kidney images. Experiments on abdominal MR images using Python image processing libraries revealed that the proposed deep learning architecture segmented the kidney images and lined up the tumors with high accuracy.

Keywords—Kidney tumor (Blob) detection; custom U-Net; mask R-CNN; semantic segmentation; deep learning; medical image processing

I. INTRODUCTION

Medical imaging provides high resolution and coverage for the visualization of specific body organs. X-Ray, CT, MRI, and PET-CT scans are some frequently used medical imaging [1] technologies. In general, physicians will manually analyze the content of medical images to identify disease information. Image processing [2] and deep learning technologies [3] have been providing disease diagnosis models for over a decade, removing human errors in disease prediction. Deep learning for medical image analysis has attracted researchers and medical analysts because it requires less human intervention in data labeling and depth processing models than traditional image processing methods. Diseased

regions (biomarkers) in a medical image differ in properties (i.e., the contrast in brightness) from their neighbor pixels and appear as blobs in nature. These biomarkers or blobs are the regions of interest (ROI) in medical image diagnosis, and they must get identified, segmented, classified, and labeled to predict disease. Image analysis models based on deep learning will assist in detecting biomarkers in medical images and provide spatial information such as location, shape, scale, inertia, and convexity. The Blob (or image ROI) detection [4] allows disease diagnosis in many instances of the medical image diagnosis such as brain tumors, kidney glomeruli, eye retina, breast lesions, and cell nuclei detection, among others. Medical image biomarkers detection models are becoming prominent applications for physicians in disease conformation, staging, and treatment planning.

Due to the importance of biomarkers detection in medical image analysis, many former researchers were focused on this topic and proposed various deep learning models for medical image blobs detection. Although many scholars have worked on medical image diagnosis, some prominent literature aided us in selecting the objectives and designing the proposed system using deep learning technologies. Parvathi et al. [5] integrated deep learning and image processing algorithms to execute the blob detection and classification operations on kidney 3D MRI images. They used the ECLAHE and IMBKM models to segment the blobs from the input images and later the deep learning IMBKM and EDCNN classifiers to classify the blobs into the selected disease categories. Xu et al. [6] created a hybrid model that used a deep U-Net model and hessian analysis to detect small blobs in 3D MRI images for kidney glomeruli detection. They designed a superset of blobs using the hessian analysis to distinguish the real-convex blobs from the noisy ones. Their custom deep learning model UH-Net integrated the hessian superset information and the U-Net pre-training knowledge to find the glomeruli through small blobs detection from the 3D kidney MRI images. Peng et al. [7] proposed a multi-scale blob detection model for automated stem cell segmentation from the underlying microscopic image set. The cell boundaries are delineated with high accuracy using blob and centerline detection.

In the literature survey, it went through many research articles as part of the medical image disease prediction and identified some research gaps, which are as follows: Because

of the morphological diversity, segmenting the kidney object from the multi-organ medical image using shape and location information yields less accuracy. The traditional semantic segmentation approach, which may detect object categories in medical images, is insufficient because the medical image contains many instances of the same object type. Therefore, the instances must be categorized as it will.

Since kidney cancer became a major cause of kidney failure in people, our primary research goal was to detect kidney tumors from MRI images. To achieve this goal, it planned to segment the kidney objects from the MR first, and the lineation of the tumors from the kidneys is later. Image processing models (such as SIFT [8] and SURF [9]) and deep learning models (such as DNNs [10], CNNs [11], and Res-Net [12], among others) are the two different technologies used to segment the kidneys from CT images. Although each model has its pros and cons for kidney segmentation, it is interested in deep learning models because they are computationally cheaper and allow for high-level automation of the segmentation process. Unlike commonly performed object segmentation from images, kidney segmentation is a unique and challenging task, as shown in Fig. 1, because diseased kidneys segmentation has issues due to morphological diversity, object overlapping, intensity variance, and integrated noise.

Kidney tumor segmentation from MR images is a two-step process that includes kidney object (with tumor) segmentation and tumor object lineation. To accomplish the kidney tumor segmentation task and address segmentation issues (research gaps), in this paper, it proposed an efficient and optimal kidney tumor segmentation architecture using the custom U-Net and Mask R-CNN [13] deep learning models. The custom U-Net model is used first for kidney segmentation, and the Mask R-CNN model is used to lineate tumors from the segmented kidney images. The custom U-Net model is used first for kidney segmentation, and the Mask R-CNN model is used to lineate tumors from the segmented kidney images. To demonstrate the efficiency of the proposed kidney tumor segmentation model, a set of MR images collected from the TCGA-KIRC dataset and a python prototype is implemented to conduct the experiments.

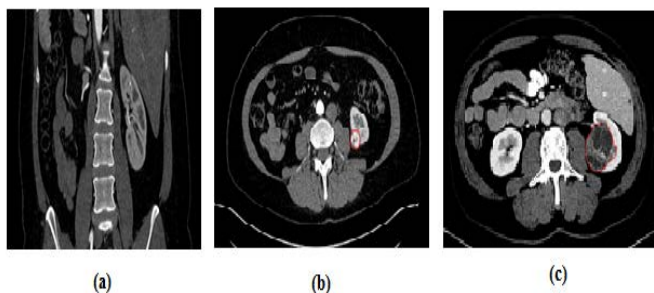


Fig. 1. Abdominal MR Scan Images. (a) Kidney with no Tumor; (b) Kidney with Mild Tumor; (c) Kidney with Moderate Tumor (Kidney Tumors Marked with Red Line in b and c).

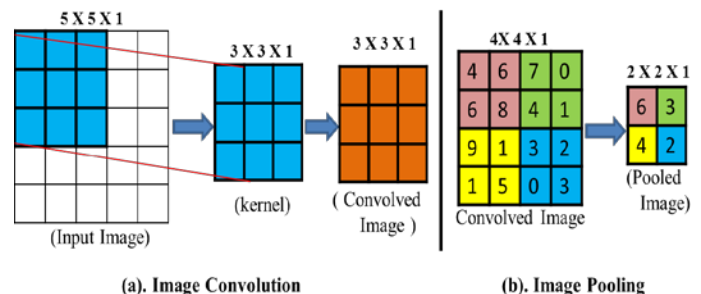
II. RELATED WORK

In this section, it will discuss the Key technologies that have been used in our kidney tumor semantic segmentation processes like CNNs [14], U-Net [15] and Mask R-CNN [13].

A. CNNs

Recent advances in high-speed internet and mobile technology have resulted in a digital multimedia world with tons of images and videos. Computer vision is an emerging future domain, which is responsible for video and image manipulation as needed. Extracting useful information from an image is a complicated task because that needs to process a high volume of pixels. For over a decade, multi-layered deep learning models have made image processing easier than traditional methods. Because of their high accuracy and fully connected layers, Convolutional Neural Networks (CNNs) have proven to be the dominant deep learning model among the various deep learning models. As a descendant of Artificial Neural Networks (ANNs) [16], CNNs [14] will automatically train the feature maps from pixel arrays and identify the receptive fields through backpropagation using Key methods like convolution, pooling, and fully connected networks (FCN) [17].

1) *Convolution*: In general, the image is a collection of pixels, and these pixels will get converted into the respective intensity (RGB and grayscale) values for representation in a binary matrix model, which is feasible for manipulations. To manipulate the images with less computational overhead, they should be resized to a small size (down sampling) while retaining their receptive field (context) information. Convolution [18] is an affine transformation model in which the selected kernel matrix (filter) elements are iteratively multiplied against the input image matrix elements to generate the small-sized output convolved matrix. Fig. 2(a) represents the convolutional model with an input image (5x5x1) and the kernel (3x3x1) with a stride value of 2, and also the output convolved image (3x3x1). When it comes to the 3D images with RGB values, three color channels map with three different kernels for computations, and the final summation value is added with the bias to generate the convolved output image.



(a). Image Convolution

(b). Image Pooling

Fig. 2. Input Image Convolution and Pooling Model.

2) *Pooling*: In CNN, the convolution is followed it by a pooling [19] process, which mimics the behavior of the convolution process to reduce the convolved image spatial size at a high rate. Using either the max or average pooling method reduces computational overhead while learning and regulates over-fit issues. In Fig. 2(b), the average pooling method with a 2x2 filter and stride value of 2 is applied on a convolved image (4x4x1) to generate a pooled feature map (2x2x1). Like the convolution process, the pooling does not support the zero-padding at input feature map borders.

3) *FCN*: The FCN [17] is a feed-forward neural network model for multilayer perceptron that enables the backpropagation to learn the key features for classification across the epochs. The high-level features generated by the final convolution/pooling process are encoded using a single (flattened) vector and fed into the FCN. The FCN calculates the loss-entropy value for decision-making against classification uncertainty to reduce false positives in classification.

B. U-Net

Ronneberger [15] designed U-Net, as it knows deep convolutional network architecture, for the semantic segmentation of objects from images, with high speed and precision. Extraction of the ROI is frequently required task in biomedical images, particularly for organ segmentation, objects localization. An efficient deep learning-based semantic segmentation model, such as U-Net, is required to achieve this ROI extraction. Compared to other CNN architectures [20], the U-Net is the most adaptive for medical image segmentation because of additional benefits such as pixel-level segmentation, limited training data, end-to-end training, pixel padding support, de-convolutions, and elastic deformation.

The two sections of the U-Net architecture are the contracting path (encoder part) and the symmetric expanding path (decoder part). The encoder part of U-Net, like convolutional networks, is continuous with convolutions and pooling methods to make the context more precise and sharper. This encoder reduces the dimensionality of the input feature without losing context, allowing the process to complete with less computation. The encoder performs the 3x3 convolutions iteratively till the pivot point. And after each convolution process, the batch normalization and the activation function [21] (Rectified Linear Unit (ReLU)) are applied with pooling strides for down-sampling, which helps in the précised context making. In contrast, the U-Net has a decoder part with a transposed convolution mechanism on the other side, making the U-Net an end-to-end FCN model. The encoder output is up-sampled [22] by the decoder using convolutions, batch normalizations, and ReLU activations. The decoder is intended to return the output with precise localization using the up-sampling process and transposed convolution.

C. Mask R-CNN

As part of their research on AI, the Facebook AI Research Team (FAIR) introduced the instance segmentation framework called Mask R-CNN [10] as an extension to the Faster R-CNN [23] by adding the ROI segmentation masks. Compared to the other models, the Mask R-CNN is fast, simple, flexible, and accurate in instance segmentation is proven by the COCO - 2016 challenge. Mask R-CNN can segment the multiple instances precisely from the images, using image localization, object detection, and segmentation methods. Mask R-CNN architecture was designed by joining the Faster R-CNN with FCN model [24] for instance segmentation process.

Initially, a set of input images with different class objects are selected for instance segmentation. Deep CNN architectures [20] with convolution and pooling operations will extract the ROI bounding boxes from the input images. Unlike the Region-based CNN model, the Mask R-CNN had the ROI alignment phase, in which the exact spatial ROI volumes are identified from input images based on the input masks, using the pixel to the pixel alignment process. Mask R-CNN evaluates the ROIs from ROI-Pool and in parallel performs the target object detection to overcome the performance issues. Mask R-CNN evaluates the ROIs from ROI-Pool and in parallel performs the target object detection to overcome the performance issues. The bounding boxes are scaled using the Intersection over Union (IoU) metrics [25] after completing the ROI alignment process, and misinterpretations get eliminated using the feature matching threshold value. At this point, various class masks are applied to the coarse-grained bounding boxes to find the fine-grained segmentation. Finally, these fine-grained segmentations are precisely lineated and masked.

III. KIDNEY TUMORS SEGMENTATION ARCHITECTURE USING CU-NET AND MASK R-CNN MODELS

In recent times, kidney tumor diagnosis from the medical images becomes a focusable research area due to its impact and importance in disease diagnosis and staging. The contribution of tumor detection is invaluable in cancer disease staging and treatment (especially in targeted therapy) planning. Researchers are interested in medical image analysis using deep learning models over traditional image processing techniques to reduce the computational (i.e., hardware) difficulties [26] in medical image processing. It is discussed in Section I that the kidney tumor diagnosis from MRI images faces several issues since this process differs slightly from the regular object segmentation and lineation process. To address the issues involved with the kidney tumor semantic segmentation process, It designed an efficient and optimal deep learning architecture (shown in Fig. 4) using the Custom U-Net [10] and Mask R-CNN models for kidney image segmentation and the tumor instance lineation from medical MR images. Kidney tumors can be segmented [27] from the medical MR images in two phases: Kidney(s) segmentation from MR images and tumors boundary lineation from kidney images.

A. Kidney Segmentation Phase

The process of extracting kidney images (with tumors) from MR scan images is known as kidney segmentation [28]. Later these extracted kidney images are used for tumor detection and its boundary lineation. For this, it selected a set of abdominal MR images and their associated ground truth values (masks) as a training dataset (shown in Fig. 3) for the experimental analysis. However, extracting the kidney context from the MR images is a complex process due to several reasons. Because of the cancer disease [29], the shape of the kidneys is inconsistent in nature and different from one other, which will make the network's training process difficult. Because the MR scan images are collected from different MR scanners, the intensity of the input images varies, which is incompatible with many deep learning networks. In addition to kidneys and other organs, noisy data is often present in MR scan images, making the object detection process more complex.

1) *Custom U-Net*: To solve these challenges in the kidney extraction process, it used the custom U-Net [10] model, a trained convolutional neural network that is suited for medical image segmentation. U-Net model [15] was selected over the other CNNs [21] because the U-Net supports the classification at pixel level and is suitable for the multi-class instance labeling if required. Due to the systematic hurdles [30] involved in data collection and processing, obtaining a dataset with tons of images and masks is impossible related to medical images. U-Net is a light-tight model because it can train efficient models with limited training datasets. Unlike trained nets [20] such as LeNet-5 and Dense DNN, the U-Net is free from dense layers and thus accepts input data with intensity variance.

It designed a custom U-Net model with additional features by extending the traditional U-Net to support kidney object segmentation with high accuracy. Our custom U-Net model is designed with a validation set to ensure test accuracy. By adjusting the hyper-parameters at validation time, the custom U-Net tunes the deep model to achieve high accuracy in test results. CU-Net was enhanced with data augmentation techniques such as image flips and others to double the size of the input dataset to generalize the training model. Dropout regularization functions it added to CU-Net during the training phase after each max-pooling operation to randomly replace neurons (pixels) with zero values and train the model with alternative neural networks to minimize overfitting.



Fig. 3. An Abdominal MR Image (356 x 356) with Kidney Tumor (Left) and its Ground Truth Image for Training (Right).

2) *Dataset model*: A set of total 'n' MR scan abdomen images $I = \{I_1, I_2, I_3 \dots I_n\}$ containing multiple organs with dimensions $D = [d_1, d_2]$, pixels $P = (p_1, p_2)$, are presented in a binary matrix model $M = [m_p \times m_q]$. In our dataset, an image I_1 is having the greyscale pixel ($i_1(P)$) with its pixel value is represented as $0 \leq i_1(P) \leq 255$. Mask image set \hat{M} is a set of total 'n' masks with information about kidneys with tumors segmentation, and it maps with their original MR images for training. The mask image set $\hat{M} = \{M_1, M_2, M_3 \dots M_n\}$ along with its label information L is presented as $M_k = \{(M_k, L) \in I_k \ \& \ L = 1\}$.

3) *Training Custom U-Net*: Once the data is defined and available in hand, the next immediate step in Custom U-Net is the data preparation. It classifies the data into a training set I_α , validation set I_β , and test set I_γ . It used the validation set I_β in the training phase to assess the model accuracy and to detect the overfitting problems [31] at the training phase itself. After partitioning the data set into train and test sets, a custom U-Net model with a contracting path and an expensive path was designed. The U-Net model is symmetric, with four layers of processing at each path. The 2D_convolution, max pooling, and dropout functions are implemented in the contracting path, whereas the transpose convolution, concatenate, and dropout functions are implemented in the expensive path, as shown in Algorithm 1. In U-Net, the contracting path's four layers are executed first, with convolution, max pooling, and dropout functions, and the results are passed to the next layer in the path. The convolution function increases the context of the input image I_{in} , which helps in target feature extraction, using the neurons (z), kernel ($k_{m \times n}$), stride ($s_{m \times n}$), activation function φ , an array of 4 channels $\mu = [1, 2, 4, 16]$, and padding p elements.

Down sampling [22] is a spatial dimensionality reduction method that reduces image height and width to make the image computationally feasible. After executing the convolution process twice, the resulted image volume is given as input to the max-pooling function to reduce the dimensionality of the image without losing the context. The ideal pool size ($e_{m \times n}$) is selected and evaluated against the convolved image C_i to create the max pooled image Q_i . After max pooling, dropout functions with a frequency rate (f_{rate}) (0.0 - 1.0) are executed during the training phase. This function randomly sets the input pixels to zero, which helps to prevent values from dropping during the training phase and keeps the model from overfitting. This step completes a layer of the contracting path, and it will take four repeats to complete the entire contracting path. Soon after the contracting path completes, the convolution process will be repeated twice with the double neurons (μ) of the contracting path's last layer to build the connection (C_m) it has two paths.

Like the contracting path, the expensive path had four layers with transposed convolution, concatenation, dropout, and convolution functions but executed in backward direction. The Con2DTrans function performs the de-convolution process to reverse the convolution processes using the specified stride $s_{m \times n}$, kernel $k_{m \times n}$, and other attributes. The

de-convolved image D_i is concatenated with its counterpart convolution image C_i to increase the dimensions. Dropout function can by the convolutions restores the image with equal dimensions of its counterpart contracting path layer. The same process will be repeated four times to conclude the expensive path execution. Finally, the single neuron and the 1x1 kernel-based convolution process will be executed to return the output image I_{out} with sharpened target context. In this manner, our proposed custom U-Net model is trained against the input image set to obtain the segmentation knowledge, which helps in validation and testing operations.

Algorithm-1: Custom U-Net Model Algorithm

```

Input:  $I_{in}, k, s, p, z, \varphi, e_{m*n}$ 
Output:  $I_{out}$ 
Method:
 $cn_1, cn_2, cn_3, cn_4, \mu = [v_1, v_2, v_3, v_4]$ 
// contracting path
for i=1 to 4 do
 $C_i = con2D((z * \mu [i - 1]), k_{m*n}, \varphi, p)(I_{in})$ 
 $C_i = con2D((z * \mu [i - 1]), k_{m*n}, \varphi, p)(C_i)$ 
 $cn_i = I_{in}$ 
 $Q_i = Max\_Pool(e_{m*n}, C_i)$ 
 $Q_i = D\_Out(f_{rate})(Q_i)$ 
 $I_{in} = Q_i$ 
end // for
// connected layers
 $C_m = con2D((z * \mu [3] * 2), k_{m*n}, \varphi, p)(I_{in})$ 
 $C_m = con2D((z * \mu [3] * 2), k_{m*n}, \varphi, p)(C_m)$ 
 $\mu = [v_4, v_3, v_2, v_1]$ 
// expensive path
for i=4 to 1 do
 $D_i = con2DTrans((z * \mu_{i-1}), k_{m*n}, s_{m*n}, \varphi, p)(C_m)$ 
 $D_i = concat(D_i, C_i)$ 
 $D_i = D\_Out(f_{rate})(D_i)$ 
 $D_i = con2D((z * \mu [i - 1]), k_{m*n}, \varphi, p)(D_i)$ 
 $D_i = con2D((z * \mu [i - 1]), k_{m*n}, \varphi, p)(D_i)$ 
 $C_m = D_i$ 
end //for
 $I_{out} = con2D(1, k_{1*1}, \varphi, p)(cn_1)$ 
return  $I_{out}$ 

```

Regular classification models treat the validation set as an optional activity because it consumes more time for validations. But in our custom U-Net segmentation process, it generated the validation set I_β to monitor the model performance and hyper parameters tuning [32] according to the requirements. After the training process designed a segmentation model ω , the validation set I_β assesses the model performance at the training phase itself and fine-tunes the parameters through the backpropagation method if required. At the test phase, these fine-tuned models will assure the précised ROI segmentation. Due to the complexity involved in pixel-level processing, the medical image training may encounter the overfitting [31] problem, which arises when the trained segmentation model performance is specific and bounded to the training dataset only. In this case the trained model yields the best results on training data I_α but it fails to segment the test data I_γ . To overcome this over fitting issue in segmentation, it customized the U-Net to compare the trained model segmentation accuracy on both the training and validation datasets. The precision difference between both

datasets will be compared against the over-fit threshold(δ) to confirm the overfit or the difference in performance \mathbb{D} is shown below.

$$\mathbb{D} = \frac{1}{k} \sum_{i=1}^k \omega(I_\alpha) - \omega(I_\beta) \{ \text{if } \mathbb{D} \geq \delta \text{ than overfit} \}$$

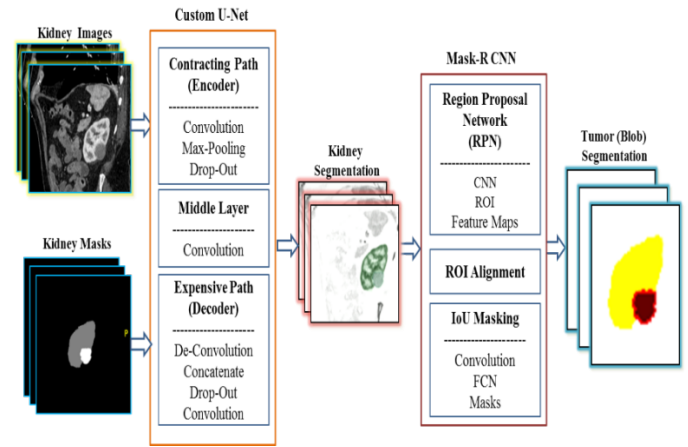


Fig. 4. Kidney Tumor Blob Instance Segmentation Architecture using CU-Net and Mask R-CNN Models.

B. Tumor Segmentation and Boundary Lineation

Because the kidney images (including tumors) it used to train the Custom U-Net based kidney segmentation model (shown in Fig. 4), the trained U-Net model returns segmented kidney images with tumors as a result. The tumor instances from the kidney images should be lineated and masked to find the tumor instance boundaries. Some prominent solutions include threshold-based segmentation, edge detection segmentation, feature clustering, bounding box, and ROI extraction. Among them, it selected Mask R-CNN [13], a fast, simple, and generalized ROI-based segmentation model for the target tumor object selection and precise segmentation (lineation) process. Stones, glomeruli, and tumors, etc. may appear as blobs in kidney imaging. Mask R-CNN detects a variety of blob objects on existing kidney images using the bounding boxes, and then the target tumors are identified using the shaded masks.

Convolution is used to extract feature maps from kidneys with tumor instances, and the Region Proposal Network (RPN) [23] is applied to the feature maps to generate bounding boxes for the target tumor blob. Based on the ROI volume, the bounding boxes are selected for further processing. ROI volume is evaluated using the Intersection over Union (IoU) approach, which compares the bounding boxes with the ground truth labels for ROI presence estimation. FCN has been used to detect the blob structures and mask them with the selected bounding boxes. Compared to the other segmentation models, this Mask R-CNN is lighter, faster, and reliable for pixel-level semantic segmentation.

IV. EXPERIMENTAL ANALYSIS

To conduct the experiments on the proposed kidney tumor semantic segmentation architecture with CU-Net and Mask R-CNN models, it collected a set of 30 kidney MR images from

the TCGA-KIRC dataset [33]. Images with 360x360 pixels and their corresponding masks (shown in Fig. 2) are extracted from these MR images for training and testing. The proposed Custom U-Net and Mask R-CNN based tumor segmentation architecture was implemented using the Keras-2.4.3 python interfaces on the TensorFlow-2.3.0 platform.

First, the MR image dataset is preprocessed and partitioned into train and test datasets, as explained in Section III. Train dataset images are transformed into two-dimensional binary arrays using the pixel data transformation methods for further processing. The images are now resized to 320x320 pixels for process compatibility with the custom U-net model. The contracting path and expansive path of the CU-Net are designed using convolutional and max-pooling methods respectively from the Keras library. The proposed Custom U-Net model with the input layer and output layer uses the binary cross-entropy [34] as loss function and Adam's optimizer [35] for accuracy calculation with the prediction results. The dataset was augmented using image flips and other techniques to generate a set of synthetic data images derived from the core MR images. This step will increase the training data size by 2x more than the actual size to handle the overfitting issue in the classification process. Along with the data augmentation techniques, early stopping feature is also introduced to stop the training process at the appropriate time to avoid the over fit and under fit issues in training. To regularize the learning rate across multi epochs the learning rate reducing techniques also applied with CU-Net model. By specifying the epochs and the batch sizes for training process, the CU-Net model is trained on MR images to generate the efficient model for kidney image detection and segmentation.

The kidney segmentation binaries obtained from the Custom U-Net have been used as input to the Mask R-CNN model, which extracts tumor data. Mask R-CNN extracts objects from input images using bounding boxes and aligns the extracted objects using ROI information. Soon after the object localization using the bounding boxes alignment process, Mask R-CNN starts the pixels level comparison using the FCN to lineate the objects with specified shade masks. In Fig. 5, the kidney tumor segmentation results are shown along with the input images, masks, CU-Net kidney segments, and Mask R-CNN tumor lineation.

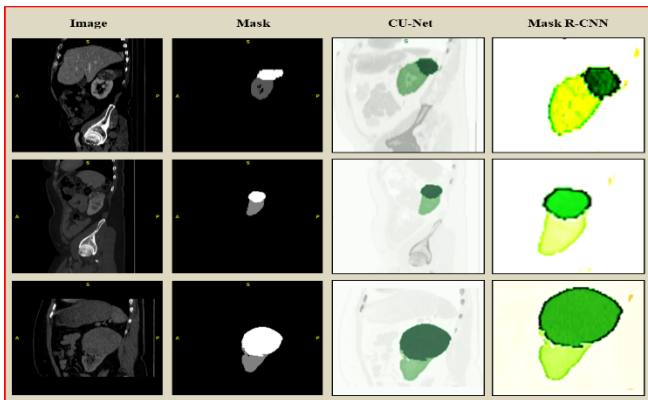


Fig. 5. Kidney Tumor Segmentation Results from the Experiments on Custom U-Net and Mask R-CNN Model.

Finally, the proposed model results have been evaluated using the loss and accuracy metrics from the prediction results on the test dataset. It adjusted the training and validation dataset proportions to test the accuracy and IoU metrics, and the results from the proposed architecture with CU-Net and Mask R-CNN are shown in Table I.

TABLE I. KIDNEY TUMOR SEGMENTATION ACCURACY AND IOU RESULTS

Data Partition	IOU	Accuracy
TD-70% and VD-6%	0.875	0.912
TD-75% and VD-8%	0.913	0.941
TD-65% and VD-15%	0.849	0.877
TD-60% and VD-20%	0.831	0.819

Fig. 6 depicts the generated validation results accuracy and loss value across multiple epochs for the proposed Custom U-Net model. The experimental results show that the proposed Custom U-Net and Mask R-CNN model is optimal, and it efficiently lineated blobs like kidney tumors with high lineation precision and segmentation accuracy.

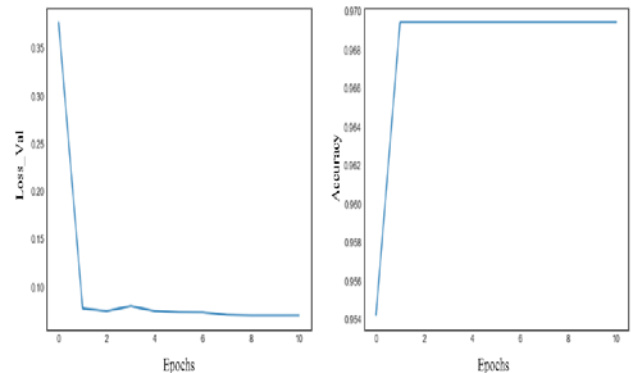


Fig. 6. Proposed Segmentation Model Results Accuracy and Loss Values across the Epochs.

V. DISCUSSION

For starters, this model allows for the use of global location and context at the same time. Second, it works with fewer training samples and outperforms other segmentation algorithms. Mask R-CNN outperforms all existing single-model entries on every task. Faster R-CNN is extremely efficient, with only a minor overhead added. Mask R-CNN can be easily adapted to other tasks.

VI. CONCLUSION

In this paper, it proposed the kidney tumor segmentation architecture with Custom U-Net and Mask R-CNN models. U-Net model is customized to overcome the kidney object segmentation issues like morphological diversity, object overlapping, intensity variance, and training overfit. Mask R-CNN is chosen to accurately lineate the tumor boundaries and segment (mask) the instances. The proposed architecture is used to train a set of MR scan images of kidney cancer, and the results are presented with the metrics IoU and accuracy. The experiments yielded high accuracy and IoU in kidney tumor segmentation and masking.

REFERENCES

- [1] Krupinski EA, Jiang Y. Anniversary paper: evaluation of medical imaging systems. *Med Phys.* 2008 Feb;35(2):645-59. doi: 10.1118/1.2830376. PMID: 18383686.
- [2] Angenent, S. & Pichon, Eric & Tannenbaum, Allen. (2006). Mathematical methods in medical image processing. *Bulletin of the American Mathematical Society.* 43. 365-396. 10.1090/S0273-0979-06-01104-9.
- [3] Razzak M.I., Naz S., Zaib A. (2018) Deep Learning for Medical Image Processing: Overview, Challenges and the Future. *Classification in BioApps. Lecture Notes in Computational Vision and Biomechanics*, vol 26. Springer, Cham. https://doi.org/10.1007/978-3-319-65981-7_12.
- [4] C. Duanggate, B. Uyyanonvara, S. Makhanov and S. A. Barman, "Enhanced support region for scale-space blob detection," in international conference on Robotics, Informatics and Intelligent control Technologies.
- [5] Sitanaboina S L Parvathi, Dr. Harikiran Jonnadula, "Small Blob Detection and Classification in 3D MRI Human Kidney Images Using IMBKM and EDCNN Classifier", Vol.12 No.5, 629-642, *Turkish Journal of Computer and Mathematics Education*, 2021.
- [6] Xu, Yanzhe, Teresa Wu, F. Gao, J. Charlton and K. Bennett. "Improved small blob detection in 3D images using jointly constrained deep learning and Hessian analysis." *Scientific Reports* 10 (2020). DOI:10.1038/s41598-019-57223-y.
- [7] Peng H, Zhou X, Li F, Xia X, Wong ST, "Integrating Multi-Scale Blob/Curvilinear Detector Techniques and Multi-Level Sets for Automated Segmentation of Stem Cell Images". *Proc IEEE Int Symp Biomed Imaging.* 2009 Summer; 2009:1362-1365. doi: 10.1109/ISBI.2009.5193318.
- [8] LoIt, D. G. "Distinctive image features from scale-invariant keypoints", *International Journal of Computer Vision* (2004).
- [9] Bay, H., Ess, A., Tuytelaars, T. & Van Gool, L. "Speeded-Up Robust Features (SURF)", *Computer Vision and Image Understanding* - 2008.
- [10] Carneiro G., Zheng Y., Xing F., Yang L. (2017) Review of Deep Learning Methods in Mammography, Cardiovascular, and Microscopy Image Analysis. In: Lu L., Zheng Y., Carneiro G., Yang L. (eds) *Deep Learning and Convolutional Neural Networks for Medical Image Computing. Advances in Computer Vision and Pattern Recognition.* Springer, Cham. https://doi.org/10.1007/978-3-319-42999-1_2.
- [11] Mortazi A., Bagci U. (2018) Automatically Designing CNN Architectures for Medical Image Segmentation. In: Shi Y., Suk HL, Liu M. (eds) *Machine Learning in Medical Imaging. MLMI 2018. Lecture Notes in Computer Science*, vol 11046. Springer, Cham. https://doi.org/10.1007/978-3-030-00919-9_12.
- [12] Zhang Q., Cui Z., Niu X., Geng S., Qiao Y. (2017) Image Segmentation with Pyramid Dilated Convolution Based on ResNet and U-Net. In: Liu D., Xie S., Li Y., Zhao D., El-Alfy ES. (eds) *Neural Information Processing. ICONIP 2017. Lecture Notes in Computer Science*, vol 10635. Springer, Cham. https://doi.org/10.1007/978-3-319-70096-0_38
- [13] He, Kaiming & Gkioxari, Georgia & Dollar, Piotr & Girshick, Ross. (2017). Mask R-CNN. 2980-2988. 10.1109/ICCV.2017.322.
- [14] A. A. M. Al-Saffar, H. Tao and M. A. Talab, "Review of deep convolution neural network in image classification," 2017 International Conference on Radar, Antenna, Microwave, Electronics, and Telecommunications (ICRAMET), 2017, pp. 26-31, doi: 10.1109/ICRAMET.2017.8253139.
- [15] Ronneberger, Olaf & Fischer, Philipp & Brox, Thomas. (2015). U-Net: Convolutional Networks for Biomedical Image Segmentation.
- [16] Filippo Amato, Alberto López, Eladia María Peña-Méndez, Petr Vaňhara, Aleš Hampl, Josef Havel, *Artificial neural networks in medical diagnosis, Journal of Applied Biomedicine*, Volume 11, Issue 2, 2013, Pages 47-58, ISSN 1214-021X, <https://doi.org/10.2478/v10136-012-0031-x>.
- [17] E. Shelhamer, J. Long and T. Darrell, "Fully Convolutional Networks for Semantic Segmentation," in *IEEE Transactions on Pattern Analysis and Machine Intelligence*, vol. 39, no. 4, pp. 640-651, 1 April 2017, doi: 10.1109/TPAMI.2016.2572683.
- [18] Minsik Cho and Daniel Brand, "MEC: memory-efficient convolution for deep neural network". In *Proceedings of the 34th International Conference on Machine Learning - Volume 70 (ICML'17)*. JMLR.org, 815-824. 2017.
- [19] V. Christlein, L. Spranger, M. Seuret, A. Nicolaou, P. Král and A. Maier, "Deep Generalized Max Pooling," 2019 International Conference on Document Analysis and Recognition (ICDAR), 2019, pp. 1090-1096, doi: 10.1109/ICDAR.2019.00177.
- [20] Alzubaidi, L., Zhang, J., Humaidi, A.J. et al. Review of deep learning: concepts, CNN architectures, challenges, applications, future directions. *J Big Data* 8, 53 (2021). <https://doi.org/10.1186/s40537-021-00444-8>
- [21] Nwankpa, Chigozie & Ijomah, Winifred & Gachagan, Anthony & Marshall, Stephen. (2020). Activation Functions: Comparison of trends in Practice and Research for Deep Learning.
- [22] A. Youssef, "Analysis and comparison of various image downsampling and upsampling methods," *Proceedings DCC '98 Data Compression Conference (Cat. No.98TB100225)*, 1998, pp. 583-, doi: 10.1109/DCC.1998.672325.
- [23] S. Ren, K. He, R. Girshick, and J. Sun. Faster R-CNN: Towards real-time object detection with region proposal networks. In *NIPS*, 2015
- [24] J. Long, E. Shelhamer, and T. Darrell. Fully convolutional networks for semantic segmentation. In *CVPR*, 2015.
- [25] Rahman, Md & Wang, Yang. (2016). Optimizing Intersection-Over-Union in Deep Neural Networks for Image Segmentation. 10072. 234-244. 10.1007/978-3-319-50835-1_22.
- [26] Scholl, Ingrid & Aach, Til & Deserno, Thomas & Kuhlen, Torsten. (2011). Challenges of medical image processing. *Computer Science - R&D.* 26. 5-13. 10.1007/s00450-010-0146-9.
- [27] Daza, Laura & Gomez, Catalina & Arbelaez, Pablo. (2019). Semantic Segmentation of Kidney Tumor using Convolutional Neural Networks. 10.24926/548719.077.
- [28] N. Goceri and E. Goceri, "A Neural Network Based Kidney Segmentation from MR Images," 2015 IEEE 14th International Conference on Machine Learning and Applications (ICMLA), 2015, pp. 1195-1198, doi: 10.1109/ICMLA.2015.229.
- [29] Nicholas J Vogelzang, Walter M Stadler, "Kidney cancer", *The Lancet*, Volume 352, Issue 9141, 1998, Pages 1691-1696, ISSN 0140-6736, [https://doi.org/10.1016/S0140-6736\(98\)01041-1](https://doi.org/10.1016/S0140-6736(98)01041-1).
- [30] Kohli MD, Summers RM, Geis JR, "Medical Image Data and Datasets in the Era of Machine Learning", Whitepaper from the 2016 C-MIMI Meeting Dataset Session. *J Digit Imaging.* 2017 Aug-30 pp:392-399. doi: 10.1007/s10278-017-9976-3.
- [31] Horwath, J.P., Zakharov, D.N., Mégret, R. et al. Understanding important features of deep learning models for segmentation of high-resolution transmission electron microscopy images. *npj Comput Mater* 6, 108 (2020). <https://doi.org/10.1038/s41524-020-00363-x>.
- [32] Schratz, Patrick & Muenchow, Jannes & Iturrutxa, Eugenia & Richter, Jakob & Brenning, Alexander. (2018). Performance evaluation and hyperparameter tuning of statistical and machine-learning models using spatial data.
- [33] Akin, O., Elnajjar, P., Heller, M., Jarosz, R., Erickson, B. J., Kirk, Filippini, J. (2016). Radiology Data from The Cancer Genome Atlas Kidney Renal Clear Cell Carcinoma [TCGA- KIRC] collection. The Cancer Imaging Archive. <http://doi.org/10.7937/K9/TCIA.2016.V6PBVTDR>.
- [34] Zhang Z, Sabuncu M. Generalized cross entropy loss for training deep neural networks with noisy labels, In *Advances in neural information processing systems* 2018 (pp. 8778-8788).
- [35] D. Kingma and J. Ba, "Adam: A method for stochastic optimization," *International Conference on Learning Representations (ICLR)* 2015, 2015.

GonioPi: Towards Developing a Scalable, Versatile, Reliable and Accurate Handheld-Wearable Digital Goniometer

Thomas Jonathan R. Garcia, Dhong Fhel K. Gom-os

Center for Research in Intelligent Systems, Department of Computer Science
University of the Philippines Cebu, Cebu, Philippines

Abstract—Range of Motion (ROM) Testing is an important physical examination performed in physical therapy used in assessing the ROM of a patient’s joint. The most commonly used instrument for ROM Testing is the universal goniometer. The most common cause for unreliable and inaccurate joint angle ROM measurements is measurement errors. Multiple studies have been done to mitigate measurement errors in clinical goniometry by designing and developing wearable digital goniometers using sensor technology. This study aims to design and develop a handheld-wearable digital goniometer called the GonioPi that is versatile, scalable, reliable and accurate when using the MPU-6050 IMU sensor and Raspberry Pi Pico as the main components. The results showed that the GonioPi is versatile and scalable as it is able to support multiple ROM Tests using multiple different positions on people with varying heights, weights, and BMI categories. The results also showed that the GonioPi is reliable and accurate as it was able to record joint angle ROM measurements of less than 5 degrees and 10 degrees which are the accepted standard values for reliability and accuracy, respectively.

Keywords—Range of Motion (ROM); goniometer; physical therapy; goniometry; wearable; sensors; MPU-6050; Raspberry Pi Pico

I. INTRODUCTION

Range of Motion (ROM) Testing is one of the important physical examinations performed in physical therapy and rehabilitative sciences. ROM Testing can be used to identify a patient’s underlying conditions to help with diagnosis and rehabilitative treatment.

A goniometer is the most used instrument for ROM Testing. It is used to measure the angle of a patient’s ROM at a joint. Goniometers have different types that vary in shape and size depending on which joint is being tested. The most used goniometer are the short arm and long arm universal goniometers. These universal goniometers are still analog which lead to the most common complication in clinical goniometry – measurement errors. Errors in measurement can be caused by systematic errors such as improper technique, improper use of the instrument, the instrument being used, or visual estimation when an instrument is not available. These measurement errors result in unreliable and inaccurate joint angle ROM measurements. A universal goniometer is considered reliable, its mean joint angle ROM measurement should be < 5 degrees [1, 2]. Moreover, it was shown that

universal goniometers have a minimum significant difference of 10 to 14 degrees which is considered unreliable and inaccurate when used to measure joint angle ROM [3].

To mitigate measurement errors in clinical goniometry, wearable digital goniometers using sensor technology has been designed and developed by some [4, 5]. Wearable devices using sensor technology in physical therapy and rehabilitative science have shown high reliability and accuracy when used for the application of clinical goniometry. However, gaps in the research can be seen with other factors of the devices such as versatility, scalability, and cost-efficiency.

Previous attempts to develop wearable digital goniometers using sensor technology are neither versatile nor scalable. These studies only considered some of the 34 different ROM tests [6] such as wrist flexion and extension, forearm supination and pronation, radial deviation, and ulnar deviation [7, 8]; elbow joint [9, 10]; hip flexion [11]; and knee flexion and extension [12]. There is no study which attempted to develop a scalable and versatile digital goniometer - one that can support all possible ROM tests in multiple different positions on people with varying heights, weights, and BMI categories.

Developing a scalable and versatile, not just an accurate and reliable, digital goniometer is important in the field of clinical goniometry [13]. Such an instrument will provide a dependable single device to users without the need to use multiple different instruments to perform different ROM tests. This reduces cost and eliminates the need to train in multiple different instruments.

Therefore, this research aims to design and develop a versatile and scalable handheld-wearable digital goniometer with the use of affordable components that is at the same time accurate and reliable in terms of joint angle ROM measurements when performing ROM Testing. The device is referred here as GonioPi – a portmanteau of the word’s goniometer and Raspberry Pi, the microcontroller used to develop the device.

II. REVIEW OF RELATED LITERATURE

A. Physical Therapy and Clinical Goniometry

Physical therapy and rehabilitative science is a field of medicine that focuses on the care of patients with medical conditions related to movement and health. Patient care in this

field is done by physical therapists by providing services that prevent or limit dysfunction.

The concepts of kinesiology and goniometry are important in the field of physical therapy and rehabilitative science as they focus on the study of human motion and joint angle measurements [6, 14]. Moreover, both these concepts are important in identifying and assessing medical conditions related to muscle performance and neurological function [14].

Clinical kinesiology and goniometry involve range of motion which is a technique used to examine the angle created at a joint to assess the need for physical rehabilitation [15, 16]. This is done through different types of range of motion tests such as flexion, extension, abduction, adduction, and rotation among others. Reliable and accurate range of motion tests are needed in diagnosing, assessing, evaluating, and tracking of a patient's physical rehabilitation progress.

B. Range of Motion Instruments

A patient's range of motion can be assessed with the use of different range of motion instruments with the universal goniometer being the most used. Other instruments include the gravity-dependent goniometer (inclinometer), electrogoniometer, and visual estimation [14]. Although these manual instruments (universal goniometer, inclinometer, and visual estimation) are inexpensive, the common issue shared by these instruments are their susceptibility to systematic errors which lead to measurement errors. Electrogoniometers on the other hand, provide better accuracy and reliability as they use electronic components. However, this instrument is often used for the purposes of research rather than in the clinical setting because it is expensive.

C. Wearable Devices using Sensor Technology for Clinical Goniometry

The emerging trend of wearable electronics has extended into the field of medicine with fitness trackers like the Fitbit being the most sold product in the commercial market. Wearable devices are categorized as electronic devices that can be worn, embedded, or implanted in a person's body or clothing. In healthcare, specifically, wearable devices should perform a specific medical function [17]. Wearable devices that monitor biochemical measurements, blood oxygen saturation, blood pressure, cardiac activity, and respiration are currently used in the clinical settings [18].

Wearable devices along with other technologies such as video games and consoles, virtual and augmented realities, exoskeletons, and robots have influenced the medical specialty of physical therapy and rehabilitative science. Over the past decade multiple studies focusing on wearable devices using sensor technology in physical therapy and rehabilitative science have been published [13]. The most used types of sensors in these studies were flex sensors, inertial measurement unit (IMU) sensors, hall-effect sensors, magnetometers, and e-textile and stitched sensors [5]. The studies presented that all these types of sensors have high accuracy and reliability when used for clinical goniometry. However, it is important to consider the advantages and disadvantages of these sensors with regards to other factors such as versatility, scalability, and cost-efficiency.

D. Applications of the MPU-6050 IMU Sensor for Clinical Goniometry

Based on the acquired information from the related literature of wearable devices using sensor technology, it was clear that IMU sensors were the most suitable type of sensor for the design and development of a digital goniometer since they were not limited in versatility, and they had high reliability and accuracy. Thus, the MPU-6050 IMU sensor was chosen as the specific IMU sensor for this research.

The MPU-6050 IMU sensor has multiple applications for both non-medical and medical purposes. The MPU-6050 IMU sensor is used widely across different fields for different purposes utilizing the sensor's 6 degrees of freedom (DOF) with its 3-axis accelerometer and 3-axis gyroscope.

Focusing specifically on the applications of the MPU-6050 IMU sensor for clinical goniometry, related literature has explored the sensor's use in devices that measure the joint angle ROM of the fingers, wrist, forearm, elbow, hip, and knee mostly focusing on the motions of flexion and extension. A data glove for finger joint measurement using three MPU-6050 IMU sensors coupled with two 2.2-inch flex sensors connected to an Arduino microcontroller with all the components sewn onto a cloth glove was used for finger joint flexion – the results showed that the use of MPU-6050 IMU sensor for the device was highly accurate as it recorded low percentage of error ranging from 0.81% to 5.41% [19]. This study only considered fingers, wrist, forearm, elbow, hip, and knee and mostly focused on the motions of flexion and extension. It can be said that the developed device is not versatile. It also did not mention testing for different body sizes, so its scalability is not proven.

Two related studies using the MPU-6050 IMU sensor on a wearable device focused on the ROM Tests of wrist flexion and extension, forearm supination and pronation, radial deviation, and ulnar deviation – the results of both studies were considered reliable since all the ROM Tests recorded joint angle ROM measurements with a standard deviation of < 5 degrees [7, 8]. Similarly, these two developed devices, although found to be reliable, are not versatile. There was also no mention in the studies if the devices were tested for scalability as only one or two test subjects were able to test them.

Another two related studies used the MPU-6050 IMU sensor on wearable devices for the elbow joint [9, 10]. The first study focused on the ROM Tests of elbow flexion and extension as well as forearm supination and pronation while the second study only focused on the ROM Tests of elbow flexion and extension. The wearable devices of both studies were also considered reliable as they were also able to record average standard deviations for joint angle ROM measurements of < 5 degrees. Both studies also did not consider versatility and scalability, although the devices are found to be reliable.

A study that focused on measuring pelvic retroversion during hip flexion used two MPU-6050 IMU sensors connected an Arduino microcontroller that were attached to elastic Velcro-like straps recorded an average angle of 7.30

degrees which is considered reliable for pelvic retroversion – with this result the researchers concluded that the MPU-6050 IMU sensor was considered reliable when performing the ROM Test of hip flexion [11]. The device, however, cannot be considered versatile or scalable. Although 12 testers tested the device, the BMI categories of the testers were not known.

Finally, a custom physical activity and knee angle measurement sensor system for patients with neuromuscular disorders and gait abnormalities was developed using two MPU-6050 IMU sensors and an 8-bit RISC microprocessor attached to a knee sleeve [12]. The wearable device was used to perform knee joint angle measurements for the ROM Tests of knee flexion and extension and the results were considered reliable as the recorded data showed a standard deviation of < 5 degrees when compared to ground truth data recorded from an electromechanical goniometer. The study did not consider versatility and scalability.

Overall, the MPU-6050 IMU sensor is highly reliable and accurate in measuring joint angle ROM for the application of clinical goniometry. However, it can also be seen with the related literature that the developed wearable devices were limited in versatility and scalability since they generally conform to only some joints or body segments.

III. METHODOLOGY

The methodology includes the design, development, testing, and evaluation of the Goniopi and its Assisted Mode feature. The design and development of the Goniopi focuses on achieving high reliability and accuracy as well as satisfying the factors and requirements of versatility and scalability.

A. Design and Development of the Goniopi

The design of the Goniopi is comprised of three parts – the digital goniometer, the acrylic case, and the wearable attachable container.

The digital goniometer is the main component of the Goniopi. It is the instrument that allows users to perform ROM Tests and measure joint angle ROM. To satisfy the factors and requirements of versatility and scalability, the design of the Goniopi's digital goniometer considered components that would allow the MPU-6050 IMU sensor to measure reliable and accurate joint angle ROM measurements. Moreover, these components would have also been of a small and compact form factor. Therefore, the components of the Goniopi's digital goniometer were composed of the Raspberry Pi Pico microcontroller, MPU-6050 IMU sensor, Waveshare Dual GPIO Expander, Waveshare 1.14" LCD Display, DIYMORE 18650 Battery Shield V8, and two 18650 Li-ion rechargeable batteries.

The Goniopi's acrylic case also aimed to satisfy the factors and requirements of versatility and scalability when the Goniopi is used for both its handheld and wearable configuration. Considering that the components of the Goniopi's digital goniometer were chosen since they satisfied the factors and requirements of versatility and scalability, then the goal was to create a case design in which its dimensions were enough to enclose the assembled digital goniometer while maintaining the versatility and scalability of the device.

Furthermore, it was taken into consideration that the components of the Goniopi's digital goniometer, especially the MPU-6050 IMU sensor, should be visible to the user in order to avoid errors in placement when positioning the Goniopi on a specific joint or body segment. Thus, the Goniopi's acrylic case was made with 3mm acrylic sheets precisely cut using a CNC machine. The dimensions of the Goniopi with its acrylic case are 7.16cm (length), 6.30cm (width), and 11.20cm (height). Fig. 1 shows the Goniopi with its assembled digital goniometer enclosed in the acrylic case.

The Goniopi's wearable attachable container still aimed in satisfying the factors and requirements of versatility and scalability.

Considering that the Goniopi's digital goniometer enclosed in its acrylic should have already satisfied the factors and requirements of versatility and scalability, then the goal was to create a wearable design that would maintain the versatility and scalability of the device. Thus, the Goniopi's wearable attachable container had a pouch-like design made of synthetic fabric, specifically spandex lined with fusible interfacing, with an adjustable buckle strap. The adjustable buckle strap of the Goniopi's wearable attachable container has a length of 133cm which allowed it to fit from the waist and chest body segments all the way down to the wrist joint. Fig. 2 shows the Goniopi inside its wearable attachable container.



Fig. 1. Goniopi with Assembled Digital Goniometer in the Acrylic Case.



Fig. 2. Goniopi's Wearable Attachable Container.

Finally, dual-axis tilt calculation was used to calculate and output the tilt angle measured by the MPU-6050 IMU sensor. Dual-axis tilt calculation was done by solving for the ratio of the inverse sine of the x-axis and inverse cosine of the y-axis [20]. Equation (1) shows the formula for dual-axis tilt calculation. Equation (2) shows the formula to solve for the angle (theta) using dual-axis tilt calculation. With this implementation, the GonioPi was able to output angle measurements from 0 degrees to 180 degrees when it is tilted either clockwise or counterclockwise on the x-axis or z-axis.

$$\frac{A_{X,OUT}}{A_{Y,OUT}} = \frac{1g \times \sin(\theta)}{1g \times \cos(\theta)} = \tan(\theta) \quad (1)$$

$$\theta = \tan^{-1} \left(\frac{A_{X,OUT}}{A_{Y,OUT}} \right) \quad (2)$$

B. Assisted Mode Feature

The Assisted Mode feature of the GonioPi has the main functionality of outputting responsive feedback to the user when the GonioPi is used to measure joint angle ROM. The feature uses the factors of age and gender to give the user feedback if the joint angle ROM measured is BELOW NORMAL, NORMAL, or ABOVE NORMAL.

The Assisted Mode feature was implemented using a finite state machine which utilized a nested switch case algorithm. The factors of age sex, type of joint, type of motion, and normal range of motion are used to assess the measured joint angle ROM.

C. Initial Device Testing

The initial device testing of the GonioPi was performed independently by the researchers with the aid of a test subject to identify the supported ROM Tests of the GonioPi. This was done using both the handheld and wearable configurations. Since the researchers are not professionals in the field of physical therapy, a criterion stating that a ROM Test was considered initially supported by GonioPi if the device was able to output a joint angle ROM with a minus 5-degree threshold from the maximum value of the full ROM of a specific joint. Fig. 3 shows the researchers performing the initial device testing on a test subject.

D. Final Device Testing

The final device testing of the GonioPi consisted of confirming which ROM Tests were supported by the GonioPi using both the handheld and wearable configurations, reliability and accuracy testing, and an evaluation of the GonioPi and its Assisted Mode feature. The final device testing of the GonioPi was performed by eight medical professionals, specifically physical therapy interns, grouped into four pairs. Fig. 4 shows the final device testing of the GonioPi performed by the testers.

E. Final Device Testing for Confirmed Supported ROM Tests

The final device testing for confirmed supported ROM Test was done by making the testers use the GonioPi to perform a specific ROM Test on their partner. The testers were then asked to record if whether a specific ROM Test was either supported or unsupported by the GonioPi. Considering that the testers were professionals in the field of physical therapy, the decision of labeling whether a specific ROM Test was

considered supported or unsupported by the GonioPi was purely based on the tester's assessment of the device when using it in both its handheld and wearable configurations respectively.

The results recorded by the medical professionals were then collected and tallied. A specific ROM Test was then confirmed to be supported by the GonioPi if 60% or five out of eight testers labeled it as supported, otherwise it was confirmed to be unsupported by the GonioPi.

F. Final Device Testing for Reliability and Accuracy

The final device testing for reliability and accuracy of the GonioPi was limited to the ROM Tests of flexion and extension for the shoulder, elbow, hip, and knee. The GonioPi's reliability and accuracy were evaluated using the statistical methods of standard deviation and significant difference, respectively.



Fig. 3. Initial Device Testing of the GonioPi.

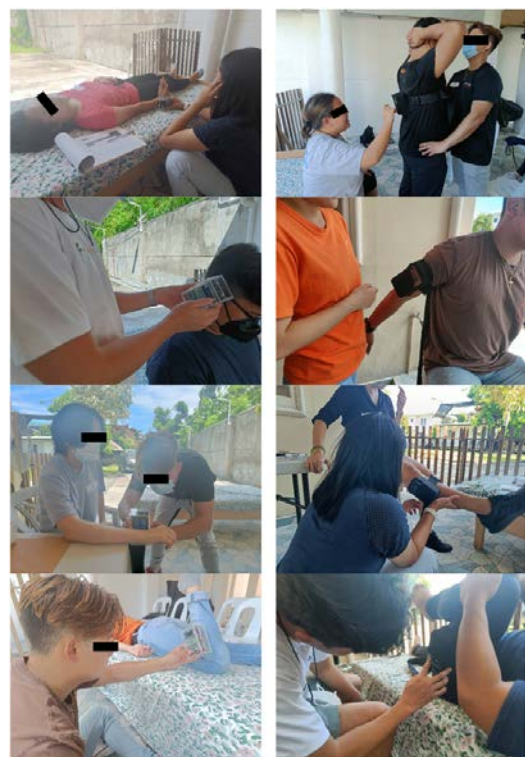


Fig. 4. Final Device Testing of the GonioPi.

It is important to note that the ROM Tests of shoulder and elbow flexion and extension were performed using the sitting position, the ROM Test of hip flexion was done using the supine position, and the ROM Tests of hip extension as well as knee flexion and extension were done using the prone position.

The testers measured the joint angle ROM of each ROM Test being tested for reliability five times on their partner. Once the data was gathered and collected, the standard deviation for a specific ROM Test of each test subject was computed by the researchers. This was done for both the handheld and wearable configuration. The average standard deviation for each ROM Test was then computed by the researchers using the values of the individual standard deviation for a specific ROM Test of each test subject.

An average joint angle ROM measurement of ≤ 5 degrees must have been achieved by the GonioPi for it to be considered reliable when performing a specific ROM Test, otherwise it was considered unreliable.

The accuracy of the GonioPi was evaluated using significant difference. A Bland Altman plot using 1.96 multiplied by the standard deviation generates a 95% confidence interval for evaluating a ROM Test [3]. Thus, the GonioPi's accuracy for each ROM Test was solved by multiplying 1.96 with the values of the average standard deviation of each ROM Test collected from the GonioPi's reliability testing.

An average joint angle ROM measurement of ≤ 10 degrees must have been achieved by the GonioPi for it to be considered accurate when performing a specific ROM Test, otherwise it was considered inaccurate.

G. Versatility and Scalability of the GonioPi

Versatility is the ability of a device to perform multiple ROM Tests on different joints using different types of motions and scalability is the ability of a device to handle different body sizes [13].

The versatility and scalability of the GonioPi were evaluated based on the results of the GonioPi's final device testing for the confirmed supported ROM Tests. Versatility of the GonioPi was evaluated based on the number of ROM Tests supported by the GonioPi – specifically considering how many out of the 11 joints and 15 motions were supported by the GonioPi using its handheld and wearable configurations, respectively. Scalability of the GonioPi was also evaluated based on the number of ROM Tests supported by the GonioPi – specifically considering the varying heights, weights, and BMI categories of the test subjects.

H. Evaluation of the GonioPi and the Assisted Mode Feature

Both the GonioPi and its Assisted Mode feature were evaluated through a survey with a series of qualitative questions. The GonioPi was evaluated based on its perceived usefulness, perceived ease of use, emotions, attitudes, and comfort. The Assisted Mode feature was evaluated based on its importance, usefulness, helpfulness, and design.

IV. RESULTS AND DISCUSSION

The results and discussion include a general overview of the results for initial device testing as well as the evaluation of the GonioPi and its Assisted Mode feature. Meanwhile, detailed results of the final device testing for the confirmed ROM Tests of the GonioPi and device reliability and accuracy testing are presented.

A. Results of the Initial Device Testing

The initial device testing of the GonioPi showed promising results for both the handheld and wearable configurations. Majority of the ROM Tests for both configurations were considered initially supported by the GonioPi using multiple different positions based on the set criterion. Specifically, the handheld configuration supported 30 out of 34 ROM Tests and the wearable configuration supported 21 out of 34 ROM Tests. With these promising results, it was evident that final device testing with medical professionals had to be performed to confirm the supported ROM Tests of the GonioPi.

B. Results of the Final Device Testing of the GonioPi for Confirmed Supported ROM Tests

The results for the final device testing of the GonioPi for the confirmed supported ROM Tests of the GonioPi showed that using its handheld configuration, the GonioPi supports 34 out of 34 ROM Tests using multiple different positions such as supine, prone, in sitting, and standing. Notably, all 34 ROM Tests were unanimously confirmed to be supported by the testers.

Furthermore, using its wearable configuration, the GonioPi supports 18 out of 34 ROM Tests using multiple different positions such as supine, prone, in sitting, and standing. The other 16 ROM Tests were confirmed by the testers to be unsupported by the GonioPi when used as a wearable device. Out of the 16 ROM Tests confirmed to be unsupported by the testers, 8 of which consists of the wrist and ankle joints – these were the ROM Tests of wrist flexion, wrist extension, ulnar deviation, radial deviation, ankle dorsiflexion, ankle plantarflexion, ankle inversion, and ankle eversion. These ROM Tests were considered unsupported by the testers because the GonioPi's size was too bulky when attached to these joints which did not allow the testers to properly position the device to perform these ROM Tests. Moreover, the testers stated that the bulkiness of the GonioPi also impeded the movement of the joint when attached to the test subject. Four ROM Tests, specifically cervical extension, cervical lateral flexion, trunk flexion, and trunk extension were considered unsupported by the testers because the GonioPi could not output joint angle ROM measurements that were satisfactory for the testers to consider them supported. Moreover, the testers stated that due to the bulkiness and weight of the GonioPi, testing these ROM Tests using the wearable configuration was greatly affected by gravity. The GonioPi in its attachable container would sag which affected the joint angle ROM measurement being outputted by the GonioPi. Also, for the ROM Tests of trunk flexion and extension the testers stated that they could not position the GonioPi using its attachable container properly on the test subject's body. Finally, the last 4 ROM Tests, specifically forearm supination, forearm pronation, hip abduction, and hip adduction – these

ROM Tests were considered unsupported by the testers because the Goniopi's sensor does not work and could not output a proper joint angle ROM measurement when attached to the body segment or joint of these ROM Tests as the sensor was oriented on the y-axis. The Goniopi's dual-axis tilt calculation implementation only allows for it to output angle measurements when the sensor is oriented on its x-axis or z-axis.

Table I shows a summary of all the confirmed supported and unsupported ROM Tests of the Goniopi both using its handheld and wearable configurations.

TABLE I. SUMMARY OF THE CONFIRMED SUPPORTED ROM TESTS FOR HANDHELD AND WEARABLE CONFIGURATIONS

GonioPi Final Device Testing Results		
Range of Motion Test	Handheld	Wearable
1. Cervical Flexion	(8/8) Supported	(7/8) Supported
2. Cervical Extension	(8/8) Supported	(1/8) Unsupported
3. Cervical Lateral Flexion	(8/8) Supported	(0/8) Unsupported
4. Cervical Rotation	(8/8) Supported	(8/8) Supported
5. Wrist Flexion	(8/8) Supported	(0/8) Unsupported
6. Wrist Extension	(8/8) Supported	(0/8) Unsupported
7. Ulnar Deviation	(8/8) Supported	(0/8) Unsupported
8. Radial Deviation	(8/8) Supported	(0/8) Unsupported
9. Shoulder Flexion	(8/8) Supported	(8/8) Supported
10. Shoulder Extension	(8/8) Supported	(8/8) Supported
11. Shoulder Abduction	(8/8) Supported	(8/8) Supported
12. Shoulder Adduction	(8/8) Supported	(8/8) Supported
13. Shoulder Lateral Rotation	(8/8) Supported	(8/8) Supported
14. Shoulder Medial Rotation	(8/8) Supported	(8/8) Supported
15. Forearm Supination	(8/8) Supported	(0/8) Unsupported
16. Forearm Pronation	(8/8) Supported	(0/8) Unsupported
17. Elbow Flexion	(8/8) Supported	(8/8) Supported
18. Elbow Extension	(8/8) Supported	(8/8) Supported
19. Trunk Flexion	(8/8) Supported	(0/8) Unsupported
20. Trunk Extension	(8/8) Supported	(0/8) Unsupported
21. Trunk Lateral Flexion	(8/8) Supported	(6/8) Supported
22. Trunk Rotation	(8/8) Supported	(5/8) Supported
23. Hip Flexion	(8/8) Supported	(7/8) Supported
24. Hip Extension	(8/8) Supported	(8/8) Supported
25. Hip Abduction	(8/8) Supported	(0/8) Unsupported
26. Hip Adduction	(8/8) Supported	(0/8) Unsupported
27. Hip Lateral Rotation (ER)	(8/8) Supported	(8/8) Supported
28. Hip Medial Rotation (IR)	(8/8) Supported	(8/8) Supported
29. Knee Flexion	(8/8) Supported	(8/8) Supported
30. Knee Extension	(8/8) Supported	(8/8) Supported
31. Ankle Dorsiflexion	(8/8) Supported	(0/8) Unsupported
32. Ankle Plantarflexion	(8/8) Supported	(0/8) Unsupported
33. Ankle Inversion	(8/8) Supported	(0/8) Unsupported
34. Ankle Eversion	(8/8) Supported	(0/8) Unsupported

C. Results of the Final Device Testing for Reliability and Accuracy

The results of the final device testing for reliability presented that the Goniopi using the handheld configuration is reliable for 6 out of the 8 ROM Tests that were evaluated. Specifically, the ROM Tests of shoulder flexion, shoulder extension, elbow flexion, hip extension, knee flexion, and knee extension. The Goniopi was considered reliable in performing these ROM Tests because their individual average standard deviations when using the Goniopi in its handheld configuration was ≤ 5 degrees. As for the ROM Tests considered as unreliable, specifically elbow extension and hip flexion – they were considered unreliable because their individual standard deviations were > 5 degrees. However, it is important to note that for the ROM Test of elbow extension the average standard deviation was only greater by 0.13 degrees and for the ROM Test of hip flexion the average standard deviation was only greater by 0.41 degrees.

Moreover, using the wearable configuration, the Goniopi is reliable for 5 out of 8 ROM Tests that were evaluated. Specifically, the ROM Tests of shoulder extension, elbow flexion, elbow extension, hip flexion, and knee extension. The Goniopi was considered reliable in performing these ROM Tests because their individual average standard deviations when using the Goniopi in its handheld configuration was ≤ 5 degrees. As for the ROM Tests considered as unreliable, specifically shoulder flexion, hip extension, and knee flexion – they were considered unreliable because their individual standard deviations were > 5 degrees. However, it is important to note that for the ROM Test of shoulder flexion the average standard deviation was only greater by 0.91 degrees. Furthermore, for the ROM Test of hip extension the average standard deviation was only greater by 0.47 degrees and for the ROM Test of knee flexion the average standard deviation was only greater by 0.35 degrees.

Table II shows a summary of the results for the Goniopi's reliability testing.

Considering the accuracy testing of the Goniopi for the 8 ROM Tests being evaluated was dependent of the average standard deviation values for the Goniopi's reliability testing, it was expected that the results would be consistent in the sense that the ROM Tests considered reliable were also accurate and the ROM Tests considered unreliable were also inaccurate.

Therefore, for the handheld configuration the 6 ROM Tests of shoulder flexion, shoulder extension, elbow flexion, hip extension, knee flexion, and knee extension the Goniopi was accurate in performing these ROM Tests because their individual significant differences were ≤ 10 degrees. As for the 2 ROM Tests of elbow extension and hip flexion, the Goniopi was inaccurate in performing these ROM Tests because their individual significant differences were > 10 degrees. However, it is still important to note that the significant difference for the ROM Test of elbow extension was only greater by 0.05 degrees and for the ROM Test of hip flexion the significant difference was only greater by 0.60 degrees.

TABLE II. SUMMARY OF THE AVERAGE STANDARD DEVIATIONS FOR RELIABILITY TESTING USING THE HANDHELD AND WEARABLE CONFIGURATIONS

GonioPi Reliability Testing Results for Handheld Configuration		
Range of Motion Test	Average Standard Deviation	Remarks
Shoulder Flexion	4.01°	Reliable
Shoulder Extension	3.64°	Reliable
Elbow Flexion	4.42°	Reliable
Elbow Extension	5.13°	Unreliable
Hip Flexion	5.41°	Unreliable
Hip Extension	4.61°	Reliable
Knee Flexion	4.06°	Reliable
Knee Extension	4.87°	Reliable
GonioPi Reliability Testing Results for Wearable Configuration		
Range of Motion Test	Average Standard Deviation	Remarks
Shoulder Flexion	5.91°	Unreliable
Shoulder Extension	4.18°	Reliable
Elbow Flexion	3.74°	Reliable
Elbow Extension	4.36°	Reliable
Hip Flexion	4.17°	Reliable
Hip Extension	5.47°	Unreliable
Knee Flexion	5.35°	Unreliable
Knee Extension	4.85°	Reliable

Moreover, for the wearable configuration, the 5 ROM Tests of shoulder extension, elbow flexion, elbow extension, hip flexion, and knee extension the GonioPi was accurate in performing these ROM Tests because their individual significant differences were ≤ 10 degrees. As for the 3 ROM Tests of shoulder flexion, hip extension, and knee flexion, the GonioPi was inaccurate in performing these ROM Tests because their individual significant differences were > 10 degrees. However, it is also still important to note that for the ROM Test of shoulder flexion the significant difference was only greater by 1.58 degrees. Furthermore, for the ROM Test of hip extension, the significant difference was only greater by 0.72 degrees. Finally, for the ROM Test of knee flexion, the significant difference was only greater by 0.49 degrees.

Table III shows the summary of the results for the GonioPi's accuracy testing.

There is no consistency with the ROM Tests considered as unreliable and inaccurate when comparing the results for both the handheld and wearable configurations. Thus, retesting these ROM Tests for reliability using the GonioPi or an improved version of the device should be considered in a future study.

Overall, it can be said that the GonioPi can be considered as reliable and accurate for the 8 ROM Tests evaluated for reliability and accuracy since most of them were considered reliable and accurate and those considered unreliable and inaccurate were only a few decimal points greater than accepted standard values of 5 degrees and 10 degrees respectively.

TABLE III. SUMMARY OF THE SIGNIFICANT DIFFERENCE FOR ACCURACY TESTING USING THE HANDHELD AND WEARABLE CONFIGURATIONS

GonioPi Accuracy Testing Results for Handheld Configuration		
Range of Motion Test	Average Significant Difference	Remarks
Shoulder Flexion	7.86°	Accurate
Shoulder Extension	7.13°	Accurate
Elbow Flexion	8.66°	Accurate
Elbow Extension	10.05°	Inaccurate
Hip Flexion	10.60°	Inaccurate
Hip Extension	9.04°	Accurate
Knee Flexion	7.96°	Accurate
Knee Extension	9.55°	Accurate
GonioPi Accuracy Testing Results for Wearable Configuration		
Range of Motion Test	Average Significant Difference	Remarks
Shoulder Flexion	11.58°	Inaccurate
Shoulder Extension	8.19°	Accurate
Elbow Flexion	7.33°	Accurate
Elbow Extension	8.55°	Accurate
Hip Flexion	8.17°	Accurate
Hip Extension	10.72°	Inaccurate
Knee Flexion	10.49°	Inaccurate
Knee Extension	9.51°	Accurate

D. Results for the Versatility and Scalability of the GonioPi

In terms of versatility, considering that 34 out of 34 ROM Tests are supported by the GonioPi using its handheld configuration and out of those 34 supported ROM Tests 11 out of 11 joints and 15 out of 15 motions are supported, then it can be said that the GonioPi is versatile when used as a handheld digital goniometer.

Furthermore, still in terms of versatility, considering that 18 out of 34 ROM Tests (52%) are supported by the GonioPi using its wearable configuration and out of those 18 supported ROM Tests, 6 out of 11 joints (54%) and 8 out of 15 motions (53%) are supported then it can be said that the GonioPi is relatively versatile when used as a wearable digital goniometer. The GonioPi's issue with versatility using its wearable configuration is due to its bulky size and improper sensor orientation when attached to a specific unsupported joint. The issue of the GonioPi's bulky size can be resolved by making the design of the GonioPi smaller and more compact. The issue of improper sensor orientation can be resolved by using triple-axis tilt calculation for solving the joint angle ROM measurement rather than the current implementation which uses dual-axis tilt calculation.

In terms of scalability, considering that the GonioPi using both its handheld and wearable configurations was tested on test subjects of varying heights, weights, and BMIs – specifically, five (5) normal, (2) overweight, and (2) obese then it can be said that the GonioPi is scalable as both a handheld and wearable digital goniometer. However, a future study can be performed to include the underweight BMI category to

better establish the GonioPi's scalability. Moreover, the GonioPi using its handheld configuration can be used to perform ROM Tests for both large and small joints of the body while the GonioPi using its wearable configuration can be used to perform ROM Tests for mostly large joints on the body. Both configurations, however, do not allow for ROM Tests for the finger joint. Finally, it is important to note that the GonioPi's wearable attachable container design can conform to all joints of the body except for the fingers.

E. Results of the Evaluation of the GonioPi and Assisted Mode Feature

The results of the survey for the evaluation of the GonioPi presented that majority of the testers found the GonioPi to be useful, easy to use, likeable, and comfortable when used as a digital goniometer by medical professionals for both its handheld and wearable configurations. Majority of the positive feedback from the testers regarding the GonioPi highlighted its efficiency, convenience, and ease of use. A tester also mentioned that it is a nice and useful innovation. Moreover, the testers mentioned that the GonioPi helps them in their profession by allowing them to get ROM measurements faster and easier. When it comes to the negative feedback of the GonioPi, the testers highlighted its size being too bulky. Moreover, the testers also stated that its wearable configuration limits some motions and that because of its weight it is greatly influenced by gravity. The testers also mentioned that the sensor is quite sensitive and picks up some unnecessary motions. A tester also mentioned that the GonioPi has a lack of visual markers such as a fulcrum and arm like the universal goniometer. Finally, as for the wearable attachable container's design, they found it a bit loose, and the adjustable buckle strap a hassle to adjust. The testers stated that the GonioPi can be improved by decreasing its size – making it less bulky and more compact. Moreover, adding visual markers such as an indicator of a fulcrum and an arm on the acrylic case could help getting joint angle ROM measurements easier in the sense that it decreases user error of overcompensating or undercompensating the tilt of the device. One tester mentioned that a bigger switch and buttons would be beneficial for them. Finally, as for the wearable attachable container, the testers suggested that the strap should be thinner and smoother while the attachable container should be more secure.

The results for the survey of the Assisted Mode feature of the GonioPi presented that majority of the testers found the Assisted Mode feature to be important, useful, helpful, and user friendly which increases the usability and relevance of the GonioPi. Moreover, the feature also makes the GonioPi a better device overall. Majority of the positive feedback from the testers regarding the Assisted Mode feature of the GonioPi highlighted how it makes it easier for a user to determine whether or not the joint angle ROM measurement of a patient is within normal range or not. Moreover, the testers mentioned that it is helpful in aiding physical therapists determine the state of a patient's ROM. Lastly, a tester stated that it is useful and effective especially for "newbies". When it comes to the negative feedback from the testers regarding the Assisted Mode feature of the GonioPi, the testers highlighted how the feature only has limited motions and joints. A couple of testers stated that the feature may be at risk for inaccuracy due to

human error when using the GonioPi. Lastly, a tester stated that the feature has no indication of the normal values of each joint. The testers stated that the GonioPi's Assisted Mode feature can be improved by adding more options of joints and motions to be tested. Moreover, a tester stated that adding the normal values of each joint for a user's awareness and knowledge can be helpful. Finally, a tester also stated that a warning message requesting the tester to immobilize patient's joint being tested may help in decreasing human errors that may lead to measurement errors in the joint angle ROM measurement.

F. Limitations of the Final Device Testing

It should be noted that the method for the final device testing of the GonioPi for confirmed supported ROM Tests was done by making each tester perform 9 ROM Tests using different positions on their partner while the other pairs observed and gave their remarks based on their observation of the ROM Test being performed. This means that all testers have not tested each ROM tests using the device. This may have effects on the collected data as actually using the device for measurement may give a different result compared with just observing.

In addition, the testers in the final device testing are physical therapy interns. While it is assumed that they have sufficient knowledge in clinical goniometry, it might provide different results if the test was carried out by experienced physical therapists.

Looking at the results for reliability of the GonioPi for both the handheld and wearable configurations, there is no consistency with the ROM Tests considered as unreliable. Moreover, comparing the individual data collected from the test subjects, the first two pairs of testers-test subjects (testers 1, 2, 3, and 4) had higher values of individual standard deviations for the different ROM Tests compared to the next two pairs of testers-test subjects (testers 3, 4, 5, and 6). The possibility of these differences in results may have been caused by tester-test subject/patient fatigue as manifested by the testers themselves during testing. Considering that the first two pairs of testers-test subjects extended their testing time during the first day, it raises the possibility that by the time they were collecting the data for reliability testing they were already tired and could not properly and consistently perform the different ROM Tests being evaluated. Compared to the next two pairs of testers-test subjects who performed the data gathering for the reliability testing during the second day of testing – they were able to perform the different ROM Tests more consistently as they were not affected by fatigue from an entire day of testing.

V. FUTURE WORKS AND RECOMMENDATIONS

The current size of the GonioPi is too bulky. An improvement that can be made to resolve this issue would be to look for and use smaller and more compact components to reduce the overall size of the GonioPi. The researchers suggest future works consider using the Pimoroni LiPo SHIM for Pico power supply. It is a small and compact power supply that can be powered by a LiPo/Li-Ion battery and soldered onto the back of the Raspberry Pi Pico microcontroller. Using this component as a substitute power supply of the battery shield

V8 would reduce the thickness of the GonioPi by about 2.70cm which would result to an overall thickness of 3.60cm for the next version of the GonioPi.

A reduction in the overall size and weight of the GonioPi would allow the attachable container to be more secure since it will be affected less by gravity due to the reduced weight of the GonioPi. Moreover, as for the adjustable straps of the wearable attachable container, an improvement can be made by reducing its thickness and changing the adjustable buckle strap to an adjustable belt strap and lock as suggested by one of the testers.

For the GonioPi to support more ROM Tests using its wearable configuration as well as improving its reliability and accuracy, it is suggested that future works pursue on implementing a triple-axis tilt calculation for measuring joint angle ROM. Implementing a triple-axis tilt calculation would allow the GonioPi to calculate and measure joint angle ROM measurements when the sensor is oriented on the y-axis. Moreover, implementing a triple-axis tilt calculation would also slightly improve the sensor's reliability and accuracy.

It is also suggested that future studies perform testing that include a participant with BMI categories of underweight and higher classes of obesity. This would mean that the scalability of the device can be evaluated for much smaller and larger participants, respectively.

An improvement can also be made by implementing a sampling window. Implementing a sampling window would allow the sensor to output stable data to the Raspberry Pi Pico microcontroller before outputting it on the display. This would mean that the joint angle ROM measurement outputted on the display won't update every second with the slightest movement but rather it will stabilize first and output an average value of a chosen number of samples.

It is also recommended to add a straight edge ruler component at the back of the acrylic case design of the GonioPi as suggested by a tester in order for them to know that they are neither undercompensating nor overcompensating the tilt of the device when performing a ROM Test. Moreover, another tester suggested that a visual marker be added to midsection of the top of the acrylic case design to act as visual marker for rotation, and deviation motions of joints.

An improvement can also be made in the Assisted Mode Feature by adding more joints and motions as the testers considered the current implementation of the feature important, useful, and helpful.

A retest of the eight (8) ROM Tests evaluated in this research should be conducted to make the results of the handheld configuration testing consistent with the wearable configuration testing. The researchers also suggest that the testing for device reliability and accuracy should be performed independently from any other device testing to avoid tester-test subject/patient fatigue.

The researchers suggest the use of other sensors such as the ADXL335 3-axis Accelerometer Module, ADXL345 Accelerometer Module, BNO055 9-DOF IMU sensor, and MPU-9250 9-Axis IMU sensor. The researchers also recommend exploring the use of the accelerometers of modern

smartphones for the application of clinical goniometry, like existing apps such as PhysioMaster.

VI. CONCLUSION

In conclusion, the design and development of the GonioPi has shown that a versatile, scalable, reliable, and accurate digital goniometer can be made using the MPU-6050 IMU sensor along with the components of the Raspberry Pi Pico microcontroller, Waveshare Dual GPIO Expander, Waveshare 1.14" LCD Display, 18650 Battery Shield V8, and two (2) 18650 Li-ion rechargeable batteries enclosed in an acrylic case with a wearable design of a pouch like attachable container with adjustable buckle straps.

In terms of versatility and scalability, the GonioPi has shown that it is versatile and scalable as it supports 34 ROM Tests of 11 different joints using 15 different motions, and 18 ROM Tests of 6 different joints using 8 different motions in multiple different positions using both the handheld and wearable configurations respectively for people of varying heights, weights, and BMIs. Improvements can be made for the wearable configuration to support more ROM Tests by using triple-axis tilt calculation and reducing the size of the GonioPi by substituting its power supply component.

In terms of reliability and accuracy, the GonioPi has shown high reliability and accuracy as it was reliable and accurate for majority of the ROM Tests of flexion and extension for the shoulder, elbow, hip, and knee joints for both the handheld and wearable configurations as its joint angle ROM measurements of $< 5^\circ$ for device reliability, and joint angle ROM measurements of $< 10^\circ$ for device accuracy. Improvements can be made for the GonioPi's reliability and accuracy by adding visual markers to the device in order to minimize user error when using the GonioPi.

Finally, regarding the Assisted Mode feature of the GonioPi – the feature has proven to be important, useful, and helpful with the feedback of the testers who also requested for more joints and motions to be added to the feature as an improvement.

ACKNOWLEDGMENT

The authors would like to thank the physical therapy interns who volunteered to participate as testers of the GonioPi. Finally, the author would also like to express his deepest appreciation to his family and friends who supported him throughout the entire research.

REFERENCES

- [1] Boone, D.C., Azen, S.P., Lin, C.-M., Spence, C., Baron, C., Lee, L., 1978. Reliability of Goniometric Measurements. *Physical Therapy* 58, 1355–1360. <https://doi.org/10.1093/ptj/58.11.1355>.
- [2] Bovens, A.M.P.M., van Baak, M.A., Vrencken, J.G.P.M., Wijnen, J.A.G., Verstappen, F.T.J., 1990. Variability and reliability of joint measurements. *Am J Sports Med* 18, 58–63. <https://doi.org/10.1177/036354659001800110>.
- [3] Hancock, G.E., Hepworth, T., Wembridge, K., 2018. Accuracy and reliability of knee goniometry methods. *J Exp Orthop* 5, 46. <https://doi.org/10.1186/s40634-018-0161-5>.
- [4] Walmsley, C.P., Williams, S.A., Grisbrook, T., Elliott, C., Imms, C., Campbell, A., 2018. Measurement of Upper Limb Range of Motion Using Wearable Sensors: A Systematic Review. *Sports Med - Open* 4, 53. <https://doi.org/10.1186/s40798-018-0167-7>.

- [5] Avila, F.R., Carter, R.E., McLeod, C.J., Bruce, C.J., Giardi, D., Guliyeva, G., Forte, A.J., 2021. Accuracy of Wearable Sensor Technology in Hand Goniometry: A Systematic Review. *Hand* (New York, N.Y.) 155894472110146. <https://doi.org/10.1177/15589447211014606>.
- [6] Houglum, P.A., Bertoti, D., Brunnstrom, S., 2012. Brunnstrom's clinical kinesiology, 6th ed. ed. F.A. Davis, Philadelphia.
- [7] Huang, S.-M., Gi, P.-Y., Wu, P.-Y., 2018. A Design of Wearable Goniometers for Measuring Carpal Angular Movement, in: 2018 IEEE International Conference on Advanced Manufacturing (ICAM). Presented at the 2018 IEEE International Conference on Advanced Manufacturing (ICAM), IEEE, Yunlin, pp. 1–4. <https://doi.org/10.1109/AMCON.2018.8615058>.
- [8] Jin Hiung, F., Mat Sahat, I., 2020. Development of wrist monitoring device to measure wrist range of motion. *IOP Conf. Ser.: Mater. Sci. Eng.* 788, 012033. <https://doi.org/10.1088/1757-899X/788/1/012033>.
- [9] Narejo, A., Baqai, A., Sikandar, N., Ali, A., Narejo, S., 2020. Physiotherapy: Design and Implementation of a Wearable Sleeve using IMU Sensor and VR to Measure Elbow Range of Motion. *IJACSA* 11. <https://doi.org/10.14569/IJACSA.2020.0110953>.
- [10] Jacob, A., Wan Zakaria, W.N., Md Tomari, M.R.B., 2016. Implementation of IMU sensor for elbow movement measurement of Badminton players, in: 2016 2nd IEEE International Symposium on Robotics and Manufacturing Automation (ROMA). Presented at the 2016 2nd IEEE International Symposium on Robotics and Manufacturing Automation (ROMA), IEEE, Ipoh, Malaysia, pp. 1–6. <https://doi.org/10.1109/ROMA.2016.7847813>.
- [11] Fenato Junior, A., Garcia, L.M., Perdoná, G.D.S.C., Maranhão, D.A., 2020. MEASUREMENT OF PELVIC RETROVERSION DURING HIP FLEXION: EVALUATION WITH ACCELEROMETERS. *Acta ortop. bras.* 28, 69–73. <https://doi.org/10.1590/1413-785220202801227237>.
- [12] Feldhege, F., Mau-Moeller, A., Lindner, T., Hein, A., Marksches, A., Zettl, U., Bader, R., 2015. Accuracy of a Custom Physical Activity and Knee Angle Measurement Sensor System for Patients with Neuromuscular Disorders and Gait Abnormalities. *Sensors* 15, 10734–10752. <https://doi.org/10.3390/s150510734>.
- [13] Wang, Q., Markopoulos, P., Yu, B., Chen, W., Timmermans, A., 2017. Interactive wearable systems for upper body rehabilitation: a systematic review. *J NeuroEngineering Rehabil* 14, 20. <https://doi.org/10.1186/s12984-017-0229-y>.
- [14] Norkin, C.C., White, D.J., 2009. Measurement of joint motion: a guide to goniometry, 4th ed. ed. F.A. Davis, Philadelphia.
- [15] American Physical Therapy Association (Ed.), 2001. Guide to physical therapist practice, 2nd ed. ed. American Physical Therapy Association, Alexandria, Va.
- [16] Kisner, C., Colby, L.A., 2012. Therapeutic exercise: foundations and techniques, 6th ed. ed. F.A. Davis, Philadelphia.
- [17] Glaros, C., I. Fotiadis, D., 2005. Wearable Devices in Healthcare, in: G. Silverman, B., Jain, A., Ichalkaranje, A., C. Jain, L. (Eds.), *Intelligent Paradigms for Healthcare Enterprises, Studies in Fuzziness and Soft Computing*. Springer Berlin Heidelberg, Berlin, Heidelberg, pp. 237–264. https://doi.org/10.1007/11311966_8.
- [18] Xiao-Fei Teng, Yuan-Ting Zhang, Poon, C.C.Y., Bonato, P., 2008. Wearable Medical Systems for p-Health. *IEEE Rev. Biomed. Eng.* 1, 62–74. <https://doi.org/10.1109/RBME.2008.2008248>.
- [19] Wa'ie Hazman, M.A., Aimi Mohd Nordin, I.N., Mohd Noh, F.H., Khamis, N., M. Razif, M.R., Athif Faudzi, A., Mohd Hanif, A.S., 2020. IMU sensor-based data glove for finger joint measurement. *IJEECS* 20, 82. <https://doi.org/10.11591/ijeeecs.v20.i1.pp82-88>.
- [20] Fisher, C.J., 2010. Using an Accelerometer for Inclination Sensing 8.

Computational Approach to Identify Regulatory Biomarkers in the Pathogenesis of Breast Carcinoma

Ghazala Sultan¹, Swaleha
Zubair^{2*}

Department of Computer Science
Aligarh Muslim University
Aligarh, India

Inamul Hasan Madar³

Department of Pharmacology
Saveetha Dental College and
Hospitals
Chennai, India

Harishchander Anandaram⁴

Centre for Excellence in
Computational Engineering and
Networking, Amrita Vishwa
Vidyapeetham, Coimbatore, India

Abstract—Breast Cancer is reckoned amongst the most common cause of morbidity and mortality among women, adversely affecting female population irrespective of age. The poor survival rate reported in invasive carcinoma cases demands the identification of early developmental stage key markers. MicroRNAs are contributing a critical role in gene regulation potential markers. Over 2000 miRNAs have been identified and considered to offer a unique opportunity for early detection of diseases. In this study, a gene-miRNA-TF interaction network was constructed from the differentially expressed genes obtained from the invasive lobular and invasive ductal carcinoma samples. The network consists of experimentally validated miRNAs and transcription factors were identified for the target genes, followed by thermodynamics studies to identify the binding free energy between mRNA-miRNA. Our analysis identified miRNA; hsa-miR-28-5p binds with MAD2L1 with unexpectedly high binding free energy equivalent to -92.54kcal/mol and also makes canonical triplex with hsa-miR-203a, which acts as a catalyst to initialize the MAD2L1 regulation. For the identified regulatory elements, we proposed a mathematical model and feed-forward loops that may serve in understanding the regulatory mechanisms in breast cancer pathogenesis and progression.

Keywords—Breast cancer; invasive lobular carcinoma; invasive ductal carcinoma; biomarkers; MicroRNA; transcription factors; feed forward loops

I. INTRODUCTION

Breast cancer is the major type of cancer affecting female population in both developed and developing countries. Breast carcinoma can be classified into ductal carcinoma in situ (DCIS) and lobular carcinoma in situ (LCIS). In the initial stages of breast cancer (i.e., DCIS), the abnormal cells are restricted to the lining of breast ducts, which may lead to invasive cancer if not treated, “In situ” type tumor is confined to the epithelial layer, where it leads to DCIS and LCIS [1]. When the tumor cells burst out from the tissues, these can be Invasive Ductal Carcinoma (IDC) and Invasive Lobular Carcinoma (ILC). IDC accounts for almost 80% of the diagnoses of breast cancer cases, while ILC is composed of another 5%-15% [2].

Most breast cancers begin as asymptomatic lump or tumor that originates from either glandular tissue of breast i.e. lobules or in the ducts that connect these lobules. Molecular subtypes of cancer have been identified by biomarkers including hormones (Estrogen (E), progesterone (P)), and

receptors (ER, PR, HER1 and HER2). In 2019, almost 62,930 and 268,600 new cases of DCIS and IDC were reported respectively in United States. Breast cancer is associated with mutations in genes like BRCA1/2, p53, ATM, and CHD1. Nearly 5-10% of breast cancers are linked to the inheritance of gene mutations, mostly BRCA1/2 mutations. Women with BRCA1/2 mutations have a 45-65% higher chance of developing breast cancer [3]. Non-genetic risk factors include first-degree family history, race and ethnicity, lifestyle, exposure to radiation, alcoholism, obesity, and hormone replacement therapies. Few reports suggest that metabolism, particularly fatty acid oxidative metabolism plays a significant role in cancer progression by reprogramming their signaling pathways [4,5].

MAD2L1 gene is known as mitotic arrest deficient 2 like 1 or mitotic spindle assembly checkpoint protein MAD2. Aliases of MAD2L1 include HSMAD2 and MAD2. MAD2L1 plays an essential role in supervising cell cycle regulation, G1/S checkpoint, cell growth and death, Oocyte meiosis and progesterone-mediated oocyte maturation [6]. Studies have reported that chromosomal instability due to aberrant expression of MAD2L1 may promote tumorigenesis, where upregulation of MAD2L1 has been reported in breast, lung, liver and stomach cancer [7,8,9].

MicroRNAs (miRNAs) are small, 18-22 nucleotide long, non-coding RNA molecules. They are the key players in RNA interference pathways causing silencing of their associated target genes. miRNAs regulate the expression of 30-50% of genes and target various elements of signaling pathways and cellular networks. Recent studies have established their role as oncogenes or anti-oncogenes in regulating multiple cellular pathways involved in breast cancer pathogenesis. Therefore, miRNA may aid in developing new methods for cancer diagnostics and therapy.

II. RELATED WORK

The expression profile of miRNAs differs in normal and tumor tissues. miRNA profiling has identified that miR-99a was dysregulated in breast cancer tissues as compared to normal tissue [10]. Furthermore, numerous studies have reported that miRNAs are dysregulated at various stages of breast cancer [11]. Therefore, they have been used to identify characteristic miRNA signatures in human breast cancers. To decipher and analyze the differential changes of oncogenes

and tumor suppressor genes, transcriptome analysis with the help of microarray expression-based studies would help in the identification of novel markers associated with the cancer progression [12].

The role of miR-28-3p is well established in different cancer types including breast cancer, colorectal cancer, B-cell lymphoma, glioma and renal cell carcinoma. Liang Ma et al. identified the inhibition property of miR-28-3p by regulating WSB2 in breast cancer [13], while in other cancer it has been found to target TRPM7, Rap1b and cyclin D1 [14, 15]. However, the potential role of miR-28-3p targeting MAD2L1 is not yet reported in breast cancer.

III. MATERIALS AND METHOD

A. Mining of Differentially Expressed Genes

In the present study, breast cancer dataset GSE36295 was retrieved from Gene Expression Omnibus database of NCBI and analyzed to identify DEGs. The dataset encompasses 50 Saudi Arabian subjects with 5 control samples, 5 ILC (Invasive Lobular Carcinoma samples), 34 IDC (Invasive Ductal Carcinoma) and the remaining 6 samples were poorly differentiated (not included in the study). Expression profiling was conducted on Human Gene 1.0 ST GeneChip arrays (Affymetrix) testing platform. In order to calculate and analyze the DEGs between Control vs. ILC and Control vs. IDC samples, we have used Bioconductor packages in R namely affy, limma and other packages included in our customized pipeline. To calculate FDR and p-values, Benjamin and Hochberg (FDR) and t-test methods were utilized respectively [16]. A volcano plot and heatmap were constructed, which represent the distribution of p-value and fold change of DEGs using R.

B. Gene-Gene Interaction Network (GGIN) Analysis for Hub Nodes and Target Genes Identification

GeneMANIA [17] and Search Tool for Retrieval of Interacting Genes/Proteins (STRING) [18] were utilized to develop GGIN. The parameters used for network generation were; all prediction sources enabled medium confidence score ≥ 0.40 and no interactors in the first and second shell. The final GGIN was downloaded in .txt format for visualization and analysis in Cytoscape 3.7.1 using CytoHubba [19]. In this study, identified hub genes were further subjected to the Oncoprint module in cBioPortal and the hub genes with the relative frequency of mutation and copy number variants < 1 were selected as target genes.

C. Enrichment Analysis of Target Genes and Functional Annotation

Enrichr [20] identified the enriched terms in a given gene list and web-based gene set analysis toolkit (WebGestalt) [21] is a data mining system. It has four modules that aid in examining gene sets for Gene Ontology terms, metabolic and signaling pathways, tissue expression and chromosome distribution. The target genes were subjected to enriched pathways and biological process enrichment analysis through Enrichr and WebGestalt, respectively.

D. Identification of Validated miRNA for Target Genes

miRTarBase provides comprehensive data on experimentally validated miRNA and target interactions [22]. It consists of more than 13,404 validated miRNA and target interactions. In our study, the genes with a lesser frequency of mutations were subjected to regulatory analysis to identify the novel targets for validated miRNA. Furthermore, Regulatory Network Repository (RegNetwork) consisting of the integration of five-types of transcriptional and post-transcriptional regulatory relationships for mice and humans, was used to identify the experimentally validated Transcription Factors.

E. Thermodynamics Estimation of Gene-miRNA Interactions and miRNA-mRNA Duplex Binding Site Prediction

miRmap is an open-source software library that ranks potential targets on the basis of repression strength. It combines evolutionary, probabilistic, thermodynamics and sequence-based features [23]. It uses four approaches to examine feature correlations using experimental data from transcriptomics, proteomics and immunopurification studies. For binding site and thermodynamics estimation, the identified target gene-miRNA duplex was subjected to miRmap web.

F. miRNA Triplex, ODE and mRNA Regulation using Feed Forward Loop

TriplexRNA is a web resource that incorporates methods for triplex structure analysis, miRNA target prediction, simulation and c. The triplex formation of target genes obtained miRNA was examined through TriplexRNA [24]. An Ordinary Differential Equation (ODE) was proposed to explain the alteration of miRNA and Transcriptional Factors (rate of change) concerning the target gene in initiating the regulatory pathogenesis of the disease. The MAD2L1 regulatory mechanism was further explained with Feed Forward Loop.

IV. RESULTS AND DISCUSSION

A. Identification of differentially Expressed Genes

The microarray expression dataset GSE36295 was obtained from GEO and was analyzed in R using bioconductor packages. The dataset comprised of 5 control, 5 ILC, and 34 IDC tissue samples of female breast cancer patients. The principal components analysis revealed the relatedness between samples of each category (Fig. 1A). The dataset was normalized using RMA normalization approach and DEGs were identified using the threshold of $|\log_{2}FC| \geq 1$ and a Benjamini & Hochberg adjusted p-value cut-off of 0.05 (Fig. 1B). The principal components analysis plots clearly classify the distinct expression of genes in Control and Cancerous samples (IDC and ILC). Each cluster represents the sample with same feature within it and differentiates from the samples in other clusters. Thus, differentiating the gene expression in normal breast to the gene expression in breast cancer samples. 1509 DEGs were identified that were further used for network construction.

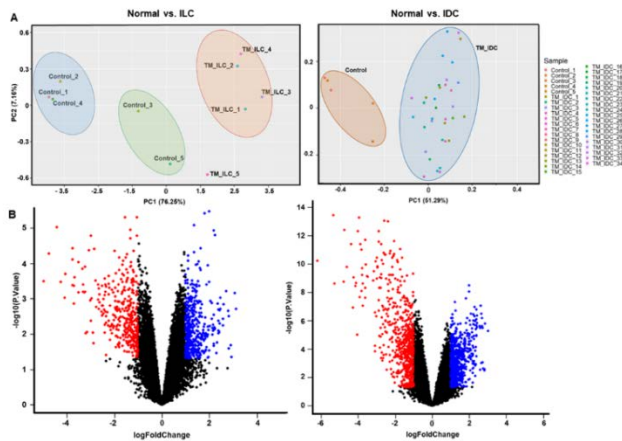


Fig. 1. (A). Principal Components Analysis of IDC and ILC Samples with Normal Samples. (B). Volcano Plots for DEGs where Red Dots and Blue Dots Represent up and Downregulated Genes Respectively.

B. The Structure of GGIN and Identification of Target Genes and Enrichment Analysis

From GeneMANIA studies, the DEGs were found to have a well-established role in the pathogenesis of cancer based on co-expression, co-localization, and pathways. The GGIN obtained from STRING consisted of 1509 nodes and 21993 edges, with average local clustering coefficient of 0.381 and average node degree of 29. CytoHubba plugin of Cytoscape 3.7.1 identified central elements of the GGIN. Hubs are nodes with maximum interactions and occupy a central position in the interaction networks. Maximum Clique Centrality measure identified the hub genes including BUB1B, CDCA8, CDK1, TOP2A, NUSAP1, MAD2L1, SPAG5, KIF2C, ASPM, CCNB2 (Fig. 2A). In cBioPortal, we examined genetic alterations in the top ten hub genes and identified that for CDCA8, CDK1, NUSAP1, TOP2A, MAD2L1 and CCNB2 the frequency of mutations and copy number variants were less than one. Since these genes showed the least genetic alterations, therefore, were selected as target genes for further study. The enrichment analysis of target genes revealed that they were associated with metabolic processes of amino acids, lipids, drugs and nucleoside bisphosphates (Fig. 2B). Furthermore, they were enriched in Progesterone mediated Oocyte mutation; Cell Cycle; p53 signaling and cellular senescence pathways (Fig. 2C). The identified biological processes and signaling pathways have a well-established role in cancer pathogenesis.

C. Identification of Validated miRNAs and Transcriptions Factors for Target Genes

The regulatory elements of the gene i.e. validated miRNAs and Transcription Factors were obtained from miRtarBase and RegNetwork (Table I). The interactions between gene-miRNA in and the interactions between gene-miRNA-cooperative miRNA in forming a triplex were given in Table II. The experimentally validated miRNAs and Transcription Factors (Table I) were identified for the target genes MAD2L1 and CDK1; for other target genes, no validated regulators were found.

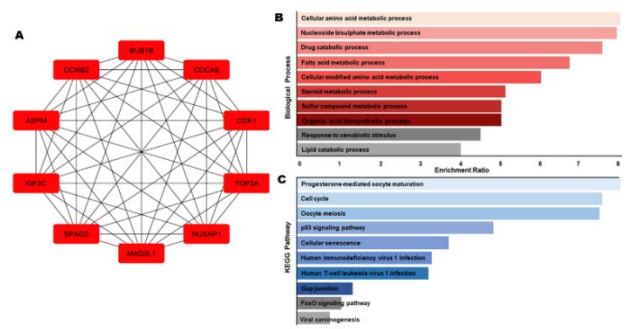


Fig. 2. (A) Top 10 Hub Genes of GGIN as Identified from CytoHubb. Functional Enrichment Analysis of Target Genes (B) Biological Processes (C) Signaling Pathways.

TABLE I. VALIDATED MIRNAs FOR CDK1 AND MAD2L1

Gene	Regulatory Elements	
	Transcription Factor	miRNA
MAD2L1	E2F4, ESR2 MYB, MYC	hsa-miR-28-5p hsa-miR-192-5p
CDK1	RB1, SP1, ATF1, E2F1, E2F4, ETS2, MYB, MYC	hsa-miR-31-5p hsa-miR-663a hsa-miR-24-3p hsa-miR-302a-3p

D. Seed Pairing and Construction of Gene Regulatory Network

In case of seed pairing CDK1-hsa-miR-31-5p form a complementarily pairing with a binding free energy of -34.33 Kcal/mol (Table II) and with triplex formation, CDK1-hsa-miR-31-5p-hsa-miR-543 forms a canonical triplex to initiate the process of regulation. Similarly, MAD2L1-hsa-miR-28-5p-hsa-miR-203 forms a canonical triplex. The interaction between the genes: CDK1, miRNAs: hsa-miR-28-5p, hsa-miR-31-5p and transcription factors (TFs): RB1, SP1, ATF1, E2F1, E2F4, ETS2, MYB and MYC is given in Fig. 3.

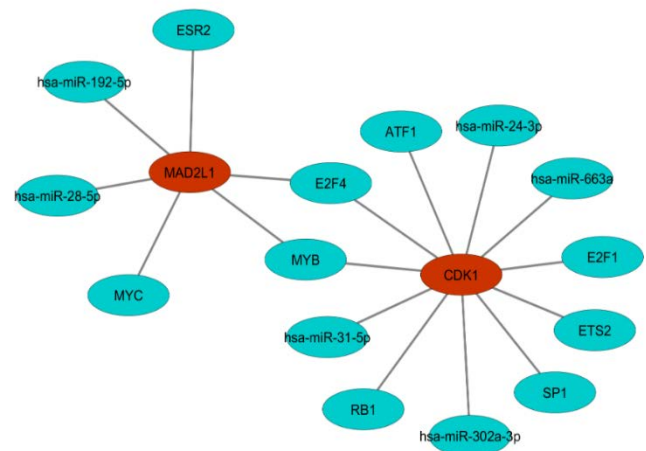


Fig. 3. Network Representing Regulation of CDK1 and MAD2L1 by miRNAs and TFs, where the Target Genes are represented in Red Color and Regulatory Elements in Blue Color.

TABLE II. INTERACTION OF GENE-MIRNA (SEED PAIRING) AND GENE-MIRNA-COOPERATIVE MIRNA (TRIPLEX)

Gene	Regulatory Element (miRNA)	Binding Free Energy (Kcal/mol)	Triplex Form-ation (cooperative miRNA)	Binding Free Energy of Triplex (Kcal/mol)	Nature of Complementarity (Self/Duplex/Triplex)
MAD2L1	hsa-miR-28-5p	-92.58	hsa-miR-203	-28.86	Canonical Triplex
CDK1	hsa-miR-31-5p	-34.33	hsa-miR-543	-33.36	Canonical Triplex
			hsa-miR-181a	-32.96	miRNA Self Complementarity
			hsa-miR-181b	-31.96	Canonical Triplex
			hsa-miR-181c	-31.76	miRNA Self Complementarity
			hsa-miR-146a	-31.16	Canonical Triplex
			hsa-miR-146b	-31.16	Canonical Triplex
			hsa-miR-494	-30.76	miRNA Self Complementarity
			hsa-miR-181d	-30.56	target self complementarity
			hsa-miR-329	-29.26	miRNA self-complementarity
			hsa-miR-362-3p	-28.16	miRNA self-complementarity

E. Analysis of miRNA-Mediated Mechanisms of Translation Repression and Gene Regulation via Transcription Factors

The gene MAD2L1 was regulated by transcription factors E2F4, ESR2, MYB and MYC and repressed by hsa-miR-192-5p and hsa-miR-28-5p. Similarly, the regulation of the gene CDK1 is a combination of activation by transcription factors RB1, SP1, ATF1, E2F1, E2F4, ETS2, MYB and repression by miRNAs hsa-miR-31-5p, hsa-miR-63a, hsa-miR-24-3p and hsa-miR-302a-3p. However, it was observed that the binding free energy of MAD2L1-hsa-miR-28-5p is less than CDK1-hsa-miR-31-5p (Table II). Therefore, the stability of MAD2L1-hsa-miR-28-5p was more than CDK1-hsa-miR-31-5p. Therefore, MAD2L1-hsa-miR-28-5p was taken forward for further understanding its role in driving the regulatory pathogenesis of Invasive Ductal and Invasive Lobular Breast Carcinoma.

F. Analytical Modeling of Gene Regulation to Understand the Regulatory Pathogenesis of Breast Cancer

In the mathematical modeling of the miRNA mediated transcriptional regulatory network which was associated with the pathogenesis of breast cancer, the involved factors are (i) gene: MAD2L1, miRNA: hsa-miR-28-5p, hsa-miR-203 and TFs: E2F4, ESR2, MYB and MYC. Hence, the regulatory pathogenesis of Breast cancer is initiated by the regulation of the gene: MAD2L1, activated by the TFs: E2F4, ESR2, MYB and MYC and repressed by the miRNAs: miRNA: hsa-miR-28-5p with the cooperation of hsa-miR-203. Since the cooperative miRNA, hsa-miR-203 act as a catalyst in driving the pathogenesis, the core miRNA hsa-miR-28-5p is preferred in the modeling and the ordinary differential equation of the mathematical model that initiates the regulatory pathogenesis in Breast Cancer is illustrated as:

$$[d(\text{MAD2L1}) / dt = k (\text{Synthesis of E2F4, ESR2, MYB and MYC}) + \text{MAD2L1} + k (\text{Up-regulation of E2F4, ESR2, MYB and MYC}) (\text{hsa-miR-28-5p}) - k (\text{Degradation of E2F4, ESR2, MYB and MYC}) (\text{E2F4, ESR2, MYB and MYC})]$$

where k represents the rate of synthesis/degradation of TFs.

Additionally, the mRNA binding sites of the corresponding miRNA hsa-miR-28-5p and hsa-miR-203a of

breast cancer-associated gene MAD2L1 were obtained by gene-miRNA mapping pair. The binding sites are shown in Fig. 4. We found that hsa-miR-28-5p has one binding site on MAD2L1 while ha-miR-203a has two binding sites on MAD2L1. For hsa-miR-192-5p, there was no binding site found on MAD2L1.

G. mRNA-miRNA-TF Regulatory Analysis through Feed-Forward Loops

Although no specific protocol has been studied for the mechanism of miRNAs, comparative studies have identified that genes regulated by miRNAs might have considerable contribution in cellular processes [25]. The available experimental shreds of evidence justify the regulation of genes due to miRNA through translational repression with or without mRNA decay. However, the variation in these contributions over time remains undefined which is also went unnoticed in case of TFs [26]. Therefore, we design a transcription network utilizing one of the most significant motifs i.e. Feed Forward Loop (FFL) motif [27]. In this study, the FFL is composed of a transcription factor (E2F4, ESR2, MYB, MYC) which regulates other or the miRNA (hsa-miR-28-5p), then TFs and miRNA both bind at the regulatory region of the target gene (MAD2L1) and jointly modulate its transcription rate. This FFL collectively has three transcription interactions, which could be either activation or repression. A recent computational analysis demonstrated that FFL, containing TF and miRNAs, are overrepresented in gene regulatory networks, assuming that they confer useful regulatory opportunities [28].

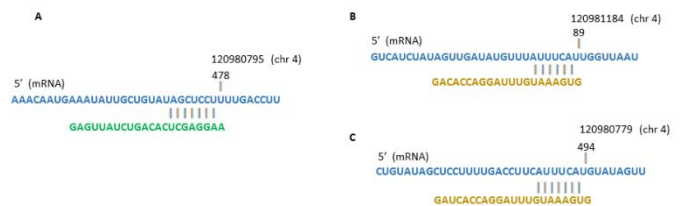


Fig. 4. Target Binding Site of miRNA (A) hsa-miR-28-5p and (B) hsa-miR-203a with MALD21.

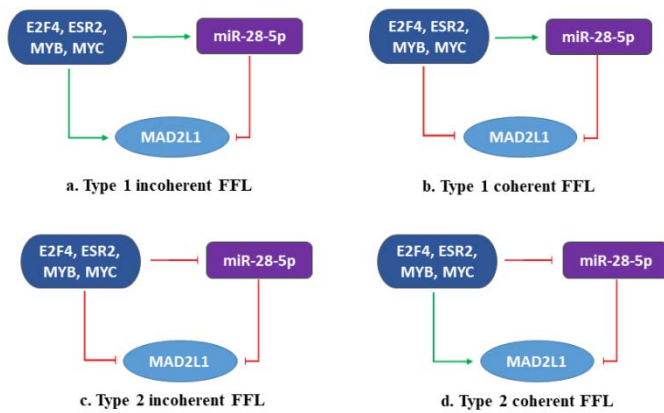


Fig. 5. The Incoherent and Coherent Feed forward Loops between the Target Gene and its Regulatory Factors is Represented; where Arrows (Green) Indicate Activation, the T-bars Indicate Repression. The Dark Blue Shape with Circular Ends Represent Transcription Factors.

The FFL has two possible structure configurations in both coherent and incoherent FFL specified as type 1 or 2 coherent FFLs and type 1 or 2 incoherent FFLs respectively as shown in Fig. 5(a, b, c, d) where miR-28-5p is miRNA and MAD2L1 is the target protein. In 5(a) represents Type 1 incoherent FFL where TF activates both target mRNA and miRNA synthesis. 5(b) Type 1 coherent FFL, miRNA and TF represses target mRNA but activates miRNA synthesis. 5(c) Type 2 incoherent FFL, TF represses both target mRNA and miRNA synthesis. 5(d) Type 2 coherent FFL, TF activates target mRNA and represses miRNA synthesis. Additionally, we emphasize that this study is carried out utilizing secondary data repositories which encompass a limited number of genes/miRNAs; hence these may provide bounded results. In this study, we performed a comprehensive analysis using various bioinformatics approaches to understand the molecular interaction between genes and miRNA and their involvement in the pathogenesis of breast cancer. The findings from this study strongly suggest that hsa-miR-28-5p might play a critical role by regulating MAD2L1 which subsequently inhibits cell cycle and p53 signaling pathway in breast cancer patients. The potential role of hsa-miR-28-5p mediating breast cancer pathogenesis on binding with MAD2L1 gene may act as a significant therapeutic target for the diagnosed subjects.

V. CONCLUSION

The systematic analysis for identification of target genes majorly contributing in the primary stage of development of invasive breast carcinoma, MAD2L1 was found to have experimentally validated miRNA and transcription factor targets from multiple databases. The regulation of MAD2L1 is a combination of activation by transcription factors E2F4, ESR2, MYB and MYC and repression by hsa-miR-28-5p and hsa-miR-192-5p. In case of seed pairing, MAD2L1-hsa-miR-28-5p forms a complementarily pairing with a binding free energy of -92.58 Kcal/mol and a canonical triplex MAD2L1-hsa-miR-28-5p-hsa-miR-203. Since, the binding free energy of MAD2L1-hsa-miR-28-5p seed pairing is 3-folds lesser than CDK1, the stability of MAD2L1-hsa-miR-28-5p will be much greater than CDK1-hsa-miR-31-5p. Therefore, the mRNA-miRNA-TF complex MAD2L1 - hsa-miR-28-5p and

associated transcription factors: E2F4, ESR2, MYB and MYC might play a vital target in driving the regulatory pathogenesis of breast cancer. The regulatory pathogenesis of breast cancer is initiated by the regulation of the gene: MAD2L1, which is activated by the TFs: E2F4, ESR2, MYB and MYC and repressed by the miRNA: hsa-miR-28-5p with the cooperation of miRNA: hsa-miR-203. Since the cooperative miRNA hsa-miR-203 act as a catalyst in driving the pathogenesis, the mathematical model that initiates the regulatory pathogenesis in Breast Cancer is illustrated as:

$$[d(\text{MAD2L1})/dt = k(\text{Synthesis of E2F4, ESR2, MYB and MYC}) + \text{MAD2L1} + k(\text{Up regulation of E2F4, ESR2, MYB and MYC})(\text{hsa-miR-28-5p}) - k(\text{Degradation of E2F4, ESR2, MYB and MYC})(\text{E2F4, ESR2, MYB and MYC})]$$

Additionally, the type 1 and type 2 coherent and incoherent feed-forward loops help to determine the regulatory mechanism of TFs and miRNA associated with MAD2L1, which further need invitro validation to determine the exact conditional mechanism of these regulators in breast cancer pathogenesis.

Since limited studies have been focused on the regulatory role of MAD2L1 associated miRNAs and their impact on tumor progression in breast cancer, this study will help in understanding the pathogenesis of MAD2L1 regulation in estimating the cascade of processes associated with breast cancer initiation and progression throughout invasive ductal carcinoma and invasive lobular carcinoma. The constructed model requires simulation with experimentally determined values in a larger time scale.

REFERENCES

- [1] J. Makki, "Diversity of Breast Carcinoma: Histological Subtypes and Clinical Relevance.", *Clin Med Insights Pathol.* 2015, pp. 8:23-31.
- [2] Y. Xiao, D. Ma, M. Ruan, S. Zhao, X. Y. Liu, Y. Z. Jiang and Z. M. Shao, "Mixed invasive ductal and lobular carcinoma has distinct clinical features and predicts worse prognosis when stratified by estrogen receptor status." *Sci Rep.* 2017, pp. 7(1):10380.
- [3] Y. Feng, M. Spezia, S. Huang, C. Yuan, Z. Zeng, L. Zhang, et al., "Breast cancer development and progression: Risk factors, cancer stem cells, signaling pathways, genomics, and molecular pathogenesis." *Genes Dis.* 2018, pp. 5(2):77-106.
- [4] A. Aiderus, M. A. Black and A. K. Dunbier, "Fatty acid oxidation is associated with proliferation and prognosis in breast and other cancers." *BMC Cancer,* 2018, pp. 18(1):805.
- [5] G. Sultan, S. Zubair, I. A. Tayubi, H. U. Dahms and I. H. Madar, "Towards the early detection of ductal carcinoma (a common type of breast cancer) using biomarkers linked to the PPAR(γ) signaling pathway." *Bioinformatics,* 2019, pp. 15(11):799-805.
- [6] Z. Wang, D. Katsaros, Y. Shen, Y. Fu, E. M. Canuto, C. Benedetto, et al., "Biological and Clinical Significance of MAD2L1 and BUB1, Genes Frequently Appearing in Expression Signatures for Breast Cancer Prognosis.", *PLoS One,* 2015, pp. 10(8):e0136246.
- [7] X. F. Zhu, M. Yi, J. Hi, W. Tang, M. Y. Lu, T. Li and Z. B. Feng, "Pathological significance of MAD2L1 in breast cancer: an immunohistochemical study and meta analysis." *Int J Clin Exp Pathol.,* 2017, pp. 10(9):9190-9201.
- [8] Y. Bian, R. Kitagawa, P. K. Bansal, Y. Fujii, A. Stepanov and K. Kitagawa, "Synthetic genetic array screen identifies PP2A as a therapeutic target in Mad2-overexpressing tumors." *Proc Natl Acad Sci U S A,* 2014, pp. 111(4):1628-33.
- [9] Y. Wang, F. Wang, J. He, J. Du, H. Zhang, H. Shi, et al., "miR-30a-3p Targets MAD2L1 and Regulates Proliferation of Gastric Cancer Cells." *Onco Targets Ther.* 2019, pp. 12:11313-11324.

- [10] X. Long, Y. Shi, P. Ye, J. Guo, Q. Zhou and Y. Tang, "MicroRNA-99a Suppresses Breast Cancer Progression by Targeting FGFR3." *Front Oncol.* 2020, pp. 9:1473.
- [11] M. Kahraman, A. Röske, T. Laufer, T. Fehlmann, C. Backes, F. Kern, et al, "MicroRNA in diagnosis and therapy monitoring of early-stage triple-negative breast cancer." *Sci Rep.* 2018, pp. 8(1):11584.
- [12] M. S. Rao, T. R. Van Vleet, R. Ciurlionis, W. R. Buck, S.W. Mittelstadt, EAG, et al, "Comparison of RNA-Seq and Microarray Gene Expression Platforms for the Toxicogenomic Evaluation of Liver From Short-Term Rat Toxicity Studies." *Front Genet.* 2019, pp. 22:9:636.
- [13] L. Ma, Y. Zhang and F. Hu, "miR-28-5p inhibits the migration of breast cancer by regulating WSB2." *Int J Mol Med.* 2020, pp. 46(4):1562-1570.
- [14] J. Wan, A. A. Guo, I. Chowdhury, S. Guo, J. Hibbert, G. Wang, et al, "TRPM7 Induces Mechanistic Target of Rap1b Through the Downregulation of miR-28-5p in Glioma Proliferation and Invasion." *Front Onco.*, 2019, pp. 9:1413.
- [15] Y. Lv, H. Yang, X. Ma and G. Wu, "Strand-specific miR-28-3p and miR-28-5p have differential effects on nasopharyngeal cancer cells proliferation, apoptosis, migration and invasion." *Cancer Cell Int.* 2019, pp. 19:187.
- [16] M. Jafari and N. Ansari-Pour, "Why, When and How to Adjust Your P Values?." *Cell J.* 2019, pp. 20(4):604-607.
- [17] M. Franz, H. Rodriguez, C. Lopes, K. Zuberi, J. Montojo, G. D. Bader, et al, "GeneMANIA update 2018." *Nucleic Acids Res.* 2018, pp. 46(W1):W60-W64.
- [18] B. Snel, G. Lehmann, P. Bork and M. A. Huynen, "String: A web-server to retrieve and display the repeatedly occurring neighbourhood of a gene." *Nucleic Acids Res.*, 2000, pp. 28(18): 3442-3444.
- [19] C. H. Chin, S. H. Chen, H. H. Wu, C. W. Ho, M. T. Ko and C. Y. Lin, "cytoHubba: identifying hub objects and sub-networks from complex interactome." *BMC Syst Biol.*, 2014, pp. Suppl 4(Suppl 4):S11.
- [20] E. Y. Chen, C. M. Tan, Y. Kou, Q. Duan, Z. Wang, G. V. Meirelles, et al, "Enrichr: interactive and collaborative HTML5 gene list enrichment analysis tool." *BMC Bioinformatics.* 2013, pp. 14:128.
- [21] Y. Liao, J. Wang, E. J. Jaehnig, Z. Shi and B. Zhang, "WebGestalt 2019: gene set analysis toolkit with revamped UIs and APIs." *Nucleic Acids Research*, 2019, pp. W199-W205.
- [22] C.H. Chou, S. Shrestha, C. D. Yang, N. W. Chang, Y. L. Lin, K. W. Liao, et al, "miRTarBase update 2018: a resource for experimentally validated microRNA-target interactions." *Nucleic Acids Res.*, 2018, pp. 46(D1):D296-D302.
- [23] C. E. Vejnar, M. Blum and E. M. Zdobnov, "miRmap web: Comprehensive microRNA target prediction online." *Nucleic Acids Res.* 2013, pp. W165-8.
- [24] U. Schmitz, X. Lai, F. Winter, O. Wolkenhauer, J. Vera and S. K. Gupta, "Cooperative gene regulation by microRNA pairs and their identification using a computational workflow." *Nucleic Acids Res.* 2014, pp. 42(12):7539-52.
- [25] R. C. Friedman, K.K.H. Farh, C.B. Burge and D. P. Bartel, "Most mammalian mRNAs are conserved targets of microRNAs." *Genome Research*, 2008, pp. 19(1), 92-105.
- [26] M. A. Duk, M. G. Samsonova and A. M. Samsonov, "Dynamics of miRNA driven feed-forward loop depends upon miRNA action mechanisms." *BMC Genomics.* 2014, pp. 15 Suppl 12(Suppl 12):S9.
- [27] W. Dubitzky, O. Wolkenhauer, K. H. Cho. and H. Yokota, "Encyclopedia of Systems Biology." Springer. 2013., pp. 2367.
- [28] G. Qin, S. Mallik, R. Mitra, A. Li, P. Jia, C. M. Eischen, et al, "MicroRNA and transcription factor co-regulatory networks and subtype classification of seminoma and non-seminoma in testicular germ cell tumors." *Sci Rep.* 2020, pp. 10(1):852.

Discourse-based Opinion Mining of Customer Responses to Telecommunications Services in Saudi Arabia during the COVID-19 Crisis

Abdulfattah Omar

Department of English

College of Science & Humanities

Prince Sattam Bin Abdulaziz University, Saudi Arabia

Department of English, Faculty of Arts, Port Saud University, Egypt

Abstract—This study used opinion mining theory and the potentials of artificial intelligence to explore the opinions, sentiments, and attitudes of customers expressed on Twitter regarding the services provided by the Saudi telecommunications companies during the COVID-19 crisis. A corpus of 12,458 Twitter posts was constructed covering the period 2020–2021. For data analysis, the study adopted a discourse-based mining approach, combining vector space classification (VSC) and collocation analysis. The results indicate that most users had negative attitudes and sentiments regarding the performance of the telecommunications companies during the pandemic, as reflected in both the lexical semantic properties and discursal and thematic features of their Twitter posts. The study of collocates and the discursal properties of the data was useful in attaining a deeper understanding of the users' responses and attitudes to the performance of the telecommunications companies during the COVID-19 pandemic. It was not possible for text clustering based on the “bag of words” model alone to address the discursal features in the corpus. Opinion mining applications, especially in Arabic, thus need to integrate discourse approaches to gain a better understanding of people's opinions and attitudes regarding given issues.

Keywords—Artificial intelligence; collocate analysis; COVID-19; discourse; opinion mining; vector space clustering

I. INTRODUCTION

In recent years, millions of users all over the world have been using social media platforms and networks in an unprecedented manner as channels for expressing their views and commenting on different issues [1, 2]. In many ways, these platforms and networks have gained such legitimacy that they have become an integral part of modern life. In the face of the increasing influence of social media networks in modern societies, institutions and organizations have begun to explore people's attitudes and responses to their policies and decisions as reflected on social media networks [2, 3].

Social media networks are used extensively to express trends and ideas within society due to their potential to offer a dialogue based on equality between the individual, the elite, and the masses; thus, the elite is no longer playing its former role in shaping and mobilizing public opinion [4, 5]. Social networks have transformed and changed from being just a means of communication between individuals and groups, or

even conveying the news or commenting on it, to a means of addressing various issues and provoking reactions based on the tremendous ability to spread messages. Indeed, sometimes news is transmitted from social networking sites (Facebook, Twitter) to newspapers, satellite programs, and official media, increasing the impact and spread of these sites [6]. Modern technologies and the information revolution have provided ease of broadcasting to all at low cost, resulting in the emergence of many actors. Indeed, anyone, even those lacking knowledge, competence, and qualifications in the relevant field, can express points of view and prejudices through social media, transmitting and using images, videos, and publications [7, 8]. In this regard, in recent years there has been increasing interest among academics, politicians, and marketing agencies in the ways social media networks and platforms can be used to measure public opinion in an approach known as opinion mining [9, 10].

However, in Arab countries, including Saudi Arabia, the potential of opinion mining has not yet been fully exploited in relation to social media content. The failure to consider people's responses and sentiments concerning given issues can lead to serious problems and challenges for organizations and institutions. Thus, this study seeks to propose a reliable model of opinion mining that takes into consideration the discursal properties of social media language, as well as the unique linguistic features of Arabic. It does so through an empirical analysis exploring and identifying the opinions, sentiments, and attitudes of Saudis regarding the services provided by telecommunications companies during the COVID-19 pandemic expressed on Twitter. The study sets out to answer two major questions: What were Saudis' opinions of and responses to telecommunications services during the COVID-19 lockdown? How can discourse-based approaches be integrated in data mining studies to offer a reliable conceptual analysis of people's opinions and sentiments as expressed on social media networks and platforms? To address the research questions, the study employed a corpus of 12,458 Twitter posts covering the period 2019–2021. The rationale is that Twitter is one of the most popular social media networks in Saudi Arabia and it was the most preferred venue for Saudis to express their views during the COVID-19 lockdown.

A. Background

During the COVID-19 pandemic, there was an urgent need for reliable and effective telecommunications services that could address the increasing demand for non-traditional methods of connecting people and ensuring businesses and government agencies performed properly. The three telecommunications companies operating in the Kingdom of Saudi Arabia (STC, Mobily, and Zain) announced different initiatives to improve their performance and increase their ability to address the needs of their users and institutions throughout the Kingdom. These initiatives included incentive packages for students, internet coverage in remote areas, and free internet access for the social distancing application "Tawakalna". The telecommunications companies announced their commitment to meeting business and private demands, whether in terms of aiding the fight against the epidemic or facilitating the work of economic sectors and supporting citizens.

In education, for instance, the telecommunications companies released an initiative whereby students were given free access to the "Your Lesson" educational platform administered by the Ministry of Education. This was meant to enable students to learn remotely with the shift from face-to-face education to distance learning. Through this initiative, the telecommunications companies intended to provide support for the local community and fulfill their social responsibilities under the exceptional circumstances suddenly being experienced in the Kingdom and globally. The initiative was also a continuation of the telecommunications companies' support for the education sector in the Kingdom, given the recognition of its importance in policy and the right of all to receive an education. The "Your Lesson" platform was launched by the Ministry of Education when it suspending in-person teaching hours and switched to distance learning at the beginning of the pandemic. More than two million students enrolled in government schools, their parents, and all those in charge of the educational process could browse the platform for free, with no effect on their data usage or allowances provided by their cellular lines or home internet subscriptions.

During the COVID-19 pandemic, the Saudi Communications and Information Technology Commission (CITC) was keen to issue a set of decisions that would contribute to ensuring the safety of citizens and residents in the Kingdom, and it launched many initiatives to enable the communications and information technology sector to perform its role in facing the pandemic. The CITC developed an action plan that would assure the performance of its tasks and mitigate the effects of the pandemic. The measures included cooperation with the competent official authorities in the country to approve the import, customs release, and field inspection of shipments of communications devices, equipment, and spare parts. The extraordinary circumstances at the time highlighted the importance of the telecommunications sector and its role in empowering other sectors through the capabilities it provides. These include facilitating links between ministries, companies, institutions, and even individuals.

Despite the policies and initiatives adopted by the CITC, telecommunications companies faced a series of complex

challenges during the COVID-19 pandemic in maintaining business sustainability and continuing to serve customers who were confined to their homes in lockdown. Moreover, they had to address the pressures of hugely increased consumption as demand for internet access on mobile networks exceeded all expectations. Not only did many employees start working remotely, but also the rates of data consumption related to entertainment increased among people unable to leave their homes.

B. Theoretical Framework

Opinion mining is a field of research in natural language processing (NLP) that includes data mining, text mining, and internet mining [11]. Research in this field extends beyond computer science to business management and sociology due to its importance for business and society [11]. Its significance has become increasingly evident with the development of social media platforms such as Twitter and Facebook [12, 13]. Opinion mining is the process of analyzing data from different perspectives and discovering anomalies, patterns, and correlations in data sets that are insightful and useful for predicting outcomes that can help users make informed decisions [14, 15]. Opinion mining refers to the use of NLP, computational linguistics, and textual analysis to reveal positive, negative, or neutral sentiments and attitudes toward given issues or products through the extraction of useful patterns from textual data, and the categorization and interpretation of data using certain analytic techniques [16, 17].

The underlying principle of opinion mining is that people tend to have biased opinions, so the aim is to build a system that analyzes individuals' feelings and opinions on certain topics and to identify what they want from a product, service, or event [18]. Data analysis is thus the process of inferring, measuring, or understanding people's opinions of a product, service, or brand in the marketplace. People express their opinions by texting images, sending personal messages, and commenting, increasingly on social media networks, such as Twitter and Facebook. Companies and governments can use the data produced by social media companies to measure opinions on a particular topic or product. In this process, opinion mining can be exploited to interpret the nuances of customer reviews, financial news reports, social media, etc. [19]. Artificial intelligence has played a key role in almost all opinion mining applications [20, 21], with algorithms specifically designed for the analysis of people's opinions on social media sites.

II. LITERATURE REVIEW

In recent years, both research and industry have paid special attention to the huge amounts of data available on the internet [22, 23]. The sources of data can be user or customer ratings of specific products, posts, comments, tweets, news articles, and various types of information on web pages. With the advent of social media, people started talking more openly about their experiences with products and services online through blogs, social media stories, reviews, recommendations, reports, hashtags, comments, direct messages, news articles, and so on [24]. Such online interactions leave a digital fingerprint of an individual's

expression of the experience. Hence there arose a need to adopt NLP approaches to organize what is circulated on social media sites, and to treat it in a short time with the least effort and cost [25, 26].

From a business point of view, opinion mining has proved useful for businesses and organizations. By analyzing users' opinions through surveys or their interactions (posts or comments about a particular product) on social media sites, companies can respond to their customers' needs, and improve their services and products to suit those needs [14, 27]. The underlying principle is that by drawing on a wide range of opinions and expressions, businesses and brands can accurately capture the voice of their target audience, understand market dynamics, and even identify their market position among end users [28]. Pazos-Rangel et al. argue that opinion mining not only helps companies and businesses understand the current context of a particular topic, but also enables them to predict the future, as well as using the information contained in the texts to calculate positive/negative feedback, which is an important indicator in decision-making processes [29]. Liu considers that adopting opinion mining and sentiment analysis techniques can aid companies, enterprises, and governments in the difficult process of making sound decisions by providing information on people's opinions and experiences of the products, services, or policies concerned [14].

In business, opinion mining has been widely used in marketing, customer services, and other areas to increase revenue, improve spending, target new customers, provide the best customer service, and address customer needs through analysis of the opinions, sentiments, and attitudes of users and customers related to services and products. Bal et al. assert that opinion mining has become one of the critical success factors for the growth and survival of organizations in an era of unprecedented global competitiveness [30].

According to Zvarevashe and Olugbara, there are many examples of the successful use of opinion mining to improve the quality of products and services. Manufacturers use opinions about a product or service as a reaction to make decisions aimed at improving quality [31]. Opinion mining and sentiment analysis are used to analyze the opinions of consumers or online customers to determine the advantages and disadvantages of a product or service, and this process saves the money that would previously have been spent on gathering information by other means.

Opinion mining has been closely associated with marketing research [32, 33]. This is one of the fields that uses sentiment analysis techniques to analyze consumer trends in relation to certain products or services, and it is also used to determine the success of an advertising campaign and study "what an individual needs from products or services that are not available in the market"; thus, it is highly significant and if used in the right way economically, it will be of great benefit to businesses [34-36].

Various opinion mining methodologies and techniques have been developed based on different models, including polarity, automatic detection, and aspect-based approaches. In the polarity model, sentiments and attitudes are automatically

identified and categorized (positive, negative, neutral). In some cases that require high accuracy, the classes of polarity are expanded, encompassing very positive, positive, neutral, negative, and very negative [17, 37].

In the emotion detection model, the goal is to identify emotions, such as happiness, fear, anger, etc. Dictionaries tend to be used in this approach (listing words with their corresponding emotions), but automatic learning algorithms can also be employed [17]. Here it is worth noting that when using dictionaries, the problem of the relation between different emotions and words arises, in particular that people can express their emotions in different ways [38].

In aspect-based opinion mining applications, the goal is to extract both the entity described in the text (in this case, attributes or components of a product or service) and the sentiment expressed toward such entities [39]. According to Moghaddam, the premise is that extracted aspects and estimated ratings clearly provide detailed information for users to make decisions and for suppliers to monitor their consumers. [40].

Despite the popularity of these methodologies and models, one major problem remains. Put simply, they do not consider the context of the texts because this adds to the complexity of the models and increases the time and cost of processing [41]. This study addresses the gap in the literature by proposing an integrated opinion mining model that takes into account the contextual aspects and features of the texts under investigation.

III. METHODS, DATA AND PROCEDURES

To explore and identify the opinions, sentiments, evaluations, and attitudes of Saudis regarding telecommunications services during COVID-19 pandemic, this study is based on a corpus of 12,458 Twitter posts over the period 2020–2021. The rationale is that Twitter is one of the most popular social media networks in Saudi Arabia. Furthermore, Twitter was the most preferred venue for Saudis to express their views and sentiments during the COVID-19 lockdown. The study is confined to tweets written in Arabic. The data include posts in both Modern Standard Arabic (MSA) and Saudi spoken Arabic. The latter is not usually considered in NLP applications in Arabic as it has typically been considered a lower variety than MSA. With the emergence of social media networks, however, colloquial and spoken dialects of Arabic have become highly prevalent. It is thus appropriate to include all the Arabic varieties in Saudi Arabia to undertake a thorough classification of Saudis' responses.

Different methodologies are used for opinion mining, including rule-based methodologies and methodologies based on machine learning techniques. In rule-based methodologies, determining polarity and identifying the sentiments and attitudes of the users are based on manually defining a set of rules in which lexicons of groups of words and expressions with corresponding feelings are predefined [42]. Two strings are usually created that directly identify polarity. Positive words can include good, great, and reliable. Negative words may include bad, failed, and unreliable. The words expressing

positive feelings and the words expressing negative feelings are then counted and calculated. If the number of positive words exceeds the number of negative words, the result is a positive feeling, and vice versa; in the event of equality, the result is neutral [43].

In machine learning methodologies, no hand-written rules are developed. The premise is that opinion mining is first a clustering issue. Thus, machine learning algorithms are used for data clustering, based on no prior assumptions about the data [44]. Text clustering is the process of automatically grouping natural language texts according to an analysis of their informational content using machine learning algorithms [45]. Clustering is one of several computational systems for carrying out data mining tasks. Document clustering has proved successful in many important operations for data mining, including NLP, feature extraction, annotation, and summarization.

Text clustering underwent considerable development in the 1990s when it emerged as a subtask of information retrieval (IR) applications. The hallmark of that development was a dramatic improvement in the effectiveness of text clustering systems. The last two decades have witnessed an unprecedented revolution in the rise of mechanized solutions for organizing the vast quantity of unstructured digital documents and of powerful tools for turning an unstructured repository into a structured one [46]. The main bulk of clustering systems or approaches can best be described under the heading vector semantics (VS) or vector space clustering (VSC). Semantic structure is essential for clustering applications. The underlying principle of VSC is that it measures or computes semantic similarity between the documents to be clustered [47].

For the purposes of this study, VSC was conducted based on the lexical semantic properties of the linguistic content of the tweets. VSC is one of the most appropriate classification methods for opinion mining applications [48-50]. The steps are described in the following sub-sections.

A. Text Preprocessing

Texts are first chopped into a list of tokens representing them. This is usually done in a straightforward way, removing punctuation and non-alphabetic characters and all extraneous material. This has the effect of converting texts into what is called a “bag of words,” in which context and word order are not considered.

B. Removing Function Words

One of the main challenges with text clustering applications is the difficulty of extracting the semantics of natural language texts. This is usually due to the occurrence of irrelevant terms within documents. In text clustering, function words are classified as irrelevant. Thus, text clustering is typically based on what can be called keyword indexing. This is the selection of only index terms, or what are traditionally called content words, within documents. The main assumption in removing function or grammatical words is that they do not carry lexical significance, so it is essential to remove them. Function words are described as “noisy” and are not considered in the analysis. Hence, they are best described as

irrelevant features. The retention of such irrelevant variables or features is useless and even misleading in clustering applications.

C. Stemming

After removing the function words, stemming is carried out. Stemming can broadly be defined as the process of conflating semantically equivalent word variants into the same root by removing derivational and inflectional affixes [51]. The basic concept of stemming is that words with the same stem or root referring to the same concept must be grouped under the same form. Stemmers are thus designed to conflate together all and only those pairs of words that are semantically equivalent and share the same stem [52]. The premise is that word endings do not have essential meanings in themselves and thus their removal is useful in text clustering applications. Conflating words that have the same root into a single term improves the performance of clustering systems by reducing the size and complexity of the data in the system [45].

Various stemmers have been developed in English. These have been concerned particularly with suffixes, i.e., derivational and inflectional endings attached to words. As noted by Stageberg, derivational suffixes affect the part of speech (act, active, activate, activation) and they can be piled up [53]. That is, it is possible to add more than one suffix to one word. Inflectional suffixes, in contrast, do not change the part of speech, but indicate a grammatical function or change within the word (play → plays, cat → cats, big → bigger). Inflectional suffixes cannot pile up, the only exception being the plural followed by the possessive. The attachment of derivational and inflectional morphemes typically leads to an increase in word variant forms. According to Stageberg, derivational morphology is one of the most means of creating new words. From an IR viewpoint, this is a problem since the increase in word variant forms leads to complexity in the data in the system. As a result, word variant forms affect the effectiveness of IR systems and it is necessary to employ stemming algorithms that can reduce the size and complexity of the corpus by conflating semantically related variant forms in a common term.

English stemmers are not appropriate for Arabic due to the morphological and linguistic differences in the languages. Arabic has its own unique morphological system that is completely different from English. For the purposes of the study, the light-based stemmer (Light10) was used.

D. Data Representation

For data representation, a matrix is built including all the lexical types of the posts. A data matrix is simply a quantitative data table that summarizes the frequencies of each word within the documents, where the documents are the rows and the words or lexical types are the columns. A collection of 500 documents can be all represented in just one matrix. The matrix includes all the lexical types in the corpus after removing the function words and carrying out stemming. The lexical frequency is weighted. A matrix of this kind is called a row vector matrix and can be represented as X_{ij} , where i represent rows and j represents columns. Thus, the data matrix X_{ij} is a representation of rows (tweets in this case), and columns (lexical types).

One problem with such a matrix is variation in document length. Posts in Twitter tend to vary in length, some being long and others very short. Variation in document length can have serious consequences for the reliability of classification applications. If not addressed, there will be a negative influence, since the classification will be based on the length of documents not the lexical properties [47]. All documents need to contribute significantly and equally to the distance in VSC, so that the distances are equitable. Otherwise, the differences between very long documents will dominate the distance calculation. One way of addressing this problem is to compensate the short texts for length through a process called normalization of text length [54]. Cosine normalization is used for this purpose. In this process, all row vectors of the matrix are transformed to have unit length and are made to lie on a hypersphere of radius 1 around the origin so that all vectors are equal in length. Accordingly, variation in the lengths of documents, and correspondingly of the vectors that represent them, are no longer a factor [55]. This has the effect of representing the variables equally in the matrix.

In this study, having carried out the normalization of text length, it was clear that high dimensionality was another problem that could have a negative impact on the reliability and validity of document classification. High dimensionality of the data is challenging for automatic classification systems as it is difficult to classify documents based on their lexical semantic properties when the number of dimensions is staggeringly high [56, 57]. In the face of this problem, term frequency-inverse document frequency (TF-IDF) can be used so that the classification is based on only and all the most distinctive features or variables. In our case, the datasets were reduced to the highest 200 TF-IDF variables thought to be the most distinctive features in the corpus, as shown in Fig. 1.

Then, the posts were clustered using Euclidean distance methods to identify and explore the responses of Saudis to the services of the telecommunications companies during the pandemic. Euclidean geometry is concerned with modelling the world as it is experienced. It describes the physical world in any finite number of dimensions using a distance formula [58]. Euclidean geometry has been used virtually unchanged for 2,000 years to understand physical reality. It used to be seen as a perfect model for logical reasoning. Despite its deficiencies, Euclidean geometry is still used in a range of disciplines, including the analysis of textual data.

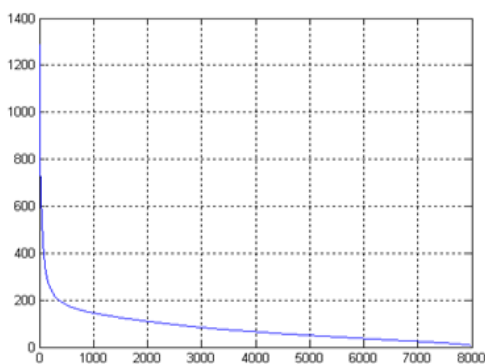


Fig. 1. Term Weighting using TF-IDF.

To overcome the limitation of machine learning algorithms in the classification process, discourse analysis methods were finally incorporated in the analysis and categorization of the data. The hypothesis here is that context is essential for understanding the polarity within the data and users' attitudes and sentiments. Failure to consider the context can result in misinterpretation of users' views.

IV. ANALYSIS AND DISCUSSION

In this study, the data matrix was first hierarchically analyzed using Euclidean distance with four clustering methods (single linkage, complete linkage, average linkage, and increase in the sum of squares), then using squared Euclidean distance with the same clustering methods. Finally, the clustering structures were compared to determine the extent to which they agreed on the data structure.

The results showed no significant difference between the Euclidean and squared Euclidean measures. For all the hierarchical cluster analyses, optimizing both functions produced almost the same order of the proximity matrix and tree. However, the Ward clustering method worked better with Euclidean distance than with squared Euclidean distance as it gave clearer results, and the groups or classes were more clearly defined. It was also apparent that all four methods agreed on the main clusters in their clustering of the matrix rows but disagreed on the detailed structure.

Single linkage clustering was not very useful in identifying meaningful clusters for this study because of the "chaining effect" feature that characterizes it. The problem with such clustering is that the texts are chained together in a way that obscures any structure beyond sequentiality. Likewise, complete linkage was not appropriate. The two complete clustering structures were uneven, producing a large number of small-membership clusters and sometimes producing a small number of large-membership clusters.

Although average linkage clustering is considered the default method in agglomerative hierarchical clustering since it overcomes the problems associated with single and complete linkages, it was not ideal in this case because of the overwhelming tendency toward left branching. One more problem with average linkage is that some classes or groups are too small to be considered distinct classes, whereas some other classes are too large to express the dataset consistently.

Thus, Ward linkage clustering (or what is usually referred to as the sum of squares) with the Euclidean distance measure seemed to be the most appropriate because it achieved the clearest partitioning of the matrix rows. Ward clustering served the purpose of the analysis, namely to discover useful associations and meaningful groups in the dataset, and thus obtain a clearer picture of the responses of the users. The study was not only concerned with identifying the yes/no or approve/disapprove dichotomy. Rather, it sought to gain a deeper understanding of the data corpus. Using the sum of squares, it was easy to identify the number of clusters (2). The matrix rows were assigned into two clearly identified classes or clusters, as shown in Fig. 2.

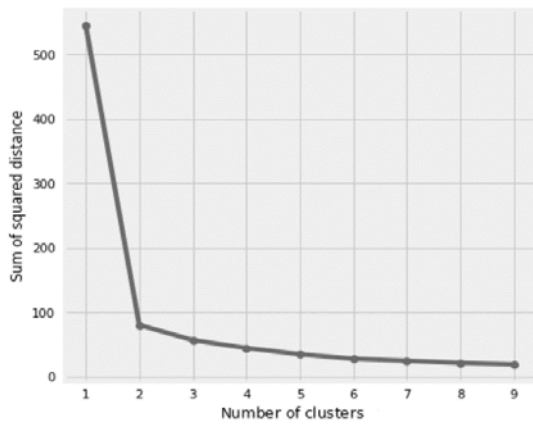


Fig. 2. Identification of the Number of Clusters.

Next, principal components analysis (PCA) was carried out. The comparisons showed a great deal of agreement in all clustering structures, supporting the validity of the results. The clustering structure most agreed on was Ward clustering with the Euclidean distance measure. The matrix rows of this structure are assigned into two groups, A and B.

A. Centroid Comparison

To measure the distance between the two clusters, centroid analysis was used, such that numerical differences between Group A and Group B specify the numerical difference between the vectors of A and B for each of the 200 variables. Based on the centroid comparison results, it is possible to determine which variables are most and least characteristic of each group, and which most differentiate them. There is too much detail here for convenient interpretation. Attention can be restricted to a smaller number of higher variance variables at the top of the tables, shown in Table I.

TABLE I. CENTROID COMPARISON

Variable index	Centroid 1 frequency Group A	Centroid 2 frequency Group B	Difference
48	2.44595E009	0.000	2.44595E009
4	2.42644E009	4.0673E006	2.42238E009
31	2.54036E009	2.79667E008	2.26069E009
65	2.91405E009	1.1363E009	1.77775E009
104	1.80511E009	6.30595E007	1.74205E009
53	4.38992E009	3.14724E009	1.24268E009
8	1.16744E009	4.12437E008	7.55E008
128	7.63672E008	9.94767E006	7.53725E008
69	9.86888E008	2.62397E008	7.2449E008
117	1.87076E009	1.15296E009	7.178E008
49	3.37362E009	2.70039E009	6.73233E008
19	1.1788E009	6.07323E008	5.71476E008
144	4.43691E008	9.60451E008	5.1676E008
5	6.67001E008	1.16991E009	5.02913E008
123	3.90971E008	8.59611E008	4.6864E008

18	0.000	3.24402E008	3.24402E008
169	8.47943E008	1.17019E009	3.2225E008
86	7.41665E008	1.04859E009	3.06928E008
98	2.92798E008	5.83877E008	2.9108E008
14	0.000	1.88799E008	1.88799E008
170	2.77724E008	4.55483E008	1.77759E008
37	2.56518E008	9.27863E007	1.63732E008
133	8.15213E007	2.43435E008	1.61914E008
109	5.88612E007	2.20095E008	1.61233E008
54	1.10216E008	2.71329E008	1.61112E008
134	1.97654E008	4.10541E007	1.56599E008
27	0.000	1.53976E008	1.53976E008
6	5.58119E007	1.64829E008	1.09017E008
89	7.12929E008	6.04511E008	1.08418E008
3	2.12619E008	1.07434E008	1.05185E008
79	0.000	9.86853E007	9.86853E007
151	1.70559E008	2.68003E008	9.74437E007
7	4.01059E007	1.33103E008	9.29971E007
184	5.98243E007	1.52622E008	9.27976E007
29	1.43507E008	2.34668E008	9.11606E007
9	1.18371E008	2.09474E008	9.11036E007
81	0.000	9.00644E007	9.00644E007
35	9.1281E007	2.32374E006	8.89573E007
2	0.000	8.86559E007	8.86559E007
147	4.71117E007	1.34375E008	8.72632E007

Based on the centroid comparison, it is clear that there are significant differences between the members of each cluster or group. A comparison of the most distinctive variables in each group reveals that the texts in Group A tend to express approval of the telecommunications and internet services, as indicated by words like good, better, free, useful, and initiative, shown in Table II.

TABLE II. DISTINCTIVE LEXICAL FEATURES OF GROUP A

Group A		
Arabic words	Transliteration	English translation
جيد	Jyid	good
أفضل	Afdil	better
مجاني	Majaani	free
مفيدة	Mufida	useful
مبادرة	Mubadara	initiative
إضافية	Iidafiatan	additional
سماح	Samah	allowance
يمكن	Yumkin	enable
حلو	Hulwa	cool
معقول	Maequl	reasonable
كويس	Kuays	well/fine

Group B, in contrast, reflects the disapproval of the users of the services provided by the companies, as indicated by words such as poor, worst, disconnected, and complaint, shown in Table III.

TABLE III. DISTINCTIVE LEXICAL FEATURES OF GROUP B

Group B		
Arabic words	Transliteration	English Translation
أسوأ	'aswa	the worst
سيئة	Sayiya	poor
عدم	Eadam	Non
شكوي	Shakwi	complaint
فصل	Fasl	disconnect
مفيش	Mufish	Nothing
بايظ	Bayiz	Down/not working
لعنة	Laena	Curse
فاشل	Fashil	loser/failure
مو	Mw	not
لا	La	no
هدر	Hadr	waste
غلا	Ghlana	expensive

Concerning the number of the tweets in each group, it is clear that most users had negative attitudes toward the services provided by the telecommunications services during the COVID-19 pandemic. The first group includes 31% of the tweets in the corpus, while the second group includes 69%. Referring to the lexical centroids, it can be claimed that the attitudes of Saudis to the services provided by the telecommunications companies during the pandemic were largely negative. Although the statistical findings of the study give broad indications about the attitudes and sentiments of the users on this issue, it is important here to look at the discourse features of the corpus to obtain a broader and more in-depth knowledge about the data. This is shown in the collocation analysis below.

B. Collocates

This section seeks to explore the distinctive discourse features of the two groups assigned through cluster analysis. For this purpose, three key words, MOBILY, ZAIN, and STC, were selected denoting the three telecommunications companies operating in Saudi Arabia. These are shown in Table IV.

TABLE IV. FREQUENCY OF KEY WORDS

KEY WORD			FREQUENCY
	موبيلي	MOBILY	1486
	زين	ZAIN	1369
	إس تي سي	STC	1199

A frequency analysis of the three key words using the KWIC concordance analysis was then carried out with the two groups, A and B, to explore the discursive and thematic features of each group.

In Group A, the three key words were associated with concepts such as shopping apps, working from home, facilitating virtual interactions, health information, access to services, social distancing, tracing apps, social connectedness, connectivity solutions, education services, and education providers, as shown in Table V.

For Group 2, the three key words MOBILY, ZAIN, and STC appeared to be associated with key concepts including service suspension, weak infrastructure, reduced network performance, congestion in mobile networks, high cost, uneconomical, high-priced, connection problems, threatened with disconnection, frustrating handling of individual complaints, remote areas, missing classes, disadvantaged neighborhoods, digital divide, poor coverage, and poor customer service. A frequency analysis of these collocates is shown in Table VI.

Based on the collocation analysis, it can be suggested that most users had negative attitudes concerning the performance of the three telecommunications companies during the pandemic. They were not happy with the high costs of the services and packages, or the connection problems that had negative implications for their commitment to classes. Many of them expressed their dissatisfaction with the companies' handling of their complaints. Others were concerned with the poor infrastructure in remote areas and disadvantaged neighborhoods. In contrast, a minority of users had positive attitudes. Referring to their tweets, they expressed their satisfaction with the services in terms of disseminating information on health, facilitating social distancing, and supporting distance learning through education platforms, and working from home. They were also happy with the initiatives and free internet services provided by the companies during the pandemic.

TABLE V. COLLOCATES IN GROUP 1

	Collocates	Frequency
تسهيل التواصل	facilitating virtual interactions	865
معلومات صحية	health information	775
الوصول إلى الخدمات	access to services	692
توافر الخدمات	availability of services	692
التواصل الاجتماعي	social connectedness	544
سرعة عالية	high speed	356
التباعد الاجتماعي	social distance	344
حلول الإتصال	connectivity solutions	311
الخدمات التعليمية	education services	289
المؤسسات التعليمية	education providers	257
التعليم الجامعي	university education	249
تطبيقات التسوق	shopping apps	199
العمل من المنزل	working from home	185
منصات التعليم	Education platforms	167

TABLE VI. COLLOCATES IN GROUP 2

	Collocates	Frequency
فصل الخدمة	service suspension	1968
بنية تحتية ضعيفة	weak infrastructure	1885
انخفاض أداء الشبكة	reduced network performance	1779
الضغط علي شبكات المحمول	congestion in mobile networks	1766
مكلفة	Costly	1693
تكلفة عالية	high-cost	1655
غير اقتصادي	Uneconomical	1588
غالي	high-priced	1579
مشاكل الإتصال	connection problems	1344
مهدة بانقطاع وفصل الخدمات	threatened with disconnection	1288
التعامل المحبط مع شكاوي العملاء	frustrating handing of individual complaints	1262
مناطق نائية	remote areas	1223
الغياب عن المحاضرات	missing classes	1175
الأحياء المحرومة	disadvantaged neighborhoods	1134
تغطية سيئة	poor coverage	988
خدمة العملاء السيئة	poor customer service	967

It can thus be argued that the study of collocates and discursive properties of the data was useful in attaining a deeper understanding of the users' responses and attitudes to the performance of the telecommunications companies during the COVID-19 pandemic. It was not possible for text clustering based on the "bag of words" model alone to address the discourse features in the corpus. Opinion mining applications, especially in Arabic, thus need to integrate discourse approaches to gain a better understanding of people's opinions and attitudes regarding given issues. Arabic is one of the most widely used languages on the internet, but it has not received sufficient attention in such applications compared to other languages, particularly English. The reason for this is that it has a complex linguistic structure and its own linguistic nature, and the availability of linguistic resources on Arabic is limited mainly to dictionaries and grammar. This is one of the challenges facing researchers working in Arabic. The proposed method addresses some of the linguistic challenges in opinion mining applications in Arabic.

V. CONCLUSION

This study has addressed the issue of using the potential of artificial intelligence to explore the sentiments and attitudes of customers concerning the performance of the Saudi telecommunications companies during the COVID-19 pandemic. It is clear that most users had negative attitudes. The study has offered an integrated approach that combines VSC and discourse analysis tools to address the limitations traditionally associated with opinion mining applications. The integration of discourse analysis tools was useful in attaining a deeper understanding of the users' responses and attitudes. Although this study was limited to the performance of telecommunications companies in Saudi Arabia during the COVID-19 pandemic, the proposed method can be usefully applied in other opinion mining applications, especially in

Arabic, which poses many challenges for researchers due to its unique linguistic features and lack of linguistic resources. Such issues tend to have negative implications for NLP applications in Arabic, including opinion mining.

ACKNOWLEDGMENT

This project was supported by the Deanship of Scientific Research at Prince Sattam Bin Abdulaziz University under research project No. 2021/02/17636.

REFERENCES

- [1] V.-A. Briciu and A. Briciu, "Social Media and Organizational Communication," in Encyclopedia of Organizational Knowledge, Administration, and Technology: IGI Global, 2021, pp. 2609-2624.
- [2] C. T. P. Duong, "Social media. A literature review," Journal of Media Research-Revista de Studii Media, vol. 13, no. 38, pp. 112-126, 2020.
- [3] J. C. Hung, N. Y. Yen, and J. W. Chang, Frontier Computing: Theory, Technologies and Applications (FC 2019). Springer Singapore, 2020.
- [4] A. Jungherr, G. Rivero, and D. Gayo-Avello, Retooling politics: How digital media are shaping democracy. Cambridge University Press, 2020.
- [5] H. Rim, Y. Lee, and S. Yoo, "Polarized public opinion responding to corporate social advocacy: Social network analysis of boycotters and advocates," Public relations review, vol. 46, no. 2, p. 101869, 2020.
- [6] H. Wimmen and M. Asseburg, Dynamics of Transformation, Elite Change and New Social Mobilization: Egypt, Libya, Tunisia and Yemen. London; New York: Routledge, 2018.
- [7] J.-C. Plantin and A. Punathambekar, "Digital media infrastructures: pipes, platforms, and politics," Media, culture & society, vol. 41, no. 2, pp. 163-174, 2019.
- [8] Y. Zhang, F. Chen, and K. Rohe, "Social Media Public Opinion as Flocks in a Murmuration: Conceptualizing and Measuring Opinion Expression on Social Media," Journal of Computer-Mediated Communication, vol. 27, no. 1, p. zmb021, 2022.
- [9] B. Bandgar, Social Networks and their Opinion Mining. GRIN Verlag, 2020.
- [10] B. Leventhal, Predictive Analytics for Marketers: Using Data Mining for Business Advantage. Kogan Page, 2018.
- [11] S. Bhatia, P. Chaudhary, and N. Dey, Opinion Mining in Information Retrieval. Springer Singapore, 2020.
- [12] F. A. Pozzi, E. Fersini, E. Messina, and B. Liu, Sentiment Analysis in Social Networks. London; New York: Morgan Kaufmann, 2017.
- [13] R. Zafarani, M. A. Abbasi, and H. Liu, Social Media Mining: An Introduction. Cambridge: Cambridge University Press, 2014.
- [14] B. Liu, Sentiment Analysis and Opinion Mining. San Rafael, California: Morgan & Claypool, 2012.
- [15] B. Liu, Sentiment Analysis: Mining Opinions, Sentiments, and Emotions. New York: Cambridge University Press, 2020.
- [16] B. Pang and L. Lee, Opinion Mining and Sentiment Analysis. Delft, the Netherlands: Now Publishers, 2008.
- [17] E. Cambria, D. Das, S. Bandyopadhyay, and A. Feraco, A Practical Guide to Sentiment Analysis. Springer International Publishing, 2017.
- [18] C. A. Iglesias and A. Moreno, Sentiment Analysis for Social Media. Basel, Switzerland: Multidisciplinary Digital Publishing Institute (MDPI), 2020.
- [19] B. Agarwal, R. Nayak, N. Mittal, and S. Patnaik, Deep Learning-Based Approaches for Sentiment Analysis. Springer Singapore, 2020.
- [20] D. Binu and B. R. Rajakumar, Artificial Intelligence in Data Mining: Theories and Applications. Elsevier Science, 2021.
- [21] F. Hemmatian and M. K. Sohrabi, "A survey on classification techniques for opinion mining and sentiment analysis," Artificial intelligence review, vol. 52, no. 3, pp. 1495-1545, 2019.
- [22] U. Sivarajah, M. M. Kamal, Z. Irani, and V. Weerakkody, "Critical analysis of Big Data challenges and analytical methods," Journal of Business Research, vol. 70, pp. 263-286, 2017/01/01/ 2017.

- [23] D. R. Anderson, D. J. Sweeney, T. A. Williams, J. D. Camm, and J. J. Cochran, *Essentials of Statistics for Business and Economics*. Cengage Learning, 2017.
- [24] R. T. Herschel, *Principles and Applications of Business Intelligence Research*. Business Science Reference, 2012.
- [25] J. Berg, M. Furrer, E. Harmon, U. Rani, and M. S. Silberman, *Digital Labour Platforms and the Future of Work: Towards Decent Work in the Online World*. International Labour Office, 2018.
- [26] C. J. Plume, Y. K. Dwivedi, and E. L. Slade, *Social Media in the Marketing Context: A State of the Art Analysis and Future Directions*. Elsevier Science, 2016.
- [27] S. K. Trivedi, S. Dey, A. Kumar, and T. K. Panda, *Handbook of Research on Advanced Data Mining Techniques and Applications for Business Intelligence*. IGI Global, 2017.
- [28] L. Botha, *Utilizing Social Media to the Benefit of Companies*. North-West University, Potchefstroom Campus, 2017.
- [29] R. A. Pazos-Rangel, R. Florencia-Juarez, M. A. Paredes-Valverde, and G. Rivera, *Handbook of Research on Natural Language Processing and Smart Service Systems*. IGI Global, 2020.
- [30] M. Bal, Y. Bal, and A. Demirhan, "Creating Competitive Advantage by Using Data Mining Technique as an Innovative Method for Decision Making Process in Business," *IJOM*, vol. 1, pp. 38-45, 07/01 2011.
- [31] K. Zvarevashe and O. O. Olugbara, "A framework for sentiment analysis with opinion mining of hotel reviews," in 2018 Conference on information communications technology and society (ICTAS), 2018, pp. 1-4: IEEE.
- [32] P. Sánchez-Núñez, M. J. Cobo, C. De Las Heras-Pedrosa, J. I. Peláez, and E. Herrera-Viedma, "Opinion mining, sentiment analysis and emotion understanding in advertising: a bibliometric analysis," *IEEE Access*, vol. 8, pp. 134563-134576, 2020.
- [33] G. S. Linoff and M. J. A. Berry, *Data Mining Techniques: For Marketing, Sales, and Customer Relationship Management*. Wiley, 2011.
- [34] J. Jacobson, A. Gruzd, and Á. Hernández-García, "Social media marketing: Who is watching the watchers?," *Journal of Retailing and Consumer Services*, vol. 53, p. 101774, 2020.
- [35] V.-D. Păvăloaia, E.-M. Teodor, D. Fotache, and M. Danileț, "Opinion mining on social media data: sentiment analysis of user preferences," *Sustainability*, vol. 11, no. 16, p. 4459, 2019.
- [36] S. Chiu and D. Tavella, *Data Mining and Market Intelligence for Optimal Marketing Returns*. London; New York: Routledge, 2008.
- [37] S. Poria, A. Hussain, and E. Cambria, *Multimodal Sentiment Analysis*. Springer International Publishing, 2018.
- [38] B. Liu, *Opinions, Sentiment, and Emotion in Text*. Cambridge University Press, 2015.
- [39] A. Secareanu, J. Schneider, and B. Schenk, *Aspect-based Opinion Mining from Online Customer Reviews Using Word Embeddings*. Universität Liechtenstein, Information Systems, 2017.
- [40] S. A. Moghaddam, *Aspect-based Opinion Mining in Online Reviews*. Simon Fraser University, 2013.
- [41] A. Omar and W. Hamouda, "A Sentiment Analysis of Egypt's New Real Estate Registration Law on Facebook," *International Journal of Advanced Computer Science and Applications*, vol. 12, no. 4, pp. 656-663, 2021.
- [42] S. Poria, E. Cambria, L.-W. Ku, C. Gui, and A. Gelbukh, "A rule-based approach to aspect extraction from product reviews," in *Proceedings of the second workshop on natural language processing for social media (SocialNLP)*, 2014, pp. 28-37.
- [43] S. Ahmed and A. Danti, "Effective sentimental analysis and opinion mining of web reviews using rule based classifiers," in *Computational Intelligence in Data Mining—Volume 1: Springer*, 2016, pp. 171-179.
- [44] R. Agrawal and N. Gupta, *Extracting Knowledge From Opinion Mining*. IGI Global, 2018.
- [45] M. W. Berry, *Survey of Text Mining: Clustering, Classification, and Retrieval*. Springer New York, 2013.
- [46] W. Wu, H. Xiong, and S. Shekhar, *Clustering and Information Retrieval*. Springer US, 2013.
- [47] H. Moisl, *Cluster Analysis for Corpus Linguistics*. Berlin: De Gruyter, 2015.
- [48] F. M. Alliheibi, A. Omar, and N. Al-Horais, "Opinion Mining of Saudi Responses to COVID-19 Vaccines on Twitter " *International Journal of Advanced Computer Science and Applications*, vol. 12, no. 6, pp. 72-78, 2021.
- [49] S. Lakshmanaprabu et al., "Ranking analysis for online customer reviews of products using opinion mining with clustering," *Complexity*, vol. 2018, 2018.
- [50] M. Kang, J. Ahn, and K. Lee, "Opinion mining using ensemble text hidden Markov models for text classification," *Expert Systems with Applications*, vol. 94, pp. 218-227, 2018.
- [51] A. Omar and W. Hamouda, "The Effectiveness of Stemming in the Stylometric Authorship Attribution in Arabic," *International Journal of Advanced Computer Science and Applications*, vol. 11 no. 1, pp. 116-122, 2020.
- [52] C. D. Manning, P. Raghavan, and H. Schütze, *Introduction to Information Retrieval*. Cambridge: Cambridge University Press, 2008.
- [53] N. C. Stageberg, *An Introductory English Grammar*. . New York; London: Holt, Rinehart and Winston, 1981.
- [54] B. He, "Document Length Normalization," in *Encyclopedia of Database Systems*, L. Liu and M. T. Özsu, Eds. Boston, MA: Springer US, 2009, pp. 940-941.
- [55] H. Moisl, "Using Electronic Corpora in Historical Dialectology Research: The Problem of Document Length Variation," in *Studies in English and European Historical Dialectology*, vol. 98, M. a. L. Dossena, R, Ed. Frankfurt: Peter Lang, 2009, pp. 67-90.
- [56] C. C. Aggarwal, *Data Classification: Algorithms and Applications*. CRC Press, 2014.
- [57] A. Omar and W. Hamouda, "Document Length Variation in the Vector Space Clustering of News in Arabic: A Comparison of Methods," *International Journal of Advanced Computer Science and Applications*, vol. 11 no. 2, pp. 75-80 2020.
- [58] R. A. Johnson, *Advanced Euclidean Geometry*. Dover Publications, 2013.

AUTHORS' PROFILE



Abdulfattah Omar is an Associate Professor of English Language and Linguistics in the Department of English, College of Science & Humanities, Prince Sattam Bin Abdulaziz University (KSA). Also, he is a standing Associate Professor of English Language and Linguistics in the Department of English, Faculty of Arts, Port Said University, Egypt. Dr. Omar received his PhD degree in computational linguistics in 2010 from Newcastle University, UK. His research interests include computational linguistics, literary computing, and digital humanities.

Building Footprint Extraction in Dense Area from LiDAR Data using Mask R-CNN

Sayed A. Mohamed*, Amira S. Mahmoud, Marwa S. Moustafa, Ashraf K. Helmy, Ayman H. Nasr
Data Reception, Analysis and Receiving Station Division, National Authority for Remote
Sensing and Space Science, Cairo, Egypt

Abstract—Building footprint extraction is an essential process for various geospatial applications. The city management is entrusted with eliminating slums, which are increasing in rural areas. Compared with more traditional methods, several recent research investigations have revealed that creating footprints in dense areas is challenging and has a limited supply. Deep learning algorithms provide a significant improvement in the accuracy of the automated building footprint extraction using remote sensing data. The mask R-CNN object detection framework used to effectively extract building in dense areas sometimes fails to provide an adequate building boundary result due to urban edge intersections and unstructured buildings. Thus, we introduced a modified workflow to train ensemble of the mask R-CNN using two backbones ResNet (34, 101). Furthermore, the results were stacked to fine-grain the structure of building boundaries. The proposed workflow includes data preprocessing and deep learning, for instance, segmentation was introduced and applied to a light detecting and ranging (LiDAR) point cloud in a dense rural area. The outperformance of the proposed method produced better-regularized polygons that obtained results with an overall accuracy of 94.63%.

Keywords—Deep learning; object detection; mask R-CNN; point cloud; light detecting and ranging (LiDAR)

I. INTRODUCTION

The identification and extraction of urban footprint has become an important research topic and tool in city planning, transportation planning, urban simulation, 3D city modelling, and building change detection [1-3]. Automatic building footprint extraction is needed to meet the rising demand for precise city building outlines. LiDAR data creates digital terrain and surface models [4]. Despite the benefits of using LiDAR to extract vegetation, essential infrastructure, and hydrography, building footprint extraction is desired for estimating population, energy demand, and quality of life [5]. Several techniques have been introduced to extract building footprints using optical sensors. These techniques include image-based, LiDAR-based, and data fusion-based [6]. For instance, Image-based technique use spectral properties. Spectral ambiguities and shadow occlusions can lead to inaccurate building footprints. [7]. Nemours approaches used LiDAR intensity, echo, and geometric attributes, but fusing LiDAR and high-resolution images improves performance and robustness.

Deep learning uses multilayer neural networks in many applications [8, 9] such as: object detection [10], image classification, image denoising [11], medical image segmentation [12], image super-resolution [13-15], and depth

prediction in stereo and monocular images [16]. Recently, several researches have investigated deep learning algorithms to improve building footprint extraction [17-19] either using CNN or a fully convolutional neural network.

CNN-based object detectors are single and two-stage. Fast R-CNN, faster R-CNN [20], and mask R-CNN are widely identified as two-stage detectors. Fast R-CNN doesn't allow end-to-end training since it uses a selective search to extract region proposals, which reduces the performance. Faster R-CNN replaces Region Proposal Network (RPN) selections, allowing end-to-end training. However, multiscale and small objects are a challenge. Despite their high inference speed [21], YOLO [22], YOLOV2, YOLOV3, and Single Shot Detector SSD [23] are single-stage networks with low detection accuracy in dense and tiny objects. Building footprint extraction requires accuracy; hence a two-stage neural network is used.

Mask R-CNN combines object detection and segmentation to improve overall accuracy and detect small and multiscale objects. But the detection speed is hardly real-time.

Class imbalance is an issue in remote sensing. This occurs when one or more classes are underrepresented in a dataset [7]. Traditional learning algorithms assume a balanced training set, which leads to a bias toward the majority classes. Consequently, the built model predicts poorly since all objects are in the dominating class regardless of the feature vector value [24]. The majority class classification bias is worse for high-dimensional data when variables exceed samples. The problem of skewed class distribution caused by uneven data was ignored. Class imbalance techniques are divided into data and algorithmic techniques. Data level approaches include data sampling, random over sampling, random under sampling, and a hybrid between them and feature selection. Algorithmic approaches are cost-sensitive and hybrid/ensemble. these approaches perform better.

In imbalanced datasets, ensemble classifiers improve single classifiers by merging them. Ensemble learning algorithms improve imbalanced data classification more than data sampling strategies. Due to precision-focused ensemble construction methods, the minority class is unrecognized. Developing ensemble learning algorithms must address class imbalances. Several approaches using ensemble learning and imbalanced learning have been reported [4]. Integrating ensemble-based techniques into an imbalanced dataset reduces overfitting and improves classification accuracy.

*Corresponding Author.

This paper used an ensemble of mask R-CNNs to effectively extract the building footprint using the LiDAR dataset in dense rural areas. The dense area in Maghagha city contains a skew distribution between structure and unstructured buildings. Datasets of GIS buildings were integrated with the collected LiDAR dataset to improve the building extraction results. The main contributions are summarized as follows:

- The mask R-CNN framework was used to effectively extract building footprints in dense areas.
- Different core mask R-CNN networks were adopted to benefit from transfer learning and different strategies (data augmentation and postprocessing).
- Class imbalance was handled in building types using a weighted voting ensemble approach.

The remainder of this work is structured as follows: Section 2 provides relevant work and a summary of point cloud classification methods. Section 3 introduces the proposed LiDAR building footprint extraction method from the point cloud. Section 4 summarizes the results of several tests done to evaluate the efficiency of the proposed LiDAR classification method on real data for Maghagha area. Section 5 concluded the findings.

II. RELATED WORK

LiDAR is an effective remote sensing technology for precisely describing terrain geometry. Thus, it is a viable solution for mapping dense urban areas to support infrastructural reconstruction, maintenance, and visibility. LiDAR technology provides very precise spatial resolution and height information [25]. Many studies have outlined the benefits of applying LiDAR data in characterizing urban structures [26, 27]. LiDAR point cloud data segmentation for automatic building extraction improves building detection and surface extraction in urban scenes [28]. A point feature based on normal vector variance is presented to extract buildings from LiDAR point cloud data by merging point- and grid-based features [29]. Building footprints using LiDAR data were needed to build a dataset for the open data portal and evaluate the minimal acceptable criteria for accurate building extraction [30]. Airborne laser scanning is a good choice in urban planning because of its capacity to determine building height, mobility, and rapid data acquisition [19, 31].

Morphology utilizes a filtering window to create an identical output image. A morphological operation compares a point's value to its neighbors. Dilation and erosion are morphological procedures that extend or diminish structures. Dilation adds border points, but erosion subtracts. The image structure dictates how many points are added or removed. The structuring element is a set of coordinates that determines the performance [1, 32].

Recently, machine learning algorithms in LiDAR have been generalized. Insufficient, complicated structure and large size limit the machine learning performance. In [4], The authors presented an effective method for combining point cloud and optical data. The method extracted points and super voxel features. The TraAdaboost algorithm with multi classes was utilised to improve LiDAR-based point cloud

classification. The results demonstrated the improved classification performance compared with nonregistered LiDAR points. In [5] Integrated spectral signatures from diverse sensors into LiDAR point cloud classification utilizing multiple feature spaces using machine learning algorithms.

Furthermore, several efforts were conducted [1, 4, 5] to assess LiDAR data in building footprint extraction, varying between semiautomatic to automatic. Extracting a building footprint can be divided into three phases: isolating nonground points, segmenting building points, and extracting the building outline from the building footprint segmentation, as shown in Fig. 1.

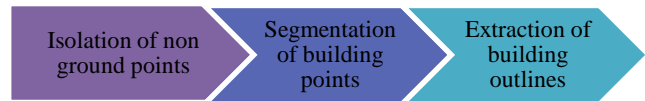


Fig. 1. Typical Building Footprint Extraction from LiDAR Data.

Different levels of filters, such as morphological filters [5, 24, 33], progressive densification [34], surface-based filters [35], and segmentation-based filtering [36], can be applied in the isolation of nonground points phase. These filtering methods work well on flat ground but poorly on undulating terrain [37]. Another common approach was to employ a nonhierarchical classification to separate land-use types. Here, point cloud intensity was used to improve classification. However, roadways and parking lots have the same intensity values as building rooftops; including them does not improve results [38].

In the segmentation phase, trees, utilities, buildings, etc. are used as nonground points. A traditional method for separating these objects uses thresholds on a digital surface model (DSM) or a normalized DSM (difference between Digital Terrain Models DTM and DSM) [39]. This isn't always successful, as trees and buildings are often comparable heights and close together [40]. Other approaches for separating trees from building points include morphological filters, texture analysis, and plane fitting [41], and hierarchical object-oriented classification [42]. Notably, the accuracy depends on study area complexity [43]. SSD is considered simple compared with other approaches that use object proposals. SSD encapsulated proposal creation and feature resampling in a single network to simplify training [23]. Mask R-CNN can distinguish the adjacent objects and extract the outline of an object [44]. Finally, an extraction technique to construct a polygon or footprint from noisy and irregular boundaries is required. Examples of most common approaches include the least squares technique [45], nonlinear least squares [46], angle histogram of boundary points [47], weighted line segmentation [5], and invariant parameters using known roof types [48]. The quality of the building footprint depends on the various factors as point density, geometry, and building density [48]. In a fully convolutional network, a Spatial Residual Inception module termed (SRI-Net) was proposed to collect and combine multiscale multilevel features. SRI-Net can detect large buildings easily while preserving global and local details [49]. Due to land-cover changes and delayed geospatial data updates, some building annotations may be missing in the ground truth building mask., thereby leading to confusion in

CNN. To address this issue, the building footprints extraction problem was formulated as a long-tailed classification. Then, a three-term joint loss function was proposed: 1) logit adjusted cross-entropy, 2) weighted dice loss, and 3) boundary alignment loss. The obtained results indicate that the proposed loss function preserves the fine-grained structure of building boundaries, effectively discriminates between building and background pixels, and increases F1-scores [50].

III. PROPOSED METHOD

An ensemble method for building footprint extraction was introduced that combines two mask R-CNNs working in tandem, followed by a postprocessing phase to enhance building footprint prediction. Two backbone architectures were adopted ResNet (101, 34). The input layer accepts images of dimensions 256×256 and 128×128 pixels, respectively. Furthermore, different augmentation approaches were adopted to enhance the results. Fig. 2 shows a graphical representation of the proposed approach.

The mask R-CNN is a versatile model used in different fields [21] and comprises two phases: region proposals generation and classification [51]. This paper adopted the mask R-CNN as the benchmark model for detecting the footprints of rural buildings in dense areas. In the following subsection, data preparation, training, and detection phases were discussed in detail.

A. Data Preparation

Six-stage workflow in extracting the building footprint was adopted a. In the first stage, DSM for the study area was generated a using LiDAR ENVI software. To automatically define the building footprint, only points designated as

buildings was filtered. The deep learning framework for the ArcGIS Pro software was incorporated in the preparation and labeling of the second stage. Thus, 150 sample buildings were chosen to serve as training data for the proposed neural network ensemble using “Label Object for Deep Learning.” In the third stage, to contain image chips and labels, the sample data were converted into training data using the “Export Training data for Deep Learning” tool. In the fourth stage, two mask R-CNN ResNet backbones (34, 101) were trained and generated models for each of them. In the fifth stage, the “Detecting Objects using Deep Learning” tool was used for testing and data inferencing. Finally, the regularization of the building footprint use was done in the sixth stage by simply removing artifacts and correcting distortions in the building footprint polygons generated using “Feature Extraction.”

B. Backbone Initialization

Image patches of size (256×256 and 128×128) were fed to ResNet-101 and ResNet-34 backbones in mask R-CNN, respectively to extract features. Table I shows a detailed description of both backbones. The residual family converges faster and achieves better training results compared with the shallow network. The image patches were fed to the backbone architecture to extract feature maps using transfer learning. These feature maps served as input for the next layer, after which the RPN was applied. This forecasts whether an object is present in that region. Here the regions obtained from RPN, which the model predicts, contain some objects and take various shapes. Hence, a pooling layer was applied to make the shape of all regions uniform. Next, these regions were fed to a fully connected network to forecast class labels and bounding boxes.

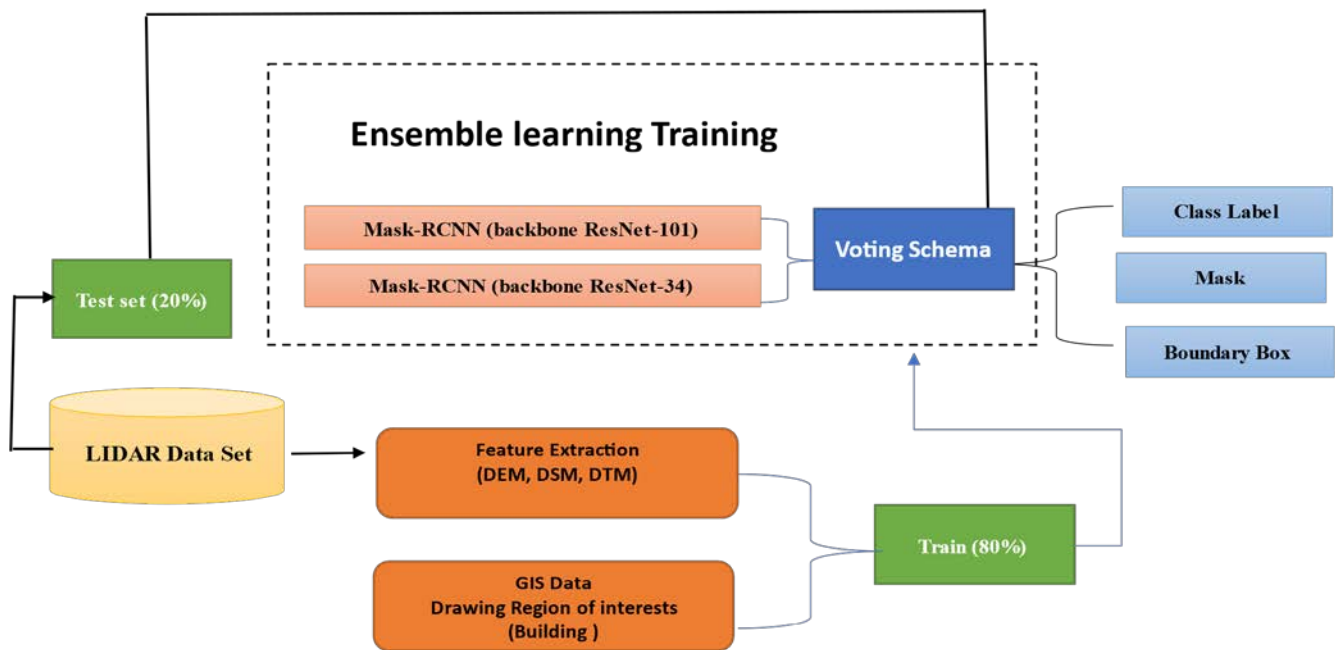


Fig. 2. Workflow of Mask R-CNN Ensemble Learning by using Two different Backbones Resnet 101 and 34.

C. The Ensemble Voting Schema

Dense urban in the Maghagha study area is considered a mix of structured and unstructured building units. However, the skew class distribution between most of the unstructured and structured buildings introduced a bias in favor of the majority class. To address this problem, a hard-weighted voting scheme of the selected models was set ranging from 0 to 1. For each roof type, each model has a class likelihood score. The scores were multiplied by the CNN weights. Then, the products for the weighting step were summed. The weights were chosen at random using the Bayesian optimization process. Finally, the output class was decided using the maximum probability index. With default parameter settings, the Bayesian optimization method was run 100 times. The weighted voting is given in Eq (1).

$$\text{weighted voting} = w_1 * \text{Model}_1 + \dots + w_n * \text{Model}_n \quad (1)$$

where n denotes the number of models and w_1 and Model_1 represent the weight and probability score of the selected Mask R-CNN model, respectively. Two models are considered in this work ($n=2$).

TABLE I. RESNET-34 AND 101 ARCHITECTURES

Layer name	Output size	ResNet-34	ResNet-101
Conv1	112 × 112	7 × 7, 64, stride 2 3 × 3 max pool, stride 2	
Conv2.X	56 × 56	$\begin{bmatrix} 3 \times 3, 64 \\ 3 \times 3, 64 \end{bmatrix} \times 3$	$\begin{bmatrix} 1 \times 1, 64 \\ 3 \times 3, 64 \\ 1 \times 1, 256 \end{bmatrix} \times 3$
Conv3.X	28 × 28	$\begin{bmatrix} 3 \times 3, 128 \\ 3 \times 3, 128 \end{bmatrix} \times 4$	$\begin{bmatrix} 1 \times 1, 128 \\ 3 \times 3, 128 \\ 1 \times 1, 512 \end{bmatrix} \times 4$
Conv4.X	14 × 14	$\begin{bmatrix} 3 \times 3, 256 \\ 3 \times 3, 256 \end{bmatrix} \times 6$	$\begin{bmatrix} 1 \times 1, 256 \\ 3 \times 3, 256 \\ 1 \times 1, 1024 \end{bmatrix} \times 23$
Conv5.X	7 × 7	$\begin{bmatrix} 3 \times 3, 512 \\ 3 \times 3, 512 \end{bmatrix} \times 3$	$\begin{bmatrix} 1 \times 1, 512 \\ 3 \times 3, 512 \\ 1 \times 1, 2048 \end{bmatrix} \times 4$
	1 × 1	Average pool, SoftMax	
FLOPs		3.6 × 10 ⁹	7.6 × 10 ⁹

IV. EXPERIMENTAL RESULTS

A. Dataset

Maghagha city is located in the north of El-Minya Governorate, Egypt. It is positioned between longitudes (30° 30': 31° E), and latitudes (28° 30': 29° N), as shown in Fig. 3, and covers an area of approximately 2,700 km² [52]. Trimble® AX60, a high-performance, adaptable, and fully integrated airborne LiDAR solution designed to fulfill most aerial survey needs were utilized. The AX60 is a complete system that provides optimum quality, operational flexibility and efficiency, and in-service reliability [53]. The dataset was acquired using an Airborne Beechcraft B200. Furthermore, another dataset of high-resolution optical data, Nikon IC65+ and 2D-RGB imagery, from the same aircraft with sensors being rigidly fixed to the same platform used. Table II shows the parameters of the system used. The collected dataset study area comprises 10 LAS files, each approximately 2.2 km in

width and 18.5 km in length. Additionally, we collected 580 TIF RGB images measuring 1.6 km in length and 1.2 km in width. Because of limited computation power, one LAS file was used to generate DSM and Digital Elevation Model DEM for the data object segmentation process. As a sample training set, only two roof types were considered: structured and unstructured, as shown in Fig. 4.

B. Evaluation Metrics

The proposed building footprint extraction workflow performance was evaluated using the overall accuracy (OA), precision, recall, and F-score. The precision computed by Eq. (2) shows the average of images that are correctly identified to the total number of structured and unstructured buildings that are correctly and non-correctly identified with the reference input.

$$\text{Precision (P)} = \frac{T_p}{T_p + F_p} \quad (2)$$

where T_p and F_p represent the true and false positives, respectively.

TABLE II. THE PARAMETERS OF THE USED SYSTEM

Trimble® AX60 System	
LiDAR point clouds	
Sensor model	Trimble AC IQ180
Laser wavelength	Near-infrared
Laser pulse repetition rate (PRR)	100–400 kHz
Scanning mechanism	Rotating polygon mirror
Scan frequency (max.)	200 Hz
Operating flight altitude	50–4700 m (164–15,500 ft) AGL
Range measurement accuracy	2 cm
Intensity capture	16-bit dynamic range for each echo
Digital aerial camera	
Model	Nikon IC 65+
Array size	80 MP
Channels	Three (RGB)
Shutter type	Electronically controlled leaf shutter
Ground sample distance	>5 cm
Calibration	Geometrically and radiometrically



Fig. 3. Location Map of the Study Area (Maghagha, El-Minya Governorate, Egypt).

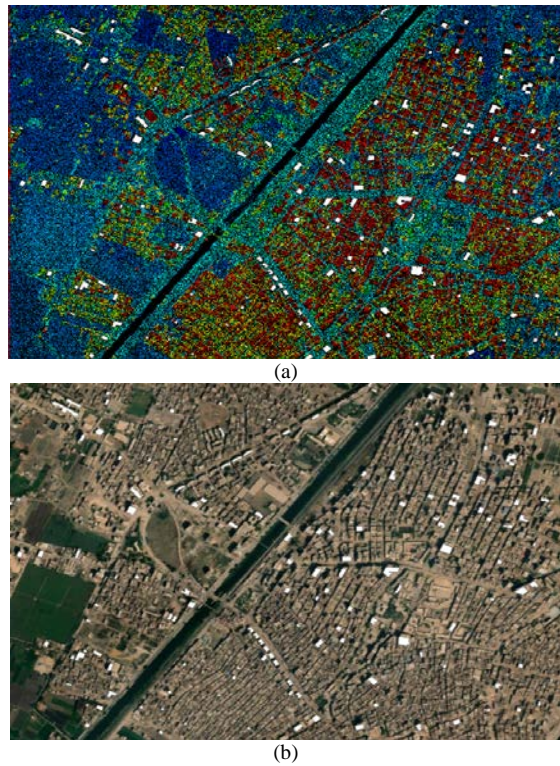


Fig. 4. Samples of Training Set Roofs, Structured and Nonstructured Covered (a) Point Clouds and (b) Very High-resolution RGB Image.

Recall, Eq. (3) defines the average number of structured and nonstructured buildings that are correctly identified of the total number of buildings that are correctly and non-correctly identified.

$$\text{Recall (R)} = \frac{T_p}{T_p + F_N} \quad (3)$$

where F_N represents the false negative.

F-score is defined in Eq. (4). If the obtained value is 1, the object detection is best and is worst when at 0.

$$\text{F-score} = \frac{2PR}{P+R} \quad (4)$$

Finally, OA represents the ratio of correctly identified structured and nonstructured buildings to the total number of buildings.

C. Experimental Setup

The suggested building footprint detection model was tested using datasets from Maghagha areas. The chosen dataset contains a mix of urban variety, including both structured and unstructured roofs. Various roofing materials, shapes, widths, and heights were used on the buildings. The LiDAR data used were collected on March 25, 2015. The system had a 30° scanning angle and a ±15° camera angle. The LiDAR data have an average point density of 7 points/m² and a point spacing of 0.38 m. Overall, the minimum and maximum elevations of the operating area were 46.83 and 90.5 m, respectively. In the working area, DSM varied from 47.15 to 104.87 m. The raw LiDAR point clouds were used to create two separate products: DEM and DSM. Furthermore, the laser

scanning equipment also captured RGB images along with the point clouds. The orthophotos collected had a spatial resolution of 20 cm.

DSM was created using Inverse Distance Weighting IDW interpolation with a spatial resolution of 0.05 m. Meanwhile, DEM was created using the multiscale curvature classification filtering algorithm in ArcGIS (MCC) [20]. This solution has several advantages, including a built-in function in ArcGIS software that simplifies the deployment and allows integration into an automated processing workflow. With a mini-batch size of 2, the models were trained with 20 epochs and a learning rate of 0.0001. All tests were run on an Intel (R) Core i7 3.40 GHz processor with an NVIDIA GeForce GTX 1080-Ti GPU. These parameters were chosen based on their experimentally high accuracy. Because of the limited computational resources, optimizing the training algorithm settings may enhance performance even further.

D. Results and Discussion

Experiments were conducted in several regions with varying numbers of buildings and roof shapes to demonstrate the detection accuracy of the framework. Fig. 5 shows the visual results. Despite the discontinuous and unclear borders in the DSM pictures, the suggested approach reliably identifies building footprints from highly populated locations. Furthermore, by overcoming the obstacles of location, form, and size, the mask R-CNN approach precisely partitioned the building footprints.

Fig. 6 shows another visual result for building footprints. From the results, the proposed method can accurately localize and segment building footprints under several settings, due to the extraction of a representative set of features by ResNet-34 and the segmentation capabilities of Mask R-CNN. Thus, the localization and segmentation ability may be slightly reduced for samples with large changes in size, particularly in dense regions. Fig. 7 shows a snapshot of results obtained from ResNet101, ResNet 34, and the proposed ensemble. One can observe the outperformance of the proposed ensemble results compared with the other two backbone architectures.

The proposed approach can precisely identify varied shapes of the building footprint with an average accuracy of 0.9463 on the dataset. Furthermore, by overcoming the differences in position, size, and shape, the suggested method can precisely segment regular and nonregular roofs. Evaluation measures (OA, precision, recall, and F-score) were applied to better understand the performance of proposed strategy. Table III shows the outcomes of the proposed approach. The results obtained show average overall accuracy, precision, recall, and F-score of 94.63%, 82%, 97.60%, and 88.46%, respectively.

TABLE III. OBTAINED ACCURACY, PRECISION, RECALL, AND F1- SCORE OF DIFFERENT BACKBONE COMPARED WITH THE PROPOSED

	OA	Precision	Recall	F-score
ResNet34	81%	32.6%	33.18%	31.4%
ResNet101	88.75%	72.19%	70.6%	71.4%
Proposed ensemble	94.63%	82%	97.60%	88.46%

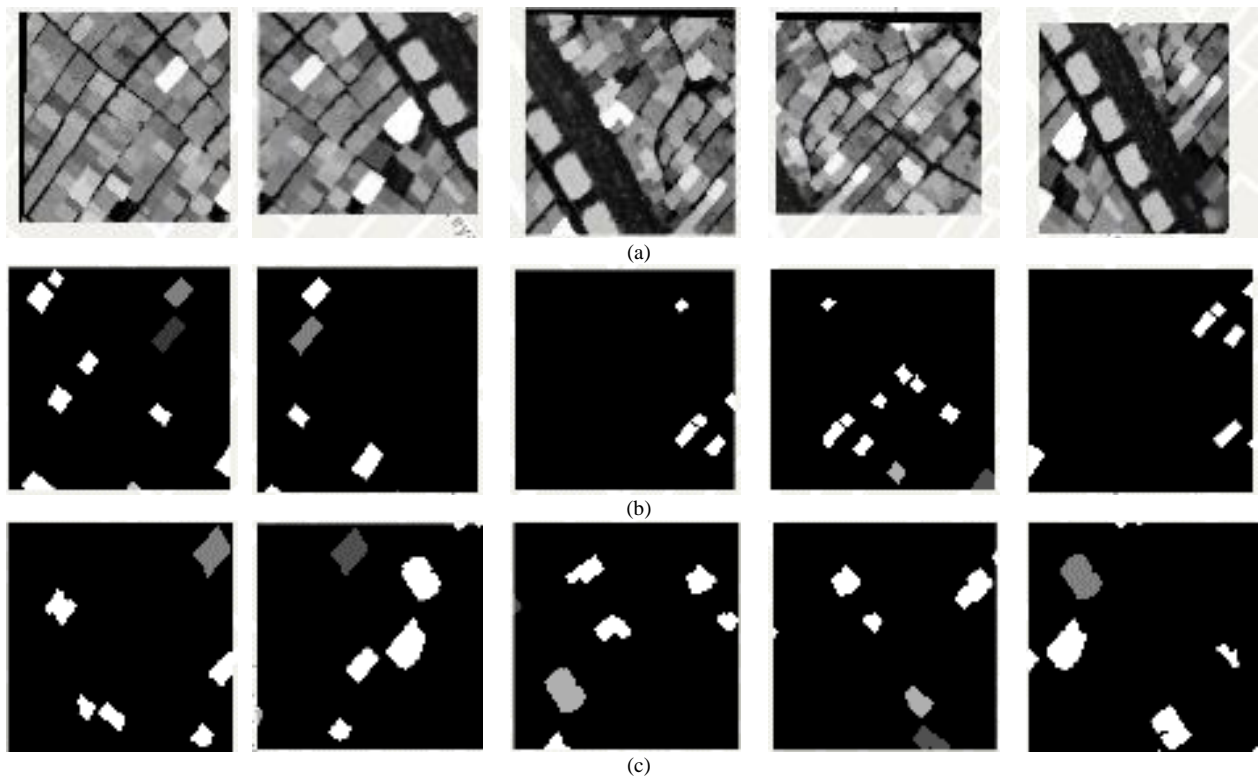


Fig. 5. Visual Results via ResNet-101 Building Footprints Extraction. (a) Input Images. (b) Ground Truth Mask Images. (c) Mask Output Images.

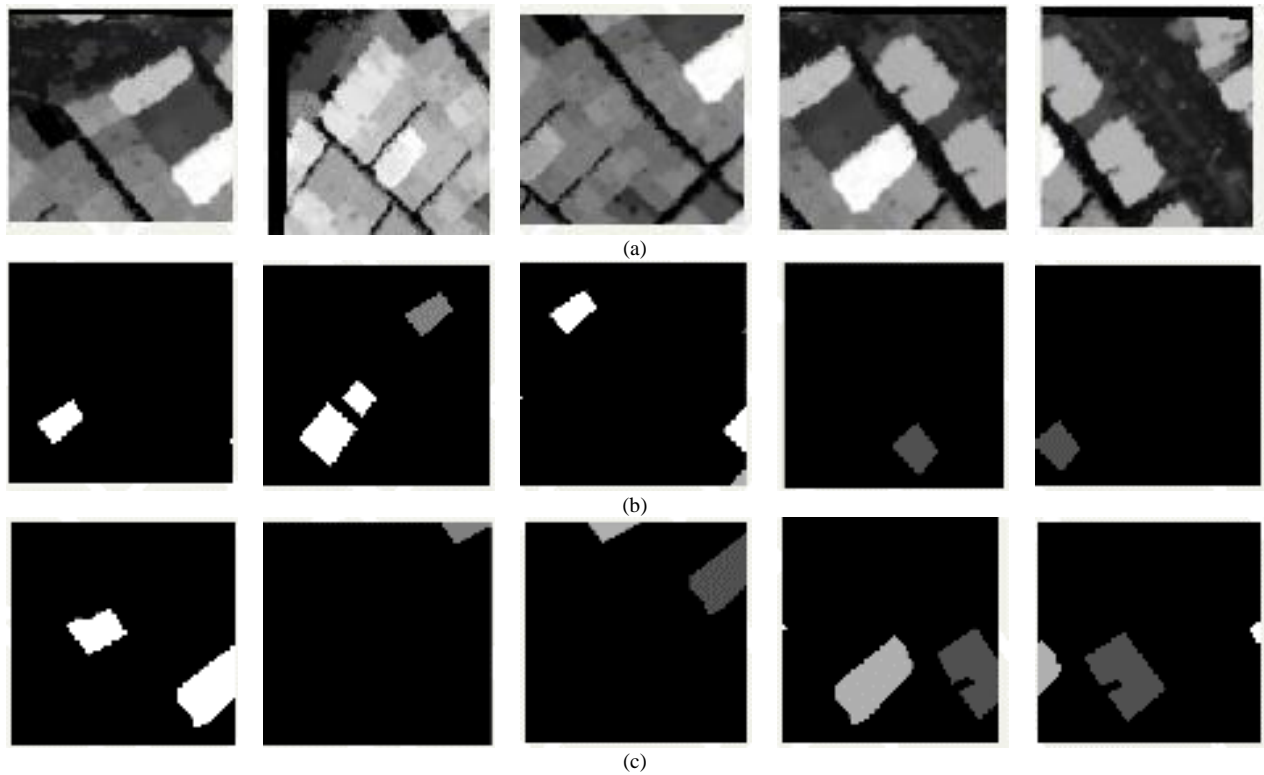


Fig. 6. Visualization Results via ResNet-34 Building Footprint Extraction. (a) Input Images. (b) Ground Truth Mask Images. (c) Mask Output.

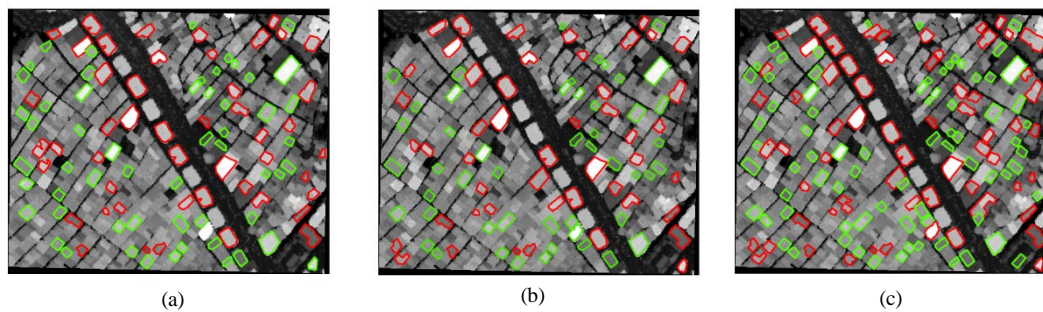


Fig. 7. Visualization Results for Building Footprint Extraction via a) ResNet-101, (b) ResNet-34, (c) Proposed Ensemble (Green and Red Colors Indicate Regular and Nonregular Roofs, Respectively).

V. CONCLUSION

Buildings are fundamental for urban planning and are essential in the development of a city. The extraction of precise building footprints from remote sensing data has been a topic of consideration. Recently, it has received much attention. Building data are useful in many geospatial applications, including urban planning, risk assessment, 3D city modeling, environmental sciences, and natural disaster damage assessment. Satellite photographs, aerial shots, radar scans, and laser scanning data can all be used to determine the footprint of a building. LiDAR provides a precise and efficient method of getting elevation data, which can be used to extract ground objects such as buildings. The ability to collect high-density point clouds quicker, great vertical precision, and low cost are all advantages of LiDAR over traditional photogrammetry. However, accurate extraction of buildings in urban dense areas with imprecise boundaries is difficult due to the presence of nearby objects. This paper proposed a building footprint extraction model tested using the LiDAR dataset. The study was chosen because the dense rural areas have a mix of urban elements, including both structured and unstructured roofs. Conclusively, the trained building footprint extraction model can detect all structured and unstructured buildings in the LiDAR data. The detected buildings could be saved as a feature layer and used for various data products to derive business value.

REFERENCES

- [1] Guo, Liang, Xingdong Deng, Yang Liu, Huagui He, Hong Lin, Guangxin Qiu, and Weijun Yang. "Extraction of dense urban buildings from photogrammetric and LiDAR point clouds." *IEEE Access* 9 2021: 111823-111832.
- [2] M. Khoshboresh-Masouleh, F. Alidoost, and H. Arefi, "Multiscale building segmentation based on deep learning for remote sensing RGB images from different sensors," *Journal of Applied Remote Sensing*, vol. 14, no. 3, 2020, p. 034503.
- [3] A. S. Mahmoud, S. A. Mohamed, M. S. Moustafa, R. A. El-Khorib, H. M. Abdelsalam, and I. A. El-Khodary, "Training Compact Change Detection Network for Remote Sensing Imagery," *IEEE Access*, vol. 9, 2021, pp. 90366-90378.
- [4] Khoshboresh-Masouleh M, Saradjian MR. Robust building footprint extraction from big multi-sensor data using deep competition network. *arXiv preprint arXiv:2011.02879*. 2020 Nov 4.
- [5] K. Zhang, J. Yan, and S.-C. Chen, "Automatic construction of building footprints from airborne LIDAR data," *IEEE Transactions on Geoscience and Remote Sensing*, vol. 44, no. 9, 2006, pp. 2523-2533.
- [6] J. Zhang and X. Lin, "Advances in fusion of optical imagery and LiDAR point cloud applied to photogrammetry and remote sensing," *International Journal of Image and Data Fusion*, vol. 8, no. 1, 2017, pp. 1-31.
- [7] K. R. Adeline, M. Chen, X. Briottet, S. Pang, and N. Paparoditis, "Shadow detection in very high spatial resolution aerial images: A comparative study," *ISPRS Journal of Photogrammetry and Remote Sensing*, vol. 80, 2013, pp. 21-38.
- [8] G. Huang, Z. Liu, L. Van Der Maaten, and K. Q. Weinberger, "Densely connected convolutional networks," in *Proceedings of the IEEE conference on computer vision and pattern recognition*, 2017, pp. 4700-4708.
- [9] Donahue, Jeff, Yangqing Jia, Oriol Vinyals, Judy Hoffman, Ning Zhang, Eric Tzeng, and Trevor Darrell. "Decaf: A deep convolutional activation feature for generic visual recognition," in *International conference on machine learning*, 2014, pp. 647-655: PMLR.
- [10] A. Mahmoud, S. Mohamed, R. El-Khoribi, and H. Abdelsalam, "Object detection using adaptive mask RCNN in optical remote sensing images," *Int. J. Intell. Eng. Syst.*, vol. 13, no. 1, 2020, pp. 65-76.
- [11] Q. Shi, X. Tang, T. Yang, R. Liu, and L. Zhang, "Hyperspectral image denoising using a 3-D attention denoising network," *IEEE Transactions on Geoscience and Remote Sensing*, vol. 59, no. 12, 2021, pp. 10348-10363.
- [12] O. Ronneberger, P. Fischer, and T. Brox, "U-net: Convolutional networks for biomedical image segmentation," in *International Conference on Medical image computing and computer-assisted intervention*, 2015, pp. 234-241: Springer.
- [13] T. Tong, G. Li, X. Liu, and Q. Gao, "Image super-resolution using dense skip connections," in *Proceedings of the IEEE international conference on computer vision*, 2017, pp. 4799-4807.
- [14] M. S. Moustafa and S. A. Sayed, "Satellite Imagery Super-Resolution Using Squeeze-and-Excitation-Based GAN," *International Journal of Aeronautical and Space Sciences*, vol. 22, no. 6, 2021, pp. 1481-1492.
- [15] S. A. Mohamed, A. S. El-Sherbeny, A. H. Nasr, and A. K. Helmy, "A New Image Super-Resolution Restoration Algorithm," *International Journal of Computer Applications*, vol. 173, 2017, pp. 5-12.
- [16] D. Eigen and R. Fergus, "Predicting depth, surface normals and semantic labels with a common multi-scale convolutional architecture," in *Proceedings of the IEEE international conference on computer vision*, 2015, pp. 2650-2658.
- [17] W. Li, C. He, J. Fang, J. Zheng, H. Fu, and L. Yu, "Semantic segmentation-based building footprint extraction using very high-resolution satellite images and multi-source GIS data," *Remote Sensing*, vol. 11, no. 4, 2019, p. 403.
- [18] J. Xing, Z. Ruixi, R. Zen, D. M. S. Arsa, I. Khalil, and S. Bressan, "Building extraction from google earth images," in *Proceedings of the 21st International Conference on Information Integration and Web-based Applications & Services*, 2019, pp. 502-511.
- [19] D. He, Q. Shi, X. Liu, Y. Zhong, and L. Zhang, "Generating 2m fine-scale urban tree cover product over 34 metropolises in China based on deep context-aware sub-pixel mapping network," *International Journal of Applied Earth Observation and Geoinformation*, vol. 106, 2022, p. 102667.
- [20] S. Ren, K. He, R. Girshick, and J. Sun, "Faster r-cnn: Towards real-time object detection with region proposal networks," *IEEE transactions on pattern analysis and machine intelligence*, vol. 39, no. 6, 2016, pp. 1137-1149.

- [21] K. He, G. Gkioxari, P. Dollár, and R. Girshick, "Mask r-cnn," in Proceedings of the IEEE international conference on computer vision, 2017, pp. 2961-2969.
- [22] J. Redmon, S. Divvala, R. Girshick, and A. Farhadi, "You only look once: Unified, real-time object detection," in Proceedings of the IEEE conference on computer vision and pattern recognition, 2016, pp. 779-788.
- [23] Liu, Wei, Dragomir Anguelov, Dumitru Erhan, Christian Szegedy, Scott Reed, Cheng-Yang Fu, and Alexander C. Berg. "Ssd: Single shot multibox detector," in European conference on computer vision, 2016, pp. 21-37: Springer.
- [24] J. Kilian, N. Haala, and M. Englich, "Capture and evaluation of airborne laser scanner data," International Archives of Photogrammetry and Remote Sensing, vol. 31, 1996, pp. 383-388.
- [25] A. Novo, N. Fariñas-Álvarez, J. Martínez-Sánchez, H. González-Jorge, and H. Lorenzo, "Automatic processing of aerial LiDAR data to detect vegetation continuity in the surroundings of roads," Remote Sensing, vol. 12, no. 10, 2020, p. 1677.
- [26] W. Y. Yan, A. Shaker, and N. El-Ashmawy, "Urban land cover classification using airborne LiDAR data: A review," Remote Sensing of Environment, vol. 158, 2015, pp. 295-310.
- [27] I. Prieto, J. L. Izkara, and E. Usobiaga, "The application of lidar data for the solar potential analysis based on urban 3D model," Remote Sensing, vol. 11, no. 20, 2019, p. 2348.
- [28] Awrangjeb, Mohammad, Guojun Lu, and C. Fraser. "Automatic building extraction from LiDAR data covering complex urban scenes." The International Archives of Photogrammetry, Remote Sensing and Spatial Information Sciences 40, no. 3, 2014, pp 25.
- [29] S. Du, Y. Zhang, Z. Zou, S. Xu, X. He, and S. Chen, "Automatic building extraction from LiDAR data fusion of point and grid-based features," ISPRS journal of photogrammetry and remote sensing, vol. 130, 2017, pp. 294-307.
- [30] J.-S. Proulx-Bourque, H. McGrath, D. Bergeron, and C. Fortin, "Extraction of Building Footprints from LiDAR: An Assessment of Classification and Point Density Requirements," in Advances in Remote Sensing for Infrastructure Monitoring: Springer, 2021, pp. 259-271.
- [31] T. Tang and L. Dai, "Accuracy test of point-based and object-based urban building feature classification and extraction applying airborne LiDAR data," Geocarto international, vol. 29, no. 7, 2014, pp. 710-730.
- [32] S. Zhang, F. Han, and S. M. Bogus, "Building Footprint and Height Information Extraction from Airborne LiDAR and Aerial Imagery," in Construction Research Congress 2020: Computer Applications, 2020, pp. 326-335: American Society of Civil Engineers Reston, VA.
- [33] K. Zhang, S.-C. Chen, D. Whitman, M.-L. Shyu, J. Yan, and C. Zhang, "A progressive morphological filter for removing nonground measurements from airborne LIDAR data," IEEE transactions on geoscience and remote sensing, vol. 41, no. 4, 2003, pp. 872-882.
- [34] J. Pérez-García, J. Delgado, J. Cardenal, C. Colomo, and M. Ureña, "Progressive densification and region growing methods for LIDAR data classification," International Archives of the Photogrammetry, Remote Sensing and Spatial Information Sciences, vol. 39, no. B3, 2012, pp. 155-160.
- [35] N. Pfeifer, S. O. Elberink, and S. Filin, "Automatic tie elements detection for laser scanner strip adjustment," International Archives of Photogrammetry and Remote Sensing, vol. 36, no. 3/W3, 2005, pp. 1682-1750.
- [36] S. Filin and N. Pfeifer, "Segmentation of airborne laser scanning data using a slope adaptive neighborhood," ISPRS journal of Photogrammetry and Remote Sensing, vol. 60, no. 2, 2006, pp. 71-80.
- [37] A. L. Montealegre, M. T. Lamelas, and J. De La Riva, "A comparison of open-source LiDAR filtering algorithms in a Mediterranean forest environment," IEEE Journal of Selected Topics in Applied Earth Observations and Remote Sensing, vol. 8, no. 8, 2015, pp. 4072-4085.
- [38] M. Ghanea, P. Moallem, and M. Momeni, "Automatic building extraction in dense urban areas through GeoEye multispectral imagery," International journal of remote sensing, vol. 35, no. 13, 2014, pp. 5094-5119.
- [39] C. Beumier and M. Idrissa, "Digital terrain models derived from digital surface model uniform regions in urban areas," International Journal of Remote Sensing, vol. 37, no. 15, 2016, pp. 3477-3493.
- [40] Q.-Y. Zhou and U. Neumann, "Complete residential urban area reconstruction from dense aerial LiDAR point clouds," Graphical Models, vol. 75, no. 3, 2013, pp. 118-125.
- [41] M. Awrangjeb and C. S. Fraser, "Automatic segmentation of raw LiDAR data for extraction of building roofs," Remote Sensing, vol. 6, no. 5, 2014, pp. 3716-3751.
- [42] M. Awrangjeb, C. S. Fraser, and G. Lu, "BUILDING CHANGE DETECTION FROM LIDAR POINT CLOUD DATA BASED ON CONNECTED COMPONENT ANALYSIS," ISPRS Annals of Photogrammetry, Remote Sensing & Spatial Information Sciences, vol. 2, 2015.
- [43] X. Liu, H. Hu, and P. Hu, "Accuracy assessment of LiDAR-derived digital elevation models based on approximation theory," Remote Sensing, vol. 7, no. 6, 2015, pp. 7062-7079.
- [44] Fang, Weili, Lieyun Ding, Peter ED Love, Hanbin Luo, Heng Li, Feniosky Pena-Mora, Botao Zhong, and Cheng Zhou. "Computer vision applications in construction safety assurance," Automation in Construction, vol. 110, 2020, p. 103013.
- [45] A. Zarea, A. Mohammadzadeh, and M. Valadanjoei, "Extraction and 3D Reconstruction of Buildings Using LiDAR Data and Aerial Image," Journal of Geomatics Science and Technology, vol. 4, no. 3, 2015, pp. 167-186.
- [46] I. Lokhat and G. Touya, "Enhancing building footprints with squaring operations," Journal of Spatial Information Science, vol. 2016, no. 13, 2016, pp. 33-60.
- [47] S. G. Salve and K. C. Jondhale, "Shape matching and object recognition using shape contexts," in 2010 3rd International Conference on Computer Science and Information Technology, vol. 9, 2010, pp. 471-474: IEEE.
- [48] H.-G. Maas and G. Vosselman, "Two algorithms for extracting building models from raw laser altimetry data," ISPRS Journal of photogrammetry and remote sensing, vol. 54, no. 2-3, 1999, pp. 153-163.
- [49] Liu, Penghua, Xiaoping Liu, Mengxi Liu, Qian Shi, Jinxing Yang, Xiaocong Xu, and Yuanying Zhang. "Building footprint extraction from high-resolution images via spatial residual inception convolutional neural network," Remote Sensing, vol. 11, no. 7, 2019, p. 830.
- [50] J. Kang, R. Fernandez-Beltran, X. Sun, J. Ni, and A. Plaza, "Deep Learning-Based Building Footprint Extraction With Missing Annotations," IEEE Geoscience and Remote Sensing Letters, 2021.
- [51] Wu, Q., Feng, D., Cao, C., Zeng, X., Feng, Z., Wu, J. and Huang, Z. "Improved Mask R-CNN for Aircraft Detection in Remote Sensing Images," Sensors, vol. 21, no. 8, 2021, p. 2618.
- [52] A. Faid and S. Mansour, "Management of Groundwater Reservoir in Maghagh Aquifer System Using Modeling and Remote Sensing Technique (Upper Egypt)," 2006.
- [53] E. van Rees, "Trimble's AX60i and AX80," GeoInformatics, vol. 17, no. 5, 2014, p. 36.

Cricket Event Recognition and Classification from Umpire Action Gestures using Convolutional Neural Network

Suvarna Nandyal¹

Department of Computer Science & Engineering
P. D. A. College of Engineering (Affiliated to Visvesvaraya
Technological University, Belagavi-590018)
Kalaburagi-585102, Karnataka, India

Suvarna Laxmikant Kattimani^{2*}

Department of Computer Science & Engineering
B.L.D.E.A's V.P.Dr.P.G.Halakatti College of Engineering
and Technology (Affiliated to Visvesvaraya Technological
University, Belagavi-590018), Vijayapur-586103
Karnataka, India

Abstract—The advancement of hardware and deep learning technologies has made it possible to apply these technologies to a variety of fields. A deep learning architecture, the Convolutional Neural Network (CNN), revolutionized the field of computer vision. One of the most popular applications of computer vision is in sports. There are different types of events in cricket, which makes it a complex game. This task introduces a new dataset called SNWOLF for detecting Umpire postures and categorizing events in cricket match. The proposed dataset will be a preliminary help, it was assessed in system development for the automatic generation of highlights from cricket sport. When it comes to cricket, the umpire has the authority to make crucial decisions about on-field incidents. The referee signals important incidents with hand signals and gestures that are one-of-a-kind. Based on detecting the referee's stance from the cricket video referee action frame, it identifies most frequently used events classification: SIX, NO BALL, WIDE, OUT, LEG BYE, and FOUR. The proposed method utilizes Convolutional Neural Networks (CNNs) architecture to extract features and classify identified frames into Umpire postures of six event classes. Here created a completely new dataset of 1040 images of Umpire Action Images containing these six events. Our method train CNNs classifier on 80% images of SNWOLF dataset and tested on 20% of remaining images. Our approach achieves an average overall accuracy of 98.20% and converges on very low cross-entropy losses. The proposed system is a influential answer for generation of cricket sport highlights.

Keywords—Cricket match; computer vision; deep learning; SNWOLF dataset; umpire recognition; umpire action images; CNN; event classification

I. INTRODUCTION

The emerging areas like Artificial intelligence (AI) and machine learning (ML) are transforming modern society. An important subset of machine learning is deep learning, which can be employed to recognize images and speech. Deep learning is rapidly being applied in sports for a variety of applications, due to the advancements in computer vision. The use of AI is ubiquitous, from helping executives match in the decision-making process to helping athletes train on physical aspects. In the last few years, advances in TV channel transmission and CCTV technology have made it possible to exploit vast volumes of data and vision in the computer

research for sporting activities is growing. CNN is a highly efficient deep learning feature extractor and classifier for detecting various details and patterns in images. Time related physical movements of the fingers, hands, arms, head, face, or torso that are expressive and significant aimed at assigning meaningful information or interacting with the environment.

In recent years, gestures have become widely used by humans to interact with computers and machines and most everyday devices such as televisions, smart phones, and car dashboards can now be controlled with simple hand gestures. Gestures of cricket sports helps the umpire to take decision, gesture recognition for event recognition, development of assistive devices for the hearing impaired, sign language recognition, patient emotional medicine that allows very young children to interact with computers. It is also used in many areas such as gesturing [1] condition or stress level, lie detection, driver attention / fatigue monitoring, etc.

Incorporating gesture recognition technology into the sport makes game play fairer and more proficient. Gestures made by sports people show what meaningful information can be derived. Gestures are intended by those who move parts of their body in a predefined way to help with specific highlights, video context labeling, and more importantly, decision making and automatic extraction of highlights. Cricket is an important sport in many countries, the second most popular sport in Asia, the fourth most popular in Europe and the second most popular sport in the world [2]. However, since the 19th century, the same old manual method has been used to update the scoreboard. This puts a lot of strain on the scoreboard. The manner of viewing the rating has modified loads in time, however the simple rating updating manner remains the equal and achieved with the aid of using a person. Therefore, in the 21st century, there is an urgent need for automated systems in this area. Automated systems are replacing many of the tedious manual tasks performed by humans five or ten years ago. Therefore, there is an urgent need to develop such a fully functional automation system. Using state-of-the-art equipment and machine learning algorithms, one can improve the accuracy of decisions and provide perfect results that are evasive to the naked eye. This has led to the design of a system that recognizes cricket referee gestures in real time. In

*Corresponding Author.

addition, the reason for choosing cricket is that there are not enough technical applications to make cricket more impartial and accurate. Therefore, cricket has become an interesting topic for deep learning researchers doing computer vision-based research to identify and recognize the referee's various postures to extract the highlights of the cricket match.

In this work there is no existing record of cricket referee behavioral gestures. Created and named own dataset- "SNWOLF"- to train and evaluate the performance of the proposed method. The dataset includes 1040 umpire action images and proposed a method which uses SNWOLF dataset for identifying the umpire event postures from umpire action images and classified into six event classes for Highlights Extraction using CNNs. Initially the Convolutional neural network classifier was pre-trained on 80% Umpire Action Event images, like SIX, NOBALL, WIDE, OUT, LEG BYE and FOUR, from SNWOLF dataset and remaining 20% Umpire Action images are tested. Our method can be noted as novel approach for state-of-the art techniques.

SNWOLF Dataset: SNWOLF is collections of Umpire Action images. We use this dataset to train CNN machine learning and computer vision algorithm. SNWOLF dataset has 1040 Umpire Action colored images. It has Six classes, and they are an SIX, NO BALL, WIDE, OUT, LEG BYE, FOUR. The images are of size 32x32 pixels. The dataset consists of 832 training and 208 testing examples. It is a database for people who want to try learning techniques and pattern recognition methods on real-world data while spending minimal efforts on preprocessing and formatting. We will use this database in our experiment.

II. RELATED WORKS

In the area of cricket activity detection, some work is being done using computer vision. For ball-by-ball cricket video classification, Dixi et al. [3] compared three separate CNN architectures. To classify each ball into distinct results, they used the VGG16-CNN framework, which had already been pre-trained for transfer learning. In a game of cricket, Batra et al. [4] suggested an automated multifaceted perceptual approach for detecting balls thrown. To extract the highlight event of the cricket match, Harry Al. [5] employed the intensity projection profile of the referee. Hari et al. [5] used the referee's intensity projection profile to extract the highlight event of the match of cricket. To recognize foot crossings, Chowdhury et al. [6] recommended using video processing technologies. Lazarescu et al. [7] categorized cricket footage in broad terms based on camera movement metrics. The batsman's motion vector was employed to detect cricket shots by Karmaker et al. [8]. Semwaletal et al. [9] used saliency and optical flow to emphasize static and dynamic cues from cricket video, and then used CNN to extract feature representations for these cues. Finally, they adopted a Support Vector Machine (SVM) [10] to categories' cricket shots premised on those characteristic representations.

There exists limited work for classification of cricket sports images to detect cricket events. It has been noticed that an approach, based on Convolutional neural networks, provides the most precise detection. Very few explorations have been conducted by experts in the of cricket event

detection. However, none of them have attempted to recognize Events – like SIX,NOBALL,WIDE,OUT,LEG BYE,FOUR - using deep learning(CNN) method. Our findings may be the basis for future research on cricket video summarization and query-oriented highlight extraction.

All the current vision systems mainly rely on deep learning approach [11] which is a part of machine learning[12] attracted many researchers and the results of applying to this technique in many fields [13], [14], [15] are becoming more encouraging. L. Y. Deng and Y. Liu [16] provides event feature manipulations at multiple levels and correctly detects interested events, video indexing with merge for what user preferences. Aravind Ravi et al.[17] used pre-trained VGG19 and Inception V3 networks for feature extraction and highest classification results are obtained using linear SVM.Rabia A. Minhas et al.[19] proposed an effective shot classification method based on AlexNet Convolutional Neural Networks (AlexNet CNN) for field sports videos and achieves the maximum accuracy of 94.07%. In [20-22] provides large scale image Net for visual recognition, umpire-signals for different activities and scene classification for video summarization. Karen Simonyan et al.[23] suggested an evaluation of networks of increasing depth using an architecture with very small (3x3) convolution filters. In deep learning, a machine models learns to perform independently, the classification tasks from images, text, or sound with almost accurate results as compared to past. The models get trained by huge labeled data templates and neural network structure with many layers.

Table I shows the Research Gaps in this. So we have carried out the work considering the current scenario of digitization of cricket sports video. In this paper umpire gestures are recognized and classified for highlights generation, video summary creation and further work is query based event retrieval from the cricket sports video at global level.

Contributions of the proposed work:

- In this work a novel deep learning framework has been designed to recognize Umpire Action Image such as SIX, NOBALL, WIDE, OUT, LEGBYE, FOUR etc which can be used for Cricket Video Highlight Summarization. It consists of 14 layers of Convolution, pooling, flattening and fully connected layer.
- A designed dataset consisting of 1040 Umpire Action Images of events like SIX, NOBALL, WIDE, OUT, LEGBYE, FOUR has been built to train and evaluate the model.
- This work mainly concentrates on calculating Feature map for each Umpire Action Image and classify it among six Umpire Event Classes- SIX, NOBALL, WIDE, OUT, LEGBYE, FOUR etc. Hence CNN has been applied to reach the acceptable accuracy of the model.
- Rigorous experimentation has been carried out to tune the model and the relationship between model accuracy and parameters is presented. 80% dataset images used for huge training set and remaining for testing to achieve model accuracy of 96.48%.

TABLE I. IDENTIFICATION OF RESEARCH GAPS AND LIMITATIONS FROM EXISTING MODEL

Sl.No.	Author	Algorithm	Merits	Research Gaps	Accuracy
1	Kalpiti Dixit et al.[3]	Single Frame Based architecture using softmax probabilities	Softmax function translates these raw scores into softmax scores which helps for classification	The model can be extended to more general problem of commentary generation	80%
2	N. Batra et al.[4]	Trajectory Approximation Algorithm	Detection of no-ball and wide ball making accurate decisions	Technique could be extended to check for faults, order of service in doubles and aces.	85%
3	M.Lazar escu et al.[7]	Incremental learning Algorithm	Camera motion parameters define the trajectory of the ball.	straight drive shot was unable to accurately classify the shot	77%
4	Md Nafee Al Islam et al.[18]	CNN model with transfer learning	Model classifies Cricket bowlers based on bowling actions	Extend our work and include bowlers from all the cricket playing nations.	93%
5	Shahid Karim et al.[24]	Inverted residual network architecture	SSD method quickly and accurately recognize the multi-gesture hands in video	Design more advanced CNN network to improve the accuracy of gesture recognition.	90%

III. PROPOSED MODEL FOR CLASSIFYING UMPIRE ACTION FRAMES

A. SNWOLF Dataset

The existing image dataset for event classification of the umpire action frame could not be found. Work accumulated pictures of Umpire completing a variety of tasks actions related to types of events as an example: “SIX”, “NO BALL”, “OUT”, “LEG BYE”, “FOUR” and “WIDE”. There are six types of data in the dataset. To train and test the model, we had to create our own dataset called "SNWOLF". Each class is made up of 174 images, and each of the six classes provides a total of 1040 images. Fig. 2 depicts some of the photographs from the dataset for each of the six types of events. From the dataset, we trained the model with 832 images and remaining 208 images were used as a validation set to achieve test accuracy.

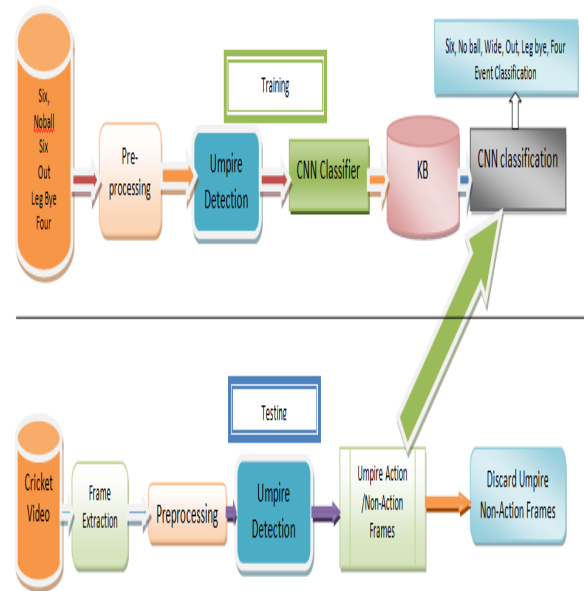


Fig. 1. System Architecture for Cricket Event Classification.



Fig. 2. An Example of a SNWOLF Dataset showing an Image of a Referee for Actions such as: “Six”, “No Ball”, “Wide”, “Out”, “Leg Bye” and “Four”.

Fig. 1 shows the proposed model is a deep learning based model which makes use of convolution neural networks. There are two phases, one is training phase and another is testing phase. During training, the model is trained on 80% of SNWOLF dataset images and knowledge base is created to test remaining Umpire Action Images for classification among six classes of events. The CNN and its layers are explained in Section subsequent sections.

B. Convolution Neural Network

CNNs (Convolutional Neural Networks) [11, 12] are a deep learning architecture that is being used to classify images [13]. Yann Le Cunetal. [14] first, introduced the idea of a Convolutional neural network that can be trained by back propagation. Jing Yu, Hang Li, Shou-Lin Yin, and Shahid Karim [24] offer a deep learning method for recognizing dynamic gestures in Human-Computer Interfaces using Transfer learning and to recognize different gestures quickly and effectively but the accuracy improvement is required in gesture recognition. Convolutional neural network's design became well-known with researchers that specialize in deep learning, with the introduction of LeNet5 in [15] and demonstrated outstanding performance in handwriting recognition and our proposed framework of Convolutional Neural Network is as shown in Fig. 3.

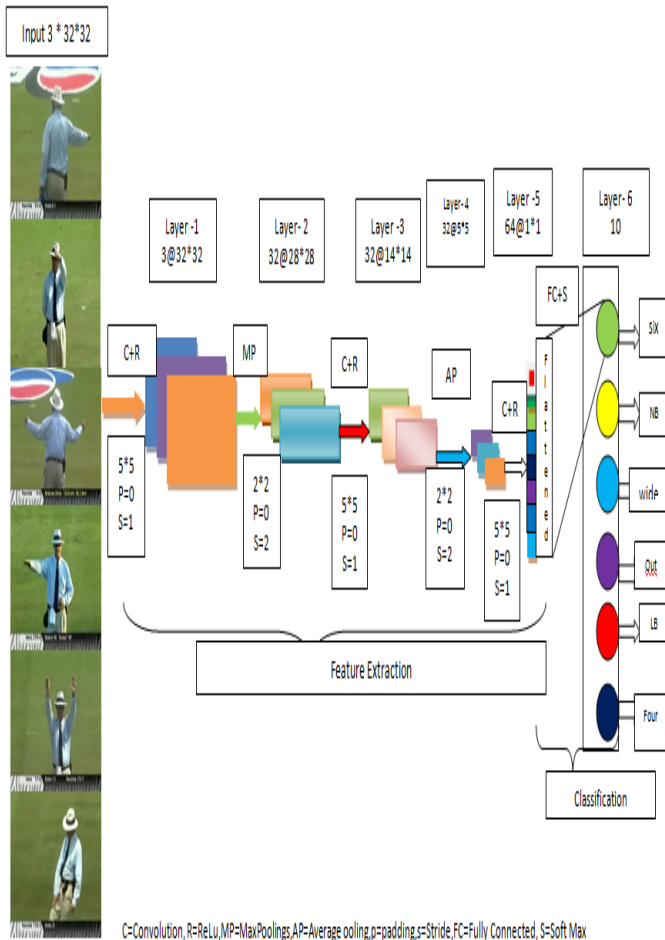


Fig. 3. Framework of Convolutional Neural Networks.

Convolutional Neural Network has four layers. They are convolution, pooling, flattening and fully connected layer. We assume a gray scale or RGB image 'I' represented by size n1 * n2 denoted by function given in Eq. (1).

$$I: \{1, \dots, n_1\} * \{1, \dots, n_2\} \rightarrow W \in \mathbb{R}, (i, j) \rightarrow I_{i,j} \quad (1)$$

Given the filter $K \in \mathbb{R}^{2h_1 + 1 * 2h_2 + 1}$, the discrete convolution of the image I with filter K is given by Eq. (2)

$$I \times K = \sum_{u=-h_1}^{h_1} \sum_{v=-h_2}^{h_2} K_{u,v} I_{r+u, s+v} \quad (2)$$

Where the filter K is given by Eq. (3).

$$K = \begin{matrix} K_{-h_1, -h_2} & \dots & K_{-h_1, h_2} \\ \dots & K_{0,0} & \dots \\ K_{h_1, -h_2} & \dots & K_{h_1, h_2} \end{matrix} \quad (3)$$

A filter which is most familiar for smoothing is the discrete Gaussian filter $K_G(\sigma)$ which is given by Eq. (4).

$$K_G(\sigma) = \frac{1}{\sqrt{2\pi\sigma^2}} \exp\left(-\frac{r^2+s^2}{2\sigma^2}\right) \quad (4)$$

Convolution Layer: The small window with width and height spatially convolves through the input volume and dot products are computed between the entries of the filter during the forward pass. Assume layer 1 be a Convolutional layer. The input to this layer constitutes m1 (I-1) feature maps from the preceding layer with m2 (I-1) * m3 (I-1) size. When I=1, image I is an input consisting of one or more mediums. This is how raw images are fed as input to the convolution neural network. The output from the layer 1 constitutes m1 (I) feature maps m2 (I) * m3 (I) sized Eq. (5) is used to compute the feature map (ith) of layer l.

$$Y_i^{(l)} = B_i^{(l)} + \sum_{j=1}^{m_1^{(l-1)}} K_{i,j}^{(l)} * Y_j^{(l-1)} \quad (5)$$

Where, B is a bias and K is the filter of size 2h1+1*2h2+1 coupling the jth activation map in layer(I-1) with the ith activation map in layer l. m2 (I) and m3 (I) are determined by border influences. If layer l is not linear, m1(I) activation maps are the inputs to it and m1(I) = m1(I-1) activation maps are the outputs, each of size m2(I) * m2(I) along with m3(I) * m3(I-1), given by Eq. (6).

$$Y_i^{(l)} = f(Y_i^{(l-1)}) \quad (6)$$

Pooling layer: Pooling is nothing but a down-sampling with non-linearity. The output of pooling is maximum value of such sub-region and reduces size of representation, memory, computation in network and controls the over fitting.

Flattening Layer: Flatten our pooled feature map into a column and insert the data into Artificial Neural Network.

Fully Connected Layer: It takes the output from several convolution and max pooling layers and performs affine transformation with matrix multiplication and bias offset to compute its activations. The output of this layer is calculated using Eq. (7).

$$Y_i^{(l)} = f(Z_i^{(l)}) \quad (7)$$

C. Model Implementation

The provided training data set was being used to train the CNN model. Initially the image features are extracted from each umpire action training images and model creates feature map- knowledge base - for testing. If the image in the frame was categorized as being one of the six classifications as : SIX, NO BALL, WIDE, OUT, LEG BYE or FOUR, then the processed frame is accumulated in one of the six classes and further used for generating the Event video summary of Cricket Sport. Algorithm 1 depicts the way in which the model is created for the purpose.

Algorithm 1 : Proposed work Model

Input: Upload dataset- SNWOLF-consisting of 80% images for training purpose

Output: trained CNN model

Begin

Step1: Data Pre-processing

Step2: Input Layer

This step reshapes the image into 3*32*32 pixels

Step3: Convolution and Pooling layers

P=32

For i = 1 to 4 do

1.Add six convolution layer with P feature maps of size 3*3 and a rectifier activation function. Also dropout layer at 20% in between these six layers

2. Add 2*2 is the greatest pool layer size and stride 3

3. P=P*2

End

Step4: Flatten Layer

It is going to flatten our pooled feature map into a column. Set dropout layer at units and a 20%

Step5: Dense layer:

Create a 512-unit completely linked layer with a rectifier activation function.

Also set dropout layer at 20%

Step6: layer output

With 50 units and a softmax activation mechanism, create a fully connected output layer.

Step7: logic layer

The final step is the prediction.

End

IV. RESULTS AND EVALUATION OF SNWOLF DATASET

After the model has been trained, we tried to achieve almost 100% performance using the validity set. Fig. 4 displays the accuracy of instruction and verification progressively improves with the range maximum iteration. Our system was able to achieve an exactness of 98.2% which demonstrates classification ability on the practice set. Fig. 5

depicts the model's confusion matrix after being put through its paces with the test set. A matrix of uncertainty was used to measure the Accuracy, Precision and Recall of each class. The model's macro was then used to determine the F1 score average of the fit rate score and the recall score. Table I provides a summary of the model evaluation.

Table II shows the summary result of the classification assessment of the model on the practice set (SNWOLF).

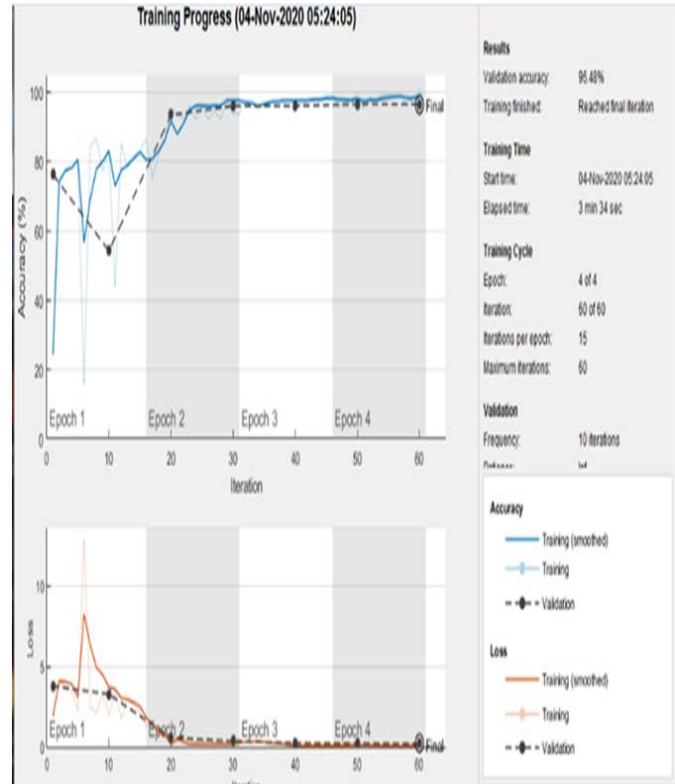


Fig. 4. Training and Validation Accuracy.

TABLE II. SUMMARY RESULT OF THE CLASSIFICATION ASSESSMENT OF THE MODEL ON THE PRACTICE SET –SNWOLF

Event Name	Accurac y for individu al event	Error rate for individu al Event	Precisi on	Reca ll	F1 scor e	Accura cy
1.Action.No Ball	83.3 %	16.7%	83	52	92%	98.20%
2.Action.Wid e	98.5%	1.5%	97	96		
3.Action.Out	97.9%	2.1%	97	99		
4.Action.Fou r	98.7%	1.3%	98	100		
5.Action.Six	100%	0%	100	100		
6.Action.Leg Bye	98.2%	1.8%	100	91		

Results of CNN Classification

		Confusion Matrix						
Output Class	01	02.1Action	02.2Action	02.3Action	02.4Action	02.5Action	02.6Action	
		114 5.1%	2 0.1%	0 0.0%	1 0.0%	8 0.4%	0 0.0%	0 0.0%
02.1Action	2 0.1%	10 0.4%	0 0.0%	0 0.0%	0 0.0%	0 0.0%	0 0.0%	83.3% 16.7%
02.2Action	2 0.1%	0 0.0%	131 5.9%	0 0.0%	0 0.0%	0 0.0%	0 0.0%	98.5% 1.5%
02.3Action	4 0.2%	0 0.0%	0 0.0%	191 8.6%	0 0.0%	0 0.0%	0 0.0%	97.9% 2.1%
02.4Action	8 0.4%	7 0.3%	5 0.2%	1 0.0%	1687 75.8%	0 0.0%	1 0.0%	98.7% 1.3%
02.5Action	0 0.0%	0 0.0%	0 0.0%	0 0.0%	0 0.0%	41 1.8%	0 0.0%	100% 0.0%
02.6Action	0 0.0%	0 0.0%	0 0.0%	0 0.0%	0 0.0%	0 0.0%	11 0.5%	100% 0.0%
	87.7% 12.3%	52.6% 47.4%	96.3% 3.7%	99.0% 1.0%	99.5% 0.5%	100% 0.0%	91.7% 8.3%	98.2% 1.8%
	01	02.1Action	02.2Action	02.3Action	02.4Action	02.5Action	02.6Action	
	Target Class							

Fig. 5. Confusion Matrix.

V. CONCLUSION AND FUTURE WORK

A CNN deep feature model is proposed in this research that can identify and classify six unique cricket EVENTS (SIX, NO BALL, WIDE, OUT, LEG-BY, FOUR) based on the Umpire Action Frame of the dataset. Using SNWOLF as a dataset, we trained the model on 80% of the images to identify and classify six events related to a cricket match between the two countries. Our model, shown in Fig. 6, test set was 98.2% accurate and the F1 score was 92.0%, which worked very well. The sample outputs of six classes Gestures are shown in Fig. 7. We intend to broaden our scope of study in the future to cover all forms of cricket competition country events where different types of cricket matches are played.

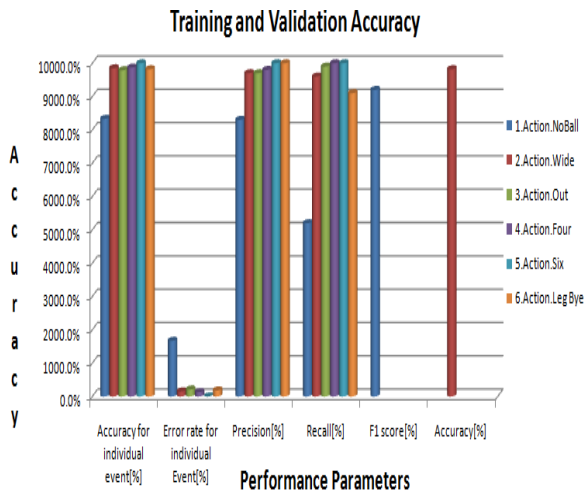


Fig. 6. Classification Model Evaluation Results on Accuracy, Error, Precision, Recall, F1 Score and Accuracy.



Fig. 7. Sample Images of Output Classes Six, No Ball, Wide, Out, Leg Bye and Four Events.

We intend to broaden our scope of study in the future for detection of other events, like Ball Catch, Baler Detection, Boundary, Third Umpire Decision, etc. will be suggested. Further covering all forms of cricket competition country events where different types of cricket matches are played. In this work open problems identified for future work are Text Tagging for events detected and Audio Annotation with Commentary.

REFERENCES

- [1] S. Mitra and T. Acharya, "Gesture recognition: A survey, IEEE Transactions on Systems, Man, and Cybernetics", Part C (Applications and Reviews), vol. 37, no. 3, pp. 311-324, 2007. DOI: 10.1109/TSMCC.2007.893280.
- [2] Top10 list of the internet world's most popular sports,http://www.topendsports.com/world/lists/popular-sport/fans.htm.
- [3] K.Dixit and A.Balakrishnan, Deep learning using CNNs for ball-by-ball outcome classification in sports, Report on the course: Convolutional Neural Networks for Visual Recognition, Stanford University, 2016.
- [4] Batra et al."an automated multi-dimensional visual system which detected no-balls bowled in a cricket match". DOI:10.1109/ICACCI.2014.6968378.
- [5] R.Hari and M.Wilsey, Event detection in cricket videos using intensity projection profile of umpire gestures, in 20/4 Annual IEEE India Conference (INDICaN). IEEE, 2014, pp.1-6. DOI: 10.1109/INDICON.2014.7030519.
- [6] A.E.Chowdhury,M.S. Rahim, and M.A.U. Rahman, Application of computer vision in cricket: Foot over step no-ball detection, in 2016 3rd International Conference on Electrical Engineering and information Communication Technology(ICEEICT). IEEE, 2016, pp.1-5. DOI: 10.1109/CEEICT.2016.7873086.
- [7] M.Lazarescu,S.Venkatesh,and G.West, Classifying and learning cricket shots using camera motion, in Australasian Joint Conference on Artificial Intelligence. Springer, 1999, pp.13-23. DOI: 10.1007/3-540-46695-9_2.
- [8] D. Karmaker, A. Chowdhury, M.Miah, M.Imran, and M.Rahman, "Cricket shot classification using motion vector", in 2015 2nd International Conference on Computing Technology and Information Management (ICCTIM). IEEE, 2015, pp.125-129. DOI: 10.1109/ICCTIM.2015.7224605.
- [9] A.Semwal,D. Mishra,V.Raj, J.Sharma, and A.Mittal, Cricket shot detection from videos, in 2018 9th International Conference on Computing, Communication and Networking Technologies(ICCCNT). IEEE,2018,pp.1-6. DOI: 10.1109/ICCCNT.2018.8494081.
- [10] C.J.Burges, A tutorial on support vector machines for pattern recognition, Data mining and knowledge discovery, vol.2,no.2,pp.121-167,1998. doi.org/10.1023/A:1009715923555.

- [11] James Wang, DEEP LEARNING: An Artificial Intelligence Revolution, A white ARK Invest, 2011, pp.1-41.
- [12] V.N.Pawar and S.N.Talbar, Machine learning approach for object recognition, International Journal of Modeling and Optimization, Vol.2, No.5, pp.622-628, October 2012. DOI:10.7763/IJMO.2012.V2.196.
- [13] Y.LeCun,K.Kavukvuoglu, and C. Farabet., Convolutional Networks and Applications in Vision. In Circuits and Systems, International Symposium on, pages 253-256, 2010. DOI: 10.1109/ISCAS.2010.5537907.
- [14] Simonyan, K., Zisserman, A.: Very deep Convolutional Networks for large-scale image recognition. arXiv:1409.1556 (2014).
- [15] He, K., Zhang, X., Ren, S., Sun, J.: Deep residual learning for image recognition. In: Proceedings of the IEEE Conference on Computer Vision and Pattern Recognition, pp. 770–778 (2016). DOI:10.1109/CVPR.2016.90.
- [16] Deng, L.Y., Liu, Y.: Semantic analysis and video event mining in sports video. In: 22nd International Conference on Advanced Information Networking and Applications-Workshops (aina workshops2008), Okinawa,pp.1517–1522(2008). <https://doi.org/10.1109/WAINA.2008.167>.
- [17] Ravi, A., Venugopal, H., Paul, S., Tizhoosh, H.R.: A Dataset and Preliminary Results for Umpire Pose Detection Using SVM Classification of Deep Features. ArXiv: 1809.06217 (2018).
- [18] Islam, M.N.A., Hassan, T.B., Khan, S.K.: A CNN-based approach to classify cricket bowlers based on their bowling actions. arXiv:1909.01228 (2019).
- [19] Minhas, R.A., Javed, A., Irtaza, A., Mahmood, M.T., Joo, Y.B.: Shot classification of field sports videos using alexnet Convolutional neural network. Appl. Sci. 9(3), 483 (2019).
- [20] Russakovsky, O., et al.: Image net large scale visual recognition challenge. Int. J. Comput. Vis. 115(3), 211–252 (2015).
- [21] Different activities in cricket. 2015, [Online].Available: <http://www.open.ac.uk/ouclub/main/six-sidecricket/umpire-signals>.
- [22] Rafiq, M., Rafiq, G., Agyeman, R., Jin, S.I., Choi, G.S.: Scene classification for sports video summarization using transfer learning, Sensors 20(6), 1702 (2020), <https://doi.org/10.3390/s20061702>.
- [23] Karen Simonyan and Andrew Zisserman, Very deep Convolutional networks for large-scale image recognition, arXiv preprint arXiv: 1409.1556, 2014.
- [24] Jing Yu, Hang Li, Shou-Lin Yin and Shahid Karim :Dynamic Gesture Recognition Based on Deep Learning in Human-to-Computer Interfaces, 2020 - Volume 23 Volume 23, Issue 1 01 March 2020 Reach: 769 ,DOI.org/10.6180/jase.202003_23(1).0004.

Optimization Performance Analysis for Adaptive Genetic Algorithm with Nonlinear Probabilities

Wenjuan Sun¹

College of Information Engineering
Chaohu University
HeFei, China

Qiaoping Su²

School of Intelligent Manufacturing
Anhui Xinhua University
HeFei, China

Hongli Yuan³, Yan Chen⁴

School of Big Data and Artificial
Intelligence, Anhui Xinhua
University, HeFei, China

Abstract—Genetic Algorithm (GA) has been proven to be easy in falling into local optimal value due to its fixed crossover probability and mutation probability, while Adaptive Genetic Algorithm (AGA) has strong global search capability because the two probabilities adjust adaptively. There are two categories of AGA according to the different adjustment methods for crossover and mutation probabilities: probabilistic linear adjustment AGA and probabilistic non-linear adjustment AGA. AGA with linear adjustment of probability values cannot solve the problems of local optimal value and premature convergence. The nonlinear adaptive probability adjustment strategy can avoid premature convergence, poor stability and slow convergence speed. The typical AGA with nonlinear adjustment of probabilities are compared and analyzed through benchmark functions. The optimization performance of typical AGA algorithms is compared and analyzed by 10 benchmark functions. Compared with traditional GA and other AGA algorithms, AGA with crossover and mutation probabilities adjusted nonlinearly at both ends of the average fitness value has higher computational stability and is easy to find the global optimal solution, which provides ideas for the application of adaptive genetic algorithm.

Keywords—Adaptive genetic algorithm; genetic algorithm; nonlinear adjustment; probability

I. INTRODUCTION

Genetic Algorithm (GA) was first put forwarded by Professor Holland [1]. GA is a highly parallel random search algorithm developed from natural selection and evolution mechanism in biology, providing a solution to complex optimization problems. It has the characteristics of fast search speed, simple process and the flexibility is strong [2]. However, the optimization results easily fall into local optimal values due to its fixed crossover probability and mutation probability [3-4].

For this reason, many researchers put forward an improved method of GA to enhance its global search ability. Generally speaking, there are three categories of these improvements [5]:

The first category is a hybrid optimization algorithm based on GA [6-8]. Combining GA with other optimization algorithms to improve the performance is meaningful for solving different types of optimization problems. However, because different methods are relatively independent, their improvement work can only be carried out in their respective fields.

The second category is to improve the crossover operator [9] or mutation operator [10] in GA, which improves the optimization performance of GA to some extent, but the improvement is not significant [11].

The third category is Adaptive Genetic Algorithm (AGA) [11-14], which adaptively adjusts crossover probability (P_c) and mutation probability (P_m). Because the P_c and P_m adapted to the population are used in each evolutionary generation, instead of the fixed probability value, the adaptive ability of GA can be greatly improved, and the algorithm can converge to the global optimal solution more easily. Moreover, this improved method has wide application range and strong universality [5].

AGA was first proposed by Srinivas et al. [15]. In AGA algorithm proposed by Srinivas et al., when the fitness value of an individual is equal to the maximum fitness value of the individual in this generation, the values of P_c and P_m will be zero, which will lead to premature optimization calculation. For this reason, many scholars have put forward improved methods for AGA. Several different versions of improved AGA have been found. There are two categories of improved AGA methods: linear adjustment and nonlinear adjustment according to the different adjustment methods of crossover and mutation probabilities. This paper focuses on AGA algorithm for nonlinear adjustment of probability.

II. ADAPTIVE GENETIC ALGORITHM

The adaptive ability of genetic algorithm should be reflected in that individuals in the population automatically discover the characteristics and rules of the environment according to the changes of the environment. The most obvious environmental feature is the individual's adaptability to the environment, and the most obvious evolutionary law is the relationship between the individual's fitness value and the average fitness value of all individuals in the population and the minimum fitness value and the maximum fitness value in the population.

In evolution, individuals don't remember which generation they evolved into, only whether they improved their ability to adapt to their environment. If there are improvements, then a better evolutionary pattern will be found, and as much as possible this pattern will be preserved in the algorithm design. Otherwise, the model is likely to become obsolete by nature.

The main difference between GA and AGA is the choice of P_c and P_m values. In GA, these two probabilities are randomly determined or based on insufficient prior knowledge reference, while AGA depends on the state of population in the evolution process to select the optimal value. The optimization process of AGA is in Fig. 1.

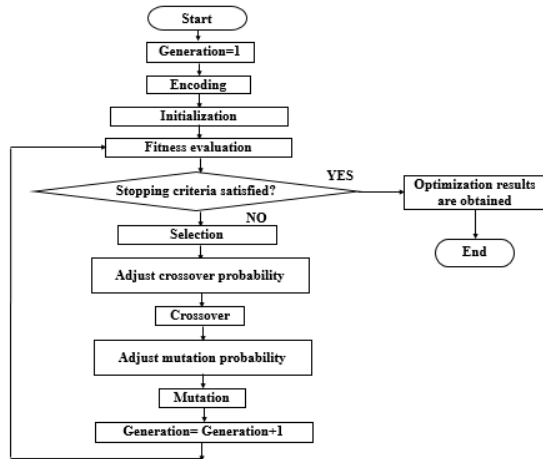


Fig. 1. The Flowchart for AGA.

III. LITERATURE REVIEW ABOUT NONLINEAR ADJUSTMENT AGA

There are two categories of AGA according to the different adjustment methods for P_c and P_m : probabilistic linear adjustment AGA [16-18] and probabilistic nonlinear adjustment AGA [19-22]. AGA with linear adjustment of probability values cannot solve the problems of local optimal value and premature problem [19-22]. The nonlinear adaptive probability adjustment strategy can avoid premature problem, poor stability and slow convergence speed. According to whether the probability is adjusted at two branches of the average fitness value, the AGA with nonlinear adjustment can be divided into three types: one end is fixed and the other end is nonlinear adjustment (taking the average fitness value as the cutoff point) [18-19]; linear adjustment at one end and nonlinear adjustment at the other [21-22]; nonlinear adjustment at two ends.

A. One Branch is Fixed and the Other is Adjusted Nonlinearly [19-22]

1) *Nonlinear adjustment of probability value by exponential function*[19]: Equation (1) and equation (2) give the adjustment formulas of P_c and P_m through exponential function [19] in solving the minimum optimization problem, respectively. This AGA is labeled as AGA-1.

$$P_c = \begin{cases} P_{cmax} - (P_{cmax} - P_{cmin}) \exp\left(1 - \frac{f_{avg} - f_{min}}{f_{avg} - f}\right), & f' \leq f_{avg} \\ P_{cmax}, & f' > f_{avg} \end{cases} \quad (1)$$

$$P_m = \begin{cases} P_{mmax} - (P_{mmax} - P_{mmin}) \exp\left(1 - \frac{f_{avg} - f_{min}}{f_{avg} - f}\right), & f \leq f_{avg} \\ P_{mmax}, & f > f_{avg} \end{cases} \quad (2)$$

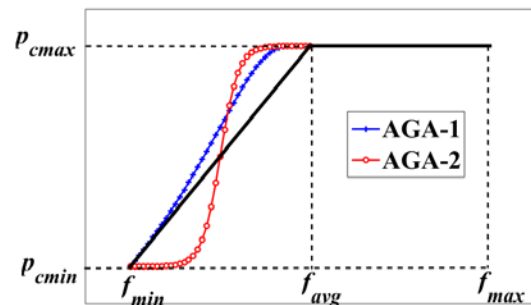
where f_{max} , f_{min} and f_{avg} represent the maximum, minimum and average fitness values, respectively; f' is the larger fitness value of the selected individuals participating in crossover for P_c [18], and f is the fitness value of selected individual participating in mutation for P_m [18], and $P_{max} > P_{min} \in (0,1)$. If $f' = f_{avg}$ OR $f = f_{avg}$, $P_c = 0.01$ and $P_m = 0.001$.

2) *Nonlinear adjustment of probability value by sigmoid function*[20]: The adjustment formulas of P_c and P_m through sigmoid function ($A=9.903438$) [20] in solving the minimum optimization problem are given in Equation (3) and Equation (4), respectively. This AGA is labeled as AGA-2.

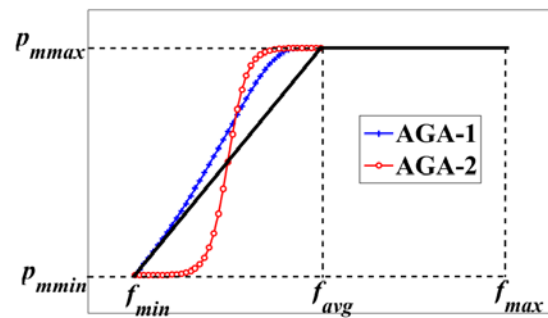
$$P_c = \begin{cases} \frac{(P_{cmax} - P_{cmin})}{1 + \exp\left(\frac{A \cdot 2(f_{avg} - f')}{f_{avg} - f_{min} - 1}\right)} + P_{cmin}, & f' \leq f_{avg} \\ P_{cmax}, & f' > f_{avg} \end{cases} \quad (3)$$

$$P_m = \begin{cases} \frac{(P_{mmax} - P_{mmin})}{1 + \exp\left(\frac{A \cdot 2(f_{avg} - f)}{f_{avg} - f_{min} - 1}\right)} + P_{mmin}, & f \leq f_{avg} \\ P_{mmax}, & f > f_{avg} \end{cases} \quad (4)$$

Fig. 2 shows the adaptive curves of P_c and P_m for AGA-1 and AGA-2. P_c and P_m will adjust nonlinearly according to the fitness of individuals between f_{avg} and f_{min} .



(a) P_c .



(b) P_m .

Fig. 2. Adaptive P_c and P_m of AGA-1 and AGA-2.

B. One Branch is Linear and the other is Nonlinear (Mark as AGA-3) [22]

Although AGA-1 and AGA-2 can avoid the local optimization and the premature convergence problem to some extent due to the adoption of a nonlinear adjustment strategy on one branch, it may still lead to the algorithm to fall into local optimum solution easily when the individuals' fitness value are larger than average fitness value and P_c and P_m are both fixed. For this reason, Wang [21] proposed the following improved adjustment strategy as shown in equation (5) and equation (6).

$$P_c = \begin{cases} P_{c3} + (P_{c2} - P_{c3}) \exp\left(\frac{10(f' - f_{avg})}{f_{avg} - f_{min}}\right), f' \leq f_{avg} \\ P_{c2} - \frac{(P_{c1} - P_{c2})(f_{avg} - f')}{f_{max} - f_{avg}}, f' > f_{avg} \end{cases} \quad (5)$$

$$P_m = \begin{cases} P_{m3} + (P_{m2} - P_{m3}) \exp\left(\frac{10(f - f_{avg})}{f_{avg} - f_{min}}\right), f \leq f_{avg} \\ P_{m2} - \frac{(P_{m1} - P_{m2})(f_{avg} - f)}{f_{max} - f_{avg}}, f > f_{avg} \end{cases} \quad (6)$$

Adjustment curves of P_c and P_m for AGA-3 are in Fig. 3.

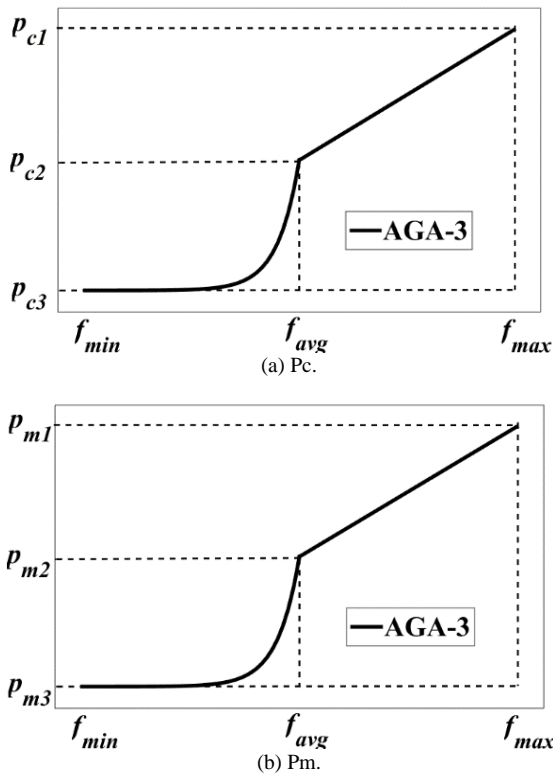


Fig. 3. Adaptive P_c and P_m of AGA-3.

C. Two Branches are Nonlinear (Mark as AGA-4) [22]

The values of P_c and P_m are adjusted adaptively and nonlinearly at both branches by sigmoid function [22]:

$$P_c = \begin{cases} P_{c3} + \frac{(P_{c2} - P_{c3})}{1 + \exp\left(A \frac{2(f_{avg} - f')}{f_{avg} - f_{min} - 1}\right)}, f_{min} < f' \leq f_{avg} \\ P_{c2} + \frac{(P_{c1} - P_{c2})}{1 + \exp\left(A \frac{\left(\frac{f_{avg} + f_{max} - f'}{2}\right)}{(f' - f_{avg})(f_{max} - f')}\right)}, f_{avg} < f' < \frac{f_{avg} + f_{max}}{2} \\ P_{c2} + \frac{(P_{c1} - P_{c2})}{1 + \exp\left(A \left(1 - \frac{2(f' - f_{avg})}{f_{max} - f_{avg}}\right)\right)}, \frac{f_{avg} + f_{max}}{2} < f' \leq f_{max} \end{cases} \quad (7)$$

[22]

$$P_m = \begin{cases} P_{m3} + \frac{(P_{m2} - P_{m3})}{1 + \exp\left(A \frac{2(f_{avg} - f)}{f_{avg} - f_{min} - 1}\right)}, f_{min} < f \leq f_{avg} \\ P_{m2} + \frac{(P_{m1} - P_{m2})}{1 + \exp\left(A \frac{\left(\frac{f_{avg} + f_{max} - f}{2}\right)}{(f' - f_{avg})(f_{max} - f)}\right)}, f_{avg} < f < \frac{f_{avg} + f_{max}}{2} \\ P_{m2} + \frac{(P_{m1} - P_{m2})}{1 + \exp\left(A \left(1 - \frac{2(f - f_{avg})}{f_{max} - f_{avg}}\right)\right)}, \frac{f_{avg} + f_{max}}{2} < f \leq f_{max} \end{cases} \quad (8) [22]$$

Adjustment curves of P_c and P_m for AGA-4 are presented in Fig. 4.

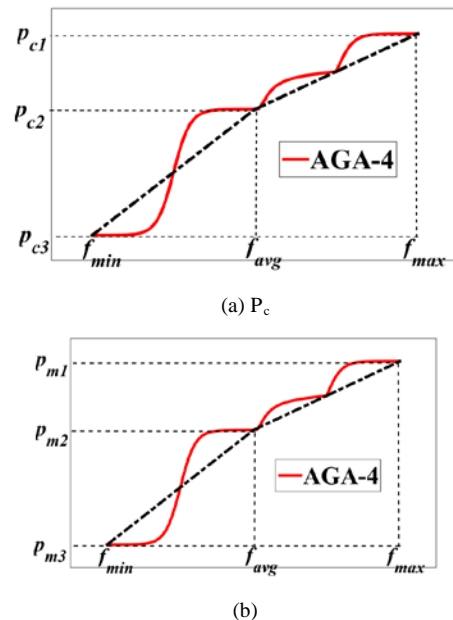


Fig. 4. Adaptive P_c and P_m of AGA-4.

IV. ANALYZE ALGORITHM PERFORMANCE BY BENCHMARK FUNCTION

The performance of the above four AGAs for minimum optimization problems is examined in this section. In order to analyze the results, basic GA is used as a benchmark for comparison. Ten standard benchmark functions commonly

used in literatures are selected for numerical simulation analysis.

A. Parameters Setting of Algorithm

GA and the above four AGAs have the same parameters except P_c and P_m . All parameters are exhibited in Table I.

TABLE I. PARAMETERS OF GA AND AGAS

Parameters	Value	Parameters	Value
Population(P)	50	P_{cmax} for AGA-1 and AGA-2	0.75
Generation(G)	500	P_{cmin} for AGA-1 and AGA-2	0.3
P_c for GA	0.85	P_{m1} for AGA-3 and AGA-4	0.1
P_m for GA	0.01	P_{m2} for AGA-3 and AGA-4	0.05
P_{c1} for AGA-3 and AGA-4	0.9	P_{m3} for AGA-3 and AGA-4	0.01
P_{c2} for AGA-3 and AGA-4	0.6	P_{mmax} for AGA-1 and AGA-2	0.075
P_{c3} for AGA-3 and AGA-4	0.3	P_{mmin} for AGA-1 and AGA-2	0.01

B. Benchmark Function

Ten benchmark functions [23] are used here to evaluate the performance of AGA. Their expressions, search ranges and global optimum values are listed in Table II. f_1 - f_5 are multimodal functions, and f_6 - f_{10} are singlemodal functions. GOV stands for global optimum value, and D stands for dimensions in Table II.

C. Numerical Results

The numerical results are presented in Table III and IV. Table III gives the average optimum value of 20 calculations using basic GA and the four different AGAs, and Table IV provides the standard deviations.

The results in Table III show that the optimized values obtained by AGA-4 are the smallest among the five algorithms, showing the advantage of AGA-4 in solving the minimum optimization problem. It can be seen from Table IV that the standard deviation values of AGA-4 in the 20 calculations are also the smallest, which indicates the stability and the optimization consistency. Numerical results demonstrated that the adaptive probability of nonlinearly tuning P_c and P_m can avoid the problems of premature maturation and slow convergence, as well as poor stability of AGA-4.

TABLE II. BENCHMARK FUNCTION

Objective function	Search range	GOV ¹	D ²
$f_1(x) = \sum_{i=1}^D \frac{x_i^2}{4000} - \prod_{i=1}^D \cos\left(\frac{x_i}{\sqrt{i}}\right) + 1$	[-600,600]	0	10
$f_2(x) = -20 \exp\left(-0.2 \sqrt{\frac{1}{D} \sum_{i=1}^D x_i^2}\right) - \exp\left(\frac{1}{D} \sum_{i=1}^D \cos(2\pi x_i)\right) + 20 + e$	[-32.768, 32.768]	0	10
$f_3(x) = 418.9829D - \sum_{i=1}^D x_i \sin(\sqrt{ x_i })$	[-500,500]	0	10
$f_4(x) = \left(\sum_{i=1}^5 i \cos((i+1)x_1 + i)\right) \left(\sum_{i=1}^5 i \cos((i+1)x_2 + i)\right)$	[-10,10]	-186.731	2
$f_5(x) = -0.0001 \left(\sin(x_1) \sin(x_2) \exp\left(\left 100 - \frac{\sqrt{x_1^2 + x_2^2}}{\pi} \right \right) + 1 \right)^{0.1}$	[-10,10]	-2.0626	2
$f_6(x) = \sum_{i=1}^{D-1} \left[100(x_{i+1} - x_i^2)^2 + (x_i - 1)^2 \right]$	[-2.048, 2.048]	0	10
$f_7(x) = (x_i - 1)^2 + \sum_{i=2}^D i(2x_i^2 - x_{i-1})^2$	[-10,10]	0	10
$f_8(x) = \sum_{i=1}^D ix_i^2$	[-10,10]	0	10
$f_9(x) = \sum_{i=1}^D x_i ^{i+1}$	[-1,1]	0	10
$f_{10}(x) = \sum_{i=1}^D x_i^2$	[-5.12, 5.12]	0	10

¹ Global optimum value.

² Dimension.

TABLE III. AVERAGE OPTIMUM VALUE

	f_1	f_2	f_3	f_4	f_5	f_6	f_7	f_8	f_9	f_{10}
GOV	0	0	0	-186.731	-2.0626	0	0	0	0	0
GA	0.747	4.262	335.36	-169.591	-2.0604	42.754	54.017	2.213	0.001	0.453
AGA-1	0.696	2.237	31.884	-177.974	-2.0615	9.661	1.875	0.128	9.879e-5	0.026
AGA-2	0.668	2.221	21.878	-180.060	-2.0621	9.122	1.724	0.122	7.272e-5	0.020
AGA-3	0.707	2.414	29.548	-164.344	-2.0609	9.171	2.105	0.124	7.806e-5	0.024
AGA-4	0.581	1.860	21.072	-184.722	-2.0622	5.670	1.638	0.068	2.841e-5	0.017

TABLE IV. STANDARD DEVIATION

	f_1	f_2	f_3	f_4	f_5	f_6	f_7	f_8	f_9	f_{10}
GOV	0.2619	0.8444	213.232	27.7019	0.0024	27.7788	90.221	1.9592	0.0015	0.2438
GA	0.1976	0.5892	30.0707	18.2699	0.0028	10.6393	0.9642	0.1247	1.354e-4	0.0240
AGA-1	0.2194	0.5436	18.5877	13.4561	0.0011	9.5237	0.8206	0.1124	1.291e-4	0.0163
AGA-2	0.2328	0.8642	38.3224	21.6508	0.0019	7.6770	1.5144	0.1138	1.525e-4	0.0266
AGA-3	0.1589	0.5008	10.0260	2.4383	3.737e-4	2.2428	0.7944	0.0450	3.366e-5	0.0107
AGA-4	0.2619	0.8444	213.232	27.7019	0.0024	27.7788	90.221	1.9592	0.0015	0.2438

D. Discussion

In order to improve the comparative analysis of different AGAs, the probability adjustment curves of different AGAs are drawn in Fig. 5. Fig. 5 exhibit that the curves of P_c and P_m in AGA-3 become steeper when f_{avg} and f_{min} are closer to each other. As a result, the probabilities of these individuals are greatly different each other even if there is little difference in individual fitness values. Thus, most individuals only have lower P_c and P_m , causing the evolution to stagnate. In order to avoid the occurrence of the above situation, firstly, the adaptive adjustment curves of P_c and P_m should be changed slowly at f_{avg} so as to greatly enhance P_c and P_m of individuals with fitness closer to f_{avg} . Secondly, to ensure that better individuals in contemporary population still have a certain crossover and mutation probabilities, the adaptive adjustment curve at f_{min} should be smoothed. Although AGA-1's adaptive adjustment curve is relatively smooth in the near area f_{avg} , it retains a large probability value in the near area f_{min} , which is not conducive to the retention of dominant individuals in the late stage of evolution. However, in AGA-2, the P_c and P_m vary slowly in the near area f_{avg} , and P_c and P_m values close to f_{avg} are significantly improved. At the same time, since the patterns of nearby f_{min} individuals are preserved as much as possible, their values are low but greater than zero, which explains why the algorithm tries to get out of local convergence.

On the other hand, the results of AGA-2 are obviously better than AGA-1 and AGA-3, which indicates that a good nonlinear adjustment curve can greatly improve the performance of AGA. However, to some extent, it is easy for AGA to fall into the local optimal solution because AGA-2 adopts a fixed probability value between f_{avg} and f_{max} . AGA-4

makes the P_c and P_m curves change nonlinear slowly through nonlinear adjustment, and makes the curves smooth at any point. When the individual population is in a comparable state, AGA-4 pulls apart most individuals near f_{avg} , thus promoting the process of evolution. It is of positive significance to eliminate local convergence and prevent the algorithm from falling into stagnation.

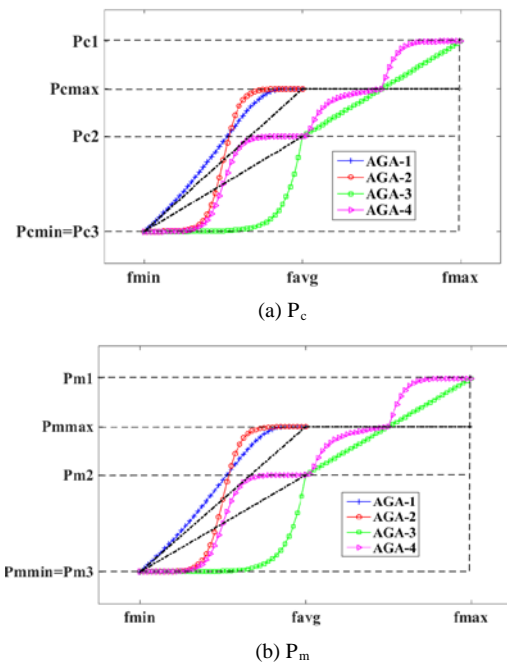


Fig. 5. Adaptive P_c and P_m of AGA-1, AGA-2, AGA-3 and AGA-4.

V. CONCLUSION

AGA algorithms with nonlinear adjustment of P_c and P_m are systematically summarized, and the optimization performance of typical AGA algorithms is compared and

analyzed by 10 benchmark functions. The optimization calculation results of benchmark functions show the superiority of AGA-4 which has crossover probability and mutation probability that are nonlinear adjusted at both ends of f_{avg} . Compared with traditional GA and other AGA algorithms, AGA-4 has higher computational stability and it's easy to find the global optimal solution.

In the future, we will study the crossover operator and mutation operator of AGA in order to further improve the performance of the optimization algorithm.

ACKNOWLEDGMENT

This research was funded by Anhui province university outstanding young talents support fund, grant number gxyq2020077.

REFERENCES

- [1] Holland J, Adaptation in natural and artificial systems : an introductory analysis with application to biology. Control & Artificial Intelligence 1975.
- [2] Meng Siyuan, Zhang Chuancheng, Composition of Web Services of Multi-Population Adaptive Genetic Algorithm Based on Cosine Improvement, Journal of Computer and Communications 09(06),2021, pp.109-119.
- [3] Lu H, Qiao F. An efficient adaptive genetic algorithm for energy saving in the hybrid flow shop scheduling with batch production at last stage[J]. Expert Systems, 2022, 39(2): e12678.
- [4] Mahjoob M, Fazeli S S, Milanlouei S, et al. A modified adaptive genetic algorithm for multi-product multi-period inventory routing problem[J]. Sustainable Operations and Computers, 2022, 3: 1-9.
- [5] ALI M Z, AWAD N H, SUGANTHAN P N, et al, An improved class of real-coded genetic algorithms for numerical optimization, Neurocomputing 275(JAN.31), 2017 ,pp.155-166.
- [6] LENO I J, SANKAR S S, PONNAMBALAM S, MIP model and elitist strategy hybrid GA-SA algorithm for layout design, Journal of Intelligent Manufacturing 29(2),2018, pp.369-387.
- [7] HU Y, LI J, HONG M, et al, Short term electric load forecasting model and its verification for process industrial enterprises based on hybrid GA-PSO-BPNN algorithm—A case study of papermaking process, Energy 170,2019, pp.1215-1227.
- [8] Yin F M, Xu H H, Gao H H, et al, Research on weibo public opinion prediction using improved genetic algorithm based BP neural networks, Journal of Computers 30(3),2019, pp.82-101.
- [9] PAVAI G, GEETHA T, New crossover operators using dominance and co-dominance principles for faster convergence of genetic algorithms, Soft Computing ,2018, pp.1-26.
- [10] ALBAYRAK M, ALLAHVERDI N, Development a new mutation operator to solve the traveling salesman problem by aid of genetic algorithms, Expert Systems with Applications 38(3),2011, pp.1313-1320.
- [11] SUN N, LU Y, A self-adaptive genetic algorithm with improved mutation mode based on measurement of population diversity, Neural Computing and Applications 31(5),2019, pp.1435-1443.
- [12] MOKSHIN A V, MOKSHIN V V, SHARNIN L M, Adaptive genetic algorithms used to analyze behavior of complex system, Communications in Nonlinear Science and Numerical Simulation 71,2019, pp.174-186.
- [13] So C , Ho I M , Chae J S , et al, PWR core loading pattern optimization with adaptive genetic algorithm, Annals of Nuclear Energy 159(9),2021, pp.108331.
- [14] Denis R , Madhubala P., Hybrid data encryption model integrating multi-objective adaptive genetic algorithm for secure medical data communication over cloud-based healthcare systems, Multimedia Tools and Applications (11) ,2021.
- [15] Srinivas M., Patnaik L M., Adaptive probabilities of crossover and mutation in genetic algorithms, IEEE Transactions on Systems Man & Cybernetics 24(4),2002, pp.656-667.
- [16] SUNG W.T., HSIAO C. L., IHPG algorithm for efficient information fusion in multi-sensor network via smoothing parameter optimization, Informatica 24(2),2013, pp.291-313.
- [17] SONG J, HOU C, XUE G, et al, Study of constellation design of pseudolites based on improved adaptive genetic algorithm, Journal of Communications 11(9),2016, pp.879-885.
- [18] YAN M, HU H, OTAKE Y, et al, Improved adaptive genetic algorithm with sparsity constraint applied to thermal neutron CT reconstruction of two-phase flow, Meas. Sci. Technol. 29(5),2018, pp.055404.
- [19] DONG Z, YANG M., Optimal design of a double-vibrator ultrasonic motor using combination method of finite element method, sensitivity analysis and adaptive genetic algorithm, Sens. Actuators A Phys.266,2017, pp.1-8.
- [20] YAN B, YAN C, LONG F, et al., Multi-objective optimization of electronic product goods location assignment in stereoscopic warehouse based on adaptive genetic algorithm, J. Intell. Manuf. 29(6),2018, pp.1273-1285.
- [21] L. Wang, Research on emergency management capability evaluation of hazardous chemical supply chain, Chemical Engineering Transactions, 62,2017, pp.1369-1374.
- [22] Wenjuan SUN, Yingqing HUANG, Haiibo CHEN, An improved adaptive genetic algorithm for optimizing pyroshock acceleration synthesis, IEEE Access (99),2019, pp.132682 -132693.
- [23] K. Deep, J.C. Bansal, K.N. Das, A.K. Lal, H. Garg, A.K. Nagar, M. Pant, On the hybridization of spider monkey optimization and genetic algorithms, Proceedings of Sixth International Conference on Soft Computing for Problem Solving (volume 546),2017, pp.185-196.

Improved Particle Swarm Approach for Dynamic Automated Guided Vehicles Dispatching

Radhia Zaghoud¹, Marwa Amara²

Computer Science Department, Faculty of Science
Northern Border University, Arar 91431, Saudi Arabia^{1,2}
LARIA, National School of Computer Science
Manouba University, Tunis, Tunisia^{1,2}

Khaled Ghedira³

Université Centrale de Tunis
Tunis, 1002, Tunisia

Abstract—The automated guided vehicles dispatching is one of the important operations in containers terminal because it affects the loading/unloading process. This operation has become faster and more complex until the automation advent. Although this evolution, the environment has become dynamic and uncertain. This paper aims to propose an improved particle swarm approach for solving the bi-objective problem of automated guided vehicles dispatching and routing in a dynamic environment of containers terminal. The objectives are to minimize the total travel distance of all automated guided vehicles and maximize the workload balance between them. The application of particle swarm algorithm in its basic form, shows a premature convergence. To ameliorate this convergence, the authors proposed the application of a method to escape the worst particles from the local optimum. The new Hybrid Guided Particle Swarm approach consists of hybridization between Dijkstra algorithms and a Guided Particle Swarm Algorithm. The routing problem is solved with Dijkstra algorithm and the dispatching problem with guided particle swarm approach. As a first step, this approach has been applied in a static environment where the dispatching parameters and the routing parameters are fixed in advance. The second step consists of applying this approach in a dynamic environment where the number of containers associated with each automated guided vehicles can change, the shortest path and the container locations can also change during the algorithm execution. The numeric results in a static environment show a good Hybrid Guided Particle Swarm performance with a faster and more stable convergence, which surpasses previous approaches such as Hybrid Genetic Approach and the efficiency of its extension approach Dynamic Hybrid Guided Particle Swarm in a dynamic environment.

Keywords—Dispatching; automated guided vehicles; dynamic; containers; particle swarm; genetic algorithm

I. INTRODUCTION

The productivity of maritime transportation has significantly advanced with the advent of automation. Automated container terminals have become crucial intermediaries between the marine and land transportation systems. As the number of ships entering and exiting daily from terminals has greatly increased, the number of containers loaded by ships has become very large [1]. Following this revolution, many maritime ports worldwide have established automated equipment to manage the increase in container traffic. They also installed an automated control system to achieve an optimal performance. The equipment in ACT is classified into three principal types: quayside equipment, quay

cranes (QCs) used to load or unload containers from or to the ship; landside equipment, yard cranes (YCs) employed for container loading or unloading in the yard storage depots; and intermediate zone equipment, automated guided vehicles (AGVs) used to transport containers from the two sides of the port. An AGV is a mobile robot that follows markers or wires on the floor or uses vision, magnets, or lasers for navigation. It is extensively employed in industry to transport goods from an origin location to a target location [2, 3, 4]. AGVs are widely used in manufacturing, medicine, and logistics industries. Although this equipment has accelerated the ACT operations, any working failure of any one of them may cause a late or partial blockage or global blockage of the whole system in the ACT. The most critical goal of an automated container terminal is to increase productivity by minimizing the berthing duration of ships. This objective can be accomplished by finishing the main ship loading/unloading operation at its scheduled time because any lateness can affect the synchronization of the entire system. This operation includes four types of sub-operations: (1) loading/unloading containers from/to the ship, (2) AGV dispatching and routing, and (3) loading/unloading containers to the yard storage zone. The container loading/unloading process began after ship berthing. The containers are unloaded from the ship by the quay cranes and are then transported by the AGVs to the landside of the port. They are then unloaded by yard cranes and stocked in the corresponding yard storage zone. Conversely, the ship-loading operation begins by assigning containers to AGVs for transfer to the quayside to be loaded by the quay cranes to the ship. These loading and unloading operations have become faster with the advent of container terminal automation and a high number of equipment in the port [5]. Nevertheless, with this important evolution of the container terminal, the risk of breakdown of any element in the system increases. This failure can have some consequences, such as the lateness of the loading/unloading operation; therefore, the berthing duration of the ship increases, which will indirectly disturb the productivity of the port. The latency of the ship berthing duration may cause the unavailability of container terminal equipment, which will delay the loading/unloading operation of all ships after this disruption. This paper studies the problem of AGVs dispatching in a static and dynamic environment of containers terminal. In the first step, the authors investigate to solve the static problem. They choose to optimize the total travel distance of all AGVs and the workload balance between them. By studying these two

criteria; the total travel distance depends on AGV's path and the balance workload depends on AGV's autonomy. The first criteria were optimized by using an exact algorithm to search the shortest path for each AGV and the second criteria were optimized by maximizing the autonomy of each AGV. The workload balance makes the AGVs system more robust because the AGV working more tasks than other AGVs will lose its autonomy early. Because the AGV's autonomy is limited to its battery energy, the breakdown of AGVs can be frequent with absence of workload balance. In a static environment, this problem parameters are fixed in advance; the number of road network nodes, and the number of AGVs, and the number of containers. However, the real situation in maritime ports is completely different because the number of equipment is big, so the possibility of breakdown of any equipment is also big. A breakdown of any equipment can make a delay in the corresponding sub-process which can affect the loading /unloading operation. A new ship arriving to the port may haven't the necessary equipment of its unloading/loading operation available. An extension of the proposed approach in the first step, was developed to solve the problem of dispatching AGVs to containers in a dynamic environment. The remainder of this paper is organized as follows: the second Section presents a literature review of this problem. The problem description and mathematical formulation are presented in the third Section. In the fourth Section, we present the proposed approaches in a static environment. In the fifth section, the authors propose an extension of the proposed approach for the dynamic environment. The numerical study results are cited in the sixth section, and finally, a discussion of the results and conclusions is given in the seventh section.

II. LITERATURE REVIEW

A. Related Work

In ACTs, the operations can be grouped into two classes of processes: loading and unloading. The loading process consists of transferring containers from the yard location area to AGVs via yard cranes to be transported to the ship to be loaded by the quay cranes. The unloading process involves unloading containers from the ship using quay cranes, and transportation by AGVs to the corresponding storage locations in the yard. Many studies have focused on ACT operations. Most studies were concerned with global loading and unloading operations. They proposed simultaneous scheduling systems including QCs, AGVs, and YCs. Despite the importance of dispatching containers to AGVs and AGV routing in the unwinding of loading and unloading processes, few studies have independently focused on this problem. Several literature reviews were developed [7, 8, 9, 10] studying yard and quay side operations, examining independently studied problems, as well as combined problems. They also revised the literature on yard crane scheduling, transport vehicle dispatching and scheduling, quay crane assignment and scheduling problems for the yard, vehicle routing and traffic control, and storage location and space planning problems. [11] considered the global ACT system and proposed an integrated scheduling model for handling equipment coordination and AGV routing. The optimization goal was to minimize the makespan of the global

process. The authors developed a Congestion Prevention Rule-based bi-level genetic algorithm (CPR-BGA) to solve the proposed model. [12] proposed a new method for optimizing the ASC and AGV scheduling and a collaborative AGV and ASC scheduling model in automatic terminal. The proposed model is designed based on a genetic algorithm (GA) and aims to minimize the AGV waiting time and ASC running time. The dispatching problem of AGVs to containers was studied by [6], where the AGVs scheduling was assimilated as a process of allocating AGVs to tasks, considering the cost and time of operations. The objectives chosen were makespan maximization and minimization of the number of AGVs, while considering the battery charge of the AGVs. A fuzzy GA, PSO optimization algorithm, and a hybrid GA-PSO were developed to optimize the proposed model. [13] proposed an approach named the modified memetic particle swarm optimization (MMPSO) algorithm based on PSO integrated with the memetic algorithm (MA). This approach is applied to generate the initial feasible solutions for scheduling multi-load AGVs to minimize travel and waiting time in manufacture system (FMS). [14] studied the problem of work transport organization and control. They proposed an approach based on a non-changeable path during travel and a fuzzy logic to order the set of stations requesting transport services. GA is applied to stations sequence optimization. [15] studied the problem of resource optimization in AGV-served FMS. They proposed a scheduling model integrating machines and AGVs. The objective function is the makespan of jobs from raw material storage to finished parts storage. [16] consider the problem of dispatching multiple-load AGVs in an FMS. A PDER rule based on pickup-or-delivery-in-route is proposed to address the task determination problem, which indicates whether the next task of an AGV partially loaded should be picking up a new job or dropping off a carried load. A workload-balancing (WLB) algorithm was developed to address the pickup-dispatching problem that determines which job should be assigned to an AGV. [17] investigated the multiple-AGV path planning. The authors proposes a GA approach with two innovations; a three-exchange crossover heuristic operators, used to produce better offspring and a double-path constraint for minimizing the total path distance of all AGVs and the single path distances of each AGV. [18] studied the autonomous driving system that uses dynamic path planning to avoid static and moving obstacles. To determine the optimal path, acceleration, and vehicle speed, the proposed method generated a set of path candidates. The optimum path selection is based on the total cost of static safety, comfortability, and dynamic safety, with the identification of acceleration and speed. [19] proposed a Q-learning method to find the AGVs shortest-time routes. To improve the selecting action policy for this method, the authors developed an improved anisotropic Q-learning routing algorithm with vehicle-waiting-time estimation. The performance of these methods was tested based on simulations. [20] considered the dynamic scheduling process to solve the AGV scheduling and planning problems. The authors proposes a two stage mixed integer model for AGVs cost transportation optimization with lay time constraint. They developed an approach based on heuristic, and DIK algorithm, and Q-learning algorithm for solving the proposed model. A strategy for avoidance conflict of AGVs

was also proposed. [21] investigated the dynamic AGVs scheduling problem with AGVs and machines having specific speed. They proposed a biological intelligent approach (BIA) inspired by hormone regulation in endocrine system. The objectives were to minimize the makespan and maximize the shop floor work efficiency. To solve this problem in a static environment, many approaches have been proposed, and metaheuristics perform well for this type of problem [6]. The PSO algorithm is one of the best algorithms cited in the literature, although the disadvantage of its premature convergence. To the authors' best knowledge, the problem of dispatching containers to AGVs in container terminals has been studied in general, in an integrated manner with other dispatching problems, such as the dispatching of quay cranes and yard cranes. The weakness of the combination of this problem of dispatching with the other problems of dispatching in container terminals in the same system management can propagate any disruption from one phase to the following phase. For example, if there is a problem in quay crane dispatching, it will propagate to AGV dispatching. So, the resolution becomes more complex. The study of this problem separately can easily detect any disruption and facilitate its resolution. Many studies investigate the problem of AGV dispatching and routing in a static environment, but this approach is different of the real situation in container terminals so its application will not be efficient. A scarce number of researchers are interested in this problem in a dynamic environment. All the previous studies don't combine the two criteria of travel distance and workload balance, although the combination of these two criteria can be more attached and applicable to the real situation. The hybridization of particle swarm with Dijkstra algorithm make a good guide to PSO approach to find the best solution and the re-initialization of worst particles parameters help these particles to avoid from local optimum. The PSO approach has the advantage of the fast convergence in comparison with genetic algorithm. In this paper, the authors propose a guided hybrid particle swarm algorithm (GHPSO) to solve this problem in a static environment. Because the accurate situation in the container terminal is not static, they propose an extension of this approach to apply in the dynamic environment.

B. Particle Swarm Optimisation

A particle swarm is a metaheuristic algorithm presented in 1995 by Kennedy and Eberhart, and it was developed under the inspiration of the behavior laws of bird blocks, fish schools, and human communities. To achieve the optimum solution, PSO starts from a group of random groups of solutions and then repeatedly searches. It has proven to be a highly efficient optimization algorithm in numerous studies and experiments [22]. As a metaheuristic, PSO does not guarantee that the optimal solution is obtained. The basic particle swarm optimization is described as follows:

Assuming N is the number of particles, the i^{th} particle position $i = (1, 2, \dots, N)$ in dimension space d can be denoted as $X_i = [x_{i,1}, x_{i,2}, \dots, x_{i,d}]$, its velocity is defined as the moving distance between the particles in each iteration, and is denoted as $V = [v_{i,1}, v_{i,2}, \dots, v_{i,d}]$.

The objective function consists of determining the optimal position of the particle, and the local optimal particle position P_{best} in the t^{th} iteration is denoted as $P_i = [p_{i,1}, p_{i,2}, \dots, p_{i,d}]$. The global optimal position g_{best} in the t^{th} iteration is denoted as $P_g = [p_{g,1}, p_{g,2}, \dots, p_{g,d}]$. In the $(t + 1)^{th}$ iteration, the flight velocity $V_{i,j}(t + 1)$ of the i^{th} particle in the j dimensional space, $j = (1, 2, \dots, d)$, and its position $X_{i,j}(t + 1)$ can be derived from the following equations:

$$V_{i,j}(t + 1) = W * V_{i,j}(t) + C_1 * R_1 * [P_{i,j} - X_{i,j}(t)] + C_2 * R_2 * [P_{g,j} - X_{i,j}(t)] \quad (1)$$

$$X_{i,j}(t + 1) = X_{i,j}(t) + V_{i,j}(t + 1), j = 1, 2, \dots, d \quad (2)$$

W is the inertia coefficient; C_1 and C_2 are the cognitive coefficient and social learning coefficient, R_1 and R_2 denote random numbers between 0 and 1; $P_{i,j}$ is the local optimal particle position of the i^{th} particle in the j dimension space, $P_{g,j}$ is the global optimal particle position of the i^{th} particle in the j dimension space. PSO achieves its optimum solution by starting from a group of random solutions and then repeatedly searching [23, 24, 25, 26]. PSO has a good level of particle convergence because of the fast transmission of information among the particles. For this reason, swarm diversity decreases very quickly after the iterations and can lead to a suboptimal solution. This evolution process can trap in a local optimum or premature convergence.

Many variants of the PSO algorithm have been proposed to solve the diversity loss problem. The problem of decreasing diversity can be attributed to several factors. The population diversity of PSO is an important feature that demonstrates the exploration or exploitation ability of the algorithm. It is a technique used to determine the degree of convergence or divergence of PSO in the search process. As example, ARPSO is a method used to control the degree of diversity. It consists of an algorithm called ARPSO, which tests if the diversity is above the predefined threshold d_{low} , then particles attract each other, and if it is below d_{low} , then the particles repel each other until they meet the required high diversity d_{high} . LOD is also a method for local optima detectors; it consists of computing the number of iterations in which the neighbor does not improve, that is, if the fitness value (FV) of the best particle remains unchanged for a specific number of iterations, the particle optimization sub-process is trapped in a local optimum [27, 28, 29, 30, 31, 32]. To increase the diversity of swarms, several methods have been cited in the literature as particle re-initialization and particle mutation. Inspired from the idea of LOD, the authors apply this method to escape the worst particles from the local optimum.

C. Scheduling/Rescheduling System

The goal of this system is to plan the production of a collection of jobs assigned to multiple machines given the production environment specifications. The scheduling problem has been demonstrated in the literature as a non-polynomial (NP-hard) [33]. In a multi-AGV system, n containers are available: $\{C_1, C_2, C_3, \dots, C_n\}$ to be transferred by k AGVs $\{V_1, V_2, V_3, \dots, V_k\}$, and the main objective is to determine the optimal schedule for n containers to be transported by the system. Each AGV can transfer only one

container within a specific time interval. According to literature the selection of AGV can be based on one of the following methods: [34, 35]

- Longest travel distance
- Shortest travel distance
- Random
- Minimum AGV queue size

In its standard form, the scheduling problem can be described as a set of known tasks assigned to a set of available machines, considering the technological limitations of the system. This class of approach is called static scheduling. In this scheduling type, the tasks to be assigned and system parameters are known in advance and are invariant in time [36, 37, 38]. Multiple events, such as new task arrivals, machine breakdowns, task priority changes, and preventive machines, can affect the system in real situations. These changes in circumstances result from a dynamic environment that necessitates task reassignment. Rescheduling is defined as the process of updating existing production scheduling to react to any event. The literature explains three different strategies [39]. The Predictive-reactive strategy consists of providing an initial predictive schedule and changing it to reply to the disturbances that appear within the system. The proactive (or robust) strategy based on developing a schedule that absorbs any disturbances that may occur in the system. The dynamic strategy does not provide an initial schedule, but the assignment is performed dynamically. The authors choose the proactive rescheduling because the proposed approach was applied for static environment in first step, then it was extended for dynamic environment in second step.

III. PROBLEM FORMULATION

Assume a set of containers $C = \{C_1, C_2, C_3, \dots, C_m\}$ stored in different locations $L = \{L_1, L_2, L_3, \dots, L_n\}$ at the port. These containers must be transferred to unloading locations to be transported by trucks and trains to clients, or inversely to a charging location to be loaded on a ship. A set of AGVs, $V = \{V_1, V_2, V_3, \dots, V_k\}$ should/will be available for transporting containers. The problem consists of assigning this set of containers to a set of AGVs and planning the path to each AGV. This problem can be decomposed into two sub-problems: A dispatching problem of AGVs to containers and a routing problem of AGVs. Many factors intervene in this optimization problem, such as distance traveled by AGVs, stability of the road network in the port, availability of AGVs, and utilization ratio of AGVs. For these reasons, the problem is considered as multi-objective problem. The authors choose to optimize the AGVs total travel distance and the balancing workload of AGVs. The AGVs dispatching and routing system can be assimilated to a scheduling system where a job is equivalent to the task of transferring the container from its origin location to its target location and the machine is equivalent to the AGV. In a static environment, the initial scheduling is sufficient for carrying a set of containers from their initial locations to their target locations. However, with the appearance of port automation, the number of pieces of equipment has become very

important, and many events can appear and change the system situation. For example, new arrival of containers, changes in container priorities, breakdown of any equipment or AGV, AGV battery changes, and AGV preventive maintenance lead to system disruption. This change in the port situation requires system rescheduling. To develop an efficient scheduling system, it is necessary to study this problem in a dynamic environment. In first step, the authors study the problem of AGVs dispatching and routing in a static environment. In the second step they consider the cases of new containers arrival, the breakdown of AGVs, and the disruption of the road network in the port and proposed an extension of the first approach for resolving the problem in the dynamic environment.

A. Mathematic Model in a Static Environment

$C = \{C_1, C_2, C_3, \dots, C_m\}$: Set of containers.

$L = \{L_1, L_2, L_3, \dots, L_n\}$: Set of container locations (nodes).

$V = \{V_1, V_2, V_3, \dots, V_k\}$: Set of vehicles (AGV).

d_{ij} : Distance between nodes i and j

S : Speed of AGV

t_{ijk} : Travel time of vehicle V_k from node i to node j

$[tb_i, te_i]$: Time window of node i

tb_i : Beginning time of task in node i

te_i : Ending time of task in node i

td_i : Departure time from node i

ta_i : Arrival time at node i

tw_i : Waiting time at node i

S : Speed of AGV

q_{ik} : Load of AGV

Twt_k : Total work time of vehicle V_k

X_{ijk} : Decision variable $\begin{cases} 1 & \text{if the vehicle } V_k \text{ is busy} \\ 0 & \text{otherwise} \end{cases}$ (3)

The objective function is an aggregation of two sub-functions to be optimized: The function F1 for the total travel distance of all AGVs and the function F2 for the balance of AGVs workload.

$$F = \alpha * F_1 + \beta * F_2 \quad (4)$$

The objective function value depends on two coefficients α and β associated respectively to F1 and F2 which values are fixed by a domain specialist.

$$F \equiv \begin{cases} F_1 = \sum_{i \in N} \sum_{j \in N} \sum_{k \in V} X_{ijk} * \frac{d_{ijk}}{S} \\ F_2 = \sqrt{\left(\frac{1}{k} - \frac{1}{k^2}\right) * \left(\sum_{k \in V} Twt_k^2 - 2 * \prod_{k \in V} Twt_k\right)} \end{cases} \quad (5)$$

$$\sum_{i \in N} \sum_{k \in V} X_{ijk} = 1, \forall j \in N \quad (6)$$

$$\sum_{i \in N} X_{i0k} = 1, \forall k \in V \quad (7)$$

$$\sum_{j \in N} X_{0jk} = 1, \forall k \in V \quad (8)$$

$$\sum_{i \in N} X_{ijk} - \sum_{i \in N} X_{jik} = 0, \forall k \in V, \forall j \in N \quad (9)$$

$$Q_k = \sum_{i \in N} \sum_{j \in N} q_{ijk} = 1, \forall k \in V \quad (10)$$

$$X_{ijk} = 1 \rightarrow tb_i \leq ta_i < te_i, \forall i \in N, \forall j \in N, \forall k \in V \quad (11)$$

$$X_{ijk} = 1 \rightarrow tb_i \leq td_i < te_i, \forall i \in N, \forall j \in N, \forall k \in V \quad (12)$$

$$X_{ijk} = 1 \rightarrow ta_i - t_{ijk} + Tw_i \leq_i tb_i, \forall i \in N, \forall j \in N, \forall k \in V \quad (13)$$

$$X_{ijk} = 1 \rightarrow td_i - t_{ijk} + Tw_i \leq_i te_i, \forall i \in N, \forall j \in N, \forall k \in V \quad (14)$$

(6) The transport cost from node i to node j is equal to 1.

(7) and (8): the possibility of moving from node zero to any other node.

(9): bi-directionality of each edge.

(10): AGV load equals 1

(11): The AGV must arrive at node i within the arrival time window.

(12): The container must be moved within the departure time window of the node.

(13) and (14): The AGV must arrive before the beginning of the node time window, and must move before the end of the node time window.

B. Dynamic Environment Parameters

In containers terminal, the real situation is dynamic and uncertain. Any equipment such as quay crane, truck, AGV, road can breakdown at any moment of time. A lateness of the loading/unloading operation for the corresponding ship can appear. This tardiness will propagate for all the ships coming after. Three cases was investigated in this study:

a) New Arrival Containers: This case can change the number of containers. Assume C' the set of containers of the new arriving ship. For the current process, the total number of containers to be loaded/unloaded will be $C_T = C \cup C'$. Each AGV will have an extra number of containers to transfer.

$C = \{C_1, C_2, C_3, \dots, C_m\}$: set of containers for current ship

$C' = \{C'_1, C'_2, C'_3, \dots, C'_n\}$: set of containers for new ship

$C_T = \{C_1, C_2, C_3, \dots, C_m, C'_1, C'_2, C'_3, \dots, C'_n\}$: Total set of containers to be loaded/unloaded

b) Road Network Disturbance: This case appear when there is a breakdown in some nodes of road network. Assume $L1$ and $L2$ are unavailable, all the paths containing these two nodes will be modified. Assume $L = \{L_1, L_2, L_3, \dots, L_n\}$, the initial set of nodes, the new set of nodes will be $L' = L \setminus \{L_1, L_2\}$. As consequence the AGV will travel a path other than the shortest path proposed initially.

c) AGVs Breakdown: If an AGV is unavailable, the set of containers corresponding to this AGV will be assigned to other AGVs. Assume $V = \{V_1, V_2, V_3, \dots, V_k\}$, if V_1 and V_3 are unavailable, the new set of available AGVs will be $V' = V \setminus \{V_1, V_3\}$. This event will have an effect on the workload balance of AGVs.

IV. PROPOSED APPROACHES

To increase the diversity of swarms, several methods have been cited in the literature as particle re-initialization and particle mutation. The main of particle re-initialization method is to increase the possibility of "jumping out" of local optima and to maintain the ability of the algorithm to find the "good enough" solution. After several iterations, some particles were selected to reinitialize their position and velocity. The number of chosen particles can be either constant or fuzzy. Three methods to select particles: 1) The random selection consists of selecting randomly a set particles to reinitialize its position and velocity. This method can obtain great exploration ability owing to the possibility that all particles have the chance to be reinitialized. 2) The elitist selection based on choosing a set of the best particles, having the best fitness value, to reinitialize its position and velocity. When the population diversity decreases, most particles have the best fitness values. When these elitists are reinitialized, the exploration ability of the algorithm increases but the good particles can be lost. 3) The worst particle selection consists of choosing a set of the worst particles to reinitialize its position and velocity. This idea can increase the ability of the algorithm to explore space and find the "good enough" solution by ameliorating bad particles. The particle mutation method is based on applying the mutation feature of GA to change one or more features of a particle to achieve better particles quality. This is a common method for increasing the population diversity. It can improve exploration abilities, which can be applied to different elements of a particle swarm.

The authors propose a new hybrid PSO approach called HPSO based on a heuristic and PSO algorithm. This approach did not show a clear convergence. It presents a very quick convergence which risks premature convergence. To improve the approach results, the authors propose a second approach guided particle swarm called GPSO. It consists of guiding the HPSO approach in the routing problem by choosing the shortest path for each AGV by applying the Dijkstra algorithm. This approach presents acceptable convergence. In comparing its results with previous results, it appears acceptable, but it's necessary to verify the problem of premature convergence. A third approach is proposed, named GHPSO, which combines the ameliorations of the two previous approaches (Fig. 1).

A. Hybrid Particle Swarm Approach (HPSO)

This approach is a hybridization between a heuristic, the Dijkstra algorithm, and the particle swarm algorithm; it is called the HPSO approach. It uses a heuristic based on assigning each container to the nearest AGV.

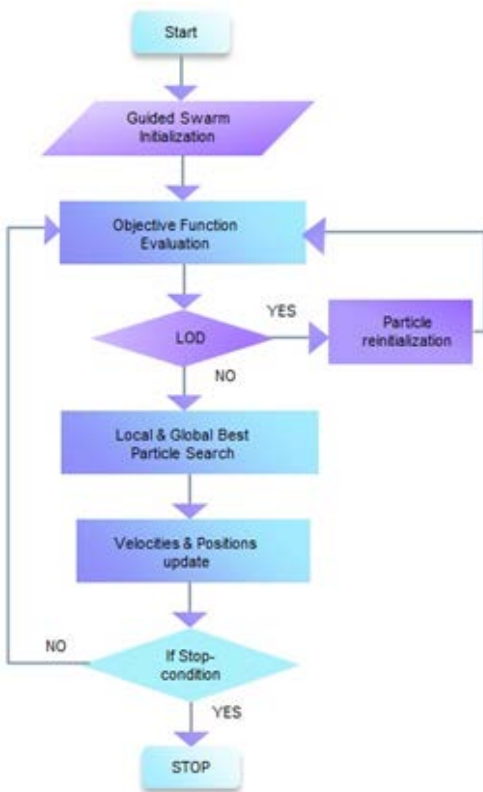


Fig. 1. GHPSO Flowchart.

The AGV travels the shortest distance to arrive at a container location. The shortest path problem is solved using the Dijkstra algorithm, and the optimal solution is determined by applying the PSO algorithm through a fixed number of iterations. The HPSO algorithm is as follows (Fig. 2).

Algorithm1: HPSO

Results: GBest

Iterations = 1;

Guided_Swarm_Initialization();

While (Iterations <= Nb_iterations)

```

{
    Objective_Function_Evaluation();
    Best_Positions_Search();
    Particles_Updates();
    Iteration = Iteration + 1;
}
    
```

End Algo

Procedure1: Guided_Swarm_Initialization()

Sort_List_Containers();

While (List_Containers # ϕ)

```

{
    Assign_container_AGV();
    Choose_shortest_path();
}
    
```

End proc

Fig. 2. HPSO Algorithm.

B. Guided Hybrid particle Swarm Approach (GHPSO)

The HPSO approach and the GPSO approach show a fast convergence which risks the premature convergence. To surpass this deficiency, the authors propose to study the diversity of PSO population. The population diversity was computed to prevent premature convergence. They choose to control the activity of particles to detect which particles were responsible for the diversity of population loss. LOD (local optimum detector) for each particle to determine whether the particle is inactive for an important number of iterations. The authors selected a threshold value for the number of iterations.

After detecting these particles, they re-initialize the positions and velocities for all particles to jump out of the local optimum.

C. Robustness of the GHPSO in a Dynamic Environment

In a dynamic container terminal environment, any disturbance can cause an increase in the number of containers in depots or Quays, because the waiting time for loading or unloading increases. The number of AGVs in the port is fixed but may decrease due to any breakdown (Fig. 3).

Algorithm2: GHPSO

Results: GBest

Iterations = 1;

Guided_Swarm_Initialization();

While (Iterations <= Nb_iterations)

```

{
    While (List_Particles #  $\phi$ )
        if (LOD(Particle) == true)
        {
            Particle_reinitialization();
            Go to EV;
        }
        else
        {
            Best_Positions_Search();
            Particles_Updates();
        }
        Iteration = Iteration + 1;
}
    
```

Procedure2: LOD(Particle, limit_repetition)

if (nb_repetition_Particle == limit_repetition)

```

{
    nb_repetition_Particle = 0;
    return true;
}
else
{
    nb_repetition_Particle = nb_repetition_Particle + 1;
    return false;
}
    
```

End proc

Fig. 3. GHPSO Algorithm.

The authors propose an extension of the GHPSO approach for a dynamic environment, dynamic guided hybrid particle swarm called DGHPPO approach, which studies three disturbance cases:

a) *Arrival of New Containers*: To solve the problem of new container arrivals, DGHPPO proposes to add the new containers to the AGVs queues during the Algorithm execution. The number of containers associated to each AGV will increase. An AGV_i can begin the dispatching process with n containers and finishes it with n+m containers. The solution will be optimized after completing the iterations.

b) *AGV Breakdown*: The DGHPPO approach proposes a new distribution of containers associated with a broken AGV for other AGVs. The number of containers for the available AGVs increases. New dispatching was proposed and optimized after completing the iterations.

c) *Network Road Disruption*: The unavailability of any node in the road network affects the set of paths proposed for the AGVs. This disturbance can cause inaccessibility of any path. AGVs must stop the transfer of the associated container. The DGHPPO approach proposes a new path to travel, then the solution will be optimized.

V. EXPERIMENTAL STUDIES

The application of these approaches was performed with a computer having 8 GOs of RAM and a processor speed of 2.4 GHz. The proposed approaches were implemented with a swarm population of 50 particles, the number of AGVs is 4 and the number of containers is 20. The PSO parameter values chosen after several tests were C1=2, C2=2, Wmin=0.4, and Wmax=0.9. R1 and R2 were randomly chosen such that $R_1 + R_2 = 1$. The threshold value chosen after several tests was 5. After several numeric tests, the genetic algorithm parameters chosen are as follows: 70% of the population was selected for crossing over and 10% for mutation.

Numerical tests were applied to two previous versions of the GA approach [40] and four new versions of the PSO approach.

Fig. 4 shows a comparative graph between the two previous genetic algorithm approaches: genetic algorithm (GA) and hybrid genetic algorithm (HGA: GA + Dijkstra). The initial solutions of the two approaches are very different. This demonstrates the importance of hybridization with the Dijkstra algorithm in the second approach. The convergence of the GA with an optimum solution value is 2.51, but it is not significant because of the random paths chosen for the AGVs. The HGA graph shows good convergence with an optimum solution value of 1.5 because the paths are optimized using the Dijkstra algorithm.

Fig. 5 presents a comparative graph of the PSO approaches. The basic PSO algorithm (PSO curve in blue) shows quick convergence from the first iterations with an optimum solution value of 2.6, and it becomes almost stable at 2.5.

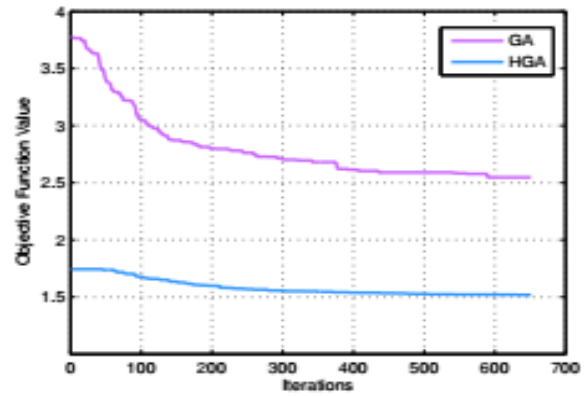


Fig. 4. GA Approaches Comparison.

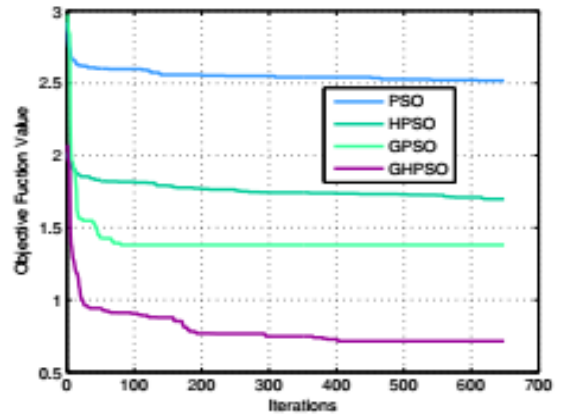


Fig. 5. PSO Approaches Comparison.

The hybridization with Dijkstra's algorithm and the insertion of a heuristic for choosing the nearest AGV with the standard PSO (HPSO curve in green) considerably improves the optimum solution value from 2.5 to 1.7, but the convergence is again not very remarkable. It is clear that the population diversity quickly decreases. The guided particle swarm approach GPSO (PSO+ re-initialization: curve in light green) shows a slight improvement in the solution value. Its value decreases from 1.7 to 1.4, and the convergence appeared significant. The last curve represents the GHPSO model. Its solution value is 0.7, which is the optimum among all proposed approaches. This convergence becomes significant in comparison with previous approaches. It is clear that the problem of a faster decrease in population diversity is solved by the insertion of LOD and the re-initialization of particles.

To determine the best approach, the authors performed a final comparison between the best GA and PSO approaches, as shown in Fig. 6. The graphs show good convergence of the PSO approach in comparison with the previous GA approach.

A comparison of the running times computed for each approach is shown in Fig. 7. The GHPSO presented an acceptable running time of 19.510-3 s in comparison with other proposed approaches.

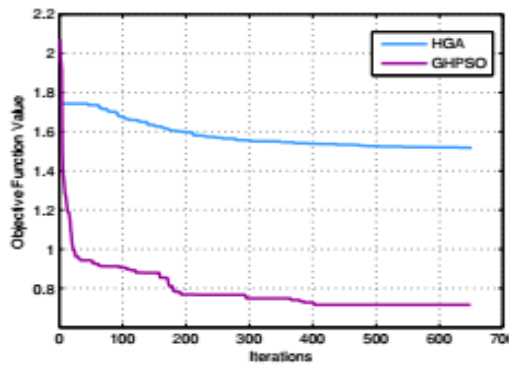


Fig. 6. GA and PSO Approaches Comparison.

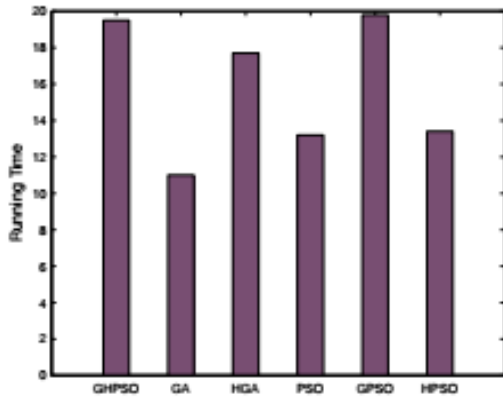


Fig. 7. Running Time Comparison.

The numerical results show the good performance of the GHPSO as the best PSO approach in a static environment. This approach also surpasses the performance of GA. This deduction encourages the authors to apply this approach in a dynamic environment, where the number of containers, AGVs, and nodes in the road network are not fixed.

Fig. 8 shows the approach convergence after the insertion of new containers. The authors propose the insertion of 20 containers at 50 iterations. It is clear that the approach begins by improving the initial solution to determine the optimum solution. The initial solution objective function value is 3, and at iteration 50, it becomes 1. When new containers were inserted, the solution value increased to 1.65. Subsequently, it was again in decreasing order to find the best solution. It reached notable convergence at almost 120 iterations with an optimum solution value of 0.6. This result demonstrates the robustness of the GHPSO approach in determining the optimum solution in the case of new container arrivals.

Fig. 9 presents the numerical results of an AGV breakdown at iteration 100, when the guided hybrid particle swarm approach (GHPSO) begins to converge. The solution value increases again because of the distance traveled by each AGV, but after 140 iterations, it converges again with a solution value of 1.25, which was greater than the initial optimum solution value due to increasing of workload of each AGV. These results demonstrate the GHPSO approach efficiency in reaching the optimum solution.

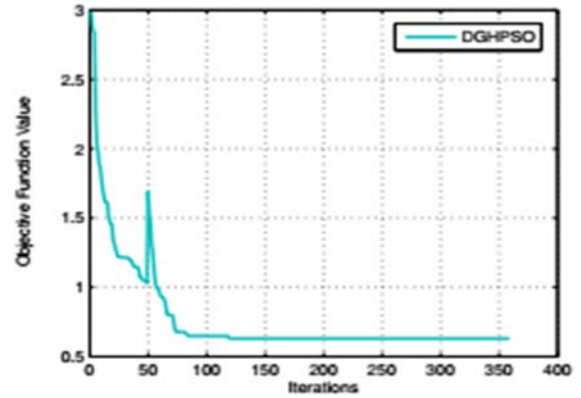


Fig. 8. New Containers Arrival.

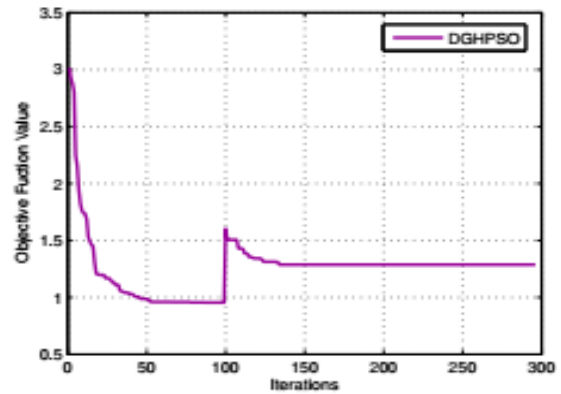


Fig. 9. AGV Breakdown

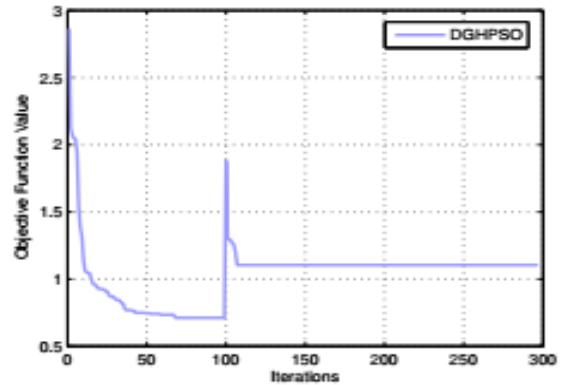


Fig. 10. Unavailable Path.

Fig. 10 shows the numerical results when some paths become unavailable. The solution value increased again and then decreased to converge to a solution value of 1.2, which was greater than the optimum solution before path breakdown due to unavailability of shortest path.

VI. CONCLUSION AND PERSPECTIVES

In this study, the problem of dispatching containers to AGVs in a container terminal in static and dynamic

environments was investigated using an improved PSO algorithm. A new guided PSO approach named GHPSO was proposed for optimizing the total travel distance and balancing the workload between AGVs. The first idea was to combine heuristic and Dijkstra with the PSO algorithm to obtain the optimum solution. The numerical results show an acceptable solution, but the convergence is not significant because an important number of particles cannot ameliorate their best local solution. The idea was to apply the insertion of the LOD parameter and reinitialize the particles to achieve good results. The convergence became significant for the GPSO, and the best optimum solution value was obtained using the GHPSO. This work showed a very good GHPSO performance compared to other approaches, although the running time was acceptable. The proposed approach was tested in a dynamic environment (DGHPSO), where the number of containers, number of AGVs, and network road nodes were not fixed. To demonstrate the robustness of this approach, the authors proposed an extension to study the arrival of new containers during approach execution. The numerical results show good convergence for the approach. In addition, for the two AGV breakdown and node breakdown cases, the proposed approach shows good convergence. This approach shows good robustness in static and dynamic environments for finding the optimum solution within a reasonable running time. In future work, the authors will study the efficiency of this approach for the multi-objective problem with the AGV energy constraint and its effect on task allocation in a static and uncertain environment.

ACKNOWLEDGMENT

The authors gratefully acknowledge the approval and the support of this research study by the grant no SAO-2018-3-9-F-7766 from the deanship of scientific research at Northern Border University, Arar, Kingdom of Saudi Arabia.

REFERENCES

- [1] Zakaria Z, Petrovic S. (2012). Genetic algorithms for match-up rescheduling of the flexible manufacturing systems. *Computers & Industrial Engineering*, 62(2), 670-686.
- [2] Oyekanlu EA, Smith AC, Thomas WP, Mulroy G, Hitesh D, Ramsey M, Sun D. (2020). A review of recent advances in automated guided vehicle technologies: Integration challenges and research areas for 5G-based smart manufacturing applications. *IEEE access*, 8, 202312-202353.
- [3] De Ryck M, Versteyhe M, Debrouwere F. (2020). Automated guided vehicle systems, state-of-the-art control algorithms and techniques. *Journal of Manufacturing Systems*, 54, 152-173.
- [4] Bae J, Chung W. (2018). A heuristic for path planning of multiple heterogeneous automated guided vehicles. *International Journal of Precision Engineering and Manufacturing*, 19(12), 1765-1771.
- [5] Luo J, Wu Y. (2020). Scheduling of container-handling equipment during the loading process at an automated container terminal. *Computers & Industrial Engineering*, 149, 106848.
- [6] Mousavi M, Yap HJ, Musa S N, Dawal SZM. (2017). A fuzzy hybrid GA-PSO algorithm for multi-objective AGV scheduling in FMS. *a*, 1(1), 1.
- [7] Fazlollahab H, Saidi-Mehrabad M. (2015). Methodologies to optimize automated guided vehicle scheduling and routing problems: a review study. *Journal of Intelligent & Robotic Systems*, 77(3), 525-545.
- [8] Kizilay D, Eliyi DT. (2021). A comprehensive review of quay crane scheduling, yard operations and integrations thereof in container terminals. *Flexible Services and Manufacturing Journal*, 33(1), 1-42.
- [9] Vancea AP, Orha I. (2019). A survey in the design and control of automated guided vehicle systems. *Carpathian Journal of Electronic and Computer Engineering*, 12(2), 41-49.
- [10] Hyla P, Szpytko J. (2017). Automated guided vehicles: the survey. *Journal of KONES*, 24.
- [11] Yang Y, Zhong M, Dessouky Y, Postolache O. (2018). An integrated scheduling method for AGV routing in automated container terminals. *Computers Industrial Engineering*, 126, 482-493.
- [12] Zhang Q, Hu W, Duan J, Qin J. (2021). Cooperative Scheduling of AGV and ASC in Automation Container Terminal Relay Operation Mode. *Mathematical Problems in Engineering*, 2021.
- [13] Chawla V, Chanda A, Angra S. (2018). Scheduling of multi load AGVs in FMS by modified memetic particle swarm optimization algorithm. *Journal of Project Management*, 3(1), 39-54.
- [14] Gola A, K losowski G. (2017, June). Application of fuzzy logic and genetic algorithms in automated works transport organization. In *International symposium on distributed computing and artificial intelligence* (pp. 29-36). Springer, Cham.
- [15] Mishra N, Roy D. and, van Ommeren JK. (2017). A stochastic model for inter terminal container transportation. *Transportation science*, 51(1), pp.67-87.
- [16] Li MP, Kuhl ME. (2017, December). Design and simulation analysis of PDER: A multiple load automated guided vehicle dispatching algorithm. In *2017 winter simulation conference (wsc)* (pp. 3311-3322). IEEE. Scheduling of container-handling equipment during the loading process at an automated container terminal.
- [17] Han Z, Wang D, Liu F, Zhao Z. (2017). Multi-AGV path planning with double-path constraints by using an improved genetic algorithm. *PLoS one*, 12(7), e0181747.
- [18] Hu X, Chen L, Tang B, Cao D, He H. (2018). Dynamic path planning for autonomous driving on various roads with avoidance of static and moving obstacles. *Mechanical systems and signal processing*, 100, 482-500.
- [19] Zhou P, Lin L, Kim KH. (2021). Anisotropic Q-learning and waiting estimation based real time routing for automated guided vehicles at container terminals. *Journal of Heuristics*, pp.1-22.
- [20] Yue L, Fan H, Ma M. (2021). Optimizing configuration and scheduling of double 40 ft dual trolley quay cranes and AGVs for improving container terminal services. *Journal of Cleaner Production*, 292, p.126019. 17.
- [21] Gu W, Li Y, Zheng K, Yuan M. (2020). A bio-inspired scheduling approach for machines and automated guided vehicles in flexible manufacturing system using hormone secretion principle. *Advances in mechanical engineering*, 12(2), p.1687814020907787.
- [22] Yan X, Zhang C, Luo W, Li W, Chen W, Liu H. (2012). Solve traveling salesman problem using particle swarm optimization algorithm. *International Journal of Computer Science Issues (IJCSI)*, 9(6), 264.
- [23] Cheng S, Sh Y. (2011, April). Diversity control in particle swarm optimization. In *2011 IEEE Symposium on Swarm Intelligence* (pp. 1-9). IEEE.
- [24] Ding J, Liu J, Chowdhury KR, Zhang W, Hu Q, Lei J. (2014). A particle swarm optimization using local stochastic search and enhancing diversity for continuous optimization. *Neuro computing*, 137, 261-267.
- [25] Bonyadi MR, Michalewicz Z. (2017). Particle swarm optimization for single objective continuous space problems: a review. *Evolutionary computation*, 25(1), 1-54.
- [26] Freitas D, Lopes LG, Morgado-Dias F. (2020). Particle swarm optimization: a historical review up to the current developments. *Entropy*, 22(3), 362.
- [27] Li N, Li YX. (2012). A Diversity Guided Particles Swarm Optimization. In *Advanced Materials Research* (Vol. 532, pp. 1429-1433). Trans Tech Publications Ltd.
- [28] Han F, Liu Q. (2014). A diversity-guided hybrid particle swarm optimization based on gradient search. *Neuro-computing*, 137, 234-240.
- [29] Wang D, Tan D, Liu L. (2018). Particle swarm optimization algorithm: an overview. *Soft Computing*, 22(2), pp.387-408.

- [30] Abdel-Kader RF. 2018. An improved PSO algorithm with genetic and neighborhood-based diversity operators for the job shop scheduling problem. *Applied Artificial Intelligence*, 32(5), pp.433-462.
- [31] Ayari A, Bouamama S. (2019). ACD3GPSO: automatic clustering-based algorithm for multi-robot task allocation using dynamic distributed double-guided particle swarm optimization. *Assembly Automation*.
- [32] Song Z, Liu B, Cheng H. (2019). Adaptive particle swarm optimization with population diversity control and its application in tandem blade optimization. *Proceedings of the Institution of Mechanical Engineers, Part C: Journal of Mechanical Engineering Science*, 233(6), 1859-1875
- [33] Ahmadian, M.M., Khatami, M., Salehipour, A. and Cheng, T.C.E., 2021. Four decades of research on the open-shop scheduling problem to minimize the makespan. *European Journal of Operational Research*, 295(2), pp.399-426.
- [34] Chin IL, Ioannou PA. (2002). A Comparison of Different AGV Dispatching Rules in an Automated Container Terminal. *The IEEE 5th International Conference on Intelligent Transportation Systems*, IEEE, Si.
- [35] Heger, Jens, and Thomas Voß. "Dynamic priority based dispatching of AGVs in flexible job shops." *Procedia CIRP* 79 (2019): 445-449.ngapore, pp. 880-885.
- [36] Valledor P, Gomez A, Priore P, Puente J. (2018). Particle swarm optimization algorithm: an overview. *Soft Computing*, 22(2), 387-408.
- [37] Cai, B., Huang, S., Liu, D. and Dissanayake, G., 2014. Rescheduling policies for large-scale task allocation of autonomous straddle carriers under uncertainty at automated container.
- [38] Xin, J., Negenborn, R.R. and Lodewijks, G., 2014. Rescheduling of interacting machines in automated container terminals. *IFAC Proceedings Volumes*, 47(3), pp.1698-1704.
- [39] Kuster J, Jannach D, Friedrich G. (2010). Applying local rescheduling in response to schedule disruptions. *Annals of Operations Research*, 180(1), 265-282.
- [40] Zaghdoud, R., Mesghouni, K., Dutilleul, S. C., Zidi, K., Ghedira, K. A Hybrid Method for Assigning Containers to AGVs in the Dynamic Environment of Container Terminals. *Studies in informatics and control*, 2015, Vol. 24, No. 1, pp. 43-50. ISSN 1220-1766.

A New Approach for Detecting and Mitigating Address Resolution Protocol (ARP) Poisoning

Ahmed A.Galal^{1*}

Department of Network
Misr University for Science and
Technology Giza, Egypt

Atef Z.Ghalwash²

Department of Computer Science
Faculty of Computers and Artificial
Intelligence, Helwan University
Cairo, Egypt

Mona Nasr³

Department of Information Systems
Faculty of Computers and Artificial
Intelligence, Helwan University
Cairo, Egypt

Abstract—Address Resolution Protocol (ARP) Poisoning attack is considered as one of the most devastating attacks in a network context. As a result of its stateless nature and lack of authentication, this protocol suffers from many spoofing attacks in which attackers poison the cache of hosts on the network. By sending spoofed ARP requests and replies. This paper proposes an approach for detecting and mitigating ARP poisoning. This approach includes three modules: Module 1 for giving permission for first time and to store information in the database. There a security measure using MD5 hash is used. Module 2 is for avoiding internal ARP. Module 3 is for detecting whether a MAC has two IPs or an IP has two MACs. The architecture includes a database that gives a great facility and support for storing ARP table information. As ARP table entries generally expire after a short amount of time. To ensure changes in the network are accounted for. Experiments were conducted on real life network environment using Ettercap to check the functionality of the proposed mechanism. The results of experiments show that the proposed approach was able to detect and mitigate ARP poisoning. Especially, whether a MAC has two IPs or an IP has two MACs.

Keywords—Address Resolution Protocol (ARP); ARP detecting; ARP mitigation; ARP spoofing

I. INTRODUCTION

The security of the network is becoming a major concern for network managers and engineers. Traditional networks are vulnerable to a variety of security flaws and assaults. In order to identify the attacks or infections, anti-virus software or an intrusion detection system (IDS) might be used. Inconsistency in communications between hosts, on the other hand, exacerbates security concerns. Security techniques that can be effectively used in network innovation are in short supply.

The fundamental reason for such assaults is a breakdown in communication between security innovation engineers and network designers [1]. A programmer will concentrate on the communication channel, collect data, decode it, and re-insert a copy message. The most important aspects to consider while constructing a secure network are confidentiality and integrity. The variety of attacks, on the other hand, continues to grow with the passage of time [2].

Address Resolution Protocol (ARP) is a mechanism for mapping Internet Protocol (IP) addresses to Media Access Control (MAC) addresses that is widely used. ARP, on the other hand, has a number of flaws. For example, there is no

built-in way for a receiving node to verify the sender of a packet [3]. The ARP process excludes any authentication or integrity verification and is unconcerned whether the packet originates from a legitimate source. Any packet that has its fields filled from the allowed set of values is right.

As a result, ARP is a stateless protocol. The nodes can send ARP answers without receiving an ARP request first. Attackers use these weaknesses in ARP to carry out the ARP Cache Poisoning attack. This attack is carried out in traditional networks by poisoning a host's cache through introducing bogus or spoofed IP to MAC address mappings into the victim's ARP cache table.

The detection and mitigation of ARP Poisoning attacks are critical. Because attackers can use this attack to launch other attacks as Denial of Service (DoS), Distributed Denial of Service (DDoS) and Man-In-The-Middle (MITM) attacks. Attackers can use ARPs to communicate with the system they want to attack since they allow links between networks using IP and MAC addresses. ARP Spoofing leads to simply intercepting or dropping and not forwarding the target's packets.

The paper is organized as follows: Section II presents the related work. Section III introduces the proposed ARP approach. Testing and recorded results are shown in Section IV. Section V has the conclusion and future work.

II. RELATED WORK

The research publications relevant to ARP attack detection and prevention will be presented in this section. A framework has been introduced in [4] to detect any rogue user in the network attempting to impersonate another user. The framework included a built-in security measures to prevent attacks on the framework itself and to prevent having a single point of failure. The framework also used robust security mechanisms including RSA. This initializes the random time intervals to prevent other devices from sending client messages. AES encryption has been used for all subsequent messages.

Authors in [5] have examined the conditions for conducting a Man in the middle (MITM) attack in networks using the Address Resolution Protocol (ARP). In addition to, methods for detecting and preventing such attacks. They presented an implementation of an ARP spoofing attack using Python and

*Corresponding Author.

C# (scapy) languages. They have provided Man-in-the-middle attacks examples such as DHCP spoofing and ICMP redirection. While authors in [6] proposed a detection algorithm that looks for differences between the real MAC Address and the response MAC Address of the ARP Packet sniffed. In addition to, a prevention algorithm for ARP Poisoning attacks using static entries in ARP table. The implementation for both algorithms has been done using Python Programming language using scapy library.

A survey study for the theory of ARP spoofing attacks and the various existing techniques proposed to defend ARP against them was presented in [7]. The study has shown that for best security measures, both detection and prevention systems should be implemented in the network with consideration to minimize the cryptography processes. They also recommended the four security requirements to develop a mechanism approach to detect/prevent ARP spoofing attacks shown in Fig. 1.

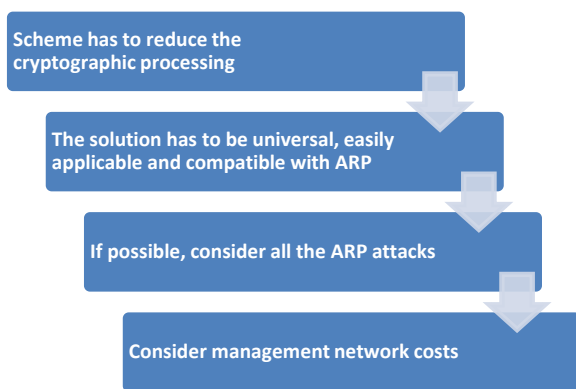


Fig. 1. ARP Detection and Prevention Requirements.

The description of ARP and how it works was discussed in [8]. The topic of ARP Spoofing and its many attacks then has been discussed. Finally, it compared several detection and mitigation approaches, as well as their benefits and drawbacks, in order to combat ARP attacks.

In [9], the authors offered three methods for detecting and preventing ARP spoofing. These methods may have few flaws or disadvantages. Within a LAN, these strategies are simple to implement. Method 1 is the most effective, Method 2 necessitates the creation of a new protocol, and Method 3 is costly and time-consuming owing to software or server deployment. Depending on the needs of the business, any of these strategies can be used.

The authors in [10], looked at various tools and strategies for detecting and preventing Address Resolution Protocol Spoofing attacks. To learn more about how a host maintains the address resolution protocol cache table with a spoofed or false media access control, MAC cache table, the ARP spoof tool was used to send a spoofed Address Resolution Protocol reply packet to a host in a local area network. Lastly, they compared the detection and prevention tools and approaches against the Address Resolution Protocol Spoofing assault in terms of their efficiency in detecting and preventing the attack as well as system performance requirements.

The ARP spoofing attack in traditional networks was investigated in [11]. They first performed ARP spoofing in an SDN network and discovered that the threat of an ARP attack is still present and has a significant impact on the network. They suggested a unique protection method for ARP spoofing based on the OpenFlow platform. The mechanism was given a theoretical analysis, and it was implemented as a module of the POX controller. On the OpenFlow platform and related SDN platforms, this significantly decreased the security danger of ARP spoofing.

A detailed survey on various solutions to mitigate ARP Cache Poisoning attack in SDN was carried out in [12]. Flow graph-based solutions, traffic pattern-based solutions, and IP-MAC Address Bindings-based solutions were all characterized in this survey. All of these solutions were assessed rigorously in terms of their functioning principles, benefits, and drawbacks. Another key element of this study was the ability to compare different systems based on numerous performance measures, such as attack Detection time, ARP response time, delay calculation at the controller, and so on.

Thus, all the pervious related works solutions considered ARP cache table in switch for either detecting or mitigating ARP poisoning. Without resolving the problem in which, the ARP cache table may be destroyed. If the switch is restarted or if an administrator action is performed.

III. PROPOSED ARP APPROACH

The proposed ARP approach in this paper consisted of three modules that will effectively detect and mitigate ARP cache poisoning in real life network. The proposed approach overview is shown in Fig. 2. Module 1 is responsible for initialization of eligible new user. Where information will be stored in the database; in addition, checking information of eligible users before going to module 2. Detecting and mitigating internal ARP will be occurred in module 2. While external ARP detection and mitigation will be in module 3. Where intruder is either an IP with two MACs or a MAC has two IPs.

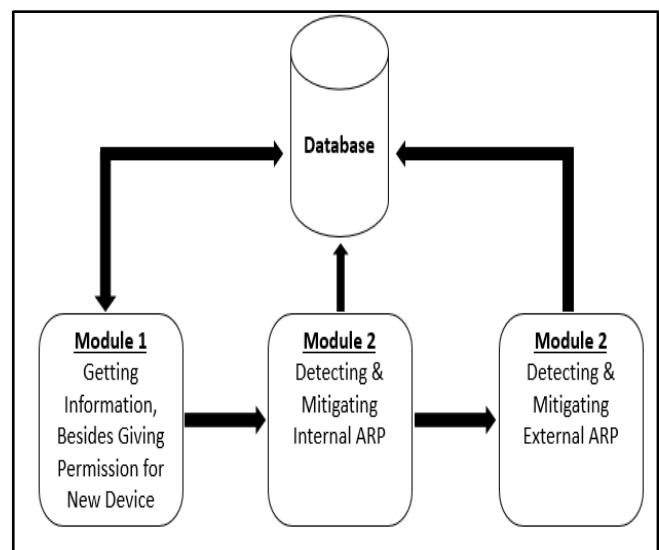


Fig. 2. Proposed Approach Overview.

The database was added to check and compare ARP table content. As the typical timeout for ARP cache is from 10 to 20 minutes [13] [14] [15], thus this made the cache to be cleared automatically. In addition to, the ARP cache table may be deleted due to switch restarting or an admin action. The database was designed to store the following ARP information:

- IP Address.
- MAC Address.
- Hash for IP + MAC.
- Port Number.
- Time.
- Date.
- Switch IP.

The database facilitates the detection of whether a MAC has two IPs or an IP has two MACs.

A. Module 1

Fig. 3 represented the flowchart for module 1. Module 1 was designed for getting and checking device data in database to decide whether forwarding device packets or not. In case which data was found, and then move to module 2. While if not found, an admin has to decide whether to give permission for that device to join network or to block device. In addition module 1 included adding a device that first time asks to join network. After assigning IP to joined device MAC, the proposed approach pop up a message showing this IP with its MAC.

If yes the following information will be stored in the database <IP, MAC, Hash for IP + MAC, Port Number, Time, Date, Switch IP> (first-give-permission) this scenario repeated each new device joined. The hash for IP and MAC has been done using MD5. A 128-bit fingerprint is generated by encoding a string of arbitrary length into an MD5 hash. The MD5 algorithm will always provide the same 128-bit hash value when encoding the same string. When storing sensitive data in databases like MySQL, MD5 hashes are typically utilized with smaller strings [16].

B. Module 2

To avoid internal ARP, module 2 was proposed as in Fig. 4. After checking device data in the database, Module 2 has to check IP and mac stored in switch ARP table. If found, the hash for that IP and MAC would be compared with the stored in the database. If the comparison result was match then, forward packet otherwise go to module 3. While if the hash for IP and MAC was not found in switch ARP table. Check for hash of IP and MAC in the database. If found, switch ARP table will be updated, then return to the start of module 2. If not found, move to module 3.

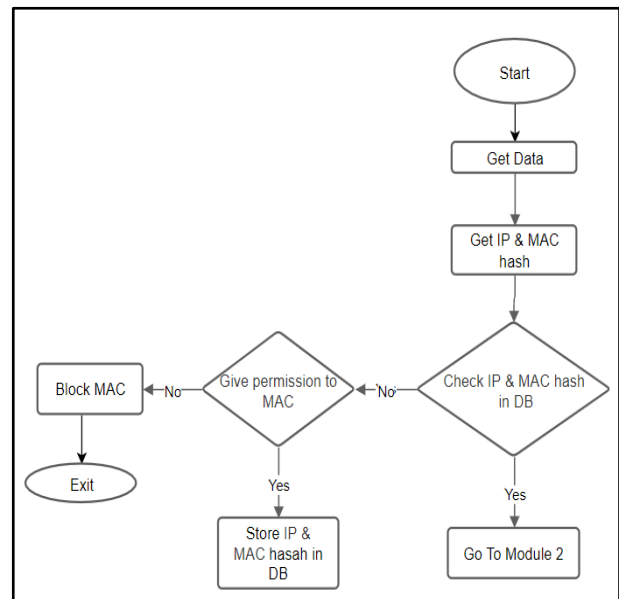


Fig. 3. Module 1 Flowchart.

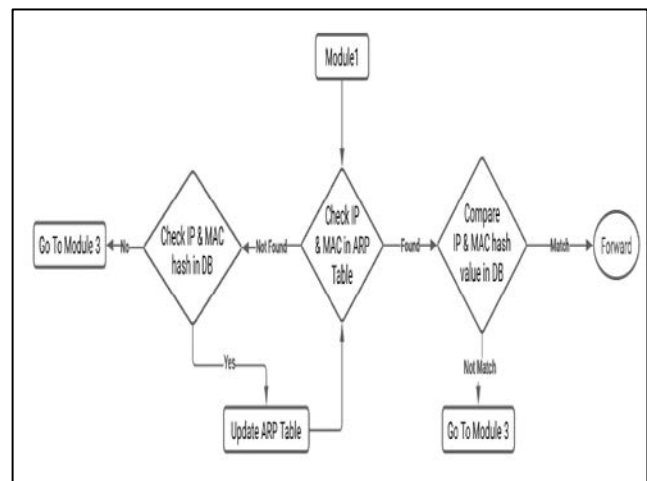


Fig. 4. Module 2 Flowchart.

C. Module 3

Module 3 as shown in Fig. 5, was designed to detect whether a MAC has two IPs or an IP has two MACs. In case of an IP has more than one MAC. The module will retrieve all MAC hashes from the database. Then it will check which MAC belongs to that IP from the database. The packet will be forwarded if MAC belongs to that IP was matched in the database. Otherwise an admin has to decide either to block MAC or to forward packet. The second case is in which a MAC has two IPs. All IPs hashes will be retrieved from the database. Checking which IP belongs to that MAC hash in the database. Besides checking which IP is active. If the result is matched and active then forward the packet. If not matched the admin has to choose either to update the database with new IP, or to block this MAC.

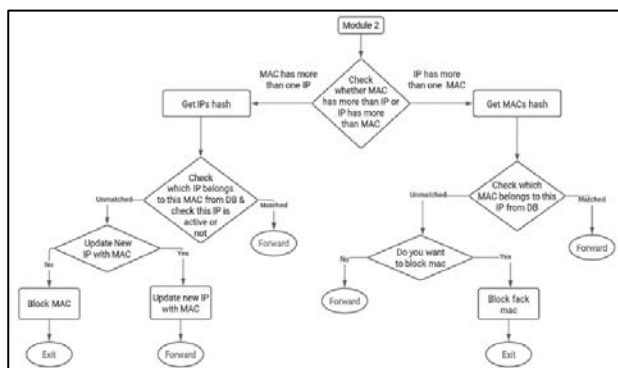


Fig. 5. Module 3 Flowchart.

IV. TESTING AND RESULTS

This section will illustrate environment setup for the proposed approach. Besides presenting test cases and results, the proposed approach architecture is shown in Fig. 6. In which, two eligible devices were connected. The attacker (intruder) was trying to control the switch that was synchronized with database.

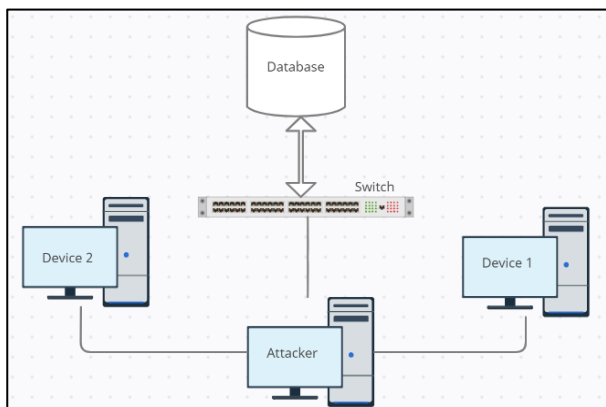


Fig. 6. Proposed Approach Architecture.

A. Environment Setup

The following tools and libraries are required to build up the environment for the suggested approach:

- VMware Workstation Pro [17]: is a hosted hypervisor that works with x64 versions of Windows and Linux. Users can create Virtual Machines on a single device with VMWare Workstation Pro. The Virtual Machines can then be used with the physical machine at the same time.
- Kali Linux [18]: Kali Linux is a Debian-based Linux distribution operating system designed for digital forensics and penetration testing.
- Scapy [19]: is a computer network packet manipulation tool. Using scapy, packets can be faked, decoded, sent over the wire, captured, and Requests and responses can be matched.
- Netmiko [20]: is a multi-vendor library that makes it easier for Paramiko to connect to network devices via SSH.

- Ettercap [21]: can deconstruct various protocols (even encrypted ones) both actively and passively, and it has a lot of features for network and host investigation.

One kali Linux virtual machine was created to work as attacker using Ettercap.

- MySQL Database [22]: gives consumers the flexibility, scalability, and availability they need to handle the database problems of next-generation web, cloud, and communications services. The database was connected with the proposed approach using mysql.connector.
- Python [23]: Python is a general-purpose programming language with a high level of abstraction. Its design philosophy priorities code readability and makes extensive use of indentation.

B. Phase 1 “Initialization” Testing and Results

In this phase, module 1 checked the database to either allow or deny connecting a new node. Fig. 7 represented that the database was empty. In addition, the proposed approach popped up a message for adding new node. Fig. 8 presented the database after storing a new device information in which, MAC [00:0c:29:dd:29:c8] with IP [172.19.15.18] was successfully added.

C. Phase 2 “Authentication” Testing and Results

Besides matching between the database and the ARP table for authenticating IP and MAC, Phase 2 included checking for IP and MAC in the ARP table or not, which was happened in module 2. Check for IP with its MAC in ARP table. If it is found in the ARP table then the hashed value for IP and MAC is compared with the database.

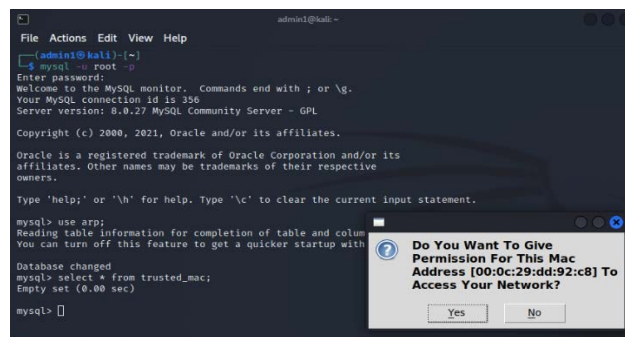


Fig. 7. Empty Database.

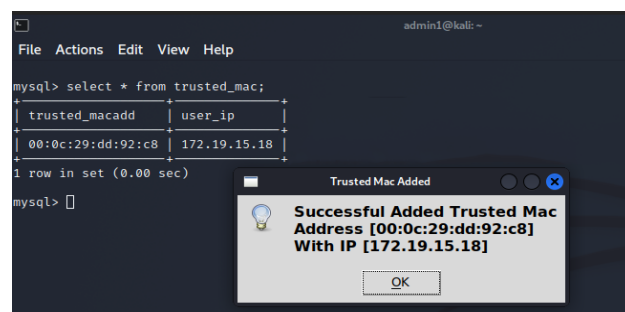


Fig. 8. Adding New Device in the Database.

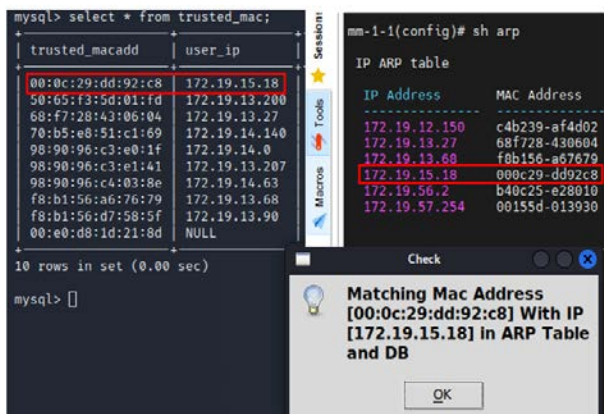


Fig. 9. Check for MAC with IP in Both ARP Table and Database.

The proposed approach popped up a message for MAC [00:0c:29:dd:92:c8] with IP [172.19.15.18] in case of matching and founding in both ARP table and the database as in Fig. 9. If not matched go to module 3.

Fig. 10 shows the case in which MAC [50:65:f3:5d:01:fd] with IP [172.19.13.200] was not found in ARP table. The proposed approach would check for stored MAC and IP hashes in the database. If not found then, it would move to module 3. While in case of found, the proposed approach would update the ARP table automatically in Fig. 11.

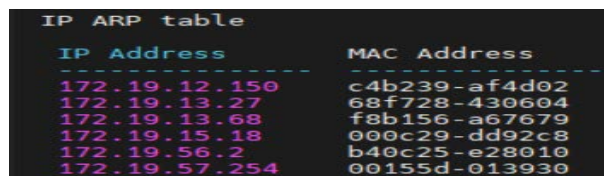


Fig. 10. ARP Table before Update.

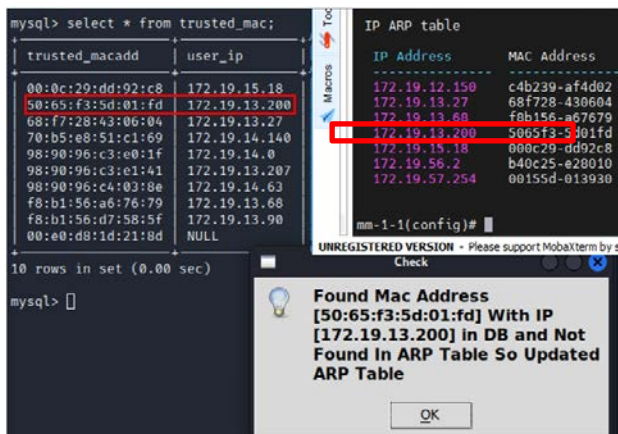


Fig. 11. ARP Table after Updating.

D. Phase 3 “Poisoning Detection & Classification” Testing and Results

Module 3 where classification and detection of whether an IP has two MACs or a MAC has two IPs, was tested in this phase. The first case included testing of a MAC has more than one IP. All IPs hashes was retrieved from the database. Then, the original IP belonged to this MAC was checked in the database as in Fig. 12. Where the ARP table showed MAC

[f8:b1:56:a6:76:79] with IP [172.19.12.201] and [172.19.13.68]. While the database showed that IP for MAC [f8:b1:56:a6:76:79] was [172.19.13.68]. The packet of the active and original IP would be forwarded and the other IP would be released. While if not active the admin has to decide either to update the database with new IP or to block the MAC as in Fig. 13.

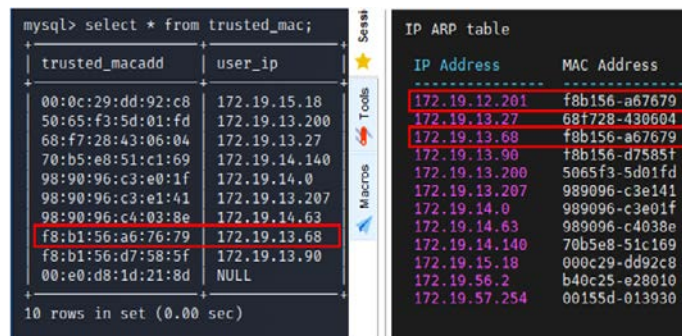


Fig. 12. Check for Original IP.

The second case was for one IP with more than one MAC. The original MAC was checked from the database after getting all MACs hashes. The packet of the matched one was forwarded. But if not matched, the proposed approach popped up a message alerting that ARP poisoning was happened as in Fig. 14. Where IP [172.19.13.207] has original MAC [98:90:96:c3:e1:41] and fake MAC [00:0c:29:dd:92:c8]. Thus, the admin has to decide either to block fake MAC or not.

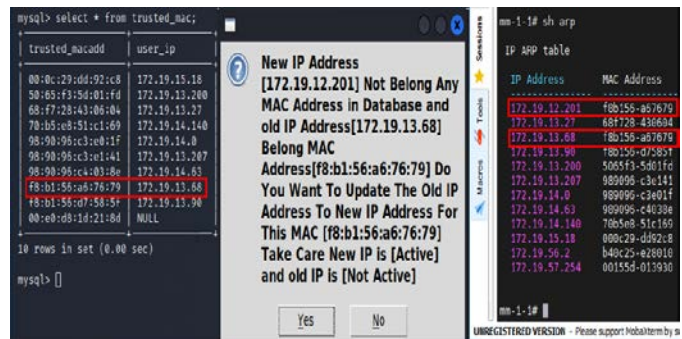


Fig. 13. Update IP or Block MAC.

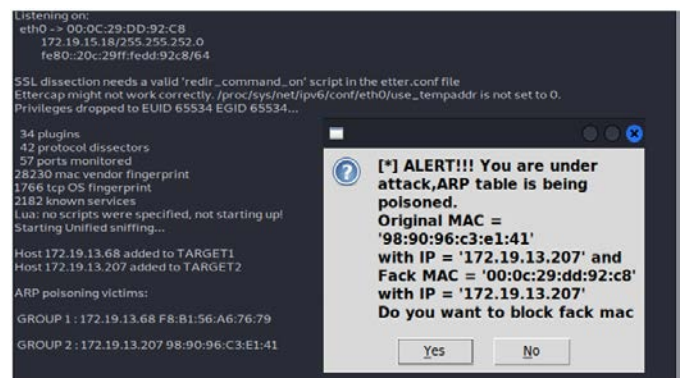


Fig. 14. IP with Two MACs.

V. CONCLUSION AND FUTURE WORK

This research proposed a new approach for detecting and mitigating ARP poisoning attack. The database was added to the proposed approach architecture for storing information from switch. Avoiding missing the data as typical timeout for ARP cache is from 10 to 20 minutes. Furthermore, the ARP cache table may be deleted due to switch restarting or an admin action. The proposed approach has included three modules. The first one was for getting data and storing it in the database. Besides giving permission for new joining device, the second one was for checking IP and MAC in both ARP table and comparing them with the stored records in the database.

The comparison has been done for hashing of IPs and MACs that were stored in the database. The used function for hashing IP and MAC was MD5 function. The third module was to detect either a MAC has more IPs or an IP has more MACs. Where a successful detection for both cases has been done and presented in testing and results shown in Fig. 12, 13 and 14. The ARP poisoning attack was generated using Ettercap.

For future work, the proposed approach may be applied for detecting ARP poisoning in Software Defined Network (SDN). The proposed approach may also apply for other attacks as Man-In-The-Middle (MITM) attack.

REFERENCES

- [1] C. D.Francis Xavier and C.Divya, "Address Resolution Protocol Based Attacks: Prevention and Detection Schemes," in *Proceeding of the International Conference on Computer Networks, Big Data and IoT (ICCBi - 2018)*, Springer, 2019, p. 247–256.
- [2] M. Conti, N. Dragoni and V. Lesyk, "A Survey of Man In The Middle Attacks," *IEEE Communications Surveys & Tutorials*, vol. 18, no. 3, pp. 2027 - 2051, 2016.
- [3] Z. Shah and S. Cosgrove, "Mitigating ARP Cache Poisoning Attack in Software-Defined Networking (SDN): A Survey," *Electronics*, 2019.
- [4] K. D. Bhattacharya, N. S. H. Karthick, P. Suresh and N. Bhalaji, "DetecSec: A Framework to Detect and Mitigate ARP Cache Poisoning Attacks," in *Evolutionary Computing and Mobile Sustainable Networks*, Springer, 2022, p. 997–1007.
- [5] P. P. Stepanov, G. V. Nikonova, T. S. Pavlychenko and A. S. Gil, "The problem of security address resolution protocol," *Journal of Physics: Conference Series*, 2021.
- [6] A. Majumdar, S. Raj and T.Subbulakshmi, "ARP Poisoning Detection and Prevention using Scapy," *Journal of Physics: Conference Series*, 2021.
- [7] S. Hijazi and M. S. Obaidat, "Address resolution protocol spoofing attacks and security approaches: A survey," Wiley, 2019.
- [8] R. Vaishnavi and S. Goyal, "A Detailed Survey for Detection and Mitigation Techniques against ARP Spoofing," in *2020 Fourth International Conference on I-SMAC (IoT in Social, Mobile, Analytics and Cloud) (I-SMAC)*, Palladam, India, 2020.
- [9] G. Agrawal and V. Chennai, "Detection and Prevention of ARP-Spoofing Attacks," *International Journal of Engineering Research & Technology (IJERT)*, vol. 8, no. 10, 2019.
- [10] T. A. ASSEGIE and P. S. NAIR, "COMPARATIVE STUDY ON METHODS USED IN PREVENTION AND DETECTION AGAINST ADDRESS RESOLUTION PROTOCOL SPOOFING ATTACK," *Journal of Theoretical and Applied Information Technology*, vol. 97, no. 16, 2019. J. Clerk Maxwell, *A Treatise on Electricity and Magnetism*, 3rd ed., vol. 2. Oxford: Clarendon, 1892, pp.68–73.
- [11] X. Jing, C. Zhiping, H. Gang and X. Ming, "An Active Defense Solution for ARP Spoofing in OpenFlow Network," *Chinese Journal of Electronics*, vol. 28, no. 1, 2019. K. Elissa, "Title of paper if known," unpublished.
- [12] Z. Shah and S. Cosgrove, "Mitigating ARP Cache Poisoning Attack in Software-Defined Networking (SDN): A Survey," *Electronic*, 2019.
- [13] "The Windows Club," 8 September 2021. [Online]. Available: <https://www.thewindowsclub.com/how-to-clear-arp-cache-in-windows>. [Accessed 29 March 2022].
- [14] "Network Command Reference," [Online]. Available: [https://netref.soe.ucsc.edu/node/20#:~:text=The%20typical%20lifetime%20of%20an.20%20minutes\)%20have%20been%20observed..](https://netref.soe.ucsc.edu/node/20#:~:text=The%20typical%20lifetime%20of%20an.20%20minutes)%20have%20been%20observed..) [Accessed 29 March 2022].
- [15] "parsons-technology.com," [Online]. Available: <https://parsons-technology.com/how-do-i-scan-arp-on-windows/>. [Accessed 29 March 2022].
- [16] "MD5 Hash Generator," [Online]. Available: <https://www.md5hashgenerator.com/>. [Accessed 1 August 2021].
- [17] [Online]. Available: <https://www.vmware.com/products/workstation-pro/workstation-pro-evaluation.html?msclkid=035ab3aeb19811ecbf27f7efbb37856b>. [Accessed 28 July 2021].
- [18] [Online]. Available: <https://www.kali.org/docs/installation/?msclkid=e7d930bab19a11ecb69ac0998f02a7ce>. [Accessed 29 July 2021].
- [19] [Online]. Available: <https://scapy.net/?msclkid=0a6c51adb19c11eca81cb4bd35facb34>. [Accessed 29 July 2021].
- [20] [Online]. Available: <https://pypi.org/project/netmiko/?msclkid=dde5ec40b19c11ecbfdcce04f1742acf>. [Accessed 29 July 2021].
- [21] [Online]. Available: <https://www.ettercap-project.org/?msclkid=c140605fb19d11ec9eb5e091e216729e>. [Accessed 30 July 2021].
- [22] [Online]. Available: <https://www.mysql.com/?msclkid=79374b5ab19e11ec807d6d6e8b4f38b6>. [Accessed 30 July 2021].
- [23] [Online]. Available: <https://www.python.org/?msclkid=fb10350cb1a211ec86584fd4b5ede560>. [Accessed 30 July 2021].

Cross-Layer based TCP Performance Enhancement in IoT Networks

Sultana Parween, Syed Zeeshan Hussain

Department. of Computer Science
Jamia Millia Islamia
New Delhi, India

Abstract—Transmission Control Protocol (TCP) used multiple paths for performing transmission of data simultaneously to improve its performance. However, previous TCP protocols in Internet of Things (IoT) networks experienced difficulty to transmit a greater number of subflows. To overcome the above issues, we introduced cross-layer framework to perform efficient packet scheduling and congestion control for increasing the performance of TCP in IoT networks. Initially, the proposed IoT network is constructed based on grid topology using Manhattan distance which improves the scalability and flexibility of the network. After network construction, packet scheduling is performed by considering numerous parameters such as bandwidth, delay, buffer rate, etc., using fitness based proportional fair (FPF) scheduling algorithm and selecting best subflow to reduce the transmission delay. The scheduled subflow is sent over an optimal path to improve the throughput and goodput. After packet scheduling, congestion control in TCP is performed using cooperative constraint approximation 3^+ (CoCoA 3^+ -TCP) algorithm in which three stages are employed namely congestion detection, fast retransmission, and recovery. The congestion detection in TCP-IoT environment is performed by considering several parameters in which cat and mouse-based optimization (CMO) is utilized to adaptively estimate retransmission timeout (RTO) for reducing the delay and improving the convergence during retransmission. Fast retransmission and recovery are performed to improve the network performance by adjusting the congestion window size thereby avoiding congestion. The simulation of cross-layer approach is carried out using network simulator (NS-3.26) and the simulation results show that the proposed work outperforms high TCP performance in terms of throughput, goodput, packet loss, and transmission delay, jitter, and congestion window size.

Keywords—Internet of things (IoT); transmission control protocol (TCP); cross-layer approach; packet scheduling; congestion control; fast retransmission; recovery

I. INTRODUCTION

In recent days, Internet of Things (IoT) is an emerging technology that provides connectivity between various heterogeneous devices to send data through the network. Various sensor nodes act as IoT devices that are interconnected and it is applied for various applications such as health care, home automation, environmental monitoring, transportation, and management of infrastructure [1], etc. Several IoT protocols are used for performing data transmission between heterogeneous IoT devices such as AMQP (advanced message queuing protocol), MQTT (message queuing telemetry transport) and CoAP (constrained

application protocol), HTTP (HyperText Transfer Protocol), and XMPP (Extensible Messaging and Presence Protocol). These protocols are provided effective communication among IoT devices that are used in applications such as embedded systems and industrial 4.0 [2]. However, various challenges are present in IoT data transmission between sensor nodes due to their individual transmission rate which leads to high network congestion [3]. To overcome such challenges Transmission Control Protocol (TCP) which is a transport layer protocol is introduced for efficient data transmission because it transmits huge amount of data traffic globally and is constrained to handle network blockage by reducing the congestion in the IoT environment and also enhances the quality of service (QoS) [4], [5]. This protocol provides effective data transmission with better performance in terms of load, connectivity, reliability, low latency, and speed when compared with user datagram protocol (UDP) [6], [7].

However, several challenges are present in TCP protocol which affects the data transmission by fixed round trip time (RTT) and retransmission timeout (RTO), transmission delay, high buffer rate, bandwidth consumption, etc. that leads to high data congestion. The challenges in TCP affect the performance of the network [8], [9]. Several approaches are introduced to control the congestion occurred in TCP by implementing CoCoA, CoCoA $^+$, etc. algorithm [10] for classifying weak RTT. However, these algorithms are suffered from severe issues in affecting the network performance, so there would be an improvement in those algorithms must be needed and perform exponential backoff by estimating RTT and RTO however, the frequent retransmission in the network leads to congestion in the network [11]. Congestion control is performed by adjusting the size of congestion window (CWND) after successful recovery. The precise changes in congestion window with respect to the available bandwidth improve the throughput. Some of the works focused on adjusting the congestion window size by considering only limited assumptions. However, the precise analytical justification was not provided which affects the reliability [12]. Retransmission is performed if RTO is expired. After duplicate acknowledges, retransmission is performed. Several works need high retransmission attempts for better recovery [13]. Packet scheduling is performed to avoid congestion by selecting optimal paths and sub-flows [14]. Queue scheduling and path scheduling are also performed for congestion avoidance [15]. Several challenges are present in packet scheduling such as high consumption of bandwidth, high transmission delay, and degradation of throughput which

affects the efficiency of congestion control [16]. However, efficient packet scheduling with congestion control is still in demand.

A. Motivation and Objectives

In this study, the transmission control protocol for cross-layer approach in IoT is designed for improving the performance of the network. This research also addresses the problems of high bandwidth consumption, high packet loss, high transmission latency, and low throughput to enhance TCP performance. The performance of TCP is affected by high packet loss, throughput degradation, high transmission latency, and bandwidth consumption. The existing works address these problems but, still, it does not provide a proper solution for TCP performance improvement. We are motivated by the major problems of this research which are listed below:

- **Inappropriate Congestion Control:** The existing works perform congestion control by considering RTT and RTO information; however, they did not estimate based on the current network status which leads to high packet loss and transmission delay. In addition, the count of duplicate acknowledgement (DACK) also affects the process of fast retransmission and fast recovery which degrades the throughput and Goodput.
- **High Bandwidth Consumption:** The existing work utilizes fixed RTO for congestion control mechanism which consumes high bandwidth when the packet transmission is completed before RTO expired; the completed packets need to wait until the RTO gets over. Further, the existing path selection methods consume high bandwidth as the initial data was sent over multiple paths in the network to find the optimal path.
- **Inefficient Scheduling:** In scheduling, most of the works only consider limited parameters (RTT, loss rate, and bandwidth) for packet scheduling and optimal path selection which provides inefficient scheduling which increases high jitter and packet loss. In addition, existing random subflow selection achieves high packet loss due to no consideration of completion time.

The above major gaps in the existing works motivated us to provide an effective objective in TCP. The major objective of this research is to reduce packet loss, and transmission latency and increase throughput and Goodput by performing packet scheduling and congestion control using cross-layer approach [17]. The other sub-objective of this research is listed as follows,

- To reduce jitter and transmission latency by performing efficient packet scheduling by considering several metrics such as transmission rate, queue length, completion time, etc. which improves the performance of congestion control.
- To increase the performance of TCP by performing cross layer-based congestion control in which the RTO is estimated by considering the current status of the

network which increases the performance of congestion control.

- To increase the performance of fast retransmission and fast recovery by reducing the count of DACK that reduces transmission latency during data transmission.

B. Research Contribution

The proposed CoCoA3⁺-TCP approach introduced cross-layer framework to improve the performance of TCP in IoT environment. The major contributions of this research are sorted as follows,

- Firstly, network construction is performed based on grid topology to increase the flexibility and scalability of the network which leads to high communication efficiency with low transmission delay.
- Secondly, packet scheduling is performed by implementing fitness based proportional fair (FPF) scheduling algorithm and selecting of best subflows and optimal path to reduce the jitter and transmission delay efficiently.
- Finally, congestion control in TCP is performed using CoCoA3⁺-TCP algorithm by congestion detection and avoidance, fast retransmission, and recovery to improve the throughput and goodput which reduces the packet loss.

The performance of the proposed CoCoA3⁺-TCP method is evaluated by considering several performance metrics to illustrate the performance of TCP such as throughput, goodput, packet loss, transmission delay, jitter, and congestion window size.

C. Paper Organization

The rest of the paper is organized as follows, Section II provides the existing works and its research gaps, section III emphasizes some specific problems in this field, and corresponding solutions are also provided. Section IV illustrates the proposed work with detailed explanation, relevant diagrams, equations, and pseudocodes. Section V explains the experimental analysis which consists of simulation setup, comparative analysis, and summary of the research are provided. Section VI tells about the conclusion and possible future direction of the proposed method.

II. LITERATURE SURVEY

This section represents the literature survey of the previous approaches to increase the performance of TCP in terms of packet scheduling and congestion control. In addition, the research gaps in the previous methods are also described in this section.

A. Packet Scheduling Schemes

This sub-section describes the related works which were proposed for performing packet scheduling to increase the performance of TCP.

Authors in [18], proposed novel congestion control method for multipath TCP. The proposed work performed congestion control and scheduling for improving the performance of TCP.

This research used explicit congestion notification method for detection of shared bottleneck, which includes two processes such as subflow monitoring noticing the segment of TCP and estimating the congestion degree, and verification of shared bottleneck. Based on the shared bottleneck, congestion control is performed. Then packet scheduling is performed by considering fastest subflow, which is arranged based on RTT. Finally, simulation result shows that the proposed work achieved better performance in terms of throughput and detection accuracy. For subflow scheduling, this research only considers RTT which is not enough for optimal subflow scheduling leading to inefficient scheduling, therefore it degrades the performance of multipath TCP.

In [19], authors proposed an efficient packet scheduling method for improving the performance of multipath TCP. The proposed scheduling algorithm computes the number of packets is sent for every path. For that, optimal path is selected by considering buffer rate and completion time, and RTT. In addition, congestion control is performed based on the size of congestion window. For every path selection, congestion window size is evaluated and updated. The experimental results demonstrate that the proposed work achieved superior performance compare to existing approaches. Here, optimal path is selected by considering limited parameters which are not enough for selecting optimal path; hence it leads to degradation of throughput and Goodput.

Authors proposed coupled bottleneck bandwidth and round-trip propagation time (BBR) for improving the performance of multipath TCP by performing congestion control in [20]. The proposed work includes two phases such as congestion control and adaptive scheduling. Initially, coupled BBR evaluates the bandwidth for allocating the sending rate for every subflow for performing congestion control. Then scheduler selects the optimal path by considering the RTT and bandwidth to increase reliability and robustness. Here, packets are scheduled using pre-scheduling algorithm. The experimental result shows that the proposed work achieved better performance in terms of throughput and Goodput. Here, packet scheduling is performed by using pre-scheduling algorithm. However, it considers only limited parameters for scheduling which is not enough for optimal scheduling, in addition, random subflow based scheduling is performed which leads to high transmission latency and low throughput.

Authors proposed an approach to perform congestion control based on cross-layer in the wireless sensor network using fuzzy sliding method for controlling the modes [21]. Initially, signal to noise ratio (SNR) was applied to the channel in the TCP model with cross-layer-based congestion control in the middle of MAC layer, and transmission layer. Then integrating the sliding-mode control with fuzzy control for designing the Fuzzy-Sliding Mode Controller (FSMC) manages the buffer queue length in the congested nodes adaptively. Finally, NS-2.35 was used to perform simulation for comparing the proposed approach with several state-of-the-art methods in terms of packet loss, throughput, convergence, and delay. Here congestion control was performed using FSMC. However, lack of considering the priority of packets leads to high packet loss.

In [22], authors proposed an approach to perform congestion control and scheduling in the wireless network dynamically for reducing the delay. Initially, scheduling of selected data flow was performed to minimize the end-to-end delay using virtual rate scheduling algorithm which modifies the scheduling scheme. Flow control was performed based on windows to reduce the buffer overflow. In scheduling, each slot is decoupled into various mini-slots for low complexity. In addition, the congestion control was effectively performed by separating the mini-slots into numerous micro slots. Adjustment of virtual rate was performed to identify the priority of every flow link.

Authors proposed multi-path scheduling and congestion control by implementing deep reinforcement learning approach [23]. Initially, packet scheduling and congestion control framework was proposed by implementing deep Q learning (DQL) for the multipath TCP. The DQL technique was used to perform congestion control and scheduling optimally by the intelligent agents based on experience using policy gradients. Dynamic scheduling and congestion control were performed across all network paths by integrating the DQL with policy gradients. Recurrent neural network and long-short term memory algorithm were used to learn the behavior of paths and adjusts the scheduling and congestion control appropriately. Finally, experimental analysis was performed by comparing the performance of this approach with existing multipath TCP algorithms.

B. Congestion Control Schemes

This sub-section describes the related works which were proposed for controlling the congestion to increase the performance of TCP.

A dynamic congestion window algorithm for IoT environment was proposed by the authors in [24]. The main objective of this research is to minimize the delay and maximize the packet delivery ratio. In this research, congestion window size is dynamically changed based on the transmission rate, and bandwidth. The congestion window is adjusted only when the paths need to transmit the data. The simulation results demonstrate that the proposed work achieved superior performance in terms of packet delivery ratio, delay, and throughput. Here, the congestion window is adjusted based on the transmission rate and bandwidth which is not enough for congestion control due to lack of significant parameters such as RTO, RTT, and queue status, hence it leads to poor congestion.

A novel congestion control algorithm to improve the performance of improved multipath TCP was proposed in [25]. The main aim of this research is to reduce the delay and increase the throughput. The proposed work includes four processes such as startup, drain, probe bandwidth, and probe RTT which estimate the size of the congestion window considering pacing rate, congestion window, and send quantum. In this way, congestion control is performed for improving the performance of multipath TCP. The simulation result shows that proposed work achieved better performance in terms of throughput compared to existing approaches.

A novel method to improve the performance of TCP was proposed in [26] by considering queue size, retransmission, medium access control (MAC) overhead, and node energy. Here, the contention window is adjusted based on residual energy, queue size, slot time, and congestion window. Scheduling is done by estimating backoff time in a dynamic manner which improves the performance of TCP. The experimental result shows that the proposed work achieved better performance in terms of throughput, overhead, and energy consumption.

The congestion control mechanism for multipath TCP based on the flow control of the data was proposed by the authors in [27]. The proposed congestion control algorithm includes two main goals; first one is enhancing the throughput compared to single-path TCP. Second one is collecting the subflows by shared bottleneck. The bottleneck detection is performed based on RTT, packet loss, and congestion notification. For that purpose, this research proposed three filters such as RTT filter, congestion notification filter, and packet loss filter. Based on these filters the proposed work performed congestion control for multipath TCP. The simulation result shows that the proposed work achieved better performance in terms of detection accuracy and latency. Here, congestion window is adjusted based on three parameters that perform well, but the values are not considered based on the current network status, hence it leads to performance degradation of multipath TCP.

Authors in [28], proposed a congestion control method to improve the performance of TCP. The proposed work used window-based congestion control for resolving the limitations of the TCP in wireless networks. Here, congestion control is performed by considering queue level, sending rate, and flow utilization rate. This research includes three processes such as congestion window growth, congestion control, and recovery. In which the window growth is estimated based on threshold value (i.e., maximum window size). Congestion control is performed by considering two-level notifications. Finally, stability of the throughput is estimated based on transmission rate, and utility rate. The simulation shows that the proposed work achieved superior performance in terms of throughput, end-to-end delay, and Goodput. Authors proposed an approach to perform multipath scheduling of packets for controlling the network congestion concerning buffer acknowledgment in [29]. This method consists of two major entities a multi-path-packet scheduler (MPS), and a multi-path-congestion controller (MCC) in which the MPS was used to schedule the path based on three delay probabilities such as transmission delay and In-Out delay, and congestion delay. The MCC was used to manage the congestion control by considering the transmission control rate with respect to buffer availability, and packet delivery rate for increasing the throughput with low packet loss. Finally, simulation was performed to prove the performance of this approach in terms of buffer utilization, and throughput. Here, path scheduling was performed to reduce the transmission delay. However, lack of considering the data priority leads to high data loss.

The related works from [18 to 23] represents the packet scheduling schemes of the state-of-the art works whereas, the works [24 to 29] describes the congestion control schemes of

the previous approaches. These methods have several limitations which are described at the end of each previous method. These limitations pave the way for the proposed CoCoA3⁺-TCP method.

III. PROBLEM STATEMENT

The retransmission-based effective TCP congestion control method for IoT was introduced in [30]. Bottle-neck bandwidth round trip propagation time improves the fairness of RTT for congestion control was introduced in [31]. The major problems employed in this research are,

- Authors performed RTT estimation to calculate RTO for exponential backoff to improve congestion control of TCP. However, fixed RTO increases the waiting time of packets which leads to high latency and bandwidth consumption.
- Authors considered only queue status and delivery rate for adjusting CWND to perform congestion control. However, these parameters are not enough to perform effective congestion control leading to high jitter and low Goodput.
- Authors performed retransmission after obtaining three duplicate ACKs for reducing packet delivery failure. However, it increases the total delay of transmission which degrades the performance of TCP.

The packet scheduling and congestion control framework based on BBR to enhance the fairness of multipath TCP wireless networks was introduced in [32]. The major problems employed in this research are:

- Authors considered RTT to adjust the CWND for the improvement of congestion control. However, lack of considering RTO that leads to degradation of throughput.
- Two or more subflows share the same bottleneck set simultaneously for congestion control. However, these subflows are selected randomly without considering buffer rate and data size which leads to high transmission delay and packet loss.
- Several parameters such as bottleneck bandwidth, RTT, loss rate, and subflows are considered for packet scheduling. However, these parameters are not enough for optimal scheduling of packets which leads to high transmission delay.

The cross-layer congestion control framework for IoT environment was introduced in [33]. The major problems employed in this research are:

- Authors selected paths by considering only path bandwidth for congestion avoidance. However, single parameter is not enough to select the optimal path that leads to high jitter and packet loss.
- The proposed congestion control policy is used for performing fast retransmission based on adaptive data rate with respect to the path. However, lack of

considering RTO leads to high bandwidth consumption and high retransmission delay.

A. Research Solutions

To overcome the above problems faced by the existing works, the proposed work initially constructed the network as grid topology based on Manhattan distance which increases the flexibility and scalability of the network. After that, efficient packet scheduling is performed to reduce the latency during transmission and jitter using fitness based proportional fair scheduling algorithm which calculates the fitness value for every scheduling slot. The subflow and optimal path selection is done after packet scheduling to improve the throughput. The congestion control is performed to improve the performance using CoCoA3⁺-TCP Algorithm that consists of three sub-processes namely congestion detection and avoidance, fast retransmission, and fast recovery. Here, congestion is detected by several metrics in that RTO is adaptively estimated using CMO algorithm. After congestion is detected fast transmission

and fast recovery are performed by reducing the count of duplicate acknowledgment which reduces the transmission latency during data transmission. The overall proposed work improves the throughput, and goodput, and reduces the jitter and transmission latency in the TCP IoT environment.

IV. PROPOSED WORK

This section provides the research methodology of the proposed cross-layer CoCoA3⁺-TCP. The proposed work mainly focuses on improving the performance of the TCP using the cross-layer approach in an IoT environment. The performance of TCP is affected by high packet loss, Round Trip Time (RTT), and maximum segment size which lead to high latency and low throughput. The proposed work uses cross-layer design which allows the interaction between the data link layer and transport layer to transfer the information. Fig. 1 denotes the overall architecture of the proposed work in which cross-layer approaches among two layers is depicted.

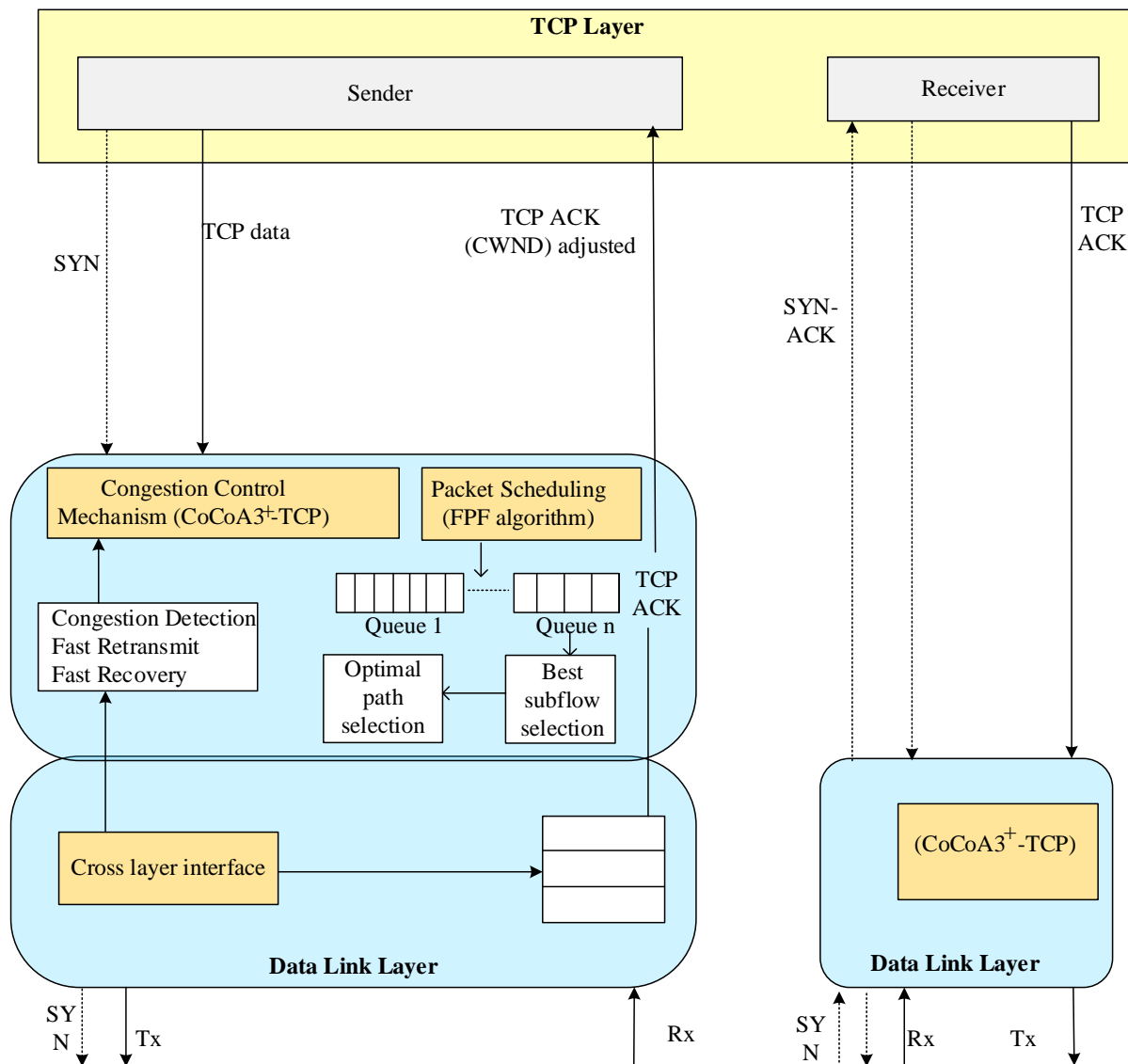


Fig. 1. CoCoA3⁺-TCP Architecture.

Initially, the network is constructed by Manhattan distance-based grid topology which is a simpler grid topology that increases the flexibility and scalability of the network. The nodes are arranged in grid size of order 10×10 . The proposed work assumes that the nodes in the network have stable range of communication range and that there are no crashes among the IoT nodes. Each node can communicate with each other, which are in the range of their respective communication. The range of transmission is constrained so that there is immediate communication among the nodes is established. Let (C^{n_i}, D^{n_i}) be the coordinates of node n_i , hence the distance (Dis) among the node n_i and node n_j can be formulated as.

$$Dis_{n_i, n_j} = |C^{n_i} - C^{n_j}| + |D^{n_i} - D^{n_j}| \quad (1)$$

The above equation denotes the arrangement of IoT nodes in the environment in 10×10 by Manhattan distance measure. This research improves the TCP performance by providing two processes which are listed as follows,

- Efficient Packet Scheduling
- TCP Congestion Control

A. Efficient Packet Scheduling

The main aim of packet scheduling is to reduce the jitter and transmission latency and improve the Goodput and throughput. Here, packets are scheduled and transmitted to the receiver which reduces transmission delay and congestion. For packet scheduling, we proposed FPF by considering bandwidth, energy (En), delay (dl), transmission rate (TXr), queue length (QL), buffer rate (BR), completion time (cti) and data size (dz) which can be formulated as,

$$P^\blacksquare = arg \max_p \left(\frac{SR_{k,b}}{(W-1)T_k + \sum_{b=1}^B I_{k,b} SR_{k,b}} \right) \quad (2)$$

Where, P^\blacksquare denotes the important value of each user which is used for effective packet scheduling, $SR_{k,b}$ rate of service for the k^{th} user at b^{th} time index based on the above-mentioned packet scheduling metrics, T_k indicates the $k - th$ user throughput, W is the window size, $I_{k,b}$ denotes the indicator variable which indicates the, when $I_{k,b} = 1$ the $k - th$ user packet is scheduled at $b - th$ time index else 0. The T_k can be formulated as.

$$T_k(t+1) = \begin{cases} \left(1 - \frac{1}{W}\right)T_{k,b}(t) + \frac{1}{W}A_k(t), V = P^\blacksquare \\ \left(1 - \frac{1}{W}\right)T_{k,b}(t), V \neq P^\blacksquare \end{cases} \quad (3)$$

Where, T_k denotes the past throughput that is dispensed to users in the previous transmission time interval. $T_k(t+1)$ denotes the current throughput which is calculated based on the T_k . V denotes the index of the user packets, A_k indicates the user throughput in current transmission time interval. Based on the importance value of each user fitness value is calculated. Here, fitness value is used to enhance long-term fairness and throughput in every scheduling slot which can be formulated as,

$$Fit(U) = \begin{cases} \max_{SR} (En, TXr, QL) \\ \min_{SR} (dl, cti, dz, BR) \end{cases} \quad (4)$$

The above equation denotes the fitness value of each user packet. The user packets are scheduled based on the above-mentioned equation.

After completed packet scheduling best subflow is selected for scheduling which reduces the transmission delay during data transmission. The best subflow is selected based on the priority and fitness values of the user packets. The user packet with highest $Fit(U)$ are given more priority which can be formulated as

$$SF = \begin{cases} \uparrow Fit(U), SF_1 \\ \vdots \\ \downarrow Fit(U), SF_n \end{cases} \quad (5)$$

From the above equation, the $\uparrow Fit(U)$ indicates the user packet with higher fitness value who is given more priority and selected as first subflow while $\downarrow Fit(U)$ denotes the user packet with lower fitness value who is given less priority and selected as $n - th$ subflow. Finally, optimal path is selected from multiple paths for sending scheduled subflows. For optimal path selection, we consider congestion rate, transmission delay, and high throughput. Finally, TCP performances are improved by sending the scheduled subflow through optimal path. Fig. 2 represents the efficient packet scheduling, sub scheduling, and optimal path selection of the proposed work.

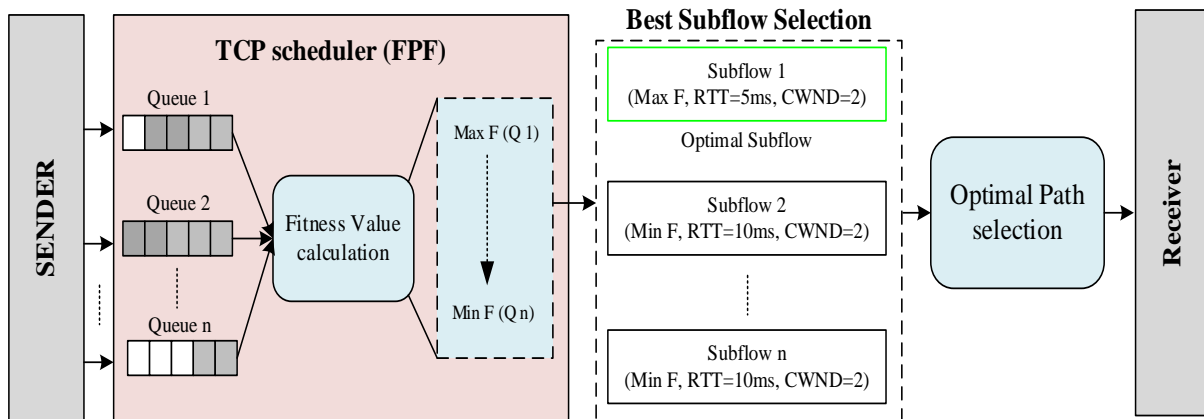


Fig. 2. FPF based Efficient Packet Scheduling.

B. TCP Congestion Control

In general, the network has congestion due to many packets being sent by the senders at a particular time, which affects the performance in terms of throughput, and packet delivery rate in TCP. To improve the performance of TCP, we need to avoid congestion in the network. The proposed congestion control CoCoA3⁺-TCP Algorithm includes three sub-processes such as congestion detection and avoidance, fast retransmission, and fast recovery.

Initially, congestion is detected by considering RTT, Retransmission Timeout (RTO), transmission rate, delay, bandwidth, delivery rate, and queue status.

1) *Round trip time (RTT)*: The amount of time taken for data to reach its destination and return the acknowledgment is known as RTT. The RTT can be formulated as,

$$RTT = 2 \times Pd \quad (6)$$

Where Pd denotes the propagation delay. The good protocol must have less Pd thereby having less RTT.

2) *Transmission rate (TXr)*: The TXr is defined as the amount of data transmitted in a specific channel over a unit of time. In TCP the TXr is dependent on the size of the window which can be formulated as,

$$W = \frac{trf_t}{speed} \quad (7)$$

Where W is window size, generally TXr depends on W in TCP, trf_t indicates the time of transfer, and $speed$ denotes the speed of transfer, respectively.

3) *Delay (dl)*: The delay is defined as the amount of time taken for data to transmit from source to destination. Generally, unit of delay depends on the time is taken nature of data. The delay must be less for a good communication protocol.

4) *Bandwidth(BW)*: The BW is defined as the capacity of the network to withstand with high amount of data over a medium of transmission. The BW can be formulated as,

$$BW = \frac{W}{RTT} \quad (8)$$

Where W denotes the size of the window, and RTT denotes the round-trip time.

5) *Delivery rate (DR)*: The amount of data packet delivered to the destination in a period is known as DR . Generally, a good TCP must have high DR .

6) *Queue status (QS)*: The QS is defined based on the queue length. Higher the Queue length greater the congestion rate. The QS can be formulated as,

$$Ql = (1 - W) \times Ql + W \times Q_{sam} \quad (9)$$

Where, W is the window size, Q_{sam} is the sample queue that denotes the actual queue length of the packet arrival.

Here, the RTO value is estimated dynamically rather than fixed as a static value based on the current status of the environment. Then overall RTO value is estimated which is optimally calculated by CMO which is presented in CoCoA3⁺-TCP. The CMO algorithm is a nature-inspired algorithm that mimics cat and mouse behaviours. This algorithm consists of two phases namely missing acknowledgment modelling and packet retransmission modelling. The population of packets in the TCP-IoT network is determined as,

$$R = \begin{bmatrix} R_1 \\ \vdots \\ R_i \\ \vdots \\ R_n \end{bmatrix}_{n \times m} = \begin{bmatrix} R_{1,1} & \cdots & R_{1,d} & \cdots & R_{1,m} \\ \vdots & & \vdots & & \vdots \\ R_{i,1} & & R_{i,d} & & R_{i,m} \\ \vdots & & \vdots & & \vdots \\ R_{n,1} & & R_{n,d} & & R_{n,m} \end{bmatrix}_{n \times m} \quad (10)$$

From the above equation, R denotes the packets population matrix, R_i denotes the exploration agent (i -th), n indicates the number of packets transmitted in the network, and the problem variable is denoted as m . In the network, each transmitted packet must be objective function which can be formulated as,

$$OF = \begin{bmatrix} OF_1 \\ \vdots \\ OF_i \\ \vdots \\ OF_n \end{bmatrix}_{n \times 1} \quad (11)$$

Where, OF is the objective function vector, and OF_i is the exploration agent objective function. From the above OF values the best and worst transmitted packets are selected that can be formulated as,

$$OF_{alt} = \begin{bmatrix} OF_1^{alt} & Mini(OF) \\ \vdots & \vdots \\ OF_n^{alt} & Maxi(OF) \end{bmatrix}_{n \times 1} \quad (12)$$

From the above equation, OF_{alt} denotes the altered transmitted packet objective function based on equation (11). The transmitted packet with minimum objective function is considered as the best member else worst member. The overall packet population matrix consists of two groups namely missing acknowledgment packets and retransmitted packets. From that, the population of missing acknowledgment packets and retransmitted packets can be formulated as follows:

$$Mi(R) = \begin{bmatrix} Mi(R)_1 = R_1^{alt} \\ \vdots \\ Mi(R)_i = R_i^{alt} \\ \vdots \\ Mi(R)_{nR} = R_{nR}^{alt} \end{bmatrix}_{nR \times m} = \begin{bmatrix} R_{1,1}^{alt} & \cdots & R_{1,d}^{alt} & \cdots & R_{1,m}^{alt} \\ \vdots & & \vdots & & \vdots \\ R_{i,1}^{alt} & & R_{i,d}^{alt} & & R_{i,m}^{alt} \\ \vdots & & \vdots & & \vdots \\ R_{nR,1}^{alt} & & R_{nR,d}^{alt} & & R_{nR,m}^{alt} \end{bmatrix}_{nR \times m} \quad (13)$$

$$rt(R) = \begin{bmatrix} rt(R)_1 = R_{nR+1}^{alt} \\ \vdots \\ rt(R)_j = R_{nr+j}^{alt} \\ \vdots \\ rt(R)_{nrt} = R_{nR+nrt}^{alt} \end{bmatrix}_{nrt \times m} = \begin{bmatrix} R_{nR+1,1}^{alt} & \dots & R_{nR+1,d}^{alt} & \dots & R_{nR+1,m}^{alt} \\ \vdots & & \vdots & & \vdots \\ R_{nR+j,1}^{alt} & & R_{nR+j,d}^{alt} & & R_{nR+j,m}^{alt} \\ \vdots & & \vdots & & \vdots \\ R_{nR+nrt,1}^{alt} & & R_{nR+nrt,d}^{alt} & & R_{nR+nrt,m}^{alt} \end{bmatrix}_{nrt \times m} \quad (14)$$

From the above equations (13) and (14), $Mi(R)$ denotes the missing acknowledge packets and $rt(R)$ denotes the retransmitted packets respectively. Therefore, in first phase, the missing acknowledgment packets are found by,

$$Mi(R)_i = \begin{cases} Mi(R)_i^{new}, |OF_i^{Mi(R),new} < OF_i^{Mi(R)} \\ Mi(R), else \end{cases} \quad (15)$$

Where, $Mi(R)_i^{new}$ is missing acknowledgment based on current network status, and $OF_i^{Mi(R),new}$ denotes the objective of missing acknowledgment. In second phase, the retransmitted packet is found by,

$$rt(R)_j = \begin{cases} rt(R)_j^{new}, |OF_i^{rt(R),new} < OF_i^{rt(R)} \\ rt(R), else \end{cases} \quad (16)$$

Where, $rt(R)_j^{new}$ new retransmitted packets based on current network status, and $OF_i^{rt(R),new}$ denote the objective function of new retransmitted packets. From the equation (15) and (16), the RTO is adaptively determined by,

$$RTO = Mi(R)_i^{new} - rt(R)_j^{new} \quad (17)$$

The pseudocode for adaptive RTO estimation based on cat and mouse optimization algorithm is given below:

```

Pseudocode
Adaptive RTO selection ()
Start CMO
    Initialize R using (10)
    Set exploration agents (n) and iterations (T)
    Compute OF using (11)
    Alter the OF using (12)
    Set the Mi(R) population using (13)
    Set the rt(R) population using (14)
Stage 1: Missing ACK stage
    For i=1: nR;
        Find the missing acknowledged packets using (15)
    End
Stage 2: packet retransmission modelling
    For j=1: nrt;
        Find retransmitted packets using (16)
    End
    Calculate RTO using (17)
End
    
```

Due to congestion, the network has high packet loss; hence we need to perform fast retransmission and fast recovery. The basic goal of fast retransmission is to minimize the count of duplicate acknowledgment (DACK) which reduces the transmission latency during data transmission. The steps involved in fast retransmission are:

- Step 1: Sender sent some packets to the receiver, and receiver receives the packets and gives acknowledgment.
- Step 2: If correct acknowledgment, the sender sends another packet. Else, sender sends acknowledge message along with lost packets to sender.
- Step 3: Along with lost packets, sender continuously sends another packet which leads to two DACK.
- Step 4: After getting two DACK, the sender retransmits the missing packets (i.e., Fast recovery) without exceeding RTO based on the current network status which is evaluated by RTT for every packet given in equation (6).

The proposed algorithm adjusts the congestion window size that reduces the delay which is illustrated in Fig. 3. The current network status is determined based on RTT. If the RTT increases beyond network limit then there is congestion in the network, and when RTT gets decreased there is no congestion, at that time size of congestion window must be increased to avoid the congestion further.

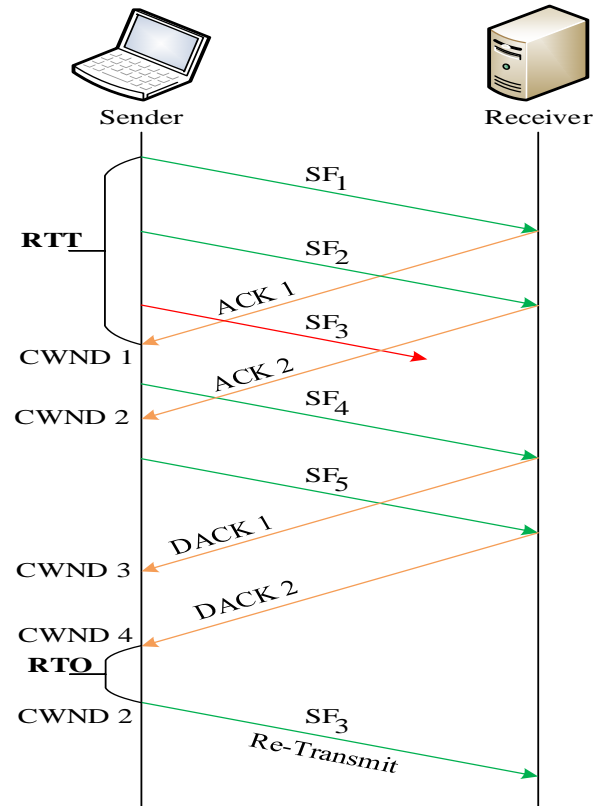


Fig. 3. CWND Adjustment for Fast Retransmission and Recovery.

V. EXPERIMENTAL RESULTS

In this section, the proposed CoCoA3⁺-TCP is experimented with and validated. This section is further subdivided into four sub-sections such as simulation setup, application scenario comparative analysis, and research summary.

A. Simulation Setup

This sub-section describes the simulation of the proposed work. Initially, the network is constructed as grid topology based on Manhattan distance for improving the scalability of the network. This work utilizes the system with hardware configuration of random-access memory (RAM) 8GB, hard disk 256GB, and processor of Intel(R) Core (TM) i5-3210M CPU @ 2.50GHz; the software configuration of network simulator with version 3.26, and operating system of Ubuntu Linux 18.04. Table I denotes the various simulation parameters used for simulating the proposed model. Fig. 4 represents the simulation grid topology of the proposed CoCoA3⁺-TCP.

The above figure represents the simulation grid topology of the proposed CoCoA3⁺-TCP. The proposed work constructs the grid as size of 10 × 10 using Manhattan distance which is flexible and mitigates the scalability issues. By this grid topology construction, the proposed work achieves high transmission efficiency, high throughput and less delay during packet scheduling and congestion control, respectively.

TABLE I. SIMULATION CONFIGURATION

Simulation Parameter	Values
Network Simulator	NS-3.26
Routing Protocol	AODV
Type of Traffic	TCP
Area of Simulation	1500m × 1500m
No. of IoT nodes	100
No. of Base station	1
Size of the window	2 ⁸
Size of the packet	2000 bytes
Size of the Queue	30 packets
Placement of IoT node	Grid topology
Topology Size	10 × 10
Time for Total Simulation	300ms

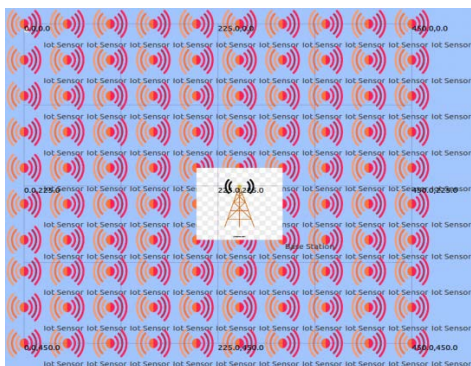


Fig. 4. Simulation Grid Topology of CoCoA3⁺-TCP.

B. Application Scenario

The proposed TCP-IoT model can be adopted in medical environment (i.e. patient monitoring system). The medical environment consists of numerous patients and each patient are equipped with IoT sensors (i.e. heart beat sensor, blood pressure sensor, etc.). The improper counter measure in the medical environment leads to severe threats to the patients. To take correct medical counter measure at correct time period, the sensed data are optimally report to the doctors. For that we propose, reliable TCP-IP congestion control fast and reliable mechanism in which every sensor data is forwarded to the server where it performs scheduling using FPF algorithm based on several metrics such as bandwidth, delay, buffer rate, etc. The scheduled data are selected best sub flow using CoCoA3⁺-TCP algorithm. The proposed work can be applied in the medical environment for patient monitoring reduces the latency, and congestion issues.

C. Comparative Analysis

In this sub-section, the comparative analysis is performed for the proposed CoCoA3⁺-TCP method with several previous approaches such as ICC-TCP (28), and BC-CPS (30) methods for evaluating the performance of these methods. Various performance metrics are considered in terms of throughput, goodput, packet loss, transmission delay, jitter, and congestion window size respectively to evaluate the performance of the proposed CoCoA3⁺-TCP method and other previous works.

1) *Impact of throughput:* This metric is used to evaluate the total number of data packets received (\hat{p}) at a certain period (t) by the receiver. Throughput (ϵ) is denoted in terms of bits per second. The formulation of this metric is described as follows,

$$\epsilon = \frac{\hat{p}}{t} \quad (18)$$

Fig. 5 illustrates the comparison of throughput between the proposed CoCoA3⁺-TCP method with several previous methods such as ICC-TCP, and BC-CPS methods with respect to the packet size. A network with high throughput achieves better communication between the source and destination. Throughput increases with increasing the packet size.

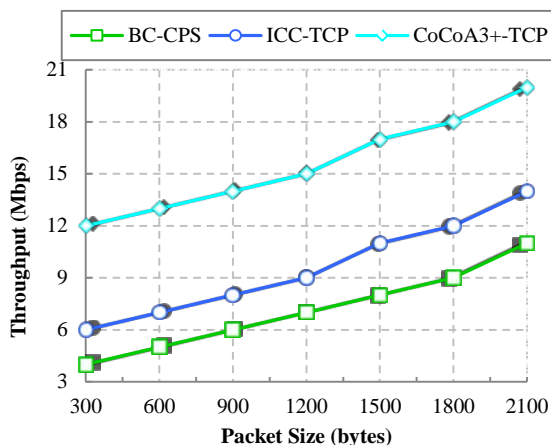


Fig. 5. Throughput Vs. Packet Size.

In the existing BC-CPS approach, congestion control and packet scheduling are statically performed with poor RTO measurement, and retransmission was performed after several ACK which increases the latency that leads to low throughput. In the proposed CoCoA3⁺-TCP method, adaptive RTO estimation is performed and retransmission of packets is performed after receiving two DACK which reduces the latency that increases the throughput of the proposed CoCoA3⁺-TCP method. The comparative results show that the proposed CoCoA3⁺-TCP method achieves high throughput (12-20 Mbps) when compared with ICC-TCP (6-14 Mbps) method and BC-CPS (4-11 Mbps) method.

Similarly, Fig. 6 shows the comparison of throughput with respect to simulation time. From this figure, it is clearly shown that the proposed CoCoA3⁺-TCP method achieves high throughput of 20 Mbps for the packet size of 2100 bytes which is 6 Mbps higher than the ICC-TCP method and 9 Mbps higher than BC-CPS method.

2) *Impact of goodput*: It is one of the important metrics which is the other form of throughput in the application level to evaluate the performance of the proposed algorithm for performing accurate and efficient communication, especially during huge data transmission. Goodput (β) is formulated by the ratio between the amount of particular data (u) to the time taken for reaching the receiver (f) which is expressed as follows:

$$\beta = \frac{u}{f} \quad (19)$$

Fig. 7 represents the goodput comparison for the proposed CoCoA3⁺-TCP method and several previous works in terms of packet size. A network with low transmission delay achieves high goodput which increases the communication efficiency. The goodput increases with respect to increase of packet size. In the existing BC-CPS method, lack of considering the RTO when evaluating the RTT for the communication increases the latency which reduces the performance of the TCP by attaining low goodput.

In the proposed CoCoA3⁺-TCP method, the RTO is estimated based on current status of the network which increases the TCP performance by achieving high goodput. From the graphical results, it is proved that the proposed CoCoA3⁺-TCP method achieves high goodput when compared with state-of-the-art methods. The proposed CoCoA3⁺-TCP attains high goodput of 800 Kbps at 2100 bytes. The difference of goodput between the proposed CoCoA3⁺-TCP method and the ICC-TCP method is 120 Kbps, and 200 Kbps for the BC-CPS method.

Similarly, Fig. 8 represents the comparison of goodput to the simulation time. The comparative results show that the proposed CoCoA3⁺-TCP method achieves high goodput of 800 Kbps which is 140 Kbps higher than ICC-TCP method and 200 Kbps higher than BC-CPS method at 300ms.

3) *Impact of packet loss*: It is used in the network to evaluate communication reliability. Packet loss is defined as the ratio of the number of data packets that are not received to the total amount of packets which is formulated as follows:

$$\eta = \frac{\dagger}{\partial} \quad (20)$$

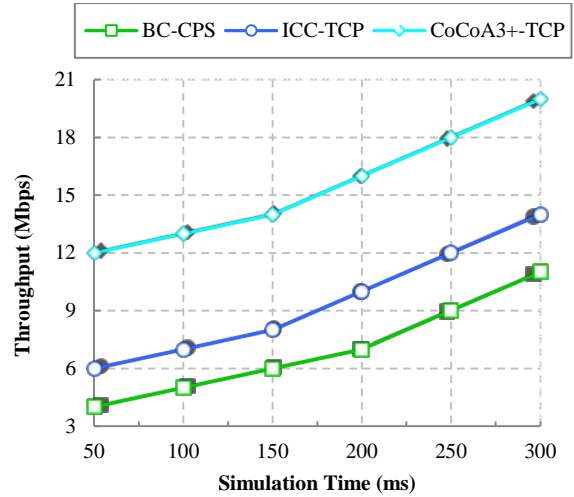


Fig. 6. Throughput Vs. Simulation Time.

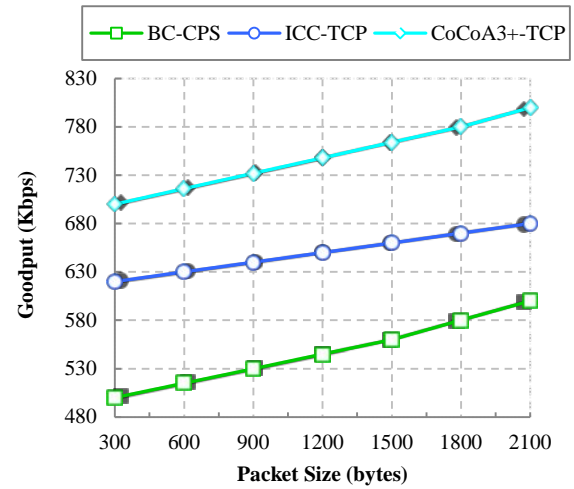


Fig. 7. Goodput Vs. Packet Size.

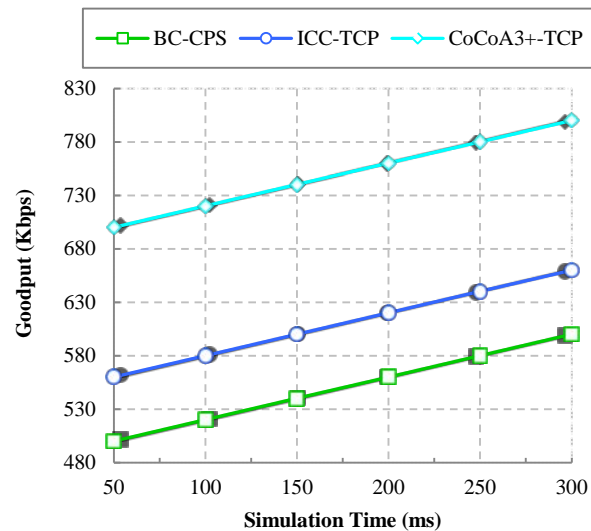


Fig. 8. Goodput Vs. Simulation Time.

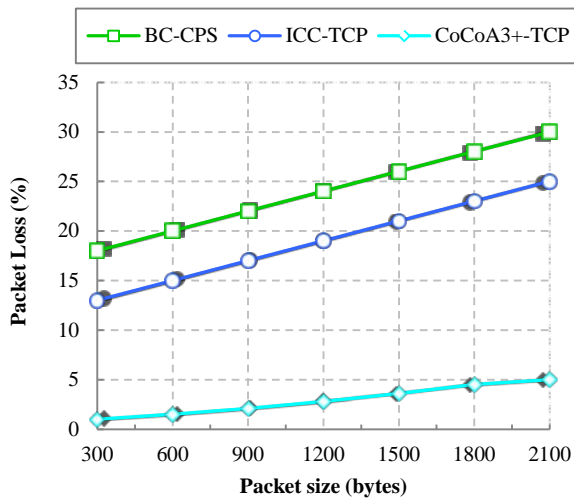


Fig. 9. Packet Loss Vs. Packet Size.

Where η shows the packet loss, \uparrow represents the non-received data packets and ∂ denotes the total amount of packets. Fig. 9 shows the comparison of packet loss between the proposed CoCoA3⁺-TCP method and several previous approaches. A network with low packet loss reduces the number of retransmissions which decreases the network congestion. The packet loss increases with increase in packet size. In the ICC-TCP methods, the congestion control is performed by evaluating the RTT without considering the present network status that increases the DACK which leads to high packet loss. In the proposed method, congestion control is performed by adaptively implementing CoCoA3⁺-TCP algorithm. In addition, the congestion window is increased by one when more than two DACK reduces the packet loss.

The comparative results illustrate that the proposed CoCoA3⁺-TCP method achieves low packet loss when compared with other previous methods. The proposed CoCoA3⁺-TCP method achieves low packet loss of about 5% for 2100 bytes of packet size which is 20% lower than ICC-TCP method, and 25% lower than BC-CPS method. Table II describes the packet loss variation of the proposed CoCoA3⁺-TCP method and other existing approaches.

4) *Impact of transmission delay:* Transmission delay (\jmath) represents the amount of additional time taken by the proposed CoCoA3⁺-TCP method to transmit the packets from the source to the destination. It is formulated by the difference between the actual packet received time (ϑ) and the expected time (ζ) which is expressed as follows:

$$\jmath = \vartheta - \zeta \tag{21}$$

TABLE II. NUMERICAL ANALYSIS OF PACKET LOSS

Methods	Packet Size
BC-CPS	24.3 ± 0.5
ICC-TCP	19.5 ± 0.4
CoCoA3 ⁺ -TCP	2.92 ± 0.1

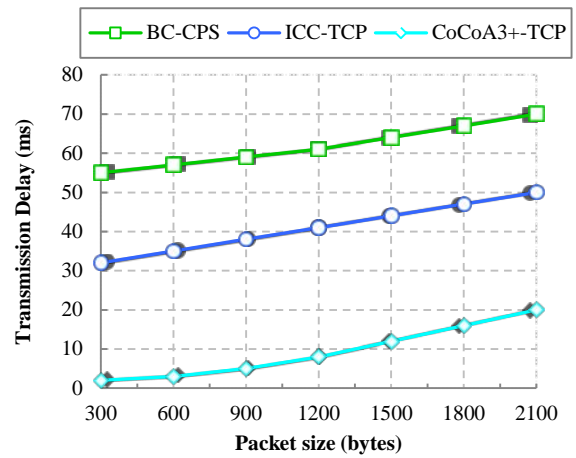


Fig. 10. Transmission Delay Vs. Packet Size.

Fig. 10 illustrates the comparison of transmission delay for the proposed CoCoA3⁺-TCP method and other existing methods in terms of packet size. A network with low transmission delay increases the throughput as well as goodput. The transmission delay increases with increasing the packet size. In the BC-CPS method, random selection of subflows is performed with insufficient parameters such as RTT, loss rate, etc., for data transmission which increases the transmission delay and also leads to high packet loss. In the proposed CoCoA3⁺-TCP work, Optimal selection of subflows is performed by considering buffer rate, queue length, etc. which improves the fairness for long term that reduces the transmission delay when compared with other previous methods. From this figure, it is clearly shown that the proposed CoCoA3⁺-TCP method achieves low transmission delay of about 20ms for 2100 bytes of packet size which is 30ms faster than ICC-TCP method and 50ms faster than BC-CPS method.

Similarly, Fig. 11 shows the comparison of transmission delay with respect to simulation time between the proposed CoCoA3⁺-TCP method and existing methods. The results show that the proposed CoCoA3⁺-TCP method achieves low transmission delay of about 20ms for 300ms of simulation time which is 28ms faster than ICC-TCP method and 48ms faster than BC-CPS method.

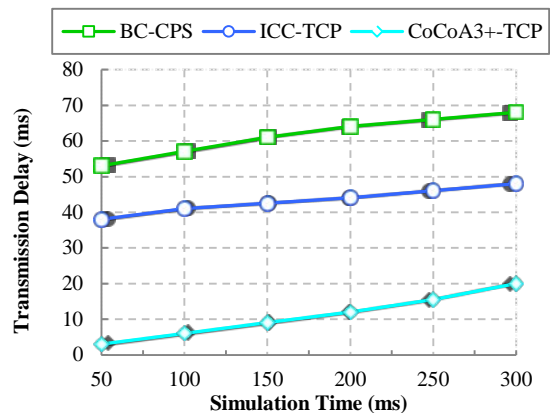


Fig. 11. Transmission Delay Vs. Simulation Time.

5) *Impact of jitter*: This metric is used to evaluate the difference between the transmitting time and receiving time. The formulation of jitter is defined as the time variation between the current and previous data packets which is expressed as follows:

$$\lambda = \xi - \kappa \tag{22}$$

Where λ denotes the jitter, ξ represents the current packet receiving time, κ shows the previous packet receiving time.

Fig. 12 shows the comparison of jitter between the proposed CoCoA3⁺-TCP method and several state-of-the-art approaches in terms of packet size. A network with low jitter increases the performance of TCP. The jitter increases with increasing the packet size. In the ICC-TCP method, DACK was not considered during retransmission which increases the latency of data recovery that leads to high jitter. In addition, lack of considering RTO in the BC-CPS method during congestion control also increases the jitter.

In the proposed CoCoA3⁺-TCP method, fast data recovery is performed by considering the DACK more than two and reducing the congestion window to half of the present status of congestion window with respect to RTT and RTO is considered based on the network's current status that reduces the jitter effectively when compared with other previous works. The graphical results illustrate that the proposed CoCoA3⁺-TCP method achieves low jitter of about 15ms for 2100 bytes of packet size. Whereas, the ICC-TCP and BC-CPS methods achieve jitter of about 50ms and 60ms for the same packet size which is 35ms and 45ms greater than the proposed CoCoA3⁺-TCP method.

Similarly, Fig. 13 illustrates the comparison of jitter between the proposed CoCoA3⁺-TCP method and other previous methods with respect to simulation time. The results show that the proposed CoCoA3⁺-TCP method achieves low jitter of about 15ms which is 32ms faster than ICC-TCP method and 43ms faster than BC-CPS method.

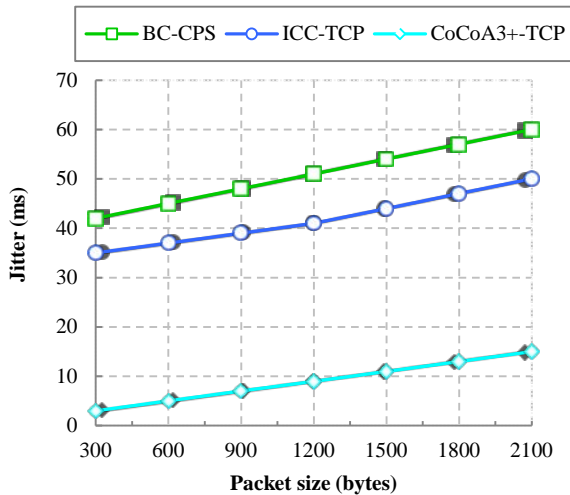


Fig. 12. Jitter Vs. Packet Size.

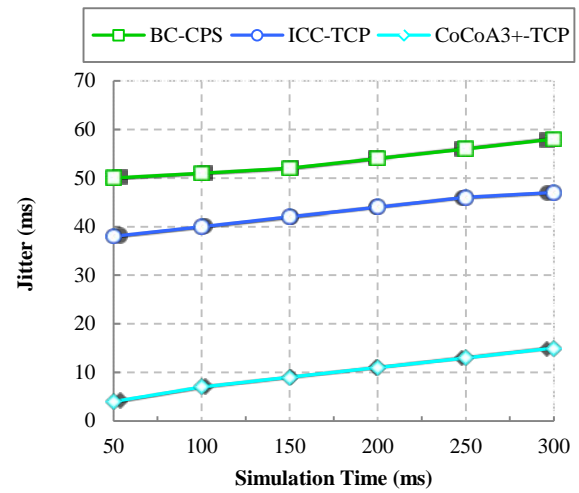


Fig. 13. Jitter Vs. Simulation Time.

6) *Impact of congestion window size*: This metric is used to evaluate the number of data packets transmitted from the source to the destination without any traffic. A network with large congestion window size increases the throughput of the network. Whenever DACK occurs, the size of the congestion window decreases to half of its size to perform fast retransmission and recovery.

Fig. 14 represents the comparison of congestion window size for the proposed CoCoA3⁺-TCP method and other existing methods with respect to simulation time. The size of the congestion window increases when normal data transmission and decreases when retransmission occurs with increasing simulation time. In the state-of-the-art approaches, the size of the congestion window is randomly changed to send the data packets with lack of considering the RTO which increases the congestion that leads to high complexity in congestion control.

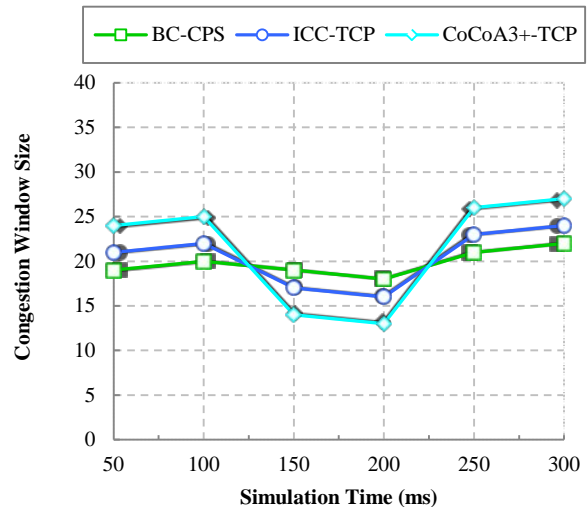


Fig. 14. Congestion Window Size Vs. Simulation Time.

In the proposed CoCoA3⁺-TCP method, the congestion window is adaptively changed, i.e. whenever the DACK increased, the congestion window is increased by one. For faster data recovery, the congestion window is reduced by half with respect to RTT which reduces the congestion and increases the control of congestion. In addition, estimation of dynamic RTO is performed based on the network's current status which also reduces the retransmission of packets. The comparative results illustrate that the proposed CoCoA3⁺-TCP method achieves better congestion window size when compared with other previous methods.

The proposed CoCoA3⁺-TCP method attains high congestion window size of about 27 which is 4 larger than ICC-TCP method and 6 larger than the BC-CPS method. When retransmission occurs, the size of the congestion window decreases by about 13 which is 5 lower than BC-CPS method and 3 lower than ICC-TCP method. Table III illustrates the changes in congestion window size between the proposed CoCoA3⁺-TCP method and several previous works.

TABLE III. NUMERICAL ANALYSIS OF CONGESTION WINDOW SIZE

Methods	Simulation Time
BC-CPS	19.3 ± 0.5
ICC-TCP	20.5 ± 0.3
CoCoA3 ⁺ -TCP	21.5 ± 0.1

D. Research Summary

This sub-section summarizes the overall performance of the proposed CoCoA3⁺-TCP method in terms of throughput, goodput, packet loss, transmission delay, jitter, and congestion window size respectively from Fig. 5 to 14. The major highlights of the proposed CoCoA3⁺-TCP method are described in this sub-section. Fitness based Proportional Fair (FPF) scheduling algorithm is proposed for performing efficient packet scheduling which improves throughput and Goodput by reducing the transmission delay and jitter. The CoCoA3⁺-TCP algorithm is proposed for improving congestion control and avoidance with CMO by considering multiple parameters such as delay, transmission rate, RTT, RTO, and bandwidth. DACK count is minimized by performing fast retransmission and recovery which retransmits the packets before the threshold of RTO depending upon the current network status. Table IV represents the ablation study between the existing and proposed approaches which consists of the average values of the corresponding performance metrics. From this table, it is proved that the proposed CoCoA3⁺-TCP method achieved high TCP performance when compared with other existing works.

TABLE IV. NUMERICAL ANALYSIS OF PROPOSED AND EXISTING METHODS

Performance Metrics		BC-CPS	ICC-TCP	CoCoA3 ⁺ -TCP
Throughput (Mbps)	Packet Size (bytes)	7.14 ± 0.5	9.58 ± 0.3	15.57 ± 0.1
	Simulation Time (ms)	7.15 ± 0.4	9.5 ± 0.2	15.5 ± 0.1
Goodput (Kbps)	Packet Size (bytes)	547.14 ± 0.5	650.20 ± 0.4	748.57 ± 0.1
	Simulation Time (ms)	550.20 ± 0.4	610.15 ± 0.3	750.18 ± 0.1
Transmission Delay (ms)	Packet Size (bytes)	61.85 ± 0.4	41.23 ± 0.2	9.42 ± 0.1
	Simulation Time (ms)	61.5 ± 0.5	43.25 ± 0.4	10.91 ± 0.1
Jitter (ms)	Packet Size (bytes)	51.5 ± 0.5	41.85 ± 0.2	9.3 ± 0.1
	Simulation Time (ms)	53.5 ± 0.4	42.83 ± 0.3	9.83 ± 0.1

VI. CONCLUSION AND FUTURE WORK

The cross-layer approach is proposed in this research to perform efficient packet scheduling and congestion control for improving the TCP performance in IoT networks. Initially, network construction is performed which improves the flexibility and scalability of the network. After network construction, packet scheduling is performed by considering numerous parameters using FPF scheduling algorithm, and best subflow is selected which reduces the transmission delay and jitter. Optimal path selection is performed by considering several parameters to increase the throughput and goodput. The congestion control in TCP is performed by proposing CoCoA3⁺-TCP algorithm which consists of three sub-stages such as congestion control, fast retransmission, and fast recovery to reduce the transmission delay and improve the network performance. Fast retransmission is achieved by estimating the RTO dynamically using a cat and mouse based optimization (CMO) algorithm and fast recovery is performed by reducing the congestion window. The simulation is performed by network simulator (NS-3.26) and the results illustrate that the proposed CoCoA3⁺-TCP method achieved high performance of TCP in IoT network when compared with other previous works.

In future, this research will be improved by providing security for TCP protocol in IoT environment with low complexity that reduces the transmission delay. In addition, the security increases the throughput and goodput with low retransmission.

REFERENCES

- [1] V. Vijaya Kumar et al., "Design of peer-to-peer protocol with sensible and secure IoT communication for future internet architecture," *Microprocess. Microsyst.*, vol. 78, no. February, p. 103216, 2020.
- [2] N. Nikolov, "Research of MQTT, CoAP, HTTP and XMPP IoT Communication protocols for Embedded Systems," 2020 29th Int. Sci. Conf. Electron. 2020 - Proc., pp. 18–21, 2020.
- [3] S. Parween, S. Z. Hussain, and M. A. Hussain, "A Survey on Issues and Possible Solutions of Cross-Layer Design in Internet of Things," *Int. J. Comput. Networks Appl.*, vol. 8, no. 4, p. 311, 2021.
- [4] M. Prakash and A. Abdrabou, "Performance Insights on Using Multipath TCP for Wireless Multihomed IoT Gateways," *Proc. 2020 Int. Conf. Comput. Inf. Telecommun. Syst. CITIS 2020*, pp. 1–5, 2020.
- [5] S. Z. Hussain and S. Parween, "Comparative Study of TCP Congestion Control Algorithm in IoT," In 2021 3rd International Conference on Advances in Computing, Communication Control and Networking (ICAC3N), pp. 1428–1431, IEEE, 2022.
- [6] J. Wirges and U. Dettmar, "Performance of TCP and UDP over narrowband internet of things (NB-IoT)," *Proc. - 2019 IEEE Int. Conf. Internet Things Intell. Syst. IoTaIS 2019*, pp. 5–11, 2019.
- [7] Y. Yang and L. Hanzo, "Permutation-Based TCP and UDP Transmissions to Improve Goodput and Latency in the Internet of Things," *IEEE Internet Things J.*, vol. 8, no. 18, pp. 14276–14286, 2021.
- [8] M. A. Alrshah, M. A. Al-Maqri, and M. Othman, "Elastic-TCP: Flexible Congestion Control Algorithm to Adapt for High-BDP Networks," *IEEE Syst. J.*, vol. 13, no. 2, pp. 1336–1346, 2019.
- [9] K. Miyazawa, S. Yamaguchi, and A. Kobayashi, "A study on cyclic performance fluctuation of CUBIC TCP and TCP BBR considering estimated RTT and bandwidth," *Proc. - 2019 7th Int. Symp. Comput. Netw. Work. CANDARW 2019*, pp. 478–480, 2019.
- [10] S. Parween and S. Z. Hussain, "A Comparative analysis of CoAP based Congestion Control in IoT," pp. 321–324, 2021.
- [11] S. Kishimoto, S. Osada, Y. Tarutani, Y. Fukushima, and T. Yokohira, "A TCP Incast Avoidance Method Based on Retransmission Requests from a Client," *ICTC 2019 - 10th Int. Conf. ICT Converg. ICT Converg. Lead. Auton. Futur.*, pp. 153–158, 2019.
- [12] G. Luan and N. C. Beaulieu, "Accurate mathematical modeling and solution of TCP congestion window size distribution," *Comput. Commun.*, vol. 163, pp. 195–201, 2020.
- [13] H. M. Noman, A. A. Abdulrazzaq, M. M. Kareem, and A. H. Ali, "Improvement Investigation of the TCP Algorithms with Avoiding Network Congestion Based on OPNET," *IOP Conf. Ser. Mater. Sci. Eng.*, vol. 518, no. 5, 2019.
- [14] P. Dong, J. Xie, W. Tang, N. Xiong, H. Zhong, and A. V. Vasilakos, "Performance Evaluation of Multipath TCP Scheduling Algorithms," *IEEE Access*, vol. 7, pp. 29818–29825, 2019.
- [15] A. Marin, S. Rossi, and C. Zen, "Size-based scheduling for TCP flows: Implementation and performance evaluation," *Comput. Networks*, vol. 183, no. September, p. 107574, 2020.
- [16] V. Adarsh, P. Schmitt, and E. Belding, "MPTCP performance over heterogenous subpaths," *Proc. - Int. Conf. Comput. Commun. Networks, ICCCN*, vol. July, 2019.
- [17] S. Parween and S. Z. Hussain, "A review on cross-layer design approach in WSN by different techniques," *Adv. Sci. Technol. Eng. Syst.*, vol. 5, no. 4, pp. 741–754, 2020.
- [18] W. Wei, K. Xue, J. Han, D. S. L. Wei, and P. Hong, "Shared Bottleneck-Based Congestion Control and Packet Scheduling for Multipath TCP," *IEEE/ACM Trans. Netw.*, vol. 28, no. 2, pp. 653–666, 2020.
- [19] R. K. Chaturvedi and S. Chand, "An Adaptive and Efficient Packet Scheduler for Multipath TCP," *Iran. J. Sci. Technol. - Trans. Electr. Eng.*, vol. 8, 2020.
- [20] J. Han et al., "Leveraging coupled BBR and adaptive packet scheduling to boost MPTCP," *IEEE Trans. Wirel. Commun.*, vol. 20, no. 11, pp. 7555–7567, 2021.
- [21] S. Qu, L. Zhao, and Z. Xiong, "Cross-layer congestion control of wireless sensor networks based on fuzzy sliding mode control," *Neural Comput. Appl.*, vol. 32, no. 17, pp. 13505–13520, 2020.
- [22] K. Malarvizhi and L. S. Jayashree, "Dynamic scheduling and congestion control for minimizing delay in multihop wireless networks," *J. Ambient Intell. Humaniz. Comput.*, vol. 12, no. 3, pp. 3949–3957, 2021.
- [23] S. R. Pokhrel and A. Walid, "Learning to Harness Bandwidth with Multipath Congestion Control and Scheduling," *IEEE Trans. Mob. Comput.*, vol. 1233, no. c, pp. 1–14, 2021.
- [24] R. Chappala, C. Anuradha, and P. S. R. C. Murthy, "Adaptive Congestion Window Algorithm for the Internet of Things Enabled Networks," *Int. J. Adv. Comput. Sci. Appl.*, vol. 12, no. 2, pp. 105–111, 2021.
- [25] I. Mahmud, T. Lubna, Y. J. Song, and Y. Z. Cho, "Coupled multipath BBR (c-MPBBR): A efficient congestion control algorithm for multipath TCP," *IEEE Access*, vol. 8, pp. 165497–165511, 2020.
- [26] R. M. Bhavadharini, S. Karthik, N. Karthikeyan, and A. Paul, "Wireless Networking Performance in IoT Using Adaptive Contention Window," *Wirel. Commun. Mob. Comput.*, vol. 2018.
- [27] I. Mahmud, T. Lubna, G. H. Kim, and Y. Z. Cho, "Ba-mpcubic: Bottleneck-aware multipath cubic for multipath-tcp," *Sensors*, vol. 21, no. 18, 2021.
- [28] M. Joseph Auxilius Jude, V. C. Diniesh, and M. Shivaranjani, "Throughput stability and flow fairness enhancement of TCP traffic in multi-hop wireless networks," *Wirel. Networks*, vol. 26, no. 6, pp. 4689–4704, 2020.
- [29] A. Kumar, P. V. S. Srinivas, and A. Govardhan, "A Multipath Packet Scheduling Approach based on Buffer Acknowledgement for Congestion Control," *Procedia Comput. Sci.*, vol. 171, pp. 2137–2146, 2020.
- [30] C. Lim, "Improving congestion control of TCP for constrained IoT networks," *Sensors (Switzerland)*, vol. 20, no. 17, pp. 1–16, 2020.
- [31] W. Pan, H. Tan, X. Li, and X. Li, "Improved RTT fairness of BBR congestion control algorithm based on adaptive congestion window," *Electron.*, vol. 10, no. 5, pp. 1–18, 2021.
- [32] W. Wei, K. Xue, J. Han, Y. Xing, D. S. L. Wei, and P. Hong, "BBR-Based Congestion Control and Packet Scheduling for Bottleneck Fairness Considered Multipath TCP in Heterogeneous Wireless Networks," *IEEE Trans. Veh. Technol.*, vol. 70, no. 1, pp. 914–927, 2021.
- [33] L. P. Verma and M. Kumar, "An IoT based Congestion Control Algorithm," *Internet of Things*, vol. 9, p. 100157, 2020.

Sena TLS-Parser: A Software Testing Tool for Generating Test Cases

Rosziati Ibrahim¹

Department of Software Engineering
Universiti Tun Hussein Onn Malaysia
Parit Raja, Malaysia

Sapiee Jamel³

Department of Information Security
Universiti Tun Hussein Onn Malaysia
Parit Raja, Malaysia

Samah W.G. AbuSalim²

Department of Computer Information Sciences
Universiti Teknologi PETRONAS (UTP)
Perak, Malaysia

Jahari Abdul Wahab⁴

Engineering R&D Department
SENA Traffic Systems Sdn. Bhd.
Kuala Lumpur, Malaysia

Abstract—Currently, software complexity and size has been steadily growing, while the variety of testing has also been increased as well. The quality of software testing must be improved to meet deadlines and reduce development testing costs. Testing software manually is time consuming, while automation saves time and money as well as increasing test coverage and accuracy. Over the last several years, many approaches to automate test case creation have been proposed. Model-based testing (MBT) is a test design technique that supports the automation of software testing processes by generating test artefacts based on a system model that represents the system under test's (SUT) behavioral aspects. The optimization technique for automatically generating test cases using Sena TLS-Parser is discussed in this paper. Sena TLS-Parser is developed as a Plug-in Tool to generate test cases automatically and reduce the time spent manually creating test cases. The process of generating test cases automatically by Sena TLS-Parser is be presented through several case studies. Experimental results on six publicly available java applications show that the proposed framework for Sena TLS-Parser outperforms other automated test case generation frameworks. Sena TLS-Parser has been shown to solve the problem of software testers manually creating test cases, while able to complete optimization in a shorter period of time.

Keywords—Software testing; schema parser; software under test (SUT); model based testing (MBT); java applications

I. INTRODUCTION

Before a software can be released to consumers, it needs to pass the software testing phase. Software testing covers the aspect of testing the software to meet its functional requirements as well as discovering errors before the software is released. Two main factors are usually used to determine whether tests will show failures: test inputs and test oracles [1]. A statement in JUnit test is an example of a test oracle. Software testing is important not only for the software company, but also for consumers. Many consumers are currently worried about how software companies ensure software quality, the mechanisms used to do so, and so on. Although the types, frequency and activities of tests vary from program to program, most of the common activities used in

each test cycle are: requirements testing, test planning, writing test cases, test execution, testing feedback and defect testing.

The development of test cases is a difficult aspect of software testing [2]. Creating test cases manually is time consuming. Creating test cases manually should address the aspects of the test objective. Therefore, creating test cases automatically is more efficient and consumes less time. The techniques for automated test case generation aim to efficiently identify a limited number of cases that satisfy an adequacy criterion, reducing the cost and resulting in more effective software product testing. One of the well-known techniques for software testing is Model-based testing (MBT). MBT is a testing technique that creates test cases automatically from models derived from existing application artifacts [3]. MBT is a promising approach for automatic testing to increase testing performance and effectiveness [4]. MBT can perform and complete test tasks in a more cost-effective and reliable manner than conventional test methods. A description of the MBT method is presented in [5]. This paper addresses the problem of manually creating test cases that consume more time. By introducing Sena TLSParser, test cases can be automatically created and generated. Sena TLS Parser can reduce time in generating test cases manually.

The next section will discuss related works followed by details of the proposed Sena TLS-Parser Framework. Subsequently, the implementation of Sena TLS-Parser is discussed followed by the comparison of the proposed framework with other frameworks.

II. RELATED WORK

With the development of model-based engineering technology [6], MBT has attracted more and more interest in research. In the past few years, several MBT tools have been developed to support MBT activities [7]. Li et al. [4] proposed and applied a set of test case generation criteria, as well as surveying new methods that have not been used in previous research or have not been analyzed using test case generation criteria. From 2000 to 2018, a review study on requirement-based test case generation was presented in [8]. The study was

conducted to gain information in the areas of requirements-based test case generation and future studies. In addition, authors in [9] present a systematic mapping study (SMS) by analyzing 87 studies in this field. They discovered that the majority of the studies were devoted to test generation activities. Utting et al. [10] presented model-based research literature over the last ten years including MBT methodology and the industry's current level of MBT adoption. The Unified Modeling Language (UML) is a diagrammatical modeling language that enables developers to identify, visualize, create, analyze and document system features. It is the most popular and widely accepted language in the software industry, to the point that its spread and popularity may have reached a point where it is impossible to imagine a software working without it. There are many UML diagrams used for this purpose such as class diagram, use case diagram, activity diagram and others. One of these diagrams, the UML activity diagram is used to describe behavior while modeling the sequence of activities in the system. It is closely related to use case diagram, which shows the sequence of steps the system performs in order to carry out a use case. By using it, any software process is simplified and improved by identifying complex use cases. Therefore, many research works concentrate on generating test cases from UML [11 - 16].

Many researchers have created a variety of tools for test case generation, but the features of these tools vary greatly. This makes it difficult for the user to identify the right tool for the testing process. TCG, an open-source LoTuS modelling tool plugin was developed by Muniz et al. [17] to generate test cases. EvoSuite [18, 19] is a tool that generates test suites automatically for Java programs with high code coverage and assertions. EvoSuite employs a number of innovative techniques that result in increased structural coverage and efficient assertion selection based on seeded defects, both of which are important features that other Java tools are lacking. Another tool called EPiT was developed by Ibrahim et al. [20], which is shown to be effective in generating test cases automatically. With the increase in Android mobile devices, there is growing interest in automated testing for Android applications. GUI testing is one of the most used techniques for detecting errors in mobile applications and for testing app functionality and usability. Salihu et al. [21] proposed AMOGA which is an alternative model-based testing approach for mobile apps. Their proposed method uses a combination of the UI element's event list and each event to dynamically exercise event ordering at run time. Another tool called APE is presented by Gu et al. [22] for Android apps testing. PLATOOL [23] is another tool that has been proven effective in creating useful functional tests to deal with events involved in mobile applications during the automatic testing phase. More details about various software testing techniques applied for testing mobile applications are shown in [24].

The Synchronized Depth First Search (SDFS) introduced by Pinkal and Niggemann [25] to automate test case generation is proven to efficiently execute testing with less effort and time compared to other techniques. Based on research, it is possible to generate test cases automatically using Timed Synchronizable I/O Automation. Genetic algorithms have been used successfully in software testing. Mishra et al. [26, 27]

shows how genetic algorithms are used for software testing in generating random test cases. Du et al. [28] presents a combination of genetic algorithms with mutation testing to increase coverage and mutation score within test cases. To assess output in terms of generating test cases, the proposed algorithm by Wang and Liu [29] shows that it is capable of achieving both high performance and low time cost in the automated generation of software test cases.

One significant approach is the generation of test cases from UML models. Shin and Lim [30] propose an approach in reducing time and resources required for testing embedded software. Ma and Provost [31] suggest a testing process that ensures that a system's nominal behavior is fully covered while still allowing for the consideration of defective behavior. Elqortobi et al. [32] describe the components of an automated Modified Condition/Decision Coverage MC/DC Test Generation Tool (TGT) for avionics software test sequence generation. Their method incorporates three coverage parameters to increase the performance and error detection capacity of the derived tests. The criteria are selected to satisfy the industrial needs for avionics software certification.

III. SENA TLS-PARSER

Sena TLS-Parser consists of four main steps. Fig. 1 shows the flowchart for Sena TLS-Parser.

Based on Fig. 1, Sena TLS-Parser can be used to generate test cases automatically in Eclipse Integrated Development Environment (IDE). The source code is the input for Sena TLS-Parser. The schema parser will read the source codes line by line. The token will be used to detect classes and methods using code smell. The algorithm for code smell is discussed in [33]. MBT is used for generating the test cases. The algorithm for generating the test cases is discussed in [20]. However, for the time being, Sena TLS-Parser can only generate test cases for Java applications only. The output for Sena TLS-Parser is the generated test cases as shown in Fig. 2.

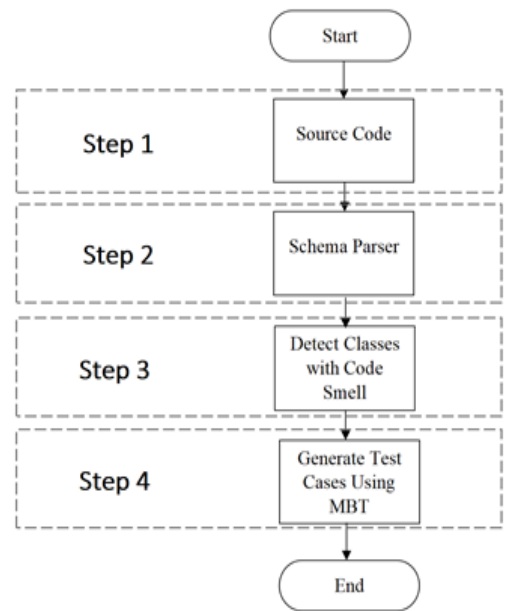


Fig. 1. The Flowchart for Sena TLS-Parser.

```

Console SenaTLSParser
Start Time: 2022/06/22 14:24:58
### Working in project linux-core-service-5 ###

Package

Package CVS

Package com

Package com.CVS

Package com.senatraffic

-----
Source file Constants.java
Has number of lines: 154

-----
Source file ItrafficService.java
Has number of lines: 63

Method name :main
Signature :(QString;)V
Return Type :V
Input variable :
args
Generate Test Cases:
Test Case 1 : valid [args]are input with :1
Test Case 2 : invalid [args]are input with :-1
Test Case 3 : null [args]are input with :null
    
```

Fig. 2. Test Cases Generated from Sena TLS-Parser.

IV. IMPLEMENTATION OF SENA TLS-PARSER

The tool is executed in four steps and this section discusses the steps. The first step is importing the java project to an Eclipse environment as a Plug-in Tool. Fig. 3 shows an example of how Sena TLS-Parser is imported as a Plug-in Tool. By clicking the in-help tab menu, Sena TLS-Parser can be installed as a new software option in Eclipse environment. Sena TLS-Parser will then analyze the codes by right clicking the project and selecting the SenaTLSParser-2.0 as shown in Fig. 4.

Based on Table II, Sena TLS-Parser successfully generated test cases automatically for each application. The duration also depends on the line of code (LOC) for the application. If the LOC is smaller, less time is taken to generate the test cases; for example the Calculator application. If, however, the LOC is much bigger, more time is required to generate the test cases. However, the generation of the test cases also depends on the complexity of the algorithm and the number of methods the application has; for example the Elevator application.



Fig. 3. Installation of Sena TLS-Parser as a Plug-in Tool.

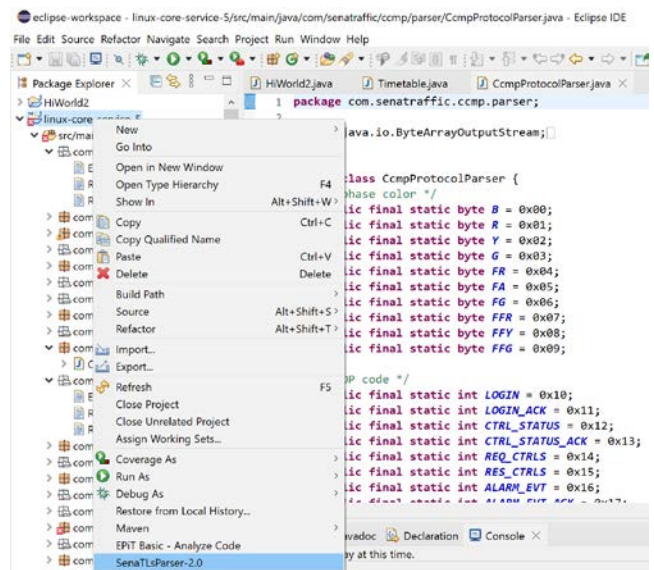


Fig. 4. Sena TLS-Parser as a Plug-in Tool.

Fig. 4 shows the second step for selecting Sena TLS-Parser to analyze source code. The third step is for Sena TLS-Parser to begin analyzing and detecting all of the classes in the source code. The class will be detected by the parser node by node. Sena TLS-Parser then identifies a method within each node. Sena TLS-Parser will save all detected method classes in a variable. Finally, for the fourth step, test cases are generated based on the identified attributes. When Sena TLS-Parser has finished analyzing the source codes, a success popup menu will appear. Fig. 5 shows the popup menu appearing, which indicates the time used to analyze the source code.

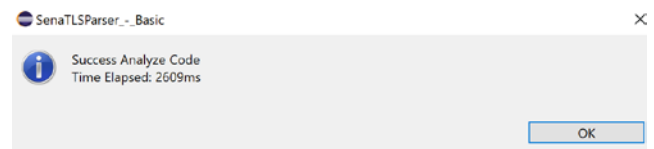


Fig. 5. Time Taken to Generate Test Cases from Sena TLS-Parser.

After the code analysis process is complete, the results will be shown in the Sena TLS-Parser console. The console contains all project information such as project name, test cases created for each class, and the time and date of when the test was conducted. Fig. 2 shows the Sena TLS-Parser console.

V. RESULTS AND DISCUSSION

Case studies are used for testing the performance of Sena TLS-Parser. The case studies are completed by testing Java applications only by developing test cases for each case study to evaluate performance in execution time. For the case studies, performance evaluation regarding Java applications is tested using Eclipse IDE Version 4.5. The six case studies were selected and downloaded from GitHub website [34]. The six case studies are Calculator [35], ATM Machine [36], BlackJack [37], Traffic Light Simulation [38], Airline Reservation [39] and Elevator [40]. Table I describes the case studies used in this paper by providing a summary of the number of classes for each application and a description for each case study.

TABLE I. THE CASE STUDIES

Application	Number classes	Description
Calculator [35]	1	The application contains mathematical methods like add, subtract, multiply, divide methods.
ATM Machine [36]	5	The application has financial transactions such as cash deposits, withdrawals and transfer funds.
BlackJack [37]	5	Simple Blackjack implemented in Java. Creates a random deck of cards, or takes in a file with a list of cards, and plays a round. Prints the winner and the resulting hands of the player and the dealer.
Traffic Light Simulation [38]	5	A traffic light has three lenses, green, orange and red mounted in a panel. Simulates a set of traffic lights (N, S), (E, W) at an intersection.
Airline Reservation [39]	7	Provide online ticket and seat booking for national and international flights as well as flight departure information.
Elevator [40]	9	A small Java project to simulate the evolution of an elevator.

The source codes from all applications are uploaded in Eclipse environment. Subsequently, Sena TLSParser is used as a Plug-in Tool to generate test cases for each application listed in Table I. The results for each case study are shown in Table II. Sena TLSParser shows the duration taken to analyze the source code and generate test cases based on the number of classes detected in the LOC for each application. The results show that the Calculator application is the fastest with 1ms. Meanwhile, the slowest is the ATM Machine application, which is 89ms. The comparison is based on the time required to generate test cases using Sena TLS-Parser.

Based on Table II, Sena TLS-Parser successfully generated test cases automatically for each application. The duration taken also depends on the LOC for each application. If the LOC is smaller, less time is required to generate the test cases; for example the Calculator application. If, however, the LOC is much bigger, more time is required to generate the test cases. However, the generation of the test cases will also depend on the complexity of the algorithm and the number of methods in the application; for example the Elevator application.

TABLE II. THE RESULTS USING SENA TLS-PARSER

APPLICATION	Number classes	LOC	Duration Time (ms)
Calculator	1	63	1
ATM Machine	5	635	89
BlackJack	5	458	51
Traffic Light Simulation	5	185	46
Airline Reservation	7	154	15
Elevator	9	1150	75

Testing the software manually requires effort and is time consuming. Automation saves time and money while also increasing test coverage and accuracy, which is beneficial to both developers and testers. Choosing the right automation framework is critical to assist with various types of testing such

as unit, functional, and regression testing. For comparison purposes, three automated testing frameworks are reviewed compared to the proposed framework, Sena TLS-Parser. These frameworks are JUnit [41], TestNG [42] and Epit [20], which are widely used in the generation of test cases.

A. Junit Testing Framework

JUnit [41] is a well-known Java unit testing framework. It is easy to understand, simple to integrate, and best of all, it is open-sourced. For writing test cases, JUnit employs annotations and assertions. It includes a test-runner for identifying and running all test methods in a project. The JUnit process is done through setting fixed states for objects and running tests by using Fixtures, Test suites, Test runners and JUnit classes are the main features offered by JUnit. The work of these Fixtures aims to provide a good environment for the conduct and implementation of the test. Test suites are a collection of unit test cases that are compiled together. Before testing a code, annotations are used in order to run the test suite. Test runners are used to carry out test cases while JUnit classes are used for testing and writing JUnits, with assert, test case, and test result.

B. TestNG Framework

Cédric Beust created TestNG [42], an open-source test automation framework inspired by JUnit and NUnit for the Java language. The goal of TestNG's design is to provide more powerful and easy-to-use functionalities for a broad range of test categories such as unit, functional, end-to-end, integration, and so on. TestNG's advanced and useful features make it a more robust framework than its competitors. In this framework, the executing of the methods is determined by a set of codes called annotations. Using these annotations demonstrates the usage of Java language new features in a real-world production environment.

C. EPiT Plug-in

EPiT [20] was created to reduce the time spent manually generating test cases by utilizing code smell technique for automated test case generation. EPiT begins by reading the code line by line before applying code smell technique to detect all classes in the Java application. Following that the tool determines the method's name, input parameter, and return type and stores them in variables for use in generating test cases. EPiT has demonstrated its ability to optimize automated test case generation using the code smell technique in a short period of time and with high efficiency.

D. Comparisons of Results

Each framework is used to test the generation of test cases for the case studies. Table III presents the result comparison of the test cases generation framework for each case study based on execution time.

A JUnit test is a method in a class that is only used for testing. This is known as a Test class. To indicate that a method is a test method, @Test annotation is used. This function executes the code being tested. An assert method is used which is provided by Junit.

TestNG covers all categories of tests such as unit, functional, and integration testing. In this research, TestNG has

been integrated with eclipse to generate the test report and execute multiple test cases in parallel. TestNG uses various Annotations for test cases generation, such as @BeforeSuite, @AfterSuite, @BeforeTest, and @AfterTest. Annotations in TestNG are lines of code that can control how the method below them will be executed. Annotations are preceded by “@” symbol.

TABLE III. THE RESULTS FOR DIFFERENT FRAMEWORKS

Application	JUnit	TestNG	EPiT	Sena TLS-Parser
Calculator	32	9	8	1
Airline Reservation	96	57	59	15
Traffic Light Simulation	4201	4101	91	46
BlackJack	93	60	111	51
ATM Machine	179	76	94	89
Elevator	339	67	95	75

The comparison between the testing frameworks has been done based on duration required to generate test cases for each application. The results demonstrate the effectiveness of the proposed tool (Sena TLS-Parser) in automatically and quickly producing test cases. Oshin et al. [43] compared JUnit framework with TestNG framework. Based on Table III, TestNG gives better results as compared with JUnit. The results shown are consistent with the comparison done by [43]. The results show that the Calculator application is the fastest with 32ms for JUnit, 9ms for TestNG, 8ms for EPiT and 1ms using Sena TLS-Parser. For Calculator application, Sena TLS-

Parser gives the best result compared to JUnit, TestNG and EPiT. Meanwhile, for the Traffic Light simulation, both JUnit and TestNG have more execution time as compared to EPiT and Sena TLS-Parser. Sena TLS-Parser is an automation testing tool dedicated for Sena Traffic Light System (TLS) with MBT embedded in its algorithm. Therefore, the results show it has better performance. Meanwhile, EPiT with its technique for code smell [33] improved the generation of test cases compared to the JUnit and TestNG frameworks.

For more clarification, Fig. 6 shows the graph for the applications and duration time for each of the frameworks. It is noticeable that the time taken by each framework to generate test cases depends on the complexity of the algorithm and the number of methods of the application. For example, the traffic light simulation application has more complexity for the algorithm as compared with the Elevator application. Therefore, it takes a lot of time to generate test cases using JUnit and TestNG frameworks. Comparing with EPiT and Sena TLS-Parser, traffic light simulation application takes less time than Elevator application in generating test cases. In addition, the line of codes for the ATM Machine application is less than the Elevator application, however it takes more time using EPiT framework when applying code smell algorithm for the purpose of reducing the redundancy of test cases generation.

To summarize, there are numerous factors that contribute to inconsistent results, including project code complexity, CPU usage, and memory usage. Despite inconsistencies in the results, the results of the case studies demonstrated that Sena TLS-Parser is faster than conventional manually generated test cases and other testing frameworks.

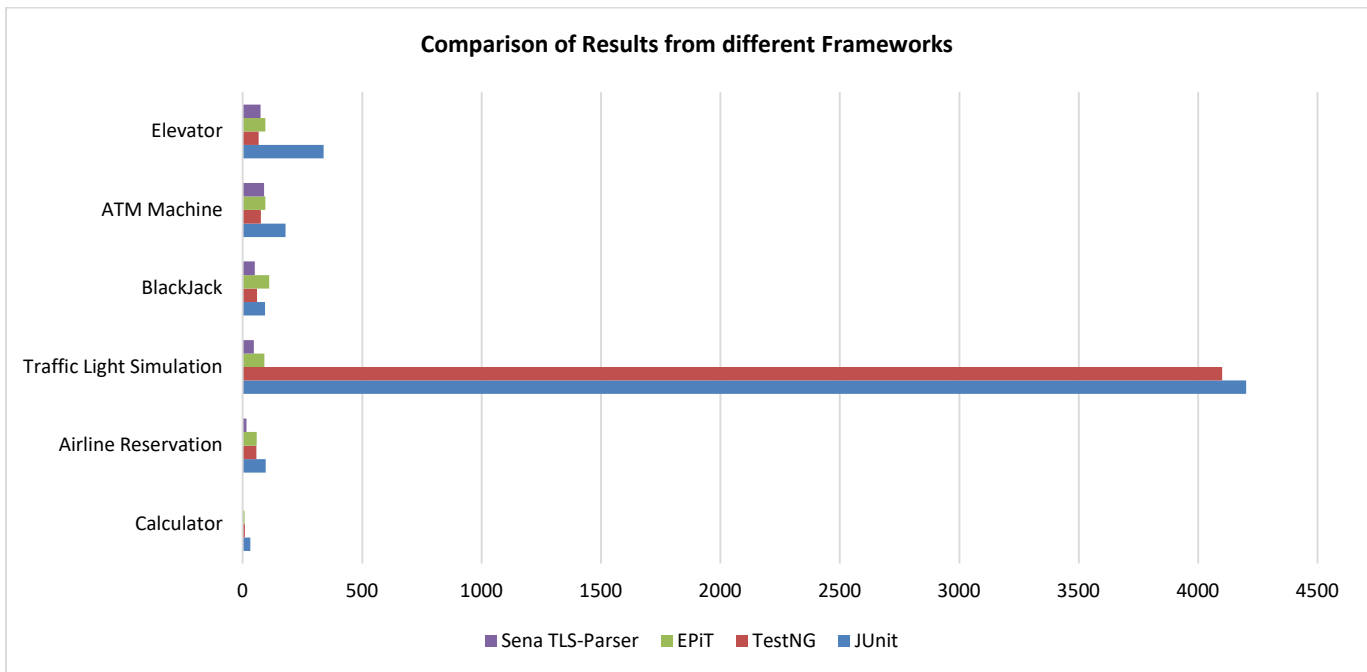


Fig. 6. Comparison of Results from different Frameworks.

VI. CONCLUSION AND FUTURE WORK

During the software testing process, automatic test data generation is critical. Unit-level testing is more successful because test cases cover all the essential paths of the software being tested. The process of creating test cases automatically by Sena TLS-Parser in an Eclipse setting was discussed in this paper. Based on the results presented in this paper, it is shown that Sena TLS-Parser has successfully generated test cases automatically and has a faster response time than traditional manual testing as well as JUnit testing and TestNG. Also, using the MBT technique to create test cases is a very powerful way to do so. For future work related to this research, Sena TLS-Parser framework can be extended to work with other programming languages such as C and C++. Adding other features would also be an interesting direction for future work using Sena TLS-Parser. Sena TLS-Parser can also be generalized to cover mobile applications for software testing. A convertor can be used to convert the source codes of mobile application in “.apk” format into source codes of java programming in “.java” format. By having the convertor, Sena TLSParser will also be able to generate test cases for mobile applications.

ACKNOWLEDGMENT

The authors would like to thank Universiti Tun Hussein Onn Malaysia (UTHM) for supporting this research. The authors received funding for this study from Industry Grant under Grant Vote No M081.

REFERENCES

- [1] N. Li and J. Offutt, “Test Oracle Strategies for Model-Based Testing,” *IEEE Transactions on Software Engineering*, 43(4), 372–395. doi:10.1109/tse.2016.2597136, 2017.
- [2] M. Keyvanpour, H. Homayouni, and H. Shirazee, “Automatic Software Test Case Generation: An Analytical Classification Framework,” *International Journal of Software Engineering and Its Applications* Vol. 6, No. 4, October, 2012.
- [3] G. De Cleve Farto and A. T. Endo, “Evaluating the Model-Based Testing Approach in the Context of Mobile Applications,” *Electronic Notes in Theoretical Computer Science*, 314, 3–21. doi:10.1016/j.entcs.2015.05.002, 2015.
- [4] W. Li, F. Le Gall and N. Spaseski, “A Survey on Model-Based Testing Tools for Test Case Generation,” In: *Itsykson V., Scedrov A., Zakharov V. (eds) Tools and Methods of Program Analysis*. TMPA 2017. Communications in Computer and Information Science, vol 779. Springer, Cham. https://doi.org/10.1007/978-3-319-71734-0_7.
- [5] M. Utting, B. Legeard, F. Bouquet, E. Fournieret, F. Peureux and A. Verotte, “Recent Advances in Model-Based Testing,” *Advances in Computers*, 53–120, January 2016. doi:10.1016/bs.adcom.2015.11.004.
- [6] Model-Based Engineering Forum. [Online]. Available: <http://modelbasedengineering.com/>.
- [7] R. Marinescu, C. Seceleanu, H. Le Guen, P. Pettersson, “A research overview of tool supported model-based testing of requirements-based designs,” In: *Advances in Computers*, pp. 89–140. Elsevier (2015).
- [8] A. Mustafa, W. M. Wan-Kadir, N. Ibrahim, M. A. Shah, M. Younas et al., “Automated test case generation from requirements: a systematic literature review,” *Computers, Materials & Continua*, vol. 67, no.2, pp. 1819–1833, 2021.
- [9] M. Bernardino, E. M. Rodrigues, A. F. Zorzo and L. Marchezan, “Systematic mapping study on MBT: tools and models,” *IET Software*, 11(4), 141–155. doi:10.1049/iet-sen.2015.0154, 2017.
- [10] M. Utting, B. Legeard, F. Bouquet, E. Fournieret, F. Peureux, and A. Verotte, “Chapter two - recent advances in model-based testing,” *ser. Advances in Computers*, A. Memon, Ed. Elsevier, 2016, vol. 101, pp. 53 – 120.
- [11] F. G. C. Ribeiro, C. E. Pereira, A. Rettberg, M. S. Soares, “Model-based requirements specification of real-time systems with UML, SysML, and MARTE,” *Software & Systems Modeling*, vol. 17, no. 1, pp. 343-361, 2018.
- [12] M. L. van Eck, N. Sidorova, W. M. van der Aalst, “Guided interaction exploration and performance analysis in artifact-centric process models,” *IEEE 19th Conference on Business & Information Systems Engineering*, pp. 1-5, 2018.
- [13] N. Khurana, R. S. Chhillar, U. A. Chhillar, “A novel technique for generation and optimization of test cases using use case, sequence, activity diagram and genetic algorithm,” *Journal of Software*, vol. 11, no. 3, pp. 242-250, 2016.
- [14] T. A. Alrawashed, A. Almomani, A. Althunibat, A. Tamimi, “An Automated Approach to Generate Test Cases from Use Case Description Model,” *CMES-Computer Modeling in Engineering & Sciences*, 119(3), 409–425, 2019.
- [15] Meiliana, I. Septian, R. Alianto, Daniel, & F. Gaol, “Automated Test Case Generation from UML Activity Diagram and Sequence Diagram using Depth First Search Algorithm,” *ICSCSI*, 2017.
- [16] M., I. Septian, R. S. Alianto, D. and F. L. Gaol, “Automated Test Case Generation from UML Activity Diagram and Sequence Diagram using Depth First Search Algorithm,” *Procedia Computer Science*, 116, 629–637. doi:10.1016/j.procs.2017.10.029.
- [17] L.L. Muniz, U.C. Nett and P. Maia, “TCG - A Model-based Testing Tool for Functional and Statistical Testing,” *ICEIS*, 2015.
- [18] J. Campos, A. Panichella and G. Fraser, “EvoSuite at the SBST 2019 Tool Competition,” *2019 IEEE/ACM 12th International Workshop on Search-Based Software Testing (SBST)*, Montreal, QC, Canada, 2019, pp. 29-32, doi: 10.1109/SBST.2019.00017.
- [19] G. Fraser and A. Arcuri, “EvoSuite: automatic test suite generation for object-oriented software,” In *Proceedings of the 19th ACM SIGSOFT symposium and the 13th European conference on Foundations of software engineering*, 2011.
- [20] R. Ibrahim, A.A. Amin, S. Jamel, J. Abdul Wahab, “EpiT: A Software Testing Tool for Generation of Test Cases Automatically,” *International Journal of Engineering Trends and Technology*, 68(7), 8-12, 2020.
- [21] I.A. Salihu, R. Ibrahim, B. S. Ahmed, K. Z. Zamli and A. Usman, “AMOGA: A Static-Dynamic Model Generation Strategy for Mobile Apps Testing,” *IEEE Access*, 1–1. doi:10.1109/access.2019.2895504, 2019.
- [22] T. Gu, C. Sun, X. Ma, C. Cao, C. Xu, Y. Yao, ... Z. Su, “Practical GUI Testing of Android Applications Via Model Abstraction and Refinement,” *2019 IEEE/ACM 41st International Conference on Software Engineering (ICSE)*. doi:10.1109/icse.2019.00042.
- [23] E. H. Marinho and E. Figueiredo, “PLATOOL: A Functional Test Generation Tool for Mobile Applications,” In *Proceedings of the 34th Brazilian Symposium on Software Engineering (SBES '20)*. Association for Computing Machinery, New York, NY, USA, 548–553. DOI:<https://doi.org/10.1145/3422392.3422508>, 2020.
- [24] S.W.G. AbuSalim, R. Ibrahim, J. Abdul Wahab, “Comparative Analysis of Software Testing Techniques for Mobile Applications,” In: *Phys.: Conf. Ser.* 1793 012036, 2020.
- [25] K. Pinkal and O. Niggemann, “A new approach to model-based test case generation for industrial automation systems,” *2017 IEEE 15th International Conference on Industrial Informatics (INDIN)*, Emden, 2017, pp. 53-58, doi: 10.1109/INDIN.2017.8104746.
- [26] D. Mishra, S. Bilgaiyan, R. Mishra, A. A. Acharya, ... S. Mishra, “A Review of Random Test Case Generation using Genetic Algorithm,” *Indian Journal of Science and Technology*, 10(30), 1–7. doi:10.17485/ijst/2017/v10i30/107654, 2017.
- [27] D. Mishra, R. Mishra, K. Das and A. Acharya, “Test Case Generation and Optimization for Critical Path Testing Using Genetic Algorithm,” *SocProS*, 2017.
- [28] Y. Du, Y. Pan, H. Ao, N. Ottinah Alexander and Y. Fan, “Automatic Test Case Generation and Optimization Based on Mutation Testing,” *2019 IEEE 19th International Conference on Software Quality*,

- Reliability and Security Companion (QRS-C)*. doi:10.1109/qrs-c.2019.00105, 2019.
- [29] Z. Wang and Q. Liu, "A Software Test Case Automatic Generation Technology Based on the Modified Particle Swarm Optimization Algorithm," *2018 International Conference on Virtual Reality and Intelligent Systems (ICVRIS)*. doi:10.1109/icvr.2018.00045, 2018.
- [30] K.-W. Shin and D.-J. Lim, "Model-based automatic test case generation for automotive embedded software testing," *International Journal of Automotive Technology*, 19(1), 107–119. doi:10.1007/s12239-018-0011-6, 2017.
- [31] C. Ma and J. Provost, "A model-based testing framework with reduced set of test cases for programmable controllers," *2017 13th IEEE Conference on Automation Science and Engineering (CASE)*. doi:10.1109/coase.2017.8256225.
- [32] M. Elqortobi, A. Rahj, J. Bentahar, and R. Dssouli, "Test Generation Tool for Modified Condition/Decision Coverage: Model Based Testing," *In Proceedings of the 13th International Conference on Intelligent Systems: Theories and Applications (SITA'20)*. Association for Computing Machinery, New York, NY, USA, Article 38, 1–6. DOI:<https://doi.org/10.1145/3419604.3419628>, 2020.
- [33] R. Ibrahim, M. Ahmed, R. Nayak and S. Jamel, "Reducing Redundancy of Test Cases Generation using Code Smell Detection and Refactoring". *Journal of King Saud University - Computer and Information Science*, Volume 32, Issue 3, March 2020.
- [34] GitHub. *GitHub Repository*. [Online]. Available: <https://github.com/>
- [35] Клуб анонимных айтишников, *GitHub repository for calculator-unit-test-example-java*. [Online]. Available: <https://github.com/kranonit/calculator-unit-test-example-java>
- [36] Samah AbuSalim. *GitHub repository for ATMMachine*. [Online]. Available: <https://github.com/samahwaleed/ATMMachine>
- [37] Danish Mohd, *GitHub repository for Blackjack-game-in-java*, <https://github.com/DanisHack/Blackjack-game-in-java>
- [38] Yvan Martin. *GitHub Repository for traffic-light-simulation*. [Online]. Available: <https://github.com/ymartin/traffic-light-simulation>
- [39] Annu Dalal. *GitHub Repository for Airline-Reservation-System*. [Online]. Available: <https://github.com/annudalal/Airline-Reservation-System>
- [40] Khesualdo Condori. *GitHub Repository for Elevator-Scheduling-Simulator*. [Online]. Available: <https://github.com/00111000/Elevator-Scheduling-Simulator>
- [41] JUnit. *JUnit4*. [Online]. Available: <https://junit.org/junit4/>
- [42] Cédric Beust and Hani Suleiman. "Next Generation Java Testing: TestNG and Advanced Concepts." Addison-Wesley Professional, 2007.
- [43] Oshin and V. Chaudhary, "Comparison Analysis of TestNG and JUnit frameworks for Automation with Java," *Journal of Emerging Technologies and Innovative Research (JETIR)*, June 2018, Vol 5. Issue 6.

Deep Sentiment Extraction using Fuzzy-Rule based Deep Sentiment Analysis

SIREESHA JASTI¹

Research Scholar, Computer Science and Engineering
GITAM School of Technology
Visakhapatnam, India

G.V.S. RAJ KUMAR²

Professor, Computer Science and Engineering
GITAM School of Technology
Visakhapatnam, India

Abstract—In the world of social media, the amount of textual data is increasing exponentially on the internet, and a large portion of it expresses subjective opinions. Sentiment Analysis (SA) also named as Opinion mining, which is used to automatically identify and extract the subjective sentiments from text. In recent years, the research on sentiment analysis started taking off because of a huge amount of data is available on the social media like twitter, machine learning algorithms popularity is increased in IR (Information Retrieval) and NLP (Natural Language Processing). In this work, we proposed three phase systems for sentiment classification in twitter tweets task of SemEval competition. The task is predicting the sentiment like negative, positive or neutral of a twitter tweets by analyzing the whole tweet. The first system used Artificial Bee Colony (ABC) optimization technique is used with Bag-of-words (BoW) technique in association with Naive Bayes (NB) and k-Nearest Neighbor (kNN) classification techniques with combination of various categories of features in identifying the sentiment for a given twitter tweet. The second system used to preserve the context a Rider Feedback Artificial Tree Optimization-enabled Deep Recurrent neural networks (RFATO-enabled Deep RNN) is developed for the efficient classification of sentiments into various grades. Further to improve the accuracy of classification on n-valued scale Adaptive Rider Feedback Artificial Tree (Adaptive RiFAT)-based Deep Neuro fuzzy network is devised for efficient sentiment grade classification. Finally, this research work proposed a Fuzzy-Rule Based Deep Sentiment Extraction (FBDSE) Algorithm with Deep Sentiment Score computation. Accuracy measure is considered to test the proposed systems performance. It was observed that the fuzzy-rule based system achieved good accuracy compared with machine learning and deep learning based approaches.

Keywords—Sentiment analysis; SemEval; recurrent neural networks; LSTM; word embeddings; accuracy; f1-score; fuzzy – rule; deep sentiment extraction

I. INTRODUCTION

Nowadays, online social media platforms like Twitter or Face book provide a valuable framework for individuals to share and discuss ideas and opinions regarding various topics including health related issues. Within the past decade these kinds of platforms have spread globally and witnessed a rapid growth in the number of users reaching people from various demographic groups, ethnicity and occupations. Twitter is a social media platform that was used by millions of active users to share their opinion, sentiments and their thoughts on any issue. In this platform, the users are interacted through

messages which are called tweets. The estimation of the organizers of the twitter is around 500 million tweets are forwarded in every day. These tweet messages are restricted in size which can contain at most 140 characters. Twitter allow for an exhaustive aggregation and analysis of user generated content which facilitates monitoring of public opinions and sentiment over time towards certain topics of interest. Keeping track of these developments can be crucial for health professionals in order to understand and address the public opinion and behavior with regard to health related topics.

Due to the importance of sentiment analysis to business, the interest has shifted from computer science to management, economics and to the whole society. Nowadays, almost all of the big companies and organizations are having a sort of voice of the customer channel such as emails or call centers and a mean to analyze it. This will help organizations to reshape their services and re-engineer their business processes into the best practice ones. Recently, business has realized the important role that voice of the customer plays in their organizations. The need to have classification systems that are able to handle their feedback data efficiently is emerged. Sentiment analysis is considered as branch of social information where retrieved text is intended to be classified into many classes depending on the detected emotions [1].

Sentiment analysis is the science of extracting, studying and investigating people's sentiments, experience and point of view that documented into a piece of text called, *review*. This extracted information could express general feelings of the authors or extracting sentiments regarding entities such as service, or a product [2]. In computer science, it is about modeling a system that classifies the polarity of a given review. Sentiment analysis model trying to classify reviews into labeled polarities like negative or positive and some adding neutral class [3]. The significant definition for an opinion is a quadruple of four components (G, S, H, T). G is sentiment target, also known as entity or aspect such as camera, product or service under review. S is the sentiment with respect to a target. Opinion's holder is representing by H, whereas T is the time that the opinion was given in. Analyzing the sentiment of given input could be done on three different levels. In the literature, document level sentiment analysis is investigated when calculating the sentiment of the total document, having that the document is about single entity. Another level of a scope is the sentence level when each sentence is analyzed and given a polarity [3]. In this level, it is assumed that the review consists of several opinionated

targets, aspects or entities and their polarities. Finally, aspect level sentiment analysis, where the sentiment is determined on the aspects of an entity. Sentiment analysis has many end-user applications such as monitoring news and social media to look for biased opinions, monitor attitudes towards political candidates or controversial topics during an election, or keeping track of company reputation and consumer response. Sentiment analysis can also be useful for researchers in other fields such as political science and media studies by providing a quantitative method of analyzing public opinion. The internet is growing by the minute and most of the content is in the form of unstructured text. A lot of this data, like blogs, social media and product reviews, are subjective and opinionated. Market analysis is one of the most prominent use cases of SA. Companies used sentiment analysis to keep track of customer relationships, company reputation, consumer response to products and more. Another use of SA is intelligence, where governments can monitor and flag potential threats to national security. There are also many political uses like identifying ideological shifts on social media or identifying which topics engage the public. SA is also used to analyze twitter for public opinion on some topic analysing the plot of fiction, tracking how emotions change throughout the story.

Many of sentiment analysis systems focus on a single language, typically English. However, as the Internet spreads around the world, users are leaving comments in a variety of their native languages. Sentiment analysis in a single language increases the possibility of missing sensitive details in texts written in other languages. Multi-lingual sentiment classification techniques were developed to evaluate data in multiple languages [10]. Sentiment classification frameworks and techniques for various languages are being developed as a result of this. The majority of research in sentiment classification based on the usage of machine learning techniques, unsupervised and supervised. The supervised methods used machine learning algorithms to train with labeled sentiment data and to determine the sentiment of unlabeled test documents. A machine learning method is used in the training phase to learn a prediction model, which is then utilized in the testing or prediction phase to classify documents that the model has never seen before. Feature engineering is likely the most important of these components for classification. People express their negative feelings in sarcastic text by using positive words. Because of this, sarcasm can easily fool sentiment analysis models unless they are specifically designed to account for its possibility. English is considered Majority of the digital platforms and articles are using.

Traditional approaches take the input text, process it and find the sentiment classifications like positive and/or negative based on users one-dimensional reviews. But, these are failed to look into multidimensional perspective of the users review like sarcastic reviews. So, there is very much need for the approaches which are capable to understand the user's multidimensional perspective in giving the reviews.

In this work, machine learning based approaches are used for sentiment analysis at the initial phases. Deep leaning based architectures are developed in the next phases to tokenize the

input as word embeddings for the sentiment analysis task. Finally, this research demonstrates the fuzzy rule based approaches to compute the degree of sentiment using polarity and deep sentiment score. This study is experimented on SemEval competition sentiment classification dataset contains small micro-blog twitter messages.

This work is structured in six sections. The Section 2 explains the existing work of the sentiment analysis. The dataset details and evaluation measures are presented in Section 3. The machine learning based approach described in Section 4 with experiment results. The Section 5 explains the deep neural architectures and experimental results for sentiment classification. Section 6 concludes this work.

II. RELATED WORK

The automated process of splitting and categorizing units of texts into separate, specified categories, also known as classes, is referred to as text categorization. Text classification can be used to extract a text's topic, but it can also be used to classify sentiment. Sentiment classification, often known as sentiment analysis, is the process of determining whether a text is negative, positive, or neutral. NLP methods are used to systematically analyze and evaluate the sentiment expressed in text and assign it to a sentiment class.

Topic classification, i.e. determining whether a text is about politics or sports, is usually done using machine-learning approaches. Pang et al. (2002) adopted [1] these machine-learning methods and regarded positive or negative sentiment as topics of their own. With this approach they managed to achieve performances hovering around 80% when analyzing movie reviews. However, the experiments conducted only contained reviews that were considered positive or negative. Agarwal et al. conducted [4] the accuracy of sentiment analysis on Tweets using a Support Vector Machine (SVM) was around 60% depending on the features employed. They also pre-processed the Tweets by replacing acronyms with full meanings and emoticons with their emotional states. When doing binary classification, the proposed method achieved an accuracy of roughly 75% when omitting the neutral class and just having positive or negative classes.

Bhayani et al. conducted [5] experiments that utilized distant supervision on data extracted from Twitter. Distant supervision relates to gathering and labelling training data automatically. They worked on the notion that any Tweet with a positive emoticon likewise has positive emotion, and any Tweet with a negative emoticon has negative sentiment. They could construct an annotated classifier training set without hand-labeling data using these assumptions. They regarded emoticons to be noise; therefore they removed them from the data set. Given the importance of emoticons in expressing moods and their widespread use in sentiment analysis, a feasible upgrade to this approach would be to appropriately integrate emoticons and their emotional connotations.

Edilson Anselmo et al., explained [6] a multi-view ensemble approach for the task of SA also specifically named as Message Polarity Classification in SemEval-2017 challenge. In this ensemble approach, different types of

features are used to train every base classifier. The first base classifier is Linear SVM which uses bag-of-words model as a feature space. The second base classifier is another Linear SVM which uses the averaging of word embeddings of tweets. The third base classifier is Logistic Regressor where in the tweets are represented as averaging of weighted word embeddings. In the first classifier, the tweets are represented with the TF-IDF (Term Frequency and Inverse Document Frequency) weights of bag-of-words. In the third classifier the word embeddings weight is represented with TF-IDF measure. In case of F1-score and recall, their proposed system got an 18th rank and 20th respectively among 38 participants in the competition.

Tzu-Hsuan Yang et al., implemented [7] a system for SA task in twitter dataset. This system is a combination of two deep neural networks based models such as LSTM Recurrent Neural Network and convolution neural network (CNN) through interpolation. These models take the input as distributional words representations of tweets as vectors and the output is the sentiment of a tweet. They observed that the word embeddings performance is good in RNN for computing Recall and accuracy when compared with one-hot vectors. They identified that LSTM model performance is good for predicting all classes but the RNN fails to predict the negative class. They also observed that the performance of LSTM is good on neutral and positive classes and the performance of CNN is good on negative class compared with LSTM. The proposed system obtained an average F1 score of 0.587, average recall rate of 0.618 and the accuracy of 0.618 for sentiment analysis task of SemEval 2017 Competition.

Recently, the implementation of SA in twitter using neural networks become one of the state of the art techniques because they took less number of features when compared with traditional techniques. Yichun Yin et al., proposed [8] an effective and simple ensemble method to boost the performance of neural network models. They collected the several sets of word embeddings which are constructed by using skip-gram model or released publicly or learned from different corpus. They assume that the usage of these embeddings increases the performances and generalizations of neural network models. They identified different types of neural networks like RNN, CNN, LSTM and GRU for implementing their method, but they used RCNN [9] in their method. The aim of RCNN is to capture non-consecutive and longer range patterns in a weighted manner by using adaptive gated decay and non-consecutive convolution. The proposed method achieved 1st rank in Accuracy and 5th rank in average recall in the SemEval 2017 sentiment analysis competition.

Traditional techniques used a different type of hand crafted features such as semantic, surface-form and sentiment lexicons for sentiment classification of twitter [10]. The performance of these techniques mainly depends on the quality work of feature construction and developing a popular system for these features. Moreover, the one-hot representation of these features proposes the sparsity problem in the representation and the semantic information also not captured in the representation. To overcome this problem, Tang et al. induced [11] real-valued, sentiment-specific and low-dimensional embedding features for sentiment

classification of twitter which encode the combination of sentiments and semantics of words. They identified that the hand-crafted features and embedding features achieved similar results.

AbeedSarker et al., presented [12] a system by combining the dense and sparse vector representations of words and clusters are used for generalized words representations for supervised text classification. The neural networks are trained by using the dense vectors which are represented with word embeddings in a large unlabeled dataset to predict the neighboring words. The sequences of word n-grams (n range is 1-3) are used for generating the sparse vectors. The Support Vector Machines (SVMs) with an RBF kernel is used for classification of a text segment by concatenating the different vector representations. This system is specifically proposed for non-experts of machine learning and natural language processing and doesn't require any manual tuning of weights or parameters. The system generates the classification model by automatically optimizing the relevant hyper-parameters and producing the training vectors for SVM classifier from a given training dataset. This system is evaluated on the sentiment analysis task of SemEval 2017 English dataset. The proposed system achieved F1-score of 0.632, accuracy of 0.646 and average recall of 0.637.

Raphael Troncy et al., proposed [13] a SentiME++ system which is an ensemble approach for the SA task of SemEval 2017 competition. The aim of this system is to classify the English tweets based on the type of sentiment like negative, positive or neutral sentiments they have. SentiME++ merge the predictions of five popular sentiment classifiers such as NRC-Canada [10], GU-MLT-LT [14], KLUE [14], TeamX [15] and Stanford Sentiment System (subsystem of the Stanford NLP Core toolkit). In SentiME++ approach, a bootstrap sampling (a uniform random sampling with replacement) technique is used to produce four different training sets from the initial training set T. These training sets are used to train the four sub classifiers separately. SentiME++ trains four classifiers separately and fifth classifier Stanford Sentiment System is not trained with training data. The outputs of five classifiers are represented as a feature vector and this is directed to stack supervised learner. This system produced a F1-score of 0.613 for sentiment classification and obtained 12th rank in the competition.

Chukwuyem Onyibe explained [16] a supervised system which uses lexical features (Uni-grams, Tweet length, Tweet length binned, Bi-grams, SentiStrength, Removed URL, Stop words) and optimized Conditional Random Fields to predict the tweet sentiment. We used CRF++ which is implemented with the primary machine learning component as Conditional Random Fields (CRF). They were inspired by the work of Yang et al. (2007) who used CRFs to identify the sentiment in web blogs by giving training at sentence level and classifying at the document level by considering the sequences of sentences. In their work, they optimized the parameters of CRF++ as well as lexical features for the task of sentiment classification in twitter of SemEval 2017. The combination of SentiStrength and unigrams performed well to obtain good results. They obtained good results for sentiment classification when the parameters of CRF are f value 1, c value 8.5 and

features are uni-grams. The proposed system achieved an average F1-score of 0.54226, average recall of 0.59024 and accuracy of 0.61519.

Mohammed Jabreel et al., proposed [17] a system named as SiTAKA for SemEval 2017 twitter SA task for both Arabic and English languages tweets. In this system, the tweets are represented with a set of novel features which includes the information generated by five lexicons (NRC hashtags lexicon [10], General Inquirer [T8], TSLex [18], Hu-Liu opinion lexicon (HL) [19] and SenticNet [20]) and a bag of negated words. It was observed that the combination of these features with some basic features (syntactic, basic text, lexicon, Word Embeddings and cluster) increases the performance of the classification. The SVM classifier is used to identify the sentiment of tweets. The proposed system achieved 2nd rank in Arabic and 8th rank English language tweets.

SymeonSymeonid is proposed [21] an approach based on a Majority Vote scheme and combined the classical linguistic resources such as sentiment lexicon features and bag-of-words with supervised machine learning methods for sentiment classification task. The usage of lexicons and bag-of-words representation has a predefined sentiment for each uni-gram and bi-gram. We used different types of classifiers such as Ridge, Logistic Regression, Stochastic Gradient Descent, Nearest Centroid, Bernoulli Naive Bayes, Linear SVC, Passive-Aggressive for testing the performance of the proposed approach. It was observed that among the set of all three combination classifiers one set of classifiers such as the Nearest Centroid, the Stochastic Gradient Descent (SGD) and Bernoulli Naive Bayes achieved best results. They also identified that Nearest Centroid is a weak classifier when alone but it gives best contribution when combined with other two classifiers.

Sentiment classification is one of the major issues of NLP and become more popular among many research fields. Typically, sentiment classification predicts the sentiment of a text into various discrete classes like negative, positive or neutral. Ming Wang et al., explained [22] a deep learning system to classify 2-polarity, 3-polarity and 5-polarity in tweets by combining SVM with GRU. In their system, first they used pre-trained word embeddings to train a gated recurrent neural network, and then they extracted features from GRU layer and forwarded these features to SVM to perform quantification and classification sub-tasks. Joosung Yoon et al., proposed [23] a sentiment analyzer for sentiment classification to predict the sentiment at document level of English tweets for SemEval 2017 competition. This method is based on lexicon integrated CNNs with attention (LCA). The proposed method achieved an average recall of 58.9%, an average F1-score of 55.2% and an accuracy of 61.4% for the task of sentiment classification.

MickaelRouvier et al., explained [24] a system which is an ensemble model of Deep Neural Networks (DNN) such as RNN-LSTM and CNN. We used four different types of pre-trained embeddings such as three different sentiment embeddings and one lexical embedding on large datasets to initialize the input representation of DNN. These models can capture word level information only. We injected some

sentence level features like Emoticons, Elongated units, Lexicons, All-caps and Punctuation into the system. They used a score-level fusion approach to combine the ensemble of DNNs. The proposed system got 2nd rank at SemEval 2017 competition and achieved an average recall of 67.6%. It was identified that the CNN model obtained best results for sentiment classification when compared with RNN-LSTM models. Haowei Zhang et al., proposed [25] a multichannel model named as CNN-LSTM to predict the sentiment of English language twitter tweets and this model is a combination of two parts such as multi-channel LSTM and CNN. Unlike a CNN, a multi-channel strategy is applied in the proposed model to extract different scales of active local n-gram features and various filters of different length are used in this strategy. Then LSTM is used to compose the information sequentially. In the classification process, they considered both long distance dependencies across tweets and local information within tweets by combining both CNN and LSTM. This multi-channel approach achieved an accuracy of 0.640 for sentiment classification.

AmitAjitDeshmane et al., proposed [26] a system for SemEval 2017 twitter sentiment analysis task. The system is an ensemble of three different deep learning architectures. The first architecture used CNN to perform the text classification. The second architecture implemented with gated RNN. In third subsystem, the opinion lexicons are integrated directly with CNN architecture. The proposed ensemble system obtained a macro-averaged recall of 64.3%. It was observed that the first architecture is crucial to improve the results of sentiment classification. Iv'an Castro et al., proposed [27] a system for SemEval-2017 twitter sentiment analysis task. In this system, they studied about how the relationships among sense n-grams and sentiment polarities like negative, neutral or positive are contributed to this task. They also tested the effect of removing a large set of char n-grams features reported in previous works. Based on these observations, they explore a SentiWordNet as a polarity lexicon and constructed a SVM system. The proposed system got 10th rank in the competition and achieved an F1-score of 0.624.

Yunxiao Zhou et al., reported [28] a system for SA in twitter task of SemEval-2017 competition. They investigated various traditional Natural Language Processing (NLP) features (Word RF n-grams, POS tag, Negation), domain specific features (All-caps, Bag-of-Hashtags, Elongated, Emoticon, Punctuation) and word embedding features (GoogleW2V, GloVe, sentiment word vector (SWV), sentiment-specific word embedding (SSWE)) along with supervised machine learning techniques ((SVM), AdaBoost, Logistic Regression (LR) and SGD) to address this task.

III. PROPOSED FUZZY-RULE BASED SYSTEM AND METHODOLOGY

In this section an automated framework for deep sentiment extraction is proposed with the components described in (Fig. 1).

Initially, the framework will accept the reviews from any dataset and then text processing steps like stemming and stop word removal are performed. The process of feature selection is carried out as second step for the process using novel

machine learning methods, which is elaborated in this work. Pre-processed data is given as input in the feature extraction stage, where extraction of significant features, namely spam words-based features, SentiWordNet features, emoticon-based features and TF-IDF features takes place for decreasing the processing of data. Further, the key phrases from the review text are extracted using feature fusion methods. This section elaborates the procedure of identification of parameter μ based on decision tree. At first, review data is trained for finding the parameter after that, rule is induced and categorized. Feature fused output is taken as input for classification of sentiment grade. Here, a classifier named Deep learning network is used to perform the classification of the sentiment grade. Moreover, deep learning network is trained based on devised Adaptive RFATO technique. This proposed Adaptive RFATO algorithm is devised by combining ROA [29] and FAT scheme [30] with adaptive concept.

On the other hand, ROA involves four riders, namely follower, bypass rider, attacker and overtake racing besides others for reaching destination. Finally, fuzzy rule based approaches are used to analyze the degree of sentiment using polarity and to extract the opinion. The combination of ROA and FAT scheme, named as RFATO technique offers best solution to solve optimization issues. However, this method consumes more computational time. Hence, this research included the adaptive mechanism with RFATO method for obtaining less computational time.

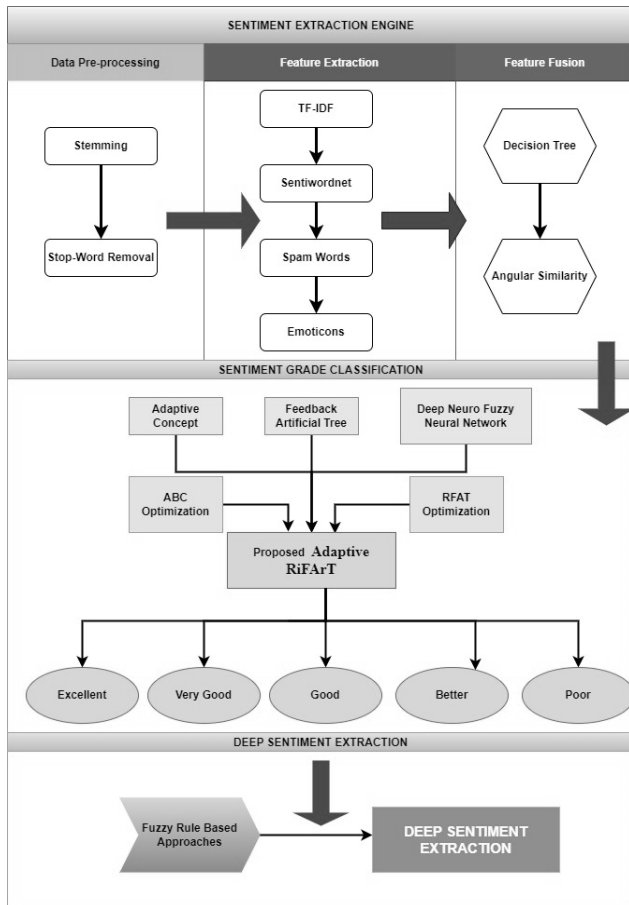


Fig. 1. Proposed Frameworks for Deep Sentiment Extraction.

A. Gated Recurrent Units (GRU) for Sentiment Analysis

By using the gating mechanism the gradient stays high for long time-steps and thus overcome the problem of vanishing gradient. Despite its effectiveness, the complexity found in the gating mechanism make the architecture expensive to execute and hard to analyze. As a result, many variations have been proposed but Gated Recurrent Unit (GRU) introduced by [32] is one of the strongest competitors to LSTM. Compared to LSTM, it is much simpler and faster and needs fewer gates to calculate. In sentiment classification task, RNN based layer could be used to generate sentence hidden representation and then, this representation could be used as input to the classification function to find a polarity of a given tweet [33, 34].

For the proposed models, GRU layer is used rather than LSTM as its GRU works better in this experiment as the validation loss on the dataset was lesser and it was faster also. Compared with standard RNN, GRU cell uses two gates to handle the flow of the data, z_t to represent update gate and r_t to represent reset gate. z_t determines the amount of previous information to keep while r_t determines the methodology of combining the old memory with the new input. The entire internal memory is output without an additional activation. At each step, each word-distributed representation is given as an input word x_t , the current cell state c_t and hidden state h_t can be updated with the previous cell state c_{t-1} and previous hidden state h_{t-1} . The equations (1) (2) (3) and (4) are used to compute the z_t , r_t , c_t and h_t respectively.

$$z_t = \sigma(x_t U_z + h_{t-1} W_z) \tag{1}$$

$$r_t = \sigma(x_t U_r + h_{t-1} W_r) \tag{2}$$

$$c_t = \tanh(x_t U_c + W_c(h_{t-1} \odot r_t)) \tag{3}$$

$$h_t = (1 - z_t \odot c_t + z_t \odot h_{t-1}) \tag{4}$$

The output of this layer is the hidden representation of the given tweet that is going to be fed into the attention layer to highlight the most informative words and to generate the final tweet representation.

B. Attention Layer for Sentiment Orientation

The attention mechanism is used to amplify the most informative words in a given tweet with higher weights inspired by [31]. The attention layer is placed after GRU layer to point out the most influence words to the tweet meaning and then the specific word representations are combined to form a vector representation for tweets. To generate the final tweet representation, the attention layer uses the following mathematical formulas.

Using each hidden state h_t and dot product with its weights is producing the hidden representation u_t . The equation (5) is used to compute u_t .

$$u_t = \tanh(h_t w_t + b_t) \tag{5}$$

The un-normalized hidden representation of the current word u_t is passed to softmax function to get the normalized importance weight α_t . The ' α_t ' is computed using equation (6).

$$\alpha_i = \frac{\exp(u_i)}{\sum_{i=1}^T \exp(u_i)} \quad (6)$$

Where, T is count of time-steps in the input, w_t and b_t are the weights of attention layer which are optimized during training to allocate more weights to the most important words of a sentence. Finally, the high level vector representation of a tweet S is produced based on the weights by using weighted sum of the word annotations. The S is computed using equation (7).

$$S = \sum_{i=1}^T h_{it} \alpha_{it} \quad (7)$$

To classify the tweets into the sentiment labels, the final vector representation of tweet is fed into fully connected Sigmoid logistic regression layer. It produces an output in the range between 0 and 1 by using the probability distributions of all sentiment classes.

This result into a semantic orientation of the word or the phrase using the Point_wise Mutual Information:

$$SO(S) = PMI(S, Excellent) - PMI(S, poor) \quad (8)$$

Here,

$SO(S)$, denotes the semantic orientation of the phrase.

$PMI(S, Excellent)$, denotes the PMI for the phrase with positive sentiment.

$PMI(S, poor)$, denotes the PMI for the phrase with negative sentiment.

IV. PROPOSED MODEL FOR SENTIMENT EXTRATION

This section elaborates on the proposed mathematical model for the deep sentiment extraction process. Firstly, the generic set of positive and negative words accumulated in two different classes. The words are collected based on the popular vocabulary of the most commonly used phrases for consumer product review systems.

$$[P] = \langle Good, Excellent, Amazing, Incredible, Great, \dots \rangle \quad (9)$$

and

$$[N] = \langle Bad, Poor, Terrible, \dots \rangle \quad (10)$$

Here, the Positive and Negative reference words are represented by the sets P and N.

$$SO(S) = PMI(S, [P]) - PMI(S, [N]) \quad (11)$$

Further, only the phrases or the words are considered with the highest correlation as $SO(S) > 1$

Finally, perform the iterative classification of the phrases in the review or feedback for identifying the sentiment score and calculate the total score based on the weighted calculation of rating and text feedback, the mathematical model is

converted into the workable algorithm as discussed in Algorithm-1.

Algorithm-1: Fuzzy-Rule Based Deep Sentiment Extraction (FBDSE)

- Step -1. Create collection of positive and negative word sets
 Step -2. Accept the list of products and analyse
- A. For each product
 - B. Break the sentences into phrases
 - i. For each zone
 - a. Calculate the correlation score
 - b. if the score is higher than 1
 - Then consider the phrase
 - c. else
 - Reject the phrase from the set
 - d. Repeat for minimal set
 - C. Consider the Compound score- Deep Sentiment can be measured by Compound Score and it lies between -1 to +1
 - D. Calculate the Deep Sentiment Score = rating *0.8 + text score * 0.2
 - E. Deep Sentiment score ≥ 0.5 = Positive (P)
 neutral if $0 < \text{Deep Sentiment score} < 0.5$ = Neutral(Nu)
 negative if $-1 \geq \text{Deep Sentiment score} \leq -0.5$ = Negative(N)
-

V. DATASET CHARACTERISTICS AND EVALUATION MEASURES

In this work, the experiment conducted on the dataset provided by the organizers of SemEval competition task of twitter sentiment analysis at tweet level. This dataset is a combination of the twitter datasets and the characteristics of a dataset are specified in the Table I.

In the training dataset, the number of tweets in neutral class is more compared to other two classes. The dataset is not balanced which means the three classes contain varying number of tweets. The researchers of sentiment analysis used various measures such as F1-Score, recall, precision and accuracy for evaluating the machine learning techniques. In this work, accuracy is used to test the efficiency of the machine learning techniques. Accuracy is the ratio of the number of test tweets are correctly classified their sentiment and the number of test tweets considered in the experiment. Precision and recall metrics are highly recommended especially if the dataset is unbalance. Precision measures the probability that a positive prediction is really positive. Recall measures the efficiency of a model to find all positive reviews in a dataset. Here, the detailed classifications of sentiment types based on given user ratings are shown in Table II.

TABLE I. THE DATASET CHARACTERISTICS

Dataset	Total	Positive	Negative	Neutral
SemEval train	47831	18377	7442	22012
SemEval dev	5653	2412	1056	2185
SemEval test	12284	2375	3972	5937

TABLE II. USER RATINGS AND SENTIMENT TYPE MAPPING

User Rating (Given)	Sentiment Type
-2	Poor
-1	Better
0	Good
1	Very Good
2	Excellent

The following Table III consists of sample of tweets classified into different feature types rated in between -2 and 2.

TABLE III. EXTRACTION OF SENTIMENT FEATURES AND TYPES

Company Name	Total tweets	Poor (-2)	Better (-1)	Good (0)	Very Good (1)	Excellent (2)
Microsoft	100	12	34	20	31	3
Amazon	100	6	12	12	55	15
Bentley	100	1	2	32	62	3
David Cameron	100	7	31	37	24	1
Donald trump	100	2	42	40	15	1
Google	100	0	8	59	33	0
Harry Potter	100	2	0	18	64	16
i-phone	100	0	5	30	56	9
Jurassic World	100	0	5	11	62	22
Madonna	100	0	2	21	73	4

User sentiment score have been calculated as three categories Negative(N), Positive(P) and Neutral (Nu) following table (Table IV) consists of sample of tweets classified into different feature types rated in between -2 and 2.

Next, Deep sentiment score discussed in the proposed approach for the above mentioned three sentiment types is calculated and shown in Table V.

Next, the comparison between the extracted user sentiment score and deep sentiment score have been composed and the observations are shown in Table VI.

TABLE IV. USER SENTIMENT SCORE

Company Name	Negative(N)	Neutral(Nu)	Positive(P)
Microsoft	0.46	0.2	0.34
Amazon	0.18	0.12	0.7
Bentley	0.03	0.32	0.65
David Cameron	0.38	0.37	0.25
Donald Trump	0.44	0.4	0.16
Google	0.08	0.59	0.33
Harry Potter	0.02	0.18	0.8
i-phone	0.05	0.3	0.65
Jurassic World	0.05	0.11	0.84
Madonna	0.02	0.21	0.77

TABLE V. DEEP SENTIMENT SCORE

Company Name	Negative	Neutral	Positive
Microsoft	0.092	0.04	0.068
Amazon	0.036	0.024	0.14
Bentley	0.006	0.064	0.13
DavidCameron	0.076	0.074	0.05
Donald Trump	0.088	0.08	0.032
Google	0.016	0.118	0.066
Harry Potter	0.004	0.036	0.16
i-phone	0.01	0.06	0.13
Jurassic World	0.01	0.022	0.168
Madonna	0.004	0.042	0.154

TABLE VI. COMPARISON OF EXTRACTED USER AND DEEP SENTIMENT SCORE

Company Name	Negative(N)		Neutral(Nu)		Positive(P)	
	USER	DEEP	USER	DEEP	USER	DEEP
Microsoft	0.46	0.092	0.2	0.04	0.34	0.068
Amazon	0.18	0.036	0.12	0.024	0.7	0.14
Bentley	0.03	0.006	0.32	0.064	0.65	0.13
David Cameron	0.38	0.076	0.37	0.074	0.25	0.05
Donald Trump	0.44	0.088	0.4	0.08	0.16	0.032
Google	0.08	0.016	0.59	0.118	0.33	0.066
Harry Potter	0.02	0.004	0.18	0.036	0.8	0.16
i-phone	0.05	0.01	0.3	0.06	0.65	0.13
Jurassic World	0.05	0.01	0.11	0.022	0.84	0.168
Madonna	0.02	0.004	0.21	0.042	0.77	0.154

The graphical illustration of the above calculations is made visible using the following graph as shown in Fig. 2.

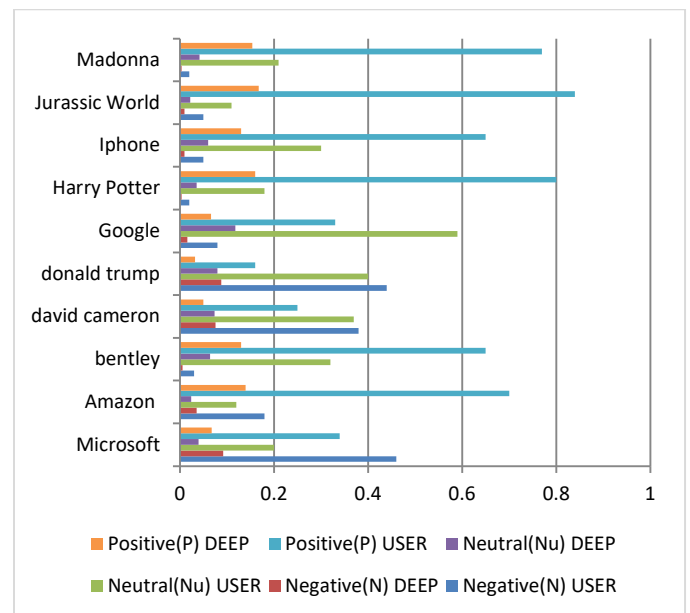


Fig. 2. Comparison between User and Deep Sentiment Score.

TABLE VII. COMPOUND SCORE

Company Name	Compound Score	Final Opinion (Towards)
Microsoft	0.552	Positive
Amazon	0.84	Positive
Bentley	0.78	Positive
David Cameron	0.456	Neutral
Donald Trump	0.528	Neutral
Google	0.708	Positive
Harry Potter	0.96	Positive
i-phone	0.78	Positive
Jurassic World	1	Positive
Madonna	0.924	Positive

Finally, as discussed in the proposed Fuzzy-Rule Based Deep Sentiment Extraction (FBDSE) Algorithm; the compound score of the sentiments have been calculated as shown in Table VII to understand the sentiment orientation which helps in identification of the polarity of the opinion.

Next, as we discussed in the proposed algorithm extracts the opinion based on the Compound Score (CS). If the $CS \geq 0.5$, neutral if $0 < CS < 0.5$ and negative if $-1 \geq CS < -0.5$. The graph represents the final compound score is shown in Fig. 3.

The Precision, Recall and F1-Score of the proposed Fuzzy-Rule Based Deep Sentiment Extraction (FBDSE) are compared with the earlier proposed algorithms as shown in Table VIII.

Finally, observed that there is a remarkable enhancement in the performance as shown in Fig. 4.

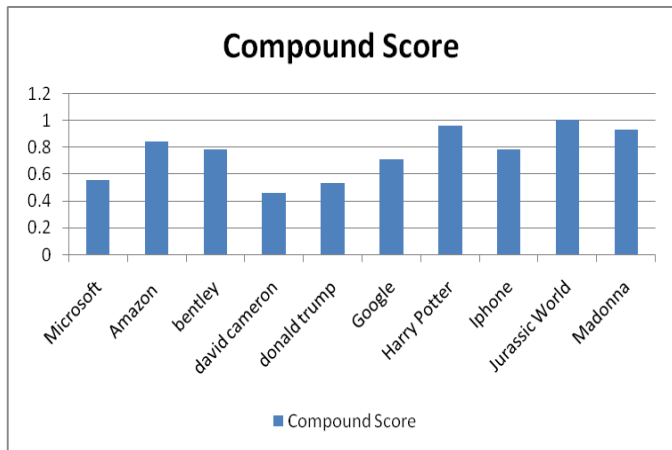


Fig. 3. Compound Score.

TABLE VIII. COMPOUND SCORE

Model Performance	ABC Bi-Gram Model	Proposed RFATO Enabled Deep-RNN	Adaptive RFATO Based Deep Neuro Fuzzy Network	Proposed FBDSE Approach
Recall	0.823	0.887	0.889	0.937
Precision	0.797	0.8	0.801	0.897
F1-Score	0.81	0.841	0.843	0.917

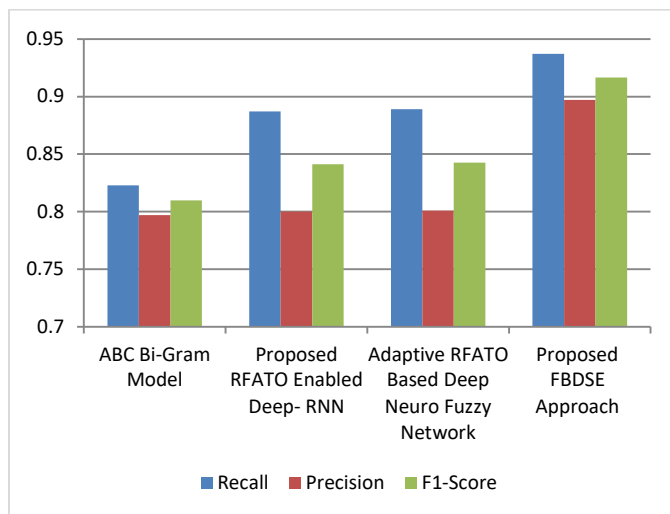


Fig. 4. Comparison of Performance.

VI. CONCLUSION

This research work proposed two approaches for sentiment classification task of SemEval competition. The first approach used machine learning techniques like NB, RF and SVM by using a set of stylistic, syntactic and semantic features. Among these techniques, the SVM obtained good accuracy for sentiment classification. The second approach used deep neural architectures like RNN, LSTM and GRU for sentiment classification. Two word embedding models are used for generating word vectors. The deep learning based approach performance is good compared with machine learning based approach.

A new methodology is proposed to deep sentiment extraction and grading on N-Scale by developing a fuzzy rule based system for sentiment analysis, which can offer more refined outputs through the use of fuzzy membership degrees. The experimental results indicate that our fuzzy-based approach performs marginally better than the other algorithms. In addition, the fuzzy approach allows the definition of different degrees of sentiment without the need to use a larger number of classes and almost 91% of accurate deep sentiments extracted on the given products. Future scope of this work is focused on Multi-Lingual Deep Sentiment Extraction using semantic annotations and AI-based reasons.

REFERENCES

- [1] Pang, Bo, Lillian Lee, and ShivakumarVaithyanathan. "Thumbs up?: sentiment classification using machine learning techniques." Proceedings of the ACL-02 conference on Empirical methods in natural language processing-Volume 10. Association for Computational Linguistics, 2002.
- [2] Abbasi, Ahmed, Hsinchun Chen, and Arab Salem. "Sentiment analysis in multiple languages: Feature selection for opinion classification in Web forums." ACM Transactions on Information Systems (TOIS) 26.3 (2008): 12.
- [3] Pang, Bo, and Lillian Lee. "Opinion mining and sentiment analysis." Foundations and Trends® in Information Retrieval 2.1-2 (2008): 1-135.
- [4] Agarwal, B. Xie, I. Vovsha, O. Rambow, R. Passonneau, "Sentiment Analysis of Twitter Data", In Proceedings of the ACL 2011 Workshop on Languages in Social Media, 2011, pp. 30-38.

- [5] Go, R. Bhayani, L.Huang. "Twitter Sentiment Classification Using Distant Supervision". Stanford University, Technical Paper, 2009.
- [6] Edilson Anselmo Corrêa Junior, Vanessa Marinho, and Leandro Santos. 2017. NILC-USP at SemEval-2017 Task 4: A Multi-view Ensemble for Twitter Sentiment Analysis. In Proceedings of the 11th International Workshop on Semantic Evaluation. Vancouver, Canada, SemEval '17, pages 610–614.
- [7] Tzu-Hsuan Yang, Tzu-Hsuan Tseng, and Chia-Ping Chen. 2017. deepSA at SemEval-2017 Task 4: Interpolated deep neural networks for sentiment analysis in Twitter. In Proceedings of the 11th International Workshop on Semantic Evaluation. Vancouver, Canada, SemEval '17, pages 615–619.
- [8] Yichun Yin, Yangqiu Song, and Ming Zhang. 2017. NNEMBs at SemEval-2017 Task 4: Neural Twitter sentiment classification: a simple ensemble method with different embeddings. In Proceedings of the 11th International Workshop on Semantic Evaluation. Vancouver, Canada, SemEval '17, pages 620–624.
- [9] Tao Lei, Hrishikesh Joshi, Regina Barzilay, Tommi S. Jaakkola, Katerina Tymoshenko, Alessandro Moschitti, and Lluís M.´arquez. 2016. Semi-supervised question retrieval with gated convolutions. In NAACL HLT 2016, The 2016 Conference of the North American Chapter of the Association for Computational Linguistics: Human Language Technologies, San Diego California, USA, June 12-17, 2016. pages 1279–1289.
- [10] Saif Mohammad, Svetlana Kiritchenko, and Xiaodan Zhu. 2013. Nrcanada: Building the state-of-the-art in sentiment analysis of tweets. In Proceedings of the 7th International Workshop on Semantic Evaluation, SemEval@NAACL-HLT 2013, Atlanta, Georgia, USA, June 14-15, 2013. pages 321–327.
- [11] Duyu Tang, Furu Wei, Nan Yang, Ming Zhou, Ting Liu, and Bing Qin. 2014. Learning sentiment-specific word embedding for twitter sentiment classification. In Proceedings of the 52nd Annual Meeting of the Association for Computational Linguistics (Volume 1: Long Papers). Association for Computational Linguistics, Baltimore, Maryland, pages 1555–1565.12.
- [12] Abeed Sarker and Graciela Gonzalez. 2017. HLP@UPenn at SemEval-2017 Task 4A: A simple, self-optimizing text classification system combining dense and sparse vectors. In Proceedings of the 11th International Workshop on Semantic Evaluation. Vancouver, Canada, SemEval '17, pages 639–642.
- [13] Raphael Troncy, Enrico Palumbo, Efstratios Sygkounas, and Giuseppe Rizzo. 2017. SentiME++ at SemEval-2017 Task 4: Stacking state-of-the-art classifiers to enhance sentiment classification. In Proceedings of the 11th International Workshop on Semantic Evaluation. Vancouver, Canada, SemEval '17, pages 647–651.
- [14] Thomas Proisl, Paul Greiner, Stefan Evert, and Besim Kabashi. 2013. KLUE: Simple and robust methods for polarity classification. In 7th International Workshop on Semantic Evaluation (SemEval).
- [15] Yasuhide Miura, Shigeyuki Sakaki, Keigo Hattori, and Tomoko Ohkuma. 2014. TeamX: A Sentiment Analyzer with Enhanced Lexicon Mapping and Weighting Scheme for Unbalanced Data. In 8th International Workshop on Semantic Evaluation (SemEval). T8 Philip Stone, Dexter C Dunphy, Marshall S Smith, and DM Ogilvie. 1968. The general inquirer: A computer approach to content analysis. *Journal of Regional Science* 8(1):113–116.
- [16] Chukwuyem Onyibe and Nizar Habash. 2017. OMAM at SemEval-2017 Task 4: English sentiment analysis with conditional random fields. In Proceedings of the 11th International Workshop on Semantic Evaluation. Vancouver, Canada, SemEval '17, pages 669–673.
- [17] Mohammed Jabreel and Antonio Moreno. 2017. SiTAKA at SemEval-2017 Task 4: Sentiment analysis in Twitter based on a rich set of features. In Proceedings of the 11th International Workshop on Semantic Evaluation. Vancouver, Canada, SemEval '17, pages 693–698.
- [18] Duyu Tang, Furu Wei, Bing Qin, Ting Liu, and Ming Zhou. 2014a. Coooolll: A Deep Learning System for Twitter Sentiment Classification. In Proceedings of the 8th International Workshop on Semantic Evaluation (SemEval 2014). Association for Computational Linguistics and Dublin City University, Dublin, Ireland, pages 208–212.
- [19] Mingqing Hu and Bing Liu. 2004. Mining and summarizing customer reviews. In Proceedings of the tenth ACM SIGKDD international conference on Knowledge discovery and data mining. ACM, pages 168–177.
- [20] Erik Cambria, Daniel Olsher, and Dheeraj Rajagopal. 2014. SenticNet 3: a common and common-sense knowledge base for cognition-driven sentiment analysis. In Twenty-eighth AAAI conference on artificial intelligence.
- [21] Symeon Symeonidis, Dimitrios Effrosynidis, John Kordonis, and Avi Arampatzis. 2017. DUTH at SemEval-2017 Task 4: A voting classification approach for Twitter sentiment analysis. In Proceedings of the 11th International Workshop on Semantic Evaluation. Vancouver, Canada, SemEval '17, pages 703–707.
- [22] Ming Wang, Biao Chu, Qingxun Liu, and Xiaobing Zhou. 2017. YNUDLG at SemEval-2017 Task 4: A GRU-SVM model for sentiment classification and quantification in Twitter. In Proceedings of the 11th International Workshop on Semantic Evaluation. Vancouver, Canada, SemEval '17, pages 712–716.
- [23] Joosung Yoon, Hyeoncheol Kim, and Kigun Lyu. 2017. Adullam at SemEval-2017 Task 4: Sentiment analyzer using lexicon integrated convolutional neural networks with attention. In Proceedings of the 11th International Workshop on Semantic Evaluation. Vancouver, Canada, SemEval '17, pages 731–735.
- [24] Mickael Rouvier. 2017. LIA at SemEval-2017 Task 4: An ensemble of neural networks for sentiment classification. In Proceedings of the 11th International Workshop on Semantic Evaluation. Vancouver, Canada, SemEval '17, pages 759–764.
- [25] Haowei Zhang, Jin Wang, Jixian Zhang, and Xuejie Zhang. 2017. YNU-HPCC at SemEval 2017 Task 4: Using a multi-channel CNN-LSTM model for sentiment classification. In Proceedings of the 11th International Workshop on Semantic Evaluation. Vancouver, Canada, SemEval '17, pages 795–800.
- [26] Amit Ajit Deshmane and Jasper Friedrichs. 2017. TSA-INF at SemEval-2017 Task 4: An ensemble of deep learning architectures including lexicon features for Twitter sentiment analysis. In Proceedings of the 11th International Workshop on Semantic Evaluation. Vancouver, Canada, SemEval '17, pages 801–805.
- [27] Iván Castro, Sebastián Oliva, José Abreu, Claudia Martínez, and Yoan Gutiérrez. 2017. UCSC-NLP at SemEval-2017 Task 4: Sense n-grams for sentiment analysis in Twitter. In Proceedings of the 11th International Workshop on Semantic Evaluation. Vancouver, Canada, SemEval '17, pages 806–810.
- [28] Yunxiao Zhou, Man Lan, and Yuanbin Wu. 2017. ECNU at SemEval-2017 Task 4: Evaluating effective features on machine learning methods for Twitter message polarity classification. In Proceedings of the 11th International Workshop on Semantic Evaluation. Vancouver, Canada, SemEval 2017, pages 811–815.
- [29] Peter F Brown, Peter V Desouza, Robert L Mercer, Vincent J Della Pietra, and Jenifer C Lai. 1992. Class-based ngram models of natural language. *Computational linguistics* 18(4):467–479.
- [30] Olutobi Owoputi, Brendan O'Connor, Chris Dyer, Kevin Gimpel, Nathan Schneider, and Noah A Smith. 2013. Improved part-of-speech tagging for online conversational text with word clusters. Association for Computational Linguistics.
- [31] Bengio, Yoshua, Aaron Courville, and Pascal Vincent. "Representation learning: A review and new perspectives." *Pattern Analysis and Machine Intelligence*, IEEE Transactions on 35.8 (2013a): 1798-1828.
- [32] Chung, Junyoung, Caglar Gulcehre, KyungHyun Cho, and Yoshua Bengio. "Empirical evaluation of gated recurrent neural networks on sequence modeling." *arXiv preprint arXiv:1412.3555* (2014).
- [33] Lin, Zhouhan, Minwei Feng, Cicero Nogueira dos Santos, Mo Yu, Bing Xiang, Bowen Zhou, and Yoshua Bengio. "A structured self-attentive sentence embedding." *arXiv preprint arXiv:1703.03130* (2017).
- [34] Wang, Yequan, Minlie Huang, and Li Zhao. "Attention-based lstm for aspect-level sentiment classification." *Proceedings of the 2016 conference on empirical methods in natural language processing*. 2016.

RS Invariant Image Classification and Retrieval with Pretrained Deep Learning Models

D. N. Hire¹

E&TC Dept, Research Scholar, DYPCOE, Pune, India

Dr. A. V. Patil²

E&TC Dept, Principal, DYPIEMR, Pune, India

Abstract—CBIR deals with seeking of related images from large dataset, like Internet is a demanding task. Since last two decades scientists are working in this area in various angles. Deep learning provided state-of-the-art result for image categorization and recovery. But pre-trained deep learning models are not strong enough to rotation and scale variations. A technique is proposed in this work to improve the precision and recall of image retrieval. This method concentrates on the extraction of high-level features with rotation and scaling invariant from ResNet18 CNN (Convolutional Neural Network) model. These features used for segregation of images using VGG19 deep learning model. Finally, after classification if the class of given query image is correct, we will get the 100% results for both precision and recall as the ideal requirement of image retrieval technique. Our experimental results shows that not only our proposed technique outstrip current techniques for rotated and scaled query images but also it has preferable results for retrieval time requirements. The performance investigation exhibit that the presented method upgrades the average precision value from 76.50% for combined features DCD (Dominant Color Descriptor), wavelet and curvelet to 99.1% and average recall value from 14.21% to 19.82% for rotated and scaled images utilizing Corel dataset. Also, the average retrieval time required is 1.39 sec, which is lower than existing modern techniques.

Keywords—CBIR; CNN; deep learning; ResNet18; rotation; scale; VGG19

I. INTRODUCTION

Since last two decades due to usage of mobile phones and easily availability of Internet on likely smart devices the data generated per year is increasing day by day. Usually, the data is in the form of images and figures as it is said that “A picture is worth a thousand words”. So, the large amount of image data produced and given for various applications like multimedia, e-commerce, medical, agriculture, etc. Managing of that image dataset, for finding, scanning, describing and diving is the tedious task. Managing that large dataset manually may create difficulties like mishandling and wastage of time. In June 2011, Google included the search by image feature as an application to image retrieval [1]. Before that it was search by text method which includes searching of images by its name but as the annotation of every image is difficult task and it varies from ones to others perspective so, the Content Based Image Retrieval (CBIR) invented in 1990s which make use of the low-level description of images like shape, texture, color [2,3] and now a days with deep learning model high level features [4,5] utilized to improve the retrieval result.

From Fig. 1 and 2, it proved that if the image rotated by 90-degree and given as query image, Google can't retrieve similar correct similar images. Google treating image of building as horizontal cylindrical rods and providing images as per this prediction is incorrect. So, there is a need for geometrically transformed efficient image retrieval method. So, for summarizing, features used for image comparison in these current methods are not robust to rotation and scaling factor.

In this paper, we proposed a technique of image retrieval with deep learning which is robust to rotation and scaling by introducing rotated and scaled images in training dataset. And for extracting high-level features from images ResNet18 model utilized whereas for classification VGG19 used.

The remaining part of paper arranged as mentioned: Section II describes the similar work on this research work. Section III provides information related to VGG19 and ResNet18 models used in proposed technique. The proposed RS invariant image retrieval technique explained in Section IV. The proposed method investigation results and discussion mentioned in Section V. The article concluded with conclusion in Section VI.

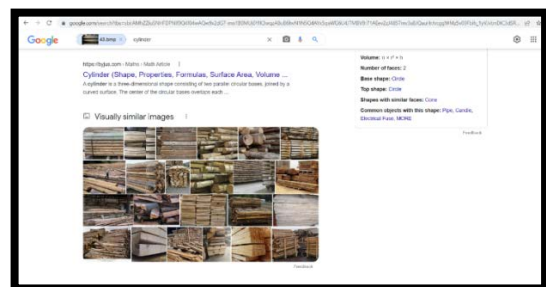


Fig. 1. Result of Google Search for Corel Dataset Image under Category Building with 90-Degree Rotation.

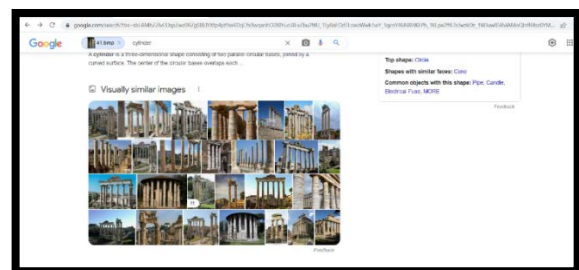


Fig. 2. Result of Google Search for Corel Dataset Original Image under Category Building.

II. SIMILAR WORK

The heart of CBIR is representation of image with its features. In that manner the feature extraction process plays vital role in image retrieval. Low level features were considered at the beginning of CBIR system, viz., color, texture, shape, etc. Out of which color is the most prominent feature which will be considered as invariant to scale and rotation. Many researchers already worked on that feature and came up with different techniques as mentioned in [14]. The combination of features like texture and color provided in paper [18] further improved the performance of image retrieval by developing method called RSHD. In [6][7] author collected color and texture features from images with color histogram and Gabor filter algorithm and selected only prominent features for retrieving similar images to reduce the computational complexity. In [8] color and texture feature called CCM and DBPSP respectively and third feature called based on color histogram called CHKM used for image retrieval. [12][13][14] [17] describes the use DCD features in various means to improve accuracy of image retrieval. Use of curvelet features also provided improvement in accuracy of image retrieval as referenced in [15][16][17]. Wavelet features applied in image retrieval as reflected in [9][10][11][17]. Deep Learning technique evolved in 1943 in the form of computer model developed by Walter Pitts and Warren McCulloch using neural networks derived from the human brain. But the deep learning usage started in real manner after the invention of high-speed computer and GPUs to fulfill the memory requirement of deep learning models. In [4][5] deep learning model provided state-of-the-art result in case of image recognition for large image dataset containing approximately 2.5 million images. So, there is a scope of research in this field of deep learning to further improve image retrieval performance by considering rotation and scale invariant features.

III. DEEP LEARNING MODELS

There are various deep learning models invented out of which CNN prominently used for image related applications. Using CNN models various algorithms developed out of that we choose ResNet18 and VGG19 by comparing performance related to computational complexity and accuracy.

A. ResNet18

ResNet-18 is an 18-layer deep convolutional neural community. The community can classify snap shots into 1001 kind of item categories, consisting of keyboards, mice, pencils, and a number of animals. As a result, the community has found out a number of wealthy characteristic representations for a number of images. The community's image enter length is 224 × 224 pixels. We can do the modifications in network by transfer learning as per our requirement.

ResNet18 model is used to create bag of features in our proposed technique due to its advantageous properties.

- Networks with a large number of layers (even thousands) may be easily taught without raising the training error rate.

- ResNets can aid with identity mapping to solve the vanishing gradient problem.

Fig. 3 describes the working of ResNet18 model. The output of a specific layer is linearized and used as a feature vector given the network. We experiment with two alternative layers of the network: the output of the average pooling layer and the linearized output of the fifth convolutional stage (that is conv5x) (that is average pool). The size of the feature vector for the conv5x layer is 25,088 (77512), and for the average pool layer, it is 512. Since the feature vector's size influences computation costs, dimensionality reduction techniques like Principal Component Analysis are used to lower the feature vector's size.

Layer Name	Output Size	ResNet-18
conv1	112 × 112 × 64	7 × 7, 64, stride 2
conv2_x	56 × 56 × 64	3 × 3 max pool, stride 2
		$\begin{bmatrix} 3 \times 3, 64 \\ 3 \times 3, 64 \end{bmatrix} \times 2$
conv3_x	28 × 28 × 128	$\begin{bmatrix} 3 \times 3, 128 \\ 3 \times 3, 128 \end{bmatrix} \times 2$
conv4_x	14 × 14 × 256	$\begin{bmatrix} 3 \times 3, 256 \\ 3 \times 3, 256 \end{bmatrix} \times 2$
conv5_x	7 × 7 × 512	$\begin{bmatrix} 3 \times 3, 512 \\ 3 \times 3, 512 \end{bmatrix} \times 2$
average pool	1 × 1 × 512	7 × 7 average pool
fully connected	1000	512 × 1000 fully connections
softmax	1000	

Fig. 3. ResNet18 Architecture [19].

B. VGG19

This network shown in Fig. 4, received a fixed size RGB image (224 * 224) as input, indicating that the matrix has shape (224,224,3). The only pre-processing is to subtract the average RGB value of each pixel, which was calculated throughout the training set. They used kernel with size (3*3) and step size of 1 pixel to cover the whole concept of image. To maintain the spatial resolution of the image, spatial padding was applied on 2*2 pixel window. Then, the adjusted linear unit (ReLU) is used to introduce nonlinearity into the model to improve classification and save processing time (previous models used tanh or sigmoid). Three fully connected layers have been implemented, the first two having size 4096, followed by a 1000 channel layer for 1000 line ILSVRC classifier and finally a softmax function.

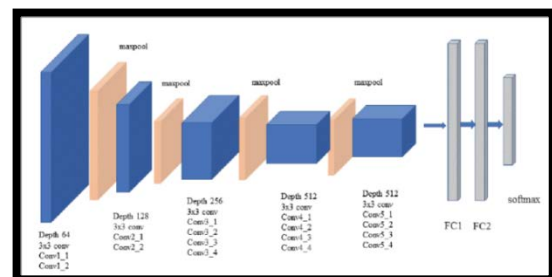


Fig. 4. VGG19 Architecture [20].

IV. RS INVARIANT IMAGE RETRIEVAL SYSTEM

To make the system Rotation and scale (RS) invariant we trained the VGG19 model of classification with images containing rotated images with 45-degree and 90-degree and scaled images with scaling factor 0.4 and 0.6. So, the Corel-1k original dataset which consist of 10 classes and in each class 100 images now transformed to 5k dataset as each image in 1k dataset is rotated with 45-degree, 90-degree and scaled with scaling factor 0.4 and 0.6. In that way 1 image in 1k dataset will have another 4 images. Fig. 5 illustrates the detailed working model of proposed system. Firstly, the dataset divided into training and testing parts. Then training dataset trained with ResNet18 model and features of that dataset collected from pooling layer 5 of this model. Then these collected features acts as the input to the VGG19 model and used for classification of query images to find the class of given query image.

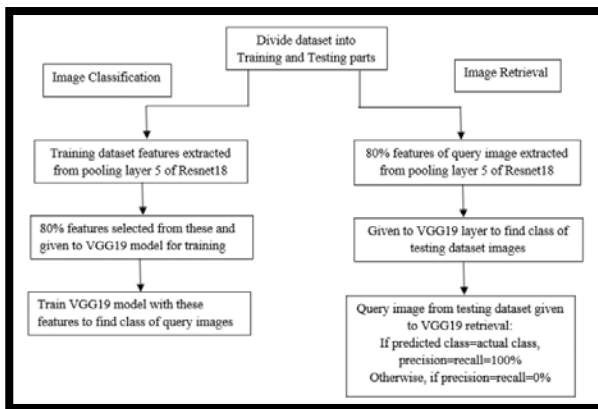


Fig. 5. The Proposed RS Invariant Image Retrieval System.

In the image retrieval part, 80% features of query image extracted from pooling layer 5 of ResNet18 model and given to VGG19 model to find class of query image. Then after classification for output class top 12 images will be retrieved at the output. If predicted class is same as actual class of query image then precision and recall parameter values will be 100% but if predicted class is wrong then precision and recall values goes down to 0%.

V. EXPERIMENTAL STRUCTURE AND RESULTS

To visualize the practicality of our proposed system analyzed using datasets corel-1k, corel-1k scale and rotate dataset with 45-degree and 90-degree rotated and scaled images including images with scaling factor 0.4 and 0.6, Corel-1k rotated dataset which includes images rotated with angle 0-degree, 90-degree, 180-degree and 270-degree as well as Corel-1k scaled dataset which consists of images scaled with factor 0.5, 0.75, 1, 1.25, and 1.5.

Table I describes the dataset with their categories, classes, total images and total images per class in detail. VGG19 model trained for classification of images in dataset. The dataset divided into training and testing dataset as 70% and 30% respectively. The classification accuracy for every dataset is given in Table II. The classification accuracy is for all dataset is more than 96% which is providing better results for image retrieval.

TABLE I. DETAILS OF DATASET USED

Name of dataset	Description	Classes	Total images	Images per class
Corel-1k	Original dataset	10	1000	100
Corel-1k Scale	Scaled by factor 0.5, 0.75, 1, 1.25, 1.5	10	5000	500
Corel-1k rotate	Rotated by degree-0, 90, 180, 270	10	4000	400
Corel -1k scale & rotate	Scaled by factor 0.4, 0.6 and rotated by angle 45 & 90	10	5000	500

TABLE II. CLASSIFICATION ACCURACY OF SELECTED DATASET

Dataset	No. of Training Images	No. of Testing Images	Classification accuracy (%)
Corel-1k	700	300	97
Corel-1k Scale	3500	1500	98.3
Corel-1k rotate	2800	1200	96.8
Corel -1k scale & rotate	3500	1500	96.5

Fig. 6 implies the confusion matrix for Corel-1k scale dataset. After analysing this, our model gives 100% classification accuracy for 5 classes bus, dinosaurs, elephant, food and horse whereas minimum accuracy for class building in which out of 150 testing images, 140 classified correctly but 5 classified as African people and 5 as beach due to the features extracted from images.

Correctly classified and retrieved images for query image from Corel-1k rotate dataset and class African People illustrated in Fig. 7. Fig. 8 shows the evidence of wrong classification of query image which actually belongs to African people category classified under elephant category and resulting in 0% precision and recall values.

Fig. 9 and 10 demonstrate the analysis of proposed technique in the form of precision and recall for all query images from dataset Corel-1k, which is highest in all the previous CBIR methods. For the proposed technique the precision values lies between 99% and 100%, whereas recall values lies between 19% and 20% (the maximum value of recall is 20% as retrieving top 20 images).

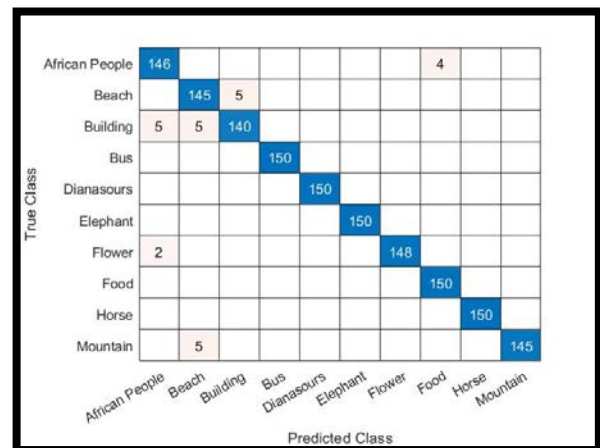


Fig. 6. Confusion Matrix for Corel-1k Scale Dataset.

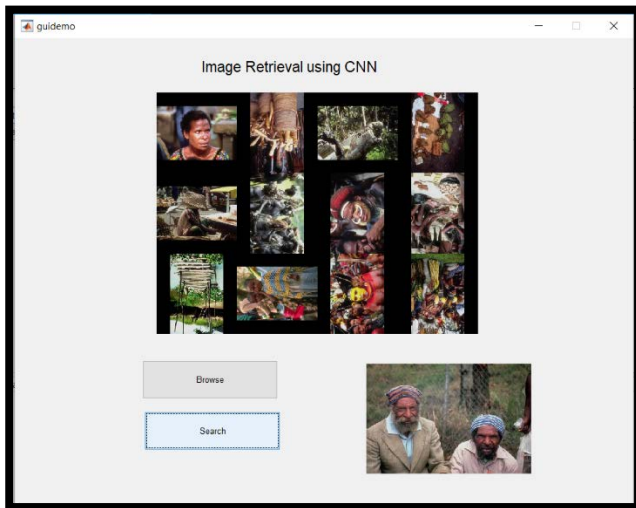


Fig. 7. Correctly Classified & Retrieved Image of Category 'African People' from Corel-1k Rotate Dataset.

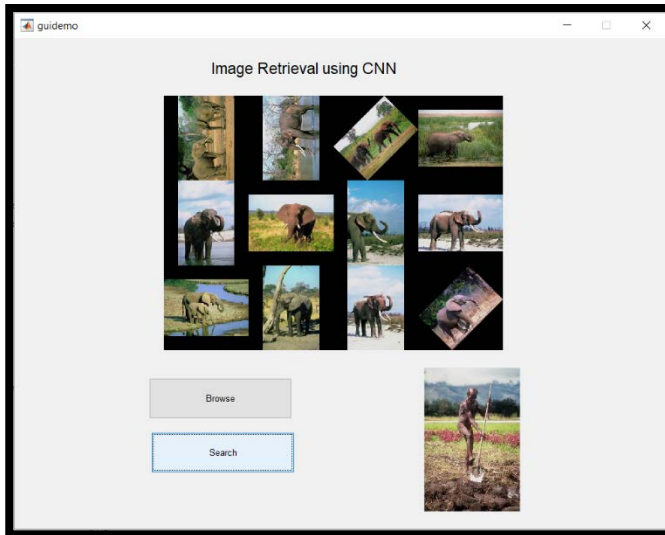


Fig. 8. Wrongly Classified & Retrieved Image of Category 'African People' from Corel-1k Scale & Rotate Dataset.

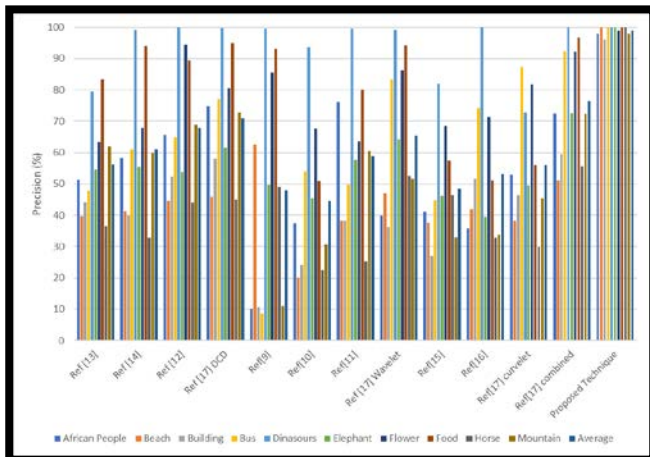


Fig. 9. Comparison of Proposed Technique % Precision with Previous Techniques using Corel-1k Dataset.

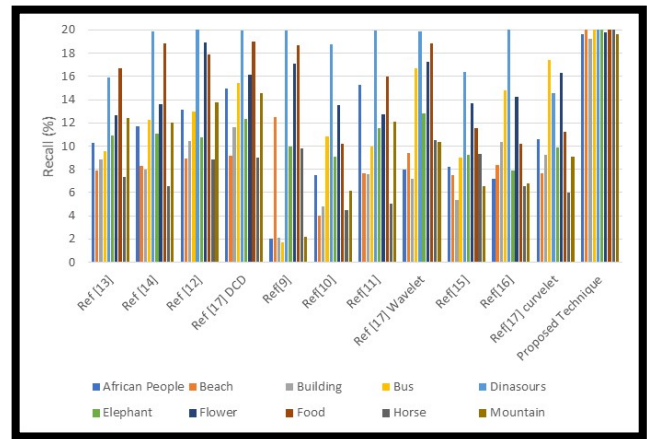


Fig. 10. Comparison of Proposed Technique % Recall with Previous Techniques using Corel-1k Dataset.

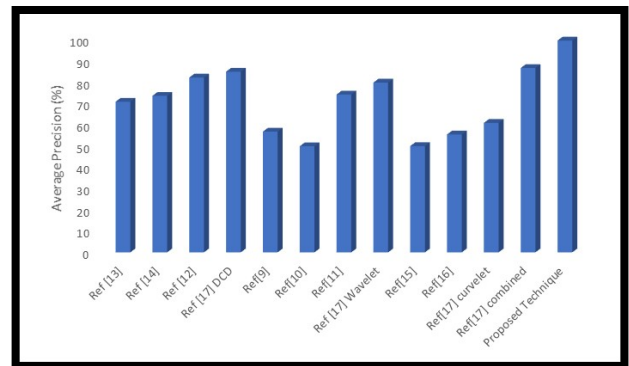


Fig. 11. Comparison of Proposed Technique % Precision with Previous Techniques using Corel-1k scale Dataset.

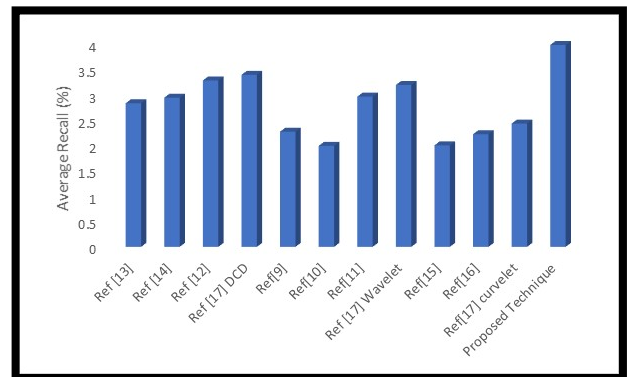


Fig. 12. Comparison of Proposed Technique % Recall with Previous Techniques using Corel-1k scale Dataset.

In case of Corel-1k scale dataset comparison for parameters precision and recall with previous techniques proves our system as scale invariant image retrieval as illustrated in Fig. 11 and 12. Fig. 13 shows the performance of proposed system for various datasets. The system gives best result for Corel-1k scale dataset which shows robustness of system for scale invariance. Average retrieval time for proposed system calculated by randomly considering 100 query images and averaging their retrieval time and plotted in Fig. 14 which shows that the retrieval time is less for proposed system except retrieval time of system mentioned in [18].

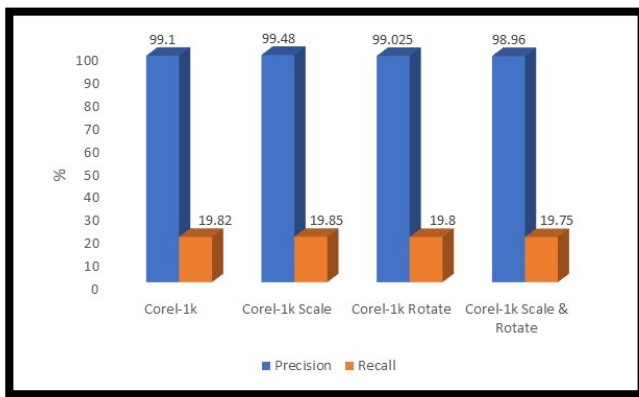


Fig. 13. Performance of Proposed Technique for Selected Dataset.

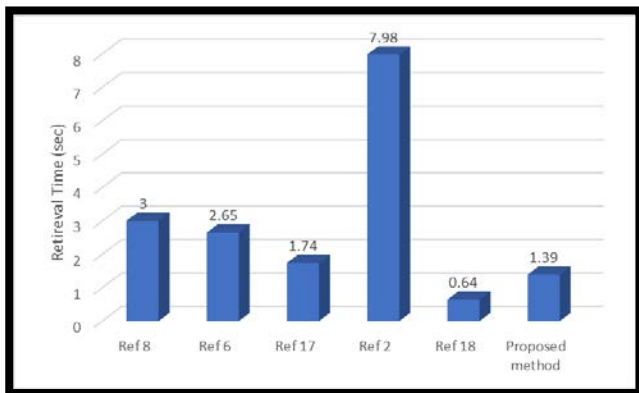


Fig. 14. Average Retrieval Time of Image Retrieval Systems.

VI. CONCLUSION

We present a deep learning-based feature extraction, classification, and retrieval approach that is resistant to scale and rotation fluctuations in this paper. The most important 80% of collected features are chosen, reducing the computational complexity of the classification and retrieval procedure. In comparison to existing state-of-the-art systems, the experimental findings demonstrated that the suggested CBIR system had the highest precision and recall rate for all datasets, including rotated and scaled images. In addition, compared to previous approaches, there is a lower demand for average retrieval time. Because it has to display the images at output from a selected class rather than the entire database, the classification procedure before retrieval reduces image retrieval time. When the query image is correctly classified, retrieval accuracy is 100 percent.

ACKNOWLEDGMENT

This work supported by Dr. D. Y. Patil Institute of Engineering, Management & Research, Akurdi, Pune by providing access to latest research articles.

REFERENCES

[1] Accessd on 19th February, 2022 https://en.wikipedia.org/wiki/Google_Images.

[2] Kundu, Malay Kumar, Manish Chowdhury, and Samuel Rota Bulo, "A graph-based relevance feedback mechanism in content-based image retrieval", *Knowledge-Based Systems*, 2015, 73, pp. 254–264.

[3] Yue, Jun, Zhenbo Li, Lu Liu, and Zetian Fu.: "Content-based image retrieval using color and texture fused features", *Mathematical and Computer Modelling*, 2011, 54, (3), pp. 1121–1127.

[4] K. Simonyan and A. Zisserman, "Very deep convolutional networks for large-scale image recognition," *arXiv preprint arXiv:1409.1556*, 2014.

[5] C. Szegedy, W. Liu, Y. Jia, P. Sermanet, S. Reed, D. Anguelov, D. Erhan, V. Vanhoucke, and A. Rabinovich, "Going deeper with convolutions," in *IEEE Conference on Computer Vision and Pattern Recognition (CVPR)*, 2015.

[6] ElAlami, M. Esmel., "A novel image retrieval model based on the most relevant features", *Knowledge-Based Systems*, 2011, 24, (1), pp. 23–32.

[7] Wang, Xiang-Yang, Hong-Ying Yang, and Dong-Ming Li., "A new content-based image retrieval technique using color and texture information", *Computers & Electrical Engineering*, 2013, 39, (3), pp. 746–761.

[8] Chuen-Horng Lin, Rong-Tai Chen and Yung-Kuan Chan, "A smart content-based image retrieval system based on color and texture feature", *Image and Vision Computing*, 2009, 27, (6), pp. 658–665.

[9] Farsi, Hassan, and Sajad Mohamadzadeh, "Colour and texture feature-based image retrieval by using Hadamard matrix in discrete wavelet transform", *IET Image Processing*, 2013, 7, (3), pp. 212–218.

[10] Shiv Ram Dubey, Satish Kumar Singh and Rajat Kumar Singh, "Local Wavelet Pattern: A New Feature Descriptor for Image Retrieval in Medical CT Databases", *IEEE Transaction on Image Processing*, 2015, 24, (12), pp. 5892–5903.

[11] Murala, Subrahmanyam, Anil Balaji Gonde, and Rudra Prakash Maheshwari, "Color and texture features for image indexing and retrieval", *IEEE International Advance Computing Conference (IACC)*, 2009, pp. 1411–1416.

[12] Dubey, Shiv Ram, Satish Kumar Singh, and Rajat Kumar Singh, "Local neighbourhood-based robust colour occurrence descriptor for colour image retrieval", *IET Image Processing*, 2015, 9, (7), pp. 578–586.

[13] Talib, Ahmed, Massudi Mahmuddin, Husniza Husni, and Loay E. George, "A weighted dominant color descriptor for content-based image retrieval", *Journal of Visual Communication and Image Representation*, 2013, 24, (3), pp. 345–360.

[14] Deng, Y., Manjunath, B. S., Kenney, C., Moore, M. S., & Shin, H., "An efficient color representation for image retrieval", *IEEE Transactions on Image Processing*, 2001, 10, (1), pp. 140–147.

[15] Sumana, I. J., Islam, M. M., Zhang, D., and Lu, G., "Content based image retrieval using curvelet transform", *10th Workshop on IEEE Multimedia Signal Processing*, Cairns, Qld, 2008, pp. 11–16.

[16] Anil Balaji Gonde, R.P. Maheshwari and R. Balasubramanian, "Modified curvelet transform with vocabulary tree for content based image retrieval", *Digital Signal Processing*, 2013, 23, (1), pp. 142–150.

[17] Sadegh Fadaei, Rassoul Amirfattahi, Mohammad Reza Ahmadvadeh, "A New Content-Based Image Retrieval System Based on Optimized Integration of DCD, Wavelet and Curvelet Features" Feb-2017, *IET Image Processing*, Vol 11, issue 2, 89-98.

[18] Shiv Ram Dubey, Satish Kumar Singh, and Rajat Kumar Singh, "Rotation and scale invariant hybrid image descriptor and retrieval", *Computers & Electrical Engineering*, 2015, 46, pp. 288–302.

[19] Paolo Napoletano, Flavio Piccoli, Raimondo Schettini, "Anomaly Detection in Nanofibrous Materials by CNN-Based Self-Similarity", accessd on 19th February, 2022 https://www.researchgate.net/figure/ResNet-18-Architecture_tbl1_322476121.

[20] Roland Hewage, "Extract Features, Visualize Filters and Feature Maps in VGG16 and VGG19 CNN Models", accessd on 19th February, 2022 <https://towardsdatascience.com/extract-features-visualize-filters-and-feature-maps-in-vgg16-and-vgg19-cnn-models-d2da6333edd0>.

Accuracy Enhancement of Prediction Method using SMOTE for Early Prediction Student's Graduation in XYZ University

Ainul Yaqin*, Majid Rahardi, Ferian Fauzi Abdulloh

Computer Science Faculty, University of AMIKOM Yogyakarta, Yogyakarta, Indonesia

Abstract—According to the Minister of Education and Culture of the Republic of Indonesia's regulations from 2014, one of the essential elements in implementing higher education is the student's study duration. Higher education institutions will use early graduation prediction as a guide when developing policy. According to XYZ University data, the student study period is Grade Point Average (GPA), Gender, and Age are all aspects to consider. Using a dataset of 8491 data, the Prediction of Early Graduation of Students based on XYZ University data was examined by this study, particularly in the information systems and informatics study program. The aim is to find significant features and compare three prediction models: Artificial Neural Networks (ANN), K-Nearest Neighbor (K-NN) method, and Support Vector Machines (SVM). The Challenge in the development of a prediction model is imbalanced data. The Synthetic Minority Oversampling Technique (SMOTE) handles the class imbalance problem. Next, the machine learning models are trained and then compared. Prediction results increase. The best test accuracy value is on ANN with a data Imbalance of 62.5% to 70.5% after using SMOTE, compared to the accuracy test on the K-NN method with SMOTE 69.3%, while the SVM method increased to 69.8%. The most significant increase in recall value to 71.3% occurred in the ANN.

Keywords—Prediction study period; SMOTE; neural network; k-nearest neighbors; support vector machine

I. INTRODUCTION

A. Background

One of the criteria that can be used to determine a student's performance in higher education is the student's study duration. The information about the study session is recorded in the academic database in this case, and management can utilize it to assess decision-making. The Informatics and Information Systems Study Program at XYZ University is an example of a study program with the maximum number of active students and continues to increase every year. Management can identify early prevention strategies connected to Drop Out (DO) instances by using the prediction model for the student study period, which will have a domino effect on accreditation.

Undergraduate students must take at least 144-semester credits with a study period of four years or less to meet learning outcomes, as expressly stated in the Regulation of the Minister of Education and Culture of the Republic of Indonesia in 2014, a section on graduate competency standards article 17 [1]. Consequently, the study program

manager is required to keep track of student progress to reduce the number of dropouts. The development of prediction models for students' study periods using machine learning models has been done using several parameters Gender[2], GPA [3][4], Number of semester credit units (credits), parents' job, high school major, high school city[2][5]. In this study, a prediction model for the study period was constructed utilizing semester 1 to 4 GPA values based on XYZ University's educational program, which highlights concentration selection in semester four lectures, ages, and Gender.

The K-Nearest Neighbor technique (K-NN), Artificial Neural Networks (ANN), and Support Vector Machines are some examples of popular machine learning methods for Prediction (SVM) [6]. The Challenge in the development of a prediction model is imbalanced data. This situation prompted us to use the Synthetic Minority Oversampling Technique (SMOTE) to improve prediction utilizing balance data [7] to handle the class imbalance problem. University XYZ datasets are used in an experimental study to validate the suggested approach, including selecting a prediction model and performance indicators. In the following areas, this study adds to the existing body of knowledge:

- 1) ANN, K-NN, and SVM were used to create an effective model.
- 2) To analyze the relevant features extracted from the dataset that has an impact on the machine learning algorithm's performance.
- 3) Performance of ANN, K-NN, and SVM models using Imbalance data is compared using SMOTE.

Thirty percent of machine learning methods used in predicting student performance are artificial neural networks and vector machines at 6,20%. Other methods used are decision tree, nave Bayes, and k-Nearest Neighbor 17% each [6].

B. Related Work

Agustin [8] used class year, GPA, and grades from nine courses as parameters with the Naive Bayes Classification Technique, K-Nearest Neighbor, and Neural Network to predict student study period. His research divided predictions into three classes: fast, precise, and slow. And using the most influential attribute selection, namely, GPA, using the classifier attribute.

*Corresponding Author.

Prediction of students' graduation time using the K-Nearest Neighbor Algorithm with the parameter GPA of students during the seventh semester will be used as training data. Data of students who pass are used as sample data. K-Nearest Neighbor works according to the given data sample. The highest level of Accuracy can be achieved when $k = 3$ [9].

The fundamental purpose of SVM is to separate the data set into classifications to find the most negligible Hyperplane. The gamma value used varies from 0 to 1, but a good default gamma value is 0.1 and can be achieved Accuracy of 73% [10].

The rest of the paper is organized as follows: Section II outlines the proposed approach, the dataset, preprocessing, and data visualization to uncover the dataset's hidden pattern. It also explains the various algorithms employed in this study. The discussion and analysis of the results, performance metrics, and experimental study design are all described in Section III. In Section IV, the findings are discussed. Section V concludes with a discussion of future work.

II. RESEARCH METHODOLOGY

This research will use a method divided into three stages: preprocessing, predictive Process, and evaluation. The research flow is shown in Fig. 1.

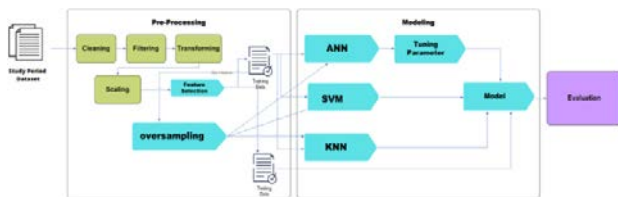


Fig. 1. Research Methodology.

A. Synthetic Minority Oversampling Technique (SMOTE)

Several approaches to dealing with data imbalances include *undersampling*, *oversampling*, and *hybrid* methods [11]. Oversampling technique is often adopted to overcome the problem by generating new synthetic sample data [12][7][13]. In comparison, the *Undersampling technique* has an approach of removing data from the majority class to balance the class distribution [14].

B. Artificial Neural Networks (ANN)

A Neural Network (ANN) is a group of small processing units based on a human neural network in general [15]. The learning system is a never-ending process of adding to the NN's knowledge (continuity). When used to recognize an object, the inside will be fully utilized. The anatomy of neural networks [16] is shown in Fig. 2.

The following data is provided by the ANN Structure shown in Fig. 2. The "Input Layer" is made up of input nodes that transmit data from the outside world to the network. A "hidden layer" is formed when a group of hidden nodes is combined [17]. The hidden layer nodes of the ANN have an activation function that allows for a curvilinear fit between the input and output units (layers). The activation function you choose has a big impact on how well your network works. [18].

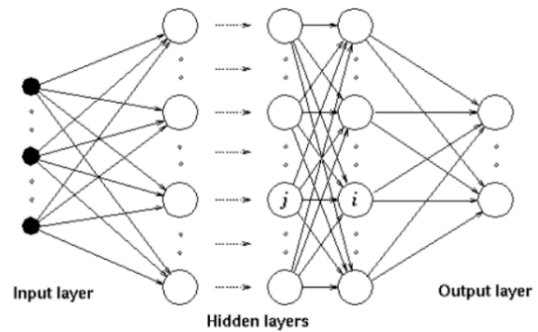


Fig. 2. Arsitektur ANN.

C. K-Nearest Neighbor method (K-NN)

K-NN is a statistical classification technique that uses the closest training samples in Feature Space to classify objects. It's a lazy learning algorithm in which the K-NN function is approximated locally and all calculations are postponed until classification is completed [19]. The K-NN algorithm generally uses the Euclidean distance formula, such as the formula 1:

$$D_{xy} = \sqrt{\sum_{i=1}^n (X_i - y_i)^2} \quad (1)$$

The transition from distances to weights should follow some kernel functions. Typical examples of this function include rectangular kernel, triangular kernel, cosine kernel, Gauss kernel, and inversion kernel [20].

D. Support Vector Machines (SVM)

Support Vector Machines (SVM) is a supervised learning algorithm that uses a learning algorithm that analyzes data related to classification and regression analysis [21]. In SVM modeling, there are several different kernels, including Radial Base (RBF), linear (LIN), sigmoid (SIG), and polynomial (POLM melakrefrefPOL) [22]. SVM reformats non-linear into linear by generating a Hyperplane and converting it to a straightforward form that can be processed [23].

The support vector is the closest training point to the Hyperplane, so maximizing the margin is considered a rule by minimizing the value of w [22]. The Decision Function Formula of SVM as in formula 2 and the SVM Scheme is shown in Fig. 3.

$$f(x) = \text{sign}(w \cdot x + b) \quad (2)$$

E. Evaluation

At this stage, an Evaluation or Model Evaluation is carried out on each model based on the accuracy score using the *Confusion Matrix* to determine the Accuracy of Prediction, *recall*, *precision*, and *F-Measure* [24].

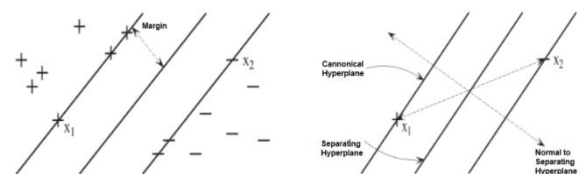


Fig. 3. Skema SVM.

III. EXPERIMENTAL STUDY

To test the proposed technique, this experiment chooses a diverse range of prediction algorithms, datasets, and performance metrics. Data sources, classification methods, performance measurements, and experimental design are all discussed in this subsection.

A. Data Source

The data was obtained by using query study data for students of the informatics and information systems study program in the class of 2004 to 2015 from the XYZ University database with a total data of 10,274. The dataset obtained consists of NIM, Gender, SMA, Date of Birth, Date of graduation, and GPA 1 to GPA 4. Summary dataset is shown in Table I.

TABLE I. SUMMARY DATASET

COLUMN	TYPE	DATA NULL/ISNA()
NIM	object	0
GENDER	object	0
Senior High School	object	569
Birth Date	datetime64[ns]	38
Graduation Date	datetime64[ns]	458
GPA 1	float64	8
GPA 2	float64	258
GPA 3	float64	406
GPA 4	float64	766

B. Prediction Model

This section discusses the algorithms used in this study. The prediction Model use ANN, K-NN, and SVM algorithm. The feature selection phase used the ONE-HOT algorithm, and an enhanced version of SMOTE was used in the rebalancing phase.

The first architectural model will be built with the ANN Algorithm in this study uses 1 hidden layer [25] with 1 to 100 neurons and a learning rate of 0.1 to 0.5, and a maximum iteration of 1000. The second model uses the K-NN algorithm by comparing and testing various K values from 2 to 1000. The third model uses SVM Algorithm by choosing the kernel between RBF and Linear [26].

C. Performance Measures (Evaluation)

Accuracy, true positive rate (Recall), true negative rate, precision, G-Mean, F-measure, and computation time are all popularly used performance indicators in classification. The following are the definitions for these metrics.

- 1) True Positive (TP): TP is the number of instances that are correctly positive.
- 2) True Negative (TN): TN stands for the number of instances that are correctly negative.
- 3) False Positive (FP): The number of positive events that have been misclassified as negative.
- 4) False Negative (FN): the number of negative instances that have been misclassified as positive.

5) TP rate (TPR) is also called sensitivity measure or Recall like formula 3.

$$\text{sensitivity} = TP / (TP + FN) \quad (3)$$

6) TN rate is called specificity measure like the formula 4.

$$\text{specificity} = TN / (TN + FP) \quad (4)$$

7) FP rate is called Type-I error like the formula 5.

$$\text{Type - I error} = FP / (FP + TN) \quad (5)$$

8) Type-II error is another term for the FN rate. Like the formula 6

$$\text{Type - II error} = FN / (FN + TP) \quad (6)$$

9) Overall Accuracy: The percentage of accurately anticipated instances, such as formula 7, is referred to as accuracy.

$$\text{Accuracy} = (TN + TP) / (TP + FP + TN + FN) \quad (7)$$

10) Precision: This is the Number of fault-prone modules that are fault-prone modules like formula 8.

$$\text{Precision} = TP / (FP + TP) \quad (8)$$

11) G-Mean: it is the geometric mean of sensitivity and precision like the formula 9.

$$\text{G Mean} = \sqrt{\text{sensitivity} * \text{Precision}} \quad (9)$$

12) The harmonic mean of precision and recall is known as the F-Measure. The F-measure, like the formula 10, has been frequently utilized in information retrieval.

$$\text{F Measure} = (2 * \text{Precision} * \text{TPR}) / (\text{Precision} + \text{TPR}) \quad (10)$$

D. Experimental Design

The following procedure was used to carry out the experiment:

Input: Dataset University XYZ

Tool: Jupyter - Python Base

Step 1: Pre-Processing Data

In this Phase, several processes are carried out, namely:

1. The Process of cleaning null data from 10,274 data to 8491 data
2. The filtering process is carried out by:
 - a. The value of the study period is obtained through the difference between the year of study and the date of graduation by labeling the study period on time if the study period is ≤ 48 months with a label 1 and late study with a label 0 if the study period > 48 months
 - b. Get the student's age (years) during semester 4 by calculating the difference between the start date of college and the date of birth plus 2 years.
3. The transformation process is carried out by:
 - a. Categorize data from school and age
 - b. Combining age group data with Gender

4. The scaling process is carried out on Semester 1 GPA data into Semester 4 GPA data using MinMax Scaler(MMS)[27] like formula 11 [28]:

$$MMS = (X - X_{min}) / (X_{min} - X_{max}) \quad (11)$$

Step 2: Correlation Analysis

Correlation analysis was used to determine the degree of relationship between GPA 1, GPA 2, GPA 3, GPA 4, Age, Gender, Year of Class, and Senior High School during the study period.

Step 3: Features Selection

In this stage, feature determination is carried out, which will be used in the prediction model

Step 4: Split Data Train and Testing and Balancing using SMOTE

In this Step, Data distribution is divided into 80% training data and 20% testing data. Then, the training data is balanced with SMOTE and then stored in other variables

Step 5: Training Prediction Model

In this Phase, the prediction model was built with ANN, K-NN, and SVM trained using the Imbalanced training data and SMOTE training data. So it produces six models.

Step 6: Evaluation

In this Phase, evaluate the results of testing data as much as 20% of the dataset on six models (in the model training

phase) such as Accuracy, recall, precision, G-Means, and F-Measure.

IV. RESULTS

A. Dataset

The results of the preprocessing of the dataset are shown in Table II.

B. Correlation Analysis

Fig. 4 shows that the GPA 1 to 4 has a correlation value of >0.3 with the Study Period. Then the Gender-Age value data with Study Period also indicates a negative relationship with a correlation value of -0.13

C. Features Selection

At this stage, the features are determined by setting a GPA 1 to 4, and Gender-Age is the feature and the Study Period is the target. Then Categorical Features Encoding is carried out for Gender-Age data. So that the resulting features selection data includes as many as 12 features. The result of feature selection is shown in Table III.

D. Split Data

In this Phase, the data was obtained from 6792 training data and 1699 testing data. The summary of training data is shown in Fig. 5. Training Balance data is shown in Fig. 6.

TABLE II. DATASET

Num	Nim	Lblgender	Lblschool	GPA1	GPA2	GPA3	GPA4	YEAR	LblAge	LblGender-Age	Study Period
0	13.11	0	2	3.5	3.833333	4	3.5	2013	19-23	7	1
1	13.11	0	2	3.5	3.75	3.333333	3.25	2013	19-23	7	1
2	13.11	0	1	3.166667	3.083333	3.333333	3.25	2013	19-23	7	1
3	13.11	1	0	3.5	3.25	3.5	3.416667	2013	19-23	6	1
4	13.11	0	1	3.25	3.166667	3.25	3.166667	2013	19-23	7	1
...
8488	04.12.	1	1	2.5	2.923077	3	2.923077	2004	19-23	6	1
8489	04.12.	0	0	2.833333	2.923077	3	2.615385	2004	19-23	7	1
8490	04.12.	0	1	3.5	3.285714	3.307692	3.153846	2004	19-23	7	1
8491	04.12.	0	1	3.5	3.357143	3.538462	2.833333	2004	19-23	7	1

TABLE III. RESULT OF FEATURE SELECTION

Num	GPA1	GPA2	GPA3	GPA4	L_19-23	L_23-27	L_<19	L_>27	P_19-23	P_23-27	P_<19	P_>27	STUDY PERIOD
0	0.85	0.9575163	1	0.87209	1	0	0	0	0	0	0	0	1
1	0.85	0.9362745	0.8300	0.80813	1	0	0	0	0	0	0	0	1
2	0.75	0.7663399	0.8300	0.80813	1	0	0	0	0	0	0	0	1
3	0.85	0.8088235	0.8725	0.85077	0	0	0	0	1	0	0	0	1
4	0.775	0.7875817	0.8088	0.78682	1	0	0	0	0	0	0	0	1
...
8488	0.55	0.7254902	0.7450	0.72450	0	0	0	0	1	0	0	0	1
8489	0.65	0.7254902	0.7450	0.64579	1	0	0	0	0	0	0	0	1
8490	0.85	0.8179272	0.8235	0.78354	1	0	0	0	0	0	0	0	1
8491	0.85	0.8361345	0.8823	0.70155	1	0	0	0	0	0	0	0	1

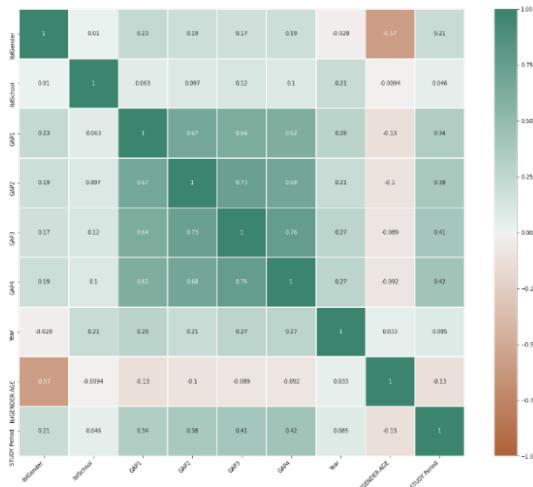


Fig. 4. Correlation Analysis.

```

1 X_train, X_test, y_train, y_test = train_test_split(dtfix[features], dtfix[target], test_size=0.20, random_state=42)
2 print("Training data", X_train.shape)
3 # print(y_train.shape)
4 print("Testing data", X_test.shape)
5 # print(y_test.shape)

Training data (6792, 12)
Testing data (1699, 12)
    
```

Fig. 5. Split Data.

```

1 y_train.STATUS.value_counts()

0    3792
1    3000
Name: STATUS, dtype: int64
    
```

Fig. 6. Imbalance Data.

Then, the training data is balanced with SMOTE. It is shown in Fig. 7.

```

1 print("Imbalance Training data : ", y_train.value_counts())
2 print("Balance Data using SMOTE: ", y_train_smote.value_counts())

Imbalance Training data : STATUS
0    3792
1    3000
dtype: int64
Balance Data using SMOTE: STATUS
0    3792
1    3792
dtype: int64
    
```

Fig. 7. SMOTE.

E. Results of Artificial Neural Network Training Model

Network modeling is done by finding the best model with the GridSerachCV function in sklearn. Modeling is based on several parameters of the activation function, namely, tanh, relu, and logistics, with the Number of neurons in the hidden layer ranging from 1 to 100 neurons, a learning rate of 0.1 to 0.5, and a maximum iteration of 1000. The best model of ANN obtained activation function = "tanh", learning rate = 0.1, alpha = 0.1 and neuron = 99 in the hidden layer. The result of the ANN Training Model is shown in Table IV.

F. Results of K-Nearest Neighbors (K-NN) Training Model

K-NN modeling is carried out with uniform and distance and testing various K values from 2 to 1000. The Result of the Highest Accuracy is shown in Fig. 8 and Table V.

G. Results of Support Vector Machine (SVM) Training Model

SVM modeling is done by choosing a kernel between RBF and linear, with the results shown in Fig. 9.

TABLE IV. RESULT OF ANN TRAINING MODEL

Training Data	Study Period (Target)		ANN training accuracy	ANN testing accuracy
	0	1		
Imbalance	3792	3000	0.7005	0.6250
SMOTE	3792	3792	0.6969	0.7080

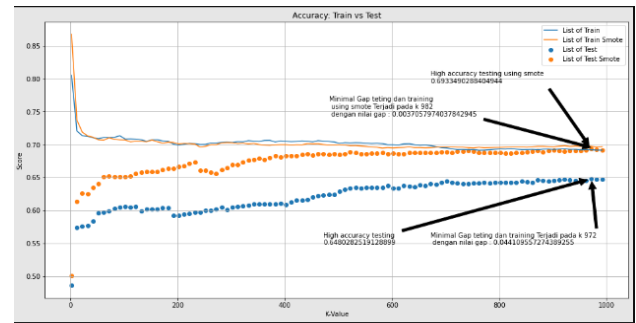


Fig. 8. Result of Highest K-NN Accuracy.

TABLE V. RESULT OF THE K-NN TRAINING MODEL

Training Data	Study Period		K-NN training accuracy	K-NN testing accuracy
	0	1		
Imbalance	3792	3000	0.6921	0.6972
SMOTE Balance	3792	3792	0.6480	0.6933

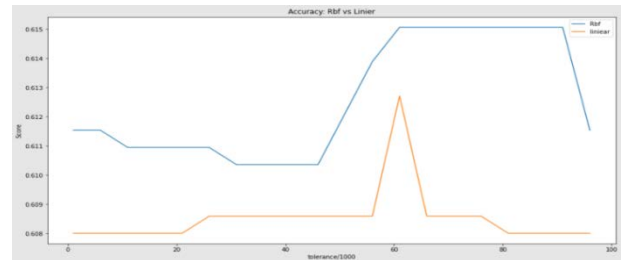


Fig. 9. Result of Comparison SVM Kernel.

The results of training and testing the SVM model with the RBF kernel using Balance data and SMOTE Balance data are shown in Fig. 10 and Table VI.

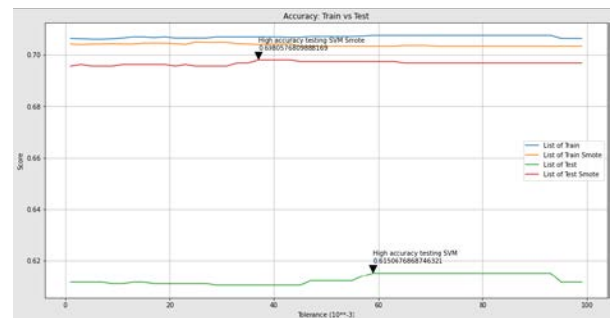


Fig. 10. Result of Highest Accuracy of SVM.

TABLE VI. RESULT OF THE SVM TRAINING MODEL

Training Data	Study Period (Target)		SVM training accuracy	SVM testing accuracy
	0	1		
Imbalance	3792	3000	0.7077	0.6150
SMOTE	3792	3792	0.7051	0.6980

TABLE VII. EVALUATION OF PERFORMANCE PREDICTION MODEL

	Imbalance-ANN	SMOTE-ANN	Imbalance-K-NN	SMOTE-K-NN	Imbalance-SVM	SMOTE-SVM
Training Accuracy	0.700530035	0.696993671	0.692137809	0.697257384	0.707744405	0.705168776
Testing Accuracy	0.625073573	0.708063567	0.648028252	0.693349029	0.615067687	0.698057681
TP	591	805	661	768	558	676
FP	471	398	440	410	483	452
FN	100	173	131	161	88	119
TN	537	323	467	360	570	452
Recall	0.52393617	0.713652482	0.585992908	0.680851064	0.494680851	0.59929078
Precision	0.8552822	0.823108384	0.83459596	0.826695371	0.86377709	0.850314465
G-Mean	0.657402861	0.705288613	0.671977086	0.699197609	0.646871565	0.688763242
F-Measure	0.649807587	0.764482431	0.688541667	0.746718522	0.629086809	0.703068123

REFERENCES

H. Evaluation

The evaluation phase, this study uses data testing as much as 1699 data on six models that have been trained. The results can be seen in Table VII.

Based on Table VII, the results of conformity testing are performed using a confusion matrix, and the test results are displayed in graphical form as follows in Fig. 11.

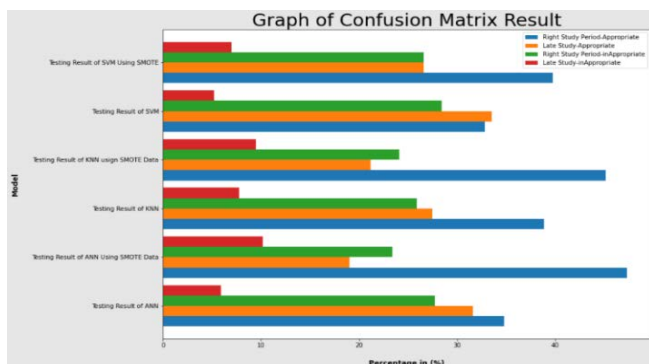


Fig. 11. Confusion Matrix Test Result.

V. CONCLUSION

Based on the results, this study can be formulated as follows. SMOTE can increase the recall value and test the accuracy of ANN, K-NN, and SVM models with relevant features extracted, namely GPA 1 to 4, and Encoding of Gender-Age based on correlation values. Prediction results have the best increase in the value of accuracy testing on ANN with a data Imbalance of 62.5% to 70.5% after using SMOTE, compared to the accuracy test on the K-NN method with SMOTE 69.3%. In comparison, the SVM method increased to 69.8%. The most significant increase in recall value to 71.3% occurred in the ANN.

ACKNOWLEDGMENT

This research has been fully supported by grants from the University of AMIKOM (#RP-1615185701000).

- [1] Kementerian Pendidikan dan Kebudayaan RI, "Peraturan Menteri Standar Nasional Pendidikan Tinggi," Ban-PT, 2015. [Online]. Available: https://www.banpt.or.id/?page_id=80.
- [2] A. Maulana, "Prediction of student graduation accuracy using decision tree with application of genetic algorithms," IOP Conf. Ser. Mater. Sci. Eng., vol. 1073, no. 1, p. 012055, Feb. 2021, DOI: 10.1088/1757-899X/1073/1/012055.
- [3] A. Yaqin, A. D. Laksito, and S. Fatonah, "Evaluation of Backpropagation Neural Network Models for Early Prediction of Student's Graduation in XYZ University," Int. J. Adv. Sci. Eng. Inf. Technol., vol. 11, no. 2, pp. 610-617, 2021, DOI: 10.18517/IJASEIT.11.2.11152.
- [4] M. Anwar, "Prediction of the graduation rate of engineering education students using Artificial Neural Network Algorithms," Int. J. Res. Couns. Educ., vol. 5, no. 1, pp. 23-31, Jun. 2021, DOI: 10.24036/00411ZA0002.
- [5] M. Wati, W. H. Rahmah, N. Novirasari, Haviluddin, E. Budiman, and Islamiyah, "Analysis K-Means Clustering to Predicting Student Graduation," J. Phys. Conf. Ser., vol. 1844, no. 1, p. 012028, Mar. 2021, DOI: 10.1088/1742-6596/1844/1/012028.
- [6] Y. Baashar, G. Alkawsy, N. Ali, H. Alhussian, and H. T. Bahbouh, "Predicting student's performance using machine learning methods: A systematic literature review," 2021 Int. Conf. Comput. Inf. Sci., pp. 357-362, Jul. 2021, DOI: 10.1109/ICCOINS49721.2021.9497185.
- [7] D. Gonzalez-Cuaute et al., "Synthetic Minority Oversampling Technique for Optimizing Classification Tasks in Botnet and Intrusion-Detection-System Datasets," DOI: 10.3390/app10030794.
- [8] D. Agustin, D. Zaenal Abidin, and E. Rasywir, "Kajian Komparasi Teknik Klasifikasi Naive Bayes, K-Nearest Neighbor, Dan Jaringan Saraf Tiruan Pada Prediksi Lama Masa Studi Mahasiswa Jurusan Teknik Informatika (Studi Kasus : Stikom Dinamika Bangsa Jambi)."
- [9] R. Muliono, J. H. Lubis, and N. Khairina, "Analysis K-Nearest Neighbor Algorithm for Improving Prediction Student Graduation Time," Sink. J. dan Penelit. Tek. Inform., vol. 4, no. 2, pp. 42-46, Mar. 2020, DOI: 10.33395/SINKRON.V4I2.10480.
- [10] I. Rodrigues, A. Parayil, T. Shetty, and I. Mirza, "Use of Linear Discriminant Analysis (LDA), K Nearest Neighbours (K-NN), Decision Tree (CART), Random Forest (RF), Gaussian Naive Bayes (NB), Support Vector Machines (SVM) to Predict Admission for Post Graduation Courses," SSRN Electron. J., 2020, DOI: 10.2139/ssrn.3683065.
- [11] M. Koziarski, "CSMOUTE: Combined Synthetic Oversampling and Undersampling Technique for Imbalanced Data Classification."

- [12] S. Feng et al., "COSTE: Complexity-based OverSampling TEchnique to alleviate the class imbalance problem in software defect prediction," *Inf. Softw. Technol.*, vol. 129, pp. 950–5849, Jan. 2021, DOI: 10.1016/j.infsof.2020.106432.
- [13] F. Kamalov and D. Denisov, "Gamma distribution-based sampling for imbalanced data," *Knowledge-Based Syst.*, vol. 207, p. 106368, Nov. 2020, DOI: 10.1016/j.knosys.2020.106368.
- [14] T. Liu, X. Zhu, W. Pedrycz, and Z. Li, "A design of information granule-based under-sampling method in imbalanced data classification," *Soft Comput.*, vol. 24, no. 22, pp. 17333–17347, 2020, DOI: 10.1007/s00500-020-05023-2.
- [15] S.-C. Wang, "Artificial Neural Network," in *Interdisciplinary Computing in Java Programming*, Boston, MA: Springer US, 2003, pp. 81–100.
- [16] B. S. Santoso, J. P. Tanjung, U. P. Indonesia, B. Gandum, and A. N. Network, "Classification of Wheat Seeds Using Neural Network Backpropagation," *JITE (J. Informatics Telecommun. Eng.)*, vol. 4, no. January 2021.
- [17] O. Ahmed and A. Brifcani, "Gene Expression Classification Based on Deep Learning," *4th Sci. Int. Conf. Najaf, SICN 2019*, pp. 145–149, 2019, doi: 10.1109/SICN47020.2019.9019357.
- [18] M. A. Mercioni and S. Holban, "Soft-Clipping Swish: A Novel Activation Function for Deep Learning," pp. 225–230, Jun. 2021, DOI: 10.1109/SACIS1354.2021.9465622.
- [19] R. Harikumar and K. P. Sunil, *K-NN Classifier and K-Means Clustering for Robust Classification of Epilepsy ... - Harikumar Rajaguru, Sunil Kumar Prabhakar - Google Books*. Hamburg: Anchor Academic Publishing, 2017.
- [20] L. Cui, Y. Zhang, R. Zhang, and Q. H. Liu, "A Modified Efficient K-NN Method for Antenna Optimization and Design," *IEEE Trans. Antennas Propag.*, vol. 68, no. 10, pp. 6858–6866, 2020, DOI: 10.1109/TAP.2020.3001743.
- [21] J. Smith, *Support Vector Machine: Examples With Matlab*. CreateSpace Independent Publishing Platform, 2017.
- [22] D. J. Armaghani, P. G. Asteris, B. Askarian, M. Hasanipanah, R. Tarinejad, and V. Van Huynh, "Examining hybrid and single SVM models with different kernels to predict rock brittleness," *Sustain.*, vol. 12, no. 6, pp. 1–17, 2020, DOI: 10.3390/su12062229.
- [23] M. N. Jebur, B. Pradhan, and M. S. Tehrany, "Optimization of landslide conditioning factors using very high-resolution airborne laser scanning (LiDAR) data at catchment scale," *Remote Sens. Environ.*, vol. 152, pp. 150–165, 2014, DOI: 10.1016/j.rse.2014.05.013.
- [24] J. Xu, Y. Zhang, and D. Miao, "Three-way confusion matrix for classification: A measure driven view," *Inf. Sci. (Ny)*, vol. 507, pp. 772–794, Jan. 2020, DOI: 10.1016/J.INS.2019.06.064.
- [25] I. Diakonikolas, D. M. Kane, V. Kontonis, and N. Zarfis, "Algorithms and SQ Lower Bounds for PAC Learning One-Hidden-Layer ReLU Networks," *Proceedings of Machine Learning Research*, vol. 125, PMLR, pp. 1514–1539, 15-Jul-2020.
- [26] B. Yekkehkhany, A. Safari, S. Homayouni, and M. Hasanlou, "A comparison study of different kernel functions for SVM-based classification of multi-temporal polarimetry SAR data," *Int. Arch. Photogramm. Remote Sens. Spat. Inf. Sci. - ISPRS Arch.*, vol. 40, no. 2W3, pp. 281–285, 2014, DOI: 10.5194/ISPRSARCHIVES-XL-2-W3-281-2014.
- [27] H. Shaheen, S. Agarwal, and P. Ranjan, "MinMaxScaler Binary PSO for Feature Selection," *Adv. Intell. Syst. Comput.*, vol. 1045, pp. 705–716, 2020, DOI: 10.1007/978-981-15-0029-9_55.
- [28] T. T. Dien, S. H. Luu, N. Thanh-Hai, and N. Thai-Nghe, "Deep learning with data transformation and factor analysis for student performance prediction," *Int. J. Adv. Comput. Sci. Appl.*, vol. 11, no. 8, pp. 711–721, 2020, DOI: 10.14569/IJACSA.2020.0110886.

Research on the Classification Modeling for the Natural Language Texts with Subjectivity Characteristic

Chen Xiao Yu¹, Song Ying³

Computer School
Beijing Information Science & Technology University
Beijing, China

Gao Feng², Zhang Xiao Min⁴

Academy of Agricultural Planning and Engineering
Ministry of Agriculture and Rural Affairs
Beijing, China

Abstract—The methods of natural language text classification have the characteristic of diversification, and the text characteristics are the basis of the method effectiveness; this paper takes the car service complaint data as an example to study the classification modeling for the texts with subjectivity characteristic. The effective handling of car service complaints is important for improving user experience and maintaining brand reputation; manual classification commonly has the disadvantages of experience dependence, prone to error, heavy workload and so on; corresponding automatic classification modeling research is of great practical significance. The core links of the research method in this study include word segmentation, text vectorization, feature selection and dimensionality reduction based on correlation, classification modeling based on progressive method and random forest, and model reliability analysis; the research results show that the car service complaint texts could be effectively classified based on the method in this study, which could provide a reference for related further research and application.

Keywords—Car service complaint; text classification; machine learning; natural language texts

I. INTRODUCTION

Car service complaints widely exist in the use of cars of different types, brands, and use times. Effective classification of service complaint texts is an important part of the basis for the efficient and reasonable handling of corresponding complaints. The classification of service complaints could be done by users or receiving staff, if this work is handed over to the users, on one hand, it might increase the user's irritability and dissatisfaction, and on the other hand, the users possibly make mistakes because they might don't know much about the professional field; if the complaint receiving staff conducts manual classification, there are also problems such as heavy workload, experience dependence, and error-prone; therefore, it is of great practical value to carry out the automatic classification modeling and realize automatic classification of service complaint.

Machine learning methods are widely used in data processing such as classification and regression, and they are also quite widely used in automatic classification of natural language texts [1-4]. The text classification modeling methods based on machine learning have the characteristics of

diversification and different applicability. In recent years, related researchers have carried out a lot of studies on different types of texts, which provides a well foundation for follow-up text classification modeling research. In general, it has the necessary theoretical basis and important practical significance to carry out automatic classification modeling for car service complaint texts so as to realize automatic classification of the complaints, through reasonably using machine learning methods based on the characteristics of the complaint texts.

Chinese text classification modeling based on machine learning commonly involves data preprocessing, text vectorization, classification modeling, and model reliability analysis, among which, text vectorization and classification modeling are commonly the core links. In related research, the methods used in text vectorization mainly involve three categories, including word frequency-based methods such as TF-IDF and Bag-of-words [5-7], distributed static word vector-based methods such as Word2vec [8-11], distributed dynamic word vector-based methods such as BERT [12-13]. Different types of methods commonly have different characteristics and applicable scenarios; the methods based on word frequency is relatively simple in principle and convenient to implement, but text vectorization based on this kind of methods would lose context information; the distributed static word vector methods and the distributed dynamic word vector methods both understand and represent words based on context, and could effectively retain context information in the process of text vectorization; the main difference between the static word vector methods and the dynamic word vector methods is the polysemy distinction of a word, the static word vector methods couldn't distinguish the different interpretations of a word in different contexts, while the dynamic word vector methods have the ability to distinguish. In text classification modeling, after the texts are converted to vectors, it is commonly necessary to furtherly process classification information so as to obtain text classification prediction results; in related researches, the basic methods used in classification information processing mainly involve two categories, including classical machine learning methods [14], such as Naive Bayes and random forests, and various neural network methods [15-19]. The neural network methods used in text classification have the characteristic of diversification, including basic neural network methods such as CNN, RNN,

Funding Project: Promote the Classification Development of College-Construction of Professional Degree Sites of Electronic Information (Intelligent Computing) (5112211039).

LSTM, BILSTM, and various improved neural network methods suitable for different application scenarios. At the same time, the neural network method has the characteristic of flexible superposition, different kinds of neural networks could be stacked up for use. Applying the methods based on different types of neural networks stacking to the classification information processing, the effect of multi-layer classification information processing could be achieved, which commonly could improve the quality of classification information extraction and the classification accuracy of the model. In addition, ensemble learning methods are gradually being used in natural language text classification research in recent years [20]. Ensemble learning methods could comprehensively use a variety of basic methods, which could firstly build multiple individual models based on different kinds of basic methods, and then perform horizontal integration of basic models through certain strategies, obtaining prediction results through two-stage process processing. In general, the natural language text classification modeling based on machine learning has the characteristics of multi-link research process and diversified research methods; different types of basic methods commonly have different characteristics and applicability differences; in text classification modeling, technical routes and technical methods could be designed and selected based on actual text characteristics.

The basic characteristics of car service complaint texts include quite rich emotional expressions and professional vocabularies. After data preprocessing and basic analysis, based on the characteristics of the service complaint texts, this study uses the Jieba word segmentation tool for word segmentation, word frequency-based method for text vectorization, and correlation method for feature selection; the classification model is trained based on progressive training method and random forest, and the feature dimension is adjusted through the modeling feedback; model reliability is assessed based on the effect of data amount on the modeling and the effect of text length on the probability distribution of classification predictions. It is expected that this study could provide effective reference for subsequent related research and application.

II. TECHNICAL ROUTE

The technical route of this study includes data sorting, data characteristic analysis, splitting words, feature extraction, classification modeling, model reliability analysis, conclusion and outlook. In feature extraction, the method based on word frequency and correlation analysis is used; in classification modeling, random forest and progressive method are used to construct classification model.

The technical route is shown as Fig. 1.

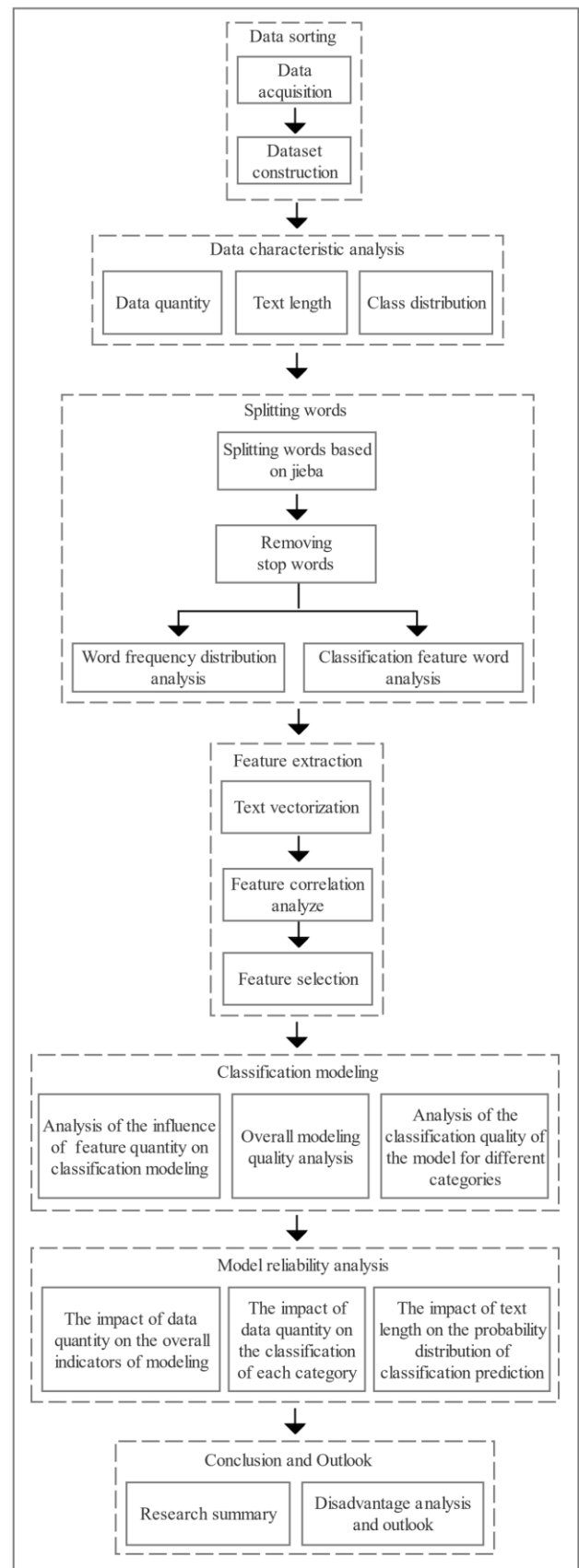


Fig. 1. Technical Route Figure.

III. DATA

The research data of this study is from the Beijing Car Quality Net Information Technology Limited Company. The dataset used includes seven classes of car service complaint text data, which includes service attitude, personnel technology, service charge, not keeping promise, sale fraud, accessory dispute, service process is not perfect. The total data amount of the dataset is 2100, and the data amount of each class is 300.

The characteristics of data amount and text length of the dataset are shown in Table I.

The data distribution of the dataset in terms of car type, purchase and use time, and brand is shown in Fig. 2. The coverage of the dataset in terms of car type, purchase and use time, and brand is relatively comprehensive, and the overall distribution uniformity is quite well.

TABLE I. DATA DESCRIPTION

No.	Class	Data amount	Average length of text	Maximum length of text	Minimum length of text	Text length standard deviation
1	Service attitude	300	18.5033	24	15	1.8352
2	Personnel technology	300	19.1167	26	15	1.9806
3	Service charge	300	18.6133	24	14	1.9156
4	Not keeping promise	300	18.5500	24	13	1.8670
5	Sale fraud	300	18.7100	29	14	2.2065
6	Accessory dispute	300	18.5267	30	15	1.9618
7	Service process is not perfect	300	18.7033	26	14	2.2193
8	All	2100	18.6748	30	13	2.0098

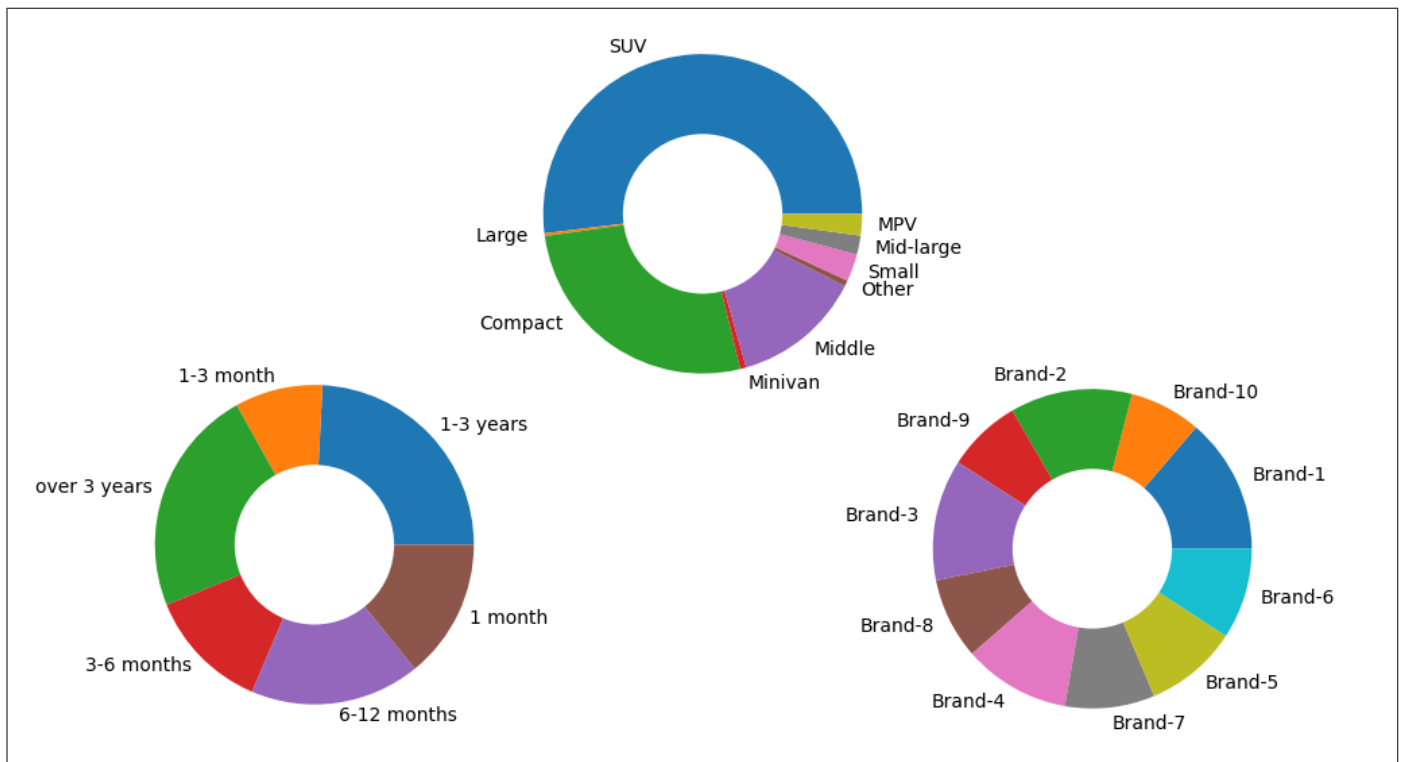


Fig. 2. Data Distribution Characteristics.

IV. WORD SEGMENTATION

Chinese text classification commonly needs to separate the texts into words, in this study, Jieba tool is used for word segmentation, which is widely used in Chinese text segmentation. After word segmentation, the data process of removing stop words is conducted to remove the feature words with low classification relevance. After removing stop words, the word segmentation result is shown in Table II. In the different classes, the highest word amount is 2865 and the lowest amount is 2611; the highest unique word amount is 743 and the lowest amount is 516; the highest value of repetition rate is 0.8129 and the lowest value is 0.7154.

The distribution differences of the global high frequency words in different classes could reflect the applicability of the

data processing method based on word frequency in the classification modeling for the corresponding text data to a large extent. The analyze result for the word frequency distribution of the global high frequency words of the dataset in the different classed is shown in Fig. 3. Overall, the higher the global word frequency value, the higher the difference of the word frequency distribution of the feature words in the different classes; the distribution of the global high frequency feature words of the dataset in different classes shows a high degree of discrimination as a whole, which shows that the data processing method based on word frequency is suitable for the classification modeling scene targeted in this study. The class high frequency feature words are shown in Table III.

TABLE II. WORD SEGMENTATION RESULTS

No.	Class	Number of characters	Number of separated words	Number of unique words	Repetition rate
1	Service attitude	5551	2611	743	0.7154
2	Personnel technology	5735	2788	719	0.7421
3	Service charge	5584	2682	618	0.7696
4	Not keeping promise	5565	2758	516	0.8129
5	Sale fraud	5613	2865	558	0.8052
6	Accessory dispute	5558	2802	620	0.7787
7	Service process is not perfect	5611	2731	544	0.8008
8	All	39217	19237	2092	0.8913

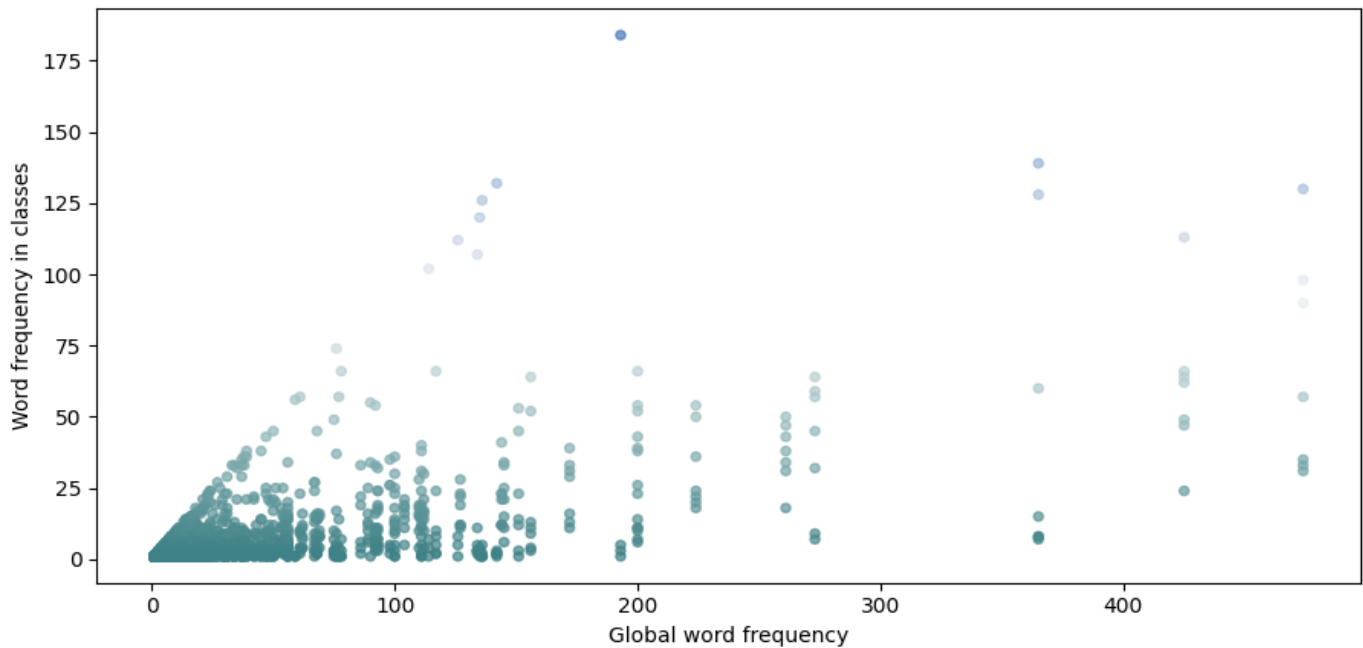


Fig. 3. Word Frequency Distribution.

TABLE III. CLASS HIGH FREQUENCY FEATURE WORDS

No.	Service attitude	Personnel technology	Service charge	Not keeping promise	Sale fraud	Accessory dispute	Service process is not perfect
1	4S shop	Repair	Dealer	Fulfill	Publicity	Accessory	Upgrade
2	Dealer	4S shop	Return	Promise	Inconsistent	Repair	Machine system
3	Repair	Dealer	4S shop	Dealer	Sell	Replace	Car
4	Factory	Maintenance	Car purchase	Not receive	Dealer	Factory	Car machine
5	*	Accident	Charge	Maintenance	Factory	4S shop	*
6	Not	*	Deposit	Car purchase	Car	Dealer	*
7	Vehicle	*	*	Not yet	*	Original factory	*
8	After sale	Cause	Charge	*	Function	Accident	Factory
9	*	Vehicle	Not yet	Car	*	*	Not yet
10	Bad	*	Deposit	Subsidy	*	Not	Update
11	Not yet	Damage	*	4S shop	*	Cause	4S shop
12	Attitude	Change	*	Delivering car	Sale	*	Version
13	When	Bad	Sale	Deposit	Suspected	Vehicle	Solve
14	Solve problem	*	*	*	*	*	*
15	Accident	Specification	When	Replace	4S shop	*	Provide
16	Delay	*	Maintenance	Order car	*	Accessory	*
17	*	Engine	Purchase	When	Light	After sale	Dealer
18	*	Not yet	*	Factory	*	Quality	Navigation
19	Fault	Personnel	Pay	Presentation	Parking	Damage	*
20	*	Record	*	*	New car	*	*

V. FEATURE EXTRACTION AND CLASSIFICATION MODELING

Based on basic analysis for the data characteristics, this study adopts the bag-of-words method based on word frequency for text vectorization, and operates feature word correlation analysis for the feature selection and word vector dimensionality reduction.

Based on correlation analysis, feature words with a degree of correlation higher than 0.95 are partly removed to reduce the dimension of the word vectors and improve the efficiency of model training, model classification. Through the feature selection, 257 features with high relevance are removed, and 1689 features are reserved. Fig. 4 shows the correlation matrix of part global high frequency features in the dataset.

In this study, the random forest combined with progressive model training method is used for the classification model training. In the model training, the features involved are gradually increased for obtaining the optimal amount of the modeling features by comparing the results of multiple rounds of training, in order to avoid too little features used do not contain enough classification information for supporting high quality classification modeling, or the model prediction accuracy, model classification efficiency are negatively affected due to too much features used. The research results show that in this study, the optimal modeling effect is obtained when using 1689 features.

Table IV shows the comparison of the progressive multi-round training results from the aspects of feature selection ratio, feature amount, overall accuracy, overall precision, overall recall, overall f1-score, highest f1-score in the classes, and lowest f1-score in the classes.

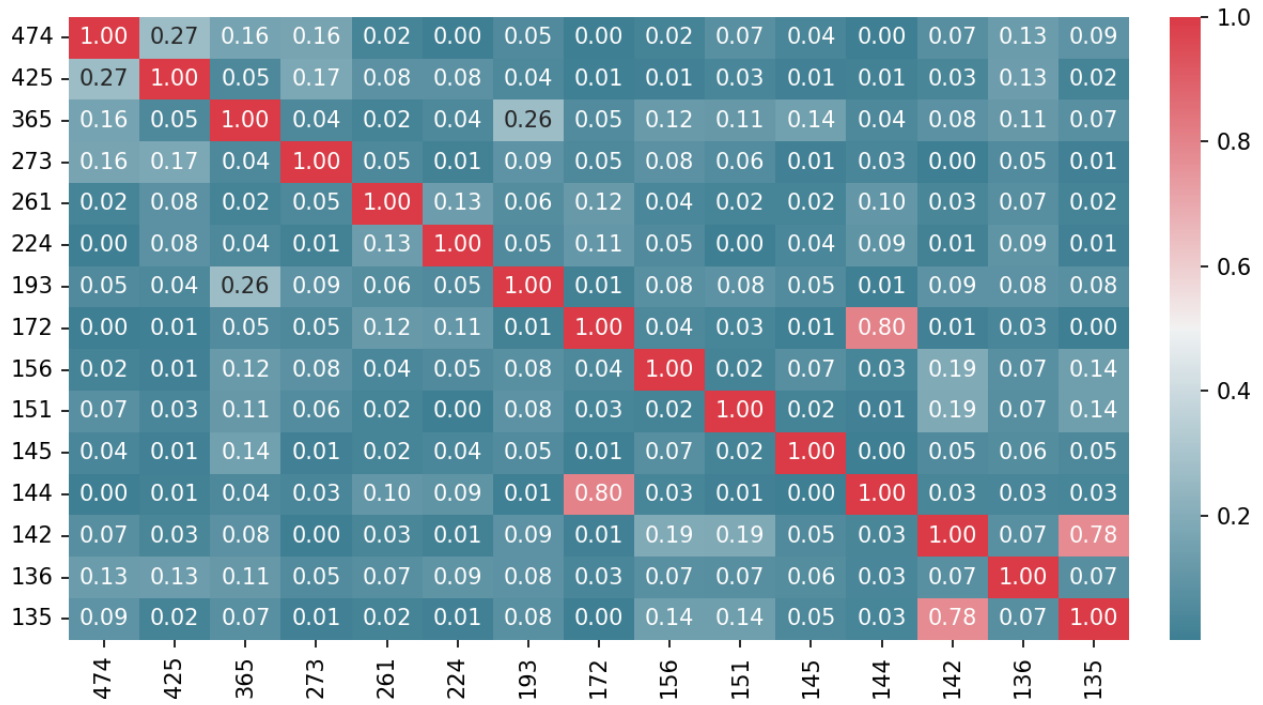


Fig. 4. Correlation Matrix Heatmap.

TABLE IV. CLASSIFICATION MODEL TRAINING

No.	Feature selection ratio	Feature amount	Accuracy	Precision	Recall	F1-score	Highest f1-score in the classes	Lowest f1-score in the classes
1	10%	169	0.8000	0.8041	0.8000	0.8008	0.8966	0.7119
2	20%	338	0.8000	0.8041	0.8000	0.8008	0.8966	0.7119
3	30%	507	0.8000	0.8041	0.8000	0.8008	0.8966	0.7119
4	40%	676	0.8000	0.8041	0.8000	0.8008	0.8966	0.7119
5	50%	845	0.8000	0.8041	0.8000	0.8008	0.8966	0.7119
6	55%	929	0.8333	0.8423	0.8333	0.8358	0.8966	0.7188
7	60%	1013	0.8333	0.8418	0.8333	0.8352	0.8814	0.7213
8	65%	1098	0.8333	0.8482	0.8333	0.8368	0.9123	0.7188
9	70%	1182	0.8333	0.8404	0.8333	0.8346	0.8852	0.7213
10	75%	1267	0.8286	0.8336	0.8286	0.8298	0.8929	0.7097
11	80%	1351	0.8381	0.8438	0.8381	0.8396	0.9180	0.7302
12	85%	1436	0.8238	0.8274	0.8238	0.8249	0.8667	0.7619
13	90%	1520	0.8286	0.8326	0.8286	0.8296	0.8772	0.7213
14	95%	1605	0.8333	0.8436	0.8333	0.8359	0.9153	0.7419
15	100%	1689	0.8476	0.8550	0.8476	0.8495	0.9123	0.7619

VI. MODEL RELIABILITY ANALYSIS

Model reliability analysis is of great significance to the classification modeling, since the modeling is commonly based on limited data, and the modeling indexes mainly reflect the overall quality of the model. The applicability of the model to new data and the reliability of the model classification under specific condition are commonly difficult to evaluate based on the overall modeling result indexes.

This study evaluates the reliability of the model from two aspects: the effect of data amount on the modeling and the effect of text length on the model prediction probability distribution. In term of the effect of data amount, Table V shows the comparison of the multi-round model training result parameters under the condition of increasing data amount. In term of the effect of text length, the first 8 and last 8 text data in the global text length rank are selected for model classification prediction probability distribution analysis. The model classification prediction probability distribution is shown in Table VI.

TABLE V. THE EFFECT OF DATA AMOUNT ON MODEL TRAINING

No.	Data use ratio	Data amount	Accuracy	Precision	Recall	F1-score	Highest f1-score in the classes	Lowest f1-score in the classes
1	10%	210	0.7143	0.7381	0.7143	0.7197	1.0000	0.3333
2	20%	420	0.7143	0.7381	0.7143	0.7197	1.0000	0.3333
3	30%	630	0.7143	0.7381	0.7143	0.7197	1.0000	0.3333
4	40%	840	0.7143	0.7381	0.7143	0.7197	1.0000	0.3333
5	50%	1050	0.7143	0.7381	0.7143	0.7197	1.0000	0.3333
6	55%	1155	0.7845	0.7953	0.7815	0.7829	0.9714	0.5625
7	60%	1260	0.7381	0.7475	0.7381	0.7398	0.9143	0.6061
8	65%	1365	0.8175	0.8357	0.8169	0.8199	0.9189	0.6977
9	70%	1470	0.8571	0.8678	0.8571	0.8580	0.9767	0.7755
10	75%	1575	0.8165	0.8243	0.8156	0.8171	0.8980	0.6667
11	80%	1680	0.7917	0.7928	0.7917	0.7908	0.8571	0.6939
12	85%	1785	0.8715	0.8777	0.8716	0.8714	0.9630	0.8077
13	90%	1890	0.8466	0.8510	0.8466	0.8466	0.9310	0.7241
14	95%	1995	0.8100	0.8220	0.8103	0.8126	0.8772	0.6667
15	100%	2100	0.8476	0.8550	0.8476	0.8495	0.9123	0.7619

TABLE VI. THE PREDICTION PROBABILITY DISTRIBUTION FOR THE FIRST 8 AND LAST 8 TEXTS IN THE GLOBAL TEXT LENGTH RANK

No.	Service attitude	Personnel technology	Service charge	Not keeping promise	Sale fraud	Accessory dispute	Service process is not perfect
F-1	0.0700	0.1300	0.0300	0.0000	0.0000	0.7200	0.0500
F-2	0.1000	0.3700	0.0500	0.1000	0.1450	0.1000	0.1350
F-3	0.0500	0.9100	0.0000	0.0000	0.0200	0.0000	0.0200
F-4	0.1000	0.6800	0.0000	0.0000	0.1000	0.0800	0.0400
F-5	0.0100	0.0500	0.1700	0.0000	0.0700	0.0100	0.6900
F-6	0.0100	0.0500	0.1700	0.0000	0.0700	0.0100	0.6900
F-7	0.0700	0.8000	0.0800	0.0100	0.0000	0.0100	0.0300
F-8	0.7500	0.0800	0.0100	0.0200	0.0000	0.0400	0.1000
L-1	0.0100	0.0400	0.0000	0.9300	0.0000	0.0100	0.0100
L-2	0.0300	0.0600	0.7100	0.1300	0.0500	0.0100	0.0100
L-3	0.0000	0.0200	0.9600	0.0000	0.0100	0.0100	0.0000
L-4	0.0000	0.0200	0.9600	0.0000	0.0100	0.0100	0.0000
L-5	0.0000	0.0000	0.0000	0.0000	0.9900	0.0100	0.0000
L-6	0.0000	0.0100	0.0000	0.0000	0.0300	0.0100	0.9500
L-7	0.0300	0.0400	0.0000	0.0000	0.0200	0.0300	0.8800
L-8	0.9700	0.0000	0.0000	0.0000	0.0100	0.0200	0.0000

VII. CONCLUSION AND OUTLOOK

This study focus on the issue of car service complaint classification modeling, the dataset used involves 7 classed of service complaint texts, and the data amount of every class is all 300; the core links of the research process include word segmentation, text vectorization, the feature selection and dimensionality reduction based on correlation analysis, the classification modeling based on random forest and progressive method, and the model reliability analysis based on data

amount and text length; the results show that based on the method of this study, the effective classification for the car service complaint texts could be realized. In this study, when the feature amount reaches 1689, the optimal modeling effect is obtained, the values of overall accuracy, overall precision, overall recall, overall f1-score, the highest f1-score in the classes, the lowest f1-score in the classes respectively reach 0.8476, 0.8550, 0.8476, 0.8495, 0.9123 and 0.7619; in the model reliability analysis, when the data use ratio reaches 85%, the modeling effect is generally stable; the analysis results of

the effect of text length on the model classification prediction probability distribution show that the distribution is overall high discriminative.

In summary, the car service complaint data could be effectively classified based on the method of this study, which could provide reference for the classification modeling of the natural language texts with subjectivity characteristic; at the same time, this study still belongs to theoretical research, and has not been applied to practice.

REFERENCES

- [1] Zhu Fang Peng, Wang Xiao Feng, Text classification for ship industry news [J], *Journal of Electronic Measurement and Instrumentation*, 2020, 34 (01): 149-155.
- [2] Zhao Ming, Du Hui Fang, Dong Cui Cui, Chen Chang Song, Diet health text classification based on word2vec and LSTM [J], *Transactions of the Chinese Society for Agricultural Machinery*, 2017, 48 (10): 202-208.
- [3] Bao Xiang, Liu Gui Feng, Yang Guo Li, Patent text classification method based on multi-instance Learning [J], *Information Studies: Theory & Application*, 2018, 41 (11): 144-148.
- [4] Wen Chao Dong, Zeng Cheng, Ren Jun Wei, Zhang Yan, Patent text classification based on ALBERT and bidirectional gated recurrent unit [J], *Journal of Computer Applications*, 2021, 41 (02): 407-412.
- [5] Hu Jing, Liu Wei, Ma Kai, Text categorization of hypertension medical records based on machine learning [J]. *Science Technology and Engineering*, 2019, 19 (33): 296-301.
- [6] Yu Hang, Li Hong Lian, Lü Xue Qiang, Text classification of NPC report contents [J], *Computer Engineering and Design*, 2021, 42 (06): 1772-1778.
- [7] Wang Xiang Xiang, Fang Hui, Chen Chong Cheng, Classification technique of cultural tourism text based on naive Bayes [J]. *Journal of Fuzhou University (Natural Science Edition)*, 2018, 46 (05): 644-649.
- [8] Zhou Qing Hua, Li Xiao Li, Research on short text classification method of railway signal equipment fault based on MCNN [J]. *Journal of Railway Science and Engineering*, 2019, 16 (11): 2859-2865.
- [9] Feng Shuai, Xu Tong Yu, Zhou Yun Cheng, Zhao Dong Xue, Jin Ning, et al. Rice knowledge text classification based on deep convolution neural network [J]. *Transactions of the Chinese Society for Agricultural Machinery*, 2021, 52 (03): 257-264.
- [10] Niu Zhen Dong, Shi Peng Fei, Zhu Yi Fan, Zhang Si Fan, Research on classification of commodity ultra-short text based on deep random forest [J]. *Transactions of Beijing Institute of Technology*, 2021, 41 (12): 1277-1285.
- [11] Zhang Yu, Liu Kai Feng, Zhang Quan Xin, Wang Yan Ge, Gao Kai Long, A combined-convolutional neural network for Chinese news text classification [J]. *Acta Electronica Sinica*, 2021, 49 (06): 1059-1067.
- [12] Li Ke Yue, Chen Yi, Niu Shao Zhang, Social E-commerce text classification algorithm based on BERT [J], *Computer Science*, 2021, 48 (02): 87-92.
- [13] Tian Yuan, Yuan Ye, Liu Hai Bin, Man Zhi Bo, Mao Cun Li, BERT pre-trained language model for defective text classification of power grid equipment [J]. *Journal of Nanjing University of Science and Technology*, 2020, 44 (04): 446-453.
- [14] Zhao Yan, Li Xiao Hui, Zhou Yun Cheng, Zhang Yue. A study on agricultural text classification method based on naive bayesian [J]. *Water Saving Irrigation*, 2018(02):98-102.
- [15] Chen Ping, Kuang Yao, Hu Jing Yi, Wang Xiang yang, Cai Jing. Text categorization method with enhanced domain features in power audit field [J]. *Journal of Computer Applications*, 2020, 40 (S1): 109-112.
- [16] Liu Zi Quan, Wang Hui Fang, Cao Jing, Qiu Jian, A classification model of power equipment defect texts based on convolutional neural network [J]. *Power System Technology*, 2018, 42 (02): 644-651.
- [17] Ge Xiao Wei, Li Kai Xia, Chen Ming, Text classification of nursing adverse events based on CNN-SVM [J]. *Computer Engineering & Science*, 2020, 42 (01): 161-166.
- [18] Wang Meng Xuan, Zhang Sheng, Wang Yue, Lei Ting, Du Wen, Research and application of improved CRNN model in classification of alarm texts [J]. *Journal of Applied Sciences*, 2020, 38 (03): 388-400.
- [19] Wang Si Di, Hu Guang Wei, Yang Si Yu, Shi Yun, Automatic transferring government website e-mails based on text classification [J]. *Data Analysis and Knowledge Discovery*, 2020, 4 (06): 51-59.
- [20] Zhang Bo, Sun Yi, Li Meng Ying, Zheng Fu Qi, Zhang Yi Jia, et al. Medical text classification based on transfer learning and deep learning [J]. *Journal of Shanxi University (Natural Science Edition)*, 2020, 43 (04): 947-954.

Multi-layer Stacking-based Emotion Recognition using Data Fusion Strategy

Saba Tahseen¹

PhD Scholar

Dept. of Computer Science and Engineering
Christ University, Bangalore, India

Ajit Danti²

Professor

Dept. of Computer Science and Engineering
Christ University, Bangalore, India

Abstract—Electroencephalography (EEG), or brain waves, is a commonly utilized bio signal in emotion detection because it has been discovered that the data recorded from the brain seems to have a connection between motions and physiological effects. This paper is based on the feature selection strategy by using the data fusion technique from the same source of EEG Brainwave Dataset for Classification. The multi-layer Stacking Classifier with two different layers of machine learning techniques was introduced in this approach to concurrently learn the feature and distinguish the emotion of pure EEG signals states in positive, neutral and negative states. First layer of stacking includes the support vector classifier and Random Forest, and the second layer of stacking includes multilayer perceptron and Nu-support vector classifiers. Features are selected based on a Linear Regression based correlation coefficient (LR-CC) score with a different range like n_1, n_2, n_3, n_4 a, for d_1 used n_1 and n_2 dataset, for d_2 dataset, combined dataset of n_3 and n_4 are used and developed a new dataset d_3 which is the combination of d_1 and d_2 by using the feature selection strategy which results in 997 features out of 2548 features of the EEG Brainwave dataset with a classification accuracy of emotion recognition 98.75%, which is comparable to many state-of-the-art techniques. It has been established some scientific groundwork for using data fusion strategy in emotion recognition.

Keywords—Electroencephalograph (EEG); linear regression based correlation coefficient; feature selection; multi-layer stacking model; machine learning techniques; emotion recognition

I. INTRODUCTION

With the rapid advancement of computers and human contact technology, there is a significant demand in the area of human interaction for a more intelligent and humanized human-machine interface (HMI). A (BCI) brain-computer interface transforms a way of transforming brain processes that are connected directly to the brain of a living organism, such as a human or an animal. BCI serves as a bridge for communication between both the human brain and as a tool to detect different applications, such as emotion identification and different applications [1].

Human communication, daily life, and work all rely heavily on emotional expressiveness. It can be characterized as positive, neutral, or negative experiences arising from a variety of physiological activities, and it includes a wide range of emotions such as sadness, happiness, surprise, anger, and disgust [2][3][4].

Emotion recognition research has become more common among researchers with the development of sensor-based technology and processes and accessibility have improved. Emotion recognition can have important applications, whether professional, personal, or personal [5] such as in the fields of medicine [6], education, psychology, computer games, driving, security, entertainment [7], and workload evaluation, and many others [8].

Emotions can be detected in a variety of ways, including brain waves and facial expressions. Brain waves are a means of obtaining emotion that can be both intrusive and non-invasive. In wires and an intrusive Brain-computer-interface (BCI) are surgically implanted on the accessible brain surface. The non-invasive method is known as BCI, and it provides a simple, fast, and beneficial method for collecting the brainwaves, which comprises functional magnetic resonance imaging (fMRI), Magnetoencephalogram (MEG), Electroencephalogram (EEG), and numerous signaling have already been approved, recognized, and classified as non-physiological and physiological signals, respectively. In the practical application of emotion recognition, Gesture, Text, movement, speech, voice intonation, and facial expression, among other non-physiological signals, are indeed the original concept is a term that has been used a lot in the past. More studies have recently been conducted using physiological signals such as electrocardiogram (ECG) and electroencephalogram (EEG) [9].

This study proposes an electroencephalography (EEG) signal analysis technique for recognizing and classifying emotional states, as well as a correlation-based data reduction strategy coefficient score between features with a different range and developed a new dataset. Machine learning models are grouped into three types: supervised, unsupervised, and reinforcement learning, as well as a specific form termed ensembles learning, based on the methodology utilized [10].

An ensemble machine learning algorithm is often known as stacking. Stacking is the process of learning how to aggregate the prediction of participating ensemble components using a machine learning model and minimize the variation. In this paper extension of Stacking Classifier with two layers of learning models i.e., Multi-layer Stacking Classifier is developed.

In this research article there are four contributions:
1) Calculated the correlation coefficient score of features

based on linear regression model. 2) Prepared a different dataset with a particular range and applied a data fusion strategy. 3) Developed a method which has already been tested through a developed dataset. 4) Calculated the time complexity of each classifier.

This manuscript's structure is as follows: Section II describes the related work on emotion recognition, data reduction, and on machine learning techniques. Section III describes about possible approach for reducing data in an EEG analysis by generating restricted electrode correlations zones. Section IV explains the configuration for the classification procedure as well as the methods used to carry out the experiments. The results of executing the proposed solutions are discussed in Section V, and the work's conclusions are discussed in Section VI.

II. RELATED WORK

A method for classifying emotional states using wavelet compression, EEG data, and sensor classification procedure, links electrodes in a 10/20 model to Brodmann n areas and reduces computational load. The emotions modelling is based on hold value of an adjusted space from the Russell Arousal Valence Space and the Geneva model, and the classification procedure was accomplished using an SVM Classification process, which achieved an 81.46%, classification performance for a multi-class problem [11].

Researchers used the zero-time window-based using the numerator group-delay to derive immediate frequency features function to correctly detect the periods in each emotional situation. Using QDC and RNN, as well as the DEAP database, separate class systems were constructed used to test them [12].

There are two types of network entropy metrics calculated: nodal degree entropy and clustering coefficient entropy. The effective characteristics are fed into the SVM classifier using the AUC method to accomplish emotion recognition across participants. The findings of the experiment revealed that the properties of 18 channels selected by AUC were significant ($p < 0.005$) for the EEG signals of 62 channels [13].

The program collects features from EEG data and uses machine learning techniques to classify emotions, with different segments of a trial being utilized to train the proposed model and examine its impact on emotion detection outcomes. Second, using the classification performance and two emotion coefficients, namely, the correlations and entropy coefficients, a unique activation curve for emotions is created. The activation curve can not only define emotions, but it may also indicate the emotional activating mechanism to some extent. Next, the two factors are combined to provide a weight coefficient, which improves emotion recognition accuracy. Experiments on the DEAP and SEED datasets were conducted to validate the suggested technique [14]. Based on the SJTU emotion EEG datasets (SEED) and the ResNet50 and Adam

optimizer, the CNN model is being used to train the features and recognize the emotions of positive, negative and neutral states of real EEG signals in a single model [15]. This study presented a new model called the "hybrid model" that merged three ensemble models. For classification challenges, a set of features is retrieved from raw IoT datasets from various IoT domains utilizing linear discriminant analysis (LDA), Principal component analysis (PCA), and Isomap. The classifiers' accuracy, area under the curve (AUC), and F1 score are used to compare their performances [16].

A feature extraction subsystem and a classifier subsystem are created in this paper for an EEG-based emotion recognition system. 9 features extracted from the time and frequency domain from the EEG sign were used because the greater performance of the feature extraction module may result in higher recognition accuracy [17]. Authors have created a machine learning algorithm based on ensembles. The data was cleaned using a pre-processing technique, and feature selection was done using wrapper-based methods; additionally, a stacking-based ensemble learning model was used to identify the MDD participants in the final stage [18]. The proposed research makes a significant addition by presenting an enhanced version of the agent-based data reduction algorithm that incorporates the stacking generalization mechanism for data reduction. Enhancing the performance of the categorization results in the model discussed in [19]. Considering the aforementioned factors and applying the skills in this sector, it is inspired to write this research to address the following problem.

- How accuracy and prediction performance can be improved?
- How to overcome from overfitting problem?
- How precise can the EEG waves be classified?
- What are other essential features can derive using EEG data?

III. DATASET DETAILS

Performed thorough analysis on the EEG Brainwave Dataset, which is publicly available, in each state: happy, neutral, and negative - data was collected for 3 minutes from two subjects (1 male, 1 female). To record the TP9, AF7, AF8, and TP10 EEG placements, the author employed a Muse EEG headgear with dry electrodes.

IV. PROPOSED METHODOLOGY

In this section, discussed about a possible approach for reducing data in an EEG analysis by generating restricted electrode correlations zone and explains about the configuration for the classification procedure as well as the methods used to carry out the experiments.

A. Data Preprocessing

In Machine Learning, data preprocessing relates to the procedure of organizing and managing basic information to make it appropriate for creating and training Machine Learning models. First libraries are required for data preprocessing, identifying missing values, so, the EEG

brainwave dataset has no missing values, and provides the label for each category like positive, negative, and neutral.

B. Feature Selection

For features, correlation coefficient score is determined with a linear regression model. For each feature set, selected the subset of features based on the range and created a new dataset.

C. Correlation Coefficient Score

To calculate the correlation coefficient, the linear regression model is used. The linear relationship between multiple Correlations is used to assess variables. Correlation is used to predict one variable from the other. Because the good variables are so closely related to the aim, using correlation to pick features stands to reason. Furthermore, variables should really be relevant to the goal yet unrelated to each other. It anticipates one from the other if the two variables are correlated. As a result, if features are correlated, the model only needs one among them because the other provides no additional information. The linear correlation coefficient is a mathematical expression that measures the degree and direction of a relationship between two variables:

$$r = \frac{\sum \frac{(x_i - \bar{x})(y_i - \bar{y})}{s_x s_y}}{n-1} \quad (1)$$

Where \bar{x} and s_x are represented, the sample mean and sample deviation of the x 's. And \bar{y} and s_y are represented the mean and standard deviation of the y 's.

A different method of calculating the correlation coefficient is as follows:

$$r = \frac{s_{xy}}{\sqrt{s_{xx}s_{yy}}} \quad (2)$$

Where,

$$s_{xx} = \sum x^2 - \frac{(\sum x)^2}{n}$$

$$s_{xy} = \sum xy - \frac{(\sum x)(\sum y)}{n}$$

$$s_{yy} = \sum y^2 - \frac{(\sum y)^2}{n}$$

The properties of "r" are as follows:

- It is always in the range of -1 to +1.
- Because it is a dimensionless quantity measure, "r" would have been the same that whether two variables were measured in pounds and inches or grams and centimeters.
- Favorable "r" levels are linked to positive connections.
- Bad "r" values are linked to negative relationships.

First, Linear Regression model is used to find the feature importance of each feature. Then correlation coefficient Score is determined for each feature. Following ranges are considered for each dataset.

$$n_1 = 0.0 \text{ to } 0.3;$$

$$n_2 = 0.31 \text{ to } 0.5;$$

$$n_3 = 0.51 \text{ to } 0.75;$$

$$n_4 = 0.76 \text{ to } 1.0.$$

Based on the Correlation Coefficient score value, it is found that 610 features importance score are within 0.0-0.3, 179 features are within 0.31-0.5, 136 features are within the range 0.51-0.75 and 77 features are within 0.76 to 1.0. After applying the data fusion technique for the EEG brainwave dataset, 997 features are selected. At this stage developed a four set of datasets with different feature values. Then selected all the unique features from n_1 and n_2 and generated the new dataset called d_1 which has 787 columns excluding the label. The same procedure has been applied on n_3 and n_4 and after combining the features and filtering the unique features, around 211 are considered, i.e., d_2 . And finally, by considering d_2 and d_3 determined 997 unique features and that is final dataset to work on.

$d_1, d_2,$ and d_3 are the final combined dataset of $d_1,$

and $d_2,$ which details as follows:

$$n_1 = (2132 \text{ trails} \times 610 \text{ features})$$

$$n_2 = (2132 \text{ trails} \times 179 \text{ features})$$

$$d_1 = n_1 + n_2 = (2132 \text{ trails} \times 787 \text{ features})$$

$$n_3 = (2132 \text{ trails} \times 136 \text{ features})$$

$$n_4 = (2132 \text{ trails} \times 77 \text{ features})$$

$$d_2 = n_3 + n_4 = (2132 \text{ trails} \times 211 \text{ features})$$

$$d_3 = d_1 + d_2 = (2132 \text{ trails} \times 997 \text{ features}).$$

D. Machine Learning Classifiers

The method of feature selection, the LR-CC algorithm chooses the most essential features for predicting emotional states. The next step is to classify the emotions by using a dataset using a machine learning technique. Multilayer stacking Classifier is developed based on Stacking Classifier 1 and Stacking Classifier 2 method on Support vector classifier, Random Forest for a Stacking Classifier 1 (layer1), and Nu-Support vector classifier, r, and Multi-Layer Perceptron for Stacking Classifiers 2 (layer 2) as low-level base learners and Random Forest as meta learner algorithm. This section examines step-by step working of the suggested model and overall design. Fig. 1 establishes the framework. First, there are the EEG signals that have been pre-processed from the dataset based on correlation coefficient score; the feature selection stage selects the features based on the data fusion technique and makes a new dataset, i.e., d_3

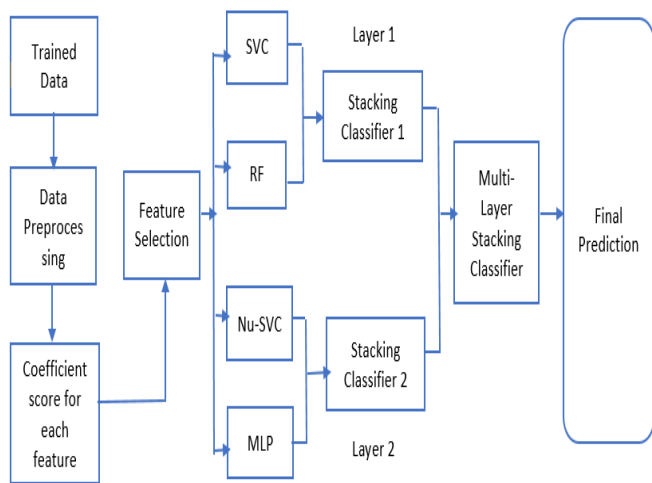


Fig. 1. Architecture Diagram of Multi-layer Stacking Model based on different Machine Learning Classifier Called as Learners and Meta Classifier.

Two layers of Classifiers are implemented separately first and created as a Stacking Classifiers 1 and 2 with a random forest as a meta learner, after implementation of these stacking 1 and 2, developed a multi-layer Stacking Classifier which is based on the predictions of Stacking Classifier 1, and Stacking Classifier 2 as an input and generate a final prediction. A feedforward artificial neural network is a multilayered perceptron in which the functions and structure of the ANN are like the brain's activities and structure [20]. Neurons are basic components that are connected and work in tandem. These neurons are linked by a vital link that contains the information to solve difficulties [21]. For regression and classification issues, a support vector machine (SVM) is a supervised machine learning technique. Each property is represented by a point in n -dimensional space (n = number of features). A hyperplane is created to do linear classification, which effectively separates the two classes. Kernel approaches such as Gaussian kernel, Laplace kernel, and Polynomial kernel are utilized for non-linear classification [22]. Random forest is a decision tree-based learning technique that combines numerous decision trees. It forecasts by aggregating decision tree forecasts [23]. The resilience of SVC and Nu-SVC isn't always the best option, and random forest is suitable in situations [24]. It is difficult to acquire using a Multilayer Perceptron to find the best parameters. Developed a multi-layer stacking ensemble model to address these concerns and increase forecast accuracy. Support Vector Classifier (SVC), Nu-Support Vector Classifier (NuSVC), Multi-layer Perceptron (MLP), and Random Forest classifier, layer 1, and layer 2 will be trained and tested individually. These four models will compensate for shortcomings and provide superior outcomes when stacking. The following shows the algorithm for multilayer stacking with 2 layers. SVC, RF classifier for Stacking 1 or layer 1 as L_1 Classifier and for Stacking 2 or layer 2 as L_2 has Nu-SVC and MLP. After implementation of these classifiers, developed a new model i.e., multi-layer stacking which is based on L_1 and L_2 and for meta classifier M used Random Forest with cross validation K and generate a prediction P . Confusion matrix will be used to evaluate each classifier's performance. Finally, results are compared by stacking the predictions of different classifiers.

Algorithm: Multilayer Stacking Classification

Input:

Training Datasets $D, L_1, L_2, L_3, M, SVC, RF, MLP, Nu-SVC$

Output: An Ensemble Classifiers, L_3, P

Step 1: Load SVC, RF Model

load (SVC, RF)

Step 2: Train First Level Classifiers L_1

Apply First level Classifier on dataset D

$L_1 <- (SVC, RF)$

Step 3: Load MLP, Nu-SVC Model

Load (MLP, Nu-SVC)

Step 4: Train a Second Level Classifier L_2

Apply Second level Classifier on dataset D

$L_2 <- (MLP, Nu-SVC)$

Step 5: Construct a new training model based on L_1 and L_2

Adopt a Cross-validation approach K in preparing a new training set for Meta classifier M

Step 6: Learn a meta-Classifiers M

Return Multi-Layer Stacking model L_3

Return P

Where,

D : Dataset

L_1 : Layer 1 Classifiers

L_2 : Layer 2 Classifiers

L_3 : Multi-layer Stacking Model

M : Meta Classifiers

P : Prediction

V. EXPERIMENTAL RESULTS

The main source of dataset consists of 2132 records and 2548 features, after data pre-processing, feature selection is made based on the Linear Regression-Correlation Coefficient (LR-CC) with a Correlation coefficient score of features, 997 features have been selected by applying the data fusion technique, The data fusion method focuses on a group of features that need to be improved, refined, or obtained. on the original dataset. Data fusion techniques are applied with feature level for selecting the features from the same source, i.e., the EEG Brainwave dataset to develop a single dataset.

The classification is divided into 3 parts, in the first part i.e., base learners are learned, and findings are predicted after selecting the features separately in the second part layer 1 and layer 2 are learned and findings are predicted separately, and in the third part, to solve the problems with the individual implements Stacking Classifiers 1 and 2 are developed and made a new prediction as input for the multilayer stacking classifier. In the multi-layer stacking, classifiers are trained layer 1(SVC+RF) and layer 2(Nu-svc+MLP) and the base learners predicted output to the multi-layer stacking as an input.

Developed different datasets and combined them into one dataset by using data fusion techniques. Proposed models are tested on different datasets and accuracy of the algorithms are shown in Fig. 2. It is observed the accuracy of the existing algorithm and Proposed algorithm i.e., multi-layer stacking with n_1 dataset which has 610 features.

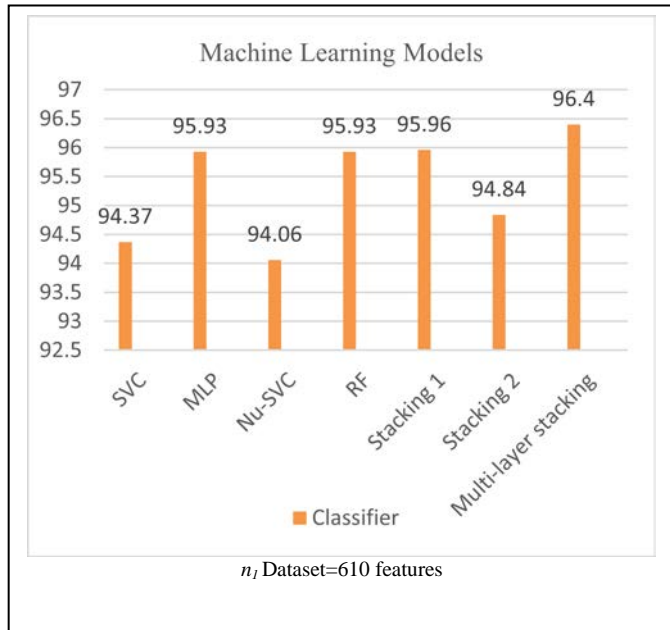


Fig. 2. Machine Learning Model Performance of Dataset $n_1=610$ Features.

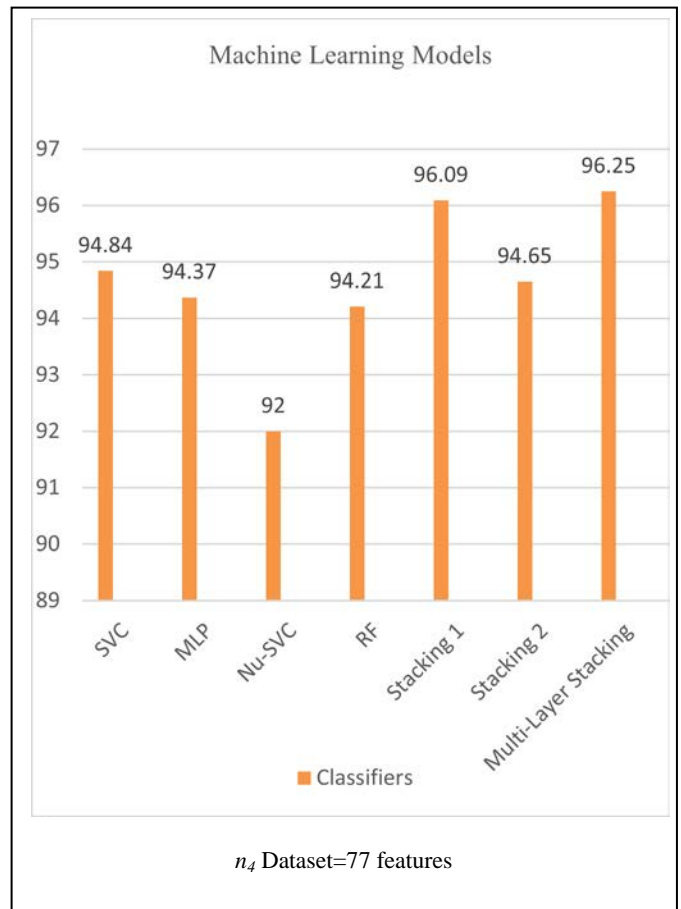


Fig. 4. Machine Learning Models Performance of Dataset $n_3=136$ Features.

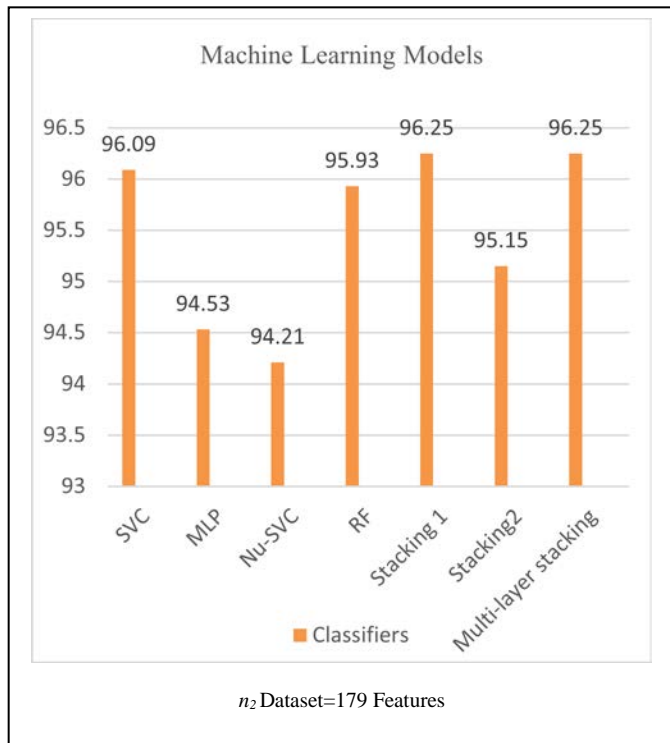


Fig. 3. Machine Learning Models Performance of Dataset $n_2=179$ Features.

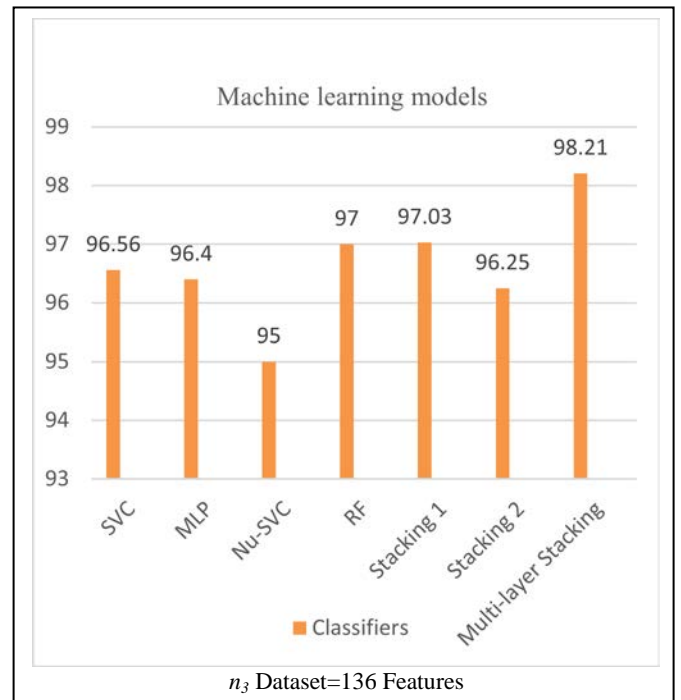


Fig. 5. Machine Learning Models Performance of Dataset $n_4=77$ Features.

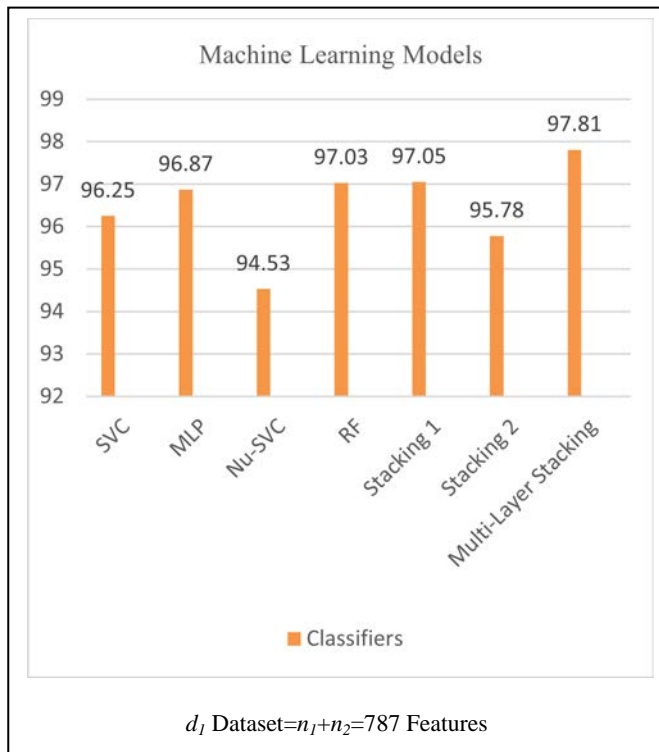


Fig. 6. Machine Learning Models Performance of Dataset $d_1=787$ Features.

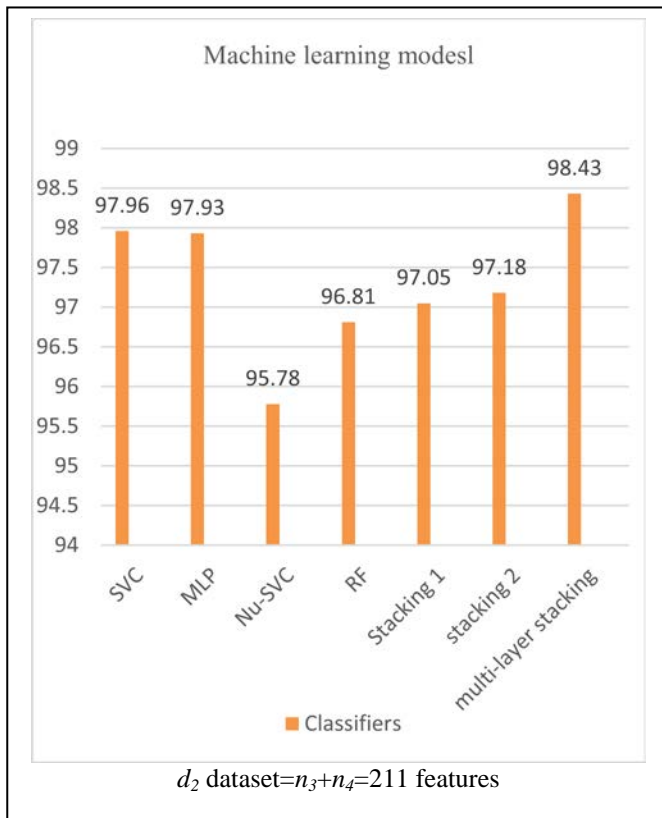


Fig. 7. Machine Learning Models Performance of Dataset $d_2=211$ Features.

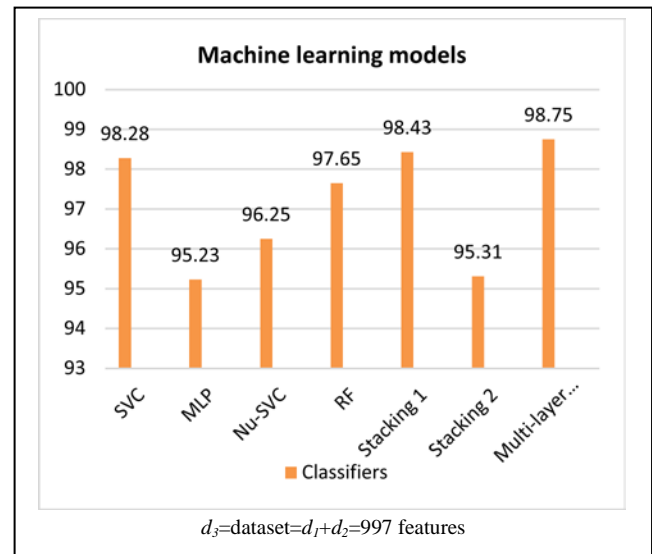


Fig. 8. Machine Learning Models Performance of Dataset $d_3=997$ Features.

Represented the summary of Fig. 2 to Fig. 8 in the form of Table I, in this table, in which proposed model achieved highest accuracy with the unique combination of datasets.

A. Performance Evaluation

To evaluate the developed models, confusion matrix is determined. A confusion matrix is a table that shows how well a classification model (or "classifier") performs on a set of test data for which the true values are known. This is a list of rates that are frequently generated using a binary classifier's confusion matrix:

- Accuracy: What percentage of the time does the classifier get it right?

$$\frac{TP+TN}{N} \quad (3)$$

- Precision: When it predicts yes, how often does it get it right?

$$\frac{TP}{TP+FP} \quad (4)$$

- Recall: The number of true positives divided by the total number of true positives and false negatives equals recall.

$$\frac{TP}{TP+FN} \quad (5)$$

- F1-score: The genuine general positive rate (recall) and precision are weighted averages.

B. Confusion Matrix for Each Classifier

The confusion matrix, which includes metrics such as Sensitivity, Accuracy, Precision, Specificity, and measure, is used to evaluate the algorithm's efficiency after it has been implemented. Fig. 9 to 14 are the confusion matrix of SVC, MLP, Nu-SVC, RF, stacking 1, stacking 2 and Multi-Layer stacking are shown in Fig. 15. Similarly, ensembles models.

TABLE I. ACCURACY OF CLASSIFIERS

Models \ Dataset	n_1	n_2	n_3	n_4	d_1	d_2	d_3
SVC	94.37	96.09	96.56	94.84	96.25	97.96	98.28
RF	95.93	94.53	96.40	94.37	96.87	97.03	95.23
Nu-SVC	94.06	94.21	95	92	94.53	95.78	96.25
MLP	95.93	95.93	97	94.21	97.03	96.81	97.65
Stacking 1	95.96	96.25	97.03	96.09	97.05	97.05	98.43
Stacking 2	94.84	95.15	96.25	94.65	95.78	97.81	95.31
Multi-layer stacking	96.4	96.25	98.24	96.25	97.81	98.43	98.75

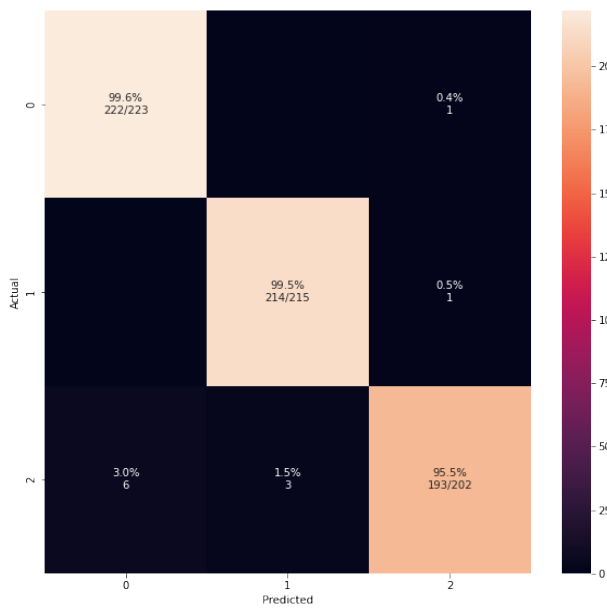


Fig. 9. Confusion Matrix for Support Vector Classifier Model.

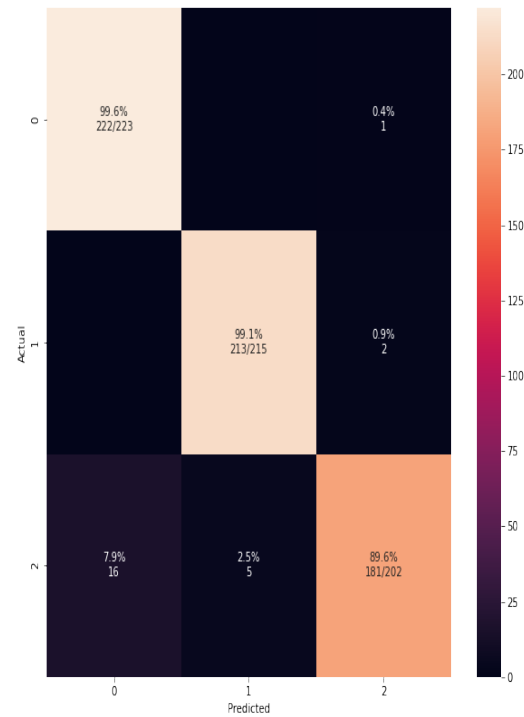


Fig. 11. Confusion Matrix of Nu-SVC Model.

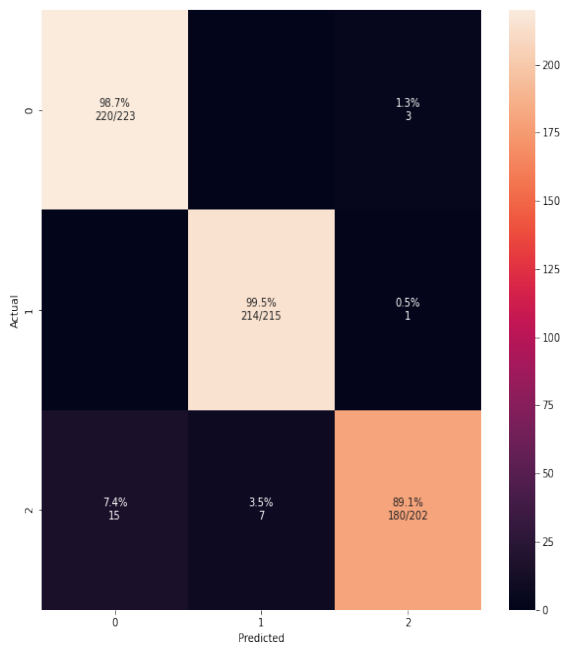


Fig. 10. Confusion Matrix of Multilayer Perceptron Model.

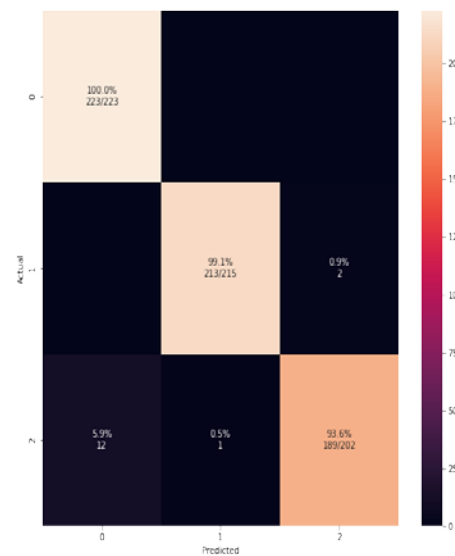


Fig. 12. Confusion Matrix of Random Forest Model.

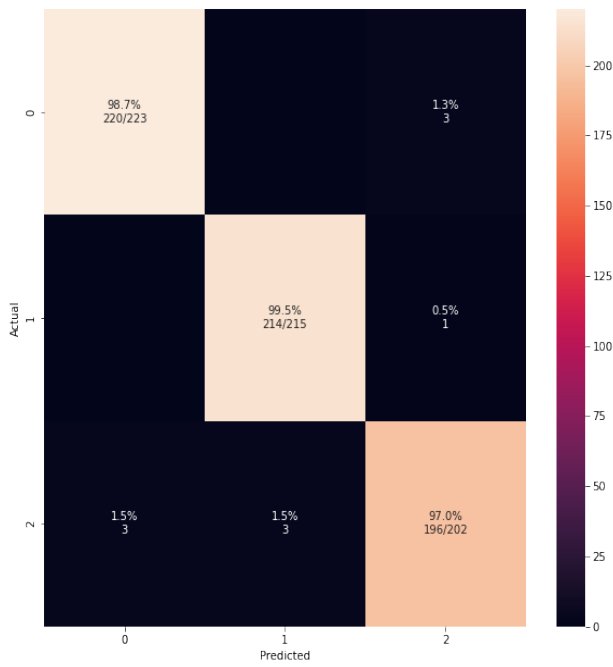


Fig. 13. Confusion Matrix of Stacking 1 Model.

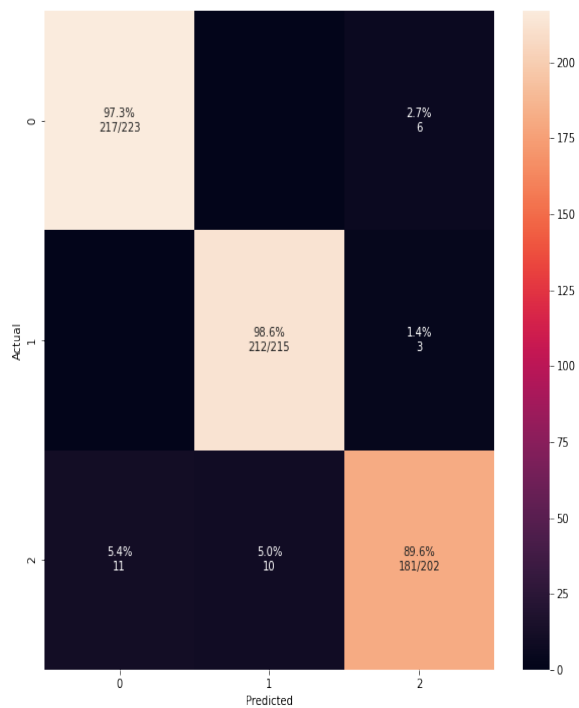


Fig. 14. Confusion Matrix of Stacking 2 Model.

As a result of the increased focus on boosting prediction performance, multi-layer stacking ensembles depicted to improved predictive performance in this investigation. Various classifications are used such as SVC, MLP, Nu-SVC, RF as a base learner and divided these into two layers stacking 1 and stacking 2, and Random Forest as a meta learner. Eventually, merged these four different models to trade-off various constraints and which provided higher performance. Fig. 8 is a summary of the findings. Evaluated the developed

multilayer stacking model to establish state strategies and discovered that suggested approach outperforms them by a wide margin. In contrast, tested proposed models on different datasets and found that proposed method works better compared to other state-of-the-art methods upon these datasets, it's helpful to improve forecast accuracy. Table II shows the comparison state of the art methods for the recognition of neutral, negative, and positive emotions. Accuracy comparison of this research method with other methods of data reduction strategies or feature selection is the recognition of neutral, negative, and positive emotions.

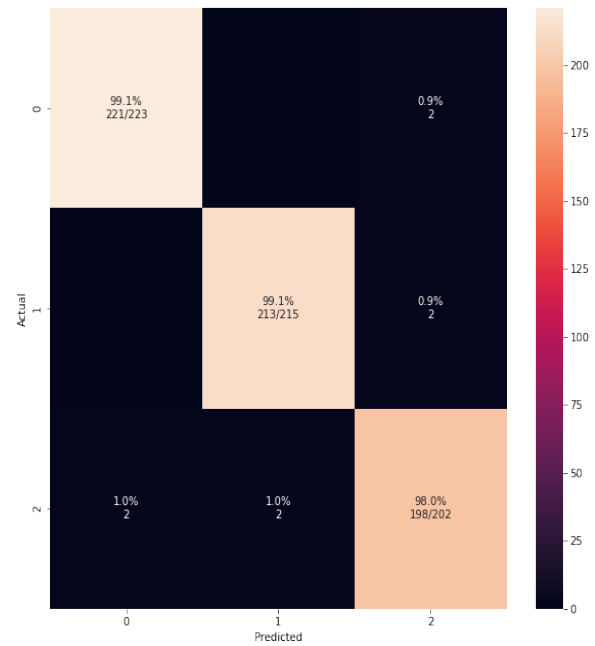


Fig. 15. Confusion Matrix for Multi-layer Stacking.

TABLE II. COMPARISON OF THE PROPOSED MODEL

Study	Classifiers	Dataset	Feature Selection	Accuracy
Proposed method	Multi-Layer Stacking	EEG brainwave Data	997 features selected based on LR-CC	98.75
[26]	Deep neural network	EEG brainwave dataset	63 features with information gain	94.89
[17]	Random Forest	DEAP dataset	Features Selected from the time and frequency domains	62.85
[25]	KNN	EEG Brainwave dataset	PCA used for feature selection	96.22
[13]	SVM	DEAP Dataset	Select features based on network entropy measures	68.44

TABLE III. ACCURACIES OF EMOTIONS

Emotions	accuracy	Emotional State (0,1,2)
Happy	99.66	Positive-2
Fear	68.00	Positive-2
Surprise	77.00	positive-2
Sad	98.00	Negative-0
Angry	71.00	Negative-0
Disgust	61.00	Negative-0
Neutral	100	Neutral-1

Table III represents the average accuracy of recognition of emotions in positive, negative, and neutral state using the multi-layer classification approach. Highest accuracy achieved in neutral state as compared to other emotional state.

C. Time Complexity

The amount of time needed for an algorithm to run as a function of the length of the input is known as temporal complexity. It calculates how long each statement of code in an algorithm takes to execute. Calculated time for each and every model and proposed multi-layer stacking model which shown in Table IV.

TABLE IV. TIME COMPLEXITY OF EACH MODEL

Model	Time
SVC	0.76 sec
MLP	1.83 sec
Nu-SVC	1.27 sec
RF	0.27 sec
Stacking 1	4.69 sec
Stacking 2	6.70 sec
Multi-Layer Stacking	19.09 sec

VI. CONCLUSION

In this study, a multi-layer stacking model for boosting the prediction accuracy of emotion recognition using several machine learning techniques to solve a multi-classification problem even with a small dataset. In the first step, Linear Regression-Correlation Coefficient (LR-CC) method is applied for selecting features based on their content which assists in improving forecast accuracy. An original dataset has 2548 features after applying the data fusion technique final dataset of 997 features are selected. The data has been divided into two categories: training and Testing. The training data is used to train the multi-layer stacking, and the testing data is used to make the predictions. Multi-Layer stacking is implemented by two layers, in each layer two base learners or machine learning algorithms are considered like SVM, MLP, Nu-SVC, RF, and set meta learner as a Random Forest. Individual classifiers are also implemented to make comparisons. The 98.75% accuracy is obtained for Multi-Layer Stacking. As compared to the single base learners, the results indicate that the multi-layer stacking model improves the predictive performance. However, proposed method took much time during the training process. In Future, planning to

work on these issues to improve the computational cost and focus on multimodal data fusion strategy with higher classification performance.

ACKNOWLEDGMENT

This study received no financing help from public, private, or nonprofit organizations. Our Sincere acknowledgement goes to faculty members of Department of computer science engineering from Christ University.

REFERENCES

- [1] Kanjo, L. Al-Husain, and A. Chamberlain, "Emotions in context: examining pervasive affective sensing systems, applications, and analyses," *Personal and Ubiquitous Compu* 2015, ting, vol. 19, no. 7, pp. 1197-1212.
- [2] A. Raheel, M. Majid, M. Alnowami, and S. M. Anwar, "Physiological sensors based emotion recognition while experiencing tactile enhanced multimedia," *Sensors*, 2020, vol. 20, no. 14, p. 4037.
- [3] S. Paul, A. Banerjee, and D. Tibarewala, "Emotional eye movement analysis using electrooculography signal," *International Journal of Biomedical Engineering and Technology*, 2017, vol. 23, no. 1, pp. 59-70.
- [4] W.-L. Zheng, W. Liu, Y. Lu, B.-L. Lu, and A. Cichocki, "Emotionmeter: A multimodal framework for recognizing human emotions," *IEEE transactions on cybernetics*, 2018, vol. 49, no. 3, pp. 1110-1122.
- [5] S. Farashi and R. Khosrowabadi, "EEG based emotion recognition using minimum spanning tree," *Physical and Engineering Sciences in Medicine*, 2020, vol. 43, no. 3, pp. 985-996.
- [6] J. Z. Lim, J. Mountstephens, and J. Teo, "Emotion Recognition Using Eye-Tracking: Taxonomy, Review and Current Challenges," *Sensors*, 2020, vol. 20, no. 8, p. 2384.
- [7] H. Ullah, M. Uzair, A. Mahmood, M. Ullah, S. D. Khan, and F. A. Cheikh, "Internal emotion classification using EEG signal with the sparse discriminative ensemble," *IEEE Access*, 2019, vol. 7, pp. 40144-40153.
- [8] J. Li, Z. Zhang, and H. He, "Hierarchical convolutional neural networks for EEG-based emotion recognition," *Cognitive Computation*, 2018, vol. 10, no. 2, pp. 368-380.
- [9] X. Chai et al., "A fast, efficient domain adaptation technique for cross-domain electroencephalography (EEG)-based emotion recognition," *Sensors*, 2017, vol. 17, no. 5, p. 1014.
- [10] J. Huang, Y.-F. Li, and. Xie, "An empirical analysis of data preprocessing for machine learning-based software cost estimation," *Inf. Softw. Technol.*, vol. 67, pp. 108-127, Nov. 2015, DOI: 10.1016/j.infsof.2015.07.004.
- [11] Adrian Rodriguez Aguinaga, Miguel Angel Lopez Ramir,ez, EZnerd Maria del Rosario Baltazar Flores, "Cl, classification model of arousal and valence mental states by EEG signals analysis and Brodmann correlations" *International Journal of Advanced Computer Science and Applications(IJACSA)*, 6(6), 2015. <http://dx.doi.org/10.14569/IJACSA.2015.060633>.
- [12] Gannouni, S., Aledaily, A., Belwafi, K. et al. Emotion detection using electroencephalography signals and a zero-time windowing-based epoch estimation and relevant electrode identification. *Sci Rep* 11, 7071 (2021). <https://doi.org/10.1038/s41598-021-86345-5>.
- [13] L. Yao, M. Wang, Y. Lu, H. Li, and X. Zhang, "EEG-Based Emotion Recognition by Exploiting Fused Network Entropy Measures of Complex Networks across Subjects," *Entropy*, vol. 23, no. 8, p. 984, Jul. 2021, DOI: 10.3390/e23080984.
- [14] Qing, R. Qiao, X. Xu, and Y. Cheng, "Interpretable Emotion Recognition Using EEG Signals," in *IEEE Access*, vol. 7, pp. 94160-94170, 2019, DOI: 10.1109/ACCESS.2019.2928691.
- [15] Isah Salim Ahmad, Shuai Zhang, Sani Saminu, Lingyue Wang, Abd El Kader Isselmou, Ziliang Cai, Imran Javaid, Souha Kamhi, Ummay Kulsum, "Deep Learning Based on CNN for Emotion Recognition Using EEG Signal," *WSEAS Transactions on Signal Processing*, vol. 17, pp. 28-40, 2021.

- [16] Mr. Vijay, M. Khadse. "A Novel Approach of Ensemble Learning with Feature Reduction for Classification of Binary and Multiclass IoT Data." (2021).
- [17] Kusumaningrum, T & Faqih, Akhmad & Kusumoputro, Benyamin. (2020). Emotion Recognition Based on DEAP Database using EEG Time-Frequency Features and Machine Learning Methods. *Journal of Physics: Conference Series*. 1501. 012020. 10.1088/1742-6596/1501/1/012020.
- [18] N. Mahendran, P. M. Durai Raj Vincent, K. Srinivasan, V. Sharma, and D. K. Jayakody, "Realizing a Stacking Generalization Model to Improve the Prediction Accuracy of Major Depressive Disorder in Adults," in *IEEE Access*, vol. 8, pp. 49509-49522, 2020, DOI: 10.1109/ACCESS.2020.2977887.
- [19] Czarnowski and P. Jędrzejowicz, "An approach to machine classification based on stacking generalization and instance selection," 2016 IEEE International Conference on Systems, Man, and Cybernetics (SMC), 2016, pp. 004836-004841, DOI: 10.1109/SMC.2016.7844994.
- [20] S. Mabu, M. Obayashi, and T. Kuremoto, "Ensemble learning of rule-based evolutionary algorithm using multi-layer perceptron for supporting decisions in stock trading problems," *Appl. Soft Comput.*, vol. 36, pp. 357-367, Nov. 2015, DOI: 10.1016/j.asoc.2015.07.020.
- [21] J. Huang, Y.-F. Li, and Xie, "An empirical analysis of data preprocessing for machine learning-based software cost estimation," *Inf. Softw. Technol.*, vol. 67, pp. 108-127, Nov. 2015, DOI: 10.1016/j.infsof.2015.07.004.
- [22] Y. Hou, J. Xu, Y. Huang, and Ma, "A big data application to predict depression in the university based on the reading habits," in *Proc. 3rd Int. Conf. Syst. Information. (ICSAI)*, Nov. 2016, pp. 1085-1089, DOI: 10.1109/ICSAI.2016.7811112.
- [23] Y. Zhou and Qiu, "Random forest for label ranking," *Expert Syst. Appl.*, vol. 112, pp. 99-109, Dec. 2018.
- [24] J. Xiao, "SVM and KNN ensemble learning for traffic incident detection," *Phys. A Stat. Mech. Appl.*, vol. 517, pp. 29-35, Mar. 2019, DOI: 10.1016/j.physa.2018.10.060.
- [25] Saxena A., Tripathi K., Khanna A., Gupta D., Sundaram S. (2020) Emotion Detection Through EEG Signals Using FFT and Machine Learning Techniques. In: Khanna A., Gupta D., Bhattacharyya S., Snael V., Platos J., Hassanien A. (eds) International Conference on Innovative Computing and Communications. *Advances in Intelligent Systems and Computing*, vol 1087. Springer, Singapore. https://doi.org/10.1007/978-981-15-1286-5_46.
- [26] J. J. Bird, D. R. Faria, L. J. Manso., A. Ekárt, & C. D. Buckingham "Mental Emotional Sentiment Classification with an EEG-based Brain-machine Interface.:2019.

The Implementation of a Solution for Low-Power Wide-Area Network using LoRaWAN

Nicoleta Cristina GAITAN¹, Floarea PITU²

Faculty of Electrical Engineering and Computer Science, Stefan cel Mare University of Suceava^{1,2}
Integrated Center for Research, Development and Innovation in Advanced Materials, Nanotechnologies
and Distributed Systems for Fabrication and Control (MANSiD), Stefan cel Mare University, Suceava, Romania¹

Abstract—In recent years, there has been an increasing emphasis on low-power wide-area network also knowns as LPWAN (Low-Power Wide-Area Networks) technologies that allow efficient and fast data transfer, thus desiring a large-scale integration of various devices facilitating long-distance communications in various fields such as agriculture, logistics, or infrastructure. This category of technologies includes SigFox, LoRa, NB-IoT and others. One area where these low-power technologies can be used successfully is agriculture, in which monitoring the humidity and temperature are crucial. The social-economic context of 2022 highlights as one of the main priorities the security of the food and the raw materials provided by the agriculture field, so the desire is to obtain a large, efficient, and traceable production. Starting from this context, in this paper an architecture based on LoRa (Long-Range) technology and the LoRaWAN protocol it is proposed. We will place special emphasis on monitoring the extremely important parameters in agriculture, namely temperature, humidity and pressure. Although there are multiple works of research in this direction or in similar directions in other fields of activity, we should mention that each of them focuses on certain strictly geographical area and most of the times the results are purely theoretical. The gain that comes with this paper consists first in the fact that there is a practical support implementable and secondly the solution described can be adapted to different geographical regions. Moreover, at the end of this paper, we will focus on the comparison and analysis at the architectural level of two LPWAN technologies, namely SigFox vs. LoRa implemented in the same context in order to find the best results.

Keywords—LoRa; low-power; LoRaWAN protocol; SigFox; LPWAN

I. INTRODUCTION

In the current social and economic context, the field of agriculture is once again proving to be an area of great global importance. With the onset of the COVID 19 pandemic in 2020, agriculture returned to the table of global discussions and thus brought up the issue of crop efficiency and how agriculture is divided globally into different production sectors. The main problem that deepened in this sector started with the COVID 19 pandemic and was related to the food supply chain and the level of agricultural productivity in each country [1]. Another problem facing the agricultural sector today is related to the military conflict between Ukraine and Russia. Both countries have a critical role to play globally in producing cereals and vegetable oils. Thus, with the sanctions imposed by the West on Russia and the fact that Ukraine can no longer export and produce the usual quantities of agricultural products

[2], we can say that agriculture needs particular attention, and the need to research in this field is justified. Investments in research in this field usually have technologies such as the Internet of Things (IoT) as a starting point.

When we refer to the IoT, we refer to the billions of devices interconnected by certain communication technologies that ensure the collection and exchange of data between them remotely without the need for a person's direct presence or intervention. IoT includes the family of low-power wide-area networks (LPWAN), which consists of several technologies such as LoRa, SigFox, NB-IoT (Narrow Band - Internet of Things), LTE-M (Long Term Evolutions for Machines), and so on [3]. These LPWAN technologies aim to reduce or even cushion the disadvantages of traditionally used communications networks, such as Zig-Bee, WiFi, Bluetooth, or even LTE. The applications of LPWAN technologies cover a wide range of fields. Still, the main ones are agriculture, logistics applications, infrastructure monitoring, personal and commercial applications, medical, etc. LoRa is a complex technology composed of two main components. The LoRa alliance [19] specifications present these components as two distinct levels: the physical LoRa level and the MAC protocol level, namely LoRaWAN [4].

A. LoRa Physical Layer

LoRa is based on a radio modulation technique developed and patented by Semtech [5], which operates in the unlicensed spectrum of frequency bands. This technique is used especially when the power consumption is low and extended coverage is needed. The name refers to the long-distance data links covered by this technology. LoRa is one of the best choices when communication requires a very high range. LoRa covers up to 5 km in urban areas and 15 km or more in rural areas.

A vital feature of this type of technology is that it does not require considerable power resources, so devices that are operated on batteries can be used. The energy needed to transmit a data packet is very low, and this is because the data packets are small and are not transmitted continuously but only a few times a day. Moreover, when the end devices are asleep, the power consumption is of the order of mW and thus allows the operation of the same battery even for several years. LoRa uses the proprietary of spread spectrum modulation technology derived from Chirp Spread Spectrum technology, providing a trade-off between sensitivity and data rate while operating in a 125 kHz fixed bandwidth channel. In addition, LoRa uses orthogonal spread factors. This technique allows the network to

preserve the battery life of connected end devices by making adaptive optimizations based on each node's power level and data transmission at the individual level. The higher the spreading factor, the higher the processing gain and the reception sensitivity, but the data transmission rate will undoubtedly be lower [4][5].

B. LoRaWAN MAC Layer

LoRaWAN is standardized by the LoRa Alliance and defines a MAC protocol and a system architecture for networks based on the physical LoRa layer. LoRaWAN provides an environment access mechanism that allows multiple end devices to communicate with a LoRa modulation gateway.

LoRa communications networks operate under a star-like topology where communication between end-devices and a central network server is done through gateway nodes that transparently transmit messages. The final devices communicate data taken from sensors to gateways, and these gateways will connect to a server through a network connection other than LoRaWAN. Usually, this connection is made through the WiFi protocol. Communications are bidirectional under this protocol, and uplink messages have priority. The LoRaWAN protocol operates in the free frequency band, between 863MHz and 870 MHz in Europe and 433 MHz in the United States [4].

In Fig. 1, it is presented the main stack layers of the LoRa architecture that are related to each other and how the ISM bands are used based on the geographical area. The Application layer does not directly relate to the MAC layer and the physical layer, so it is realized at a higher level based on the data saved on the server.

This paper presents a study about LoRa architecture with practical implementation in agriculture. Section II reviews state of the art in this area, while Section III describes the architecture we proposed. In Section IV, we made a comparison about LoRa vs SigFox, and the conclusions are drawn in Section V.

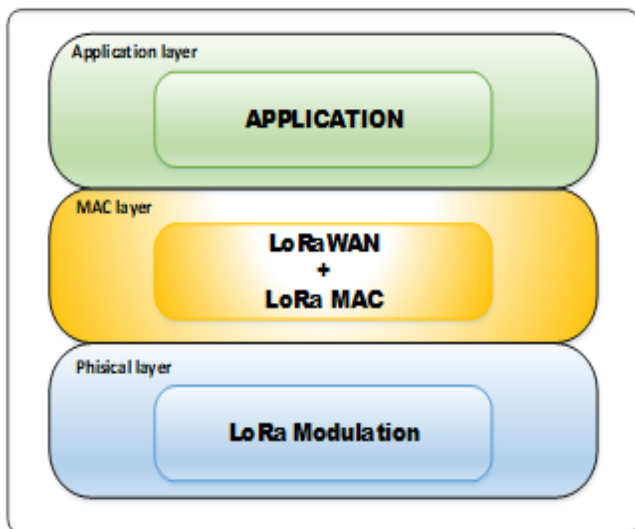


Fig. 1. The Main Stack Layers for LoRa Architecture.

II. RELATED WORK

Integrating IoT technology into agriculture is not new; it has been introduced and implemented repeatedly but not on a vast scale but usually at the prototype level. The geographical areas with the greatest need for these technologies typically do not have people specialized in this direction or financial support. Interest in IoT technologies in agriculture has continued an upward trend in recent years, evidenced by outstanding research. One such work is [6], where the authors implemented a system based on a WSN architecture. In this paper, the researchers focus on real-time monitoring of temperature, light intensity, and humidity parameters. Once collected, this data is transmitted further through the LoRa-based gateway, and then visual processing and tracking are performed using a cloud tool. They concluded that the proposed architecture did not cover more than 600 meters following their research.

In [7], Klaina et al. propose a multi-scenario-focused approach to large-scale monitoring using multiple LPWAN technologies. This paper focuses on a network of sensors and various communications links. These sensors are mounted on both tractors and farmers. They came up with this proposal to evaluate and improve the equipment's performance and to monitor and manage them as efficiently as possible. At the level of this paper, different data links were tested to take into account the impact of soil, spatial distribution and infrastructure elements present. Their study showed that LPWAN networks provide better performance in the range covered. Still, better communication links were observed than in the traditional ZigBee network.

The study by Miles et al. [8] presents an evaluation of the performance of a LoRaWAN network using an NS-3 simulator. The authors propose and validate in this paper a mathematical model that focuses on estimating as accurately as possible the successful delivery of data packets on the network presented in a pilot farm starting from the transmission intervals and the number of nodes that make up the network. The conclusion they reached after conducting this study, consisting of a single network gateway and up to 1000 nodes, is that the proposed LoRaWAN architecture is suitable for various implementations in agriculture.

The performance and implementation of LoRa technology are not limited to agriculture, so there are many areas in which this technology has been successfully addressed. An example of such an implementation is made in [9], which proposes a street lighting monitoring system in a smart-city approach. Remote management and control of LED lights are done through LoRa technology. In another research paper [10], the authors propose a system for remote monitoring of forest fires in areas that are difficult to access through LoRa technology. The authors of this paper emphasize the importance of the distance covered by the system but also the reliability of the implementation.

Another proposal in which LoRa technology occupies a prominent place is the authors of Maftei et al. [11], in which a health application is implemented. In this paper, the authors designed a device to monitor the main health parameters such as heart rate, body temperature, blood oxygen saturation, and

the battery level that powers this system. This information is transmitted to a gateway via the LoRaWAN protocol, and then this information is processed and stored in a blockchain network. The achieved conclusion of this study shows that the LoRa protocol can be integrated well into the remote healthcare system but also in applications based on blockchain technologies.

In this section we have noticed that the LoRa technology and LoRaWAN protocol have multiples areas of application but although each study adds to the whole research ecosystem it should be noted that there are gaps. Some of these would be the fact of the distance covered; can this technology cover the expected distance in the agricultural sector as well? Or the values remain valid only for other types of applications in different fields, so this paper addresses and disseminates this fact. Another question that arises as a result of the research is how accurate is the data? Thus, even if the data obtained in the mentioned studies fall within reliable data, in the agricultural sector there is a danger that depending on the device used, the data will not correspond to reality, so in this study, we want to combat this phenomenon.

III. SYSTEM DESCRIPTION

To demonstrate the reliability of the LoRaWAN communications protocol in terms of implementation in agriculture, we propose a system architecture consisting of three main blocks: the final device or end node, the gateway, and the application server. The functionality of each component that composes our system will be described below.

A. The End Node

In our paper the development board from STMicroelectronics, namely the NUCLEO-L973RZ board [12] represents the end node. This board is especially notable for its low-power MCU. This tool can also be used with other development boards such as Arduino or other similar devices. In our case, we used this board together with the expansion board I-NUCLEO-LRWAN1 [13]. This board contains the LoRaWAN USI WM-SG-SM-42 module and the ST HTS221 temperature and humidity sensor but also the ST LPS22HB pressure sensor as well as the sensor that incorporates both an accelerometer and an ST LSM303AGR gyroscope; however, in this paper, we focused only on the use of the temperature and humidity sensor as well as the pressure one.

In Fig. 2, we can see the end node device, which is in use in this application.

LPS22HB [14] is an ultra-compact piezo resistive sensor that works like a digital barometer. This device consists of a sensitive element that detects absolute pressure consisting of a suspended membrane. By certain specific STMicroelectronics methods, which are not open-sourced, it measures the desired values and then communicates them further to the main application via either I2C (Inter-Integrated Circuit) or SPI (Serial Peripheral Interface) interface. LPS22HB operates at -40°C to $+85^{\circ}\text{C}$ and can measure pressure values between 260 hPa to 1260 hPa.

ST HTS221 [15] is an ultra-compact sensor for measuring relative temperature and humidity, and it consists of a sensitive

element such as a polymeric dielectric planar capacitor. The temperature detection range is between -40°C and $+120^{\circ}\text{C}$, and a mixed-signal ASIC (application-specific integrated circuit) is used to transmit the measured information further to the main application via digital serial interfaces.

B. The Gateway

The gateway includes two boards supplied by the same manufacturer, namely STMicroelectronics. The first board is the NUCLEO-F746ZG development board [16], which is the support on which the LoRa protocol-specific gateway expansion board will be attached, developed by Semtech.

C. The Server

The server used in this implementation and to which data is transmitted through the gateway is from The Things Network (TTN) [17]. This IoT server is designed especially for the LoRaWAN protocol, being a free tool that promises maximum security, is used globally in over 151 countries and whose members exceed the number of 168 thousand.

D. System Functionality

For the application to become functional, each of the three main components has to be configured, so the software utilities offered by STMicroelectronics were used for the development boards, namely, STM32CubeProgrammer and STM32CubeIDE.

For the gateway configuration, the devices used must be set in gateway mode, a setting done by programming the firmware. This operation is done as seen in Fig. 3.

Once the gateway firmware is programmed, it has to be configured in such a way that the parameters related to the frequency in which the device will work match the geographical area we are located. At this level, particular attention should be paid to the MAC address parameter of the device. The address is required later in establishing the connectivity with the server.

Fig. 4 presents the main parameters of the gateway as seen from a connection to the TeraTerm terminal. In this terminal, we have the opportunity to modify the main specifications, such as the MAC address or the frequency band.



Fig. 2. The End Node Device used in this Application.

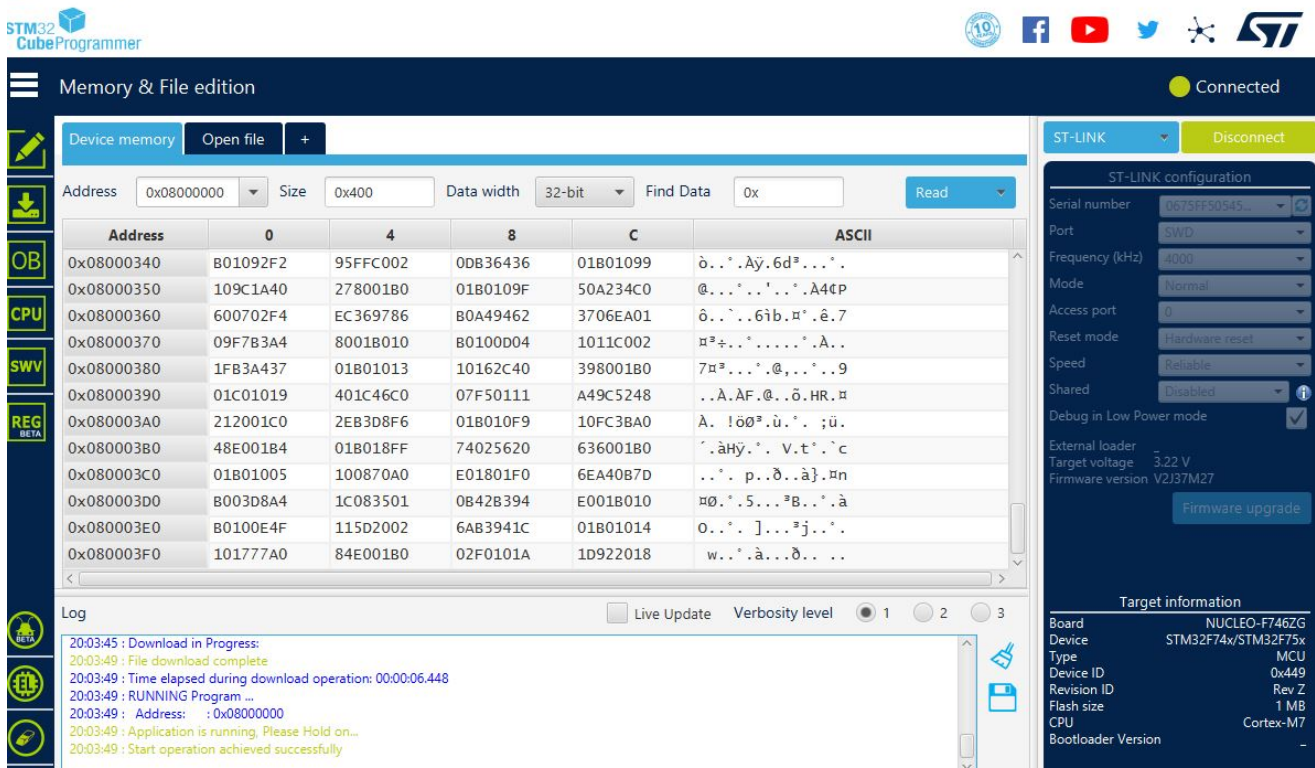


Fig. 3. The Firmware Programming in STM32 Cube Programmer.

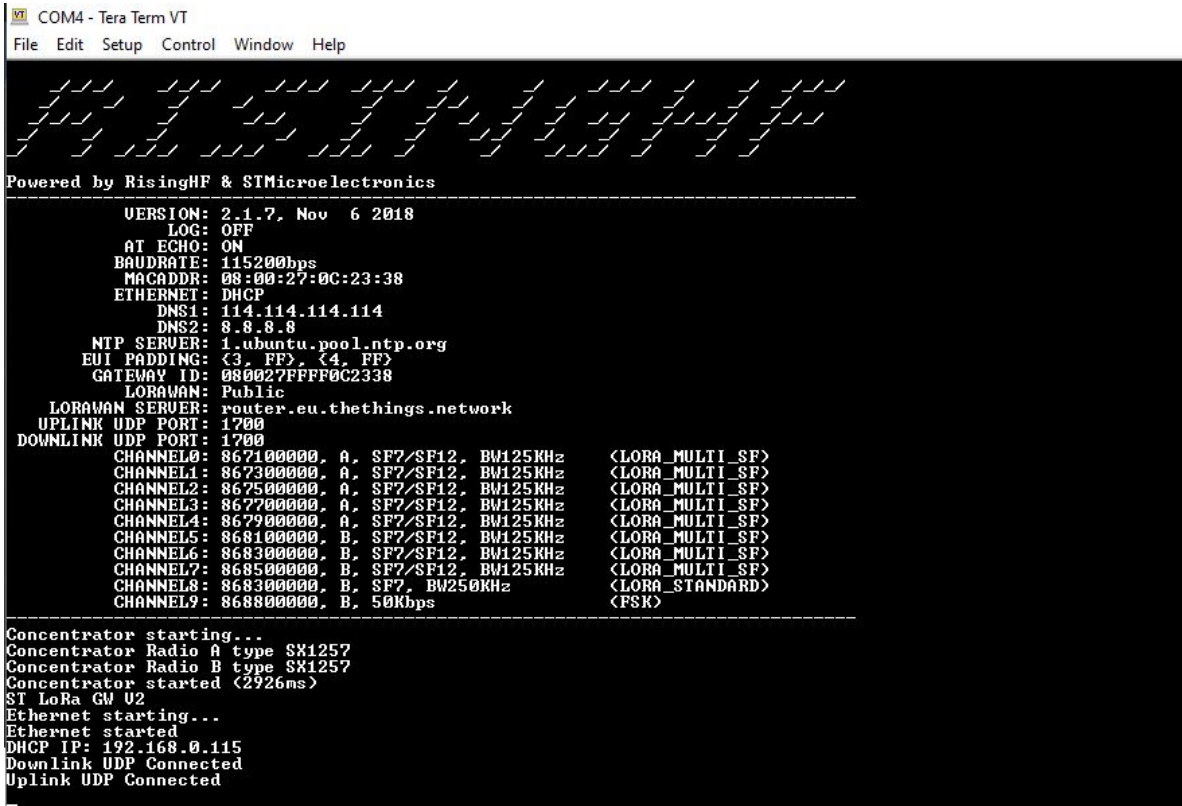


Fig. 4. The Gateway Configuration Terminal in TeraTerm.

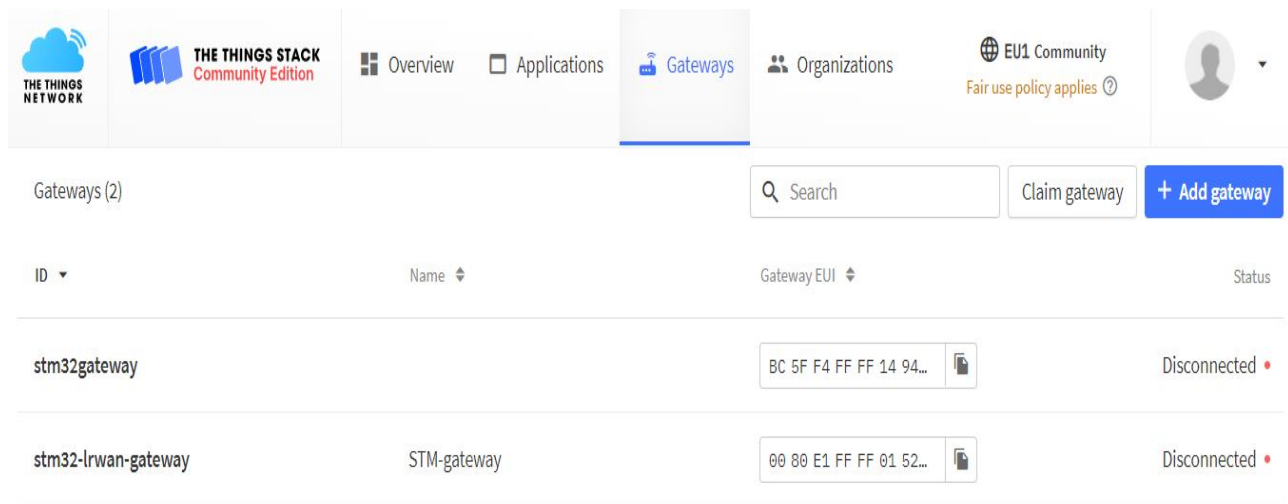


Fig. 5. The Gateways Registered on TTN Server.

In order to be able to connect the application to the server, firstly, it is necessary to create an account on the server site and then add a device either as an end node or as a gateway. After completing these steps and verifying the connection functionality, the values received from the end node located in the remote area can be viewed and processed from the final application in TTN.

In Fig. 5, it can be seen the main interface of the gateways registered on the server. Here we can add another gateway or end device, and we can see the status at the time being. The gateways are displayed based on the MAC addresses enrolled initially.

IV. LORA VS SIGFOX

Both the LoRaWAN protocol and SigFox are part of the same category of IoT technologies, namely LPWAN technologies, but the principle of operation differs. Our paper started from the premise of using such a system in agriculture. In this paper and in the previous one [18], both devices were integrated into the environment, but the particular emphasis was placed on how the data was transmitted and processed.

Thus, after making and completing all the necessary connections, we could see a significant advantage that the LoRaWAN protocol has compared to SigFox, namely, the coverage.

If in the previous paper, due to our geographical position, namely the northeastern region of Romania, we could not connect the system to a gateway and then to the actual SigFox server, this time using LoRa, we were able to configure our gateway. We also connected to a server that would allow the recording and processing of transmitted data. In addition to connecting to an already created server, the advantage of LoRa is that with the necessary hardware components, we can create our own server and integrate it into an application.

In this study, the emphasis was on creating a complete system for the agricultural sector for implicit monitoring of the main factors influencing the evolution of various crops, starting with the network node or end device and creating the final application as a result of data obtained from the server. This

system was created to see how the LoRa infrastructure, which consists of the LoRa modulation technique and the LoRaWAN communication protocol [19][20], relates to the environment in which it is used and the additional benefits that this technology brings.

V. CONCLUSION

In the introduction of this paper, we started from the premise of comparing it with another work conducted in a different paper in the same field of agriculture but which is based on a different communication protocol, namely the LoRaWAN protocol compared to the SigFox protocol. The conclusion we have reached is that LoRa technology has a clear advantage ensuring a better connection. Once a gateway is configured, the data transmission does not depend strictly on the manufacturer's servers, as in the case of the SigFox protocol. Still, it can use open-source servers or even you can set up your own servers.

Another aspect that should be mentioned is that using the development boards mentioned in this paper, STMicroelectronics offers considerable support when it comes to configuring, programming and viewing the code used in different instances of the application.

Finally, we can conclude that as a LPWAN technology, LoRa, is a reliable solution in the field of agriculture and offers advantages from superior to traditional technologies. Also, an important thing to note is that this protocol allows users from everywhere to contribute to the development of its effectiveness.

REFERENCES

- [1] R. Siche, "What is the impact of COVID-19 disease on agriculture?," *Scientia Agropecuaria*, vol. 11, pp. 3-6, 2020.
- [2] F. Harvey, "Ukraine war piles pressure on global food system already in crisis," *The Guardian*, 9 March 2022. [Online]. Available: <https://www.theguardian.com/food/2022/mar/09/ukraine-war-piles-pressure-on-global-food-system-already-in-crisis>. [Accessed 15 March 2022].
- [3] M. Sarika, "LPWAN's – Overview, Market Scenario and Performance Analysis of Lora, Sigfox Using NB-Fi Range Calculator," in 2021 International Conference on Smart Generation Computing, Communication and Networking (SMART GENCON), 2021.

- [4] "A technical overview of LoRa® and LoRaWAN™," November 2015. [Online]. Available: <https://loro-alliance.org/wp-content/uploads/2020/11/what-is-lorawan.pdf>. [Accessed 20 March 2022].
- [5] Semtech, "What Is LoRa®?," [Online]. Available: <https://www.semtech.com/loro/what-is-lora>. [Accessed 20 March 2022].
- [6] W. Chanwattanapong, S. Hongdumnuen, B. Kumkhet, S. Junon and P. Sangmahamad, "LoRa Network Based Multi-Wireless Sensor Nodes and LoRa Gateway for Agriculture Application," 2021 Research, Invention, and Innovation Congress: Innovation Electricals and Electronics (RI2C), pp. 133-136, 2021.
- [7] H. Klaina, I. P. Guembe, P. Lopez-Iturri, M. Á. Campo-Bescós, L. Azpilicueta, O. Aghzout, A. V. Alejos and F. Falcone, "Analysis of low power wide area network wireless technologies in smart agriculture for large-scale farm monitoring and tractor communications," Measurement, vol. 187, pp. 1-18, 2022.
- [8] B. Miles, E.-B. Bourennane, S. Boucherkha and S. Chikhi, "A study of LoRaWAN protocol performance for IoT applications in smart agriculture," Computer Communications, vol. 164, pp. 148-157, 2020.
- [9] E. Bingöl, M. Kuzlu and M. Pipattanasompom, "A LoRa-based Smart Streetlighting System for Smart Cities," in 2019 7th International Istanbul Smart Grids and Cities Congress and Fair (ICSG), Istanbul, 2019.
- [10] N. C. Gaitan and P. Hojbota, "Forest Fire Detection System using LoRa Technology," (IJACSA) International Journal of Advanced Computer Science and Applications, vol. XI, no. 5, pp. 18-21, 2020.
- [11] A. A. Maftei, P. M. Mutescu, V. Popa, A. Petrariu and A. Lavric, "Internet of Things Healthcare Application: a Blockchain and LoRa Approach," in The 9th IEEE International Conference on E-Health and Bioengineering - EHB 2021, Iasi, 2021.
- [12] STMicroelectronics, "STM32 Nucleo-64 development board with STM32L073RZ MCU," [Online]. Available: https://www.st.com/en/evaluation-tools/nucleo-1073rz.html?ecmp=tt9470_gl_link_feb2019&rt=db&id=DB2196#st_all-features_sec-nav-tab. [Accessed 15 March 2022].
- [13] STMicroelectronics, "USI® STM32™ Nucleo expansion board for LoRa™," [Online]. Available: <https://www.st.com/en/evaluation-tools/i-nucleo-lrwan1.html>. [Accessed 15 March 2022].
- [14] "MEMS nano pressure sensor: 260-1260 hPa absolute digital output barometer," [Online]. Available: <https://www.st.com/en/mems-and-sensors/lps22hb.html>. [Accessed 16 March 2022].
- [15] "Capacitive digital sensor for relative humidity and temperature," [Online]. Available: <https://www.st.com/en/mems-and-sensors/hts221.html>. [Accessed 16 March 2022].
- [16] "STM32 Nucleo-144 development board," [Online]. Available: <https://www.st.com/en/evaluation-tools/nucleo-f746zg.html>. [Accessed 16 March 2022].
- [17] "The Things Network," [Online]. Available: <https://www.thethingsnetwork.org/>. [Accessed 20 January 2022].
- [18] F. Pitu and N. C. Gaitan, "Surveillance of SigFox technology integrated with environmental monitoring," 2020 International Conference on Development and Application Systems (DAS), 2020, pp. 69-72, doi: 10.1109/DAS49615.2020.9108957.
- [19] "LoRa Alliance," [Online]. Available: <https://loro-alliance.org/>. [Accessed 23 March 2022].
- [20] Gaitan, N. C., "A long-distance communication architecture for medical devices based on LoRaWAN protocol," Electronics, 10(8), 940, 2021.

Chaos Detection and Mitigation in Swarm of Drones using Machine Learning Techniques and Chaotic Attractors

Emmanuel NEBE¹, Mistura Laide SANNI², Rasheed Ayodeji ADETONA³
Bodunde Odunola AKINYEMI⁴, Sururah Apinke BELLO⁵, Ganiyu Adesola ADEROUNMU⁶
Department of Computer Science and Engineering, Obafemi Awolowo University, Ile-Ife, Nigeria^{1, 2, 4, 5, 6}
Department of Mathematics, Obafemi Awolowo University, Ile-Ife, Nigeria³

Abstract—Most existing identification and tackling of chaos in swarm drone missions focus on single drone scenarios. There is a need to assess the status of a system with multiple drones, hence, this research presents an on-the-fly chaotic behavior detection model for large numbers of flying drones using machine learning techniques. A succession of three Artificial Intelligence knowledge discovery procedures, Logistic Regression (LR), Convolutional Neural Network (CNN), Gaussian Mixture Models (GMMs) and Expectation–Maximization (EM) were employed to reduce the dimension of the actual data of the swarm of drone’s flight and classify it as non-chaotic and chaotic. A one-dimensional, multi-layer perceptive, deep neural network-based classification system was also used to collect the related characteristics and distinguish between chaotic and non-chaotic conditions. The Rössler system was then employed to deal with such chaotic conditions. Validation of the proposed chaotic detection and mitigation technique was performed using real-world flight test data, demonstrating its viability for real-time implementation. The results demonstrated that swarm mobility horizon-based monitoring is a viable solution for real-time monitoring of a system’s chaos with a significantly reduced commotion effect. The proposed technique has been tested to improve the performance of fully autonomous drone swarm flights.

Keywords—Chaos detection; swarm of drones; machine learning; autoencoder; Rössler system

I. INTRODUCTION

A swarm of drones is a group of two or more drones that exchange data and work as a single cooperative unit to accomplish a specific mission objective. Drone coordination has been extensively researched in the fields of surveillance systems, precision agriculture, transportation, disaster management, and entertainment [1] [2].

A swarm of small aircraft allows for a larger mission area, more flexible mission capabilities, greater resilience against single-point failure, and lower costs. Swarm drone research has covered a wide range of topics, including collision avoidance [3], [4], [5], [6], mission-level planning and control to enable high-level autonomy [7], [8], the human operator’s communication with a swarm of drones [9], [10], ad hoc backbone network customized for a swarm operation, and the construction of small-scale airborne vehicles [11], [12]. Previously, technology-oriented research focused on how to

improve performance and capacity [13], [14], [15], but more recent research has focused on making such swarm systems more safe, secure, and reliable to operate [7], [16], [17]. Studies in the development of new coordination algorithms that combine biological processes are based on self-regulation [18], [19], and environmental adaptability to allow a swarm of drones to work with greater sophistication, reliability, scalability, and flexibility [20].

A number of practical issues that might disrupt the successful completion of the swarm mission could arise during the operation of a swarm of drones. For example, the energy consumption limitation of drones, which limits drones in their ability to handle long-term flight, may cause one or more drones in the swarm to experience failure, necessitating the development of an intelligent, efficient power failure mechanism. Alternatives for aerial path loss should also be considered while maintaining drone security and safety. When considering a multi-drone environment, where a small or large group should operate together or act in the same aerial environment, various flight problems and obstacles, in addition to the aforementioned chaotic difficulties, may arise, such as weather conditions and signal loss. These chaotic issues, however, impose a number of constraints on the use of swarms of drones and must be addressed in real-time.

The ability to monitor or manage the disorder or instability of the drones in a swarm, and take predictive and critical steps as needed for the safe and dependable operation of swarm drones, is referred to as chaos handling. Many factors can have an impact on the system’s health, such as issues with the drone system’s actuators and sensors, communication connection flaws, and possibly hostile cyberattacks. Determining such causes requires a thorough understanding of the system, mission, and surroundings. Therefore, detecting chaos in swarm system behavior is the first step toward managing the system’s health. This is crucial even when the source or type of chaos is unknown.

Despite extensive research into traditional model-based approaches for fault handling, identification, and isolation, particularly in aircraft safety systems, there are no known existing solutions for dealing with chaos among drones [21] [22]. Failure Detection, Identification, and Recovery (FDIR) has recently been extended to swarms of drone systems in terms of operations [23], and resistance against cyberattacks

[23], [24], [25], but there is still a need to address chaos among the swarm of drones, regardless of whether the causes of such chaos are known or unknown. In [26], evaluation of drones that use onboard sensor data for Failure Detection, Identification, and Recovery (FDIR) using a cooperative virtual sensor system for the design and experimental verification of techniques and procedures for handling chaos in swarm drone systems was done. Furthermore, compared to large aircraft, drone swarms are a new market entry; thus, failure mechanisms and chaos are not widely implemented or in use. Therefore, statistical methods which do not rely solely on the physical-based model of the drones may be a more viable option for detecting and mitigating chaos in the current swarm of drone systems. Thus, in this study, an attempt was made to develop a machine learning-based model for chaos detection in a swarm of drones; and a mitigation technique to deal with such chaotic conditions is also proposed.

The remaining sections of the paper are organized as follows: Section II discusses related works, while Section III describes the machine learning methods used in detecting and mitigating chaos in real-time swarm dataset. Section IV describes the chaos detection modeling process, while Section V presents the results of the model evaluations to demonstrate the effectiveness of the chaos detection and mitigation strategies for swarms of drones. Finally, the conclusion was presented in Section VI.

II. RELATED WORK

Several significant studies have been conducted in order to apply data-driven machine-learning algorithms for detecting faults and anomalies in aerial vehicles. Some researchers combined chaotic dynamics with powerful swarm-based algorithms used in mobility models such as Ant Colony Optimization (ACO), Artificial Bee Colony (ABC), and Particle Swarm Optimization (PSO) [27], [28], [29]. The Lorenz and Rössler attractors are time-discretized, and the three-dimensional chaotic maps are addressed via a three-dimensional solvable chaos graph built from general chaos solutions.

A three-dimensional path planning for Unmanned Aerial Vehicles (UAVs) based on chaos particle swarm optimization, which addresses the shortcomings of particle swarm optimization (PSO) was proposed in [30]. However, the solution quickly falls into a local optimum and gradually converges with poor precision in a motion phase. The concept of the Chaos Optimization (CO) algorithm was incorporated into the PSO algorithm through in-depth analysis based on the conventional update operations on the velocity and location of the mobile nodes in the swarm. As a result, track preparation searches are eliminated and rapidity followed by convergence precision is enhanced.

In [31], a basic two-dimensional solvable chaos map was used to mathematically analyze chaotic modeling and simulation on a dynamic coordinate. Also in [32], a chaotic-based approach was used to maintain coordinated flight formation of swarm unmanned aerial vehicles at a low input cost. A study in [33] focuses on a discrete dynamic map (logistic map) to generate a chaotic sequence of bits [33]. The bits are then translated into locations that allow the robots to

construct a deterministic route plan. Meanwhile the R-UAVs are fractional three-dimensional when using the Qi system [34]. As a result, a three-dimensional chaotic dynamic solution should be used to model the mobility model of swarm UAVs.

The 3D chaotic-based-approach is used in ASIMUT to implement dynamic system mobility models for UAVs in an unpredictable regime. This mobility model is supplemented by a hybrid mobility model called Chaotic Ant Colony Optimization for Coverage (CACOC), which combines the ACO with the system's three ordinary differential equations. The mobility model is data-centric in a multi-level swarm perception networked on the multi-layer FANET architecture [35], [36]. Also, a collision avoidance technique was incorporated into a predictive mobility model, based on the assumption that all UAVs were flown at different altitudes to avoid collisions [37]. However, this may not be realistic in some UAV swarm applications.

For real-time detection and monitoring of aviation system abnormalities, a Multivariate Gaussian Mixture Model (MGMM) was proposed [38]. Also proposed was a Recurring Neural Network (RNN) method for events and trends which can reduce the security margins of a system using a dataset from a Flight Data Recorder (FDR) [39].

A K-nearest neighbor (KNN) methodology was introduced in [40] to identify the reasons and factors for drone failures and potential deteriorations in drone performance on the ground in order to assess the causes of failure and potential deterioration in drone performance during flight. An actual flight dataset was used in [41] to validate the developed Anomaly Detection (AD) model, which shows if there is any abnormality in the swarm drone flight. For the generation model, the AD model created a training model using a Deep Neural Network.

Most of the work done has focused only on the health management of a single drone; no methodological approach for the reliable detection of chaos in swarm flights has been proposed, with the goal of overcoming the aforementioned swarm drone behavior constraint. For example, an end to end fault analysis framework for a single micro aerial vehicle that only considers anomalies with obstacle detections [54]. Some studies used artificial neural network for sensor-based fault detection [55]. As a result, this current study proposes a machine learning-based, data-driven methodology for detecting chaotic anomalies in swarm flights. The proposed method aimed to address both the lack of marked recorded information in swarm flights and the disparity between non-chaotic and pathological data. This study investigates the use of moving average-based monitoring with a limited time frame to reduce noise in continuous monitoring while also allowing for responsive chaos detection.

In general, supervised learning approaches outperform unsupervised learning methods in classification problems. However, in the case of chaos detection, a relatively new type of self-supervised knowledge extraction that outperforms the fully supervised technique has been reported. As a result, this method can be used to detect chaos in in-flight data. A highly sophisticated self-supervised framework that outperforms all other unsupervised methods, and demonstrated that the

completely controlled approach ranks better and outperforms the other methods was developed in [42].

This paper backs up this claim by demonstrating that supervised learning is still a viable core framework when a significant amount of labeled data is available, and an adequate labeling process can be produced. This study makes three significant contributions: It (a) proposes a systematic process for data-driven chaos identification in swarm flights, (b) generates a real-time solution to such chaos, and (c) validates the method using real flight test data.

III. METHODOLOGY

The following methods were used in this study to detect chaos in a swarm of drone flights: First, a set of unsupervised learning methods were employed: An Autoencoder (AE) was used to reconstruct and reduce the time series dimensionality of flight data, and then an Expectation–Maximization (EM) clustering by Gaussian Mixture Model (GMM) separated the flight data time series dimension into four categories: true chaos, unsure chaos, doubtful normal, and truly normal. Then, a Deep Neural Network was trained to extract features and detect chaos, which is a 1D-CNN concatenation of a single, multi-layer logistic regression perceptron neural network [43].

To properly identify chaos and handle it, three decisions must be made: (a) detecting chaos symptoms in the swarm, (b) identifying which drone is in chaos, and (c) providing a solution to such drones in a state of chaos. The chaotic detection technique makes these decisions by observing the kinematic characteristics of the drones, such as a drone's location and velocity. This chaos detection scheme is located at the ground station or controller, which monitors the health and the flying status of all swarm vehicles; thus, it transfers drone data to the ground station, where it is processed by the chaos detection scheme to show flight normality.

In this study, the swarm system employed a real-time Kinematic Velocity (KV) GPS-based precision navigation method as described by [44]. The dataset used as learning data for recognizing chaotic behavior during swarm mission execution was sourced from a series of swarm drone flight tests conducted by the Korean Aerospace Research Institute, in which up to 30 quadcopter drones were deployed [41].

A total of 50 tests were conducted, with individual and multiple groups of test drones. The output data from each drone trajectory consists of 248 parameters presented as time series, some of which include numerous observations of various parameters. As critical characteristics in detecting chaos in motion, three sites were chosen: the drone location and set point values, three-vehicle speed components, and vehicle status. The KV-GPS data, in which the accuracy was validated in [44] was used to calculate the location coordinates (x_t, y_t, z_t) and velocity components in three dimensions for the drones. The following three parameters in Equation 1 are also considered chaotic, as they can be associated with errors between intended and actual behavior during drone movement coming from mission control.

$$x = x_t - x_s$$

$$y = y_t - y_s$$

$$z = z_t - z_s \tag{1}$$

Also, inertial navigation system readings labeled GA from accelerometers and gyro sensors may also cause mechanical faults in drone systems because they can cause unexpected acceleration and angular rate behavior. Thus, the drone status indicator is used to verify the data consistency and calibration. Since this research aimed to develop a chaos detection and mitigation method that is independent of drone type and features, datasets are not tagged with drone identifiers as a result. Fig. 1 depicts an illustrative view of the swarm system configurations.

It should be noted that these topological indicators are not always the whole set of characteristics required to identify all potential chaos in swarm flights. These are, nevertheless, crucial indicators for sensing chaos produced by specific kinds of errors and failures. As a result, this research detects and identifies chaotic behavior using topological indicators and produces a solution to such a problem using a chaotic attractor. Also, the flight trajectory dataset is only partially labeled. Some of the incorrect events discovered during the flight test are classified as chaos. Table I lists the features of the indicators utilized in this paper.

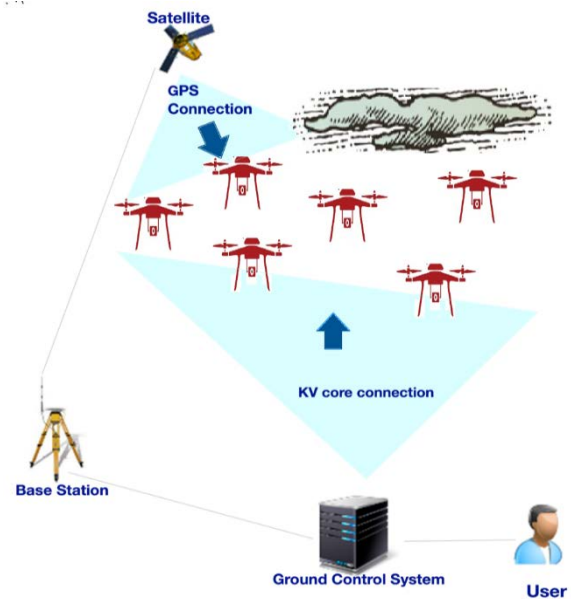


Fig. 1. Configuration of the Swarm of Drone System.

TABLE I. PARAMETERS EXTRACTED FOR DRONE SWARM FLIGHT ANALYSIS

Drone Parts	Parameter Description	Attribute
Drone state	Hovering Navigating	Discrete
Trajectory	Position (x_t, y_t, z_t)	Continuous
GA	Gyro (Rate and integrals of drone body frame) Accelerometer (Axis (x,y,z) values and integrals of accelerometer)	Continuous
KV-GPS	Inertial Velocity Vectors and Positions	Continuous

A. Machine Learning Algorithms

This section discusses four machine learning methods that were used in this study to develop a data-driven chaos detection strategy. The first two are unsupervised learning algorithms that work with unlabeled data, whereas the last two are supervised classification algorithms that work with labeled data. The details are as follows:

1) *Autoencoder and Chaos Detection (AECD)*: Autoencoder-based chaos detection (AECD) is a semi-supervised learning-based chaos identification technique. As part of this study, an autoencoder was used to compress the raw flight input data. Autoencoders (AE) are neural networks that are statistically based on a given probability distribution [45]. The autoencoder consists of two sub-models: encoder and decoder. The encoder compresses the input, while the decoder attempts to reconstruct the input from the encoder's compressed form. After training, the encoder model is saved, whereas the decoder is destroyed. For machine learning training, the encoder is then used as a data preparation tool, to extract features from raw data.

A single-layered neural network has an encoder and a decoder, as shown in Equations (2) and (3). This is the nonlinear transformation function of the autoencoder. Equation 2 depicts how an affine mapping uses nonlinearity to convert an input vector d to a hidden vector h . In Equation 3, the decoder uses the same transformation as the encoder to rebuild the cached representation h back to the initial input space. As shown in Equation 4, the reconstruction error is defined as the difference between the original input vector d and the reconstruction z . The reconstruction error is minimized via the autoencoder.

$$h = \sigma(W_{dh}d + b_{dh}) \quad (2)$$

$$z = \sigma(W_{hd}d + b_{hd}) \quad (3)$$

$$\text{Reconstruction error} = \|d - z\| \quad (4)$$

where, w and b are the weights and biases of the neural network.

By adding noise to the original input vector d , the autoencoders use a noisy input vector d' as the input vector. In other words, a noisy input d' was fed into the autoencoder in order to recreate the original input d . In this way, the autoencoder is protected from white noise in the data and collects only significant patterns in swarm flight data [46]. The reconstruction error is then calculated by measuring the difference between the final output and the noisy input reconstruction. The reconstruction error is then used to determine the chaos score.

Data points with a high degree of reconstruction are described as chaos. To train the autoencoder, only data with normal occurrences is utilized. The autoencoder will successfully reconstruct normal data after training but will fail to reconstruct chaotic data that the autoencoder has never seen. Algorithm 1 depicts the chaos detection technique based on autoencoder reconstruction errors.

Algorithm 1 Autoencoder and Chaos Detection Algorithm

INPUT: Normal dataset $D = \{d^1, \dots, d^n\}$, Chaos dataset $d^{(i)}$
 $i=1, \dots, n$, threshold α
OUTPUT: reconstruction error $\|d - d'\|$
 $\theta, \varphi \leftarrow$ Initialize parameter
repeat
 $E = \sum_{i=1}^n \|d^{(i)} - g_{\theta}(f_{\varphi}(d^{(i)}))\|$ Calculate the total amount of reconstruction error, where g_{θ} and f_{φ} are the autoencoder's multilayered neural networks.
 $\theta, \varphi \leftarrow$ update parameters using Stochastic Gradient Descent
until parameters θ, φ convergence
then
 $\theta, \varphi \leftarrow$ Using the normal dataset D , train the autoencoder
for all values $i=1$ to n **do**
reconstruction error(i) = $\|d^{(i)} - g_{\theta}(f_{\varphi}(d^{(i)}))\|$
if $\alpha <$ the reconstruction error(i) **then**
 $d^{(i)}$ is in chaos
else
 $d^{(i)}$ is not in chaos
end if
end for

2) *Clustering using Gaussian Mixture Models (GMMs) and Expectation–Maximization (EM)*: The flight data points were assumed to be distributed randomly in a Gaussian manner. Gaussian Mixture Models (GMMs) were used to simulate the data. Each flight data cluster's Gaussian parameters were determined using two parameters derived from an optimization technique called Expectation–Maximization (EM): the mean and standard deviation. Therefore, drone clusters can have any elliptical shape since the standard deviations in the x and y axes are obtained. As a result, each Gaussian distribution has exactly one cluster. The hidden variables were used to find the Maximum Likelihood Estimators (MLEs). Since the AECD model contains latent variables, maximum likelihood estimates of the model were sought using the EM method. As a result, the log-likelihood is as shown in Equation 5.

$$\log(P(D|\theta)) = \log(\sum_z P(D, Z|\theta)) \quad (5)$$

Where, D represent the total number of observable variables

Z represent the total number of latent variables, marginalized from the joint distribution.

Assuming datasets D and Z , were selected at the same time, the entire dataset is referred to as $\{D, Z\}$ and the incomplete dataset is referred to as D . From the original dataset, Z , is unknown, but the posterior $P(Z|D, \theta)$ contains the information about Z . Therefore, the log-likelihood expectation was analyzed by using the M-step process to evaluate the posterior probabilities. The expectation of the entire data log-likelihood was maximized to get a new estimated parameter via the E-step process. The current value of the parameters θ^0 was used in the E-step to obtain the posterior distribution of the latent variables, which is provided by $P(Z|D, \theta^0)$. This expectation, represented by $Q(\theta, \theta^0)$ is shown in Equation 6. The new parameter θ' is then determined in the M-step by maximizing Q as shown in Equation 7.

$$Q(\theta, \theta^0) = E_{(Z|D, \theta^0)}[\log((D, Z|\theta))] = P \sum_Z P(Z|D, \theta^0) \log(P(D, Z|\theta)) \quad (6)$$

$$\theta' = \operatorname{argmax}_{\theta} Q(\theta, \theta^0) \quad (7)$$

where

$\theta = \mu_1, \dots, \mu_k, \sigma_1, \dots, \sigma_k, \pi_1, \dots, \pi_k$ are the unknown parameters used in deriving the MLE Gaussian Mixture Model. The relevant quantities for GMM are then derived to form the complete likelihood as shown in Equations 8 and 9.

$$\log(P(D, Z|\mu, \sigma, \pi)) = \sum_{i=1}^n \sum_{k=1}^m I(Z_i = k)(\log(\pi_k) + \log(N(D_i|\mu_k, \sigma_k))) \quad (8)$$

$$E_{(Z|D)} \log(P(D, Z|\mu, \sigma, \pi)) = \sum_{i=1}^n \sum_{k=1}^m Y_Z(k) (\log \pi_k + \log(N(D_i|\mu_k, \sigma_k))) \quad (9)$$

The posterior probabilities $\gamma_{Z_i}(k)$ was evaluated from the current values of μ_k and σ_k . Since $E_{Z|D}[I(Z_i=k)] = P(Z_i=k|D)$, marginal probability distribution can thus be replaced with the posterior probability $\gamma_{Z_i}(k)$.

Hence, Expectation-Maximization is derived as follows: first, initial values were chosen for the parameters μ , σ , and π , these parameters were employed in the E-step to evaluate the posterior probability $\gamma_{Z_i}(k)$. With fixed $\gamma_{Z_i}(k)$, the expected complete log-likelihood is maximized as shown in Equation 9 with respect to μ_k , σ_k , and π_k .

3) *Convolutional Neural Network (CNN)*: Convolutional Neural Network concept was used to extract features from drones' trajectories. It was noted that CNN has made great strides in handling two-dimensional image data and thus for one-dimensional time series data, locality/dispersion may also be used [43]. The CNN network structure employed in this study for cataloguing and classification comprises a stack of one-dimensional convolutional and max-pooling layers, including an additional global-pooling or flattening layer connected to the max-pooling layers. A Multi-layer Perceptron (MLP) is linked to the output layer of the one-dimensional CNN and then stochastic gradient descent is used to maximize the weights of both the MLP and CNN simultaneously [47]. A nonlinear activation function is used to transform a perception y into a linear combination that uses its weighted inputs to generate a single output which is dependent on many real-valued inputs (from the GMM and EM outputs). The perceptron is expressed in Equation 10.

$$y = \varphi(\sum_{i=1}^n \omega_i D_i + b) = \varphi(w^T x + b) \quad (10)$$

4) *Logistic Regression (LR)*: Logistic Regression (LR) was used for two-class classification in this study. LR is one of the easiest and most widely used methods of machine learning that can be used for two-class classification. It is a statistical method for predicting binary classes with intrinsically dichotomous values or target variables like one and zero. Equation 11 can be used to express the logistic regression hypothesis.

$$y = (1 + \exp(-(\beta_0 + \beta_1 D_1 + \beta_2 D_2 + \dots, \beta_m D_m)))^{-1} \quad (11)$$

where, D_m denotes the explanatory features of the flight data and; β_m denotes the related coefficients that will be optimized via a learning process.

Because y has a value between 0 and 1, the result can be interpreted as the likelihood of fitting to class 1. As shown in Equation 12, the most common loss function for optimizing coefficients is maximization of output probability.

$$\text{loss}(z, y) = -\sum_{i=1}^n (z_i \log y_i + (1 - z_i) \log(1 - y_i)) \quad (12)$$

where, n represents the amount of data points and;

z represents the desired outcome.

Equation 12 illustrates how the loss function can also be viewed as the cross-entropy between z and y . Instead of using a neural network, this sigmoidal activation function is commonly used for categorization. In this scenario, the network is trained to minimize the cross-entropy loss.

B. Rössler System (RS)

The Rössler System (RS) was used to handle any drone's trajectory in the swarm that remains in a state of chaos. As shown in Equation 13, the numerical solution for a drone's three-dimensional trajectories is given as a fractional order of the Rössler System [34]. The data for the a drone's three coordinates in the (x, y, z) axis is given by a time step t .

$$\begin{cases} D_t x = y - z \\ D_t y = x + ay \\ D_t z = b + z(x - c) \end{cases} \quad (13)$$

The RS is composed of three Ordinary Differential Equations (ODEs) with only one non-linear term, with constant values $a = 0.2$, $b = 0.2$, and $c = 9.0$; thus, each ODE can represent a dimension of a drone's flight trajectory [36], [48]. The synchronization of the RS with machine learning algorithm for trajectories in chaos was achieved after eliminating the leading drone's trajectory flight data observations. In order to remove the transient states, a numerical solution was constructed for this system using the fourth-order Runge-Kutta approach and record time points with each time step being $t = 0.1$.

IV. CHAOS DETECTION AND MITIGATION MODEL DESCRIPTION

The details of the model description are as follows:

A. Model Architecture

Fig. 2 depicts the general architecture of the model for detecting and mitigating chaos in a swarm of drones. The flight test data used for this study were collected in advance but when swarm flight data is provided in real time, it is not automatically labeled. This is normal in chaos detection instances since the data can only be plainly labeled in the presence of a functioning chaos detector or if human investigators have thoroughly examined the data. As a result, the data was initially grouped and labeled into various relevant

groups using a clustering method. Four criteria are addressed in this study's labeling method because of the ambiguity in chaos judgments: Normal (N), chaos (C), tentative normal (N⁺), and tentative chaos (C⁻). The last two categories were included because there are times when it's unclear whether the data provided is sufficient to determine whether a flight's behavior is chaotic or normal. After the labeled data has been secured, a binary classifier based on CNN was trained and validated on a set of training data to understand the critical characteristics in identifying chaos in swarm flight data. The trained model may then be utilized for both post-flight analysis and real-time chaos monitoring as a chaos detection technique. Meanwhile, as a chaos handling technique, the Rössler system was used to generate new flight paths for drones in the swarm that are in a chaotic state.

B. Data Preparation

A total of 73,749-time series dataset were generated as a result of the data preprocessing analysis, which includes data cleaning, integration, and transformation.

1) *Data cleaning*: The data cleaning process includes the completion of missing values, the filtering of excessive noise, the elimination of outliers, and the resolution of solution discrepancies. The difference between the real and reference positions of the drones in the swarm, as well as the actual velocity, are used as input data. To correspond to the timestamps of the two distinct data sources, a linear interpolation approach was used. In order to get a different value to real data at the same time, a linear interpolation of reference data with low noise relative to actual signals was performed. Excessively high values, possibly due to the training dataset, remove noise aberrations.

2) *Data integration*: Data from multiple drones were combined to create a dataset containing drone identification numbers. The drone identification numbers are not explicitly used in the learning process, but they are necessary for evaluating the performance of the learned model. One label, a one-time stamp, and six kinematic variables are also included in the input data.

3) *Data normalization*: The goal of data normalization is to keep the array of values for the specified parameters within a certain range. The well-known standardizing approach was used in this study. As shown in Equation 14, the standardization approach normalized each data sequence by

computing the mean (D_{mean}) and standard deviation (D_{std}) values.

$$D_{normalized} = (D - D_{mean})/D_{std} \quad (14)$$

C. Data Labelling and Clustering

Sensors mounted on drones produces multidimensional data which is characterized by a complex correlation, making it difficult to define the system's status. An autoencoder and chaos detection (AECD) algorithm was used to reduce the dimensionality of the data by identifying the primary correlation pattern between the variables. AECD is based on the assumption that the majority of system states can be adequately described by the characteristics of a few key components, and it has proven to be a successful feature extraction technique in a variety of situations [49]. The encoded kinematic information is represented by a six-dimensional AECD algorithm to produce the rate of cumulative dispersion to encode the component axes of a swarm of drones.

The clustering approach was used to facilitate labeling of unlabeled data in its raw form. Labeling data aids supervised learning processes in chaos classification by grouping data based on some kind of similarity or distance measure, making it easier for human specialists to classify the data.

This study employed clustering on the smaller space created by the AECD algorithm using Gaussian Mixture Models (GMMs) and Expectation-Maximization (EM). The time-series data for AECD was based on six variables for drone trajectories in the (x, y, z) axes and the velocity vectors (vx, vy, vz), with one drone label presented after AECD. Because the principal component axis was chosen to have a cumulative dispersion rate of 90% or higher, the number of dimensions reduced as a result of AECD may vary depending on the available flight data.

Specifically, clustering was performed on data that had been dimension-reduced, and the EM technique was used to maximize the number of clusters [50]. Based on the clustered findings, the state of each drone in the swarm was classified as Normal (N) or Chaos (C). The associated variables were obtained by categorizing them into two groups.

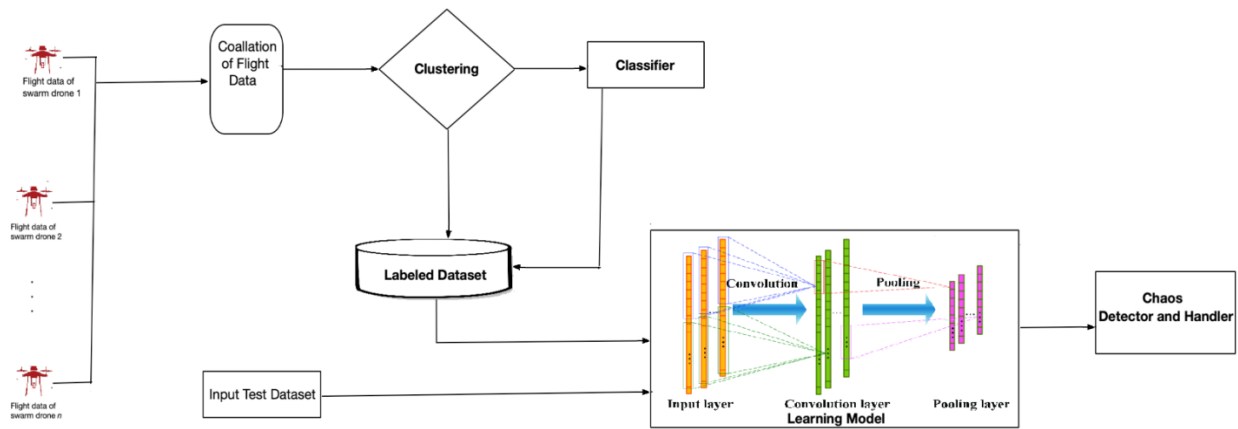


Fig. 2. Chaos Detection and Mitigation Model Architecture for Swarm of Drones.

It first examined the outcome of a swarm of drones in completing a specific scenario as a mission using KV-GPS data and trajectory location data. It finally checked the sensor signals to detect any chaos in the drone using the GA data. AECD, GMMs, and EM clustering are the three techniques that label unlabeled datasets into two categories: Normal (N) with a data sample of 23,501 and Chaotic (C) with a data sample of 20,266.

D. Optimization and Classification of Data Sample

The data sample was classified and optimized in three stages. First, the data sample was standardized, then the data was classified using a CNN classifier, and finally, the classified data was optimized using Stochastic Gradient Descent with the AdaDelta optimization technique.

1) *Standardization of data samples:* After categorizing the normal and chaotic states, the drone-label information was deleted, leaving a total of six variables. To standardize the range of input variable values, a data standardization approach similar to pre-processing for clustering was used. In the labeled data, the Logistic regression technique was used for the binary categorized variables. The two-potential dependent-variable values of 0 and 1 represent the "normal" and "abnormal" results. Binary logistic models were used to assess the likelihood of a binary answer based on one or more predictor (or independent) functions.

2) *CNN Classifier:* To normalize the time sequence data of the kinematic variables specified in this study, the Gaussian Mixture Models and Expectation-Maximization technique were used. The data was first transferred through a one-dimensional Convolutional Neural Network (CNN) with six hidden layers, which was then linked to a dense multilevel perceptron with sigmoid activation at the output end. The sigmoid activation function result was compared to the target label value by reversing this error and its cross-entropy error (Equation 5), and was used to learn the overall neural network. A Stochastic Gradient Descent technique combined with minibatch was used for learning. Table II shows the details about the neural network layers and the parameters used to train the network, while Table III shows more details about

the design, it was created by first building a sufficiently large network and then controlling it with batch normalization [51].

3) *Stochastic and mini batch gradient descent in adadelta optimization:* Most neural network methods are designed to improve accuracy; they work best when each class studies the same (or comparable) amount of data. However, when the number of normal and chaotic drones is significantly different, a varied binary classification, such as in defect classification or chaotic detection, does not produce excellent results [52]. This method generates additional samples in order to achieve a one-to-one relationship between normal and abnormal data for batches in order to optimize AdaDelta to compensate for the imbalance used in the network's training [53].

The AdaDelta optimization method is a stochastic optimization methodology for Stochastic Gradient Descent with a per-dimension learning rate method. It aims to slow down the monotonously fast rate of learning. Rather than gathering all past squared gradients, AdaDelta limits the window of accumulated past gradients to a specific size. Only one example was analyzed at a time to perform a single step in Stochastic Gradient Descent (SGD). Using the SGD, the following steps were taken for each epoch:

- a) Take the sample data,
- b) Insert it to Convolutional Neural Network,
- c) Find its gradient,
- d) Use the computed gradient in step 3 for weight updates,
- e) Repeat steps (a)–(d) for all of the items in the data sample.

Because only one example was considered at a time, the cost will fluctuate rather than decrease over the training examples. Considering, mN and mC denoting the number of data points labeled as normal (N) and chaotic (C), respectively. If the sampling required to produce a minibatch in the stores' gradient is carried out consistently, the predicted data quantity ratio for the two classes is mN/mC .

TABLE II. ONE-DIMENSIONAL CONVOLUTIONAL NEURAL NETWORK PARAMETER

Layer	Input Variables (<i>n</i> , timestamp, 5)	Output (<i>n</i> , 160, 5)	Operation Standard
1	(<i>n</i> , 160, 5)	(<i>n</i> , 80, 10)	One-dimensional Convolutional, Rectified Liner Unit (ReLU), one-dimensional batch normalization
2	(<i>n</i> , 80, 10)	(<i>n</i> , 40, 20)	One-dimensional Convolutional, ReLU, one-dimensional batch normalization
3	(<i>n</i> , 40, 20)	(<i>n</i> , 20, 40)	One-dimensional Convolutional, ReLU, one-dimensional batch normalization
4	(<i>n</i> , 20, 40)	(<i>n</i> , 10, 80)	One-dimensional Convolutional, ReLU, one-dimensional batch normalization
5	(<i>n</i> , 10, 80)	(<i>n</i> , 5, 160)	One-dimensional Convolutional, ReLU, one-dimensional batch normalization
6	(<i>n</i> , 5, 160)	(<i>n</i> , 5, 128)	One-dimensional Convolutional, ReLU, one-dimensional batch normalization
7	(<i>n</i> , 5, 160)	(<i>n</i> , 160)	Global pooling average
8	(<i>n</i> , 160)	(<i>n</i> , 64)	Batch standardization, Dense, ReLU
9	(<i>n</i> , 80)	(<i>n</i> , 2)	Dense, Sigmoid

TABLE III. LEARNING MODEL HYPER-PARAMETERS

Size of Batch	Length of Batch in Seconds	Number of Epoch	Learning rate
128	160	50	0.00005

E. Handling Drones in Chaos

The optimized classified chaos based on the trajectories of the drones in the swarm were addressed in real time using the Poincare map from the Rössler system, with the data sample classified and labeled as chaos, mC. The Poincaré map was created by charting the function's value each time it crosses a specified plane in a specific direction.

Plotting the *x*, *y*, and *z* coordinates every time it passes through the *x*=0 plane, where *x* changes from negative to positive. As a result, the Poincaré map converts the solutions of the three Ordinary Differential Equations of the Rössler system into the coordinates that best remove such drones from the chaotic state.

V. RESULT AND DISCUSSION

The detailed results are as follows:

A. Clustering and AECD

The flight data from a swarm of six drones was evaluated using the Autoencoder and Chaos Detection algorithms, as well as Gaussian Mixture Models and Expectation-Minimization for clustering. Fig. 3 and Fig. 4 depict the clustering results for a swarm of drones on a specific illustrative flight test day using

AECD and Gaussian Mixture Models. The first and second autoencoder components generated the distribution of data points in the reduced space; Fig. 3 is based on KV-GPS data, while Fig. 4 is based on GA data. The dimension was reduced to auto-decoded axes with a cumulative dispersion rate of at least 93% using the AECD process, and the clusters were discovered using Gaussian Mixture Models clustering with Expectation-Maximization. Fig. 4 depicts the distribution of data points in the reduced space formed by the autoencoder encoder and decoder components. A drone's data is disseminated in a very different way than data from other drones. As a result, it's reasonable to assume that data from the fourth drone in the swarm (Drn 4) will contain the chaotic time series. However, it is unclear how the clustering result is related to chaos, given that all data from a potentially problematic drone is unlikely to belong to a single cluster. The scatter plot for each cluster is shown in Fig. 5. This depicts the swarm's data point cluster. The plot aids in identifying the points of the root causes of chaos in a swarm, as well as the dependability of such points in relation to the rest of the swarm. Fig. 6 shows the percentage of data from each drone that belongs to a specific cluster. This depicts the effectiveness of such clusters of data points in relation to each drone in the swarm in order to identify the chaotic drone.

The majority of flight data from all drones falls into Clusters 4 and 9, but the distributions for the swarm's fourth drone (Drn 4) and the other drones differ. Drn 4 differs from the others in the ratio of data belonging to Clusters 4 and 9, with significantly more data belonging to Cluster 4 than Cluster 9 when compared to the other drones in the swarm. Another intriguing discovery is that data from Drn 4, a potentially chaotic drone, does not belong in Clusters 1, 2, 3, or 8. As a result, while the clustering does not indicate which drone may have exhibited chaotic behavior, the distribution of data among the clusters may indicate chaos in the flight data. Clusters 5, 6, and 7 may indicate chaos flight data, whereas Clusters 1, 2, 3, 8, and 9 indicate normal data. For the remainder of the clustering method, data from each drone in Clusters 4-6 was labeled "C," while data from Clusters 1-4, 8, and 9 was labeled "N." In cases of indistinct data, such as Cluster 3, and questionable data, such as the first drone (Drn 1) in Cluster 6, a human expert may examine the flight data to use as labeled data.

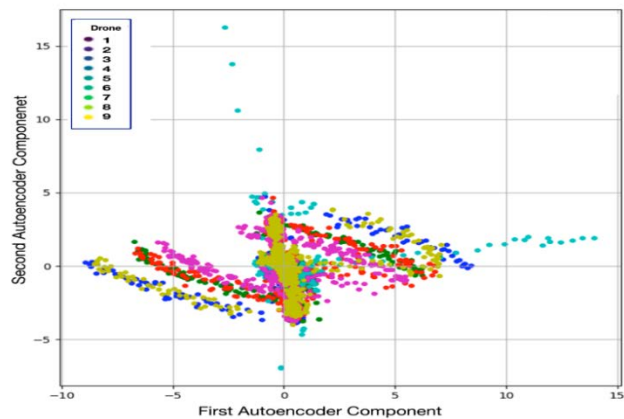


Fig. 3. Autoencoder KV-GPS Set Points Data Results.

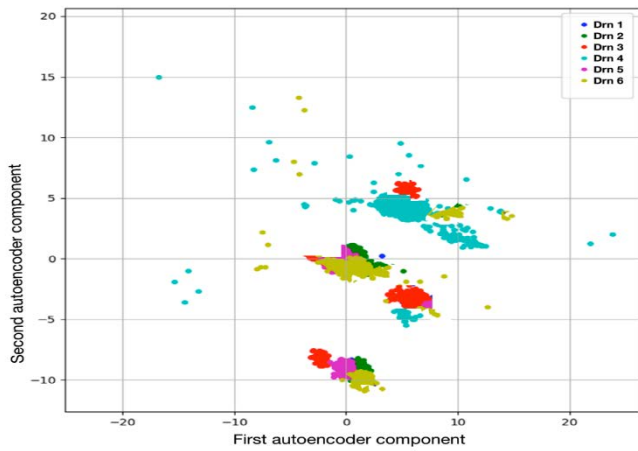


Fig. 4. Autoencoder GA Data Results.

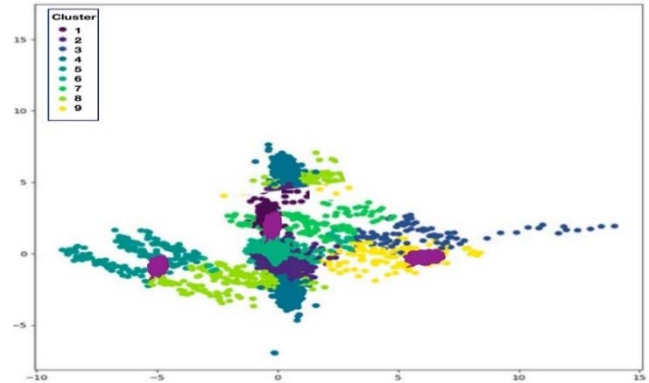


Fig. 5. Cluster Scatter Plot.

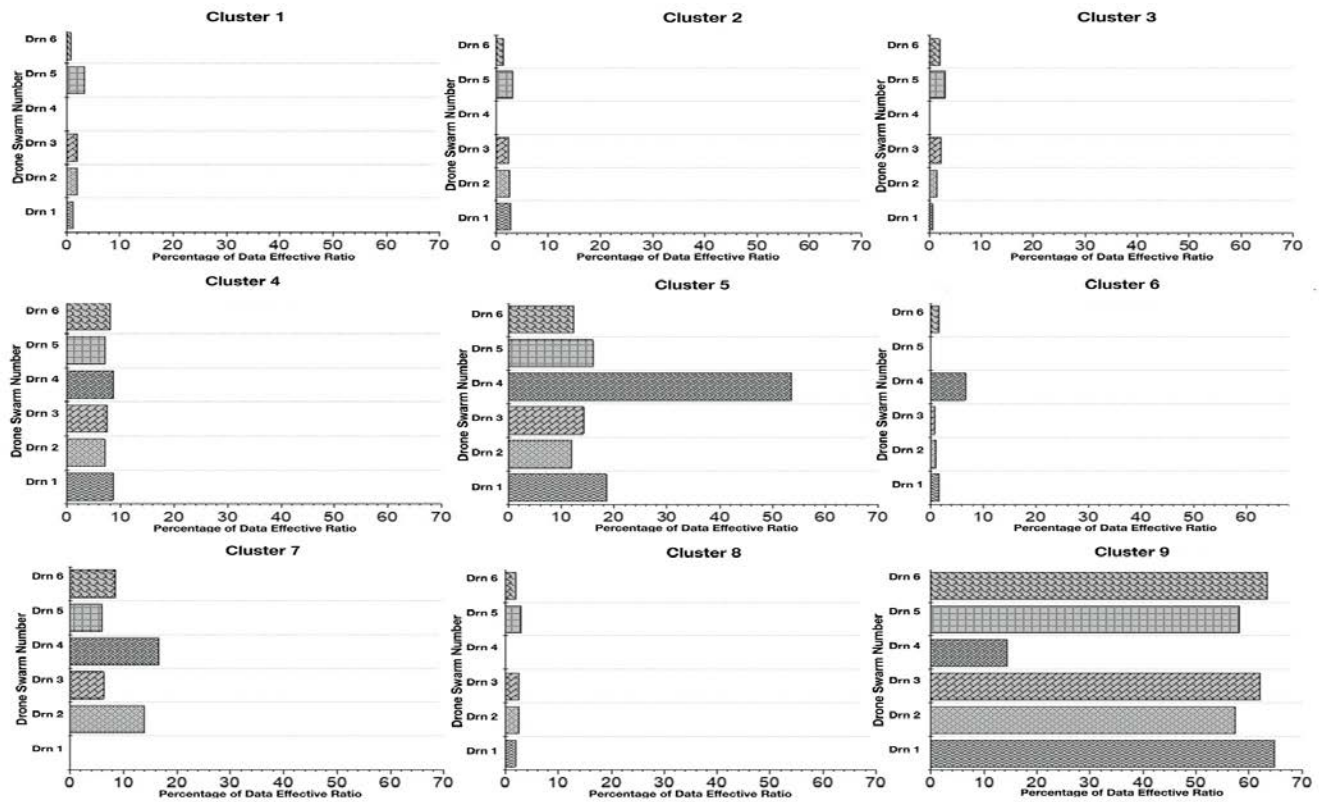


Fig. 6. Clustering Results for Swarm Flight Data using Gaussian Mixture Models.

B. Classification Results

The developed Convolutional Neural Network (CNN) classifier was trained until its cross-entropy and loss value converged on the learning parameters listed in Table II. The data from the test flight obtained from the swarm of drones was used as the training set of size 43,767; 70% of this dataset was used for training the neural network and 30% for model validation.

The dataset contains all of the drone's flight data, which was used to generate a test set with a size of 8,753. To validate the applicability of the sampling method, the test accuracy was equated with the variable rate of imbalance, resulting in the

chaos data ratio versus the non-chaotic data in the initial dataset. If the recommended sampling is not used, chaotic swarm flight data is used in the learning process with the rate of imbalance relative to non-chaotic data. The chaos swarm flight dataset was replicated by the factor of the rate of inverse imbalance when samplings are used. The classification data accuracy was compared by the accurate classification out of all cases, which is dependent on the use of the sampling scheme to detect the differential imbalance of the original swarm flight data set. Fig. 7 compares the chaos findings of the case for the original rate of imbalance. This is the scenario when the swarm's sixth drone (Drn 6) exhibits chaotic flying behavior; only the sampling result clearly identifies chaos in the Drn 6

flight data. It is clear that the suggested sampling strategy significantly improves classification accuracy, achieving zero classification error. It should also be noted that when the sampling technique is not used, the classification accuracy is approximately 50%. One thing to keep in mind is that even with a higher imbalance rate of 0.5, there was no improvement as shown in Fig. 8.

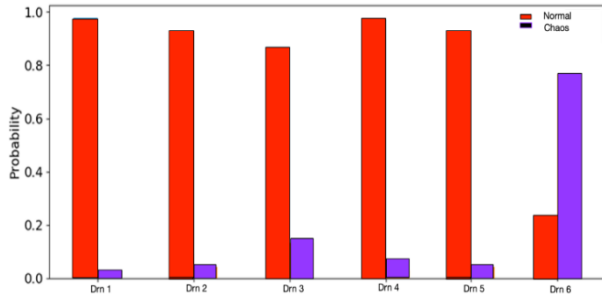


Fig. 7. Drone Imbalance Percentage (with Sampling).

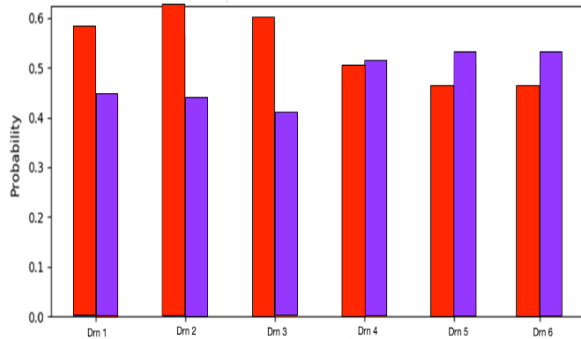


Fig. 8. Drone Imbalance Percentage (without Sampling).

C. Discussion

The proposed chaos detection methods were tested to see if the trained neural network classifier was useful for time series entry using real flight test data. If the input time series did not belong to the training set, the results for a sample drone flight test data and probability were computed [43]. The swarm flight test data was used, with clustering findings shown in Fig. 5 and Fig. 6. When the time series of the entry was constantly fed into the network, the neural network's output value corresponds to the sixth drone (Drn 6). The first output comes in response to the Kinematic variables [44] in the first 16 seconds segment, as the Convolutional Neural Network (CNN) takes a length of 160 input at a data rate of 10 Hz. The neural network calculates the output in real-time in response to the most recent 160-times segment points. The possibility of being normal has been determined to fluctuate over time until it reaches zero. When the average was achieved over the entire duration of the swarm flight, the average probability value of the six drones flown in that swarm flight test was compared. There's a much higher chance that this troublesome drone will be in a state of chaos than usual. According to Drn 6, the time history of the film input variables revealed that the drone does not respond effectively to changes in the x- and z-direction in the 90s and 75s, respectively; thus, the chaos detection schema revealed that the system cannot be normal at 85 seconds from the

original data point, based on the behavior. Drn 6 crashed during the flight test, according to the original flight log. As a result of the application of the Rössler system's algorithm, the drone was sent on alternate routes assuming the chaos is in the trajectory flight data. This prevents drone 6 (Drn 6) from crashing in the test flight log. In terms of online chaos monitoring, the results showed that there were two extreme approaches to monitoring. Constant monitoring of the non-chaotic or chaotic probability allows for a high frequency assessment of system chaos. This method enables effective responsiveness in chaos detection because it constantly delivers updated information about the system's normalcy.

The output signal, on the other hand, was noticeably noisy during the transient period, as shown in Fig. 8. As shown, the average probability over the entire time duration provides a cooperative judgment on the system's chaos. Despite the fact that the decision frequency may be too low, this method may be the least noisy susceptible method. The non-chaotic/chaotic probabilities are averaged over a set period of time, and the dataset was then updated with new values.

The adjacent averaging window's time frame may overlap. The average non-chaotic probability was computed over 30 seconds and updated every 20 seconds, implying that one-third of the data is overlapped between time frames. The chaotic probability of 70 is around 40% in the first time segment window, increases to around 55% in the second time frame, and finally exceeds 90% in the third time window. This enables the chaos to be observed at a relatively high frequency while avoiding data noise.

VI. CONCLUSION

This study proposed a machine learning-based chaos detection and a mitigation technique for the flight paths of a swarm of drones. The proposed techniques consist of three major steps: a labeling phase that uses lower-dimensional features to label unlabeled data, a binary/dual classification step that employs a 1-D CNN with a cross-entropy-based loss function, and a mitigation step that employs the Rössler system to generate new non-chaotic trajectories for drones in chaos. The deep neural network was trained using real flight test data. In this paper, Swarm mobility horizon-based monitoring was demonstrated to be a viable solution for real-time monitoring of a system's chaos with significantly reduced commotion effect. This technique can be used to mitigate the effects of drone crashes and failures in a fully autonomous swarm of drones.

A future focus will be the integration of network intrusion detection, monitoring, and mitigation into the overall health-management architecture of swarm drones. This could result in a more reliable fully autonomous swarm of drones by mitigating the effects of network intrusions, which can cause chaos and anomaly in a swarm of drones.

ACKNOWLEDGMENT

This Research was funded by the TETFund Research Fund and Africa Centre of Excellence OAK-Park, Obafemi Awolowo University, Ile-Ife, Nigeria.

REFERENCES

- [1] A. Otto, N. Agatz, J. Campbell, B. Golden, E. Pesch, "Optimization approaches for civil applications of unmanned aerial vehicles (UAVs) or aerial drones: A survey". *Networks*, vol. 72, no. 4, pp. 411-458, 2018. doi: 10.1002/net.21818.
- [2] Y. Li, C. Liu, "Applications of multirotor drone technologies in construction management". *International Journal of Construction Management*, vol. 19, no. 5, pp. 401-412, 2019. doi: 10.1080/15623599.2018.1452101.
- [3] K. Loayza, P. Lucas, E. Peláez, "A centralized control of movements using a collision avoidance algorithm for a swarm of autonomous agents". In *proceedings of the 2017 IEEE Second Ecuador Technical Chapters Meeting (ETCM)*, pp. 1-6, 2017. doi: 10.1109/ETCM.2017.8247496.
- [4] J. N. Yasin, S. A. Mohamed, M. H. Haghbayan, J. Heikkonen, H. Tenhunen, J. Plosila, "Navigation of autonomous swarm of drones using translational coordinates". In *proceedings of the International Conference on Practical Applications of Agents and Multi-Agent Systems*, pp. 353-362, 2020, doi: 10.1007/978-3-030-49778-1_28.
- [5] G. Ahmed, T. Sheltami, A. Mahmoud, A. Yasar, "IoD swarms collision avoidance via improved particle swarm optimization". *Transportation Research Part A: Policy and Practice*, vol. 142, pp. 260-278, 2020. doi: 10.1016/j.tra.2020.09.005.
- [6] R. Ourari, K. Cui, H. Koepl, "Decentralized Swarm Collision Avoidance for Quadrotors via End-to-End Reinforcement Learning". *arXiv preprint, arXiv:2104.14912*, 2021.
- [7] A. Majd, M. Loni, G. Sahebi, M. Daneshtalab, "Improving motion safety and efficiency of intelligent autonomous swarm of drones". *Drones*, vol. 4, no. 3, pp. 48, 2020. doi: 10.3390/drones4030048.
- [8] A. Atyabi, Z. S. Mahmoud, S. Nefti-Meziani, "Current advancements on autonomous mission planning and management systems: An AUV and UAV perspective". *Annual Reviews in Control*, vol. 46, pp. 196-215, 2018. doi: 10.1016/j.arcontrol.2018.07.002.
- [9] J. Cleland-Huang, A. Agrawal, "Human-drone interactions with semi-autonomous cohorts of collaborating drones". *arXiv preprint*, arXiv:2010.04101, 2020.
- [10] J. R. Cauchard, M. Khamis, J. Garcia, M. Kljun, A. M. Brock, "Toward a roadmap for human-drone interaction". *Interactions*, vol. 28, no. 2, pp. 76-81, 2021. doi: 10.1145/3447889.
- [11] M. A. Khan, A. Safi, I. M. Qureshi, I. U. Khan, "Flying ad-hoc networks (FANETs): A review of communication architectures, and routing protocols. In 2017 First International Conference on Latest trends in Electrical Engineering and Computing Technologies (INTELLECT)", pp. 1-9, 2017, doi: 10.1109/INTELLECT.2017.8277614.
- [12] Z. Chu, F. Hu, E. S. Bentley, S. Kumar, "Model and simulations of multipath bridge routing for inter-swarm UAV communications in EMANE/CORE", *International Journal of Modelling and Simulation*, 2021. doi: 10.1080/02286203.2021.1931789.
- [13] A. A. Akintola, G. A. Aderounmu, L. A. Akanbi, M.O Adigun, "Modeling and performance Analysis of Dynamic Random Early Detection (DRED) Gateway for Congestion Avoidance". *Journal of Issues in Informing Science and Information Technology*, vol. 2, pp. 623-636, 2005, doi: 10.28945/2920.
- [14] A. A. Akintola, G. A. Aderounmu, A. U. Osakwe, M.O. Adigun, "Performance Modelling of an Enhanced Optimistic Locking Architecture for Concurrency Control in a Distributed Database". *Journal of Research and Practice in Information Technology*, vol. 37, no. 4, pp. 365-380, 2005.
- [15] O. A. Oluwatope, D. Iyanda, G. A. Aderounmu, E. R. Adagunodo, "Computational Modelling of Collaborative Resources Sharing in Grid System". *The Journal of Computer Science and Its Application*, vol. 19, no. 1, pp. 74-83, 2012.
- [16] Z. Yuan, J. Jin, L. Sun, K. W. Chin, G. M. Muntean, "Ultra-reliable IoT communications with UAVs: A swarm use case". *IEEE Communications Magazine*, vol. 56, no. 12, pp. 90-96, 2018. doi: 10.1109/MCOM.2018.1800161
- [17] S. A. Bello, G. A. Aderounmu, M. L. Sanni, K. A. AbdulSalam. S.I. Eludiora., A. D. Akinde, "Estimation of Optimal Frequency and Antennae Length between Resource Interface and Mobile Terminal in Wireless ATM", *Ife Journal of Technology*, vol. 19, no. 2, pp. 55-58, 2010.
- [18] S.U. Otor, B.O. Akinyemi, T.A. Aladesanmi, G.A. Aderounmu, B.H. Kamagaté, "An Adaptive Bio-Inspired Optimisation Model Based on the Foraging Behaviour of a Social Spider". *Cogent Engineering*, vol. 6, no. 1, 2019. doi: 10.1080/23311916.2019.1588681.
- [19] S.U. Otor, B.O. Akinyemi, T.A. Aladesanmi, G.A. Aderounmu, B.H. Kamagaté, "An Improved Bio-inspired based Intrusion Detection Model for a Cyberspace". *Cogent Engineering*, vol. 8, no. 1, 2021. doi: 10.1080/23311916.2020.1859667.
- [20] P. Petráček, V. Walter, T. Báča, M. Saska, "Bio-inspired compact swarms of unmanned aerial vehicles without communication and external localization". *Bioinspiration & Biomimetics*, vol. 16, no. 2, 2020.
- [21] Y. Albayram, T. Jensen, M. M. H. Khan, R. Buck, E. Coman, "Investigating the Effect of System Reliability, Risk, and Role on Users' Emotions and Attitudes toward a Safety-Critical Drone System". *International Journal of Human-Computer Interaction*, vol. 35, no. 9, pp.761-772, 2019. doi: 10.1080/10447318.2018.1491665.
- [22] V. Kkarchenko, "Big data and internet of things for safety critical applications: challenges, methodology and industry cases". *International Journal on Information Technologies and Security*, vol.10, no.4, 2018.
- [23] B. Hu, P. J. Seiler, "Certification analysis for a model-based UAV fault detection system". In *proceedings of the AIAA Guidance, Navigation, and Control Conference*, pp. 0610, 2014. doi:10.2514/6.2014-0610.
- [24] E. Ordoukhanian, A. M. Madni, "System Trade-offs in Multi-UAV Networks". In *proceedings of the AIAA SPACE 2015 Conference and Exposition*, pp. 4542, 2015. doi: 10.2514/6.2015-4542.
- [25] L. Negash, S. H. Kim, H. L. Choi, "Distributed observes for cyberattack detection and isolation in formation-flying unmanned aerial vehicles". *Journal of Aerospace Information Systems*, vol. 14, no. 10, pp. 551-565, 2017. doi: 10.2514/1.1010531.
- [26] A. Suarez, G. Heredia, A. Ollero, "Cooperative sensor fault recovery in multi-UAV systems". In *proceedings of the 2016 IEEE International Conference on Robotics and Automation (ICRA)*, pp. 1188-1193, 2016. doi: 10.1109/ICRA.2016.7487249.
- [27] M. C. Boutalbi, M. A. Riahl, A. Ahriche. "Enhanced UAVs Mobility Models for Surveillance and Intruders Detection Missions." *Arabian Journal for Science and Engineering*, pp. 1-17, 2022. Doi: 10.1007/s13369-021-06541-3.
- [28] R. A. Saeed, M. Omri, S. Abdel-Khalek, E.S. Ali, M. F. Alotaibi. "Optimal path planning for drones based on swarm intelligence algorithm." *Neural Computing and Applications* vol. 34, no. 12, pp. 10133-10155, 2022. Doi: 10.1007/s00521-022-06998-9.
- [29] W. He, X.Q. Wenjian, L. Lifang. "A novel hybrid particle swarm optimization for multi-UAV cooperate path planning." *Applied Intelligence*, vol. 51, no. 10, pp. 7350-7364, 2021. Doi: 10.1007/s10489-020-02082-8.
- [30] Z. Cheng, Y. X. Tang, Y. L. Liu, "3-D Path Planning for UAV Based on Chaos Particle Swarm Optimization". *Applied Mechanics and Materials*, vol. 232, no. 1, pp. 625-630, 2012. doi: 10.4028/www.scientific.net/AMM.232.625.
- [31] S. Kawamoto, "2-D and 3-D solvable chaos maps". *Chaotic Modeling and Simulation (CMSIM)*, vol. 1, pp. 107-118, 2017.
- [32] W. Zhu, H. Duan, "Chaotic biogeography-based optimization approach to receding horizon control for multiple UAVs formation flight". *IFAC-Papers OnLine*, vol.48, no.5, pp.35-40, 2015. doi: 10.1016/j.ifacol.2015.06.460.
- [33] C. K. Volos, I. M. Kyprianidis, I. N. Stouboulos, "A chaotic path planning generator for autonomous mobile robots". *Robotics and Autonomous Systems*, vol. 60, no.4, pp. 651-656. 2012. doi: 10.1016/j.robot.2012.01.001.
- [34] H. Wang, S. He, K. Sun, "Complex dynamics of the fractional-order rössler system and its tracking synchronization control". *Complexity*, 2018. doi: 10.1155/2018/4019749.
- [35] L. Ouvre, G. Masson, F. Hameau, B. G. Gaillard, B. Caillat, "A CMOS duty-cycled coherent RF front-end IC for IR-UWB systems". In *proceedings of the 2015 IEEE International Conference on Ubiquitous*

- Wireless Broadband (ICUWB), pp. 1-5, 2015. doi: 10.1109/ICUWB.2015.7324396.
- [36] M. Rosalie, E. Kieffer, M. R. Brust, G. Danoy, P. Bouvry, "Bayesian optimisation to select Rössler system parameters used in Chaotic Ant Colony Optimisation for Coverage". *Journal of computational science*, vol. 41, no.2, 2020. doi: 10.1016/j.jocs.2019.101047.
- [37] J. Dentler, M. Rosalie, G. Danoy, P. Bouvry, S. Kannan, M. Olivares-Mendez, H. Voos, "Collision avoidance effects on the mobility of a UAV swarm using chaotic ant colony with model predictive control". *Journal of intelligent and robotic systems*, vol. 93, pp. 227-243, 2019. doi: 10.1007/s10846-018-0822-8.
- [38] G. Li, A. Rai, H. Lee, A. Chattopadhyay, "Operational anomaly detection in flight data using a multivariate gaussian mixture model". In proceedings of the 10th Annual Conference of the Prognostics and Health Management Society, 2018. doi: 10.36001/phmconf.2018.v10i1.474.
- [39] A. Nanduri, L. Sherry, "Anomaly detection in aircraft data using Recurrent Neural Networks (RNN)". In proceedings of the 2016 Integrated Communications Navigation and Surveillance (ICNS), pp. 5C2-1, 2016. doi: 10.1109/ICNSURV.2016.7486356.
- [40] A. Manukyan, M. A. Olivares-Mendez, H. Voos, M. Geist, "Real time degradation identification of UAV using machine learning techniques". In proceedings of the 2017 International Conference on Unmanned Aircraft Systems (ICUAS), pp. 1223-1230, 2017. doi: 10.1109/ICUAS.2017.7991445.
- [41] H. Ahn, "Deep Learning based Anomaly Detection for a Vehicle in Swarm Drone System". In proceedings of the 2020 International Conference on Unmanned Aircraft Systems (ICUAS), pp. 557-561, 2020. doi: 10.1109/ICUAS48674.2020.9213880.
- [42] D. Hendrycks, M. Mantas, K. Saurav, S. Dawn. "Using self-supervised learning can improve model robustness and uncertainty." arXiv preprint: arXiv:1906.12340, 2019.
- [43] S. Kiranyaz, O. Avci, O. Abdeljaber, T. Ince, M. Gabbouj, D. J. nman, "1D convolutional neural networks and applications: A survey". *Mechanical systems and signal processing*, vol. 151, 2021. doi: 10.1016/j.ymsp.2020.107398.
- [44] H. Moon, C. Kim, W. Lee, "A UAV based 3-D positioning framework for detecting locations of buried persons in collapsed disaster area". *International Archives of the Photogrammetry, Remote Sensing & Spatial Information Sciences*, vol. 41, 2016. doi: 10.5194/isprs-archives-XLI-B8-121-2016.
- [45] J. An, S. Cho, "Variational autoencoder based anomaly detection using reconstruction probability". *Special Lecture on IE*, vol. 2, no. 1, pp. 1-18, 2015.
- [46] K. Kashima, "Nonlinear model reduction by deep autoencoder of noise response data". In proceedings of the 2016 IEEE 55th conference on decision and control (CDC), pp. 5750-5755, 2016. doi: 10.1109/CDC.2016.7799153.
- [47] F. Chollet, *Deep learning mit Python und Keras: Das Praxis-Handbuch vom Entwickler der Keras-Bibliothek*. MITP-Verlags GmbH & Co. KG., 2018).
- [48] T. F. Weng, X. X. Cao, H. J. Yang, "Complex network perspective on modelling chaotic systems via machine learning". *Chinese Physics B*, vol. 30, no. 6, 2021. doi: 10.1088/1674-1056/abd9b3.
- [49] M. Ramamurthy, Y. H. Robinson, S. Vimal, A. Suresh, "Auto encoder based dimensionality reduction and classification using convolutional neural networks for hyperspectral images". *Microprocessors and Microsystems*, vol. 79, 2020. doi: 10.1016/j.micpro.2020.103280.
- [50] Z. Tirandaz, G. Akbarizadeh, H. Kaabi, "PolSAR image segmentation based on feature extraction and data compression using weighted neighborhood filter bank and hidden Markov random field-expectation maximization". *Measurement*, vol. 153, 2020. doi: 10.1016/j.measurement.2019.107432.
- [51] S. Loffe, C. Szegedy, "Batch normalization: Accelerating deep network training by reducing internal covariate shift". In proceedings of the International conference on machine learning, pp. 448-456, 2015. doi: 10.5555/3045118.3045167.
- [52] M. Buda, A. Maki, M. A. Mazurowski, "A systematic study of the class imbalance problem in convolutional neural networks". *Neural Networks*, vol. 106, pp. 249-259, 2018. doi: 10.1016/j.neunet.2018.07.011.
- [53] E. Yazan, M. F. Talu, "Comparison of the stochastic gradient descent based optimization techniques". In proceedings of the 2017 International Artificial Intelligence and Data Processing Symposium (IDAP), pp. 1-5, 2017. doi: 10.1109/IDAP.2017.8090299.
- [54] Y. S. Hsiao, Z. Wan, T. Jia, R. Ghosal, A. Raychowdhury, D. Brooks, G. Y. Wei, V. J. Reddi "Mavfi: An end-to-end fault analysis framework with anomaly detection and recovery for micro aerial vehicles." arXiv preprint arXiv:2105.12882, 2021.
- [55] M. Ullah, C. Zhao, H. Maqsood, M. U. Hassan, M. Humayun "Improved neural network-based sensor fault detection and estimation strategy for an autonomous aerial vehicle." *International Journal of Intelligent Unmanned Systems*, 2021. Doi: 10.1108/IJUS-09-2021-0109.

Integrating Big Data Analytics into Business Process Modelling: Possible Contributions and Challenges

Zaeem AL-MAdhrah, Dalbir Singh, Elaheh Yadegaridehkordi

Center for Software Technology and Management

Faculty of Information Science and Technology

Universiti Kebangsaan Malaysia, 43600 Bangi, Selangor, Malaysia

Abstract—Business Process Modelling (BPM) is a set of organised, structured, and related activities that boost the development and evolution of an organisation's success by understanding, improving, and automating existing business processes. Recently, the integration of Big Data Analytics (BDA) into BPM has widely gained more attention as a unique opportunity for organisations to enhance their efficiency, effectiveness, added value, and competitive advantage. However, some organisations still rely on old data-driven strategies and are late in integrating BDA into their BPM. This study aims to explore the possible contributions and challenges of integrating BDA into BPM. This study discovered that better decision making, embracing the organisation's performance, upgrading business process capabilities, and supporting supply chain management are the main contributions of BDA to BPM in organisations. However, poor data quality, shortage of BDA professionals, and data security and protection are the main challenges that hinder organisations from implementing BDA. This study provides valuable insights for organisations that intend to implement big data technologies in their business processes.

Keywords—Big data analytics; business process modeling; BPM; organisation's performance

I. INTRODUCTION

Business Process Modelling (BPM) is a set of organised, structured, and related activities that operate together to accomplish an organisation's end goals. BPM is an essential factor in developing and evolving an organisation's success since it encourages understanding, improving, and automating existing business processes [1]. Additionally, Business process models must be efficiently modelled to generate a good functioning of the organisations [2].

BPM assures that the business processes are consistent and pushes business execution toward accomplishing the overall strategy and goals of the organisation. BPM enables the communication and documentation of an organisation's business processes [3]. It gives a united language and methodology for communicating procedures, information, and guidelines about the business processes within organisations. Also, BPM helps to ensure that business processes and rules are well-designed by formalising existing processes that may not be well-documented and adjusting them to be well-designed [4]. That leads to getting rid of the guesswork and confirming that these documented processes match the organisation's guidelines and legal regulations. BPM gives a clear understanding of the process's flow that influence

decision making process [5]. That helps managers figure out if there is a chance for further optimisation by improving the process's cycle time, utilising better resources, and allowing testing models before implementing them [6].

Big data provides excellent advantages for organisations as it gives accurate and consistent business insights, automated decisions for real-time processes, and the detection of fraud operations [7]. Besides that, big data helps organisations gain more leverage and return on investments and risk qualifications. Big data is currently a significant factor in the world of technology. Organisations use big data to increase revenues by targeting specific customers and retaining existing customers [8]. With the proper integration of big data, organisations can determine precisely what their customers are looking for, which gives them leverage to meet customers' needs. In addition, big data nowadays is used to target specific markets instead of spending tremendous money on advertising which reduces the costs for the organisations. Identifying risks and foreseeing potential opportunities are now possible by using big data [9]. Eventually, big data will be in almost every industry with significant advantages [10].

In recent years, using Big Data Analytics (BDA) to operate and manage business processes properly has widely gained more importance [11]. Therefore, integrating BDA into BPM represents a unique opportunity for organisations to enhance their efficiency and effectiveness along with the business to achieve added value and competitive advantage [12]. BDA can make a remarkable improvement in multiple aspects of BPM. One of the benefits BDA can bring to organisations is wastage management. According to previous studies, wastage consumes a massive chunk of an organisation's resources. BDA can help organisations develop efficient and effective waste management strategies [13]. As the measurement is at the centre of data analytics for waste management, it facilitates observing the business processes and, consequently, identifying the processes that generate the most waste. Based on that, the organisation can take actions to reduce wastage which leads to greater BMP. In addition, integrating BDA into BPM can develop powerful talent management for the organisations [14]. It can identify the problems in the production processes and propose solutions based on data analytics. Also, it can help the organisations in the process of recruitment and acquire talents that fit the business's needs and values. Besides that, it enables the organisations to foresee any turnover changes in process modelling.

Moreover, big data can generate patterns based on data to BPM to enhance customer management. When these generated patterns are integrated with business processes, they can evaluate the quality of customer services, bring up an accurate customer classification, acquire new customers and retain the current customers, predict customer behaviours, and improve customer value [15]. All these benefits will be significant advantages for the organisations.

However, the IT industry has significantly improved BDA's scope, while BPM societies haven't been really up to date with the massive jump in IT. BPM's societies keep relying on old modelling-based approaches, which are at a disadvantage [16]. In addition, a high percentage of companies feared the disruption of data-driven competitors, which led them to forge the adoption of embracing BDA. Besides that, many organisations believe that if they don't utilise the data appropriately and nimble, data analytics might compromise threats to them instead of being assets [17]. Additionally, some companies hesitate to change into data-driven companies due to the possibility of failure in changing business culture transformation. Hence, no accomplishments will be achieved with old BPM approaches to manage an organisation's processes because data is always limited.

Consequently, with the old BPM, the value of information is often insufficient for decision making, long time to analyse behaviours of products, services or customers, requires more cost for hardware, software and maintenance, and is always a step behind the other modernised organisations [18]. Moreover, as technology is constantly evolving, BPM faces the pressure of keeping up with the latest data and upgrades in terms of social media and unstructured data [19]. So, all of this must be put in perspective in pursuing a better rapport with the new technical world so that better decisions result in more outstanding outcomes.

BDA has raised the profit edges of businesses that have embraced it by enhancing efficiency and reducing costs. Indeed, the world is moving toward the Internet of Things (IoT) [20] and data analytics; organisations must integrate BDA into business process modelling before it's too late [21] [22]. Also, organisations should use BDA in BPM to enhance data-driven decisions which improve business-related outcomes [23]. That would come up with more new revenue opportunities, effective marketing strategies, customer's personalisation, and improved operational efficiency. Therefore, this study aims to explore (i) integration of BDA into BPM and (ii) related possible contributions and challenges.

II. LITERATURE REVIEW

Various studies have been conducted, with the main focus being on why a diverse number of companies are not interested in embracing BDA to support BPM. In this section of the study, multiple arguments from different perspectives will be presented to demonstrate why some companies support adopting BDA in BPM and other companies do not support that.

Some companies believe the intense, increasing volume of data from new sources – mostly unstructured data – requires

new approaches to process management [24]. Acquiring these approaches requires a new storage level, a higher level of computing power, and very skilled analytical expertise if companies want to reap valuable information and insights. For some companies, this is considered as a complexity that requires both talents and experience [25]. It can be a valid argument here if there was an abundant amount of data, and it would require much more work to filter the valuable data from the invaluable data.

In contrast, companies had the challenging mission to dig deep to explore the opportunities and the effect on the business of big data in managing business processes. Big data is evolving as a corporate criterion for business modelling. Big data is considered a tool that provides opportunities for creativity and innovation due to its high agility for the companies [26]. It can load a large amount of data, recognise links and understand patterns. Embracing big data to make digital transformation in organisations enables them to add digital content to the business processes [27]. This enhances the quality of decision-making based on real customers' relationship data. Furthermore, digital transformations will improve the management processes that allow the business to expand and gain more outstanding production and distribution.

On the other hand, moving to the digitisation of business modelling concerns companies worldwide [28]. Digitalisation has ruined the business management ways in several industries. For instance, in retail, companies such as Amazon strongly damaged the classic commerce like shopping malls. In some cases, business processes in companies require a tremendous amount of data to gain value rather than the size [28], [29]. Companies are allocating a lot of resources to collecting a massive amount of data that might not be as valuable as expected once they seek the correct data. Many barriers make organisations hesitate to chase big data related opportunities [30]. These barriers might include outdated IT infrastructure, complexity of processing big data, messiness and randomisation of big data, lack of data experiences and skills to coordinate with business processes, privacy concerns, and eventually, the organisation's cultures, which may not be conducive operationally for data-driven decision making.

According to previous research, businesses need quicker and more precise insights into growing volumes of transactional data [31]. BDA technology serves to achieve high efficiency in business processes and raises organisations' effectiveness to another level [32]. Digitalising organisations with BDA technology will add value to the organisations. To clarify, analysing big data in real-time supports the organisation to optimise the organisational vision by reviewing the past and foreseeing the future [33]. Besides that, acquiring BDA and coordinating it with BPM speeds up the processes like modelling, monitoring, measuring, redesigning, reengineering, process analysis, process enactment, enterprise application integration, and business intelligence [34]. Overall, these qualities possess great benefits for the organisations in various aspects.

Furthermore, the financial benefits of BDA in marketing and business increasingly rise year after year compared to the other organisations that are not implementing BDA technology

[35]. They also mentioned that the percentage of failure of embracing BDA is low, and it is caused by the lack of proper strategies to implement BDA. Thereupon, acquiring BDA technology requires companies to enhance their business process management.

Based on the conducted arguments, integrating BDA technology in an organisation is a risk that companies should take due to the intense pace of advanced technology. Accordingly, it might be a privilege and advantage if it is properly utilised, or it might be a loss of money if misused. BPM is a system that is based on data. Therefore, feeding up this system with more valuable and accurate data will strengthen the outcome of the system and produce supportive approaches that enhance business processes. In addition to that, based on the statistical studies, organisations that operate their business processes based on data analytics are exceptionally ahead of other organisations that don't use BDA until now.

III. CONTRIBUTIONS OF BDA TO BPM

A. Better Decision Making

BDA can assist in better decision-making by collecting, storing, and analysing data across a collaborative network [36]. Integrating BDA in BPM enhances the user's experiences with a powerful realisation of what has happened in the past. It assesses what is happening currently and predicts the process's behaviours in the future [33]. Besides that, decision-making with BDA provides organisations with more accurate process models and better performance. BDA plays a prominent role in improving decision-making for organisations [37].

Four types of BDA enhance business processes to ensure efficiency in decision-making [38] [39] (Table I). BDA works majorly to provide a clearer insight to model the organisation's processes, which helps the organisations enhance their productivity and creativity. Modelling business processes based on clear visions and accurate patterns support the organisation's growth and stability [40].

TABLE I. FOUR TYPES OF BDA TO ENHANCE BUSINESS PROCESSES

Data Analytics Type	Description
Descriptive Analytics	Describe what happened and what went wrong, and at which stage? Based on the provided answers, organisations can detect obstacles and avoid mistakes during process modelling.
Diagnostic Analytics	Historical data can be measured against other data to answer why something happened. Comparing old data and recent data helps to give organisations a greater idea of their business's growth and stability.
Predictive Analytics	Predicting what is likely to happen in the future based on the data analysed. Creating patterns based on predictions gives the organisations a very supportive advantage to plan for improvement in every aspect of the business. Also, predicting what issues the organisations may face greatly benefits the organisations.
Prescriptive Analytics	Prescribing what action to be taken to eliminate a future problem. Make probabilities for each situation that might happen and create a backup plan to handle it.

B. Embracing BDA in BPM Shapes the Organisation's Performance

BDA significantly boosts customer deployment and superior organisational performance. BDA plays a vital role in shaping organisations' performance [41]. One of BDA's benefits is that it differentiates between high and low-performing organisations; therefore, those firms that apply BDA become proactive and future-oriented. In addition, big data can increase the likelihood of innovation performance, leading to the creation of patterns and behaviours in business processes [42]. Furthermore, BDA can build benefits for any organisation by improving its performance (process performance, financial performance, production performance, marketing performance, and partnership performance) and competitive advantage. Also, decisions in data-driven organisations are more likely to outcome positively and give more insights into business processes [43]. Hence, big data gives extra leverage for improving organisation performance. An organisation's performance is measured by various factors such as finance, quality, improvement, and value of the organisation in the market [44]. BDA is a major participant in each of these factors once it helps to enhance them in various ways [45]. Process modelling using BDA will strengthen the organisation's strategies, resulting in better revenue and financial stability.

Additionally, organised models in business enhance the quality and lead to improvement of the organisations [46]. Besides that, when the organisation is financially improving and its quality is enhanced, its value is raised in the market. Hence, the organisational performance is supported by using BDA.

C. BDA Upgrades Business Process Capabilities

Big Data Analytics Capabilities (BDAC) is defined as the company's capabilities to influence technology and talented skills to take advantage of BD regarding the generation of perceptions essential to overperform competitors. To clarify, BDAC is the ability of organisations to come up with insights that support organisations using big data management [47].

Managing BDA is a challenging and complicated task for companies due to the variety of resources and types of data. Still, when the company is capable of managing that big data and utilising the outputs of BDA to enhance modelling business processes, then the organisations are taking greater advantages compared to others who can't manage BDA [48]. The ability to manage big data and extract value data differentiates successful firms from non-successful ones. Based on an organisation's financial welfare, big data is defined and evolved more technologically in organisations. In addition to that, BDA's capabilities assist in offering advantages such as optimising the data generation process, suggesting data integration from diverse sources, incorporating different types of findings into the business process, and data visualisation capability to facilitate the decision-making process [49].

Based on the expert's experience in using BDA techniques, organisations can precisely predict the market's needs and requirements and then develop their strategies and structures to accomplish the best insights about market needs and reveal future market objectives [50].

D. BDA Supports Supply Chain Management (SCM) in Organisations

Embracing big data support supply chain management (SCM) in an organisation reflects significant advantages on business process models [51]. Applying big data improves existing business processes by focusing on current business needs and challenges, and data can be investigated to create saleable products and services as new value propositions. As the range of supply chains is global, the volume of data collected from its various processes and the rate at which it is being generated can be qualified as Big Data [52]. Also, marketing and sales are now counting on analysis of the unstructured and structured data to get more significant insights into customer needs and improve the cost aspects of supply chain processes [53]. The utilisation of BDA provides an incredible value in product development, market demand predictions, supply decisions, distribution optimisation, and customer feedback [54].

Moreover, big data can be applied in SCM for operational and development purposes, value discovery, value creation, and value capture [55]. There are several areas primary for applying big data for SCM. Fig. 1 illustrates the areas as the source, make, move, and sell [56].

BDA and SCM in Organizations.	
Source	Big data may be used to integrate with suppliers, evaluate sourcing channel options, and portion supplier negotiations.
Make	It involves reduction of capacity constraints, warehousing optimisation, performance reporting, facility location/layout, and workforce analytics.
Move	The application of big data involves routing, scheduling, using transportation alternatives, optimising, and maintaining vehicles.
Sell	Big data enables micro segmentations of customers, the capture and prediction of customers demand and behaviours, as well as the price and the assortment optimisation.

Fig. 1. Main Areas for BDA in SCM.

IV. CHALLENGES OF INTEGRATION OF BD INTO BPM

Initially, organisations will need to gather vast amounts of data through mobile, social networks, digital videos, and sensors. Organisations then will need to integrate them into their business processes [57]. Therefore, they must be aware of the challenges of big data to have an intelligent and efficient BPM that aims to bring great value to process decision-makers and process modellers. Organisations have to manage many challenges and obstacles when they decide to integrate BDA into BPM, as explained in the following sections.

A. Poor Data Quality

One of the most common challenges to embracing BDA in business organisations is poor data quality. When business organisations intend to be data-driven, data quality must be concerned cautiously because data quality directly impacts business outcomes [58]. Poor data quality leads to poor insights, which lead to poor decisions, and vital decisions based on low-quality data can have disastrous effects [59]. Poor data quality causes inefficiencies in business processes that rely on it. Instead of focusing on essential activities, these inefficiencies may result in very costly redo efforts validating and correcting data inaccuracies. Besides that, poor data quality leads to distrust [60]. Maintaining high-quality data might differ between complying with regulations and paying millions

in fines. Time, money, and reputations can be wasted if the data is incorrect, negatively impacting business organisations and eroding client confidence [61]. Therefore, it is critical to be aware of the importance of data quality because good data quality will enhance BPM, and poor data quality will lead to significant damage to BPM in any business organisation.

B. Shortage of Professionals who Understand BDA

Business organisations that seek to integrate BDA into BPM will have to deal with large data sets that keep growing in size and variety. Incorporating data sets into an analytical platform becomes increasingly difficult because the volume and variety of data available today can overwhelm even the most experienced data engineers [62]. Therefore, the market has significantly demanded big data scientists and analysts. Because the position of a data scientist is multidisciplinary, businesses organisations must select someone with a diverse set of talents related to BDA. Another big issue that organisations confront is a shortage of professionals who are familiar with BDA [63]. Compared to the vast amount of data created, data scientists have a severe scarcity. For instance, when someone who is not an expert data engineer tries to merge unstructured and inconsistent data from several sources, mistakes occur and wrong insights are produced, resulting in missing data, inconsistent data, logic conflicts, duplicate data, and bad decisions [64]. Therefore, if there are no expert professionals to deal with this massive volume of big data efficiently and effectively, then integrating them with BPM is not helpful and it may bring wrong insights and false signals for business modelling, which will impact business organisations negatively as all the decisions will be based on inaccurate and useless insights.

C. Data Security and Protection

Integrating BDA in BPM requires business organisations to seek massive data sets to develop enhanced business models and visions. More data brings more opportunities and potential threats simultaneously, especially when the data sets are less organised [65]. As businesses expand and add new tools to their software stacks and install new technologies to make sense of their data, the risk of security breaches increases. Therefore, business organisations that indiscriminately collect data from many sources may be gathering fraudulent (and so invalid and perhaps damaging) data [66]. Fake and inaccurate data will impact any analysis that a company can perform. Additionally, when businesses gather data without using precautions like encryption, access control, and firewalls, the data becomes subject to leaks, viruses, and data harvesting, which may be incredibly destructive to businesses and compromise customer privacy [67]. Thus, if the data are not well-protected and secured, the business will be damaged and lose its value in the market. As a result, data protection and security are important conditions to integrate BDA into BPM.

D. Confusing a Variety of Big Data Technologies

Nowadays, there are many technologies specialised for BDA in the market. Acquiring the right technology for big data is a real challenge for organisations [68]. Each BDA technology has different processing, storing, cleaning, and reporting features. For instance, the speed of processing big data is essential for organisations. Therefore, some companies

will choose Spark technology to process because of its high speed, while others will be settled with Hadoop MapReduce's speed. Hence, if an organisation has less data and embraces Spark technology, it would lead to money wastage and vice versa [69]. Also, data storage makes a big difference in the organisation's big data processing. For instance, some organisations tend to go for Cassandra to store their data, while others would prefer to embrace Hbase to store their data. Therefore, the features of BDA technology may significantly impact organisations either positively or negatively, depending on selecting the right technology [70]. Choosing an appropriate technology for big data plays a significant role in enhancing the BPM. When the suitable technology is adopted, the business processes will be well strategised and organised, resulting in optimised business insights [71]. On the other hand, if the BDA technology is poorly chosen, the business processes will have unexpected outcomes and false foreseen.

E. Managing Large Volume of Data

Managing large volumes of data is the first challenge for organisations to consider when integrating BDA into BPM [72]. These large volumes of data which are extracted from customer relationship management (CRM), enterprise resource planning (ERP), and other data sources, need to be consolidated and pulled into a unified manageable big data [73]. Besides that, the correct storage of these vast amounts of knowledge is one of the most critical concerns of big data. Data saved in data centers and company databases are continually growing [74]. Thus, it becomes difficult to manage large data sets as they increase rapidly over time. The majority of the data is unstructured and comes from various sources, including documents, movies, audio, text files, and other media. [75].

V. CONCLUSION

This study discussed the possible contributions and challenges of integrating BDA into BPM. It illustrated the importance of BPM and how organisations pose the BPM as the backbone for their businesses to succeed. Also, how BPM participates in ensuring the business processes modelling is a consistent technique and pushes business execution toward accomplishing the overall strategy and goals of the organisation. Besides that, this study demonstrates the roles of BPM and how it organises and operates all the processes in an organisation to come out with the best possible performance. Another part of this study had closer attention to the value of BDA in today's technology world and how organisations embrace it to support their businesses. It explained how data is the core component of any organisation's success. More of BDA was illustrated in terms of the enhancement and encouragement BDA brings to any organisation. Multiple studies with different perspectives were argued in this study to demonstrate why some organisations strive to embrace BDA and others consider it a waste of time and effort. These studies concluded that embracing BDA strongly supports BPM and enhances the value of the organisations. Next, the study provides multiple contributions of BDA in BPM, such as how integrating BDA into BPM helps to understand the business and support decision-making efficiently and effectively. Another contribution was that the relationship between BDA

and business performance had been illustrated precisely. Furthermore, how BDA can support SCM and optimise its process lifecycle to enhance the operations in an organisation. It generally concentrates on implementing BDA with BPM to improve existing business processes by focusing on current business needs and challenges. In this way, data can be investigated to create saleable products and services as new value propositions. Then, BPM's capabilities with the existence of BDA were indicated to be at a very different level with BDA than without BDA. This study demonstrated that BDA's capabilities support BPM to provide advantages such as incorporating different types of findings into the business process, optimising the data generation process, data visualisation capability facilitating the decision-making process, and suggesting data integration from diverse sources. Additionally, the study explained the challenges of embracing BDA in organisations to support BPM. Three significant challenges were identified in this study to predict what organisations may need to manage if they decide to integrate BDA in BPM.

The first challenge is poor data quality, which generates false insights in modelling processes, resulting in wrong decisions. This challenge can be solved by fixing the data in the source system to correct data issues such as missing data and incomplete data. Therefore, data must be set and cleaned in the Extract, Transform and Load (ETL) phase before it is used to make any analytics and predictions [76]. Besides that, data analytics leaders must set data quality standards that can be applied across the organisation's business units. They must then establish a clear connection between business processes, organisational performance, and data assets [77]. Make a list of the organisation's current data quality challenges and how they affect the business. Then, data and analytics professionals may start creating a specific data quality improvement plan that is the "best fit" for the company [78].

The second challenge is the shortage of professionals who understand the BDA in BPM. This challenge can be solved by paying extra attention while interviewing BDA professionals to ensure these professionals understand the structures of the organisation's requirements and strategies in terms of business processing and data. In addition, automating data-related tasks is a new approach followed by companies to solve this challenge. Automated data management, data science, and analytics tools and platforms such as Alteryx and DataRobot have also come on to the scene. However, some experts have warned that inexperienced staff can pose a risk to data science automation [79]. Also, companies are looking into ways to democratise data science by upskilling and reskilling their staff to become less reliant on small teams of pricey experts to see a return on their data science investments [80].

The third challenge is data protection and security. It cannot be fully tackled, but organisations usually improve their safety to decrease the threat rate. Many companies take data discovery and classification as a new approach to protect their data. Data discovery and classification is a process that involves scanning data repositories for the types of data that organisations consider significant, sorting it into categories, and clearly labelling it with a digital signature indicating its classification [81]. Besides that, firewalls are very significant

tech to protect data in an organisation. To prevent unwanted traffic from entering the network, firewalls are used. Furthermore, organisations can only open particular ports, giving hackers less freedom to move to gain access to or download sensitive data [82].

In addition, there are other challenges, such as a variety of big data technologies in the market. This challenge can be avoided by understanding the needs and requirements of the organisations and then adopting a technology with specific features to meet the organisations' needs and requirements. Besides that, managing large volumes of data is considered a challenge in some organisations. This challenge can be avoided by targeting the correct data and focusing on the quality instead of the quantity of data. Eventually, the summary of this study supports the embracing of BDA in BPM to make organisations a better place in today's world. The efficiency and effectiveness that BDA brings to the organisations increase the value and enhance the performance of the organisations. Another finding in this study is that the fear and hesitation of embracing BDA by some organisations was because they think they may not be able to utilise the generated structured and unstructured data properly to support BPM. While in fact, the study proved how embracing BDA could strongly support BPM. Indeed, integrating BDA and BPM is a risk that should be taken due to its value to the organisations from different aspects. Furthermore, the study proved that BDA could increase productivity, encourage creativity, and enhance performance modelling. Additionally, the findings showed how integrating BDA and BPM assures understanding of the business processes and supports decision-making. To conclude, this paper recommends organisations take a step forward and embrace BDA to help positively organise process modelling and raise the business value.

Eventually, integrating BDA in BPM is an opportunity that every organisation should seek due to the valuable benefits it brings. BDA assists organisations in finding more efficient ways to organise businesses processes and increase their customer acquisitions and retention. Besides that, organisations will gain more opportunities to develop innovative new products to meet customers' changing needs with BDA. In addition, businesses use big data to plan their advertising by observing online activity, monitoring point-of-sale transactions, and assuring on-the-fly detection of dynamic changes in client behaviours. These are then utilised to determine the target group, the most crucial factor to consider while planning a campaign.

Moreover, reliance on BDA could manage an organisation's risk plan and create a clear vision to minimise potential risks. Also, businesses can achieve contextual intelligence across the supply chain by using BDA. Therefore, BDA will make a significant impact on BPM and these impacts will raise the quality of the organisation's performance.

The next phase of this technology development is a complete automation strategy. Researchers should conduct many studies to increase the automation of BDA within organisations. Automating BDA is an advanced strategy that can make a difference in the positive side of organisations. Some researchers have attempted to make theories about full

automation for BDA in BPM. Still, they discovered that experts are not optimistic about this strategy because they believe that full automation in such an early stage may lead to many errors, negatively affecting BPM in organisations [83].

ACKNOWLEDGMENT

This research has been funded by Universiti Kebangsaan Malaysia Internal Funding.

REFERENCES

- [1] K. Guizania, S.A. Ghannouchi, "An approach for selecting a business process modeling language that best meets the requirements of a modeler", *Procedia Computer Science*, vol. 181, no. , pp. 843–851, 2021.
- [2] Diana Sola, Christian Meilicke, et al, "A rule-based recommendation approach for business process modeling", *33rd International Conference on Advanced Information Systems Engineering (ICSOC)*, vol. 63, no. 16, pp. 428 – 434, 2021.
- [3] Luise Pufahl and Mathias Weske, "Batch activity: enhancing business process modeling and enactment with batch processing", *Computing*, vol. 101, pp 1909–1933, 2019.
- [4] Julia Bräker, Martin Semmann, "How does business process modeling reflect augmented reality-based processes?", *25th Pacific Asia Conference on Information Systems (PACIS)*, vol. 75, no. 3, 2021.
- [5] Mohamad. R. Rosman, "The Role of Business Processes In Influencing the Decision Support Capabilities of Enterprise Content Management System (ECMS): Towards A Framework." *Asia-Pacific Journal of Information Technology and Multimedia*, vol. 9, no. 1, pp. 58 – 68, 2020.
- [6] David Santiago, "Key Benefits of Business Process Modeling" *Industrial Engineering, Universidade de Vigo, Spain*, no. 74, 2017.
- [7] Elisabetta Raguseo, "Big data technologies: An empirical investigation on their adoption, benefits and risks for companies", *International Journal of Information Management*, vol. 38, no. 1, pp. 187-195, 2018.
- [8] Feras M. Awaysheh, and Mamoun Alazab, "Big data resource management & networks: Taxonomy, survey, and future directions", *IEEE Communications Surveys & Tutorials*, vol. , no. , 2021.
- [9] Apurva Mhatre, Vantika Mahalingam, et al, "Predicting employee attrition along with identifying high risk employees using big data and machine learning", *2nd International Conference on Advances in Computing, Communication Control and Networking (icaccn)*, vol. 8, no. 3, pp.351, 2021.
- [10] Ong Kiat Xin1, Dalbir Singh, "Development of Learning Analytics Dashboard based on Moodle Learning Management System", *International Journal of Advanced Computer Science and Applications (IJACSA)*, vol. 12, no 7, pp. 838-843, 2021.
- [11] Asma Hassania, Sonia A. Gahnouchi, "A framework for Business Process Data Management based on Big Data Approach", *Procedia Computer Science*, vol. 121, pp. 740–747, 2017.
- [12] Silva Robak, and Bogdan Franczyk, "Business Process Optimisation with Big Data Analytics Under Consideration of Privacy", *Proceedings of the Federated Conference on Computer Science (ACSSIS)*, vol. 8, pp. 1199–1204, ISSN 2300-5963, 2017.
- [13] Weisheng Lu, Jinying Xu, "Is the private sector more efficient? Big data analytics of construction waste management sectoral efficiency", *Resources, Conservation and Recycling*, vol. 155, 2020.
- [14] Javaid Butt, "A conceptual framework to support digital transformation in manufacturing using an integrated business process management approach", *Designs, Multidisciplinary Digital Publishing Institute*, vol. 4, no. 3, 2020.
- [15] Maria Holmlunda, Yves V. Vaerenbergh, et al, "Customer experience management in the age of big data analytics: A strategic framework", *Journal of Business Research*, vol. 116, pp. 356-365, 2020.
- [16] Sherif Sakr, Zakaria Maamar, et al, "Business Process Analytics and Big Data Systems: A Roadmap to Bridge the Gap", *Institute of Computer Science, IEEE Access*, vol. 8, no. 7, pp. 322-333, 2018.

- [17] Kal Raustiala and Christopher J. Sprigman, "The second digital disruption: Streaming and the dawn of data-driven creativity", *New York University Law (NYUL) Rev.* 94, p. 1555, 2019.
- [18] Fosso Wamba, "Big data analytics and business process innovation", *Business Process Management Journal*, vol. 23 no. 3, pp. 470-476, 2017.
- [19] Meena Jha, Sanjay Jha, Liam O'Brien, "Combining Big Data Analytics with Business Process using reengineering", *IEEE Tenth International Conference on Research Challenges in Information Science (RCIS)*, 2017.
- [20] Jacentha Maniam Nur Afifah Mohd Shai, Dalbir Singh, "Adaptation of Internet of Things (IOT) Application in Business Process Management (BPM) for Improved Data Management", *Pertanika Journal of Scholarly Research Reviews (PJSRR)*, vol. 5, no. 2, pp. 1-9, 2019.
- [21] Mohammad K. Hasan, Ali Alkhalifah, et al, "Blockchain Technology on Smart Grid, Energy Trading, and Big Data: Security Issues, Challenges, and Recommendations" *Wireless Communications and Mobile Computing*, vol. 2022, no. 28, 2022.
- [22] Parisa Maroufkhani, W. Ismail, "Big data analytics adoption model for small and medium enterprises", *Journal of Science and Technology Policy Management*, vol. , no. , 2020.
- [23] Fosso W. Samuel, and Queiroz Maciel, et al, "Big data analytics-enabled sensing capability and organisational outcomes: Assessing the mediating effects of business analytics culture", *Journal Annals of Operations Research*, vol. , no. , 2020.
- [24] Nedelcu, "About big data and its challenges and benefits in manufacturing", *Database Systems Journal*, vol. 4, no. 3, pp. 10-19, 2016.
- [25] Gökalp, Mert Onuralp, et al, "A process assessment model for big data analytics", *Computer Standards & Interfaces*, vol. 80, p. 103585, 2022.
- [26] Thomas H. Davenport and Randy Bean, "Big Data Business Impact: Achieving Business Results through Innovation and Disruption", *New Vantage Partners (NVP)*, vol. , no. , 2017.
- [27] Ancarani, Carmela D. Mauro, "Successful digital transformations need a focus on the individual", *Digitalisierung im Einkauf. Springer Gabler, Wiesbaden*, pp. 11-26, 2018.
- [28] Michael Rachinger, "Digitalization and its influence on business model innovation", *Journal of Manufacturing Technology Management Open Access*, vol. 30, no. 8, pp. 1143-1160, 2018.
- [29] Maxwell Wessel, "You Don't Need Big Data - You Need the Right Data", *Harvard Business Review*, 2016.
- [30] Dai, Hong-Ning, et al, "Big data analytics for manufacturing internet of things: opportunities, challenges and enabling technologies", *Enterprise Information Systems*, vol. 14, no. 9-10, pp.1279-1303, 2020.
- [31] Ajah, Ifeyinwa Angela, et la, "Big Data and Business Analytics: Trends, Platforms, Success Factors and Applications", *Big Data Cognitive Computing*, vol. 3, no 2, p. 32, 2019.
- [32] Aleš Popovič, and Ray Hackney, et al, "The impact of big data analytics on firms' high value business performance", *Business intelligence and analytics*, 2016.
- [33] Uthayasankar Sivarajah, and Muhammad M. Kamal, et al, "Critical analysis of Big Data challenges and analytical methods", *Journal of Business Research*, vol. 8, pp. 263-286, 2017.
- [34] Grace Park, and Lawrence Chung, et al, "A modeling framework for business process reengineering using big data analytics and a goal-orientation", *11th International Conference on Research Challenges in Information Science (RCIS)*, pp. 21-32, 2017.
- [35] Barbara A. Manko, "Big data: The effect of analytics on marketing and business", *Journal of Information Technology Teaching Cases*, vol. 0(0) 1-7, 2021.
- [36] Saggi, Mandeep Kaur, and Sushma Jain, "A survey towards an integration of big data analytics to big insights for value-creation", *Information Processing & Management* vol. 54, no 5, pp.758-790, 2018.
- [37] AlNuaimi, Bader Khamis, et al, "The role of big data analytics capabilities in greening e-procurement: A higher order PLS-SEM analysis", *Technological Forecasting and Social Change*, vol. 169, no 120808, 2021.
- [38] Deshpande, Prachi S, et all, "Predictive and prescriptive analytics in big-data era"; *Security and data storage aspect in cloud computing*, Springer, Singapore, vol.52, no pp. 71-81, 2019.
- [39] Martin Wallner, Tomáš Peráček, "Usage of advanced data analysis in Austrian industrial companies", *International Conference on Innovations in Science and Education (economics and business)*, vol. 2, pp. 265-273, 2021.
- [40] Riccardo Rialti, Giacomo Marzi, "From Big Data to Performance: The Importance of Ambidexterity, Agility and BDA Integration in Business Processes, A Theory-Based Framework", *Ambidextrous Organizations in the Big Data Era*, Palgrave Pivot, Cham, vol. 13, pp. 39-67, 2020.
- [41] Awan, Usama, et al, "Big data analytics capability and decision-making: The role of data-driven insight on circular economy performance", *Technological Forecasting and Social Change*, vol. 168, p.120766, 2020.
- [42] Rialti, Riccardo, et al, "Big data analytics capabilities and performance: Evidence from a moderated multi-mediation model", *Technological Forecasting and Social Change*, vol. 149, p.119781, 2019.
- [43] Carillo, Kevin Daniel André, et al, "How to turn managers into data-driven decision makers: Measuring attitudes towards business analytics", *Business Process Management Journal*, vol. 25, Issue 3, ISSN: 1463-7154, 2018.
- [44] Ali, Saqib, et al, "How big data analytics boosts organizational performance: The mediating role of the sustainable product development", *Journal of Open Innovation: Technology, Market, and Complexity*, vol. 6, no. 4, 2020.
- [45] Bouranta, Nancy, et al, "The key factors of total quality management in the service sector: a cross-cultural study", *Benchmarking: An International Journal*, vol. 26, no. 3, 2019.
- [46] Raut, Rakesh D., et al, "Linking big data analytics and operational sustainability practices for sustainable business management", *Journal of cleaner production*, vol. 224, pp. 10-24, 2019.
- [47] Ciampi, Francesco, et al, "Exploring the impact of big data analytics capabilities on business model innovation: The mediating role of entrepreneurial orientation", *Journal of Business Research*, vol. 123, pp. 1-13, 2021.
- [48] Mikalef, Patrick, et al, "Big data analytics capabilities and innovation: the mediating role of dynamic capabilities and moderating effect of the environment", *British Journal of Management*, vol. 30, no. 2, pp. 272-298, 2019.
- [49] Shah, Tushar R, "Can big data analytics help organisations achieve sustainable competitive advantage? A developmental enquiry", *Technology in Society*, vol. 68, p. 101801, 2022.
- [50] Ghasemaghaci, Maryam, "Does big data enhance firm innovation competency? The mediating role of data-driven insights", *Journal of Business Research*, vol. 104, pp. 69-84, 2019.
- [51] Morten Brinch, Jan Stentoft, "Big Data and its Applications in Supply Chain Management: Findings from a Delphi Study", *Proceedings of the 50th Hawaii International Conference on System Sciences*, vol. 13, no. 5, pp. 1351-1360, 2018.
- [52] Sumit Maheshwari, Prerna Gautam, "Role of big data analytics in supply chain management: current trends and future perspectives", *International Journal of Production Research*, vol. 59, no .6, pp.1875-1900, 2021.
- [53] Wamba, Samuel Fosso, et al, "The performance effects of big data analytics and supply chain ambidexterity: The moderating effect of environmental dynamism", *International Journal of Production Economics*, vol. 222, no. 5, p.107498, 2020.
- [54] Mahya Seyedan, Fereshteh Mafakheri, "Predictive big data analytics for supply chain demand forecasting: methods, applications, and research opportunities", *journal of Big Data*, vol. 53, no.7, 2020.
- [55] S. Chehbi-Gamoura, Ridha Derrouiche, et al, "Insights from big Data Analytics in supply chain management: an all-inclusive literature review using the SCOR model", *Production Planning & Control*, vol. 3, no. 5, pp. 355-382, 2018.
- [56] Nada R. Sanders, "How to use big data to drive your supply chain", *California Management Review*, vol. 58, no. 3, 2017.

- [57] Verma, Jai Prakash, et al, "Big data analytics: Challenges and applications for text, audio, video, and social media data", *International Journal on Soft Computing, Artificial Intelligence and Applications (IJSCAI)*, vol. 5, no. 1, pp. 41-51, 2016.
- [58] Kirill Kovalenko, "Common data quality management issues and their business impact", *BizData*, 2019.
- [59] Nkonyana, Thembinkosi, et la, "Impact of poor data quality in remotely sensed data", *Artificial Intelligence and Evolutionary Computations in Engineering Systems*, Springer, Singapore, vol. 765, pp. 79-86, 2018.
- [60] Lisa C. Günther, Eduardo Colangelo, "Data quality assessment for improved decision-making: a methodology for small and medium-sized enterprises", *Procedia Manufacturing*, vol. 29, pp. 583-591, 2019.
- [61] Chmielewski, M., "An MTurk crisis? Shifts in data quality and the impact on study results", *Social Psychological and Personality Science*, vol. 11, no. 4, pp. 464-473, 2020.
- [62] Nwokeji, Joshua C, et al, "Panel: Addressing the Shortage of Big Data Skills with Inter-Disciplinary Big Data Curriculum", *IEEE Frontiers in Education Conference (FIE)*, pp. 1-4, 2019.
- [63] Iqbal, Muhammad, et al, "A study of big data for business growth in SMEs: Opportunities & challenges", *International Conference on Computing, Mathematics and Engineering Technologies (iCoMET)*, *IEEE*, vol. 18, 2018.
- [64] Lee, In, "Big data: Dimensions, evolution, impacts, and challenges", *Business horizons*, vol. 60, no. 3, pp. 293-303, 2017.
- [65] Flesca, Sergio, et al, "A comprehensive guide through the Italian database research over the last 25 years", *Berlin/Heidelberg, Germany: Springer International Publishing*, vol. 31, pp. 425-439, 2018.
- [66] Khan, Mudassir, et al, "Security and privacy issue of big data over the cloud computing: a comprehensive analysis", *IJRTE-Scopus*, vol. 7, no. 6s, pp. 413-417, 2019.
- [67] Muskan Parihar, "Big Data security and privacy", *International Journal of Engineering Research & Technology*, vol. 10, no. 07, pp. 323-327, 2021.
- [68] Nitin Singh, "Big data technology: developments in current research and emerging landscape", *Enterprise Information Systems*, vol. 13, no. 6, pp. 801-831, 2019.
- [69] Alex Bekker, "The 'Scary' Seven: big data challenges and ways to solve them", *ScienceSoft*, 2018.
- [70] Du, Guansan, et al, "Application of innovative risk early warning mode under big data technology in Internet credit financial risk assessment", *Journal of Computational and Applied Mathematics*, vol. 386, p.113260, 2021.
- [71] Wright, Len Tiu, et al, "Adoption of big data technology for innovation in B2B marketing", *Journal of Business-to-Business Marketing*, vol. 26, no. 3-4, pp. 281-293, 2019.
- [72] Rossi, & HIRAMA, et al, "Characterizing Big Data Management", *Issues in Informing Science and Information Technology*, vol. 12, no. 03, pp. 165-180, 2015.
- [73] Mohammadi, Mehdi, et al, "Enabling cognitive smart cities using big data and machine learning: Approaches and challenges", *IEEE Communications Magazine*, vol. 56, no. 2, pp. 94-101, 2018.
- [74] Josh Fruhlinger, Zeus Kerravala, "What are data centers? How they work and how they are changing in size and scope", *Network World*, vol. 34, no. 5, 2020.
- [75] Chandan Gaur, "Top 6 Big Data Challenges and Solutions to Overcome", *Enterprise Data Management, XENONSTACK*, 2020.
- [76] Wahyudi, Agung, et al, "A process pattern model for tackling and improving big data quality", *Information Systems Frontiers*, vol. 20, no. 3, pp. 457-469, 2018.
- [77] Manasi Sakpal, "How to Improve Your Data Quality", *Experience Data and Analytics conferences, Gartner*, 2021.
- [78] Ravi, Akash, "If we didn't solve small data in the past, how can we solve Big Data today?", *Certified Network Infrastructure Technician*, vol. 2111, no. 0442, 2021.
- [79] Jen DuBois, "The Data Scientist Shortage in 2020", *QuantHub*, 2020.
- [80] Ramgopal Kashyap, "Big data analytics challenges and solutions", *Amity School of Engineering & Technology, Raipur, India*, vol. 19, no. 08, 2019.
- [81] Tahir, Hassane, and Patrick Brézillon, "Considering Context in Procedures of Personal Data Discovery", *International Conference on Electrical, Computer, Communications and Mechatronics Engineering (ICECCME)*, *IEEE*, pp. 1-5, 2021.
- [82] Terentyev, Olexander, "Data protection by means of firewalls of new generation", *International scientific journal Transfer of Innovative Technologies*, vol. 3, no. 1, pp. 90-92, 2020.
- [83] Novak, Andrej, et, al, "Product decision-making information systems, real-time sensor networks, and artificial intelligence-driven big data analytics in sustainable Industry 4.0", *Economics, Management and Financial Markets*, vol. 16, no. 2, pp. 62-72, 2021.

K-Means Customers Clustering by their RFMT and Score Satisfaction Analysis

Doae Mensouri, Abdellah Azmani, Monir Azmani
Intelligent Automation Laboratory, FST of Tangier
Abdelmalek Essaadi University, Tetouan, Morocco

Abstract—Businesses derive more revenue from building and maintaining long-term relationships with their customers. Therefore, it is essential to build refined strategies based on customer relationship management, with the purpose of increasing their turnover and profits while retaining their customers. In this context, customer segmentation, which is at the heart of marketing strategy, makes it possible to determine the answers to questions relating to the number of investments to be released, the marketing campaigns to be organized, and the development strategy to be implemented. This paper develops an extended RFMT (Recency, Frequency, Monetary, and Interpurchase Time) model, namely the RFMTS model, by introducing a new dimension as satisfaction ‘S’. The aim of this model is to analyze online consumer satisfaction over time and discern changes to implement customer segmentation. This article proposes an approach to a segmentation, by client clustering along the unsupervised machine learning method k-means based on data generated using the proposed RFMTS model, in order to improve the customer relationship and develop more effective personalized marketing strategies. The study shows that including satisfaction to the existing RFM model for customer clustering has a major impact and helps identify customers who are satisfied and those who are not, unlike previous attempts to develop new RFM models. By ignoring the “satisfaction” indicator, what went well and what didn't went well cannot be understood. Consequently, the business loses its unsatisfied, loyal, and profitable customers and either fails or relies only on the satisfied ones to continue making profits for an indefinite period of time.

Keywords—Customer segmentation; customer satisfaction; RFMT model; machine learning; k-means

I. INTRODUCTION

As modern economies are primarily service-based, businesses increasingly derive revenue from building and maintaining long-term relationships with their customers. The key to a sustainable e-commerce business is understanding customer characteristics for personalized marketing strategies [1]. In such an environment, marketing aims to maximize customer value [2] and satisfaction, as well as the equity that characterizes the sum of these for all customers of the company.

This study focuses on customer segmentation based on behavioral data due to its availability and evaluation with time. RFM analysis is one of the most renowned techniques used to evaluate customers based on their buying behavior. After collecting and pretreating the data, a new model named RFMTS by adding a new dimension is proposed, which is

satisfaction, to the shopping behavior characteristics. Once the values of the new RFMTS model are calculated, k-means the most well-known and widely used clustering method [3], [4] is applied to variables to segment customers. Finally, the behavior of each cluster is analyzed to derive insights and help retailers make the right decisions for each cluster. Grouping customers into different groups on one hand helps to understand customers' needs [5]. On the other hand it allows a company to operate its subsequent segmentation in order to optimize its resources, as well as its sales and marketing efforts [6]. Furthermore, taking customer satisfaction into consideration helps to develop effective marketing strategies and reinforce customers loyalty. Customer satisfaction reflects the difference between the expected and perceived quality of a service [7]. In order to benefit from a large share of the market, companies try their best to reach higher levels of customer satisfaction, which is an important driving force for revenue growth [8], by improving their services [9]. The level of satisfaction determines whether a customer would like to order once again, and become loyal or leave the company [10]. Thus, the motivation for this study to include the satisfaction factor. The application of this approach is made on the e-commerce public dataset, which connects small businesses, but it can be applied to any set of data from which the five RFMTS variables can be extracted.

II. RELATED WORK

A. RFM (Recency, Frequency, Monetary)

RFM was first developed by A. M. Hughes [11] as a method of analyzing customer value. Over the past few decades this models have become a widespread paradigm for behavioral segmentation [12]–[14]. RFM makes it possible to distinguish, at a given moment, customers according to a value which is determined from their time interval since the recording of their last order, their frequency of purchases and the amount spent on their purchases.

- Recency (R): represents the value of the period between a customer's last purchase and current moment. A smaller value of recency implies that the customer purchase frequently. Similarly, a big value implies that the customer won't make a purchase shortly.
- Frequency (F): represents the number of purchases made by the customer. It is equal to the total number of purchases. A high value of frequency implies a high level of customer loyalty.

- Monetary value (M): represents the average value of a given customer's purchases. This is equal to the sum of all customer's purchases divided by the total number of purchases. A customer with a high monetary value, is a customer who provides high revenue to the company.

Several publications have attempted to develop new RFM models, taking into account additional variables, to test whether they perform better than the traditional RFM model. For example, Yeh et al. [14] extended the RFM model, namely RFMTC, by adding two parameters time since first purchase (T) and churn probability (C). In 2012, Alvandi et al. and Wei et al. [15] have developed LRFM model taking into account the duration (L) between the first and the last purchase of a customer. Based on the previous model, Peker et al. proposed a new one (LRFMP) by including the customer visit period (P) [16]. In 2017, Moghaddam et al. developed a new RFM model, namely RFMV, by adding a variable of variety of products (V) [17]. In 2018, Yoseph and Heikkila [18] introduced purchase rate of change (C) to show the quantity and sign of change in customer buying behavior. In 2021, a new parameter was introduced, the inter-purchase Time (T), defined as the time interval between two consecutive purchases by a customer in the same store or on the same website [1]. However, these expanded RFM models lack information revealing customer satisfaction ratings. In this regard, in this paper, RFMT model is extended as RFMTS model by taking satisfaction (S) into account.

B. Customer Satisfaction

The existence of many service providers depends heavily on their competitive advantage in terms of customer satisfaction (CS) [19]. Existing studies [20], [21] have argued that modeling CS is an important research topic. Fornell defined CS as the overall evaluation of the quality of a product or service by a customer based on his purchase and consumption experience [22]. While R. L. Oliver [23] defined it as a judgment of the comfort level of a product/service feature or the product or service itself provides (or is providing) satisfaction related to consumption, including levels of underachievement or overachievement. Customer satisfaction has been examined extensively in past research, which includes the impacts of customer satisfaction [24], [25] and identify the determinants of CS [20], [26]. Customer satisfaction has not been introduced into the extant RFM model for customer segmentation. This article intended to introduce Satisfaction into the RFMT model to create a better performed model, namely RFMTS. Natural language processing is generally used to increase knowledge concerning customer satisfaction [27]. In this study S is equal to the sum of all customer's review score divided by the total number of reviews, since the review score is already defined in the database. Let $RS_0 \dots RS_n$ be the review scores given by a customer c, thus the Sc value can be calculated as follows (Equation 1).

$$Sc = \frac{\sum_{i=0}^n RS_i}{n+1} \quad (1)$$

C. Decision Making

RFMTS model can be used to segment customers in order to identify which customers are satisfied, unsatisfied, active, promising, lost, basic, low-value purchasers, loyal high spenders, at risk. Understanding segments can help retailers better tailor their products, marketing strategies and investments. Several combinations of R, F, M, T, S are possible, some canceling out in front of the others. Table I shows the characteristics of the segments and the actions to take into account when dealing with some of them.

TABLE I. SEGMENTS CHARACTERISTICS

Segment characteristics	Action
High R, High F, High M, Short T, High S	Loyal customers: improve their value by enticing them to place a few more orders. Increase their loyalty by offering exclusive perks that only the best customers can access.
High R, High F, High M, Short T, Low S	Loyal unsatisfied customers: solve their problems as fast as possible, can't lose them at any cost.
High R, Low F, Low M, Short T, High S	Promising customers: turn them into loyal customers by earning their trust, providing great service, and making them lives easier.
Weak R, Low F, Low M, Long T, Low S	Lost customers: identify their cause of dissatisfaction, learn from it and design campaigns to reactivate them
High R, Low F, High M, Moderate T, High S	Active customers: just like basic ones, keep them interested and active by personalizing their offers.
Weak R, Low F, Moderate M, Short T, High S	Basic customers: maximize their value by personalizing the offers intended for them. Take responsibility and offer a sincere apology if an error has occurred

III. IMPLEMENTATION

A. Data Origin

The application of the approach presented in this article, is based on a dataset provided by Olist Store, the largest store in Brazilian markets that connects small businesses. Therefore, this dataset contains many purchases made between the periods 2016-2018 in different stores that used the Olist service. It is an open-source database, downloadable from the Kaggle site (<https://www.kaggle.com>), known as "Brazilian E-Commerce Public Dataset" and whose Fig. 1 illustrates its model with its different objects and their associations. In the application of the approach presented here, only the Payments, Customers, Orders and Reviews sub datasets (described by Tables II, III, IV and V) are used because they contain the variables necessary for the different variables' calculations.

Initially the number of rows of the Customers, Orders, Payments, and Reviews sub datasets is 99.441, 99.478, 99.478 and 98.410 respectively. A first filter was performed to keep only the orders already concluded (order_status column) reducing their size to 96,478. For the customer data subset, after a first filtering only clients of the concluded orders were kept, its cardinality is no more than 93357. As for the payment, it had to be adapted to that of the orders with the same number of elements.

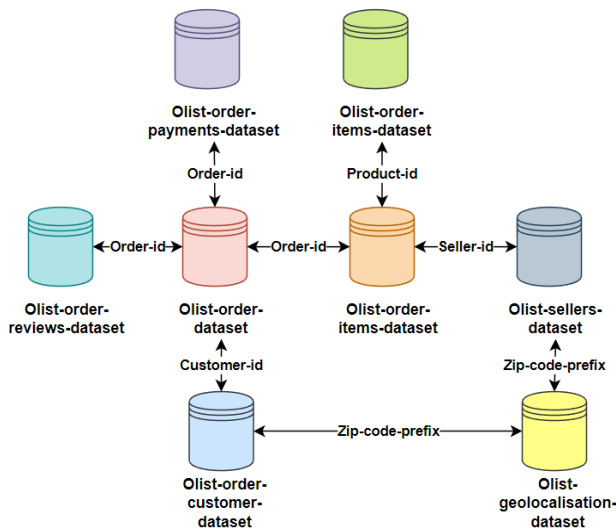


Fig. 1. The Dataset.

TABLE II. PAYMENTS DATASET

Column	Description
Order_id	Order id
Payment_sequential	Sequences of the payments made in case of EMI
Payment_type	Mode of payment
Payment_installments	Number of installments in case of EMI purchase
Payment_value	Total amount paid for the purchase order

TABLE III. CUSTOMERS DATASET

Column	Description
Customer_id	Customer id
Customer_unique_id	Unique id of the Customer
Customer_zip_code_prefix	Zip code of customer's location
Customer_city	Customer's City
Customer_state	Customer's State

TABLE IV. ORDERS DATASET

Column	Description
Order_id	Order id
Customer_id	Customer id
Order_status	Order status.i.e shipped, delivered
Order_purchase_timeslamp	Timeslamp of the purchase
Order_approved_at	Timeslamp of the order approval

TABLE V. REVIEWS DATASET

Column	Description
review_id	Id of the review given on the product ordered by the order id.
order_id	A unique id of order made by the consumers.
review_score	review score given by the customer for each order on the scale of 1–5.
review_comment_title	Title of the review
review_comment_message	Review comments posted by the consumer for each order.

B. Data Preparation

Once the three sub datasets have been filtered and prepared, the next step is to merge them by their respective primary keys (customer_id, order_id) into a single dataset (Table VI) that will be used to generate other data including the CLV of each customer. However, the generation of CLVs which is done from the models of the Lifetimes library requires, as mentioned above, the application of the RFMTS model with the determination, for each of the 93357client its five variables: recency R, frequency F, monetary value M, regularity of purchase T (Time) and satisfaction S.

C. Generation of Customer Data by Application of the RFMTS Model

At this level, the set of data constituted above (Table VI) will be enriched by the generation for each customer of the five aforementioned factors: Recency, Frequency, Monetary, and Regularity of purchase and Satisfaction value.

To be able to carry out certain calculations, it is necessary to specify the date during which this calculation must be carried out to simulate an immediate study of the transactions of the company. To be consistent with the initial dataset, August 29, 2018, is chosen as the last purchase made. As explained before, recency of each customer is equal to the period between the last purchase and August 29, 2018. Frequency is equal to the total number of purchases made by a customer. Monetary value is equal to the sum of all customer's purchases divided by the total number of purchases. Inter-purchase Time is equal to the period between the last and the first purchase divided by the frequency. The fifth variable, Satisfaction (S), measures the average customer's satisfaction S, it is equal to the sum of all review score divided by the total number of reviews given by a customer.

Table VII presents the new configuration of the study dataset after the generation of R, F, M, T and S for each customer.

D. Clustering Customers based on RFMTS Model

After calculating the variables, Recency, Frequency, Monetary value, Inter-purchase time and satisfaction (Table VII), the next step is grouping the consumers based on the RFMTS model. For this an unsupervised Machine Learning method K-Means is using here.

TABLE VI. INITIAL DATASET

Customer ID	Order ID	Order Purchase Time	Payment Value	Review Score
0a0a...a872	e481f...d6af7	10/2/2017 10:56	10.11	4
c846...84a1	9c5de...053c	10/2/2017 10:56	18.12	4
763c...2b93	11c17...7b62	10/2/2017 10:56	25.59	3
...
9b7f...77d6	53cdb2...3451	7/24/2018 20:41	142.14	4
455c...ba1b	4777...ec65d	8/8/2018 8:38	20.46	1

TABLE VII. DATA AFTER CALCULATION F,R,M,T AND S

Customer ID	R	F	M	T	S
0a0a...a872	411.96	2	46.31	121.66	4.34
c846...84a1	140.34	2.17	83.06	121.66	4.77
763c...2b93	210.55	2.30	220.76	91.25	3.17
...
9b7f...77d6	210.54	1.87	5675.43	170	4.05
455c...ba1b	1350.29	2.15	130.89	320.27	1.24

1) About K-means: As shown in Fig. 2, the k-means algorithm procedure is a simple and easy way to classify a data set through a specified number K of clusters a priori [28], [29]. Each cluster is characterized by its center of gravity, that is, its central point whose coordinates are obtained by calculating the average of each of the coordinates of the sample points assigned to the clusters.

2) K-means customers clustering: Before using it, it was necessary to normalize the variables, because since it is a model that works with the distances of the data, the dimensions and magnitudes play a very important role in its implementation. As an example. Table VIII presents the array of normalized data.

In the case of this study, the “elbow method” was used to indicate the number of clusters which reduces the inertia (proximity of points to their centroid) to a relevant point [30].

Initialization
 Choosing the starting points that are used as initial estimates of cluster centroids. They are taken as initial starting values.

Loop:

- **Build k clusters:** examine each point of the data set and assign it to the cluster whose centroid is closest.
- **The new centroids are calculated:** when each point in the data set is assigned to a cluster, it is necessary to recalculate the new centroids k.

Until

- No point changes its cluster assignment or until the centroids no longer move.

Fig. 2. K-means Clustering Algorithm.

TABLE VIII. ARRAY OF NORMALIZED DATA

```
array ([[[-0.82886279, -0.84339079, -0.19094101, -0.10203975, -2.29586173],
[-0.80920189, -0.82379511, -0.19094101, -0.60932832, -0.06528104],
[ 1.96298496, 1.9391955, -0.19094101, -0.34827659, 0.67824586],
...,
[ 2.16614759, 2.14168417, -0.19094101, -0.23223394, 0.67824586],
[-0.77643372, -0.79113565, -0.19094101, -0.1383473, 0.67824586],
[ 1.6156424, 1.59300518, -0.19094101, -0.41310834, 0.67824586]])
```

TABLE IX. NUMBER OF CUSTOMERS PER CLUSTER

Cluster	Customer
0	14203
1	41730
2	30313
3	5167
4	1994

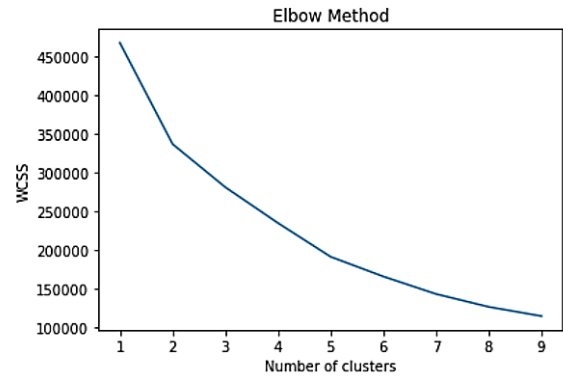


Fig. 3. Elbow Method.

Fig. 3 shows that the number five is the most appropriate for the segmentation. With this number of clusters, the model was trained with the scaled database and attaches the created labels to the initial Table VII.

At first glance, it can be seen from Table IX that the “0” cluster clearly refers to the group with the highest shopping users. A better visualization, of these new segments, can have place by using PCA to reduce the variables into two and be able to translate them into a scatter plot.

K-Means model did a good job of clustering the customers, but from the result of the graph (Fig. 4) and the number of customers per cluster (Table IX), it can be noticed that the order of the clusters does not really represent the importance of the customer versus profitability. This mini theory can be corroborated by looking at the R, F, M, T, S of each cluster (Table X).

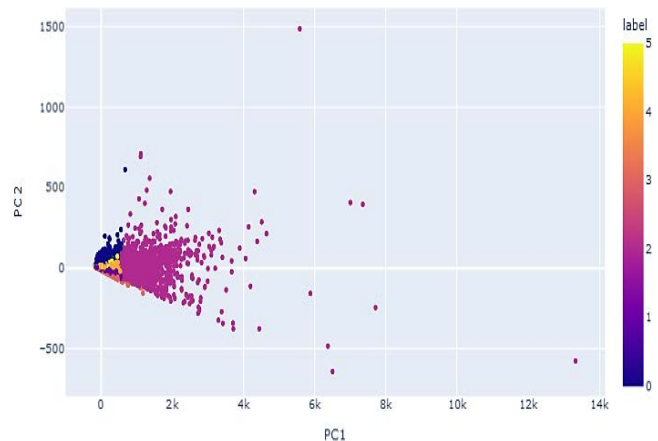


Fig. 4. PCA Dataset Visualization.

TABLE X. AVERAGE RFMTS OF EACH CLUSTER

Cluster	R	F	M	T	S
0	212.91	2.25	204.84	273.75	3.15
1	152.08	2.19	70	30.41	4.65
2	395.41	2	28.33	10.34	4.51
3	1216.66	2.05	100.85	395.41	1.51
4	212.91	1.50	281.91	152.08	4.08

3) *Visualisation and analysis of the result:* Each cluster represents a segmentation of the market. To make the right decisions and develop efficient marketing strategies, it's necessary to analyze and understand the characteristics of each cluster. The RFMTS characteristics of each cluster are analyzed in this section. Table X lists the average RFMTS values of each cluster. Fig. 5, to Fig. 9 represent the distribution of the five clusters according to the respective distributions R, F, M, T, and S. The x axis of these figures represents the different clusters of customers, while the y axis represents the respective RFMTS values. The height of each rectangle is the range of y value variation, while the y value that lines up exactly with the line inside the rectangle represents the average value. The dataset used in this study contains 93357 customers. Fig. 10 shows the number of customers included in each one of the five clusters (C0, C1, C2, C3, and C4). Among the five clusters, cluster 0 (C0) has the highest percentage of the customers, equal to 44.7%, while cluster 4 (C4) has the lowest percentage of the customers, equal to 2.1%.

Cluster 0: contained 15.2% of the total customers (Fig. 10). It's characterized by a high R (7.95 months), low F (2.25), high M (\$204,84), moderate T (9.46 months) and moderate S (3.15). Most customers in this cluster spend around \$204.84. The last shopping date was around 9,46 months ago. The average satisfaction rating is around 3,15. Therefore, this cluster can be labeled as an active satisfied group.

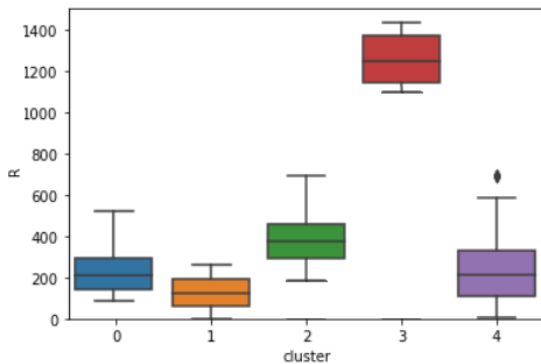


Fig. 5. Distribution of the Five Clusters According to R.

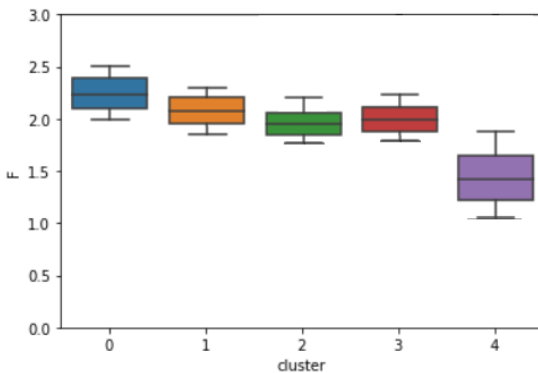


Fig. 6. Distribution of the Five Clusters According to F.

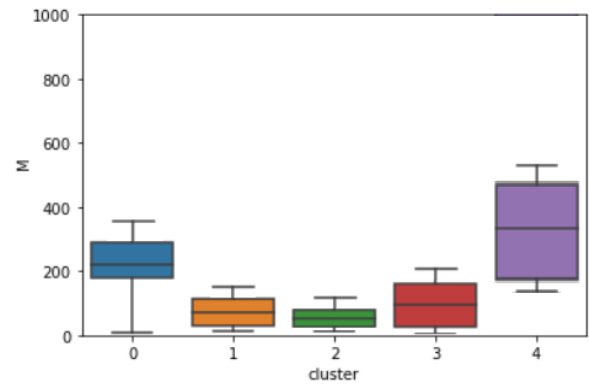


Fig. 7. Distribution of the Five Clusters According to M.

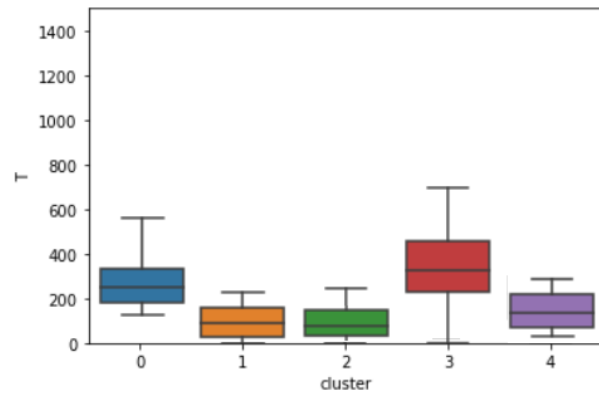


Fig. 8. Distribution of the Five Clusters According to T.

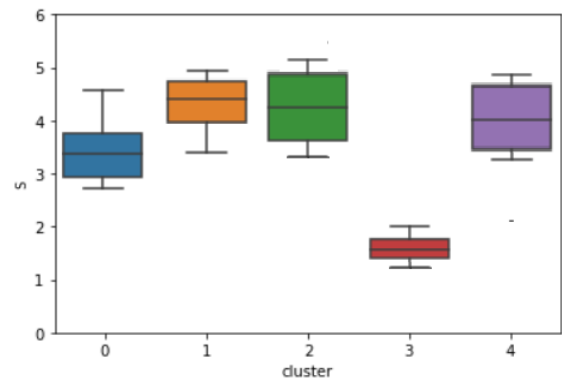


Fig. 9. Distribution of the Five Clusters According to S.

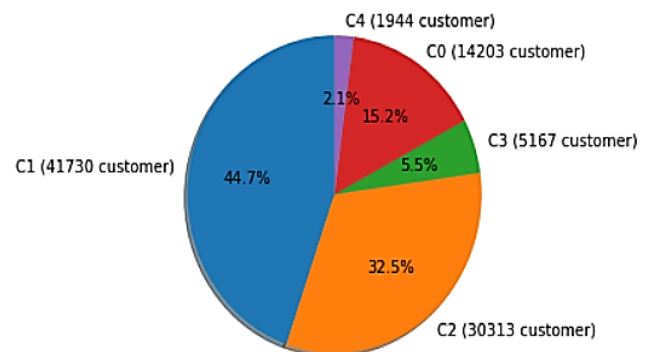


Fig. 10. Clusters Size.

Cluster 1: as the largest sized group, Cluster 0 represents 44.7% of all customers (Fig. 10). It's characterized by a high R (5.17 months), low F (2.19), low M (\$70), short T (1.17 months) and a high S (4.65). The last purchase date was about 5.17 months ago. Even if M is low, the satisfaction is high, and T is short. Therefore, cluster 0 can be considered as a promising satisfied group.

Cluster 2: represents 32.5% of the total customers (Fig. 10). This cluster is characterized by a low R (13.05 months), low F (2), low M (\$28.33), short T (0.34 months) and a high S (4.51). Customers in this cluster spent an average of \$28.33, shopped twice in a short time, and their last purchase was around a year ago, and gave high ratings. Therefore, cluster 2 can be considered as the basic group.

Cluster 3: contained 5.5% of the total customers (Fig. 10). It is characterized by a weak R (40.03 months), a low F (2.05), a moderate M (\$100.85), a long T (13.05 month) and a low S (1.51). It is the only cluster that simultaneously had low R, F, and S. Even if the average expense is around \$100,85, the last purchase in this cluster was about 40,03 months ago, and the satisfaction is really low. Therefore, Cluster 3 can be considered as lost unsatisfied group.

Cluster 4: as the smallest sized group, cluster 4 represents 2,1% of all customers (Fig. 10). This cluster is characterized by a high R (7.56 months), low F (1.50), high M (\$281.91), moderate T (5.66) and a high S (4.08). The most recent shopping date was about 7.56 months ago, the average spend is around \$281.91, and the ratings are high. For these reasons, this cluster can be labeled as a gold profitable group.

Table XI represent the final table after assigning the corresponding cluster label to each customer.

TABLE XI. FINAL DATASET

Customer ID	R	F	M	T	S	Cluster
0a0a...a872	411.96	2	46.31	121.66	4.34	Basic
c846...84a1	140.34	2.17	83.06	121.66	4.77	Promising satisfied
763c...2b93	210.55	2.30	220.76	91.25	3.17	Active satisfied
...
9b7f...77d6	210.54	1.87	5675.43	170	4.05	Gold profitable
455c...ba1b	1350.29	2.15	130.89	320.27	1.24	Lost unsatisfied

IV. DISCUSSION AND RECOMMENDATIONS

This study is a sort of monograph on the importance of customer satisfaction. Its purpose is to segment customers, the heart of marketing strategy [31]. After pretreating the e-commerce dataset, RFMTS values were calculated for each customer. K-means was then used to segment the customers into five clusters. Finally, a cluster analysis was conducted to identify the characteristics of each customer's cluster. Cluster 0 is regarded as the active satisfied group. C1 is the promising group. While C2 contains basic customers, C3 is thought to be

a lost unsatisfied group. C4 is the gold-loyal group. Every company is trying its best to make their customers happy in a business environment that's highly competitive [32], [33]. Compared to previous work based on the RFMT model [1], the clusters obtained (lost group, promising, profitable, active profitable, and loyal) value the profitability of customers but neglect their satisfaction, which is a key factor for any successful and sustainable business. In turbulent markets, a company's reputation largely depends on customer satisfaction [34]. Failing to take customer satisfaction into account can lead to a marketing strategy that is not in line with the interests of customers and therefore have a negative effect on the business. Even if, in the case of this study, the satisfaction rate is high, the company should not rest on its laurels because everything can change, since trade is an area in perpetual transformation (competition, influence, exchange rate).

Finding new customers for the enterprise is essential, but retaining existing customers [35] can be even more important and profitable. Therefore, the company should develop marketing strategies to retain its customers.

- Increase the trust: trust is the belief that the other party of the exchange will not take advantage of opportunistic behavior and will act in a good manner [36]. It has been proven that trust has an important impact on customer purchase intention [37] and that it's a critical factor for online enterprises' success. Keeping the promises made to customers is essential to increasing customer trust and loyalty.
- Increase the net benefits: net benefit of online shopping includes both utilitarian and hedonic value [38]. It's the global benefits received from customers while shopping online. It includes enjoyment, monetary gain, delivery time and after sales service.
- Improve system quality: System quality has a significant impact on online customer satisfaction and decision-making [39], [40]. System quality includes the elements that evaluate the performance of a website, website design, page loading speed, website crashing, interruption, flexibility, and ease of navigation between pages.
- Increase customer reacquisition: customer defection is the decision to end a contract with a specific company [5], [41], [42]. Customer reacquisition provides companies with high economic benefits. An average business has a 60-70% chance of successfully reselling to active buyers, 20-40% to lost customers, and only a 5-20% chance of successfully sale to new prospects [43].

V. CONCLUSION AND OUTLOOK

Segmentation helps to identify potential customers and understand their needs, which increases business revenue. Based on the existent RFMT (i.e., Recency, Frequency, Monetary, and Time) model, satisfaction (S) value was added to create a new model called RFMTS for better customer segmentation. The new model created can be applied to any

dataset from which the 5 variables (recency, frequency, monetary, time, and satisfaction) can be extracted. This study started with a typical relational database of an e-commerce site and ended with a segmentation of each of its customers according to their purchasing behaviors and satisfaction. After the customers' clusters are defined, business strategies can be generated to improve customer relationships.

Grouping customers into different groups based of the proposed RFMTS model helps decision makers identify market segments more clearly and thus develop more effective marketing and sales strategies to build customer loyalty [44]. This study opens the door to many outlooks, for example: Reinforced learning can be based on the results obtained in order to identify the cluster target of each type of offers. Being able to identify the best target for a specific offer allow the company to win at several levels, whether it be at the investment level, that the level of customer satisfaction, knowing that they prefer to receive that the adequate offers to their preferences.

ACKNOWLEDGMENT

This research is supported by the Ministry of Higher Education, Scientific Research and Innovation, the Digital Development Agency (DDA) and the National Center for Scientific and Technical Research (CNRST) of Morocco (Smart DLSP Project - AL KHAWARIZMI IA-PROGRAM).

REFERENCES

- [1] Z. Jinfeng, W. Jinliang, and X. Bugao, "Customer segmentation by web content mining," *Journal of Retailing and Consumer Services*, vol. 61, p. 102588, Jul. 2021, doi: 10.1016/j.jretconser.2021.102588.
- [2] S. Gupta et al., "Modeling Customer Lifetime Value," *Journal of Service Research*, vol. 9, no. 2, pp. 139–155, Nov. 2006, doi: 10.1177/1094670506293810.
- [3] K. P. Sinaga and M.-S. Yang, "Unsupervised K-Means Clustering Algorithm," *IEEE Access*, vol. 8, pp. 80716–80727, 2020, doi: 10.1109/ACCESS.2020.2988796.
- [4] J. MacQueen, "Some methods for classification and analysis of multivariate observations," *Proceedings of the Fifth Berkeley Symposium on Mathematical Statistics and Probability, Volume 1: Statistics*, vol. 5.1, pp. 281–298, Jan. 1967.
- [5] M. Chandar, A. Laha, and P. Krishna, "Modeling churn behavior of bank customers using predictive data mining techniques.," 2006, pp. 24–26.
- [6] R. Lefébure and G. Venturi, *Gestion de la relation client: Edition 2005*. Eyrolles, 2011.
- [7] P. Padma and J. Ahn, "Guest satisfaction & dissatisfaction in luxury hotels: An application of big data," *International Journal of Hospitality Management*, vol. 84, p. 102318, Jan. 2020, doi: 10.1016/j.ijhm.2019.102318.
- [8] D. Gursoy and C. Chi, "Effects of COVID-19 pandemic on hospitality industry: review of the current situations and a research agenda," 2020.
- [9] R. Dabestani, A. Shahin, and M. Saljoughian, "Evaluation and prioritization of service quality dimensions based on gap analysis with analytic network process," 2017, doi: 10.1108/IJQRM-04-2015-0050.
- [10] M. A. Shbool, A. Al-Bazi, and R. Al-Hadeethi, "The effect of customer satisfaction on parcel delivery operations using autonomous vehicles: An agent-based simulation study," *Heliyon*, vol. 8, no. 5, p. e09409, May 2022, doi: 10.1016/j.heliyon.2022.e09409.
- [11] A. M. Hughes, *Strategic database marketing: the masterplan for starting and managing a profitable, customer-based marketing program*. Chicago, Ill: Probus Pub. Co., 1994.
- [12] I. Maryani, D. Riana, R. D. Astuti, A. Ishaq, Sutrisno, and E. A. Pratama, "Customer Segmentation based on RFM model and Clustering Techniques With K-Means Algorithm," in 2018 Third International Conference on Informatics and Computing (ICIC), Oct. 2018, pp. 1–6. doi: 10.1109/IAC.2018.8780570.
- [13] A. J. Christy, A. Umamakeswari, L. Priyatharsini, and A. Neyaa, "RFM ranking - An effective approach to customer segmentation," *J. King Saud Univ. Comput. Inf. Sci.*, 2018, doi: 10.1016/j.jksuci.2018.09.004.
- [14] I.-C. Yeh, K.-J. Yang, and T.-M. Ting, "Knowledge discovery on RFM model using Bernoulli sequence," *Expert Systems with Applications*, vol. 36, no. 3, Part 2, pp. 5866–5871, Apr. 2009, doi: 10.1016/j.eswa.2008.07.018.
- [15] M. Alvandi, S. Fazli, and F. Abdoli, "K-Mean Clustering Method For Analysis Customer Lifetime Value With LRFM Relationship Model In Banking Services," 2012. <https://www.semanticscholar.org/paper/K-Mean-Clustering-Method-For-Analysis-Customer-With-Alvandi-Fazli/54ac58708a608bee195e9f60825a61da51ebbcf1> (accessed May 17, 2022).
- [16] S. Peker, A. Kocyigit, and P. E. Eren, "LRFMP model for customer segmentation in the grocery retail industry: a case study," *Marketing Intelligence & Planning*, vol. 35, no. 4, pp. 544–559, Jan. 2017, doi: 10.1108/MIP-11-2016-0210.
- [17] S. Q. Moghaddam, N. Abdolvand, and S. Rajaee Harandi, "A RFMV model and customer segmentation based on variety of products," *Journal of Information Systems and Telecommunication*, vol. 5, pp. 155–161, Jun. 2017.
- [18] F. Yoseph and M. Heikkila, "Segmenting Retail Customers with an Enhanced RFM and a Hybrid Regression/Clustering Method," 2018 International Conference on Machine Learning and Data Engineering (iCMLDE), 2018, doi: 10.1109/ICMLDE.2018.00029.
- [19] A. P. Darko and D. Liang, "Modeling customer satisfaction through online reviews: A FlowSort group decision model under probabilistic linguistic settings," *Expert Systems with Applications*, vol. 195, p. 116649, Jun. 2022, doi: 10.1016/j.eswa.2022.116649.
- [20] A. Ahani et al., "Revealing customers' satisfaction and preferences through online review analysis: The case of Canary Islands hotels," *Journal of Retailing and Consumer Services*, vol. 51, pp. 331–343, Nov. 2019, doi: 10.1016/j.jretconser.2019.06.014.
- [21] J.-W. Bi, Y. Liu, Z.-P. Fan, and E. Cambria, "Modelling customer satisfaction from online reviews using ensemble neural network and effect-based Kano model," *International Journal of Production Research*, vol. 57, no. 22, pp. 7068–7088, Nov. 2019, doi: 10.1080/00207543.2019.1574989.
- [22] C. Fornell, "A National Customer Satisfaction Barometer: The Swedish Experience," *Journal of Marketing*, vol. 56, no. 1, pp. 6–21, 1992, doi: 10.2307/1252129.
- [23] R. L. Oliver, *Satisfaction: A Behavioral Perspective on the Consumer*. McGraw Hill, 1997.
- [24] D. Lee, J. Moon, Y. J. Kim, and M. Y. Yi, "Antecedents and consequences of mobile phone usability: Linking simplicity and interactivity to satisfaction, trust, and brand loyalty," *Information & Management*, vol. 52, no. 3, pp. 295–304, Apr. 2015, doi: 10.1016/j.im.2014.12.001.
- [25] C. Liao, H.-N. Lin, M. M. Luo, and S. Chea, "Factors influencing online shoppers' repurchase intentions: The roles of satisfaction and regret," *Inf. Manag.*, 2017, doi: 10.1016/j.im.2016.12.005.
- [26] E. Park, Y. Jang, J. Kim, N. J. Jeong, K. Bae, and A. P. del Pobil, "Determinants of customer satisfaction with airline services: An analysis of customer feedback big data," *Journal of Retailing and Consumer Services*, vol. 51, pp. 186–190, Nov. 2019, doi: 10.1016/j.jretconser.2019.06.009.
- [27] Y. Piris and A.-C. Gay, "Customer satisfaction and natural language processing," *Journal of Business Research*, vol. 124, pp. 264–271, Jan. 2021, doi: 10.1016/j.jbusres.2020.11.065.
- [28] A. Banumathi and A. Pethalakshmi, "Refinement of K-Means and Fuzzy C-Means," *International Journal of Computer Applications*, vol. 39, no. 17, Feb. 2012, Accessed: Oct. 21, 2021. [Online]. Available: <https://www.ijcaonline.org/archives/volume39/number17/4911-7441>.

- [29] R. J. Bharati and V. V. Gohokar, "A Comparative Analysis of Fuzzy C-Means Clustering and K Means Clustering Algorithms," *International Journal Of Computational Engineering Research*, Jun. 2012.
- [30] M. A. Syakur, B. K. Khotimah, E. M. S. Rochman, and B. D. Satoto, "Integration K-Means Clustering Method and Elbow Method For Identification of The Best Customer Profile Cluster," *IOP Conf. Ser.: Mater. Sci. Eng.*, vol. 336, p. 012017, Apr. 2018, doi: 10.1088/1757-899X/336/1/012017.
- [31] M. S. Kahreh, M. Tive, A. Babania, and M. Hesani, "Analyzing the Applications of Customer Lifetime Value (CLV) based on Benefit Segmentation for the Banking Sector," *Procedia - Social and Behavioral Sciences*, vol. 109, pp. 590–594, Jan. 2014, doi: 10.1016/j.sbspro.2013.12.511.
- [32] K. Hellen and M. Saaksjarvi, "Happiness as a predictor of service quality and commitment for utilitarian and hedonic services," *Psychology & Marketing*, vol. 28, no. 9, pp. 934–957, 2011.
- [33] A. Kumar, J. Paul, and S. Starčević, "Do brands make consumers happy?- A masstige theory perspective," *Journal of Retailing and Consumer Services*, vol. 58, p. 102318, Jan. 2021, doi: 10.1016/j.jretconser.2020.102318.
- [34] R. U. Khan, Y. Salamzadeh, Q. Iqbal, and S. Yang, "The Impact of Customer Relationship Management and Company Reputation on Customer Loyalty: The Mediating Role of Customer Satisfaction," *Journal of Relationship Marketing*, vol. 21, no. 1, pp. 1–26, Jan. 2022, doi: 10.1080/15332667.2020.1840904.
- [35] L. Tong, Y. Wang, F. Wen, and X. Li, "The research of customer loyalty improvement in telecom industry based on NPS data mining," *China Communications*, vol. 14, no. 11, pp. 260–268, Nov. 2017, doi: 10.1109/CC.2017.8233665.
- [36] D. Gefen, E. Karahanna, and D. Straub, "Trust and TAM in Online Shopping: An Integrated Model," *MIS Q.*, 2003, doi: 10.2307/30036519.
- [37] M. Tajvidi, Y. Wang, N. Hajli, and P. E. D. Love, "Brand value Co-creation in social commerce: The role of interactivity, social support, and relationship quality," *Computers in Human Behavior*, vol. 115, p. 105238, Feb. 2021, doi: 10.1016/j.chb.2017.11.006.
- [38] T. L. Childers, C. L. Carr, J. Peck, and S. Carson, "Hedonic and utilitarian motivations for online retail shopping behavior," *Journal of Retailing*, vol. 77, no. 4, pp. 511–535, Dec. 2001, doi: 10.1016/S0022-4359(01)00056-2.
- [39] H. H. Bauer, T. Falk, and M. Hammerschmidt, "eTransQual: A transaction process-based approach for capturing service quality in online shopping," *Journal of Business Research*, vol. 59, no. 7, pp. 866–875, Jul. 2006, doi: 10.1016/j.jbusres.2006.01.021.
- [40] D. M. Szymanski and R. T. Hise, "E-satisfaction: an initial examination," *Journal of Retailing*, vol. 76, no. 3, pp. 309–322, Jul. 2000, doi: 10.1016/S0022-4359(00)00035-X.
- [41] K. Stewart, "An exploration of customer exit in retail banking," *International Journal of Bank Marketing*, vol. 16, no. 1, pp. 6–14, Jan. 1998, doi: 10.1108/02652329810197735.
- [42] G. Capponi, N. Corrocher, and L. Zirulia, "Personalized pricing for customer retention: Theory and evidence from mobile communication," *Telecommunications Policy*, vol. 45, no. 1, p. 102069, Feb. 2021, doi: 10.1016/j.telpol.2020.102069.
- [43] J. Griffin and M. W. Lowenstein, *Customer Winback: How to Recapture Lost Customers--And Keep Them Loyal*. Wiley, 2001.
- [44] A. Hiziroglu and S. Sengul, "Investigating Two Customer Lifetime Value Models from Segmentation Perspective," *Procedia - Social and Behavioral Sciences*, vol. 62, pp. 766–774, Oct. 2012, doi: 10.1016/j.sbspro.2012.09.129.

Indoor Positioning System: A Review

N. Syazwani C.J.¹, Nur Haliza Abdul Wahab²
School of Computing, Faculty of Engineering
Universiti Teknologi Malaysia (UTM)
Johor, Malaysia

Noorhazirah Sunar³, Sharifah H. S. Ariffin⁴
School of Electrical, Faculty of Engineering
Universiti Teknologi Malaysia (UTM)
Johor, Malaysia

Keng Yinn Wong⁵
School of Mechanical, Faculty of Engineering
Universiti Teknologi Malaysia (UTM)
Johor, Malaysia

Yichiet Aun⁶
Faculty of Information and Technology,
Universiti Tunku Abdul Rahman (UTAR)
Perak, Malaysia

Abstract—Global Positioning System (GPS) has been developed in outdoor environments in recent years. GPS offers a wide range of applications in outdoor areas, including military, weather forecasting, vehicle tracking, mapping, farming, and many more. In an outdoor environment, an exact location, velocity, and time can be determined by using GPS. Rather than emitting satellite signals, GPS receivers passively receive them. However, due to No Line-of-Sight (NLoS), low signal strength, and low accuracy, GPS is not suitable to be used indoors. As consequence, the indoor environment necessitates a different Indoor Positioning System (IPS) approach that is capable to locate the position within a structure. IPS systems provide a variety of location-based indoor tracking solutions, such as Real-Time Location Systems (RTLS), indoor navigation, inventory management, and first-responder location systems. Different technologies, algorithms, and techniques have been proposed in IPS to determine the position and accuracy of the system. This paper introduces a review article on indoor positioning technologies, algorithms, and techniques. This review paper is expected to deliver a better understanding to the reader and compared the better solutions for IPS by choosing the suitable technologies, algorithms, and techniques that need to be implemented according to their situation.

Keywords—Global positioning system (GPS); indoor positioning system (IPS); real-time location system (RTLS)

I. INTRODUCTION

The positioning system is a method to determine the position of the object in space. In today's economy, many positioning systems are employed in all areas. In general, the positioning system can be divided into three types which are Global Positioning System (GPS), Local Positioning System (LPS), and Hybrid Positioning System (HPS) which have been highly useful in a wide variety of outdoor and indoor environments [1]. GPS is one of many satellites orbiting around the universe. GPS has several uses in a variety of fields in outdoor environments such as military, weather forecasting, vehicle tracking, mapping, farming, etc. [2]. An exact location, velocity, and time can be determined by using GPS. Rather than emitting satellite signals, GPS receivers passively receive them. The object's precision ranges from 2 to 6 meters. However, GPS is not suitable to determine the location indoors because there is

No Line-of-Sight (NLoS), low signal strength, and low accuracy.

LPS is one of the positioning technologies included in electronic performance and tracking systems, as it determines the position of an object in the Cartesian coordinate system [3]. It usually allows users to collect data to keep track of external load needs. Zone (up to 20 meters) and precise placement (from 0.1 to 3 meters) are types of LPS. The use of optimal LPS in an indoor environment becomes necessary with good accuracy, precision, cost, power consumption, and coverage. Wireless Fidelity (Wi-Fi), Bluetooth Low Energy (BLE), Radio Frequency Identification (RFID), and Ultrawideband (UWB) are an example of common wireless communication that is involved in LPS. However, LPS is more complex and expensive compared to GPS due to the deployment of infrastructure and hardware.

Meanwhile, HBS is a combination of GPS with LPS to track items in both outdoor and indoor environments. These systems were created to address the limitations of GPS, which is extremely accurate in open spaces but fails to perform well indoors or between tall buildings. Better position estimations can be determined by hybridizing the positioning information from different technologies. This way, the combination can enhance the system's accuracy and availability in diverse locations [4]. The solution is highly optimized, with opportunistic fingerprint selection and floor change detection minimizing time-consuming processing and a battery-saving subsystem reducing power consumption by turning off unnecessary technologies.

Through all of the positioning systems available, it can be divided into outdoor positioning and indoor positioning. For outdoor positioning, the GPS can always support with high accuracy, but Indoor Positioning Systems (IPS) face more challenges than outdoor positioning due to pervasive hindrances and interaction interference [5], multi-path effect, fading, reflecting, deep shadowing effect, and delay deterioration.

IPS refers to the technology that helps to locate the position of people or objects inside the buildings. The location data is sent into some sort of application software to make the data useful. The design of IPS depends on what type of indoor positioning technologies, indoor positioning algorithms, and

indoor positioning techniques are used in the system. IPS technologies provide a variety of location-based indoor tracking solutions [6], such as Real-Time Location Systems (RTLS), navigation, inventory management, and first-responder location systems.

IPS also can be divided into self-positioning and remote-positioning systems. A self-positioning happened when a system the positioning was measured by the node (device) itself. The node will act as a receiver and the transmitter will be the anchor node surrounding. By using this system, it guarantees privacy, but in another way, it burdens the node with the computational service to measure its location or position. The example of this system should have a reference sensor node also known as an anchor node with a known position and a target such as a node, object or people to be located (device). The reference sensor node sends a range request to the target's compatible mobile device such as a smartphone. Smartphones receive the signals and respond to the reference sensor node with a response. Sensors will calculate the traveling time between sensors and smartphones. The computed time sent by the sensors will then be received by the calculating center. A computation center is often a Personal Computer (PC) or a Base Station (BS). The calculating center, which had a strong computational capability, used a positioning algorithm to process the provided data and obtain the target's location result.

While, for the remote-positioning, the receiver will be placed at the anchor node surrounding while the node (device) will be reacted as the transmitter. The computational system will be a burden on the infrastructure (the server) while the node (device) can have lower power consumption. In this positioning system, the node (device) uses signals, transmitted by the anchor node to calculate its position.

IPS can be divided into two phases which is signal measurement is the first phase. The physical position of the target node will be calculated in the second phase using the signal characteristics collected in the first phase. The most frequent approach is ranging, which involves obtaining distance or angle estimations. Geometric techniques will be used to determine the target node's position as the intersection of position lines derived from position-related parameters at reference nodes. The two most popular geometric approaches are Trilateration and Triangulation. To filter the measurement noise and improve the accuracy, optimization-based statistical techniques are often used. The communication entity associated with individuals is represented in the first phase by certain signals transmitted between the target node and sensor nodes, as well as the number of reference nodes represented by the sensor nodes. At this moment, receivers will be gathering information about the signal's characteristics such as arrival time, signal intensity, and direction.

II. LITERATURE REVIEW

Recently, Wi-Fi technologies in indoor positioning system have been topic of interest among researchers. The subsections that follow present some existing works for indoor positioning that implemented RSSI algorithm and Trilateration technique. RSSI algorithm are the most popular range-based. The primary concept is to use the power of the received signal, knowledge of the broadcast power, and the route loss model to estimate the

distance between a transmitter and the receiver [7]. Trilateration technique is used to determine an object position using simultaneous range measurements from at least three reference APs at known locations.

The BLE with RSSI algorithm were proposed in [7]. Positioning algorithm were implemented in Java using Android SDK and been tested in Huawei B199 smartphone. Four Beacon devices were placed in one room and mobile device were placed in four different positions. The distance between mobile devices with Beacon devices were calculated by using RSSI and filtered by using Kalman Filter. Triangulation was used to calculated the current location of mobile devices. The average accuracy achieved in this system was 0.2 – 0.4m.

Researchers in [8] presented a Beacon Bluetooth device to overcome the limitation of other technologies. The distance estimation of the beacons, the number of signals collected by Android devices, and the internet connection from the Android smartphone all impact the accuracy of the user position. The Trilateration technique was employed in this study, along with a measuring methodology based on RSSI value. The result shows that accuracy achieved is 84%. According to the findings of the test, objects with thickness and density have a significant impact on the RSSI of the Beacon devices. Calibration on Beacons is important for fine-tuning RSSI values at a distance of 1 meter in order to improve the accuracy of the estimated distance between the beacon and the device. Disadvantages of using Bluetooth beacon is, to get high accuracy, more beacon devices need to be installed and resulting high in cost.

Therefore, after reviewing the limitations of other projects, this review suggests an implementation of existing Wi-Fi infrastructure with received signal strength values. In addition, the integration of RSSI algorithm and Trilateration technique with been suggested to determine the improvement of accuracy in the system.

III. INDOOR POSITIONING TECHNOLOGIES

There are many different types of technologies that can be implemented in IPS. It is important to use the correct technology based on the type of positioning that needs to be developed. Satellite-Based, Magnetic-Based, Inertial Sensor-Based, Sound-Based (Audible Sound, Ultrasonic Sound, Acoustic Sound), Optical-Based, Radio Frequency-Based (Wi-Fi, BLE, RFID, and UWB), and Vision-Based [9] are examples of technologies as shown in Fig. 1.

A. Satellite-based

The most popular system for outdoor systems is the Satellite-Based. It is based on a global network of satellites that transmit radio signals in medium-earth orbit. The basic GPS service provides users with an approximately average User Range Error (URE) of less than 7.8 meters 95 percent of the time, anywhere on or near the surface of the earth [10]. Satellite control systems take little effort and cost to set up, but their operation necessitates the installation of monitoring systems and dispatching software.

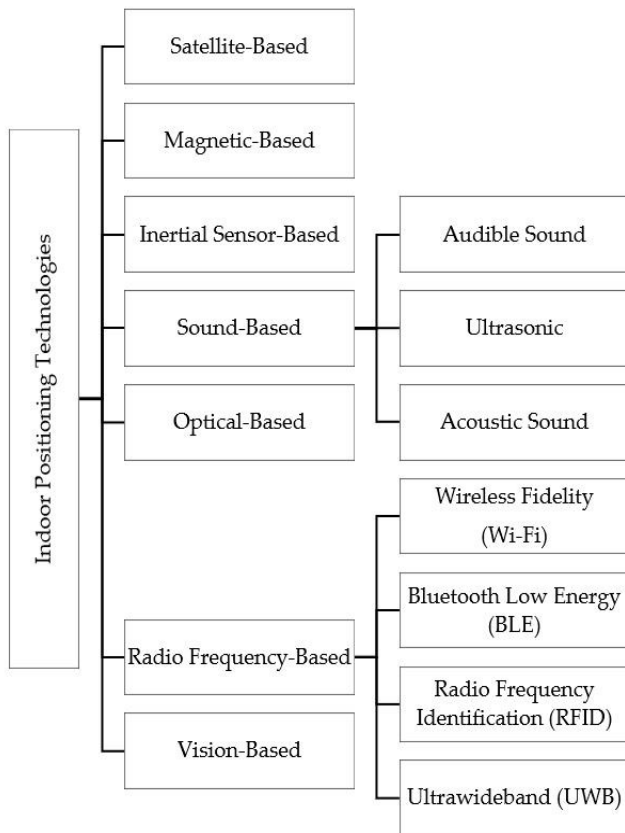


Fig. 1. Types of Indoor Positioning Technologies.

Despite all of the benefits, GPS only works in open areas where satellite signals are consistently received. The scope of the global system is limited to transport and in some cases, mobile personnel [11]. However, due to technological limits of signal re-reflection in the premises, even with wide windows, satellite technologies will not be useful for premises, manufacturing, or deep mining.

B. Magnetic-based

To determine the locations which relate to magnetic indoor positioning, the use of geomagnetic fields has been distorted [12]. Magnetic fields can be used in IPS in two methods [13]. The first method is when one makes use of anomalies induced by disruptions in the earth's magnetic field to perform positioning. Another method is using artificially generated magnetic fields in which coils of current-carrying wire are installed in strategic areas throughout the structure. On receiving node, each coil's magnetic field strength is measured.

To build an efficient magnetic field map, a map-building system for magnetic fields is needed. The magnetic field system consists of sensors such as an array, odometry, and a data alignment system. The position of the system is estimated by using odometry when the system is moving in a test area. At the same time, magnetic field data is measured. Finally, a magnetic field map is built when the data are aligned with the position. Earth's geomagnetic-based positioning system which is based on Earth does not require any additional hardware because it enables a smartphone compass to locate the position in an

indoor environment [14]. It also has a stable signal [15]. The robustness can be obtained when using magnetic fields as fingerprinting in indoor environments [16]. When constructing indoor positioning systems, resilience is important since it may significantly minimize the number of measurements and time required to create a large fingerprint database.

External factors such as device diversity and user diversity need to be aware. Magnetic sensors may be made using a variety of sensing technologies and materials. As a result, multiple magnetic sensors at the same position may produce different results. Magnetic reading might be slightly different when using different sensors [17]. In addition, the different user has different step lengths; hence they generate different magnetic fingerprints.

C. Inertial Sensor-based

Sensors based on inertia and associated measurement principles are known as inertial sensors. Accelerometers and gyroscopes are an example of inertial sensors. It does not require any external references [18] and installation since it does not depend on the environment.

The orientation inaccuracy will develop with time owing to sensor drift and recursive computation. Because accurate orientation information is a requirement for personal tracking/positioning and movement monitoring, incorrect orientation will impair the calculated accuracy of position. Magnetic field sensors are fused with inertial sensors using a Kalman filter to offer a long-term stable orientation solution.

In addition, the Inertial Navigation System (INS) is another localization navigation technology that is capable of calculating the location by a self-contained navigation technique that uses the existence of computers, motion sensors, and rotation sensors to be as the reference point. INS is normally used for a wide range of applications such as navigation of aircraft, tactical and strategic missiles, and submarines.

D. Sound-based

Another technology used for localization systems is Sound-Based which is normally used in underwater monitoring and tracking. This technology can be classified into three categories which are Audible Sound, Ultrasonic, and Acoustic Sound. Sound waves travel at a slower rate than electromagnetic waves leading to the major problem which is to make time synchronization easier.

1) *Audible sound*: Due to its intrinsic qualities, Audible Sound has recently been studied as an emergent technique. Audible Sound can be used to store the data for location systems [19]. It has similar qualities to ultrasound but is less expensive and more acceptable for use in everyday life because of the availability of off-the-shelf equipment with broader coverage, such as loudspeakers and mobile phones, which may be utilized with just modest modifications. Audible Sound was assumed that it would disrupt the acoustic environment unfavorably [20], so it was not tackled.

2) *Ultrasound*: Ultrasonic systems employ sound frequencies above the hearing range (above 20 kHz) to establish the user's location by measuring the time an

ultrasonic signal takes to travel from a transmitter to a receiver.

“Active” and “Passive” are types of ultrasonic systems. The ultrasonic positioning system can be implemented in various applications such as healthcare, hotel business, offices, and other indoor building. The Time-of-Flight (ToF) approach, which involves measuring the signal propagation time from the sensor to the receiver, is the basis for ultrasonic positioning. Special tags use to transmit ultrasound impulses are applied to measure the distance. The receiver network analyses these signals and delivers data to the central system, which calculates the position with a 3 cm precision using multilateration.

The advantage of ultrasonic is it can work in real-time. The frequency of the signal varies can be up to 3 seconds. It also can carry out the system's operational deployment with fine-tuning. Apart from that, the accuracy of ultrasound can be identified within several centimeters.

However, an ultrasound signal is only slightly influenced by its surroundings and has very little penetration through walls [21], which might help it be more useful in the suggested ultrasonic indoor locating system.

3) *Acoustic sound*: Due to its unique benefits, audio-based indoor positioning technology, which functions by producing and receiving acoustic signals between nodes and the placement target, has recently gotten a lot of attention. An Angle of Arrival (AoA), Time of Arrival (ToA), Time Difference of Arrival (TDoA), and Frequency Difference of Arrival (FDoA) are measurements that depend on acoustic signal measurement. The measurements have been implemented in audio-based indoor positioning.

E. Optical based

Optical-Based positioning used for localization is normally in the form of an Electro-Magnetic (EM) spectrum since the techniques and challenges are quite different. This system is a flexible navigation system for deep space operations. Optical positioning can be characterized into two, which are Infrared (IR) and Visible Light Communications (VLC).

1) *Infrared (IR)*: An IR communication technology is extensively used, low-cost, and widely available [22]. Infrared signals are employed in a variety of applications, from consumer remote controls to data transmission. In [22], the researcher proposed a low-range IR signal with AoA estimation. The proposed concept is applied to overcome the localization problem that prevents NLoS issues. It has been applied to navigate a grocery cart in a difficult environment. The results of the tests range from centimeter-level accuracy in a static 1 Dimension (1D) environment to 1 m mean localization error in a 2 Dimension (2D) setup for a mobile cart moving at 140 cm/s. These findings suggest that utilizing easily accessible IR technology and low-cost hardware components, suitable localization precision, and real-time navigation support may be accomplished in the supermarket.

Other than that, [23] stated that IR Light Emitting Diode (LED) with a wide emitting angle is less complex than a laser-based. However, to have a sufficiently high Signal-to-Noise Ratio (SNR) for effective demodulation, a complex sensor design is required.

2) *Visible light communications (VLC)*: VLC has been deemed an appealing alternative for indoor location systems. Triangulation is one of the algorithms that has been applied in the VLC positioning system due to its low cost and accuracy. The location can be estimated using the geometric properties of the triangle, where the light-emitting diodes (LEDs) serve as anchors and the receivers serve as agents in VLC systems, by measuring the distances between multiple reference anchors. In harsh environments, however, the triangulation positioning algorithm may fail.

The advantages of VLC are illuminance that can be dimmed [24], intrinsic security, and a spectrum that is generally available. Furthermore, because VLC-based systems are less susceptible to multipath propagation and disturbance from other wireless devices, they should give superior location accuracy to radio-wave alternatives. VLC does not produce electromagnetic interference and it can be implemented in restricted buildings such as hospitals [25].

F. Radiofrequency

Radiofrequency (RF) technology was commonly used in IPS. It is a mixes narrow-band with spread-spectrum transmissions and is based on signal strength technologies [26], which are especially useful for wireless communication devices.

Wi-Fi, BLE, RFID, and UWB are among the common wireless communication technologies involved in RF. While RF-based systems offer various advantages for positioning, they have a severe flaw in the indoor environment. Accuracy, cost of implementation, and power consumptions are the important parameters that need to evaluate to choose the best and most affordable technologies.

1) *Wireless fidelity (Wi-Fi)*: Now-a-days, Wi-Fi, which is based on the IEEE 802.11 standard, is well-known and widely used in radio technology. When there are enough Wi-Fi access points and no dedicated infrastructure is required, Wi-Fi-based procedures are employed in interior scenarios; alternatively, existing building infrastructure may be utilized because most current buildings are equipped with Wi-Fi access points. Wi-Fi-based indoor navigation systems commonly used RSS Fingerprinting, Triangulation, or Trilateration techniques [27] for location estimation.

Access points are commonly utilized in a building's planned or current Wi-Fi wireless networking capacity whose position has been optimized for data connection. It calculates the distances between three or more Wi-Fi access points using the Wi-Fi receiver in a smartphone.

The accuracy of Wi-Fi for interior locating is normally 5-15 meters. The precision of this measurement is determined by the amount of shielding provided by walls, ceilings, and people, as well as the number of entry points. The inclusion of smartphone

sensors can enhance the findings, and the floor level can also be determined. The implementation of Wi-Fi might be low due to the existing Wi-Fi structure in each building; however, power consumption for a Wi-Fi-based positioning system is high.

2) *Bluetooth low energy (BLE)*: BLE is a kind of wireless communication optimized for short-range communication. It is virtually as accurate as Wi-Fi-based systems, and they employ RF signal sources to monitor users' whereabouts via proximity sensing or RSSI fingerprinting.

Smartphones are now often utilized as receivers for both Bluetooth and Wi-Fi signals, following recent advancements. Beacons are small devices for BLE that be mounted on the walls [28]. Beacons device use battery power supply, as for that, it requires battery placement.

For BLE, complex signal processing is needed to reach good accuracy. The implementation cost for BLE is low as it is one of the most popular and easily used in indoor positioning. The power consumption for BLE can be high due to high data throughput.

3) *Radiofrequency identification (RFID)*: RFID is a traditional method of automated identification that is based on RF wireless communication technology. A typical RFID system contains tags such as transponders, smart tags, a reader, and a host computer and software/ infrastructure. A wired or wireless connection connects the reader to the host computer. For tracking reasons, on electromagnetic transfer between RFID readers and RFID tags [29]. It mixes narrow-band with spread-spectrum transmissions and is based on signal strength technologies, which are especially useful for wireless communication devices. The electromagnetic field of sources or equipment produces radio waves.

The accuracy of RFID can be determined in a short range of 0.5 to 1m and does not suitable for high-range scale location usage. The batteries of RFID tags also have to be replaced if it needs to do a large coverage. The complexity is getting high due to the implementation of complex algorithms such as the Kalman filter, K-Nearest Neighbor (KNN), and Radio map. RFID has low power consumption.

4) *Ultra-wideband (UWB)*: UWB is a radio technique that uses a wide section of the radio spectrum to distribute high-bandwidth communications. It allows UWB to transmit large amounts of data with consuming minimal energy for short-range communication [30]. UWB pulses have a low frequency that allows them to travel through walls, equipment, and other impediments. It also will not interact with current Radio Frequency (RF) systems if it were properly constructed. Since reflected signals do not overlay directly with received signals, UWB's brief transmission pulses make it easy to differentiate between direct and reflected signals. As a result, multipath interference is not a problem with UWB. Fixed-location sensors receivers and tags are used in UWB.

The accuracy of UWB can be achieved by 0.1 to 0.3 meters which is much better than Wi-Fi and BLE. However, this technology is a unique solution that necessitates the use of certain components that it is best suited to industrial applications. Compared to other positioning technology systems, UWB utilizes less power, allowing for greater power efficiency and longer device battery life. The implementation of UWB is quite complex because it requires signal acquisition, synchronization, and tracking with high precision.

G. Vision-based

This method is based on video data processing and assessment. In general, there are two ways [31] to conduct video-based localization which are fixed camera systems and mobile camera systems.

1) *Fixed camera system*: Fixed camera systems are used when they can be mounted in fixed locations. For example, the moving objects have been captured using one or more cameras. The tracking target's characteristics must be utilized. If the target's prominent characteristics show in the camera's field of vision, the target's location may be determined by the camera's fixed position. The target's location is determined by its location inside the recorded picture and the spatial distribution of its conspicuous characteristics.

2) *Mobile camera system*: The camera in the mobile camera system is already equipped to perform the localization with the known position in several landmarks. There are two stages in localization to determine the mobile camera's location and orientation; the offline stage and the online stage. Images of the environment are captured at predefined locations and each image is processed to extract its unique features that are stored in a database in the offline stage. During the online stage, the camera captures a picture, which is then extracted and matched to previously recorded attributes to determine the camera's position.

IV. INDOOR POSITIONING TECHNOLOGIES DISCUSSION

Each one of the technologies has its specialty. From the table below, we can conclude that GPS is not suitable to use in an indoor environment. Magnetic-based is suitable to determine the accuracy of position; however, it is complex and high in cost. In addition, inertial-based also can be used to determine the high accuracy and can be developed in a wide range of applications. However, fused with magnetic-based to get a long-term stabilization, it makes the system complex. Due to the high cost and its complexity, sound-based is the least suitable for indoor positioning systems. Optical-based and visual-based are low in cost system; however, it is complex and less accurate compared to other technologies.

Recently, the RF communication technologies such as Wi-Fi, BLE, RFID, and UWB are widely used in indoor positioning to develop location estimation. Their characteristic such as power consumption, accuracy, and cost are the factors that have been evaluated due to the benefits of an indoor positioning system as shown in Table I.

TABLE I. SUMMARY OF TECHNOLOGIES IN IPS

Technologies	Advantages	Disadvantages
Satellite-Based	<ul style="list-style-type: none"> • GPS easy to navigate • Low-cost implementation 	<ul style="list-style-type: none"> • Cannot be implemented in an indoor environment • Less accurate
Magnetic-Based	<ul style="list-style-type: none"> • High accuracy 	<ul style="list-style-type: none"> • High-cost implementation • Complex
Intertial-Based	<ul style="list-style-type: none"> • High accuracy • Wide range application • Does not require hardware installation • High accuracy 	<ul style="list-style-type: none"> • Fused with magnetic to get long-term stabilization • Complex
Sound-Based		
Audible Sound	<ul style="list-style-type: none"> • Less expensive • Easy to implement 	<ul style="list-style-type: none"> • High-cost implementation
Ultrasonic	<ul style="list-style-type: none"> • Close range distance measurement 	<ul style="list-style-type: none"> • High-cost implementation
Acoustic sound	<ul style="list-style-type: none"> • Low-cost implementation • Easy to implement 	<ul style="list-style-type: none"> • Complex
Optical-Based	<ul style="list-style-type: none"> • Low-cost implementation 	<ul style="list-style-type: none"> • Complex • Low accuracy
Radio Frequency (RF)-Based		
Wi-Fi	<ul style="list-style-type: none"> • Low-cost implementation 	<ul style="list-style-type: none"> • High power consumption
BLE	<ul style="list-style-type: none"> • Low power consumption • High accuracy 	<ul style="list-style-type: none"> • Complex • High-cost implementation
RFID	<ul style="list-style-type: none"> • Small size • High accuracy • Low power consumption 	<ul style="list-style-type: none"> • High-cost implementation • Complex
UWB	<ul style="list-style-type: none"> • High-in accuracy • Low power consumption 	<ul style="list-style-type: none"> • High-cost implementation
Vision-Based	<ul style="list-style-type: none"> • Low-cost implementation 	<ul style="list-style-type: none"> • Low accuracy • Complex

V. INDOOR POSITIONING ALGORITHMS

Signal characteristics with geometrical parameters made up of metrics like angle, distance, and the signal may be used to compute the position of an object or user. The algorithms for indoor positioning as displayed in Fig. 2 are divided into two which are directly based and distance-based. The Angle of Arrival (AoA) and Angle Difference of Arrival (ADoA) can be categorized as direction-based. In addition, distance-based [32] are Phase of Arrival (PoA), Phase Difference of Arrival (PDoA), Reference Signal Received Power (RSRP), Received Signal Strength Indicator (RSSI), Channel State Information (CSI), ToA, TDoA, and Round-Trip Time (RTT).

A. Direction-based

1) Angle of arrival (AoA)/ angle difference of arrival (ADoA): The word ‘Angle of Arrival’ (AoA) is used in a simplified technique for 2D operation, calculating angles in a single plane [33]. Using multiple AoAs with known receiver absolute position, any multilateration approach may be used to determine the sender's absolute coordinate. An equipment

upgrades at receiver AoA [34] and error in non-linear dependent are primary difficulties.

The localization of AoA is determined by using directional antennas or antenna arrays as shown in Fig. 3. An antenna array may be used to determine the angle at which the broadcast signal impacts directly on the receiver by leveraging and measuring the difference in time of arrival at selected antennae array members. The position of the source is restricted along a line along the predicted line of bearing by a single AoA measurement. A triangulation technique may be implemented to produce position estimation when numerous AoA measurements are collected concurrently according to the environment.

To determine mobile node location, at least two reference nodes are required to perform the AoA algorithm. An equation for AoA is as follows [35]:

$$x = d_i \cos(\theta_i) + x_i,$$

$$y = d_i \sin(\theta_i) + y_i, i = 1, 2, 3 \tag{1}$$

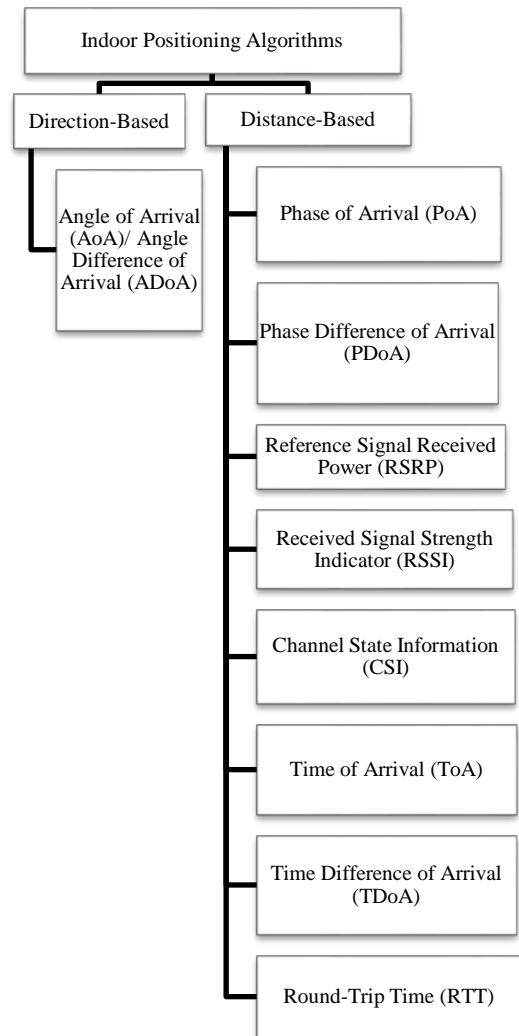


Fig. 2. Types of Indoor Positioning Algorithms.

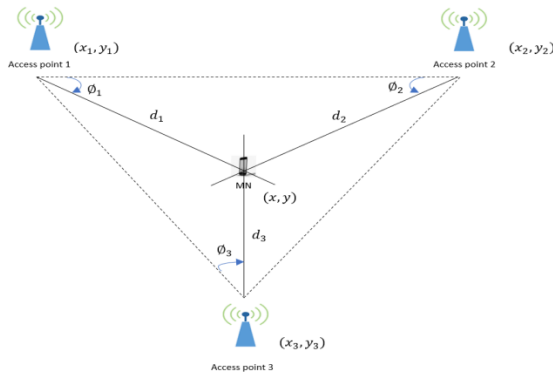


Fig. 3. AoA based Localization.

B. Distance-based

1) *Phase of arrival (PoA)*: The phase of the carrier signal is used to calculate the distance in PoA ranging methods [36]. In a passive RFID 2D localization system, the PoA positioning approach was applied to improve the accuracy [37] and reduce the disruptions caused by multipath propagation.

To improve their effectiveness, PoA techniques can be used with other techniques like ToF, TDoA, and RSSI. However, for great accuracy, PoA positioning techniques may require LoS.

2) *Phase difference of arrival (PDoA)*: PDoA methods, which employ the delta between phases of the receiver to determine the angle between receivers and transmitters, were originally used in radar systems [38]. PDoA only requires two antennas. It does not need time to synchronize among base stations compared to TDoA positioning.

3) *Reference signal received power (RSRP)*: RSRP variables are physical layer data from a 4G cellular system that are used to anticipate a user's position with absolute precision [39]. RSSI algorithm is used to determine RSRP. It uses cell-specific reference signals to compute the mean achievable strength. As a result, compared to regular RSSI, it may provide more signal strength information linked with varied locations.

4) *Received signal strength indicator (RSSI)*: The Received Signal Strength (RSS), also known as the Received Signal Strength Indicator (RSSI), is a measurement of the strength of a radio signal that has been received. [40]. RSSI is also known as a measurement to show the condition of received power in the anchor nodes and it is used in most wireless communication methods [41]. RSSI-based localization has the advantage of simplicity [42]. RSS-based target localization is a popular issue in wireless sensor networks, with several applications [43]. This method is based on video data processing and assessment.

The traditional approach to RSS-based localization is to use RSS data to derive distance information between the sensor and the target. Unfortunately, when the number of sensors is insufficient, the traditional RSS-based localization approach fails to attain adequate accuracy due to the deteriorating effects of fading, shadowing, and reflections of the radio signal.

Furthermore, many targets are active at the same time in multiple target localization settings, and target signals overlap at each sensor. The traditional approach is no longer practicable since it is difficult for a sensor to directly extract distance information from every target. As a result, developing an effective RSS-based localization technique for various targets is quite important.

Hardware modifications such as the smartphone's form factor, receiver module due to a number, internal circuitry architecture, and antenna design such as built-in signal processing and data loss can all affect RSSI readings [44]. RSS readings may be acquired with little effort and without additional circuitry, resulting in significant cost and energy savings for sensors. With the estimation, position information can be acquired. Fig. 4 shows an overview of how signal strength affects distance. The user node is to be estimated. RN₁, RN₂, and RN₃ as reference nodes. There are three processes to determine the user position [45]. First, collect and measure RSSI. The second process is determining the RSSI distance using the path-loss equation. Lastly, position estimation uses the Trilateration method.

The distance between Mobile Node (MN) and each APs can be determined using RSSI from the Distance Power Law equation [46]:

$$P_r(d_i) = P_r(d_0) - 10n \log\left(\frac{d_i}{d_0}\right) + (-T) \times WAF \quad (dBm) \quad (2)$$

$P_r(d_0)$ represent the initial value, d_0 is received power at a close-in reference distance of one meter, d_i is the distance between transmitter and receiver, n is the path loss exponent between 0 to 5, T is several walls between transmitter and receiver, WAF is Wall Attenuation Factor. Based on the equation above, the distance d_i can be calculated as follows:

$$d = e^{\frac{P_r(d_0) - P_r(d_i) - T \cdot WAF}{10}} \quad (3)$$

5) *Channel state information (CSI)*: In Wi-Fi indoor positioning, Channel State Information (CSI) is commonly been applied. It is because of the features based on the physical layer and descriptions of amplitude and phase information; CSI can represent fine-grained channel information. As a result, most researchers are interested in CSI-based positioning [47]. Signals are propagated in a Wi-Fi network using Orthogonal Frequency Division Multiplexing (OFDM) modulation. The signal is received by the terminal after being broadcast across the multipath channel by OFDM, which divides the communication channel into orthogonal sub-channels of various frequencies [48]. The properties of the communication link between the transmitter and the receiver are represented by CSI. CSI can be expressed as [48]:

$$Y = HX + N \quad (4)$$

Y represents the received signal vector. H is the channel information matrix, X is the transmitted signal vector, and N is additive white Gaussian noise. CSI also can be expressed as:

$$\hat{H} = \frac{Y}{X} \quad (5)$$

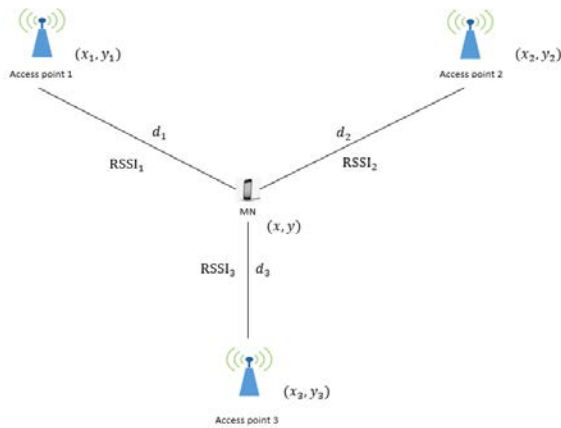


Fig. 4. RSSI-based Localization.

\hat{H} represents the Channel Frequency Response (CFR) for each subchannel. Researchers in [49] proposed deep learning-based indoor fingerprinting using CSI named as DeepFi. The system architecture is divided into offline and online training. Deep learning is used to train all the weights in offline training. Moreover, to decrease complexity, a greedy learning technique is employed to train all the weights layer by layer. During online training, the researcher used the probabilistic method to obtain the location. The result shows that DeepFi successfully minimizes location error when compared to three current approaches.

The extreme multipath and shadow fading effects, as well as the sensitivity to the dynamic environment, are two major obstacles to a functional CSI-based indoor positioning system. Short and long-term interference will cause the signal unavailable:

6) *Time of arrival (ToA)*: The absolute time when a radio signal from a transmitter reaches a distant receiver is known as the Time of Arrival (ToA) [50]. The simplest and most popular ranging approach is a ToA, which is most famously utilized in the GPS [51]. This algorithm is based on determining the time when the signal was sent to the target, the time when the signal arrives at the target, and the speed at which the signal travels. When all of these are known, the distance can be calculated by using [51]:

$$d = c * (t_{arrival} - t_{sent}) \quad (6)$$

C is the speed of light. The set of probable target locations may be identified using this distance. Many radiolocation systems employ ToA readings to accomplish true-range multilateration geo-positioning. When signals move at a constant velocity, the real range or distance may be determined directly from the ToA. The measured ToA depicts a circle with its center at the receiver in two-dimensional (2D) space, and the source must be on the circumference. In 2D, an equation is as follows [51]:

$$d = \sqrt{(x_{ref} - x)^2 + (y_{ref} - y)^2} \quad (7)$$

(x_{ref}, y_{ref}) is a known position of reference point. At least 3 or more reference points are needed to determine the target

position by finding the intersection. Fig. 5 states that 2D location estimation required a minimum of three sensors where A, B, and C are the distances between transmitter and receiver. An intersection can be required if there are at least three sensors. Meanwhile, for 3-Dimensional (3D) position estimation, it required at least four sensors [52] as shown in Fig. 5.

The clocks of the tag and the reader must be synchronized to get a perfect measurement of elapsed time. However, the cost for implementation is high and it is more complex.

7) *Time difference of arrival (TDoA)*: TDoA is a common approach for identifying targets using a set of sensor nodes with known positions. [53]. It is the second most used range technique, and it is more versatile than ToA in some ways. The time signal was received and the speed at which it traveled is all that is required for this technique. It is not the time when the signal was transmitted from the destination. Unlike previous geolocation methods, TDoA delivers accurate geolocation even for signals with power levels below the noise floor.

To achieve high-accuracy TDoA, precise synchronization between receivers is required. Anchors must be precisely synced, which necessitates the usage of synchronization beacons. Fig. 6 shows the working principle of TDoA.

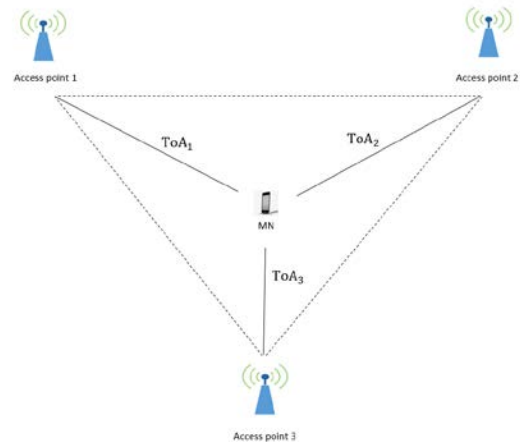


Fig. 5. ToA-based Localization.

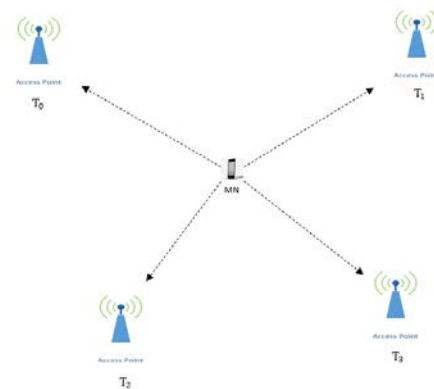


Fig. 6. TDoA-based Localization.

At a specific moment of timestamp at reception, T_0 , the tag will blink and four access points receive the message at various times ($T_1 \dots T_4$). The difference time of arrival has to be computed to estimate the position of the tag using this equation [51]:

$$\Delta d = c * (\Delta t) \tag{8}$$

where c is the speed of light, Δt is the difference in arrival times at each reference point. Meanwhile, for 2D, the equation is as follows [54]:

$$\Delta d = \sqrt{(x_2 - x)^2 + (y_2 - y)^2} - \sqrt{(x_1 - x)^2 + (y_1 - y)^2} \tag{9}$$

where (x_1, y_1) and (x_2, y_2) is a known position. This equation may be changed to the form of a hyperbola via nonlinear regression. After calculating a sufficient number of hyperbolas, the intersection may be used to determine the target's location.

8) *Round-trip time (RTT)*: Indoor positioning systems based on distance estimates were given Wi-Fi Round-Trip Timing (RTT). Unlike the Wi-Fi fingerprint approach, which necessitates the creation of a massive database known as a radio map, this protocol may be readily implemented in an indoor positioning system using only the AP's installation coordinates. In addition, Wi-Fi RTT is determined by Fine Timing Measurement (FTM).

Fig. 7 shows the FTM is a ping-pong technique that measures the signals of RTT. Firstly, a smartphone needs to transmit the request to RTT AP [55]. The AP and smartphone then begin sending the FTM message and recording the transmission timestamp, as well as waiting for the acknowledgment packet and recording the receipt timestamp. As a result, ToA and Time of Departure (ToD) may be acquired and used to determine the ToF of the signal from transmitter to receiver. The distance between the AP and the smartphone is calculated using ToF.

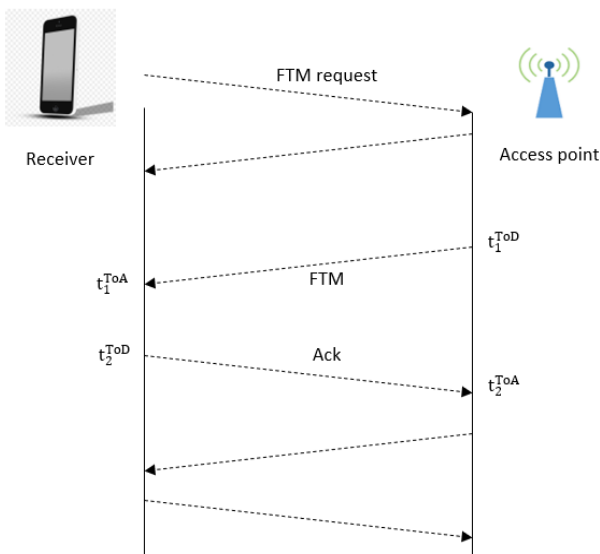


Fig. 7. RTT-based Localization.

An Android system has RTT Application Programming Interface (API). It is used to obtain ToF using [55]:

$$ToF = \frac{(t_2^{ToA} - t_2^{ToD}) + (t_1^{ToA} - t_1^{ToD})}{2} \tag{10}$$

where t_i^{ToA} ($i = 1, 2, 3, \dots$) and t_i^{ToD} ($i = 1, 2, 3, \dots$) is ToA and ToD measurements. The distance between transmitter and smartphone then been calculated using the equation as follows:

$$d_{rtt} = ToF * c \tag{11}$$

c is representing the speed of light. Meanwhile, d_{rtt} is the distance between transmitter and smartphone.

VI. INDOOR POSITIONING ALGORITHMS DISCUSSION

In summary, the signal-based is critical in determining position since it is used in the computation and estimation of a location. The algorithms that are commonly involved are AoA, ToA, TDoA, and RSSI positioning-based. However, due to complexity, high cost, and required additional hardware for AoA, ToA, and TDoA compared to RSSI. Therefore, the RSSI algorithm is the best solution for determining the user/ object position. The comparison of the indoor positioning algorithm is shown in Table II.

TABLE II. SUMMARY OF ALGORITHMS IN IPS

Algorithms	Advantages	Disadvantages
AoA	<ul style="list-style-type: none"> • Easy to implement • Required at least two APs for localization 	<ul style="list-style-type: none"> • Low accuracy in a large area • Specialized antenna • High-cost implementation • Complex
ADoA	<ul style="list-style-type: none"> • No need for an angle phase 	<ul style="list-style-type: none"> • Required additional sensor
PoA	<ul style="list-style-type: none"> • Signal change is easy to obtain 	<ul style="list-style-type: none"> • Require LoS for high accuracy
PDoA	<ul style="list-style-type: none"> • High accuracy • Reduce multipath effects 	<ul style="list-style-type: none"> • Accuracy is depending on the multipath effect
RSRP	<ul style="list-style-type: none"> • Provide more signal strength 	<ul style="list-style-type: none"> • Station interference and thermal noise have an influence
RSSI	<ul style="list-style-type: none"> • Low-cost implementation • Easy to implement 	<ul style="list-style-type: none"> • Low accuracy in a large area
CSI	<ul style="list-style-type: none"> • Good stability • High accuracy 	<ul style="list-style-type: none"> • High-cost implementation • Complex
ToA	<ul style="list-style-type: none"> • Easy to implement • Time measurement required for TDMA/CDMA network 	<ul style="list-style-type: none"> • Need a synchronized network • High-cost of implementation • Complex
TDoA	<ul style="list-style-type: none"> • The receiver does not need the time of transmission • Time measurement required for TDMA/CDMA network 	<ul style="list-style-type: none"> • Need a synchronized network • Complex
RTT	<ul style="list-style-type: none"> • High range measurement • No need a synchronize between nodes 	<ul style="list-style-type: none"> • Multipath effects • Complex

VII. INDOOR POSITIONING TECHNIQUES

The current position or location of the target item was calculated using positioning techniques [56]. The algorithm and the output of the position are processed by the positioning technique. Triangulation, Trilateration, Proximity, Scene Analysis, Fingerprinting, and Pedestrian Dead Reckoning are the main technique for indoor positioning as shown in Fig. 8.

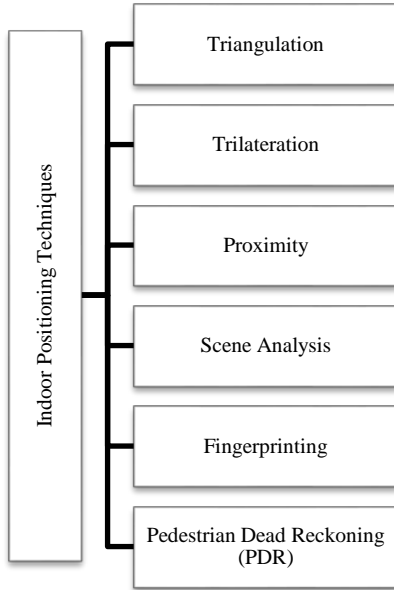


Fig. 8. Types of Indoor Positioning Technique.

A. Triangulation

Triangulation is a method of calculating a position based on the predetermined distance between three measuring devices and the measured angles from those three locations of an object [57]. Triangulation provides high accuracy if AoA has good precision. By increasing the number of access points, high precision may be obtained. However, a small error in angle calculation may affect the location accuracy.

This technique is particularly well suited to line-of-sight communication [58]. Calculating the angles and distance between reference points, as well as determining the position of a transmitter, are used to determine the position of an object. Triangulation can be divided into two categories: a) Lateration and b) Angulation. The basic localization for triangulation is shown in Fig. 9. From three access points, an angle measurement was made by the lines from distant points intersecting with the baseline.

These angles are then utilized to calculate unknown distances and, as a result, distance place was found [59]. The equation is as follows [60]:

$$\begin{aligned}
 x &= d_1 \sin(\theta_1) + x_1 \\
 y &= d_1 \cos(\theta_1) + y_1 \\
 x &= -d_2 \sin(\theta_2) + x_2 \\
 y &= d_2 \cos(\theta_2) + y_2
 \end{aligned}
 \tag{12}$$

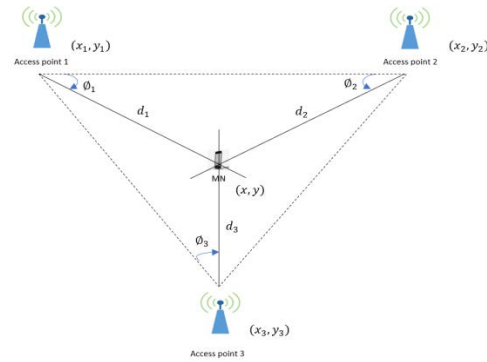


Fig. 9. Triangulation Technique Localization.

B. Trilateration

Trilateration is a more widely used technology that GPS also employs [59]. Trilateration is a method to determine an object's position using simultaneous range measurements from at least three reference nodes at known locations [61]. Measurements of angle do not involve trilateration [62]. Fig. 10 shows the three access points used in the trilateration technique in an indoor positioning system.

In practice, the edge-to-edge intersection of all reference circles is difficult to obtain due to the continuously changing in an indoor environment. The dependence of all three or more circles on edge-to-edge intersection reduces the estimation accuracy [63] of the trilateration technique.

The distance can be estimated using this equation [60]. It can be solved by using the matrix method:

$$\begin{aligned}
 d_1^2 &= (x - x_1)^2 + (y - y_1)^2 \\
 d_2^2 &= (x - x_2)^2 + (y - y_2)^2 \\
 d_3^2 &= (x - x_3)^2 + (y - y_3)^2
 \end{aligned}
 \tag{13}$$

C. Proximity

Localization based on proximity is a type of range-free localization. Proximity is the simplest method for localization [64]. It also might be the primary option if the user doesn't know the specific Mobile Devices (MD) radio settings or the architecture of the surroundings. Many researchers have utilized proximity-based localization to locate objects in ad hoc and wireless sensor networks.

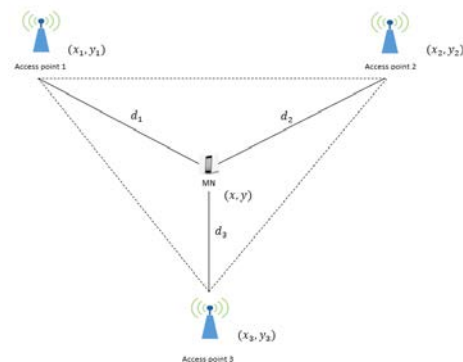


Fig. 10. Trilateration Technique Localization.

Fig. 11 shows the proximity method for indoor positioning. In proximity methods, the MD's position is determined relative to the AN position instead of explicit distances to the ANs. The precision needed for proximity detection in interior contexts is less than one meter, while it is roughly 5-10 meters for GPS [65]. This is because 5-10 meters precision is possible for street-level navigation, and the substantial localization/ proximity mistake such as meter-wide library aisle cannot be tolerated.

In contrast to triangulation and trilateration, proximity offers location information, not an absolute or relative position prediction. A grid of antennas with known positions is used to identify the location. When a mobile device detects mobility, the closest antenna is used to compute the position. If a mobile device detects more than one antenna, the location is calculated using the strongest signal. To calculate the access distance between mobile devices and determine mobile location, RSSI is used.

Apart from that, proximity is used in various systems that use Wi-Fi, Bluetooth, RFID, and UWB and requires minimal calibration. Larger spread readers are required to produce a dependable and wider coverage area. With huge spread readers, there is a risk of increased complexity.

D. Scene Analysis

Scene analysis is one of the most popular approaches, as it is based on the observation of space features, is independent of direct sight, and produces good results even in contexts with many impediments [66].

Most of the scene analysis that has been proposed is based on the IEEE 802.11 standard due to its broad application. The scene analysis technique has several benefits over previous techniques, including increased resistance to the multi-path fading problem and the fact that it is not dependent on spatial-temporal variables like propagation time and signal reception angle. When there is NLoS between the radios in the network [67], these properties are extremely vulnerable to mistakes.

However, memory requirements for data storage and the human effort necessary [66] to execute the training step in the operational environment are the technique's key flaws.

E. Fingerprinting

Environmental surveys are frequently required for scene analysis-based localization approaches to acquire fingerprints or properties of the environment where the localization system will be employed. One of the most often recommended ways for indoor positioning is the location fingerprinting approach. The potential of location fingerprinting is to reduce multipath and NLoS propagation difficulties [68]. Fingerprinting also has high accuracy compared to other methods [69]. Furthermore, because Wi-Fi access points (APs) are already installed indoors, and the RSSI data are easily available from mobile devices, Application Programming Interface (API), requires no new infrastructure gear.

Fingerprinting technique includes offline (training) and online (positioning) stages [70]. It's necessary to develop a reliable fingerprinting database. Fig. 12 shows an illustration of fingerprinting in the offline and online stages. At an offline stage, each AP was collected at the Reference Point (RP) and

extracted to generate fingerprints, which are then entered into a fingerprinting database. It is designed to learn the RSSI at each reference point.

During the online stage, the RSS of the test point is measured in real-time and compared to the offline fingerprints to establish location. The set is then orthogonalized to fulfill the essential criteria for the compressive sensing technique. The RSSD between APs is used to determine the processed set. The distance between offline and online values can be determined using [69]:

$$D_j = \sum_{i=1}^m \sqrt{(RSSI_{i(online)} - RSSI_{i(offline)})^2} \quad (14)$$

where, i is the number of beacons ranging from 1 to the total number around tags, m . To compare the measured value to the database, determine the most similar fingerprint, and achieve localization, the RSSD value is utilized as the new fingerprint. Finally, precise localization is achieved using the compressive sensing theory.

F. Pedestrian Dead Reckoning (PDR)

The PDR positioning technique is a self-contained positioning system. Its main premise is to use an accelerometer, gyroscope, and geomagnetic meter to acquire real-time motion direction and step information to determine the location information of the moving target. PDR positioning achieves excellent positioning accuracy in a short amount of time; however, it can only produce relative positioning findings, and cumulative mistakes exist [71]. If the heading inaccuracy in PDR can be corrected, it is dependable for consistently precise positioning.



Fig. 11. Proximity Technique Localization.

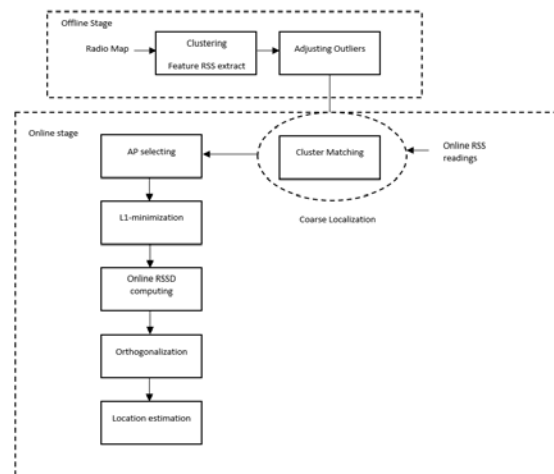


Fig. 12. Illustration of Fingerprinting Technique.

Researchers in [72] proposed to enhance PDR with RSSI. Erroneous headings will be corrected based on linear regression of locations computed using RSSI data derived from Wi-Fi signals to assure PDR's high dependability for extended duration placement. The outcomes of the experiment proved that the proposed strategy is practicable.

The user's position is calculated by combining the user's step length, several steps, and heading angle [73]. The step of the walking pedestrian can be expressed in [74]:

$$\begin{bmatrix} \hat{x}_k \\ \hat{y}_k \end{bmatrix} = \begin{bmatrix} x_0 \\ y_0 \end{bmatrix} + \sum_{i=1}^k \hat{L}_i \cdot \begin{bmatrix} \sin(\hat{\theta}_i) \\ \cos(\hat{\theta}_i) \end{bmatrix} \quad (15)$$

Where $\begin{bmatrix} \hat{x}_k \\ \hat{y}_k \end{bmatrix}$ represent the estimated position of the step, $\begin{bmatrix} x_0 \\ y_0 \end{bmatrix}$ represent an initial position, \hat{L}_i is estimated step length, and $\hat{\theta}_i$ is estimated heading angle.

VIII. INDOOR POSITIONING TECHNIQUES DISCUSSION

According to the discussion above, the signal property used in a positioning technique has a big impact on how effective the positioning approach is. As a result, it is critical to comprehend positioning algorithms and techniques to employ the most relevant attribute. The comparison of the indoor positioning technique is shown in Table III. The table stated that triangulation, proximity, scene analysis, and PDR techniques are complex.

In addition, fingerprinting technique is complex because it involved offline (training) and online (positioning). Therefore, in this review, the Trilateration technique is suggested due to its low cost, ease of implementation, and high accuracy.

TABLE III. SUMMARY OF TECHNIQUES IN IPS

Technologies	Advantages	Disadvantages
Triangulation	<ul style="list-style-type: none"> Low-cost implementation High accuracy within room level 	<ul style="list-style-type: none"> Low accuracy in a large area Complex Required angle measurement
Trilateration	<ul style="list-style-type: none"> Simple Low-cost implementation High accuracy 	<ul style="list-style-type: none"> Accuracy may occur due to environmental changes
Proximity	<ul style="list-style-type: none"> High accuracy 	<ul style="list-style-type: none"> High-cost implementation Complex
Scene Analysis	<ul style="list-style-type: none"> High performance 	<ul style="list-style-type: none"> High-cost implementation Complex Medium accuracy
Fingerprinting	<ul style="list-style-type: none"> No infrastructure needed 	<ul style="list-style-type: none"> Accuracy is depending on fingerprinting data resolution Complex
PDR	<ul style="list-style-type: none"> Accuracy within a short amount of time 	<ul style="list-style-type: none"> Complex

IX. CONCLUSION

The overview of the positioning system and indoor positioning system was introduced. This review aims to provide a full understanding of indoor positioning technologies, algorithms, and techniques involved in an indoor environment. RF communication technologies such as Wi-Fi, BLE, RFID, and UWB are widely used in indoor positioning recently to develop location estimation. RSSI algorithm is the best algorithm to determine the user location estimation compared to AoA, ToA, and TDOA which required additional hardware, high cost, and are complex. Trilateration technique is suggested due to its low cost, ease of implementation, and high accuracy. However, the use of technology, algorithm, and technique of indoor positioning are depending on many factors such as cost, available resources, type of environment, and the level of accuracy.

ACKNOWLEDGMENT

This research was supported by the Ministry of Education (MOE) through Fundamental Research Grant Scheme (FRGS/1/2021/ICT10/UTM/02/3). We also want to thank the Government of Malaysia which provides the MyBrain15 program for sponsoring this work under the self-fund research grant and L0022 from the Ministry of Science, Technology, and Innovation (MOSTI).

This research was supported by a UTM Encouragement Research Grant Q.J130000.3851.19J08.

REFERENCES

- Hameedah Sahib Hasan, Mohamed Hussien, Shaharil Mad Saad, and Mohd Azuwan Mat Dzahir, "An Overview of Local Positioning System: Technologies, Techniques, and Applications," *International Journal of Engineering & Technology*, vol. 7, no. 3.25, pp. 1-5, 2018.
- Francis Olawale Abulude, Akinyinka Akinnusote, and Adewale Adeyemi, "Global Positioning System and It's Wide Application," *Continental J. Information Technology*, vol. 9, no. 1, pp. 22-32, 2015.
- Filipe Manuel Clemente, Jose Pino Ortega, Asier Loc Arcos and Markel Rico-Gonzalez, "Chapter 4: Local Positioning System," in *The Use of Applied Technology and Recovery in Sports*, 2021, p. 13.
- Pedro J. Fernandez, Jose Santa, and Antonio F. Skarmeta, "Hybrid Positioning for Smart Spaces: Proposal and Evaluation," *Applied Sciences MDPI*, vol. 10, no. 12, p. 4083, 2020.
- Xuyu Wang, Shiwen Mao, Santosh Pandey, and Prathima Agrawal, "CA2T: Cooperative Antenna Arrays Technique for Pinpoint Indoor Localization," *Procedia Computer Science*, vol. 34, pp. 392-399, 2014.
- Brian Ray, "How An Indoor Positioning System Works," *RTLS Technologies*, 16 August 2018. [Online]. Available: <https://www.link-labs.com/blog/indoor-positioning-system>. [Accessed 31 January 2022].
- Zhenghua Chen, Qingchang Zhu, and Yeng Chai Soh, "Smartphone Inertial Sensor-Based Indoor Localization and Tracking With iBeacon Corrections," *IEEE Transactions on Industrial Informatics*, vol. 12, no. 4, pp. 1540-1549, 2016.
- A. Noertjahyana, Ignatius Alex Wijayanto, and Justinus Andjarwirawan, "Development of Mobile Indoor Positioning System Application Using Android and Bluetooth Low Energy with Trilateration Method," *2017 International Conference on Soft Computing, Intelligent System and Information Technology (ICSIIT)*, pp. 185-189, 2017.
- Nur Haliza Abdul Wahab, Sharifah Hafizah Syed Ariff, Liza A Latiff, and Sarerusaenye Ismail, "Indoor Location Assistant by Integrated Localized Routing in Proxy Mobile," *Journal of Advanced Research in Dynamic and Control Routing in Proxy Mobile*, vol. 11, no. 10, pp. 1108-1115, 2019.
- Huthaifa Ahmad Obeidat, Wafa Shuaieb, Omar Obeidat and Raed Abd-Alhameed, "A Review of Indoor Localization Techniques and Wireless

- Technologies," *Wireless Personal Communications*, vol. 119, pp. 289-327, 2021.
- [11] "OBJECT POSITIONING TYPES. THE APPLICATION OF EACH POSITIONING TECHNOLOGY," *RealTrac*, 26 March 2019. [Online]. Available: <https://real-trac.com/en-my/company/blog/the-types-of-position-objects-what-applies-each-of-the-positioning-technologies/>. [Accessed 31 January 2022].
- [12] Namkyoung Lee and Dongsoo Han, "Magnetic indoor positioning system using deep neural network," 2017 International Conference on Indoor Positioning and Indoor Navigation (IPIN), pp. 1-8, 2017.
- [13] Kyle Wroble, "Performance Analysis of Magnetic Indoor Local Positioning System," Western Michigan University, 2017.
- [14] Greg Sterling, "Magnetic Positioning: The Arrival of 'Indoor GPS'," *opusresearch*, San Fransisco, 2014.
- [15] Namkyoung Lee, Sumin Ahn, and Dongsoo Han, "AMID: Accurate Magnetic Indoor Localization Using Deep Learning," *Sensors MDPI*, vol. 18, p. 16, 2018.
- [16] Myeongcheol Kwak, Chorom Hamm, Soobin Park, and Ted Taekyoung Kwon, "Magnetic Field based Indoor Localization System: A Crowdsourcing Approach," 2019 International Conference on Indoor Positioning and Indoor Navigation (IPIN), pp. 1-8, 2019.
- [17] Myeongcheol Kwak, Youngmong Park, Junyoung kim, Jinyoung Han, and Taekyoung Kwon, "An Energy-efficient and Lightweight Indoor Localization System for Internet-of-Things (IoT) Environment," *Proceedings of the ACM on Interactive Mobile Wearable and Ubiquitous Technologies*, vol. 2, no. 1, pp. 1-28, 2018.
- [18] Rui Zhang, Fabian Hoflinger, and Leo Reindl, "Inertial Sensor Based Indoor Localization and Monitoring System for Emergency Responders," *IEEE Sensors Journal*, vol. 13, no. 2, pp. 838-848, 2013.
- [19] Ramon F. Brena, Juan Pablo García-Vázquez, Carlos E. Galván-Tejada, David Muñoz-Rodríguez, Cesar Vargas-Rosales, and James Fangmeyer, "Evolution of Indoor Positioning Technologies: A Survey," *Journal of Sensors*, vol. 2017, p. 21, 2017.
- [20] J. N. Moutinho, R. E. Araujo, and D. Freitas, "Indoor localization with audible sound — Towards practical implementation," *Pervasive and Mobile Computing*, vol. 29, pp. 1-16, 2016.
- [21] Jun Qi and Guo-Ping Liu, "A Robust High-Accuracy Ultrasound Indoor Positioning System Based on a Wireless Sensor Network," *Sensors MDPI*, vol. 17, no. 2554, p. 17, 2017.
- [22] Damir Arbula and Sandi Ljubic, "Indoor Localization Based on Infrared Angle of Arrival Sensor Network," *Sensors MDPI*, vol. 20, no. 21, p. 6278, 2020.
- [23] Ernesto Martin-Gorostiza, Francisco Javier Meca-Meca, Jose Luis Lazaro-Galilea, David Salido-Monzu, Eduardo Martos-Naya, and Andreas Wieser, "Infrared local positioning system using phase differences," 2014 Ubiquitous Positioning Indoor Navigation and Location Based Service (UPINLBS), pp. 238-247, 2015.
- [24] Tiantian Zhang, Ji Zhou, Zhenshan Zhang, Yueming Lu, Fei Su, and Yaojun Qiao, "Dimming Control Systems Based on Low-PAPR SCFDM for Visible Light Communications," *IEEE Photonics Journal*, vol. 10, no. 5, pp. 1-11, 2018.
- [25] Wenbo Ding, Fang Yang, Hui Yang, Jintao Wang, Xiaofei Wang, Xun Zhang, and Jian Song, "A hybrid power line and visible light communication system for indoor hospital applications," *Computer Industry*, vol. 68, pp. 170-178, 2015.
- [26] Tan Kim Geok, Khaig Zar Aung, Moe Sandar aung, Min Thu Soe, Azlan Avdaziz, Chia Pao Liew, Ferdous Hossain, Chih P. Tso, and Wong Hin Yong, "Review of Indoor Positioning: Radio Wave Technology," *Applied Sciences MDPI*, vol. 11, no. 279, p. 44, 2021.
- [27] Suining He, S. -H. Gary Chan, "Wi-Fi Fingerprint-Based Indoor Positioning: Recent Advances and Comparisons," *IEEE Communications Surveys & Tutorials*, vol. 18, no. 1, pp. 466-490, 2015.
- [28] "Indoor Positioning Systems based on BLE Beacons," *Locatify*, [Online]. Available: <https://locatify.com/blog/indoor-positioning-systems-ble-beacons/>. [Accessed 1 December 2021].
- [29] "RFID for Indoor Asset Tracking," *Leverage*, 4 April 2019. [Online]. Available: <https://www.ietfforall.com/rfid-indoor-asset-tracking/>. [Accessed 27 November 2021].
- [30] Ray Bernard, "Applying Indoor Positioning Systems: A Primer for Integrators and Security Specialists," *Security Industry Association (SIA)*, 21 November 2017. [Online]. Available: <https://www.securityindustry.org/2017/11/21/indoor-positioning-systems/>. [Accessed 1 December 2021].
- [31] Luca Mainetti, Luigi Patrono, and Ilaria Sergi, "A Survey on Indoor Positioning Systems," 2014 22nd International Conference on Software, Telecommunications and Computer Networks (SoftCOM), pp. 111-120, 2015.
- [32] Marina Md Din, Norziana Jamil, Jacenitha Maniam and Mohamad A Mohamed, "Review of indoor localization techniques," *International Journal of Engineering & Technology*, vol. 7, no. 2, pp. 201-204, 2018.
- [33] Stijn Wielandt and Lieven De Strycker, "Indoor Multipath Assisted Angle of Arrival Localization," *Sensors (MDPI)*, vol. 17, no. 11, p. 2522, 2017.
- [34] "Angle of Arrival," *eTutorials.org*, [Online]. Available: <http://etutorials.org/Mobile+devices/mobile+location+services/Part+2+The+Mobile+Location+Server/Chapter+5.+Mobile+Positioning/Angle+of+Arrival/>. [Accessed 21 June 2021].
- [35] David Munoz, Frantz Bouchereau, Cesar Vargas, and Rogerio Enriquez, "Location Information Processing," *Position Location Techniques and Applications*, pp. 67-102, 2009.
- [36] Faheem Zafari, Athanasios Gkelias, and Kin K. Leung, "A Survey of Indoor Localization Systems and Technologies," *IEEE Communications Surveys & Tutorials*, vol. 21, no. 3, pp. 2568-2599, 2019.
- [37] Martin Scherhauff, Markus Pichler, Erwin Schimback, Dominikus J. Muller, Andreas Ziroff, and Andreas Stelzer, "Indoor Localization of Passive UHF RFID Tags Based on Phase-of-Arrival Evaluation," *IEEE Transactions on Microwave Theory and Techniques*, vol. 61, no. 12, pp. 4724-4729, 2013.
- [38] Yan Zhang and Linfu Duan, "A phase-difference-of-arrival assisted ultra-wideband positioning method for elderly care," *Measurement*, vol. 170, 2021.
- [39] Nithayanathan Poosamani and Injong Rhee, "Towards a practical indoor location matching system using 4G LTE PHY layer information," 2015 IEEE International Conference on Pervasive Computing and Communication Workshops (PerCom Workshops), pp. 284-287, 2015.
- [40] "What is the RSS (Received Signal Strength)," *Accuware Support*, [Online]. Available: <https://accuware.com/support/knowledge-base/what-is-the-signal-strength-rss/>. [Accessed 27 June 2021].
- [41] Alireza Shojaifar, "Evaluation and Improvement of the RSSI-based Localization Algorithm," *Blekinge Tekniska Hogskola (BTH)*, 2015.
- [42] Suhui Jeong, Halim Lee, Taewon and Jiwon Seo, "RSS-based LTE Base Station Localization Using Single Receiver in Environment with Unknown Path-Loss Exponent," 2020 Internatooal Conference on Information and Communication Technology Convergence (ICTC), 2020.
- [43] Peng Qian, Yan Guo, Ning Li and Sixing Yang, "Localization in WSNs With Quantized Received Signal Strength," *IEEE Access*, vol. 7, pp. 60228-60241, 2019.
- [44] Harsh Agarwal, Navyata Sanghvi, Vivek Roy and Kris Kitani, "DeepBLE: Generalizing RSSI-based Localization Across Different Devices," *Association for Computing Machinery*, 2021.
- [45] Kiattisak Sengchuai, Nattha Jindapetch, and Apidet Booranawong, "EFFECTS OF SAMPLING PERIODS ON THE COMMUNICATION RELIABILITY AND THE ESTIMATION ACCURACY OF AN RSSI-BASED INDOOR LOCALIZATION SYSTEM," *Suanaree J. Sci. Technol.*, vol. 27, no. 1, pp. 1-9, 2020.
- [46] Nur Haliza Abdul Wahab, N. Syazwani C. J, Sharifah Hafizah Syed Ariffin, Nuraini Huda Abdul Kadir, and Noorhazirah Sunar, "Three Dimension (3D) Indoor Positioning via Received Signal Strength Indicator in Internet of Things," *Lecture Notes in Electrical Engineering*, vol. 842, pp. 1081-1092, 2021.
- [47] Zhang Yong and Wu Chengbin, "An indoor positioning system using Channel State Information based on TrAdaBoost Transfer Learning," 2021 4th International Conference on Advanced Electronic Materials, Computers and Software Engineering (AEMCSE), pp. 1286-1293, 2021.
- [48] Wen Liu, Qianqian Cheng, Zhongliang Deng, Hong Chen, Xiao Fu, Xinyu Zheng, Shixuan Zheng, Cunzhe Chen, and Shuo Wang, "Survey

- on CSI-based Indoor Positioning Systems and Recent Advances," 2019 International Conference on Indoor Positioning and Indoor Navigation (IPIN), pp. 1-8, 2019.
- [49] Xuyu Wang, Lingjun Gao, Shiwen Mao, and Santosh Pandey, "DeepFi: Deep learning for indoor fingerprinting using channel state information," 2015 IEEE Wireless Communications and Networking Conference (WCNC), pp. 1666-1671, 2015.
- [50] "Time of arrival," Wikipedia, 24 February 2021. [Online]. Available: https://en.wikipedia.org/wiki/Time_of_arrival. [Accessed 28 June 2021].
- [51] Brian O'Keefe, "Finding Location with Time of Arrival and Time Difference of Arrival Techniques," 2017.
- [52] Xinya Li, Zhiqun Daniel Deng, Lynn T. Rauchenstein, Thomas J. Carlson, "Contributed Review: Source-localization algorithms and applications using time of arrival and time difference of arrival measurements," Review of Scientific Instruments, vol. 87, no. 4, 2016.
- [53] Peng Wu, Shaojing Su, Zhen Zuo, Xiaojun Guo, Bei Sun and Xudong Wen, "Time Difference of Arrival (TDoA) Localization Combining Weighted Least Squares and Firefly Algorithm," Sensors - MDPI, vol. 19, p. 2554, 2019.
- [54] Guowei Shi and Ying Ming, "Survey of Indoor Positioning Systems Based on Ultra-wideband (UWB) Technology," Wireless Communications, Networking and Applications, pp. 1269-1278, 2016.
- [55] Ke Wang, Ampalavanapillai Nirmalathas, Christine Lim, Kamal Alameh, Hongtao Li, and Efstratios Skafidas, "Indoor infrared optical wireless localization system with background light power estimation capability," Optics Express, vol. 25, no. 19, pp. 22923-22931, 2017.
- [56] Siye Wang, Chang Ding, Weiqing Huang, Yanfang Zhang, Jianguo Jiang, Shaoyi Zhu, Yue Cui, and Jun-yu Lin, "Determination of an Indoor Target Position: An Accurate and Adaptable Approach Based on Differential Positioning," International Journal of Antennas and Propagation, vol. 2019, p. 19, 2019.
- [57] "Trilateration vs. Triangulation for Indoor Positioning Systems," IoT For All, 22 March 2019. [Online]. Available: <https://www.iotforall.com/trilateration-vs-triangulation-indoor-positioning-systems>. [Accessed 4 July 2021].
- [58] Zeynep Turgut, Gulsum Zeynep Gurkas Aydin and Ahmet Sertbas, "Indoor Localization Techniques for Smart Building Environment," The 7th International Conference on Ambient Systems, Networks and Technologies (ANT 2016), pp. 1176-1181, 2016.
- [59] Ipshita Biswas, "Triangulation vs Trilateration vs Multilateration – for Indoor Positioning Systems," PATHPARTNER, 6 June 2019. [Online]. Available: <https://www.pathpartnertech.com/triangulation-vs-trilateration-vs-multilateration-for-indoor-positioning-systems/>. [Accessed 15 November 2021].
- [60] Tran Trong Khanh, VanDung Nguyen, Xuan-Quy Pham, and Eui Nam Huh, "Wi-Fi indoor positioning and navigation: a cloudlet-based cloud computing approach," Human-centric Computing and Information Sciences volume, vol. 10, no. 32, 2020.
- [61] Hanwang Qian, Fu Pengcheng, Baoqing Li, Jianpo Liu, and Xiaobing Yuan, "A Novel Loss Recovery and Tracking Scheme for Maneuvering Target in Hybrid WSNs," Sensors (MDPI), vol. 18, no. 2, p. 341, 2018.
- [62] Upasana Chaunan, "Indoor Positioning System (Trilateration)," 6 August 2015. [Online]. Available: <https://www.tothenew.com/blog/indoor-positioning-systemtrilateration/>. [Accessed 15 November 2021].
- [63] Simeon Pande and Kwame S Ibwe, "Robust Trilateration Based Algorithm for Indoor Positioning Systems," Tanzania Journal of Science, vol. 47, no. 3, pp. 1195-1210, 2021.
- [64] Islam Alyafawi, "Real-Time Localization using Software Defined Radio," 2015.
- [65] Faheem Zafari, Ioannis Papapanagioutou and Konstantinos Christidis, "Micro-location for Internet of Things equipped Smart Buildings," IEEE Internet of Things Journal, vol. 3, no. 1, pp. 96-112, 2016.
- [66] Vahideh Moghtadaiee and Andrew G. Dempster, "Design protocol and performance analysis of indoor fingerprinting positioning systems," Physical Communication, vol. 13, pp. 17-30, 2014.
- [67] E. S. Pino, C. Montez. O. T. Valle, E. Leao, and R. Moraes, "An Indoor Positioning System Using Scene Analysis in IEEE 802.15.4 Networks," IECON 2019 - 45th Annual Conference of the IEEE Industrial Electronics Society, pp. 2817-2822, 2019.
- [68] Vahideh Moghtadaiee, Seyed Ali Ghorashi and Mohammad Ghavami, "New Reconstructed Database for Cost Reduction in Indoor Fingerprinting Localization," IEEE Access, vol. 7, pp. 104462-104477, 2019.
- [69] Snatosh Subedi and Jae-Young Pyun, "Practical Fingerprinting Localization for Indoor Positioning System by Using Beacons," Journal of Sensors - Hindawi, p. 16, 2017.
- [70] Shuai Huang, Kun Zhao, Zhengqi Zheng, Wenqing Ji, Tianyi Li and Xiaofei Liao, "An Optimized Fingerprinting-Based Indoor Positioning with Kalman Filter and Universal Kriging for 5G Internet of Things," Wireless Communications and Mobile Computing, p. 10, 2021.
- [71] Fei Lu, Jian Wang, Jixian Zhang, and Houzeng Han, "An Indoor Localization Method for Pedestrians Base on Combined UWB/ PDR/ Floor Map," Sensors (MDPI), vol. 19, no. 11, p. 2578, 2019.
- [72] Liew Lin Shen and Wallace Wong Shung Hui, "Improved Pedestrian Dead-Reckoning-Based Indoor Positioning by RSSI-Based Heading Correction," IEEE Sensors Journal, vol. 16, no. 21, pp. 7762-7773, 2016.
- [73] Ryoji Ban, Katsuhiko Kaji, Kei Hiroi and Nabuo Kawaguchi, "Indoor Positioning Method Integrating Pedestrian Dead Reckoning with Magnetic Field and Wi-Fi Fingerprints," 2015 Eight International Conference on Mobile Computing and Ubiquitous Networking (ICMU), pp. 167-172, 2015.
- [74] Mei Wang, Nan Duan, Zou Zhou, Fei Zheng, Hongbing Qiu, Xiaopeng Li, and Guoli Zhang, "Indoor PDR Positioning Assisted by Acoustic Source Localization, and Pedestrian Movement Behavior Recognition, Using a Dual-Microphone Smartphone," Wireless Communications and Mobile Computing, vol. 2021, p. 16, 2021.

A Lightweight ECC-based Three-Factor Mutual Authentication and Key Agreement Protocol for WSNs in IoT

Meriam Fariss, Hassan El Gafif, Ahmed Toumanari

Laboratory of Applied Mathematics and Intelligent Systems Engineering (MAISI)
National School of Applied Sciences (ENSA)
Agadir, Morocco

Abstract—The Internet of Things (IoT) represents a giant ecosystem where many objects are connected. They collect and exchange large amounts of data at a very high speed. One of the main parts of IoT is the Wireless Sensor Network (WSN), which is deployed in various critical applications such as military surveillance and healthcare that require high levels of security and efficiency. Authentication is a primary security factor that ensures the legitimacy of data requests and responses in WSN. Moreover, sensor nodes are characterized by their limited resources, which raise the need for lightweight authentication schemes applicable in IoT environments. This paper presents an informal analysis of the security of X. Li et al.'s protocol, which is claimed to be efficient and resistant to various attacks. The analysis results show that the reviewed protocol does not provide user anonymity and it is vulnerable to session key disclosure attack, many-time pad attack, and insider attack. To address all these requirements, a new three-factor authentication protocol is presented, which guarantees higher security using Physically Unclonable Function (PUF) and Elliptic Curve Cryptography (ECC). This protocol does not only withstand the security weaknesses in X. Li et al.'s scheme but also provides smart card revocation and is resistant to cloning attack. In terms of both computational and communicational costs, results demonstrate that the proposed scheme provides higher efficiency in comparison with other related protocols, which makes it notably suitable for IoT environments.

Keywords—Mutual authentication; elliptic-curve cryptography; Physically Unclonable Function; wireless sensor networks; key-agreement; internet of things

I. INTRODUCTION

It is widely believed that the Internet of Things (IoT) [1, 2] is the upcoming promising technology that will bring many revolutionary changes in different life sides. The IoT architecture connects a set of heterogeneous things belonging to our daily life use and enables them to exchange a huge amount of data, which are also processed and stored. One of the principal application domains of IoT is Wireless Sensor Networks (WSN)[3]. WSNs are generally deployed in unattended areas and consist of widely distributed autonomous sensing devices, gateway nodes (GWNs), and remote users communicating over the public channel. The GWN represents a bridge of communication between sensors and users. Sensors play an important role in WSN by monitoring environmental and physical conditions and providing real-time data, which are

directly accessed by users as and when demanded. Therefore, a secure mutual authentication process represents a primary concern in WSNs allowing only legitimate users to access the sensed data. Moreover, WSN consists of many resource-constrained sensor nodes having limited power, low bandwidth and battery, small storage space, and limited computational abilities. These two main issues related to security concerns and performance limitations in WSN deployment represent an important challenge that must be taken into consideration in every proposed protocol. ECC represents an important security solution in WSN [4] by offering the same security level compared to other cryptography mechanisms (e.g. RSA) with much smaller key size and less computational power requirements, which makes it suitable for resource-constrained environments.

Contribution. Many authentication protocols are designed to ensure higher and efficient security in WSNs. However, some security and performance challenges are still not solved which makes these protocols vulnerable to several security attacks and not applicable in resource-constrained environments such as WSN. In this paper, an efficient three-factor mutual authentication and key agreement protocol is proposed that overcomes critical security concerns found in the studied protocols such as impersonation attacks, cloning attacks, and insider attacks. In addition, it guarantees user and sensor anonymity and untraceability. In contrast with the existing protocols, no secure channel assumption is required by this protocol. It is also more efficient than all the studied schemes in terms of communications cost. It is also computationally more efficient than most of the studied protocols. As a result, it is more suitable for WSN than the studied schemes. Additionally, this protocol provides smart card revocation (in case of lost/stolen smart card) and identity and password update feature. Another interesting feature provided by this protocol, that does not exist in the studied protocols, is that the GWN cannot decrypt the communicated messages between the user and the sensor since it does not possess the session key.

Organization of the paper. The remainder of this paper is organized as follows: Section II presents the related work. In Section III, an overview of the main preliminaries of the present paper is provided. Section IV, describes the principal weaknesses of X. Li et al.'s scheme [5]. The proposed protocol is described in detail in Section V. The security analysis of this

This work is supported by the National Center for Scientific and Technical Research (CNRST) [scholarship number: 4UIZ2017].

protocol and its performance analysis are described in Sections VI and VII respectively. Finally, some concluding remarks are given in Section VIII.

II. RELATED WORK

In the literature, there are various mutual authentication protocols designed to address the security and performance challenges in WSNs. In 2009, Das [6] proposed a hash-based two-factor user authentication protocol for WSN using the smart card. Subsequently, many authentication protocols have been proposed to improve the security of Das' scheme [7–9]. He et al. (2010) [10] proposed an enhancement of [6] that overcomes insider and impersonation attacks. However, Kumar and Lee (2011) [11] have identified that He et al.'s protocol [10] lacks many security features such as no user anonymity and it does not establish a session key between the user and the sensor. In 2011, Yeh et al. [8] proposed an ECC-based authentication protocol for WSN to improve security with higher efficiency. Unfortunately, this protocol cannot provide mutual authentication and key agreement. To overcome the weaknesses detected in [8], Shi et al. (2013)[12] proposed a user authentication protocol based on ECC which improves security features, communicational, and computational costs. Nonetheless, [12] contains other weaknesses. Choi et al. (2014) [13] presented a review of [12] and have found that it is not secure since it cannot withstand session key attack and smart card attack. In the same year, Jiang et al. [14] proposed a two-factor authentication scheme for WSN. In 2015, Wu et al. [15] pointed out some weaknesses in [13] and [14] such as being vulnerable to off-line guessing attack and user forgery attack. Wu et al. presented an enhanced protocol based on ECC that addresses the security weaknesses detected and provides higher security. Nam et al. (2014) [16] proposed an authentication scheme for WSN using ECC that provides user anonymity and perfect forward secrecy. In 2015, Jiang et al. [17] designed an ECC-based two-factor authentication protocol. After reviewing He et al.'s scheme (2015) [18] and presenting its main security weaknesses such as stolen smart card attack and tracking attack, Jiang et al. proved that their proposed scheme achieves mutual authentication and key agreement between the user and the sensor, it also guarantees user anonymity and untraceability. In 2016, Lu et al. [19] proposed a two-factor mutual authentication and key agreement protocol using a smart card. They claimed that their proposition is resistant to insider attack due to the use of the hashed value of the password. It is also claimed to be resistant to many attacks such as known session-specific temporary information attack and a denial-of-service attack. In 2022, Chander et al. [20] proposed an improved two-factor authentication scheme for WSN using ECC.

To improve the security of two-factor authentication protocols, three-factor authentication has drawn researchers' attention and many three-factor authentication protocols are proposed [5, 21–25]. Moreover, biometric recognition [26] presents many advantages that guarantee a higher security level in WSNs compared with passwords. For this reason, many biometric-based authentication protocols have been proposed [27, 28]. In 2016, Park et al. [22] proposed a three-factor ECC-based authentication protocol using biometric information to overcome security weaknesses detected in Chang et al.'s

scheme (2015) [23] such as incorrectness of password change and off-line guessing attack. Later on, Jung et al. (2017) [24] pointed out that [23] is vulnerable to password guessing attack and user impersonation. They also demonstrated that this protocol does not provide session key verification. To overcome these security weaknesses, Jung et al. proposed an improved authentication and key agreement protocol using the user's biometric information. In the same year, S.Challa et al. [25] proposed a signature-based authentication and key agreement protocol in IoT using ECC. They claimed that their protocol is secure against several attacks such as privileged insider attack and stolen smart card attack. In 2018, X. Li et al.[5] proposed a fingerprint-based mutual authentication protocol for WSN, which they claimed provides user and sensor anonymity and untraceability and many other security features.

As you can notice from the aforementioned literature, important research work has been done to detect and overcome security weaknesses in WSN environments for secure communication between different entities. Moreover, security issues are not the only factor that should be taken into consideration. Each security protocol should be efficient enough to be applied and suitable for IoT applications due to the resource-constrained feature of different devices used. To address the security and efficiency issues raised in the previous work, this paper proposes a three-factor mutual authentication and key agreement protocol for WSN based on ECC.

III. PRELIMINARIES

This section gives an overview of the main preliminary concepts used in the present paper.

A. Physical Unclonable Function (PUF)

A PUF [29–31] is a low-cost technology that extracts entropy from uncontrollable manufacturing variations in the physical structure of identically produced devices. Typically, it is physically impossible to recreate the same conditions in another device even if the same manufacturing process is performed again, and it is mathematically impossible to accurately predict the PUF's behavior as well. PUF uses this entropy to generate a unique sequence of bits (response) for each device given an input (challenge) acting as the device's fingerprint that does not need to be stored in the device's memory. To measure the performance of a given PUF, researchers use two main metrics:

- Uniqueness (μ_{inter}): the average fraction of dissimilar bits between responses of different PUFs to a given challenge. The ideal value of μ_{inter} is 0.5 (random).
- Reliability (μ_{intra}): the average fraction of dissimilar bits between responses of a fixed PUF to a given challenge. This metric measure the average error resulted in PUF's output due to the undesirable noise. The ideal value of μ_{intra} is 0 (no error).

In our protocol, we use a recently proposed PUF scheme. HBN-PUF [32] is a strong, chaos-enhanced, and asynchronous PUF. According to [33], the creators of HBN-PUF aim to move quickly to commercialize this technology.

B. Fuzzy Commitment Scheme

The fuzzy commitment scheme was introduced by Juels and Wattenberg in 1999[34]. This technique is commonly used in biometric authentication schemes and it combines error-correcting code techniques and cryptography. For an error-correcting code over a message space $M = \{0,1\}^k$, we consider a set of codewords $C \subseteq \{0,1\}^n$ where $n > k$ to achieve redundancy. Before transmission, each message $m \in M$ is mapped to a codeword $c \in C$. We define the translation function $g: M \rightarrow C$, and the decoding function $f: \{0,1\}^n \rightarrow CU\{\emptyset\}$ that maps arbitrary an n -bit string to the nearest codeword, else it outputs \emptyset . Biometric-based applications use a reference template generated firstly at the registration phase. At the authentication phase, a new biometric sample is provided and compared to the reference template which needs to be securely and secretly stored. Due to many reasons, the provided biometric sample is not the same as the reference template.

Let's consider the secure one-way hash function $h: \{0,1\}^n \rightarrow \{0,1\}^l$. The fuzzy commitment scheme is defined as follows: $F: \{0,1\}^n, \{0,1\}^n \rightarrow \{0,1\}^l, \{0,1\}^n$. F commits a random codeword $c \in C$ to the biometric template b provided at the registration phase to the server. The server computes then $F(c,b) = (\alpha,\delta)$, where $\alpha=h(c)$ and $\delta=c \oplus b$. The server stores (α,δ) in its database. At the authentication phase, a noisy biometric data b' is input by the user. To open the commitment F using b' , the server computes $c' = f(b' \oplus \delta)$, using the decoding function f . Then, it compares $h(c')$ with the stored value of α . If $h(c') = \alpha$, the commitment is opened successfully and the user is authenticated.

IV. WEAKNESSES OF X. LI ET AL.'S SCHEME [5]

This section describes the functional and security flaws of X.Li et al.'s three-factor anonymous authentication scheme [5]. It involves three main types of entities: the user U_i , the trusted gateway node GWN , and the sensor node S_j .

A. GWN Master Key Update

In the reviewed protocol, the GWN has its private key x and the master key K_{GWN} . When the GWN updates K_{GWN} , it must recalculate $B_i = h(ID_i \parallel K_{GWN}) \oplus h(RPW_i \parallel c_i)$ for each U_i and $K_{GWN-S} = h(SID_j \parallel K_{GWN})$ for each S_j . Moreover, when the GWN updates its private key x it must recalculate its public key X and send it to all users to be updated on their smart cards. Hence, the GWN master key update is a very expensive process.

B. No Smart Card Revocation

When a user's smart card is lost/stolen, he/she should be able to send a revocation request to the GWN . However, X. Li et al.'s protocol does not provide this feature.

C. No user Identity Change

In real life, the user needs to change his identity but X. Li et al.'s scheme does not provide this feature.

D. Insider Attack

The protocol of X. Li et al. is exposed to an insider attack by a legitimate user, who can start by performing successfully a usual login phase by inputting his valid biometric information, ID_i and PW_i . Then the login request message $\{M_2, M_4, M_5, M_6, M_7\}$ is sent to the GWN , which calculates

$M_8 = ID_i \oplus K_{GWN-S}$ and sends it explicitly over the public channel to S_j . Since the U_i knows his own ID_i , he can compute the secret key $K_{GWN-S} = M_8 \oplus ID_i$. By knowing this secret information, the adversary can perform many other attacks that we detail in the following paragraphs.

E. Many-time Pad Attack

In X. Li et al.'s scheme, the same sensor node S_j uses the One-Time Pad K_{GWN-S} for all the users with whom it communicates: for user U_1 we have $M_8^1 = ID_1 \oplus K_{GWN-S}$, for user U_2 we have $M_8^2 = ID_2 \oplus K_{GWN-S}$, etc. If an attacker intercepts the message M_8 corresponding to at least two different users U_1 and U_2 , he can perform the Many-Time Pad attack ($M_8^1 \oplus M_8^2 = ID_1 \oplus ID_2$). Generally, the ID_i chosen by users is a low entropy information, hence the attacker can perform a dictionary attack to recover ID_1 (or ID_2) and can then calculate $K_{GWN-S} = M_8^1 \oplus ID_1$.

F. User Anonymity

X. Li et al. presumed that the user's real identity ID_i is shielded in their protocol; however, we proved in the aforementioned attack that user anonymity is not guaranteed. The adversary who has the secret key K_{GWN-S} (from previous attacks) can easily reveal each user's identity by catching the exchanged message $\{M_8, M_9, M_{10}, M_{11}\}$ between the legitimate user and the GWN and computing $ID_i = M_8 \oplus K_{GWN-S}$.

G. Session Key Disclosure Attack

From the insider attack, the adversary, who also knows SID_j , gets the sensor node secret key K_{GWN-S} that allows him to calculate the session key as follows: the adversary obtains ID_i from the user anonymity flaw, and calculates the GWN random number $r_g = M_9 \oplus h(ID_i \parallel K_{GWN-S})$ from the message $\{M_8, M_9, M_{10}, M_{11}\}$ sent by the GWN . The legal sensor S_j generates its private random number r_j and calculates $M_{12} = r_j \oplus K_{GWN-S}$ that it sends explicitly over the public channel to the GWN . The adversary can retrieve $r_j = M_{12} \oplus K_{GWN-S}$ from M_{12} and $r_i = r_g \oplus M_{10}$ from M_{10} . Hence, the attacker can easily calculate the session key $SK = h(ID_i \parallel SID_j \parallel r_i \parallel r_j \parallel r_g)$.

H. Sensor Impersonation Attack

X. Li et al. presumed that S_j cannot be impersonated since the S_j 's secret key $K_{GWN-S} = h(SID_j \parallel K_{GWN})$ is unknown. Through the previous attacks, we have shown that K_{GWN-S} can be calculated, thus an attacker can impersonate S_j .

I. Sensor Node Untraceability

Any adversary can trace different sessions between a particular user U_i and a sensor node S_j since the exchanged message $M_8 = ID_i \oplus K_{GWN-S}$ stays the same in all sessions.

V. PROPOSED PROTOCOL

To overcome the functional and security flaws described in the previous section, the current paper proposes this improved protocol that involves three main entities: the Gateway Node (GWN) as a trusted entity, the Sensor Node (S_j), and the User (U_i). It consists of six phases: initialization phase, user and sensor registration, login and mutual authentication, user's identity update, user's password update, and smart card revocation. Table I summarizes the notations used throughout this section.

TABLE I. NOTATIONS USED IN THE PRESENT PAPER AND THEIR DESCRIPTIONS

Parameter	Description
U_i	User
S_j	Sensor node
GWN	Gateway node
F_p	Finite field of order p
$E(F_p)$	Elliptic Curve
P	Generator Point
n	Order of P
$h()$	Hash function
C	Set of codewords
pn_i	U_i 's phone number
$PUF()$	Physical Unclonable Function
x_{GWN}	GWN 's private key (master key)
$X_{GWN} = x_{GWN}P$	GWN 's public key
y_i	U_i 's private key
$Y_i = y_iP$	U_i 's public key
$E_{AES}(.)_S$	AES Encryption using the key S
$D_{AES}(.)_S$	AES Decryption using the key S
TS	Timestamp
$status_i$	The status of the user (active or inactive)
ID_i	U_i 's identity (64 bits)
SID_j	Sensor identity (64 bits)
SC	Smart Card
DB	Database

A. Initialization Phase

Before the execution of the protocol, the initialization phase must be performed by the GWN . It selects an additive group G

and its generator point P of order n (a large prime number) on an elliptic curve $E(F_p)$ where F_p is a finite field. GWN chooses randomly its private key $x_{GWN} \in \mathbb{Z}_n^*$ and computes the corresponding public key $X_{GWN} = x_{GWN}.P$. At last, GWN stores its private key and publishes the system parameters $\{E(F_p), G, P, h(), X_{GWN}\}$ where $h()$ is a 128-bit hash function.

B. Registration Phase

Unlike the reviewed scheme, the registration phase in this protocol does not require a secure channel to exchange data with the GWN neither for the user nor for the sensor.

1) *User registration:* In the user registration phase, it is assumed that U_i already possesses a private key y_i and published its corresponding public key $Y_i=y_i.P$. This key pair is needed to encrypt/decrypt the parameters $ID_i, b_i,$ and pn_i . This phase involves U_i and GWN . At the end of this phase, U_i becomes a legitimate user. The details of this phase are shown in Fig. 1.

2) *Sensor registration:* This phase involves GWN and S_j . GWN should store some data in each S_j 's memory before deploying the sensors in the WSN. First, GWN selects SID_j for each S_j , generates a random number u_j , and stores SID_j and u_j in S_j 's memory. Moreover, each S_j has its own pre-implemented $PUF_j()$. GWN calculates $K_{GWN-S}=PUF_j(u_j)$ and stores $\{SID_j, K_{GWN-S}\}$ in its DB.

C. Login and Mutual Authentication

To remotely access the sensed data of S_j , U_i should perform a successful login. Moreover $U_i, S_j,$ and GWN must be mutually authenticated to exchange data. This phase is performed over a public channel as shown in Fig. 2.

D. User's Password Update

The password update phase allows a legitimate user U_i to change his/her old password PW_i^{old} to a new one PW_i^{new} . The steps of this phase are shown in Fig. 3.

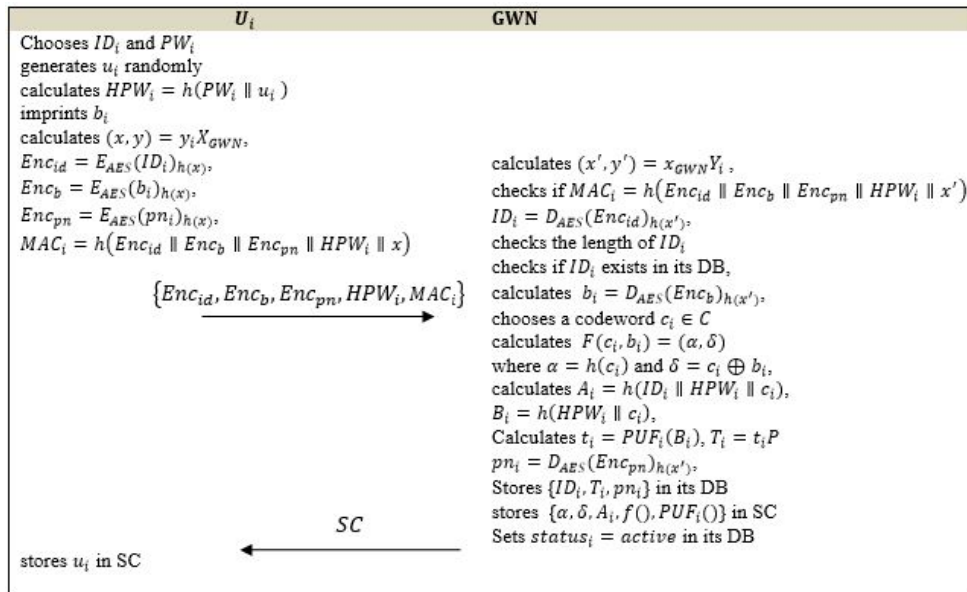


Fig. 1. User Registration Phase.

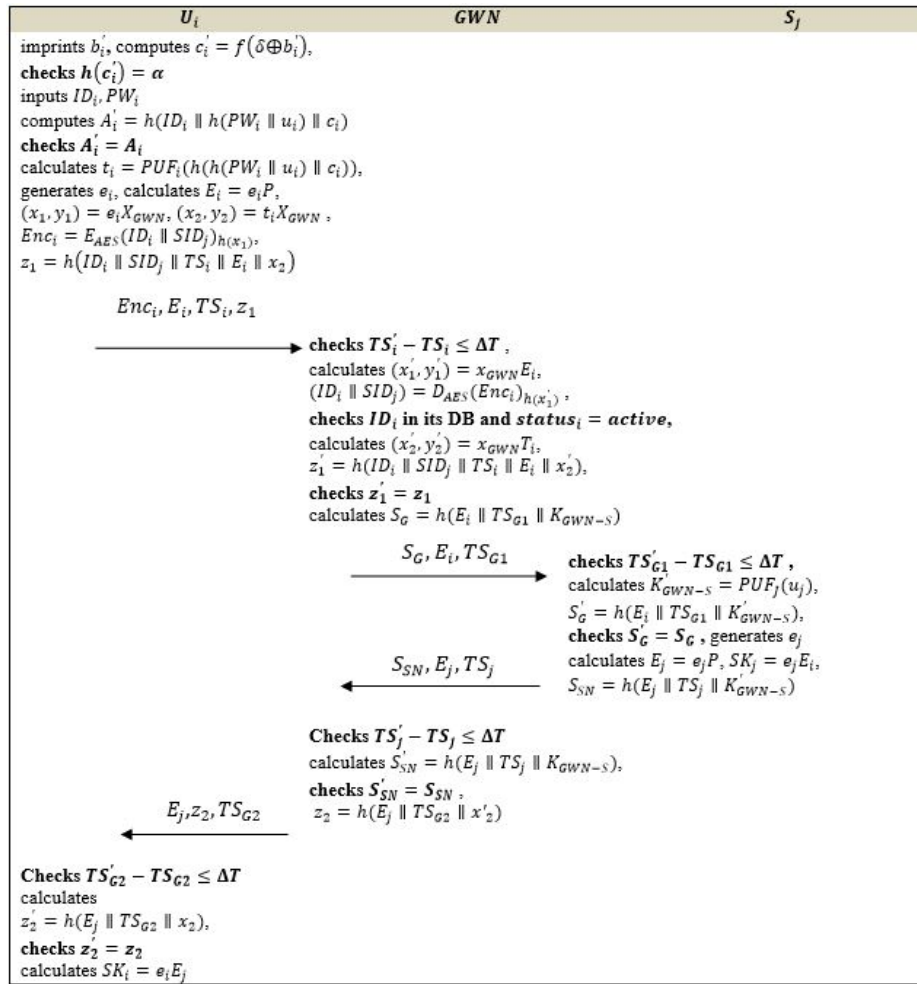


Fig. 2. Login and Mutual Authentication Phase.

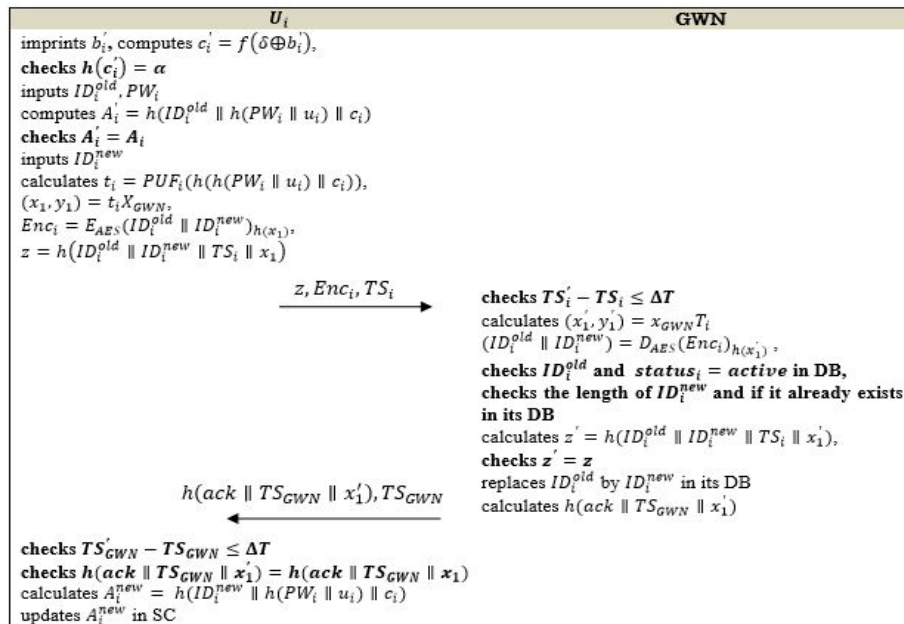


Fig. 3. User's Identity Update Phase.

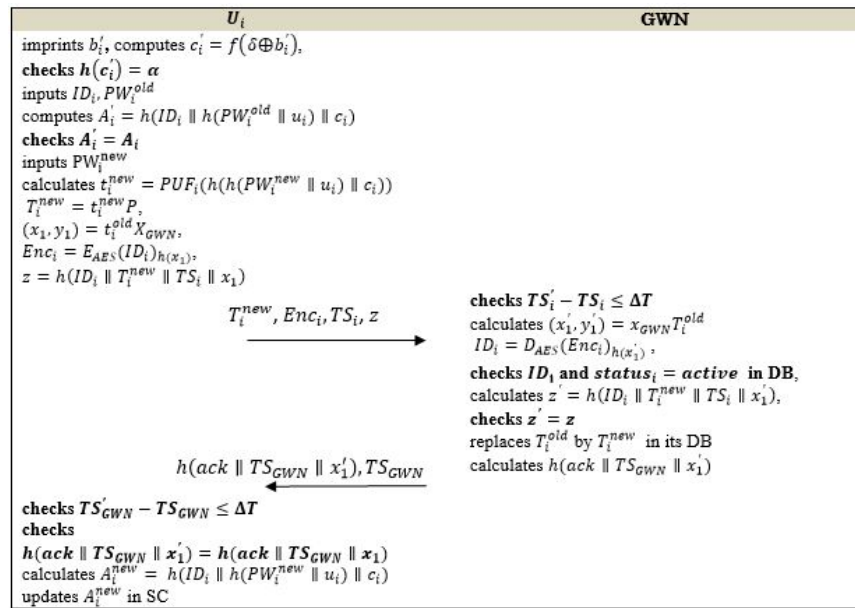


Fig. 4. User's Password Update Phase.

E. User's Identity Update

In addition to password update, this scheme allows each legitimate user U_i to change his/her ID_i whenever he/she wants, following the steps shown in Fig. 4.

F. Smart Card Revocation and Re-registration

A legal user U_i can revoke his/her lost or stolen SC through a secure process. Once U_i realizes the loss of his/her SC, he/she informs GWN to obtain a new one. SC revocation and re-registration phase steps are described below:

- **Revocation request:** it is performed remotely over the public channel. The main purpose of this step is to deactivate the stolen/lost SC immediately when the U_i sends a revocation request to the GWN. Therefore, the re-registration step can be performed later on. First, the revocation request is sent by U_i to GWN which verifies the user's identity through a one-time password mechanism using U_i 's phone number p_{ni} which was already stored in the GWN's database at the user's registration phase. Then, GWN checks if $status_i = active$. If it holds, GWN updates $T_i = Null$ and $status_i = inactive$ in its DB. Else, the revocation request is terminated. From then on, the lost/stolen SC is no more valid.
- **Re-registration:** this step aims to securely authenticate U_i who wants to re-register in the system after the revocation of his/her old SC. At the end of this step, a new active SC is delivered to the legitimate user by the GWN. First, U_i presents in person his/her Personal Identification Card to GWN for verification. Then the authenticated user inputs his ID_i , chooses PW_{inew} , and calculates $HPW_{inew} = h(PW_{inew} \parallel u_{inew})$ (u_{inew} is generated randomly). Then, U_i imprints $binew$. The GWN checks if ID_i exists in its DB and $status_i = inactive$. If this is true, GWN chooses a codeword $cinew \in C$, calculates $F(cinew, binew) = (\alpha_{new},$

$\delta_{new})$ where $\alpha_{new} = h(cinew)$ and $\delta_{new} = cinew \oplus binew$. Then GWN computes $A_{inew} = h(ID_i \parallel HPW_{inew} \parallel cinew)$, $B_{inew} = h(HPW_{inew} \parallel cinew)$, and $T_{inew} = PUF_{inew}(B_{inew})P$. After performing these operations, GWN updates T_{inew} and sets $status_i = active$ in its DB. Then GWN stores the parameters $\{\alpha_{new}, \delta_{new}, A_{inew}, PUF_{inew}(), f()\}$ in the new SC. Finally, GWN delivers the new SC to U_i . When receiving the SC, U_i stores the random number u_{inew} in his/her new SC. From then on, U_i can use his new active SC securely over the public channel.

VI. SECURITY ANALYSIS OF THE PROPOSED PROTOCOL

A. Informal Security Analysis

This section informally discusses the security features of the current protocol. This scheme provides important security features and resists many security attacks in WSN. Remember that all communications in this protocol are performed over the public channel and no secure channel assumption is required. Moreover, Table II presents the security features comparison between the proposed protocol and the following schemes: X.Li et al. [5], Choi et al. [13], Zhang et al. [35], and S.Challa et al. [25]. The first 12 evaluation criteria are proposed in [36]. In addition, proposed three new criteria are provided:

- **C13. SN Anonymity:** the sensor's identity is protected and its activity cannot be traced.
- **C14. Freely Identity Change:** the identity is memorable, and can be chosen freely and changed by the user.
- **C15. Suitable for IoT:** no direct communication between the users and sensors, the communication should be through a gateway.

Table II shows that all the studied schemes satisfies $C1, C2,$ and $C3$ except [35] that does not satisfies $C2$ since it does not support password update feature. Except for [35] that does not

support smart cards, all the studied protocols are resistant to SC loss attack (C4). For instance, in the current protocol, when an adversary steals a legitimate user’s smart card, he needs B_i to calculate $t_i = PUF(B_i)$. However, $B_i = h(h(PW_i || u_i) || c_i)$ is not stored in SC, so the attacker has to compute it. This is not possible, because he needs to know the password PW_i and the codeword c_i . Moreover, when U_i ’s SC is stolen, the GWN changes the parameter $status_i$ to *inactive* after performing a SC revocation, as explained previously, making it no more valid.

TABLE II. COMPARISON OF SECURITY FEATURES OF THE STUDIED PROTOCOLS

Evaluation Criteria	[5]	[13]	[35]	[25]	Our protocol
C1. No password verifier-table	Yes	Yes	Yes	Yes	Yes
C2. Password friendly	Yes	Yes	No	Yes	Yes
C3. No password exposure	Yes	Yes	Yes	Yes	Yes
C4. No smart card loss attack	Yes	Yes	-	Yes	Yes
C5. Resistance to known attacks					
- Replay Attack	Yes	Yes	Yes	Yes	Yes
- Offline Password Guess	Yes	Yes	Yes	Yes	Yes
- User Impersonation attack	Yes	No	Yes	Yes	Yes
- SN Impersonation attack	No	Yes	Yes	Yes	Yes
- GWN Impersonation attack	Yes	Yes	Yes	Yes	Yes
- Cloning Attack	No	No	No	No	Yes
- Insider Attack	No	Yes	Yes	Yes	Yes
C6. Sound repairability	No	No	-	Yes	Yes
C7. Provision of key agreement	Yes	Yes	Yes	Yes	Yes
C8. No clock synchronization	Yes	No	No	No	No
C9. Timely typo detection	Yes	Yes	No	Yes	Yes
C10. Mutual authentication	Yes	Yes	Yes	Yes	Yes
C11. User anonymity	No	No	No	Yes	Yes
C12. Forward secrecy	Yes	Yes	Yes	Yes	Yes
C13. SN anonymity	No	No	No	Yes	Yes
C14. Freely identity change	No	No	No	No	Yes
C15. Suitable for IoT	Yes	No	Yes	No	Yes

The C5 criteria consist of the following attacks:

- **Replay attack:** as shown in Table II, all the studied schemes are resistant to replay attack. In this protocol, timestamps are used to prevent this attack.
- **Offline password guess:** Table II shows that all the studied protocols are resistant to the offline password guess. In this protocol, if an attacker has U_i ’s SC, this means that he has access to four elements: $\alpha = h(c_i)$, $\delta = c_i \oplus b_i$, $A_i = h(ID_i || h(PW_i || u_i) || c_i)$, and u_i . The goal of the attacker in this attack is to get PW_i (we suppose that he already knows the ID_i of SC owner). To guess PW_i by performing a password dictionary attack on A_i , the attacker needs to know c_i first. However, according to Juels and Wattenberg [34], it’s impossible to retrieve c_i from α and δ . In addition, the attacker cannot guess c_i from A_i using a dictionary attack because c_i is a random number with high entropy. As a result, the current protocol resists the offline password attack.

- **User, GWN, and SN impersonation attack:** this protocol is resistant to user, GWN, and SN impersonation attacks since the attacker cannot compute $z1 = h(ID_i || SID_i || TS_i || Ea || x2)$, $z2 = h(Ea || TSG2 || x2)$, $SG = h(Ea || TSG1 || KGWN - S_j)$, or $SSN = h(Ea || TS_j || KGWN - S_j)$. That is because he is not able to get $KGWN - S_j$ or to compute $x2$ as long as he does not have access to U_i ’s private key t_i or GWN’s master key $xGWN$. In contrast, [5] is vulnerable to the SN impersonation attack as showed in the “Weaknesses of X.Li et al.’s scheme” section above and [13] suffers from user impersonation attack.
- **Cloning attack:** In contrast with the other studied schemes, this protocol is resistant to cloning attack. To protect SC from the cloning attack, PUF is used to compute U_i ’s private key t_i . Suppose that an attacker somehow succeeded to get the PW_i and c_i and cloned U_i ’s SC, then the attacker will try to compute $t_i' = PUF_{cloned}(h(h(PW_i || u_i) || c_i))$. However, the computed t_i' will be different from U_i ’s private key t_i because the cloned PUF_{cloned} is different from the original PUF_i as explained previously in the preliminaries. Moreover, the current protocol is resistant to sensor cloning attack since if an attacker clones the sensor he will get u_j and will try to compute $K'GWN - S = PUF_{cloned}(u_j)$. However, the computed $K'GWN - S$ will be different from the original $KGWN - S$ because the cloned PUF_{cloned} is different from the original PUF_j .
- **Insider attack:** This attack is performed by a legitimate user U_a to gain additional privileges. The author in [5] is the only scheme that suffers from insider attack as we described in the “Weaknesses of X.Li et al.’s scheme” section above. In the following, a proof that this scheme is resistant to the insider attack is given. In this analysis, the goal is to prove that an insider attacker has no advantage compared with an outsider attacker. That is, all the insider attacker’s additional information, that an outsider attacker does not possess, does not give him any additional power as an attacker. First, all the data that an insider attacker U_a possesses and outsider attackers do not have are specified as follows: ID_a , PW_a , $ba, \alpha = h(ca), \delta a = ca \oplus ba, u_a, A_a = h(ID_a || h(PW_a || u_a) || ca), ta = PUF_a(h(h(PW_a || u_a) || ca))$, and in each session he has: ea and SID_j of the targeted sensor S_j . Notice that these data, except SID_j , are unique to U_a and do not consist of any information that is used by other users, sensor nodes, or GWN. Thus, these data give U_a no advantage to attack other users, sensor nodes, or GWN compared to an outsider attacker. Next, it is important to make sure that these data do not help U_a to extract some useful information from the messages exchanged in his sessions. In the following, the messages exchanged in each session of U_a are cited (excluding the messages generated by U_a): $SG = h(E_i || TSG1 || KGWN - S), E_i, TSG1, SSN = h(E_j || TS_j || KGWN - S), E_j, TS_j, z2 = h(E_j || TSG2 || x2), TSG2$. Obviously, the public elements $E_i, TSG1, E_j, TS_j$, and $TSG2$ can be retrieved by any attacker not only an insider attacker; thus, they represent no advantage of an insider attacker

over the outsider attackers. Besides, since the messages SG, SSN, and z_2 are unique to each session, the insider attacker cannot use them to attack other sessions. Additionally, assuming that the used hash function is secure, the insider attacker cannot extract KGWN-S or x_2 from SG, SSN, or z_2 . As a result, you can conclude that an insider attacker does not possess and cannot extract any additional useful information as an attacker compared to an outsider attacker. Thus, insider and outsider attackers have the same capabilities.

According to [36], sound repairability (C6) means that the scheme provides SC revocation without requiring the user to change her identity. As you can see in the smart card revocation and re-registration sub-section, this protocol perfectly fits to this criteria and does not require any identity update after SC revocation. The authors in [5] and [13] do not support the SC revocation feature at all and [35] does not support smart cards. Table II also shows that all the studied schemes guarantee mutual authentication (C10) and provision of a key agreement (C7). In [5], the generated session key consists of a hash of the user ID, the sensor SID, and three fresh nonces that are new for each session. As a result, if an attacker disclosed one or more session keys, he would not be able to guess the other session keys as long as the hash function is secure. Thus, [5] satisfies the forward secrecy criteria (C12). The rest of studied protocols, including our protocol, satisfy C12 as well since the generated session key depend on a fresh ECDH shared key and by knowing some session keys the attacker will not be able to affect the other sessions except if he can resolve the ECDH problem which is cryptographically hard.

Only [5] satisfies the “No clock synchronization” (C8) criteria since all the other protocols employ timestamps to prevent replay attacks. Timely typo detection criteria (C9) require that the user will be timely notified if she inputs wrong credentials by mistake when login. This is satisfied by all the studied schemes except [35] which do not employ any checking locally in the login phase. The credentials in [35] are checked afterward by the gateway node. The current protocol and [25] meet the user and sensor node anonymity criteria (C11 and C13). In this protocol, The user and sensor anonymity is guaranteed by the fact that ID_i and SID_j are not sent clearly over the public channel, and they are encrypted $Enc_i = E_{AES}(ID_i || SID_j)_{h(x_1)}$. Thus, no adversary can reveal the user’s or sensor’s real identity from the exchanged messages. The untraceability of the user and the sensor node is provided in this scheme through the fact that all exchanged data vary from one session to another. This is because E_i and E_j are generated in each session randomly, thus Enc_i , z_1 , S_G , S_{SN} , and z_2 vary from a session to another since they are computed based on E_i or ID_j . In contrast, [5] does not fulfill this criteria as showed in the “Weaknesses of X.Li et al.’s scheme” section above. The authors in [13] and [35] do not guarantee this criteria either since they communicate the user’s ID and sensor’s SID in clear during the authentication phase.

In addition to the abovementioned features, the current protocol is the only protocol that supports freely identity change (C14). Besides, it is suitable for IoT (C15) since there

is no direct data exchange between the user and the sensor node, unlike [13] and [25], where the sensor node contacts the user directly.

B. Formal Security Analysis using AVISPA Tool

This section formally analyzes the security and authentication logic of the current protocol using the widely used AVISPA Tool. The implementation of this protocol in the HLPSL is provided. The analysis results will show that this protocol is safe. In this HLPSL specification, three basic roles representing the protocol’s principals are defined: user, gateway, and sensor. In addition, there are two composed roles, session and environment, and a goals section where the security goals are specified. Table III contains the notations used in the specification and their corresponding notations in the protocol’s login and authentication phase provided in Fig. 2.

TABLE III. HLPSL SPECIFICATION’S NOTATIONS AND THEIR CORRESPONDING PROTOCOL NOTATIONS

HLPSL Specification’s Notations	Corresponding Protocol’s Notations
U, GWN, and S	The agents’ IDs
TS1, TS2, TS3, TS4	$TS_i, TS_{G1}, TS_{G2}, TS_j$
UU, US	u_i, u_j
DELTA	δ
B, PW	b_i, PW_i
P	The generator point P
XGWN, PXGWN	x_{GWN}, X_{GWN}
Hash, F, PUFU, PUFs	h, f, PUF_i, PUF_j
E1, PE1, E2, PE2	e_i, E_i, e_j, E_j
C, A	c_i, A_i
T, PT	t_i, T_i
SK	SK
KGWNS	K_{GWN-S}

```

role user(U, GWN, S: agent,
          TS1, TS4, UU, DELTA, B, PW: text,
          P: nat,
          PXGWN: message,
          Hash, F, PUFU: hash_func,
          SND, RCV: channel(dy))
played_by U def=
local
  State: nat,
  E1, C, A, T: text,
  SK, PE2, X: message
init
  State := 0
transition
  1.State = 0 ^ RCV(start) =>
  State:=1
  ^ C' := F(xor(DELTA, B))
  ^ A' := Hash(U.Hash(PW.UU),C)
  ^ T' := PUFU(Hash(Hash(PW.UU.C)))
  ^ E1' := new()
  ^ X' := exp(PXGWN,T')
  ^ SND(exp(P.E1'),(U.S)_Hash(exp(PXGWN,E1')).TS1.
Hash(U.S.TS1.exp(P.E1').X'))
  ^ witness(U,GWN,gateway_user_e1,Hash(U.S.TS1.exp(
P.E1').X'))
  2.State = 1 ^ RCV(PE2'.TS4.Hash(PE2'.TS4.X)) =>
  State:=2
  ^ SK' := exp(PE2',E1)
  ^ request(U,GWN,user_gateway_e2,Hash(PE2'.TS4.X))
end role
    
```

Fig. 5. User Role's HLPSL Specification.

Fig. 5 describes the user role specification. The gateway role's specification is provided in Fig. 6. The sensor role's specification is described in Fig. 7. In Fig. 8, the HLPSSL specification of the session and environment roles is provided. Fig. 9 shows the analysis results obtained using the OFMC and CL-AtSe backends. Currently, AVISPA Tool provides four backends: OFMC, CL-AtSe, SATMC, and TA4SP. However, SATMC, and TA4SP do not support operations like xor() and exp(). Both OFMC and CL-AtSe analysis results show that this protocol is safe against active and passive attacks.

```

role gateway(
  U, GWN, S: agent,
  KGWNS: message,
  TS1, TS2, TS3, TS4, XGWN: text,
  PT: message,
  Hash: hash_func,
  SND, RCV: channel(dy) )
played_by GWN def=
local
  State: nat,
  PE1, PE2: message
init
  State := 0
transition
  1.State = 0 ∧ RCV(PE1'.{U,S} Hash(exp(PE1',
  XGWN)),TS1.Hash(U.S.TS1.PE1'.exp(PT,XGWN))) =>
  State' := 1
  ∧ SND(PE1'.TS2.Hash(PE1'.TS2.KGWNS))
  ∧ request(GWN,U,gateway_user_e1,Hash(U.S.TS1.PE1'.
  exp(PT,XGWN)))
  ∧ witness(GWN,S,sensor_gateway_e1,Hash(PE1'.TS2.
  KGWNS))
  2.State = 1 ∧ RCV(PE2'.TS3.Hash(PE2'.TS3.KGWNS))
=>
  State' := 2
  ∧ SND(PE2'.TS4.Hash(PE2'.TS4.exp(PT,XGWN)))
  ∧ request(GWN,S,gateway_sensor_e2,Hash(PE2'.TS3.
  KGWNS))
  ∧ witness(GWN,U,user_gateway_e2,Hash(PE2'.TS4.
  exp(PT,XGWN)))
end role
    
```

Fig. 6. Gateway Node Role's HLPSSL Specification

```

role sensor(
  U, GWN, S: agent,
  P : nat,
  TS2, TS3, US: text,
  Hash, PUFs: hash_func,
  SND, RCV: channel(dy))
played_by S def=
local
  State: nat,
  E2 : text,
  SK, PE1 : message,
  KGWNS : message
init
  State := 0 ∧ KGWNS := PUFs(US)
transition
  1.State = 0 ∧ RCV(PE1'.TS2.Hash(PE1'.TS2.KGWNS))
=>
  State' := 1
  ∧ E2' := new()
  ∧ SK' := exp(PE1', E2')
  ∧ SND(exp(P,E2').TS3.Hash(exp(P,E2').TS3.KGWNS))
  ∧ request(S,GWN,sensor_gateway_e1,Hash(PE1'.TS2.
  KGWNS))
  ∧ secret(SK', sk, {U,S})
  ∧ witness(S,GWN,gateway_sensor_e2,Hash(exp(P,E2').
  TS3.KGWNS))
end role
    
```

Fig. 8. Sensor Node Role's HLPSSL Specification.

<pre> % OFMC % Version of 2006/02/13 SUMMARY SAFE DETAILS SAFE BOUNDED_NUMBER_OF_SESSIONS TYPED_MODEL BOUNDED_NUMBER_OF_SESSIONS PROTOCOL /home/span/span/testsuite/results/MAKA- Login-Auth.if GOAL As Specified BACKEND CL-AtSe OFMC COMMENTS STATISTICS parseTime: 0.00s searchTime: 5.96s visitedNodes: 550 nodes depth: 14 plies </pre>	<pre> SUMMARY SAFE DETAILS BOUNDED_NUMBER_OF_SESSIONS TYPED_MODEL PROTOCOL /home/span/span/testsuite/results/MAKA- Login-Auth.if GOAL As Specified BACKEND CL-AtSe STATISTICS Analysed : 119282 states Reachable : 89374 states Translation: 0.05 seconds Computation: 67.03 seconds </pre>
--	---

Fig. 9. Analysis Result using OFMC and CL-AtSe Backends.

```

%%SESSION ROLE %%%
role session(
  U, GWN, S: agent,
  P : nat,
  TS1, TS2, TS3, TS4, XGWN, UU, DELTA, B, PW, US: text,
  Hash, F, PUFU, PUFs: hash_func)
def=
local
  SU, RU, SGWN, RGWN, SS, RS: channel(dy)
composition
  user(U, GWN, S, TS1, TS4, UU, DELTA, B, PW, P, exp(P, XGWN),
  Hash, F, PUFU, SU, RU)
  ∧ gateway(U, GWN, S, PUFs(US), TS1, TS2, TS3, TS4, XGWN,
  exp(P,PUFU(Hash(Hash(PW,UU).F(xor(DELTA, B))))), Hash, SGWN, RGWN)
  ∧ sensor(U, GWN, S, P, TS2, TS3, US, Hash, PUFs, SS, RS)
end role
%%ENVIRONMENT ROLE %%%
role environment() def=
const
  u, gwn, s: agent,
  p: nat,
  xgwn, ts11, ts21, ts31, ts41, ts12, ts22, ts32, ts42, ts13, ts23, ts33, ts43,
  ts14, ts24, ts34, ts44, uu, deltau, bu, pwu, us, ui, deltai, bi, pwi, ui: text,
  sk, gateway_user_e1, user_gateway_e2, sensor_gateway_e1,
  gateway_sensor_e2: protocol_id,
  h, f, pufu, pufs, pufi: hash_func
intruder_knowledge = {u, gwn, s, i, p, exp(p, xgwn), ui, deltai, bi, pwi,
  exp(p,pufu(h(pwu,uu).f(xor(deltai, bu))))}, h, pufi, f, ts11, ts21, ts31, ts41,
  ts12, ts22, ts32, ts42, ts13, ts23, ts33, ts43, ts14, ts24, ts34, ts44}
composition
  session(u,gwn,s,p, ts11, ts21, ts31, ts41, xgwn, uu, deltau, bu, pwu, us, h,
  f, pufu, pufs)
  ∧ session(u, gwn, s, p, ts12, ts22, ts32, ts42, xgwn, uu, deltau, bu, pwu, us,
  h, f, pufu, pufs)
  ∧ session(u, gwn, i, p, ts13, ts23, ts33, ts43, xgwn, uu, deltau, bu, pwu, ui,
  h, f, pufu, pufi)
  ∧ session(i, gwn, s, p, ts14, ts24, ts34, ts44, xgwn, ui, deltai, bi, pwi, us, h,
  f, pufi, pufs)
end role
%%GOALS %%%
goal
  authentication_on_gateway_user_e1
  authentication_on_user_gateway_e2
  authentication_on_sensor_gateway_e1
  authentication_on_gateway_sensor_e2
  secrecy_of_sk
end goal
environment()
    
```

Fig. 7. Session, Environment, and Goals' HLPSSL Specification.

VII. PERFORMANCE COMPARISON

This section presents the computational and communicational costs of this proposed protocol in comparison with other related schemes [5, 13, 25, 35]. To calculate the communication costs of the current protocol in comparison with the other related schemes, assume that the length of each element is as follows: user identity (64 bits), sensor identity (64 bits), hash (128 bits), timestamp (64 bits), ECC point (320 bits), AES (128 bits). From Table IV, you can obviously see that this protocol communication cost is the best compared to the other protocols. In terms of computation costs, the following notations are used: T_{EPM} denotes the time cost of one point multiplication computation on ECC, T_h denotes the time cost of one hash function computation and T_{AES} denotes the time cost of one AES encryption/decryption operation [37]. Note that T_{AES} requires much less time compared to T_{EPM} [38]. Note also that compared to hash functions, PUFs require much less hardware overhead to implement [39], thus the negligible execution time of PUF will not be included in the comparison. Table IV provides a summary of the computation costs comparison. The computation cost of this protocol is considerably higher than the computation cost of X.Li et al.'s scheme [5]. This is explained by the fact that the reviewed protocol does not use ECC point multiplication operations in all steps of the mutual authentication phase, which makes it vulnerable to many attacks as previously discussed in Section IV. This protocol requires slightly more computational costs than Choi et al.'s scheme [13], but it is more secure as

shown previously in Table IV. In addition, note that at the sensor side, which is a resource-constrained device, the current protocol generates less computation cost compared to Choi et al.'s scheme. Compared to the protocols proposed by S.Challa et al. [25] and Zhang et al. [35], this protocol achieves a better efficiency level since it only requires the execution of 8 ECC point-scalar multiplications in total, while the former protocols require the execution of 14 ECC point-scalar multiplications.

VIII. CONCLUSION

After reviewing X.Li et al.'s protocol and finding it to be vulnerable to many serious attacks such as insider attack, many time pad attack, lack of anonymity, and impersonation attacks, this paper presented a new mutual authentication and key agreement scheme that strengthens its security using three factors: password, smart card, and biometrics. The informal security analysis proved that this protocol resists all the attacks found in the studied protocol including X.Li et al.'s protocol. Additionally, a formal security analysis was given using AVISPA tool, which shows that the protocol is safe. In contrast with the studied protocols, this protocol also provides a freely identity change feature in addition to the password update.

TABLE IV. COMPARISON OF COMPUTATION AND COMMUNICATION COSTS OF THE STUDIED PROTOCOLS

	[5]	[13]	[35]	[25]	Our protocol
Computation time of U_i	$2T_{EPM} + 8T_h$	$3T_{EPM} + 9T_h$	$5T_{EPM} + 4T_h$	$5T_{EPM} + 5T_h$	$4T_{EPM} + 8T_h + T_{AES}$
Computation time of GWN	$T_{EPM} + 9T_h$	$T_{EPM} + 5T_h$	$5T_{EPM} + 5T_h$	$5T_{EPM} + 4T_h$	$2T_{EPM} + 5T_h + T_{AES}$
Computation time of S_j	$4T_h$	$2T_{EPM} + 6T_h$	$4T_{EPM} + 4T_h$	$4T_{EPM} + 3T_h$	$2T_{EPM} + 2T_h$
Total of computation costs	$3T_{EPM} + 21T_h$	$6T_{EPM} + 20T_h$	$14T_{EPM} + 13T_h$	$14T_{EPM} + 12T_h$	$8T_{EPM} + 15T_h + 2T_{AES}$
Communication costs (bits)	2368	3072	3168	2464	2176

On the other side, the proposed protocol achieved better results in terms of communication compared to the studied protocols. Computationally, X.Li et al.'s protocol is the most efficient. However, this efficiency advantage comes at the expense of security as shown previously. In terms of security-efficiency ratio, the current protocol can be considered better than all the studied schemes. In the future, it will be interesting to improve this protocol to be suitable for mobile IoT applications where objects can jump from a gateway node zone to another in the same session without repeating the authentication process.

REFERENCES

[1] Ammar, M., Russello, G., Crispo, B.: Internet of Things: A survey on the security of IoT frameworks. *J. Inf. Secur. Appl.* 38, 8–27 (2018).
 [2] Atzori, L., Iera, A., Morabito, G.: The Internet of Things: A survey. *Comput. Networks.* 54, 2787–2805 (2010).
 [3] Ray, P.P.: A survey on Internet of Things architectures. *J. King Saud Univ. - Comput. Inf. Sci.* 30, 291–319 (2018).
 [4] Suárez-Albela, M., Fernández-Caramés, T.M., Fraga-Lamas, P., Castedo, L.: A practical evaluation of a high-security energy-efficient

gateway for IoT fog computing applications. *Sensors (Switzerland)*. 17, 1–39 (2017).
 [5] Li, X., Niu, J., Kumari, S., Wu, F., Sangaiah, A.K., Choo, K.K.R.: A three-factor anonymous authentication scheme for wireless sensor networks in internet of things environments. *J. Netw. Comput. Appl.* 103, 194–204 (2018).
 [6] Das, M.L.: Two-factor user authentication in wireless sensor networks. *IEEE Trans. Wirel. Commun.* 8, 1086–1090 (2009).
 [7] Nyang, D., Lee, M.-K.: Improvement of Das's Two-Factor Authentication Protocol in Wireless Sensor Networks. *IACR Cryptol. ePrint Arch.* 2009, 631 (2009).
 [8] Yeh, H.L., Chen, T.H., Liu, P.C., Kim, T.H., Wei, H.W.: A secured authentication protocol for wireless sensor networks using Elliptic Curves Cryptography. *Sensors*. 11, 4767–4779 (2011).
 [9] Chen, T.H., Shih, W.K.: A robust mutual authentication protocol for wireless sensor networks. *ETRI J.* 32, 704–712 (2010).
 [10] He, D., Gao, Y., Chan, S., Chen, C., Bu, J.: An enhanced two-factor user Authentication Scheme in Wireless Sensor Networks. *Ad-Hoc Sens. Wirel. Networks*. 10, 361–371 (2010).
 [11] Kumar, P., Lee, H.J.: Cryptanalysis on two user authentication protocols using smart card for wireless sensor networks. *2011 Wirel. Adv. WiAd* 2011. 241–245 (2011).
 [12] Shi, W., Gong, P.: A new user authentication protocol for wireless sensor networks using elliptic curves cryptography. *Int. J. Distrib. Sens. Networks*. 2013, (2013).
 [13] Choi, Y., Lee, D., Kim, J., Jung, J., Nam, J., Won, D.: Security enhanced user authentication protocol for wireless sensor networks using elliptic curves cryptography. *Sensors (Switzerland)*. 14, 10081–10106 (2014).
 [14] Jiang, Q., Ma, J., Lu, X., Tian, Y.: An efficient two-factor user authentication scheme with unlinkability for wireless sensor networks. *Peer-to-Peer Netw. Appl.* 8, 1070–1081 (2015).
 [15] Wu, F., Xu, L., Kumari, S., Li, X.: A new and secure authentication scheme for wireless sensor networks with formal proof. *Peer-to-Peer Netw. Appl.* 10, 16–30 (2017).
 [16] Nam, J., Kim, M., Paik, J., Lee, Y., Won, D.: A provably-secure ECC-based authentication scheme for wireless sensor networks. *Sensors (Switzerland)*. 14, 21023–21044 (2014).
 [17] Jiang, Q., Ma, J., Wei, F., Tian, Y., Shen, J., Yang, Y.: An untraceable temporal-credential-based two-factor authentication scheme using ECC for wireless sensor networks. *J. Netw. Comput. Appl.* 76, 37–48 (2016).
 [18] He, D., Kumar, N., Chilamkurti, N.: A secure temporal-credential-based mutual authentication and key agreement scheme with pseudo identity for wireless sensor networks. *Inf. Sci. (Ny)*. 321, 263–277 (2015).
 [19] Lu, Y., Li, L., Peng, H., Yang, Y.: An energy efficient mutual authentication and key agreement scheme preserving anonymity for wireless sensor networks. *Sensors (Switzerland)*. 16, 1–21 (2016).
 [20] Chander, B., Kumaravelan, G.: An Improved 2-Factor Authentication Scheme for WSN Based on ECC. *IETE Tech. Rev.* 1–12 (2022).
 [21] Jiang, Q., Zeadally, S., Ma, J., He, D.: Lightweight three-factor authentication and key agreement protocol for internet-integrated wireless sensor networks. *IEEE Access*. 5, 3376–3392 (2017).
 [22] Park, Y.H., Park, Y.H.: Three-factor user authentication and key agreement using elliptic curve cryptosystem in wireless sensor networks. *Sensors (Switzerland)*. 16, (2016).
 [23] Chang, I.P., Lee, T.F., Lin, T.H., Liu, C.M.: Enhanced two-factor authentication and key agreement using dynamic identities in wireless sensor networks. *Sensors (Switzerland)*. 15, 29841–29854 (2015).
 [24] Jung, J., Moon, J., Lee, D., Won, D.: Efficient and security enhanced anonymous authentication with key agreement scheme in wireless sensor networks. *Sensors (Switzerland)*. 17, (2017).
 [25] Challa, S., Wazid, M., Das, A.K., Kumar, N., Goutham Reddy, A., Yoon, E.J., Yoo, K.Y.: Secure Signature-Based Authenticated Key Establishment Scheme for Future IoT Applications. *IEEE Access*. 5, 3028–3043 (2017).
 [26] Delac, K., Grgic, M.: A survey of biometric recognition methods. *Proc. Elmar - Int. Symp. Electron. Mar.* 184–193 (2004).

- [27] Althobaiti, O., Al-Rodhaan, M., Al-Dhelaan, A.: An efficient biometric authentication protocol for wireless sensor networks. *Int. J. Distrib. Sens. Networks*. 2013, (2013).
- [28] Chaudhry, S.A., Naqvi, H., Farash, M.S., Shon, T., Sher, M.: An improved and robust biometrics-based three factor authentication scheme for multiserver environments. *J. Supercomput.* 74, 3504–3520 (2018).
- [29] Herder, C., Yu, M.D., Koushanfar, F., Devadas, S.: Physical unclonable functions and applications: A tutorial. *Proc. IEEE*. 102, 1126–1141 (2014).
- [30] Maiti, A., Gunreddy, V., Schaumont, P.: A systematic method to evaluate and compare the performance of physical unclonable functions. *Embed. Syst. Des. with FPGAs*. 9781461413, 245–267 (2013).
- [31] Suh, G.E., Devadas, S.: Physical unclonable functions for device authentication and secret key generation. *Proc. - Des. Autom. Conf.* 9–14 (2007).
- [32] Charlot, N., Canaday, D., Pomerance, A., Gauthier, D.J.: Hybrid Boolean Networks as Physically Unclonable Functions. *IEEE Access*. 9, 44855–44867 (2021).
- [33] Jeff Grabmeier: Scientists harness chaos to protect devices from hackers, <https://news.osu.edu/scientists-harness-chaos-to-protect-devices-from-hackers/>.
- [34] Juels, A., Wattenberg, M.: A fuzzy commitment scheme. In: *Proceeding CCS '99 Proceedings of the 6th ACM conference on Computer and communications security*, pp. 28–36 (1999).
- [35] Zhang, K., Xu, K., Wei, F.: A provably secure anonymous authenticated key exchange protocol based on ECC for wireless sensor networks. *Wirel. Commun. Mob. Comput.* 2018, (2018).
- [36] Wang, D., Wang, P.: Two Birds with One Stone: Two-Factor Authentication with Security beyond Conventional Bound. *IEEE Trans. Dependable Secur. Comput.* 15, 708–722 (2018).
- [37] Salman, R.S., Farhan, A.K., Shakir, A.: Lightweight Modifications in the Advanced Encryption Standard (AES) for IoT Applications: A Comparative Survey. In: *2022 International Conference on Computer Science and Software Engineering (CSASE)*. IEEE, pp. 325–330 (2022).
- [38] De La Piedra, A., Braeken, A., Touhafi, A.: A performance comparison study of ECC and AES in commercial and research sensor nodes. *IEEE EuroCon 2013*. 347–354 (2013).
- [39] Bolotnyy, L., Robins, G.: Physically unclonable function -based security and privacy in RFID systems. *Proc. - Fifth Annu. IEEE Int. Conf. Pervasive Comput. Commun. PerCom 2007*. 211–218 (2007).

Threshold Segmentation of Magnetic Column Defect Image based on Artificial Fish Swarm Algorithm

Wang Jun¹, Hou Mengjie^{2*}, Zhang Ruiran³
Jiangxi University of Science and Technology
School of Mechanical and Electrical Engineering
Ganzhou, China

Xiao Jingjing⁴
Jiangxi Applied Technology Vocational College
School of Mechanical and Electrical Engineering
Ganzhou, China

Abstract—Aiming at the low efficiency of magnetic column surface defect detection, the vulnerability to human influence, and the insufficient anti-noise performance of existing 2D-OTSU threshold segmentation algorithm, an improved artificial fish swarm algorithm combined with 2D-OTSU algorithm was proposed to improve the accuracy and real-time of magnetic column surface defect detection. Firstly, the weight coefficient was added on the basis of the original 2D-OTSU algorithm, and the distance function was set to optimize the weight coefficient. The objective function was established by combining the inter-class discrete matrix and the intra-class discrete matrix, and the optimal threshold was obtained. Secondly, logistic model was used to optimize the perceptual range and moving step size of the artificial fish swarm algorithm, so as to balance the local and global search ability of the algorithm and improve the convergence speed of the algorithm. Finally, the optimal segmentation threshold is used to segment the image, and compared with other algorithms on four benchmark functions. Experimental results show that the improved algorithm can effectively reduce the time complexity of threshold segmentation and improve the efficiency of the algorithm. At the same time, the segmentation accuracy of the improved algorithm for magnetic column defects reaches 93%, which has good practicability.

Keywords—Defect detecting; threshold segmentation; artificial fish swarm algorithm; improved 2D-OTSU algorithm

I. INTRODUCTION

In the process of magnetic column production, the surface of magnetic column will produce scarring, edge drop, black film and crack. At present, magnetic column surface defects are mainly detected and classified by inspection, which may result in missed detection and error detection in the detection process, affecting the economic benefits of enterprises [1-2].

In recent years, image processing technology has developed vigorously, and defect detection using image processing technology has the advantages of security, reliability and strong adaptability. How to rapidly and accurately segment images by using image processing technology has become a hot topic [3]. Otsu [4] proposed the dynamic threshold method, also known as Otsu segmentation algorithm, to determine the threshold value of image segmentation by the maximum variance between the target region and background region. Zhang et al. [5] used Canny edge detection and Otsu to segment the filtered image, effectively removing the noise of abnormal points. Bo et al. [6] and Wang et al. [7] proposed to use the maximum entropy method to select segmentation

threshold, when the image background is more complex, image segmentation is easy to cause partial information loss in the image and requires a large amount of calculation. The traditional Otsu algorithm only calculates the gray level of a single pixel without using the surrounding pixels, so there is a large error in the image threshold segmentation. On the basis of one-dimensional Otsu algorithm, 2D-OTSU algorithm is proposed to establish two-dimensional histogram based on the original image and the surrounding pixel smoothing information, which reduces the error in image segmentation and improves the accuracy of the algorithm.

In this paper, a threshold segmentation method of 2D-OTSU magnetic column image based on DLAFFSA is proposed. By adding weight coefficient, the performance of 2D-OTSU algorithm is improved. The artificial fish swarm intelligence algorithm was introduced to improve its sensing range and moving step size, and the effectiveness of the improved artificial fish swarm intelligence algorithm was verified through performance test experiments.

II. RELATED WORK

Liu et al. [8] proposed 2D-OTSU algorithm, which extended Otsu method to the case of two-dimensional histogram. The optimal segmentation threshold was obtained by taking the maximum straight of two-dimensional measure criterion. As the one-dimensional space changed to two-dimensional space, the amount of computation increased and the calculation speed slowed down. He et al. [9] established the one-dimensional straight-line intercept histogram and the corresponding threshold selection criterion, which improved the anti-noise performance of the algorithm, but could not distinguish the low-light position information well. Xiao et al. [10] reduced the search space of threshold by mapping the pixel set of two-dimensional histogram to the trapezoidal region, thus improving the computing efficiency. However, some information was lost when the threshold space was compressed, which reduced the segmentation accuracy. Zeng et al. [11] combined the directional fuzzy reciprocal with the straight intercept histogram, replaced the gray information of the neighborhood with the fuzzy reciprocal, strengthened the details of the weak light position, and improved the segmentation accuracy of the model. Yang et al. [12] added local variance into 2D-OTSU, which not only took into account the degree of data dispersion between each pixel point and the central pixel point, but also improved the segmentation

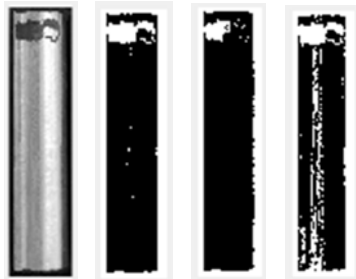
*Corresponding Author.

accuracy while reducing noise interference, but its operation speed was still slow.

In order to solve such problems, many studies [13-15] use swarm intelligence to improve the traditional algorithm. For example, Ma [16] proposed the swarm intelligence whale algorithm, which uses swarm intelligence to conduct local search for threshold mechanism and then further search for global extreme value, thus improving the operation speed of the algorithm. Liu et al. [17] proposed to use the improved firefly algorithm to optimize the two-dimensional Otsu algorithm. In order to enable each firefly to find its own optimal position in the global, the mobile strategy was improved and global information was introduced in the iteration to enable firefly to have global search ability, avoid falling into local extremum and improve the operation efficiency.

III. THRESHOLD SEGMENTATION

Threshold segmentation model has three parts, including establishing segmentation model, determining threshold criterion and solving threshold. As shown in Fig. 1(a) is the image of magnetic column surface defect to be segmented, and Fig. 1(b) is the result of segmentation of magnetic column surface image by selecting an appropriate threshold value. When the threshold value of image segmentation is an appropriate value, the target area of image defect is obvious, and the defect is completely separated from the background. When the segmentation threshold is too small, the defect region of magnetic column cannot be completely segmented, and the defect target region of magnetic column surface defect image is smaller than the actual defect area, as shown in Fig. 1(c). When the segmentation threshold is too large, the magnetic column surface defect image is over-segmented, and part of the background region of the magnetic column image is segmented into the defect region, as shown in Fig. 1(d). Therefore, determining the appropriate threshold algorithm is the key to image threshold segmentation.



(a)Image1 (b)Image2 (c)Image3 (d)Image4.

Fig. 1. Segmentation Results of different Thresholds.

A. Improved 2D-OTSU Algorithm

In order to get the best threshold value, threshold segmentation method is very important. OTSU method is the maximum inter-class variance method, which is the criterion to determine the threshold of image segmentation [18]. However, the noise resistance of this method is weak, and the magnetic column image with low contrast is easily affected by noise, so the image segmentation effect is not obvious. In view of this,

one-dimensional OTSU (1D-OTSU) method has no significant effect. Compared with 1D-OTSU, 2D-OTSU has lower sensitivity to noise and is more significant for defect image segmentation on magnetic column surface [19]. In order to eliminate the influence of isolated noise, weight coefficient is introduced, 2D-OTSU algorithm is improved to optimize the image segmentation effect.

Digital image $f(x, y)$, its field smooths the image for $g(x, y)$, $f(x, y)$ is the abscissa in a two-dimensional histogram, $g(x, y)$ is the ordinate, two-dimensional element (i, j) is composed of pixel gray value i and field gray value j . The probability is $p_{ij} = \frac{f_{ij}}{N}$. f_{ij} is the number of (i, j) 's, therefore.

$$\sum_{i=0}^{L-1} \sum_{j=0}^{L-1} f_{ij} = N, \sum_{i=0}^{L-1} \sum_{j=0}^{L-1} p_{ij} = 1 \quad (1)$$

If two-dimensional element is selected as the threshold value in the two-dimensional histogram, the two-dimensional histogram can be divided into four types of regions. Region 1 and region 3 are target and background region respectively, and region 2 and region 4 are noise and edge region, respectively. The two-dimensional histogram is shown in Fig. 2.

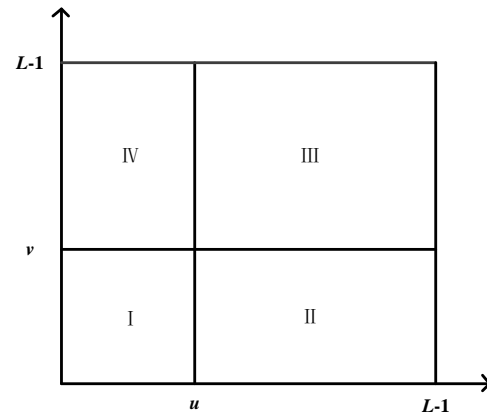


Fig. 2. Two-dimensional Histogram.

Set the probability of target and background area as ω_0 and ω_1 , then

$$\omega_0 = \sum_{i=0}^{u-1} \sum_{j=0}^{v-1} p_{ij}, \omega_1 = \sum_{i=u}^{L-1} \sum_{j=v}^{L-1} p_{ij} \quad (2)$$

The corresponding mean values η_0 and η_1 are

$$\eta_0 = (\eta_{0i}, \eta_{0j})^T = \left[\sum_{i=0}^{u-1} \sum_{j=0}^{v-1} ip_{ij}, \sum_{i=0}^{u-1} \sum_{j=0}^{v-1} jp_{ij} \right]^T \quad (3)$$

$$\eta_1 = (\eta_{1i}, \eta_{1j})^T = \left[\sum_{i=u}^{L-1} \sum_{j=v}^{L-1} ip_{ij}, \sum_{i=u}^{L-1} \sum_{j=v}^{L-1} jp_{ij} \right]^T \quad (4)$$

The mean value of the total gray scale is

$$\bar{\eta} = (\bar{\eta}_i, \bar{\eta}_j)^T = \left[\sum_{i=0}^{L-1} \sum_{j=0}^{L-1} ip_{ij}, \sum_{i=0}^{L-1} \sum_{j=0}^{L-1} jp_{ij} \right]^T \quad (5)$$

The various internal discrete matrices is

$$S_k = \sum_{h=0}^{L-1} \omega_k \left[(h - \eta_k)(h - \eta_k)^T \right] \quad k = 0, 1 \quad (6)$$

The discrete matrix between classes is

$$S = \sum_{k=0}^1 \omega_k \left[(\eta_k - \bar{\eta})(\eta_k - \bar{\eta})^T \right] \quad (7)$$

The distance function between ω_0 and ω_1 is

$$r_{rr}(S) = \frac{\sum_{k=0}^1 \omega_k \left[(\eta_{ki} - \bar{\eta}_i)(\eta_{kj} - \bar{\eta}_j)^2 \right]}{\omega_0(1 - \omega_0)} \quad (8)$$

When $r_{rr}(S)$ is the maximum of (i, j) , two-dimensional element (u, v) is selected as the optimal threshold. However, isolated noise still exists. In order to eliminate the influence of isolated noise, this paper introduces weight coefficient β on the basis of 2D-OTSU algorithm to determine the final comprehensive objective function and obtain the optimal threshold. The objective function is determined by studying the inter-class discrete matrix and the intra-class discrete matrix:

$$r_{rr}(S) = r_{rr}(S)_{\max} - \beta r_{rr}(S_k)_{\min} \quad (9)$$

$r_{rr}(S)$ is the maximum value of $r_{rr}(S)$ between classes, $r_{rr}(S_k)_{\min}$ is the minimum value of $r_{rr}(S_k)$ within classes, and β is the weight coefficient, which is related to the grayscale characteristics of the image and can be described by ω_k . The calculation formula of weight coefficient β is as follows:

$$\beta = 1 + \frac{1 - \exp(a - b\omega_k)}{1 + \exp(a - b\omega_k)} \quad (10)$$

Through 200 experiments, when $a=0.6$, $b=0.045$, the best weight coefficient β is obtained, and the weight coefficient β is added into the 2D-OTSU algorithm to eliminate the influence of isolated noise.

B. 2D-OTSU Image Threshold Segmentation Method based on DLAFA

Artificial fish swarm algorithm has strong ability to solve the optimal solution, high precision and fast convergence speed[20]. However, due to the characteristics of magnetic column defects, the traditional artificial fish swarm algorithm cannot completely meet the threshold segmentation of magnetic column surface defect image. In this paper, the artificial fish swarm algorithm is improved to improve the

accuracy of threshold segmentation algorithm of magnetic column surface defect image.

1) *Adjustment of perception range:* The size of visual represents the size of the search area of the individual fish. When the perceptual range of visual is larger, the search range of individual fish will be larger, which is conducive to the global search. When the perceptual range is small, the local range search is more accurate.

Carry on dynamic adjustment to visual, use dynamic change form to change visual original determination way. At the beginning of the algorithm, the whole magnetic column surface image is searched globally, and the range of Visual should be enlarged to improve the convergence of the algorithm. In the later stage of the algorithm, the local search is carried out in the magnetic column surface image, and the range variation of Visual should be reduced to improve the search speed of the algorithm. The Logistic model with dynamic transformation is used to dynamically adjust Visual, set the maximum and minimum value of visual change range as $visual_{\max}$ and $visual_{\min}$, visual dynamic adjustment formula is:

$$\begin{cases} \frac{dvisual}{dt} = \alpha \left(1 - \frac{visual}{visual_{\min}} \right) visual \\ visual(0) = visual_{\max} \end{cases} \quad (11)$$

According to the logistic model, formula (11) is simplified as

$$visual(t) = \frac{visual_{\min}}{1 + \left(\frac{visual_{\min}}{visual_{\max}} - 1 \right) e^{-\alpha t}} \quad (12)$$

Where, α is the initial decay rate, and t is the number of iterations of the algorithm. The initial decay rate α is used to adjust the speed of visual descent. When α is larger, it indicates that visual attenuation speed is faster, when α is smaller, it indicates that visual attenuation speed is slow.

According to (11), when the number of iterations is zero, the value of Visual is the maximum $visual_{\max}$. After t iterations, Visual approaches from the maximum value $visual_{\max}$ to the minimum value $visual_{\min}$. With the increasing number of iterations, Visual slowly converges from the maximum value $visual_{\max}$ to the minimum value $visual_{\min}$. Thus realized the algorithm from the beginning to the end of the visual value by the larger value dynamic conversion to the smaller value function.

2) *Move step size adjustment:* In the process of algorithm iteration, the larger step is, the faster the search speed is in the same visual. The smaller step is, the slower the search speed is and the more iterations are. At the beginning of the algorithm, visual range is larger, at this time, take a larger value of step, reduce the workload of searching the best position state, improve the convergence speed of the algorithm; In the later stage of the algorithm, the local area of the best position state has been determined, visual is a smaller search range, a

smaller step is needed to carry out a more detailed local search, improve the accuracy of the algorithm.

The adjustment requirements of parameter step are the same as those of Visual, in that a larger value is required at the beginning and a smaller value is required later. The parameters change dynamically during the algorithm, from large to small. Logistic model is also used to dynamically adjust parameter step, and the formula is as follows:

$$\begin{cases} \frac{dstep}{dt} = \alpha(1 - \frac{step}{step_{min}})step \\ step(0) = step_{max} \end{cases} \quad (13)$$

According to the Logistic model, formula (13) is simplified as:

$$step(t) = \frac{step_{min}}{1 + (\frac{step_{min}}{step_{max}} - 1)e^{-\alpha t}} \quad (14)$$

Where, $step_{max}$ is the maximum value of step and $step_{min}$ is the minimum value of step.

According to the experiment, $visual_{max} = 10$, $visual_{min} = 1$, $step_{max} = 8$, $step_{min} = 0.5$, $\alpha = 0.1$, that is, the transformation range of Visual is [1,10], and the change range of step is [0.5,8]. The dynamic transformation curve of Visual and STEP is shown in Fig. 3.

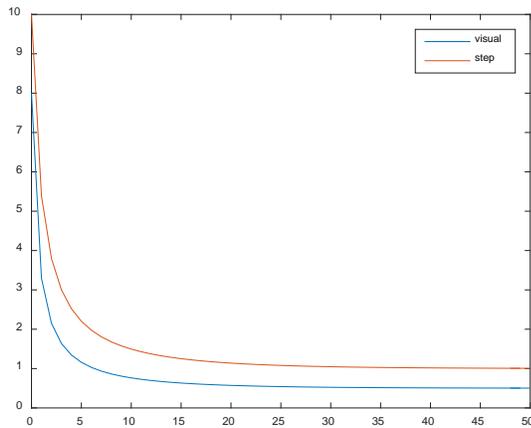


Fig. 3. Dynamic Transformation Curve of Visual and Step.

In an iterative cycle of 50, when 10 generations, visual and step convergence to the minimum, that is to say, in the first ten generations for global search, the rest of the iteration cycle for local search, this artificial fish algorithm can quickly locate the optimal solution is not at the early stage of the iteration into local optimal solution, and can improve the accuracy of solution in the late iterations.

In the 2D-OTSU algorithm, an optimal threshold (u, v) should be found for image segmentation, and the optimal threshold (u, v) should be found through the distance measure function in the maximum inter-class variance method to achieve the purpose of image segmentation of magnetic

column surface defects. In this paper, 2D-OTSU algorithm is improved by adding DLAFA algorithm to improve the accuracy and anti-noise of 2D-OTSU algorithm. The objective function of 2D-OTSU algorithm was used as DLAFA algorithm to obtain the optimal threshold of fish food concentration $f(X)$, so as to carry out the threshold segmentation of magnetic column surface defect image.

The specific steps of 2D-OTSU image threshold segmentation based on DLAFA are as follows:

- Initialize the algorithm parameters.
- Take the objective function of 2D-OTSU algorithm as the food concentration of DLAFA algorithm to find the maximum distance function.
- Update the searcher position in the bulletin board to find the best position.
- Judge whether the optimal position or the condition of maximum iteration value of the algorithm is reached, and output the result; otherwise, continue to perform the previous step.
- Image threshold segmentation of magnetic column surface defects is carried out according to the optimal threshold value.

The 2D-OTSU image threshold segmentation flow chart based on DLAFA is shown in the Fig. 4.

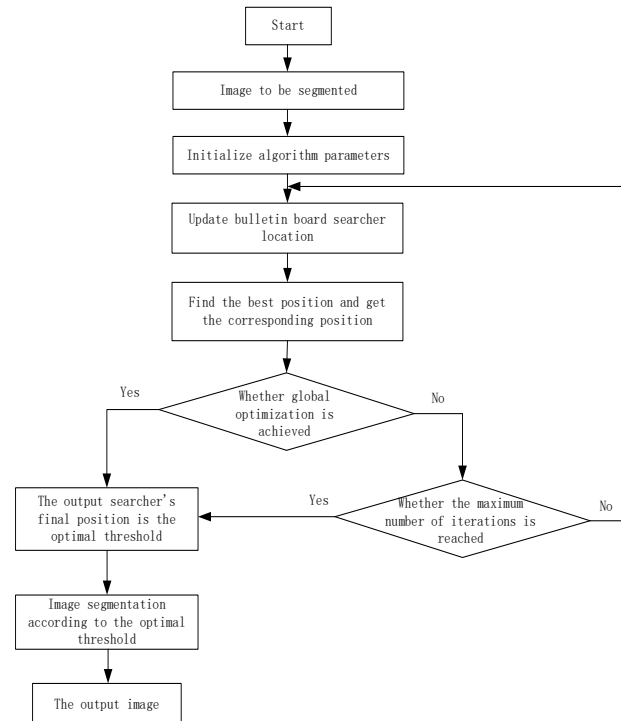


Fig. 4. 2D-OTSU Image Threshold Segmentation Flow Chart based on DLAFA.

IV. ALGORITHM PERFORMANCE TEST

In order to verify the effectiveness of the improved artificial fish swarm algorithm, the improved adaptive artificial

fish swarm algorithm DLAFFSA and the standard artificial fish swarm algorithm AFSA are compared and tested by Benchmark function [19]. In DLAFFSA algorithm, set parameters, $n = 20$, $visual_{max} = 10$, $visual_{min} = 1$, $step_{max} = 8$, $step_{min} = 0.5$, $\lambda = 2$. In the AFSA algorithm, $visual = 2$, $step = 2$, and other parameter settings are the same as those in the DLAFFSA algorithm. The four selected test benchmark functions are shown in Table I.

TABLE I. SELECTED FOUR TEST BENCHMARK FUNCTIONS

The function name	Test functions	Variable scope	The optimal value
Rastrigin	$f_1(x) = \sum_{i=1}^n [x_i^2 - 10 \cos(2\pi x_i) + 10]$	[-5.12, 5.12]	0
Ackley	$f_2(x) = -20e^{-0.2 \sqrt{\frac{1}{n} \sum_{i=1}^n x_i^2}} - e^{\frac{1}{n} \sum_{i=1}^n \cos(2\pi x_i)} + 20 + e$	[-50, 50]	0
Rosenbrock	$f_3(x) = \sum_{i=1}^{n-1} [100(x_{i+1} - x_i^2)^2 + (x_i - 1)^2]$	[-32, 32]	0
Schaffer	$f_4(x) = 0.5 + \frac{\sin^2 \sqrt{x^2 + y^2} - 0.5}{[1 + 0.001(x^2 + y^2)]^2}$	[-10, 10]	0

The parameters of DLAFFSA algorithm and AFSA algorithm are set. During the performance comparison test, both algorithms are executed for 30 times. The performance of DLAFFSA algorithm is verified by comparing the mean and variance of solutions obtained by DLAFFSA algorithm and AFSA algorithm after the test of four selected benchmark functions, as well as the number of successful iterations of algorithm on the benchmark function and the average number of iterations required after successful iteration.

In the four classical benchmark functions, DLAFFSA and AFSA algorithms set the number of iterations to 2000. $f_1(x)$ is a unimodal function $f_2(x)$, $f_3(x)$, and $f_4(x)$ are multimodal functions. Test results of DLAFFSA and AFSA on the benchmark function are shown in Table II.

As can be seen from the data results in Table II, the mean values of solutions obtained from four different benchmark functions are smaller than those obtained from AFSA algorithm. Compared with AFSA algorithm, the variance of solutions obtained by DLAFFSA algorithm in four different benchmark functions is smaller. From the comparison of mean and variance, DLAFFSA algorithm has higher accuracy, and DLAFFSA algorithm is better than AFSA algorithm.

TABLE II. TEST RESULTS OF DLAFFSA AND AFSA ON THE BENCHMARK FUNCTION

Benchmark functions	DLAFFSA		AFSA	
	The mean	The variance	The mean	The variance
f_1	1.4203	0.2912	12.6237	2.7212
f_2	5.6e-16	8.1e-16	2.8e-10	1.9e-12
f_3	1.7e-28	2.7e-72	0.00681	0.0143
f_4	3.5231	2.7873	6.6372	3.8221

TABLE III. SUCCESSFUL ITERATION RESULTS OF DLAFFSA AND AFSA

Benchmark functions	DLAFFSA		AFSA	
	Number of successful	Average number of iterations	Number of successful	Average number of iterations
f_1	21	1074	15	1829
f_2	16	1527	9	1672
f_3	23	982	23	1082
f_4	28	609	19	695

Table III shows the average iteration times required by DLAFFSA algorithm and AFSA algorithm for successful iteration on benchmark functions when the test results and algorithm convergence are successful. It can be seen from the table that the successful iteration times of DLAFFSA algorithm on four benchmark functions are more than the successful iteration times of AFSA algorithm on four benchmark functions. The average iteration times of DLAFFSA algorithm on the successful iteration of the four benchmark functions are also less than that of AFSA algorithm on the successful iteration of the four benchmark functions. The performance of DLAFFSA algorithm is better than that of AFSA algorithm.

V. EXPERIMENTAL RESULTS AND ANALYSIS

In order to verify the effect and accuracy of the improved 2D-OTSU image threshold segmentation method on magnetic column surface defect image threshold segmentation, the 2D-OTSU image threshold segmentation method based on DLAFFSA was compared with the traditional 2D-OTSU method and the improved firefly algorithm in literature [21]. The image segmentation of four magnetic column surface defects, namely, magnetic column scar, black slice, edge drop and crack, was analyzed by comparative experiment. The image threshold segmentation and comparison effect of magnetic column surface defects is shown in Fig. 5.

As can be seen from the comparison figure, magnetic column surface defects are complex and have many kinds of defects. For scarring and black spot defects, the traditional 2D-OTSU algorithm will produce many noise points. Although the algorithm in [21] effectively reduces noise points, the edge segmentation effect of magnetic column is poor. For side drop defects, the 2D-OTSU algorithm has more noise points, and both the algorithm in [21] and the algorithm in this paper can be well segmented. However, for crack defects with low contrast, the traditional 2D-OTSU image segmentation algorithm and the algorithm in [21] are still affected by isolated noise and cannot effectively extract magnetic column surface defects. However, the algorithm in this paper can effectively eliminate isolated noise and extract magnetic column surface defects. Table IV shows the comparison of optimal thresholds and time for processing magnetic columns with different defects using three threshold segmentation algorithms. It can be seen that the running time of 2D-OTSU using firefly algorithm is 32.2% of that of traditional 2D-OTSU. Although it can effectively reduce the running time, the running speed is still relatively slow. The proposed algorithm reduces the running time of the traditional 2D-OTSU algorithm by 82.45%, and ensures the accuracy of the algorithm while reducing the running time.

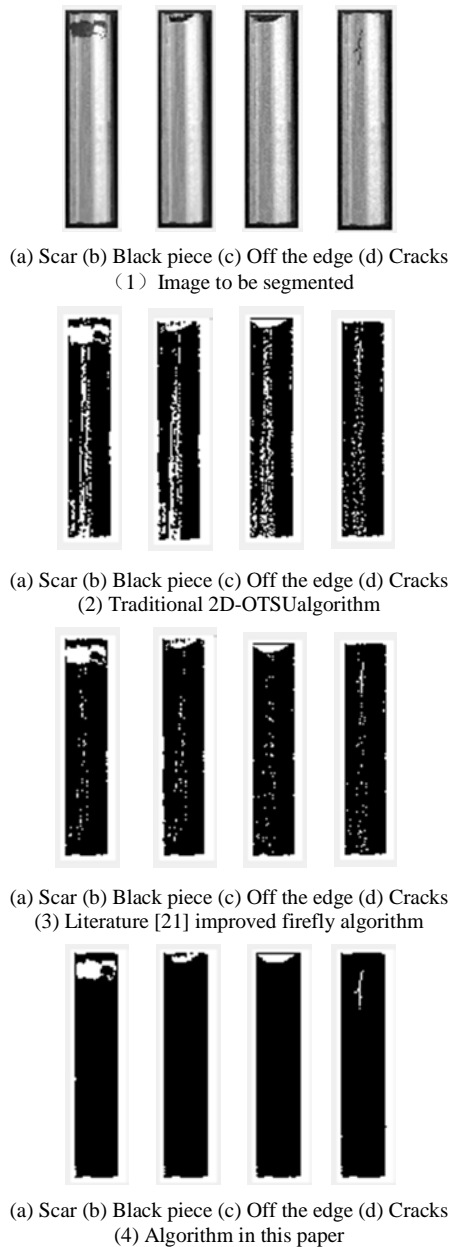


Fig. 5. Threshold Segmentation Effect of different Methods.

TABLE IV. THE OPTIMAL THRESHOLD AND SEGMENTATION TIME OF DIFFERENT ALGORITHMS ARE COMPARED

Algorithm	Scar	Black piece	Off the edge	Cracks	Mean Spent time/ms
2D-OTSU	(96,109)	(102,123)	(94,115)	(103,117)	508.43
Firefly algorithm + 2D-OTSU	(103,112)	(109,120)	(106,112)	(102,115)	163.59
Ours	(103,108)	(113,119)	(108,112)	(107,111)	89.23

The threshold segmentation of 500 magnetic column images with defects is carried out by the method in this paper, and the images obtained are used as classification recognition samples after feature extraction. 300 of them are selected as

KNN classifier training sample set, and the remaining 200 as KNN classifier test sample set. The test samples are classified by the KNN classifier successfully trained. The classification recognition results are statistically analyzed, and the classification results are shown in Table IV.

TABLE V. CLASSIFICATION RESULTS

	Scar	Black piece	Off the edge	Cracks	total
Actual sample size	45	55	48	52	200
Correct identification number	41	52	44	49	186
Leaving out the number	0	0	0	0	0
Mistakenly identified several	2	2	1	1	6
Recognition accuracy%	91.1	94.5	91.7	94.2	93

Table V shows that the classification accuracy of four types of magnetic column surface defects reaches 93%, including 94.5% for black piece defects, the accuracy of cracks defect classification was 94.2%. Due to the difficulty in distinguishing edge defect from scar defect, the classification accuracy is lower than the other two defect types, but the recognition accuracy can reach more than 90%. The recognition accuracy of scar is 91.1%, the recognition accuracy of off the edge is 91.7%. In particular, the missing rate is 0, and all defects can be detected, which can meet the requirements of magnetic column surface defect detection.

VI. CONCLUSION

Aiming at the problems of low segmentation efficiency and weak anti-noise ability of traditional 2D-OTSU algorithm, this paper proposes a 2D-OTSU image threshold segmentation algorithm based on DLAFFSA. In this paper, a weight coefficient is added to 2D-OTSU algorithm to eliminate isolated noise and distinguish background and target effectively. The artificial fish swarm algorithm is improved to improve the convergence and search speed of the algorithm and effectively reduce the time complexity of threshold segmentation by adjusting the perceived range and moving step size of fish swarm. By comparing the performance of adaptive artificial fish swarm algorithm DLAFFSA with the standard artificial fish swarm algorithm AFSA using the benchmark function, it is concluded that the improved algorithm has higher accuracy, shorter convergence time and stronger overall performance than the original algorithm. Finally, the proposed algorithm is compared with the traditional 2D-OTSU method and the improved firefly algorithm in terms of segmentation accuracy and running time. Experimental results show that the proposed algorithm can better segment magnetic column edge, effectively eliminate isolated noise, improve the running speed of the algorithm, and ensure the segmentation accuracy.

ACKNOWLEDGMENT

This work is supported by science foundation of Education Department of Jiangxi Province(GJJ150676), and Natural science foundation of Jxust(NSFJ2015-G15).

REFERENCES

- [1] Song Ke, Xie Weicheng, Xia Xinyang, and Jiang Wenbo. Research on Wallpaper Defect Detection Method Based on improved Otsu [J]. *Manufacturing Automation*, 2019, Vol. 41 (6): 12-15.
- [2] Da Yihui, Dong Guirong, Wang Bin, Liu Dianzi, and Qian Zhenghua. A novel approach to surface defect detection[J]. *International Journal of Engineering Science*, 2018, 133(DEC.):181-195.
- [3] Zhao Feng, Kong Lingrun, and Ma Geni. Threshold image segmentation algorithm based on hybrid optimization of multi-objective particle swarm optimization and artificial bee swarm optimization [J]. *Computer engineering and science*, 2020, 42(02):281-290.
- [4] Aditya Raj, Gunjan Gautam, Siti Norul Huda Sheikh Abdullah, Abbas Salimi Zaini, and Susanta Mukhopadhyay. Multi-level thresholding based on differential evolution and Tsallis Fuzzy entropy[J]. *Image and Vision Computing*, 2019, 91: 103792.
- [5] Zhang Zhenhai, Jia Zhengman, Ji Kun. Research on Crack Identification Method of Subway tunnel based on improved Otsu Method [J]. *Journal of Chongqing Jiaotong University (Natural Science Edition)*, 2022, Vol. 41 (1): 84-90.
- [6] Lei Bo, Fan Jiulun. Image thresholding segmentation method based on minimum square rough entropy[J]. *Applied Soft Computing*, 2019, 84(1):105687.
- [7] Wang Yun, Zhang Guangbin, and Zhang Xiaofeng. Multilevel Image Thresholding Using Tsallis Entropy and Cooperative Pigeon-inspired Optimization Bionic Algorithm[J]. *Journal of Bionic Engineering*, 2019, 16(5): 954-964.
- [8] Liu Jianzhuang, Li Wenqing. Two-dimensional Otsu Automatic Threshold Segmentation method for Gray Image [J]. *Acta Automatica Sinica*, 1993(01):101-105.
- [9] He Zhiyong, Sun Lining, Huang Weiguo. Thresholding segmentation method based on Otsu Criterion and line Intercept histogram[J]. *Optics and Precision Engineering*, 2012, 20(10):2315-2323.
- [10] Xiao Leyi, Ouyang Honglin, Fan Chaodong. An improved Otsu method for threshold segmentation based on set mapping and trapezoid region intercept histogram[J]. *Optik*, 2019, 196:163106.
- [11] Zeng Yanyang, Xie Gaosen, and Zhang Jianchun. Low-light image segmentation based on intercept histogram and Otsu fusion [J]. *Laser & Optoelectronics Progress*, 2021, vol 58 (20): 219-227.
- [12] Yang Huixian, Yan Wei, Tan Zhenghua, Li Miao, and Cai Yongyong. Image segmentation based on improved gray local variance[J]. *Computer Engineering and Applications*, 2017, 53(4):209-213.
- [13] Cao Shuang, An Jiancheng. Wolf Optimized 2D Otsu Fast Image Segmentation Algorithm [J]. *Computer Engineering and Science*, 2018, Vol. 40 (7):1221-1226.
- [14] Zhang Lin, Wang Tinghua, and Zhou Huiying. Research Progress of SVR Parameter Optimization Based on Swarm Intelligence Algorithm [J]. *Computer Engineering and Applications*, 2021, Vol 57 (16):50-64.
- [15] Yan Yuanyuan, Chen Hua, and Jiang Bo. Identification of tomato diseases based on swarm intelligence algorithm classification model [J]. *Jiangsu Agricultural Sciences*, 2020, Vol 48 (1): 219-224.
- [16] Ma Guoyuan, Yue Xiaofeng. An improved whale optimization algorithm based on multilevel threshold image segmentation using the Otsu method[J]. *Engineering Applications of Artificial Intelligence*, 2022, Vol. 113: 104960.
- [17] Liu Peijin, Wang Xi, and He Ning. Improved multi-threshold infrared image segmentation method based on FUSION of GSO and TWO-DIMENSIONAL OTSU [J]. *Journal of Applied Optics*, 2021, Vol. 42 (4):671-677.
- [18] Numan Saeed , Nelson King , Zafar Said , and Mohammed A. Omar. Automatic defects detection in CFRP thermograms, using convolutional neural networks and transfer learning[J]. *Infrared Physics & Technology*, 2019, 102:103048.
- [19] Cao Yiqin, Duan Yeyu, and Wu Dan. Image segmentation method of 2d-otsu rail defects based on WFSOA [J]. *Computer science*, 2020, 47(5):154-160.
- [20] Cui Liqun, Song Xiao, Li Hongxu, Zhang Mingjie. Multi-threshold image segmentation based on improved fish swarm algorithm [J]. *Computer science*, 2014, 41(08):306-310+321.
- [21] Liu Xinjing, Liu Yanlong, and Xu Xinxin. Membrane mechanism Firefly algorithm optimization of Multi-threshold Otsu image Segmentation [J]. *Journal of Small And Micro Computer Systems*, 2020, Vol 41 (2): 410-415.

Deep Separable Convolution Network for Prediction of Lung Diseases from X-rays

Geetha. N¹

(Reg No. BDU2120412778980) Research Scholar in
Computer Science, J.J college of Arts and Science
(Autonomous), Sivapuram Post, Pudukkottai (Affiliated to
Bharathidasan University, Tiruchirapalli)
Tamil Nadu, India

Dr. S. J. Sathish Aaron Joseph S. J²

Assistant Professor and Research Advisor in Computer
Science, (Ref.No:05526/Ph.D.K 10/Dir/Computer
Science/R.A), P.G and Department of Computer Science
J.J.College of Arts and Science (Autonomous)
Sivapuram, Pudukkottai, Tamil Nadu, India

Abstract—Accurate diagnosis of lung cancer has been critical, and image segmentation and deep learning (DL) techniques have made it easier for medical people. Yet, the concept's effectiveness is extremely limited due to a scarcity of skilled radiologists. Although emerging DL-based methods frequently necessitate accordance with the regulation, such as labelled feature map, to train such networks, which is difficult to terminate on a big scale. This study proposed a swarm intelligence based modified DL model called MSCOA-DSCN to classify and forecast various Lung Diseases through anterior X-rays. Image enhancement with a modified median filter and edge enhancement with statistical range applied for better image production. The disparity between min and max pixels focused on the Statistical range from each 3×3 input image cluster. Utilized Enriched Auto-Seed Fuzzy Means Morphological Clustering for segmentation (EASFMC); they could function together to identify edges in X-Ray imaging. Used A deep separable convolution network (DSCN) was in the created system to predict the class of lung cancer, and Modified Butterfly Optimization Algorithm (MBOA) applied for the feature selection procedure. This present study compared with various state-of-the-art classification algorithms using the NIH Chest-Xray-14 database.

Keywords—Lung diseases; X-rays; deep learning; filtering; edge detection; segmentation and swarm intelligence

I. INTRODUCTION

In recent times, Lung cancer (LC) is the main leading causes of mortality among the most dangerous tumours that can harm a person's health. It has the highest mortality rate, including all tumours, and is the prominent basis of cancer death in human [1]. LC accounts for roughly 1.8 million people infected each year, or 13% of all cancer cases, and 1.6 million fatalities globally, or 19.4% of all cancer-related deaths. In 2020, the expected mortality of cancer patients in developing countries [2] was 679,421 men and 712,758 females, particularly in India. Around one in 68 men suffers this form of LC; about one in 29 women suffer breast cancer, therefore around one in nine Indians suffering cancer between the decades of 0 and 74. Increasing the risk of LC, the discovery in the early stages will improve survival rates significantly. Still, it is also impossible to discern the early-stage prediction of LC due to fewer symptoms [3].

Computer-based technology has significantly grown in importance around the globe. As of early January 2019,

COVID-19 causes causing substantial respiratory problems and severe health issues, leading to the possibility of the COVID-19 pathogenic virus and other such bacterial or viral infections [4]. As a result, the accurate intervention of lung disorders is rather critical than ever. Machine learning (ML) and DL can be beneficial throughout this case. The recognition of medical images in ML-based detection approaches necessitates a specific stage to isolate malignancies, automatic localization, and identification in internal organs, as well as particular processing, which is highly useful [5]. "DL approaches" that perform well in cancer categorization advance current trends.

Various studies have focused on how DL schemes might be used [6,7] with both the expansion of computer programming for medicine and social research initiatives, this approach has the potential to lower medical expenditures. The NIH chest X-ray image database is obtained mainly from the Kaggle repository [8] for use in development. A number of research works have been carried out on the diagnosis of chest diseases using artificial intelligence methodologies. In [9], multilayer, probabilistic, learning vector quantization, and generalized regression neural networks have been used for diagnosis chest diseases. The diagnosis of chronic obstructive pulmonary and pneumonia diseases was implemented using neural networks and artificial immune system [10]. In [11], the detection of lung diseases such as TB, pneumonia, and lung cancer using chest radiographs is considered. The histogram equalization in image segmentation was applied for image preprocessing, and feed forward neural network is used for classification purpose. The above research works have been efficiently used in classifying medical diseases; however, their performance was not as efficient as the deep networks in terms of accuracy, computation time, and minimum square error achieved. Deep learning-based systems have been applied to increase the accuracy of image classification [12]. These deep networks showed superhuman accuracies in performing such tasks. This success motivated the researchers to apply these networks to medical images for diseases classification tasks, and the results showed that deep networks can efficiently extract useful features that distinguish different classes of images [13]. Most commonly used deep learning architecture is the convolutional neural network (CNN). CNN has been applied to various medical images classification due to its power of extracting different level features from images

[14] [15]. This work presents a novel hybrid method for classifying lung illness in the aforementioned dataset. The research's significant contribution is the invention of a different hybrid DL system appropriate for detecting lung illness from X-ray pictures.

The study discusses the architectures of DSCN further with MBOA to help determine whether use individuals to diagnose LC in this research would work. The NIH chest X-ray image database is initially pre-processed images after that trained using the suggested DSCN-MBOA model to assess the percentage of lungs directly impacted by cancer and network image preparedness for LC. The networks in this translucent classification structure have achieved equivalent performance, latency (time), recall, f-measure, precision, and accuracy metrics. The following is the work's main contribution:

- The input x-ray images are first pre-processed with a modified median filter for noise reduction and statistical range edge detection.
- Enriched Auto-Seed Fuzzy Means Morphological Clustering is used for segmentation (EASFMC).
- By using DSCN and the MBOA for feature selection, the created method identifies a certain kind of lung illness.

The following is a conceivable structure for the manuscript: The second section discusses relevant research on lung classification and nodule identification and classification. Section 3 discusses the methodology of this study and a complete examination of the implemented dataset. Section 4 describes the findings and experimental discussion with their appropriate outcome results, while Section 5 finishes the research work with recommendations for further research.

II. RELATED WORK

A complete examination of numerous LC detection approaches for forecasting cancer is an uncontrolled development in the lung region, notably in lung X-ray images described in this literature review. Liu et al. [16] developed a Convolutional Neural Network (CNN)-based cascade technique for lesion classification. To get the localization of the focal liver lesions, initially utilize the transfer learning (TL) method to learn the automatic recognition network on the experimental dataset. Peng et al., [17] utilized a parallel genetic algorithm (GA) to detect LC in chest X-ray images. The approach combines pattern matching and localized search strategies, and experiments have shown promising outcomes.

The 121-layer CNN (DenseNet121) and the TL algorithm being investigated by Ausawalaithong et al., [18] are mechanisms for diagnosing LC via chest X-ray data. This classifier trained on the sample until moving on to the LC image database to overcome the difficulty of a short dataset. Yan et al. [19] suggested a weakly supervised DL architecture

comprising squeeze-and-excitation blocks, multi-map transfer, and max-min pooling for grouping similar respiratory diseases, including identifying anomalous lesion locations on Chest X-ray14 dataset for diagnosing major lumbar spinal disorders. The extensive simulation shows that the proposed model has high effectiveness than the existing methods.

Yan et al. [20] described a new weakly-supervised learning model for classifying pulmonary diseases based on the analysis of given chest X-rays and localizing disease patches on X-rays at pixel-level refinement. The suggested network's benefits come from the acquisition of disease-specific characteristics during multi-map transfer layers and the cross-channel feature realignment provided by squeeze-and-excitation blocks somewhere between dense partitions. Heat maps, which are the raw material for producing the network's range of processes, are another way to display it.

The above X-ray scans are massive, containing 110,120 images and weighing almost 44 GB. Including the Chest X-ray-based LC expert systems, in [21] performed a thorough statistical study of different DL network models. The main objective is to obtain a performance evaluation for each DL network structure. It includes aspects of measurement, including accuracy performance, examination of training and validation time, memory utilization analysis, CPU and memory observation, graphics processing energy consumption, and some enhancement ideas.

In [22] suggested a Modified AlexNet (MAN) DL architecture to assess the lung abnormalities, where a threshold filter to reduce artifacts from Lung CT images is applied. Besides combining in-depth features with handcrafted features, this study introduces a new Ensemble-Feature-Technique (EFT). However, serial fusion and Principal Component Analysis (PCA)-based design to identify the significant feature set used. Compared to the other existing framework methods, experimental data show that MAN outperforms them. Bharati et al. [22] created new hybrid DL architecture (By merging data augmentation, VGG, and spatial transformer network (STN) into CNN) and denoted as VDSNet. Table I show the proposed methods' advantages and disadvantages in this literature review.

Here the Inference from the existing works is considered as conventional DL algorithms are robust, they underachieve when images are slanted, flipped or otherwise abnormally oriented. Again, hybrid approaches to evaluate the accuracy while reducing the learning rate are applied. The presented hybrid technique named DSCN- MSCOA may detect suspicious problematic regions using chest X-ray images that are highly effective and enhance diagnosis when compared to standard methods. In a way, it can improve the therapy's effectiveness for the affected individual in terms of accuracy, precision, etc.

TABLE I. EXISTING PROPOSED METHODS WITH THEIR ADVANTAGES AND DISADVANTAGES

Author	Dataset	Method	Advantages	Disadvantages	Performance metrics
Liu et al., [9]	2594 chest x-rays and JSRT dataset	Cascaded CNN	Reduce the number of actions required to detect the condition and increase the learning duration.	The issue with using CNN to diagnose LC is that it is highly effective when the sample size is too small.	JSRT dataset: Precision of 0.885 and recall of 0.858 Chest x-ray: Precision of 0.985 and recall 0.958
Peng et al., [10]	154 pieces of medical images	GA	This results in more accurate learning without having to spend more time on it.	The reality that all tumor spots on chest X-rays were genetic conditions is overlooked because GA will not handle various diseases sequentially.	optimal solutions 100% execution time 14814s
Ausawalaithong et al., [11]	JSRT Dataset and ChestX-ray14 Dataset	CNN with TL	This suggested scheme is capable of resolving the issue of a small dataset.	Owing to the unavailability of features which include genetic factors and tobacco consumption rate in learning, as well as images, accuracy is reduced.	mean accuracy: 74.43±6.01%, mean specificity: 74.96±9.85%, and mean sensitivity: 74.68±15.33%
Yan et al., [13]	ChestX-ray14 dataset	weakly-supervised DL framework	As more of a result, using minimal samples can yield high accuracy.	Using the minimal number of bounding boxes, re-investigate an effective representation of lesion regions.	Average AUC 0.8302
Wibisono et al., [13]	110,120 images	five different CNN models	In terms of execution rate and accuracy, this might be the most efficient DL conceptual model.	The availability of sufficient labeling by a medical expert is a key barrier to applying DL models to serious health concerns.	AUROC scores 0.80 - 0.82, CPU utilization 527% - 940% memory usage 23.39 GB - 38 GB and execution time 2.91 hours - 7.6 hours.
Bhandary et al., [14]	chest X-Ray images and LIDC-IDRI	modified AlexNet	It is essential because it could be viewed as a program that helps physicians in doing further diagnostic procedures.	Though the recognition rate was improved by 0.05 on the ROC-AUC scoring system, there was always scope for change.	classification accuracy 97.27%
Bharati et al., [15]	NIH chest X-ray	VDSNet	It takes a lot less time to train, but the accuracy rate is significantly worse.	Unfortunately, this should result in a lengthy period of training.	validation accuracy of 73%

III. PROPOSED METHOD

An optimized DL-based technique opts to classify and extract LC regions on X-ray images. The proposed framework is composed of various successive components shown in Fig. 1. After pre-processing X-ray images using a modified median filter, the undesired LC components are masked using Enriched Auto-Seed Fuzzy Means Morphological Clustering (EASFMC) based segmentation and removal. After that, the features are extracted from the final fully-connected layers for the DSCN architecture, which are then optimized using MBOA. The optimized feature set input for DSCN for LC classification. Pre-processing is required because this technique requires an X-Ray image representation that could have noise, inappropriate blurring, or being out of perspective.

A. Dataset Description

The dataset [8] file comprises a random sample of 5% of the whole dataset, with 5606 photos with a resolution of 1024 x 1024 pixels each. To build a .csv (comma-separated values) file with patient data in addition class labels for the entire dataset. The following is a description of the class. There are 15 "No findings" classes, as well as 14 diseases such as Edema type images (118), Emphysema type images (127), Cardiomegaly type images (141), Fibrosis type images (84), Pneumothorax type images (271), Consolidation type images (226), Pleural Thickening type images (176), Mass type images (284), Effusion type images (644), Infiltration type images (967) and Nodule type images (313). Also, technique classifies "No finds" for 3044 images.

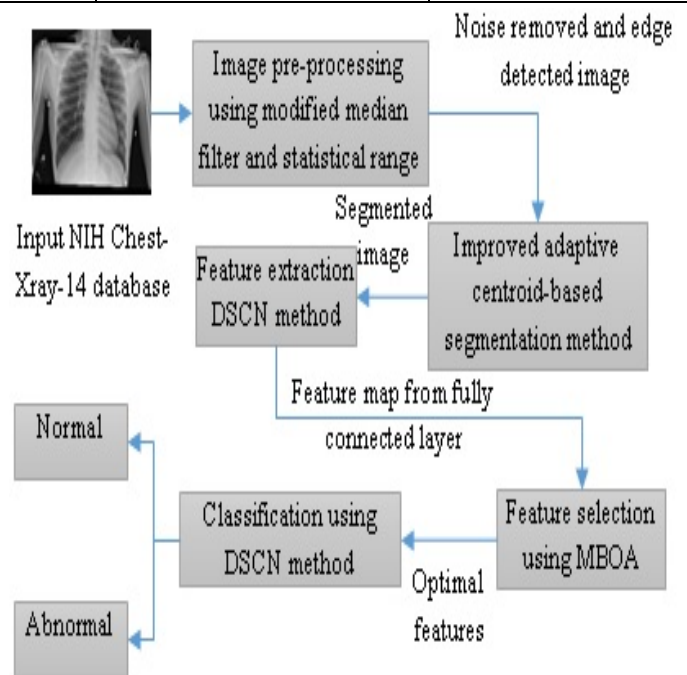


Fig. 1. General Framework Diagram.

B. Image pre-processing and Edge Detection

Modified Median Filter for noise Removal: The median filter [23] is the most widely utilized image-enhancing filter. It blurs and distorts images by modifying noisy, denoted as

corrupted pixels, and noiseless, indicated as uncorrupted pixels. The modified median filters incorporate a switching mechanism to replace several pixels when it is determined to be contaminated. These results of pixels in an image are computed by Algorithm 1. A three × three window across the image stretches by starting in the upper left corner. Its function is associated with the maximum and minimum image pixels within the window to determine whether a pixel remains uncorrupted or corrupted. When a pixel's value is between the top and minimum, it is uncorrupted. A refined pixel is left alone within a specified filtering window, whereas corrupted pixels swap by the median image pixel or an effectively understood immediate adjacent pixel; is done for each pixel value. Determine the absolute value ϑ by the difference between both the window's centre pixel as well as its neighboring pixels with $n=8$, which is expressed as in Eq. (1-2):

$$\vartheta = \frac{\sum_{i=1}^n |\varphi(i,j)|}{n} \text{ where } i, j = 1, 2, \dots, n \quad (1)$$

$$\text{threshold} = \mu \left[\frac{\text{avg}}{\text{avg} + \text{var}} \right] \quad (2)$$

where the *threshold* is the ideal threshold in the proposed algorithm and is the mean of (i,j). In the filtering window, the mean avg, as well as variance var of n neighbor pixels nearest to the center pixel, as well as variance var of n neighbor points adjacent to the center pixel is determined. It can be explained simply:

$$\text{var} = \sqrt{\frac{(\sum_{i=1}^n x(i,j) - \text{ave})^2}{n}} \text{ and } \text{avg} = \frac{\sum_{i=1}^n x(i,j)}{n} \quad (3)$$

Algorithm 1. The modified median filtering algorithm

- Input:** Corrupted Input chest X-ray Image by noise
Output: Noise removed Image, using a $M \times N$ window
1. The $M \times N$ window is skimmed in excess of the entire image.
 2. Category the pixels, denoted by S_{ij} inside the window in ascending order.
 3. Find minimum S_{min} , maximum S_{max} and median S_{med} of the pixel values
 4. If ($S_{min} < S_{epicenter} < S_{max}$)
 5. denote the medium pixel as uncorrupted such that no filtering required
 6. Else
 7. denote the medium pixel as corrupted
 8. If ($S_{epicenter}$ is not an noise which is margin significance)
 9. Substitute $S_{epicenter}$ through S_{med}
 10. Else
 11. Substitute $S_{epicenter}$ through $S_{i-1,j}$
 12. End If
 13. End If
 14. Recurrence step 2 to 9 for the complete image and obtain noise removed image.
-

Statistical Range for Edge detection: The measures of dispersion between every maximum and minimum value of a specified collected data, matrix, or linear data in massive volumes of data, the variety can be used to detect edges. Every pixel is supplanted with a variety of grey values from the

surrounding area. The variety also gives meaning to the mean, median, as well as mode, it can gain a piece of deeper knowledge through a variety of facts. In this study, the statistical range (SR) from each of the 3×3 matrix partitions from the lung input image was examined. The equation for determining SR is as follows:

$$SR = S_{med} - S_{min} \quad (4)$$

C. EASFMC for Segmentation

The lung segmentation technique is a prerequisite in classifying lung images and yet is essential for effective cancer diagnoses. Earlier, used Otsu's approach [24] to determine a global specified threshold, then image edge detection was employed to extract the bounding box of the image's centre, i.e., the malignancy location on an image. The region is segmented using regions of interest with an EASFMC clustering methodology, a density-based technique for detecting spontaneously generated clusters in more extensive coverage of large databases with imperfection. EASFMC additionally clusters sites only in high-density areas, whereas endpoints in specific areas are considered outliers or interference. So the amount of segments is determined dynamically.

Based on EASFMC, the study proposes a method for extracting the characteristic features of cancer areas. The fuzzy concept, commonly employed in the classification process, is being used here for segmentation—the given image segments into several clusters due to specific fuzzified data clusters by keeping their geometric placements—the measure of similarity of each pixel to the precedent cluster's centre value using the membership degree. The method has indeed been designed in this study to determine its initial centroids reference value on its own, making the segmentation procedure automatic. The EASFMC Segmentation steps are explained in detail as follows.

Step 1: The ROI $I(x,y)$ was obtained initially, which comprises the cancer area and the ordinary location, two reference cluster numbers must be specified for this. Those two main clusters c were generated sequentially in an attempt to implement this segmentation quickly and easily.

$$c_1 = \frac{\sum (\sum_{m=1}^i \max(I(m, :)))}{N}$$

$$c_2 = \frac{\sum (\sum_{n=1}^j \max(I(m, :)))}{N}$$

Where $m = 1, 2, \dots, i$ and $n = 1, 2, \dots, j$. (5)

Where i is the amount of rows, j is the amount of columns in image $I(m, n)$ and N is the complete number of non-zero pixels.

Step 2: The differentiation between each pixel as well as clusters was computed, therefore two distance matrices, $dist_1$ and $dist_2$, respectively built for both c_1 and c_2 using the formulae below.

$$dist_1 = [c_1 - I(m, n)]^2 \text{ and}$$

$$dist_2 = [c_2 - I(m, n)]^2 \quad (6)$$

Step 3: The distance matrices acquired in the initial state were smooth fuzzified using the following equations, and even the coefficients were therefore normalised as well as fuzzified using a constant variable $r > 1$ as then their summation was 1, as well as the resultant smooth fuzzified output was preserved in F_1 and F_2 .

$$F_1 = \frac{1}{\frac{2}{(dist_1)^{r-1}}} \text{ and}$$

$$F_2 = \frac{1}{\frac{2}{(dist_2)^{r-1}}} \quad (7)$$

This seems to be comparable to simply normalising the coefficients to achieve their summation 1 for $r = 2$.

Step 4: Around an image $F(m, n)$, fuzzy rule-based assignment was conducted prior to F_1 and F_2 , as well as the segmented images seg_1 (the segmented image with respect to initial cluster c_1) and seg_2 (another segmented image with respect to cluster c_2) were generated as follows:

$$seg_1(i, j) = I(m, n), \text{ if } F_2(i, j) < F_1(m, n) \text{ and}$$

$$seg_2(i, j) = I(m, n), \text{ if } F_2(m, n) > F_1(m, n) \quad (8)$$

Step 5: These seg_1 and seg_2 were refined through updating the cluster value c_1 and c_2 consuming the subsequent equations.

$$c_{1_update} = \frac{\sum(seg_1(i, j) \neq 0)}{N_1} \text{ and}$$

$$c_{2_update} = \frac{\sum(seg_2(i, j) \neq 0)}{N_2} \quad (9)$$

Where N_1 and N_2 are the complete amount of non-zero pixels in seg_1 and seg_2 correspondingly.

Step 6: Step 1 to 5 were repetitive once more with the new cluster centre values such as c_{1_update} and c_{2_update} up to the difference between two sequential restructured clusters were minimum.

Step 7: Mathematical morphology is used for the binary image, and the cancer regions are improved in the processed binary image. Formerly, DSCNN is applied for feature extraction yields the final results of feature extraction then also classification after X-ray image segmentation.

D. Feature Extraction and Classification using DSCNN

In DSCNN, image features are extracted from the fully connected (FC) layers and then optimized utilizing the MSCOA method. The system gave a 2-dimensional feature map containing the retrieved image features as input. Provide N filters to every convolutional network layer to identify cancer region abnormalities across data points. Every neural inference produced a probability function in maintaining the likelihood of every output class. Fig. 3 depicts the DSCNN classifier's architectural framework. The network's initial layer was a normal convolutional layer throughout all situations. Another batch-normalization layer including activation function (rectified linear unit (ReLU) [25]) followed the convolutional layer.

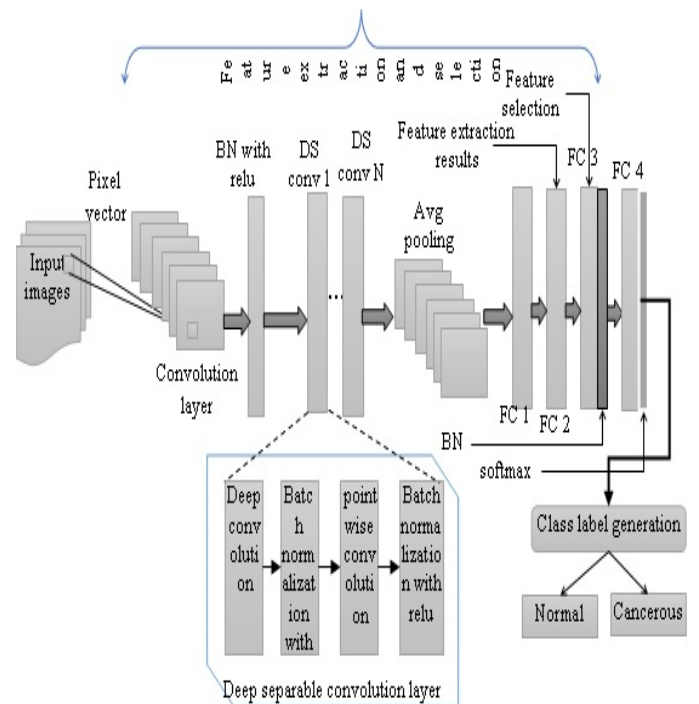


Fig. 2. General Architecture of the DSCNN for LC Detection.

Sophisticated features are represented efficiently by DSCNNs. Meanwhile, the number of convolution layers (Conv) and its type, pooling function, kernel size and activation function, and fully connected layers model. The primary goal is to acquire outstanding raw pixel information to identify the detection efficiency of the overall architecture. Following the DSCNN process of learning, MSCOA is used to isolate the optimal feature selection, just the most essential attributes that maximize classification performance. The DSCNNs fundamental aim of sharing weights over multiple layers is to reduce the curse of dimensionality. Can summarize entire network as (Conv1: $1 \times 3@64$) \rightarrow (DSConv2: $1 \times 3@64$) \rightarrow (FC1: 128) \rightarrow (FC2: 128) \rightarrow (FC3: 64) \rightarrow (BN: 64) \rightarrow (FC4: 64) and Fig. 2 shows the suggested DSCNN architecture into four layers: (1) Conv (2) Deep Separable Convolution layer (DS Conv), (3) Pooling layers, and (4) FC.

Conv: This is the first conv, with 64 filters, a kernel of dimension 3, as well as a stride of value 1, and it employs the ReLU as a non-linear function, followed by dropout regularization with a rate of 0.5 and then a size two max-pooling operations.

DS Conv: This is the second DS Conv, similar to Conv1, except that instead of max-pooling, this uses an adaptive average pooling layer.

FC: FC1, FC2, and FC3 are feature extraction and feature selection layers that output learned features from raw input, with 128, 128, and 64 neurons.

BN and FC4: FC4 is the final FC layer to produce the classification predictions, and BN (batch normalization) operation.

BN was used to speed up the training process while also reducing the risk of overloading due to regularization. After BN and ReLU activations, the input image array to the first conv layer. each of the DS conv layers 1 to N starts with a deep convolution, then BN and ReLU, before moving on to a pointwise conv, BN, and ReLU activation again. The application determines average pooling and FC layer containing soft max activations after the conv layers. Great learning rates can be employed when the activation patterns since the strength of the biases of each layer are much more equivalent, resulting in rapid system divergence.

The small number of features in the mini-batch creates a regularization effect since the activations of a single image file are not normalized by the mean and variance of each image file but rather by the mean and variance of the mini-batch wherein it occurs. Following the BN layer, a series of DS convs consisted of a deep wavelet convolution (DW conv) and a pointwise convolution (PW conv). A BN followed each one with ReLU activation. After that, an average pooling layer decreases the number of activations by introducing an averaging window to every input cable network's complete time-frequency feature map. Finally, the probabilities for every class label using an FC layer with softmax activations.

E. Feature Selection using MBOA

The food gathering behavior of butterflies [26] inspired the Butterfly Optimization Algorithm (BOA) used to find and identify the best solution in a multi-dimensional domain. To reach a local and global optimum solution, certain unique places are allocated to butterflies in the ecosystem, including some input values. The calibration period starts after this, and the method runs like a virtual environment, optimizing the location of the features (butterflies) by tweaking its parameter. The primary three variables of the butterfly algorithm are used to move features (butterflies) from its random position to the optimal solution whereas butterflies use their keen sense of smell and scent to detect the presence of other butterflies.

Each scent in BOA has its unique distinct, enticing aroma and unique touch. This is one of the guiding features that set BOA apart from other meta-heuristics. To understand how fragrance is regulated in BOA [26], first understand how a technology such as music, lighting, or warmth is computed. The entire concept of identifying and managing the method is based on three key terms: stimulus intensity (\mathcal{J}), power exponent (\mathcal{E}) and sensory modality (\mathcal{M}). Sensation implies measuring the variety of energy and processing it by comparing methods in sensory modality technique, while methodology implies the basic information used by the sensors.

Currently, numerous modalities include lighting, music, and warmth. In BOA, while sI is the strength of the physical stimulus, when a butterfly emits a more visible smell, other butterflies in the area can sense be drawn towards it. The power of the butterfly or rational response represents an improvement in intensity, where pE is the parameter that

considers regular expression, which accounts for fluctuating levels of absorption. This part conducted several stimuli estimating experiments on bugs, critters, and individuals, and they have hypothesized that as the number increases, insects become less sensitive to changes in the environment. Using these ideas, the fragrance \mathfrak{FR}_i (fragrance is smell by i th butterfly) in BOA is computed as [27]:

$$\mathfrak{FR} = \mathcal{M} * \mathcal{J}^{\mathcal{E}} \quad (10)$$

The global and the local search stage are utilized to assert that fragrance levels rise in a well-liked situation. A butterflies B would produce a smell that may be sensed from every location in the region in this manner. The butterfly finds the fitness values \mathcal{F} , which can be depicted as in the global search stage.

$$x_i^{iter+1} = x_i^{iter} + (\mathcal{R}^2 \times \mathcal{F} - x_i^{iter}) \times \mathfrak{FR}_i \quad (11)$$

where x_i^{iter} is the way out vector x_i for i th butterfly in iteration number $iter$. Fragrance of i th butterfly is represented by $frag_i$ and \mathcal{R} is a random number which would be in between 0 and 1, also here $\mathcal{R} < \mathcal{P}$, where \mathcal{P} is the switching probability. Neighborhood or local search stage can be represented as

$$x_i^{iter+1} = x_i^{iter} + (\mathcal{R}^2 \times x_j^{iter} - x_k^{iter}) \times \mathfrak{FR}_i \quad (12)$$

where x_j^{iter} and x_k^{iter} are j th and k th butterflies from the search space. On the off chance that x_k^{iter} has a place with a similar swarm and x_i^{iter+1} turns into a neighborhood random walk. Scan for nourishment and mating accomplice by butterflies can happen at both neighborhood and global level and thus \mathcal{P} is utilized as a part of BOA to switch between normal globe searches to concentrate local search.

By researching the scent and separating it from the poor one, the DSCNN-based feature findings contribute in the examination of fragrance in the movement of numerous butterflies and the transmittance of smell to interact to each other and go beyond the optimal butterfly. A butterfly with a little more fragrance and a higher fitness value can attract more butterflies in that region, and a butterfly with plenty of fragrance and sometimes a based on the fitness value can attract more butterflies in that area. Particles in the region can compress their replies by using the parameter \mathcal{E} . The \mathfrak{FR} and \mathcal{J} are the main issues to get the variance of \mathcal{J} and formulation of \mathfrak{FR} . The values of \mathcal{J} which are encoded with objective function and \mathfrak{FR} is relative which is calculated as

$$\mathfrak{FR} = \mathcal{M} * \mathcal{J}^{\mathcal{E}} \left(1 - \frac{N_{tf} - N_{fs}}{N_{tf}} \right) \quad (13)$$

The accuracy of the DSCNN classifier has been employed as an efficiency analyzer in the creation of objective functions with a large number of features. Where (N_{tf}) denotes the overall quantity of features (tf), (N_{fs}) denotes the dimension of the feature subset (fs). The BOA's Sensory Modality \mathcal{M} parameter instructs the butterflies to sense the fragrance

generated from other butterflies within the search region and direct their search to those providing the most scent [23]. Like the value of the \mathcal{M} , the parameter is increased, and the algorithm's performance improves throughout execution. As the number of iterations increases, the algorithm's performance improves for the period of the iterative search process. A significant impact on the efficiency of BOA and the performance will be enhanced considerably in comparison to the conventional BOA with Eq. (14), it is analyzed that the new values of \mathcal{M} will have.

$$\mathcal{M}^{iter} = \mathcal{M}^{iter-1} * \frac{(10.0 - \frac{5}{0.9})^2}{MaxGen} \quad (14)$$

where $iter$ is the current iteration number and $MaxGen$ is the maximum number of iteration in the algorithm. In this suggested work, the adaptive mechanism of \mathcal{M} is designed and used in the algorithm, which adds useful elements to the algorithm's performance and aids in acquiring alternative discoveries in the search space, enabling the BOA approach to achieve better results. The flowchart of MBOA is given in Fig. 3 and the pseudo code of MBOA is clarified in Algorithm 1.

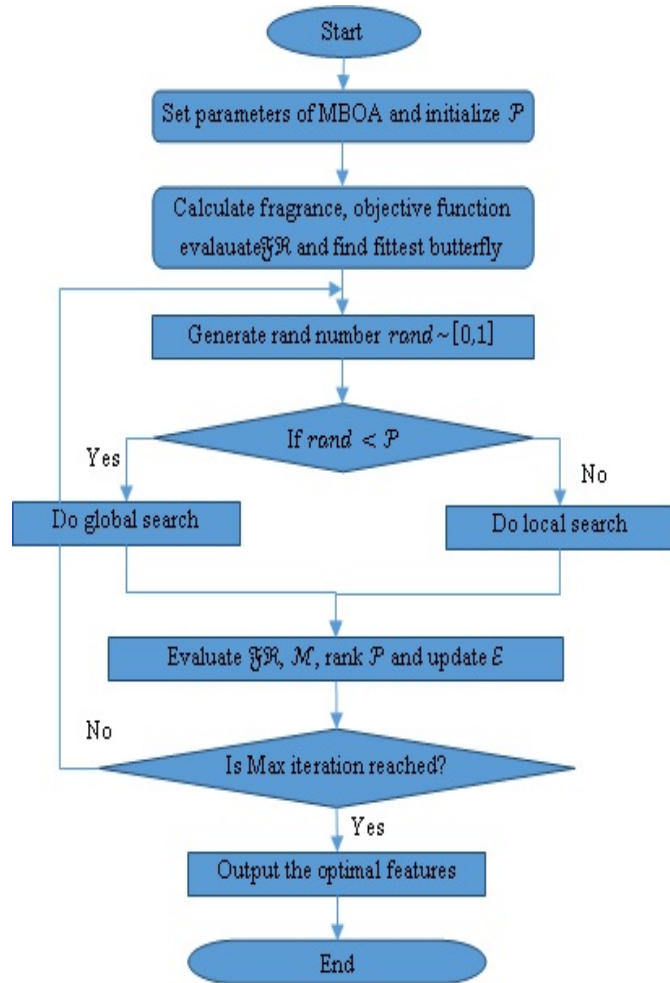


Fig. 3. Flowchart of Proposed MBOA based Optimal Feature Selection.

Algorithm 2. Pseudo-Code for MBOA for optimal feature selection

Input: Features extracted by DSCNN
Output: Feature subset selection (optimal features)

Begin
 Do initial population of N butterflies $x_i = (i = 1, 2, \dots, n)$
 Determine \mathcal{J} at x_i is determined by $\mathfrak{FR}(x_i)$
 Outline \mathcal{M} , \mathcal{E} and \mathcal{P}
 while ending criteria not encountered do
 for each butterfly in population do
 Determine \mathfrak{FR} for butterfly using Eq. (10)
 end for
 Discover the paramount \mathcal{F}
 ensure for each butterfly in population
 Derive a random number $rand$ from $[0, 1]$
 if $rand < \mathcal{P}$
 Interchange in the direction of best solution using Eq. (10)
 else
 Interchange arbitrarily using Eq. (13)
 end if
 end for
 Apprise the worth of \mathcal{M}
 end while
 while ending criteria reached do
 Determine objective function (accuracy of the test set by DSCNN classifier) of butterflies are evaluated depend on Eq. (15);
 return optimal butterflies (the selected optimal feature subset);
 End while
 End

IV. EXPERIMENTAL RESULTS AND DISCUSSION

The proposed work DSCNN-MBOA classifies the collected features into two class labels: normal and cancerous. The lung X-ray images are generally contained the noise, so, the first step of the work is applying pre-processing techniques to remove unwanted and noisy information for further analysis. After that, these images will be passed via an operation of segmentation in which the cancer region is extracted. Then the segmented image will be the given input of the proposed DSCNN-MBOA for detection of the LC, MBOA used for feature selection and various parameters are then utilized to assess the performance of the proposal such as accuracy, precision, F1-score, execution time, specificity and sensitivity and compare with exiting methods such as VDSNet [22], modified AlexNet [21] and CNN with TL [20].

$$Accuracy = \frac{TP+TN}{TP+TN+FP+FN} * 100 \quad (15)$$

$$Precision = \frac{TP}{TP+FP} * 100 \quad (16)$$

$$F1\ score = \frac{2*Precision*Recall}{Precision+Recall} \quad (17)$$

$$Specificity = \frac{TN}{TN+FP} * 100 \quad (18)$$

$$Sensitivity = \frac{TP}{TP+FN} * 100 \quad (19)$$

Here, FP described as False Positive, which is the total number of lung images that are presently negative and classified as positive. Where TP described as True Positive, which is the total number of lung images that are currently positive and classified as cancerous, FN described as False Negative, which is the total number of lung images that are presently positive and classified to be harmful as normal. TN described as True Negative, which is the total number of lung images that are currently negative and classified to be negative.

A. Accuracy Comparison Results

Fig. 4 gives the accuracy of proposed and existing models for the number of features in a shared database. The proposed DSCNN-MBOA increases the accuracy with a value of 98.45%. The reason for this is that the threshold is primarily used to alter the size of the sub training dataset, but it is also utilized for other purposes. The lower the value, the more likely the raw dataset samples are dispersed among the sub training datasets. The incorporation of the MBOA mechanism in the proposed model improves accuracy performance because it increases the convergence speed of DSCNN.

B. Precision Comparison Results

Fig. 5 indicates the precision of proposed and existing models for the number of features in a given database. As increasing the number of features, the precision is also maximized. E.g., the DSCNN-MBOA attains a precision of 98.5% compared to the VDSNet, modified AlexNet and CNN with TL. Because the DSCNN-MBOA combines feature extraction and classification into a single DSCNN-MBOA structure, it decreases the time necessary to compute the derived factors, resulting in a higher precision rate. DSCNN-MBOA performs best with high-speed converges, which is likely due to a lack of data on the features of the huge images, speeding up convergence time over the entire dataset.

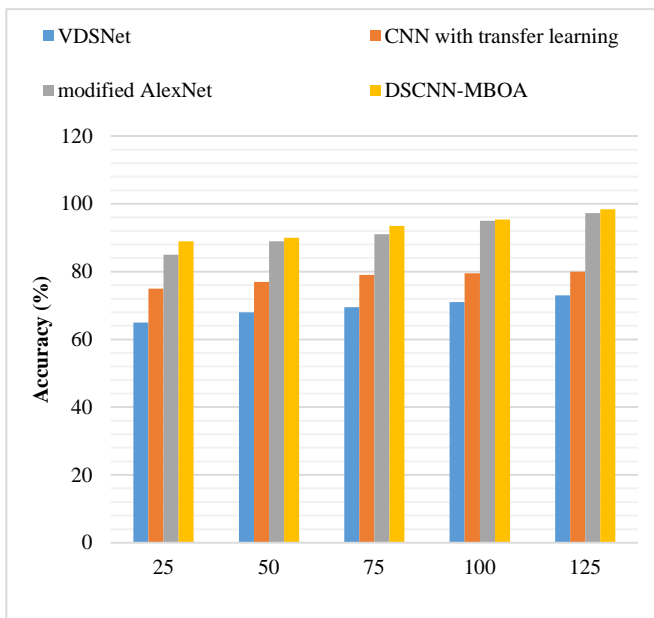


Fig. 4. Accuracy Performance Comparison.

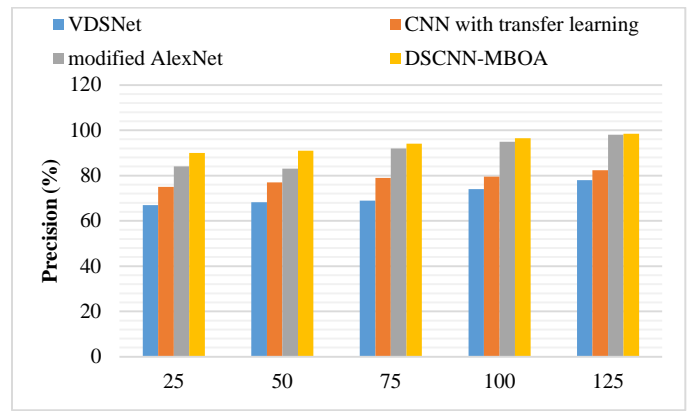


Fig. 5. Precision Performance Comparison.

1) *F1-score comparison results:* From Fig. 6, it indicates the F1-score of proposed and existing models for the number of features in given databases. E.g., the DSCNN-MBOA provides an f-measure of 98.85% compared to all other models such as VDSNet, modified AlexNet and CNN with TL. The reason is that the MBOA is effectively optimizing the features with high convergence speed, and thus DSCNN-MBOA has good validation results with a high F1-score rate. The combined power of CNN, modified AlexNet and attention mechanism prove advantageous in LC detection.

2) *Execution time comparison results:* From Fig. 7, it indicates the execution time of proposed and existing models for the number of features in a given database. As increasing the number of features, the execution time is also maximized. E.g., the DSCNN-MBOA attains a recall of 527.15s compared to the VDSNet, modified AlexNet and CNN with TL. Because the proposed model can reduce more bias in all datasets and reduce minor variance and thus the model is simple to process the LC.

3) *Specificity comparison results:* From Fig. 8, it indicates the recall of proposed and existing models for the number of features in a given database. As increasing the number of features, the recall is also maximized. E.g., the DSCNN-MBOA attains a recall of 89.65% compared to the VDSNet, modified AlexNet and CNN with TL. Because existing methods are simple models that are ineffective for high-dimensional datasets, they are under fitting. EASFMC has the advantage of good segmentation of cancer regions, thus increasing the classification rate of the proposed DSCNN-MBOA. Existing techniques generally perform not well when images are rotated, tilted, or otherwise strangely oriented. As a result, hybrid approaches have improved accuracy while decreasing training time. The study's findings imply that DL models can be utilized to strengthen diagnosis when compared to standard methods.

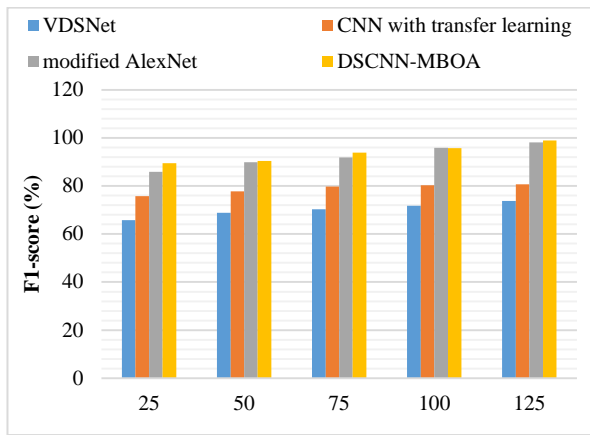


Fig. 6. F1-score Performance Comparison.

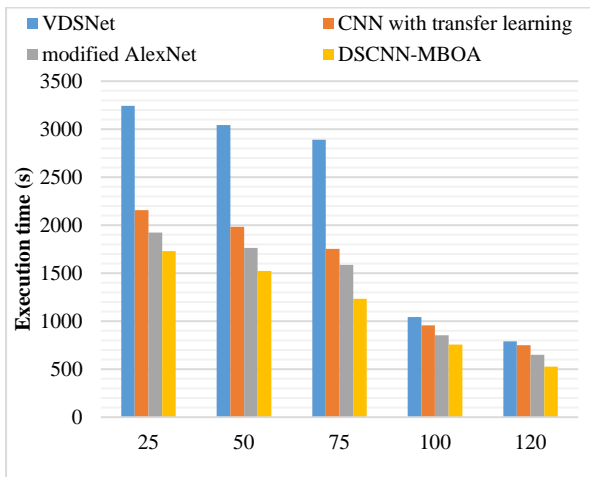


Fig. 7. Execution Time Performance Comparison.

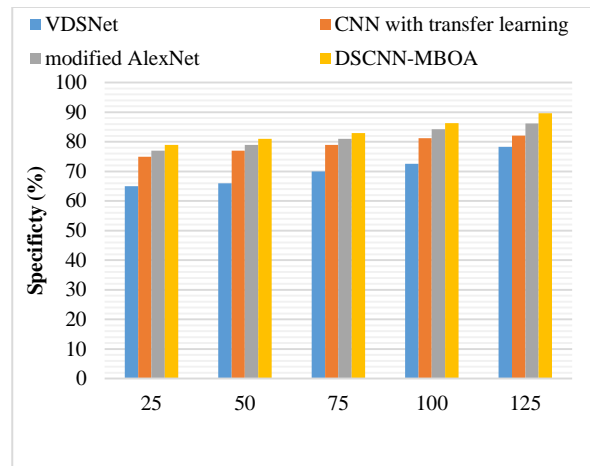


Fig. 8. Specificity Performance Comparison.

4) *Sensitivity comparison results:* From Fig. 9, it gives the accuracy of proposed and existing models for the number of features in a shared database. The DSCNN-MBOA increases the accuracy and attains the sensitivity 95% when compared to VDSNet, modified AlexNet and CNN with TL. Thus the

proposed algorithm is more significant than the existing algorithms for better good validation results for predicting cancer. The proposed DSCNN-MBOA model was utterly independent of the abrupt feature changes. Thus, it could be helpful for LC n X-ray images. As can be seen from the results, the average max pooling is beneficial for the DSCNN model. Better performance can be achieved can reduce the influence of class imbalance on the training process and making the model pay more attention to classes that are difficult to recognize.

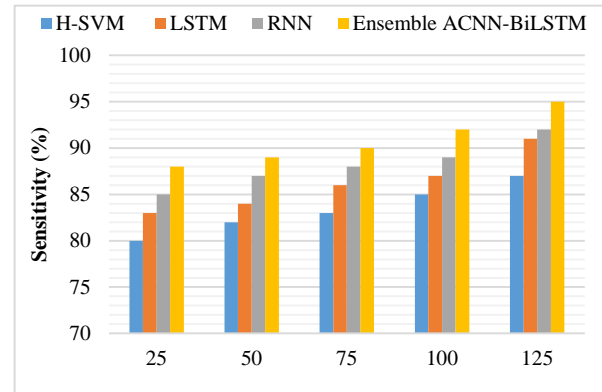


Fig. 9. Sensitivity Performance Comparison.

V. CONCLUSION AND FUTURE WORK

On the basis of chest X-ray images, this study presents a hybrid DL (DSCNN-MBOA) based approach for LC identification. In order to improve cancer detection performance, the phases of background segmentation, feature set extraction, feature optimization, and DSCNN-based LC classification are used. The proposed method achieves a precision of 98.45% and a time complexity of 527.15s while maintaining a tradeoff with network performance. In chest X-ray images, the proposed hybrid technique may effectively detect the cancer zone. When working with a large dataset, this research project faces a number of problems. As a result, while small datasets can generate great accuracy, they are impractical for real-world applications. Besides applying improved DL or other innovative TL algorithms for the sample, then combining GoogLeNet, AlexNet, and ResNet-152 architecture to create a hybrid algorithm in the future, this study will combine GoogLeNet, AlexNet, and ResNet-152 architecture to create a hybrid algorithm. The use of image data augmentation techniques such as color space augmentations, feature space augmentations, hyper parameter optimization, and other methods to improve the accuracy of automated chest X-ray diagnosis systems will be explored. In future research, even though the dual dataset method is successful, a more advanced deep learning method will be proposed for lung disease detection. In the first study, more datasets will be collected to increase efficacy. As is common knowledge, deep learning success is strongly influenced by the quantity of labeled data available. So this research will combine hybrid deep neural networks. A study is also planned to develop novel robust optimization based hybrid CNN-based lung segmentation with multiple datasets.

REFERENCES

- [1] Siegel, R. L., Miller, K. D., Fedewa, S. A., Ahnen, D. J., Meester, R. G., Barzi, A., & Jemal, A. (2017). Colorectal cancer statistics, 2017. *CA: a cancer journal for clinicians*, 67(3), 177-193.
- [2] Mathur, P., Sathishkumar, K., Chaturvedi, M., Das, P., Sudarshan, K. L., Santhappan, S., & ICMR-NCDIR-NCRP Investigator Group. (2020). Cancer statistics, 2020: report from national cancer registry programme, India. *JCO Global Oncology*, 6, 1063-1075.
- [3] Valente, I. R. S., Cortez, P. C., Neto, E. C., Soares, J. M., de Albuquerque, V. H. C., & Tavares, J. M. R. (2016). Automatic 3D pulmonary nodule detection in CT images: a survey. *Computer methods and programs in biomedicine*, 124, 91-107.
- [4] Yang, L., Xu, H. Y., & Wang, Y. (2020). Diagnostic and therapeutic strategies of LC patients during the outbreak of 2019 novel coronavirus disease (COVID-19). *Zhonghua zhongliu zazhi [Chinese journal of oncology]*, 42(4), 292-295.
- [5] Kadir, T., & Gleeson, F. (2018). LC prediction using machine learning and advanced imaging techniques. *Translational LC research*, 7(3), 304.
- [6] Sun, W., Zheng, B., & Qian, W. (2017). Automatic feature learning using multichannel ROI based on deep structured algorithms for computerized LC diagnosis. *Computers in biology and medicine*, 89, 530-539.
- [7] Sun, W., Zheng, B., & Qian, W. (2016, March). Computer aided LC diagnosis with DL algorithms. In *Medical imaging 2016: computer-aided diagnosis* (Vol. 9785, pp. 241-248). SPIE.
- [8] NIH sample Chest X-rays Dataset Available at: <https://www.kaggle.com/nih-chest-xrays/sample>, Accessed 28th Jun 2020.
- [9] O. Er, N. Yumusak, and F. Temurtas, "Chest diseases diagnosis using artificial neural networks," *Expert Systems with Applications*, vol. 37, no. 12, pp. 7648–7655, 2010.
- [10] O. Er, C. Sertkaya, F. Temurtas, and A. C. Tanrikulu, "A comparative study on chronic obstructive pulmonary and pneumonia diseases diagnosis using neural networks and artificial immune system," *Journal of Medical Systems*, vol. 33, no. 6, pp. 485–492, 2009.
- [11] S. Khobragade, A. Tiwari, C. Y. Pati, and V. Narke, "Automatic detection of major lung diseases using chest radiographs and classification by feed-forward artificial neural network," in *Proceedings of 1st IEEE International Conference on Power Electronics, Intelligent Control and Energy Systems (ICPEICES-2016)*, pp. 1–5, Delhi, India, 2016.
- [12] G. Litjens, T. Kooi, E. B. Bejnordi et al., "A survey on deep learning in medical image analysis," *Medical Image Analysis*, vol. 42, pp. 60–88, 2017.
- [13] S. Albarqouni, C. Baur, F. Achilles, V. Belagiannis, S. Demirci, and N. Navab, "Aggnet: deep learning from crowds for mitosis detection in breast cancer histology images," *IEEE Transactions on Medical Imaging*, vol. 35, no. 5, pp. 1313–1321, 2016.
- [14] G. E. Hinton, S. Osindero, and Y. W. Teh, "A fast learning algorithm for deep belief nets," *Neural Computation*, vol. 18, no. 7, pp. 1527–1554, 2006.
- [15] H.-C. Shin, K. Roberts, L. Lu, D. Demner-Fushman, J. Yao, and R. M. Summers, "Learning to read chest X-rays: recurrent neural cascade model for automated image annotation," *Cornel University library*, 2016.
- [16] Liu, C., Wang, B., Jiao, Q., & Zhu, M. (2019, June). Reducing false positives for lung nodule detection in chest X-rays using cascading CNN. In *2019 14th IEEE Conference on Industrial Electronics and Applications (ICIEA)* (pp. 1204-1207).
- [17] Peng, G., Liu, L., Zeng, K., Li, T., & Nakayama, S. (2012, December). LC Detection in Chest X-Ray Images with Parallel Genetic Algorithm. In *2012 13th International Conference on Parallel and Distributed Computing, Applications and Technologies* (pp. 189-192).
- [18] Ausawalaithong, W., Thirach, A., Marukatat, S., & Wilaiprasitporn, T. (2018, November). Automatic LC prediction from chest X-ray images using the DL approach. In *2018 11th Biomedical Engineering International Conference (BMEiCON)* (pp. 1-5).
- [19] Yan, C., Yao, J., Li, R., Xu, Z., & Huang, J. (2018, August). Weakly supervised DL for thoracic disease classification and localization on chest x-rays. In *Proceedings of the 2018 ACM international conference on bioinformatics, computational biology, and health informatics*, pp. 103-110.
- [20] Wibisono, A., Adibah, J., Priatmadji, F. S., Viderisa, N. Z., Husna, A., & Mursanto, P. (2019, November). Performance Analysis of DL Network Models of Localized Images in Chest X-ray Decision Support System. In *Proceedings of the 2019 3rd International Conference on Big Data Research* (pp. 54-59).
- [21] Bhandary, A., Prabhu, G. A., Rajinikanth, V., Thanaraj, K. P., Satapathy, S. C., Robbins, D. E. & Raja, N. S. M. (2020). DL framework to detect lung abnormality—A study with chest X-Ray and lung CT scan images. *Pattern Recognition Letters*, 129, 271-278.
- [22] Bharati, S., Podder, P., & Mondal, M. R. H. (2020). Hybrid DL for detecting lung diseases from X-ray images. *Informatics in Medicine Unlocked*, 20, 100391.
- [23] Maheswari, D., & Radha, V. (2010). Noise removal in compound image using median filter. *IJCSE International Journal on Computer Science and Engineering*, 2(04), 1359-1362.
- [24] Huang, M., Yu, W., & Zhu, D. (2012, August). An improved image segmentation algorithm based on the Otsu method. In *2012 13th ACIS International Conference on Software Engineering, Artificial Intelligence, Networking and Parallel/Distributed Computing* (pp. 135-139).
- [25] Hara, K., Saito, D., & Shouno, H. (2015, July). Analysis of function of rectified linear unit used in DL. In *2015 international joint conference on neural networks (IJCNN)* (pp. 1-8).
- [26] Arora, S., & Singh, S. (2019). Butterfly optimization algorithm: a novel approach for global optimization. *Soft Computing*, 23(3), 715-734.
- [27] Tubishat, M., Alswaitti, M., Mirjalili, S., Al-Garadi, M. A., & Rana, T. A. (2020). Dynamic butterfly optimization algorithm for feature selection. *IEEE Access*, 8, 194303-194314.

Face Recognition System Design and Implementation using Neural Networks

Jamil Abedalrahim Jamil Alsyayadeh^{1*}, Chang Kai Xin⁴

Department of Electronics & Computer Engineering Technology, Fakulti Teknologi Kejuruteraan Elektrik & Elektronik (FTKKE), Universiti Teknikal Malaysia Melaka (UTeM), Melaka, Malaysia

Irianto²

Department of General Education, Faculty of Resilience
Rabdan Academy, Abu Dhabi, United Arab Emirates

Azwan Aziz³

Department of Industrial Technology, Faculty of
Mechanical and Manufacturing Engineering Technology
Universiti Teknikal Malaysia Melaka (UTeM)
Melaka, Malaysia

A. K. M. Zakir Hossain⁵

Centre for Telecommunication Research & Innovation
(CeTRI), Fakulti Teknologi Kejuruteraan Elektrik &
Elektronik (FTKKE), Universiti Teknikal Malaysia Melaka
(UTeM), Melaka

Safarudin Gazali Herawan⁶

Industrial Engineering Department, Faculty of Engineering
Bina Nusantara University, Jakarta, Indonesia 11480

Abstract—Face recognition technology is used in biometric security systems to identify a person digitally before granting the access to the system or the data in it. There are many kidnappings or abduction cases happen around us, however, the kidnap suspects will be set free if there is lack of evidence or when the victims are not able to testify in court because they suffer from post-traumatic stress disorder (PTSD). The objectives of this study are, to develop a device that will capture the image of a kidnapper as evidence for future reference and send the captured image to the family of the victim through email, to design a face recognition system to be used in searching kidnap suspects and to determine the best training parameters for the convolution neural network (CNN) layers used by the proposed face recognition system. The accuracy of the proposed system is tested with three different datasets, namely the AT&T database, face database from [23] and a custom face dataset. The results are 87.50%, 92.19% and 95.93% respectively. The overall face recognition accuracy of the proposed system is 98.48%. The best training parameters for the proposed CNN model are kernel size of 5x5, 32 and 64 filters for first and second convolutional layers and learning rate of 0.001.

Keywords—Face recognition system; biometric identification; face detection; image processing; convolutional neural networks

I. INTRODUCTION

There are many kidnappings or abduction cases happen around us. The fate of the victim remains unknown until the suspect is found and arrested. In the cases of victims being rescued in time by the authorities, it is likely that the victims who suffer from post-traumatic stress disorder (PTSD) could not recognise or remember the face of the kidnapper during their testimony in court. Therefore, the purpose of this work is to develop a device to capture the image of a kidnapper and reduce the time taken for the authorities to find the suspect.

One of the most widely used technologies in the world today is the facial recognition technology. With the use of

facial recognition, a biometric system can identify a person digitally before granting the access to it or the data in it. Complicated and unrealistic biometric security systems are often portrayed by computer graphics in many futuristic movies; however, Apple had taken one step forward and release a face unlock feature for its iPhone X in 2017. This breakthrough uses a sensor to scan the face of the user and saves it as the face ID. The phone can be unlocked when the face of the person unlocking the phone matched with the face ID. The release of this new authentication method has made a big impact in the smartphone industry and all the latest smartphones have started to implement the same face unlock feature in their systems. Facial recognition technology is also used in other systems, for instance, it is used in airport security, law enforcement, attendance systems and to search for a person. This system uses neural network in the development and implementation of face recognition system. Neural network can be trained to process and analyse data, recognise patterns, and make prediction about specific operations. Generally, the programmer needs to provide numerous examples to train neural network, in order for it to learn the patterns [1].

We proposed an idea which combines both hardware and software, where the hardware will capture image of the suspect and the software will perform facial recognition. Our approach allows the hardware to not only capture the image of the suspect but also send the captured image to notify the victim's family that the victim is in danger so that the family can report to the authorities and rescue the victim in a shorter period. The image is then be used as an input to the face recognition system to identify the suspect. The accuracy of the proposed system is 87.50% when tested with the AT&T database, 92.19% with face database from [23] and 95.93% with custom face database. The potential users of the proposed system could be women and children as they are often the target of abduction.

*Corresponding Author.

The device can be attached to the users' belongings and the users can press the button to activate the device when they are in danger and their family will be notified in no time. In addition to all this, the best training parameters for the convolutional neural network layers used by the proposed face recognition system will be determined.

The remain of this paper has been organized as follows: Section 2 discusses the related works. The background of the study is described in Section 3. Section 4 described the results and discussion and finally, the conclusion is described in Section 5.

II. RELATED WORK

In [2], the factors that might affect the accuracy of face recognition systems are classified into two main categories, intrinsic and extrinsic factors. Physical conditions of the human faces are considered as intrinsic factors, for example, aging and facial expressions. Extrinsic factors are made up of partial occlusion, pose variance and illumination. The authors in [3] stated that a useful face recognition system must fulfill the following characteristics: firstly, it must be able to work well with both images and videos, secondly, it must be capable to process in real time, thirdly, it must be robust in illumination variation, fourthly it needs to perform its task without being affected by hair, ethnicity or gender of a person and lastly, it must be able to work with faces detected from all angles. They also stated that a robust face recognition system is made up of three basic steps: face detection, feature extraction and face recognition. There are various techniques that can be used for face recognition, such as Eigenface, Neural Network, Hidden Markov Model (HMM) and Support Vector Machine (SVM).

The Eigenface technique is used in [4] for building face recognition software and the average accuracy for their face recognition software is 85%. Next, a hybrid approach which consists of the Haar Cascades and Eigenface methods that can detect multiple faces in a single detection process is proposed in [5]. The accuracy of this proposed solution was reported to be 91.67%.

Another technique that can be used to develop a face recognition system is called the neural networks. This technique was used in [6] and the average accuracy of the proposed system was 96.84%. The authors in [7] proposed to improve the backpropagation artificial neural network (BP-ANN) for a better performance of the face recognition system. The proposed system yielded a success ratio of 82%. In [8], the researchers used a hybrid approach which includes Elman Neural Network, Curvelet transform and HSI colour space. The resulting accuracy obtained by the authors was 94%. In addition, the authors of [9] proposed an effective method for face recognition that uses Principal Component Analysis (PCA) and models trained with Feed Forward Back Propagation Learning (FFBPL) and Elman Neural Network. The results of FFBPL were 98.33% and 98.80% while the results of Elman Neural Networks were 98.33% and 95.14%.

Next, convolutional neural networks are widely used in research these days, in [10], a real-time face recognition system is built using CNN. The maximum accuracies of the proposed system are 98.75% for standard datasets and 98.00% for real-

time inputs. An algorithm for face detection and recognition based on the same concept in [11][12] gives the accuracy of 97.9%. Besides, to develop a face recognition with small dataset, the authors proposed a method that uses a modified deep learning neural network in [13][14]. The accuracy of the proposed system achieved 99.6%. A deep convolutional neural network-based face recognition system that uses transfer learning approach is proposed in [15][16]. The accuracy of the proposed algorithm was 99.06%. In [17], an attendance system with face recognition based on deep learning technique. The overall accuracy obtained by the proposed system in a real-time environment was 95.02%. Similarly, an intelligent face recognizing attendance system that can identify several people simultaneously that is built based on CNN is proposed in [18]. The proposed system was tested with frontal view, side view and downwards view. The accuracies obtained for these three conditions were 81.25%, 75.00% and 43.75% respectively. A multi-face recognition system is proposed by the researchers in [19][20] to detect the prisoners in jail and the accuracy was 87%. Next, the researchers proposed a face recognition using a CNN model in [21][22]. The highest accuracy achieved by the proposed system was 98.3%. The authors in [23] proposed a deep CNN based face recognition system that can identify an individual in all possible conditions that might affect the accuracy of the face recognition system. The accuracies of the proposed system were 99.7% and 94.02% respectively. The authors of [24] proposed a home security system that uses face recognition technology developed by CNN. The Raspberry Pi was used as a microcontroller so that when the face of the homeowner was detected, the door will be unlocked automatically. The proposed system was able to achieve 97.5% accuracy.

A combination of 2D Hidden Markov Model (2DHMM) and Expectation-Maximalization (EM) algorithm is used in the face recognition system in [25] and its recognition rate was 99%. Besides that, in [26], two-dimensional Hidden Markov Models was used for face recognition. The recognition rates for 2D images were 93% and 95%. Next, the recognition rates for 3D images achieved 94% for both UMB-DB and FRGC databases. Lastly, the recognition rate for 2D+3D images was 96% for both databases.

By using wavelet Gabor filter and SVM, the authors in [27] have successfully built a 3D facial recognition system. The highest accuracy that the proposed system achieved was 97.3%. The authors in [28] proposed a face recognition that uses SVM with implementation of kernel as the classification method to identify lookalike faces. Two types of kernels were used in the proposed system, namely, the Radial Basis Function kernel and the polynomial kernel. The accuracy for both kernels is 94%.

III. BACKGROUND OF THE STUDY

This system two uses publicly available face databases, namely AT&T database and a database provided by the author of [29]. Besides, a hardware device is used to capture the image of the kidnapper, the image will be used as input to the face recognition system, therefore a custom face dataset needs to be created to test the accuracy of the proposed system. The components used for the hardware are the ESP32-CAM, FTDI

adapter and push button. The block diagram of the ESP32-CAM is shown in Fig. 1. The hardware is programmed using Arduino IDE while the face recognition system is built in MATLAB.

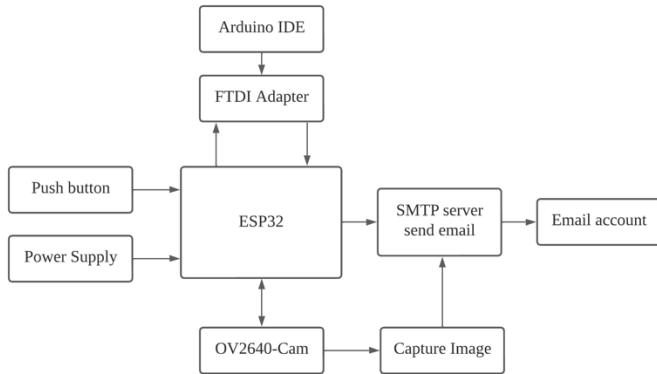


Fig. 1. ESP32-CAM Block Diagram.

The proposed system is developed according to the flowcharts shown in Fig. 2 to Fig. 4. Fig. 2 shows the flowchart of creating a custom face dataset. A custom face dataset is created because an ESP32-cam will be used to capture images of people, it is certain that during the testing process, the face captured by the device is not in the pre-curated face databases, such as the AT&T Database that contains a total of 400 images of 40 individuals. Hence, in order to yield higher accuracy, other than using the publicly available face dataset, we decided to create a custom face dataset for the system. After creating a face dataset, the face recognition system can be trained. The images in the face dataset created manually will be separated into two folders, one for testing purpose and another for training purpose. The same image cannot exist in both folders, in other words, all images of each individual in both folders must be different in terms of postures, lighting condition, facial expressions. The proposed system will be trained and tested with the images available before testing with the image captured directly from the ESP32-CAM.

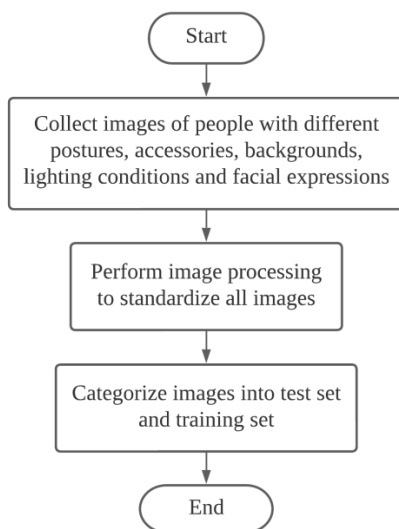


Fig. 2. Flowchart of Creating a Custom Face Dataset.

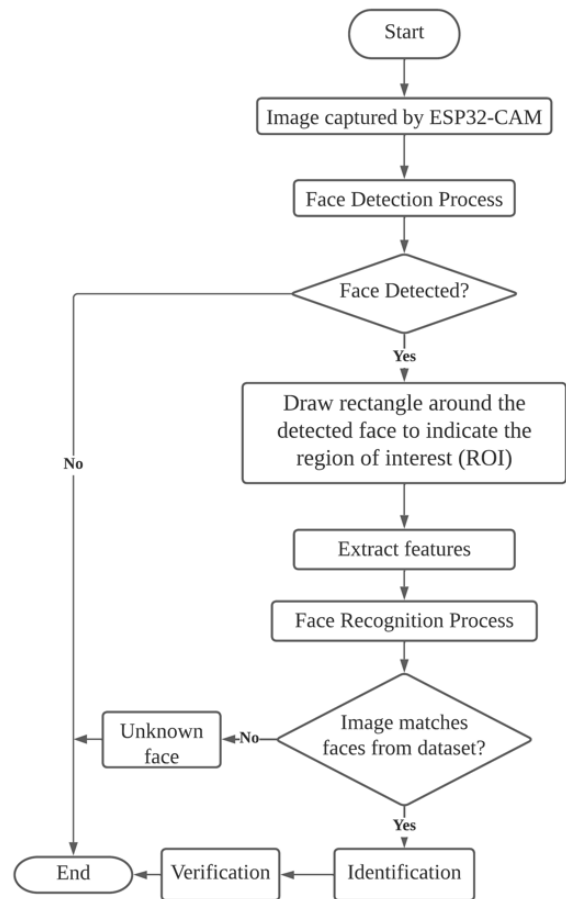


Fig. 3. Face Recognition System Programming Flowchart.

Fig. 3 shows the programming flowchart of the ESP32-CAM using Arduino IDE. The initialization process includes assigning the SSID and password to the device so that it can connect to the Wi-Fi or mobile hotspot and setting up the email account that will be receiving the captured image. Initially, the device will be in deep sleep mode and when it is triggered by a button, it will wake from the deep sleep mode to perform its function, which is capturing images. After an image is captured, the image will be sent to the assigned email account through SMTP server. After sending the email successfully, the device will go back to deep sleep mode again.

Fig. 4 shows the programming flowchart of the proposed face recognition system. Firstly, the image captured by the ESP32-CAM must be downloaded from the email account before it can go through the face detection process. In face detection process, if the program detected a face, it would draw a rectangle around the face to mark it as a region of interest (ROI) so that the program can omit other unwanted parts to focus on features extraction. After extracting the facial features, the program will perform the face recognition process which uses the Neural Network as foundation. When the captured image matches the faces from dataset, the system will identify and verify the identity of the person being captured in the image. If the image does not match any of the faces from the dataset, it is an unknown face to the system and the program will terminate.

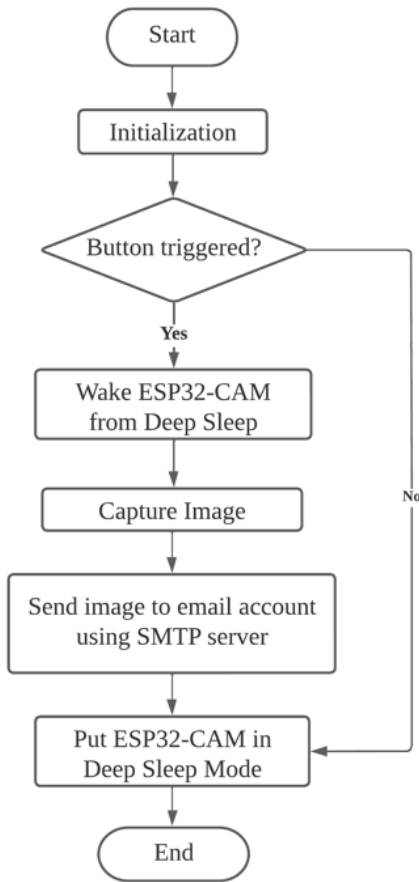


Fig. 4. ESP32-CAM Programming Flowchart.

Fig. 5 shows the circuit connection between ESP32-CAM, FTDI Adapter and an external push button. A jumper wire is connected from GPIO 0 to GND for programming purpose and can be removed once the programming is finished. The push button is used to wake the ESP32-CAM from deep sleep mode and it is connected to the GPIO 13 pin. The TX pin of ESP32-CAM is connected to the RX pin of the FTDI Programmer and the RX pin of ESP32-CAM is connected to the TX pin of the FTDI Programmer so that data can be exchanged between these two devices in serial communication.

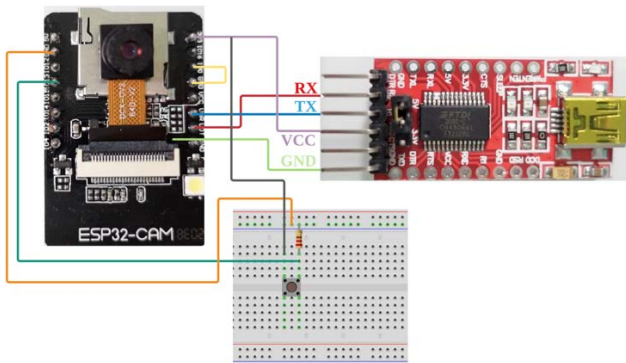


Fig. 5. Circuit Design.

IV. RESULTS AND DISCUSSION

A good face recognition system must fulfill several criteria; the most important is the accuracy of the result. Face recognition systems are widely used in law enforcement, a slightly inaccurate result might cause an innocent person being wanted and wrongly accused of crime that he or she did not commit. To test the functionality of a face recognition system, face datasets are used. There are many different face datasets available publicly such as LFW, Yale and AT&T databases. This system uses AT&T databases and a custom face dataset. This section explains the development of a face recognition system and the combination of the system with some hardware that will be discussed in the following section.

A. Hardware Implementation

The hardware device is configured so that when the external button is pressed, the ESP32-CAM will take a picture, connect to the internet and send the picture to an assigned email address. Fig. 6 shows the image taken by the ESP32-CAM being sent to the assigned email address.

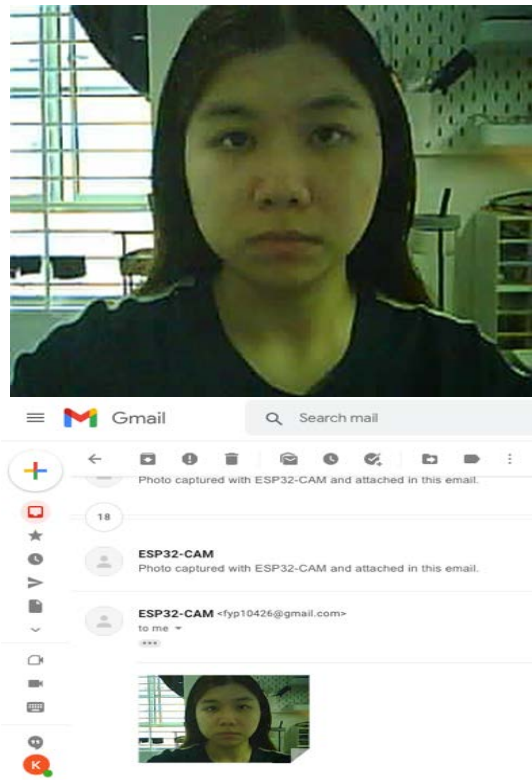


Fig. 6. Image Taken by the ESP32-CAM Sent to an Assigned Email Address.

B. Training Parameters for the Proposed System

The researcher carried out an experiment to find out the values of the parameters that will give the CNN model the best accuracy in face recognition. The parameters chosen are the kernel size, the number of filters for convolutional layers and the learning rate.

Fig. 7 shows the validation accuracy and average elapsed training time of the CNN model. For easier understanding, the four values of the x-axis from the graph will be referred as set

A, B, C and D in the following discussion. From the graph, it can be concluded that in general, the validation accuracy for learning rate of 0.03 is the lowest compared to other learning rates, except for set B because the learning rate that gives the lowest validation accuracy for set B is 0.001. Thus, learning rate of 0.03 is the first to be eliminated.

Next, the total time elapsed for training range between 4 minutes and 9 minutes. The CNN model that uses the shortest average training time is set A while the longest is set D. Set C has the second shortest average training time, and compared to set A, the validation accuracy of set C is higher in overall. The aim is to find the value that will give the highest accuracy without compromising the training speed, set C meets the requirements, and from all the learning rates in set C, 0.001 gives the highest accuracy, 90.48%. Therefore, the parameters that will be used for training the CNN model are, kernel size of 5x5, 32 filters on the first convolutional layer and 64 filters on the second convolutional layer and learning rate of 0.001.

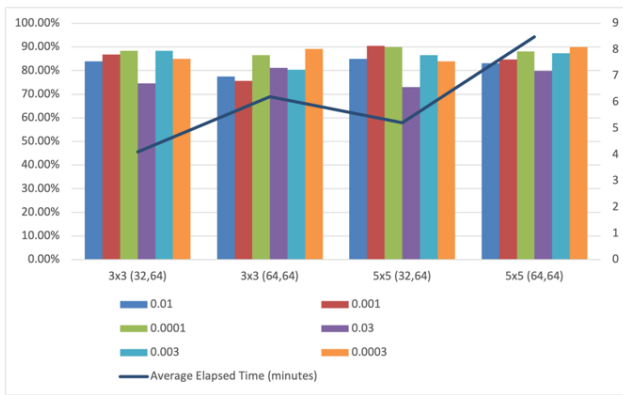


Fig. 7. Validation Accuracy and Average Training Time of the CNN Model with different Training Parameters.

TABLE I. LAYERS OF THE PROPOSED CNN MODEL

Layer	Type	Activations	Learnable
1	Input	112 x 92 x 1	-
2	Convolution	112 x 92 x 32	Weights 5 x 5 x 1 x 32 Bias 1 x 1 x 32
3	Batch Normalization	112 x 92 x 32	Offset 1 x 1 x 32 Scale 1 x 1 x 32
4	ReLU	112 x 92 x 32	-
5	Max Pooling	56 x 46 x 32	-
6	Convolution	56 x 46 x 64	Weights 5 x 5 x 32 x 64 Bias 1 x 1 x 64
7	Batch Normalization	56 x 46 x 64	Offset 1 x 1 x 64 Scale 1 x 1 x 64
8	ReLU	56 x 46 x 64	-
9	Max Pooling	28 x 23 x 64	-
10	Fully Connected	1 x 1 x 57	Weights 57 x 41216 Bias 57 x 1
11	Softmax	1 x 1 x 57	-
12	Classification Output	1 x 1 x 57	-

Table I shows the CNN structure made up of 12 layers, which are the input layers, two convolutional layers, two batch normalization layers, two ReLU layers, two pooling layers, a fully connected layer, a Softmax layer and an output layer.

C. Software Implementation

Face detection is the first task to be done by a face recognition system after getting the input image. The proposed system uses the built-in cascade object detector for face detection. This detector uses Viola-Jones algorithm and it can be called by the vision.CascadeObjectDetector function. By default, the classification model of this function detects upright face that is facing forward, the classifiers used in this model are the weak classifiers based on classification and regression tree analysis (CART). There is another classification model that detects the same object but with classifiers which use local binary patterns (LBP) for facial features encoding. The difference between CART and LBP based classifiers is, the classification model that uses CART has the ability to model higher-order dependencies between facial features while the classification model that uses LBP is more robust to variation in illumination. There are others classification models to detect upper body, eyes, mouth and nose. Since the proposed system focuses on the face area, therefore the default classification model is used.

Next, to test the accuracy of the proposed face recognition system, folders of testing images which are not seen by the trained model were created. Fig. 8 shows some of the face recognition outcomes of the proposed system. The results obtained for testing the proposed system with three different face databases are recorded in Table II to Table IV while the comparison of the results is shown in Table V.

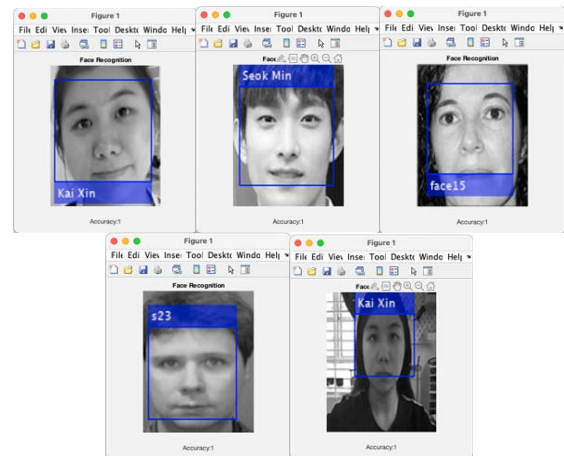


Fig. 8. Face Recognition Outcomes of the Proposed System.

The results of the proposed system are classified into three groups, the true positive (TP), false negative (FN) and false positive (FP). The result is a TP when the predicted identity matches the actual identity. FP happens when the system predicted person A but the actual identity is person B, or in other words, the input image is the face of person B but the output result returns person A. Lastly, the FN result is caused by failure in detecting and recognising faces that are known by the system, that is, when the input image is person A which is known by the system, the proposed system failed to detect and

recognise the face of the person and return the face recognition result as “Unknown”.

The face recognition accuracy is calculated by the following formula.

$$Accuracy = \frac{TP+TN}{TP+TN+FP+FN} \quad (1)$$

There are two classes in the custom face dataset, Class 1 is made up of images of celebrity while Class 2 is made up of the images of one of the authors. From Table II, Class 1 is tested by 20 images and the accuracy is 100%. On the other hand, the proposed system is able to recognise 239 out of 250 testing images correctly from Class 2, the accuracy is 95.60%. There are four FN results, and these might be caused by the low image resolution as the images are taken by a 2-megapixel ESP32-CAM. The average accuracy of the proposed system when tested with custom face dataset is 95.93%.

The proposed software system is also tested with two different pre-curated face databases that are publicly available. Table III shows the face recognition result when the system is tested with the dataset from reference [23]. The dataset is made up of 16 classes and the proposed system is tested by four images of each class. There are 59 TP and 5 FN results, yielding an average accuracy of 92.19%. Lastly, Table IV shows the face recognition result of AT&T database with total of 40 classes. The proposed system was tested with two images of each class and successfully recognized 70 out of 80 images. The average accuracy is 87.50%.

TABLE II. FACE RECOGNITION RESULT OF CUSTOM FACE DATASET

Class	Testing Images	TP	FN	FP	Accuracy
1	20	20	0	0	100.00%
2	250	239	4	7	95.60%
Total		259	4	7	-
Average Accuracy					95.93%

TABLE III. FACE RECOGNITION RESULT OF DATASET FROM REFERENCE [23]

Class	Testing Images	TP	FN	FP	Accuracy
1	4	3	1	0	75.00%
2	4	4	0	0	100.00%
3	4	4	0	0	100.00%
4	4	4	0	0	100.00%
5	4	4	0	0	100.00%
6	4	4	0	0	100.00%
7	4	4	0	0	100.00%
8	4	4	0	0	100.00%
9	4	4	0	0	100.00%
10	4	4	0	0	100.00%
11	4	4	0	0	100.00%
12	4	4	0	0	100.00%
13	4	2	2	0	50.00%
14	4	2	2	0	50.00%
15	4	4	0	0	100.00%
16	4	4	0	0	100.00%
Total		59	5	0	-
Average Accuracy					92.19%

TABLE IV. FACE RECOGNITION RESULT OF AT&T DATABASE

Class	Testing Images	TP	FN	FP	Accuracy
1	2	2	0	0	100.00%
2	2	2	0	0	100.00%
3	2	1	1	0	50.00%
4	2	2	0	0	100.00%
5	2	2	0	0	100.00%
6	2	2	0	0	100.00%
7	2	2	0	0	100.00%
8	2	1	1	0	50.00%
9	2	2	0	0	100.00%
10	2	2	0	0	100.00%
11	2	2	0	0	100.00%
12	2	2	0	0	100.00%
13	2	2	0	0	100.00%
14	2	2	0	0	100.00%
15	2	2	0	0	100.00%
16	2	1	1	0	50.00%
17	2	2	0	0	100.00%
18	2	2	0	0	100.00%
19	2	1	1	0	50.00%
20	2	2	0	0	100.00%
21	2	2	0	0	100.00%
22	2	2	0	0	100.00%
23	2	2	0	0	100.00%
24	2	2	0	0	100.00%
25	2	2	0	0	100.00%
26	2	1	1	0	50.00%
27	2	2	0	0	100.00%
28	2	2	0	0	100.00%
29	2	2	0	0	100.00%
30	2	2	0	0	100.00%
31	2	1	1	0	50.00%
32	2	2	0	0	100.00%
33	2	2	0	0	100.00%
34	2	0	2	0	0.00%
35	2	1	1	0	50.00%
36	2	2	0	0	100.00%
37	2	1	1	0	50.00%
38	2	2	0	0	100.00%
39	2	2	0	0	100.00%
40	2	2	0	0	100.00%
Total		70	10	0	-
Average Accuracy					87.50%

TABLE V. COMPARISON BETWEEN THE FACE RECOGNITION ACCURACY OF DIFFERENT FACE DATABASES

Face Database	Total Training Images	Total Testing Images	Accuracy
AT&T	320	80	87.50%
Dataset from reference [23]	244	64	92.19%
Custom face dataset	1250	250	95.93%

From Table V, the face recognition result for the images from the custom dataset is the highest, with the accuracy of 95.93%, while face recognition result using AT&T database is the lowest, with 87.50%. The accuracy of the face recognition for the custom face dataset is the highest because the two other face databases were trained with less than 20 images for a subject while the custom face dataset created by the researcher has 90 training images for the first class and 1160 for the second class. This is to ensure the result for images taken by the ESP32-CAM to have a higher accuracy. Therefore, with the face recognition result, it can be concluded that the goal is achieved. In short, the overall accuracy of the proposed system is 98.48%.

Furthermore, an experiment is carried out to find out the maximum distance between the camera and the face so that the face can be detected and recognised by the proposed system. The ESP32-CAM is placed at a certain distance from the face and five images are taken for each distance. The effect of distance between face and the ESP32-CAM on face detection rate and face recognition accuracy is recorded in Table VI. The results show that when the distance is beyond 200 cm, the face cannot be detected by the proposed system and the face recognition process cannot be carried out. This limitation could be overcome in future research by using a higher resolution camera module.

Table VII shows the accuracies of different face recognition systems that use custom face dataset. The proposed system is made up of hardware to capture the image of a kidnap suspect and software to identify the kidnap suspect, therefore a custom face dataset is created to test the functionality of the whole system. The accuracy of the proposed system is higher than the previous studies shown in Table VII.

TABLE VI. EFFECT OF DISTANCE BETWEEN THE FACE AND THE ESP32-CAM ON FACE DETECTION RATE AND FACE RECOGNITION ACCURACY

Distance (cm)	Testing Images	Images with detected face	Face detection success rate	Face recognition Accuracy
30	5	5	100.00%	100.00%
40	5	5	100.00%	100.00%
50	5	5	100.00%	100.00%
60	5	5	100.00%	100.00%
70	5	5	100.00%	100.00%
80	5	5	100.00%	100.00%
90	5	5	100.00%	100.00%
100	5	5	100.00%	100.00%
110	5	5	100.00%	100.00%
200	5	5	100.00%	100.00%
300	5	0	0%	0%

TABLE VII. ACCURACY OF FACE RECOGNITION SYSTEMS WITH CUSTOM FACE DATASET

Method	Accuracy
Eigenface [3]	85.00%
BPANN [6]	82.00%
ENN, Curvelet transform, HSI Colour Space [7]	94.00%
Deep learning [13]	95.02%
Deep CNN [14]	81.25% (Frontal view) 75.00% (Side view) 43.75% (Downwards) view)
CNN [15]	87.00%
Proposed method	95.93%

V. CONCLUSION

This article presents the development and implementation of face recognition system using neural networks. The proposed system is made up of a hardware that can capture a picture and send it to an assigned email; and a software built in MATLAB for face recognition process. The findings of this research suggested that the best training parameters for the proposed system are kernel size of 5x5, number of filters of 32 for first convolutional layer, number of filters of 64 for second convolutional layer and initial learning rate of 0.001. The proposed system is robust as its overall face recognition accuracy is 98.48%. The limitation of the system is when the distance between face and ESP32-CAM is beyond 200 cm, face detection and recognition process cannot be carried out. The recommendations for future research include, using a higher resolution camera module, larger custom face dataset and hybrid approach of face recognition techniques that can increase the face recognition accuracy of the system.

ACKNOWLEDGMENT

The authors would like to thank Centre for Research and Innovation Management (CRIM) for the support given to this research by Universiti Teknikal Malaysia Melaka (UTeM). We thank also those who contributed in any other forms for providing their continuous support throughout this work.

REFERENCES

- [1] M. S. B. Maind and M. P. Wankar, "Research Paper on Basic of Artificial Neural Network", IJRITCC, vol. 2, no. 1, pp. 96-100, Jan. 2014.
- [2] M. Sharif, F. Naz, M. Yasmin, M. A. Shahid and A. Rehman, "Face Recognition: A Survey", Journal of Engineering Science and Technology Review, vol. 10, no. 2, p.p 166-177, 2017.
- [3] Y. Kortli, M. Jridi, A. Al Falou, M. Atri, "Face Recognition Systems: A Survey", Sensors, vol. 20, no. 2, p.p 342, 2020.
- [4] R. Rosnelly, M. S. Simanjuntak, A. Clinton Sitepu, M. Azhari, S. Kosasi, and Husen, "Face Recognition Using Eigenface Algorithm on Laptop Camera," in 2020 8th International Conference on Cyber and IT Service Management, CITSM 2020, 2020, pp. 1-4.
- [5] T. Mantoro, M. Ayu, Suhendi, "Multi-Faces Recognition Process Using Haar Cascades and Eigenface Methods", 2018 6th International Conference on Multimedia Computing and Systems (ICMCS), pp. 1-5.
- [6] T. H. Le, "Applying Artificial Neural Networks for Face Recognition", Advances in Artificial Neural Systems, vol. 2011, Article ID 673016, 16 pages, 2011. <https://doi.org/10.1155/2011/673016>.
- [7] M. M. Hussein, A. H. Mutlag, H. Shareef, "Developed artificial neural network based human face recognition", Indonesian Journal of Electrical Engineering and Computer Science, vol. 16, no. 3, pp 1279-1285, 2019.

- [8] A. S. Abdullah, M. A. Abed, I. Al_Barazanchi, "Improving face recognition by elman neural network using curvelet transform and HSI color space", *Periodicals of Engineering and Natural Sciences*, vol. 7, no. 2, pp 430-437, 2019.
- [9] S. A. Baker, H. H. Mohammed, H.A. Aldabagh, "Improving face recognition by artificial neural network using principal component analysis", *TELKOMNIKA Telecommunication, Computing, Electronic and Control*, vol. 18, no. 6, pp 3357-3364, 2020.
- [10] K.B Pranav, J. Manikandan, "Design and Evaluation of a Real-Time Face Recognition System using Convolutional Neural Networks", *Procedia Computer Science*, vol. 171, pp 1651-1659, 2020.
- [11] M. Z. Khan, S. Harous, S. U. Hassan, M. U. Ghani Khan, R. Iqbal, and S. Mumtaz, "Deep Unified Model for Face Recognition Based on Convolution Neural Network and Edge Computing," *IEEE Access*, vol. 7, pp. 72622–72633, 2019.
- [12] Fedorchenko, I., Oliinyk, A., Stepanenko, A., Zaiko, T., Korniienko, S., Burtsev, N. "Development of a genetic algorithm for placing power supply sources in a distributed electric network". *European Journal of Enterprise Technologies*, issue 5/101, 6–16 (2019), doi: 10.15587/1729-4061.2019.180897.
- [13] U. Aiman, V. Vishwakarma, "Face recognition using modified deep learning neural network", 2017 8th International Conference on Computing, Communication and Networking Technologies (ICCCNT), pp. 1-5.
- [14] Fedorchenko, I., Oliinyk, A., Stepanenko, A., Svyrydenko, A., Goncharenko, D. "Genetic method of image processing for motor vehicle recognition". 2019 2nd International Workshop on Computer Modeling and Intelligent Systems, CMIS, 2019, Zaporizhzhia, April 15-19, CEUR Workshop Proceedings, Vol. 2353, pp. 211-226.
- [15] S. AbdELminaam D, Almansori AM, Taha M, Badr E, "A deep facial recognition system using computational intelligent algorithms", *PLoS ONE*, vol. 15, no. 12, pp. 1-27, 2020.
- [16] Oliinyk, A., Fedorchenko, I., Stepanenko, A., Katschan, A., Fedorchenko, Y., Kharchenko, A., Goncharenko, D. "Development of genetic methods for predicting the incidence of volumes of emissions of pollutants in air". 2019 2nd International Workshop on Informatics and Data-Driven Medicine, IDDM, CEUR Workshop Proceedings, 2019, Vol.2488, pp. 340–353.
- [17] M. Arsenovic, S. Sladojevic, A. Anderla, S. Darko, "FaceTime—Deep learning-based face recognition attendance system," 2017 IEEE 15th International Symposium on Intelligent Systems and Informatics (SISY), 2017, pp. 53-58, doi: 10.1109/SISY.2017.8080587.
- [18] Nurkhamid, P. Setialana, H. Jati, R. Wardani, Y. Indrihapsari, N. Norwawi, "Intelligent Attendance System with Face Recognition using the Deep Convolutional Neural Network Method", *Journal of Physics: Conference Series*, 1737, 012031, 2021.
- [19] I. G. S. M. Diyasa, A. Fauzi, M. Idhom and A. Setiawan, "Multi-face Recognition for the Detection of Prisoners in Jail using a Modified Cascade Classifier and CNN", 2020 2nd International Conference on Science & Technology, 1884, 012005, 2021, doi:10.1088/1742-6596/1844/1/012005.
- [20] Oliinyk, A., Fedorchenko, I., Stepanenko, .Rud M., Goncharenko, D. Implementation of evolutionary methods of solving the travelling salesman problem in a robotic warehouse // *Lecture Notes on Data Engineering and Communications Technologies*, 2021, 48, P. 263–292.
- [21] P. Kamenecay, M. Benco, T. Mizdos, R. Radil, "A New Method for Face Recognition using Convolutional Neural Network", *Advances in Electrical and Electronic Engineering*, vol. 15, no. 4, pp. 663.672, 2017, DOI: 10.15598/aeee.v15i4.2389.
- [22] Fedorchenko, I., Oliinyk, A., Stepanenko, Zaiko, T., Korniienko S., Kharchenko, A. Construction of a genetic method to forecast the population health indicators based on neural network models // *Eastern-European Journal of Enterprise Technologies*, 2020, 1 (4-103), P. 52–63. DOI: 10.15587/1729-4061.2020.197319.
- [23] M. Alghaili, Z. Li, H. Ali, "FaceFilter: Face Identification with Deep Learning and Filter Algorithm", *Hindawi Scientific Programming*, 7846264, pp. 1-9, 2020, doi.org/10.1155/2020/7846264.
- [24] N. S. Irjanto and N. Surantha, "Home Security System with Face Recognition based on Convolutional Neural Network", *International Journal of Advanced Computer Science and Applications*, vol. 11, no. 11, p.p 408-412, 2020.
- [25] M. Srivasan and N. Ravichandran, "A new technique for Face Recognition using 2D-Gabor Wavelet Transform with 2D-Hidden Markov Model approach", *International Conference on Signal Processing, Image Processing and Pattern Recognition 2013, ICSIPR 2013*, vol. 1, p.p 151-156.
- [26] J. Bobulski, "Multimodal face recognition method with two-dimensional hidden Markov model", *Bulletin of the Polish Academy of Sciences Technical Sciences*, vol. 65, no. 1, p.p 121-128, 2017.
- [27] J. Moreano and N. Palomino, "Global Facial Recognition Using Gabor Wavelet, Support Vector Machines and 3D Face Models", *Journal of Advances in Information Technology*, vol. 11, no. 3, p.p 143-148, 2020.
- [28] Z. Rustam and R. Faradina, "Face Recognition to Identify Look-Alike Faces using Support Vector Machine", *Journal of Physics: Conference Series*, vol. 1108, 012071, 2018.
- [29] F. Hashmi (2021), Face recognition using deep learning CNN in python [Online]. Available: <https://thinkingneuron.com/face-recognition-using-deep-learning-cnn-in-python/>. [Accessed: 11-Dec-2021].

Sparse Feature Aware Noise Removal Technique for Brain Multiple Sclerosis Lesions using Magnetic Resonance Imaging

Swetha M D¹

Department of Information Science and Engineering
B.M.S College of Engineering, Bangalore, India

Aditya C R²

Department of Computer Science and Engineering
Vidyavardhaka College of Engineering, Mysore, India

Abstract—Medical Resonance Imaging (MRI) is non-radioactive-based medical imaging that provides a super-resolution of tissues. However, because of its complex nature using existing Deep Learning-based noise removal (i.e., Denoising) techniques, the reconstruction quality is poor and time-consuming. An extensive study shows very limited work has been done on Brain Multiple Sclerosis (MS) Lesions MRI. Designing an efficient noise removal technique will aid in improving MRI quality; thereby will aid in achieving better segmentation classification performance. In reducing computing time and enhancing image quality (i.e. reduce noise) this paper presents the Sparse Feature Aware Noise Removal (SFANR) technique for Brain MRI using Convolution Neural Network (CNN) architecture. A sparse-aware feature is incorporated into the patch-wise morphology learning model for removing noise in large-scale MRI MS lesion datasets. Experimental results demonstrated that our model SFANR outperforms all other state-of-art noise removal techniques in terms of Peak-Signal-Noise-Ratio (PSNR), Structural Similarity Index Metric (SSIM) with less running time.

Keywords—Convolution neural networks; deep learning; denoising; magnetic resonance imaging; morphology learning; multiple sclerosis; sparse features

I. INTRODUCTION

With the advancement in sensor and computer technologies, medical imaging such as MRI, Positron Emission Tomography (PET), and Computed Tomography (CT) plays a very significant part in diverse diagnostic applications such as treating a serious ailment, radiosurgery, clinical diagnosis [1]. This MRI is used to obtain detailed information on soft tissues, and CT is used to obtain information on implants and bones. This work focuses on Multiple Sclerosis (MS) Lesion brain MRI data. Generally, the multi-contrast MRI provides the radiologists with additional information for studying different pathologies. In [1] demonstrated that for reducing time and redundancy, multi-echo saturation recovery MRI sequences are obtained at different inversion times and echo times to reconstruct a single MRI sequence [1]. Further, different parameter-map (PM) and parameter weighted (PW) contrasts can altogether be reconstructed. The state-of-art reconstruction methodologies employ pixel-wise least-square fitting of motion of macroscopic nuclear magnetization equation for obtaining relaxation parameter (i.e., by summing up all nuclear magnetic moment). Later, the PW contrasts are reconstructed through

PMs. However, due to patient motion, over-simplified models, non-linear fitting operations, flow, and partial volume significantly impact the quality of MS lesion brain MRI reconstruction [2]. In particular, the T2-FLAIR (T2-weighted fluid-attenuated inversion recovery) MS lesion brain MRI, low SNR (Signal-to-Noise-Ratio), chemical shift artifacts, and edge-enhancement are seen [3].

The CNNs-based model has attained very good results in medical imaging, especially for CT and MRI. In improving the quality of the image cross-modality between MR/PET [4], [5] and MR/CT [6] has been emphasized. Further, CNN is applied for MRI contrast enhancement. In [7], [8] contrast of T2-weighted MRI is improved using T2-weighted MRI, similarly, in [9] using T1-weighted and T2-weighted the FLAIR MRI is generated, and in [10] using 3T inputs construct 7T high-resolution MRI. All the above-mentioned methods use an encoder-decoder framework using Deep learning Techniques such as ResNets [11] and U-net [12].

In [13] for representing neighborhood features introduced localized network. In [14] the author enhances the texture of the image employed generative adversarial network (GAN). Further, in increasing the sharpness the author in [8] introduced an edge similarity loss function into the generative adversarial network. In [15] reduced the scanning time by combining contrast and under-sampling reconstruction. Additionally, [16] introduce feature structure to resolve unknown contrast problem during image reconstruction [17]. In [18] presented a new noise removal technique through multi-task deep GAN; However, poor correlation among different layers impacts the quality of the feature constructed. In addressing [1] designed an ensemble convolution neural network [19] to obtain high-quality feature sets [20], [21]. However, weights of a convolutional network [22] are updated individually for the entire MRI information; thus, the final reconstructed image exhibit higher noise, poor contrast, and limited sparse feature representation. In [23] addressed the above issues by employing morphology-based [24] feature construction using CNN. The model is efficient in eliminating noise with very good reconstruction quality; however, there exist optimization constraints in obtaining good quality sparse features.

In addressing the research problem, this paper presents sparse feature-aware noise removal technique for MS lesion MRI data. The patch-wise CNN framework can extract features in a parallel manner aiding in reducing training overheads.

Further, the SFANR model can remove different types of noise such as Rician, Gaussian, and Speckle more efficiently through the adoption of the morphological-based feature construction mechanism adopted in SFANR. The proposed noise removal technique helps in reducing redundant features and computation overheads; thus, significantly SFANR improves PSNR and SSIM.

The significance of SFANR is described below:

- The work presented a CNN-based noise removal technique using sparsity-aware morphological features.
- No prior work has considered denoising the brain MS lesions MRI.
- The SFANR achieves much higher PSNR and SSIM in comparison with existing denoising methodologies.
- The model achieves very less running time in comparison with other noise removal methodologies.

The rest of the manuscript is arranged as described. In Section II, the literature survey is discussed. In Section III, the proposed sparse feature aware noise removal technique for MS lesion Brain MRI is presented. In Section IV, the outcome i.e., MS lesion brain MRI reconstruction quality achieved using proposed SFANR and existing noise removal models is studied. In Section V, the significance of SFANR is concluded and future enhancement of the SFANR model is given.

II. LITERATURE SURVEY

This section presents a survey of various noise removal techniques presented in recent times for brain MS lesions MRI. In [1], the author presented a fully-connected CNN-based denoising method by optimizing the loss layer. The three-dimensional CNN and residual network are merged for extracting multi-dimensional features. Finally, ensemble feature extraction along two models constructed by varying noise levels. The model is efficient in eliminating Gaussian-like noise.

In [17], the author designed a deep learning model through multi-task learning for extracting association among spatial and relaxation features. The model utilizes association mapping among different T2-weighted MRI with varying contrast for enhancing the reconstruction quality such as low SNR (Signal-to-Noise-Ratio), chemical shift artifacts, and edge-enhancement are seen [3] as shown in Fig. 1. Similarly, [18] designed a denoising model using GAN by extracting features from Multi-Contrast MRI.

In [20], the author designed a denoising method using end-to-end residual CNN. The image is reconstructed using a loss function employing mean square error to optimize the feature extraction process. In [21] an autonomous CNN-based model has been employed for removing noise in Diffusion tensor MRI data. The model denoising accuracies are not dependent on high SNR MRI input. Similarly, [22] presented a new noise removal technique that works with a single-subject dataset encompassing with low-noise of voxel-by-voxel Diffusion tensor MRI sequence by employing one-dimensional CNN and deep learning models.

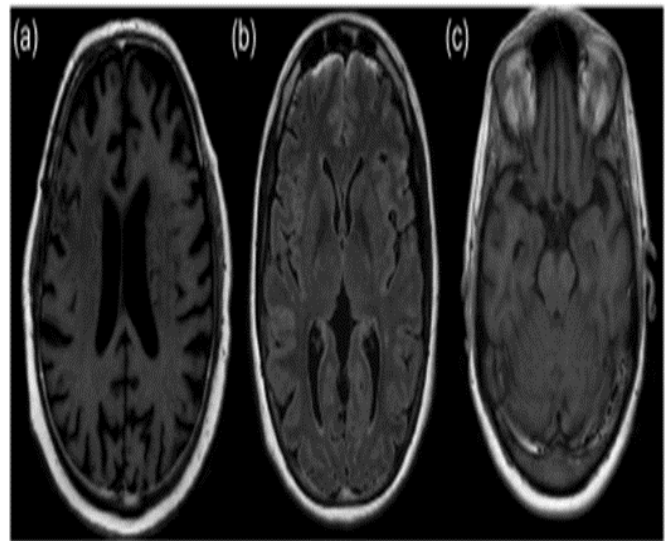


Fig. 1. Low-quality Reconstruction Outcome Obtained using Standard Noise Removal Technique (a): T1-FLAIR (b): T2-FLAIR (c): T1-weighted [1].

In [23] a denoising model is presented to remove Rician noise from MRI using a sparse dictionary learning mechanism. The dictionary is constructed leveraging Maximum posterior combined using noisy MRI. Similarly, [24] used morphological features to address the impact of noise due to non-uniform illumination. Further, employed principal component analysis retains detailed features such as textures, smooth edges, etc. during RGB to grey conversion. The extracted features are trained using CNN. However, poor feature correlation during training significantly impacts noise removal accuracies.

An extensive survey shows exploiting sparse features and morphology construction, and CNN aided in improving noise removal performance; however, existing models are not efficient in adaptively removing different noises such as speckle, Rician, and Gaussian. In addressing the limitation in the next section, a novel methodology namely the sparse feature aware noise removal technique has been presented.

III. PROPOSED METHODOLOGY

The proposed methodology for efficiently removing noise from brain MS lesions MRI is given. The proposed methodology employs a convolution neural network for eliminating noise in brain MS lesions MRI. A sparse feature-aware noise removal technique using CNNs improve the quality of MS lesion MRI data. The proposed methodology is composed of three stages morphology construction stage, aggregating sparsity-aware features into the patch-wise morphology stage, and validating the quality of image reconstructed image. First, in the morphological construction stage, a different sparsity feature-aware layer is created by subdividing the input MRI (i.e., each MRI is segmented into multiple patches; then, those patches are given as input to the SFANR-CNN model). The outcome i.e., sparse feature weight variance among different layers is used during the training process for the construction of morphology structure. In the subsequent stage, the sparsity-aware feature is used for the creation of morphology, and the information is trained with CNN and later used during the testing stage for removing noise

from MS lesion MRI data; thus, aiding in improving the quality of reconstructed MS lesion MRI images. In our work, the quality of noise removal technique is validated using Peak-Signal-to-Noise-Ratio (PSNR) and Structural Similarity Index Metric (SSIM). A significant amount of work has been done for removing noise in MRI datasets. Nonetheless, the standard noise removal methodologies exhibit poor performance due to issues like large dataset size, time consumption, high slew rate, large power absorption, and temporal dimension. The aforementioned issues are addressed through the construction of sparsity feature-aware CNN architecture using patch-wise morphological learning for designing an effective noise removal model with good processing efficiency.

A. Convolution Neural Network

The CNN is widely used for removing noise from MRI and CT [19], [20]. The CNN-based noise removal techniques [21], [22], provide an effective way of eliminating a different kind of noise [23] from MRI and improving its reconstruction quality [24], [25], and enhancing segmentation [26], [27] and classification outcomes as well [28], [29]. The CNN employs a hierarchical learning mechanism where a feed-forward network is used for the extraction of different features and a hidden layer is used to optimize the feature learning weights. However, in this work sparsity-aware feature using CNN is modeled as shown in Fig. 2 shows removing noise from brain MS lesion MRI data. The proposed SFANR-CNN adopts a patch-wise morphological learning mechanism using prior information; thus, is very fast and efficient in removing a different kind of noise present in brain MS lesion MRI.

B. Noise Removal Framework

This section presents a framework for removing noise from brain MS lesion MRI as shown in Fig. 2. Initially, the brain MS lesion MRIs are segmented into different patches. Later, the segmented brain MS lesion MRI is given as input to SFANR-CNN for extraction of sparsity-aware features. The sparsity-aware feature weights are optimized during the training process for the construction of morphology. Later, during the testing process, the constructed morphology is used for removing noise from brain MS lesion MRI. The quality of reconstructed brain MS lesion MRI using SFANR-CNN is measured in terms of PSNR and SSIM.

C. Patch-wise Learning Model

Patch-wise morphological learning technique is presented for eliminating noise from MS lesion MRI data. Let noise k be aggregated to the input brain MS lesion MRI patch signal i ,

$$\mathbb{Y} = i + k, \quad (1)$$

where the value of parameter k is generally set in the range of 8 and 12. Here, the patch-wise noise removal method is established considering the patch size of $m \times m$. The noise in MS lesion MRI data is individually removed from all the patches, and later MRI is reconstructed through the integration of entire patches within a frame; later, using the averaging function, the overlapped patches are optimized. In this work, the size of Morphology \mathbb{D} is set to $m^2 \times n$ where n is greater than m^2 .

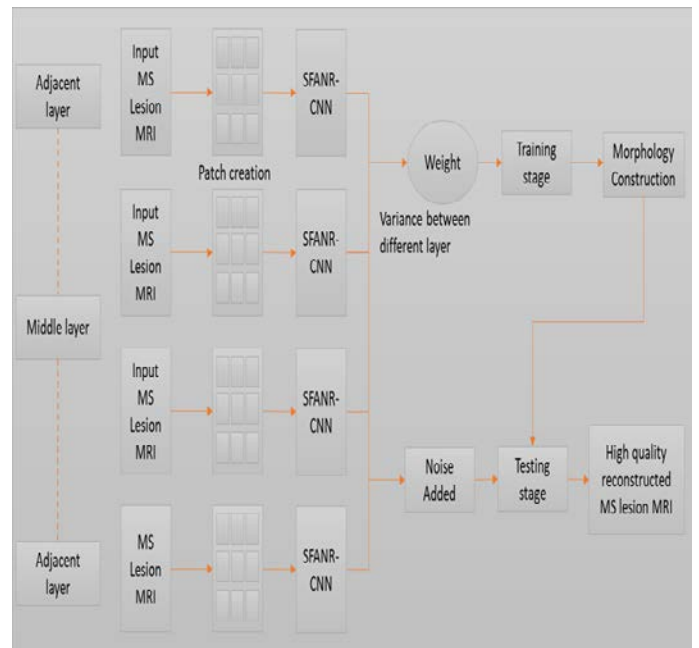


Fig. 2. Architecture of Sparse Feature aware Noise Removal (SFANR) Technique.

D. Sparse Feature Aware Patch-wise Learning Model

In a patch-wise morphology construction-based noise removal mechanism the atomic element [28] is used as the basis function. A sparsity-aware linear noise removal mechanism is used to remove the noise within entire patches constructed from brain MS lesion MRI data. The additive white Gaussian noise error is minimized through the following mathematical representation.

$$\min \|\alpha\|_0 \text{ s.t. } \|\mathbb{D}_\alpha - \mathbb{Y}\|_2 \leq \epsilon, \quad (2)$$

where \mathbb{Y} represents brain MS lesion MRI patch with the presence of noise, l_0 defines a pseudo normalization parameter that is used for estimating $\|\cdot\|_0$, and ϵ defines pre-defined. Using l_0 the sparsity-aware feature can be optimized at the cost of convex normalization problem. The parameter ϵ is optimized for approximating the normalization error $\|\mathbb{D}_\alpha - \mathbb{Y}\|_2$ through its variance. Then, using a sliding window the quality of denoised brain MS lesion MRI can be enhanced; similarly, the optimization of overlapping patches is done by employing averaging function as defined.

$$\mathbb{D} \leftarrow \eta \Delta \frac{\Delta \|i - \mathbb{D}_\alpha\|_2}{\Delta \mathbb{D}}, \quad (3)$$

where η defines a parameter of the sliding window. Using the below equation the minimization of overlapping patches is done.

$$\min \|i - \mathbb{D}_\alpha\|_2 \text{ s.t. } -1 \leq \alpha \leq 1, \quad (4)$$

Here, we evaluate the pixel mean of different patch sizes of $m \times k$, where m and k are hyper-parameters and \bar{i} denotes local mean estimates for an image.

$$\bar{i} = \mathbb{F}\{i\} = \mathbb{F}\{\mathbb{Y} - k\} = \mathbb{F}\{\mathbb{Y}\} - \mathbb{F}\{k\} = \mathbb{F}\{\mathbb{Y}\} = \bar{\mathbb{Y}}, \quad (5)$$

where \mathbb{F} is function to obtain pixel mean $\bar{\mathbb{Y}}$. We estimate that the actual input image is corrupted using Rician, Speckle, and Additive White Gaussian noise and which can be described using equation (6).

$$\log q(\mathbb{Y}|i) = \frac{1}{2\sigma^2} \sum_{r,n} (\mathbb{Y}_{r,n} - i_{r,n})^2, \quad (6)$$

Here, the indexes r and n represent all positions of an MS lesion MRI data.

$$\min_{\beta} \mathcal{P} = \mathbb{F} \left\{ \left(i - \bar{i} - \beta(\mathbb{Y} - \bar{i}) \right) \right\}, \quad (7)$$

where β is a decision factor that defines if β is close to 1 then the MS lesion MRI data will be noisy type \mathbb{Y} and if β is near to 0 then it is the de-noised image \bar{i} . Equation (7) demonstrates the minimization of squared error.

Patch-wise morphology learning is constructed encompassing distinctive sparse-aware features for both noiseless and noisy brain MS lesion MRI datasets. The patch-wise morphology learning methodology is very efficient in solving the complexity of optimization of sparsity feature construction; thus, improving brain MS lesion MRI reconstruction outcomes. The morphology construction is extremely fast which takes about 20% time and remaining time it takes for training the model for removing noise from brain MS lesion MRI. No heuristic knowledge is required for the construction of morphology; thus, one can learn sparse feature-based morphologies more adaptively. The constructed morphology is later used during the testing process to obtain a very good denoised brain MS lesion MRI.

E. Training Patch-wise Learning Model for Removing Noise in MRI

Designing an efficient training model aid in detecting a different kind of noise and improves the brain MS lesion MRI reconstruction quality. However, the brain MS lesion MRI is extremely large and complex; thus, is time-consuming for performing the training process. In this work, the training time is reduced by adopting parallel execution of patch-wise morphology construction. The parameter selection for training is set as a random process where parameter estimation is carried out considering different patches and noise types. The small normalization vectors can be optimized easily where the regularization parameter is optimized using pre-training. Using CNN variance among different layers to optimize weight and morphology is constructed. The training efficiency for removing noise from brain MS lesion MRI is measured using PSNR and SSIM.

F. The Testing Patch-wise Learning Model for Removing Noise in MRI

In the testing for removing noise from brain MS lesion MRI in this work the noise is detected patch-wise. Further, in avoiding the over-fitting problem the patch-wide weight variance is minimized. The morphology constructed during the training stage is used during the testing process for reducing noise in brain MS lesion MRI.

$$\hat{i} = \bar{i} + \frac{(\mathbb{F}\{(\mathbb{Y}-\bar{\mathbb{Y}})^2\} - \sigma^2)(\mathbb{Y}-\bar{i})}{\mathbb{F}\{(\mathbb{Y}-\bar{\mathbb{Y}})^2\}}, \quad (8)$$

where σ defines the level of noise present in brain MS lesion MRI and the Eq. (8) defines noise removed MS lesion dataset mathematical representation. The testing process encompasses the estimation of \bar{i} and $\mathbb{F}\{(\mathbb{Y}-\bar{\mathbb{Y}})^2\}$. The effectiveness of estimation of \bar{i} is enhanced through reduction of noise from brain MS lesion MRI using patch-wise morphology information with a patch size of $m \times k$. The model aids in minimizing sparse error and overhead reduction. The improved probability distribution function using logarithm for removing noise in brain MS lesion MRI is given as.

$$i^{(t+1)} = i^{(t)} + \eta \left[\sum_{r=1}^K N_r^- * \psi_r(N_r^- * i^{(t)}) + \frac{\lambda}{\sigma^2} (\mathbb{Y} - i^{(t)}) \right] \quad (9)$$

where η defines step size estimation, convolution is defined by $*$ sign, and N_r^- describes the central pixel. To bring trade-off among likelihood and prior λ is used. The outcome of λ depends according to the presence of noise level σ . The experiment conducted in the next section shows the proposed SFANR-CNN is effective in removing a different kind of noise and enhancing the quality of brain MS lesion MRI in terms of PSNR and SSIM.

IV. SIMULATION ANALYSIS AND RESULTS

This section studies the performance efficiency of the proposed SFANR technique and existing noise removal techniques [1], [17]. This work uses brain MS lesion MRI data used in [30] which is very similar to brain MRI used [1], [17]. In this work noise such as Speckle, Gaussian, and Rician is added to the brain MS lesion MRI. The performance of different noise removal techniques is measured in terms of PSNR and SSIM. The PSNR and SSIM are computed using the equation defined in [1]. The experiment is conducted on Windows 10 operating system running an I-5 quad-core processor with 16 GB RAM equipped with a dedicated 4GB CUDA GPU. Fig. 3 shows the input, MRI with noise, and reconstructed MS lesion brain MRI using the SFANR technique.

The graphical representation of PSNR is shown in Fig. 4. The graphical representation of SSIM is shown in Fig. 5. A higher value indicates better performance; thus, the SFANR achieves much better outcomes than existing methods, namely, a U-NET [1], Multi-Task Deep Learning (MTDL) [1], Deep Parallel Ensemble Denoising (DPED) [17]. Thus, are very efficient in removing Gaussian, Speckle, and Rician noise from MS lesion MRI.

The Table I shows the computation outcome achieved using proposed SFANR over existing noise removal methods such as DPED [1], Morphology learning CNN (ML-CNN) [24], and noise removal using dictionary learning (NRDL) [1]. The SFANR achieves much lesser running time than other existing methodologies; thus, are very efficient.

The Table II shows the SSIM and PSNR performance achieved using SFANR considering different noise. No prior work has considered such evaluation.

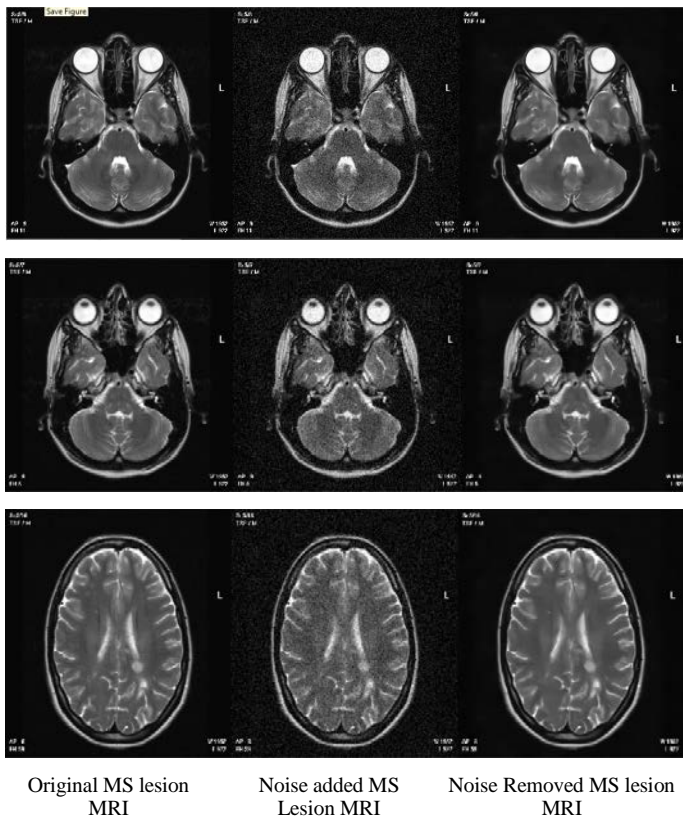


Fig. 3. The Outcome was achieved using the SFANR-CNN Model.

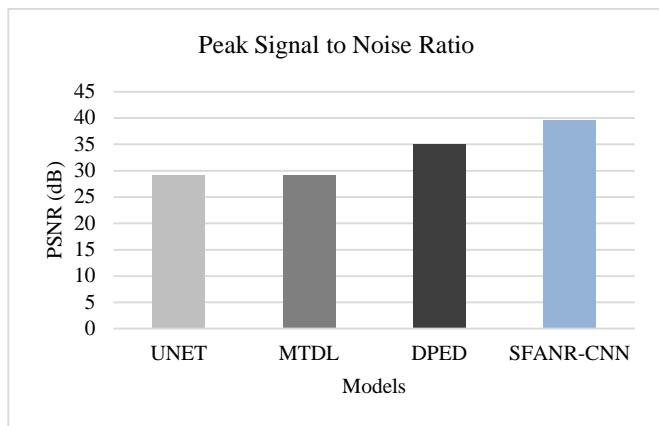


Fig. 4. PSNR achieved using SFANR-CNN and other Noise Removal Technique.

TABLE I. COMPUTATION TIME STUDY

Methodology	Running time (seconds)
NRDL [23], 2019	143.97
DPED [1] 2021	3.11
ML-CNN [24], 2022	11.3
SFANR	2.98

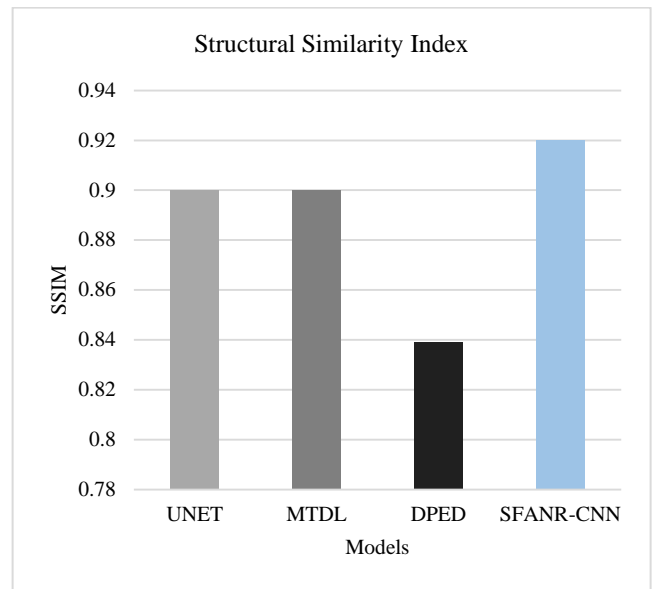


Fig. 5. SSIM achieved using SFANR-CNN and other Noise Removal Technique.

TABLE II. NOISE STUDY OF SFANR

Methodology	PSNR (dB)	SSIM
Speckle	37.34	0.901
Gaussian	39.63	0.925
Rician	38.54	0.903

The Table III shows comparative study of proposed SFANR with other methodologies. The table shows no prior work have worked on detecting and removing noise for brain MS lesion MRI. Then, each method is modeled to remove only one particular noise; however, SFANR are trained with multiple noise type such as Rician, Speckle, and Gaussian; thus, are adaptive to remove different noise.

TABLE III. COMPARATIVE ANALYSIS

Methodology	Method	Noise Type	Metrics	MS Lesion MRI
Jian et al., [23], 2019	Dictionary learning	Rician	SSIM, PSNR, & time	No
Aetesam et al., [1], 2021	Parallel Ensemble Denoising	Gaussian-Impulse	SSIM, PSNR, & running time	No
Wang et al., [17], 2020	Multi-task deep learning model	Gaussian	HFEN, SSIM, & PSNR	No
Bhutto et al., [24], 2022	Morphology learning and CNN	Background noise	SNR & time	No
SFANR	Sparse-morphology using CNN	Rician, Speckle, and Gaussian	SSIM, PSNR, running time	Yes

V. CONCLUSION

MRI is a widely used detection technique; however, image detection is a complex and time-consuming procedure as data is not clear because of its noisy nature. Therefore, we have implemented a sparsity-based noise removal technique using CNN architecture for the high-quality reconstruction of thermal and ultrasound images with improved time efficiency. In our model SFANR-CNN, we implemented a patch-wise morphology learning algorithm by producing morphology while training for efficient denoising for various types of noises. We have used various parameters to define the high quality of our reconstructed MS lesion MRI namely PSNR and SSIM. Experimental outcomes show that our model SFANR-CNN outperforms all other state-of-art-algorithms in terms of PSNR and SSIM. Our model produces high PSNR results of 39.63 dB which is much higher than any other algorithm. Similarly, SSIM outcomes are 0.92 using our model SFANR-CNN. Alongside, a running time of 2.98 seconds is attained for removing noise. These results demonstrate the superiority of our model SFANR-CNN.

Future work would consider evaluating performance by introducing a different kind of noise. Designing a better noise removal technique will aid in detecting and segmenting MS lesions more efficiently which in the future will be considered.

REFERENCES

- [1] Aetesam, Hazique & Maji, Suman. Noise dependent training for deep parallel ensemble denoising in magnetic resonance images. *Biomedical Signal Processing and Control*. 66. 102405, 10.1016/j.bspc.2020.102405, 2021.
- [2] Ryu K, Nam Y, Gho SM, Jang J, Lee HJ, Cha J, Baek HJ, Park J, Kim DH. Data-driven synthetic MRI FLAIR artifact correction via deep neural network. *J Magn Reson Imaging*. Vol. 50(5), p. 1413-1423. doi: 10.1002/jmri.26712., 2019.
- [3] Tanenbaum LN, Tsiouris AJ, Johnson AN, Naidich TP, DeLano MC, Melhem ER, Quarterman P, Parameswaran SX, Shankaranarayanan A, Goyen M, Field AS. Synthetic MRI for Clinical Neuroimaging: Results of the Magnetic Resonance Image Compilation (MAGiC) Prospective, Multicenter, Multireader Trial. *AJNR Am J Neuroradiol*. Vol. 38(6). pp. 1103-1110. doi: 10.3174/ajnr.A5227. Epub. PMID: 28450439; PMCID: PMC7960099, 2017.
- [4] Y. Pan, M. Liu, C. Lian, T. Zhou, Y. Xia, and D. Shen, "Synthesizing missing PET from MRI with cycle-consistent generative adversarial networks for Alzheimer's disease diagnosis," in *Proc. Int. Conf. Med. Image Comput. Comput.-Assist. Intervent. Granada, Spain: Springer*, pp. 455-463, 2019.
- [5] Andrew P. Leynes1, Jaewon Yang, Florian Wiesinger, Sandeep S. Kaushik, Dattesh D. Shanbhag, Youngho Seo1, Thomas A. Hope, Peder E. Z. Larson "Direct pseudoCT generation for pelvis PET/MRI attenuation correction using deep convolutional neural networks with multi-parametric MRI: Zero echo-time and dixon deep pseudoCT (ZeDD-CT)," *J. Nucl. Med.*, vol. 59, no. 5, pp. 852-858, 2019.
- [6] Maspero M, Savenije MHF, Dinkla AM, Seevinck PR, Intven MPW, Jurgeniemi-Schulz IM, Kerkmeijer LGW, van den Berg CAT. Dose evaluation of fast synthetic-CT generation using a generative adversarial network for general pelvis MR-only radiotherapy. *Phys Med Biol*. 2018 vol. 18; pp. 63, Art. no. 185001. doi: 10.1088/1361-6560/aada6d. PMID: 30109989, 2019.
- [7] S. U. Dar, M. Yurt, L. Karacan, A. Erdem, E. Erdem, and T. Cukur, "Image synthesis in multi-contrast MRI with conditional generative adversarial networks," *IEEE Trans. Med. Imag.*, vol. 38, no. 10, pp. 2375-2388, 2020.
- [8] B. Yu, L. Zhou, L. Wang, Y. Shi, J. Fripp, and P. Bourgeat, "Ea-GANs: Edge-aware generative adversarial networks for crossmodality MR image synthesis," *IEEE Trans. Med. Imag.*, vol. 38, no. 7, pp. 1750-1762, 2019.
- [9] T. Abe and N. Salamon, "A deep learning approach to synthesize flair image from T1WI and T2WI," in *Proc. 26th Annu. Meeting (ISMRM)*, Paris, France, p. 3130, 2018.
- [10] Dong Nie, Roger Trullo, Jun Lian, Li Wang, Caroline Petitjean, Su Ruan, Qian Wang, and Dinggang Shen, Medical Image Synthesis with Deep Convolutional Adversarial Networks [published correction appears in *IEEE Trans Biomed Eng*. 2020 Sep;67(9):2706]. *IEEE Trans Biomed Eng*. Vol. 65(12), pp. 2720-2730. doi:10.1109/TBME.2018.2814538, 2018.
- [11] Christian Ledig, Lucas Theis, Ferenc Huszar, Jose Caballero, Andrew Cunningham, Alejandro Acosta, Andrew Aitken, Alykhan Tejani, Johannes Totz, Zehan Wang, Wenzhe Shi "Photo-realistic single image super-resolution using a generative adversarial network," in *Proc. IEEE Conf. Comput. Vis. Pattern Recognit. (CVPR)*, vol. 2, no. 3, pp. 4, 2018.
- [12] O. Ronneberger, P. Fischer, and T. Brox, "U-net: Convolutional networks for biomedical image segmentation," in *Proc. Int. Conf. Med. Image Comput. Comput.-Assist. Intervent. Munich, Germany: Springer*, pp. 234-241, 2016.
- [13] H. Van Nguyen, K. Zhou, and R. Vemulapalli, "Cross-domain synthesis of medical images using efficient location-sensitive deep network," in *Proc. Int. Conf. Med. Image Comput. Comput.-Assist. Intervent. Munich, Germany: Springer*, pp. 677-684, 2016.
- [14] A. Sharma and G. Hamarneh, "Missing MRI pulse sequence synthesis using multi-modal generative adversarial network," arXiv:1904.12200. [Online]. Available: <http://arxiv.org/abs/1904.12200>, 2019.
- [15] Xiang, Lei & Chen, Yong & Chang, Weitang & Zhan, Yiqiang & Lin, Weili & Wang, Qian. Deep-Learning-Based Multi-Modal Fusion for Fast MR Reconstruction. *IEEE Transactions on Biomedical Engineering*. PP. 1-1. 10.1109/TBME.2018.2883958, 2019.
- [16] A. Chartsias, T. Joyce, M. V. Giuffrida, and S. A. Tsaftaris, "Multimodal MR synthesis via modality-invariant latent representation," *IEEE Trans. Med. Imag.*, vol. 37, no. 3, pp. 803-814, 2019.
- [17] Wang, Guanhua & Gong, Enhao & Banerjee, Suchandrima & Martin, Dann & Tong, Elizabeth & Choi, Jay & Chen, Huijun & Wintermark, Max & Pauly, John & Zaharchuk, Greg. Synthesize High-Quality Multi-Contrast Magnetic Resonance Imaging From Multi-Echo Acquisition Using Multi-Task Deep Generative Model. *IEEE Transactions on Medical Imaging*. PP. 1-1. 10.1109/TMI.2020.2987026, 2020.
- [18] Zhang, H.; Li, H.; Dillman, J.R.; Parikh, N.A.; He, L. Multi-Contrast MRI Image Synthesis Using Switchable Cycle-Consistent Generative Adversarial Networks. *Diagnostics*, 12, 816. <https://doi.org/10.3390/diagnostics12040816>, 2022.
- [19] Zuo, W., Zhang, K., Zhang, L. Convolutional Neural Networks for Image Denoising and Restoration. In: Bertalmio, M. (eds) Denoising of Photographic Images and Video. Advances in Computer Vision and Pattern Recognition. Springer, Cham. https://doi.org/10.1007/978-3-319-96029-6_4, 2018.
- [20] S. Gai and Z. Bao, "New image denoising algorithm via improved deep convolutional neural network with perceptive loss," *Expert Systems with Applications*, vol. 138, pp. 112815, 2019.
- [21] Qiyuan Tian, Ziyu Li, Qiuyun Fan, Jonathan R. Polimeni, Berkin Bilgic, David H. Salat, Susie Y. Huang, SDnDTI: Self-supervised deep learning-based denoising for diffusion tensor MRI, *NeuroImage*, Volume 253, 119033, ISSN 1053-8119, <https://doi.org/10.1016/j.neuroimage.2022.119033>, 2022.
- [22] Hu Cheng, Sophia Vinci-Booher, Jian Wang, Bradley Caron, Qiuting Wen, Sharlene Newman, Franco Pestilli., "Denoising diffusion weighted imaging data using convolutional neural networks" *bioRxiv* 2022.01.17.476708; doi: <https://doi.org/10.1101/2022.01.17.476708>, 2022.
- [23] Jian Lu, Jiapeng Tian, Lixin Shen, Qingtang Jiang, Xueying Zeng, Yuru Zou, "Rician Noise Removal via a Learned Dictionary", *Mathematical Problems in Engineering*, vol. 2019, Article ID 8535206, 13 pages. <https://doi.org/10.1155/2019/8535206>, 2019.
- [24] Bhutto, J.A.; Tian, L.; Du, Q.; Sun, Z.; Yu, L.; Tahir, M.F. CT and MRI Medical Image Fusion Using Noise-Removal and Contrast Enhancement

- Scheme with Convolutional Neural Network. Entropy 24, 393. <https://doi.org/10.3390/e24030393>, 2022.
- [25] Khalid, Noor & Ismail, Muhammad & Manaf, Muhammad & Fadzil, Ahmad & Ibrahim, Shafaf. MRI brain tumor segmentation: A forthright image processing approach. Bulletin of Electrical Engineering and Informatics. Vol. 9, No. 3. pp. 1024~1031. 10.11591/eei.v9i3.2063, 2020.
- [26] Pavana H R ,Swetha M D, "Predicting the Multiple Sclerosis Lesions of Brain Using Convolutional Neural Network", in International Journal of Innovative Research in Computer and Communication Engineering, Volume 8, Issue 7, 2020.
- [27] Swetha. M.D, Dhanush et.al,"A Survey on Identification of Multiple Sclerosis Lesions from Brain MRI",Published in 25 International Journal for Research in Applied Science Engineering Technology (IJRASET) with ISSN: 2321-9653,Pgs- 1386-89, Volume 8 Issue V 2020.
- [28] Hamiane, Madina & Saeed, Fatema. SVM Classification of MRI Brain Images for Computer-Assisted Diagnosis. International Journal of Electrical and Computer Engineering. 7. 10.11591/ijece.v7i5.pp2555-2564, 2017.
- [29] Saeed, Soobia & Abdullah, Afnizanfaizal. Recognition of brain cancer and cerebrospinal fluid due to the usage of different MRI image by utilizing support vector machine. Bulletin of Electrical Engineering and Informatics. 9. 10.11591/eei.v9i2.1869, 2020.
- [30] K. P. Constantinou, I. P. Constantinou, C. S. Pattichis and M. S. Pattichis, "Medical Image Analysis Using AM-FM Models and Methods," in IEEE Reviews in Biomedical Engineering, vol. 14, pp. 270-289, doi: 10.1109/RBME.2020.2967273, 2021.

Sentiment Analysis of Covid-19 Vaccination using Support Vector Machine in Indonesia

Majid Rahardi^{1*}, Afrig Aminuddin², Ferian Fauzi Abdulloh³, Rizky Adhi Nugroho⁴
Faculty of Computer Science, Universitas Amikom Yogyakarta, Yogyakarta, Indonesia

Abstract—Along with the development of the Covid-19 pandemic, many responses and news were shared through social media. The new Covid-19 vaccination promoted by the government has raised pros and cons from the public. Public resistance to covid-19 vaccination will lead to a higher fatality rate. This study carried out sentiment analysis about the Covid-19 vaccine using the Support Vector Machine (SVM). This research aims to study the public response to the acceptance of the vaccination program. The research result can be used to determine the direction of government policy. Data collection was taken via Twitter in the year 2021. The data then undergoes the preprocessing methods. Afterward, the data is processed using SVM classification. Finally, the result is evaluated by a confusion matrix. The experimental result shows that SVM produces 56.80% positive, 33.75% neutral, and 9.45% negative. The highest model accuracy was obtained by RBF kernel of 92%, linear and polynomial kernels obtained 90% accuracy, and sigmoid kernel obtained 89% accuracy.

Keywords—Covid-19; vaccination; support vector machine; twitter

I. INTRODUCTION

World Health Organization (WHO) announced that the Covid-19 virus has spread to countries since 2019. WHO officially set Covid-19 as a global pandemic on March 11, 2020 [1][2]. Various steps were taken to overcome this pandemic. One of them is the manufacture of vaccines. In Indonesia, President Joko Widodo inaugurated Perpres Nomor 99 Tahun 2020 About Vaccine Procurement and Vaccination Implementation In the Context of Combating the Corona Virus Pandemic Disease 2019 (Covid-19) [3].

The pros and cons of vaccination have attracted various groups to express opinions. Social media is a medium that is easy and fast to access. So, it is not uncommon for people to express their views on social media. According to APJII, around 51.5% of internet users in Indonesia use social media daily [4]. One of the social media that is often used in Indonesia is Twitter. Twitter has 152 million registered users worldwide and more than 500 million unregistered users per month[5].

The number of opinions and the ease of accessing social media allow researchers to research cyberspace. One of these studies is sentiment analysis. Sentiment analysis is a classification process to classify the text in the document into positive, negative, and neutral classes [6][7]. The results from sentiment analysis can be used for various purposes [8].

Based on that problem, this research will compare the sentiment analysis results regarding the Indonesian people's

point of view towards Covid-19 vaccination activities from Twitter. First, the data are taken from Twitter in Bahasa. Afterward, the data is preprocessed. Then, sentiment analysis is carried out using the Support Vector Machine.

II. LITERATURE REVIEW

A. Sentiment Analysis

The opinion is a point of view or attitude of humans to a situation, entity, and others. The statement of each individual has a subjective nature. So that it can provide different points of view [9]–[12]. Differences of opinion can then be investigated, giving rise to a generalization of the field of study in the form of sentiment analysis. Sentiment analysis is an area of study that studies opinions, sentiments, evaluations, judgments, attitudes, and emotions towards an entity such as an organization, event, person, and goods [13].

B. Preprocessing

Preprocessing is an activity that is carried out before further analysis of the data. In this process, entities and unnecessary information are removed. Preprocessing is done through several stages: cleaning, case folding, tokenizing, normalization, stopwords, and stemming[14]. Preprocessing aims to convert raw data into more structured data to be recognizable to the machine[15], [16].

C. TF-IDF

TF-IDF consists of two interrelated matrices, namely TF and IDF. TF or Term-Frequency is a matrix that counts the number of times a word appears in a document [17]. IDF or Inverse Document Frequency is a matrix that counts the frequency of a word that appears throughout the document [17]. The purpose of TF-IDF is to calculate the importance level of words in a document [18][19]. The equation in TF-IDF can be seen in (1).

$$TFIDF(t,d) = T(t,d) \times IDF(t) \quad (1)$$

t = the number of a term or word in the document.

d = the number of document.

D. Synthetic Minority Oversampling Technique

The total of each dataset class determines the level of validity and accuracy of a model. The quality of a good dataset can be obtained with consistency and good trustworthiness. The imbalanced class dataset can be overcome by using SMOTE [20]. This technique utilizes the concept of K-Nearest Neighbor, which then SMOTE plays a role in making synthetic data from minority classes [21]. A new minority sample is

*Corresponding Author.

created using this method by linear interpolation between two minority samples [22].

E. Support Vector Machine

Support Vector Machine is a method of machine learning used for data classification. This method is included in supervised learning. Therefore, labeling is required in the data [23][24]. Support Vector Machine works to separate data by finding the best hyperplane and margin maximum [25]. The hyperplane is a plane separator or differentiator between two classes, while the margin is the distance between the outermost samples of the class or which is called the Support Vector. The equation of Support Vector Machine can be seen in (2) [24].

$$w \cdot x - b = 0 \tag{2}$$

where w represents the weight vector, x denotes the input vector, and b indicates the bias.

F. Performance Evaluation Measure

Performance Evaluation Measure is a process for evaluating the performance or capability of a classification system or model [26]. Evaluations are displayed in a table with several entities called the confusion matrix. These entities include accuracy, precision, recall, and F1-Score.

Precision is the match value between the answers system and the user’s information. The recall is the value of the accuracy of the unit of data with a previously called up team of information. Accuracy results from a comparison between correct information by the whole information. F1-Score is the value obtained from the weighted average between precision and recall. The equation of performance evaluation measure can be seen in (3), (4), (5), and (6) [27]–[29].

$$Precision = \frac{TP}{TP+FP} \tag{3}$$

$$Recall = \frac{TP}{TP+FN} \tag{4}$$

$$Accuracy = \frac{TP+TN}{TP+TN+FP+FN} \tag{5}$$

$$F1\ Score = \frac{2(Precision)(Recall)}{(Precision+Recall)} \tag{6}$$

The table is known as the Confusion Matrix used to describe PEM. This table contains the results of the dataset test with the model that has been made in the prediction class and actual class. The table of Confusion Matrix can be seen in Table I [30].

True Positive indicates that the model previously predicted true proved true. True Negative suggests that the previous model was predicted wrong and proved wrong. False Positive shows that the previously predicted model true is proven false. False Negative indicates that the previously predicted model was proven wrong correct [27]–[29].

TABLE I. CONFUSION MATRIX

	Actual True	Actual False
True Predicted	True Positive (TP)	False Positive (FP)
False Predicted	False Negative (FN)	True Negative (TN)

III. METHODS

A. System Overview

The system takes data through Twitter in Bahasa Indonesia with a total of 2000 tweets and the timeline between October 19, 2021, and October 22, 2021. After that, the data is manually labeled after cleaning the tweet. Then, do the preprocessing to clean up data noise and simplify the classification process. After that, word weighting was done using the TF-IDF method and sentiment dataset class balancing using the SMOTE method. Then, divide the dataset into data training and data testing. Next, classification sentiment is done using the Support Vector Machine and Evaluating the value indicated through Confusion Matrix. The system of this sentiment analysis process can be seen in Fig. 1.

B. Data Collection and Cleaning

Data collection is done through Twitter using the Twitter API. Twitter API consists of Access Token, Access Token Secret, API Key, and API Key Secret. This process is written in Python using Tweepy library. Researchers use the keywords “vaksin” and “vaksinasi” as a reference for searching and used in a CSV file or Comma Separated Values. Results of the Crawling Tweets process can be seen in Table II.

The next process that needs to be done is cleaning to simplify the labeling process. Also, removes URLs, punctuation, and numeric, including in the cleaning process. In addition, eliminating mentions of users by @ and deleting duplicate tweets are included in the cleaning process. The results of the cleaning process can be seen in Table III.

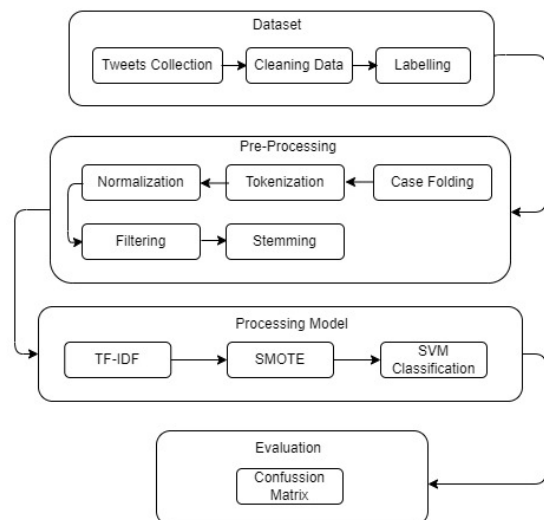


Fig. 1. System Overview of Sentiment Analysis.

TABLE II. RESULTS OF THE CRAWLING TWEETS

Date and Time	User	Tweet
2021-10-19 22:58:43	COVID PASTI BERLALU	Para pelajar menyampaikan rasa terima kasih atas program vaksinasi yang terus dilakukan oleh pemerintah. #AyoVaksin #KaltaraSuksesVaksinasi #VaksinasiPulihkanRI #IndonesiaSehat #IndonesiaHebat https://t.co/h5x41UO3tF

TABLE III. RESULTS OF THE CLEANING PROCESS

Tweet before Cleaning	Tweet After Cleaning
Para pelajar menyampaikan rasa terima kasih atas program vaksinasi yang terus dilakukan oleh pemerintah. #AyoVaksin #KaltaraSuksesVaksinasi #VaksinasiPilihkanRI #IndonesiaSehat #IndonesiaHebat https://t.co/h5x41UO3tF	Para pelajar menyampaikan rasa terima kasih atas program vaksinasi massal yang terus dilakukan oleh pemerintah

C. Data Labelling

The labeling process needs to be done before the sentiment analysis process. This process is done manually conducted by researchers with several parameters. The parameter used is the positive sentiment with the number two symbol, a neutral sentiment with the number symbol one, and negative sentiment with zero. Results of the labeling process can be seen in Table IV.

TABLE IV. RESULTS OF THE LABELLING PROCESS

Tweet after Cleaning	Label
Para pelajar menyampaikan rasa terima kasih atas program vaksinasi massal yang terus dilakukan oleh pemerintah	2

D. Data Preprocessing

This stage is one of the most important carried out in sentiment analysis. At this stage, data is cleaned of noise to form the data according to the standard. This process makes it easier for the system to recognize and analyze a word.

1) *Case Folding*: This process is changing each letter in the sentence to lowercase. The result of Case Folding process can be seen in Table V.

TABLE V. RESULTS OF CASE FOLDING PROCESS

Tweet before Case Folding	Tweet after Case Folding
Para pelajar menyampaikan rasa terima kasih atas program vaksinasi massal yang terus dilakukan oleh pemerintah	para pelajar menyampaikan rasa terima kasih atas program vaksinasi massal yang terus dilakukan oleh pemerintah

2) *Tokenizing*: This process is splitting sentences into a piece of the word called tokens. The result of the Tokenizing process can be seen in Table VI.

3) *Normalization*: This step is converting each word or token into a common phrase. The standard used in this case is the standard Indonesian word. This method was based on research published in the journal by Salsabila et al. [31]. The results of the Normalization process can be seen in Table VII.

4) *Stopwords or filtering*: This process removes words or tokens that are unnecessary and unrelated for further analysis. The result of the Stopwords process can be seen in Table VIII.

TABLE VI. RESULTS OF THE TOKENIZING PROCESS

Tweet before Tokenizing	Tweet after Tokenizing
para pelajar menyampaikan rasa terima kasih atas program vaksinasi massal yang terus dilakukan oleh pemerintah	['para', 'pelajar', 'menyampaikan', 'rasa', 'terima', 'kasih', 'atas', 'program', 'vaksinasi', 'massal', 'yang', 'terus', 'dilakukan', 'oleh', 'pemerintah']

TABLE VII. RESULTS OF THE NORMALIZATION PROCESS

Tweet Tokens	Normalization
['betul', 'vaksinasi', 'itu', 'penting', 'sbg', 'benteng', 'pertahanan', 'diri', 'dr', 'dalam']	['betul', 'vaksinasi', 'itu', 'penting', 'sebagai', 'benteng', 'pertahanan', 'diri', 'dalam']

TABLE VIII. RESULTS OF THE STOPWORDS PROCESS

Normalization	Stopwords
['para', 'pelajar', 'menyampaikan', 'rasa', 'terima', 'kasih', 'atas', 'program', 'vaksinasi', 'massal', 'yang', 'terus', 'dilakukan', 'oleh', 'pemerintah']	['pelajar', 'menyampaikan', 'rasa', 'terima', 'kasih', 'atas', 'program', 'vaksinasi', 'massal', 'terus', 'dilakukan']

5) *Stemming*: This process changes words or tokens into a word form base. The results of the stemming process can be seen in Table IX.

TABLE IX. RESULTS OF THE STEMMING PROCESS

Stopwords	Stemming
['pelajar', 'menyampaikan', 'rasa', 'terima', 'kasih', 'atas', 'program', 'vaksinasi', 'massal', 'terus', 'dilakukan']	['ajar', 'sampai', 'rasa', 'terima', 'kasih', 'atas', 'program', 'vaksinasi', 'massal', 'terus', 'laku']

E. Feature Extraction

Feature extraction or TF-IDF will calculate each word by the value against the number of documents used at this stage. This process aims to carry out the classification process easily and recognize words in the form of numbers. The results of the implementation of TF-IDF are as follows:

- Document 1: Ayo dukung program vaksinasi massal capai target herd immunity nasional untuk Indonesia sehat.
- Document 2: Mau sehat Ayo vaksinasi Indonesia bangkit.

The calculation of TF-IDF can be seen in Table X.

TABLE X. RESULTS OF TF-IDF PROCESS

Word	TF		IDF	TF-IDF Score	
	D1	D2		D1	D2
Ayo	$\frac{1}{13}$	$\frac{1}{13}$	$\log\left(\frac{2}{2+1}\right) = 0.18$	0.013	0.013
Dukung	$\frac{1}{13}$	0	$\log\left(\frac{2}{1+1}\right) = 0$	0	0
Program	$\frac{1}{13}$	0	$\log\left(\frac{2}{1+1}\right) = 0$	0	0
Vaksinasi	$\frac{1}{13}$	$\frac{1}{13}$	$\log\left(\frac{2}{2+1}\right) = 0.18$	0.013	0.013
Masal	$\frac{1}{13}$	0	$\log\left(\frac{2}{1+1}\right) = 0$	0	0
Capi	$\frac{1}{13}$	0	$\log\left(\frac{2}{1+1}\right) = 0$	0	0
Target	$\frac{1}{13}$	0	$\log\left(\frac{2}{1+1}\right) = 0$	0	0
Herd	$\frac{1}{13}$	0	$\log\left(\frac{2}{1+1}\right) = 0$	0	0

Immunity	$\frac{1}{13}$	0	$\log\left(\frac{2}{1+1}\right) = 0$	0	0
Nasional	$\frac{1}{13}$	0	$\log\left(\frac{2}{1+1}\right) = 0$	0	0
Untuk	$\frac{1}{13}$	0	$\log\left(\frac{2}{1+1}\right) = 0$	0	0
Indonesia	$\frac{1}{13}$	$\frac{1}{13}$	$\log\left(\frac{2}{2+1}\right) = 0.18$	0.013	0.013
Sehat	$\frac{1}{13}$	$\frac{1}{13}$	$\log\left(\frac{2}{2+1}\right) = 0.18$	0.013	0.013
Mau	0	$\frac{1}{13}$	$\log\left(\frac{2}{1+1}\right) = 0$	0	0
Bangkit	0	$\frac{1}{13}$	$\log\left(\frac{2}{1+1}\right) = 0$	0	0

IV. RESULT

A. Sentiment Analysis

Researchers analyze sentiment by manually labeling each tweet. The labeled sentiment is done after the cleaning process. As a result, there are 1136 tweets (56.80%) with positive sentiment, 675 tweets (33.75%) with the neutral sentiment, and 189 (9.45%) tweets with negative sentiment. In the case of the imbalanced dataset, researchers implement SMOTE to balance the minority class and majority class.

B. Performance Evaluation Measure

The evaluation of the model in this research is presented in a confusion matrix table which consists of prediction class and actual class. The comparison of each kernel also becomes an evaluation parameter in this research.

1) *Linear kernel*: Parameters used in the test of the linear kernel, i.e., the complexity and maximum iterations. Increased complexity causes accuracy to decrease, and increasing the maximum iteration value tends to give a constant value with low volatility. The best accuracy result is 90% with C = 1 and max iteration = "default". The confusion matrix table of the linear kernel can be seen in Table XII, and the performance evaluation measure can be seen in Table XIII.

2) *RBF Kernel*: Parameters used in the test of RBF kernel, i.e., complexity and gamma. Testing the complexity value of more than five tends to produce high accuracy values constant, and increases in the value of gamma cause accuracy to decrease. The best accuracy result is 92% with C = 1 and gamma = 1. The confusion matrix table of the RBF kernel can be seen in Table XIV, and the performance evaluation measure can be seen in Table XV.

F. Synthetic Minority Oversampling Technique

SMOTE will balance the dataset by taking advantage of the TF-IDF value. Balancing dataset class is a must because there is a gap in data between positive, neutral, and negative classes. SMOTE will create class neutral and negative belonging to the minority class synthetic data to match the majority class, positive class. Before and after the implementation of SMOTE can be seen in Fig. 2 and 3.

```
[ ] df["Label"].value_counts()

2    1136
1     675
0     189
Name: Label, dtype: int64
```

Fig. 2. Before Implementation of SMOTE.

```
[52] from imblearn.over_sampling import SMOTE
sm_combine = SMOTE(random_state=10)
x_vect, y = sm_combine.fit_resample(x_vect, df['Label'])
y.value_counts()

1    1136
2    1136
0    1136
Name: Label, dtype: int64
```

Fig. 3. After Implementation of SMOTE.

G. Support Vector Machine

This research tested the model using four Support Vector Machine kernels, i.e., linear, polynomial, RBF, and sigmoid. Various kernels are utilized to change the level of data dimensions to be different depending on the kernel used. The equation of each Support Vector Machine kernel can be seen in Table XI [32].

TABLE XI. SUPPORT VECTOR MACHINE KERNEL EQUATION

Kernel	Equation	
Linear	$K(x_i, x) = x_i^T x$	
Polynomial	$K(x_i, x) = (\gamma \cdot x_i^T x + r)^p$	$p = \text{degree}$ $r = \text{coef}()$
RBF	$K(x_i, x) = \exp(-\gamma x_i^T x ^2)$	$\gamma = \text{gamma}$
Sigmoid	$K(x_i, x) = \tanh(\gamma \cdot x_i^T x + r)$	$r = \text{coef}()$

TABLE XII. CONFUSION MATRIX OF LINEAR KERNEL

Actual	Predicted		
	Negative	Neutral	Positive
Negative	88	0	0
Neutral	4	117	13
Positive	3	15	101

TABLE XIII. PERFORMANCE EVALUATION MEASURE OF LINEAR KERNEL

Sentiment	Precision	Recall	F1-Score
Negative	0.93	1.00	0.96
Neutral	0.86	0.87	0.88
Positive	0.89	0.85	0.87

TABLE XIV. CONFUSION MATRIX OF RBF KERNEL

Actual	Predicted		
	Negative	Neutral	Positive
Negative	88	0	0
Neutral	2	115	17
Positive	1	8	110

TABLE XV. PERFORMANCE EVALUATION MEASURE OF RBF KERNEL

Sentiment	Precision	Recall	F1-Score
Negative	0.97	1.00	0.98
Neutral	0.93	0.86	0.89
Positive	0.87	0.92	0.89

3) *Polynomial Kernel*: Parameters used in the test of Polynomial kernel, i.e., complexity, gamma, and degree. Testing on three parameters causes a decrease in accuracy as the value increases. The best accuracy result is 90% with C = 1, gamma = "scale", and degree = 1. The confusion matrix table of the Polynomial kernel can be seen in Table XVI, and the performance evaluation measure can be seen in Table XVII.

TABLE XVI. CONFUSION MATRIX OF POLYNOMIAL KERNEL

Actual	Predicted		
	Negative	Neutral	Positive
Negative	88	0	0
Neutral	4	118	12
Positive	3	16	100

TABLE XVII. PERFORMANCE EVALUATION MEASURE OF POLYNOMIAL KERNEL

Sentiment	Precision	Recall	F1-Score
Negative	0.93	1.00	0.96
Neutral	0.88	0.88	0.88
Positive	0.89	0.84	0.87

4) *Sigmoid Kernel*: Parameters used in the test of the sigmoid kernel, i.e., complexity and gamma. Increasing the value of complexity and gamma produces an accuracy value that tends to decrease. The best accuracy result is 89%, with C = 1 and gamma = "scale". The confusion matrix table of the sigmoid kernel can be seen in Table XVIII, and the performance evaluation measure can be seen in Table XIX.

TABLE XVIII. CONFUSION MATRIX OF SIGMOID KERNEL

Actual	Predicted		
	Negative	Neutral	Positive
Negative	88	0	0
Neutral	7	114	13
Positive	5	13	101

TABLE XIX. PERFORMANCE EVALUATION MEASURE OF SIGMOID KERNEL

Sentiment	Precision	Recall	F1-Score
Negative	0.88	1.00	0.94
Neutral	0.90	0.85	0.87
Positive	0.89	0.85	0.87

V. CONCLUSION

Sentiment class classification generates positive sentiment 1136 tweets (56.80%), neutral sentiment 675 tweets (33.75%), and negative sentiment 189 tweets (9.45%). The dataset class number gap is balanced through the SMOTE method, which generates 1136 tweets in all class sentiments. The classification results using the Support Vector Machine have the best accuracy result obtained on the RBF kernel by 92%, followed by Linear kernel and Polynomial kernel by 90%; lastly, the Sigmoid kernel by 89%.

REFERENCES

- [1] Cucinotta and M. Vanelli, "WHO declares COVID-19 a pandemic," *Acta Biomed.*, vol. 91, no. 1, pp. 157–160, 2020, doi: 10.23750/abm.v91i1.9397.
- [2] H. Chen et al., "Clinical characteristics and intrauterine vertical transmission potential of COVID-19 infection in nine pregnant women: a retrospective review of medical records," *Lancet*, vol. 395, no. 10226, pp. 809–815, 2020, doi: 10.1016/S0140-6736(20)30360-3.
- [3] Presiden Republik Indonesia, "Peraturan Presiden No. 99 Tahun 2020 tentang Pengadaan Vaksin dan Pelaksanaan Vaksinasi dalam Rangka Penanggulangan Pandemi Corona Virus Disease 2019 (Covid-19)," *Peratur. Pres.*, vol. 2019, no. 039471, pp. 1–13, 2020.
- [4] Asosiasi Penyelenggara Jasa Internet Indonesia, "Laporan Survei Internet APJII 2019 – 2020," Asos. Penyelenggara Jasa Internet Indonesia, 2020. <https://apjii.or.id/survei>.
- [5] K. Garcia and L. Berton, "Topic detection and sentiment analysis in Twitter content related to COVID-19 from Brazil and the USA," *Appl. Soft Comput.*, vol. 101, p. 107057, 2021, doi: 10.1016/j.asoc.2020.107057.
- [6] A. J. Nair, G. Veena, and A. Vinayak, "Comparative study of Twitter Sentiment on COVID - 19 Tweets," *Proc. - 5th Int. Conf. Comput. Methodol. Commun. ICCMC 2021*, no. Iccmc, pp. 1773–1778, 2021, doi: 10.1109/ICCMC51019.2021.9418320.
- [7] M. S. Akhtar, D. Gupta, A. Ekbal, and P. Bhattacharyya, "Feature selection and ensemble construction: A two-step method for aspect based sentiment analysis," *Knowledge-Based Syst.*, vol. 125, pp. 116–135, 2017, doi: 10.1016/j.knosys.2017.03.020.
- [8] L. C. Cheng and S. L. Tsai, "Deep learning for automated sentiment analysis of social media," *Proc. 2019 IEEE/ACM Int. Conf. Adv. Soc. Networks Anal. Mining, ASONAM 2019*, pp. 1001–1004, 2019, doi: 10.1145/3341161.3344821.
- [9] M. Wongkar and A. Angdresey, "Sentiment Analysis Using Naive Bayes Algorithm Of The Data Crawler: Twitter," *Proc. 2019 4th Int. Conf. Informatics Comput. ICIC 2019*, pp. 1–5, 2019, doi: 10.1109/ICIC47613.2019.8985884.
- [10] L. Kurniasari and A. Setyanto, "Sentiment Analysis using Recurrent Neural Network," *J. Phys. Conf. Ser.*, vol. 1471, no. 1, Mar. 2020, doi: 10.1088/1742-6596/1471/1/012018.
- [11] E. Y. Sari, A. D. Wierfi, and A. Setyanto, "Sentiment Analysis of Customer Satisfaction on Transportation Network Company Using Naive Bayes Classifier," *2019 Int. Conf. Comput. Eng. Network, Intell. Multimedia, CENIM 2019 - Proceeding*, vol. 2019-November, Nov. 2019, doi: 10.1109/CENIM48368.2019.8973262.
- [12] M. Rosanensi, M. Madani, R. T. P. Wanggono, A. Setyanto, A. A. Selameto, and S. N. Wahyuni, "Analysis sentiment and tourist response to rinjani mountain tour based on comments from photo upload in instagram," *Proc. - 2018 3rd Int. Conf. Inf. Technol. Inf. Syst. Electr. Eng. ICITISEE 2018*, pp. 184–188, Jul. 2018, doi: 10.1109/ICITISEE.2018.8720960.
- [13] B. Liu, "Sentiment Analysis and Opinion Mining," *Synth. Lect. Hum. Lang. Technol.*, vol. 5, no. 1, pp. 1–167, May 2012, doi: 10.2200/S00416ED1V01Y201204HLT016.
- [14] J. H. Jaman and R. Abdulrohman, "Sentiment Analysis of Customers on Utilizing Online Motorcycle Taxi Service at Twitter with the Support Vector Machine," *ICECOS 2019 - 3rd Int. Conf. Electr. Eng. Comput.*

- Sci. Proceeding, pp. 231–234, 2019, doi: 10.1109/ICECOS47637.2019.8984483.
- [15] U. Makhmudah, S. Bukhori, J. A. Putra, and B. A. B. Yudha, "Sentiment Analysis of Indonesian Homosexual Tweets Using Support Vector Machine Method," Proc. - 2019 Int. Conf. Comput. Sci. Inf. Technol. Electr. Eng. ICOMITEE 2019, pp. 183–186, 2019, doi: 10.1109/ICOMITEE.2019.8920940.
- [16] H. Hairani, M. Innuddin, and M. Rahardi, "Accuracy Enhancement of Correlated Naive Bayes Method by Using Correlation Feature Selection (CFS) for Health Data Classification," 2020 3rd Int. Conf. Inf. Commun. Technol. ICOIACT 2020, pp. 51–55, Nov. 2020, doi: 10.1109/ICOIACT50329.2020.9332021.
- [17] R. Hassan and M. R. Islam, "Impact of Sentiment Analysis in Fake Online Review Detection," 2021 Int. Conf. Inf. Commun. Technol. Sustain. Dev. ICICT4SD 2021 - Proc., pp. 21–24, 2021, doi: 10.1109/ICICT4SD50815.2021.9396899.
- [18] R. Ahuja, A. Chug, S. Kohli, S. Gupta, and P. Ahuja, "The impact of features extraction on the sentiment analysis," Procedia Comput. Sci., vol. 152, pp. 341–348, 2019, doi: 10.1016/j.procs.2019.05.008.
- [19] M. Rathi, A. Malik, D. Varshney, R. Sharma, and S. Mendiratta, "Sentiment Analysis of Tweets Using Machine Learning Approach," in 2018 Eleventh International Conference on Contemporary Computing (IC3), Aug. 2018, pp. 1–3, doi: 10.1109/IC3.2018.8530517.
- [20] G. Yang and L. Qicheng, "An over Sampling Method of Unbalanced Data Based on Ant Colony Clustering," IEEE Access, vol. 9, pp. 130990–130996, 2021, doi: 10.1109/ACCESS.2021.3114443.
- [21] E. dwi nurindah Sari, "Analisis Sentimen Nasabah Pada Layanan Perbankan Menggunakan Metode Regresi Logistik Biner , Naïve Bayes Classifier (NBC), dan Support Vector Machine (SVM)," J. Sains Dan Seni Its, vol. 8, no. 2, p. 177, 2019.
- [22] F. Wang, J. Zhang, Y. Bu, and B. Chen, "Research on imbalanced data set preprocessing based on deep learning," Proc. - 2021 Asia-Pacific Conf. Commun. Technol. Comput. Sci. ACCTCS 2021, pp. 75–79, 2021, doi: 10.1109/ACCTCS52002.2021.00023.
- [23] K. R. Kavitha, A. Gopinath, and M. Gopi, "Applying improved SVM classifier for leukemia cancer classification using FCBF," 2017 Int. Conf. Adv. Comput. Commun. Informatics, ICACCI 2017, vol. 2017-Janua, pp. 61–66, 2017, doi: 10.1109/ICACCI.2017.8125817.
- [24] S. Zahoor and R. Rohilla, "Twitter Sentiment Analysis Using Machine Learning Algorithms: A Case Study," Proc. - 2020 Int. Conf. Adv. Comput. Commun. Mater. ICACCM 2020, pp. 194–199, 2020, doi: 10.1109/ICACCM50413.2020.9213011.
- [25] S. Rani and S. Bhatt, "Sentiment Analysis on twitter data using Machine Learning," J. Xidian Univ., vol. 14, no. 12, pp. 1–4, Dec. 2020, doi: 10.37896/jxu14.12/039.
- [26] A. Imron, "Analisis Sentimen Terhadap Tempat Wisata di Kabupaten Rembang Menggunakan Metode Naive Bayes Classifier," pp. 10–13, 2019.
- [27] K. Kusriani, E. T. Luthfi, M. Muqorobin, and R. W. Abdullah, "Comparison of naive bayes and K-NN method on tuition fee payment overdue prediction," 2019 4th Int. Conf. Inf. Technol. Inf. Syst. Electr. Eng. ICITISEE 2019, vol. 6, pp. 125–130, 2019, doi: 10.1109/ICITISEE48480.2019.9003782.
- [28] F. Ernawan, A. Aminuddin, D. Nincarean, M. F. A. Razak, and A. Firdaus, "Three Layer Authentications with a Spiral Block Mapping to Prove Authenticity in Medical Images," Int. J. Adv. Comput. Sci. Appl., vol. 13, no. 4, pp. 211–223, 2022, doi: 10.14569/IJACSA.2022.0130425.
- [29] A. Aminuddin and F. Ernawan, "AuSR1: Authentication and self-recovery using a new image inpainting technique with LSB shifting in fragile image watermarking," J. King Saud Univ. - Comput. Inf. Sci., Feb. 2022, doi: 10.1016/J.JKSUCI.2022.02.009.
- [30] A. C. Emcha, Widyawan, and T. B. Adji, "Quotation extraction from Indonesian online news," 2019 Int. Conf. Inf. Commun. Technol. ICOIACT 2019, pp. 408–412, 2019, doi: 10.1109/ICOIACT46704.2019.8938558.
- [31] N. Aliyah Salsabila, Y. Ardhito Winatmoko, A. Akbar Septiandri, and A. Jamal, "Colloquial Indonesian Lexicon," Proc. 2018 Int. Conf. Asian Lang. Process. IALP 2018, pp. 226–229, 2019, doi: 10.1109/IALP.2018.8629151.
- [32] H. C. Husada and A. S. Paramita, "Analisis Sentimen Pada Maskapai Penerbangan di Platform Twitter Menggunakan Algoritma Support Vector Machine (SVM)," Teknika, vol. 10, no. 1, pp. 18–26, 2021, doi: 10.34148/teknika.v10i1.311.

Application of Optimized SVM in Sample Classification

Xuemei Yao

School of Data Science and Information Engineering, Guizhou Minzu University, China

Abstract—Support vector machines (SVM) have unique advantages in solving problems with small samples, nonlinearity and high dimension. It has a relatively complete theory and has been widely used in various fields. The classification accuracy and generalization ability of SVMs are determined by the selected parameters, for which there is no solid theoretical guidance. To address this parameter optimization problem, we applied random selection, genetic algorithms (GA), particle swarm optimization (PSO) and K-fold cross validation (k-CV) method to optimize the parameters of SVMs. Taking the classification accuracy, mean squared error and squared correlation coefficient as the goal, the K-fold cross validation method is chosen as the best way to optimize SVM parameters. In order to further verify the best performance of the SVM whose parameters are optimized by the K-fold cross validation method, the back propagation neural network and decision tree are used as the contrast models. The experimental results show that the SVM-cross validation method has the highest classification accuracy in SVM parameter selection, which lead to SVM classifiers that outperform both BP neural networks and decision tree method.

Keywords—Support vector machine; parameter optimization; K-fold cross validation; sample classification

I. INTRODUCTION

Support Vector Machine (SVM) is a theory that studies the rule of machine learning in the case of limited sample based on the statistical learning theory including Vapnik-Chervonenkis Dimension (VCD) and Structural Risk Minimization (SRM). SVM has many unique advantages in solving the problem of high-dimensional pattern recognition. It can use the limited sample information to compromise the complexity and learning ability of the model, and avoid the problems caused by over-learning and under-learning as much as possible, so that the system has a better ability to extend. SVM has attracted the attention and research interests of experts and scholars in various fields, and made a lot of research results in practical application, which has promoted the development of various fields [1-3].

Although SVM has been widely used in text classification [4], image recognition[5], prediction[6] and so on, its performance is mainly dependent on the selection of penalty factor and kernel parameter. So far, SVM parameter selection still does not have a complete set of theory and standards, but in practical application, the choice of parameter directly determines the classification accuracy and generalization ability of SVM [7-8]. The common methods of optimizing parameters are as follows, experimental method, grid search and numerical method. The first way means that you need to

select different parameters for multiple experiments, and then select a pair of parameters for the best results, which is not only time consuming and too random; the second method is feasible in the case of small samples, but the efficiency and feasibility is lower when the data is large; the third method is more sensitive to the selection of the initial value. With the development of artificial intelligence, some groups of intelligent optimization algorithm such as ant colony optimization algorithm (ACO), genetic algorithm (GA), particle swarm algorithm (PSO) and so on are used to optimize the parameters of SVM.

Rajeshwari et al [9] proposed a new Weighted-SVM kernel by applying a suitably transformed weight vector derived from particle swarm optimized neural networks. Yang et al [10] envisaged the analysis of the dissolved oxygen fault of the water quality monitoring system using the GA-SVM and the result exhibited a good accuracy. Faris et al [11] proposed a robust approach based on a recent nature-inspired metaheuristic called multi-verse optimizer for selecting optimal features and optimizing the parameters of SVM simultaneously and it can effectively reduce the number of features while maintaining a high prediction accuracy. John et al [12] proposed a detection technique using SVM with Grid search algorithm and recognized the disorder with an accuracy rate of 89%.

In the above research, it is for a specific field to select a suitable way to optimize the parameters of SVM, but it does not compare these parameter optimization algorithms in the same application to select the best way. To address this issue, based on the identification of Italian wine, random selection, GA, PSO and cross validation (CV) are used to optimize the parameters of SVM, and the best way was selected. In order to verify that the SVM which is optimized by the best way has a good classification accuracy, the neural network and decision tree are used as contrast model for analysis.

II. METHODOLOGY

A. Introduction of SVM

SVM is a statistical learning method proposed by Vapnik in 1992 based on VCD theory and SRM principle [13]. SVM maps the input space into a high dimensional kernel space by introducing the kernel function. In order to classify the sample, the optimal classification hyperplane with lower VCD is obtained in the high dimensional kernel space, so that one class is located on the side of the hyperplane and the other side of the hyperplane is another class. Take the Two-Dimensional (2D) space as an example showed in Fig. 1. There are many samples, some with five-pointed star and some with a circle.

This work is supported by the Natural Science Foundation of the Guizhou Province (No. [2020]1Y263).

Classification by SVM is to find a hyperplane (the red line in Fig. 1), according to the classification requirements, the sample will be divided into class 1 with five-pointed star and class 2 with circle. The point falling on the classification boundary is called support vector

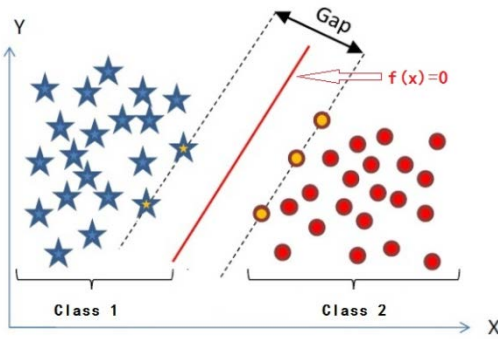


Fig. 1. Schematic Diagram of SVM in 2D Space.

The main idea of SVM is to establish a classification hyperplane $f(x) = 0$ as a decision surface for a multidimensional space to be classified, for any positive case x satisfying $f(x) > 0$, and the counter example is satisfied with $f(x) < 0$. The purpose of SVM is to find the appropriate $f(x)$ to maximize the isolation edge (Gap) and minimize the training error between the positive and negative examples. Through the decision-making surface to achieve the classification of the sample, the decision-making function can be written as:

$$f(x) = \text{sign}(\sum_{x_i \in S_V}^n a_i y_i k(x_i, x) + b) \quad (1)$$

where a_i : Lagrange multiplier, s.t. $0 < a_i < c$

S_V : Support vector.

$K(x_i, x)$: Kernel function.

x_i : The positive examples.

y_i : The negative examples.

b : Threshold.

n : The number of samples.

In practical application, SVM has a complete theoretical basis, but it needs to choose different parameters and kernel functions for different conditions in order to obtain the desired results. Different support vector classifiers can be generated by using different kernel functions. Commonly used kernel functions are linear kernel function, radial basis function (RBF), polynomial kernel function and so on. Since it is only necessary to determine a parameter in RBF, which is beneficial to parameter optimization, RBF is chosen as the kernel function of SVM in this article. The expression can now be written as:

$$K(x_i, x) = \exp\left(\frac{1}{2g^2} \|x_i - x\|^2\right) \quad (2)$$

Where g is the nuclear parameter to be determined. The penalty factor c is an important parameter in SVM. It is used to control the weight of the loss and sorting interval. The bigger the value of c , the higher the fit degree of the model, but its generalization ability is reduced. According to SVM regression

theory, c and g have a great influence on the classification results. Therefore, it is necessary to choose the best c and g to obtain the superior performance of SVM.

Definition 1

The mathematical model of SVM parameter will be written as: $P = \{bestc, bestg\}$.

Definition 2

The objective function of SVM parameter optimization is the accuracy of prediction model.

In this paper, the problem of SVM parameter optimization can be described mathematically:

For $\forall p = \{c, g\}$, satisfied $P = \max(\text{Accuracy})$

$$\text{s.t.} \begin{cases} P \subset p \\ c > 0 \\ g > 0 \end{cases} \quad (3)$$

SVM solves the practical puzzles such as small sample, nonlinearity and high dimension. It has strong versatility, robustness and effectiveness and it is widely used in classification and regression. The SVM is originally designed for two classification problems. When dealing with multiple classification, it is necessary to combine multiple two classifiers to construct the appropriate multi-classifier. In this paper, the tool used in constructing the forecasting model is the LibSVM software package developed by Chih-Jen Lin of Taiwan University.

B. SVM Parameter Optimization Method

1) *Random selection*: Random selection belongs to the experimental method. According to the theory of SVM, we randomly select different parameters to test and analyze the samples, and then choose a set of parameters with the highest classification accuracy. The method is too random and lacks of authoritative theoretical guidance.

2) *Genetic Algorithm (GA)*: GA is proposed by Professor J. Holland of the United States in 1975. Its main feature is the direct operation of the structure of the object; there is no limit of derivation and continuity of the function; it has better global optimization ability [14]. GA is a computational model for simulating the natural selection and genetic mechanism of Darwin's theory of biological evolution. It is a method for searching the optimal solution by simulating natural evolutionary processes [15]. It introduces the principle of "survival of the fittest" in the process of coding of parameter optimization. According to the selected fitness function, the individuals are selected by the selection, crossover and mutation of the genetic process, so that the individuals with good fitness value are retained, the remaining are eliminated. The new group not only inherited the previous generation of information, but also better than it. It is repeatedly until the conditions are satisfied. Genetic algorithm has been widely used in combinatorial optimization, machine learning, adaptive control and other fields. The process of GA shows in Fig. 2.

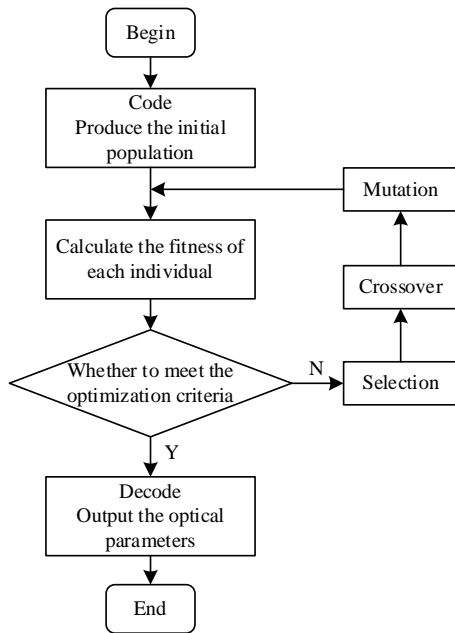


Fig. 2. Flow Chart of GA.

3) *Particle Swarm Optimization (PSO)*: PSO is an optimization algorithm based on population intelligence in computing intelligence [16]. It is first proposed by Kennedy and Eberhart in 1995 and its basic concept comes from the study of predatory behavior of birds. PSO initializes a group of particles in the solvable space first. Each particle represents a potential optimal solution of the search space and the characteristics of particle are displayed by three indexes of position, velocity and fitness value. The particle moves in the solution space [17]. By tracking the trajectories of the particle, it updates the position and speed of individual constantly to follow the optimal output. The process of PSO algorithm shows in Fig. 3.

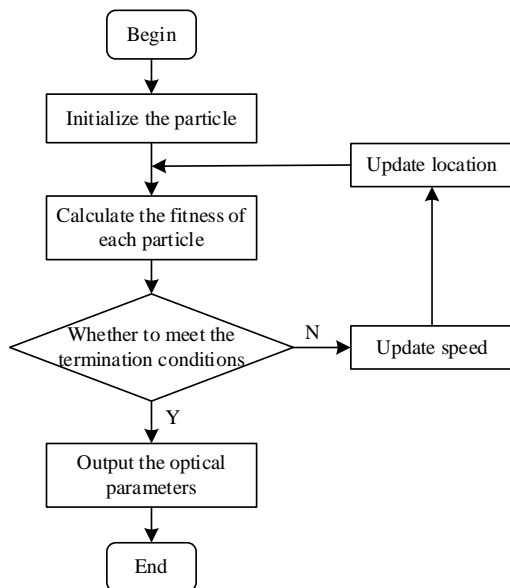


Fig. 3. Flow Chart of PSO.

4) *Cross-Validation (CV)*: CV is a statistical analysis method used to verify the performance of a classifier. The basic idea is to divide the original data into two parts in a certain sense, one is the training set and the other is validation set [18-19]. Firstly, the training set is used to train the classifier, then the validation set is used to test the model to obtain the classification accuracy as the performance index of the classifier. The optimal parameters obtained by CV can effectively avoid the occurrence of over learning and less learning, and finally get the ideal prediction accuracy for the testing set. The Hold-out method, K-fold CV, Leave-one-out CV are commonly used methods. The second method is adopted in the article that is K-CV. Its basic idea is to divide the original data into K disjoint subsets, then it selects one of them as the validation set and the other K-1 subsets as the training set. The K models can be obtained in this way, and the average of the final classification accuracy of the K models as the performance index of the K-CV classifier. Generally speaking, K is greater than or equal to 2. But in practice, K is taken from 3. K will try to take 2 only when the original data is very small.

C. Classification Forecasting Model Based on SVM

1) *Data preprocessing*: Raw data usually has a different order of magnitude, which directly affects the results of the data analysis. In order to eliminate the influence, data standardization is required to address the comparability between data indicators. The data is in the same order of magnitude after processing and it is suitable for comprehensive evaluation. Two commonly used normalized methods are as follows.

a) *Normalized between [0,1]*: The normalized mapping used in this method is as follows.

$$f: x \rightarrow y = \frac{x-x_{min}}{x_{max}-x_{min}} \tag{4}$$

where $x, y \in R^*$; $x_{min} = \min(x)$; $x_{max} = \max(x)$. The result of the normalization is that the raw data is scaled to [0,1].

b) *Normalized between [-1,1]*: The normalized mapping used in this method is as follows.

$$f: x \rightarrow y = 2 * \frac{x-x_{min}}{x_{max}-x_{min}} - 1 \tag{5}$$

where $x, y \in R^*$; $x_{min} = \min(x)$; $x_{max} = \max(x)$. The result of the normalization is that the raw data is scaled to [-1, 1].

2) *Classification forecasting model*: The classification prediction model based on SVM is divided into two stages: parameter optimization and prediction classification. The first stage is parameter optimization. The training set and testing set are separated from the original data, then the normalized preprocessing method makes the data samples in the same order of magnitude with the same dimension. The parameters of SVM are optimized by random selection, GA, PSO and K-fold CV method. The optimal parameters are selected from

three angles: accuracy, MSE and r^2 . The second stage is prediction classification. The K -CV-SVM model is established with the best parameters to find the support vector of the training sample and determine the optimal classification hyperplane, and then forecast the testing set. In order to further verify the superior performance of K -CV-SVM model, neural network and decision tree are designed as contrast model. The overall structure of the paper is shown in Fig. 4.

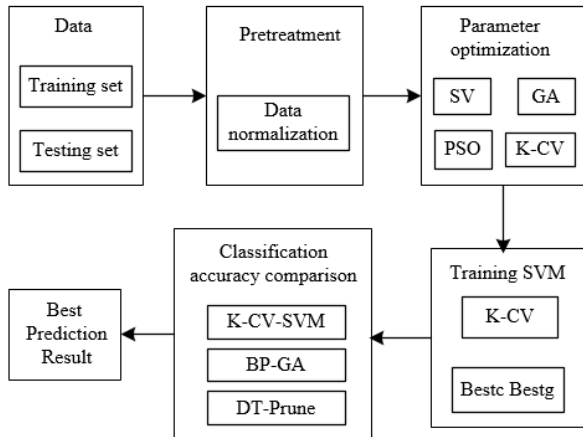


Fig. 4. Diagram of SVM Classification.

III. EXPERIMENTAL DISCUSSION

A. Experimental Data Description

In order to verify the validity of the method proposed in this paper, we use the wine data to carry out the experimental. Wine data is from the UCI dataset and it can be download from the link: <http://archive.ics.uci.edu/ml/datasets/Wine>. These data are the results of a chemical analysis of wines grown in the same region in Italy but derived from three different cultivars. The analysis determines the composition of each wine. The data contains 178 samples and each contains 13 attributes and 1 label. The attributes which are the main chemical composition of wine donated by Riccardo Leardi are: 1) Alcohol; 2) Malic acid; 3) Ash; 4) Alcalinity of ash; 5) Magnesium; 6) Total phenols; 7) Flavanoids; 8) Nonflavanoid phenols; 9) Proanthocyanins; 10) Color intensity; 11) Hue; 12) OD280/OD315 of diluted wines; 13) Proline. Wine data is divided into two parts on average, one as a training set, and one as a testing set. The classification model is obtained by training the SVM, and then the model is used to predict the label of testing set. It is necessary to note that the selection of training set and testing set is fixed at the time of parameter optimization, but it is random selected when the classification prediction accuracy of SVM, BP and DT is analyzed.

B. Parameter Optimization of SVM

In order to test the effectiveness of different methods for SVM parameter optimization, four kinds of prediction models are designed to compare and analyze, such as classification model of random selection parameters of support vector machine (RS-SVM), classification model of genetic algorithm optimization parameters of support vector machine (GA-SVM), classification model of particle swarm algorithm

optimization parameters of support vector machine (PSO-SVM), classification model of K -fold cross validation algorithm optimization parameters of support vector machine (K -CV-SVM).

1) *RS-SVM*: Random selection parameter refers to the absence of any restrictions, without any theoretical support, completely by the operator according to their own wishes to randomly specify the value of the parameter. If you do not manually set the parameters, SVM will use the default value to perform. In this paper, c is 13 and g is 17 by manual setting. The prediction accuracy of the model is 74.1573%, as shown in Table I. The classification prediction error of the model is shown in Fig. 9(a), and the classification chart is shown in Fig. 10(a).

2) *GA-SVM*: GA is a search heuristic algorithm used in solving the optimization problem in the field of artificial intelligence. The GA-SVM uses GA to find the best parameters for SVM. The parameters of GA are set as follows.

The number of iterations: 200.

The size of population: 20.

The probability of crossover: 0.4.

The probability of mutation: 0.2.

The result of model is that bestc is 3.2703, bestg is 3.6738, and classification accuracy is 97.7528%. They are showed in Table I. The best fitness curve is showed in Fig. 5. In the GA with the number of iterations of 200, it can be seen that the speed of parameter optimization converges faster. It is obvious that the average fitness of the population is stable between 85% and 93% after 10 generations of evolution, and tends to be stable. In this way, the classification prediction error of the model is shown in Fig. 9(b), and the classification chart is shown in Fig. 10(b).

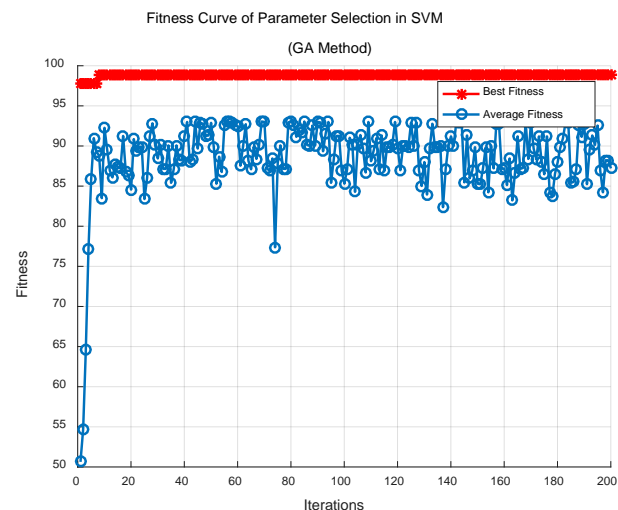


Fig. 5. Fitness Curve of GA-SVM.

3) *PSO-SVM*: PSO is an optimization algorithm based on group intelligence. Compared with GA, PSO has no selection, crossover and mutation operation, but it searches the result

through the particles in the solution space to follow the optimal way. The PSO-SVM uses PSO to find the best parameters for SVM. The parameters of PSO are set as follows.

The number of iterations: 200.

The size of population: 20.

The result of model is that bestc is 32.7842, bestg is 4.4621, and classification accuracy is 97.7528%. They are showed in Table I. The best fitness curve is showed in Fig. 6. Obviously, the stability of model fitness is poor and the variation range is large. The average fitness of the population fluctuates greatly between 50% and 80% after the population begins to evolve. It can be seen that there is still no steady trend with the number of iterations of 200. In this way, the classification prediction error of the model is shown in Fig. 9(c), and the classification chart is shown in Fig. 10(c).

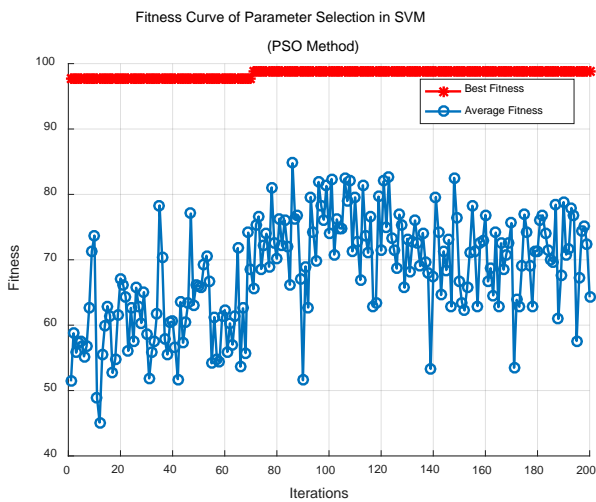


Fig. 6. Fitness Curve of PSO-SVM.

4) *K-CV-SVM*: The model is designed using the *K-CV* method to obtain the best parameters of SVM and divides into two phases. The first stage is a rough choice. Let us set the value of c and g in a certain range ($2^{-10} < c < 2^{10}$ and $2^{-10} < g < 2^{10}$). When the value of c and g is selected, the training set is taken as the original data and the classification accuracy is obtained by the *K-CV* method. Finally, a pair of c and g with the highest classification accuracy are selected as the optimal parameter. If there are multiple sets of c and g corresponding to the highest classification accuracy, then select the combination with the smallest c as the optimal parameters; if the corresponding c has multiple g , then select the first group of c and g as the best parameter. The reason is that the larger c will lead to the occurrence of the over learning, that is, the classification accuracy of training set is high, but the testing set is very low. So in all combinations that can achieve the highest classification accuracy, the smaller c is considered a better choice for the object. The rough selection of the parameters gives the contour map as shown in Fig. 7.

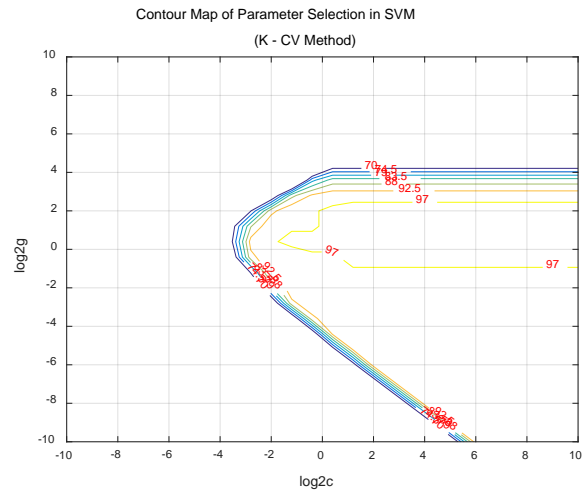


Fig. 7. Contour Map of Parameter Selected Roughly.

In the Fig. 7, the x -axis represents the value of c , which is the logarithm of 2, and the y -axis represents the value of g , which is the logarithm of 2, and the contour line indicates the classification accuracy with corresponding c and g which are gained by *K-CV* method. As can be seen from the Fig. 7, the range of c can be reduced to $2^{-2} \sim 2^4$, the range of g can be reduced to $2^{-2} \sim 2^4$, so that the fine selection can be made on the basis of rough selection. The fine selection of the parameters gives the contour map as shown in Fig. 8.

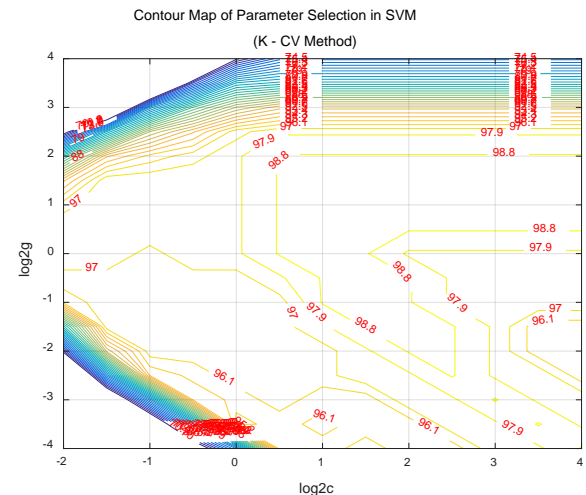
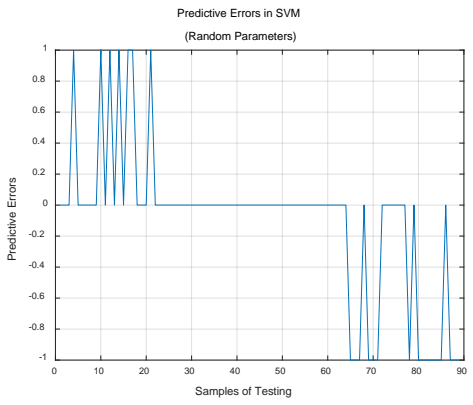


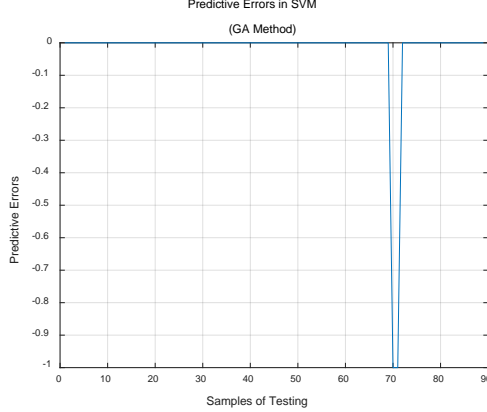
Fig. 8. Contour Map of Parameter Selected Finely.

The result of fine selection of parameters is that c is 1.4142 and g is 1. In this way, the classification accuracy of model is 98.8764 showed in Table I, the classification prediction error of the model is shown in Fig. 9(d), and the classification chart is shown in Fig. 10(d).

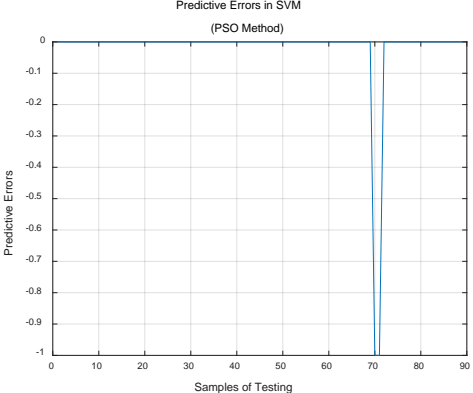
The prediction error curve showed in the Fig. 9 indicates that the prediction error of RS-SVM is the largest, while the prediction error of k-CV-SVM is the smallest. The prediction error of GA-SVM and PSO-SVM are equal. The classification accuracy showed in Table I also illustrates it.



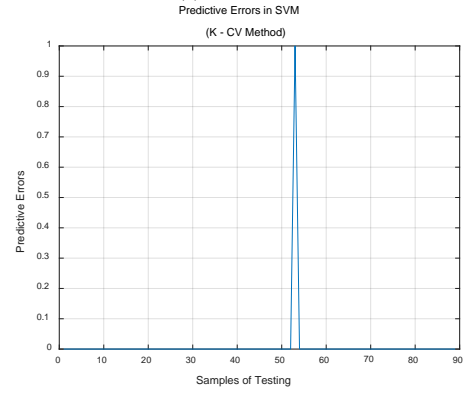
(a) Random Selected.



(b) GA Method.

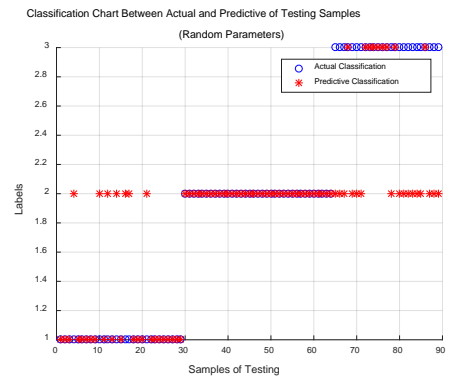


(c) PSO Method.

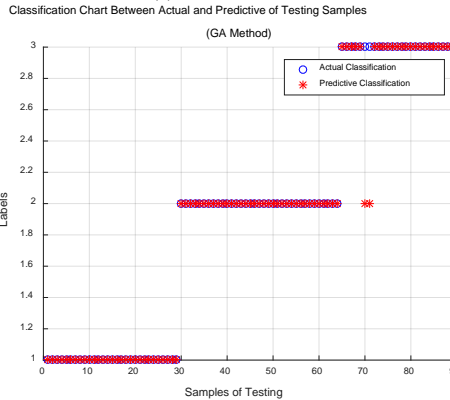


(d) K-CV Method.

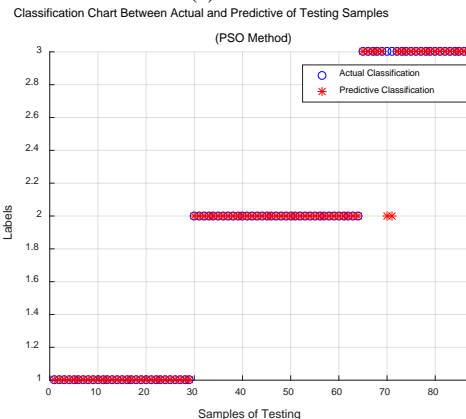
Fig. 9. Predictive Error Curve of Different Parameter Optimization Methods.



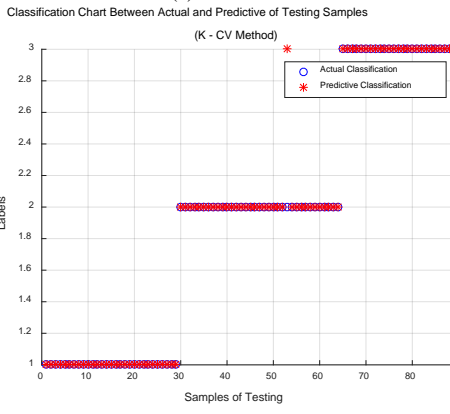
(a) Random Selected



(b) GA Method



(c) PSO Method



(d) K-CV Method

Fig. 10. Predictive and Practical Classification of different Parameter Optimization Methods.

Fig. 10 shows that the number of right classification is 66 and the number of wrong classification is 23 in the RS-SVM model. The number of misclassifications is the highest among the four models, that is, the prediction error of the model is the largest, which is consistent with Fig. 9(a). In the GA-SVM model, the number of right classification is 87 and the number of wrong classification is 2. The classification result of PSO-SVM model is equivalent to GA-SVM and the prediction error is similar, which is consistent with Fig. 9(b) and (c). In the K-CV-SVM model, the number of right classification is 88 and the number of wrong classification is 1. The number of misclassifications is the least among the four models, that is, the prediction error of the model is the least, which is consistent with Fig. 9(d). Overall, the K-CV-SVM model has the highest number of correct classification and the highest classification accuracy.

The other two parameters can also be obtained while the model is running. One is mean squared error (MSE), the other is squared correlation coefficient (r^2). Generally speaking, the accuracy is considered in the problem of classification and the MSE and r^2 are considered in regression issues. MSE is an indicator of the distance between the estimated and true values of the parameter. The smaller the value of MSE, the closer the results of the prediction model are to the real state and the model will have a better accuracy. r^2 is a statistical indicator used to describe the correlation and closeness between the variables. The larger the value of r^2 , the closer is the relationship between the variables. The model optimizes the parameters of SVM with four different methods and carries out the prediction of classification. Table I shows that K-CV-SVM has the highest classification accuracy in four models. On the other hand, K-CV-SVM has the smallest MSE and maximum r^2 , indicating that the prediction results of K-CV-SVM model are the closest to the real state. At the same time, compared with GA-SVM and PSO-SVM, the K-CV-SVM model consumes the least time when the classification accuracy is similar. Therefore, K-CV method is the best way to optimize the parameters of SVM, whether it is classification or regression.

C. The Application of Optimized SVM in Classification

In order to further verify the best effect of SVM by the K-CV method to optimize the parameter, the back propagation

neural network (BP) and decision tree (DT) are used as contrast model based on the same data set. In order to eliminate the influence of the random probability on model, the BP and DT model are run 50 times, and the best and the worst state are selected to increase the contrast effect. The results of prediction are showed in Table II.

It can be seen from Table II that the highest classification accuracy is 100% and the worst case is only 75.28% in the BP prediction model, and the number of wrong samples reached 22 which reflects the natural defect that the BP is easy to fall into the local optimum. In order to overcome the defect, the GA is used to optimize the initial weights and thresholds of the BP (GA-BP), and then the training and prediction are carried out. The classification accuracy of the GA-BP is improved to 93.62%. Similarly, the performance of the DT is also uneven, the best accuracy of the classification is 97.75% and the worst is only 78.65% and the number of wrong samples is 19. The reason is that the original DT is flourishing, which contains a lot of noise and boundary nodes, which is prone to over-fitting. In general, pruning is performed on the DT to improve the classification accuracy. The result in Table II shows that the classification accuracy of the DT after pruning (DT-Prune) is improved to 96.63%, which further confirmed the effect of pruning. Compared with K-CV-SVM, GA-BP and DT-Prune found that the classification accuracy of K-CV-SVM model is 98.88%, and only one sample is wrong. The K-CV-SVM model has the best performance in three models.

TABLE I. PARAMETER OPTIMIZATION RESULT CONTRAST

	Random	GA	PSO	K-CV
c	13	3.2708	32.7842	1.4142
g	17	3.6738	4.4621	1
Accuracy (%)	74.1573	97.7528	97.7528	98.8764
MSE	0.2584	0.0225	0.0225	0.0112
r^2	0.5907	0.9637	0.9637	0.9820
Time(s)	0.9340	12.6566	16.7837	5.2956

TABLE II. COMPARISON WITH OVERALL PERFORMANCE OF THREE PREDICTION METHOD

	SVM		BP		DT		DT-Prune
	K-CV	Best	Worst	GA-BP	Best	Worst	
Right Number	88	89	67	83	87	70	86
Wrong Number	1	0	22	6	2	19	3
Accuracy (%)	98.88	100	75.28	93.26	97.75	78.65	96.63
Time(s)	5.36	1.22	2.76	0.96	1.56	1.55	2.65

IV. CONCLUSION

SVM classification prediction model solves the problem of nonlinear and small sample, but the effect of classification has a great relationship with the parameter setting. According to the theory of SVM, the penalty factor (c) and the kernel parameter (g) have the greatest influence on the classification result. Therefore, the paper analyzes the efficiency of the four methods to optimize the parameters of SVM. Experiments show that the optimal parameters of SVM can be obtained by K-CV and the classification accuracy is highest. In order to further illustrate the conclusion, the BP and DT are designed as the contrast model. The final results show that K-CV-SVM model has a good overall performance both in classification and regression, and it is an effective method for classification and prediction.

Parameter optimization is of great significance to ensure the accuracy of the prediction model. At the same time, the convergence speed of the algorithm and the running time of the program are also a factor that cannot be ignored, especially in the case of huge samples. The results in Table II show that the K-CV-SVM model has the highest classification accuracy, but the running time of system is also the most. Therefore, the next step is to study how to ensure the accuracy rate at the same time to speed up the convergence rate and reduce the time consumption.

REFERENCES

- [1] Liu J , Hu Y , Yang S . A SVM-Based Framework for Fault Detection in High-Speed Trains[J]. *Measurement*, 2020, 172:108779.
- [2] Zhang H . Intelligent Detection of Small Faults Using a Support Vector Machine[J]. *Energies*, 2021, 14.
- [3] Peng Q , Lin X , Shi H , et al. An SVM Classification based Signal Detection Method in UHF RFID Systems[J]. *IEEE Transactions on Industrial Informatics*, 2020, (99):1-1.
- [4] Bajard J C , Martins P , Sousa L , et al. Improving the Efficiency of SVM Classification With FHE[J]. *IEEE transactions on information forensics and security*, 2020, 15:1709-1722.
- [5] Wang W , Zhang B , Wang Z Q , et al. Garbage image recognition and classification based on hog feature and SVM-Boosting[J]. *Journal of Physics Conference Series*, 2021, 1966(1):012002.
- [6] Kowalczyk A , Raskutti B . One class SVM for yeast regulation prediction[J]. *ACM SIGKDD Explorations Newsletter*, 2002, 4(2):99-100.
- [7] Balachandran M , Shin T H , Gwang L . PVP-SVM: Sequence-Based Prediction of Phage Virion Proteins Using a Support Vector Machine[J]. *Frontiers in Microbiology*, 2018, 9:476.
- [8] Mohamed, Goudjil, Mouloud, et al. A Novel Active Learning Method Using SVM for Text Classification[J]. *International Journal of Automation and Computing*, 2018, v.15(03):44-52.
- [9] Rajeshwari R , Mandal S , Rajasekaran. Compressive strength prediction of SCC containing fly ash using SVM and PSO-SVM models[J]. *Journal of Structural Engineering (Madras)*, 2021, 48(1):1-11.
- [10] Yang P , Li Z , Yu Y , et al. Studies on fault diagnosis of dissolved oxygen sensor based on GA-SVM[J]. *Mathematical Biosciences and Engineering*, 2021, 18(1):386-399.
- [11] Faris, H., Hassonah, M.A., Al-Zoubi, A.M., Mirjalili, S. and Aljarah, I. A multi-verse optimizer approach for feature selection and optimizing SVM parameters based on a robust system architecture. *Neural Computing & Applications*. 2017. pp.1-15.
- [12] John R G , Ramachandran K I , Valavan K K , et al. Detection of Obstructive Sleep Apnea from ECG Signal using SVM based Grid Search[J]. *International Journal of Electronics and Telecommunications*, 2021, 67(1):5-12.
- [13] Xia J , Wang Z , Yang D , et al. Performance optimization of support vector machine with oppositional grasshopper optimization for acute appendicitis diagnosis[J]. *Computers in Biology and Medicine*, 2022, 143:105206-.
- [14] Liang B , Mao Z , Zhang K , et al. Analysis and Optimal Design of a WPT Coupler for Underwater Vehicles Using Non-Dominated Sorting Genetic Algorithm[J]. *Applied Sciences*, 2022, 12(4):2015.
- [15] Wu Y , Li X , Liu Q , et al. The Analysis of Credit Risks in Agricultural Supply Chain Finance Assessment Model Based on Genetic Algorithm and Backpropagation Neural Network[J]. *Computational Economics*, 2021:1-24.
- [16] Liu G , Zhu H . Displacement Estimation of Six-Pole Hybrid Magnetic Bearing Using Modified Particle Swarm Optimization Support Vector Machine[J]. *Energies*, 2022, 15.
- [17] Alajmi M S , Almeshal A M . Least Squares Boosting Ensemble and Quantum-Behaved Particle Swarm Optimization for Predicting the Surface Roughness in Face Milling Process of Aluminum Material[J]. *Applied Sciences*, 2021, 11(5):2126.
- [18] Rhoads T , Neale A C , Resch Z J , et al. Psychometric implications of failure on one performance validity test: a cross-validation study to inform criterion group definition[J]. *Journal of Clinical and Experimental Neuropsychology*, 2021(6):1-12.
- [19] Sheppard L . Deployment, Calibration, and Cross-Validation of Low-Cost Electrochemical Sensors for Carbon Monoxide, Nitrogen Oxides, and Ozone for an Epidemiological Study[J]. *Sensors*, 2021, 21.

A Distributed Intrusion Detection System using Machine Learning for IoT based on ToN-IoT Dataset

Abdallah R. Gad¹, Mohamed Haggag², Ahmed A. Nashat³, Tamer M. Barakat⁴

Department of Communication and Electronics Engineering

October High Institute for Engineering & Technology, 6th of October City 12596, Egypt¹

Department of Electronics and Communication Engineering

Misr University for Science and Technology, 6th of October City 12566, Egypt²

Electrical Engineering Department, Faculty of Engineering, Fayoum University, Fayoum, 63514, Egypt^{1,3,4}

Abstract—The internet of things (IoT) is a collection of common physical things which can communicate and synthesize data utilizing network infrastructure by connecting to the internet. IoT networks are increasingly vulnerable to security breaches as their popularity grows. Cyber security attacks are among the most popular severe dangers to IoT security. Many academics are increasingly interested in enhancing the security of IoT systems. Machine learning (ML) approaches were employed to function as intrusion detection systems (IDSs) to provide better security capabilities. This work proposed a novel distributed detection system based on machine ML approaches to detect attacks in IoT and mitigate malicious occurrences. Furthermore, NSL-KDD or KDD-CUP99 datasets are used in the great majority of current studies. These datasets are not updated with new attacks. As a consequence, the ToN-IoT dataset was used for training and testing. It was created from a large-scale, diverse IoT network. The ToN-IoT dataset reflects data from each layer of the IoT system, such as cloud, fog, and edge layer. Various ML methods were tested in each specific partition of the ToN-IoT dataset. The proposed model is the first suggested model based on the collected data from the same IoT system from all layers. The Chi2 technique was used to pick features in a network dataset. It reduced the number of features to 20. Another feature selection tool employed in the windows dataset was the correlation matrix, which was used to extract the most relevant features from the whole dataset. To balance the classes, the SMOTE method was used. This paper tests numerous ML approaches in both binary and multi-class classification problems. According to the findings, the XGBoost approach is superior to other ML algorithms for each node in the suggested model.

Keywords—Intrusion detection system (IDS); internet of things (IoT); ToN-IoT dataset; machine learning (ML)

I. INTRODUCTION

The internet of things (IoT) is a network of everyday physical objects which can communicate and synthesize data utilizing the current network infrastructure by connecting to the internet. These things are networked digital appliances or sensors that can collect data and transmit it across the internet. New applications and services are created as a result of the interplay between sensors, connectivity, people, and processes. In the IoT, these digital sensors or devices are known as "things" [1].

As IoT networks become more prevalent, they become more prone to security breaches. Cyber security attacks are one of the most common serious threats to IoT security. These attacks take several forms and target various resources on a wide range of IoT devices. These cyberattacks frequently target a large number of devices in an IoT network, which may then be utilized as a "resource" or "platform" for attacks such as distributed-denial-of-service (DDoS) and fraudulent operations such as ransomware and password attacks. As a result, securing IoT devices and building malicious (intrusion) detection models for IoT systems is becoming increasingly vital for protecting sensitive data[2].

Because the security of broad IoT is vital, it is critical for identifying IoT risks and defining current prevention methods. This work outline and categorize IoT security threats categories and common defense methods to give the reader the security foundation they need to understand the work[2]. The following are some of the reasons why IoT security procedures vary from those used in traditional security systems:

- IoT systems' computational power, memory capacity, battery life, and network bandwidth are all restricted. As a result, existing standard security solutions, which are often expensive in terms of resources, cannot be installed.
- IoT systems are widely scattered and heterogeneous. As a result, traditional centralized solutions may be ineffective. Furthermore, the distributed nature of IoT introduces new obstacles and restrictions to its security.
- IoT solutions are employed in an ever-changing physical context. Physical attacks, as a result, have been added to the list of typical security issues.

One of the IoT security protection solutions is IDS. An IDS [3] is software and/or hardware that monitors a network or system for hostile activity and issues quick alarms. Since 1970 IDSs have been used. They are divided into two categories: i) deployment and ii) detecting methods. There are two types of IDS deployments: HIDS and NIDS. HIDS (Host-based Intrusion Detection System) is an intrusion detection system installed on a host machine (i.e., a device or a Thing). They keep track of and evaluate system application files and the operating system. Insider intrusion detection and prevention are best accomplished through HIDS. NIDS (Network-based

Intrusion Detection System) captures and analyzes network packet traffic. To put it another way, they are sniffing packets. NIDSs are effective against external intrusion attacks. After the intrusion has occurred, the following situation will explore. An exemplary detection system is one that rapidly recognizes the compromised condition and minimizes the loss (s). IDSs come in many different forms. all categories of IDSs are presented in [4].

Signature detection(knowledge-based)[5], Anomaly detection (behavior-based) [6], and Hybrid detection are the different detection types of IDSs.

An intrusion prevention system (IPS) [7] is used to keep off intruders. An IPS reacts quickly and prevents harmful traffic from passing through by deleting sessions, restarting sessions, blocking packets, or proxying traffic. On the other hand, an IDS replied once an attack has been detected. Inline detection, layer seven switches, deceptive systems, application firewalls, and hybrid switches are all examples of IPS.

During the study experimentation, the following stages will be followed:

1) Choosing ToN-IoT as a new dataset [8]. The dataset was thoroughly analyzed by removing the flow identification attributes to eliminate bias and overfitting and preprocessing the data.

2) The ToN-IoT dataset also has many issues, including class imbalance, categorical attributes, and missing values. For challenges using the ToN-IoT dataset, a hybrid approach was provided.

3) The ToN-IoT dataset was utilized to test several machine learning (ML), which are: naïve bias (NB), logistic regression (LR), decision tree (DT), k-Nearest Neighbor (KNN), support vector machine (SVM), random forest (RF), XGBoost, Adaboost.

The subsequent are the research's major contributions:

1) Propose a distributed machine learning IDS for IoT with comparison to another research.

2) Most existing detection algorithms are evaluated using the NSL-KDD, KDD-CUP99, and UNSW-NB15 datasets. These databases are out of date and do not cover current IoT threats. However, the effectiveness of the proposed model is evaluated using an actual ToN-IoT dataset. As assessment measures, accuracy, precision, recall, F1-Score, and false-positive rate (FPR) are utilized.

3) Resolving issues with the ToN-IoT dataset, such as class imbalance, missing values, and irrelevant attributes that impact the IDS model's performance.

4) The Chi² and correlation matrix were used to select the most important attributes.

5) The class imbalance problem was solved using the SMOTE approach.

The paper organization is as follows: The sections below provide a short overview of IDS for IoT. The ToN-IoT dataset is briefly described in Section III. In Section IV is described the experimental techniques. In Section 5, the findings of the

experiments are discussed. Finally, in Section VI, the conclusion is offered.

II. RELATED WORK

Previously, many machine learning methods were used to malicious datasets in malicious intrusion detection research. IoT devices, as previously stated, are lightweight and low-powered devices with limited computing ability to run traditional antimalware solutions [9]. As a result, research is undertaken to address these issues.

Alhanahnah et al [10] set out to solve this problem by developing IoT malware detection technologies that could operate effectively on any platform while being lightweight despite resource limits. Lightweight signatures were created from high-level code to create the suggested solution. The investigation proved that the signature generating mechanism is effective. The proposed method was found to have an 85.2 % detection rate with zero false positives using analytical approaches.

Ngo and Nguyen [11] also investigated the increase of malware targeting IoT sensors and enhanced the efficacy of current malicious software detection techniques. The research looked at several prior studies on IoT security. The pros and cons of various malware detection technologies were examined and contrasted. The study discovered that the ELF-header approach had a low false detection rate of 0.2 % using tabular comparisons. Furthermore, employing the coding scheme to combine malware samples enhanced detection accuracy to over 98 %, according to the data.

Su et al. [12] suggested a lightweight technique to detect and classify DDoS malware and normal IoT applications. The research used a convolutional neural network to conduct experiments, allowing resource-constrained IoT devices to function normally. The correctness of the suggested design was tested using a five-fold validation technique. With an average accuracy of 94 %, the recommended design predicted malware.

Nguyen et al. [13] also assessed the efficacy of three deep learning-based techniques in identifying IoT malicious software. The models were developed using attributes 1) fixed-size-byte series, 2) fixed-size-color image, and 3) variable sized-sequence data. The fixed-size byte sequence strategy was less accurate than the variable-sized and fixed-size color picture approaches, with an accuracy of 90.58 %. However, the study was regarded as initial, and the authors recommended that further tests be conducted to increase the accuracy.

Alasmay et al. [14] used multiple datasets to see the relationships and variations between malicious software on various systems. A method was constructed and utilized for categorizing android malware, IoT malware, and non-threatening samples using control flow graphs. A 10-fold validation procedure was used to assess the performance of these models. The convolutional neural network (CNN) model was shown to have a 99.66 % accuracy in detecting IoT malware from normal samples in the study.

Hasan et al. [15] used artificial neural networks (ANN), SVM, and LR as machine learning algorithms to identify attacks and abnormalities in IoT sensors at IoT sites. With a

99.4 % accuracy, the experiment suggests that CNN is the preferable approach to apply in IoT for intrusion detection systems.

Authors [16] suggested a revolutionary real-time, distributed, and lightweight IDS, efficiently combining edge, fog, and cloud computing. It enables sophisticated data processing at the intermediaries' level, decreasing the amount of data sent to the cloud. As a result, processing occurs at hubs, routers, or gateways. The IDS's AIS architecture is made up of three parts:

A training engine: trains detectors using data from an initial learning dataset. Because it necessitates complicated and powerful processing units, this stage is handled on the cloud layer.

An analyzer examines abnormalities provided by detectors in order to warn and reject false positive signals. To increase precision, the authors apply memory cell detectors and genetic algorithms. The analyzer engine is installed at the fog layer since this stage necessitates a greater connection between the infected edge nodes and the main engine.

Detector sensors: Each node in the network is equipped with detecting logic. Various detectors might recognize each form of attack in the suggested IDS, which is intelligent and distributed. When a threshold is exceeded, the anomaly is transmitted to the analyzer engine, resulting in an intrusion warning.

The essential work strengths are as follows: a) Combination of innovative analysis in the cloud with lightweight analysis in the fog-layer; b) botnet attacks are detected using a smart strategy, and c) detection of zero-day attacks and unknown attacks based on an online self-training method. The lightweight IDS efficiency was evaluated using two datasets: SSH Brute Force dataset, and KDD-Cup99. According to testing data, the three-layered suggested approach achieves a 3.51 % false-positive rate (FPR) with 98.35% and 97.83% precision.

A real-time combination of specification-based and anomaly-based IoT IDS was proposed by Bostani and Sheikhan [17]. It may be used to identify sinkholes and selective-forwarding attacks in 6LowPAN networks. This IDS operates in two stages: router-level specification detection and root-level anomaly detection. First, the routers examine aspects of the traffic of a network and host nodes on a local level. The first phase's findings are forwarded to the root node for the second step and then deleted from routers to save memory and CPU resources. At the root node, the second phase is global intrusion detection, which involves performing anomaly-based analysis on entering data packets. To demonstrate appropriate real-time detection, they use three main experimental tests, each with ten simulations: the first contracts with assessment values, the second with network scale (small and medium-size) to confirm independent scale-network IDS, and the third with the option to extend detected attacks such as wormhole. According to the results of simulated situational experiments, the proposed hybrid technique may reach a true positive rate of 76.19 % and a FPR of 5.92 %.

Moustafa et al. [9] introduced an ensemble NIDS based on existing statistical characteristics to reduce harmful events, including botnet cyberattacks against HTTP, MQTT, and DNS protocols in IoT systems. The model has three phases: a) Using a thorough study of the TCP/IP model, a collection of attributes is derived from the network traffic protocols. The authors used the Bro-IDS tool for the basic characteristics and created a new extractor module (that collaborates with Bro-IDS) to derive further statistical aspects of transactional processes. b) The correlation coefficient is applied to the result attributes in this step-in order to obtain the essential ones. This phase allows NIDS's computational cost to be reduced. An ensemble technique using the AdaBoost (Adaptive Boosting) algorithm disperses the network data. Then, to identify attacks, Decision Tree (DT), NB, and ANN ML algorithms are used. When compared to individual ML algorithms, the AdaBoost technique improves detection performance. It is capable of dealing with any situation through the computation of an error function, the minor differences of the feature vectors are used to learn and select which learners can correctly categorize each instance of the input data, and the error function is assigned to each occurrence. They used the UNSW-NB15 and NIMS botnet datasets. The ensemble approach achieved between 95.25 % and 99.86 % of DR and 0.01 % to 0.72 % of FPR.

Nguyen et al. [18] presented a self-learning anomaly-based IDS (DoT) that was autonomous. Their solution consists of Security Gateways that monitor system devices, as well as an IoT security service (which might be a service provider) that detects abnormalities in a device-type-specific mode. Network devices are automatically grouped based on their manufacturer's hardware and software specifications. Then, for each device type, anomaly models will be created. According to the authors, the used algorithm is Gated Recurrent Units (GRU), which is a recurrent neural network (RNN) that can train efficiently with little training data. As a result, final GRU models result from a collective learning process involving multiple Security Gateways while maintaining privacy. This IDS approach appears to be communication-efficient and ideal for distributed systems such as the internet of things. In order to identify the Mirai virus, the authors test their approach in a real-world smart home deployment. They have a DR with 95.6 % and no false alarms in 257 ms.

Illy et al. [19] presented a fog-to-things IDS architecture. The detecting method is implemented on two levels: the fog and cloud layers of the system. On the one hand, this design enables the authors to deal with their computationally demanding ML detection induced by ensemble learning (a combination of ML algorithms). On the other side, owing to fog detection provides for low latency detection and, consequently, quick reaction. As a result, anomaly detection is conducted first in the fog layer; if the traffic is detected as an attack, an alert is delivered to the security administrator. Additional analysis is performed in the cloud to categorize the kind of attack and provide it to him. They used a multi-expert mode and a multi-stage technique to evaluate alternative ML combinations. On the NSL-KDD dataset, they achieved 85.81 % overall accuracy for binary classification and 84.25 % overall accuracy for attack classification, respectively.

TABLE I. A SUMMARY OF APPROACHES FOR IoT MALICIOUS DETECTION

Authors	Study purpose	ML-methods	Data used for Evaluation
Alhanahnah [10]	Developing IoT malware detection technologies that could operate effectively on any platform while being lightweight despite resource limits.	Statistical technique	IoT malware dataset
Su [12]	Detecting and classifying DDoS	CNN	IoT DDoS malware dataset
Nguyen [13]	Identifying IoT malware.	Deep learning	They prepare their own data
Alasmary [14]	Detection of IoT network attacks.	KNN- ID3- Random Forest- AdaBoost- Multi-layer perceptron (MLP)- Naïve Bayes (NB)	Bot-IoT
Hasan [15]	Identifying attacks and anomalies	Neural Networks (NN), SVM, and logistic regression	Data collected from Kaggle
Hosseinpour [16]	Distributed IDS	Artificial Immune System (AIS)	KDD99 and SSH Brute Force from ISCX
Bostani [17]	A mixture of specification-based and Anomaly-based IDS	Unsupervised-Optimum Path Forest	NSL-KDD
Moustafa[9]	An ensemble NIDS	Decision Tree (DT), NB, and ANN	UNSW-NB15
Nguyen [18]	A self-learning anomaly-based IDS	a recurrent neural network	Real-world smart home
Illy [19]	A fog-to-things IDS	ensemble learning	NSL-KDD
Gonzalo et al. [20]	Detecting IoT attacks	CNN, LSTM	KDD99, NSL-KDD, CISC2010
Shafiq [21]	A new-feature selection algorithm.	Decision Tree (C4.5)- SVM-RF-NB	BoT-IoT

Gonzalo et al. [20] demonstrated an embedded IoT micro-security that uses a CNN prototype to identify URL-based cyberattacks on a client's IoT devices. For botnet detection, the add-on works in concert with an RNN-LSTM model housed on the back end servers. With an accuracy of 94.30 % and an F-1 score of 93.58 %, CNN can detect phishing attacks. Botnet attacks are detected using LSTM with a 94.80% accuracy when all malicious in the dataset are utilized.

Shafiq et al. [21] demonstrated a malicious intrusion model for IoT. this study developed a new feature selection technique and tested the newly developed technique on several machine learning techniques such as s, C4.5 decision tree, and Random Forest classifiers; they got more than 95% accuracy. A summary of algorithms that are used to construct IDS for IoT is presented in Table I.

III. STATE-OF-THE-ART DATASETS

KDD99 and NSL-KDD are the most extensively used NIDS/HIDS datasets. For assessment and testing, public attack datasets such as CAIDA [22], DEFCON [23], ADFA IDS[24] , KYOTO [25], and ISCX 2012 [26] are accessible. The most recent are either unlabeled data or unavailable data from certain nations, or data exclusive to a domain.

KDD99 [27] is a dataset used for constructing the robust NIDS for detecting "dangerous" connections from "great" ones. The dataset is a feature-extracted edition of the DARPA dataset. KDD99 comprises data from a military network with

inserted attacks that are divided into four categories: i) DoS; ii) remote to user; iii) user to root; iv) probing. Using the Bro-IDS tool, KDD99 is based on 41 attributes for each sample+, as well as the class label. The attributes are divided into four categories [27]:

- 1–9: the fundamental attributes of each TCP connection.
- 10-22: attributes suggested by domain knowledge.
- 23-31: a two-second time frame was used to calculate traffic attributes.
- 32-42: host capabilities are intended to evaluate cyberattacks lasting longer than two seconds.

KDD99 is common and widely used for experimental analysis by security researchers. Various efforts [28, 29] were created to minimize the number of characteristics by picking the most important ones from the initial 41. However, numerous studies, such as [30, 31], have found KDD99 to have drawbacks, a few of the most notable ones:

The probability distributions of the testing and training sets diverge. To put it another way, KDD99 has imbalanced categorization.

- The data set is no longer current (1999).
- New attacks are not available.
- The data collected are not from an IoT system.

NSL-KDD [32] is an improved version of KDD99 that addresses its shortcomings. First, duplicate entries are deleted from the whole dataset. Second, a range of samples from the original KDD99 was chosen to acquire accurate findings from classifier systems. Third, the issue of an uneven probability distribution is no longer an issue. The lack of current low-footprint attack scenarios is a fundamental flaw in this collection.

UNSW-NB15 [33] was built by the Australian Centre for Cyber Security in 2015. Its purpose is to create a mixture of modern real-world activities and synthetic modern attacks behaviors. There are around two million and 540,044 records in four CSV files. Those records were created from 100GB of raw data recorded using the tcpdump utility (in pcap files).

The IoT dataset by Sivanathan et al. [34, 35]. Deals with categorization for IoT sensors based on network traffic characteristics. The authors provide a brilliant ecosystem for 28 IoT sensors, including cameras, lighting, plugs, motion sensors, appliances, and health-monitoring devices. They use statistical analysis to provide essential insights into network traffic patterns utilizing attributes such as port numbers, activity cycles, signaling patterns, and encryption suites. They also synthesized network traffic traces from their infrastructure for six months and provided them to the scholarly community.

The CICIDS database [36] is a recent Intrusion dataset provided by the Canadian Institute for Cyber-security, to represent the most recent attacks similar to real-world data. It was created using HTTP, HTTPS, FTP, SSH, and e-mail protocols to model the abstract behavior of 25 users. CIC-FlowMeter examines the data, including labeled data based on timestamps, starting, and ending IP addresses, ports, protocols,

and attacks. The authors developed the B-Profile technique to describe the behavior of FTP, SSH, HTTP, HTTPS, and e-mail protocols in order to simulate realistic traffic. While capturing the data, the authors used Brute Force FTP, SSH Heartbleed, and DDoS attacks. Unlike current standard IDS datasets, the assessment system [37] identified eleven critical attributes required to develop a valid benchmark dataset.

The CSE-CIC-IDS 2018 [38] dataset is a one-of-a-kind IDS dataset that has emerged to replace poor datasets that restrict IDS/NIDS experimental assessments. CSE-CIC-IDS2018 is an anomaly-based dataset containing intrusions in the network to overcome the usage of signature datasets: a) dos; b) Heartbleed; c) botnet; d) brute-force; e) DDoS; f) and web attacks were among the seven attack scenarios mentioned by the authors. The attack architecture consists of 50 nodes, whereas the target organization is divided into five departments, each with 30 servers and 420 hosts. CICFlowMeter-V3 was used to extract 80 characteristics from network traffic and system logs.

BoT-IoT [39] The ACCS Cyber Range Lab created a network environment based on IoT that includes both regular and botnet traffic. The Ostinato and Node-red tools were used to create IoT and non-IoT network traffic, respectively. The Argus program was used for extracting the dataset's original 42 attributes from a total of 69.3GB of pcap files. The collection comprises 477 normal flows (0.01 %) and 3,668,045 assault flows (99.99 %), totaling 3,668,522 flows. The dataset contains traffic from DDoS, DoS, OS, Data exfiltration, Keylogging attacks, and further DDoS and DoS operations put up on the protocol utilized. The main lack in this dataset is that it comprises over 99 % botnet traffic but just about 1% regular traffic.

TABLE II. AVAILABLE DATASETS

Dataset	Dataset Advantages	Dataset Disadvantages
KDD99	<ul style="list-style-type: none">KDD99 is the most widely deployed dataset.Data that has been labeled and has 41 attributes for each connection and the class description.DOS, remote-to-user, user-to-root, and probing attacks are all used.(PCAP) network traffic is provided.	<ul style="list-style-type: none">The dataset is out of date, and KDD99 has imbalanced classes.Not for the internet of things (IoT) systems.
NSL-KDD	<ul style="list-style-type: none">It is an upgraded version of KDD99 that addresses the limitations of KDD99.no duplicated records in the training and test sets.	<ul style="list-style-type: none">There are not enough current low-footprint attack scenarios.Not for the internet of things (IoT).
UNSWNB15	<ul style="list-style-type: none">It offers real-world modern regular activities and synthetic modern attack behaviors.Network traffic (PCAP) and CSV files are available.	<ul style="list-style-type: none">Because recent attacks and typical network traffic behave similarly, it is more complicated than the KDD99 dataset.
Sivanathan Dataset	<ul style="list-style-type: none">This IoT network traffic dataset is based on a real-world IoT network.CSV and PCAP files are available.	<ul style="list-style-type: none">Data that has not been tagged.No attack data is required for the IoT device proliferation and traffic characterization.
CICIDS	<ul style="list-style-type: none">labeled network flows used for building IDS based on machine learning.PCAP and CSV files are available.Brute Force, DoS, Heartbleed, Web-Attack, Botnet, and DDoS cyberattacks.	<ul style="list-style-type: none">Not public.Not for the internet of things (IoT).
CSE-CICIDS2018	<ul style="list-style-type: none">PCAP, CSV, and log files are available.Brute-force, Botnet, DoS, DDoS, and Web attacks are all implemented.It is a dynamically produced dataset that may be modified, extended, and replicated.	<ul style="list-style-type: none">Not public.Not for the internet of things (IoT).
BoT-IoT	<ul style="list-style-type: none">IoT network traffic dataset.PCAP and CSV files are available.	<ul style="list-style-type: none">The main lack in this dataset is that it comprises over 99 % botnet traffic but just about 1% regular traffic.

KDD99 is the most often used network dataset, as indicated in Table II. Since 1999, it has been in use. It is, unfortunately, out of date. NSL-KDD was built to overcome the limitations of KDD99. There are no duplicate records, and the data is balanced. UNSW-NB15 was proposed as a replacement for NSL-KDD, which lacks contemporary attacks. It is a well-known dataset that has been subjected to recent attacks. Meanwhile, when it comes to similarities between new attacks and normal activities, it is more complicated than KDD99. The Sivanathan et al. dataset, CSE-CIC-IDS 2018, and CICIDS are examples of more recent network datasets. Compared to the other datasets offered, Sivanathan's work is the only one that includes IoT network traffic. It is, however, intended for the proliferation of IoT devices rather than intrusion detection. CICIDS and CSE-CIC-IDS 2018 have labeled records but do not target IoT system security despite having an up-to-date attack list.

IV. ToN-IoT DATASET

The ToN-IoT dataset was used in this investigation. The ToN-IoT includes telemetry data from linked devices, Linux operating system data, Windows operating system logs, and IoT network traffic, among other data sources acquired from the entire IoT system. A medium-scale IoT network provides diverse data. ToN-IoT was designed by the UNSW Canberra IoT Labs and the Cyber Range. The ToN-IoT repository contains the ToN-IoT dataset [40]. Furthermore, the ToN-IoT was represented in CSV format with a labeled column indicating attack or normal and a sub-category attack-type. Various types of cyberattacks, such as ransomware, password attack, scanning, denial of service (DoS), distributed denial of

service (DDoS), data injection, backdoor, Cross-site Scripting (XSS), and Man-In-The-Middle (MITM) were represented. Various IoT and IIoT sensors were targeted in these attacks, launched, and gathered across the IIoT network. The dataset's details may be found in [40].

1) *ToN-IoT network dataset*: The network ToN-IoT dataset contains 44 attributes and a label classified as normal or attack for each data point. Fig. 1 shows the statistics for network data samples in the train-test ToN-IoT dataset.

2) *ToN-IoT Linux dataset*: Linux datasets are partitioned into three categories disk, memory, and process CSV files. The first CSV file contains attributes for disk usage in normal behavior and attack. The second CSV file is related to memory activity, containing ten attributes, a label column labeled as normal or attack, and an attack-type containing attack type (DoS, DDoS). The last file belongs to processes in Linux operating system. The Linux process ToN-IoT contains 14 attributes and an attack type for each data point. Fig. 1 shows the statistics for all Linux data records in ToN-IoT.

3) *ToN-IoT Windows dataset*: Windows datasets are contained records for windows 7 & 10. Windows 7 CSV file contains 133 attributes, labeled as normal or attack, and attack-type containing attack type (DoS, DDoS). Windows 10 CSV file contains 125 attributes, labeled as normal or attack and attack-type, which contain attack type (DoS, DDoS). The statistics for all Windows data in the ToN-IoT were presented in Fig. 1.

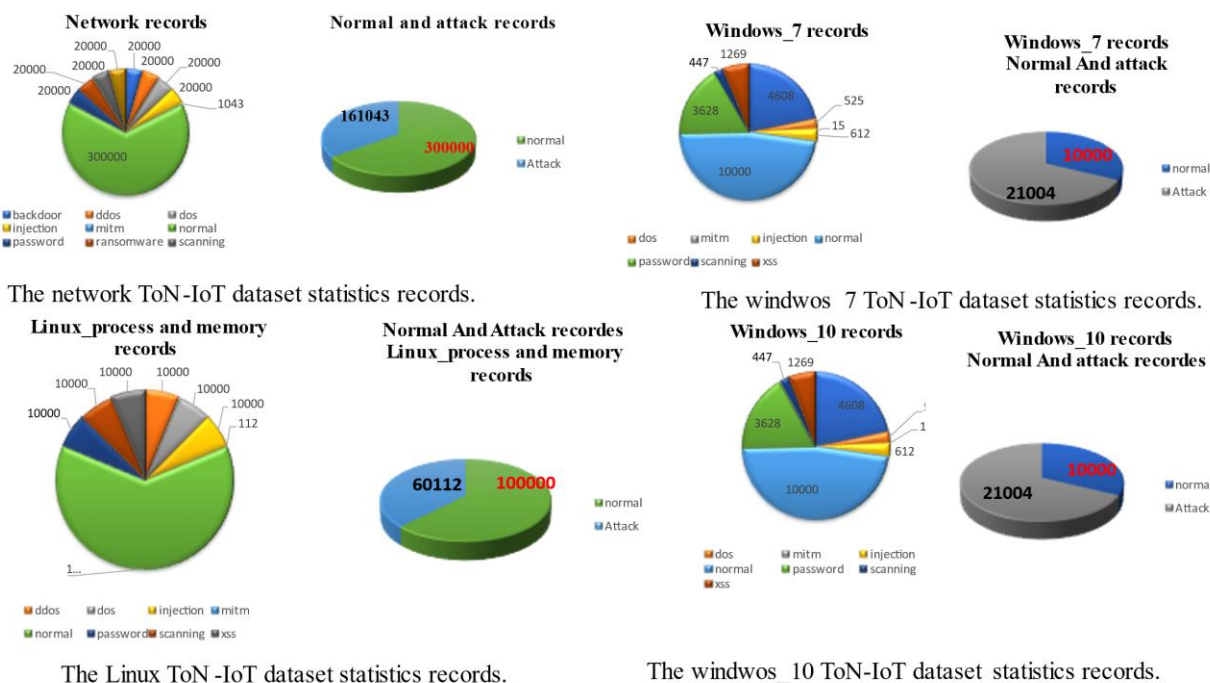


Fig. 1. ToN-IoT Statistics.

V. DISTRIBUTED IDS

This part of work discusses the architecture of the proposed model, system components of the proposed detection model, and the various detection nodes in proposed model.

A. Model Architecture

The primary purpose of the suggested detection system for IoT networks is to make on-demand security services more convenient while also preventing attacks. The proposed detection system employs a machine learning for detecting attacks in the network traffic within the IoT network and in all other nodes in IoT systems. As shown in Fig. 2, the proposed detection system functions primarily in various stages/phases - cloud phase, fog-network-detection phase, and a fog-host detection phase.

B. Machine Learning Methods

The ToN-IoT dataset has been used to evaluate various machine learning (ML) approaches. The chosen algorithms are utilized for training, and testing ML approaches with various parameters in the preprocessing phase of data for intrusion detection. The accuracy, precision, recall, F1-Score, false-positive rate (FPR), and confusion matrix were used to evaluate the different classifiers. The methodologies utilized have demonstrated great performance in the production of IDSs and have proven to be successful in various industries. This study look at the logistic regression (LR), naïve bias (NB), support vector machine (SVM), decision tree (DT), random forest (RF), k-Nearest Neighbor (KNN), Adaboost, and XGBoost techniques, among others [41], [42].

C. Model Nodes

In this section each node in the proposed model will be discussed.

1) *Malicious network detection node (Cloud layer):* The framework for malicious/intrusion detection comprises the default procedure in machine learning:

- a) Data preprocessing and feature engineering.
- b) Training machine learning models.
- c) Evaluate the selected model.

The deployed IDS in the cloud was established using various feature-engineering techniques discussed in the next section.

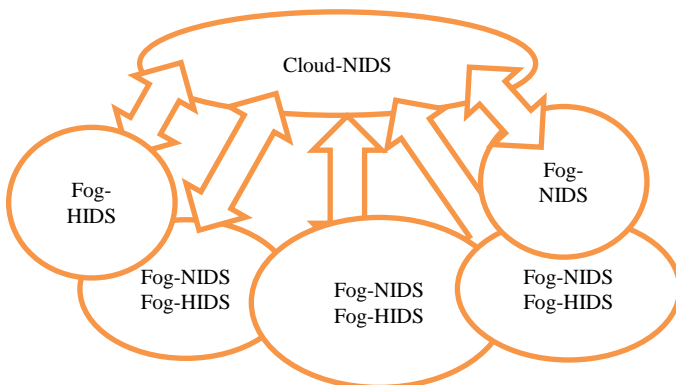


Fig. 2. The Proposed Detection System.

ToN-IoT preprocessing: Filtering and preparing are the most critical steps before supplying data into machine learning in order to achieve high performance. The used dataset has numerous obstacles, including missing values, categorical characteristics, and class imbalance. Unnecessary attributes may impact the performance of the chosen ML algorithms. Using permutations of multiple preprocessing and normalizing strategies, this work tested the selected ML algorithms using several preprocessing techniques.

- **Missing value imputation:** Missing values are common in the ToN-IoT. These missing values must be addressed appropriately. In the proposed model, the imputation of missing values is substituted with the most frequent value in each feature containing missing data. A second an approach was imputed numerical features using mean value.
- **Converting categorical attributes to numerical:** There are various categorical attributes in the ToN-IoT dataset. Numerical values must be assigned to the category characteristics. One-hot encoding was used to achieve this goal.
- **Class-imbalance:** The SMOTE technique was utilized to balance the classes in the used dataset. The ToN-IoT dataset is plagued with class imbalance distributions. Solutions to the imbalanced problem, oversampling, under-sampling, and hybrid techniques were proposed. Oversampling is the practice of duplicating the minority class points. Several researchers utilized it. However, this approach has the drawback of overfitting these spots. Others employ under-sampling, which reduces the dominating class's score. The problem with this method is that some of the elements that have been removed may be necessary for accurately portraying the class. A hybrid strategy was used; it duplicates minority class points while removing certain majority class points. Synthetic Minority Oversampling Technique (SMOTE) [43], [44] enhances basic random oversampling by providing synthetic minority class samples, addressing the overfitting problem that can occur with simple random oversampling. SMOTE creates new data points instead of replicating old ones. A linear combination of two comparable minority samples is used to generate extra minority data points.
- **Several attributes such as timestamp, IP-address, source-port, and destination_port were removed from the dataset since they may cause overfitting.**

The two key steps used during feature-engineering development are preprocessing based on the mentioned dataset challenges and data normalization. For high performance, ML approaches are evaluated using a variety of feature-engineering techniques:

Feature selection: Various aspects must be checked for intrusion detection, some of features will be valuable while others will be useless. The feature selection procedure is assigning a score to each potential feature and picking the best (k) attributes. A function of both is obtained by counting the frequency of a feature in training for each positive and negative

class occurrence separately. Non-essential attributes are removed, increasing accuracy, decreasing computation time, and reducing the overfitting problem, resulting in better performance. The used feature selection technique was χ^2 , which is a filter method.[31], [45].

$$\chi^2 = \sum_{i=1}^m \sum_{j=1}^n \frac{(O_i - E_i)^2}{E_i} \quad (1)$$

where m indicates the no of attributes, n indicates the no of classes, O_i is the observed frequency, and E_i is the expected frequency.

- **Data normalization:** The ToN-IoT contains attributes with varying values, and some attributes have larger values than others. Because a technique may be slanted toward characteristics with larger values, differing values out of range might lead to inaccurate results. As a result, data normalization is critical in preventing outweighing attributes with greater values over attributes with smaller values by scaling the feature vector. Min-Max is used to scale data between [0:1] as presented in Eq. (2).

$$Z = \frac{x - x_{min}}{x_{max} - x_{min}} \quad (2)$$

where x reflects the feature-value, Z reflects the feature-value after normalization, the maximum and minimum values of the feature are x_{max} and x_{min} .

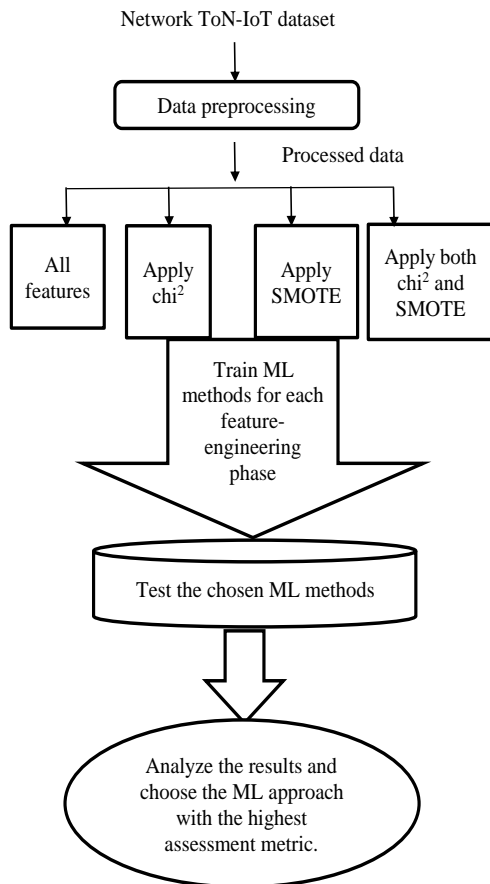


Fig. 3. The Procedure to Evaluate Network Dataset [41].

The training process: All ToN-IoT datasets are in CSV extension; initially, the ToN-IoT dataset was divided into two sets. The first set comprises training with 70% of the dataset. The second set contains unseen data for evaluating the performance of the selected ML algorithms. Before employing any preprocessing to the ToN-IoT, the splitting step was completed to avoid data leaking. The effectiveness of the chosen machine learning algorithms is evaluated using a variety of assessment measures, which will be provided in the next section. The previous steps associated with evaluating the performance of various ML algorithms utilizing ToN-IoT datasets are summarized in Fig. 3 and 4.

Classifier performance evaluation: Based on the ToN-IoT dataset, numerous metrics were utilized to assess the efficacy of various machine learning approaches. The chosen assessment techniques were chosen because they provide a detailed explanation of the outcomes for machine learning-based malicious detection [46].

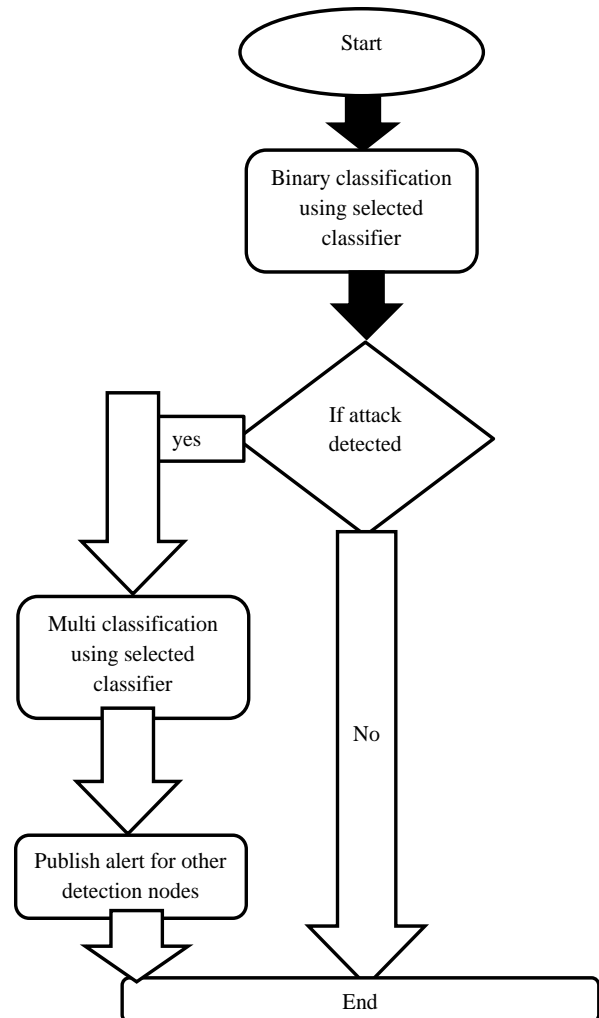


Fig. 4. The Overall Process for Malicious Detection.

The first metric is accuracy, which measures a technique's overall efficiency as a proportion of instances accurately identified as normal or attacks. The precision metric, which shows the proportion of accurately recognized attacks out of all

detected attacks, is the second metric. The third metric is recall, which represents the proportion of properly recognized attacks in the test dataset as a fraction of all attacks. The fourth metric is the F1-score. The final metric was the false-positive rate (FPR) [46]. These carefully chosen metrics are defined as follows:

$$\text{Accuracy} = \frac{TP+TN}{TP+TN+FP+FN} \quad (3)$$

$$\text{Precision} = \frac{TP}{TP+FP} \quad (4)$$

$$\text{Recall} = \frac{TP}{TP+FN} \quad (5)$$

$$\text{F1 - score} = 2 \times \frac{(\text{precision} * \text{recall})}{(\text{precision} + \text{recall})} \quad (6)$$

$$\text{FPR} = \frac{FP}{FP+TN} \quad (7)$$

Where true positive (TP) is the total number of actual attack records that are correctly identified as attacks. True Negative (TN) refers to the total number of real records that are correctly classified as normal records. False Negative (FN) refers to the total number of real attack samples that are incorrectly detected as normal. False Positive (FP) refers to the total number of normal samples that are incorrectly identified as attacks.

2) *Malicious network detection node (Fog layer):* In the fog computing layer, this work offer an IDS in the proposed architecture. Devices in this tier have more effective attributes than those on the IoT edge layer. It is feasible to use intrusion\malicious detection to monitor the IoT system without sending the data to the cloud, eliminating the latency issue that has plagued several studies advocating cloud layer analysis. The fog layer has processing nodes nearest to the physical IoT system, processing instruments, and edge storage to identify threats more quickly. A binary classification approach and a multi-class classification method are used in the architecture to detect intrusions.

The process is shown in Fig. 5.

1) The fog node connects each terminal device to the network using various protocols and collects data created by each terminal sensor in real-time[47].

2) The original data is preprocessed and trained by the cloud server: The entire training dataset is collected on the cloud server, and the entire training procedure is completed there, including the generation, and saving of a training model.

3) The fog node transmits a detection command: After establishing a communication link with the terminal device, the fog node gathers a considerable quantity of network data and sends a detection instruction to the cloud server.

4) The cloud server provides the training phase: The cloud server sends the data preprocessing pipeline and the trained classification prototype to the fog node after receiving the detection instruction.

5) Fog-node detection: The fog-node receives the model and utilizes it for data preprocessing and detection, producing detection results.

6) Malicious response: The discovered anomalous data are forwarded to the malicious response module, which performs the necessary processing [47].

In the fog layer, the same malicious network IDS model was used, it was trained in the cloud layer.

3) *The host malicious detection node (fog layer):* The fog layer contains the operating system (OS) devices in the IoT system. a malicious detection model was deployed for each device in the fog layer in the IoT system. The deployed model is called a host intrusion detection system. A host IDS is considered to run on a single machine and protect it from interruptions or malicious attacks that could harm the device – or data. A HIDS uses the measurements in the host environment. These supplies are sent into the HIDSs as input.

Based on the selected ToN_IoT dataset, two operating systems (Linux and Windows 10&7) were included in the dataset. Based on these data, an intrusion model was designed for each partition of data to detect included attacks.

a) *Windows dataset (preprocessing):* The correlation study significantly influences the applicability of attributes in defining security events using machine learning models. We built a correlation coefficient function [43] for ranking the attributes powers into a range of [-1, 1] in order to estimate the correlation coefficient between the attributes without the label characteristics on the Windows 7 and 10 datasets. The direction of the link is indicated by the sign of the correlation coefficient, while the magnitude (i.e., how near it is to -1 or +1) reflects the strength of the relationships between the characteristics [43]. The correlation matrix was tweaked to find the most associated attributes with a cut-off value of 0.85 % or above. Table III shows the top ten most associated traits in each dataset. As presented in Table III illustrate the most linked attributes of the Windows 7 and 10 datasets, respectively. Machine/deep learning algorithms would.

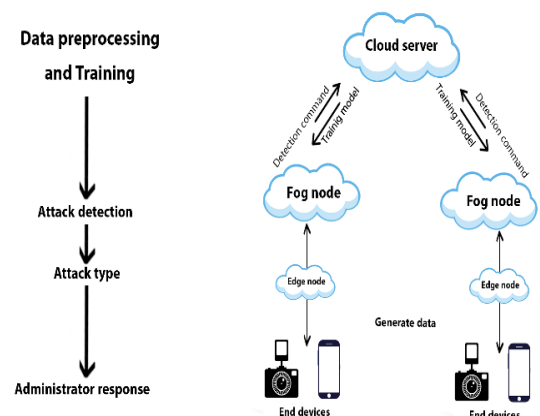


Fig. 5. Cloud-Fog Intrusion Detection Scheme.

TABLE III. THE TOP TEN ATTRIBUTES

Attributes (win_7)	Attributes (win_10)
Process_Total_IO Other_Bytes_sec	Network_I.Intel_R.._82574_L_GNC_ Current_Bandwidth
Network_-_I.Intel_R_Pro- _000MT)_Bytes_Received_sec	Network_I_Intel.R_82574L GNC_Packets_Sent_Unicast_sec
Process_Total_IO_ Other_Operations_sec	Memory_Pool_Paged_Bytes
Process_Total_IO Data_Bytes_sec	Logical_Disk_Total Disk_Read_Bytes.sec
Process_Total_IO_Read_Bytes _sec	Memory_Page_Reads_sec
Network_I.Intel.R_ Pro_1000MT_Bytes_Received_sec	Network_I.Intel.R 82574L_GNC.Packets_Sent.sec
Process_Pool_Paged_Bytes	Memory.Modified_Page_List_Bytes
Process_Pool_Paged_Bytes	Process_IO_Data_Operations_sec
Network_I.Intel.RPro_ 1000MT.Packets_Received_sec	LogicalDisk_Total._Avg.Disk.Bytes_ Transfer
Process_Total_IO_Data__Operat ions_sec	Processor_pct_Processor_Time

b) *Preprocessing of Linux dataset:* Linux datasets are partitioned into three categories: disk, memory, and process. Timestamp and CMD attributes were eliminated from the dataset for obtaining high performance and far away from overfitting. The Correlation-matrices of the most critical attributes in the Win_7 dataset and Win_10 are extracted from another paper [48].

VI. DATASET EVALUATION

In this part, the architecture of the suggested model was evaluated; the evaluation is based on binary classification and multi-class classification.

The presented results in this section are based on the best outcomes from the experimentations, other outcomes for classifiers such LR, NB, Adaboost, and SVM are neglected since these classifiers have poor results.

Malicious detection for network dataset evaluation (cloud layer):

Based on the newly available ToN-IoT dataset, the efficiency of the deployed machine learning approaches were investigated for malicious identification. The best parameters stated in the literature were selected [49], [50]. The experiments for this work were carried out in Python 3.8. All trials were run on a Windows 10 computer with a Core i7 processor and 16 GB of RAM. An experimental methodology was utilized to evaluate the effectiveness of the selected ML algorithms using the ToN-IoT network.

- Binary classification [41]: The results for the network dataset are introduced in this section. In addition to the confusion matrix, the accuracy, precision, recall, F1-score, and FPR are offered to evaluate the chosen ML algorithms. In general, the XGBoost produces considerable results for binary classification depending on multiple feature engineering strategies applied to the dataset.

Using all attributes, for XGBoost, the training accuracy is 0.992 %, the testing accuracy is 0.991 %, the recall is 0.984 %, the precision is 0.991 %, and the F1-score is 0.987 %, according to the results. With a significance of 0.007, k-Nearest Neighbor (KNN) exhibits relevance in the scenario of false-positive rate (FPR). The findings for the best ML techniques are shown in Table IV. The kNN, on the other hand, was the second-best technique. The training accuracy is 0.989 %, the testing accuracy is 0.988 %, the recall is 0.986 %, the precision is 0.979 %, and the F1-score is 0.983 %, according to the kNN findings. Naive bias is the poorest technique (NB). The heterogeneity of data in ToN-IoT datasets might explain the ML technique's performance variances. The findings of RF and DT are practically identical.

As a feature selection strategy, the Chi² was used. After using Chi² to evaluate ML algorithms based on a variety of criteria, because the optimum assessment measure is obtained with only 20 features, the best 20 attributes were selected from the total 108 attributes. After Chi², XGBoost provides considerable results, almost identical to testing with all characteristics. The training accuracy is 0.984 %, the testing accuracy is 0.983 %, the recall is 0.984 %, the precision is 0.967 %, the F1-score is 0.975 %, and the FPR is 0.008 %, according to the findings. The KNN approach was the second-best technique. Naive bias is the poorest technique (NB).). The findings for the ML techniques are shown in Table IV.

Because ToN-IoT has an issue with class imbalance, another testing approach based on SMOTE was used; XGBoost and KNN also have the same best outcome with 0.990 % accuracies. Recall is 0.976 %, accuracy is 0.997 %, F1-score is 0.986 %, and FPR is 0.013 % for XGBoost in terms of other assessment criteria. KNN has a recall of 0.981 %, accuracy of 0.990 %, F1-score of 0.985 %, and FPR has the highest score of 0.001 % to other ML algorithms. XGBoost is superior to KNN since it requires less training and testing time.

Finally, the selected ML algorithms were assessed using Chi² and SMOTE for binary classification. With Chi² and SMOTE, KNN produces considerable results. The findings for the ML techniques are shown in Table IV.

- Multi-class classification: The dataset contains an attribute type that displays the attack sub-class for multi-class classification tasks, as stated before. There are ten sub-classes in ToN-IoT. In this part, candidates' ML methods will be analyzed for evaluating multi-classification tasks. When assessing prospective ML methods for a multi-class classification task, several factors must be considered. To begin, LR is most commonly employed to solve binary classification task and cannot be immediately used for multi-class classifications. As a result, to construct LR for multi-class classification, the one-vs-rest (OvR) approach is applied. Accuracy, precision, recall, F-score, and confusion matrix are the assessment measures used to compare all models. The multi-classification findings are summarized in Table V. When comparing all ML algorithms, XGBoost achieves decent results. The training accuracy for XGBoost is 0.986 percent, the testing accuracy is 0.983 %, the recall is 0.953 %, the

F1-score is 0.949 percent, and the FPR is 0.008 %. KNN comes in second with scores of 0.981 % for training accuracy and 0.979 % for testing accuracy, and the AdaBoost classifier has the worst metrics of all tested ML methods. SVM is the most time-consuming in terms of training and testing.

The Chi² feature selection methodology after was used evaluating all of the specified ML algorithms over the whole dataset. Chi² will assess all ML algorithms with the best 20 attributes from all 108 attributes. XGBoost achieves considerable results in binary classification, for example. The training accuracy is 0.985 percent, the testing accuracy is 0.982 %, the recall is 0.950 %, the precision is 0.943 %, the F1-score is 0.946%, and the FPR is 0.008 %. Table V. displays the results of all ML techniques applied with the Chi² approach.

KNN was the second-best approach, AdaBoost is the poorest model.

Another approach based on the SMOTE technique was used. As seen in Table V, XGBoost outperforms other commonly used ML algorithms. Finally, the selected ML algorithms were assessed using the Chi² and SMOTE methodologies on the basis of the multi-class classification issue. With the Chi² and SMOTE methods, XGBoost achieves considerable results. The training accuracy of XGBoost is 0.980 %, while the FPR is 0.019 %. Table V. displays the outcomes of chosen ML approaches using the Chi² and SMOTE techniques.

In the cloud layer, the network intrusion detection was suggested to be deployed in the cloud for binary and multi-class classification problems, as shown in Fig. 6.

TABLE IV. THE RESULTS OF THE BINARY CLASSIFICATION (NETWORK_DATA)

Data	Models	Train Acc	Acc	Precision	Recall	F1-score	FPR	Confusion Matrix
Network All attributes	DT	0.981	0.980	0.960	0.982	0.971	0.022	[[88032 1966] [851 47464]]
	RF	0.980	0.979	0.959	0.984	0.971	0.023	[[87949 2049] [792 47523]]
	KNN	0.989	0.988	0.986	0.979	0.983	0.007	[[89325 673] [995 47320]]
	XGB	0.992	0.991	0.984	0.991	0.987	0.009	[[89220 778] [442 47873]]
Network Chi ²	KNN	0.984	0.982	0.983	0.965	0.974	0.009	[[89170 828] [1694 46621]]
	XGB	0.984	0.983	0.984	0.967	0.975	0.008	[[89247 751] [1598 46717]]
Network SMOTE	KNN	0.991	0.990	0.981	0.990	0.985	0.001	[[89067 931] [504 47811]]
	XGB	0.993	0.990	0.976	0.997	0.986	0.013	[[88789 1209] [125 48190]]
Network Chi ² & SMOTE	KNN	0.985	0.982	0.959	0.989	0.974	0.023	[[87960 2038] [515 47800]]
	XGB	0.986	0.982	0.954	0.996	0.975	0.026	[[87670 2328] [190 48125]]

TABLE V. THE OUTCOMES OF THE MULTI-CLASS CLASSIFICATION (NETWORK_DATA)

DATA	Models	Train Acc	Acc	Precision	Recall	F1-score	FPR
Network All attributes	AdaBoost	0.399	0.399	0.339	0.229	0.274	0.505
	KNN	0.981	0.979	0.933	0.925	0.929	0.009
	XGB	0.986	0.983	0.945	0.953	0.949	0.008
Network Chi ²	AdaBoost	0.498	0.497	0.352	0.363	0.358	0.424
	KNN	0.980	0.977	0.929	0.928	0.929	0.014
Network SMOTE	KNN	0.976	0.976	0.901	0.956	0.928	0.018
	XGB	0.980	0.979	0.907	0.968	0.937	0.018
Network Chi ² & SMOTE	KNN	0.971	0.976	0.899	0.956	0.927	0.019
	XGB	0.980	0.978	0.911	0.967	0.939	0.019

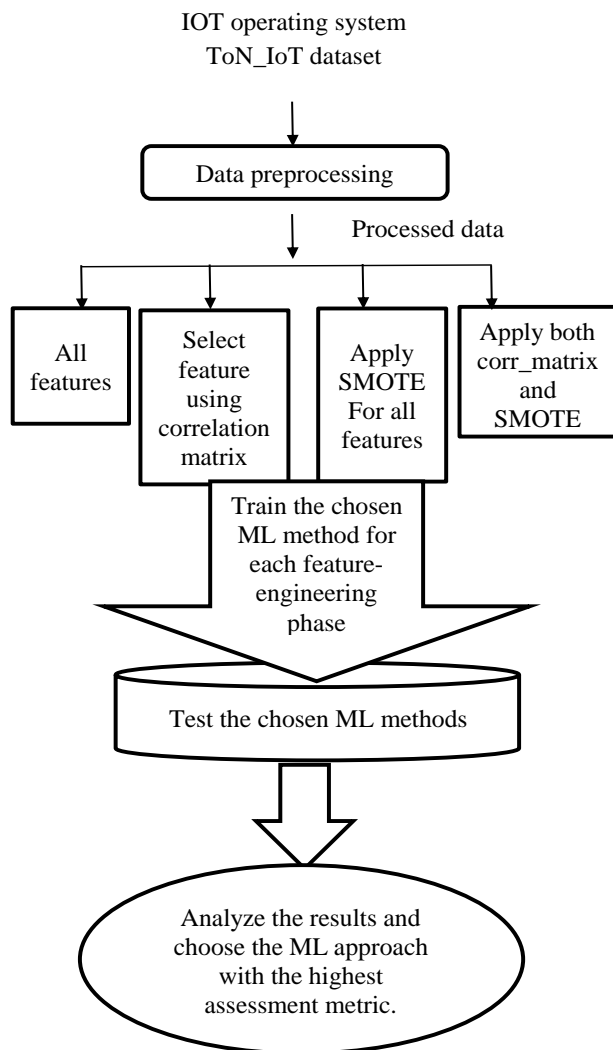


Fig. 6. The Process for Evaluating ML Methods on the OS ToN-IoT Dataset.

After applying various feature engineering techniques for the network ToN_IoT dataset, the XGBoost classifiers obtains optimal results using chi2 and SMOTE techniques that were used for class balancing and feature selection.

- Malicious detection for Linux dataset evaluation (fog layer): The same intrusion model was deployed in the fog layer with the same specification as discussed in earlier sections.
- Linux dataset evaluation (fog layer): This section focuses on the effectiveness of the used ML techniques for host malicious detection using the newly released Linux ToN-IoT dataset. Linux dataset was partitioned into three categories process, disk, and memory.
- Process_Linux (Binary classification): This section showed the findings for the Linux ToN-IoT dataset. In general, XGBoost is useful for binary classification. This experiment begin by impute missing values and then use the Min-Max normalization approach. Training accuracy is 0.994 %, testing accuracy is 0.993

%, recall is 0.990 %, precision is 0.991 %, and F1-score is 0.991 %, according to the findings. In terms of false-positive rate (FPR), XGBoost is significant at 0.005%. Table VI displays the results of all ML techniques applied without the SMOTE approach. The KNN approach, on the other hand, was the second-best methodology.

Because ToN-IoT has a class imbalance issue, another testing methodology based on SMOTE approach was used; RF and DT had the same better outcome with 0.992 % accuracies. In terms of other assessment measures, F1-score is 0.989 % for DT and RF, and FPR is 0.007 % for DT, which is superior to RF. Table VI displays the outcomes for several ML algorithms.

Multi-class classification (Process_Linux): For multi-class classification tasks, the Linux ToN-IoT dataset includes a feature type that displays the attack sub-category. When assessing prospective ML algorithms for a multi-class classification issue, several factors must be taken into account. The multi-classification findings are summarized in Table VII.

When compared to other ML algorithms, XGBoost achieves decent results. The training accuracy for XGBoost is 0.962 %, the testing accuracy is 0.954 %, the recall is 0.870 %, the precision is 0.909 %, the F1-score is 0.889 %, and the FPR is 0.004 %. DT and RF come in second with scores of 0.981 % for training accuracy and 0.979 % for testing accuracy, and the AdaBoost classifier has the worst statistics of all tested ML methods.

Another procedure was used based on the SMOTE method. As stated in Table VII. DT has the greatest outcomes compared to other used ML techniques.

- Memory_Linux (Binary classification): In this section, the results for memory-based Linux ToN-IoT dataset were presented. In general, RF is significant for binary classification. To begin with, the results reveal that the training accuracy is 0.999 %, the testing accuracy is 0.997 %, the recall is 0.993 %, the precision is 0.997 %, the F1- score is 0.995 %, and the FPR is 0.001 percent, with XGBoost achieving the best second result. Table VIII displays the results of all ML techniques applied without the SMOTE approach. NB is the worst approach.

Because ToN-IoT has a class imbalance problem, another approach based on SMOTE was used; RF produced the best result with 0.997 % accuracy.

- Multi-class classification (Memory_Linux): For multi-class classification tasks, the Linux memory ToN-IoT dataset includes a feature type that displays the attack sub-class. The multi-classification findings are summarized in Table IX.

When compared to other ML algorithms, XGBoost achieves decent results. The training accuracy for XGBoost is 0.986 %, the testing accuracy is 0.982 %, the recall is 0.922 %, the precision is 0.965 %, the F1-score is 0.943 %, and the FPR is 0.001 %. RF comes in second with scores of 0.988 % for training accuracy and 0.982 % for testing accuracy.

TABLE VI. THE OUTCOMES OF THE BINARY CLASSIFICATION (LINUX_PROCESS_DATA)

DATA	Models	Train Acc	Acc	Precision	Recall	F1-score	FPR	Confusion Matrix
process All attributes	KNN	0.992	0.990	0.988	0.985	0.986	0.007	[[29549 215] [281 17989]]
	XGB	0.994	0.993	0.991	0.990	0.991	0.005	[[29606 158] [181 18089]]
process SMOTE	DT	0.997	0.992	0.989	0.989	0.989	0.007	[[29555 209] [192 18078]]
	RF	0.997	0.992	0.988	0.990	0.989	0.008	[[29540 224] [181 18089]]
	XGBOOST	0.994	0.992	0.985	0.995	0.990	0.009	[[29483 281] [88 18182]]

TABLE VII. THE OUTCOMES OF THE MULTI-CLASS CLASSIFICATION (LINUX_PROCESS_DATA)

DATA	Models	Train Acc	Acc	Precision	Recall	F1-score	FPR
process All attributes	DT	0.969	0.952	0.901	0.889	0.895	0.005
	RF	0.969	0.950	0.875	0.839	0.857	0.006
	XGBOOST	0.962	0.954	0.909	0.870	0.889	0.004
Process SMOTE	DT	0.943	0.950	0.838	0.881	0.859	0.01
	RF	0.943	0.948	0.831	0.871	0.851	0.011
	XGBoost	0.934	0.949	0.811	0.884	0.846	0.017

TABLE VIII. THE OUTCOMES OF THE BINARY CLASSIFICATION. (MEMORY_LINUX)

DATA	Models	Train Acc	Acc	Precision	Recall	F1-score	FPR	Confusion Matrix
Memory All attributes	DT	0.999	0.996	0.995	0.991	0.993	0.002	[[29867 66] [104 11997]]
	RF	0.999	0.997	0.997	0.993	0.995	0.001	[[29891 42] [83 12018]]
	XGBoost	0.998	0.997	0.996	0.992	0.994	0.002	[[29887 46] [93 12008]]
Memory SMOTE	DT	0.999	0.996	0.992	0.993	0.993	0.003	[[29837 96] [79 12022]]
	RF	0.999	0.997	0.995	0.995	0.995	0.002	[[29867 66] [64 12037]]
	XGBoost	0.998	0.996	0.991	0.996	0.993	0.004	[[29818 115] [49 12052]]

TABLE IX. THE RESULTS OF THE MULTI-CLASS CLASSIFICATION (LINUX MEMORY)

DATA	Models	Train Acc	Acc	Precision	Recall	F1-score	FPR
process All attributes	DT	0.988	0.982	0.947	0.928	0.937	0.002
	RF	0.988	0.982	0.964	0.918	0.941	0.001
	XGBoost	0.986	0.982	0.965	0.922	0.943	0.001
Process SMOTE	DT	0.972	0.981	0.874	0.947	0.909	0.003
	RF	0.972	0.981	0.878	0.938	0.907	0.003
	XGBoost	0.968	0.978	0.877	0.933	0.904	0.008

Another approach was used based on the SMOTE method. As stated in Table IX, DT has the top outcomes compared to other employed ML methods.

- Malicious detection for windows dataset evaluation (fog layer): This work focuses on the efficiency of the chosen ML methods for malicious detection using the

newly released Windows ToN-IoT dataset. The Windows dataset was partitioned into two categories, Win_10 and Win_7.

- Win_10 dataset (Binary classification): In this part, the outcomes for the Windows ToN-IoT were presented.

In general, XGBoost shows significance. Training accuracy is 1.0%, testing accuracy is 1.0%, and F1-score is 1.0%, according to the results. In the case of false-positive rate (FPR), XGBoost shows significance with 0.0. Table X. shows the results for the selected ML methods. Since ToN-IoT suffers from a class imbalance problem, another testing methodology was done based on SMOTE technique, XGBoost has the best result. Table X. shows the results for all used ML methods using SMOTE technique.

Another testing technique was based on the best selected attributes that were selected from a correlation matrix. XGBoost obtains the best result with and without SMOTE. Tables X shows the outcomes for all selected ML methods.

- Multi-class classification (Win_10): For multi-class classification issues, the ToN-IoT dataset includes a feature type that displays the attack sub-category. The multi-classification findings are summarized in Table XI.

When compared to other ML algorithms, XGBoost achieves decent results. XGBoost training accuracy is 1.0, its testing accuracy, recall, precision, and F1-score are all 1.0%, and its FPR is 0.00 %. Another testing approach based on the SMOTE technique was used. As seen in Table XI. XGBoost outperforms other commonly used ML algorithms.

- Win_7 dataset (Binary classification (Win_7): In general, for binary classification, XGBoost shows significant results for windows 7 dataset. Table XII displays the outcomes for the selected ML method.

ToN-IoT has a class imbalance problem, another testing methodology was done based on SMOTE technique, XGBoost has the best result.

XGBoost obtains the best result with and without SMOTE for multi-class classification. XGBoost shows significant outcomes. Table XIII displays the outcomes for the selected ML method.

TABLE X. THE OUTCOMES OF THE BINARY CLASSIFICATION. (WIN_10)

DATA	Models	Train Acc	Acc	Precision	Recall	F1-score	FPR	Confusion Matrix
WIN_10 All attributes	XGBoost	1.0	1.0	1.0	1.0	1.0	0.0	[[3045 0] [0 3287]]
WIN_10 All attributes (SMOTE)	XGBoost	1.0	1.0	1.0	1.0	1.0	0.0	[[3045 0] [0 3287]]
(10) Selected attributes	XGBoost	1.0	1.0	1.0	1.0	1.0	0.001	[[3043 2] [1 3286]]
(10) Selected attributes SMOTE	XGBoost	1.0	0.999	0.999	1.000	0.999	0.001	[[3042 3] [1 3286]]

TABLE XI. THE RESULTS OF THE MULTI-CLASS CLASSIFICATION FOR NORMAL RECORDS AGAINST ATTACK RECORDS (WIN_10)

DATA	Models	Train Acc	Acc	Precision	Recall	F1-score	FPR
WIN_10 All attributes	XGBoost	1.0	1.0	1.0	1.0	1.0	0.0
WIN_10 All attributes (SMOTE)	XGBoost	1.0	1.0	1.0	1.0	1.0	0.0
(10) Selected attributes	XGBoost	1.0	0.989	0.977	0.911	0.943	0.001
(10) Selected attributes SMOTE	XGBoost	1.0	0.986	0.868	0.912	0.890	0.001

TABLE XII. THE OUTCOMES OF THE BINARY CLASSIFICATION. (WIN_7)

DATA	Models	Train Acc	Acc	Precision	Recall	F1-score	FPR	Confusion Matrix
WIN_7 All attributes	XGBoost	1.0	0.999	0.999	0.998	0.999	0.00	[[3000 1] [3 1790]]
WIN_7 All attributes (SMOTE)	XGBoost	1.0	1.0	1.0	1.0	1.0	0.0	[[3000 1] [0 1793]]
(10) Selected attributes	XGBoost	1.0	0.987	0.988	0.977	0.982	0.007	[[2979 22] [42 1751]]
(10) Selected attributes SMOTE	XGBoost	0.999	0.986	0.979	0.983	0.981	0.012	[[2964 37] [31 1762]]

TABLE XIII. THE RESULTS OF THE MULTI-CLASS CLASSIFICATION (WIN_7).

DATA	Models	Train Acc	Acc	Precision	Recall	F1-score	FPR
WIN_7 All attributes	XGBoost	1.0	1.0	1.0	1.0	1.0	0.0
WIN_7 All attributes (SMOTE)	XGBoost	1.0	1.0	1.0	1.0	1.0	0.0
(10) Selected attributes	XGBoost	1.0	1.0	1.0	1.0	1.0	0.0
(10) Selected attributes SMOTE	XGBoost	1.0	1.0	1.0	1.0	1.0	0.0

VII. CONCLUSION

Based on the ToN-IoT dataset, this study proposed a unique malicious detection technique for IoT. The ToN-IoT dataset was employed for training and testing, and the suggested model incorporates several essential aspects. There is a problem with a class imbalance in the ToN-IoT dataset, as well as missing values. This work which deal with ToN-IoT can cover more attacks than prior work with obsolete datasets like KDD-CUP99, NSL-KDD, and UNSW-NB15. The ToN-IoT contains nine types of attacks (Scanning, Cross-Site Scripting (XSS), Denial of Service (DoS), Distributed Denial of Service (DDoS), Backdoor, Injection Attack, Password Cracking Attack, Man-In-The-Middle (MITM), Ransomware.

Exploring, preprocessing, feature selection, class imbalance solution, training ML methods, and testing ML methods are the various system blocks. In a network dataset, the Chi² approach was utilized to select attributes. It lowered the number of attributes to 20, resulting in a quicker training time, lower model complexity, and the highest performance over the whole dataset. Another feature selection methodology was the correlation matrix which was used in the windows dataset to obtain the most relevant attributes from the whole dataset. The SMOTE approach was utilized to balance the classes. It improved performance by reducing dominant class bias, reducing overfitting, and improving the overall performance. A good evaluation metric was achieved by using Chi², SMOTE, and correlation matrix as preprocessing approaches. For evaluating the performance of the deployed ML algorithms, many evaluation metrics (accuracy, precision, recall, F1-score, FPR, and confusion matrix) were used. The results determined that XGBoost outperforms all other ML approaches in binary classification and multi-class classification tasks after assessing the selected ML methods. The main contributions of this work are that it uses a new benchmark dataset that is updated with new attacks and gathered from a real IoT system. The gathered dataset reflects data from each layer of the IoT system, such as (the cloud, fog, and edge layers). The proposed model is a distributed malicious model based on a multi-layer for IoT system. Various ML methods were tested in each specific parathion of the ToN-IoT dataset. The prosed model is the first suggested model that is based on the collected data from the same IoT system from all layers and devices (sensors).

In the future, Deep learning methods such as (recurrent neural network, auto-encoder, and convolution neural network) will be used in the ToN-IoT dataset. More work might be done in the future to enhance the performance of the baseline techniques on the datasets. Advanced parameter optimization

approaches (for example, Bayesian optimization and the genetic algorithm) can be used to optimize the model's hyperparameters and get superior outcomes.

REFERENCES

- [1] M. Lombardi, F. Pascale, and D. Santaniello, "Internet of Things: A General Overview between Architectures, Protocols and Applications," *Information*, vol. 12, no. 2, p. 87, 2021.
- [2] X. Yao et al., "Security and privacy issues of physical objects in the IoT: Challenges and opportunities," *Digital Communications*, vol. 7, no. 3, pp. 373-384, 2021.
- [3] A. S. Ashoor and S. Gore, "Difference between intrusion detection system (IDS) and intrusion prevention system (IPS)," in *International Conference on Network Security and Applications*, 2011, pp. 497-501: Springer.
- [4] E. P. Nugroho, T. Djatna, I. S. Sitanggang, A. Buono, and I. Hermadi, "A Review of Intrusion Detection System in IoT with Machine Learning Approach: Current and Future Research," in *2020 6th International Conference on Science in Information Technology (ICSITech)*, 2020, pp. 138-143: IEEE.
- [5] L. Thomas and S. Bhat, "Machine Learning and Deep Learning Techniques for IoT-based Intrusion Detection Systems: A Literature Review," *International Journal of Management, Technology Social Sciences* vol. 6, no. 2, pp. 296-314, 2021.
- [6] A. A. Cook, G. Mısırlı, and Z. Fan, "Anomaly detection for IoT time-series data: A survey," *IEEE Internet of Things Journal*, vol. 7, no. 7, pp. 6481-6494, 2019.
- [7] V. Pandu, J. Mohan, and T. P. Kumar, "Network intrusion detection and prevention systems for attacks in IoT systems," in *Countering Cyber Attacks and Preserving the Integrity and Availability of Critical Systems: IGI Global*, 2019, pp. 128-141.
- [8] N. M. T.-I. D. [Online]. Available: <https://cloudstor.aarnet.edu.au/plus/s/ds5zW91vdgjEj9i>.
- [9] N. Moustafa, B. Turnbull, and K.-K. R. Choo, "An ensemble intrusion detection technique based on proposed statistical flow features for protecting network traffic of internet of things," *IEEE Internet of Things Journal* vol. 6, no. 3, pp. 4815-4830, 2018.
- [10] M. Alhanahnah, Q. Lin, Q. Yan, N. Zhang, and Z. Chen, "Efficient signature generation for classifying cross-architecture IoT malware," in *2018 IEEE Conference on Communications and Network Security (CNS)*, 2018, pp. 1-9: IEEE.
- [11] Q.-D. Ngo, H.-T. Nguyen, V.-H. Le, and D.-H. Nguyen, "A survey of IoT malware and detection methods based on static features," *ICT Express*, vol. 6, no. 4, pp. 280-286, 2020.
- [12] J. Su, D. V. Vasconcellos, S. Prasad, D. Sgandurra, Y. Feng, and K. Sakurai, "Lightweight classification of IoT malware based on image recognition," in *2018 IEEE 42Nd annual computer software and applications conference (COMPSAC)*, 2018, vol. 2, pp. 664-669: IEEE.
- [13] K. D. T. Nguyen, T. M. Tuan, S. H. Le, A. P. Viet, M. Ogawa, and N. Le Minh, "Comparison of three deep learning-based approaches for IoT malware detection," in *2018 10th international conference on Knowledge and Systems Engineering (KSE)*, 2018, pp. 382-388: IEEE.
- [14] H. Alasmay et al., "Analyzing and detecting emerging internet of things malware: A graph-based approach," *IEEE Internet of Things Journal*, vol. 6, no. 5, pp. 8977-8988, 2019.

- [15] M. Hasan, M. M. Islam, M. I. I. Zarif, and M. Hashem, "Attack and anomaly detection in IoT sensors in IoT sites using machine learning approaches," *Internet of Things* vol. 7, p. 100059, 2019.
- [16] F. Hosseinpour, P. Vahdani Amoli, J. Plosila, T. Hämäläinen, and H. Tenhunen, "An intrusion detection system for fog computing and IoT based logistic systems using a smart data approach," *International Journal of Digital Content Technology its Applications* vol. 10, 2016.
- [17] H. Bostani and M. Sheikhan, "Hybrid of anomaly-based and specification-based IDS for Internet of Things using unsupervised OPF based on MapReduce approach," *Computer Communications*, vol. 98, pp. 52-71, 2017.
- [18] T. D. Nguyen, S. Marchal, M. Miettinen, H. Fereidooni, N. Asokan, and A.-R. Sadeghi, "DfIoT: A federated self-learning anomaly detection system for IoT," in *2019 IEEE 39th International Conference on Distributed Computing Systems (ICDCS)*, 2019, pp. 756-767: IEEE.
- [19] P. Illy, G. Kaddoum, C. M. Moreira, K. Kaur, and S. Garg, "Securing fog-to-things environment using intrusion detection system based on ensemble learning," in *2019 IEEE Wireless Communications and Networking Conference (WCNC)*, 2019, pp. 1-7: IEEE.
- [20] G. D. L. T. Parra, P. Rad, K.-K. R. Choo, and N. Beebe, "Detecting Internet of Things attacks using distributed deep learning," *Journal of Network Computer Applications* vol. 163, p. 102662, 2020.
- [21] M. Shafiq, Z. Tian, A. K. Bashir, X. Du, and M. Guizani, "IoT malicious traffic identification using wrapper-based feature selection mechanisms," *Computers Security* vol. 94, p. 101863, 2020.
- [22] CAIDA: Center for Applied Internet Data Analysis. CAIDA Data - Overview of Datasets, Monitors, and Reports Available: (<https://www.caida.org/data/overview/index.xml>).
- [23] D. R. H. C.-C. t. F. Archive. Available: (<https://www.defcon.org/html/links/dc-ctf.html>).
- [24] A. -IDS-DATASET. Available: (<https://www.unsw.adfa.edu.au/unsw-canberra-cyber/cybersecurity/ADFA-IDS-Datasets/>).
- [25] J. Song, H. Takakura, Y. Okabe, M. Eto, D. Inoue, and K. Nakao, "Statistical analysis of honeypot data and building of Kyoto 2006+ dataset for NIDS evaluation," in *Proceedings of the first workshop on building analysis datasets and gathering experience returns for security*, 2011, pp. 29-36.
- [26] D. R. C. I. f. C. UNB. Available: (<https://www.unb.ca/cic/datasets/index.html>).
- [27] S. D. Bay, D. Kibler, M. J. Pazzani, and P. Smyth, "The UCI KDD archive of large data sets for data mining research and experimentation," *ACM SIGKDD explorations newsletter*, vol. 2, no. 2, pp. 81-85, 2000.
- [28] N. Chandoliker and V. Nandavadekar, "Selection of relevant feature for intrusion attack classification by analyzing KDD Cup 99," *International Journal of Computer Science Information Technology* vol. 2, no. 2, pp. 85-90, 2012.
- [29] H. G. Kayacik, A. N. Zincir-Heywood, and M. I. Heywood, "Selecting features for intrusion detection: A feature relevance analysis on KDD 99 intrusion detection datasets," in *Proceedings of the third annual conference on privacy, security and trust*, 2005, vol. 94, pp. 1723-1722: Citeseer.
- [30] J. Granjal, E. Monteiro, and J. S. Silva, "Security for the internet of things: a survey of existing protocols and open research issues," *IEEE Communications Surveys Tutorials* vol. 17, no. 3, pp. 1294-1312, 2015.
- [31] A. A. Olusola, A. S. Oladele, and D. O. Abosede, "Analysis of KDD'99 intrusion detection dataset for selection of relevance features," in *Proceedings of the world congress on engineering and computer science*, 2010, vol. 1, pp. 20-22: WCECS.
- [32] NSL-KDD | Datasets | Research | Canadian Institute for Cybersecurity | UNB.
- [33] N. Moustafa and J. Slay, "UNSW-NB15: a comprehensive data set for network intrusion detection systems (UNSW-NB15 network data set)," in *2015 military communications and information systems conference (MilCIS)*, 2015, pp. 1-6: IEEE.
- [34] A. Sivanathan et al., "Characterizing and classifying IoT traffic in smart cities and campuses," in *2017 IEEE Conference on Computer Communications Workshops (INFOCOM WKSHPS)*, 2017, pp. 559-564: IEEE.
- [35] A. H. A. Sivanathan, Hassan Habibi, and V. Sivaraman., "UNSW Proliferation Dataset," ed.
- [36] Canadian Institute for Cybersecurity (CIC). IDS 2017 | Datasets | Research | Canadian Institute for Cybersecurity | UNB, ed.
- [37] A. Gharib, I. Sharafaldin, A. H. Lashkari, and A. A. Ghorbani, "An evaluation framework for intrusion detection dataset," in *2016 International Conference on Information Science and Security (ICISS)*, 2016, pp. 1-6: IEEE.
- [38] CSE-CIC-IDS2018 | Datasets | Research | Canadian Institute for Cybersecurity | UNB, ed.
- [39] N. Koroniotis, N. Moustafa, E. Sitnikova, and B. Turnbull, "Towards the development of realistic botnet dataset in the internet of things for network forensic analytics: Bot-iot dataset," *Future Generation Computer Systems*, vol. 100, pp. 779-796, 2019.
- [40] T.-I. D. N. Moustafa, 2020, [online] Available: <https://cloudstor.aarnet.edu.au/plus/s/ds5zW91vdgjEj9i>.
- [41] A. R. Gad, A. A. Nashat, and T. M. Barkat, "Intrusion Detection System Using Machine Learning for Vehicular Ad Hoc Networks Based on ToN-IoT Dataset," *IEEE Access*, vol. 9, pp. 142206-142217, 2021.
- [42] A. R. Gad, N. Hassan, R. A. A. Seoud, and T. M. J. A. Nassef, "Automatic machine learning classification of Alzheimer's disease based on selected slices from 3D magnetic resonance imaging," vol. 67, pp. 10-15.
- [43] J. Wang, M. Xu, H. Wang, and J. Zhang, "Classification of imbalanced data by using the SMOTE algorithm and locally linear embedding," in *2006 8th international Conference on Signal Processing*, 2006, vol. 3: IEEE.
- [44] S. Bagui and K. Li, "Resampling imbalanced data for network intrusion detection datasets," *Journal of Big Data*, vol. 8, no. 1, pp. 1-41, 2021.
- [45] H. Liu and R. Setiono, "Chi2: Feature selection and discretization of numeric attributes," in *Proceedings of 7th IEEE International Conference on Tools with Artificial Intelligence*, 1995, pp. 388-391: IEEE.
- [46] M. Haggag, M. M. Tantawy, and M. M. El-Soudani, "Implementing a deep learning model for intrusion detection on apache spark platform," *IEEE Access* vol. 8, pp. 163660-163672, 2020.
- [47] R. Du, Y. Li, X. Liang, and J. Tian, "Support vector machine intrusion detection scheme based on cloud-fog collaboration," *Mobile Networks Applications* pp. 1-10, 2022.
- [48] N. Moustafa, M. Keshk, E. Debie, and H. Janicke, "Federated TON_IoT Windows datasets for evaluating AI-based security applications," in *2020 IEEE 19th International Conference on Trust, Security and Privacy in Computing and Communications (TrustCom)*, 2020, pp. 848-855: IEEE.
- [49] J. Han, J. Pei, and M. Kamber, *Data mining: concepts and techniques*. Elsevier, 2011.
- [50] A. Alsaedi, N. Moustafa, Z. Tari, A. Mahmood, and A. Anwar, "TON_IoT telemetry dataset: A new generation dataset of IoT and IIoT for data-driven intrusion detection systems," *IEEE Access*, vol. 8, pp. 165130-165150, 2020.

COVID-19 Detection on X-Ray Images using a Combining Mechanism of Pre-trained CNNs

Oussama El Gannour¹, Soufiane Hamida², Shawki Saleh³, Yasser Lamalem⁴, Bouchaib Cherradi⁵, Abdelhadi Raihani⁶
EEIS Laboratory, ENSET of Mohammedia, Hassan II University of Casablanca, Mohammedia, Morocco^{1,2,3,5,6}
Computer research laboratory (L@RI), Ibn Tofail University of Kenitra, Kenitra, Morocco⁴
STIE Team, CRMEF Casablanca-Settat, El Jadida, Morocco⁵

Abstract—The COVID-19 infection was sparked by the severe acute respiratory syndrome SARS-CoV-2, as mentioned by the World Health Organization, and originated in Wuhan, Republic of China, eventually extending to every nation worldwide in 2020. This research aims to establish an efficient Medical Diagnosis Support System (MDSS) for recognizing COVID-19 in chest radiography with X-ray data. To build an ever more efficient classifier, this MDSS employs the concatenation mechanism to merge pretrained convolutional neural networks (CNNs) predicated on Transfer Learning (TL) classifiers. In the feature extraction phase, this proposed classifier employs a parallel deep feature extraction approach based on Deep Learning (DL). As a result, this approach increases the accuracy of our proposed model, thus identifying COVID-19 cases with higher accuracy. The suggested concatenation classifier was trained and validated using a Chest Radiography image database with four categories: COVID-19, Normal, Pneumonia, and Tuberculosis during this research. Furthermore, we integrated four separate public X-Ray imaging datasets to construct this dataset. In contrast, our mentioned concatenation classifier achieved 99.66% accuracy and 99.48% sensitivity respectively.

Keywords—COVID-19; deep learning; transfer learning; feature extraction; concatenation technique

I. INTRODUCTION

A group of viruses named Coronaviruses, which includes MERS-CoV, SARS-CoV, and finally SARS-CoV-2, are likely reasons for mild to severe respiratory illnesses [1]. As reported in the report from the World Health Organization, the COVID-19 infection was espoused by the severe acute respiratory syndrome SARS-CoV-2 and originated in Wuhan, Republic of China, before spreading to every country and territory throughout the world in 2020 [2]–[4]. Furthermore, in the preliminary days of SARS-CoV-2, various respiratory symptoms including hyperthermia, cough, shortness of breath, exhaustion, and finally pneumonia are frequent [5], [6]. COVID-19 influences the cardiovascular and respiratory systems, and in extreme situations, it might result in multiple organ dysfunction syndrome or acute respiratory distress.

As a necessary consequence, COVID-19 diseases have become a major health concern that has spread globally. As a result, emerging innovations are important in preventing the outbreak of the epidemic. For these reasons, researchers throughout the world collaborate and work on strategies to overcome the virus's obstacles. In particular, new Artificial Intelligence (AI)-based methods can eliminate interpersonal physical-contact [7]–[11]. Drones, for instance, might be used

to sterilize public areas and thermal cameras could be used to detect rising temperatures.

In reality, the two subsets of AI are employed to health data analysis: the first subset is Machine Learning (ML) and the second is Deep Learning (DL) approaches, including radiography images or computed tomography scans, have been shown to be useful on detection of illness and monitoring [12]–[14], [15]–[17]. As a result, various types of human maladies, like as Parkinson's disease [18]–[21], brain tumor segmentation [22], [23], breast cancer [24], diabetes [25], medical image segmentation [26], and heart disease prediction [27]–[30], atherosclerosis diseases [31], could be identified using such techniques. AI advancements have also contributed in the development of a wide range of other scientific fields [32]–[34], [35]–[39].

This research focuses to establish a consistent MDSS [40] for monitoring COVID-19 in Chest Radiography data from a variety of virus diseases and pulmonary infections [41]–[44]. The essential innovation of this MDSS is the employment of the concatenation mechanism to merge pretrained convolutional neural networks (CNNs) predicated on Transfer Learning (TL) techniques to generate an efficient classifier. As a result, we integrated four separate X-Ray image databases in this work to introduce a further dataset, containing four categories: COVID-19, Viral Pneumonia, Normal, and finally Tuberculosis. Our suggested classifier was trained and validated using this novel dataset.

The remainder of this paper is organized as follows: The materials and methods are presented in Section II. The experimental results and discussion are presented in Section III. Finally, in Section IV, we conclude our work with some future research prospects.

II. MATERIALS AND METHODS

A. Schematic of the Planned COVID-19 Monitoring MDSS

We present, in this research, an automated method for classifying COVID-19 cases predicated on different TL classifiers (Fig. 1). This automated approach proposed is founded on the concatenation mechanism among two pretrained classifiers of the TL approach. This approach integrates the information taken from both Base-Models to construct the final classification result, which improves performance. To begin, we use the Keras library to choose two pre-trained classifiers (VGG16 and VGG19). The training and testing datasets of chest X-Ray images were produced using

four main public databases. COVID-19, Normal, Pneumonia, and Tuberculosis cases are included in this dataset. The pictures in the produced database are subjected to a series of preprocessing operations. By using the default channel of the network's input structure, all the Chest Radiography images were standardized to similarly input sizes ($224 \times 224 \times 3$).

In this architecture, the X-Ray training dataset is used to train our proposed concatenation classifier. We employ a cross-validation approach to validate the training phase after we have constructed the classifier to prevent the over-fitting problem. Our proposed classifiers' classification results were then evaluated using the testing dataset. Finally, the suggested concatenation classifier's performance was assessed using confusion matrices and a variety of score measures.

B. Dataset Description

This subsection gives a summary of the datasets used during this research. This work was focused on the gathering and analysis of four public databases separated into four classifications: "COVID-19", "Tuberculosis", "Normal", and finally "Viral Pneumonia". The final dataset employed is mentioned in Table I. We exhibit different exemplary instances of the obtained dataset in Fig. 2.

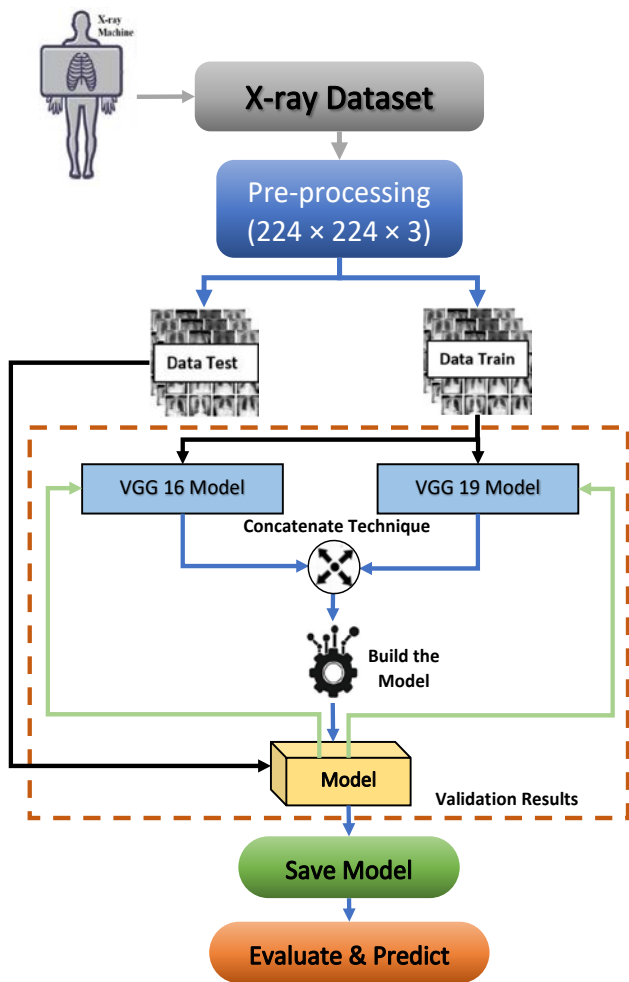


Fig. 1. Schematic Depicting the Planned Classification MDSS Design.

TABLE I. OVERVIEW OF THE MEDICAL X-RAY IMAGES DATABASE SAMPLES

Dataset	Class	Training (90%)	Testing (10%)	Total (100%)
Ref. Dataset ^{a,b,c,d}	COVID-19	1206	134	1340
	Viral Pneumonia	1581	176	1757
	Tuberculosis	3150	350	3500
	Normal	2024	225	2249
Total		7961	885	8846

^a. "COVID-19 Radiography Database"
^b. "COVID-19 Detection X-Ray Dataset"
^c. "COVID-19 Patients Lungs X-Ray Images"
^d. "Tuberculosis (TB) Chest X-Ray Database"

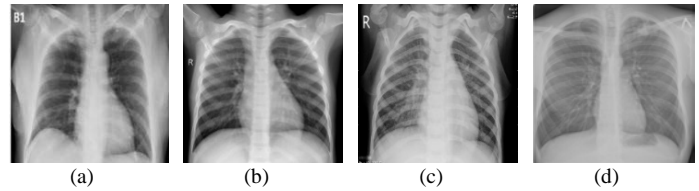


Fig. 2. Specimens of Chest Radiography Images from the Four Categories: (a) COVID-19 Specimen; (b) Normal Specimen; (c) Viral Pneumonia Specimen; (d) Tuberculosis Specimen.

C. Background on TL Algorithms

Instead of developing and learning a CNN from scratch, the TF technique can be used. This technique is a paradigm of machine learning and as such, it is concerned with the knowledge and expertise gained while performing a task. In deep learning, this strategy is applied where the beginning points are saved as pretrained classifiers. This makes it easier for training and accurate efficiency. VGG16 and VGG19 are two pre-trained CNN classifiers that are shareable, and available. They had already been trained on a number of databases, including ImageNet. On a vast scale, it's a massive hierarchical image database. The technical structure of the TL classifiers is depicted in Fig. 3.

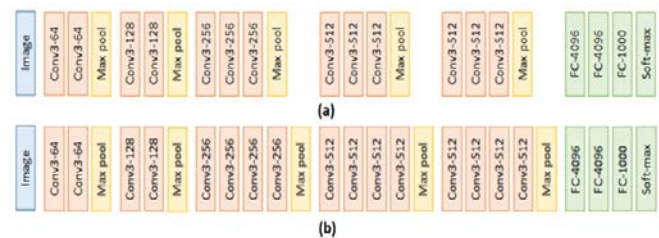


Fig. 3. The Detailed Structure of the TL Classifiers: (a) VGG16 Classifier; (b) VGG19 Classifier.

D. Planned Concatenation Classifier Depending on TL Technique

This subsection explains the technical structure of our classifier, which is shown in Fig. 1. In fact, we used two modified pre-trained TL classifiers, VGG16 and VGG19, both having an identical configuration input dimension, to build our recommended classifier with an initial input size of 3 channels, and 224×224 dimension ($224 \times 224 \times 3$). The entire flowchart of this classifier is shown in Fig. 4.

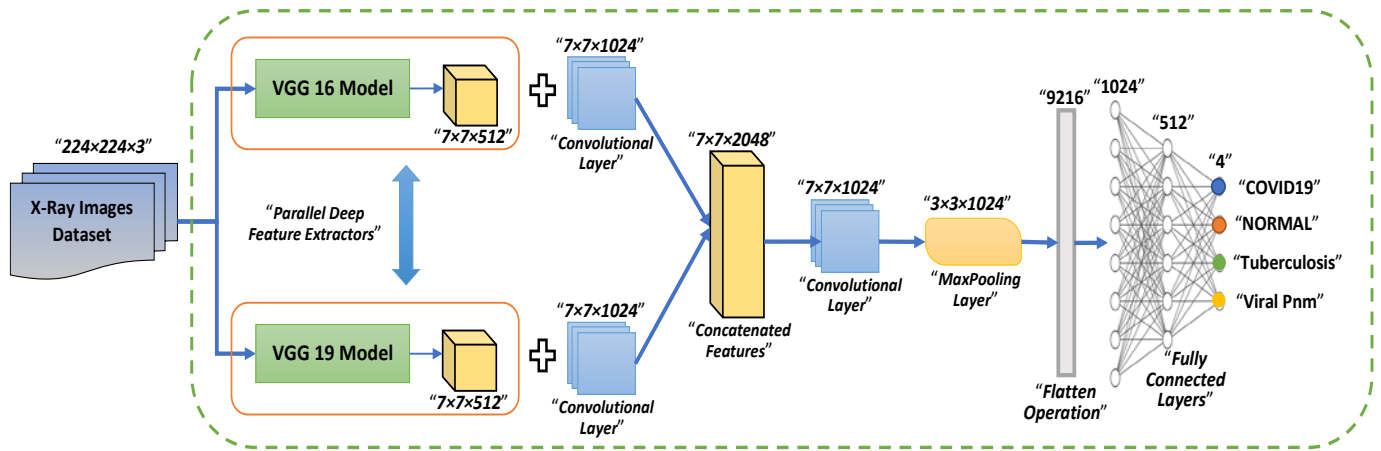


Fig. 4. The Suggested Concatenated Classifier's Design.

III. RESULTS AND DISCUSSION

A. Classifier Performance Evaluation

1) *Confusion matrix and evaluation metrics:* The confusion matrix gives additional feedback about the performance of a classification algorithm, including properly predicted classes, incorrect classes, and the types of errors made. This will help to gather four critical factors for calculating the accuracy of the proposed classifier. TP (True Positive), TN (True Negative), FP (False Positive), and finally FN (False Negative) are the four elements. Expressions below give the confusion factors for the “COVID-19” class as depicted in Table II.

The five indicators employed in this work to evaluate our proposed classifier: Precision, Specificity, Sensitivity, Negative Predictive Value (NPV), and the last indicator is Accuracy.

2) *Cross-validation technique:* In the ML challenge, the Cross-Validation (CV) technique employs the K-Fold CV method. In fact, we begin by separating the data into training and testing sets. Folds have been generated from our training set, which have been divided into K subsets. Thereafter, we repeatedly fit the model K times, training the data on folds K-1 and assessing fold K each time. At the completion of the training, we average the performance on each of the folds to determine the classifier's final validation metrics. Fig. 5 provides a CV method implementation example.

TABLE II. DEFINITION OF CONFUSION MATRIX FACTORS

Confusion Factors	Definition
TP	The number of Chest Radiography images that are forecast exactly as COVID-19.
TN	The number of Chest Radiography images that are forecast exactly as not COVID-19.
FN	The number of Chest Radiography images that are forecast erroneously as not COVID-19.
FP	The number of Chest Radiography images that are forecast erroneously as COVID-19.

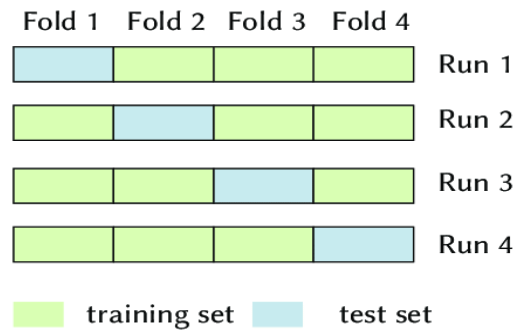


Fig. 5. Example of the Cross-validation Method Implementation with a K-Fold Equal to 4.

B. Experimental Results

1) *Results of the planned classifier training:* The planned concatenation classifier was built on the Google Collab platform, in this work. It's an AI virtualization technology (Cloud Computer Service) for AI research. An Intel Xeon Processor with 2 cores running at 2.20 GHz, 13GB of RAM, and finally a Tesla K80 GPU with 12GB of GDDR5 VRAM were used in this workstation. To validate this work, we used 4-fold cross-validation to build our planned concatenation classifier over 25 epochs to assure similar results. The charts for our Chest Radiography image datasets training and validation for fold 4 are described in Fig. 6.

2) *Results of the planned classifier testing:* We may infer that our suggested classifier gives a robust classification of the four classes based on the results of our research. For all classification k-fold classifiers, the TP value for all categories, is higher than either the FP and FN numbers. In all k-fold classifiers, the COVID-19 class of FP and FN values is lower than the other classes. This indicates that our concatenation classifier has a low risk of confusing COVID-19 infected instances. The confusion matrix of the concatenated classifier for all folds is shown in Fig. 7.

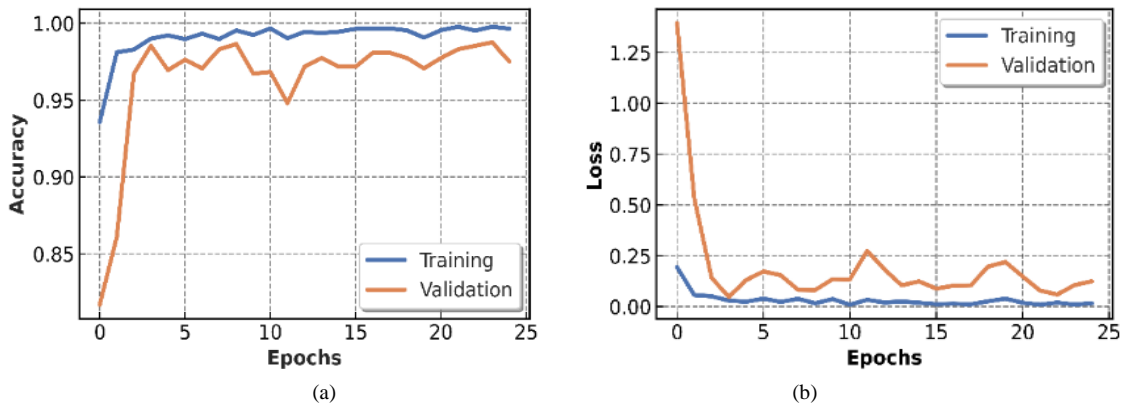


Fig. 6. Curves Produced in Fold 4: (a) Accuracy; (b) Loss.

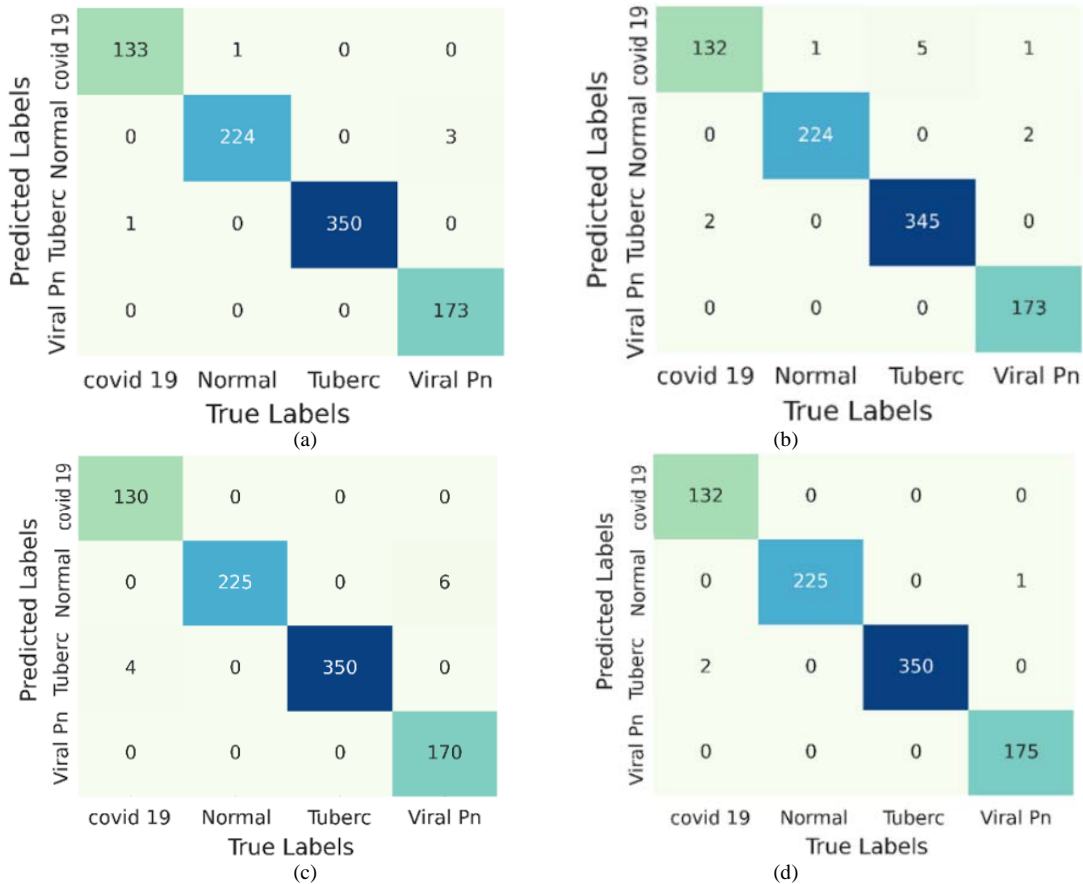


Fig. 7. The Confusion Matrix of the Concatenated Classifier: (a) 1-Fold CM, (b) 2-Fold CM, (c) 3-Fold CM and (d) 4-Fold CM.

A ROC curve could be used to examine these results. This diagnostic test depicts the ratio of False Positive Rate against True Positive Rate as represented by this curve. A ROC curve, in general, helps to compare several classifiers based on the AUC variable's value. The ROC curve for our concatenation classifier in fold four is shown in Fig. 8.

Table III presents the performance evaluation scores of our proposed concatenation classifier for each fold to help elucidate these results.

C. Discussion

In this paper, we developed an innovative COVID-19 diagnostic classifier based on a concatenation mechanism and two pre-trained TL classifiers. The goal of this proposed classifier is to provide the best algorithm possible for the detection of COVID-19 cases. This classifier was built and tested applying a dataset of produced Chest Radiography images from four different databases. Tuberculosis, Pneumonia, Normal and COVID-19 are the four classes in this dataset. In fact, we noticed in the experimental results section that our proposed classifier had a 99% accuracy for all folds. Furthermore, this classifier has a loss value of less than 3%.

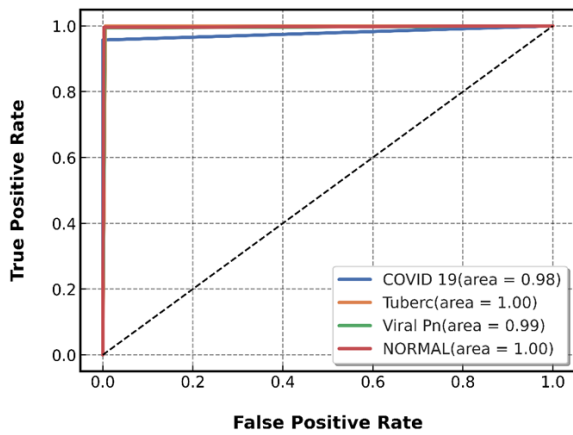


Fig. 8. ROC Curves Findings for the Concatenated Classifier in Fold 4.

Many specialists from around the world have written and published articles on the coronavirus that causes COVID-19 disease in the previous two years. In recently published findings, AI Algorithms have been utilized to examine X-Ray images and assist in the diagnosis of infected cases. DL algorithms are the most frequent in image categorization because they produce better results than classical ML methods. In this subsection, we will examine the research published that applies DL approaches to detect COVID-19 by employing innovative methodologies.

COVIDetection-Net is a classifier used in the categorization of Chest Radiography images proposed by the authors in [45]. To extract the features, this classifier uses ShuffleNet and SqueezeNet networks, as well as Multiclass SVM to classify them. The suggested classifier had a 99.44% accuracy using a multi-class database (COVID-19, normal, Bacterial pneumonia, and Viral pneumonia).

Another paper published in [46], proposed a classifier called SARS-Net, by combining Graph CNN and CNN. X-Ray pictures from five different datasets were used to create this classifier, which had a classification accuracy of 97.6%.

A concatenation classifier was suggested in the scientific paper [47], to merge features retrieved employing the CNN with two pretrained models based on TL approaches like as ResNet-18 and GoogleNet. The two datasets used in this study: X-Ray images, and CT scans, contained binary classes: COVID-19, and non-COVID-19 for each dataset. The proposed classifier archived an accuracy of 98.9% and 99.3% for CT and X-Ray images.

The authors published a comparison analysis depending on TL approaches in [48]. This study proposes two modified models: MobileNetV3, and ResNet18. These models were developed using a database that included five categories: “COVID-19”, “Tuberculosis”, “Normal”, “Bacterial Pneumonia”, and finally “Viral Pneumonia”. The accuracy of the proposed models was 99.3% and 99.6% for ResNet18 and MobileNetV3, respectively.

The mentioned works in this section show an improved recognition models by focusing on the analysis of the dataset used, the optimization of hyper-parameters, or the combination of the performance of several models based on various algorithms. However, feature engineering is an intriguing phase in recognition system development. Indeed, using extracted characteristics improves the performance of a recognition system. Indeed, the success of the categorization system is directly reliant on the recovered primitives. In Table IV, we summarized the performances finding of concatenation-based classifiers in comparison to our proposed classifier.

TABLE III. PERFORMANCE OF THE PROPOSED CONCATENATED CLASSIFIER ON EACH FOLD

Folds	Loss	Accuracy	Precision	Sensitivity	Specificity	NPV
F1	0.027	99.43%	99.41%	99.28%	99.81%	99.82%
F2	0.030	98.75%	98.38%	98.73%	99.60%	99.56%
F3	0.051	98.87%	99.07%	98.40%	99.59%	99.66%
F4	0.015	99.66%	99.75%	99.48%	99.87%	99.90%

TABLE IV. COMPARATIVE RESULTS FOR THE PROPOSED CLASSIFIER WITH RELATED STUDIES

Studies	Classifiers used	Accuracy	Precision	Sensitivity
[45]	COVIDetection-Net	99.44%	94.42%	94.45%
[46]	SARS-Net	97.6%	N/A	92.9%
[47]	Concatenation CNN_ResNet18_GoogleNet	99.3%	99.79%	98.8%
[48]	ResNet18	99.3%	99.23%	99.36%
	MobileNetV3	99.6%	99.5%	99.5%
Proposed classifier	Concatenation VGG16_VGG19	99.66%	99.75%	99.48%

IV. CONCLUSION

In conclusion, using the X-Ray images dataset, we provide a COVID-19 detection mechanism. The proposed concatenation classifier was built and tested utilizing a dataset of Chest Radiography images divided into four categories: COVID-19, Viral Pneumonia, Normal, and Tuberculosis. We integrated four separate online X-Ray picture collections to create this dataset. Concerning the novelty of this work, we use in the feature extraction phase a parallel deep feature extraction approach based on the TL models. This feature extraction approach increases the accuracy of our proposed models, thus identifying COVID-19 cases with higher accuracy. The proposed concatenation classifier achieved 99.6% accuracy and 99.48% sensitivity, respectively.

In future studies, we hope to use the proposed design to classify other illnesses, such as Parkinson's disease, heart disease, and cancer. Nonetheless, we want to use Artificial Intelligence of Things (AIoT) to enhance the resilience and accuracy of our MDSS for monitoring pandemics and tumors. This field is referred to as AIoT, and it integrates IoT infrastructure with artificial intelligence (AI) technology.

REFERENCES

- [1] Astuti and Ysrafil, 'Severe Acute Respiratory Syndrome Coronavirus 2 (SARS-CoV-2): An overview of viral structure and host response', *Diabetes & Metabolic Syndrome: Clinical Research & Reviews*, vol. 14, no. 4, pp. 407–412, Jul. 2020, doi: 10.1016/j.dsx.2020.04.020.
- [2] C. Sohrabi et al., 'World Health Organization declares global emergency: A review of the 2019 novel coronavirus (COVID-19)', *International Journal of Surgery*, vol. 76, pp. 71–76, Apr. 2020, doi: 10.1016/j.ijssu.2020.02.034.
- [3] H. Turki and K. Khrouf, 'Data Analysis of Coronavirus CoVID-19: Study of Spread and Vaccination in European Countries', *IJACSA*, vol. 13, no. 1, 2022, doi: 10.14569/IJACSA.2022.0130185.
- [4] S. Khan and A. Alfaifi, 'Modeling of Coronavirus Behavior to Predict it's Spread', *IJACSA*, vol. 11, no. 5, 2020, doi: 10.14569/IJACSA.2020.0110552.
- [5] J. R. Larsen, M. R. Martin, J. D. Martin, P. Kuhn, and J. B. Hicks, 'Modeling the Onset of Symptoms of COVID-19', *Front. Public Health*, vol. 8, p. 473, Aug. 2020, doi: 10.3389/fpubh.2020.00473.
- [6] V. Sherimon et al., 'Covid-19 Ontology Engineering-Knowledge Modeling of Severe Acute Respiratory Syndrome Coronavirus 2 (SARS-CoV-2)', *IJACSA*, vol. 11, no. 11, 2020, doi: 10.14569/IJACSA.2020.0111115.
- [7] R. Vaishya, M. Javaid, I. H. Khan, and A. Haleem, 'Artificial Intelligence (AI) applications for COVID-19 pandemic', *Diabetes & Metabolic Syndrome: Clinical Research & Reviews*, vol. 14, no. 4, pp. 337–339, Jul. 2020, doi: 10.1016/j.dsx.2020.04.012.
- [8] Q. Khurma, K. Nairoukh, A. Hussein, M. Abualhaj, and Q. Shambour, 'Online Learning Acceptance Model during Covid-19: An Integrated Conceptual Model', *IJACSA*, vol. 12, no. 5, 2021, doi: 10.14569/IJACSA.2021.0120561.
- [9] O. El Gannour, B. Cherradi, S. Hamida, M. Jebbari, and A. Raihani, 'Screening Medical Face Mask for Coronavirus Prevention using Deep Learning and AutoML', in *2022 2nd International Conference on Innovative Research in Applied Science, Engineering and Technology (IRASET)*, Meknes, Morocco, Mar. 2022, pp. 1–7. doi: 10.1109/IRASET52964.2022.9737903.
- [10] S.-W. Chen, X.-W. Gu, J.-J. Wang, and H.-S. Zhu, 'AIoT Used for COVID-19 Pandemic Prevention and Control', *Contrast Media & Molecular Imaging*, vol. 2021, pp. 1–23, Oct. 2021, doi: 10.1155/2021/3257035.
- [11] F. Albogamy, 'IoT-based e-Health Framework for COVID-19 Patients Monitoring', *IJACSA*, vol. 12, no. 9, 2021, doi: 10.14569/IJACSA.2021.0120961.
- [12] O. El Gannour, S. Hamida, B. Cherradi, A. Raihani, and H. Moujahid, 'Performance Evaluation of Transfer Learning Technique for Automatic Detection of Patients with COVID-19 on X-Ray Images', in *2020 IEEE 2nd International Conference on Electronics, Control, Optimization and Computer Science (ICECOCS)*, Kenitra, Morocco, Dec. 2020, pp. 1–6. doi: 10.1109/ICECOCS50124.2020.9314458.
- [13] H. Moujahid, B. Cherradi, M. Al-Sarem, and L. Bahatti, 'Diagnosis of COVID-19 Disease Using Convolutional Neural Network Models Based Transfer Learning', in *Innovative Systems for Intelligent Health Informatics*, vol. 72, F. Saeed, F. Mohammed, and A. Al-Nahari, Eds. Cham: Springer International Publishing, 2021, pp. 148–159. doi: 10.1007/978-3-030-70713-2_16.
- [14] S. Hamida, O. E. Gannour, B. Cherradi, H. Ouajji, and A. Raihani, 'Optimization of Machine Learning Algorithms Hyper-Parameters for Improving the Prediction of Patients Infected with COVID-19', in *2020 IEEE 2nd International Conference on Electronics, Control, Optimization and Computer Science (ICECOCS)*, Kenitra, Morocco, Dec. 2020, pp. 1–6. doi: 10.1109/ICECOCS50124.2020.9314373.
- [15] S. Chokri, W. B. Daoud, W. Hanini, S. Mahfoudhi, and A. Makhlof, 'AI-based System for the Detection and Prevention of COVID-19', *IJACSA*, vol. 13, no. 1, 2022, doi: 10.14569/IJACSA.2022.0130171.
- [16] E. Fayyumi, S. Idwan, and H. AboShindi, 'Machine Learning and Statistical Modelling for Prediction of Novel COVID-19 Patients Case Study: Jordan', *IJACSA*, vol. 11, no. 5, 2020, doi: 10.14569/IJACSA.2020.0110518.
- [17] W. Alawad, B. Alburaidi, A. Alzahrani, and F. Alflaj, 'A Comparative Study of Stand-Alone and Hybrid CNN Models for COVID-19 Detection', *IJACSA*, vol. 12, no. 6, 2021, doi: 10.14569/IJACSA.2021.01206102.
- [18] A. Ouhmida, A. Raihani, B. Cherradi, and Y. Lamalem, 'Parkinson's disease classification using machine learning algorithms: performance analysis and comparison', in *2022 2nd International Conference on Innovative Research in Applied Science, Engineering and Technology (IRASET)*, Meknes, Morocco, Mar. 2022, pp. 1–6. doi: 10.1109/IRASET52964.2022.9738264.
- [19] A. Ouhmida, A. Raihani, B. Cherradi, and O. Terrada, 'A Novel Approach for Parkinson's Disease Detection Based on Voice Classification and Features Selection Techniques', *Int. J. Onl. Eng.*, vol. 17, no. 10, p. 111, Oct. 2021, doi: 10.3991/ijoe.v17i10.24499.
- [20] A. Ouhmida, O. Terrada, A. Raihani, B. Cherradi, and S. Hamida, 'Voice-Based Deep Learning Medical Diagnosis System for Parkinson's Disease Prediction', in *2021 International Congress of Advanced Technology and Engineering (ICOTEN)*, Taiz, Yemen, Jul. 2021, pp. 1–5. doi: 10.1109/ICOTEN52080.2021.9493456.
- [21] M. Alissa et al., 'Parkinson's disease diagnosis using convolutional neural networks and figure-copying tasks', *Neural Comput & Applic*, Sep. 2021, doi: 10.1007/s00521-021-06469-7.
- [22] H. Moujahid, B. Cherradi, and L. Bahatti, 'Convolutional Neural Networks for Multimodal Brain MRI Images Segmentation: A Comparative Study', in *Smart Applications and Data Analysis*, vol. 1207, M. Hamlich, L. Bellatreche, A. Mondal, and C. Ordonez, Eds. Cham: Springer International Publishing, 2020, pp. 329–338. doi: 10.1007/978-3-030-45183-7_25.
- [23] A. Jijja and Dr. Dinesh, 'Efficient MRI Segmentation and Detection of Brain Tumor using Convolutional Neural Network', *IJACSA*, vol. 10, no. 4, 2019, doi: 10.14569/IJACSA.2019.0100466.
- [24] S. Laghmati, B. Cherradi, A. Tmiri, O. Daanouni, and S. Hamida, 'Classification of Patients with Breast Cancer using Neighbourhood Component Analysis and Supervised Machine Learning Techniques', in *2020 3rd International Conference on Advanced Communication Technologies and Networking (CommNet)*, Marrakech, Morocco, Sep. 2020, pp. 1–6. doi: 10.1109/CommNet49926.2020.9199633.
- [25] O. Daanouni, B. Cherradi, and A. Tmiri, 'Diabetes Diseases Prediction Using Supervised Machine Learning and Neighbourhood Components Analysis', in *Proceedings of the 3rd International Conference on Networking, Information Systems & Security*, Marrakech Morocco, Mar. 2020, pp. 1–5. doi: 10.1145/3386723.3387887.
- [26] N. Ait Ali, B. Cherradi, A. El Abbassi, O. Bouattane, and M. Youssfi, 'GPU fuzzy c-means algorithm implementations: performance analysis

- on medical image segmentation', *Multimed Tools Appl*, vol. 77, no. 16, pp. 21221–21243, Aug. 2018, doi: 10.1007/s11042-017-5589-6.
- [27] O. Terrada, B. Cherradi, S. Hamida, A. Raihani, H. Moujahid, and O. Bouattane, 'Prediction of Patients with Heart Disease using Artificial Neural Network and Adaptive Boosting techniques', in 2020 3rd International Conference on Advanced Communication Technologies and Networking (CommNet), Marrakech, Morocco, Sep. 2020, pp. 1–6. doi: 10.1109/CommNet49926.2020.9199620.
- [28] O. Terrada, S. Hamida, B. Cherradi, A. Raihani, and O. Bouattane, 'Supervised Machine Learning Based Medical Diagnosis Support System for Prediction of Patients with Heart Disease', *Adv. sci. technol. eng. syst. j.*, vol. 5, no. 5, pp. 269–277, 2020, doi: 10.25046/aj050533.
- [29] B. Cherradi, O. Terrada, A. Ouhmida, S. Hamida, A. Raihani, and O. Bouattane, 'Computer-Aided Diagnosis System for Early Prediction of Atherosclerosis using Machine Learning and K-fold cross-validation', in 2021 International Congress of Advanced Technology and Engineering (ICOTEN), Taiz, Yemen, Jul. 2021, pp. 1–9. doi: 10.1109/ICOTEN52080.2021.9493524.
- [30] I. Javid, A. Khalaf, and R. Ghazali, 'Enhanced Accuracy of Heart Disease Prediction using Machine Learning and Recurrent Neural Networks Ensemble Majority Voting Method', *IJACSA*, vol. 11, no. 3, 2020, doi: 10.14569/IJACSA.2020.0110369.
- [31] O. Terrada, B. Cherradi, A. Raihani, and O. Bouattane, 'A novel medical diagnosis support system for predicting patients with atherosclerosis diseases', *Informatics in Medicine Unlocked*, vol. 21, p. 100483, 2020, doi: 10.1016/j.imu.2020.100483.
- [32] S. Hamida, B. Cherradi, O. Terrada, A. Raihani, H. Ouajji, and S. Laghmati, 'A Novel Feature Extraction System for Cursive Word Vocabulary Recognition using Local Features Descriptors and Gabor Filter', in 2020 3rd International Conference on Advanced Communication Technologies and Networking (CommNet), Marrakech, Morocco, Sep. 2020, pp. 1–7. doi: 10.1109/CommNet49926.2020.9199642.
- [33] A. Alsaeedi and M. Al-Sarem, 'Detecting Rumors on Social Media Based on a CNN Deep Learning Technique', *Arab J Sci Eng*, vol. 45, no. 12, pp. 10813–10844, Dec. 2020, doi: 10.1007/s13369-020-04839-2.
- [34] W. Sun, P. Bocchini, and B. D. Davison, 'Applications of artificial intelligence for disaster management', *Nat Hazards*, vol. 103, no. 3, pp. 2631–2689, Sep. 2020, doi: 10.1007/s11069-020-04124-3.
- [35] F. M. Alliheibi, A. Omar, and N. Al-Horais, 'Opinion Mining of Saudi Responses to COVID-19 Vaccines on Twitter', *IJACSA*, vol. 12, no. 6, 2021, doi: 10.14569/IJACSA.2021.0120610.
- [36] A. R. Mahlous and A. Al-Laith, 'Fake News Detection in Arabic Tweets during the COVID-19 Pandemic', *IJACSA*, vol. 12, no. 6, 2021, doi: 10.14569/IJACSA.2021.0120691.
- [37] P. V. Sagar, T. Pavan, G. Krishna, and M. Nageswara, 'COVID-19 Transmission Risks Assessment using Agent-Based Weighted Clustering Approach', *IJACSA*, vol. 11, no. 11, 2020, doi: 10.14569/IJACSA.2020.0111167.
- [38] H. Ghandorh et al., 'An ICU Admission Predictive Model for COVID-19 Patients in Saudi Arabia', *IJACSA*, vol. 12, no. 7, 2021, doi: 10.14569/IJACSA.2021.0120764.
- [39] S. Hamida, B. Cherradi, O. El Gannour, O. Terrada, A. Raihani, and H. Ouajji, 'New Database of French Computer Science Words Handwritten Vocabulary', in 2021 International Congress of Advanced Technology and Engineering (ICOTEN), Taiz, Yemen, Jul. 2021, pp. 1–5. doi: 10.1109/ICOTEN52080.2021.9493438.
- [40] M. Fernandes, S. M. Vieira, F. Leite, C. Palos, S. Finkelstein, and J. M. C. Sousa, 'Clinical Decision Support Systems for Triage in the Emergency Department using Intelligent Systems: a Review', *Artificial Intelligence in Medicine*, vol. 102, p. 101762, Jan. 2020, doi: 10.1016/j.artmed.2019.101762.
- [41] B. I. Khaleel and M. Y. Ahmed, 'Pneumonia detection using butterfly optimization and hybrid butterfly optimization algorithm', *Bulletin EEI*, vol. 10, no. 4, pp. 2037–2045, Aug. 2021, doi: 10.11591/eei.v10i4.2872.
- [42] H. Moujahid et al., 'Combining CNN and Grad-Cam for COVID-19 Disease Prediction and Visual Explanation', *Intelligent Automation & Soft Computing*, vol. 32, no. 2, pp. 723–745, 2022, doi: 10.32604/iasec.2022.022179.
- [43] O. El Gannour et al., 'Concatenation of Pre-Trained Convolutional Neural Networks for Enhanced COVID-19 Screening Using Transfer Learning Technique', *Electronics*, vol. 11, no. 1, p. 103, Dec. 2021, doi: 10.3390/electronics11010103.
- [44] S. Hamida, O. El Gannour, B. Cherradi, A. Raihani, H. Moujahid, and H. Ouajji, 'A Novel COVID-19 Diagnosis Support System Using the Stacking Approach and Transfer Learning Technique on Chest X-Ray Images', *Journal of Healthcare Engineering*, vol. 2021, pp. 1–17, Nov. 2021, doi: 10.1155/2021/9437538.
- [45] A. S. Elkorany and Z. F. Elsharkawy, 'COVIDetection-Net: A tailored COVID-19 detection from chest radiography images using deep learning', *Optik*, vol. 231, p. 166405, Apr. 2021, doi: 10.1016/j.ijleo.2021.166405.
- [46] A. Kumar, A. R. Tripathi, S. C. Satapathy, and Y.-D. Zhang, 'SARS-Net: COVID-19 detection from chest x-rays by combining graph convolutional network and convolutional neural network', *Pattern Recognition*, vol. 122, p. 108255, Feb. 2022, doi: 10.1016/j.patcog.2021.108255.
- [47] W. Saad, W. A. Shalaby, M. Shokair, F. A. El-Samie, M. Dessouky, and E. Abdellatef, 'COVID-19 classification using deep feature concatenation technique', *J Ambient Intell Human Comput*, Mar. 2021, doi: 10.1007/s12652-021-02967-7.
- [48] G. Jia, H.-K. Lam, and Y. Xu, 'Classification of COVID-19 chest X-Ray and CT images using a type of dynamic CNN modification method', *Computers in Biology and Medicine*, vol. 134, p. 104425, Jul. 2021, doi: 10.1016/j.compbiomed.2021.104425.

Sentiment Analysis of Tweets using Unsupervised Learning Techniques and the K-Means Algorithm

Orlando Iparraguirre-Villanueva¹, Victor Guevara-Ponce², Fernando Sierra-Liñan³

Saul Beltozar-Clemente⁴, Michael Cabanillas-Carbonell⁵

Facultad de Ingeniería y Arquitectura, Universidad Autónoma del Perú, Lima, Perú¹

Escuela de Posgrado, Universidad Ricardo Palma, Lima, Perú²

Facultad de Ingeniería, Universidad Privada del Norte, Lima, Perú³

Universidad Científica del Sur, Lima, Perú⁴

Vicerrectorado de Investigación, Universidad Norbert Wiener, Lima, Perú⁵

Abstract—Today, web content such as images, text, speeches, and videos are user-generated, and social networks have become increasingly popular as a means for people to share their ideas and opinions. One of the most popular social media for expressing their feelings towards events that occur is Twitter. The main objective of this study is to classify and analyze the content of the affiliates of the Pension and Funds Administration (AFP) published on Twitter. This study incorporates machine learning techniques for data mining, cleaning, tokenization, exploratory analysis, classification, and sentiment analysis. To apply the study and examine the data, Twitter was used with the hashtag #afp, followed by descriptive and exploratory analysis, including metrics of the tweets. Finally, a content analysis was carried out, including word frequency calculation, lemmatization, and classification of words by sentiment, emotions, and word cloud. The study uses tweets published in the month of May 2022. Sentiment distribution was also performed in three polarity classes: positive, neutral, and negative, representing 22%, 4%, and 74% respectively. Supported by the unsupervised learning method and the K-Means algorithm, we were able to determine the number of clusters using the elbow method. Finally, the sentiment analysis and the clusters formed indicate that there is a very pronounced dispersion, the distances are not very similar, even though the data standardization work was carried out.

Keywords—Techniques; machine learning; classification; twitter

I. INTRODUCTION

The analysis of data derived from social media is of growing importance from various points of view, including academic and economic ones. Currently, there are 4.2 billion users on social networks worldwide, equivalent to 53.6% of the total population [1]. In Peru, there are 26.41 million social network users, equivalent to 81.4% of the population [2].

On Twitter, an average user makes six comments on all types of tweets, follows one user, and shares two tweets on average in 30 days; the number of likes and comments on social media tweets influences users' self-presentation [3]. Social networks are new spaces where groups of users with specific characteristics are centered, allowing them to share expressions, and opinions, these are considered the new means of communication and exchange of web content [4], [5], and the amount of data provided by users and feedback is

enormous, however, there is no predefined method or tool to sort and classify the comments, since knowing the opinions of users is of utmost importance to generate knowledge and make better decisions in the different areas [6],[5],[7].

The AFPs are private institutions whose sole purpose is to manage pension funds in the form of personal accounts that provide retirement, disability, and survivor's pensions and funeral expenses [8]. The objective of the AFP is to protect the older population from the risk of poverty and allow citizens to save for their retirement. This study aims to classify and analyze the sentiments of Twitter users (affiliates) using machine learning models, for this case we will work with the hashtag #afp.

Comments are composed of positive opinions that create a contagion effect, while criticism or negative comments also influence users' decisions [9], by which, it is important to classify and analyze users' sentiments to know their reactions to a certain topic or tweet. Supported by association rule learning and machine learning algorithms, it is possible to discover the relationships between words that associate sentiments [10],[11].

The article is organized as follows. Section II describes the main works related to sentiment analysis. Section III presents the method and case implementation. Section IV describes and discusses the results and discussions. Finally, Section V presents the conclusions.

II. RELATED WORK

Currently, the Internet and social networks are environments in which large amounts of user data are collected [12]. Comments can negatively affect the reputation of a person or company and be harmed socially and/or economically, it is for this reason, that [13] argues that to generate social capital, it is necessary to work on the feedback generated by users on social networks.

The authors in [14],[15],[16] implemented an analysis model using machine learning classifiers, to measure and predict user profile credibility, the implemented model was evaluated on two different datasets with term frequency and three inverse document frequency variables. Similarly, in [17],[18],[19] identified features that can be useful for predicting whether a tweet or comment is a rumor or

information, using a rule-based approach involving regular expressions to categorize sentences.

In addition, [20] analyzed the existence of malicious users spreading malware or phishing in tweet comments, for which six classifiers were used: random tree, random forest, Naïve Bayes, Kstar, decision table, and decision stump. Likewise, [21] proposed an approach to extract from Twitter the image content, classify it and verify the authenticity of digital images and discover manipulation. Also [22] recommended a topic analysis and sentiment polarity classification with machine learning techniques for emergency management, finding that the most suitable classification model is random forests.

Likewise, [23] developed a system that employs sentiment analysis for product reviews (e.g., the company shares a photo of a new product in a tweet and it receives a thousand new product comments), the system classifies the comments as positive or negative.

Machine learning employs two types of techniques: supervised learning, which trains a model on known input and output data so that it can predict future results. Unsupervised learning finds hidden patterns or intrinsic structures in the input data. In the same context, in [24],[25],[26] the authors used natural language processing methods to detect fake news in social media posts, and also created a semi-supervised learning model for early detection.

In addition, in [27],[28] a supervised learning model for rumor verification using contextual features based on contextual word embeddings, speech acts, and the writing style was presented. In [29] the authors collected unstructured data from social networks, using an application implementing different supervised and unsupervised learning classification algorithms. Similarly, in [30] a novel method for generating opinion summaries in social networks was proposed, using the unsupervised learning technique, in [31] content analysis of textual Twitter data was performed using a set of supervised and unsupervised machine learning methods to appropriately cluster and classify traffic-related events.

Although previous studies considered many aspects of sentiment analysis in social networks, according to the review conducted, there is a gap to be investigated in the use of clustering rules to classify and analyze user sentiments, considering that these results would be of great use to stakeholders, as it would allow them to make better decisions supported with ML.

III. METHOD AND IMPLEMENTATION OF THE CASE

This section presents the construction of the machine learning terminology, the method, and the detailed implementation of the proposed case study that seeks to predict members' sentiments regarding AFP of Peru.

Machine learning (ML) is a discipline of artificial intelligence that, through algorithms, teaches computers to build models from experience [32]. ML is divided into three types: supervised learning, unsupervised learning, and reinforcement learning, and these in turn are classified into different learning models, as shown in Fig. 1. The study uses

unsupervised learning, and the k-means algorithm, for which we will address only this category.

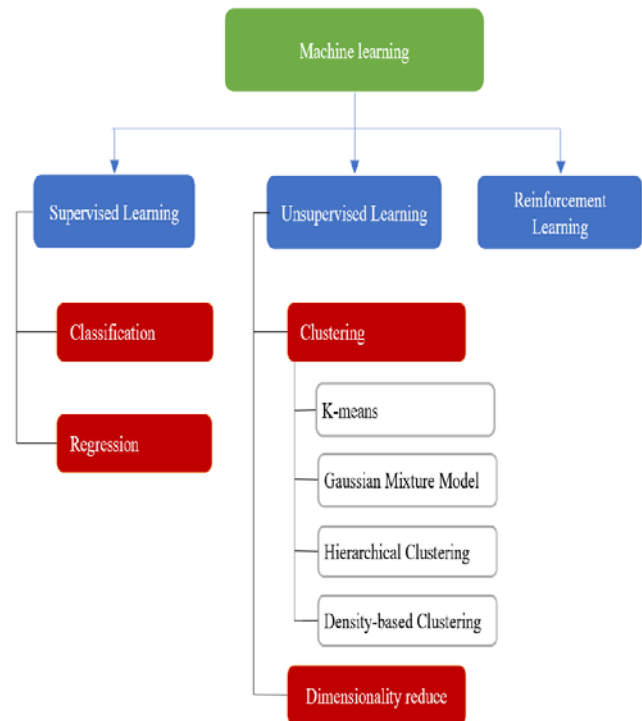


Fig. 1. Types of Learning.

Unsupervised Learning: It does not require labeled data and can be processed by clustering methods. Clustering is a typical example of unsupervised learning that finds visual classifications that match the hypothesis [14]. The goal of clustering is to find similarities, regardless of the kind of data. Therefore, a clustering algorithm needs to know how to calculate similarity, and then start running.

K-Means: It is a clustering algorithm that combines the "n" observations into "k" clusters that are aggregated together according to specific similarities [33], as shown in Fig. 2.

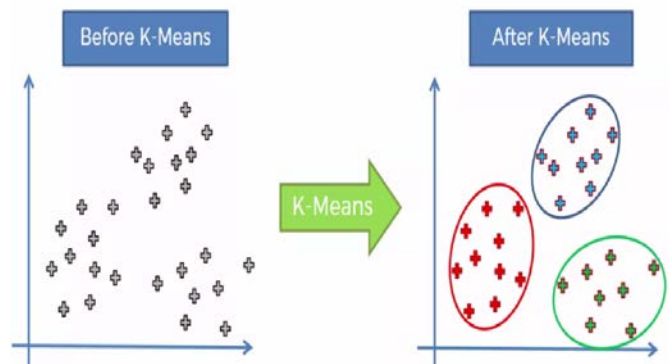


Fig. 2. Grouping of K-Means.

The K-Means algorithm follows the following steps:

- **Initiation:** The location of the centroids of the k clusters is chosen randomly.

- Assignment: Each datum is assigned to the nearest centroid.
- Updating: The centroid position is updated to the arithmetic mean of the data positions assigned to the cluster.

Steps 2 and 3 are followed iteratively until there are no more changes in the location of the centroids, or they move below a threshold distance from each step. The K-means algorithm seeks to solve an optimization problem, the function to be optimized being the sum of the quadratic distances from each object to the centroid of its cluster. The objects are represented by d dimensional real vectors (x_1, x_2, \dots, x_n) and the algorithm constructs k clusters where the sum of the distance of the objects, within each object $s = \{s_1, s_2, \dots, s_k\}$, to its centroid is minimized. The problem is formulated as follows:

$$\frac{\min}{s} E(\mu_i) = \frac{\min}{s} \sum_{i=1}^k \sum_{x_j \in s_i} |x_j - \mu_i|^2 \quad (1)$$

Where S is the data set whose elements are the objects represented by vectors, where each of its elements represents an attribute. We have k cluster with its corresponding centroid μ_i . On each centroid update, from the mathematical point of view, we impose the necessary condition of extrema to the function $E(\mu_i)$ which, for the quadratic function (1) is.

$$\frac{\partial E}{\partial \mu_i} = 0 \Rightarrow \mu_i^{(t+1)} = \frac{1}{|S_i^{(t)}|} + \sum_{x_j \in S_i^{(t)}} x_j$$

The k-means algorithm is simple and fast, however, it is necessary to decide the value of K and the final result will depend on the initialization of the centroids.

The Cross-Industry Standard Process for Data Mining (CRISP-DM) methodology was chosen for the development of the case. It is a model that divides the process into six main phases: business understanding, data compression, data preparation, modeling phase, evaluation, and implementation. CRISP-DM has a structured approach, establishing a set of tasks and activities for each phase.

A. Business Understanding

The AFP is a private institution in charge of managing people's provisional savings. Like any company, with the arrival of COVID-19, the economy of the region has been severely affected and, therefore, the annualized profitability of the AFP has not been favorable. This has led the Congress of the Republic to promote laws such as free disaffiliation, 100% of contributions for those over 55 years of age, among other authorizations for controlled withdrawals under the context of a pandemic for the years 2020 to 2022. Peruvians' perception of the AFP has never been positive, probably because retirement pensions do not meet expectations, among other factors. In this context, the sentiment analysis of the case study aims to analyze and classify the opinions of AFP members. This analysis can help the AFP to make better decisions in its offerings to the market. Fig. 3 shows the general process of sentiment analysis.

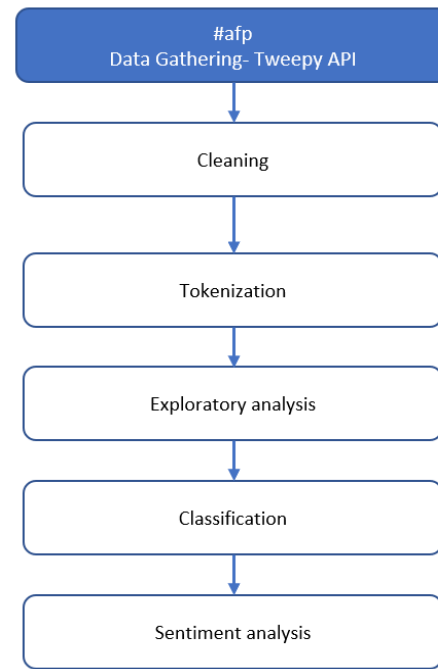


Fig. 3. General Sentiment Analysis Process.

Fig. 3 shows the general process of sentiment classification and analysis. It starts with extraction supported by libraries, then we move on to cleaning and tokenization, this process consists of removing from the text everything that does not provide information about the subject matter. For example, on Twitter, users can write in a way that they consider convenient, such as abbreviations, punctuation marks, web page URLs, single characters, numbers, etc.

Tokenization consists of dividing the text into its constituent units, in this case, words. Next, we perform the exploratory analysis, in this stage, we try to understand and study which words and how often they are used, as well as their meaning. In the Python or R language, one of the structures that facilitate the exploratory analysis is the DataFrame, which is where the information of the tweets is stored. The next step is to perform the classification, in this phase, to be able to apply classification algorithms to the text (tweets), a numerical representation of the text is created.

One of the most used ways is known as the Bag of words, this method consists of identifying the set formed by all the words (tokens) that arise in the corpus. Finally, we proceed with the sentiment analysis, for which it is necessary to have a dictionary in which a sentiment or sentiment level is associated with each word.

B. Data Comprehension

The dataset for the case study has been collected on recent Tweets from May 2022, related to the hashtag #afp, with coordinates -12.062152, -77.0361328 corresponding to the city of Lima. The dataset is composed of 18k tweets. The data we collected contains relevant information about most of the tweets such as their attributes (user_id, status_id, created_at, screen_name, text, source, display_text_width,

reply_to_status_id, favorite_count, replay_to_user_id, replay_to_screen_name, is_quote, retweet_count, quote_count, media_url, media_t.co, media_expanded_url, etc.) which, in sum, are 90 attributes with 18k tweets to be processed, as shown in Fig. 4.

```

38 tweets_afp <- search_tweets(
39   q = "AFP",
40   geocode = "-12.062152,-77.0361328,20mi",
41   include_rts = FALSE,
42   n = 18000
43 )
    
```

Fig. 4. Tweet Search and Download Code.

1) *DataSet preparation*: This is an essential step before applying any machine learning model. The DataSet preparation phase starts with a crucial previous step, known as extraction, loading, and transformation, to load the extracted data to a source or data warehouse, in this case, it will be processed in a single computer with the necessary characteristics to support the processing of 18k tweets represented in a DataSet. The phases, as a whole, are described below:

2) *Extraction, loading, and transformation*: This process was implemented with the code illustrated in Fig. 4, the data were stored in a text file, then, supported with the *stringr* library, we performed the first preliminary cleaning, then the text file was converted to a csv file (`write.csv()`), then we applied tokenization with the libraries *tidyverse*, *tibble* and a personal dictionary in Spanish loaded with the *readxl* library. And then we used lemmatization, that is, the root of a word that can be written in several forms and refer to the same thing. For example, if the words *pueblo*, *pueblito*, *pueblano* are found, the root of these three words is *pueblo*, thus avoiding redundancy in the analysis, this process is supported in a pre-trained model with the *udpipe* library, as shown in Table I.

In the next step, we performed an exploratory analysis of the data, using the bag-of-words(bow) model to obtain the most common words in the lexicon, obtaining a list of the most frequent words in the hashtag #afp. Fig. 5 shows a dense word cloud with some of the most used words in the generated corpus, also, it can be seen that several words are found in different positions.

TABLE I. LEMMATIZATION OF WORDS

senten ce_id	sentence	token_ id	token	lemma
1	chabelitacongre	1	chabelitacongre	chabelitacongre
1	ayudas	1	ayudas	ayudas
1	pueblo	1	pueblo	pueblo
1	quitando	1	quitando	quitando
1	jubilación	1	jubilación	jubilación
1	problema	1	problema	problema

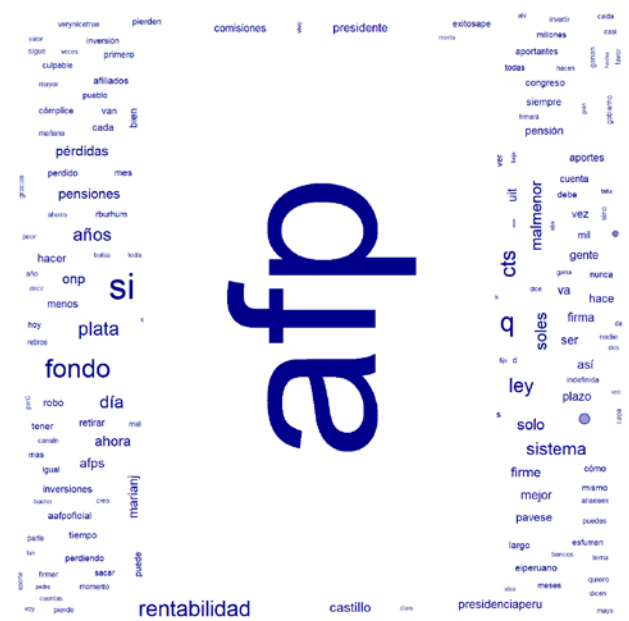


Fig. 5. Most Popular Words Related to #afp from our Corpus.

Next, the *syuzhet* dictionary package is used, this package works with four sentiment dictionaries, such as: Bing, Afinn, Stanford, and NRC, in our case, we will work with NRC, since it is the only one available in several languages, including Spanish. This dictionary has 14182 words with categories of feelings, positive, negative, and the emotions of anger, anticipation, disgust, fear, joy, sadness, surprise, confidence, etc. This dictionary is used with the purpose of analyzing and grouping the words of the corpus and to know in which category the feelings are grouped. Fig. 6 shows that the negative sentiment of affiliates is most frequently repeated in the tweets, followed by positive sentiment, fear, confidence, anger, disgust, etc.

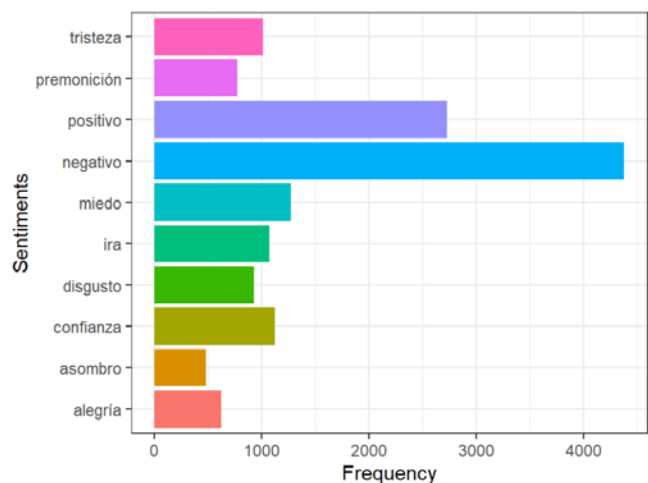


Fig. 6. Frequency of Terms in Sentiment Analysis.

Fig. 7 shows the words of the tweets grouped by sentiment, in it, we can analyze each of the words associated with a particular feeling. For example, the word *money* is the one that mostly generates the feeling of joy, followed by astonishment, confidence, anger, positive and premonition. In

the same line, the word congress is the one that mostly generates disgust, likewise, the word government is the one that mostly generates the feeling of fear.

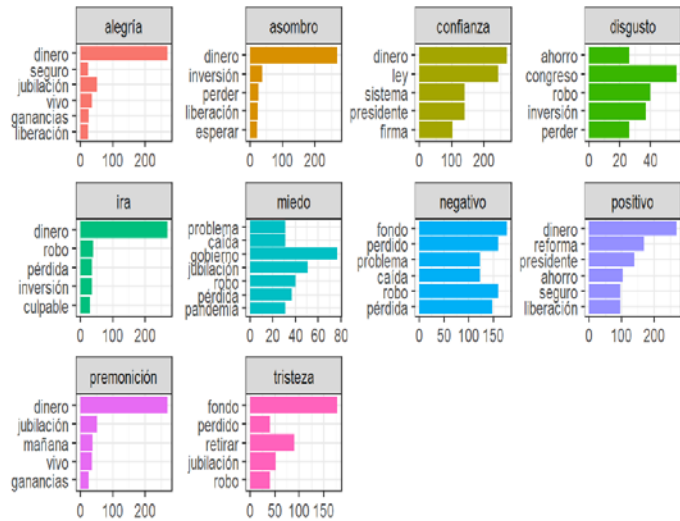


Fig. 7. Words for Sentiment.

C. Preparation and Clustering with K-means

At this stage, we have already extracted, cleaned the data and stored it in a text file. Next, we use the TM package, to call the functions VectorSource (), inspect () and removeSparseTerms (), the latter function to remove words that are not very frequent, and finally we convert the text into a word frequency matrix with the TermDocumentMatrix () function. The k-means clustering is a vector quantization method, which tends to find clusters of comparable spatial extent. Part of the code is shown in Fig. 8.

```

407 library(tm)
408 corpus <- Corpus(VectorSource(texto))
409 corpus
410 inspect(corpus)
411 # Printout of a corpus line
412
413 writeLines(as.character(corpus[[100]])) # basic package
414 content(corpus[[100]])
415
416 d <- tm_map(corpus, tolower)
417 inspect(d)
418 # Remove custom empty words
419 d <- tm_map(d, removewords, sw.es)
420 inspect(d)
421
422 # Create Term Matrix with TermDocumentMatrix()
423 tdm <- TermDocumentMatrix(d)
424 tdm
...

```

Fig. 8. Use of Libraries in R.

D. Modeling Phase

In this context, it is very important to analyze the relationship between words with the findAssocs () function of the tm package. The calculation of the findAssocs () function is performed at the document level. Then, for each specific document containing the word in question, the other terms in those documents are associated, the other search terms are ignored. The function returns a list of all the other terms that meet or exceed the minimum threshold (findAssocs (tdm, "afp", 0.40)). The minimum correlation values are usually

relatively low due to the diversity of words. The tweets of the hashtag #afp have been cleaned and organized with tweets_tdm. For the case study, the function findAssocs () searches for the association of terms and manipulates the results with list_vect2df () from the qdap package and then creates the diagram with the ggplot2 library. Fig. 9 shows the strong association represented by the thickness of the lines between the words. The word afp is the root for the association of the other words, such as afp-money, afp-withdrawal, afp-funds, afp-system, afp-years, afp-law, afp-now, funds-withdrawal, withdrawal-law, afp-castle, etc. This association process allows us to know the words most associated and expressed by AFP members.

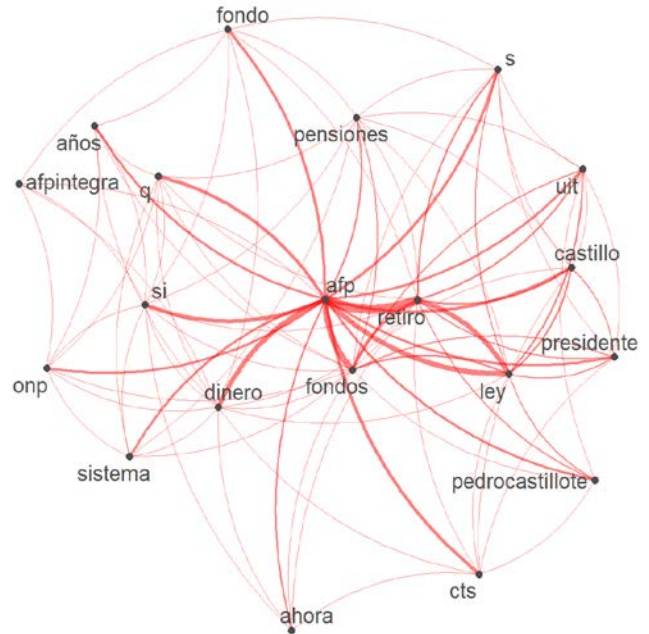


Fig. 9. Frequency Represented in Line Thickness.

In Fig. 10, the sentiment classification is presented with the overall percentage of each positive, negative and neutral tweet found in the dataset. It can be seen that the sentiment classes are unequal, as a large part of the affiliates express themselves negatively or neutral concerning the hashtag #afp.

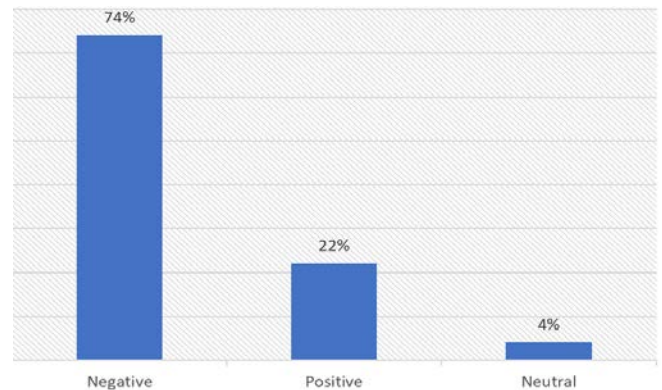


Fig. 10. Sentiment Distribution of the Three Polarity Classes along with the Percentage of Tweets Referring to the #afp Hashtag.

IV. RESULTS AND DISCUSSION

In this section, we present the performance of the k-means algorithm to obtain the best number of clusters and the results of the case study. In general, most clustering algorithms, including k-means, employ different numbers of clusters, and are evaluated by multiple validity measures to determine the most meritorious clustering results. To measure clustering performance, we use a precision index (IP), where $IP = \sum_{k=1}^c n(c_k)/n$, where c_k is the number of data points that obtain the correct clustering for cluster k and n is the total number of data points.

The higher the accuracy index, the better the clustering performance. K-Means clustering is based on data partitioning, data that have the same features are grouped into one cluster, while data that have different features are grouped into other clusters. The steps of K-Means clustering are three: deciding the cluster number k, centroid initialization and assigning the data to the nearest cluster, the determination of the closeness of objects/data is determined based on the distance of objects/data, to calculate the distance of all data to each centroid point, the Euclidean distance theory is used, which is represented as follows.

$$D(i, j) = \sqrt{(x_{i1} - x_{j1})^2 + (x_{i2} - x_{j2})^2 + \dots + (x_{ip} - x_{jp})^2}$$

Where:

$D(i, j)$ = distance of the data to the cluster center j.

X_{ik} = i^{th} in the k^{th} data attribute.

X_{ij} = j^{th} center point in the k^{th} data attribute.

The centroid is the average of all data/objects within a particular cluster. Each data/object is reassigned using the new cluster centroid, the cluster does not change, then the clustering process is finished, otherwise, repeat the steps until there is no change for each cluster.

To determine the number of clusters in which the data are grouped, we use the elbow method, this method uses the mean of the observations to their centroid, i.e., it looks at the intra-cluster distances. The larger the number of clusters k, the intra-cluster variance tends to decrease. The smaller the intra-cluster distance the better.

The elbow method searches for the k value which satisfies that an increase of k does not substantially improve the mean intra-cluster distance. To find the number k, 15 clusters were assigned, in Fig. 11 it can be seen that the elbow(k) is formed at point 3, this means that the number of clusters that we will process will be k=3.

Once the number of clusters (k = 3) has been determined, we can start with the data processing. For this, the tweets had to be converted to numerical data, using one-hot encoding for the transformation, as shown in Table II.

It is advisable to scale values and not to introduce variables that are highly correlated or that are linear combinations of other variables, i.e., to avoid multicollinearity. The objective of scaling variables is to make them comparable, that is, to have a mean equal to zero and a standard deviation equal to one. The scaled method is achieved by using the following formula:

$$z(x) = \frac{x_i - cen\ tr\ o(x)}{deviation(x)}$$

Where, center(x) is a measure of centrality with mean or median and variance (x) is a measure of dispersion such as standard deviation. The standardization of data is important as it makes the distances similar to that without scaling. Fig. 12 shows a representation by dimensions and the clusters formed. It is clearly observed that a cluster of comments or tweets are very homogeneous, with low values in cluster 1, we refer to the negative sentiment and high values in cluster 2, cluster 3 is presented in the central part with intermediate values in both cluster 1 and 2 corresponding to the positive and neutral sentiments.

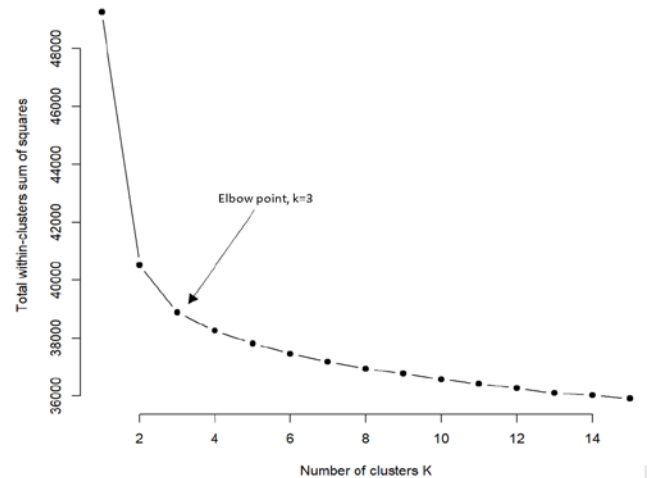


Fig. 11. Elbow Method - Number of Clusters.

TABLE II. SUMMARY OF ONE HOT CODING

Docs	afp	casa	hasta	los	que	seguro	son	tienes	todos	vida
1	0	0	0	0	0	0	0	0	0	0
10	1	0	0	2	2	0	0	0	0	1
2	1	0	0	3	1	0	1	0	1	0
3	0	2	1	1	0	0	1	0	1	0
4	1	0	0	0	1	0	0	0	0	0
5	1	0	0	0	0	0	0	1	0	0
6	1	0	0	0	0	0	0	0	0	0
7	1	0	0	0	1	0	0	0	0	0
8	1	0	0	0	0	3	1	1	0	3
9	1	0	1	1	3	0	0	1	0	0

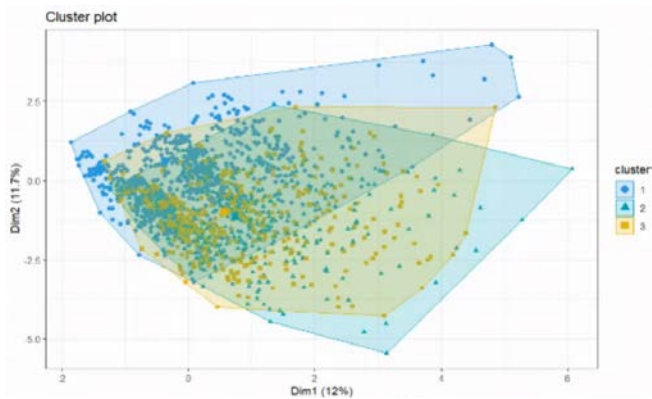


Fig. 12. Sentiment Analysis of #afp.

V. CONCLUSION

In recent years, several approaches have been developed for sentiment analysis on social network data, specifically on Twitter. The process of sentiment analysis is often complex due to the huge amount of data and the need to achieve a high level of accuracy. This study presents the sentiment analysis of Twitter hashtag #afp data, for which the k-means algorithm was used. This algorithm is based on data partitioning, data having the same features that are grouped into a cluster. In this study, eight types of feelings (sadness, foreboding, positive, negative, fear, anger, disgust, confidence, amazement and joy) were used. After applying unsupervised learning with K-Means, it is seen that the negative feeling is the most recurrent, followed by positive feeling, fear, confidence, etc. As shown in Fig. 6 out of a total of 18000 tweets related to the hashtag #afp, tweets with sentiments, positive, neutral and negative represent 22%, 4% and 74% respectively. This means, that machine learning applying the K-Means algorithm proves to be efficient and practical, and can be easily applied for sentiment classification on related topics, where we do not have input and output tags.

This study provides theoretical and practical scopes. Regarding the theoretical scope, the study applies a machine learning approach, with the unsupervised learning method for sentiment analysis of AFP members, using Twitter data with the hashtag #afp. Also, sentiment analysis with machine learning can be applied in different industries such as marketing, services and academia, etc. In terms of practical scope, this study recommends machine learning with the unsupervised method to be applied in cases similar to the study, allowing it to be adapted and improved to achieve a better level of accuracy, especially in complex situations when performing textual analysis.

In this study, from the classification to the analysis of feelings, there was evidence of certain feelings that were most repeated, with negative feelings being the predominant one, with which we can conclude that the members do not feel represented or reject the actions of the AFP, followed by positive feelings, fear, trust, anger, sadness, disgust, premonition, joy and amazement, in that order. This study is not without limitations. Attribute mapping was applied to the initial data set; within this, there may be a diversity of factors, combinations that may affect the classification results. In

future work, machine learning with the unsupervised method and the K-Means algorithm can be optimized to improve the accuracy of sentiment detection, classification and analysis.

REFERENCES

- [1] P. Lara-Navarra, A. López-Borrull, J. Sánchez-Navarro, and P. Yànez, "Measuring the influence of users on social networks: SocialEngagement proposal," p. 899, 2018, doi: 10.3145/epi.2018.jul.18.
- [2] H. Xiang, K. Y. Chau, W. Iqbal, M. Irfan, and V. Dagar, "Determinants of Social Commerce Usage and Online Impulse Purchase: Implications for Business and Digital Revolution," *Frontiers in Psychology*, vol. 13, Feb. 2022, doi: 10.3389/FPSYG.2022.837042.
- [3] C. Marino, C. Lista, D. Solari, M. M. Spada, A. Vieno, and L. Finos, "Predicting comments on Facebook photos: Who posts might matter more than what type of photo is posted," *Addictive Behaviors Reports*, vol. 15, p. 100417, Jun. 2022, doi: 10.1016/J.ABREP.2022.100417.
- [4] O. R. Seryasat, I. Kor, H. G. Zadeh, and A. S. Taleghani, "Predicting the number of comments on facebook posts using an ensemble regression model," *International Journal of Nonlinear Analysis and Applications*, vol. 12, no. Special Issue, pp. 49–62, Dec. 2021, doi: 10.22075/IJNAA.2021.4796.
- [5] C. P. Chandrika and J. S. Kallimani, "Classification of Abusive Comments Using Various Machine Learning Algorithms," *Advances in Intelligent Systems and Computing*, vol. 1040, pp. 255–262, 2020, doi: 10.1007/978-981-15-1451-7_28.
- [6] J. Biswas, M. M. Rahman, A. A. Biswas, M. A. Z. Khan, A. Rajbongshi, and H. A. Niloy, "Sentiment Analysis on User Reaction for Online Food Delivery Services using BERT Model," *2021 7th International Conference on Advanced Computing and Communication Systems, ICACCS 2021*, pp. 1019–1023, Mar. 2021, doi: 10.1109/ICACCS51430.2021.9441669.
- [7] H. Deng, D. Ergu, F. Liu, Y. Cai, and B. Ma, "Text sentiment analysis of fusion model based on attention mechanism," *Procedia Computer Science*, vol. 199, pp. 741–748, 2021, doi: 10.1016/J.PROCS.2022.01.092.
- [8] "Asociación de AFP." <https://www.asociacionafp.pe/> (accessed May 19, 2022).
- [9] F. Erlandsson, A. Borg, H. Johnson, and P. Bródka, "Predicting user participation in social media," *Lecture Notes in Computer Science (including subseries Lecture Notes in Artificial Intelligence and Lecture Notes in Bioinformatics)*, vol. 9564, pp. 126–135, 2016, doi: 10.1007/978-3-319-28361-6_10.
- [10] L. Parisi, R. Ma, N. RaviChandran, and M. Lanzillotta, "hyper-sinh: An accurate and reliable function from shallow to deep learning in TensorFlow and Keras," *Machine Learning with Applications*, vol. 6, p. 100112, Dec. 2021, doi: 10.1016/J.MLWA.2021.100112.
- [11] D. C. Gkikas, K. Tzafilkou, P. K. Theodoridis, A. Garmpis, and M. C. Gkikas, "How do text characteristics impact user engagement in social media posts: Modeling content readability, length, and hashtags number in Facebook," *International Journal of Information Management Data Insights*, vol. 2, no. 1, p. 100067, Apr. 2022, doi: 10.1016/J.JJIMEI.2022.100067.
- [12] N. A. Awad and A. Mahmoud, "Analyzing customer reviews on social media via applying association rule," *Computers, Materials and Continua*, vol. 68, no. 2, pp. 1519–1530, Apr. 2021, doi: 10.32604/CMC.2021.016974.
- [13] A. Wang and K. Potika, "Cyberbullying Classification based on Social Network Analysis," *Proceedings - IEEE 7th International Conference on Big Data Computing Service and Applications, BigDataService 2021*, pp. 87–95, 2021, doi: 10.1109/BIGDATASERVICES52369.2021.00016.
- [14] E. A. Afify, A. S. Eldin, and A. E. Khedr, "Facebook Profile Credibility Detection using Machine and Deep Learning Techniques based on User's Sentiment Response on Status Message," *International Journal of Advanced Computer Science and Applications*, vol. 11, no. 12, pp. 622–637, 2020, doi: 10.14569/IJACSA.2020.0111273.
- [15] M. Khalid, I. Ashraf, A. Mehmood, S. Ullah, M. Ahmad, and G. S. Choi, "GBSVM: Sentiment classification from unstructured reviews

- using ensemble classifier,” *Applied Sciences* (Switzerland), vol. 10, no. 8, Apr. 2020, doi: 10.3390/APP10082788.
- [16] S. Adonai, H. Morales, M. Fabiola, M. Antayhua, and L. Andrade-Arenas, “Development of Predictions through Machine Learning for Sars-Cov-2 Forecasting in Peru,” *IJACSA) International Journal of Advanced Computer Science and Applications*, vol. 12, no. 11, p. 2021, doi: 10.14569/IJACSA.2021.0121188.
- [17] D. Sharma and S. Singhal, “Detection of fake news on social media using classification data mining techniques,” *International Journal of Engineering and Advanced Technology*, vol. 9, no. 1, pp. 3132–3138, Oct. 2019, doi: 10.35940/IJEAT.A1637.109119.
- [18] R. Moin, Zahoor-ur-Rehman, K. Mahmood, M. E. Alzahrani, and M. Q. Saleem, “Framework for rumors detection in social media,” *International Journal of Advanced Computer Science and Applications*, vol. 9, no. 5, pp. 439–444, 2018, doi: 10.14569/IJACSA.2018.090557.
- [19] M. Cabanillas-Carbonell, R. Verdecia-Peña, E. Medina-Rafaile, J. Luis, H. Salazar, and O. Casazola-Cruz, “Data Mining to Determine Behavioral Patterns in Respiratory Disease in Pediatric Patients,” *IJACSA) International Journal of Advanced Computer Science and Applications*, vol. 12, no. 7, p. 2021, doi: 10.14569/IJACSA.2021.0120749.
- [20] N. Alias, C. F. M. Foozy, and S. N. Ramli, “Video spam comment features selection using machine learning techniques,” *Indonesian Journal of Electrical Engineering and Computer Science*, vol. 15, no. 2, pp. 1046–1053, Aug. 2019, doi: 10.11591/IJECS.V15.I2.PP1046-1053.
- [21] N. M. AlShariah and A. K. Jilani Saudagar, “Detecting fake images on social media using machine learning,” *International Journal of Advanced Computer Science and Applications*, vol. 10, no. 12, pp. 170–176, 2019, doi: 10.14569/IJACSA.2019.0101224.
- [22] H. Park, H. Seo, K. J. Kim, and G. Moon, “Application of machine learning techniques to tweet polarity classification with news topic analysis,” *International Journal of Engineering and Technology(UAE)*, vol. 7, no. 4, pp. 40–41, 2018, doi: 10.14419/IJET.V7I4.4.19606.
- [23] U. Suleymanov, B. K. Kalejahi, E. Amrahov, and R. Badirkhanli, “Text classification for azerbaijani language using machine learning,” *Computer Systems Science and Engineering*, vol. 35, no. 6, pp. 467–475, 2020, doi: 10.32604/CSSE.2020.35.467.
- [24] S. G. Taskin, E. U. Kucuksille, and K. Topal, “Detection of Turkish Fake News in Twitter with Machine Learning Algorithms,” *Arabian Journal for Science and Engineering*, vol. 47, no. 2, pp. 2359–2379, Feb. 2022, doi: 10.1007/S13369-021-06223-0.
- [25] P. M. Konkobo, R. Zhang, S. Huang, T. T. Minoungou, J. A. Ouedraogo, and L. Li, “A Deep Learning Model for Early Detection of Fake News on Social Media*,” *Proceedings of 2020 7th IEEE International Conference on Behavioural and Social Computing, BESC 2020*, Nov. 2020, doi: 10.1109/BESC51023.2020.9348311.
- [26] R. Shima, H. Yunan, O. Fukuda, H. Okumura, K. Arai, and N. Bu, “Object classification with deep convolutional neural network using spatial information,” *ICIBMS 2017 - 2nd International Conference on Intelligent Informatics and Biomedical Sciences*, vol. 2018-January, pp. 135–139, Feb. 2018, doi: 10.1109/ICIBMS.2017.8279704.
- [27] Z. Jahanbakhsh-Nagadeh, M. R. Feizi-Derakhshi, and A. Sharifi, “A semi-supervised model for Persian rumor verification based on content information,” *Multimedia Tools and Applications*, vol. 80, no. 28–29, pp. 35267–35295, Nov. 2021, doi: 10.1007/S11042-020-10077-3.
- [28] V. González-Gutierrez et al., “Multitasking Behavior and Perceptions of Academic Performance in University Business Students in Mexico during the COVID-19 Pandemic,” *International Journal of Mental Health Promotion*, vol. 24, no. 4, pp. 565–581, 2022, doi: 10.32604/ijmhp.2022.021176.
- [29] S. K. Punia, M. Kumar, T. Stephan, G. G. Deverajan, and R. Patan, “Performance analysis of machine learning algorithms for big data classification: ML and ai-based algorithms for big data analysis,” *International Journal of E-Health and Medical Communications*, vol. 12, no. 4, pp. 60–75, Jul. 2021, doi: 10.4018/IJEHMC.20210701.OA4.
- [30] A. Rao and K. Shah, “An Unsupervised Technique to Generate Summaries from Opinionated Review Documents,” *Advances in Intelligent Systems and Computing*, vol. 1199, pp. 388–397, 2021, doi: 10.1007/978-981-15-6353-9_35.
- [31] K. Kokkinos and E. Nathanail, “Exploring an Ensemble of Textual Machine Learning Methodologies for Traffic Event Detection and Classification,” *Transport and Telecommunication*, vol. 21, no. 4, pp. 285–294, Dec. 2020, doi: 10.2478/TTJ-2020-0023.
- [32] D. Solyali, “A comparative analysis of machine learning approaches for short-/long-term electricity load forecasting in Cyprus,” *Sustainability* (Switzerland), vol. 12, no. 9, May 2020, doi: 10.3390/SU12093612.
- [33] J. A. Hartigan and M. A. Wong, “Algorithm AS 136: A K-Means Clustering Algorithm,” *Applied Statistics*, vol. 28, no. 1, p. 100, 1979, doi: 10.2307/2346830.

Registration Methods for Thermal Images of Diabetic Foot Monitoring: A Comparative Study

Doha Bouallal^{1*}, Hassan Douzi², Rachid Harba³
IRF-SIC Laboratory, Ibn Zohr University, Agadir, Morocco^{1,2}
PRISME Laboratory, Orléans University, Orléans, France^{1,2,3}

Abstract—This paper presents a comparative study of image registration techniques for Diabetic Foot (DF) thermal images. Four registration methods (Intensity-based algorithm, Iterative closest point (ICP), subpixel registration algorithm, which is mainly based on Fast Fourier Transform (FFT), and the pyramid approach for subpixel registration) have been implemented and analyzed. The performances of the four algorithms were evaluated using several overlap and symmetry metrics such as the Dice similarity coefficient (DSC), Root Mean Square Error (RMSE) and peak signal to noise ratio (PSNR). The methods were analyzed in a first step on the images of contralateral feet (right and left) of the same subject, which is called in this paper "contralateral registration" and in a second step on a pair of images of the same subject but acquired in two different times T0 and T10 after applying a cold stress test, which is called "multitemporal registration". Results showed that the intensity-based approach and the pyramid approach for subpixel registration algorithm give the best results in both types of registration (contralateral / multitemporal) and can be used efficiently for the registration of these types of images even under changing conditions.

Keywords—Medical imaging; diabetic foot; thermography; registration; mobile health

I. INTRODUCTION

According to the World Health Organization (WHO) [1], by 2030 diabetes will be ranked the 7th leading cause of death worldwide. Type II diabetes (formerly known as non-insulin dependent diabetes or mature diabetes) results from a misuse of insulin by the body. It represents the majority of diabetes cases. It is largely the result of being overweight and not being physically active. A poorly controlled diabetes has a damaging impact on several organs of the body, namely the eyes (blindness), the kidneys (nephropathy) or renal failure, the heart (cardiac accident), the nervous system (neuropathy), the blood vessels (ischemia, stroke) and complications in the feet as ulcers that can lead to amputation of the lower limbs, known by the diabetic foot (DF) [2] which represents the core of our study. Diabetic foot ulcers are invariably preceded by inflammation, the presence of infection and pain. However, in the early stages of wound development, patients with diabetes may have difficulty experiencing pain due to neuropathic sensory loss [3]. On the other hand, inflammation can be identified by assessing the temperature of the affected foot. Thus, temperature assessment using a thermal camera appears to be a useful predictor of foot ulceration. Research shows that there is a significant relationship between increased temperature and diabetic foot complications [4][5].

Increased temperature can be detected up to a week before foot ulceration occurs. The most commonly used criterion is that if the point to point temperature difference ΔT of the corresponding area of the right and left foot is greater than 2.2°C [6], there is a high risk of infection or ulceration in diabetic feet. This is called hyperthermia (see Fig. 1) and this temperature difference map is calculated point-to-point between the left and right foot after the process of registration and overlap.

Thermography is a non-invasive technology and does not require any contact with the patient's skin. This allows using it to avoid any undesirable pressures that could affect the temperature measurement, as well as the transmission of pathological organisms. For all these reasons, it has been adopted as the main technology in our study.

In the literature, there are similar works for detecting hyperthermia areas in DF. Fraiwan et al. [7], used intensity-based registration after segmenting the two plantar surfaces using Histogram shape thresholding, to align the two feet and detect the hyperthermia areas. In [8] they used ICP to register the two feet and calculate the point-to-point temperature difference.

Except that in these works the authors did not detail the performance of these methods or provide quantitative evaluations to assess the accuracy of the registration.

Kaabouch et al [9] separated the original image into two (left foot, right foot), identified the centroid and the farthest heel points of each foot, in order to calculate the angle of the feature line with respect to the vertical direction, finally they apply translation and rotation to adjust both feet in the center of the image and this technique is limited because it assumes that both feet are on the same plane in the image and have the same shape and size.

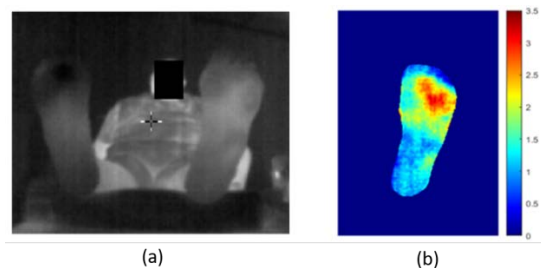


Fig. 1. Original Thermal Image, (b) Thermal difference Map $|\Delta T|$ for a Subject with an Ulcer.

*Corresponding Author.

In this paper, we analyze four different registration methods to obtain foot images aligned with high accuracy, in order to perform the thermal monitoring analysis, namely, the calculation of $|\Delta T|$ between the contralateral feet as shown in Fig. 1. This registration step requires high precision, because any deviation between the feet images will have a direct impact on the accuracy of detecting abnormal plantar temperature.

The rest of the paper is organized as follows. Section 2 called materials and methods describes the acquisition protocol of our data, the used equipment, and subjects who participated to our acquisition campaign. It presents also the existing thermal analysis for DF assessment, as well as the compared registration techniques. The third section is dedicated to the quantitative and qualitative results of the tested methods. Finally, the conclusion is presented in the last section.

II. MATERIALS AND METHODS

A. Image Acquisition

In this section, we first explain the choice of the smartphone thermal camera, then, we describe the acquisition protocol of our images and the recruitment of participants.

1) *The chosen camera:* is the FlirOne Pro camera, designed to be connected to a smartphone. This camera consists of two sensors. A thermal sensor that measures heat through infrared emission, and an RGB sensor designed to acquire visible images in parallel with the thermal core. The camera has a thermal image resolution of 160x120 pixels and a spectral range of 8-14 μm . FlirOne Pro can detect temperature differences of 0.1°C, which is sufficient to detect possible hyperthermia variations. It was used with a smartphone Samsung Galaxy S8.

2) *Acquisition protocol:* To collect our images, we adopted two acquisition protocols, the first one allows to obtain a single thermal image of the patient's feet, after letting him rest for 15 min (Fig. 2). The second one called Cold Stress test [10] is a protocol that consists in taking two acquisitions of the same patient in two different moments (Fig. 3).

As shown in Fig. 2, after the medical examination, Patients are requested to rest barefoot for a 15 minutes interval to allow the feet to regain their normal temperature. Finally, thermal and RGB images are acquired.

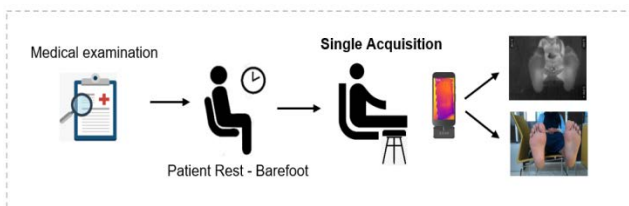


Fig. 2. Acquisition Protocol (Single Acquisition).

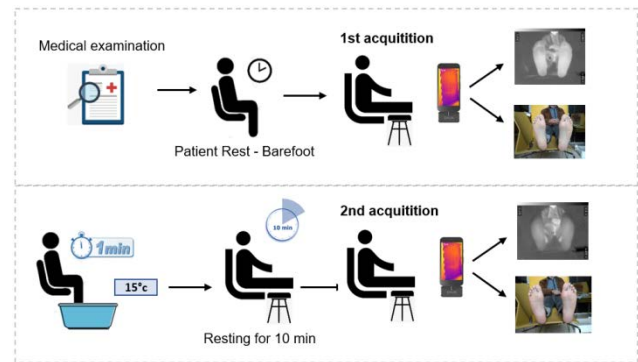


Fig. 3. Cold Stress Test Protocol (Multitemporal Acquisition).

Participants are asked to remove their shoes and socks. After a 15 minutes interval to allow the feet to recover their normal temperature, the person laid down on a stretcher or chair and placed his/her feet at the end of the stretcher, in a vertical position, and 10 cm apart. The baseline thermal image was taken freehandedly using a Samsung Galaxy S8 and a FLIR ONE Pro camera. After that, the patient is asked to immerse the feet, which are protected with thin plastic for 60 seconds in water at 15°C. After 10 minutes, a new plantar thermal image is recorded. Fig. 3 illustrates the protocol step by step.

3) Subjects:

a) *Control group:* Composed of 82 healthy (non-diabetic) individuals who participated in two acquisition campaigns. The first one was conducted at the University of Orleans, France. Participants were members of Prisme staff. A total of 22 people participated in this first acquisition campaign. The second acquisition campaign was organized at the IBN Zohr University in Agadir, Morocco. In which volunteer students and members of the IRF-SIC laboratory without a history of diabetes participated. In this campaign, two acquisitions were carried out for 43 people in two different moments applying the protocol of the cold stress test described in Fig. 3. In addition to 17 people who participated in a single acquisition (Fig. 2). The criteria for recruiting individuals were simple: any adult volunteer who is non-diabetic and does not have a foot problem.

b) *Diabetic group:* 145 diabetic persons accepted to participate to our study within the diabetic Foot Service of the national hospital Dos De Mayo de Lima in Perou, and signed the informed consent form. For this campaign, we exclude patients with ulcers, partial or total amputations. All acquisitions and tests were carried out under the supervision of specialists and diabetologists, who performed a set of clinical examinations on the patients to monitor neuropathy and ischemia. Two images were captured for each patient at two different moments after applying the cold stress test (Fig. 3).

B. DF Thermal Analysis Methods

The analyses of diabetic foot thermograms can be divided into three main categories, according to existing works in the literature. The first is the asymmetric analysis between the two feet of the patient. As several studies have shown [11][3][6], there is contralateral symmetry in the distribution of skin temperature in healthy individuals, and any asymmetry in this distribution may be indicative of an abnormality. Therefore, many scientific experiments are conducted on diabetic patients [4][8][12][13][14][10][15][16] in which they found that a temperature variation of 2.2°C or more between the two feet (right and left) was detected in diabetic patients who are at risk of developing ulcers in these hyperthermic areas (see Fig. 1). The second type of thermal analysis is temperature distribution analysis [17]. The advantage of this type of analysis is that the temperature difference between the contralateral feet is no longer used and each foot can be analyzed separately. In the majority of the works based on this type of analysis, they divide the feet into several regions called angiosomes [18] by which they classify the patient's foot as being at risk of ulceration [19] [20]. The last type of analysis is based on external stress; the purpose of this analysis is to observe the response of the body thermoregulation system after applying a specific stress. This stress can vary from immersing limb in hot or cold water [10] [21], or it can be a mechanical stress such as walking or running [22]. This evaluation was presented in [21] by the thermal recovery index (TRI) which is calculated between the feet of the same patient in two different moments before and after stress). As in the study [10], they evaluated the relationship between plantar foot temperature variation and cold stress test applied on diabetic patients, by calculating the difference in temperature of the same foot at two different times, which is called a multitemporal analysis.

These thermal analyses require a series of pre-processing steps of the foot thermograms, to prepare these zones of interest which are the plantar soles. The first task consists in segmenting the two feet and separating them from the rest of the background (Fig. 4), and in this study the images we are going to present are previously segmented using a neural architecture that is detailed in our previous work [23].

Once the feet have been segmented, a primordial step is to align the feet in order to calculate the temperature difference either by applying the contralateral analysis (asymmetry) or the analysis based on the external stress (multitemporal). This step is the core of this work. Our objective is to find the most suitable registration method for our problem, which can be defined by two essential challenges;

- Variation in shape and position between the patient's feet, which complicates the registration.
- Dissimilarity between two images of the same patient foot taken at different times (in our case instant T_0 before cold stress test and instant T_{10} after cold stress test), from different distances, or from different viewpoints.

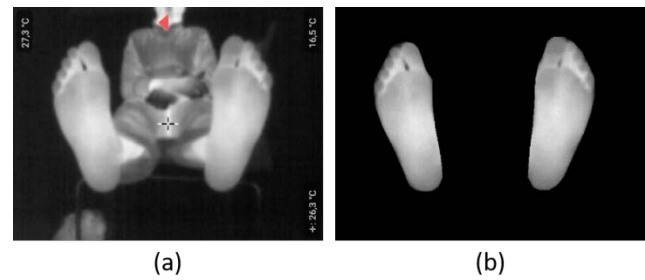


Fig. 4. (a) Thermal Image, (b) Segmented Feet.

C. Image Registration

1) *Registration types*: In this work we conducted two types of experiments. The first one is a contralateral registration, which consists of aligning the right and left feet of the same patient image. And the second is a multitemporal registration applied on a pair of images of the same feet acquired in two different moments with the cold stress test.

a) *Contralateral registration*: the first dataset consists of thermal images of segmented feet as shown in Fig. 4(b). The image of the two feet is divided into two (left foot and right foot), the right foot is considered as the reference image (fixed) and the left foot (moving) is flipped horizontally to register it with the reference image, in order to calculate the temperature difference between the two feet after aligning them. The process is detailed in Fig. 5.

b) *Multitemporal registration*: this type consists of registering a pair of thermal images of the same patient taken at two different times. A first acquisition at time T_0 captured before the application of the cold stress test [10] and a second acquisition at time T_{10} made 10 min after the application of the cold stress test.

This is a multitemporal registration in which the goal is to align the two images of the same foot at two different times T_0 and T_{10} . The image of the right foot at time T_{10} , which is considered as a target (moving image), is aligned with the image of the right foot at T_0 , which is considered as a reference image (fixed image), and the same for the left foot. The process is shown in Fig. 6.

2) *Registration techniques*: In our research, the objective is not to make the foot images identical. We are looking for the transformation that minimizes the distance between the information contained in one image and its correspondence on the other image. As well as studying the significant differences that will allow us to localize the region at risk of ulceration. In our case, the registration must not modify the size of potential anomalies, or make local deformations on the foot, since this could, for example, mask the detection of a hyperthermia area. Therefore, the registration methods chosen in this paper are linear, either rigid transformations (translation-rotation) such as the ICP [24] and the Sicairos et al. method [25], or affine transformations, namely intensity-based algorithm [26] and pyramid approach [27]. In the following, we will present the registration techniques that we have compared and evaluated on our database.

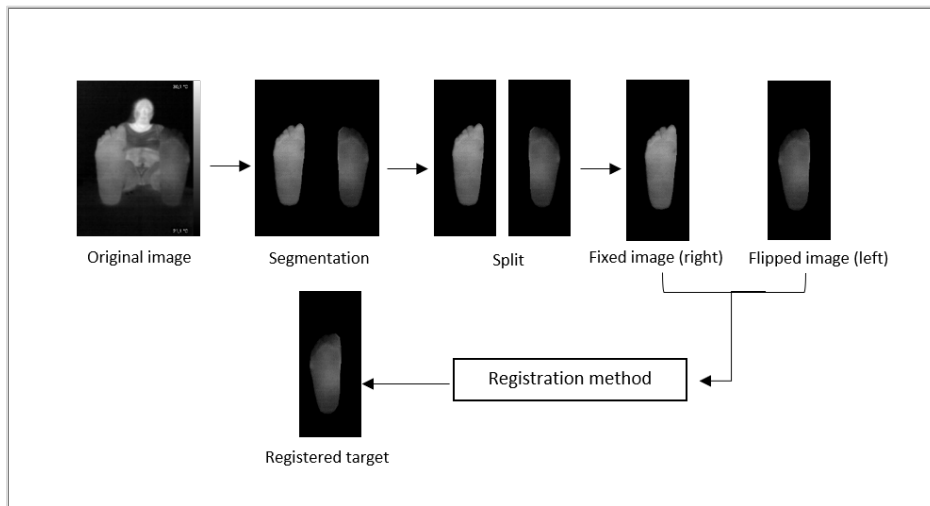


Fig. 5. Contralateral Registration Process.

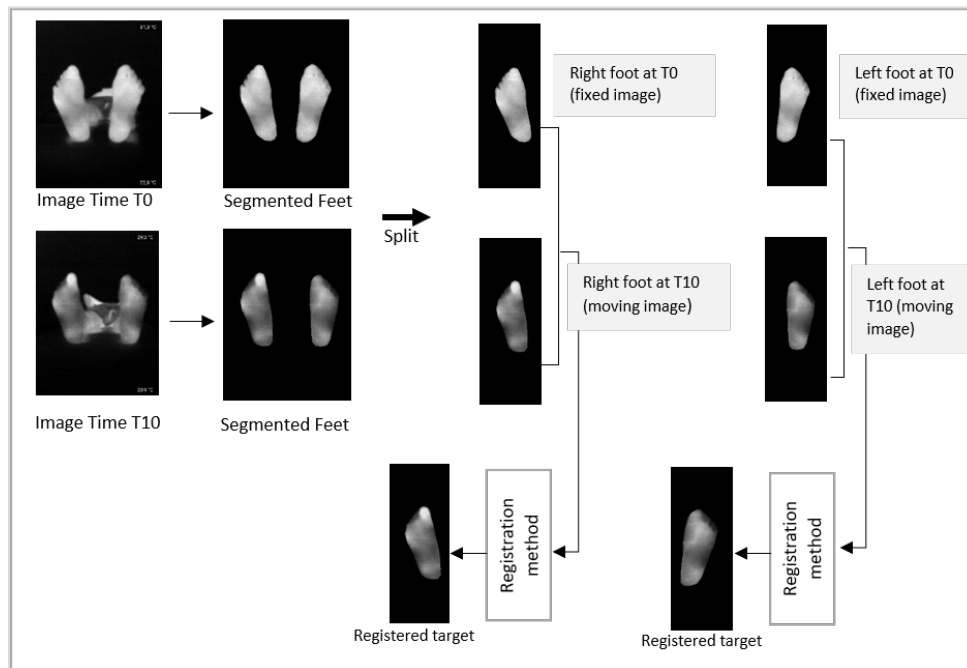


Fig. 6. Multitemporal Registration (after Applying Cold Stress Test).

a) *Iterative Closest Point (ICP)*: The Iterative Closest Point (ICP) algorithm is used to match two sets of data, most often in the form of point clouds or meshes corresponding to two partial views of the same object. Iteratively, the algorithm revises the transformation (combination of translation and rotation) needed to minimize an error metric, usually a distance between the source and target point clouds, such as the sum of squared differences between the coordinates of the matched pairs.

In this work, we used a maximum number of iterations of 300 and a minimum difference in the correspondence measure between two successive iterations of $1e^{-5}$. These values were chosen empirically, after a number of tests, as it was observed that no more than 300 iterations were required in any of the studied cases to converge to an optimal solution.

b) *Sicairos et al approach*: To perform a simple translation between two images, the usual technique for solving this problem is to compute an oversampled cross-correlation between the image to be registered and a reference image, using a Fast Fourier Transform (FFT), and locate its peak. The computational burden associated with this approach increases as the accuracy required for the registration increases, especially in terms of memory.

Therefore, as an alternative Guizar-Sicairos et al. [25] have developed different algorithms that significantly improve performance without sacrificing accuracy. These algorithms start with an initial estimation of the location of the cross-correlation peak obtained by the FFT method with an upsampling factor of $k_0=2$. This initial upsampling is used for the purpose of selecting an appropriate starting point for cross-

correlations that might have more than one peak of similar magnitude. This type of algorithm, as in the FFT upsampling approach, always uses all the information available in the images to compute the initial estimate and each point of the upsampled cross-correlation grid, which makes it very robust to noise. It has been demonstrated in [25] that these new registration refinement algorithms can achieve subpixel image registration with the same or better accuracy than traditional FFT oversampling but with significantly reduced computation time and memory requirements.

c) *Intensity-based registration:* The intensity-based registration method operates directly on the gray values of the images. The main goal of this technique is to find the right transformation that maximizes (or minimizes) the similarity metric between the corresponding voxels.

The most frequently used similarity measures are the sum of squared differences of pixel intensities, the regional correction or the mutual information.

As shown in the Fig. 7, the algorithm takes two images in input, the image to be registered (moving image) and the reference image (fixed image). It requires four other essential parameters, namely; a similarity metric, an optimizer and the type of transformation.

The process begins with the transformation type we specify and an internally determined transformation matrix. They jointly determine the specific image transformation which is applied to the moving image with a bilinear interpolation. Then the metric compares the transformed moving image to the fixed image and a metric value is returned.

Finally, the process stops when it has reached a point of decreasing efficiency or has reached the maximum number of iterations. If there is no stopping condition, the optimizer adjusts the transformation to start the next iteration.

In this experiment, we ran the intensity-based algorithm using One Plus One Evolutionary optimizer with an initial radius of $6,25 e^{-3}/3,5$, growth factor of 1,05 and a maximum iterations number of 300. The similarity metric used is a mattes mutual information metric. For the initial transformation type, we used affine transformation. These chosen parameters are the ones that gave the best results after several tests.

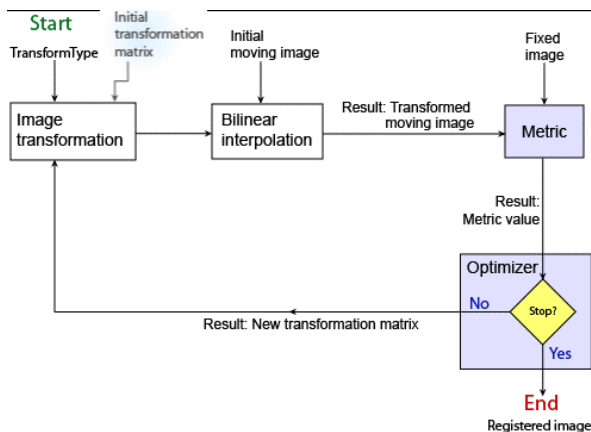


Fig. 7. Intensity-based Registration Algorithm [23].

d) *Pyramid Approach for subpixel registration:* Thévenaz et al. [27] proposed an automatic sub-pixel registration algorithm that minimizes the mean square intensity difference between a reference data set and a test data set, which can be images (two-dimensional) or even volumes (three-dimensional). This method uses an explicit spline representation of the images in conjunction with spline processing, and is based on a coarse-to-fine iterative strategy (pyramid approach).

The minimization is performed according to a new variation (ML*) of the Marquardt-Levenberg algorithm [28] for nonlinear least squares optimization. The geometric deformation model consists of a global three-dimensional (3D) affine transformation that can optionally be restricted to rigid body motion (rotation and translation), combined with isometric scaling. It also includes an optional adjustment of the contrast differences of the images.

According to [27], this algorithm has shown excellent results for the registration of intramodal positron emission tomography (PET) and functional magnetic resonance imaging (fMRI) data.

III. RESULTS

In order to assess the best approach for registering the thermal infrared images of the diabetic foot application, we have tested the four registration methods on our two types of acquisitions, the first “Contralateral” (Fig. 5) containing one image of the feet of each patient (left, right) and the second “Multitemporal” (Fig. 6) containing a pair of images of the same feet acquired at two different times. The purpose is to evaluate the robustness of these approaches in both cases of registration (contralateral/multitemporal) and under the changes that can occur in the position of the subject’s feet, changes in the distance of acquisition or viewpoints, especially for the images captured at two different times.

A. Evaluation Metrics

To quantitatively evaluate the performance of these algorithms, we adopted three evaluation metrics that are most commonly used in the field of registration evaluation. The first one is the Dice similarity Coefficient (DSC) [20], the second one is the RMSE (Root Mean square error) and the last one is PSNR (Peak Signal to Noise Ratio).

- Dice similarity coefficient (DSC): is a statistical indicator that measures the similarity of two samples.
- This score quantifies the overlap between the fixed foot and the registered one.

$$DSC = \frac{2 * |X \cap Y|}{|X| + |Y|} \quad (1)$$

X is the reference image and Y is the registered image.

- Root Mean Square error (RMSE): used to measure the difference per pixel between the moving image and reference image. The lower the value of RMSE, the better the registration performance.

$$RMSE(X, Y) = \sqrt{\frac{\sum_{i=1}^n (X_i - Y_i)^2}{n}} \quad (2)$$

where, X and Y are respectively the reference image and the registered image. n is the total number of pixels in the image.

- Peak Signal to noise ratio (PSNR) : is identified as a numerical measure for image registration quality based on the pixel differences between two images [29]. The Mathematical equation is provided as in equation 3 based on [29]. Where MAX_I is the maximum possible pixel value of the image and MSE is mean square error between reference and target image. A higher PSNR value indicates a higher similarity between registered images. Contrarily, the smaller PSNR value indicates poor similarity between images.

$$PSNR = 10 \cdot \log_{10} \left(\frac{MAX_I^2}{MSE} \right) \quad (3)$$

$$MSE = \frac{1}{n} \sum_{i=1}^n (X_i - Y_i)^2 \quad (4)$$

B. Comparative Results

From the results in Tables I and II, on one hand we deduce that the intensity-based method gives the best value for the Dice coefficient (0.97) followed by the pyramid method (0.96). (The best results are highlighted in bold). On the other hand, we notice that the four algorithms are more robust in the first type of registration (contralateral registration), which is reasonable, since in these acquisitions the two feet to be registered (right and left) are positioned at the same distance from the camera. So generally, in this case we are in front of geometrical transformations that can be considered as a combination of translation and rotation.

TABLE I. COMPARATIVE RESULTS FOR CONTRALATERAL REGISTRATION BETWEEN RIGHT AND LEFT FEET

Methods \ Metrics	Intensity based registration	ICP	Sicairos et al	Pyramid approach
DSC	0,97	0,95	0,93	0,96
RMSE	0,245	0,315	0,34	0,23
PSNR	25,85	23,62	22,90	26,41

TABLE II. COMPARATIVE RESULTS FOR MULTITEMPORAL REGISTRATION

Methods \ Metrics	Intensity based registration	ICP	Sicairos et al	Pyramid approach
DSC	0,968	0,905	0,89	0,94
RMSE	0,344	0,445	0,442	0,318
PSNR	22,24	19,85	19,85	23

Contrary to multi-temporal registration, in which we can clearly see that in some cases, the acquirer can change the distance and position of the camera between time T0 and T10 (ex: Fig. 12). With smartphone, freehandedly, the distance between the feet and the camera may slightly change. This generates a change of scale between the two feet, making the task of registration more complicated.

Based on the results of the two previous tables (Tables I and II) and the charts in the two Fig. 8, 9 and 10, we can see that the performance of the compared methods has decreased

between the contralateral and the multitemporal registration. For example, in Fig. 9 we have the ICP method with a DSC of 0.95 as a result of final overlap of the registered feet (right and left), this value decreased to 0.90 when applying ICP on the images of the same feet acquired at two different times, a difference of 5%.

And this is expected, since the transformation applied by ICP cannot perform perspective corrections. While in the images of the cold stress test the person making the acquisitions often changes the distance and position of the camera between the two instants. The only method that kept the same performance between the two types of registration is the intensity-based method. As shown in Fig. 9 dice values for multitemporal and contralateral registration are almost identical for this method, unlike the other algorithms.

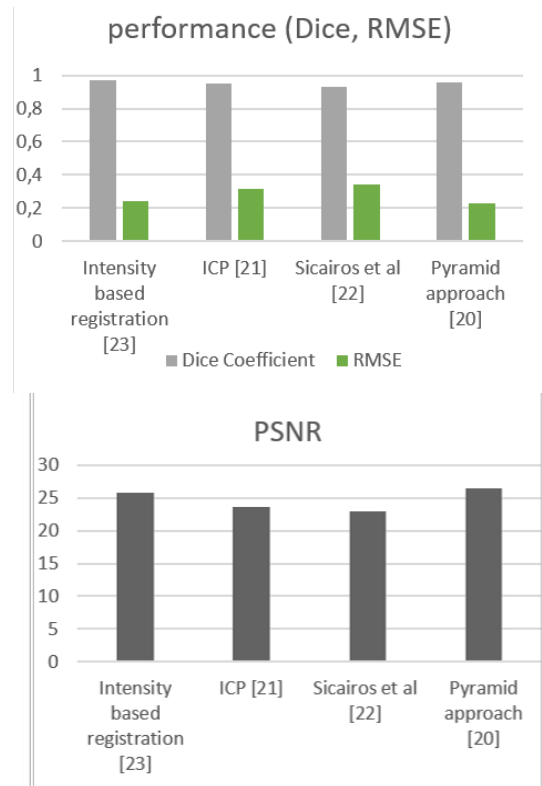


Fig. 8. Dice Coefficient, RMSE and PSNR Metrics for the Four Registration Methods Obtained with Images of Contralateral Feet (Registration between Right and Left Foot).

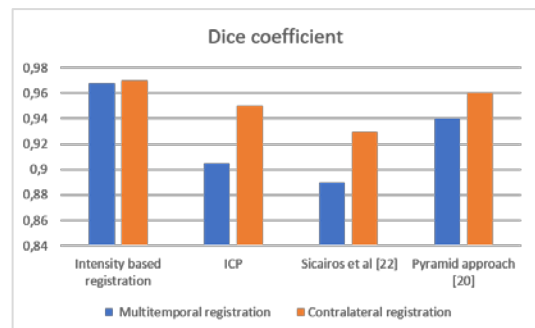


Fig. 9. Dice Coefficient of the Four Registration Methods to Evaluate their Performance in Both Type of Registration (Contralateral and Multitemporal).

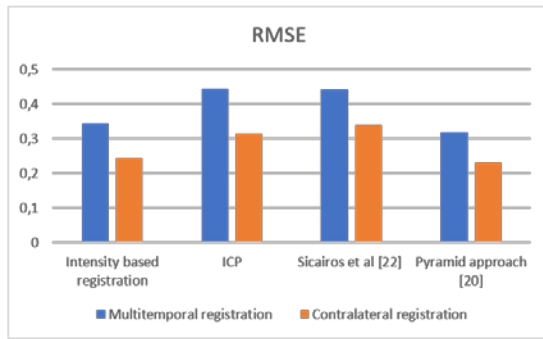


Fig. 10. RMSE of the Four Registration Methods to Evaluate their Performance in Both Type of Registration (Contralateral and Multitemporal).

The qualitative results are in total agreement with the results calculated above (Tables I and II), we see that in Fig. 11 All four registration methods obtain a visually correct overlap between the fixed thermal image and the registered foot when both feet of the subject are located at the same distance from the camera. And the two algorithms based on the intensity and the one of Th evenaz et al [27] (pyramid registration approach) give the best performances.

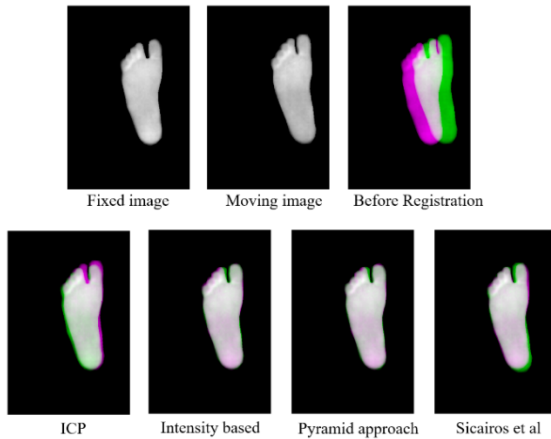


Fig. 11. Example of Contralateral Registration (Left Foot and Right Foot). in All Images, the Foot in Pink is the Fixed Foot (Right) and the Foot in Green is the Moving Foot (Left).

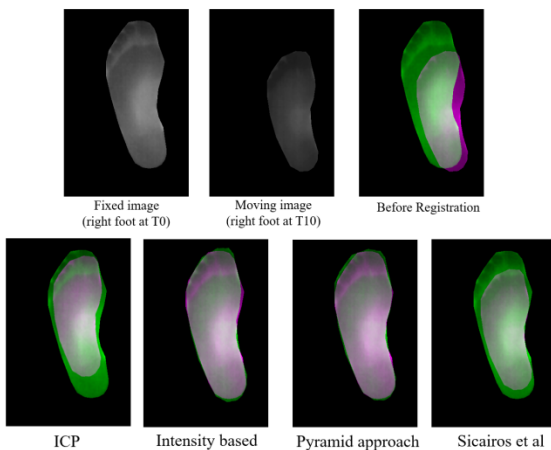


Fig. 12. Example of Multitemporal Registration (Right Foot at Time T0 and Right Foot at Time T10). in All Images, the Foot in Green is the Fixed Foot (Right Foot T0) and the Foot in Pink is the Moving Foot (Right Foot T10).

For multitemporal registration, as shown in Fig. 12 and 13, the added challenges to the algorithms are the change of the capturing view point and the difference distance from the camera between the acquisition at time T0 and the second acquisition at time T10. The methods that have proven their robustness in these cases are intensity based and pyramid approach. They align the images, where the feet don't have the same size and shape. Unlike the method of [9] which is limited and only works in the case where both feet are on the same plane in the image and have the same shape and size.

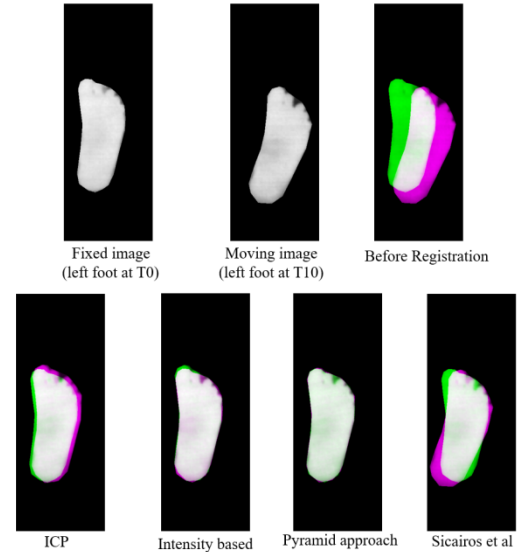


Fig. 13. Example of Multitemporal Registration (Left Foot at Time T0 and Left Foot at Time T10). in All Images, the Foot in Green is the Fixed Foot (Left Foot T0) and the Foot in Pink is the Moving Foot (Left Foot T10).

IV. CONCLUSION

To diagnose the DF problem at an early stage and to detect the areas at risk of ulceration, it is necessary to have a fast and non-contact procedure with simple and low-cost devices. In order to achieve this goal, it is important to implement an approach with a high-level accuracy in diagnosis, ensuring that the acquisition and processing of data does not introduce systematic errors that can be avoided at the time of conception.

Medical diagnostic devices of DF supposed to perform these thermal analyses; such as the computation of temperature difference between contralateral feet or between feet after application of external stresses, require a correct alignment of the acquired images. Because any deviation between the images of the feet will have a direct impact on the accuracy of the subsequent abnormal temperature detection. Hence, the need to evaluate the performance of the registration techniques is used at the heart of this alignment.

In this work, a group of registration methods was implemented and evaluated to match thermal images for diabetic foot application. For the registration of contralateral feet, the methods compared in this paper gave satisfying results. However, when applying the multitemporal registration which consists in aligning the same foot captured in two different instants (T0 and T10), we notice that the performances of ICP and Sicairos et al method have decreased.

- _tid=srchtitle_intensity%20based%20registration_1 (consulté le 6 janvier 2022).
- [27] P. Thévenaz, U. E. Ruttimann, et M. Unser, « A pyramid approach to subpixel registration based on intensity », *IEEE Trans. Image Process. Publ. IEEE Signal Process. Soc.*, vol. 7, n° 1, p. 27-41, 1998, doi: 10.1109/83.650848.
- [28] D. W. Marquardt, « An Algorithm for Least-Squares Estimation of Nonlinear Parameters », *J. Soc. Ind. Appl. Math.*, vol. 11, n° 2, p. 431-441, 1963.
- [29] Y. Tanabe et T. Ishida, « Quantification of the accuracy limits of image registration using peak signal-to-noise ratio », *Radiol. Phys. Technol.*, vol. 10, n° 1, p. 91-94, mars 2017, doi: 10.1007/s12194-016-0372-3.

Op-RMSprop (Optimized-Root Mean Square Propagation) Classification for Prediction of Polycystic Ovary Syndrome (PCOS) using Hybrid Machine Learning Technique

Rakshitha Kiran P¹

Assistant Professor, Dept of MCA
Research Scholar Dept of ISE, Dayananda Sagar College of
Engineering, Bengaluru-78, affiliated to VTU

Naveen N. C²

Professor and Head, Dept of CSE
JSS Academy of Technical Education
Bengaluru-60, affiliated to VTU

Abstract—Polycystic Ovary Syndrome is a common women's health problem caused by the imbalance in the reproductive hormones which causes problems in the ovaries. An appropriate machine learning (ML) algorithm can be applied to analyze the datasets and validate the performance of the algorithm in terms of accuracy. In this paper, a unique hybrid and optimized methodology are proposed which uses SVM linear kernel with Logistic Regression functionalities in a different way. The output of this model is passed on to the RMSprop optimizer. Optimization will train the model iteratively to get better output. For this research 1600 datasets were collected from the leading hospital in Bangalore Urban region. This optimized hybrid method is tested over PCOS datasets and it exhibited 89.03% accuracy. The results showed that the optimized-hybrid model works efficiently when compared to other existing ML Algorithms like SVM, Logistic regression, Decision tree, KNN, Random forest, and Adaboost. Also, the results of the optimized-hybrid SVLR model showed good results in terms of F-measure, precision, and recall statistical criteria. Overall this paper summarizes the working of the proposed optimized-SVLR hybrid model and prediction of PCOS.

Keywords—SVM; decision tree; logistic regression; RM Sprop; frameworks

I. INTRODUCTION

In the present world, there are very large innovations in the field of medicine which help clinical experts to predict any disease in a better and faster way. The research by Kirschner MA [2] shows that around 60-70% of the Indian young women population suffers from polycystic ovary syndrome (PCOS). PCOS is an endocrinopathy caused because of an imbalance of the reproductive hormones affecting women of reproductive age, which creates complications in the ovaries [1] [26]. The ovaries produce eggs which will be released every month in case of a healthy menstrual cycle. But ladies with PCOS will end up with irregular menstrual cycles as the egg may not develop as it should or it may not be released during ovulation [4]. Most women develop PCOS in their 20s and 30s but it can arise at any age after puberty [1]. Obesity is one of the root causes of PCOS and other infertility-related problems [5]. Women with PCOS have a number of obstacles to successful lifestyle improvement. For weight management,

the intrinsic factors range is changed in PCOS, which is indicated by recent research. This has an impact on how well PCOS-affected women can control their weight, although there is currently insufficient and conflicting evidence.

Computational model-based frameworks constructed with ML techniques are now widely regarded as valuable tools for predicting and analyzing a wide range of diseases. Around-the-clock ML approaches are sufficient to successfully and proficiently predict the disease [7]. ML models, in contrast to traditional techniques, do not require in-depth knowledge of data insights. SVM, Nave Bayes, Decision Tree, and Artificial Neural Network (ANN) is classifier models of ML approaches that are commonly used in medical services.

Due to the expensive computational tasks, and overfitting conditions, high dimensional data can have an impact on classifier accuracy in the majority of the existing research. The multiple characteristics are used by the previous research for classifying the PCOS problem, which affects the effectiveness of the classification results. To overcome these challenges, a novel Op-RMSprop algorithm has been proposed. The overfitting problem is reduced by selecting the most significant data by using the proposed model, and also it enhances the classification performance and processing time.

The proposed research's primary goal is to provide a unique and accurate prediction model which could predict the possibility of PCOS patients becoming infertile soon. Here a hybrid model is built combining the functionality of the two models Support Vector Machine and Logistic Regression Algorithms and the model is optimized using the RMSprop optimizer. One of the most important aspects of ML is optimization [6]. The optimization model is created and the features of the optimization method from the input data are learned by the ML-based algorithms [8]. The popularization and implementation of ML models are significantly influenced by the efficiency and effectiveness of quantitative optimization algorithms in the era of large databases [9]. For this research RMSProp Optimization model [33] has been used, which is one of the best optimization techniques available and provides optimal output, also this technique reduces the learning rate monotonically.

This paper summarizes various first-order optimization techniques in Section II, a Literature review on the application of ML in the healthcare domain in Section III, criteria for evaluation of ML algorithms in Section IV, the proposed framework in Section V, and Results of the proposed framework in Section VI and finally in Section VII Conclusion.

II. LITERATURE REVIEW

In [16], Prof. Keshavaraj GK, and Prof.SuryaSukumran explain about Data mining process where knowledge is extracted from huge datasets. Three main modules of Data mining are Clustering/ Classification, Association Rules, and Sequence Analysis. In classification/clustering data set is analyzed and a set of grouping rules is generated which is used to classify future data. In DM information is extracted from data sets and transformed into an understandable structure. It follows a computational methodology for discovering patterns in large data sets involving different approaches like AI, ML, statistics, and database systems. All DM tasks are either automatic or semi-automatic used for the examination of huge amounts of datasets. There are six common classes of tasks in DM they are: Anomaly detection, Regression, Classification, Clustering, Association rule learning, and Summarization. Classification is a prime methodology in data mining and is widely used to predict relationships for data instances. In this paper, a few basic classification techniques like DT induction, KNN classifier, and Bayesian networks are discussed. This paper aims to give an insight into various classification techniques in data mining.

In [17], the author summarizes the caused deaths due to heart disease which has become a major issue. With the rise in heart stroke rates at younger ages, there is a need to put in place an early-stage device to identify the signs of a heart attack and thereby avoid it. It is not possible for a common man to undergo ECG frequently and as a result, there must be an application to detect chances of heart stroke at an early stage. In this paper, the authors have proposed a model which can predict the chances of a heart stroke using basic attributes like BP, age, gender, pulse rate, etc. An Artificial Neural network algorithm has given the most accurate result.

In [18] the author gives insights into the constructive examination of different chronic diseases. ML algorithms provide a large impact on health care by giving an effective inspection of problems for accurate diagnosis. In this paper, the authors talk about the kidney problem which is associated with other numerous factors like hypertension, aging, and diabetes, and its effects on people in the age group 60 and above. The authors used ML techniques to analyze chronic kidney disease (CKD). Around 400 data sets were collected from the UCI repository and Apriori algorithm with 10-fold-cross validation. Six classification different algorithms like ZeroR, Naïve Bayes, J48, OneR, and IBK were applied to the datasets. Data were preprocessed and normalization of missing data was done before analyzing datasets. The results shown were 99% detection accuracy for CKD datasets using the Apriori algorithm [13]. This study examines different ML methods, especially classification and association techniques.

The paper also analyses the impacts of utilizing feature determination procedures in amalgamation with classification. This was carried out using the ANACONDA python tool. The outcomes were cross-checked with correctly classified instances, mean absolute value, and kappa statistic, with or without the feature_selection methodology. Datasets are processed with the Apriori_Association algorithm and the best results were achieved with IBk and Apriori associative algorithm with an accuracy of 99%.

Diabetes is considered to be the worst and perhaps most chronic illness that causes sugar levels to increase. If diabetes remains untreated and unidentified, a lot of problems can happen [24]. To address the common yet crucial problem, the ML concept was used. In this paper likelihood of diabetics was predicted using a high precision value obtained from the model built using ML techniques. Thus classification algorithms DT, SVM, and NB are used here, to detect diabetes at an early phase. Using Pima Indians Diabetes Database (PIDD) from the UCI system observation was done. The performance of all algorithms is measured on different parameters such as Precision, Accuracy, F-Measure2, and Recall. The values obtained from the experiments were verified using Working Characteristic Receiver (ROC) [24].

Breast cancer (BC) is the most often observed problem faced by women worldwide, causing cancer-related deaths [20]. To enhance the prediction and probability of survival considerably breast cancer must be detected at an early stage. Accurately classification of benign tumors can help patients avoid unwarranted treatments. In this paper, the author reviews ML techniques in breast cancer detection, and diagnosis. Artificial neural networks (ANNs), support vector machines (SVMs), decision trees (DTs), and k-nearest neighbors (k-NNs) were applied to the cancer datasets [20].

Daqqa, Khaled A. S. Abu et al [21], used data mining techniques for getting patterns and models which are undiscovered in datasets. Leukemia is a condition that affects blood status. Blood_Cell_Counter (CBC) is employed to determine Leukemia detection. Leukemia is determined by examining the blood cell relations, gender, age, and also current health condition of patients using ML techniques. Datasets of 4,000 patients were involved in this study. Three classification algorithms like SVM, k-NN, and DTs were used in this study. From the experimental results, while comparing the models 77.30% accuracy is achieved by the DT algorithm than the other methods.

The main research gap of the previous methods includes the lower performance results of the detection and diagnosis of the PCOS problem, high processing time, high overfitting problem, and high computational cost. The proposed model solves these problems, reduces the overfitting risk, and improves the classification performance and processing time of the model.

III. NEED FOR OPTIMIZATION IN MACHINE LEARNING

Building a model hypothesis, describing the objective function, and the model parameters are determined by solving the minimum and maximum of the objective function, these steps are important aspects of ML [10]. The first two steps of

these three crucial processes are ML modeling problems, and the desired model is solved by using the third step with optimization methods. The optimization problems are formulated in almost every ML algorithm. The optimization model is created and the features of the optimization method from the input data are learned by the ML based algorithms.

The most commonly used optimization technique is a first-order method. An extensive survey done on optimization methods by Sun et al [33] says that ML frequently employs first-order optimization algorithms. The commonly utilized first-order optimization algorithms that are used in the ML journey are summarized in Table I.

TABLE I. SUMMARIZATION OF FIRST-ORDER OPTIMIZATION TECHNIQUES [33]

Method	Properties	Advantages	Disadvantages
Gradient Descent	Here With every update, the model finds the target and gradually converges to the objective function's optimal values.	the objective function is convex	The cost of calculation is high since it operates by dynamically adjusting elements in the reverse direction of the objective function's gradient.
Stochastic Gradient Descent	Here, each iteration is based on a random sample that updates the gradient (theta) rather than directly calculating the gradient itself.	The cost of calculation is reduced since the time it takes to calculate each update is independent of the total number of training samples.	Determining the suitable learning rate is difficult.
Adagrad	Here the learning rate will be low if the high gradient, and vice versa	The approach can be used to solve problems with sparse gradients. Each parameter's learning rate is adaptively adjusted.	For addressing non-convex problems, it is not suitable.
RMSprop	It changes the way from total gradient accumulation to an exponential moving average.	It can be used to solve non-stationary and non-convex issues. Also, suitable for large and multidimensional space	The update procedure is reshaped around the local minimum within the late training period.
Adam	Combines the momentum method and adaptive methods	With large amounts of data and larger feature space, it is effective for solving most non-convex optimization problems	In some instances, the approach may fail to converge.
ADMM (alternating direction method of multipliers)	The approach addresses optimization problems with linear constraints.	Divide and rule methodology	Difficult to calculate the penalty

From Table I, we can infer that the RMSprop optimization technique is one of the best techniques which can be applied to medical datasets. It's one of the good and fast optimizers when compared to the existing optimizers. RMSProp is an algorithm that aims to find the global minima where the cost function reaches the smallest possible value. The technique relies on the concept of the Exponentially Weighted Average (EWA) of the gradients. The exponentially weighted average (EWA) is used to determine the moving average. It consists in keeping the previous values in a memory buffer. This is achieved by using this recursive formula:

$$V_t = \beta V_{t-1} + (1 - \beta) \theta_t \tag{1}$$

Where V_t : Moving average value at 't' i.e. averaging θ_t over $1/(1-\beta)$ units (approx).

IV. BACKGROUND

PCOS is a famine problem faced mostly by young women between the ages of 19-35yrs. The risk of PCOS is higher if a woman is obese or if her mother, her sister, or her aunt had PCOS [2][27]. A few common signs of PCOS are as follows:

- Women undergoing PCOS may have an Irregular menstrual cycle i.e. they will fail to get periods or may have fewer periods (less than 8 times/ year) or they may have periods every 21 days or more frequently. Few ladies may even stop getting periods [11][25].

- Excessive hair on the facial hair or various body parts that men normally have. This phenomenon is named "Hirsutism", which affects about 70-80% of women having PCOS.
- Acne may be developed on the face, chest, or upper back.
- Hair thinning or loss of hair can happen on the scalp resulting in baldness.
- Increase in the weight or problem in losing weight
- Skin darkening in the neck region or other parts of the body.
- Skin tags are tiny flaps of excess skin in the neck section or armpits.

PCOS is caused because of two main reasons:

1) More production of androgens hormones, at times, is called "male hormones". Every woman contributes towards making a small number of androgens. Androgens are responsible for the overall development of male features such as male-pattern baldness in the female body [2][34]. Women having PCOS have higher androgens. Two major signs of androgens are it stops the egg from releasing during each menstrual cycle and extra growth of hair and acne [12][28].

2) An increase in insulin levels results in PCOS. Insulin is a hormone that is responsible for converting food into energy. Insulin resistance is a condition in which cells of the body fail to respond adequately to insulin, resulting in higher levels of insulin blood [3][35]. Most women with PCOS undergo insulin resistance when they are obese or overweight [14].

3) Multiple key factors include poor eating habits, less physical activity, and having a diabetes family background (usually type 2 diabetes). This can lead to type 2 diabetes over time. Fig. 1 shows the complex interaction with the underlying problem of PCOS. The figure describes the root cause of PCOS [29].

This section presents the results obtained through experimentation. It is important to find the best fitting classification algorithms [19] [22]. There are various criteria to measure the performance of the algorithms; they are listed as follows [23]:

- Classification accuracy: is the potential of the design to effectively foresee the class labels. It is given in the form of percentage.
- Speed: is the time taken to bring up the model.
- Robustness: to predict the system correctly with missing data and noisy observations.
- Scalability: A model can be precise and efficient when managing a growing quantity of data.
- Interpretability: the degree of interpretation that the algorithm provides.
- Rule Structure: Understanding the rule structure of the algorithm.

The second stage is to inspect performance criteria like measurements, the speed, and frequency of the working model, and intelligibility.

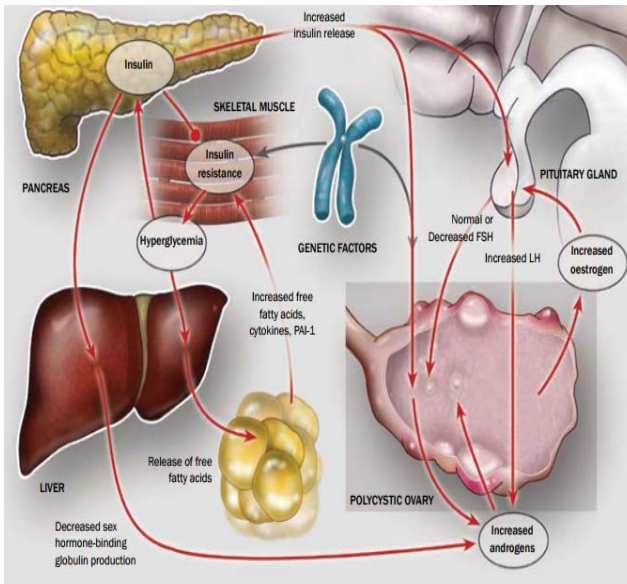


Fig. 1. Complex Interaction Underlying PCOS.

Accuracy (AC): is the percentage of correct predictions. It is calculated as per the confusion matrix.

$$AC = \frac{TN + TP}{TP + FP + FN + TN} \quad (2)$$

- TN --> true “-”
- TP --> true “+”
- FP --> false “+”
- FN --> false “-”

Precision (P): reflects the fraction of positive observations of “+” observations correctly predicted among the total “+” observations predicted.

$$P = \frac{TP}{TP + FP} \quad (3)$$

Recall (R): calculates the proportion of accurately projected positives in each class.

$$R = \frac{TP}{TP + FN} \quad (4)$$

F-measure: The criteria for Recall and Precision are taken together than individually. Thus the F-Measure values that are obtained by the Harmonic Mean (HM) of both methods are considered. F-measure thus provides two levels of classification accuracy.

$$F - \text{measure} = \frac{2 \times P \times R}{P + R} \quad (5)$$

Where R is the recall and P is the precision.

ROC area: The curve shows how different classification algorithms perform in terms of prediction value. It is important for selection criterion for finding the correct methodology for classification. If the value approaches 1, it demonstrates that the classification was done properly.

RMSE: The RMSE is determined as the Mean Squared Error's square root. To calculate the dissimilarity between actual values and estimated values, RMSE is used. It shows the difference between expected and observed values' standard deviation. The RMSE value is desirable to a small.

$$RMSE = \sqrt{MSE} = \sqrt{\frac{\sum_{i=1}^n (y_i - \hat{y}_i)^2}{n}} \quad (6)$$

V. RESEARCH METHODOLOGY

The main purpose of this paper is to examine classification ML techniques based on the accuracy of prediction for PCOS detection. The paper explores different detection methodologies with different techniques using classification algorithms and analyses them for events that have been accurately described. These classification algorithms give early-stage PCOS analysis standards.

In the proposed methodology, a prediction model is built, and also the comparison of various classification algorithms is shown in Fig. 5. The main goal of this research is to propose the best classification technique using ML to predict PCOS. A comparative study of the proposed method is carried out using other cutting-edge techniques. Fig. 2 describes the different phases in brief:

1) *Dataset selection process:* The PCOS [30][32] is detected by selecting the dataset for analyzing data to extract necessary information. Datasets to implement the ML technique should be in large numbers to get accurate results. The dataset for this research is obtained from ESIC Hospital, Bangalore urban region. The data was collected from ladies within the age group of 19-40, working in different firms.

2) *Data Preprocessing and feature selection step:* The dataset retrieved from Survey had 20 attributes, out of which only 17 attributes are applicable for this research. The few missing records, invalid values, duplicate values, and unnecessary fields were removed. Based on the attribute-relation file format, the dataset is created using 17 attributes. It is then transformed into binomial form.

3) *Data:* A dataset stored in CSV format contained 1800 PCOS patient details containing 17 selected attributes. The final "class" attribute has the value "0/1", which shows that an individual with PCOS, like 1, and normal patients as "0". The PCOS dataset's standards, representations, and attributes are described in Table III. The dataset has 735 "non PCOS" and 1065 "PCOS" cases.

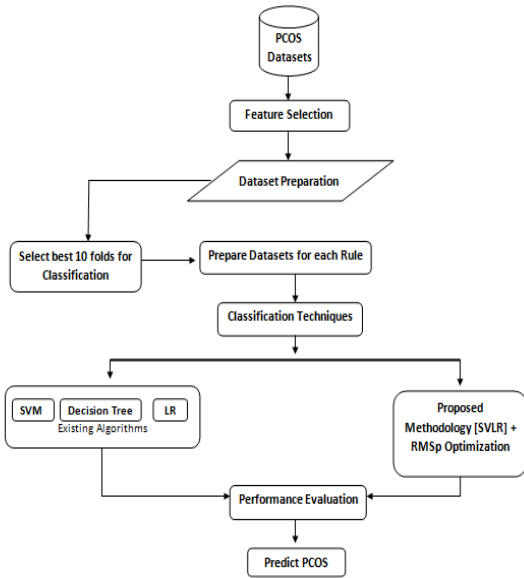


Fig. 2. Proposed Methodology.

A. Proposed Optimized-Hybrid SVLR Classification Technique

This is a hybrid classifier combining the two classifiers i.e. Support vector machine and Logistic regression classifiers.

SVM can be used as a regression method by maintaining a few characteristics that characterize the algorithm. SVLR uses the same principles as the SVM for classification but with minor changes. This SVLR technique performs two stage classifications. The training and testing stages have a distinct window to extract the features from the datasets. The dataset after preprocessing is passed on to the SVLR machine model to analyze the dataset. The schematic diagram of the proposed method is given in Fig. 3.

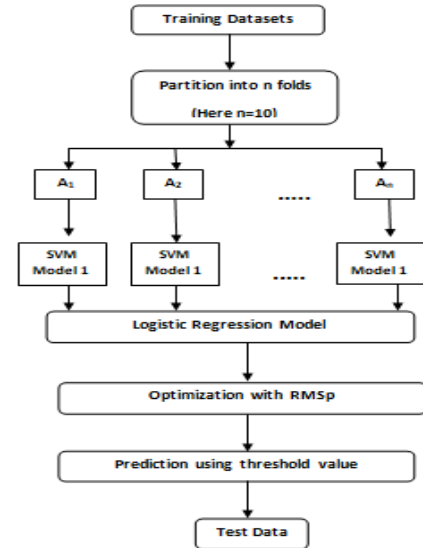


Fig. 3. Working on Proposed Optimized-SVLR Model.

B. SVLR Algorithm

Let's represent the Dataset in the form (A_1, A_2, A_N) where N represents N - samples and where $= 1, 2, \dots, 10$.

Step 1: There is an 'N' number of SVM Classifier models, represented as SV_i running over 'N' sets of datasets. For every run, SVM Classifier will form a Hyperplane to say h_i to SV_i .

Step 2: The distance d_R to the hyperplane must be calculated for 'N' samples in the data set. Therefore the vector with 'n' dimension where $d = d_{k,1} \dots d_{k,n}$ is obtained.

Step 3: The 'd' vector is then prepared to be given to the Logistic Regression Model which will take all responses of the SVM model.

Step 4: After the evaluation with the LR model, the prediction is done and necessary parameters are evaluated using the threshold value. In the proposed method, the description of the attributes is given in Table II.

TABLE II. DESCRIPTION OF ATTRIBUTES

SL.No	Attributes	Description
1	Are your periods regular? (YES/NO)	two nominal values "yes" and "no"
2	Are you gaining weight Rapidly? (YES/NO)	two nominal values "yes" and "no"
3	Are you facing an excess of facial or Body Hair? (YES/NO)	two nominal values "yes" and "no"
4	Do you have patches of dark areas on your skin? (Yes/No)	two nominal values "yes" and "no"
5	Do You suffer from pimples? (YES/NO)	two nominal values "yes" and "no"
6	Do you face depression and anxiety? (YES/NO)	two nominal values "yes" and "no"
7	Do you have any family history of Hyper Tension? (YES/NO)	two nominal values "yes" and "no"
8	Are you finding any difficulty in maintaining your body weight? (YES/NO)	two nominal values "yes" and "no"
9	Do you have oily skin? (YES/NO)	two nominal values "yes" and "no"
10	Are you losing a lot of hair or has it become thinner in its strength? (YES/NO)	two nominal values "yes" and "no"
11	Do you exercise regularly?	two nominal values "yes" and "no"
12	Are you mentally stressed due to the following exercise? (Are you newly admitted to the hostel?)	two nominal values "yes" and "no"
13	Are you mentally stressed due to the following exercise? (Do you have personal problems?)	having two nominal values "yes" and "no"
14	Are you mentally stressed due to the following exercise? (Peer pressure?)	two nominal values "yes" and "no"
15	Are you mentally stressed due to the following exercise? (Change in dietary habits?)	two nominal values "yes" and "no"
16	How often do you eat fast food?	two nominal values "yes" and "no"
17	Any Family history of diabetes?	two nominal values "yes" and "no"
18	Class Label	PCOS suffering patient-Yes (1) else No(0)

C. RMSprop Optimization

Root Mean Squared Propagation is an extension to the gradient descent optimization algorithm [31] and is designed to speed up the optimization process, by decreasing the number of function evaluations that are needed to improve the functionality of the optimization algorithm to obtain the best. RMSprop is similar to gradient descent with momentum in that it employs an exponentially weighted average of gradient, but the distinction is that it updates the parameters [15].

Implementation: The algorithm works better results by updating the model parameters such as the Weight (W) and bias (B).

Consider the parameters W_i and W_j which are used to update the parameters W and B. During the backward propagation:

$$\text{Weight} = W - \text{learning rate} * W_i$$

$$\text{Bias} = B - \text{learning rate} * W_j$$

The weighted averages of W_i and W_j 's squares are exponentially weighted in the RMSprop algorithm.

$$\Delta W_i = \beta * \Delta W_i + (1 - \beta) * W_{i2}$$

$$\Delta W_j = \beta * \Delta W_j + (1 - \beta) * W_{j2}$$

Here, ' β ' momentum is a separate hyperparameter that ranges from 0 to 1.

Then a new weighted average of observed and previous values must be calculated. After that the parameters are updated.

$$\text{Weight} = W - \text{learning rate} * W_i / \sqrt{\Delta W_i}$$

$$\text{Bias} = b - \text{learning rate} * W_j / \sqrt{\Delta W_j}$$

ΔW_i is comparatively small so it is divided by W_i and ΔW_j is comparatively large, so W_j is divided with a relatively larger number to slow down the changes on a vertical dimension.

VI. EXPERIMENTAL RESULTS

A. Performance Evaluation of Existing ML Algorithms for PCOS Datasets

The PCOS datasets have been tested over different ML Algorithms. The performance measures of the paper have been summarized in Table III.

F-measure, Recall, Precision, ROC area, RMSE, and Accuracy value was calculated and compared.

The highest classification accuracy of 87.39 percent is obtained by Logistic Regression and SVM classifiers, as seen in the tables above. While comparing the RMSE values, also the SVM and LR classifiers achieve the reduced results of 0.35 then the other classifiers, and Decision Tree (DT) obtains the worst performance results with a value of 0.361. The LR algorithm has the largest ROC area, with a value of 0.87, therefore it has the best classification performance. SVM and LR are the best methods when precision and F-measure are considered. According to the recall criterion, the SVM and LR show a good value of 0.874. In terms of recall, precision, F-measure, and accuracy evaluation metrics, SVM and logistic regression are the best algorithms.

TABLE III. EVALUATION OF ML ALGORITHMS

Algorithm	F-measure	Recall	Precision	ROC area	RMSE	Accuracy (%)
KNeighbors Classifier	0.827	0.84	0.827	0.883	0.32	84.032
Support Vector Machine (SVM) Classifier	0.871	0.874	0.869	0.788	0.355	87.395
Decision Tree (DT) Classifier	0.832	0.832	0.82	0.77	0.361	83.1
Random Forest (RF) Classifier	0.717	0.798	0.839	0.933	0.334	79.8319
AdaBoost Classifier	0.844	0.849	0.841	0.884	0.3291	84.87
Gaussian Naïve base Classifier	0.832	0.832	0.832	0.896	0.3365	83.1933
Logistic Regression (LR)	0.875	0.874	0.876	0.844	0.3572	87.395

B. Performance Evaluation of Optimized RMSprop-SVLR Hybrid Algorithm for PCOS Datasets

The paper proposes a new optimized and hybrid ML Model which combines the features of both Support Vectors Machine as well as Logistic Regression Algorithms and performs optimization to enhance the output. The optimized-SVLR Model takes PCOS Datasets as input and checks for performance metrics.

The output value is accurately determined by the proposed method as per the results. Fig. 4(b) depicts the RMSE reduction curve of the gradient descent method during training and testing. The expected and observed outputs of the test signal are also shown in Fig. 4(a). The RMSE values can

steadily decrease with iteration when relatively modest learning rates are utilized due to an effective network setup.

The average precision score and the recall trade-off were then shown. The Precision-Recall Curve depicts the distribution of values in detail. When there is a major deficiency in the dataset, the Precision-Recall Curve is performed and the PCOS problem is identified based on the performance of the curve because depending on a single metric is damaging and not a sufficient measure of selecting the algorithm

The Precision-Recall Curve and Average Precision Score are depicted in Fig. 5. Precision Score is the AP at the top of each graph. The AP for the Precision-Recall Curve is Average Precision Score is shown below in the figure.

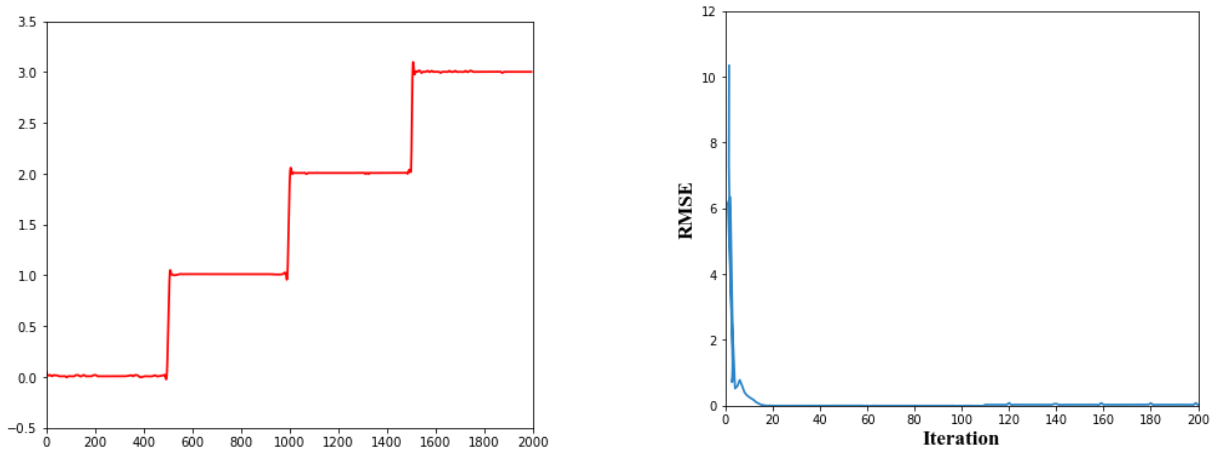


Fig. 4. Numerical Labels are used to calculate the RMSE in the Training Phase. Classification Results using the Provided (a) Over Modeled Labels as Output Labels and (b) RMSE Value based on Numerical Labels during the Training Process.

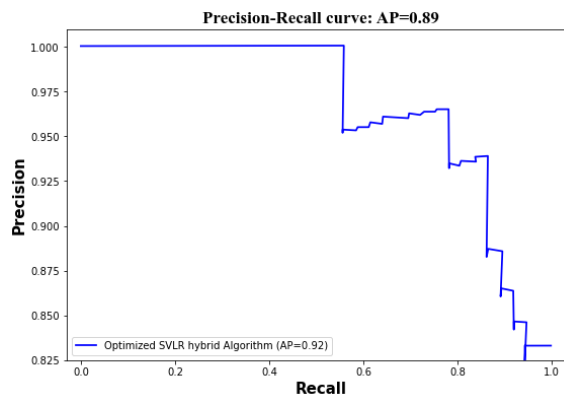


Fig. 5. With Average Precision, the Precision-Recall Curve for Hybrid-SVLR Algorithm.

Table IV shows the performance of an optimized-SVLR algorithm. The optimized SVLR Algorithm is a hybrid algorithm that combines the features of Support Vector Machine and Logistic Regression. The model is optimized with RMSprop optimized algorithm. It is observed that Optimized-SVLR performed well for the given datasets for all the performance measures.

C. Results and Discussion

The higher accuracy of 89% is achieved by the proposed Optimized-SVLR algorithm based on input images with feature extraction and PCOS diagnosis as per the results. The performance of each classifier is shown by the ROC curve for a better representation of this comparison. The true-positive and false-positive rates are compared by forming the curve. Based on this curve, the best classifier has the lowest false positive rates and highest true-positive rates. Fig. 6 illustrates the ROC curve.

As per the results, the developed SVLR model is the best classifier for PCOS diagnosis. Moreover, the Random Forest Classifier and the Gaussian Nave basis Classifier are the second and third high-performance classifiers, respectively.

The accuracy comparison of several existing classifiers with the proposed classifiers is given in Fig. 7. The optimized-hybrid SVLR model produces better accuracy than the prior classifiers; the SVLR model effectively diagnoses the PCOS problem.

TABLE IV. PERFORMANCE MEASURES OF OPTIMIZED SVLR HYBRID ALGORITHM

Optimized SVLR Algorithm	Performance measures
Accuracy	89 %
Recall	0.92
Precision	0.89
ROC area	1.0
RMSE	0.29
F-measure	0.91

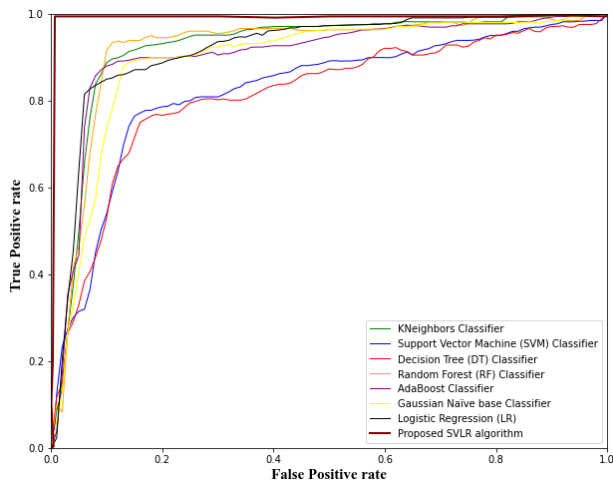


Fig. 6. The ROC Curve of the Classifiers for Diagnosis of PCOS.

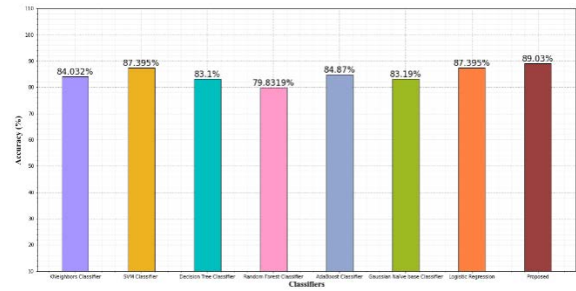


Fig. 7. Accuracy Comparison Graph.

PCOS is a significant medical problem among women caused by the imbalance in the reproductive hormones which causes problems in the ovaries. An appropriate ML algorithm can be applied to analyze the datasets and validate the performance of the algorithm in terms of accuracy. A different hybrid and optimized methodology are proposed in this paper, which uses SVM linear kernel with Logistic Regression functionalities in a different way. The RMSprop optimizer receives the output of this model. The performance of the diagnosis is improved by training the model iteratively using optimization. 1600 datasets from the top hospital in Bangalore's urban area were gathered for this research.

VII. CONCLUSION AND FUTURE REFERENCE

This paper addresses women's fertility problems caused because of polycystic ovary syndrome (PCOS). PCOS is a very common problem faced by women of the reproductive age. These risk factors causing this problem are unhealthy food habits, lack of exercise, hereditary, diabetes, prolonged medications, etc. The ML technique is applied to 1800 datasets that were collected from ESIC hospital, Bangalore. Various classification algorithms like, SVM, Decision Tree, Logistic Regression, Random forest, NB, Adaboost, and KNN were applied to the datasets collected. Accuracy, RMSE, ROC, Precision, Recall, and F-measure were calculated for the classification algorithm. Optimizing improves the performance of the algorithm and thus improves the overall performance. It is observed that the optimized hybrid SVLR performs well when compared with all other classification algorithms. The Optimized SVLR algorithms give an accuracy of 89.03, which is comparatively better than other classification algorithms. Also this new proposed optimized SVLR Algorithm could be applied to other healthcare domains to obtain better results in both medical as well as ML domains.

ACKNOWLEDGMENT

We declare that this manuscript is original, has not been published before, and is not currently being considered for publication elsewhere.

CONFLICTS OF INTEREST

The authors declare that they have no known competing financial interests or personal relationships that could have appeared to influence the work reported in this paper.

Funding: The authors received no specific funding for this study.

Availability of Data and Material: Not applicable.

Code Availability: Not applicable.

Authors' Contributions: The author confirms sole responsibility for the following: study conception and design, data collection, analysis and interpretation of results, and manuscript preparation.

Ethics Approval: This material is the authors' own original work, which has not been previously published.

Elsewhere: The paper reflects the authors' own research and analysis in a truthful and complete manner.

REFERENCES

- [1] Stein, Irving F. Amenorrhea associated with bilateral polycystic ovaries, "Am J Obstet Gynecol 1935", vol. 29, pp. 181-191.
- [2] Kirschner MA, "Obesity, androgens, oestrogens, and cancer risk", *Cancer Res* 1982, Vol. 42, pp. 3281-3285.
- [3] Ehrmann, A. David, "Polycystic ovary syndrome," *New England Journal of Medicine* 2005, 352, no. 12, pp. 1223-1236. 10.1056/NEJMr041536.
- [4] Professor Cindy Farquhar, Associate Professor Neil Johnson, Department of Obstetrics and Gynaecology, University of Auckland Understanding polycystic ovary syndrome Issue 12 April 2008, ISSN 1177-5645 (Print) ISSN 2253-1947 (Online).
- [5] N. Pise and P. Kulkarni, "Algorithm selection for classification problems", *SAI Computing Conference (SAI)*, London 2016, pp. 203-211, 10.1109/SAL2016.7555983.
- [6] Jiawei Han and Kamber "Data Mining Concepts and techniques".
- [7] S. Taneja, C. Gupta, K. Goyal and D. Gureja, "An Enhanced K-Nearest Neighbor Algorithm Using Information Gain and Clustering," *Fourth International Conference on Advanced Computing & Communication Technologies, Rohtak* 2014, pp. 325-329, 10.1109/ACCT.2014.22.
- [8] L. Jiang, Z. Cai, D. Wang, and S. Jiang, "Survey of Improving K-Nearest-Neighbor for Classification.Proc", *4th International Conference on Fuzzy Systems and Knowledge Discovery (FSKD 2007)*, vol. 1, Aug. 2007, pp. 679-683, 10.1109/FSKD.2007.552.
- [9] N. Cristianini, J. Shawe-Taylor, "Support Vector Machines. In *An Introduction to Support Vector Machines and Other Kernel-based Learning Methods*", Cambridge: Cambridge University Press 2000, pp. 93-124, 10.1017/CBO9780511801389.008.
- [10] Burges, JC. Christopher, "A tutorial on support vector machines for pattern recognition", *Data mining and knowledge discovery*, vol. 2, no. 2, 1998, pp. 121-167, <https://doi.org/10.1023/A:1009715923555>.
- [11] R. C. Barros, M. P. Basgalupp, A. C. P. L. F. de Carvalho, and A. A. Freitas, "A Survey of Evolutionary Algorithms for Decision-Tree Induction," *Systems Man & Cybernetics Part C Applications & Reviews IEEE Transactions on* 2012, vol. 42, pp. 291-312, <https://doi.org/10.1023/A:1009715923555>.
- [12] L. Breiman, "Random Forests, Machine Learning", vol. 45, no. 1, 2001 pp. 5-32, <https://doi.org/10.1023/A:1010933404324>.
- [13] Mohammed, Mohssen & Khan, Muhammad & Bashier, Eihab. (2016). *Machine Learning: Algorithms and Applications*. 10.1201/9781315371658.
- [14] Muhamad Hariz B. Muhamad Adnan, Wahidah Husain and Nur Aini "Abdul Rashid, Parameter Identification and Selection for Childhood Obesity Prediction Using Data Mining", *2nd International Conference on Management and Artificial Intelligence 2012*, Vol.3.
- [15] L. Liu, "Research on Logistic Regression Algorithm of Breast Cancer Diagnose Data by Machine Learning", *International Conference on Robots & Intelligent System (ICRIS)*, Changsha 2018, pp. 157-160, 10.1109/ICRIS.2018.00049.
- [16] G K, G. Kesavaraj and Sukumaran, Surya, "A study on classification techniques in data mining. 2013 4th International Conference on Computing, Communications and Networking Technologies, ICCCNT 2013, Pp. 1-7, 10.1109/ICCCNT.2013.6726842.
- [17] A. Gavhane, G. Kokkula, I. Pandya and K. Devadkar, "Prediction of Heart Disease Using Machine Learning", *Second International Conference on Electronics, Communication and Aerospace Technology (ICECA)* Coimbatore 2018, pp. 1275-1278, 10.1109/ICECA.2018.8474922.
- [18] Z. Wang, J.W. Chung, X. Jiang, Y. Cui, M. Wang, A. Zheng, "Machine learning-based prediction system for chronic kidney disease using associative classification technique", *International Journal of Engineering & Technology* 2018, Vol. 7, Pp. 1161-1167, 10.14419/ijet.v7i4.36.25377.
- [19] Çiğşar, Begümand Unal, Deniz, "Comparison of Data Mining Classification Algorithms Determining the Default Risk," *Scientific Programming* 2019, Pp. 1-8, 10.1155/2019/8706505.
- [20] W. Yue, Z. Wang, H. Chen, A. Payne, X. Liu, "Machine learning with applications in breast cancer diagnosis and prognosis", *Designs* 2018, vol. 2, no. 2, pp. 13.
- [21] Daqqa, Khaled AS Abu, Ashraf YA Maghari, and Wael FM Al Sarraj. "Prediction and diagnosis of leukemia using classification algorithms," *2017 8th international conference on information technology (ICIT)*, IEEE 2017, pp. 638-643.
- [22] I. Nguyen, E. Frank, and M. Hall, "Data Mining Practical Machine Learning Tools and techniques", Morgan Kaufmann, Burlington, MA, USA, 2011.
- [23] J. Stefanowski, *Data Mining- Evaluation of Classifiers*, "Institute of Computing Sciences Poznan University of Technology," Poland, 2010.
- [24] Deepti Sisodia, Dilip Singh Sisodia, "Prediction of Diabetes using Classification Algorithms", *Procedia Computer Science*, Vol. 132, 2018, Pages 1578-1585, ISSN 1877-0509, <https://doi.org/10.1016/j.procs.2018.05.122>.
- [25] Setji TL, Brown AJ, "Polycystic ovary syndrome: update on diagnosis and treatment," *Am J Med*. 2014 Oct vol. 127, no.10, pp. 912-9, 10.1016/j.amjmed.2014.04.017.
- [26] R. Azziz "Polycystic Ovary Syndrome. *Obstet Gynecol*," 2018 Aug; vol. 132, no. 2, pp. 321-336, 10.1097/AOG.0000000000002698.
- [27] Silva IS, Ferreira CN, Costa LBX, Soter MO, Carvalho LML, de C Albuquerque J, Sales MF, Candido AL, Reis FM, Veloso AA, Gomes KB. "Polycystic ovary syndrome: clinical and laboratory variables related to new phenotypes using machine-learning models," *J Endocrinol Invest*. 2021 Sep 15, 10.1007/s40618-021-01672-8.
- [28] Silva IS, Ferreira CN, Costa LBX, Soter MO, Carvalho LML, de C Albuquerque J, Sales MF, Candido AL, Reis FM, Veloso AA, Gomes KB. "Polycystic ovary syndrome: clinical and laboratory variables related to new phenotypes using machine-learning models." *J Endocrinol Invest*. 2021 Sep 15, 10.1007/s40618-021-01672-8.
- [29] Shaziya, Humera. "A Study of the Optimization Algorithms in Deep Learning," 2020, 10.1109/ICISC44355.2019.9036442.
- [30] S. Chang and A. Dunaif, "Diagnosis of polycystic ovary syndrome: which criteria to use and when?," *Endocrinology and Metabolism Clinics* 2021, vol. 50, no.1, pp.11-23.
- [31] Mustapha, Aatila & Lachgar, Mohamed and Ali, Kartit. "Comparative study of optimization techniques in deep learning: Application in the ophthalmology field Comparative study of optimization techniques in deep learning: Application in the ophthalmology field," *Journal of Physics: Conference Series* 2021, 1743. 10.1088/1742-6596/1743/1/012002.
- [32] K. Soucie, T. Samardzic, K. Schramer, C. Ly and R. Katzman, "The diagnostic experiences of women with polycystic ovary syndrome (PCOS) in Ontario", *Canada. Qualitative Health Research* 2021, vol. 31, no.3, pp.523-534.
- [33] S. Sun, Z. Cao, H. Zhu and J. Zhao, "A Survey of Optimization Methods From a Machine Learning Perspective," in *IEEE Transactions on Cybernetics*, vol. 50, no. 8, pp. 3668-3681, Aug. 2020, doi: 10.1109/TCYB.2019.2950779.
- [34] P. Rao, and P. Bhide, "Controversies in the diagnosis of polycystic ovary syndrome", *Therapeutic Advances in Reproductive Health* 2020, vol. 14, p.2633494120913032.
- [35] E. Khashchenko, E. Uvarova, M. Vysokikh, T. Ivanets, L. Krechetova, N. Tarasova, I. Sukhanova, F. Mamedova, P. Borovikov, I. Balashov, G. Sukhikh, "The relevant hormonal levels and diagnostic features of polycystic ovary syndrome in adolescents," *Journal of Clinical Medicine* 2020, vol. 9, no. 6, p.18-31.

Influence of Management Automation on Managerial Decision-making in the Agro-Industrial Complex

Sergey Dokholyan¹, Evgeniya Olegovna Ermolaeva², Alexander Sergeyevich Verkhovod³, Elena Vladimirovna Dupliy⁴, Anna Evgenievna Gorokhova⁵, Vyacheslav Aleksandrovich Ivanov⁶, Vladimir Dmitrievich Sekerin⁷

Institute of Socio-Economic Research, Dagestan Federal Research Center of the Russian Academy of Sciences¹
Makhachkala, Russia¹

Kemerovo State University, Kemerovo, Russia²

Moscow Aviation Institute, Moscow, Russia³

Russian State Social University, Moscow, Russia⁴

Moscow Polytechnic University, Moscow, Russia^{5,7}

Russian State University of Tourism and Service, Moscow, Russia⁶

Abstract—The preservation and rational use of the grown harvest, obtaining the maximum product output from raw materials today is one of the most important state tasks. Automation of production processes is the main area in which production is currently advancing around the world. Everything that was previously performed by the person himself, his functions, not only physical but also intellectual, are gradually transferred to automation systems that perform technological cycles and exercise control over them. The purpose of the article is to analyze the effect of automation on the ability to store grain in elevators. The main research question is what factors should be considered when introducing an automation system into the grain storage process at elevators to improve the efficiency of process control at enterprises. To solve the question posed, a qualitative study was conducted using the method of an expert survey. The article reveals the factors that affect the quality of grain; the tasks implemented in the computerized process control system (CPCS) and management information and control system (MICS); the factors that hinder the grain elevator automation; the tasks solved by the automation of grain elevators in the framework of autonomous subsystems and integrated automatic control systems (ACS). It is concluded that the implementation of automation in the process of grain storage in elevators leads to an increase in grain quality, increased productivity, reduction or elimination of losses caused by theft and the peculiarities of grain storage, saving energy resources, minimizing the impact of the human factor, as well as the risks of accidents. At that, the inclusion of non-standard tools in the MICS and CPCS makes it easier to solve several current automation problems. Creating standard problem-oriented complexes of responsible decision-makers based on an integrated ACS, with the inclusion of certified object-oriented non-standard tools in their composition, is the most rational way to further improve the efficiency of the automated control system of the industry.

Keywords—Grain elevator; automation; grain quality; grain storage; grain drying; grain losses

I. INTRODUCTION

Storage of grain products without losses is of great national importance and serves to solve several strategic tasks, such as guaranteeing the country's food security, providing raw materials for the processing industry, strengthening the feed base of animal agriculture, and creating appropriate conditions

for effective export-import. Grain storage is one of the main factors of stabilization and increase of grain production not only in Russia. In the context of the global logistics crisis, it is necessary for grain to be able to be stored for as long as possible, without the deterioration of the consumer characteristics of grain quality. To do this, it is necessary that during its production, technological processes are carried out at the highest quality level, even if the enterprise does not have significant labor and financial resources.

In the broad sense of the term, storage means a system of technical and technological, regulatory, and economic-legal measures aimed at extending the shelf life of grain and seeds [1]. Technical and technological measures include a network of granaries/elevators, and a set of processes for accepting grain, preparing it for storage, as well as the storage technology itself [1].

An important part of the storage system is grain elevators, which represent complexes of structures designed for receiving, cleaning, drying, processing grain, and shipping it to consumers. A grain elevator is a complex system with a large number of operations that require precise accounting and control.

It should be noted that in agricultural enterprises, where the shortage of highly qualified labor is most noticeable, there is a fairly high need for partial or complete automation of technological processes, which in the contemporary conditions is an integral part of rising the competitive advantage of the enterprise because it will allow competing quite successfully both on the domestic and the world market [2]. Thus, according to a study by the California Farm Bureau, more than 40% of farmers over the past five years have not been able to employ all the workers needed to grow the main crop. It was revealed that about 56% of farmers started using mechanization in the last five years, and of the total, more than half noted this was initiated by a lack of skilled labor [3].

However, according to the researchers [4], the construction of grain elevators primarily focuses on equipment, its efficiency, and cost, while automation of grain elevator operations, as a rule, is postponed, although, with its implementation, agricultural enterprises could have saved

significant funds. Thus, the researchers [4] claim that the payback period of a fully automated newly built grain elevator is 1.5 years less than that of a similar non-automated grain elevator due to minimizing personnel costs, reducing energy consumption, and optimizing technological routes. At that, automation of an already operating grain elevator with a capacity of 40 thousand tons of one-time grain storage takes 3-4 months (from the programming process flows to the assembly of equipment and installing software).

Therefore, the grain elevator is the most relevant research object of automation systems in the industry.

II. LITERATURE REVIEW

According to the researchers [5] the grain quality and properties are influenced by various factors that need to be taken into account already at the growing stage, during harvesting, primary processing of grain, and subsequent storage. A detailed description of these factors is presented in Table I.

TABLE I. FACTORS AFFECTING GRAIN QUALITY

Stage	Factor
Grain cultivation	The quality of the seed grain, in particular, the sowing and varietal characteristics. Thus, the grain of different wheat varieties has different flour-milling and baking qualities; different varieties of corn differ in feed properties; varieties of barley have various brewing qualities; different varieties of rapeseed and soy differ in oil content and the like.
	Reducing infestation of fields and the impact of pests
	Application of mineral fertilizers
Harvesting	Weather and climatic conditions. Thus, in the case of a large amount of precipitation, grain receiving plants receive highly moisture grain, which requires additional costs for drying. In dry years, during the grain maturation period the grain filling stage grows short reduced; in early frosts, grain is characterized by lower technological qualities and less resistance to storage.
	Harvesting with a combine. In Soviet times, as a basis for solving grain quality issues, namely, drying, maturing in rolls, and the ability to start harvesting 6-7 days earlier, a separate combining method was used. But with high prices for fuel and lubricants, as well as in adverse weather conditions, a separate combining method is often economically inefficient and can lead to a significant loss of grain. Therefore farms often use the direct combining method. Currently, the energy component is the main criterion for choosing the grain harvesting method.
	Grain fractionation by moisture. If the grain was harvested in different weather conditions, it is advisable to carry out grain fractionation by moisture (dry, medium-dry, wet and sodden grain) to facilitate post-harvest processing and storage of grain, and reduce energy costs.
Post-harvest grain processing	Grain cleaning and drying allows bringing the grain to the requirements of regulatory documents in terms of the foreign matter and moisture content of grain for further storage in granaries or further processing.
	Complete set for the quality of individual grain batches
Grain storage	Disinfection against pests
	Required temperature and humidity (climate control) in the granary

Source: Compiled based on [6-9]

According to the researchers [10], the greatest influence on the grain quality has heat treatment, namely, grain drying, which, if the process is not properly conducted, downplays all measures to obtain a high quality of the crop.

At the present development stage of grain drying equipment, the convective drying method is most often used in continuously operating grain dryers of column, tower, vertical, and drum types. Also, for drying grain in small volumes, or grain for seed purposes, periodic grain dryers in a fixed layer or bunkers for venting grain are used [11]. The automation level of the drying process allows controlling and measuring the grain feed, level, moisture, and temperature, as well as heat carrier temperature in the grain dryer [12].

Recent practices in the field of automated process control systems make it possible to automatically predict the process of self-heating of grain, which is necessary to improve the efficiency of grain storage [12, 13].

However, the use of serial standard tools in automated enterprise control systems and automated process control systems of enterprises in the grain storage and processing industry has practically exhausted its potential [14, 15]. The inclusion of non-standard tools in standard automated enterprise management systems and automated process control systems makes it possible to simplify the solution of several topical automation problems [16, 17]. The creation of typical problem-oriented complexes of responsible decision-makers based on an integrated ACS, with the inclusion of certified object-oriented non-standard tools in their composition, is the most rational way to further improve the efficiency of the industry's automated control system [18, 19].

Thus, the issues of introducing control automation for grain storage at elevators relevant in Russia remain unresolved. They include factors constraining the automation of elevator operation and the possibility of creating an integrated ACS (ACS of technological processes and ACS of the enterprise).

The research hypothesis is formulated as follows. The implementation of automation in the grain storage process in elevators allows improving grain quality, increasing productivity, reducing or eliminating losses caused by theft and the grain storage peculiarities, saving energy resources, minimizing the impact of the human factor, and the risks of accidents.

The article reveals the factors affecting the grain quality; as well as the tasks implemented in the computerized process control system (CPCS) and management information and control system (MICS); the factors that hinder the automation of grain elevators; the tasks solved by the automation of grain elevators in the framework of autonomous subsystems and integrated automatic control systems.

III. RESEARCH OBJECTIVES

The following research objectives were set:

1) To determine the factors affecting the quality of the grain should be taken into account already at the stage of grain cultivation, harvesting, primary processing, and subsequent storage.

- 2) To determine the factors that hinders the complex automation of grain elevators.
- 3) To specify the tasks implemented in the CPCS and grain elevator MICS using standard and non-standard means.
- 4) To consider the tasks solved by the integrated ACS of the grain elevator, whose solution within the local subsystems is difficult or impossible.

The article consists of an introduction, a literature review, research methods, results, discussion, and conclusion.

IV. METHODS

A. Research Design

To achieve the set goals, the following research methods were used in the article:

- Theoretical methods (generalization, analysis, and synthesis theoretical basis of the study). The theoretical basis of the study was grouped depending on the type of documents. The first group of sources of information consisted of studies devoted to the problem of grain quality and storage factors affecting it. The second group of information sources was devoted to the problem of automation of grain storage complexes. The considered sources of information were mainly articles from scientific peer-reviewed journals indexed in Scopus and Web of Science over the past 15 years (57 publications).
- Empirical methods (expert survey method) were employed to determine the factors that hinder the automation of grain elevators, as well as tasks implemented through CPCS and MICS, and solved using the integrated ACS of the grain elevator.

B. The Procedure and Research Tools

The expert online survey was held as part of the annual comprehensive monitoring of the development of agriculture in Russia in 2021. The annual comprehensive monitoring was supported by six universities (Dagestan Federal Research Center of the Russian Academy of Sciences, Kemerovo State University, Moscow Aviation Institute, Russian State Social University, Moscow Polytechnic University, and Russian State University of Tourism and Service). The selection criteria for the work of experts included experience in the field of agricultural automation for at least seven years, a position at a level below a middle manager in engineering companies engaged in the design and maintenance of elevators, as well as heads of agricultural enterprises, whose interests include the use of ACS of technological processes and ACS of the enterprise of the elevator.

The expert online survey was attended by 35 experts' distribution by status and length of service is presented in Table II.

The experts were asked several questions concerning the automation of the grain elevator performance:

- 1) What are the main deterrents to the automation of elevator operation?

- 2) What tasks are subject to automation in the first place in the ACS of technological processes and the ACS of the enterprise?
- 3) What tasks can be solved by the integrated ACS of the elevator?

All participants were warned about the purpose of the survey and the planning of the organizers of the study to publish the survey results in a generalized form.

TABLE II. DISTRIBUTION OF EXPERTS BY STATUS AND WORK EXPERIENCE

Status	Work experience	Number, persons
Heads of engineering companies	7 to 12 years	9
	Over 12 years	10
Heads of agricultural enterprises	7 to 12 years	4
	Over 12 years	12

C. Statistical Analysis

During the mathematical processing of the research results, the percentage of expert mentions of the factors hindering the automation of grain elevators, as well as the tasks solved by the integrated ACS, was determined.

The ranking of the entire set of expert opinions consisted in their arrangement by each of the experts in the form of a sequence according to their decreasing preference.

At that, each of the opinions was evaluated by the rank (number) under which they were arranged in this sequence. The final rank represented the arithmetic mean of all the expert ranks in the sample of experts.

V. RESULT

According to experts, despite the huge potential opportunities of the current market, the provision of a variety of automation services, the complex automation of grain elevator operations is constrained by the following factors (Table III).

According to experts, these factors predetermine the situation in which solutions to automation problems are performed within the established document flow with the same automation functions and a simple transfer, as a rule, only the technical support of the ACS to a more modern level.

TABLE III. FACTORS HINDERING THE GRAIN ELEVATOR AUTOMATION

Factors	%	Rank
Lack of objective knowledge about the potential capabilities of the ACS on the part of the customer; as a rule, decision-makers underestimate the importance of automation or, sometimes, have excessively high expectations	74.3%	1
The lack of subject orientation of developer enterprises and, as a result, the lack of knowledge about the subject area on the part of specialists of leading enterprises specialized in providing IT services (technologies) using standard design solutions	68.6%	2

Note: compiled based on an expert survey.

Initially, the experts considered standard already functioning CPCS and MICS. According to experts, with respect to the CPCS of the grain elevator, automation should concern tasks implemented using standard (SCADA) and non-standard tools. In the MICS, tasks are implemented, as a rule, using 1C (Table IV).

TABLE IV. TASKS IMPLEMENTED BY THE CPCS AND MICS

Means	List of tasks
CPCS	
Standard	Controlling grain movement routes (several hundred, sometimes thousands of input/output signals); weighing, dosing (usually implemented using strain gauges); management of aspiration, ventilation, i.e. typical CPCS tasks implemented using SCADA systems.
Nonstandard	Measuring the temperature field of grain storage array (several thousand control points); grain drying control (a few dozen of the input-output signals); measuring the grain humidity in the flow; continuous grain level measurement in silos, etc.
MICS	
Standard	Accounting, tax, production accounting; as well as issues, such as personnel, salary, warehouse, trade, etc., i.e. typical MICS tasks, which are implemented using the 1C complex
Nonstandard	Quantitative and qualitative analysis of grain and grain accounting, grain movement accounting, decision-making support systems, etc.

Note: compiled based on an expert survey

At that, in standard solutions, noted systems function locally, the CPS and MICS continue to remain autonomous and have no links. Meanwhile, according to experts, some automation tasks are successfully solved within the framework of autonomous subsystems.

However, the creation of an integrated ACS will allow solving problems that are difficult or impossible to solve within local subsystems (Table V).

TABLE V. TASKS SOLVED BY THE INTEGRATED ACS

No	Tasks	%	Rank
1	Grain drying in automatic mode	82.6%	1
2	Performing grain acceptance and shipment operations with a given performance	77.1%	2
3	Reducing or eliminating grain losses due to theft	71.4%	3
4	Eliminating losses caused by the grain storage peculiarities	62.9%	4

Note: compiled based on an expert survey

VI. DISCUSSION

Speaking about the automation of grain elevators in the framework of implementing autonomous subsystems, the majority of experts (82.6% of respondents) note that as a rule standard design solutions are developed by organizations that are official dealers of large developer enterprises. Thus, automated control systems are implemented using SCADA systems, which are collecting real-time information from remote points for processing, analyzing, and possibly managing remote objects. The requirements of real-time processing are determined by the need to deliver all the necessary events and data to the central interface of the

operator (dispatcher). All contemporary SCADA systems include three main structural components:

- RTU (Remote Terminal Unit), which is the lower level of the CPCS: industrial computers, programmable logic controller (PLC).
- MTU (Master Terminal Unit), which is supervisory control center (upper level).
- CS (Communication System) [13].

The SCADA system solves the following main tasks: providing data exchange with controllers, terminal devices, and real-time data processing; visualization of the technological process progress on monitors and terminals; ensuring the storage of technical information in a real-time database; monitoring technological parameters; implementing warning alarm and alarm event protocol; generating reports on the progress of technological processes; providing data to external systems at the enterprise management level [14]-[16].

The characteristics of alternative SCADA systems are given in Table VI.

Free technical support is provided by the Russian company AdAstra Research Group LLC (TraceMode V6) – the only 100% Russian company in the SCADA systems market, as well as by JSC Klinkmann SPb, a distributor of AVEVA (InTouch V10), which has been trying to enter the Russian market since 2019.

According to experts, that is confirmed also in the works of researchers [17], the main drawback of standard design solutions is the replication of universal proposed tools without the proper orientation to a specific subject area. Besides, the functionality of the supplied equipment (software product) is due to the versatility, and therefore the excess of the means used, which leads to a decrease in reliability, the inability to take into account the specifics of the grain elevator, and leads to a lower level of automation.

TABLE VI. CHARACTERISTICS OF ALTERNATIVE SCADA SYSTEMS FOR RUSSIA

Name of the SCADA	The function of the process execution module	Cost of technical support, thousand USD	Availability of a free development environment	Price of the process execution module, thousand USD
InTouch V10	Monitoring, management, archiving	Free of charge	-	10.84
Trace Mode V6	Monitoring, management	Free of charge	+	1.62
Master SCADA V3.1	Monitoring, management, archiving	0.25 per year	+	2.03
iFix V4	Monitoring, management, archiving	2.2 per year	+	8,64
GENESIS32 V9	Monitoring, management, archiving	4.8 per year	+	11.92

The second class of tasks is handled by small IT companies. Their products, as noted by one of the experts (Nikolai K., 12 years of experience), "are subject-oriented, often unique and belong to non-standard equipment". This allows them to create competitive, subject-oriented, non-redundant, unique, and in some cases significantly more reliable products that have no analogs in terms of price/quality ratio [18]. However, non-standard equipment requires additional costs for verification and metrological certification, which significantly narrows the scope of its application and, in the face of the risk of uncertainty of the final result, in the assessment of the customer, leads to insufficient funding and is usually limited to a small-scale or single-item production [19].

According to one of the experts (Alexander, 12 years of experience) "systems that are implemented using serial standard and unique non-standard tools today function locally and do not interact with each other in any way. Integrated systems that have proven themselves and are implemented using both standard and non-standard tools into a single integrated ACS will make it possible to minimize the disadvantages of each approach and maximize the benefits of each of them".

Speaking about the tasks solved by the integrated ACS of the grain elevator, experts put in the first place the possibility of drying grain in automatic mode (Table IV), since drying grain, according to one of the respondents, is "the most important stage of storage and processing technological processes, whose results depend on both consumer and technological characteristics of grain quality". As an argument, the fact is given that a deviation from the target value of the grain moisture towards increase can lead to fire-fanging of grain mass during storage, while a deviation towards decrease –to a deterioration in consumer characteristics, weight, etc. and thus, to the lost profit.

At that, the operator judges the technological process progress and the quality of grain subjectively, based on own experience. The reason for this is the inability to measure grain quality indicators directly during the technological process. This conclusion can be explained by the results of the study [20]. The operator monitors the technological process based on the current values of temperature and, in the best case, humidity, and can control the process only by setting the drying cycle time and the burner operating mode. Automatic control of the burner is impossible without an adequate control model.

Therefore, it is extremely difficult to build an adequate model for controlling the technological process of grain drying, which would allow judging the expected consumer characteristics of grain quality by the observed technological parameters, without the knowledge and experience of a qualified operator. According to experts, the drying process management using deterministic control models in practice is currently unknown. As a result, the grain drying process is controlled manually and depends entirely on the operator's qualifications.

Building a control model that would allow performing grain drying in an automated or automatic mode is an urgent task, whose solution would allow excluding unskilled actions

of the operator, and therefore reducing the likelihood of deterioration of consumer characteristics of grain quality [21]. The solution of this problem is associated with the determination of the relationship between the observed parameters of the technological process and grain quality indicators, and the significance of these relationships [22]. The technological process parameters are controlled by the CPCS of the grain drying process, while the grain quality indicators are controlled by the laboratory assistant at his workstation in the quality laboratory.

According to one of the experts (Mikhail, 16 years of experience), a real alternative to deterministic models, is "building a knowledge model using the fuzzy logic instrument, which provides a link between the controlled technological parameters and the grain quality characteristics, determined in laboratory conditions. Therefore, the timely inclusion in the grain drying model of the quality characteristics of grain at the dryer inlet simplifies building a proper model and allows solving the main problem of grain drying: obtaining (or improving) the quality characteristics of grain according to their specified values".

At present, in the ACS, operating at grain elevators, there are no connections between local subsystems. Creating a knowledge model of a qualified operator, which would take into account the quality indicators and technological parameters, is an urgent task, whose solution will significantly improve the quality of grain drying [23].

Experts point out that executing grain receiving and shipping operations (Table IV) requires controlling the route of grain movement at given productivity. The grain shipment regulations require maximum possible specified performance, which can lead to congestion in problematic areas of transportation. To eliminate congestion, it is necessary to install conveyor (sectional) weighers on sections of the actuator control loop (ACL), which are functioning as intelligent shipment performance sensors. Depending on the measurement result, it is necessary to increase or decrease the shipment intensity by adjusting the rotation of the actuating mechanism (speed of the conveyor belt on the route). The solution of this problem within the framework of the ACS does not always lead to the necessary result [24]. The efficiency of solving the above-mentioned problem is significantly increased when applying a control model using data from grain movement control (MICS) and a subsystem for continuous grain level measurement in storage silos (CPCS), which is difficult or impossible to solve in the framework of SCADA systems [25].

Besides, the integration of the grain movement control subsystem and the route management subsystem allows performing technological operations providing the optimal route in terms of minimizing energy consumption, taking into account the state of technological equipment, the possibility of bypassing equipment units that have failed, by creating an alternative route, and suchlike.

According to experts, an effective solution to the problem of losses caused by theft (Table IV) is impossible without creating integrated systems based on a single information base CPCS and MICS, logical models for checking the grain movement starting from its reception operation through the

shipment operation, taking into account the identified bottlenecks and taking appropriate comprehensive measures to ensure mutual control of employees responsible for production process accounting and the technology of reception, cleaning, drying, movement, storage, and shipment (production).

In the course of grain storage, pockets of self-heating may appear (losses due to the storage peculiarities, Table IV), which can be revealed by the thermometry system indicators and eliminated by moving grain from one grain storage container to another with simultaneous cooling.

The integration of some subsystems (thermometry, grain movement, grain movement control, ventilation, and electricity metering subsystems taking into account the daily tariff variations) will allow identifying automatically the hotbeds of self-heating, determining the availability of free containers; finding the optimal route of grain movement and the time of its execution, and performing grain storage control processes in automatic mode [26]. All these measures will allow minimizing the impact of the human factor, leading to the exclusion of unjustified losses, improving grain quality, reducing energy consumption required for its movement, as well as significantly reducing the costs of controlling the systems of the ventilation system, aspiration, etc.

VII. CONCLUSION

The research results confirmed the hypothesis that the implementation of automation in the grain storage process in elevators leads to an improvement of grain quality, increase in productivity, reduction or elimination of losses caused by theft and the grain storage peculiarities, saving energy resources, minimizing the impact of the human factor, as well as the risks of emergency situations.

The results of the study show that the main tasks solved by the integrated ACS are drying grain in automatic mode, performing operations of receiving and unloading grain with a given capacity, and reducing or eliminating losses caused by theft and features of grain storage.

The most effective practical implementation of these tasks is possible through the cooperation of organizations that specialize in the development of systems using standard tools, as well as organizations that develop non-standard automation tools.

A promising area for further research is the analysis of technologies based on reducing the volume of grain drying, ensuring high quality and reliable storage of grain products.

ACKNOWLEDGMENT

The study was carried out with the financial support of the RFBR, project No. 20-010-00965A.

REFERENCES

- [1] Z. Chen, W. Wu, J. Dou, Z. Liu, K. Chen, Y. Xu, "Design and analysis of a radio-frequency moisture sensor for grain based on the difference method," *Micromachines*, vol. 12(6), 708, 2021. DOI: 10.3390/mi12060708.
- [2] Rosinformagrotech, "Departmental project "Digital agriculture"," Official publication, Moscow: Rosinformagrotech, 2019.
- [3] J. Daniels, "California farmers increasingly turning to mechanization due to labor shortages, says a survey", CNBC, 2019. Retrieved from <https://www.cnbc.com/2019/05/01/farmers-turning-to-mechanization-due-to-labor-shortages-says-survey.html>.
- [4] R. Bucklin, S. Thompson, M. Montross, A. Abdel-Hadi, "Grain storage systems design", in: *Handbook of Farm Dairy and Food Machinery*, M. Kutz Ed, Cambridge: Academic Press, 2013, pp. 123-175. DOI: 10.1016/B978-081551538-8.50008-X.
- [5] J. G. Nuttall, G. J. O'Leary, J. F. Panozzo, C. K. Walker, K. M. Barlowb, G. J. Fitzgerald, "Models of grain quality in wheat. A review," *Field Crops Research*, vol. 202, pp. 136-145, 2017. DOI: 10.1016/j.fcr.2015.12.011.
- [6] A. Challinor, T. Wheeler, P. Craufurd, J. Slingo, "Simulation of the impact of high-temperature stress on annual crop yields", *Agricultural and Forest Meteorology*, vol. 135, pp. 180-189, 2005. DOI: 10.1016/j.agrformet.2005.11.015.
- [7] N. Fernando, J. Panozzo, M. Tausz, R. Norton, G. Fitzgerald, S. Seneweera, "Rising atmospheric CO2 concentration affects mineral nutrient and protein concentration of wheat grain," *Food Chemistry*, vol. 133, pp. 1307-1311, 2012. DOI: 10.1016/j.foodchem.2012.01.105.
- [8] M. Hruskova, I. Svec, "Wheat hardness in relation to other quality factors," *Czech Journal of Food Sciences*, vol. 27, pp. 240-248, 2009. DOI: 10.17221/71/2009-CJFS.
- [9] L. Kong, J. Si, B. Zhang, B. Feng, S. Li, F. Wang, "Environmental modification of wheat grain protein accumulation and associated processing quality: A case study of China," *Australian Journal of Crop Science*, vol. 7(2), pp. 173-181, 2013.
- [10] V. G. S. Raghavan, V. Sosle, "Grain drying", in: *Handbook of Industrial Drying*, A. S. Mujumdar Ed., Boca Raton, USA: CRC Press, 2007, pp. 563-573. DOI: 10.1201/9781420017618.ch23.
- [11] Ó. Reykdal, "Drying and storing of harvested grain. A Review of Methods," *Matis Report*, Skýrsla Matis, 2018.
- [12] Y. Evdokimova, "Digitalization and automation of the agricultural sector," *IOP Conf. Series: Earth and Environmental Science*, vol. 723, pp. 032002, 2021. DOI: 10.1088/1755-1315/723/3/032002.
- [13] D. Daluyen, K. Yaptenco, E. Peralta, D. Suministrado, "Microcontroller-based control system for safe grain storage in a silo," *IOP Conf. Series: Earth and Environmental Science*, vol. 230, pp. 012020, 2019. DOI: 10.1088/1755-1315/230/1/012020.
- [14] Z. Yaozu, L. I. U. Hong, "Application of PLC and SCADA in auto-control systems for silo grain handling," *Proceedings of the 7th International Conference on stored-product protection*, vol. 2, pp. 1919-1922, 2010.
- [15] D. S. Belaits, M. S. Vyshegurov, A. P. Balashov, N. N. Konova, A. A. Samokhvalova, A. I. Golikov, "A promising mechanism for the material support of the farming industry (A case study of the Novosibirsk Region)," *Scientific Papers, Series "Management, Economic Engineering in Agriculture and Rural Development"*, vol. 18(1), pp. 85-102, 2018.
- [16] C. Lalhriatpuia, M. Kimi, T. K. Hazarika, "Influence of crop regulations on growth, yield, and quality of grapes (*Vitis vinifera*) in North-East India," *Res. On Crops*, vol. 22(1), pp. 96-103, 2021.
- [17] N. V. Lyasnikov, "Digital agricultural sector of Russia: A review of breakthrough technologies of the fourth technological mode," *Food Policy and Security*, vol. 5(4), pp. 169-182, 2018.
- [18] S. Himesh, "Digital revolution and Big Data: A new revolution in agriculture," *CAB Reviews*, vol. 13, pp. 1-7, 2018. DOI: 10.1079/PAVSNNR201813021.
- [19] A. N. Anishchenko, A. A. Shutkov, "Agriculture 4.0 as a promising model of scientific and technological development of the agricultural sector of contemporary Russia," *Food Policy and Security*, vol. 6(3), pp. 129-140, 2019.
- [20] V. Saiz-Rubio, F. Rovira-Más, "From smart farming towards agriculture 5.0: A Review on Crop Data Management," *Agronomy*, vol. 10, pp. 207, 2020. DOI: 10.3390/agronomy10020207.
- [21] G. Mbofung, S. Goggi, L. Leandro, R. Mullen, "Effects of storage temperature and relative humidity on viability and vigor of treated soybean seeds," *Crop Science*, vol. 53, pp. 1086-1095, 2013. DOI: 10.2135/cropsci2012.09.0530.

- [22] G. A. Mosher, N. Keren, S.A. Freeman, C. R. Hurburgh, "Management of safety and quality, and the relationship with employee decisions in country grain elevators," *Journal of Agricultural Safety and Health*, vol. 18(3), pp. 195-215, 2012. DOI: 10.13031/2013.41957.
- [23] A. I. Altukhov, M. N. Dudin, A. N. Anishchenko, "Digital transformation as a technological breakthrough and transition to a new development level of the agro-industrial sector of Russia," *Food Policy and Security*, vol. 7(2), pp. 81-96, 2020. DOI: 10.1051/e3sconf/202022201012.
- [24] D. C. Lopes, A. J. Steidle Neto, J. K. Santiago, "Comparison of equilibrium and logarithmic models for grain drying," *Biosystems Engineering*, vol. 118, pp. 105-114, 2014. DOI: 10.1016/j.biosystemseng.2013.11.011.
- [25] G. G. Atungulu, G. A. Olatunde, "Assessment of new in-bin drying and storage technology for soybean seed," *Drying Technology*, vol. 36, pp. 383-399, 2017. DOI: 10.1080/07373937.2017.1335751.
- [26] S. Navaratne, A. M. Saja Sheriff, "Fabrication of a hydro cooling system to mitigate dry matter loss of stored wheat grains in silos," *The International Journal of Engineering Science*, vol. 5(4), pp. 572-577, 2014.

Enhancing the Security of Data Stored in the Cloud using customized Data Visualization Patterns

Archana M¹

Research scholar, School of CSE
REVA UNIVERSITY, Bengaluru-560064

Dr. Gururaj Murtugudde²

Professor, School of CSE
REVA University, Bengaluru-560064

Abstract—Cloud Computing is getting popularized with the invention of latest technologies like Big Data, Artificial Intelligence, Data Science etc. The biggest challenge faced by researchers is efficient ways of accessing the data and acquiring the required results. The efficiency of the system will help the researchers to go one step further in the field of cloud computing. Alongside of storing the data in an optimal way, one biggest challenge faced by the researchers is security. How best security can be enhanced for this data in order to protect the end system from data thefts and illegal attacks. In this paper the proposed research concentrates on customized data visualization techniques that have been developed in order to store the data and also enhance the data security. These visualization patterns are dynamic in nature and can be further extended based on the need and level of the security required by the application. The proposed research in this paper will help researchers to implement the data visualization techniques with enhanced security in the real time data stored in the cloud from unauthorized access and various attacks like Malware etc. and these data patterns are dynamic in nature which will be selected based on the number of fragments need to be stored pertaining to particular cluster or region. The patterns will be selected based on two factors basically, one is the number of fragments and another important factor is how many nodes are available in the pattern. This proposed research will give an additional strength to the Cloud Computing Platforms like AWS and Google Cloud where the customers can feel that their data is in safe hands. Today when we are living in the data world, the need of this system is very much essential as it enhances the security of the data.

Keywords—Artificial intelligence; big data; cloud computing; data science; data visualization

I. INTRODUCTION

Data is the today's heart of IT companies and as data is growing day by day the major issue faced is what are the best ways to store data in order to later access it easily. The data has grown from KB's to MB's and MB's to GB, today the data produced is in Zeta and Peta Bytes from each individual source. There are two major issues faced by the cloud service providers when data is growing day by day. [15] The first one is how to store this data and the second one is what the possible ways to secure the data are. On top of it how fast the data can be accessed when needed. In olden days as the size of the data was not so huge and also the data which was getting produced was not so drastic, the industries were using servers and later moved to data centers etc., The problem again here is how fast the data can be accessed and how many data centers should be

established when data keeps on getting increased. So instead of working on physical resources, the concept of cloud computing has been introduced. In this cloud computing there is no limit on how much data is going to be stored and it's easy to access the data as data is stored virtually on the cloud.[3] The data which is getting generated might be structured or unstructured or semi structured. It might be string data or numerical or image data. And most of the cloud providers prefer third party to protect the data. The third party protection though it is preferred but cannot work all the times as it is difficult to trust the third party vendors. On top of it the data has to be protected again from these third party service providers. By considering all of the above scenarios and after extensive research, it is found that there is a need for a system which will help the cloud service providers easily to Store, Secure and Access the data easily from cloud [4].

The proposed research methodology utilizes the various data visualization techniques that are implemented in such a way that the data can be stored easily for providing highest level of security and also for the ease of access. The entire data will be stored in the cloud after proper conversion of quasi and unstructured data to structured data [5].

The final structured data will be stored in the form of fragments and these fragments will be stored in the form of customized patterns and preexisting patterns for providing high level security for the data [3]. In the proposed system if there is a need for third party, same can be involved without any hesitation. Though the third party is involved in controlling the cloud but they don't have any access to final data that is stored for future requirements, so the proposed system will work effectively to store and process the data when there is a need. [7].

II. LITERATURE SURVEY

1) This Paper is referred to understand the data encryption techniques using code book.

2) This paper gives a clear insight on the how data visualization techniques can be implemented in light weight web pages and also scientific applications as a micro service.

3) The main take away from this paper is how data visualization techniques will be used for rain fall predictions and also understand what are the various default visualization images that can be used for this. The default visualization images are not up to the mark due to various reasons.

4) In this paper the main discussion is on how the sequential patterns will be recorded. And the sequential patterns of the objects will be stored for future data visualization patterns. It includes various objects which are static and dynamic in nature.

5) This paper gives an idea on how the data can be fragmented for easy storage. And also, how to encrypt this fragment to store in the cloud for security. And also gives an insight on how easily these fragments can be accessed.

6) In this paper the main take away is how d3 visualization can be used while decoding and storing the data. And once the data is stored how it can be extracted for future use. They built a search engine where user can give visual based inputs which will be stored in the form graphs, charts and data will be stored in that, in encoding format.

7) In this paper the main idea is how to generate evolutionary patterns using original data. These evolutionary patterns are like data visualizations which will help in future for the urban planning.

8) This paper gives a clear idea on Data Visualization. Starting from what is data visualization to how these techniques can be useful in real time applications. What are the different ways this data visualization can be used like for predicting, analyzing, result, reports etc..

9) This paper is used to understand data encryption techniques using Siribhoovalaya and how data fragments can be encoded and decoded using such techniques.

10) This paper researches how the data stored in cloud can be utilized further for data visualization. In this paper the data taken is traffic data which can be used to generate data visualization patterns. After researching on this paper it is also clearly understood that most of the researches give much preference for data visualization while working on real-time data.

11) The main take away from this paper is how to work on behavioral lines which are getting generated in data visualization. These behavioural lines really help to understand the behaviors of objects or phenomena which is happening in real time. And also give insight on how to access cloud data for the same.

The literature survey on various papers gave clearly an idea to implement proposed research by avoiding few drawbacks faced by them.

III. IMPLEMENTATION

In order to provide high level security for the data, the data has been encrypted using the concept of Siribhoovalaya. Once the encryption process has been done the first level of security is provided for the data [5]. The next level will be how and best the data can be stored and further accessed when it is required. To do this the concept of data visualization is used in which the data will be stored in various patterns [8]. And the patterns or either the fixed or customized patterns.

Algorithm to Read and Store the Encrypted Data in Patterns:

1. Start
 2. Read the Encrypted Data
 3. Load the Encrypted Data
 4. Selection of Pattern based on Selection Function
 5. Store the data as per the pattern technique.
 6. Verify the final pattern.
 7. Stop
-

In order to retrieve the data when needed just choose the pattern saved and get back the data.

Pseudo Code to Read and Store the Encrypted Data in Patterns:

Procedure RS_Encrypt()

Input: Encrypted Data

Output : Pattern Based on Encrypted Data

While not end of this document

 Data[]=datastore.getinstance()

if (Data[]!=null)

 for Data[] do

 count =count+1

 else

 exit()

 selection (count)

 Nodes=count

 Select pattern based on count value

 For each node do

 Store(data[])

End procedure

Algorithm to extract the data from the Pattern:

1. Start
2. Select the solution pattern from which data needs to be extracted
3. Verify once again the pattern with Select Function.
4. Retrieve the data which is stored.
5. Cross check the Encrypted data.
6. Stop

Pseudo Code to extract the data from the Pattern:

Procedure Read(data[])

Select the pattern

 For each node

 read data at every node

 store(data[])

End Procedure

After these steps the data decryption algorithm will be applied in order to retrieve the original data. The main thing to observe here is that the data is not going to be stored as it is, instead, it will be stored in the form of fragments and each fragment will be assigned with a particular node in the data visualization pattern and in particular order so that it will be very easy to retrieve back the data when it is needed [9].

IV. DATA VISUALIZATION PATTERNS

The data visualization patterns will really help in storing the data securely. And these patterns can be created and stored, which can be used basis the number of fragments and level of the security required and based on the Select Function as discussed later. Let us consider an example if the data is public that is should be shown to every customer in the organization, then normal data visualization patterns [6] will be chosen. If the data is a secured one which needs to be hid from all except the administrators, then it can use high level data visualization pattern in order to provide additional security [8].

Low Level Data visualization patterns and High-Level Data Visualization patterns will be decided basis the number of nodes available in the patterns and also it depends on the number of nodes available in the particular pattern to store the data [10].

The sample data considered here is already encrypted data using the code book algorithm pertaining to one particular category [1].

The Fragments might be a single letter or word, depending on the application it will be selected. Once the fragments are generated, in the next step data is encrypted using code book. The encrypted fragments are considered one by one to store it in the visualization pattern [12]. And for every fragment an individual ID will be generated to access it back easily when required. So the existing technology problems like Storing and Processing of cloud data will be solved in this system [1]. Also the performance of the system is tested with various factors like size of the fragment, number of fragments and Indexing. [6].

There are total 50 fragments which are encrypted. Each fragment has the encrypted data as per code book algorithm. By considering the number of fragments the following patterns are generated as a reference,

Fragment No	Fragment Data
1	!#\$^&
2	*&\$%#@
3	!\$&*##
4)@#&*#
5	!\$&*#(
6	^\$&*##
8	@&*##
9	@%&#(
10	*##!\$
11	!#\$^&
12	*&\$%#@
13	!\$&*##
14)@#&*#
15	!\$&*#(
16	^\$&*##
17	@&*##
18	@%&#(
19	*##!\$
20	!#\$^&
21	*&\$%#@
22	!\$&*##
23)@#&*#
24	!\$&*#(
25	^\$&*##
26	@&*##
27	@%&#(
28	*##!\$
29	!#\$^&
30	*&\$%#@
31	!\$&*##
32)@#&*#
33	!\$&*#(
34	^\$&*##
35	@&*##
36	@%&#(
37	!#\$^&
38	*&\$%#@
39	!\$&*##
40)@#&*#
41	!\$&*#(
42	^\$&*##
43	@&*##
44	@%&#(
45	*##!\$
46	!#\$^&
47	*&\$%#@
48	!\$&*##
49)@#&*#
50	!\$&*#(

Fig. 1. Sample Encrypted Fragment Data for Data Visualization.

Based on the above encrypted fragments (Fig. 1), the below various visualization patterns (Fig. 2 to Fig. 8) are generated for the reference.

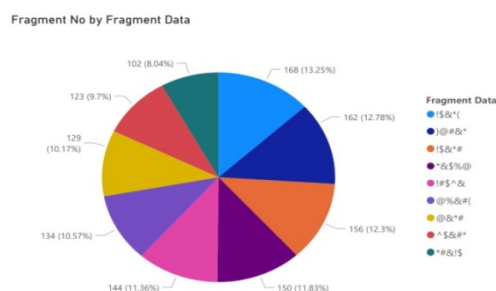


Fig. 2. Sample Data Visualization Pattern_Circular Structure.



Fig. 3. Sample Data Visualization Pattern_Sequential Steps Architecture.

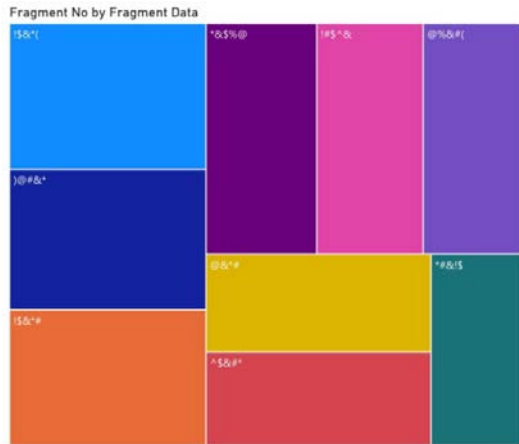


Fig. 4. Sample Data Visualization Pattern_Block Structure.

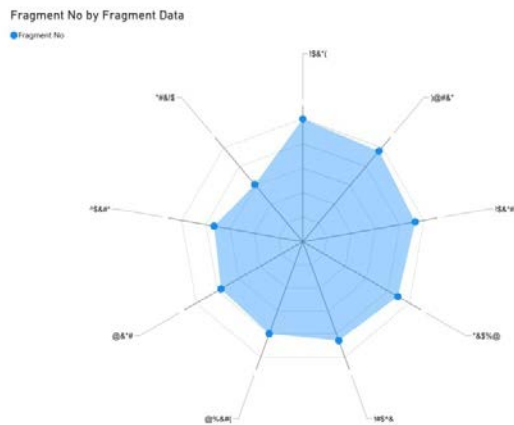


Fig. 5. Sample Data Visualization Pattern_Spiral Structure.

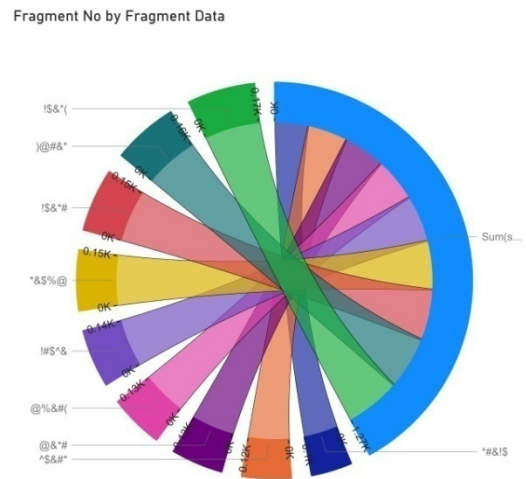


Fig. 6. Sample Data Visualization Pattern_Circular Architecture with Divisions.

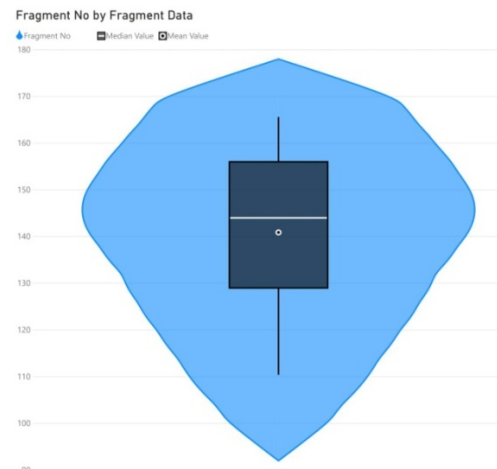


Fig. 7. Data Visualization Pattern_Leaf Architecture.

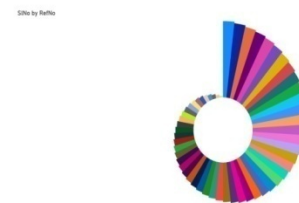


Fig. 8. Data Visualization Pattern_Snail Architecture.

Fig. 2 to Fig. 8 are the sample visuals generated based on the encrypted fragment data based on the above sample data.

The above proposed method is an optimized way of storing the data into the cloud and also provides the enhanced security for the fragments in the cloud. [1].

The Encrypted Data will be stored into the cloud based on the size using either available visualization patterns or customized patterns. This data will be stored into the particular pattern based on the randomization algorithm [11].

Optimization

The optimization in this system is achieved by choosing the exact pattern which will store the data at various nodes depending on the size of the data. Here it is evident that the space will not be wasted unnecessarily by choosing the pattern of 100 nodes to store only three fragments data. And the level security plays very vital role while doing the optimization process.

V. PATTERN SELECTION ALGORITHM FOR OPTIMIZATION

The pattern selection algorithm in this research is used to perform the optimization process on the secured data fragments which need to be stored in the cloud for further access [13]. The pattern selection algorithm will work on the select function which is defined as $f(x)$. Based on this select function only the corresponding pattern is selected and fragments will be stored into the corresponding location of the nodes in the patterns for further accessing when it is required [7]. The select function is defined as:

$$f(x) = \text{Number of Fragments (N)} / \text{Number of nodes available in the pattern (NP)}$$

The Number of Nodes should be always greater than Number of Fragments.

The final randomization function is defined as

$$f(x) = N/NP \text{ where } NP > N$$

This Select function will be used to decide the optimization factor while storing the data into the cloud compared to the existing methods.

VI. CUSTOMIZED PATTERN GENERATION

In the previous step the procedure of selecting the existing pattern has been discussed with respect to storing the data into the cloud. While doing the above process one more limitation the system faces after quite some time is that when all the available patterns are completed then the system is going to repeat same patterns or any new patterns are going to get generated. The proposed method will generate the customized data patterns and same will be stored in the system for further use. And also there is no harm in repeating the same patterns also as the data storing will be changed though the pattern is same.

In order to generate and store customized patterns various factors will be considered. The first and foremost factor is number of fragments which need to be stored in the pattern. Then comes the level of complexity or security. The pattern generation algorithm will consider above parameters majorly while generating the pattern.

Pattern Generation Algorithm

- Start.
- The number of fragments needs to be stored (n) (the value of n starts from 1,2,3,4,5...)
- Identify the Level of Complexity (L-Low Complexity, M-Medium Complexity, H- High Complexity)
 - The complexity level can be fixed based on the level of security needs to be provided for example, L=3, M=5, H=7.
- Calculate the value of $f(x)$, where $f(x) = n * \text{Level of Complexity}$
- Generate the pattern based on the value of $f(x)$
- Store the pattern into the system

- Stop

Once the new pattern stored into the system, again the pattern selection algorithm procedure applied in order to select the pattern based on number of fragments need to be stored.

Consider an example $n=1$ and $L=3$ then the value of $f(x) = n * L = 1 * 3 = 3$, means total 3 arcs need to be generated with 3 node places, out of which one is original node and remaining two will be dummy nodes.

So the default pattern will be generated and it can be customized as per the requirements. While generating the customized patterns based on the value of $f(x)$, elements can be selected by the users like either they can use lines, boxes, QR-Codes, Circles, Some Special Images etc.,

Are the elements limited while generating pattern? Not really the user can choose various types of elements as it will be generated before storing the data, so that the system will be trained with the sample customized patterns as shown in Fig. 9, Fig. 10 and Fig. 11.

As shown above the customized data patterns can be generated by considering the $f(x)$ value thereby storing the data further using pattern selection and randomization algorithm.



Fig. 9. Multi QR Code Based Pattern.



Fig. 10. Basket Ball Half Court Pattern.

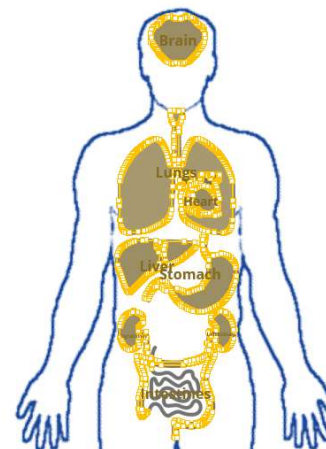


Fig. 11. Human Body – Pattern and Data can be Stored in various Parts.

VII. COMPARATIVE STUDY

As most of the researchers working on cloud based data access and security, most of the researchers are using graph coloring process after data fragmentation process [2]. The main drawback of this algorithms is that the complexity will increase with the increase of degree of nodes (Number of Nodes) due to which the process of storing the data will be a hectic process and accessing also not so easy which will lead to NP-Hard problem [14]. To overcome this in the proposed method the pattern selection algorithm is defined in such a way that the complexity remains same though the degree of nodes will get increased continuously. Whatever might be the degree of nodes based on select function defined in Pattern selection algorithm, the pattern will be selected but the procedure to store and retrieve the data will remain the same. That means the select function can be used with various degree of nodes represented as Δ , where the value of Δ varies from 1 to n. After the process and various experiments performed are based on Δ values that the Select function derives as.

$$f(x) = \sum_{\Delta=1}^n N/NP \text{ where } NP > N$$

The proposed method will never lead to the NP-Hard problem as the procedure followed to generate patterns is independent to the Degree of Nodes [14].

The proposed method is very much optimized compared to the existing algorithms in order to store and access the data from cloud. Each and every pattern when storing in the cloud will be stored with a key reference for better access [5]. For example if the fragments are related to a company called A the key used to store these company fragments are represented as A_Frag_1.

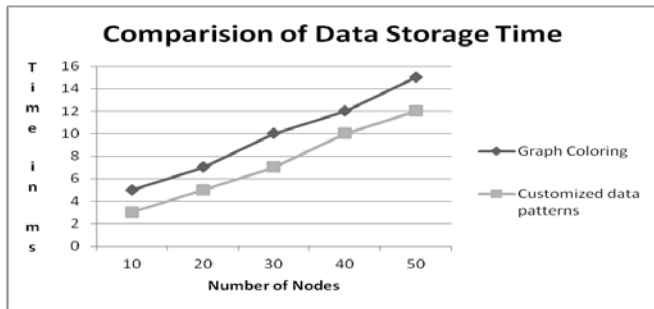


Fig. 12. Comparison of Data Storage Time.

This graph (Fig. 12) depicts the time taken for storing the data onto the cloud based in the form of number of nodes. Ex: to store 10 nodes in Customized Data Pattern technique it will take 3ms whereas to do the same in existing graph coloring algorithm it will take 5ms.

This graph (Fig. 13) represents the time taken to retrieve back the nodes from cloud. Ex: in existing graph coloring algorithm it took approximately 12-13ms to retrieve 10 nodes whereas in the proposed system it took 6 to 7 ms to retrieve 10 nodes.

Fig. 12 and Fig. 13 clearly show that the results of the proposed system are satisfactory compared to existing methods.

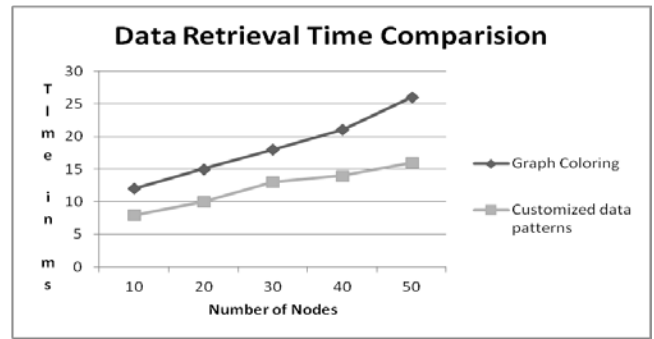


Fig. 13. Data Retrieval Time Comparison.

VIII. ENHANCED SECURITY

Coming to security as the hackers try to hack the data, the Encrypted data position is not known to the hackers as the size of the pattern i.e. number of node places will be decided by the service provider so that the select function value will be very difficult to identify. If suppose the hacker identified the random function again, he needs to work on decrypting the data as the encryption algorithm used in this paper is very secured which is called as Code Book based algorithm [1]. The proposed system compared to existing methods is optimized and enhances the security for fragments which are getting stored in the cloud. Fig. 14 gives the encryption time for different algorithms.

In the Table I the proposed Code Book (ref. Table II) algorithm is compared with the existing algorithms with respect to encryption time. And it is found that the code book algorithm will give very good results compared to existing algorithms with respect to encryption.

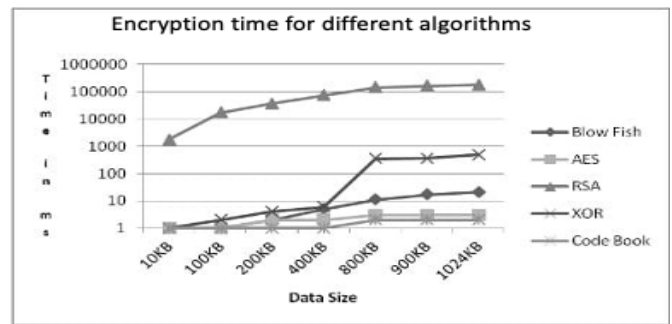


Fig. 14. Encryption Time for different Algorithms.

TABLE I. AVERAGE TIME TAKEN FOR ENCRYPTION OF DATA FRAGMENTS (BASED ON SIZE)

Time in (ms)	10K B	100K B	200K B	400K B	800K B	900K B	1024K B
Blow Fish	1	1	2	5	11	17	21
AES	1	1	2	2	3	3	3
RSA	1743	17177	36814	73216	143206	162905	181246
XOR	1	2	4	6	356	358	489
Code Book	1	1	1	1	2	2	2

TABLE II. SAMPLE CODE BOOK

S. No	Letter/Number	Symbol
1.	A	↓
2.	a	€
3.	B	¥
4.	b	α
5.	1	∩
6.	2	¶
8.	3	ə
9.	,	Υ
10.	.	✓

IX. REAL TIME TESTING OF THE PROPOSED RESEARCH

In order to test the encryption technique used and data visualization techniques, the data has been shared with the certified ethical hackers to test it. The ethical hackers tried for almost 10 to 15 days and came back and said it is very difficult to crack the final data, so it is evident that the proposed research provides best security for the data which is getting stored in the cloud. The proposed method will provide multi-level security for the data which is getting stored on the cloud. One method is in the form of Encryption and another way using data visualization [6].

X. CONCLUSION

It is evident that from the proposed research whatever data is getting stored on the cloud is very well protected from all the attacks which are expected while working in real time. And also the proposed solution will give ease of access to the data which is stored on the cloud. The patterns are selected basis the pattern selection algorithm based on the number of fragments and also the number of data node representations available in the particular pattern. So it is very clear that the data storing and processing will be an easy process with the proposed procedure.

XI. FUTURE ENHANCEMENT

At present the proposed solution is working very well for the data which is stored as either individual data set or as a fragment without any limitation. In future, same system can be used to store the images for providing security. And also the data visualization patterns can be drawn in much more complex way in order to increase the level of security.

REFERENCES

- [1] M. Archana, P. M. Mallikarjuna Shastry, "Hierarchical encryption algorithm to secure data fragments in cloud computing," in International Journal of Future Generation Communication and Networking, vol. 14, no. 1, 2021.
- [2] M. Raji, A. Hota, T. Hobson, J. Huang, "Scientific Visualization as a Microservice", in IEEE Transactions on Visualization and Computer Graphics, vol. 26, no. 4, pp. 1760-1774, 2020. doi: 10.1109/TVCG.2018.2879672.
- [3] Y. K. Joshi, U. Chawla, S. Shukla, "Rainfall Prediction Using Data Visualisation Techniques," 2020 10th International Conference on Cloud Computing, Data Science & Engineering (Confluence), pp. 327-331, 2020. doi: 10.1109/Confluence47617.2020.9057928.
- [4] T. Wiktorski, A. Królak, K. Rosińska, P. Strumillo, J. C. Lin, "Visualization of Generic Utility of Sequential Patterns", in IEEE Access, vol. 8, pp. 78004-78014, 2020. doi: 10.1109/ACCESS.2020.2989165.
- [5] M. Archana, P. M. Mallikarjun Shastry, "A Method for Text Data Fragmentation to Provide Security in Cloud Computing," International Journal of Engineering and Advanced Technology (JEAT) ISSN, vol. 9, no. 2, pp. 2249 – 8958, 2019.
- [6] E. Hoque, M. Agrawala, "Searching the Visual Style and Structure of D3 Visualizations", in IEEE Transactions on Visualization and Computer Graphics, vol. 26, no. 1, pp. 1236-1245, 2020, doi: 10.1109/TVCG.2019.2934431.
- [7] X. Shi, F. Lv, D. Seng, B. Xing, J. Chen, "Exploring the Evolutionary Patterns of Urban Activity Areas Based on Origin-Destination Data", in IEEE Access, vol. 7, pp. 20416-20431, 2019. doi: 10.1109/ACCESS.2019.2897070.
- [8] M. Islam, S. Jin, "An Overview of Data Visualization", 2019 International Conference on Information Science and Communications Technologies (ICISCT), pp. 1-7, 2019. doi: 10.1109/ICISCT47635.2019.9012031.
- [9] T. M. Aruna, M. S. Satyanarayana, G. N. Divyaraj, "A Unique Work of Out of Sight Epigraphy Creation for Data Security", Journal of Advanced Research in Dynamical and Control Systems, vol. 11, no. 7, 2019.
- [10] Jia Chaolong, Wang Hanning, Wei Lili, "Research on Visualization of Multi-Dimensional Real-Time Traffic Data Stream Based on Cloud Computing", Procedia Engineering, vol. 137, pp. 709-718, 2016. ISSN 1877-7058. doi:10.1016/j.proeng.2016.01.308.
- [11] C. Muelder, B. Zhu, W. Chen, H. Zhang, K. Ma, "Visual Analysis of Cloud Computing Performance Using Behavioral Lines", in IEEE Transactions on Visualization and Computer Graphics, vol. 22, no. 6, pp. 1694-1704, 2016, doi: 10.1109/TVCG.2016.2534558.
- [12] L. Battle, P. Duan, Z. Miranda, D. Mukusheva, R. Chang, M. Stonebraker, "Beagle: Automated extraction and interpretation of visualizations from the Web", Proc. of SIGCHI, vol. 594, no. 8, pp. 1-594, 2018.
- [13] E. Glassman, T. Zhang, B. Hartmann, M. Kim, "Visualizing API usage examples at scale," Proc. of SIGCHI, vol. 580, no. 12, pp. 1-580, 2018.
- [14] M. A. Borkin, A. A. Vo, Z. Bylinskii, P. Isola, S. Sunkavalli, A. Oliva, et al., "What makes a visualization memorable?", IEEE Transactions on Visualization and Computer Graphics, vol. 19, no. 12, pp. 2306-2315, 2013.
- [15] "www.datapine.com [Online].

Incremental Learning based Optimized Sentiment Classification using Hybrid Two-Stage LSTM-SVM Classifier

Alka Londhe, P.V.R.D. Prasada Rao

Department of Computer Science and Engineering
Koneru Lakshmaiah Education Foundation, Vaddeswaram, AP, India

Abstract—Sentiment analysis is a subtopic of Natural Language Processing (NLP) techniques that involves extracting emotions from unprocessed text. This is commonly used on customer review posts to automatically determine if user / customer sentiments are negative or positive. But quality of these analysis is completely dependent on its quantity of raw data. The conventional classifier-based sentiment prediction is not capable to handle these large datasets. Hence, for an efficient and effective sentiment prediction, deep learning approach is used. The proposed system consists of three main phases, such as 1) Data collection and pre-processing, 2) Count vectorizer and dimensionality reduction is used for feature extraction, 3) Hybrid classifier LSTM-SVM using incremental learning. Initially the input raw data is gathered from the e-commerce sites for product reviews and collected raw is given to pre-processing, which do tokenization, stop word removal, lemmatization for each review text. After pre-processing, features like keywords, length, and word count are extracted and given to feature extraction stage. Then a hybrid classifier using two-stage LSTM and SVM is developed for training the sentimental classes by passing new features and classes for incremental learning. The proposed system is developed using python and it is compared with the state-of-the-art classification techniques. The performance of the proposed system is compared based on performance metrics such as accuracy, precision, recall, sensitivity, specificity etc. The proposed model performed an accuracy of 92% which is better compared to the state-of-the-art existing techniques.

Keywords—Sentiment analysis; natural language processing; incremental learning; long short-term memory; support vector machine; hybrid; dimensionality reduction; principal component analysis

I. INTRODUCTION

Sentiments play an important role in rational decision making, perception, memory, creativity, human intelligence, social interaction, learning and more. Sentiment analysis and Opinion mining is a subtopic of text mining and NLP (Natural Language Processing) that deals with the extraction of knowledge and automated discovery about people's opinions, evaluation and sentiments from textual data such as review websites, customer feedback forms and personal blogs [1,2]. Sentiment analysis and opinion mining is a region, which has received significant interest in recent times because of its application and practical usage in today's environment. Emotion analysis of text involves cautious modelling of context, association of words with different emotions and

contexts with changing levels of magnitude making the identification of words for document representation. Emotions are categorized into surprise, sadness, anger, fear, excitement and disgust [3]. For example, a sentence containing beautiful morning #amazing, the word amazing could be related strongly with emotion joy, morning could be weakly associated with emotion joy and beautiful will be related moderately to emotions such as joy and love. Emotion lexicons capture such word-emotion associations [4]. To organize the data and improve classification performance, lexicon dependent holoentropy is applied. It is created to reduce the computational risk associated with solving a multidimensional problem. The similarity score between the keywords of all sentiment classes and semantic words is determined using combined holoentropy [5]. However, these methods rely on lexical resources (external) which are concerned with mapping words to a numerical sentiment score or categorical (positive, negative, and neutral). Clearly, the efficiency of the entire method intensely depends on one of the best lexical resources, which relies on it [6]. As a significance, the efficiency of certain widespread is available on lexical resources, which is in the task for classification of microblog posts.

Sentiment analysis (SA) using supervised machine learning algorithms is popular and provides better results compared to unsupervised machine learning algorithms. However, supervised approaches require a labelled training set, which is time and labor-intensive operation [7, 8]. Whereas, the unsupervised approaches don't need labelled training set. The emotions can also be acquired by the reviews, which can be collected not only from applications but also provide comment features such as Google Play Store [9]. Platforms like Amazon, Flipkart are regularly used by users/customers to give their sentiments about numerous subjects, including the product quality [10, 11]. Nevertheless, social media does not have rating system and companies being observed cannot instantly detect the sentiment of these remarks. As a result, many businesses and companies have a strong claim for sentiment classification. By using a machine learning method, computer can learn emotion form text. In machine learning, computers cannot solve problems by applying pre-programmed rules, but rather by creating a model that can evaluate an example [12]. Hence, it can anticipate a sentiment or emotion. Machine learning is also a part of AI (Artificial Intelligence), which is a subset of deep learning.

Deep neural networks are utilized by deep learning to obtain input data that can be used for improved representation and to complete a task precisely [13, 14]. Likewise, sentiment analysis using deep learning techniques has a better accuracy compared to the traditional machine learning techniques such as SVM and Naïve Bayes (NB). Multiple or hybrid classifiers are mainly used for better training and better performance metrics than the single classifier. The error of single classifier will be greater than hybrid classifier because in hybrid, the trained data of one classifier will be given to the input of another. so, the trained net will be effective compared to the single classifier. Incremental learning technique is necessary to develop the learning models or trained net, which is capable of adding newly available classes without the need of retraining the models. Though many techniques had performed better but the error rate and performance of the existing technique is not achieved well [15]. So, in the proposed research effective feature selection is designed to enhance the classification performance.

The contribution of the paper is as below:

- To acquire extraction of data from the raw data, pre-processing technique is used that consists of sentence splitting, tokenization, spell correction, stop-word removal and lemmatization.
- To extract datasets more conveniently and effectively, the count vectorizer and dimensionality deduction is used.
- To attain an effective classification, the hybrid two-stage LSTM-SVM approach is used.

The upcoming portion of the paper is organized as follows; Section II illustrates certain research articles related to existing methods used for sentiment analyzing. Section III describes briefly about the proposed methodology. Section IV explains the results and performance metrics of the proposed framework. Section V concludes the entire research work.

II. RELATED WORK

Several feature selection algorithms have been introduced for choosing the most relevant features that are required for better classification. The most commonly used feature selection techniques are SVM and LSTM. Some of the existing feature selection technique used in sentiment analysing is reviewed below.

Fu X et al. [17] has performed sentiment analysis using long short-term memory networks (LSTMs). This method is based on combination of LSTM with embedded words for representation of text. However, embedded words carry more semantic data than the sentiment data, so that the embedded word will cause inaccuracy to the sentiment analysis. To solve these issues, a lexicon-improved LSTM model is developed, which uses the sentiment-based lexicon as an additional data for sentiment classifier to pre-train a word and then include embedded sentiment words that are not inside the lexicon. The usage of a hybrid sentiment embedding and word embedding can improve word representation accuracy. Furthermore, without the intention of improving the LSTM's ability to gather global sentiment data, a new method for identifying the

sensitivity vector in common sentiment analysis is developed. The outcomes of this model have comparative or better results than the existing models. Londhe A et al. [18] proposed incremental approach using LSTM-RNN for aspect level sentiment analysis. Major outcome of the paper was automated aspect extractions with comparable accuracy.

Long F et al. [19] aim to investigate the sentiment interpretation of social media in Chinese text by incorporating the Multi-head Attention (MHAT) mechanism with Bidirectional Long-Short Term Memory (BiLSTM) networks, in order to overcome the lack of Sentiment Analysis, which is currently carried out using old machine learning techniques. BiLSTM networks retain the text's actual context and resolve the issue of long-term dependency. By performing numerous dispersed calculations, the MHAT process can obtain related data from a distinct illustration subspace, and impact weights are added to the generated text sequence. The numerical experiments reveal that the suggested model outperforms existing well-established approaches. Rhanoui M et al, [25] also investigate CNN-BiLSTM model for document level sentiment analysis.

Khanvilkar, G et al. [20] has designed sentiment analysis for product recommendation using random forest algorithm. Sentiment analysis is a tool for analysing natural language and determining human emotions. The purpose of emotion analysis is to identify the polarity of a person's textual opinion and it can also be used to provide product suggestions. Products can be recommended to another user based on user reviews. Sentiment analysis is used by major product websites to analyse the difficulties and popularity of the product. Sentiment analysis is usually described as a task with two classification classes: negative and positive. Using ordinal classification, this approach calculates the polarity of user-provided reviews. Using machine learning methods SVM and Random Forest, the system will determine polarity. Users will be given recommendations based on the polarity that has been attained.

Can, E. F et al. [21] has designed Multilingual Sentiment Analysis using RNN-Based Framework for Limited Data. Sentiment analysis is a type of NLP work that evaluates a user's feelings, opinions, and ratings of a product. The fact that sentiment analysis is primarily reliant on language is one of the most difficult parts of it. Language-specific word embedding's, sentiment lexicons, and even annotated data exist. Optimizing models for each language is very time consuming and labour intensive, especially for RNN (Recurrent Neural Network) models. From a resource aspect, gathering data for several languages is relatively difficult. A sentiment analysis approach based on RNN is trained with reviews in English and translated into other languages to do this. As a result, the model may be used to assess feelings in different languages. According to the experimental results, the robust technique of a single model trained on English reviews statistically achieves the benchmarks in other languages.

Anitha Elavarasi S. et al., [22] In the age of big data and internet technology, organisations can use sentimental analysis or opinion mining to collect feedback on their services or goods in a more accurate and effective manner. In this paper

linear regression and support vector machine are applied to the IMDB data sets. There are 50000 movie reviews in the dataset, with both negative and positive polarity remarks. SVM classifier and logistic regression were used as machine learning algorithms. The outcomes were analysed through accuracy, precision and recall. In comparison to SVM, which has an accuracy of 81%, logistic regression has a higher accuracy of 90 percent, making it more successful than SVM.

From the above-mentioned literature studied, various feature selection methods are designed based on LSTM [17, 18, 26], BiLSTM [19, 25], RF [20], RNN [21, 27], SVM [22] and hybrid LSTM-SVM [23] techniques. But rate of error is high and accurate prediction is lesser while using this existing method. At the same time optimal feature selection subset is not attained in the existing algorithm. Therefore, selection of hybrid feature algorithm is designed in this proposed research for effective selection of features from the dataset.

III. PROPOSED METHODOLOGY

Natural Language Processing (NLP) technique is a Sentiment analysing process that contain extracting of sentiments associated with some raw texts.

Generally, on social media, people used to post customer reviews in order to automatically understand, whether it is positive or negative review but quality of these analysis is completely dependent on its quantity of raw data. So recently, researchers are trying to utilize large dataset for modelling the sentiment prediction. The conventional classifier-based sentiment prediction is not capable to handle these large datasets. So, for an effective and efficient sentiment prediction, hybrid models on hybrid platforms need to be used [16]. In this paper an efficient deep learning-based hybrid model for sentiment prediction is proposed.

Fig. 1 illustrates the architecture of proposed model. It consists of three phases: 1) Data collection and pre-processing, 2) dimensionality reduction and feature extraction, 3) classification and incremental learning are the three primary steps of the proposed system. The raw data for the input is initially obtained from the online platforms for product reviews such as Amazon, Flipkart and Snapdeal. The data is pre-processed to eliminate superfluous information as keywords, length, and word count are extracted after pre-processing. After pre-processing techniques, emotional features are extracted with count vectorizer and dimensionality reduction, which is used for extracting the unwanted words for reliable sentiment analysis and converting it to vector format. Then, for sentimental class prediction, hybrid two-stage LSTM-SVM approach is used for training the sentimental classes. The new classes and features are introduced during training phase for incremental learning.

A. Data Collection and Pre-processing

By reviewing the literature, it is found that aspect extraction and sentiment classification have not been studied satisfactorily on Yelp dataset [29]. This dataset is well described in results section. Pre-processing phase involves filtering noisy text using a variety of pre-processing techniques [24], such as sentence splitting, tokenization, spelling correction, lemmatization, case-conversion, stop-word removal

and anaphoric reference resolution. These steps are used to omit irrelevant phrases to offer better categorization.

- **Splitting:** The technique of breaking up a text string in a systematic way so that the individual parts of the text may be processed is known as string splitting. For example, a timestamp can be divided into hours, minutes, and seconds. So that those values can be used in the numeric analysis.
- **Tokenization:** Tokenization is an action of dividing a sequence of strings into pieces such as symbols, phrases, keywords, words, and other elements called tokens. Tokens can be individual phrases, words or even whole sentences.
- **Stop word removal:** Stop words are a group of terms that are regularly employed in any language. In English, “and”, “is” and “the” would easily qualify as stop words. Stop words removal phase is used in NLP and text mining applications to remove unnecessary terms, enabling applications to concentrate on the subsequent words accordingly.
- **Lemmatization:** Lemmatization describes the process of gathering words with the same lemma or root, but different meaning derivatives so that they can be analysed as a single item.
- **Spell correction:** Spelling correction is a well-known task in NLP. It uses techniques of “noisy and correct word mappings” data from numerous sources for automated spell correction.

B. Pre-processed Data Extraction for New Features

The new features are updated with the pre-processed data by using the below mentioned feature extraction process.

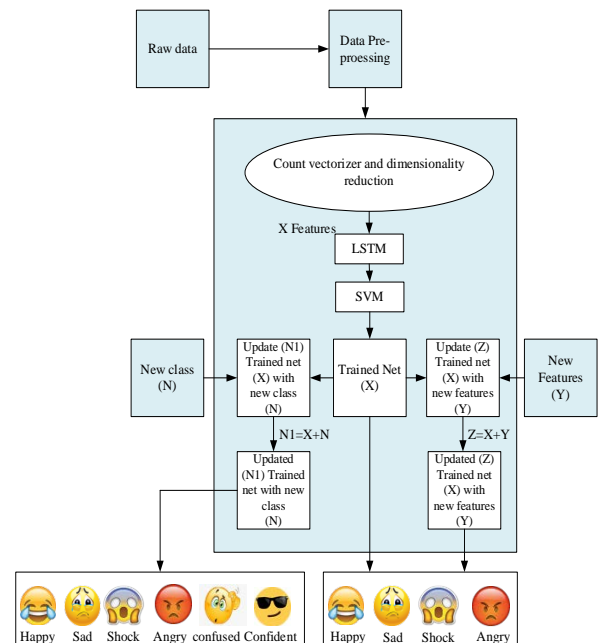


Fig. 1. Proposed Model of Sentimental Analysis and Text Classification.

- Words and Their Frequencies: The frequency counts of unigrams, bigrams, and n-gram models are considered as features. Additional research has been done to properly characterize this feature using the word presence rather than frequencies.
- Parts of Speech Tags: Adjectives, adverbs, and certain groups of verbs and nouns are excellent indicators of subjectivity and sentiment.
- Opinion Words and Phrases: Apart from individual words, phrases and idioms that can convey emotion as features. For example. Someone's arm and a leg,
- Position of Terms: The placement of a term in a text can have an impact on how much the term affects the overall theme of the text.
- Negation: Negation is a significant feature that can be difficult to interpret. When a negation is present, the polarity of opinion is usually altered.
- Syntax: Many academics employ syntactic patterns such collocations are used as features to learn subjective patterns.

If the pre-processed data is "best coffee" then the feature extraction of parts of speech will be 1, 1. This is because "best" is an adjective and "coffee" is a noun, both the parts of speech contain one word. So, the outcome of these pre-processed data is 1, 1. Likewise the other method such as opinion words and phrases, position of terms, negation and syntax are used for extracting the features. These extracted and the features are updated to the class.

C. Feature Extraction

Feature extraction is a process of extracting the required features for sentimental classes. The features are retrieved using a countvectorizer and dimensionality reduction, which reduces a large amount of raw data into smaller groups for analysis. A disadvantage of huge data sets is that processing a higher number of variables which demands a lot of computational resources. So that, the dimensionality reduction technique is utilised to solve this issue.

1) *Countvectorizer*: Countvectorizer is a major tool used in the python for converting the given text into vector with the frequency of each word that occurs in the entire text. This is helpful in converting multiple texts into each vector [24]. Each text sample and unique word is represented in row matrix and column matrix. Though the sentences of data may be in different size, the conversion of word to vector will be of same rows and columns for each and every other sentence.

2) *Dimensionality reduction*: It is necessary to smooth the input text dataset before applying a feature extraction and reduction model using Principal Component Analysis (PCA). PCA's primary goal is to extract important features from a big dataset and produce a lower-dimensional feature space. It may be used to extract data from a large number of different datasets. In addition, if we use a bigger dataset for analysis, the classifier will take longer to run. For this reason, feature

extraction and dimension reduction are used to reduce the size and complexity of the data representation.

3) *Hybrid two-stage LSTM-SVM classifier*: In this proposed model, the hybrid two-stage LSTM-SVM approach is used for sentiment classification. Extracted features from dimensionality reduction are given as an input to this hybrid model.

a) *SVM Classification*: SVM is a state-of-the-art supervised ML algorithm which can be used for both regression and classification tasks. The SVM finds hyperplanes that differentiate the classes to perform classification task. For a set of training vectors belonging to separate classes, shown in (1):

$$\{(x^1, y^2), \dots, (x^m, y^m)\}, \quad x \in R^n, y \in \{1, -1\} \quad (1)$$

Mathematically a hyperplane for separating two classes can be represented as shown in (2):

$$\sum_{i=1}^M X_{ij}^l y_i^l + Bias^l \quad (2)$$

This can be written more in vector format as $\langle W, X \rangle + b = 0$. Here X is "an input vector or document", W is known as "a weight vector and corresponds to the normal vector" for separating hyperplane 'H', m represents "the number of input variables, in the case of text, this can be viewed as the number of words (or phrases, etc.) that are used to describe a document" and b denotes "the perpendicular distance from the hyperplane to the origin".

$$\min |(w, x^i) + b| = 1 \quad (3)$$

From the above equation, it be evaluated that the optimal separating hyperplane given by:

$$w^* = \sum_{i=1}^l \alpha_i y_i x_i \quad (4)$$

$$b^* = -0.5(w^*, x_r + x_s) \quad (5)$$

α_i is the multiplier, x_s and x_r are support vectors that satisfies each class $\alpha_r > 0, y_r = -1; \alpha_s > 0, y_s = 1$.

b) *LSTM Classification*: LSTM is a variant of RNN, it deals with the vanishing and exploding gradient problems. LSTM unit is consisting of a cell, forget gate, an input gate and an output gate.

$$f_i = \sigma(W_f x_i + U_f h_{i-1} + b_f) \quad (6)$$

$$i_i = \sigma(W_i x_i + U_i h_{i-1} + b_i) \quad (7)$$

$$o_i = \sigma(W_o x_i + U_o h_{i-1} + b_o) \quad (8)$$

$$c_i = f_i * c_{i-1} + i_i * \tan h(W_c x_i + U_c h_{i-1} + b_c) \quad (9)$$

$$h_i = o_i * \tan h(c_i) \quad (10)$$

Here, h_i represents hidden state, c_i is the central state, o_i is the output gate, i_i is the input gate and f_i is the forget gate.

Fig. 2 illustrates the combined architecture of the hybrid two-stage LSTM-SVM model. Extracted features are given to input layer. The hidden layer of the LSTM consists of N layers. These layers will get interacted and given to the fully connected layer. LSTM is similar to RNN, but it has only one

tanh layer. The LSTM has two tanh layers and 3 sigmoid layers. The output from the hidden layer is given to the fully connected layer. The softmax layer of the LSTM is replaced with SVM for classification. Softmax layer is a softmax function, which is mainly used for multi-class classification. The SVM first finds hyperplanes that differentiate the classes to perform classification task. Thus, the prediction of sentiment class will be acquired as an output from the classifier.

c) *Incremental Learning*: In incremental learning, first trained-net produces a classification of sentiment with a set of extracted features. The output from the trained-net (X) will be sentiment classes e.g. happy, sad, shock and angry as shown in algorithm.

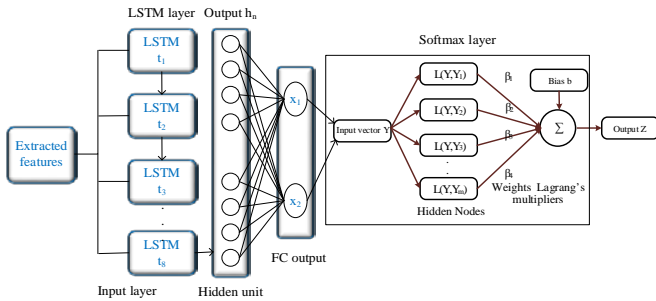


Fig. 2. Hybrid Two-Stage LSTM-SVM Architecture.

Then for incremental learning the new features (Y) are added to the trained-net (X), it produces an updated trained-net output ($Z=X+Y$). This updated trained-net will predict the new features according to the sentiment classes such as happy, sad, shock and angry. Likewise, the new classes (N) are added to the trained net (X) for producing an updated trained-net (N1), these updated trained-net ($N1=X+N$) will be addition of new classes and existing classes. The new class consists of confident and confused and the existing class consists of happy, sad, shock and angry. These classes are added and produce an updated trained net (N1) output, which consist of happy, sad, shock, angry, confused and confident as mentioned in Fig. 1.

IV. RESULT AND DISCUSSION

The acquired datasets consists of special characters, uppercase and keywords. These characters in the sentence are extracted by using the pre-processing technique, which consist of spell correction, tokenization, stop word removal, splitting and lemmatization. Next process is feature extraction for removing the unwanted words because large data will take more processing time, to overcome this issue the dimensionality reduction is used. The extracted features from the countvectorizer and dimensionality reduction are given to the hybrid two-stage LSTM-SVM classifier for sentimental analysis.

Algorithm: Incremental Hybrid Two-Stage LSTM-SVM Classifier for Sentiment Classification

Input raw dataset = A

For all data in dataset

#Pre-processing (A)

- A1 = Splitting (A) // Sentence splitting into words for processing
- A2 = Tokenization (A1) // Breaking sequence of strings into pieces
- A3 = Stop word removal (A2) // stop words such as “the”, “an”, “a” are removed
- A4 = Lemmatization (A3) // Changing words with different derivatives
- A5 = Spell correction (A4) // auto correction of noisy to proper words for misspelled words

#Feature extraction

- A6 = Countvectorizer (A5) // Conversion of string to numerical
- A7 = Dimensionality reduction (A6)

#Hybrid Two-stage LSTM-SVM Classifier

- L = LSTM (A7) // Numerical value from Countvectorizer is classified with LSTM
- S = SVM (L) // Last layer output of LSTM is classified with SVM

#Incremental Learning

- Trained-net = S
- For (i=0, i=i+n, i++) // Initial value = 0, number of features = n, new features = i
 - { Z=S+i // Adding trained-net and new features, Updated trained-net (Z)
 - }
- For (j=0, j=j+n, j++) // Initial value = 0, number of features = n, new classes = j
 - { N=S+j // Adding trained-net and new classes, Updated trained-net (N)
 - }

Output: Prediction of sentiment classes based on reviews with incremental learning

a) *Datasets*: For Model evaluation four separate datasets were used. 1) Sentiment Labelled Sentences Data Set [28]: in this dataset, sentences are selected from three different websites: {imdb.com, amazon.com, yelp.com}. From each website, 500 positive and 500 negative sentences are randomly selected. 2) Large Movie Review Dataset [29]: this dataset is taken from Kaggle - IMDB dataset of 50000 movie reviews. 3) Amazon product review dataset [30]: this dataset contains product reviews (ratings, text, helpfulness votes). 4) The Yelp dataset [31, 32] is a subset of reviews, businesses and user data for use in personal, academic purposes and educational. This dataset consists of 8,635,404 reviews, 160,585 businesses, 200,000 pictures and 8 metropolitan areas.

Fig. 3 illustrates the extraction of input in the preprocessing step. Datasets is acquired and converted to lower case. Sentence will be extracted by the special character removal, which removes the special characters such as '@', '#', '_'. Then splitting and localization process will take place, this is used to split each and every word and localize it. After splitting and localization, the next step is removal of the stop words such as is, are, a, an, the etc. These are the steps involved in the pre-processing technique and the next step is data partitioning and feature extraction. The feature extraction is implemented by the Yake tool [33]. The extracted features are classified by a two-level classifier, which is a hybrid model that is combination of LSTM and SVM. The performance of state-of-the-art existing feature selection approaches is compared with proposed feature selection process. The performance attained

using Accuracy, Precision, Recall, F-1 score, Specificity, False Negative Rate (FNR), False Positive Rate (FPR), Negative Predictive Value (NPV) and Error.

Table I and Table II illustrate the results obtained on datasets 1, 2, 3 & 4 for various metrics using the existing and proposed sentiment classification model. The values for parameters such as Error, FNR, FPR are smaller as compared to existing techniques and the metrics such as accuracy, precision, recall, F-1 score and NPV are greater as compared to existing techniques. The below section will explain graphical representation for the comparison of proposed and existing models.

Input Review	Output Tokens
The food is always great here. The service from both the manager as well as the staff is super. Only draw back of this restaurant is it's super loud. If you can, snag a patio table!	'food', 'always', 'great', 'service', 'manager', 'well', 'staff', 'super', 'draw', 'back', 'restaurant', 'super', 'loud', 'sang', 'ratio', 'table'
This place used to be a cool, chill place. Now its a bunch of neanderthal bouncers hopped up on steroids acting like the can do whatever they want. There are so many better places in davis square where they are glad you are visiting their business. Sad that the burren is now the worst place in davis.	'place', 'used', 'cool', 'chill', 'place', 'bunch', 'neanderthal', 'bounce', 'hoped', 'osteoide', 'acting', 'like', 'whatever', 'want', 'many', 'better', 'place', 'davis', 'square', 'glad', 'visiting', 'business', 'sad', 'burden', 'worst', 'place', 'davis'
The setting is perfectly adequate, and the food comes close. The dining chains like Chilis and Victoria Station do barbecue better. It's no surprise you can always pick up coupons for Linwood at restaurant.com.	'setting', 'perfectly', 'adequate', 'food', 'come', 'close', 'dining', 'chain', 'like', 'child', 'victoria', 'station', 'barbecue', 'better', 'surprise', 'always', 'pick', 'coupon', 'linwood', 'restaurant', 'com'

Fig. 3. Input and Output Obtained after Pre-Processing.

TABLE I. PERFORMANCE BASED COMPARISON FOR DATASET BETWEEN PROPOSED AND EXISTING TECHNIQUES ON DATASET 1 & 2

Performance Metrics	Techniques									
	DATA 1					DATA 2				
	RF	ANN	SVM	LSTM	LSTM-SVM	RF	ANN	SVM	LSTM	LSTM-SVM
Accuracy	0.42	0.68	0.75	0.78	0.85	0.80	0.82	0.84	0.84	0.92
Error	0.58	0.32	0.25	0.22	0.15	0.20	0.18	0.16	0.16	0.08
Precision	0.20	0.40	0.49	0.66	0.88	0.78	0.74	0.76	0.80	0.85
Recall	0.18	0.15	0.30	0.45	0.71	0.25	0.36	0.40	0.68	0.78
Specificity	0.50	0.78	0.82	0.84	0.96	0.84	0.86	0.86	0.88	0.93
F1_Score	0.70	0.76	0.84	0.88	0.92	0.70	0.76	0.82	0.86	0.91
Negative Predictive Value (NPV)	0.52	0.78	0.82	0.84	0.92	0.84	0.84	0.89	0.93	0.94
False Negative Rate (FNR)	0.32	0.30	0.29	0.25	0.20	0.20	0.20	0.17	0.14	0.05
False Positive Rate (FPR)	0.23	0.17	0.09	0.06	0.05	0.35	0.30	0.22	0.17	0.10

TABLE II. PERFORMANCE BASED COMPARISON FOR DATASET BETWEEN PROPOSED AND EXISTING TECHNIQUES ON DATASET 3 & 4

Performance Metrics	Techniques									
	DATA 3					DATA 4				
	RF	ANN	SVM	LSTM	LSTM-SVM	RF	ANN	SVM	LSTM	LSTM-SVM
Accuracy	0.63	0.68	0.68	0.77	0.86	0.60	0.73	0.76	0.78	0.89
Error	0.37	0.32	0.32	0.23	0.14	0.40	0.27	0.24	0.22	0.11
Precision	0.64	0.69	0.70	0.71	0.87	0.60	0.76	0.76	0.83	0.90
Recall	0.63	0.68	0.69	0.69	0.87	0.60	0.73	0.75	0.71	0.89
Specificity	0.63	0.68	0.69	0.84	0.86	0.60	0.73	0.76	0.85	0.89
F1_Score	0.67	0.69	0.71	0.75	0.91	0.70	0.73	0.74	0.83	0.86
Negative Predictive Value (NPV)	0.68	0.69	0.72	0.77	0.85	0.71	0.73	0.81	0.83	0.89
False Negative Rate (FNR)	0.30	0.21	0.20	0.15	0.10	0.24	0.20	0.17	0.13	0.08
False Positive Rate (FPR)	0.39	0.31	0.29	0.19	0.12	0.20	0.19	0.16	0.10	0.08

Fig. 4 illustrates the comparison metrics as mentioned in Table II and Table III, for proposed approach with the existing approaches. In this the existing approach such as LSTM, SVM, ANN, and RF are compared with the proposed approach of hybrid two-stage LSTM-SVM. It is observed that hybrid two-stage LSTM-SVM performs well in comparison with approaches.

Table III illustrates the comparison of performance metrics for incremented classes and features on the proposed model.

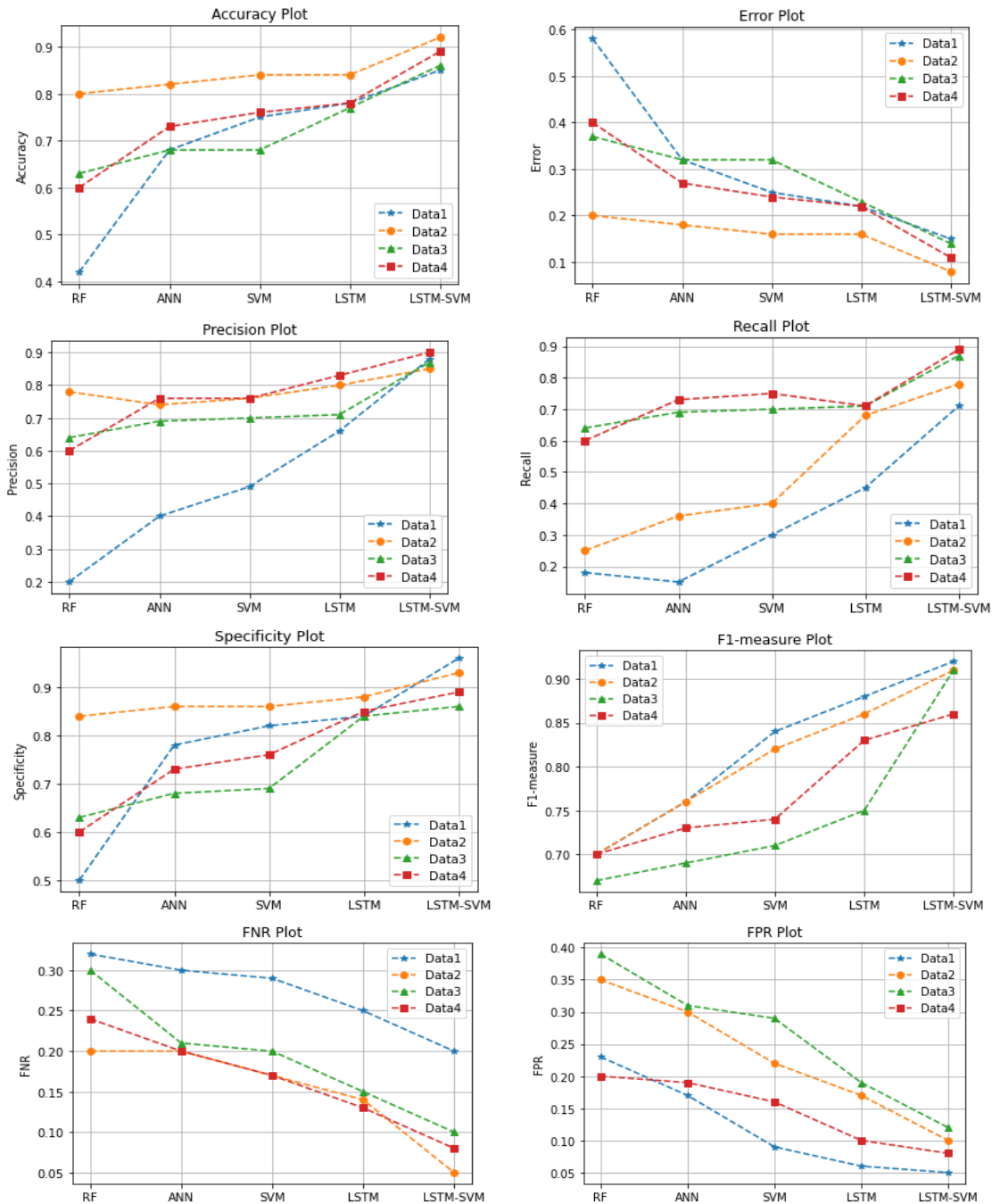


Fig. 4. Comparison of Accuracy, Error, Precision, Recall, Specificity, F1-Measure, FNR and FPR Metric.

Fig. 5 illustrates the accuracy comparison of incremented values for the proposed model. In this figure, the performance metrics for three class 50 features is smaller compared to incremented three class 75 features. The performance metrics of the incremented five class 50 features is smaller compared to the five class 75 features. From this, the incremented class and features of the proposed model attains a best performance metrics.

TABLE III. COMPARISON OF PERFORMANCE METRICS FOR INCREMENTED CLASSES AND FEATURES ON THE PROPOSED MODEL

Proposed method	3 class with 50 features	3 class with 75 features	5 class with 50 features	5 class with 75 features
Accuracy	0.895	0.99	0.85	0.88
Error	0.11	0.01	0.15	0.12
Precision	0.83	0.98	0.51	0.61
Recall	0.80	0.98	0.53	0.63

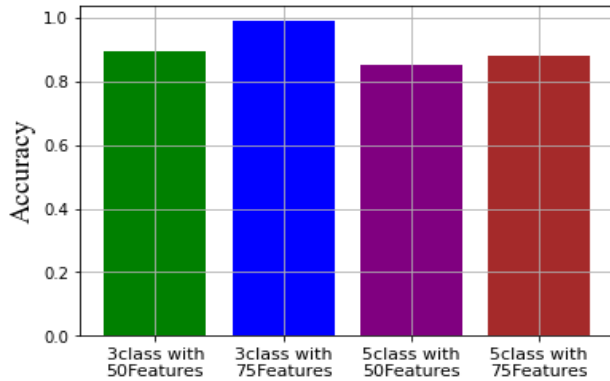


Fig. 5. Comparison of Accuracy Metrics for Incrementing Features and Incrementing Classes.

V. CONCLUSION

This paper aims to design best sentiment analysis for social media posts and review comments. Many researchers are trying to utilize the large datasets for sentiment analysis but the performance of conventional techniques is not satisfactory. In this technique, features are extracted and converted by the countvectorizer, then for classification a hybrid two-stage LSTM-SVM model is used to predict sentiments. The proposed hybrid two-stage algorithm is validated and compared with the state-of-the-art existing sentiment classification technique. The comparison analysis revealed that the proposed model has excellent performance metrics. The accuracy of the proposed model varies according to the incremental leaning, the accuracy for three class 50 and 75 features is 89 and 99 then, the accuracy for five class 50 and 75 features is 85 and 88. This analysis reveals that the incremented class and features attain a better accuracy.

REFERENCES

[1] Kurnia, Rafly, Y. Tangkuman, and A. Girsang. "Classification of user comment using word2vec and svm classifier." *Int. J. Adv. Trends Comput. Sci. Eng* 9, no. 1 (2020): 643-648.

[2] Xu, Dongliang, Zhihong Tian, Rufeng Lai, Xiangtao Kong, Zhiyuan Tan, and Wei Shi. "Deep learning based emotion analysis of microblog texts." *Information Fusion* 64 (2020): 1-11.

[3] Apte, Prathamesh, and Saritha Sri Khetwat. "Text-based emotion analysis: feature selection techniques and approaches." In *Emerging Technologies in Data Mining and Information Security*, pp. 837-847. Springer, Singapore, 2019.

[4] Kratzwald, Bernhard, Suzana Ilić, Mathias Kraus, Stefan Feuerriegel, and Helmut Prendinger. "Deep learning for affective computing: Text-based emotion recognition in decision support." *Decision Support Systems* 115 (2018): 24-35.

[5] Krommyda, Maria, Anastasios Rigos, Kostas Bouklas, and Angelos Amditis. "An experimental analysis of data annotation methodologies

for emotion detection in short text posted on social media." In *Informatics*, vol. 8, no. 1, p. 19. MDPI, 2021.

[6] Haryadi, Daniel, and Gede Putra Kusuma. "Emotion detection in text using nested long short-term memory." *International Journal of Advanced Computer Science and Applications* 10, no. 6 (2019).

[7] Rajasegaran, Jathushan, Munawar Hayat, Salman Khan, Fahad Shahbaz Khan, and Ling Shao. "Random path selection for incremental learning." *Advances in Neural Information Processing Systems* 3 (2019).

[8] Yang, Li, Ying Li, Jin Wang, and R. Simon Sherratt. "Sentiment analysis for E-commerce product reviews in Chinese based on sentiment lexicon and deep learning." *IEEE access* 8 (2020): 23522-23530.

[9] Jagdale, Rajkumar S., Vishal S. Shirsat, and Sachin N. Deshmukh. "Sentiment analysis on product reviews using machine learning techniques." In *Cognitive informatics and soft computing*, pp. 639-647. Springer, Singapore, 2019.

[10] Nguyen, Heidi, Aravind Veluchamy, Mamadou Diop, and Rashed Iqbal. "Comparative study of sentiment analysis with product reviews using machine learning and lexicon-based approaches." *SMU Data Science Review* 1, no. 4 (2018): 7.

[11] Muhammad, Waqar, Maria Mushtaq, Khurum Nazir Junejo, and Muhammad Yaseen Khan. "Sentiment analysis of product reviews in the absence of labelled data using supervised learning approaches." *Malaysian Journal of Computer Science* 33, no. 2 (2020): 118-132.

[12] Bose, Rajesh, Raktim Kumar Dey, Sandip Roy, and Debabrata Sarddar. "Sentiment analysis on online product reviews." In *Information and Communication Technology for Sustainable Development*, pp. 559-569. Springer, Singapore, 2020.

[13] Almestekawy, Abdulwahab, and Mustafa Abdulsalam. "Sentiment analysis of product reviews using bag of words and bag of concepts." *International Journal of Electronics and Information Engineering* 11, no. 2 (2019): 49-60.

[14] Güner, Levent, Emilie Coyne, and Jim Smit. "Sentiment analysis for amazon. com reviews." *Big Data in Media Technology (DM2583) KTH Royal Institute of Technology* 9 (2019).

[15] Tang, Duyu, and Meishan Zhang. "Deep learning in sentiment analysis." In *Deep learning in natural language processing*, pp. 219-253. Springer, Singapore, 2018.

[16] Londhe, Alka, and Pvrđ Prasada Rao. "Platforms for big data analytics: Trend towards hybrid era." In *2017 International Conference on Energy, Communication, Data Analytics and Soft Computing (ICECDS)*, pp. 3235-3238. IEEE, 2017.

[17] Fu, Xianghua, Jingying Yang, Jianqiang Li, Min Fang, and Huihui Wang. "Lexicon-enhanced LSTM with attention for general sentiment analysis." *IEEE Access* 6 (2018): 71884-71891.

[18] Londhe, Alka, and P. V. R. D. Rao. "Aspect Based Sentiment Analysis–An Incremental Model Learning Approach Using LSTM-RNN." In *International Conference on Advances in Computing and Data Sciences*, pp. 677-689. Springer, Cham, 2021.

[19] Long, Fei, Kai Zhou, and Weihua Ou. "Sentiment analysis of text based on bidirectional LSTM with multi-head attention." *IEEE Access* 7 (2019): 141960-141969.

[20] Khanvilkar, Gayatri, and Deepali Vora. "Sentiment analysis for product recommendation using random forest." *International Journal of Engineering & Technology* 7, no. 3 (2018): 87-89.

[21] Can, Ethem F., Aysu Ezen-Can, and Fazli Can. "Multilingual sentiment analysis: An RNN-based framework for limited data." *arXiv preprint arXiv:1806.04511* (2018).

[22] AnithaElavarasi, S., J. Jayanthi, and N. Basker. "A comparative study on logistic regression and svm based machine learning approach for analyzing user reviews." *Turk. J. Physiother. Rehabil* 32 (2021): 3564-3570.

[23] Londhe, Alka, and P. V. R. D. Rao. "Incremental Learning Based Optimized Sentiment Classification using Hybrid Two-Stage LSTM-SVM Classifier" In *International Journal of Advanced Computer Science and Applications*, in Press.

[24] Onan, Aytuğ. "Sentiment analysis on product reviews based on weighted word embeddings and deep neural networks." *Concurrency and Computation: Practice and Experience* 33, no. 23 (2021): e5909.

- [25] Rhanoui, Maryem, Mounia Mikram, Siham Yousfi, and Soukaina Barzali. "A CNN-BiLSTM model for document-level sentiment analysis." *Machine Learning and Knowledge Extraction* 1, no. 3 (2019): 832-847.
- [26] Murthy, G. S. N., Shanmukha Rao Allu, Bhargavi Andhavarapu, Mounika Bagadi, and Mounika Belusonti. "Text based sentiment analysis using LSTM." *Int. J. Eng. Res. Tech. Res* 9, no. 05 (2020).
- [27] Agarap, Abien Fred. "Statistical analysis on E-commerce reviews, with sentiment classification using bidirectional recurrent neural network (RNN)." *arXiv preprint arXiv:1805.03687* (2018).
- [28] Sentiment Labelled Sentences Data Set - <https://archive.ics.uci.edu/ml/datasets/Sentiment+Labelled+Sentences> accessed on 2-Jan-2022.
- [29] Large Movie Review Dataset - <https://ai.stanford.edu/~amaas/data/sentiment/> accessed on 2-Jan-2022.
- [30] Amazon product data - <https://cseweb.ucsd.edu/~jmcauley/datasets.html> accessed on 2-Jan-2022.
- [31] Yelp restaurant review dataset - url: <https://www.yelp.com/dataset> accessed on 2-Jan-2022.
- [32] Alamoudi, Eman Saeed, and Norah Saleh Alghamdi. "Sentiment classification and aspect-based sentiment analysis on yelp reviews using deep learning and word embeddings." *Journal of Decision Systems* 30, no. 2-3 (2021): 259-281.
- [33] Campos, Ricardo, Vítor Mangaravite, Arian Pasquali, Alípio Mário Jorge, Célia Nunes, and Adam Jatowt. "Yake! collection-independent automatic keyword extractor." In *European Conference on Information Retrieval*, pp. 806-810. Springer, Cham, 2018.

Data Recovery Approach with Optimized Cauchy Coding in Distributed Storage System

Snehalata Funde*, Gandharba Swain

Department of Computer Science and Engineering
Koneru Lakshmaiah Education Foundation
Vaddeswaram-522302, Guntur, Andhra Pradesh, India

Abstract—In the professional world, the impact of big data is pulsating to change things. Data is currently generated by a wide range of sensors that are part of smart devices. It necessitates data storage and retrieval that is fault tolerant. Data loss can be caused by natural calamities, human error, or mechanical failure. Several security threats and data degradation attacks attempt to destroy storage disks, causing partial or complete data loss. The data encoding and data recovery mechanisms is proposed in this research. To produce a set of matrices utilizing matrix heuristics, the suggested system proposes an efficient Optimized Cauchy Coding (OCC) approach. In this paper, the Cauchy matrix is used as a generator matrix in Reed Solomon (RS) code to encode data blocks with fewer XOR operations. It reduces the encoding algorithm's time complexity. Furthermore, in the event of a disk failure, missing data from any data block is made available through the Code word. In terms of data recovery, it outperforms the Optimal Weakly Secure Minimum Storage Regenerating (OWSPM-MSR) and Product-Matrix Minimum Storage Regenerating (PM-MSR) methods. For data coding, a 1024KB file with various combinations of data blocks l and parity blocks m is evaluated. In the first scenario, m is 1 and l ranges from 4 to 10. The value of l is 4 in the second scenario, while m ranges from 1 to 10. The existing OWSPM-MSR approach takes an average of 0.125 seconds to encode and 0.22 seconds to decode, whereas the PM-MSR approach takes an average of 0.045 seconds to encode and 0.16 seconds to decode. The proposed OCC approach speeds up data coding by taking an average of 0.035 seconds to encode and 0.116 seconds to decode data.

Keywords—Optimized cauchy coding; fault tolerant; data availability; reed solomon code

I. INTRODUCTION

Nowadays, social media is the primary source of data generation that we refer to as "big data," and it generates tremendous amounts of data. It is both enormous in size and intricate in nature. As a result of the current pandemic crisis, the use of the internet and smart phones is increasing every day. As a result, numerous businesses generate a high volume of records in the Petabyte or Exabyte range. Traditional systems are limited in their ability to capture, store, and analyze such large amounts of data, according to Wang et al. [1]. Large datasets can now be stored, compiled, and evaluated because of advancements in processing and storage capabilities. Big data analytics offers novel approaches to analyzing massive datasets. Few applications are rigorously found in the domains of healthcare, finance, traffic management, education, and retail [2]. Furthermore, the

increase in data necessitates attention to several difficulties such as privacy, integrity, and access control, all of which are required to protect data from various attacks such as data degradation attacks and man-in-the-middle attacks. The current research uses a Cauchy matrix generation method to build and create models that can be used to manage data recovery for dispersed datasets.

Yang et al. [3] describe a multi-cloud storage system that optimizes security and affordability. Chervyakov et al. [4] proposed a distributed data storage system for processing encrypted data and controlling calculations. Furthermore, the Redundant Residue Number System is used to discover and remedy errors. For distributed cloud storage, a block chain approach to security architecture is being investigated. Li et al. [5] used a genetic algorithm to solve file block duplication among numerous users and data centers. Bhuvaneshwari & Tharini [6] argue that scalable and dependable distributed storage systems are essential due to the growing volume of data. For massive data storage, Low Density Parity Check (LDPC) codes are being investigated. Tang & Zhang [7] demonstrate how a Vander-monde matrix is concatenated with an identity matrix to ease encoder and decoder design. Furthermore, in bit matrices of the Cauchy matrix, several finite fields are explored to decrease one. Erasure-resilient codes are Cauchy Reed-Solomon (RS) codes. Makovenko et al. [8] describe the use of heuristic perturbation to optimize coding bit-matrices for fault tolerant data storage. The ability to serve multiple clients at the same time is one of the most significant requirements of cloud storage solutions. The help rate region is a new addition to the map. Kazemi et al. [9] defines a Quality of Service (QoS) metric for coded, distributed setups. It's a collection of information access requests that the system manages all at once.

Dai & Boroomand [10] offered a combination of big data and man-made consciousness technologies to improve security by detecting attacks on internet-connected devices. Ravikumar & Kavitha [11] demonstrate how to use adaptive hybrid mutation to optimize a black widow clustering approach. To improve remote sensing retrieval mechanisms, Li & Zhang [12] propose widely open datasets with evaluation metrics. Xiao & Zhou [13] propose classifiers based on resource optimization and framework to minimize data repair and update concerns in erasure coding schemes. Gong & Sung [14] introduce zig-zag codes as erasure codes for data decoding. The dependability vs. storage trade-off is examined. Dau et al. [15] consider the Cauchy and Vander-monde

*Corresponding Author.

matrices while constructing maximum distance separable codes to tackle coding challenges. This method is used to select arbitrary Vander-monde/Cauchy matrix evaluation points. It necessitates the use of very small finite fields. The dimensions of the generator matrix are polynomial. Additional design limitations are implemented, rendering the Vander-monde/Cauchy matrix ineffective for code construction. Wu et al. [16] show how to use Cauchy RS codes to improve the efficiency of distributed storage systems. It starts by calculating the best post scaling encoder matrix based on the data migration policy. Following that, the data transfer process is optimized using the chosen post scaling encoder matrix. The Solomon code protocol for multi-party authentication is thought to improve the security of the system. When data is large, it can be difficult to construct Solomon code as matrix creation since it takes a long time. Another difficulty with several portions is space complexity. Information is securely stored in a wireless network using both local and geographic replication. It aids in the recovery after a disaster. Zhang et al. [17] discuss the architecture, as well as resource supply and replication technologies. It reduces the time it takes to deploy software and increases customer adoption. The disadvantage is that it necessitates a larger development pool.

Chen & Ma [18] present a disk recovery strategy that is both efficient and cost-effective. It decreases the amount of data that is read from the disk. Furthermore, the workload quantity on all surviving disks is the same. To recover the failed disk, only a few disk reads are needed. Recovery of all the data takes a long time. Shen et al. [19] demonstrate how to determine the optimal number of code word pictures for any XOR-based erasure code. It produces recapture rosters with the least amount of data possible. It also improves I/O performance for cloud document frameworks that use large square sizes. For the length of recuperation, it reduces the amount of data read. Its drawback is that it necessitates a significant amount of area. On database servers, it causes a heating problem. Burihabwa et al. [20] suggest using a flat XOR-code for data recovery. Recovery schedules are also generated. As a result, the execution time is minimized. Periodic system backup is not included in this system's configuration. Hadoop is a platform for storing and analyzing massive data sets. Hadoop Distributed File System (HDFS) is used to store the large amount of data. Partitioning a large record into blocks is considered a block position strategy. Following that, it was assigned to the homogenous cluster. Shah & Padole [21] offer a novel approach to updating the information blocks on explicit hubs. Total nodes are split into two categories: homogenous and heterogeneous, and high and low performing nodes. It improves node burden revision. Its drawback is that it requires a capacity approach that can work on both homogeneous and heterogeneous clusters. It requires apps that can run in a diverse and homogenous environment in a short amount of time.

Information is stored in a NoSQL database in a hub-like way. As a result, the information becomes skewed. These data sets should store information that is extremely accessible. It also has no reservations about the parcel's adaptability and durability. Pandey [22] introduces this strategy for balancing load in a circulating environment. It divides data into small

parts, making it easier to move things around on their own. As erasure codes, Cauchy RS codes are gaining in use. It is preferred in Redundant Array of Independent Disks (RAID) arrays that use Solid-State Drives (SSDs). The use of Galois Field (GF) math to accomplish matrix-vector multiplication is necessary for such coding on a processor-based RAID regulator. The erasure coding performance of resistive RAM (ReRAM) can be improved. RAID controllers and SSD controllers use it as core memory. The Cauchy-Vandermonde matrix is used by Han et al. [23] as the encoding generating matrix. SSDs are used to distribute rebuilding efforts for a single failure. It boosts the speed of encoding and decoding. More memory accesses result from increased computation complexity. It has a high level of durability while requiring less storage space. To improve failure recovery performance, Xu et al. [24] introduce a PBD-based Data Layout (PDL). In the event of part failures, it clearly gives superior assistance to front-end applications. For mixed erasure codes, it provides a uniform data layout. Each lump containing different symbols from a coding strip resides in a different node and on a different disk in distributed storage. Pirahandeh & Kim [25] present a scalable, multisector scheduler that allows for three levels of adaptability to non-critical failure over time, plates, and nodes. It can now recover from multiple levels of failure. The innermost assembly of each node, which consists of total disks and segments for each node, is alarming. It raises encoder and decoder average performance. It has been determined that it is suitable for use in a distributed storage environment that is adaptive. To determine parity chunks, our approach uses fewer XOR tasks. It provides a consistent information layout for integrated Erase Code (EC).

The rest of the paper is written in the following format. The related work is discussed in Section II. The proposed Optimized Cauchy Coding (OCC) method is detailed in Section III. The evaluation findings are given in a real-time scenario in Section IV. The proposed OCC system benefits and potential scope are summarized in Section V.

II. RELATED WORK

A. Related Work

This section discusses relevant work in the data storage domain for fault tolerant systems that addresses time, space, and complexity issues in matrix formation.

In light of the equipment execution system for decoding, Wu et al. [26] suggested a novel high-speed Cauchy algorithm to construct an encoding calculation. To achieve the same results as Cauchy, this technique requires a less sophisticated calculating process. Ca-Co, a useful Cauchy coding method for information storage in distributed systems, was proposed by Zhang et al. [27]. To produce a scheduling sequence, it uses a Cauchy matrix with XOR operations. In comparison to existing systems, the system provides an effective data storage approach. It can quickly generate a Ca-Co matrix using the XOR operation. Tang & Cai [28] offer a novel erasure decoding approach. To protect against capacity node disappointments, erasure coding is preferred in the appropriate stockpiling framework. The data is first separated into data blocks, which are then coded to create encoding blocks. The decoding method is used to recover the lost data blocks. In

light of the changing system of the translating change matrix, the decoding failures are acknowledged. Erasure coding improves interpreting effectiveness while requiring less bandwidth for modernization. The hypothetical examination, on the other hand, demonstrates the method's accuracy. The system of data restoration benefits from available erasure-coded data insertion strategies. To recover data, the operator first replaces all unproductive nodes with one new node. The Node Replacement Process (NRP) takes hours or days in practice. Due to the lack of durability, the enhanced statistics are lost once more. Information accessibility and dependability are maintained by a few methods in circulating record systems.

The Erasure Coding (EC) method is popular for increasing space efficiency. It has incalculable execution encoding, decoding, and input/yield corruption elements in general. Kim [29] proposes a buffering and joining method in which several I/O demands that occur during encoding are combined and treated as one. It offers four recovery options for distributing the disk input/yield loads generated during decoding. Erasure coding is a generally complex technology used in the allocated storage framework to protect against capacity node disk failure. It improves resilience while also reducing repetitiveness. First, the data is separated into b chunks. The encoding technique is then used to convert the b blocks into c blocks. The decoding technique recovers the $c - b$ blocks that were missed. Clients of distributed storage typically assign different redundancy configurations to the repetitiveness settings (b , c , and d) of EC. It is based on the perfect balance of execution and internal failure adaption. This work aids in the observation of a very low likelihood encoding approach for a design with available configurations that produces superior results. With low data repetition, EC codes are used in the cloud. Just a hypothetical investigation demonstrates the Ca-Co technique's accuracy.

The Optimal Weakly Secure Minimum Storage Regenerating (OWSPM-MSR) [31] approach was proposed by Bian et al. Its implementation is based on Jerasure, and the test was run on a Linux machine with an Intel Core i5 CPU and 4GB RAM. A Galois field size of 28 and a block size of 1024 are used in the implementation. They compared many factors, such as calculation time and storage overhead, with the previous system. This method use the Cauchy-network based RS coding algorithm. Over constrained fields, division and multiplication may be converted into subtraction and addition tasks, and they can be recognized by XOR tasks. Furthermore, they calculated the aforementioned during data recovery in terms of translating time. In the most pessimistic case, it takes a little longer than Product-Matrix Minimum Storage Regenerating (PM-MSR). The time between techniques became longer as the number of data blocks (k) and parity blocks (p) increased (m). Because it takes longer to invert a matrix, the time consumed by the OWSPM-MSR approach is longer than the time necessary to encode the data.

Shah et al. [32] proposed a technique which is based on a product matrix structure. PM-MSR uses the Vandermonde network to reconstruct information that has been lost due to a disc crash. Two special characteristics of the Product-Matrix structure make the codes used in this system desirable from a

security standpoint. For starters, several standards in the literature, including those in, take functional repair into account. The data placed in the replacement node might vary from the data stored in the failed node in this form of repair as long as the replacement node meets the system's rebuilding and appropriate working requirements. This enables a snoop to get a greater amount of data by examining the information stored in a core over several instances of repair. PM codes, on the other hand, provide a precise fix, with information stored in the substitute node indistinguishable from that stored in the bombed node. Second, regardless of whether the fix is exact, the information downloaded during the repair of a given server may be dependent on the arrangement of n nodes cooperating in the maintenance with handling, and therefore may alter between fixes of that node. By default, the PM system ensures that the data retrieved by the substitute node is independent of the helper nodes' personalities. The Vandermonde-based has a high level of complexity in terms of duplication and division in a Galois field, resulting in a long calculation time.

The approach proposed by Wang et al. [30] involves replacing some submatrices of the polarizing change with networks on the decoder side, resulting in a less difficult evaluation of log-probability proportions. This strategy allows for a reduction in complexity for the sequential termination, list, and successive translation calculations. Later, it was suggested that an improved decoding technique for polar codes with large kernels be used. It entails replacing the instances of large kernels in the polarizing change with more straightforward frameworks in a specified way. The methodology does not require any sideways encoder enlargements and has no effect on decoder operation. It can also be used in conjunction with list and consecutive translation calculations. For efficient polar codes, many encoding computations are addressed. In comparison to previous non-recursive algorithms, an improved encoding approach reduces the number of calculations due to an iterative property of the generating matrix and a specific lower three-sided design of the lattice. When compared to current non-recursive approaches, it reduces the number of XOR processing units, which is advantageous for numerous executions over existing algorithms. Many limiting or figure units haven't been changed. This makes the framework less stable.

B. Problem Identification

In the above related work, many techniques are introduced to find a way to deal with fault tolerance with Cauchy matrix in combination with RS code. Several existing approaches require a long computation time to conduct XOR operations in encoding and decoding user data. In existing work, erasure codes like Cauchy RS use Galois Field (GF) to accomplish matrix-vector multiplication, which causes CPU overhead due to an exponential increase in read/write operations. We present an Optimized Cauchy Coding method with RS coding to overcome this problem. Proposed method makes it easier to create Cauchy matrices because it reduces the number of XOR operations in data recovery.

C. Research Contribution

The main objectives of this paper are as per the following:

- To reduce the number of read/write operations in the encoding process while storing data in a distributed environment with a certain redundancy configuration.
- To minimize XOR operations for various combinations of matrices as well as schedule fewer iterations for data recovery on the data blocks with logarithmic functions.
- To handle unnecessary resource utilization problems in a distributed environment, replica formation of the same block is replaced with a single block with fault tolerance ability to recover data.

III. METHODOLOGY

The Optimized Cauchy Coding (OCC) technique proposed is based on RS coding. The OCC paradigm for data recovery is depicted in Fig. 1. The encoding and decoding procedure here involves a number of different entities.

The entities engaged in the coding process are listed below:

- 1) Client
- 2) Data files
- 3) Data blocks
- 4) Parity blocks
- 5) Server nodes

In the block diagram of OCC approach at first when a client wants to write a data file, the write data request will first

travel via the encoding block, where the files from the client side F1, F2, F3, and F4 can be written on server nodes.

The source file that the client wants to write on the server node will no longer be written in the original format of the source data file, but will instead be translated into a different format to secure the data. The encoding procedure encodes the file received from the client to make the system fault resistant and increases data availability in the event of a disk failure. To produce a check matrix, the OCC technique examines redundancy configurations (l, m, n) during the encoding process. The number of data blocks is represented as one, the number of parity blocks is represented as m, and the number of coding unit bits per word is represented as n in this system. The experiment considers the trade-off between matrix creation time and resource utilization. In a distributed environment, the system is emulated. XOR operations are used to produce each Ca-Co coding matrix for each chunk. Cauchy matrices are built on GF. Using the Cauchy matrix and XOR operations, GF additions and multiplications are also minimized. In terms of time, the Cauchy matrix density determines encoding performance. Algorithm 1 explains the check matrix construction process. Data blocks and parity blocks for the input files will be written on the servers S1 through S6 after the encoding procedure is completed. When clients want to read the files, the data is decoded by the decoding process. If any data blocks are missing, the data can be recovered using the decoding process, which uses the check matrix established during the encoding process to reassemble the data.

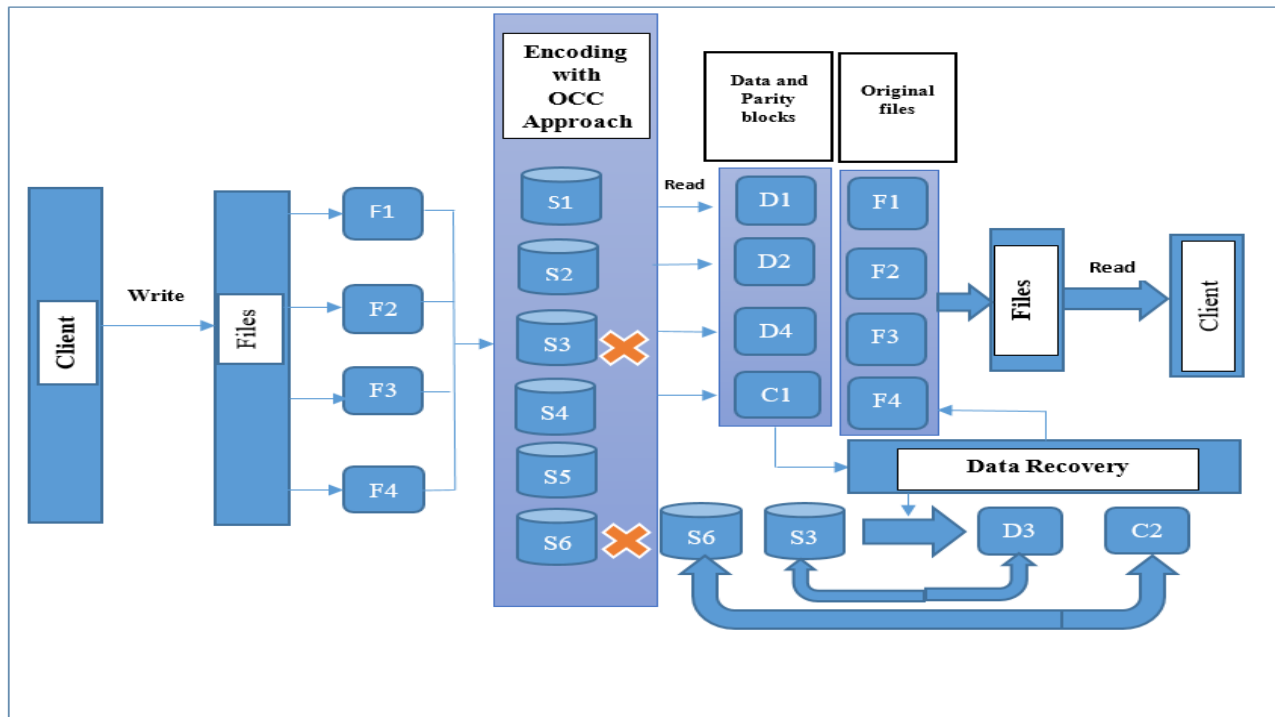


Fig. 1. OCC Data Recovery Approach.

The suggested method lets users control their access in a safe and private way. Algorithm 1 shows how to make an optimized Cauchy matrix and encode data blocks in a data write operation in a step-by-step way.

The proposed OCC data recovery technique converts the Cauchy encoding entities into Boolean form and stores them as a binary matrix. Further binary XOR operations are performed for the elements obtained from Galois Field $GF(2^n)$. It helps in reducing the time complexity of XOR calculations. Here in the encoding algorithm, three parameters l , m and n are considered to generate the Cauchy matrix, where l is the number of data blocks, m is the number of parity blocks and n is the coding unit bits per word.

Algorithm 1: OCC encoding algorithm

Input: $\{l, m, n\}$ where $l = \text{data blocks}$, $m = \text{parity blocks}$ and $n = \text{coding unit bits per word}$

Output: Code word check matrix

The following are the steps for the encoding strategy.

Step 1: We need to generate elements of $GF(2^n)$ with the help of specific polynomial then generate its binary form matrix. So first we need to generate polynomial to generate a $GF(2^n)$.

For different value of n different polynomials are there as below. If we have prime polynomial of degree n over $GF(2)$ then $GF(2^n)$ can be constructed. For $n = 3$ generate $GF(2^3)$ from $GF(2)$ using prime polynomial $p(x) = x^3 + x + 1$.

To calculate elements of $GF(2^3)$: As $p(x) = x^3 + x + 1$, polynomial elements over $GF(2^3)$ is as below:

$$GF(8) = GF(2^3)$$

z^0	1
z^1	z
z^2	z^2
z^3	$z + 1$
z^4	$z^2 + z$
z^5	$z^2 + z + 1$
z^6	$z^2 + 1$
$z^7 \equiv z^0$	1

This shows set of elements generated on $GF(2^n)$ using polynomial.

As per binary matrix rules $BM(d)$ is generated using d elements of polynomial and coefficient vector $V(d)$.

Step 2: Generate a Cauchy coding matrix.

In the binary Cauchy coding matrix, the count of ONES decides how many operations of XOR will be required. A lower number of ONES yields better performance. In this matrix generation, the Cauchy Good (CG) method is used for enhancing the performance because the generated matrix will have a lower number of ONES as compared to other heuristic methods.

With the help of CG, constructing the Cauchy matrix, which is defined as MG. Furthermore, we divide each element of MG, as in column j by $MG_{0,j}$: MG is modified and row 0 elements are all ONES. For other rows like row i , present number of ONES are calculated which are considered as N . Further by dividing row i , elements by $MG_{i,j}$ and record the number of ONES count, which is represented as $N_j (j \in [0, l - 1])$.

Select a minimum of $\{N_0, N_1, \dots, N_{l-1}\}$ which generates CG position one. Repeat step 2 for the remaining matrix elements of CG.

Step 3: Expand the Cauchy coding matrix of size $l \times m$ to the binary matrix of size $ln \times mn$. Consider the extended matrix as a matrix E .

Step 4: Create an array.

Divide m data blocks into n parts similar to d_1, d_2, \dots, d_m into $d_{1,1}, d_{1,2}, \dots, d_{m,n}$.

$$C = E \times D$$

$$C = \begin{bmatrix} E_{1,1} & E_{1,2} & \dots & E_{1,mn} \\ E_{2,1} & E_{2,2} & \dots & E_{2,mn} \\ \vdots & \vdots & \vdots & \vdots \\ E_{ln,1} & E_{ln,2} & \dots & E_{ln,mn} \end{bmatrix} \times \begin{bmatrix} d_{1,1} \\ d_{1,2} \\ \vdots \\ d_{m,n} \end{bmatrix} = \begin{bmatrix} C_{1,1} \\ C_{1,2} \\ \vdots \\ C_{l,n} \end{bmatrix} \quad (1)$$

$$C_{1,1} = (E_{1,1} \cdot d_{1,1}) \oplus (E_{1,2} \cdot d_{1,2}) \oplus (E_{1,mn} \cdot d_{m,n})$$

The result array is as below:

$$R1 = \begin{bmatrix} d_{1,1} & d_{2,1} \dots & d_{m,1} C_{1,1} & C_{2,1} \dots & C_{m,1} \\ d_{1,2} & d_{2,2} \dots & d_{m,2} C_{1,2} & C_{2,2} \dots & C_{m,2} \\ \vdots & \vdots & \vdots & \vdots & \vdots \\ d_{1,n} & d_{2,n} \dots & d_{m,n} C_{1,n} & C_{2,n} \dots & C_{l,n} \end{bmatrix} \quad (2)$$

Further XOR operations are calculated then sorted. Further result is replaced with new data as $R2$.

Algorithm 2 shows how to write data to a cloud storage service using the OCC approach.

Algorithm 2: Data recovery algorithm

Input: Code word check matrix

Output: Plain text

Step 1: The client sends a request to the server for data extraction.

Step 2: The decoding matrix generation phase.

As $R1$ has been partitioned into the blocks of $(m + 1) \times n$ and matrix $BM(d)$ which has $(m + 1) \times n \times (m + 1) \times n$ in size is formed.

$$BM(d) = \frac{\text{Identity matrix} \mid \text{Zero matrix}}{\text{Parity matrix of } R1} \quad (3)$$

Step 3: Evaluate the missing data blocks.

i: When a data node fails, the information for the whole segment is lost. So while re-establishing information, a relating list L of missing components is made for the missing node.

ii: The component d in the missing component list L is iterated through. Assuming it has a place in the data component; continue to step iii.

If it has a place in the redundant component, skip it.

iii: The r is the row set whose element d is one in the parity check matrix H . Assume that there is no component in r , set row d to zero. In case there is a component in r , then, at that point, we select the row with the little load of hamming subsequent to eliminate the missing component from r as r_1 . The row corresponding to the component in r and the row d performs XOR with r_1 and r_1 is set to 0.

iv: After handling each component of the list L , the values in the column corresponding to the redundant components in the list can be set to zero.

Step 4: Data recovery phase

Now, line r_d is an analogous row to the component d of the missing component list with the name L which is the relating matrix $BM(d)$. C_d is a set of columns with 1 in r_d . The information block relating to the component in C_d is the data block expected for restoring the component d .

As per the above component list with the name L and the binary matrix $BM(d)$, all missing records can be recovered as before. Lost data can be recovered with XOR operations with available dataset.

IV. RESULT

This section examines performance in terms of the amount of time it takes to encode and decode data in a distributed system. The requirement to run a test-engine to evaluate system performance is shown in Table I.

At the output, it encodes these data blocks into m parity blocks. The storage system is resistant to numerous disk failures in this case. The OCC code works with binary data. Each word consists of n bits such that $2^n \geq 1 + m$. For data encoding, redundancy configuration (l, m, n) varies by keeping different combinations of data blocks and parity blocks.

TABLE I. SYSTEM REQUIREMENT

Particulars	Specifications
CPU with RAM	Pentium 2.5 GHz with 4 GB RAM
Language	Java
Operating system	Linux

The work of the proposed system is compared to that of the present system in terms of encoding and decoding times, utilizing various redundancy configurations. Encoding time refers to the time it takes to convert the contents of a file into a specified format that allows data to be securely sent and stored in a specific data node. The time it takes to convert an encoded data sequence back to its native format is known as decoding time. Table II demonstrates the time necessary to code files ranging in size from 1MB to 50MB using the proposed OCC coding technique in seconds.

TABLE II. ENCODING AND DECODING TIME FOR VARIOUS SIZE INPUT FILE FOR PROPOSED OCC (L=10, M=20)

File size	Encoding Time	Decoding Time
1 MB	0.12	0.145
5 MB	0.26	0.31
10 MB	0.54	1.3

In the event of a disk failure, Table III outlines the various criteria, such as data availability, recoverability, efficiency, and storage overhead. It displays great data availability, high recoverability, and high efficiency for the inputs $l = 4$ and $m = 1$. For the same arrangement, the storage overhead is minimal. The amount of storage space required grows as the number of parity blocks grow.

TABLE III. PERFORMANCE ANALYSIS OF PROPOSED OCC FOR VARIOUS INPUT PAIR VALUES (L, M)

Encoding	Availability	Recoverability	Efficiency	Storage Overhead
$l=4, m=1$	High	High	High	Low
$l=5, m=1$	High	High	Medium	Low
$l=6, m=1$	High	High	High	Low
$l=7, m=1$	High	High	High	Medium
$l=4, m=2$	High	High	High	Low
$l=4, m=3$	High	Medium	High	Low
$l=4, m=4$	High	High	Medium	Low
$l=4, m=5$	High	Medium	Low	High

V. DISCUSSION

Table IV demonstrates the encoding time required for various ways to encode the data when different numbers of data blocks ($l = 4$ to $l = 10$) and parity block ($m = 1$) are examined. For comparison of the proposed OCC with the existing approaches of Optimal Weakly Secure Minimum Storage Regenerating (OWSPM-MSR) [31] and Product-Matrix Minimum Storage Regenerating (PM-MSR) [32], a total of seven different combinations are evaluated.

TABLE IV. ENCODING TIME FOR VARIOUS NUMBER OF DATA BLOCK (L)

Techniques	Encoding Time(s)						
	$l=4, m=1$	$l=5, m=1$	$l=6, m=1$	$l=7, m=1$	$l=8, m=1$	$l=9, m=1$	$l=10, m=1$
OWSPM-MSR	0.0065	0.0065	0.0082	0.0119	0.0125	0.0119	0.0135
PM-MSR	0.0065	0.0077	0.039	0.053	0.098	0.27	0.38
Proposed OCC	0.006	0.0063	0.008	0.0084	0.009	0.0096	0.01

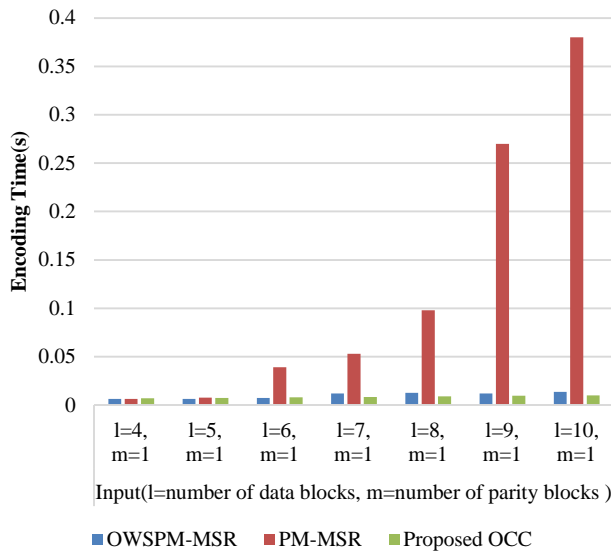


Fig. 2. Comparison of Encoding Time with Various Number of Data Blocks.

Fig. 2 depicts an encoding time plot, with the X axis representing input and the Y axis representing encoding time for a single input. The inputs are the number of data blocks ($l = 4$ to 10) and the number of parity blocks ($m = 1$). The OCC encoding procedure outperforms the previous OWSPM-MSR and PM-MSR algorithms for various combinations of one and m . Fig. 3 depicts an encoding time plot, with the X axis representing input and the Y axis representing encoding time for a single input. The number of data blocks ($l = 4$) and the number of parity blocks ($m = 1$ to 10) are used as inputs. The OCC encoding procedure outperforms the previous OWSPM-MSR and PM-MSR algorithms for various combinations of l and m .

Table V shows the encoding time required for various approaches to encode the data when $m = 1$ to $m = 10$ parity

blocks and data blocks $l = 4$ are examined. For comparison of the proposed OCC with the existing approaches OWSPM-MSR and PM-MSR, a total of seven different combinations are explored.

Table VI demonstrates the decoding time necessary for various ways to decode the data when different numbers of data blocks ($l = 4$ to $l = 10$) and parity block ($m = 1$) are examined. For a comparison of the new OCC with the existing OWSPM-MSR and PM-MSR approaches, seven different combinations are tried.

Fig. 4 depicts a plot for decoding time, with the X axis representing input and the Y axis representing decoding time for a certain input. The inputs are the number of data blocks ($l = 4$ to 10) and the number of parity blocks ($m = 1$). OCC outperforms the previous OWSPM-MSR and PM-MSR algorithms for various combinations of l and m decoding.

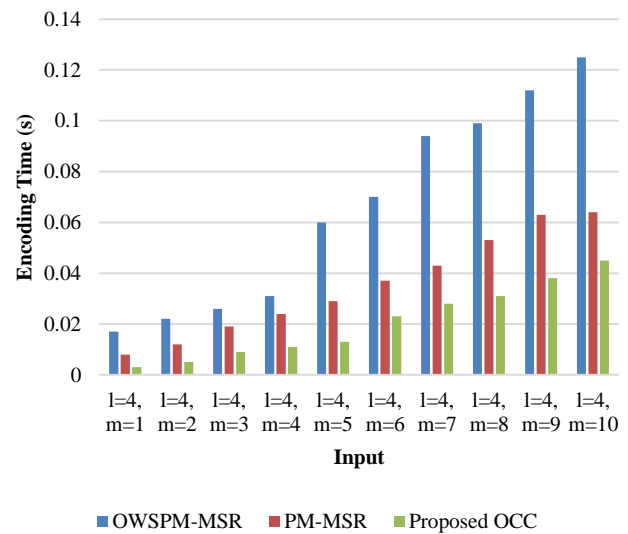


Fig. 3. Comparison of Encoding Time for Various Number of Parity Blocks.

TABLE V. ENCODING TIME (IN SECONDS) FOR VARIOUS NUMBER OF PARITY BLOCKS

Techniques	Encoding Time(s)									
	$l=4, m=1$	$l=4, m=2$	$l=4, m=3$	$l=4, m=4$	$l=4, m=5$	$l=4, m=6$	$l=4, m=7$	$l=4, m=8$	$l=4, m=9$	$l=4, m=10$
OWSPM-MSR	0.017	0.022	0.026	0.031	0.06	0.07	0.094	0.099	0.112	0.125
PM-MSR	0.008	0.012	0.019	0.024	0.029	0.037	0.043	0.053	0.063	0.064
Proposed OCC	0.003	0.005	0.009	0.011	0.013	0.023	0.028	0.031	0.038	0.045

TABLE VI. DECODING TIME (IN SECONDS) FOR VARIOUS NUMBER OF DATA BLOCKS

Techniques	Decoding Time(s)						
	$l=4, m=1$	$l=5, m=1$	$l=6, m=1$	$l=7, m=1$	$l=8, m=1$	$l=9, m=1$	$l=10, m=1$
OWSPM-MSR	0.010	0.023	0.045	0.075	0.12	0.19	0.26
PM-MSR	0.0092	0.015	0.035	0.050	0.070	0.085	0.13
Proposed OCC	0.0077	0.0083	0.0089	0.0097	0.010	0.016	0.018
PM-MSR	0.0092	0.015	0.035	0.050	0.070	0.085	0.13

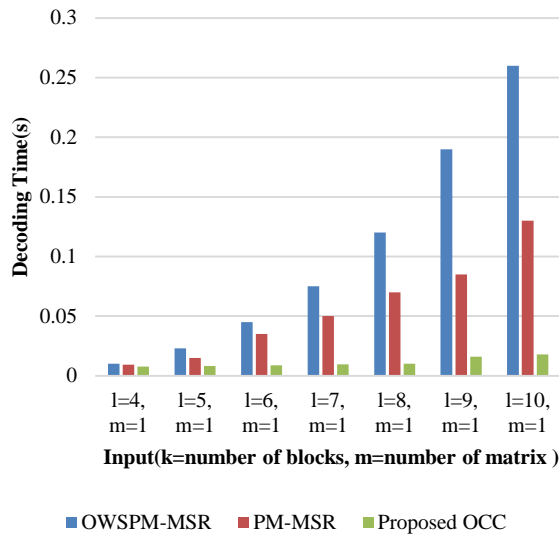


Fig. 4. Comparison of Decoding Time for Various Number of Data Blocks.

Table VII compares the average time required for encoding and decoding 1024KB of data using different approaches. In comparison to the existing two methodologies, the proposed system takes less time.

Table VIII demonstrates the decoding time required for various ways to decode the data when $m = 1$ to $m = 10$ parity blocks are used in combination with data block $l = 4$. For a comparison of the new OCC with the existing OWSPM-MSR and PM-MSR approaches, seven different combinations are tried.

TABLE VIII. DECODING TIME FOR VARIOUS NUMBER OF PARITY BLOCKS

Techniques	Decoding Time(s)									
	$l=4, m=1$	$l=4, m=2$	$l=4, m=3$	$l=4, m=4$	$l=4, m=5$	$l=4, m=6$	$l=4, m=7$	$l=4, m=8$	$l=4, m=9$	$l=4, m=10$
OWSPM-MSR	0.03	0.045	0.065	0.080	0.11	0.13	0.15	0.16	0.19	0.22
PM-MSR	0.02	0.035	0.050	0.070	0.08	0.085	0.095	0.010	0.12	0.16
Proposed OCC	0.0086	0.0092	0.0099	0.0103	0.0135	0.0156	0.0187	0.0256	0.0285	0.0321

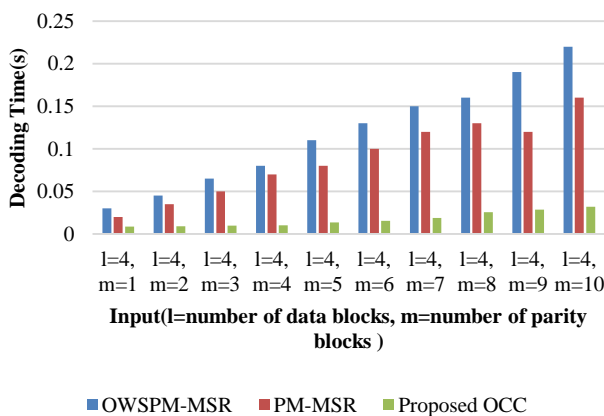


Fig. 5. Comparison of Decoding Time for Various Number of Parity Blocks.

TABLE VII. AVERAGE ENCODING AND DECODING TIME OF DIFFERENT METHODS (FILE SIZE 1024KB, L=4, M=10)

Techniques	Encoding Time(s)	Decoding Time(s)
OWSPM-MSR	0.125	0.22
PM-MSR	0.045	0.16
Proposed OCC	0.035	0.116

Fig. 5 depicts a plot for decoding time, with the X axis representing input and the Y axis representing encoding time for a certain input. As inputs, the data block count ($l = 4$) and the m parity block count ($m = 1$ to 10) are used. OCC outperforms the previous OWSPM-MSR and PM-MSR algorithms for various combinations of l and m decoding.

Fig. 6 and Fig. 7 provide a comparison graph for average data encoding and decoding times for various techniques, showing that the proposed OCC outperforms existing techniques with a 0.035 second encoding time and 0.116 second decoding time for a 1024KB data file.

The OCC data recovery strategy outperforms the OWSPM-MSR and PM-MSR data recovery strategies. Because PM-MSR employs the Vandermonde matrix in the encoding process, the encoding time is longer than the OCC technique, which uses the Cauchy matrix in conjunction with the RS code. In the encoding process, the OCC technique employs a Cauchy Good matrix with fewer ONES, which decreases the time required for the XOR operation. Ultimately it optimized overall processing time for encoding and decoding. As a result, the OCC technique outperforms the OWSPM-MSR and PM-MSR strategy.

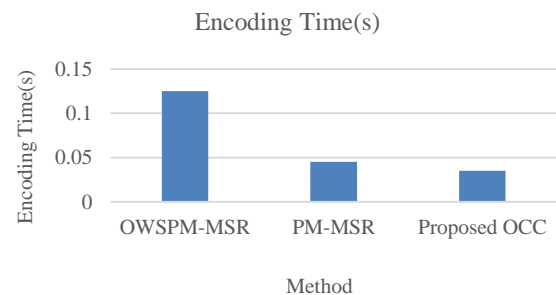


Fig. 6. Comparison of Average Encoding Time of Different Methods.

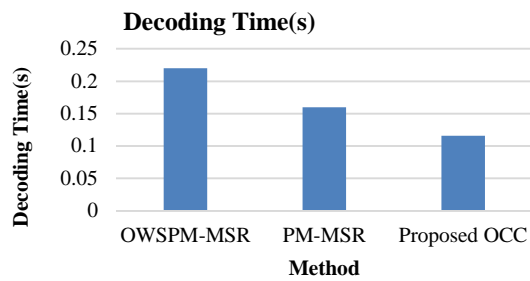


Fig. 7. Comparison of Average Encoding and Decoding Time of Different Methods.

VI. CONCLUSION AND FUTURE WORK

This paper proposed an optimized Ca-Co approach to utilize matrix as well as schedule heuristics to attain an optimal coding structure. In terms of data recovery, it outperforms the OWSPM-MSR and PM-MSR approaches. For data coding, a 1024KB file with various combinations of data blocks l and parity blocks m is evaluated. For coding, two data block and parity block combinations are evaluated. In the first scenario, m equals 1 and l ranges from 4 to 10. The value of l is 4 in the second scenario, while m ranges from 1 to 10. The existing OWSPM-MSR approach takes an average of 0.125 seconds to encode and 0.22 seconds to decode, whereas the PM-MSR approach takes an average of 0.045 seconds to encode and 0.16 seconds to decode. The proposed OCC enhances data coding performance by taking an average of 0.035 seconds to encode and 0.116 seconds to decode data. In future, we intend to use the system in a hybrid cloud environment to balance energy savings with resource virtualization using punctured Cauchy RS code, which can further optimize network resources like power and bandwidth.

REFERENCES

[1] J. Wang, Y. Yang, T. Wang, R. S. Sherratt, J. Zhang, "Big Data Service Architecture: A Survey," *Journal of Internet Technology*, vol. 21, no. 2, pp. 393-405, Mar. 2020.

[2] N. A. Ghani, S. Hamid, I. A. T. Hashem, E. Ahmed, "Social Media Big Data Analytics: A Survey", *Computers in Human Behavior*, Vol. 101, pp. 417-428, 2019, ISSN 0747-5632, <https://doi.org/10.1016/j.chb.2018.08.039>.

[3] J. Yang, H. Zhu, T. Liu, "Secure and Economical Multi-Cloud Storage Policy with NSGA-II-C", *Applied Soft Computing*, Vol. 83, 2019, 105649, ISSN 1568-4946, <https://doi.org/10.1016/j.asoc.2019.105649>.

[4] N. Chervyakov, M. Babenko, A. Tchernykh, N. Kucherov, V. Miranda-Lopez, J. M. Cortes-Mendoza, "AR-RRNS: Configurable Reliable Distributed Data Storage Systems for Internet of Things to Ensure Security", *Future Generation Computer Systems*, Vol. 92, 2019, Pages 1080-1092, ISSN 0167-739X, <https://doi.org/10.1016/j.future.2017.09.061>.

[5] J. Li, J. Wu, L. Chen, "Block-secure: Blockchain Based Scheme for Secure P2P Cloud Storage", *Information Sciences*, Vol. 465, pp. 219-231, 2018, ISSN 0020-0255.

[6] P. V. Bhuvaneshwari & C. Tharini, "Review on LDPC Codes for Big Data Storage", *Wireless Personal Communications*, Vol. 117, Issue 2, pp. 1601-1625, 2021.

[7] Y. J. Tang and X. Zhang, "Fast En/Decoding of Reed-Solomon Codes for Failure Recovery", *IEEE Transactions on Computers*, vol. 71, no. 3, pp. 724-735, 1 March 2022, <https://doi.org/10.1109/TC.2021.3060701>.

[8] M. Makovenko, M. Cheng and C. Tian, "Revisiting the Optimization of Cauchy Reed-Solomon Coding Matrix for Fault-Tolerant Data Storage," *IEEE Transactions on Computers*, <https://doi.org/10.1109/TC.2021.3110131>.

[9] F. Kazemi, S. Kurz, Soljanin and A. Sprintson, "Efficient Storage Schemes for Desired Service Rate Regions", *2020 IEEE Information Theory Workshop (ITW)*, pp. 1-21, 2020.

[10] D. Dai and S. Boroomand, "A Review of Artificial Intelligence to Enhance the Security of Big Data Systems: State-of-Art, Methodologies, Applications, and Challenges", *Archives of Computational Methods in Engineering*, pp. 1291-1309, 2022.

[11] S. Ravikumar and D. Kavitha, "A New Adaptive Hybrid Mutation Black Widow Clustering Based Data Partitioning for Big Data", *Analysis Wireless Pers Commun*, Vol. 120, pp. 1313-1339, 2021, <https://doi.org/10.1007/s11277-021-08516-x>.

[12] Y. Li, J. Ma, Y. Zhang, "Image Retrieval from Remote Sensing Big Data: A Survey", *Information Fusion*, Vol. 67, pp. 94-115, 2021, ISSN 1566-2535, <https://doi.org/10.1016/j.inffus.2020.10.008>.

[13] Y. Xiao, S. Zhou and L. Zhong, "Erasure Coding-Oriented Data Update for Cloud Storage: A Survey," in *IEEE Access*, vol. 8, pp. 227982-227998, 2020, doi: 10.1109/ACCESS.2020.3033024.

[14] X. Gong, C. Wan Sung, Zigzag, "Decodable Codes: Linear-Time Erasure Codes with Applications to Data Storage", *Journal of Computer and System Sciences*, Vol. 89, pp. 190-208, 2017, ISSN 0022-0000, <https://doi.org/10.1016/j.jcss.2017.05.005>.

[15] S. H. Dau, W. Song, A. Sprintson and C. Yuen, "Constructions of MDS Codes via Random Vandermonde and Cauchy Matrices over Small Fields," *2015 53rd Annual Allerton Conference on Communication, Control, and Computing (Allerton)*, 2015, pp. 949-955, <https://doi.org/10.1109/ALLERTON.2015.7447110>.

[16] S. Wu, Y. Xu, Y. Li and Z. Yang, "I/O-Efficient Scaling Schemes for Distributed Storage Systems with CRS Codes," *IEEE Transactions on Parallel and Distributed Systems*, Vol. 27, No. 9, pp. 2639-2652, 1 Sept. 2016, <https://doi.org/10.1109/TPDS.2015.2505722>.

[17] Y. Zhang, J. Yang, A. Memaripour and S. Swanson, "Mojim: A Reliable and Highly-Available Non-Volatile Memory System", *SIGARCH Comput. Archit. News*, Vol. 43, No. 1, pp. 3-18, 2015, <https://doi.org/10.1145/2786763.269437>.

[18] X. Chen and X. Ma, "Optimized Recovery Algorithms for RDP $(p, 3) S$ Code," in *IEEE Communications Letters*, vol. 22, no. 12, pp. 2443-2446, Dec. 2018, <https://doi.org/10.1109/LCOMM.2018.2875468>.

[19] Z. Shen, J. Shu and P. P. C. Lee, "Reconsidering Single Failure Recovery in Clustered File Systems," *2016 46th Annual IEEE/IFIP International Conference on Dependable Systems and Networks (DSN)*, 2016, pp. 323-334, doi: 10.1109/DSN.2016.37.

[20] D. Burihabwa, P. Felber, H. Mercier, and V. Schiavoni, "A Performance Evaluation of Erasure Coding Libraries for Cloud-Based Data Stores: (Practical Experience Report)", *In Distributed Applications and Interoperable Systems: 16th IFIP WG 6.1 International Conference, DAIS 2016*, Proceedings. Springer-Verlag, Berlin, Heidelberg, pp. 160-173, 2016, https://doi.org/10.1007/978-3-319-39577-7_13.

[21] A. Shah and M. Padole, "Load Balancing through Block Rearrangement Policy for Hadoop Heterogeneous Cluster," *2018 International Conference on Advances in Computing, Communications and Informatics (ICACCI)*, 2018, pp. 230-236, doi: 10.1109/ICACCI.2018.8554404.

[22] Sudhakar and S. K. Pandey, "An Approach to Improve Load Balancing in Distributed Storage Systems for NoSQL Databases: MongoDB", *In: Pattnaik, P., Rautaray, S., Das, H., Nayak, J. (eds) Progress in Computing, Analytics and Networking. Advances in Intelligent Systems and Computing*, Vol. 710, pp. 529-538, Springer, Singapore, https://doi.org/10.1007/978-981-10-7871-2_51.

[23] L. Han, S. Tan, B. Xiao, C. Ma and Z. Shao, "Optimizing Cauchy Reed-Solomon Coding via ReRAM Crossbars in SSD-based RAID Systems," *2019 IEEE Non-Volatile Memory Systems and Applications Symposium (NVMSA)*, 2019, pp. 1-6, <https://doi.org/10.1109/NVMSA.2019.8863519>.

[24] L. Xu, M. Lyu, Z. Li, C. Li and Y. Xu, "A Data Layout and Fast Failure Recovery Scheme for Distributed Storage Systems with Mixed Erasure Codes" in *IEEE Transactions on Computers*, no. 01, pp. 1-1, 2021, <https://doi.org/10.1109/TC.2021.3105882>.

[25] M. Pirahandeh and D. Kim, "MS Scheduler: New, Scalable, and High-Performance Sparse AVX-2 Parity Encoding and Decoding Technique

- for Erasure-Coded Cloud Storage Systems”, *Future Generation Computer Systems*, Vol. 126, 2022, pp. 123-135, ISSN 0167-739X, <https://doi.org/10.1016/j.future.2021.08.002>.
- [26] R. Wu, L. Wang, and Y. Wu, “A High-Speed Cauchy CODEC Algorithm for Distributed Storage System”, In *Proceedings of the 2020 International Conference on Internet Computing for Science and Engineering (ICICSE '20)*. Association for Computing Machinery, New York, NY, USA, pp. 20–24, 2020, <https://doi.org/10.1145/3424311.3424313>.
- [27] G. Zhang, G. Wu, S. Wang, J. Shu, W. Zheng and K. Li, "CaCo: An Efficient Cauchy Coding Approach for Cloud Storage Systems," in *IEEE Transactions on Computers*, vol. 65, no. 2, pp. 435-447, 1 Feb. 2016, doi: 10.1109/TC.2015.2428701.
- [28] D. Tang and H. Cai, "A Novel Decoding Method for the Erasure Codes", *Security and Communication Networks*, vol. 2021, Article ID 8755697, pp. 1-12, 2021, <https://doi.org/10.1155/2021/8755697>.
- [29] J-J Kim, “Erasure-Coding-Based Storage and Recovery for Distributed Exascale Storage Systems”, *Applied Sciences*, Vol. 11, No. 8:3298, <https://doi.org/10.3390/app11083298>.
- [30] X. Wang, Z. Zhang, L. Shan, J. Li, Y. Wang, H. Cao, Z. Li, “An Optimized Encoding Algorithm for Systematic Polar Codes”, *J Wireless Com Network 2019*, 193 (2019), pp. 1-12, <https://doi.org/10.1186/s13638-019-1491-4>.
- [31] J. Bian, S. Luo, Z. Li and Y. Yang, "Optimal Weakly Secure Minimum Storage Regenerating Codes Scheme," in *IEEE Access*, vol. 7, pp. 151120-151130, 2019, <https://doi: 10.1109/ACCESS.2019.2947248>.
- [32] N. B. Shah, K. V. Rashmi and P. V. Kumar, "Information-Theoretically Secure Regenerating Codes for Distributed Storage," *2011 IEEE Global Telecommunications Conference - GLOBECOM 2011*, 2011, pp. 1-5, <https://doi: 10.1109/GLOCOM.2011.6133754>.

Impact of COVID-19 Pandemic Measures and Restrictions on Cellular Network Traffic in Malaysia

Sallar Salam Murad¹, Salman Yussof²
Institute of Informatics and Computing in Energy
Universiti Tenaga Nasional (UNITEN)
Kajang, 43000, Malaysia

Rozin Badeel³, Reham A. Ahmed⁴
Department of Communication Technology and Network
University Putra Malaysia (UPM)
Seri Kembangan, 43300, Malaysia

Abstract—Due to the COVID-19 pandemic, intensive controls were put in place to prevent the pandemic from spreading. People's habits have been altered by the COVID-19 measures and restrictions imposed such as social distance and lockdown measures. These unexpected changes created a significant impact on cellular networks, such as increased use of online services and content streaming, which increased the burden on wireless networks. This research work is basically a case study that aims to examine and investigate cellular network performance, including upload speed, download speed, and latency, during two periods (MCO, CMCO) in three different regions, including Kuala Lumpur, Selangor (Cheras), and Johor Bahru, to observe the effects of lockdown enforcement and other restrictions in Malaysia on cellular network traffic. We used the phone application Speedtest™ as a tool for data collection within different times during the day, considering the peak times, including morning, evening, and night times. The research findings show how COVID-19 has affected internet traffic in Malaysia significantly. This research would help perspective developers and companies to better understand and be prepared for tough times and higher load on cellular networks in future pandemics such as COVID-19.

Keywords—Cellular networks; COVID-19; network performance; pandemic

I. INTRODUCTION

COVID-19 has shifted public perceptions about pandemics, with far-reaching repercussions for the global health and economic systems that was started in Wuhan, China [1]. In barely six months (from January to June 2020), 210 nations and territories worldwide reported more than ten million sick persons, including more than 500 thousand deaths [2]. COVID-19 has caused huge economic losses in addition to the worldwide health catastrophe (e.g., a projected 25% unemployment rate in the United States) [3], as a result of that, one million Canadians lost their jobs in March 2020 [4]. The Australian economy shed 1.4 million jobs [5], as well as a global GDP loss of 3% [6]. Because of this, several analysts have projected a worldwide recession [7], [8]. Since there was no cure or vaccine back in 2020 and the virus was spreading rapidly, many countries have implemented various measures of social distancing [9], [10], [11], [12] to slow the spread of the pandemic and give more time for the pharmaceutical industry to develop a cure or vaccine. Few of these scenarios are contact tracing [13], tracking and monitoring [14], quarantine [15], and lockdown [16]. Specifically, such scenarios aim to reduce the

transmission of illness by limiting the frequency and closeness of human physical contacts, such as closing public locations (e.g., schools and universities workplaces), avoiding large crowds and maintaining a safe gap among the people [9], [15]. However, the closure of schools and businesses means that many more people will have to work or study online, which will lead to an overwhelming rise in Internet traffic and online service needs, such as new Zoom users. Therefore, the load on the cellular networks has increased significantly [12], [17].

The social distancing and measures have a significant impact in reducing the spread of the virus. Malaysia was one of the countries that implemented social distancing solutions in early March 2020 [18], such as lockdown and restricted movement and measurements for individuals in outdoor areas, namely Movement Control Order (MCO) and Conditional Movement Control Order CMCO [18]. During that time, a substantial increase happened in data traffic and this has adverse effects on the network experience for the users in Malaysia. Note that Umobile, Maxis, Celcom, and Digi are the cellular networks providers in Malaysia. As soon as the MCO was launched, Malaysian smartphone users' average mobile data usage hit the roof, and this was followed by dramatic declines in the consumers' average 4G Download Speed Experience. Fig. 1 shows the recent social distancing scenarios [12] that were deployed during COVID-19 pandemic around the world.

In [19], Comcast, one of the major US operators, claims a 32% rise in upstream traffic growth and an 18% increase in downstream traffic growth outside of Europe as shown in Fig. 2, and Fig. 3 shows the increase of gaming downloads, streaming, and web video consumption and video conferencing.

It's worth noting that throughout that period in Malaysia, 4G Download Speeds for U Mobile customers increased by almost two times compared to pre-MCO levels. Until the week of May 18, data usage on most Malaysian networks was at its highest point. On average, Celcom's network experienced a 44 percent rise in data usage, followed by Maxis's 36 percent increase [18]. Compared to the beginning of the year, U Mobile subscribers' 4G download speeds were more than twice as fast by September 30th. According to [20], U Mobile has been bolstering its network infrastructure in recent months to keep up with the soaring demand for data by expanding its capacity and fine-tuning the performance of its current cells.

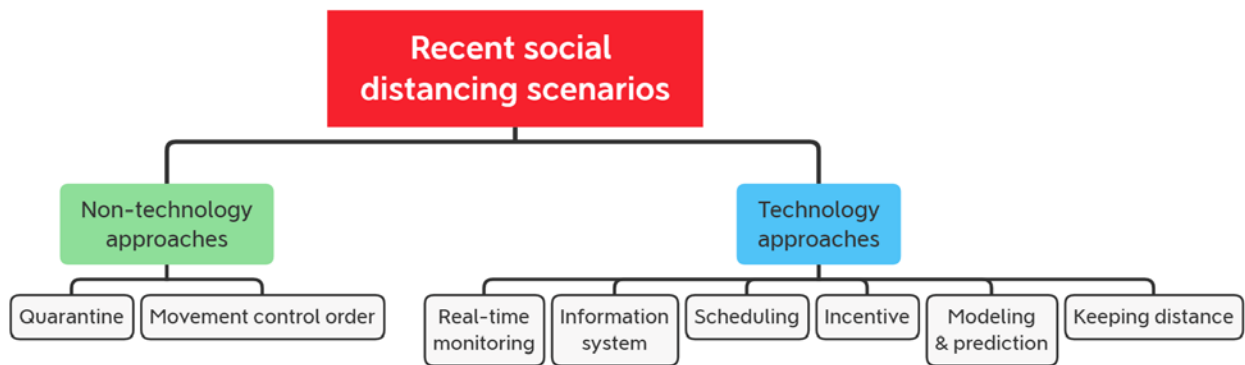


Fig. 1. COVID-19 Measures and Social Distancing Scenarios.

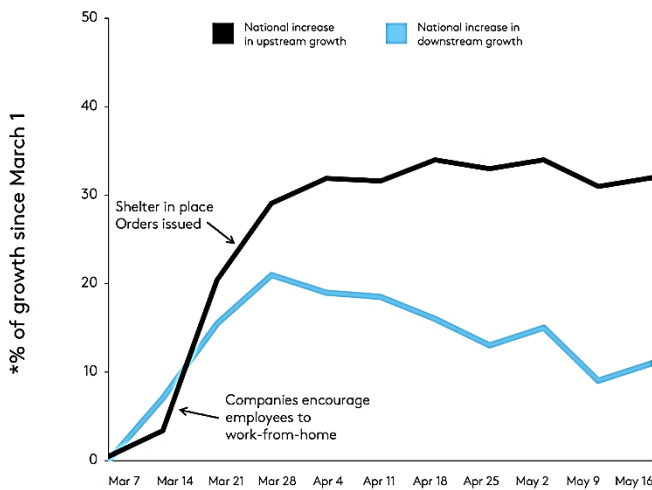


Fig. 2. Network Growth Over Time.



Fig. 3. Entertainment, Streaming, and Gaming Increase Rates.

This study aims to investigate and analyze the usage of internet services, including networks traffics, latency and speed of internet, to understand the pandemic's impact on our daily use of internet applications and services and to support future researchers and developers for maintaining and improving the digital infrastructure or services. By doing this, countries and authorities can avoid the negative side of social distancing in the future pandemic, such as negative economic impacts and disturbances of services provided by companies that rely on online connections.

The rest of the paper is organized as follows: Section II shows related research works. Section III introduces an overview of mobile data in response to the COVID-19 measures and cellular network service providers in Malaysia. Section IV presents the methodology and data collection method of this research. Section V illustrates the results and discussion. Limitations and future directions are shown in

Section VI. Finally, Section VII summarizes the work as a conclusion.

II. RELATED WORK

Microsoft claims that there has been an increase of 755% in the use of cloud servers [21], which means an increase in usage during the pandemic. Moreover, companies such as Netflix and YouTube concentrated the streaming quality in Europe to prevent network overload [22]. Moreover, since the shutdown in Italy, Cloudflare [23] and Fastly [24], two of the world's largest content delivery networks, have reported a 20–40 percent spike in daily traffic. Furthermore, according to ISPs, the rise in network traffic has been reported in public news and blog reports.

According to Vodafone [25], fixed broadband use has increased by more than 50% in Italy and Spain. With a 100% increase in upstream traffic and a 44% increase in downstream traffic during the pandemic. In [26], Telefonica IP networks had a traffic growth of about 40%, while mobile phone usage rose by approximately 50% and data usage increased by about 25% [27]. Moreover, in [26] and [28], traffic increased by 10–40% at European Internet Exchange Points. In [27], Malaysia's internet traffic increased by 23.5 percent during the first stage of the pandemic due to the additional burden of online education and video conferencing. Many cities have started using online shopping such as Lazada and grab car for food delivery and many people used streaming video services like Netflix to pass the time while they were confined to their homes.

Few studies have considered reporting some variations and statistics during COVID-19 pandemic. In the research work [29], the authors investigated the impact of the lockdown on Politecnico di Torino's campus network in Italy. They also noticed that inbound traffic had fallen significantly, but it has more than doubled outgoing traffic.

In [30], using data from a diverse set of vantage points (one ISP, three IXPs, and one metropolitan educational network), the authors examined the effect of these lockdowns on traffic shifts. We can observe that the Internet infrastructure was able to handle the new volume, as most traffic shifts occur outside of traditional peak hours. While many networks saw increased traffic demands, in particular, those providing services to residential users, academic networks experience major overall

decreases. Yet, in these networks, we can observe substantial increases when considering applications associated to remote working and lecturing. The study also included the effect that government-mandated lockdowns had on the Internet by analyzing network data. Since all data sources exhibit vastly differing traffic characteristics and volumes, the authors normalized the data to make it easier to compare.

The Internet was a gateway to the world; the study [31] used data from Internet speed tests, consumer complaints, search engine optimization tools, and logs of Internet use from public libraries to understand the effects of the pandemic on Internet use and performance. Despite reports that the Internet handled the surge in traffic well, we find that complaints about Internet speed nearly tripled, and performance was degraded. The study stated that many people without Internet at home turned to public Wi-Fi hotspots during the pandemic. We find that this occurred disproportionately in neighborhoods with more students. Future distance learning initiatives should consider the challenges some students face in obtaining Internet access.

Mobile sensing has played a key role in providing digital solutions to aid with COVID-19 containment policies, primarily to automate contact tracing and social distancing measures. Many COVID-19 technology solutions leverage positioning systems, generally using Bluetooth and GPS, and can theoretically be adapted to monitor safety compliance within dedicated environments. However, they may not be the ideal modalities for indoor positioning. The study [32] conjectures that analyzing user occupancy and mobility via deployed WiFi infrastructure can help institutions monitor and maintain safety compliance according to the public health guidelines. Using smartphones as a proxy for user location, their analysis demonstrated how coarse-grained WiFi data can sufficiently reflect the indoor occupancy spectrum when different COVID-19 policies were enacted. They have demonstrated how their data source can be a practical application for institutional crowd control and discussed the implications of their findings for policy-making.

The study [33] evaluated the impact on the Internet latency caused by the increased number of human activities that was

carried out on-line. Their analysis of the impact of COVID-19 pandemic relied on the results generated by both Anchoring Measurements (AMs) and User-Defined Measurements (UDMs). Beside ICMP-based latency, an evaluation of latency as seen at the HTTP level was provided. Latency is particularly important not only because it has a profound effect on some classes of applications, but also because it is, by itself, an excellent indicator of the health status of the network. We believe that the provided numbers and the related analysis will definitely help in better understanding this previously unseen event in the history of the Internet.

The article [34] provided a perspective of the scale of Internet traffic growth and how well the Internet coped with the increased demand as seen from Facebook's edge network. They have used this infrastructure serving multiple large social networks and their related family of apps as vantage points to analyze how traffic and product properties changed over the course of the beginning of the Covid-19 pandemic.

The pandemic has significantly changed people's mobility and habits, subsequently impacting how they use telecommunication networks. The study [35] has investigated the effects of the COVID-19 emergency on a UK Mobile Network Operator (MNO). The authors have quantified the changes in users' mobility and investigate how this impacted the cellular network usage and performance. Their findings brought insights at different geo-temporal granularity on the status of the cellular network, from the decrease in data traffic volume in the cellular network and lower load on the radio network, counterposed to a surge in the conversational voice traffic volume.

Table I shows a summary of related works. The motivation for this study is that no study has investigated the impact of COVID-19 restrictions and measures on cellular network traffic in different times during the day and through the year 2021 in Malaysia. Moreover, the COVID-19 restrictions and measures such as social distancing and lockdowns have increased our daily use of internet services and applications; therefore it is important to study the variations of data speeds and usage.

TABLE I. RELATED WORK SUMMARY

Ref.	Focus	Findings	Location	Time frame		Network type
				From	To	
[29]	Analyzed the changes in the traffic patterns.	<ol style="list-style-type: none"> 1. Reveals the importance of using different lenses to fully understand the COVID-19 pandemic's impact at the traffic level: Mornings and late evening hours see more traffic. 2. Conclude that the Internet did its job and coped well with unseen and rapid traffic shifts. 	The Politecnico di Torino campus network / Italy.	February 2020.	April 2020	WiFi
[30]	Analyzed network flow data from multiple vantage points, including a large academic network and a large ISP at the edge, and, at the core.	<ol style="list-style-type: none"> 1. They found that the traffic volume increased by 15-20% almost within a week-while overall still modest, this constitutes a large increase within this short time period. 2. Traffic increases in applications that people use when at home, such as Web conferencing, VPN, and gaming. 	Three IXPs located in Europe and the US.	January 1, 2020.	June 24, 2020.	The core of the Internet (IXPs), and at the edge (a metropolitan university network).
[31]	To understand the effects of the pandemic on Internet use and performance.	<ol style="list-style-type: none"> 1. Downstream data rates changed little, but median upstream data rates at midday dropped by about a third. 2. Significant increases in the use of many important categories of online content, including those used for work communications, education, grocery shopping, social media, news, and job searches. 	Wi-Fi in 73 public libraries in Western Pennsylvania/ US.	December, 2019.	September, 2020.	WiFi
[32]	Analyzes staff and students' mobility data. Seeks to investigate if location data that is passively sensed from existing WiFi infrastructure can, in fact, show the real-world effects of various COVID-19 policies on institutions.	Show that online learning, split-team, and other space management policies effectively lower occupancy. However, they do not change the mobility for individuals transitioning between spaces.	2 campuses in Singapore, and 1 in the Northeastern United States.	January 6, 2020.	April 7, 2020.	WiFi
[33]	Analyzed the impact of the COVID-19 pandemic on the latency of the Internet. The analysis focuses on Italy.	<ol style="list-style-type: none"> 1. The analysis of a large set of measurements shows that the impact on the network can be significant, especially in terms of increased variability of latency. 2. The impact is not negligible also for Italy and the other countries in the whole of Europe. 3. The major changes have been observed in the evening, the time of the day when most of the on-line activities are related to entertainment. 	Italy, Spain, France, Germany, Sweden, and whole of Europe.	February 08, 2020.	March 28, 2020.	Not specified
[34]	Used Facebook's edge network serving content to users across Facebook's family of apps to provide a perspective on how the Internet coped with and reacted to the surge in demand induced by Covid-19. Assessed the impact of this traffic surge on network stress and performance.	<ol style="list-style-type: none"> 1. Showed that there have been changes in traffic demand, user behavior and user experience. 2. Different regions of the world saw different magnitudes of impact with predominantly less developed regions exhibiting larger performance degradations. 3. North America and Europe did not show any signs of stress in their networks, India and parts of Sub-Saharan Africa and South America did witness signs of network stress translating into degraded video experience, higher amount of traffic overflowing to indirect links and secondary CDN locations, and higher network round trip times. 4. Found that traffic increases occurred mainly on broadband networks. 	Facebook servers around the world with 2.5 billion monthly active users.	January, 2020.	Late July, 2020	Facebook's Edge Network
[35]	The study focused on presenting an analysis of the changes in mobility and their impact on the cellular network traffic.	<ol style="list-style-type: none"> 1. An overall decrease of 50%, with non- uniform changes across different geographical areas and social backgrounds. 2. Despite significant pattern changes, the MNO was able to provide service maintaining quality standards: the radio load was below common values and per user throughput was likely application limited. 3. Identified one issue in voice traffic packet loss due to excess of congestion in the interconnection infrastructure MNOs use to exchange voice traffic. 	The entire country to specific regions (London).	February 23, 2020.	May 31, 2020.	Cellular network

III. MALAYSIA'S RESPONSE TO COVID-19: PROBLEM DEFINITION

On March 18, the Malaysian government issued a continuous Movement Control Order (MCO) [36]. Throughout the crisis, as more Malaysians stayed at home to obey the order, they rely on mobile networks for business, education, information, and pleasure expanded. The Malaysian Communications and Multimedia Commission (MCMC) detected a significant rise in data traffic and suspected that this has significantly impacted consumers' network services in a variety of ways; furthermore, with students and staff working from home [37], as well as variations in user activity during the lockdown [38], [39]. Normal internet speed may have reduced during non-peak hours, reducing total speeds. Furthermore, in order to avoid being confined in the city and to save expenses, many city workers returned to their home towns in the suburbs or rural regions.

This swing in mobile usage geography suggests that users were spending additional time in places where the network infrastructure was not designed to support such a large number of users and their increasing mobile data consumption. Following that, Beginning April 1, 2020, until restrictions were reduced, the MCMC announced that few cellular companies such as Celcom, Digi, Maxis, and U Mobile would offer all of their customers (prepaid and postpaid) 1GB of free data each day between 8 a.m. and 6 p.m., while Unifi offered various unlimited plans to support its customers [1].

As data demand grew during the early months of the outbreak [40], more users experienced poorer average 4G download rates. Given the challenges, Malaysia's mobile operators have supplied consistent coverage to their customers in this extraordinary situation. However, mobile network service is not always steady or of high quality. Several basic Quality of Service (QoS) requirements for mobile broadband have been defined by the MCMC. While there was significant dissatisfaction with network speeds, Malaysians mainly accepted their situation until the COVID-19 epidemic triggered the MCO, which restricted people to their homes and increased their dependency on high-speed internet connection for business, school, and entertainment [2]. Malaysia's internet traffic grew by 23.5 % in the first week of the MCO. Median download speed fell from 13.7 Mbps in early February to 8.8 Mbps in late March, as each additional activity imposed at strain on the entire digital infrastructure. Local telecommunications and internet service companies moved quickly to upgrade wireless backhaul to fiber optic connections in order to reduce internet disruptions and increase network performance.

Malaysian internet traffic had shifted to residential areas and increased by 30-70% by September 2020, yet internet speed had declined by 30-40% [2]. Malaysia's internet speed has significantly decreased as a result of increased bandwidth demand since the MCO's implementation [3]. Congestion may

occur as a result of increased data usage, resulting in slower speeds. This has had an effect on the user experience, with longer loading times noted, particularly when accessing bandwidth-intensive media such as High-Definition (HD) streaming services. However, comparable trends have been reported worldwide, according to MCMC, with operators experiencing an unprecedented increase in bandwidth demand as a result of this behavioral shift. The vast majority of today's leisure activities, such as streaming services [41], video chats, and online gaming, take a significant amount of data. All of this puts a considerable strain on existing infrastructure.

Furthermore, E-commerce is a massive platform that is expanding at an unprecedented rate around the world. E-commerce has experienced a huge increase in sales [42], as more shoppers turn to online grocery platforms to purchase their daily necessities. Digital media providers such as Netflix are becoming popularity [43]. Malaysia ranks fifth in the world and first in Southeast Asia in terms of social media adoption, according to Hootsuite's Digital 2020 research [44]. Fig. 4 shows meaningful statistical data on internet users as well as other important elements.

The employees who are working from home rely heavily on various online conference call platforms to continue their business discussion. Every day, the ordinary Malaysian internet user spends 7 hours and 57 minutes online, which equivalent to roughly 100 days per year. This is greater than the global average user time spent. Google, YouTube, Facebook, WhatsApp, and Maybank2u are the leading five most visited websites in Malaysia [44].

The use of E-wallets in Malaysia such as Touch and Go, Grab, Fave, Samsung Pay, and others has grown [45]. The ratio dipped to 55% at the beginning of 2020, but due to the "new normal, 70% of users now feel they will use e-wallet services even if no benefits are offered [46]–[48]. Fig. 5 shows the number of payments and E-wallets statistics as well as types of E-wallets in Malaysia. People are turning to online grocery platforms to purchase their daily requirements, which have resulted in a significant surge in e-commerce sales.

In China, for example, Carrefour China recorded a 600 percent year-over-year rise in vegetable deliveries during the Lunar New Year period, and JD.com observed a 215 percent growth in online grocery sales to 15,000 tonnes in just the first ten days of February 2020 [44].

Note that the growth of ecommerce before the crises of COVID-19 has increased significantly. According to the Worldwide Ecommerce Report 2019, global retail e-commerce sales are worth US\$3.535 trillion and are predicted to hit US\$6.5 trillion by 2023. Malaysia is among the top five fastest-growing e-commerce countries, indicating that the country has significant e-commerce potential. Fig. 6 presents some fast facts about online shopping growth in some countries [46].



Fig. 4. State of Internet in January 2020 Around the World and in Malaysia.

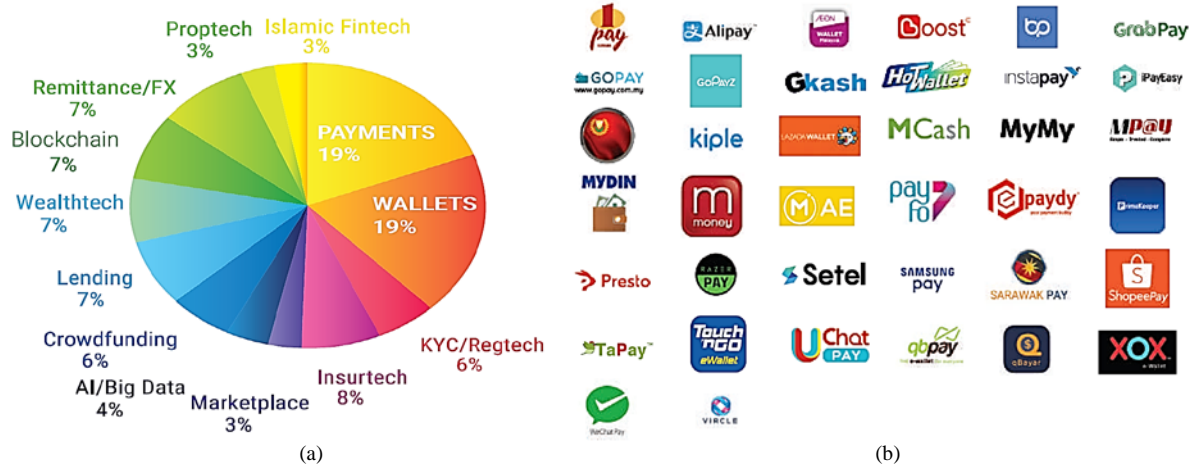


Fig. 5. (a): Payments and E-Wallets against other Elements during 2019 according to Fintech Report [42], (b) Most Popular E-Wallets in Malaysia.

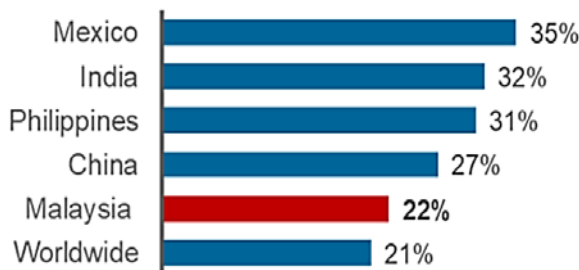


Fig. 6. State of Internet in January 2020 Around the World and in Malaysia.

IV. METHODOLOGY

In this section, the methodology process details are presented. In addition, the tool used for the data collection process with the details is explained. In this work, we have by used Speedtest phone application Ookla [49] for the data collection. Every day, approximately ten million individual tests are performed by users in places and at times when their connectivity is vital to them. Speedtest has delivered almost 35 billion tests since its establishment in 2006. After the data collection process, all data gathered and analyzed using Excel sheets, then converted to graphs as results. Customers are

linking to networks everywhere such as on the road, in their cars, at home, at work, and everywhere else.

When paired with data on cell site locations, tools to priorities optimization and rollout efforts, and competitor comparisons, Cell Analytics offers an entire solution for mobile network operators to examine their networks and determine areas that demand upgrading. The data collected for this study was conducted by using different phone types.

The data were collected in three different times during the day, namely morning, afternoon, and evening. The data collection for the morning time starts from 10 am to 12pm, afternoon time 4pm to 6pm and evening 10 pm to 12 pm. An iPhone 12, Samsung galaxy s8 and Poco F2 Xiaomi were used. Details of data are summarized in Table II.

Fig. 7(a) and (b) shows a snapshot of an example of the application used in this study during the data collection process including testing the download speed and upload speed. The coverage areas of Umobile cellular networks in Kuala Lumpur and Johor Bharu provided by Speedtest are shown in Fig. 7(c) and (d), respectively. Fig. 8 shows the methodology steps and details. All the data were collected and analyzed using excel sheets.

TABLE II. DATA COLLECTION DETAILS

Matrices		Details
Country		Malaysia
Cities		Johor Bahru, Kuala Lumpur, and Cheras (Selangor)
Network type		Umobile
Performance matrices		Download speed, upload speeds, and latency
Smartphone types		iPhone 12, Samsung galaxy S8, and Poco F2 Xiaomi
Time of collection	Morning time	10-11:50 am
	Afternoon time	4-6 pm
	Evening time	10-11:59 pm
Date of collection	Phase 1	13 January – 13 February
	Phase 2	5 March – 2 April
Data collection tool		Speedtest phone App
Lockdown periods		MCO and CMCO



Fig. 7. (a): Snapshot of Speedtest Application showing the Collection of Download Speed Data, (b) Collection of Upload Speed Data, (c): UMobile Cellular Network Coverage in Kuala Lumpur, and (d): UMobile Cellular Network Coverage in Johor Bahru.

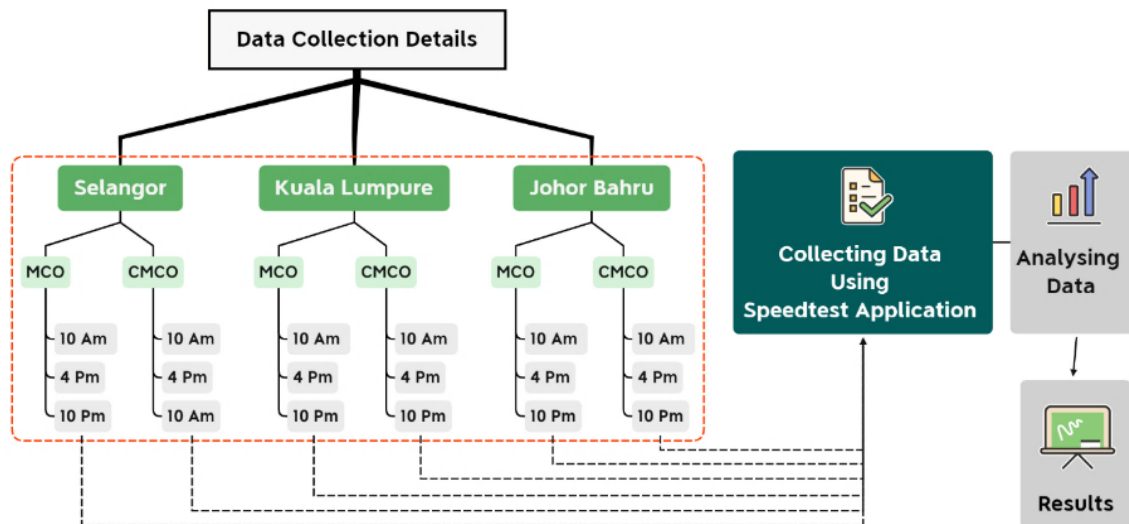


Fig. 8. Snapshot Methodology Process Details.

V. RESULTS AND DISCUSSION

This section presents the results and discussion. The main data gathered for this study including the download speed rate and upload speed rate. In addition, the latency was also measured. All data were collected, transformed to readable graphs then analyzed. We evaluate the performance of cellular networks during two time periods, namely MCO and CMCO. In order to describe the data being studied, all data were analyzed and compared. Specifically, download speed in the morning is compared with afternoon and evening time within same period, same for the upload speed, then the latency. In addition, all performance metrics during MCO is compared with the performance during CMCO. Finally, an overall comparison is presented as final findings.

The first period, MCO started from 13 January 2021 to 13 February 2021, and the second-period CMCO began from 5 March 2021 to 2 April 2021.

Microsoft Excel was used to combine and compare the data from three cite to measure the network speed and latency in (LTE cellular, U-mobile). It should be noted that the variations of data taken into consideration may be caused by the traffic volume and the peak hours for people using the internet for example work, online study or video streaming.

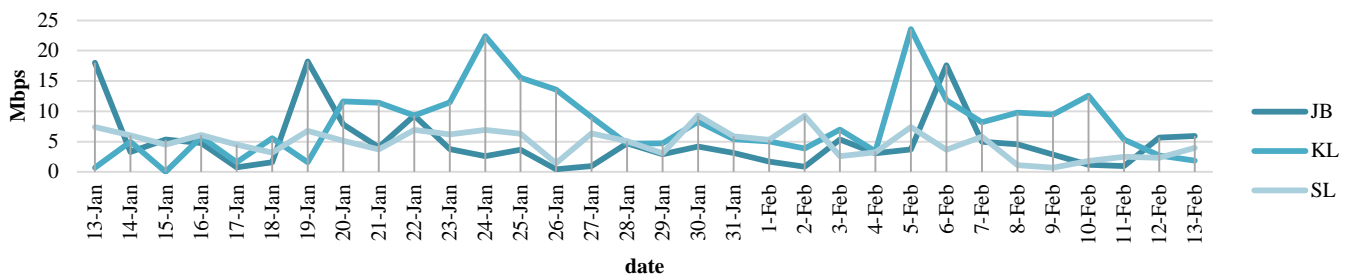
Since the performance of the considered cellular networks presented in this study is highly dependent on network parameters and a few other variables such as i) number of users connected to the BS [50], ii) time of data collection where speed and data traffic varies from time to time based on the density of users which relies on population when comparing different cellular networks performance from different areas. The data rate requirements per user also play an important role in load variations on the BS which represents the data usage [51]. In the data collection phase, we had to collect data from

three different cities in Malaysia in order to make a fair comparison of cellular networks within different user density, and to simulate diverse network conditions and verify the impact of COVID-19 measures and restrictions.

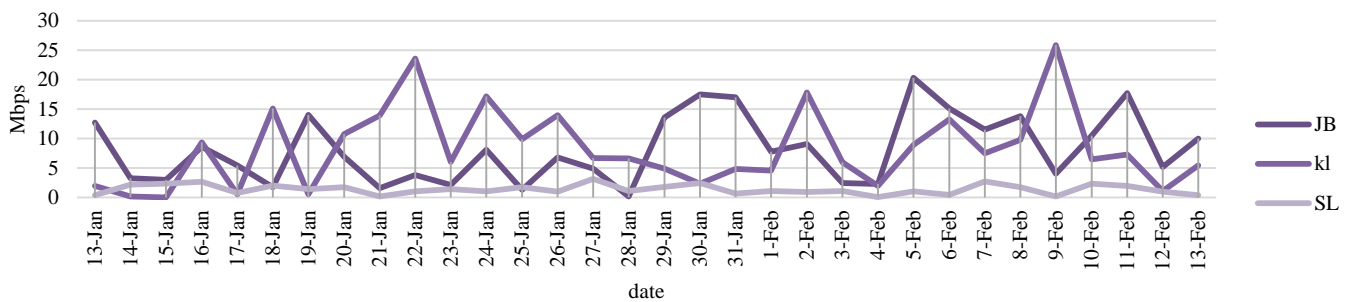
All data collection were conducted on smartphones (iPhone 13, Samsung S8), with 60 GB of RAM memory. Exceptionally in this scenario, since the phone application used by the client is making calculations and data measurements, it is affected only by network conditions and the server connected nearby the cellular BS. To verify the use of different smartphone types, we had to utilize all smartphones on same network operators that is popular in Malaysia and subscribed to the same broadband subscription which is Umobile. Note that the average download speed while using a cellular network during normal times (before the crises of COVID-19) was around 4-8Mb/s.

Since download speed rates are the most important aspect of the network speed, our focus will be on the download speed rates in this discussion. Fig. 9 describes the network performance during MCO at 10 am from 13 of January to 13 of February.

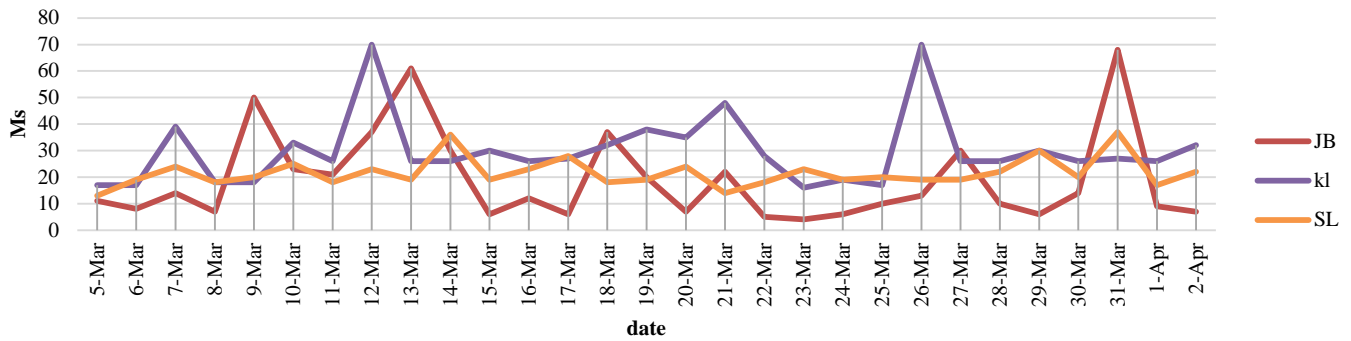
It is shown that the download and upload speed in KL and JB increases in some days especially weekends, and decreases in weekdays. This is because the necessity for services and applications for business, education, and/or online meetings is higher on weekdays; therefore the load on the network is higher. In addition, it can be seen the download and upload speed rates are higher in KL. This is because the population there is much higher than other areas in Malaysia, thus there are more cellular networks installed in the area. The highest download speed during this period is around 23Mbps in KL, while the lowest is near to 0 Mbps on some days for KL and JB.



(a) Download Speed at 10 AM.



(b) Upload Speed at 10 AM.

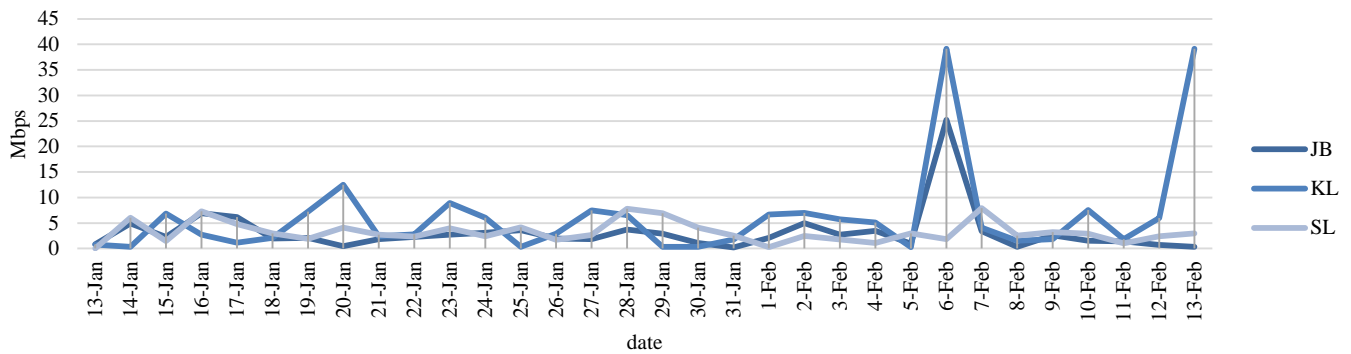


(c) Latency at 10 AM.

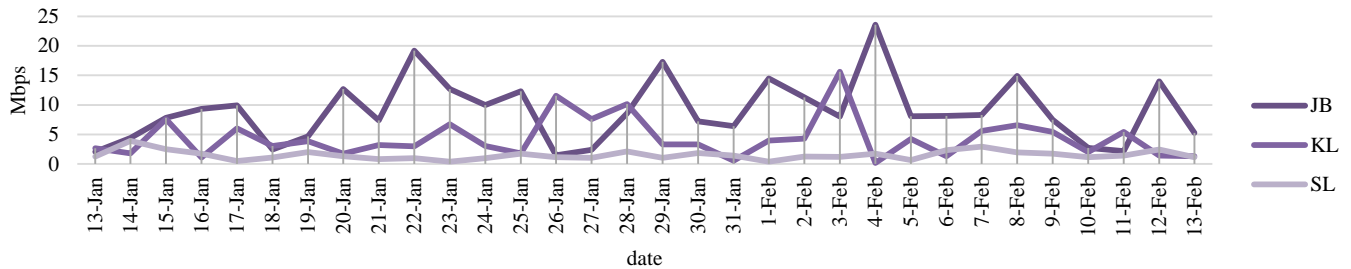
Fig. 9. Network Performance during MCO at 10AM.

Fig. 10 presents the network performance during MCO at 4 pm from 13 of January to 13 of February. It is obvious that there is performance differences compared with the 10 am rates. Specifically, during this period all rates were quite low

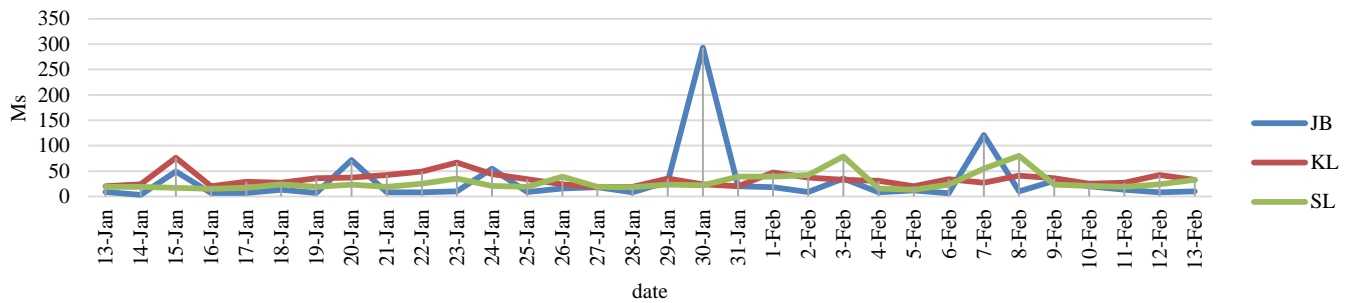
except in 6 of February and 13 of February (weekends) in KL and JB. The highest rate measured during this period was 30-40Mbps for download speed.



(a) Download Speed at 4:00 PM.



(b) Upload Speed at 4:00 PM.



(c) Latency at 4:00 PM.

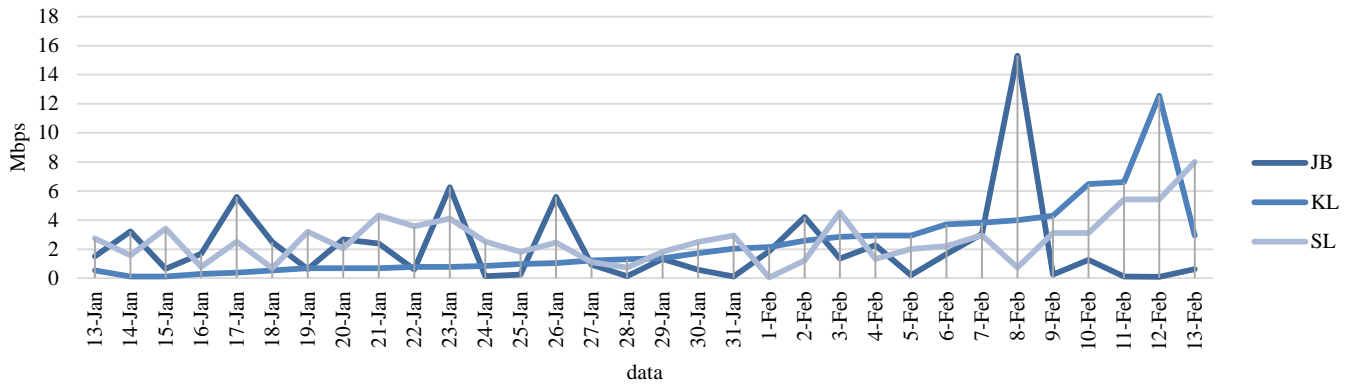
Fig. 10. Network Performance during MCO at 4PM.

On the other hand, most of the weekdays during this peak time (4 pm) has the lowest rates, this is because most services and online meetings shifted afternoon in MCO.

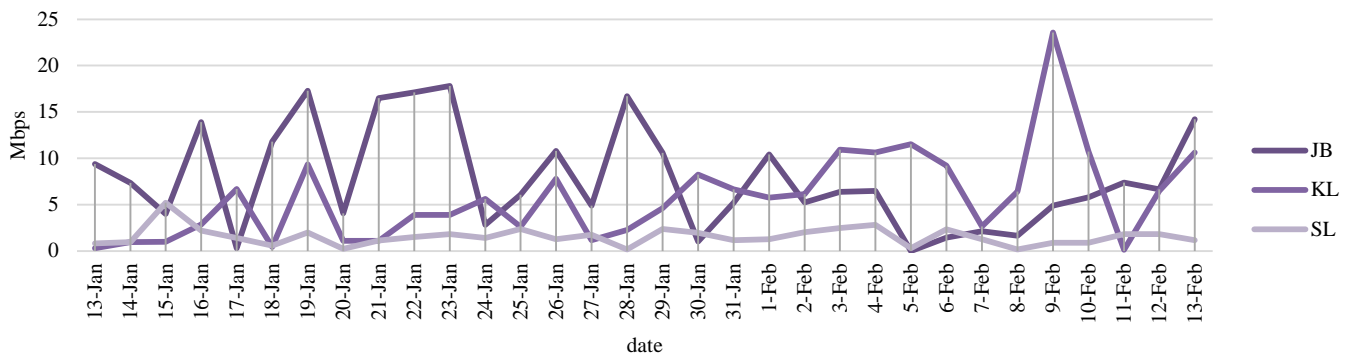
Fig. 11 presents the network performance during MCO at 10 pm from 13 of January to 13 of February. The download speed is low overall, mostly in KL. This is because the usage of online services and streaming such as Netflix has risen after the pandemic, especially in the evening. Moreover, it can be seen that the rates are lower when comparing it with the morning and afternoon rates. This is because the government of Malaysia ordered people not to go out in the evening, and most of the markets were closed, therefore the usage of the internet has increased. It can be seen that from 8 of February,

the download speed rates increase as the MCO period is about to finish.

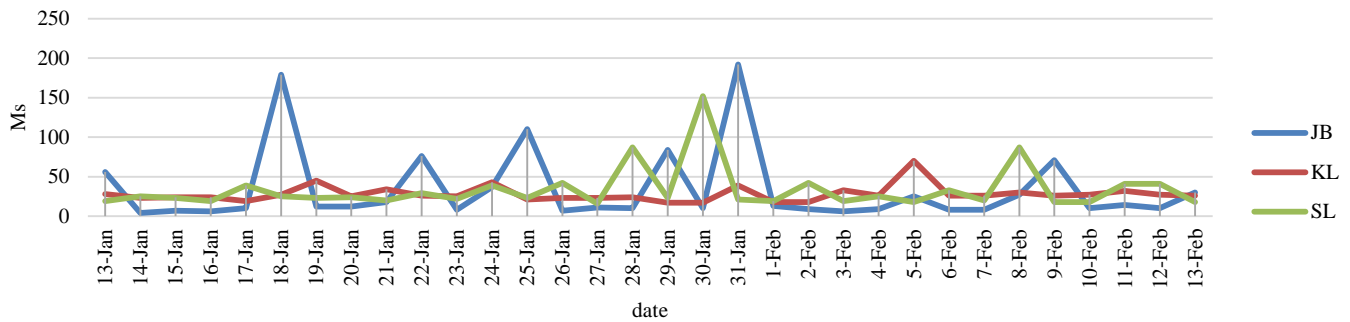
Fig. 12 presents the network performance during CMCO at 10 am from 5 of March to 2 of April. This figure shows the decreased download speed rate in the morning time (10 am) compared with the morning time of MCO. This is because the restrictions were less during CMCO and people could go out shopping and more businesses opened after the MCO period. In addition, during CMCO, the users of cellular networks service increased compared with MCO due to the fact that in the MCO period, people spent more time at home which means most of the users change their connection to WiFi network.



(a) Download Speed at 10 PM.

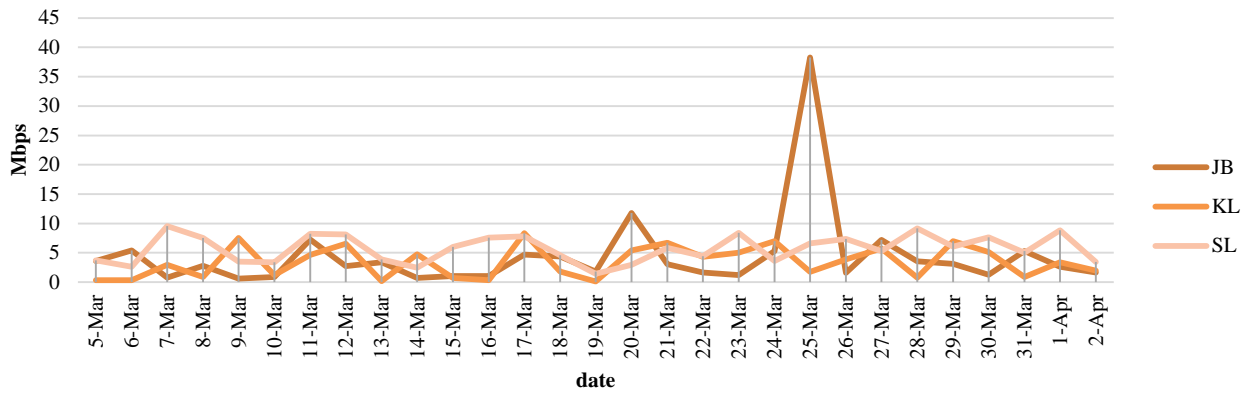


(b) Upload Speed at 10 PM.

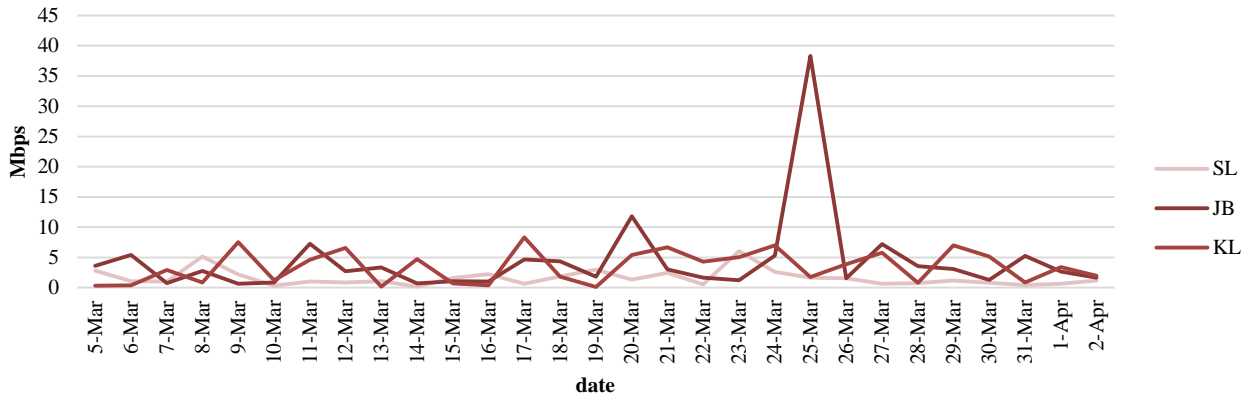


(c) Latency at 10 PM.

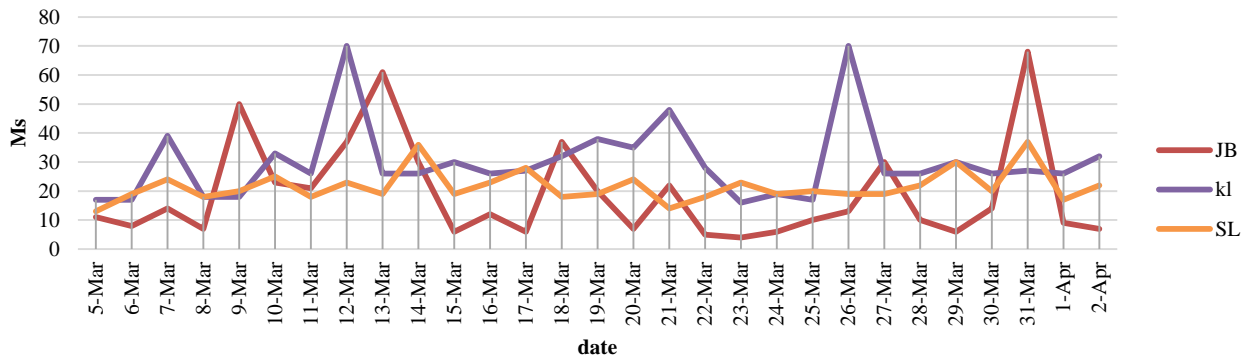
Fig. 11. Network Performance during MCO at 10PM.



(a) Download Speed at 10:00 AM.



(b) Upload Speed at 10:00 AM.

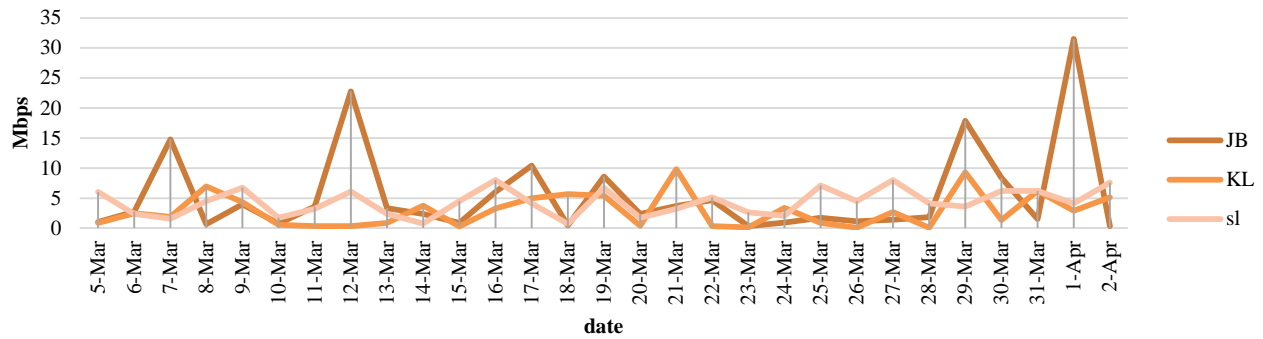


(c) Latency at 10:00 AM.

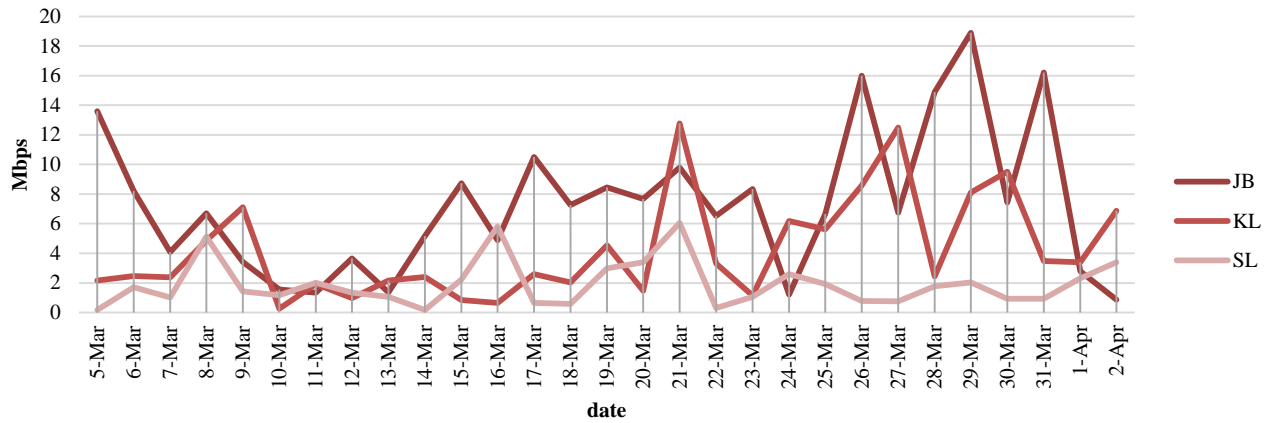
Fig. 12. Network Performance during CMCO at 10AM.

While in the CMCO period when people had the chance to go out, they shifted back to the cellular network connections. The rates of the download speed for the morning time were more stable than MCO, as well as for the upload speed. The highest value measured was on 20 of March (weekend) and 25 of March. On the other hand, the latency value increased near and on the weekend as well on 12, 21 and 26 of March for KL, and on 13 and 31 of March JB. Overall latency in this period is higher than the latency measured in the morning of MCO due to the increased usage during the CMCO.

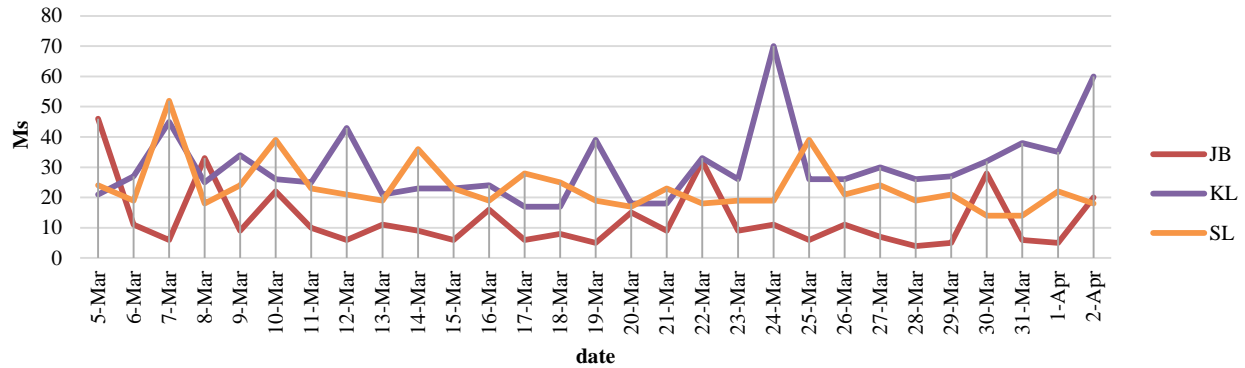
Fig. 13 presents the network performance during CMCO at 4 PM from 5 of March to 2 of April. The download speed during this period has slightly increased compared with the morning time. This is because in the CMCO time, the peak time has shifted mostly in the morning to the afternoon because the measures and restrictions has been minimized by the government, therefore the load on the network is expected to be less in the afternoon and evening times. The highest rate achieved by the network for the download speed is around 25-30Mbps on 12 of March and 1 of April during the weekend (Saturday and Sunday) and in Friday.



(a) Download Speed at 04:00 PM.



(b) Upload Speed at 04:00 PM.



(c) Latency at 04:00 PM.

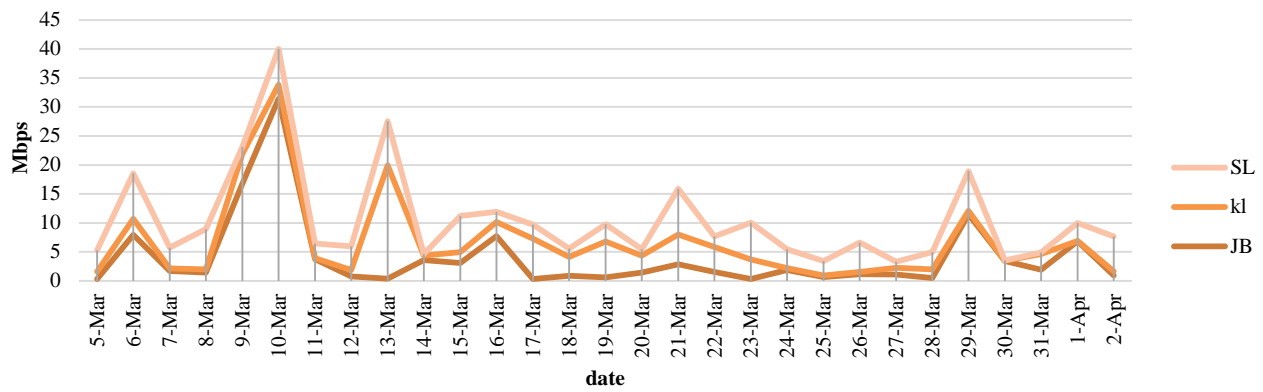
Fig. 13. Network Performance during CMCO at 4PM.

For the latency, due to the increased number of users of the cellular networks, the rates of latency have increased significantly, especially in KL in 24 of March and 2 of April.

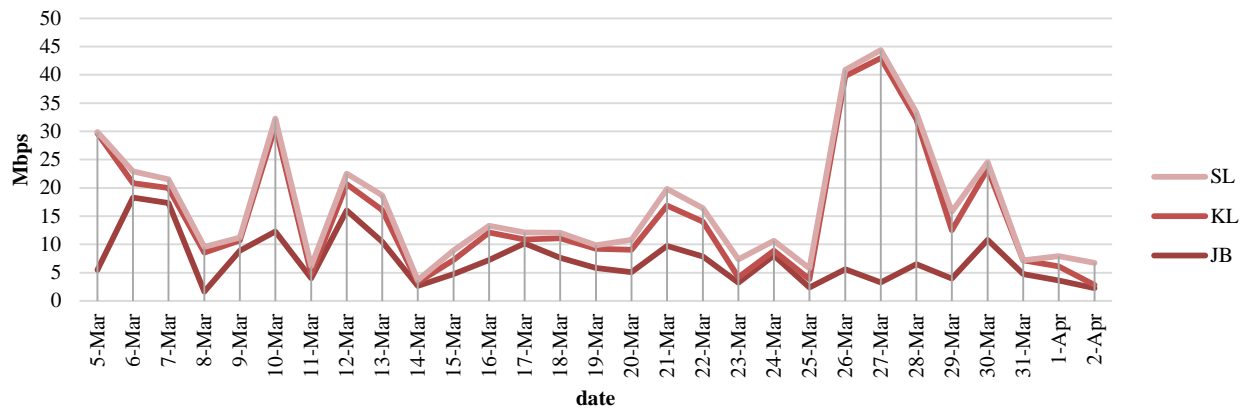
Fig. 14 presents the network performance during CMCO at 10 PM from 5 of March to 2 of April. Overall rates including download, upload and latency are higher than the morning and afternoon times. The download speed rate in this period is slightly higher when comparing it with the evening time of the MCO period. This is because people had to go home after 8 pm, which means the number of cellular users decreased

significantly. The highest upload speed rate achieved was around 45Mbps on 27 of March (weekend) in KL and Cheras. The lowest value of latency is around 0-50ms, and the highest has reached 200ms same as the value of latency in the MCO evening time.

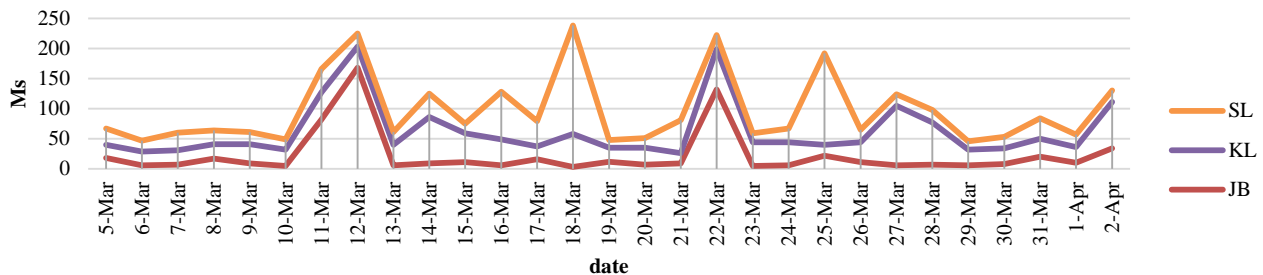
This is because of the increased number of users during the CMCO than the MCO period. In addition, the number of people subscribed to a broadband subscription plan has increased during CMCO.



(a) Download Speed at 10:00 PM.



(b) Upload Speed at 10:00 PM.



(c) Latency at 10:00 PM.

Fig. 14. Network Performance during CMCO at 10PM.

To summarize and extract the findings from all the above results, the average rates are presented in Fig. 15. In addition, the highest and the lowest values of all times for all cities are shown and highlighted in red and yellow colours, respectively. The highest value of all rates within all times among the three cities is highlighted in blue colour. While the lowest values are highlighted in yellow color. Specifically, the average rates of the download speed are presented in Fig. 15(a). As shown in the figure, the highest value in the MCO period was in KL in the morning time. This is because, as mentioned earlier, the cellular towers and BS deployed in that area are much more than in other areas, and the peak time of workers who relied on the internet connection in the morning time of the MCO was shifted to work from home in fixable times. The lowest value

was in the evening time in JB. On the other hand, the highest value in the CMCO period was in SL (Cheras) in the morning time. While the lowest value was in KL in the evening time.

Fig. 15(b) shows the upload speed rates. The highest value in the MCO period was in JB in the Afternoon time and the lowest value was in SL (Cheras) in the morning time. On the other hand, the highest value in the CMCO period was in JB during morning time, and the lowest value was in SL (Cheras) during the evening time.

Fig. 15(c) presents the latency values for all cities in all times. The longest time of latency in the MCO period was in JB during the morning time, which expresses the best value, and the highest time of latency was in SL (Cheras) in the

morning time as well, which was the worst value. The highest time of latency in the CMCO period was in KL in the evening time, while the lowest time was in JB during the afternoon time.

In Fig. 16, the total volume values of downloads, uploads, and latency in a percentage manner are presented. In Fig. 16(a) during MCO, the biggest volume of downloads was in KL which is 45%, while the rates in JB and SL are almost the same. On the other hand, during CMCO, the biggest overall value of downloads was in SL which is 42%, and the lowest value was in KL which is 25%. In Fig. 16(b), the upload speed total value is presented. During MCO, the higher values were in both KL and JB which are 46%, and the lowest was in SL which is 8%. In addition, during the CMCO, the greatest value of upload speed total value was in JB which is 54%, and the lowest was in SL at 10%. In Fig. 16(c), the overall latency is shown. The highest volume of latency during the MCO was in SL at 42%, and the lowest was in JB at 22%. Moreover, the greater value during the CMCO was in KL at 42%, and the

least value was in JB at 27%. That means the total volume of downloads was at the highest value in KL during MCO at 45%, and the biggest total volume of uploads was in JB during CMCO at 54%. In addition, the worst value of total latency was in the SL during MCO and in KL during CMCO at 42%. Therefore, to accelerate the performance of cellular networks, and to decrease the burden, it is important to use another wireless technology such as WiFi, visible light communication, and other types of optical wireless communications to support the network and to deliver higher data rates [52].

To conclude, for the overall evaluation of cellular networks during the two periods, it can be seen that the performance of cellular networks has decreased especially in the peak times and during weekdays during the CMCO more than the MCO times. The speed rates depend on the number of computing devices that work concurrently in addition to the user requirements and the usage of data. The processing of such a big amount of data requires intensive computing tasks.

Times		Download rate		
		JB	KL	SL
MCO	10AM	4.94	7.88	4.83
	4PM	3.15	6.24	3.23
	10PM	2.16	2.31	2.66
CMCO	10AM	4.43	3.43	5.69
	4PM	5.35	2.83	4.20
	10PM	4.04	2.71	3.69

Times		Upload rate		
		JB	KL	SL
MCO	10AM	8.19	8.26	1.37
	4PM	8.96	4.35	1.51
	10PM	8.07	5.79	1.55
CMCO	10AM	9.17	6.16	1.61
	4PM	7.34	4.24	1.92
	10PM	7.24	7.92	1.60

Times		Latency		
		JB	KL	SL
MCO	10AM	18.41	30.72	36.22
	4PM	29.44	33.72	28.09
	10PM	34.03	27.88	33.44
CMCO	10AM	19.10	29.97	21.59
	4PM	12.83	30.17	23.34
	10PM	22.69	38.86	35.76

Fig. 15. Network Performance Average Values during MCO and CMCO in All Times for All Cities.

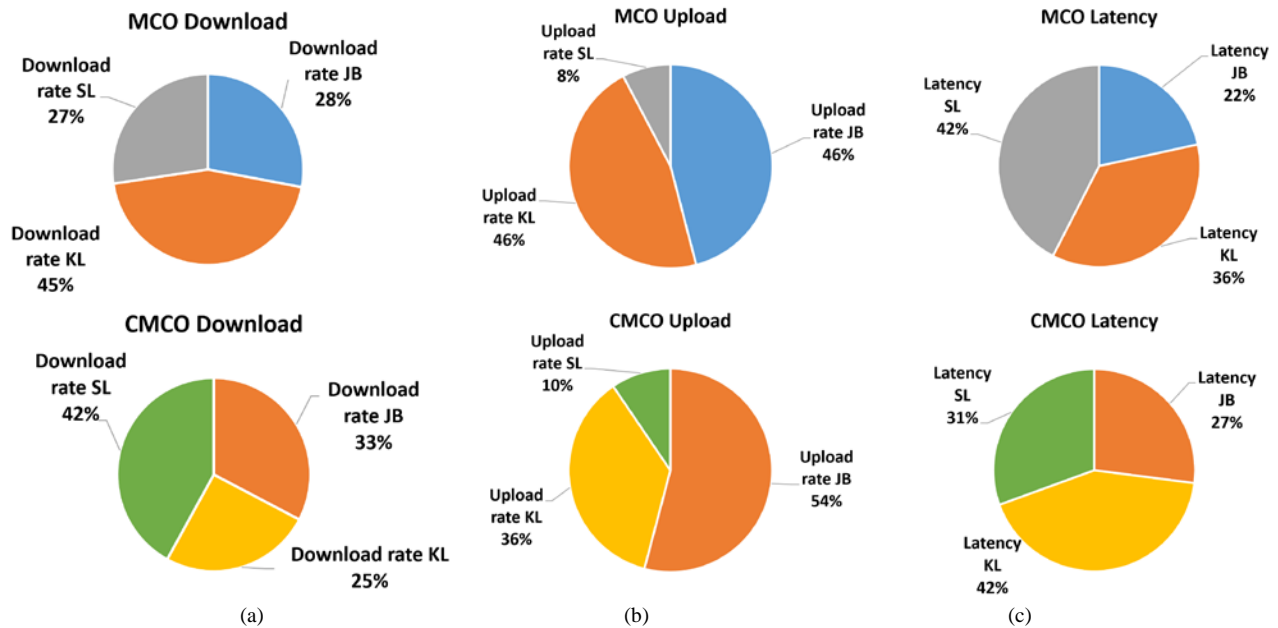


Fig. 16. Overview of Total Values of All Rates during MCO and CMCO.

VI. LIMITATIONS AND FUTURE DIRECTIONS

The main limitation of the study can be divided into few points as follows: i) data collection: only three cities were taken into account, ii) only Umobile network service provider was considered, iii) the exact location of users and distance to the cellular BS was neglected due to some difficulties, especially during the mobility around the city in the CMCO period. According to the above limitations, it is only possible to make further steps for future directions related to this study, where similar situations and circumstances would be available during a pandemic similar to COVID-19. Therefore, when studying cellular network traffic during a pandemic in Malaysia or any other country, more cities can be taken into account in addition to other factors. However, when a pandemic happens, lockdown and other types of movement restrictions take place immediately which makes it hard to conduct such research study.

VII. CONCLUSION

A new age in wireless networks has been accompanied in by the COVID-19 pandemic. Computer wireless communications is a complex challenge since multiple features are involved. The present pandemic situation and the debate in this paper clearly describe the need for efficient impact analysis in this digital era. In this paper, we investigate the effect of COVID-19 measures and restrictions on cellular network traffic in Malaysia. The results show a significant impact on our daily use of network services and applications including download speed, upload speed, and latency. Moreover, three cities were taken into account which is Kuala Lumpur, Johor Bahru, and Selangor (Cheras) using Speedtest phone applications during two periods namely MCO and CMCO. In addition, Umobile was taken into account as a cellular network provider which is one of the most popular network service providers in Malaysia. This study used a simple approach as a method of calculation and analysis of cellular networks performance. The proposed analysis is presented as a case study that consists of different components and factors for the presented findings. Companies will also be required to optimize budgets and accelerate their digital revolutions as they adjust to the new normal post-crisis. By leveraging the emerging technologies and service models transformed to do more with less, communications leaders would have to embrace these initiatives.

ACKNOWLEDGMENT

The publication of this research is supported by the UNITEN BOLD Refresh publication fund. The authors declare that they have no conflicts of interest.

REFERENCES

- [1] World Health Organization. Timeline of WHO's Response to COVID-19. 2020. Available online: <https://www.who.int/news-room/detail/29-06-2020-covid-timeline> (accessed on 29 June 2021).
- [2] World Health Organization. Coronavirus (COVID-19). 2020. Available online: <https://covid19.who.int/> (accessed on 20 August 2021).
- [3] E. Lempinen. COVID-19: Economic Impact, Human Solutions. Berkeley News. Available online: <https://news.berkeley.edu/2020/04/10/covid-19-economic-impact-human-solutions/> (accessed on 20 April 2021).
- [4] Evans, P. Canada Lost More Than 1 Million Jobs Last Month as

- COVID-19 Struck. CBC News. 2020. Available online: <https://www.cbc.ca/news/business/canada-jobs-march-covid-19-1.5527359> (accessed on 20 April 2021).
- [5] Sullivan, K. ABC News. Unemployment Rate Predicted to Reach 10 Per Cent Amid Coronavirus Pandemic, Pushing Australia Into Recession. 2020. Available online: <https://www.abc.net.au/news/2020-04-13/coronavirus-unemploy> (accessed on 22 April 2021).
- [6] Gopinath, G. International Monetary Fund Blog. The Great Lockdown: Worst Economic Downturn Since the Great Depression. 2020. Available online: <https://blogs.imf.org/2020/04/14/the-great-lockdown-worst-economic-downturn> (accessed on 26 April 2021).
- [7] Pickert, R.; Qiu, Y.; McIntyre, A. Bloomberg. U.S. Recession Model at 100% Confirms Downturn is Already Here. 2020. Available online: <https://www.bloomberg.com/graphics/us-economic-recession-tracker/> (accessed on 28 April 2021).
- [8] BBC News. Coronavirus: World Economy May Face Double Recession. 2020. Available online: <https://www.bbc.com/news/business-52306001> (accessed on 11 May 2021).
- [9] N.M. Ferguson, D.A. Cummings, S. Cauchemez, C. Fraser, S. Riley et al., "Strategies for containing an emerging influenza pandemic in Southeast Asia," *Nature*, vol. 437, no. 7056, pp. 209–214, 2005.
- [10] C. Fraser, S. Riley, R. M. Anderson and N. M. Ferguson, "Factors that make an infectious disease outbreak controllable," *Proceedings of the National Academy of Sciences*, vol. 101, no. 16, pp. 6146–6151, 2004.
- [11] N. M. Ferguson, D. A. T. Cummings, C. Fraser, J. C. Cajka and P. C. Cooley, "Strategies for mitigating an influenza pandemic," *Nature*, vol. 442, no. 7101, pp. 448–452, 2006.
- [12] S. S. Murad, S. Yussof and R. Badeel, "Wireless Technologies for Social Distancing in The Time Of COVID-19: Literature Review, Open Issues, and Limitations," *Sensors*, vol. 22, no. 6, p. 2313, 2022.
- [13] Safer Together. TraceTogether. Available online: <https://www.tracetogogether.gov.sg/> (accessed on 13 May 2021).
- [14] MIT. PACT: Private Automated Contact Tracing. Available online: <https://pact.mit.edu/> (accessed on 14 May 2021).
- [15] C. Adlhoj, European centre for disease prevention and control. In Considerations Relating to Social Distancing Measures in Response to COVID-19, Second Update; ECDC: Stockholm, Sweden, 2020. Available online: <https://www.ecdc.europa.eu/en/covid-19-social-distancing> (accessed on 16 May 2021).
- [16] M. Jancowicz, At Least 6 Countries Reimposed Lockdown Measures as New Coronavirus Cases Flared Up Again. Here's What they Looked Like. *Business Insider*. 2020. Available online: <https://www.businessinsider.com/countries/> (accessed on 02 June 2021).
- [17] S. Williams, IT Brief. COVID-19: Zoom Downloads Explode as People Work From Home. 2020. Available online: <https://itbrief.com.au/story/covid-19-zoom-downloads-explode-as-people-work-from-home/> (accessed on 02 June 2021).
- [18] H. Khatri. Analyzing Malaysia's mobile data consumption, and its effects on 4G Download Speed. Available online: <https://www.opensignal.com/2020/10/29/analyzing-malysias-mobile-data-consumption-and-its-effects-on-4g-download-speed/> (accessed on 08 June 2021).
- [19] COVID-19 RESPONSE. COVID-19 Network Update. Available online: <https://corporate.comcast.com/covid-19/network/may-20-2020/> (accessed on 03 July 2021).
- [20] R. Gong. Malaysia's Response to COVID-19: Mobile Data and Infrastructure. Available online: <https://blogs.lse.ac.uk/seac/2020/11/23/malysias-response-to-covid-19-mobile-data-and-infrastructure/> (accessed on 11 June 2021).
- [21] S. S. Murad, R. Badeel, N. S. A. Alsandi *et al.*, "Optimized Min-Min Task Scheduling Algorithm for Scientific Workflows in A Cloud Environment," *Journal of Theoretical and Applied Information Technology*, vol. 100, no. 2, p. 408-506, 2022.
- [22] Netflix. Available online: <https://edition.cnn.com/> (accessed on 14 June 2021).
- [23] Cloudflare. A global network built for the cloud. Available online: <https://blog.cloudflare.com/> (accessed on 16 June 2021).
- [24] Fastly. How COVID-19 is affecting internet performance. Available

- online: <https://www.fastly.com/blog/how-covid-19-is-affecting-internet-performance/> (accessed on 19 June 2021).
- [25] Vodafone. An update on Vodafone's networks. Available online: <https://www.vodafone.com/news/technology/update-on-vodafone-networks/> (accessed on 23 June 2021).
- [26] Telefonica. Operators advise a rational and responsible use of telecommunication networks to cope with traffic increases. Available online: <https://www.telefonica.com/en/communication-room/operators-advise-a-rational-and-responsible-use-of-telecommunication-networks-to-cope-with-traffic-increases/> (accessed on 23 June 2021).
- [27] R. Gong. Malaysia's Response to COVID-19: Mobile Data and Infrastructure. Available online: <https://blogs.lse.ac.uk/seac/2020/11/23/malysias-response-to-covid-19-mobile-data-and-infrastructure/> (accessed on 11 June 2021).
- [28] AMS-IX NEWS. 17% traffic increase on the AMS-IX platform due to Corona/ COVID-19 crisis. Available online: <https://www.ams-ix.net/ams/news/17-traffic-increase-on-the-ams-ix-platform-due-to-corona-covid-19-crisis/> (accessed on 26 June 2021).
- [29] T. Favale, F. Soro, M. Trevisan, I. Drago and M. Mellia, "Campus traffic and e-Learning during COVID-19 pandemic" *Computer networks*, 176, 107290, 2020.
- [30] A. Feldmann *et al.*, "The Lockdown Effect: Implications of the COVID-19 Pandemic on Internet Traffic," *Proceedings of the ACM Internet Measurement Conference*, pp. 1–18, 2020.
- [31] S. Dahiya, L. N. Rokanas, S. Singh, M. Yang, and J. M. Peha, "Lessons From Internet Use and Performance During Covid-19," *J. Inf. Policy*, vol. 11, pp. 202–221, 2021.
- [32] C. Zakaria, A. Trivedi, E. Cecchet, M. Chee, P. Shenoy, and R. Balan, "Analyzing the Impact of COVID-19 Control Policies on Campus Occupancy and Mobility via WiFi Sensing," *ACM Trans. Spat. Algorithms Syst.*, vol. 1, no. 1, 2022.
- [33] M. Candela, V. Luconi, and A. Vecchio, "Impact of the COVID-19 pandemic on the Internet latency: A large-scale study," *Comput. Networks*, vol. 182, no. August, p. 107495, 2020.
- [34] T. Böttger, G. Ibrahim, and B. Vallis, *How the Internet reacted to Covid-19: A perspective from Facebook's Edge Network*, vol. 1, no. 1. Association for Computing Machinery, 2020.
- [35] A. Lutu, D. Perino, M. Bagnulo, E. Frias-Martinez, and J. Khangosstar, "A Characterization of the COVID-19 Pandemic Impact on a Mobile Network Operator Traffic," *Proc. ACM SIGCOMM Internet Meas. Conf. IMC*, pp. 19–33, 2020.
- [36] The Malaysian Communications and Multimedia Commission. Available online: <https://www.mcmc.gov.my/en/home/> (accessed 11 February 2022).
- [37] E. Bolisani, E. Scarso, C. Ipsen, K. Kirchner, and J. P. Hansen, "Working from home during COVID-19 pandemic: lessons learned and issues," *Management & Marketing. Challenges for the Knowledge Society*, vol. 15, no. s1, pp. 458–476, 2020.
- [38] A. Lutu, D. Perino, M. Bagnulo, E. Frias-Martinez, and J. Khangosstar, "A characterization of the COVID-19 pandemic impact on a mobile network operator traffic," in *Proceedings of the ACM internet measurement conference*, 2020, pp. 19–33.
- [39] G. Heiler, T. Reisch, J. Hurt, M. Forghani, A. Omani et al., "Country-wide mobility changes observed using mobile phone data during COVID-19 pandemic," in *2020 IEEE International Conference on Big Data (Big Data)*, 2020, pp. 3123–3132.
- [40] V. Bhandari, "Improving internet connectivity during Covid-19," *Digital Pathways at Oxford Paper Series*, no. 4, 2020.
- [41] N. Wlömert and D. Papies, "On-demand streaming services and music industry revenues—Insights from Spotify's market entry," *International Journal of Research in Marketing*, vol. 33, no. 2, pp. 314–327, 2016.
- [42] S. Dinesh and Y. MuniRaju, "Scalability of e-commerce in the COVID-19 era," *International journal of research*, vol. 9, no. 1, pp. 123–128, 2021.
- [43] M. Batool, H. Ghulam, M.A. Hayat, M.Z. Naeem, A. Ejaz et al., "How COVID-19 has shaken the sharing economy? An analysis using Google trends data," *Economic Research-Ekonomska Istraživanja*, vol. 34, no. 1, pp. 2374–2386, 2021.
- [44] Hootsuite. A quick assessment of malysias internet usage according to the Digital, 2020. Available online: <https://27.group/a-quick-assessment-of-malysias-internet-usage/> (accessed on 10 December 2021).
- [45] H. M. Aji, I. Berakon and M. Md Husin, "COVID-19 and e-wallet usage intention: A multigroup analysis between Indonesia and Malaysia," *Cogent Business & Management*, vol. 7, no. 1, p. 1804181, 2020.
- [46] Fintech Malaysia Report 2021. Fintech Reaches an Inflection Point in Malaysia. Available online: <https://fintechnews.my/27070/malaysia/fintech-malaysia-report-2021/> (accessed 13 February 2022).
- [47] Opptus. Full-service Bespoke Market Research Company in Malaysia. Available online: <https://www.opptus.com/> (accessed 15 February 2022).
- [48] D. Portal. Available online: <https://datareportal.com/reports/digital-2021-malaysia/> (accessed 15 February 2022).
- [49] Okkla. Available online: <http://www.speedtest.net/apps/android/> (accessed 17 February 2022).
- [50] M. Z. Shafiq, L. Ji, A. X. Liu, J. Pang, S. Venkataraman et al., "A first look at cellular network performance during crowded events," *ACM SIGMETRICS Performance Evaluation Review*, vol. 41, no. 1, pp. 17–28, 2013.
- [51] F. Hu, Y. Deng, W. Saad, M. Bennis, and A. H. Aghvami, "Cellular-connected wireless virtual reality: Requirements, challenges, and solutions," *IEEE Communication Magazine*, vol. 58, no. 5, pp. 105–111, 2020.
- [52] R. Badeel, S. K. Subramaniam, Z. M. Hanapi, and A. Muhammed, "A Review on LiFi Network Research: Open Issues, Applications and Future Directions," *Applied Sciences*, vol. 11, no. 23, p. 11118, 2021.

A Deep Learning Classification Approach using Feature Fusion Model for Heart Disease Diagnosis

Bhandare Trupti Vasantrao¹

PhD Scholar

Department of Computer Science
and Engineering
Alliance College of Engineering and
Design, Alliance University
Bangalore, India

Dr. Selvarani Rangasamy²

Professor

Department of Computer Science
and Engineering
Alliance College of Engineering and
Design, Alliance University
Bangalore, India

Dr. Chetan J. Shelke³

Associate Professor

Department of Computer Science
and Engineering
Alliance College of Engineering and
Design, Alliance University
Bangalore, India

Abstract—Early Diagnosis has a very critical role in medical data processing and automated system. In medical diagnosis, automation is focused in different area of applications, in which heart disease diagnosis is a prominent domain. An early detection of heart disease can save many lives or criticality issues in diagnosing patients. In the process of heart disease diagnosis spatial and frequency domain features are used in making decision by the automation system. The processing features are observed to time variant or invariant in nature and the criticality of the observing feature varies with the diagnosis need. Wherein, the current automation system utilizes the features extracted in a large count to attain a higher accuracy, the processing overhead, and delay are considerable. Different regression approaches were developed in recent past to minimize the processing feature overhead the features are optimized based on gain performance or distance factors. The characteristic variation of feature and the significance of the feature vector are not addressed. This paper outlines a method of feature selection for heart disease diagnosis, based on weighted method of feature vector in consideration of feature significance and probability of estimate. A new optimizing function for feature selection is proposed as a dual function of probability factor and feature weight value. Simulation results illustrate the improvement of accuracy and speed of computation using proposed method compared to other existing methods.

Keywords—Deep learning approach; heart disease diagnosis; feature fusion model; ECG analysis; weighted clustering; F-Score

I. INTRODUCTION

The real time world is tending towards automation with the emergence of new technologies. To improve the system performance, different technologies were proposed to attain higher performance in the process of technologies in automation. The medical data processing is an emerging area of automation. In processing the medical data in making decision, the diagnosis systems were developed based on the captured samples which were passed to the processing unit using advanced processing algorithms. In the processing of medical data for automation, heart disease diagnosis has evolved as an area of interest in recent past. Various approaches have evolved in recent time in diagnosis of an early prediction of heart disease using electrocardiogram (ECG) or physiological parameters defined in Cleveland data set. Cardiac activity is measured as a rapid variation in the process

of heart which is based on the physical or mental working condition of a person. ECG signals are measured for the variation of electrical impulses in the heart operation based on the contraction or expansion of heart functioning. This is one of the most dominantly used observations in the diagnosis of heart disease. The process of ECG signal processing requires a high precision of storage and computation to provide an exact prediction of the heart condition. ECG processing has been now observed as a most common observation of various heart disease diagnosing such as arterial fibrillation, post-operative complication in cardio surgery [1,2], etc. The post diagnosis complications and delay in diagnosis results in longer hospitalization leading to critical illness and increases a high cost of treatments as well [3]. High risk of heart disease is observed in older age persons [4], however in recent time a rapid increase in the cases of aged between 40 and 50 is also observed. Different diagnoses of heart disease use ECG signal were presented in literature. R-peak detection for ECG analysis is outlined in [5] square double difference method for the QRS segment localization was outlined. This process is developed for feature extraction from ECG using three steps of operations. Process of sorting, thresholding and approximation of the relative region is presented. The R-peak detection is developed based on the magnitude difference of the RR peak values. The external inference has however limited the decision performance. In [6] a feature extraction process with signal denoising is presented. This method proposed soft thresholding approach in processing of ECG signal. Wavelet based method is used in the extraction of feature vectors and processed for signal denoising. The spectral decomposed bands are processed using soft threshold. The selection of feature vector is improved using K-nearest neighbor (KNN) approach outlined in [7]. This approach developed a classifier model using KNN approach in categorizing QRS patterns in ECG signal analysis. This approach applied a band pass filter in selection of feature vector and noise filtration process. In [8] band pass FIR filter was used in extracting the feature vectors. Totally six features were extracted for QRS pattern using a sliding window approach. An approach of signal denoising using modified Weibull distribution for ECG is presented in [9]. This is a blind method defined for the extraction of signal from the source using independent component analysis. In deriving line patterns Hilbert transformation were used. The extraction of

feature vector was processed with normalized multi derivative wavelet used for detection and denoising. The classification of the extraction feature is developed using Euclidian distance where a Nyman Pearson classification is developed in [10]. In [11] a wavelet-based transformation is developed for feature extraction and a temporal relation is used in the developing the feature selection. A feature extraction and selection approach are outlined in [12] where P, T peaks were used in diagnosis of heart disease. The presented approach develops a multi classification for heart disease diagnosis. A geometrical feature extraction is outlined in [13]. These approaches extract the feature based on the structural representation of ECG signal. The structural variations were derived using 1-D discrete wavelet transformation. The extracted features are however biased with noise effects which lead to misclassification. In classification model, various classifier such as support vector machine (SVM), probabilistic neural network (PNN) and multi-layer perceptron (MLP) back propagated network is outlined in [14, 15, 25]. Artificial intelligence (AI) methods have been used in the diagnosis and early alarming of cardiovascular diseases. The usage of AI in the diagnosis of cardiology application is outlined in [16,17]. These approaches significantly eliminate the baseline wandering and using the linear mapping the classification is performed. In [18] a new classifier model based on kernel driven classifier is presented. The authors in [19, 20] outlines the application of artificial neural network (ANN) and SVM model in classification. Similarly, a cross wavelet transform (XWT) is outlined in [21], where two distinct signals are correlated in deriving the correlation. Other method such as wavelet entropy [22, 23] and signature descriptors [24] were presented in automation of heart diseases diagnosis. In [28, 29] different deep learning techniques based on MRI sample processing for early detection of brain tumors and gliomas is presented. However, the feature overhead, accuracy of feature selection and a proper relation of trained features is constraint. In developing a new feature representation for heart disease diagnosis, a new approach of feature fusion using the property of discrete monitored data with the continuous ECG signals features. The overhead of feature representation is addressed ad significant feature vectors were selected in processing the system faster and more accurate. The contribution to the presented work is listed as:

- 1) Developed a new feature fusion approach using regression and weighted clustering.
- 2) Developed a classifier model using deep neural network model using feature selected.
- 3) Integrated electronic record data with ECG feature vector.

The rest of this paper is outlined in seven sections. Characteristic of the features for a heart disease diagnosis is presented in Section II. Section III outlines the existing approach of feature representation and the proposed approach is outlined in Section IV. Section V present the simulation result obtained for developed work. Section VI outlines the conclusion for the developed work.

II. FEATURE REPRESENTATION IN HEART DISEASE DIAGNOSIS

The diagnoses of heart diseases are affected by multiple factors. There are multiple observations which are inter-relative in nature. A proposed selection others feature can improve the estimation performance as well, the accuracy of estimation. The two dominant features used in the diagnosis of the heart disease are the discrete monitoring vector and the continuous varying ECG signal. The observation of the discrete feature vector is presented with 14 dominant feature representations. These features are listed as:

- 1) *Age*: Patients age in year.
- 2) *Sex*: represent the patient is Male/female gender.
- 3) *Chest pain (CP)*: define type of chest pain in a patient.
 - a) Patient having a past record of chest pain referred as typical angina (angina).
 - b) The patient past record is not effective however current observation of chest pain termed as atypical angina (abnang).
 - c) Patient with short period chest pain with painful condition termed as non-anginal pain (notang).
 - d) Patient with illness but with low possibility of heart disease termed as Asymptomatic (asympt).
- 4) *Trestbps*: Resting blood pressure of a patient at initial monitoring.
- 5) *Chol*: patient's density of cholesterol in mg/dl.
- 6) *Fbs*: it is a Boolean representation reflecting the fast state of blood sugar with higher value of 120mg/dl.
- 7) *Restecg*: Reflect patient ECG on rest state. This is reflected in 3 states having normal, abnormal or hypertrophy.
- 8) *Thalach*: this represents the patient maximum value of heart rate obtained.
- 9) *Exang*: this is s Boolean value which indicates the angina pain when exercise.
- 10) *Oldpeak*: value of ST variation when rested from exercise.
- 11) *Slope*: indicates the variation in the slope when in exercise.
- 12) *Ca*: indicate major vessels numbers.
- 13) *Thal*: indicate the status of heart condition which could be reversible or non-reversible condition.
- 14) *Num*: indicate the class attributes which indicate patient health condition which varies from 0-4 value.

These UCI features are readily available at (<https://archive.ics.uci.edu/ml/datasets/Heart+Disease>) Cleveland database, which describe the measured discrete coefficient of automation system. A feature selection approach of the monitoring feature of Cleveland data set is presented in our past work [27]. In addition to the measured discrete parameter, a continuous signal monitoring of ECG is used for representation. ECG reads the impulse of heart muscle variations. This reflects the functionality of the heart and the rhythmic repetition indicates the variation of heart movements. A typical ECG signal is measured for a continuous monitoring which could extend from 24-48 hours. For a detail monitor

about 12 different observations can be used with different placed sensors. The ECG signals are recorded for a 125Hz to 500 Hz sampling rate which are buffered in 8–12bit binary representation. The volume of discrete samples buffered into a file for processing could range from few Kb's to a large Mb. The interference during the capturing of ECG or buffering is an additional overhead to the buffered data. Basically a ECG signal is captured a 0.05-100Hz frequency range for a value of 1-10mV. ECG signal is characterized by five peaks and valleys which are termed as P, Q, R, S, and T representing the variation of heart movement. The estimation of ECG features defining the PQRST time period, peak values etc. the variation of a P-R interval could extend for 0.2 to 0.2 seconds for a normal heart condition. The duration of the ECG peaks and the amplitude variations in QRST representation diagnosis different heart disease cases such as cardiac arrhythmias, ventricular hypertrophy, myocardial infection, Arterial fibrillation etc. A representation of an ECG is signal is presented in "Fig. 1".

The ECG signal is characterized by the varying coordinates of the signal and the 12 features used in the process of diagnosis are as listed:

- 1) R_pk_cnt – Number of R peaks in the signal
- 2) Q_Dur – Q time period
- 3) R_Dur – Period of R-R time interval
- 4) R_Ampl – Amplitude for R peak
- 5) Q_Ampl - Amplitude for Q peak
- 6) S_Ampl - Amplitude for R peak
- 7) P_Loc – location of P
- 8) Q_Loc - location of Q
- 9) R_Loc - location of R
- 10)S_Loc - location of S
- 11)T_Loc - location of T
- 12)ST_dev- ST deviation

The variations of these parameters reflect the variation in heart movement which is used in the diagnosis of heart disease. The automation system developed in diagnosis of heart disease read these features as an input parameter in making decisions and diagnosis of different heart disease. In recent [26] a fusion model for ECG feature and medical record data is presented. The feature fusion model is developed based on the cluster information gain for a normalized factor. The presented approach of feature fusion is presented in following section.

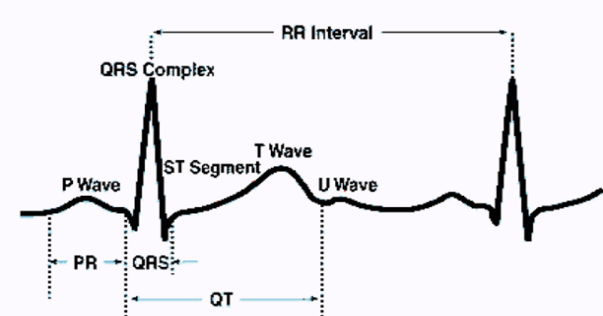


Fig. 1. Figure Illustrate ECG Signal Representation with Feature Representation. different Segment of ECG Shown in Figure P Wave, PR Interval, QRS, ST Segment and T Wave [25].

III. EMBEDDED FEATURE FUSION APPROACH

The representing features for diagnosis are very important in representing the variations in observing data. Features for heart disease diagnosis are observed by recording sensor interface or by recording physical or medical history of a patient. As multiple sources of feature vector exist developing different processing and classification system is very complex and overhead for automation system. Fusion of multiple observations can reduce the overhead in automation process. Fusion can be developed based on data, feature or decision level. A feature based fusion approach is proposed in [26]. This approach attempts to fuse the patient record data with the sensor monitoring features. The framework for feature fusion approach proposed in [22] shown in "Fig. 2". An integration of physiological data observed via sensors with the electronic recorded data is developed.

The data recorded are preprocessed for its representation and improve the quality of representation. A signal denoising, missing data filtering and normalization. The presented approach developed a feature fusion selection method based on information gain and entropy of information. Here, a set of feature vectors are structured obtained from sensors and record data. The feature selection is optimized by observing the information gain factor (IGF). IGF of the feature vector is represented as,

$$IGF(f, f') = v(f) - v(f, f') \quad (1)$$

Where f, f' are the feature vectors of sensor and recorded data, respectively. $v(\cdot)$ is the entropy function of the variable. The entropy (v) of a feature set is measured based on the redundancy parameters of the feature vectors in a class given by,

$$v(f_i) = -\sum_{i=1}^k P(f_i) \log_2(P(f_i)) \quad (2)$$

Where $P(\cdot)$ is the probability factor for a feature entering into cluster. The selection of the feature vector is governed by the distance metric of the entropy value of the two observing feature vectors. An optimization is observed when the distance is minimal. The information gain is then defined by,

$$IGF(f, f') = -\sum_{i=1}^k P(f_i) \log_2(P(f_i)) - (-\sum_{i=1}^k P(f_i) - \sum_{i=1}^k P(f_i) \log_2(P(f_i, f_i))) \quad (3)$$

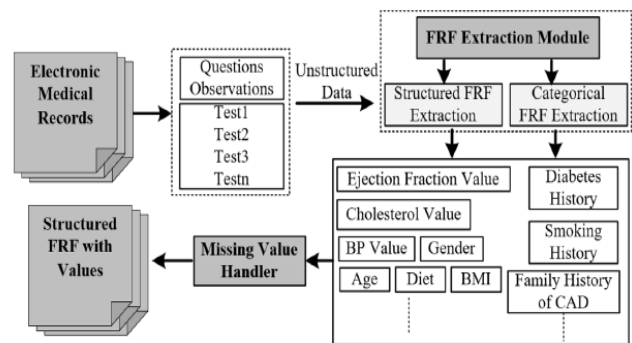


Fig. 2. Work Flow for Feature Fusion and Decision for Heart Disease Analysis. Figure Illustrate the Extraction of Features from Unstructured Electronic Medical Record.[26].

The presented work discards the features with low information gain and select only features with high information gains. The selection is based on the higher values of *IGF* which is relative to the entropy of a feature value. The presented work discards the features based on the redundancy of the feature vector in the set. A weight-based feature selection is also presented in prioritization of feature selection. However, the outlined work though improves estimation accuracy discard the features with reference to redundancy factor. The process of low entropy feature elimination reduces the processing overhead but, the criticality of the feature set is not observed. Secondly, the redundancy wrt. Vector magnitude is observed but the diversity in feature vector in fusion is not considered. This discard features of importance due to similar magnitude values. To overcome the addressed issue, a new regression model with divergence factor is presented. The outlined method is presented in the following section.

IV. WEIGHTED FEATURE FUSION MODEL AND CLASSIFICATION

Feature fusion based on entropy eliminates features of low magnitude or higher redundancy; however, the significance of such features was not observed with the criticality of heart disease. Elimination of feature of higher critical features having higher entropy could lead to lower estimation performance and hence should be selected based on feature criticality. An approach based on the divergence of feature vector and its importance based on its criticality called weighted feature fusion model (WFM) is presented. The proposed feature selection is developed based on an auto regressive model. The auto regression approach has a significant means of selecting appropriate fusion of record data with ECG features simultaneously. The auto regression method is developed based on the information theory approach where the optimization is achieved using burg's method. The method minimizes the information loss based on feature vectors and the approximation of test feature with the registering group (G_i). For a given set of feature vector $\{f, f'\}$, where f is the features derived from the grouping of ECG signal (f_{ECG}) and the record values (f_R) of patient physiological details and f' is the feature set of other classes.

$$f = \{f_{ECG}, f_R\} \quad (4)$$

An auto regression for the feature set is computed to derive the variation (γ_i) using distance metric for all 'j' features set in the group given as,

$$\gamma_i = (f_i - f'_{i,j})^2 \quad (5)$$

To observe the criticality of the feature vector a weight value is associated with different class of heart disease based on the severity factor. Severity of the heart disease is defined in 5 different classes as listed in Table I, where each class group is associated with a weight value indicating its criticality. The weight value of each class is allotted based on its criticality. Here a higher value of 0.5 is given to class-4 type of heart disease and 0.1 is given to the healthy class. The associated weight value for each class is presented in Table I.

TABLE I. WEIGHT ASSOCIATION WITH CLASS ATTRIBUTE FROM ELECTRONIC RECORD DATA. THE WEIGHT VALUE OF EACH CLASS IS ALLOTTED BASED ON ITS CRITICALITY

Group (G_i)	Class	Infection level in %	Categorize	Weight allotted (ω_i)
G_0	Healthy	Nil	Healthy	0.1
G_1	class -1	0-20%	starting level	0.2
G_2	class -2	20-40%	Effective with-Low	0.3
G_3	class -3	40-60%	Effective with - High	0.4
G_4	class -4	60-max%	Significant level	0.5

A regression model is developed for the selection of fusion feature where a Bergman divergence approach is applied for selecting the best suitable feature values. The optimization of feature selection is defined as a minimization function given as,

$$Arg \min(P[\gamma_i(f, f')]) \quad (6)$$

Features with minimum probability of diversity are eliminated and features with higher diversity are considered for selection. The two-feature set f and f' are processed for computing diversity (γ_i) based on squared distance. The Probability function $P(\cdot)$ defines the probability of diversity among the set of fusion features. The diversity factor is computed as,

$$\gamma_i(f, f') = (f - f')^2 \quad (7)$$

The features with higher diversity factor have a higher probability of selection. However, the proposed approach measures the criticality of the feature in selection based on the class of severity. For the measure of class severity, a weight value is associated listed in Table I.

The features are processed for computing an aggregated weight factor ($A\omega$) for all k-classes given by,

$$A\omega = \sum_{i=1}^k \omega_i \quad (8)$$

Where, ω_i are the associated weight values for each class value. An aggregated class weight (ω_{kc}) for each group (c) is computed given by,

$$\omega_{kc} = \sum_{i=1}^k \omega_{i_c} \quad (9)$$

The selection of feature vector in fusion is optimized by the minimization of divergence factor and having feature vector with relative higher weight value. the optimization for feature selection is given by,

$$Fsel \Rightarrow \{arg \min(P[\gamma_i(f, f')]), ((\sum_{i=1}^k \omega_{i_c}) > \frac{A\omega}{k})\} \quad (10)$$

The process of feature selection presented optimizes the features with higher diversity and having weight associated higher than the relative weight value of all class $A\omega/k$. This condition selects features which has a variation in feature and are of more significance. The proposed feature fusion approach based on divergence factor and aggregated weight is outlined in the algorithm below.

ALGORITHM

Input: Feature set (f, f')

Result: selected fusion features

Process 1: Diversity feature selection

1. for each class,
2. Compute fusion feature for each patient 'i',
 $f_i = \{f_{ECGi}, f_{Ri}\}$
3. Compute divergence of feature vector,
 $\gamma_i(f, f') = (f - f')^2$
4. Converge the feature with the minimal factor
 $\arg \min(P[\gamma_i(f, f')])$
5. Update the feature fusion for each group with minimal divergence,

$$G_u = f_i \Rightarrow G_u$$

Where 'u' define the group label varying 1-5.

6. Update the feature selection using weight allocation using process 2.

Process 2: Weighted selection approach (G_u, ω_i)

1. Associate weight (ω_i) for each group G_u

$$G_u \Leftrightarrow \omega_i$$

2. Compute aggregated weight factor $(A\omega)$,

$$A\omega = \sum_{i=1}^k \omega_i$$

3. compute each class aggregated weight,

$$\omega_{kc} = \sum_{i=1}^k \omega_{i_c}$$

4. Converge the feature selection of fusion,

$$Fsel \Rightarrow \{ \arg \min(P[\gamma_i(f, f')]), (\sum_{i=1}^k \omega_{i_c}) > \frac{A\omega}{k} \}$$

end Process1

end Process0

end

Selected features are distinct with variations and higher weight associated which is passed to a classifier unit. The classification operation is developed based on Ensemble deep learning model. The Neural Network is developed with training and testing phase. The network is trained for minimum class error and the NN model is developed with multiple layers with input, hidden and output layers. The network layout of the NN model is show in "Fig. 3".

The input to the NN model is the selected fusion features x_i and weight value v_i . For a given input set a set of weight is associated given as, $v = [v_1, v_2, \dots, v_v]$ for the input $X = [x_1, x_2, \dots, x_v]$

The output of the network is given by,

$$Y = f(v_i x)$$

or

$$Y = \sum_{i=1}^v v_i x_i \quad (11)$$

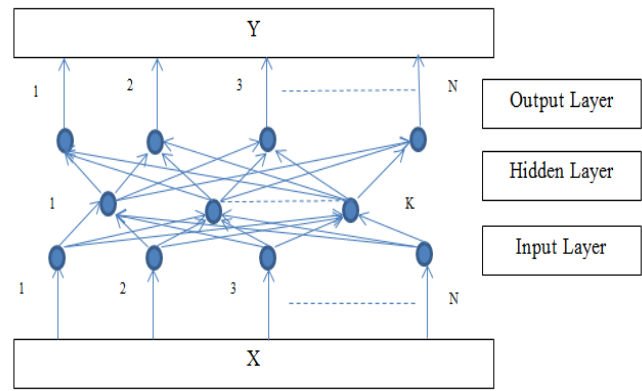


Fig. 3. Network Layout of the NN Model. Figure Illustrate the General Form of Neural Network with n-Input Nodes, N-Output Nodes and K Hidden Layers.

The output of the network is given as a bipolar representation of the NN model output given by,

$$Y = f(vt x) \quad (12)$$

$$Y = \begin{cases} -1, & x < 0 \\ 1, & x \geq 0 \end{cases} \quad (13)$$

A multi-level NN model is used for transition as illustrated in "Fig. 4".

The multi-level model process for error minimization based on the weight updation where a feed forward back propagated network for error minimization is developed. A weighted input-output relation with bias (g) passed to activation function (a) is used for mapping the output to input based on the updation. The relation of the input to output is given as,

$$Y_i = f\left(\sum_{i=1}^n \omega_i a\left(\sum_{i=1}^k \Phi_i x_i + g_i\right)\right) \quad (14)$$

The output is obtained as a function of updating weight variable Φ and bias value (g) and the class weight value is applied with the weight updation of NN model.

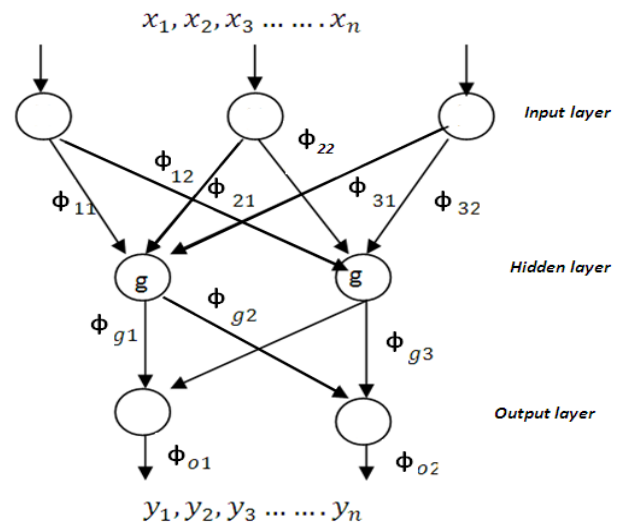


Fig. 4. Multi-Layer Network for Classification is Shown in Figure with Input X_1-X_n and Output y_1-y_n .

V. EXPERIMENTAL RESULTS

The presented approach of weighted feature fusion model (WFM) is tested for the presence or absence of heart disorderness. Simulation is developed for electronic records (ER) from updated Cleveland database consisting of 600 patient records, where each patient has 14 records of entry. The records are updated for time line observation and selected for fusion. ECG signals of 600 patients are taken from MIT database. ECG features are computed for peak values and time periods, which are used for fusion with the ER data. The proposed approach WFM is compared with the existing approach of embedded fusion model [26] and classifier models for performance evaluation. Few sets of ECG signals and ER used in training the network is shown in “Fig. 5” and Table II, respectively.

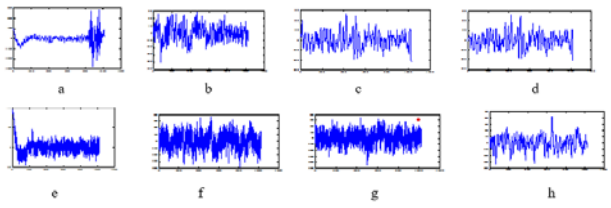


Fig. 5. ECG Signals from Database used for Training. The ECG Signals from MIT Database are used to Compute Peak Values and Time Periods.

Feature for each ECG signal is computed and fusion approach is applied with selective approach as outlined in Section IV. For testing an ECG signal is randomly selected from the database and corresponding ER record is read.

The ECG signal is processed for feature extraction, where the features are processed for fusion and selection and mapped to classifier model. NN classifier performs the classification for detection of disease diagnosis. The processing ECG signal is shown in “Fig. 6”.

The ECG signal is processed for peak detection and time period computation. Magnitude and time interval in reference to QRST measurement is computed. The magnitude plot for the peak values is illustrated in “Fig. 7”.

Computed features for the processing ECG signal are listed and a Mean value is computed to observe the variation of computing features for different ECG signals. Table III list the feature values for different test samples where the R peak counts (F1), Q-duration(T1), RR interval (T2), R-peak(F2), Q-peak(F3), S-peak(F4), P-location(F5), R-location(F6), S-location(F7), T-location(F8) and ST deviation(F9) is computed.

TABLE II. ER RECORD FOR THE PATIENTS USED IN TRAINING. THIS ER RECORD CONTAIN 14 DIFFERENT ATTRIBUTES FIELDS

ER-Values	ER-filed													
	age	sex	Chest pain	Trestbps	Chol	Fbs	Restecg	Thalach	Exang	Oldpeak	Slope	Ca	Thal	Num
P1	64	0	3	140	313	0	0	133	0	0.2	1	0	7	0
P2	43	1	4	110	309	0	0	161	0	0	2	0	7	3
P3	45	1	4	128	259	0	2	143	0	3	2	3	3	1
P4	58	0	3	144	312	1	0	152	1	0	1	2	3	4
P5	50	0	2	142	200	0	2	134	0	0.9	1	0	7	1

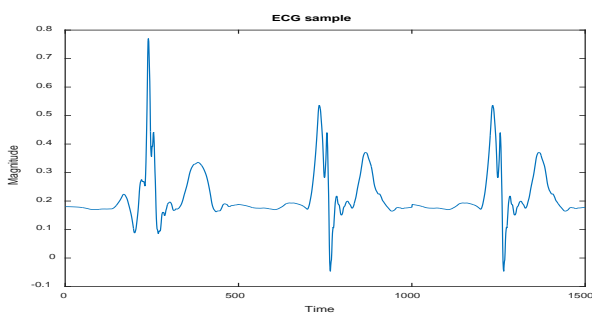


Fig. 6. Test Sample for Classification. Figure shows ECG Input Signal for Classifier.

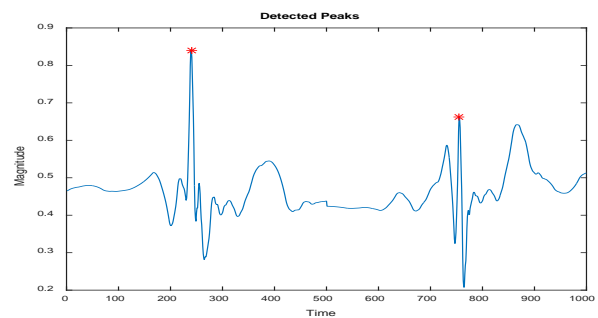


Fig. 7. Peak Level Representation of the Processing ECG Signal. Figure Illustrate that the Computed Peak Value of the Signal.

TABLE III. OBSERVATION FOR DIFFERENT FEATURE VECTORS COMPUTED FROM ECG SIGNAL. TABLE SHOWS THE LIST OF THE FEATURE VALUES FOR THE DIFFERENT TEST SAMPLES.

Sample	T1 (ms)	T2(ms)	F1	F2	F3	F4	F5	F6	F7	F8	F9	Mean
S1	585	578	2	0.86	0.62	0.66	273	351	347	361	0.13	227.2
S2	576	567	0.392	0.81	0.62	0.61	254	323	332	323	0.14	216.14
S3	534	573	0.37	0.85	0.62	0.66	251	356	343	334	0.12	217.60
S4	561	543	0.395	0.83	0.62	0.62	276	376	346	367	0.15	224.69
S5	588	571	0.36	0.89	0.62	0.69	212	398	323	369	0.16	223.97
S6	579	577	0.31	0.81	0.62	0.63	265	312	364	362	0.12	223.77
S7	565	567	0.67	0.80	0.62	0.67	223	353	368	367	0.16	222.35

The features are processed for fusion with ER and selection using WFM approach. The selected features passed to classifier model result in the classification of heart diseases. To observe the performance of the developed method retrieval accuracy, recall rate, precision and F-Score of the system is computed for 5-random test iterations. The accuracy of the system is measured as,

$$\text{Accuracy} = \frac{TP+TN}{TP+TN+FP+FN} \quad (15)$$

The four parameters of observation (TP, TN, FP, FN) is derived from the confusion matrix presented in Table IV given as,

Where,

TP is the true positive.

TN is true negative

FP is false positive and

FN is false negative.

The precision for the developed system is defined by,

$$P = \frac{TP}{TP+FP} \quad (16)$$

Recall factor for the system is computed by,

$$R = \frac{TP}{TP+FN} \quad (17)$$

and the F-Score of the system is measured given by,

$$F = \frac{2 \cdot R \cdot P}{R+P} \quad (18)$$

Observation for the developed system is listed in Tables V to VIII.

System accuracy of the proposed approach is shown in “Fig. 8” and it is observed to be improved by 0.7%. The accuracy is observed based on the selected feature due to divergence and weighted feature. As the features of critical observations are retained rather than entropy measure the accuracy of the proposed system is improved.

TABLE IV. CONFUSION MATRIX FOR THE ANALYSIS

Diagnosis	Effective	Not-Effective
Effective	TP	FN
Not-Effective	TN	FP

TABLE V. SYSTEM ACCURACY OF THE WFM APPROACH. THE PROPOSED WFM APPROACH HAS 99.2% ACCURACY, WHICH SHOWS 0.71% INCREASE IN ACCURACY THAN THAT OF FUSION MODEL

SVM [26]	L-Regression [26]	Decision Tree [26]	Naïve Bayes [26]	Fusion model [26]	Proposed WFM
84.4	92.2	77.6	83.4	98.5	99.2

TABLE VI. SYSTEM RECALL RATE OF THE DEVELOPED APPROACH. THE PROPOSED WFM APPROACH HAS 1.97% INCREASE IN RECALL THAN THAT OF FUSION MODEL

SVM [26]	L-Regression [26]	Decision Tree [26]	Naïve Bayes [26]	Fusion model [26]	Proposed WFM
81.5	95.2	77.7	78.5	96.4	98.3

TABLE VII. SYSTEM PRECISION OF THE DEVELOPED APPROACH. THE PROPOSED WFM APPROACH HAS 98.9% PRECISION

SVM [26]	L-Regression [26]	Decision Tree [26]	Naïve Bayes [26]	Fusion model [26]	Proposed WFM
87.5	89.2	84.6	88.8	98.2	98.9

TABLE VIII. SYSTEM F-SCORE OF THE DEVELOPED APPROACH. THE PROPOSED WFM APPROACH HAS 98.4% F-SCORE

SVM [26]	L-Regression [26]	Decision Tree [26]	Naïve Bayes [26]	Fusion model [26]	Proposed WFM
84.5	92.2	77.6	83.4	97.2	98.4

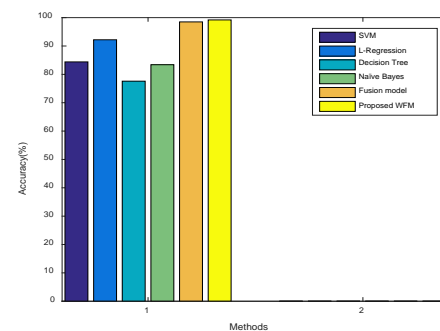


Fig. 8. Figure shows the Accuracy Plot for WFM Approach. The Developed System Achieves 99.2% Accuracy.

System recall, and precision shown in “Fig. 9, 10” is observed to have an improved by 2%, and 0.7% respectively. The selective approach by weighted method results in improvement of the system parameters. The F-Score of the system is improved by 1.2% as shown in “Fig. 11”.

Observation for the developed approach for different time period of observation is listed in Table IX. The variation of time period in ECG monitoring has significance on the classification performance is shown in “Fig. 12”. For a short period, observation of 10ms the accuracy obtained is 97%, wherein for 15ms observation it is obtained to 98% and for a higher time period observation of 20ms the accuracy is retained to 98%, signifying an average period observation has a maximum accuracy and long period observation has same effect as redundant features are observed. The time period for longer period is observed to be higher compared to short period observation. Selection of the features with high divergence and weight parameter result in selection of feature vectors which result in lower time for classification.

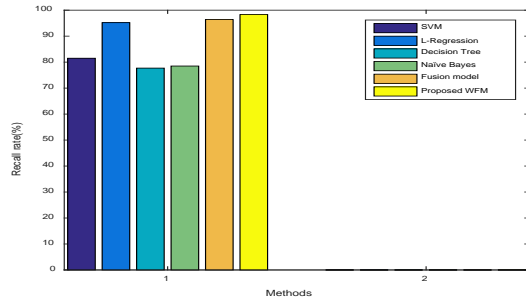


Fig. 9. Recall Rate Plot for WFM Approach. Figure shows the Recall Rate of Developed System Up to 98.3%.

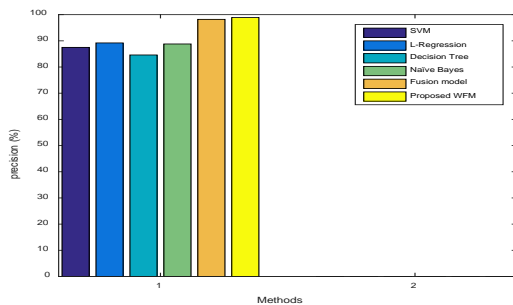


Fig. 10. Precision Plot for WFM Approach. Figure Shows the System Precision of Developed System Up to 98.9%.

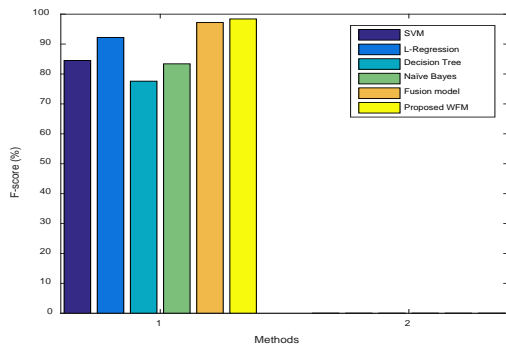


Fig. 11. F-Score Plot for WFM Approach. Figure shows the F-Score of Developed System Up to 98.4%.

TABLE IX. OBSERVATION FOR ECG SIGNAL WITH DIFFERENT TIME PERIODS. THE OBSERVATIONS OF ECG SIGNAL WITH TIME PERIODS 10MS, 15MS, 20MS

Observing time period	Accuracy (%)	Recall	Precision	F-Measure	Time (sec)
10ms	97.3	95.3	98.1	96.8	10.6
15ms	98.6	97.4	98.6	98.2	14.5
20ms	98.7	97.6	98.8	98.4	18.3

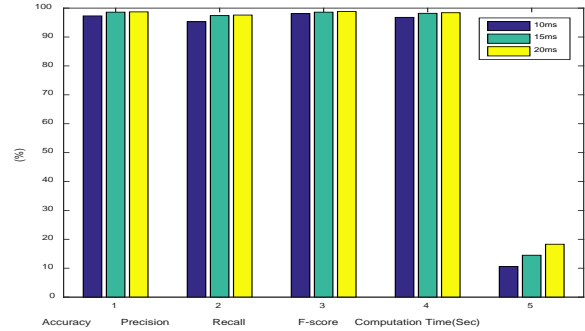


Fig. 12. Observation for different Time Period of Sample. The Figure Illustrates the Observations of ECG Signal with Time Periods 10ms, 15ms, 20ms.

VI. CONCLUSION

An approach for feature fusion based on the selection of feature vector and class attribute is presented. The process of weighted clustering based on information gain and updated feature is presented. This approach illustrated an enhancement of feature selection and improvement in accuracy of the system based on the observations obtained. The system accuracy is obtained to be improved based on the selected feature and fusion of multiple parameters in observation. The significant illustration of feature selection has given dual advantage of feature selection and classification performance for heart disease diagnosis. The selective method of feature selection based on divergence and weighted method provide a more accurate selection of fusion feature as the criticality factor is monitored based on associated weight factor which results in the improvement of system performance. In future, the proposed approach will be extended with varying conditions of heart monitoring with patient having multiple diseases and varying signal input conditions such as magnitude variations and signal wandering distortions.

REFERENCES

- [1] Cochet H, Dubois R, Sacher F, Derval N, Sermesant M, Hocini M, Montaudon M, Haïssaguerre M, Laurent F, Jaïs P. Cardiac arrhythmias: multimodal assessment integrating body surface ECG mapping into cardiac imaging. *Radiology* 2014; 271:239 doi: 10.1148/radiol.13131331.
- [2] S. Mandal, A. H. Roy and P. Mondal, Detection of Cardiac Arrhythmia based on feature fusion and Machine Learning algorithms, 2021 International Conference on Intelligent Technologies (CONIT) 2021; doi: 10.1109/CONIT51480.2021.9498352.
- [3] Park J, An J, Kim J, Jung S, Gil Y, Jang Y, Lee K, Oh IY. Study on the use of standard 12-lead ECG data for rhythm-type ECG classification problems. *Computer Methods Programs Biomed* 2022; 214:106521. doi: 10.1016/j.cmpb.2021.106521.

- [4] Lyon A, Mincholé A, Martínez JP, Laguna P, Rodriguez B. Computational techniques for ECG analysis and interpretation in light of their contribution to medical advances. *J R Soc Interface* 2018; 15:20170821. doi: 10.1098/rsif.2017.0821.
- [5] Hossain, Adibalbnat, SabitriSikder, Annesha Das, and Ashim Dey. Applying Machine Learning Classifiers on ECG Dataset for Predicting Heart Disease. *International Conference on Automation, Control and Mechatronics for Industry 4.0 (ACMI), IEEE* 2021.
- [6] Skala T, Tudos Z, Homola M, Moravec O, Kocher M, Cerna M, Ctvrlik F, Odstreil F, Langova K, Klementova O, Taborsky M. The impact of ECG synchronization during acquisition of left-atrium computed tomography model on radiation dose and arrhythmia recurrence rate after catheter ablation of atrial fibrillation - a prospective, randomized study. *Bratisl Lek Listy* 2019; 120:177. doi: 10.4149/BLL_2019_033.
- [7] Diwakar, Manoj, Amrendra Tripathi, Kapil Joshi, Minakshi Memoria, and Prabhishkek Singh. Latest trends on heart disease prediction using machine learning and image fusion. *Materials Today* 2021; 3213.
- [8] Xu, Yang, Mingzhang Luo, Tao Li, and Gangbing Song. ECG signal denoising and baseline wander correction based on CEEMDAN and wavelet threshold. *Sensors* 2017; 2754.
- [9] Adam, A. M., B. S. El-Desouky, and R. M. Farouk. "Modified Weibull distribution for Biomedical signals denoising." *Neuroscience Informatics* 2, no. 1 (2022): 100038.
- [10] Fan Liang, WeihongXie, Yang Yu. Beating Heart Motion Accurate Prediction Method Based on Interactive Multiple Model: An Information Fusion Approach. *BioMed Research International* 2017; 1279486. <https://doi.org/10.1155/2017/1279486>.
- [11] Saeed, Jwan Najeeb, and Siddeeq Y. Ameen. Smart Healthcare for ECG Telemonitoring System. *Journal of Soft Computing and Data Mining* 2021; 75.
- [12] Yildirim O, Talo M, Ciaccio EJ, Tan RS, Acharya UR. Accurate deep neural network model to detect cardiac arrhythmia on more than 10,000 individual subject ECG records. *Comput Methods Programs Biomed* 2020; 197:105740. doi: 10.1016/j.cmpb.2020.105740.
- [13] Ullah A, Anwar SM, Bilal M, Mehmood RM. Classification of Arrhythmia by Using Deep Learning with 2-D ECG Spectral Image Representation. *Remote Sensing* 2020; 12:1685. <https://doi.org/10.3390/rs12101685>.
- [14] Sahoo, Santanu et al. Machine Learning Approach to Detect Cardiac Arrhythmias in ECG Signals: A Survey. *Irbm* 2020; 41:185.
- [15] Solbiati M, Trombetta L, Sacco RM, Erba L, Bozzano V, Costantino G et al. A systematic review of noninvasive electrocardiogram monitoring devices for the evaluation of suspected cardiovascular syncope. *Journal of Medical Devices, Transactions of the ASME* 2019 Jun 1; 13:024001-1. <https://doi.org/10.1115/1.4042795>.
- [16] Sujith, A. V. L. N., Guna Sekhar Sajja, V. Mahalakshmi, Shibili Nuhmani, and B. Prasanalakshmi. "Systematic review of smart health monitoring using deep learning and Artificial intelligence." *Neuroscience Informatics* 2, no. 3 (2022): 100028.
- [17] Sardar, Partha, J. Dawn Abbott, Amartya Kundu, Herbert D. Aronow, Juan F. Granada, and Jay Giri. "Impact of artificial intelligence on interventional cardiology: from decision-making aid to advanced interventional procedure assistance." *JACC: Cardiovascular Interventions* 12, no. 14 (2019): 1293-1303.
- [18] Balasaheb H. Patil, Dr. P. M. Patil. Crow search algorithm with Discrete Wavelet Transform to aid Mumford Shah inpainting model. *Springer Journal Evolutionary Intelligence* 2018; 11:73. <https://doi.org/10.1007/s12065-018-0160-6>.
- [19] Zhao W, Sampalli S. Sensing and Signal Processing in Smart Healthcare. *Electronics* 2020; 9:1954. <https://doi.org/10.3390/electronics9111954>.
- [20] Fontaine GH, Li G, Saguner AM, Frank R. Mechanisms of torsade de pointes tachycardia in patients with spontaneous high-degree atrioventricular block: A modern look at old data. *J Electrocardiol* 2019; 56:55. doi: 10.1016/j.jelectrocard.2019.05.007.
- [21] Joshi, Aashna, Maitrik Shah. Coronary Artery Disease Prediction Techniques: A Survey. *Lecture Notes in Networks and Systems* 2020; 203:593.
- [22] Padeletti M, Bagliani G, De Ponti R, Leonelli FM, Locati ET. Surface Electrocardiogram Recording: Baseline 12-lead and Ambulatory Electrocardiogram Monitoring. *Card Electrophysiol Clin*. 2019; 11:189. doi: 10.1016/j.ccep.2019.01.004.
- [23] Ayon, Safial Islam, Md Milon Islam, Md Rahat Hossain. Coronary artery heart disease prediction: a comparative study of computational intelligence techniques. *IETE Journal of Research* 2020; 67:1.
- [24] Korra, Seena& Sudarshan, E. Smart healthcare monitoring system using raspberry Pi on IoT platform. *ARPN Journal of Engineering and Applied Sciences* 2019; 14:872.
- [25] Almustafa, K.M. Prediction of heart disease and classifiers' sensitivity analysis. *BMC Bioinformatics* 2020; 21:278. <https://doi.org/10.1186/s12859-020-03626-y>.
- [26] Farman Ali, Shaker El-Sappagh, S.M. Riazul Islam, Daehan Kwak, Amjad Ali, Muhammad Imran, Kyung-Sup Kwak, A smart healthcare monitoring system for heart disease prediction based on ensemble deep learning and feature fusion, *Information Fusion* 2020; 63:208 <https://doi.org/10.1016/j.inffus.2020.06.008>.
- [27] Bhandare Trupti Vasantrao & Rangasamy Selvarani., Weighted Clustering for Deep Learning Approach in Heart Disease Diagnosis. *International Journal of Advanced Computer Science and Applications*. Vol.12, No.10, 2021.
- [28] Disha Wankhede, Dr Selvarani Rangasamy, Review on Deep learning approach for brain tumor glioma analysis, *International Conference on Convergence of Smart Technologies IC2ST-2021*, <https://doi.org/10.17762/itii.v9i1.144>
- [29] Disha Wankhede, Dr. Selvarani Rangasamy, Dynamic Architecture Based Deep Learning Approach for Glioblastoma Brain Tumor Survival Prediction, *Neurosci. Informatics*, vol. 2, no. 4, p. 100062, 2022, doi: 10.1016/j.neuri.2022.100062.

An Effective Demand based Optimal Route Generation in Transport System using DFCM and ABSO Approaches

Archana M. Nayak^{1*}

Research Scholar
Computer Engineering Department
Gujarat Technological University, Gujarat, India

Nirbhay Chaubey²

Associate Professor
Dean of Computer Applications
Ganpat University, Gujarat, India

Abstract—The transportation network service quality is generally depends on providing demand based routing. Different existing approaches are focused to enhance the service quality of the transportation but them fails to satisfy the demand. This work presents an effective demand based objectives for optimal route generation in public transport system. The importance of this work is providing demand based optimal routing for large city transportation. The proposed demand based optimal route generation process is described in subsequent stages. Initially the passengers in each route are clustered using Distance based adaptive Fuzzy C-means clustering approach (DFCM) for collecting the passengers count in each stop. Here the number of cluster members in each cluster is equivalent to the passenger count of each stop. After the clustering process, adaptive objectives based beetle swarm optimization (ABSO) approach based routing is performed with the clustered data. Then re-routing is performed based on the demand based objectives such as passenger's count, comfort level of passengers, route distance and average travel time using ABSO approach. This ABSO approach provides the optimal routing based on these demand based objectives. The presented methodology is implemented in the MATLAB working platform. The dataset used for the analysis is Surat city transport historical data. The experimental results of the presented work is examined with the different existing approaches in terms of root mean square error (9.5%), mean error (0.254%), mean absolute error (0.3007%), correlation coefficient (0.8993), vehicle occupancy (85%) and accuracy (99.57%).

Keywords—Clustering; optimization; demand based objectives; comfort level; optimal routing

I. INTRODUCTION

The increased population rate in large cities is one of the major transportation issues in developing countries. The unplanned organization in those cities increases the mobility demand and improves the tendency of private vehicle transport ownerships [1, 2]. This issue is common for all large cities have to deal with hundreds of vehicles running through their street each day. The congestion of traffic is increasing day by day even in rural areas also. Moreover, the traffic congestion associated delays are happening more often [3, 4]. A public transport network plays an important role in changing the demand from private to effective transportation and reduced traffic congestion [5]. The better public transportation can avoid the traffic congestion. To enhance the

cooperation in public transport systems, different demand based models are introduced. Passenger comfort [6] is one of the vital indexes used to validate the quality of public transport system.

The quality of the public transport system is depends on increasing the passenger comfort. Therefore, enhancing the bus comfort is a great attention by the public transport to attract the passengers [7-9]. The passenger's choice of transport is depends on various factors like comfort ability, travelling time, expense and reliability. Therefore, transport authorities are making attention to attract the passengers by providing passengers demand based transportation [10, 11]. The comfort of transportation is categorized into two classes. One is based on the performance of vehicle and the other one is depends on the operation of transport. Various studies are presented for providing demand based public transportation [11]. The investigated works states that uncertainties in travel times and traffic increases the passenger's stress level and reduces the passenger's quality [12, 13]. Some of the researchers proved that the comfort is depends on the passenger's load. So, accurately determining the bus comfort and providing demand based effective bus routing is important for improving the quality of transportation [14]. The load factor of passenger's and the bus travel time is an important and foremost for the quality of transportation [15]. The proficient public transport system can lessen the negative issues of private transport network.

Moreover, the quality of transport is mainly depends on minimization of travel time and waiting time. This effectively increases the performance of transportation [16]. The transportation authorities are responsible for generating the optimal routes. Based on the different objectives, transport authorities are determining the demanded bus routes and schedules [17]. The main concern of public transport is satisfying the public needs and the transport authorities are focussing on their profit. Moreover, different constraints are considered in the existing researches for the generation of transportation routes [18]. But the optimal route generation is still in demand.

Numerous optimization approaches are utilized in the existing works to enhance the transportation framework. Some of the existing optimization approaches are, genetic algorithm

*Corresponding Author.

(GA) [19, 20], simulated annealing (SA), Tabu search (TS) and Swarm intelligence (SI) [21]. These optimization approaches are proved their capability, effectiveness in optimal route generation in transportation network. But all the major issues of transportation are not solved as a whole and optimal route generation is still in demand. Moreover, demand based optimal route generation is not performed in the existing works.

The main motivation of proposed work is providing demand based transportation in large cities. Therefore, the quality of transportation can be achieved by considering major objectives such as passenger's count, comfort level of passengers, route distance and average travel time. In the presented work, demand based optimal route generation is proposed to improve the quality of transportation network. The major contributions of the presented methodology is described as,

- To effectively cluster the passengers in the transportation network, distance based fuzzy c-means clustering (DFCM) approach is utilized. This approach is utilized to gather the accurate passenger's count of each station in the transportation network.
- Optimal routing is generated by using effective objective based adaptive beetle swarm optimization. Re-routing is performed based on the different objectives such as comfort level of passengers, passenger's count, route distance and average travel time.
- Demand based effective routing is obtained by the proposed ABSO optimal routing approach. Here, the performance of the proposed approach is enhanced based on the considered effective objectives. This enhances the quality of the transportation by providing demand based vehicles.

The organization of this research work is described as: Section 2 surveys the recent related works, the presented approach is described in section 3, results and their discussion is provided in section 4 and the section 5 concludes the paper respectively.

II. RELATED WORK

Ovidiu Cosma et al. [22] presented an innovative methodology for two-stage transportation issues with fixed costs related to the routes. The developed heuristic algorithm solves the investigated transportation issues and it was attained by integrating the linear programming optimization issue within the genetic optimization process. Moreover, an effective local search process was incorporated with genetic optimization algorithm able to enhancing the global search. The proposed methodology effectively solves the transportation issue and enhances the quality in transportation. The performance can be enhanced further by using other optimization approaches in transportation.

Jiangtao Liu et al. [23] developed a routing based on the integration of travel demand, vehicle supply and restricted

infrastructure. Based on these constraints, vehicles were optimally assigned in the routes to satisfy the passenger's. Various decomposition techniques were adapted in this research. Vehicle based integer linear programming model was presented for space time state (STS) with Dantzig Wolfe decomposition methodology. The presented methodology effectively increases the efficiency and reduces the congestion in transportation. But the proposed methodology was challenging to predict the optimal routes based on the travel demand.

Jishnu Narayan et al. [24] developed an integrated bus route selection and scheduling framework for static and dynamic public transport networks. The introduced framework based on the dynamic demand based route generation using an iterative learning framework. The effective routing based on this proposed approach effectively reduces the average waiting time of passengers. The combination of fixed and flexible transport networks enhances the routing ability and satisfies the passengers. Moreover, the day to day learning was considered to effective selection of routes and allocation of transport vehicles. The proposed approach can be improved in future by incorporating the time and reliability of passenger's.

Mahmoud Owais and Abdullah Alshehri [25] developed a pareto optimal route generation in transportation networks. Instead of considering the travel time like existing approach, the presented approach considered the relation among the traffic flow and the respective trip time. Based on the demand based information, the initialized routes were changed and select the traffic allocation approach. Finally, different objectives based approach was conducted with pareto optimal route generation. Further, the research performance can be enhanced by using effective recent techniques in future.

Philipp Heyken Soares [26] developed a zone based optimized routing in an urban network. Node based optimization was introduced on transportation routes by predicting the passenger trips for each stops. Here, the hybrid methodology was utilized for evaluate the journey times of source to destination. The travel time of each stop was determined by the node based procedures. The developed optimization procedure was applied on input considered real world database and the enhancement was shown existing routing framework. Further enhancements were possible in various factors based on passenger's comfort and satisfaction.

The investigated existing approaches are tried to solve the issues in the transportation system. But still, the existing approaches are not reached the satisfaction level by solving all the issues. Some of the approaches are focused on increasing the passenger's while decreasing the comfort of passengers. Therefore, the quality of transportation is needs to be enhanced by considering major objectives. The proposed work considered the four effective objectives such as passenger's count, comfort level of passengers, route distance and average travel time to provide the demand based routing. This resolves the issues present in the existing routing. Based on the proposed demand based routing, the service quality of the transportation can be increased.

III. PROPOSED METHODOLOGY

This work presents an effective demand based optimal route generation in transport system. At first, Distance based adaptive Fuzzy C-means clustering approach (DFCM) is utilized for clustering the passengers in each stop. Here, the number of cluster members in each cluster is equivalent to the passenger's count of every station. Afterwards, adaptive beetle swarm optimization approach based routing is performed based on the clustered data. Further, re-routing is performed based on the effective objectives such as passenger's count, comfort level of passengers, route distance and average travel time using ABSO approach. In the optimal route generation approach, objectives are analysed in each pair of stations in the route using the ABSO approach. This ABSO approach enhances transportation system by providing demand based routing. The schematic diagram of the presented methodology is depicted in Fig. 1.

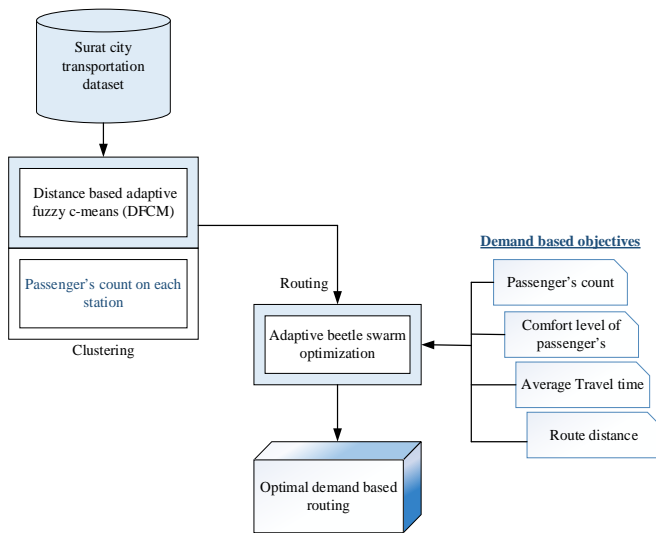


Fig. 1. Schematic Diagram of Presented Methodology.

The process of demand based optimal routing in the transportation system is described in the subsequent sections. Initially, the input Surat city transportation history data is considered and the passenger of each station is obtained by the proposed DFCM clustering. Afterwards, routing is performed by the proposed ABSO approach and demand based objectives are updated in this optimization approach to effectively performs the re-routing. This methodology effectively provides the demand based routing.

A. Distance based Adaptive Fuzzy C-Means (DFCM) Clustering

The proposed DFCM clustering approach minimizes the objective function through the iterative process. Consider, $Q = \{q_1, q_2, q_3, \dots, q_p\}$ represents the vectors of cluster centre, $\bar{U} = [\bar{\mu}_{kp}]^{m \times p_{opt}}$, $\bar{\mu}_{kp}$ represents the membership degree of input data y_k to the cluster centre q_p , $\bar{\mu}_{kp} \in (0, 1)$. The objective function of the presented DFCM approach is described as,

$$\bar{J}_{DFCM} = \sum_{p=1}^{p_{opt}} \sum_{k=1}^m \bar{\mu}_{kp} \|y_k - q_p\|^N + D(k) \quad (1)$$

Here, N represents the constant to control the fuzzy function of clustering results $N \in [1, +\infty)$. Here, the cluster membership function is updated by the subsequent condition (2),

$$\bar{\mu}_{kp} = \frac{1}{\sum_{l=1}^{p_{opt}} \left(\frac{D_{kp}}{D_{kl}} \right)^{\frac{2}{n-1}}} \quad (2)$$

The cluster centre vectors are updated by the subsequent condition (3),

$$q_p = \frac{\sum_{k=1}^m (\bar{\mu}_{kp})^n y_k}{\sum_{k=1}^m (\bar{\mu}_{kp})^n} \quad (3)$$

The fuzzy c-means clustering is processed into different steps to minimize the objective function \bar{J}_k with the update of \bar{U} and \bar{Q} .

The effectiveness of the fuzzy c-means clustering is based on the initial means. The means are having great impact on the final clustering. The existing FCM approaches are based on the arbitrary initialization to examine the centroid for clustering. But, the proposed DFCM approach centroids are selected according to the dense nodes positioning. The nearest neighbouring nodes are considered as a dense nodes. The nearest neighbouring nodes are the nodes with minimum distance. The distance of the nodes is evaluated based on the dense nodes to estimate the passenger's count in each station. Distance is evaluated by the subsequent condition (4),

$$D(k) = \sum_{l=1}^M \exp \left[-\|y_k - y_l\|^2 * \left(\frac{1}{Dense\ cluster} \right)^2 \right] \quad (4)$$

$$Dense\ cluster = \frac{M}{P_{opt}} \quad (5)$$

Here, P_{opt} represents the optimal cluster center. Based on these evaluations, the high dense data points are considered as a first cluster centre, and the farthest from the first centre is considered as a second centre and so on. The P^{th} cluster centroid is satisfied with the condition $Maximum \left\{ \prod_{k=1}^{p-1} (q_p - q_k) \right\}$.

The evaluated distance using condition (4) is updated in the condition (1). Then, the objective function satisfies the

condition $|\bar{J}_k^{(t)} - \bar{J}_k^{(t-1)}| < \delta$, and then forms the optimal clustering. Here, δ represents the threshold function. The

initial cluster centre is needs to be changed to overcome the issue of distance among the node position and the cluster centre is zero. The cluster centres are updated based on the consideration that if the neighbouring node centre is far from $q_1, q_2, q_3, \dots, q_p$ is then considered as the updated cluster centroid. Clusters are formed by assigning nearest sensor nodes to the cluster based on this DFCM approach. The nearest sensor nodes are considered based on the minimum distance of sensor nodes. The pseudo code of the DFCM clustering is described in algorithm 1.

In algorithm 1, the proposed DFCM clustering steps are provided. This effectively clusters the historical data of passengers. Evaluate the objective function \bar{J}_{DFCM} as per the condition (1), if the condition satisfies $|\bar{J}_k^{(t)} - \bar{J}_k^{(t-1)}| < \delta$ then the optimal clustering is obtained. The passenger's count details of each station are obtained in this clustering approach.

Algorithm 1: Pseudo code of DFCM clustering

Input: Initialize the passenger data in the transportation network $S = \{s_1, s_2, \dots, s_n\}$ and the initial centres $Q = \{q_1, q_2, \dots, q_p\}$

Output: Optimal clustering

Begin

Initialization of passenger's data $S = \{s_1, s_2, \dots, s_n\}$ and centroids $Q = \{q_1, q_2, \dots, q_p\}$.

Compute the objective function (\bar{J}_{DFCM}) utilizing condition (1).

Evaluate membership nodes and cluster centres with conditions (2) and (3) at \bar{J}_{DFCM} computation step.

Compute the adaptive distance evaluation for passenger data using the condition (4)

Update the cluster centroids by utilizing the condition (3),

If the clustering process attains best outcome at maximum iterations, then the iteration is terminated.

Else

Repeat the above procedure until reaches the best solution.

Return optimal clustering

End

B. Demand based Optimal Routing in Transportation System

The demand based optimal routing is attained by the proposed adaptive objectives based beetle swarm optimization approach. Optimal re-routing is performed by updating the demand based objectives such as passenger's count, comfort level of passengers, route distance and average travel time are described in the subsequent sub sections.

1) *Demand based objective measures:* In this section, effective objectives are evaluated based on the transportation demand is described in the subsequent sections,

a) *Comfort Level of Passengers:* The passenger's comfort level is depends on the number of passenger's in the vehicle and the capacity of the vehicle. Comfort level of passenger is estimated by the subsequent condition (6),

$$\bar{C}_\alpha = \frac{\bar{P}_N}{\bar{V}_C} \quad (6)$$

Here, α represents the passenger's comfort level, \bar{P}_N represents the number of passengers in the vehicle and \bar{V}_C represents the vehicle's capacity.

b) *Passenger's Count:* The number of passengers in each station is computed based on the count between source and destination. Passenger's count is computed by the subsequent condition (7),

$$\bar{P}_m = \frac{\bar{K}}{\sum_i \bar{K}_i} \quad (7)$$

Here, \bar{P}_{count} represents the passenger's count, \bar{K} represents the number of passengers arriving in the station in a specified time. Similarly, number of passengers in vehicle based on the passenger count is computed by the subsequent condition (8).

$$V_m = V_{m-1} (1 - \bar{P}_m) + \frac{R_m \bar{K}}{N} \quad (8)$$

Here, N represents the average number of trips in a specified time, R_m is computed by the subsequent condition (9),

$$R_m = \begin{cases} \frac{M-m}{M-1} & \text{for direction : } m \rightarrow M \\ \frac{m-1}{M-1} & \text{for direction : } m \rightarrow 1 \end{cases} \quad (9)$$

Here, m and M represents the two consecutive stations.

c) *Route Distance:* Route length represents the sum of the distance among all the mid stations. The route distance is estimated by calculating the distance among each stop from source and destination. The distance between two adjacent nodes are computed by the subsequent condition (10),

$$\bar{D}_{route} = a \frac{\bar{S}_j \bar{D}_k}{dist_{j,k}} \quad (10)$$

Here, \bar{D}_{route} represents the route distance, a signifies the adjustment factor, \bar{S}_j represents the source point of trip at j ,

\bar{D}_k represents the destination point trip at k , and $dist_{j,k}$ signifies the distance between the two station points.

d) *Average Travel Time*: The travel time is the starting and stopping time of vehicle from source to destination. The travel time of passenger is varies based on the different stations. The average travel time is computed by the various transport stations. The travel time of passengers are computed by the subsequent condition (11),

$$\bar{T}_{avg} = \sum_{i=1 to n} TS_{\kappa} \quad (11)$$

Here, \bar{T}_{avg} represents the average travel time, TS represents the travel time between two stations. The travel time is increases based on the increasing distance.

2) *Optimal routing in transport network using adaptive objective based beetle swarm optimization (ABSO)*

Initially, starting and target points are initialized in the transport network. Moreover, the general attributes of beetle swarm optimization approach is initialized. The beetle swarm optimization approach is the combination of beetle foraging mechanism and swarm optimization. Two beetle antennae of the beetles are used to explore the nearby regions. If the one side antenna finds the more valuable data, then the beetle will move to that antenna side. This optimization approach is based on the behaviour of beetles. The flow diagram of the presented ABSO process is depicted in Fig. 2.

Initially, the input optimization parameters are initialized and the fitness is evaluated based on the average weight of four objectives by utilizing the condition (17). Then the swarm attributes of the optimization algorithm is updated. If the maximum iteration is reached then the optimal global best solution is considered as the optimal routing.

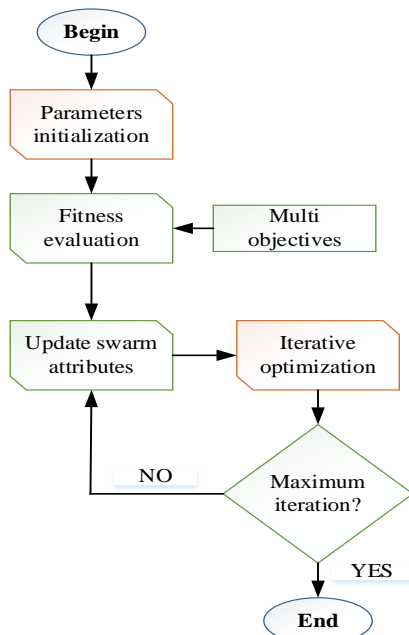


Fig. 2. Flow Diagram of ABSO Routing.

a) *Parameters Initialization*: The input population of optimization approach is expressed as $\bar{Y} = (\bar{Y}_1, \bar{Y}_2, \bar{Y}_3, \dots, \bar{Y}_m)$. Here, m represents the population size. The position (\bar{P}_a) and speed attribute (\bar{S}_a) of beetle is first arbitrarily initialized in a m dimensional search space. Speed attributes of beetle k is expressed as $\bar{V}_k = (v_{k1}, v_{k2}, v_{k3}, \dots, v_{ks})^T$. The set of individual best is expressed as $b_i = (b_{i1}, b_{i2}, b_{i3}, \dots, b_{is})^T$. The global best set signified as $\bar{b}_g = (b_{g1}, b_{g2}, b_{g3}, \dots, b_{gs})^T$. The speed update of the optimization approach is described in the subsequent condition (12),

$$y_{js}^{t+1} = y_{js}^t + \bar{\lambda} v_{js}^t + (1 - \bar{\lambda}) \in_{js}^t \quad (12)$$

Here, $\in_{js}^{t+1} = \delta^t \times v_{js}^t \times F(\bar{Y})$ (13)

$$y_{rs}^{t+1} = y_{rs}^t + v_{rs}^t \times \frac{\bar{d}^t}{2} \quad (14)$$

$$y_{ls}^{t+1} = y_{ls}^t - v_{ls}^t \times \frac{\bar{d}^t}{2} \quad (15)$$

The position attribute of every beetle individual is updated by the subsequent condition (16),

$$v_{js}^{t+1} = \bar{\omega} v_{js}^t + \bar{c}_1 \bar{r}_1 (p_{is}^t - \bar{y}_{is}^t) + \bar{c}_2 \bar{r}_2 (p_{gs}^t - \bar{y}_{gs}^t) \quad (16)$$

Here, $s = 1, 2, \dots, S$ and $j = 1, 2, \dots, m$, t represents the iteration time, \in_{js} signifies the displacement increment examined by the strength of data predicted by the beetle antennae, $\bar{\lambda}$ signifies the decrement factor, $\bar{\omega}$ signifies the inertia weight, \bar{r}_1 and \bar{r}_2 are arbitrary function with value ranging from 0 to 1, \bar{c}_1 and \bar{c}_2 signifies the degree of impact of individual and global best on the beetle, δ^t signifies the searching step size of beetle, \bar{d} represents the predicted distance of antennae, $F(\bar{Y})$ signifies the fitness function, y_{ls}^{t+1} signifies the predicted distance of left antennae, y_{rs}^{t+1} signifies the predicted distance of right antennae.

b) *Fitness Evaluation*: Fitness function is evaluated based on four different objectives such as, passenger's count, comfort level of passengers, route distance and average travel time. Fitness of optimal route generation using the proposed optimization approach is described in the subsequent condition (17),

$$F(\bar{Y}) = \min \left(\frac{\bar{P}_m + \bar{D}_{route} + \bar{C}_a + \bar{T}_{avg}}{4} \right) \quad (17)$$

Here, \bar{P}_m represents the passenger count computed by the condition (6), \bar{D}_{route} represents the route distance computed by the condition (10), \bar{T}_{avg} represents the average travel time computed by the condition (11), \bar{C}_α represents the comfort level of passengers computed by the condition (9), $F(\bar{Y})$ represents the fitness function for the evaluation of optimal route. The minimum values of fitness function are considered as the global best value (\bar{b}_g).

c) *Update of Optimization Attributes in Beetle Swarm Optimization:* The position and speed attributes of every beetle swarm is updated by the conditions in (12) to condition (16). Further, the fitness function is computed for each updated beetle individuals. Also, the individual best (\bar{b}_i) solutions are updated and attains the global (\bar{b}_g) solution.

d) *Iterative Optimization:* The variables ∂^t and \bar{d} of the optimization is updated by the subsequent conditions (18) and (19).

$$\partial^t = 0.95\partial^{t-1} \tag{18}$$

$$\bar{d}^t = 0.95\bar{d}^{t-1} + 0.01 \tag{19}$$

Here, \bar{d} represents the predicted distance of antennae, and ∂^t signifies the searching step size of beetle. Iterations are performed to the maximum by updating these variables to end optimization. Finally, optimal demand based routing is obtained according to the global best output.

IV. RESULTS AND DISCUSSION

The experimental results of the proposed demand based on the optimal route generation in transport system is implemented in the working platform of MATLAB. The dataset used for the implementation is Surat city historical transport data. The performance of the presented technique is analyzed with the existing Inverse distance weighting (IDW), and Empirical Bayesian Kriging (EBK) [27], XGBoost, gradient boosting regression model (GDBR), support vector machine regression (SVR), and multiple linear regression model (MLR) [28], agent based scheduled routing [29] techniques in terms of Root mean square error, mean square error, mean absolute error, correlation coefficient, accuracy, vehicle occupancy. The performance metrics utilized for analyzing the presented work is described in the subsequent sections.

A. Dataset Description: Surat City Historical Data

Surat city transportation system historical data is considered for the evaluation of optimal demand based routing performance in the presented work. The passenger detail for this prediction process is taken from Surat city dataset. The passenger details are taken for one year (June 2017 to June 2018) for passenger flow prediction in transportation. The passenger details are taken for one year (June 2017 to June

2018) for optimal route prediction in transportation. The presented DFCM clustering approach output is depicted in Fig. 3.

In Fig. 3, the proposed DFCM clustering output of passenger's count is provided. This provides the accurate details of passengers in every station. The number of passengers in each station is gathered by using this clustering process. Each cluster provides the passenger details of each station. Based on the predicted passenger's count, each route passenger's flow for august month is depicted in Fig. 4.

In Fig. 4, august month data of Surat city transportation dataset is examined for evaluating the Passenger's count variations of route 1. The passenger count of route 1 is depicted in Fig. 4 for each day in a month. Here, RAST, SAHD, KADB, UDHD and ADGS represent the different stations in the considered route 1. The passenger count of each day is calculated by adding the passenger details of each trip of the day. The passenger count in RAST station is higher than the other stations. Similarly, passenger's count variations of route 2 are analyzed with august month data and it are depicted in Fig. 5.

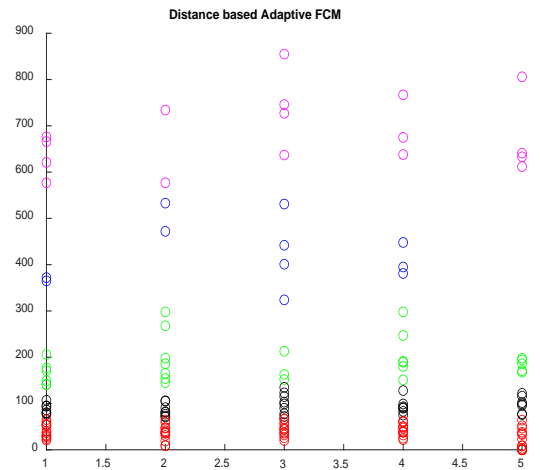


Fig. 3. DFCM Clustering Output.

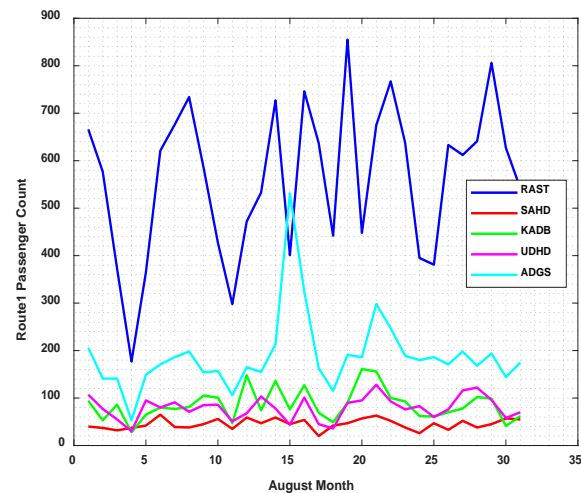


Fig. 4. Passenger's Count Variations of August Month with Route 1.

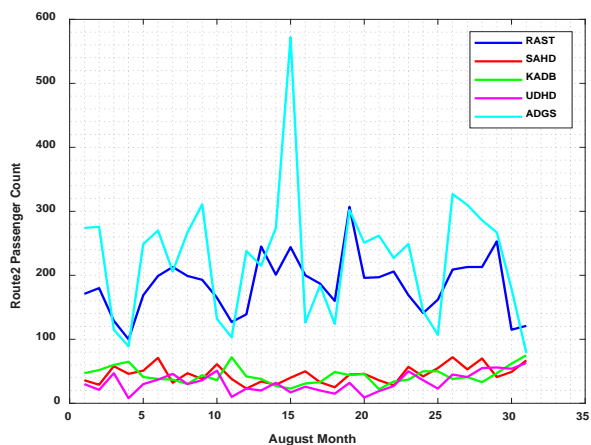


Fig. 5. Passenger's Count Variations of August Month with Route 2.

In Fig. 5, Passenger's count variations of route 2 are examined for evaluating the august month data of Surat city transportation dataset. In Fig. 5, the passenger count of each station of route 2 is depicted. Here, RAST, SAHD, KADB, UDHD and ADGS characterize the different stations of the considered route 2. The passenger counts in route 2 with different stations are provided. This demonstrates that the passenger count in station name ADGS is higher than other stations. Similarly, the daily passenger flow is analyzed for different stations with various trip timings are depicted in Fig. 6.

In Fig. 6, daily passenger's flow of different stations such as, 10, 1003, 1015, 2040, and 2799 is analyzed with various bus timings from morning 6 O' clock to night 9 O'clock. This demonstrates that the daily passenger flow of the station number 10 is higher than the other stations. Moreover, the passenger count is at peak at 9 o'clock timing than other timings. Here, the daily passenger flow of each trip timing details is demonstrated for a month. The passenger count of each trip for one month is illustrated for various stations. Moreover, the passenger's demand for one month data is depicted in Fig. 7.

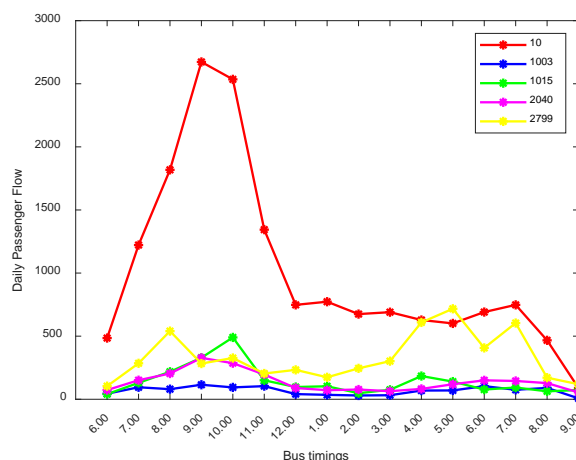


Fig. 6. Daily Passenger's Flow of different Stations with Various Trip Timings.

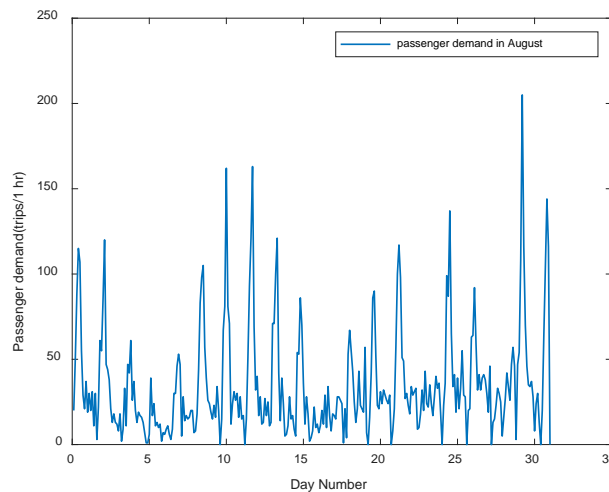


Fig. 7. Passenger Demand in August Month.

The Fig. 7 depicts that the demand of passengers for a month. Based on the passengers demand, transport needs to be allocated with optimal routing approach. Here, the passenger demand is calculated based on the passenger data for 30 days. Furthermore, routing is performed based on the adaptive beetle swarm optimization approach for august month data. The effective objectives such as passenger count, travel time, comfort level and distance are considered for re-routing. In this way, an optimal demand based routing is generated to enhance the quality of service. Moreover, the passenger demand for a week based data for a month is depicted in Fig. 8.

In Fig. 8, passenger demand is evaluated for an august month data. Here, the passenger demand is evaluated for each day in a week for a month. This figure provides the passenger demand data for a month on weekly basis. The demand based objectives are considered for each pair of stops in the transportation system. The demand based objective measure for the pair of stations 1 and station 5 is depicted in Fig. 9.

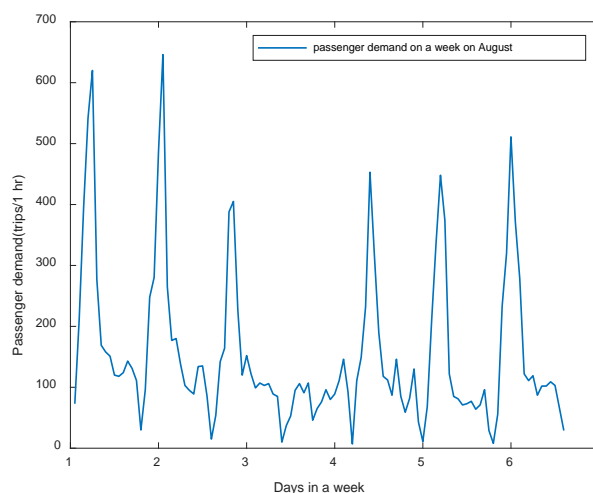


Fig. 8. Passenger Demand of Week based Data for an August Month.

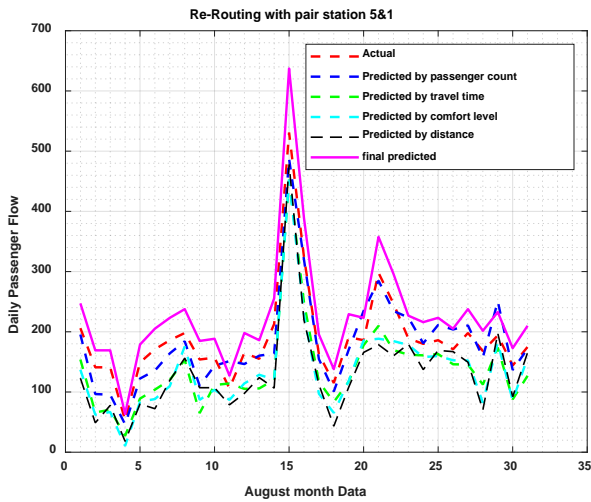


Fig. 9. Demand based Routing with Pair of Station 1 & 5.

In Fig. 9, august month data is considered to predict the demand based routing. Here, the daily passenger flow is illustrated by considering various parameters like passenger count data, travel time, comfort level and distance. Finally, daily passenger is depicted by considering all these parameters. Here, pair of stations 1 and station 5 is illustrated to prove the effectiveness of proposed demand based routing. The proposed route 2 is obtained as an optimal routing. Similarly, optimal routing based on the effective objectives with pair of station 3 and station 4 is depicted in Fig. 10.

In Fig. 10, demand based routing with pair of station 3 and station 4 is provided. Here, august month data is considered to analyze the routing based on different objectives. The combined objectives output is providing higher performance than the single objectives. This illustration proved that the effectiveness of proposed demand based routing. Similarly, optimal routing based on the effective objectives with pair of station 1 and station 2 is depicted in Fig. 11.

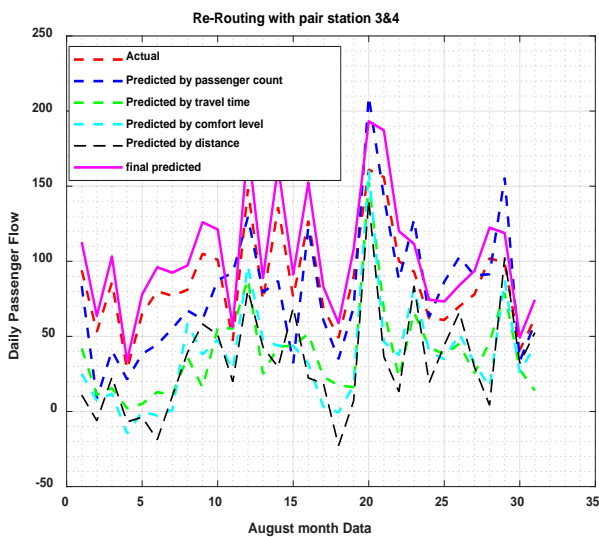


Fig. 10. Demand based Routing with Pair of Station 3 & 4.

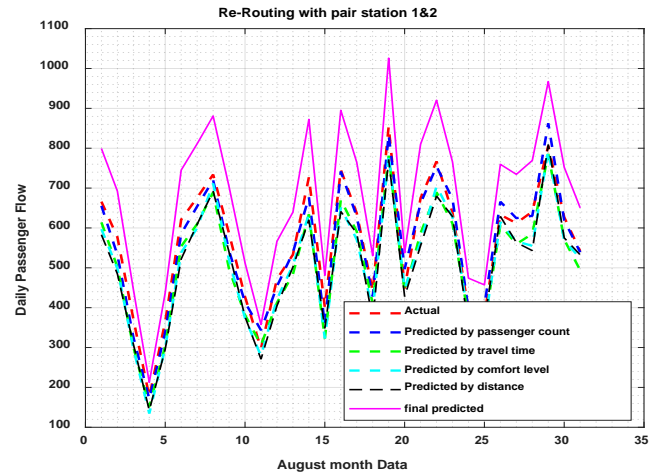


Fig. 11. Demand based Routing with Pair of Station 1 & 2.

In Fig. 11, optimal routing is evaluated with pair of station 1 and station 2. Here, the prediction performance is analyzed without objectives and with objectives such as passenger count, travel time, comfort level, distance. The final predicted output is based on all the combined objectives. Optimal routing based on the effective demand based objectives for the pair of station 4 and station 5 is depicted in Fig. 12.

In Fig. 12, routing performance is evaluated with the pair of stations 4 and station 5. This proves that the proposed demand based optimal routing achieves enhanced performance than the single objective based predictions. The passenger's flow with the proposed demand based routing is enhanced. This enhancement proves that the service quality of the transportation system.

B. Performance Metrics

In this section, different performance metrics such as Root mean square error, mean square error, mean absolute error, correlation coefficient, accuracy, vehicle occupancy are described in the subsequent sub sections.

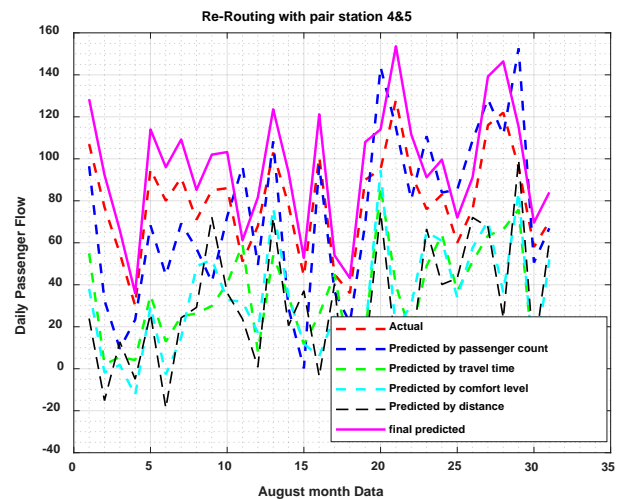


Fig. 12. Demand based Routing with Pair of Station 4 & 5.

1) *Correlation coefficient*: Correlation coefficient is evaluating the correlation among the considered variables. The correlation coefficient range is 0 to 1. The performance is proved by obtaining the value closer to 1. The correlation is estimated between the attained optimal route and the other existing routes. It is computed by the subsequent condition (20),

$$\bar{C}_c = \frac{Cov(y_k, z_k)}{\sqrt{Var[y_k] - Var[z_k]}} \quad (20)$$

Here, y_k and z_k represents the predicted optimal and original routing, $Cov(y_k, z_k)$ represents the covariance of y_k and z_k , $Var[y_k]$ represents the variance of y_k and $Var[z_k]$ represents the variance of z_k . In the optimal routing prediction, correlation coefficient is used to examine the linear correlation among the predicted optimal data and original data.

2) *Root means squared error (RMSE)*: This RMSE measure is used to examine the variation between predicted and the original values. This demonstrates the model accuracy from the perception of predicted deviation. This is computed by the subsequent condition (21).

$$\bar{R}_{MSE} = \sqrt{\frac{\sum_{k=1}^m |y_k - z_k|^2}{m}} \quad (21)$$

Here, \bar{R}_{MSE} represents the root mean squared error. This measure is used to prove the prediction accuracy rate by minimizing the error in optimal routing.

3) *Mean absolute error (MAE)*: The mean absolute error performance is the average of absolute values of the variation among all the predicted values and the original values. This accurately predicts the error of the predicted output. The MAE measure is computed by the subsequent condition (22).

$$\bar{M}_{AE} = \frac{1}{m} \sum_{k=1}^m |y_k - z_k| \quad (22)$$

Here, \bar{M}_{AE} represents the mean absolute error. The minimum value of mean absolute error proves that the proposed demand based optimal routing is effective technique demand based optimal route prediction.

4) *Mean squared error (MSE)*: This measure is similar to the MAE performance metric but only the difference is taking square in the mean differences of the input and predicted data. It is calculated with the mean of the square difference among the original input and the predicted data. It is evaluated with the subsequent condition (23).

$$\overline{MsE} = \frac{1}{T} \sum_{k=1 \dots T} (z_k - \tilde{z}_k)^2 \quad (23)$$

Here, \overline{MsE} represents the MSE, T represents the total considered data, z_k and \tilde{z}_k denotes the original data and predicted data correspondingly.

5) *Accuracy*: Accuracy measure is the ratio of correctly predicted data to the total number of observations. Moreover, it is the percentage of accurateness for predicting the data. It is evaluated utilizing the subsequent condition (24).

$$\bar{A}_y = \frac{\bar{C}_p}{T_p} \quad (24)$$

Here, \bar{A}_y represents the accuracy, \bar{C}_p represents the correct predictions, and T_p represents the total predictions.

6) *Vehicle occupancy*: Vehicle occupancy is determined by the occupancy rate and it is equivalent to average number of passengers in the vehicle. It is computed based on the average numbers of passengers used the vehicles in the same route. The average computation is attained from the number of trips in the same route for a day. The passenger's count of each trip is estimated to attain the vehicle capacity. The vehicle occupancy is computed by the subsequent condition (25).

$$V_o = \frac{\sum T_N(P_C)}{N} \quad (25)$$

Here, V_o represents the vehicle occupancy, T_N represents the number of vehicle trips, N represents the Trips number, and P_C represents the passengers in each trip.

C. Performance Analysis

In this section, performance of the presented approach is examined with the existing strategies in terms of Root mean square error, mean square error, mean absolute error, correlation coefficient, accuracy, vehicle occupancy. The performance metrics and their validations are examined with the various existing approaches. The RMSE performance evaluation is analyzed with the existing approaches for each station is depicted in Fig. 13.

In Fig. 13, the RMSE performance demonstration is provided with existing approaches for each station. The RMSE value of the presented approach for each station is station 1 (0.2629), station 2 (0.2217), station 3 (0.2474), station 4 (0.2629), and station 5 (0.0768) respectively. The presented demand based route prediction is examined with the existing XGBoost, gradient boosting regression model (GDBR), support vector machine regression (SVR), and multiple linear regression model (MLR) approaches. Here, the RMSE performance is evaluated for 5 stations with the

existing approaches. The RMSE performance on varying stations is portrayed in Table I.

In Table I, RMSE measure values are lesser than the different existing approaches. The obtained RMSE of presented approach for each station is station 1 (0.2629), station 2 (0.2217), station 3 (0.2474), station 4 (0.2629), and station 5 (0.0768) correspondingly. The performance analysis of the proposed demand based routing with existing approaches is depicted in Fig. 14.

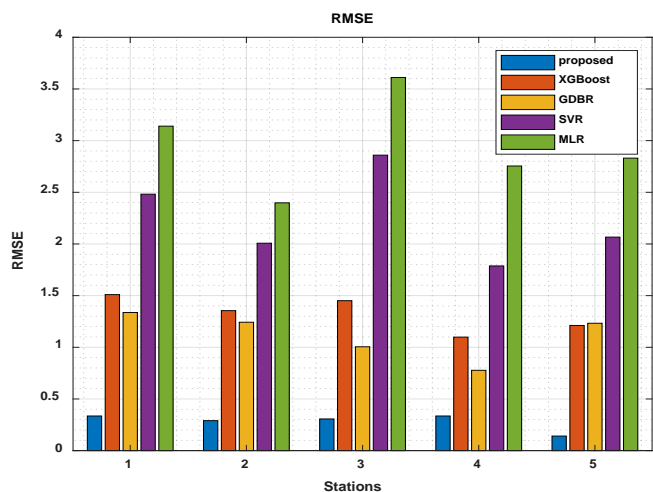


Fig. 13. Performance Analysis on RMSE for Each Station.

TABLE I. RMSE PERFORMANCE ON DIFFERENT STATIONS

Technique	XGBoost	GDBR	SVR	MLR	Proposed
STATION 1	1.1043	1.1131	2.5570	3.0657	0.2629
STATION 2	1.4011	1.0558	1.6021	3.1922	0.2217
STATION 3	0.8773	1.3297	1.3851	3.0004	0.2474
STATION 4	0.6586	0.9369	3.0113	2.7080	0.2629
STATION 5	1.0901	1.5924	2.7080	3.5162	0.0768

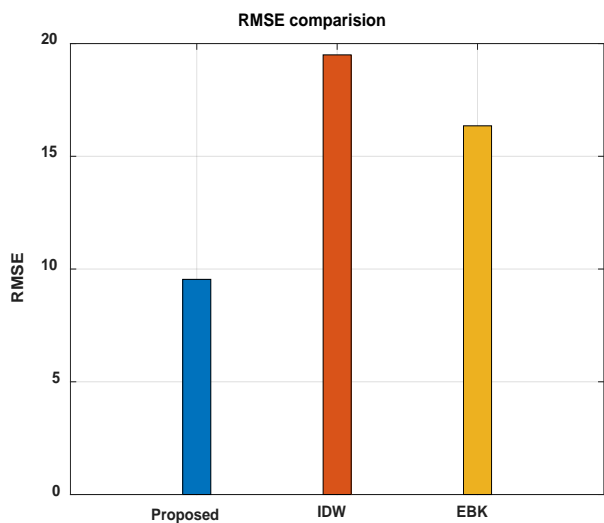


Fig. 14. Performance Analysis on RMSE.

In Fig. 14, RMSE performance evaluation is provided with existing Inverse distance weighting (IDW), and Empirical Bayesian Kriging (EBK) [27] approaches. The existing EBK, and IDW approaches are used Orissa dataset, which is overcome by the proposed approach with surat city dataset. Here, the RMSE value of presented approach is 9.5. This error value is much lesser than the existing IDW (19.4994) and EBK (16.3527) approaches. This demonstrates that the presented approach provides reduced RMSE than the existing approaches to prove the efficiency of the proposed approach. The comparison analysis on RMSE is mentioned in Table II.

In Table II, the RMSE of the presented approach is compared with the existing approaches. The proposed approach attains reduced RMSE than the existing IDW, EBK [27] approaches. The presented approach attains enhanced performance than the existing techniques by reducing the error rate. The comparison analysis of MSE is examined with the existing approaches are depicted in Fig. 15.

In Fig. 15, performance of the presented approach in terms of MSE is analyzed with the different existing approaches like XGBoost, GDBR, SVR, and MLR. The MSE value of presented approach for each station is station 1 (0.3007), station 2 (0.2548), station 3 (0.2500), station 4 (0.3007), and station 5 (0.2544) respectively. This clearly demonstrates that the presented demand based optimal routing approach provides enhanced performance with less error. The performance comparison on MSE is mentioned in Table III.

TABLE II. COMPARISON ANALYSIS ON RMSE

Techniques	Dataset	Root Mean squared error (%)
Inverse distance weighting	Orissa dataset	19.4994
Empirical Bayesian Kriging	Orissa dataset	16.3527
Proposed	Surat city historical dataset	9.5

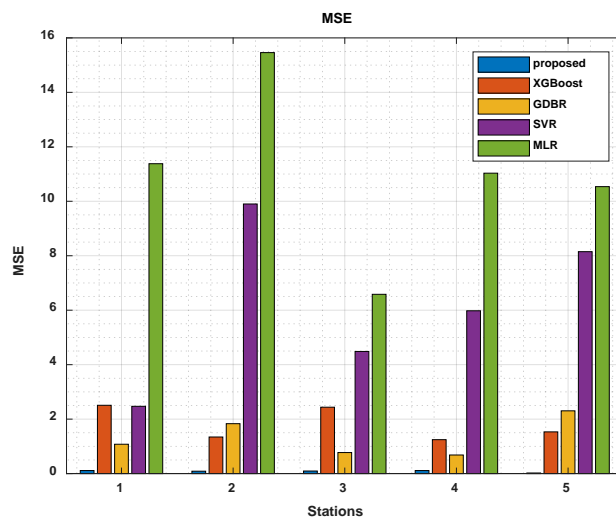


Fig. 15. Performance Analysis on MSE.

In Table III, the performance comparison on MSE is provided. Here, the performance of the presented approach is compared with the different existing approaches like GDBR, SVR, XGBoost, and MLR. The attained MSE value of presented approach for each station is station 1 (0.3007), station 2 (0.2548), station 3 (0.2500), station 4 (0.3007), and station 5 (0.2544) correspondingly. Moreover, the comparison on mean absolute error is depicted in Fig. 16.

In Fig. 16, mean absolute error performance of the proposed and the existing strategies for each station is provided. This proves that the presented demand based routing provides enhanced performance than the existing XGBoost, GDBR, SVR, and MLR approaches. The attained MAE value of presented approach for each station is station 1 (0.2007), station 2 (0.3548), station 3 (0.2500), station 4 (0.5007), and station 5 (0.3544) correspondingly. The performance on MAE for varying stations is portrayed in Table IV.

TABLE III. MSE PERFORMANCE ON DIFFERENT STATIONS

Technique	XGBoost	GDBR	SVR	MLR	Proposed
STATION 1	1.2195	1.2390	6.5384	9.3988	0.3007
STATION 2	1.9630	1.1147	2.5669	10.1900	0.2548
STATION 3	0.7697	1.7681	1.9185	9.0023	0.2500
STATION 4	0.4338	0.8778	9.0681	7.3333	0.3007
STATION 5	1.1884	2.5357	4.9333	12.3639	0.2544

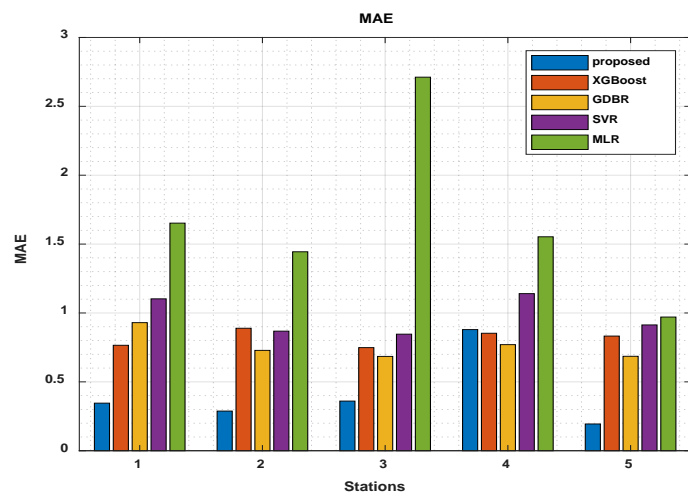


Fig. 16. Performance Analysis on MAE (%).

TABLE IV. MAE PERFORMANCE ON DIFFERENT STATIONS

Technique	XGBoost	GDBR	SVR	MLR	Proposed
STATION 1	0.7415	0.5089	0.8601	2.0907	0.2007
STATION 2	0.7542	0.6676	0.8905	2.3933	0.3548
STATION 3	0.8470	0.5624	1.2911	1.4605	0.2500
STATION 4	0.8975	0.8437	1.4642	0.9596	0.5007
STATION 5	0.8760	0.5943	0.9015	1.2081	0.3544

The Table IV proves that the presented methodology provides enhanced performance in terms of MAE than the XGBoost, GDBR, SVR, and MLR approaches. Moreover, the performance efficiency is examined by the vehicle occupancy is depicted in Fig. 17.

In Fig. 17, vehicle occupancy performance is demonstrated with the existing agent based scheduled routing [29]. Here, the vehicle occupancy is evaluated based on the number of passengers used the vehicle for a month. This illustrates that the presented routing process increases the usage of passengers. This proved that the performance of demand based optimal routing is effective than the other transportation routings. The vehicle occupancy is enhanced by the better quality service of the transportation based on the presented methodology. The performance on accuracy for varying stations is portrayed in Table V.

The Table V proves that the presented methodology provides enhanced performance in terms of accuracy than the deep neural network (DNN), Random forest (RF), Linear regression (LR) approaches. The attained accuracy of presented approach for each station is station 1 (99.51%), station 2 (98.14%), station 3 (98.69%), station 4 (97.61%), and station 5 (98.19%) correspondingly. The accuracy performance of the proposed optimal routing is depicted in Fig. 18.

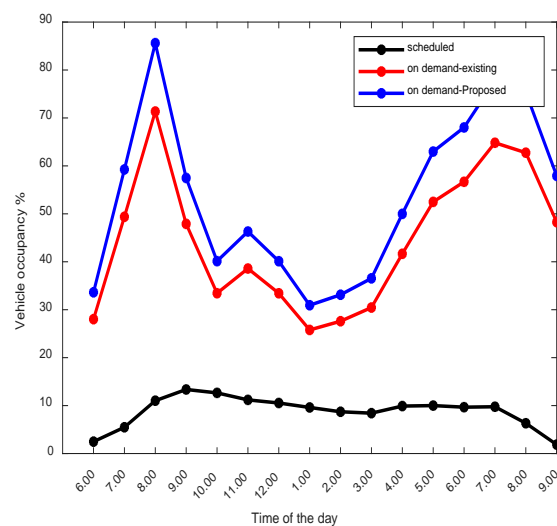


Fig. 17. Performance Analysis on Vehicle Occupancy (%).

TABLE V. ACCURACY PERFORMANCE ON DIFFERENT STATIONS

Technique	DNN (%)	LR (%)	RF (%)	Proposed (%)
STATION 1	98.26	94.52	94.08	99.51
STATION 2	98.58	94.52	94.08	98.14
STATION 3	98.5858	94.52	94.088	98.69
STATION 4	98.58	94.52	94.087	97.61
STATION 5	98.58	94.52	94.089	98.19

In Fig. 18, the presented approach is analyzed with the existing approaches in terms of accuracy performance. This proved that the presented approach provides enhanced accuracy performance than the existing strategies. The performance on correlation coefficient for varying stations is mentioned in Table VI.

The Table VI proves that the presented methodology provides enhanced performance in terms of correlation coefficient than the XGBoost, GDBR, SVR, and MLR approaches. The attained correlation coefficient of presented approach for each station is station 1 (0.8993) station 2 (0.1000), station 3 (0.2800), station 4 (0.2000), and station 5 (0.4800) correspondingly. The comparison analysis in terms of correlation coefficient is depicted in Fig. 19.

In Fig. 19, the correlation coefficient performance is examined with the different existing approaches. The correlation coefficient of presented approach for each station is station 1 (99.51%), station 2 (98.14%), station 3 (98.69%), station 4 (97.61%), and station 5 (98.19%) correspondingly. Here, the proposed approach achieved a high correlation coefficient for each station than the existing the XGBoost, GDBR, SVR, and MLR approaches. Here, this validation is evaluated for each station in the considered Surat city transportation dataset. This proposed methodology provides enhanced results in demand based optimal routing. Furthermore, this methodology enhances the quality of transportation service.

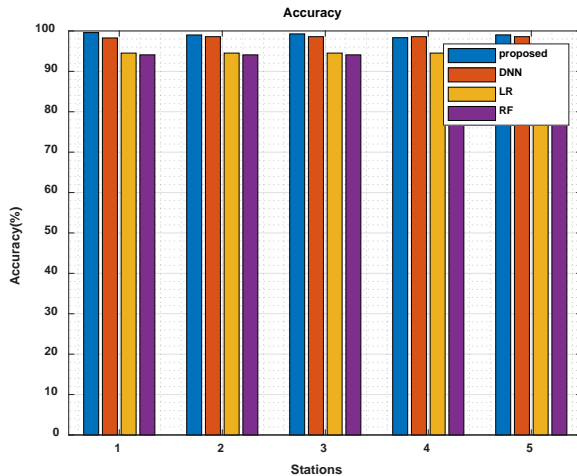


Fig. 18. Performance Analysis on Accuracy (%).

TABLE VI. CORRELATION COEFFICIENT PERFORMANCE ON DIFFERENT STATIONS

Technique	XGBoost	GDBR	SVR	MLR	Proposed
STATION 1	0.6259	0.6529	0.5598	0.2788	0.8993
STATION 2	0.5876	0.3125	0.5281	0.1164	0.1000
STATION 3	0.6263	0.4114	0.5977	0.2863	0.2800
STATION 4	0.4736	0.6480	0.2810	0.2754	0.2000
STATION 5	0.5624	0.5944	0.4928	0.1643	0.4800

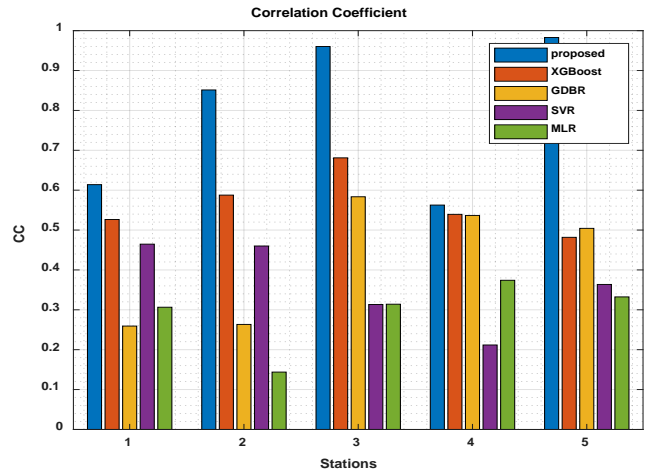


Fig. 19. Performance Analysis on Correlation Coefficient.

V. CONCLUSION

This paper presented a demand based effective routing in transportation network. At first, Distance based adaptive Fuzzy C-means clustering approach (DFCM) is utilized for clustering the passengers in each stop. Here, the number of cluster members in each cluster is equivalent to the passenger’s count of every station. Afterwards, adaptive beetle swarm optimization approach based routing is performed based on the clustered data. Further, re-routing is performed based on the effective objectives such as passenger’s count, comfort level of passengers, route distance and average travel time using ABSO approach. In the optimal route generation approach, objectives are analysed in each pair of stations in the route using the ABSO approach. This ABSO approach enhances transportation system by providing demand based routing. The presented work is examined with the various existing approaches in terms of different performances like RMSE (9.5%), Mean error (0.254%), vehicle occupancy (85%), MAE (0.3007%), correlation coefficient (0.8993), and accuracy (99.57%). This proved that the presented approach provides better performance than the existing routing approaches in transportation system. In future, this demand based transportation is further enhanced with improved deep learning based approaches to decrease the time consumption. Increasing number of objectives will further improve the performance of demand based routing. Moreover, the demand based transportation will be examined with other larger datasets.

ACKNOWLEDGMENT

I sincerely thank Nirbhay Chaubey for their guidance and encouragement in carrying out this research work.

REFERENCES

- [1] M. Nassereddine, H. Eskandari, “An integrated MCDM approach to evaluate public transportation systems in Tehran, Transportation Research Part A: Policy and Practice,” vol. 106, pp. 427-439, 2017.
- [2] X. Wan, H. Ghazzai, Y. Massoud, “Mobile Crowdsourcing for Intelligent Transportation Systems: Real-Time Navigation in Urban Areas,” IEEE Access, vol. 7, pp. 136995-137009, 2019.
- [3] T. Afrin, N. Yodo, “A Survey of Road Traffic Congestion Measures towards a Sustainable and Resilient Transportation System,” Sustainability, vol. 12, pp. 4660, (2020).

- [4] H. Xiong, A. Vahedian, X. Zhou, Y. Li, J. Luo, "Predicting traffic congestion propagation patterns: A propagation graph approach," In Proceedings of the 11th ACM SIGSPATIAL International Workshop on Computational Transportation Science, pp. 60-69, 2018.
- [5] H. Xiong, A. Vahedian, X. Zhou, Y. Li, J. Luo, "Predicting traffic congestion propagation patterns: A propagation graph approach," In Proceedings of the 11th ACM SIGSPATIAL International Workshop on Computational Transportation Science, pp. 60-69, 2018.
- [6] J. Weng, X. Di, C. Wang, J. Wang, L. Mao, "A bus service evaluation method from passenger's perspective based on satisfaction surveys: A case study of Beijing," *China, Sustainability*, vol. 10, no. 8, pp. 2723, 2018.
- [7] S. Güner, "Measuring the quality of public transportation systems and ranking the bus transit routes using multi-criteria decision making techniques," *Case studies on transport policy*, vol. 6, no. 2, pp. 214-224, 2018.
- [8] M. Javid, S. Hussain, M. Anwaar, "Passenger's Perceptions on Prospects of Qingqi Paratransit Public Transport Service in Lahore," *Iranian Journal of Science and Technology, Transactions of Civil Engineering*, vol. 44, pp. 185-195, 2020.
- [9] Y. Wang, Z. Zhang, M. Zhu, H. Wang, "The Impact of Service Quality and Customer Satisfaction on Reuse Intention in Urban Rail Transit in Tianjin," *China. SAGE Open*, vol. 10, pp. 215824401989880, 2020.
- [10] A. Alkharabsheh, S. Moslem, S. Duleba, "Evaluating Passenger Demand for Development of the Urban Transport System by an AHP Model with the Real-World Application of Amman," *Applied Sciences*, vol. 9, pp. 4759, 2019.
- [11] Ö. Bilişik, Ş. Şeker, N. Aydın, N. Güngör, H. Baraçlı, "Passenger Satisfaction Evaluation of Public Transportation in Istanbul by Using Fuzzy Quality Function Deployment Methodology," *Arabian Journal for Science and Engineering*, vol. 44, pp. 2811-2824, 2019.
- [12] V. Cacchiani, J. Qi, L. Yang, "Robust optimization models for integrated train stop planning and timetabling with passenger demand uncertainty," *Transportation Research Part B: Methodological*, vol. 136, pp. 1-29, 2020.
- [13] Ş. İmre, D. Çelebi, "Measuring Comfort in Public Transport: A case study for İstanbul," *Transportation Research Procedia*, vol. 25, pp. 2441-2449, 2017.
- [14] C. Zhang, Y. Liu, W. Lu, G. Xiao, "Evaluating passenger satisfaction index based on PLS-SEM model: Evidence from Chinese public transport service," *Transportation Research Part A: Policy and Practice*, vol. 120, pp. 149-164, 2019.
- [15] X. Shen, S. Feng, Z. Li, B. Hu, "Analysis of bus passenger comfort perception based on passenger load factor and in-vehicle time," *SpringerPlus*, vol. 5, 2016.
- [16] F. Kurtulmuşoğlu, F. Pakdil, K. Atalay, "Quality improvement strategies of highway bus service based on a fuzzy quality function deployment approach," *Transportmetrica A: Transport Science*, vol. 12, pp. 175-202, 2016.
- [17] S. Ordonez Medina, B. Wang, "Public transport routing including fixed schedule, shared on-demand and door-to-door services," *Procedia Computer Science*, vol. 151, pp. 846-851, 2019.
- [18] I. Katsaragakis, I. Tassopoulos, G. Beligiannis, "Solving the Urban Transit Routing Problem Using a Cat Swarm Optimization-Based Algorithm," *Algorithms*, vol. 13, pp. 223, 2020.
- [19] T. Vlachopanagiotis, K. Grizos, G. Georgiadis, I. Politis, "Public Transportation Network Design and Frequency Setting: Pareto Optimality through Alternating-Objective Genetic Algorithms," *Future Transportation*, vol. 1, pp. 248-267, 2021.
- [20] M. Owais, M. Osman, "Complete hierarchical multi-objective genetic algorithm for transit network design problem," *Expert Systems with Applications*, vol. 114, pp. 143-154, 2018.
- [21] M. Owais, M. Osman, "Complete hierarchical multi-objective genetic algorithm for transit network design problem," *Expert Systems with Applications*, vol. 114, pp. 143-154, 2018.
- [22] O. Cosma, P. Pop, D. Dănciulescu, "A novel matheuristic approach for a two-stage transportation problem with fixed costs associated to the routes," *Computers & Operations Research*, vol. 118, pp. 104906, 2020.
- [23] J. Liu, P. Mirchandani, X. Zhou, "Integrated vehicle assignment and routing for system-optimal shared mobility planning with endogenous road congestion," *Transportation Research Part C: Emerging Technologies*, vol. 117, pp. 102675, 2020.
- [24] J. Narayan, O. Cats, N. van Oort, S. Hoogendoorn, "Integrated route choice and assignment model for fixed and flexible public transport systems," *Transportation Research Part C: Emerging Technologies*, vol. 115, pp. 102631, 2020.
- [25] M. Owais, A. Alshehri, "Pareto Optimal Path Generation Algorithm in Stochastic Transportation Networks," *IEEE Access*, vol. 8, pp. 58970-58981, 2020.
- [26] P. Heyken Soares, "Zone-based public transport route optimisation in an urban network," *Public Transport*, vol. 13, pp. 197-231, 2020.
- [27] K.K.R. Samal, K.S. Babu, S.K. Das, "ORS: The optimal routing solution for smart city users," In *Electronic systems and intelligent computing*, Springer, Singapore, pp. 177-186, 2020.
- [28] X. Kong, M. Li, T. Tang, K. Tian, L. Moreira-Matias, F. Xia, "Shared Subway Shuttle Bus Route Planning Based on Transport Data Analytics," *IEEE Transactions on Automation Science and Engineering*, vol. 15, pp. 1507-1520, 2018.
- [29] S. Liyanage, H. Dia, "An Agent-Based Simulation Approach for Evaluating the Performance of On-Demand Bus Services," *Sustainability*, vol. 12, pp. 4117, 2020.

Implementation of Electronic Health Record and Health Insurance Management System using Blockchain Technology

Lincy Golda Careline S, Dr.T.Godhavari
Dr. MGR Educational and Research Institute, Chennai, India

Abstract—Electronic health records (EHR) play an important role in digital health transition. EHRs contain medical information such as demographics, laboratory test results, radiological images, vaccination status, insurance policy, and claims. EHR is essential for doctors and healthcare organizations to analyze a patient's profile and provide appropriate therapy. Despite this, current electronic health record (EHR) systems lag with difficulties such as Interoperability and security. Better and faster care may be provided with an integrated and secure health record for each patient that can be transmitted easily in real-time across countries. People having health insurance policies are often confronted by insurance jargon and the insurer's cumbersome requirements while filing a claim for treatment. There are times when the claims processing takes longer than expected. The insurer, Third-Party Administrators (TPAs), and network provider hospitals examine, approve, and initiate the sum claimed. The use of blockchain in the process allows for more efficient information sharing at a lower cost and with more security. Only authorized individuals have access to the shared ledger on a blockchain, making it more confidential and secure. All parties engaged in a health insurance policy, including the insurer, the insured, the TPA, and the network provider hospital, may be members of the blockchain network and have access to the same set of policy data. In our proposed work we implemented a Blockchain-based EHR and Health insurance management system using Ethereum and deployed smart contracts using solidity and created a web application with web3js and React Framework.

Keywords—*Electronic health records; insurance policy and claim processing; smart contracts; Ethereum; homomorphic encryption; edge computing*

I. INTRODUCTION

Blockchain transforms the healthcare sector by storing and sharing patients' electronic health records, insurance policies, and claims to provide more secure, transparent, and traceable data [1]. The technology integrates diverse data management systems resulting in an electronic health record system that is connected and interoperable. The doctor treats the patient and enters the patient's report into their existing health information system, which includes tests, prescriptions, and significant notes. The data fields connected with the patient's public ID are then redirected to the blockchain using APIs. In the blockchain, each transaction is authenticated and given a unique identity (public key). APIs can be used by doctors and health organizations to make a query and retrieve encrypted patient data using the patient's public key. Patients can give

the doctor or the healthcare facility permission to decrypt their data by supplying the private key (which functions as a password). The data remains encrypted for those who do not have access to the private key [4]. Blockchain is a distributed network of computers that is governed by a time-stamped collection of immutable data records that are not held by a single person, company, or government entity. Because the blockchain network is decentralized, data may be exchanged and updated, but it cannot be copied, modified, or erased, making it public and accountable [2]. As a result, the best platform for storing and distributing electronic medical records is blockchain. An Electronic Health Record (EHR) is an electronic representation of a patient's medical history [6]. Blockchain is the next big thing in healthcare and it will revolutionize how it is supplied and administered. The fundamental issue is information asymmetry, which means that not everyone has the same easy access to the data [5]. Blockchain and smart contracts safeguard data, increase interoperability, and allow numerous entities to access the medical information that makes up the EHR by providing a secure distributed network, a shared ledger, and the ability to add independent blocks of medical transactions [3]. Blockchain has four main benefits in an EHR system.

- Longitudinal patient records: Data is assembled progressively, ensuring that no data is lost or tampered with.
- Master patient indices: A single master patient file contains all of the different blocks of information, reducing the chances of medical errors or mismatches.
- Claims adjudication: Instead of relying on a central authority, automated smart contracts can assist handle claims more quickly and efficiently.
- Interoperability: Only approved authorized providers have access to the data and the capacity to edit it, allowing for greater data reconciliation and care quality improvement.

The advantages of electronic health records extend far beyond cost savings. An EHR system provides quick access to accurate and up-to-date patient information. This lowers long-term healthcare costs and improves efficiency, especially if a patient is transferred between departments during treatment [11]. Blockchain technology ensures that every participant has their own copy of the digital ledger, which is updated in real-time as transactions occur. Hacking is nearly impossible due

to the lack of a centralized server. Because a recorded transaction cannot be reversed in theory, the ledger is an immutable source of truth, regardless of how many copies are kept by participants [10]. It is possible to confirm data, records, and participant identities while keeping their identities disguised. Our digital environment is rapidly changing in the pursuit of excellence. Without a doubt, technology has a significant impact on our daily lives and other elements of our lives, with the potential to dramatically improve them. One of the industries that potentially benefits from the adoption of blockchain is insurance [17]. Many blockchain insurance firms are working to improve the end-user experience as well as the businesses that handle people's insurance. Because most underwriting and claims work requires collaboration among numerous parties, blockchain will assist the insurance sector [18]. While blockchain adoption is still in its infancy, the applications covered here are a good place to start for insurers interested in taking advantage of its potential. When it comes to technology, it has the potential to affect the lives of millions of people all over the world. Because life insurance procedures differ from country to country, finding a consistent manner to manage all claims and processes is vital [22].

II. LITERATURE SURVEY

More than 4,000 years ago, the Sumerians penned medical data on a clay tablet. The Egyptian papyrus was next, followed by the thick folders. The first medical electronic information system was established by Lockheed in 1960. The Decentralized Hospital Computer Program (DHCP) and the Computerized Patient Record System (CPRS) were implemented by the Department of Veterans Affairs in the 1970s. President Bush first mentioned the term "Electronic Health Record" in 2004. The usage of the EHR system allowed increased payments to physicians and hospitals under President Obama's American Recovery and Reinvestment Act of 2009, which was part of the Health Information Technology for Economic and Clinical Health Act (HITECH) [10]. In Estonia, 99 percent of health records have been digitized. E-Health Records are even accessible to first responders and paramedics [7]. It's useful for non-responsive individuals when further information about their medical history and probable sensitivities is needed quickly. Currently, systems in many countries are scattered and do not communicate with one another. By integrating scattered systems across countries and regions, a blockchain-based electronic health record can enable real interoperability [14]. Instead of being saved in a single database, healthcare data can be stored immutably in a decentralized fashion using blockchain. As a result, a hacker would not be able to access the data through a single point of entry. This is how blockchain improves the security of health-related data. Homomorphic encryption can be used since blockchains do not provide anonymity [12], [16]. However, complete anonymity in healthcare is neither essential nor desirable. Instead, alternatives should be found that allow patients to choose who to reveal their name to, whether to remain pseudonymous and what data to provide. They can, however, be improved to improve patient care and accessibility to information. An electronic health record (EHR) is a collection of patient-related data that is maintained

electronically [15]. The growth of screening tests, medical imaging, and diagnostics has resulted in an avalanche of information on patient health. EHR (electronic health record) systems are a fantastic approach to boosting patient care. As more patient data becomes digital and an increasing number of consumers seek mobile access to health records, the function of EHR is improving and digitizing in healthcare [13]. In general, electronic health records (EHR) features and frameworks have long been seen as a surefire means to improve medical care delivery systems. The current life insurance claims system is inefficient, as it might take a long time to process a claim. It means that the claimant will have to deal with a lot of red tapes before their claims are handled [24]. All of these issues can be mitigated with blockchain life insurance. To ensure that claims are processed more quickly and efficiently, a good blockchain-based life insurance model can work in combination with the hospital, insurance company, death certificates, and burial licenses.

III. CHALLENGES IN EXISTING ELECTRONIC HEALTH RECORDS AND HEALTH INSURANCE

According to research, 50-60% of physicians experience burnout, which results in lower patient satisfaction, decreased patient safety, and more malpractice claims [23]. A large amount of time is necessary to incorporate data into EHR systems. As a result, physicians are unable to devote sufficient time to improving patient communication. As a result, the quality of patient treatment declines, and physicians grow increasingly frustrated and dissatisfied. Furthermore, EHRs are believed to be a cost burden on both providers and practitioners in some cases. Interoperability refers to an EHR's capacity to communicate data and information to other devices so that it can be used by a large number of individuals. The systems must communicate well with one another to obtain a complete picture of a patient's medical history as in Fig. 1. Data communication in an EHR is frequently delayed due to a lack of interoperability between segments of the same EHR or between the EHR and another system. The information held in an EHR and shared on a blockchain's distributed ledger would be updated and secured, ready to be used by anybody with authorization [8]. A blockchain-based EHR solution will improve data quality and interoperability thus reducing the time it takes to obtain a patient's information [9]. Furthermore, using blockchain for electronic health records will help to reduce costs, especially in terms of software development and health record system maintenance.

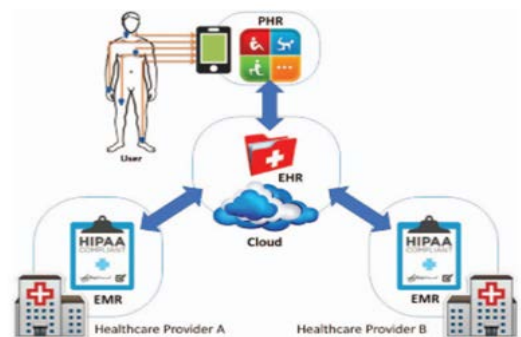


Fig. 1. EHR Framework.

When information is maintained within an EHR and shared on a distributed blockchain ledger, it may be updated, safeguarded, and made ready for use by anybody authorized to access it [12]. A blockchain-based EHR system reduces the amount of time it takes to get information on a patient. It will also improve data quality and provide seamless and safe interchange. As a result, blockchain for EHRs (electronic health records) may result in lower costs [19]. Insurance clients, who are frequently perplexed by plans, have grown skeptical of insurers and have developed a rising suspicion of them. The issue of trust is a huge one for insurance companies. The majority of the time, insurance companies do not have access to all of a patient's information, resulting in higher processing costs or incorrect plan assignments. Documents are occasionally incorrectly filled or not submitted, and sometimes lost, due to the distributed paperwork and filings among the numerous parties in the insurance network [24]. Customers are dissatisfied when insurance firms fail to process claims within specified deadlines [25]. Insurers are under increasing pressure to decrease administrative expenses, and blockchain technology have the potential to assist by upgrading fragmented legacy IT systems, improving efficiency, and increasing competitiveness [26]. Increased automation is required in the insurance industry, which blockchain technologies can help with. New systems, processes, security protocols, and business models are necessary to meet rising customer demands for tailored services, increased privacy, innovative products, added value, and competitive pricing from their insurers.

IV. BLOCKCHAIN IMPLEMENTATION IN ELECTRONIC HEALTH RECORDS AND HEALTH INSURANCE SYSTEMS

The IoT healthcare sensors such as temperature, humidity, airflow, pressure, SpO2, heart rate, and pulse sensors are used to collect the patient's real-time data and store it in edge computing devices [12]. The data stored in the edge device is then retrieved and the transaction is processed in the blockchain as shown in Fig. 2 and Fig. 3. This might lead to healthcare providers and academics having access to enormous amounts of anonymized patient data for research reasons. Every blockchain node has a copy of the data that is constantly updated. As a result, any tampering or manipulation of health information will be discovered right away. Every transaction is also signed with a cryptographic stamp, allowing each piece of data to be traced back to its source. This means that a doctor can monitor a patient's recovery from surgery or sickness in real-time recognizing potential problems or concerns with eating, exercise, and vital indicators like heart rate without having to see them in person. It allows a doctor to monitor a patient's recovery after surgery or illness in real-time.

```
lincygoldacareline@DESKTOP-EQ55Q8H: ~/Blockchain
lincygoldacareline@DESKTOP-EQ55Q8H:~$ cd Blockchain
lincygoldacareline@DESKTOP-EQ55Q8H:~/Blockchain$ python3 main.py
Block 0 <block.Block object at 0x7f23dde5beb8>
Timestamp: 2022-06-21 22:26:24.298762
Transactions: []
Current Hash: d07f907292bb5a9f1d178cb9d30f27db1d98f6e5a3d8bc409f5117e254ab8cd3
Previous Hash: 0
Block 1 <block.Block object at 0x7f23dde5bef0>
Timestamp: 2022-06-21 22:26:24.298935
Transactions: {'id': 1, 'temp_sensor': 23.0}
Current Hash: 080be0f9c9da0fc3ff450cf397218da5cb36d5ce442dc2136c247e55727c4ed2
Previous Hash: d07f907292bb5a9f1d178cb9d30f27db1d98f6e5a3d8bc409f5117e254ab8cd3
Block 2 <block.Block object at 0x7f23dde822e8>
Timestamp: 2022-06-21 22:26:24.299595
Transactions: {'id': 2, 'temp_sensor': 25.0}
Current Hash: 65b53d8e13da1d4778eb71393011a8194d6be6522c4c79ce13fd085bb8715f98
Previous Hash: 080be0f9c9da0fc3ff450cf397218da5cb36d5ce442dc2136c247e55727c4ed2
True
lincygoldacareline@DESKTOP-EQ55Q8H:~/Blockchain$
```

Fig. 2. Sensor Data is Stored in the Blockchain.

```
lincygoldacareline@DESKTOP-EQ55Q8H:~/Blockchain
lincygoldacareline@DESKTOP-EQ55Q8H:~/Blockchain$ python3 main.py
Block 0 <block.Block object at 0x7f23dde5beb8>
Timestamp: 2022-06-21 22:26:24.298762
Transactions: []
Current Hash: d07f907292bb5a9f1d178cb9d30f27db1d98f6e5a3d8bc409f5117e254ab8cd3
Previous Hash: 0
Block 1 <block.Block object at 0x7f23dde5bef0>
Timestamp: 2022-06-21 22:26:24.298935
Transactions: {'id': 1, 'temp_sensor': 23.0}
Current Hash: 080be0f9c9da0fc3ff450cf397218da5cb36d5ce442dc2136c247e55727c4ed2
Previous Hash: d07f907292bb5a9f1d178cb9d30f27db1d98f6e5a3d8bc409f5117e254ab8cd3
Block 2 <block.Block object at 0x7f23dde822e8>
Timestamp: 2022-06-21 22:26:24.299595
Transactions: {'id': 2, 'temp_sensor': 25.0}
Current Hash: 65b53d8e13da1d4778eb71393011a8194d6be6522c4c79ce13fd085bb8715f98
Previous Hash: 080be0f9c9da0fc3ff450cf397218da5cb36d5ce442dc2136c247e55727c4ed2
True
lincygoldacareline@DESKTOP-EQ55Q8H:~/Blockchain$
```

Fig. 3. Transaction is processed and Hash is generated for the Appended Sensor Data in the Blockchain.

Customers may encounter time-consuming paper forms when applying for insurance or reporting a claim. They may need to talk with the insurance companies and hospital employees to get medical insurance claims reimbursed [17]. Claims processing, data verification and reconciliation, and documentation procedures are shown in Fig. 4 and Fig. 5. Blockchain can help make selling and servicing insurance better, faster, and cheaper by improving fraud detection [19], claims administration, health insurance, and reinsurance. As a result, customers may see lower costs and have a better experience. The Blockchain has the potential to assist in the resolution of present property and casualty insurance issues. The strategy is to digitally manage physical assets. Smart contracts allow claims to be processed automatically. All modifications can also be tracked for authenticity, making them auditable. Smart contracts are crucial because they provide the functionality of converting paper contracts into programmable code [20]. The smart contracts, in turn, can be automatically performed by ingesting all of the data and acting on it as needed [21].

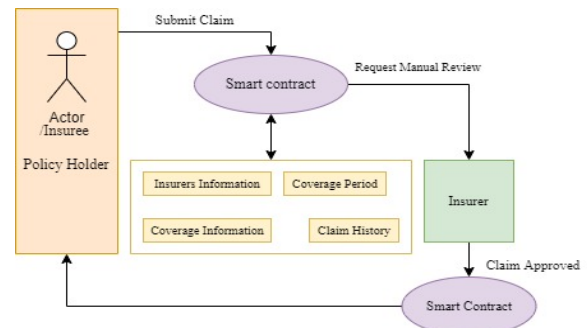


Fig. 4. Proposed Insurance Claim Processing.

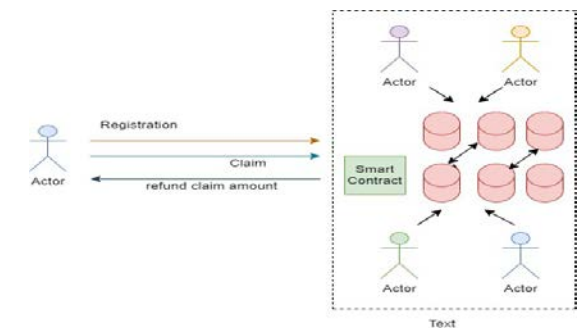


Fig. 5. Health Insurance Framework.

Deploying blockchain on healthcare networks will improve patient diagnostics and medical expenditures by expediting and improving patient diagnosis. The patient is the owner of his or her medical information and has the right to give it as needed without relying on any other parties. Because hospitals and clinicians would have immediate and complete access to a patient's data, the need for additional testing and long or incorrect diagnoses would be greatly reduced. Smart contracts will automatically initiate transactions, making claim processing and denial even easier and faster. This would greatly boost the level of trust in insurance companies. Sharing data across the network's many providers on a distributed ledger ensures that data will be retrieved quickly at any time, while also reducing the danger of improper documentation and data/documentation loss to nearly zero. This would help insurance firms save money on processing costs. The widespread adoption of blockchain by insurance companies throughout the world brings up a slew of prospects for distributed ledger technology validation services.

Blockchain is quickly gaining attraction as a technology that has the potential to alter the insurance sector. For accuracy and credibility, insurers rely largely on information and data acquired by various devices. Insurers should make sure that blockchain is linked with IoT as the best way to assure that the data captured is accurate. The interplay of blockchain, IoT, and big data in this way has the potential to transform the insurance sector. The idea is to automate the entire process, including premiums, claims, and other issues. With the ability to streamline the insurance sector while simultaneously increasing transparency and confidence.

V. RESULTS AND DISCUSSION

In our proposed work we implemented a Blockchain-based electronic health record and Health insurance management system using Ethereum Framework, smart contracts are deployed using a solidity debugger and the transaction are processed through truffle-based Ganache Test network. Created a web application with React framework as shown in Fig. 6.

Patients' and recipients' electronic health records such as demographics, laboratory test results, vaccination status, insurance policy and claims are stored in the React framework as in Fig. 7 and Fig. 8. Delegations are created and the electronic health records can be updated using the React framework as shown in Fig. 9 and Fig. 10.

The electronic health records are stored in the blockchain using Django REST Framework. The promise of blockchain technology is enormous, and integrating it with EHR will ensure that we all benefit from a better, more equitable, and healthier future.

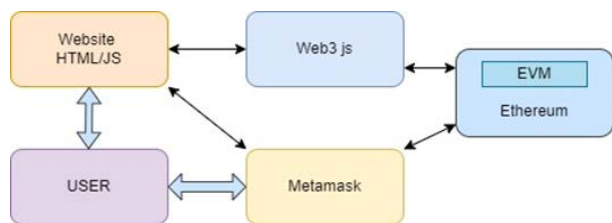


Fig. 6. Block Diagram of Proposed Work.

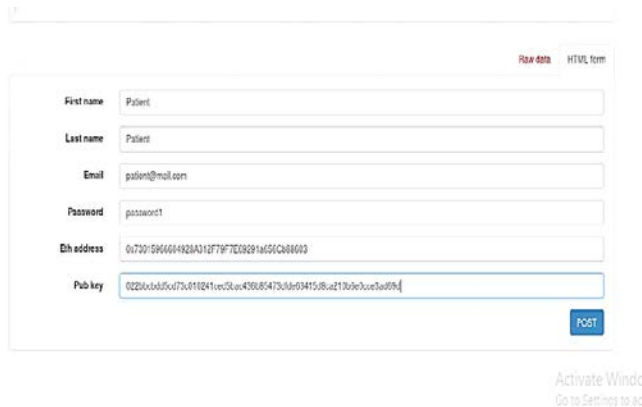


Fig. 7. Patients Signup Webpage using React Framework.



Fig. 8. Recipients Signup Webpage using React Framework.



Fig. 9. Delegations are created in React Framework.

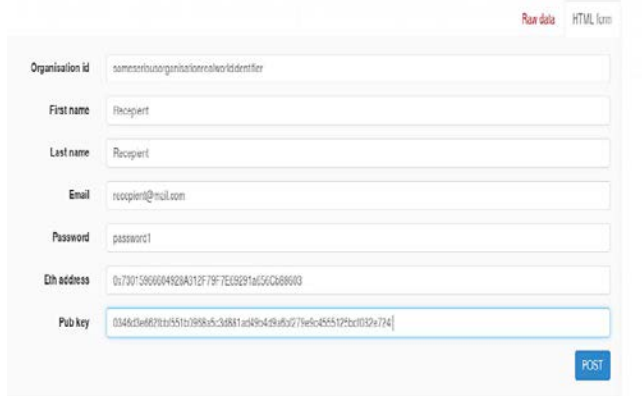


Fig. 10. Patients Health Records are Uploaded in React Framework.

VI. ADVANTAGES AND LIMITATIONS OF PROPOSED SYSTEM

There are major advantages that blockchain can offer to the traditional health record system. Patients have more control over their data because they can provide just the relevant authorities access to the data. Health data may be collected, saved, secured, and shared using blockchain for EHRs, which also allows for real-time utilization. It might lead to the selection of anonymized patient records for use in research by healthcare practitioners and researchers. When a blockchain is used to maintain electronic medical records, it offers a long-awaited standardized solution for the management of digital health data. To access patient data, hospitals and care providers will no longer need separate software or databases. EHRs give clinicians access to a patient's medical history. Patients no longer need to fill out the same paperwork at each visit to the doctor. The convenience of e-prescriptions provided straight to pharmacies is increased. The usage of a dashboard also makes it easier for patients to communicate with their doctors and streamlines their care. Patients and doctors can communicate directly because they use the same platform. Different specialists, hospitals, laboratories, and even pharmacists will be able to share the same information. Treatment providers will have a better understanding of how to improve patients' care if data is less scattered. Automated claim management aids in the seamless processing of reimbursements. It also reduces the administrative expenditures of hospitals or offices. Efficiency and expenses are improved by automating administrative processes and automatic clinical documentation.

The advantages of electronic health records are vast, but they also have a few limitations, most of which are related to the implementation and learning of EHR systems. The cost of implementing an EHR system is not insignificant. The majority of these costs are directly tied to the implementation of hardware and software. When new systems are implemented, the workflow is inevitably disturbed, resulting in a temporary loss of productivity. In the end, these losses will be only temporary, and revenues will rise. Because of increased productivity and faster claim reimbursements. The entire medical history of a patient is readily available, which is beneficial for diagnostic purposes but possibly dangerous for keeping sensitive information private.

VII. CONCLUSION AND FUTURE WORK

The potential of blockchain technology has already been recognized by the majority of forward-thinking healthcare industries. More importantly, blockchain will improve patient care by standardizing how parties manage and access electronic medical records. It can aid in the detection of health trends and the improvement of treatment. Blockchain technology has enormous and thought-provoking possibilities and the deployment of EHR on the blockchain has the potential to alter the healthcare industry. Using blockchain to standardize the management and access to electronic medical records, on the other hand, would elevate patient care to new heights. Patients will receive more accurate diagnoses and have complete ownership over their digital health information. And, if electronic health metadata has been collected and reconciled securely, it can be used to identify health patterns,

improve treatment, and eradicate diseases. Insurance is no exception, and blockchain has a lot of potentials. The most prevalent use cases are fraud detection and prevention, claims management. The 'quickest win' for blockchain in the insurance sector is cost savings. The enhanced security of blockchain, as well as its capacity to establish trust between entities, are two reasons why it may be able to tackle the interoperability challenge more effectively than current solutions. Existing EHRs in hospitals and physician offices would most likely be used to create a blockchain-based interoperable and comprehensive health record.

Combining Electronic Health Records (EHR) with Artificial Intelligence and Voice Recognition is beneficial to EHR systems because it allows clinicians to enter information and patient data. Artificial Intelligence has a history of transforming the healthcare industry by supporting clinicians in analyzing prior trends in a patient's condition and establishing a diagnosis. The predictive analytics application has a significant impact on the healthcare industry. Predictive analytics technology is being employed in a wide range of applications, from cancer treatments to emergency staffing optimization, and it will soon be embraced even more widely. With features like real-time data monitoring, telemedicine, and more, 5G has a lot of potential in the healthcare sector. Healthcare personnel will be able to access data via a tablet or smartphone through mobile computing and cloud-based infrastructure to securely store and retrieve data. As a result, devices like smartwatches will be used in the healthcare industry to automatically upload and track patient data as well as enable remote patient monitoring.

REFERENCES

- [1] G. Yang, C. Li, and K. E. Marstein, "A blockchain-based architecture for securing electronic health record systems," *Concurr. Comput.*, vol. 33, no. 14, 2021, DOI: 10.1002/cpe.5479.
- [2] K. Shuaib, J. Abdella, F. Syllabi, and M. A. Serhani, "Secure decentralized electronic health records sharing system based on blockchains," *J. King Saud Univ. - Comput. Inf. Sci.*, no. xxxx, 2021, doi: 10.1016/j.jksuci.2021.05.002.
- [3] A. Khatoun, "A blockchain-based smart contract system for healthcare management," *Electron.*, vol. 9, no. 1, 2020, DOI: 10.3390/electronics9010094.
- [4] F. A. Regu, S. Mohd, Z. Hakami, K. K. Reegu, and S. Alam, "Towards Trustworthiness of Electronic Health Record system using Blockchain," *Ann. Rom. Soc. Cell Biol.*, vol. 25, no. 6, pp. 2425–2434, 2021.
- [5] H. M. Hussien, S. M. Yasin, N. I. Udzir, and M. I. H. Ninggal, "Blockchain-based access control scheme for secure shared personal health records over decentralized storage," *Sensors*, vol. 21, no. 7, pp. 1–36, 2021, DOI: 10.3390/s21072462.
- [6] S. Alla, L. Soltanisehat, U. Tatar, and O. Keskin, "Blockchain technology in electronic healthcare systems," *IISE Annu. Conf. Expo 2018*, no. June, pp. 901–906, 2018.
- [7] A. A. Abd-al Razzaq *et al.*, "Blockchain technologies to mitigate COVID-19 challenges: A scoping review," *Comput. Methods Programs Biomed. Update.*, vol. 1, no. November 2020, p. 100001, 2021, DOI: 10.1016/j.cmpbup.2020.100001.
- [8] M. Antwi, A. Adnane, F. Ahmad, R. Hussain, M. Habib ur Rehman, and C. A. Kerrache, "The Case of HyperLedger Fabric as a Blockchain Solution for Healthcare Applications," *Blockchain Res. Appl.*, p. 100012, 2021, DOI: 10.1016/j.bcr.2021.100012.
- [9] M. Prokofieva and S. J. Miah, "Blockchain in healthcare," *Australas. J. Inf. Syst.*, vol. 23, no. July, pp. 1–22, 2019, DOI: 10.3127/axis.v23i0.2203.
- [10] D. A. S. Vinotha and G. Monisha, "Health Record Transaction in

- Hospital Management Using Blockchain,” pp. 707–710, 2020.
- [11] L. Ismail, H. Materwala, and A. Hennebelle, “A scoping review of integrated blockchain-cloud (Bcc) architecture for healthcare: Applications, challenges, and solutions,” *Sensors*, vol. 21, no. 11, 2021, DOI: 10.3390/s21113753.
- [12] H. Guo, W. Li, M. Nejad, and C. C. Shen, “Access control for electronic health records with hybrid blockchain-edge architecture,” *Proc. - 2019 2nd IEEE Int. Conf. Blockchain, Blockchain 2019*, no. June, pp. 44–51, 2019, DOI: 10.1109/Blockchain.2019.00015.
- [13] R. W. Ahmad, K. Salah, R. Jayaraman, I. Yaqoob, S. Ellahham, and M. Omar, “The role of blockchain technology in telehealth and telemedicine,” *Int. J. Med. Inform.*, vol. 148, no. January, p. 104399, 2021, DOI: 10.1016/j.ijmedinf.2021.104399.
- [14] A. Shahnaz, U. Qamar, and A. Khalid, “Using Blockchain for Electronic Health Records,” *IEEE Access*, vol. 7, pp. 147782–147795, 2019, DOI: 10.1109/ACCESS.2019.2946373.
- [15] S. E. E. Profile, “Electronic Health Records (EHR),” no. June, 2016, DOI: 10.19030/ajhs.v3i3.7139.
- [16] C. Shen and M. Nejad, “Attribute-based Multi-Signature and Encryption for EHR Management : A Blockchain-based Solution.”
- [17] J. Kuckreja, P. Nigde, and P. Patil, “Health insurance claim using blockchain,” no. May, pp. 2406–2409, 2021.
- [18] P. K. M. S. S. K. P. K. Sravan Nukala Poorna Viswanadha; Baruah, “Use of Blockchain Technology in integrating Health Insurance Company and Hospital,” *Int. J. Sci. Eng. Res.*, vol. 9, no. 10, pp. 1664–1669, 2018.
- [19] C. Kudumula, “Blockchain in Insurance Industry,” *Int. J. Comput. Trends Technol.*, vol. 69, no. 3, pp. 5–9, 2021, doi: 10.14445/22312803/ijctt-v69i3p102.
- [20] V. Aleksieva, H. Valchanov, and A. Huliyan, “Application of smart contracts based on Ethereum blockchain for insurance services,” *Proc. Int. Conf. Biomed. Innov. Appl. BIA 2019*, pp. 1–4, 2019, DOI: 10.1109/BIA48344.2019.8967468.
- [21] V. Gatteschi, F. Lamberti, C. Demartini, C. Pranteda, and V. Santamaria, “Blockchain and smart contracts for insurance: Is the technology mature enough?,” *Futur. Internet*, vol. 10, no. 2, pp. 8–13, 2018, DOI: 10.3390/fi1002020.
- [22] J. Gera, A. R. Palakayala, V. K. K. Rejeti, and T. Anusha, “Blockchain technology for fraudulent practices in insurance claim process,” *Proc. 5th Int. Conf. Commun. Electron. Syst. ICCES 2020*, no. Icces, pp. 1068–1075, 2020, DOI: 10.1109/ICCES48766.2020.09138012.
- [23] I. Nath, “Data Exchange Platform to Fight Insurance Fraud on Blockchain,” *IEEE Int. Conf. Data Min. Work. ICDMW*, vol. 0, pp. 821–825, 2016, DOI: 10.1109/ICDMW.2016.0121.
- [24] C. Oham, R. Jurdak, S. S. Kanhere, A. Dorri, and S. Jha, “B-FICA: BlockChain based Framework for Auto-Insurance Claim and Adjudication,” *Proc. - IEEE 2018 Int. Congr. Cybermatics 2018 IEEE Conf. Internet Things, Green Comput. Commun. Cyber, Phys. Soc. Comput. Smart Data, Blockchain, Comput. Inf. Technol. iThings/Gree*, pp. 1171–1180, 2018, DOI: 10.1109/Cybermatics_2018.2018.00210.
- [25] B. Lakshma Reddy, A. Karthik, and S. Prayla Shyry, “A blockchain framework for insurance processes in hospitals,” *Int. J. Recent Technol. Eng.*, vol. 7, no. 5, pp. 116–119, 2019.
- [26] G. Saldamli, V. Reddy, K. S. Bojja, M. K. Gururaja, Y. Doddaveerappa, and L. Tawalbeh, “Health Care Insurance Fraud Detection Using Blockchain,” *2020 7th Int. Conf. Softw. Defin. Syst. SDS 2020*, pp. 145–152, 2020, DOI: 10.1109/SDS49854.2020.9143900.

Predicting Blocking Bugs with Machine Learning Techniques: A Systematic Review

Selasie Aformaley Brown¹, Benjamin Asubam Weyori²
Adebayo Felix Adekoya³, Patrick Kwaku Kudjo⁴, Solomon Mensah⁵

Department of Computer Science, University of Energy and Natural Resources, Sunyani-Ghana^{1,2,3}

Department of Information Technology, University of Professional Studies Accra-Ghana^{1,4}

Department of Computer Science, University of Ghana, Legon-Ghana⁵

Abstract—The application of machine learning (ML) techniques to predict blocking bugs have emerged for the early detection of Blocking Bugs (BBs) in software components to mitigate the adverse effect of BBs on software release and project cost. This study presents a systematic literature review of the trends in the application of ML techniques in BB prediction, existing research gaps, and possible research directions to serve as a reference for future research and an application insight for software engineers. We constructed search phrases from relevant terms and used them to extract peer-reviewed studies from the databases of five famous academic publishers, namely Scopus, SpringerLink, IEEE Xplore, ACM digital library, and ScienceDirect. We included primary studies published between January 2012 and February 2022 that applied ML techniques to building Blocking Bug Prediction models (BBPMs). Our result reveals a paucity of literature on BBPMs. Also, previous researchers employed ML techniques such as Decision Trees, Random Forest, Bayes Network, XGBoost, and DNN in building existing BB prediction models. However, the publicly available datasets for building BBPMs are significantly imbalanced. Despite the poor performance of the *Accuracy* metric where imbalanced datasets are concerned, some primary studies still utilized the *Accuracy* metric to assess the performance of their proposed BBPM. Further research is required to validate existing and new BBPM on datasets of commercial software projects. Also, future researchers should mitigate the effect of class imbalance on the proposed BB prediction model before training a BBPM.

Keywords—Blocking bugs; systematic review; software maintenance; bug report; reliability; machine learning

I. INTRODUCTION

Software bugs are inevitable occurrences in the development and maintenance of software products. Hence, software engineers rely on bug reports generated by bug tracking tools such as Bugzilla, BugHead, and Trac to manage and resolve errors in software components, an activity aimed at improving and maintaining the quality of software projects. In Bugzilla, for instance, errors encountered by a software tester or user are logged in the bug tracking system and assigned the state NEW. The state of the bug report then changes to ASSIGNED when the bug is allocated to a suitable developer to resolve. Once the bug is fixed, a developer other than the one to whom the bug was assigned then ascertains the fixing and closes the bug report. At this point, the state of the bug report changes to CLOSED. However, the status of a bug report may remain at the ASSIGNED state for a long time because of another bug preventing the bug from being resolved. This type of bug is

referred to as a Blocking bug [1]. In this context, blocking bugs are defined as bugs that prevent other bugs from being fixed. Thus, the time for fixing such a bug depends greatly on how long it will take to detect and resolve the blocking bug. Previous work by Valdivia-Garcia and Shihab [2] confirms that fixing a BB is almost three times the amount of time needed to fix a non-BB. Consequently, the debugging process may be impacted negatively, affecting software release and increasing the cost of software maintenance. Furthermore, Bohm et al. [3] found that locating and fixing a bug in a software product after the deployment stage is about 100 times more expensive than addressing it during the early phase of the software development life cycle. Hence, the early detection of Blocking Bugs (BBs) in software projects is critical to software maintenance. While there are criteria for detecting BBs in bug reports, the method is manual and heavily reliant on the bug reporters' and the developer assigned's competence in providing suitable labels [1]. However, the skills of the software user or bug reporter to accurately label a bug as BB is intrinsically in doubt, hence the heavy dependence on the developer (i.e., to whom the bug was assigned) to label such bugs.

Additionally, the unstructured nature of the text in some bug reports makes the manual BB classification process by developers laborious and error-prone. Meanwhile, large software projects are likely to have enormous bug reports; for instance, Valdivia-Garcia et al. [1] collected 609,800 bugs from eight software projects, out of which 77,448 were blocking bugs and 532,352 non-blocking bugs. The researchers further discovered that manually identifying blocking bugs takes 3–18 days. Therefore, the over-reliance on software developers prolongs the process of identifying BBs in bug reports and is also time-consuming as the number of bug reports increases. These fundamental challenges present the opportunity to apply ML techniques to predicting BBs (i.e., classifying and detecting BBs). Although some peer-reviewed articles have been published on using ML techniques to predict BBs [1], [2], [4]–[7], there is a dearth of literature on the subject. For instance, a thorough search in databases of well-known publishers such as Scopus, SpringerLink, IEEE Xplore, ACM digital library, and ScienceDirect produced only six papers. Unfortunately, none of these six papers was an SLR. Yet, SLR is crucial in a specific domain of studies for discovering research questions and rationalizing future research [8]. Even though a recent SLR[9] on the broader topic of bug severity acknowledged BBs as a severe bug, there has been no SLR published on the specific area of applying ML techniques to predicting BBs since the

field was first found introduced in 2014 [1]. Thus, to promote further research and increase the quality of literature in this domain, a systematic review that comprehensively discusses the existing BBPMs, research gaps, and possible research directions to serve as a point of reference for research and practice is critically important. Additionally, this research will contribute to a better understanding of the trends in characterizing and predicting blocking bugs. In other words, the goal of this study is to find out the recent trends and directions in this field and to identify opportunities for future research by researchers and practitioners within the software engineering domain and also to appreciate how the research space has evolved over time with regards to BBs. Finally, the approach presented in this study can serve as a guide for researchers and practitioners (e.g. Ph.D. Student, Master students) when seeking to predict instances of bugs that are BBs based on various data miners.

Based on the aforementioned needs and motivations, in this work, we systematically present a detailed analysis of the trends in the application of ML techniques in BB prediction. Thus, the study aims at answering the following five research questions (RQs):

RQ1: What are the publication trends in BB prediction research?

RQ2: Which datasets are used to train the proposed prediction model?

RQ3: What kind of ML learning techniques is adopted in building the proposed BB prediction model?

RQ4: Which evaluation criterion is used to measure the performance of the BB prediction model?

RQ5: Which ML classifiers are used as baselines to benchmark the proposed model?

The remainder of study is organized as follows: Section 2 describes the proposed research method, including the overall process and the goal and research questions addressed in this study. Section 3 discusses the findings of the meta-analysis of the study. Section 4 presents the results of the systematic. Section 5 summarizes and concludes the study and provides future research directions.

II. RESEARCH METHOD

This SLR follows the software evidence-based engineering (SEBE) guidelines proposed by kitchenham and Charters [10]. The SEBE guidelines have increasingly gained popularity and acceptance in the software engineering research space [11]-[16]. The SEBE provides an all-inclusive outline of how software engineering researchers can conduct SLR using evidence-based research and practice models. Therefore, we segmented the SLR into four major phases with subdivisions to conform with the prescriptions by kitchenham and Charters [10]: plan search, search procedure, search, and report. Fig. 1 depicts the SLR process of this study.

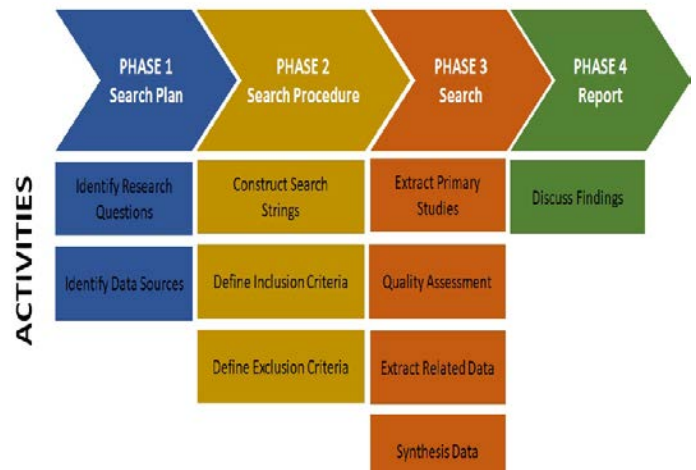


Fig. 1. Process Flow Diagram.

A. Phase 1: Search Plan

This phase of the SLR process presents the research questions addressed in this study and the databases where primary studies were collected.

1) *Data sources*: This section captures the academic databases and repositories where the search was conducted. Five databases of famous academic publishers, namely Scopus, SpringerLink, IEEE Xplore, ACM digital library, and Science Direct, were the data sources for the collection of primary studies for this paper. Also, a few portions of publications were retrieved from Google Scholar to achieve thorough coverage of article collection. Table I displays sampled data sources and the number of results returned by search queries in those academic databases on 18th February 2022.

B. Phase 2: Search Procedure

This phase of the SLR describes how search strings were constructed. It also captures the inclusion and exclusion criteria used in selecting primary studies.

TABLE I. DATA SOURCES AND SEARCH RESULTS

Data Source	URL	Result
Scopus	https://scopus.com	61
SpringerLink	https://link.springer.com	246
IEEE Xplore	https://ieeexplore.ieee.org	20
ACM Digital Library	https://dl.acm.org	152
ScienceDirect	https://ieeexplore.ieee.org	31
Google Scholar	https://scholar.google.com	169
	Total Result	679

1) *Search string*: Keywords were extracted from research questions and related papers. Then synonyms and alternate words were identified for creating search strings by using Boolean *OR* for alternative words and Boolean *AND* for linking search keywords. The keywords and their alternatives are shown in Table II. The resulting search phrases were tweaked to conform with the format required by each online database. Table III shows the search string for each database. Additionally, the Table IV shows the search strings per the data sources that were used in this study.

2) *Inclusion criteria*: Peer-reviewed articles about blocking bugs published in journals, conferences, technical reports, or book chapters from 2012 to 2022 were targeted for review. Whereas 2014 marked the first application of machine learning to predict blocking bugs [1], 2012 was chosen as the start date to widen the scope of our search. Also, the focus was on publications in English that used ML to detect and classify blocking bugs or predict a phenomenon related to blocking bugs. Moreso, studies that constructed prediction models based on binary data classification of blocking bugs were selected. The authors ensured that all selected publications reported their data source, performance evaluation, baseline techniques, and the challenges and limitations of their studies.

3) *Exclusion criteria*: Mendeley [17], a reference management software, was used to delete duplicate papers which were 274 in number. Next, the papers that were not peer-reviewed and for which the complete text was not available in English were excluded. An article that was not about blocking bugs in computer software or was not written regarding predicting a phenomenon of blocking bugs with machine learning was not considered. Articles were mainly excluded based on titles and abstracts, full-text reading, and later quality evaluation. The data sources and the corresponding number of publications after the exclusion criteria are captured in Table III.

TABLE II. KEYWORDS AND ALTERNATIVE WORDS/PHRASES

Keyword	Alternative word/phrase
Blocking Bug	(‘blocker bugs’ OR ‘severe bugs’ OR ‘Bug Severity’)
Prediction	(‘Identifying’ OR ‘Classifying’ OR ‘Detection’ OR ‘Characterizing’)
Machine Learning	(‘machine technique’ OR ‘method’ OR ‘model’ OR ‘algorithm’)

TABLE III. NUMBER OF PUBLICATIONS AFTER EXCLUSION CRITERIA

Data Source	Number of shortlisted Publications
Scopus	2
SpringerLink	0
IEEE Xplore	3
ACM Digital Library	1
ScienceDirect	0
Google Scholar	0
Total	6

TABLE IV. SEARCH STRINGS PER DATA SOURCE

Data Source	Search String
Scopus	("Blocking Bug" OR "Severe Bugs" OR "Bug Severity" OR "Blocker Bug") AND ("Identifying" OR "Prediction" OR "Classifying" OR "Detection" OR "Characterizing") AND ("machine learning" OR "method" OR "model" OR "algorithm")
SpringerLink	("Blocking Bug" OR "Severe Bugs" OR "Bug Severity" OR "Blocker Bug") AND ("Identifying" OR "Prediction" OR "Classifying" OR "Detection" OR "Characterizing") AND ("machine learning" OR "method" OR "model" OR "algorithm")
IEEE Xplore	("Blocking Bug" OR "Severe Bugs" OR "Bug Severity" OR "Blocker Bug") AND ("Identifying" OR "Prediction" OR "Classifying" OR "Detection" OR "Characterizing") AND ("machine learning" OR "method" OR "model" OR "algorithm")
ACM Digital Library	[[All: "blocking bug"] OR [All: "severe bugs"] OR [All: "bug severity"] OR [All: "blocker bug"]] AND [[All: "identifying"] OR [All: "prediction"] OR [All: "classifying"] OR [All: "detection"] OR [All: "characterizing"]] AND [[All: "machine learning"] OR [All: "method"] OR [All: "model"] OR [All: "algorithm"]]
ScienceDirect	("Blocking Bug" OR "Severe Bugs" OR "Blocker Bug") AND ("Prediction" OR "Classifying" OR "Detection" OR "Characterizing") AND ("machine learning" OR "algorithm")
Google Scholar	("Blocking Bug" OR "Blocker Bug") AND ("Identifying" OR "Prediction" OR "Classifying" OR "Detection" OR "Characterizing") AND ("machine learning" OR "method" OR "model" OR "algorithm")

C. Phase 3: Search

This phase of the SLR explains the approach adopted for sampling relevant primary studies.

1) *Study selection*: To sample relevant primary studies that meet the needs of this study, the tollgate method proposed by Afzal et al. [16] was adopted. Fig. 2 depicts the tollgate approach used. This approach is made up of five steps which were traced by the authors as follows:

Step 1: Data was collected from selected online data sources via the use of search strings generated in Table III.

Step 2: Duplicate studies were excluded using Mendeley.

Step 3: Inclusion/ exclusion criteria were applied by perusing the titles and abstracts.

Step 4: Inclusion/ exclusion criteria were applied by reading the introductions and conclusions.

Step 5: Inclusion/ exclusion criteria were applied by reading the full text of sampled studies.

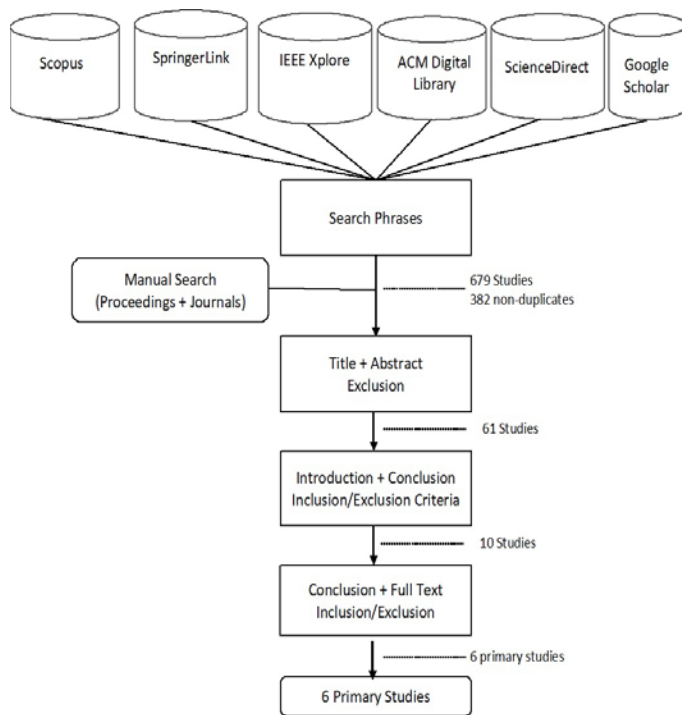


Fig. 2. The Tollgate Approach.

The search strings established in Table III were used to collect 679 from the selected data sources for this study (i.e. Table I) in the first step. At the end of the tollgate approach, six primary studies [1], [4]-[7] were selected. Table VII shows the shortlisted primary studies.

2) *Quality assessment of selected studies*: The purpose of the study quality assessment was to ensure that the sampled primary studies could adequately answer the research questions. It also aids in interpreting findings for data analysis and synthesis [18]. Hence, each quality criterion was designated by the prefix ‘QC’ and a number. The QC and data extraction activities were performed at the same time. Table V shows a quality assurance checklist for selected primary studies. A mathematical approach was used to assign quality scores, as in Kitchenham [10]. Thus, attributes of the quality criteria outlined in **Table V** were extracted for each primary study and scored on how well they met the requirements. For each attribute there are three possible values: Yes (Y) = 1 point, Partial (P) = 0.5 point, No (N) = 0 point. A study is allocated a score of 1 if the article clearly answers the QC question and a score of 0.5 if it partially answers the QC. Studies that do not answer the QC questions receive a score of 0. The six QC scores were added together to get the total quality score. As a result, the overall quality score of each selected study ranged from 0 (extremely poor) to 6 (very good). This approach to quality score has been widely used by SLR researchers in the software engineering domain [14], [19], [20], and related domains [21]. Each selected article in this study received a score greater than 70%. This percentage score shows that the primary studies can sufficiently answer the research questions.

TABLE V. QUALITY CHECKLIST FOR SELECTING PRIMARY STUDIES

Serial Number	QC Checklist
QC1	Does the selected study give details of the machine learning techniques applied in the study to answer RQ1?
QC2	Does the selected study give details of the dataset and the data source used in the study to answer RQ2?
QC3	Does the selected study benchmark its results with the performance of other prediction techniques to answer RQ3?
QC4	Does the selected study provide information about the performance metrics used to evaluate results to answer RQ4?
QC5	Does the selected study report the ML classifiers used as baselines to benchmark the proposed model to answer RQ5?

3) *Data extraction*: A structured extraction form created with Microsoft Excel was used to extract the information needed for data synthesis. Table VI indicates the items extracted from each primary study.

TABLE VI. DATA EXTRACTION FORM ITEMS

Data Item	Description
Reference	Title, Author, Type (i.e Journal/conference/workshop)
Technique	ML technique was applied in building the proposed model in the study.
Pre-processing	Preprocessing methods for machine learning technique
Dataset	Source of datasets used in training ML models
Evaluation	Metrics used for model evaluation
Results	The outcome of the model performance evaluation
Baseline	Baseline techniques with which proposed models were compared
Future works	Future works proposed by the study

TABLE VII. SHORTLISTED PRIMARY STUDIES

Ref.	Year	Library	Journal/Conference
Valdivia-Garcia and Shihab [23]	2014	ACM	Conference: MSR'14, May 31 – June 1, 2014, Hyderabad, India
Xia et al	2015	Elsevier	Journal: Information and Software Technology
Valdivia-Garcia et al[2]	2018	Elsevier	Journal: Journal of Systems and Software
Din et al.	2020	IEEE Xplore	Conference: 2018 IEEE 42nd Annual Computer Software and Applications Conference (COMPSAC)
Cheng et al. [24]	2020	IEEE Xplore	Conference: IEEE 44th Annual Computers, Software, and Applications Conference (COMPSAC)
Brown et al. [25]	2021	IEEE Xplore	Conference: 2021 International Conference on Cyber Security and Internet of Things (ICSIoT)

4) *Data synthesis*: At this stage, the relevant extracted data were synthesized using the thematic approach [22] to answer the research questions outlined in Table V.

D. Phase 4: Report

The final phase of the SLR summarizes and examines the review results. Then, in distinct sub-sections, the full summary of the findings of this review is discussed and interpreted in relation to the research questions.

III. FINDINGS

RQ1: What are the publication trends in BB prediction research?

Our search following the SEBE SLR methodology identified six primary studies that applied ML to predicting BB. The publication period of these studies spans from January 2014 to February 2022. Table VII presents the selected publications, while Fig. 3 depicts the publications over the years or distribution of primary studies. Observing Table VII, conference publications or proceedings seem to dominate the publications over the period with four articles, while journal articles account for two publications. This distribution further suggests the paucity of publications on the use of ML for predicting BBs over the years.

RQ2: Which datasets are used to train the proposed prediction model?

The performance of a machine learning technique is heavily reliant on the quality of the dataset used in training the prediction model. To train BBPM, all the six selected primary studies in this work utilized datasets extracted from publicly available bug reports about specific software projects. These bug reports were retrieved from Bugzilla, IssueTracker, and monorail issue tracking systems. The ones obtained from Bugzilla are Eclipse, NetBeans, Gentoo, Fedora, Mozilla, and NetBeans. While bug reports of Chromium and OpenOffice were retrieved from Montrail and IssueTracker. Table IX shows the web locations where these bug reports about the various projects were extracted. Also, studies used bug reports from authentic projects with actual proportions of blocking bugs (BBs) and non-blocking bugs (Non-BBs). Table VIII and Fig. 4 show blocking bug and non-blocking bug distribution within the extracted datasets and the distribution of projects from which datasets were extracted per the studies, respectively.

From Table VIII, it is observed that the chosen primary studies made use of at least two sets of datasets from the open-source application domain. For instance, Ding et al. [5] validated their method on two open-source projects, namely, Mozilla Firefox and Netbeans, which contained 132,584 bugs. 18900 were Blocking Bugs and 113,684 Non-Blocking Bugs. Also, Cheng et al. [7] gathered a total of 214873 bugs from Eclipse, FreeDesktop, NetBeans, and OpenOffice, of which 16,402 were Blocking Bugs. Both Valdivia-Garcia and Shihab [1] and Xia et al. [4] selected a total of 402,962 bugs from six (6) open-source projects (i.e. Chromium, Eclipse, FreeDesk Mozilla, NetBeans, and OpenOffice). 18,422 of the total bugs were blocking bugs. Similarly, Valdivia-Garcia et al. [2] and Brown

et al. [6] mined a total of 609,800 bugs which had 77,448 blocking bugs from eight projects (i.e., Chromium, Eclipse, FreeDesktop, Mozilla, NetBeans, OpenOffice, Gentoo, and Fedora) in their studies. The open-source projects used by the selected primary studies in this paper, as well as their corresponding bug tracking systems, are as follows:

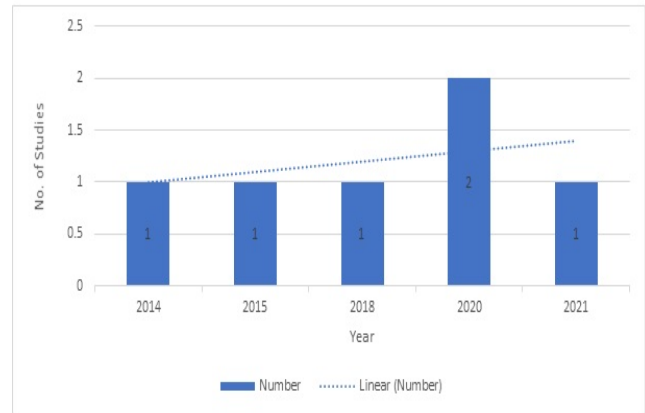


Fig. 3. Distribution of Primary Studies.

TABLE VIII. DISTRIBUTION OF DATASET UTILIZED BY PRIMARY STUDIES

Studies	No. of Projects	Projects	No. of Bbs	No. of Non-Bbs
Valdivia-Garcia and Shihab [1]	6	Chromium, Eclipse, FreeDesktop, Mozilla, NetBeans, and OpenOffice	18,422	384,540
Xia et al. [12]	6	Chromium, Eclipse, FreeDesktop, Mozilla, NetBeans, and OpenOffice	18,422	384,540
Valdivia-Garcia et al. [11]	8	Chromium, Eclipse, FreeDesktop, Mozilla, NetBeans, OpenOffice, Gentoo, and Fedora	77,448	532,352
Cheng et al. [14]	4	Eclipse, FreeDesktop, NetBeans, and OpenOffice	34,892	229,729
Ding et al. [13]	2	Mozilla Firefox and Netbeans	16,402	198,471
Brown et al. [15]	8	Chromium, Eclipse, FreeDesktop, Mozilla, NetBeans, OpenOffice, Gentoo, and Fedora	18,900	113,684

TABLE IX. SOURCES WHERE DATASETS OF OPEN-SOURCE PROJECTS WERE EXTRACTED

Project	Source
Chromium	https://bugs.chromium.org/p/chromium/issues/list
Eclipse	https://bugs.eclipse.org/bugs/
NetBeans	https://netbeans.org/bugzilla/
OpenOffice	https://bz.apache.org/ooo/
Gentoo	https://bugs.gentoo.org/buglist
Fedora	https://bugzilla.redhat.com/ss
Mozilla	https://bugzilla.mozilla.org/
free desktop	https://bugzilla.freedesktop.org/

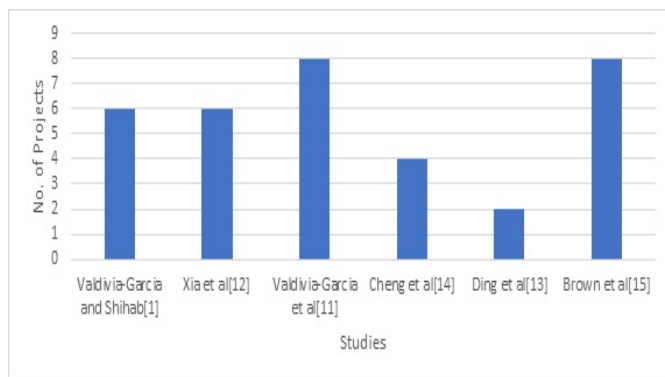


Fig. 4. Distribution of Projects Studied by the Selected Studies.

- Chromium is a popular open-source web browser developed by Google and used mainly as the codebase for Google Chrome. C++ and C programming languages dominate it; however, it comprises other programming languages such as JavaScript and Python, amongst others. Chromium has its bug tracking mechanism in Google code, called Monorail, which has a feature called "Blocking." The "blocking" feature can identify if a bug is a blocking bug or not.
- Eclipse is a well-known integrated development environment (IDE) developed mainly with Java yet supports many programming languages, including Python, Ruby, and C/C++. In addition, eclipse uses Bugzilla for reporting and tracking bugs. This issue tracking system has a feature called "Blocks." This is used for identifying a bug as a blocking bug. GNU/Linux or FreeBSD. Gentoo also uses Bugzilla in reporting and tracking bugs; hence the "Blocks" field identifies a blocking bug.
- Mozilla is an open-source project that hosts and develops products such as Firefox, Thunderbird, Bugzilla, Gecko layout engine, and others. The programming languages used in its development are C, JavaScript, and C++. In addition, Mozilla tracks its bugs in Bugzilla software and uses the "Blocks" field to show if a bug is a blocking bug.
- NetBeans is an open-source IDE for developing applications in the java programming language for Win-

dows, Mac, Linux, and Solaris. However, it supports PHP, C, and C++, amongst others. NetBeans was developed with the Java programming language. Bugzilla is an issue tracking system used by Netbeans; hence the "Blocks" field indicates whether a reported bug is a blocking bug or not.

- OpenOffice is an office suite created by Sun Microsystems and is now maintained by Apache. It is maintained with its programming language called OpenOffice.org Basic. IssueTracker, a derivative of Bugzilla, was used by OpenOffice when these primary studies were undertaken. Just like Bugzilla, it has a "Blocks" feature which indicates whether a bug is a blocking bug or not. At the time of this study, Bugzilla had succeeded IssueTracker, which was also known as IssueZilla.

Valdivia-Garcia et al. [2] and Brown et al. [6] used the most extensive dataset with the most bugs (i.e. 609,800 bugs), which they extracted from Chromium, Eclipse, Free Desktop, Mozilla, NetBeans, OpenOffice, Gentoo, and Fedora. The open-source project that most of the studies included in their dataset is Netbeans, while Gentoo and Fedora were the least utilized by the studies, as captured in Fig. 6. Although the six primary studies used datasets from popular and well-supported open-source projects with a substantial number of bug reports, the distribution of dataset sizes in Fig. 5, coupled with the unequal distribution of Blocking bugs and non-blocking bugs in Table VIII, suggests the challenge of class imbalance. Thus, in most studies, BBs account for less than 12% of the total available dataset [2]. However, extensive research exists about the challenges an imbalanced dataset, also referred to as the class imbalance phenomenon [23], poses to the performance of classifiers that use them in training. Also, it is worth noting that all the studies considered in this work used datasets related to open-source projects; hence their findings may not apply to closed and commercial software projects.

RQ3: What kind of ML learning techniques is adopted in building the proposed BB prediction model?

The primary studies considered in this SLR proposed new methods for identifying a bug as blocking bugs or non-blocking bugs based on an existing classification technique. Fig. 7 shows the distribution of the classification techniques employed in the various studies.



Fig. 5. Distribution of Datasets by Selected Studies.

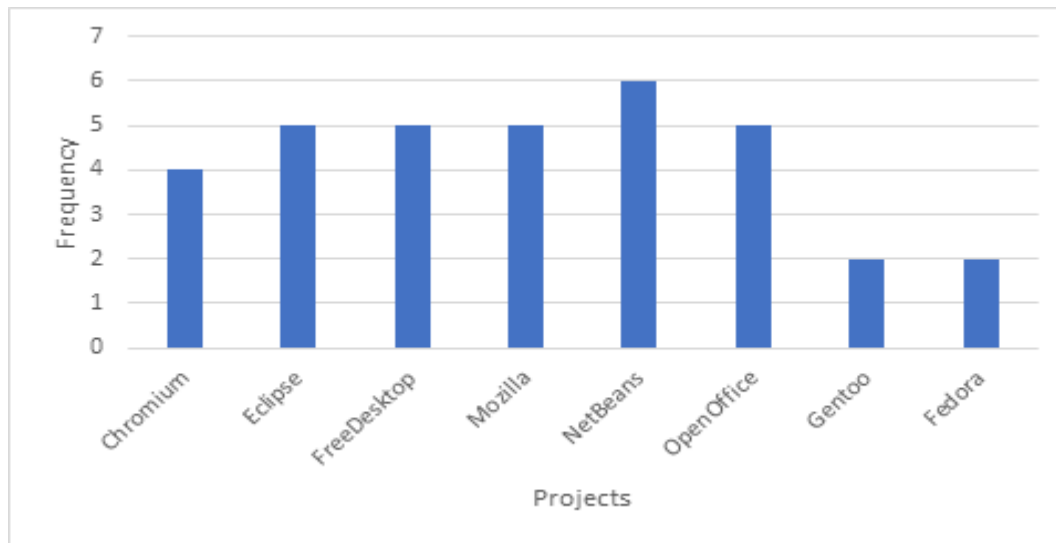


Fig. 6. Distribution of Projects and their Frequency of use in Primary Studies.

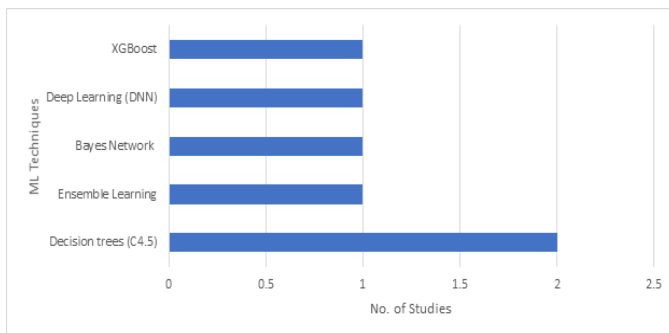


Fig. 7. Distribution of Classification Techniques.

TABLE X. DISTRIBUTION OF ML TECHNIQUES UTILIZED BY PRIMARY STUDIES

ML Techniques	Studies
Decision trees (C4.5)	Valdivia-Garcia and Shihab[1], Valdivia-Garcia et al [11]
Ensemble learning	Xia et al. [12]
Bayes Network	Ding et al. [13]
Deep Learning (DNN)	Brown et al. [15]
XGBoost	Cheng et al. [14]

Valdivia-Garcia and Shihab [1] and Valdivia-Garcia et al. [2] used a re-sampling technique to pre-process the training data to resolve the data imbalance issue; non-blocking bugs outnumber blocking bugs. Even though random forest performed better in terms of F1 measure than their proposed model, which was based on Decision trees (C4.5), they recommended their model as the most appropriate for practitioners.

Xia et al. [4] built a classifier called ELBlocker based on the random forest technique. They separated the training data into many disjoint sets and developed different classifiers, which they then merged to identify an appropriate threshold for classifying bugs as blocking or non-blocking. Also, Cheng et al. [7] presented a new classification framework called XGBlocker, consisting of two stages. XGBlocker captures more features from bug reports in the first stage to construct an improved dataset. In the second stage, XGBlocker employs the XGBoost technique to build an efficient model for performing the prediction task. Ding et al. [5] proposed a Bayes Network-based classifier for forecasting the breakability of the blocking bug pairs.

The classifier is identical to the Bayes Network classifier; as the threshold lowers from 0.5 to 0, the classifier becomes

stricter and removes more boundary instances to improve precision. In Brown et al. [6], researchers proposed a DeepLabB classifier based on deep neural networks for predicting blocking bugs. Three deep neural networks were developed and trained independently, each with a different number of hidden layers. The first DNN had two hidden layers, the second DNN had three hidden layers, and the third DNN had four hidden layers. Bayesian optimization was used to estimate the best learning rate for each model. It is worth mentioning that apart from Brown et al. [6], who employed a deep learning approach in this domain, at the time of this work, the rest used Decision Trees, Random Forest, Bayes Network, and XGBoost for building Blocking bug prediction models in the selected primary studies. Table X shows the studies and the classification techniques adopted in building their classifiers. While the most frequently used ML technique in building BB classifiers is based on the Decision Trees, Random Forest was reported by two studies [1][11] to have performed better than Zero-R, Naive Bayes, and KNN.

RQ4: Which evaluation criterion is used to measure the performance of the BB prediction model?

The primary studies assessed the prediction abilities of their proposed BB prediction model using various combinations of evaluation metrics. Fig. 8 depicts the distribution of research based on performance metrics. In Valdivia-Garcia and Shihab [2], Precision, Recall, F1-Score, and Accuracy were used to measure the effectiveness of their proposed classifier and reported 9-29% precision, 47-76% recall, and 15-42% F1-Score.

The F1 score and cost-effectiveness were used to assess the efficiency of ELBlocker in Xia et al. [12], which attained an F1-Score up to 0.482 and EffectivenessRatio@20% scores of 0.831. In Valdivia-Garcia et al. [11], the researchers utilized Precision, Recall, and F1-Score to evaluate the performance of their proposed model. The proposed model achieved 13%–45% precision, 47%–66% Recall, and 21%–54% F1-Score. Ding et al. [13] used ROC Area, Accuracy, F1-Score, Recall, and Precision to assess the efficiency of the classifier they recommended. In Mozilla Firefox the proposed BayesNet model achieved 0.629, 0.729, 0.676, 0.831, and 76.54 % for Precision, Recall, F-measure, Roc Area, and Accuracy, respectively. However, it recorded Precision, Recall, F-measure, Roc Area, and Accuracy of 0.488, 0.583, 0.531, 0.764, and 73.45%, respectively, in the case of the NetBeans dataset. To compare the performance of XGBlocker to other classifiers, Cheng et al. [14] employed AUC, Cost-Effectiveness, and F1-Score. XGBlocker reported an F1-score of 0.808, ER@20% of 0.944, and AUC of 0.975.

Brown et al [15] used MCC, F1, and AUC to compare DeepLaBB with other classifiers. DeepLaBB recorded an MCC of 0.8504%, F1 Score of 0.4292%, and AUC of 2.9459%.

The following is a summary of the various performance metrics used in the primary studies considered in this work:

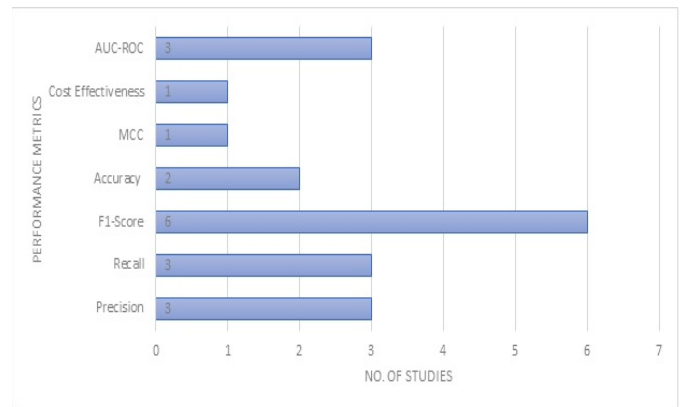


Fig. 8. Performance Metrics and the Corresponding Number of Primary Studies.

Accuracy refers to the proportion of correctly categorized instances to the total number of instances. It can be calculated using the formula below with the aid of True positives (TP), False negative (FN), False positives (FP), and True negative (TN) extracted from the confusion matrix.

$$\text{Accuracy} = \frac{TP+TN}{TP+FP+TN+FN}$$

MCC refers to Matthew's Correlation Coefficient. To measure the quality of binary categorization, MCC examines all true and false positives and negatives [29]. It can be computed as:

$$\text{MCC} = \frac{TP*TN-FP*FN}{\sqrt{((TP+FP)(TP+FN)(TN+FP)(TN+FN))}}$$

Recall is the ratio of accurately categorized positive cases to the total number of positive instances. Recall can be calculated as:

$$\text{Recall} = \frac{TP}{TP+FN}$$

Precision is a measure of the proportion of correctly categorized positive instances among all positive samples. It can be computed as follows:

$$\text{Precision} = \frac{TP}{TP+FP}$$

F1-Score is the harmonic mean of precision and recall. F1's best value is 1, and its worst value is 0. It can be represented mathematically as:

$$\text{F1-Score} = \frac{2*Precision*Recall}{Precision+Recall}$$

The AUC-ROC refers to AUC (Area under Curve)-ROC (Receiver Operating Characteristic). It is a trade-off between the True Positive Rate (TPR) and the False Positive Rate (FPR) and represents the classifier's ability to predict classes correctly.

It can be generated by charting TPR (True Positive Rate), i.e., Sensitivity or recall vs. FPR (False Positive Rate), i.e., 1-Specificity, at different threshold values.

Cost-Effectiveness [24] is a cost-sensitive indicator of prediction performance. It assesses a method's prediction performance under a cost limit. Even though research findings [25] discourage the use of Accuracy for evaluating classifiers trained with an imbalanced dataset, Valdivia-Garcia and Shihab [1] and Ding et al. [24] employed Accuracy in their works; the F1 score is the most common evaluation metric utilized among the studies in this SLR, followed by Precision and Recall. The least common measure employed is cost-effectiveness.

RQ5: Which ML classifiers are used as baselines to benchmark the proposed model?

The studies considered in this work compared the performance of proposed BB prediction models to baseline techniques to assess their efficacy. Fig 8 shows the baselines to which the proposed techniques were compared. After reviewing the primary studies in this work, it can be concluded that the proposed BB prediction models outperformed individual baseline classifiers in the vast majority of cases at the time of this study. The C4.5 Decision tree algorithm-based BB prediction model proposed in Valdivia-Garcia and Shihab [1] and Valdivia-Garcia et al. [2] performed better than Naive Bayes, kNN, and Zero-R baselines.

The C4.5 based model was chosen over the random forest because it is an explainable model that practitioners can easily understand. To forecast the possibility of a blocking bug, Xia et al. [4] used an ensemble of various classifiers. The ELBlocker showed a significant improvement compared with Valdivia-Garcia and Shihab's methods [1], SMOTE, one-sided selection (OSS), and bagging. In Cheng et al. [7], the proposed XGBBlocker was compared with Gradient Boosting Decision Tree (GBDT), AdaBoost, ELBlocker, XGB_14, CART, Logistic Regression, and Valdivia-Garcia and Shihab's approaches. The proposed method displayed superior performance in all instances. Ding et al. [5] offered a method for describing and forecasting the breakability of the blocked bug pairs, which performed better compared with the Zero-R Classifier's performance, Naive Bayes, BayesNet, KNN, and Random Forest. Brown et al. [6] introduced DeepLaBB for predicting blocking bugs in open-source projects. DeepLaBB showed improved performance compared with the performance of Random Forest, KNN, CART, and ANN on the same datasets. The performance of proposed BB predicting models was compared with that of base classifiers such as RF, KNN, NB, Zero classifier, and Valdivia-Garcia and Shihab's approaches in the majority of the research articles. Generally, the choice of baseline varied from one study to another. However, as shown in Fig. 9, RF was the most utilized baseline classifier in most studies, closely followed by KNN. Even though most of the proposed BB prediction models in the various studies performed better than the baseline classifiers, some BB prediction models have not improved performance compared with traditional classifiers. For instance, in Valdivia-Garcia and Shihab [1], when it comes to chromium and Eclipse data sets, the proposed model had recall values of 49% and 47%, slightly below the 50% recall value of the baseline. In the same paper, random forest performed better than the proposed model in precision across all project datasets. Also, Zero-R outperformed all the classifiers in terms of Accuracy. Similarly, in Valdivia-Garcia et al. [1], the Zero-R model

had the highest Accuracy across all project datasets except for Fedora. Also, in Brown et al. [6], a baseline classifier, Random Forest, performed better than the proposed DeepLaBB in the FreeDesktop dataset in terms of MCC and F1-Score.

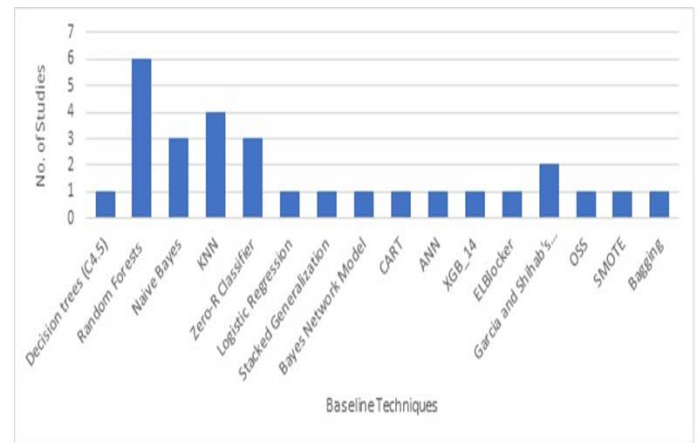


Fig. 9. Distribution of Baseline Classifiers and Primary Studies.

IV. SUMMARY

This SLR traced the research advances in applying ML techniques to predict Blocking Bugs. After a rigorous analysis of the most pertinent research papers published between January 2012 to February 2022 in the databases of five famous academic publishers, namely Scopus, SpringerLink, IEEE Xplore, ACM digital library, and Science Direct, six (6) BB primary papers/studies were identified and reviewed. The findings regarding the research trend, variety of proposed ML techniques, baseline classifiers, evaluation metrics, and sources of datasets for predicting BBs during this study are captured in Fig. 3, Table X, Fig. 9, Fig. 8, and Table IX, respectively. The existing studies confirm that proposed ML techniques (i.e. BBPMS) significantly improve the detection of BBs in software bug reports and that they generally outperform the traditional classifiers. Also, this study concludes that there is a paucity of literature on the application of ML to BB prediction. Further research is required to validate existing and new prediction models on bug reports of commercial or closed software projects. In addition, new researchers should explore the effect of parameter tuning and the efficiency of ML approaches such as deep learning and ensemble learning in improving the classification of BBs. Furthermore, before training a classifier, researchers should take steps to mitigate the effect of class imbalance on the proposed BB prediction model.

REFERENCES

- [1] H. Valdivia Garcia and E. Shihab, "Characterizing and predicting blocking bugs in open source projects," in Proceedings of the 11th working conference on mining software repositories, 2014, pp. 72-81.
- [2] H. Valdivia-Garcia, E. Shihab, and M. Nagappan, "Characterizing and predicting blocking bugs in open source projects," Journal of Systems and Software, vol. 143, pp. 44-58, 2018.
- [3] B. W. Boehm, "Software engineering economics," in Software pioneers, ed: Springer, 2002, pp. 641-686.
- [4] X. Xia, D. Lo, E. Shihab, X. Wang, and X. Yang, "Elblocker: Predicting blocking bugs with ensemble imbalance learning," Information and Software Technology, vol. 61, pp. 93-106, 2015.
- [5] H. Ding, W. Ma, L. Chen, Y. Zhou, and B. Xu, "Predicting the breakability of blocking bug pairs," in 2018 IEEE 42nd Annual Computer

- Software and Applications Conference (COMPSAC), 2018, pp. 219-228.
- [6] S. A. Brown, B. A. Weyori, A. F. Adekoya, P. K. Kudjo, S. Mensah, and S. Abedu, "DeepLaBB: A Deep Learning Framework for Blocking Bugs," in 2021 International Conference on Cyber Security and Internet of Things (ICSIoT), 2021, pp. 22-25.
- [7] X. Cheng, N. Liu, L. Guo, Z. Xu, and T. Zhang, "Blocking Bug Prediction Based on XGBoost with Enhanced Features," in 2020 IEEE 44th Annual Computers, Software, and Applications Conference (COMPSAC), 2020, pp. 902-911.
- [8] P. V. Torres-Carrión, C. S. González-González, S. Aciar, and G. Rodríguez-Morales, "Methodology for systematic literature review applied to engineering and education," in 2018 IEEE Global engineering education conference (EDUCON), 2018, pp. 1364-1373.
- [9] L. A. F. Gomes, R. da Silva Torres, and M. L. Côrtes, "Bug report severity level prediction in open source software: A survey and research opportunities," *Information and software technology*, vol. 115, pp. 58-78, 2019.
- [10] B. Kitchenham, R. Pretorius, D. Budgen, O. P. Brereton, M. Turner, M. Niazi, et al., "Systematic literature reviews in software engineering—a tertiary study," *Information and software technology*, vol. 52, pp. 792-805, 2010.
- [11] M. Niazi, A. M. Saeed, M. Alshayeb, S. Mahmood, and S. Zafar, "A maturity model for secure requirements engineering," *Computers & Security*, vol. 95, p. 101852, 2020.
- [12] M. Galster, D. Weyns, D. Tofan, B. Michalik, and P. Avgeriou, "Variability in software systems—a systematic literature review," *IEEE Transactions on Software Engineering*, vol. 40, pp. 282-306, 2013.
- [13] M. Ilyas, S. U. Khan, and N. Rashid, "Empirical validation of software integration practices in global software development," *SN Computer Science*, vol. 1, pp. 1-23, 2020.
- [14] R. Hoda, N. Salleh, J. Grundy, and H. M. Tee, "Systematic literature reviews in agile software development: A tertiary study," *Information and software technology*, vol. 85, pp. 60-70, 2017.
- [15] V. Garousi, G. Giray, E. Tüzün, C. Catal, and M. Felderer, "Aligning software engineering education with industrial needs: A meta-analysis," *Journal of Systems and Software*, vol. 156, pp. 65-83, 2019.
- [16] J. dos Santos, L. E. G. Martins, V. A. de Santiago Júnior, L. V. Povia, and L. B. R. dos Santos, "Software requirements testing approaches: a systematic literature review," *Requirements Engineering*, vol. 25, pp. 317-337, 2020.
- [17] "Search | Mendeley." <https://www.mendeley.com/search/> (accessed Apr. 04).
- [18] B. Kitchenham and S. Charters, "Guidelines for performing systematic literature reviews in software engineering," 2007.
- [19] P. Achimugu, A. Selamat, R. Ibrahim, and M. N. r. Mahrin, "A systematic literature review of software requirements prioritization research," *Information and software technology*, vol. 56, pp. 568-585, 2014.
- [20] M. Goulão, V. Amaral, and M. Mernik, "Quality in model-driven engineering: a tertiary study," *Software Quality Journal*, vol. 24, pp. 601-633, 2016.
- [21] A. Qazi and N. A. Fayaz Hussain, "Rahim, Glenn Hardaker, Daniyal Alghazzawi, Khaled Shaban, Khalid Haruna 2019," *Towards Sustainable Energy: A Systematic Review of Renewable Energy Sources, Technologies, and Public Opinions*, *IEEE Access*, vol. 7, pp. 63837-63851.
- [22] D. S. Cruzes and T. Dyba, "Recommended steps for thematic synthesis in software engineering," in 2011 international symposium on empirical software engineering and measurement, 2011, pp. 275-284.
- [23] H. He, "Member, IEEE, and Edwardo A. Garcia," *Learning from Imbalanced Data*, *IEEE Transactions on knowledge and data engineering*, vol. 21, pp. 1041-4347, 2009.
- [24] F. Rahman and P. Devanbu, "How, and why, process metrics are better," in 2013 35th International Conference on Software Engineering (ICSE), 2013, pp. 432-441.
- [25] T. Menzies, J. DiStefano, A. Orrego, and R. Chapman, "Assessing predictors of software defects," in *Proc. Workshop Predictive Software Models*, 2004.

Trace Learners Clustering to Improve Learning Object Recommendation in Online Education Platforms

Zriaa Rajae¹

Informatics and Applications
Laboratory (IA), Faculty of Sciences
Moulay Ismail University of Meknes
Morocco

Amali Said²

Informatics and Applications
Laboratory (IA), FSJES
Moulay Ismail University of Meknes
Morocco

El Faddouli Nour-eddine³

RIME Team, MASI Laboratory
E3S Research Center, EMI
Mohammed V University
Morocco

Abstract—E-learning platforms propose pedagogical pathways where learners are invited to mobilize their autonomy to achieve the learning objectives. However, some learners face a set of cognitive barriers that require additional learning objects to progress in the course. A mediating recommendation system is one of the efficient solutions to reinforce the resilience of online platforms, while suggesting learning objects that will be interesting for them according to their needs. The objective of this contribution is to design a new mediator recommendation model for e-learning platforms to suggest learning objects to the learner based on collaborative filtering. To this end, the proposed system relies on the implicit behaviors estimation function as an underlying technique to convert tacit traces into explicit preferences allowing to compute the similarity between learners.

Keywords—e-learning; recommendation system; learning objects; tacit behaviors

I. INTRODUCTION

E-learning has become, in recent years, the fundamental pillar of any educational system [1], as it allows everyone to learn easily, at any time, from any place and through any tool (laptops, smart phones, ...). In addition, several universities, institutes and schools have started using e-learning platforms to evolve their educational systems under any circumstances.

E-learning is considered as a process by which a set of educational activities and resources are delivered through digital devices to help learners achieve their learning objectives in the best possible conditions [2]. Moreover, these platforms are based on two fundamental aspects: the technological aspect (platform infrastructure) and the pedagogical aspect (learning content and its exploitation) [3], moreover, they are generally designed for heterogeneous learners with diverse pedagogical characteristics, including those related to experience levels, preferences, learning styles, etc. To this end, it is necessary to take full advantage of new technologies to improve the context of the pedagogical tool and also to adapt the learning strategies according to the learners' profiles.

Today, the application of recommender systems in e-learning has become an important field of research, as learning platforms have grown considerably, resulting in a massive increase in online digital resources. As a result, learners face

great difficulty in choosing the most relevant and useful learning resources. Recommender systems are promising new technologies in online learning environments, as they can mitigate the problem of information overload [4-5], while highlighting what is most relevant and interesting based on the learner's profile. The recommendation of personalized learning resources is based on the different types of knowledge identified in the learner's profile, such as: preferences, learning styles and contextual information [6]. Several works have been proposed in the application of recommender systems, which help users to get the desired information through some filtering processes, such as: recommending movies on Netflix, videos on Youtube, articles on Amazon and courses on Byju and Gooru.

This paper presents a recommendation system based on Tacit Learner Preferences (TLP), supported by a new methodological approach for extracting their tacit preferences, in order to provide learners with learning resources that perfectly match their preferences without the tutor's intervention. The recommendation system is based on a learner model that gathers all personal information (age, education level, language, ...), pedagogical characteristics (learning styles, ...) and competency profiles (prerequisites, performance, expertise level, ...). All this information is extracted from the learner's interactions within the online platform. However, the problem is the difficulty of extracting tacit traces from the learning platform.

The objective of this paper is to convert the tacit traces into explicit ratings, in order to estimate the learner's preferences for a resource in the learner model of the recommender system.

The rest of the paper is organized as follows. In Section II, we highlight the main techniques proposed in the literature. In Section III, we represent related research work. In Section IV, we describe our proposed approach: Model for Converting Tacit Behaviors into Explicit Behaviors and in Section V, we conclude the paper and suggest possible future work.

II. TYPES FOR RECOMMENDER SYSTEMS

Recommender system is defined as a strategy that helps users make decisions in complex and evolving information

spaces [7-8]. The recommender system suggests items for the user to evaluate based on their profile and the target domain. In addition, recommender systems address the problem of information overload and lack of domain knowledge, which users usually encounter, by providing personalized and exclusive content and service recommendations [9]. Recommender systems are classified into three main categories namely: Content-Based Filtering (CBF), Collaborative Filtering (CF), Hybrid Filtering (HF).

A. Content-Based Filtering

Content-based filtering (CBF) is used to suggest articles similar to those previously liked by the user [10]. For example, the recommendation of research articles is based on the content-based approach, where the procedure uses the descriptive content of the articles and the users' needs without considering the ratings of other users [11]. The main problem with the content-based filtering recommender method is serendipity

1) *This problem of serendipity* is more known in content-based recommender systems, as these systems only recommend items that match the user's profile. At this point, the user has no chance to receive unexpected recommendations, which leads to a certain weariness with the proposed recommendations.

B. Collaborative Filtering

Collaborative filtering (CF) is the most common and effective technique in recommender systems, as it compares users' ratings with other users' ratings to find the users who are "most similar" based on a similarity criterion and to recommend the articles that similar users have previously liked [12]. In 2016, QusaiShambour et al. developed a personalized recommendation system based on collaborative multi-criteria filtering of articles, while exploiting multi-criteria ratings and semantic information of articles, to overcome the problem of data sparsity and cold start of articles [13]. Collaborative filtering is considered the most popular and widespread method in recommender systems. They have been massively exploited in companies and universities. Some of these systems include PHOAKS [14], which helps users find accurate and relevant information on the web, GroupLens [15], BellcoreVideoRecommender [16], etc.

The main problem with the collaborative filtering recommendation method is data sparsity and the cold start problem:

1) *The cold start problem [17-18]*: is caused by the lack of data on new items or new users. Indeed, a new item cannot be recommended until a user has evaluated it. Similarly, for a new user, we cannot predict his preferences without knowing his item evaluation history.

2) *The sparsity problem [19-20-21]*: is generated when the number of items rated by users is very small compared to the total number of items available in the system. Parity results in a very low density of the matrix (items/user). This

affects the ability of the system to recommend less accurate items.

C. Hybrid Filtering

Hybrid filtering (HF): aims at combining the strengths of the previously explained recommendation approaches in order to benefit from their complementary advantages and to overcome the problems identified before. Several techniques have been proposed to combine the basic techniques to create a new hybrid system. In 2018, R. Shanthi and colleagues proposed a hybrid recommender system to recommend products to users based on users' opinions and ratings [22]. In 2002, Burke describes a taxonomy that proposes seven ways of hybridization: weighted, switching, mixed, feature combination, cascade, feature augmentation, and meta-level [23].

III. RELATED WORK

Several recommender systems have been developed for online learning, such as: In 2018, Feng Zhang et al. proposed a recommender system based on the collaborative filtering approach to recommend learning resources that are valued by learners most similar to the active learner [24]. In 2018, Hayder Murad et al. designed a recommender system that detects students' profiles and knowledge levels, with the aim of automatically recommending online video learning materials that are perfectly suited to students' needs [25]. In 2017, Tarus et al. propose a hybrid ontology-based recommender system with sequential pattern mining to recommend online learning resources to learners [26]. In 2015, Bokde et al. develop an academic recommender system, which provides engineering school students with recommendations that meet their past preferences, based on a hybrid technique that combines article-based multi-criteria collaborative filtering with a dimensionality reduction approach [27]. In addition, a tutoring system based on a recommendation engine Protus (ProgrammingTutoring System) [28] was designed to recommend materials of interest to learners, while taking into account their pedagogical differences such as: preferences, knowledge, learning goals and learner progress, etc. The initial recommendation in Portus is based on the default sequence of lessons and the surveys previously assigned to the lessons.

Most of the works proposed in e-learning context are based on collaborative filtering, with the aim of recommending educational resources based on the profile and explicit evaluations of similar learners. These recommendation systems are designed to provide a personalized list of suggestions (educational resources, learning activities or videos). However, these systems ignore the importance of assisting learners in their learning journey, through the recommendation of additional resources to help them overcome cognitive difficulties and also to maintain their perseverance throughout the online training. Moreover, these recommender systems only exploit explicit user ratings to make recommendations.

Explicit evaluations are sometimes poorly expressed or ignored by users, which leads to a decrease in the performance of recommender systems [29]. In other words, implicit user

feedback is poorly considered in most existing recommender systems compared to explicit feedbacks, knowing that implicit behaviors can serve as a means to overcome several problems that plague recommender systems, such as: data sparsity and cold start.

Moreover, to improve the accuracy of recommendations, several works have been done to better capture and know users' preferences based on their behaviors in the system; In 2009, Rendle et al. proposed an article recommendation system based on users' implicit comments to predict a personalized ranking on a set of articles [30]. In 2008, Hu et al. developed a recommender system based mainly on implicit user interactions which are considered as user preferences, the proposed approach is based on converting expressed trust into user preference [31]. In 2006, Zigoris et al. proposed a Bayesian model technique to combine implicit and explicit user behaviors [32]. In 2005, Adomavicius et al. focused on exploiting implicit user interactions to make relevant recommendations [33].

Designing a recommender model based on a preference matrix that generates the different implicit interactions and explicit evaluations of learners is one of the challenges. Indeed, implicit feedbacks represent an objectivity towards a learning resource, while explicit feedbacks indicate a subjectivity, through the learners' rating of the learning objects. This combination allows for a more personalized learning environment that is more appropriate to the learners' expectations.

IV. PROPOSED MODEL

The model proposed illustrates the general recommendation process that is based on the tacit behaviors (objective preferences) and explicit evaluations (subjective preferences) of learners in e-learning, in order to build a preference matrix that represents the set of learning objects with their ratings. In addition, this model also allows to suggest learning objects that help learners to overcome cognitive obstacles and to progress easily in their training path, without any personal experience required in the search of alternatives (see Fig. 1).

First, the implicit user data is extracted from the log files. Then, this data is processed in such a way that it is combined with the explicit evaluations stored in the database of the LMS used. Subsequently, the prepared data are used in a learner preference matrix for learning objects "LPLO" that combines objective and subjective learner preferences. Then, a classification of learners into virtual communities of similar interest is done, using the clustering approach. Finally, the recommended learning objects are presented to the learner in order to help him in his learning path. In this way, the learner can interact with the recommended learning objects and start to exploit the ones that match his cognitive level and preferences.

A. Model of Conversion from Tacit to Explicit Behaviors

Our proposal is based on the exploration of the log files and the database of the used LMS, which record the learners'

traces during their interactions with the e-learning system. Furthermore, the preference matrix is generated based on these interactions, in order to select the most relevant learning objects. Tacit behavioral indicators and explicit ratings are used to build a model of the learner in an e-learning system by analyzing the learner's interactions with the learning objects implicitly or explicitly.

In order to maintain interoperability of CEHL, a set of standards have been considered in the literature to model learners [34] such as:

- The PAPI Learner Model (Public and Private Information for Learner) is a standard developed by the IEEE P1484.2 Learner Model Working Group and is one of the first proposals to model the learner. Various information is presented in this model: personal or demographic information, relational information, information on preferences, information on the learner's history and learning progress, etc.
- The IMS-LIP Learner Model ((IMS Learner Information Package), is a standard that allows the necessary characteristics of a learner to be modeled using XML technology in order to ensure interoperability between CEHL. The characteristics presented in this model are the learner's personal information, acquired skills, information related to qualifications, information about the learner's preferences and interests, etc.

Our system is based on the PAPI model for modeling the learner in the learning system, because, the objective of this contribution is to collect and exploit the information about the learner's history in the recommendation process (see Fig. 2). Thus, we used the demographic information as initial information to start the learner profiling process, and the behavioral information to describe the objective preferences in his profile [35].

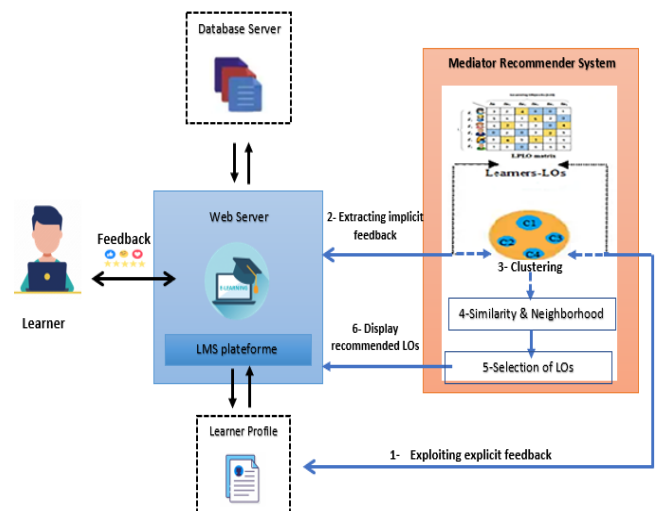


Fig. 1. Recommender System Model.

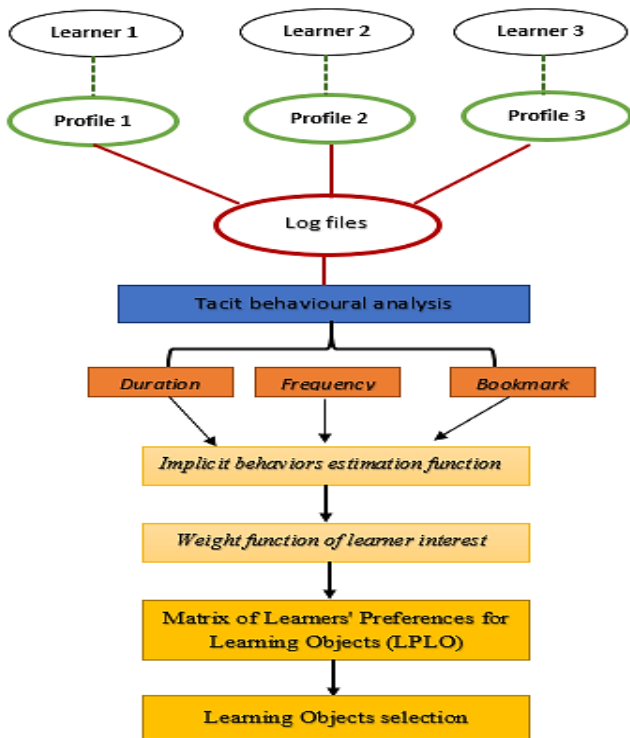


Fig. 2. Behavioural Analysis for LOs Selection.

1) *Learner demographic information*: name, gender, age, nationality, languages, education level, etc. This type of information is used during the learner's first interactions with the system, in order to overcome the cold start problem. Demographic filtering is used to begin the process of building the learner's profile.

2) *Behavioral information*: duration of use of a learning object, frequency of access to a learning object, learning object marked as important to the learner. This type of information is used to transform tacit behaviors into explicit preferences.

3) *Estimation function for implicit behaviors*: The learner's browsing history is recorded in a log file, hence the need to prepare the log file (their extraction and analysis), in order to generate a scoring matrix based on the following indicators:

- Duration (D): indicates the time a learner spends when operating a learning object.
- Frequency (F): indicates how often the learner requests the learning object.
- Bookmark(s): indicates the learning objects that are marked by the learner as important.

The implicit interest estimation function (1) allows to define the implicit score for each learning object, visited or consulted by the learner through the use of the indicators mentioned above; In this respect, we have relied on the "Page

InterestEstimator" formula, to compute the implicit scores defined by Philip K. Chan in 2003, in an e-learning context, which uses the user traces to define the interest of a user for an article (web page) [36-37]. In our context, the implicit interest estimation function is defined as follows:

$$Imp(l_a, lo_k) = D(l_a, lo_k) + F(l_a, lo_k) + B(l_a, lo_k) \quad (1)$$

Where:

l_a is active learner, lo_k is a learning Object, $D(l_a, lo_k)$ indicate the duration, $F(l_a, lo_k)$ the frequency and $B(l_a, lo_k)$ denotes the bookmarks.

4) *Learner interest weighting function*: The learner interest weighting function (Wli) (2) is used to combine tacit behavioral indicators and variant ratings between 1 and 5 (see Table I).

TABLE I. THE LEARNING OBJECT RATING SCALE

Linking	Rating scale
Very like	5
Like	4
Normal	3
Not like	2
Do not like	1

On the other hand, the value 0 indicates that the learning object is not evaluated by the learner.

The learner interest weights function (2) is defined as follows:

$$Wli(l_a, lo_k) = 1/2 (Imp(l_a, lo_k) + Exp(l_a, lo_k)) \quad (2)$$

Where:

$Exp(l_a, lo_k)$ l_a is the current learner and lo_k is the learner's explicit score, where k is the number of learning object, the rating is normalized according to the scale [1-5], in case the lo_k is no longer rated by the learner, the value assigned to the $Exp(l_a, lo_k)$ function is '0'.

5) *Matrix of learner preferences for learning objects (LPLO)*: After the normalization of ratings, the basic matrix LRLO (Learners' Ratings for Learning Objects) contains the explicit ratings of the learners, this matrix is transformed into matrix LPLO (Learners' Preferences for Learning Objects) contains the implicit and explicit preferences of the learners, where the rows represent the learners L {l1,l2,l3,...}. And the columns represent the learning objects LO {lo1,lo2,lo3,...}. Moreover, the unknown notations are defined by the function $Wli(l_a, lo_k)$, which is computed based on the implicit interest estimation function (1), with the aim of defining the implicit score for each learning object, visited or accessed by the learner through the exploitation of the following indicators: Duration, frequency and bookmark (see Fig. 3).

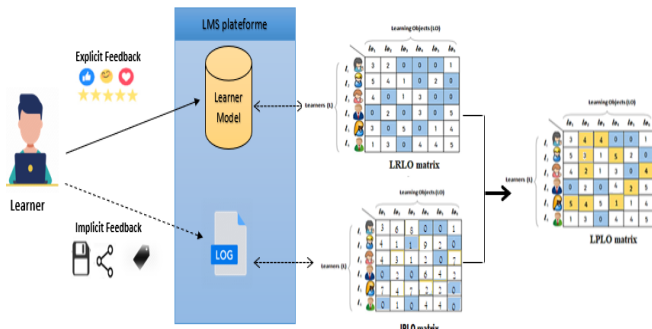


Fig. 3. Matrix Transformations.

The LPLO matrix is less sparse compared to the basic LRLO matrix, the sparsity level (3) is calculated as the ratio of the number of unevaluated learning objects (empty entries) to the total number of learning objects in the matrix (Matrix Size).

$$levelofsparsity = \frac{UnratedLOsnumbers}{MatrixSize} \quad (3)$$

The number of missing ratings for the LRLO matrix is 14, while for the LPLO matrix is 7, moreover the size of both matrices is 36. The level of sparsity for the LRLO matrix is 39%, however for the LPLO matrix is 19%. Also, when the matrix is less sparsity data, i.e. the number of missing ratings is low; the recommendations will be more accurate.

6) *Preference matrix weighted by educational criteria:* Learning objects are tagged with a set of pedagogical criteria, which are defined by the course designer. These criteria are transcribed by values and are used to personalize the recommendations according to the learner's level of involvement in the learning system and his preferences expressed in his profile.

The Table II illustrates the different educational criteria with their values.

So, for each learner 'cl', there exists in his profile a set of learning objects $LO_{cl} = \{lo_i^{cl} \in LO, i=1...m_{cl}\}$, where lo_i^{cl} are the learning objects consulted by the current learner 'cl', the values of the pedagogical criteria are described by v_i^{cl} and the notations generated on the basis of the function Wli (2) for the pair {learner, learning object} are expressed by r_i^{cl} . (see Table III).

B. Classification of Learners into Clusters

1) *Pearson correlation coefficient (PCC):* is one of several measures such as: Manhattan distance, Jaccard similarity, Cosine similarity and Euclidean distance [38], all these measures are used to calculate the degree of similarity between learners based on a set of criteria, where similar learners are assigned to the same cluster; each of these measures has been applied to millions of clustering applications in the measure of creating virtual communalities of similar interest.

TABLE II. EDUCATIONAL CRITERIA AND THEIR ASSOCIATED VALUES

Function	Criteria	Values
Content $f(c)$	Duration (D)	5,10, 15, ... min
	Difficulty level (DL)	
	LOT(Lower Order Thinking)	1
	MOT (Middle Order Thinking)	2
	HOT (Higher Order Thinking)	3
	Objective Level (OL)	
	Remember	1
	Comprehension	2
	Application	3
	Analysis	4
Evaluation	5	
Presentation $f(p)$	Preferences(P)	
	Theory	1
	Exercises	2
	Examples	3
	Real-life applications/ Simulation	4
	case study	5
	Demonstration	6
Assessment tests	7	
Media $f(m)$	Learning material (LM)	
	Text	1
	Image	2
	Audio	3
	Video	4

TABLE III. LEARNING OBJECTS-PEDAGOGICAL CRITERIA-RATING MATRIX BY LEARNER

	c_1	c_2	c_3	c_p	r_{cl}
lo_1	v_1^1	v_2^1	v_3^1			v_p^1	r_{cl}^1
lo_2	v_1^2	v_2^2	v_3^2			v_p^2	r_{cl}^2
lo_3	v_1^3	v_2^3	v_3^3			v_p^3	r_{cl}^3
lo_4	v_1^4	v_2^4	v_3^4			v_p^4	r_{cl}^4
..
..
lo_m	v_1^m	v_2^m	v_3^m			v_p^m	r_{cl}^m

In our context, we use the Pearson correlation; given that the variables of the matrix are associated in a linear way, i.e. when a change is made to one variable, a proportional change is made to the other variable. Moreover, since the values of the variables are quantitative and have a Gaussian distribution, the use of the Pearson correlation is adequate to define the degree of similarity between the learners. On the other hand, the De Jaccard similarity coefficient is sufficiently appropriate for use in documents or word similarity measurement.

Pearson Correlation Coefficient (PCC) known as Pearson Product-Moment Correlation Coefficient "r", PCC is one of the most popular coefficients for measuring the dependence of two variables, i.e. the relationship between two quantitative variables and the degree of similarity between these two variables.

- Dependency Coefficient (DC): is calculated through the Pearson Correlation Coefficient in order to identify the degree of association between the ratings provided by the learner for all the learning objects consulted.
- Pearson Correlation Coefficient (PCC) (8): is a statistical measure of the linear relationship between two variables and it ranges between [-1,+1]; the positive correlation indicates that the variables increase or decrease in parallel, however a negative correlation means that one variable increases while the other decreases. Furthermore, correlation (4) is a measure of effect where the strength of the correlation is described as follows, with $-1.0 \leq r \leq +1.0$ (see Table IV).

TABLE IV. INTERPRETATION OF R VALUES

r value	Interprétation
+ .80 to +1.0	Very strong positive relationship
+ .60 to +.79	Strong positive relationship
+ .40 to +.59	Moderate positive relationship
+ .20 to +.39	Weak positive relationship
+ .01 to+.19	Negligible relationship
0	No relationship
- .01 to -.19	Negligible relationship
- .20 to -.39	Weak negative relationship
- .40 to -.59	Moderate negative relationship
- .60 to -.79	Strong negative relationship
- .80 to -1.0	Very strong negative relationship

The correlation value 'r' is calculated as follows:

$$r_{x,y} = \frac{\delta xy}{\delta x \delta y} \tag{4}$$

Where:

$$\delta xy = \frac{1}{n} \sum_{i=1}^n x_i y_i + \bar{x} \bar{y} \tag{5}$$

$$\delta x = \sqrt{\sum_{i=1}^n \frac{x_i^2}{n} - \bar{x}^2} \tag{6}$$

$$\delta y = \sqrt{\sum_{i=1}^n \frac{y_i^2}{n} - \bar{y}^2} \tag{7}$$

Based on the formula proposed by Manuel J. Barranco and Luis Martinez, the Pearson correlation coefficient is associated with two variables (see Table V):

- r_{cl} : The ratings assigned by the current learner 'cl' for the learning objects.
- v_{cl} : The pedagogical criteria of the learning objects consulted by the current learner.

$$PCC_{clj} = \frac{\sum_i r_{i}^{cl} v_{ij}^{cl} - \frac{\sum_i r_{i}^{cl} \sum_i v_{ij}^{cl}}{n_{cl}}}{\sqrt{(\sum_i (r_{i}^{cl})^2 - \frac{(\sum_i r_{i}^{cl})^2}{n_{cl}})} \sqrt{(\sum_i (v_{ij}^{cl})^2 - \frac{(\sum_i v_{ij}^{cl})^2}{n_{cl}})}} \tag{8}$$

TABLE V. DETAILS OF NOTATIONS USED IN PCC METRIC

Notation	Description
r_{i}^{cl}	Score assigned by the learner 'cl' for the learning object 'lo _i '
v_{ij}^{cl}	Pedagogical criterion 'vj' for the learning object 'lo _i ' consulted by the learner 'cl'
n_{cl}	Number of learning objects consulted by the current learner 'cl'

7) *K-means clustering*: The main goal of clustering is to divide learners into groups based on similarity characteristics with the aim of recommending learning objects that the active learner has never visited [39]. In a first step, learners with similar interests will be grouped in the same cluster, in order to recommend them appropriate learning objects, for this purpose, we opt for the K-means algorithm which refers to the preference matrix "LPLO" (learner-learning object) generated in the previous step.

The K-means algorithm is well known for its efficiency and power in clustering a large data set compared to other k-nearest neighbors' algorithm [40]. Moreover, it is considered one of the most popular clustering algorithms for unsupervised learning.

The procedure for assigning learners into clusters via the k-means algorithm is done according to the following pseudo code:

Input: k // Number of desired clusters
 $L = \{l_1, l_2, l_3, \dots, l_n\}$ // Set of learners

Output: a set of k clusters

Process:

Arbitrarily select k learners form L as the initial cluster centers;

Repeat:

- 1-(re) assign each learner to the clusters with the most similar interests based on the Pearson correlation coefficient 'PCC' of the current learner and the mean value of the learners in the cluster
- 2-Update the cluster means; calculate new mean value of learners for each cluster;

Until no change;

8) *Selecting learning objects*: The learning objects recommended to the current learner is made, by the association between the profile of the current learner and the learning objects repository. Moreover, the learning objects that are well evaluated by the closest neighbors' to the active learner and having a score higher than three will be recommended to the current user (see Fig. 4).

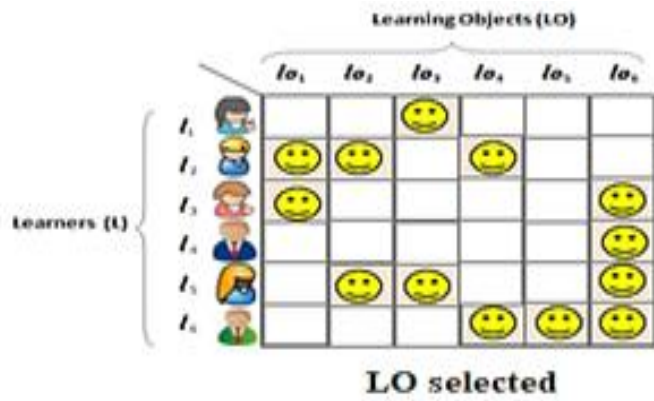


Fig. 4. The Selected Learning Objects.

Rate [lo20] = 4 ✓ Rate [lo6] = 1

Rate [lo12] = 2 Rate [lo15] = 5 ✓

Rate [lo29] = 6 ✓ Rate [lo80] = 2

V. EXPERIMENTATION

This section presents a performance analysis of the proposed methodology. The performance of this work is evaluated against the recommendation based only on the explicit preferences of the users.

The participants in this experiment are 100 learners from a high school in the delegation of Chefchaouen, Morocco. However, the learners had to study four modules in the computer science subject, namely: "Generalities of Computer Systems", "Software", "Algorithms and Programming" and "Networks and the Internet"; each module consists of a set of lessons, which are well defined in the pedagogical guidelines of computer science in high school. Our first experiment is based on the first module "Generalities of Computer Systems", which contains three lessons: lesson 1 "Basic Definitions and Vocabulary", lesson 2 "Basic Structure of a Computer" and lesson 3 "Software and Application Areas of Computer Science" (see Table VI).

The Table VII expresses the degree of depth of the concepts for each notion.

Our approach is tested on learning objects stored in the LMS database. The first module "General Computer Systems" provides an assessment dataset of 50 learning objects containing 36 ratings from 26 learners. The ratings are integers ranging from 1 to 5. The experiments are performed on an HP computer with CORE i5 processors.

The Sum Squared Error (SSE) (8) is used to find an appropriate k by plotting the number of clusters against the SSE, while evaluating SSE for different values of k.

$$SSE = \sum_{i=1}^n (y_i - \hat{y}_i)^2 \tag{9}$$

Where:

i is test set, y_i is predicted value and \hat{y}_i is actual value.

TABLE VI. MODULE NO. 1: GENERALITIES ON COMPUTER SYSTEMS

Content	Schedule	Common Core			
		Letter & Arts	Original	Science	Technologies
Definition and basic Vocabulary	2h				
Definition of information		2	2	2	2
Definition of treatment		2	2	2	2
Definition of computer Science		2	2	2	2
Definition of the computer system		2	2	2	2
Basic structure of a computer	4h				
Functional diagram of a Computer		2	2	3	3
Peripherals		2	2	3	3
Central processing unit		2	2	3	3
Types of software	1h				
Basic software		2	2	2	2
Application software		2	2	2	2
Fields of application	1h	2	2	2	2

TABLE VII. THE DEGREE OF DEPTH

Degree of depth	Descriptor
1	Initiation
2	Appropriation
3	Master

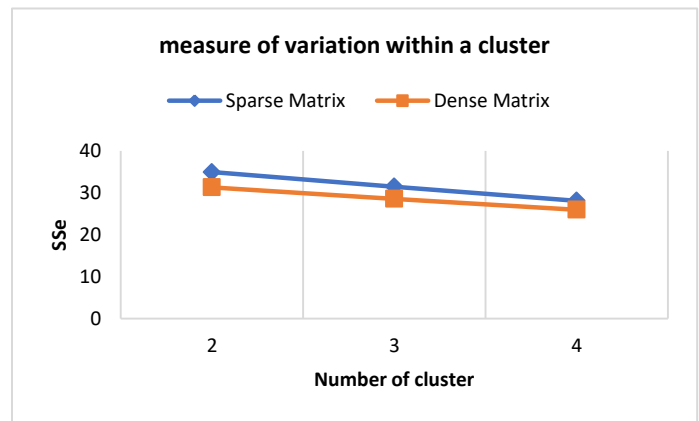


Fig. 5. The Appropriate Number of Clusters in respect to the Matrices.

From the above graph (see Fig. 5), we notice that the SSE value is high in the sparse matrix unlike the dense matrix. For both matrices, when the number of cluster increases, the SES

value decreases. This means that the number of clusters is independent to the type of matrix. For this distribution of 100 learners, the most appropriate number of clusters for both matrix types (sparse or dense) is 4 clusters.

The silhouette is used to determine the degree of separation between clusters. The silhouette plot in (Fig. 6), illustrates the proximity of learners in neighboring clusters using a measure of [-1, +1]. A value of +1 indicates that the learners are far apart, 0 indicates that the observations are very close, and -1 indicates that the learners can be assigned to the wrong cluster.

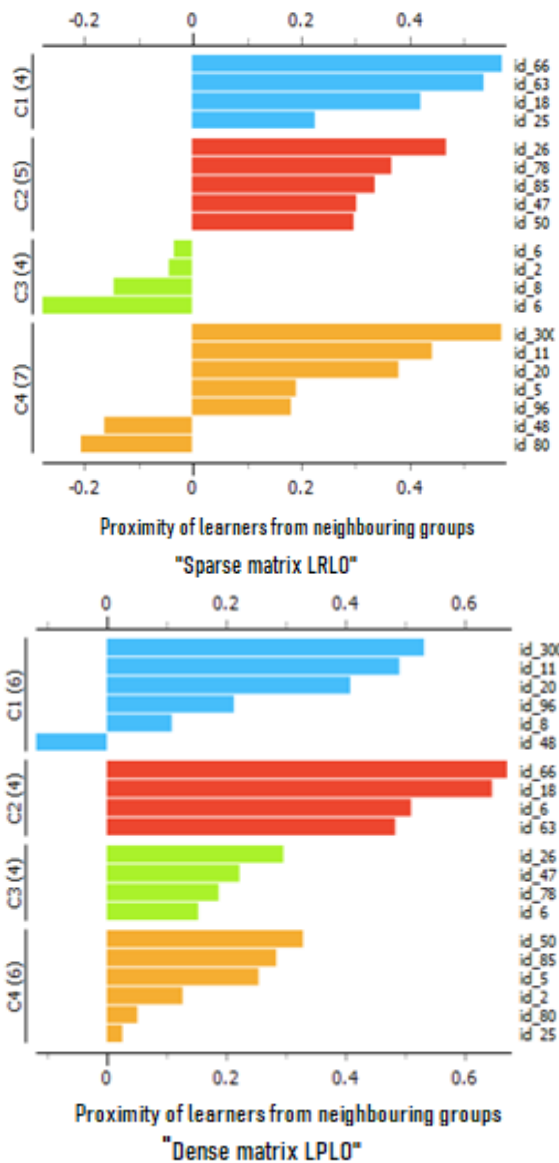


Fig. 6. Silhouette Analysis for Sparse and Dense Matrix.

For the sparse matrix LRLO "Learners Ratings for Learning Objects", we find that some learners are assigned to the wrong cluster, due to lack of ratings of learning objects in this Matrix. Since, some learners do not rate all these objects, their assignments to some clusters may be inappropriate. However, for the dense matrix LPLO "Learners Preferences

for Learning Objects", the majority of learners are classified in the appropriate clusters, thanks to the elicitation of preferences through the combination of explicit ratings and implicit interactions of learners with the learning objects.

The mean absolute error (MAE) "(10)" is a measure of prediction accuracy. It indicates the absolute value of the difference between the predicted value and the actual value.

This measure is used to indicate the effectiveness of our recommendation system based on implicit and explicit learner feedback and recommendation systems based on explicit feedback only. The lower the MAE value, the smaller the magnitude of the error.

$$MAE = \frac{\sum_{(u,i) \in test} |prediction_{u,i} - real_{u,i}|}{n_{test}} \quad (10)$$

Where:

n is the total number of ratings-prediction pairs in the test set, $prediction_{u,i}$ is the predicted rating for learner u on learning object j, and $real_{u,i}$ is the actual rating in the real dataset (see Table VIII).

In the graph (see Fig. 7), we see that with the variation of the number of clusters, the magnitude of the error is gradually decreased for the dense matrix "LPLO", which is based on the implicit and explicit preferences of the learners; contrary to the LRLO matrix where the magnitude of the error gradually increases. This is due to the insufficient ratings explicitly expressed by the learner, which leads to a loss of accuracy when assigning learners to clusters. This is also shown in Fig. 6, where we can infer that the less sparse the matrix is, the better the learners are assigned to clusters with similar learning needs. Therefore, the recommendations will be more appropriate.

TABLE VIII. MAE VALUE ACCORDING TO THE TYPE OF MATRIX

Number of cluster	Mean Absolute Error	
	Dense Matrix LPLO	Sparse Matrix LRLO
2	0.18386	1.7154
3	0.08716	2.4421
4	0.06501	2.6225

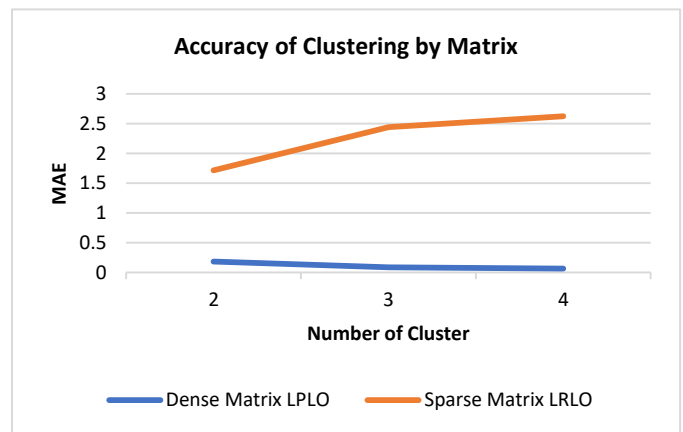


Fig. 7. The Accuracy of Clustering the Learners by Matrix.

VI. CONCLUSION AND FUTURE WORK

Recommender systems have become a promising solution for improving the efficiency of e-learning systems. Preference matrices are the basic inputs of recommender systems, because based on these matrices, systems can suggest personalized learning objects and adapt them to the learner's profile. On the other hand, the lack of ratings in the preference matrices can handicap their functioning and consequently the recommendations will be less personalized.

To this end, we have proposed a model of a mediating recommendation system based on a matrix that combines the tacit and explicit behaviors of the learner. Through the exploration of the log file, while exploiting some indicators such as duration, frequency and bookmarks in the preference matrix, in order to obtain better performances.

The k-means clustering algorithm is used to group learners with similar preferences into clusters, in order to recommend to the active learner new learning objects that have not yet been viewed or visited by him and that have been well rated by his closest neighbors.

The results obtained in the experimentation phase illustrate the importance of hybridizing implicit traces and explicit ratings of learners to improve the accuracy of assignment of learners to appropriate clusters.

In our future work, we plan to study the recommendation of sequences of objects and learning activities, based on the dynamic prediction of the learning strategy adapted to the active learner, through evolutionary meta-heuristic algorithms such as: Ant Colony Optimization (ACO) and Particle Swarm Optimization (PSO). This will allow recommending the learner a personalized learning path (scenario).

REFERENCES

- [1] Bezovski, Z., & Poorani, S. (2016, March). The evolution of e-learning and new trends. In *Information and Knowledge Management* (Vol. 6, No. 3, pp. 50-57). IISTE.
- [2] Clark, R. C., & Mayer, R. E. (2016). *E-learning and the science of instruction: Proven guidelines for consumers and designers of multimedia learning*. John Wiley & sons.
- [3] Devedžić, V. (2006). *Semantic web and education* (Vol. 12). Springer Science & Business Media.
- [4] Maes, P. (1995). Agents that reduce work and information overload. In *Readings in human-computer interaction* (pp. 811-821). Morgan Kaufmann.
- [5] Sarwar, B., Karypis, G., Konstan, J., & Riedl, J. (2000, October). Analysis of recommendation algorithms for e-commerce. In *Proceedings of the 2nd ACM Conference on Electronic Commerce* (pp. 158-167).
- [6] Joshi, N., & Gupta, R. May (2020). "A personalized web based e-learning recommendation system to enhance and user learning experience", *International Journal of Recent Technology and Engineering (IJRTE)* ISSN 2277-3878, 9(1),1186-1195.
- [7] Rashid, A. M., Albert, I., Cosley, D., Lam, S. K., McNee, S. M., Konstan, J. A., & Riedl, J. (2002, January). Getting to know you: learning new user preferences in recommender systems. In *Proceedings of the 7th international conference on Intelligent user interfaces* (pp. 127-134).
- [8] Nafea, S. M., Siewe, F., & He, Y. (2019). On Recommendation of Learning Objects using Felder-Silverman Learning Style Model. *IEEE Access*, 7, 163034-163048.
- [9] Lalitha, T. B., & Sreeja, P. S. (2020). Personalised Self-Directed Learning Recommendation System. *Procedia Computer Science*, 171, 583-592.
- [10] Javed, U., Shaukat, K., Hameed, I. A., Iqbal, F., Alam, T. M., & Luo, S. (2021). A Review of Content-Based and Context-Based Recommendation Systems. *International Journal of Emerging Technologies in Learning (IJET)*, 16(3), 274-306.
- [11] Philip, S., Shola, P., & Ovy, A. (2014). Application of content-based approach in research paper recommendation system for a digital library. *International Journal of Advanced Computer Science and Applications*, 5(10).
- [12] Shi, Y., & Yang, X. (2020). A Personalized Matching System for Management Teaching Resources Based on Collaborative Filtering Algorithm. *International Journal of Emerging Technologies in Learning (IJET)*, 15(13), 207-220.
- [13] Shambour, Q., Hourani, M., & Fraihat, S. (2016). An item-based multi-criteria collaborative filtering algorithm for personalized recommender systems. *International Journal of Advanced Computer Science and Applications*, 7(8), 274-279.
- [14] Felfernig A., Friedrich G., Jannach D., and Zanker M. (2006) An Integrated Environment for the Development of Knowledge-Based Recommender Applications, *International Journal of Electronic Commerce*, 11(2), 11-34.
- [15] Resnick P., Iacovou N., Suchak M., Bergstrom P., and Riedl J., (1994), GroupLens: An Open Architecture for Collaborative Filtering of Netnews, In *Proceedings of ACM Conference on Computer Supported Cooperative Work*, Chapel Hill, NC, USA, 175-186.
- [16] Shih Y. and Liu D., 2005, Hybrid Recommendation Approaches: Collaborative Filtering via Valuable Content Information, In the *Proceedings of the 38th Annual Hawaii International Conference HICSS '05*, 217-223.
- [17] Adomavicius G, Tuzhilin A, 2005 June, Toward the next generation of recommender systems: a survey of the state-of-the-art and possible extensions. *Knowledge and Data Engineering, IEEE Transactions on*; 17(6):734-749.
- [18] Schein AI, Popescul A, Ungar LH, et al. 2002, Methods and metrics for cold-start recommendations. In: *SIGIR '02: Proceedings of the 25th annual international ACM SIGIR conference on Research and development in information retrieval*. New York, NY, USA: ACM; p. 253-260.
- [19] Da Silva, J. F. G., de Moura Junior, N. N., & Caloba, L. P. (2018, July). Effects of data sparsity on recommender systems based on collaborative filtering. In *2018 International Joint Conference on Neural Networks (IJCNN)* (pp. 1-8). IEEE.
- [20] F. Ricci, L. Rokach, B. Shapira, and P. B. Kantor, 2010, *Recommender Systems Handbook*. Springer.
- [21] Arwar, B., Karypis, G., Konstan, J., & Riedl, J. (2000, October). Analysis of recommendation algorithms for e-commerce. In *Proceedings of the 2nd ACM Conference on Electronic Commerce* (pp. 158-167).
- [22] Shanthi, R., & Rajagopalan, S. P. (2018). A Personalized Hybrid Recommendation Procedure for Internet Shopping Support. *International Journal Of Advanced Computer Science And Applications*, 9(12), 363-372.
- [23] Burke, R. (2002). Hybrid recommender systems: Survey and experiments. *User modeling and user-adapted interaction*, 12(4), 331-370.
- [24] Feng Zhang, Victor E. Lee, Ruoming Jin, Saurabh Garg, Chi Cheng, Privacy-aware smart city: A case study in collaborative, 2018. *filtering recommender systems*, in: *Journal of Parallel and Distributed Computing*.
- [25] Murad, H., & Yang, L. (2018). Personalized e-learning recommender system using multimedia data. *International Journal of Advanced Computer Science and Applications*, 9(9), 565-567.
- [26] Tarus, J. K., Niu, Z., & Yousif, A. (2017). A hybrid knowledge-based recommender system for e-learning based on ontology and sequential pattern mining. *Future Generation Computer Systems*, 72, 37-48.
- [27] Bokde, D. K., Girase, S., & Mukhopadhyay, D. (2015, December). An approach to a university recommendation by multi-criteria collaborative filtering and dimensionality reduction techniques. In *2015 IEEE International Symposium on Nanoelectronic and Information Systems* (pp. 231-236). IEEE.
- [28] Vesin, B., Ivanović, M., Klačnja-Milićević, A., & Budimac, Z. (2012).

- Protus 2.0: Ontology-based semantic recommendation in programming tutoring system. *Expert Systems with Applications*, 39(15), 12229-12246.
- [29] Kulkarni, P. V., Rai, S., & Kale, R. (2020). Recommender system in elearning: a survey. In *Proceeding of International Conference on Computational Science and Applications* (pp. 119-126). Springer, Singapore.
- [30] Rendle, S., Freudenthaler, C., Gantner, Z., & Schmidt-Thieme, L. (2012). BPR: Bayesian personalized ranking from implicit feedback. *arXiv preprint arXiv:1205.2618*.
- [31] Hu, Y., Koren, Y., & Volinsky, C. (2008, December). Collaborative filtering for implicit feedback datasets. In *2008 Eighth IEEE International Conference on Data Mining* (pp. 263-272). IEEE.
- [32] Zigoris, P., & Zhang, Y. (2006, November). Bayesian adaptive user profiling with explicit & implicit feedback. In *Proceedings of the 15th ACM international conference on Information and knowledge management* (pp. 397-404).
- [33] Adomavicius, G., & Tuzhilin, A. (2005). Toward the next generation of recommender systems: A survey of the state-of-the-art and possible extensions. *IEEE transactions on knowledge and data engineering*, 17(6), 734-749.
- [34] Oubahssi, L., & Grandbastien, M. (2007, June). Un modèle pour améliorer l'interopérabilité des données pédagogiques apprenant. In *3ième conférence en Environnement Informatique pour l'Apprentissage Humain-EIAH 2007* (pp. 437-448). INRP.
- [35] Zriaa, R., & Amali, S. (2020, December). Recommendation of Learning Objects Through Dynamic Learning Style Identification and k-means Clustering Algorithm. In *International Conference on Advanced Intelligent Systems for Sustainable Development* (pp. 730-748). Springer, Cham.
- [36] Kim, H. R., & Chan, P. K. (2003, January). Learning implicit user interest hierarchy for context in personalization. In *Proceedings of the 8th international conference on Intelligent user interfaces* (pp. 101-108).
- [37] Núñez-Valdez, E. R., Quintana, D., Crespo, R. G., Isasi, P., & Herrera-Viedma, E. (2018). A recommender system based on implicit feedback for selective dissemination of ebooks. *Information Sciences*, 467, 87-98.
- [38] Egghe, L., & Leydesdorff, L. (2009). The relation between Pearson's correlation coefficient r and Salton's cosine measure. *Journal of the American Society for information Science and Technology*, 60(5), 1027-1036.
- [39] DUBEY, Ankita and CHOUBEY, Asso Prof Dr Abha, "A Systematic Review on K-Means Clustering Techniques", *International Journal of Scientific Research Engineering & Technology (IJSRET)*, ISSN, vol.6, 6, pp. 2278-0882, June 2017.
- [40] Zriaa, R., & Amali, S. (2020, October). A Comparative Study Between K-Nearest Neighbors and K-Means Clustering Techniques of Collaborative Filtering in e-Learning Environment. In *The Proceedings of the Third International Conference on Smart City Applications* (pp. 268-282). Springer, Cham.

DDoS Intrusion Detection Model for IoT Networks using Backpropagation Neural Network

Jasem Almotiri

Department of Computer Science, College of Computers, and information Technology
Taif University, Taif, Saudi Arabia

Abstract—In today's digital landscape, Internet of Things (IoT) networking has grown dramatically broad. The major feature of IoT network devices is their ability to connect to the internet and interact with it through data collecting and exchanging. Distributed Denial of Service (DDoS) is one form of cyber-attacks in which the hackers penetrate a single connection and then multiple machines are operating together to attack one target. The direct connectivity of IoT devices to the internet makes DDoS attacks worse and more dangerous. The more businesses adapted IoT networks to streamline the operations, the more allowing of DDoS intrusions at small and large scales to take place. Therefore, the intrusion detection module in the IoT networks is not optional in today's business environment. To achieve this objective, in this paper, an intelligent intrusion detection model is proposed to detect DDoS attacks in IoT networks. The intelligent model is a backpropagation neural network-based framework. The results are analyzed using different performance measures. The proposed model proves a detection rate of 99.46% and detection accuracy of 95.76% using the up-to-date benchmark CICDDoS2019 dataset. Furthermore, the proposed model has been compared with the most recent DDoS intrusion detection schemes and competitive performance is achieved.

Keywords—DDoS; backpropagation neural network; IoT network; intrusion detection; CICDDoS2019

I. INTRODUCTION

IoT networks are considered a considerable movement in the world of networking and data communication. This movement is majorly driven by the fifth-generation network (5G), which is expected to broaden today's IoT functionalities. As the adaption of IoT networks is in a dramatic increase, IoT network is expected to be a huge growing market.

However, this growth is thwarted by DDoS attacks which are the most prevalent cyber threats. Some cybersecurity experts consider IoT networks as the major force behind DDoS attacks. These types of attacks have a distributive nature; in particular, they depend on one vulnerable device in the IoT network to create an opening for intruders to make use of any other IoT devices to drive a huge amount of traffic.

IoT platform security is embedded in the process of product development of IoT-based devices. However, when it comes to cybersecurity, no data processing unit is an island. From data production, data transmission, data processing, data visualization to data analysis and prediction, all of these major stages of IoT networking are considered open gates for intrusions and hackers to perform their attacks especially

DDoS and Botnet attacks. The botnet is a collection of hijacked internet-connected devices that are used to execute a large-scale attack. The infected devices are controlled by attacks actors who often cybercriminals and are used to perform particular malicious duties in an unobserved manner from the user. One of the major tasks to be done by a botnet is to generate malicious traffic for DDoS attacks.

DDoS attacks are carried out when multiple machines (devices) are operating together for sake of attacking one target device. Using control and command software, DDoS attacker avails of the weaknesses and security vulnerabilities of one IoT device to control several IoT network devices. Once the target device is in control, DDoS attack admits exponentially requests to be sent to the target device, which enhances the power of attack on one hand and boosts the difficulty of detecting attribution on the other hand, where due to the distributive nature of the DDoS attack, the original source of the attack becomes harder to be identified. DDoS attacks are easy to deal with in the short term, but it becomes very difficult in the long term. Due to the distributed nature of the DDoS attack, it is considered one of the most fatal enemies of the internet of things platform. In principle, if internet-connected devices get hacked, the DDoS malware could easily spread to other devices in the network [1], [2].

Although IoT has used a variety of protocols for security purposes, hackers and intruders developed more complex and intelligent techniques to fulfill their penetrations ending up with misalignment between the speed of IoT development and IoT cybersecurity. In the case of dealing with sensitive data processing and management through IoT platforms, there is a pressure to close the gap that caused an increased vulnerability, especially for crucial data where security becomes the single most cardinal factor that companies, and organizations consider when purchasing IoT products.

In response, a new generation of artificial intelligence-based intrusion detection techniques to address the limitations of the conventional intrusion detection techniques has emerged and adapted as a major building block of IoT security systems. Recently, the awareness to use the machine learning in general and artificial neural networks in particular to secure network traffic against DDoS attacks has increased rapidly. DDoS Detection systems based on artificial neural networks are such typical solutions to model and predict malicious behavior over network traffic flows and Backpropagation neural network are considered one of the powerful yet flexible supervised training algorithms.

In the context of supervised neural networks, backpropagation neural network is considered one of the powerful classifying and filtering engines in this field. Much of the power of backpropagation arises from the fact that the repeated composition of specific types of nonlinear functions boosts the abstract representation power of the neural network. Moreover, an efficient computation of the gradient at each layer can be highly performed by the backpropagation training algorithm. Therefore, backpropagation neural network can efficiently learn the abstract representation of the behavior of network flows in general, and the pattern of the malicious flows in particular.

Some researchers, in this field, deployed backpropagation in its original form to design and develop different schemes for intrusion detection systems. However, the majority of researchers tend to use the enhanced versions of backpropagation in order to address the shortcomings of the classical backpropagation algorithm in an attempt to lower the time and the computational overhead of the training phase or to remedy the convergence difficulties of the classical version. Other scenarios use a standard backpropagation neural network that heavily depends on a variety of features engineering techniques in prior.

These scenarios come at the expense of higher design complexity associated with new born issues related to time cost and resources. Furthermore, in the context of intrusion detection, the overall performance of many of the predictive models based on the enhanced versions do not exceed that can be achieved by the classical one.

With minimal neural network architecture, and without any features preprocessing, the main aim of this work is to prove that the conventional standard backpropagation can be used to build an accurate yet robust predictive model for DDoS attacks. We have achieved this by conducting the training using modern up-to date DDoS dataset and conducting rigorous testing analysis while the performance of the predictive model is benchmarked using highly indicative standard performance metrics.

The major improvements that we presented in this article are reviewed as follows:

- Propose an intelligent DDoS intrusion detection system that can predict DDoS malicious network traffic in IoT networks by exploiting the predictivity power of the standard backpropagation neural network.
- In this work, CICDDoS2019 dataset is used to verify that the proposed detection model applies to different types of DDoS malicious traffic flows.
- We have proved that using low-complexity standard version of backpropagation based neural network can achieve comparable detection performance even though no form of features engineering (such as feature weighting or features selection), was considered.

The rest of the paper is organized as follows: Section II presents related works; Section III describes our proposed DDoS intrusion detection methodology followed by the

experimental performance evaluation in Section IV and Section V concludes this paper and suggests future directions.

II. RELATED WORK

Exploiting the very basic form of backpropagation algorithm applied on multi-layered perceptron neural network, an intrusion detection model seeking a reduction in false alarm rate as a major performance aspect was proposed by [3] where it shows the intrusion recognition capability of the backpropagation algorithm despite the rudimentary framework.

Using internet packet traces as an experimental dataset, authors in [4] used the standard backpropagation neural network to thwart DoS and DDoS attacks in IoT environments.

As a precise and efficient classifier [5] used a standard backpropagation network to classify DDoS traffic after an initial judgment of the characteristics of the abnormal network traffic.

Using a backpropagation-based autoencoder, [6] designed a joint anomaly and signature-based DDoS intrusion detector implemented in the cloud. Based on a behavioral study that collected a variety of DDoS signatures in one database, the targeted traffic was first compared to the known DDoS attacks. If no matching has occurred, then the traffic fed to the backpropagation autoencoder to be classified into DDoS or benign. If a DDoS attack was detected, the signature of this attack was used to update the database of DDoS signatures.

Despite the vivid versatility of backpropagation in designing intelligent intrusion detection models/systems, it has some downsides such as local minima, slow convergence, and network paralysis. These downsides moving the wheel of extension around the axle of standard backpropagation were enhanced versions of backpropagation emerged and implemented for harder predictive tasks such as DDoS/DoS detection. As an example of using an enhanced version of backpropagation in the domain of intelligent intrusion detection, [7] presented an intrusion detection system composed of hybrid phases of misuse detection and anomaly detection by applying the Levenberg-Marquardt algorithm as a technique to optimize the backpropagation-based network that was used as the classification engine of the proposed predictive system.

Applying the same backpropagation customization, authors in [8] used multi-core technology to detect DDoS intrusions via neural networks. Multi-core uses one CPU that combines a couple or more independent cores into a single circuit. Their IP flow-based DDoS intrusion detection technique is built based on the idea that an IP packet holds information of the upper layer which can be exploited into special attributes representing the special characteristics of DDoS attacks in a well-posed manner. Then, attributes vectors are fed into a Levenberg-Marquardt based backpropagation neural network as input to be classified into DDoS or benign traffic.

Authors in [9] proposed a DDoS intrusion detection algorithm composed of two main phases: a training phase and a detection phase. In the training phase, a non-linear time series model called GARCH was used to evaluate the normal traffic

prediction, whereas a feed-forward backpropagation neural network was used as the benign/DDoS classifying engine.

For cloud security, based on backpropagation neural networks, authors in [10] proposed a DDoS detector model that offered a solution to tracing back a given cloud traceback for the sake of finding the source of the real attack. Moreover, they introduced a cloud protector built using a feedforward backpropagation neural network.

III. METHOD

As IoT networks are broad, the attack surface for this type of network is even broader. This has been reflected in various methodologies and techniques designed to fall under the umbrella of IoT network security. Public Key Infrastructure (PKI) authentication, securing Application Program Interface (API), and network intrusion detection systems, the lists long are just a few of the techniques IT leaders can use to combat the growing malicious penetrations rooted in vulnerable devices of IoT networks. As a rule of thumb, as the ways available for devices to be able to connect, the more ways attackers and hackers can intercept them.

Therefore, one of the most harmonious security techniques that can be deployed for IoT network security is the security gateways, which act as intermediary units between the IoT network devices and the outside world (internet, cloud computing, etc.). These units are equipped with processors chips with more computational capabilities, memory, and processing power rather than that exists in the IoT devices themselves. These additional features enable gateway units to run artificial neural network-based intelligent intrusion detection systems to ensure intruders cannot access the IoT network devices they connect.

Fig. 1 shows the general high-level framework of our proposed DDoS intrusion detection model in the context of IoT networking where at the heart of the IoT securing gateway lies

the proposed intrusion detection model. Fig. 2 illustrates the flow pipeline of our proposed system, which is built using the backpropagation feedforward artificial neural network that trained, validated, and tested using a real benchmark CICDDoS2019 dataset [11]. As illustrated in Fig. 2, once the dataset is pre-processed in a way harmonious to the format accepted by the neural network, it is split into two datasets: training and testing. Then, a backpropagation neural network is trained to obtain the optimal parameters and meta parameters of the network structure. Afterward, the network is ready to be used as intelligent DDoS intrusion detection, where a new set of flow traffic (DDoS and normal traffic) is presented to the network, where it detects the DDoS attack traffic and raises an alarm. The following subsections elaborate each module of our proposed model shown in Fig. 2 in detail.

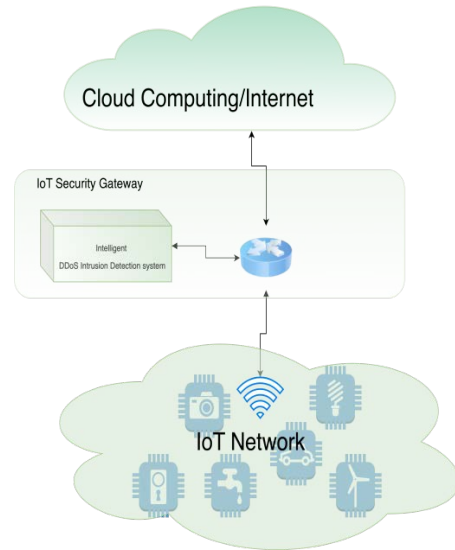


Fig. 1. High-Level Framework of the Proposed DDoS Intrusion Detection System in the Framework of IoT Networks.

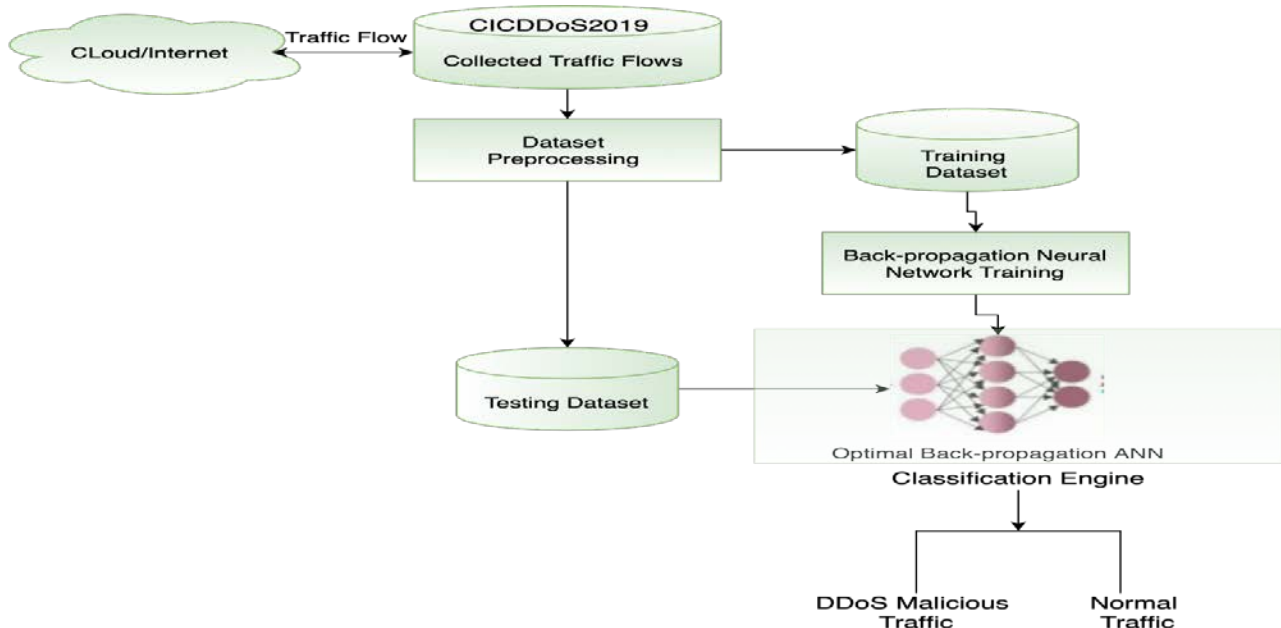


Fig. 2. Proposed DDoS Intrusion Detection System using Standard Backpropagation Neural Network.

A. Dataset Pre-Processing

To evaluate our backpropagation network-DDoS detection model, the real benchmark CICDDoS2019 dataset [11] is used. This dataset is composed of two types of DDoS attacks: reflection and exploitation in form of both malicious and normal network packets.

Even though the CICDDoS2019 dataset is major consists of numerical values, dataset preprocessing is an essential step to validate its suitability for both: as input to the neural network and for the classification task of the model. Fig. 3 illustrates the basic steps that applied to the raw CICDDoS2019 dataset which include: dataset cleansing, features selection, and dataset normalization.

Initially, the total number of raw dataset features is 81, in the dataset cleansing, we select the features that have zero values, which have no impact on the classification output of the neural network and dropped them out resulting in 22 unique features. Moreover, all dataset samples that contain infinity or misleading values have been removed as well. The label column of the dataset is converted into a numerical representation where 0 represents the benign traffic and 1 represents the DDoS one.

As the last step of dataset preprocessing, the dataset values are normalized using the standard min-max normalization [12], [13] as illustrated in (1):

$$\hat{v}_i = \frac{v_i - \min_{DB}}{\max_{DB} - \min_{DB}} \cdot (\text{new}_{DB}^{\max} - \text{new}_{DB}^{\min}) + \text{new}_{DB}^{\min} \quad (1)$$

where (1) represents the min-max normalization step that linearly transformed the raw database $DB = \text{CICDDoS2019}$ values $v_i \in DB$ into new values \hat{v}_i in the range $[\text{new}_{DB}^{\max}, \text{new}_{DB}^{\min}]$.

B. Proposed Model

At the core of the proposed model, a backpropagation feedforward neural network is used to model the behavior of the flows of the network traffic. The basic annotated structure of the backpropagation neural network is shown in the simplest form of the feedforward network structure composed of input units at the left, any number of intermediary hidden layers, and a layer of output units at the right.

Connections from the second hidden layer to the last L hidden layers are hidden whereas the connections from higher layers to lower layers are forbidden. Backpropagation comprises two major phases: (1) Forward phase, and (2) Backward phases. In the forward phase, the outputs of all nodes are computed, the local derivatives of the nodes 'activation function relative to the net inputs are computed as well.

On the other hand, the main task of the backward phase is to aggregate the products of these local values over all paths from the nodes to the network outputs. In the forward phase, the components of an input training vector are fed into the neural network. This results in driving a forward cascade of computations across network layers using the current state of weights to yield the network output, which represents the predicted output of the network. Afterward, the predicted output is compared to the label associated with the training instance and the derivative of the loss function concerning the output is computed.

The derivative of the resulting loss is fed to the backward phase where it is used to compute the loss concerning the weights in all layers in the backward path.

As pictorially illustrated in Fig. 4, Let $\mathcal{D} = \{y, d\}$ refers to the training dataset composed of the input-output (label) pairs and let x_j refers to the net input of the j^{th} unit where x_j is a linear combination function of the i^{th} weighted outputs y_i of i^{th} layer as in (2):

$$x_j = \sum_i^I y_i w_{ji} \quad (2)$$

Where

I : refers to the number of features of input vector (for our case, $I = 63$).

w_{ji} : is the weight of the connection between the layer (j) and the layer (i).

y_i : is the output of the layer (i).

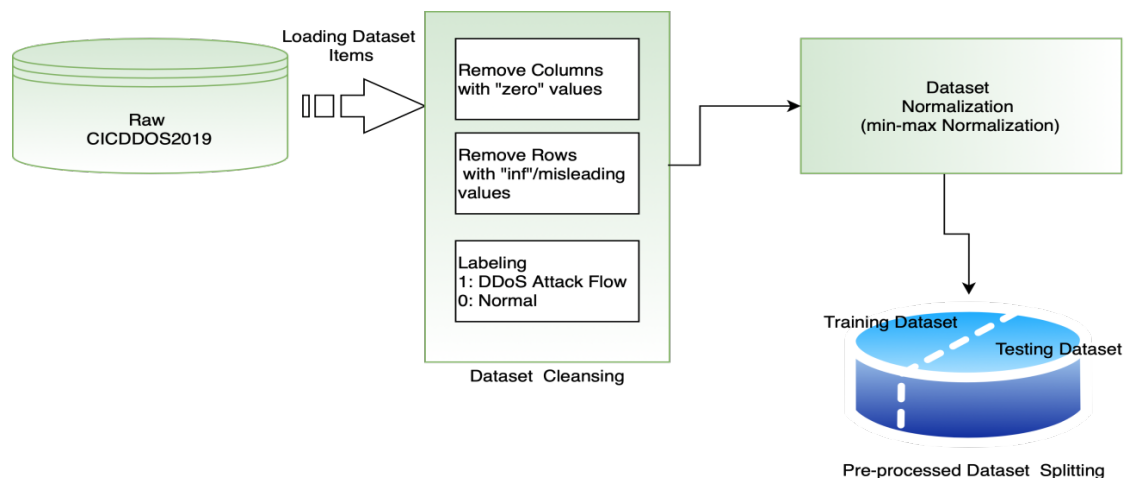


Fig. 3. CICDDoS2019 Dataset Pre-Processing Steps.

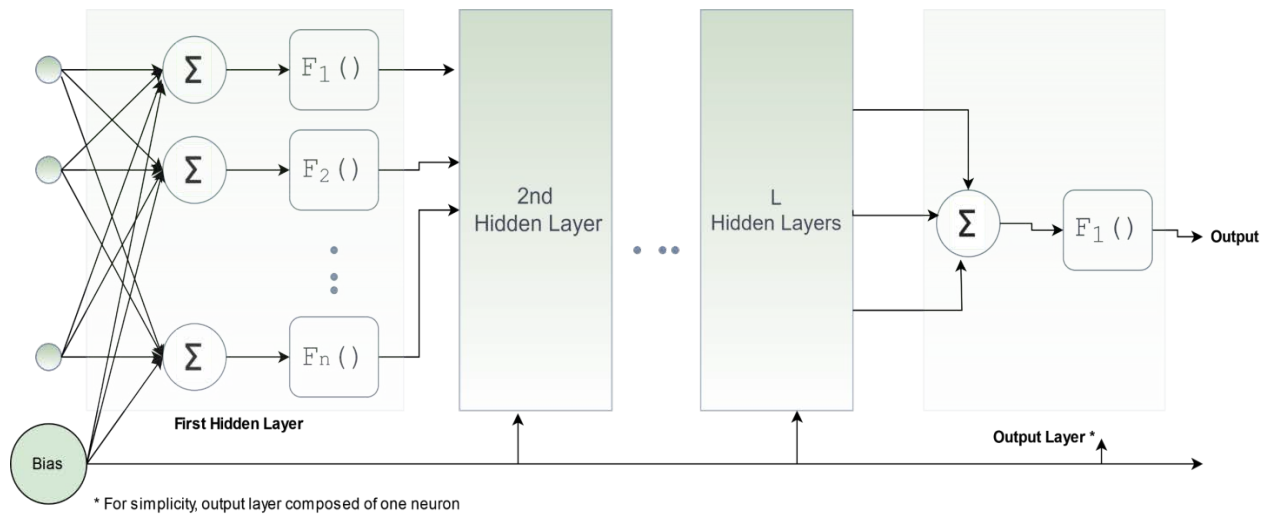


Fig. 4. Backpropagation Neural Network Layers Structure.

As shown in Fig. 4, all neurons are given biases by introducing an extra input line with no input but of a constant output (always has a value of 1) and it treated as an extra weighted input connection. Each neuron in the network has a real valued nonlinear function of its total input as in (3):

$$y_j(x) = \frac{(1-e^{-\alpha x_j})}{(1+e^{-\alpha x_j})} \quad (3)$$

where :

Δw : represents the updated value of the weight vector w .

γ : is a positive learning step (learning rate) parameter.

The target is to find a set of weights parameters generated the network that is same as (or sufficiently close to) the desired output, the network model has the given set of weights parameters which used to make predictions and the differences between those predictions and the actual outputs are computed as error values. Typically, we seek to minimize the error of the function given by in (4):

$$x_j = \sum_i^l y_i w_{ji} \quad (4)$$

Where, E is the error function, d is the index over target outputs, j is an index over the output units of the output layer.

Gradient decent of the error function ∇E lies at the heart of backpropagation, where it seeks to change the weights parameters through multiple evaluations where the optimization algorithm ($\nabla E = 0$) navigates down the gradient of error function till the minimum is found.

IV. EXPERIMENTAL RESULTS AND DISCUSSION

This section analyzes the performance of the proposed DDoS intrusion detection framework using backpropagation-based predictive model. This system is implemented, and experimentation is performed on Intel(R) Core (TM) i7-4500U CPU @ 1.80GHz and 2.40 GHz with 8GB of RAM and 64-bit Windows operating system. For more deeper experimental analysis and more controllability, we use MATrix LABratory (MATLAB)®2021b to build the back propagation neural

network-based model from scratch where the available built-in neural network toolbox has not been used.

A. Performance Metrics

For purpose of model analysis, we used a subset of CICDDoS2019 dataset [11] we conducted many simulation trials, where the training dataset volume almost equals the volume testing dataset. In order to evaluate the detection performance of the system, we first established the confusion matrix, as shown in Table I. Then, the confusion matrices of the training and testing results are obtained. Based on the confusion matrices we considered the performance metrics that include Accuracy, Precision, F1-measure, False Positive Rate (FPR), Recall, Mathew Correlation coefficient and Kappa coefficients as in (5)-(11).

$$\text{Accuracy (Acc)} = \frac{(TP+TN)}{(TP+TN+FP+FN)} \quad (5)$$

$$\text{Precision (Pr)} = \frac{TP}{TP+FP} \quad (6)$$

$$\text{Mathew Correlation Coefficient (Mcc)} = \frac{TP*TN-FP*FN}{\sqrt{(TP+FP)(TP+FN)(TN+FP)(TN+FN)}} \quad (7)$$

$$\text{Kappa Coefficient (K)} = \frac{Obs^{agree}-Expect^{agree}}{1-Expect^{agree}} \quad (8)$$

Where

$$Obs^{agree} = ACC = \frac{(TP + TN)}{(TP + TN + FP + FN)},$$

$$Expect^{agree} = \frac{A + B}{(TP + TN + FP + FN)},$$

TABLE I. CONFUSION MATRIX

Actual	Predicted	
	Normal	DDoS
Normal	TN	FP
DDoS	FN	TP

$$A = \frac{(TP + FN)(TP + FP)}{(TP + TN + FP + FN)}$$

$$B = \frac{(FP + TN)(FN + TN)}{(TP + TN + FP + FN)}$$

$$FPR = \frac{FP}{FP+TN} \tag{9}$$

$$F\text{-Measure (F1)} = \frac{2}{\frac{1}{Recall} + \frac{1}{Pr}} \tag{10}$$

$$Recall \text{ (Sensitivity)} = \frac{TP}{TP+FN} \tag{11}$$

where, False Positive (FP) and False Negatives (FN) refers to misclassified events. In contrary, True Positive (TP) and True Negative (TN) refers to the events that are correctly predicted by the model, i.e., if the model predicts normal events as normal, then, it is recorded as TN, whereas, if the model predicts the DDoS attack traffic flow as a DDoS malicious attack traffic, then it is recorded as TP.

B. Results

In this section we performed a series of experiments to determine the optimal network model architecture of the proposed backpropagation-based model along with varying many networks' hyper-parameters.

Afterwards, we performed another set of experiments that analyze the impacts of varying specific network parameters on the detection performance of the proposed intrusion detection model. We used four layers backpropagation neural network with two hidden layers of 64 neurons with $tanh(x) = (\frac{2}{1+exp(-ax)} - 1)$ as activation function, where the optimal value of the sigmoid slope α parameter is to be determined through the experimental analysis.

Table II shows the architecture of this network whereas Table III shows the optimal values of hyper-parameters of the backpropagation neural network used in our proposed intrusion detection model. Dataset was normalized via min-max normalization with [0.5, +0.5] range and then have been split

into training and testing sub-datasets with normal/DDoS distribution as shown in Fig. 5.

Although in the real-time applications, the number of DDoS attack traffic is much less than the normal one, for a robust intrusion detection system, we used a training dataset composed of about 50% DDoS attacks and the same scenario was used for test dataset as can be noted from Fig. 5.

Table IV and Table V show the confusion matrices of both training and testing phases respectively, meanwhile, Table VI represents the detection performance of both stages in terms of performance metrics listed in (5)-(11).

From Table IV, Table V, TPR and TNR are high whereas FPR and FNR are low. Moreover, besides the high detection performance shown in Table VI, it is noticeable that there is a subtle difference in the detection performance between the training and testing phases, therefore, our backpropagation model is not underfit or overfit.

In terms of True positive rate, True negative rate, False positive rate, and False negative rate illustrated in (12)-(15), Table VII summarizes a comparison between our approach and a recent work proposed by Liu et al. [14].

TABLE II. NETWORK LAYERS ARCHITECTURE

Layer	Neurons number	Activation Function
Input	64	none
Hidden #1	44	Tanh
Hidden #2	20	Tanh
Output	1	Tanh

TABLE III. HYPER-PARAMETERS OF NETWORK MODEL

Parameter	Value
Learning rate γ	-10
Number of Epochs	4000
Training batch size	50,000
Loss Function	Mean Square Error (MSE)

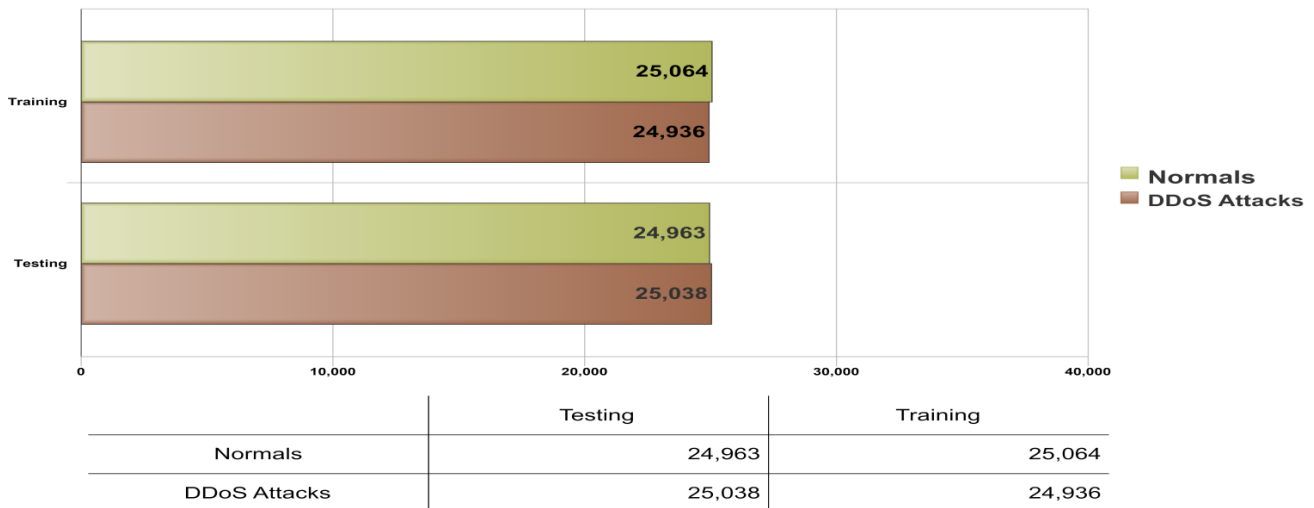


Fig. 5. Frequency of DDoS Intrusions for Training and Testing Datasets for the 2-Labels (Normal/DDoS) Scenario.

TABLE IV. CONFUSION MATRIX OF TRAINING PHASE

	Predicted	
Actual	Normal	DDoS
Normal	23092	1893
DDoS	134	24881

TABLE V. CONFUSION MATRIX OF TESTING PHASE

	Predicted	
Actual	Normal	DDoS
Normal	23022	1984
DDoS	136	24859

TABLE VI. AVERAGE DETECTION PERFORMANCE OF THE PROPOSED BACKPROPAGATION NN-BASED DDoS INTRUSION DETECTION MODEL

Performance Metric	Training Phase	Testing Phase
Accuracy	0.9595	0.9576
Detection Rate (Recall)	0.9946	0.9945
Specificity	0.9242	0.9207
Precision	0.9293	0.9261
FPR	0.0758	0.0793
F1-Score	0.9609	0.9591
MCC Coefficient	0.9212	0.9177
Kappa Coefficient	0.9189	0.9152

$$\text{True Positive Rate} = \frac{TP}{TP+FN} \quad (12)$$

$$\text{True Negative Rate} = \frac{TN}{TN+FP} \quad (13)$$

$$\text{False Positive Rate} = \frac{FP}{FP+TN} \quad (14)$$

$$\text{False Negative Rate} = \frac{FN}{FN+TP} \quad (15)$$

As can be noted from Table VII, detection performances achieved by our proposed BP-based model were higher compared to those achieved by the different ML-based listed in Table VII. Although Liu *et al.* [14] had considered only the results of the neural network and disregarded the other approaches due to the unacceptable results, our proposed model still has higher performance. On the other hand, In contrary to the simple preprocessing of neural network inputs required by our proposed model, Liu *et al.* [14] used the Fast Fourier Transform (FFT) coefficients and the information entropy as input features to the input layer of the neural network which entails extra computational overhead and preprocessing of the network traffic before the detection takes place.

Furthermore, we compare our proposed DDoS intrusion detection model with various related Machine Learning approaches as shown in Table VIII.

TABLE VII. THE AVERAGE PERFORMANCE OF OUR PROPOSED BACKPROPAGATION ANN MODEL IN TERMS OF FPR, FNR, TPR, TNR METRICS

	Year	FPR	FNR	TPR	TNR
Random Forest [14]	2021	0.844	0.0001	0.999	0.156
Gaussian Naive Bayes [14]	2021	1.0	0.0	1.0	0.0
Neural Network [14]	2021	0.0222	0.0069	0.9930	0.9777
Proposed BP ANN-Model	-	0.0793	0.0054	0.9946	0.9207

TABLE VIII. AVERAGE PERFORMANCE EVALUATION OF THE PROPOSED MODEL WITH OTHER CLASSICAL ML-BASED TECHNIQUES

Machine Learning-based Method	Year	Acc	Recall	F1 Score	Precision
ID3 [11]	2019	-	0.65	0.69	0.78
Random Forest(RF) [11]	2019	-	0.56	0.62	0.77
Naive Bayes (NB) [11]	2019	-	0.11	0.05	0.41
Multinomial Logistic Regression (LR) [11]	2019	-	0.02	0.04	0.25
Bandwidth Control Mechanism + Extreme Gradient Boosting Algorithm (XGBoost) [15]	2020	0.997	1.000	1.0000	1.0000
Logistic Regression [15],[16]	2020	0.8000	0.8000	0.8000	0.8500
Naive Bayes [15],[17]	2020	0.7700	0.7700	0.7600	0.8400
ID3 [15],[18]	2020	0.9850	0.9990	0.9900	0.9900
Random Forest [15],[19]	2020	0.9855	0.9900	0.9900	0.9900
Autoencoder [20]	2021	0.8945	-	-	-
Restricted Boltzmann [20]	2021	0.5651	-	-	-
K-means [20]	2021	0.7538	-	-	-
Expectation-Minimization (EM) [20]	2021	0.7096	-	-	-
Proposed Model	-	0.9576	0.9946	0.9591	0.9261

As shown in Table VIII The obtained results show that the detection performance of our proposed BP-based DDoS predictive model is far superior to that had been reported by the authors of the CICDDoS2019 dataset [11] using ID3, RF, NB, and LR algorithms owing to the nonlinear modeling power of the backpropagation neural network. The same findings can be noticed if the detection performance of our proposed BP-model is compared to Autoencoder, Restricted Boltzmann, K-means, and Expectation-minimization machine learning algorithms adopted by [20].

Even though ID3, RF, NB, and LR algorithms were re-generated by [15], they have achieved superior detection performance to that had been achieved by [11]. Authors in [15] attributed their higher results to the performed preprocessing steps they adapted. However, in comparing our results to that reported by [15] for LR and NB-based algorithms, we can conclude that the influence of the pre-processing is limited because our BP-model that processed by the simple classical pre-processing steps was able to achieve superior results in comparison with these algorithms.

A regular BP-based detection model and the detection performance of [15] built is based on sequential steps of preprocessing and a combination of the bandwidth control mechanism and Extreme gradient boosting algorithm.

C. Experiments on Different Network Parameters Tuning

Since backpropagation network is a gradient-descent based learning algorithm, the first steps that come into consideration while building the network architecture is the initial state of the network as well as the network parameters tuning of the network in order to converging to the optimal minima of loss function gradient in least number of epochs.

Therefore, in the following subsections, we investigate the influence of the required number of Epochs, learning rate γ and sigmoid slope α on the detection performance of the system in training and testing phases and then analyze for the most appropriate values of these parameters.

It is worthy to mention that the backpropagation network is highly sensitive to the initial state of their weight's metrics, we have turned the initial weights to random values in the

range $-0.285 \leq w^{ini} \leq -1.06$ before we are conducting these experiments. Otherwise, improper weights initialization can drive the network to saturate at a static accuracy threshold and stuck in a static local minimum.

1) *Impact of increasing number of epochs:* To examine the effect of increasing epochs number of the training phase on the detection performance in the prediction phase of the proposed BP-based model in terms of accuracy, recall, FPR, Precision, Kappa and MCC coefficient. First, we set the span of epoch to be from 200 to 9000 and fix other parameters such as learning rate, initial weights, and sigmoid slope, then a comparative analysis between the impact of epochs number on the detection performance on both training and testing phases is conducted as illustrated in Fig. 6. and Fig. 7.

As illustrated in Fig. 6 and Fig. 7 the predictive behavior of the proposed model in training and testing phases is almost the same, which ensures that our model is not underfitting or overfitting. To emphasize this behavior further and to ensure the stability and robustness of the prediction performance, the difference of accuracy performance between these phases are zoomed in as illustrated in Fig. 8 where it can be noted that the differential behavior decreases steadily to less than $0.1e-3$ and in unison manner as the number of the training epochs increases.

As can be noted from Fig. 6, the accuracy of detection increases steadily as the training epochs increases until it hits $Epoch = 2000$, where beyond this value, the rate of change in detection is saturated and cannot be traced without zooming in effect. At $Epoch = 4500$, the accuracy behavior shows a temporary tenuous decrease; however, it is not exhibited by the Recall and FPR performance behavior. It is clear that by epoch 4000, almost accuracy, recall, and FPR performances start to converge quickly to a steady-state behavior, therefore 4000 is a sufficient number of training epochs for sake of optimal performance. Although FPR, as shown in Fig. 6, reaches the minimum at $Epochs = 2000$, the accuracy and sensitivity of the predictive model do not show the same characteristic, and as a compromised solution, Epochs = 2000 was not adapted.

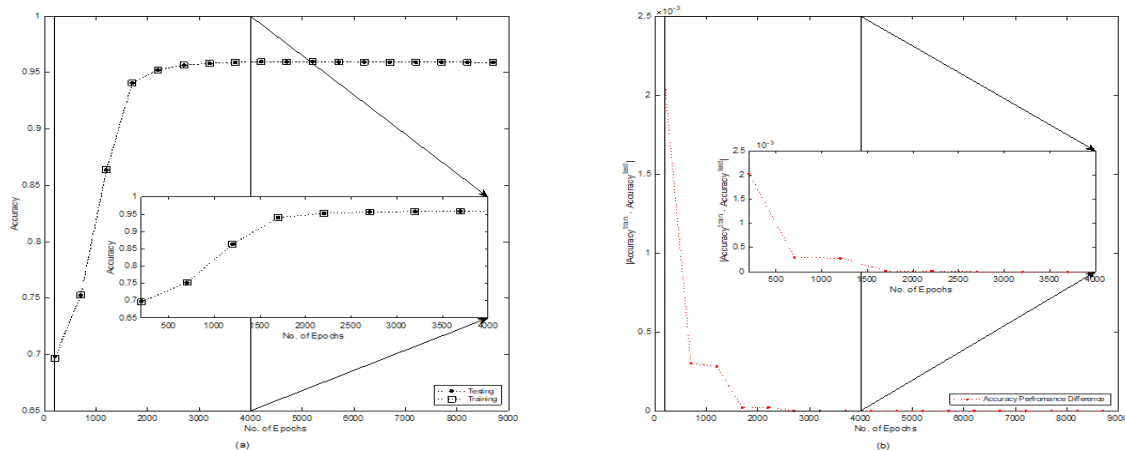


Fig. 6. (a) Accuracy Performance of the Proposed Model in Training and Testing Phases Versus Number of Training Epochs Zoomed in from Epoch No = 4000 to 8000. (b) Difference between the Accuracy Detection of Training and Testing Phases Zoomed in from Epoch No =4000 to 8000.

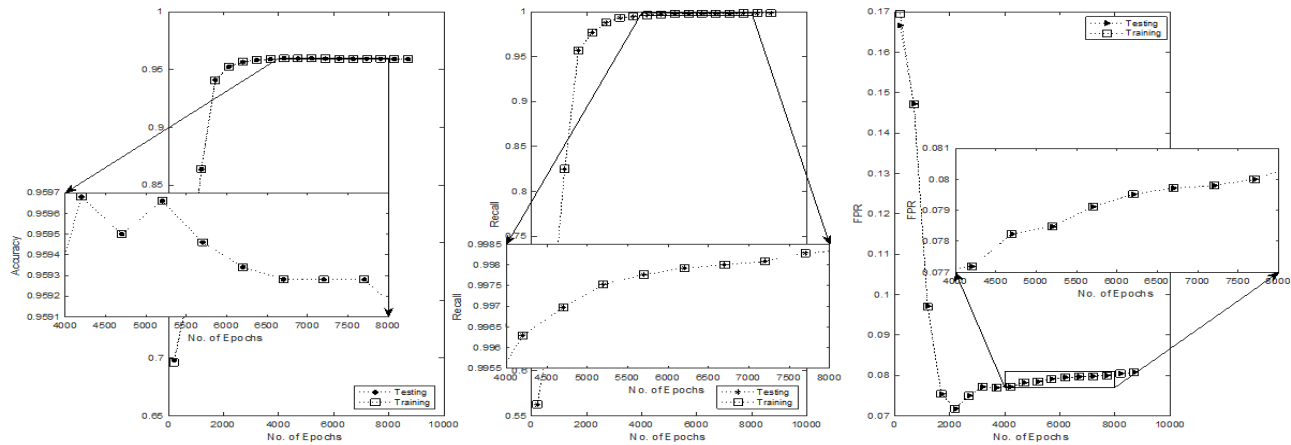


Fig. 7. Accuracy, Recall (Sensitivity), and FPR Performance of the Proposed Model in Training and Testing Phases Versus Number of Training Epochs Zoomed in from Epoch No = 4000 to 8000.

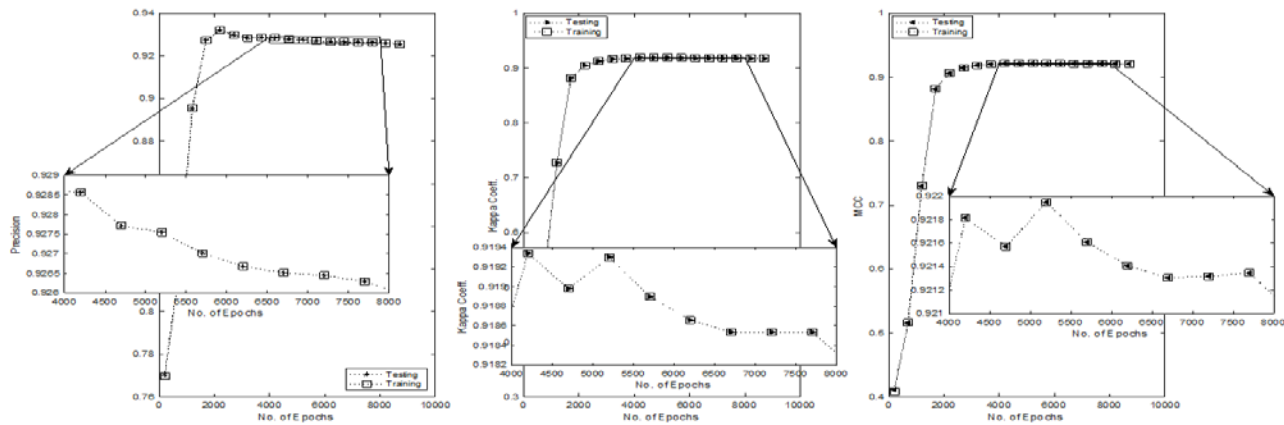


Fig. 8. Precision, Kappa and MCC Coefficients based Performance of the Proposed Model in Training and Testing Phases Versus Number of Training Epochs Zoomed in from Epoch No = 4000 to 8000.

Epochs number of 4000 may appear as a large number of training iterations that required for the neural network to reach a steady detection performance which insinuates a computational challenge appertains to the running time required to train the network. However, due to the simple and efficient network architecture, the entire training phase takes less than five minutes (299 seconds at rate of 13 seconds per epoch). On the other hand, the prediction stage of the system is more time-crucial in comparison to the training phase. Most of the computational overhead is front-loaded during the training phase, the prediction process for 50,000 traffic flows takes less than 0.068 second (in a rate of 1e-6 second per each traffic flow), which is considered as highly computational efficient.

2) *The variation of sigmoid slope experiment:* In this experiment, the slope of sigmoid function (activation function used in all network neurons) was changed in the range $0 \leq \alpha \leq 1$ and the detection accuracy, sensitivity and FPR metrics were recorded.

As shown in Fig. 9, the performance of the system shows a noticeable enhancement as α parameter is increased from

0.1 to 0.2, however, as the value of α transcends 0.2, the system shows a degradation in terms of accuracy and FPR. Furthermore, as the value of α transcends 0.5, the network fails to converge.

On the other hand, even though detection rate shows an enhancement as value of α transcends 0.2, it is unnoticeable and in comparison, to the FPR-based behavior, it cannot be adapted. Thus, based on the experiment we have adapted $\alpha = 0.2$.

3) *The variation of learning rate experiment:* In this experiment, the effect of learning rate on the system performance is investigated. As shown in Fig. 10, the detection performance is decremental as the learning rate exceeds $\gamma > -10$, whereas, system performance, for all metrics, shows almost a saturated behavior against increasing learning rate in the range $-30 \leq \gamma \leq -10$. Therefore, $\gamma = -10$, was adapted.

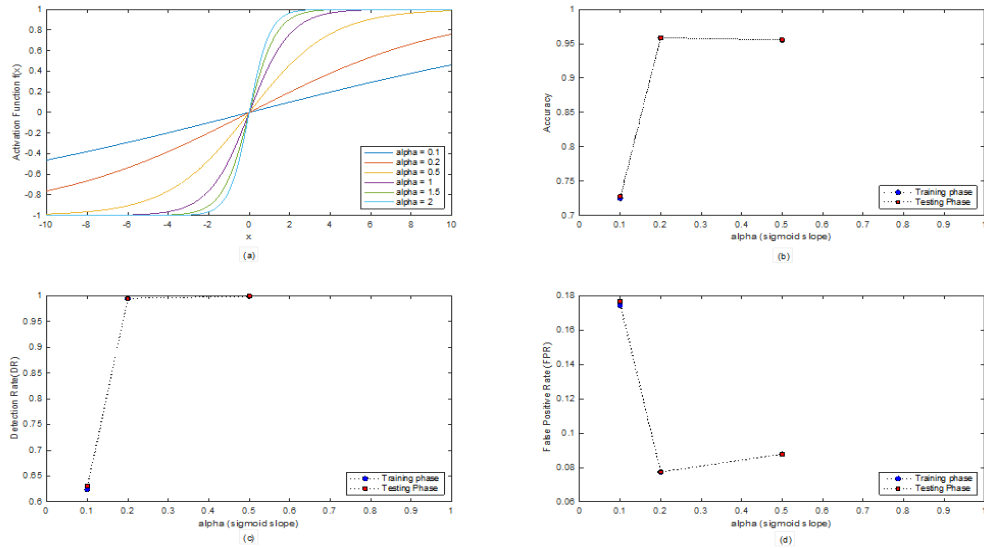


Fig. 9. System Performance (in Terms of Accuracy, Detection Rate and FPR) Under different Values of Sigmoid Slope α . (a) Sigmoid Activation Function Profiles for Different Values of Slope α . (b) Detection Accuracy versus Changing Sigmoid Slope α Parameter. (c) Detection Rate versus Changing Sigmoid Slope α Parameter. (d) FPR versus Changing Sigmoid Slope α Parameter.

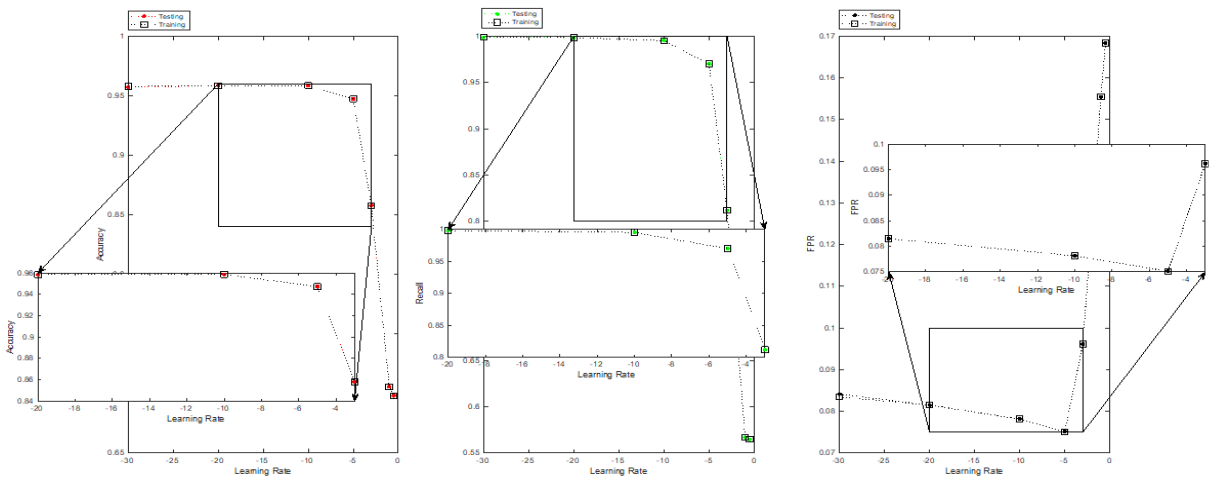


Fig. 10. Accuracy, Recall (Sensitivity), and FPR Performance of the Proposed Model in Training and Testing Phases Under Different Values of Learning Rate Parameter γ .

V. CONCLUSION

In this paper, we have proposed a backpropagation neural network-based methodology for DDoS attacks detection in IoT networks. CICDDoS2019 dataset has comprehensive categories of reflective DDoS attacks that have been considered, so our scheme uses this dataset for model training and evaluation. In contrast to many machines learning-based DDoS intrusion detection models that adapt numerous preprocessing steps and multiple stages and hybrid types of machine learning algorithms to attain high detection performance, our proposed model requires a simple preprocessing step used the standard backpropagation neural network only as a detection engine where we have achieved competitive detection performance. Results show that our model achieves a recall of 0.9946 and accuracy and FPR of

0.9576 and 0.0793 respectively. In our experimental results, we have conducted extensive comparisons with other up-to-date DDoS intrusion detection schemes, and we examined the effect of changing epoch parameter on the overall performance of the backpropagation neural network, however, for further detection performance amelioration, tuning other hyperparameters and examining their impact can be offered as a future work where different approaches such as Bayesian optimization and Random search can be utilized for this purpose.

REFERENCES

- [1] CISA, "Understanding Denial-of-Service Attacks," Cybersecurity and Infrastructure Security Agency. [Online]. Available: <https://www.cisa.gov/uscert/ncas/tips/ST04-015>.
- [2] A. Dahiya and B. Gupta, "How IoT is Making DDoS Attacks More Dangerous?," Insights2Techno. [Online]. Available:

- <https://insights2techinfo.com/how-iot-is-making-ddos-attacks-more-dangerous/>.
- [3] M. darkaie and R. Tavoli, "Providing a method to reduce the false alarm rate in network intrusion detection systems using the multilayer perceptron technique and backpropagation algorithm," in 2019 5th Conference on Knowledge Based Engineering and Innovation (KBEL), Tehran, Iran, Feb. 2019, pp. 001–006. doi: 10.1109/KBEL.2019.8735024.
- [4] E. Hodo et al., "Threat analysis of IoT networks using artificial neural network intrusion detection system," in 2016 International Symposium on Networks, Computers and Communications (ISNCC), Yasmine Hammamet, Tunisia, May 2016, pp. 1–6. doi: 10.1109/ISNCC.2016.7746067.
- [5] X. Wu and Y. Chen, "Validation of Chaos Hypothesis in NADA and Improved DDoS Detection Algorithm," IEEE Commun. Lett., vol. 17, no. 12, pp. 2396–2399, Dec. 2013, doi: 10.1109/LCOMM.2013.102913.130932.
- [6] S. Alzahrani and L. Hong, "Detection of Distributed Denial of Service (DDoS) Attacks Using Artificial Intelligence on Cloud," in 2018 IEEE World Congress on Services (SERVICES), San Francisco, CA, Jul. 2018, pp. 35–36. doi: 10.1109/SERVICES.2018.00031.
- [7] Ming-Qing Ling and Wei-Wei Liu, "Research on intrusion detection systems based on Levenberg-Marquardt algorithm," in 2008 International Conference on Machine Learning and Cybernetics, Kunming, China, Jul. 2008, pp. 3684–3688. doi: 10.1109/ICMLC.2008.4621045.
- [8] Dongqi Wang, Zhu yufu, and Jia Jie, "A multi-core based DDoS detection method," in 2010 3rd International Conference on Computer Science and Information Technology, Chengdu, China, Jul. 2010, pp. 115–118. doi: 10.1109/ICCSIT.2010.5564969.
- [9] O. P. Badve, B. B. Gupta, S. Yamaguchi, and Z. Gou, "DDoS detection and filtering technique in cloud environment using GARCH model," in 2015 IEEE 4th Global Conference on Consumer Electronics (GCCE), Osaka, Japan, Oct. 2015, pp. 584–586. doi: 10.1109/GCCE.2015.7398603.
- [10] B. Joshi, A. S. Vijayan, and B. K. Joshi, "Securing cloud computing environment against DDoS attacks," in 2012 International Conference on Computer Communication and Informatics, Coimbatore, India, Jan. 2012, pp. 1–5. doi: 10.1109/ICCCI.2012.6158817.
- [11] I. Sharafaldin, A. H. Lashkari, S. Hakak, and A. A. Ghorbani, "Developing realistic distributed denial of service (DDoS) attack dataset and taxonomy," 2019, pp. 1–8.
- [12] Data Mining. Elsevier, 2012. doi: 10.1016/C2009-0-61819-5.
- [13] A Machine-Learning Approach to Phishing Detection and Defense. Elsevier, 2015. doi: 10.1016/C2014-0-03762-8.
- [14] Z. Liu, C. Hu, and C. Shan, "Riemannian manifold on stream data: Fourier transform and entropy-based DDoS attacks detection method," Computers & Security, vol. 109, p. 102392, Oct. 2021, doi: 10.1016/j.cose.2021.102392.
- [15] H. A. Alamri and V. Thayananthan, "Bandwidth Control Mechanism and Extreme Gradient Boosting Algorithm for Protecting Software-Defined Networks Against DDoS Attacks," IEEE Access, vol. 8, pp. 194269–194288, 2020, doi: 10.1109/ACCESS.2020.3033942.
- [16] S. Menard, Logistic regression: From introductory to advanced concepts and applications. Sage, 2010.
- [17] H. Zhang, "Exploring conditions for the optimality of naive Bayes," International Journal of Pattern Recognition and Artificial Intelligence, vol. 19, no. 02, pp. 183–198, 2005.
- [18] H. H. Patel and P. Prajapati, "Study and analysis of decision tree based classification algorithms," International Journal of Computer Sciences and Engineering, vol. 6, no. 10, pp. 74–78, 2018.
- [19] M. Denil, D. Matheson, and N. De Freitas, "Narrowing the gap: Random forests in theory and in practice," 2014, pp. 665–673.
- [20] V. Odumuyiwa and R. Alabi, "DDoS Detection on Internet of Things Using Unsupervised Algorithms," Journal of Cyber Security and Mobility, pp. 569–592, 2021.

Analysis and Evaluation of Two Feature Selection Algorithms in Improving the Performance of the Sentiment Analysis Model of Arabic Tweets

Maria Yousef¹

Department of Computer Science
Al-al Bayt University
Mafraq, Jordan

Abdulla ALali²

Department of Computer Science
Isra University
Amman, Jordan

Abstract—Recently, Sentiment analysis from Twitter is one of the most interesting research disciplines; it combined data mining technologies with natural language processing techniques. The sentiment analysis system aims to evaluate the texts that are posted on social platforms to express positive, negative, or neutral feelings of people regarding a certain domain. The high dimensionality of the feature vector is considered to be one of the most popular problems of Arabic sentiment analysis. The main contribution of this paper is to solve the dimensionality problem by presenting a comparative study between two feature selection algorithms, namely, Information Gain (IG), and Chi-Square to choose the best one which may lead to improve the classification accuracy. In this paper, the Arabic Jordanian sentiment analysis model is proposed through four steps. First, a preprocessing step has been applied to the database and includes (Remove Non-Arabic Symbols, Tokenizing, Arabic Stop Word Removal, and Stemming). In the second step, the TF-IDF algorithm is used as a feature extraction method to represent the text into feature vectors. Then, we utilized IG and Chi-Square as feature selection steps to obtain the best subset of features and decrease the total number of features. Finally, different algorithms have been used in the classification step such as (SVM, DT, and KNN) to classify the views people have shared on Twitter, into two classes (positive, and negative). Several experiments were performed on Jordanian dialectal tweets using the AJGT database. The experimental results show the following: 1) The information acquisition algorithm outperformed the Chi-Square Algorithm in the feature selection step, as it was able to reduce the number of features from 1170 to 713 and increase the accuracy of the classifiers by 10%, 2) SVM classifier shows the greatest classification performance among all the classifiers tested which gives the highest accuracy of 85% with IG algorithm.

Keywords—Sentiment analysis; Information Gain (IG); Chi-Square; AJGT database

I. INTRODUCTION

In the past few years, people have been able to interact and share comments across a variety of social media platforms. People all around the world use social media websites to share their ideas and feelings, exchange information, and share news in an easy way. Twitter is a social media website that was launched in 2006 and quickly grew in popularity throughout the world, with over 313 million monthly active users and more than 40 languages supported [1].

The Twitter platform allows users to upload short posts known as tweets to share their feelings, opinions, and thoughts on a wide range of topics. The number of Twitter users in the Arab world is growing rapidly, and a huge amount of Arabic tweets are generated daily. Because of the Extensive use of the Twitter website, media organizations and companies are interested in learning what people think and feel about their commodities, services, and products through their tweets by using sentiment analysis systems.

Sentiment analysis (SA), often defined as opinion mining, is a Natural Language Processing (NLP) process that contains automatically detecting an attitude from a text that is connected to a specific issue. Oueslati et al. in [2] described sentiment analysis as a "method used to determine favorable and unfavorable opinions toward specific products and services using large numbers of textual data sources". The main purpose of SA is to discover people's feelings, opinions, beliefs, emotions, and attitudes expressed in natural language whether positive, negative, or neutral about a person, an organization, a product, a location, or an event, and how this changes over time.

Machine learning and lexicon-based techniques are the two main strategies used in the literature to create SA systems. The lexicon-based technique uses a predetermined vocabulary with weighted terms and their sentiment inclination to estimate the sentiment tendency of text data. In this strategy, the process of classifying the text is done using its set dictionary as described in [3]. While the Machine Learning (ML) strategy uses well-known ML algorithms to solve SA as a classification problem [3]. In several literatures, we discovered that the two methodologies were blended to create a hybrid approach.

Sentiment analysis research in English has made significant progress, but it is still restricted in the Arabic language. The Arabic language has a complicated structure, according to its ambiguity and extensive morphological properties. This, along with having wide range of dialects and resource scarcity, makes progress in Arabic SA research difficult. Because of the significance of the Arabic language, this research focusing on assessing the sentiment of Arabic tweets shared by a huge number of users on Twitter by using machine learning approach.

One of the difficult issues that machine learning methods encounter in sentiment analysis and more generally in text classification is a large number of the features in the using dataset. Where a feature can have a favorable or negative impact on classification performance based on its relevance and redundancy with regard to the class labels. Therefore, feature selection approaches are necessary to enhance the accuracy and efficiency of classification algorithms by picking the most relevant and discriminating feature vectors. Feature selection methods determine the most useful features by measuring the quality of a features subset with which the best performance can be obtained.

This work examined the impact of two feature selection techniques (Chi-Square, and Information Gain (IG)) on the performance of three classifiers (DT, KNN, and SVM) that trained on Jordanian Arabic Tweets to create a sentiment analysis model. The Arabic Jordanian General Tweets (AJGT) Dataset is used in this study to classify Jordanian tweets in two classes (negative, and positive). The AJGT dataset involves 1,800 tweets that are categorized as (900 positives, 900 negatives) represent people's opinions on different topics.

The study is conducted as follows. The associated study is discussed in Section II. The technique of the proposed model is explained in Section III. Section IV discusses the experiments and their outcomes. Section V concludes with a summary of the study's findings.

II. RELATED WORK

In the sentiment analysis literature, a variety of machine learning techniques have been utilized [4-6]. In the classification task, the feature selection approach is used to increase performance by reducing dimensionality. There is a substantial amount of published work in the English language that uses several feature selection techniques to increase the performance of the sentiment analysis model [7]. On the converse, the influence of feature selection on dialectal Arabic sentiment analysis has received less attention.

Duwairi and El-Orfaily [8] examined the effect of feature correlation, stemming, and n-gram models on sentiment analysis of Arabic text. For text representation, several N-gram models of words and characters were utilized. In this research, two datasets were utilized to conduct experiments. The first dataset is named the Politics dataset it contains 300 reviews of which 164 are categorized as positive reviews and 136 are categorized as negative reviews. The authors gathered these reviews from Aljazeera webpage. While the second dataset is known as the Movie dataset and is open to the public. Three classification algorithms were employed to classify the reviews (SVM, Naïve Bayes, and K-NN). From the result, SVM and Naïve Bayes classifiers achieve better performance. Substantial improvement has been achieved by using the top 1200 correlated features and word N-gram with Naïve Bayes algorithm to produce the most increased accuracy with 97.2%.

Baker et al., [9] introduced the first research of epidemic illnesses based on tweets in the Arabic language by developing a novel sentiment analysis system that aims to identify Influenza from Arab countries' tweets. The authors of this work obtained, labeled, filtered, and analyzed Arabic-language

influenza-related tweets. The following algorithms were used to evaluate the system's quality and performance: DT, K-NN, NB, and SVM. From the tests, the best accuracy value of detecting influenza was 83.20%, which was achieved in the NB algorithm.

Altaher Taha [10] proposed a novel technique for sentiment analysis of Arabic tweets using features weighting and deep learning. In this work, stop word removal, tokenization, and stemming are utilized as preprocessing methods, followed by the use of two feature weighting methods (Chi-Square and Information Gain) to give high weights to the most important features of Arabic tweets. Second, the deep learning approach is used to efficiently and correctly classify Arabic tweets as either positive or negative. The suggested methodology was compared to the performance of different classification algorithms such as Neural Networks (NN), Support Vector Machine (SVM), and Decision Tree (DT) using the same data gathered from Arabic tweets. The suggested method exceeds the others, achieving the maximum precision and accuracy of 93.7% and 90%, respectively.

El Rahman et al., [11] developed a model that can classify tweets as negative, positive, or neutral using different techniques to improve the classification accuracy. The authors of this study used Twitter API to extract Tweets on two topics: KFC and McDonald's, in order to determine which restaurant is more popular. This presented methodology combined the use of both unsupervised and supervised machine learning techniques. Firstly lexicon-based algorithms have been used to create previously unlabeled data. After that data was input into several supervised models for training purposes, including (SVM, NB, DT, and RF). Different testing measurements, such as f-score and cross-validation, were used to test the outcomes of the suggested models. As a consequence, both positive and negative reviews show that McDonald's is more popular than KFC.

Ghallab et al., [12] presented a deep survey of the current literature related to Arabic sentiment analysis (ASA). The major aims of this review are to encourage research and to identify new areas for future study in ASA, Analyze and compare the methods used in each study and its results, also to make it easier for other researchers to find similar works. After filtering, this review focused to analyzed 108 published studies from 22 conferences and 11 journals proceedings. The conclusions of the review indicate that there is little study on creating standard datasets and using promising classifiers. Furthermore, the review shows limited research interested in designing a novel feature representation that appropriates for the Arabic language characteristics. Finally, the review highlights future research in the development of recommender systems in several areas with the goal of an improved framework for ASA.

III. PROPOSED METHODOLGY

In this part, we will clarify the parts of the suggested sentiment analysis model for Twitter in more detail. As seen in Fig. 1, the suggested model is divided into two parts: Training and Classification. The goal of the training part is to create a classification model that can discriminate between negative and positive tweets based on input labeled tweet collections.

Then during the classification part, the previously trained classification model will apply to assign a negative or positive label to the new unlabeled tweets. This proposed model includes four steps: Preprocessing, Feature Extraction, Feature Selection, and the Classification Model for Sentiment Analysis. The overall steps of the proposed model are shown in Fig. 1.

A. Arabic Jordanian General Tweet (AJGT) Dataset

Arabic Jordanian General Tweets is a new dataset Created 6in 2017 by Alomari et al., [13] for the purpose of sentiment analyses, and it contains 1,800 tweets that are categorized as (900 positives, 900 negatives) represent people's opinions on different topics. The AJGT has been written in Jordanian dialect and MSA, and it's publicly available as a Github project.

B. Preprocessing

The major goal of this step is to process the input tweet text by using natural language processing approach to prepare it for the next step of appropriately extracting the features. In this study, there are different preprocessing steps adapted in the data like filtering, tokenization, and stemming. These steps are clarified in more detail as below:

1) *Remove non-arabic symbols*: Most Arabic tweets on Twitter involve noise, like elongations, diacritical marks, mixed language, and special characters. Therefore, one of the

most crucial stages in preparing Arabic text for Twitter is to clean up the tweets by eliminating this kind of noise [14]. AJGT dataset has some special characters like (!, ,, ?, %). To eliminate the noise from the text, non-Arabic characters are removed by using the cleaning method. As illustrated in Fig. 2, The cleaning procedure checks if each character in the text of the tweet belongs to the Arabic alphabet by reading it character by character. If a character belongs to the Arabic alphabet, it is chosen; otherwise, it is replaced with white space by.

2) *Tokenizing*: Tokenization is only a segmentation technique of the sentences. The goal of this process is to divide sentences into smaller pieces called "tokens", whether that is words or phrases [15]. There are several ways for dividing the phrases in RapidMiner, including using the n-gram approach. The n-gram is a type of graph that is based on the number of letters in a word (n-number-of-tokens) and is utilized to keep the sentences at its meaning [16]. When n=2, it's referred to as diagrams, and when n=3, it's referred to as trigrams. For n=3, a sequence of three consecutive words (tokens) is created for every Arabic tweet in the dataset. In this study, we used a unigram option which means dividing the sentence into single words, each part representing a word.

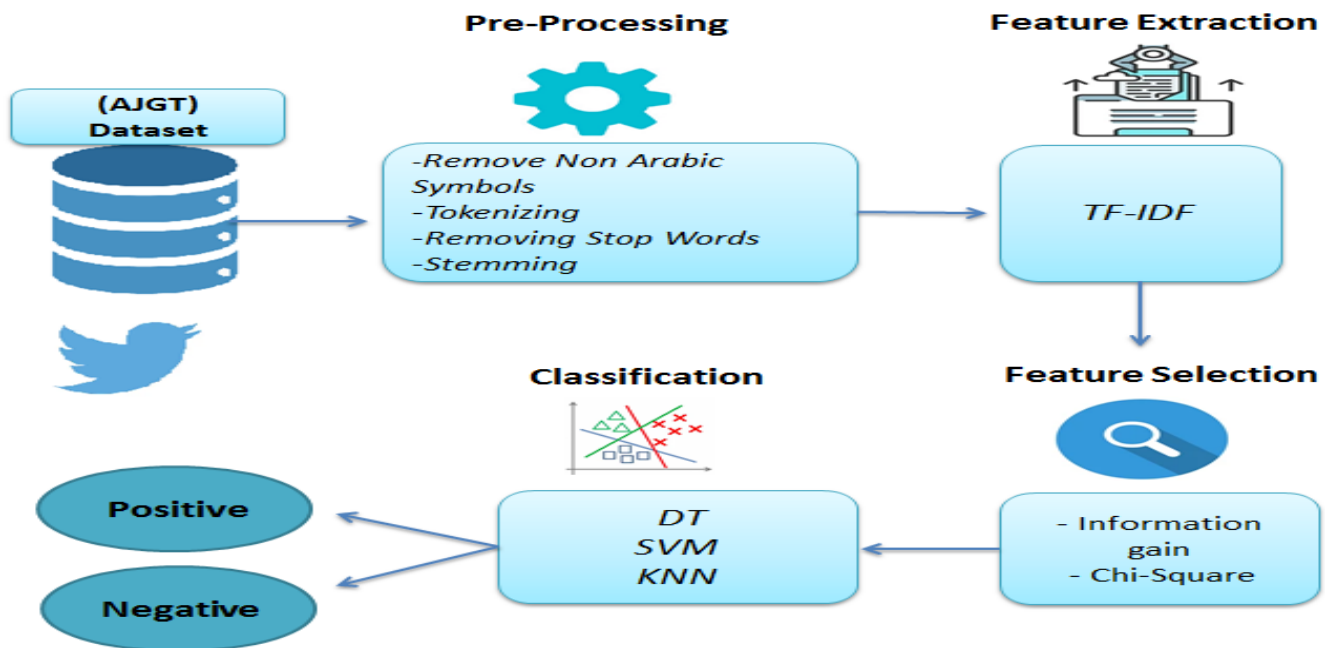


Fig. 1. The Proposed Model Framework.

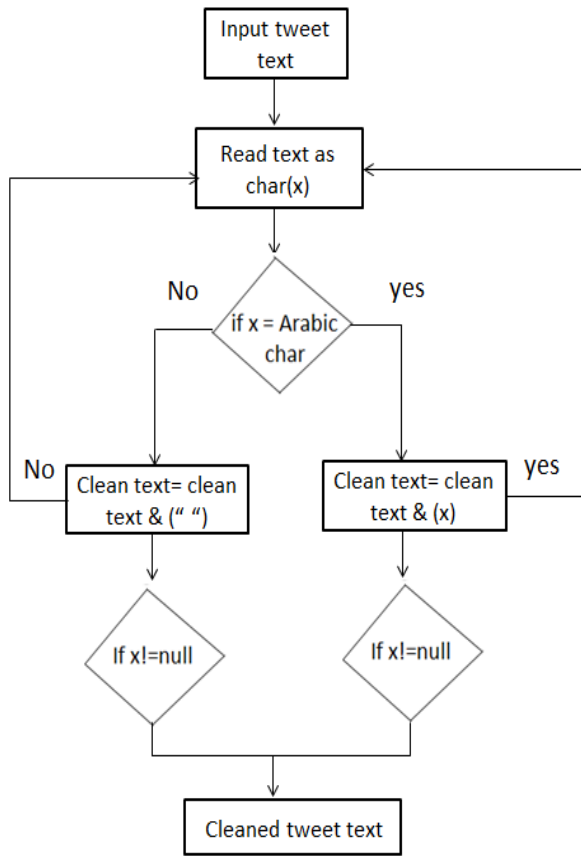


Fig. 2. Cleaned Method.

3) *Arabic stop word removal*: This step is one of the most popular used preprocessing techniques in different NLP applications. This task is employed to eliminate unnecessary and meaningless words [17]. Stop words refer to phrases that appear frequently in Arabic writings, such as (i.e. , الى , بعد , من , لهم , كما , قد). In this step, each token is compared to the stop word list that already exists. If it's on the list, it will be removed.

4) *Stemming*: Replacing a word with its stem means returning it to its original form. this strategy has a significant influence on reducing storage requirements and eliminating redundant terms. Because many Arabic words have the same stem, converting words with the same stem will eliminate redundant terms, for example, the words يعملون , يعمل , تعمل have the same stem which is عمل so all of these words will be replaced with the word عمل. There are two ways to stem a word: reducing it to its three-letter root and light stemming, which eliminates frequent suffixes and prefixes but does not reduce it to its root. In this study, we used root stemming (Porter's Stemmer algorithm).

C. Feature Extraction

After the preprocessing step, the text should be converted into a numeric representation that the ML classifier can interpret. A vector model, often called a feature model, is a model that is represented by a matrix of word weights. Weighting Word is a method of assigning a score to the

frequency with which a phrase occurs in a text document [18]. TF-IDF (Term Frequency-Inverse Document Frequency) is one of the popular methods for weighting words. The idea of TF-IDF is that it calculates the frequency of each token in a tweet [19]. Because each tweet is varied in length, a term may occur more frequently in a long tweet than in a short tweet. As a result, term frequency is frequently split by the document's length (the total words in the document). The TF-IDF value shows how important a token is to a document in the tweets.

D. Feature Selection

The classification's performance is heavily influenced by the feature vector. Notably, that features if, by excluding or including them, the performance would improve or decrease. The relevant features are critical to the training phase because it has an informative aspect that would enhance the classification. On the other hand, the irrelevant ones are less informative, thus including them may have an adverse effect on performance. Determine which of the features are irrelevant or relevant is the objective of this step [20]. In this section, two feature selection strategies were used to extract the most relevant and meaningful features which are Information Gain and Chi-Square (IG).

1) *Information Gain (IG)*: IG is a useful feature selection method that assesses how informative a feature is about the class. IG denotes the reduction of uncertainty in selecting a category by knowing when the value of the feature. IG is a ranking score algorithm which can be computed for a term as shown in (1) [21]:

$$IG = \sum_{i=0}^m P(c_i) \log(P(c_i)) + P(t) \sum_{i=0}^m P(c_i | t) \log(P(c_i | t)) + P(\bar{t}) \sum_{i=0}^m P(c_i | \bar{t}) \log(P(c_i | \bar{t})) \quad (1)$$

c_i Represent the i th category, the probability of the i th category is $P(c_i)$. The probability that the word t will occur or not appear in the documents are represented by $P(t)$ and $P(\bar{t})$. $P(c_i | t)$ Represents the probability of the i th category if the term t appeared, while $P(c_i | \bar{t})$ represents the likelihood of the i th category if the word t did not exist.

2) *Chi-Square*: The Chi-Square of independence is a statistical hypothesis test that calculates the difference between predicted and observed frequencies for two events [22]. The purpose of this test is to see if a difference between observed and predicted data is due to chance or if there is a link between the events. In feature selection, the two events to know the relationship between are the occurrence of the term and the occurrence of the class. Few studies have looked into the impact of utilizing the Chi-Square feature selection approach in Arabic sentiment analysis, such as [23]. In this study, The value for each term concerning the value of the class is calculated as shown in (2).

$$X^2(t, c) = \frac{D \times (PN - MQ)^2}{(P+M) \times (Q+N) \times (P+Q) \times (M+N)} \quad (2)$$

Where D represented the total number of tweets, P denotes the count of tweets in class c that include the term t . Q is the number of Arabic tweets containing t occurring without c .

While the number of tweets in class c that occur without t is M . While, N is the number of tweets from other classes that do not include term t .

E. Classification Algorithms

1) *Decision Tree (DT)*: It is a hierarchical tree that divides data into groups depending on attribute value conditions. according to another definition, it is the technique of recursively partitioning training data into smaller pieces based on a series of tests that are displayed at each branch of the tree [24]. Every node in the tree represented a feature training test, and each branch dropping from the node matched the feature value. For example, to categorize an instance, start with the parent node, verify its feature, and then move down the tree branch to the value of the feature for the specific instance which knows the leaf node (or terminal node) and represents the class label [25]. In the text situation, decision tree nodes are usually represented by words in tweets. several techniques are employed in the decision tree to improve classification accuracy. We used a DT with a maximum depth of 10 in this work. This algorithm is based on a gain ratio-based selection criterion for deciding which characteristics to separate.

2) *K-Nearest neighbor (K-NN)*: It's a ranking approach that uses a method based on the number of nearest neighbors and the distance between both the training data and the target data. [26]. Therefore, to make a prediction task, kNN utilizes similarity measures to make a comparison between a particular test entry and the training data set An n -featured record is displayed for each data entity. Each data entity displays an n -featured record. To guess a class label for an unidentified record, The kNN algorithm selects k recodes from the training data set that are the nearest to the unknown records. One of the most widely used for calculating this distance is called Euclidean measurement. In this study, the value of k is set at 5 and the used distance measure is Mixed Euclidean Distance.

3) *Support vector machine (SVM)*: The SVM method was chosen because it is one of the most well-known classifiers in latest years. In the sentiment analysis research area, the SVM classifier outperformed other classifiers in several studies such as in [27,28]. The goal of SVM is to discover the Highest Marginal Hyperplane, which is the maximum margin between the hyperplane and the points on the hyperplane border. In general, SVM provides the benefit of overfitting protection and the ability to handle huge feature spaces. In this study, a radial basis function kernel SVM (RBF SVM) was used.

IV. PERFORMANCE EVALUATION METRIC

To analyze the efficiency of the suggested strategy, the following standard assessment measures were used:

1) *Accuracy*: It's an important metric to assess the achievement of the classification task. It is represented as the percentage of correctly classified samples to the total samples. thus, it can be calculated mathematically by using the formula shown in (3) [29]:

$$Accuracy = \frac{TP+FP}{TP+FP+TN+FN} \quad (3)$$

2) *Precision*: It determines how strict the classification output is. It is described as the percentage of samples accurately classified as positive compared to the total number of samples classified as positive. thus, it can be calculated mathematically by using the formula shown in (4) [30]:

$$Precision = \frac{TP}{TP+FP} \quad (4)$$

3) *Recall*: this metric is used to determine the quality of the classifier's output. It can be calculated mathematically by using the formula shown in (5) [30]:

$$Recall = \frac{TP}{TP+FN} \quad (5)$$

Where:

(TP) is the number of Arabic tweets properly classified as belonging to the correct class by the classifier.

(TN) is the number of Arabic tweets successfully classified as not belonging to the right class by the classifier.

(FP) is the number of Arabic tweets wrongly classified as belonging to the correct class by the classifier.

(FN) is the number of Arabic tweets wrongly classified as not belonging to the correct class by the classifier.

V. RESULT AND DISCUSSION

In this work, three experiments were undertaken to examine the Impact of feature selection techniques and some classification algorithms on the dialectal Arabic sentiment analysis. In the first experiment, we applied classification algorithms directly to the AJGT database, while we applied two methods of feature selection (information acquisition and Chi-Square) in the second and third experiments to compare them and choose the best method that enhances the accuracy of sentiment classification. In the next part, the experiments are explained in more detail.

A. First Experiment

The goal of this experiment is to It is to find the most accurate classification algorithm based on all the features in the database. In this experiment, we compare the accuracy of the most used classifiers in sentiment analysis systems without employing feature selection methods. First, we prepared the data set using the preprocess approaches mentioned in Section B. After that, numerous classifiers were used, including SVM, DT, and k-NN for sentiment classification. To avoid dataset overfitting and improve model performance, we verified the models using the cross-validation approach, which randomly separates the dataset into a training dataset and a testing dataset depending on the k -fold value [31].

The first experiment employed a different number of K -fold that was chosen as (5, 10, 15, and 20). Whereat each time the tweets are tested with various folds and various classifiers. Fig. 3 shows the average accuracy for the various folds (5, 10, 15, and 20) using the DT, KNN, and SVM classifiers. The results are as follows: the average accuracy of the DT is 62.8%, 62.4%, 62.8%, and 62.4%, respectively. The average accuracy

of the KNN is 62.6%, 62.6%, 62.7%, and 62.8%, respectively. Also, the average accuracy of the SVM is 62%, 62.6%, 62.7%, and 63.2% respectively. After comparing all of the accuracy values, we observed that the SVM RBF method achieved the greatest accuracy value of 63.2% at 20-folds.

B. Second Experiment

The purpose of this experiment is to study the effect of employing the Information Gain approach on the suggested system in two aspects: accuracy improvement and dimension reduction. In the first portion of the experiment, the accuracy of the classifiers (DT, KNN, and SVM) is computed after applying the Information Gain approach as a feature selection algorithm to obtain the best subset of features from all features. In the second portion of the experiment, we are interested in assessing the reduction ratio achieved by using the IG strategy, because the IG technique is primarily utilized to choose features that better match the given classes. Based on that, the IG algorithm was able to reduce the total number of features from 1170 to 713 and the results were presented in Table II. Table II demonstrates the performance of the proposed approach for Arabic sentiment analysis based on the IG feature selection algorithm at 20-folds (determined based on previous experience as in 4.1).

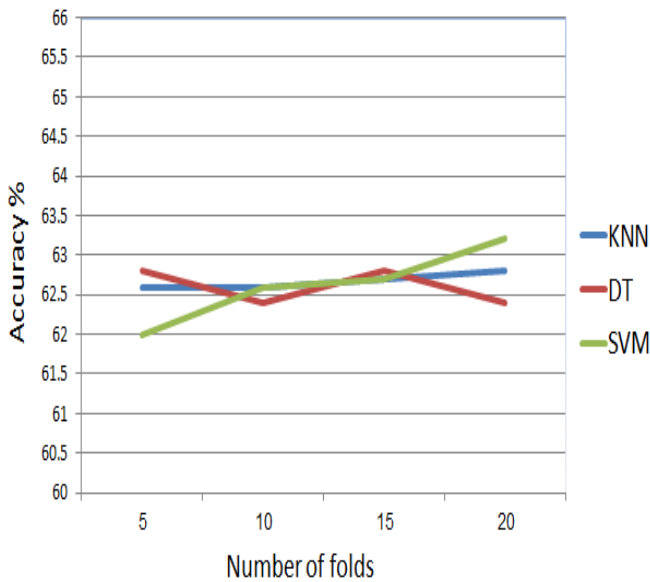


Fig. 3. Accuracy Comparison of Different Classifiers before using Feature Selection.

TABLE I. EXAMPLE OF THE CLEANING ALGORITHM OUTCOMES

Tweet text before cleaning	Tweet text after cleaning
"ما شاء الله ... ونعم التعليم في الاردن ابداعوا الشباب !!!"	"ما شاء الله ونعم التعليم في الاردن ابداعوا الشباب"
"الجمال : ليس فقط شينا نراه بل هو شيء نكتشفه ، روح جميله ، وفكر جميل ، اخلاق جميله ، وادب جميل"	"الجمال ليس فقط شينا نراه بل هو شيء نكتشفه روح جميله وفكر جميل اخلاق جميله وادب جميل"
"وانا 100% بس شكلها هاي مو مدرسه"	"وانا بس شكلها هاي مو مدرسه"

TABLE II. COMPARISON OF ACCURACY AFTER USING IG WITH SEVERAL CLASSIFIERS

Algorithms	Accuracy %	Precision %	Recall %
DT	75	74	75
KNN	72	75	70
SVM	85	85	84

As demonstrated in Table III, using the IG technique increased the accuracy of the proposed model by about 15% on average in all employed classifiers. Furthermore, utilizing the IG approach decreases the AJGT dataset's feature vector length by around 61%. This allows the classifiers to distinguish efficiently between positive and negative classes with lower computational requirements. Furthermore, applying the IG approach in the feature selection step reduces the feature vector length for the AJGT dataset by around 61%. This enables the classifiers to discriminate between positive and negative classes more effectively while using fewer computational requirements. Based on the findings in Table I, we can observe that using the IG technique not only reduces the dimension of the feature vector but also significantly improves the performance of all classifiers.

C. Third Experiment

In this experiment, we aim to evaluate the performance of the proposed model after using the Chi-Square approach as a feature selection method. After applying the same evaluation process described in the second experiment on the AJGT dataset, the Chi-Square Algorithm was able to reduce the total number of features from 1170 to 750 features and the results were presented in Table III. Table III shows the performance of the proposed approach for Arabic sentiment analysis based on the Chi-Square feature selection algorithm at 20-folds (determined based on previous experience as in Section 4.1).

After comparing the results of previous experiments, we conclude the following:

- The SVM classifier shows the greatest classification performance among all the classifiers tested, but its performance decreases as the number of features increases. In the second and third tests, the D-tree classifier's performance appears to remain stable, despite the low number of features. In all experiments, K-NN had the worst results.
- The proposed approach based on the Information Gain Algorithm in the feature selection step achieved a 2% improvement overall classifiers compared to the Chi-Square Algorithm.

TABLE III. COMPARISON OF ACCURACY AFTER USING CHI-SQUARE WITH SEVERAL CLASSIFIERS

Algorithms	Accuracy %	Precision %	Recall %
DT	73	73	71
KNN	70	72	70
SVM	83	84	82

- The efficiency of this proposed approach is due to two main factors: First, we utilized a preprocessing step to improve the quality of the data we used, which leads to an increase in the quality of the results. Second, using feature selection algorithms to select the best subset of features reduces the total number of features and improves the classification model's accuracy. An IG algorithm outperformed the Chi-Square Algorithm as it was able to reduce the number of features from 1170 to 731, whereas the Chi-Square Algorithm reduced it to 750.

VI. CONCLUSION

This study examined the impact of two feature selection approaches (IG, and chi-square) on the performance of the (DT, KNN, and SVM) classifiers for dialectal Arabic sentiment analysis. The experiments are implemented in the RapidMiner data mining tool by using an AJGT dataset and a 20-fold cross-validation technique. The dataset consists of 1800 Arabic Jordanian tweets labeled by two different classes (negative and positive). The experimental results showed the Information Gain Algorithm outperformed the Chi-Square Algorithm in the feature selection step, as it was able to reduce the number of features by 61% and increase the accuracy of the classifiers by 10%. Moreover, the SVM classifier shows the greatest classification performance rather than DT, and KNN among all the experiments which give the highest accuracy of 85% with the IG algorithm.

REFERENCES

- [1] T. Singh, & M. Kumari, "Role of text pre-processing in twitter sentiment analysis. *Procedia Computer Science*", vol. 89, pp. 549-554, 2016.
- [2] O., E. Cambria., M. B. HajHmida, and H. Ounelli, "A review of sentiment analysis research in Arabic language". *Future Generation Computer Systems*, vol. 112, pp. 408-430, 2020.
- [3] M. Ahmad, S. Aftab, S. S. Muhammad, and S. Ahmad, "Machine learning techniques for sentiment analysis: A review," *Int. J. Multidiscip. Sci. Eng.*, vol. 8, no.3, pp.27, 2017.
- [4] A. Elnagar, S. Yagi, A. B Nassif., I. Shahin, & S. A. Salloum, "Sentiment analysis in dialectal Arabic: a systematic review". In *International Conference on Advanced Machine Learning Technologies and Applications*, pp. 407-417, Springer, 2021.
- [5] R. S. Jagdale, V. S. Shirsat, and V. S. Deshmukh, "Sentiment analysis on product reviews using machine learning techniques," In *Cognitive Informatics and Soft Computing*, pp. 639-647, 2019.
- [6] R. B. Shamantha, S. M. Shetty, and P. Rai, "Sentiment analysis using machine learning classifiers: evaluation of performance". In *2019 IEEE 4th International Conference on Computer and Communication Systems (ICCCS)*, pp. 21-25, IEEE, February.2019 .
- [7] Koncz, and J. Paralic, "An approach to feature selection for sentiment analysis," In *2011 15th IEEE International Conference on Intelligent Engineering Systems*, pp. 357-362, IEEE, June.2011.
- [8] R. Duwairi, and M. El-Orfali, "A study of the effects of preprocessing strategies on sentiment analysis for Arabic text,". *Journal of Information Science*, vol.40, no.4, pp. 501-513, 2014.
- [9] Q. B. Baker, F. Shatnawi, S. Rawashdeh, M. Al-Smadi, and Y. Jararweh, "Detecting Epidemic Diseases Using Sentiment Analysis of Arabic Tweets," *J. Univers. Comput. Sci.*, vol.26, no.1, pp.50-70, 2020.
- [10] A. Altaher, "Hybrid approach for sentiment analysis of Arabic tweets based on deep learning model and features weighting," *International Journal of Advanced and Applied Sciences*, vol.4, no.8, pp.43-49, 2017. <https://doi.org/10.21833/ijaas.2017.08.007>.
- [11] S. A. El Rahman, F. A. AlOtaibi, and W. A. AlShehri, "Sentiment analysis of twitter data," In *2019 International Conference on Computer and Information Sciences (ICCIS)*, pp. 1-4, IEEE, April. 2019.
- [12] A. Ghallab, A. Mohsen, and Y. Ali, "Arabic sentiment analysis: A systematic literature review," *Applied Computational Intelligence and Soft Computing*, 2020.
- [13] K. M. Alomari, H. M. ElSherif, and K. Shaalan, "Arabic tweets sentimental analysis using machine learning," In *International Conference on Industrial, Engineering and Other Applications of Applied Intelligent Systems*, pp. 602-610, Springer, Cham, June. 2017.
- [14] A. Krouska, C. Troussas, and M. Virvou, "The effect of preprocessing techniques on Twitter sentiment analysis," In *2016 7th international conference on information, intelligence, systems & applications (IISA)*, pp. 1-5, IEEE, July. 2016.
- [15] S. Vijayarani, and R. Janani, (2016). "Text mining: open source tokenization tools-an analysis," *Advanced Computational Intelligence: An International Journal (ACIJ)*, vol. 3, no.1, pp.37-47,2016.
- [16] F. Aisopos, G. Papadakis, and T. Varvarigou, "Sentiment analysis of social media content using n-gram graphs," In *Proceedings of the 3rd ACM SIGMM international workshop on Social media*, pp. 9-14, November.2011.
- [17] A. W. Pradana, and M. Hayaty, "The effect of stemming and removal of stopwords on the accuracy of sentiment analysis on Indonesian-language texts," *Kinetik: Game Technology, Information System, Computer Network, Computing, Electronics, and Control*, pp.375-380, 2019.
- [18] J. Kumar, J. K. Rout, and S. K. Jena, "Sentiment analysis using weight model based on SentiWordNet 3.0.," In *Recent Findings in Intelligent Computing Techniques*, pp. 131-139, Springer, Singapore, 2018.
- [19] A. Mee, E. Homapour, F. Chiclana, and O. Engel, "Sentiment analysis using TF-IDF weighting of UK MPs' tweets on Brexit," *Knowledge-Based Systems*, vol.228, pp.107238,2021
- [20] B. Agarwal, and N. Mittal, "Optimal feature selection for sentiment analysis," In *International conference on intelligent text processing and computational linguistics*, pp. 13-24, Springer, Berlin, Heidelberg, March.2013.
- [21] B. Azhagusundari, and A. S. Thanamani, "Feature selection based on information gain," *International Journal of Innovative Technology and Exploring Engineering (IJITEE)*, vol. 2, no.2, pp.18-21, 2013.
- [22] A. M. Bidgoli, and M. N. Parsa, "A hybrid feature selection by resampling, chi squared and consistency evaluation techniques," *World Academy of Science, Engineering and Technology*, vol.68, pp. 276-285, 2012.
- [23] A. Sharma, and S. Dey, "A comparative study of feature selection and machine learning techniques for sentiment analysis," In *Proceedings of the 2012 ACM research in applied computation symposium*, pp. 1-7, October.2012.
- [24] S. B. Kotsiantis, I. Zaharakis, and P. Pintelas, "Supervised machine learning: A review of classification techniques," *Emerging artificial intelligence applications in computer engineering*, vol.160, no.1, pp.3-24, 2007.
- [25] M. Du, S. M. Wang, and G. Gong, "Research on decision tree algorithm based on information entropy," In *Advanced Materials Research*, vol. 267, pp. 732-737, Trans Tech Publications Ltd, 2011.
- [26] H. A. Abu Alfeilat, A. B. Hassanat, O. Lasassmeh, A. S. Tarawneh, M. B. Alhasanat, H. S. Eyal Salman, and V. S. Prasath, (2019). "Effects of distance measure choice on k-nearest neighbor classifier performance: a review," *Big data*, vol.7, no.4, pp.221-248, 2019.
- [27] M. Ahmad, S. Aftab, M. S. Bashir, N. Hameed, I. Ali, and Z. Nawaz, "SVM optimization for sentiment analysis," *Int. J. Adv. Comput. Sci. Appl.*, vol. 9, no.4, pp.393-398, 2018.
- [28] R. M. Duwairi, and I. Qarqaz, "Arabic sentiment analysis using supervised classification," In *2014 International Conference on Future Internet of Things and Cloud*, pp. 579-583, IEEE, August. 2014.
- [29] M. Shahrokh Esfahani, and E. R. Dougherty, (2014). "Effect of separate sampling on classification accuracy," *Bioinformatics*, vol.30, no.2, pp. 242-250, 2014.
- [30] D. M. Powers, (2020). "Evaluation: from precision, recall and F-measure to ROC, informedness, markedness and correlation," *arXiv preprint arXiv:2010.16061*, 2020.
- [31] M. W. Browne, "Cross-validation methods," *Journal of mathematical psychology*, vol.44, no.1, pp. 108-132, 2000.

Domain Human Recognition Techniques using Deep Learning

Dr. Seshaiiah Merikapudi¹, Dr. Murthy SVN², Manjunatha.S³, R.V.Gandhi⁴

Associate Professor, Department of CSE, SJC Institute of Technology, Chickballapur, India^{1,2,3}

Assistant Professor, Department of CSE(DS)⁴

Keshav Memorial Institute of Technology, Hyderabad, Telangana, India⁴

Abstract—As a key research subject in the fields of health and human-machine interaction, human activity recognition (HAR) has emerged as a major research focus over the past few decades. Many artificial intelligence-based models are being created for activity recognition. However, these algorithms are failing to extract spatial and temporal properties, resulting in poor performance on real-world long-term HAR. A drawback in the literature is that there are only a small number of publicly available datasets for physical activity recognition that contain a small number of activities, owing to the scarcity of publicly available datasets. In this paper, a hybrid model for activity recognition that incorporates both convolutional neural networks (CNN) are developed. The CNN network is used for extracting spatial characteristics, while the LSTM network is used for learning time-related information. Using a variety of traditional and deep machine learning models, an extensive ablation investigation is carried out in order to find the best possible HAR solution. The CNN approach can achieve a precision of 90.89%, indicating that the model is suitable for HAR applications.

Keywords—Human recognition; deep learning; hybrid model; CNN; HAR

I. INTRODUCTION

Human activity recognition (HAR) is a well-established research topic that requires the correct identification of a wide range of activities that are collected in a variety of ways. Sensor-based HAR makes use of inertial sensors such as accelerometers and gyroscopes to measure the acceleration and rotational velocity of a body. There are numerous advantages to employing sensors to capture a person movement rather than cameras and microphones, including the fact that they are less sensitive to noise, less invasive for the user, and less expensive. Sensors are also less expensive than cameras and microphones [1]-[5]. Furthermore, as a result of the growing use of sensors embedded in cellphones, these devices have become virtually ubiquitous in our lives.

Aspects of sensor-based HAR that are particularly challenging are the encoding of information and the representation of time. Previous classification systems depended on features extracted from kinetic signals that were first constructed and then implemented into the system. Please keep in mind that these characteristics are largely picked on the basis of heuristics, which are determined by the nature of the work at hand. If you have a deep grasp of the application area or extensive human experience, you may find that when you extract the characteristics from the data collection, you only get a shallow set of characteristics. As previously stated,

standard HAR techniques do not scale well to complex motion patterns and do not perform well on dynamic data, which is defined as data gathered from streams that remain forever outside of the lab [6]-[9].

Automated and deep approaches to human-computer interaction are becoming increasingly prevalent in the field of human-computer interaction. Most deep learning research in biometrics has been focused on face and speaker recognition [12]. The selection of significant characteristics from the data is delegated to the learning model through the use of data-driven signal classification methods, which are used to train the learning model on the data. CNNs are particularly useful when it comes to detecting spatial and temporal correlations between signals [10]. Efficient features are first extracted from raw data. The features include mean, median, autoregressive coefficients, etc. [11].

This paper presents the construction of an activity recognition model that incorporates convolutional neural networks (CNNs). The CNN network is used to extract spatial features, whereas the LSTM network is used to learn about time-related information. It is necessary to do a thorough ablation analysis utilizing a variety of classical and deep machine learning models in order to determine the most effective HAR solution possible. The CNN technique can be employed for HAR applications because of its high precision of 90.89%.

II. RELATED WORK

When it comes to common supervised machine learning techniques, the generic Activity Recognition Chain [13] includes steps such as preprocessing, extraction of features, and classification. When it comes to deep learning (DL), CNNs are an example of a technique that does not require the extraction of features from raw data before classification [14]. CNN feature extraction is accomplished through the convolution of the input signal with a kernel [15]. The outcome of the convolution technique is a feature map that contains information about the data.

Both advantages and drawbacks arise from the ability of CNNs to automatically learn properties. It streamlines the ARC [14] by automating jobs that would otherwise require domain-specific expertise, like the identification of a suitable feature collection. In contrast to the feature selection approach, which starts with the largest number of features feasible and narrows it down to only those that provide the

best discrimination across target classes, CNNs do not require any of these phases. Instead, the use of a CNN incorporates the feature extraction phase into the classifier model, requiring an extended training period to generate adequate features and exposing the approach to problems such as those arising from cold starts. In order to mitigate this problem, it is common in computer vision to use pre-trained CNN models for feature extraction, such as those developed by Raja Raman et al. [16].

In the MLP classifier, there are numerous dense, fully connected layers that lead to an output layer with as many nodes as the number of target classes present in the input. A vector of HCF is used as an input to a regular MLP in order to feed it (a). In the CNN scenario (b), convolutional layers are employed to extract features from the data [17].

An alternative is to do a max-pooling operation after each of the convolutional layers, which will result in a further reduction in the feature map size due to down sampling of the data [17]. A 1D vector that has been flattened from the output of the previous convolutional layer is supplied into the MLP layer just as it was in the HCF example. While IMU signals frequently contain a temporal component, 2D convolution is more commonly used in the processing of picture audio [18] and video audio [19].

Rectified Linear Unit (ReLU) activation functions are one of the most frequently used activation functions for convolutional layers, while Softmax activation functions are commonly applied in multi-class classification settings [15]. It is possible to employ alternative activation functions in the case of multi-label classification, such as the sigmoid function [20].

III. PROPOSED METHOD

A two-pronged approach will be used to experiment with CNN in this section. In the first phase of this work, CNN automatically retrieved features with a variety of hyper parameters and topologies, which are then analyzed and the results were presented. A real-world dataset was utilized for the second aim, which investigated the viability of employing a pre-trained CNN feature extractor for HAR. It is useful to take advantage of a CNN ability to automate feature extraction while avoiding the cold-start difficulty.

Two steps in a case study were recommended, which are depicted in Fig. 1.

In the first stage, a CNN feature extractor is trained to extract features from images [Fig. 1(a)]. This step involves experimenting with different topologies and hyper parameter combinations. The best-performing HAR models have been discovered as a result of this research. It is only used as a feature extractor in the second stage, in order to convert raw data into a suitable input vector for a second classifier model in the third phase. The flattening layer generates feature vectors as a result of a succession of convolutional processes, and the weights of the CNN networks are fixed at the beginning of the first phase.

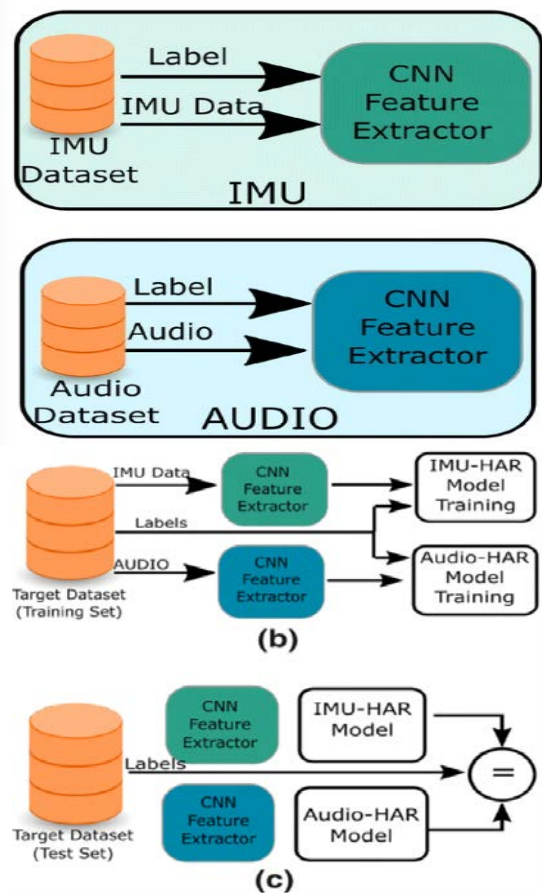


Fig. 1. Two-pronged Approach will be used to Experiment with CNN.

Following an aim similar to transfer learning, the feature vector formed by taking the output of the flattening layer can be used to represent raw data in a different context by using the feature vector created by taking the output of the flattening layer. As seen in Fig. 1(b), the characteristics generated by the pre-trained classifier are utilized to train the second model, which is subsequently used to train the first model. Finally, as illustrated in Fig. 1(c), the second model is put to the test.

In several preliminary experiments, HCF and CNN were compared. However, the breadth of the current case study was restricted due to the nature of the data. For example, CNN feature extractor for HAR is used in this work to explain how to use the tool, and some additional data and analysis are included that was not included in the previous study to demonstrate how to utilize the tool.

As a result of the prior investigation, several key data requirements for the case study were identified. For the first phase, it was found that data collected in controlled environments was the most appropriate choice. The likelihood of noisy labels being introduced into these datasets is low due to the fact that they are developed in a controlled laboratory environment. Consider that the comparison with HCFs may be influenced by issues such as label noise, which could result in an incorrect rating.

A. Network Architecture

Because each sensor samples six different signal components, the type of input examples that the network receives is determined by the sensor design. These six different signal components are then organized into a single channel image matrix of size $6 \times 204 \times N$, which is the largest size available. Consequently, the network input takes the shape of $6 \times 204 \times N$, where N is the number of channels and is equivalent to the number of sensors used for sampling in the network. Model-driven input adaptation is the term used to describe this technique, which is capable of recognizing both spatial and temporal patterns within the signal components.

The convolutional model is illustrated in its entirety in Fig. 3. Following the input layer, there are three convolutional layers and three max-pooling layers. Following this procedure, each input channel receives a collection of multiple feature maps, each with kernels of sizes 3×5 , $2,4 \times 2$, and 2×2 according to the size of the input channel. It is necessary to pad the input of each convolutional layer correctly in order to ensure that there is no resolution loss caused by the convolutional process. A batch normalization procedure is employed during the creation of each convolutional layer. In the three max-pooling layers, kernels with sizes of 3×3 , 2×2 , and 3×2 are employed. Following that there are three dense layers of 500, 250, and 125 units apiece, which together form a network that is entirely connected. During the training phase, neurons have a 0.5% chance of being dropped from the thick layers.

It is true that the cross-entropy function is used to measure loss; however, it is also used as an activation function for all of the network nodes as well. The Adam optimizer is a stochastic approach to optimization that uses a random number generator. Units in the output layer correspond to the number of actions performed by each group, and there are m units in total. The softmax method will return the class of the input windows that is the most likely to be encountered.

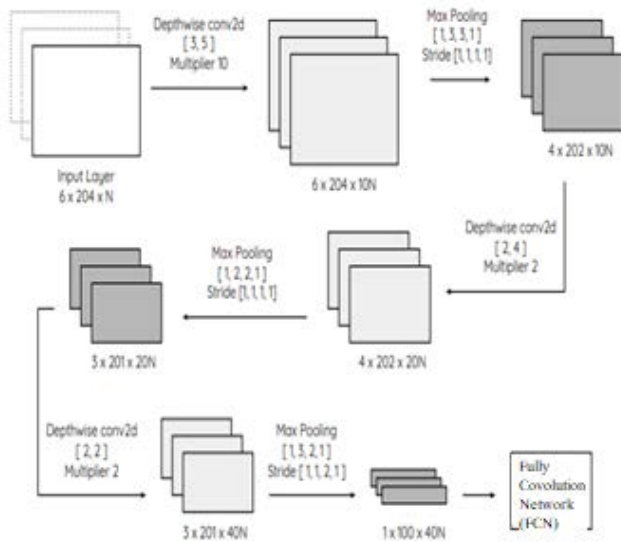


Fig. 2. CNN Architecture.

The Fig. 2 represents the CNN Architecture. The input results in fully convolutional network (FCN). We have chosen a set of hyper parameters that are consistent across all activity groups and sensor configurations. These parameters were chosen based on best practices in the literature and empirical evidence. It has been discovered that a batch size of 1024 can significantly speed up the learning process when compared to smaller batches, while not being computationally prohibitively complex to maintain.

Depending on the behavior of specific combinations, there are between 150 and 300 training epochs available. The starting rate of learning is set at 0.005% each minute. Rather than attempting to construct the most efficient network, our goal is to assess the classification potential of various sensor technologies.

We make our architectural decisions as a result of a very normal network configuration, which is based on modest kernels, standard regularisation methods, and a small number of hyperparameters. If no regularisation process is employed, three convolutional layers will result in overfitting if no regularisation procedure is used. The inclusion of extra convolutional or dense layers has little effect on the performance of the network, but the introduction of dropout helps to stabilise learning and improve stability.

IV. RESULTS AND DISCUSSION

The Tensor Flow 1.7 framework is utilized in the construction of the network. Following the recording of the activity, the signal is decomposed into 204 points, each of which corresponds to roughly two seconds of movement, with a stride of five points between each point. Reduced window sizes are associated with enhanced classification performance, and in the context of CNNs, the limited structure of the network input data makes the training process easier. The shape of the generated matrix is determined by the number of sensors employed to sample the window: $6N \times 204$ in this case. This has resulted in a significant increase in the quantity of training and testing samples available. It is uneven because the activities have varying execution periods and because different subjects may complete the same activity at various rates, which makes the dataset unbalanced.

For the purpose of evaluating the performance of our classification system, we employ a typical 5-fold cross-validation approach. To separate the accessible datasets, we employ topics rather than windows as a division method. As a result, this prevents overfitting and enhances the generalization of model outputs as a result. In order to produce each fold, an 80/20 split is achieved by separating four people from a group of 19, as mentioned previously.

Through this case study, which is shown in Fig. 3 to Fig. 7 were able to investigate the impact of various hyper parameters and CNN settings on the feature learning capabilities of our model. Regarding feature learning in HAR, this experiment provided an excellent overview of the main elements that determine a CNN ability to learn new features and how these aspects interact with one another. While the results from the first phase of the case study demonstrated that CNNs can perform at least as well as the best HCFs, the

results from the second step demonstrated that CNNs can perform at least as well as the best HCFs. This is why CNNs must be trained before being used, and as a result, they are susceptible to the cold-start problem.

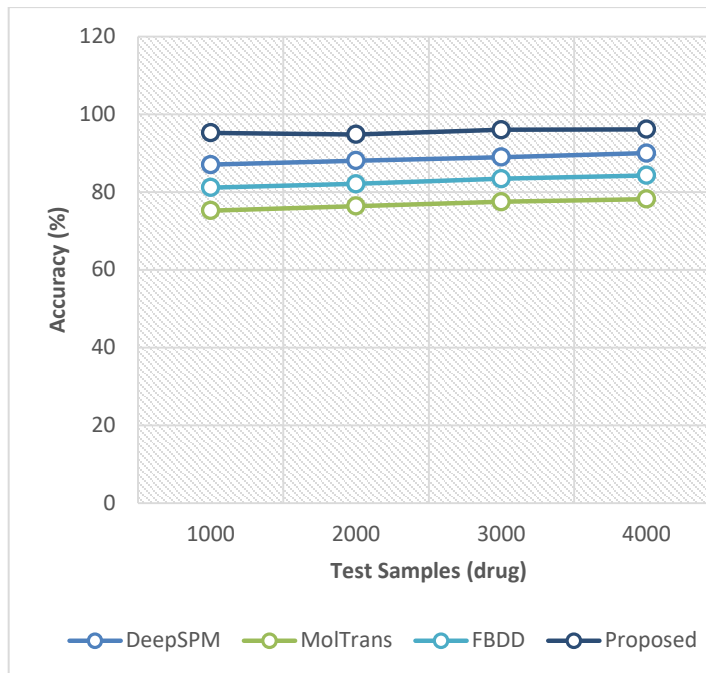


Fig. 3. Accuracy.

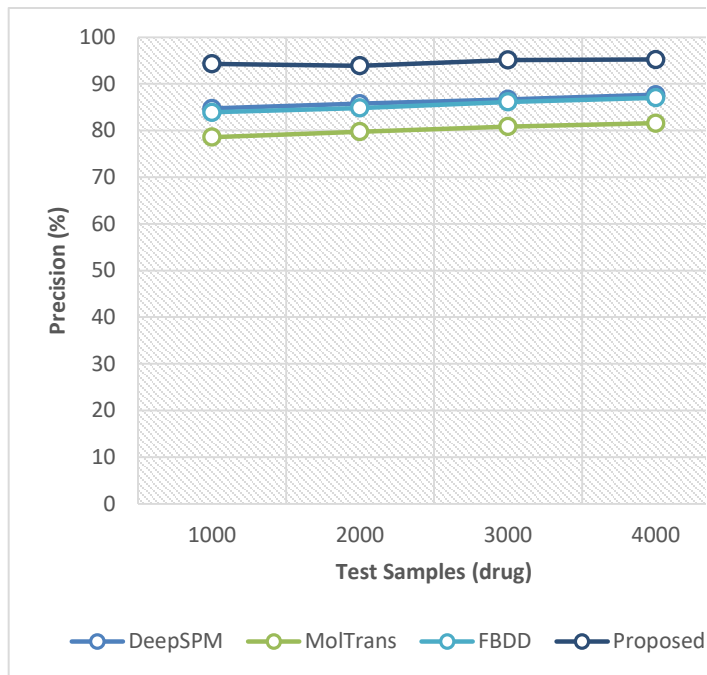


Fig. 4. Precision.

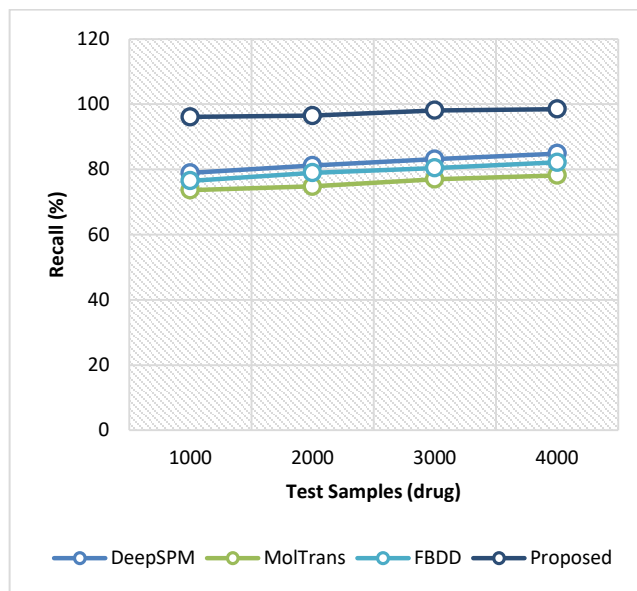


Fig. 5. Recall.

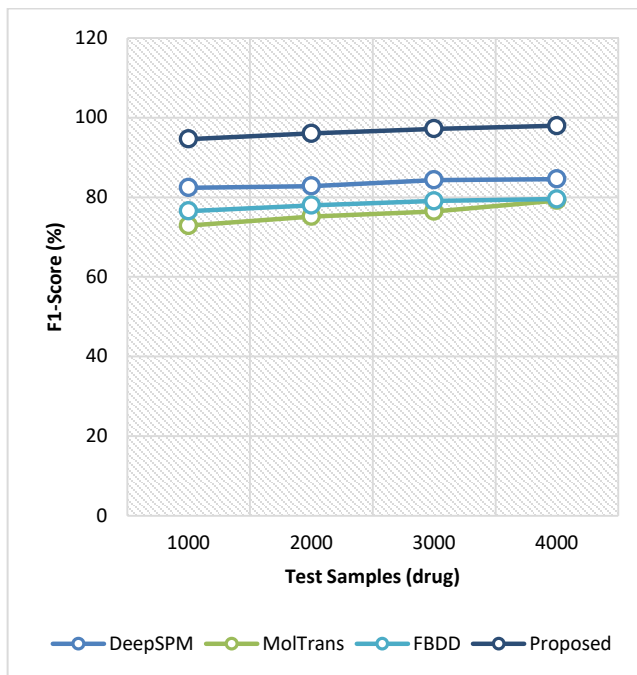


Fig. 6. F1-Measure.

To evaluate CNN feature learning methods for dataset test cases, a pre-trained CNN feature extractor was employed on a real-world dataset to extract features from it. Real-world datasets enable the evaluation of CNN automatic features in a more realistic environment than was previously possible. The problem of dealing with uncontrolled environments was brought to light through realism-based testing.

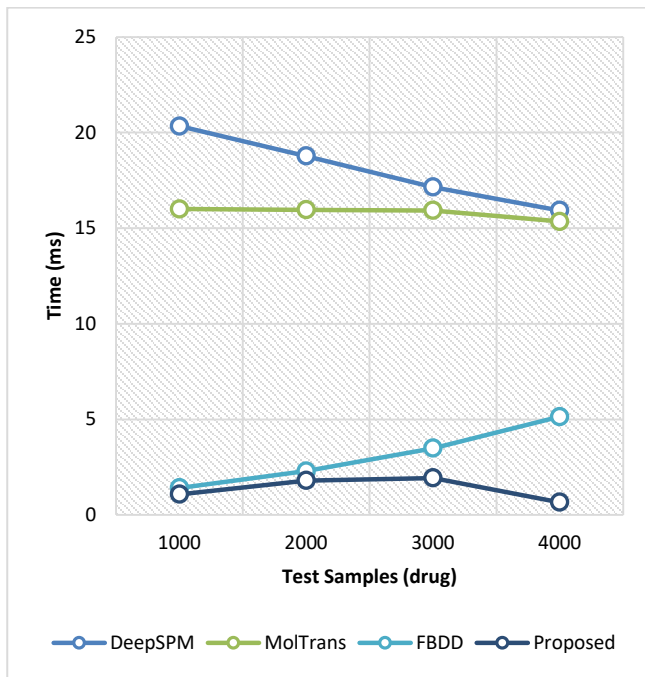


Fig. 7. Computational Time.

Although a larger number of training epochs were required, it was demonstrated that SGD enabled the model to be trained with greater accuracy on the test set, leading to an F-Score of 94% in the more challenging target activities, which included transitions as a NULL class. We were successful in identifying a suitable network architecture that matched our feature learning criteria while also keeping the model complexity under control. The architecture was evaluated using data from a large real-world dataset that was made available to the public.

V. CONCLUSION

This paper presents the construction of an activity recognition model that incorporates both convolutional neural networks (CNNs) and convolutional neural networks (CNNs). This work was primarily intended to demonstrate the usage of a CNN pre-trained feature extractor rather than to provide a comprehensive analysis of the hyper parameters and settings used in the training process. The optimization of models, on the other hand, is subject to several restrictions. When analyzing designs with varied numbers of convolutional layers and convolution kernel sizes, for example, only the ReLU activation function was used to achieve the best results.

Other modes of activation may be investigated in future investigations. In a similar vein, the default Keera's learning rate of 0.001 was employed. The CNN network is used to extract spatial features, whereas the LSTM network is used to learn about time-related information. It is necessary to do a thorough ablation analysis utilising a variety of classical and deep machine learning models in order to determine the most effective HAR solution possible. The CNN technique can be employed for HAR applications because of its high precision of 90.89%.

REFERENCES

- [1] Ramasamy Ramamurthy, S., & Roy, N. (2018). Recent trends in machine learning for human activity recognition—A survey. *Wiley Interdisciplinary Reviews: Data Mining and Knowledge Discovery*, 8(4), e1254.
- [2] Chen, K., Zhang, D., Yao, L., Guo, B., Yu, Z., & Liu, Y. (2021). Deep learning for sensor-based human activity recognition: Overview, challenges, and opportunities. *ACM Computing Surveys (CSUR)*, 54(4), 1-40.
- [3] Nweke, H. F., Teh, Y. W., Al-Garadi, M. A., & Alo, U. R. (2018). Deep learning algorithms for human activity recognition using mobile and wearable sensor networks: State of the art and research challenges. *Expert Systems with Applications*, 105, 233-261.
- [4] Zhang, J., Yin, Z., Chen, P., & Nichele, S. (2020). Emotion recognition using multi-modal data and machine learning techniques: A tutorial and review. *Information Fusion*, 59, 103-126.
- [5] Antar, A. D., Ahmed, M., & Ahad, M. A. R. (2019, May). Challenges in sensor-based human activity recognition and a comparative analysis of benchmark datasets: a review. In *2019 Joint 8th International Conference on Informatics, Electronics & Vision (ICIEV) and 2019 3rd International Conference on Imaging, Vision & Pattern Recognition (icIVPR)* (pp. 134-139). IEEE.
- [6] Rashid, K. M., & Louis, J. (2019). Times-series data augmentation and deep learning for construction equipment activity recognition. *Advanced Engineering Informatics*, 42, 100944.
- [7] Pouyanfar, S., Sadiq, S., Yan, Y., Tian, H., Tao, Y., Reyes, M. P., ... & Iyengar, S. S. (2018). A survey on deep learning: Algorithms, techniques, and applications. *ACM Computing Surveys (CSUR)*, 51(5), 1-36.
- [8] Purwins, H., Li, B., Virtanen, T., Schlüter, J., Chang, S. Y., & Sainath, T. (2019). Deep learning for audio signal processing. *IEEE Journal of Selected Topics in Signal Processing*, 13(2), 206-219.
- [9] Ghosh, S., Das, N., Das, I., & Maulik, U. (2019). Understanding deep learning techniques for image segmentation. *ACM Computing Surveys (CSUR)*, 52(4), 1-35.
- [10] Khalil, R. A., Jones, E., Babar, M. I., Jan, T., Zafar, M. H., & Alhussain, T. (2019). Speech emotion recognition using deep learning techniques: A review. *IEEE Access*, 7, 7327-117345.
- [11] Hassan, M. M., Uddin, M. Z., Mohamed, A., & Almogren, A. (2018). A robust human activity recognition system using smartphone sensors and deep learning. *Future Generation Computer Systems*, 81, 307-313.
- [12] Sundararajan, K., & Woodard, D. L. (2018). Deep learning for biometrics: A survey. *ACM Computing Surveys (CSUR)*, 51(3), 1-34.
- [13] Bulling, A., Blanke, U., & Schiele, B. (2014). A tutorial on human activity recognition using body-worn inertial sensors. *ACM Computing Surveys (CSUR)*, 46(3), 1-33.
- [14] LeCun, Y., Bengio, Y., & Hinton, G. (2015). Deep learning. *nature*, 521(7553), 436-444.
- [15] Ordóñez, F. J., & Roggen, D. (2016). Deep convolutional and lstm recurrent neural networks for multimodal wearable activity recognition. *Sensors*, 16(1), 115.
- [16] Rajaraman, S., Antani, S. K., Poostchi, M., Silamut, K., Hossain, M. A., Maude, R. J., ... & Thoma, G. R. (2018). Pre-trained convolutional neural networks as feature extractors toward improved malaria parasite detection in thin blood smear images. *PeerJ*, 6, e4568.
- [17] Baldominos, A., Cervantes, A., Saez, Y., & Isasi, P. (2019). A comparison of machine learning and deep learning techniques for activity recognition using mobile devices. *Sensors*, 19(3), 521.
- [18] Moya Rueda, F., Grzeszick, R., Fink, G. A., Feldhorst, S., & Ten Hompel, M. (2018, June). Convolutional neural networks for human activity recognition using body-worn sensors. In *Informatics* (Vol. 5, No. 2, p. 26). Multidisciplinary Digital Publishing Institute.
- [19] Saeed, A., Ozcelebi, T., Trajanovski, S., & Lukkien, J. (2018). Learning behavioral context recognition with multi-stream temporal convolutional networks. *arXiv preprint arXiv:1808.08766*.
- [20] Huang, S. J., Gao, W., & Zhou, Z. H. (2018). Fast multi-instance multi-label learning. *IEEE transactions on pattern analysis and machine intelligence*, 41(11), 2614-2627.

Tourist Reviews Sentiment Classification using Deep Learning Techniques: A Case Study in Saudi Arabia

Banan A. Alharbi, Mohammad A. Mezher, Abdullah M. Barakeh
Dept. of Computer Science, Fahad Bin Sultan University, Tabuk, Saudi Arabia

Abstract—Now-a-days, social media sites and travel blogs have become one of the most vital expression sources. Tourists express everything related to their experiences, reviews, and opinions about the place they visited. Moreover, the sentiment classification of tourist reviews on social media sites plays an increasingly important role in tourism growth and development. Accordingly, these reviews are valuable for both new tourists and officials to understand their needs and improve their services based on the assessment of tourists. The tourism industry anywhere also relies heavily on the opinions of former tourists. However, most tourists write their reviews in their local dialect, making sentiment classification more difficult because there are no specific rules to control the writing system. Moreover, there is a gap between Modern Standard Arabic (MSA) and local dialects. One of the most prominent issues in sentiment analysis is that the local dialect lexicon has not seen significant development. Although a few lexicons are available to the public, they are sparse and small. Thus, this paper aims to build a model capable of accurate sentiment classification in the Saudi dialect for Arabic in tourist place reviews using deep learning techniques. Machine learning techniques help classifying these reviews into (positive, negative, and neutral). In this paper, three machine learning algorithms were used, Support -Vector Machine (SVM), Long short-term memory (LSTM), and Recurrent Neural Network (RNN). These algorithms are classified using Google Map data set for tourist places in Saudi Arabia. Performance classification of these algorithms is done using various performance measures such as accuracy, precision, recall and F-score. The results show that the SVM algorithm outperforms the deep learning techniques. The result of SVM was 98%, outperforming the LSTM, and RNN had the same performance of 96%.

Keywords—Sentiment classification; Saudi dialect; support -vector machine; recurrent neural network; long short-term memory

I. INTRODUCTION

Due to the astounding and quick expansion of social networking sites, an increasing number of individuals are sharing their experiences and opinions on various issues, including travel, hotels, physical items, movie reviews, and health. One cannot deny that social media sites play a role in people's daily and social lives. Additionally, they assist tourists in selecting the appropriate destination via their comments on tourist destinations' social media sites, as mentioned by [1].

Moreover, social media sites have gained a significant attraction on the web. These sites have evolved into an indispensable resource for travelers whose decisions are influenced by the reviews and opinions of other travelers. Human emotions and emotional cognition influence purchasing

decisions, travel, and other variables. Online reviews can help researchers and business owners understand tourists' needs and preferences correctly. It was further noted that the tourism industry's primary reliance on the opinions and perceptions of former travelers is universal. They emphasized that [2] the views expressed by tourists in the comments play a role in influencing the choices of other tourists for their travel destinations.

Moreover, travelers frequently desire to know the attractions for which a city they wish to visit is renowned. They research social media sites for recommendations, opinions, and reviews to visit tourist destinations. Given the plethora of information and evaluations, it is difficult for travelers to obtain reliable judgments and select the best hotels, restaurants, and attractions. Many people share their experiences and views spontaneously and more credibly about the tourist places they visit without a financial return. Therefore, it will be challenging for the reader to locate relevant websites when researching, rewriting, and summarizing the facts and viewpoints vital to them.

Consequently, the significance of sentiment classification reduces the time and effort required to extract relevant information for travellers. The sentiment classification process studies people's emotional state and their assessments of a particular topic or their attitudes towards a specific event, and sentiment classification is used in tourism applications, products, shopping and other areas of life. Consumers place greater credence on online reviews, personal recommendations, and comments and thus are more likely to provide product reviews after purchasing. The classification process aims to determine the polarity of the text and determine whether a person feels optimistic about a particular product, negative or neutral. Classifying reviews (positive or negative) is the goal of sentiment classification, and like the use of text, analysis has proven cost-effective. The classification is mainly based on an explained supervised learning approach [3].

As a result, sentiment classification is one of the most active and prosperous research areas in Natural Language Processing (NLP). Many researchers and those interested in this field use deep learning for sentiment classification. Data technologies reduce sentiment classification errors to ensure the highest accuracy on social media [4]. This study aims to develop a model capable of accurate sentiment classification in the Saudi dialect of Arabic by analyzing tourist location reviews using deep learning techniques.

A. Sentiment Classification

Sentiment classification refers to analyzing textual data on social media and extracting people's sentiments about different topics. The sentiment classification also provides a more understanding of people's views on a particular topic. We can observe the sentiment classification in action when determining consumer satisfaction with a specific product based on their input. In addition, we may learn about people's preferences for top attractions through their recommendations on social networking sites and by assessing the quality of hotels through reviews. These reviews can also classify opinions as positive, negative or neutral. Many English, Chinese and other languages have made remarkable progress and are high-performance using sentiment classification [5]. Likewise, as the volume of unstructured data generated by social media grows, the demand for sentiment classification has skyrocketed. There are three different levels of sentiment classification: document level, sentence level, and feature level.

- Document-level: The document is classified by general feeling, either positive, negative or neutral, and the paper is supposed to contain an opinion on one topic.
- Sentence level: At the sentence level, the classification determines whether the opinion in this sentence is positive, negative or neutral.
- Feature level: Feature level makes a more accurate analysis. Instead of looking at the structure of language (documents, paragraphs, sentences, or phrases), it directly looks at the same opinion.

It is also called aspect-based sentiment analysis. This level examines multi-opinionated sentences to determine the attitude towards entities or their aspects by examining the opinion and the entity's purpose or one of its features.

B. Sentiment Classification Techniques

It has developed classification methods in machine learning. There are roughly three classification strategies for sentiment: machine learning, lexicon-based, and hybrid.

- Machine Learning-based approach: Two proposed sets of classification sentiment problems are traditional and deep learning models [6]. Traditional models apply to classic machine learning algorithms: Naïve Bayes (NB) classifier, Maximum Entropy (ME) or SVM. Algorithm inputs also use language features such as N-grams, bi-grams, bag-of-words, parts of speech, or adjectives and adverbs. Consequently, choosing features in traditional models can affect the accuracy of the results. In contrast, sentiment analysis employing deep learning models such as Deep Neural Networks (DNN), Convolutional Neural Networks (CNN), and RNN can get better results than conventional methods. Accordingly, we can address classification problems at the document level, Sentence level, or Aspect or Feature level.
- Lexicon-based approach: this technique was the first to use sentiment analysis [6]. It consists of a set of sentiment terms that are translated and pre-known. It is also divided into two approaches: dictionary-based and

corpus-based. In the first form of sentiment classification, a dictionary of terms is used to locate the first sentiment words, using a synonym and antonym dictionary such as WordNet SentiWordNet. In the second type, the sentiment classification corpus-based does not depend on the dictionary of pre-defined sentiment terminology but on statistical or semantic analysis for the polarity sentiment. The corpus-based uses a technique such as neighbours (k-NN), Conditional Random Field (CRF).

- A hybrid approach is prevalent and confuses both approaches, and sentiment dictionaries play a significant role in most methods [7]. The more effectively the classifier is trained, the easier and better is the future predictions. We can divide text classification methods into supervised and unsupervised learning using machine learning. Conversely, unsupervised learning is used when it is challenging to find classified training documents.

C. Deep Learning

Deep learning is a branch of machine learning as it depends on neural networks that resemble the human brain. Deep learning refers to the deep neural network introduced in 2006 by G.E. Hinton. Accordingly, deep learning can recognize speech, analyse images, and process natural language. Deep learning networks also provide supervised and unsupervised groups. Consequently, many companies have been interested in machine learning in handling big data, and models have been created to analyse big and complex data faster and more accurately [8]. However, there are many networks in deep learning, such as CNN and Deep Belief Network, and there are many benefits for neural networks in vector representation, sentence classification, sentence modelling, and text creation.

D. Models

1) *Long short-term memory model*: LSTM is a developer version of RNN. They were developed to overcome the problems of RNN in the vanishing and exploding gradient. They were introduced by [9]. Consequently, LSTM has achieved great success in various NLP tasks. Accordingly, [10] designed to model temporal sequences and their long-range dependencies more accurately than conventional RNNs of three basic gates: the input gate, the output gate o_t , and the forget gate f_t .

- The input gate controls the amount of information transferred from the input to the current cell.
- Forget gate f_t . This gate decides what information should be thrown away or kept. Data from the previous hidden state and information from the current input are passed through the sigmoid function. Values come out between 0 and 1—the closer to 0 means to forget, and the closer to 1 means to keep.
- The output gate o_t controls the amount of information transferred to the output.

2) *Recurrent neural network model*: RNNs are artificial neural networks that process and use sequential data. In a

conventional neural network, each input and output is treated as independent of the other, which might result in poor performance. Hence, the idea of a repetitive neural network predicts the following word in the sentence based on the previous word. RNNs have the concept of 'memory' that helps them store the states or information of prior inputs to generate the following output of the sequence. In this way, the network can use history to understand the sequential nature of the data. According to this, RNNs have shown great success in many NLP tasks. Mainly concentrating on sequential data applications, such as text classification and speech recognition. On the other hand, RNNs have also shown notable success in image processing.

3) *Support vector machine model*: SVM algorithm is one of the supervised machine learning algorithms used for classification and regression, developed by Vapnik. SVM is used to solve various classification problems, such as the recognition of fonts, images, text classification, and other fields [11]. The concepts used in SVMs, like hyperplane, optimal margin, Kernels, etc. There are two types of SVM: linear classification and non-linear classification. Linear classification: divides the two groups of data linearly. SVM picks the hyperplane with the most significant margin to achieve maximum separation between the two classes. The margin equals the sum of the shortest distances between the separating hyperplane and the closest data point of both categories. Non-linear classification in SVM has been extended using Kernels. Kernels are mathematical functions that transform the data from a given space (known as Input Space) to a new high dimensional space (known as Feature Space) where data can be separated with a linear surface (called hyperplane).

II. RELATED WORK

Social media sites generate vast reviews about travel, products, movies, etc. In addition, social media sites provide a suitable space for people to share their experiences more freely. Today, people are increasingly making their views and experiences available online. Therefore, millions of web pages will appear when you search for any topic online. It is challenging and time-consuming to gain an overall understanding of these reviews. A few reviews may influence an individual's perspective. Accordingly, sentiment classification aims to solve such problems by automatically classifying people's views into negative, positive, and neutral opinions. This makes it an important field of research for consumers, companies and Governments. However, resources are not always available for all areas or languages. While there has been a great deal of study on sentiment classification in English, very few scholars have examined sentiment classification in Arabic, despite the growing number of Arabic speakers.

A. Tourist Place Reviews Sentiment Classification

With the radical change in social lifestyle and people's general decisions, sentiment classification has become the subject of long-term research. A study analyzing sentiment

classification revealed that numerous studies use movie or restaurant reviews as a proxy for sentiment categorisation. [12] stated that traditional sentiment classification methods often require significant human efforts. With the growing volume of web reviews, people have a big problem increasing information. The author in [1] has focused on analyzing and organising unstructured data from social media sites. In light of this, unstructured data from social media has increased the demand for sentiment analysis. The author in [13] explained that sentiment analysis could be at different levels, such as document level, sentence level, and aspect-based. The results of experimental studies [14] also showed that one of the tasks of sentiment classification at the document level is to consider the importance of sentences.

Moreover, as explained by [15], many studies use classification algorithms such as NB, ME, and, particularly, SVM to classify the polarity of reviews. Accordingly, [16] compared two approaches to supervised machine learning methods regarding sentiment classification of reviews between SVM and NB, which was highly accurate. The results indicated that NB outperformed SVM, as the training data set consists of many reviews. The approach of NB has reached a high degree of accuracy compared to SVM.

In addition, [17] compared five machine learning algorithms, K-Nearest Neighbors (KNN), Decision Tree, Artificial Neural Networks (ANNs), Naïve Bayes and SVM are used for the classification of sentiments. These algorithms are analysed on Twitter's dataset, and the performance of these methods has been compared based on different performance metrics such as accuracy, precision, recall and F measure. The results showed that SVM outperforms others and has a higher predictive ability than other algorithms. So, all the metrics, Accuracy, Precision, Recall and F-score, are high in the case of SVM.

The author in [18] compared the accuracy of LSTM and CNN by looking at the different designs of each. The training sample was taken from Booking and TripAdvisor. Thus, the results showed that LSTM neural networks outperform CNN in performance. LSTM produces higher accuracy. They also show that combining convolutional layers with recurrent LSTM layers does not benefit.

The author in [19] suggested a hybrid model using LSTM and a profound CNN model named hybrid CNN-LSTM model. Suggested results showed hybrid CNN-LSTM model outperforms traditional deep learning and machine learning techniques in precision, recall, f-measure, and accuracy. The training sample was IMDB movie and Amazon movie reviews.

The author in [20] has widely explained the importance of online reviews. The authors in [21], [22] have also dealt with the impact of online comments on tourist decision-making. The author in [23] shows the importance of recognizing the impact of online reviews on tourist behaviour. The intensity and effects of internet reviews on users' purchasing behaviour and decision-making have been demonstrated [24], [25]. Furthermore, [26] presented several tourists' satisfaction, while some studies employed internet reviews. Hotel visitors'

satisfaction [27] and feelings about a film [28]. Others also stated that traveller reviews are more up-to-date, entertaining, and trustworthy than those published by travel service providers [29].

B. Deep Learning Sentiment Classification

In recent years, deep learning has become an effective way to solve sentiment classification problems. Consequently, several studies have recommended deep learning-based models for sentiment classification that outperform conventional machine learning models [30]. Many deep learning models include DNN, CNN, and deep Restricted Boltzmann Machine (RBM).

One study suggested CNN for sentiment classification. The sample of training datasets was divided into three groups (movie review data, customer review data, and Stanford Sentiment Treebank data). Experimental results showed that CNN layers contributed to better performance of relatively long texts [31].

Another compared traditional models such as Logistic Regression, SVM, and deep learning models such as CNN and the simple LSTM. The results showed that the larger the data set, the better the deep learning models were than traditional models, as the LSTM results were 95.55% better accurate. The training sample was Amazon reviews [32].

C. Reviews Arabic Language Sentiment Classification

Research has been done on sentiment classification in English. Although Arabic is one of the most widely used languages on social media, few studies have focused on sentiment classification in Arabic. According to statistics Internet World Stats, Arabic is the fourth most commonly used language online after English, Chinese and Spanish [33]. Although Arabic-speaking users have increased online in recent years, sentiment analysis research in Arabic has not yet evolved.

The author in [34] applied the sentiment analysis of Arabic tweets from Twitter. They used unsupervised methods. They examined preprocessing methods of text and similarity to compile algorithms and discussed how they affected the results. Moreover, they used a k-means algorithm. Therefore, the brevity of the language in this context presents a challenge to the likelihood of ambiguity. In this investigation, root-based derivation yielded the best degree of accuracy, as indicated by the findings.

The author in [35] compared two supervised learning algorithms, SVM, and RNN, in terms of ability to face the challenges of Aspect-Based sentiment analysis. The training sample was Arabic hotel reviews. The results showed that the SVM approach outperformed the RNN approach in all tasks in terms of accuracy, but RNN was faster at implementation.

The author in [36] analyse the collected twitter posts in different Arabic dialects and compare the various algorithms. The measurement of performance of different algorithms is evaluated in terms of recall, precision, f-measure, and accuracy. Experimental results showed that unigram gives a higher accuracy of 99.96%, with Passive-Aggressive (PA) or Ridge Regression (RR).

The author in [37] uses two models of deep learning, CNN and LSTM. The training sample was the Arabic Sentiment Tweets Dataset (ASTD) dataset. The best results for an LSTM model. Sayed et al., 2020 used nine supervised machine learning algorithms: namely, Gradient Boosting, Logistic Regression, Ridge Classifier, SVM, Decision Tree, Random Forest, KNN, Multi-layer Perceptron (MLP) and NB. The training data sample on evaluations written in Arabic was manually prepared through hotel evaluations from Booking.com. The Experimental results showed that the Ridge Classifier (RC) appears to have the best performance in accuracy, recall, precision, training time and F1 score.

The author in [38] applied K-means and Hierarchical unsupervised learning approaches. The training sample was sentiment analysis from the tourism website TripAdvisor for Arabic reviews of Saudi hotels. Used clustering, features and preprocessing strategies to find the best models. The results showed that k-means clustering achieved the best accuracy. The author in [39] suggested combining linguistic and statistical features and sentiment classification using a tweets dataset in Arabic. They used three classifiers: SVM, KNN and ME. The results showed that SVM achieved the highest accuracy in the classification.

D. Saudi Dialect for Arabic Review Sentiment Classification

We have been increasingly interested in analyzing Arabic texts on social media sites over the past few years. However, most social media users write their comments in the local dialect of their countries rather than MSA. In addition, some work has been done to build MSA sentiment lexicons. There has been a limitation in building a dialectal Arabic lexicon, especially for the Saudi dialect. This is mainly due to the limitation in the existing natural language processing tools and the resources available for Arabic, which is developed to deal with MSA only.

The author in [5] applied deep learning to sentiment classification Saudi dialect data on Twitter. Deep learning techniques were used to compare LSTM and Bidirectional Long Short-Term Memory (Bi-LSTM) and algorithm SVM. The data sample was from 32,063 tweets. The results showed that deep learning techniques outperform the algorithm SVM. The experimental result of Bi-LSTM was 94% exceeding the LSTM's 91%, while the SVM had the lowest performance of 86.4%.

The author in [40] presented a new sentiment dictionary in the Saudi dialect called the Saudi Dialect Sentiment lexicon (SauDiSenti). The SauDiSenti comprises 4,431 words, a hybrid between MSA and Saudi dialects. They compared SauDiSenti performance to that of AraSenTi. The first experience, which used only positive and negative tweets, showed the first experiment AraSenTi outperformed SauDiSenti in precision, recall, and F measure. The second experiment evaluated SauDiSenti and AraSenTi using positive, negative, and neutral tweets. The results showed that SauDiSenti outperformed AraSenTi for two values because AraSenTi identified most neutral tweets as either positive or negative. Despite the small size of SauDiSenti, they also added promising results in sentiment analysis of the Saudi dialect tweets.

The author in [41] they introduced a system to analyse the tweets of Saudi users on Twitter about Saudi universities. They used two different models suggesting sentiment analysis on Twitter. The first model depends on the use of SVM. The second model is based on using different classifier models. The results showed that SVM outperformed all other classification models.

The author in [42] compared two strategies. The first applied a translation that transforms from dialect to MSA. The second involved the designing of sentiment analysis on the resulting MSA text. Use tweets in the Saudi dialect. Use seven classifiers Logistic Regression, Passive Aggressive, SVM, Perceptron, Multinomial NB, SGD and KNN. The results showed that they proved that applying sentiment analysis techniques yields better results on MSA data than on dialect data.

In addition, there are studies on sentiment classification reviewed in other dialects such as Jordanian, Algerian, Sudanese and Egyptian. The author in [43] studied the effect of five methods of testing features on the performance of the SVM classifier. Sentiment classification was carried out on dialectical Jordanian reviews using an SVM classifier. The feature selection methods are Information Gain (IG), correlation, SVM, Gini Index (GI), and Chi-Square. He integrated some test methods to explore their ability to improve and choose the feature. The results showed that the best performance of the SVM and correlation feature selection methods was produced by combined with the uni-gram model.

The author in [44] compared the results of accurate deep learning models with classic models CNN, LSTM, SVM, and NB. They used two datasets: posts and comments collected from Algerian Facebook pages, and the second was the corpus of Algerian labelled tweets. The results showed that deep learning models are accurate compared to the classical approaches.

The author in [45] used machine learning methods for sentiment classification for text in the Sudanese dialect on Facebook. The Sudanese colloquial has no grammatical or morphological rules, as they have been made clear. Moreover, they used two different classifiers were applied SVM and NB. The results showed that SVM with lemmatisation libraries improved sentiment classification accuracy, as SVM achieved a measurement accuracy of 68.6%, while NB achieved 63.1%.

The author in [46] provided a sentiment analysis system MSA and Egyptian dialect. A different dataset (tweets, product reviews, TV program comments and Hotel reservations) was used. They demonstrated that expanding the polarity lexicon automatically affects sentiment classification. They also showed that exploitation idioms and saying lexicon with a high coverage polarity lexicon have the most significant impact on classification accuracy. Experimental results showed that the SVM classifier indicates high-resolution performance levels.

III. METHODOLOGY

A. Sentiment Classification

Many social media sites have gained tremendous popularity in the tourism and hospitality industry, such as TripAdvisor,

Citysearch, Virtual Tour, Booking, and Foursquare. Consequently, these sites provided space and opportunity for people to express their opinions freely [47]. These reviews written by people across social media sites are a unique opportunity for sentiment analysis. According to this, sentiment classification aims to classify reviews into three (positive, negative, neutral) or more (positive, very positive, very negative, negative, neutral). However, without human intervention, it is difficult for a machine to discern the polarity and strength of a feeling.

B. Pseudocode of Model Sentimental Classification

Sentiment classification for tourism reviews has been accomplished by developing an algorithm called Sentiment_classification. Firstly, text Preprocessing on reviews data & lexicon, cleaning, tokenising, removing stopword, stemming text. Secondly, reviews that have been preprocessed will determine the sentiment polarity using the Saudi Sentiment Lexicon. The polarity values will determine every word in the reviews, and then the value is calculated to know the reviews' sentiment (negative, neutral or positive). We no longer need to manually label sentiments to each review (because there are too many reviews). The dataset that has been processed will be used for sentiment classification with deep learning models.

```
Algorithm.1: Sentimental_Classification
1. Start
2. Load Raw Data
3. Load Saudi Lexicon
4. Text Preprocessing:
5. Raw Data & Lexicon → cleaning text, text tokenisation, removing
   stop word, Stemming, normalisation
6. # Determine Sentiment Polarity of Reviews Dataset
7. Score=0
8. for word in text:
9.     if (word in lexicon_positive)
10.        score = score + lexicon_positive[word]
11. for word in text:
12.     if (word in lexicon_negative):
13.        score = score + lexicon_negative[word]
14. # Calculation of Polarity reviews
15. if (score >0)
16.     polarity = 'positive'
17. elif (score <0)
18.     polarity = 'negative'
19. else
20.     polarity= 'neutral'
21.     return score, polarity
22. Modelling (Reviews Dataset):
23. # Split the Data (with composition Training Data 80%, Testing Data 20%)
24. Classifier ← Training Data
25. Predict Model ← Testing Data
26. # Model is evaluated using its confusion matrix of test data
27. Confusion matrix → Accuracy, Precision, Recall, F1-score
28. End
```

C. Proposed Modification

The flowchart in Fig. 1 shows the methodology followed in this research, which begins with extracting data for Arabic reviews in the Saudi dialect from Google Maps, including 14 cities in Saudi Arabia and 55 different places. After that

processing and cleaning are done for the extracted reviews. The processing process for the lexicon. The polarity of reviews is calculated. Hence, the dataset is ready for classification. Splitting the dataset is used for 80% of training data and 20% of test data. Finally, predict the model and results.

D. Dataset

Dataset is the first step of sentiment classification. The paper aims to classify Arabic reviews of tourist places in the Saudi dialect. According to this, Google Map web scraping was used to collect the dataset containing 22433 reviews and save it in a fixed format CSV [48]. The dataset included 14 cities in Saudi Arabia, thus covering most dialects in Saudi Arabia (Hijazi, Najdi, Northern, Eastern, and Southern). Given the dataset, it turned out that most of the comments were written in Najdi, Hijazi dialect and MSA. Tourist places in every city included museums, archaeological sites, Islamic places, exhibitions, parks, and recreational places. Reviews were automatically classified as positive, negative, and neutral.

E. Text Preprocessing

The text preprocessing process plays a vital role by applying the steps:

- **Cleaning Text:** Removing non-Arabic letters, numbers, punctuation marks, replacing newlines into space, remove characters space from both left and right text.
- **Text Tokenisation:** Divides text into words, for example (يستحق الزيارة منتزه جميل) after the tokenisation process ('جميل', 'منتزه', 'الزيارة', 'يستحق').
- **Removing Stop-word:** non-semantic words are called stop words, such as (ampersand pronouns, prepositions, and nouns). In addition, it does not affect the meaning and overall feeling of the text.
- **Normalisation:** The scientific of replacing some letters with other letters standardises the character forms used in writing. For example, the letters (ا،آ،أ،أا) are replaced by (ا), (ي) is replaced by (ى), (ة) is replaced by (ة), (ء) are replaced by (ئ،ئ) and (ك) is replaced by (گ). Replace some characters that appear more than once with a two-character such as (ممتاااااااا) converted to (ممتاز).
- **Stemming:** Stemming of words is one of the essential steps in text preprocessing; for example: removing suffixes and prefixes from words.
- **Remove Prefixes:** ال، وال، بال، كال، فال، لل
- **Remove Suffixes:** ها، ان، ات، ون، ين، ية، ه، ي

F. Polarity of Reviews

This study used a Lexicon-based method to identify polarity, and evaluations are classified as positive, negative, and neutral, Table I. Although more polarity categories might more precisely define the polarity of the evaluation, the model has been limited to the three categories of positive, negative, and neutral. According to this, the polarity of reviews is determined based on the majority of opinion words. If the number of positive words in the review is more, it will be classified as positive.

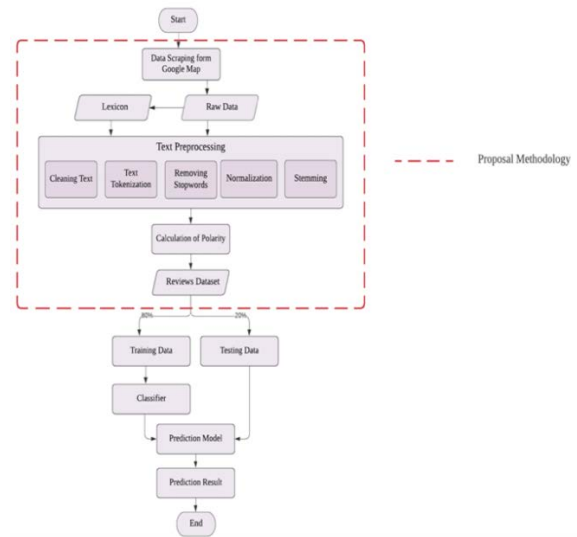


Fig. 1. Main Methodology Flowchart.

Conversely, if the number of negative words is high, the polarity of the review will be rated negatively. If the number of positive and negative words is equal, the review is neutral. In addition, if the opinion word is preceded by negation "مش، غير، لا", then the polarity of that review is reversed. Finally, the polarity of sensations is computed using the remaining poles and gathered in order to forecast the polarity of positive, negative, and neutral emotions. The Fig. 2 shows how the model calculates the scores polarities of sentiments to sentiment score calculation in reviews. Each positive word is greater than 0, and every negative word is smaller than 0. If neutral, it is equal to 0.

TABLE I. SAMPLE OF POSITIVE, NEGATIVE, NEUTRAL REVIEW

حديقة هادئة وجدا خلابة	Positive
لا يستحق الزيارة مبالغ في قيمة التذكرة	Negative
بحيرة جميلة تحتاج إلى صيانة أفضل	Neutral

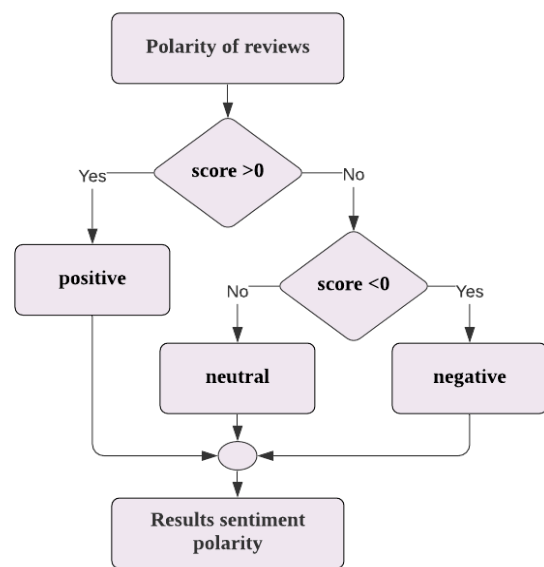


Fig. 2. Polarity of Reviews.

IV. RESULTS AND DISCUSSION

The dataset consists of 68.8% positive, 14.6% negative, 16.6% neutral. Fig. 3 shows the number of reviews for each class.

In the Fig. 3 above, positive reviews are far more than negative and neutral reviews in the dataset. When one category is greater than the other, the data is skewed. Therefore, classification accuracy is not an appropriate statistic to optimise when dealing with imbalanced categories. Thus, accuracy may be artificially relatively high. Majority categories are favoured, while minority categories are not recognized. They result in a biased model for a particular category. Most machine learning algorithms work best when the number of samples in each category is almost equal. There are different ways to balance data: random oversampling and SMOTE. To balance the data, random oversampling was utilised to replicate the minority class samples. It also does not result in any data loss.

Evaluating the model after applying all stages is one of the most critical steps. In addition to this, there are many metrics to assess the quality of deep learning models. This research used two methods to evaluate the confusion matrix, K-Fold Cross-Validation. Indeed, the confusion matrix is one of the most informative performance measures a multi-class learning system can rely on [49]. The most commonly used measure for sentiment classifications is accuracy, precision, recall, and F1-score. They are briefly described below. There it is indicated as True Positives (TP), False Positives (FP), True Negative (TN) and False Negative (FN).

Accuracy is one of the most frequently used metrics. The ratio is expected reviews relative to the total number of reviews correctly. Calculation of the accuracy is made according to the equation.

$$Accuracy = \frac{TP+TN}{TP+FP+FN+TN} \tag{1}$$

The ratio of properly expected positive reviews to the total expected positive reviews. The precision measure is calculated using an equation.

$$Precision = \frac{TP}{TP+FP} \tag{2}$$

It tells what fraction of all positive samples was correctly predicted as positive by the classifier. This value is calculated according to the equation.

$$Recall = \frac{TP}{TP+FN} \tag{3}$$

It combines precision and recall into a single measure. Mathematically it is the harmonic mean of precision and recall.

$$F1\ Score = \frac{2*Precision*Recall}{Precision+Recall} \tag{4}$$

The results shown in Table II proved that some machine learning algorithms outperform each other in terms of accuracy, precision, recall, and F1-score, their ability to classify, discriminate and recognize reviews to be classified into (positive-negative-neutral). It was noted that the SVM model was more accurate than other classification models, with 98% accuracy.

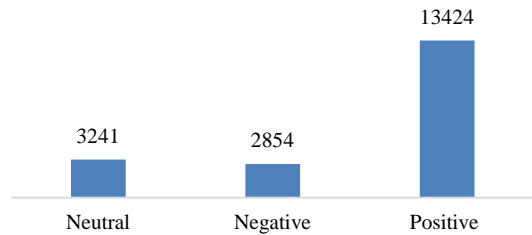


Fig. 3. Number of Reviews for Each Class.

TABLE II. CLASSIFICATION METHODS

Classification Method	Accuracy	Precision	Recall	F1-score
SVM	98%	98.16	98.08	98.09
LSTM	96%	95.63	95.58	95.58
RNN	96%	95.99	95.96	95.95

The Fig. 4 below shows the results of Table II of the models used and compares the best results in terms of accuracy, precision, recall and F1-score. It also shows the superiority of the SVM model over the models used.

K-Fold Cross-Validation is one of the most common ways to validate ML models and bolster and corroborate our findings. The available dataset is partitioned into subsets of approximately equal size. The "K" refers to the number of producing several subsets. The first subset serves as a validation set, and the remaining four subsets serve as a training set.

Table III represents the accuracy obtained by implementing the Stratified K-Fold Cross Validation Technique on the dataset used: 99% accuracy for the SVM model, 94.7% for the LSTM model, and 93.9% for the RNN model. The accuracy obtained by each algorithm is almost similar to our findings from this confusion matrix.

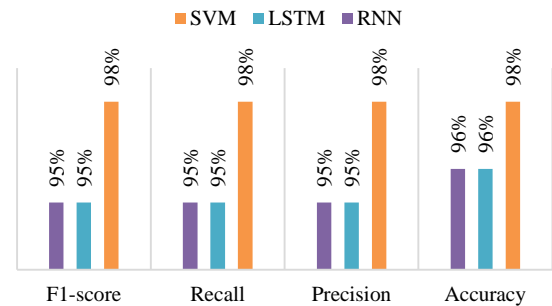


Fig. 4. A Comparison of Various Performance Measurements.

TABLE III. ILLUSTRATION OF K-FOLD CROSS-VALIDATION

Model	1-Fold	2-Fold	3-Fold	4-Fold	5-Fold
SVM	97.5%	98.51%	99.6%	99.7%	99.7%
LSTM	94.2%	95.3%	95.2%	94.5%	94.5%
RNN	90.0%	91.0%	90.5%	99.4%	99.2%

One of the functions of machine learning is the prediction and classification of data, for which we employ one of the many machine learning models. Are tuning the parameters of models so that their behaviour can be adjusted for a given problem. According to this, a parameter can be described as a configuration variable intrinsic to the model. Multiple experiments are performed to obtain the best parameters. Table IV shows the best parametric settings for models used in the paper.

The Fig. 5 shows the training and testing accuracy score of the classifiers used in this paper.

Fig. 5 shows that the highest training accuracy score was 99% for the SVM model, and the training accuracy score for the LSTM and RNN models was 98%. Finally, the highest testing accuracy is 99% of the SVM model. Accordingly, the SVM model outperformed the rest of the classification models, as the training and testing data ratio was the highest among the classifiers; consequently, the SVM model was the best model performing among the models used.

Accordingly, almost all prior research has used machine learning algorithms to classify the Arabic text into positive, neutral or negative. Since this paper focuses on Arabic reviews in the Saudi dialect, Table V below shows the results obtained by other researchers.

TABLE IV. PARAMETRIC SETTINGS FOR THE USED MODELS

Model	Parametric settings
SVM Model	kernel='rbf'
	degree=3
	gamma=0.5
	C=1.0
	class_weight='balanced'
LSTM Model	dropout_rate=0.002
	embed_dim = 32
	hidden_unit = 160
	optimizers = RMSprop
	epochs=50
	batch_size=1500
RNN Model	dropout_rate=0.002
	embed_dim = 32
	hidden_unit = 160
	optimizers = RMSprop
	epochs=50
	batch_size=1500

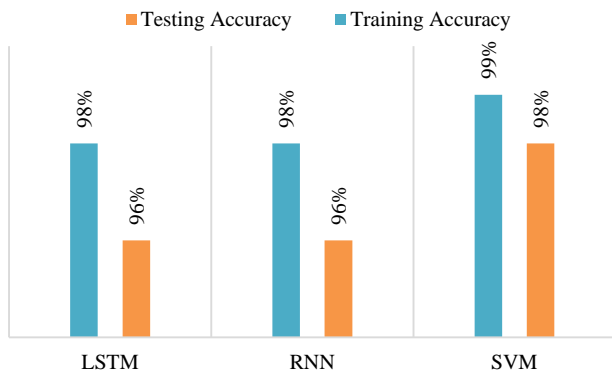


Fig. 5. A Comparison of the Training and Testing Accuracy Scores.

TABLE V. A BENCHMARK OF STUDIES USING SAUDI DIALECT DATASETS

Paper Name	Model Name	Accuracy
Sentiment Analysis of Saudi Dialect Using Deep Learning Techniques [5].	Bi-LSTM	94%
Arabic tweets sentiment analysis – a hybrid scheme [50].	SVM	84%
SDCT: Multi-Dialects Corpus Classification for Saudi Tweets [51].	SGC and LSVM	91.5%
Effect of Saudi dialect preprocessing on Arabic sentiment analysis [52].	KNN	73.3%
Sentiment Analysis of Twitter Data for Saudi Universities [41].	SVM	93.5%
Tourist Reviews Sentiment Classification Using Deep learning Techniqnes: A Case Study in Saudi Arabia	SVM	98%

Table V shows that all previous studies dealt with the problem of classifying reviews in the Saudi dialect. It also shows that the highest accuracy was 94 for the model Bi-LSTM [5]. Previous studies used the same models used in this paper with varying degrees of accuracy, and that is naturally due to how they processed the data. In this paper, we compared the three models after processing the dataset to see which model gives the highest accuracy results in addressing the problem of sentiment classification in the Saudi dialect. We noticed that SVM gave the best results in different places such as accuracy, precision, recall and F1-score. In addition, although the dataset used in this paper was very poor compared to previous research, the study achieved good results. Most prior research has shown that Twitter, as well as Amazon and Tripadvisor, is the most often utilized dataset source in sentiment categorization.

V. CONCLUSION

There is continued growth in tourists' search for online tourist services. This has led to an increase in the volume of online reviews, but manual reviews are time-consuming and useless. Reading a few reviews provides an incomplete understanding. Accordingly, this paper aimed to build a model capable of accurately sentiment classification in the Saudi dialect for Arabic review in the tourist place reviews using deep learning techniques. A Saudi dialect lexicon was created. The created lexicon was used to classify web scraping reviews from Google Map.

The classification of reviews was limited to (positive, negative, and neutral). This article has also provided: a summary of how-to sentiment categorization. The second section of the study is a literature survey on machine learning approaches. Thirdly, the study introduced three classification algorithms: SVM, LSTM, and RNN. The proposed algorithms' performance was measured and compared through performance metrics such as accuracy, precision, recall, and F1-score. The results showed that SVM achieved the highest classification accuracy of 98%, outperforming RNN and LSTM. All the metrics: Accuracy, Precision, Recall and F1-score high in case of SVM.

Future study will entail locating the optimal method to categorise the Saudi tone with greater precision and gathering

additional tourism ratings to expand the dataset. In addition, more classifications are needed than positive, negative, or neutral as they do not provide sufficient information about the reaction given by people and classify phrases with different emotions such as sadness, neutral, worry, love, fun, hate, happiness, and anger. This would help extract the person's natural feelings and hope to expand our lexicon by adding more slang terms for the Saudi dialect.

REFERENCES

- [1] Ain, Q.T., Ali, M., Riaz, A., Noureen, A., Kamran, M., Hayat, B., & Rehman, A.U. (2017). Sentiment Analysis Using Deep Learning Techniques: A Review. *International Journal of Advanced Computer Science and Applications*, 8.
- [2] Asghar, M.Z., Kundi, F.M., Ahmad, S., Khan, A., & Saddozai, F.K. (2018). T-SAF: Twitter sentiment analysis framework using a hybrid classification scheme. *Expert Syst. J. Knowl. Eng.*, 35.
- [3] Humphreys, A., & Wang, R.J. (2018). Automated Text Analysis for Consumer Research. *Journal of Consumer Research*, 44, 1274-1306.
- [4] Singh, J., Singh, G., & Singh, R. (2016). A review of sentiment analysis techniques for opinionated web text. *CSI Transactions on ICT*, 4, 241-247.
- [5] Alahmary, R.M., Al-Dossari, H., & Emam, A.Z. (2019). Sentiment Analysis of Saudi Dialect Using Deep Learning Techniques. 2019 International Conference on Electronics, Information, and Communication (ICEIC), 1-6.
- [6] Medhat, W., Hassan, A.H., & Korashy, H. (2014). Sentiment analysis algorithms and applications: A survey. *Ain Shams Engineering Journal*, 5, 1093-1113.
- [7] Pandey, A.C., Rajpoot, D.S., & Saraswat, M. (2017). Twitter sentiment analysis using hybrid cuckoo search method. *Inf. Process. Manag.*, 53, 764-779.
- [8] Chen, W., Xu, Z., Zheng, X., Yu, Q., & Luo, Y. (2020). Research on Sentiment Classification of Online Travel Review Text. *Applied Sciences*, 10, 5275.
- [9] Hochreiter, S., & Schmidhuber, J. (1997). Long Short-Term Memory. *Neural Computation*, 9, 1735-1780.
- [10] Sak, H., Senior, A.W., & Beaufays, F. (2014). Long Short-Term Memory Based Recurrent Neural Network Architectures for Large Vocabulary Speech Recognition. *ArXiv*, abs/1402.1128.
- [11] Mustafa Abdullah, D., & Mohsin Abdulazeez, A. (2021). Machine Learning Applications based on SVM Classification A Review.
- [12] Guan, Z., Chen, L., Zhao, W., Zheng, Y., Tan, S., & Cai, D. (2016). Weakly-Supervised Deep Learning for Customer Review Sentiment Classification. *IJCAI*.
- [13] Rezapour, M. (2020). Sentiment classification of skewed shoppers' reviews using machine learning techniques, examining the textual features.
- [14] Choi, G., Oh, S., & Kim, H. (2020). Improving Document-Level Sentiment Classification Using Importance of Sentences. *Entropy*, 22.
- [15] Catal, C., & Nangir, M. (2017). A sentiment classification model based on multiple classifiers. *Appl. Soft Comput.*, 50, 135-141.
- [16] [16] Wawre, S.V., & Deshmukh, S.N. (2016). Sentiment Classification using Machine Learning Techniques.
- [17] Godara, N., & Kumar, S. (2019). Opinion Mining using Machine Learning Techniques. *International Journal of Engineering and Advanced Technology*, 9(2).
- [18] Martin, C. A., Torres, J. M., Aguilar, R. M. & Diaz, S. (2018). Using Deep Learning to Predict Sentiments: Case Study in Tourism. *Complexity*, 2018. DOI: <https://doi.org/10.1155/2018/7408431>.
- [19] Rehman, A.U., Malik, A.K., Raza, B., & Ali, W. (2019). A Hybrid CNN-LSTM Model for Improving Accuracy of Movie Reviews Sentiment Analysis. *Multimedia Tools and Applications*, 1-17.
- [20] Litvin, S.W., Goldsmith, R.E., & Pan, B. (2008). Electronic word-of-mouth in hospitality and tourism management. *Tourism Management*, 29, 458-468.
- [21] Camilleri, A.R. (2017). The Presentation Format of Review Score Information Influences Consumer Preferences through the Attribution of Outlier Reviews. *ERN: Marketing (Including Charities & the Private Sector) (Sub-Topic)*.
- [22] Yang, Y., Park, S., & Hu, X. (2018). Electronic word of mouth and hotel performance: A meta-analysis. *Tourism Management*.
- [23] Ernst, D., & Dolnicar, S. (2018). How to Avoid Random Market Segmentation Solutions. *Journal of Travel Research*, 57, 69 - 82.
- [24] Park, D., Kim, S., & Han, I. (2007). The Effects of Consumer Knowledge on Message Processing of Electronic Word of Mouth via Online Consumer Reviews. *ECIS*.
- [25] Gursoy, D. (2019). A critical review of determinants of information search behavior and utilization of online reviews in decision making process (invited paper for 'luminaries' special issue of International Journal of Hospitality Management). *International Journal of Hospitality Management*.
- [26] Xiang, Z., Du, Q., Ma, Y., & Fan, W. (2017). A comparative analysis of major online review platforms: Implications for social media analytics in hospitality and tourism. *Tourism Management*, 58, 51-65.
- [27] Crotts, J.C., Mason, P., & Davis, B. (2009). Measuring Guest Satisfaction and Competitive Position in the Hospitality and Tourism Industry. *Journal of Travel Research*, 48, 139 - 151.
- [28] Mohamed Ali, N., El Hamid, M.M., & Youssif, A.A. (2019). SENTIMENT ANALYSIS FOR MOVIES REVIEWS DATASET USING DEEP LEARNING MODELS. *International Journal of Data Mining & Knowledge Management Process*.
- [29] Gretzel, U., Kyung, Y., & Melanie, P. (2007). "Online Travel Reviews Study: Role and Impact of Online Travel Reviews." *Laboratory for Intelligent Systems in Tourism*, Texas A&M University.
- [30] Abdi, A., Shamsuddin, S.M., Hasan, S., & Piran, J. (2019). Deep learning-based sentiment classification of evaluative text based on multi-feature fusion. *Inf. Process. Manag.*, 56, 1245-1259.
- [31] Kim, H., & Jeong, Y. (2019). Sentiment Classification Using Convolutional Neural Networks. *Applied Sciences*.
- [32] Katić, T., & Milićević, N. (2018, September). Comparing sentiment analysis and document representation methods of amazon reviews. In *2018 IEEE 16th International Symposium on Intelligent Systems and Informatics (SISY)* (pp. 000283-000286). *IEEE*.
- [33] Oueslati, O., Cambria, E., Hajhmid, M.B., & Ounelli, H. (2020). A review of sentiment analysis research in Arabic language. *ArXiv*, abs/2005.12240.
- [34] Abuaiadah, D., Rajendran, D., & Jarrar, M. (2017). Clustering Arabic Tweets for Sentiment Analysis. *2017 IEEE/ACS 14th International Conference on Computer Systems and Applications (AICCSA)*, 449-456.
- [35] Al-Smadi, M., Qawasmeh, O., Al-Ayyoub, M., Jararweh, Y., & Gupta, B.B. (2018). Deep Recurrent neural network vs. support vector machine for aspect-based sentiment analysis of Arabic hotels' reviews. *J. Comput. Sci.*, 27, 386-393.
- [36] Gamal, D., Alfonse, M., El-Horbaty, E.M., & Salem, A.M. (2019). Implementation of Machine Learning Algorithms in Arabic Sentiment Analysis Using N-Gram Features. *Procedia Computer Science*.
- [37] Heikal, M., Torki, M., & El-Makky, N.M. (2018). Sentiment Analysis of Arabic Tweets using Deep Learning. *ACLING*.
- [38] Alosaimi, S., Alharthi, M.A., Alghamdi, K.K., Alsubait, T., & Alqurashi, T. (2020). Sentiment Analysis of Arabic Reviews for Saudi Hotels Using Unsupervised Machine Learning. *Journal of Computer Science*, 16, 1258-1267.
- [39] AL-Jumaili, A. S. (2020). A Hybrid Method of Linguistic and Statistical Features for Arabic Sentiment Analysis. *Baghdad Science Journal*, 17(1 (Suppl.)), 0385-0385.
- [40] Al-Thubaity, A.O., Alqahtani, Q., & Aljandal, A. (2018). Sentiment lexicon for sentiment analysis of Saudi dialect tweets. *ACLING*.
- [41] Alraily, M., & Shahin, O.R. (2020). Sentiment Analysis of Twitter Data for Saudi Universities. *International Journal of Machine Learning and Computing*, 10, 18-24.
- [42] Rizkallah, S., Atiya, A.F., Mahgoub, H.E., & Heragy, M. (2018). Dialect Versus MSA Sentiment Analysis. *AMLTA*.

- [43] Al-Harbi, O. (2019). A Comparative Study of Feature Selection Methods for Dialectal Arabic Sentiment Classification Using Support Vector Machine. ArXiv, abs/1902.06242.
- [44] Moudjari, L., & Akli-Astouati, K. (2020). An Experimental Study on Sentiment Classification of Algerian Dialect Texts. KES.
- [45] Heamida, I., S, Ahmed, E., S., Mohamed, M., N., Salih, A., A. (2020). Applying Sentiment Analysis on Arabic comments in Sudanese Dialect. International Journal of Computer Science Trends and Technology (IJCT) – Volume 8 Issue 3, May-Jun 2020.
- [46] Ibrahim, H.S., Abdou, S., & Gheith, M.H. (2015). Sentiment Analysis For Modern Standard Arabic And Colloquial. ArXiv, abs/1505.03105.
- [47] Zhang, Y., Sun, M., Ren, Y., & Shen, J. (2020). Sentiment Analysis of Sina Weibo Users Under the Impact of Super Typhoon Lekima Using Natural Language Processing Tools: A Multi-Tags Case Study. Procedia Computer Science, 174, 478-490.
- [48] <https://github.com/Banan6/Dataset-Tourist-places-reviews>.
- [49] Koço, S., & Capponi, C. (2013). On multi-class classification through the minimization of the confusion matrix norm. ACML.
- [50] Aldayel, H. K., & Azmi, A. M. (2016). Arabic tweets sentiment analysis—a hybrid scheme. Journal of Information Science, 42(6), 782-797.
- [51] Bayazed, A., Torabah, O., AlSulami, R., Alahmadi, D., Babour, A., & Saeedi, K. (2020). SDCT: Multi-Dialects Corpus Classification for Saudi Tweets. methodology, 11(11).
- [52] Al-Harbi, W. A., & Emam, A. (2015). Effect of Saudi dialect preprocessing on Arabic sentiment analysis. International Journal of Advanced Computer Technology, 4(6), 91-99.

An Outlier Detection and Feature Ranking based Ensemble Learning for ECG Analysis

Venkata Anuhya Ardeti¹

Research Scholar

Dept. of ECM, Koneru Lakshmaiah Education Foundation
Vaddeswaram, Andhra Pradesh, India

Venkata Ratnam Kolluru²

Associate Professor

Dept. of ECM, Koneru Lakshmaiah Education Foundation
Vaddeswaram, Andhra Pradesh, India

George Tom Varghese³

Associate Professor

Dept. of EIE, St. Joseph's College of Engineering and
Technology, Palai, Kottayam, Kerala, India

Rajesh Kumar Patjoshi⁴

Associate Professor

Dept. of ECE, National Institute of Science and Technology
Berhampur, Odisha, India

Abstract—Automated classification of each heartbeat class from the ECG signal is important to diagnose cardiovascular diseases (CVDs) more quickly. ECG data acquired from the real-time or clinical databases contains exceptional values or extreme values called outliers. The separation and removal of outliers is very much useful for improving the data quality. The presence of outliers will influence the results of machine learning (ML) methods such as classification and regression. Outlier identification and removal plays a significant role in this area of research and is a part of signal denoising. Also, most of the traditional ECG-signal processing methods are facing the difficulty in finding the essential key features of recorded signal. In this work, an extreme outlier detection technique known as improved inter quartile range (IIQR) filtering method is used to find the outliers of the signal for the feature ranking process. In addition, an optimized random forest (ORF) based heterogenous ensemble classification model is proposed to improve the true positive and runtime on the ECG data. The classification of each heartbeat type is classified with majority voting technique. Ensemble learning and majority voting rule is used to enhance the accuracy of heart disease prediction. The proposed feature ranking based ORF ensemble classification model (LR + SVM + ORF + XGBoost + KNN) is evaluated on the MITBIH arrhythmia database and produces an overall accuracy of 99.45% which significantly outperforms the state-of-the-art methods such as, (LR + SVM + RF + XGBoost + KNN) with 96.17% accuracy, ensemble deep learning accuracy of 95.81% and ensemble SVM accuracy of 94.47%.

Keywords—Feature ranking; improved inter quartile range; majority voting; outlier detection; optimized random forest

I. INTRODUCTION

World health organization (WHO) reported that globally cardiovascular diseases (CVDs) are the leading cause of death, having a significant impact on the nation's financial and health-care systems. The people residing in low-and middle-income countries are most affected with CVDs due to lack of access to effective and equitable healthcare services, resulting the increased mortality rate at a younger age [1]. An electrocardiogram (ECG) is a non-invasive tool for detecting CVDs that produces reliable findings with affordable cost. But

the beat-by-beat analysis of ECG waveform data manually is tedious, inaccurate, and overwhelming [2]. So, efficient, and precise automated methods for beat classification have gotten significant interest recently. Due to the enormous data quantity and sparseness of medical data, obtaining an essential feature set for classification problems is becoming increasingly difficult. The performance of most classifiers is improved by eliminating the irrelevant or redundant features [3, 4]. Feature selection helps to avoid overfitting and high dimensionality problems in machine learning by reducing the number of features in the model and tries to optimize the model performance [5]. Most conventional classification methods are independent of dynamic feature selection due to large data size and high dimensionality. Feature selection through ranking tries to reduce the computational complexity of the model by compromising the classifier performance [6]. ECG “feature ranking and classification” are the significant tasks to medical and scientific researchers due to its higher-dimension feature space and small sample size. Existing techniques reviewed in the literature concentrates on using single base classifiers and independent of feature ranking process for feature selection. These models are limited to small data size and suffer with high dimensional feature space.

In this study, an extreme level outlier detection filtering approach is proposed for the detection of outliers from the ECG data taken from MITBIH Arrhythmia dataset [7]. The proposed outlier technique is an improvement to the traditional inter-quartile range outlier detection method [8, 9]. The extreme level outliers are removed to improve the error rate in the classification. After filtering, a hybrid kernel-based feature selection approach is developed to find the ranks of the features. The features with highest ranks having highest probability are considered for classification and the features with lowest ranks are neglected. These optimal set of features are used to predict the abnormality using classification model. In this research, we have developed an ensemble learning model involves five base classifiers with majority voting mechanism. The proposed ensemble method outperforms the state-of-the-art base classification techniques with an accuracy of 99.45%.

The rest of the paper is organized as follows: Section 2 gives a comprehensive review on various feature extraction and classification techniques reported in the literature. Section 3 discusses the proposed extreme level outlier detection-based hybrid random forest ensemble classification model. This section is divided into four subsections, where Section 3.1 deals with the ECG dataset used for training and testing the model. Section 3.2 explains the extreme outlier detection-based filtering approach used to find the outliers present in the data, while Section 3.3 describes the enhanced entropy-based feature ranking process, and Section 3.4 discusses the proposed optimized random forest ensemble learning model to classify the individual classes of ECG heartbeats. Section 4 report the results and discussions obtained for proposed ensemble classification model. Finally, the conclusions are drawn in Section 5.

II. MOTIVATION TOWARDS ENSEMBLE LEARNING

High dimensional biomedical data includes large amount of redundant and irrelevant features. If all the features are considered of equal importance, then the accuracy, time and spatial complexity of the model can be severely impacted. Hence, feature selection is considered as a significant step in the diagnosis of diseases based on high-dimensional biomedical data. The idea behind feature selection is to select an appropriate feature subset [10] which will act as a suitable foundation for future classification. It enhances the generalization capability of the prediction model, optimizes the homogeneity of the prediction algorithm, improves the computational performance, and avoid overfitting.

Feature selection algorithms are categorized into three types i.e., filters, wrappers, and embedded methods. Filter methods evaluate each feature independently of the classifier, rank the features according to some evaluation criterion and select the best ones [11]. This evaluation can be performed by using entropy for instance [12]. Wrappers methods evaluate the classifier's performance on various subsets of features and select the subset with maximum performance. These approaches are slower than filter methods and are dependent on the classifier used. Furthermore, feature subset selection is an NP-hard process that requires significant computation time and memory [13]. Genetic algorithm, Random search and greedy stepwise are some traditional algorithms used for feature subset selection. Embedded approaches on the other hand select the features during the learning process like artificial neural networks do [14]. Some studies on the other hand, applied various dimensionality reduction techniques on high dimensional database to diminish the size of the feature space. Most popular techniques such as principal component analysis (PCA) [15], singular value decomposition (SVD) [16] and linear discriminant analysis (LDA) [17] are used for biometric authentication applications.

The optimized feature set is given as input to the classifier to recognize the information about cardiac diseases from ECG. Abnormal classification has become a valuable and promising technique for early assessment of arrhythmia. Mohebbanazz et al., [18] proposed an optimized decision tree (DT) and adaptive boosted optimized decision tree method for classification of six types of ECG beats and evaluated the

performance of the model on MITBIH arrhythmia database achieved an effective accuracy of 98.77% compared to state-of-the-art techniques. [19] introduced a time-efficient, reliable, and low-complexity resource-saving architecture with random forest (RF) classifier to classify two major types of arrhythmias such as supraventricular ectopic beats ventricular ectopic beats (VEB) and (SVEB). Classification performance of the model reaches to the f1 scores of 81.05% for SVEB and 97.07% for VEB. Another popular classifier known as, Support Vector Machine (SVM), [20] is a linear classifier that separates the classes linearly by creating a hyperplane from high-dimensional space. It captures the non-linear relationships of the ECG signal, detects the heartbeats, and classifies the data as normal/abnormal with high accuracy. Researchers proposed several SVM based classification techniques to detect arrhythmias in literature which involves Multi-class SVM [21], SVM with NN [22]. However, due to its high dimensionality space, it suffers with computational constraints. An efficient real-time time series cardiac disease prone weight (CDPW) Naive Bayes classification technique is implemented in [23] that estimate the posterior probability of different features using fuzzy rule and measures the CDPW value. The model performance was evaluated using 15000 records of real-time ECG data, and greater precision values were produced with less time complexity. The author in [24] employed K-Nearest Neighbour classifier on MITBIH arrhythmia database to classify five types of ECG beats and attained an accuracy of 98.40% for isolating the signals. A robust extreme gradient boosting technique is utilized in [25] to classify five ECG beat classes from both MITBIH data and self-collected single-lead wearable ECG dataset. The developed model outperforms the traditional models with an accuracy of 99.14% on MITDB and 98.68% on wearable ECG dataset. Ahmed et al., in [26] employed artificial neural network (ANN) to classify the ECG heartbeats from two imbalanced datasets MITBIH arrhythmia and PTB databases. They focus on penalising the loss value of ANN by assigning the class weights which outperforms the state-of-the-techniques. However, researchers have demonstrated that the ensemble system can increase the performance of a base classifier.

Motivated by the development of several ML models, and a bid to improve accuracy, we propose a heterogeneous ensemble learning framework. Ensemble learning is the process of integrating various learners together to improve the stability and prediction ability of the classification model. It has been successfully applied in solving various machine learning problems includes feature selection, classification, and prediction. Fig. 1 shows a typical block diagram of an ensemble classification model, which includes three primary blocks: training datasets, base classifiers, and a combiner. In recent studies, researchers have proved that performance of the base classifier can be improved with ensemble classification method. Jose et al., [27] proposed random forest ensemble classification technique to diagnose cardiac arrhythmia. In this model the more informative features were selected using ranking criteria on training dataset. The performance of the learning model is evaluated on MITBIH arrhythmia database and obtained an accuracy of 96.14% and f1-score of 97.7%, 90.5% and 73% for normal, ventricular and

supraventricular beats. An ensemble of random forest and support vector machine is implemented in [28], to classify five types of cardiac arrhythmia's and obtained an accuracy of 98.21%. Recent advances in technology proposed deep learning-based ensemble classification technique for improved cardiac diagnosis [29]. Experimentation is carried out on PTBDB and MITBIH database and found an accuracy, F1 score and area under curve (AUC) of 0.98, 0.93 and 0.92 for MITBIH datasets and 0.99, 0.986 and 0.995 for PTB dataset. A hybrid heterogeneous ensemble classification model for the prediction of heart disease is proposed in [30]. The performance of the model is evaluated on the Kaggle dataset and reports 98% accuracy which outperforms the weak learners. As many ensemble classification techniques reported in the literature, developing a robust ensemble learning model with lowest error and greater accuracy is still becoming a challenging task.

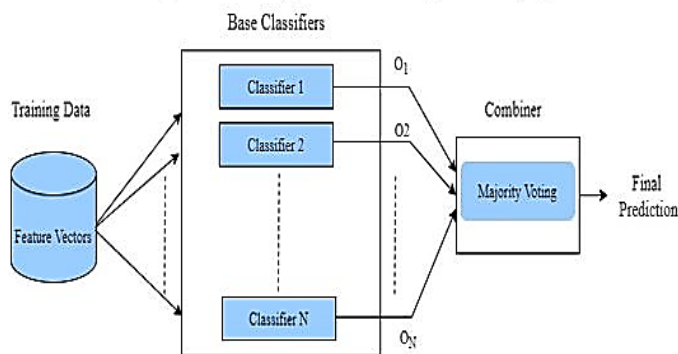


Fig. 1. Architecture of Ensemble Learning System.

III. EXTREME LEVEL OUTLIER DETECTION AND ORF BASED ENSEMBLE CLASSIFICATION

The outlier detection-based ensemble classification framework is shown in Fig. 2. It includes the following stages: 1) Data Acquisition, 2) Preprocessing, 3) Feature Ranking and 4) Classification.

A. Data Acquisition

The ECG data used for this proposed framework is taken from the clinical pre-recorded MITBIH Arrhythmia database. It consists of 48 ECG recordings, each spanning 30 minutes and captured at 360 Hz per channel with an 11-b resolution and a 10-mV range. In this work, we have evaluated the proposed model on two datasets i.e., dataset1 and dataset2. The dataset1 is the DWT processed training data taken from [24] having the specified features of amplitude, RR intervals, Speed, etc., and dataset2 consists of raw DWT processed coefficients of MITBIH arrhythmia dataset. Most recent studies concentrated on the evaluation of four classes such as N (Normal), S (Supraventricular), V (Ventricular) and F (Fusion) beats. In this work, we focus on detecting the N (Normal Synus Rhythm), and three arrhythmia's such as B (Ventricular Bigeminy), T (Ventricular Trigeminy) and VT (Ventricular Tachycardia). The waveform representation of ventricular bigeminy, ventricular tachycardia and ventricular trigemini is shown in Fig. 3(a), 3(b) and 3(c), respectively.

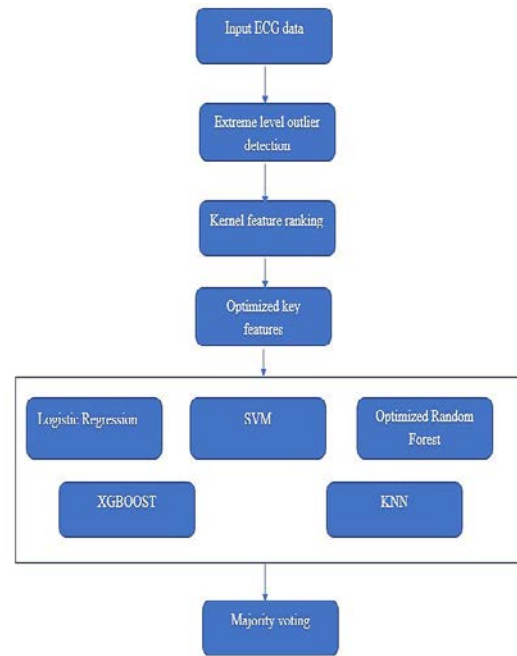


Fig. 2. Framework for Extreme Outlier Detection-and ORF based Heterogenous Ensemble Learning.

B. Data Preprocessing

Data preprocessing is the foremost step before implementing any machine learning technique. It improves the quality of data and makes it useful for modelling. The outlier technique used in this model is extreme value outlier detection. In this approach, the extreme level outliers are removed to improve the error rate in the classification problem. This approach is an extension to the traditional quartile-based filtering approach. The mathematical equation for finding the outliers is represented as follows:

At first, the data is sorted in ascending and split into three quartiles,

$$A[] = \text{SortedAttIndices}(); \quad (1)$$

The 25th, 50th and 75th percentile of data represented in three quartiles in the form of $\lambda_1, \lambda_2, \lambda_3$, and is represented as,

$$\lambda_1 = V(F(|A|/4)); \quad (2)$$

$$\lambda_2 = (V(F(|A|/2) + V(F(|A|/2+1))) / 2; \quad (3)$$

$$\lambda_3 = (V(F(|A| - |A|/4 - 1)) + V(F(|A| - |A|/4))) / 2; \quad (4)$$

Inter Quartile Range (IQR) between the first and third quartiles can be calculated as,

$$\theta = \lambda_3 - \lambda_1; \quad (5)$$

The upper and lower extreme values of the outliers can be detected using,

$$UE[] = \lambda_3 + \eta \cdot \log(\Gamma\theta) \quad (6)$$

$$LE[] = \lambda_1 - \eta \cdot \log(\Gamma\theta) \quad (7)$$



Fig.3(a). Wave representation for ECG signal record 105 of MITDB representing Bigeminy condition.



Fig.3(b). Wave representation for ECG signal record 106 of MITDB representing ventricular tachycardia condition.

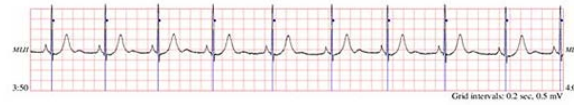


Fig.3(c). Wave representation for ECG signal record 106 of MITDB representing ventricular trigeminy condition.

Fig. 3. Waveform Representation of Bigeminy, Ventricular Tachycardia and Ventricular Trigeminy Conditions.

$$\Gamma(v/2, x/2) = \int_x^{\infty} r^{v-1} \cdot e^{-r} dr \quad (8)$$

$$U_{Outlier} = \lambda_3 + \eta \cdot \max(\Gamma(\lambda_3 + \lambda_1, 9)), \log(\Gamma\theta) \quad (9)$$

$$L_{Outlier} = \lambda_3 - \eta \cdot \max(\Gamma(\lambda_3 + \lambda_1, 9)), \log(\Gamma\theta) \quad (10)$$

C. Feature Ranking

After filtering approach, feature rankings are evaluated for better classification accuracy in the machine learning algorithms (e.g., support vector machines, logistic regression, Naive Bayes, random forest and artificial neural networks). For each feature, the usual technique of calculation is to estimate the distribution mean and standard deviation. Feature selection is a technique of eliminating redundant and nonessential data from the dataset discovering those features from those which have a significant effect on the outcome (e.g. higher accuracy in learning, lower computational cost, and better model interpretability).

In the proposed feature selection approach, an advanced kernel estimator is used to improve the hyper-parameters of the algorithm. The kernel estimator calculates the correlation values of each individual feature corresponding to the input dataset. In the proposed model, the hyperparameters were initialized using the kernel estimator and probabilistic based entropy measure. Here, each feature is ranked using the probability algorithm. The subset of top k features is selected as essential key features of the classification problem. Gaussian Estimator uses the kernel probability function to estimate the conditional variance of input data features.

$$B_f = \text{uniqueCV}(D); // \text{Unique column values} \quad (11)$$

$$HB_f = \text{Histobins}[] = \text{histogrambin}(D) \quad (12)$$

$$\text{GaussianKernel} : GK(f, \theta) = e^{-\theta^2 / (2 * f^2)} \quad (13)$$

$$\psi = gkv = GK(\sum HB_f, \sum B_f); \quad (14)$$

$$\text{KernelProbability} = KP(D) = |\sum HB_f / (\sum \psi * HB_f)| \quad (15)$$

$$\text{GaussianEntropy} : GE(d_i) = -GK(\sum_i d_i \cdot \log(d_i), \mu_d) \quad (16)$$

The Conditional Gaussian Estimator (CGE) can be calculated as,

$$\text{CGE} : CGE(d_i) = -GK(\sum_i d_i \cdot \log(d_i), \mu_d) - GE(\sum_i d_i) \quad (17)$$

$$\text{KernelProbEstimation}(kp) : \text{IPSO}(kp) = GE(\sum_i kp) - CGE(kp) \quad (18)$$

Gaussian entropy is used to find the entropy value of the feature based on the Gaussian Estimator. Conditional Gaussian Estimator is used to check the conditional probability of each feature value based on the Gaussian probability estimator. Finally, improved optimization hyperparameters are computed using the Gaussian Kernel Estimator and Conditional Gaussian Estimator.

D. Ensemble Classification

In this phase, an optimized random forest approach is proposed by using the key features. A heterogenous ensemble learning model is implemented by using a set of base classifiers. we have developed an ensemble learning model comprised of four base classifiers and one optimized random forest (ORF) classifier with majority voting mechanism. The standard random forest (RF) technique employs its own entropy measure for classification, but the proposed ORF uses an enhanced entropy measure for beat classification. Ensemble learning and majority voting rule is used to enhance the accuracy of heart disease prediction.

Algorithm Steps:

- Step 1: Input ECG data
- Step 2: Pre-process input data for missing values.
- Step 3: Gradient filter is used to transform the data from unequal distribution
- Step 4: For each randomized sample S_i
 - Do
 - Enhanced entropy:
 - $Pr = -\text{Prob}(D_i) \cdot \log(\text{Prob}(D_i))$
 - $\text{Ent}(D) = \sum_i Pr$
 - $PE = \text{Math.cbrt}(\text{entropy}(\text{data}) * \text{total} * \text{GHDSplitCriterion} \cdot \text{computeHellinger}(\text{data})) * Pr / (\text{chiVal}(\text{data}))$.
- for each sample in the test data check
 - If $(PE > 0)$
 - Then
 - $S' = \text{Classify}((D_i, D_j));$
 - else
 - continue
 - end for

IV. RESULTS AND DISCUSSION

On the heart ECG dataset, experiments are run in the python environment. On large, high-dimensional datasets, the extreme level outlier detection technique is used improve the true positive rate and accuracy. A hybrid heterogeneous ensemble classification framework is developed in this work to improve the overall classifier performance. Majority voting technique is employed to find the appropriate decision of individual base classifiers.

The proposed ensemble learning method compares the results using the entire training data set. As a result, each cross-validation model's prediction accuracy tends to be higher than base classification models. The proposed kernel-based feature selection-classification model outperforms conventional models, according to experimental results. A confusion matrix contains information about a classification model's actual and predicted classifications. The data in the matrix is commonly used to evaluate the performance of such a model. The classification results are displayed in the Confusion matrix shown in Table I. It depicts the connection between the actual and predicted classes. It also demonstrates how many true features were predicted as true as well as false.

TABLE I. CONFUSION MATRIX

Actual Values		
Predicted Values	TN	FP
	FN	TP

True Negative (TN): The predicted values were correctly identified as true negatives.

True Positive (TP): The predicted values turned out to be true positives.

False Positive (FP): The predicted values were misinterpreted as true positives. i.e., the negative values were predicted to be positive.

False Negative (FN): The predicted values were incorrectly predicted as actual negatives, i.e., positive values were incorrectly predicted as negatives.

We can deduce the following statistical measures from the confusion matrix:

1) *Precision*: Refers to the percentage of correct positive cases.

$$\text{Precision} = \frac{TP}{(TP + FP)} \tag{19}$$

2) *Recall or sensitivity*: Represents the number of correctly identified positive cases.

$$\text{Recall} = \frac{TP}{(TP + FN)} \tag{20}$$

3) *F1 score*: Defined as the harmonic mean of precision and recall.

$$\text{F - measure} = 2 * \left[\frac{\text{Precision} * \text{Recall}}{\text{Precision} + \text{Recall}} \right] \tag{21}$$

4) *Accuracy*: It is the percentage of correct predictions out of a total number of predictions.

$$\text{Accuracy} = \frac{(TP + TN)}{(TP + TN + FP + FN)} \tag{22}$$

The following figures and tables show the experimental results of the MIT-ECG Data

Table II describes the sample ECG signal data with specified number of features such as RR, speed, age, sex, medicine, and class. This dataset is used to train the model using the proposed classification framework.

Fig. 4 illustrates the existing ensemble learning model on the input MITDB dataset. From the figure, it is observed that the experimentation is carried out on the dataset with ensemble of several base classifiers such as LR, SVM, RF, XGBoost and KNN. The learning model correctly classifies the instances of bigeminy, normal tachycardia and ventricular tachycardia beats with 96.17% accuracy.

Fig. 5 explains the proposed ensemble learning model on the input MITDB dataset. Here an optimized random forest (ORF) based heterogeneous ensemble learning model is developed and experiment is conducted on the dataset. From the figure, it is observed that the ORF ensemble learning model optimizes the relevant and redundant features based on entropy value and correctly classifies the instances with 99.455accuracy compared to existing ensemble learning models.

Table III lists out the comparison of proposed ensemble learning method with state-of-the-art classification techniques. The proposed optimized random forest-based ensemble model exhibits the superior performance among all the state-of-the-art methods stated.

Fig. 6 shows the comparative analysis of proposed ensemble heat-beat detection to the conventional models for accuracy metric. In this figure, as the number of samples increases along with features space, proposed model has better heat-beat detection accuracy than the previous models. Here, the cross validation is performed for 10 samples, 20 samples, 30 samples, 40 samples and 50 samples and accuracy performance for proposed model is observed.

TABLE II. DWT PROCESSED MITBIH ARRHYTHMIA DATA TAKEN FROM [24]

Amplitude	RR	Speed	Age	Sex		Medicine	Arrhythmia
0.915824	1.841667	0.49728	24	F		Yes	(B
0.794527	1.541667	0.515369	24	F		Yes	(B
0.764521	1.377778	0.554894	24	F		Yes	(B
1.039003	1.591667	0.652777	24	F		Yes	(B
2.003128	1.563889	1.280863	24	F		Yes	(B
1.688101	0.772222	2.18603	24	F		Yes	(B
1.668218	1.852778	0.900388	24	F		Yes	(B
1.995825	2.258333	0.88376	24	F		Yes	(B
0.976473	1.766667	0.55272	24	F		Yes	(B
1.191556	1.725	0.690757	24	F		Yes	(B
0.674095	1.847222	0.364924	24	F		Yes	(B
1.404964	2.263889	0.620598	24	F		Yes	(B
0.804747	1.841667	0.436967	24	F		Yes	(B
0.805688	1.880556	0.428431	24	F		Yes	(B
0.561085	1.711111	0.327907	24	F		Yes	(B
0.816213	1.702778	0.479342	24	F		Yes	(B
2.284514	1.680556	1.35938	24	F		Yes	(B
1.343283	1.85	0.726099	51	F		Yes	(B
1.346042	1.827778	0.736437	51	F		Yes	(B
1.295921	1.847222	0.701551	51	F		Yes	(B
1.171628	1.891667	0.619363	51	F		Yes	(B
1.205873	1.841667	0.654773	51	F		Yes	(B
1.198081	1.805556	0.663553	51	F		Yes	(B
1.147332	1.888889	0.607411	51	F		Yes	(B
1.354347	1.833333	0.738734	51	F		Yes	(B
1.469106	1.805556	0.813659	51	F		Yes	(B
1.350584	1.85	0.730046	51	F		Yes	(B
1.22675	1.838889	0.667115	51	F		Yes	(B
1.274882	1.811111	0.703922	51	F		Yes	(B
1.200385	1.819444	0.659753	51	F		Yes	(B
1.16124	1.894444	0.612971	51	F		Yes	(B
1.21954	1.897222	0.642803	51	F		Yes	(B
1.302295	1.886111	0.690466	51	F		Yes	(B
1.216297	1.886111	0.64487	51	F		Yes	(B
1.679835	1.522222	1.103542	51	F		Yes	(B
1.194743	1.852778	0.644839	51	F		Yes	(B
1.253372	1.791667	0.699556	51	F		Yes	(B
2.019494	1.683333	1.199699	51	F		Yes	(B
0.646879	1.736111	0.372602	51	F		Yes	(B
1.531183	1.930556	0.793131	51	F		Yes	(B
1.133171	1.847222	0.613446	51	F		Yes	(B
1.231869	1.830556	0.672948	51	F		Yes	(B

0.931352	0.813889	1.144323	69	M		Yes	(N
0.926876	0.813889	1.138824	69	M		Yes	(N
0.874316	0.813889	1.074244	69	M		Yes	(N
0.799794	0.788889	1.013823	69	M		Yes	(N
0.751938	0.788889	0.953161	69	M		Yes	(N
0.811479	0.788889	1.028636	69	M		Yes	(N
0.905821	0.816667	1.109169	69	M		Yes	(N
0.835362	0.652778	1.279703	69	M		Yes	(N
0.656436	0.991667	0.661952	69	M		Yes	(N
0.836695	0.841667	0.994093	69	M		Yes	(N
0.8435	0.808333	1.043506	69	M		Yes	(N
0.789682	0.794444	0.994005	69	M		Yes	(N
0.757089	0.769444	0.983943	69	M		Yes	(N
0.880419	0.838889	1.049507	69	M		Yes	(N
0.841678	0.855556	0.983779	69	M		Yes	(N
0.740295	0.822222	0.900359	69	M		Yes	(N
0.795441	0.830556	0.957721	69	M		Yes	(N
0.854628	0.819444	1.042936	69	M		Yes	(N
0.772212	0.794444	0.972015	69	M		Yes	(N
0.947551	0.8	1.184439	69	M		Yes	(N
0.838421	0.788889	1.062787	69	M		Yes	(N
0.945943	0.822222	1.150471	69	M		Yes	(N
0.837924	0.869444	0.963746	69	M		Yes	(N
0.808701	0.822222	0.983555	69	M		Yes	(N
0.866462	0.786111	1.102213	69	M		Yes	(N
1.041742	0.794444	1.311283	69	M		Yes	(N
0.806761	0.772222	1.044726	69	M		Yes	(N
0.846139	0.786111	1.07636	69	M		Yes	(N
0.898411	0.813889	1.10385	69	M		Yes	(N
0.79059	0.813889	0.971374	69	M		Yes	(N
0.685813	0.827778	0.828499	69	M		Yes	(N
0.777621	0.844444	0.920867	69	M		Yes	(N
1.035218	0.808333	1.280682	69	M		Yes	(N
0.80213	0.772222	1.03873	69	M		Yes	(N
0.724004	0.8	0.905005	69	M		Yes	(N
0.827432	0.788889	1.048857	69	M		Yes	(N
0.908186	0.858333	1.058081	69	M		Yes	(N
0.82578	0.841667	0.981125	69	M		Yes	(N
0.740944	0.825	0.898114	69	M		Yes	(N
0.839793	0.802778	1.046109	69	M		Yes	(N
1.005817	0.836111	1.202971	69	M		Yes	(N
0.756791	0.791667	0.955947	69	M		Yes	(N
0.799774	0.788889	1.013798	69	M		Yes	(N
0.780397	0.819444	0.952349	69	M		Yes	(N

0.886177	0.847222	1.045979	69	M		Yes	(N
0.774806	0.877778	0.882691	69	M		Yes	(N
0.751943	0.822222	0.914525	69	M		Yes	(N
0.864779	0.777778	1.111859	69	M		Yes	(N
0.865518	0.802778	1.078154	69	M		Yes	(N
0.707004	0.811111	0.871649	69	M		Yes	(N
0.709407	0.797222	0.889849	69	M		Yes	(N
0.828879	0.836111	0.99135	69	M		Yes	(N
0.81786	0.830556	0.984714	69	M		Yes	(N
0.74823	0.825	0.906946	69	M		Yes	(N
0.761216	0.811111	0.938485	69	M		Yes	(N
0.963256	0.788889	1.221029	69	M		Yes	(N
0.971116	0.783333	1.239722	69	M		Yes	(N
0.717338	0.805556	0.890489	69	M		Yes	(N
0.80705	0.841667	0.958871	69	M		Yes	(N
0.89964	0.833333	1.079568	69	M		Yes	(N
1.034261	0.830556	1.245265	69	M		Yes	(N
0.733918	0.805556	0.911071	69	M		Yes	(N
0.792855	0.777778	1.019385	69	M		Yes	(N
0.751469	0.797222	0.942609	69	M		Yes	(N
0.737086	0.783333	0.940961	69	M		Yes	(N

```

=== Classifier model (full training set) ===

Existing Ensemble Classifier((LR+SVM+RF+XGBOOST+KNN) For ECG MIT Data
====
Correctly Classified Instances      2819      96.1788 %
Incorrectly Classified Instances    112       3.8212 %
Kappa statistic                    0
Mean absolute error                 0.0377
Root mean squared error             0.1364
Relative absolute error             100 %
Root relative squared error         100 %
Total Number of Instances          2931

=== Detailed Accuracy By Class ===

          TP Rate  FP Rate  Precision  Recall  F-Measure  MCC      ROC Area  PRC Area  Class
          0.000    0.000    ?          0.000    ?          ?        0.481    0.014    (B
          1.000    1.000    0.962     1.000    0.981     ?        0.493    0.961    (N
          0.000    0.000    ?          0.000    ?          ?        0.488    0.013    (T
          0.000    0.000    ?          0.000    ?          ?        0.485    0.010    (VT
Weighted Avg.   0.962    0.962    ?          0.962    ?          ?        0.492    0.925

=== Confusion Matrix ===

 a  b  c  d  <-- classified as
0  42  0  0 |  a = (B
0 2819 0  0 |  b = (N
0  39  0  0 |  c = (T
0  31  0  0 |  d = (VT

```

Fig. 4. Existing Ensemble Learning Result.

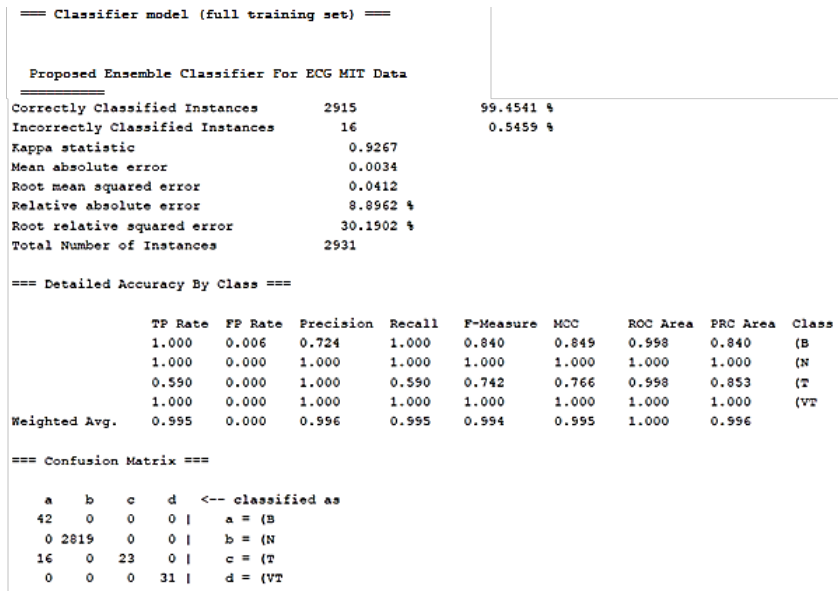


Fig. 5. Optimized Random Forest based Ensemble Learning Result.

TABLE III. COMPARISON OF PROPOSED ENSEMBLE MODEL WITH OTHER STATE-OF-THE-ART METHODS

Ref	Dataset	Classifier	Performance metrics
[18]	MITBIH	ODT+ Adaptive boosted ODT	98.77% _{ACC}
[24]	MITBIH	KNN	98.40% _{ACC}
[25]	MITBIH, Wearable dataset	XGBOOST	99.14% _{ACC} MITBIH, 98.68% _{ACC} Wearable dataset
[26]	MITBIH	KNN+DT	97.64% _{Acc}
		SVM	97.58% _{Acc}
		Ensemble Approach	97.78% _{Acc}
		ANN with Class Weights	98.06% _{Acc}
[27]	452 samples of sample data	RF Ensemble	90% _{Acc}
[28]	MITBIH	RF+SVM	98.2% _{Acc}
[29]	MITBIH	DL Ensemble	98% _{Acc} 0.93 _{F1score} 0.92 _{AUC}
[30]	Kaggle	LR+SVM+DT+NB+KNN	98% _{Acc}
Proposed Ensemble Method	MITBIH	LR+SVM+RF+XGBOOST+KNN	96.1% _{Acc}
		LR+SVM+ORF+XGBOOST+KNN	99.45%_{Acc}

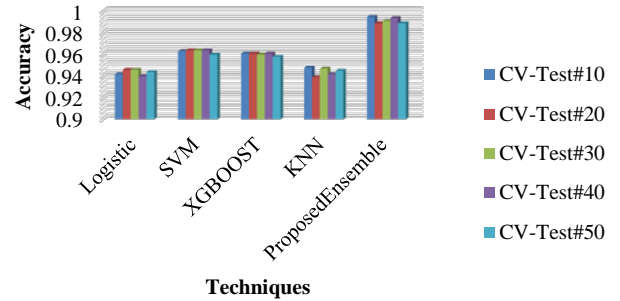


Fig. 6. Comparative Analysis of Proposed Framework to the Conventional Frameworks for ECG Heartbeat Detection for Accuracy Metric.

Fig. 7 depicts the comparative analysis of proposed ensemble heartbeat detection to the conventional models for recall metric. In this figure, as the number of samples increases along with features space, proposed model has better recall than the previous models. Here, the cross validation is performed for 10 samples, 20 samples, 30 samples, 40 samples and 50 samples and the recall for proposed model is observed.

Fig. 8 presents the comparative analysis of proposed ensemble heart-beat detection to the conventional models for F-measure metric. In this figure, as the number of samples increases along with features space, proposed model has better heart-beat detection F-measure than the previous models.

Table IV lists the comparative analysis of proposed ensemble heartbeat detection to the conventional models for AUC metric. Here, the cross-validation test of 10 samples to 50 samples is done and classification result is observed over various classifiers. In this table, as the number of samples increases along with features space, proposed model has better heartbeat detection AUC than the previous models.

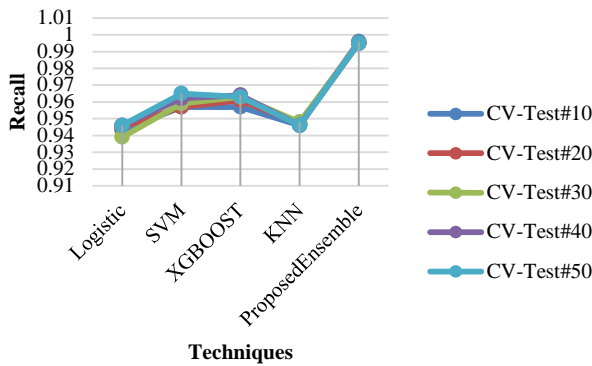


Fig. 7. Comparative Analysis of Proposed Framework to the Conventional Frameworks for ECG Heartbeat Detection for Recall Metric.

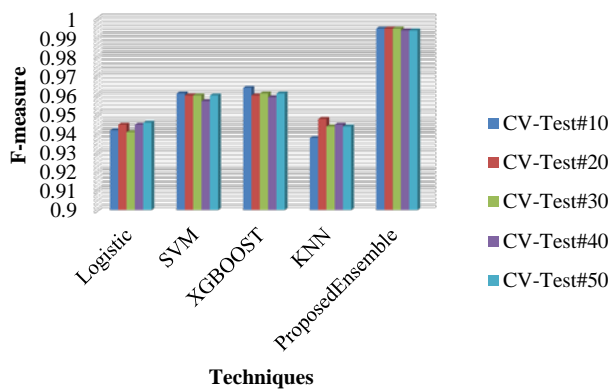


Fig. 8. Comparative Analysis of Proposed Framework to the Conventional Frameworks for ECG Heartbeat Detection for F1-Score Metric.

Table V lists the comparative analysis of proposed ensemble heartbeat detection to the conventional models for precision metric. In this table, as the number of samples increases along with features space, proposed model has better heartbeat detection precision than the previous models.

TABLE IV. COMPARISON OF PROPOSED FRAMEWORK IN TERMS OF AUC METRIC

CV-Test	Logistic	SV M	XGBOOS T	KN N	HRF Ensemble Learning
CV-Test#10	0.943	0.963	0.961	0.94	0.995
CV-Test#20	0.942	0.964	0.964	0.942	0.975
CV-Test#30	0.941	0.965	0.965	0.942	0.974
CV-Test#40	0.939	0.963	0.965	0.942	0.985
CV-Test#50	0.941	0.961	0.963	0.942	0.971

TABLE V. COMPARISON OF PROPOSED FRAMEWORK IN TERMS OF AUC METRIC

CV-Test	Logistic	SV M	XGBOOS T	KN N	Proposed Ensemble
CV-Test#10	0.943	0.958	0.959	0.939	0.995
CV-Test#20	0.945	0.961	0.963	0.941	0.985
CV-Test#30	0.945	0.96	0.959	0.944	0.974
CV-Test#40	0.939	0.962	0.962	0.94	0.985
CV-Test#50	0.94	0.961	0.963	0.939	0.978

V. CONCLUSION

In this paper, an optimized ensemble learning approach is implemented on the MITBIH arrhythmia dataset for better decision making. Since most of the base classifiers are independent of data size and outliers, the proposed improved inter quartile range outlier detection-based optimized random forest ensemble learning model has better efficiency in terms of outliers filtering and data classification problem. This outlier technique proposed in this work is an improvement to the traditional inter quartile range outlier detection method which removes the extreme level outliers and improves the accuracy in the classification process. After filtering, a kernel-based feature selection approach is implemented to find the ranks of the features. In addition, this paper proposed an enhanced entropy measure used in decision trees of random forest algorithm to get the optimal set of features. Finally, the ensemble learning classifies each class of heartbeat by majority voting principle and achieved an accuracy of 99.45% which outperforms the various state-of-the-methods.

ACKNOWLEDGMENT

This research did not receive any specific grant from funding agencies in the public, commercial, or not-for-profit sectors.

REFERENCES

- [1] Shreya Bhattacharyya, Souvik Majumder, Arrhythmic Heartbeat Classification Using Ensemble of Random Forest and Support Vector Machine Algorithm, IEEE Transactions on Artificial Intelligence, Volume 2, Issue 3, June 2021.
- [2] Aurore Lyon, Ana Mincholé, Juan Pablo Martínez, Pablo Laguna, and Blanca Rodríguez Computational techniques for ECG analysis and interpretation in light of their contribution to medical advances, Journal of the Royal Society Interface, vol. 15(138), 2018, <https://dx.doi.org/10.1098%2Frsif.2017.0821>.
- [3] Asir Antony Gnana Singh Danasingh, Identifying Redundant Features using Unsupervised Learning for High-Dimensional Data, SN Applied Sciences, July 2020.
- [4] Jafar Abdollahi & Babak Nouri-Moghaddam, A Hybrid Method for Heart Disease Diagnosis utilizing Feature Selection based Ensemble Classifier Model Generation, Iran Journal of Computer Science, May 2022, <https://dx.doi.org/10.1007/s42044-022-00104-x>.

- [5] Utkarsh Mahadeokhaire, R. Dhanalakshmi, Stability of Feature Selection Algorithm: A review, Journal of King Saud University - Computer and Information Sciences, June 2019.
- [6] Pierre Michel, Nicolas Ngo, Jean-Francois Pons, A Filter Approach for Feature Selection in Classification: Application to Automatic Atrial Fibrillation Detection in Electrocardiogram Recordings, BMC Medical Informatics and Decision Making, 21, Article Number 130, May 2021.
- [7] A. Venkata Anuhya, Venkata Ratnam Kolluru and Rajesh Kumar Patjyoshi, A Deep Learning Approach for Detection and classification of QRS Contours using Single-lead ECG, International Journal of Pharmaceutical Sciences and Research, Vol. 12, No. 2, pp. 75-91, June 2020.
- [8] Alex Barros, Paulo Resque, Joao Almeida, Renato Mota, Data Improvement Model based ECG Biometric for User Authentication and Identification, Sensors, Vol.20, Issue 10, May 2020.
- [9] John Hart, Inter-quartile Analysis of Resting heart rate and heart rate Variability following Spinal Adjustment; A Case Study, Neuroscience Discovery, January 2019, <http://dx.doi.org/10.7243/2052-6946-7-1>.
- [10] Bingtao Zhang, Peng Cao, Classification of High Dimensional Biomedical Data Based on Feature Selection using Redundant Removal, PLOS ONE, April 2019.
- [11] Muhammed Rizwan, Bradley M Whitaker and David V Anderson, AF detection from ECG recordings using feature selection, sparse coding, and ensemble learning, Physiological Measurement, 39, 124007 (10pp), 2018, <https://doi.org/10.1088/1361-6579/aaf35b>.
- [12] Yuwei Zhang, Yuan Zhang, Benny Lo, Wenyao Xu, Wearable ECG Signal Processing For Automated Cardiac Arrhythmia Classification using CFASE-Based Feature Selection, Expert Systems, pp 1-13, April 2019, <https://doi.org/10.1111/exsy.12432>.
- [13] G. Angayarkanni, Dr. S. Hemalatha, Selection of Features Associated with Coronary Artery Diseases (CAD) using Feature Selection Techniques, Journal of Xi'an University of Architecture & Technology, Vol.12 (11), pp. 686-699, 2020.
- [14] Vinay Varma K, Embedded Methods for Feature Selection in Neural Networks, October 2020, <https://doi.org/10.48550/arXiv.2010.05834>.
- [15] Agnieszka Wosiak, Principal Component Analysis based on Data Characteristics for Dimensionality Reduction of ECG Recordings in Arrhythmia Classification, Open Physics, Vol. 17, Iss. 10, September 2019, <https://dx.doi.org/10.1515/phys-2019-0050>.
- [16] S. Wu, P. Chen, A. L. Swindlehurst, and P. Hung, Cancelable biometric recognition with ECGs: subspace-based approaches, IEEE Transactions Information Forensics and Security, Vol. 14, no. 5, pp. 1323-36, May 2019.
- [17] Chulseung Yang, Gi Won Ku, Jeong-Gi Lee, Sang-Hyun Lee, Interval-Based LDA Algorithm for Electrocardiograms for Individual Verification, IEEE Transactions Information Forensics and Security, Vol. 10 (17), August 2020.
- [18] Mohebbanaaz, L. V. Rajani Kumari and Y. Padma Sai, Classification of ECG beats using optimized decision tree and adaptive boosted optimized decision tree, Signal, Image and Video Processing, 16, pages 695-703, October 2021.
- [19] Bo-Han Kung, Po-Yuan Hu, Chiu-Chang Huang, Cheng-Che Lee, Chia-Yu Yao, and Chieh-Hsiung Kuan, An Efficient ECG Classification System Using Resource-Saving Architecture and Random Forest, IEEE Journal of Biomedical Health Informatics, vol. 25(6), pp 1904-1914, 2021, DOI: 10.1109/JBHI.2020.3035191.
- [20] Venkatesan, C., Karthigaikumar, P., Paul, A., Satheeskumaran, S., & Kumar, R, ECG Signal Preprocessing and SVM Classifier-Based Abnormality Detection in Remote Healthcare Applications, IEEE Access: Practical Innovations, Open Solutions, vol. 6, pp 9767-9773, 2018, <https://doi.org/10.1109/access.2018.2794346>.
- [21] Jha, C. K., & Kolekar, M. H, Cardiac Arrhythmia Classification using Tunable Q-Wavelet Transform based Features and Support Vector Machine Classifier. Biomedical Signal Processing and Control, 59(101875), 2020, <https://doi.org/10.1016/j.bspc.2020.101875>.
- [22] Sahoo, S., Kanungo, B., Behera, S., & Sabut, S, Multiresolution Wavelet Transform Based Feature Extraction and ECG Classification to Detect Cardiac Abnormalities. Measurement: journal of the International Measurement Confederation, Vol. 108, pp 55-66, 2017, <https://doi.org/10.1016/j.measurement.2017.05.022>.
- [23] S. T. Aarthy and J. L. Mazher Iqbal, Time series real time naive bayes electrocardiogram signal classification for efficient disease prediction using fuzzy rules, Journal of Ambient Intelligence and Humanized Computing, Vol. 12, pp 5257-5267, 2021.
- [24] Vedavathi Gauribidanur Rangappa, Sahani Venkata Appala Varaprasad Prasad, and Alok Agarwal, Classification of Cardiac Arrhythmia Stages using Hybrid Features Extraction with K-Nearest Neighbour Classifier of ECG Signals, International Journal of Intelligent Engineering and Systems, Vol.11, No.6, 2018.
- [25] Huaiyu Zhu, Yisheng Zhao, Yun Pan, Hanshuang Xie, Fan Wu and Ruohong Huan, Robust Heartbeat Classification for Wearable Single-Lead ECG via Extreme Gradient Boosting, Sensors, Vol. 21, 5290, 2021, <https://doi.org/10.3390/s21165290>.
- [26] Md. Atik Ahmed, Kazi Amit Hasan, Khan Fashee Monowar, Nowfel Mashnoor, ECG Heartbeat Classification Using Ensemble of Efficient Machine Learning Approaches on Imbalanced datasets, International Conference on Advanced Information and Communication Technology, 2020, <https://doi.org/10.1109/ICAICT51780.2020.9333534>.
- [27] Jose Francisco Saenz-Cogollo and Maurizio Agelli, Investigating Feature Selection and Random Forests for Inter-Patient Heartbeat Classification, Vol. 13, Issue 4, March 2020.
- [28] Shreya Bhattacharyya; Souvik Majumder; Papiya Debnath, Arrhythmic Heartbeat Classification Using Ensemble of Random Forest and Support Vector Machine Algorithm, IEEE Transactions on Artificial Intelligence, Vol. 2, Issue 3, June 2021.
- [29] Adyasha Rath, Debahuti Mishra, Ganapati Panda, Suresh Chandra satapathy and Kajjian Xia, Improved heart disease detection from ECG signal using deep learning based ensemble model", Sustainable Computing: Informatics and Systems, Vol. 35, 100732, September 2022.
- [30] Suresh Subramanian and Y Angeline Christobel, A Hybrid Machine Learning Model to Predict Heart Disease Accurately, Vol. 15, Iss. 12, pp. 527-534, March 2022, <https://doi.org/10.17485/IJST/v15i12.104>.

Improved Data Segmentation Architecture for Early Size Estimation using Machine Learning

Ms. Manisha^{1*}

Research Scholar: ECE Deptt.
MDU, India

Dr. Rahul Rishi²

Professor, UIET: ECE Deptt.
MDU, India

Dr. Sonia Sharma³

Asst. Prof.: ECE Deptt.
MDU, India

Abstract—Software size estimation plays an important role in project management. According to the report given by Standish Chaos, about 65% of software projects are beyond companies budget or overdue; which could have been saved if an early estimation was imposed. Though the software size can't be measured directly, but it is related to effort and hence a low effort will lead to low size. The calculation of effort depends upon how the data is organized or segmented. This research paper focuses on the improvement of data segmentation in order to reduce the effort and parallel the size. In order to improve the segmentation architecture, the project data is divided based on the similarity indexes which the projects have in between their attributes. Three similarity measures were used namely Cosine Similarity (CS), Soft Cosine Similarity (SC) and a hybrid similarity index which combines CS and SC. Based on these similarity indexes, the project data is divided into groups by K-means algorithm. In order to estimate the size, the co-relation between the formed groups are calculated. To calculate the correlation, Mean Square Error (MSE), Square Error (SE), and Standard Deviation (STD) is calculated and the normalized parameters are used to evaluate the software size.

Keywords—Cosine similarity; hybrid similarity; machine learning; size estimation and soft cosine similarity

I. INTRODUCTION

Software size estimation has always been a favorite area for the researchers as the wrong estimation of effort and size will lead to high computation risk and project failure. If the company does not earn from a project, even if the project is complete, it is termed as failure. Therefore, to overcome this problem, an early stage prediction model is designed based of the past project experience [1]. Underestimation and overestimation both leads to high project risk completion. In case, if size of the software project is estimated at the earliest stage, then, project handling team can provide better plan. Conventional software development mainly goes through four levels namely requirements elicitation, design, coding and testing [2]. After designing early size estimation model, most of the systems have better response. If the project estimation is terminated just after first level, then it affects directly the project management. Therefore, early size estimation of project is a crucial task not only for conventional software development but also for agile development, as it makes the projects more manageable. Software size metrics play an important role in the success of this task [3]. In the conventional approach, Lines of Code (LOC), evaluation has been a way to evaluate the size of the projects [4]. Function Point (FP) sizing also evolved as a method to acquire the

details of the project but being a object oriented concept again, the usage of FP will also require code oriented metrics [5], [6]. Early size estimation requires the attributes which does not involve post coding methods. Any estimation method, requires a learning model and as it is described earlier, code oriented metrics will be only attained once the project is complete. In order to train the system, the Ground Truth (GT) of the data is the foremost requirement. GT refers to the class label of the data. As for example, suppose a project had 5000 LOC, 10 team members, 1 team lead and 50 hours of development and the effort from the team in order to develop the project was "high", then the GT for Project Attribute(PA) \rightarrow {5000, 10, 1, 50} is high. Unfortunately, these type of metrics can be only evaluated after the development and does not suit early size estimation. In the early age of development of early size estimation, authors introduced learning methods using machine learning and its extension. [7]. used machine learning oriented neural networks to train the system based on the feedback from the engagements of the company but the generation of GT through machine learning failed here.

A. Machine Learning

The machine learning architecture needs a training data algorithm with its ground truth value. The material methods which involves statistics are called machine learning. Common machine learning algorithms are as follows.

- 1) K-means.
- 2) Regression.
- 3) Linear Propagation Model.

This research article uses K-means clustering algorithm with the enhancement of base architecture. The k-means clustering algorithm selects a random centroid out of the provided set of attributes. If there are three attributes, then the centroid of the clusters will also have three attributes. The adjustment in the centroid takes place when the co-relation between the attributes and centroids varies and goes to the adjustment into another cluster. In order to calculate the distance between centroid and attribute values, Euclidian distance is calculated. The data is always divided into 'k' number of clusters and in order to decide 'k', there are multiple ways of advisory. This research work does not focuses on the calculation of 'k' as there are two sections for the entire data namely 'high size' and 'low size' which is further subdivided into two sub-segments namely 'moderate' and 'high'. The size before the development can't be directly evaluated and hence this research article refers to the

statement that high effort will lead to high size and low co-relation will lead to high effort.

$$Effort \propto cost || size \quad (1)$$

The rest of the paper is organized as follows: Section 2 represents the related work in the field of size estimation. Section 3 presents the proposed work including technique used and process of work. The result and discussions are presented in Section 4. Conclusion is presented in Section 5.

II. RELATED WORK

Ahn et al. (2003) have presented a metric analyses based methodology tool to estimate effort at early stage of software project. Using this model, a project manager can analyzed, software system like as analyzed by FP analysis. In addition, relation between UML point and effort has also been observed [8]. Baskeles et al. (2007) have presented ML based software estimation model to resolve the problems related to cost and schedule extension. The test has been conducted on the collected data obtained from software industry in Turkey. Principle Component Analysis (PCA) has been applied as data dimension reduction approach. ML technique has been trained by 50 and 40 projects, and test later using 10 and 20 projects respectively. From the test results it has been concluded that the parametric models are not sufficient for software effort estimation [9]. Nassif et al. (2013) have presented a new logarithmic based linear regression model, which works on the basis of use case point model (UCP). This approach is used case diagram to determine software effort. To regulate the productivity factor of regression model Fuzzy logic is used as Fuzzy Interface System (FIS). Based on software size and project group productivity, neural network is design and used to estimate software effort. At last comparison between ANN and log-linear regression based model has been presented. The results show that NN outperformed compared to regression model while estimating small project, but for large scale projects regression algorithm performed better [10]. Satapathy et al. (2016) have used Random Forest (RF) as ML approach to enhance the performance of effort prediction model. UCP approach has been used for estimating project effort, the parameters of which has been improved using RF approach. Among various ML techniques like NN, log-linear regression scheme, stochastic approach, and radial function method, RF surpass among all [11]. Sharma et al. (2017) have presented a review on various ML techniques used for software effort and size estimation. LOC and FP are the two main metrics used for effort estimation. There are various validation methods that can be considered in the expansion of research to confirm the consequences of software effort assessments. The main validation methods are Cross Assessments, Jackknife method and Iterative method. In addition, research trends have shown that assessment methods need to be explored and improved. In addition, other ML approaches, such as size metrics and

regression trees, can also be utilized using real-life data sets [12]. Spikol et al. (2018) have presented ML based effort estimation model using International Software Benchmarking Standards Group (ISBSG) dataset. For cross validation, three ML techniques SVM, ANN, and generalized Linear Model has been used [13]. Lavazza et al. (2019) have empirically studied the COSMIC early size estimation scheme using historical dataset. Average Functional Process along with the Equal Size Bands methods have been used for the prediction of effort estimation. Results shows that sometimes functional process provides better results that can be accepted but sometimes the error is so large, which is not to be acceptable for better performance of any project. On the other hand, band method provides better results [14]. Nassif et al. (2019) have compared three FIS systems namely, Mamdani, Sugeno with defined output, and Sugeno with linear output. The performance of the system has been analyzed based on standard sized accuracy, error, effect size and statistical tests. The designed model is trained using ISBSG dataset, and results show that FIS are very sensitive to outliers. Authors also concluded that when fuzzy logic is used in combination to regression model, the system outperforms [15]. Silhavy et al. (2021) had proposed a method for size estimation based on the use case and the number of actors. In the process, stepwise regression was performed that minimized the number of errors adjoining the size estimation of the software system. This is also added that the predictions were independent of the use case points to avoid inaccurate estimations [16]. Daud and Malik (2021) had aimed at quantitative analysis of the effect of precise software size estimations when the project transits to the designing phase. To achieve this Analysis to Design Adjustment Factors were introduced in the proposed work that demonstrated improved accuracy of the proposed model [17]. Suresh (2022) had integrated Artificial Neural Netowrk (ANN) to generate precise estimations in the initial stages of development cycle. It was observed that the work offered optimal and automated predictions based on training and classification using ANN architecture. The work exhibited better and more accurate software effort estimations in comparison to the existing works [18].

A. Problem Formulation

It becomes easy to the train a system when the GT of the data is available but, if there is no GT, the system remains uncertain in order to make the system understand what the data represents for. In case of post size estimation, the GT is easy as the developers speaks themselves and the outcome defines the GT but, in case of early size estimation, GT is not present. This articles focuses on the development of automatic GT for improved segmented section in order to quantify low size and high size based on the co-relation between the groups as shown in Fig. 1.

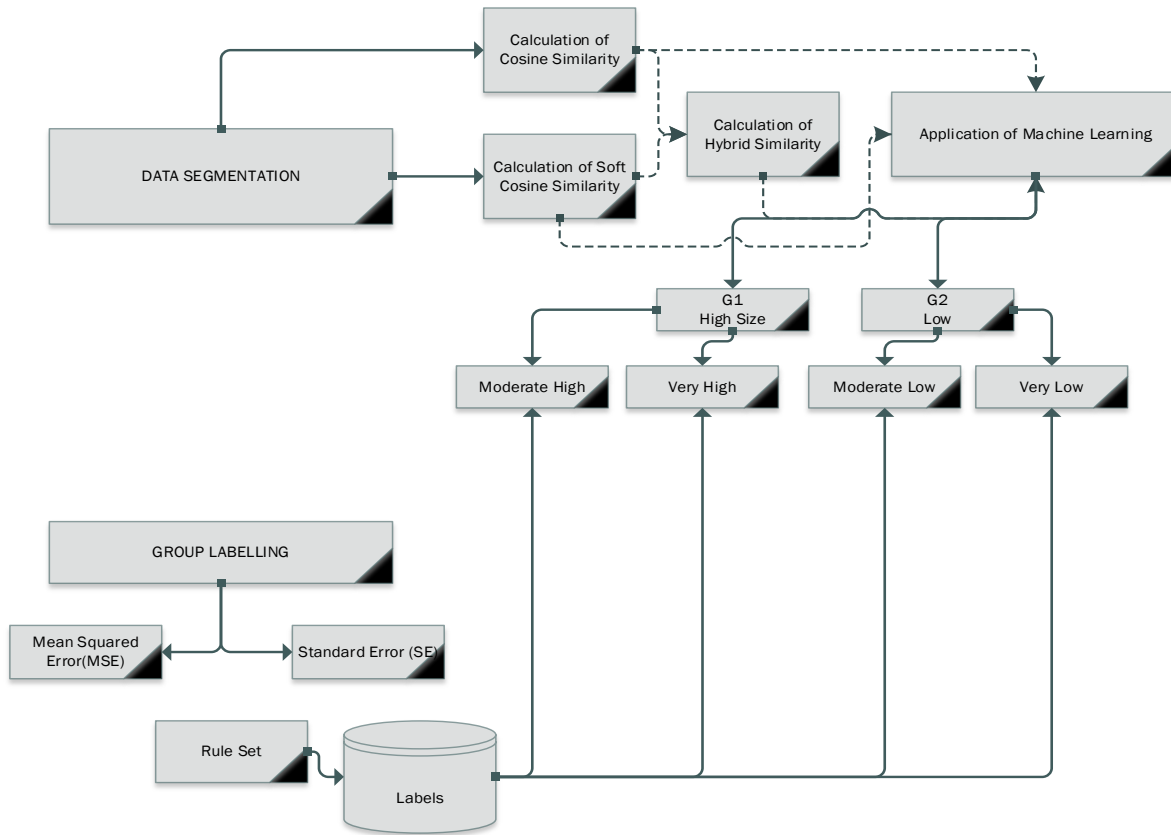


Fig. 1. The Proposed Work Model.

III. PROPOSED WORK

The proposed work is divided into two segments, namely, segment generation and group labelling. The architecture of the proposed work is illustrated using Fig. 2. The data segmentation involves the application of Cosine Similarity (CS), Soft Cosine Similarity (SC) and hybrid similarity which is a summed value of CS and SC. The formation of groups utilizing K-means is also a part of this section. The K-means algorithm divides the entire attribute set in two groups and their labelling is done by the group labelling section of the proposed algorithm.

A. Calculate Similarity Indices

Here data, segmentation is used to obtain ground truth value. Here, data is fragmented based on their size into two parts high fragments and low fragments after finding the centroid for each row in the dataset. The available dataset contains irrelevant information, therefore need to be rectified before used for analysis process. Hence, need to be isolated from the available data for any project for size estimation. Therefore clustering using K-means play an important role for cluster formation. Before applying clustering, we need to find out similarity indices, which are obtained using three

similarity measures (i) Cosine Similarity (CS), (ii) Soft Cosine (SC) measure, (iii) Hybrid similarity measure.

1) *Cosine similarity*: It is similarity measurement approach used to find out the similarity metric between two entities based on their size using the concept of the cosine angle between entities in an n-dimensional space. Exactly, to calculate the cosine similarity between two entities in an n-dimensional space, the given formula is used:

$$\text{Cos}(\theta) = \frac{\vec{M} \cdot \vec{N}}{\|\vec{M}\| \|\vec{N}\|} \quad (2)$$

Here, 'M' and 'N' are two entities may be array or vectors; cosine equation gives the angle between them using the written equation:

$$\begin{aligned} \vec{M} \cdot \vec{N} &= \sum_{k=1}^n M_k \times N_k \\ &= M_1 \times N_1 + M_2 \times N_2 + \dots + M_n \times N_n \\ \|\vec{M}\| &= \sqrt{M_1^2 + M_2^2 + \dots + M_n^2} \\ \|\vec{N}\| &= \sqrt{N_1^2 + N_2^2 + \dots + N_n^2} \end{aligned} \quad (3)$$

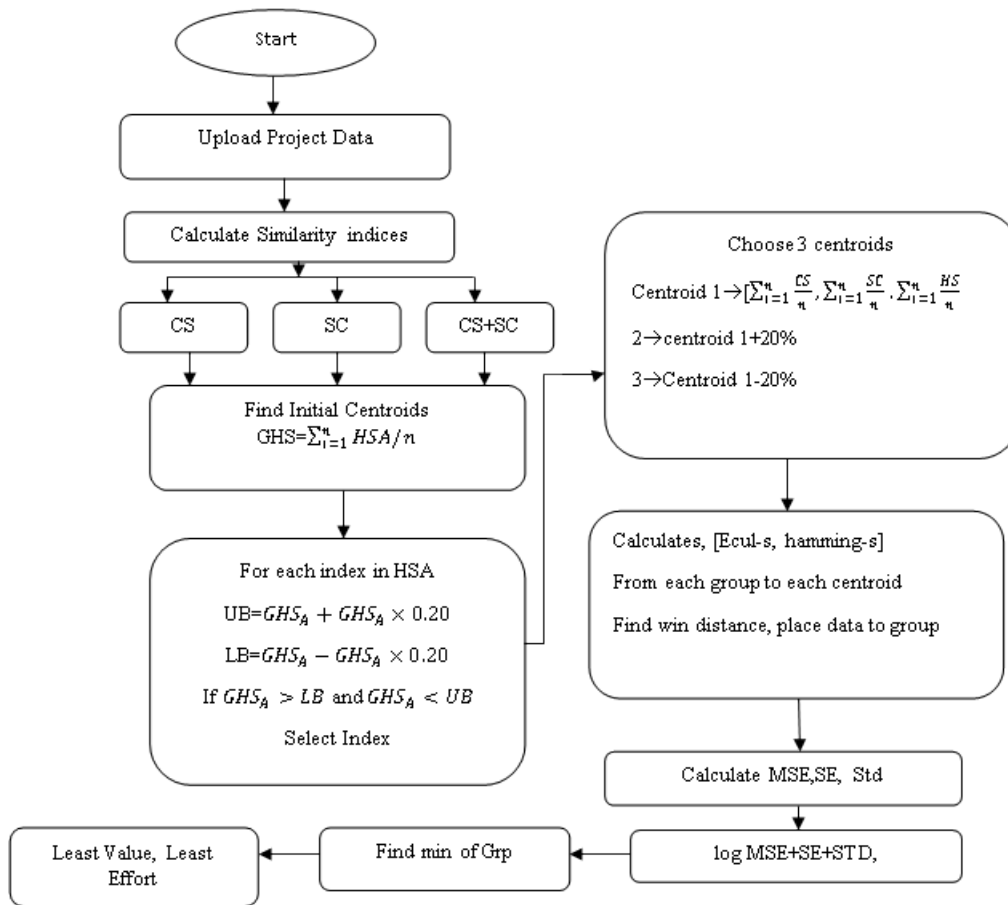


Fig. 2. Proposed Work.

We consider an example to calculate the similarity between two sample data such as M and N, where

$$M = [1, 1, 0]$$

$$N = [1, 0, 1]$$

$$\vec{M} \cdot \vec{N} = 1 \times 1 + 1 \times 0 + 0 \times 1 = 1 + 0 + 0 = 1 \quad (4)$$

$$\|\vec{M}\| = \sqrt{1^2 + 1^2 + 0^2} = \sqrt{2} \quad (5)$$

$$\|\vec{N}\| = \sqrt{1^2 + 0^2 + 1^2} = \sqrt{2} \quad (6)$$

So, the value of cosine similarity is;

$$\cos(\theta) = \frac{1}{\sqrt{2} \times \sqrt{2}} = \frac{1}{2} = 0.5 \quad (7)$$

$$\theta = \cos^{-1}(0.5) = 60^\circ \quad (8)$$

Cosine similarity is used to measure the closeness between the data elements. It is a measurement of similarity between two non-zero arrays or vectors of an inner product space that measures the cosine of the angle between them. The cosine of 0° is 1, and it is less than 1 for any angle in the interval $(0, \pi)$ radians. It is thus a judgment of orientation and not

magnitude: two vectors with the same orientation have a cosine similarity of 1, two vectors oriented at 90° relative to each other have a similarity of 0, and two vectors diametrically opposed have a similarity of -1, independent of their magnitude. These bounds apply for any number of dimensions, and the cosine similarity is most commonly used in high-dimensional positive spaces. Some important points related to the cosine similarity is written as:

- 1) Always applicable for two non-zero arrays or vectors.
- 2) The cosine similarity considers the Vector Space Model (VSM) features as independent or completely different.
- 3) The time complexity of cosine similarity is non quadratic.
- 4) Cosine similarity use the concept of Term Frequency–Inverse Document Frequency (TF-IDF) to calculate the similarity between documents
- 5) Cosine Similarity uses the Euclidean Distance to measure the closeness between two entities.

The designed algorithm for CS is written.

Algorithm: Cosine Similarity

Input: PD → Uploaded project data to calculate similarity

Output: SIM_{COS} → Cosine Similarity for PD

SIM_{COS} = [0] // to store cosine similarities values

Sim-count = 0

For m = 1 → Length (PD)

Current-PD = PD (m)

For n = m+1 → Length (PD)

Reference-PD = PD (n)

Calculate the cos similarity using given equation

$$\overrightarrow{\text{Current - PD}} \cdot \overrightarrow{\text{Reference - PD}} = \sum_{k=1}^n \text{Current - PD}_k \times \text{Reference - PD}_k$$

$$\|\overrightarrow{\text{Current - PD}}\| = \sqrt{\text{Current - PD}_1^2 + \text{Current - PD}_2^2 + \dots + \text{Current - PD}_n^2}$$

$$\|\overrightarrow{\text{Reference - PD}}\| = \sqrt{\text{Reference - PD}_1^2 + \text{Reference - PD}_2^2 + \dots + \text{Reference - PD}_n^2}$$

$$\text{Cos}(\theta) = \frac{\overrightarrow{\text{Current - PD}} \cdot \overrightarrow{\text{Reference - PD}}}{\|\overrightarrow{\text{Current - PD}}\| \|\overrightarrow{\text{Reference - PD}}\|}$$

SIM_{COS}[Sim-count]=Cos(θ)

Increment in index of array, Sim-count = Sim-count + 1

End - For

End - For

Return: SIM_{COS} as an output in terms of Cosine Similarity for PD

End - Algorithm

2) *Soft cosine similarity*: Soft cosine or the soft similarity approach is used to calculate the similarity between two entities similar to the cosine similarity approach. Cosine similarity has the VSM (Vector Space Model) features as completely different or independent whereas the soft cosine measures considers the VSM similarity features that assists in the generalization of cosine and soft cosine with similarity idea. For the computation of soft cosine, S as matrix is utilized for the indication of similarity among features. It could be measured by Levenshtein distance and Wordnet similarity. Soft cosine similarity finds the most common between two document sets.

$$\text{Soft Cosine} = \text{Cos}\left(\frac{n}{i=1} |X \cap Y|\right) \quad (9)$$

Where, X and Y are the two entities in n dimensional space and the some important points related to the soft cosine similarity is written as:

1) A soft cosine similarity between two vectors considers similarities between pairs of features.

2) The soft cosine similarity measures the similarity of features in Vector Space Model (VSM) as dependent.

3) The time complexity of Soft Cosine Similarity is quadratic, which makes it perfectly applicable to real-world tasks but it can be reduced to sub quadratic.

4) Soft Cosine similarity uses the concept of n-grams which is a contiguous sequence of n items.

5) Soft Cosine Similarity uses the Levenshtein Distance.

The algorithm for soft cosine similarity index is written below.

Algorithm: Soft Cosine Similarity

Input: PD → Uploaded project data to calculate similarity

Output: SIM_{SOFTCOS} → Soft Cosine Similarity for PD

SIM_{SOFTCOS} = [0] // to store soft cosine similarities values

Sim-count = 0

For m = 1 → Length (PD)

Current-PD = PD (m)

For n = m+1 → Length (PD)

Reference-PD = PD (n)

$$\text{SIM}_{\text{SOFTCOS}} = \text{Cos}\left(\frac{n}{i=1} |\text{Current - PD} \cap \text{Reference - PD}|\right)$$

SIM_{SOFTCOS}[Sim-count]=SIM_{SOFTCOS}

Increment in index of array, Sim-count = Sim-count + 1

End - For

End - For

Return: SIM_{SOFTCOS} as an output in terms of Soft Cosine Similarity for PD

End - Algorithm

B. Hybrid Similarity

When CS and SC measures are used in combination, then the measure form is known as hybrid similarity indices. By comparing average of each row with remaining rows, an average value is obtained. Suppose we have 100 rows in the project, therefore, to find similarity either applying CS, SC, or hybrid similarity average value obtained for each row (1st row) is compared to the remaining 99 rows. This process will provide an average value, which is used to find initial centroid of data that is given by equation (10).

$$\text{GHS}_A = \sum_{i=1}^n \text{HS} / n \quad (10)$$

Where, GHS_A represents Gross Hybrid Similarity, HS indicates hybrid similarity value.

For each index in HS, determined upper bound (UB), and Lower Bound (LB) values by multiplying 20 % of data to the obtained GHS average, adding and subtracting the obtained value to GHS. The added value is indicated by UB, and, subtracted value is represented by LB. Both UB and LB values are represented by equation (11), and equation (12), respectively.

$$UB = GHS_A + GHS_A \times 0.20 \quad (11)$$

$$LB = GHS_A - GHS_A \times 0.20 \quad (12)$$

If the obtained average values of is greater than LB or less than UB ($GHS_A > LB$ and $GHS_A < UB$), then index value is selected.

The algorithm for hybrid similarity measure is written.

Algorithm: Hybrid Similarity (Soft Cosine Similarity)

Input: PD \rightarrow Uploaded project data to calculate similarity

Output: $SIM_H \rightarrow$ Hybrid Similarity for PD

$SIM_H = [()]$ // to store cosine similarities values

Sim-count = 0

For m = 1 \rightarrow Length (PD)

Current-PD = PD (m)

For n = m+1 \rightarrow Length (PD)

Reference-PD = PD (n)

Calculate the cos similarity using given equation

$$\overrightarrow{\text{Current} - \text{PD}} \cdot \overrightarrow{\text{Reference} - \text{PD}} = \sum_{k=1}^n \text{Current} - \text{PD}_k \times \text{Reference} - \text{PD}_k$$

$$\|\overrightarrow{\text{Current} - \text{PD}}\| = \sqrt{\text{Current} - \text{PD}_1^2 + \text{Current} - \text{PD}_2^2 + \dots + \text{Current} - \text{PD}_n^2}$$

$$\|\overrightarrow{\text{Reference} - \text{PD}}\| = \sqrt{\text{Reference} - \text{PD}_1^2 + \text{Reference} - \text{PD}_2^2 + \dots + \text{Reference} - \text{PD}_n^2}$$

$$\text{Cos}(\theta) = \frac{\overrightarrow{\text{Current} - \text{PD}} \cdot \overrightarrow{\text{Reference} - \text{PD}}}{\|\overrightarrow{\text{Current} - \text{PD}}\| \|\overrightarrow{\text{Reference} - \text{PD}}\|}$$

$$SIM_{SOFTCOS} = \text{Cos}\left(\frac{n}{i=1} |\text{Current} - \text{PD} \cap \text{Reference} - \text{PD}|\right)$$

$SIM_H[\text{Sim-count}] = \{\text{Cos}(\theta) + SIM_{SOFTCOS}\}$

Increment in index of array, Sim-count = Sim-count + 1

End - For

End - For

Return: SIM_H as an output in terms of Hybrid Similarity for PD

End - Algorithm

Now, apply K means as ML approach for centroid selection.

ML is a branch of artificial intelligence (AI). In more detail, it is a method of data analysis that allows a machine / robot or any analysis system to learn independently by solving a number of similar problems. Machine learning aims to develop computer programs that can access information and use it to learn. The training process begins with a specific set of information, such as examples, direct experience, or instruction, to look for examples in the data and make better decisions in the future based on the examples we provide. The main purpose is to ensure that computers automatically learn without human intervention and outside help, and to regulate actions accordingly.

ML algorithms are often classified as supervised, semi-supervised or un-supervised. In general, these algorithms can apply past data to new data, using the noted examples to predict future events. Starting with the analysis of a known training database, the learning algorithm creates a resultant function to predict the output values. In doing so, the learning algorithm can also compare the result with specific "correct"

samples of the latest data and find errors to change the development model accordingly. In semi-supervised ML approach small amount of data (labeled) is merged to the huge dataset (unlabeled). It lies between supervised (labeled data), and un-supervised learning (un-labeled data). In contrast, unsupervised ML algorithms are used when the information used for training is not classified or marked in any way. The system examines the data and can draw conclusions from the datasets.

Improving machine learning algorithms is used to interact with the environment - trial and error search is the most important learning characteristic of this method, which allows programs to automatically detect ideal behavior in a specific context to maximize its performance.

K-means is a clustering approach used to partitioned N number of data into k number of groups known as clusters. The process is followed as:

- Initially, select K centroid, which is the center point of each fragmented data.
- Allocate data point to the closest centroid.

- Reallocate centroid value as the calculated average value for each group.
- Reallocate the data points to the adjoining centroid.
- Repeat until the data points remain in the same group.

After dividing data into different groups on the bases of boundary conditions as mentioned above, three centroids have been selected for the divided data. The process of centroid selection is as follows:

Consider an initial set of k means (centroids) $(C_1, C_2, \dots, \dots, C_n)$ in clusters (S_1, S_2, \dots, S_n) . At the first stage, the centroids of the clusters are selected randomly or according to a certain rule (for example, choose the centroids that maximize the initial distances between the clusters). We refer observations to those clusters whose mean (centroid) is closest to them. Each observation belongs to only one cluster, even if it can be assigned to two or more clusters. Then the centroid of each i-th cluster is recalculated according to the equation (13).

$$C_j = \frac{1}{S_j} \sum_{x(j) \in S_j} X(j) \quad (13)$$

Thus, the k-means algorithm consists in recalculating the centroid at each step for each cluster obtained in the previous step. The algorithm stops when the value C_j does not change the maximum and minimum value. The three centroids are formed and named as centroid 1, centroid 2, and centroid 3, each represented by equation (14), equation (15), and equation (16) respectively.

$$\text{Centroid 1} = \left[\sum_{i=1}^n \frac{CS}{n}, \sum_{i=1}^n \frac{SC}{n}, \sum_{i=1}^n \frac{HS}{n} \right] \quad (14)$$

$$\text{Centroid 2} = \text{centroid 1} + 20\% \quad (15)$$

$$\text{Centroid 3} \rightarrow \text{Centroid 1} - 20\% \quad (16)$$

The designed algorithm for K-means is written.

Algorithm: K-means

Input: PD \rightarrow Uploaded project data for clustering
Output: C-Data and C \rightarrow Clustered Data and their centroids
 Initialize an estimated Centroid C = C1, C2 and C3
 Where, $C1 = \frac{SIM_{COS}}{\text{Count of PD}} + \frac{SIM_{SOFTCOS}}{\text{Count of PD}} + \frac{SIM_H}{\text{Count of PD}}$
 $C2 = C1 + 20\% \text{ of } C1$
 $C3 = C1 - 20\% \text{ of } C1$
 Calculate size of PD in terms of [Row, Col.] = size (PD)
For i \rightarrow 1 **to all Row**
 For j \rightarrow 1 **to all column**
 If PD (i,j) == C1
 C-Data 1 = PD (i,j)
 Else if PD (i,j) == C2
 C-Data 2 = PD (i,j)
 Else
 C-Data 3 = PD (i,j)
 End
 Adjust Centroid C using their mean
 C = Average (C-Data 1, C-Data 2 and C-Data 3)
 End - For
End - For
Return: C-Data and C as a Clustered Data and their centroids respectively
End - Algorithm

After selecting centroid, next step is to calculate Euclidian distance and hamming distance as metrics. The k-means method is a method of cluster analysis, the purpose of which is to divide m observations (from space P^n) into k clusters, with each observation referring to the cluster to the center (centroid) of which it is closest. Euclidean distance is used as a measure of proximity, which is given by equation (17).

$$p(x, y) = \sqrt{(x_1 - y_1)^2 + (x_2 - y_2)^2 + \dots + (x_n - y_n)^2} \quad (17)$$

$$= \sqrt{\sum_{i=1}^n (x_i - y_i)^2}$$

Where x, y represent the Euclidean vector.

C. The Group Labelling

As shown in Fig. 1, once the group is formed, the correlation between the group elements is calculated using Mean Square Error (MSE), Standard Error (SE) and Standard Deviation (STD) for both the groups. In order to neutralize, the evaluated parameters for every group, log scale is considered which joins summative of MSE, SE and STD. A ruleset for labelling the group is designed as follows.

Algorithm Labelling

Input: Groups , Evaluated Parameters

Foreach grp in Groups

$$\text{Calculate } \frac{\sum_{i=1}^{n1} MSE}{n}, \frac{\sum_{i=1}^{n1} STD}{n}, \frac{\sum_{i=1}^{n1} SE}{n}$$

$$\text{Judgement}_{Level}.Append = \log\left(\frac{\sum_{i=1}^{n1} MSE}{n} + \frac{\sum_{i=1}^{n1} STD}{n} + \frac{\sum_{i=1}^{n1} SE}{n}\right)$$

End For

Find $\min(\text{Judgement}_{Level})$ and label it low effort as the correlation is high and viceversa.

IV. ANALYSIS AND DISCUSSION

In size and effort estimation in software project, there are a number of measures on the basis of which evaluations has performed. In this research, we have used three metrics to measure the performance of designed size estimation of software project as given by equation (18), equation (19), and equation (20). These are as follows:

Mean Square Error (MSE):

$$MSE = \frac{1}{n} \sum_{i=1}^n \varepsilon_i^2 \quad (18)$$

Standard Error (SE):

$$SE = \sum_{i=1}^n \varepsilon_i^2 \quad (19)$$

Standard Deviation (STD):

$$STD = \sqrt{\frac{1}{n-1} \sum_{i=1}^n (x_i - \tilde{x}_i)^2} \quad (20)$$

In this research, we have applied data fragmentation approach in addition to K-means approach. The results evaluated based on above mentioned parameters is listed in Table I.

TABLE I. EVALUATED PARAMETERS

Attributes	MSE	SE	STD
Project	0.0572	0.1247	0.472
TeamExp	0.0269	0.1345	0.136
ManagerExp	0.0378	0.2365	0.257
YearEnd	0.0472	0.3254	0.369
Transactions	0.0952	0.1025	0.158
Length	0.0360	0.2456	0.354
Effort	0.0761	0.6582	0.648
Entities	0.0871	0.7251	0.756
PointsNonAdjust	0.0675	0.6981	0.597
Adjustment	0.0752	0.5368	0.694
PointsAjust	0.0697	0.4865	0.486
Language	0.0315	0.3785	0.697

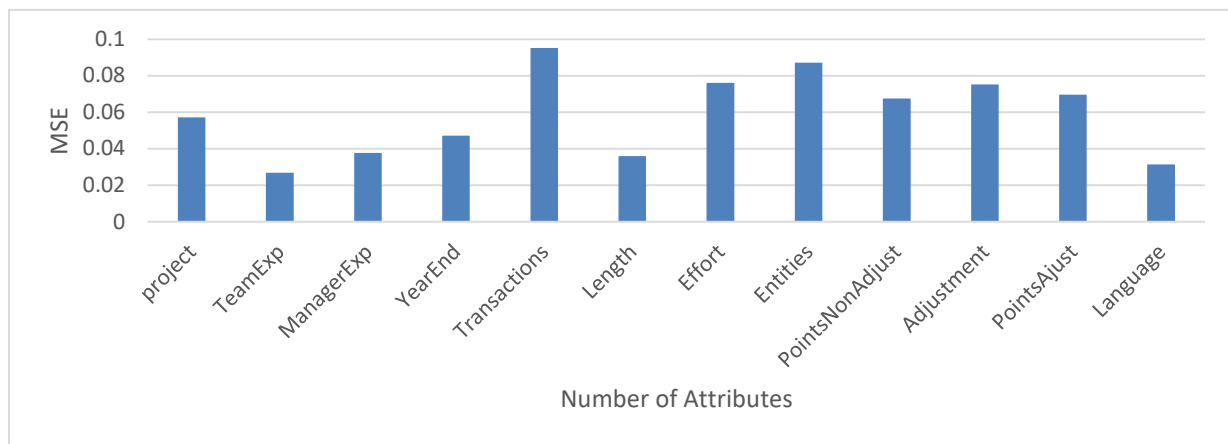


Fig. 3. MSE.

Fig. 3 represents the MSE value analysed for 12 different attributes. X-axis and y-axis represents the number of attributes taken for software project and evaluated MSE value. It is observed that for transaction attribute, designed system show highest error, whereas for team expert error is analysed as minimum. The average mean square error obtained for the designed system is observed as 0.05895, which is very small, and the system can be considered as accepted one for the early size estimation of project using ML technique.

SE is an estimate of the standard deviation of its sample distribution that roughly shows how much the value of a analyzed project rows can differ from its mean. The standard error of estimation is a value equal to the square root of the root mean square error (MSE) regression .MSE, in turn, is equal to the sum of the squares of the differences between the observed parameter (x) and the regression-estimated values (\bar{x}) calculated from all observations and referred to their number n as represented by equation (19). The standard error value has been measured to find out the degree of deviation of the values obtained using the regression, from the actually observed, and thus assess the accuracy of the corresponding

model. The deviation has been represented in Fig. 4, in which the graph shows maximum and minimum SE value of 0.7251, 0.1025 for attribute Entities and transaction respectively. Overall, the average SE analyzed for the proposed work is observed as 0.3877.

The standard deviation is a statistical characteristic of the distribution of a random variable, showing the average degree of dispersion of the values of the quantity relative to the mathematical expectation, denoted by greek σ (sigma).The standard deviation is measured in units of the random variable itself and is used to calculate the standard error of the arithmetic mean, when constructing confidence intervals , when statistically testing hypotheses , when measuring the linear relationship between random variables. It is defined as the square root of the variance of a random variable. Fig. 5 represents the examined STD for different attributes individually. The results show that for entities attribute, the designed early size estimation system using ML approach shows maximum STD, whereas, for 0.158 and 0.136 respectively.

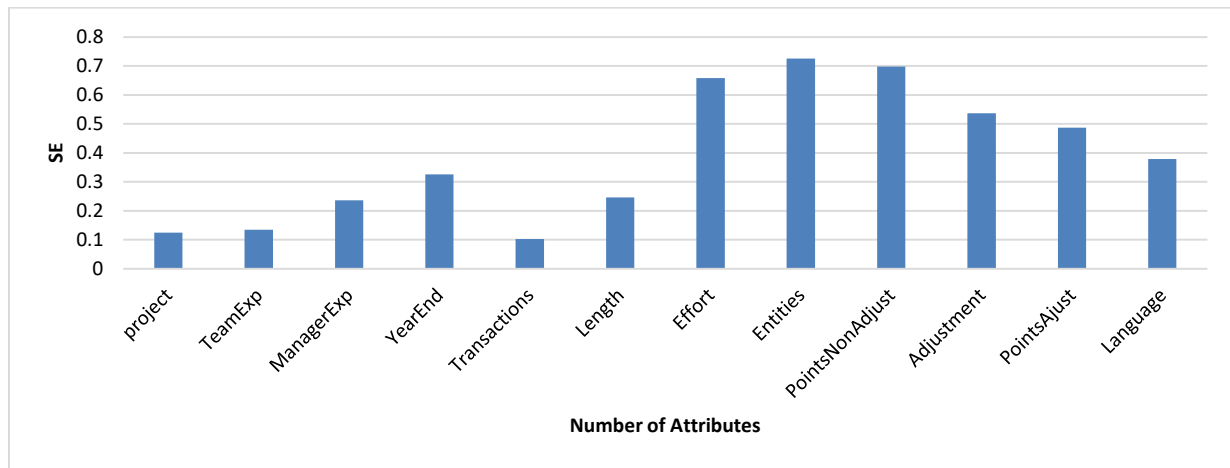


Fig. 4. SE.

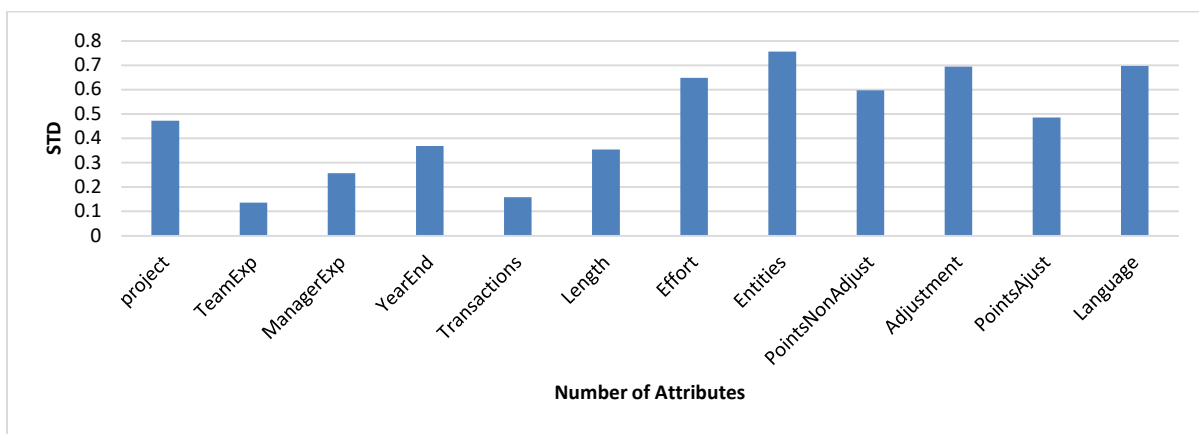


Fig. 5. STD.

V. CONCLUSION

This paper represents a novel segmentation method in order to label the projects as high size and low size. In order to do so, three similarity indexes namely CS, SC and a hybrid similarity which is a combination of CS and SC is designed. The value of 'k' which is total number of groups that can be formed from a supplied set of data is set to be 2 for "high" and "low" size. Once the data is divided, the proposed work model goes for group labelling which is based on machine learning parameters namely MSE, STD and SE. As the parameters are different in nature, a log scale neutralization is performed. A rule architecture was developed to judge the labels and over 500 projects were labelled for high and low software size. A detailed evaluation of parameters is presented in section 4 and the current segmentation architecture will help in establishing Q-Learning mechanism for future project size estimations.

REFERENCES

- [1] E. N. Regolin, G. A. De Souza, A. R. Pozo, & S. R. Vergilio, "Exploring machine learning techniques for software size estimation," In *23rd International Conference of the Chilean Computer Science Society, 2003. SCCS 2003. Proceedings*, pp. 130-136, November 2003. IEEE.
- [2] C. Zhang, S. Tong, W. Mo, Y. Zhou, Y. Xia, B. Shen, "Esse: an early software size estimation method based on auto-extracted requirements features," In *Proceedings of the 8th Asia-Pacific Symposium on Internet ware*, pp. 112-115, 2016.
- [3] D. Azar, "A genetic algorithm for improving accuracy of software quality predictive models: a search-based software engineering approach," *International Journal of Computational Intelligence and Applications*, vol. 9, no. 2, pp.125-36, 2010.
- [4] M. Kaur, S.K. Sehra, "Particle swarm optimization based effort estimation using Function Point analysis," In *2014 International Conference on Issues and Challenges in Intelligent Computing Techniques (ICICT)*, pp. 140-145, 2014.
- [5] L. J. Lazić, M. Petrović, P. Spalević, S. Serbia, "Comparative Study on Applicability of Four Software Size Estimation Models Based on Lines of Code," In *Proceedings of the 6th WSEAS EUROPEAN COMPUTING CONFERENCE (ECC'12), Prague, Czech Republic*, pp. 71-80, 2012.
- [6] P.R. PVGD, C. V. Hari, "Software Effort Estimation Using Particle Swarm Optimization with Inertia Weight," *Global Journal of Computer Science and Technology*, 1969.
- [7] B. Baskeles, B. Turhan, A. Bener, "Software effort estimation using machine learning methods," In *2007 22nd international symposium on computer and information sciences*, pp. 1-6, 2017.
- [8] Y. Ahn, J. Suh, S. Kim, H. Kim, "The software maintenance project effort estimation model based on function points," *Journal of Software maintenance and evolution: Research and practice*, vol 15, no.2, pp.71-85, 2003.
- [9] B. Baskeles, B. Turhan, A. Bener, "Software effort estimation using machine learning methods," In *2007 22nd international symposium on computer and information sciences*, pp. 1-6, 2007.
- [10] A.B. Nassif, D. Ho, L.F. Capretz, "Towards an early software estimation using log-linear regression and a multilayer perceptron model," *Journal of Systems and Software*, vol. 86, no. 1, pp.144-60, 2013.

- [11] S.M. Satapathy, B.P. Acharya, S.K. Rath, "Earl stage software effort estimation using random forest technique based on use case points," *IET Software*, vol.10, no. 1, pp. 10-7, 2016.
- [12] P. Sharma, J. Singh, "Systematic literature review on software effort estimation using machine learning approaches," *In 2017 International Conference on Next Generation Computing and Information Systems (ICNGCIS)*, pp. 43-47, 2017.
- [13] D. Spikol, E. Ruffaldi, G. Dabisias, M. Cukurova, "Supervised machine learning in multimodal learning analytics for estimating success in project-based learning," *Journal of Computer Assisted Learning*, vol. 34, no. 4, pp. 366-77, 2018.
- [14] L. Lavazza, S. Morasca, "Empirical evaluation and proposals for bands-based COSMIC early estimation methods," *Information and Software Technology*, vol.109, pp.108-25, 2019.
- [15] A.B. Nassif, M. Azzeh, A.Idri, A. Abran, "Software development effort estimation using regression fuzzy models," *Computational Intelligence and neuroscience*, pp.1-17, 2019.
- [16] R. Silhavy, P. Silhavy, & Z. Prokopova, "Using Actors and Use Cases for Software Size Estimation," *Electronics 2021*, vol. 10, p. 592, 2021.
- [17] M. Daud, & A. A. Malik, "Improving the accuracy of early software size estimation using analysis-to-design adjustment factors (ADAFs)," *IEEE Access*, vol. 9, pp. 81986-81999, 2021.
- [18] Y. Suresh, "Effective ANN Model based on Neuro-Evolution Mechanism for Realistic Software Estimates in the Early Phase of Software Development," *International Journal of Advanced Computer Science and Applications*, vol.13, no.2, 2022.

Use of Information and Computer-based Distance Learning Technologies during COVID-19 Active Restrictions

Irina Petrovna Gladilina¹, Lyudmila Nikolaevna Pankova²
Svetlana Alexandrovna Sergeeva³, Vladimir Kolesnik⁴, Alexey Vorontsov⁵
Moscow Metropolitan Governance University, Moscow, Russia^{1, 2, 4, 5}
Moscow State Institute of International Relations (MGIMO), Moscow, Russia³

Abstract—Despite the reduction of restrictive measures imposed due to the COVID-19 pandemic, the problem of organizing distance learning continues to be topical. Distance learning imposes a much greater responsibility on teachers, giving them more of a workload as learning technologies change rapidly and teachers have to actively adapt to innovations, devoting a lot of time to preparing appropriate materials to ensure the best learning outcomes. The aim of the study is to detect the use of the most effective means of organizing distance learning by teachers. The study is based on a survey of university professors who were teaching in the distance mode during 2020-2021 active administrative restrictions. Opportunities for the use of various services in the organization of distance learning are analyzed and the drawbacks and advantages of the distance learning system are highlighted. The study reveals previously unapparent issues that arose in the course of distance work in quarantine. These include, first and foremost, the high physical workload of teachers, the many technical problems that arose in the transition to distance learning, the lack of teachers' competencies, which needs to be urgently addressed, and the complicated coordination of the learning process. Despite the problems identified, the authors argue that the system of distance learning can and must be adopted and further developed as an additional supporting direction in the organization of the learning process, which will allow educational institutions to promptly shift to distance learning as needed.

Keywords—Distance learning; teachers; electronic service; online class

I. INTRODUCTION

The COVID-19 pandemic forced universities to shift to the mode of distance learning (DL), which required them to use all the powers of the infrastructure, employ specialized software, expand the functionality of the existing educational platforms, and work on the development of databases and teachers' competence [1], [2]. In essence, it was a complex systemic task that covered virtually all parts of the educational process.

Contemporary ICT and web technologies are moving to ever more advanced levels of operation, and DL is becoming more than just an online session or webinar as it incorporates many more student activities, such as data collection, data processing, communication, and interaction with the interface and the external environment [3]–[5].

Research on the peculiarities of using the DL system by teachers of information and computer technologies acquired particular significance when all educational institutions faced the need to fully shift to DL due to the introduced quarantine measures caused by the COVID-19 pandemic. In this light, of special interest are the issues of the use of various means of organizing DL by teachers and practical recommendations on the implementation of DL that could be used by universities during the period of restrictions caused by the COVID-19 pandemic [6].

II. LITERATURE REVIEW

In the course of the quarantine, there appeared a considerable amount of papers with practical advice and recommendations on the introduction of DL. For instance, one study [7] reveals that the teachers who most easily rearranged their style of work and got more enjoyment from the introduction of the DL work at the institutions that had clear systemic communications and algorithms for action formed prior to the pandemic and implemented and maintained at the level of the management of the individual educational institution.

Scientific research actively discusses new approaches to the organization of DL, which requires substantiation of such provisions as the motivational, technological, and process support for the education system as an integral pedagogical system that accounts for the individual interests, abilities, and aptitudes of students and the newest teaching strategies [8]. At present, the most acute are the issues of using electronic services and platforms to successfully employ DL in the educational process [9], [10].

In the present study, we define DL as a part of web-oriented education – a type of education that fundamentally relies on the use of ICT and in which the participants of the learning process primarily engage in individualized educational communication [11].

In accordance with the research problem, researchers consider cases of DL implementation during the COVID-19 pandemic at various universities around the world [7, 8, 9] and in various areas of study [10, 11, 12]. Researchers analyze the factors that facilitate and hinder the implementation of distance

education during the COVID-19 pandemic [13], study the perception of distance learning by students during the pandemic [14], the satisfaction of teachers and students of distance education and their understanding of the opportunities and problems of distance learning during the period of quarantine restrictions [15]; determine the existing educational and technological barriers to distance education [16] and the relationship between digital transformation, satisfaction and the intention of students to continue learning online [17] during quarantine restrictions; prove the advantages of organizing DL in order to prevent the spread of a pandemic [18]; justify the benefits of distance learning during the crisis, which are the use of technology, improving the communication skills of students and saving time on teaching and learning [19]; determine the priorities of learning after the removal of restrictions to find a balance between distance learning and full-time education [20].

Nevertheless, a full picture of the realities of DL cannot be painted without considering the position and feedback of teachers as those who put the system into operation.

In view of the above, the goal of the present study is to detect the use of the most effective means of organizing DL by teachers during the period of active restrictions caused by the COVID-19 pandemic.

Research objectives are:

- 1) To analyze the opportunities to use various services in the organization of DL during quarantine measures.
- 2) To define the advantages and drawbacks of the DL system.
- 3) To identify previously unapparent problems in the process of distance work during quarantine.

Further, the article describes the methodology of the study, presents the results of the study and analyzes their significance. In conclusion, the conclusions of the work carried out are drawn.

III. METHODS

The established research goal entails the following approximate list of theoretical and empirical research methods: the theoretical methods of analysis, synthesis, comparison, and summarization used in the study of scientific literature on the organization of DL during the period of quarantine restrictions caused by the pandemic. The theoretical base of the study was grouped depending on the type of documents. The first group of information sources consisted of studies devoted to the problem of the possibility of introducing distance learning into the educational process. The second group of information sources was devoted to the consideration of the specifics of the use of DL during the period of active restrictions caused by the COVID-19 pandemic. The considered sources of information were 30 articles from scientific peer-reviewed journals Scopus and Web of Science for the last 3 years; the empirical method of a survey employed to analyze the existing peculiarities and problems of organizing DL.

The primary method of research was an expert survey, the sample of which consisted of 100 teachers sampled by the

method of criterion-based selection. The survey method was the most appropriate for the purpose of the study, since determining the use by teachers of the most effective means of organizing distance learning during the period of active restrictions caused by the COVID-19 pandemic was most accurately feasible when analyzing the opinions of the teachers themselves, as direct participants in this process. The survey included the following questions:

“What services do you use to post educational and methodological support materials during the organization of DL?” (multiple choice possible), followed by a discussion of the experience;

“What services do you use for hosting video conferences?” (multiple choice possible);

“In your opinion, what are the main disadvantages of DL?” (multiple choice possible);

“In your opinion, what are the main advantages of DL?” (multiple choice possible);

“In your opinion, what are the major problems in the process of DL during quarantine that were not apparent beforehand?” (multiple choice possible).

Thus, the surveyed teachers were asked to identify the main resources they had used to post educational and methodological materials for students to access and the services most often used for communication with students and hosting online conferences. The survey also enabled the teachers to describe the advantages and disadvantages they see in the DL system and to identify major problems in the DL process during quarantine that were not evident beforehand. In addition, the teachers were able to give their opinions on opportunities for improvement.

Further on, the opinions of teachers about the services preferred for posting educational and methodological materials and hosting video conferences, the main drawbacks of DL, and the problems discovered in the course of distance work were ranked by popularity. The consistency of teachers' opinions was assessed by the concordance coefficient:

$$w = \frac{12S}{n^2(m^3 - m)}$$

where S is the sum of the squared deviations of all rank estimates of each evaluated object from the mean value; n – the number of respondents; m – the number of assessment objects.

Statistical processing of the survey results and calculation of descriptive statistics (percentage of expert mentions) and the concordance coefficient were performed using the SPSS software product.

IV. RESULTS

The conducted survey reveals that in posting educational and methodological materials as part of DL, the respondents give preference to Moodle (45%) and Google Classroom (44%) due to their convenient subdivision of topics and classes and easy access for students (Table I).

TABLE I. SERVICES FOR POSTING EDUCATIONAL AND METHODOLOGICAL SUPPORT MATERIALS

№	Service	Response rate*, %	Rank
1	Moodle	45%	1
2	Google Classroom	44%	2
3	Google Drive	31%	3
4	Microsoft Teams	8%	4
5	Other	29%	

multiple choice possible

An object-oriented DL environment Moodle relies on contemporary information and computer technology. The service can also be used by students to receive feedback, as they can post their completed laboratory assignments and other documents to be checked by the professor.

Google Drive as a platform for storing materials with an opportunity to share access to them ranks third in the respondents' choice (31% of the respondents choose this option). Microsoft Teams is used by only 8% of those surveyed. Meanwhile, 29% of the professors do not use any of the mentioned services.

The concordance coefficient for the question is $W = 0.78$ ($p < 0.01$), indicating strong consistency of the teachers' responses to the question.

Subsequent additional questions focus on teachers' experiences with the most popular services (Tables II and III).

TABLE II. EXPERIENCE WITH MOODLE

№	Teachers' judgment	Response rate, %
1	Use a lot	39%
2	Use little	13%
3	Not use at all	36%
4	Consider it convenient to use	43%
5	Consider it inconvenient to use	7%
6	Recommended for use	43%
7	Not recommended for use	7%

TABLE III. EXPERIENCE WITH GOOGLE CLASSROOM

№	Teachers' judgment	Response rate, %
1	Use a lot	24%
2	Use little	23%
3	Not use at all	36%
4	Consider it convenient to use	26%
5	Consider it inconvenient to use	3%
6	Recommended for use	37%
7	Not recommended for use	26%

Considering the above services from the point of convenience, 43% of the surveyed teachers consider Moodle to be quite usable and recommend it for use in the educational process (Table II). However, commenting on their experience using Moodle, 7% of the respondents do not recommend using

it as the main system for organizing DL in educational organizations (Table II), explaining their position by the fact that teachers and students voice many complaints about its operation.

The Google Classroom service is used in working with educational and methodological materials by 24% of teachers and recommended for use by only 26% (Table III). Moreover, 36% do not use Moodle and Google Classroom in the learning process at all and consider them inconvenient.

In the organization of DL, of importance are video conferencing platforms, which allow students to attend lectures in real time and actively discuss the materials presented while physically being in different places. This model approximates online learning to study in a real classroom as much as possible.

The responses of teachers to the question "What services do you use for hosting video conferences?" are presented in Table IV.

TABLE IV. SERVICES FOR HOSTING VIDEO CONFERENCES

№	Service	Response rate*, %	Rank
1	TrueConfServer	55%	1
2	VideoMost	34%	2
3	Google Meet	17%	3
4	Google Hangouts	10%	4
5	Microsoft Teams	8%	5
6	Cisco Webex Meetings	3%	6-7
7	Big Blue Button	3%	6-7
8	Skype	2%	8
9	Discord	1%	9

multiple choice possible

The survey results show that the most popular video conferencing service is TrueConfServer, which gained popularity after Russian universities ceased cooperation with Zoom, with the selection rate of 55% (Table IV). Another Russian product, VideoMost, has 34% of the vote.

Free video chat services Google Meet and Google Hangouts are used by 17% and 10% of respondents, respectively. The Microsoft Teams service is approved by 8% of university professors; such a low rate may be explained by a fairly high subscription fee charged for most Microsoft services. Among other video conferencing resources mentioned by the teachers are Cisco Webex Meetings (3%), Skype (2%), and Discord (2%).

It should be noted that conferencing directly in Moodle is not a typical solution. Only 3% of the respondents use the Big Blue Button service, which integrates with Moodle, although the previous question reveals that 39% of the respondents use Moodle to post educational and methodological materials (Table II).

The value of the concordance coefficient $W = 0.76$ ($p < 0.01$) indicates a high coherence of the teachers' opinions on this issue.

The main disadvantages of DL as viewed by teachers are presented in Table V.

TABLE V. PRIMARY DISADVANTAGES OF DL

No	Primary disadvantages of DL	Response rate*, %	Rank
1	round-the-clock load	65%	1
2	lack of a unified platform	37%	2
3	lack of unified standards and requirements, as well as unified software	35%	3
4	unequal access to high-speed Internet	19%	4
5	difficulties in objectively assessing knowledge	16%	5

multiple choice possible

The value of the concordance coefficient $W = 0.82$ ($p < 0.01$), which suggests a strong consistency of opinion on the issue.

Additionally, the survey of teachers during the DL process while in quarantine revealed problems that were not apparent beforehand (Table VI).

TABLE VI. PROBLEMS DETECTED WHILE WORKING IN THE DISTANCE MODE

No	Problem	Response rate*, %	Rank
1	teachers' technical competence	68%	1
2	optimization of class schedules and workload in the distance mode	44%	2
3	multitasking	37%	3
4	content structuring of information flows	24%	4
5	electronic deanery	20%	5

multiple choice possible

For this item, the concordance coefficient is $W = 0.75$ ($p < 0.01$), indicating a strong concordance of the teachers' views on the matter.

V. DISCUSSION

According to the survey results, the main drawback of DL for teachers is a round-the-clock load caused by the need to adjust educational and methodological materials for online classes, post them online, hold consultations and video conferences, maintain contact with students and their parents (special attention should be paid to the professor's actions in the case of prolonged absence of students who do not attend classes and do not contact them), as well as to conduct control and assessment of the level of students' knowledge, which is consistent with previous research [13]. A particular factor in the higher workload of teachers is the increased amount of reporting documents required in the course of DL.

Among the key disadvantages of the organization of DL, the teachers also note the lack of a unified platform, lack of uniform standards, requirements, and unified software, lack of student motivation, unequal access to high-speed Internet, plagiarism, and difficulties in assessing students' knowledge objectively.

Further on, the study reveals an ambiguity in the teachers' perspectives on the advantages of DL over classroom teaching, or, conversely, classroom over DL. Those advocating for the advantages of DL justify their position by the following arguments: DL provides an opportunity to learn for those unable to attend classes for objective reasons, allows saving time and money for transportation, results in more comfortable working conditions, and gives an opportunity to train the self-discipline and self-organization of students, as well as to develop their skills of independent information search and processing and self-learning.

Discussing the problems detected in the course of remote work, the teachers prioritize in the organization of DL the need for teachers to acquire specific competence, which includes: 1) knowledge of the opportunities and available resources to conduct DL: learning platforms, software, techniques, and instruments; 2) mastery of the methodology of adjusting traditional courses for the electronic format; 3) mastery of the technology of digitizing learning tasks. What can become a solution to the above problem, researchers suggest, is the organization of training and masterclasses as part of professional development programs [20], [21].

The need for content structuring of information flows owes to the fact that the transition to an exclusively distance form of work in the quarantine majorly increased the flow of information from various sources and university departments [22]. The lack of the competence and culture of online communication has resulted in too much noise and spam in professional correspondence, which made coordination and timely access to the necessary documents difficult. To resolve this issue, researchers suggest [16], [23], it is enough to develop a system of labeling documents by content according to an agreed-upon standard in order to structure them and move them to appropriate databases and to provide guidelines for professional online communication for university staff, faculty, and students.

The problem of optimization of class schedules and workload in the distance format consists in the fact that in DL, the number of students in a group does not depend on the size of the classroom and the number of seats. This gives an opportunity to optimize the schedule by merging the student groups studying in the same program. Educational platforms allow one to simultaneously engage all students in different types of tasks during the class. This measure ensures the high quality of the educational process, but also considerably increases the intensity of the teachers' work and the time required to prepare for distance classes and check students; assignments on the platform. Scholars believe that in order to alleviate these issues, it is appropriate to optimize the schedule without reducing the number of classes for students by assigning the courses of one specialty to a single professor [14], [24], [25]. Reducing the teacher's workload by merging student groups can enhance the quality of DL classes by freeing up the professor's time to prepare and check assignments on the platform.

The problem of multitasking consists in the fact that while holding classes in the form of webinars, aside from their regular function of transmitting and controlling the assimilation

of knowledge, teachers also acquire the functions of: an organizer of communication who informs and invites the group to a webinar; a webinar moderator who manages communication in a DL environment; a technical assistant who provides technical support for the process. Simultaneous performance of all these functions, which in traditional teaching are split between the professor, dean's office, and laboratory assistants and require the professional skills of a moderator, significantly increases the load and stress on one faculty member and leads to exhaustion [19].

The problem of multitasking can be solved by means of a specially developed methodology for organizing and holding webinars for systematic DL. This requires, first, to define the specific goals and functions of the participants and those responsible for the organization and support of the process; second, to automate the processes when needed and possible; third, to account for the increased workload of teachers in the remote format [14].

Finally, management of the learning process in DL necessitates the creation of an electronic deanery, which would serve the functions of information support, feedback, learning process organization, control, collection, and analysis of statistical data, sharing the experience gained, and more.

VI. CONCLUSION

In general, in the context of active restrictions caused by COVID-19, the most effective way to organize the educational process is to switch to an emergency distance learning mode. However, for both teachers and students, long-term training in this mode raises a number of problems, the solution of which requires continued research in this area. In the context of our study, we identified, first of all, the problems of the lack of a single platform, common standards and requirements, as well as unified software.

The issue of relevant organization of DL needs to be studied further since there is a need to reconsider and reorganize the entire learning process, renew the content of educational programs, and develop new integral programs for DL to support the mobile vector of learning, strengthen students' interest, and eliminate the factors of disorganization, distraction from the learning process, and loss of interest.

It is advisable to continue using DL periodically to collect teachers' feedback and recommendations to improve DL since teachers are the key objects and subjects of educational activities who experience the development of DL first-hand at its initial and early stages.

Most universities' learning systems are more oriented toward developing the organization of the in-classroom learning process rather than the DL system. Meanwhile, a system of prompt transition to DL cannot be developed without repeated practice and specialized software. The current state and prospects for the development of technology and remote work, as well as the epidemiological situation, bring to light the need for methodological support for programs, as well as technical and human resource capacity, to ensure self-sufficient DL.

The prospect of further research may be the development of recommendations for teachers on the practical solution of problems arising from the use of educational services and technologies caused by the need to switch to emergency distance learning.

REFERENCES

- [1] E. A. Smirnova, A. N. Stolyarova, K. S. Surnina, Y. M. Denenberg, and T. V. Dikova, "Impact of the COVID-19 pandemic on the development of digital technologies in academic education," *Journal of Advanced Pharmacy Education And Research*, vol. 11, no. 1, pp. 207–213, 2021, doi: 10.51847/NOMIOs9nAQ.
- [2] S. E. Shishov, "Digitalization Policy Influence: Implementation of Mobile Learning in the University Educational Process," *Webology*, vol. 18, no. Special Issue 04, pp. 687–699, Sep. 2021, doi: 10.14704/WEB/V18SI04/WEB18158.
- [3] S. Kumar Basak, M. Wotto, and P. Bélanger, "E-learning, M-learning and D-learning: Conceptual definition and comparative analysis," *E-Learning and Digital Media*, vol. 15, no. 4, pp. 191–216, Jul. 2018, doi: 10.1177/2042753018785180.
- [4] M. V. Vinichenko, M. V. Vinogradova, G. Yu. Nikiporets-Takigawa, and M. V. Rybakova, "The impact of the pandemic on the quality of education and the image of a university," *XLinguae*, vol. 14, no. 1, pp. 17–37, Jan. 2021, doi: 10.18355/XL.2021.14.01.02.
- [5] S. Evgenyevna Bobrova, E. Nikolaevna Popova, Y. Sergeevna Sizova, L. Nikolaevna Orlova, and I. Veniaminovna Polozhentseva, "Professional Foreign Language Competence Formation using Educational Multimedia Technologies," *International Journal of Education and Practice*, vol. 9, no. 1, pp. 155–170, 2021, doi: 10.18488/journal.61.2021.91.155.170.
- [6] M. v. Vinichenko, T. K. Ridho, P. Karacsony, N. P. Li, G. S. Narrainen, and O. L. Chulanova, "The Feasibility and Expediency of Gamification Activities in Higher Education," *International Journal of Education and Practice*, vol. 7, no. 4, pp. 459–468, 2019, doi: 10.18488/journal.61.2019.74.459.468.
- [7] W. Bao, "COVID - 19 and online teaching in higher education: A case study of Peking University," *Human Behavior and Emerging Technologies*, vol. 2, no. 2, pp. 113-115, 2020. <https://doi.org/10.1002/hbe2.191>
- [8] S. Katic, F.V. Ferraro, F.I. Ambra, M.L. Iavarone, "Distance Learning during the COVID-19 Pandemic. A Comparison between European Countries," *Educ. Sci.* vol. 11, no. 595, 2021. <https://doi.org/10.3390/educsci11100595>
- [9] H. Yulia, "Online Learning to Prevent the Spread of Pandemic Corona Virus in Indonesia," *ETERNAL (English Teaching Journal)*, vol. 11, no. 1, pp. 48–56, 2020.
- [10] N. Sitthimongkolchai, C. Viriyavejakul, S. Tuntiwongwanich, "Blended Experiential Learning with e-Portfolios Learning to Enhance Creative Imagination," *Emerging Science Journal*, vol. 6, Special Issue, pp. 25-39, 2022.
- [11] J. Code, R. Ralph, K. Forde, "Pandemic designs for the future: perspectives of technology education teachers during COVID-19," *Information and Learning Science*, vol. 121, no. 5/6, pp. 419-431, 2020. <https://doi.org/10.1108/ILS-04-2020-0112>
- [12] T.Y. Chang, G. Hong, C. Paganelli, P. Phantumvanit, W.J. Chang, Y.S. Shieh, M.L. Hsu, "Innovation of dental education during COVID-19 pandemic," *Journal of Dental Sciences*. 2021. <https://doi.org/10.1016/j.jds.2020.07.011>
- [13] M.P. Dewi, N.M.B. Wajdi, "Distance Learning Policy During Pandemic Covid-19," *EDUTECH Journal of Education And Technology*, vol. 4, no. 3, pp. 325-333, 2021.
- [14] F.V. Ferraro, F.I. Ambra, L. Aruta, M.L. Iavarone, "Students' perception of distanced learning: A retrospective analysis," *Eur. J. Res. Educ. Teach.* no. 19, pp. 533–543, 2021.
- [15] G.A.El Refae, A. Kaba, S. Eletter, "Distance learning during COVID-19 pandemic: satisfaction, opportunities and challenges as perceived by faculty members and students," *Interactive Technology and Smart Education*, vol. 18 (3), pp. 298-318, 2021.

- [16] F.I. Ambra, F.V. Ferraro, L. Aruta, M.L. Iavarone, "Distanced learning between educational and technological barriers A survey in the Campania region (Italy) with secondary school students," *Attual. Pedagog.* no. 2, pp. 5–26, 2020.
- [17] D.V. Vu, G.N. Tran, C.V. Nguyen, "State-of-the-Art of Digital Transformation, Student Satisfaction, Word of Mouth and Online Learning Intention in Vietnam," *Emerging Science Journal*, vol. 6, Special Issue, pp. 40-54, 2022. <https://doi.org/10.28991/ESJ-2022-SIED-04>
- [18] S.A. Madya, "Online Learning Implementation in the Covid-19 Pandemic," *Ninth International Conference on Language and Arts (ICLA 2020)*, pp. 26-31, 2021. <https://doi.org/10.2991/assehr.k.210325.005>
- [19] T. Snoussi et al., "Distance E-Learning (DEL) and Communication Studies During Covid-19 Pandemic," *Utopía y Praxis Latinoamericana*, vol. 25, no. 1, pp. 253-269, 2020.
- [20] S.A. Ahmed et al., "Model for utilizing distance learning post COVID-19 using (PACT)TM a cross sectional qualitative study," *BMC Medical Education*, 20, 400, 2020. <https://doi.org/10.1186/s12909-020-02311-1>
- [21] N. A. Belousova et al., "Digital environment components for the formation of students' information and analytical skills," *Journal of Advanced Pharmacy Education and Research*, vol. 10, no. 4, pp. 118–125, 2020.
- [22] M. V. Vinichenko, M. V. Rybakova, O. L. Chulanova, S. A. Barkov, S. A. Makushkin, and P. Karacsony, "Views on Working with Information in a Semi-Digital Society: Its Possibility to Develop as Open Innovation Culture," *Journal of Open Innovation: Technology, Market, and Complexity*, vol. 7, no. 2, p. 160, Jun. 2021, doi: 10.3390/joitmc7020160.
- [23] D. M. Kapustina, S. A. Makushkin, E. V. Danilova, T. I. Alexandrova, Y. M. Lagusev, and V. D. Sekerin, "Telework of a Company Employee: Issues of Organizing and Monitoring the Performance of Labor Duties," *Webology*, vol. 18, no. Special Issue 04, pp. 1160–1169, Sep. 2021, doi: 10.14704/WEB/V18SI04/WEB18189.
- [24] I. Korotaeva and O. Chuksina, "Perspectives on the Improving Quality of Language Education: The Case of Moscow Aviation Institute," *Universal Journal of Educational Research*, vol. 8, no. 8, pp. 3392–3397, Aug. 2020, doi: 10.13189/ujer.2020.080812.
- [25] M. S. Logachev, N. A. Orekhovskaya, T. N. Seregina, S. Shishov, and S. F. Volvak, "Information System for Monitoring and Managing the Quality of Educational Programs," *Journal of Open Innovation: Technology, Market, and Complexity*, vol. 7, no. 1, p. 93, Mar. 2021, doi: 10.3390/joitmc7010093.

Detection of COVID-19 from Chest X-Ray Images using CNN and ANN Approach

Micheal Olaolu Arowolo¹, Marion Olubunmi Adebisi², Eniola Precious Michael³
Happiness Eric Aigbogun⁴, Sulaiman Olaniyi Abdulsalam⁵, Ayodele Ariyo Adebisi⁶

Department of Computer Science, Kwara State University, Malete, Nigeria⁵
Department of Computer Science, Landmark University, Omu-Aran, Nigeria^{1, 2, 3, 4, 6}

Abstract—The occurrence of coronavirus (COVID-19), which causes respiratory illnesses, is higher than in 2003. (SARS). COVID-19 and SARS are both spreading over regions and infecting living beings, with more than 73,435 deaths and more than 2000 deaths documented as of August 12, 2020. In contrast, SARS killed 774 lives in 2003, whereas COVID-19 claimed more in the shortest amount of time. However, the fundamental difference between them is that, after 17 years of SARS, a powerful new tool has developed that could be utilized to combat the virus and keep it within reasonable boundaries. One of these tools is machine learning (ML). Recently, machine learning (ML) has caused a paradigm shift in the healthcare industry, and its use in the COVID-19 outbreak could be profitable, especially in forecasting the location of the next outbreak. The use of AI in COVID-19 diagnosis and monitoring can be accelerated, reducing the time and cost of these processes. As a result, this study uses ANN and CNN techniques to detect COVID-19 from chest x-ray pictures, with 95% and 75% accuracy, respectively. Machine learning has greatly enhanced monitoring, diagnosis, monitoring, analysis, forecasting, touch tracking, and medication/vaccine production processes for the Covid-19 disease outbreak, reducing human involvement in nursing treatment.

Keywords—Machine learning; COVID-19; ANN; CNN; X-ray images

I. INTRODUCTION

Throughout history, there has been widespread of infectious disease among our places of residence. This has caused deterioration of every aspect of our economics and well-being as a whole. This effect has caused solutions being found through the use of machine learning as a division of artificial intelligence. Over the years there has been the existence some pandemics such as the Athenian plague [1], Ebola pandemic [2], HIV pandemic [3], Zika virus [4], black death [5], etc. Coronavirus which is a happening contactable epidemic that is all over the spheres of the world is a virus belonging to the family Coronaviridae [6].

In fighting covid-19 there has been many solutions being proffered through the use of different machine learning techniques [7]. It has also aided in various studies, including the ensemble of machine learning for the simulation of covid19 deaths [8], as well as identifying who is prone to being the next victim, diagnosing suspected individuals, developing medicine vastly, and being able to predict the next occurrence of such a remerging virus.

Some computer scientists have used machine learning to test coronavirus presence such as [9] who worked on automated detection of Coronavirus disease-2019 (COVID-19) from X-ray images and used YOLO (You only look once) machine learning technique. However, his model misdiagnosed COVID-19 patients as pneumonia and predicted incorrectly in low production of X-ray images and patients with other diseases. Research uses Convolutional Neural Network (CNN) and the deep learning approach to detect multi-class brain disease using MRI images. There was no feature extraction, collection, or classification in this process because it was fully automated [10]. A system created from machine learning techniques was also created to diagnose coronavirus [11].

Artificial intelligence (AI)-based models have effectively used current noticeable data to learn the cause of current therapies on humans, provided their unique characteristics. All this will help in detecting various diseases based on each individual's characteristics. Recent advancements in machine learning models optimized for making research through noticeable information setting can be used to learn customized treatment outcomes.

However, although these models can produce correct diagnosis and predict other ailments and infectious diseases. Furthermore, regardless of how accurate most machine learning models relating to covid19 prediction appear to be, they appear to be difficult to interpret. The difficulty in detecting Covid19 infection at an early stage is also attributed to the high similarity of its symptoms to those of pneumonia. As a result, distinguishing cases of coronavirus from pneumonia is easy, which could save a patient's life.

This research uses chest X-ray images to classify Coronavirus disease using machine learning classifiers (convolutional neural networks) implemented in Python, as well as rectified linear units (ReLU) to help overcome image non-linearity (in this case chest x-ray images). This research, on the other hand, suggests using a Convolutional neural network (CNN) and Artificial Neural Network (ANN) method to develop a model to detect coronavirus disease.

II. REVIEWS OF RELATED WORK

With the support of imaging and image-based classification methods, machine learning is now a highly important and flexible technique for detecting terminal diseases in recent years.

Research that used machine learning was proposed [12] to classify skin cancer at the dermatologist stage (CNNs). The use of a single CNN qualified end-to-end from photographs directly, with only pixels and disease labels as inputs, to classify skin lesions.

An epilepsy detection system based on this technique is proposed [13]. The proposed method has an accuracy of 100% for all of the tested signals when it was used to identify electroencephalogram (EEG) recordings using EEG signals into epileptic and non-epileptic.

A deep convolutional neural network was developed with long-term ECG signals to create a system for detecting arrhythmia [14]. Instead of the hand-crafted feature extraction and selection used in conventional approaches, a full end-to-end structure was developed. Their key achievement is the development of a new 2D-convolutional neural model that can recognize 17 cardiac arrhythmia disorders with a high level of accuracy.

Deep neural networks with chest visuals were used [9] to automate the prediction of coronavirus disease instances. He proposed a model called "DarkCovidNet model," and the model does not involve any handcrafted feature extraction techniques, and it was accurate and fast. However, the model misdiagnosed COVID-19 patients as pneumonia and predicted incorrectly in bad-quality X-ray images and predicting of wrong diseases not aimed at.

A study using CNN and the deep learning approach to identify multi-class brain disease using Magnetic resonance imaging (MRI) images was proposed [15]. There was no feature extraction, collection, or classification in this process because it was fully automated.

The deep learning model was created [16] using 224 verified COVID-19 images. Their model had success rates of 98.75% and 93.48% in two and three grades, respectively.

Using chest X-ray images and the ResNet50 model, [17] achieved a COVID-19 detection accuracy of 98%.

Using X-ray images, [18] categorized features obtained from various convolutional neural network (CNN) models with the aid of a support vector machine (SVM) classifier.

A deep learning approach was proposed to detect Pneumonia in chest X-ray images efficiently [10]; transfer learning is used to fine-tune the deep learning models to achieve higher training and validation accuracy; however, large datasets for chest X-rays were not usable, and the results of the deep learning models could not be clarified properly. The final prediction of the model must also be properly explained, which is one of the disadvantages of deep learning-based models.

A study used whole-slide images and deep transfer learning to detect invasive ductal carcinoma. COVID-Net, a deep model for COVID-19 detection proposed [19], correctly identified normal, non-COVID pneumonia, and COVID-19 cases with 92.4 % accuracy.

A deep learning model for detecting covid19 in CT-scan images was proposed [20]. The Python programming language was used to carry out this research. Python Deep Learning

libraries such as Keras and TensorFlow 2.0 were used to develop and train the Convolution Neural Network (CNN) model. The open-access archive of COVID-19 chest computed tomography (CT) images was used as the dataset.

A model was developed for automated voice-based detection of severe acute respiratory syndrome coronavirus 2 (SARS-CoV-2) [21] that could help with COVID19 screening. However, the cough dataset was not included in any of his input datasets because the transformer was built on speech data and was intended to improve non-speech input efficiency.

A model to efficiently classify the COVID-19 infected patients and normally based on chest X-ray radiography using Machine Learning techniques was proposed [22]. The proposed system involves pre-processing, feature extraction, and classification. The results show that among the four classifiers, SVM has the highest accuracy of 96 % (K-Nearest Neighbors and Random Forest had 92% accuracy, Naive Bayes had 90 % accuracy, and Decision Tree had 82 % accuracy).

A study involving the use of machine learning detects COVID-19 infection from regular blood tests [23]. His model had a sensitivity of 92 to 95 % and an accuracy of 82 %. However, the study had two major limitations: the study had a small number of cases considered, and the accuracy of his test could be harmed by issues such as insufficient procedures for collecting, handling, transporting, and storing swabs, sample contamination, and the presence of interfering substances.

A deep learning model for improving the characterization of covid19 from chest X-ray images using CNN was developed [24], but their limitations include improving the proposed deep learning model's design and, most importantly, testing the model's robustness on some large-scale datasets. In addition, his qualified CNN-based deep learning model has been deployed to both web and Android applications for clinical use.

A study was proposed using used transfer learning and a convolutional neural network to detect covid19 from x-ray images automatically [25]. However, they were unable to differentiate mild symptoms from pneumonia symptoms, even though these symptoms may not be visible on x-rays or may not be visible at all.

For covid19 detection based on x-ray images, [26] proposed a concatenation technique in convolutional neural networks. The model, however, was not tested on a large number of datasets and was ineffective in medical diagnosis.

A study that used deep learning to classify covid19 in chest x-ray images was developed [27]. The accuracy of this study's classification was 99.5 %, but the dataset was too limited.

III. MATERIAL AND METHODS

A. Data Description

This study makes use of dataset retrieved from the Kaggle repository (<https://www.kaggle.com/praveengovi/coronahack-chest-xraydataset>).

Kaggle is an online data science platform for developers and techies, with a variety of crowdsourced datasets and frameworks. The dataset was found by searching for the

“corona chest x-ray dataset” on Google. It contains a corona chest x-ray dataset with 6 features and 5935 samples, as well as attributes such as the image name of the x-ray, a label that indicates x-ray (normal or healthy, and person affected with pneumonia), dataset type, and another label called label 2 that holds information about the person affected with pneumonia. This dataset of chest x-rays will be used to analyze my data with CNN and ANN to achieve the following performance metrics sensitivity, time, and speed.

The suggested model below focuses on using a convolutional neural network to implement a model. The dataset, which consists of chest x-ray (pneumonia cases included) images obtained from Kaggle, will be fed into a trained CNN model and also a trained ANN model to predict which of the model will give better accuracy results. The analysis will be evaluated using the following performance metrics: accuracies, precision, and recall.

B. Convolutional Neural Network

Convolutional Neural Networks, often known as ConvNet, are a type of deep learning used to assess visuals [28]. The employment of the layered arithmetic operations by the system is referred to as a CNN. Convolution is a unique sort of linear operation. CNN's concealed structures consist convolutional layers that convolve using multiplication and perhaps other dot multiplication. Backpropagation is done in this algorithm and it gives a better result in terms of accuracy. The Convolution layer employs small filters (e.g., 3×3 or 5×5), a stride of $S=1$, and, most significantly, padding the input volume with zeros in such a way that the convolutional layer does not alter or modify the input's spatial dimensions. That is, if $F=3$, using $P=1$ would keep the input at its original size. $P=2$ when $F = 5$. $P = (F - 1)/2$ holds the input size for a general F . It is only natural to see this on the first convolutional layer that is looking at the input image while using larger filter sizes (such as 7×7). Convolution is a numerical method for calculating the integration of the combination of two functions while one of the indicators is flipped (also known as signals). After one of two functions g and f is passed over the other, it specifies the sum of their overlap. It is a device that combines two components into one. To begin, rotate the signal g 180 degrees horizontally, then slide the flipped g across f , multiplying and maintaining all of its values.

C. Artificial Neural Network

This deals according to the neurons present in the brain of human and these neurons are arranged in layers. It makes use of similar pattern recognition that solves the problem fed to it. This algorithm mimics the operation of a human brain.

ANNs are used to predict a variety of processes. Numerous disciplines of mathematics, engineering, medicine, economics, neurology, and many others have successfully used ANNs. They can handle noisy and incomplete data, which are typical of most renewable energy data, among their many other benefits. They can handle a vast array of data and are adaptable in handling changes in parameters. They can also correlate the hidden data in a large pile, which may significantly influence the model. Once an artificial neural network (ANN) has figured out the pattern, it can carry out complicated tasks like prediction, modeling, identification, optimization, forecasting,

and control. Although this has been discussed by a number of researchers, most biomass models do not use random selection of hidden nodes, which can lead to overfitting and underfitting. The majority of biomass prediction models have been created through trial and error. An artificial neural network (ANN) is a complex network made up of interconnected neurons, which are simple processing units. Three elements—Structure, Learning Algorithm, and Activation Functions—can be used to define ANN. The input and output parameters are connected to a complex stratum of neurons in the hidden layers. A connection that is inbound has two values attached to it: an input value and a weight. The added value influences the unit's output. To learn the pattern, ANNs are trained using data sets. Once trained, they might be shown fresh patterns for prediction or classification. Whether it is a non-linear regression, classification, or optimization task, the network architecture is determined by the way in which neurons are connected to one another. The majority of modeling research up until the year 2000 were primarily based on the linear regression method, according to a summary of the studies on prediction models for the heating value of various biomass-based materials employing proximate analysis components. However, there is a nonlinear relationship between several proximate analysis biomass components and their High Heating Value, HHV. As a result, the prediction of models based on linear regression may not be accurate enough, especially when the models are tested on several data [29].

D. Development and Evaluation of Model

A variety of techniques will be used to incorporate various aspects and functionalities of the system during the implementation process. The model, which is the engine that runs the app/system, will be built/developed using the Python programming language, Kaggle, and Tensorflow software. This includes libraries such as the Keras library, Numpy, Sklearn, and Matplotlib, among others. This research will be carried out on a Windows 10 computer with a Python programming language running on an Intel Pentium Core i3 2GHz processor and 4GB RAM (64bit).

IV. RESULT AND DISCUSSION

The covid-19 dataset was gotten from the Kaggle repository (<https://www.kaggle.com/praveengovi/coronahack-chest-xraydataset>) and was implemented using goggle colab, thereafter classification techniques were performed. Specifically, this chapter shows the result of the studies for the proposed model. This study implements a coronavirus disease detection from chest x-ray images using a convolutional neural network and artificial neural network. The data contains corona chest x-ray dataset with 6 features and 5910 samples, as well as attributes such as the image name of the x-ray, label that indicates x-ray (normal or healthy, and person affected with pneumonia), dataset type, and another label called label 2 that holds information about the person affected with pneumonia. The “!pip install” keyword was used to import libraries that are not in collab by default. Different libraries were imported such as; Keras, Tensorflow, NumPy, glob, shuttle, sklearn, imutils, matplotlib, argparse.

Because of the large size dataset, the kaggle Application Programming Interface (!mkdir-p~/.kaggle/ && mv

kaggle.json ~/.kaggle/ &&chmod 600 ~/.kaggle/kaggle.json) was used in importing the dataset.

The data used was categorized into “Normal” which refers to chest x-ray images with coronavirus symptoms and “Pneumonia”. Due to the close resemblance of COVID-19 infection to Pneumonia hence a need to distinguish between them in other to have a high level of accuracy and precision as earlier discussed in the aims and objectives of this study. The COVID-19 dataset is then being passed into the ReLU activation function which is a non-linear function that solves problem of vanishing gradient associated with the use of CNN thereby giving better and faster results and known to be better than the use of sigmoid activation function. Data augmentation simply means creating prototypes of data in other to add to the quantity of the training set and to also regularize the network, classification of the images into “normal” or “COVID” is also being done.

The model is then trained with the train images and by the number of epochs which was 25 and batch size which was 32 provided. During the training, the model tries to learn and recognize patterns of a particular disease for better accuracy. During this training much is taken into consideration to avoid inaccuracy of the model as this can result in inaccurate predictions.

Fig. 1 and Fig. 2 depict the confusion matrix of the CNN trained model which is 74% respectively. For each chop, it explores the correlation among clinical specificity and sensitivity. A confusion matrix is a table that shows how well a classification model (or "classifier") performs on a number of test data for which the true data have been collected.

In this experiment coronavirus chest x-ray dataset was used to experiment with the detection of COVID-19 through chest x-ray images using CNN approach. However, it was shown that ANN outperforms CNN in terms of 95% accuracy. Table I shows the performance evaluation measures for the study.

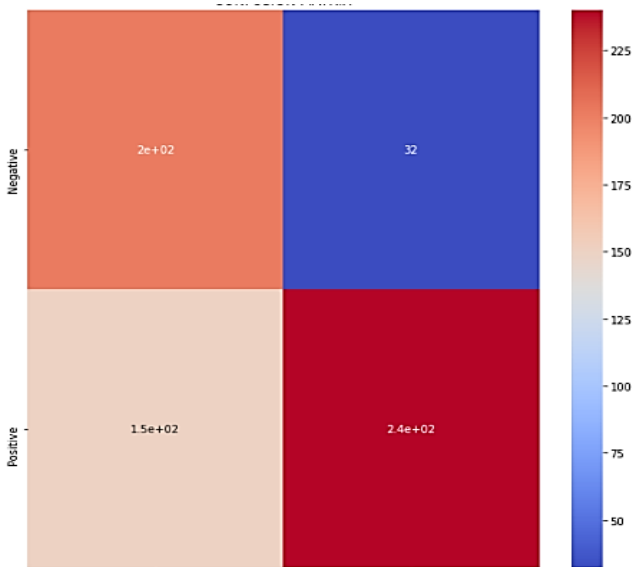


Fig. 1. Confusion Matrix for the COVID-19 Dataset using CNN (TP=32 ; TN=240 ; FP=202 ; FN=150).

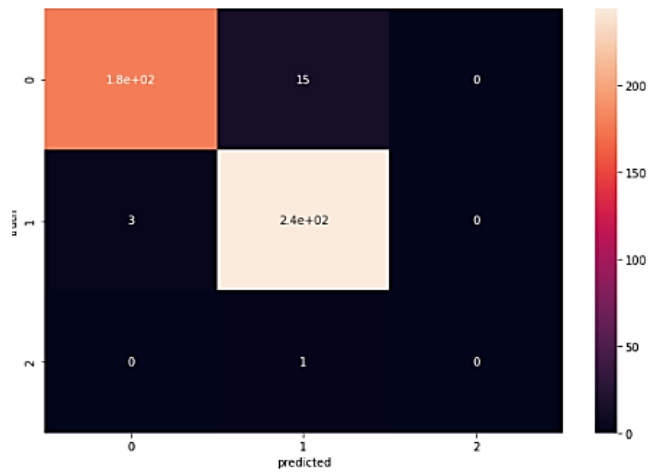


Fig. 2. Confusion Matrix of the ANN Trained Model (TP=178; TN=244; FP=16; FN=3).

TABLE I. PERFORMANCE EVALUATION OF STUDY

Performance Measures (%)	COVID-19 Data + CNN	COVID-9 Data+ ANN	Formula
Accuracy	70.83	95.69	$ACC = (TP + TN) / (P + N)$
Sensitivity	57.39	98.34	$TPR = TP / (TP + FN)$
Specificity	88.24	93.85	$SPC = TN / (FP + TN)$
Precision	86.32	91.75	$PPV = TP / (TP + FP)$
Negative Predictive Value	61.54	98.79	$NPV = TN / (TN + FN)$
False Positive Rate	11.76	6.15	$FPR = FP / (FP + TN)$
False Discovery Rate	13.68	8.25	$FDR = FP / (FP + TP)$
False Negative Rate	42.61	1.66	$FNR = FN / (FN + TP)$
F1-Score	68.94	94.93	$F1 = 2TP / (2TP + FP + FN)$
Matthew's Correlation Coefficient	46.73	91.36	$TP * TN - FP * FN / \sqrt{((TP + FP) * (TP + FN) * (TN + FP) * (TN + FN))}$

The significance of this study for medical professionals and researchers is critical. The identification of coronavirus with the help of this study will enable human radiologists to make more informed decisions about coronavirus prevention and treatment. Furthermore, since this research focuses on having a higher degree of accuracy, it will support both patients and medical professionals, as well as researchers working on further research and prediction for coronavirus care. It is life-saving for both patients and physicians, and it is much more important in countries where laboratory kits for testing are unavailable. Since there is no need for touch until diagnosing COVID-19, the protection of both uninfected individuals and medical practitioners is guaranteed. Table II compares this study with the state-of-the-art.

TABLE II. COMPARATIVE EVALUATION

Authors	Algorithm/Method	Results
Nusra Rouf et al, 2020	Logistic regression and Multinomial Naive Bayes	80% Accuracy
Wang and Wong, 2020	CovidNet from CXR images	93.3% Accuracy
Shuai Wang, 2020	Modified transfer learning technique	89.5% Accuracy
Ioannis,2020	Transfer learning and CNN	96.78% Accuracy
Chuansheng Zheng, 2020	Weak label	90% Accuracy

V. CONCLUSION

The ability to recognize COVID-19 from chest X-ray pictures is critical for both physicians and patients in order to cut testing expense. Artificial intelligence and deep learning can recognize pictures for the tasks that have been learned. Numerous tests were carried out in this paper to identify COVID-19 in chest X-ray pictures with extreme accuracy using a CNN. The classification was divided into three categories: COVID-19/Normal, COVID-19/Pneumonia, and COVID-19/Pneumonia/Normal. In this research, both CNN and ANN were employed to detect COVID-19, and the artificial neural network's accuracy was determined to be 95% greater than the convolutional neural network. To combat the challenges of vanishing gradient regarding the usage of CNN, the COVID-19 sample was fed into the rectified linear unit. Furthermore, the next system design, ANN, which has the highest accuracy, can detect COVID-19 in two classes, COVID-19/Pneumonia/Normal pictures, with a 95% accuracy. As a result, clinicians may find that using Artificial intelligence operating systems solutions can help them diagnose COVID-19. Ongoing research based on the result of this research would further to our understanding of the use of CNN architectures with COVID-19 chest X-ray images and improve the study's findings. People may also consider employing real-world data and wider samples in the long term, as well as developing new algorithms such as enhancing DCNN and RNN. A wider sample should be examined, as should the usage of other machine learning algorithms, with the goal of improving accuracy in the long term. Activation maps can be used in conjunction with the intended machine learning technique to make the findings and framework more readable.

REFERENCES

- [1] Sabbatani, S., & Fiorino, S. (2009). [The Antonine Plague and the decline of the Roman Empire]. *Le Infezioni in Medicina: Rivista Periodica Di Eziologia, Epidemiologia, Diagnostica, Clinica e Terapia Delle Patologie Infettive*, 17(4).
- [2] Kotar, T. (2014). Ebola. In *Zdravniski Vestnik* (Vol. 83, Issue 11). <https://doi.org/10.3329/kyamcj.v5i2.32357>.
- [3] Eisinger, R. W., & Fauci, A. S. (2018). Ending the HIV/AIDS pandemic. *Emerging Infectious Diseases*, 24(3). <https://doi.org/10.3201/eid2403.171797>.
- [4] Masmajan, S., Musso, D., Vouga, M., Pomar, L., Dashraath, P., Stojanov, M., Panchaud, A., & Baud, D. (2020). Zika virus. In *Pathogens* (Vol. 9, Issue 11). <https://doi.org/10.3390/pathogens9110898>.
- [5] Curtis, D. R., & Roosen, J. (2017). The sex-selective impact of the Black Death and recurring plagues in the Southern Netherlands, 1349–1450. *American Journal of Physical Anthropology*, 164(2). <https://doi.org/10.1002/ajpa.23266>.
- [6] Sharma, S., Rathod, P., & Ukey, U. (2020). An overview of coronavirus disease 19 - COVID 19. *International Journal of Research in Medical Sciences*, 8(7). <https://doi.org/10.18203/2320-6012.ijrms20202927>.
- [7] Wakefield, K. (2019). *A guide to machine learning algorithms and their applications*. Sas Uk.
- [8] Bathwal, R., Tirumala, K., Chitta, P., & Varadarajan, V. (2020). Ensemble machine learning methods for modeling Covid19 deaths. In arXiv.
- [9] Al-Hazaimeh, O. M., & Al-Smadi, M. (2019). Automated pedestrian recognition based on deep Convolutional neural networks. *International Journal of Machine Learning and Computing*, 9(5), 662-667. <https://doi.org/10.18178/ijmlc.2019.9.5.855>.
- [10] Abbasa, M. A., Bukhari, S. U., Arssalan Bokhari, S. K., & Niazi, M. (2020). The application of hybrid deep learning approach to evaluate chest ray images for the diagnosis of pneumonia in children. <https://doi.org/10.1101/2020.12.03.20243550>.
- [11] Hedman, L. R., & Felländer-Tsai, L. (2020). Simulation-based skills training in non-performing orthopedic surgeons: Skills acquisition, motivation, and flow during the COVID-19 pandemic. *Acta Orthopaedica*, 91(5), 520-522. <https://doi.org/10.1080/17453674.2020.1781413>.
- [12] Shah, D., & Mangrulkar, R. S. (2021). Machine learning techniques to classify breast cancer. *Design of Intelligent Applications Using Machine Learning and Deep Learning Techniques*, 245-256. <https://doi.org/10.1201/9781003133681-17>.
- [13] Chakraborti, S., Choudhary, A., Singh, A., Kumar, R., & Swetapadma, A. (2018). undefined. *International Journal of Information Technology*, 10(3), 257-263. <https://doi.org/10.1007/s41870-018-0088-1>.
- [14] Yıldırım, Ö., Plawiak, P., Tan, R., & Acharya, U. R. (2018). Arrhythmia detection using deep convolutional neural network with long duration ECG signals. *Computers in Biology and Medicine*, 102, 411-420. <https://doi.org/10.1016/j.compbiomed.2018.09.009>.
- [15] Perumal, V., Narayanan, V., & Rajasekar, S. J. (2022). Detection of brain tumor with magnetic resonance imaging using deep learning techniques. *Brain Tumor MRI Image Segmentation Using Deep Learning Techniques*, 183-196. <https://doi.org/10.1016/b978-0-323-91171-9.00014-4>.
- [16] Makris, A., Kontopoulos, I., & Tserpes, K. (2020). COVID-19 detection from chest X-ray images using deep learning and Convolutional neural networks. <https://doi.org/10.1101/2020.05.22.20110817>.
- [17] Narin, A. (2020). undefined. 2020 Medical Technologies Congress (TIPEKNO). <https://doi.org/10.1109/tiptekno50054.2020.9299289>.
- [18] Aurelia, J., & Rustam, Z. (2021). A hybrid Convolutional neural network-support vector machine for X-ray computed tomography images on CancerA hybrid Convolutional neural network-support vector machine for X-ray computed tomography images on cancer. *Open Access Macedonian Journal of Medical Sciences*, 9(B), 1283-1289. <https://doi.org/10.3889/oamjms.2021.6955>.
- [19] Wang, L., Lin, Z. Q., & Wong, A. (2020). COVID-net: A tailored deep convolutional neural network design for detection of COVID-19 cases from chest X-ray images. *Scientific Reports*, 10(1). <https://doi.org/10.1038/s41598-020-76550-z>.
- [20] Saleh, A. Y., & Ilango, L. (2020). Detection of covid-19 in computed tomography (Ct) scan images using deep learning. *International Journal of Advanced Trends in Computer Science and Engineering*, 9(5). <https://doi.org/10.30534/ijatcse/2020/77952020>.
- [21] Pinkas, G., Karny, Y., Malachi, A., Barkai, G., Bachar, G., & Aharonson, V. (2020). SARS-CoV-2 Detection From Voice. *IEEE Open Journal of Engineering in Medicine and Biology*, 1. <https://doi.org/10.1109/ojemb.2020.3026468>.
- [22] imad, M., Khan, N., Ullah, F., Hassan, M. A., Hussain, A., & Faiza. (2020). COVID-19 Classification based on Chest X-Ray Images Using Machine Learning Techniques. *Journal of Computer Science and Technology Studies*, 2(2).
- [23] Brinati, D., Campagner, A., Ferrari, D., Locatelli, M., Banfi, G., & Cabitza, F. (2020). Detection of COVID-19 Infection from Routine Blood Exams with Machine Learning: A Feasibility Study. *Journal of Medical Systems*, 44(8). <https://doi.org/10.1007/s10916-020-01597-4>.

- [24] Oyelade, O. N., & Ezugwu, A. E. (2020). Deep Learning Model for Improving the Characterization of Coronavirus on Chest X-ray Images Using CNN. In medRxiv. <https://doi.org/10.1101/2020.10.30.20222786>.
- [25] Apostolopoulos, I. D., & Mpesiana, T. A. (2020). Covid-19: automatic detection from X-ray images utilizing transfer learning with convolutional neural networks. *Physical and Engineering Sciences in Medicine*, 43(2), 635–640. <https://doi.org/10.1007/s13246-020-00865-4>.
- [26] Qasim, Y. R. H., Hassan, H. A. M., & Hassan, A. A. M. (2020). Concatenation Technique in Convolutional Neural Networks for COVID-19 Detection Based on X-ray Images. <https://doi.org/10.5121/csit.2020.101602>.
- [27] Karhan, Z., & Akal, F. (2020). Covid-19 Classification Using Deep Learning in Chest X-Ray Images. TIPTEKNO 2020 - Tip Teknolojileri Kongresi - 2020 Medical Technologies Congress, TIPTEKNO 2020. <https://doi.org/10.1109/TIPTEKNO50054.2020.9299315>.
- [28] Yamashita, R., Nishio, M., Do, R. K., & Togashi, K. (2018). Convolutional neural networks: An overview and application in radiology. *Insights into Imaging*, 9(4), 611–629. <https://doi.org/10.1007/s13244-018-0639-9>.
- [29] Pancholi, P. D., & Patel, S. J. (2022). Literature survey for applications of artificial neural networks. *Research Anthology on Artificial Neural Network Applications*, 669–682. <https://doi.org/10.4018/978-1-6684-2408-7.ch031>.

A Novel Region Growing Algorithm using Wavelet Coefficient Feature Combination of Image Dynamics

Tamanna Sahoo, Bibhuprasad Mohanty

Department of Electronics and Communication Engineering
ITER, Siksha 'O' Anusandhan, Deemed to be University, Bhubaneswar, India

Abstract—Moving object detection has versatile and potential applications in video surveillance, traffic monitoring, human motion capture etc., where detecting object(s) in a complex scene is vital. In the existing background subtraction method based on frame differencing, the false positive and misclassification rate increases as the background becomes more complex and also with the presence of multiple moving objects in the scene. In this piece of work, an approach has been made to enhance the detection performance of the background subtraction method by exploiting the dynamism available in the scene. The resultant differencing frame so obtained by the spatial background subtraction method is subjected to wavelet transformation. By extracting and combining wavelet features from the dynamics of the scene, a novel method of region growing technique has been further utilized to detect the moving object(s) in the scene. Simulation of various video sequences from CDnet, SBMnet, AGVS, I2R and Urban Tracker database has been applied and the method provides satisfactory detection of the moving object in a complex scene. The quantitative measure like Recall, Precision, F1-measure, and specificity computed for the algorithms, have indicated the algorithms can be a suitable candidate for surveillance applications.

Keywords—Moving object; dynamism; wavelet transformation; region growing

I. INTRODUCTION

Identification of moving objects and localizing them in a video scene has become crucial as well as an initial task for many complex visual processing algorithms such as detection, classification, tracking, and analysis. This has lead researchers to work in this area and various models (parametric and non-parametric) have been already proposed in the spatial domain.

Using the benefit of the multiresolution analysis, two moving object detection methods have been proposed. The first one being object detection based on image dynamics subtraction [1], and the second one is to develop a novel region growing algorithms by extracting the wavelet features from the resultant subtracted image frames. In both algorithms, along with the dynamics creation, traditional background subtraction has been utilized in the transformed domain. In the second method, wavelet coefficient features of image dynamics are combined selectively to obtain a seed-based region growing process [2] for detecting the moving object in the scene. The methods have been applied to different video sequences available in CDnet [3], SBMnet [4], AGVS [5], I2R [6], and UrbanTracker [7] dataset. The result obtained by extensive simulation, has been compared with the reported results of

several well-known techniques like ViBe [8], PCP [9], TD-2DDFT [10], and TD-2DUWT [11].

The rest of the paper is organized accordingly, wherein Section II provides survey papers related to both methods, Section III discusses the algorithm used in discrete wavelet transform domain and the creation of dynamics. Further in Section IV, the results of both the methods have been presented for various datasets and it has been discussed, both qualitatively and quantitatively using performance measure.

II. RELATED WORK

Various techniques have been reported for the detection of moving object(s), such as, Paisitkriangkrai et al., [12] presents a study of moving targets like humans in pedestrian detection, using local feature extraction and support vector machine. In [13], a dual model (self and neighborhood model) which is a non-parametric-based background segmentation method has been proposed.

The generation of background becomes difficult for a complex scene or when there is a sudden change in illumination. This problem is tackled by Elharrouss et al., [14], by using the block-based Sum of Absolute Difference (SAD) method for background utilization as well as block-based entropy evaluation for background modeling purposes.

In the wavelet domain, the detection problem is addressed by Huang et al., [15], [16], by using change detection methods. Tsai et al., [17] applied 2-dimensional discrete Fourier transform (2D-DFT) where each Spatio-temporal slice of the gradient image is processed to detect the foreground objects.

According to Khare et al., [18], Daubechis Complex Wavelet Transform (DCWT) along with double change detection are the techniques used for detecting moving objects. Li et al. [19], estimated the models of foreground and background in wavelet domain using the likelihood of wavelet coefficients. Huntsberger et al. has used a wavelet-based algorithm for recognition and detection of objects in anti-submarine warfare using Logan radar data [20, 21]. Wavelet packet decomposition method has been applied for the analysis of sonar images, which are of quite large formats. Further, Tian et al. [22] have used wavelet coefficient characterization, namely spectral statistics and wavelet coefficients characterization (SSWCC) in spectral images for detecting targets. Boccigone et al., [23] have used Renyi's information as well as wavelet transform and region growing process for the detection in mammographic images. The camouflaged target

images using wavelet coefficient features have also been proposed by Chennasetty et al., [24].

III. PROPOSED METHODOLOGIES

We have tried to obtain optimal detection results in the transformed domain by proposing a technique (Method I), named as Image Dynamic Subtraction (IDS). By utilizing this technique with the wavelet features, another novel region growing technique has been proposed (Method II), named as Image Dynamic Subtraction using Region Growing (IDS-RG). Below the detailed discussion has been presented.

A. Method I: Image Dynamics Subtraction (IDS)

The conventional background subtraction method suffers from the disadvantage of misdetection (detection of static object(s) along with moving object) which requires extensive further processing. First, the dynamics of the frame is created (Fig. 1) and then by using the algorithm of background subtraction, the difference is taken between the current dynamic frame and background dynamic frame.

1) *Dynamic extraction:* In a scene, when the dynamics, which is the motion of an object, are extracted by only using high-frequency components, is known as dynamic extraction. The high-frequency component gives information about the required edge and high contrast values of the moving objects.

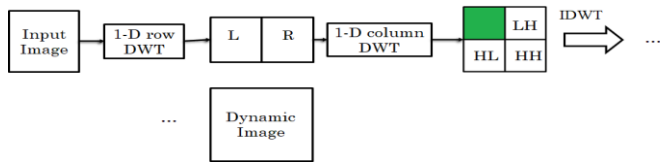


Fig. 1. Dynamic Extraction Process using Two-dimensional Discrete Wavelet Transform (2D-DWT).

Fig. 1 above depicts the dynamic extraction process using 2D-DWT where the decomposition of the image [25] is at a spatial level.

After decomposing into sub-bands (LL, LH, HL, and HH), the approximation coefficient (LL subband) is masked to zero and inverse DWT is applied to only higher frequency components to obtain the dynamics of that image. The following equation of creation of dynamics is presented below:

$$W^{-1} = [W] - F_{KA}^{-j}(x, y) \quad (1)$$

Where the F_{KA} , F_{KH} , F_{KD} , and F_{KV} represent the approximation, horizontal, diagonal, and vertical coefficient of the two-dimensional discrete wavelet transform at the j^{th} level. The W represents the wavelet decomposition and W^{-1} represents the inverse decomposition.

Fig. 2, shows the experimental setup of image dynamic subtraction (IDS) [19].

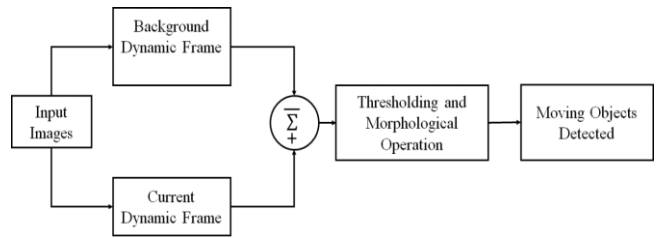


Fig. 2. Setup of Image Dynamic Subtraction using Two Dimensional Discrete Wavelet Transform (IDS-2DWT).

Group of frames is taken as input, the very first frame being referred as background frame. The dynamic extraction of background and the current frame is processed, using thresholding and morphological operation the detection result is produced. The advantage of this method is to avoid further processing of the detected result to get rid of misdetection due to the presence of a static object in the frame. The proposed method algorithm is provided below.

Step-1 Image Pre-processing

For input image

Do

- *Convert color image to grayscale image.*
- *Resize it to 512x512.*

End

Step-2 Frame selection

Do

- *Select $B(x,y)$ as the background frame.*
- *F_k as the current frame.*

End

Step-3 Dynamic extraction of both frames

Do

- *Apply 2 level 2D-DWT.*
- *Mask LL subband to zero.*
- *Apply 2 level inverse 2D-DWT*

End

Step-4 Background Subtraction

Do

- *Using frame difference method*

$$D_k(x,y) = F_{kdy} - B_{dy} \quad (2)$$

End

Step-5 Thresholding and binarize

Do

- Apply Otsu thresholding to $D_k(x,y)$.
- Get the value T_H .
- Binarize the difference image.

$$D(x,y) = \begin{cases} 1, & D_k(x,y) \geq T_H \\ 0, & \text{otherwise} \end{cases} \quad (3)$$

End

Step-6 Morphological Operation

Do

- Using dilation operation.

$$MO = D(x,y) \oplus B \quad (4)$$

- Where B is the structuring element and MO is the moving objects detected.

End

B. Method II: Image Dynamic Subtraction with Region Growing (IDS-RG)

The region growing process [26] is a technique where the regions are grown depending on some criteria. The most appropriate way to grow a region is by identifying the proper seed points.

1) *Seed point computation:* In this work, the selection of seed points is carried out based on the maximum featured value [27]. This present methodology avoids the Otsu thresholding and morphological operation that has been carried out in the previous method. After the selection, adjacent neighboring pixels which are satisfying the user-defined threshold condition, are included in the region.

A threshold value is taken to stop the region from growing and an optimal region is obtained. But one needs to keep in mind that the threshold value taken should be high enough so that the whole region is extracted [28]. This may also lead to the growth of a region much larger than the actual region, so the choice of threshold value must be a little higher than the optimal value so that the region grown is the actual region boundary.

The proposed technique of image dynamic subtraction using region growing is presented below in Fig. 3. In first step, a difference frame is computed by subtracting the reference background frame from the current frame. The difference input image of size $N \times M$ is then resized to 512×512 . Image resizing is done so that the image can be divided into sub-region, in form of power 2. Then it is converted to a gray-scale image (if the image is a color image). It is then divided into non-overlapping sub-blocks of 32×32 or 16×16 .

Each of the above non-overlapping sub-block is converted to a ‘dynamic’ sub-block by adopting the procedure enumerated previously.

Wavelet coefficient features (WCF) like contrast, cluster prominence, energy, cluster shade, maximum probability, entropy, autocorrelation, variance, inverse difference normalized are extracted by using the popular GLCM method. With lots of experimentation, the initialization of the GLCM for 0-degree orientation, and separation vector (d) as one has been taken. The normalized linear values of contrast feature values are acquired along with normalized logarithmic values of cluster shade and cluster prominence, depending upon their dynamic ranges of the features. Three of the wavelet coefficient features are combined. From extensive possible combinations, it has been found that cluster shade, cluster prominence, and contrast combination provide maximum values for each sub-block as compared to other combinations.

For seed block selection, the selection is based on the criterion that the high value of the W.C.F represents the moving object in the spatial domain. Accordingly, the maximum of combined feature values is chosen as the reference seed sub-block. The purpose of selecting the seed block is that the higher value of the wavelet coefficient feature represents that it is a part of the target region. Then the coordinate of the seed point is computed based on the criteria that it is available at the midpoint of the seed sub-block at $(r/2, c/2)$ point of the seed block [38], where r is the row and c is the column.

On selection of the seed block and subsequent seed point, the region [24] with the presence of the moving object is grown by selecting a suitable threshold value and merging the pixels with the seed points. The following Fig. 4 depicts the region growing algorithm undertaken for the purpose.

In the process, using the suitable pixel distance, pix_dist required is selected. It is done by creating a difference between the neighborhood pixels present in form of array in (k) and the R_mean (which is initially taken as the pixel value of seed point in $I(r/2, c/2)$) is satisfied for threshold. If the pixel distance is minimum of all and less than the threshold value (T) is added to the region. The next new R_mean is calculated using (5).

$$\text{New}(R_mean) = \frac{R_mean \times R_size + k(\text{index})}{R_size + 1} \quad (5)$$

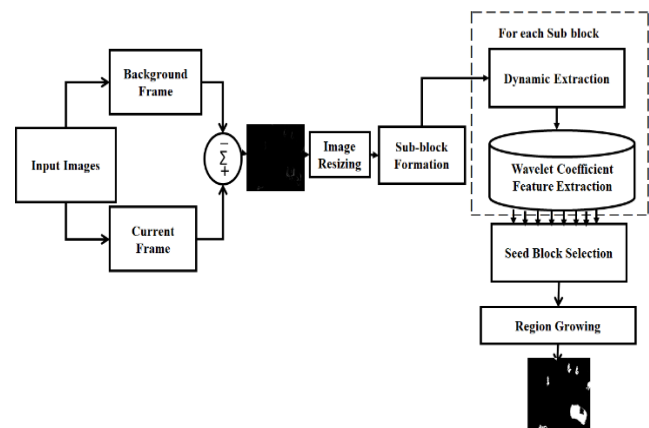


Fig. 3. General Setup of Image Dynamic Subtraction using Region Growing Algorithm.

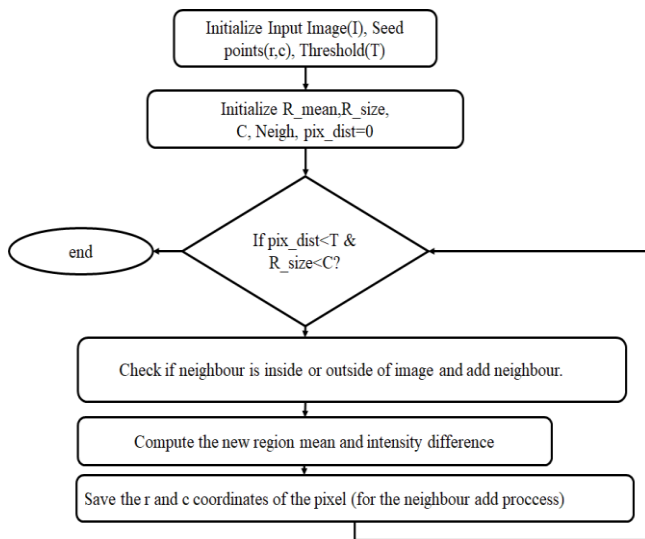


Fig. 4. Steps to Carry out Seed-based RGA.

Here R_size represents the number of pixels in the regions. The process continues until all the regions satisfying the threshold condition are added to the region.

IV. RESULT AND DISCUSSION

Extensive simulations are carried out on different video sequences with multiple and complex challenges for the detection of moving objects from a video frame. The experimentation is carried out on MATLAB environment (R2016a) by using Intel Core i5 CPU with 2.20GHz).

A. Test Sequence

Both of the methodologies are simulated on different frames of a particular test sequence, by carefully selecting the reference frames as background frames. The choice of sequence number, taken arbitrarily, but the complexity involved in the frames is considered. The major challengeable complexities are multiple moving objects, multiple static objects which changes as the sequences progress, camera movement, shadow for the static object occluding the moving object, complex background due to snowfall or rain, etc. In this paper, the detection results for different video sequences (one from CDnet [3], one each from UrbanTracker [7], I2R [6], AGVS [5], and SBMnet database [4] has been presented in this paper. Further, four more video sequences from CDnet has been compared with different state-of art methodologies.

B. Experimental Results (Method-II)

The next proposed method is image dynamic subtraction using a region growing algorithm. Here in this method, the current and reference frames are subtracted first. Then difference frame is divided into sub-blocks. The creation of dynamics (using 2D-DWT) is done on each sub-block, where wavelet coefficient features (WCF) using gray level co-occurrence matrix are extracted.

The maximum of each WCF from the sub-blocks is chosen as a seed block. The purpose of selecting the seed block is that the higher value of the wavelet coefficient feature represents

that the region is part of the target. The moving object regions are grown using the seed point region growing algorithm from where the seed block the midpoint pixels are considered as the seed point. In the proposed technique, the combination of features like contrast, cluster prominence, and cluster shade are considered and the results are presented in Fig. 5 and Fig. 6.

1) *Combined feature*: The combination of features [32] is done to strengthen multiple complementary features and yield a more powerful feature. Features like contrast, cluster prominence, and cluster shade have been used.

The Contrast feature measures the local variations present in an image where it provides a correlation between the highest and lowest value of a continuous set of pixels [29]. Cluster shade is used for measuring the skewness of the matrix and is believed to gauge the perceptual concept of uniformity [30]. If the value is high the image is asymmetric [31]. Similarly, cluster prominence is the measure of asymmetry where if it is high, it is less symmetry.

2) *Background updation*: The process of background subtraction is about the difference between the current and reference (also known as background) image. Here for the experimentation, two types of reference or background image have been used where one is like the clear background image and the other one is the background updated reference image.

The need for background updation is in the practical application where the background of the frame changes with the change of light and the motion of the local background. Thus new background of moving objects becomes static. Thus the background should be updated in real-time [33].

Challenges like illumination change have to be overcome, for which the background is updated and it is given in (6):

$$B_{t+1} = (1-\alpha) B_t + \alpha \cdot I_t \quad (6)$$

Where B_{t+1} is the updated background, I_t is the current video frame, B_t represents the previous background frame and α is the learning rate, ranging from [0, 1]. Here, the ' α ' is chosen through trials. According to [34], the higher the value of alpha, the presence of foreground in the background is a must and the lower value cannot overcome the sudden change of illumination in a scene. This background model obtains a threshold that can be applied over the distance between corresponding pixel values of I_t and B_t . The method is best in terms of speed, simplicity, and memory requirements than other methods like mean, median, histogram, and Min-max. To elaborate the idea of background updation, in the next Fig. 5, an example of Rouen video has been presented.

The first row in Fig. 5 represents the original frames (27, 50, and 173). The second and third-row represent the detection result of the proposed method without and with background updation. Using without background updation, the presence of ghostly artifacts of moving pedestrians, present in the background frame, are also present in the detection result. But while using the method with background updation, only the moving objects of the current frame have been detected in the result.

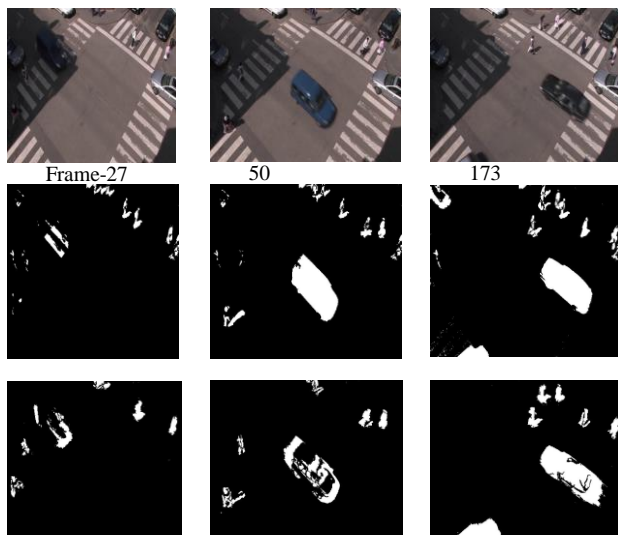


Fig. 5. Multiple Moving Object Detection using Method II. 1st Row: Test Frames in Rouen (Traffic) Sequence, 2nd Row: Corresponding Detection Results with Background Updation, and 3rd Row: Detection without Background Updation.

C. Qualitative Performance Measure

The visual comparison of the two methods of image dynamic subtraction using region growing algorithm (IDS-RG) with and without background updation with the ground truth has been presented in Fig. 6. The first row represents the

original image of the current frames of test sequences, the second row represents the ground truth of that frame. The results of all frames are quite similar in this technique, that is, only the contours of moving objects are present and even the static lines of the background image are also present in the output detection result of IDS-RG without background updation. The method-II using a combined wavelet coefficient feature (WCF) with or without background updation has been applied to test sequences: Rouen (from Urban Tracker); bungalow (from CDnet); advertisement board (from SBMnet), bootstrap (from I2R) and S1 (from AGVS). The results with background updation are quite better than without background updation in Rouen, bootstrap, and bungalow video. The experimental results of IDS-2DDWT and IDS-RG are also compared with the four state-of-art background subtraction method below from Fig. 7 and Fig. 8 respectively.

Although in advertisement board and S1 video, without updation have shown a better result than with background updation as in later one only the contour is present but the presence of ghostly artifacts like snow and few static lines in the resulting image is also present. Further, addition of three crowded video sequences having complex scenario and multiple moving objects has also been used for comparison with the state-of-art results [37]. It includes skating sequence from bad weather category where snow is regarded as dynamic background, a tramcrossroad sequence from low frame rate category from the ChangeDetection.net (CD.net) benchmark dataset [3].

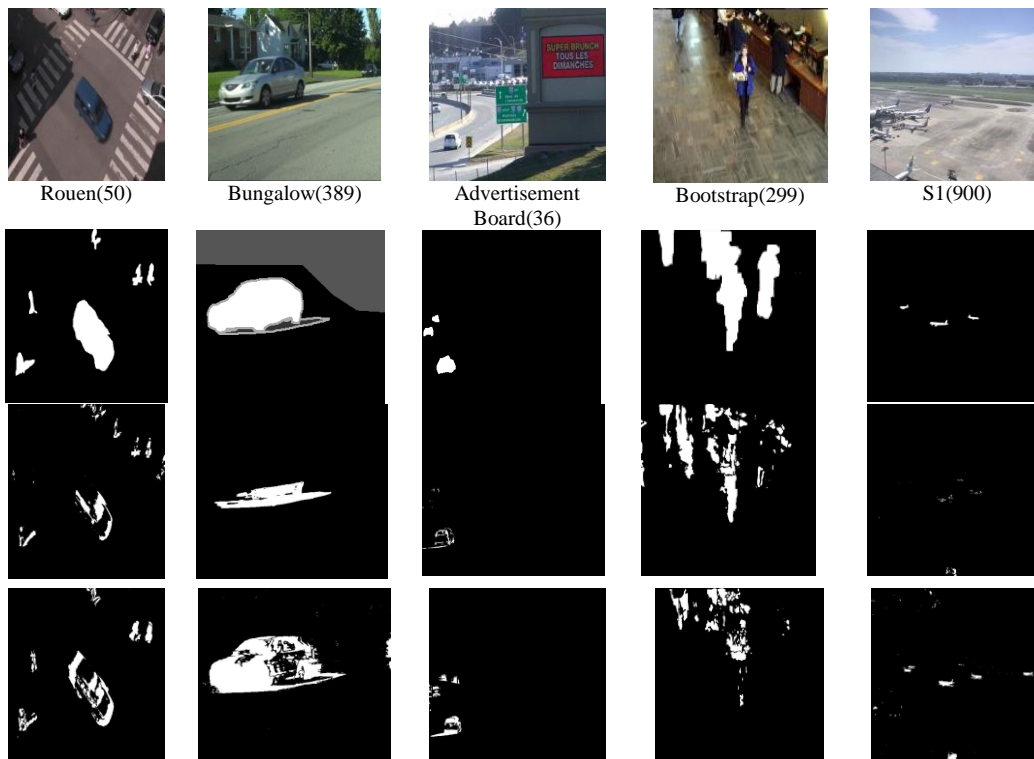


Fig. 6. More Detection Results for Algorithm II with different Datasets, 1st Row: Test Frames of Sequences (The Number in the Parenthesis Indicate the Frame Number of that Sequence), 2nd Row: Ground Truth of Frames, 3rd Row: Corresponding Detection Results without Background Updation and 4th Row: Detection with Background Updation.

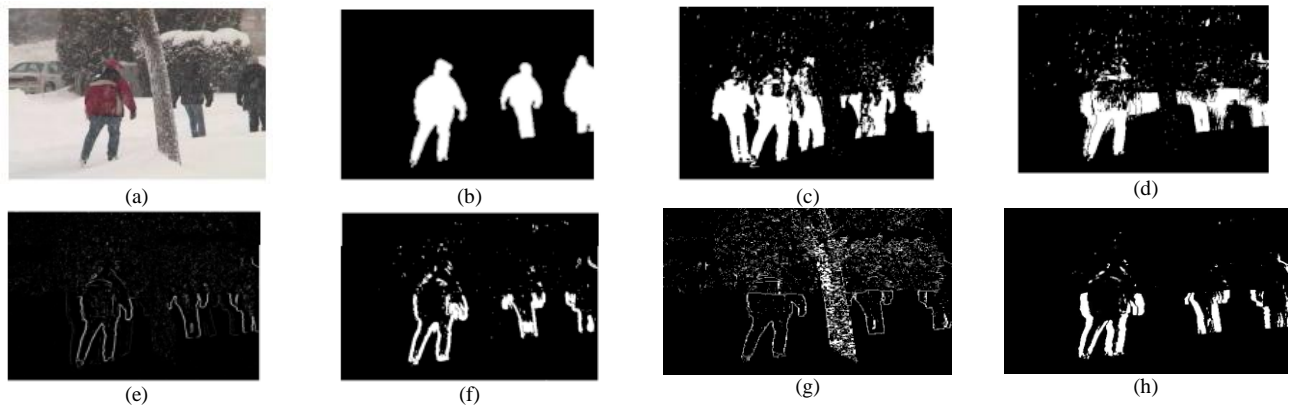


Fig. 7. Detection Result of Skating Frame (Frame Number-1953) (a) Input Frame (b) Ground Frame Reference; (c) ViBe; (d) PCP; (e) TD-2DDFT; (f) TD-2DUWT;(g) IDS-2DDWT;(h) IDS-RG + BU.

In Fig. 7 it has been shown that the proposed methodology (IDS-RG + BU) provides significantly better detection results than other methods. Since, the tree is available in the foreground, and is misdetected as in the Fig. 7(g) with IDS-2DDWT, the IDS-RG + BU method properly detects it as *not* moving object and hence clear detection of moving object (in this case, three human being in caps and gloves) are obtained. It is interesting to note that the proposed method is capable of eliminating the dynamic background due to continuous snowfall during the entire video sequence (as compared to ViBe and PCP). Due to low contrast the two human beings are not distinctly distinguishable against the black backdrops. Accordingly, the proposed method also fails to exhibit the entire contour of both persons in Fig. 7(h).

The video frame chosen for Fig. 8 is complex as it contains multiple numbers of moving small sized cars in the static background of high raising building and road with leveling as in Fig. 8(a). A careful observation of the frame reveals that the small sized moving cars are really indistinguishable against the backdrop. But the ground truth reference frame as obtained from the dataset [3], provides only the clearly visible and distinguishable three moving cars. It has been observed that both of our methods are capable of detecting almost all available moving objects [Fig. 8(g) and (h)]. But better visual representation is obtained in IDS-RG+BU method. The IDS-2DDWT method has some mis-detection and ghostly artefacts.

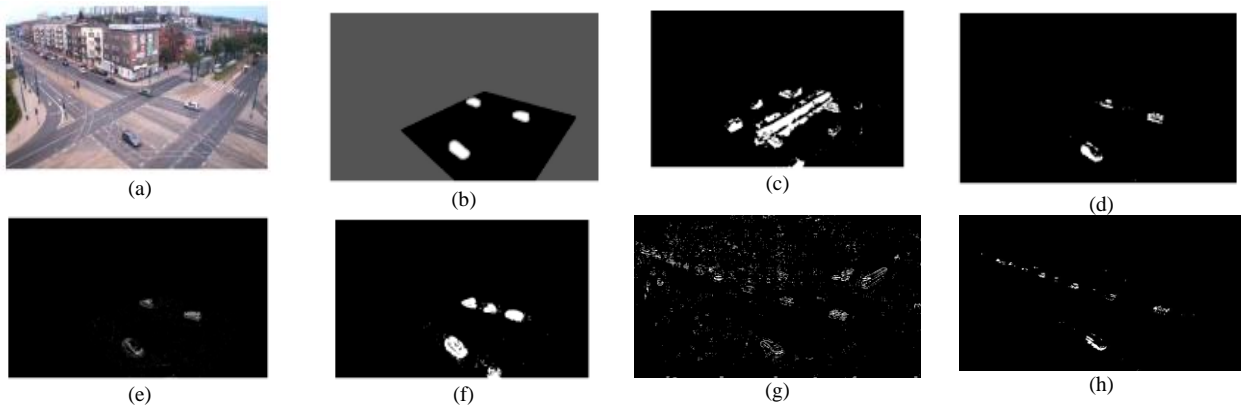


Fig. 8. Detection Result of Tramcrossroad Frame (Frame Number-502) (a) Input Frame (b) Ground Frame Reference; (c) ViBe; (d) PCP; (e) TD-2DDFT; (f) TD-2DUWT;(g) IDS-2DDWT;(h) IDS-RG + BU.

The reported results of ViBe (c), PCP(d) and TD-2DDFT(e) have significant detection errors as shown.

D. Quantitative Performance Measure (QPM) Comparison

The performance of the proposed techniques and state-of-art is measured using four generalized metrics namely: Recall, Precision, F1- measure, and Specificity. Recall [35] can be defined by the percentage of detected true positive as compared to the total number of true positive in the ground truth which is given by (7). Precision [36] presented in (8), presents the percentage of true positives detected in comparison with the total number of items detected by the method. The above-mentioned metrics are used and usually, a method is considered to be good if it gives a high recall value without sacrificing the precision. F1-measure [39] is considered as the weighted harmonic mean of recall and precision using (9). Equation 10 is specificity which is defined as the number of correct negative predictions which is divided by the total number of negatives.

$$\text{Recall} = \frac{TP}{TP + FN} \quad (7)$$

$$\text{Precision} = \frac{TP}{TP + FP} \quad (8)$$

$$\text{F1-Measure} = \frac{2 \times \text{Recall} \times \text{Precision}}{\text{Recall} + \text{Precision}} \quad (9)$$

$$\text{Specificity} = \frac{TN}{TN + FP} \quad (10)$$

Table I presents the quantitative performance measure of videos of different datasets used for the experimentation purpose. The results of QPM determine that IDS-RG with background updation shows better results in most of the video sequences (Recall value of Rouen, Bungalow Advertisement board sequences is greater than IDS and IDS-RG (without background updation)).

The results of IDS-2DDWT and IDS-RG with background updation are further compared with well-known state-of-art techniques. From skating and tramcrossroad test sequences, short clips of 96 frames are taken as input. To be specific, two

short clips consist of 96 frames from skating sequence (from frames 1905 to 2000), from tramcrossroad sequence (from frames 413 to 508) and their quantitative performance measure has been presented Table II and Table III. In all videos, the result in IDS-RG has shown better. Table II and III presents the average metrics for all 96 frames, respectively. ViBe produces very low metrics especially in tramcrossroad video (as shown in Table III); further due to foreground aperture problem TD-2DUWT method also suffer as shown in Table II. Image Dynamic Subtraction using region growing with background updation metrics shows better result in overall indicators.

TABLE I. QPM RESULTS OF ALL DATASETS USED FOR THE PROPOSED TECHNIQUES

Dataset	Method I: Image Dynamic subtraction				Method II: Image Dynamic Subtraction using Region Growing (without Back-ground Updation)				Method II: Image Dynamic Subtraction using Region Growing (with Background Updation)			
	Recall	Precision	F1-Measure	Specificity	Recall	Precision	F1-Measure	Specificity	Recall	Precision	F1-Measure	Specificity
Rouen (50)	0.9657	0.9957	0.9804	0.9960	0.9821	0.9843	0.9831	0.9845	0.9947	0.9929	0.9938	0.9931
Bungalow (389)	0.8723	0.9904	0.9276	0.9903	0.9835	0.9875	0.9855	0.9864	0.9885	0.9918	0.9357	0.9917
Advertisement (36)	0.9598	0.9793	0.9695	0.9795	0.9681	0.9944	0.9811	0.9924	0.9705	0.9969	0.9884	0.9959
Boot-Strap (299)	0.9705	0.9390	0.9532	0.9365	0.9563	0.9635	0.9493	0.9127	0.9438	0.9512	0.9963	0.9925
S1 (900)	0.9880	0.9868	0.9824	0.9965	0.9968	0.9917	0.9943	0.9915	0.9957	0.9885	0.9963	0.9925

TABLE II. COMPARISON OF AVERAGE METRICS OF SKATING SEQUENCE (96 FRAMES)

Method	Recall	Precision	F1-Measure	Similarity
ViBe	0.5210	0.3779	0.4394	0.2816
PCP	0.4654	0.5205	0.4914	0.3257
TD-2DUWT	0.2266	0.6287	0.3332	0.1999
IDS-2DDWT	0.8937	0.9313	0.9121	0.8384
IDS-RG(with BU)	0.9656	0.9526	0.9442	0.9575

TABLE III. COMPARISON OF AVERAGE METRICS OF TRAMCROSSROAD VIDEO (96 FRAMES)

Method	Recall	Precision	F1-Measure	Similarity
ViBe	0.6095	0.00982	0.1692	0.0924
PCP	0.5939	0.8300	0.6924	0.5295
TD-2DUWT	0.5940	0.5574	0.5751	0.4036
IDS-2DDWT	0.9726	0.9666	0.9696	0.9410
IDS-RG(with BU)	0.9623	0.9567	0.9241	0.9338

V. CONCLUSION

Two new methods of multiple moving object detection in a video sequences have been proposed in this paper. Instead of adopting the conventional background subtraction method by means of frame differencing in spatial domain, the present work proposed the subtraction of dynamism available in the current and reference frame, thereby making it a potential technique for video surveillance. The use of discrete wavelet transform solves the localization of motion pixels associated in a frame by keeping those into high frequency subbands on decomposition. The exploration of these pixels are the dynamics of the frame which provide the necessary information of the moving object. Hence, instead of background subtraction, we refer to it as Image Dynamic Subtraction (IDS). The method of IDS exhibit better detection results both quantitatively (Table II and III) and qualitatively (Fig. 7 and Fig. 8). By suitably choosing wavelet coefficient feature (WCF), and adopting the region growing technique over and above it, the proposed method IDS-RG+BU exhibit enhanced detection results. The second method is capable of eliminating ghostly artefacts, occlusion, static lines, cluttering due to dynamic background as has been reported in this paper. Further, it has been observed that, the method of IDS-RG +BU is capable of detecting the moving object (even multiple objects) irrespective of size (for example tramcrossroad video). However, this method fails to provide the requisite results if the colours of the moving object and the background objects are the same and if the contrast between them is insignificant (for example skating video). In addition, this method fails to provide a complete binary image of the moving object(s) in some cases. Even if it detects the moving object by eliminating occlusion due to static object, the present proposed method does not exhibit acceptable result in case of occlusion made by another moving object. Attempts are being made to address these issues.

REFERENCES

- [1] T. Sahoo, B. Mohanty, "Moving object detection using background subtraction in wavelet domain," 2nd International Conference on Data Science and Business Analytics (ICDSBA),2018.
- [2] T. Sahoo, B. Mohanty, "Novel Region Growing Mechanism for Object Detection in a Complex Background," In: Pradhan G., Morris S., Nayak N. (eds) Advances in Electrical Control and Signal Systems. Lecture Notes in Electrical Engineering, vol 665,2020.
- [3] Y. Wang, P.M Jodoin, F. Porikli, J. Konrad, Y. Benezeth, and J. Ishwar , "CDnet 2014: An Expanded Change Detection Benchmark Dataset,"in Proc. IEEE Workshop on Change Detection (CDW-2014) at CVPR-2014, pp. 387-394.
- [4] P. M Jodoin, L. Maddalena, A. Petrosino, Y. Wang Y, "Extensive benchmark and survey of modeling methods for scene background initialization," IEEE Trans. Image Process, vol. 26, no. 11, pp. 5244–5256,2017.
- [5] <http://www.agvscaac.com/pages/imagesDownload.html>.
- [6] L. Li, W. Huang, I. Y.-H. Gu, Q. Tian: "Statistical modeling of complex backgrounds for foreground object detection." IEEE Trans. Image Process., vol. 13, no. 11, pp. 1459–1472, Nov. 2004.
- [7] J.P Odoin, G.A Bilodeau, N. Saunier N, "Urban Tracker: Multiple Object Tracking in Urban Mixed Traffic," Accepted for *IEEE Winter conference on Applications of Computer Vision (WACV14)*, Steamboat Springs.
- [8] O. Barnich, M. van Droogenbroeck, "ViBe: A universal background subtraction algorithm for video sequences," IEEE Trans. Image Process. Vol-20,pp- 1709–1724,2011.
- [9] E.J Candès, X. Li, Y. Ma, J. Wright, "Robust principal component analysis?" J. ACM ,vol- 58, issue- 11,2011.
- [10] D. Tsai, W. Chiu, "Motion detection using Fourier image reconstruction," Pattern Recognit. Lett. Vol- 29, pp-2145–2155,2008.
- [11] V. Cmojevic, B. Anti ´c, D. Culibrk, "Optimal wavelet differencing method for robust motion detection," In ' Proceedings of the 16th IEEE International Conference on Image Processing (ICIP 2009), Cairo, Egypt, pp. 645–648,2009.
- [12] B. Yin, J. Zhang, Z. Wang, "Background segmentation of dynamic scenes based on dual model," IET Computer Vision, vol. 8, no. 6, pp. 545–555,2014.
- [13] W. Liu, H. Chen, L. Ma, "Moving object detection and tracking based on ZYNQ FPGA and ARM SOC,"in Proc. IET Int. Radar Conf., pp. 1–4,2015.
- [14] A.K Samantaray, P. Kanungo, B. Mohanty, "Neighborhood decision based impulse noise filter," IET Image Process, vol. 12, no. 7, pp. 1222–1227,2018.
- [15] J.C Huang, W.S Hsieh, "Wavelet-based moving object segmentation," Electron.Lett.39 (19),2003.
- [16] J. Huang, T. Su, L. Wang, W. Hsieh, "Double-change detection method for wavelet-based moving-object segmentation," IET Electronics Letters, 40(13):798–199,2004.
- [17] D.M Tsai, W.Y Chiu, "Motion detection using Fourier image reconstruction," Pattern Recognition Lett. 29 (16) 2145–2155,2008.
- [18] M. Khare, R.K Srivastava, A. Khare, "Moving object segmentation in daubechies complex wavelet domain," Signal, Image and Video Processing. Accepted, doi: 10.1007/s11760-013-0496-4, Springer,2013.
- [19] S. Li, D. Florencio, W. Li, Y. Zhao, C. Cook , "A fusion framework for camouflaged moving foreground detection in the wavelet domain,"IEEE Transactions on Image Processing, 27(8):3918–3930,2018.
- [20] T.L Huntsberger, B.D Jawerth, "Wavelet based automatic target detection and recognition," Annual Tech. Rep., University Research Initiative Program for Combat Readiness, University of South Carolina, Columbia, SC, USA,1998.
- [21] T.L Huntsberger, B.D Jawerth, "Wavelet based algorithms for acoustic and non-acoustic antisubmarine warfare," Annual Tech. Rep., University Research Initiative Program for Combat Readiness, University of South Carolina, Columbia, SC, USA,1998.
- [22] Y. Tian, H. Qi, X. Wang, "Target detection and classification using seismic signal processing in unattended ground sensor systems," in Proc. IEEE Int. Conf. Acoustics, Speech, Signal Processing (ICASSP'02),vol.4,p.4172,Orlando,Fla,USA,2002.
- [23] G. Boccignone, A. Chianese, A. Picariello, "Using Renyi's information and wavelets for target detection: an application to mammograms," Pattern Analysis and Applications, vol. 3, no. 4, pp. 303–313,2000.
- [24] N. Singh and S. Veenadhari, "Segmentation of Fuzzy Enhanced Mammogram Mass Images by using K-Mean Clustering and Region Growing," International Journal of Advanced Computer Science and Applications(IJACSA), 11(5), 2020. <http://dx.doi.org/10.14569/IJACSA.2020.0110546>
- [25] A. Jalal, V. Singh V, "A robust background subtraction approach based on Daubechies complex wavelet transform,"in: Advances in Computing and Communication, ACC 2011, pp. 516–524,2011.
- [26] S. Paisitkriangkrai, C. Shen, J. Zhang, "Performance evaluation of local features in human classification and detection,"Iet Computer Vision, vol. 2, no. 28, pp. 236–246,2008.
- [27] T. Bouwmans, "Traditional and recent approaches in background modeling for foreground detection: An overview," Computer Science Review 11 (31- 66),2014.
- [28] J. Yang, M. Shi, Q. Yi, "A New Method for Motion Target Detection by Background Subtraction and Update,"Physics Procedia, 33, pp 1768–17752012.
- [29] M. Unser, "Sum and difference histograms for texture classification," IEEE Trans. Pattern Anal. Mach. Intell. 8, 118–125 (1986).
- [30] X. Yang , S. Tridandapani, J.J Beitler, D.S Yu , E.J Yoshida, W.J Curran, T. Liu, "Ultrasound GLCM texture analysis of radiation-induced parotid-gland injury in head-and-neck cancer radiotherapy: an in vivo study of late toxicity," Med. Phys. 39 5732–9,2012.

- [31] J. Wu, S. Poehlman, M.D. Noseworthy, M.V Kamath, "Texture feature based automated seeded region growing in abdominal MRI segmentation," In Proc. Int. Conf. BioMedical Engineering and Informatics, volume 2, pages 263–267,2008.
- [32] R. Kalsotra, S. Arora, "A Comprehensive Survey of Video Datasets for Background Subtraction," IEEE Access, 2019.
- [33] G. Takhar, C. Prakash, N. Mittal, R. Kumar, "Comparative Analysis of Background Subtraction Techniques and Applications," IEEE International Conference on Recent Advances and Innovations in Engineering, pp. 1-8,2016.
- [34] J. Hou J, B.P. Zhang, N.M. Qi, Y. Yang, "Evaluating feature combination in object classification," in: International Symposium on Visual Computing, pp. 597–606,2011.
- [35] Y. Lin, Y. Tong, Y. Cao, Y. Zhou, S. Wang, "Visual-Attention Based Background Modeling for Detecting Infrequently Moving Objects," in *IEEE Transactions on Circuits and Systems for Video Technology*, vol. 27, no. 6, pp. 1208-1221,2017.
- [36] S. Arivazhagan, L. Ganesan , "Automatic target detection using wavelet transform," EURASIP Journal on Applied Signal Processing, vol. 2004, no. 17, pp. 2663–2674.
- [37] G. Han , J. Wang, X. Cai, "Background subtraction based on three-dimensional discrete wavelet transform," Sensors Basel 16(4):456,2016.
- [38] A. Afifi, "A Hybrid Technique Based on Combining Fuzzy K-means Clustering and Region Growing for Improving Gray Matter and White Matter Segmentation" International Journal of Advanced Computer Science and Applications(IJACSA), 3(7), 2012. <http://dx.doi.org/10.14569/IJACSA.2012.030716>
- [39] Mohana and H.V Ravish Aradhya, "Object Detection and Tracking using Deep Learning and Artificial Intelligence for Video Surveillance Applications," International Journal of Advanced Computer Science and Applications(IJACSA), 10(12), 2019. <http://dx.doi.org/10.14569/IJACSA.2019.0101269>.

Driver Drowsiness Detection and Monitoring System (DDDMS)

Raz Amzar Fahimi Rozali¹, Suzi Iryanti Fadilah^{2*}, Azizul Rahman Mohd Shariff^{3*}, Khuzairi Mohd Zaini^{4*}, Fatima Karim⁵, Mohd Helmy Abd Wahab⁶, Rajan Thangaveloo⁷, Abdul Samad Bin Shibghatullah⁸

School of Computer Science, Universiti Sains Malaysia (USM), Penang, Malaysia^{1, 2, 3, 5}

School of Computing, Universiti Utara Malaysia (UUM), Kedah, Malaysia⁴

Fakulti Kejuruteraan Elektrik dan Elektronik, Universiti Tun Hussein Onn (UTHM), Johor, Malaysia⁶

Faculty of Computer Science and Information Technology in Universiti Malaysia Sarawak (UNIMAS)⁷

Institute of Computer Science & Digital Innovation, UCSI University Kuala Lumpur, Malaysia⁸

Abstract—The purpose of this paper is to develop a driver drowsiness and monitoring system that could act as an assistant to the driver during the driving process. The system is aimed at reducing fatal crashes caused by driver's drowsiness and distraction. For drowsiness, the system operates by analysing eye blinks and yawn frequency of the driver while for distraction, the system works based on the head pose estimation and eye tracking. The alarm will be triggered if any of these conditions occur. Main part of the implementation of this system will be using python with computer vision, while Raspberry Pi, which is uniquely designed, for the hardware platform and the speaker for alarming. In short, this driver drowsiness monitoring system can always monitor drivers so as to avoid accidents in real time.

Keywords—Distraction; drowsiness; eye blink; yawn; head pose estimation; eye tracking; computer vision; Raspberry Pi

I. INTRODUCTION

Driver distraction and drowsiness are the major public health concerns and have led to road accident that have become one of the major causes of death and injuries in Malaysia. The Bukit Aman Investigation and Traffic Enforcement has reported that in the first six months of 2019, the country reported 281,527 road accidents, an increase of 2.5%, compared to 274,556 in the same period last year. These often stem from peoples' mistakes that occur in different activities related to vehicle driving. The term "drowsy" indicates "sleepy," as in prone to falling asleep. Drowsiness is commonly induced by a lack of sleep, certain medications, and boredom produced by driving a vehicle for extended periods of time. The driver will lose control of his vehicle when sleepy, resulting in an accident. Driver distraction is defined by the National Highway Traffic Safety Administration (NHTSA) as the process through which drivers redirect their attention away from driving duties. Drivers are often distracted by activities taking place around them, such as texting, talking on cell phones, or conversing with others. All these activities divert drivers' attention away from the road, which can lead to accidents that threaten drivers, pedestrians, and even other vehicles on the road.

Many efforts have been made to reduce all these numbers such as developments in computers that can be used to track drivers' conditions with the ability of alerting in dangerous situations [1]. Using physiological measures, ocular measures,

and performance measures, a variety of methods have been investigated and applied to describe driver drowsiness and distraction. Despite the effort, since many studies are focused on referring to the non-direct function, driver drowsiness and monitoring systems have not become widespread. Thus, this paper describes the design and development of a Driver Drowsiness and Monitoring System using Raspberry Pi minicomputer with a webcam making the system cost-effective and portable. The objective of the work is to develop driving assistant system that can help driver to stay alert while driving so that numerous accidents can be reduced or prevented. This paper is organized as follows.

In Section II, this paper presents the previous works. Section III presents the proposed Driver Drowsiness and Monitoring System. In Section IV, the paper discusses the results of the experiments to show accuracy of the system. Finally, the conclusion and future work will be explained in Section V.

II. RELATED WORK

A. Driver Drowsiness and Monitoring System

Due to large number of accidents occurring over time, the ability to detect driver's distraction and drowsiness, then alarming them in real time becomes challenging. In order to improve the system development, a few existing systems in the market have been studied and discussed. Majority of the applications are integrated with the single functionalities only. Anti-Sleep Pilot is the dashboard device that will monitor both driver and their driving condition. It will let the driver know when it's time to take a ten-minute rest and pull over. The device continuously calculates the driver's fatigue level once driving started and status displayed. Driver alertness is also maintained and measured through occasional reactive tests in which the device must be touched as soon as indicated. If the combination of variables approaching the limit, the visual and audible signals from the Pilot will be activated to the fact that the driver need to take a break- the system is adaptive to light and sound, so that its monitor and warning automatically change for cabin conditions.

In industry, systems based on near-IR are the most common. The Saab Driver Attention Warning System detects visual inattention and drowsy driving. The system uses two

*Corresponding Author.

miniature IR cameras integrated with Smart Eye technology to accurately estimate head pose, gaze, and eyelid status. When a driver's gaze is not located inside the primary attention zone (which covers the central part of the frontal windshield) for a predefined period, an alarm is triggered. When the cameras detect a pattern of long duration eye-lid closures, indicating the potential onset of drowsiness, a series of three warnings is initiated. This can only be cancelled when the driver presses a reset button in the fascia. The system is then immediately reactivated. [10] In this paper the author provides facts and figures of road accidents due to driver's drowsiness. Study reveals that in United States of America near about ten million fatal accidents occur in a year. In order to find safety precautions and road accident prevention, real time driver's drowsiness monitoring must be done. Author claimed 80% correct results of the suggested structure by focusing on the facial expressions of the driver and to propose a lightweight model using Android application.

The authors [12] used a lightweight Convolutional-Neural-Network model to categorize facial sleepiness patterns of drivers while driving on road. With glasses, the accuracy level range between 85% to 88% with and without glasses along with the overall average of 83%. [13] Driver sleepiness is one of the main reasons for road accidents and the number of such accidents can be minimized with the help of driver drowsiness monitoring system. A lot of research has been done and variety of alarm models and frameworks were deployed for this purpose including capturing facial and head movements along with yawn frequency. The paper itself is a survey and it presented a comprehensive comparative analysis for the detection of driver sleepiness and preventive measures adopted. The authors [13] reviewed multiple approaches SVM (Support Vector Machine), HMM (Hidden Markov Model) and CNN (Convolutional Neural Networks) along with their positive and negative impacts and limitations associated with each approach to help researchers in finding gaps. They concluded that SVM is comparatively cheap but doesn't work best with large data sets whereas HMM and CNN has less error ratio, but they are costly. The authors [14] presented a detailed comparison between invasive and non-invasive sleepiness detection methods. Invasive method like electrooculogram (by recording eye movements) and non-invasive method like electrocardiogram (by recording heart rhythm and activity) of the driver. The authors used hybrid approach by combining both EOG and ECG, but this strategy has limitations associated with it as there are many other reasons for change in heart rhythm except for drowsiness only.

The authors [15] proposed a framework to estimate in advance about the number of possible road accidents which could happen according to the road condition by using the random variable function and Taylor's series. The authors [16] described another approach by breaking down the proposed model in four steps. Started by capturing movements of the driver from the real time video after then categorizing different sleep conditions by considering other factors like with putting glasses on or off and movements of mouth, head, and eyes. The authors are using any two conditions to get to know the sleepiness state of the driver. Another research based on measuring heart rhythm to detect driver's sleep state as

heart-rate-variability (HRV) has already been used to determine the brain disorder [17]. Therefore, the authors recommend using HRV to detect sleep state of the driver as change in sleep state changes the involuntary physiologic process of the man which directly effects HRV. But again, the reason for change in HRV may not be only the drowsiness as presence of other factors can never be ignored and this becomes the limitation of the suggested approach.

Driver's face expressions recorded, and alert sent to the driver when found in drowsy state. It works by extraction of facial expressions and then running an algorithm to check and detect the drowsy position and finally alert sent to driver to make him/her conscious [18].

B. Eye Blink Detection Method

For the blink detection, Mandeep and Gagandeep [2] had proposed a method using Mean Shift Algorithm. In this algorithm, eyes are identified in each frame, and each eye blink is compared to a mean value. The system analyzes the eye opening at each blink to a standard mean value, and an alert is generated if the eye opening exceeds this value for a certain number of consecutive frames. Compared to the algorithm in this study, the system does not need to store information from previous frames because eye blinking measurements from a collective number of frames are utilized to assess drowsiness. The algorithm proposed is simple but efficient to detect eye blink. The system monitors the EAR which is the ratio between the height and the width of the eye contour in the real time. This value can represent the level of the eye opening by comparing to threshold value.

The research [11] was focused on capturing eye movement with the help of cameras by using CNN which is used to identify real time patterns in images and videos. The eye movement pattern from the video helps in categorizing sleepy or non-sleepy driver and consequently generates an alarm in order to provide protection from road accidents. Although, the researchers [11] provided more accuracy when compared to conventional CNN but it works with only capturing eye movement and not considering yawning and head movement. [19] This paper covered other factors along with detection of driver's drowsiness by capturing eye-blink. Upon drowsiness detection, the system sends an alarm to make the driver alert. Location monitoring was done by GPS and driver's alcohol, temperature and heart rhythm were measured to monitor health by putting a check on vehicle speed and informing about the current status to other vehicles [19]. The authors [20] advocate to smartly monitor driver drowsiness without conditioning it with other factors like steering-angle, pedal-pressure and electrocardiogram etc. In fact, it used a USB camera to capture video and extract facial traces for sleep pattern monitoring by using iris area and eye closure period. In [31] researchers presented a solution to a challenge normally faced in driver drowsiness detection that is capturing driver's different facial images like frequency of eye-closure and yawning at night or when light is low. To solve this issue, infrared camera was used to capture facial images with adequate visibility. More than 3000 facial images were used for testing purpose and researcher claims the result was more than 90% accurate for both eye-closure and yawn frequency monitoring in low light.

C. Yawn Detection Method

On the other hand, the yawn detection in [3] describes a system in which the face is found in a video frame using the Viola-Jones face detection approach. Then, from the face region, a mouth window is generated, and lips are searched using spatial fuzzy c-means (s-FCM) clustering. However, this algorithm has complex classifier, as a result, it is impractical to install the system inside the vehicle with little processing power, and training on datasets with huge samples is required. Compared to the algorithm in this study, the system utilizes some mouth geometrical characteristics to identify yawning which is detected by the ratio of mouth height and width. The authors [21] used an algorithm to record video and trace facial behavior like yawning, eye-closure period and frequency of eye-blink from that recorded video instead of measuring the functioning of any other device attached with the vehicle to simplify the algorithm. In [22] the authors tried to focus on driver drowsiness and to propose such an algorithm which not only detects driver's drowsiness but also finds a safe place nearby to park the vehicle there and inform the transportation authority about the problem to ensure road safety. The authors in [23] tried to enhance their previous work related to detect sleepiness with the help of machine learning. They suggested to capture face expressions and position to detect sleepiness of the driver by using a simple algorithm resulting 88% accuracy with driver wearing no glasses and 85% with driver wearing glasses. The authors also described that their proposed algorithm is more efficient in terms of storage, model-size and complexity than the benchmark-model and is capable of implementing in real time driver's sleep detection vehicle applications.

The authors [24] presented an approach to analyze the magnitude of relation of different facial parts to detect driver drowsiness. These facial parts include movements and changes in eyes, nose, ear, eyebrows, mouth, and face wrinkles. In analyzing the magnitude, relation of all these facial parts, the authors proposed the use of SVM classifier. In this research paper, the authors [25] endorsing the fact that use of images for driver's sleepiness detection is one of the main focus of research nowadays. Images of facial expressions and movements can be the best way to detect driver drowsiness and to ensure road safety. The researchers are using four types of CNN based image recognition and classification methods to process data containing yawn frequency along with variable mouth positioning. In this research the authors [26] proposed a model which needs prior training as it works on two main streamlines. One is to reduce light effect from the face images with the help of contrast limited adaptive histogram equalization and second one is to extract maximum information from the eye images using the 3D SE-blocks. The researchers used 3D-depthwise separable sensing framework instead of 3D image extraction to minimize overall cost. It comes with one limitation that face images may not be always clear as sometimes driver may wear cap or driver's hairs may cover the face resulting in the poor visibility of extracting sleepiness patterns from driver's facial images. In [27] proposed a framework where Support Vector Machine algorithm was used to monitor driver sleepiness by extracting facial expressions like eye-blinking frequency for a specific period of time or mouth opening due to yawning from the

pictures captured by a built-in camera in the vehicle. This proposed model sends an alert to driver upon drowsiness detection by using Euclidean-distance function to ceaselessly monitor eyes-mouth space approaching to sleepiness.

In [28] researchers advocated that road accidents can be avoided with driver drowsiness monitoring using MATLAB for image processing. System works on visual concept by using a camera for face recognition and detection. After that it focuses on eye blink and then information about eyes open/close was extracted by MATLAB using Hough-transform and Viola-Jones algorithms. Eye movement observation was recorded continuously using camera and driver was declared sleepy if more than five frames show closed eyes consecutively. It consequently sends alert to the driver with the help of alarm. Authors [29] presented a detailed analysis of recently used techniques and algorithms for driver's drowsiness monitoring/detection as drowsiness is one of the main reasons of road accidents and is more harmful than any other technical fault in vehicle. Authors used the analysis approach by dividing latest drowsiness detection algorithms and techniques into three categories. First one is to analyse the driver's driving style, secondly driver's mental state or psychological patterns are observed. Third and last is the detailed analysis of different visual monitoring systems used to scan and then to extract required information to alert driver and ensure road safety. Specifically focusing analysis on the data sets available to work on for driver drowsiness detection and results found are there is still plenty of attention required to add more driver drowsiness images to comprehensively monitor human yawning patterns. In [30] authors presented an approach to monitor real-time driver's sleepiness with the help of magnitude relation of driver's eye-closure along with yawn frequency and head positioning by observing the mouth and eyes movements. As the proposed model is intended for real-time environment, therefore, to achieve accuracy it runs 15 frames/second which is justifiable. The best results showed accuracy level of eye-movement/blinking was 97% and the results for yawn frequency was 96% and head positioning accuracy level was 63.4% detected.

D. Gaze Detection Method

Lastly, the gaze detection in [4] explained that the face detection was done using the Viola-Jones algorithm. The eye area is next localized using the integral projection function, followed by pupil detection and gaze classification. The pupil position and eye corner location information are utilized to identify the direction in which the subject is looking. The distance from pupil boundary to eye corner line segment is measured to find whether the driver is distracted or not. Compared to the algorithm in this study, the system is able to handle the head movement while this algorithm is done only for frontal face images. In [32] researchers proposed a framework to optimize gaze detection using data transfer learning with the help of deep-learning models. It used a small camera to capture images of eyes and mouth and then extract the required information from the centre of the eyes and mouth.

In [33] researchers proposed a framework for eye gaze detection with the use of Convolutional-Neural-Network

model and claimed better accuracy results when it comes to road safety. Along with this claim, the paradigm for the possible execution of proposed algorithm, real time eye gaze controlled autonomous vehicle can be used. The authors [34] described that real time road safety applications must deal with some challenges, like driver drowsiness, glass, and lighting reflections. Therefore, chance to get false result may increase when driver does not move his head and gaze an object with only eyes movement and gaze detection based only on head movement will not be sufficient and accurate. It presented a deep learning gaze detection without prerequisite of driver standardization with the help of an infrared small sensor.

III. PROPOSED SYSTEM

Fig. 1 shows the flowchart of the operation of Driver Drowsiness and Monitoring System in detecting drowsiness and distraction among the drivers. This system will be split into three modules which are blink detection, yawn detection and gaze detection. For all the module to operate, the system must successfully detect driver face. If there is any face detected, then it will go through each module simultaneously and begin the detection. If the driver shows any sign of drowsiness or distraction, the system will immediately sound the alarm to alert the driver.

Driver Drowsiness and Monitoring System is an automobile application that have the purpose to alert the driver when signs of drowsiness or distraction are detected. Based on Fig. 2, this system comprises a camera-based driver drowsiness and monitoring system aimed at the driver's face, which enables a real-time evaluation of the driver's presence and state. For the hardware part, the system will use Raspberry Pi 4 as the main component to make a compact embedded system. All the algorithms will be implemented in it. Webcam is installed on the car dashboard for video feed purpose to track features of the driver (8FPS). Portable speaker will be used as an alarm device. When the system detects drowsy or distracted driver condition, it makes a sound alert from the speaker. Image's processing algorithm is developed in Python and OpenCV to detect the drowsiness sign based on rate of eye blinking, eye closing period and rate of yawning while gaze detection to estimate where the driver is looking for the distraction sign.

A. Face Detection using Dlib Library

To detect the face in the image, HOG + LinearSVM face detector from dlib library will be used. The function that had been used for face detection is: `dlib.get_frontal_face_detector()`. This function will return the pre-trained HOG + Linear SVM face detector which is used for obtaining the face bounding box (i.e., the (x, y)-coordinates of the image's face). Given the face region in the face bounding box, the key facial structures in the face region can be detected. Facial landmark detection will be applied using pre-trained facial landmark detector inside the dlib library. This method is used to localize and labels mouth, right eyebrow, left eyebrow, right eye, left eye, nose and jaw. Each facial structure on the face has its own specific (x, y)-coordinates.

There are 68 coordinates (shown in Fig. 3). Those coordinates represent each facial structure mentioned above. These coordinates can be used to detect eyes, nose, mouth and left and right eyebrow and will be used for the next section.

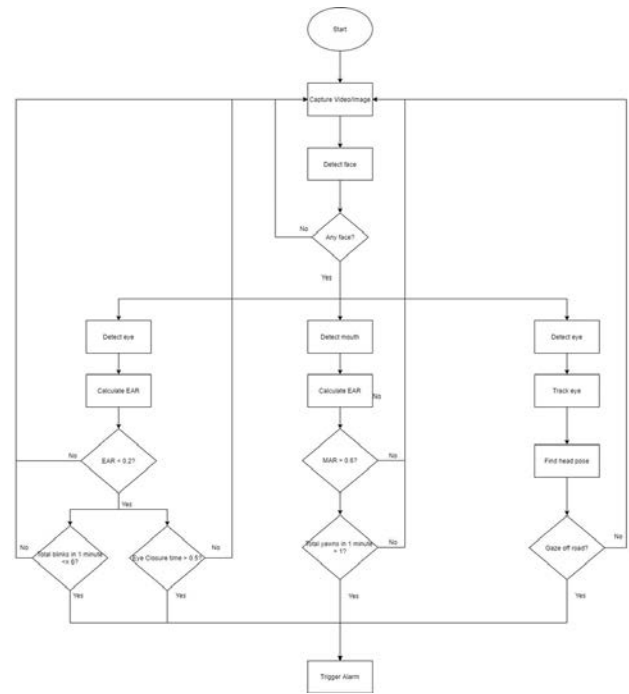


Fig. 1. Flow Chart of Driver Drowsiness and Monitoring System.

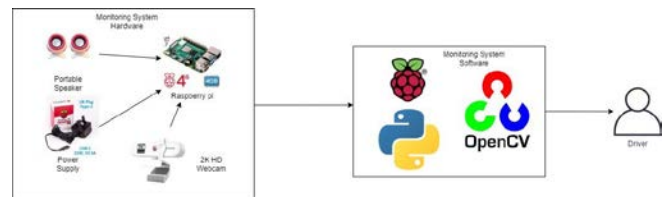


Fig. 2. System Architecture Diagram.

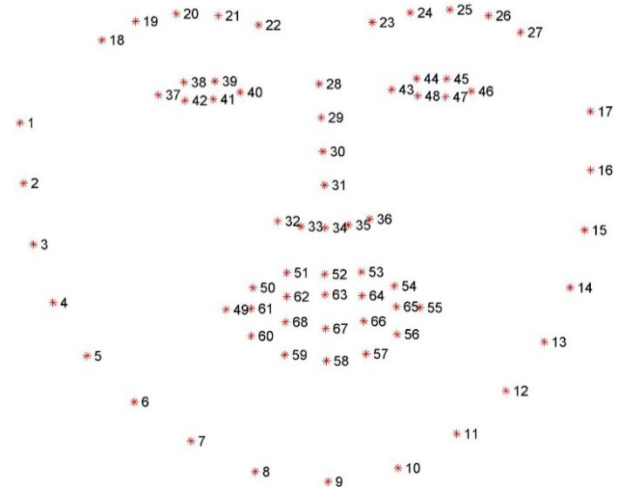


Fig. 3. 68 Facial Landmark Coordinates.

B. Blink Detection System

For the blink detection method, Eye Aspect Ratio (EAR) algorithm will be used. EAR is defined as the ratio of the height and width of the eye. First, extraction of the eye region from a set of facial landmarks. Based on Fig. 3 there are six coordinates for each eye. These six coordinates (as shown in Fig. 4) will be used for calculation of EAR value. The calculation is done for both left and right eye.

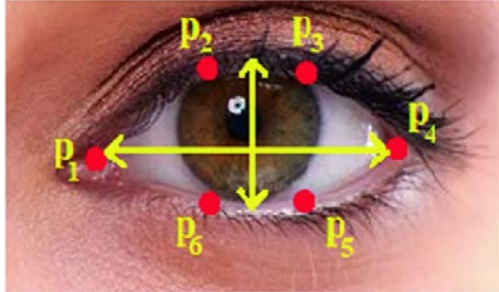


Fig. 4. The 6 Coordinates of an Eye represent in P1, P2, P3, P4, P5 and P6.

According to [5], the equation for EAR can be derived as the following:

$$EAR = \frac{|P2-P6|+|P3-P5|}{2 |P1-P4|} \quad (1)$$

Where, P1, P2, P3, P4, P5 and P6 are the facial landmark coordinates that have been obtained before. Next, the system calculates the average of two EAR together (assumption that a person blinks both eyes at the same time). EAR value will be compared with the threshold value (Te) taken as 0.2 [5]. If the EAR value is below than Te, the eye will be considered as closed. When eye is closed, the two types, which are eye closure and eye blink will be differentiated. When the duration of eye closed is more than 0.5 seconds, it will be considered as eye closure or else as eye blink.

$$EyeState = \begin{cases} Closed, EAR < Te \\ Open, EAR > Te \end{cases} \quad (2)$$

Alarm will be triggered in two conditions. Firstly, when the eye is closed for more than 0.5 seconds. This is because the typical duration of a single blink for the human eye is 0.1 to 0.4 seconds [6]. If it more than 0.5 seconds, then it is considered as eye closure. When the EAR value remains less than Te for more than 0.5 seconds, it can consider that the driver is drowsy or tired. Secondly, when the total number of blinks per minute is equal or less than six. This is because the typical blink rate for a normal individual is 10 blinks per minute, whereas it is 4-6 for a sleepy person [7].

C. Yawn Detection System

For the yawn detection method, Mouth Aspect Ratio (MAR) algorithm will be used. MAR is defined as the ratio of the height and width of the mouth. First of all, extraction of the mouth region from a set of facial landmarks. Based on Fig. 3, there total 20 coordinates for both outer and inner mouth. To calculate the MAR, only those coordinates will be used at which are at the outer mouth [8]. There are 12 coordinates (as shown in Fig. 5).

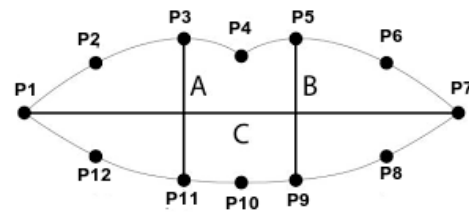


Fig. 5. The 12 Coordinates of Mouth Represent in P1, P2, P3, P4, P5, P6, P7, P8, P9, P10, P11 and P12.

According to [8], the equation for MAR can be derived as the following:

$$MAR = \frac{|P3-P11|+|P5-P9|}{2 |P1-P7|} \quad (3)$$

Where, P1, P2, P3, P4, P5, P6, P7, P8, P9, P10, P11 and P12 are the facial landmark coordinates that this study obtained before. MAR value will be compared with the threshold value (Tm) taken as 0.75. The value of Tm was established by trial and error, with several values of Tm being tested to ensure that the algorithm accurately classifies an instance of yawning and closed mouth. It shows that if the MAR value is bigger than Tm, the mouth will be considered as yawning. Every time MAR value exceeds the Tm, total threshold will be increased by 1 and will be reset back to 0 after 1 minute.

$$MouthState = \begin{cases} Close/Talking, MAR < Tm \\ Yawn, MAR > Tm \end{cases} \quad (4)$$

Alarm will be triggered when the total number of yawns per minutes is more than 1. This is because a driver becomes tired when he or she begins to yawn more than once per minute [9].

D. Gaze Detection System

For yawn detection method, the system will combine both head pose estimation and eye tracking. This combination will allow the system to detect whether the driver eyes are off the road or not. Drivers have a habit of changing their head position while driving. To determine which direction the driver is looking, 3D head pose estimation is necessary. In head pose estimation, it is typical to predict relative orientation and position with respect to camera, in calculating the Euler angles. Euler angles can be represented as roll (tilt), pitch (up and down) and yaw (left and right) as shown in Fig. 6.

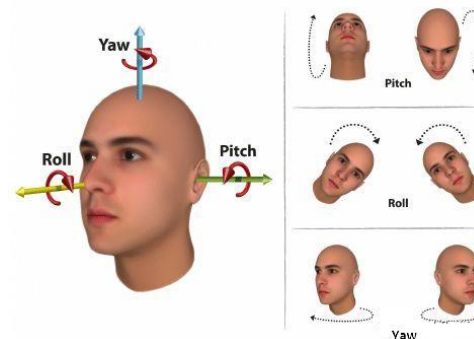


Fig. 6. Roll, Pitch, and Yaw of Euler Angles.

Out of three Euler angles, the system only extracted and used yaw angle only. This is due to the system's sole concentration on determining the left and right direction of the driver's gaze. After that, initializing the frontal face angle will be done. Frontal face is a face with a head yaw angle $\in [-15^\circ; 15^\circ]$. If the yaw angle is in between -15° and 15° it means that the driver is looking at the centre while if the yaw angle is less than -15° , it will be considered as looking in left direction and if it more than 15° , it will be considered as looking in the right direction. Eye tracking is needed because during driving, the driver's eye look is continuously shifting, based on the surroundings. As a result, identifying eyes is insufficient. Real-time tracking of eyes is required by isolating the eyes from the face using facial landmark detection mentioned. Then, detection of the iris by using image processing method such as blurring, eroding, thresholding and contour will be done. After getting the iris, the coordinate and calculate, the horizontal distance will be found to determine which direction driver is looking. The direction of the driver's gaze is determined by a combination of eye tracking and head pose estimation algorithms. Alarm will be triggered when the driver is looking other than centre for more than two seconds. This is because drivers should never move their gaze away from the road for more than two seconds at a time.

IV. RESULT AND DISCUSSION

The Driver Drowsiness and Monitoring System is tested in a variety of conditions that a driver would encounter in real life. The factors considered when developing test conditions are as follows:

- Appearance: With and without spectacles

The average frame rate of image capture throughout testing ranged between seven and eight FPS. All the people will be captured for one minutes on each function. Table I show final interpretation of the test performed on the system in terms of accuracy.

$$Truepositive = \frac{Noofframescorrectlydetected}{Totalnumbersofframes} \times 100 \quad (5)$$

The testing result in Fig. 7, Fig. 8 and Fig. 9 show that the system performs quite well under different condition that have been considered. Based on Fig. 7, the use of spectacles by driver has affected a lot in terms of accuracy. As a result, blink detection suffers from the problem of detecting false positive. This may be because system miscalculated the EAR value of the driver when he/she is wearing the spectacle. While based on Fig. 8, the system utilizes some mouth geometrical characteristics to identify yawning by detected by the ratio of mouth height and width. On the other hand, based on Fig. 9, gaze detection had lower accuracy on the spectacles driver because the system cannot track the eye properly.

TABLE I. SYSTEM ACCURACY CALCULATED FROM TESTING

	Blink/Eye closure	Yawn	Gaze
Person 1	68.3%	95%	48.3%
Person 2	91.7%	98.3%	90%
Person 3	67%	91.7%	46.7%
Person 4	96.7%	100%	93.3%
Average	80.9%	96.3%	69.6%

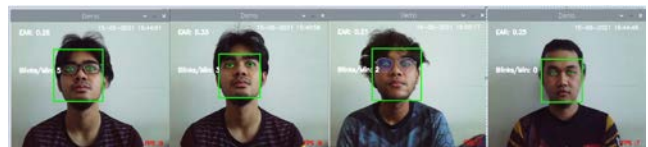


Fig. 7. Samples Testing of Eye Blink and Eye Closure.



Fig. 8. Samples Testing of Yawn.



Fig. 9. Samples Testing of Gaze.

V. CONCLUSION AND FUTURE WORK

Driver Drowsiness and Monitoring System is all in one software application for driver that can perform many functionalities in one application. This Driver Drowsiness and Monitoring System provides significant benefits to driver for them to track their behavior while driving. I really hope that this project can give benefit to driver so that driver can avoid fatal accident caused by driver negligence and sleepiness. The proposed method easily detects eye blink, yawn and gaze. Image processing provides a non-invasive method of detecting drowsiness and distraction that is free of irritation and interference. Whenever the system meets the requirement, it will set off the alarms. As a result, in this study the system is dependable, efficient, and cost-effective. The detection of drowsiness and distraction in its early phases not only assists the system in delivering timely warnings, but also warns the driver ahead of time, potentially saving lives from tragic mishaps.

In future, this Driver Drowsiness and Monitoring System could be upgraded even further when more systematic functions will be added to give ease to the vehicle driver while driving their vehicle. For instances, implementation of night vision to avoid the effect of poor detection due to insufficient light will obtain a better result that is unaffected by lack of brightness. Besides, the face detection algorithm must account for head movements and detect the face in all conceivable face orientations. So, that the system can be extended to include non-frontal face images. Then, to improve the accuracy of the system, the algorithm should include classifier that is trained on set of sample images. Lastly, to deliver a more comfortable driving experience, the system providing the function such as tire pressure monitoring, lane change assistant, etc. In a nutshell, this system will be useful to the driver by making their journey safer, more engaging, more convenient, and more fun.

ACKNOWLEDGMENT

The project is fully funded by Universiti Sains Malaysia (USM) and Ministry of Higher Education Malaysia under FRGS Grant Scheme (FRGS/1/2018/ICT03/USM/03/1).

REFERENCES

- [1] W. Zhang, B. Cheng and Y. Lin, "Driver drowsiness recognition based on computer vision technology", *Tsinghua Science and Technology*, Vol. 17, No. 3, pp. 354-362, 2012.
- [2] M. Singh, G. Kaur, "Drowsiness detection on eye blink Duration using algorithm", *International Journal of Emerging Technology and Advanced Engineering*, Vol. 2, Issue 4, April 2012.
- [3] T. Azim, M. A. Jaffar and A. M. Mirza, "Automatic Fatigue Detection of Drivers through Pupil Detection and Yawning Analysis," 2009 Fourth International Conference on Innovative Computing, Information and Control (ICICIC), 2009, pp. 441-445, doi: 10.1109/ICICIC.2009.119.
- [4] S. Maralappanavar, R. Behera and U. Mudenagudi, "Driver's distraction detection based on gaze estimation," 2016 International Conference on Advances in Computing, Communications and Informatics (ICACCI), 2016, pp. 2489-2494, doi: 10.1109/ICACCI.2016.7732431.
- [5] T. Soukupova and J. Cech, "Real-time eye blink detection using facial landmarks," *Computer Vision Winter Workshop (CVWW)*, 2016.
- [6] "Search BioNumbers - The Database of Useful Biological Numbers", *Bionumbers.hms.harvard.edu*, 2021. [Online]. Available: <https://bionumbers.hms.harvard.edu/bionumber.aspx?id=100706&ver=0>. [Accessed: 14- Aug- 2021].
- [7] M. K. Raha and A. Roy, "Fatigue Estimation through Face Monitoring and Eye Blinking", *International Conference on Mechanical Industrial and Energy Engineering*, 2014.
- [8] P. Awasekar, M. Ravi, S. Doke and Z. Shaikh, "Driver Fatigue Detection and Alert System using Non-Intrusive Eye and Yawn Detection", *International Journal of Computer Applications*, Vol. 180, No. 44, pp. 1-5, 2018.
- [9] M. U. C. J. A. Haider and A. Kassem, "Yawn Based Driver Fatigue Level Prediction", *EPiC Series in Computing*, Vol. 69, pp. 372-382, 2020.
- [10] Jabbar, R., Al-Khalifa, K., Kharbeche, M., Alhajyaseen, W., Jafari, M., & Jiang, S. (2018). Real-time driver drowsiness detection for android application using deep neural networks techniques. *Procedia computer science*, 130, 400-407.
- [11] Chirra, Venkata & Reddy, U. Srinivasulu & KishoreKolli, Venkata. (2019). Deep CNN: A Machine Learning Approach for Driver Drowsiness Detection Based on Eye State. *Revue d'Intelligence Artificielle*. 33. 461-466. 10.18280/ria.330609.
- [12] Jabbar, R., Shinoy, M., Kharbeche, M., Al-Khalifa, K., Krichen, M., & Barkaoui, K. (2020, February). Driver drowsiness detection model using convolutional neural networks techniques for android application. In *2020 IEEE International Conference on Informatics, IoT, and Enabling Technologies (ICIoT)* (pp. 237-242). IEEE.
- [13] Ramzan, M., Khan, H. U., Awan, S. M., Ismail, A., Ilyas, M., & Mahmood, A. (2019). A survey on state-of-the-art drowsiness detection techniques. *IEEE Access*, 7, 61904-61919.
- [14] Oliveira, L., Cardoso, J. S., Lourenço, A., & Ahlström, C. (2018, November). Driver drowsiness detection: a comparison between intrusive and non-intrusive signal acquisition methods. In *2018 7th European Workshop on Visual Information Processing (EUVIP)* (pp. 1-6). IEEE.
- [15] Bordel, B., Alcarria, R., Rizzo, G., & Jara, A. (2018, January). Creating predictive models for forecasting the accident rate in mountain roads using VANETs. In *International Conference on Information Technology & Systems* (pp. 319-329). Springer, Cham.
- [16] Yu, J., Park, S., Lee, S., & Jeon, M. (2018). Driver drowsiness detection using condition-adaptive representation learning framework. *IEEE transactions on intelligent transportation systems*, 20(11), 4206-4218.
- [17] Fujiwara, K., Abe, E., Kamata, K., Nakayama, C., Suzuki, Y., Yamakawa, T., ... & Kadotani, H. (2018). Heart rate variability-based driver drowsiness detection and its validation with EEG. *IEEE Transactions on Biomedical Engineering*, 66(6), 1769-1778.
- [18] Zhao, L., Wang, Z., Wang, X., & Liu, Q. (2018). Driver drowsiness detection using facial dynamic fusion information and a DBN. *IET Intelligent Transport Systems*, 12(2), 127-133.
- [19] Tiwari, K. S., Bhagat, S., Patil, N., & Nagare, P. (2019). IOT based driver drowsiness detection and health Monitoring System. *International Journal of Research and Analytical Reviews (IJRAR)*, 6(02), 163-167.
- [20] Junaedi, S., & Akbar, H. (2018, September). Driver drowsiness detection based on face feature and PERCLOS. In *Journal of Physics: Conference Series* (Vol. 1090, No. 1, p. 012037). IOP Publishing.
- [21] Deng, W., & Wu, R. (2019). Real-time driver-drowsiness detection system using facial features. *Ieee Access*, 7, 118727-118738.
- [22] Islam, M. M., Kowsar, I., Zaman, M. S., Sakib, M. F. R., & Saquib, N. (2020, June). An algorithmic approach to driver drowsiness detection for ensuring safety in an autonomous car. In *2020 IEEE Region 10 Symposium (TENSymp)* (pp. 328-333). IEEE.
- [23] Jabbar, R., Shinoy, M., Kharbeche, M., Al-Khalifa, K., Krichen, M., & Barkaoui, K. (2020, February). Driver drowsiness detection model using convolutional neural networks techniques for android application. In *2020 IEEE International Conference on Informatics, IoT, and Enabling Technologies (ICIoT)* (pp. 237-242). IEEE.
- [24] Bhargava, G. U. K., Reddy, G. K., & Rambabu, K. Supervised Learning Algorithm Driver Drowsiness Detection and Alerting System.
- [25] Salman, R. M., Rashid, M., Roy, R., Ahsan, M. M., & Siddique, Z. (2021). Driver Drowsiness Detection Using Ensemble Convolutional Neural Networks on YawDD. *arXiv preprint arXiv:2112.10298*.
- [26] Shen, Q., Zhao, S., Zhang, R., & Zhang, B. (2020, October). Robust Two-Stream Multi-Features Network for Driver Drowsiness Detection. In *Proceedings of the 2020 2nd International Conference on Robotics, Intelligent Control and Artificial Intelligence* (pp. 271-277).
- [27] Alekhya, G., Samhitha, K. V., Bhavana, P. B., & Yadav, B. V. Driver Drowsiness Monitoring System Using Visual Behaviors And Machine Learning.
- [28] Kumar, K. P., Thamanam, S. R., & Kumar, M. N. (2020). Identification of Driver Drowsiness Using Image Processing. *European Journal of Molecular & Clinical Medicine*, 7(4), 1264-1268.
- [29] sHasan, F., & Kashevnik, A. (2021, May). State-of-the-art analysis of modern drowsiness detection algorithms based on computer vision. In *2021 29th Conference of Open Innovations Association (FRUCT)* (pp. 141-149). IEEE.
- [30] Pondit, A., Dey, A., & Das, A. (2020, December). Real-time Driver Monitoring System Based on Visual Cues. In *2020 6th International Conference on Interactive Digital Media (ICIDM)* (pp. 1-6). IEEE.
- [31] Tipprasert, W., Charoenpong, T., Chianrabutra, C., & Sukjamsri, C. (2019, January). A method of driver's eyes closure and yawning detection for drowsiness analysis by infrared camera. In *2019 First International Symposium on Instrumentation, Control, Artificial Intelligence, and Robotics (ICA-SYMP)* (pp. 61-64). IEEE.
- [32] Ribeiro, R. F., & Costa, P. D. (2019, May). Driver gaze zone dataset with depth data. In *2019 14th IEEE International Conference on Automatic Face & Gesture Recognition (FG 2019)* (pp. 1-5). IEEE.
- [33] Saha, D., Ferdoushi, M., Emrose, M. T., Das, S., Hasan, S. M., Khan, A. I., & Shahnaz, C. (2018, December). Deep Learning-Based Eye Gaze Controlled Robotic Car. In *2018 IEEE Region 10 Humanitarian Technology Conference (R10-HTC)* (pp. 1-6). IEEE.
- [34] Naqvi, R. A., Arsalan, M., Batchuluun, G., Yoon, H. S., & Park, K. R. (2018). Deep learning-based gaze detection system for automobile drivers using a NIR camera sensor. *Sensors*, 18(2), 456.

BiDLNet: An Integrated Deep Learning Model for ECG-based Heart Disease Diagnosis

S.Kusuma, Dr Jothi.K. R
School of Computer Science and Engineering
Vellore Institute of Technology
Vellore, India

Abstract—Every year, around 10 million people die due to heart attacks. The use of electrocardiograms (ECGs) is a vital part of diagnosing these conditions. These signals are used to collect information about the heart's rhythm. Currently, various limitations prevent the diagnosis of heart diseases. The BiDLNet model is proposed in this paper which aims to examine the capability of electrocardiogram data to diagnose heart disease. Through a combination of deep learning techniques and structural design, BiDLNet can extract two levels of features from the data. A discrete wavelet transform is a process that takes advantage of the features extracted from higher layers and then adds them to lower layers. An ensemble classification scheme is then made to combine the predictions of various deep learning models. The BiDLNet system can classify features of different types of heart disease using two classes of classification: binary and multiclass. It performed remarkably well in achieving an accuracy of 97.5% and 91.5%, respectively.

Keywords—Heart disease; ECG; deep learning; machine learning models; discrete wavelet transform

I. INTRODUCTION

According to statistics, around half of all deaths caused by cardiovascular disease are due to sudden cardiac arrests [1,2]. The most common tool used for detecting arrhythmias is the electrocardiogram, which is a non-invasive method of monitoring the heart's activity. Unfortunately, diagnosing arrhythmias using an electrocardiogram is usually time-consuming and challenging for cardiologists. That is why a lightweight arrhythmia detection system is designed to help busy cardiologists identify and treat patients with irregular heart rhythm conditions. The ability to perform efficiently and accurately is a vital component of computer-assisted diagnosis (CAD) technology, which is used to treat cardiovascular disease.

In the past few decades, various machine learning algorithms have been extensively studied for detecting arrhythmias. These include the multi-perceptron, extreme gradient boosting, and support vector machines. The development of open-source electrocardiogram datasets such as those from MIT-BIH has greatly improved the performance of these systems. One of the most common approaches to arrhythmia detection is to identify the shape of the heartbeats in five different types according to the AAMI standard. This method usually takes three steps to implement. These include signal preprocessing, data augment, feature engineering, and linear or nonlinear classification.

Unfortunately, noise removal techniques are prone to losing valuable information about physiological signals. Also, the varying signal waveforms can lead to poor performance in the construction of features. That is why machine learning models must be designed to perform well in this field[3-6]. Due to the increasing number of data sources, the performance of machine learning models has improved significantly in detecting different types of heartbeats. This is because the increasing number of features and the complexity of the classification process have been greatly improved by the use of deep neural networks. Deep models have been able to improve the performance of various applications such as machine vision and natural language processing.

The paper shows how BiDLNet, an automatic tool for analyzing and visualizing electrocardiograms, works by taking advantage of four deep learning techniques. It first takes advantage of two different techniques to perform deep features and then combines them using a wavelet to reduce their size. BiDLNet then combines the deep learning techniques' deep features with the higher-layer features to perform a feature selection procedure. It then improves its classification performance by using an ensemble learning algorithm. BiDLNet can classify different types of heart disease from the traces of electrocardiograms. It can classify it in two categories: binary classification and multiclass classification. The first one aims to distinguish between normal and abnormal patients, while the second one focuses on the different cardiac findings.

The development of BiDLNet has been regarded as a major contribution to the advancement of the pipeline.

- It is a cost-effective, fast, and sensitive tool that can help in the detection of heart disease.
- BiDLNet can also perform a new approach to diagnosing heart disease by analyzing the 2-D image of the ECG. This method is considered to be a novel technique to perform diagnosis.
- BiDLNet is built on a network of deep learning networks that are composed of distinct structures. Due to the varying architecture of these networks, it can get two levels of deep features from each layer.
- Due to the varying dimensions of the features extracted from each layer, they are mined through deep learning techniques to reduce their size. They are then merged into a single feature in a simplified manner.

- The level of a feature that's extracted from each layer affects the performance of BiDLNet. To improve its performance, it should also consider incorporating bi-level features.

The article begins with the related literature survey in Section 2. Overview of the materials and methods used in the study in Section 3 and then moves on to introduce the experimental results. Section 4 presents the results of the study, and then Section 5 concludes with a discussion of the limitations and strengths of the proposed study.

II. LITERATURE REVIEW

Various studies have been conducted on the use of signal processing, data mining, and soft-computing techniques to analyze and visualize CADx for various applications [7]. One of these studies utilized a flexible algorithm known as FAWT to extract statistical features from the electrocardiogram signals [8]. A study conducted by Acharya et al. extracted high-order spectra from the electrocardiogram signals [9]. They then trained and tested a deep convolutional neural network for analyzing and visualizing CADx [10]. The researchers used a variety of parameters to test and improve the model's performance [11]. The researchers then explored the use of a tunable-Q wavelet transform algorithm for analyzing and visualizing CADx. They found that it performed well in the detection task [12]. In another study, the authors analyzed the performance of two deep neural networks on the same task [13].

In another study, the researchers explored the use of a joint time-frequency representation scheme for analyzing and visualizing CADx [14-16]. They found that it performed well. The results of their study led to the development of a filter bank that can be used for optimal performance. Many studies have been proposed for the analysis and visualization of CADx, CAD using HR or electrocardiogram signals. One of the techniques that is commonly used in this field is the use of multi-dimensional signal processing [17,18]. While the conventional methods of analyzing and visualizing CADx rely on matrix-based transformations and vectors, the use of tensor-based techniques can provide a powerful tool for improving the performance of these techniques [19]. In a study, the researchers proposed 33 layers of a deep convolutional neural network that can be used to classify 12 rhythm types [20]. They found that it performed well in performing diagnostic tasks on a large single-lead ECG dataset. Their models performed well in various public datasets [21]. In another study, researchers explored the use of discrete wavelet transforms to extract 3,072-dimensional features from an electrocardiogram dataset. The results of this study were superior to deep learning and ensemble learning methods [22].

In another study, the researchers proposed a CNN (Convolutional Neural Network) that was able to detect myocardial infarction using electrocardiogram beats with noise [23,24]. Unfortunately, the researchers found that the temporal properties of the signals were not taken into account properly. In some studies, the use of well-designed structures to cope with the time series has been presented. For instance, in a study, the researchers were able to distinguish five types

of arrhythmias using a deep-coded feature network and an LSTM network. They found that the LSTM network performed well under raw electrocardiograms. Despite the success of the deep model, the researchers found that the models were not able to perform well in certain types of arrhythmias. They noted that the deep model often overfits due to its lack of cross-correlation operation[25]. To improve the performance of deep models, the researchers suggested that they should be tested with more electrocardiograms.

III. MATERIALS AND METHODS

A. Algorithms and Dataset

Deep learning is a type of machine learning that involves building various structures using recurrent neural networks, belief networks, and autoencoders. These are then utilized for a particular kind of data, the most common deep learning model is the CNN. This is used in the design and construction of medical images, and it is also used in the diagnosis and classification of medical images. In this study, four CNN namely ResNet, DenseNet, Inception and Xception architectures are used to implement a proposed model for diagnosis called BiDLNet.

The PTB-XL is a recently published electrocardiogram data set that is used in this research[26]. This dataset was originally recorded from 1989 to 1996. It was made available online in 2020. The data was initially made available to the public in 2020. This dataset consists of over 20,000 electrocardiograms (ECGs) taken from 18885 individuals. The gender balance is equal between male and female patients, with ages ranging from 1 to 95 years. It also contains various heart diseases and single-disease conditions. This dataset includes a single-class label for patients with only one heart disease or a multi-class label for those with multiple heart diseases as given in Table I. The number of healthy subjects in the dataset is also impressive. A sample Heart patient dataset is shown in Fig. 1.

TABLE I. THE NUMBER OF RECORDS FOR INDIVIDUAL CLASSES

Records	Class	Description
9528	NORM	Normal ECG
2655	HYP	Hypertrophy
4907	CD	Conduction Disturbance
5250	STTC	ST/T Change
5486	MI	Myocardial Infarction



Fig. 1. Sample ECG Image.

B. Proposed BiDLNet

The paper aims to investigate the potential of deep learning techniques to diagnose heart disease using electrocardiogram data. It proposes a pipeline that aims to explore the possibility of achieving high performance in this field. The BiDLNet framework uses electrocardiogram trace images to perform the real-time clinical study. It includes four phases: Data preprocessing, Extraction of features, classification, and finally, integration. During the preprocessing stage, the image size is modified and augmented. After training four CNNs, deep features are extracted from each CNN layer. Lastly, with the fully connected layers, the obtained features are then combined in the integration stage. Through the use of deep learning techniques, such as DWT, the features can be fused seamlessly. During the feature selection stage, the number of integrated features decreases. In the classification stage, a set of schemes is then constructed to diagnose heart disease. The second scheme consists of multiple classification systems that are built on voting ensemble classification. The proposed BiDLNet Architecture is represented in Fig. 2.

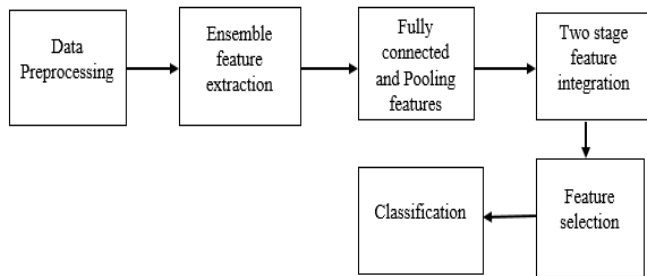


Fig. 2. BiDLNet Architecture.

1) *Data preprocessing*: The tracing image of ECG size is changed to correspond to the input layer of a deep learning model. Table II shows the sizes of the extracted features and the input layers of varied deep learning models. After extracting the features, the data augmentation procedure is applied using various approaches to improve their size and reduce overfitting issues during the training process. These include scaling, translation, and folding in y and x directions.

2) Phases of proposed methodology

a) *Phase 1: Feature Extraction*: Some problems can occur during the training of CNNs. These include convergence and overfitting. To avoid these issues, the layers should be modified to ensure that their learning rates are similar. Transfer learning can then be used to improve the performance of these layers. This study focused on a small dataset with a few images. Pre-trained CNNs are commonly used to improve the classification performance of images by training them on attributes from a large number of images. They can also be used to perform similar tasks more accurately when compared to the models that are used in the study. Four of these CNNs are currently being used with the transfer learning framework, and some of the parameters will be explained in a later section.

In this study, the size of the output layer was modified to perform multiclass and binary diagnosis tasks for heart disease

classification. After the CNNs have been trained, deep features are extracted using the method. The extracting of features is done from the CNN's two layers. The first layer is a collection of layers that accepts the raw images, while the other layers perform various functions. These include calculating the output volume, performing a convolutional process, and analyzing the regions of the image. The first layer is then joined with the other layers to form a pooling layer. This allows the CNN to minimize the size of its earlier convolutional layer and generate class scores. At last, the fully connected layers perform various functions, such as generating class scores and learning input image patterns.

Due to the different performance of deep learning techniques, the deeper layers of CNN were used in this study. The extracted sizes of the feature sets from each model were studied in Table II. To ensure that the benefits of deep learning are integrated, feature integration was also performed. The DWT method was also used to reduce the size of the features. This method can also explain the time-frequency illustration of the data. The cluster of wavelet functions in this study takes advantage of the data's low and high pass filters to produce smaller output sizes. It then passes the resulting details and approximation coefficients through various low and high pass filters. The paper uses three decomposition levels to analyze the features. The lowest level, which is known as the DWT, has a frequency range of 0 to 2.3 kHz. The cluster of wavelet functions was then combined with the deep feature sets extracted from the last layer of the CNN to perform a more accurate image classification. The "Haar" wavelet was chosen as it is an efficient tool for analyzing ECG data. The number of decomposition levels achieved by the cluster was three. The authors of the study noted that the results of the analysis of the medical signals using the approximation coefficients performed better than the details coefficients.

b) *Phase 2: Feature Selection*: After the integration step, it is important to perform a feature selection process to minimize the space occupied by various features. This process can be carried out through automated tools that can identify and eliminate redundant variables. In this step, a feature selection process is carried out using a symmetrical uncertainty method. This method takes into account the relevance of various variables and classes and computes the redundancy among them. It takes into account the information gain and the entropy of two features by measuring the relation between these two variables.

$$\text{Information Gain}(P/Q) = \text{Entropy}(P) - \text{Entropy}(Q) \quad (1)$$

$$\text{Symmetric uncertainty} = 2 \times \frac{\text{Information Gain}(P/Q)}{\text{Entropy}(P) + \text{Entropy}(Q)} \quad (2)$$

TABLE II. DEEP LEARNING ARCHITECTURES INPUT SIZE

CNN Architecture	Size of Input
ResNet 101	224X224X3
DenseNet 121	224X224X3
Inception V3	299X299X3
Xception	299X299X3

Where Entropy(P) and Entropy(Q) are the entropy of variables P and Q, and Information Gain(P/Q) is the information gain of P once examining variable Q.

c) *Phase 3: Classification:* The classification stage involves selecting three or more individual classifiers to be used for the different classification categories. These are The Linear Discriminant Analysis(LDA), Support Vector Machine(SVM), and Random Forest(RF). The process is performed using a combination of schemas that are designed to classify the various classes. The first four schemas are composed of the deep features from CNN. The next three are composed of the various features from the last average pool layer. The fourth and final version of the framework consists of the multi-classified system. Cross validation is performed on a 5-fold scale to split a dataset into two parts. For each iteration, the model is trained with 4 folds, while the 5th fold is used for testing. The average performance of the models is compared with the performance of the binary class. For the normal class, 20% of the images were used. During the multiclass classification phase, 75% of the images were used. This includes 25% of heart disease and 25% of cardiac disorders. This ensures that 25% of the images were used during every iteration of the test.

IV. RESULTS AND DISCUSSION

A. Simulation Procedure and Results

The parameters of the four CNNs are changed based on the classification category and the number of epochs. For instance, the learning rate for a multiclass and a binary class is 0.001. The mini-batch size is also changed to 4. The training process is carried out through stochastic gradient descent. The experiments are performed using Google colab. The results of the Multi-Classified System (MCS) are shown in this section. It combines the predictions of various statistical techniques such as the LDA, SVM, and RF classifiers. After feature selection, the two components were fully connected. The results of the system are shown in Fig. 3. The improved accuracy of the system is compared to that of the SVM classifier. The accuracy of the three classification techniques improved with the use of the multi-classified system. The results of the system show that the accuracy of the three techniques improved, which is higher than the result of the SVM, LDA, and the RF. The results of the system suggest that the use of the multi-classified system can improve the performance of these techniques. The classification performance of the various classes of the binary and multiclass tasks is shown in Table III. The obtained results indicate that the ensemble classification performed better than the individual classification. The accuracy of the ensemble classification was also greater than that of the individual classification as indicated in Table IV. The achieved results of the study also suggest that the use of the multi-classified system can improve the performance of these techniques.

In this the following performance measures are used to evaluate the performance of the model:

1) *Accuracy(Acc):* It is calculated by the number of successfully classified points (predictions) divided by the total number of predictions in the ratio. Its value ranges from 0 to 1.

$$Acc=(True\ Positive+True\ Negative)/(True\ Positive+False\ Positive+False\ Negative+True\ Negative)$$

2) *Sensitivity(Sen):* Calculates the number of positives returned by our model. This is also termed Recall.

$$Sen=(True\ Positive)/(True\ Positive+False\ Negative)$$

3) *Precision(Pr):* The number of successful points returned by our model can be described.

$$Pr=True\ Positive/(True\ Positive+False\ Positive)$$

4) *Specificity(Spec):* In contrast to recall, specificity can be defined as the number of negatives returned by our model.

$$Spec=(True\ Negative)/(True\ Negative +False\ Positive)$$

5) *F1 Score:* The F1 Score can be derived by taking the harmonic mean of precision and recall and giving them equal weight.

$$F1\ Score=2*((Precision*Recall)/(Precision+Recall))$$



Fig. 3. Accuracy Results of the Multi-classified System.

TABLE III. THE CLASSIFICATION PERFORMANCE OF THE VARIOUS CLASSES OF THE BINARY AND MULTICLASS TASK

Classifiers	Sensitivity	Precision	Specificity	F1 score
Binary Classification				
Linear Discriminant Analysis	0.97	0.973	0.97	0.97
Random Forest	0.965	0.965	0.966	0.965
Support Vector Machine	0.976	0.977	0.978	0.977
Voting classifier	0.976	0.977	0.978	0.977
Multi Class Classification				
Linear Discriminant Analysis	0.803	0.805	0.845	0.803
Random Forest	0.78	0.791	0.838	0.789
Support Vector Machine	0.796	0.798	0.842	0.797
Voting classifier	0.803	0.805	0.845	0.803

TABLE IV. EACH CLASS'S MULTICLASS CLASSIFICATION ACCURACY

Class	Linear Discriminant Analysis	Random Forest	Support Vector Machine	Voting classifier
Normal	87.7	87.5	87	88.2
Abnormal	90.3	88.3	87.9	91.2

B. Discussion

The literature has shown that various types of cardiovascular abnormalities can occur in patients with heart disease, such as arrhythmias and QRST anomalies. It has been suggested that the novel coronavirus could be a potential cause of these conditions, but other studies have suggested that it could also degrade them. The studies conducted on the whole electrocardiogram (ECG) data have shown that various findings have been observed. The main objective of this study is to distinguish the data from other types of ECGs and identify heart disease cases. A new tool has been proposed that can be used to perform a diagnosis of heart disease using 2D images captured from 12 leads. Although there are many studies on the use of electrocardiograms (ECGs) data for diagnosing heart disease, little is known about the techniques utilized in deep learning to analyze these images. In this study, we present a new method that uses AI techniques to analyze these images.

The proposed pipeline, BiDLNet, is based on a set of pre-trained deep learning models that are capable of extracting features from different deep layers. It was able to perform a feature extraction process by extracting large features from the former and the latter layers. The paper first looked into the various features that emerged during the recording of the ECG data. They were then studied to determine how these features affected the accuracy of diagnosis. Due to the fusion of the various features, their dimension increased. Then the feature dimensions are reduced by using the symmetric uncertainty feature selection approach to improve its classification accuracy. The paper then created a classification system that was designed to study the effects of voting on the accuracy of diagnosis. It was then used to find the optimal scheme for the BiDLNet pipeline.

The proposed tool was able to perform a multiclass classification task with good accuracy. The results of the binary task revealed that the proposed tool was able to distinguish between normal and abnormal images. The results of the study revealed that the accuracy of the classification process was significantly affected by the differences between the normal and abnormal ECGs. For instance, the accuracy of the classification for the abnormal ECG was 91.2%, while that of the classification for the normal ECG was 88.2%. The results of the study revealed that the proposed tool was able to identify an abnormal ECG compared to the other images. However, it was not able to diagnose other cardiac abnormalities. The results of the study also revealed that the proposed tool was not able to distinguish between normal and abnormal images due to the similarities between the different cardiac variations. The proposed pipeline's ability to classify heart disease electrocardiograms (ECGs) could be a promising tool for the early detection of cardiovascular variations.

V. CONCLUSION

The paper proposes a pipeline called BiDLNet that can be used to automatically diagnose heart disease using data from an electrocardiogram. It features two classification categories: multiclass and binary. The BiDLNet framework separates normal and abnormal patients by classifying them as either binary or multiclass. It then combines these features with fully connected ones. The two levels of deep features were extracted from four CNNs. To do so, it used a discrete wavelet transform to reduce the dimension of the pooling features and merge them with fully connected ones. The framework then explored the effects of integrating these features on the accuracy of its classification. It also looked into the possibility of reducing the number of features while improving its performance. After creating a multi-class classification system, the paper was able to improve the accuracy of the BiDLNet framework's classification by integrating various features. It also performed better when it selected the appropriate features. The results of the study revealed that the accuracy of the BiDLNet framework's classification was improved even further by using the multiclass classification feature, the MCS. The results of the study showed that the system achieved a sensitivity of 97.6%, specificity of 97.8%, and accuracy of 97.5% for the binary classification category. The proposed tool for analyzing cardiac variations in images was validated by an SVM classifier. The proposed pipelined system was able to correctly classify 95.2% of the abnormal ECG images as heart disease, while 91.7% of the images were categorized as normal. This means that it has been able to identify 98.8% of the patients as having heart disease. Only 1.2% of the abnormal images were misclassified as normal by the proposed pipeline while 4.8% of the images were labelled as other cardiac abnormalities. The results of the study suggest that the proposed system can accurately identify cardiac disorder ECGs. The results of the study revealed that the proposed system was able to accurately classify 95.2% of the abnormal ECG images as heart disease, while 91.7% of the images were categorized as normal. This means that it can now help identify patients with heart disease. The ability of the BiDLNet framework to distinguish between normal and abnormal findings further validates the potential of this technology to diagnose heart disease. It can be used to improve the efficiency and sensitivity of existing imaging techniques. For instance, it can be used to automatically classify images of patients with heart disease. It can also help reduce the number of unnecessary visits to the hospital. However, the tool was not able to perform a class imbalance analysis. Other deep learning techniques could also be utilized in the future to improve the accuracy of the proposed system.

REFERENCES

- [1] Wong, C. X., Brown, A., Lau, D. H., Chugh, S. S., Albert, C. M., Kalman, J. M., & Sanders, P. (2019). Epidemiology of sudden cardiac death: global and regional perspectives. *Heart, Lung and Circulation*, 28(1), 6-14.
- [2] Mendis, S., Puska, P., Norrving, B.E. and World Health Organization, 2011. *Global atlas on cardiovascular disease prevention and control*. World Health Organization.
- [3] Alizadehsani, R., Abdar, M., Roshanzamir, M., Khosravi, A., Kebria, P.M., Khozeimeh, F., Nahavandi, S., Sarrafzadegan, N. and Acharya, U.R., 2019. Machine learning-based coronary artery disease diagnosis:

- A comprehensive review. *Computers in biology and medicine*, 111, p.103346.
- [4] Alizadehsani, R., Hosseini, M.J., Sani, Z.A., Ghandeharioun, A. and Boghrati, R., 2012, December. Diagnosis of coronary artery disease using cost-sensitive algorithms. In *2012 IEEE 12th International Conference on Data Mining Workshops* (pp. 9-16). IEEE.
- [5] Alizadehsani, R., Zangoeei, M.H., Hosseini, M.J., Habibi, J., Khosravi, A., Roshanzamir, M., Khozeimeh, F., Sarrafzadegan, N. and Nahavandi, S., 2016. Coronary artery disease detection using computational intelligence methods. *Knowledge-Based Systems*, 109, pp.187-197.
- [6] Acharya, U.R., Hagiwara, Y., Koh, J.E.W., Oh, S.L., Tan, J.H., Adam, M. and San Tan, R., 2018. Entropies for automated detection of coronary artery disease using ECG signals: A review. *Biocybernetics and Biomedical Engineering*, 38(2), pp.373-384.
- [7] Acharya, U.R., Fujita, H., Lih, O.S., Adam, M., Tan, J.H. and Chua, C.K., 2017. Automated detection of coronary artery disease using different durations of ECG segments with convolutional neural network. *Knowledge-Based Systems*, 132, pp.62-71.
- [8] Patidar, S., Pachori, R.B. and Acharya, U.R., 2015. Automated diagnosis of coronary artery disease using tunable-Q wavelet transform applied on heart rate signals. *Knowledge-Based Systems*, 82, pp.1-10.
- [9] Tan, J.H., Hagiwara, Y., Pang, W., Lim, I., Oh, S.L., Adam, M., San Tan, R., Chen, M. and Acharya, U.R., 2018. Application of stacked convolutional and long short-term memory network for accurate identification of CAD ECG signals. *Computers in biology and medicine*, 94, pp.19-26.
- [10] Sharma, R.R., Kumar, M. and Pachori, R.B., 2019. Joint time-frequency domain-based CAD disease sensing system using ECG signals. *IEEE Sensors Journal*, 19(10), pp.3912-3920.
- [11] Sharma, M., Goyal, D., Achuth, P.V. and Acharya, U.R., 2018. An accurate sleep stages classification system using a new class of optimally time-frequency localized three-band wavelet filter bank. *Computers in biology and medicine*, 98, pp.58-75.
- [12] Wah, T.Y., Gopal Raj, R. and Iqbal, U., 2018. Automated diagnosis of coronary artery disease: a review and workflow. *Cardiology research and practice*, 2018.
- [13] Alizadehsani, R., Roshanzamir, M., Abdar, M., Beykikhoshk, A., Khosravi, A., Panahiazar, M., Koohestani, A., Khozeimeh, F., Nahavandi, S. and Sarrafzadegan, N., 2019. A database for using machine learning and data mining techniques for coronary artery disease diagnosis. *Scientific data*, 6(1), pp.1-13.
- [14] Anandkumar, A., Ge, R., Hsu, D., Kakade, S.M. and Telgarsky, M., 2014. Tensor decompositions for learning latent variable models. *Journal of machine learning research*, 15, pp.2773-2832.
- [15] Nesaragi, N., Patidar, S. and Aggarwal, V., 2021. Tensor learning of pointwise mutual information from EHR data for early prediction of sepsis. *Computers in biology and medicine*, 134, p.104430.
- [16] Nesaragi, N., Patidar, S. and Thangaraj, V., 2021. A correlation matrix-based tensor decomposition method for early prediction of sepsis from clinical data. *Biocybernetics and Biomedical Engineering*, 41(3), pp.1013-1024.
- [17] Hannun, A.Y., Rajpurkar, P., Haghpanahi, M., Tison, G.H., Bourn, C., Turakhia, M.P. and Ng, A.Y., 2019. Cardiologist-level arrhythmia detection and classification in ambulatory electrocardiograms using a deep neural network. *Nature medicine*, 25(1), pp.65-69.
- [18] Wang, R., Fan, J. and Li, Y., 2020. Deep multi-scale fusion neural network for multi-class arrhythmia detection. *IEEE journal of biomedical and health informatics*, 24(9), pp.2461-2472.
- [19] Yao, Q., Wang, R., Fan, X., Liu, J. and Li, Y., 2020. Multi-class arrhythmia detection from 12-lead varied-length ECG using attention-based time-incremental convolutional neural network. *Information Fusion*, 53, pp.174-182.
- [20] Fan, X., Yao, Q., Cai, Y., Miao, F., Sun, F. and Li, Y., 2018. Multiscale fusion of deep convolutional neural networks for screening atrial fibrillation from single lead short ECG recordings. *IEEE journal of biomedical and health informatics*, 22(6), pp.1744-1753.
- [21] Tuncer, T., Dogan, S., Plawiak, P. and Acharya, U.R., 2019. Automated arrhythmia detection using novel hexadecimal local pattern and multilevel wavelet transform with ECG signals. *Knowledge-Based Systems*, 186, p.104923.
- [22] Acharya, U.R., Fujita, H., Oh, S.L., Hagiwara, Y., Tan, J.H. and Adam, M., 2017. Application of deep convolutional neural network for automated detection of myocardial infarction using ECG signals. *Information Sciences*, 415, pp.190-198.
- [23] Yildirim, O., Baloglu, U.B., Tan, R.S., Ciaccio, E.J. and Acharya, U.R., 2019. A new approach for arrhythmia classification using deep coded features and LSTM networks. *Computer methods and programs in biomedicine*, 176, pp.121-133.
- [24] Gao, J., Zhang, H., Lu, P. and Wang, Z., 2019. An effective LSTM recurrent network to detect arrhythmia on imbalanced ECG dataset. *Journal of healthcare engineering*, 2019.
- [25] He, R., Liu, Y., Wang, K., Zhao, N., Yuan, Y., Li, Q. and Zhang, H., 2019. Automatic cardiac arrhythmia classification using a combination of deep residual network and bidirectional LSTM. *IEEE Access*, 7, pp.102119-102135.
- [26] Wagner P, Strodthoff N, Boussejot RD, Kreiseler D, Lunze FI, Samek W, Schaeffter T. PTB-XL, a large publicly available electrocardiography dataset. *Scientific data*. 2020 May 25;7(1):1-5.

Deep-Learning Approach for Efficient Eye-blink Detection with Hybrid Optimization Concept

Rupali Gawande, Sumit Badotra*

Department of Computer Engineering, Lovely Professional University
Phagwara, Punjab India

Abstract—In this research work, a novel eye-blink detection model is developed. The proposed eye blink detection model is modeled by following seven major phases: (a) video-to-frame conversion, (b) Pre-processing, (c) face detection, (d) eye region localization, (e) eye landmark detection and eye status detection, (f) eye blink detection and (f) Eye blink Classification. Initially, from the collected raw video sequence (input), each individual frames are extracted in the video-to-frame conversion phase. Then, each of the frames is subjected to pre-processing phase, where the quality of the image in the frames is improved using proposed Kernel median filtering (KMF) approach. In the face detection phase, the Viola-Jones Model has been utilized. Then, from the detected faces, the eye region is localization within the proposed eye region localization phase. The proposed Eye region localization phase encapsulates two major phases: Feature extraction and landmark detection. The features like improved active shape models (I-ASMs), Local Binary pattern are extracted from the detected facial images. Then, the eye region is localization by using a new optimized Convolution neural network framework. This optimized CNN framework is trained with the extracted features (I-ASM and LBP). Moreover, to enhance the classification accuracy of eye localization, the weight of CNN is fine-tuned using a new Seagull Optimization with Enhanced Exploration (SOEE), which is the improved version of standard Seagull Optimization Algorithm (SOA). The outcome from optimized CNN framework is providing the exact location of the eye region. Once the eye region is detected, it is essential to detect the status of the eye (whether open or close). The status of the eye is detected by computing the eye aspect ratio (EAR). Then, the identified eye blinks are classified based on the computed correlation coefficient as long and short blinks. Finally, a comparative evaluation has been accomplished to validate the projected model.

Keywords—Eye localization; CNN; Seagull Optimization with Enhanced Exploration (SOEE); improved active shape model (I-ASM); eye aspect ratio (EAR); eye-blink detection

I. INTRODUCTION

Recently, the Eye-tracking and/or -blinking detection algorithms are playing a significant role in the all the spheres of the world, more particularly in the smartphones that are revalorizing the entire globe. The smart phones have become ubiquities in our routing life style. We rely upon the smartphones for storing our confidential information. In the smartphones, the spoofing attacks can be avoided by utilizing the eye blink detection techniques within the face recognition systems [1-4] Moreover, the eye- blink detection systems in the smartphones provides information regarding the eye-blinking habits of the users, and provides advices [5-8]. In

fact, eye blinking is said to be the partly subconscious quick closing as well as reopening of the eyelids. The eye blinking is carried out with the aid of multiple muscles. The eye opening as well as closing is managed by the *orbicularis oculi* and *levator palpebrae superioris* [9-11]. In fact, the eye corona moistens by the eye blinking process. The frequency and duration are the prime factors for blinking. For an adult, the Average blinking frequency is 15-20 blinks/min, while the blinking frequency of the children is lower [12-15].

In literature, massive count of researchers has been devoted for eye blink detection. The outcome from them is either blink detection or eye status reorganization (open/closed eye). Most of the eye-tracking and eye-blinking detection algorithms rely upon the video input [16]. However, the techniques developed for desktop environments are not suitable for mobile/smartphone environments, owing towards the major shortcoming in terms of computational resources. A promising solution to this problem is to make use of the region of interest (ROI), wherein a smaller region is alone examined rather than searching for the location of eye in the whole image. For real-time processing, the eye localization is indeed a suitable approach for ROI-based solution. Once, the eye region is localized, its status is tracked using the deep learning models like convolutional neural network (CNN) and Artificial Neural Network (ANN) as well. Among the entire deep learning model utilized for eye blink detection, the CNN is a renowned one [17]. Although the CNN is successful in eye blink detection, it is till been considered to be a computational complexity model, owing towards its higher time consumption in training the parameters.

On the basis of this research gap is identified objective are identified as below:

- To propose an enhanced model for face localization from video frame.
- To propose an effective technique for eye pair localization from captured frame.
- To propose eye blink detection technique for left, right and double click instance.
- To evaluate effectiveness of the proposed technique.

The major contribution of this research work is: The research work Introduces a Kernel median filtering (KMF) approach for de-noising the image frames. Work also Introduces an improved active shape models (I-ASMs) in the Eye region localization phase to exactly localize the eye

*Corresponding Author.

region. It introduces an optimized CNN model for precise Eye region localization. The weight of CNN is fine-tuned using the newly projected Seagull Optimization with Enhanced Exploration (SOEE) model. This Seagull Optimization with Enhanced Exploration (SOEE) is the improved version of standard Seagull Optimization Algorithm (SOA). At the end of the research the accuracy of the system is compared with previously present technologies.

The leftover parts of this paper are arranged as: The literature review on eye blink detection is manifested in Section II. The proposed eye-blink detection framework: an overview is addressed in Section III. The video-to-frame conversion and pre-processing via proposed kernel median filtering, face detection via Viola Jones model and eye localization via optimized CNN is portrayed in Section IV, Section V and Section VI, respectively. Moreover, eye status detection and eye blink detection and classification are portrayed in Section VII and Section VIII, respectively. The results acquired as well are discussed comprehensively in Section IX. This paper is concluded in Section X.

II. RELATED WORK

In 2019, Sharmila et al. [1] have proposed a new technique for Eye Blink Detection model for preventing Computer Vision Syndrome (CVS). The proposed work uses Viola Jones algorithm for detecting the eyes, eye blink using background subtraction, gradient based corner detection and it is capable of detecting common cases of fatigued behaviour linked with prolonged computer use by tracking the eye blink rate. Hence, this proposed system could significantly reduce the symptoms among regular computer users leading to improved health habits.

In 2021, Rajamohana et al. [2] have proposed a novel automated, real-time driver's drowsiness detection framework using the proposed hybrid framework. The proposed model has formulated by blending the CNN and Bidirectional Long Term Dependencies (BiLSTM). The driver's facial image and eye blinks have been tracked using the Video camera. The projected model has encapsulated three major phases: identification of the driver's face image using a web camera, extraction of eye image features using the Euclidean algorithm and continuous eye blinks monitoring. As a n outcome, the status of the eye is exhibited as either open or close.

In 2021, Quddu et al. [3] have proposed a novel eye-tracking system using the RNN and LSTM. The authors have utilized the RNN to detect the drowsiness. In addition, the eye movements were modelled using the LSTM. Two types of LSTMs: 1-D LSTM (R-LSTM) and convolutional LSTM (C-LSTM) has been utilized.

In 2020, Liu et al. [4] have proposed a fatigue detection algorithm on the basis of the analyzed deeply-learned facial

expression. Initially, the multi block local binary patterns (MB-LBP) and Adaboost classifier has been utilized for training the face key point detection model. In addition, the 24 facial points were identified using the trained model. Moreover, the proportion of the closed eye time within the unit time (PERCLOS) and yawning frequency were computed. The driver's fatigue state was deduced using the fuzzy inference system. The projected model could detect the degree of the driver fatigue accurately as well as quickly.

In 2019, Wang et al. [5] have presented a robust fatigue detection system based on the binocular consistency using the deep learning. The eye gaze has been detected using the dual-stream bidirectional convolutional neural network (BCNN). The GP-BCNN was constructed by including the vectorized local integral projection features within the Gabor filters and the projection vectors for overcoming the orientation and scale changes. Further based on the pupil distance, the eye screening mechanism (ESM) was projected with the intention of eliminating the detected errors. The projected model has yielded a higher accuracy rate.

In 2019, Selvathi et al. [6] have proposed a fatigue and drowsiness detection system in FPGA using the deep neural network. Initially, the collected images were pre-processed via median filtering. Then, the facial regions were identified using the Viola Jones face detection algorithm. Further, the authors have extracted the Local Binary Pattern features from the detected faces, and have employed the Max pooling to lessen the level of complexity. The final detection was carried out using the SVM classifier. The results acquired had exhibited that the projected model is applicable for real time driver's vigilance monitoring.

In 2020, Lamba et al. [7] have utilized the feature level fusion (MmERMFLF) for precise multimodal eye blink recognition. The status of the eye was computed using the eye-eyebrow facet ratio (EEBFR), and eyebrow to nose facet ratio. From eye blinks, pulse rate as well as behavioral patterns (emotions), the authors have sensed the emergency state using the improved intellectual framework. Moreover, the count of eye blinks was detected using the novel multimodal method (MmERMFLF). The projected model had achieved improved reorganization accuracy.

In 2019, Zemblys et al. [8] have developed gazeNet for event detector's generation. The projected model has encapsulated an end-to-end deep learning approach, which was trained using the raw eye-tracking data and have classified it as fixations, saccades and post-saccadic oscillations. The projected model hasn't been utilized in large scale owing to its expanded training time. Table I summarizes the comparison between the existing approaches.

TABLE I. COMPARISON OF EXISTING APPROACHES

Ref No	Published Year	Approach	Advantages	Disadvantages
[2]	2021	Convolution neural Network	Convolution neural network is useful in facial recognition CNN is having higher accuracy	It is not more useful in speech and voice recognition CNN requires lots of data
[4]	2019	Facial Feature	It reduces computational cost	Vector used for facial feature finding is high
[15]	2017	Template Marching	It is easier to implement	If template used is not proper then accuracy of output is hampered
[22]	2016	Component Based	It is faster and more accurate face detection	For more accuracy larger vector should be used.
[28]	2015	Knowledge based	It reduces computational complexity	Detection rate of this technique is slower

III. PROPOSED EYE-BLINK DETECTION FRAMEWORK: AN OVERVIEW

A. Architectural Description

The proposed eye blink detection model will be modeled by following seven major phases: (a) video-to-frame conversion, (b) Pre-processing, (c) face detection, (d) eye region localization, (e) eye landmark detection and eye status detection, (f) eye blink detection and (f) Eye blink Classification. The architecture of the proposed work is manifested in Fig. 1.

- Initially, from the collected raw video sequence (input), each individual frames are extracted in the video-to-frame conversion phase.
- Then, each of the frames is subjected to pre-processing phase, where the quality of the image in the frames is improved using proposed Kernel median filtering (KMF) approach. At the end of the pre-processing phase, noiseless and higher quality video frames are acquired. These pre-processed frames are subjected to face detection phase.
- In the face detection phase, the facial region (ROI) in the pre-processed frames is detected by suppressing the rest of the regions (Non- ROI). The face detection is accomplished via Viola-Jones Model.
- Then, from the detected faces, the eye region is localization within the pro-posed eye region localization phase. The proposed Eye region localization phase encapsulates two major phases: Feature extraction and landmark detection. The features like improved active shape models (I-ASMs), LBP are extracted from the detected facial images. And then the eye region is localization by using a new optimized CNN framework. This optimized CNN framework is trained with the extracted features (I-

ASM and LBP). Moreover, to enhance the classification accuracy of eye localization, the weight of CNN is fine-tuned using a new Seagull Optimization with Enhanced Exploration (SOEE), which is the improved version of standard Seagull Optimization Algorithm (SOA) [9].

The outcome from optimized CNN framework is providing the exact location of the eye region. Once the eye region is detected, it is essential to detect the status of the eye (whether open or close).

Eye status detection: The status of the eye is detected by computing the eye aspect ratio (EAR). The aspect ratio is calculated between the points of eye to check whether eyes are opened or closed.

Eye-blink detection: It is performed onto the computed eye landmarks using the normalized cross-correlation method. Then, the identified eye blinks are classified based on the computed correlation coefficient as long and short blinks.

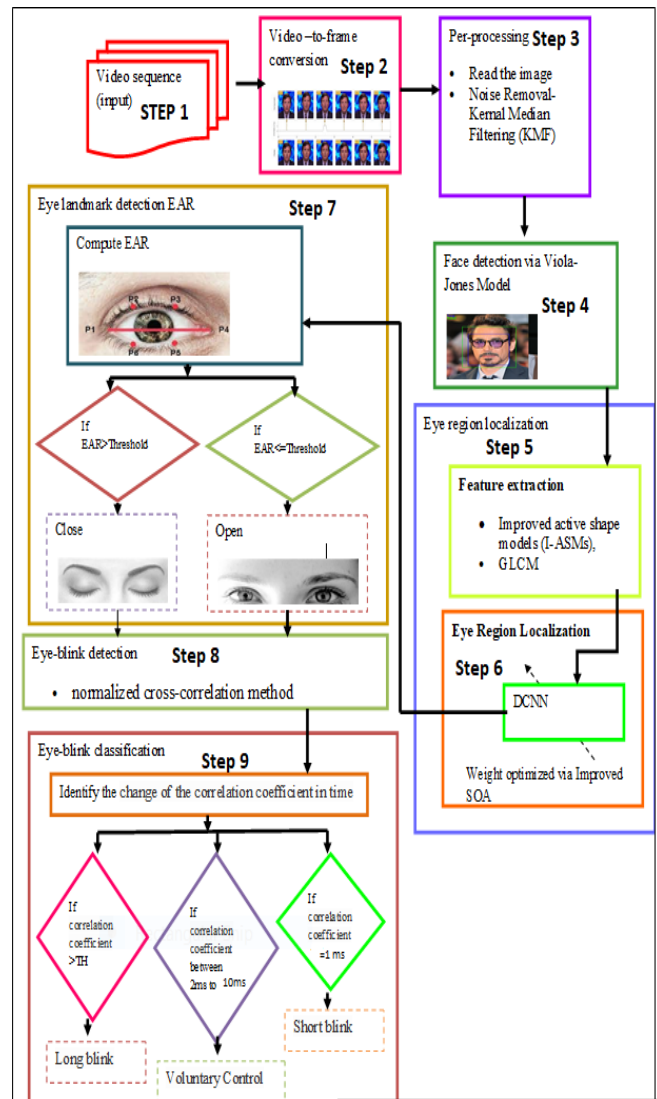


Fig. 1. Architecture of the Proposed Work.

IV. VIDEO-TO-FRAME CONVERSION AND PRE-PROCESSING VIA PROPOSED KERNEL MEDIAN FILTERING

A. Video-to-Frame Conversion

Let the collected input video sequence be denoted as, which includes count of frames. The video is indeed a medium that has become more important in today's society. It is made up of a series of frames, each of which is divided into shots and scenes, with the video being made up of a mixture of these scenes. To evaluate any video, we must first examine the features of the frames and then assess the video's attributes, which is accomplished using python' (OpenCv library) video to frame converter. Let the extracted frames be denoted as. The noise in is removed in the pre-processing stage using the proposed Kernel Median Filtering (KMF). Here, are the pixels.

B. Pre-Processing via Kernel Median Filtering

Preprocessing is a set of processes that aim to rectify or compensate for systematic mistakes in input before it is analyzed further. Owing to low collected integrity, every sort of information need pre-processing to improve it for future processing.

Pre-processing is required for the following reasons:

- 1) Light propagation qualities like scattering and absorption cause image deterioration.
- 2) Video captures with a high level of specificity, such as an unknown stiff scene, un-known hue, or poor light sensitivity. As a consequence, an initiative has been taken to discover the perfect filtering for pre-processing the frames. Filtering reduce noise by reducing statistical variances. It contributes to the reduction of visual noise. Noise affects the acquisition or capture of an image. Filtering methods are used to process the image. The ultimate focus of the filter has always been to minimize picture noise and improve the input image. Prior to further analysis and processing, it's indeed vital to optimize image quality.

The pre-processing stages utilized in this research work are

- a) Read the image in the frames
- b) De-Noise using proposed KMF

Each of the frames in is read using the OpenCV Library Cv2.imread() function From this , the noise is removed in the pre-processing stage using the proposed Kernel Median Filtering (KMF).

Median filtering is a nonlinear procedure that may be used to reduce impulsive noise, sometimes known as salt-and-pepper noise. It also is beneficial for retaining picture borders despite decreasing random noise. A random bit error in a line of communication may cause spontaneous or salt-and-pepper noise. Across an image frame, a window is moved in the median filter, and then for each pixel inside the window, its median intensity value is computed. This median intensity value is output intensity of the pixel being processed. The median filter has a significant drawback in that every outcome has always been bound by specification to have been the window's median value. The centre value substituted also isn't

evaluated to see whether it's an impulse or not. Whenever the intensity of the noise is considerable, the median filter works miserably. Therefore, a new Kernel Median Filtering (KMF) is introduced in this research work.

The steps followed in the Kernel Median Filtering (KMF) are manifested below:

- 1) The Kernel Median Filtering (KMF) detects the noisy pixels at first and then filters it as shown in Fig. 2.
- 2) Once, the noise is filtered; the pixels are validated to check whether it is a thin line or an edge pixel.
- 3) The input frame is convoluted with 4 convolutional kernels (sigmoid, RBF, Lapla-cian, Chi2). The minimal difference of these four convolutions is used for edge detection. (1)

$$C_{ij} = \min\{V^{F_i(a,b)} \otimes W_k \mid K = 1-4\} \quad (1)$$

- 4) Compare the value of with Threshold (say 1000). If the minimal value of the pixel is less than the threshold value, then the current pixel value is the same as it, else the standard median filtering is applied, and the median value is returned as the pixel value. This is mathematically shown in Eq. (2).

$$V^{KMF} = \begin{cases} Y^{MF} & ; \text{If } C_{ij} \geq T \\ V^{F_i(a,b)} & \text{Otherwise} \end{cases} \quad (2)$$

The pre-processed outcome is subjected to face detection phase, wherein the facial region is detected using the standard Viola-Jones Model.

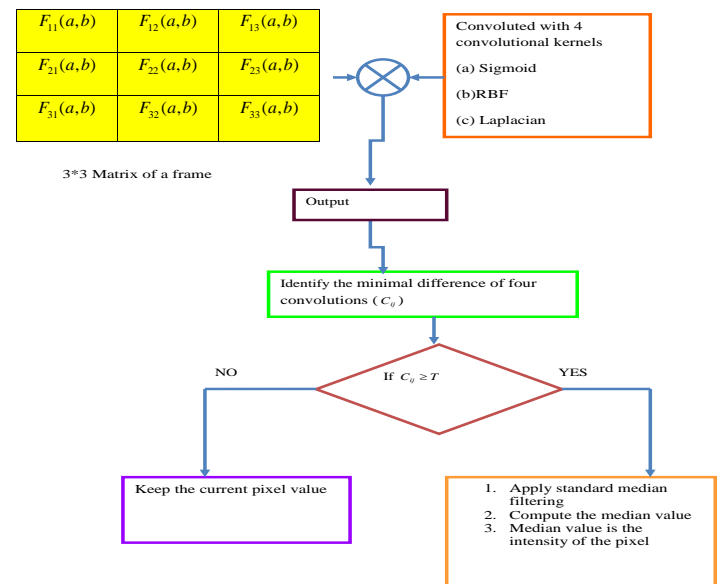


Fig. 2. Proposed Kernel Median Filtering.

V. FACE DETECTION VIA VIOLA JONES MODEL

A. Viola-Jones Model

The pre-processed image is subjected to viola-jones model for face region detection. The Viola-Jones algorithm, created by Paul Viola and Michael Jones in 2001, is indeed an object-

recognition framework that enables for real-time identification of visual properties. Although becoming an obsolete paradigm, Viola-Jones seems to be remarkably efficient, as well as its applicability in real-time face identification has conclusively demonstrated to be particularly noteworthy [10].

The Viola-Jones Algorithm has two stages:

- 1) Training
- 2) Detection

1) *Training*: Training data is the initial dataset used to train machine learning algorithms. Models create and refine their rules using this data. It's a set of data samples used to fit the parameters of a machine learning model to training it by example.

2) *Detection*: Viola-Jones had been created for frontal face images; therefore this detects them superior over face images that are oriented sideways, upwards, or downwards. The image is transformed to grayscale before its being used to recognize a face since it is necessary to focus with less data to analyze. The Viola-Jones method discovers the position on the coloured picture after detecting the face in the grayscale image. Viola-Jones constructs a box and explores for a face within it. It's obviously looking for haar-like characteristics, which would be detailed later. After moving through each and every square inside the picture, the box advances a step to the right. A multitude of boxes recognize face-like characteristics (Haar-like features) employing smaller steps, and the information from all of those boxes aggregated supports the algorithm towards determining in which the face resides.

3) *Haar-like features*: The characteristics underneath depict a box with such a dark and bright side, which the machine helps to define whatever the feature represents. As in the edge of a brow, one side may well be brighter than another at sometimes. The central area of the box may be brighter than that of the neighboring boxes, which might be misinterpreted for a nose. Viola and Jones observed three sorts of Haar-like characteristics in their research: • Four-sided features • Edge features • Line features [11]

4) *Integral images*: The integral picture aids us in performing these time-consuming computations fast enough that we may determine if a feature of a group of features meets the requirements [12].

5) *Training classifiers*: We're training the machine to recognize these characteristics. We're feeding it data and then training this to understand from it in order to make predictions. In the end, the algorithm produces whether any of the frames may be categorized as a feature or not by defining a minimal threshold [13-16].

6) *Adaptive boosting (AdaBoost)*: In general, the boosting is an Ensemble method that is formulated by means of combing several weak learners. As a resultant a strong learner is formulated. The most popularly utilized boosting models is the Adaptive Boosting approach. The adaboost solves the problem of "curse in dimensionality" issue. Even though, the formulated integral image has reduced the dimensionality of the image, still its features remain quite higher, and this tends

to lessen the training accuracy. Therefore, the adaboost has been implied [17].

7) *Cascading*: The cascading takes place next to the adaboosting model. In the cascading model, each of the sub-windows is validated to check whether the most important features are available within it or not. If the corresponding sub-window has the most important feature, then the second important features are explored, else the sub-window is discarded. This process is referred as cascading. By using this approach, the amount of computational time spends on the false windows.

From the detected facial images V^{face} , the eye region is localized in the proposed eye region localization phase.

VI. EYE LOCALIZATION VIA OPTIMIZED CNN

The proposed Eye Region Localization phase includes two major phases: (a) feature extraction and (b) face region identification. Initially, from the identified faces using viola-jones model, the facial features like improved ASM (I-ASM) and LBP (texture features) are extracted.

A. I-ASM Features

In ASM local texture feature and shape models are used. The deformation begins with the models shape. The shape is designated as a "point landmark". Eq. (3) is obtained by rotating, scaling and translating and as shown in Eq. (4).

$$G = (g_1, o_1, \dots, g_n, o_n)^H \quad (3)$$

$$g = H_{wg,wo,d,v}(G) \quad (4)$$

For ordered shapes, the average shape is formulated as in Eq. (5).

$$\bar{g} = \sum_{i=1}^m g_i$$

The differences of each shape are indicated as Eq. (6).

$$dg_i = g_i - \bar{g}$$

The covariance matrices are indicated as Eq. (7). Here, points to the count of histogram curves.

$$S = \frac{1}{m} \sum_{i=1}^m dg_i dg_i^T \quad (7)$$

The variable indicates major axes that provides divergence modes of all points of shape, and signifies the unit eigenvectors. The principal component analysis of provides eigen vectors and eigen values, and these eigen values forms the mode of variation. During the training process, the histogram curve can be modelled as the sum of the mean model and weighted modes of variation. As shown in Eq. (9), a new shape is generated using the mean of the weighted matrix sum, the mean shape of the eigenvector, and the weight vector.

$$g = \bar{g} + Eb \quad (8) \quad b = E^T (S - \bar{S}) \quad (9)$$

The initial deformation weight is set as zero.

Find a new preferred curve shape: the pixel in that is nearest to the corresponding pixel on the histogram curve of the test image is a new preferred choice of landmark.

Compute new values for the weight changes: $\Delta g = E \cdot \Delta b$
Here, $\Delta g = V^{face} - V^F$. Moreover, we acquire $b_{new} = b_{old} + \Delta b$

Limit the formulation: b is limited with the intention of guarantying the additional deformation. The weight can be chosen such that Euclidean distance is less than maximal distance.

Calculate the new shape

Repeat the process until the convergence is reached.

The extracted I-ASM feature is denoted as f^{I-ASM}

B. LBP

LBP is a measure of the correlation between pixels in a local region, which mostly represents local data. Many studies and research been published that combine more global or more local data with LBP in order to provide a more discriminative description from various feature levels. The LBP is less difficult to programme and has a higher discriminative potential. The image pixel, including the decimal numbers, is also labelled by the LBP operator. Each image pixel is computed with its surrounds during the labelling procedure by subtracting the value of the centre pixel. Furthermore, negative values are encoded as 0, and positive and zero values are encoded as 1. All of the binary codes are concatenated clockwise from the top-left to form a binary number, and these binary numbers are referred to as LBP codes [18]. The texture descriptor is used to create the local descriptions, which are then combined to create the global description. Furthermore, the distinguishable capability is used to extract characteristics from these texture objects. S_{pl} and S_{cl} in Eq. (10), respectively, denote the centre pixel intensities and the image centre pixel from the adjacent pl . The pixel's LBP descriptor is written as $LBP(\bullet)$, with NE_{pl} denoting the number of neighbours. Eq. (11) gives the LBP descriptor function f^{LBP} .

$$LBP(S_{cl}) = \sum_{pl=0}^{NE_{pl}} FE_{LBP(pl,cl)} 2^{pl-1} \quad (10)$$

$$f^{LBP} = \begin{cases} 1, & \text{if } S_{pl} - S_{cl} \geq 0 \\ 0, & \text{otherwise} \end{cases} \quad (11)$$

The final detection takes place in CNN which is trained with the extracted features $F = f^{LBP} + f^{I-ASM}$

C. CNN

The CNN is a deep learning model with three layers: "fully-connected layers, convolutional layer, and pooling

layer". A lot of convolution kernels together makeup the convolution layer, which assist in computing the feature maps. A significant number of convolution kernels are included in the convolution layer, which aid in the calculation of various feature maps. The surrounding neurons of the previous layer are linked to each of the neurons in the feature map [19]. Finally, several kernels are employed in order to acquire the whole feature maps. At location (d, e) of the B^{th} feature map residing in the A^{th} layer is $Z_{d,e,B}^A$, which is computed as per Eq. (12). In this same layer and location, the nonlinear activation function $act(\bullet)$ is computed as per Eq. (13). "Sigmoid, tanh, and ReLU" are the activation functions.

$$Z_{d,e,B}^L = W_B^{A^T} Q_{d,e}^A + bias_B^A \quad (12)$$

$$act_{d,e,B}^A = act(Z_{d,e,B}^A)$$

W and the $bias$ term denotes the weight and bias of CNN, respectively. This weight function is fine-tuned using SOEE model [20]. The patched input is denoted as $Q_{d,e}^A$. Shift-invariance has been achieved successfully by reducing feature map resolutions in the pooling layer. "The pooling layers of the CNN execute down sampling operations utilising the results collected from the convolutional layers." The pooling function is referred to as $pol()$.

The pooling function $M_{d,e,B}^A$ is then calculated for $act_{d,e,B}^A$. Here, $\mathfrak{R}_{d,e}$ denotes the local area in (d, e) . At the conclusion of the convolutional and pooling layers, there are multiple fully-connected layers.

$$M_{d,e,B}^L = pol(act_{d,e,B}^L), \forall (m,n) \in \mathfrak{R}_{d,e} \quad (14)$$

The loss() function is used to compute CNN's loss, which is represented by Eq.(15). This $Loss()$ function should be as small as possible, which is the goal of the current study. The goal function can be expressed formally as Eq. (16). A new SEEO model is used to fine-tune CNN's weight in order to achieve this objective.

$$Loss = \frac{1}{N} \sum_{n=1}^N l(\theta; M^{(n)}, O^{(n)}) \quad (15)$$

$$Obj = Min(Loss) \quad (16)$$

The total number of input-output relations $\{(J^{(n)}, M^{(n)}); n \in [1, \dots, N]\}$ is indicated by N , and the CNN's overall parameter is denoted by θ . In addition, $J^{(n)}$ represents the n^{th} input data, $M^{(n)}$ represents the matching target labels, and $O^{(n)}$ represents the CNN output.

D. Seagull Optimization with Enhanced Exploration (SOEE)

The SOA model is a novel bio-inspired algorithm that is based on the migration and attacking behaviours of a seagull.

In general, the SOA model is good in solving the complex optimization model with lower computational complexity. In literature, it has been said that the convergence speed of the solutions increases, when the adaptive meta-heuristic operators are utilized. Therefore, the Seagull Optimization with Enhanced Exploration (SOEE) is introduced in this research work. The input to SOEE is the weight of the CNN, which is fine-tuned by the SOEE to enhance the eyeblink detection accuracy. The solution fed as input to SOEE is the weight of CNN, which is shown in Fig. 3.

The steps followed in the SOEE model is furnished in the upcoming section:

Step 1: Initialize the N search agent's population P .

Step 2: Initialize the parameters A, B, itr, Max^{itr} . Here, itr, Max^{itr} points to the current iteration and the maximal iteration, respectively.

Step 3: Set the value of $f_c \leftarrow 2; u \leftarrow 1; v \leftarrow 2$

Step 4: While $itr < Max^{itr}$ do

Step 5: Compute the fitness of the search agent using Eq. (16).

Step 6: Move to the migration behaviour of SOA model. Our contribution resides in this phase. In fact, three different processes take place in the Migration (exploration) phase: Collision avoidance, Movement along the direction of the best neighbor and stay closer with the best search agent.

- With the intention of avoiding the collision amongst the search agent, a new variable A referred as the movement behaviour of search agent is added.

$$C = A * P(X) \quad (17)$$

Here, C is the search agent's non-colliding position and P is the current position of the search agent. In addition, A can be computed as per Eq. (18), wherein f_c is a variable that has been introduced to control the frequency of the employing A .

$$A = f_c - \left\{ X, \left[\frac{f_c}{Max^{itr}} \right] \right\} \quad (18)$$

- During the movement along the best neighbor's direction stage, our contribution has been included. Once the collision between the search agents is avoided, they are moved along the direction of the best neighbour. To make this movement more precise and to avoid the solutions from getting trapped into the local optima, a new mathematical model with levy function $Levy(\beta)$ has been introduced in this research work. The newly developed mathematical expression is shown in Eq. (19).

$$M = B * [P_{best}(X) - P(X)] + Levy(\beta) \quad (19)$$

Here, $Levy(\beta)$ is the levy function undergone by the search agents while searching the global best solutions. In addition, $P_{best}(X)$, $P(X)$ and M points to the global best position of the solution, current position of the search agent, position of the search agent, respectively. With the intention of having a proposed balance between the exploration as well as exploitation phase, the variable B is computed as per Eq. (20). Our contribution resides in this computational phase also. In the existing SOA model, the random variable S has been generated within the limits $[0,1]$. But, here we've computed the value of S using the newly proposed expression given in Eq. (21).

$$B = 2 * A^2 * S \quad (20)$$

$$S = 1.07(7.9S_i - 23.3S_i^2 + 28.7S_i^3 - 13S_i^4) \quad (21)$$

- Remain close to the best search agent: finally the position of the search agent is updated with respect to the best search agent as per Eq. (22) of SOA model.

$$\vec{D} = \left| \vec{C} - \vec{M} \right| \quad (22)$$

In addition, \vec{D} is the distance in between the best search agent and the current search agent.

Step 7: Move to the Attacking (exploitation) phase: in the attacking phase, the search agents undergo a spiral movement in the air. This spiral movement can be modelled in the three axes X, Y, Z as per Eq. (23)- Eq. (25), respectively.

$$x' = r * Cos(K) \quad (23)$$

$$y' = r * Sin(K) \quad (24)$$

$$z' = r * K \quad (25)$$

Step 8: The random variable K is modelled using the newly proposed expression given in Eq. (26). The proposed expression is based upon the singer map.

$$M = 1.07(7.9M_i - 23.3M_i^2 + 28.7M_i^3 - 13M_i^4) \quad (26)$$

Step 9: The updated position of the search agent is modelled as per Eq. (27). And eye region is located on that basis as shown in Fig. 4.

$$P(X) = (D * x' * y' * z') + P_{best}(x) \quad (27)$$

Step 10: Return $P(X)$

Step 11: Terminate

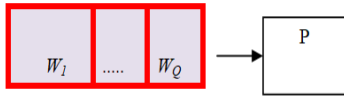


Fig. 3. Solution Encoding

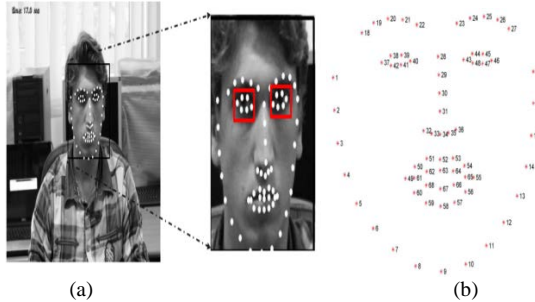


Fig. 4. An Illustration of Eye Landmark Detection: (a) Landmark Detection and (b) 68 Located Points.

VII. EYE STATUS DETECTION

Once, the eye region is localized, its status (open/ close) is identified by computing the eye aspect ratio. In this research work, the eye aspect ratio is computed between the eye points using Eq. (28). The eye computation for open and close eye is shown in Fig. 5.

$$EAR = \frac{\|P_2 - P_6\| + \|P_3 - P_5\|}{2 \cdot \|P_1 - P_4\|} \quad (28)$$

Here, P1,P2 ,P3 ,P4 ,P5 and P6 are the 2D landmark locations.

- a) The eye is considered to be open if the Eye Aspect Ratio is greater than the threshold [21].
- b) If the Eye Aspect Ratio is less than the threshold, the eye is considered closed.
- c) The EAR of both eyes is averaged since eye blinking is produced simultaneously by both eyes.

A poor monetary worth the presence of an EAR value does not imply that a person is blinking. It can happen when a person closes his or her eyes for a prolonged period of time or makes a facial expression, such as yawning, or when the EAR records a brief random fluctuation of the landmarks.

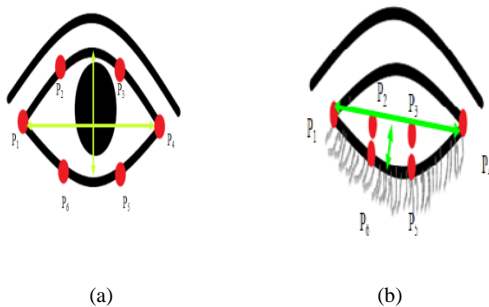


Fig. 5. EAR Computation of (a) Open and (b) Close Eye.

VIII. EYE BLINK DETECTION AND CLASSIFICATION

A. Eye Blink Detection

Once the eye's state has been determined, it is monitored for eye blink detection. For eye-blink detection, the normalized cross correlation technique is used in this study. The normalized cross correlation can be calculated using Eq. (29). In general, the correlation coefficient is used to assess the similarity of the present eye picture to the preserved template of the opened eye. As a result, the correlation coefficient is generally referred regarded as a measure of eye openness [22]. The template image matching to the user's eye is automatically obtained during the system's startup.

$$R(X',Y') = \frac{\sum_{X',Y'} [T'(X',Y') \cdot I(X+X',Y+Y')]}{\sqrt{\sum_{X',Y'} [T'(X',Y')^2 \cdot \sum_{X',Y'} I(X+X',Y+Y')^2]}} \quad (29)$$

Here, R points to the correlation coefficient of the image and T is the template image. In addition, the original image is I ; and the co-ordinates are X, Y .

B. Eye Blink Classification

To identify deliberate eye-blinks with a length more than 250 milliseconds, the correlation coefficient is shifted over time. The on-set of the eye-blink is identified whenever the value of the coefficient is less than the predetermined threshold level of TL (2ms) for consecutive frames. If indeed the correlation coefficient value is greater than the threshold value TH, the off-set of the eye-blink is discovered (250ms). Experimentation was used to determine the TL and TH threshold values. Whenever a detected eye-blink lasts more than 250 milliseconds but less than 2 milliseconds, it is considered a "control" blink [23].

IX. RESULT AND DISCUSSION

A. Experimental Setup

The proposed work has been implemented in PYTHON. The dataset for evaluation has been collected from [32]. The collected sample images are shown in Fig. 6. And open eye sample image are shown in Fig. 7. The assessment has been carried out in terms of MAE, MAPE, MSE, MSLE, RMSE and Optimization error as well. the proposed work (CNN+SOEE) has been compared over the existing models like the CNN+Bi-LSTM [2], C-LSTM [3], Bi-LSTM, RNN, MFO+CNN, GOA+CNN, SLnO+CNN and SOA+CNN, respectively. The correctly detected eye-blinks are denoted as True Positives (TP), false detections are denoted as False Positives (FP), and missed eye-blinks are denoted as False Negatives (FN) [24].

Clos e					
	sample image	Standard median filtering	proposed KMF	Viola-jones face detection model	I-ASM

Fig. 6. Sample Image for Close Eye based Eye-Blink Detection.

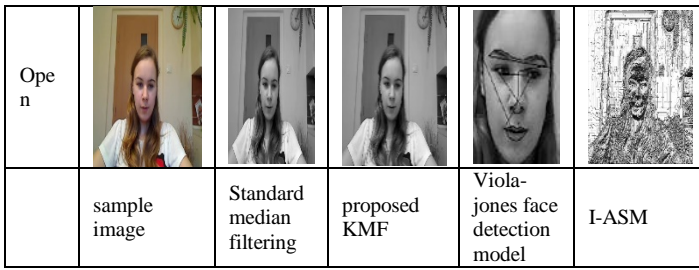


Fig. 7. Sample Image for Open Eye based Eye-Blink Detection.

B. Convergence Analysis

In literature, it has been portrayed that the convergence of the solutions increases with adaptive parameter tunings in the standard optimization model. However, it is highly significant to have a mathematical evaluation, in order to show that the newly introduced SOEE model is highly convergent over the existing ones. Therefore, a convergence analysis has been undergone for the proposed work by varying the count of iterations. Since, the prime objective behind this research work is to minimize the loss function of CNN, which localizes the eyes accurately. Once, the eyes are localized with higher accuracy then the status of the eyes can be detected more precisely [25]. Since, the objective function is a minimization function, the approach that achieves the least cost function is said to be the best approach, as it has converged sooner. The resultant of the convergence analysis of the projected model is manifested in Fig. 8.

On observing the acquired outcomes, the proposed work is identified to be successful even at the highest iteration counts. This clearly says that the projected model is applicable for huge databases. Initially, at the 0th iteration count, the cost function of the proposed as well as existing model is found to be higher. And then as the count of iterations got expanded, there seems to minimization in the cost function [26]. At the 6th iteration count, the projected model has recorded the least cost function than the existing models. Most interestingly, the proposed work has recorded the most least cost function as 4.6 at the 25th iteration count, and at this count the cost function recorded by the existing models are identified to be greater than 4.9. As a whole, the projected model is said to be highly convergent, and hence solved the optimization problems effectively.

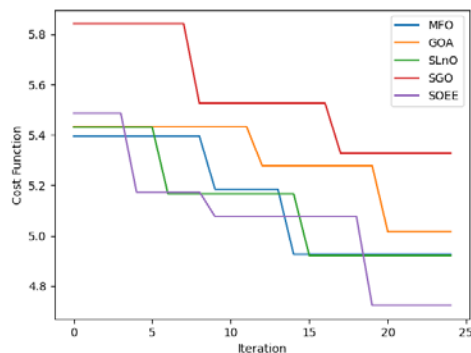


Fig. 8. Convergence Analysis of SEEO Model.

C. MAE Analysis

The MAE is the most commonly utilized for forecasting the accuracy of the model. In general, the Mean absolute error is the measure of the average absolute difference between the actual and predicted values in the eyeblink dataset. Mathematically, the MAE is given as per Eq. (30).

$$MAE = \frac{1}{N} \sum_{i=1}^N | Y_i - \hat{Y}_i | \quad (30)$$

Here, Y_i is the actual outcome and \hat{Y}_i is the predicted outcome.

In this research work, the MAE of the proposed work has been computed, and its results acquire are compared over the existing models like the CNN+Bi-LSTM [27], C-LSTM [3], Bi-LSTM, RNN, MFO+CNN, GOA+CNN, SLnO+CNN and SOA+CNN, respectively. This evaluation has been carried out by varying the learning percentage from 60, 70, 80 and 90, respectively. The results acquired are shown in Fig. 9. On observing the outcomes, the projected model has recorded the least MAE value for every variation in the learning percentage. Among the recorded results, the proposed work has recorded the least MAE value as 1.2 at 90th learning percentage. The Mae of the projected work recorded at the 60th learning percentage is 64.2%, 78.5%, 62.5%, 81.2%, 75%, 83.3%, 50% and 57.14% improved over the existing models like the CNN+Bi-LSTM [2], C-LSTM [3], Bi-LSTM, RNN, MFO+CNN, GOA+CNN, SLnO+CNN and SOA+CNN, respectively. As a whole, the projected model is said to be less prone to errors, and this is owing to the fine-tuning of the weight function of the CNN using the newly projected SOEE model. Since, the prime objective behind this research work is minimization of the loss function of the CNN, the minimized MAE acquired with the projected work has said that the defined objective has been successfully satisfied by the projected model [28].

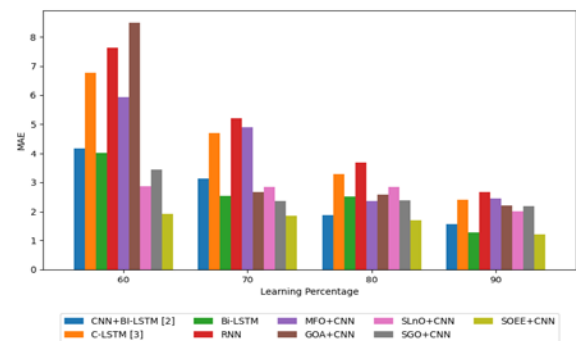


Fig. 9. MAE Analysis of SEEO Model.

D. MAPE Analysis

The MAPE also known as the mean absolute percentage deviation (MAPD) has been utilized for measuring the detection accuracy. Mathematically, the MAPE can be given as per Eq. (31).

$$MAPE = \frac{1}{N} \sum_{k=1}^N \left| \frac{Y_i - \hat{Y}_i}{Y_i} \right| \quad (31)$$

The MAPE of the proposed work has been computed, and the results acquired are manifested in Fig. 10. This evaluation has been undergone by varying the learning percentage. The graphical results acquired have exhibited a reduced MAPE value for the projected work. The projected model had recorded the minimal MAPE values as 0.03, 0.035, 0.038 and 0.015 at the 60th, 70th, 80th and 90th learning percentage. At the 60th learning percentage, the MAPE of the projected work is 37.5%, 64.2%, 34.2%, 68.75%, 69.5%, 80.7%, 41.8% and 51.9% improved over the existing models like the CNN+Bi-LSTM [2], C-LSTM [3], Bi-LSTM, RNN, MFO+CNN, GOA+CNN, SLnO+CNN and SOA+CNN, respectively.

E. MSE Analysis

MSE is the measure of the measure of the average of the squares of the errors (i.e. the averaged squared difference between the actual and the estimated value.

$$MSE = \frac{1}{N - M} \sum_{k=1}^{N-M} (Act - Pr e)^2 \quad (32)$$

The MSE of the proposed work is the lowest one for every variation in the learning percentage. The MSE of the projected work is found be below 8% for every variation in the learning percentage. The results acquired are shown in Fig. 11. The MSE value recorded by the existing works is above 15%. The proposed work has recorded the least MSE value at the 90th learning percentage. Moreover, all the existing models has recorded the MSE value as 50, 140, 42, 170, 70, 162, 19, 22 and 9 for CNN+Bi-LSTM [2], C-LSTM [3], Bi-LSTM, RNN, MFO+CNN, GOA+CNN, SLnO+CNN and SOA+CNN and proposed work, respectively. From the acquired values, it is clear that the projected model has recorded the least MSE value. On observing the overall evaluation, it is clear that the presented work is less prone to errors [29].

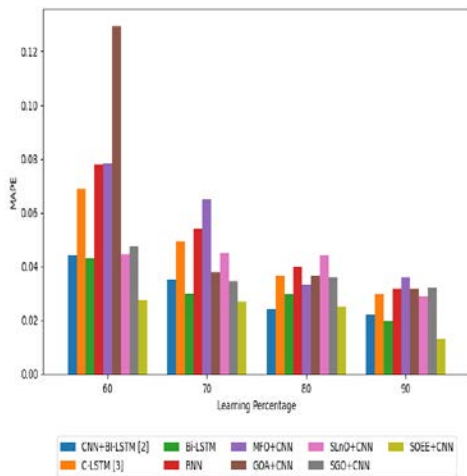


Fig. 10. MAPE Analysis of SEEO Model.

F. MSLE Analysis

The Mean squared logarithmic error (MSLE) of the projected model has been shown in Fig. 12. The MSLE is the ratio of the measure between the actual and the predicted outcomes.

$$MSLE = \frac{1}{N} \sum_{i=1}^N \left(\log(Y_i + 1) - (\log(\hat{Y}_i + 1)) \right)^2 \quad (33)$$

The results acquired are shown in Fig. 12. On observing the outcomes, the projected model had exhibited lower MSLE values. The major reason behind this reduction owes towards the fine-tuning the weight function using the newly proposed optimization model [30].

G. RMSE Analysis

“The RMSE is a frequently used measure of the differences between values (sample or population values) predicted by a model or an estimator and the values observed”. RMSE can be computed mathematically per Eq. (34).

$$RMSE = \sqrt{\frac{1}{N - M} \sum_{k=1}^{N-M} (Act - Pr e)^2} \quad (34)$$

The RMSE performance is evaluated for both the proposed and the extant techniques by varying the learning percentage. The results acquired are shown in Fig.13. The proposed work has recorded the least value for every variation in the learning percentage. The RMSE of the projected model at 60th learning percentage is 71.4%, 83.3%, 70.2%, 85.7%, 77.7%, 81.8%, 50% and 53.4% improved over the existing models like the CNN+Bi-LSTM [2], C-LSTM [3], Bi-LSTM, RNN, MFO+CNN, GOA+CNN, SLnO+CNN and SOA+CNN, respectively [31].

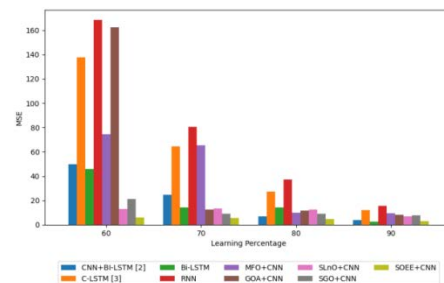


Fig. 11. MSE Analysis of SEEO Model.

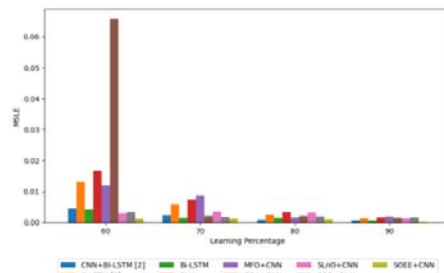


Fig. 12. MSLE Analysis of SEEO Model.

H. Performance Analysis of Proposed Work: With vs Without Optimization

The optimization algorithm deployed in this research work for eye landmark detection is said to play a major role in enhancing the detection accuracy of the eye blinks. It is essential to exhibit the supremacy of the optimization algorithms. Therefore, the proposed model has been validated with and without optimization logic. The results acquired are shown in Table II. The proposed work (KMF + I-ASM) with ESSO is compared over the existing models like Conventioanl Model (standard median filtering + Standard ASM) + ESSO and Conventioanl Model (standard median filtering +Standard ASM). The assessment has been carried out in terms of MAE, MAPE, MSE, MSLE, RMSE, respectively. The MAE of the projected model is 5.240172259, which is the least value when compared with the existing models. The MAE of the projected model is 16.3% and 15.5% better than the MAE of the conventional model + optimization and conventional model, respectively.

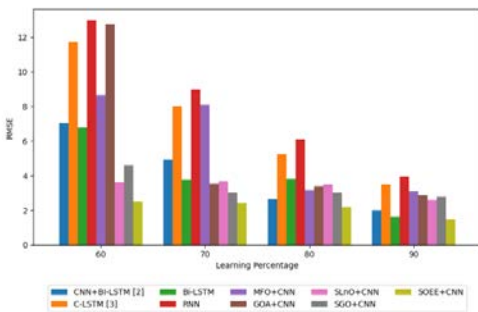


Fig. 13. RMSE Analysis of SEEO Model.

TABLE II. OVERALL PERFORMANCE ANALYSIS

	proposed work (KMF+I-ASM) with ESSO	Conventioanl Model (standard median filtering+Standard ASM)+ESSO	Conventioanl Model (standard median filtering+Standard ASM)
MSE	5.240172	6.261141	6.204798
MAE	1.754693	1.890539	1.909948
MAPE	0.025316	0.02734	0.027585
MSLE	0.001008	0.001201	0.00117
RMSE	2.289142	2.502227	2.490943

The MAPE of the projected model is 7.1% and 8.12% improved over conventional model + optimization and conventional model, respectively. In addition, the MSE of the projected model is 0.025316349, which is the least value when compared to conventional model + optimization = 0.027340005 and conventional model = 0.027584814. In addition, the projected model with optimization has recorded the least MSLE and RMSE also. Thus, from the overall evaluation, it's obvious that the major improvement behind the projected work in precisely detecting the eye blinks is only due to the fine-tuning of the weight of CNN via the optimization model [32].

I. Performance Analysis

The performance of the projected model has been validated in terms of MSE, MAE, MAPE, MSLE and RMSE,

respectively. On observing the outcomes, the projected work has recorded the least error measures. The results acquired are shown in Table II. The MSE of the projected work is 5.71662, which is indeed the least value when compared to CNN + Bi-LSTM [2] = 24.57614, C-LSTM [3] = 64.39177, Bi-LSTM = 14.25622, RNN = 80.51956, MFO + CNN = 65.42977, GOA+CNN = 12.47136, SLnO+CNN = 13.40547 and SOA+CNN = 8.938489. In addition, an improvement of 54.1%, 71.6%, 52.6%, 74.8%, 67.6%, 77.3%, 33.1% and 44.19% has been recorded by the projected model over the existing models like CNN + Bi-LSTM [2], C-LSTM [3], Bi-LSTM, RNN, MFO+CNN, GOA + CNN, SLnO + CNN and SOA+CNN, respectively in terms of MAPE. The MSE of the proposed work is 37.9%, 59.9%, 35.7%, 64.7%, 64.8%, 78.7%, 38.2% and 42.2% better than the MSE value recorded by existing models like CNN + Bi-LSTM [2], C-LSTM [3], Bi-LSTM, RNN, MFO + CNN, GOA+CNN, SLnO + CNN and SOA+CNN, respectively. The MSLE of the proposed work is 74.09%, 91.1%, 71.8%, 93.04%, 90.2%, 98.2%, 62.6% and 65.5% better than the MSE value recorded by existing models like CNN + Bi-LSTM [2], C-LSTM [3], Bi-LSTM, RNN, MFO+CNN, GOA+CNN, SLnO + CNN and SOA + CNN, respectively. Moreover, the RMSE of the projected model is also lower. The major reason behind this reduction in the error measures is owing to the utilization of the appropriate techniques for blink detection. Moreover, the prime objective of this research work is minimization of the error measures, which has been found to be achieved [33].

J. Overall Performance Analysis

The overall performance of the projected model is validated in terms of MSE, MAE, MAPE, MSLE and RMSE, respectively. The results acquired are shown in Table III. On observing the outcomes, the projected work has recorded the least error measures. The MSE value recorded by the projected model is 5.71662, which is 76.7%, 91.1%, 59.9%, 91.9%, 91.2%, 54.1% 57.3% and 36.04% better than the MSE value recorded by existing models like CNN + Bi-LSTM [2], C-LSTM [3], Bi-LSTM, RNN, MFO + CNN, GOA + CNN, SLnO + CNN and SOA + CNN, respectively. In addition, the projected model has recorded the least MAPE as 1.847275453, MSE as 0.026834139, MSLE as 0.001152411 and RMSE as 2.390945437. The major reason behind this improvement is owing to the utilization of the optimized deep learning model for eye landmark detection [34].

K. Analysis on Optimization Error

The optimization error measures recorded by the projected as well as existing models for 60, 70, 80 and 90 percent of learning are manifested in Table IV. At 60th learning percentage, the MSE value recorded by the projected model is 6.235624262, which is the least value than the existing models [35]. The MSE of the projected work at 60th learning percentage is 87.4%, 95.4%, 86.3%, 96.2%, 91.65%, 96.16%, 51.7% and 70.4% better than the MSE value recorded by existing models like CNN + Bi-LSTM [2], C-LSTM [3], Bi-LSTM, RNN, MFO + CNN, GOA + CNN, SLnO + CNN and SOA+CNN, respectively.

TABLE III. OVERALL PERFORMANCE ANALYSIS OF THE PROPOSED WORK

	CNN+BI-LSTM [2]	C-LSTM [3]	Bi-LSTM	RNN	MFO+CNN	GOA+CNN	SLnO+CNN	CNN+SGO	CNN+ISGO
MSE	24.57614	64.39177	14.25622	80.51956	65.42977	12.47136	13.40547	8.938489	5.71662
MAE	3.136789	4.703131	2.530748	5.206161	4.894731	2.660722	2.838228	2.351218	1.847275
MAPE	0.035335	0.049186	0.03004	0.053776	0.064812	0.037911	0.044808	0.034593	0.026834
MSLE	0.002347	0.005867	0.001501	0.007401	0.008796	0.002181	0.003551	0.001795	0.001152
RMSE	4.957433	8.024448	3.775741	8.973269	8.088867	3.531481	3.661348	2.989731	2.390945

TABLE IV. ANALYSIS ON OPTIMIZATION ERROR

Learning Percentage		CNN+BI-LSTM [2]	C-LSTM [3]	Bi-LSTM	RNN	MFO+CNN	GOA+CNN	SLnO+CNN	CNN+SGO	CNN+ISGO
60	MSE	49.63121	137.5381	45.80966	168.2764	74.64012	162.3975	12.9309	21.13644	6.235624
60	MAE	4.18496	6.766904	4.015798	7.63049	5.931651	8.493981	2.871482	3.441972	1.920842
60	MAPE	0.04439	0.068813	0.042835	0.078037	0.078374	0.129324	0.044625	0.047733	0.027543
60	MSLE	0.004503	0.013231	0.004145	0.016769	0.011923	0.065666	0.003121	0.003383	0.001167
60	RMSE	7.044942	11.72767	6.768283	12.97214	8.639451	12.74353	3.595957	4.597439	2.497123
70	MSE	24.57614	64.39177	14.25622	80.51956	65.42977	12.47136	13.40547	8.938489	5.71662
70	MAE	3.136789	4.703131	2.530748	5.206161	4.894731	2.660722	2.838228	2.351218	1.847275
70	MAPE	0.035335	0.049186	0.03004	0.053776	0.064812	0.037911	0.044808	0.034593	0.026834
70	MSLE	0.002347	0.005867	0.001501	0.007401	0.008796	0.002181	0.003551	0.001795	0.001152
70	RMSE	4.957433	8.024448	3.775741	8.973269	8.088867	3.531481	3.661348	2.989731	2.390945
80	MSE	7.021394	27.4651	14.35815	37.27164	10.08974	11.63154	12.38245	8.942254	4.812689
80	MAE	1.883875	3.272843	2.51215	3.682338	2.363624	2.586079	2.847396	2.376085	1.688624
80	MAPE	0.024333	0.036495	0.029784	0.040014	0.033364	0.03649	0.044139	0.03589	0.024871
80	MSLE	0.00092	0.002566	0.001488	0.003387	0.001733	0.002148	0.003147	0.002065	0.001023
80	RMSE	2.649791	5.240716	3.789215	6.105051	3.176434	3.410505	3.518871	2.99036	2.193784
90	MSE	4.077275	12.19301	2.714369	15.68119	9.575808	8.282909	6.852754	7.944575	3.126543
90	MAE	1.551431	2.413057	1.276575	2.658186	2.45427	2.206566	2.005485	2.176067	1.192031
90	MAPE	0.022036	0.029499	0.019703	0.031625	0.035901	0.031573	0.028835	0.032025	0.012821
90	MSLE	0.000757	0.001373	0.00066	0.001648	0.001956	0.001578	0.001337	0.001672	0.000127

TABLE V. ANALYSIS ON OPTIMIZATION METRICS

Learning Percentage		CNN+BI-LSTM [2]	C-LSTM [3]	Bi-LSTM	RNN	MFO+CNN	GOA+CNN	SLnO+CNN	CNN+SGO	CNN+ISGO
60	Accuracy	0.88	0.865	0.865	0.855	0.88	0.895	0.9025	0.88	0.92
60	Precision	0.88	0.865	0.865	0.855	0.88	0.895	0.9025	0.88	0.92
60	F-Measure	0.88	0.865	0.865	0.855	0.88	0.895	0.9025	0.88	0.92
70	Accuracy	0.856667	0.836667	0.846667	0.853333	0.81	0.846667	0.85	0.706667	0.89

70	Precision	0.856667	0.836667	0.846667	0.853333	0.81	0.846667	0.85	0.706667	0.89
70	F-Measure	0.856667	0.836667	0.846667	0.853333	0.81	0.846667	0.85	0.706667	0.89
80	Accuracy	0.705	0.75	0.675	0.69	0.695	0.7	0.715	0.63	0.765
80	Precision	0.705	0.75	0.675	0.69	0.695	0.7	0.715	0.63	0.765
80	F-Measure	0.705	0.75	0.675	0.69	0.695	0.7	0.715	0.63	0.765
90	Accuracy	0.75	0.84	0.94	0.92	0.88	0.81	0.87	0.77	0.85
90	Precision	0.75	0.84	0.94	0.92	0.88	0.81	0.87	0.77	0.85
90	F-Measure	0.75	0.84	0.94	0.92	0.88	0.81	0.87	0.77	0.85

L. Analysis on Optimization Metrics

The performance of the projected work is evaluated in terms of Accuracy, Precision and F-Measure, respectively. This evaluation has been carried out for varying learning percentage. The results acquired are shown in Table IV. The proposed work has attained the highest accuracy as 92% in case of eye blink detection at 60th learning percentage. The accuracy of the projected work at 60th learning percentage is 4.3%, 5.97%, 5.97%, 7.06%, 4.3%, 2.7%, 1.9% and 4.3% improved over the existing models like CNN + Bi-LSTM [2], C-LSTM [3], Bi-LSTM, RNN, MFO + CNN, GOA + CNN, SLO + CNN and SOA + CNN, respectively. In addition, at the 70th learning percentage [36-39], the projected model has recorded 89% of accuracy in eye blink detection. Moreover, at 90th learning percentage, the proposed work has recorded accuracy as 85%, which is found to be 11.7%, 1.1%, 10.5%, 8.23%, 3.5%, 4.7%, 2.3% and 9.4% improved over existing models like CNN + Bi-LSTM [2], C-LSTM [3], Bi-LSTM, RNN, MFO + CNN, GOA + CNN, SLO + CNN and SOA+CNN, respectively.

X. CONCLUSION

In this research work, a novel eye-blink detection model is developed. The proposed eye blink detection model is modeled by following seven major phases: (a) video-to-frame conversion, (b) Pre-processing, (c) face detection, (d) eye region localization, (e) eye landmark detection and eye status detection, (f) eye blink detection and (f) Eye blink Classification. Initially, from the collected raw video sequence (input), each individual frames are extracted in the video-to-frame conversion phase. Then, each of the frames are subjected to pre-processing phase, where the quality of the image in the frames are improved using proposed Kernel median filtering (KMF) approach. In the face detection phase, the Viola-Jones Model has been utilized. Then, from the detected faces, the eye region is localization within the proposed eye region localization phase. The proposed Eye region localization phase encapsulates two major phases: Feature extraction and landmark detection. The features like improved active shape models (I-ASMs), LBP are extracted from the detected facial images. Then, the eye region is localization by using a new optimized CNN framework. This optimized CNN framework is trained with the extracted features (I-ASM and LBP). Moreover, to enhance the

classification accuracy of eye localization, the weight of CNN is fine-tuned using a new Seagull Optimization with Enhanced Exploration (SOEE), which is the improved version of standard Seagull Optimization Algorithm (SOA) [31]. The outcome from optimized CNN framework is providing the exact location of the eye region. Once the eye region is detected, it is essential to detect the status of the eye (whether open or close). The status of the eye is detected by computing the eye aspect ratio (EAR). Then, the identified eye blinks are classified based on the computed correlation coefficient as long and short blinks. Finally, a comparative evaluation has been accomplished to validate the projected model.

XI. CONFLICTS OF INTEREST

There are no conflicts of interest declared by the authors.

REFERENCES

- [1] T.SreeSharmila,RSrinivasan, K K.Nagarajan, S.Athithya, "Eye Blink Detection Using Back Ground Subtraction and Gradient-Based Corner Detection for Preventing CVS", *Procedia Computer Science*, 2019.
- [2] Mani V, Manickam P, Alotaibi Y, Alghamdi S, Khalaf OI. *Hyperledger Healthchain: Patient-Centric IPFS-Based Storage of Health Records*. *Electronics*. 2021; 10(23):3003. <https://doi.org/10.3390/electronics10233003>.
- [3] Rajamohana,S.P.Radhika,E.G.Priya,S.SangeethaS., "Driver drowsiness detection system using hybrid approach of convolutional neural network and bidirectional long short term memory (CNN_BILSTM)", *Materials Today: Proceedings*, 2021.
- [4] AzharQuddus, AliShahidiZandib, LauraPrest, Felix J.E.Comeau, "Using long short term memory and convolutional neural networks for driver drowsiness detection", *Accident Analysis & Prevention*, 2021.
- [5] ZhongminLiu, YuxiPeng, WenjinHu, "Driver fatigue detection based on deeply-learned facial expression representation", *Journal of Visual Communication and Image Representation*, 2002.
- [6] Rout, R., Parida, P., Alotaibi, Y., Alghamdi, S., & Khalaf, O. I. (2021). Skin Lesion Extraction Using Multiscale Morphological Local Variance Reconstruction Based Watershed Transform and Fast Fuzzy C-Means Clustering. *Symmetry*, 13(11), 2085.
- [7] YanWang, RuiHuang, LeiGuo, "Eye gaze pattern analysis for fatigue detection based on GP-BCNN with ESM", *Pattern Recognition Letters*, 2019.
- [8] D. Selvathi, "FPGA Based Human Fatigue and Drowsiness Detection System Using Deep Neural Network for Vehicle Drivers in Road Accident Avoidance System", *Human Behaviour Analysis Using Intelligent Systems*, 2019.
- [9] Puneet Singh Lamba, Deepali Virmani& Oscar Castillo, "Multimodal human eye blink recognition method using feature level fusion for exigency detection", *Soft Computing*, 2020.

- [10] Alotaibi, Y., Malik, M. N., Khan, H. H., Batool, A., ul Islam, Saif, Alsufyani, A., & Alghamdi, S. (2021). Suggestion Mining from Opinionated Text of Big Social Media Data. *CMC-COMPUTERS MATERIALS & CONTINUA*, 68(3), 3323-3338.
- [11] RaimondasZembyls, Diederick C. Niehorster, Kenneth Holmqvist, "gazeNet: End-to-end eye-movement event detection with deep neural networks", *Behavior Research Methods*, 2019.
- [12] M. Shahbakhti *et al.*, "Simultaneous Eye Blink Characterization and Elimination from Low-Channel Prefrontal EEG Signals Enhances Driver Drowsiness Detection," in *IEEE Journal of Biomedical and Health Informatics*. doi: 10.1109/JBHI.2021.3096984.
- [13] J. Wang, J. Cao, D. Hu, T. Jiang and F. Gao, "Eye Blink Artifact Detection With Novel Optimized Multi-Dimensional Electroencephalogram Features," in *IEEE Transactions on Neural Systems and Rehabilitation Engineering*, vol. 29, pp. 1494-1503, 2021. doi: 10.1109/TNSRE.2021.3099232.
- [14] M. Shahbakhti *et al.*, "VME-DWT: An Efficient Algorithm for Detection and Elimination of Eye Blink From Short Segments of Single EEG Channel," in *IEEE Transactions on Neural Systems and Rehabilitation Engineering*, vol. 29, pp. 408-417, 2021. doi: 10.1109/TNSRE.2021.3054733.
- [15] Suryanarayana, G., Chandran, K., Khalaf, O. I., Alotaibi, Y., Alsufyani, A., & Alghamdi, S. A. (2021). Accurate Magnetic Resonance Image Super-Resolution Using Deep Networks and Gaussian Filtering in the Stationary Wavelet Domain. *IEEE Access*, 9, 71406-71417.
- [16] P. Ren *et al.*, "Dynamics of Blink and Non-Blink Cyclicality for Affective Assessment: A Case Study for Stress Identification," in *IEEE Transactions on Affective Computing*. doi: 10.1109/TAFFC.2019.2946829.
- [17] F. Wadehn, T. Weber, D. J. Mack, T. Heldt and H. -A. Loeliger, "Model-Based Separation, Detection, and Classification of Eye Movements," in *IEEE Transactions on Biomedical Engineering*, vol. 67, no. 2, pp. 588-600, Feb. 2020. doi: 10.1109/TBME.2019.2918986.
- [18] T. Jung, S. Kim and K. Kim, "DeepVision: Deepfakes Detection Using Human Eye Blinking Pattern," in *IEEE Access*, vol. 8, pp. 83144-83154, 2020. doi: 10.1109/ACCESS.2020.2988660.
- [19] Jha, N., Prashar, D., Khalaf, O. I., Alotaibi, Y., Alsufyani, A., & Alghamdi, S. (2021). Blockchain Based Crop Insurance: A Decentralized Insurance System for Modernization of Indian Farmers. *Sustainability*, 13(16), 8921.
- [20] J. Cao *et al.*, "Unsupervised Eye Blink Artifact Detection From EEG With Gaussian Mixture Model," in *IEEE Journal of Biomedical and Health Informatics*, vol. 25, no. 8, pp. 2895-2905, Aug. 2021. doi: 10.1109/JBHI.2021.3057891.
- [21] Alotaibi, Y. (2020). A New Secured E-Government Efficiency Model for Sustainable Services Provision. *Journal of Information Security and Cybercrimes Research*, 3(1), 75-96.
- [22] A. A. Jordan, A. Pegatoquet, A. Castagnetti, J. Raybaut and P. Le Coz, "Deep Learning for Eye Blink Detection Implemented at the Edge," in *IEEE Embedded Systems Letters*. doi: 10.1109/LES.2020.3029313.
- [23] Z. Wang, J. Chai and S. Xia, "Realtime and Accurate 3D Eye Gaze Capture with CNN-Based Iris and Pupil Segmentation," in *IEEE Transactions on Visualization and Computer Graphics*, vol. 27, no. 1, pp. 190-203, 1 Jan. 2021. doi: 10.1109/TVCG.2019.2938165.
- [24] X. Tian *et al.*, "iBlink: A Wearable Device Facilitating Facial Paralysis Patients to Blink," in *IEEE Transactions on Mobile Computing*, vol. 18, no. 8, pp. 1789-1801, 1 Aug. 2019. doi: 10.1109/TMC.2018.2868660.
- [25] Bharany, S., Sharma, S., Badotra, S., Khalaf, O. I., Alotaibi, Y., Alghamdi, S., & Alassery, F. (2021). Energy-Efficient Clustering Scheme for Flying Ad-Hoc Networks Using an Optimized LEACH Protocol. *Energies*, 14(19), 6016.
- [26] H. K. Wong, J. Epps and S. Chen, "Automatic Pupillary Light Reflex Detection in Eyewear Computing," in *IEEE Transactions on Cognitive and Developmental Systems*, vol. 11, no. 4, pp. 560-572, Dec. 2019. doi: 10.1109/TCDS.2018.2880664.
- [27] C. -T. Lin *et al.*, "EOG-Based Eye Movement Classification and Application on HCI Baseball Game," in *IEEE Access*, vol. 7, pp. 96166-96176, 2019. doi: 10.1109/ACCESS.2019.2927755.
- [28] K. Li, Y. Gong and Z. Ren, "A Fatigue Driving Detection Algorithm Based on Facial Multi-Feature Fusion," in *IEEE Access*, vol. 8, pp. 101244-101259, 2020. doi: 10.1109/ACCESS.2020.2998363.
- [29] Veeraiiah, N., Khalaf, O. I., Prasad, C. V. P. R., Alotaibi, Y., Alsufyani, A., Alghamdi, S. A., & Alsufyani, N. (2021). Trust aware secure energy efficient hybrid protocol for manet. *IEEE Access*, 9, 120996-121005.
- [30] C. Zhang, X. Wu, X. Zheng and S. Yu, "Driver Drowsiness Detection Using Multi-Channel Second Order Blind Identifications," in *IEEE Access*, vol. 7, pp. 11829-11843, 2019. doi: 10.1109/ACCESS.2019.2891971.
- [31] A. Sciarone, I. Bisio, C. Garibotto, F. Lavagetto, G. H. Ssstaude and A. Knopp, "Leveraging IoT Wearable Technology Towards Early Diagnosis of Neurological Diseases," in *IEEE Journal on Selected Areas in Communications*, vol. 39, no. 2, pp. 582-592, Feb. 2021. doi: 10.1109/JSAC.2020.3021573.
- [32] Z. M. Alhakeem, R. S. Ali and R. A. Abd-Alhameed, "Wheelchair Free Hands Navigation Using Robust DWT_AR Features Extraction Method With Muscle Brain Signals," in *IEEE Access*, vol. 8, pp. 64266-64277, 2020. doi: 10.1109/ACCESS.2020.2984538.
- [33] V. Skaramagkas *et al.*, "Review of eye tracking metrics involved in emotional and cognitive processes," in *IEEE Reviews in Biomedical Engineering*. doi: 10.1109/RBME.2021.3066072.
- [34] Z. Wang, Q. Hong and X. Wang, "A Memristive Circuit Implementation of Eyes State Detection in Fatigue Driving Based on Biological Long Short-term Memory Rule," in *IEEE/ACM Transactions on Computational Biology and Bioinformatics*. doi: 10.1109/TCBB.2020.2974944.
- [35] Y. Zhou, S. He, Q. Huang and Y. Li, "A Hybrid Asynchronous Brain-Computer Interface Combining SSVEP and EOG Signals," in *IEEE Transactions on Biomedical Engineering*, vol. 67, no. 10, pp. 2881-2892, Oct. 2020. doi: 10.1109/TBME.2020.2972747.
- [36] W. Deng and R. Wu, "Real-Time Driver-Drowsiness Detection System Using Facial Features," in *IEEE Access*, vol. 7, pp. 118727-118738, 2019. doi: 10.1109/ACCESS.2019.2936663.
- [37] M. Mahmood *et al.*, "Soft Nanomembrane Sensors and Flexible Hybrid Bioelectronics for Wireless Quantification of Blepharospasm," in *IEEE Transactions on Biomedical Engineering*, vol. 67, no. 11, pp. 3094-3100, Nov. 2020. doi: 10.1109/TBME.2020.2975773.
- [38] Y. Xie *et al.*, "Novel Wearable Sensors for Biomechanical Movement Monitoring Based on Electromagnetic Sensing Techniques," in *IEEE Sensors Journal*, vol. 20, no. 2, pp. 1019-1027, 15 Jan.15, 2020. doi: 10.1109/JSEN.2019.2943487.
- [39] Gaurav Dhiman, VijayKumar, "Seagull optimization algorithm: Theory and its applications for large-scale industrial engineering problems", *Knowledge-Based Systems*, Vol.165, February 2019.
- [40] Dataset collected from :” <https://www.blinkingmatters.com/research/>, Access Date: 2021-10-23.
- [41] G. Eason, B. Noble, and I. N. Sneddon, "On certain integrals of Lipschitz-Hankel type involving products of Bessel functions," *Phil. Trans. Roy. Soc. London*, vol. A247, pp. 529-551, April 1955. (*references*).
- [42] J. Clerk Maxwell, *A Treatise on Electricity and Magnetism*, 3rd ed., vol. 2. Oxford: Clarendon, 1892, pp.68-73.
- [43] I. S. Jacobs and C. P. Bean, "Fine particles, thin films and exchange anisotropy," in *Magnetism*, vol. III, G. T. Rado and H. Suhl, Eds. New York: Academic, 1963, pp. 271-350.
- [44] K. Elissa, "Title of paper if known," unpublished.
- [45] R. Nicole, "Title of paper with only first word capitalized," *J. Name Stand. Abbrev.*, in press.
- [46] Y. Yorozu, M. Hirano, K. Oka, and Y. Tagawa, "Electron spectroscopy studies on magneto-optical media and plastic substrate interface," *IEEE Transl. J. Magn. Japan*, vol. 2, pp. 740-741, August 1987 [Digests 9th Annual Conf. Magnetics Japan, p. 301, 1982].
- [47] M. Young, *The Technical Writer's Handbook*. Mill Valley, CA: University Science, 1989.

A Hybrid Quartile Deviation-based Support Vector Regression Model for Software Reliability Datasets

Y. Geetha Reddy¹, Dr. Y Prasanth²

Research Scholar¹, Professor²

Department of Computer Science and Engineering
KLEF, Guntur District, A.P., India

Abstract—Software reliability estimation using machine learning play a major role on the different software quality reliability databases. Most of the conventional software reliability estimation model fails to predict the test samples due to high true positive rate of the traditional support vector regression models. Most of the traditional machine learning based fault prediction models are integrated with standard software reliability growth measures for reliability severity classification. However, these models are used to predict the reliability level of binary class with less standard error. In this paper, a hybrid support vector regression-based quartile deviation growth measure is implemented on the training fault datasets. Experimental results are simulated on various reliability datasets with different configuration parameters for fault prediction.

Keywords—Software fault detection; reliability prediction; support vector machine; exponential distribution; quartile deviation

I. INTRODUCTION

Reliability, in its simplest form, means that a failure cannot occur within a certain period of time. The reliability concept thus stresses the probability, expected function (s), time, and operating conditions of four components. Reliability also depends on the conditions of the system that may or may not change over time. Software systems have increased significantly in size and complexity in recent decades, and the trend is expected to continue in the future [1]. Computer reliability and accessibility, usability, performance, serviceability, capabilities, and documentation are important attributes of software quality. Software reliability is difficult to achieve since software complexity seems to be high. While it is difficult to achieve a certain degree of reliability for any highly complex system, including software, system developers tend to upgrade the software layer with complexity and rapidly developing system sizes. The Software Reliability Growth Model (SRGMs) is a software reliability model (SRMs) design recognition class which is converted into a mathematical model. The reliability assessment of recent system updates is an important challenge in IT software management [2].

The probabilistic models are based on dynamic models and are represented as time-based statistical distributions. All these models are used to predict current trends and predict future trends in reliability. Probabilistic software reliability prediction models use statistical methods to estimate variables such as system error numbers, failure rates, software complexity, programme failures, etc. There are a number of

software models in the literature, but none of them is ideal. The selection of an appropriate estimate model based on a specific application is a major research problem [3]. A data set that includes instances of defined classes and a test data set for which the class must be decided must therefore be entered. The quality of the data provided for learning, and also the type of algorithm used in machine learning, depends greatly on the ability to classify successfully. Categorical labels (discrete, unordered) estimate classification results of continuously valued function models. It implies that numerical data values are expected instead of class marks to be incomplete or inaccessible. Regression analysis is the most widely used statistical method for numerical forecasting. Although other methods are available, the prediction also consists of identifying distribution trends based on available data. Genetic algorithms are also implemented to maximise the number of delayed input neurons and the number of neurons in the neural network's hidden architectural layer. We have demonstrated, using the software model for online adaptation that good-fitness and next-step predictability are better than traditional methods when cumulative software failure times are forecast because those variables' meanings are certainly not known. Many potential values can be equated to the likelihood of occurrence. Therefore, we really don't know when the next loss will happen. We know only a few possible failure times and their likelihood. "T" Two types of fault data, namely, time-domain data and interval-domain data, are widely used in software reliability modeling. The time-domain form is determined by the time the failure occurred. Learning supervised is a methodology for machine learning to build a data structure for preparation. Maximum Likelihood Assessment (MLE) is a common statistical method for the determination of the probability distribution parameters underlying a given dataset. Throughout the literature, there are many predictive models of the reliability of software-based neural networks, which are better known than certain statistical models [4-6]. Computer reliability is one of the key factors taken into account in maintaining the accuracy of the computer. Simply put, software reliability is about system failure or failure [7]. "Success and success" are two distinct variables commonly included in our software development. A fault could be identified as a fault or error during the development phase. As software constraints and modular complexity increase, the manufacture of a quality finished product is too difficult. Software defects may lose cash and time, so bugs for good performance products and decision-makers need to be predicted in advance. As a consequence, these bug accounts contain comprehensive data on bugs along

with the seriousness level [8] within different bug tracking frameworks. Generally, software bugs are defective limitations that trigger inaccurate outputs. These limitations can be described as a collection of characteristics to discover the bugs. These features affect the bug prediction model's effectiveness. Applications for software defect detection include decision trees, multifunctional regressions, neural networks, SVM, naive Bayes, and various classification types and selection models. But the relevant flaws for suitable classification could not be selected in these designs. Naive Bayes is a highly efficient method of classification for predicting flaws based on samples of practice. A naive Bayes system sees bug predictions as binary classifiers, i.e., by evaluating historical measurement information, it trains and predicts the predictor. If the attribute kinds in the metric information are blended, errors owing to lacking values or uncertain data are hard to estimate. Three separate layers of dynamic analysis can be classified. A systemic testing layer is the first layer. This layer is designed into the policy to run target programs. These strategies are designed to efficiently achieve error states. The second layer is a layer of data retrieval. In order to check programme correctness, data on the inner behaviour of the target programmes is collected. In the third level, monitors create from the information collected an abstract model of the destination programme and then check for possible errors in the programme on the abstract model. The test limits are fundamental to all dynamic analysis techniques. Dynamic analysis cannot support full target-program analysis because it uses monitored partial programme compliance. The other restriction is that it is hard to implement dynamic analysis methods except for the completion of the target programs. Executable environments and sample instances involve dynamic analysis methods. [9] the significance of various software prediction-model metrics. In this model, correlations and metric events were introduced using distinct algorithms in the bug forecast model, and bug counts were calculated in each metric. Object-oriented measurement metrics for object-oriented quality software A model for bug-projection was proposed and its levels with high, medium, and low severity defects were found to be lower than traditional models with various severe values. The technique of regression is intended to predict the quantity and density of software defects. The technique of classification aims at determining whether or not a software module (e.g. a package, code, or file) has a higher risk of defect than another. This approach [10] uses fuzzy logic with neural networks in software reliability prediction. The recurrent neural network is trained using the back-propagation algorithm. The number of failures and cumulative execution time in the failure dataset are used as inputs to the network to predict the next step failure.

The rest of the paper is organized as follows. Section II describes the related works of the SRM and its limitations. Section III describes the proposed solution to the SRM based machine learning framework on different dataset. Section IV describes the experimental results and analysis. Finally, we conclude the paper in Section V.

II. RELATED WORK

Lazarova et al. have developed various SRGMs concerning the growth rate software reliability index for error detection [11]. Li et.al, proposed a measuring method as an indicator collection, gathering data for the testing of all those metrics [12]. Mirchandani et al. suggested the non-homogeneous Poisson method-based software reliability growth pattern because the detection of these errors might also lead to detection of other errors without failure [13]. Nagaraju proposed an evolutionary model of the neural network to estimate and predict the software reliability based on a multimedia architecture input and output. In this study, the development of neural network models for software-reliability predictions was proposed using an Exponential and Logarithmic Encoding Scheme. Neural network models with the two encoding schemes above have shown a better prediction of cumulative failures than some statistical models. However, [14] the value of the encoding parameter is calculated by repeated hit / test experiments. This paper presents recommendations for encoding parameter selection, which provide consistent results for various data sets. The proposed solution is implemented using 18 separate data sets and a clear result for all datasets is observed. The method was compared to known statistical models using three sets of change points.

Rani [15] proposed a neural network approach focused on predictions of software reliability. He compared the approach to parametric model recalibration with some meaningful predictive measures with the same data sets. We concluded that better predictors are neural network methods.

Rizvi et al. [16] proposed a system in which software reliability based on the neural network would be expected. They used the reverse propagation algorithm for instructions. They used several failure times in the last 50 to estimate the next failure as output. The performance of approaches was calculated by changing the number of input nodes and hidden nodes. We concluded that the success of the strategy usually depends on the quality of the data sets.

Sagar [17] submitted a neural network approach focused on the evolutionary prediction of device reliability. They used single output architecture with multiple delayed inputs. Vojdani [18] suggested two models for cumulative system failure estimation, such as exponential neural network encoding (NNEE) and logarithmic encoding (NNLE). He encoded the data with the above two encoding scheme, i.e. the time of execution. He used the four dataset method and compared the results with some statistical models and found better results than those models.

Wang et al. [19] have proposed to reuse data from previous projects / releases for failure to boost early reliability for current projects / releases. Wang et al.[20] proposed the combinational dynamic weighted model (DWCM) based on a neural network for the prediction of device reliability. Based on the software-reliability growth model (SRGM), they used various activation functions within the secret layer. The method was used on two sets of data and the effect was compared with certain statistical models. The experimental results indicate that the DWCM approach is more successful

than traditional models. The neural network is a methodology for performance computation. The machine performance can previously be predicted on the basis of our neural network architecture. The system is also trained unless its desired output or destination can be achieved. For training purposes, we use different learning techniques that are freely described as supervised and unattended learning [21]. Software reliability is a quantitative study of every software designed since it affects directly software quality [22]. An efficient software reliability model is required in order to achieve good results. The previously developed reliability model is based on the analysis of faults linked to the code and context in which it was implemented [23]. All software reliability models are designed based on the execution time and calendar time. The time required or spent by the processor in the execution of instructions from the program is the execution time of any program [24].

Research Gaps: From the literature works, the main gaps identified for the software reliability estimation process are:

- 1) Difficult to predict the new reliability test data using machine learning approach.
- 2) Traditional SVM require different hyper parameters in order to improve the classification optimization.

III. PROPOSED GEOMETRIC PERTURBATION BASED PRIVACY PRESERVING CLASSIFIER

In this section, a statistical quartile deviation-based improved SVR prediction model is proposed on the software reliability datasets. In this work, a novel approach to predict the software reliability on the training and test software fault data. This model is integrated with the quartile deviation growth function in order to fit the S shaped curve. In the proposed model, reliability estimation is performed in two phases. In the initial phase, quartile deviation based error estimation is calculated on the training data for software reliability prediction. In the second phase, a hybrid support vector regression model is designed and implemented on the computed S-shaped training data as shown in Fig. 1.

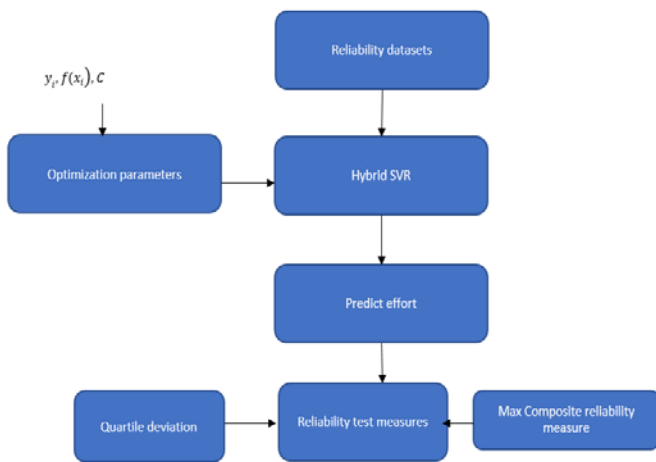


Figure 1: Max composite based SVR Framework

Fig. 1. Proposed Ensemble Deep Learning Framework for Privacy Preserving.

In the proposed model, an enhanced support vector regression is designed and implemented on the software fault dataset to improve the prediction rate and to minimize the error rate. The following proposed SVR model is implemented on the fault data. Initially, input data is given to hybrid SVR model to predict the effort rate. The prediction values of the SVR are tested using the Quartile deviation model and maximized composite reliability measures. These measures are used to find the deviation, skewness and shape of the dataset. The impact of failures on decision making is calculated using traditional software metrics. Extensive research was done using one or two software stage metrics to discover the error models. However, redundant and meaningless characteristics affect the effects of traditional designs. Also, the relationship between the new metrics and the traditional metrics is becoming too complex to make decisions as the number of software metrics increases. Generally, software metrics are used to gain quantitative insight into the software or its characteristics. The value of metrics is an ordinal, an interval, or a nominal scale. Software quality is assessed by the various features such as performance, documentation, easy maintenance and system soundness. Software reliability is considered as it is difficult to achieve with the complex nature of software. The software is therefore layered by the system developers throughout the design process to achieve a certain level of reliability, to support the later update of the software system and also to incorporate elasticity for increased system size. The reliability of software is inversely linked to the level of software complexity, since complexity is directly associated with enhanced capacity and strong software system features with enhanced functions. The main objective of this paper is to improve the software reliability prediction using the hybrid SVR model.

Let $m(x)$ be the input data, m be the estimation function. M value is estimated by using multiple linear regression method. Then the objective function of the proposed SVR model is given as

$$C(x) := \frac{1}{2} \|w\|^2 + \xi_k \cdot \psi(x) \cdot \phi(x)$$

Where

$$\psi(x) = |m(x) - \text{MLR}(x)|$$

MLR(x) = Multiple linear regression

$$\phi(x, x') = e^{-\|x-x'\|^2 / 2 \cdot \sigma^2}$$

$$\min_{\xi_k, \xi_k^*} C(x) = \frac{1}{2} \|w\|^2 + \lambda \cdot \psi(x) \cdot \phi(x) + b$$

$$\min_{\xi_k, \xi_k^*} C(x) = \frac{1}{2} \|w\|^2 + \lambda \cdot |\xi_k - \xi_k^*| \cdot \phi(x) + b$$

IV. EXPERIMENTAL RESULTS

In this work, experimental results are simulated with java environment for different software reliability datasets. The first, second, third and fourth datasets DS1, DS2, DS3, and DS4 are taken from Rome air development centre (RADC)

projects. Each dataset and its type are given in Table I, Table II, Table III and Table IV.

TABLE I. DS1 FOR FAULT PREDICTION BASED ON SEVERITY LEVEL

W	CF	Label
1	16	L
2	24	L
3	27	L
4	55	M
5	41	L
6	49	L
7	54	M
8	58	M
9	69	M
10	75	H
11	81	H
12	86	H
13	90	H
14	93	H
15	96	H
16	98	H
17	99	H
18	100	H
19	100	H
20	100	H

TABLE II. DS2 FOR FAULT PREDICTION BASED ON SEVERITY LEVEL

W	CF	Label
1	28	L
2	29	L
3	29	L
4	29	L
5	29	L
6	37	M
7	63	M
8	92	H
9	116	H
10	125	H
11	139	H
12	152	H
13	164	H
14	164	H
15	165	H
16	168	H
17	170	H
18	176	H

TABLE III. DS3 FOR FAULT PREDICTION BASED ON SEVERITY LEVEL

W	F	label
40	71	M
41	72	M
42	74	M
43	74	M
44	80	M
45	84	M
46	84	M
47	84	M
48	84	M
49	85	H
50	86	H
51	89	H
52	90	H
53	90	H
54	92	H
55	108	H
56	120	H
57	128	H
58	129	H
59	139	H
60	146	H

TABLE IV. DS4 FOR FAULT PREDICTION BASED ON SEVERITY LEVEL

W	F	Label
33	79	L
34	80	L
35	82	L
36	83	L
37	83	L
38	84	L
39	84	L
40	85	M
41	85	M
42	87	M
43	87	M
44	87	M
45	89	M
46	89	M
47	91	H
48	91	H
49	94	H

Fig. 2 represents the mean time to failure rate and its runtime for the proposed exponential distribution function. Here, the proposed exponential function is used to test the reliability of the given input parameters.

Fig. 3 represents the F-measure rate for the proposed exponential distribution function to the existing models. Here, the proposed exponential function is used to test the reliability of the given input parameters. From the figure, it is observed that the proposed approach has better improvement over the conventional model on all the datasets.

Fig. 4 represents the recall rate for the proposed exponential distribution function to the existing models. Here, the proposed exponential function is used to test the reliability of the given input parameters. From the figure, it is observed that the proposed approach has better improvement over the conventional model on all the datasets.

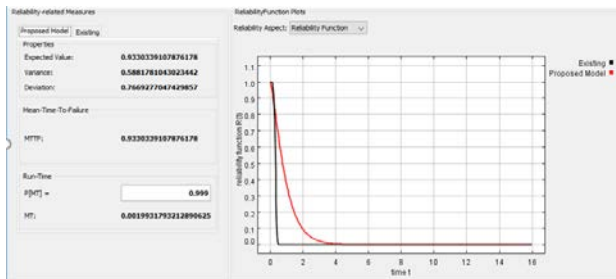


Fig. 2. Mean Time to Failure Rate and Runtime of the Proposed Model to the Exponential Model.

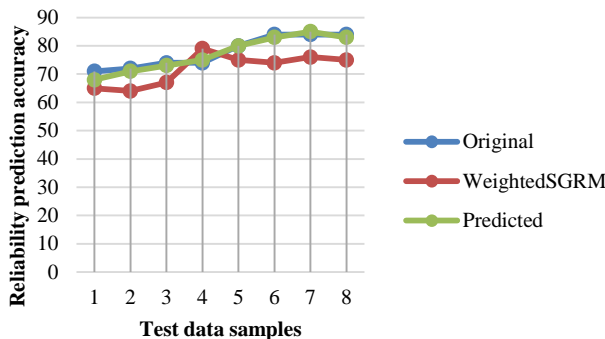


Fig. 3. Comparison of Proposed Fault Prediction Model to Existing Weighted SGRM Model on All Datasets.

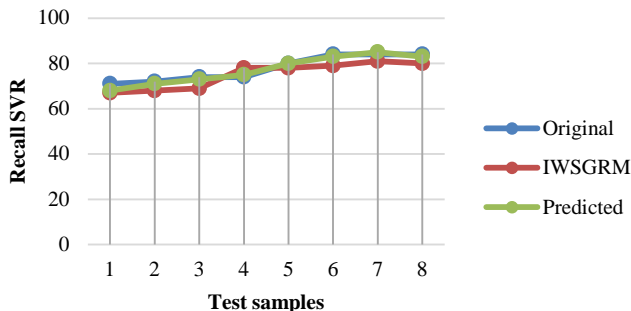


Fig. 4. Comparison of Proposed Fault Prediction Model to Existing Improved Weighted SGRM Model on All Datasets.

V. CONCLUSION

Software reliability fault prediction plays a vital role in small- and large-scale software applications. In this paper, a hybrid support vector regression-based quartile deviation model is implemented on the different software reliability datasets. Most of the traditional machine learning based fault prediction models are integrated with standard software reliability growth measures for reliability severity classification. However, these models are used to predict the reliability level of binary class with less standard error. Experimental results proved that the proposed reliability fault prediction model has better performance in terms of prediction and time is concerned.

VI. FUTURE WORK

In future work, a supervised learning model is integrated to the SVR model in order to predict the reliability for the new unclass labelled data.

REFERENCES

- [1] J. Cho, S. M. Shin, S. J. Lee, and W. Jung, "Exhaustive test cases for the software reliability of safety-critical digital systems in nuclear power plants," *Nuclear Engineering and Design*, vol. 352, p. 110151, Oct. 2019, doi: 10.1016/j.nucengdes.2019.110151.
- [2] L. V. Utkin and F. P. A. Coolen, "A robust weighted SVR-based software reliability growth model," *Reliability Engineering & System Safety*, vol. 176, pp. 93–101, Aug. 2018, doi: 10.1016/j.res.2018.04.007.
- [3] E. Abuta and J. Tian, "Reliability over consecutive releases of a semiconductor Optical Endpoint Detection software system developed in a small company," *Journal of Systems and Software*, vol. 137, pp. 355–365, Mar. 2018, doi: 10.1016/j.jss.2017.12.006.
- [4] C. Jin and S.-W. Jin, "Parameter optimization of software reliability growth model with S-shaped testing-effort function using improved swarm intelligent optimization," *Applied Soft Computing*, vol. 40, pp. 283–291, Mar. 2016, doi: 10.1016/j.asoc.2015.11.041.
- [5] M. S. Alhammadi, B. S. Almaqami, and B. Cao, "Reliability of Beta-angle in different anteroposterior and vertical combinations of malocclusions," *Orthodontic Waves*, vol. 78, no. 3, pp. 111–117, Sep. 2019, doi: 10.1016/j.odw.2019.02.002.
- [6] D. Amara and L. B. Arfa Rabai, "Towards a New Framework of Software Reliability Measurement Based on Software Metrics," *Procedia Computer Science*, vol. 109, pp. 725–730, Jan. 2017, doi: 10.1016/j.procs.2017.05.428.
- [7] J.-E. Byun, H.-M. Noh, and J. Song, "Reliability growth analysis of k-out-of-N systems using matrix-based system reliability method," *Reliability Engineering & System Safety*, vol. 165, pp. 410–421, Sep. 2017, doi: 10.1016/j.res.2017.05.001.
- [8] F. Febrero, C. Calero, and M. Ángeles Moraga, "Software reliability modeling based on ISO/IEC SQuaRE," *Information and Software Technology*, vol. 70, pp. 18–29, Feb. 2016, doi: 10.1016/j.infsof.2015.09.006.
- [9] A. Lanna, T. Castro, V. Alves, G. Rodrigues, P.-Y. Schobbens, and S. Apel, "Feature-family-based reliability analysis of software product lines," *Information and Software Technology*, vol. 94, pp. 59–81, Feb. 2018, doi: 10.1016/j.infsof.2017.10.001.
- [10] V. Ivanov, A. Reznik, and G. Succi, "Comparing the reliability of software systems: A case study on mobile operating systems," *Information Sciences*, vol. 423, pp. 398–411, Jan. 2018, doi: 10.1016/j.ins.2017.08.079.
- [11] S. Lazarova-Molnar and N. Mohamed, "Reliability Assessment in the Context of Industry 4.0: Data as a Game Changer," *Procedia Computer Science*, vol. 151, pp. 691–698, Jan. 2019, doi: 10.1016/j.procs.2019.04.092.
- [12] Q. Li and H. Pham, "NHPP software reliability model considering the uncertainty of operating environments with imperfect debugging and

- testing coverage,” *Applied Mathematical Modelling*, vol. 51, pp. 68–85, Nov. 2017, doi: 10.1016/j.apm.2017.06.034.
- [13] C. Mirchandani, “Adaptive Software Reliability Growth,” *Procedia Computer Science*, vol. 140, pp. 122–132, Jan. 2018, doi: 10.1016/j.procs.2018.10.309.
- [14] V. Nagaraju, V. Shekar, J. Steakelum, M. Luperon, Y. Shi, and L. Fiondella, “Practical software reliability engineering with the Software Failure and Reliability Assessment Tool (SFRAT),” *SoftwareX*, vol. 10, p. 100357, Jul. 2019, doi: 10.1016/j.softx.2019.100357.
- [15] P. Rani and G. S. Mahapatra, “A novel approach of NPSO on dynamic weighted NHPP model for software reliability analysis with additional fault introduction parameter,” *Heliyon*, vol. 5, no. 7, p. e02082, Jul. 2019, doi: 10.1016/j.heliyon.2019.e02082.
- [16] S. W. A. Rizvi, V. K. Singh, and R. A. Khan, “Fuzzy Logic Based Software Reliability Quantification Framework: Early Stage Perspective (FLSRQF),” *Procedia Computer Science*, vol. 89, pp. 359–368, Jan. 2016, doi: 10.1016/j.procs.2016.06.083.
- [17] B. B. Sagar, R. K. Saket, and Col. Gurmit Singh, “Exponentiated Weibull distribution approach based inflection S-shaped software reliability growth model,” *Ain Shams Engineering Journal*, vol. 7, no. 3, pp. 973–991, Sep. 2016, doi: 10.1016/j.asej.2015.05.009.
- [18] A. Vojdani and G. H. Farrahi, “Reliability assessment of cracked pipes subjected to creep-fatigue loading,” *Theoretical and Applied Fracture Mechanics*, vol. 104, p. 102333, Dec. 2019, doi: 10.1016/j.tafmec.2019.102333.
- [19] J. Wang, Z. Wu, Y. Shu, and Z. Zhang, “An optimized method for software reliability model based on nonhomogeneous Poisson process,” *Applied Mathematical Modelling*, vol. 40, no. 13, pp. 6324–6339, Jul. 2016, doi: 10.1016/j.apm.2016.01.016.
- [20] J. Wang and C. Zhang, “Software reliability prediction using a deep learning model based on the RNN encoder–decoder,” *Reliability Engineering & System Safety*, vol. 170, pp. 73–82, Feb. 2018, doi: 10.1016/j.res.2017.10.019.
- [21] J. Yang, Y. Liu, M. Xie, and M. Zhao, “Modeling and analysis of reliability of multi-release open source software incorporating both fault detection and correction processes,” *Journal of Systems and Software*, vol. 115, pp. 102–110, May 2016, doi: 10.1016/j.jss.2016.01.025.
- [22] O. Yazdanbakhsh, S. Dick, I. Reay, and E. Mace, “On deterministic chaos in software reliability growth models,” *Applied Soft Computing*, vol. 49, pp. 1256–1269, Dec. 2016, doi: 10.1016/j.asoc.2016.08.006.
- [23] M. Zhu and H. Pham, “A two-phase software reliability modeling involving with software fault dependency and imperfect fault removal,” *Computer Languages, Systems & Structures*, vol. 53, pp. 27–42, Sep. 2018, doi: 10.1016/j.cl.2017.12.002.
- [24] B. Zou, M. Yang, E.-R. Benjamin, and H. Yoshikawa, “Reliability analysis of Digital Instrumentation and Control software system,” *Progress in Nuclear Energy*, vol. 98, pp. 85–93, Jul. 2017, doi: 10.1016/j.pnucene.2017.03.006.

EAGL: Enhancement Algorithm based on Gamma Correction for Low Visibility Images

Navleen S Rekhi

Research Scholar¹ & Assistant Professor²
IKG Punjab Technical University, Kapurthala¹
DAV Institute of Engineering & Technology
Jalandhar, Punjab-India²

Jagroop S Sidhu

Associate Professor
Department of ECE
DAV Institute of Engineering & Technology
Jalandhar, Punjab-India

Abstract—Under poor light conditions or improper acquisition settings, the image degrades due to low contrast, poor brightness and suffer poor visual quality of the picture. An enhancement is required to manipulate the scale of pixel intensity for significant improvement in the image. This paper proposed the method of gamma correction with a self-adaptive value in accordance with the intensity scale of the image. After transformation to HSI (hue, saturation and intensity) channel, a multi-scale wavelet transform is implemented on the intensity component of the image. The gamma scale is computed from the combination of reformed scale constant of logarithm function and Minkowski distance measure. Lastly, wavelet based denoising technique is applied to suppress high noise coefficients to improve quality of the image. The proposed method is evaluated in terms of visual appearance, measure of information content, signal to noise ratio, and universal image quality index. It demonstrated that the proposed method showed its efficacy in terms of quality and improved visibility.

Keywords—Low scale intensity images; discrete wavelet decomposition; gamma correction; quality metrics

I. INTRODUCTION

The demand for video surveillance, medical imaging, and extensive photography has tremendously risen the challenges in the enhancement of low intensity images. Low intensity refers to illumination whose physical characteristics don't satisfy the normal image [1]. With improper light conditions and poor acquisition settings of imaging devices, the picture is affected by low contrast [2]. Such images exhibit the narrow distribution of intensity values across the intensity scale and are considered to be under/over-exposure scenes. Explicit exposure consists of a broad range of intensity values grouped narrowly into a narrow intensity range [3]. Fig. 1 displays the image with low luminance where most of its values are at the left portion of the intensity scale. Here, the intensity scale refers to the x-axis of histogram values, and the frequency of occurrence is at the y-axis. So, the intensity values at the darkest region (left portion) reflect the low visibility. Due to poor brightness, the image suffers the loss of texture features that define the content or shape of the image. The texture feature is the spatial variation of brightness across the intensity values of the pixels. With poor texture features, usability in applications like computer vision, medical analysis, and object recognition become difficult to characterize the image. So, the enhancement plays a significant role in adjusting the distribution of intensity values for better visibility in the image.

It involves modifying the intensity value for uniform distribution of pixel values at every pixel position along the intensity scale. Such processing enhances the hidden details and improves the contrast in the image. Also, the transformation to a new scale provides various advantages like suppression of noise, brightness preservation, and sharpening of the edges to make the original image more adaptable to human visual perception. The process of enhancement adjusts the luminance value. Here, the 'luminance' denotes the brightness and intensity in the single-channel obtained from RGB (red, green, and blue) color space. The various modifications had been developed taking both hardware and software methods into account. This paper presented the algorithm based on a software approach to improving picture visibility and overall quality.

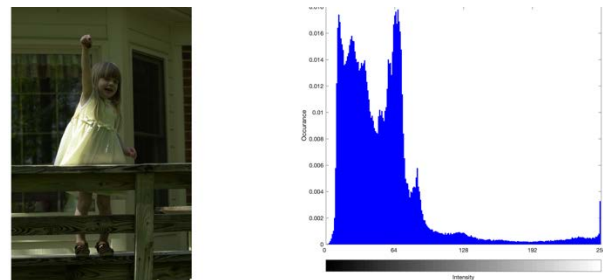


Fig. 1. The Image of Low Intensity Image.

The non-uniformity in an image occurs due to the random distribution of pixel values across the intensity scale. The uniform distribution could be obtained by applying the histogram equalization (HE). It is required to retain the maximal information for improved visibility with optimal quality. But the serious limitation of over-enhancement in HE degrades the quality of an image. Apart from HE, the point processing techniques deliberately balance the non-linear nature of pixel distribution. Most significantly, the gamma correction is the popular approach to produce quality improvement in an image. It is an intensity transformation technique to enhance the image. In simple terms, the input and output are related as: $I_{(u,v)} = I'_{x,y}$, where $I_{u,v}$ and $I_{x,y}$ represent the input and output image. The scale value ' γ ' is the scale factor in gamma correction. It modulates the luminance value to transform the image into better quality. The challenging task in gamma correction is the optimal choice of the scale factor. To overcome limitation of HE, the work is focused to auto-

adjust the scale factor of gamma for the low-intensity image. The scale factor must be automated in such a way to produce better visibility with improved contrast.

The rest of the paper is as follows: Section II discusses the related work on histogram equalization (HE) and other state-of-the-art techniques. Section III presents the key steps to the proposed method, including the conversion to HSI, multi-scale analysis, adaptive gamma correction, and auto-tuning to colour correction. Section IV describes the experimental results evaluated and compared with relevant techniques. Finally, the conclusion is followed by the future scope of the proposed method.

II. RELATED WORK

The piece-wise contrast stretching is the linear approach to scale the brightness. The image with intensity on both sides of the scale (dark and bright) is stretched to obtain the enhanced image. The stretch limit is calculated from the maximum and minimum intensity scale from the reference image. Though the linear stretching method is simple and easy but is entirely suitable for situations in which low and high scales are prominent. So, the non-linear approach of conventional histogram equalization (cHE) is implemented, defined as the frequency distribution technique based on statistical information in the image. The distinct peaks in Fig. 2 displayed the over-enhancement of the low contrast image.

The improved method of cHE based on clipping by mean-median approach on sub-division of HE is commonly used. The approach significantly improved the quality of the over-exposure images. For the image with dark scale values, this method failed to provide scalability in brightness. The MMSICHE[4] sub-divided the image based on median clipped HE. The method claimed to preserve the brightness and information contained in the image. But the method showed its inefficiency in improving the visual appearance of an image. The other method of cHE is the exposure-based sub-regions division of HE, proposed by Tan S and Isa N[2]. The sub-division of cHE in terms of very dark, dark, mid-tone, and lighter regions of a histogram's value were implemented. Most of the pixel values concentrated on the darkest region of the intensity scale. Additionally, Shiguang Liu and Yu Zhang [5] proposed the application of multi-exposure fusion to preserve the detailed information in the image. Other state-of-the-art techniques, such as Brightness Preserving Dynamic-HE (BPDHE) [6], [7] aimed to preserve the mean brightness without severe artifacts. It mapped the sub-histogram into a new dynamic range. The partitions were obtained by calculating the local maximum of the input image. The limitation of this method was that it could not handle the under/overexposed regions in the intensity values. Hence, the modified form of [8] i.e. Fuzzy HE is proposed to overcome the limitation of BPDHE through the implementation of fuzzy crisp values. In the fuzzy-based histogram approach, the partitions were calculated by computing the local maximum. The range of partitions also increased, as the number of pixels count is increased. Since illumination is non-uniform, fuzzy logic lacks a systematic approach to enhance visual appearance. Zuo C. et al [9], [10] proposed a mean-based estimation of object and background from HE. The locally

segmented approach was utilized by Hussain et al. [11] to map the shadow scales over brighter regions. The histogram equalization was implemented by dividing the images into small segments. The process of segmentation was concluded for dark images. If the dark region's scale is variable, over-enhancement could degrade the quality. As a result, the method focused on selecting segments and mapping them to more prominent regions. Recently, dynamic HE [12] was proposed for low illumination MRI images. It followed the same technique of partitions as proposed by previous two methods. Based on a novel multi-scale decomposition, bright regions were separated from dark regions with the domain as non-sub sampled transform. It is a combination of pyramid and directional filter banks. The proposed algorithm had showed the efficacy in handling MRI images. The HE approaches could be effective for natural or for images where pixel distribution is moderate. Most of the HE proposed is focused on preserving the mean brightness and improving the contrast. As shown in Fig. 2, while improving the visual appearance the image is degraded with low contrast. The application of HE and its modified approaches either under-enhanced or degraded the quality of the picture.

The alternate approach of non-linear transformation techniques are gamma correction, logarithmic and exponential function. The sigmoid is an 'S' shaped logistic function that process the image pixel by pixel to enhance the contrast. Srinvas and Bhandari [13] proposed adaptive sigmoid transfer function to achieve enhanced resolution. The sigmoid was utilized as a scale parameter to boost the lower intensity values and adjusted the high intensity values. Similarly, Gupta and Aggarwal [14] proposed a newly developed sigmoid function for contrast improvement in the image. After the transformation to YCbCr model, the normalization parameter was designed using Gaussian based sigmoid function to adjust the illumination. The contrast was enhanced for better colour compensation in the reference image. Other than sigmoid, the transformation of RGB image to extract luminance and chrominance as proposed by Priyanka S et al. [15] used principal component analysis (PCA). Due to direct analysis of raw images, there are colour saturation effects. Hence, the method could not be used for low-intensity images. The improved approach of principal component analysis was suggested by Singh and Bhandari [16]. The authors implemented PCA after the transformation of raw image into HSV channel. This fusion image had a higher quality but with a poor structure similarity index. Also, the global and local contrast adaptive model was proposed by Zhou Z et al. [17] for compensation in brightness. After transformation to HSI, the 'H' component was modified to compensate the low illumination.

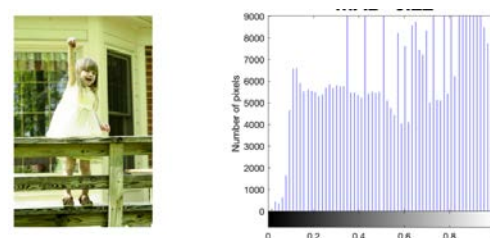


Fig. 2. Histogram Equalization of Low Intensity Image.

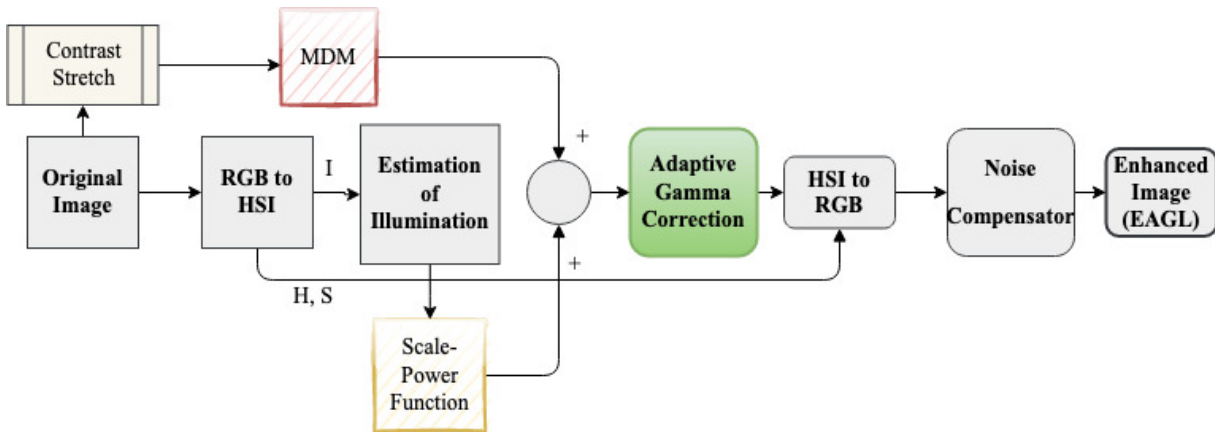


Fig. 3. Flow Diagram of EAGL

Since, the luminance is low, the computed mean could not compensate the poor brightness. Recently, algorithms developed with gamma correction had been the thrust area in image enhancement. The improved gamma correction was developed by Veluchamy and Subramani [16] and computed from cumulative density function. In this method, the detail information was preserved while the contrast was improved. In the previous published work [18], preserving the mean brightness can improve the contrast in the image. Hence, the method was effective for natural and contrast distorted images with moderate intensity values. Rahman S. et al. [19] proposed a mean-based approach to automate the selection of gamma values. The other way was proposed by Parihar [20] and Mahamdioua and Benmohammed [21] to estimate the scale through the computation of entropy and mean of the image. Wang Wencheng [22] proposed an adaptive gamma transform calculated after linear stretching of the corrected brightness in the image. Alternately, the discrete wavelet transform is utilized by Wenyung Yu et al [23] for gamma correction. The illumination was extracted from a low-light image using wavelet decomposition. The contrast value was improved with the computation of global and local spatial illumination. The recent approach for visual correction was proposed with the implementation of principal component analysis (PCA) by Singh and Bhandari [16]. In this approach principal components are adjusted to compute the gamma scale. However, PCA is widely used in image compression. Also, self-adaptive gamma scale was used in the previous work [18]. But the approach was limited to contrast distorted images.

Most of the research is focused on visibility improvement, regardless of simplicity and ease of use. The proposed work is developed to produce simple and effective algorithm for improved visibility. In this paper, multi-scale approach of enhancement is proposed with self-adjustable gamma scale. From the above discussion, the selection of scale parameters plays a significant role in improving the quality of the image. The gamma scale is computed by the combination of the Minkowski distance measure and scale-power (ScP) function. This scale parameter is further used in the gamma correction of the image. To improve the texture features, multi-scale enhancement using 2D discrete wavelet transform is implemented to estimate the intensity component in the image. Finally, the median based noise estimator suppressed high

noise coefficients to minimize the loss of information content in the image.

III. PROPOSED METHOD

A. Flow Diagram (EAGL)

The flow diagram shown in Fig. 3 illustrates the enhancement of low intensity images. It includes two stages: (1) the estimate of illumination and (2) noise correction in the final image. The purpose of the EAGL is to extract detailed information to obtain better visibility of the image. Firstly, the original image is transformed into HSI (hue, saturation and intensity) channel [24]. Mostly, global mean, variance or entropy was used to estimate luminance. Since multi-resolution preserved the maximum amount of detail (energy), a 2D-discrete wavelet transforms at a scale level of '2' [24] is used to obtain luminance value from the intensity component of the input image. The scale value is computed by combining the scale-power function and Minkowski distance measure (MDM) from the contrast stretched and wavelet coefficients of the original image. The combination provided the self-adaptive scale for gamma correction. Finally, threshold-based wavelet shrinking is implemented to suppress any noise artefacts due to transformation in the input image.

B. RGB to HSI Conversion

The image consists of sRGB (standard red, green and blue) combined to form a visual representation. Because of the non-linear nature of true colour, the image is usually transformed into other space channels like HSI [25]. Each of these parameters contains the dominance of wavelength known as hue (H), purity of colour as saturation (S) and the brightness/intensity value (I). The intensity part 'I' in the HSI (shading space) is isolated from and irrelevant to the chrominance part H, i.e., the shading data of a picture. To manipulate a shading picture independently, the 'I' can be improved while keeping the 'S' and 'H' the same. HSI is a 2D representation that approximates the way humans perceive colour. As a result, it retains a higher degree of brightness (for better visual perception). The relation is given as:

$$l_{(x,y)} = \max[R, G, B] \quad (1)$$

Where ' $l_{(x,y)}$ ' is denoted luminance component comprises of maximum intensity of red, green, and blue channel.

As it could be observed from Fig. 4, ‘I’ component is the exact brightness represented in the original image. In our experiments, hue and saturation remained unchanged and intensity value is further processed for image enhancement.

C. 2D-Discrete Wavelet Transform

After transformation to HSI, intensity component is further processed with 2D-discrete wavelet transform (DWT) to down-sample the intensity from the ‘ $l_{(x,y)}$ ’ (refer Eq. 1). The wavelet domain is considered to be high energy compaction tool for image processing. The decomposition in wavelet domain explores the directional variation (horizontal, vertical and diagonal) in image. The image is decomposed at a scale level of two to obtain wavelet coefficients as low-low pass (LL), high-low pass (HL), low-high pass (LH) and high-high (HH). The coefficients of LL are used for computation of scale-power function (as shown in Fig. 5). In our experiments, ‘sym5’ is considered as mother wavelet. The ‘sym5’ is a symmetrical mother wavelet mostly used for the non-linear content in the information.

The Fig. 5 shows the implementation of wavelet transform to separate the luminance from detail coefficients. The 2D-DWT is implemented in row- column form computed from one dimensional DWT. For a given image ‘ $l_{(x,y)}$ ’ is filtered to obtain two ‘ l_a ’ as approximation and ‘ l_d ’ detail (each of size $N \times N/2$ (N is the number of pixels)) coefficients.

The visible region in the Fig. 4 (after 1-level decomposition) is the low-low pass filter coefficients and the other dark portion is the corresponding

$$l_d^i(j',m,n) = \frac{1}{\sqrt{mn}} \sum_{\substack{1 \leq x \leq m \\ 1 < y < n}} L(x,y) d_{j',m,n}^i(x,y) \quad (2)$$

$$l_a(j',m,n) = \frac{1}{\sqrt{mn}} \sum_{\substack{1 \leq x \leq m \\ 1 < y < n}} L(x,y) a_{j',m,n}(x,y) \quad (3)$$

Where ‘ $l_d^i(j',m,n)$ ’ and ‘ $l_a(j',m,n)$ ’ are the detail and approximation coefficients of Eq. 1, j is the scale value. The decomposition is for one scale level and the mother wavelet used is ‘sym5’.

D. Scale-Power Parameter (Sc-P)

From the obtained coefficients at a level of ‘2’, scale value is computed. The value is the modified form of scale constant in logarithmic function. It is well known that logarithmic function is defined by the relation as $s=c \log(1+r)$ [3]. The scaling constant ‘c’ is chosen such that input intensity is mapped to high values and is calculated as: $c = \frac{255}{\log(1+J_m)}$, where ‘255’ is the maximum scale level, ‘ J_m ’ is the maximum intensity in the reference image. The scale constant ‘c’ produces loss of information for higher range of pixel values in the image. So, the proposed method modified the scale constant with the combination scale and power function.

Firstly, the scale is modified into the given relation as:

$$\xi^{ScP} = \frac{[J_m - l_a^i(j',m,n)]}{\log(1+l_a^i(j',m,n))} \quad (4)$$

ξ^{ScP} is the scale computed from modified scale constant of logarithmic function where in the numerator value is modified

from ‘255’ to $[J_m - l_a(j',m,n)]$ where ‘ J_m ’ is the maximum intensity in the $l_a(j',m,n)$ and $l_a^i(j',m,n)$ is the mean computed as: $l_a^i(j',m,n) = \sum_{\substack{0 \leq m \leq M-1 \\ 0 < n < N-1}} l_a(j',m,n)$. Similarly, the denominator value is modified to $\log(1+l_a^i(j',m,n))$. Next, to avoid the exaggerated intensity variation, ξ^{ScP} is further decimated to the power of 0.005. This value is taken as constant for the images whose intensity scale varies from dark to medium range of pixel distribution.

E. Minkowski Distance Measure (MDM)

For the gamma-based correction, the value of gamma greater than one will increase the intensity of the dark region. Since, the focus of the paper is to scale the intensity in the image, hence ξ^{ScP} is combined with the value of Minkowski distance measure (M^{em}). The M^{em} is a generalized form whose properties are computed from Euclidian and Manhattan distance formula. The final scale value computed for gamma is related as:

$$\gamma = \xi^{ScP} + M^{em} \quad (5)$$

F. Adaptive Gamma Correction

The gamma correction is the non-linear transformation function in which the compression and expansion is attained by changing the value of scale parameter. Finally, the improved gamma correction is implemented with the given relation as below:

$$l_{(x,y)}^{new} = (l_{(x,y)})^{1/\gamma} \quad (6)$$

where $l_{(x,y)}^{new}$ is the newly constructed luminance component of HSI channel.

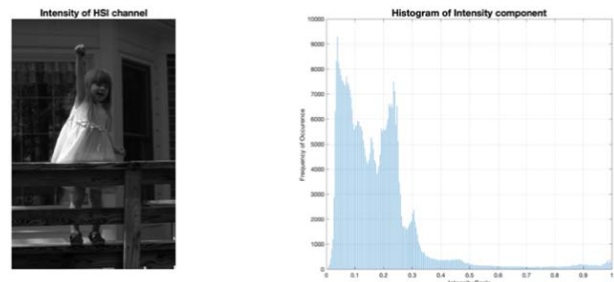


Fig. 4. Representation of ‘I’ Component of the Reference Image.

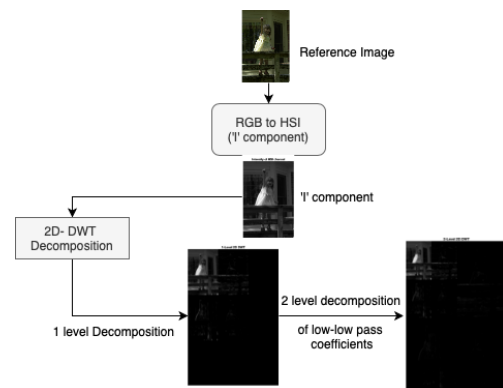


Fig. 5. 2D DWT Decomposition at a Scale Level of ‘2’.

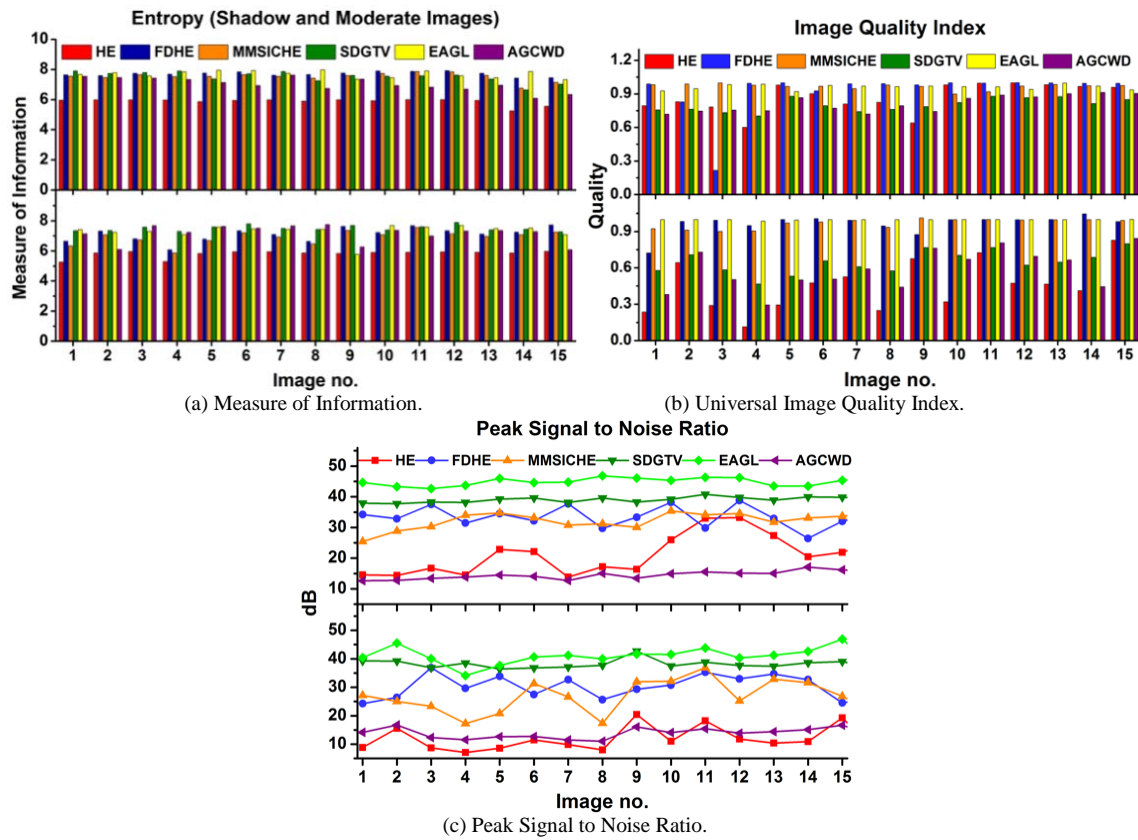


Fig. 6. Comparison of Image Quality Measures (a) Entropy, (b) Universal Image Quality Index and (c) Peak Signal to Noise Ratio for Set of Shadow (Top) and Moderate (Bottom) Images with HE, FDHE, MMSICHE, SDGTV and Proposed Method (EAGL).

G. Noise Compensation

Despite the non-uniform distribution of illumination, the hue contains the dominant wavelength of colours. Before the transformation, the hue component is adjusted from the mean square error. The self-adjusted hue compensation is computed from the mean square error between the reference and contrast stretched image. The new intensity component is transformed back to its original channel space by combining it with other channels. The transformation often degrades the quality of the image. Most of the techniques like median/mean filtering and Gaussian filter often process the noise by individual filtering. Due to high-frequency noise, the final image is blurred near the edges. So, wavelet based de-noising technique is implemented in the proposed method to effectively preserve the quality in the image. With the similar process of multi-scale 2D DWT, the adjusted threshold value is computed (Eq. 7). For any pixel value in the sub-band which is less than the threshold is set to zero and otherwise shift to the other pair of sub-bands. The threshold is calculated by the general equation as:

$$Th = \frac{\sigma^2}{\sigma_{sb}} \quad (7)$$

Where σ^2 is the median estimator computed from the sub-bands and σ_{sb} is the standard deviation of the sub-bands.

The proposed algorithm can be summarized as below:

-
- Input Image:** $l_{(x,y)}$; **Output Image:** $l_{(x,y)}^{new}$
-
- Step I: Transformation of standard (sRGB) image to HSI as given in Eq.1
 - Step II: Decompose the 'I' component using 2D- discrete wavelet transform (keeping saturation unchanged). From Eq. 2 and Eq. 3
 - Step IV: Estimate the scale parameter from image decomposition (Eq. 4) and confidence scale from contrast stretched image (Eq. 5)
 - Step V: Implement gamma correction as stated in Eq. 6 on the luminance component.
 - Step VI: The final enhanced image is obtained after conversion to sRGB channel.
 - Step VII: Perform the noise compensation using Eq. 7 and Eq. 8 to obtain output image as $l_{(x,y)}^{new}$.
-

The value obtained from Eq. 7 is used to suppress the noise coefficients through wavelet based bivariate shrinking [26]. The soft thresholding as stated in Eq. 8 is used to regulate the visibility for better texture features in the image. The Fig. 7 shows the basic illustration of threshold-based noise compensation. Since the noise is at finer level of scales, hence the wavelet coefficients represent the noise at higher scales. So, the soft thresholding scales down the coefficients that are less than the threshold value. After gamma correction, the $l_{(x,y)}^{new}$ is transformed to its original sRGB channel.

$$T^S(w|t) = \begin{cases} 0 & \text{for } |w| \leq t \\ w - t & \text{for } |w| > t \\ w + t & \text{for } |w| < -t \end{cases} \quad (8)$$

$T^S(w|t)$ is the soft-threshold equation. Where 'w' is the wavelet coefficients and 't' is the threshold value.

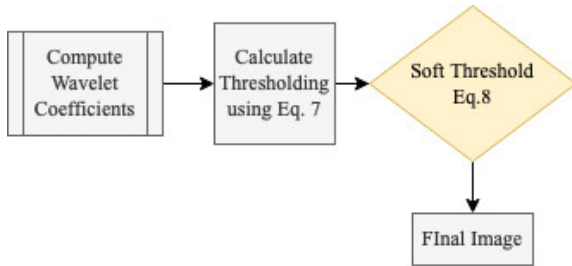


Fig. 7. Process of Wavelet Shrinking.

IV. EXPERIMENTAL RESULTS

In this paper, the experiments were conducted on Intel (R) Core (TM) i5-6th generation with 8 GB of RAM, and the software

A. Image Quality Assessment Measure (IQA)

An objective measure is based on certain criteria to assess the quality of the enhanced image. Although the quantitative metrics are not the perfect way to analyze the quality of enhancement. However, objective evaluation is usually an indicator of image quality. Because with no reference of precise image, the measure of quality is difficult to predict. To the best of our knowledge, there is no IQA method specifically designed to evaluate low-light image enhancement techniques. But, however, such metrics quantify the distortion content in the image. As a result, in various research articles [13], [16], [27], different objective assessment is used to evaluate final image. The quality measure is based on full reference methods and non-referenced methods dependant on reference image. With extensive study of research articles [29], [30], [19], [22] the following metrics were considered for our method. In our metrics, both no-reference and full reference measure had been quantified. The below listed metrics are briefly discussed.

B. Entropy (E)

It is the measure of information content in the resultant image. In cases, like low light images, higher the entropy more will be the information content in the image. With the increase in information, detail of the image too will become finer. The entropy of the image is calculated by the formula:

$$H = - \sum_{i=0}^{L-1} p(i) \log p(i). \quad (9)$$

where H is the entropy, L is the overall gray-scales of image, p(i) is the probability of gray level 'i'.

As per the measure of entropy, the higher the E value, the more information the image contains and the richer would be the image detail.

C. Peak SNR (PSNR)

It quantifies the quality of a reconstructed image with reference to the original image. The final image is compared to input image to estimate the noise content in the information signal. Higher the value of Peak SNR [29], better will be the quality of image. It is calculated from mean square error and is given as:

$$P_{SNR} = 10 \log_{10} \left(\frac{255}{\sqrt{MSE}} \right) \quad (10)$$

where MSE is the mean square error calculated between $l_{(x,y)}$ and $l_{(x,y)}^{new}$

D. Universal Image Quality Index (UIQI)

It is a quality index to measure loss of correlation, luminance and contrast distortion. It is proposed by Wang et al. [31] that quantifies the quality more effectively than mean square error. With the increase in the index value, better will the quality of image.

The visual and histogram representation of some randomly chosen images is shown in Fig. 8. The selected images were divided into three groups, viz. shadow, moderate and low intensity images. For comparison, the random selection of 15 images in each group was chosen. By shadow, it means the images have variational illumination as shown in Fig. 8(b), whereas the moderate images are represented in Fig. 8(c) and Fig. 8(d). And lastly, the low visibility image as illustrated in Fig. 1 and Fig. 8(a). The images shown in Fig. 8 showed the non-uniform distribution of histogram values. Hence, if the intensity scale is widespread, it will degrade the quality of the image. The EAGL enhanced image showed the optimal shifting of scale values to improve the visibility with the desirable amount of contrast. A bell-shaped Gaussian curve could be observed in the 'airport' image. In case of 'shadow' image, the uniform distribution of pixel values is observed. The 'cart' image has dual peaks both at the dark and light scale. The peaks were retained to avoid any loss in detail information and with the shift of intensity scale, visibility is improved. Further, Fig. 6 is the qualitative comparison of shadow and moderate intensity images. In comparison to other well-known algorithms, high PSNR, better quality and preservation of information is found in the proposed method (as summarized in Table I).

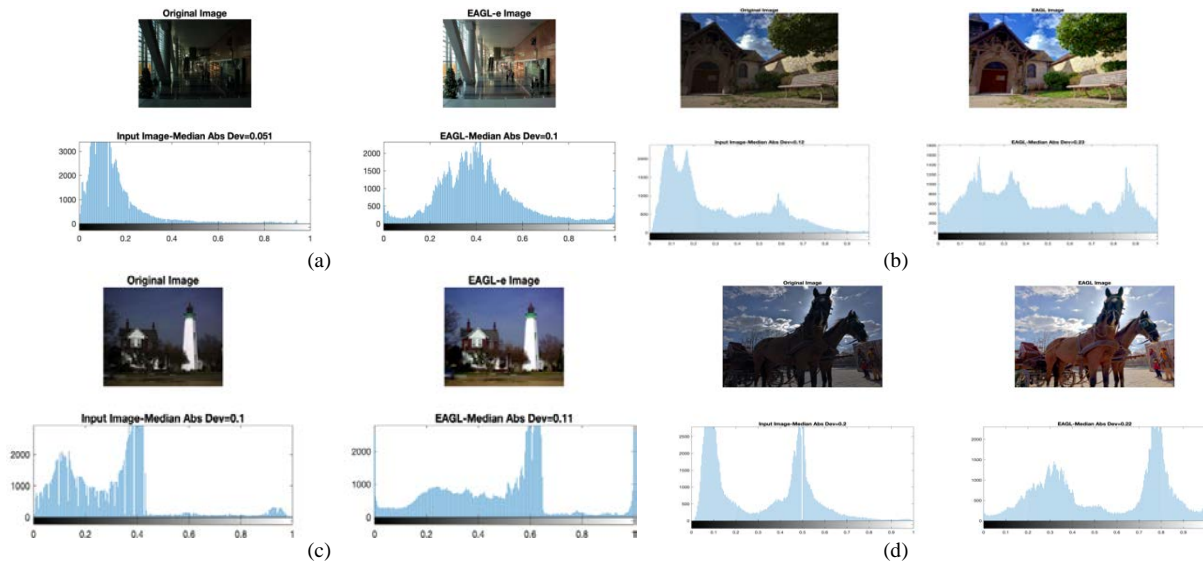


Fig. 8. Results Obtained from Proposed Method (EAGL) for Low Intensity and Low Pixel Counts (a) Airport, (b) Shadow, (c) Farmhouse and (d) Cart.

TABLE I. GROUP COMPARISON OF ALGORITHMS WITH THE PROPOSED METHOD

Group	IQA	HE	FDHE[28]	MMSICHE[4]	SDGTV[32]	AGCWD[33]	EAGL
Shad	E	5.78	7.62	7.42	7.38	6.85	7.64
	PSNR	21.29	33.12	32.40	39.14	14.85	45.18
	UIQI	0.89	0.91	0.96	0.79	0.82	0.96
Mod	E	5.80	7.02	6.82	7.49	7.22	7.36
	PSNR	11.19	29.70	26.41	37.95	13.65	40.69
	UIQI	0.41	0.96	0.96	0.61	0.57	0.99
Low	E	5.14	6.77	6.52	7.36	7.13	7.24
	PSNR	18.27	28.60	23.01	37.94	12.59	40.39
	UIQI	0.78	0.89	0.93	0.56	0.50	0.94

^{Bold indicates better results}

E. Comparison of Enhancement Algorithm with EAGL

The original image (Fig. 1) is a low intensity (mean =46.89) image with the size of 524x800, where the intensity values is concentrated on the left (dark) extrema of the intensity scale. The purpose of enhancement in the image is to scale the hidden details (background and the girl) without introducing any artificial artefacts.

Fig. 10 illustrates the comparison with the classical techniques HE, and the improved HE as developed by [4], [28] and the recent published algorithms by [13], [22], [27]. The fusion-based algorithm developed by Fu et al. [27] had quoted that the ‘girl’ image constituted both bright and dark scale (dress) that had been preserved simultaneously. But with the over enhancement, the image produced is low in sharpness. The HE is the simplest and computationally fast technique to enhance the distorted image. It statistically increases the contrast of the images having detailed intensity values. However, the finished image produced by HE and others related to HE showed poor preservation of details and contrast wrapped in the image. The similar nature of ‘dullness’ and over enhancement could be observed in the recent published

algorithm. Whereas in EAGL, the ‘girl’ in the image and its background had significantly improved the intensity of the low intensity image while preserving the details in the image. Fig. 9 is the histogram representation of enhanced image obtained from EAGL method. The shift in histogram values from dark scale to relatively bright region showed the global improvement in the image. The resultant image of the other HE based approach showed the effects of under and over-exposure of illumination which results in poor contrast. The resultant image of fuzzy-based HE (FDHE) showed under-exposure which results in poor visibility.

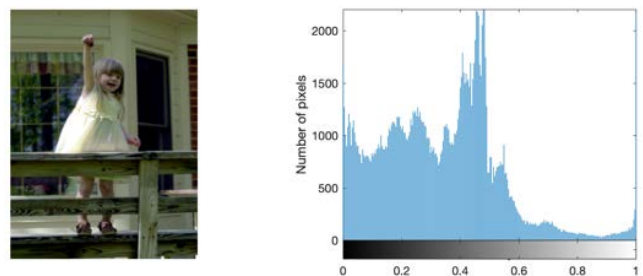


Fig. 9. Enhanced (EAGL) Image.

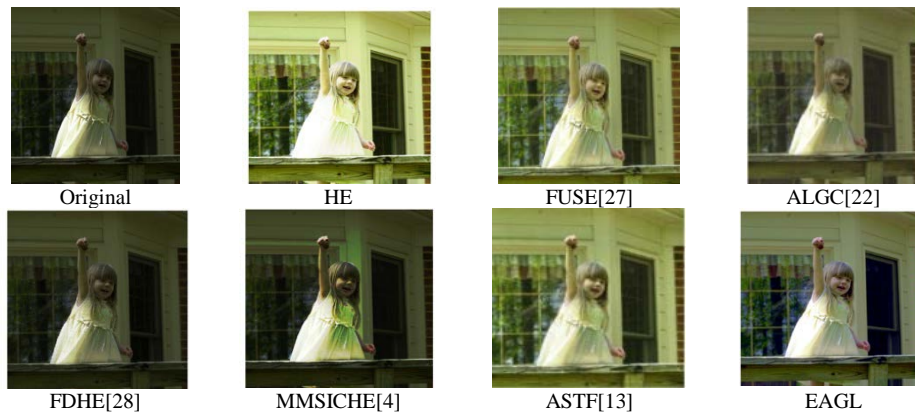


Fig. 10. Comparison of EAGL with the Recent Developed Algorithms based on Low Intensity Images.

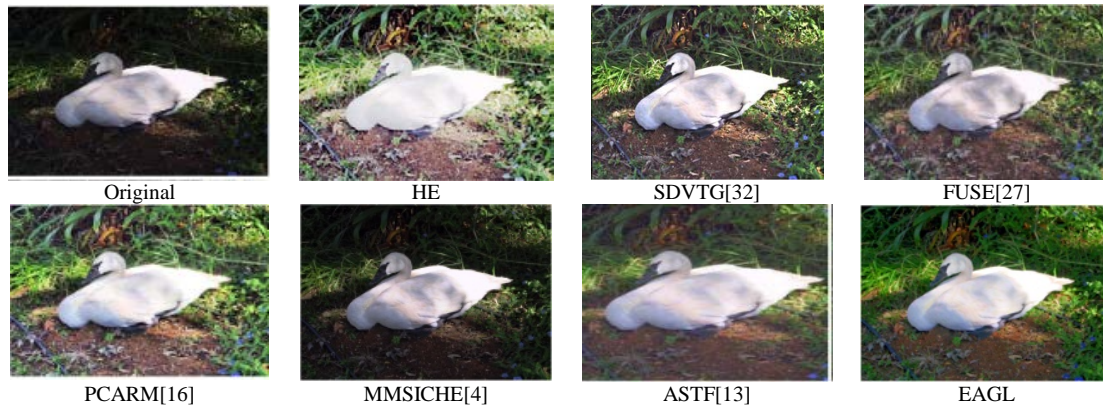


Fig. 11. Comparison of 'Swan' Image with other Relevant Algorithms.



Fig. 12. Comparison of Shadow (House) Intensity Image.

In case of MMSICHE [4], effect of color saturation had degraded the quality of the image. But in case of EAGL, the global brightness is achieved to improve the visual quality and contrast in the image. The steepness in the intensity of the pixels is improved without the loss of information (entropy). With better visibility, the background details in the image (shadow in the glass window) is improved while preserving the contrast color transition from the object with the background, whereas Fig. 12 shows the visual comparison of shadow images. The main criterion of shadow images is to produce a balance between brightness and contrast for a better visual appearance. The compared results were obtained by the default settings of the published algorithms. The method of semi-decoupled decomposition [33] produced over enhancement and degrade the quality of the image. In the case of a fusion-based algorithm [27], the haziness in the image had degraded the

overall appearance in the image. The HE and MMSICHE had not shown any significant improvement in the overall picture. With improved contrast and optimal brightness, high PSNR and quality index proved the efficacy of EAGL.

Table II summarized the comparison of visually compared images shown in Fig. 10, Fig. 11 and Fig. 12. The comparison is made with the standard enhancement technique HE, fusion based and semi-decoupled decomposition method. The proposed method is found to have high PSNR, quality index and better retention of information.

TABLE II. COMPARISON OF IMAGE 'SWAN', 'GIRL' AND 'HOUSE' WITH LOW-LIGHT ALGORITHMS

Image	IQA	SDVTG[32]	FUSE[27]	HE	EAGL
Swan(Figure 11) (513x385)	E	7.27	7.29	5.56	7.32
	UIQI	0.53	0.59	0.39	0.79
	PSNR	37.44	14.94	9.17	41.77
	TIME(sec)	3.20	1.78	0.31	0.40
Girl (Figure 10) (524x800)	E	7.34	7.35	5.95	7.09
	UIQI	0.68	0.47	0.37	0.83
	PSNR	34.01	11.78	8.73	41.09
	TIME(sec)	4.13	2.02	0.43	0.38
House(Figure 12) (1760x1160)	E	7.36	7.43	5.86	7.79
	UIQI	0.86	0.94	0.92	0.95
	PSNR	39.23	17.56	22.84	45.14
	TIME(sec)	21.08	4.02	0.95	0.41

*Bold indicates better results

F. Comparison with Recent Published Methods

Fig. 11 is ‘swan’ image that illustrated the visual comparison of the proposed algorithm with other recent published methods. The different methods were based on multi-fusion, principal component analysis, sigmoid transfer function and other HE based algorithms. The proposed method differs on its effective implementation of gamma and noise compensator. The focus is to devise the method that should be simple and effective to produce better quality in the image. From Fig. 11, the sharpness and the retention of colours produced by the EAGL outperformed the other algorithms. The HE produced over-enhancement and the MMSICHE showed a low luminance image. In case of sigmoid transfer function (ASTF) [13], the image failed to retain the sharpness and thus degraded the quality of the image. The principal component analysis is a dimensionality reduction technique to produce a scaling in brightness. But implementing principal component analysis (PCARM) [16], the loss of details could be visualized near the swan (shadow at the ground) and failed to preserve the variation of shadow to light region. The fusion method [27] lacked sharpness and failed to preserve the detailed information.

Image enhancement is a challenging task in the field of image processing. In continuing efforts of many researchers, the adaptive scale value for gamma correction is proposed. The first abstract the computation of gamma scale using log-power and Minkowski distance measure. The second abstract is the suppression of noise content using a median-based noise estimator and bivariate shrinking. The threshold is computed statistically for the optimal suppression of noise coefficients. Fig. 10, Fig. 11 and Fig. 12 showed the original image and the reconstructed image from the EAGL. The proposed algorithm is designed in a way to effectively enhance the low with a fast response time. The response time and PSNR affects the universal quality of the image.

Table III summarized the result of the proposed method with the algorithms for 100 images in terms of information preservation, quality index, suppression of noise coefficients and the response time.

TABLE III. AVERAGE COMPARISON OF EAGL

Method \ IQA	Entropy	UIQI	PSNR	Response Time (sec)
HE	5.79	0.65	16.24	0.17
SDVTG	6.90	0.67	38.34	0.65
FUSE	7.69	0.92	19.03	2.09
FPDHE	7.13	0.93	30.21	0.43
EAGL	7.36	0.98	46.46	0.29

*Bold indicates better results

V. CONCLUSION

Our experimental results focused on low visibility images due to non-uniform illumination. The prime advantage is (1) improved visibility in texture features, (2) low noise, and (3) improved contrast. In comparison to histogram equalization and other recent algorithms, the self-adaptive gamma scale had shown better improvement in retaining the texture features. The images were chosen in a way that the range of intensity

scale should lie in between extreme low to moderate values. The HE is a simple method but not effective to improve the quality of the image. The other algorithms showed low response time and PSNR which affects the universal quality of the image.

It is concluded that the adaptability to variations in shadow from moderate to low illuminated images is fast in EAGL to produce effective visibility and improved quality.

ACKNOWLEDGMENT

The authors are thankful to IKG Punjab Technical University, Kapurthala and DAV Institute of Engineering & Technology Jalandhar Punjab-India for providing necessary tools and access to peer reviewed journals for successful completion of the work.

REFERENCES

- [1] W. Wang, X. Wu, X. Yuan, and Z. Gao, “An Experiment-Based Review of Low-Light Image Enhancement Methods,” *IEEE Access*, vol. 8, pp. 87884–87917, 2020, doi: 10.1109/ACCESS.2020.2992749.
- [2] S. F. Tan and N. A. M. Isa, “Exposure Based Multi-Histogram Equalization Contrast Enhancement for Non-Uniform Illumination Images,” *IEEE Access*, vol. 7, pp. 70842–70861, 2019, doi: 10.1109/ACCESS.2019.2918557.
- [3] R. C. Gonzalez and R. E. Woods, *Digital Image Processing*. Pearson, 2018. [Online]. Available: <https://www.pearson.com/us/higher-education/program/Gonzalez-Digital-Image-Processing-4th-Edition/PGM241219.html>.
- [4] K. Singh and R. Kapoor, “Image enhancement via Median-Mean Based Sub-Image-Clipped Histogram Equalization,” *Optik (Stuttg)*, vol. 125, no. 17, pp. 4646–4651, 2014, doi: 10.1016/j.ijleo.2014.04.093.
- [5] S. Liu and Y. Zhang, “Detail-preserving underexposed image enhancement via optimal weighted multi-exposure fusion,” *IEEE Transactions on Consumer Electronics*, vol. 65, no. 3, pp. 303–311, 2019, doi: 10.1109/TCE.2019.2893644.
- [6] H. Ibrahim and N. Pik Kong, “Brightness Preserving Dynamic Histogram Equalization for Image Contrast Enhancement,” *IEEE Transactions on Consumer Electronics*, vol. 53, no. 4, pp. 1752–1758, Nov. 2007, doi: 10.1109/TCE.2007.4429280.
- [7] N. S. P. Kong and H. Ibrahim, “Color image enhancement using brightness preserving dynamic histogram equalization,” *IEEE Transactions on Consumer Electronics*, vol. 54, no. 4, pp. 1962–1968, 2008, doi: 10.1109/TCE.2008.4711259.
- [8] V. Magudeeswaran and C. G. Ravichandran, “Fuzzy logic-based histogram equalization for image contrast enhancement,” *Mathematical Problems in Engineering*, vol. 2013, 2013, doi: 10.1155/2013/891864.
- [9] C. Zuo, Q. Chen, and X. Sui, “Range Limited Bi-Histogram Equalization for image contrast enhancement,” *Optik (Stuttg)*, vol. 124, no. 5, pp. 425–431, 2013, doi: 10.1016/j.ijleo.2011.12.057.
- [10] C. Zuo, Q. Chen, X. Sui, and J. Ren, “Brightness Preserving Image Contrast Enhancement using Spatially Weighted Histogram Equalization,” 2014.
- [11] K. Hussain et al., “A histogram specification technique for dark image enhancement using a local transformation method,” *IPSA Transactions on Computer Vision and Applications*, vol. 10, no. 1, 2018, doi: 10.1186/s41074-018-0040-0.
- [12] B. S. Rao, “Dynamic Histogram Equalization for contrast enhancement for digital images,” *Applied Soft Computing Journal*, vol. 89, p. 106114, 2020, doi: 10.1016/j.asoc.2020.106114.
- [13] K. Srinivas and A. K. Bhandari, “Low light image enhancement with adaptive sigmoid transfer function,” *IET Image Processing*, vol. 14, no. 4, pp. 668–678, Mar. 2020, doi: 10.1049/iet-ipr.2019.0781.
- [14] B. Gupta and T. K. Agarwal, “New contrast enhancement approach for dark images with non-uniform illumination,” *Computers and Electrical Engineering*, vol. 70, pp. 616–630, 2018, doi: 10.1016/j.compeleceng.2017.09.007.

- [15] S. A. Priyanka, Y. K. Wang, and S. Y. Huang, "Low-light image enhancement by principal component analysis," *IEEE Access*, vol. 7, pp. 3082–3092, 2019, doi: 10.1109/ACCESS.2018.2887296.
- [16] N. Singh and A. K. Bhandari, "Principal Component Analysis-Based Low-Light Image Enhancement Using Reflection Model," *IEEE Transactions on Instrumentation and Measurement*, vol. 70, 2021, doi: 10.1109/TIM.2021.3096266.
- [17] Z. Zhou, N. Sang, and X. Hu, "Global brightness and local contrast adaptive enhancement for low illumination color image," *Optik (Stuttg)*, vol. 125, no. 6, pp. 1795–1799, 2014, doi: 10.1016/j.ijleo.2013.09.051.
- [18] N. S. Rekhi and J. S. Sidhu, "Adaptive Logarithmic-Power Algorithm for Preserving the Brightness in Contrast Distorted Images," *IJACSA) International Journal of Advanced Computer Science and Applications*, vol. 12, no. 10, pp. 197–205, 2021, [Online]. Available: www.ijacsa.thesai.org.
- [19] S. Rahman, M. M. Rahman, M. Abdullah-Al-Wadud, G. D. Al-Quaderi, and M. Shoyaib, "An adaptive gamma correction for image enhancement," *Eurasip Journal on Image and Video Processing*, vol. 2016, no. 1, pp. 1–13, 2016, doi: 10.1186/s13640-016-0138-1.
- [20] A. S. Parihar, "Entropy-Based Adaptive Gamma Correction for Content Preserving Contrast Enhancement," *International Journal of Pure and Applied Mathematics*, vol. 117, no. 20, pp. 887–893, 2017.
- [21] M. Mahamdioua and M. Benmohammed, "New Mean-Variance Gamma Method for Automatic Gamma Correction," *International Journal of Image, Graphics and Signal Processing*, vol. 9, no. 3, pp. 41–54, Mar. 2017, doi: 10.5815/ijigsp.2017.03.05.
- [22] W. Wang, X. Yuan, Z. Chen, X. Wu, and Z. Gao, "Weak-Light Image Enhancement Method Based on Adaptive Local Gamma Transform and Color Compensation," *Journal of Sensors*, vol. 2021, 2021, doi: 10.1155/2021/5563698.
- [23] W. Yu, H. Yao, D. Li, G. Li, and H. Shi, "Glargc: Adaptive dual-gamma function for image illumination perception and correction in the wavelet domain," *Sensors (Switzerland)*, vol. 21, no. 3, pp. 1–20, 2021, doi: 10.3390/s21030845.
- [24] N. S. Rekhi, J. Singh, J. S. Sidhu, and A. Arora, "Performance Evaluation of Enhancement Algorithm for Contrast Distorted Images," 2022, pp. 29–39. doi: 10.1007/978-981-16-8826-3_4.
- [25] A. Ziemba and E. Fornalik-Wajs, "Time performance of RGB to HSI colour space transformation methods," *Archives of Thermodynamics*, vol. 39, no. 1, pp. 111–128, 2018, doi: 10.1515/aoter-2018-0006.
- [26] A. Dixit and P. Sharma, "A Comparative Study of Wavelet Thresholding for Image Denoising," *International Journal of Image, Graphics and Signal Processing*, vol. 6, no. 12, pp. 39–46, Nov. 2014, doi: 10.5815/ijigsp.2014.12.06.
- [27] X. Fu, D. Zeng, Y. Huang, Y. Liao, X. Ding, and J. Paisley, "A fusion-based enhancing method for weakly illuminated images," *Signal Processing*, vol. 129, pp. 82–96, Dec. 2016, doi: 10.1016/j.sigpro.2016.05.031.
- [28] D. Sheet, H. Garud, A. Suveer, M. Mahadevappa, and J. Chatterjee, "Brightness Preserving Dynamic Fuzzy Histogram Equalization," 2010.
- [29] A. Horé and D. Ziou, "Image quality metrics: PSNR vs. SSIM," *Proceedings - International Conference on Pattern Recognition*, pp. 2366–2369, 2010, doi: 10.1109/ICPR.2010.579.
- [30] Z. Wang, A. C. Bovik, H. R. Sheikh, S. Member, E. P. Simoncelli, and S. Member, "Image Quality Assessment: From Error Visibility to Structural Similarity," vol. 13, no. 4, pp. 1–14, 2004.
- [31] Z. Wang and A. C. Bovik, "A Universal Image Quality Index," 2002. [Online]. Available: <http://anchovy.ece.utexas.edu/~zwang/re>
- [32] S. Hao, X. Han, Y. Guo, X. Xu, and M. Wang, "Low-Light Image Enhancement with Semi-Decoupled Decomposition," *IEEE Transactions on Multimedia*, vol. 22, no. 12, pp. 3025–3038, Dec. 2020, doi: 10.1109/TMM.2020.2969790.
- [33] S. C. Huang, F. C. Cheng, and Y. S. Chiu, "Efficient contrast enhancement using adaptive gamma correction with weighting distribution," *IEEE Transactions on Image Processing*, vol. 22, no. 3, pp. 1032–1041, 2013, doi: 10.1109/TIP.2012.2226047.

Approval Rating of Peruvian Politicians and Policies using Sentiment Analysis on Twitter

José Yauri¹, Luis Solis², Efraín Porras³, Manuel Lagos⁴, Enrique Tinoco⁵
School of Electrical and Computer Engineering, University of Campinas, Campinas, Brazil¹
Centro Politécnico de Ayacucho, Ayacucho, Perú¹

Dpto. de Matemática y Física, Universidad Nacional de San Cristóbal de Huamanga, Ayacucho, Perú^{2,3,4}
Dpto. de Ingeniería y Tecnología Informática, Universidad Nacional José María Arguedas, Abancay, Perú⁵

Abstract—Nowadays, using the social network Twitter, a subject can easily access, post, and share information about news, events, and incidents taking place currently in the world. Recently, due to the high number of users and the capability to transfer information instantly, Twitter had attracted the interest of politicians with the goal to interact with their followers and to communicate their policies. Fearing the disagreements and disturbances that the application of some policies might cause, usually politicians use surveys to support their actions. However, such studies still use traditional questionnaires to recover information and are costly and time-consuming. Recent advances in automatic natural language processing have allowed the extraction of information from textual data, like tweets. In this work, we present a method to analyze Twitter data related to Peruvian politicians and able to score the latent sentiment polarity of such messages. Our proposal is based on an embedding representation of tweets, which are classified by a convolutional neural network. For evaluation, we collected a new dataset related to the current President of Peru, where the model achieved 91.2% of sensibility and 94.4% of specificity. Furthermore, we evaluated the model in two politic topics, that were totally unknown for the model. In all of them, our approach gives comparable results to renowned Peruvian pollsters.

Keywords—Twitter data analytic; sentiment analysis; Peruvian politicians; approval rating; convolutional neural networks

I. INTRODUCTION

Nowadays, it is undeniable that social networks are playing an increasing role of importance in the dissemination of information. Daily, millions of people around the world access to social networks to share information and to communicate. A social network is an internet-based application that allow people to communicate between their families, friends, colleagues, circles of interest, and followers [1]. Actually, there are many social networks and usually they are oriented to specific topics, e.g., news, entertainments, movies, podcasts, professional networks, relations, etc.

Among social networks to disseminate news, Twitter registers the highest daily activity and popularity. In Twitter, a subject can easily share short messages or tweets about current events, that can be accessed by to tens of thousands of people. A subject can also reply and discuss the messages, contributing the message to become “viral”. These short messages of at most 280 characters, also named tweets, can be accompanied by a few photos and a short video. According to the report in [2], more than of 500 million of tweets are published in

a day, which highlight the importance of Twitter in people’s day-to-day communication.

Due to high popularity of Twitter and its capability to transfer information between ten of thousand people instantly, social leaders, influencer, politicians, companies, and governments have started using this social media to interact with their followers, clients, political adherents, and citizens. Once a subject gets registered in the social network, he can send and receive tweets and participate into virtual communities of his interest.

Recently, many investigations are being done aiming to analyze the stored data in social networks automatically [3]. However, the large amount of data and its non-structured nature still challenges the proposed methods [4]. The research objective is to discover hidden patterns into data and forecast trends in order to make decisions. Among the diversity of topics, the analysis of posts related to politicians becomes a hot topic of study, where the goal is to predict the approval rating of an important politician (e.g. the president, the prime minister, and others) or to measure the people satisfaction related to government policies carried out. This makes sense, actually, many governments are concerned about their approval rating. A high approval rate indicates a successful and healthy govern, both for their own citizens and foreigner’s eyes. In contrast, a low approval rate reflects a weak govern, without major importance for people, even with detriment for the state itself.

Despite the social media network offers a rich source of information, studies of approval rating of politicians still reside on traditional paper-based questionnaires, which are too slow, time-consuming and expensive studies. On the other hand, an automatic analysis system offers an agile and less expensive manner to predict approval rating. Recent advances in Natural Language Processing (NLP) had produced the technique of sentiment analysis [5]. Sentiment analysis enables to gain insights of opinions in published tweets related to a particular discussion topic [6]. Furthermore, sentiment analysis can help to reveal the psychological and mental state of the subject who wrote a particular tweet, the emotional state, level of education, and others features [7].

In this work, we present a method to predict the approval rating of politicians based on Twitter data, focusing specifically to forecast the popular endorsement the President of Peru. The proposed model consists of an embedding representation,

followed by a Convolutional Neural Network (CNN). The embedding is itself a neural network pretrained in one billion of Spanish words [8]. The model is able to learn a rich diversity of tweet messages and classify them according to their sentiment polarity content, as positive/negative or approval/disapproval. Positive and negative outcomes are weighted according to the number of messages that were fed in the model to provide the final approval or disapproval rate. The model was designed to be political agnostics, so it was trained once and tested in multiple politic topics. To evaluate the model, a new dataset of 1150 tweets was collected. Collected messages include tweet posted in Spanish related to the current President of Peru, Pedro Castillo, that were retrieved from August 2021 to February 2022. Data was manually labeled as of positive or negative sentiment, resulting in a balanced dataset.

For evaluation, the model was assessed in a hold-out validation manner, with a ratio 80:20. Testing the ability of the model to predict the approval rating of the Peruvian president, it outputs 91.2% of sensibility and 94.4% of specificity. Due to the large corpus of the pretrained embedding layer, data augmentation was not required during training. Furthermore, to assess the model agnostic feature, a new data was collected in April 2022 about two widely discussed policies in that month: the approval/disapproval rating of the Peruvian Congress and the agreement/disagreement with a new State Constitution. The model, without further training, predicts 84.0% of disapproval rating for the Peruvian Congress and 75.0% of disagreement with a new State Constitution. Comparing the obtained results against those reported by the specialized Peruvian pollsters, the model predictions correlate to the pollsters' issues. Therefore, the proposed method can be offer as an on-demand tool for text message analysis in social networks.

The remainder of this paper is organized as follows. Section II presents fundamental concepts of sentiment analysis. Section III outlines the literature review related work. Section 4 explains the proposed method. Section V details the experimental results and discussions. Finally, Section VI presents conclusions and future work.

II. FUNDAMENTALS

A. Sentiment Analysis

Sentiment analysis or opinion mining is a method into the field of NLP to teach machines to learn, detect and recognize emotional and sentimental information from a given text message [9]. Given an opinion, sentiment analysis can extract its meaning, sense, and emotional charge of the subject who wrote it. Usually, input data for opinion mining consists of text messages stored in structured spreadsheets or in unstructured repositories, such as, text document, web pages, web forums [10].

A common way to detect the sentimental charge of messages is to classify them into categories according their satisfaction or agreement scores. Typical categories can be positive, neutral, or negative sentiment, reflecting a higher satisfaction, none, or dissatisfaction of the subject related to the studied variable [11], [12]. There are many applications using sentiment analyses techniques in the social domain, including the recommendation systems [13], movie reviews

[14], identification of cyber-aggression [15], racism [16] and violence against women [17].

B. Twitter

Twitter is a messaging service in which subjects can post and interact by means of short messages or tweet [18]. Tweets consist of written opinions related to current topics of interest and can be used as a source of news and information for decision making [19]. Actually, Twitter is the social network most used by politicians because its capability to allows them to communicate massively with thousands of millions of followers [20].

C. Politician's Approval Rating

In the last decades, it has become a common practice for governments and politicians to know the opinion of people and citizens regarding their activities, decisions, and execution of policies. Such opinions are quantified and presented as a score of popular agreement or disagreement, approval or disapproval, named as approval or favorability rating.

In order to know a reliable approval rating of some politician or a government policy, specialized polling companies carry out statistical surveys in a population sample. Although these studies are reliable, they might present a delayed snapshot of the opinions of people, which are daily changing because of the massive use of communications. As an alternative, opinion mining in Twitter seems to work well like an approval rating method, as presented in Section II-A.

In this work, we study the approval rating of the president of Peru, which is presented monthly by some polling companies. This endorsement rating reflects the citizen's satisfaction related to the work of the government and the implemented policies for the country development. These ratings have many implications: it indicates the aptitude of politicians and the impact of medium and long term polices, reveals the economic strength and politic stability, and the lack or weakens of policies. Therefore, the approval rating becomes an important indicator for decision making for external agents, foreign investors, local entrepreneurs, and Peruvian citizens.

Monthly, historical approval ratings are consolidated in chart plots by several Peruvian polling companies [21], [22], [23], [24]. These results are used for making other studies and forecasting the trend curve. Downward trends indicate bad news: a government weakness and failures in the implementation of policies. For a developing country like Peru, it means capital flight, recession, economic instability, rising unemployment, and disinvestment [25].

III. LITERATURE REVIEW

The study of [26] concluded that there are high limitations when working with text data originated on Twitter, being the presence of colloquial lexicon, informal syntax, short structure, context-dependent and dynamics nature of messages are the major challenges for mining opinion [3]. NLP methods intend to solve that issues and discover meaning in human utterances and translation [27]. Moreover, the recent rising of deep learning methods in NLP has boost the Sentiment Analysis

field [28], with the goal to discover the meaning of an opinion, its context and sentimental charge.

As follows, we summarize the most relevant works related the topic investigated in this study:

The study of [29] compared a supervised learning model against a simple voting algorithm to classify tweets into three categories (positive, negative, and neutral). First, the tweet sentence is split into words (or token). Next, words are scored according to a lookup table of 2014 positive and 4783 negative words. Each positive word adds one to the sentence score, in contrast each negative word subtracts one to sentence score. The amount of positive words minus the amount of negative words provide the sentiment score of a tweet message. For classification, the voting algorithm just take in account the final score of the tweet: if the score is greater than zero, then the sentence is classified as positive; if the score is zero, then the sentence is negative; otherwise, the sentence is neutral. Following the same criteria, using a dataset of 1500 tweets, they trained a Naive Bayes (NB) classifier, achieving an average accuracy of 81%, against 74% using the simple voting algorithm. The major limitations of this work is that the scoring is strong dependent on the number of words in the lookup table.

Later, the work of [30] applied sentiment analysis in order to know the political opinions of citizens in the Indian electoral process of 2019. They proposed sentiment-based classification model to predict the electoral results. First, a dataset of 3896 tweets were collected from Twitter taking in account the two most popular political parties. Preprocessed messages were classified using the Long Short-Term Memory (LSTM) neural network, achieving a F1-Score of 0.74. In comparison against traditional machine learning (ML) methods, although relatively slow during inference time, LSTM outperforms such other methods.

The study of [9] collected data from Twitter aiming to predict the Congress election outcome in India by using sentiment analysis. To label tweets, they used the Valence Aware Dictionary and Estiment Reasoner (VADER) [31], and used a manual feature extraction [32] which are combined in a bag of words fashion (BoW). For classification, a set of MLs algorithms were compared: Logistic Regression, Decision Tree, XGBoost, Naive-Bayes and Linear Support Vector Machine [33]. Among them, the decision tree method predicted the winner political party with an accuracy of 86.3%.

Next, the study of [18] used Twitter data to analyze the opinion of people against policies of Donald Trump during the Covid-19 pandemic. First, tweet data was recovered by means of the Twitter service using the keyword DONALD TRUMP from February to May 2020. The study does not provide the number of collected tweets. Next, the collected tweets were labeled manually as either of positive or negative sentiment. And finally, for classification, they used two learning algorithms for comparison. The first one, the LSTM model achieved an average accuracy of 69%, whereas, the second one, the NB algorithm, 63%. Again, it is noticeable that LSTM outperforms the traditional ML methods due to its capability of automatic learning features.

Recently, in the context of the COVID-19 pandemic, the work of [10] used sentiment analysis to identify the

Brazilian population's perceptions about their Public Health System (named *Sistema Unificado de Saúde* in Portuguese) by analyzing Twitter content. They collected 27500 tweets using the Twitter service with the keywords SAÚDE and SUS. Data was recovered from December 2019 to October 2020. A message is scored based on the polarity of words contained in it and receives a final score, either positive, negative, or neutral. For the whole message processing and scoring, they used a dictionary of emotion lexicons [34] and its implementation in the R language programming [35]. Note that no learning model is used. As results, the authors show word clouds comparing qualitatively the sentiments of people, before and after the pandemic.

In summary, sentiment analysis is a good choice for opinion mining because it can capture underlying characteristics of messages. Among the studies, the majority of them prefer to NN models as a classifier in opposite to ML ones, which resides on hand-crafted features. However, the complex syntax, the short structure, and the use of colloquial lexicon in most of tweets still challenges current methods [3], [28].

Furthermore, yet there is scarce proposals of sentiment analysis in other languages than English, e.g., in Spanish. To the best of our knowledge, in the context of Peru, the study of [36] is a pioneering work aiming to detect cyberbullying in tweet messages written in Spanish, we assume that other works are ongoing or not published yet.

In contrast, in this work we propose a general method for approval rating of Peruvian politicians, which is evaluated in two politic scenarios to measure its generalization capability. The model trained to predict the favorability rating of the President of the Republic of Peru is used to predict the popular support of two hot topics widely discussed in Twitter: the approval rating of the Peruvian Congress and the agreement with a new State Constitution. Our method is simple, but effective, achieving high sensitivity and specificity scores in all tested cases.

IV. METHODS

The proposed framework for approval rating based on sentiment analysis in Twitter is shown in Fig. 1. This approach is designed to extract tweet posted by Twitter users related to the President of Peru. First, we gather data directly from the web page of Twitter. Next, data is preprocessed in order to prepare input data for the learning model. Then, the proposed model is trained in order to learn how discriminate positive from negative sentiment messages. Once trained the model, it is used as a classifier in order to make prediction of new unknown input data.

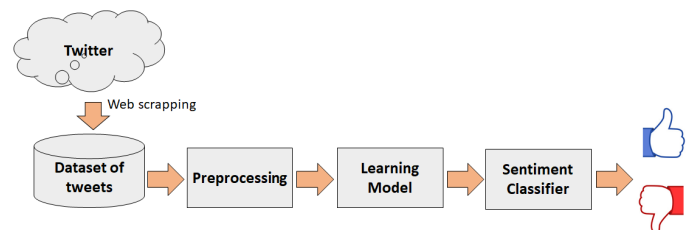


Fig. 1. The Proposed Framework.

As follows, we provide an in deep description of each module of the proposed framework:

A. Dataset

A dataset of 1150 tweets was collected from tweet messages and discussions in Spanish between Peruvian users regarding the President of the Republic of Peru. Due the cost of the Twitter service is prohibitive of us, we used the Beautiful Soup web scrapping library for Python [37].

The data collection about the Peruvian president was conducted from August 2021 to February 2022 using the tags @PEDROCASTILLO and @PRESIDENCIADelperu, and their related interactions. From August 2021 to January 2022, 900 tweets were collected (150 tweets per month), and during February 2022, 250 messages.

For each discussion topic about the Peruvian Congress (tag @CONGRESOPERU) and the new State Constitution (tag @CONSTITUCIÓN), a short dataset of 200 tweets was recovered in April 2022.

The collected tweets of the Peruvian president were labeled manually according to the perceived emotional charge in two categories. Label zero (0) was assigned for approval and label one (1) for disapproval. The Table I shows some tweets and their respective label.

TABLE I. SOME TWEETS OF THE DATASET.

Tweet	Label
This is how to govern for the people! <i>Así se gobierna para el pueblo!</i>	0
Thank you for the effort, president <i>Gracias por el esfuerzo presidente</i>	0
Get to work seriously, stupid <i>Ponte a trabajar en serio inepto</i>	1
I hope you get vacate, idiot <i>Ojalá te vaquen inútil</i>	1
Get rid him, I hate him <i>Sáquenlo lo odio</i>	1

B. Preprocessing

1) *Data Cleaning*: Raw tweet messages contain numeric digits, punctuation symbols, and special characters likewise @, #, ?, !, (,), \$, &. All of them must be deleted. Next stop-words (i.e., common words in a language) also must be removed [38]. We used the Natural Language Tool Kit (NLTK) library with stop-words in Spanish [39].

2) *Lematization*: Because tweets can use different ways of a word to express the same meaning, lemmatization intends to reduce the effect of inflectional and derived forms of words to their common base form. For instance, the words blood, bleed and bloody can be represented as the word blood [40].

3) *Tokenization*: During tokenization, each tweet is split into its smallest possible morpheme called word or token [41].

4) *Message Length Standardization*: After tokenization, tweets can have a variable length of words, so the idea is to standardize the length of each tweet. In our approach, we used the average length of words on tweets. This gives us 12.40 ± 9.08 of length, so we decided to fix the length of each tweet to the first 12 words. If a tweet contains words lesser than 12, the message is padded with empty words.

C. Learning Model

The proposed learning model is based on an end-to-end trainable deep learning neural network [42]. Fig. 2 outlines the proposed model. It consists of the learnable model itself and the sentiment classifier. Considering an input data, the model processes it aiming to predict the likelihood of belonging to the approval or disapproval class.

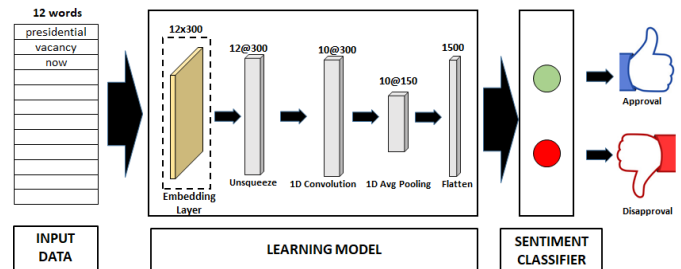


Fig. 2. The Model Architecture.

A brief description of the model is described as follows:

- **Word embedding**: In NLP, words must be encoded to be processed by the model. A common encoding method is to use an embedding, which generates a representation vector for each word. Words of the same meaning or similarity will have close feature vectors in the embedding space [5]. In this work we used the Spanish Billion Words Corpus and Embeddings (SBW). It furnishes an embedding that was pretrained on more than 1.5 billion words of the Spanish language [8]. The embedding produces a 300-dim vector for each word in the input data.
- **Squeezing**: The input data after embedding has a shape of 12×300 . To be processed in the next layer, we reshape in order to become likewise a 300-dim sequence with a feature map of 12 filters.
- **1D-Convolution**: Reshaped embedding vectors are fed to a 1D-CNN layer. The CNN has a kernel of size 3, stride 1, and padding 1. The CNN has 10 neuron filters and the Rectified Linear Unit (ReLU) is used as activation function. Also batch normalization helps us to prevent overfitting.
- **Pooling**: An average pooling layer, with a kernel of size 2 and stride 2, is used to down-sample the feature maps coming out from the CNN.
- **Flatten**: After down-sampling, feature maps are flattened and fed into a fully connected layer. The output of the flatten layer is used as feature vector and is used to perform classification.

D. Sentiment Classifier

The sentiment classifier module implements classification. Given a feature vector, to predict either the approval or disapproval likelihood, we used a fully connected layer of two neurons with a Softmax activation function to furnish prediction (see Fig. 2).

E. Model Training

In order to train the model in an end-to-end manner, we used the cross-entropy as loss function and the Adam optimizer. In our experiments, the embedding layer is not freezing, but to avoid overfitting we used a low learning rate (1e-5) and a short batch size (16), and the model was trained for just a few epochs (25).

F. Model Evaluation

To assess the model performance in the dataset of the President of Peru, we split the dataset into training and test set. Tweet data collected from August to December 2021 is the training set, whereas messages from January–February 2022 is the test set.

The model performance is scored using the metrics of sensibility and specificity, being the approval rating the true positives we want to predict.

V. RESULTS AND DISCUSSION OF RESULTS

A. Collected Dataset

We performed collection of tweet related to the President of Peru, from August 2021 to February 2022. Table II summarizes the number of tweets recovered by months.

TABLE II. DATASET ABOUT THE PRESIDENT OF PERU.

Months	N° Tweets
Aug–Dec 2021	750
Jan 2022	150
Feb 2022	250

Fig. 3 shows the word cloud or a visual representations of words with more frequency in the collected dataset of the President of Peru.



Fig. 3. The Word Cloud about the President of Peru.

Additionally, we collected a few tweets relate the Congress and the State Constitution of Peru. Table III outlines the number of tweets by the respective topic.

TABLE III. MISCELLANEOUS DATA.

Topic	Months	N° Tweets
The Congress	Apr 2022	200
The State Constitution	Apr 2022	200

B. Classification Performance

As exposed in Section IV-F, the trained model was assessed in the data of President collected during January and February 2022. Note that this data is totally unknown for the model. As a results, the model achieved 91.2% of sensitivity and 94.4% of specificity.

In order to provide a historical curve of trend likewise Peruvian pollsters furnish, we used the trained model and 40% of the data for each month to construct the trend curve of the approval/disapproval rating of the President of Peru. Fig. 4 shows the constructed historical curve with our predictions versus the surveys from IPSOS [21].

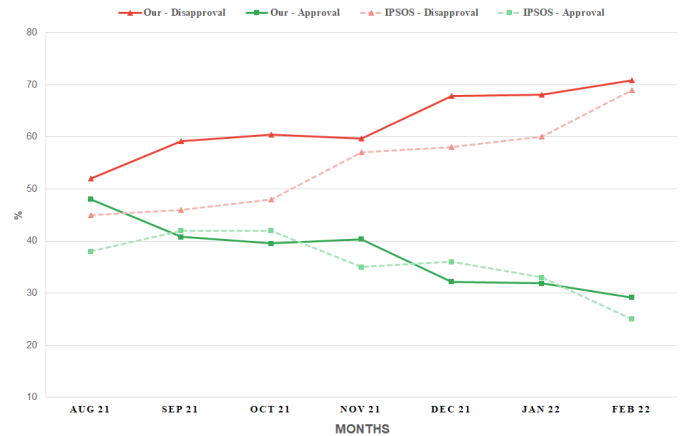


Fig. 4. Trend Curve of the Approval/Disapproval Rating of the President of Peru. Our Predictions vs IPSOS Surveys.

C. Classification of Miscellaneous Political Data

In order to evaluate the agnostic ability dealing with political data, we assessed the model in two discussions that attracted the interest of the Peruvians.

- 1) The approval rating of the Congress of Peru due to the start of the vacancy process against the president and censorship of some ministers. In this case, the predicted outputs are considered as an approval/disapproval rate. Fig. 5 outlines the approval/disapproval rating of our model related the Congress of Peru against the results of two renowned pollsters, CPI [24] and IEP [23].
- 2) The proposal of the current government to change of the state Constitution. In this case, the predicted outputs are considered as an agreement/disagreement

rate. Fig. 6 shows the outcomes of our model against the results of CPI [24].

It is worthwhile to mention that results of the pollsters were recovered from the same period of study, April 2022, aiming to compare against our proposal.

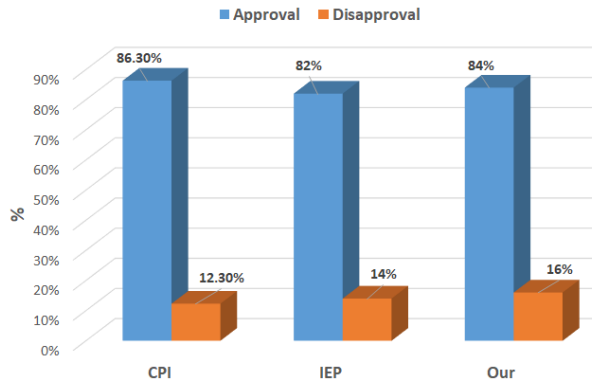


Fig. 5. Approval/Disapproval Rating of the Congress of Peru, Period April 2022.

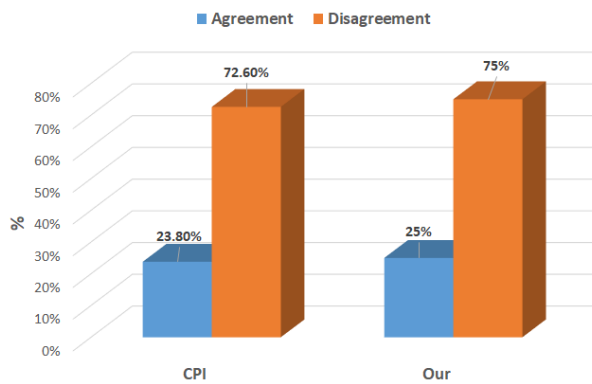


Fig. 6. Popular Agreement/Disagreement to Change the State Constitution of Peru, Period April 2022.

D. Discussion of Results

Taking into account the first experiment to predict the approval rating of the President of Peru, the proposed model achieved high performance to classify positive and negative latent sentiments in tweet messages.

In order to gain insight whether the model is working as expected, we constructed the historical trend curve of approval rating of the president and compared it with the result of one pollster. We can conclude that our model furnishes reliable predictions (see Fig. 4).

Inspecting the model architecture, although the model can seem too simple, the CNN layer improves the input features and the average pooling gives them a degree of invariance. However, it is worthwhile to mention that the simplicity of the model is compensated with the embedding layer, which was trained in a large corpus of Spanish words [8].

Besides, after analyzing the number of words of messages with politic content, we observed that in political discussions

people prefer to use short messages, usually with harsh words or words with higher sentimental polarity.

Moreover, in order to evaluate the agnostic feasibility of the model to be applied in other politic cases, we tested it in two cases without any fine tuning. In both cases, the model was able to predict close similar results likewise two Peruvian pollsters (see Fig. 5 and Fig. 6).

VI. CONCLUSION AND FUTURE WORK

In this work, we presented an approach to classify Twitter data in order to predict the approval rating of Peruvian politicians and the policies that they intend to implement. Our approach resides on a convolutional neural network model that is able to detect and score the sentiment polarity of tweet messages. To assess the model, we collected a new dataset of tweets about the current President of Peru and a miscellaneous data about discussions of two topics: the popularity of the Peruvian Congress and the possibility to change the current state Constitution. In all cases, the model provides results comparable to those offered by renowned Peruvian pollsters. So, our proposal is a low cost, agile, and reliable alternative against to the expensive and time-consuming traditional opinion surveys.

As future work, we intend to collect more data from other political discussions for more evaluation of the robustness of the model. Moreover, the model will be improved to take attention to syntactic order and semantic meaning.

ACKNOWLEDGMENT

The authors would like to thank the Research Offices of the Universidad Nacional San Cristóbal de Huamanga and Universidad Nacional José María Arguedas for their financial support.

REFERENCES

- [1] M. Mameli, M. Paolanti, C. Morbidoni, E. Frontoni, and A. Teti, "Social Media Analytics System for Action Inspection on Social Networks," *Social Network Analysis and Mining*, vol. 12, no. 1, 2022. [Online]. Available: <https://doi.org/10.1007/s13278-021-00853-w>
- [2] Statista, "Daily Social Media Usage Worldwide," accessed: 2022-05-20. [Online]. Available: <https://www.statista.com/statistics/433871/daily-social-media-usage-worldwide/>
- [3] F. A. Pozzi, E. Fersini, E. Messina, and B. Liu, *Sentiment Analysis in Social Networks*. San Francisco, CA, USA: Morgan Kaufmann Publishers Inc., 2016.
- [4] W. Aslam, W. H. Butt, and M. W. Anwar, "A Systematic Review on Social Network Analysis – Tools, Algorithms and Frameworks," *ACM International Conference Proceeding Series*, pp. 92–97, aug 2018. [Online]. Available: <https://doi.org/10.1145/3277104.3277112>
- [5] M. Sri, *Practical Natural Language Processing with Python*, 2021.
- [6] R. K. Bakshi, N. Kaur, R. Kaur, and G. Kaur, "Opinion Mining and Sentiment Analysis," in *2016 3rd international conference on computing for sustainable global development (INDIACom)*. IEEE, 2016, pp. 452–455.
- [7] B. Liu, "Many Facets of Sentiment Analysis," in *A Practical Guide to Sentiment Analysis*. Springer, 2017, pp. 11–39.
- [8] C. Cardellino, "Spanish Billion Words Corpus and Embeddings," 2016, accessed: 2022-03-20. [Online]. Available: <https://crscardellino.ar/SBWCE/>
- [9] P. Khurana Batra, A. Saxena, Shruti, and C. Goel, "Election Result Prediction using Twitter Sentiments Analysis," *PDGC 2020 - 2020 6th International Conference on Parallel, Distributed and Grid Computing*, pp. 182–185, 2020.

- [10] H. Silva, E. Andrade, D. Araujo, and J. Dantas, "Sentiment Analysis of Tweets Related to SUS before and during COVID-19 pandemic," *IEEE Latin America Transactions*, vol. 20, no. 1, pp. 6–13, 2022.
- [11] S. Poria, A. Hussain, and E. Cambria, *Multimodal Sentiment Analysis*, ser. Socio-Affective Computing. Cham: Springer International Publishing, 2018, vol. 8.
- [12] Z. Liu, Y. Lin, and M. Sun, "Representation Learning and NLP," *Representation Learning for Natural Language Processing*, pp. 1–11, 2020.
- [13] S. Bhattacharya, D. Sarkar, D. K. Kole, and P. Jana, "Recent Trends in Recommendation Systems and Sentiment Analysis," in *Advanced Data Mining Tools and Methods for Social Computing*. Elsevier, jan 2022, pp. 163–175.
- [14] U. D. Gandhi, P. Malarvizhi Kumar, G. Chandra Babu, and G. Karthick, "Sentiment Analysis on Twitter Data by Using Convolutional Neural Network (CNN) and Long Short Term Memory (LSTM)," *Wireless Personal Communications*, no. 0123456789, 2021. [Online]. Available: <https://doi.org/10.1007/s11277-021-08580-3>
- [15] G. O. Gutiérrez-Esparza, M. Vallejo-Allende, and J. Hernández-Torruco, "Classification of Cyber-Aggression Cases Applying Machine Learning," *Applied Sciences (Switzerland)*, vol. 9, no. 9, may 2019.
- [16] A. Alotaibi and M. H. Abul Hasanat, "Racism Detection in Twitter Using Deep Learning and Text Mining Techniques for the Arabic Language," in *Proceedings - 2020 1st International Conference of Smart Systems and Emerging Technologies, SMART-TECH 2020*. Institute of Electrical and Electronics Engineers Inc., nov 2020, pp. 161–164.
- [17] M. Alzyout, E. Al Bashabsheh, H. Najadat, and A. Alaiad, "Sentiment Analysis of Arabic Tweets about Violence against Women using Machine Learning," in *2021 12th International Conference on Information and Communication Systems, ICICS 2021*. Institute of Electrical and Electronics Engineers Inc., may 2021, pp. 171–176.
- [18] N. Shaghghi, A. M. Calle, J. Manuel Zuluaga Fernandez, M. Hussain, Y. Kamdar, and S. Ghosh, "Twitter Sentiment Analysis and Political Approval Ratings for Situational Awareness," *Proceedings - 2021 IEEE International Conference on Cognitive and Computational Aspects of Situation Management, CogSIMA 2021*, pp. 59–65, may 2021.
- [19] P. H. Prastyo, A. S. Sumi, A. W. Dian, and A. E. Permanasari, "Tweets Responding to the Indonesian Government's Handling of COVID-19: Sentiment Analysis Using SVM with Normalized Poly Kernel," *Journal of Information Systems Engineering and Business Intelligence*, vol. 6, no. 2, p. 112, 2020.
- [20] D. Kydros and G. Magoulios, "Twitter content analysis on Greek political leaders," vol. 13, no. 1, pp. 30–44, 2019.
- [21] IPSOS, "IPSOS Peru," Tech. Rep., accessed: 2022-05-20. [Online]. Available: <https://www.ipsos.com/es-pe>
- [22] DATUM, "Datum Internacional," accessed: 2022-05-20. [Online]. Available: <https://www.datum.com.pe/estudios>
- [23] IEP, "Instituto de Estudios Peruanos," accessed: 2022-05-20. [Online]. Available: <https://iep.org.pe/>
- [24] CPI, "CPI Research," accessed: 2022-05-20. [Online]. Available: <https://www.cpi.pe>
- [25] L. G. Rodríguez, C. G. and Tule, "Honduras 2019: Persistent economic and social instability and institutional weakness," *Revista de Ciencia Política*, vol. 40, pp. 379–400, 2020. [Online]. Available: www.scopus.com
- [26] S. Kumar, F. Morstatter, and H. Liu, *Twitter Data Analytics*, 2013.
- [27] D. Jurafsky and J. H. Martin, *Speech and Language Processing*, 2nd ed. Prentice-Hall, 2009.
- [28] B. Agarwal, R. Nayak, N. Mittal, and S. Patnaik, "Deep Learning-based Approaches for Sentiment Analysis," p. 326, 2020.
- [29] A. S. Al Shammari, "Real-time Twitter Sentiment Analysis using 3-way classifier," *21st Saudi Computer Society National Computer Conference, NCC 2018*, pp. 1–3, 2018.
- [30] M. Z. Ansari, M. B. Aziz, M. O. Siddiqui, H. Mehra, and K. P. Singh, "Analysis of Political Sentiment Orientations on Twitter," *Procedia Computer Science*, vol. 167, pp. 1821–1828, jan 2020.
- [31] C. J. Hutto and E. Gilbert, "VADER: A Parsimonious Rule-Based Model for Sentiment Analysis of Social Media Text," in *ICWSM*, 2014.
- [32] D. Yan, K. Li, S. Gu, and L. Yang, "Network-Based Bag-of-Words Model for Text Classification," *IEEE Access*, vol. 8, pp. 82 641–82 652, 2020.
- [33] K. P. Murphy, *Machine Learning: A Probabilistic Perspective*. The MIT Press, 2012.
- [34] S. M. Mohammad and P. D. Turney, "Crowdsourcing a Word-emotion Association Lexicon," *Computational Intelligence*, vol. 29, no. 3, pp. 436–465, aug 2013. [Online]. Available: <https://onlinelibrary.wiley.com/doi/full/10.1111/j.1467-8640.2012.00460.x>
- [35] R. I. amd Robert Gentleman, "R: The R Project for Statistical Computing," accessed: 2022-05-20. [Online]. Available: <https://www.r-project.org>
- [36] X. M. Cuzzano and V. H. Ayma, "A Comparison of Classification Models to Detect Cyberbullying in the Peruvian Spanish Language on Twitter," *International Journal of Advanced Computer Science and Applications*, vol. 11, no. 10, pp. 132–138, 2020.
- [37] L. Richardson, "Beautiful Soup Documentation," 2007, accessed: 2022-05-20. [Online]. Available: <https://www.crummy.com/software/BeautifulSoup/>
- [38] S. Ferilli, F. Esposito, and D. Grieco, "Automatic Learning of Linguistic Resources for Stopword Removal and Stemming from Text," *Procedia Computer Science*, vol. 38, no. C, pp. 116–123, 2014. [Online]. Available: <http://dx.doi.org/10.1016/j.procs.2014.10.019>
- [39] S. Bird, E. Klein, and E. Loper, "Natural Language Processing with Python: Analyzing Text with the Natural Language Toolkit," *O'Reilly*, 2009.
- [40] C. D. Manning, P. Raghavan, and H. Schütze, *Introduction to Information Retrieval*. USA: Cambridge University Press, 2008.
- [41] A. Rai and S. Borah, "Study of Various Methods for Tokenization," *Lecture Notes in Networks and Systems*, vol. 137, pp. 193–200, 2021.
- [42] I. Goodfellow, Y. Bengio, and A. Courville, *Deep Learning*. MIT Press, 2016.

Construction of a Repeatable Framework for Prostate Cancer Lesion Binary Semantic Segmentation using Convolutional Neural Networks

Ian Vincent O. Mirasol, Patricia Angela R. Abu, Rosula S.J. Reyes

Department of Information
Systems and Computer Science
Ateneo de Manila University
Loyola Heights, Philippines

Abstract—Prostate cancer is the 3rd most diagnosed cancer overall. Current screening methods such as the prostate-specific antigen test could result in overdiagnosis and overtreatment while other methods such as a transrectal ultrasonography are invasive. Recent medical advancements have allowed the use of multiparametric MRI — a noninvasive and reliable screening process for prostate cancer. However, assessment would still vary from different professionals introducing subjectivity. While convolutional neural network has been used in multiple studies to objectively segment prostate lesions, due to the sensitivity of datasets and varying ground-truth established used in these studies, it is not possible to reproduce and validate the results. In this study, we executed a repeatable framework for segmenting prostate cancer lesions using annotated apparent diffusion coefficient maps from the QIN-PROSTATE-Repeatability dataset — a publicly available dataset that includes multiparametric MRI images of 15 patients that are confirmed or suspected of prostate cancer with two studies each. We used a main architecture of U-Net with batch normalization tested with different encoders, varying data image augmentation combinations, and hyperparameters adopted from various published frameworks to validate which combination of parameters work best for this dataset. The best performing framework was able to achieve a Dice score of 0.47 (0.44-0.49) which is comparable to previously published studies. The results from this study can be objectively compared and improved with further studies whereas this was previously not possible.

Keywords—Convolutional neural networks; binary semantic segmentation; prostate cancer; computer vision; deep learning

I. INTRODUCTION

Prostate cancer (PCa) is the 3rd most diagnosed and the 8th leading cause of death among all cancers; this constitutes to a 7.3% incidence rate and 3.8% mortality rate from 2020 worldwide cancer cases [1].

While the Prostate-Specific Antigen (PSA) test remains to be an effective test at detecting prostate cancer [2], approximately 40% from this screening method were found to be an occurrence of overdiagnosis [3]. This increases the risk of overtreatment leading to unnecessary procedures which yielded conflicting results in terms of benefit [4].

Recent developments in multiparametric magnetic resonance imaging (mpMRI) have provided a reliable non-invasive screening process for detecting clinically significant cancer with great specificity [5], [6] while being non-inferior to a

systematic biopsy [7]. This allows the lesion to be classified in a more specific manner through objective metric scoring measures such as the Prostate Imaging and Reporting Archiving Data System (PI-RADS) [8]. However, the process for scoring requires a qualified professional to observe various images and manually assess the presence and severity of the lesion. It is also worth noting that due to the subjectivity of the assessment, results may vary for different professionals.

Various convolutional neural network (CNN) algorithms have allowed applications in MRI images specific to PCa through prostate organ segmentation and volume estimation, lesion detection, and lesion segmentation [9]. These studies explore the viability of creating an aid for professionals to use as basis and potentially lessen the subjective component of the assessment. But in training and comparing results, the ground-truth is set forth by the professionals' assessment which poses the problem of a standardized ground-truth.

The QIN-PROSTATE-Repeatability (QPR) Dataset [10] is a publicly available annotated dataset. This dataset includes mpMRI images of 15 patients of two studies each with confirmed or suspicion of prostate cancer. These images can be utilized as input and ground-truth.

This study aims to create a pipeline to execute the task of prostate lesion detection and segmentation from an ensemble of frameworks from recent CNN studies to be applied on the QPR dataset for validation.

II. STATEMENT OF THE PROBLEM

Results from mpMRI images need to be assessed by a qualified professional (e.g. trained radiologist). The procedure remains to be subjective [6] and may vary from person-to-person. The Prostate Imaging and Reporting Archiving Data System (PI-RADS) provides a systemic scoring for image interpretation and lesion detection [8] but does not completely eliminate the subjectivity of human interpretation.

There have been various studies involving the implementation of CNN to prostate mpMRI images [9]. However, most of the datasets used are not publicly available. Moreover, the ground-truth for various studies involving CNN applications for PCa also varies depending on the qualified professional assigned for the assessment. This results in a lack of stan-

standardization. The results from these studies also could not be objectively compared, reproduced, nor improved.

III. SCOPE AND LIMITATIONS

The study focused on PCa specifically found in the peripheral zone (PZ) only. About 70% of all PCa are found to be in the PZ having the most amount of prostatic glandular tissue [11]. Patients whose lesions were not found within the PZ were not considered. For sequences and views, only the apparent diffusion coefficient (ADC) map was considered. In PI-RADS scoring for PZ PCa, ADC along with diffusion-weighted imaging (DWI) images are used as references for scoring while dynamic contrast-enhanced (DCE) images are used to distinguish between PI-RADS 3 and 4 having T2-Weighted images used as a supplementary [12]. The DICOM files acquired from the QPR dataset for this study is limited to the ADC map only as the DWI images do not contain any available annotated lesion segmentation. However, these images are closely related wherein the ADC map removes the T2-weighting aspect inherent to the DWI. T2-Weighted images were also not considered as these are used as supplementary in PZ PI-RADS scoring.

IV. REVIEW OF RELATED LITERATURE AND STUDIES

PCa biomedical images are not only scarce and hard to obtain, but they require a lot of resources to manually annotate. While this is the avenue that most studies implement, this introduces variability among datasets. "An overview of publicly available patient-centered prostate cancer datasets" is a paper that summarizes all of publicly available patient-centered PCa datasets with the goal of providing researchers an avenue to select the appropriate dataset needed for their specific field of study [13]. Among the list of datasets within the article, under the imaging category, only the QIN-PROSTATE Repeatability (QPR) dataset had annotated images.

Data image augmentation is a technique used to expand the quantity of images by altering existing images from a dataset. This has been shown to prevent over-fitting and improve the overall accuracy while also being more advantageous to weight decay and dropout which both require fine-tuning of parameters [14]. Isensee et al. achieved the highest score among participants that utilized the U-Net architecture and 2nd place overall for the multi-class brain-tumor segmentation from MRI in the Brain Tumor Segmentation (BraTS) 2018 challenge [15]. This was achieved by using the baseline U-net model while focusing on aggressive data augmentation.

For training modern deep neural networks, it was shown that best results were consistently obtained through smaller batch sizes (2,32) [16]. This was further validated with an experiment on the effects of different batch sizes on a histopathology dataset [17]. Kandel and Castelli ran their model on both Adam and SGD optimizers with a learning rate (LR) set to 1×10^{-4} and 1×10^{-3} . The best AUC was achieved with a batch size of 16, Adam optimizer, and LR set at 1×10^{-4} .

The U-Net architecture showcased in a paper published in 2015 by Ronneberger et al. proposed a model that can be trained with limited images offset by data augmentation [18]. It tackled the main issues presented with working with medical data such as scarcity of an annotated dataset and the

importance of proximal location assessment. Advancements in CNN have allowed the option of combining U-Net with a different backbone for the encoder such as ResNet as well as the inclusion of batch normalization.

Multiple studies have applied U-Net on prostate-related tasks. Three U-Net models were applied to prostate MRI in a study by Bardis et al. in segmenting the prostate, PZ, and TZ separately [19]. The ground-truth was set by a radiologist and achieved Dice scores of 0.94, 0.91, and 0.76 for the prostate, TZ, and PZ segmentation respectively. A paper published in 2019 by Yoon et al. [20] used a CNN pipeline for segmenting the prostate organ, lesion detection, and then make a PI-RADS scoring. The study utilized U-Net for prostate organ segmentation then used R-CNN for lesion detection and segmentation. Moreover, a single board-certified radiologist was used as the ground truth for the manual lesion segmentation. The study achieved lesion segmentation with a Dice score of 0.76. The study by Sanford et al. published in 2020 was a development study that used CNN with the goal of predicting PI-RADS classification [21]. The lesions were segmented and bounded by a professional radiologist which was then the input for the CNN model. A study by Youn et al. published in 2021 [22] explored the viability of using deep learning algorithms for PI-RADS scoring. The study reaffirmed that at varying levels of experience of professional radiologists, the assessment would also vary. The study utilized a deep-learning based software called Prostate AI version 1.2.1 which is currently not available for commercial use.

Specific to lesion segmentation, Liu et al. implemented fuzzy Markov random fields and attained a Dice score of 0.62. A pathologist was used as the baseline for ground-truth and the PZ was manually outlined to be used for segmentation [23]. Kohl et al. used U-Net implemented with adversarial network and achieved a Dice score of 0.41. They used a radiologist for this study to establish their ground-truth. [24]. Dai et al. implemented Mask R-CNN and achieved a Dice score of 0.46 while using a clinician to establish their ground-truth [25]. These studies all have varying ways of establishing their ground-truth and the results show that lesion segmentation remains to be an area with promise for improvement.

V. METHODOLOGY

A. Image Dataset

The relevant DICOM files were acquired through the QPR dataset [10] which includes segmented mpMRI images of 15 patients with two studies per patient done two months apart. Images extracted that appear to be completely black were removed.

3D Slicer, an open source image computing platform developed for image analysis and visualization [26], was used to view the DICOM files. Within 3D Slicer, the ADC map with their corresponding segmentations were extracted. For each extracted image, the lesion segmentation was set to red within 3D Slicer. This is to maintain a high contrast of the lesion from the original grayscale image to assist in creating the mask.

Even if the patient has a confirmed lesion in the PZ, the lesion can only be seen during specific frames in the ADC sequence. Specifically, only 14.98% of the total images

have the lesion present in them. Only images with the lesion showing was used. The summary of images with lesion and the distribution from the total images can be seen in Table I.

TABLE I. PERCENT DISTRIBUTION OF IMAGES WITH LESION

Total Images	With Lesion	Distribution
434	65	14.98%

The ADC maps are available in grayscale of dimensions 272x672 and was cropped into 256x256. Using OpenCV and HSV threshold, the grayscale images with red lesion segmentations were transformed to images with binary masking having a white mask for the lesion on top of a black background. These masks served as the ground-truth for model training.

The Albumentations library [27] was used to implement the various data augmentations. To assess the effect of varying augmentation techniques for the segmentation model, we trained the model with varying levels of augmentation. The augmentations are categorized as the Isensee et al., and extended realistic augmentations.

The following augmentations were adopted from the Isensee et al., (2018) paper:

- 1) Horizontal Flip - This flips the image horizontally on the y-axis. This particular augmentation is applicable for the prostate as the original MRI scans are symmetric in nature as opposed to medical images wherein regional location is critical (e.g. images with the heart on the left side of an image).
- 2) Rotate - This rotates the image randomly in degrees within a lower and upper threshold. The threshold was set at -45 to 45 as to maintain realistic scenarios for mpMRI prostate scans (e.g. It would be unlikely to have a scan that would be 90 degrees).
- 3) Random Sized Crop - This crops the image and scales it back to its original dimensions. The minimum height was set at 162 and the maximum at 192. This allowed the PZ to be captured regardless of where the cropping would occur. This would then be scaled back to 256x256.
- 4) Random Gamma - This applies a random gamma pixel-wise adjustment on the image. This augmentation technique is viable for the prostate mpMRI scans caused by varying equipment used by different hospitals.
- 5) Elastic Transform - This applies a more liberal distortion to the image. This can simulate the varying transformations that naturally occur within the prostate.

Other realistic augmentation techniques were implemented to the dataset. These are augmentations that are realistic scenarios for variations in mpMRI scans.

- 1) Brightness, (BC) - This alters the image's brightness and contrast. This accounts for the variation in the equipment used.
- 2) Blur - This blurs the input image using a median filter with a random aperture linear size. This accounts

for the variation in quality of scans from different equipment.

- 3) Grid Distortion (GD) - Random distortions are applied per grid width and height with a maximum magnitude. This accounts for the patient's natural movement during breathing as well as expansion and contraction of body parts such as the rectum.

B. Segmentation

Due to similarities in the dataset and problem being tackled, we chose U-Net as the main architecture for this study. The flexible architecture also allowed us to modify the encoder with ResNet. The architecture comprises of two major segments: the encoding path which consists of four down-convolutions of 2x2 max pooling and a decoding path which is a set of four 2x2 up-convolutions. Batch normalization was applied before each activation. The γ and β initializers were set to their default values of 1 and 0.

For the model parameters, we used an Adam optimizer with batch size set to 16 and learning rate set at 1×10^{-4} . The initial epoch was set at 300. For the image sampling, we used a train-test-validation split of 70-15-15.

To avoid overfitting the model, EarlyStopping was added to the training on the validation loss metric with a patience of 30 epochs. This meant that if validation loss did not decrease for 30 straight epochs, training will prematurely terminate and not continue to train for the remaining epochs.

A larger learning rate could possibly result in non-convergence of the model. This was mitigated by adding ReduceLROnPlateau which decreases the learning rate if there is no improvement on the validation loss with a patience of 20 epochs. The maximum decreased learning rate was set at 1×10^{-7} with a reduction factor of 0.1.

Dice score (F1 Score) is a segmentation performance metric that compares the similarity of the predicted mask with the ground-truth mask. This is calculated by having double the intersection of the pixels of the predicted and ground-truth mask divided by the total number of pixels of the predicted mask and the ground-truth mask as shown in (1). The lesion segmentation performance of the model was measured with the average Dice score for the test images.

$$Dice = \frac{2|A \cap B|}{|A| + |B|} \quad (1)$$

VI. RESULTS AND DISCUSSION

Different encoders and model variations were applied to the dataset with Isensee augmentations applied. The results can be seen in Table II.

TABLE II. SUMMARY OF SCORES FOR DIFFERENT MODELS

Model + Backbone	Dice
U-Net	0.39
U-Net + ResNet34	0.36
U-Net + SE-ResNet152	0.30
U-Net + SE-ResNet18	0.26
U-Net + ResNet152	0.26
U-Net + Attention	0.06

The baseline U-Net still outperformed the other variations. The addition of Attention was also not beneficial to this dataset. The decrease in scores when the model gets more complicated could be attributed to the low quantity of images in the dataset. This further validated the statement from the Isensee et al. paper that the generic U-Net architecture can be competitive in segmentation given a proper framework [15].

The model was trained on all possible combinations of Isensee (base augmentation), random brightness and contrast (BC), blur, and grid distortion (GD) augmentations to the base U-Net. The effects of adding augmentations to the base U-Net can be seen in Table III.

TABLE III. SUMMARY OF SCORES FOR DIFFERENT AUGMENTATIONS

Augmentations	Dice
Isensee	0.392
Isensee + BC	0.411
Isensee + Blur	0.466
Isensee + GD	0.467
Isensee + BC + Blur	0.416
Isensee + BC + GD	0.411
Isensee + Blur + GD	0.256
Isensee + BC + Blur + GD	0.403

Adding realistic augmentations improved the overall score compared to the baseline. However, the combination of using blur and GD together did not result in an increase in score. We believe that the generated training set from the combination of blur and GD augmentations became too distant from the features that were present within the original images while the BC augmentations were not enough to significantly alter them.

The highest Dice score of 0.467 was achieved with Isensee + GD augmentations followed closely by the Isensee + blur augmentations with a Dice score of 0.466. To verify the performance of the framework with Isensee + GD and Isensee + Blur augmentations, each model was trained thrice. Each cycle had new sets of training augmentations with randomized rotations and distortion values fit within the range and tested on the same test images. Dice scores from the Isensee + GD and Isensee + blur runs can be seen in Table IV and Table V, respectively. The results show that the Isensee + GD runs were more consistent than the Isensee + blur runs and implies that the more aggressive augmentation works better for this particular dataset.

TABLE IV. COMBINATION OF ISENSEE AND GD DICE SCORE

Dice 1	Dice 2	Dice 3	Average
0.47	0.44	0.49	0.47

TABLE V. COMBINATION OF ISENSEE AND BLUR DICE SCORE

Dice 1	Dice 2	Dice 3	Average
0.47	0.37	0.40	0.41

The average Dice score of the Isensee + GD model was then compared to previously done studies. This can be seen in

Table VI. For this comparison, only the segmentation results that had a similar approach and methodology were considered. The result from the Liu et al. paper [23] was not considered since their methodology included a preliminary process of manually outlining the PZ while only considering said pixels for segmentation.

TABLE VI. SUMMARY OF SCORES COMPARED TO LITERATURE

Model	Dice
Mask R-CNN (Yoon et al., 2019)	0.76
U-Net in this study	0.47
Mask R-CNN (Dai et al., 2020)	0.46
U-Net (Kohl et al., 2017)	0.41

While this comparison involved studies that were established using different ground-truths, the aim was to have a more standardized comparison with this framework with potential areas for improvement.

VII. CONCLUSION

In this study, we provided a repeatable framework for prostate lesion segmentation that can be improved and compared with future studies. We used the ADC map and isolated the images that contained lesion as the input for the model trained using various encoders and augmentation combinations. The baseline U-Net with batch normalization trained on images augmented with a combination of Isensee (horizontal flip, random rotation, random sized crop, random gamma, elastic transform) and grid distortion augmentations with batch size of 16 and LR set at 1×10^{-4} using Adam optimizer for Dice loss performed best and achieved an average Dice score of 0.47 (0.44-0.49). Furthermore, the QPR dataset shows promise in being a viable standardized dataset for future testing and benchmarking as shown by the comparison of results to other published studies.

VIII. RECOMMENDATIONS FOR FUTURE WORK

Due to hardware limitations, the study only implemented a hold-out method. However, it is worth considering to implement a k-fold cross-validation technique for performance metrics evaluation and fine-tuning of parameters. Moreover, other models with different encoders could be considered. For the dataset, new augmentation techniques and various combinations may be further explored. Lastly, the use of other mpMRI views aside from the ADC map could be looked into.

REFERENCES

- [1] Hyuna Sung, Jacques Ferlay, Rebecca L. Siegel, Mathieu Laversanne, Isabelle Soerjomataram, Ahmedin Jemal, and Freddie Bray. Global cancer statistics 2020: Globocan estimates of incidence and mortality worldwide for 36 cancers in 185 countries. *CA: A Cancer Journal for Clinicians*, 71(3):209–249, 2021.
- [2] C Tempany, P Carrol, and M Leapman. The role of magnetic resonance imaging in prostate cancer. *UpToDate. Waltham (MA): UpToDate*, 2018.
- [3] Fritz H Schröder, Jonas Hugosson, Monique J Roobol, Teuvo LJ Tammela, Marco Zappa, Vera Nelen, Maciej Kwiatkowski, Marcos Lujan, Lissa Määttänen, Hans Lilja, et al. The european randomized study of screening for prostate cancer—prostate cancer mortality at 13 years of follow-up. *Lancet*, 384(9959):2027, 2014.

- [4] Ian E Haines and George L Gabor Miklos. Prostate-specific antigen screening trials and prostate cancer deaths: the androgen deprivation connection. *Journal of the National Cancer Institute*, 105(20):1534–1539, 2013.
- [5] Jared S Winoker, Peter A Pinto, and Ardeshir R Rastinehad. Mri to guide biopsies or avoid biopsies? *Current opinion in urology*, 28(6):522–528, 2018.
- [6] Sangeet Ghai and Masoom A Haider. Multiparametric-mri in diagnosis of prostate cancer. *Indian journal of urology: IJU: journal of the Urological Society of India*, 31(3):194, 2015.
- [7] Martin Eklund, Fredrik Jäderling, Andrea Discacciati, Martin Bergman, Magnus Annerstedt, Markus Aly, Axel Glaessgen, Stefan Carlsson, Henrik Grönberg, and Tobias Nordström. Mri-targeted or standard biopsy in prostate cancer screening. *New England Journal of Medicine*, 385(10):908–920, 2021.
- [8] Andrei S Purysko, Ronaldo H Baroni, Francesco Giganti, Daniel Costa, Raphaële Renard-Penna, Chan Kyo Kim, and Steven S Raman. Pi-rads version 2.1: a critical review, from the ajr special series on radiology reporting and data systems. *American Journal of Roentgenology*, 216(1):20–32, 2021.
- [9] Michelle D Bardis, Roozbeh Houshyar, Peter D Chang, Alexander Ushinsky, Justin Glavis-Bloom, Chantal Chahine, Thanh-Lan Bui, Mark Rupasinghe, Christopher G Filippi, and Daniel S Chow. Applications of artificial intelligence to prostate multiparametric mri (mpmri): Current and emerging trends. *Cancers*, 12(5):1204, 2020.
- [10] Andriy Fedorov, Michael Schwier, David Clunie, Christian Herz, Steve Pieper, Ron Kikinis, Clare Tempny, and Fiona Fennessy. An annotated test-retest collection of prostate multiparametric mri. *Scientific data*, 5(1):1–13, 2018.
- [11] Guan Huang, Gerald Lebovic, and Paraskevi A Vlachou. Diagnostic value of ct in detecting peripheral zone prostate cancer. *American Journal of Roentgenology*, 213(4):831–835, 2019.
- [12] Jeffrey C Weinreb, Jelle O Barentsz, Peter L Choyke, Francois Cornud, Masoom A Haider, Katarzyna J Macura, Daniel Margolis, Mitchell D Schnall, Faina Shtern, Clare M Tempny, et al. Pi-rads prostate imaging-reporting and data system: 2015, version 2. *European urology*, 69(1):16–40, 2016.
- [13] Tim Hulslen. An overview of publicly available patient-centered prostate cancer datasets. *Translational Andrology and Urology*, 8(Suppl 1):S64, 2019.
- [14] Alex Hernández-García and Peter König. Further advantages of data augmentation on convolutional neural networks. In *International Conference on Artificial Neural Networks*, pages 95–103. Springer, 2018.
- [15] Fabian Isensee, Philipp Kickingereder, Wolfgang Wick, Martin Bendzus, and Klaus H Maier-Hein. No new-net. In *International MICCAI Brainlesion Workshop*, pages 234–244. Springer, 2018.
- [16] Dominic Masters and Carlo Luschi. Revisiting small batch training for deep neural networks. *arXiv preprint arXiv:1804.07612*, 2018.
- [17] Ibrahem Kandel and Mauro Castelli. The effect of batch size on the generalizability of the convolutional neural networks on a histopathology dataset. *ICT express*, 6(4):312–315, 2020.
- [18] Olaf Ronneberger, Philipp Fischer, and Thomas Brox. U-net: Convolutional networks for biomedical image segmentation. In *International Conference on Medical image computing and computer-assisted intervention*, pages 234–241. Springer, 2015.
- [19] Michelle Bardis, Roozbeh Houshyar, Chanon Chantaduly, Karen Tran-Harding, Alexander Ushinsky, Chantal Chahine, Mark Rupasinghe, Daniel Chow, and Peter Chang. Segmentation of the prostate transition zone and peripheral zone on mr images with deep learning. *Radiology: Imaging Cancer*, 3(3):e200024, 2021.
- [20] Choongheon Yoon, Jasper Van, Michelle Bardis, Param Bhatte, Alexander Ushinsky, Justin Glavis-Bloom, Chanon Chantaduly, Daniel S Chow, Roozbeh Houshyar, and Peter Chang. Automated prostate lesion detection and pi-rads assessment with deep learning., 2019.
- [21] Thomas Sanford, Stephanie A Harmon, Evrim B Turkbey, Deepak Kesani, Sena Tuncer, Manuel Madariaga, Chris Yang, Jonathan Sackett, Sherif Mehralivand, Pingkun Yan, et al. Deep-learning-based artificial intelligence for pi-rads classification to assist multiparametric prostate mri interpretation: A development study. *Journal of Magnetic Resonance Imaging*, 52(5):1499–1507, 2020.
- [22] Seo Yeon Youn, Moon Hyung Choi, Dong Hwan Kim, Young Joon Lee, Henkjan Huisman, Evan Johnson, Tobias Penzkofer, Ivan Shabunin, David Jean Winkel, Pengyi Xing, et al. Detection and pi-rads classification of focal lesions in prostate mri: Performance comparison between a deep learning-based algorithm (dla) and radiologists with various levels of experience. *European Journal of Radiology*, 142:109894, 2021.
- [23] Xin Liu, Deanna L Langer, Masoom A Haider, Yongyi Yang, Miles N Wernick, and Imam Samil Yetik. Prostate cancer segmentation with simultaneous estimation of markov random field parameters and class. *IEEE Transactions on Medical Imaging*, 28(6):906–915, 2009.
- [24] Simon Kohl, David Bonekamp, Heinz-Peter Schlemmer, Kaneschka Yaqubi, Markus Hohenfellner, Boris Hadaschik, Jan-Philipp Radtke, and Klaus Maier-Hein. Adversarial networks for the detection of aggressive prostate cancer. *arXiv preprint arXiv:1702.08014*, 2017.
- [25] Zhenzhen Dai, Eric Carver, Chang Liu, Joon Lee, Aharon Feldman, Weiwei Zong, Milan Pantelic, Mohamed Elshaikh, and Ning Wen. Segmentation of the prostatic gland and the intraprostatic lesions on multiparametric magnetic resonance imaging using mask region-based convolutional neural networks. *Advances in radiation oncology*, 5(3):473–481, 2020.
- [26] Steve Pieper, Michael Halle, and Ron Kikinis. 3d slicer. In *2004 2nd IEEE international symposium on biomedical imaging: nano to macro (IEEE Cat No. 04EX821)*, pages 632–635. IEEE, 2004.
- [27] Alexander Buslaev, Vladimir I Iglovikov, Eugene Khvedchenya, Alex Parinov, Mikhail Druzhinin, and Alexandr A Kalinin. Albumentations: fast and flexible image augmentations. *Information*, 11(2):125, 2020.

Methods and Directions of Contact Tracing in Epidemic Discovery

Mohammed Abdalla¹

Faculty of Computers and Artificial
Intelligence, Beni-Suef University, Egypt

Amr M. AbdelAziz²

Faculty of Computers and Artificial
Intelligence, Beni-Suef University, Egypt

Louai Alarabi³

Department of Computer Science, Umm
Al-Qura University, Mecca, Saudi Arabia

Saleh Basalamah⁴

Department of computer Engineering, Umm
Al-Qura University, Mecca, Saudi Arabia

Abdeltawab Hendawi⁵

Department of Computer Science and Statistics
at the University of Rhode Island, USA

Abstract—The contact tracing process is a mitigation and monitoring strategy that aims to capture infectious diseases to control their outbreak in a practical time. Various applications have been proposed and developed contact tracing process; most of these applications utilize the smartphone technologies to record all movements of contacts and send notifications to the expected infected ones, either high-risk or low-risk. On the other side, several challenges limit the functionality of contact tracing applications and processes; these limitations include (1) privacy concerns, (2) lack to fully identify contacts, and (3) delays in identification. In this paper, we survey the functionality of the contact tracing process, how its works, open directions and challenges, applications, and its domain of use.

Keywords—Contact tracing; routes analysis; epidemic discovery; big spatial health applications

I. INTRODUCTION

In December 2019, the world would witness an unprecedented outbreak disease struck Wuhan's city, China [1]. This mysterious disease reveals itself to the globe as Coronavirus disease 2019 (COVID-19). This contagious disease dramatically spread and affected millions of people world wide [2]. This threat leads the World Health Organization (WHO) to trigger an international emergency warning to this unprecedented virus [3]. At the time of writing this paper, WHO reported that the number of people lost their lives is over 500 thousand, and over 10 million others are still struggling and fighting for their survival. This virus is extremely infectious, where it can easily pass from person to person. Hence, to cope with the coronavirus's spread, authorities around the world implemented lockdown measures for months. However, these measurements have significantly affected global economic and social activity.

Governments started to find alternatives to ease the socio-economic catastrophes, the authorities have gradually started to partially lift the lockdowns. However, they are still struggling to find efficient techniques to monitor the mobility of potentially COVID-19 infected patients and who have been in contact with a virus infected person. Since people in close contact with someone who is infected with the virus are at higher risk of becoming infected themselves, and of potentially further infecting others, closely monitoring these contacts can prevent further transmission of the virus. This process of this monitoring is known as contact tracing.

The contact tracing process is a mitigation and monitoring strategy that aims to capture infectious diseases to control their outbreak in adequate time. The contact tracing process's main objective is to prevent the onward transmission of infectious diseases by examining the infected individuals and then identifying and examining each individual's contacts. Contacts are defined as all individuals who made direct physical connections to the infected ones; thus, all next-generation suspected cases will be controlled. Various applications have been proposed and developed to serve this process, the majority of these applications utilize the smartphone technologies to record all contacts mobility and send notifications to the expected infected ones, either high-risk or low-risk. On the other side, several challenges limit the functionality of contact tracing applications and processes. These limitations include (1) privacy concerns, (2) lack to fully identify contacts, and (3) delays in identification.

In this paper, we survey the functionality of the contact tracing process, its mechanisms, open directions, challenges, applications, and its domain of use. The survey reviews an extensive collection of models adopted based on the contact tracing process output and serves this domain. Mainly, the contribution of this paper is presenting an integrated view of the contact tracing process as a whole, which will help the researchers understand the functions of the process, identify the challenges and open issues, and inspire them to develop new applications, methods, and models in this domain.

The articles mentioned in the survey have been carefully collected to reflect the impact of applying contact tracing in controlling the spread of epidemics. The main keywords in the search have been formalized to select articles that focus on the definition of contact tracing, the applications of contact tracing in epidemics, the usage of contact tracing to developing statistical models that can predict the spread of the epidemic, and the technologies of contact tracing. These keywords include contact tracing, epidemics, Covid-19, infectious diseases, and epidemic models. The targeted articles have been published between 2003 and 2020. Also, publishers with high reputation have been targeted, such as IEEE, Springer, BMC, and journals of medical internet research (JMIR).

The rest of the paper is organized as follows. Section II presents the standard definitions of contact tracing according to

different perspectives. Section III highlights the importance of contact tracing and main applications that use contact tracing. Section V tries to shed the new directions of contact tracing and the main challenges that face these directions. Section VI presents the typical models that have proposed to simulate the outbreak of epidemics and the impact contact tracing in preventing the spread of epidemics.

II. DEFINITION OF CONTACT TRACING

This section explores several definitions of the contact tracing process and highlights the different functions that must exist in this process.

In [4], authors define the COVID-19 contact tracing as the process that controls and manages the prevention of the onward transmission of COVID-19 disease by accurately determine and evaluate individuals that had direct physical contact with COVID-19 patient during the past period.

In [5], the authors define the contact tracing process, as the strategies that ensure and confirm the monitoring and controlling of the infectious disease. In [6], [7] authors define the contact tracing process is the process of following and capturing the course of infectious disease, this process starts from investigating the diagnosed cases that confirm their infection to all other individuals that were in physical contact with the patients in the recent past. In [8], authors define contact tracing as an essential procedure needed to fight the outbreak of infectious diseases; like the COVID-19 epidemic.

In [9], the authors define the contact tracing as a process of following up with the contacts that recently reacts with infected people physically. Also, the authors considered the contact tracing process as a mitigation methodology to controls the spread of infectious diseases by identifying, examining, and taking precautions the next-generation cases in a timely fashion.

In [10], the authors define the contact tracing process as a robust disease control strategy that contains and controls the disease by preventing and reducing the disease from transmissions from individual to another. In this regard, this strategy is working by following up infected cases reported, and suspected ones, then isolate them. In addition to, tracing all contacts that come into close physical contacts with these cases; either infected or suspected. Fig. 1 presents the contact tracing process. This process traces all contacts that deal with an infected patient. Then, the process categorizes these contacts into two categories: (1) infected and (2) not infected. After that, the infected patients are classified into two categories: (1) high-risk contacts; which are contacts that are exposed to death and need special care, and (2) low-risk contacts.

III. IMPORTANCE AND APPLICABILITY

This section presents the importance of contact tracing in preventing the spread of epidemics and recent applications of this technique.

Authors in [11], [12], [13] explore various methods for contact tracing including pairwise-approximation and fully random simulations methods to tackle and investigate the infected and suspicious cases. Therefore, these methods start by examining the network of contacts that belongs to the

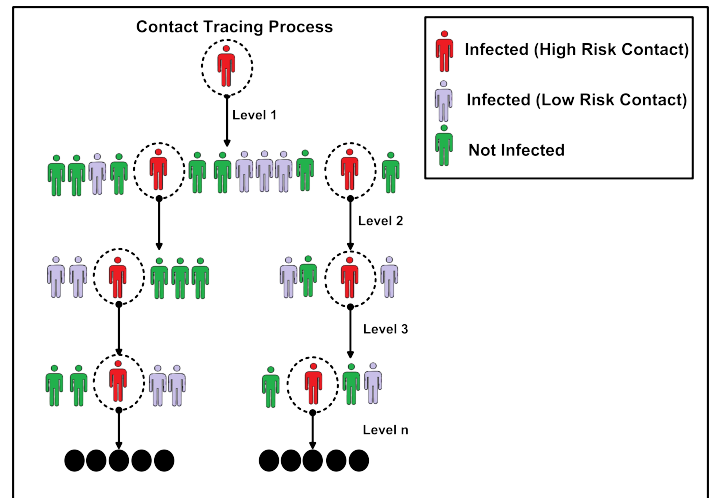


Fig. 1. Contact Tracing Process

infected and suspicious cases. Particularly, This research focus on the significance of studying well the disease-transmission pathways for each person and how to model the contact tracing approaches accurately based on disease-transmission pathways information. In the end, results show that there is a strong relationship between the accuracy of modeling the contact tracing and reproductive ratio of the disease by alert and deal with the infected and suspicious cases by either immediate treatment or isolation.

In [4], the authors highlight and investigate community surveillance roles and guidelines to reduce and prevent the spread of COVID-19 disease. Besides, the authors study how to apply the contact tracing and quarantine for COVID-19. Overall, the spread of COVID-19 disease from individual to another through nasal or oral spray or exhalation or cough of COVID-19 infectious persons. The authors mentioned the importance and criticality of contact and this for performing the quarantine in a good manner and timely fashion. Additionally, the authors classified the contacts that deal with a COVID-19 infectious human into two categories: (1) high-risk contacts, and (2) low-risk contacts. The high-risk contacts are persons that made direct physical contact with COVID-19 infected person or live with the with COVID-19 infected person in the same house. The lower cases are persons that are with COVID-19 infected persons in the same workplace or same environment or travel with the patient through any means of transportation such as; train or bus. Furthermore, the authors highlight the significance of quarantine to prevent and limit the spread of COVID-19 disease, quarantine is the process that restricts the movement of individuals that deal with COVID-19 patients in the past period. The quarantine duration of the COVID-19 identified by the World Health Organization is 28 days. Finally, the authors mentioned challenges that limit the contact tracing process in general. These challenges include: (1) the tracing difficulty of contacts who are traveled via bus or train or any other means of transportation, (2) the inability to track and remember all contacts that deal with COVID-19 patient in the last 14 days, (3) it is difficult to track and find all people that directly contact the COVID-19 patient, particularly if the patient visited wide gatherings like marriage or religious

gatherings or market, and (4) the common fear between the health care staff to trace contacts, as they are thinking they will become infected.

In [14], the authors studied the Ebola virus and concluded that the virus is transmitted from individual to another via physical interaction with the infected patients such as body fluids. Additionally, authors in [15], introduced a study that investigates the Ebola virus contact tracing process, this study aims to perform surveillance for persons that were in exposure for infected patients during 21 days. For this purpose, in [9], the authors propose and develop an Ebola transmission model that adopted contact tracing. This model investigates the perfect timing for contact tracing actions to be done. Also, the authors differentiate the contact tracing delays into three types: (1) initiation delays, (2) contact identification delays, and (3) hospitalization delays. Results showed that quick contact identification and hospitalization can lead to decreasing the spread of the epidemic to 50% compared to delayed identification. In this regard, the authors concluded that starting the contact tracing process at an early stage is a must.

In [16], [17], the authors shed light on using social networking sites (SNS) for contact tracing activities. Additionally, the authors ask the official health sectors and specialized authorities to adopt SNS for controlling and monitoring the evolution of diseases. The authors pay the attention for using SNS because SNS is considered as a significant source of data and knowledge, also the growing popularity of these sites and enriching on several easy portable devices such as; smartphones and tablets, this will provide great opportunities for health sectors to perform the contact tracing in a well-manner.

Mainly, the contact tracing process depends on studying well the contacts network of proximity interactions between persons during the Epidemic period spread. Several attempts have been done to obtain the knowledge of these physical interactions to be investigated. For example in [18], authors get a large scale Facebook data of the interaction between individuals, authors investigate this data to clarify and present the disease dynamics in the community. Additionally, in [19] authors employ wireless sensors to capture face-to-face interactions. In [20], authors describe these attempts as a costly and resources used can be not available or limited to be owned for the majority of people. For this purpose, authors a model for contact tracing based on a mobile phone, and describe the mobile phone as a powerful tool to capture communication traces for the contacts with the proximity interactions. Authors conclude that effective contact tracing can significantly reduce the impact of the Embedic outbreak. Moreover, the contact tracing becomes more effective at the beginning of the Embedic outbreak because the number of contacts that need to be traced is much less than contacts need to be traced after the Embedic evolution. Finally, the authors mentioned that the use of mobile phones to trace contacts can be a valuable option to stop the Embedic outbreak.

In [21], the authors purpose two models for reducing the spread of HIV, these models consider the stochastic screening and contact tracing strategies, these models include (1) differential infection model (DI), and (2) staged-progression model (SP). Overall, the DI model focuses on the individuals'

differences during the disease transmission, while the SP model focuses on more on the time differences for the same infected person. The authors define the stochastic screening and contact tracing as intervention strategies to fight the spread of disease transmission. In this study, the authors formulate various formulas to generate reproductive numbers and identify the equilibrium points during the embedic outbreak. Then, the results produced from either the stochastic screening or the contact tracing are compared in both models. Results showed that in the DI model, the contact tracing strategies are powerfully effective tools to determine and bound the superspreaders of the diseases, and therefore this can assist in reducing the final size of the embedic. This feedback is also consistent with the feedback provided in the following studies [22], [23], [24], [25]. On the other side, the authors highlight that in the SP model the stochastic screening is more effective and has a large effect than contact tracing in limiting and slowing the spread of the disease. Finally, the authors conclude that the effectiveness of the intervention strategies can be determined mainly by the underlying reasons for disease transmission.

In [26], [27] authors presents that due to the incubation long period of Ebola virus, which is 11 days, a massive number can come to physical contacts with infected case and the spread of the disease will grow rapidly. For this purpose, in [10], the authors propose a model that incorporates the contact tracing for prediction and monitoring the reproduction rates for Ebola infection diseases. The purposed model considers various control scenarios, to perform a perfect analysis for Ebola disease characteristics and investigates how these characteristics affect on the effectiveness of the contact tracing process to control the Ebola outbreak. These characteristics include: (1) Ebola disease characteristics, (2) surveillance protocols for infected and suspected cases, (3) reporting time of the infected cases, (4) epidemic incubation period, and (5) intervention time to handle reported cases. Additionally, the authors purpose formula to highlights the critical cases from contacts that are traced to obtain reproduction number (R_e) less than one. The formula is as follows: $R_e = k \frac{1-q}{q} + k_m$, where k represents the count of infected contacts that determined in the second iteration per un-traced contacts identified in the first phase, k_m represents the count of infected contacts that determined in the second iteration per traced contacts identified in first phase, $\frac{1-q}{q}$ is the odds that probabilities that the reported contact is not traced. To conclude, R_e production number represents the observation of reported cases per number of contacts traced (observed cases/total number of contacts traced).

Table I summarizes the main papers with their purposes and description in this direction.

IV. DOMAINS OF USE AND APPLICATIONS

This section presents the importance of contact tracing in preventing the spread of epidemics and recent applications of this technique.

To construct an effective contact tracing application that can identify contacts of infected individuals, the system should be loaded over handheld devices. Mobile phones are used by most people, so developing a mobile application for individuals will enable authorities to effectively identify contacts. Fig.

TABLE I. IMPORTANCE AND APPLICABILITY (SUMMARY)

Paper	Rational	Information Sources	Study Selection	Keywords	Year
Contact tracing and disease control	introduced methods for contact tracing including pairwise approximation and fully random simulations methods	Sexual relationships in Manitoba, Canada that contain sexual partnerships between 82 connected individuals together with the presence of chlamydia and gonorrhea infection (A model to predict the spread)	Importance and applicability of Contact racing	tracing efficiency; transmission networks; pairwise approximations; stochastic simulation	2003
Modeling the impact of random screening and contact tracing in reducing the spread of HIV	Purposed two models for reducing the spread of HIV, these models consider the stochastic screening and contact tracing strategies, these models include (1) differential infection model (DI), and (2) staged-progression model (SP)	Synthetic dataset	Importance and applicability of Contact racing	AIDS; Mathematical modeling; Epidemic modeling; Screening; Contact tracing; Reproductive number; Endemic equilibrium; Sensitivity	2003
A high resolution human contact network for infectious disease transmission	Employed wireless sensors to capture face-to-face interactions	US 2009 absentee data because of the influenza (H1N1). The dataset covers CPIs of 94% of the entire school population, representing 655 students, 73 teachers, 55 staff, and 5 other persons, and it contains 2,148,991 unique close proximity records	Importance and applicability of Contact racing	disease dynamics; network topology; public health; human interactions	2010
Dynamics and control of diseases in networks with community structure	Investigated a large-scale Facebook data to clarify and present the disease dynamics in the community	Synthetic dataset	Importance and applicability of Contact racing	dynamics of infectious diseases spread; immunization interventions	2010
1) Social Networking Sites as a Tool for Contact Tracing: Urge for Ethical Framework for Normative Guidance. 2) Using Social Networking Sites for Communicable Disease Control: Innovative Contact Tracing or Breach of Confidentiality?	Investigated using social networking sites (SNS) for contact tracing activities to control and monitor the evolution of diseases.	None	Importance and applicability of Contact racing	disease control and surveillance; Social media applications	2013
Modeling contact tracing in outbreaks with application to Ebola	Proposed a model that incorporates the contact tracing for prediction and monitoring the reproduction rates for Ebola infection diseases.	Data collected from the West Africa (Sierra Leone and Guinea) Ebola outbreak	Importance and applicability of Contact racing	Contact tracing; Ebola; Epidemiology; Mathematical modeling	2015
Quantifying the impact of early-stage contact tracing on controlling Ebola diffusion	Developed an Ebola transmission model that adopted contact tracing. This model investigates the perfect timing for contact tracing actions to be done	Synthetic dataset (A model to predict the spread)	Importance and applicability of Contact racing	Contact tracing; Ebola; activity-driven network; compartmental model; epidemic model	2018
Contact Tracing and Quarantine for Covid 19: Challenges in community surveillance	Highlighted and investigated community surveillance roles and 109 guidelines to reduce and prevent the spread of COVID-19 disease	None	Importance and applicability of Contact racing	Quarantine; Contact Tracing	2020

2 shows an example of an effective framework that uses an application loaded over individuals' mobile phones. An individual mobile application can automatically connects with another application in case they are in a specific distance. This can identify the contacts of each individual. The application sends these data to the server to store such data. In case an individual is identified as infected with Covid-19, the contacts of this person will be notified to isolate themselves and to have medical attention. Also, the systems gives the statistics of the spread of Covid-19 for decision makers to decide whether to force quarantine, isolation, or lock-down for specific regions, identified by the application.

On 20-March-2020, the government of Singapore published an application named TraceTogether which uses Bluetooth to track and trace contacts. The TraceTogether application works when two users who use the application are nearby, and a user alerts that he is a COVID-19 patient, the application starts to notify the Ministry of Health to identify the network of contacts logged to be near to them. Additionally, the application communicates with those contacts and reports them with the proper follow-up actions [28].

In [29], the authors utilize the power of smartphone application technology and develop a novel peer-to-peer smartphone application that performs the contact tracing process effectively. The authors sheds the light on the significance of the contact tracing as it is an essential process that restricts the transmission of COVID-19 pandemic. The main objective behind this study is developing a smartphone application that performs the contact tracing and similarly preserves user privacy by not collecting any personal information or any location data. The method adopted in this study that performs contact tracing with preserving the privacy mainly depends on a novel data structure named transmission graph, which

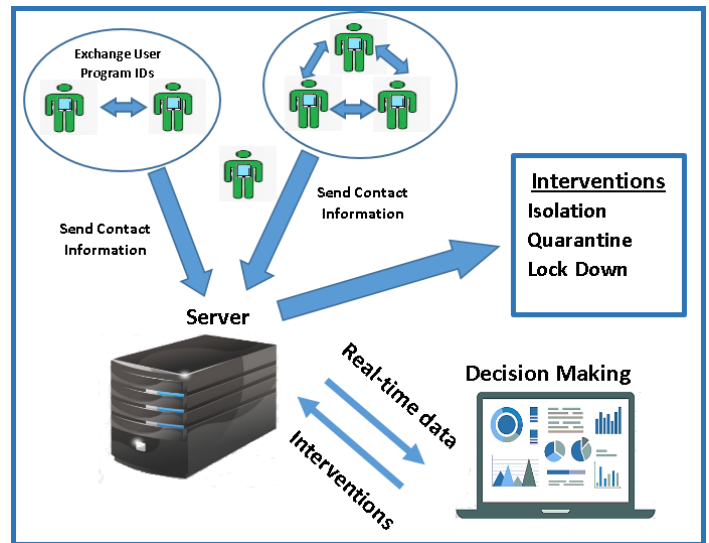


Fig. 2. A Depiction of Contact Tracing Framework based on Real-Time Monitoring of Individuals

consists of nodes and edges, the nodes represent the contact points between the persons, while the edges represent the transmission vectors between contact points. Specifically, each contact point is represented by a node and captures the physical interaction between two or more persons at a particular time and location. Finally, the transmission graph has created a network of interactions between persons and preserves user privacy at the same time.

In [30], [6], the authors describe several procedures for performing the contact tracing process. These procedures include (1) first-order tracing, (2) single-step contact tracing, (3)

iterative contact tracing, and (3) retrospective contact tracing. The first order tracing procedure identifies the individuals that make an immediate direct physical connection with the patient, these individuals require self-isolation and specific medical care handle. Furthermore, the first order tracing procedure does not care about tracing the contacts of the contacts and leave this to happen in the next step “second-order” after the first order has been done successfully. The single-step contact tracing procedure identifies all individuals that contact with the confirmed infected person, and all these individuals are considered as infected, also their contacts are identified and the procedure continues. The Iterative contact tracing procedure, this procedure performs diagnostic tests for all individuals in an iterative way, these tests include symptom screening, and the purpose of this is to discover the infection before its occurrence. The last type is retrospective contact tracing procedure, it follows the same steps of the single-step or iterative procedures, additionally, it investigates the recent past of the infected person and operates in a reverse way to identify all individuals that the patient makes a contact with them. The retrospective contact tracing procedure aims to identify who was the infected person by the disease.

The Australian government has released an application named COVIDSafe. This application aims to control the spread of COVID-19 epidemic, by communication with the expected individuals who are exposures for the infection. the application notifies these individuals and alerts them to take all required immediate precautions [31], [32].

The following studies[5], [29], [33] summarized that the effectiveness of the contact tracing approaches must consider the following: (1) contacts identification, (2) contact notifications, (3) utilizing mobile applications technology for performing automatic contact recording of the movements and direct physical communications, and (4) narrowcast communication via messages.

During the period between 2014 and 2016, the Ebola virus disease (EVD) outbreak has a dangerous effect on the following countries in Africa; such as Liberia, Guinea, and Sierra Leone. As a result, 28,000 cases are reported as infected and above 11,000 deaths as per the study introduced in [34]. In [35], authors developed a smart-phone application named Ebola Contact Tracing application (ECT app), to monitor and trace infected individuals by Ebola in Sierra Leone. This application is integrated with an alert system to report symptomatic individuals and their districts to the response center.

This study [36], discusses how contact tracing is employed by the Liberian authorities to prevent the spread of Ebola during (2014-2015). They uses the official reports of number of cases, provided by the counties, to evaluate the efficiency of the method. Authors build a model that classified the cases into: potential cases to represent cases that had previous symptoms, recovered or died, and Positive Predictive Value (PPV) to represent traced contacts. It applies their analysis over 25,830 contact tracing records of suspected cases during the period from June 4, 2014 to July 13, 2015. These cases represent 26.7% of total EVD cases. Contact tracing showed its ability to detect 3.6% of new cases during its operational time.

Authors in [37] study the spread of the severe acute respiratory syndrome (SARS) in Hong Kong in 2003. The

authors apply contact tracing over index-cases that have been in hospitals based on questionnaires. Nurses run these questionnaires to identify contacts of index-cases to inform them to isolate themselves and to have medical care. Also, the questionnaires were used to identify the transmission paths to index-cases. Analyzing the questionnaire results allows the authorities to cluster index-cases using multiple criteria, such as demographic (housing and working locations), age (friends and schools), and workplaces. These data allow the authorities to locate the hot-spots to quarantine them and to prevent the spread of the epidemic.

Authors provide a case study analysis for the spread of the Severe Acute Respiratory Syndrome CoronaVirus 2 (SARS-CoV-2) in Wuhan, China. The paper analyzes a dataset of patients in the Shenzhen provenance to identify the efficacy of applying the contact tracing in preventing the spread of the epidemic. The study focuses on applying the contact tracing to detect transmission paths and prevent new infections. The Shenzhen Center for Disease Control and Prevention (CDC) applies contact tracing to track the contacts of infected individuals. Results shows that the prediction of new cases based on contact tracing was very similar to those cases found through traditional surveillance and from hospital records [38].

In [39], the authors provide a study for different non-pharmaceutical interventions (NPI) to mitigate and suppress the spread of Covid-19 epidemic. They classifies the NPIs into two classes: mitigation and suppression interventions. The mitigation interventions aim to reduce the need of healthcare system by protecting people from severe infection. The mitigation interventions include: isolation, quarantine, and social distancing. The suppression aims to minimize the number of new cases and keeps that situation for a long time. Examples of the suppression interventions are: school and university closure and social distancing for long time. The authors provide a study for the impact of each NPI on the spread of Covid-19 and the impact of combining multiple interventions. The authors conduct the study over data collected from China, United Kingdom, and United States. Results show that combining multiple interventions can have a substantial impact in preventing the spread of the epidemic. These interventions affect the economy of the countries on both short and long terms, so countries should choose carefully the suitable NPIs for them.

A. Sexual Disease Monitoring

The Human Immunodeficiency Virus (HIV) is a serious virus that damages the immune system. It damages and kills the CD4 cells, which makes the patient body vulnerable to get infected with different infections and cancers. The HIV can be transmitted through body fluids, such as blood, semen, breast milk, and rectal fluids [40]. The early detection of the HIV gives a higher probability of patients to get treated.

Dennis et al. [40] propose an integration between contact tracing and phylogenetics to control the spread of HIV in North Carolina (NC). They initiate a routine public screening test for HIV. These tests allow the authorities to identify individuals with acute HIV infection (AHI) [41]. After identifying the infected individuals, they will be investigated to construct networks of suspicious individuals to identify transmission paths and warn infected contacts to get medical care. This

enables the authorities to control the outbreak of the epidemic. Contact tracing enables the authorities to construct a spatiotemporal clustering of infected individuals, which resulted into identifying the increase of AHI among Men that had sex with Men in two regions in NC.

Lin et al. [42] proposed another application of contact tracing in controlling the spread of sexual diseases. They employ contact tracing to identify infected individuals with HIV in Taizhou Prefecture, Zhejiang Province in China. They study collected the data in the period (2008–2010). Data were gathered from volunteers that were subjected to the HIV test. Individuals that have HIV-positive are subjected to surveys to construct a network about their contacts using surveys. The study enables the authorities to identify 463 new HIV-infected cases. The contact tracing starts with 398 as index-cases to construct their network using surveys. Tracking the 398 index-cases results into tracking 1,403 sexual contacts. The early identification of HIV-infected individuals enables the authorities to inform suspicious individuals to have medical care, which decrease the number of late diagnosis that may acquire immunodeficiency syndrome (AIDS).

B. Social Networking

In [43], the authors discuss how to construct an efficient model that can simulate the dynamics of an epidemic spread in large social contact networks (SCN)s. Large SCNs need huge computation capability to run the simulation algorithms. The authors proposed applying parallel models to simulate huge SCNs to get results in an affordable time. The authors use the high performance computing clusters to run their model in parallel. Running algorithms in parallel needs the SCN to be partitioned. The main problem of SCNs is the distribution skew in these networks as there are some nodes, which are connected to multiple nodes (hubs) and normal nodes connected to a small number of nodes. To partition the hubs, the authors propose splitting the hubs (malls and metros) into fixed splits to run the algorithm over each split in parallel. Also, they propose partitioning the agents (visitors) to mimic the dynamics of the network. The authors test their method over multiple datasets and result show the efficiency of the method.

In [44] the authors propose constructing a model that can simulate the spread of an epidemic. They focus on the social networks of contacts and how can an epidemic propagate in such networks. They consider the heterogeneity of social networks and do not give the same probability to all social network members to get infected at the beginning of the epidemic. They consider the “crowding” or “protection effect” in their model. They develop an Infected-Susceptible-Infected-Recovered (ISIR) model to simulate the spread of an epidemic. Results show that only networks with multiple links have high probability to get infected. Also, they evaluate four immunization strategies and find that the high-degree set and critical set immunization strategies are the best techniques to prevent the spread of the epidemic.

Mainly, to ensure that all contact tracing applications working effectively, they must pass through four stages. Fig. 3 summarize these stages.

The next section describes the new directions of applying contact tracing and the challenges that faces these directions.

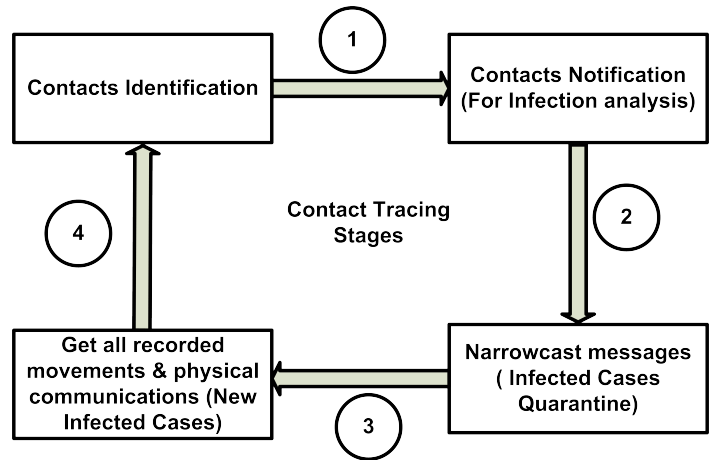


Fig. 3. Contact Tracing Stages

V. OPEN DIRECTIONS AND CHALLENGES

This section highlights the main challenges of applying contact tracing for real-life applications.

In [8], the authors highlight the privacy concerns as the constraints that limit the functionality of contact tracing applications, and they analyze the implications of these concerns and discussed the ways of improvements. The authors summarized the privacy concerns as following: (1) protection of contacts privacy from the snoopers, (2) ensuring the privacy from contacts, and (3) ensuring the privacy from authorities.

The authors in [45], [46], [47], discussed as classified the challenges in contact tracing process as follows: (1) Inability to fully identify contacts, (2) the lack in reporting systems that adopted on papers, (3) incomplete contact lists, (4) inefficiencies in data collection, (5) transcription errors during the early-stage of the contact tracing, specifically during the contact’s identification, and (6) delays in identification and isolation of the suspected individuals from these contacts.

In [48], the authors highlight some challenges that face the contact tracing process such as; the need to involve large labor to trace the contacts efficiently and accurately. For example, (1) the Canadian Health Sector opens the door for a volunteer workforce to perform the tasks of contact tracing and other relevant tasks [49], (2) In South Korea, the governments employed a huge number of medical staff and other workers at the peak of COVID-19 disease outbreak to trace contacts and controls this epidemic [50].

In [51], the authors classify the individual contact tracing methods into two categories: static and dynamic contact tracing methods. Fig. 4 shows a categorization of contact tracing devices according to contact tracing methods. The authors consider that static individual contact tracing to include: questionnaires and surveys. Although these methods have been effective in dealing with sexual diseases [52], [52], they have certain drawbacks that can be summarized into: (1) not giving an online assessment of the epidemic spread, (2) need of labor force (3) time consuming, (4) need to find contacts one by one. Online versions of these methods, such as online questionnaires and online surveys have been proposed to provide an online assessment of the spread of an epidemic [53], [54],

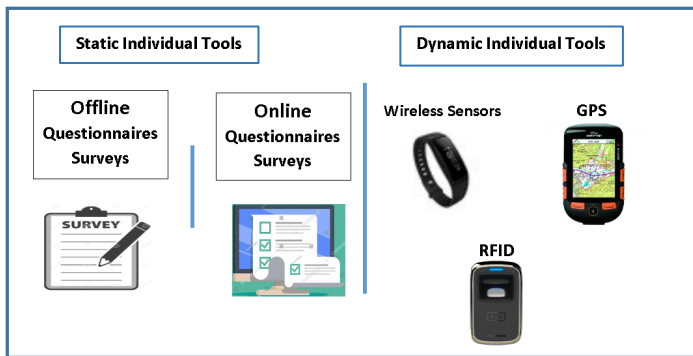


Fig. 4. Categorization of Devices used in Contact Tracing

[55]. Despite of their advantages, the authors consider that the online methods still do not give a real-time information for decision makers and users sometimes fill them with incorrect information [56]. Considering the dynamic contact tracing methods, the authors focus on mobile applications, wireless sensors, and GPS [57], [58], [59], [60], [61], [62], [63]. They identify different challenges of these methods. Considering mobile applications, the battery of mobiles represent a great challenge as it has a limited life-time. The wearable sensors are expensive to track a huge number of people and participants do not like to wear them because of privacy issues. The Radio Frequency Identification Devices (RFID)s have a limited range for sending and receiving data. Even the Global Positioning Systems (GPS) devices have limitations as they are not effective to be used in closed areas, such as schools and universities [51].

VI. MODELS

This section discusses how researchers can construct models that can describe the spread of epidemics and the impact of applying contact tracing in limiting the outbreak of epidemics.

Models are developed to predict the spread of epidemics, they can be classified into two categories: deterministic and stochastic models [64]. The deterministic model is formulated as a system of differential equations, which generates the same solution each time in case the conditions and parameters' values are the same. The main advantage of deterministic models is their ability to show how the initial conditions can affect over the behavior of the model. A stochastic model can be constructed based on differential equations. It has at least one probabilistic parameter, which makes the output changes each time the model is run [64].

In [65], the authors introduce conceptual models to simulate the outbreak of COVID-19 in Wuhan, these models consider the reaction of human behaviors and actions needed from the governments. The objective of these models is to distinguish and understand the future trends of the outbreak and predict the future ratio. Finally, these models can catch the COVID-19 paths and logged all anticipated future trends of the outbreak. The authors use important information about the COVID-19 to build the model correctly. These information include incubation time, time from onset to discharge from hospital or die. Fig. 5 shows the important stages of each

person when he gets an infection until he becomes non-infectious again.

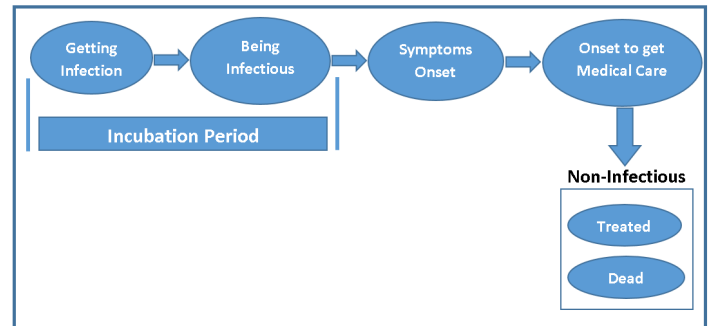


Fig. 5. Infection Progress of Covid-19

In [66], the authors propose an epidemiological model that depicts reality. This objective of this model is to describe and control the evolution of the diseases and predict individuals with high-risk exposures. The authors admit that the leverage of this model lies in generating the prediction results within a short time and how this will be useful in emergency response systems.

In [67], the authors propose an epidemiological model named "Susceptible-Infectious-Recovered-Dead (SIDR)" model, this model is designed to monitor the evolution of COVID-19 epidemic. The monitoring of the COVID-19 epidemic outbreak is done by providing and predicting the following estimates: (1) estimates about infection cases, (2) estimates about mortality, (3) estimates about recovery rates, and (4) estimates about basic reproduction number. These estimates are generated daily. The objective behind this model is to expect the outbreak evolution of the COVID-19 epidemic three weeks ahead before it happens.

In [30], the authors investigate how the effectiveness of contact tracing can limit the evolution of infectious diseases. The authors investigate a contact tracing model that is appropriate for most infections. Several cases are investigated using this model and result concluded that: (1) the variability of detection time leads to an effective contact tracing, and (2) the iterative tracing can increase the effectiveness, and (3) in general, there is no specific formula to predict the proportion that will be traced.

In [68], the authors focus on constructing a stochastic network-based simulator that can predict the spread of the Covid-19 epidemic. They develop the simulator based on the data gathered from Republic of Kazakhstan, taken as case study. The simulator is based on Susceptible-Exposed-Infectious-Recovered (SEIR) model to represent the transition of individuals among different infection states. To verify the efficacy of the model, authors run the simulator over data collected from Lombardy (Italy). Different parameters have been tuned and the simulator was helpful in predicting the duration and number of infected individuals during the spread of the epidemic.

In [69], the authors develop a stochastic model based on the susceptible-infectious-removed to discuss the effect of applying contact tracing to mitigate the spread of the epidemic.

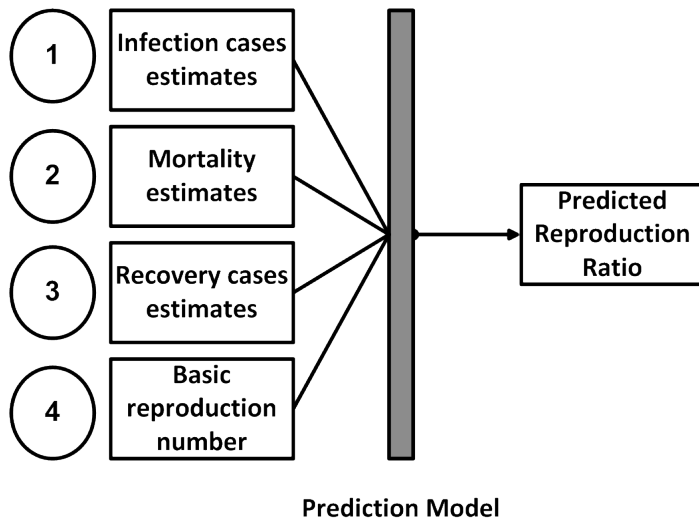


Fig. 6. Prediction Models (Reproduction Ratio)

They represent the spread of the epidemic in social networks with a graph. This facilitates the task of contact tracing in identifying new suspicious individuals. The model shows the effectiveness of contact tracing in stopping the exponential growth of the epidemic, especially in medium states. Also, the model shows the effectiveness of random screening of individuals in limiting the spread of the epidemic.

In [70], the authors provide a statistical model to evaluate the severity of Covid-19 based on the data collected from Wuhan, Hubei. The data was collected from national and provincial health commissions in Wuhan. They extend their work by including the data of 37 countries to study the fatality of Covid-19 in these countries. The data has been used to provide an estimation for important characteristics of the epidemic, such as time from onset to death or to discharge from hospital, and case fatality ratio. The model applies first over the data collected from China, then the model is applied over the data gathered from other countries. Results shows that the estimations generated from model were very similar to real data collected from the authorities in China and other countries.

In [64], the authors focus on developing a stochastic susceptible-infected-recovered (SIR) model that combines contact tracing to analyze the effect of contact tracing in controlling the spread of epidemics. The methods used the tree structure to simulate the spread of the epidemic. The authors derive equations that can describe the spread of the epidemic and the effect of the intervention tools over the spread rate. These equations are then applied over non-tree contact graphs.

In [71], the authors present an analysis of different models, proposed to simulate the spread of two epidemics: SARS and Middle East Respiratory Syndrome (MERS). The authors defines and discusses the important parameters that can affect on the efficiency of the models, such as the basic reproduction number, incubation period, latent period and infectious period. Also, they extend their work to study the effect of the intervention techniques in mitigating or stopping the spread of the epidemic, such as quarantine, isolation, and contact tracing.

Basically, the output of the contact tracing process includes the following: (1) infection cases, (2) mortality cases, and (3) recovery cases. These outputs can be considered as an input for any prediction model that anticipates the reproduction ratio of the infection. Fig. 6 concludes inputs and outputs for prediction models that try to predict the production ratio of infection.

VII. CONCLUSION

The contact tracing process is a mitigation and monitoring strategy that aims to capture infectious diseases to control their outbreak in adequate time. In this paper, we reviewed various applications developed contact tracing process, discussed in great detail the challenges that limit contact tracing applications, such as privacy concerns, lack of identifying contacts, and delays in identification fully. In this survey, we have shown how researchers can construct models that can describe the spread of epidemics and the impact of applying contact tracing in limiting the outbreak of epidemics. Finally, We have surveyed and listed open directions, applications, and its domain of use.

ACKNOWLEDGMENT

This work is supported by King Abdulaziz City for Science & Technology (KACST), Kingdom of Saudi Arabia for the (COVID-19 Research Grant Program) under Grant no. 5-20-01-007-0006.

REFERENCES

- [1] L. Li, Q. Zhang, X. Wang, J. Zhang, T. Wang, T.-L. Gao, W. Duan, K. K.-f. Tsoi, and F.-Y. Wang, "Characterizing the propagation of situational information in social media during covid-19 epidemic: A case study on weibo," *IEEE Transactions on Computational Social Systems*, 2020.
- [2] P. Jandrić, "Postdigital research in the time of covid-19," *Postdigital Science and Education*, pp. 1–6, 2020.
- [3] "World health organization," <https://www.who.int/emergencies/diseases/novel-coronavirus-2019>, 2020, accessed: 20-Apr-2020.
- [4] G. G. R. H. Ramraj and K. S. Gudogowda, "Contact Tracing and Quarantine for Covid 19: Challenges in community surveillance," *Indian Journal of Community Health*, 2020.
- [5] G. M. V.-P. B. L. M. P. H. J. A. Clennon and S. A. Ritchie, "Combining contact tracing with targeted indoor residual spraying significantly reduces dengue transmission," *Science Advances*, 2017.
- [6] K. T. D. EAMES, "Contact tracing strategies in heterogeneous populations," *Epidemiology & Infection*, 2006.
- [7] B. Armbruster and M. Brandeau, "Contact tracing to control infectious disease: When enough is enough," *Health Care Management Science*, 2007.
- [8] H. C. D. Ippolito and Y. W. Yu, "Contact tracing mobile apps for covid-19: Privacy considerations and related trade-offs," *ArXiv*, 2020.
- [9] N. M. S. T. F. C. Scoglio and F. D. Sahneh, "Quantifying the impact of early-stage contact tracing on controlling ebola diffusion," *Mathematical Biosciences and Engineering*, 2018.
- [10] C. B. H. Gulbudak and G. Webb, "Modeling contact tracing in outbreaks with application to ebola," *Journal of Theoretical Biology*, 2015.
- [11] K. T. D. Eames and M. J. Keeling, "Contact tracing and disease control," *The Royal Society*, 2003.
- [12] L. A. S. B. A. Hendawi, , and M. Abdalla, "Traceall: A real-time processing for contact tracing using indoor trajectories," *Information*, vol. 12, pp. 2078–2489, 2021.
- [13] L. A. S. B. M. Abdalla and A. Hendawi, "A holistic spatial platform for managing infectious diseases, case study on covid-19 pandemic," *2021 IEEE International Conference on Big Data (Big Data)*, pp. 3721–3730, 2021.

- [14] M. G. Dixon and I. J. Schafer, "Ebola viral disease outbreak - west africa," *MMWR Morb Mortal Wkly Rep*, 2014.
- [15] E. G. by the World Health Organization, "Implementation and management of contact tracing for ebola virus disease," <https://www.cdc.gov/vhf/ebola/pdf/contact-tracing-guidelines.pdf>, accessed: 2015.
- [16] K. T. M. M. H. H. L. T. Y. Chow and C. Seng, "Using social networking sites for communicable disease control: Innovative contact tracing or breach of confidentiality?" *Public Health Ethics*, 2014.
- [17] M. L. S. B. O. R. M. Kretzschmar and J. E. van Steenberg, "Social networking sites as a tool for contact tracing: Urge for ethical framework for normative guidance," *Public Health Ethics*, 2013.
- [18] M. Salathe and J. JH, "Dynamics and control of diseases in networks with community structure," *PLoS Comput Biol*, 2010.
- [19] M. S. K. M. L. J. L. P. F. MW, "A high resolution human contact network for infectious disease transmission," *Proceedings of the National Academy of Sciences*, 2010.
- [20] M. C. Katayoun Farrahi, Remi Emonet, "Epidemic contact tracing via communication traces," *PLoS ONE*, 2014.
- [21] J. M. H. J. Li and E. A. Stanley, "Modeling the impact of random screening and contact tracing in reducing the spread of hiv," *Mathematical Biosciences*, 2003.
- [22] S. E. L. V. J. S. D. J. W. M. M. B. K. K. Lewis and G. G. Koch, "Results of a randomized trial of partner notification in cases of hiv infection in north carolina," *New England J. Med.* 326, 1992.
- [23] C. Norwood, "Mandated life versus mandatory death: New yorks disgraceful partner notification record," *J. Commun. Health* 20, 1995.
- [24] R. GW and W. JM, "Contact tracing to control the spread of hiv-reply," *JAMA The Journal of the American Medical Association*, 1988.
- [25] R. F. W. C. W. H. S. L. H. S. T. L. C. B. Q. J. L. J. M. Artzrouni and R. L. Parker, "Contact tracing to identify human immunodeficiency virus infection in a rural community," *JAMA The Journal of the American Medical Association*, 1998.
- [26] W. E. R. Team, "Ebola virus disease in west africa the first 9 months of the epidemic and forward projections," *N Engl J Med*, 371(16):1481-95, 2014.
- [27] C. F. S. R. R. M. Anderson and N. M. Ferguson, "Factors that make an infectious disease outbreak controllable," *Proceedings of the National Academy of Sciences of the United States of America*, 2004.
- [28] S. G. Blog, "Help speed up contact tracing with tracetogether," <https://www.gov.sg/article/help-speed-up-contact-tracing-with-tracetogether>, accessed: March 2020.
- [29] T. M. Y. B. M. Lechrich and R. Sahyouni, "Peer-to-peer contact tracing: Development of a privacy-preserving smartphone app," *JMIR Mhealth Uhealth*, 2020.
- [30] D. K. C. Fraser and H. Heesterbeek, "The effectiveness of contact tracing in emerging epidemics," *PLoS ONE*, 2020.
- [31] A. G. D. of Health: COVIDSafe App, "Covidsafe app," <https://www.health.gov.au/resources/apps-and-tools/covidsafe-app>, accessed: April 2020.
- [32] M. Woodley, "Racgp releases covidsafe factsheet. royal australian college of general practitioners," <https://www1.racgp.org.au/newsgp/professional/racgp-releasescovidsafe-fact-sheet?feed=RACGPnewsGPArticle>, accessed: May 2020.
- [33] H. S. Maghdid and K. Z. Ghafoor, "A smartphone enabled approach to manage covid-19 lockdown and economic crisis," *Social and Information Networks*, 2020.
- [34] W. H. Organization, "Contact tracing during an outbreak of ebola virus disease," *Geneva: WHO*, 2014.
- [35] L. O. D. N. H. M. M. F. E. C. F. M. A. A. T. A. J. D. A. Ross and H. A. Weiss, "Use of a mobile application for ebola contact tracing and monitoring in northern sierra leone: a proof-of-concept study," *BMC Infectious Diseases volume*, 2019.
- [36] K. C. S. C. A. C. S. W. T. N. T. A. N. E. E. L. H. J. L. D. H. PetersID and M. Altmann, "Contact tracing performance during the ebola epidemic in liberia, 2014-2015," *Neglected Tropical Diseases*, 2018.
- [37] C. A. D. A. C. G. G. M. L. A. J. H. C. F. S. R. L. J. A.-R. L.-M. H. T.-Q. T. P. C. K.-P. C. T.-H. L. L.-Y. T. T. T. S.-H. L. J. H. B. K. E. M. C. L. N. M. Ferguson and R. M. Anderson, "Epidemiological determinants of spread of causal agent of severe acute respiratory syndrome in hong kong," *THE LANCET*, 2003.
- [38] T. M. J. L. Qifang Bi, Yongsheng Wu, Shujiang Mei, Chenfei Ye, Xuan Zou, Zhen Zhang, Xiaojian Liu, Lan Wei, Shaun A Truelove, Tong Zhang, Wei Gao, Cong Cheng, Xiujuan Tang, Xiaoliang Wu, Yu Wu, Binbin Sun, Suli Huang, Yu Sun, Juncen Zhang and T. Feng, "Epidemiology and transmission of covid-19 in 391 cases and 1286 of their close contacts in shenzhen, china: a retrospective cohort study," *The Lancet Infectious Diseases*, 2020.
- [39] A. Okolie and J. Muller, "Report 9: Impact of non-pharmaceutical interventions (npis) to reduce covid-19 mortality and healthcare demand," *Imperial College*, 2020.
- [40] A. M. D. D. K. P. R. B. S. B. V. M. A. C. J. K. J. S. C. Walworth and P. A. Leone, "Integration of contact tracing and phylogenetics in an investigation of acute hiv infection," *Sexually Transmitted Diseases*, 2018.
- [41] B. G. B. M. R. J.-P. R. D. M. M. N. C. M. J.-G. B. R. T. D. R. J. B. R. L. M. L. C. T. H. Charest and M. A. Wainberg, "High rates of forward transmission events after acute/early hiv-1 infection," *The Journal of Infectious Diseases*, p. 951-959, 2007.
- [42] H. L. N. H. Y. D. D. Q. W. Z. X. L. T. Zhang and R. Detels, "Tracing sexual contacts of hiv-infected individuals in a rural prefecture, eastern china," *Public Health*, 2012.
- [43] Y. W. W. C. Z. L. W. J. TAN and X. HOU, "Efficient parallel simulation over large-scale social contact networks," *Transactions on Modeling and Computer Simulation*, 2019.
- [44] Z. Z. H. W. C. WANG and H. FANG, "Modeling epidemics spreading on social contact networks," *EMERGING TOPICS IN COMPUTING*, 2020.
- [45] M. L. S. I. N. L. G. Y. R. J. L. T. E. E. H. O. D. BA, and O. Morgan, "Ebola surveillance -guinea, liberia and sierra leone," *MMWR Suppl*, 2016.
- [46] I. OS, "Learning from the challenges of ebola virus disease contact tracers in sierra leone," *The Pan African Medical Journal*, 2015.
- [47] S. J. Z. E. R. C. B. A. C. K. C. M. D. A. G. A. D. RS and L. A, "Introduction of mobile health tools to support ebola surveillance and contact tracing in guinea," *Global Health: Science and Practice*, 2015.
- [48] B. N. W. S. Armstrong and C. del Rio, "Contact tracing for covid-19: An opportunity to reduce health disparities and end the human immunodeficiency virus/aids epidemic in the united states," *Clinical Infectious Diseases*, 2020.
- [49] G. of Canada, "Covid 19: How you can make a difference," <https://www.canada.ca/en/public-health/services/diseases/2019-novel-coronavirusinfection/make-a-difference.html>, accessed: April 2020.
- [50] E. COVID-19 National Emergency Response Center, K. C. f. D. C. Case Management Team, and Prevention, "Coronavirus disease-19: Summary of 2,370 contact investigations of the first 30 cases in the republic of korea," *Osong Public Health Res Perspect*, 2020.
- [51] H. C. B. Y. H. PEI and J. LIU, "Next generation technology for epidemic prevention and control: Data-driven contact tracking," *IEEE Access*, 2018.
- [52] N. M. R. L. S. A. M. G. P. C. F. Garcia and B. F. Polk, "Hiv-1, sexual practices, and contact with foreigners in homosexual men in colombia, south america," *Johns Hopkins University*, pp. 330-334, 1990.
- [53] —, "Prevalence of unsafe sexual behavior among hiv-infected individuals: The swiss hiv cohort study," *Journal Acquired Immune Deficiency Syndromes*, vol. 33, pp. 494-499, 2003.
- [54] C. D. S. C. M. B. D. C. S. C. J. Fejsa and D. Durrheim, "Insights from flu-tracking: Thirteen tips to growing a web-based participatory surveillance system," *JMIR Public Health Surveill.*, vol. 3, 2017.
- [55] C. D. D. D. J. F. L. F. S. C. E. T. d'Espaignet and F. Tuyl, "Flutracking: A weekly australian community online survey of influenza-like illness in 2006, 2007 and 2008," *Communicable Diseases Intelligence Quarterly Report*, vol. 33, 2009.
- [56] G. K. L. A. M. S. F. B. R. A. C. M. E. E. K. D. J. J. Heederik and A. Huss, "Mobility assessment of a rural population in the netherlands using gps measurements," *International Journal of Health Geographics*, 2017.

- [57] E. Yoneki, "Fluphone study: Virtual disease spread using huggle," *ACM Mobile Communication Workshop Challenged Network*, 2011.
- [58] E. Yoneki and J. Crowcroft, "Epimap: Towards quantifying contact networks and modelling the spread of infections in developing countries," *Ad Hoc Networks*, vol. 13, 2014.
- [59] M. S. M. K. J. W. L. P. L. M. W. Feldman and J. H. Jones, "A high-resolution human contact network for infectious disease transmission," *Proceedings of the National Academy of Sciences of the United States*, vol. 107, pp. 22 020–22 025, 2010.
- [60] D. B. S. Bruin and A. K. Bregt, "Value of information and mobility constraints for sampling with mobile sensors," *Computers & Geosciences*, vol. 49, pp. 102–111, 2012.
- [61] K. M. J. K. P. J. G. M. TylerWard and D. S. Young, "A geophone wireless sensor network for investigating glacier stick-slip motion," *Computers & Geosciences*, vol. 105, pp. 103–112, 2017.
- [62] M. D. E. Hood and C. Connor, "Seamonster: A demonstration sensor web operating in virtual globes," *Computers & Geosciences*, vol. 37, pp. 93–99, 2011.
- [63] M. A. J. R. J. A. Taboada and J. M. Cotos, "Virtual integration of sensor observation data," *Computers & Geosciences*, vol. 81, pp. 12–19, 2015.
- [64] A. Okolie and J. Muller, "Exact and approximate formulas for contact tracing on random trees," *Mathematical Biosciences*, 2020.
- [65] Q. L. S. Z. D. G. Y. L. S. Y. S. S. M. M. H. W. Y. C. W. W. L. Yang and D. He, "A conceptual model for the coronavirus disease 2019 (covid-19) outbreak in wuhan, china with individual reaction and governmental action," *international journal of infectious disease*, 2020.
- [66] H. S. Rodrigues, "Application of sir epidemiological model: new trends," *International Journal of Applied Mathematics and Informatics*, 2016.
- [67] C. A. L. R. A. Tsakris and C. Siettos, "Data-based analysis, modelling and forecasting of the covid-19 outbreak," *PLoS ONE*, 2020.
- [68] A. K. D. B. A. K. B. I. A. M. M. N. M. Lewis and H. A. Varol, "A network-based stochastic epidemic simulator: Controlling covid-19 with region-specific policies," *medRxiv*, 2020.
- [69] R. Huerta and L. S. Tsimring, "Contact tracing and epidemics control in social networks," *PHYSICAL REVIEW*, 2002.
- [70] R. V. L. C. O. I. D. P. W. C. W. N. I. G. C.-D. H. T. P. G. T. W. H. F. A. D. J. T. G. M. B. S. B. A. B. A. C. Z. C. R. F. K. G. W. G. A. H. W. H. D. L. G. N.-G. S. R. S. van Elsland, Erik Volz, Haowei Wang, Yuanrong Wang, Xiaoyue Xi, Christl A Donnelly, Azra C Ghani and N. M. Ferguson, "Estimates of the severity of coronavirus disease 2019: a model-based analysis," *The Lancet*, 2020.
- [71] K. O. K. A. T. V. W. H. P. E. K. Yeoh and S. Riley, "Epidemic models of contact tracing: Systematic review of transmission studies of severe acute respiratory syndrome and middle east respiratory syndrome," *Computational and Structural Biotechnology Journal*, 2019.

Emergency Decision Model by Combining Preference Relations with Trapezoidal Pythagorean Fuzzy Probabilistic Linguistic Priority Weighted Averaging PROMETHEE Approach

Xiao Yue

Chongqing Key Laboratory of Spatial
Data Mining and Big Data Integration
for Ecology and Environment,
Chongqing Iflytek Artificial Intelligence,
Chongqing Finance and Economics College,
Chongqing, 401320, China

Li Jianhui

Chongqing Finance and
Economics College, Chongqing, China
Liu Zhancen and Chen Dan
Chongqing Finance and Economics College,
Chongqing, China

Abstract—The outbreak of COVID-19 in 2019 has brought greater international attention to emergency decision making and management. Since emergency situations are often uncertain, prevention and control are crucial. For better prevent and control, according to the characteristics of emergency incidents, the paper proposes a new form of linguistic expression trapezoidal Pythagorean fuzzy probabilistic linguistic variables to express decision-making information. Next, the paper develops the operational rules, value index and ambiguity of trapezoidal Pythagorean fuzzy probabilistic linguistic variables. Then, the new trapezoidal Pythagorean fuzzy probabilistic linguistic priority weighted averaging PROMETHEE approach is introduced to aggregate the trapezoidal Pythagorean fuzzy probabilistic linguistic information combining with preference relation. Finally, an emergency decision making case of prevention of infectious diseases analysis illustrate the necessity and effectiveness of this method, the results of comparative and experimental analyses demonstrate that the constructed new trapezoidal Pythagorean fuzzy probabilistic linguistic priority weighted averaging PROMETHEE approach owns better performances in terms of effectiveness and reasonability.

Keywords—COVID-19; emergency decision model; trapezoidal Pythagorean fuzzy probabilistic linguistic variables; preference relations; PROMETHEE approach

I. INTRODUCTION

COVID-19 first appeared in Wuhan, China, on December 30, 2019. Due to its pandemic characteristics, long incubation period and strong transmission capacity, COVID-19 is now expanding globally, with more than 133.14 million people infected worldwide as of April 5, 2021, a lot of researchers have done a lot of research on this [1], [2], [3], [4]. This poses a great threat to people all over the world. After the COVID-19 incident happened, China and the international community have paid more attention to emergency management. Hence, how to choose an effective emergency response plan and organize it quickly to reduce casualties and property losses has been reconsidered by governments, public and scholars all over the world. But in real life, all kinds of sudden events occur frequently, and the evolution of abrupt events is often

uncertain. This may lead to multiple emergency scenarios. Considering the urgency of emergencies and the complexity of the matter, the emergency command department often organizes many experts from the relevant departments, and the expert may prefer to express their opinion by linguistic terms, just like [5], [6], [7], [8]. For instance, the linguistic term "good", "bad" or "very bad" can be used to express the alternative. Due to the ambiguity and complexity of human cognition, one issue of emergency decision making is how to express the experts evaluations or preference information accurately [9], [10], [11].

In several real situations, professional judgments could not be expressed and interpreted as certain qualitative numbers; In other words, data and certain numbers are insufficient for modeling the real-world systems because of ambiguity and uncertainty in the judgment of decision-makers. In previous researches on emergency management, the linguistic term set (LTS) has been introduced into various emergency decision-making processes, like [12], [13], [14]. Whereafter, Xu et al.[9] applied the probabilistic linguistic term set(PLTS) to emergency management. But the trapezoidal Pythagorean fuzzy probabilistic linguistic term set(TrPFPLTS) has not been applied to emergency management events so far, even the application of PTS to emergency management is rare. In fact, TRPFPLTS has greater flexibility and wider applicability than other PLTS or LTS. It not only allows experts to use more than one linguistic term to express their preference, but also reflects the different probability of occurrence of all possible linguistic terms. At the same time, it is more comprehensive in the expression of fuzzy information. In this study, the paper will select the TRPFPLTS to represent the fuzzy decision information and uncertainty probability of the decision makers(DMs) for the emergency event. Take prevention and control of a local outbreak of infectious diseases as an example. When an infectious disease breaks out somewhere and its source is unknown, the emergency command department invites several experts to assess and judge the infectious ways: population density, air pollution index, number of parks and entertainment equipment,

density of restaurants, density of cultural and educational centers. In different cases, the proportion of influencing factors is different, for that reason it is very necessary to introduce TRPFPLTS to represent the real situation and the behavior of DMs.

It is unlikely that a single expert will consider all aspects of infectious disease control. Multiple attribute group decision making (MAGDM) is to find a collective solution to a decision-making problem in which a group of experts express their opinions regarding multiple alternatives. However even in a friendly environment, a lot of differences across the expert group are generated inevitably, and greatly discordant opinions are aggregated and this may lead to an intermediate opinion with which no expert totally agrees. In MAGDM, the information provided by the experts has different forms. Because of the nature of infectious diseases, it is difficult for emergency response authorities to provide an accurate assessment and determine the route of transmission among the many influencing factors. Therefore, in order to determine the cause of the outbreak of the infectious disease, we introduced a preference relationship (PR) to make a pairwise comparison of the influencing factors. Because linguistic variables are the natural expressions of DMs, researchers often use linguistic preference relations (LPR) to express DMs' subjective preferences. Herrera et al. [15], Liu et al. [16], Liu et al. [17] and Dong [18] respectively apply the LPR to multi-attribute group decision making (MAGDM). Due to the neglect of the probabilistic nature of linguistic terms in DMs' judgment, the linguistic preference relation has some limitations. Hence Zhang et al. [19], [20], Alonso et al. [21], Wang et al. [22] put forward different probabilistic linguistic preference relations respectively and applied them to different fields.

It's important to find proper way to aggregate the PRs. So far, various formats of aggregation approach have been put forward to aggregate decision making preferences. Due to the increasing complexity of social problems, more and more researchers are using PROMETHEE approach to provide solutions for DMs through priority relationships, which is based on pairwise comparisons between alternatives. The PROMETHEE method is extremely useful in complex decision making processes, especially real world MAGDM problems involving human perception and subjective judgment of experts. It is worth noting that the PROMETHEE method has considerable advantages when collaboration among specialists are restricted by their distinct fields of expertise. The PROMETHEE method is a robust decision making approach since it determines the relative merits of alternatives by comparing them in pairs, rather than ranking all of them directly. This approach can avoid the round off error which may occur during data normalization. Lolli et al. [23] defined the elicitation of criteria weights in PROMETHEE based ranking methods. Gul et al. [24] proposed a fuzzy logic based PROMETHEE method for material selection problems.

From the previous research, with the diversity, complexity of the MAGDM problem, although a lot of researches on the PRs at this stage, there are still many defects:

(1) They are limited in their depiction of each person's point of view, using only a single linguistic term to express an evaluation of an object. It can be seen that due to the limited knowledge and the complexity of reality, people often carry

out the evaluation with a certain degree of uncertainty. For example, one may use "very good", "good", "somewhat good" to describe the quality of a product, rather than simply "good" or "bad".

(2) They did not fully take into account the poor structural of the information itself, and only considers the fuzziness of the MAGDM problem. Therefore, the paper have made several innovations on the basis of previous studies.

(3) When a simple aggregation operator aggregates group decision information, it retains less information and loses the original information, which seriously leads to the loss of fuzzy information.

Based on the above investigation, we've improved and expanded on previous methods. This paper makes significant contributions on the probabilistic linguistic MAGDM problems:

(1) The paper proposes a new form of linguistic expression trapezoidal Pythagorean fuzzy probabilistic linguistic variables (TrPFPLVs) and trapezoidal Pythagorean fuzzy probabilistic linguistic preference relations (TrPFPLPRs) to express decision-making information.

(2) The paper develop the operational rules, value index and ambiguity index of trapezoidal Pythagorean fuzzy probabilistic linguistic variables (TrPFPLVs).

(3) The paper introduce the new trapezoidal Pythagorean fuzzy probabilistic linguistic priority weight (TrPFPLPW) PROMETHEE approach to aggregate the trapezoidal Pythagorean fuzzy probabilistic linguistic information.

The remainder of this paper is organized as follows. Section 2 reviews the concept of linguistic term sets, probabilistic linguistic term set and probabilistic linguistic preference relationship. Section 3 proposes the TrPFPLVs and TrPFPLPRs to express the MAGDM information, and proposed the operations and operational rules of TrPFPLVs. Section 4 develops TrPFPLPWA-PROMETHEE approach to aggregate the trapezoidal Pythagorean fuzzy probabilistic linguistic information. An emergency decision making model is introduced in Section 5. Section 6 presents a case study: prevention of infectious diseases. The paper ends with some concluding remarks in Section 7.

Xiao yue

June 28, 2022

II. PRELIMINARIES

This section present some basic definitions to facilitate our presentation.

A. The Linguistic Term Sets

A linguistic value is less precise than a number, however it is closer to human cognitive process. Therefore it is used to solve uncertain problems successfully. The LTSs are used to express the DMs' opinion over the considered objects, which is initial and totally ordered. It can be defined as follows [25]:

Definition 1. Suppose that $S = \{s_i | i = -\tau, \dots, -1, 0, 1, \dots, \tau\}$ be a pre-established finite and totally ordered discrete linguistic term set, where s_i denotes the i th linguistic value of S and τ represents the cardinality of S .

In which $s_i < s_j$ iff $i < j$. Usually, in these cases, it is often required that the linguistic term set satisfies the following additional characteristics [26], [28], [27], [29]:

- (1) There is the negation operator, $Neg(\tilde{s}_i) = s_j, j = \tau - i + 1$.
- (2) The maximum operator: $Max(s_i, s_j) = s_i$ if $s_i \geq s_j$.
- (3) The minimum operator: $Min(s_i, s_j) = s_i$ if $s_i \leq s_j$.

Example 1. The set of nine terms S could be given as follows[30], [31]:

$S = \{s_{-4} = \text{extremely bad}(EB), s_{-3} = \text{very bad}(VB), s_{-2} = \text{bad}(B), s_{-1} = \text{little bad}(LB), s_0 = \text{general}(G), s_1 = \text{little good}(LG), s_2 = \text{good}(G), s_3 = \text{extremely good}(EG), s_4 = \text{perfect}(P)\}$,

B. Probabilistic Linguistic Term Sets

In LTSs, each linguistic term value is equally important by default while ignoring the preference information in group decision making. Then Pang et al. [32] defined the PLTS to solve this problem.

Definition 2. Let $S = \{s_i | i = -\tau, \dots, -1, 0, 1, \dots, \tau\}$ be a LTS, the PLTS can be defined as:

$$L(p) = \{L^{(k)}(P^{(k)}) | L^{(k)} \in S, P^{(k)} \geq 0, k = 1, 2, \dots, \#L(p)\}, \quad (1)$$

and

$$\sum_{l=k}^{\#L(p)} P^{(k)} \leq 1 \quad (2)$$

where $L^{(k)}(P^{(k)})$ denotes the k th linguistic term $L^{(k)}$ with the probability $P^{(k)}$, and $\#L(p)$ is the number of linguistic terms in $L(p)$. For the PLTS $L(p)$, let $p^{N(k)} = P^{(k)} / \sum_{k=1}^{\#L(p)} P^{(k)}$ ($k = 1, 2, \dots, \#L(p)$), then get the normalized PLTS (NPLTS), denoted as $L(p)^N = \{L^{N(k)}(p^{N(k)}) | k = 1, 2, \dots, \#L(p)\}$. The PLTS is composed of the linguistic terms and the corresponding probabilities rather than the linguistic terms only. To be concise, the elements in the PLTS, i.e., $L^{(k)}(p^{(k)})$ ($k = 1, 2, \dots, \#L(p)$), are called probabilistic linguistic elements (PLEs).

To conduct computation, some operations are defined[32]:

(1) $L(p)_1 \oplus L(p)_2 = \{L_3^{(k_3)} p_3^{(k_3)} | k_3 = 1, \dots, \#L(p)_3\}$, where $L_3^{(k_3)} = L_1^{(k_1)} \oplus L_2^{(k_2)}$, $p_3^{(k_3)} = p_1^{(k_1)} p_2^{(k_2)}$ ($k_1 = 1, \dots, \#L(p)_1; k_2 = 1, \dots, \#L(p)_2$);

(2) $\lambda L(p)_1 = \{\lambda L_1^{(k_1)} p_1^{(k_1)} | k_1 = 1, \dots, \#L(p)_1\}$.

The operational laws related to the linguistic terms in PLTS satisfy[30]:

- (1) $s_\alpha \oplus s_\beta = s_{\alpha+\beta}$, , where $\lambda \in [0, 1]$;
- (2) $neg(s_\alpha) = s_{-\alpha}$, especially, $neg(s_0) = s_0$.
- (3) $\lambda s_\alpha = s_{\lambda\alpha}$

C. Probabilistic Linguistic Preference Relations

In many MAGDM problems, the experts use the PLTSs to express their preference degrees of one alternative over another. The preference relation with the PLTSs is called PLPR. For a finite set of alternatives $X = x_1, x_2, \dots, x_n$ ($n \geq 2$), the PLPR is defined on the linguistic evaluation scale $S = \{s_\alpha | \alpha = -\tau, \dots, -1, 0, 1, \dots, \tau\}$.

Definition 3. [33]. Given a PLPR $B = (L(p)_{ij})_{n \times n} \subset X \times X$, $L(p)_{ij}$ indicates the preference degrees of the alternative x_i over x_j and $L(p)_{ij}$ satisfies the following conditions: (1) $p_{ij}^{(k)} = p_{ji}^k$, $L_{ij}^{(k)} = neg(L_{ji}^{(k)})$, $L(p)_{ii} = \{s_0(1)\} = \{s_0\}$, $\#L(p)_{ij} = \#L(p)_{ji}$; (2) $L_{ij}^k p_{ij}^k \neq L_{ij}^{(k+1)} p_{ij}^{(k+1)}$ for $i \neq j$, $L_{ji}^k p_{ji}^k \geq L_{ji}^{(k+1)} p_{ji}^{(k+1)}$ for $i \geq j$.

III. TRAPEZOIDAL PYTHAGOREAN FUZZY PROBABILISTIC LINGUISTIC VARIABLES AND TRAPEZOIDAL PYTHAGOREAN FUZZY PROBABILISTIC LINGUISTIC PREFERENCE RELATIONS

In this part, TrPFPLVs and PPLPRs are introduced.

A. Trapezoidal Pythagorean Fuzzy Probabilistic Linguistic Variables

In order to describe the uncertain, complexity and poor structural probabilistic linguistic information more accurately and completely, the paper propose TrPFPLVs to express making decision information.

Definition 4. Let $\hat{t}_k = ([s_{\varphi_{\hat{t}_k}}]; \mu_{\hat{t}_k}(x_k), \nu_{\hat{t}_k}(x_k); p_{\hat{t}_k})$ for all $k = 1, 2, \dots, n$ be a PFPLVs, where $s_{\varphi_{\hat{t}_k}}$ represents a possible value for a linguistic label, If $s_{\varphi_{\hat{t}_k}} = s_{(\alpha_k, \beta_k, \gamma_k, \theta_k)}$, that is $\hat{t}_k = ([s_{(\alpha_k, \beta_k, \gamma_k, \theta_k)}]; \mu_{\hat{t}_k}(x_k), \nu_{\hat{t}_k}(x_k); p_{\hat{t}_k})$ be the TrPFPLV. If $s_{\varphi_{\hat{t}_k}} = s_{(\alpha_k, \beta_k, \gamma_k, \theta_k)}$ and $\beta_k = \gamma_k$, which is triangle Pythagorean fuzzy probabilistic variables (TPFPVs). $\mu_{\hat{t}_k}(x_k)$ and $\nu_{\hat{t}_k}(x_k)$ represent the degrees of membership and nonmembership respectively, and satisfy $0 \leq \mu_{\hat{t}_k}(x_k) \leq 1$, $0 \leq \nu_{\hat{t}_k}(x_k) \leq 1$ and $0 \leq \mu_{\hat{t}_k}^2(x_k) + \nu_{\hat{t}_k}^2(x_k) \leq 1$. $\pi_{\hat{t}_k}^2(x_k) = 1 - \mu_{\hat{t}_k}^2(x_k) - \nu_{\hat{t}_k}^2(x_k)$ is interpreted as indeterminacy degree or a hesitancy degree. $p_{\hat{t}_k}$ indicates the degree of certainty of his/her preference for the decision problem.

Such as his/her preference can be expressed as $([\hat{s}_3]; \mu_{\hat{t}_k}(x_k), \nu_{\hat{t}_k}(x_k); 0.5)$, it can be interpreted as he/she is 50% sure that the alternative is bad in comparison with other alternative.

if a decision maker prefers the alternative, he/she will use "positive" linguistic labels, such as "bad" or "little bad", to describe his/her degree of preference. Different "positive" linguistic labels reflect different preference degrees of the DMs. Inspired by [34], [31], the TrPFPLVs set of nine terms T can be given follows:

$$\begin{aligned} \hat{T} &= \{\hat{t}_1 = ([s_0, s_1, s_2, s_3]; \mu_{\hat{t}_k}(x_k), \nu_{\hat{t}_k}(x_k); p_{\hat{t}_k}) \\ &= \text{extremely bad}(EB), \\ \hat{t}_2 &= ([s_1, s_2, s_3, s_4]; \mu_{\hat{t}_k}(x_k), \nu_{\hat{t}_k}(x_k); p_{\hat{t}_k}) \\ &= \text{very bad}(VB), \\ \hat{t}_3 &= ([s_2, s_3, s_4, s_5]; \mu_{\hat{t}_k}(x_k), \nu_{\hat{t}_k}(x_k); p_{\hat{t}_k}) \\ &= \text{bad}(B), \\ \hat{t}_4 &= ([s_3, s_4, s_5, s_6]; \mu_{\hat{t}_k}(x_k), \nu_{\hat{t}_k}(x_k); p_{\hat{t}_k}) \\ &= \text{little bad}(LB), \\ \hat{t}_5 &= ([s_4, s_5, s_6, s_7]; \mu_{\hat{t}_k}(x_k), \nu_{\hat{t}_k}(x_k); p_{\hat{t}_k}) \\ &= \text{general}(G), \\ \hat{t}_6 &= ([s_5, s_6, s_7, s_8]; \mu_{\hat{t}_k}(x_k), \nu_{\hat{t}_k}(x_k); p_{\hat{t}_k}) \\ &= \text{little good}(LG), \\ \hat{t}_7 &= ([s_6, s_7, s_8, s_9]; \mu_{\hat{t}_k}(x_k), \nu_{\hat{t}_k}(x_k); p_{\hat{t}_k}) \\ &= \text{good}(G), \\ \hat{t}_8 &= ([s_7, s_7, s_9, s_9]; \mu_{\hat{t}_k}(x_k), \nu_{\hat{t}_k}(x_k); p_{\hat{t}_k}) \\ &= \text{extremely good}(EG), \\ \hat{t}_9 &= ([s_8, s_9, s_9, s_9]; \mu_{\hat{t}_k}(x_k), \nu_{\hat{t}_k}(x_k); p_{\hat{t}_k}) \\ &= \text{perfect}(P)\} \end{aligned}$$

Inspired by Xian's work [35], the paper further propose operational laws for TrPFPLVs to facilitate the calculation.

Definition 5. Let $\hat{T} = (\hat{t}_1, \hat{t}_2, \dots, \hat{t}_n)$ be the set of all TrPFPLVs, and $\hat{t}_1 = ([s_{\alpha_1}, s_{\beta_1}, s_{\gamma_1}, s_{\theta_1}]; \mu_{\hat{t}_1}, \nu_{\hat{t}_1}; p_{\hat{t}_1})$, $\hat{t}_2 = ([s_{\alpha_2}, s_{\beta_2}, s_{\gamma_2}, s_{\theta_2}]; \mu_{\hat{t}_2}, \nu_{\hat{t}_2}; p_{\hat{t}_2})$, $\hat{t} = ([s_{\alpha}, s_{\beta}, s_{\gamma}, s_{\theta}]; \mu_{\hat{t}}, \nu_{\hat{t}}; p_{\hat{t}}) \in \hat{S}$, $\lambda, \lambda_1, \lambda_2 \in [0, 1]$, their operational laws and properties are defined as follow:

$$\begin{aligned} (1) \hat{t}_1 \oplus \hat{t}_2 &= ([s_{\alpha_1+\alpha_2}, s_{\beta_1+\beta_2}, s_{\gamma_1+\gamma_2}, s_{\theta_1+\theta_2}]; \\ &\sqrt{\mu_{\hat{t}_1}^2 + \mu_{\hat{t}_2}^2 - \mu_{\hat{t}_1}^2 \mu_{\hat{t}_2}^2}, \nu_{\hat{t}_1} \nu_{\hat{t}_2}; p_{\hat{t}_1} p_{\hat{t}_2}); \\ (2) \lambda \odot \hat{t} &= ([s_{\lambda\alpha}, s_{\lambda\beta}, s_{\lambda\gamma}, s_{\lambda\theta}]; \sqrt{1 - (1 - \mu_{\hat{t}}^\lambda)^\lambda}, \nu_{\hat{t}}^\lambda; p_{\hat{t}}); \\ (3) \hat{t}_1 \oplus \hat{t}_2 &= \hat{t}_2 \oplus \hat{t}_1; \hat{t}_1 \otimes \hat{t}_2 = \hat{t}_2 \otimes \hat{t}_1; \\ (4) \lambda \odot (\hat{t}_1 \oplus \hat{t}_2) &= \lambda \odot \hat{t}_1 \oplus \lambda \odot \hat{t}_2; \\ (5) (\lambda_1 + \lambda_2) \odot \hat{t} &= \lambda_1 \odot \hat{t} \oplus \lambda_2 \odot \hat{t}. \end{aligned}$$

In order to rank alternatives, it is necessary to consider how to compare two TrPFPLVs. Pang et al. [32] defined the comparison between PLTSs, Xian et al. [35] defined the concepts of the compare the TrPFLVs, but there is some set of information can not be compared by the TrPFPLVs. Consequently we put forward a method to compare multiple TrPFPLVs. In order to do so, in the following, we define the score of TrPFPLVs:

Definition 6. Suppose Let $\hat{t}_k = ([s_{\varphi_{\hat{t}_k}}]; \mu_{\hat{t}_k}(x_k), \nu_{\hat{t}_k}(x_k); p_{\hat{t}_k})$ for all $k = 1, 2, \dots, n$ be a TrPFPLVs, the value index of TrPFPLVs are defined as:

$$\begin{aligned} L_{\mu_i}(\varphi^+(A_i)) &= (m_1\alpha_i + m_2\beta_i + m_3\gamma_i + m_4\theta_i)\mu_i(\varphi^+(A_i)) \quad (3) \\ L_{\nu_i}(\varphi^+(A_i)) &= (m_1\alpha_i + m_2\beta_i + m_3\gamma_i + m_4\theta_i)\nu_i(\varphi^+(A_i)) \quad (4) \\ L_{\mu_i}(\varphi^-(A_i)) &= (m_1\alpha_i + m_2\beta_i + m_3\gamma_i + m_4\theta_i)\mu_i(\varphi^-(A_i)) \quad (5) \end{aligned}$$

$$\begin{aligned} L_{\nu_i}(\varphi^-(A_i)) &= (m_1\alpha_i + m_2\beta_i + m_3\gamma_i + m_4\theta_i)\nu_i(\varphi^-(A_i)) \quad (6) \\ P_{\mu_i}(\varphi^+(A_i)) &= (-m_1\alpha_i - m_2\beta_i + m_3\gamma_i + m_4\theta_i)\mu_i(\varphi^+(A_i))p(A_i) \quad (7) \\ P_{\nu_i}(\varphi^+(A_i)) &= (-m_1\alpha_i - m_2\beta_i + m_3\gamma_i + m_4\theta_i)\nu_i(\varphi^+(A_i))p(A_i) \quad (8) \\ P_{\mu_i}(\varphi^-(A_i)) &= (-m_1\alpha_i - m_2\beta_i + m_3\gamma_i + m_4\theta_i)\mu_i(\varphi^-(A_i))p(A_i) \quad (9) \\ P_{\nu_i}(\varphi^-(A_i)) &= (-m_1\alpha_i - m_2\beta_i + m_3\gamma_i + m_4\theta_i)\nu_i(\varphi^-(A_i))p(A_i) \quad (10) \end{aligned}$$

where $m_1, m_2, m_3, m_4 \in [0, 1]$, $m_1 + m_2 + m_3 + m_4 = 1$. The value of m_1, m_2, m_3, m_4 is different and they depend on the degree of preference of the DMs for MAGDM problems. $\varphi^+(A_i)$ and $\varphi^-(A_i)$ are respectively trapezoidal Pythagorean fuzzy positive dominant flow and trapezoidal Pythagorean fuzzy negative dominant flow, they are introduced in Section 4, which will not be repeated here.

On the basic of the concept of Definition 6, a method compare between two TrPFPLVs is introduced in detail.

Definition 7. Let $\hat{t}_k = ([s_{\alpha}, s_{\beta}, s_{\gamma}, s_{\theta}]; \mu_{\hat{t}_k}, \nu_{\hat{t}_k}; p_{\hat{t}_k})$, $\hat{t}_1 = ([s_{\alpha_1}, s_{\beta_1}, s_{\gamma_1}, s_{\theta_1}]; \mu_{\hat{t}_1}, \nu_{\hat{t}_1}; p_{\hat{t}_1})$, $\hat{t}_2 = ([s_{\alpha_2}, s_{\beta_2}, s_{\gamma_2}, s_{\theta_2}]; \mu_{\hat{t}_2}, \nu_{\hat{t}_2}; p_{\hat{t}_2})$ be any three TrPFPLVs.

$$E(\varphi^+(A_i)) = \rho_i L_{\mu_i}(\varphi^+(A_i)) + (1 - \rho_i) L_{\nu_i}(\varphi^+(A_i)) \quad (11)$$

$$E(\varphi^-(A_i)) = \rho_i L_{\mu_i}(\varphi^-(A_i)) + (1 - \rho_i) L_{\nu_i}(\varphi^-(A_i)) \quad (12)$$

$$E(\varphi(A_i)) = \frac{E(\varphi^+(A_i))}{E(\varphi^+(A_i)) + E(\varphi^-(A_i))} \quad (13)$$

$$P(\varphi^+(A_i)) = \rho_i P_{\mu_i}(\varphi^+(A_i)) + (1 - \rho_i) P_{\nu_i}(\varphi^+(A_i)) \quad (14)$$

$$P(\varphi^-(A_i)) = \rho_i P_{\mu_i}(\varphi^-(A_i)) + (1 - \rho_i) P_{\nu_i}(\varphi^-(A_i)) \quad (15)$$

$$P(\varphi(A_i)) = \frac{P(\varphi^+(A_i))}{P(\varphi^+(A_i)) + P(\varphi^-(A_i))} \quad (16)$$

Where ρ_i is a parameter used to demonstrate the different degrees between two alternatives, $\rho_i \in [0, 1]$. Then the paper have

(1) If $E(\varphi(A_1)) < E(\varphi(A_2))$, then A_1 is smaller than A_2 , denoted by $A_1 < A_2$.

(2) If $E(\varphi(A_1)) = E(\varphi(A_2))$, then:

(a) If $P(\varphi(A_1)) < P(\varphi(A_2))$, then A_1 is smaller than A_2 , denoted by $A_1 < A_2$.

(b) If $P(\varphi(A_1)) = P(\varphi(A_2))$, then A_1 and A_2 represent the same information, denoted by $A_1 \sim A_2$.

Example 2. If $\varphi^+(A_1) = ([s_{3.3}, s_{3.9}, s_{4.3}, s_{4.75}]; 0.8329, 0.1000; 0.0039)$, $\varphi^-(A_1) = ([s_{1.5}, s_{2.05}, s_{2.65}, s_{3.25}]; 0.8944, 0.1861; 0.0059)$, $\varphi^+(A_2) = ([s_{2.35}, s_{2.85}, s_{3.4}, s_{3.95}]; 0.8456, 0.1414; 0.0020)$, $\varphi^-(A_2) = ([s_{2.45}, s_{3.05}, s_{3.55}, s_{4.1}]; 0.8372, 0.1414; 0.0013)$, be four TrPFPLVs, Though Definition 6, we can get

$$\begin{aligned} L_{\mu_1}(\varphi^+(A_1)) &= 3.2418, L_{\nu_1}(\varphi^+(A_1)) = 0.4108, \\ L_{\mu_1}(\varphi^-(A_1)) &= 2.1093, L_{\nu_1}(\varphi^-(A_1)) = 0.4389, \end{aligned}$$

$$\begin{aligned} L_{\mu_2}(\varphi^+(A_2)) &= 2.6495, L_{\nu_2}(\varphi^+(A_2)) = 0.4430, \\ L_{\mu_2}(\varphi^-(A_2)) &= 2.7557, L_{\nu_2}(\varphi^-(A_2)) = 0.4654, \end{aligned}$$

Then though Definition 7, we can get $E(\varphi^+(A_1)) = 0.9770$, $E(\varphi^-(A_1)) = 0.7730$

$$E(\varphi^+(A_2)) = 0.8843, E(\varphi^-(A_2)) = 0.9235,$$

$E(\varphi(A_1)) = 0.5583$ and $E(\varphi(A_2)) = 0.4892$, we can clearly see that $0.5583 > 0.4892$, that is to say $E(\varphi(A_1)) > E(\varphi(A_2))$.

B. Trapezoidal Pythagorean Fuzzy Probabilistic Linguistic Preference Relations

In the actual decision-making process, the DMs usually need to express their preference information through pairwise comparison. Because of the ambiguity of information and the incomplete understanding of the preference degree between any pair of alternatives, the DMs can not give the exact membership degree of the preference information. On the basis of Zhang et al. [33], the paper defined the trapezoidal Pythagorean fuzzy probabilistic linguistic preference relations (TrPFPLPRs).

Definition 8. A Trapezoidal Pythagorean fuzzy probabilistic linguistic preference relations (TrPFPLPRs) on the set $X = x_1, x_2, \dots, x_n$ is represented by a matrix $\tilde{R} = (\tilde{r}_{ij})_{n \times n}$, where $\hat{t}_k = \tilde{r}_{ij} = ([s_{\varphi_{\tilde{r}_{ij}}}; \mu_{\tilde{r}_{ij}}(x_{ij}), \nu_{\tilde{r}_{ij}}(x_{ij}); p_{\tilde{r}_{ij}})$ for all $i, j, k = 1, 2, \dots, n$, where $\mu_{\tilde{r}_{ij}}(x_{ij})$ denotes the degree to which the object x_i is preferred to the object x_j , $\nu_{\tilde{r}_{ij}}(x_{ij})$ indicates the degree to which the object x_i is not preferred to the object x_j , and $\pi_{\tilde{r}_{ij}}(x_{ij}) = 1 - \mu_{\tilde{r}_{ij}}^2(x_{ij}) - \nu_{\tilde{r}_{ij}}^2(x_{ij})$ is interpreted as indeterminacy degree or a hesitancy degree, where $s_{\varphi_{\tilde{r}_{ij}}}$ represents a possible value for a linguistic label, if a decision maker prefers A to B, he/she will use "positive" linguistic labels, such as "good" or "little good", to express his/her preference. Different "positive" linguistic labels reflect different preference degrees of the DMs. $p_{\tilde{r}_{ij}}$ represents the credibility of $s_{\varphi_{\tilde{r}_{ij}}}$ given by the experts when evaluating alternatives and $s_{\varphi_{\tilde{r}_{ij}}} = s_{(\alpha_i, \beta_i, \gamma_i, \theta_i)}$.

For convenience, let $\hat{t}_k = \tilde{r}_{ij} = \langle [s_{\varphi_{\tilde{r}_{ij}}}; \mu_{ij}, \nu_{ij}; p_{ij}] \rangle$ is TrPFPLVs, with the conditions:

$$\begin{cases} S = \{s_{\varphi_{\tilde{r}_{ij}}} | \varphi_{\tilde{r}_{ij}} = -\tau, \dots, -1, 0, 1, \dots, \tau\} \\ \mu_{ij}, \nu_{ij} \in [0, 1], \mu_{ji}, \nu_{ji} \in [0, 1], \mu_{ij} = \nu_{ji}, \mu_{ii} = \nu_{ii} = \sqrt{0.5}, \\ \pi_{ij}^2 = 1 - \mu_{ij}^2 - \nu_{ij}^2 \\ p_{ij} \in [0, 1], p_{ij} = p_{ji} \end{cases} \quad (17)$$

where the for all $i, j = 1, 2, \dots, n$. Specially, the TrPF-PLPR, in which each TrPFPLTS is normalized, is called the normalized TrPFPLPR (NTrPFPLPR), denoted as $\tilde{R}^N = (\tilde{r}_{ij}^N)_{n \times n}$.

Remark 1.

- (1) If neglect the linguistic $s_{\varphi_{\tilde{r}_{ij}}}$ and $p_{\tilde{r}_{ij}}$, that is $\tilde{R} = (\tilde{r}_{ij})_{n \times n} = (\hat{t}_k)_{n \times n} = (\mu_{\tilde{r}_{ij}}(x_{ij}), \nu_{\tilde{r}_{ij}}(x_{ij}))_{n \times n}$, we can get trapezoidal Pythagorean fuzzy preference relations (TrPFPRs).
- (2) If $0 \leq \mu_{\tilde{r}_{ij}}(x_{ij}) + \nu_{\tilde{r}_{ij}}(x_{ij}) \leq 1$, we can get trapezoidal fuzzy probabilistic linguistic preference relations (TrFPLPRs).
- (3) If neglect the linguistic $s_{\varphi_{\tilde{r}_{ij}}}$ and $p_{\tilde{r}_{ij}}$, $0 \leq \mu_{\tilde{r}_{ij}}(x_{ij}) + \nu_{\tilde{r}_{ij}}(x_{ij}) \leq 1$, we can get intuitionistic fuzzy preference relations (IFPRs).

- (4) If neglect the probabilistic linguistic term set $p_{\tilde{r}_{ij}}$, we can get trapezoidal Pythagorean fuzzy linguistic preference relations (TrPFLPRs).

IV. TRAPEZOIDAL PYTHAGOREAN FUZZY PROBABILISTIC LINGUISTIC PRIORITY WEIGHTED AVERAGING PROMETHEE APPROACH

In this part, we propose trapezoidal Pythagorean fuzzy probabilistic linguistic priority weighted averaging PROMETHEE (TrPFPLPWA-PROMETHEE) approach. In dealing with trapezoidal Pythagorean fuzzy probabilistic linguistic making decision problems, it is not enough for traditional aggregation approach to consider only the fuzziness of preference, but it is very important to consider the fuzzy weight among attributes for poor structural making decision problems, so that we develop the TrPFPLPWA-PROMETHEE approach.

A. Trapezoidal Pythagorean Fuzzy Probabilistic Linguistic Priority Weighted Averaging PROMETHEE

The PROMETHEE method is a classic method to deal with making decision problems. The PROMETHEE method is a sorting method based on levels above relationships. By defining the priority function, it can judge the degree of superiority between alternative according to the difference between the attribute values of each alternative. The value of the priority function is $0 \sim 1$, the smaller the function value is, the smaller the priority degree between the two schemes under the same attribute, and the larger the function value is, the greater the priority degree between the two schemes under the same attribute. It not only considers the fuzzy preference among alternatives, but also considers the weight among attributes. At present, many scholars have done a lot of research on the PROMETHEE, for instance, Le Teno et al.[36]. Therefore in this part, we develop the TrPFPLPWA-PROMETHEE approach.

Definition 9. Let $\hat{t}_k = \tilde{r}_{ij} = ([s_{\varphi_{\tilde{r}_{ij}}}; \mu_{\tilde{r}_{ij}}(x_{ij}), \nu_{\tilde{r}_{ij}}(x_{ij}); p_{\tilde{r}_{ij}})$ for all $i, j, k = 1, 2, \dots, n$, then we can get TrPFPLPWA-PROMETHEE approach:

$$\varphi^+(A_i) = \frac{1}{m-1} \oplus_{k=1, k \neq i}^m r(A_i, A_k) = \frac{1}{m-1} \oplus_{k=1, k \neq i}^m r_{ik} \quad (18)$$

$$\varphi^-(A_i) = \frac{1}{m-1} \oplus_{k=1, k \neq i}^m r(A_k, A_i) = \frac{1}{m-1} \oplus_{k=1, k \neq i}^m r_{ki} \quad (19)$$

where

$$\begin{aligned} r(A_k, A_i) &= \oplus_{j=1}^n (w_j \oplus r_{ik}^{(j)}) = \\ & \left\{ [s_{\sum_{i=1}^n \omega_j \alpha_i}, s_{\sum_{i=1}^n \omega_j \beta_i}, s_{\sum_{i=1}^n \omega_j \gamma_i}, s_{\sum_{i=1}^n \omega_j \theta_i}]; \right. \\ & \left. \sqrt{1 - \prod_{j=1}^n (1 - \mu_{ik}^{2(j)} w_j), \prod_{j=1}^n \nu_{ik}^{w_j(j)}; p_i^{(j)} p_k^{(j)}} \right\} \quad (20) \end{aligned}$$

and $\varphi^+(A_i)$ is a trapezoidal Pythagorean fuzzy positive dominant flow, the larger $\varphi^+(A_i)$ is, the higher A_i is relative to other alternatives. $\varphi^-(A_i)$ is a trapezoidal Pythagorean fuzzy negative dominant flow, the smaller $\varphi^-(A_i)$ is, and the

TABLE I. PREFERENCE RELATIONS OF THE EXPERT 1

	A_1	A_2	A_3	A_4	A_5
A_1	—	$([s_3]; 0.7, 0.6; 0.8)$	$([s_4]; 0.7, 0.2; 0.9)$	$([s_{-1}]; 0.6, 0.3; 0.4)$	$([s_2]; 0.8, 0.3; 0.6)$
A_2	$([s_{-3}]; 0.6, 0.7; 0.8)$	—	$([s_3]; 0.6, 0.3; 0.7)$	$([s_1]; 0.5, 0.4; 0.4)$	$([s_{-2}]; 0.5, 0.4; 0.5)$
A_3	$([s_{-4}]; 0.2, 0.7; 0.9)$	$([s_{-3}]; 0.3, 0.6; 0.7)$	—	$([s_{-1}]; 0.8, 0.5; 0.6)$	$([s_2]; 0.6, 0.4; 0.8)$
A_4	$([s_1]; 0.3, 0.6; 0.4)$	$([s_{-1}]; 0.4, 0.5; 0.4)$	$([s_1]; 0.5, 0.8; 0.6)$	—	$([s_3]; 0.7, 0.2; 0.4)$
A_5	$([s_{-2}]; 0.3, 0.8; 0.6)$	$([s_2]; 0.4, 0.5; 0.5)$	$([s_{-2}]; 0.4, 0.6; 0.8)$	$([s_{-3}]; 0.2, 0.7; 0.4)$	—

TABLE II. PREFERENCE RELATIONS OF THE EXPERT 2

	A_1	A_2	A_3	A_4	A_5
A_1	—	$([s_1]; 0.8, 0.5; 0.7)$	$([s_2]; 0.4, 0.6; 0.8)$	$([s_0]; 0.1, 0.8; 0.4)$	$([s_4]; 0.6, 0.7; 0.6)$
A_2	$([s_{-1}]; 0.5, 0.8; 0.7)$	—	$([s_{-4}]; 0.6, 0.3; 0.7)$	$([s_3]; 0.5, 0.7; 0.3)$	$([s_{-1}]; 0.4, 0.6; 0.6)$
A_3	$([s_{-2}]; 0.6, 0.4; 0.8)$	$([s_4]; 0.3, 0.6; 0.7)$	—	$([s_2]; 0.4, 0.7; 0.6)$	$([s_1]; 0.5, 0.4; 0.7)$
A_4	$([s_0]; 0.8, 0.1; 0.4)$	$([s_{-3}]; 0.7, 0.5; 0.3)$	$([s_{-2}]; 0.7, 0.4; 0.6)$	—	$([s_{-3}]; 0.2, 0.7; 0.4)$
A_5	$([s_{-4}]; 0.7, 0.6; 0.6)$	$([s_1]; 0.6, 0.4; 0.6)$	$([s_{-1}]; 0.4, 0.5; 0.7)$	$([s_3]; 0.7, 0.2; 0.4)$	—

TABLE III. PREFERENCE RELATIONS OF THE EXPERT 3

	A_1	A_2	A_3	A_4	A_5
A_1	—	$([s_2]; 0.6, 0.6; 0.6)$	$([s_0]; 0.7, 0.4; 0.7)$	$([s_{-3}]; 0.7, 0.8; 0.5)$	$([s_4]; 0.9, 0.4; 0.8)$
A_2	$([s_{-2}]; 0.6, 0.6; 0.9)$	—	$([s_{-1}]; 0.5, 0.3; 0.8)$	$([s_2]; 0.9, 0.9; 0.7)$	$([s_4]; 0.3, 0.9; 0.4)$
A_3	$([s_0]; 0.4, 0.7; 0.7)$	$([s_1]; 0.3, 0.5; 0.8)$	—	$([s_3]; 0.6, 0.7; 0.7)$	$([s_{-3}]; 0.4, 0.8; 0.8)$
A_4	$([s_3]; 0.8, 0.7; 0.5)$	$([s_{-2}]; 0.9, 0.9; 0.7)$	$([s_{-3}]; 0.7, 0.6; 0.7)$	—	$([s_{-2}]; 0.6, 0.3; 0.7)$
A_5	$([s_{-4}]; 0.4, 0.9; 0.8)$	$([s_{-4}]; 0.8, 0.3; 0.4)$	$([s_3]; 0.8, 0.4; 0.8)$	$([s_2]; 0.3, 0.6; 0.7)$	—

TABLE IV. DECISION MATRIX OF THE ATTRIBUTES (1)

	A_1	A_2
A_1	—	$([s_{3.6}, s_{4.2}, s_{4.6}, s_{5.2}]; 0.8072, 0.1800; 0.3360)$
A_2	$([s_{1.2}, s_{1.8}, s_{2.4}, s_3]; 0.8887, 0.3360; 0.5040)$	—
A_3	$([s_{1.2}, s_{1.8}, s_{2.4}, s_3]; 0.9360, 0.1960; 0.5040)$	$([s_{2.8}, s_{3.4}, s_{3.8}, s_{4.2}]; 0.9721, 0.1800; 0.3920)$
A_4	$([s_{3.2}, s_{3.6}, s_{4.2}, s_{4.8}]; 0.8075, 0.0420; 0.0800)$	$([s_{1.2}, s_{1.8}, s_{2.4}, s_3]; 0.7756, 0.2250; 0.0840)$
A_5	$([s_{0.4}, s_1, s_{1.6}, s_{2.2}]; 0.9101, 0.4320; 0.2880)$	$([s_{2.2}, s_{2.8}, s_{3.4}, s_4]; 0.8485, 0.0600; 0.1200)$

smaller the possibility that other alternatives are better than A_i is. Thus, $\varphi^+(A_i)$ and $\varphi^-(A_i)$ can be used to determine the level between alternatives, p_i and p_j can be interpreted as he/she is p_i or p_j sure that the alternative is bad in comparison with other alternative.

Theorem 1. Let $\hat{t}_k = \hat{r}_{ij} = ([s_{\varphi_{\hat{r}_{ij}}}], \mu_{\hat{r}_{ij}}(x_{ij}), \nu_{\hat{r}_{ij}}(x_{ij}); p_{\hat{r}_{ij}}) \in \hat{T}(i, j, k = 1, 2, \dots, n)$ be a collection of TrPFPLVs, the trapezoidal Pythagorean fuzzy positive dominant flow and trapezoidal Pythagorean fuzzy negative dominant flow are also TrPFPLV by Definition 9.

$$\varphi^+(A_i) = \frac{1}{m-1} \oplus_{k=1, k \neq i}^m r(A_i, A_k) \quad (21)$$

$$\varphi^-(A_i) = \frac{1}{m-1} \oplus_{k=1, k \neq i}^m r(A_k, A_i) \quad (22)$$

where $r(A_i, A_k) = \left\{ \left[s_{\sum_{i=1}^n \omega_j \alpha_i}, s_{\sum_{i=1}^n \omega_j \beta_i}, s_{\sum_{i=1}^n \omega_j \gamma_i}, s_{\sum_{i=1}^n \omega_j \theta_i} \right]; \right.$

$$\left. \sqrt{1 - \prod_{j=1}^n (1 - \mu_{ik}^{2(j)})^{w_j}, \prod_{j=1}^n \nu_{ik}^{w_j(j)}; p_i, p_k} \right\} \quad (23)$$

$r(A_k, A_i) = \left\{ \left[s_{\sum_{i=1}^n \omega_j \alpha_k}, s_{\sum_{i=1}^n \omega_j \beta_k}, s_{\sum_{i=1}^n \omega_j \gamma_k}, s_{\sum_{i=1}^n \omega_j \theta_k} \right]; \right.$

$$\left. \sqrt{1 - \prod_{j=1}^n (1 - \mu_{ki}^{2(j)})^{w_j}, \prod_{j=1}^n \nu_{ki}^{w_j(j)}; p_k, p_i} \right\} \quad (24)$$

Proof 1. According to Definition 5, we can get first result. In the next, we only prove the above formula by using mathematical induction on n .

For $n = 2$, since $\hat{t}_1 = ([s_{\alpha_1}, s_{\beta_1}, s_{\gamma_1}, s_{\theta_1}]; \mu_{\hat{t}_1}, \nu_{\hat{t}_1}), \hat{t}_2 = ([s_{\alpha_2}, s_{\beta_2}, s_{\gamma_2}, s_{\theta_2}]; \mu_{\hat{t}_2}, \nu_{\hat{t}_2})$,

then

$$\oplus_{k=1, k \neq i}^m r(A_1, A_2) = \omega_1 \odot \hat{s}_1 + \omega_2 \odot \hat{s}_2 = ([s_{\omega_1 \alpha_1 + \omega_2 \alpha_2}, s_{\omega_1 \beta_1 + \omega_2 \beta_2}, s_{\omega_1 \gamma_1 + \omega_2 \gamma_2}, s_{\omega_1 \theta_1 + \omega_2 \theta_2}]; \sqrt{1 - (1 - \mu_1^2)^{\omega_1} (1 - \mu_2^2)^{\omega_2}}, \nu_1^{\omega_1} \nu_2^{\omega_2})$$

Suppose that, if Eq 20-23 holds for $n = k, k \in N$, that is

$$\oplus_{i=1}^k \omega_i \odot \hat{t}_i = ([s_{\sum_{i=1}^k \omega_i \alpha_i}, s_{\sum_{i=1}^k \omega_i \beta_i}, s_{\sum_{i=1}^k \omega_i \gamma_i}, s_{\sum_{i=1}^k \omega_i \theta_i}]; \sqrt{1 - \prod_{i=1}^k (1 - \mu_{\hat{t}_i}^2)^{\omega_i}, \prod_{i=1}^k \nu_{\hat{t}_i}^{\omega_i}}).$$

Then, according to the operational laws of Definition 5, when $n = k + 1$, we have

TABLE V. DECISION MATRIX OF THE ATTRIBUTES (2)

	A_3	A_4
A_1	$([s_{3.6}, s_{4.2}, s_{4.6}, s_5]; 0.8589, 0.0480; 0.5040)$	$([s_{1.6}, s_{2.2}, s_{2.8}, s_{3.4}]; 0.8932, 0.1920; 0.0800)$
A_2	$([s_2, s_{2.4}, s_3, s_{3.6}]; 0.8888, 0.0270; 0.3920)$	$([s_{3.6}, s_4, s_{4.6}, s_{5.2}]; 0.7996, 0.2520; 0.0840)$
A_3	—	$([s_{3.2}, s_{3.6}, s_{4.2}, s_{4.8}]; 0.8485, 0.0245; 0.2520)$
A_4	$([s_{1.6}, s_{2.2}, s_{2.8}, s_{3.4}]; 0.8492, 0.1920; 0.2520)$	—
A_5	$([s_{2.4}, s_{2.8}, s_{3.4}, s_4]; 0.8719, 0.1200; 0.4480)$	$([s_{2.8}, s_{3.2}, s_{3.8}, s_{4.4}]; 0.9223, 0.0840; 0.1960)$

TABLE VI. DECISION MATRIX OF THE ATTRIBUTES (3)

	A_5
A_1	$([s_{4.4}, s_5, s_{5.2}, s_{5.4}]; 0.7314, 0.0840; 0.2880)$
A_2	$([s_{2.6}, s_{3.2}, s_{3.6}, s_4]; 0.9459, 0.1920; 0.1200)$
A_3	$([s_{2.4}, s_3, s_{3.6}, s_{4.2}]; 0.9132, 0.1280; 0.4480)$
A_4	$([s_2, s_{2.4}, s_3, s_{3.6}]; 0.8904, 0.0420; 0.1120)$
A_5	—

TABLE VII. TRAPEZOIDAL PYTHAGOREAN FUZZY DOMINANT FLOW

	$\varphi^+(A_i)$	$\varphi^-(A_i)$
A_1	$([s_{3.3}, s_{3.9}, s_{4.3}, s_{4.75}]; 0.8329, 0.1000; 0.0039)$	$([s_{1.5}, s_{2.05}, s_{2.65}, s_{3.25}]; 0.8944, 0.1861; 0.0059)$
A_2	$([s_{2.35}, s_{2.85}, s_{3.4}, s_{3.95}]; 0.8456, 0.1414; 0.0020)$	$([s_{2.45}, s_{3.05}, s_{3.55}, s_{4.1}]; 0.8372, 0.1414; 0.0013)$
A_3	$([s_{2.4}, s_{2.95}, s_{3.5}, s_{4.05}]; 0.8981, 0.1000; 0.0223)$	$([s_{2.4}, s_{2.9}, s_{3.45}, s_4]; 0.6424, 0.1000; 0.0002)$
A_4	$([s_2, s_{2.5}, s_{3.1}, s_{3.6}]; 0.6424, 0.1000; 0.0002)$	$([s_{2.8}, s_{3.25}, s_{3.85}, s_{4.45}]; 0.8196, 0.1000; 0.0003)$
A_5	$([s_{1.95}, s_{2.45}, s_{3.05}, s_{3.65}]; 0.8456, 0.1189; 0.0030)$	$([s_{2.8}, s_{3.25}, s_{3.85}, s_{4.45}]; 0.8456, 0.1000; 0.0003)$

TABLE VIII. VALUE INDEX OF A_i

	$L_{\mu_i}(\varphi^+(A_i))$	$L_{\nu_i}(\varphi^+(A_i))$	$L_{\mu_i}(\varphi^-(A_i))$	$L_{\nu_i}(\varphi^-(A_i))$
A_1	3.2418	0.4108	2.1093	0.4389
A_2	2.6495	0.4430	2.7557	0.4654
A_3	2.9864	0.3225	2.0450	0.3183
A_4	1.8266	0.2843	2.9301	0.3575
A_5	2.3394	0.3290	3.0230	0.3575

$$\begin{aligned} & \omega_1 \odot \hat{t}_1 \oplus \omega_2 \odot \hat{t}_2 \oplus \dots \oplus \omega_k \odot \hat{t}_k \oplus \omega_{k+1} \odot \hat{t}_{k+1} \\ &= \left(\left[s_{\sum_{i=1}^k \omega_i \alpha_i}, s_{\sum_{i=1}^k \omega_i \beta_i}, s_{\sum_{i=1}^k \omega_i \gamma_i}, s_{\sum_{i=1}^k \omega_i \theta_i} \right]; \right. \\ & \sqrt{1 - \prod_{i=1}^k (1 - \mu_{\hat{t}_i}^2)^{\omega_i}}, \prod_{i=1}^k \nu_{\hat{t}_i}^{\omega_i} \left. \right) \\ & \oplus \left(\left[s_{\omega_{k+1} \alpha_{k+1}}, s_{\omega_{k+1} \beta_{k+1}}, s_{\omega_{k+1} \gamma_{k+1}}, s_{\omega_{k+1} \theta_{k+1}} \right]; \right. \\ & \sqrt{1 - (1 - \mu_{\hat{t}_{k+1}}^2)^{\omega_{k+1}}}, \nu_{\hat{t}_{k+1}}^{\omega_{k+1}} \left. \right) \\ &= \left(\left[s_{\sum_{i=1}^{k+1} \omega_i \alpha_i}, s_{\sum_{i=1}^{k+1} \omega_i \beta_i}, s_{\sum_{i=1}^{k+1} \omega_i \gamma_i}, s_{\sum_{i=1}^{k+1} \omega_i \theta_i} \right]; \right. \\ & \left. \sqrt{1 - \prod_{i=1}^{k+1} (1 - \mu_{\hat{t}_i}^2)^{\omega_i}}, \prod_{i=1}^{k+1} \nu_{\hat{t}_i}^{\omega_i} \right). \end{aligned}$$

We can see $\oplus_{k=1, k \neq i}^m r(A_i, A_k)$ is still a TrPFPLV, because

$$\begin{aligned} \varphi^+(A_i) &= \frac{1}{m-1} \oplus_{k=1, k \neq i}^m r(A_i, A_k) \\ \varphi^-(A_i) &= \frac{1}{m-1} \oplus_{k=1, k \neq i}^m r(A_k, A_i) \end{aligned}$$

Then the aggregating value by TrPFPLWA-PROMETHEE approach $\varphi^+(A_i)$ and $\varphi^-(A_i)$ is still a TrPFPLV.

Theorem 2. (Commutativity) $(\hat{t}_1^*, \hat{t}_2^*, \dots, \hat{t}_n^*)$ is any permutation of the TrPFPLVs vector $(\hat{t}_1, \hat{t}_2, \dots, \hat{t}_n)$, then $TrPFPLWA-PROMETHEE(\hat{t}_1^*, \hat{t}_2^*, \dots, \hat{t}_n^*) =$

$$TrPFPLWA - PROMETHEE(\hat{t}_1, \hat{t}_2, \dots, \hat{t}_n) \quad (25)$$

Proof 2. Let

$$TrPFPLWA - PROMETHEE(\hat{t}_1^*, \hat{t}_2^*, \dots, \hat{t}_n^*) = \frac{1}{m-1} \oplus_{i=1}^n \omega_i \odot \hat{t}_i^*$$

$$TrPFPLWA - PROMETHEE(\hat{t}_1, \hat{t}_2, \dots, \hat{t}_n) = \frac{1}{m-1} \oplus_{i=1}^n \omega_i \odot \hat{t}_i$$

Since $(\hat{t}_1^*, \hat{t}_2^*, \dots, \hat{t}_n^*)$ is any permutation of $(\hat{t}_1, \hat{t}_2, \dots, \hat{t}_n)$, then we have $\hat{t}_i^* = \hat{t}_i$ for all $i(i = 1, 2, \dots, n)$. Consequently

$$TrPFPLWA - PROMETHEE(\hat{t}_1^*, \hat{t}_2^*, \dots, \hat{t}_n^*) = TrPFPLWA - PROMETHEE(\hat{t}_1, \hat{t}_2, \dots, \hat{t}_n)$$

Theorem 3. (Idempotency) If $\hat{t}_i, \hat{t} \in \hat{T}$, and $\hat{t}_i = \hat{t}$ for all $i(i = 1, 2, \dots, n)$, where $\hat{t} = ([s_\alpha, s_\beta, s_\gamma, s_\theta]; \sqrt{1 - (1 - \mu_{\hat{t}}^2)}, \nu_{\hat{t}})$, then

$$TrPFPLWA - PROMETHEE(\hat{t}_1, \hat{t}_2, \dots, \hat{t}_n) = \frac{1}{m-1} \odot \hat{t}$$

Proof 3. Since $\hat{t}_i = \hat{t}$ for all $i(i = 1, 2, \dots, n)$, let

$$\begin{aligned} TrPFPLWA - PROMETHEE(\hat{t}_1, \hat{t}_2, \dots, \hat{t}_n) &= \frac{1}{m-1} \odot \omega_1 \odot \hat{t}_1 \otimes \omega_2 \odot \hat{t}_2 \otimes \dots \otimes \omega_n \odot \hat{t}_n \\ &= \frac{1}{m-1} \odot \omega_1 \odot \hat{t} \otimes \omega_2 \odot \hat{t} \otimes \dots \otimes \omega_n \odot \hat{t} \\ &= \frac{1}{m-1} \odot (\omega_1 + \omega_2 + \dots + \omega_n) \odot \hat{t}. \end{aligned}$$

$$\begin{aligned} & \text{According to and } \sum_{i=1}^n \omega_i = 1, \text{ we have } (\omega_1 + \omega_2 + \dots + \omega_n) \odot \hat{t} \\ &= \left(\left[s_{\sum_{i=1}^n \omega_i \alpha}, s_{\sum_{i=1}^n \omega_i \beta}, s_{\sum_{i=1}^n \omega_i \gamma}, s_{\sum_{i=1}^n \omega_i \theta} \right]; \sqrt{1 - \prod_{i=1}^n (1 - \nu_i^{\omega_i})}, \prod_{i=1}^n \nu_i^{\omega_i} \right) \\ &= ([s_\alpha, s_\beta, s_\gamma, s_\theta]; \sqrt{1 - (1 - \mu_{\hat{t}}^2)^{\sum_{i=1}^n \omega_i}}, \nu_{\hat{t}}^{\sum_{i=1}^n \omega_i}) \\ &= ([s_\alpha, s_\beta, s_\gamma, s_\theta]; \sqrt{1 - (1 - \mu_{\hat{t}}^2)}, \nu_{\hat{t}}) \\ &= \hat{t}. \end{aligned}$$

$$\text{Hence, } TrPFPLWA - PROMETHEE(\mu_1, s_1, \dots, \mu_n, s) = \frac{1}{m-1} \odot \hat{t}.$$

TABLE IX. VALUE INDEX OF A_i

	$E(\varphi^+(A_1))$	$E(\varphi^-(A_1))$
A_1	0.9770	0.7730
A_2	0.8843	0.9235
A_3	0.8552	0.6636
A_4	0.5928	0.8720
A_5	0.7311	0.8906

TABLE X. RANKING RESULTS OF A_i

	$E(\varphi(A_1))$
A_1	0.5583
A_2	0.4892
A_3	0.5631
A_4	0.4047
A_5	0.4508

TABLE XI. RANKING RESULTS BY AGGREGATE METHOD

	$TrPFLECOWA$	$TrPFLECOWMD$
A_1	2.6756	0.0005
A_2	2.2082	0.0003
A_3	2.4536	0.0043
A_4	1.5181	0.0001
A_5	1.9373	0.0002

Theorem 4. (Monotonicity) Let $(\hat{t}_1^*, \dots, \hat{t}_n^*)$ and $(\hat{t}_1, \dots, \hat{t}_n)$ are two TrPFPLVs vector, if $\hat{t}_i < \hat{t}_i^*$ for all $i(i = 1, 2, \dots, n)$, then

$$TrPFPLPWA - PROMETHEE(\hat{t}_1, \dots, \hat{t}_n) < TrPFPLPWA - PROMETHEE(\hat{t}_1^*, \dots, \hat{t}_n^*) \quad (26)$$

Proof 4. Let $TrPFPLPWA - PROMETHEE(\hat{t}_1^*, \dots, \hat{t}_n^*) = \frac{1}{m-1} \oplus_{i=1}^n \omega_i \odot \hat{t}_i^*$
 $= \frac{1}{m-1} \odot \hat{t}_a^* TrPFPLPWA - PROMETHEE(\hat{t}_1, \dots, \hat{t}_n) = \frac{1}{m-1} \oplus_{i=1}^n \omega_i \odot \hat{t}_i$
 Since $\hat{t}_i < \hat{t}_i^*$ for all $i(i = 1, 2, \dots, n)$, it follows that $\hat{t}_a < \hat{t}_a^*, i = 1, 2, \dots, n$. Then $TrPFPLPWA - PROMETHEE(\hat{t}_1, \dots, \hat{t}_n) < TrPFPLPWA - PROMETHEE(\hat{t}_1^*, \dots, \hat{t}_n^*)$.

Theorem 5. (Boundedness) Let $\hat{t}_m = \min_i(\hat{t}_1, \hat{t}_2, \dots, \hat{t}_n), \hat{t}_M = \max_i(\hat{t}_1, \hat{t}_2, \dots, \hat{t}_n)$, then

$$\frac{1}{m-1} \odot \hat{t}_m \leq TrPFPLPW - PROMETHEE(\hat{t}_1, \dots, \hat{t}_n) \leq \frac{1}{m-1} \odot \hat{t}_M \quad (27)$$

Proof 5. Since $\hat{t}_m \leq \hat{t}_i \leq \hat{t}_M$ for all $i = (i = 1, 2, \dots, n)$ and $\sum_{i=1}^n \omega_i = 1$, according to Theorem 1-4, we have

$$TrPFPLPWA - PROMETHEE(\hat{t}_1, \dots, \hat{t}_n) = \frac{1}{m-1} \odot \oplus_{i=1}^n \omega_i \odot \hat{t}_i \geq \frac{1}{m-1} \odot \omega_1 \odot \hat{t}_m \oplus \omega_2 \odot \hat{t}_m \oplus \dots \oplus \omega_n \odot \hat{t}_m = \frac{1}{m-1} \odot (\sum_{i=1}^n \omega_i) \odot \hat{t}_m = \frac{1}{m-1} \odot (\omega_1 + \omega_2 + \dots + \omega_n) \hat{t}_m = \frac{1}{m-1} \odot \hat{t}_m.$$

$$TrPFPLPWA - PROMETHEE(\hat{t}_1, \dots, \hat{t}_n) = \frac{1}{m-1} \odot \oplus_{i=1}^n \omega_i \odot \hat{t}_i \leq \frac{1}{m-1} \odot \omega_1 \odot \hat{t}_M \oplus \omega_2 \odot \hat{t}_M \oplus \dots \oplus \omega_n \odot \hat{t}_M =$$

$$\frac{1}{m-1} \odot (\sum_{i=1}^n \omega_i) \odot \hat{t}_M = \frac{1}{m-1} \odot (\omega_1 + \omega_2 + \dots + \omega_n) \hat{t}_M = \frac{1}{m-1} \odot \hat{t}_M.$$

Consequently $\frac{1}{m-1} \odot \hat{t}_m \leq TrPFPLPWA - PROMETHEE(\hat{t}_1, \dots, \hat{t}_n) \leq \frac{1}{m-1} \odot \hat{t}_M$.

Remark 2. Let $(\hat{t}_1, \hat{t}_2, \dots, \hat{t}_n)$ be a collection of the TrPFPLVs and $W = (\omega_1, \omega_2, \dots, \omega_n)^T$ be the weighting vector of the TrPFPLPWA-PROMETHEE with $\omega_i \in [0, 1], \sum_{i=1}^n \omega_i = 1$. Thus,

(1) If $W = (\omega_1, \omega_2, \dots, \omega_n)^T = (\frac{1}{n}, \frac{1}{n}, \dots, \frac{1}{n})^T$, then we get the TrPFPLPA-PROMETHEE approach as follows: $TrPFPLPA - PROMETHEE(\hat{t}_1, \dots, \hat{t}_n) = \frac{1}{m-1} \oplus_{i=1}^n \frac{1}{n} \odot \hat{t}_i = \frac{1}{m-1} \odot ([s_{\frac{1}{n} \sum_{i=1}^n \alpha_i}, s_{\frac{1}{n} \sum_{i=1}^n \beta_i}, s_{\frac{1}{n} \sum_{i=1}^n \gamma_i}, s_{\frac{1}{n} \sum_{i=1}^n \theta_i}], \sqrt{1 - [\prod_{i=1}^n (1 - \mu_{\hat{t}_i}^2)]^{\frac{1}{n}}, (\sum_{i=1}^n \nu_{\hat{t}_i})^{\frac{1}{n}}})$.

(2) If $W = (\omega_1, \omega_2, \dots, \omega_n) = (1, 0, \dots, 0)^T$, then $TrPFPLPA - PROMETHEE(\hat{t}_1, \dots, \hat{t}_n) = \frac{1}{m-1} \odot \max_i \hat{t}_i$.

(3) If $W = (\omega_1, \omega_2, \dots, \omega_n) = (0, 0, \dots, 1)^T$, then $TrPFPLPA - PROMETHEE(\hat{t}_1, \dots, \hat{t}_n) = \frac{1}{m-1} \odot \min_i \hat{t}_i$.

(4) If $\omega_i = 1, \omega_j = 0, i \neq j$, then $TrPFPLPA - PROMETHEE(\hat{t}_1, \dots, \hat{t}_n) = \frac{1}{m-1} \odot \hat{t}_{a_i}$, where \hat{t}_{a_i} is the i th largest of $\mu_{\hat{t}_i}$.

Remark 3. Let $\hat{t}_k = \tilde{r}_{ij} = ([s_{\varphi_{\tilde{r}_{ij}}}], \mu_{\tilde{r}_{ij}}(x_{ij}), \nu_{\tilde{r}_{ij}}(x_{ij}); p_{\tilde{r}_{ij}})$ be TrPFPLVs, if $0 \leq \mu_{\tilde{r}_{ij}}(x_{ij}) + \nu_{\tilde{r}_{ij}}(x_{ij}) \leq 1$, we can get TrIFPLVs.

Remark 4. Let $\hat{s} = ([s_{\alpha_i}, s_{\beta_i}, s_{\gamma_i}, s_{\theta_i}], \mu_{\hat{s}_i}, \nu_{\hat{s}_i})$ be the TrPFPLV, if $s_{\beta_i} = s_{\gamma_i}$, we have triangle Pythagorean fuzzy probabilistic linguistic variables (TPFPLVs).

Remark 5. If $\hat{t}_k = \tilde{r}_{ij} = ([s_{\varphi_{\tilde{r}_{ij}}}], \mu_{\tilde{r}_{ij}}(x_{ij}), \nu_{\tilde{r}_{ij}}(x_{ij}))$ be

TrPFLSs, we have trapezoidal Pythagorean fuzzy linguistic variables (TrPFLVs).

Remark 6. If $\hat{t}_k = \hat{r}_{ij} = (\mu_{\hat{r}_{ij}}(x_{ij}), \nu_{\hat{r}_{ij}}(x_{ij}); p_{\hat{r}_{ij}})$ be PFPLSs, we have Pythagorean fuzzy probabilistic linguistic variables (PFPLVs).

Remark 7. If $\hat{t}_k = \hat{r}_{ij} = ([s_{\varphi_{\hat{r}_{ij}}}], p_{\hat{r}_{ij}})$ is a linguistic sets (LSs), if $s_{\varphi_{\hat{r}_{ij}}} = s_{\alpha_i}, s_{\beta_i}, s_{\gamma_i}, s_{\theta_i}$; we have trapezoidal probabilistic linguistic sets (TrPLSs).

V. AN EMERGENCY DECISION MAKING MODEL IN THE POOR STRUCTURAL'S TRAPEZOIDAL PYTHAGOREAN FUZZY PROBABILISTIC LINGUISTIC ENVIRONMENT

Step 1. In an emergency decision making problem, there are l alternatives $X = x_1, x_2, \dots, x_l$ and q attributes $A = A_1, A_2, \dots, A_q$, whose weight vector is $W = (\omega_1, \omega_2, \dots, \omega_q)$ be the set of attributes, where the $\sum_{i=1}^q \omega_i = 1$. Let $E = e_1, e_2, \dots, e_m$ be the set of decision makers.

$$R^{(z)} = \begin{bmatrix} \hat{r}_{11}^{(z)} & \hat{r}_{12}^{(z)} & \dots & \hat{r}_{1q}^{(z)} \\ \hat{r}_{21}^{(z)} & \hat{r}_{22}^{(z)} & \dots & \hat{r}_{2q}^{(z)} \\ \cdot & \cdot & \dots & \cdot \\ \cdot & \cdot & \dots & \cdot \\ \cdot & \cdot & \dots & \cdot \\ \hat{r}_{l1}^{(z)} & \hat{r}_{l2}^{(z)} & \dots & \hat{r}_{lq}^{(z)} \end{bmatrix}$$

where $\hat{r}_{ij}^{(z)} = ([s_{\alpha}, s_{\beta}, s_{\gamma}, s_{\theta}]; \mu_{\hat{r}_{ij}}, \nu_{\hat{r}_{ij}}; p_{ij})$ be a TrPFPLV, and $\mu_{\hat{r}_{ij}}, \nu_{\hat{r}_{ij}}, p_{ij} \in [0, 1], 0 \leq (\mu_{\hat{r}_{ij}})^2 + (\nu_{\hat{r}_{ij}})^2 \leq 1$. $\hat{r}_{ij}^{(z)} = ([s_{\alpha}, s_{\beta}, s_{\gamma}, s_{\theta}]; \mu_{\hat{r}_{ij}}, \nu_{\hat{r}_{ij}}; p_{ij})$ represents expert z 's preference for attribute x_i in attribute x_j .

Step 2. By formula (19): $r(A_k, A_i) = \oplus_{j=1}^n (w_j \oplus r_{ik}^{(j)}) = \left\{ \left[s_{\sum_{i=1}^n w_j \alpha_i}, s_{\sum_{i=1}^n w_j \beta_i}, s_{\sum_{i=1}^n w_j \gamma_i}, s_{\sum_{i=1}^n w_j \theta_i} \right]; \sqrt{1 - \prod_{j=1}^n (1 - \mu_{ik}^{2(j)}) w_j}, \prod_{j=1}^n \nu_{ik}^{w_j(j)}; p_i^{(j)} p_k^{(j)} \right\}$ to obtain the collective overall preference TrPFPLV and construct the TrPFPLPR matrices of the attributes $T^{(z)} = (\hat{t}_{ij}^{(z)})_{l \times l}$:

$$T^{(z)} = \begin{bmatrix} \hat{t}_{11}^{(z)} & \hat{t}_{12}^{(z)} & \dots & \hat{t}_{1l}^{(z)} \\ \hat{t}_{21}^{(z)} & \hat{t}_{22}^{(z)} & \dots & \hat{t}_{2l}^{(z)} \\ \cdot & \cdot & \dots & \cdot \\ \cdot & \cdot & \dots & \cdot \\ \cdot & \cdot & \dots & \cdot \\ \hat{t}_{l1}^{(z)} & \hat{t}_{l2}^{(z)} & \dots & \hat{t}_{ll}^{(z)} \end{bmatrix}$$

where $\hat{t}_{pn}^{(z)} = ([s_{\alpha}, s_{\beta}, s_{\gamma}, s_{\theta}]; \mu_{\hat{t}_{pn}}, \nu_{\hat{t}_{pn}}; p_{pn})$ be a TrPFPLV, and $\hat{t}_{pn}^{(z)}$ represents the degree to which attribute A_p is superior to attribute A_n .

Step 3. By Definition 9, further calculate trapezoidal Pythagorean fuzzy positive dominant flow and trapezoidal Pythagorean fuzzy negative dominant flow.

$$\varphi^+(A_i) = \frac{1}{m-1} \oplus_{k=1, k \neq i}^m r(A_i, A_k) = \frac{1}{m-1} \oplus_{k=1, k \neq i}^m r_{ik}$$

$$\varphi^-(A_i) = \frac{1}{m-1} \oplus_{k=1, k \neq i}^m r(A_k, A_i) = \frac{1}{m-1} \oplus_{k=1, k \neq i}^m r_{ki}$$

Step 4. Calculate $L_{\mu_i}(\varphi^+(A_i)), L_{\nu_i}(\varphi^+(A_i)), L_{\mu_i}(\varphi^-(A_i)), L_{\nu_i}(\varphi^-(A_i))$ by Definition 6.

Step 5. Calculate $E(\varphi^+(A_i))$ and $E(\varphi^-(A_i))$ by Definition 7.

Step 6. Finally, we can calculate $E(\varphi(A_i))$ to obtain the ranking results by Definition 7.

VI. CASE STUDY: APPLICATION TO PREVENTION OF INFECTIOUS DISEASES

In this section, we apply the above method to an application in emergency decision support for the prevention of infectious diseases to illustrate the proposed method, and supplies some discussions about the results. In late December 2019, the outbreak of COVID-19 in Wuhan, China, brought global attention to infectious diseases. An epidemic of infectious diseases appears somewhere and is difficult to control. To address the problem, the local health organization invited five experts (e_1, e_2, e_3, e_4) to make decisions on population density (A_1), air pollution index (A_2), number of parks and entertainment equipment (A_3), density of restaurants (A_4), density of cultural and educational centers (A_5) in a certain area to prevent and control the spread the disease.

Step 1. The experts made a decision based on the factors that might affect the infectious disease and established a decision matrix, as shown in Table I to Table III:

Step 2. Constructing the matrix by formula (7), and supposed $\omega_1 = (0.2), \omega_2 = (0.2), \omega_3 = (0.2), \omega_4 = (0.2), \omega_5 = (0.2)$, the decision matrix of the attributes which is shown in Tables IV, V and VI:

Step 3. Calculate trapezoidal Pythagorean fuzzy positive dominant flow and trapezoidal Pythagorean fuzzy negative dominant flow:

$$\begin{aligned} \varphi^+(A_1) &= \frac{1}{m-1} \oplus_{k=1, k \neq i}^m r(A_1, A_k) = \frac{1}{m-1} \oplus_{k=1, k \neq i}^m r_{1k} \\ &= \frac{1}{5-1} * \{ ([s_{3.6}, s_{4.2}, s_{4.6}, s_{5.2}]; 0.8072, 0.1800; 0.3360) \oplus \\ &([s_{3.6}, s_{4.2}, s_{4.6}, s_5]; 0.8589, 0.0480; 0.05040) \\ &\oplus ([s_{1.6}, s_{2.2}, s_{2.8}, s_{3.4}]; 0.8932, 0.1920; 0.0800) \oplus \\ &([s_{4.4}, s_5, s_{5.2}, s_{5.4}]; 0.7314, 0.0840; 0.2880) \} \\ &= ([s_{3.3}, s_{3.9}, s_{4.3}, s_{4.75}]; 0.8329, 0.1000; 0.0039) \end{aligned}$$

$$\begin{aligned} \varphi^-(A_1) &= \frac{1}{m-1} \oplus_{k=1, k \neq i}^m r(A_k, A_1) = \frac{1}{m-1} \oplus_{k=1, k \neq i}^m r_{k1} \\ &= \frac{1}{5-1} * \{ ([s_{1.2}, s_{1.8}, s_{2.4}, s_3]; 0.8887, 0.3360; 0.5040) \oplus \\ &([s_{1.2}, s_{1.8}, s_{2.4}, s_3]; 0.9360, 0.1960; 0.5040) \\ &\oplus ([s_{3.2}, s_{3.6}, s_{4.2}, s_{4.8}]; 0.8075, 0.0420; 0.0800) \oplus \\ &([s_{0.4}, s_1, s_{1.6}, s_{2.2}]; 0.9101, 0.4320; 0.2880) \} \\ &= ([s_{1.5}, s_{2.05}, s_{2.65}, s_{3.25}]; 0.8944, 0.1861; 0.0059) \end{aligned}$$

Similarly, we can get

$$\varphi^+(A_2) = ([s_{2.35}, s_{2.85}, s_{3.4}, s_{3.95}]; 0.8456, 0.1414; 0.0020)$$

$$\varphi^-(A_2) = ([s_{2.45}, s_{3.05}, s_{3.55}, s_{4.1}]; 0.8372, 0.1414; 0.0013)$$

$$\varphi^+(A_3) = ([s_{2.4}, s_{2.95}, s_{3.5}, s_{4.05}]; 0.8981, 0.1000; 0.0223)$$

$$\varphi^-(A_3) = ([s_{2.4}, s_{2.9}, s_{3.45}, s_4]; 0.8099, 0.1000; 0.0223)$$

$$\begin{aligned} \varphi^+(A_4) &= ([s_2, s_{2.5}, s_{3.1}, s_{3.86}]; 0.6424, 0.1000; 0.0002) \\ \varphi^-(A_4) &= ([s_{2.8}, s_{3.25}, s_{3.85}, s_{4.45}], 0.8196, 0.1000; 0.0003) \\ \varphi^+(A_5) &= ([s_{1.95}, s_{2.45}, s_{3.05}, s_{3.65}]; 0.8456, 0.1189; 0.0030) \\ \varphi^-(A_5) &= ([s_{2.8}, s_{3.25}, s_{3.85}, s_{4.45}], 0.8456, 0.1000; 0.0003) \end{aligned}$$

Hence, the trapezoidal Pythagorean fuzzy dominant flow can be shown in Table VII.

Step 4. Calculate $L_{\mu_i}(\varphi^+(A_i))$, $L_{\nu_i}(\varphi^+(A_i))$, $L_{\mu_i}(\varphi^-(A_i))$, $L_{\nu_i}(\varphi^-(A_i))$ by Definition 6, which is shown in Table VIII.

Step 5. Calculate $E(\varphi^+(A_i))$ and $E(\varphi^-(A_i))$ by Definition 9.

Therefore, Value index of A_i is shown in Table IX.

Step 6. Finally, we can calculate $E(\varphi(A_i))$ to obtain the ranking results by Definition 9.

Obviously, from Table X, the ranking order is shown as

$$A_3 > A_1 > A_2 > A_5 > A_4$$

We can see that the third influencing -number of parks and entertainment equipment-is the biggest for infectious diseases. the second is the effect of population density. Thus it can be seen that the prevention and control of infectious diseases should be prioritized from the park recreation facilities. Under certain control, then start from the population mobility, because of the high population density.

To illustrate the rationality of our proposed approach in dealing with emergent decision problems, some comparative analysis is performed for the above example if we use the aggregate method shown in Table XI.

The results calculated by different methods are shown in the Fig. 1.

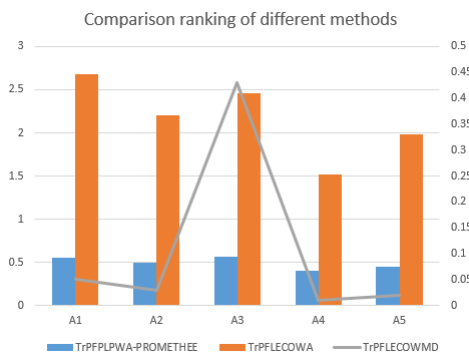


Fig. 1. Ranking Results

We can obtain $A_1 > A_3 > A_2 > A_5 > A_4$ by TrPFLECOWA and $A_3 > A_1 > A_2 > A_5 > A_4$ by TrPFLECOWMD. It can be seen from the results that the influencing factors A_1, A_3 of infectious diseases have different order. The reason is that some information is lost in the fuzzy linguistic environment due to indeterminacy, the relationship between influencing factors is ignored, and the occurrence probability of each influencing factor is not considered in

the emergency situation. It is difficult for experts to make reasonable evaluation when making uncertain decisions in emergency situations, hence it is very important to introduce probability language in the poor structural's emergency decisions. Compared with other decision making methods, this paper proposed method has the following advantages:

(1) The TrPFPLVs can describe the fuzzy probability language and its probability, and it is reasonable to make decision in the uncertain environment of emergency.

(2) The TrPFPLPWA-PROMETHEE approach mainly considers the deviation measure between alternatives or attributes, hence it can deal with the decision information with incomplete structure. It is more malleable and applicable in the poor structural's emergency decisions.

VII. CONCLUSION

The existing methods are limited and defective in terms of tackling MAGDM problems with TrPFPLVs. In addition, the researches on the aggregate operator for TrPFPLV are blank. The aim of this paper is to solve these problems. The case analysis show that the new decision-making approach can not only derive the ideal alternative efficiently, but conquer demerits of the existing methods. The contributions of this paper are summarized in the following:

(1) Compared with trapezoidal Pythagorean fuzzy linguistic variables in [37], [38], [39], [40], [41], a finer variable has been introduced to deal with complex decision-making environment, a new form of linguistic expression trapezoidal Pythagorean fuzzy probabilistic linguistic variables (TrPFPLVs) have been presented to express decision-making information.

(2) Compared with fuzzy linguistic weight averaging operator in [30], [31], [37], [35], a more complete operator has been introduced to aggregate the trapezoidal Pythagorean fuzzy probabilistic linguistic information, which is the new trapezoidal Pythagorean fuzzy probabilistic linguistic priority weight averaging (TrPFPLPWA) PROMETHEE approach.

(3) Relying on trapezoidal Pythagorean fuzzy probabilistic linguistic variables, this paper develop the operational rules, value index and ambiguity index of trapezoidal Pythagorean fuzzy probabilistic linguistic variables (TrPFPLVs).

In future studies, the TrPFPLPWA-PROMETHEE approach shall further combine with different decision-making models and extend the applications of the proposed method to other domains.

ACKNOWLEDGMENT

The authors express their gratitude to the Editor and the anonymous Reviewers for their valuable and constructive comments. And this work was supported by the General program of Chongqing Natural Science Foundation(cstc2020jcyj-msxmX0522).

ETHICAL STATEMENT

(1) This paper is an original research achievement independently obtained by the authors. The content of the paper

does not involve state secrets; It has not been published in any form in any language at home or abroad; The contents of the paper shall not infringe the copyright and other rights of others. In case of multiple submissions, infringement, disclosure and other problems, the authors of the paper will bear all the responsibilities.

(2) This work was supported by the General program of Chongqing Natural Science Foundation(cstc2020jcyj-msxmX0522).

(3) The authors declare that they have no conflict of interest.

(4) The authors are aware of and consent to the publication of this manuscript in the International Journal of Advanced Computer Science and Applications(IJACSA).

AUTHORSHIP CONTRIBUTIONS

(1) This paper propose a new form of linguistic expression trapezoidal Pythagorean fuzzy probabilistic linguistic variables (TrPFPLVs) and trapezoidal Pythagorean fuzzy probabilistic linguistic preference relations (TrPFPLPRs) to express decision-making information.

(2) This paper develop the operational rules,value index and ambiguity index of trapezoidal Pythagorean fuzzy probabilistic linguistic variables (TrPFPLVs).

(3) This paper introduce the new trapezoidal Pythagorean fuzzy probabilistic linguistic priority weight(TrPFPLPW) PROMETHEE approach to aggregate the trapezoidal Pythagorean fuzzy probabilistic linguistic information.

REFERENCES

- [1] G. Alfano; A. Ferrari; F. Fontana(2021). Hypokalemia in Patients with COVID-19. *Clinical and experimental nephrology*. 2021.
- [2] Y. X. H. Sun; V. Koh; K. Marimuthu(2020). Epidemiological and Clinical Predictors of COVID-19. *Clinical Infectious Diseases*. 71(12):786-792.
- [3] T. N. Chao; B. M. Braslow; N. D. Martin(2020).Tracheotomy in Ventilated Patients With COVID-19. *Annals of surgery*. 272(1):30-32.
- [4] J. H. Chai; S. D. Xian; S. C. Lu(2020). Z-Uncertain Probabilistic Linguistic Variables and Its Application in Emergency Decision Making for Treatment of COVID-19 Patients. *International Journal of Intelligent Systems*.
- [5] L. A. Zadeh(1975). The concept of a linguistic variable and its application to approximate reasoning-I. *Inf Sci* 8(3):199-249.
- [6] S. S. Wu; J. Lin; Z. Y. Zhang(2021). New distance measures of hesitant fuzzy linguistic term sets. *Physica Scripta*. 96(1):125002.
- [7] Y. Y. Liu; R. M. Rodriguez; H. Hagra(2019). Type-2 Fuzzy Envelope of Hesitant Fuzzy Linguistic Term Set: A New Representation Model of Comparative Linguistic Expression. *IEEE Transactions on Fuzzy Systems*. 27(12):2312-2326.
- [8] X. J. Yuan; L. Huang; X. J. Zhao; M. F. Zheng(2020). The general formula of entropy and similarity measures for hesitant fuzzy linguistic term sets. *Journal of Physics: Conference Series*. 1544:012040.
- [9] J. Gao; Z. S. Xu; P. J. Ren; H. C. Liao(2019). An emergency decision making method based on the multiplicative consistency of probabilistic linguistic preference relations. *International Journal Of Machine Learning And Cybernetics*. 10(7):1613-1629.
- [10] I. Diaz; Y. Nojima(2020). Fuzzy sets for decision making in emerging domains. *Fuzzy Sets and Systems*. 395:197-198.
- [11] M. O. Barrios; J. J. AlfaroSaiz(2020). A Hybrid Fuzzy Multi-Criteria Decision-Making Model to Evaluate the Overall Performance of Public Emergency Departments: A Case Study. *International Journal of Information Technology Decision Making*. 19(6):1485-1548.
- [12] G. Q. Zhang; J. Ma; J. Lu(2009). Emergency management evaluation by a fuzzy multi-criteria group decision support system. *Emergency Management Evaluation By a Fuzzy Multi-criteria Group Decision Support*. 23(4):517-527.
- [13] Q. Zhou; W. L. Huang; Y. Zhang(2011). Identifying critical success factors in emergency management using a fuzzy DEMATEL method. *Safety Science*. 49(2):243-252.
- [14] Y. Li; Y. Hu; X. G. Zhang; Y. Deng; S. Mahadevan(2014). An evidential DEMATEL method to identify critical success factors in emergency management. *Applied Soft Computing*. 22:504-510.
- [15] E. V. Herrera; L. Martinez; F. Mata; F. Chiclana(2005). A consensus support system model for group decision-making problems with multi-granular linguistic preference relations. *IEEE Trans Fuzzy System*. 13:644-658.
- [16] Y. Liu; Z. P. Fan; X. Zhang(2016). A method for large group decision-making based on evaluation information provided by participators from multiple groups. *Information Fusion*. 29:132-141.
- [17] P. D. Liu; F. Teng(2018). Some Muirhead mean operators for probabilistic linguistic term sets and their applications to multiple attribute decision-making. *Safety Science*. 49(2): 243-252.
- [18] Y. C. Dong; Y. F. Xu; S. Yu(2009). Linguistic multi-person decision making based on the use of multiple preference relations. *Fuzzy Sets System*. 160:603-623.
- [19] Y. X. Zhang; Z. S. Xu; H. Wang; H. C. Liao(2016). Consistency-based risk assessment with probabilistic linguistic preference relation. *Applied Soft Computing*. 49 (2016):817-833.
- [20] Y. X. Zhang; Z. S. Xu; H. C. Liao(2017). A consensus process for group decision making with probabilistic linguistic preference relations. *Information Sciences*. 414:260-275.
- [21] S. Alonso; F. Chiclana; F. Herrera; E. V. Herrera; J. F. Alcalá(2008). A consistency-based procedure to estimate missing pair-wise preference values. *International Journal of Intelligent Systems*. 23(2):155-175.
- [22] H. Wang; Z. S. Xu(2016). Interactive algorithms for improving incomplete linguistic preference relations based on consistency measures. *Applied Soft Computing*. 42:66-79.
- [23] F. Lolli; E. Balugani; A. Ishizaka(2019). On the elicitation of criteria weights in PROMETHEE based ranking methods for a mobile application. *Expert Systems with Applications*. 120:217-227.
- [24] Gul M, Celik E, Gumus AT, Guneri AF(2018). A fuzzy logic based PROMETHEE method for material selection problems. *Beni-Suef University Journal of Basic and Applied Sciences*. 7:68-79.
- [25] F. Herrera; E. V. Herrera(1995). A sequential selection process in group decision making with a linguistic assessment approach. *Information Sciences*. 85(4):223-239.
- [26] F. Herrera; E. V. Herrera; L. Verdegay (1996). Direct approach processes in group decision making using linguistic OWA operators. *Fuzzy Sets and Systems*. 79(2): 175-190.
- [27] F. Herrera; E. V. Herrera (1997). Aggregation operators for linguistic weighted information. *Systems, Man and Cybernetics*. 27: 646-656.
- [28] F. Herrera; E. V. Herrera (2000). Linguistic decision analysis: steps for solving decision problems under linguistic information. *Fuzzy Sets and Systems*. 115: 67-82.
- [29] L. Martinez; F. Herrera (2012). An overview on the 2-tuple linguistic model for computing with words in decision making under uncertain linguistic environment. *Information Sciences*. 168: 178-181.
- [30] S. D. Xian (2012). Fuzzy linguistic induced ordered weighted averaging operator and its application. *Journal of Applied Mathematics*. 2012:853-862.
- [31] S. D. Xian; W. J. Sun (2014). Fuzzy linguistic induced euclidean OWA distance operator and its application in group linguistic decision making. *International Journal of Intelligent Systems*. 29(5): 478-491.
- [32] Q. Pang; H. Wang; Z. S. Xu(2016). Probabilistic linguistic term sets multi-attribute group decision making. *Science*. 369:128-143.
- [33] X. Zhang; Z. S. Xu (2016). Extension of TOPSIS to multiple criteria decision making with Pythagorean fuzzy sets. *International Journal of Intelligent Systems*. 29(12): 1061-1078.
- [34] S. D. Xian (2012). Fuzzy linguistic induced ordered weighted averaging operator and its application. *Journal of Applied Mathematics*. 2012, 210-392.

- [35] S. D. Xian; Y. Xiao; Z. J. Yang; Y. H. Lia (2018). A New Trapezoidal Pythagorean Fuzzy Linguistic Entropic Combined Ordered Weighted Averaging Operator and Its Application for Enterprise Location. *International Journal of Intelligent Systems*. 33(9):1880-1899.
- [36] Le Teno J F; Mareschal B(1998). An interval version of PROMETHEE for the comparison of building products' design with ill-definrd data on environmental quality. *European Journal of Operational Research*. 109:522-529.
- [37] S. D. Xian; Y. Xiao; L. Li; D. X. Yu(2019). Trapezoidal Pythagorean fuzzy linguistic entropic combined ordered weighted Minkowski distance operator based on preference relations. *International Journal of Intelligent Systems*. 34(9):2196-2224.
- [38] T. G. Chen; A. C. Ova; W. Z. Hung(2022). A Digital Capability Maturity Model Based on the Hesitant Fuzzy Linguistic Variables. *Lecture Notes in Networks and Systems*. 307:687-695.
- [39] T. Tomas; N. Y. Lin; H. Michal; K. Ales; D. Hana(2022). Quarterly sales analysis using linguistic fuzzy logic with weather data. *Expert Systems with Applications*. 203:117-345.
- [40] A. Kushal(2022). Dempster-shafer theory and linguistic intuitionistic fuzzy number-based framework for blending knowledge from knowledge repositories: An approach for knowledge management. *Expert Systems with Applications*. 199:117-142.
- [41] V. Rajkumar; A. Nikunj(2022). Multiple attribute group decision-making based on generalized aggregation operators under linguistic interval-valued Pythagorean fuzzy environment. *Granular Computing*. 7(3):591-632.

Analysis of the Influence of De-hazing Methods on Vehicle Detection in Aerial Images

Khang Nguyen, Phuc Nguyen, Doanh C. Bui, Minh Tran, Nguyen D. Vo
University of Information Technology, Ho Chi Minh City, Vietnam
Vietnam National University, Ho Chi Minh City, Vietnam

Abstract—In recent years, object detection from space in adverse weather, incredibly foggy, has been challenging. In this study, we conduct an empirical experiment using two de-hazing methods: DW-GAN and Two-Branch, for removing fog, then evaluate the detection performance of six advanced object detectors belonging to four main categories: two-stage, one-stage, anchor-free and end-to-end in original and de-hazed aerial images to find the best suitable solution for vehicle detection in foggy weather. We use the UIT-DroneFog dataset, a challenging dataset that includes a lot of small, dense objects captured in various altitudes, as the benchmark to evaluate the effectiveness of approaches. After experiments, we observe that each de-hazing method has different impacts on six experimental detectors.

Keywords—Foggy weather; vehicle detection; DWGAN; two-branch; YOLOv3; sparse R-CNN; deformable det; cascade R-CNN; crossDet; adverse weather

I. INTRODUCTION

Nowadays, with the significant development of information and communication technology, especially the surging growth of the deep learning era, vehicles detection and surveillance have become extremely important and necessary. Along with that development, the prevalence of UAVs (Unmanned Aerial Vehicles) makes vehicle surveillance extremely simple and effective. Traffic surveillance from aerial images is a particular interest to researchers because it serves many essential different purposes, such as being used in the military or monitoring traffic conditions, urban management, or simply helping us know where to park in the parking lot. Compared to detecting ground view vehicles, detecting vehicles from the aerial image is more complicated and challenging due to multiple frames, various backgrounds, small objects appearing with a variety of shapes. In addition, there is a critical factor that directly affects the model's performance: the weather.

Recently, by applying deep convolution neural network CNN [1], a significant number of studies have been done to tackle this problem, such as the proposal of the Double focal loss convolutional neural network framework (DFL-CNN) model [2] with the combination of feature CNN and the focal loss function [3] or [4] carried out experiments on YOLO [5] for vehicle detection based on aerial images datasets COWC [6], VEDAI [7] and DOTA [8]. These articles have one thing in common: they were all experimented with in clear-weather conditions and achieved excellent results.

However, in reality, the weather conditions are constantly changing (rain, snow, smog, night, thunderstorms, fog, etc.), which significantly affects the accuracy and learning ability of the models.

We choose the scope of our research to detect vehicles from aerial images under foggy weather. We choose the fog scene because it is often seen in the early morning. Sometimes, the appearance of dense fog may seriously affect the ability to monitor the traffic situation. Prior studies such as SFA-Net [9] used to detect objects in the rain or solve the problem of semantic foggy scene understanding (SFSU) by de-fogging of convolutional neural networks [10].

In this study, we focus on investigating advanced object detection methods Cascade R-CNN [11], Casdou [12], YOLOv3 [13], CrossDet [14], Deformable DETR [15], Sparse R-CNN [16] for object detection in foggy conditions that limit visibility. At the same time, the evaluation of visibility improvement through 2 de-fogging (Image Dehazing) methods, which are DW GAN [17] and Two-branch Dehazing [18], also implemented on the UIT-DroneFog [12].

We summarize our contributions in this paper as:

- Using image dehazing methods to filter foggy images from the challenging dataset UIT-DroneFog.
- Experimenting with one-stage, two-stage, and the latest end-to-end deep learning methods on dehazed datasets.
- Providing in-depth evaluation of dehazing methods on experimental deep learning models to choose the best models.

The rest of the paper is: Section II is Related work; Section III is Experimental Methods; Section IV is Experimental Results; and finally, Section V is Conclusion and Future Work.

II. RELATED WORK

Object detection in the foggy condition in particular and in adverse weather conditions has been addressed in two directions: domain adaption and condition-based object detection. In domain adaptation approaches, many studies proposed to improve the more robust detector based on Faster R-CNN [19], [20], [21] to help it be adapted with other domains of images, which could be different from the original dataset. These domain-adapted detectors were trained on the source dataset, which might include images with normal, original conditions. Then, the detectors were then evaluated the performance on images with foggy, rainy or other adverse weather conditions. The characteristic of this approach was focusing on the model's architecture and did not affect the images. On the other hand, condition-based approaches tended to propose the specific detectors in concrete contexts [22], [23]. Therefore, these

detectors include processing modules such as rainy and foggy removal to transform condition-adverse images into normal images. Then the transformed images were then used for training and testing.

A. Domain Adaptation in Adverse Weather

The author in [19] tackled the adaptive domain problem by focusing on two levels: the image-level shift and the instance-level shift. The image-level shift could be described as style, illumination, etc., while the instance-level shift was object appearance and size. Based on Faster R-CNN, the authors designed H-divergence theory-based adaption module on image-level shift and instance-level shift to decrease domain discrepancy. In detail, a domain classifier was built and trained in an adversarial training manner at each level. Those two classifiers then incorporated a consistency regularizer to train a domain-invariant Regional Proposal Network in Faster R-CNN, which then could be adapted with other domains of images. The authors used the Cityscapes dataset as one of the experimental datasets. They trained on the normal version of Cityscapes and evaluated on its foggy version. Experiments proved that the performance increased by combining the proposed adaption module.

The author in [20] proposed a robust Faster R-CNN and the Noisy Labeling strategy for domain adaptation. In detail, the authors split the pipeline into three phases. In the first phase, the Faster R-CNN was trained on the source dataset then used as the base detector. Next, the authors used the base detector to obtain noisy bounding boxes. At the same time, all ground-truth instances in the source dataset were also extracted. After that, noisy bounding boxes and all extracted ground-truth boxes were fit into a classification module. The classification module would be trained on the exact ground-truth boxes from the source dataset and refine the class categories of the noisy boxes. Finally, the upgrade version of Faster R-CNN was trained on both datasets: the source dataset with human-annotated ground-truth boxes and the target dataset with annotations refined via a classification module. The proposed approach was evaluated by training on the Cityscapes and evaluating on Foggy Cityscapes dataset. Through experiments, the authors proved that using the Noisy Labeling strategy and their improved Faster R-CNN could help achieve better results than normal training, original Faster R-CNN, and other approaches 36.45% AP. Notably, this result was 7.07% lower than the result obtained via training Faster R-CNN on the Foggy Cityscapes Dataset.

The author in [21] defined a novel prior-adversarial loss function that utilized the additional knowledge from images in foggy, rainy images to correlate the amount of degradation directly. In detail, the proposed loss was used to train a prior estimation network to predict condition-specific prior from features map and minimize the weather information present in the features. This approach helped the main detection network features become invariant, decreasing the effects of adverse weather such as foggy or rainy. Furthermore, to avoid distortions caused by weather-based degradation, the authors proposed a set of residual feature recovery blocks in the detection network for de-distorting features leading to better performance. The proposed method was evaluated by training Cityscapes and evaluating on Foggy-Cityscapes dataset, the

highest result was 39.3%, which extremely outperformed the previous approaches.

B. Condition-based Object Detection Methods

To handle the problem of vehicles in foggy images that are difficult to recognize, [22] proposed a feature recovery module, which was considered as a restoration subnet and integrated with the main backbone of the detection model. The feature recovery (FR) module was designed by sharing feature extraction layers with the backbone. So, this proposed module learned to restore the clean image from the foggy image via the MSE loss in the training time. Notably, the aim was not fitting the restored image to the detection model. They trained the external FR module to help improve the weights in the main backbone, which helped enhance the quality of the features extracted from foggy images. The proposed approach was evaluated on the FOD and Foggy Driving dataset, proving the effectiveness of other detection methods.

The author in [23] proposed an encoder-decoder U-shaped network with residual connection from one layer to another for fog removal. Then, the authors employed the PP-YOLO [24] detection model for training object detection. The authors also created a dataset of foggy images by synthesizing them based on the existing dataset. Their ablation studies proved that the detection performance increased when including the proposed fog removal module.

The author in [12] proposed a synthesized foggy dataset named UIT-DroneFog based on a normal-weather dataset. Then, they experimented with the existing detectors on the new dataset to observe the performance. In their study, no fog removal techniques were recommended or used, but the authors proposed the combination of Double Heads and Cascade R-CNN, which achieved better results compared to the other methods.

C. Discussion

The adaptive domain approaches encourage object detectors to operate well on cross-domain datasets, which is suitable if we can not collect the images belonging to the domain we expect. Furthermore, adaptive object detectors also help us not to retrain the model for the new domain dataset, which is time-consuming. However, adaptive detectors still have limitations because they can not perform well as their counterparts trained and evaluated on the same domain data. Therefore, we suppose that if we have the images belonging to the domain data we need, it is unnecessary to employ adaptive detectors. So, in this study, we focus on exploring the performance of normal two-stage, one-stage and end-to-end object detection methods combined with de-hazing methods on the foggy dataset.

III. EXPERIMENTAL METHODS

A. Object Detectors

Object Detection is a complex, challenging problem in computer vision used to localize and classify objects based on images and videos. With the surging growth of Deep Learning in recent years, feature extraction from data is straightforward to implement and time-efficient, leading to the emergence

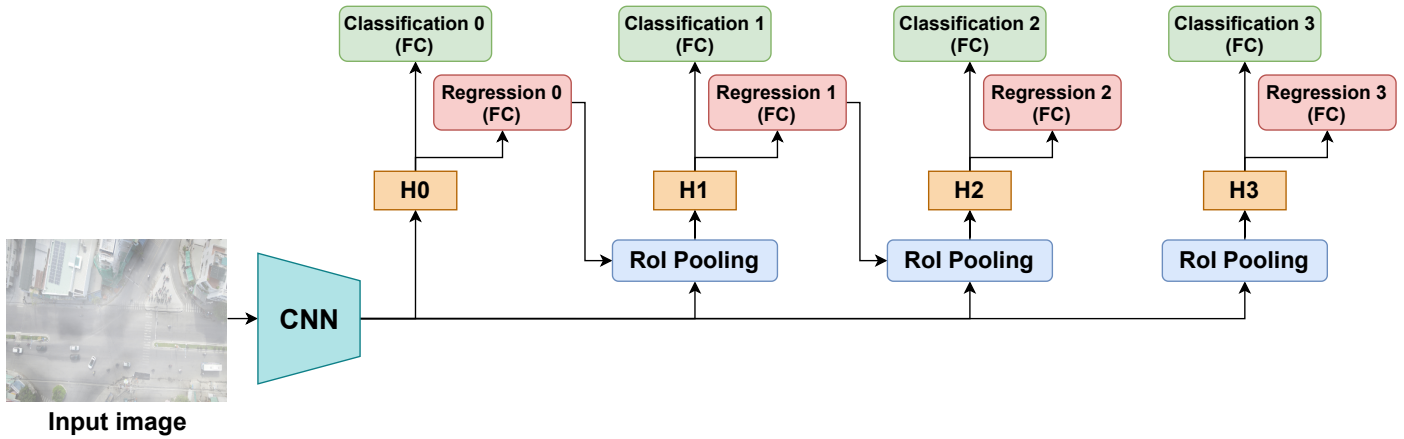


Fig. 1. Illustration of Two-Stage Cascade R-CNN Object Detection Method

of intensive studies of Object Detection. In addition to improvements in classification, researchers conduct many in-depth studies in localization to reduce computational costs and memory to make the model work more efficiently. Therefore, the research on the following detection frameworks happens to meet nowadays's needs: Two-stage, One-stage, Anchor-free and End-to-end object detection.

1) *Two-Stage Detectors*: The framework is also known as the region-based framework. Region proposals generated from input images pass through CNN where features are extracted. Then, based on the extracted features, category-specific classifiers are used to classify labels for the region proposals. There are many well-established two-stage methods that we are going to carry out the experiment on, like Cascade RCNN and Casdou.

Cascade R-CNN. In 2018, [11] proposed the high-quality detection model Cascade R-CNN. Multi-stage object detection architecture with set detectors trained in turn with the current detector's output as the input to the next detector used to solve not only the mismatch in quality between the output and the detector but also the overfitting problem caused by the sensitive IoU threshold (when the IoU is large). However, creating a high-quality detector is not simply increasing the IoU during the training phase. As we increase the IoU threshold, it also means that a significant decrease is witnessed in the number of active training samples. Different heads in the architecture designed for a particular IoU threshold, from small to large, are used at different stages (H1, H2, H3). Cascade regression is a resampling process, providing positive samples for further processing stages:

$$f(x, b) = f_T \circ f_{T-1} \circ \dots \circ f_1(x, b)$$

T : total number of refining bounding box stages. Each f_T regressor in the cascade optimized for the respective distribution b_T . Fig. 1 illustrates the architecture of Cascade R-CNN.

CasDou (Cascade R-CNN and DoubleHead). In the year 2021, [12] proposed Casdou with the combination of Cascade R-CNN, Double Heads [25], and Focal Loss [3]. The method tested on the high-quality aerial foggy outdoor vehicle dataset UIT-DroneFog achieved 34.70% on the mAP score. The author

used the Cascade R-CNN backbone instead of the Faster R-CNN because it helps the model attain high-quality detection with structural cascade regression. What's more, the Double Heads detector can be flexibly attached to various models to achieve higher detection results. In addition, based on their analysis and assumption, the author uses Focal Loss to help the model converge and have a more apparent distinction between class objects than Cross-Entropy Loss. Focal Loss is defined as follows:

$$L_{FL}(p_T) = -\alpha(1 - p_T)^\gamma \log(p_T)$$

With (α) is the balanced form of the Focal Loss function, and (γ) is used to calculate the modulating factor.

Fig. 2 illustrates the architecture of CasDou.

2) *One-Stage Detector*: Although achieving high accuracy, the two-stage methods are computationally expensive and have high resources-consumption. One-stage method - the YOLO was born for incredible processing speed while maintaining high accuracy to achieve real-time object detection. One-stage architecture directly predicts class probabilities and regress bounding-box offset values with a single feed-forward CNN network instead of heavily depending on generated region proposals.

YOLO-v3. (You Only Look Once v3) YOLO-v3 was proposed by [13] with the help to improve the accuracy of the object detection problem while keeping the inference time at the appropriate speed. YOLOv3 uses Darknet-53 (ImageNet [26] Trained Network) and Residual Network (ResNet)[27] consisting of 53 convolutional layers built with consecutive convolutional 3x3, and 1x1 layers, followed by ResNet connection skips to activate propagating through deeper layers without diminishing the gradient. Finally, the average pooling layer, 1000 fully connected layers, and Softmax activation function are added to perform classification. With this robust structure, DarkNet-53 has a much higher speed than other platforms like ResNet-101 or ResNet-152. Initially, the image is passed through a block of convolutional layers to extract features. Then, it is divided into a grid of size $S \times S$. When the image is divided into a grid, each cell in the image is responsible for detecting the object whose center locates on that cell. After selecting the anchor box, the model uses the

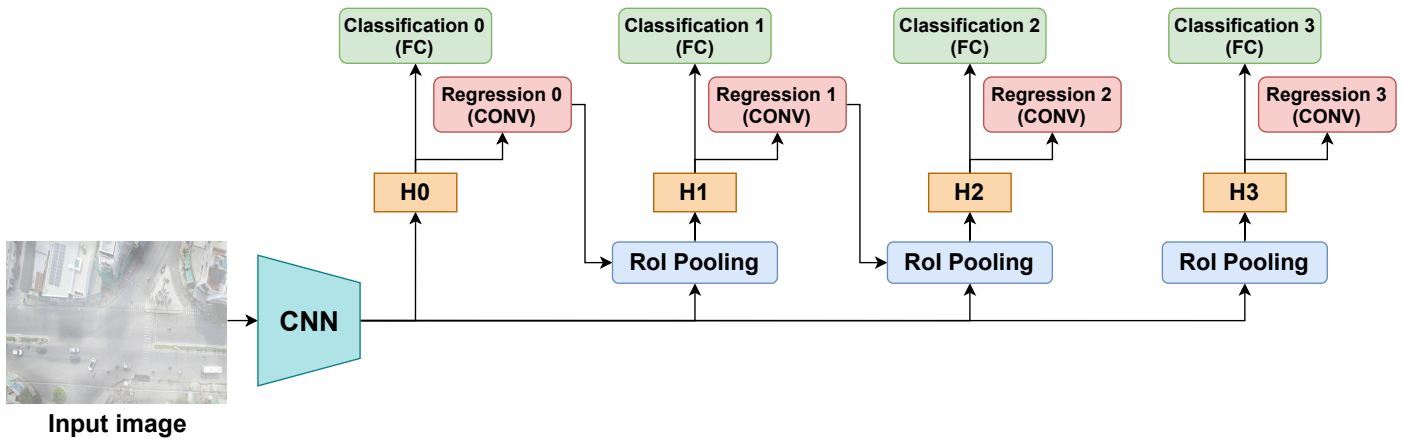


Fig. 2. Illustration of Two-Stage CasDou Object Detection Method

Direct Position Prediction formula to regress the size of the true bounding box. The model then predicts the bounding box's label using Multiple Classification. The illustration of the YOLOv3 method is shown in Fig. 3.

3) *Anchor-Free Detector*: Anchor-free detectors find the object without the preset anchors. It helps the model become less dependent on anchor-related hyperparameters and generalize more easily. CrossDet stands out to be the effective anchor-free detector that considers continuous object information and reduces noise interference.

CrossDet. CrossDet was proposed by [14] in 2021. Instead of using anchor-based methods and point-based methods that are inclined to produce noise feature output, the author proposed the CrossDet helping extract the information continuously and accurately. CrossDet-an anchor-free detector using a set of cross lines to represent objects consists of two main phases: (1) Generating the coarse crossline representation (2) Refining the crossline representation based on the extracted features on the horizontal and vertical lines. Based on trained cross lines features, feature maps $I \in R^{C \times W \times H}$ generated from backbone FPN are processed to crossline extract module (CEM). CEM is then trained to extract horizontal and vertical features. The model uses decoupled regression mechanism to optimize cross lines growth along with vertical or horizontal features. CrossDet yields the results on the two data VOC2007 [28] and MS-COCO [29], with the results, are 52.8 and 48.4 respectively on the AP score. Fig. 4 shows the architecture of CrossDet method.

4) *End-to-End Detectors*: The End-to-end approach aims to build a complex deep learning model, removing hand-designed components like pre-processing (anchor generation) and post-processing (Non-maximum suppression) and integrating them into a single model. Today's famous End-to-end methods are Deformable DETR or Sparse R-CNN. They work on sparse candidates which are progressively processed and refined through various stages.

Deformable DETR. In 2021, [15] proposed the Deformable DETR method as an improved version of the prior DETR [30]. However, achieving results as high as Faster R-CNN, DETR witnesses slow convergences and problems in detecting small objects due to the limitation of the attention

mechanism in the Transformer. The Deformable DETR is a combination of a Deformable convolution [31] and a Transformer [32]. It combines the effectiveness of the sparse spatial sampling of Deformable convolution and the relation modeling capability of Transformers. From there, it was formed into a Deformable attention module to focus on the part of "sampling spatial" as a pre-filter to focus on prominent areas instead of every location on the feature maps. Moreover, thanks to the fast convergence and flexibility of Deformable DETR, the authors also experimented with some methods to optimize the predict bounding box on the MS COCO dataset such as iterative bounding box refinement mechanism on region proposals proposed by the model. Experiments show that Deformable DETR converges faster and gives more accurate results than DETR with x10 fewer training epochs. Fig. 5 shows the architecture of Deformable DETR method.

Sparse R-CNN. In 2021, the Sparse R-CNN method, proposed by [16], is a sparse object detection method. Sparse R-CNN is an End-to-End object detection method because it eliminates the post-processing mechanism of non-maximum suppression, which is different from prior R-CNN models. Object detection methods such as the Dense method in the YOLO family where locations of anchor boxes densely cover spatial positions, scales, and aspect ratios in a single-shot way. A typical Dense-to-sparse approach is Faster R-CNN, which uses RPN [33] to derive region proposals from the dense region of candidates and refine those bounding boxes and class-specific features. The sparse method applied by Sparse R-CNN replaces RPN with a set of learnable region proposals and proposal features. Input is an image with a set of region proposals and proposal features that are randomly initialized and optimized with other parameters in the whole network. Features are extracted and fed into the backbone along with region proposals and proposal features, eventually generating outputs classification and localization. Sparse R-CNN shows its accuracy, run-time and convergence in training on the challenging COCO dataset, yielding a 45.0 AP score at 22 fps using the ResNet-50 FPN backbone. Fig. 6 shows the architecture of Sparse R-CNN object detection method.

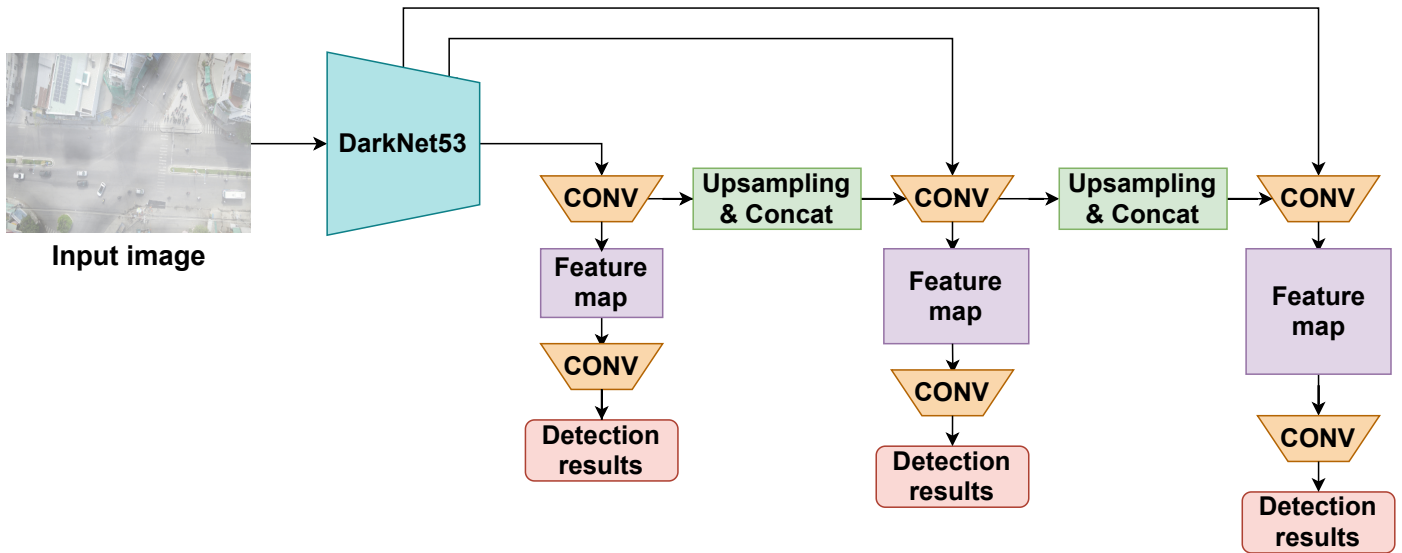


Fig. 3. Illustration of One-Stage YOLOv3 Object Detection Method

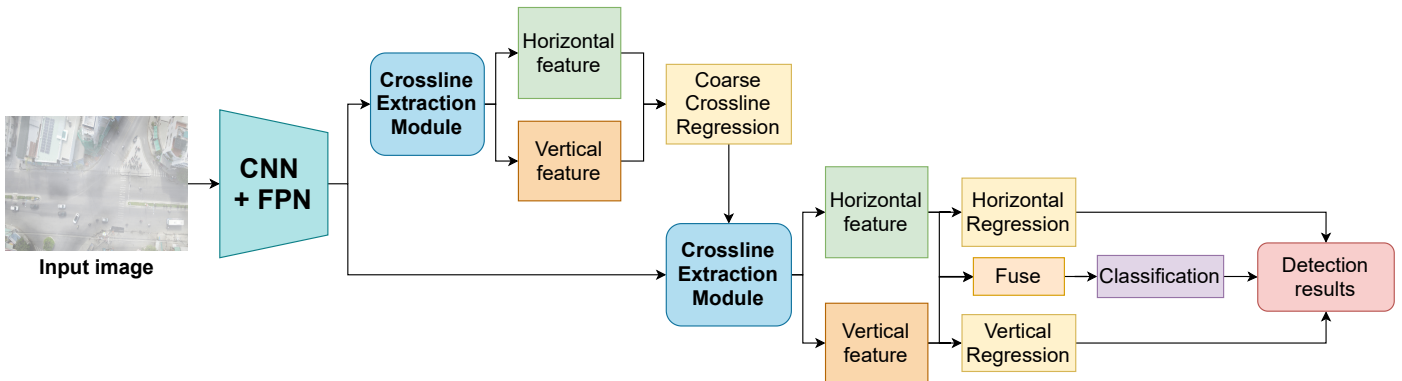


Fig. 4. Illustration of Anchor-Free CrossDet Object Detection Method

B. Image Dehazing Methods

1) *DW GAN (Discrete Wavelet Transform GAN)*: DW-GAN was proposed by [17] in 2021. This method was designed to tackle two problems that some existing CNN-based dehazing methods have when working with non-homogeneous cases. These problems are the loss of texture details when images are being dehazed due to the complicated haze distribution and over-fitting problems because of the lack of training data. The architecture of this method is a novel two-branch generative adversarial network. For the first branch, called the DWT branch, they proposed the idea of directly embedding the frequency domain knowledge into the dehazing network by utilizing wavelet transform. Therefore more high-frequency knowledge in the feature map can be retained. In terms of the knowledge adaptation branch, the Res2Net was employed with the pre-trained ImageNet weights as initialization in order to prevent overfitting and improve the generalization ability of the network. Finally, they add a basic 7×7 convolution layer as a fusion operation to map the features from two branches to clear images. Furthermore, they also introduced the final loss blend function shown in Equation 1. (L_1) is L1 loss, (L_{SSIM}) denotes MS-SSIM [34] loss, ($L_{perceptual}$) represents

perceptual loss [35] and, for the adversarial loss (L_{adv}), the discriminator in [36] is employed.

$$\mathcal{L}_{total} = L_1 + \alpha L_{SSIM} + \beta L_{perceptual} + \gamma_4 L_{adv} \quad (1)$$

Where (α) = 0.2, (β) = 0.001 and (γ) = 0.005 are the hyper-parameters weighting for each loss functions.

2) *Two-Branch Dehazing*: [18] proposed another two-branch neural network for non-homogeneous dehazing via ensemble learning. The authors found that a carefully built CNN frequently fails on a non-homogeneous dehazing dataset introduced by NITRE challenges [37] even though it performs well on large-scaled dehazing bench-marks. Therefore, they introduced a two-branch neural network to deal with the aforementioned problems separately, followed by a learnable fusion tail to map their different features. The first branch, the transfer learning sub-net, is based on an ImageNet pre-trained Res2Net. This branch extracts robust global representations from input images with pre-trained weights and then helps the network address the problem of lacking training data. In the second

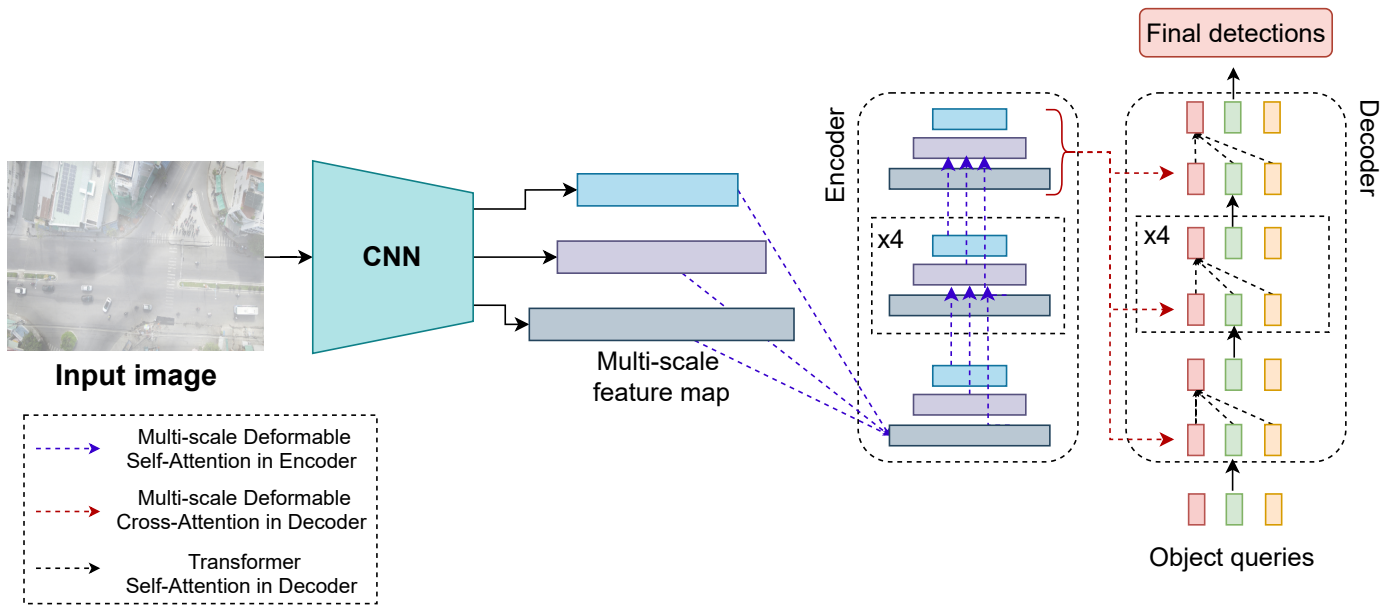


Fig. 5. Illustration of End-to-End Deformable DETR Object Detection Method

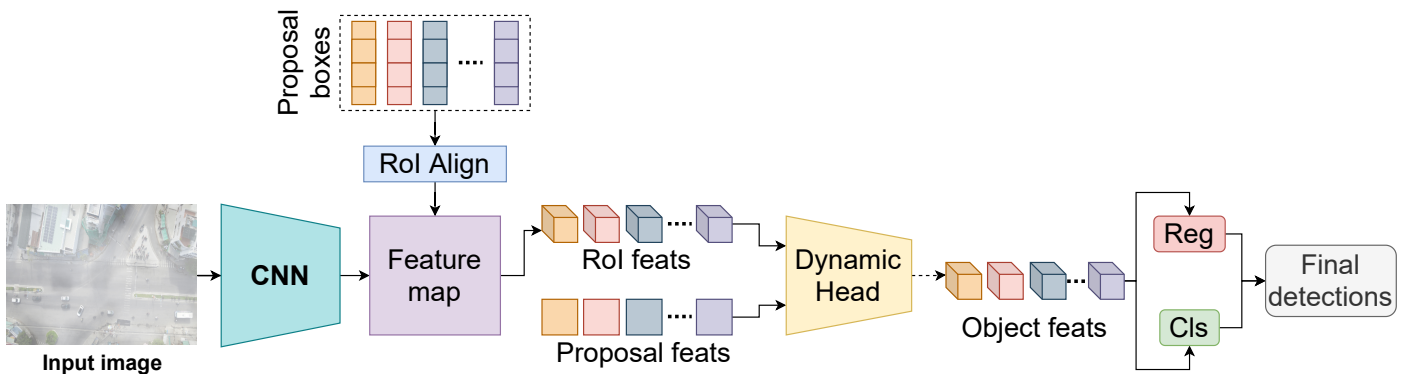


Fig. 6. Illustration of End-to-End Sparse R-CNN Object Detection Method

branch, [18] used residual channel attention network to design the current data fitting sub-net. This branch has five residual groups; each has ten residual blocks. However, the second branch always maintains the input image's original resolution and avoids using any downsampling operation. Finally, a fusion layer generates the entire network's final output. The fusion layer, in particular, takes the concatenation of features from the branches and maps them to clear outputs. Besides, they also applied the adversarial loss with the discriminator in [36] because of its effectiveness in helping restore photo-realistic photos [38], especially for a small-scaled dataset.

IV. EXPERIMENTAL RESULTS

A. Benchmark Suite

In this study, the UIT-DroneFog dataset, which was created by [12], was employed to evaluate the performances of detectors in foggy aerial images. This dataset consists of 15,370 foggy aerial images captured by drones with about 0.6 million bounding boxes of various means of transportation and pedestrians. This dataset has four classes: Pedestrian, Motor,

Car, and Bus. We also used the default subsets provided by the authors, which include: Training set (8,580 images), Validation set (1,061 images), and Testing set (5,729 images). The numbers of each class are shown in Fig. 7.

There are several reasons why we choose this dataset. Firstly, the images in this dataset are of high quality, which helps the detectors work more efficiently. Secondly, the context of these images is diverse and especially, there is an imbalance in this dataset with a vast majority of motor objects. This can be a tough challenge for our detectors.

Example images of this dataset are shown in Fig. 8.

B. Experimental Settings

The experimental processes were conducted on a GeForce RTX 2080 Ti GPU with 11018 MiB memory. We trained the models by employing the MMDetection framework V2.10.0[39]. For each model, we used the highest mAP score configuration, provided on the MMDetection GitHub website¹

¹<https://github.com/open-mmlab/mmdetection>

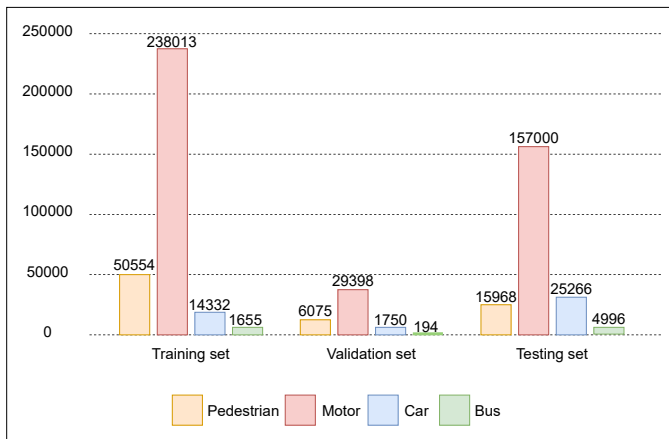


Fig. 7. Statistics of UIT-DroneFog Dataset.

or author's GitHub. We conducted every training process on a single GeForce RTX 2080 Ti GPU.

To evaluate the detectors, we used the best weights of each model on the validation set to predict and report the results on the testing set via the mAP measure to evaluate the performance of models, which is the same as the object detection contest on the MS COCO dataset. The AP score was calculated for 10 IoU varied from 50% to 95% with steps of 5%. Besides, the results of two specified values of 50% and 75% were also reported.

C. Experimental Results

The experimental results are reported in Table I, Table II, Table III. In Table I, we report the performance of five experimental object detectors on original foggy images. Overall, CasDou - a two-stage method - shows the best performance (34.7% AP) while YOLOv3 performs the worst. These results reflect the characteristic of two-stage and one-stage detectors correctly: two-stage methods often perform better than one-stage methods about accuracy. However, Deformable DETR, an end-to-end detector, has the highest results on Pedestrian and Motor class objects, which are 0.5% and 2.8% higher than CasDou. Moreover, Deformable DETR is exceptionally competitive with CasDou about AP score (33.7% AP compared to 34.7% AP), proving that end-to-end detectors that may have higher FPS can perform as well as two-stage detectors.

In Table II, we report the results of five object detectors but use DW-GAN to de-haze images before training. In general, there is a variation in the order of accuracy between the methods. Cascade R-CNN, again a two-stage method, becomes the detector that shows the best performance among the experimented detectors, but the AP score is not higher than CasDou trained on original foggy images. However, Cascade R-CNN trained on images de-hazed by DW-GAN has a noticeable improvement than its counterpart trained on synthetic hazy images (+1.3% AP, +2.5% AP@50, +1.9% AP@75). Furthermore, DW-GAN also helps YOLOv3 and Sparse R-CNN enhance the AP score compared to their results in Table I (+1.4% AP and +0.3% AP, respectively). Therefore, de-hazing images using DW-GAN significantly and positively affect the performance of five object detectors.

Table III reports the results using Two-Branch as the de-hazing method. It can be seen that this de-hazing method can not help object detectors improve the results compared to their counterparts trained on original hazy images. However, the accuracy between the methods is the same as Table I: CasDou shows the best performance (33.1% AP) and YOLOv3 performs the worst (20.4% AP); CasDou also indicates the best AP on Car and Bus classes (57.4% AP and 40.1% AP) while Deformable DETR shows the best AP on Pedestrian and Motor (2.7% AP and 35.8% AP). Notably, the CrossDet detector using the Two-Branch de-hazing method shows a slight improvement compared to its results in Table I (+0.5% AP, +0.3% AP@50, +1.3% AP@75).

Through three experimental results, we can notice that two-stage methods, especially CasDou and Cascade R-CNN, have the ability to perform better than one-stage and end-to-end detectors on both original and dehazed datasets. Besides, from these experiments, it can be seen that resurfacing objects from hazy aerial images by dehazing them is a tough challenge and not always effective due to color deviation and the loss of information compared to haze-free images. In fact, the Two-branch dehazing method significantly reduces the detection results of CasDou's detection result (-1.6% AP), while the DW-GAN is proved to be more effective when helping Cascade R-CNN improve its detection results were improved. This could be explained by the fact that DW-GAN has higher results than Two-branch dehazing when both of these two methods use the same dataset [37]. In addition, although the AP result is not so high, the DETR shows that this method can outperform all other methods by a large margin when detecting small objects, which are Pedestrian and Motor, on all three datasets (shown in Fig. 9). This means that although the small objects are blurred by fog, this method learns the features of this kind of object better. On the other hand, when detecting objects in big sizes such as Bus and Car - many times bigger than Motor and Pedestrian, a two-stage method will be an appropriate choice because the AP scores of Car and Bus detected by two-stage methods in three report tables always ranks top. Fig. 10 and Fig. 11 show the detection results of CasDou and Cascade R-CNN methods with and without using de-hazing techniques.

V. CONCLUSION

This study has provided experimental results and a thorough analysis of condition-based approaches to the problem of vehicle detection on aerial images in foggy weather. In short, we evaluate the effectiveness of advanced object detectors on aerial images with and without foggy removal. DW-GAN and Two-Branch are used for de-hazing. CasDou achieves the highest performance among experiments when the AP is recorded at 34.7% on original images. Experimental results also show that detectors trained on de-hazed methods can not achieve the best results. Still, with some detectors such as YOLOv3, CrossDet, Sparse R-CNN, foggy removal help them slightly improve the detection performance compared to their counterparts trained on original images. As we reported, the approaches using a GAN-based model to remove foggy images somehow can not achieve the result of using original images. Therefore, in the future, we plan to conduct more experiments on other recent GAN-based methods to explore their effectiveness in de-hazing. Besides, we also plan to



Fig. 8. Example Images of UIT-DroneFog Dataset.

TABLE I. EXPERIMENTAL RESULTS WITH THE DEFAULT CONFIGURATION. THE BEST PERFORMANCE IS MARKED IN BOLDFACE (NOT DEHAZED).

Method	Pedestrian	Motor	Car	Bus	AP	AP@50	AP@75
Cascade R-CNN	2.10	34.50	56.80	38.40	32.90	45.80	38.50
CasDou	2.70	34.20	59.30	42.50	34.70	50.20	40.30
CrossDet	1.60	27.30	51.10	31.80	27.90	45.60	30.30
YOLOv3	1.10	21.50	41.10	15.80	19.90	32.10	21.10
Deformable DETR	3.20	37.00	56.30	38.30	33.70	51.60	38.00
Sparse R-CNN	2.70	23.80	30.80	28.80	21.50	32.90	23.20

TABLE II. EXPERIMENTAL RESULTS ON UIT-DRONE21 DEHAZED BY DWGAN. THE BEST PERFORMANCE IS MARKED IN BOLDFACE.

Method	Pedestrian	Motor	Car	Bus	AP	AP@50	AP@75
Cascade R-CNN	2.20	32.90	58.80	42.80	34.20	48.30	40.40
CasDou	2.30	32.70	58.30	39.60	33.20	47.80	38.10
CrossDet	1.30	27.20	50.60	29.40	27.10	44.00	29.70
YOLOv3	1.20	21.10	41.50	21.30	21.30	33.30	23.60
Deformable DETR	2.10	35.10	55.40	36.20	32.20	48.60	37.30
Sparse R-CNN	2.30	22.70	33.90	28.30	21.80	32.50	24.20

TABLE III. EXPERIMENTAL RESULTS DEHAZED BY TWO-BRANCH. THE BEST PERFORMANCE IS MARKED IN BOLDFACE.

Method	Pedestrian	Motor	Car	Bus	AP	AP@50	AP@75
Cascade R-CNN	1.90	32.40	57.30	38.60	32.60	45.50	38.40
CasDou	1.90	33.00	57.40	40.10	33.10	46.60	39.10
CrossDet	2.00	25.60	51.00	33.50	28.00	44.40	31.00
YOLOv3	8.00	20.20	40.30	20.20	20.40	32.40	22.40
Deformable DETR	2.70	35.80	54.70	32.80	31.50	48.40	35.30
Sparse R-CNN	2.40	23.20	32.20	27.90	21.40	32.70	23.40

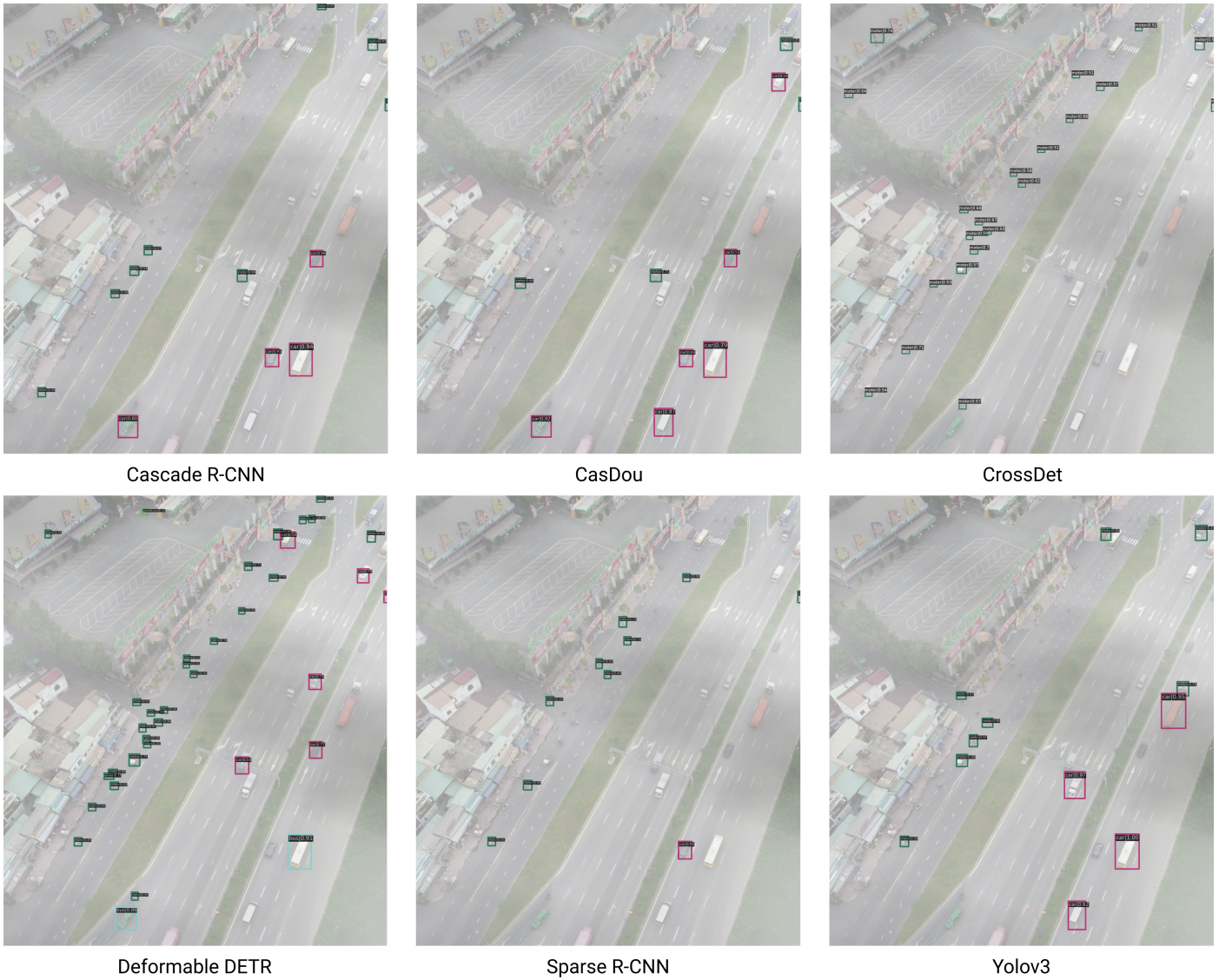


Fig. 9. Visualization Images of Detectors on UIT-DroneFog Dataset. (In Order to See the Image Clearly, Please Zoom in 2×.)

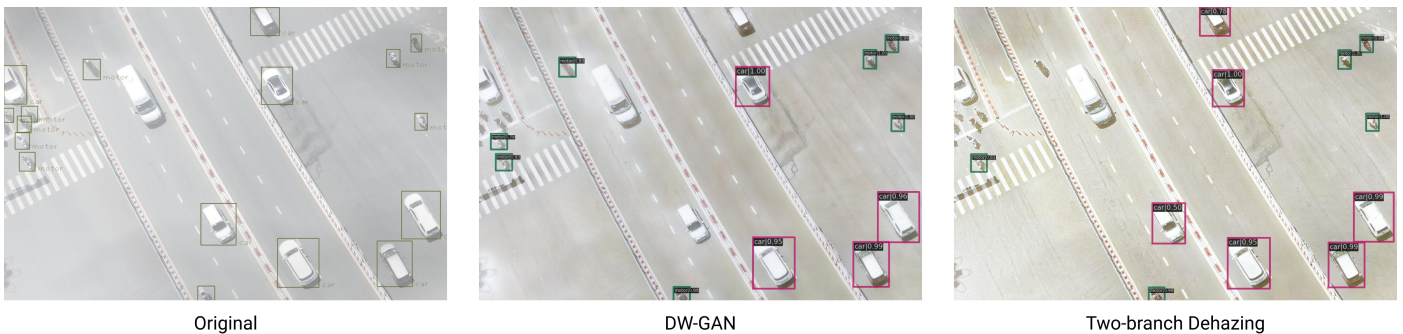


Fig. 10. CasDou on 3 Types of Dataset. The Dark Green Bounding Boxes are Motor, The Purple Bounding Boxes are Car, Light Green Bounding Boxes are Pedestrian and Bus are Cyan. (In Order to See the Image Clearly, Please Zoom in 2×.)

propose a new approach that can adaptively predict foggy images using a model trained on original images.

ACKNOWLEDGMENT

This research is funded by Vietnam National University HoChiMinh City (VNU-HCM) under grant number DS2021-

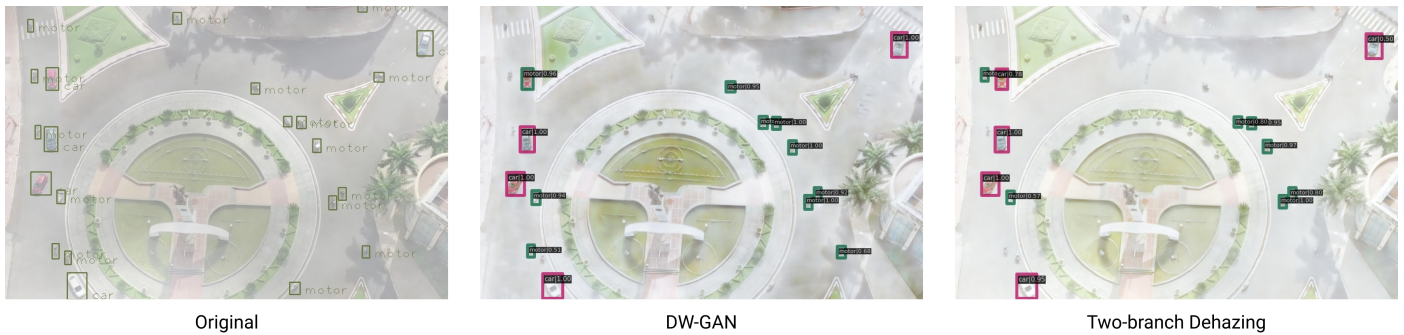


Fig. 11. Cascade R-CNN on 3 Types of Dataset. (In Order to See the Image Clearly, Please Zoom in 2×.)

26-01. We also would like to show our gratitude to the UIT-Together research group for sharing their pearls of wisdom with us during this research.

REFERENCES

- [1] Y. LeCun, Y. Bengio, and G. Hinton, "Deep learning," *nature*, vol. 521, no. 7553, pp. 436–444, 2015.
- [2] M. Y. Yang, W. Liao, X. Li, Y. Cao, and B. Rosenhahn, "Vehicle detection in aerial images," *Photogrammetric Engineering & Remote Sensing*, vol. 85, no. 4, pp. 297–304, 2019.
- [3] T.-Y. Lin, P. Goyal, R. Girshick, K. He, and P. Dollár, "Focal loss for dense object detection," in *Proceedings of the IEEE international conference on computer vision*, 2017, pp. 2980–2988.
- [4] J. Lu, C. Ma, L. Li, X. Xing, Y. Zhang, Z. Wang, and J. Xu, "A vehicle detection method for aerial image based on yolo," *Journal of Computer and Communications*, vol. 6, no. 11, pp. 98–107, 2018.
- [5] J. Redmon, S. Divvala, R. Girshick, and A. Farhadi, "You only look once: Unified, real-time object detection," in *Proceedings of the IEEE conference on computer vision and pattern recognition*, 2016, pp. 779–788.
- [6] T. N. Mundhenk, G. Konjevod, W. A. Sakla, and K. Boakye, "A large contextual dataset for classification, detection and counting of cars with deep learning," in *European conference on computer vision*. Springer, 2016, pp. 785–800.
- [7] S. Razakarivony and F. Jurie, "Vehicle detection in aerial imagery: A small target detection benchmark," *Journal of Visual Communication and Image Representation*, vol. 34, pp. 187–203, 2016.
- [8] G.-S. Xia, X. Bai, J. Ding, Z. Zhu, S. Belongie, J. Luo, M. Datu, M. Pelillo, and L. Zhang, "Dota: A large-scale dataset for object detection in aerial images," in *Proceedings of the IEEE conference on computer vision and pattern recognition*, 2018, pp. 3974–3983.
- [9] S.-C. Huang, Q.-V. Hoang, and T.-H. Le, "Sfa-net: A selective features absorption network for object detection in rainy weather conditions," *IEEE Transactions on Neural Networks and Learning Systems*, 2022.
- [10] C. Sakaridis, D. Dai, and L. Van Gool, "Semantic foggy scene understanding with synthetic data," *International Journal of Computer Vision*, vol. 126, no. 9, pp. 973–992, 2018.
- [11] Z. Cai and N. Vasconcelos, "Cascade r-cnn: Delving into high quality object detection," in *Proceedings of the IEEE conference on computer vision and pattern recognition*, 2018, pp. 6154–6162.
- [12] M. T. Tran, B. V. Tran, N. D. Vo, and K. Nguyen, "Uit-dronefog: Toward high-performance object detection via high-quality aerial foggy dataset," in *2021 8th NAFOSTED Conference on Information and Computer Science (NICS)*. IEEE, 2021, pp. 290–295.
- [13] J. Redmon and A. Farhadi, "Yolov3: An incremental improvement," *arXiv preprint arXiv:1804.02767*, 2018.
- [14] H. Qiu, H. Li, Q. Wu, J. Cui, Z. Song, L. Wang, and M. Zhang, "Crossdet: Crossline representation for object detection," in *Proceedings of the IEEE/CVF International Conference on Computer Vision*, 2021, pp. 3195–3204.
- [15] X. Zhu, W. Su, L. Lu, B. Li, X. Wang, and J. Dai, "Deformable detr: Deformable transformers for end-to-end object detection," *arXiv preprint arXiv:2010.04159*, 2020.
- [16] P. Sun, R. Zhang, Y. Jiang, T. Kong, C. Xu, W. Zhan, M. Tomizuka, L. Li, Z. Yuan, C. Wang *et al.*, "Sparse r-cnn: End-to-end object detection with learnable proposals," in *Proceedings of the IEEE/CVF Conference on Computer Vision and Pattern Recognition*, 2021, pp. 14454–14463.
- [17] M. Fu, H. Liu, Y. Yu, J. Chen, and K. Wang, "Dw-gan: A discrete wavelet transform gan for nonhomogeneous dehazing," in *Proceedings of the IEEE/CVF Conference on Computer Vision and Pattern Recognition*, 2021, pp. 203–212.
- [18] Y. Yu, H. Liu, M. Fu, J. Chen, X. Wang, and K. Wang, "A two-branch neural network for non-homogeneous dehazing via ensemble learning," in *Proceedings of the IEEE/CVF Conference on Computer Vision and Pattern Recognition*, 2021, pp. 193–202.
- [19] Y. Chen, W. Li, C. Sakaridis, D. Dai, and L. Van Gool, "Domain adaptive faster r-cnn for object detection in the wild," in *Proceedings of the IEEE conference on computer vision and pattern recognition*, 2018, pp. 3339–3348.
- [20] M. Khodabandeh, A. Vahdat, M. Ranjbar, and W. G. Macready, "A robust learning approach to domain adaptive object detection," in *Proceedings of the IEEE/CVF International Conference on Computer Vision*, 2019, pp. 480–490.
- [21] V. A. Sindagi, P. Oza, R. Yasarla, and V. M. Patel, "Prior-based domain adaptive object detection for hazy and rainy conditions," in *European Conference on Computer Vision*. Springer, 2020, pp. 763–780.
- [22] S.-C. Huang, T.-H. Le, and D.-W. Jaw, "Dsnet: Joint semantic learning for object detection in increment weather conditions," *IEEE transactions on pattern analysis and machine intelligence*, vol. 43, no. 8, pp. 2623–2633, 2020.
- [23] P. Sen, A. Das, and N. Sahu, "Object detection in foggy weather conditions," in *International Conference on Intelligent Computing & Optimization*. Springer, 2021, pp. 728–737.
- [24] X. Long, K. Deng, G. Wang, Y. Zhang, Q. Dang, Y. Gao, H. Shen, J. Ren, S. Han, E. Ding *et al.*, "Pp-yolo: An effective and efficient implementation of object detector," *arXiv preprint arXiv:2007.12099*, 2020.
- [25] Y. Wu, Y. Chen, L. Yuan, Z. Liu, L. Wang, H. Li, and Y. Fu, "Rethinking classification and localization for object detection," in *Proceedings of the IEEE/CVF conference on computer vision and pattern recognition*, 2020, pp. 10186–10195.
- [26] J. Deng, W. Dong, R. Socher, L.-J. Li, K. Li, and L. Fei-Fei, "Imagenet: A large-scale hierarchical image database," in *2009 IEEE conference on computer vision and pattern recognition*. Ieee, 2009, pp. 248–255.
- [27] K. He, X. Zhang, S. Ren, and J. Sun, "Deep residual learning for image recognition," in *Proceedings of the IEEE Conference on Computer Vision and Pattern Recognition (CVPR)*, June 2016.
- [28] D. Hoiem, S. K. Divvala, and J. H. Hays, "Pascal voc 2008 challenge," *World Literature Today*, vol. 24, 2009.

- [29] T.-Y. Lin, M. Maire, S. Belongie, J. Hays, P. Perona, D. Ramanan, P. Dollár, and C. L. Zitnick, "Microsoft coco: Common objects in context," in *European conference on computer vision*. Springer, 2014, pp. 740–755.
- [30] N. Carion, F. Massa, G. Synnaeve, N. Usunier, A. Kirillov, and S. Zagoruyko, "End-to-end object detection with transformers," in *European conference on computer vision*. Springer, 2020, pp. 213–229.
- [31] J. Dai, H. Qi, Y. Xiong, Y. Li, G. Zhang, H. Hu, and Y. Wei, "Deformable convolutional networks," in *Proceedings of the IEEE international conference on computer vision*, 2017, pp. 764–773.
- [32] A. Vaswani, N. Shazeer, N. Parmar, J. Uszkoreit, L. Jones, A. N. Gomez, E. Kaiser, and I. Polosukhin, "Attention is all you need," *Advances in neural information processing systems*, vol. 30, 2017.
- [33] S. Ren, K. He, R. Girshick, and J. Sun, "Faster r-cnn: Towards real-time object detection with region proposal networks," 2016.
- [34] Z. Wang, A. C. Bovik, H. R. Sheikh, and E. P. Simoncelli, "Image quality assessment: from error visibility to structural similarity," *IEEE transactions on image processing*, vol. 13, no. 4, pp. 600–612, 2004.
- [35] J. Johnson, A. Alahi, and L. Fei-Fei, "Perceptual losses for real-time style transfer and super-resolution," in *European conference on computer vision*. Springer, 2016, pp. 694–711.
- [36] J.-Y. Zhu, T. Park, P. Isola, and A. A. Efros, "Unpaired image-to-image translation using cycle-consistent adversarial networks," in *Proceedings of the IEEE international conference on computer vision*, 2017, pp. 2223–2232.
- [37] C. O. Ancuti, C. Ancuti, F.-A. Vasluianu, and R. Timofte, "Ntire 2021 nonhomogeneous dehazing challenge report," in *Proceedings of the IEEE/CVF Conference on Computer Vision and Pattern Recognition*, 2021, pp. 627–646.
- [38] C. Ledig, L. Theis, F. Huszár, J. Caballero, A. Cunningham, A. Acosta, A. Aitken, A. Tejani, J. Totz, Z. Wang *et al.*, "Photo-realistic single image super-resolution using a generative adversarial network," in *Proceedings of the IEEE conference on computer vision and pattern recognition*, 2017, pp. 4681–4690.
- [39] K. Chen, J. Wang, J. Pang, Y. Cao, Y. Xiong, X. Li, S. Sun, W. Feng, Z. Liu, J. Xu *et al.*, "Mmdetection: Open mmlab detection toolbox and benchmark," *arXiv preprint arXiv:1906.07155*, 2019.

Designing a Mobile Application using Augmented Reality: The Case of Children with Learning Disabilities

Misael Lazo-Amado, Leoncio Cueva-Ruiz, Laberiano Andrade-Arenas
Facultad de Ciencias e Ingeniería
Universidad de Ciencias y Humanidades, Lima, Peru

Abstract—The learning disorder has several difficulties to learn correctly; in many cases they have more stress because they do not understand the subjects proposed by the teacher. The aim of the research is to propose an innovative plan to design a mobile application for the treatment of learning disabilities using augmented reality in primary education. In this way, we used a methodology called Design Thinking that has five phases, empathize, define, devise, prototype and testing, which facilitates us in identifying the problems for itself to have solutions to these problems. For the prototype we used tools such as Marvel App, which is responsible for the layout of the mobile application. TinkerCad allows us to design the 3D model of the educational games and finally App Augmented Class to create the augmented reality model. The results obtained were through a survey about the prototype; identifying the acceptance about the prototype by parents for the usefulness of this idea for their children with learning disabilities, with 76% that the prototype is ideal for children. In addition, the prototype was validated by five experts, resulting in 85.4% acceptance. As a conclusion of the research is the achievement of a good design for a solution to the problems of children with learning disabilities to have a better understanding and to be free from stress.

Keywords—App augmented class; design thinking; marvel App; learning disorder; TinkerCad

I. INTRODUCTION

The learning disorder makes it difficult for the child to learn these causes correctly. These are presented worldwide, as there are various problems of language, comprehension or dyscalculia. In Jordan, it indicates that their primary school students have a lack of attention to classes, as they have a bad use of the internet, causing them to be completely distracted and prevent them from developing in their student process [1]. COVID-19 also had an impact on primary education, students were studying from home, avoiding the physical approach; they had no control over their virtual classes and were easily distracted by video games [2]. In the United States, multilingual children in most American schools are found to have language and learning disabilities [3].

In rural areas of Latin America there are difficulties in children's learning. In this way they obtain a low level in their subjects, as they do not have any learning method [4]. By the end of 2021, students in Latin America will be affected by the COVID-19 pandemic, making a rapid shift from face-to-face to digital learning [5]. Brazil has 55 million people living in extreme poverty and has pre-school boys with illiteracy problems [6]. This developing, resource-poor

country also analyses that 21 families believe that difficulties in learning development stem from poor social interactions, peer relationships, stress levels and communication [7].

In Peru, there were educational problems in the teaching of children during the COVID-19 pandemic [8]. They had student delays because virtual classes were not proposed. When these methods were declared, in Ayacucho and indigenous populations, they did not have these materials to carry out their classes at a distance, and also because of poor learning, the children had various problems of learning disorders [9] [10]. In this way, many children, especially in rural areas of Peru, have problems learning mathematics [11]. This also increases the level of stress, as they do not have the strategic methods for the child to be able to understand these subjects in an easy and simple way [12]. Also, dyscalculia which is a learning disorder can cause many problems at primary level and many mistakes in performing logical operations, lack of attention and concentration makes children unable to perform these functions [13].

According to these problems at international and national level, we can see the importance of having new innovative and strategic models for students at primary level to have ease in their understanding so that they can improve these learning disorders and prepare themselves to not have any difficulties in their future life. With the proposed design for the solution of the problems of children with learning problems is helping parents where their children have these difficulties. So also with the teachers since in this way the learning of the students will be much better.

The objective proposed in this project is to develop a strategic and innovative model to solve these problems, designing a mobile application for the treatment of learning disorders, using augmented reality in primary education. Cognitive games were used to improve student learning. The structure of the paper is as follows: in Section II the literature review is explained, in Section III the methodology to be developed, in Section IV the results of our work, in Section V the discussions, in Section VI the conclusions and finally in Section VII the future work.

II. LITERATURE REVIEW

Augmented reality in education allows us to do didactic work as well as help us to discover new skills in children. It also implements an analysis of the impact of augmented reality in education, which indicates that teachers enable children to learn quickly and relieve their stress with the help of

augmented reality [14]. Similarly, this research analyses by Likert scale that students have more problems in the subject of geometry, and also evaluates a development of augmented reality to improve learning, indicating that 92.50% are satisfied with the use of technology and it is suitable for use in Indonesian schools [15].

In the same way, it indicates that augmented reality is used to enjoy and live a better educational experience. Therefore, the use of augmented reality was developed for the teaching of mathematics, helping to obtain a better visualisation and understanding in secondary school students. This was developed with Unity and was accompanied by the Vuforia software development kit in order to develop the augmented reality application. At the end they obtained as a result, a mobile application with augmented reality accessible to all devices that are installed in each classroom to improve the understanding of students in an easy and simple way [16].

At Sebelas Maret University, form-based tests were used with students and teachers to indicate problems in their programming education. A multimedia with augmented reality was also developed to improve critical thinking, resulting in a better understanding of basic and advanced programming [17]. Something similar happens in this case, on the subject of biological education that develops an augmented reality application with Unity 3D for the training of its medical and veterinary students. Students indicate that augmented reality technology enhances their learning by demonstrating that virtual technology is a great support in their practices in human and animal anatomy [18].

On the other hand, he designed a mobile application with augmented reality, indicated that it will be the future of education. With the use of the Assembly application, he proposes that primary education can improve their learning in their computer, tablet and mobile assembly laboratories. This is done virtually, as during this pandemic, health restrictions prevented students from having contact with other people, which affected their face-to-face teaching. As a result, a survey of students showed that augmented reality design would be of great help in their laboratories [19]. Similarly, in this research, it helps students to develop their knowledge in chemistry with intuitive games to learn science-related topics. This is done by combining three-dimensional objects from the virtual world to a real one, 87.90% of Indonesian students validate their improvement in their understanding of chemistry [20].

In the same way, in the business field, a mobile application is designed with the use of augmented reality to provide a multimedia marketing method with augmented reality. As a result, it was possible to improve advertising and impact users with the use of these technologies [21]. This research also used Unity with the c# programming language, Blender 3D to develop a catalogue list application for the purchase of food and beverages with augmented reality. As a result, it improved the visualisation of customers observing in detail the quality of the product, gaining confidence in their purchase [22]. Finally, this article proposes to improve communications in companies, implementing an augmented reality design in animated infographics to improve their presentations, using Unity 3D to optimise communications processes resulting in the interest of new clients for their future projects [23].

The augmented reality identified by different authors in the fields of education, medicine, security, business among others, indicate the improvements that people can have when interacting with technologies. In this way, it provides ease of understanding, thus releasing stress, containing best practices in its development, so that its usefulness should be considered in problem solving. These aspects facilitate augmented reality solutions for children with learning disabilities. In this way, we will make a model for children, aiming to improve concentration in an efficient way in their cognitive development.

III. METHODOLOGY

For the development of the methodology we will use Design Thinking which will be divided into five phases (Empathise, Define, Ideate, Prototype and Test), as well as explaining the survey tools and the design of the prototype that was used.

A. Design Thinking

This methodology is focused on presenting creative solutions, generating ideas to improve society, and the methodology is of great interest to professionals because of their ability to adapt their innovative ideas [24]. The processes of Design Thinking are shown in Fig. 1. They are used to improve business environments by complementing the help of users in identifying their problems and thus solving them [25].

- 1) Parent survey: A survey of parents about learning difficulties was formulated at the beginning.
- 2) Do children have learning difficulties? In this first conditional we asked if they found the problems, if it was confirmed we took it into account and proceeded to the next step, if not we went back to the survey.
- 3) Identification of learning difficulties: In this process the children's learning problems were identified.
- 4) Solutions for learning disorders: In this process the identified problems are proposed to be solved.
- 5) Definition of the ideas of the prototype: Based on the proposed ideas, the final prototype is defined.
- 6) Surveys about the prototype: A survey about the prototype was formulated to parents for acceptance and development.
- 7) Is it an ideal prototype for children? In this second conditional it was asked if it is the ideal prototype, if it is ideal it is taken into account and if it is not, the new prototype is implemented again.
- 8) Innovation accepted: Finally, the prototype defined by the parents was accepted.

1) *Empathise*: In this first stage, it is focused on observing the needs of the users continuously through the use of interviews and surveys giving the facility to gain a better understanding of their needs [26].

2) *Define*: In this second stage, the focus is on defining the user problems that are in the empathise phase so that the innovation team must consider the biggest problem impacted by the users [27].

3) *Ideate*: This is the third stage, which is responsible for generating innovative ideas for the problems of the defined stage, allowing the team to name the best solution [28].

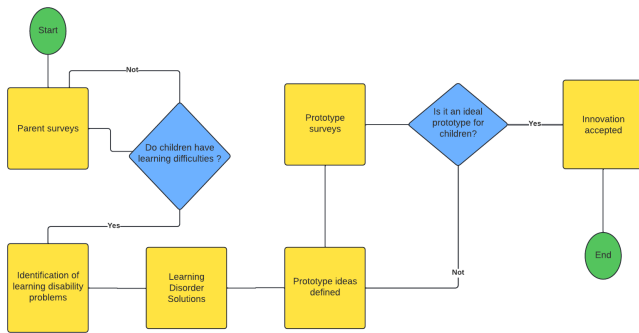


Fig. 1. Process Design Thinking.

4) *Prototype*: The fourth stage, prototyping, is responsible for designing the innovative solutions chosen by the working team in such a way that it uses prototyping tools [29]. Fig. 2 will show the procedure for the development of the mobile prototype with Marvel App, accompanied by a 3D modelling with TinkerCad and finally show the augmented reality with App Augmented Class.

a) *Tinkercad*: Tinkercad is a free tool that is used in education to design 3D objects online, its designs are made in an intuitive and easy to use way [30].

b) *MarvelAPP*: MarvelApp is a tool for the design of prototypes, with simple steps for its use, as well as limited templates for the user [31].

c) *App Augmented Class*: This application is used to design augmented reality models, it is free to use and can be downloaded from the Play Store [32].

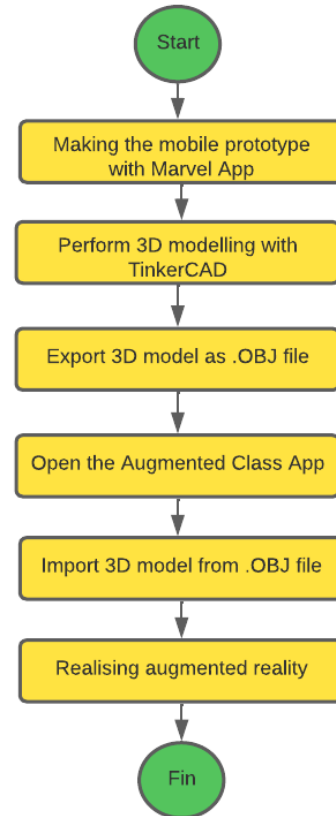


Fig. 2. The Process of Making an Augmented Reality Model.

- 1) Mobile prototyping with Marvel Apps: The start of this process is to make the mobile prototype to get the idea of the app's functions.
- 2) Make the 3D modelling with TinkerCAD: The second process was done using 3D models in TinkerCad in order to design the dynamic games for augmented reality.
- 3) Export the 3D model as an .OBJ file: The third process is to export the 3D models in a file called .OBJ.
- 4) Open the Augmented Class App : The fourth process will open the mobile application called the Augmented Class App to make the augmented reality model.
- 5) Import the 3D model from an .OBJ file : In the fifth process, the 3D modelling in the OBJ file was imported into the Augmented Class App application.
- 6) Realisation of the augmented reality: In the last process the augmented reality was realised by displaying the 3D model in the Augmented Class App.

5) *Test*: This is the last stage which involves surveying users about the solution and prototyping so that they give the go-ahead for development [33].

IV. RESULTS

This section shows the results of the proposed methodology and the validation of the prototype by the experts. We will also

tell the advantages, disadvantages and comparison of Design Thinking.

A. Result of the Empathise Stage

Table I contains the questions (Q1 to Q6) for the survey of primary school children, asking about grade, gender, district, learning difficulty, learning stress and type of learning disability.

TABLE I. PRIMARY CHILDREN SURVEY

Questions	
ID	Questions
Q1	Primary Child's Grade
Q2	Sex ?
Q3	In which district of Lima are you located?
Q4	Learning Difficulty?
Q5	Stress when studying?
Q6	What type of learning disability does the child have?

B. Result of the Define Stage

Table II indicates the 70 questionnaire responses (R1 to R6) from the first stage of Table I for parents. They are also responsible for identifying their children's learning problems at school.

TABLE II. PARENTS' RESPONSE TO THEIR CHILDREN

Answers	
ID	Answers
R1	First Grade 8.6%, Second Grade 24.3%, Third Grade 38.6%, Fourth Grade 14.3%, Fifth Grade 5.7%, Sixth Grade 8.6%.
R2	Female 40% Male 60%
R3	Puente Piedra 8.6%, Los Olivos 27.1%, Carabayllo 28.6%, San Martín de Porres 15.7%, Comas 17.1%, Rimac 2.9%
R4	Yes 85.7% , No 14.3%
R5	Yes 81.4% , No 18.6%
R6	Dyslexia 15.7%, Dyscalculia 54.3%, Dysgraphia 21.4%, Dysphasia 8.6%.

a) R1: According to the 70 responses, this indicates the number of pupils surveyed in primary school, Grade 1 has 8.6%, Grade 2 has 24.3%, Grade 3 has 38.6%, Grade 4 has 14.3%, Grade 5 has 5.7% and Grade 6 has 8.6%.

b) R2: It indicates that in the survey 60% are male students and 40% are female students.

c) R3: The students from Lima-Peru with the highest percentage are from the district of Carabayllo with 28.6%, Los Olivos 27.1%, Comas 17.1%, San Martín de Porres 15.7%, Puente Piedra 8.6%, Rimac 2.9%.

d) R4: 85.7% of students in primary education have learning difficulties and the other 14.3% have no learning difficulties.

e) R5: 81.4% of students in primary education have increased stress in their studies and the other 18.6% have no stress.

f) R6: This indicates that the students surveyed have different learning disorders and that the greatest impact of the students is Dyscalculia with 54.3%, Dysgraphia 21.4%, Dyslexia 15.7% and Dysphasia 8.6%.

C. Result of the Ideate Stage

Table III indicates the solutions (S1 to S3) proposed by the innovation team. Giving an estimated score for the choice of the best idea and completing its development in the next phase.

TABLE III. SCORING IDEAS

Solutions	Punctuation of the Ideas	
	Innovation Team	Total
S1	Making a mobile application with augmented reality	58 points .
S2	To realise a website for your learning development	34 points .
S3	Implementing new learning methods in classrooms	20 points.

a) S1: The first solution will be the chosen one, as it has a high score of 58 points scored by the innovation team. This solution proposes the creation of a mobile application with augmented reality.

b) S2: The second solution that was not chosen but can be taken into account in future projects; it has a score of 34 points scored by the innovation team. Proposing to create a website for the development of their learning.

c) S3: The third solution that was not chosen but can be taken into account in future projects has a score of 20 points scored by the innovation team. Proposing to implement new learning methods in the classroom.

D. Result of the Prototyping Stage

Fig. 3 shows the model of the mobile application so that users who have a registered account can log in. If they do not have an account, they can register correctly, and if the user forgets their password, they will have the opportunity to recover it by sending an email to change their password.



Fig. 3. Mobile System Login

Fig. 4 shows the model of the mobile prototype so that the user can request a change of password by sending an e-mail for modification. Once the user has accepted the request, a new password can be set.



Fig. 4. Password Recovery

Once logged in to the mobile application the user can choose the learning disorder problem that counts, Dyslexia, Dysgraphia, Dyscalculia and Dysphasia as shown in Fig. 5.

Fig. 6 shows the level of the game so that the child can carry out his or her treatments by showing his or her name and age. The word-forming game consists of the child with dyslexia problems observing the letters and being able to form the word.

Fig. 7 shows the level of the game for the child with his name and age with his respective Dysgraphia problem. It consists of drawing the line of the picture using a pencil; the child can also count on a stable treatment.

Fig. 8 shows the level of the game so that the child with his name and age with his respective problem Dyscalculia. It consists of performing operations, in this case subtraction, so that the child can strengthen his knowledge dynamically and select the correct option.

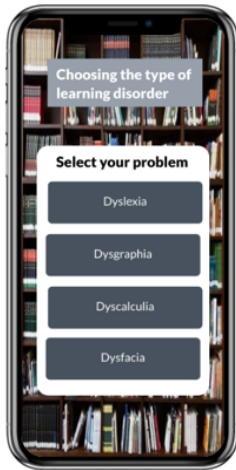


Fig. 5. Selection of Learning Disability



Fig. 6. Educational Game for Dyslexia

In Fig. 9 shows the level of the game for the child with his name and age with his respective problem Dysphasia, which consists of the child speaking slowly, pronouncing each letter, with the aim of improving the form of communication .

E. Responses from the Testing Phase

Table IV show the questions for the parents about the final prototype that was used for the input and improvement of their children with learning disabilities. Also, this interaction will serve to know the opinion, as well as the importance of the application on their stress treatment and cognitive improvement.

Fig. 10 shows the answers to the questions in the testing phase. In Q1, 76% responded that it is the ideal prototype for the children, 76% of the respondents found it very interesting and 24% did not, in Q2 they responded that the application will help in the treatment of learning disabilities, 76% agreed and 24% disagreed, in Q3 it indicates the improvement of stress, and in Q4 it indicates that 74% of the parents are confident that it does improve stress and 30% do not, in Q4

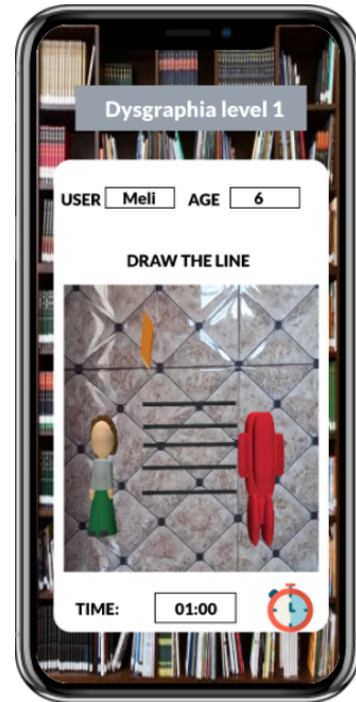


Fig. 7. Educational Game for Dysgraphia

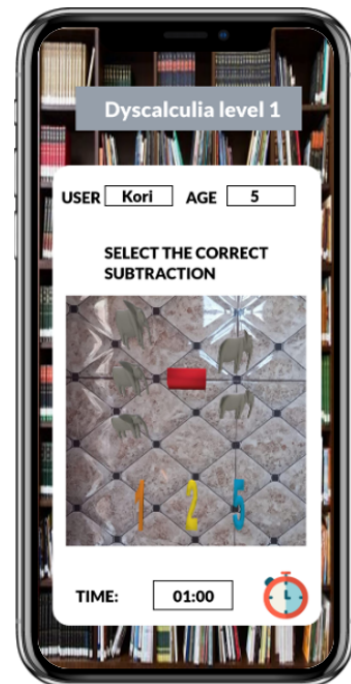


Fig. 8. Educational Game for Dyscalculia



Fig. 9. Educational Game for Dysphasia

TABLE IV. QUESTIONS FOR PARENTS ABOUT THE PROTOTYPE

Question about the prototype with augmented reality	
ID	Questions
Q1	Is the prototype ideal for your children?
Q2	Do you think it will help in their treatment of children?
Q3	Will this application improve children's stress?
Q4	Do you recommend a family member to use this application to improve the treatment of the learning disability?
Q5	Do you recommend private and public schools to implement this mobile application with augmented reality?

it indicates that 74% of the parents are confident that it does improve stress and 30% do not, in Q4 it indicates that the application will help in the treatment of learning disabilities. Likewise, 70 per cent are confident that it does improve stress and 30 per cent are not, in Q4 it indicates that 74 per cent of parents recommend that family members or close friends use the application for the treatment of learning disorders and 26 per cent do not, and finally in Q5 they responded that 78 per cent would recommend public and public schools in Peru to implement the mobile application with augmented reality and 22 per cent responded that they would not.

F. Expert Validation of the Prototype

This validation was carried out with 5 experts who will be in charge of scoring the four criteria (Functionality, Usability, Consistency and Integration). These validations were carried out on the final prototype, ensuring that it will be acceptable by the experts.

In Table V the scales Low, Moderate and High were considered. Low will have a range of 0% to 49% indicating that it would not be accepted, Moderate will have a range of

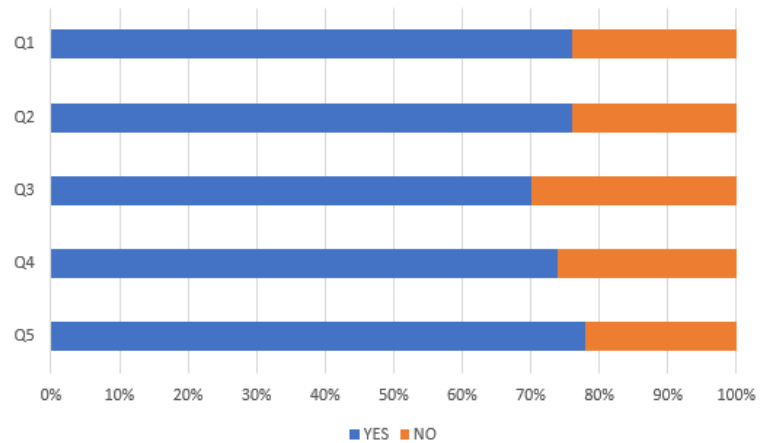


Fig. 10. Response from the Testing Phase

50% to 79% indicating that the prototype can be improved and High will have a range of 80% to 100% indicating that it would be an acceptable prototype.

TABLE V. LEVEL OF ACCEPTANCE

Level		
Under	Moderate	High
0% - 49%	50% - 79%	80% - 100%

Likewise, to find the total percentage, it was calculated as the average of the four criteria, in percentages.

Table VI shows the scores of the five selected experts, so each expert will have to score each validation from 1 to 100, and finally the result shows the level of acceptance of the prototype.

TABLE VI. QUESTIONS TO EXPERTS

Question about the prototype with augmented reality						
Experts	Functionality	Usability	Consistency	Integration	Total	Level
Expert 1	80%	85%	83%	90%	85%	High
Expert 2	90%	85%	95%	80%	88%	High
Expert 3	73%	89%	85%	90%	82%	High
Expert 4	89%	92%	90%	97%	92%	High
Expert 5	75%	76%	86%	84%	80%	High

Finally, Fig. 11 shows the 5 validating experts with a high level, i.e. the prototype has a level of acceptance by each expert. Expert 1 indicates a high level with 85%, expert 2 indicates a high level with 88%, expert 3 indicates a high level with 82%, expert 4 indicates a high level with 92% and expert 5 indicates a high level with 80%. The overall average is 85.4% acceptance.

G. About the Methodology

1) *Advantages:* The Design Thinking methodology was used to bring innovative ideas to meet user needs. This allowed us to have a dynamic teamwork to be able to bring new ideas to society and to improve the decision making process. This also allows us to see the creativity of the team and also the analysis that leads to the understanding of the problems towards the users.

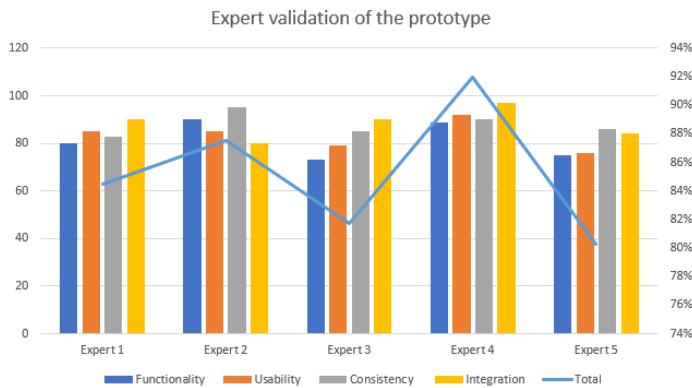


Fig. 11. Expert Validation of the Prototype

2) *Disadvantages:* The disadvantages of the Design Thinking methodology is that it is more dedicated to the prototyping of innovative ideas and not to the development of the application. In this sense, it should be considered that this methodology can go hand in hand with another methodology for the development of the proposal.

3) *Comparison:* The 5-phase methodology helped us to speed up the process of analysis and creative ideas for prototyping. Compared to other methodologies that focus on the development of the application, these include proposing innovative plans for the contribution to society.

V. DISCUSSION

It is analysed that our proposal as a solution with the use of augmented reality is a good strategy, it is also integrated that the survey method that was effective for stakeholders to analyse their problems is valid for the search for solutions, this coincides with the author [15], who evaluated the problems based on surveys, proposing the use of technology to improve student learning. Similarly in the author [19], who conducted an analysis of the respondents, finding serious problems in students with learning disabilities so he proposes the use of augmented reality for computer, tablet and mobile assembly labs. In addition, the proposed design of a mobile application with augmented reality is a perfect combination as nowadays people handle their mobile devices anywhere, which results in user satisfaction. These results agree with the author [21], as he proposes a variety of mobile designs with augmented reality for advertisements in order to impact your customers with the use of technologies. In the same way, he indicates that the intuitive games with augmented reality in the [20] leads to a good result, validating an increase in learning and comprehension in his students.

VI. CONCLUSION

This model of an augmented reality application is developed to improve learning disabilities. In the prototype educational games were made to have a better understanding, since the survey identified that children have problems with Dyslexia, Dyscalculia, Dysgraphia and Dysphasia. Design Thinking allows us to have a greater analysis of the problems in search of the needs of users, helping us to have a variety

of creative and innovative solutions. This contribution of the design of a mobile application for the treatment of learning disorders using augmented reality in primary education would be of great help to have an adequate treatment in children with the use of technologies, allowing to improve their stress level and to have a greater understanding in their subjects. A limitation of the research that was identified was the development of mobile application and augmented reality, since the methodology used only focuses on the design of innovative prototypes for problem solving.

VII. FUTURE WORK

It is suggested that the proposed research be considered for future work and that a virtual reality application be developed. In this way, children with learning disabilities can have a maximum technological experience. In addition, the research should be carried out in an interdisciplinary and multidisciplinary way, i.e. it is suggested that specialists in learning disabilities such as a psychologist, among others, be incorporated.

ACKNOWLEDGMENT

This work was sponsored by the University of Sciences and Humanities and the research direction. Thank for the unconditional support.

REFERENCES

- [1] Z. J. Rahaleh, M. A. Sakarneh, M. A. Hyassat, and N. S. al Zyouid, "Internet use among jordanian students with and without learning difficulties at primary schools," *Journal of Educational and Social Research*, vol. 11, no. 2, pp. 74–74, 2021.
- [2] M. Barr and A. Copeland-Stewart, "Playing video games during the covid-19 pandemic and effects on players' well-being," *Games and Culture*, vol. 17, no. 1, pp. 122–139, 2022.
- [3] J. M. Goodrich, L. Fitton, J. Chan, and C. J. Davis, "Assessing oral language when screening multilingual children for learning disabilities in reading," *Intervention in School and Clinic*, p. 10534512221081264, 2022.
- [4] K. Pacheco-Barrios, A. Navarro-Flores, A. Cardenas-Rojas, P. S. de Melo, E. Uygur-Kucukseymen, C. Alva-Diaz, F. Fregni, and J. G. Burneo, "Burden of epilepsy in latin america and the caribbean: a trend analysis of the global burden of disease study 1990–2019," *The Lancet Regional Health-Americas*, vol. 8, p. 100140, 2022.
- [5] G. M. Gómez and G. Andrés Uzín P, "Effects of covid-19 on education and schools' reopening in latin america," in *COVID-19 and International Development*. Springer, 2022, pp. 119–135.
- [6] T. Flenik, T. S. Bara, and M. L. Cordeiro, "Family functioning and emotional aspects of children with autism spectrum disorder in southern brazil," *Journal of Autism and Developmental Disorders*, pp. 1–8, 2022.
- [7] —, "Family functioning and emotional aspects of children with autism spectrum disorder in southern brazil," *Journal of Autism and Developmental Disorders*, pp. 1–8, 2022.
- [8] A. R. Bernaola, M. A. Tipula, J. E. Moltalvo, V. S. Sandoval, and L. Andrade-Arenas, "Analysis of the use of technological tools in university higher education using the soft systems methodology," *International Journal of Advanced Computer Science and Applications*, vol. 11, no. 7, pp. 412–420, 2020, 10.14569/IJACSA.2020.0110754.
- [9] I. O. Yahuarcani, L. A. S. Llaja, A. M. N. Satalaya, L. A. S. Bitulas, E. G. Gómez, K. D. J. Lagos, C. A. G. Cortegano, G. A. M. Alcantara, G. S. Atuncar, A. R. Pezo *et al.*, "A digital educational tool for learning the aymara language in the region of ayacucho, peru," in *2021 IEEE World Conference on Engineering Education (EDUNINE)*. IEEE, 2021, pp. 1–5.
- [10] A. Carrion-Silva, C. Diaz-Nunez, and L. Andrade-Arenas, "Admission exam web application prototype for blind people at the university of sciences and humanities," *International Journal of Advanced Computer Science and Applications*, vol. 11, no. 12, pp. 377–382, 2020, 10.14569/IJACSA.2020.0111246.

- [11] L. Andrade-Arenas and C. Sotomayor-Beltran, "On the perspectives of graduated engineering students on three dimensions of the integrated curriculum from a peruvian university," in *Proceedings of the 2019 International Symposium on Engineering Accreditation and Education, ICACIT 2019*, 2019, doi:10.1109/ICACIT46824.2019.9130268.
- [12] K. Willemse, T. Venketsamy, and N. Swanepoel, "Support teachers need to assist learners experiencing mathematical learning difficulties," *BOOK OF PROCEEDINGS—LONG PAPERS*, p. 179, 2022.
- [13] Á. Salvatierra Melgar, W. A. Quispe-Cutipa, I. Reyes-Blácido, L. S. Rodríguez-Baca, M. F. Guevara-Duarez, and M. A. Alarcón-Díaz, "Cognitive reflections in children with adhd and proposals to promote logical thinking," 2021.
- [14] M. F. A. Hanid, M. Said, and N. Yahaya, "Learning strategies using augmented reality technology in education: meta-analysis," *Universal Journal of Educational Research*, vol. 8, no. 5A, pp. 51–56, 2020.
- [15] N. P. Dinayusadewi and G. N. S. Agustika, "Development of augmented reality application as a mathematics learning media in elementary school geometry materials," *Journal of Education Technology*, vol. 4, no. 2, pp. 204–210, 2020.
- [16] R. Fernández-Enríquez and L. Delgado-Martín, "Augmented reality as a didactic resource for teaching mathematics," *Applied Sciences*, vol. 10, no. 7, p. 2560, 2020.
- [17] A. Syawaludin, P. Rintayati *et al.*, "Development of augmented reality-based interactive multimedia to improve critical thinking skills in science learning," *International Journal of Instruction*, vol. 12, no. 4, pp. 331–344, 2019.
- [18] R. Arslan, M. Kofçöglu, and C. Dargut, "Development of augmented reality application for biology education," *Journal of Turkish Science Education*, vol. 17, no. 1, pp. 62–72, 2020.
- [19] N. I. M. Enzai, N. Ahmad, M. A. H. A. Ghani, S. S. Rais, and S. Mohamed, "Development of augmented reality (ar) for innovative teaching and learning in engineering education," *Asian Journal of University Education*, vol. 16, no. 4, pp. 99–108, 2021.
- [20] I. J. Fitriyah, A. Setiawan, M. F. Marsuki, and E. Hamimi, "Development of augmented reality teaching materials of chemical bonding," in *AIP Conference Proceedings*, vol. 2330, no. 1. AIP Publishing LLC, 2021, p. 020043.
- [21] D. Renaldi and E. S. Aziz, "The design of basic computer networking simulation learning using multimedia development life cycle method based on augmented reality at smkn 1 tangerang," *Tech-E*, vol. 4, no. 2, pp. 30–35, 2021.
- [22] R. R. Wijayanti, "Implementasi augmented reality sebagai media promosi interaktif untuk katalog food and beverage pada hokcafe," *JIKA (Jurnal Informatika)*, vol. 2, no. 2, 2019.
- [23] S. Doukianou, D. Daylamani-Zad, and K. O'Loingsigh, "Implementing an augmented reality and animated infographics application for presentations: effect on audience engagement and efficacy of communication," *Multimedia Tools and Applications*, vol. 80, no. 20, pp. 30 969–30 991, 2021.
- [24] B. Ku and E. Lupton, *Health design thinking: creating products and services for better health*. MIT Press, 2022.
- [25] S. Magistretti, C. Dell'Era, R. Verganti, and M. Bianchi, "The contribution of design thinking to the r of r&d in technological innovation," *R&D Management*, vol. 52, no. 1, pp. 108–125, 2022.
- [26] J. E. McLaughlin, E. Chen, D. Lake, W. Guo, E. R. Skywark, A. Chernik, and T. Liu, "Design thinking teaching and learning in higher education: Experiences across four universities," *Plos one*, vol. 17, no. 3, p. e0265902, 2022.
- [27] V. Manna, M. Rombach, D. Dean, and H. G. Rennie, "A design thinking approach to teaching sustainability," *Journal of Marketing Education*, p. 02734753211068865, 2022.
- [28] B. Matthews, S. Doherty, P. Worthy, and J. Reid, "Design thinking, wicked problems and institutioning change: a case study," *CoDesign*, pp. 1–17, 2022.
- [29] D. Staehelin, M. Dolata, and G. Schwabe, "Managing tensions in research consortia with design thinking artifacts," in *Design Thinking for Software Engineering*. Springer, 2022, pp. 137–153.
- [30] S. Eryilmaz and G. Deniz, "Effect of tinkercad on students' computational thinking skills and perceptions: A case of ankara province," *Turkish Online Journal of Educational Technology-TOJET*, vol. 20, no. 1, pp. 25–38, 2021.
- [31] M. L. Amado, L. C. Ruiz, and L. Andrade-Arenas, "Prototype of an augmented reality application for cognitive improvement in children with autism using the desingscrum methodology," *Advances in Science, Technology and Engineering Systems*, vol. 6, no. 1, pp. 587–596, 2021.
- [32] A. P. Kłos, "Project of an it system supporting the analysis of players in an amateur football league," Ph.D. dissertation, Zakład Zarządzania Publicznego, 2022.
- [33] L. Vendraminelli, L. Macchion, A. Nosella, and A. Vinelli, "Design thinking: strategy for digital transformation," *Journal of Business Strategy*, 2022.

Implementation of a Web System: Prevent Fraud Cases in Electronic Transactions

Edwin Kcomt Ponce, Katherine Escobedo Sanchez, Laberiano Andrade-Arenas
Facultad de Ciencias e Ingeniería
Universidad de Ciencias y Humanidades
Lima, Perú

Abstract—The purpose of this project is to prevent cases of fraud in e-commerce of purchase and sale from person to person through social networks. For the development of the research work, the Scrum methodology was used to allow the project to be carried out in an agile and flexible way, adapting to the changes that could arise along the way. The technological tools that made this project possible were SQL Server, C++, Visual Studio and Marvel app, the latter for prototype design. In addition, there was the support of an artificial intelligence software known as Optical Character Recognition that allowed the document recognition process to be completed. The social network Facebook was also relevant for the development process since the data set for the training of the system was obtained from there, guaranteeing its functionality. The results obtained benefit both parties, sellers/suppliers and consumers, reducing the impact of fraud cases and guaranteeing safer online operations. In addition, a validation was carried out by experts in the development of web applications, taking usability, feasibility, scalability, innovation, and technology as criteria. Obtaining as a result the approval in all its criteria; with the total mean value of 2.76.

Keywords—Artificial intelligence; e-commerce; fraud; optical character recognition; scrum; social networks; web system

I. INTRODUCTION

Digital transformation has become more relevant in recent years as a result of the pandemic, although this process brings with it greater benefits and a positive impact on the development of a country, it also poses certain risks for a large number of the population. According to the World Economic Forum in a survey presented in its Global Risks Report 2021 [1], it indicates that cybersecurity flaws rank 7th out of a total of 37 risks presented. In Latin America, the growth of e-commerce due to the pandemic had an exponential increase, which meant a greater use of devices with internet access to carry out various operations such as payments or purchases of goods and services online [2]. Approximately 10 million Latinos have purchased consumer goods through electronic stores, however, one of the most relevant problems is the criminal activities carried out through computerized means as a consequence of this new normal [3].

Peru also adds to this growth, with e-commerce operations reaching an increase of 86% in June 2020 and reaching its highest point in July with 160%. This represents approximately 6 billion dollars, which covers the size of the e-commerce market as detailed in the report by the Peruvian Chamber of Electronic Commerce. However, this led to an increase in claims related to online transactions due to the few regulations and measures in this area. Let's take into account that before

the pandemic, Peru had around 65,700 businesses that sold online, but by the end of 2020 there were 263,200 businesses. We must add that this also brought with it the increase in informality in the digital sector [4].

In Peru there is a high rate of informality and this has been increasing according to the latest data provided by the National Institute of Statistics and Informatics, reaching an informality rate of approximately 75%, also affecting electronic commerce [5]. It is mainly social networks that are used for this type of informal trade, where many independent workers offer their products and services at very attractive prices. In this way they manage to capture even more the attention of the public, this activity through social networks represents an opportunity to generate income without discounts or commissions when carrying out their transactions. However, it is also an opportunity for fraudsters to carry out their criminal activities hiding behind anonymity and lack of security [6] [7]. These types of crimes are carried out through online transactions for advance payments without the guarantees or security that a platform of a formal company offers. The purchase and sale operation through social networks is based solely on trust between the seller/supplier and the customer, thus exposing themselves to being a victim of fraud [8].

Given the foregoing, the aim is to offer users the alternative of carrying out their online purchase and sale operations with greater security, thus avoiding and reducing computer fraud rates. This not only benefits the buyer but also the seller as it is an opportunity to demonstrate that their services and/or products can be requested with complete confidence. Thus, it also contributes to the security of the assets and personal assets of the citizen covered by the Law on Computer Crimes, thus being a reference to avoid fraud either by advertisements on a website or by social networks.

The objective of this research work is to implement a web system to prevent fraud in online transactions carried out by people through social networks. The platform will be available free of charge, allowing users to register and contribute by reporting fraud cases in order to expand the database, which in turn favors the system by improving its efficiency and accuracy. So that the reports by complaint are valid and avoid cases of misinformation; The user will be asked to attach the respective complaint so that their report can be considered. In this way, the aim is for users to have a system that helps them guarantee greater security in their payment transactions or online purchases for a requested product. As well as independent workers or business owners, they can avoid loss of resources and time by ensuring that their sale

is finalized and that it is not canceled at the last minute.

The article is organized as follows: in Section II the review of the literature, Section III the methodology, Section IV the case study, Section V results and discussions, Section VI the conclusions and finally Section VII future work.

II. LITERATURE REVIEW

The investigation addressed the issue of fraud prevention through electronic commerce, through the development of a web system. The studies of different authors on the research topic are analyzed in order to have information on trends, limitations, among others.

According to the authors [9], their application allows identifying customers who may pose a risk of fraud for an electronic commerce, through the information of cookies or IP configured in the devices used for online transactions. Normally, fraudulent clients do not make changes to their laptop, smartphone or computer, so the application manages to keep a record and identify the devices with a history linked to these criminal acts. To achieve their objective, the developers of the project use three main components for their fraud detection system, which are PC identifier, Address identifier and Asset Classifier. These methods are based on data extraction and statistical analysis. A total of 8,020 purchase requests were analyzed, efficiently detecting suspicious transactions compared to traditional methods that use data mining, but with poor performance.

For the [10] authors, the most frequent fraud operations are carried out through the use of a credit card through e-commerce. His proposal consists of applying the Support Vector Machine (SVM) algorithm, allowing fraudulent operations to be identified and classified from safe operations. The methodology for its system includes using fingerprint scanning as a measure to reinforce security during registration and access to online operations. If a transaction is classified as fraud, the payment process will be canceled and the fraudulent user's information will be sent to the database. Finally, it can be concluded that the SVM is an efficient algorithm with an accuracy of 99.9% according to a comparison table of several models prepared by the authors. These qualities of the algorithm make an accurate classification in the process of online fraud unlike other methods.

In the work developed by [11], the authors propose a new data intelligence technique with the aim of maximizing the model in the detection of fraudulent operations, without having to depend on the data variation that may exist. As in the previous article, this project focuses on operations carried out through online payments through e-commerce. The proposed system works with the Multiple Prudential Consensus model that uses and integrates the efficiency of different classification algorithms through a double criterion, probabilistic and majority. The final algorithm is determined to classify authorized or fraudulent operations according to the previously determined model and according to the analysis of criteria elaborated. The results obtained demonstrate the effectiveness of the model, compared to other systems used to detect cases of fraud. Of a total of 492 fraud samples, the developed model was able to correctly detect 394 compared to the 349 cases that were detected by the model that ranked second. The results confirm

that the proposal stands out among many other solutions both in terms of models and classification.

The authors [12] use Blockchain-based technology which is quite secure and efficient. One of its great advantages is that once the data has been registered, it is possible to alter or delete it. In addition, it is a fairly simple technology and easy to understand. Blockchain is a chain of blocks which consists of a single registry network where information from the previous block is stored and thus passes the information to the following blocks. Based on this they decide to implement this technology to support online fraud detection and thus qualify a valid purchase. Blockchain will store verified transactions and their associated qualifications, making "verified" labels no longer necessary. It is concluded that blockchain systems are quite efficient in detecting online user fraud compared to traditional methods. In addition, the system allows better control of false accounts or information and has a reputation system to effectively reduce the number of fraudulent ratings.

In the research work developed by the authors [13], they propose a proposal based on Machine Learning in order to improve the existing fraud detection systems. They consider that there is an urgency for a better detection and prevention of cases of electronic fraud. Its model is based on the use of Machine Learning algorithms integrating big data, allowing it to predict the probability that an electronic operation is safe or fraudulent. The model was trained with a dataset composed of history of credit card transactions through electronic commerce; in order to predict any probability of fraudulent operations. Specifically, supervised learning algorithms such as Random Forest, Support Vector Machine, Gradient Boost and combinations of these were used, comparing their performance. The results obtained confirm the accuracy and precision of the proposal by combining the Gradient Boost + Logistic Regression algorithms. In addition, the model, being based on Machine Learning, has an addition that is Active Learning. This new addition allows solving data labeling problems, which means an improvement in learning for fraud detection.

After analyzing the different proposals developed by the cited authors, it is considered that the use of technologies and application of engineering is of the utmost importance to combat the growing increase in cases of computer fraud. Although most of the works focus on the use of algorithms and models for more sophisticated systems, none addresses the problem of fraud when both parties involved are natural persons. The approaches and initiatives apply to companies already established and that have the economic factor to implement the systems in their respective businesses. However, in our country there is a large percentage of independent workers who offer products through social networks. Merchants do not have their own payment system and are also responsible for making deliveries in person via delivery. For this reason, what we are looking for is to develop a web system that facilitates the safe use of this type of electronic commerce. Thus, users can make their purchases with the security of knowing if they are dealing with someone reliable for their transactions.

III. METHODOLOGY

In the research carried out, an agile methodology was used, which allows the development team to have constant

communication and be able to carry out work efficiently, quickly adapting to the changes that may occur during the project. Next, the methodology used and the technological tools that were necessary for this project are described in detail.

A. SCRUM Methodology

It is a methodology that offers a personalized and flexible way of working that is suitable for software development projects with a variety of requirements [14]. This iterative work model establishes the delivery of project progress incrementally, thus achieving more efficient results and greater productivity. In Fig. 1, we graphically observe the process followed by this methodology and its respective work phases.

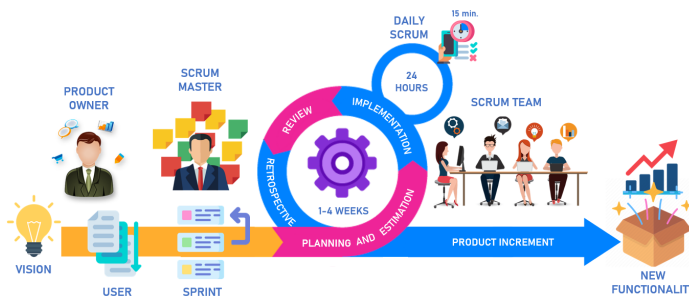


Fig. 1. Scrum Methodology Workflow.

1) *Beginning*: It is the first phase where the roles and functions of each member of the development team are identified and defined, these are assigned according to the skills and contributions of each member to the project, in the process the Scrum Master, Product Owner and the Scrum Team intervene [15]. Where the Scrum Master is mainly responsible for removing obstacles to the development of the project while the Scrum team is made up of developers, evaluators and other professionals necessary to guarantee the quality of the product.

2) *Planning and Estimation*: It is the next phase, the user stories are proposed and chosen according to the client's requirements, the product backlog is also carried out taking into account an estimation process for an adequate order of the stories. Once the requirements are organized, the sprint backlog is created. These are selected by priority and will go through the development and execution process. With the defined sprints, the team is responsible for between 1 and 4 weeks of the process to program, design and execute the sprint after the product increment is finished, the team continues with the next sprint.

3) *Implementation*: It is the third phase of the Scrum workflow, the objective is to deliver each sprint of the product organized, error-free and potentially operational, and generally at the beginning of the day during this phase small meetings are held [16]. These meetings are known as Daily Scrum that can last 15 minutes where the progress of the previous day is communicated and at the same time what impediments may be occurring for the progress of the project are discussed.

4) *Review and Retrospective*: It is the fourth and final phase of the work method, once the sprint is potentially deliverable at the end, a review of said sprint is carried out with

the Product Owner to show the increase in the product. The increment is inspected and its functionalities are demonstrated. Sometimes the product list must be adapted according to the possible new requirements that the Product Owner indicates [17]. After the review, we proceed with the retrospective; where the Scrum Team makes an analysis of itself with the possibility of proposing strategies to execute improvements in the way of working for the following advances.

B. Technological Tools

For the research work, it was considered to use specialized applications and programs for this type of project with the intention of having an adequate development environment; thus achieving the correct implementation of the proposed system.

1) *SQL Server*: It is a relational database management system that uses the Transact-SQL development language. It is ideal because it allows you to store all the information you want with a wide variety of processes and with different utilities. Plus, easily integrate application data and leverage a rich set of cognitive services to power AI processes at any data scale.

2) *Visual Studio*: It is a program that provides us with an integrated development environment which facilitates the creation, design and development of web sites and applications, at the same time allowing us to work in environments that support the .NET framework. It is compatible with a wide variety of programming languages, such as C#, C++, Visual Basic, Python, Java, PHP among others.

3) *Python*: It is a high-level programming language that processes all kinds of data. Its software is free, that is, it has no cost, allowing it to be used and distributed even for commercial use. It is accessible and multiplatform, it has an extensive library, as well as a varied repertoire of frameworks, also standing out for its simplicity of syntax.

4) *Marvel App*: It is a web application to work online that allows us to make layouts and prototypes of both web pages and applications on mobile devices. The tools it makes available are sufficient to create designs that allow developers to have clear ideas of the final product.

5) *Artificial Intelligence (AI)*: This technology aims to allow software to have the ability to learn based on data, which arise from patterns and opportunities provided by developers. Once the necessary data set is obtained, performance tests are carried out to measure and calculate the efficiency and accuracy of the AI software based on the number and quantity of hits and misses [18]. Deep Learning is a type of AI that uses multiple processing steps, also known as layers, to learn and then recognize data representations with multiple levels of abstraction. It is based on artificial neural networks, one of the specialties of this AI is image processing.

In Fig. 2, it can be seen how AI is classified, while in Fig. 3, we see the main classes of neural networks used by deep learning. For the development of this project, we worked with the Recurrent Neural Networks architecture because it was the one that best adapted to the required functionalities of the web system.

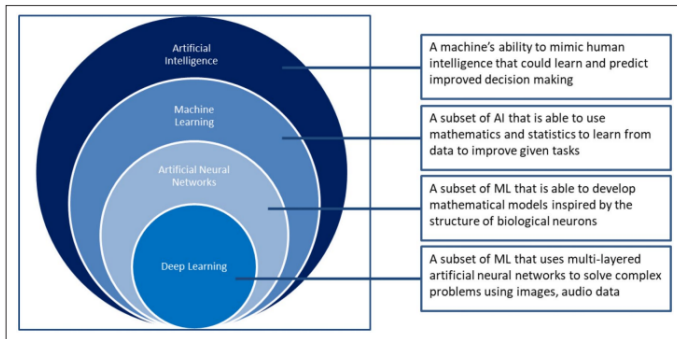


Fig. 2. Graphic that Shows how Artificial Intelligence is Classified in its Different Subfields [19].

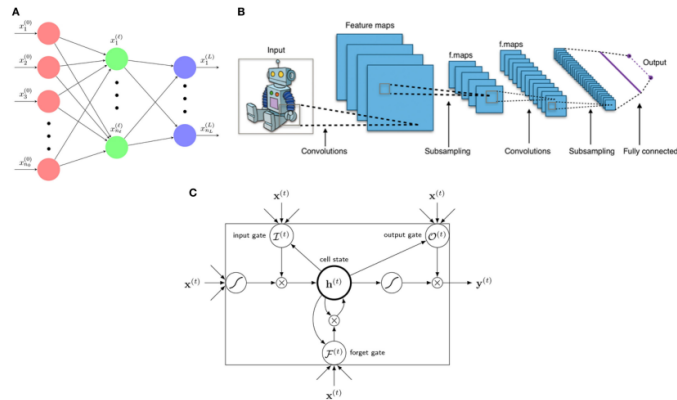


Fig. 3. The 3 Main Architectures of Deep Learning, A) Artificial Neural Network, B) Convolutional Neural Networks and C) Recurrent Neural Networks [20].

IV. CASE STUDY

A. Planning

With the roles already defined and assigned among the team members, the planning continues. Where we choose the user stories, these determine the desired features and functions of the web system requirements. For this project, a total of 10 user stories are proposed, in Table I you can see the description of each story, which allows us to better understand the operation of the system.

B. Estimate

Here the user stories are organized through the product backlog, in this list certain criteria are taken into consideration so that the stories are properly ordered. The estimation process is carried out through planning poker, when putting this technique into practice the team must assign a number (Fibonacci series) to each of the user stories. The assigned numbers are chosen from lowest to highest according to the level of difficulty that the team members consider for the development of each user story.

In Table II, we can see the product backlog developed and ordered by priority, this is defined by the effort and difficulty of development as well as its relevance in the project. As a reference to choose the priority of each story, story number

TABLE I. USER HISTORY

History No.	Description
H1	As an administrator, I want a web platform that through its design is intuitive and friendly to be used easily.
H2	As an administrator, I want the web platform to allow the user to know if a seller/supplier has a history to avoid being scammed.
H3	As an administrator, I want the web platform to have a wide database to be more efficient and precise in the search for results.
H4	As an administrator, I want the platform to allow users to write reviews to better understand the type of fraud that the accused uses.
H5	As a user, I want to contribute by registering duly substantiated complaints to improve the prevention capacity of the web.
H6	As a user, I want to be able to register on the web platform in order to be prevented from various cases of fraud.
H7	As an administrator, I want the platform to have a section where information related to computer crimes is displayed to keep users informed and warned.
H8	As an administrator, I want the web system to validate the attached file that will be uploaded as evidence by the user to detect if it is a police report.
H9	As an administrator, I want the platform to have a section with external links to government pages to provide support and guidance to victims of fraud.
H10	As administrator, I want the web platform to allow knowing a ranking of fraud complaints by number of complaints and type of fraud so that users can better and easily manage the information.

9 has been selected as its development is considered the least difficult.

TABLE II. PRODUCT BACKLOG

History No.	Estimate	PRIORITY	Sprint
H3	5	1	3
H8	8	2	3
H2	3	3	3
H5	3	4	2
H10	5	5	2
H4	2	6	2
H6	2	7	2
H9	1	8	1
H7	2	9	1
H1	2	10	1

The project is divided into 3 sprints, the first sprint has a total of 5 story points, because it requires less effort. When starting with the development of the sprints, the work team begins to integrate allowing better team work as each iteration progresses. The second and third sprints receive 12 and 16 story points respectively. Likewise, the points have increased due to the time and effort required by the requirements corresponding to these sprints. At this point in the project, the team is able to communicate and organize much better, thus achieving good coordination in the development of the web system and minimizing errors. Fig. 4 graphically shows the order by effort from lowest to highest of the user stories and the sprints to which they have been assigned.

C. Implementation and Development Stage

In this stage, the use of the technologies to be implemented and the procedure proposed for the web system are explained in detail.

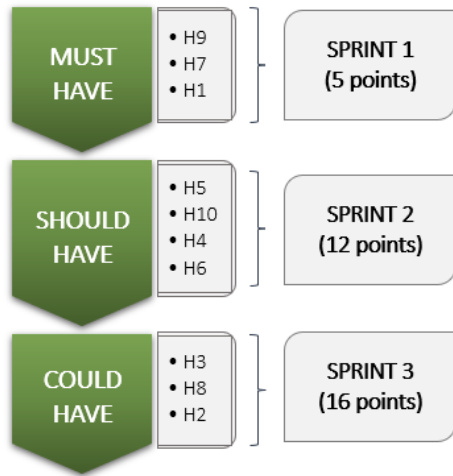


Fig. 4. Story Points and Number of Sprints.

1) *Software Development:* The web system was developed applying the use of the Model View Controller (MVC), which is a software architecture style based on three layers or levels. This type of model has proven its worth over several years and across various types of applications, a variety of programming languages, and development platforms. The model separates an application's data, user interface, and control logic into three distinct components:

a) *Model:*

Also known as the data layer, it is where the data is located and is responsible for accessing it, it is made up of one or more database managers that perform storage. It has a representation of the data used by the system, its business logic and records of the controls and views of the system.

b) *View:*

It is the user interface also known as the presentation layer, it shows the system to the user and interacts with it through mechanisms. It also integrates and organizes the information that is sent from the model through the controller, that is, it receives the data and shows it to the user.

c) *Controller:*

Also known as the business layer or business logic because it is here where all the rules that must be met are established. It acts as an intermediary between the Model and the View, managing the flow of information between them to request the database to store or retrieve data. That is, it receives requests from the user and sends responses after the process. This is also where the programs that run are located.

In Fig. 5, we can see graphically a basic scheme of how the chosen model is structured.

2) *Data Set Preparation and Extraction:* For the present project, a set of data was needed to be used for training and testing the different functionalities that were sought to be implemented.

In Fig. 6, we observe the process to obtain the data in image format, the social network Facebook served as the basis for extracting said information. By accessing a personal account, they entered communities called groups that the social network

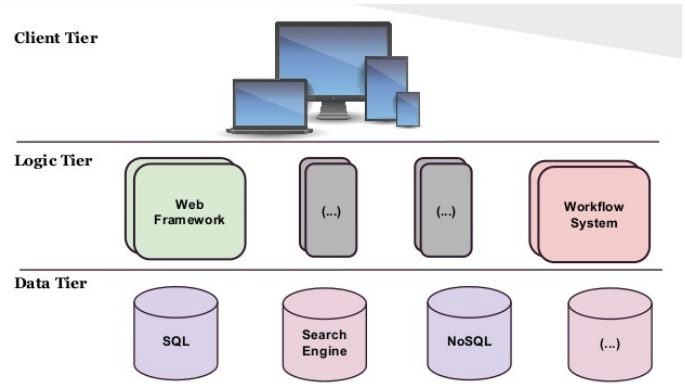


Fig. 5. Three Layer Architecture.



Fig. 6. Flowchart for Obtaining the Data Set.

offers where its users can exchange or share common interests. Then we began with the search for public publications where users of the social network made reports of having been victims of fraud.

Finally, only those publications with support were considered where images of police reports were extracted to form the data set needed by the project. This meant dividing the data into two groups, allowing training and then checking the correct functioning of the web system. In this way, it was also possible to correctly identify the types of attached files in image format that are uploaded to the system by users.

3) *Optical Character Recognition (OCR):*

a) *Definition:*

It is a software that allows us to recognize text in digital documents including images, it has become a very useful tool due to its precision, speed and efficiency to classify documents and/or extract information from them [21]. For the present research work, the Optical Character Recognition software was implemented as part of the web system for the desired function of classifying the information provided by users. In Fig. 7, we can see the process and threads carried out by the software for text extraction, once the results are obtained they can have various applications as indicated in the graph.

b) *Recurrent Neural Network (RNN) and Tesseract OCR:*

From simple image classification to medical scans, speech

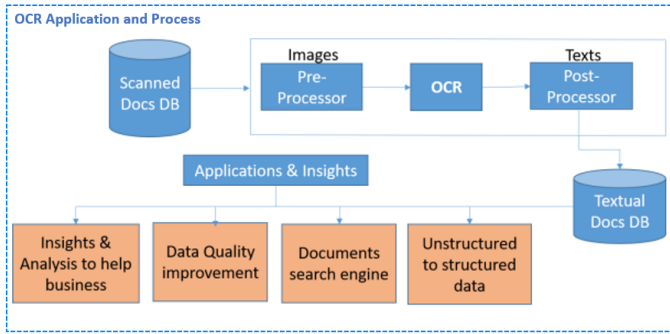


Fig. 7. Basic Flowchart of how OCR Works.

recognition and text-in-image recognition are among the many essential functions of deep learning. The RNN is a kind of neural network that is part of deep learning, it allows input data to flow in any direction along a time sequence through the layers that make up the network. The Long short-term memory (LSTM) is a type of RNN that has feedback connections, managing to process not only individual data but also complete sequences of data, avoiding loss of information over time [22].

For the proposed system, we worked with the Tesseract software, which is open source, which uses OCR and is complemented by LSTM to achieve a more efficient result in the field of text recognition through digital images. In addition, it has an extensive library that facilitates its training with a certain set of data. In Fig. 8, we can see the architecture of the Tesseract software in conjunction with the LSTM neural network.

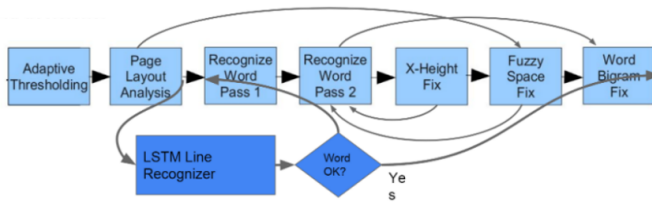


Fig. 8. Tesseract Architecture where it is Noted that there are Many Revisions of Old Decisions [23].

c) Operation:

OCR software is normally composed of four stages that are pre-processing, segmentation, character extraction and final recognition of the text, the mentioned sequence can vary depending on the results that are desired to obtain. For the present research work, since they are simple documents and in the format of a police report, the process for text recognition did not imply difficulty.

Fig. 9 shows the operation and the stages carried out by the OCR, once it manages to recognize the text in the digital document, it can also extract said information for later use, which depends on the purpose of each system that uses this technology [25].

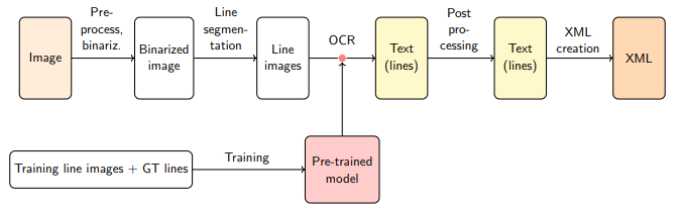


Fig. 9. Flowchart of the Process Performed by the OCR Software [24].

d) Execution and Process:

With the developed web system, the recognition software was implemented, the steps to be followed by the system as a whole were verified according to the proposal to confirm its viability and correct use. It was considered to focus a greater effort on the function of the system that requires the support of artificial intelligence because its operation is essential for the rest of the processes.

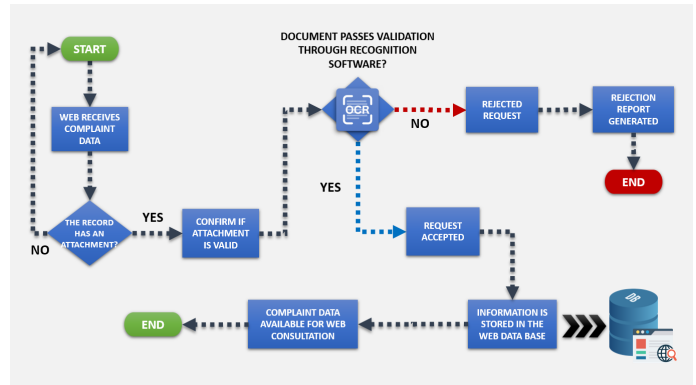


Fig. 10. Flowchart Showing Web System Working with OCR Software.

As shown in Fig. 10, the step to register a case of fraud involves attaching evidence to support it, the user through the web system must upload their respective police report in image format. Once the system receives the information of the complaint with the attached image, the recognition software will validate whether or not the image is valid by extracting the text and classifying it. If the validation result is positive, all the information entered is stored in the web system database for later use in user queries.

V. RESULTS AND DISCUSSION

Finally, each sprint and its respective user stories are explained in detail, as well as the operation of the complete web system and we verify the importance and viability of the project through statistical data.

A. Design and Prototypes

The prototypes were developed based on user stories, these allow us to understand graphically and in detail each function implemented in the web system, as well as its importance in this project. This section shows the main prototypes organized by sprints which make up the research work carried out.

1) *First Sprint:* This sprint mainly covers interfaces that do not require much effort and time, with a total of three deliverables. In Fig. 11, we see the prototype that represents the home page of the web system, in it the user has the option of being able to log in or register by creating an account. You can also see a brief description of the objective of the platform and at the top is the design of the created logo.

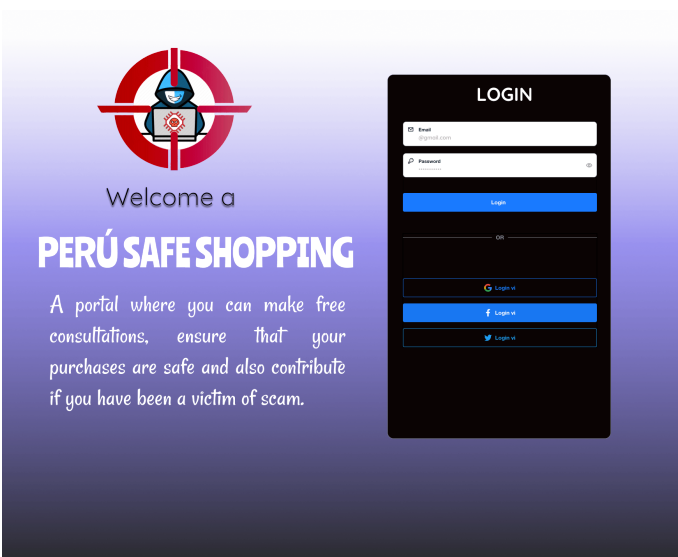


Fig. 11. Prototype based on User Story 1

In Fig. 12, we see the prototype designed for the informative section of the platform, this section includes news and advice to guide the user so that they can stay informed and prevented from the main cases of fraud and fraud at the national level.

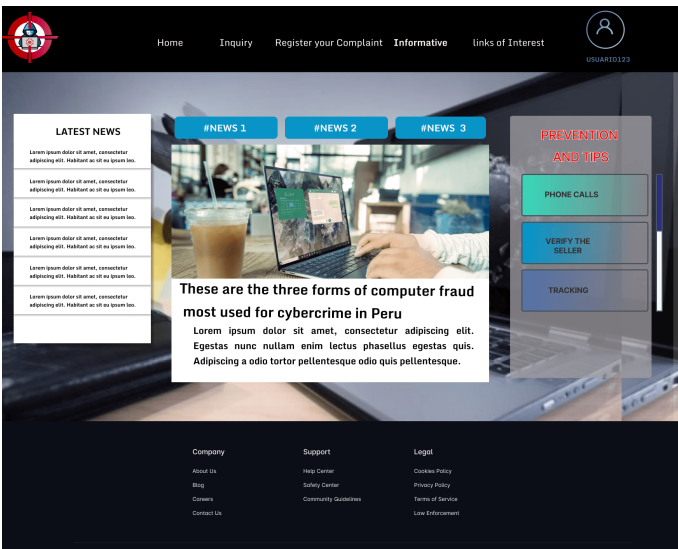


Fig. 12. Prototype based on User Story 7

2) *Second Sprint:* In this sprint, interfaces were mainly developed whose function is to show relevant information on fraud cases, which have been duly validated and stored in the system's database. In Fig. 13, the prototype shows the interface

where the user must fill out the complaint form, an important requirement in this step is to attach the document where the police complaint is certified.

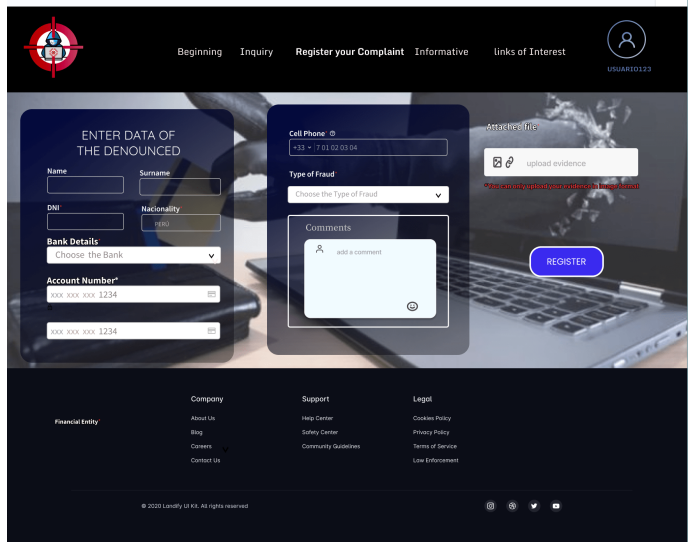


Fig. 13. Prototype based on User Story 5

The prototype in Fig. 14 shows the interface where the most reported cases of fraud can be queried, through predetermined filters such as payment method, number of reported cases and by city. In the section on the right of the interface, an easy-to-understand graph for the user is shown, where relevant information on the registered cases appears.

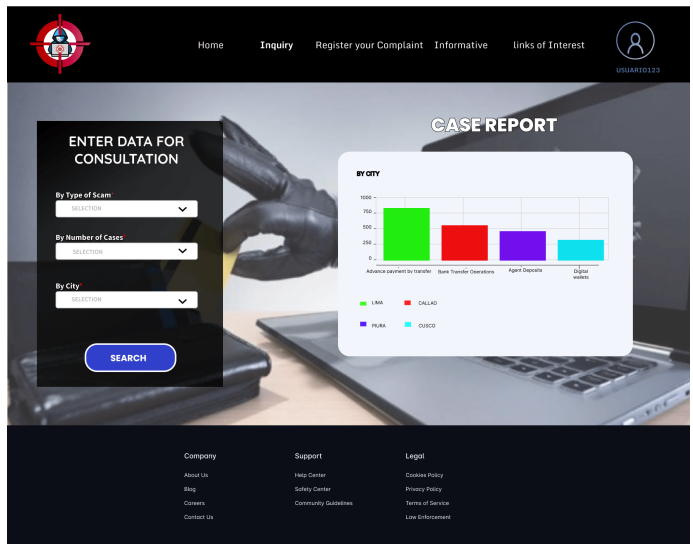


Fig. 14. Prototype based on User Story 10

In Fig. 15, we see the prototype for the user registration interface, basic data is requested for the creation of an account on the platform, also giving the alternative of being able to use a username instead of the personal name.

3) *Third Sprint:* This sprint is mostly related to internal processes and the logic of the web system, for that reason it is the sprint that requires the most time and effort in the

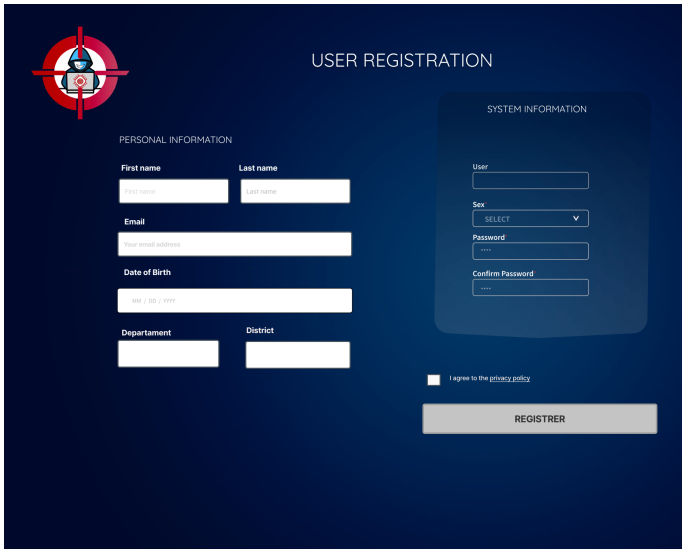


Fig. 15. Prototype based on User Story 6

development of the project. The database was initially filled manually in order to carry out the first tests of the system and detect possible errors.

Subsequently, the filling of the base continued, taking advantage of the learning process that the OCR software needed for optimal performance in the recognition of the entered documents. As mentioned in the Case Study section, the document in image format will allow the complaint record to be considered as valid or not.

Fig. 16 shows the interface where the user can check if a seller/supplier has been reported on the platform as a fraudster. Some of the requested data must be entered so that the system searches the database and displays the information of the accused in the section on the right.

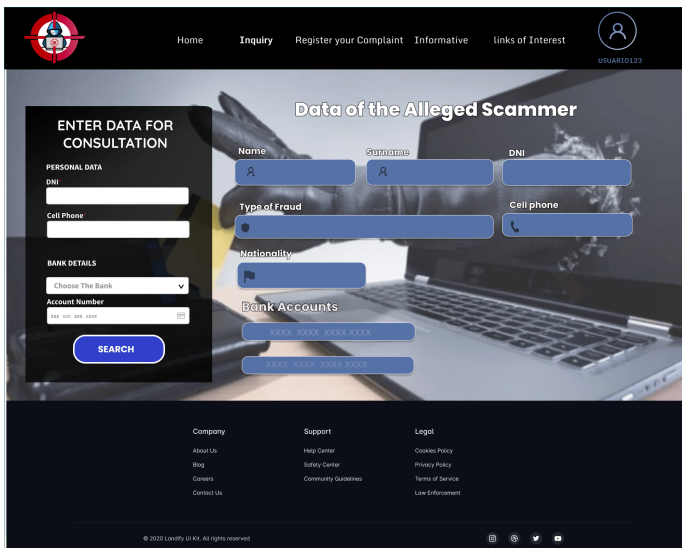


Fig. 16. Prototype based on User Story 2

B. Complaints Registered for Computer Crimes

Cybercrime in the current context is on the rise and the most affected are the consumers who have to deal with the loss of their property as a result of this type of crime. Although measures are being taken in the country and laws are being applied to regularize this situation, the efforts and policies applied have not worked properly or have not been sufficient. In Table III, we see a comparative table of the complaints made in the last five years in terms of computer crimes. Where computer fraud represents 78.2% of the reported cases, these cases are investigated by the High Technology Crimes Investigation Division (DIVINDAT).

TABLE III. COMPLAINTS OF COMPUTER CRIMES INVESTIGATED BY DIVINDAT

Crime	2015	2016	2017	2018	2019	2020	Total	%
Computer Fraud	414	610	1219	1928	2097	2615	9515	78.2
Card cloning	46	44	30	120	25	4	394	4
Fraudulent online purchases	-	-	-	287	431	261	979	8
Unauthorized electronic and/or fund transactions and transfers	368	566	1189	1521	1641	2350	8142	86

The crimes were classified according to the type of complaint: card cloning, fraudulent online purchases and unauthorized electronic and/or fund transactions and transfers, the latter being the one that forms part of this research work. The notorious increase in cases of this type of fraud was verified, registering a total of 8,142 complaints from 2015 to 2020. It was also identified that this type of fraud represents 86% of this type of computer crime, thus occupying the first place among the 3 types of cases [26].

C. Informality and Social Commerce

Informality in the country remains high, according to the Institute of Statistics and Informatics (INEI) in a study carried out in 2020. With a sample of 15,224, it was confirmed that approximately 30% of them are in the category of workers, self-employed in the informal sector [12]. With these data we can have a better picture of how broad the group of independent informal workers is, even more so if we consider that 75.3% of workers are informal at the national level, as can be seen in Fig. 17.

Informality in Peru originates mostly from tax evasion and limited resources by independent workers who fail to comply with all the requirements and procedures established to formally set up a business as required by law [12]. The limitation of resources also affects the possibility of not investing in infrastructure or having your own online store. For the aforementioned reasons, informality has also moved towards electronic commerce where sellers/suppliers establish their businesses online.

They mainly carry out their commercial activities through social networks since these do not imply any type of cost, giving greater facilities to position themselves in the digital

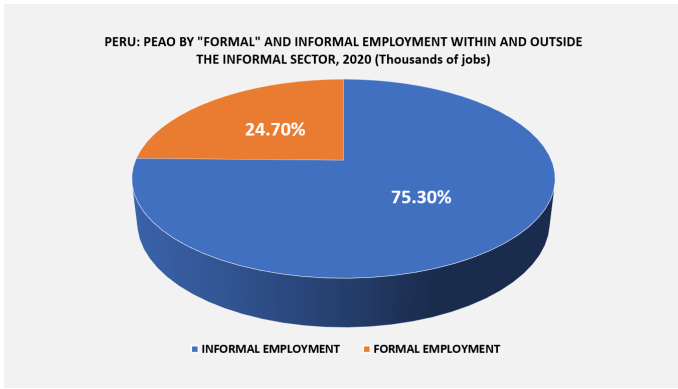


Fig. 17. The Participation of the Formal and Informal Economically Active Employed Population (PEAO) for the Year 2020 is Shown.

market. The independent worker or business owner offers their products/services describing their characteristics through Instagram or Facebook. The purchase/sale is made directly through these platforms or transferred to WhatsApp where the date and place of delivery are agreed.

D. Fraud and Social Networks

There are a large number of purchase and sale operations carried out through social networks such as Facebook, WhatsApp and Instagram where there are informal businesses with good intentions to comply with what is offered. But there are still risks for buyers since it is not the same to buy in a known establishment than to buy through a social network from a stranger. Fraudsters and/or computer criminals take advantage of the anonymity of social networks to commit their crimes, their way of operating involves creating false personal or business accounts as a facade. Then, through deception, they promise supposed products or services that they offer if they are previously paid in advance to cover the expenses involved in the delivery or fulfillment of what is offered.

TABLE IV. REQUESTS FOR ACTIVE JUDICIAL ASSISTANCE

Requirements	Number
Facebook account information	45
Email account information	18
Request information from Facebook, Messenger, WhatsApp	3
Request information from Google	2
Request information from a website	2
Arrested user identity, intervention information in the Russian social network account	1
Request information from various companies that provide social networks	1
Request removal of communications and traffic information and content of a Facebook account	1

According to the report on Cybercrime in Peru [26] prepared by the Public Ministry, 45% of active judicial assistance has been aimed at requesting information from Facebook accounts and 9% has involved social networks. In Table IV we can observe some of the requested requirements where requesting information from social networks for the cases in question stands out. These requests were made with the intention of helping the competent entities to clarify investigations and criminal proceedings that implicate social networks as a means of criminal acts related to computer fraud.

E. Risk Prevention and Minimization

Through social networks, mainly through Facebook, it was found that there is an interest on the part of citizens to make public their complaints, reports or report cases where they have been victims of fraud. However, the information through this platform is not centralized or organized, which makes access to said information difficult. In addition, through social networks there are no terms and conditions that guarantee 100% secure purchase and sale transactions. For these reasons, this project seeks to organize the data and minimize the risks due to computer fraud as a result of social commerce.

Both parties, both consumers/buyers and suppliers/sellers, can benefit from this initiative. On the one hand, the consumer/buyer who makes sure that the other party involved in the transaction has not been reported for any type of fraud. And on the other hand, the supplier/seller that manages to generate greater confidence in its clients and gain a better reputational image for its business by not being reported in the base of the proposed system.

F. Web System

The web system was designed and developed with the objective of executing a set of tasks that allow users to take preventive measures before carrying out any operation and to carry out their transactions online safely. Next, the operations of the web system are explained, grouped by their functionality, as well as the results obtained through a survey carried out on experts to validate the quality of the system.

a) Registry Functionality:

Made up of the User Registration and Complaint Registration sections, these have the function of allowing the entry and registration of data within the system. The first section mentioned authorizes access to the platform and the second section allows you to report cases of fraud by attaching your respective police report.

b) Query Functionality:

Made up of the Home, Search, Informative and Links of interest sections, these have the function of allowing the user to see information related to the topic of prevention through the different interfaces of the platform. In the particular case of the search section, it grants access to consult information on the cases reported in the system.

c) Tesseract OCR Performance:

The free software Tesseract with its LSTM-based OCR engine complemented the development of the system by facilitating the recognition of attachments provided by users; managing to identify and classify the documents as valid or not and confirming that they were a police report. The accuracy of the LSTM Recurrent Neural Network for text recognition in Urdu script was evidenced in the [27] investigation. This type of writing is based on an Arabic cursive style and due to its nature makes the text recognition process even more difficult.

However, in Fig. 18, the results obtained from this investigation are verified where the LSTM model achieves an accuracy of 98.38% despite the difficulty in recognizing the aforementioned writing. In the present research work, it was decided to use the Tesseract software precisely because of the good performance and precision that it has shown in

TABLE V. RESULT OF VALIDATION BY EXPERTS

Criterion	Questions	Media	S.D
Usability	The web system runs responsively through any type of browser.	2.87	0.35
Usability	The web system has a friendly and easy-to-use interface for users.	2.75	0.46
Usability	The web system is properly organized for users to understand.	2.87	0.35
Usability	The design of the web system works according to a programming structure.	3	0
Feasibility	The web system development budget covers cloud storage.	2.62	0.51
Feasibility	For the development of the web system there was a certain cost or budget.	2.50	0.75
Feasibility	Business strategies have been designed so that the web system generates profitability.	2.75	0.46
Scalability	The web system is stable even with the increase in user load.	2.62	0.51
Scalability	The web system has a fast response time in relation to its database.	2.87	0.35
Scalability	System processes are well established and function properly.	2.87	0.35
Innovation	The web system performs quick queries regarding information on fraud complaints.	2.87	0.35
Innovation	The web system has been created to be able to implement more information modules on computer crimes.	2.62	0.51
Innovation	The web system constantly obtains knowledge and/or relevant information.	2.75	0.46
Technology	A transactional database was used for queries and storage of information.	2.62	0.51
Technology	A specialized programming language for web systems with artificial intelligence support was used.	2.87	0.35
Technology	A framework was used for interface design and programming of the web system that is adaptable.	2.87	0.35
Technology	The web system can be adapted to any type of device.	2.75	0.46

Average Performance of Three Models

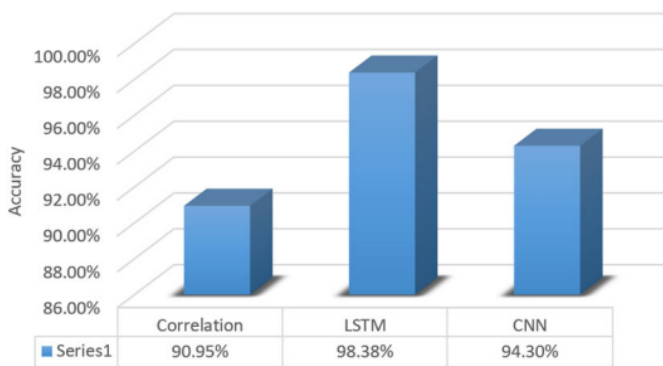


Fig. 18. Comparison between 3 Models of Artificial Neural Networks to Recognize Text in Urdu Script [27].

best OCR today.

d) Validation of the Proposed Model with Experts:

This section specifies the results obtained through a survey of 8 experts to validate the quality level of the web system. The criteria used were: Usability, Feasibility, Scalability, Innovation and Technology. The questions raised were made using the Likert scale with the answer option: 1 (very low), 2 (intermediate), 3 (very high). The questions that were applied in the validation measure the level of acceptance of the web system by experts in the development of these applications. Table V shows the result of the validation, which is divided by different criteria as well as the proposed questions and the level of quality obtained based on the calculations for the mean and standard deviation (S.D.) of each question. The calculation of the mean allowed to establish the range of the quality level, it was obtained as a result of the total mean of all the criteria of 2.76. In that sense we can say that it has been approved by the experts.

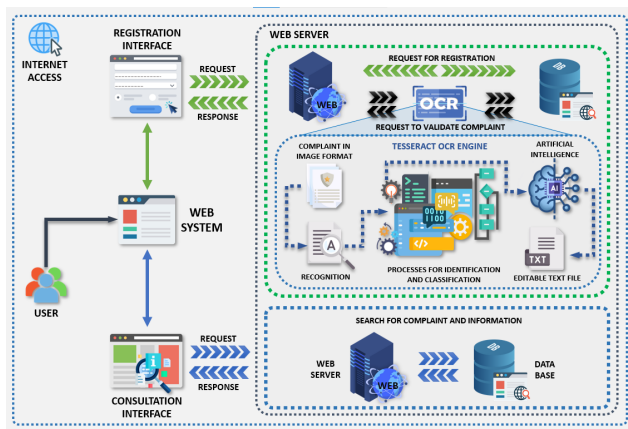


Fig. 19. Web Application Architecture.

more complex cases to identify texts in documents with image format. In addition, the software has several advantages such as having an extensive library with features that facilitate rapid learning. It also has models for several languages, covering 116 languages including Spanish, it is even recognized among the

As mentioned at the beginning of this project, the use of fraud prevention systems reduces the impact of these crimes. In the research work of [28], the favorable results were confirmed with figures when implementing a web system with the same purpose. In just 1 year, the number of computer fraud cases was reduced from 30% to 28% through its proposed model, which is also supported by artificial intelligence.

On the other hand, the investigations of [9] and [10] focus on reducing cases of fraud when purchases and payments are made through electronic commerce platforms that are part of formally constituted companies. In addition [11], [12] and [13] seek to improve the existing systems of companies that have the resources to pay for more sophisticated projects. However, the works in question do not focus or have an alternative solution for cases where purchase or sale transactions are made from person to person and that is the most used type of commerce in Peru. The proposal does not seek to favor formality, on the contrary, it seeks to offer an option for safer transactions, giving these informal businesses the opportunity and time to have enough capital to later be able to go formal.

In Fig. 19, we can see graphically the architecture of the proposed web system and the aforementioned functionalities. You can also observe in detail the support given by the OCR

tool to validate the entry of a complaint into the system, which allows the automation of this process. In this way, manual reviews of the complaints were avoided, saving time, reducing possible costs, searching for quick information and improving the management of the web system.

VI. CONCLUSION

Finally, the research work demonstrated how the proposed system contributes to the prevention of computer fraud caused by the digital informality present in social networks. The results of the project show how the system can reduce and minimize the risks of online purchase and sale transactions through advance payments which are made by bank transfers or the use of digital wallets. In this way, safer and more reliable operations are guaranteed in favor of the consumer/buyer who is the main affected in this new and growing digital commerce. The development of the web system aims to provide an easy-to-use tool, within the reach of the population and that allows them to be alert to situations of possible fraud. Reducing the impact caused by this type of computer crime until the competent entities can implement better measures to reinforce the computer security of citizens in the country.

VII. FUTURE WORK

As future work, it is suggested to continue investigating and incorporating different disciplines such as computer security, computer risks, cryptography. Also apply another methodology that is related to risk management. At the same time, it is recommended to delve into OCR technology to take advantage of the features it offers much more and to improve the productivity of the system by automating it. Likewise, it is possible to combine specialists in the areas of computing and electronics so that together they can contribute even more to the research project.

REFERENCES

- [1] World Economic Forum, *The Global Risks Report 2022 17th Edition*, 2022. [Online]. Available: <https://www.weforum.org/reports/global-risks-report-2022>
- [2] Apoyo Consultoría, “Agenda Digital para el Perú 2021-2026,” Sociedad de Comercio Exterior del Perú, Tech. Rep., 2021. [Online]. Available: <https://www.comexperu.org.pe/upload/articles/publicaciones/agenda-digital-2021-2026.pdf>
- [3] R. V. Vereau, “Los delitos informáticos y su relación con la criminalidad económica,” *Ius et Praxis*, pp. 95–110, 12 2021. [Online]. Available: <https://doi.org/10.26439/iusetpraxis2021.n053.4995>
- [4] Cámara Peruana de Comercio Electrónico (CAPECE), “Impacto del COVID-19 en el comercio electrónico en Perú y perspectivas al 2021,” CAPECE, Lima, Tech. Rep., 2021. [Online]. Available: <https://www.capece.org.pe/wp-content/uploads/2021/03/Observatorio-Ecommerce-Peru-2020-2021.pdf>
- [5] Instituto Nacional de Estadística e Informática (INEI), “Producción y Empleo Informal en el Perú 2007 - 2020,” INEI, Lima, Tech. Rep., dec 2021. [Online]. Available: <https://www.inei.gob.pe/media/MenuRecursivo/publicaciones-digitales/Est/Lib1828/libro.pdf>
- [6] C. Leyva Serrano, “Estudio de los delitos informáticos y la problemática de su tipificación en el marco de los convenios internacionales,” *Lucerna Iuris et Investigatio*, no. 1, pp. 29–47, apr 2021. [Online]. Available: <https://doi.org/10.15381/lucerna.v0i1.18373>
- [7] F. Andrade-Chaico and L. Andrade-Arenas, “Projections on insecurity, unemployment and poverty and their consequences in lima’s district san juan de lurigancho in the next 10 years,” in *SHIRCON 2019 - 2019 IEEE Sciences and Humanities International Research Conference*, 2019.
- [8] L. Mayer Lux and G. Oliver Calderón, “El delito de fraude informático: concepto y delimitación,” *Revista Chilena de Derecho y Tecnología*, vol. 9, no. 1, p. 151, jun 2020. [Online]. Available: <https://doi.org/10.5354/0719-2584.2020.57149>
- [9] K. Yoshida, K. Tsuda, S. Kurahashi, and H. Azuma, “Online shopping frauds detecting system and its evaluation,” vol. 2. IEEE Computer Society, 9 2017, pp. 649–653. [Online]. Available: <https://doi.org/10.1109/COMPSAC.2017.182>
- [10] K. K. M. Priyadharsini and M. S. F. I. M. Mary, “Online transaction fraud detection system,” *2021 International Conference on Advance Computing and Innovative Technologies in Engineering (ICACITE)*, 2021. [Online]. Available: <https://doi.org/10.1109/ICACITE51222.2021.9404750>
- [11] S. Carta, G. Fenu, D. R. Recupero, and R. Saia, “Fraud detection for e-commerce transactions by employing a prudential multiple consensus model,” *Journal of Information Security and Applications*, vol. 46, pp. 13–22, 6 2019. [Online]. Available: <https://doi.org/10.1016/j.jisa.2019.02.007>
- [12] Y. Cai and D. Zhu, “Fraud detections for online businesses: a perspective from blockchain technology,” *Financial Innovation*, vol. 2, 12 2016. [Online]. Available: <https://doi.org/10.1186/s40854-016-0039-4>
- [13] R. Jhangiani, D. Bein, and A. Verma, “Machine learning pipeline for fraud detection and prevention in e-commerce transactions,” *2019 IEEE 10th Annual Ubiquitous Computing, Electronics & Mobile Communication Conference (UEMCON)*, pp. 0135–0140, 10 2019. [Online]. Available: <https://doi.org/10.1109/UEMCON47517.2019.8992993>
- [14] A. Srivastava, S. Bhardwaj, and S. Saraswat, “Scrum model for agile methodology,” *2017 International Conference on Computing, Communication and Automation (ICCCA)*, pp. 864–869, 5 2017. [Online]. Available: <https://doi.org/10.1109/CCAA.2017.8229928>
- [15] F. Hayat, A. U. Rehman, K. S. Arif, K. Wahab, and M. Abbas, “The influence of agile methodology (scrum) on software project management.” *IEEE*, 7 2019, pp. 145–149. [Online]. Available: <https://doi.org/10.1109/SNPD.2019.8935813>
- [16] P. Ounsrimuang and S. Nootyaskool, “Introducing scrum process optimization.” *IEEE*, 7 2017, pp. 175–181. [Online]. Available: <https://doi.org/10.1109/ICMLC.2017.8107761>
- [17] A. Ramos-Romero, B. Garcia-Yataco, and L. Andrade-Arenas, “Mobile application design with iot for environmental pollution awareness,” *International Journal of Advanced Computer Science and Applications*, vol. 12, no. 1, pp. 566–572, 2021, doi:10.14569/IJACSA.2021.0120165.
- [18] R. A. Kacprzyk, J. Pedrycz, W. Jamshidi, M. Babanli, M. B. & Sadikoglu, and F. M. Aliev, *10th International Conference on Theory and Application of Soft Computing, Computing with Words and Perceptions - ICSCCW-2019*. Springer International Publishing, 2020, vol. 1095. [Online]. Available: <http://link.springer.com/10.1007/978-3-030-35249-3>
- [19] G. Delanerolle, X. Yang, S. Shetty, V. Raymont, A. Shetty, P. Phiri, D. K. Hapangama, N. Tempest, K. Majumder, and J. Q. Shi, “Artificial intelligence: A rapid case for advancement in the personalization of gynaecology/obstetric and mental health care,” *Women’s Health*, vol. 17, p. 174550652110181, 1 2021. [Online]. Available: <https://doi.org/10.1177/17455065211018111>
- [20] H.-H. Tseng, Y. Luo, R. K. T. Haken, and I. E. Naqa, “The role of machine learning in knowledge-based response-adapted radiotherapy,” *Frontiers in Oncology*, vol. 8, 7 2018. [Online]. Available: <https://doi.org/10.3389/fonc.2018.00266>
- [21] H. Singh and A. Sachan, “A proposed approach for character recognition using document analysis with ocr.” *IEEE*, 6 2018, pp. 190–195. [Online]. Available: <https://doi.org/10.1109/ICCONS.2018.8663011>
- [22] S. S. Bukhari, S. Francis, C. N. N. Kamath, and A. Dengel, “An investigative analysis of different lstm libraries for supervised and unsupervised architectures of ocr training,” vol. 2018-August. *IEEE*, 8 2018, pp. 447–452. [Online]. Available: <https://doi.org/10.1109/ICFHR-2018.2018.00084>
- [23] S. M. Shithil, A. R. M. Kamil, S. Tasnim, and A. A. M. Faudzi, “Container iso code recognition system using multiple view based on google lstm tesseract,” in *Computational Intelligence in Machine Learning*. Springer, 2022, pp. 433–440. [Online]. Available: https://doi.org/10.1007/978-981-16-8484-5_41

- [24] S. Drobac and K. Lindén, "Optical character recognition with neural networks and post-correction with finite state methods," *International Journal on Document Analysis and Recognition (IJ DAR)*, vol. 23, pp. 279–295, 12 2020. [Online]. Available: <https://link.springer.com/10.1007/s10032-020-00359-9>
- [25] Hubert, P. Phoenix, R. Sudaryono, and D. Suhartono, "Classifying promotion images using optical character recognition and naïve bayes classifier," *Procedia Computer Science*, vol. 179, pp. 498–506, 2021. [Online]. Available: <https://doi.org/10.1016/j.procs.2021.01.033>
- [26] Ministerio Público Fiscalía de la Nación, "Cibercriminalidad en el Perú: Pautas para una investigación fiscal especializada," pp. 1–70, 2021. [Online]. Available: www.mpfj.gob.pe
- [27] A. Naseer and K. Zafar, "Meta features-based scale invariant ocr decision making using lstm-rnn," *Computational and Mathematical Organization Theory*, vol. 25, pp. 165–183, 6 2019. [Online]. Available: <http://link.springer.com/10.1007/s10588-018-9265-9>
- [28] J. C. Moreno, C. M. S. M. Sánchez, J. Salavarieta, and L. M. Vargas, "Soluciones tecnológicas para la prevención de fraude y diseño de un modelo de prevención del riesgo transaccional para el botón de pago," *Entre Ciencia e Ingeniería*, pp. 36–42, 12 2019. [Online]. Available: <https://doi.org/10.31908/19098367.1154>

Benchmarking of Motion Planning Algorithms with Real-time 3D Occupancy Grid Map for an Agricultural Robotic Manipulator

Seyed Abdollah Vaghefi, Mohd Faisal Ibrahim, Mohd Hairi Mohd Zaman
Department of Electrical, Electronic and Systems Engineering
Faculty of Engineering and Built Environment, Universiti Kebangsaan Malaysia
43600 Bangi, Selangor, Malaysia

Abstract—The performance evaluation of motion planning algorithms for agricultural robotic manipulators is commonly performed via benchmarking platforms. However, creating a realistic benchmarking scene that constrains the motion planning algorithms with the characteristic of a real-work environment has always been a challenge worthy of research. In this paper, we present a lab-setup benchmarking platform to evaluate Open Motion Planning Library (OMPL) motion planners for the application of a robotic harvester of a palm-like tree using a real-time 3D occupancy grid map. First, three motion problems were defined with different levels of complexity based on a real oil palm fruit harvesting task. To achieve reliable outcomes, the benchmarking scene was modeled by converting point cloud data from a stereo-depth sensor into a 3D occupancy grid map using the Octomap algorithm. Then the benchmarking was performed, all within a real-time process. According to the results, a fair performance evaluation was achieved by modeling a realistic benchmarking scene, which can help in choosing a high-performing algorithm and efficiently conducting such harvesting tasks in real practice.

Keywords—Motion planning; agricultural; harvesting; robot manipulator; benchmarking; oil palm

I. INTRODUCTION

Over the last few decades, intelligent robots for fruit harvesting have been actively developed to bridge the increasing gap between feeding a fast-growing population and limited labor resources. Moreover, the recent international travel restrictions due to the COVID-19 pandemic in 2019-2021 have exacerbated the limited labor resources issue, leading to the unavailability of seasonal migrant workers [1]. A robotic harvester can significantly boost productivity by reducing labor and production expenses, increasing yield and quality, and improving environmental management [2]. However, current harvesting robots are limited in their capabilities in motion planning, designed for specific plant structures. This limitation is due to the target crops' unstructured and dynamic nature and obstructions within their working environment [3], [4]. Environment obstructions, such as branches and leaves, reduce the performance efficiency of harvesting robotic manipulators. In addition, they are likely to collide with those obstacles when performing harvesting tasks. Therefore, establishing a benchmarking approach to accurately evaluate a collision-free motion planning algorithm for a given task is crucial to increasing the performance of robotic harvesting manipulators.

This study aimed to perform a benchmarking of different

motion planning algorithms based on real-time perception, i.e., 3D occupancy grid mapping for a robotic harvester of a palm-like tree application. In general, palm-like trees, such as oil palm, dates, and coconut trees, have unique morphological characteristics that challenge motion planning algorithms differently from other crops. The benchmarking of motion planning algorithms based on real-time 3D occupancy mapping should achieve reliable outcomes due to the actual characteristics of the working environment, which is mimicked from the real working environment into the benchmarking scene and constrains the motion planning algorithms. In this work, four motion planning algorithms from the OMPL library, namely, RRTConnect, BiTRRT, BFMT, and FMT, were benchmarked using ROS and MoveIt platform. The process outlined in this study contributes significantly to performing the motion planning benchmarking based on realistic environmental conditions. Furthermore, it can help adopt a high-performing motion planning algorithm and effectively execute such harvesting tasks in actual works.

II. RELATED WORK

In this section, we discuss the role of various benchmarking platforms in evaluating motion planning algorithms for different applications in the literature. In addition, a brief overview and application of 3D occupancy grid mapping in robotic real-time perception will also be presented.

A. Motion Planning Benchmarking

Motion planning is a fundamental topic in robotics that deals with finding an optimal path that satisfies a target specification subject to constraints [5]. The issue of “which planner to choose” could be hard to answer, given the wide range of applications that robotic manipulators are used for [6]. During the last few years, several works have compared and analyzed the motion planning algorithms via benchmarking for different applications during the last few years. Iversen and Ellekilde [7] presented a benchmark for a set of motion planning algorithms based on three different scenarios for bin-picking applications. Despite longer planning time, the algorithms integrated with optimization outperformed due to faster execution. Morgan et al [8] proposed three different robot benchmarking protocols, namely the Modified Box and Block Test (BBT), Targeted-BBT, and Standard-BBT, for assessing various aspects of the system separately and the results compared with human performance. Chatzilygeroudis et al. [9] represented a new

benchmarking protocol to evaluate algorithms for bi-manual robotic manipulation of semi-deformable objects. Therefore, the work makes the benchmark accessible to various related fields, from adaptive control and motion planning to learning the tasks through trial-and-error learning. Jedrzejczyk et al. [10] have investigated a tomato harvesting application and suggested a benchmark of optimally configured motion planners available within Robot Operating System (ROS) and MoveIt platforms. The results indicated a comparison of efficiency and repeatability of particular planners for a planning scene imitating conditions in a greenhouse or similar pick-and-place tasks. Magalhães et al. [11] suggested benchmarking path planner algorithms from Open Manipulator Planning Library (OPML) for tree pruning tasks. Thus, the results demonstrated good agreement for the BiTRRT algorithm compared with other algorithms from the OMPL library, such as BKPIECE, LBKPIECE, SBL, and others. Despite the numerous studies that benchmarked motion planning algorithms for robotic manipulators in industrial applications, few works focused on agricultural applications. Accordingly, this paper studied benchmarking motion planning algorithms for a palm-like tree harvesting application.

B. 3D Occupancy Grid Mapping

Robotic perception is understood as a system that endows the robot with the ability to perceive, comprehend, and reason about the surrounding environment. In addition, robotic perception is crucial for a robot to make decisions, plan, and operate in real-world environments, through numerous functionalities and operations ranging from occupancy grid mapping to object detection algorithms [12]. Fryc et al. [13] proposed a robust multi-stage pipeline for efficient, collision-free brick picking given the pose of a target object. In this case, Octomap represented the realistic simulated environment as inputs to generate a set of motion plans for the robot. Terasawa et al. [14] presented a novel framework that combines a sampling-based planner and deep learning for faster motion planning, focusing on heuristics. For this purpose, the HM-TS-RRT algorithm obtained a heuristic map of the environment information from the Octomap for motion planning and generating collision-free paths within a reasonable time. Hence, the results based on HM-TS-RRT outperform the existing planners, especially in terms of the average planning time with smaller variance. Gai et al. developed a vision-based system for under-canopy navigation of agricultural robotic vehicles using a Time-of-Flight (ToF) camera [15]. A novel algorithm was used to detect parallel crop rows from occupancy grids taken under crop canopies. Therefore, the proposed system was able to map the crop rows with mean absolute errors (MAE) of 3.4 cm and 3.6 cm in corn and sorghum fields, where are provided lateral positioning data with MAE of 5.0 cm and 4.2 cm owing to the position in corn and sorghum crop rows. Chao and Chen [16] proposed a framework of visual perception, scenario mapping, and fruit modeling for robotic harvesters in orchard environments. The scenario mapping module applied the Octomap to represent the multiple classes of objects within the environment. The experiment results were shown that the localization and pose estimation of fruits, which are obtained at 0.955 and 0.923 values for the accuracy of visual perception and modeling algorithm. However, not many studies use real-time 3D occupancy grid mapping for benchmarking scenes. In

this work, we create a real-time realistic benchmarking scene based on sensor information. This approach could help the evaluation of motion planning algorithms more accurately and obtain more reliable results.

III. METHODOLOGY

The assessment of motion planning algorithms is commonly performed using benchmarking platforms for robotic manipulators [16]. However, the outcomes can be reliable when the scene is more to reality [17]. Thus, developing methods for replicating real-work environment specifications in benchmarking scenes is crucial, e.g., the “sensed representation” of test scenes which are built from sensor information. This study established a lab-setup environment as benchmarking scene modeled by converting point cloud data from a stereo-depth camera into a 3D occupancy grid map using the Octomap algorithm [18]. The experiment was then conducted to benchmark the motion planning algorithms for the three motion problems with different levels of complexity based on the oil palm tree harvesting task. The process mentioned above, including generating the 3D occupancy grid map and the benchmarking task, was implemented sequentially. All the system components worked together simultaneously in real-time. Thus the experimental results were obtained for performance assessment of the motion planning algorithms. The overall methodology procedure for this study is indicated in Fig. 1.

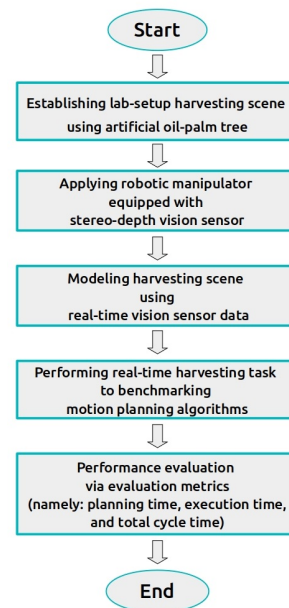


Fig. 1. Overall Methodology Procedure.

The methodology procedure of this work was performed through experimental work, as shown in Fig. 1. First, an artificial oil palm tree was utilized to establish an oil palm fruit harvesting scene. Furthermore, a robotic manipulator equipped with a stereo-depth camera (Intel RealSense D435) was used to conduct the harvesting task. The harvesting task was performed using four motion planning algorithms from the OMPL library, namely RRTConnect, BiTRRT, BFMT, and FMT. Therefore,

the experimental findings evaluated the motion planning algorithms' performance via evaluation metrics, namely planning time, execution time, and total time.

A. Experiment Setup Environment

A laboratory-based experimental setup was established using an artificial palm-like tree and a four DoF robot manipulator to mimic the characteristic of a real oil palm tree harvesting environment, as shown in Fig. 2. In addition, a stereo-depth vision sensor was mounted on the robot manipulator's end-effector to model the working environment in the benchmarking scene.

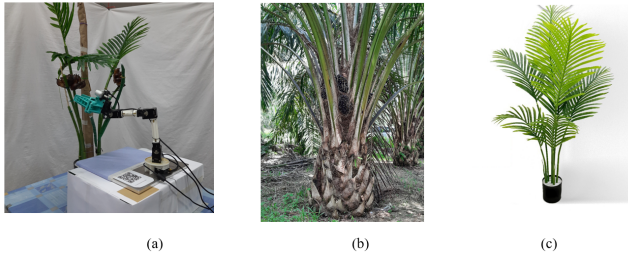


Fig. 2. (a) Laboratory-Scale Experimental Setup with a Robot Arm Attached to a Camera and Artificial Tree (b) Real Oil Palm Tree (c) Artificial Tree.

B. Robot Arm Kinematics

This work used an open-hardware robotic manipulator, model OpenManipulator made by Robotis, as shown in Fig. 3, to develop a generic and low-cost harvesting platform [19]. This robot platform allows the users to optimize its morphology, modify the length of the links, or design the robot for their specific purposes [20]. Furthermore, the robotic manipulator has four DoF, which, based on previous studies, met the minimum requirement in terms of degree of freedom for a palm-like tree harvesting application [21].

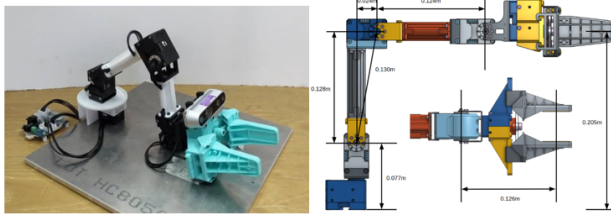


Fig. 3. OpenManipulator Robot Arm from Robotis.

Meanwhile, Fig. 4 illustrates the kinematics model of the robot manipulator, which was utilized to obtain the Denavit-Hartenberg parameters convention [22], as depicted in Table I. Besides, the robot manipulator was also modeled within Robot Operating System (ROS) platform using a domain-specific modeling language called Unified Robotic Description Format (URDF). The robot model was stored in a URDF file to represent the properties of the robot in the ROS Visualization (RVIZ) platform [18]. The URDF file format is based on XML language, which allows for encoding the robot's components such as links, joints, shapes, and physical appearance, as shown in Fig. 5.

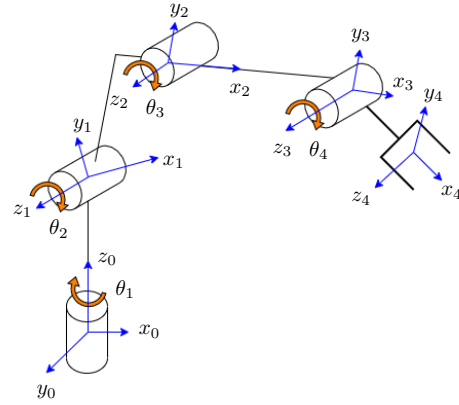


Fig. 4. Kinematic Model of Robotis OpenManipulator Robot Manipulator.

TABLE I. DH PARAMETERS FOR ROBOTIS OPENMANIPULATOR.

Joint	θ_i ($^\circ$)	d_i (m)	a_i (m)	α_i ($^\circ$)
1	θ_1	L_1	0	90
2	$\theta_2 + (90^\circ - \theta_0)$	0	L_6	0
3	$\theta_3 - (90^\circ - \theta_0)$	0	L_4	0
4	θ_4	0	L_5	90

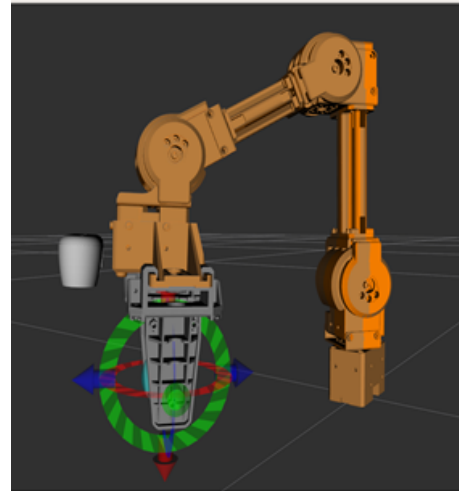


Fig. 5. Robotis Open-Manipulator Model in RVIZ Software based on its URDF File.

C. Modeling the Test Scene into a 3D Occupancy Grid Map

This work used an Intel Realsense D435i stereo-depth sensor, integrated with a point cloud library (PCL), to generate point cloud data [23] to replicate a real-work environment for the test scene. The camera is equipped with two left/right image sensors, OmniVision OV2740, which can produce full-high-definition (FHD) at 60 frames per second (fps). In addition, the Octomap library was implemented to convert the point cloud data of the lab-setup environment into a 3D occupancy grid map in real-time. Fig. 6 depicts a sample of a 3D occupancy grid map of the scene, including the tree leaves, which was generated using the Octomap algorithm.

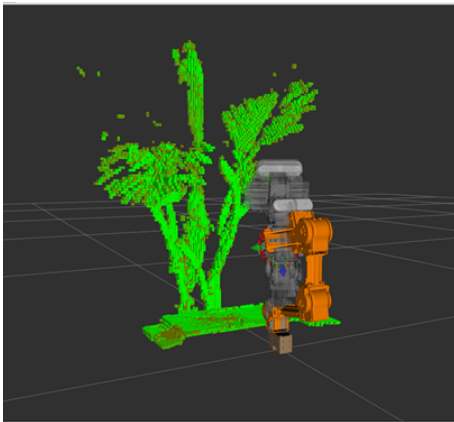


Fig. 6. A Sample of a 3D Occupancy Grid Map Including the Robot Manipulator and Artificial Oil Palm Tree.

D. Generating the Harvesting Motion Planning Problems

In this benchmarking, three motion problems with different levels of complexity in terms of collision avoidance were defined based on a real oil palm harvesting task to measure the performance of the motion planning algorithms. Each of the motion problems contains a pair of initial and goal states. The initial robot arm's configuration and position are identical for all three motion problems. The gray-colored robot arm represents the initial state, while the orange-colored robot arm indicates the goal state, as shown in Fig. 7a, 7b, and 7c. The use of the gripper was beyond the scope of this work. Therefore, it is not included in these motion planning problems.

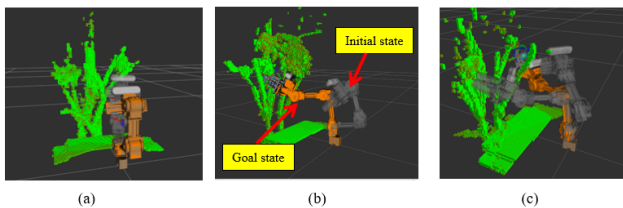


Fig. 7. Three Different Test Scenarios in this Work.

1) *Right-Side Fruit Bunch Problem*: The initial state of this problem is located in a less constrained space than the goal state, as illustrated in Fig. 8. The goal state is a stretched robot arm's configuration with the robot arm's end-effector approaching the right side of the fruit bunch from the bottom. Furthermore, the goal state represents the 'ready to cut' pose of the fruit bunch for the robot arm.

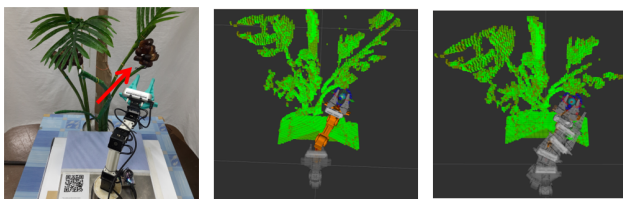


Fig. 8. Right Side of the Fruit Bunch Problem.

2) *Left-Side Fruit Bunch Problem*: The goal state of this problem is situated in a more constrained space than the previous motion problem due to the narrow passage that the robot arm should pass through to reach the target, as shown in Fig. 9. As in the previous motion problem, The goal state is a stretched robot arm's configuration with the robot arm's end-effector approaching the right side of the fruit bunch from the bottom. In addition, the goal state represents the 'ready to cut' pose of the fruit bunch for the robot arm.

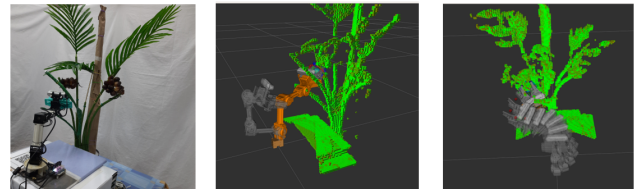


Fig. 9. Left Side of the Fruit Bunch Problem.

3) *Left-Side Fruit Bunch to Right-Side Fruit Bunch Problem*: This motion problem defines the left side of the fruit bunch as the initial state and the right side of the fruit bunch as the goal state, as shown in Fig. 10. Furthermore, the motion path needs to be created from a highly constrained space, traveling through a narrow passage and finally reaching another highly constrained space, as illustrated in Fig. 10. Thus, a higher level of complexity in terms of obstacle avoidance is provided by this motion problem than the previous motion problems.

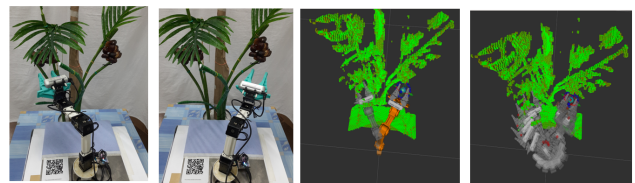


Fig. 10. Left Side to the Right Side of the Fruit Bunch Problem

E. Performance Evaluation

The experiment was performed within the ROS MoveIt platform on a computer with Ubuntu 18.04.6 LTS Operating System, Intel® Core™ i7-9750H CPU, 16 GB Memory, Nvidia GeForce RTX 2060, and ROS Melodic distribution. The ROS MoveIt platform integrates a 3D occupancy grid map of the working environment with motion planning algorithms to generate feasible paths and solve motion problems for a given task.

In order to evaluate the performance of the motion planning algorithms for solving and executing the motion planning problems, three metrics, namely planning time, execution time, and total cycle time, were defined. All the metrics were analyzed individually to demonstrate the higher performance algorithm within each of them. Planning time is considered when it takes for a motion planner to find a viable path for a given motion problem. Furthermore, The time it takes for the robot arm to move from its initial state to its goal state for a given motion path is known as execution time. Finally,

the addition of planning and execution time is considered total cycle time.

The motion planning algorithms, RRTConnect, BiTRRT, BFMT, and FMT, were implemented to solve and conduct the motion problems. For each specific problem, the problem was solved and executed 10 times by each of the algorithms for 40 runs per problem. Given the three motion problems, 120 runs were performed to conduct the benchmarking task. Furthermore, each algorithm was given 5 seconds time-out to solve the respective motion problem since such harvesting applications need to be conducted quickly in real practice. The successful cycles only were used in the analysis.

IV. RESULTS AND DISCUSSION

Fig. 11 illustrates the results of the planning time for the three motion planning problems solved by the algorithms mentioned above. In the first problem, the right-side fruit bunch, RRTConnect achieves the shortest planning time with the lowest mean of 0.11 s and also the lowest standard deviation of 0.0215 s. In contrast, FMT had the worst performance among the others. This outcome indicates that for straight forward motion planning problems, with the minimum need for curvature to avoid colliding with obstacles, RRTConnect algorithm can be considered a fast algorithm for creating motion paths.

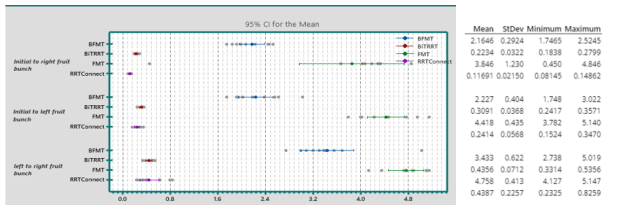


Fig. 11. Planning Time for the Three Planning Motion Planning Problems.

In the second motion planning problem, the left-side fruit bunch, more complexity in terms of collision avoidance was provided by the motion problem to the algorithms. In this problem, RRTConnect outperformed the other algorithms again (slightly faster than BiTRRT) with the lowest mean of 0.2414 s and the lowest standard deviation of 0.0568 s. Meanwhile, in the third motion planning problem, from the left-side fruit bunch to the right-side fruit bunch, RRTConnect had the shortest mean. In contrast, BiTRRT, which had a slightly higher mean, demonstrated a lower standard deviation than RRTConnect. Again, the FMT had the longest computation time among all.

Meanwhile, Fig. 12 represents the execution time of motion planning generated by the algorithms within the three motion problems. For example, in the first problem, from the initial position to the right-side fruit bunch, RRTConnect achieved the fastest execution time with the lowest mean of 4.9455 s and the lowest standard deviation of 0.1932 s. Meanwhile, FMT was the slowest, with the highest mean and highest standard deviation with more outliers than other algorithms.

In the second problem, from the initial position to the left-side fruit bunch position, RRTConnect achieved the lowest mean of 5.257 s while obtaining the highest standard deviation

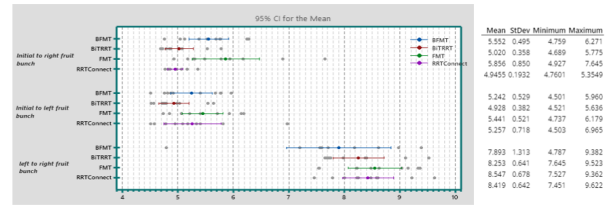


Fig. 12. Execution Time for the Three Planning Motion Planning Problems.

of 0.718 s. In contrast, FMT had the highest mean of 5.441 s and the most significant number of outliers. In the third problem, from the left side to the right side fruit bunch, the most complicated motion within this benchmarking work was provided to the motion planning algorithms. The lowest mean of 7.893 s and the highest standard deviation of 1.313 s was achieved by the BFMT. In contrast, FMT obtained the highest mean of 8.547 s but a lower standard deviation for the motions execution time.

Furthermore, Fig. 13 shows the results for the total cycle time, including motion planning times and the respective motion execution times. In the first problem, the right-side fruit bunch, RRTConnect achieved the highest performance in motion planning time and the respective execution time with the mean of 5.062 s and standard deviation of 0.1889 s. In contrast, the lowest performance was obtained by FMT with a mean of 9.702 s and a standard deviation of 0.803 s.

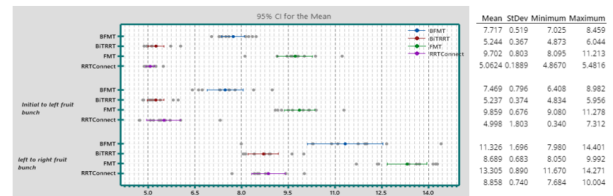


Fig. 13. Total Cycle Time for the Three Planning Motion Planning Problems.

In the second problem, despite the lowest mean of 4.998 s for RRTConnect, its standard deviation is significantly higher than the second-lowest mean, which BiTRRT achieved. To this extent, BiTRRT can be considered a more consistent algorithm for such motion problems. In the third problem, where a more complicated motion problem than the first and the second one was provided, BiTRRT achieved the highest performance with the lowest mean and standard deviation of 8.689 s and 0.683 s, respectively. In contrast, FMT demonstrated the lowest performance concerning its mean of 13.305 s and a number of outliers.

Due to the smaller size of the palm-like artificial tree, which was used in our experimental setup, compared to actual palm-like trees, the Octomap resolution was increased. Thus, the generated 3D occupancy map contains all the necessary details of the artificial tree. However, the increase in resolution would result in high computational cost leading to a rise in the planning and execution time accordingly. On the other hand, with regard to the much larger size of real palm-like trees, which would result in less computational cost for generating a 3D occupancy map with lower resolution, a

considerable decrease in motion planning time and execution time is expected for real palm-like tree harvesting applications.

V. CONCLUSION

In this study, a benchmarking of OMPL motion planning algorithms for a robotic harvester of a palm-like tree application was performed using the ROS and MoveIt platform. An experimental harvesting application setup was established using an artificial palm tree and a four DoF robotic manipulator equipped with a stereo-depth sensor. A 3D occupancy map was constructed using the Octomap algorithm to replicate the features and characteristics of the working environment based on the point cloud data produced by the stereo-depth sensor, which is imported into the benchmarking scene. The benchmarking was then performed within three harvesting scenarios, each including a motion planning problem with different levels of complexity, all as real-time experimental work. The motion planning performance was studied by defining three evaluation metrics: planning time, execution time, and total cycle time. RRTConnect demonstrated the highest performance in the first harvesting scenario according to the outcomes. However, for the second and third scenarios, BiTRRT outperformed the other algorithms. The work presented in this study can be extended to include methods for optimally configuring the OMPL motion planning algorithms based on the features and characteristics of a palm-like tree harvesting application to achieve the highest performance for a given motion planning algorithm.

ACKNOWLEDGMENT

This work was financially supported by Universiti Kebangsaan Malaysia (grant no. GUP-2019-018 and GGPM-2019-051).

REFERENCES

- [1] H. Zhou, X. Wang, and C. Chen, "Intelligent robots for fruit harvesting: Recent developments and future challenges background," 2021, Available online: <https://doi.org/10.21203/rs.3.rs-497056/v1> [accessed on 1 June 2022].
- [2] D. Sepulveda, R. Fernandez, E. Navas, M. Armada, and P. Gonzalez-De-Santos, "Robotic aubergine harvesting using dual-arm manipulation," *IEEE Access*, vol. 8, pp. 121889–121904, 2020.
- [3] L. van Herck, P. Kurtser, L. Wittemans, and Y. Edan, "Crop design for improved robotic harvesting: A case study of sweet pepper harvesting," *Biosyst. Eng.*, vol. 192, pp. 294–308, 2020.
- [4] C. W. Bac, E. J. van Henten, J. Hemming, and Y. Edan, "Harvesting Robots for High-value Crops: State-of-the-art Review and Challenges Ahead," *J. F. Robot.*, vol. 31, no. 6, pp. 888–911, 2014.
- [5] M. Moll, I. A. Sukan, and L. E. Kavraki, "Benchmarking Motion Planning Algorithms: An Extensible Infrastructure for Analysis and Visualization," *IEEE Robot. Autom. Mag.*, vol. 22, no. 3, pp. 96–102, 2015.
- [6] D. Youakim and P. Ridao, "Motion planning survey for autonomous mobile manipulators underwater manipulator case study," *Rob. Auton. Syst.*, vol. 107, pp. 20–44, 2018.
- [7] T. F. Iversen and L. P. Ellekilde, "Benchmarking motion planning algorithms for bin-picking applications," *Ind. Rob.*, vol. 44, no. 2, pp. 189–197, 2017.
- [8] A. S. Morgan, K. Hang, W. G. Bircher, F. M. Alladkani, A. Gandhi, B. Calli, and A. M. Dollar, "Benchmarking cluttered robot pick-and-place manipulation with the box and blocks test," *IEEE Robot. Autom. Lett.*, vol. 5, no. 2, pp. 454–461, 2020.
- [9] K. Chatzilygeroudis, B. Fichera, I. Lauzana, F. Bu, K. Yao, F. Khadivar, and A. Billard, "Benchmark for bimanual robotic manipulation of semi-deformable objects," *IEEE Robot. Autom. Lett.*, vol. 5, no. 2, pp. 2443–2450, 2020.
- [10] F. Jedrzejczyk, J. Bajer, G. Gawdzik, J. Glowka, and A. Sprońska, "Benchmark and analysis of path planning algorithms of 'ROS MoveIt!' for pick and place task in tomato harvesting," *Adv. Intell. Syst. Comput.*, vol. 1390, pp. 272–284, 2021.
- [11] S. A. Magalhães, F. N. dos Santos, R. C. Martins, L. F. Rocha, and J. Brito, "Path planning algorithms benchmarking for grapevines pruning and monitoring," *Lect. Notes Comput. Sci. (including Subser. Lect. Notes Artif. Intell. Lect. Notes Bioinformatics)*, vol. 11805 LNAI, pp. 295–306, 2019.
- [12] C. Premebida, R. Ambrus, and Z.-C. Marton, "Intelligent robotic perception systems," *Appl. Mob. Robot.*, 2019.
- [13] S. Fryc, L. Liu, and T. Vidal-Calleja, "Robust pipeline for mobile brick picking," *Australas. Conf. Robot. Autom. ACRA*, 2019.
- [14] R. Terasawa, Y. Ariki, T. Narihira, T. Tsuboi, and K. Nagasaka, "3D-CNN based heuristic guided task-space planner for faster motion planning," in *Proceedings of the IEEE Int. Conf. Robot. Autom.*, pp. 9548–9554, 2020.
- [15] J. Gai, L. Xiang, and L. Tang, "Using a depth camera for crop row detection and mapping for under-canopy navigation of agricultural robotic vehicle," *Comput. Electron. Agric.*, vol. 188, no. June, p. 106301, 2021.
- [16] H. Kang and C. Chen, "Visual perception and modelling in unstructured orchard for apple harvesting robots," pp. 1-23, 2019, Available online: <http://arxiv.org/abs/1912.12555> [accessed on 1 June 2022].
- [17] A. Hornung, K. M. Wurm, M. Bennewitz, C. Stachniss, and W. Burgard, "OctoMap: An efficient probabilistic 3D mapping framework based on octrees," *Auton. Robots*, vol. 34, no. 3, pp. 189–206, 2013.
- [18] X. Ling, Y. Zhao, L. Gong, C. Liu, and T. Wang, "Dual-arm cooperation and implementing for robotic harvesting tomato using binocular vision," *Rob. Auton. Syst.*, vol. 114, pp. 134–143, 2019.
- [19] M. A. M. Adzeman, M. H. M. Zaman, M. F. Nasir, M. F. Ibrahim, and S. M. Mustaza, "Kinematic modeling of a low cost 4 DOF robot arm system," *Int. J. Emerg. Trends Eng. Res.*, vol. 8, no. 10, pp. 6828-6834, 2020.
- [20] M. H. M. Zaman, M. F. Ibrahim, and A. M. Moubark, "Dimensional optimization of 4-DOF robot manipulator using artificial bee colony algorithm," in *Proceedings of the Int. Conf. Electr. Eng. Informatics*, pp. 5-8, 2021.
- [21] A. A. Aljanobi, S. A. Al-Hamed, and S. A. Al-Suhaibani, "A setup of mobile robotic unit for fruit harvesting," in *Proceedings of the 19th Int. Work. Robot. Alpe-Adria-Danube Reg.*, pp. 105–108, 2010.
- [22] H. Z. Ting, M. H. M. Zaman, M. F. Ibrahim, and A. M. Moubark, "Kinematic analysis for trajectory planning of open-source 4-DoF robot arm," *Int. J. Adv. Comput. Sci. Appl.*, vol. 12, no. 6, pp. 769-777, 2021.
- [23] R. B. Rusu and S. Cousins, "3D is here: Point cloud library (PCL)," in *Proceedings of the IEEE Int. Conf. Robot. Autom.*, pp. 1-4, 2011.

Unsupervised Domain Adaptation using Maximum Mean Covariance Discrepancy and Variational Autoencoder

Fabian Barreto¹
Department of
Electronics and Telecommunication
Xavier Institute of Engineering
Mumbai, India

Dr Jignesh Sarvaiya²
Department of Electronics,
Sardar Vallabhbhai
National Institute of Technology
Surat, India

Dr Suprava Patnaik⁴
School of Electronics,
Kalinga Institute of Industrial Technology
Bhubaneswar, India

Sushilkumar Yadav³
Jio Platforms Limited
Navi Mumbai, India

Abstract—Face Recognition has progressed tremendously from its initial use of holistic learning models to using hand-crafted, shallow, and deep learning models. DeepFace, a nine-layer Deep Convolutional Neural Network (DCNN), reached near-human performance on unconstrained face recognition for the Labeled Faces in the Wild (LFW) dataset. These models performed very well on the benchmark datasets, but their performance sometimes deteriorated for real-world applications. The problem arose when there was a domain shift due to different distribution spaces of the training and testing models. Few researchers looked at Unsupervised Domain Adaptation (UDA) to find the domain-invariant feature spaces. They tried to minimize the domain discrepancy using a static loss of maximum mean discrepancy (MMD). From MMD, the researchers delved into the higher-order statistics of maximum covariance discrepancy (MCD). MMD and MCD were combined to get maximum mean and covariance discrepancy (MMCD), which captured more information than MMD alone. We use a Variational Autoencoder (VAE) with joint mean and covariance discrepancy to offer a solution for domain adaptation. The proposed MMCD-VAE model uses VAE to measure the discrepancy in the spread of variance around the mean value and uses MMCD to measure the directional discrepancy in the variance. Analysis was done using the TinyFace benchmark dataset and the Bollywood Celebrities dataset. Three objective image quality parameters, namely SSIM, pieAPP, and SIFT feature matching, demonstrate the superiority of MMCD-VAE over the conventional KL-VAE model. MMCD-VAE shows an 18 % improvement in SSIM and a remarkable improvement in the perceptual quality of the image over the conventional KL-VAE model.

Keywords—Deep learning; domain adaptation; face recognition; maximum mean covariance discrepancy; transfer learning; variational autoencoders

I. INTRODUCTION

In the past decade, Face Recognition (FR) research has achieved high accuracy using Deep Learning (DL) approaches. It has matched that of the humans and even transcended it. Advances in DL have facilitated the growth of large training datasets required to implement DL algorithms effectively. Presently we have datasets that use large amounts of labeled

data from the internet, consisting of face images in an unconstrained environment, with a marked diversity of ethnicity, gender, and age.

At times, in real-world applications, one notices a certain discrepancy. The target face image dataset is acquired in different settings compared to the source. There is a difference in the performance of a learned model on a source dataset and a target dataset. Also, in some applications, it is not possible to have large datasets from a particular domain to train a deep learning model. So can one borrow pre-trained models from similar domains? This can help to improve the learning process. However, the caveat is that the performance is boosted only for trained and tested datasets with identical data distributions.

It is interesting to understand the learning process between the deep networks and the human person in this context. The way that learning happens in deep networks and human persons is different. Humans learn from a limited set of labeled data. The other advantage humans possess is that they can generalize their learning and apply it to new conditions or situations.

The authors in [1] have shown the theoretical limitations on the performance by studying the error bounds for different source and target data distributions. The term “data shift”, as first used in 2009, in [2], is the change of distribution of features [3]. The change in the distributions is referred to as covariate shift in [4]. Even a Deep CNN can experience domain shift [5]. Domain Adaptation (DA) algorithms attempt to understand these different shifts in statistical distributions for adaptation in domains.

The paper is organized as follows. Section II presents a review of domain adaptation techniques. Section III describes the metrics for measuring distribution discrepancy. Section IV focuses on the deep domain adaptation for face recognition. Section V presents the proposed MMCD-VAE latent feature extraction model. Section VI elaborates the experimental results, and finally Section VII provides the conclusion and

future work of this study.

II. A REVIEW OF DOMAIN ADAPTATION

A. Domain Adaptation and Transfer Learning

The authors in their landmark paper [6] gave an overview of the Transfer Learning (TL) process, where they situated the DA task in the context of TL. Tasks were Inductive Transfer Learning, Transductive Transfer Learning or Unsupervised Transfer Learning based on label availability for the source and target domain. A summary is shown in Fig. 1 as in [6], which shows how DA is a subset of TL.

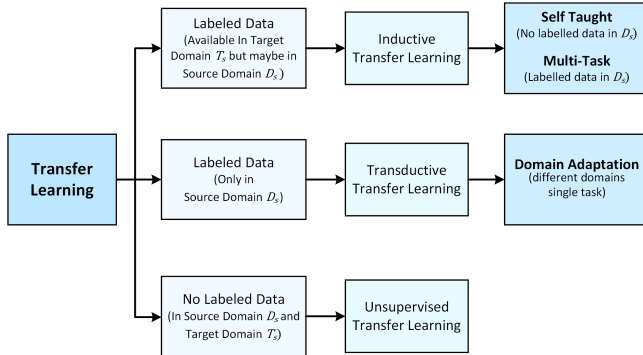


Fig. 1. The Relationship of Domain Adaptation to Transfer Learning [10].

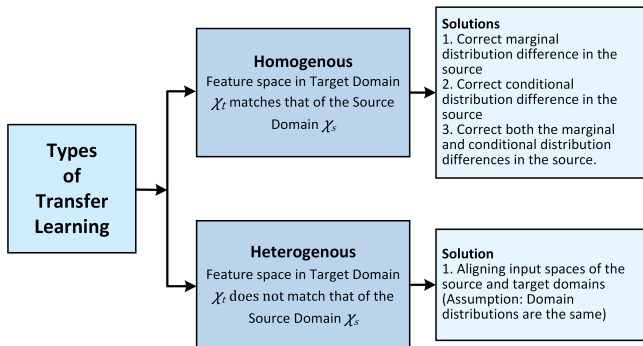


Fig. 2. Types of Transfer Learning.

The authors in [7] define TL in terms of the domains and the given tasks. They classify TL as being homogenous when the feature space is the same and heterogeneous when the feature spaces are different, as shown in Fig. 2. They also clarify that the domain adaptation process seeks to change a source domain to match more closely with the target domain. The terms supervised or unsupervised refer to the source domain availability of labeled data. And for the target domain, as informed or uninformed. A word of caution is also given on Negative transfer when the learned information detrimentally affects the target domain.

The authors in [8] elaborate on the transfer learning categories and present about forty representative approaches to transfer learning along with experimental verification. The broad categories are shown in Fig. 3.

The notations given in [6] and [7] are used to explain the concepts of DA.

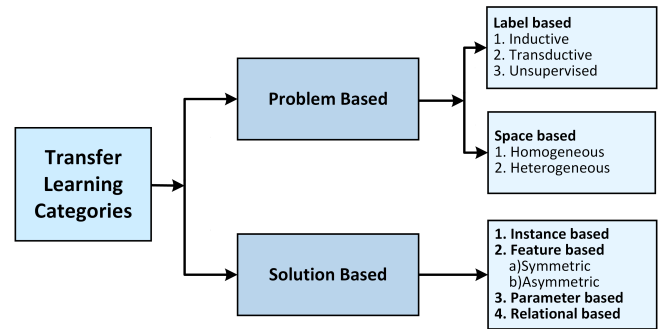


Fig. 3. Transfer Learning Categories.

Let the source domain labeled data be given by $D_s = \{x_i^s, y_i^s\}_{i=1}^M$, with i th sample x_i^s , and label y_i^s . The number of source images is given by M .

Let target domain unlabeled data be given by $D_t = \{x_i^t\}_{i=1}^N$, with i th sample x_i^t . The number of target images is given by N . The difference in data distributions as shown in Fig. 4, is given by $P(X_s, Y_s) \neq P(X_t, Y_t)$.

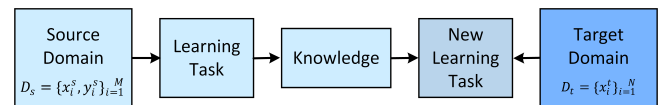


Fig. 4. A Simplified Transfer Learning Model for Domain Adaptation.

Many researchers have done surveys on TL [6], [7], [9], [10] [8] and DL [11], [12], [13], [14] and [15]. Beginning from Machine learning to Deep learning, the authors have methodically explained the nuanced terminology and clarified any inconsistencies in the terms that are used to explain the concepts of TL and DL.

III. METRICS FOR MEASURING DISTRIBUTION DISCREPANCY

A. Maximum Mean Discrepancy (MMD)

The distribution variations are found using metrics that measure distribution discrepancy. The ones often used are Kullback–Leibler divergence [16], the maximum mean discrepancy (MMD) [17], [18], the Bregman divergence [19], and the Wasserstein distance [20].

Among the most commonly used is MMD. It finds the measure between the mean of the two distributions into a reproducing kernel Hilbert space (RKHS). Maximum Mean Discrepancy (MMD) [17], [21], [22] is thus a distribution distance metric. The MMD [23] between two distributions s and t , is given by

$$L_M(s, t) = \sup_{\|\phi\|_{\mathcal{H}} \leq 1} \|E_{x^s \sim s} [\phi(x^s)] - E_{x^t \sim t} [\phi(x^t)]\|_{\mathcal{H}}^2 \quad (1)$$

Sup (“supremum”) is the largest, least upper bound (generalizations of “max”), E is the expectation of the distribution. ϕ maps original data to RKHS. The detailed proofs are given in [24].

B. Maximum Covariance Discrepancy (MCD)

The notations for MCD are taken from [24] where one can find the detailed proofs.

$$\begin{aligned} \text{MCD}[p, q, \mathcal{H}] &= \sup_{\|a\| \leq 1} \sum_{i, j \in I} a_{ij} (\text{cov}[e_i(x), e_j(x)] - \text{cov}[e_i(y), e_j(y)]) \end{aligned} \quad (2)$$

where \mathcal{H} is RKHS over X and $\{e_i \mid i \in I\}$ is an orthogonal basis of \mathcal{H} , $\|a\| = \left(\sum_{i, j \in I} a_{ij}^2\right)^{1/2}$, with cov given by: $\text{cov}[e_i(x), e_j(x)] = E_x[e_i(x)e_j(x)] - E_x[e_i(x)]E_x[e_j(x)]$.

C. Maximum Mean and Covariance Discrepancy (MMCD)

The authors in [24] have shown that the MMCD-based domain adaptation achieves better results for image classification. MMCD has both the first- and second-order statistical information in the RKHS. The notations for MMCD are taken from [24], where one can find detailed proofs.

$$\text{MMCD}[p, q, \mathcal{H}] = (\|\mu[p] - \mu[q]\|_{\mathcal{H}}^2 + \beta\|C[p] - C[q]\|_{\mathcal{HS}}^2)^{1/2} \quad (3)$$

where $\mu[p] = E_x[\phi(x)]$ and β , used to balance the MCD term, is a non-negative parameter, and C is a centered covariance operator. They show that MMD and MCD of MMCD measures the difference between means and covariances of the distributions with the degree $d = 1$ of the polynomial kernel.

IV. DEEP DOMAIN ADAPTATION FOR FACE RECOGNITION

The authors in [25], [26], [23] discuss the approaches and challenges to deep domain adaptation in the context of face recognition which indeed is a challenging task. In real-life face recognition applications, there are domain shifts due to changing conditions, like background, location, change of pose, occlusion, illumination, and other factors.

In [25], the authors have used the TaoMM dataset created using face images of Chinese fashion models. They combined the CASIA-WebFace [27] and VGGFace-Good [28] datasets and used about 1.3 million images to train their model. They also trained the model on their TaoMM dataset. These trained models were then tested on the LFW dataset [29] which has a different distribution than the TaoMM dataset. The learned weights of labeled data are transferred to initialize the training model. They also refine all weights using face verification loss in an end-to-end framework.

Their system architecture consisted of a modified inception-v2 [30] model that enhanced training using Stochastic Gradient Descent. They used an NVIDIA GTX TITAN X GPU and pre-trained for 25 epochs that lasted 89.4 hours with a learning rate of 0.2 and decay half for every five epochs. A learning rate of 0.04 and decay half for every ten epochs was used and performed on two similar GPUs for 20 epochs that lasted 18.6 hours. The two GPUs were needed as the model was complex, and the mini-batch size was 360. Their

results are comparable to the state-of-the-art single models like DeepFace [31], DeepID [32] and BaiduFace [33].

The authors in [23] use clustering-based domain adaptation (CDA). They elaborate on how the unsupervised domain adaptation methods for object classification are not applicable to face recognition tasks. The reasons are that a larger discriminating power for the classification of faces is required, and the classes in both domains are non-overlapping. CDA generates pseudo-labels and uses cosine-similarity to form a cluster. They also use deep domain confusion network (DDC) [34] and deep adaptation networks (DAN) [35]. Here MMD estimator is integrated into the CNN error to minimize domain divergence. Thus the end classification is done based on features invariant to domain changes.

They trained the CNN with labeled source data and fine-tuned it with clustered target pseudo-labeled data, which helps determine the target data's discriminative representation. They evaluated their method on GBU [36], IJB-A/B/C [37], [38], [39] and RFW [40] datasets. The architectures that they used were VGGNet [41] and ResNet-34 [42]. Both architectures are trained on CASIA-WebFace, the former tuned using Softmax loss and later with Arcface loss [43]. They preprocessed the images of datasets by resizing, aligning and augmenting them. A Gaussian kernel is used in the MMD.

Their results outperform LRPCA-face [36], Fusion [44], VGG [44], Arcface [43] DDC [34] and DAN [35] for the GBU dataset. They remark that a uniform face-aligned algorithm can achieve good FR performance. Also, incorporating MMD helps in minimizing domain discrepancy. Similarly, better performance is obtained for IJB-A/B/C and RFW datasets. They also showed the visual representations of the learned features using t-distributed stochastic neighbor embedding (t-SNE) [45].

V. PROPOSED MMCD-VAE LATENT FEATURE EXTRACTION MODEL

A. Architectures

1) *Deep Autoencoder (DAE)*: In a Deep Autoencoder (DAE) feature selection function is carried out by an encoder. Later a decoder reconstructs the best image corresponding to the selected features. Deep CNN models are very powerful in feature extraction of the images generated from deep CNN AE. These decoders are noise-free and have competent low-dimensional feature space representation. However, only CNN-based generation requires uniform samples from all the categories.

2) *Variational Autoencoder (VAE)*: Variational Autoencoder (VAE), as shown in Fig. 5 is an unsupervised probabilistic deep-neural network model consisting of an encoder-decoder pair. The encoder carries out dimension reduction and domain adaptation by having a progressively lesser number of neuronal units in a feed-forward architecture. The decoder does the reverse and brings back the compressed domain representations to their original shape by gradually increasing the number of neuronal processors. Variational autoencoders are the fabrication of a CNN Autoencoder with regularized training to avoid over-fitting. It results in a latent space favorable for the generative process. VAE is unique in the way

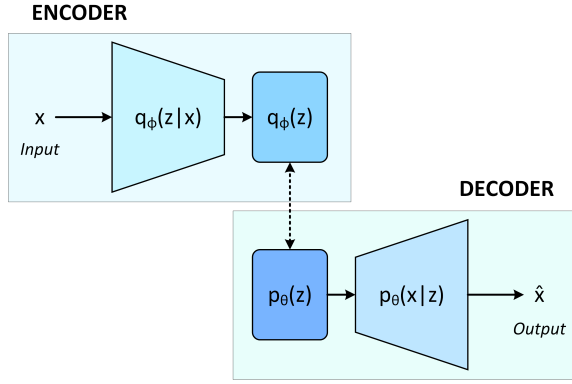


Fig. 5. Mapping Distribution of a Variational Autoencoder (VAE).

it uses the selected features for latent representation shared between encoder-decoder pairs.

Latent representation is nothing but the distribution of collected traits used as the communication protocol between the encoder-decoder pair. In practice, encoding and decoding distributions are parametric models. Joint optimization leading to reliable reconstruction ensures latent features contain the most salient statistical features and capture variations over main features.

The Face Recognition task falls under categorical marginal distribution. Assuming that ϕ and θ are parameter sets for encoder and decoder, optimized for minimum reconstruction loss, then VAE objective function can be written as:

$$L_{VAR_ELBO} = -\gamma D(q_\phi(z)||p_\theta(z)) + E(x)E_{q_\phi(z|x)}[\log p_\theta(x|z)] \quad (4)$$

where D is any strict divergence and $\gamma > 0$ is a scaling coefficient, E is the expectation operator, q_ϕ and p_θ are the distribution functions of encoder and decoder, respectively. The selection of divergence can play a crucial role. Traditionally evidence lower bound (ELBO) criterion is used in VAEs. The goal of the encoder is to obtain a simplified approximate distribution q and optimize the variational parameter ϕ such that q_ϕ be as similar as possible to the true distribution of inputs. One of the approaches is to minimize Kullback-Leibler (KL) divergence. It is defined as:

$$KL[q_\phi(w|D), p(w|D)] = \int q_\phi(w|D) \frac{q_\phi(w|D)}{p(w|D)} dw \quad (5)$$

where $p(w|D)$ is the actual distribution of input samples w . Intractability due to the integration term present in equation 5, is resolved by substituting an approximation for p in terms of q_ϕ . This substitution results in the popular Bayes by Backprop [46], a tractable objective function. ELBO suffers from uninformative latent code and variance overestimations in the feature space. Also, ELBO-VAE tends to over-fit data,

and as a result of the over-fitting, it learns a $q_\phi(z)$ whose variance tends to infinity.

3) Proposed MMCD-VAE Model for Domain Adaptation:

The proposed MMCD-VAE Model for Domain Adaptation is shown in Fig. 6. The encoder generates the same distribution for all possible variations in a sample's inputs, which works for learning good features. Regularization is possible as the input is encoded to a distribution with some variance instead of a point. Regularization aims to have continuity and completeness in the generative process. Distributions are forced to be as close as to a standard normal distribution.

MMD evaluates the distribution as identical if and only if all their first moments are the same. Therefore, MMD divergence is a metric of differential moments of $p(z)$ and $q(z)$ distributions and is accomplished using the kernel embedding trick [47]. MMD prefers to maximize the mutual information between an input x and the latent representation z . Training ELBO on a dataset with complimentary samples will still try to obtain encoder q_ϕ and decoder p_θ as Gaussian distributions with non-zero variance. For ELBO regularization term $\gamma D(q_\phi(z)||p_\theta(z))$ is not strong enough as against the loss function term $E(x)E_{q_\phi(z|x)}[\log p_\theta(x|z)]$. Complimentary samples will have class means way apart, and accordingly, MMD optimization will end up by having two modes of q_ϕ , pushed to stay far from each other. This will reduce ambiguity in reconstruction. In practice, this matters for datasets with fewer samples.

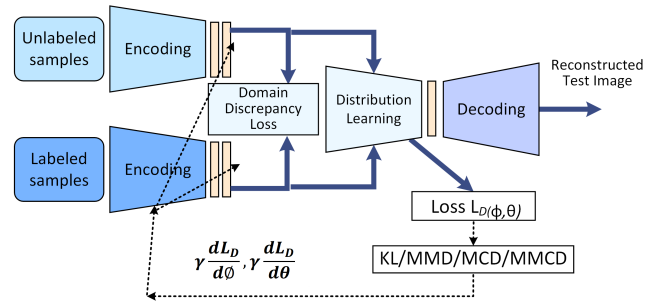


Fig. 6. Proposed MMCD-VAE Model for Domain Adaptation

The Loss function (objective function) indicates the degree to which the test image has been reconstructed and is given by:

$$l_i(\phi, \theta) = -E_{z \sim q_\phi(z|x_i)}[\log P_\theta(x_i|z)] + MMCD[Q_\phi(z|x_i)||P_\theta(z)] \quad (6)$$

Given two distributions p, q in RHKS

$$MMCD[p, q, H] = (\|\mu[p] - \mu[q]\|_H^2 + \beta \|C[p] - C[q]\|_H^2)^{1/2} \quad (7)$$

where $\mu[p] = E_x[\phi(x)]$ and β is a non-negative parameter. But $C[p] = E[w_p w_p^T] - E[w_p] E[w_p]^T$ and $C[q] = E[w_q w_q^T] - E[w_q] E[w_q]^T$

Algorithm 1: The Proposed MMCD-VAE Algorithm

Data:
 Training Dataset = $\{X_i^n\}_{i=1}^N$
 Testing Dataset = $\{Y_i^n\}_{i=1}^N$
 Encoder Network = q_ϕ
 Decoder Network = p_θ
 Batch Size = B
 Epochs = S
 Learning Rate = α

Result:
 Reconstructed Test Image

- 1 Initialize parameters of the Encoder and Decoder
- 2 **for** $epochs = i \leftarrow 1$ **to** S *Randomly select batches of Input images from the Training dataset* **do**
- 3 **for** $i \leftarrow 1$ **to** N $\mu_z(i), \sigma_z(i) = q_\phi(z | x_i)$ *Draw L samples from $z \sim N(\mu_z(i), \sigma_z(i))$* **do**
- 4 **for** $j \leftarrow 1$ **to** L $\mu_{\hat{x}}(i), \sigma_{\hat{x}}(i) = p_\theta(x_i | z)$ **do**
- 5 **end**
- 6 **end**
- 7 Define Objective function (L) using Log likelihood and MMCD distance
- 8 Update
- 9 $\phi = \phi_{old} + \alpha * \nabla_\phi_{ADAM}(\frac{\partial L}{\partial \phi})$;
- 10 $\theta = \theta_{old} + \alpha * \nabla_\theta_{ADAM}(\frac{\partial L}{\partial \theta})$
- 11 **end**
- 12 Return trained encoder = q_ϕ and trained decoder = p_θ

$$MMCD[p, q] = \left[\|E[x] - E[y]\|_2^2 + \beta \left[\|E[xx^T] - E[x]E[x]^T - (E[yy^T] - E[y]E[y]^T)\| \right]^2 \right]^{1/2} \quad (8)$$

where $x \sim p, y \sim q$. Given limited X and Y sampled from p and q respectively there is

$$MMCD[p, q] : \left(\|\mu_p - \mu_q\|_2^2 + \beta \|\Sigma_p - \Sigma_q\|_F^2 \right)^{1/2} \quad \text{where } \mu_p = \frac{1}{n}X \text{ is the mean vector and } \Sigma_p = \frac{1}{n}X\mu_n X^T \text{ is the covariance matrix of } X.$$

Substituting Equation (8) in (6) we get:

$$l_i(\phi, \theta) = -E_{z \sim \theta_\phi(z|x_i)} [\log P_\theta(x_i|z)] + \left[\|E[x] - E[y]\|_2^2 + \beta \left[\|E[xx^T] - E[x]E[x]^T - (E[yy^T] - E[y]E[y]^T)\| \right]^2 \right]^{1/2} \quad (9)$$

The authors in [24] have experimented with different kernel and non-kernel based cases. The kernels used were linear, polynomial, Gaussian, and Exponential. When a linear kernel is adopted, MMD, MCD, and MMCD measure the difference between the mean and covariance of the distributions, respectively.

B. Datasets

1) *Bollywood Celebrities Dataset*: The Bollywood Celebrities dataset [48] contains the localized face of 100 Bollywood Celebrities. A class has 80 to 150 samples of size 64×64 pixels. These are in wild conditions with different orientations, illuminations, age transitions. The sample images are shown in Fig. 7. Experimentation is carried out on 64×64 size RGB images.



Fig. 7. Sample Images from Bollywood Celebrities Dataset.

2) *TinyFace Dataset*: The TinyFace dataset contains 5,139 labeled facial identities given by 169,403 native Low Resolution face images (average 20×16 pixels) designed for the 1:N recognition test. The sample images are shown in Fig. 8. These are from public web data across a large spectrum and unconstrained environment.

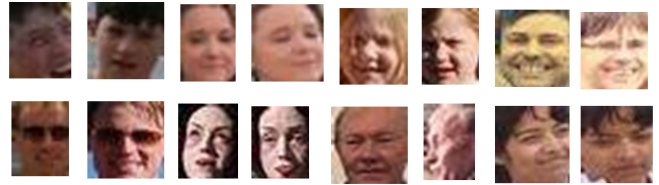


Fig. 8. Sample Images from TinyFace Dataset.

C. Objective Image Quality Comparison Metrics

The quality of the images needs to be evaluated using either a subjective or objective method. The former is based on human judgment, and the latter is by explicit numerical statistical parameters.

1) *SSIM*: Traditionally the most popular metric for image quality assessment was Peak Signal to Noise Ratio (PSNR). A standard metric is Structural Similarity Index (SSIM) which measures the similarity between two images. It was developed by Wang [49], and looked at structural information changes in the images. SSIM considers three factors, loss of correlation, luminance distortion, and contrast distortion [50]. For the SSIM index, a value of 0 means no correlation between images, and 1 means the two images are the same.

2) *PieAPP*: PieAPP [51] is a perceptual image-error metric that robustly predicts visual differences like humans. It uses pairwise preference as a robust way to create large Image quality assessment (IQA) datasets and uses a new pairwise-learning framework to train an error-estimation function. A reference image and a distorted image are given as input resulting in a PieAPP value as an output. Lower the value of the PieAPP error metric better the image perceptual quality.

3) *SIFT Features*: Face recognition is challenging compared to many other object recognition tasks as face features in the two domains are often non-overlapping. Global alignment of the source and target samples is not feasible for unconstrained face images. The goal of the proposed unsupervised domain adaptation model is to discover novel domain-invariant representations using scale-invariant features transform (SIFT) [52], as a parametric evaluation entity for the domain adaptation. Some authors [53], [54] have worked using SIFT for face recognition but have not used VAE. The challenge is to maximize scale-invariant features and thus get the corresponding match.

Many domain adaptation algorithms match the distribution without understanding the goodness in preserving key spatial features. This work analyses domain adaptation by optimizing encoder and decoder parameters. We use training samples and utilize unlabeled testing samples.

VI. RESULTS AND DISCUSSION

A. Experimental Setup

The domain adaptation experiments were conducted on NVIDIA GeForce RTX 2070 SUPER GPU. The PC configuration consists of a Multi-core (8 total) and Hyper-threaded (16 total) 3.80 gigahertz Intel Core i7-10700K. The memory is 32 GB, and the SSD hard drive has a 1TB capacity. The software used was Python version 3.8.5 (64-bit), libraries NumPy and Matplotlib, TensorFlow, and Keras.

The Bollywood Celebrities dataset was used for training. As the images for this dataset are 64×64 , the target images were resized to 64×64 . 300 epochs were used to train the model.

B. Experimental Results and Discussion

1) *Training and Testing on Bollywood Celebrities Dataset*: In [24], the authors used MMCD and compared the classification performance using two benchmark datasets PIE and Office-Caltech. Their performance was better than nearest neighbor, principal component analysis, correlation alignment transfer component analysis, geodesic flow kernel, and joint domain adaptation. We have combined MMCD with VAE and the training and testing details are mentioned below.

The MMCD-VAE model was first trained with the Bollywood Celebrities dataset for 300 epochs and then tested on different images from that dataset. The generated images for KL-VAE and MMCD-VAE models with the Training and Testing on Bollywood Celebrities dataset are shown in Fig. 9. SSIM and PieAPP error metric comparison is shown in Table I.

MMCD-VAE performs better than KL-VAE. MMCD-VAE shows an average of 20 % improvement in SSIM and a remarkable improvement in perceptual quality of the image, as seen from the PieAPP error metric, over the conventional KL-VAE model.

Fig. 10 demonstrates the SIFT features for the Bollywood Celebrities generated images. The proposed MMCD-VAE method is also applied to face images of the same class, but varying domains and generated face images are tested for



Fig. 9. Results for Bollywood Celebrities Dataset Images (a) Original (b) KL-VAE Generated Image (c) MMCD-VAE Generated Image.

TABLE I. SSIM AND PIEAPP COMPARISON FOR KL-VAE AND MMCD-VAE WITH TRAINING AND TESTING ON BOLLYWOOD CELEBRITIES DATASET

Face Images (Bollywood Dataset)	SSIM		PieAPP error metric	
	Original vs KL-VAE	Original vs MMCD-VAE	Original vs KL-VAE	Original vs MMCD-VAE
	Actor 1	0.719202	0.915040	3.537072
Actor 2	0.646112	0.859116	2.928503	0.365942
Actor 3	0.567586	0.811546	3.581390	0.940700
Actor 4	0.571617	0.790679	3.197515	1.132178
Actor 5	0.660647	0.883705	4.058572	1.056081
Actor 6	0.575935	0.808702	3.890267	1.467767
Actor 7	0.596703	0.881254	2.642451	0.065619
Actor 8	0.677114	0.916528	2.971156	0.904211
Average	0.626865	0.858321	3.350866	0.788718

inter-class similarity, as shown in Fig. 11. It can be seen that MMCD-VAE generated images have comparatively more SIFT key points than conventional KL-VAE generated images. More scale-invariant features assure that the proposed MMCD-VAE can capture more information.

The reconstruction loss gives the measure of how well the test image has been reconstructed and is shown in Fig. 12. We

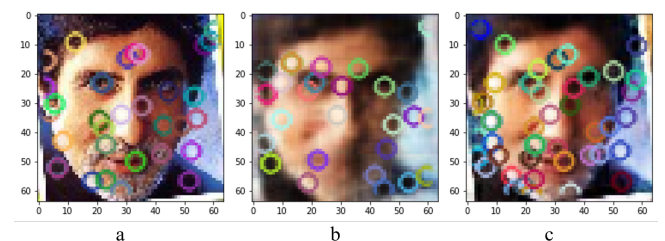


Fig. 10. SIFT Features for Bollywood Celebrities Dataset Images for Same Class (a) Original Image 36 SIFT Features (b) KL-VAE Image 27 SIFT Features (c) MMCD-VAE 49 SIFT Feature.

TABLE II. SSIM AND PieAPP COMPARISON FOR KL-VAE AND MMCD-VAE WITH TRAINING ON BOLLYWOOD CELEBRITIES AND TESTING ON TINYFACE DATASET

Face Images (TinyFace Dataset)	SSIM		PieAPP error metric	
	Original vs KL-VAE	Original vs MMCD-VAE	Original vs KL-VAE	Original vs MMCD-VAE
Face 1	0.472164	0.671485	1.819303	1.429740
Face 2	0.527809	0.668509	3.577199	2.522136
Face 3	0.559499	0.735055	1.111426	1.166033
Face 4	0.477758	0.650393	2.297195	1.644578
Face 5	0.529925	0.754939	1.154995	0.967473
Face 6	0.377013	0.618141	4.915103	1.919206
Face 7	0.508398	0.664005	1.727580	1.665994
Face 8	0.530098	0.667237	3.178573	1.667042
Average	0.497833	0.678721	2.472672	1.622775

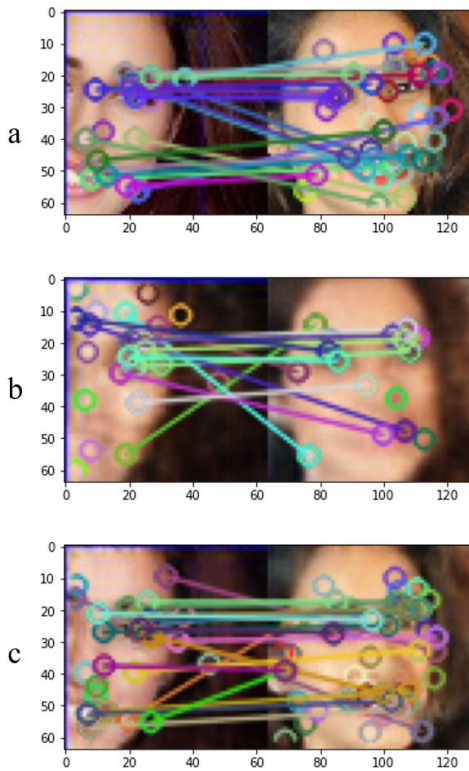


Fig. 11. Results for Bollywood Celebrities Dataset Images for Same Class Different Domain (a) Original Image 18 SIFT Matching Features (b) KL-VAE Image 12 SIFT Matching Features (c) MMCD-VAE 25 SIFT Matching Features.

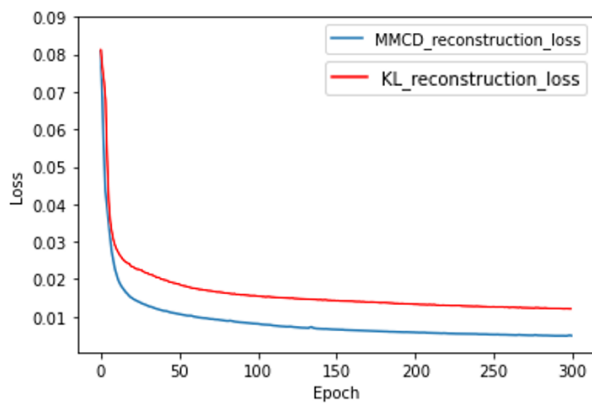


Fig. 12. Reconstruction Loss for the Conventional KL-VAE v/s Proposed MMCD-VAE.

observe that the MMCD-VAE model training is stable like the conventional KL-VAE, and demonstrates that the MMCD-VAE reconstruction loss is a meaningful metric of progress.

2) *Training on Bollywood Celebrities Dataset and Testing on TinyFace Dataset:* In VAE networks, the latent representations correspond to different levels of abstraction mapped to multifarious face attributes. Better the hidden representations, the greater is the adaptation quality. The MMCD-VAE model trained with Bollywood Celebrities dataset for 300 epochs was tested on TinyFace data. The total dataset was not tested but only a sample was used to check the results. The MMCD-VAE model performs better than the KL-VAE model, as seen from the subjective quality of the generated face images given in Fig. 13. The TinyFace dataset images are low resolution images. Even in the case of an original blurry image, the generated image has clearer features of eyes, nose, and mouth. As seen in Fig. 14, there are more SIFT key points in MMCD-VAE than KL-VAE generated images.

SSIM and PieAPP error metric comparison is shown in Table II. MMCD-VAE performs better than KL-VAE. MMCD-VAE shows an average of 18 % improvement in SSIM and an improvement in perceptual quality of the image over the conventional KL-VAE model. In this case, the PieAPP error metric difference between KL-VAE and MMCD-VAE is smaller than the one observed with the Bollywood Celebrities dataset images as the TinyFace are low-resolution images.

VII. CONCLUSION AND FUTURE WORK

This study reviewed the literature on domain adaptation, especially in Face Recognition. It began by looking into the challenging problem of how models trained on benchmark datasets, at times, fail in real-world scenarios. One example is test images collected from the online web. The benchmark dataset on which a model is trained is often high resolution and performs poorly for low-resolution target images. This happens because the source and target domain experience shifts due to changing conditions. Hence the need for domain adaptation and the various metrics for determining the distribution discrepancy.

CONFLICT OF INTEREST

The authors declare that they have no conflict of interest.

REFERENCES

- [1] S. Ben-David, J. Blitzer, K. Crammer, F. Pereira *et al.*, "Analysis of representations for domain adaptation," *Advances in neural information processing systems*, vol. 19, p. 137, 2007.
- [2] J. Quiñero-Candela, M. Sugiyama, N. D. Lawrence, and A. Schwaighofer, *Dataset shift in machine learning*. Mit Press, 2009.
- [3] J. G. Moreno-Torres, T. Raeder, R. Alaiz-Rodríguez, N. V. Chawla, and F. Herrera, "A unifying view on dataset shift in classification," *Pattern recognition*, vol. 45, no. 1, pp. 521–530, 2012.
- [4] H. Shimodaira, "Improving predictive inference under covariate shift by weighting the log-likelihood function," *Journal of statistical planning and inference*, vol. 90, no. 2, pp. 227–244, 2000.
- [5] J. Donahue, Y. Jia, O. Vinyals, J. Hoffman, N. Zhang, E. Tzeng, and T. Darrell, "Decaf: A deep convolutional activation feature for generic visual recognition," in *International conference on machine learning*. PMLR, 2014, pp. 647–655.
- [6] S. J. Pan and Q. Yang, "A survey on transfer learning," *IEEE Transactions on knowledge and data engineering*, vol. 22, no. 10, pp. 1345–1359, 2009.
- [7] K. Weiss, T. M. Khoshgoftaar, and D. Wang, "A survey of transfer learning," *Journal of Big data*, vol. 3, no. 1, pp. 1–40, 2016.
- [8] F. Zhuang, Z. Qi, K. Duan, D. Xi, Y. Zhu, H. Zhu, H. Xiong, and Q. He, "A comprehensive survey on transfer learning," *Proceedings of the IEEE*, vol. 109, no. 1, pp. 43–76, 2020.
- [9] J. Zhang, W. Li, and P. Ogunbona, "Transfer learning for cross-dataset recognition: a survey," *arXiv preprint arXiv:1705.04396*, vol. 5, 2017.
- [10] C. Tan, F. Sun, T. Kong, W. Zhang, C. Yang, and C. Liu, "A survey on deep transfer learning," in *International conference on artificial neural networks*. Springer, 2018, pp. 270–279.
- [11] V. M. Patel, R. Gopalan, R. Li, and R. Chellappa, "Visual domain adaptation: A survey of recent advances," *IEEE signal processing magazine*, vol. 32, no. 3, pp. 53–69, 2015.
- [12] S. Sun, H. Shi, and Y. Wu, "A survey of multi-source domain adaptation," *Information Fusion*, vol. 24, pp. 84–92, 2015.
- [13] G. Csurka, "A comprehensive survey on domain adaptation for visual applications," *Domain adaptation in computer vision applications*, pp. 1–35, 2017.
- [14] M. Wang and W. Deng, "Deep visual domain adaptation: A survey," *Neurocomputing*, vol. 312, pp. 135–153, 2018.
- [15] G. Wilson and D. J. Cook, "A survey of unsupervised deep domain adaptation," *ACM Transactions on Intelligent Systems and Technology (TIST)*, vol. 11, no. 5, pp. 1–46, 2020.
- [16] X. Cao, D. Wipf, F. Wen, G. Duan, and J. Sun, "A practical transfer learning algorithm for face verification," in *Proceedings of the IEEE international conference on computer vision*, 2013, pp. 3208–3215.
- [17] A. Gretton, K. Borgwardt, M. Rasch, B. Schölkopf, and A. Smola, "A kernel method for the two-sample-problem," *Advances in neural information processing systems*, vol. 19, pp. 513–520, 2006.
- [18] A. Gretton, K. M. Borgwardt, M. J. Rasch, B. Schölkopf, and A. Smola, "A kernel two-sample test," *The Journal of Machine Learning Research*, vol. 13, no. 1, pp. 723–773, 2012.
- [19] S. Si, D. Tao, and B. Geng, "Bregman divergence-based regularization for transfer subspace learning," *IEEE Transactions on Knowledge and Data Engineering*, vol. 22, no. 7, pp. 929–942, 2009.
- [20] J. Shen, Y. Qu, W. Zhang, and Y. Yu, "Wasserstein distance guided representation learning for domain adaptation," in *Thirty-Second AAAI Conference on Artificial Intelligence*, 2018.
- [21] Y. Li, K. Swersky, and R. Zemel, "Generative moment matching networks," in *International Conference on Machine Learning*. PMLR, 2015, pp. 1718–1727.
- [22] G. K. Dziugaite, D. M. Roy, and Z. Ghahramani, "Training generative neural networks via maximum mean discrepancy optimization," *arXiv preprint arXiv:1505.03906*, 2015.
- [23] M. Wang and W. Deng, "Deep face recognition with clustering based domain adaptation," *Neurocomputing*, vol. 393, pp. 1–14, 2020.
- [24] W. Zhang, X. Zhang, L. Lan, and Z. Luo, "Maximum mean and covariance discrepancy for unsupervised domain adaptation," *Neural Processing Letters*, vol. 51, no. 1, pp. 347–366, 2020.



Fig. 13. Results for TinyFace Dataset (a) Original Image (b) KL-VAE Generated Image (c) MMCD-VAE Generated Image.

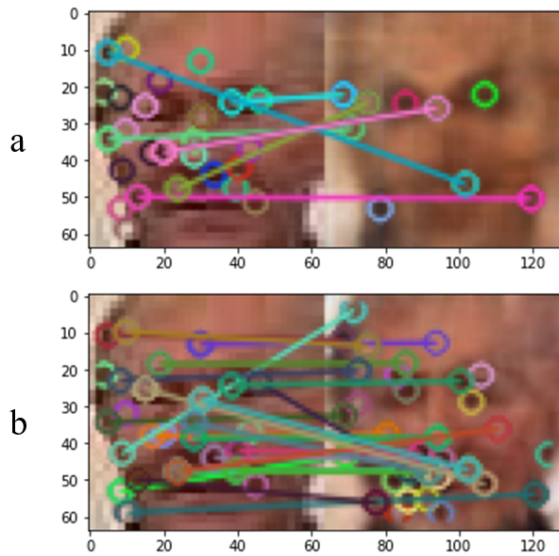


Fig. 14. SIFT Matching Features (a)Original and KL-VAE (b)Original and MMCD-VAE.

In the experimental part, we compared the performance of the proposed MMCD-VAE model. Results are compared for sample images taken from the Bollywood Celebrities dataset and TinyFace dataset. TinyFace is a challenging dataset, because it is low-resolution and recognition performance drops with the decrease in resolution. Quantitative comparisons are shown for matching SIFT key points and SSIM. The MMCD-VAE domain adaptation method rendered images with better Objective Image Quality, as seen in the SSIM, pieApp, and SIFT key-points metrics.

The future scope is to look at detailed testing of RFW datasets to better understand how to improve face recognition across diverse races. The low-resolution surveillance face images of the QMUL-SurvFace dataset is another area to pursue further research. An emerging area of research is adversarial discriminative domain adaptation, which reduces the difference between the source and target domain distributions using adversarial learning methods.

- [25] G. Wen, H. Chen, D. Cai, and X. He, "Improving face recognition with domain adaptation," *Neurocomputing*, vol. 287, pp. 45–51, 2018.
- [26] Z. Luo, J. Hu, W. Deng, and H. Shen, "Deep unsupervised domain adaptation for face recognition," in *2018 13th IEEE International Conference on Automatic Face & Gesture Recognition (FG 2018)*. IEEE, 2018, pp. 453–457.
- [27] D. Yi, Z. Lei, S. Liao, and S. Z. Li, "Learning face representation from scratch," *arXiv preprint arXiv:1411.7923*, 2014.
- [28] O. M. Parkhi, A. Vedaldi, and A. Zisserman, "Deep face recognition," in *British Machine Vision Conference*, 2015.
- [29] G. B. Huang, M. Ramesh, T. Berg, and E. Learned-Miller, "Labeled faces in the wild: A database for studying face recognition in unconstrained environments," University of Massachusetts, Amherst, Tech. Rep. 07-49, October 2007.
- [30] C. Szegedy, V. Vanhoucke, S. Ioffe, J. Shlens, and Z. Wojna, "Rethinking the inception architecture for computer vision," in *Proceedings of the IEEE conference on computer vision and pattern recognition*, 2016, pp. 2818–2826.
- [31] Y. Taigman, M. Yang, M. Ranzato, and L. Wolf, "Deepface: Closing the gap to human-level performance in face verification," in *Proceedings of the IEEE conference on computer vision and pattern recognition*, 2014, pp. 1701–1708.
- [32] Y. Sun, X. Wang, and X. Tang, "Deep learning face representation from predicting 10,000 classes," in *Proceedings of the IEEE conference on computer vision and pattern recognition*, 2014, pp. 1891–1898.
- [33] J. Liu, Y. Deng, T. Bai, Z. Wei, and C. Huang, "Targeting ultimate accuracy: Face recognition via deep embedding," *arXiv preprint arXiv:1506.07310*, 2015.
- [34] E. Tzeng, J. Hoffman, N. Zhang, K. Saenko, and T. Darrell, "Deep domain confusion: Maximizing for domain invariance," *arXiv preprint arXiv:1412.3474*, 2014.
- [35] M. Long, Y. Cao, J. Wang, and M. Jordan, "Learning transferable features with deep adaptation networks," in *International conference on machine learning*. PMLR, 2015, pp. 97–105.
- [36] P. J. Phillips, J. R. Beveridge, B. A. Draper, G. Givens, A. J. O'Toole, D. Bolme, J. Dunlop, Y. M. Lui, H. Sahibzada, and S. Weimer, "The good, the bad, and the ugly face challenge problem," *Image and Vision Computing*, vol. 30, no. 3, pp. 177–185, 2012.
- [37] B. F. Klare, B. Klein, E. Taborsky, A. Blanton, J. Cheney, K. Allen, P. Grother, A. Mah, and A. K. Jain, "Pushing the frontiers of unconstrained face detection and recognition: Iarpa janus benchmark a," in *Proceedings of the IEEE conference on computer vision and pattern recognition*, 2015, pp. 1931–1939.
- [38] C. Whitelam, E. Taborsky, A. Blanton, B. Maze, J. Adams, T. Miller, N. Kalka, A. K. Jain, J. A. Duncan, K. Allen *et al.*, "Iarpa janus benchmark-b face dataset," in *proceedings of the IEEE conference on computer vision and pattern recognition workshops*, 2017, pp. 90–98.
- [39] B. Maze, J. Adams, J. A. Duncan, N. Kalka, T. Miller, C. Otto, A. K. Jain, W. T. Niggel, J. Anderson, J. Cheney *et al.*, "Iarpa janus benchmark-c: Face dataset and protocol," in *2018 International Conference on Biometrics (ICB)*. IEEE, 2018, pp. 158–165.
- [40] M. Wang, W. Deng, J. Hu, X. Tao, and Y. Huang, "Racial faces in the wild: Reducing racial bias by information maximization adaptation network," in *Proceedings of the IEEE/CVF International Conference on Computer Vision*, 2019, pp. 692–702.
- [41] K. Simonyan and A. Zisserman, "Very deep convolutional networks for large-scale image recognition," *arXiv preprint arXiv:1409.1556*, 2014.
- [42] K. He, X. Zhang, S. Ren, and J. Sun, "Deep residual learning for image recognition," in *Proceedings of the IEEE conference on computer vision and pattern recognition*, 2016, pp. 770–778.
- [43] J. Deng, J. Guo, N. Xue, and S. Zafeiriou, "Arcface: Additive angular margin loss for deep face recognition," in *Proceedings of the IEEE/CVF Conference on Computer Vision and Pattern Recognition*, 2019, pp. 4690–4699.
- [44] L. Van der Maaten and G. Hinton, "A cross benchmark assessment of a deep convolutional neural network for face recognition," in *2017 12th IEEE International Conference on Automatic Face & Gesture Recognition (FG 2017)*. IEEE, 2017, pp. 705–710.
- [45] L. Van der Maaten and G. Hinton, "Visualizing data using t-sne," *Journal of machine learning research*, vol. 9, no. 11, 2008.
- [46] C. Blundell, J. Cornebise, K. Kavukcuoglu, and D. Wierstra, "Weight uncertainty in neural network," in *International Conference on Machine Learning*. PMLR, 2015, pp. 1613–1622.
- [47] V. Vapnik, *The nature of statistical learning theory*. Springer science & business media, 1999.
- [48] Y. Sushilkumar, "Bollywood celebrities localized face dataset," <https://www.kaggle.com/sushilyadav1998/bollywood-celeb-localized-face-dataset>, Nov. 2017, [Online; accessed 1-July-2021].
- [49] Z. Wang, A. C. Bovik, H. R. Sheikh, and E. P. Simoncelli, "Image quality assessment: from error visibility to structural similarity," *IEEE transactions on image processing*, vol. 13, no. 4, pp. 600–612, 2004.
- [50] A. Hore and D. Ziou, "Image quality metrics: Psnr vs. ssim," in *2010 20th international conference on pattern recognition*. IEEE, 2010, pp. 2366–2369.
- [51] E. Prashnani, H. Cai, Y. Mostofi, and P. Sen, "Pieapp: Perceptual image-error assessment through pairwise preference," in *Proceedings of the IEEE Conference on Computer Vision and Pattern Recognition*, 2018, pp. 1808–1817.
- [52] D. G. Lowe, "Distinctive image features from scale-invariant keypoints," *International journal of computer vision*, vol. 60, no. 2, pp. 91–110, 2004.
- [53] C. Geng and X. Jiang, "Face recognition using sift features," in *2009 16th IEEE international conference on image processing (ICIP)*. IEEE, 2009, pp. 3313–3316.
- [54] L. Lenc and P. Král, "Automatic face recognition system based on the sift features," *Computers & Electrical Engineering*, vol. 46, pp. 256–272, 2015.

Prediction of Quality of Water According to a Random Forest Classifier

Shahd Maadi Alomani¹, Najd Ibrahim Alhawiti², and A'aeshah Alhakamy³ 

Faculty of Computers and Information Technology, Master of Artificial Intelligence at University of Tabuk, Saudi Arabia^{1,2,3}
Industrial Innovation & Robotics Center (IIRC), and Faculty of Computers and Information Technology,
Department of Computer Science at University of Tabuk, Saudi Arabia³

Abstract—Potable or drinking water is a daily life necessity for humans. The safety of this water is a concern in many regions around the world, since polluted waters are increasing and causing the spread of disease among populations. Continuous management and evaluation of the water which is meant for drinking is very essential and must be taken seriously. Often, the quality of water is evaluated through regular laboratory testing and analysis which can be tiresome and time consuming. On the other hand, advanced technologies using big data with the help of machine learning can have better results in terms of potability evaluation. For this reason, several studies have been conducted on predicting the quality of water and the several factors and classification that affect the prediction model. In this study, a random forest model was developed using PySpark classification to predict the potability of river water by relying on ten different features: pH, hardness, presence of solids, presence of chloramines, presence of sulfate, conductivity, organic carbon, trihalomethanes, turbidity, and finally potability. In addition, The developed model was able to predict water potability classification with a 1.0 accuracy, and 1.0 F1-score.

Keywords—Big data; machine learning; classification; random forest; water quality; PySpark

I. INTRODUCTION

When there is no water, there's no life. Freshwater is the most essential natural resource without which life, all forms of life, would not exist. Humans of all the other living organisms rely on the water not just for drinking but also for various aspects of their lives such as bathing, cooking, and watering their agricultural fields. In fact, there's even increased demand for water due to the increase in wide spreading urbanization, the development and expansion of the economic movement, and the general rapid increase in human population [1].

However, the water quality and its safety for use for different purposes is a complex issue. The overuse of the water both underground and on the surface in addition to other factors are causing the deterioration of water quality. One of the factors that are having a significant impact on water is the global climate change since it doesn't just affect the availability of water resources but also affects their future quality. Add to that the dangerous pollution resulting from the human activities where individual humans don't only dump their waste into rivers and wells, but also large factories could pollute rivers and underground water as a result of their chemical wastes [2]. As a matter of fact, the poor-quality water is the source of many water-borne illnesses such as diarrhea. This means that using non-clean water especially for drinking raises health issues that can be avoided but choosing the appropriate water to drink [3].

The most common estimation of water quality has been the laboratory analysis which is time-consuming, expensive, and not very practical. The laboratory analysis of water requires the collection of water samples from different areas over a period of time, then transporting these samples in suitable conditions before they can be analyzed. Of course, this method is still being applied, but with the current development of technology, these processes can be made much more efficient by applying machine learning and big data tools [4]. Machine learning ML is a method of programming software in a way that allows them to learn from historical data and adapt accordingly such that they learn, assess their performance, and improve. Machine learning algorithms are often used to detect patterns in data and the non-visible behavior of data. There are several algorithms already in ML divided into classes: unsupervised, semi-supervised, supervised, and reinforced algorithms [5].

Random Forest RF is one of the machine learning algorithms through which several decision trees are merged together to achieve more accurate results. The term random forest also corresponds to the randomness of the method where the choice of samples is random. More specifically, a number of samples are randomly chosen from the training dataset in order to form what is called the "root node" samples. Furthermore, the choice of attributes in RF is also random, where the candidate attributes are selected at random, and after that the most suitable attribute is picked to be the "split node". The RF model starts with shuffles input sample data, creates many training sets that make up the decision trees, and finally chooses the output prediction results based on the majority of votes from the collection of decision trees [6].

In this paper, PySpark for the classification is utilized to evaluate water potability using a well-known Water Quality dataset. The Random Forest Classifier was used to build a model that assesses various properties, including temperature, acidity, turbidity, and hardness, to arrive at an accurate decision. The developed model is evaluated to answer the following research questions for a better understanding of the presented work.

- **RQ1:** *What factors directly affect the potability of the water?*
- **RQ2:** *Can a random forest model effectively predict the quality of water based on these factors?*

The topic of water quality assessment was chosen due to its importance, and we have selected the Random Forest model to be our predictive model for the quality of water after reviewing the literature. Through literature, it was evident that

Random Forest provides the most effective and accurate results in evaluating the quality of water.

II. RELATED WORK

A lot of studies discuss the quality of potable water and quality of river waters or near-shore water, and many of them also focus on finding the relationships between several factors affecting the quality of water and which of them have the greatest influence. Numerous studies applied machine learning algorithms to predict the influential factors affecting water quality, including the Random Forest algorithm.

The term water potability refers to the characteristic that the water is safe for human consumption, specifically drinking or cooking. For example, potable water must be free from micro-organisms or harmful chemicals [7]. Other factors that indicate the quality of water are shown in Fig. 1, such as the chemical pH, the clarity of the water, abundance of nutrients, presence or absence of pest animals and vegetation, etc. [8].

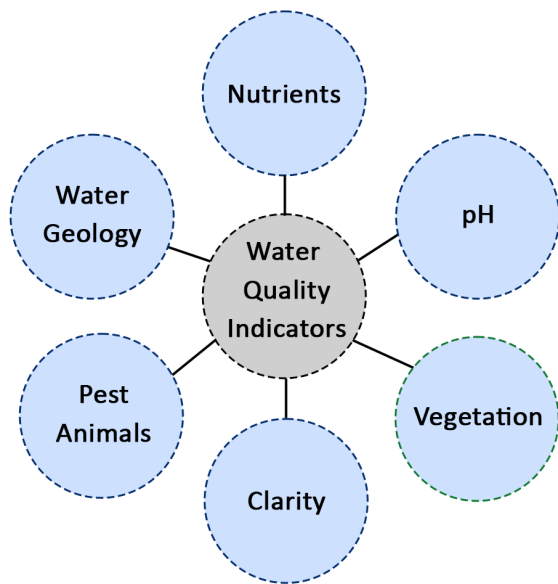


Fig. 1. Some of the Factors that Indicate Water Quality.

Back in 1960, a water quality index was created as a means to evaluate the safety of water [9]. After that period, many water assessment and quality management programs have been developed. In order to make appropriate decisions about drinkable water, one must be educated about the many factors that affect the safety of the water. Among other factors, potable water is affected by the source of origin, as well as whether it was treated before being delivered to houses, and the storage containers or water pumps and pipelines [10]. That's in addition to the factors within the water itself such as its temperature, its content of certain salts and minerals, its electrical conductivity, its pH, and other features [11]. The various water quality indicators can be divided into four classes: biological, chemical, physical, and radiological, as described in the Table I.

The aim of Xu, et al. research [12] is to design a framework for the prediction of the water quality in two

TABLE I. CLASSIFICATION OF WATER INDICATORS INTO BIOLOGICAL, CHEMICAL, PHYSICAL AND RADIOLOGICAL

Classes of Water Quality Indicators	Examples
Biological	Bacteria, parasites
Chemical	pH, dissolved oxygen, salts
Physical	Temperature, electric conductivity
Radiological	Radioactive elements like Uranium

regions, inland river water and nearshore water, based on different factors. The researchers were investigating the effect of several factors such as turbidity, temperature, dissolved gasses, ammonia concentrations, and dissolved solids on the total nitrogen level in the tested water. Inland water testing occurred at 2-hour intervals and total nitrogen levels were also collected at 4-hour intervals. The collected samples made a total of 1917 creating the dataset which was then subjected to normalization and correlation analysis. 90% of these data were used to train machine learning algorithms including Decision Tree, KNN, SVR, MLR, Random Forest, Ridge Regression, and GBRT. On the other hand, 10% were used to evaluate the models by comparing the predicted results of total nitrogen with the actual collected results.

This evaluation was based on correlation coefficient as well as the following metrics: Root Mean Square Error (RMSE), Mean Absolute Percentage Error, Nash–Sutcliffe efficiency coefficient, Mean Square Error, and Mean Absolute Error. The evaluation results showed that Random Forest achieves the best prediction results with 0.967 correlation coefficient and 0.509 RMSE, and that the ensemble models in general outperformed the non-ensemble models. Random Forest was also the focus when testing nearshore waters in comparison to the other ML models, where 147 new data were gathered and only three metrics were used since the acquired data differ from before (only temperature and salinity). The results of the second testing also came in favor of Random Forest compared to the other algorithms, achieving the lowest MAE and MAPE values.

In another study, Bachir Sakaa and his colleagues developed a Random Forest model as well as a Sequential Minimal Optimization-Support Vector Machine method for the determination of water quality in Saf-Saf river [13]. The researchers chose to collect the data from 35 areas in wet and dry seasons in order to gather 70 total samples that make up their dataset. The dataset was divided into training and testing subsets made up of 80% and 20% of data respectively. It was decided that the two models will be evaluated according to the root mean square error (RMSE), relative absolute error, mean absolute error, and root relative square error. In addition to these values, sensitivity analysis was carried out to assess how the independent variables (factors) are affecting the dependent variable (water quality). In order to determine the effector factors, a method called recursive feature elimination-linear “RFEL” was used where 15 different features were selected including suspended solids, ammonium, chemical, and biochemical oxygen demand, temperature, oxygen saturation, conductivity, and pH. Upon analyzing the results, it was evident that the results greatly differ in the upstream river area compared to the downstream river area. The same was noticed between data from wet seasons vs. dry seasons. RFEL was also used to determine a subset of combinations of some features

to notice their effects as a group. In this regard, for Random Forest the third created combination scored the best values (RMSE=5.17 and correlation R2=0.82) whereas for SMO-SVM the fourth input was better than the rest (RMSE=7.43 and R2=0.71). When comparing the overall performance of RF compare to SMO-SVM, it was concluded that they have similar results even though the error metrics show the superiority of RF.

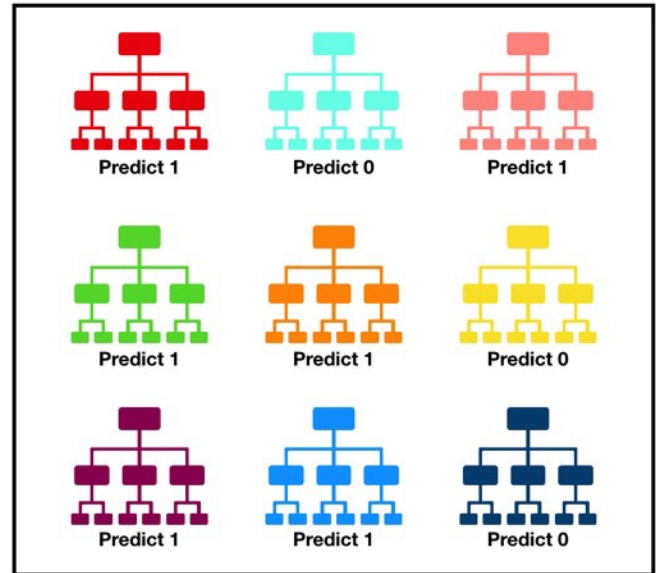
RF was also employed in another study to predict the concentration of dissolved oxygen in the water of Potomac River [14]. More specifically, the purpose of the study was to determine the most important factors influencing the concentration of oxygen and to evaluate the efficiency of the Random Forest model in predicting the latter with respect to a varying combination of factors. Dissolved oxygen data were collected from a publicly available water quality database by the USGS. The variables chosen in this study are the gauge height, water temperature, turbidity, water pH, instantaneous discharge, and specific conductance. As a method of data preparation and pre-processing, a noise removal process was done by eliminating the individual predictor with its respective co-measured factors in order to avoid missing data. The Kolmogorov-Smirnov test was used to check the normality of each predictor variable, and also Box-Cox transform was used on the datasets. Furthermore, the water temperature was transformed into the Kelvin metric, and the data were standardized with the Z-score technique. After pre-processing, the data were divided 80-20 for training and testing respectively and the performance of two models: RF and MLR was evaluated through RMSE and R2 values. The correlation matrix revealed a significantly strong correlation with water temperature, and a significantly weak correlation with water salinity. There is also a strong multi-collinearity in the data due to correlation between the multiple variables. In conclusion, temperature, pH, and salinity were able to explain 98.7% of the data variance.

III. METHOD

The main purpose of this study is to be able to assess the quality of rivers' water and whether it is drinkable or not based on a machine learning technique, namely Random Forest.

Quite literally, the random forest is a large collection of several decision trees that are used in unity, where the group of decisions can be collected to come up with one decision as an output. This happens after each decision tree dictates a specific class as its prediction result, and the class that collects the most votes from the tree ensemble is finally chosen as an output of the model. Fig. 2 shows a simple example of how a random forest chooses a prediction based on the collective results from each decision tree.

Machine learning is the automated data analysis process. Instead of being conventionally performed by a data scientist, nowadays, machines can replace manual analysis while using the same math and statistical techniques. The main difference though is that in machine learning, the techniques are integrated into algorithms that are capable of learning and improving themselves on their own. Machine learning has become the key to facilitating artificial intelligence (AI), where automated decisions can replace human decisions. And even though data science, machine learning, and artificial



Tally: Six 1s and Three 0s
Prediction: 1

Fig. 2. Example of Decision Making using Random Forest Model by Tony [15].

intelligence are puzzle pieces in the same field, yet each has its own applications and its own meaning.

Machine learning approaches in general can be divided into supervised and unsupervised machine learning. In the unsupervised models such as Principle Component Analysis of K-mean clustering, the algorithm finds hidden patterns within the data without them being labeled. On the other hand, supervised machine learning like Decision Tree or Random Forest, operates on previously labeled data and it is their objective to perform classification predictions based on how they were trained with the respective labels [16].

In machine learning, often several steps are done in sequence starting with data pre-processing, extraction of features, fitting of the model, and finally the evaluation of the performance of the developed model. These steps require a lot of transformation for data, which can be easily done by the machine learning pipeline to keep everything in order. The role of a pipeline is to keep the data flowing properly and that the transformations are adequately done to make sure that the result reached is accurate and without error.

Machine learning is one of the very effective methods by which Big Data can be processed, visualized, and interpreted [17], [18]. In this study, for the execution of our model, we relied on the Spark framework since spark is capable of performing large processing tasks quickly and allows the distribution of tasks over several computers for processing [19]. More specifically, PySpark was utilized as it allows the use of Python as a programming language. In Apache Spark, machine learning algorithms can be employed through Spark MLlib which we also relied on.

The ML pipeline requires a chain of command where the stages are assigned and it can run smoothly on Spark.

The stages involved within a pipeline can be transformers or estimators that have different functions. The function of a transformer is to convert one type of data frame into another type of data frame which can be done through updating the categorical values within one column into numeric values, or through user-defined logic to map the data in the column to other values. On the other hand, an estimator is capable of developing a model based on a fit method. Here, for instance, the Random Forest classifier is an estimator.

There are several steps to be done for the completion of the study. These involve exploring the data after acquiring the dataset, preparing the data, and performing correlation analysis. After that, model design and testing are followed by model assessment or evaluation, see Fig. 3.

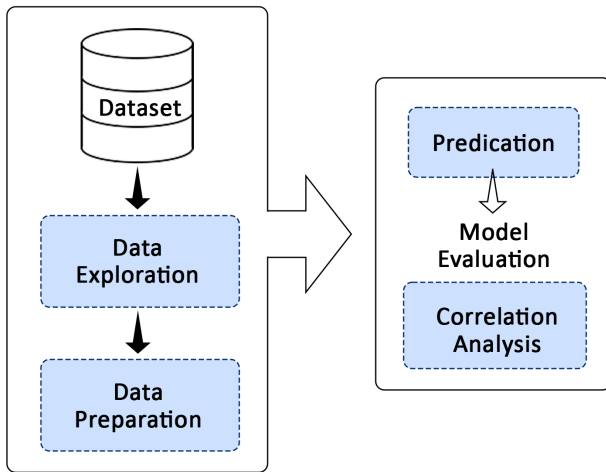


Fig. 3. Flowchart Explaining the Steps Followed in this Study: Data Exploration and Preparation, Correlation Analysis, Model Design and Evaluation.

IV. DATA

The chosen dataset comprises a total of ten features that will be used to predict the quality of water and whether it is good for drinking or not. Fig. 4 shows the ten values that describe the quality of the water, which are: pH, hardness, presence of solids presence of chloramines, presence of sulfate, conductivity, organic carbon, trihalomethanes, turbidity, and finally potability. The corresponding definitions and values of these features are described below.

pH. The pH metric is an evaluation of the concentration of hydrogen ions within a solution, and it allows the differentiation between acid media, basic media, and neutral media as water [20]. The pH recommended by the world health organization determines that the pH of drinkable water must range between 6.52 and 6.83.

Hardness. Hardness is the resultant of both magnesium and calcium salts that deposit from the geologic surrounding of running water [21]. The period of time in which the water is in contact with hardness-producing material determines how much hardness there is in raw water [22].

Total Dissolved Solids. Dissolved solids in water refer to the salts that can be present including potassium, magnesium, calcium, bicarbonates, sodium, chlorides, etc. [23]. The presence of these dissolved solids in water leads to changing its flavor in addition to affecting its safety [24]. The ideal concentration for TDS is 500 mg/l and should not go above 1000 mg/l for drinking water.

Chloramines. Chloramine alongside chlorine is often used for the treatment of water and disinfecting it from bacteria and other microorganisms [25], [26]. For safety, the amount of chloramine in drinkable water should not exceed 4 mg per liter.

Sulfate. Sulfates are natural elements present in the soil, minerals, food, groundwater, plants, and rocks. Yet they are heavily used in the chemical industry. The sulfate concentration in freshwater should be between 3 and 30 mg per liter [27].

Conductivity. Electric conductivity is a measure of conducting electricity through water. Pure water does not conduct electricity, rather it is considered an insulator [28]. However, ionic water has an increased electric conductivity as a result of the ionic compounds in it [29]. The safe electric conductivity level should be less than 400 $\mu S/cm$.

Organic Carbon. Total organic Carbon TOC resembles the total quantity of carbon from organic matter within the water [30]. This organic carbon can originate from either the decay of natural organic matter or from an unnatural synthetic source. The normal values of organic carbon should be less than 2 mg per liter for drinkable water, and less than 4 mg per liter for the water to be treated.

Trihalomethanes. Trihalomethanes are referred to as THMs in short, and these are molecules abundant in the case of chlorine treatment of water [31]. The factors that affect the amount of THMs are the temperature of treated water, the required chlorine concentration, and the level of organic matter within the water [32]. In order for water to be drinkable, the THM value must be below 80 ppm.

Turbidity. Turbidity is a description of the state of water and whether solids are suspended in it or not [33]. The turbidity of water can be calculated by the light emitting characteristics of water, which represents the quality of waste discharge in regard to the colloidal matter. The turbidity value recommended by the World Health Organization is turbidity=5.00 NTU.

Potability. Potability is a term given to describe whether the water is safe for human consumption or drinking or not [34]. In fact, it should also be considered if the same water is good for watering plants. If the given value=1 then the water is potable or drinkable, whereas value=0 means the water is not suitable for consumption.

A. Data Exploration and Preparation

As part of data pre-processing, the data were converted into float after being in a string. In addition, the data that were in repetition were deleted, so only the necessary data were kept, see Fig. 5.

Initially, we will check whether there are NULL values or not. This is important to ensure that the algorithm can run smoothly without any missing data since null values indicate

	ph	Hardness	Solids	Chloramines	Sulfate	Conductivity	Organic_carbon	Trihalomethanes	Turbidity	Potability
	null	204.8904554713363	20791.318980747026	7.300211873184757	368.51644134980336	564.3086541722439	10.3797830780847	86.9909704615088	2.9631353806316407	0
	3.71608007538699	129.42292051494425	18630.057857970347	6.635245883862	null	592.8853591348523	15.180013116357259	56.32907628451764	4.500656274942408	0
	8.099124189298397	224.23625939355776	19909.541732292393	9.275883602694089	null	418.6062130644815	16.868636929550973	66.42009251176368	3.0559337496641685	0
	8.316765884214679	214.37339408562252	22018.417440775294	8.05933237743854	356.88613564305666	363.2656161642437	18.436524495493302	100.34167436500808	4.628770536837084	0
	9.092223456290965	181.10150923612525	17978.98633892625	6.546599974207941	310.13573752420444	398.4108138184466	11.558279443446395	31.9979927272424737	4.075075425430034	0
	5.584086638456089	188.313327696164	20748.68773904612	7.54486878877965	326.6783629116736	280.4679159314077	8.309734640152758	54.917861841994466	2.5597082275565217	0
	10.223862164528773	248.07173527013992	28749.716543528233	7.5134084658313025	393.66339551509645	283.6516335078445	13.789695317519886	84.60355617402357	2.672988736934779	0
	8.635848718500734	203.36152258457054	13672.091763901635	4.563008685599703	303.3097711592812	474.60764494244853	12.36381669870525	62.798308962925155	4.401424715445482	0
	null	118.98857909025189	14285.583854224515	7.804173553073094	268.646940746221	389.3755658712614	12.70604896865791	53.928845767512236	3.5950171809576155	0
	11.180284470721592	227.23146923797458	25484.50849098786	9.077200016914393	404.04163468400896	563.8854814810949	17.92788641128502	71.9766810321915	4.370561936655497	0
	7.360648105838258	165.52079725952862	32452.614409143884	7.550700906704114	326.62435345560164	425.38341949538733	15.586810438033126	78.74001566430479	3.6622917828524573	0
	7.974521648923869	218.69330048866644	18767.65668181348	8.110384501123875	null	364.09823046204866	14.525745697593209	76.48591117965157	4.011718108339787	0
	7.119824384264552	156.70499334039215	18730.813653342713	3.6060360905057203	282.3440584739606	347.71502726194376	15.929535988825699	79.5007783369744	3.445756223321899	0

Fig. 4. The Ten Feature for Assessing the Potability of Water.

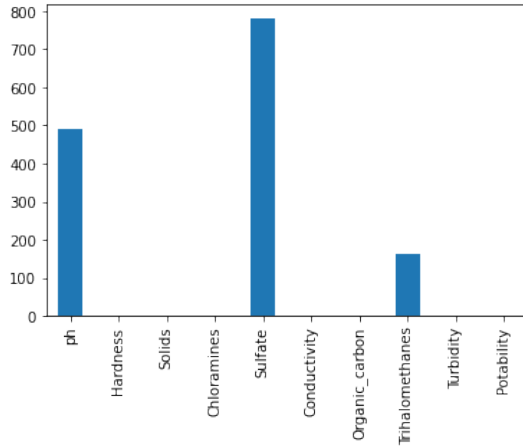


Fig. 5. The Value of Necessary Data Needed for our Model.

missing data. Furthermore, the algorithm can obtain more accurate results when the null values are replaced. As can be seen in the image below, pH, Sulfate, and Trihalomethanes have NULL values. As a solution, the null values are usually replaced by the average or mean of the specific category. After that the information in the dataset is checked again.

The mean value is calculated by measuring the sum of the available values divided by the total number of values in the categories. This mean calculation is used to handle the missing data relative to NULL values, see Fig. 6.

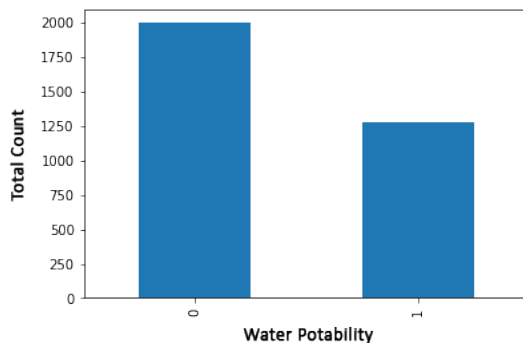


Fig. 6. The Sum of the Available Values for Water Potability in the Dataset: 0 Water is not Potable, 1 Water is Potable.

The value of feature probability density is also measured

for each feature. This function describes the probability of a certain feature falling between a range of values. It is also described as density as it shows the mass distribution of said feature over the total scale. Continuous variables or features would produce a curvature shape, either described as a normal distribution or non-normal distribution. In Fig. 7, the distribution probability of all ten features is shown (as continuous bar graphs mixed into a curve).

V. RESULT

At the beginning of the study, we presented the first research question **RQ1: What factors directly affect the potability of the water?** To which the answer can be deduced from the correlation analysis. The correlation is done using the heat map function of seaborn, see Fig. 8. This function shows the degree that which two factors affect each other. The correlation matrix below shows that each feature is only strongly correlated with itself (scoring +1). On the other hand, when seeing the correlation between the features with potability, no strong correlations exist. Yet there exists a weak correlation between two of the factors: pH and hardness (0.08). This analysis means that the dimensions can't be reduced in this study due to the absence of correlations between the variables. Further, the data are divided into independent and dependent features. All are independent features except Potability because Potability is our dependent feature.

Answering the second research question **RQ2: Can a random forest model effectively predict the quality of water based on these factors?** The dataset was divided into 80% training, and 20% testing on a Random Forest Classifier model (Fig. 9). At first, the model was trained, then it was fed the testing dataset to observe and assess the predictions. The answer to our second research question can be found by evaluating the model through numbers. The most commonly used metrics for model evaluation are accuracy, precision, recall, and f1-score.

The accuracy is the measurement of how close the predicted value is to the actual value, whereas the precision is the measure of how much the model can produce a repeated prediction value. The recall shows how much the model is good at identifying true positives. Based on both precision and recall, the F1-score value is calculated, and the greater the value the better. The results obtained by our Random Forest model can be summed up in Table II. These results show good performance by our Random Forest model, and they are very satisfactory.

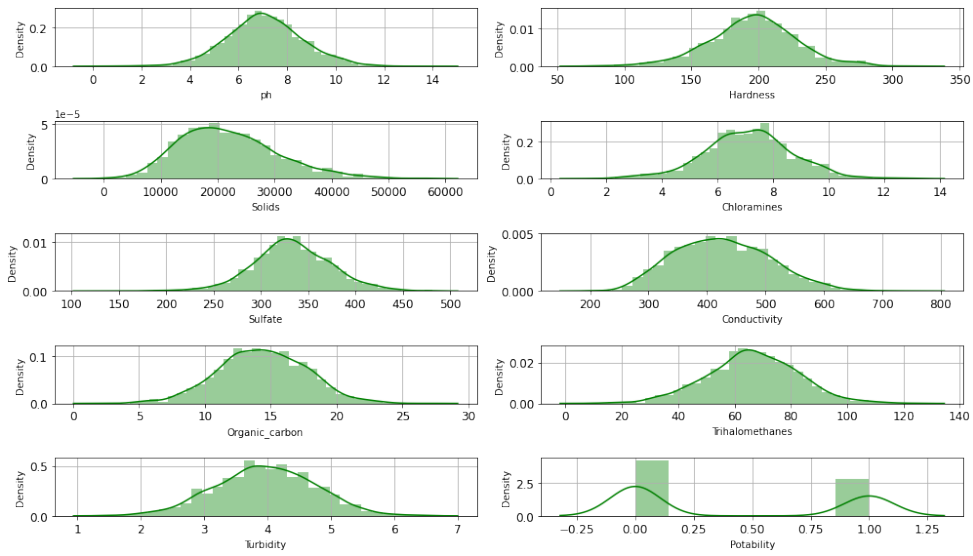


Fig. 7. Feature Probability Distribution as Calculated for each Feature.



Fig. 8. Correlation Matrix Showing no Correlations between the Different Variables.

TABLE II. MODEL PERFORMANCE EVALUATION BASED ON ACCURACY, RECALL, PRECISION, AND F1-SCORE

Test accuracy	1.0
Test recall	1.0
Test F1-score	1.0
Test Precision	1.0

VI. DISCUSSION

In this study, water quality prediction model was designed using machine learning classification in form of random forest classifier in predicting the water potability. Various variables are considered to perform a variety of calculations related to the water quality. These included pH, hardness, presence of solids, presence of chloramines, presence of sulfate, conductivity, organic carbon, trihalomethanes, turbidity. The results of the study revealed that different machine learning models performed differently when it came to predicting water potability. In order to compare our model with previous work presented by Xu, et al. [12] and Devi [35], we used RMSE (Root Mean Square Error) as metrics to evaluate the accuracy of random forest model in each study with ours. We can visually compare the accuracy of these models using Fig. 10.

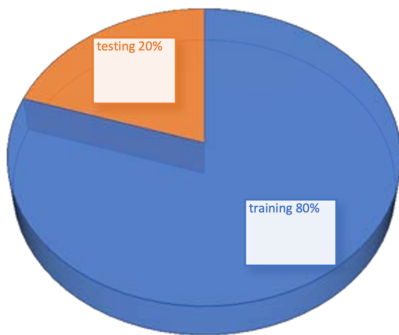


Fig. 9. Distribution of Dataset into Testing and Training.

One of the main advantages of ensemble learning is its ability to improve the system's overall performance. In addition, random forest methods can also reduce the likelihood of overfitting due to their random nature.. After successfully completing the water random forest prediction task, we then used remote sensing bands to perform water quality prediction. The previous variables were used as targets, while the independent variables were used as the distribution of the data. Through the use of the Jupyter platform, we were able to perform an inverted analysis of the data to fit the water quality prediction model. As it can be seen, our model provide a better performance score.

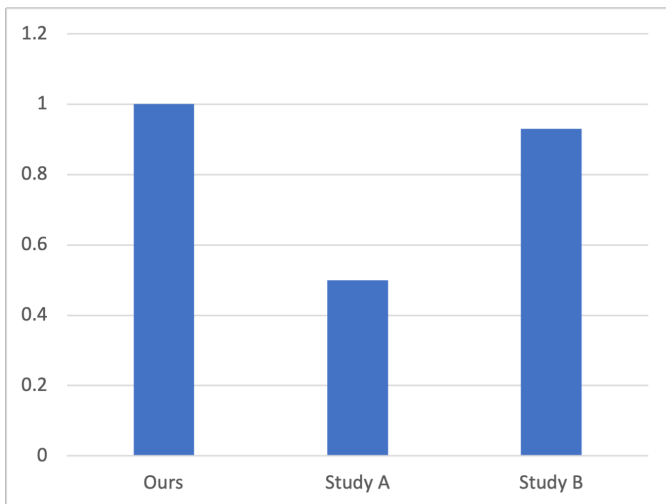


Fig. 10. Accuracy Histograms of Different Models: Ours, Study A [12] and Study B [35].

VII. CONCLUSION

The safety of our drinking water is a very essential matter, which should be monitored and managed effectively due to its importance. The quality of water that we used for drinking or cooking has a direct effect on our own health, which is why having perfectly safe water is not only a right for humans but also extremely critical. Several protocols and assessment criteria were developed to keep an eye on the safety and potability of water of different origins (underground, surface, inshore waters, etc.).

Using machine learning and PySpark classification for collection, storage, and analysis of water samples is a much more effective and efficient method for water quality evaluation than regular laboratory tests. This motivated us to create a machine learning model based on the Random Forest algorithm to evaluate the quality of river water based on 10 distinctive features: pH, hardness, presence of solids, presence of chloramines, presence of sulfate, conductivity, organic carbon, trihalomethanes, turbidity, and finally potability. The obtained results show that the developed RF model is capable of predicting whether the collected water sample is potable or not with a 100% accuracy and 1.0 F1-score.

The water quality prediction model that we designed can be used in the field of water quality monitoring. In the future, it can be used to provide an online tool that allows users to monitor the water quality of their local waterways. This method can be used to collect the necessary data using sensors to perform the prediction. The next step in the development of the water quality prediction model will be to collect the stream data necessary to perform the prediction. This method will be carried out through a dynamic update of the model.

REFERENCES

[1] M. Kachroud, F. Trolard, M. Kefi, S. Jebari, and G. Bourrié, "Water quality indices: Challenges and application limits in the literature," *Water*, vol. 11, no. 2, 2019. [Online]. Available: <https://www.mdpi.com/2073-4441/11/2/361>

[2] S. H. Ewaid, S. A. Abed, N. Al-Ansari, and R. M. Salih, "Development and evaluation of a water quality index for the iraqi rivers," *Hydrology*, vol. 7, no. 3, 2020. [Online]. Available: <https://www.mdpi.com/2306-5338/7/3/67>

[3] O. T. Opafola, K. T. Oladepo, F. O. Ajibade, and A. O. David, "Potability assessment of packaged sachet water sold within a tertiary institution in southwestern nigeria," *Journal of King Saud University - Science*, vol. 32, no. 3, pp. 1999–2004, 2020. [Online]. Available: <https://www.sciencedirect.com/science/article/pii/S1018364720300537>

[4] U. Ahmed, R. Mumtaz, H. Anwar, A. A. Shah, R. Irfan, and J. García-Nieto, "Efficient water quality prediction using supervised machine learning," *Water*, vol. 11, no. 11, 2019. [Online]. Available: <https://www.mdpi.com/2073-4441/11/11/2210>

[5] D. Poudel, D. Shrestha, S. Bhattarai, and A. Ghimire, "Comparison of machine learning algorithms in statistically imputed water potability dataset," *preprint*, 2022.

[6] J. H. Lee, J. Y. Lee, M. H. Lee, M. Y. Lee, Y. W. Kim, J. S. Hyung, K. B. Kim, Y. K. Cha, and J. Y. Koo, "Development of a short-term water quality prediction model for urban rivers using real-time water quality data," *Water Supply*, vol. 22, no. 4, pp. 4082–4097, 02 2022. [Online]. Available: <https://doi.org/10.2166/ws.2022.038>

[7] M. Kejarawal, C. Patil, A. B. Tiwari, and S. K. Sahani, "Water potability testing case study of mumbai region," *Journal of Harmonized Research in Applied Science*, 2018.

[8] D. T. Burns, E. L. Johnston, and M. J. Walker, "Authenticity and the Potability of Coconut Water - a Critical Review," *Journal of AOAC INTERNATIONAL*, vol. 103, no. 3, pp. 800–806, 03 2020. [Online]. Available: <https://doi.org/10.1093/jaoacint/qsx008>

[9] E. Ochungo, G. Ouma, J. Obiero, and N. Odero, "Water quality index for assessment of potability of groundwater resource in langata sub county, nairobi-kenya," *American Journal of Water Resources*, vol. 7, no. 2, pp. 62–75, 2019.

[10] Z. Jamshidzadeh and M. T. Barzi, "Groundwater quality assessment using the potability water quality index (pwqi): a case in the kashan plain, central iran," *Environmental earth sciences*, vol. 77, no. 3, pp. 1–13, 2018. [Online]. Available: <https://doi.org/10.1007/s12665-018-7237-5>

[11] P. Li and J. Wu, "Drinking water quality and public health. exposure and health, 11 (2), 73–79," 2019.

[12] J. Xu, Z. Xu, J. Kuang, C. Lin, L. Xiao, X. Huang, and Y. Zhang, "An alternative to laboratory testing: Random forest-based water quality prediction framework for inland and nearshore water bodies," *Water*, vol. 13, no. 22, 2021. [Online]. Available: <https://www.mdpi.com/2073-4441/13/22/3262>

[13] B. Sakaa, A. Elbeltagi, S. Boudibi, H. Chaffai, A. R. M. Islam, L. C. Kulimushi, P. Choudhari, A. Hani, Y. Brouziyne, Y. J. Wong *et al.*, "Water quality index modeling using random forest and improved smo algorithm for support vector machine in saf-18 river basin," *Environmental Science and Pollution Research*, pp. 1–18, 2022. [Online]. Available: <https://doi.org/10.1007/s11356-022-18644-x>

[14] M. H. Ahmed, "Prediction of the concentration of dissolved oxygen in running water by employing a random forest machine learning technique," *Preprints*, 2020.

[15] T. Yiu, "Understanding random forest: How the algorithm works and why it is so effective," *Towards Data Science*, 2019. [Online]. Available: <https://towardsdatascience.com/understanding-random-forest-58381e0602d2>

[16] J. McArthur, N. Shahbazi, R. Fok, C. Raghubar, B. Bortoluzzi, and A. An, "Machine learning and bim visualization for maintenance issue classification and enhanced data collection," *Advanced Engineering Informatics*, vol. 38, pp. 101–112, 2018. [Online]. Available: <https://www.sciencedirect.com/science/article/pii/S1474034617305049>

[17] N. Deshai, S. Venkataramana, B. V. D. S. Sekhar, K. Srinivas, and G. P. Saradhi Varma, "A study on big data processing frameworks: Spark and storm," in *Smart Intelligent Computing and Applications*, S. C. Satapathy, V. Bhateja, J. R. Mohanty, and S. K. Udgata, Eds. Singapore: Springer Singapore, 2020, pp. 415–424.

[18] S. Chen, "Research on big data computing model based on spark and big data application," *Journal of Physics: Conference Series*, vol. 2082, no. 1, p. 012017, nov 2021. [Online]. Available: <https://doi.org/10.1088/1742-6596/2082/1/012017>

- [19] L. Chen and L. A. Coulbaly, "Data science and big data practice using apache spark and python," in *Intelligent Analytics With Advanced Multi-Industry Applications*. IGI Global, 2021, pp. 67–95. [Online]. Available: <https://doi.org/10.4018/978-1-7998-4963-6.ch004>
- [20] K. Myeong-ryul and L. Wontae, "Effects of water temperature and ph on water quality improvement by a mixture of beneficial microorganisms," *J Korean Soc Environ Eng*, vol. 40, no. 1, pp. 1–6, 2018. [Online]. Available: <http://www.jksee.or.kr/journal/view.php?number=4088>
- [21] D. Shvachko, "Hardness of water and its impact on the human body," Ph.D. dissertation, Sumy State University, 2017.
- [22] Z. K. Jabbar-Lopez, C. Y. Ung, H. Alexander, N. Guring, J. Chalmers, S. Danby, M. J. Cork, J. L. Peacock, and C. Flohr, "The effect of water hardness on atopic eczema, skin barrier function: A systematic review, meta-analysis," *Clinical & Experimental Allergy*, vol. 51, no. 3, pp. 430–451, 2021. [Online]. Available: <https://doi.org/10.1111/cea.13797>
- [23] J. Warrack and M. Kang, "Challenges to the use of a base of fresh water in groundwater management: Total dissolved solids vs. depth across california," *Frontiers in Water*, vol. 3, 2021. [Online]. Available: <https://www.frontiersin.org/article/10.3389/frwa.2021.730942>
- [24] M. Jamei, I. Ahmadianfar, X. Chu, and Z. M. Yaseen, "Prediction of surface water total dissolved solids using hybridized wavelet-multigene genetic programming: New approach," *Journal of Hydrology*, vol. 589, p. 125335, 2020. [Online]. Available: <https://www.sciencedirect.com/science/article/pii/S0022169420307952>
- [25] J.-L. Boudenne, F. Robert-Peillard, and B. Coulomb, "Chapter two - inorganic chloramines analysis in water;" in *Analysis and Formation of Disinfection Byproducts in Drinking Water*, ser. Comprehensive Analytical Chemistry, T. Manasfi and J.-L. Boudenne, Eds. Elsevier, 2021, vol. 92, pp. 31–49. [Online]. Available: <https://www.sciencedirect.com/science/article/pii/S0166526X21000027>
- [26] Z. T. How, I. Kristiana, F. Busetti, K. L. Linge, and C. A. Joll, "Organic chloramines in chlorine-based disinfected water systems: A critical review," *Journal of Environmental Sciences*, vol. 58, pp. 2–18, 2017, water treatment and disinfection by-products. [Online]. Available: <https://www.sciencedirect.com/science/article/pii/S1001074216311822>
- [27] H. Tahraoui, A.-E. Belhadj, A.-E. Hamitouche, M. Bouhedda, and A. Amrane, "Predicting the concentration of sulfate (so4 2-) in drinking water using artificial neural networks: A case study: Médéa-algeria," *Desalination and Water Treatment*, vol. 217, pp. 181–194, 2021. [Online]. Available: <https://hal.archives-ouvertes.fr/hal-03225482>
- [28] Y. Xianhong, L. Shijun, H. Jian, and X. Jie, "Application analysis of conductivity in drinking water quality analysis," *IOP Conference Series: Earth and Environmental Science*, vol. 784, no. 1, p. 012028, may 2021. [Online]. Available: <https://doi.org/10.1088/1755-1315/784/1/012028>
- [29] T. Manzoor, S.Iqbal, F.Somorro, S.Imran, H. Alvi, and S. S. Haider, "Analysis of fluoride ion concentration in drinking water of karachi in relation with conductivity and ph," *Pakistan Journal of Chemistry*, vol. 9, no. 1-4, pp. 1–5, may 2019. [Online]. Available: <https://doi.org/10.15228/2019.v09.i01-4.p01>
- [30] K. I.A., S. D.A., K. E.A., P. E.G., and B. L.A., "Approaches to regulating organic carbon and the necessity of its obligatory monitoring in drinking water," *Public Health and Life Environment – PH&LE.*, vol. 9, pp. 61–66, may 2020. [Online]. Available: <https://doi.org/10.35627/2219-5238/2020-330-9-61-66>
- [31] S. Sriboonnak, P. Induvesa, S. Wattanachira, P. Rakruam, A. Siyasukh, C. Pumas, A. Wongrueng, and E. Khan, "Trihalomethanes in water supply system and water distribution networks," *International Journal of Environmental Research and Public Health*, vol. 18, no. 17, 2021. [Online]. Available: <https://www.mdpi.com/1660-4601/18/17/9066>
- [32] Y. Wang, G. Zhu, and B. Engel, "Health risk assessment of trihalomethanes in water treatment plants in jiangsu province, china," *Ecotoxicology and Environmental Safety*, vol. 170, pp. 346–354, 2019. [Online]. Available: <https://www.sciencedirect.com/science/article/pii/S0147651318312910>
- [33] D. Wang, X. Chang, K. Ma, Z. Li, and L. Deng, "Estimating effluent turbidity in the drinking water flocculation process with an improved random forest model," *Water Supply*, vol. 22, no. 1, pp. 1107–1119, 07 2021. [Online]. Available: <https://doi.org/10.2166/ws.2021.213>
- [34] V. Pradhan, "Assessment of potability of water with respect to physical parameters," *International Journal of Life Sciences*, vol. 2, no. 4, pp. 382–388, 2014.
- [35] S. Devi, "Random forest advice for water quality prediction in the regions of kadapa district," *Int. J. Innov. Technol. Explor. Eng*, vol. 8, pp. 1–3, 2019.

Virtual Reality Platform for Sustainable Road Education among Users of Urban Mobility in Cuenca, Ecuador

Gabriel A. León-Paredes¹, Omar G. Bravo-Quezada¹, Erwin J. Sacoto-Cabrera¹, Wilson F. Calle-Siavichay¹
Ledys L. Jiménez-González², and Juan Aguirre-Benalcazar³

Universidad Politécnica Salesiana, Cuenca - Ecuador¹

Instituto Tecnológico Sudamericano, Cuenca - Ecuador²

Empresa Pública Municipal de Movilidad, Tránsito y Transporte de Cuenca, Cuenca - Ecuador³

Abstract—A traffic accident is an event generated in an unforeseen way that is beyond the control of the people involved, which can produce bodily, functional, or organic injuries, leading to death or disability in the worst cases. According to the *Empresa Pública Municipal de Movilidad, Tránsito y Transporte de Cuenca (EMOV-EP)*, the total accidents recorded in 2021 were, 24.97% due to ignoring traffic signs, 21.11% due to not paying attention to traffic, and 16.94% due to driving under the influence of alcohol. The EMOV-EP, is the responsible for the regulation of human mobility. Thus, the EMOV-EP in conjunction with the *Universidad Politécnica Salesiana (UPS)* have introduced the next research question: How can a road safety education strategy, supported by Information and Communication Technologies (ICTs), can be developed to contribute to the improvement of the behavior of citizens to increase their knowledge of the traffic laws and regulations, and thus reduce the number of accidents in the city of Cuenca? Furthermore, in this paper we present the development of a Virtual Reality (VR) platform designed for road safety education. The platform is composed of a Web system, and 4 VR systems (games) that have been designed for 4 common causes of accidents respectively (drunk drivers, high-speed drivers, cyclists riding in bicycle lanes, and users of the tram transport system), using a serious games approach and the Oculus Rift/Quest technology. We have found that more than 80% of users have had a very good experience of playing and learning through the VR systems. Hence, this virtual reality platform constitutes a technological proposal with social impact because it creates an entertainment environment that can raise awareness among citizens, thereby strengthening road safety education and reducing the number of accidents in the city of Cuenca.

Keywords—Virtual reality; road safety education; virtual scenarios; serious games; educational experience

I. INTRODUCTION

Traffic education is a widely topic addressed worldwide but is not well understood. It refers to demographic elements, educational levels and even individual and collective identities. As it directly concerns road safety and the coexistence of actors, it requires a set of coresponsibilities in addition to the establishment, knowledge and socialization of rules of conduct among both pedestrians and drivers [1].

Currently, road safety education is considered a general problem whose responsibility falls to an entire society [2]. Its objective is increasing the awareness of citizens for the development of reasonable road behavior, but it is fundamentally responsible for the knowledge of the laws and regulations

in force regarding public use and road safety. In this sense, road safety includes the absence of danger and risks from the existence of regulatory mechanisms in the context of traffic, which translate to the prevention of accidents [3].

Therefore, a traffic accident is an event generated in an unforeseen way that is beyond the control of the people involved, which can produce bodily, functional or organic injuries, leading to death or disability in the worst cases [4]. Since the end of the twentieth century, the Pan American Health Organization (PAHO) has shown that traffic accidents are among the main causes of injuries (serious or minor), disabilities and death in both developed and underdeveloped countries [5] [6]. Currently, they have become a kind of epidemic worldwide that has cost the lives of more than 1.24 million people—a public health problem for the World Health Organization (WHO) due to the high percentage of mortality among young people aged 15 to 29 years; indeed, by the year 2030, traffic accidents will be one of the five leading causes of death worldwide [5] [7].

In the context of Latin America and the Caribbean, the figures are alarming; even though the percentage of traffic accidents is well below that of developed countries, the rate of injuries and deaths due to road accidents is comparable to the levels in the United States and Canada. Specifically, countries with lower incomes have higher fatality rates in traffic accidents, 90 percent of which stand out as among pedestrians and cyclists, corresponding to the most underdeveloped countries. Hence, the PAHO has expressed the need not only for a continuous and systematic evaluation of road safety worldwide but also joint efforts involving different sectors of society to address road safety in a comprehensive manner through road safety education.

Ecuador is among the ten countries with the highest mortality rate in traffic accidents, despite being among the 5 countries on the continent with the lowest rate of registered vehicles [8]. Regarding the traffic accidents that occur daily in Ecuador, they are generally caused by citizens who take improper actions in their driving; pedestrians also regularly ignore current traffic and transportation laws, causing road accidents in which about half of the fatalities are pedestrians themselves [9]. On the other hand, the expansion of the means of transport for the mobilization of citizens in large masses has been a topic of high demand in most cities of Ecuador

due to the population growth that has been recorded in recent decades. In the city of Cuenca, the capital of the province of Azuay, located in the Andean highlands in the south of the country, which has been declared a Cultural Heritage of Humanity by UNESCO, the “*Tranvía 4 Ríos de Cuenca*” project has been carried out a public transport alternative. Its planning and construction began in 2012, and its commercial operation began on September 25, 2020 following a long and complex construction process, and many economic and technical problems that had been overcome [10].

Currently, the tram for the city of Cuenca is in full operation, and the contribution of this service has been noted to a large extent. However, there is a process requiring adaptation and education for mobility users to learn to coexist with this new means of transport. In addition to the accidents related to other means of internal transportation, there have been a variety of accidents involving this means of transport that have generated a notable increase in the accident rate [11]. According to an interview with officials at the *Empresa Pública Municipal de Movilidad, Tránsito y Transporte de Cuenca* (EMOV-EP), amid the increase in traffic accidents in the city, in recent years, multiple strategies have been created to increase the awareness of citizens of the rules and mechanisms for accident prevention [12]. However, these entail the necessary intervention of all agents and social sectors related to mobility, i.e., without excluding the academy as a fundamental element for intervening in this problem with research, all training proposals and road safety education strategies. Their purpose is to educate the public in the options for avoiding and preventing traffic accidents. All of their aspects should therefore be taken into account to reduce the high accident rates that have been shown in the previous research carried out by the authors of this scientific article [7].

Accordingly, the following question arises: How can a road safety education strategy, supported by information and communication technologies (ICTs), be developed to contribute to the improvement of the behavior of citizens to increase their proper use of traffic routes and thus reduce the number of accidents?

To address this question, a joint work by the EMOV-EP, Universidad Politécnica Salesiana (UPS), and UPS’s Cloud Computing, Smart Cities & High Performance Computing Research Group (GIPH4C), has proposed creating a Virtual Reality (VR) platform for sustainable road safety education in the city of Cuenca. The novelty of the proposal is mainly the possibility of reducing traffic accidents within the city through an educational technological platform that recreates environments similar to those of the city, providing an alternative with a novel approach to society that is completely different from previously developed VR platforms.

The use of VR as a learning technology allows the visualization of educational scenarios in all areas from a three-dimensional perspective. Computer-generated scenarios transform educational concepts via a new rapid sensory perception of individuals. The results obtained in the test phase of this project show a high index of motivation toward road safety education; users become the new protagonists for their own education, a fundamental requirement of the concept of gamification that has been introduced in the educational field of so-called Serious Games (SGs). Similarly, the potential of

virtual reality is confirmed by the serious games perspective in the adaptive learning process and through its contribution to the development of a more responsible road culture through games [13].

From a theoretical point of view, the importance of the use of this technology is demonstrated by not only the interaction that a user has with it but also this technology’s ability to activate all the human senses—especially touch, vision and hearing—whereby learning becomes more productive [14]. Hence, the proposal to use virtual reality technology for road training and awareness comprises a great milestone in the environment of road safety education.

Below, the main theoretical and empirical works related to the use of information and communication technologies for road safety education are presented. Next, we describe the development phases of the development of the virtual reality platform based on serious games for sustainable traffic education among mobility users in the city of Cuenca, Ecuador. In addition, the article presents the results from the test phase, which was carried out in conjunction with the EMOV-EP. Finally, we present the conclusions of the study and some recommendations for the platform’s implementation.

II. BACKGROUND

According to research at the *Universidad de Guayaquil*, since traffic accidents in Ecuador are one of the main causes of death in the population, especially among children and adolescents, road safety education should be considered a national problem that all social actors are directly responsible for [2]. Some of the main causes of traffic accidents are the recklessness of pedestrians and drivers, ignorance of current regulations, and so-called road complexity factors. Accordingly, the development of a virtual teaching-learning platform with 3D animation has been proposed as a strategy for increasing the awareness of citizens through education in road behavior rules. This proposal was initially limited to the training of high school students. Also, does not contemplate real spaces for the simulation of accidents, nor strategies of continuity and permanent implementation of the strategy. As for the techniques used for the development of the platform, it is not detailed in depth.

Similarly, the *Universidad Espíritu Santo* of Ecuador has proposed the development of an interactive T-Learning application [15] for road safety education. The platform is based on the ISDBT-Tb digital TV standards that allow the dissemination of road safety issues. Despite being a novel proposal for the education of road culture among citizens, its implementation as a strategy for reducing traffic accidents is based on the establishment of alliances between public and private television operators and educational institutions to provide generalized training throughout the country. This proposal is limited to the use of tools offered by the internet, which, although it has the capacity to generate changes in the behavior of citizens, does not offer the possibility of interacting face to face, and the research does not delve into the mechanisms for the update of the contents.

In correspondence with [3] the results of the study places Ecuador as one of the Latin American countries with the highest rate of traffic accidents. Among the causes of this

situation, the increase in the number of automobiles and the lack of knowledge about road safety by pedestrians and drivers stand out. Also, after analyzing the public policies and mechanisms established to reduce accident levels, the authors maintain that these have been ineffective because they focus mainly on the imposition of sanctions, without considering that the traffic accidents are a consequence of the lack of road education. In this sense, they warn about the need to overcome coercive policies. Despite the fact that the study assumed the city of Guayaquil as the field of action, the analysis of the results obtained after the application of theoretical and empirical methods allows the researchers to conclude that all of Ecuador requires educational programs based on accident prevention.

On the other hand, the *Instituto Tecnológico Bolivariano* in the city of Guayaquil, Ecuador, has proposed to use social marketing to increase the awareness of road safety among university technology students [16]. This research is a response to national statistics that show a lack of education in this area drives its accident rates and that young people are one of the groups with the greatest tendency to suffer irreparable consequences. According to this study, the main causes of road accidents are drivers' alcohol consumption, reckless actions, speeding, ignoring and disrespecting traffic signs and using cell phones. The proposed marketing strategy thus focuses on awareness-raising actions that are disseminated through social networks, cell phones and other personal channels to allow users to understand that road safety education is a way of life. The research establishes novel actions based on the promotion of road education, however, it is only aimed at technology students and does not present alternatives for the use of advanced information and communication technologies as part of the strategy.

This literature review of related works shows that most of the research and proposals from higher education institutions for the road training of citizens have been developed in the city of Guayaquil. However, statistical sources show that there has been a growing and accelerating accident rate in the city of Cuenca in recent years. The largest number of traffic accidents that occur in Cuenca are a consequence of the active or passive ignorance of the citizenry of the traffic and transportation laws and regulations that are in force in Ecuador. Such accidents are produced by the recklessness and speeding of drivers of light and heavy vehicles among other factors. Although in recent years higher fines have been established and a series of radar sites have been placed on both high- and low-speed roads with the purpose of warning citizens about the established speed limits, there is no evidence of a reduction in the number of accidents; on the contrary, they have increased. As a result, the city of Cuenca continues to experience a climate of road insecurity involving large numbers of accidents and deaths from various causes [17].

Notably, regarding the causes of road accidents in Cuenca, although Ecuador is not in the top 10 countries that consume the most liquor, driving under the influence of alcohol has become a highly recidivist factor in the city of Cuenca, causing countless traffic accidents; thus, the EMOV-EP considers alcohol consumption a necessary factor in its relevant analyses [18]. In addition to vehicle drivers, a fundamental component in road education and culture is obviously pedestrians, whose

behavior directly affects the processes of the regularization of daily mobility. For example, it has been empirically observed that in areas of large agglomeration in the city, especially the most commercial and concurrent sectors such as the main markets [19], passers-by do not respect traffic signals at all, crossing through prohibited crossings such as pedestrian crossings and tram lines without being aware of the consequences that these actions may have for their physical well-being and that of the rest of the citizens who use public highways.

In addition, the city of Cuenca has a high rate of traffic accidents involving two-wheeled vehicles. The vast majority of these accidents are related to the lack of respect for traffic signs by cyclists, motorcyclists and/or pedestrians [20]. This situation results in accidents that put people's lives at risk; due to their recurrence, a decline in road safety is generated that affects all citizens as well as the foreigners who throughout the year come to know and enjoy Cuenca. In this point it should be mentioned that, this capital of the province of Azuay in the Ecuadorian mountain range has been recognized by UNESCO as a cultural heritage of humanity due to its culture and the natural and architectural beauty that represent it.

Moreover, notably, according to the high figures from the EMOV-EP regarding the total accidents recorded in 2021, 24.97% were due to ignoring traffic signs, 21.11% were due to not paying attention to traffic, and 16.94% were due to driving under the influence of alcohol. These data coincide with the previously cited research. Collectively, such data show that in accidents where material losses are relatively high, injuries or human losses are also unfortunately present, thereby positioning this issue as of the utmost most importance—one that must be resolved in the medium and short term [7].

Therefore, the EMOV-EP, as the body responsible for the regulation of human mobility in the city, in conjunction with the education system, promoted a series of road safety education campaigns to reach the greatest number of people in Cuenca's population. It thus allied with the *Universidad Politécnica Salesiana*, specifically with the research group GIPH4C, to create a greater number of frequent traffic drills throughout the city to involve the citizenship in these without people knowing that they have been drilled as such. However, due to its infeasibility, this option has been discarded; it was deemed economically in sustainable due to the numerous logistics involved. Specifically, it was found that emergency calls to 911 would cease to be important while the drill was implemented and thus the time allotted should not exceed 15 minutes to create spaces where citizens could intervene. Hence, such education implies assuming the costs that these drills represent and considering the logistics that all these processes entail; these are too high and numerous for the drills to be viable factors in producing the benefits that were the goals of this proposal.

Thus, based on an analysis of human mobility in the city of Cuenca and their joint discussion of alternatives for its regulation, the EMOV-EP and *Universidad Politécnica Salesiana*, through the research group GIPH4C, have proposed the following objective: to intervene through virtual reality technology via a virtual platform that allows creating environments similar to the environments of the city, creating the most appropriate alternative to try to resolve all the problems that have been discussed.

Furthermore, the antecedents analyzed in the first part of this research allow us to maintain that until now, the impact of platforms based on virtual reality on road training in Ecuador has been unknown. However, these new technological trends have been implemented in educational environments in general, such as virtual laboratories and learning based on serious games, with excellent results. The novelty of this proposal is thus the implementation of virtual reality technology with serious games in the field of road safety education to generate processes and new information and communication tools in regard to the road education of citizens in general [21].

That is, this paper entails the creation of a virtual reality system based on serious games for the training and awareness of citizens regarding aspects of road safety education.

Virtual reality is the simulation of a certain environment in which users are immersed and have the actual sensation of being there. Although its origins date to the 1960s, the costs of the equipment necessary for its operation have long been one of the main barriers to its distribution. However, the emergence of more affordable virtual reality hardware for games and entertainment has promoted a resurgence of virtual reality in recent years [22], sparking great interest in the field of education, especially concerning the imminent need to incorporate new technologies to improve teaching-learning processes [23] [24].

Thus, we analyze VR's properties of presence and immersion, which are considered key factors to strengthen learning. Presence allows the user to have the perception of being and existing in the virtual environment, while immersion entails the veracity that technology can evoke. However, for a true immersion of the user in the virtual environment, an additional factor is needed: interactivity. Since games are the most natural means for interactivity to be achieved, this is where SGs—those activities whose approach is innovative because they are designed for entertainment purposes but can also be used to educate or train users in certain areas—are salient [23] [25].

In the framework of this research project proposal, through the virtual platform, specific environments of the city of Cuenca are rendered in 3D within a virtual reality scenario to present the experience and various causes of a traffic accident to a user. The development of each scenario involves the use of virtual reality glasses with Oculus Rift/Quest technology [26] to overcome difficulties in the game while promoting learning through these experiences.

III. METHODOLOGY

The development of the project was structured into three stages based on the organization of serious games. The actions included in each of the stages are as follows:

- 1) **Living the Experience:** In this first stage, The player experiences a traffic accident in the first and/or third person, where emotions play a very important role. The idea is for people to reflect on what has happened. Thus, an introductory scenario is presented that allows them to understand the history of and know the causes that trigger the accident, generating greater awareness in each of the participants.

- 2) **Learning:** The accident that was experienced in the previous stage is repeated, but now a bank of questions is presented whenever a traffic violation occurs in the animation. At this stage, it is possible to measure the concentration of people while educating them about the violations presented. The responses to the questions are saved and then used to analyze the process later. To obtain a final score, a virtual driver's license is presented where a total of 30 points is accumulated. Each time a question is answered incorrectly, the score is reduced, depending on the violation committed. Thus, when the score is zero or the question bank segment has ended, feedback is presented on the questions that have been poorly answered.
- 3) **Free will:** In this stage, the player has the freedom to move around and interact with different objects that make up the virtual reality scenario without any restriction. The decisions that the players make during this stage experience, directly influence their final result. In theory, with the learning obtained in the previous stages, the participant at this time should make the appropriate decisions to avoid the same traffic accident in order not to repeat the game. Hence, the system successfully fosters their participation. The "Tranvía Cuatro Rios de Cuenca" scenario has a more informative purpose than simply recreation or gaming *per se*. Therefore, in the third phase, the player has the possibility of approaching two different stops or tram stations, and overcoming various obstacles of daily life, such as pedestrian crossings, traffic signals, or traffic lights, with the aim of traveling to where a ticketing and ticket validation machine is located and interacting with it. Similarly, the players can recharge their balance and buy tickets for their subsequent boarding of the tram system. In this case, if a player commits an offense, a representative fine is given to train him or her in the proper use of the actual system by reducing inconveniences in its use. This is because the fine for not paying for this service has a current value of USD \$ 120.00.

Notably, prior to the development of the three above mentioned stages, the identification of the places in the city, where the greatest number of problems arise was based on the agglomeration of pedestrians and traffic accidents. The sites with the highest recurrence were selected for the development of the virtual environments, as detailed in Table I:

TABLE I. PLACES CHOSEN FOR THE DEVELOPMENT OF VIRTUAL ENVIRONMENTS

No.	Location	Problem found / Chosen scenario
1	Ave. Huayna Capac between Calle Bolívar and Calle Larga	Driving a vehicle under the influence of alcohol.
2	Ave. Américas entrance to Quinta Chica and Hospital del Río.	Driving vehicles at high speeds.
3	Ave. Fray V. Solano between Los tres puentes sector and Virgen de Bronce Church	Users of bicycles and cycle paths.
4	Ave. Américas, Feria Libre - El Arenal sector	Users of the tramway system.

Once the sectors to be displayed in the platform were selected, a photographic survey was performed. The use of the Street View tools of Google Maps and Sketchup allowed the development of all the 3D virtual scenarios. Subsequently, the information obtained was exported to the Unity 3D tool; by manipulating lighting, shadows and other factors, the desired images of the scenarios for the game experiences were obtained. Below, these images are presented in Fig. 1, 2, 3, and 4.

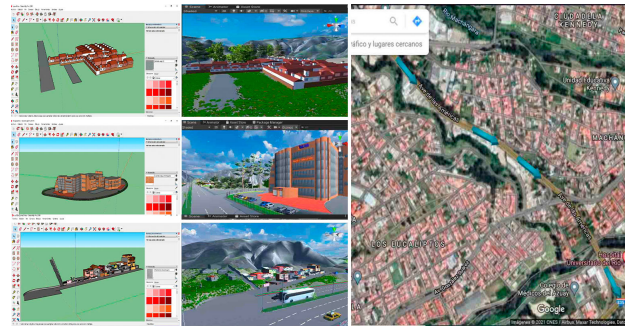


Fig. 4. Avenue of the Americas Scenario.



Fig. 1. El Arenal Virtual Scenario.

After developing the scenarios in a three-dimensional way with the tools described before, the next step was to establish all these places using Sketchup, Make Human, Adobe Fuze, Mixamo, and Blender, obtaining additional pre-designed images from 3D Warehouse. Humanoid characters and vehicles, which were positioned in various spaces within each scenario, were also created with their respective animations to approach the reality of each sector, as shown in Fig. 5, 6, and 7.

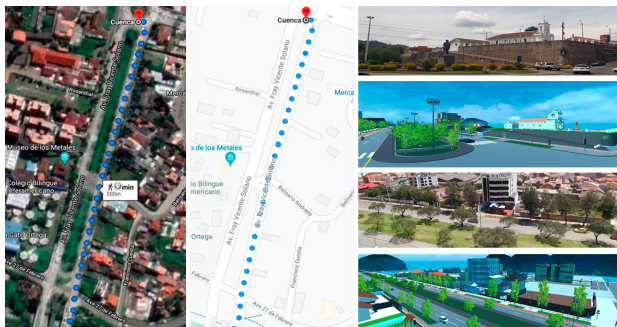


Fig. 2. Los Tres Puentes Sector and Virgen de Bronce Church Virtual Scenario.



Fig. 5. Diversity of Vehicles Designed in the Local Context.



Fig. 3. Huayna Cápac Avenue Scenario.

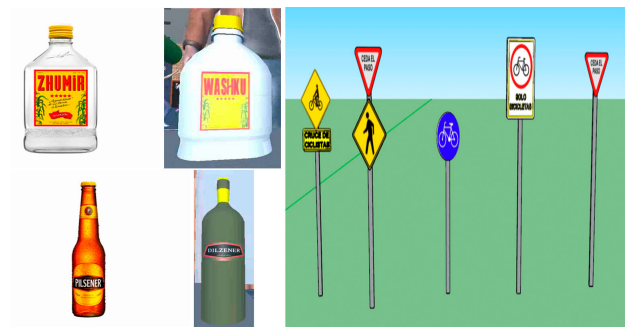


Fig. 6. Various Objects are Designed Similarly to the Originals.

An important factor throughout the research process and the development of the virtual reality proposal was the possibility of maintaining the effective representation of each place. Hence, common characters and vehicles to the city of Cuenca were included in the setting, such as the “Cholita cuencana” from Cuenca, a typical character of the city, visualized in Fig. 8.

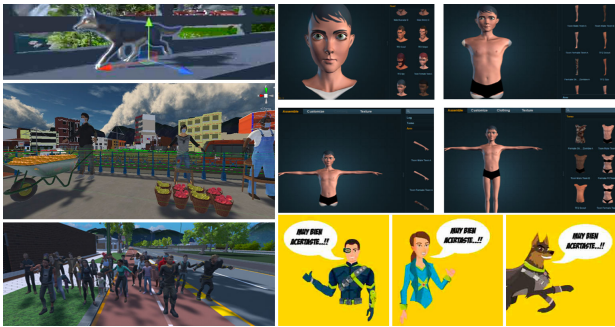


Fig. 7. Design of Varied Characters.



Fig. 8. Design of a “Cholita Cuencana” in 3D to be Included in the Scenarios.

To maintain the same criteria, street vendors were also included (see Fig. 9), as well as characters who are commonly found in different parts of the city and security personnel, such as police, citizen guards, traffic agents, and civilians.



Fig. 9. Design of Street Vendors in the City in 3D.

After creating these scenarios according to their local context, we designed a script in which the traffic accident that occurs in each sector is narrated, necessitating our investigation of the different accidents that usually occur in real life. This information was obtained from various local media, such as the *El Tiempo*¹, and *El Mercurio*² newspapers, the social

¹<https://www.eltiempo.com.ec>

²<https://www.elmercurio.com.ec>

networks of public security companies, such as *ECU-911*³, and news websites. This information allowed us to determine the problems to be addressed in the scenarios and to identify the infractions that should be implemented in the context of serious games.

To better understand all the procedures that are carried out after traffic accidents and the reactions they generate among pedestrians and other security entities, the research team participated in drills conducted by the EMOV-EP during 2020. Through the observation of these drills, the different attitudes of people toward an accident involving a driver under the influence of alcohol and a cyclist on a cycle track were observed and recorded, as shown in Fig. 10. In this way, relevant conclusions were obtained to more realistically depict the specific scenario that we developed and presented.



Fig. 10. Simulation of Transit Accident Held in the City of Cuenca. Where Members of the EMOV-EP and UPS Participate.

Furthermore, the EMOV-EP constantly interacts with citizenship to transmit knowledge and education on road issues; these interactions became opportunities for the socialization of the research project (see Fig. 11). In these spaces, it was possible to present the serious game proposal to the public, interact with users and obtain useful feedback for the enrichment of the proposal and assure a better actual user experience, i.e., for users to effectively learn about the proper use of roads and the consequences of poor decision-making when driving a vehicle or traveling on the streets and avenues of the city.



Fig. 11. Socialization of the System with Citizens.

Another important component within the proposal concerns the mechanisms for evaluating learning among the platform’s users. Therefore, a web platform has been developed. This platform allows the visualization of the reference question bank for each scenario and ensures that these are modified

³<https://twitter.com/ecu911austro?lang=es>

according to any needs or changes that occur, especially regarding cases of the application of fines.

In a complementary manner, the platform generates the data and statistics recorded by the entire system in graphical format. Through these data, it is possible to detect what questions are the most familiar to users and, in turn, the scenarios where the population has more difficulties or ignores more traffic laws (see Fig. 12 and 13).

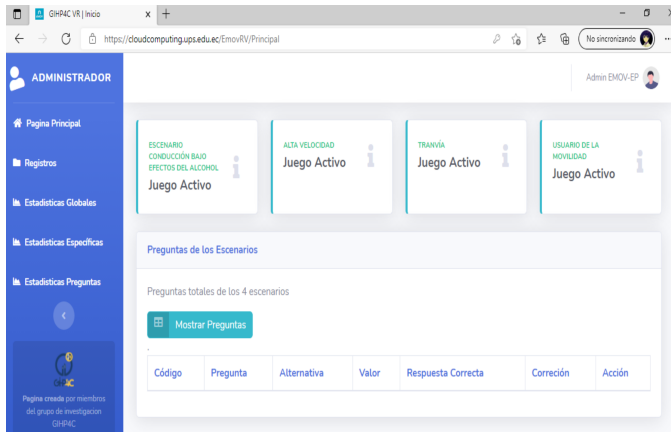


Fig. 12. Visualization of the Web Platform: Main Page.

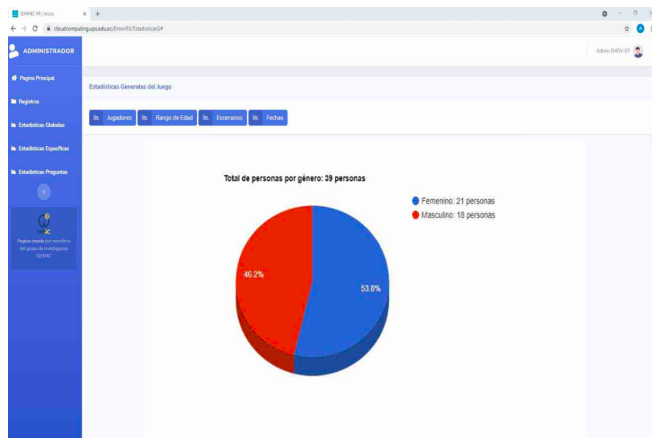


Fig. 13. Visualization of the Web Platform: Statistical Results.

Moreover, the storage system of the question bank is two MySQL databases, one local and one at the cloud level. Both databases maintain a master-master relationship. However, during the socialization of the project, it was observed that on some occasions, it is possible that there is no internet connection. Hence, the backup of the generated records must be stored on the local disk, but when there is a connection, they are uploaded to the cloud. To perform this procedure in the cloud, it is necessary to be connected to the internet through a static IP address that is assigned within the facilities of the EMOV-EP, guaranteeing the required information security.

IV. RESULTS

A. Hardware and Software

To provide a greater understanding of the results of this project, developed jointly between the EMOV-EP, the *Univer-*

sidad Politécnica Salesiana and the UPS's GIPH4C research group, we provide the following basic characteristics of the necessary computer and the installation of the platform for use: computer with Windows 10 or higher operating system; video card Nvidia GTX1060/GTX 1660 or equivalent of AMD - Ryzen 2600/3600 or Intel i5 8600 or equivalent; Memory of 16 GB of DDR3 or DDR4 RAM; and, solid-state hard drive of at least 512 GB and a mechanical hard drive of at least 1 TB.

Nevertheless, in terms of performance and functionality, a certain latency has been observed in the fluidity and execution of the developed scenarios. Among the most important causes for this delay that we have detected are the following:

- **Lighting:** Lighting is an important factor when using many system resources since it visually depends on how much coloring and how many objects (including the addition of shadows) are added to each figure in the virtual scenarios.
- **Vertices and Groups of Objects and Rendering:** A surplus of groups and vertices to present very detailed objects causes the rendering to become slow when interpreting many points and details. It is thus advisable to make them more simple without too many details to improve the speeds of the processes.
- **Colliders:** It is better to generate these with fewer vertices and avoid their use; otherwise, it is necessary to include Mesh Colliders.
- **Occlusion:** How and when both objects and animations are visualized play a very important role in performance because they cause slowness and latency within the execution. It is advisable to use the parameter called Occlusion Map, since it gives different qualities in the rendering of the same object; the further away it is, the less its quality and thus fewer resources are used. In contrast, as you approach it, its quality and detail increase, using more resources in less time. This same parameter, due to the unified visual field of the camera, allows a rendering of a scene to be fixed as the viewer views it. Specifically, what the visual field of the camera captures is what is rendered and animated—such rendering and animation stops once the object or fraction of the scene with respect to the visual field of the scene is outside the camera's focus.
- **Scripts:** Script optimization is important for making the project work correctly because if there are infinite or constant loops, these will generate resource consumption.
- **Animations:** Within the animations, a factor to account for is the generation of the exoskeleton of the character to be animated. The greater the number of bones generated, the more fluid the animation will be and, in turn, the more graphic resources will be consumed. Hence, it is recommended that if a character does not perform movements that require complete control of all his or her joints, only a basic exoskeleton (control of head, neck, back and extremities) is rendered. Similarly, if the character does not

perform movements in terms of facial expressions, it is unnecessary to generate them, as these increase the weight of an animation due to unused resources.

Regarding the process of executing the scenarios in the computer, when executing the four scenarios at the same time, the consumption of video resources, RAM and cache memory of the computer is extensive; they are working at their maximum capacity, which causes an increase in hardware temperatures. In many cases, the programs can become “frozen”; therefore, they should be executed one scenario at a time, because a computer can only connect to a single Oculus device. By having only one scenario thus executed, everything functions without problems. A quick and timely solution, however, would be to expand the capacity of the computer’s video card and RAM.

B. The Use of the System by Users

Due to the ongoing COVID-19 pandemic, declared worldwide by WHO [27] in late 2019, the socialization phase of the research project was reduced. However, given the obligation to understand the acceptance (or not) of the virtual platform by its end users, a group of 30 people was randomly chosen. The platform was presented to them and they experienced all four virtual scenarios. This entire validation process was carried out under strict biosafety measures. Once the presentation was completed, the group responded to a survey that was formulated to obtain feedback on the proposal via their comments and suggestions. Some of the most important questions and its answers of the survey are presented in Table II, which concern the user’s level of knowledge generated by a traffic accident scenario, perception of virtual reality, identification of the sector of the city and evaluation of the experience of learning through play.

It is important to note at this point that the limitations presented in the validation phase of the proposal did not affect the process of verifying the usefulness and operation of the platform. Indeed, the answers to the questions for all four scenarios were favorable. As shown in Table II, an average of more than 60 percent of the people surveyed rated them with the highest score. Notably, moreover, the contributions, observations and suggestions from those who interacted with the platform, in addition to the recommendations of the specialized staff at the EMOV-EP, will be considered in the construction of the next stages of improvement and implementation of the virtual platform project.

V. DISCUSSION

The literature review on the use of information and communication technologies to promote road education, previously detailed shows on one hand a growing concern about the accelerated increase in the rate of traffic accidents in Ecuador. On the other hand, it is also notorious the emergence of proposals from higher education institutions in order to promote actions that lead to the training of citizens in terms of knowledge, respect, and compliance with current laws and regulations on the matter.

Therefore, in the following paragraphs, we discuss the meeting points and differences between this proposed and the main related works addressed.

Research work in [1] contributes to our paper from the theoretical point of view which exposes the aspects related to road education, its relationship with road safety, and the necessary participation of the different actors of society; in the generation of articulated actions, from the roles and responsibilities of each instance. As for the work proposal mentioned above, it is restricted to the exposition of government actions implemented in Guadalajara-Mexico for the education of adults in respect of traffic laws. As a result, the authors propose the implementation of a road education subject as an elective course at the *Universidad de Jalisco*. Finally, the work does not detail in depth the methodology used to generate the proposals. Likewise, it is limited to adult education, which greatly differentiates it from the proposal for the use of serious games in our research, which can be aimed at children, youth, and adults.

In the local context, another similar study is presented by [2], which concur with the gathering of its empirical information and the results of our paper regarding to the high accident rate in several cities of Ecuador. However, the study is limited to the city of Guayaquil. Similarly, our research coincides with the consideration of road education in Ecuador as a national problem, which makes it necessary to generate joint and multidisciplinary actions to reduce what they define as a technological scourge. Regarding the methodology, they are based on a training process through interactive websites with 3D animations but are only aimed at young high school students. Last, the study does not expose the methodology for the development of the applications used. Nor does it detail the results obtained in the implementation of the proposal.

In the same way, the authors in [3] agree with our study regarding the approach of traffic accidents in Ecuador as a public health problem, due to their accelerated growth in the last two years. However, among the causes of this growth, the authors point out the lack of government commitment to complement effective politics in the mobility area. Whereas, in our proposal, we have recognized mechanisms for road education in the city of Cuenca in which we have involved public and private, social, academic, and governmental actors. Also, the analyzed research is limited to proposing the development of road safety educational projects in the field of educational institutions. However, the components of the training or techniques and instruments for its application are not exposed. As result, the identification of accident statistics in the city of Guayaquil stands out, in addition to the characterization of the training undertaken by the educational units in road education.

Moreover, the authors in [16], address the city of Guayaquil as a field of action and they have the same point of view as previous and our investigations in considering that traffic accidents constitute one of the main causes of death in Ecuador, mainly for young people. Another point of agreement between the investigations has to do with affirming that the lack of road education is a fundamental factor in accident rates. In relation to the research proposal, revolves around marketing strategies and is addressed only to students of Technological Institutes. In the results, the research coincides with the data obtained in our paper by pointing out recklessness, disrespect for traffic signs, alcohol consumption, and the use of cell phones while driving as causes of main accidents.

TABLE II. COMMON QUESTIONS AN ITS ANSWERS FOR EACH SCENARIO USED FOR THE VALIDATION AND ACCEPTANCE OF THE PROJECT

Scenarios	Questions				
	<i>Question 1</i>				
<i>How much did you correctly appreciate and understand the theme of the accident presented in each scenario? On a range from 1 to 3, where 1 is Nothing and 3 is Everything.</i>					
	Option 1	Option 2	Option 3		
<i>Driving a vehicle under the influence of alcohol</i>	0	0	30		
<i>Driving vehicles at high speeds</i>	0	0	30		
<i>Users of bicycles and cycle paths</i>	1	3	26		
<i>Users of the tramway system</i>	0	8	22		
<i>Question 2</i>					
<i>How did you find the Virtual Reality experience? On a range from 1 to 5 (1 as very bad and 5 as very good)</i>					
	Option 1	Option 2	Option 3	Option 4	Option 5
<i>Driving a vehicle under the influence of alcohol</i>	0	0	1	7	22
<i>Driving vehicles at high speeds</i>	0	0	1	4	25
<i>Users of bicycles and cycle paths</i>	0	0	7	10	13
<i>Users of the tramway system</i>	0	0	6	9	15
<i>Question 3</i>					
<i>Were you able to identify the sector of the city where you were?</i>					
	Option Yes		Option No		
<i>Driving a vehicle under the influence of alcohol</i>	29		1		
<i>Driving vehicles at high speeds</i>	29		1		
<i>Users of bicycles and cycle paths</i>	22		8		
<i>Users of the tramway system</i>	22		8		
<i>Question 4</i>					
<i>How would you rate the experience of playing and learning through these virtual means? On a range from 1 to 5 (1 as very bad and 5 as very good)</i>					
	Option 1	Option 2	Option 3	Option 4	Option 5
<i>Driving a vehicle under the influence of alcohol</i>	0	0	0	3	27
<i>Driving vehicles at high speeds</i>	0	0	0	2	28
<i>Users of bicycles and cycle paths</i>	0	0	3	6	21
<i>Users of the tramway system</i>	0	0	0	7	23

VI. CONCLUSION

The use of ICTs to promote road education in Ecuador evidences the development of several research papers in which traffic accidents and their consequences are considered a public health problem that cannot be addressed only by establishing public policies, but with the cooperation of different sectors of society (public and private). The research papers studied are limited to the analysis of the causes and not the presentation of innovative proposals that go beyond the traditional methods of training in road culture. Similarly, the bibliographic review found a diversity of research applied in Ecuador, however, most are developed in the context of the city of Guayaquil, and for the city of Cuenca, there is no evidence of research proposals of great impact for reduce the number of accidents through road education.

The development of road education proposals based on virtual reality with a focus on serious games is currently a highly relevant topic. Through our review of the theoretical and empirical background of this research, it is evident that first, traffic accidents have become one of the main causes of death not only in Ecuador but also globally. Second, the growing number of accidents in the city of Cuenca, Ecuador is mainly generated by high speed, driving under the influence of alcohol, recklessness of drivers and pedestrians, and ignorance of traffic rules and signals. Accordingly, the need to articulate interinstitutional efforts is evident, a prerequisite to generating proposals that mediated by new information and communication technology, can contribute to the formation of a road culture in the city of Cuenca.

The social impact of the project developed jointly by the EMOV-EP and the GIPH4C, made up of professor-researchers from *Universidad Politécnica Salesiana*, derives from the cre-

ation of a 3D virtual platform based on entertainment through the simulation of environments. Its purpose is to train, educate and raise awareness among citizens about the proper use of roads for the prevention of the traffic accidents that according to official statistics typically result in irremediable situations. Hence, it is proposed that through the use of new technologies for learning and the serious games approach, citizens will understand and learn about traffic education in the city of Cuenca.

For the structuring of this 3D virtual platform of traffic education, the sites in the city of Cuenca where there is a greater occurrence of accidents due to pedestrian agglomerations or traffic incidents were identified. In each of these scenarios, the various situations that lead to accidents or fines for failing to comply with traffic regulations were simulated. The virtual environments also included the “*Tranvía Cuatro Rios de Cuenca*”, a means of mass transportation that has been operational since 2020. Given the novelty of the service it provides, citizens remain unaware of the rules for its proper use and do not grasp that the failure to comply with them carries fines and other penalties.

The validation of the virtual platform for road safety education with an Social Group focus was carried out through tests performed on citizens. A group of 30 randomly selected people experienced the 4 virtual environments, witnessing common situations related to mobility within the city. Once their simulation was complete, these users of the platform answered a series of questions about its operation, composition and usefulness. The results of the survey show that 91 percent of people fully understood the context presented in each scenario. After the survey, the personnel in charge of the EMOV-EP asked a question about road safety that was addressed in the

scenarios presented and obtained 100 percent correct answers. Thus, this project clearly has great educational, technological and innovation potential; it can therefore be implemented as an education and road awareness strategy in the city of Cuenca.

The results obtained in this first phase of the project are considered theoretical and empirical background for the continuity of this and other research that aims to promote road culture through the use of immersive technology as an education tool.

REFERENCES

- [1] C. M. Pacheco Cortés, "Educación vial en la era digital: cultura vial y educación permanente," *Diálogos sobre educación. Temas actuales en investigación educativa*, vol. 8, no. 15, 2017.
- [2] J. E. Fernández Escobar, A. M. Ávila Portuondo, and R. Milánés Gómez, "La educación vial asistida por tecnología 3d: un modelo de su enseñanza-aprendizaje," *Revista Universidad y Sociedad*, vol. 9, no. 3, pp. 130–134, 2017.
- [3] D. C. Anchaluiza Iza and A. L. Sellan Naula, "Accidentes de tránsito como consecuencia de la falta de educación vial en la ciudad de guayaquil," B.S. thesis, Universidad de Guayaquil, Facultad de Jurisprudencia Ciencias Sociales y Políticas, 2020.
- [4] M. E. Salinas Cabrera and L. H. Vele Figueroa, "Estudio científico de la accidentalidad de tránsito en el cantón cuenca," 2014.
- [5] O. P. de la Salud, "Los accidentes de tránsito son la primera causa de mundial de muerte entre jóvenes de 15 a 29 años, 2013," 2013.
- [6] W. H. Organization, "Informe sobre la situación mundial de la seguridad vial : es hora de pasar a la acción," p. 287 p., 2009.
- [7] G. A. León-Paredes, O. G. Bravo-Quezada, E. J. Sacoto-Cabrera, O. F. Pizarro-Gordillo, P. E. Vintimilla-Tapia, J. F. Bravo-Torres, and W. P. Cabrera-Chica, "Virtual reality and data analysis based platform for urban mobility awareness as a tool for road education," in *2020 IEEE ANDESCON*. IEEE, 2020, pp. 1–6.
- [8] O. P. de la Salud and O. M. de la Salud, "La seguridad vial en la región de las americas," 2016.
- [9] J. L. Rivas Luna and D. Santos Rodríguez, "Factores de riesgo que inciden en los accidentes de tránsito en el ecuador," 2019.
- [10] S. Rumé, "Sobre imposiciones y adecuaciones infraestructurales. el caso del tranvía en cuenca, ecuador," Master's thesis, 2018.
- [11] C. T. de Cuenca. (2021) Camión causa daños en la ruta del tranvía de cuenca. [Online]. Available: <http://tranvia.cuenca.gob.ec/content/cami{\o}n-causa-da{\~n}os-en-ruta-del-tranv{\i}a-de-cuenca>
- [12] J. D. Arévalo Peña, "La eficacia publicitaria en las campañas de prevención en seguridad vial," Master's thesis, Universidad del Azuay, 2016.
- [13] E. R. Escartín, "La realidad virtual, una tecnología educativa a nuestro alcance," *Pixel-Bit. Revista de Medios y Educación*, 15, 5-21., 2000.
- [14] E. C. Andrade Andrade and E. J. Velázquez Guerrero, "La biblioteca de la facultad de ingeniería en la plataforma educativa de la udelar-uruguay: implementando un servicio de formación de usuarios virtual," *Revista Interamericana de Bibliotecología*, vol. 37, no. 2, pp. 171–178, 2014.
- [15] S. Encalada Chérrez and I. Silva Feraud, "Aplicativo t-learning para tdt en el ecuador," *Investigatio Research Review*, no. 6, pp. 67–80, 2021.
- [16] M. S. Tolozano Lapierre, "Marketing social para promover la seguridad vial en estudiantes de institutos tecnológicos, caso: Instituto superior tecnológico bolivariano-guayaquil 2019." Ph.D. dissertation, 2018.
- [17] G. R. Zambrano and V. E. Senti, "Marco de trabajo para el diseño de una arquitectura its en ecuador que mejore la interoperabilidad y el despliegue de los sistemas de control de tráfico vehicular/[framework for designing an its architecture in ecuador that improves the interoperability and deployment of vehicular traffic control systems]," *International Journal of Innovation and Applied Studies*, vol. 14, no. 4, p. 886, 2016.
- [18] C. L. C. Morocho, "Análisis de la percepción que tienen los infractores de tránsito sobre conducir en estado de embriaguez en la ciudad de cuenca," Ph.D. dissertation, Universidad De Cuenca, 2016.
- [19] A. Cárdenas-Rebello and J. A. Orozco-Toro, "Publicidad social y su influencia en la percepción de las campañas sociales de prevención de accidentes de tránsito en ecuador," *RETOS. Revista de Ciencias de la Administración y Economía*, vol. 10, no. 20, pp. 219–231, 2020.
- [20] P. A. Chimbo Cárdenas and C. S. Jadán Loja, "Determinación de los factores de riesgo en accidentes de tránsito donde están involucrados vehículos de la categoría 1 en la ciudad de cuenca," B.S. thesis, 2017.
- [21] I. Aznar Díaz, J. M. Trujillo Torres, and J. M. Romero Rodríguez, "Estudio bibliométrico sobre la realidad virtual aplicada a la neurorrehabilitación y su influencia en la literatura científica," *Revista Cubana de Información en Ciencias de la Salud*, vol. 29, no. 2, pp. 0–0, 2018.
- [22] I. Wohlgenannt, A. Simons, and S. Stieglitz, "Virtual reality," *Business & Information Systems Engineering*, vol. 62, no. 5, pp. 455–461, 2020.
- [23] D. Checa and A. Bustillo, "A review of immersive virtual reality serious games to enhance learning and training," *Multimedia Tools and Applications*, vol. 79, no. 9, pp. 5501–5527, 2020.
- [24] G. Mariscal, E. Jiménez, M. D. Vivas-Urias, S. Redondo-Duarte, and S. Moreno-Pérez, "Aprendizaje basado en simulación con realidad virtual," *Education in the Knowledge Society (EKS)*, vol. 21, pp. 15–15, 2020.
- [25] Z. Feng, V. A. González, R. Amor, R. Lovreglio, and G. Cabrera-Guerrero, "Immersive virtual reality serious games for evacuation training and research: A systematic literature review," *Computers & Education*, vol. 127, pp. 252–266, 2018.
- [26] C. Hillmann, "Comparing the gear vr, oculus go, and oculus quest," in *Unreal for Mobile and Standalone VR*. Springer, 2019, pp. 141–167.
- [27] W. H. Organization et al., "Brote de enfermedad por coronavirus (covid-19)," *Recuperado de <https://www.who.int/emergencies/diseases/novel-coronavirus-2019>*, 2020.

An E2ED-based Approach to Custom Robot Navigation and Localization

Andrés Moreno, Daniel Páez, Fredy Martínez
Universidad Distrital
Francisco José de Caldas
Bogotá D.C., Colombia

Abstract—Simultaneous mapping and localization or SLAM is a basic strategy used with robots and autonomous vehicles to identify unknown environments. It is of great attention in robotics due to its importance in the development of motion planning schemes in unknown and dynamic environments, which are close to the real cases of application of a robot. This is why, in parallel with research, they are also important in specialized training processes in robotics. However, access to robotic platforms and laboratories is often complex and costly, with high demands on time and resources, particularly for small research centers. A more efficient and affordable approach to working with autonomous algorithms and motion planning schemes is often the use of the ROS-Gazebo simulator, which allows high integration with customized non-commercial robots, and the possibility of an end-to-end design (E2ED) solution. This research addresses this approach as a training and research strategy with our ARMOS TurtleBot robotic platform, creating an environment for working with navigation algorithms, in localization, mapping, and path planning tasks. This paper shows the integration of ROS into the ARMOS TurtleBot project, and the design of several subsystems based on ROS to improve the interaction in the development of service robot tasks. The project's source code is available to the research community.

Keywords—End-to-End design; localization; navigation; path planning; robotics; SLAM

I. INTRODUCTION

Robotics is a field of research in constant growth, the need for support, cost reduction, safety, and reliability drives the development and study of problems related to its application in real tasks. There are major unsolved problems that hinder its wide use in applications such as service robotics (the area closest to our research), in general, related to interaction, autonomy, safety, and reliability [1]. Many research centers around the world are actively working in these niches, but in many cases, access to robotic platforms and specialized laboratories is restricted for reasons of cost, availability, and resources related to this activity. A working scheme of good acceptance in the scientific community is the use of high-performance simulators, which can replicate very faithfully the behavior of a robot, one of the most popular platforms today in this regard is ROS OS (Robotic Operating System).

The operating system has more than 10 years of growth and interaction in robotic programming, and its particular details such as interoperability and open source generation provide services comparable to those of an operating system, such as hardware abstraction, low-level device control, inter-process message passing and packet management [2]. Though is not

an operating system, it provides the same services to its users as an operating system does.

In today's social development, the implementation of mobile robots for problem-solving in industrial and non-industrial environments is of great relevance [3]. Applications in rural or agricultural areas, as well as those involving direct interaction with humans [4], [5], are of great current interest. In this respect, mobile robotic platforms have been proposed that can be used in a greenhouse to transport vegetables [6], [7], in some cases with safe interaction systems with humans. Another study proposes the control and tracking of trajectories based on simulations and experiments in real-time on the ROS platform, where the objective is to validate the effectiveness of the proposed control algorithm and compare it with a modified hybrid PID dynamic controller with feedback [8]. In these cases, ROS was fundamental in the design and performance evaluation stages. As for the concrete problem of mapping and navigation, whether in the land, water, or air vehicles, ROS allows SLAM simulation in the working environment, thus reconstructing the map and dynamically planning a trajectory to the target destination [9], [10].

The use of this type of software tool becomes essential when control schemes integrate a large variety of sensors [11]. Not only does it facilitate the preliminary performance evaluation of the scheme (reducing costs and implementation time), but it also speeds up the overall implementation time of the schemes. In assistive robotics, this is key, as new interaction schemes and control algorithms are continually being developed and need to be evaluated quickly [12]. These applications involve both the interaction problem and the navigation problem, which in many cases involve complex control algorithms, whose performance and coordination must be evaluated before implementation on real platforms [13], [14]. The emulation under ideal conditions, therefore, allows having an additional design tool that guarantees time and design reduction throughout the whole process [15].

Our research project is part of a macro project aimed at the development of robotic solutions for assistance tasks, particularly in applications related to the care of people (elderly and children). In previous years, we have developed a modular mobile platform with load capacity for integration with a manipulator robot (industrial application) and/or an anthropomorphic robot for services [16], [17]. Previous prototypes of this robot had been integrated with ROS to provide ease of handling and simulation of behaviors [18], [19]. At the time, the use of the platform with ROS in structured motion planning applications was justified due to the simplification

in the integration of navigation algorithms. This project seeks the same benefit in a more complex robot, which additionally requires greater availability of access for members of the research group. However, the application of ROS in more complex robot also opened the door to new problems [20].

Similar projects to the one proposed in this research have been previously developed on other platforms [21]. ROS is commonly used to facilitate the design, analysis, and tuning of control algorithms by taking advantage of its modularity and master-slave scheme of work. Our work differs from some of them, such as [22], [23], in the sense that it prefers coding in an open environment with Python support, unlike MatLab, which conforms to a closed platform with expensive licensing. Still, as in its previous uses, it allows the easy use of simulators such as Gazebo. We did not solve all the issues mentioned above, but we did accomplish our goal: We programmed robots using the ROS framework.

II. PROBLEM STATEMENT

The ARMOS TurtleBot robot is a robotic platform designed and implemented by the ARMOS research group to develop assistance tasks and human support (service robot) (Fig. 1). Although it was conceived as a mobile platform for other systems, it has load restrictions (maximum value defined as 10 kg), and movement restrictions derived from its structure and motors. It has four 9 V DC motors with geared motors, driving a caterpillar on a differential structure. Each of the motors has a starting torque of 9.5 kg, no-load speed of 150 RPM (revolutions per minute), starting current of 4.5 A, and nominal working current of 1.2 A (200 mA no-load). These motors have a Hall sensor for shaft position estimation.



Fig. 1. ARMOS TurtleBot Robot.

The working model of the motors is in pairs, i.e., the same control signal activates simultaneously the two motors on the right side, and another signal activates simultaneously the two motors on the left side. This scheme improves the robot's total torque while also simplifying its model and control scheme without sacrificing displacement capacity.

The structure is composed of an aluminum base, a material chosen for its lightweight, which reduces the total weight of the platform. Object detection is done through sensors around the robot. The robot has nine SHARP GP2Y0A21YK IR infrared sensors, which are distributed throughout the robot structure. Other peripherals included in the robot are:

- Four contact buttons, that function as impact detectors.
- A TCS3200 color sensor located at the bottom of the robot.
- An inductive sensor LJ12A3-4-Z/BY located in the lower part of the robot to detect metallic elements.

For the control system, two STM32L432KCU6 microcontrollers are used to process sensor and actuator signals, and a Raspberry Pi 4 card is used as the control unit, which will also have the ROS OS operating system.

The ARMOS TurtleBot robot was designed with diversity and a wide variety of peripherals capable of interacting and communicating with each other through the master-slave level configuration. In addition, it allows the simple integration of new peripherals with a LiDAR sensor. The initial tasks of the robot contemplate navigation problems in dynamic and unknown environments, the reason why in this project we intend to implement ROS in the platform and evaluate its performance in basic navigation tasks that contemplate the use of these peripherals in a real environment.

III. METHODS

The ARMOS TurtleBot vehicle platform can be analyzed by separating it into two sections. The first one is composed of position sensors. These are in charge of identifying bodies or objects close to the trajectory performed by the robot. Additionally, the drives of these devices prevent damage to the robot's electronic circuits (Fig. 2).

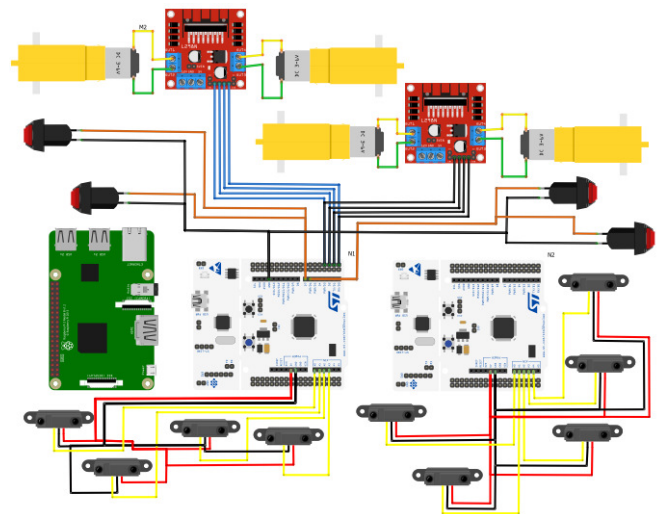


Fig. 2. Proximity Sensor Connection.

The second section is composed of proximity sensors. The main purpose of these devices is to specify the characteristics of the materials that are in the path (floor) and that could

modify their behavior according to the programmed task. There is the detection of metallic materials, and the characterization of materials according to their color (Fig. 3).

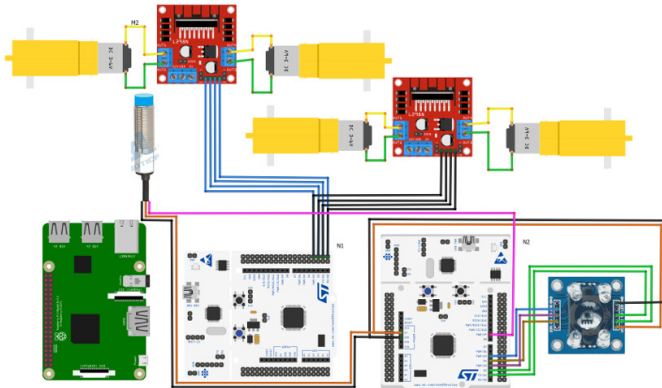


Fig. 3. Connection of Color and Inductive Sensors.

To integrate ROS into the robotic platform we have sought to replicate its structure within the software. All the physical components, considering their specific capabilities, as well as the communication, signal collection, and handling capabilities, have been programmatically replicated on ROS. The correct description of the robot requires a correct description of each peripheral, which was linked to specific laboratory tests. In this way the robot architecture was developed, starting from its control unit, the Raspberry Pi 4 board, which is responsible for managing all the information. Fig. 4 shows the complete architecture of the main systems and subsystems involved in the robotic platform.

The first step is to establish serial communication with the devices or peripherals of the ARMOS TurtleBot platform. To start the interaction with the ROS OS framework, the following command is entered in a Raspberry Pi 4 terminal (on the robot):

```
$ roscore
```

In this way, the operating system starts the communication. The initial part corresponds to the user generated to work on this terminal (pi@raspberrypi:). Thus, if the connection is successful, the system responds as shown in Fig. 5.

This corresponds to the workspace and communication verification process of the master node in ROS OS. At this moment is when the communication or start of the ROS OS system is successfully obtained. The next step is to continue with the opening of the workspace defined for the nodes and commands that are entered, this can be done through the command line as follows.

```
$ cd ~/catkin_ws/ &&source devel\setup.bash
$ cd rosrn roserial_server serial_node _port:=dev/ttyACM0
```

The command line corresponding to roserial is the one that indicates the communication through language or programs generated through Arduino IDE 18.2, which is the version implemented for the project.

The next step consists of the communication of the peripherals or sensors, both position, and proximity. For this mobile application, the programming is done under the C++ language, where it should be noted the confirmation of one of the main objectives of the ROS OS system, the recycling of code and interoperability between the various programming options available at the moment.

For the inductive sensor LJ12A3-4-Z/BY whose function, as detailed above, is to enable the robot to determine the existence (detection) of metallic material on the surface on which the ARMOS TurtleBot robot is moving (floor), the corresponding command line is as follows:

```
$ rostopic echo inductive_sensor
```

The metal detection and the message received by ROS OS are shown in Fig. 6.

The contact sensor or pushbutton has the objective of detecting contact with an object, which should produce a change in the speed and direction of the robot according to the navigation strategy. The command line to control this sensor is as follows:

```
$ rostopic echo switch_limit
```

The response or communication by ROS OS in case of contact detection is shown in Fig. 7.

The proximity sensor used is the Sharp GP2Y0A21YK IR. There are a total of nine of these sensors, which are in charge of establishing the distances to obstacles or objects around the robot. Their signal is visualized through a graph generated by the operating system, the tool is called rqt_plot. The following are the lines of code and their corresponding response for three sensors (Fig. 8 and 9).

```
$ rqt_plot / sensor3/range: /sensor4/range: /sensor5/range
```

The last sensor coupled to the system is the TC3200 color sensor. The color identification method consists of 64 photodiodes equally distributed in four colors (red, green, blue, and white). Its operating principle is based on the conversion of signals (electronic circuit) from current to frequency, where a specific frequency is assigned to the detected color, thus with the constant determination of three frequencies (red, green, and blue) and the determination of the frequency range during the three readings, the conditions to be programmed in the control unit are obtained. The frequency ranges are specified in Table I.

TABLE I. FREQUENCY RANGE FOR COLOR DETERMINATION BY THE SENSOR

Colors according to frequency range			
Red	R<50	V>90	A>90
Blue	R>85	V>80	A<50
Green	R>90	V<120	A>58

In the robot, the color sensor is managed by a STM32L432KCU6 microcontroller. This microcontroller establishes the communication with ROS OS. To query the

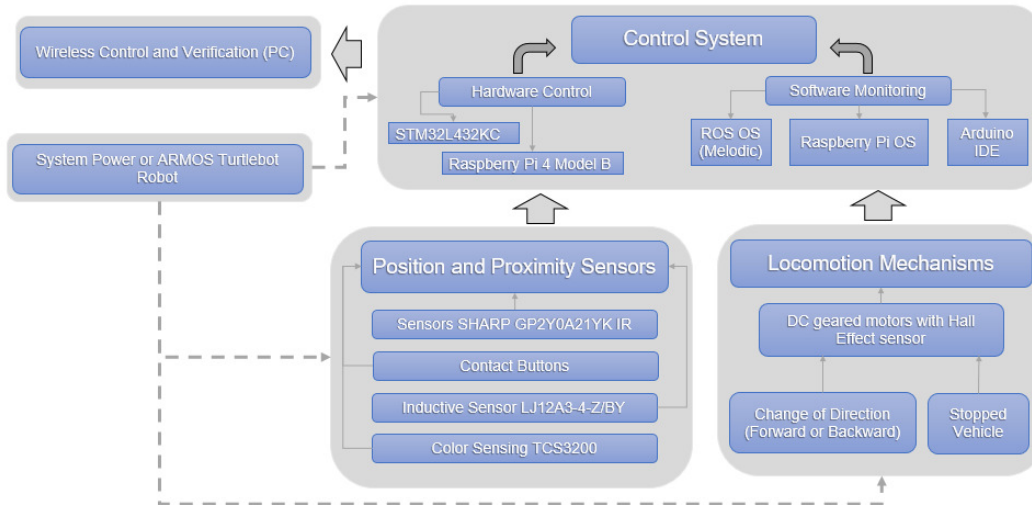


Fig. 4. Control Scheme: Hardware and Software.

```

roscore http://raspberrypi11311/
roscore http:// pi@raspberrypi:~$ roscore
... logging to /home/pi/.ros/log/dec31f2e-dba0-11ec-90fd-e45f010909f7/roslaunch
-raspberrypi-1238.log
Checking log directory for disk usage. This may take a while.
Press Ctrl-C to interrupt
Done checking log file disk usage. Usage is <1GB.

started roslaunch server http://raspberrypi:45585/
ros_comm version 1.14.11

SUMMARY
=====
PARAMETERS
 * /rostdistro: melodic
 * /rosversion: 1.14.11

NODES
auto-starting new master
process[master]: started with pid [1248]
    
```

Fig. 5. Roscore Start.

```

pi@raspberrypi:~/catkin_ws
roscore http:// pi@raspberrypi:~$ rostopic echo Inductive_sensor
data: "Metal Detected!"
---
data: "Metal Detected!"
---
data: "Metal Detected!"
---
    
```

Fig. 6. Metal Detection Report from the Inductive Sensor.

reading, a message is sent from ROS similar to the one shown below.

```
$ rostopic echo color_sensor
```

Actuator management is also configured from ROS. The monitoring and instructions of the DC motors, as well as the Hall effect sensors coupled to each of them, can also be easily managed from this environment. These sensors prove to be an essential tool that allows the feedback of the movement of each motor, thus reducing errors in autonomous navigation tasks in real environments. Three basic commands were designed for its operation: go forward, stop and reverse. These commands are translated into specific movements performed by each of the motors, and controller through Hall effect sensors. The instruction for their execution is as follows:

```
$ rostopic pub forward std_msgs/empty
```

IV. RESULTS AND DISCUSSION

To evaluate the performance of the system, a test environment was built to assess the behavior of each of the robot's sensors, as well as its actuators and communication characteristics. The following is a brief description of this test environment, as well as the expected interaction with the ARMOS Turtlebot robot, its displacement parameters, and the defined trajectory path.

The scenario where the peripheral integration tests are performed on the ARMOS Turtlebot robot has a flat surface (Fig. 10). In the center of the area, there is a box composed of different materials with characteristics recognizable by the devices embedded in the robot. The navigation of the robot was programmed with restrictions on its displacement, to evaluate the interaction of sensors and actuators in the ROS OS operating system. The navigation conditions for the execution of the experiment are detailed below.

The displacement of the robot starts with the control signal generated from the control unit installed on the robot

```

pi@raspberrypi: ~/catkin_ws
roscore http://... pi@raspberr... pi@raspberr...
pi@raspberrypi:~/catkin_ws $ rostopic echo switch_limit
data: "CRASH!"
---
data: "CRASH!"
---
data: "CRASH!"
---
data: "CRASH!"
---
data: "CRASH!"
---
data: "CRASH!"
---
data: "CRASH!"
---
data: "CRASH!"
---
data: "CRASH!"
---
data: "CRASH!"

```

Fig. 7. Impact Report from the Contact Sensor.

```

pi@raspberrypi:~/catkin_ws $ rqt_plot /sensor1/range: /sensor7/range: sensor9/r
range
pi@raspberrypi:~/catkin_ws $ rqt_plot sensor1/range
pi@raspberrypi:~/catkin_ws $ rqt_plot sensor2/range
pi@raspberrypi:~/catkin_ws $ rqt_plot sensor3/range
pi@raspberrypi:~/catkin_ws $ rqt_plot /sensor1/range: /sensor7/range: sensor9/r
range
pi@raspberrypi:~/catkin_ws $ rqt_plot /sensor3/range: /sensor4/range: sensor5/r
ange

```

Fig. 8. IR Sensors Report.

itself. From there, the ROS connection is established with the peripherals as described above. As soon as the communication is established and the work folder is opened, the trajectory is started with the instruction from the corresponding command line. At this point, the ROS connection has been established between the control unit and other peripherals.

The specific mechanism to intervene during the whole test is the caterpillar wheels equipped with geared motors and coupled to Hall effect sensors. These devices are used to

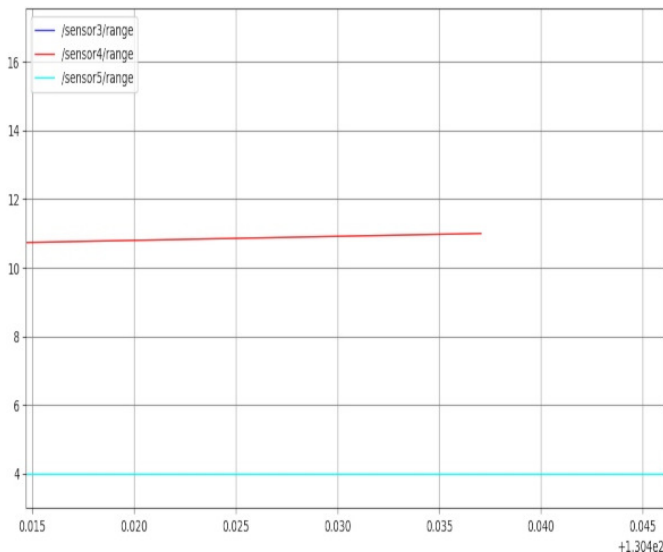


Fig. 9. Distance Curves Reported by the IR Sensor



Fig. 10. Test Environment Setup.

move the robot to carry out the trajectory. The path is defined on a surface adapted with characteristic colored materials, recognizable by the TC3200 color sensor. The first zone corresponds to the blue material, the sensor acquires this information and transmits it directly to ROS OS, which is in charge of processing the data and sending a color detection message. In this case, the text specifying the color of the detected object is displayed on the terminal.

Sharp GP2Y0A21YK IR infrared proximity sensors have a maximum detection range of 80 cm. For the proposed test application, this detection is conditioned to a maximum of 20 to 25 cm, and the control is done graphically in real-time through the rqt_plot tool of ROS OS, making the recognition of object or obstacle and its distance. Once this condition is met, the programmed instruction is the change of direction, and to perform this action by the robot, a rotation is performed on its axis (right) which occurs whenever the motors on each side rotate at the same speed and in opposite directions (one side of the robot moves forward and the other backward).

Starting up in the new direction, the surface on which it is running is colored green, which is detected by the TC3200 color sensor. Thereupon the system and its programming will issue a message on the terminal indicating that the second green area has been detected. While the vehicle is running, a green-colored area is detected by the TC3200 color sensor.

When a metallic material is detected, it is time for the intervention of the inductive sensor LJ12A3-4-Z/BY, which causes two different interactions in the programming and control of the robot. The first consists of the ROS instruction that indicates the detection of metal, performing a change of direction or rotation on the axis. Additionally, the data of the metal material is sent so that a message is transmitted to the terminal indicating the detection of this element.

It changes direction in a 90-degree turn with a new rotation on its axis in relation to its previous position. The robot is moving over a third displacement zone, this time in red. As before, this information is reflected through ROS OS using a message indicating the detection of a colored area.

The test or experiment ends with the intervention of the contact sensors that aim to detect the impact of an obstacle on the robot. These are activated when changing state (bi-valued sensor), which complements the reading of the distance sensor formed by the nine infrared sensors IR Sharp GP2Y0A21YK, or even substitute it when the obstacle is below the line of sensing of the infrared. The action defined at this point is that the robot stops immediately.

This navigation circuit was developed by the robot multiple times to verify the consistency of operation and results. One of these tests can be seen in the following link (Fig. 11).

<https://youtu.be/uh5wzhIwi6g>

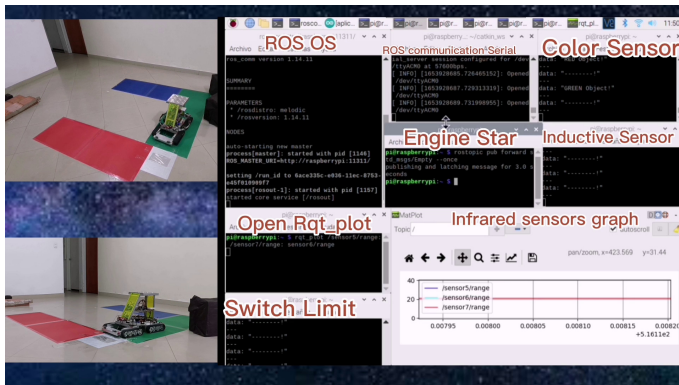


Fig. 11. ROS-Controlled Robot Performance Test.

Communication between ROS OS and the sensors allows it to know where they are and allows for these devices to communicate between them automatically, as a message that is generated by one device will be transmitted automatically to all other devices. When running all the peripherals and devices associated with the robot, it is evident that the communication between ROS OS and these works correctly because there are no crashes or failures when all these devices are communicating at the same time in the system. This feature guarantees the robustness of the system and allows for validating it for evaluation tests of more complex navigation algorithms.

The inductive sensor detects the metal correctly, and the message display transmitted by ROS OS through the terminal shows the warning message approximately one second after the sensor detected the metal surface. In the case of the contact sensor, it was triggered immediately when the robot

had a collision with the obstacle that was not detected by the IR ranger sensors located at the front of the robot. The warning message displayed by the ROS system was almost instantaneous when the collision occurred (about a 120 ms delay).

As for the motors, when the command was executed in ROS OS on the terminal to move the wheels of the robot and produce forward motion, it was evident in all tests that there was a delay in the response of the motors of approximately three seconds after the command was executed. The same was true for moving the wheels backward or for stopping the movement of the motors completely. After almost three seconds of waiting to start or stop the movement, the motors responded appropriately.

The most important sensor in the reactive control tasks is the ranger IR sensor. Each sensor in the system was individually tested for interaction with ROS OS. The object detection tests were verified in the rqt_plot tool that is integrated in ROS OS, which allows to view two-dimensional plots. In this tool, a distance vs. time graph is displayed, where a continuous line appears referring to the distance in cm, in which the ranger sensor is detecting an obstacle. The individual tests showed that the sensors detected the objects acceptably with an error of approximately one to two centimeters. Back in the test application, where the sensors were acting in conjunction with the other devices on the robot, it was found that the reading accuracy error increased to almost three centimeters for some sensors. When trying to visualize the nine signals detected by each of the sensors in the rqt_plot tool, the operating system of the raspberry pi generated delay in the response and sometimes even total crash of the system. So to avoid this problem, it was decided to visualize in the rqt_plot tool only some of the IR, but to use all of them for mapping tasks. In the tests, the response of the three ranger sensors located at the front of the robot is visualized. The ranger sensors were programmed to detect objects within a range of 0.2 to 0.25 m, and then instantly generate action on the robot's motors. Furthermore, when they detected an object in this distance range, the motors reacted within two to three seconds after the sensor had detected the object.

The color sensor was evaluated individually with ROS OS before being incorporated with the other devices and sensors on the robot. The ROS readings were accurate over the three colors that the sensor measures. When the sensor was incorporated into the test task, the color readings began to differ significantly from the previous ones, resulting in erroneous readings in the application. The possible interference of communication delays on the performance of this sensor is evaluated in this case.

In this study, the results of implementing ROS as a handling strategy for the ARMOS TurtleBot robot were achieved and shown. The strategies used can be generalized and further investigated on this platform as well as on other custom robotic platforms not initially designed with ROS in mind. This work can be further enhanced with the use of navigation algorithms and optimization techniques that reflect the comparative performance of each case. This study shows that ROS can be used as a suitable programming environment for a robot and should be the one platform from which further work is done

V. CONCLUSION

The constant innovation in design, programming, and control in mobile robotics leads to the generation of a wide variety of algorithms, compromising the understanding and suitability of robotic applications as a whole. A design methodology already proven and widely studied is the versatility offered by the ROS OS operating system in the different stages of the development of control schemes for robots. This tool combines the ease of code recycling and the interaction and communication of different types of programming languages. This paper presents and explains the integration of the ROS OS (Melodic) operating system on the ARMOS TurtleBot mobile robot and its peripherals. The platform is designed to perform navigation tasks or activities, thus obtaining synchronization, data transfer, and information management in real-time on surfaces with suitable characteristics to be detected by the different devices that make up the robot. The proposed purpose corresponds to the integration of the devices that make possible the displacement and recognition of the robot in a given environment. The systems involved according to the architecture are Raspberry Pi OS, ROS OS (Melodic), and some microcontrollers as embedded systems that directly manipulate sensors and motors, with this architecture the compatibility and possibility of integration of peripherals are confirmed. The simultaneous interaction of the proximity peripherals and position sensors through the ROS OS operating system is visualized through windows or terminals utilizing messages or interactively in 2D graphics, confirming the interoperability and real-time control of the environment surrounding the robot when it performs navigation tasks. The presence of windows and graphic interfaces for its control demonstrates the possibility of remote real-time observation and monitoring, providing immediate feedback about the robot's environment. No communication problems are detected that could prevent its use as a general strategy in the development of navigation algorithms. On the contrary, the possibility of integrating additional peripherals such as a LiDAR sensor or a digital camera onboard is observed.

ACKNOWLEDGMENT

This work was supported by the Universidad Distrital Francisco José de Caldas, specifically by the Technological Faculty. The views expressed in this paper are not necessarily endorsed by Universidad Distrital. The authors thank all the students and researchers of the research group ARMOS for their support in the development of this work.

REFERENCES

- [1] B. Liu and C. Liu, "Path planning of mobile robots based on improved RRT algorithm," *Journal of Physics: Conference Series*, vol. 2216, no. 1, p. 012020, mar 2022.
- [2] R. Alonso, A. Bonini, D. R. Recupero, and L. D. Spano, "Exploiting virtual reality and the robot operating system to remote-control a humanoid robot," *Multimedia Tools and Applications*, vol. 81, no. 11, pp. 15 565–15 592, feb 2022.
- [3] A. Shahoud, D. Shashev, and S. Shidlovskiy, "Visual navigation and path tracking using street geometry information for image alignment and servoing," *Drones*, vol. 6, no. 5, p. 107, apr 2022.
- [4] M. Quiroz, R. Patiño, J. Diaz-Amado, and Y. Cardinale, "Group emotion detection based on social robot perception," *Sensors*, vol. 22, no. 10, p. 3749, may 2022.
- [5] P. Wang, R. Ye, J. Zhang, and T. Wang, "An eco-driving controller based on intelligent connected vehicles for sustainable transportation," *Applied Sciences*, vol. 12, no. 9, p. 4533, apr 2022.
- [6] E.-T. Baek and D.-Y. Im, "ROS-based unmanned mobile robot platform for agriculture," *Applied Sciences*, vol. 12, no. 9, p. 4335, apr 2022.
- [7] R. Xu and C. Li, "A modular agricultural robotic system (MARS) for precision farming: Concept and implementation," *Journal of Field Robotics*, vol. 39, no. 4, pp. 387–409, jan 2022.
- [8] A. D. Sabiha, M. A. Kamel, E. Said, and W. M. Hussein, "ROS-based trajectory tracking control for autonomous tracked vehicle using optimized backstepping and sliding mode control," *Robotics and Autonomous Systems*, vol. 152, p. 104058, jun 2022.
- [9] M. Facerias, V. Puig, and E. Alcalá, "Zonotopic linear parameter varying SLAM applied to autonomous vehicles," *Sensors*, vol. 22, no. 10, p. 3672, may 2022.
- [10] H. M. P. C. Jayaweera and S. Hanoun, "Path planning of unmanned aerial vehicles (UAVs) in windy environments," *Drones*, vol. 6, no. 5, p. 101, apr 2022.
- [11] Y. Guo, X. Fang, Z. Dong, and H. Mi, "Research on multi-sensor information fusion and intelligent optimization algorithm and related topics of mobile robots," *EURASIP Journal on Advances in Signal Processing*, vol. 2021, no. 1, nov 2021.
- [12] J. A. C. Panceri, É. Freitas, J. C. de Souza, S. da Luz Schreider, E. Caldeira, and T. F. Bastos, "A new socially assistive robot with integrated serious games for therapies with children with autism spectrum disorder and down syndrome: A pilot study," *Sensors*, vol. 21, no. 24, p. 8414, dec 2021.
- [13] A. A. Umar and J.-S. Kim, "Nonlinear model predictive path-following for mecanum-wheeled omnidirectional mobile robot," *The transactions of The Korean Institute of Electrical Engineers*, vol. 70, no. 12, pp. 1946–1952, dec 2021.
- [14] B. Boroujerdian, R. Ghosal, J. Cruz, B. Plancher, and V. J. Reddi, "RoboRun: A robot runtime to exploit spatial heterogeneity," in *2021 58th ACM/IEEE Design Automation Conference (DAC)*. IEEE, dec 2021.
- [15] S. Chen, W. Zhou, A.-S. Yang, H. Chen, B. Li, and C.-Y. Wen, "An end-to-end UAV simulation platform for visual SLAM and navigation," *Aerospace*, vol. 9, no. 2, p. 48, jan 2022.
- [16] C. Penagos, L. Pacheco, and F. Martínez, "Armos turtlebot 1 robotic platform: Description, kinematics and odometric navigation," *International Journal of Engineering and Technology*, vol. 10, no. 5, pp. 1402–1409, 2018.
- [17] C. Hernández, D. Giral, and F. Martínez, "Kinematic and dynamic analysis of a differential robotic platform with caterpillar tracks," *(JATIT) Journal of Theoretical and Applied Information Technology*, vol. 99, no. 24, pp. 5993–6003, 2021.
- [18] A. Moreno and D. Páez, "Performance evaluation of ros on the raspberry pi platform as os for small robots," *Tekhnê*, vol. 14, no. 1, pp. 61–72, 2017.
- [19] F. Martínez, "Turtlebot3 robot operation for navigation applications using ros," *Tekhnê*, vol. 18, no. 2, pp. 19–24, 2021.
- [20] A. Yilmaz, E. Sumer, and H. Temeltas, "A precise scan matching based localization method for an autonomously guided vehicle in smart factories," *Robotics and Computer-Integrated Manufacturing*, vol. 75, p. 102302, jun 2022.
- [21] S. Abdul-Rahman, M. S. A. Razak, A. H. B. M. Mushin, R. Hamzah, N. A. Bakar, and Z. A. Aziz, "Simulation of simultaneous localization and mapping using 3d point cloud data," *Indonesian Journal of Electrical Engineering and Computer Science*, vol. 16, no. 2, p. 941, 2019.
- [22] Z. Chen, S. Yan, M. Yuan, B. Yao, and J. Hu, "Modular development of master-slave asymmetric teleoperation systems with a novel workspace mapping algorithm," *IEEE Access*, vol. 6, no. 1, pp. 15 356–15 364, 2018.
- [23] N. Sadeghzadeh-Nokhodberiz, A. Can, R. Stolkin, and A. Montazeri, "Dynamics-based modified fast simultaneous localization and mapping for unmanned aerial vehicles with joint inertial sensor bias and drift estimation," *IEEE Access*, vol. 9, no. 1, pp. 120 247–120 260, 2021.

Identifying Community-Supported Technologies and Software Developments Concepts by K-means Clustering

Farag Almansoury, Segla Kpodjedo, Ghizlane El Boussaidi

Department of Software Engineering and Information Technology, École de Technologie Supérieure(ETS)
University of Quebec, Montreal, QC, Canada

Abstract—Working on technologies that have community support is one of the most important factors in software development. Software developers often face difficulties during software development, and community support from other software developers help them significantly. This paper presents an approach based on K-mean clustering technique to identify the level of community support for software technologies and development concepts using Stack Overflow discussion forums. To test the approach, a case study was performed by gathering data from SO and preparing a dataset that contains over a million of Java developers' questions. Then, K-mean clustering was applied to identify the community support levels. The goal is to find the best features that group community-supported software technologies and development concepts and identify the number of groups to determine the community support levels. Statistical error, clustering and classification evaluation metrics were applied. The results indicate that the best features to formulate community supported technologies and development concept levels are Failure Rate and Wait Time. The results show that the approach identifies two groups of community supported and development concept levels based on the best silhouette index value of 97%. According to the results the majority of Java technologies and development concepts are labeled with less community supported technologies and development concepts (Cluster 2). Random Forest classifier was applied to indirectly evaluate the approach to detect the identified community support class. The result shows that RF classifier presents a good performance and shows high accuracy value of 99.49% which indicates that the identified groups improve the performance of the classifier. The approach can be utilized to assist software developers and researchers in utilizing the SO platform in developing SO-based recommendation systems.

Keywords—Stack overflow; unsupervised machine learning; k-means clustering; empirical study; machine learning; random forest; software development; Java; classification; community support

I. INTRODUCTION

Developing a software from scratch with standard libraries is no longer a viable option for most meaningful software projects. Thus, some of the key decisions for a software project are about which technology to turn to, or which APIs or projects to depend on. Choosing the right technology is very important as it can significantly impact a project's quality and velocity. Depending on the particularities of their projects, software developers may have to sift through a wide range of rapidly evolving technologies (be it frameworks or libraries) across various platforms (PC, Mobile, Web). To inform their decision, they try to get guidance from online articles or blogs about which technologies are the best. For example, a developer may be looking for an IDE for his project and

end up on a website or a forum post about the "10 Best IDE Software"¹. These online resources, though valuable, often provide opinion-driven commentary, sometimes informed by the experience of a single writer or blogger. Moreover, they run the risk of being outdated, given the fast pace of many technologies. For up-to-date, interactive discussions, developers sometimes turn to Stack Overflow (SO), the leading Q&A website for software development. However, their questions about API or technology recommendations are systematically dismissed as seeking opinions², which is explicitly banned by Stack Overflow. For example, "What IDE to use for Python?"³, "What good, C++ programming IDE is available for Linux?"⁴, "What is the best IDE for PHP?"⁵, and "What programming language to create and format book?"⁶

Community-supported technologies used among software developers are important and help speed up software productivity. For this reason, we have turned to SO since it contains big data from software developers' discussions. SO has more than 20,000,000 questions related to different topics dealing with developers' issues in different domains and platforms. Hence, it become a target to developers since it enables them to find solutions for their problems. SO has also been utilized by researchers to carry out their studies [1], [2], [3], [4], [5]. Software developers and researchers are trying to find a mechanism to organize the data to facilitate and speed up the search processes and find the appropriate answers to the questions raised [6]. Thus, we turned to SO to identify which technologies and software development concepts have community support.

This study aims to provide an approach that help software developers and the software engineering research community to identify the technologies and development concepts that have the most and least community support by leveraging SO and the unsupervised machine learning technique k-means clustering. The study aims to answer the two following questions:

¹<https://websitesetup.org/best-ide-software/>

²There are good reasons to ban opinion and recommendation-seeking questions on a Q&A forum as they may devolve into never-ending discussions or be fodder for bitter arguments about which technologies are the best. Moreover, entities behind those technologies may participate and recommend their own products.

³<https://stackoverflow.com/questions/81584>

⁴<https://stackoverflow.com/questions/24109>

⁵<https://stackoverflow.com/questions/116292>

⁶<https://stackoverflow.com/questions/68275077>

RQ1:What are the features that identify clusters of technologies and software development concepts that have community support?

RQ2:What is the clusters quality and if the identified clusters consistent to increase the ability to differentiate between community-supported technologies and development concepts?

To gain more insight into the potential application of the approach, it has been applied to all Java-related postings on SO from 2014 to 2021 and studied the distribution of technologies and development concepts among community support levels. We chose to concentrate on Java ecosystem to demonstrate that the technique is applicable. If the approach is effective, it is simpler to generalise it to a wider range of domains and technologies than to determine that a technique designed for multiple domains at once would not work. Java ecosystem was utilized as a case study since Java is one of the programming language that is gaining the most traction among software developers on SO.

To apply the approach and analyze data, we turned to the most useful and popular library for machine learning in Python Scikit-learn [7] and the full-featured AI and ML integrated tool that supports multiple scripting languages and is easy to work with huge datasets Tableau [8]. Scikit-learn ML is a high-level API built on data frames and datasets that allows pipelines and is easier to build. Tableau features an analytics pane with drag-and-drop machine learning that allows us to forecast future outcomes based on historical data, discover future trends for your data using multiple models, or understand the relationships between data points using clustering. Cluster validity technique for the k-means clustering algorithm had already been proposed in the literature, thus, statistical error techniques the sum of squares within each cluster (WSS) and the sum of squares between clusters (BSS) in addition to and silhouette index were used.

The paper's primary contributions can be summarised as follows:

- The novel approach introduced in this paper can be used as a decision support based on K-Mean Clustering, for community-supported techniques and development concepts detection.
- We built a clustering model to identify community-supported software technologies and development concepts level of community support based on new features namely Failure rate (FR) and wait time (WT).

The rest of the paper is organized as follows: Section II introduces the theoretical background. Section III reviews the literature related to the study. Section IV outlines the approach overview and its application on Java ecosystem. Section V evaluates the approach based on clustering evaluation techniques. Section VI provides results and discussion. Section VII provides concluding remarks. Finally, Section VIII provides the future work.

II. THEORETICAL BACKGROUND

A. Stack Overflow and its Tagging System

“*Stack Overflow (SO)* is a question and answer website for amateur programmers and professionals programmers”⁷. It is a privately owned website that was established in 2008 by Atwood and Spolsky. Users are encouraged to participate as they can earn points towards their reputation and other privileges (e.g. editing), for being actively involved on the site. Users can vote for questions and answers, both upvotes (positive feedback) and down votes (negative feedback) are allowed. The number of the upvotes minus the number of downvotes represent the score. It is the largest Software development Q&A community, according to the SO Annual developer survey 2019⁸ which reported that SO had 80 million visit, of which 25% are developer professionals and university students, and more than 80% rely on SO for educational purposes and also 65% of Stack Overflow's professional developers contribute to open source projects.

Tagging System: According to Stack Overflow's tagging system, a question must have between one and five tags. A tag is a single word or compound words (for example, WebGL, vertex-shader, respectively) that define the technical term at the centre of the question [9] (see Fig. 1 for an example). Tags on Stack Overflow include a broad variety of technical terminology [10], [11], from definitions to programming languages, IDE, frameworks, libraries/tools/, and individual APIs (at class or module level). Researchers frequently use these tags as a starting point for investigating the issues addressed on SO.

B. Clustering

Clustering is the breaking down of a set of data or objects into a number of clusters. Each cluster consists of a group of similar facts that behave identically. Clustering is equivalent to classification, except that the classes in clusters are not defined and determined in advance, and data grouping is performed with no supervision [12], [13]. Different techniques used for clustering include partitioning based, hierarchical, density and grid [14]. K-means [15], which is the most basic and widely used partitioning procedure among scientific clustering algorithms [16], [17] was utilized.

C. Classification

Classification is an important aspect of data mining as a technique for forecast modelling. Simply put, classification is the process of breaking down data into dependent or independent categories [18]. Based on previous decisions, classification is utilised to make some future decisions. Different techniques used for classification include Random Forest, support vector machine, decision tree learning, neural networks, nearest neighbour, and Naves Bayes method [19]. In the experiment, the Random Forest classifier was employed.

III. RELATED WORK

In recent years, Stack Overflow questions and answers have been the topic of extensive research. One of the goals of

⁷<https://stackoverflow.com>

⁸<https://insights.stackoverflow.com/survey/2019>

Display wireframe and solid color

Asked 5 years, 9 months ago Active 1 month ago Viewed 28k times

▲
21
▼
Is it possible to display the wireframe of the object and also the solid color of its faces on the same object? I found a way using a clone of the object and assign different materials e.g

```
var geometry = new THREE.PlaneGeometry(plane.width, plane.height,width - 1, height - 1);  
var materialWireframe = new THREE.MeshPhongMaterial({color:"red",wireframe:true});  
var materialSolid = new THREE.MeshPhongMaterial({color:"green",wireframe:false});  
var plane = new THREE.Mesh(geometry, materialWireframe );  
var plane1 = plane.clone();  
plane1.material = materialSolid ;  
plane1.material.needsUpdate = true;
```

any thoughts?

three.js mesh

Fig. 1. Post Example ob Satck Overflow.

these studies is to track developers' interest in various topics and how it evolves over time, as well as their relationship to current technology trends[10], [20]. The majority of research also emphasizes how challenging it is to maintain the quality of SO Q&A [11].

Stack Overflow has received a lot of attention from the research community in the recent years. The rapid increase in the number of studies are a result of two main reasons: 1) the influx of new technologies that generated discussions on Q&A forums/websites; and 2) the increased use of these technologies by software developers due to their capability of solving problems, knowledge sharing, and learning.

The popularity of SO and its sheer volume of questions and answers have made it a platform of interest for research on specific areas such as mobile development [1], web development [21], [22], [3],web 3d [23], security [24], [4], [25]. In [21], for instance, used data from Stack Overflow to obtain a better understanding of the challenges faced by web developers. Their results show there was an increase in the number of questions related to web-development, concurrently with a downtrend for cross-browser related posts. In particular, [21] used data from SO to get a better understanding of the challenges faced by web developers. It extracted questions tagged with JavaScript, HTML5, CSS and found that cross browser issues were trending down. Another study in [22] investigated web developers' concerns pertaining to Web APIs. It found that "known issue/bug" is a dominant topic of discussion, and observed that discussions are majoritarily (three times out of four) about occasional concerns that disappear quickly, which would suggest that "Web API providers tend to timely address most problems encountered by client developers". Finally, [3] focused on popularity and difficulty of issues related to the web frameworks Laravel and Django and found that half the issues are shared by both, with installation being a popular

but difficult issue for both. The study by [9] reported that the key technologies that the question is about can typically be deduced from the question tags. These research studies are the basis for the approach, which uses Stack Overflow's crowd sourced expertise to answer information needs in technology community support inquiries.

IV. THE APPROACH OVERVIEW AND ITS APPLICATION ON JAVA ECOSYSTEM

The aim of this research consists of two parts, the first part is to what extent we can leverage K-means clustering to distinguish and group the community-supported technologies and development concepts based on the stack overflow platform to identify Which features contribute significantly to the the clusters formation. The second goal is to examine to which extent is the discovered community supported level consistent enough to increase the ability to distinguish between community-supported technologies and development concepts? it can be used as a detection tool based on machine learning classifier model. Fig. 2 introduces the approach that starts from select targeted technologies to identify the community supported technologies and development concepts. Then data from the questions tagged with the targeted technologies was extracted after the topics based on tags co-occurrence with the target technologies were grouped. We then identified the most important features to be used as an input to the model. Later, the K-mean Clustering algorithm was applied and the model was evaluated to check the quality of the resulting clusters based on the classification and evaluation-clustering quality techniques. In the next section, we demonstrated the approach on 1297109 Java questions asked by Java developers as a case study to examine it.

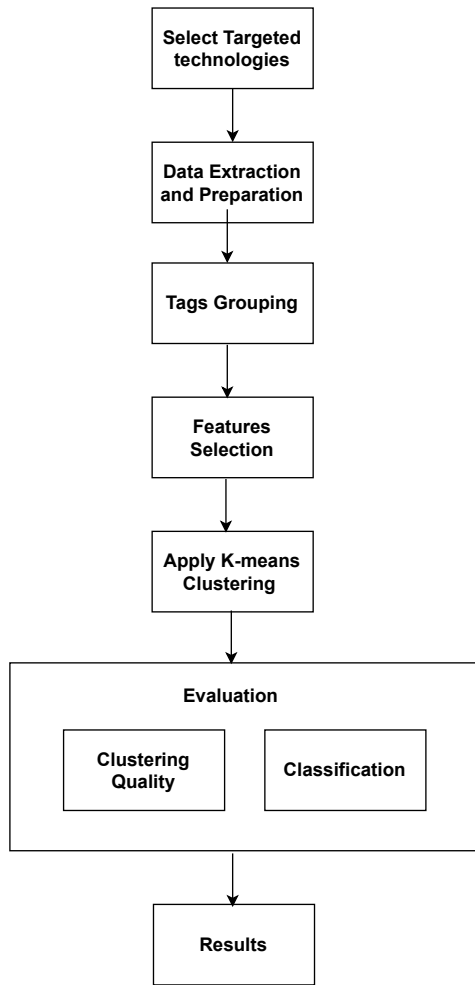


Fig. 2. An Approach to Identify Community Supported Techniques and Development Concepts.

A. Data Extraction and Preparation

In this step, data preparation refers to reprocessing the dataset for the modelling phase. We present a dataset obtained by analyzing 1297109 questions from the SO platform. The data set used in this study includes all Java discussions on SO. Over 782 topics of the million questions found, are unique to Java ecosystem. Since we are interested in identifying community-supported technologies and development concepts of the java ecosystem, hence tags with more than 30 questions were included. Table I shows data set information. Table II present the list of features to be used during clustering should be revised.

B. K-mean Clustering to Identify Supporting Level

Clustering analysis is a well-known concept in the field of data mining [26]. Clustering is a popular method for grouping data based on shared patterns or similarities. Numerous applications [27], [28], including science, technology, biology, social science economics, medicine, smart farming, geospatial,

TABLE I. GENERAL INFORMATION OF THE DATA-SET USED

Data set info	Items	Description
Java Questions	1297109	All questions related to the java ecosystem on SO from 2015 to 2021
All paired tags (Topics)	980	All co-occurrence topics with java questions related to software technologies and development concepts
paired tags >=30 Questions	794	All co-occurrence topics with java questions that have at least 30 questions as threshold related to software technologies and development concepts

TABLE II. FEATURES AND MEASURES.

Features and metrics	Description
Questions	The number count of the questions related to tag x.
Tag Name	keywords provided for the questions by developers that define the technical term at the center of the question.
Views	Number of views for the question, extracted by metadata ViewCount attribute of the post.
Score	Number of upvotes minus number of downvotes, extracted by metadata upvotes and downvotes attributes of the post.
Favorite	Number of Favorites For the question, extracted by metadata Favorites Count attribute of the post.
Comment	Number of comments For the question, extracted by metadata CommentCount attribute of the post.
Answers	Number of answers For the question, extracted by metadata AnswerCount attribute of the post.
Failure rate (FR)	The percentage of questions that do not have an accepted answer.
Wait Time (WT)	The median time for satisfactory answers (in these cases where the question got an answer that its asker accepted).

stock market, and many more, have made extensive use of cluster analysis.

In this paper k-means clustering was performed. The K-Means algorithm is an unsupervised learning approach for classifying/grouping objects based on their features. The technique splits the data into k clusters for a specified number of clusters k. Each cluster has a centre (centroid), which is defined as the mean value of all its points. K-means locates cluster centres iteratively by minimising the distance between individual cluster points and the cluster centre. K-means requires the specification of cluster centers from the outset. The method begins with a single cluster and selects a variable whose mean is used as a threshold for splitting the data in half. The centroids of these two components are then utilized to initialize k-means in order to optimize the two clusters' membership. Following that, one of the two clusters is chosen for splitting and a variable within it is picked whose mean is utilized as a threshold for splitting the cluster in half. K-means is then used to partition the data into three clusters, each of which is initialized with the centroids of the two split clusters and the remaining cluster's centroid. This procedure is repeated until a predetermined number of clusters has been attained [29], [30].

To compute the k-means clustering for each k. Assume a given a sample dataset $T = \{T_w | w = 1, 2, 3, \dots, n\}$. Each sample data in T contains f features of continuous data, denoted by $f_1, f_2, f_3, \dots, f_n$. The algorithmic approach used in K-Means is as follows: To begin, k initial clustering centres are chosen at random from T, denoted by $C_i (1 < i < k)$. The Euclidean distance between C_i and the sample data is then calculated and divided by C_i in T, and find the sample data closest to C_i . The sample data is then assigned to the

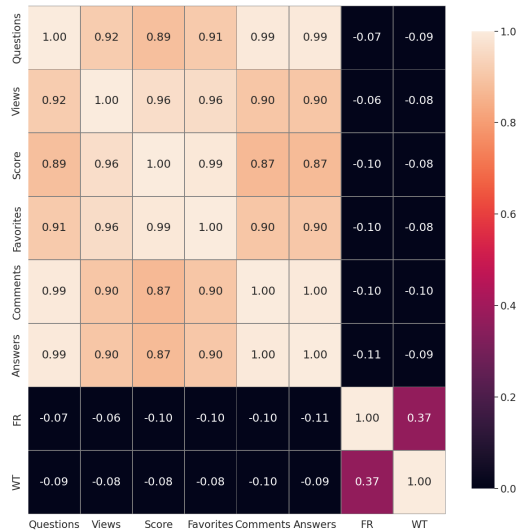


Fig. 3. Covariance Heatmap.

cluster corresponding to C_i , and the average of the sample data in each cluster is recalculated as the new clustering centre. Repeat these steps until the Cluster centre no longer changes or the maximum number of iterations is reached. The Euclidean distance computation formula is as follows:

$$d(t, C_i) = \sqrt{\sum_{j=1}^n (t_j - C_{ij})^2} \quad (1)$$

Note: T is the sample data, C_i is the i th cluster center, n is the number of features, t_j and C_{ij} , are the j th attribute values of T and C_i respectively. The result of clustering can be judged by the sum of square error of the data set. The formula for calculating the sum of squares of errors is as follows:

$$SSE = \sum_{i=1}^n \sum_{n \in C_i} |(t, C_i)|^2 \quad (2)$$

Before applying k-means clustering, the scale and variance of the features, as well as the multi-linearity between the features must be examined as significant correlations between features may lead to erroneous conclusions by overemphasizing one or more underlying components. Pearson correlations between features were calculated, and it was determined that the current data set has a multilinearity effect. A 2D correlation matrix was shown in Fig. 3 to show the relationships between the features.

K-means cluster analysis was carried and the number of clusters was chosen as two. the number of software technologies and development concepts are 353 for the most community supported ones (Cluster1) and 441 of software technologies and development concepts. The distance between

the centers of the clusters was determined to FR be 49.45% and 62.79% for of the clusters1 and cluster2, respectively. where the WT the centers are 89.44 minutes and 365.77 minutes for Clusters 1and 2, respectively. After deciding on the number of clusters, some tests must be carried out to check stability, the relative size of the clusters, and external validity.

V. CLUSTER EVALUATION

A good clustering algorithm should achieve high similarity between the data points within the same cluster. To assess cluster quality: The criteria for determining the appropriate number of clusters were as follows: two strategies were employed to assess the quality of the clustering based on criteria for determining the appropriate number of clusters, including Cohesion and Separation metrics, classification and Silhouette index.

A. Cluster Cohesion and Separation

Separation and Cohesion are internal metrics. Cluster Separation quantifies how distinct or well-separated one cluster is from others. Whereas Cluster Cohesion measures the degree to which objects inside a cluster are connected. Separation is calculated by the sum of squares between clusters (BSS). Cohesion is measured by the sum of squares within each cluster (WSS). We can therefore take WSS to be the measure of density and BSS to be the measure of separation. For clustering to be effective, a lower WSS and a larger BSS [31] are required.

B. Silhouette Index

The silhouette index [32] is used to study validity of the separation distance between the generated clusters. It is one of the most well-known techniques for clustering validation [33], [34], [35]. It shows the closeness of points in one cluster is to points in nearby clusters and thus provides a visual way to examine factors such as cluster number. The range of this metric is [-1, 1]. Silhouette coefficients of near +1 (as these values are known) suggest that the sample is far distant from the surrounding clusters. A value of 0 denotes that the sample is on or very near the decision boundary between two neighbouring clusters. However, negative values suggest that the samples might be assigned to the incorrect cluster [36], [37]. This is how the silhouette index is computed:

$d(i; j)$ represents the distance between cluster C_i data points and j . We read $a(i)$ as an indication of how well i is allocated to its own cluster (the smaller the value, the better the assignment).

$$a(i) = \frac{1}{|c_i| - 1} \sum_{j \in C_i, j \neq i} d_{i \neq j}(i, j) \quad (3)$$

Then, we present the mean dissimilarity $b(i)$ of point i to a cluster C_k as the average distance between i and all C_k points (where $C_k \neq C_i$). For each data point, $i \in C_i$.

$$b(i) = \min_{k \neq i} \frac{1}{|c_k|} \sum_{j \in C_k} d_k(i, j) \quad (4)$$

The value of silhouette of one data point i is defined as follows:

$$S(i) = \frac{b(i) - a(i)}{\max\{a(i), b(i)\}}, \text{ if } |c_i| > 1 \quad (5)$$

Consequently, the $s(i)$ present in the dataset is a measure of the clustering accuracy of the data.

1) *Evaluation by Classification* : Clustering is performed on unlabeled data to label each cluster. After data has been clustered into groups, a classification technique can be employed. When each cluster's classification model is built separately, there's a good probability of getting better results in terms of accuracy.

Classification based on the clustering process can be indirectly used to evaluate the quality of the clustering process. The evaluation uses the set of Java technologies and development concepts to train model that automates the classification of java technologies and development concepts topics using the supervised machine learning algorithms Random Forest (RF) [38]. RF was chosen since it has been effectively used in many research-related tasks. As a result, the RF approach will be utilised in this study to classify and discriminate between supported and less supported java technologies and development concepts.

VI. RESULTS AND DISCUSSION

In this section reports results of the clustering formulation based on test analysis of variance (ANOVA) and the quality of clustering using the statistical error and silhouette score techniques. Additionally, the clustering assessed indirectly by a classification technique, namely, RF.

A. Features to Formulate K-mean Clustering

Fig. 4 shows the result of k-mean clustering. It is important to note that before the application of cluster analysis, the scale and variance of the variables and multilinearity among the variables should be checked. According to the results, the calculated Pearson correlations between the features proved that multilinearity effect exists in the current data set. The correlation matrix is presented in Table III.

The results show that there are features that significantly contribute to the formation of the clusters. The failure rate and Wait time features were found to be the best features that formulate the community support technologies and development concepts clustering. The ANOVA results depicted in Tables X and V and the model Summary diagnostics as shown in Table III and VIII demonstrate the features that significantly contribute to the formation of the clusters. In Table III when clustering model was fed with all features (Views, Score, Favorite, Comment, Answers, FR and WT) there was a high correlation with these features and the clustering model. We further found that Within-group Sum of Squares (WSS) is higher than Between-group Sum of Squares (BSS). As mentioned before that WSS means the sum of distances between the points and the corresponding centroids for each cluster and BSS means the sum of distances between the centroids and the total sample mean multiplied by the number

TABLE III. INPUTS FOR CLUSTERING AND DIAGNOSTICS BASED ON FR AND WT

Inputs for Clustering	
Features	Sum of FR Sum of WT
Summary Diagnostics	
Number of Clusters:	2
Number of Points	794
Between-group Sum of Squares	10.039
Within-group Sum of Squares	9.3994
Total Sum of Squares	19.438

TABLE IV. THE AVERAGE VALUE WITHIN EACH CLUSTER BASE ON FR AND WT

Centers	Cluster1	Cluster 2
Number of Items	353	441
Sum of FR	49.45	62.798
Sum of WT	89.446	365.77

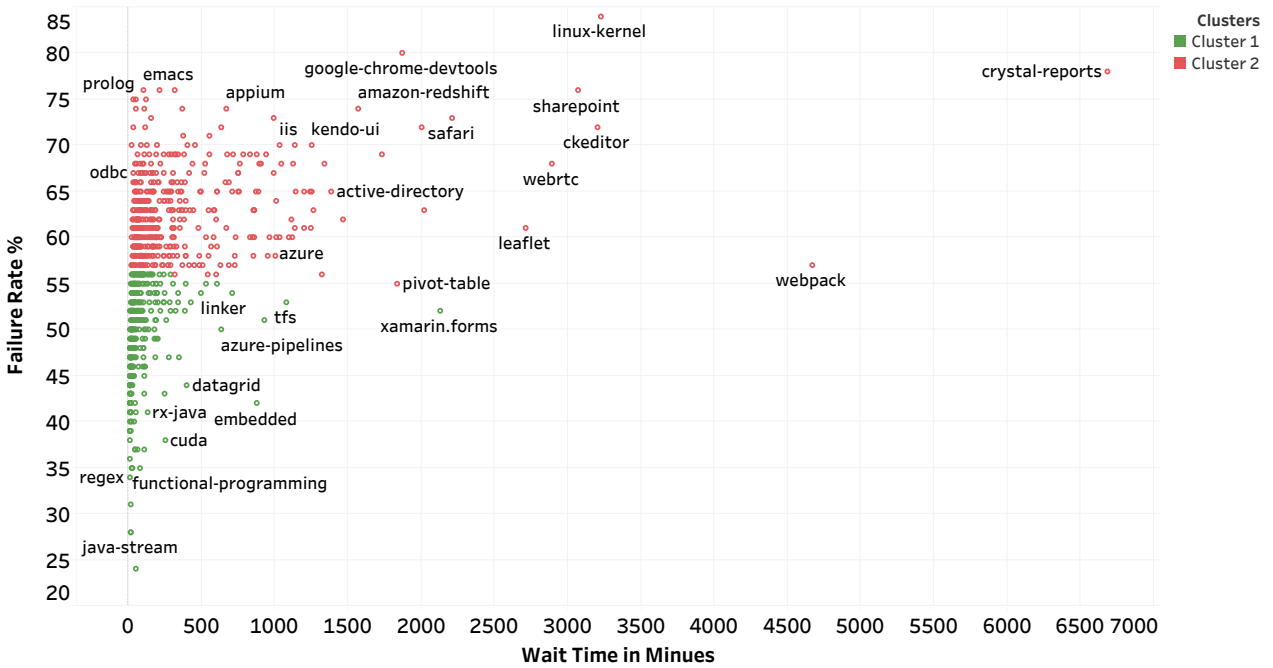
of points within each cluster. After performing the experiments by inserting the features into the model, the best results were obtained only when using the two features FR and WT after achieving a value of WSS lower than BSS as shown in Tables III and VIII. It is also noted that the Table VIII has a value of WSS greater than BSS, and this indicates that the features that achieve the best results for the k-mean clustering formation to determine the levels of community supported technologies and development concepts are FR and WT. Cluster 1 represents the best community supported technologies and development concepts for java developers. Whereas Cluster 2 represents the less community supported technologies and development concepts for java developers. Table IV shows that 44% of the technologies and development concepts in cluster 1 are more supported than the items in cluster 2 that comprises 55.5% of the Java technology and development concepts. The majority of the technologies and development concepts in cluster 2 have less wait time and failure rate. the result help developers gain insights about the community supported technologies and development concepts.

B. Assets the Quality of K-means Clustering

Extra evaluation technique was used to examine the cohesiveness of the quality matrices that is computed using the findings of the average global silhouette. Fig. 5 illustrates a silhouette curve for estimating the ideal number of clusters, gauging each cluster's quality cohesiveness. Fig. 5 reveals that the average silhouette score is (97%). This is a reasonable value because the clustering is predicated on the silhouette index, which is already high. The result shows that the two group clustering is an optimal number, thus the resulted clustering can be used as a new feature as an input of the classification models.

TABLE V. ANOVA ANALYSIS OF K-MEANS CLUSTER ANALYSIS BASED ON FR AND WT

Variable	F-statistic	p-value	Model	Error
			Sum of Squares	Sum of Squares
FR	498.6	0.0	9.703	15.41
WT	66.05	1.67E-15	0.3357	4.026



Z
 Fig. 4. Sum of WT vs. Sum of FR. Color Shows Details about Clusters. The Marks are Labeled by Software Technologies and Development Concepts of Java Ecosystem.

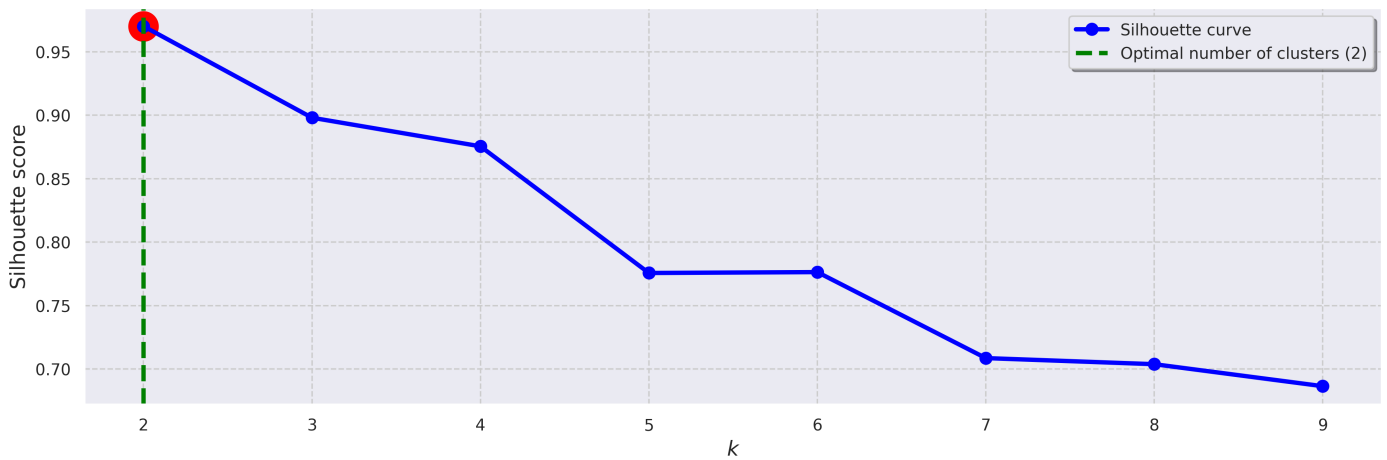


Fig. 5. Silhouette Curve for Predict Optimal Number of Clusters

C. Experimental Setup Using the RF classification

The RF model was run based on the most commonly-used method to explore hyper-parameter configuration space called Grid search (GS) [39] to tune the model to fit the best result that is provided by the respective implementation of python. GS operates by calculating the Cartesian product of a finite set of user-specified values. The code developed by [40] was used, which implements hyper-parameter optimization for machine learning algorithms, the values for the parameters of the RF ML algorithm considered in this paper are summarized in Table VI.

TABLE VI. RF CONFIGURATION HYPER-PARAMETER SPACE.

Hyper-parameter	Type	Search Space	best values
n_estimators	Discrete	[10,100]	20
max_depth	Discrete	[5,50]	15
min_samples_leaf	Discrete	[1,11]	1
criterion	Categorical	gini, entropy	gini

This study will employ a different metric of evaluation to assess this RF algorithm. These metrics are calculated based on four primary areas. In a supervised classification issue, a true output and a predicted or model-generated output exist. Therefore, each data point’s result will be categorised as one of the following:

- True Positive (TP): both the label and the prediction are positive.
- True Negative (TN): both the label and the prediction are negative.
- False Positive (FP): describes a situation in which the label is negative but the prediction is positive.
- False negative (FN): although the label is positive, the prediction is negative.

These four categories are the foundation of the majority of classification evaluation metrics. Performance parameters were used to evaluate the model: Accuracy, precision, recall and F-measure.

- Accuracy: It represents the proportion of correctly classified supported technologies and development concepts. It is technically defined as:

$$Accuracy = \frac{TP + TN}{(TP + FN) + (FN + TN)} \quad (6)$$

- Precision: It is the proportion of correctly identified supported technologies and development concepts relative to the total number of supported technologies and development concepts in a X class. The range of values is from 0 (poor precision) to 1 (high precision). The weighted average precision is determined as the mean of Precision of the true class and false class in relation to the number of tags predicted for each class. It is described as:

$$Precision = \frac{TP}{TP + FP} \quad (7)$$

- Recall: It is the proportion of successfully classified tags relative to the number of observed true instances.

The values vary from 0 (poor recall) and 1 (high recall). The weighted average recall is derived as the mean of recall of the true class and recall of the false class, weighted by the number of tags tagged with each class.

$$Recall = \frac{TP}{TP + FN} \quad (8)$$

- F1-Measure: It denotes a performance indicator that considers both the precision and recall of the classification obtained. The formula is as follows:

$$F - Measure = \frac{2 * recall * precision}{recall + precision} \quad (9)$$

- Area under ROC-Curve (AUC): It’s a measure of the classifier’s predictive strength, essentially telling us how well the model can distinguish between classes. AUC of 1 shows the best performance, while 0.5 indicates that the performance is comparable to that of a random classifier.

The dataset was divided into a training set and a testing set. In the training phase, cross validation is used 80% of the time, and 20% of the time in the testing phase. Cross-validation of 20% is used to test the model. RF algorithm was found to be achieving an average accuracy score of 99.49%. Table VII summarizes the results of the RF classifier based on these results, the configurations are shown in Table VI

TABLE VII. DETAILED ACCURACY BY CLASS

	Precision	Recall	F-Measure	ROC Area	Class
	0,994	0,994	0,994	0,999	Cluster 1
	0,995	0,995	0,995	0,999	Cluster 2
Weighted Avg.	0,995	0,995	0,995	0,999	

VII. CONCLUSION

In this paper, we introduced an approach based on K-mean clustering techniques to identify the level of community supported software technologies and development concepts leveraging software developer’s discussions on SO. The approach is based on tags explicitly assigned to questions. we identified how community supported and development concepts of java technologies based on java developers questions on SO. First, we created data set and used it to automate the clustering of software technologies and development concepts. In the

TABLE VIII. INPUTS FOR CLUSTERING AND DIAGNOSTICS BASED ON ALL FEATURES.

Inputs for Clustering	
Features	Sum of FR
	Sum of WT
	Sum of Answers
	Sum of Comments
	Sum of Views
	Sum of Favorites
	Sum of Score
Summary Diagnostics	
Number of Clusters:	2
Number of Points	794
Between-group Sum of Squares	10.188
Within-group Sum of Squares	21.245
Total Sum of Squares	31.433

TABLE IX. THE AVERAGE VALUE WITHIN EACH CLUSTER BASED ON ALL FEATURES

Centers	Cluster1	Cluster 2
Number of Items	355	439
Sum of FR	49.535	62.79
Sum of WT	88.6	367.71
Sum of Answers	5892.7	1693.9
Sum of Comments	10657	3275.3
Sum of Views	7.06E+06	2.55E+06
Sum of Favorites	1398.2	444.91
Sum of Score	5132.5	1588.6

TABLE X. ANOVA ANALYSIS OF K-MEANS CLUSTER ANALYSIS BASED ON ALL FEATURES

Features	F-statistic	p-value	Model	Error
			Sum of Squares	Sum of Squares
Sum of FR	492.3	0.0	9.58	15.41
Sum of WT	67.47	8.88E-16	0.3429	4.026
Sum of Answers	21.21	4.80E-06	0.04448	1.661
Sum of Comments	20.09	8.48E-06	0.0437	1.723
Sum of Score	17.47	3.24E-05	0.06513	2.952
Sum of Favorites	17.27	3.60E-05	0.0549	2.518
Sum of Views	14.44	1.56E-04	0.05726	3.141

first approach, we identified which feature can formulate clustering the community supported and development concepts. We implemented correlation analysis, ANOVA and diagnosis the K-mean model to get the best features to formulate the levels of groups of community supported and development concepts. we found that features that formulate the two clusters to determine the community supported software technologies and development concepts levels are failure rate, that is the percentage of its questions that do not have an accepted answer, and its median wait time, that is the median time to get accepted answers;are the best features. We found that the majority of Java technologies and development concepts are labeled with cluster 1 most community supported technologies and development concepts and cluster 2 less community supported technologies and development concepts.The approach was evaluated in two steps. The quality of clustering shows that the best value is 97%, the higher the silhouette index value, the more effective the construction of clusters. To assess the approach, the identified technologies and development concept groups were added as new features to the dataset and then RF was applied. The evaluation with the java data set showed that the approach outperforms the RF with an average precision and recall of 0.995 and 0.995, respectively.

VIII. FUTURE WORK

In the future, we are planning to apply and compare the classification of results based on different types of clustering algorithms to choose the right supported technologies. Also building detailed user interface development to maximize the benefits of a decision support system (DSS) in the software development sector.

REFERENCES

[1] C. Rosen and E. Shihab, "What are mobile developers asking about? a large scale study using stack overflow," *ESEM*, vol. 21, no. 3, pp. 1192–1223, 2016.
 [2] M. Linares-Vásquez, B. Dit, and D. Poshvanyk, "An exploratory analysis of mobile development issues using stack overflow," in *Proceedings of the 10th Working Conference on Mining Software Repositories*. IEEE Press, 2013, pp. 93–96.

[3] Z. e. a. Mehrab, "Mining developer questions about major web frameworks," in *WEBIST*, 2018, pp. 191–198.
 [4] F. Fischer, K. Böttinger, H. Xiao, C. Stransky, Y. Acar, M. Backes, and S. Fahl, "Stack overflow considered harmful? the impact of copy&paste on android application security," in *2017 IEEE Symposium on Security and Privacy (SP)*. IEEE, 2017, pp. 121–136.
 [5] C. Chen, Z. Xing, and L. Han, "Techland: Assisting technology landscape inquiries with insights from stack overflow," in *2016 IEEE International Conference on Software Maintenance and Evolution (ICSME)*. IEEE, 2016, pp. 356–366.
 [6] Y. Wu, S. Wang, C.-P. Bezemer, and K. Inoue, "How do developers utilize source code from stack overflow?" *Empirical Software Engineering*, vol. 24, no. 2, pp. 637–673, 2019.
 [7] F. Pedregosa, G. Varoquaux, A. Gramfort, V. Michel, B. Thirion, O. Grisel, M. Blondel, P. Prettenhofer, R. Weiss, V. Dubourg *et al.*, "Scikit-learn: Machine learning in python," *Journal of machine learning research*, vol. 12, no. Oct, pp. 2825–2830, 2011.
 [8] L. Beard and N. Aghassibake, "Tableau (version 2020.3)," *Journal of the Medical Library Association: JMLA*, vol. 109, no. 1, p. 159, 2021.
 [9] S. M. Nasehi, J. Sillito, F. Maurer, and C. Burns, "What makes a good code example?: A study of programming q&a in stackoverflow," in *2012 28th IEEE International Conference on Software Maintenance (ICSM)*. IEEE, 2012, pp. 25–34.
 [10] A. Barua, S. W. Thomas, and A. E. Hassan, "What are developers talking about? an analysis of topics and trends in stack overflow," *Empirical Software Engineering*, vol. 19, no. 3, pp. 619–654, 2014.
 [11] C. Treude, O. Barzilay, and M.-A. Storey, "How do programmers ask and answer questions on the web?: Nier track," in *Software Engineering (ICSE), 2011 33rd International Conference on*. IEEE, 2011, pp. 804–807.
 [12] J. Han, J. Pei, and M. Kamber, *Data mining: concepts and techniques*. Elsevier, 2011.
 [13] R. Kiani, S. Mahdavi, and A. Keshavarzi, "Analysis and prediction of crimes by clustering and classification," *International Journal of Advanced Research in Artificial Intelligence*, vol. 4, no. 8, pp. 11–17, 2015.
 [14] T. Sajana, C. S. Rani, and K. Narayana, "A survey on clustering techniques for big data mining," *Indian journal of Science and Technology*, vol. 9, no. 3, pp. 1–12, 2016.
 [15] J. A. Hartigan and M. A. Wong, "Algorithm as 136: A k-means clustering algorithm," *Journal of the royal statistical society. series c (applied statistics)*, vol. 28, no. 1, pp. 100–108, 1979.
 [16] S. Naeem and A. Wumaier, "Study and implementing k-mean clustering algorithm on english text and techniques to find the optimal value of k," *Int. J. Comput. Appl.*, vol. 182, no. 31, pp. 7–14, 2018.
 [17] P. Berkhin, "A survey of clustering data mining techniques," in *Grouping multidimensional data*. Springer, 2006, pp. 25–71.
 [18] S. Joshi and B. Nigam, "Categorizing the document using multi class classification in data mining," in *2011 International Conference on Computational Intelligence and Communication Networks*. IEEE, 2011, pp. 251–255.
 [19] G. Kesavaraj and S. Sukumaran, "A study on classification techniques in data mining," in *2013 fourth international conference on computing, communications and networking technologies (ICCCNT)*. IEEE, 2013, pp. 1–7.
 [20] A. Ahmad, C. Feng, S. Ge, and A. Yousif, "A survey on mining stack overflow: question and answering (q&a) community," *Data Technologies and Applications*, 2018.
 [21] K. Bajaj, K. Pattabiraman, and A. Mesbah, "Mining questions asked by web developers," in *MSR 2014*, 2014, pp. 112–121.
 [22] V. et al., "What do client developers concern when using web apis? an empirical study on developer forums and stack overflow," in *ICWS '16*. IEEE, 2016, pp. 131–138.
 [23] F. Almansoury, S. Kpodjedo, and G. E. Boussaidi, "Investigating web3d topics on stackoverflow: a preliminary study of webgl and three.js," in *The 25th International Conference on 3D Web Technology*, 2020, pp. 1–2.

- [24] X.-L. Yang, D. Lo, X. Xia, Z.-Y. Wan, and J.-L. Sun, "What security questions do developers ask? a large-scale study of stack overflow posts," *JCST*, vol. 31, no. 5, pp. 910–924, 2016.
- [25] N. Meng, S. Nagy, D. Yao, W. Zhuang, and G. A. Argoty, "Secure coding practices in java: Challenges and vulnerabilities," in *ICSE'18*, 2018, pp. 372–383.
- [26] K. A. Nazeer and M. Sebastian, "Improving the accuracy and efficiency of the k-means clustering algorithm," in *Proceedings of the world congress on engineering*, vol. 1. Citeseer, 2009, pp. 1–3.
- [27] A. Bansal, M. Sharma, and S. Goel, "Improved k-mean clustering algorithm for prediction analysis using classification technique in data mining," *International Journal of Computer Applications*, vol. 157, no. 6, pp. 0975–8887, 2017.
- [28] B. Aubaidan, M. Mohd, and M. Albared, "Comparative study of k-means and k-means++ clustering algorithms on crime domain," 2014.
- [29] T. Kanungo, D. M. Mount, N. S. Netanyahu, C. D. Piatko, R. Silverman, and A. Y. Wu, "An efficient k-means clustering algorithm: Analysis and implementation," *IEEE transactions on pattern analysis and machine intelligence*, vol. 24, no. 7, pp. 881–892, 2002.
- [30] M. E. Celebi, H. A. Kingravi, and P. A. Vela, "A comparative study of efficient initialization methods for the k-means clustering algorithm," *Expert systems with applications*, vol. 40, no. 1, pp. 200–210, 2013.
- [31] K. M. Lee, K. M. Lee, and C. H. Lee, "Statistical cluster validity indexes to consider cohesion and separation," in *2012 international conference on fuzzy theory and its applications (ifuzzy2012)*. IEEE, 2012, pp. 228–232.
- [32] P. J. Rousseeuw, "Silhouettes: a graphical aid to the interpretation and validation of cluster analysis," *Journal of computational and applied mathematics*, vol. 20, pp. 53–65, 1987.
- [33] S. Chaimontree, K. Atkinson, and F. Coenen, "Best clustering configuration metrics: towards multiagent based clustering," in *International Conference on Advanced Data Mining and Applications*. Springer, 2010, pp. 48–59.
- [34] S. A. Burney and H. Tariq, "K-means cluster analysis for image segmentation," *International Journal of Computer Applications*, vol. 96, no. 4, 2014.
- [35] A. R. Mamat, F. S. Mohamed, M. A. Mohamed, N. M. Rawi, and M. I. Awang, "Silhouette index for determining optimal k-means clustering on images in different color models," *Int. J. Eng. Technol.*, vol. 7, no. 2, pp. 105–109, 2018.
- [36] A. Starczewski and A. Krzyżak, "Performance evaluation of the silhouette index," in *International conference on artificial intelligence and soft computing*. Springer, 2015, pp. 49–58.
- [37] X. Wang and Y. Xu, "An improved index for clustering validation based on silhouette index and calinski-harabasz index," in *IOP Conference Series: Materials Science and Engineering*, vol. 569, no. 5. IOP Publishing, 2019, p. 052024.
- [38] L. Breiman, "Random forests," *Machine learning*, vol. 45, no. 1, pp. 5–32, 2001.
- [39] J. Bergstra, R. Bardenet, Y. Bengio, and B. Kégl, "Algorithms for hyperparameter optimization," *Advances in neural information processing systems*, vol. 24, 2011.
- [40] L. Yang and A. Shami, "On hyperparameter optimization of machine learning algorithms: Theory and practice," *Neurocomputing*, vol. 415, pp. 295–316, 2020.

On the Role of Text Preprocessing in BERT Embedding-based DNNs for Classifying Informal Texts

Aliyah Kurniasih

Department of Computer Science
University of Nusa Mandiri
Jakarta, Indonesia

Lindung Parningotan Manik

Research Center for Data and Information Sciences
National Research and Innovation Agency
Cibinong, Indonesia

Abstract—Due to highly unstructured and noisy data, analyzing society reports in written texts is very challenging. Classifying informal text data is still considered a difficult task in natural language processing since the texts could contain abbreviated words, repeating characters, typos, slang, et cetera. Therefore, text preprocessing is commonly performed to remove the noises and make the texts more structured. However, we argued that most tasks of preprocessing are no longer required if suitable word embeddings approach and deep neural network (DNN) architecture are correctly chosen. This study investigated the effects of text preprocessing in fine-tuning a pre-trained Bidirectional Encoder Representations from Transformers (BERT) model using various DNN architectures such as multilayer perceptron (MLP), long short-term memory (LSTM), bidirectional long-short term memory (Bi-LSTM), convolutional neural network (CNN), and gated recurrent unit (GRU). Various experiments were conducted using numerous learning rates and batch sizes. As a result, text preprocessing had insignificant effects on most models such as LSTM, Bi-LSTM, and CNN. Moreover, the combination of BERT embeddings and CNN produced the best classification performance.

Keywords—Natural language processing; bert embeddings; deep neural network; text preprocessing

I. INTRODUCTION

Societies often generate informal texts in the form of complaints, aspirations, and ideas. Therefore, it is crucial to follow up on most of the reports received by the various applications to increase service quality. However, the fluid, social, and dynamic written language that continues to develop becomes a challenge in natural language processing (NLP) research field. Furthermore, other challenges in text data such as typos, slang words, and informal vocabularies, followed by various hashtags and emoticons, remain to continue.

In order to overcome these problems, text preprocessing is performed to manage text data before building an NLP model using machine learning. For example, removing hashtags, URLs, stopwords, punctuations, @annotation, ASCII, and duplicate characters in a word is common in text mining [1]. Furthermore, tokenization, case-folding, stemming, and lemmatization were also performed preprocessing texts [2]. These steps are important in conventional machine learning since preprocessing can decrease vocabulary size by removing unhelpful parts of data or noise [3]. Thus, it can reduce the

text data size and enhance the effectiveness and efficiency of the machine learning algorithms.

However, these approaches could be problematic. Some preprocessing steps could make semantic meaning between tokens or words in sentences disappear. For example, removing some stopwords could affect the contexts and generate ambiguous results. Sometimes, emoticons and hashtags could be helpful when analyzing emotions or sentiments within texts. Moreover, mistakes could be made if done manually or even automatically. To the best of our knowledge, no stemmer has 100% accuracy. Thus, in addition to losing the meaning, over stemming and under stemming could occur.

There are several techniques for extracting text features. Within text mining, feature extraction means converting texts to vectors. In conventional machine learning, the Bag-of-Word (BOW) method and Term Frequency-Inverse Document Frequency (TF-IDF) are commonly used [4]. The deficiency of these approaches is that they do not capture the position in the text, co-occurrences in different documents, and the semantics. Some of these problems were solved with word embeddings, which are learned text representations in which words with related meanings are represented similarly. It is considered one of the breakthroughs in deep learning. Studies in [5], [6], [7] suggested the Word2Vec approach to extract text features, while others suggested Glove [8]. Nevertheless, both approaches are context-independent, and they could not catch all semantic information such as Out-Of-Vocabulary (OOV) and some opposite word pairs.

Now-a-days, the NLP model that could perfectly capture almost all semantic contextual meanings is the Bidirectional Encoder from Transformers (BERT) [9]. It takes a sequence (typically a sentence) as input rather than a single word to generate contextual embeddings. Before BERT can build word embeddings, the context provided by surrounding words has to be shown. Word2Vec generates only one vector representation for each word. If there are any different word meanings, they are combined into one single vector. Meanwhile, BERT generates different vectors of a single word in different contexts. It is a leap in text mining techniques where pre-trained models are utilized in transfer learning with Transformers network [10]. Some pre-trained BERT models are already available in some languages other than English, such as AnchiBERT for ancient Chinese language [11], PhoBERT for Vietnamese [12], and

IndoBERT for the Indonesian language [13], [14].

In previous studies, BERT has been applied in text classification and generated passably result [15], [16], [17], [18], [19]. With many noises in the data, such as slang words, non-standard abbreviations, and typos, experiments conducted in [20] to analyze the sentiments of flood disaster-related texts using a pre-trained BERT model showed promising results. The study claimed that the noises had great effects on accuracy. However, the authors did not experiment with text preprocessing to prove that claim. We hypothesized that choosing the suitable word embeddings approach and DNN architecture makes most text preprocessing steps no longer required.

The contribution of this study is twofold. First, we investigated the effect of text preprocessing in the BERT embedding-based deep neural networks (DNNs) when classifying informal texts. While NLP studies suggested that text preprocessing was required most of the time, we argued that these tasks do not affect classification performance nowadays. Second, we also aimed to find and propose DNN architecture with the best classification performance in fine-tuning BERT embeddings. Therefore, we conducted experiments with or without most text preprocessing tasks using five DNN architectures, including long short-term memory (LSTM), bidirectional long short-term memory (Bi-LSTM), convolutional neural network (CNN), multi-layer perceptron (MLP), and gated recurrent unit (GRU). In addition, each model was also tuned with various optimization methods and hyperparameters, such as learning rate and batch size.

The remainder of this paper is organized as follows. First, Section II presents the dataset and research methods. Then, the results and discussions are explained in Section III and Section IV, respectively. Finally, conclusions and future research recommendations are provided in Section V.

II. MATERIALS AND METHODS

The research method in this study is shown in Fig. 1. First, we collected a dataset in the Indonesian language from society reports taken from a Citizen Relation Management (CRM) application in the Water Resources Agency of Jakarta, Indonesia. There were 3,217 instances obtained from 1 January to 31 July 2021. Initially, the CRM administration staff performed the manual classifications of the text reports into five handling categories, namely flood mitigation, waterways, drain closure, infiltration well, and others. The distribution of data is displayed in Table I.

TABLE I. NUMBER OF LABELED DATA

Category	Amount of Data
Flood mitigation	1360
Waterways	1071
Others	423
Drain closure	343
Infiltration well	20

We performed text preprocessing semi-automatically before conducting one of our sequences of experiments. Correcting abbreviated vocabulary, removing repeated syllable alphabet, repairing typos, and formalizing slang words to

standard words based on Indonesian dictionary rules were done manually. Meanwhile, case-folding and removing numbers, mentions, hashtags, as well as emoticons were performed automatically.

The IndoBERT model released by IndoNLU [13] was used to create the BERT embeddings of the dataset. The model was pre-trained using Masked Language Modelling (MLM) and Next Sentence Prediction (NSP), consisting of 124.5M parameters in the base architecture. A text data collection which consists of 4 billion words called Indo4B with a size of 23.43 GB, was used to train the model.

Furthermore, we divided the dataset into 70% training data, 15% validation data, and 15% test data. Training data used to build model, validation data used to test the trained networks to validate model, and testing data used to test model that was built. Validation and test data used were not part of training data to produce an objective evaluation result. Moreover, five DNN architectures were trained. The LSTM, Bi-LSTM, CNN, MLP, and GRU were chosen since they performed well in previous studies [1], [8], [21].

TABLE II. HYPERPARAMETERS OF DNN ALGORITHMS

Parameter	Parameter Value
IndoBERT	Indobenchmark/indobert-base-p1
Max length	512
Neuron	1024, 512, 256
Batch size	16, 32
Dropout	0.2
Activation function	ReLU
Output function	Softmax
Loss function	Categorical_crossentropy
Epoch	20
Number of layer	1-5
Type of layer	LSTM, BiLSTM, CNN, GRU, MLP
Optimization	Adam
Learning rate	5×10^{-5} , 3×10^{-5} , 2×10^{-5}

TABLE III. MODELS' ARCHITECTURE

Architecture	Layer
MLP	One input layer, three dense layer (neuron 1024, 512, 256), dropout layer (0.2), one output layer
LSTM	One input layer, one lstm layer (1024), two dense layer (512, 256), dropout layer (0.2), one output layer
BiLSTM	One input layer, one bi-lstm layer (1024), two dense layer (512, 256), dropout layer (0.2), one output layer
CNN	One input layer, one convolutional layer (1024), one pooling layer, two dense layer (512, 256), dropout layer (0.2), one output layer
GRU	One input layer, one gru layer (1024), two dense layer (512, 256), dropout layer (0.2), one output layer

Hyperparameter values such as maximum length, the number of neurons, learning rates, batch sizes, and epochs were determined based on previously conducted research related to BERT fine-tuning [15]. Moreover, the ReLu activation function was used on the hidden layer and the Softmax activation function on the output layer. The categorical cross-entropy was used as a loss function since target label classification has more than two classes. The dropout value was set to 0.2 used on the last hidden layer before the output layer to regularize the model to decrease overfitting from happening on the model.

Each model was built and experimented with a variation

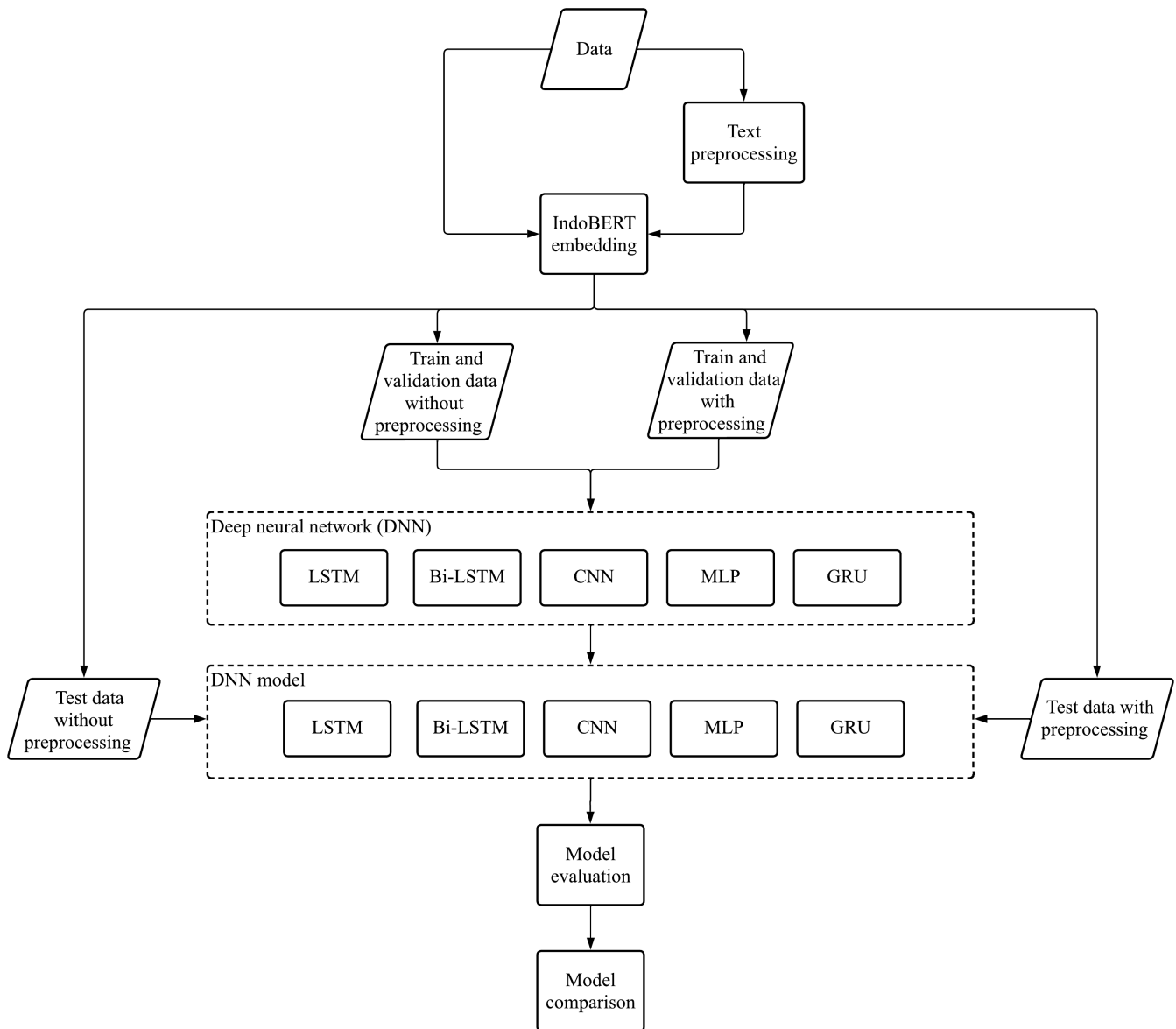


Fig. 1. Research Method.

amount of batch size of 16 as well as 32, learning rates of 5×10^{-5} , 3×10^{-5} , 2×10^{-5} , and an epoch of 20. Moreover, Adam is used to optimizing the model since it is the best adaptive optimizer in most cases. The summary of the hyperparameter values is shown in Table II. Meanwhile, all DNN architectures were composed of one input layer, one output layer, and at least one hidden layer. The detail of the five architectures and the used parameters on the layers is represented in Table III.

Standard performance metrics, such as *TP* (True Positive), *TN* (True Negative), *FP* (False Positive), and *FN* (False Negative), were used as primary building blocks to evaluate classification models. A *TP* is measured when the model predicts the positive class correctly. A *TN*, on the other hand, is a result in which the model correctly classifies the negative class. Conversely, a *FP* occurs when the model predicts the

positive class inaccurately. Meanwhile, a *FN* is an outcome in which the model classifies the negative class inaccurately.

Furthermore, other classification metrics, such as accuracy, F1-score, precision, and recall, were used to evaluate the models' performances. The accuracy, calculated using Equation 1, is the ratio of the number of correct predictions divided by the total number of input samples. Meanwhile, recall, calculated using Equation 2, measures the model's ability to detect positive samples. On the other hand, precision, calculated using Equation 3, measures the model's accuracy in classifying a sample as positive. Lastly, F1-score, which summarizes a model's predictive performance by combining two previously opposing variables — precision and recall, is calculated using Equation 4. F1-score could be considered the best metric in this study since the dataset has an uneven class distribution.

TABLE IV. TEXT PREPROCESSING RESULTS

Without Text Preprocessing	With Text Preprocessing	English Version
mohon bantuannya got mampet , sudah saya bersihkan sebagian kotorannya tapi masih mampet dan sampai mengalir ke jalan #gotmampet #gotkotor	mohon bantuannya got mampat , sudah saya bersihkan sebagian kotorannya tetapi masih mampat dan sampai mengalir ke jalan.	please help the gutter is clogged, i have cleaned some of the dirt but it is still clogged and the water flows into the street
jl Taman malaka selatan 3, duren sawit, jakarta timur	jalan taman malaka selatan tiga duren sawit jakarta timur	street of south malaka park three duren sawit east jakarta
laporan pak .di wilayah Cakung tepat nya di keluarahan rawa Terate kali sudah dangkal pak mohon untuk segera di keruk lumpur bir dlm.sudh mengadu ke lurah rawa Terate ttp blm ada tanggapan smpi skrng	laporan pak, di wilayah cakung tepatnya di keluarahan rawa terate kali sudah dangkal pak. mohon untuk segera di keruk lumpur biar dalam . sudah mengadu ke lurah rawa terate tetap belum ada tanggapan sampai sekarang .	sir, in the cakung area, to be precise, in the rawa terate sub-district, the river is already shallow. please immediately dredge the mud. i have complained to the village head, still no response until now
jln cipinang lontar rt13rw06 dekat bekas hotel ahmad mas .. mohon solusi nya bapak ibu yg terhormat karena setiap hujan kami kebanjiran karena GOT yg susah untuk di bersihkan nya karena sebagian warga depan rumah nya itu di tinggikan di atas GOT	jalan cipinang lontar rukun tetangga 013 rukun warga 006 dekat bekas hotel ahmad mas. mohon solusinya bapak ibu yang terhormat karena setiap hujan kami kebanjiran karena got yang susah untuk di bersihkannya karena sebagian warga depan rumahnya itu ditinggikan di atas got .	cipinang lontar street, rt 013 rw 006 near the former hotel ahmad. please provide a solution, because every time it rains we are flooded, the sewers are difficult to clean because the front part of some of the residents' houses are elevated above the sewers.
@TMC Polda Metro @Radio Elshinta @DKI Jakarta Kerusakan penutup gorong-gorong yang sama yang diperbaiki tgl 5 maret lalu. Jelek banget kualitasnya, bikin macet panjang di pertigaan Tipar Cakung - RGTC sampai 1 KM @DKI Jakarta kok tidak ditindak lanjuti kerusakan penutup gorong-gorong ini?	kerusakan penutup gorong-gorong yang sama yang diperbaiki tanggal 5 maret lalu. jelek banget kualitasnya, bikin macet panjang di pertigaan tipar cakung rgtc sampai satu kilometer, ko tidak ditindak lanjuti kerusakan penutup gorong-gorong ini?	same damage to the culvert cover which was repaired on 5 march. very bad quality, causing a long traffic jam at the tipar cakung rgtc junction for up to one kilometer, how come no action is taken to fix the damage on this culvert cover?
Pak, mohon dibuatkan sumur resapan sepanjang jalan ini, selalu rawan banjirrrrrrr	pak, mohon dibuatkan sumur resapan di sepanjang jalan ini, selalu rawan banjir .	sir, please make an infiltration well along this road, it is always prone to flooding.

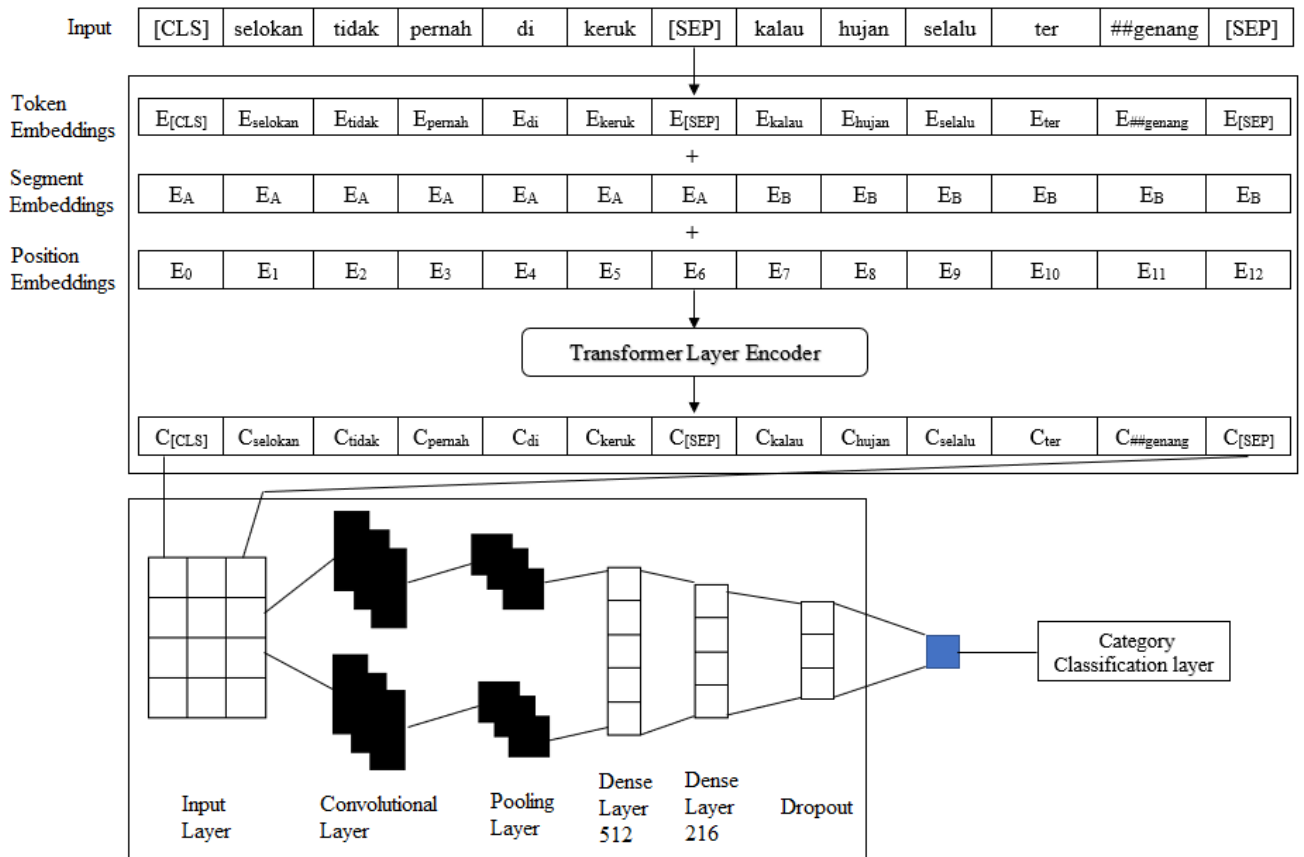


Fig. 2. Representation of BERT Embeddings and CNN.

$$Accuracy = \frac{TP + TN}{TP + TN + FP + FN} \quad (1)$$

$$Recall = \frac{TP}{TP + FN} \quad (2)$$

$$Precision = \frac{TP}{TP + FP} \quad (3)$$

$$F1 - score = \frac{2 \times precision \times recall}{precision + recall} \quad (4)$$

Finally, the performance results of DNN models with and without text processing were compared to see if there is a significant difference between both approaches using a statistical t-Test, Paired Two Sample for Means. The test statistic is calculated using Equation 5 where \bar{d} is the sample mean of the differences, s is the sample standard deviation of the differences, n is the sample size, and t is the Student t quantile with $n-1$ degrees of freedom used to define the p-value. In statistical significance testing, it is the likelihood of receiving a test statistic at least as extreme as the observed one, assuming that the null hypothesis is true. The null hypothesis is rejected when the p-value is smaller than the predetermined significance level, suggesting that the observed result would be highly implausible under the null hypothesis.

$$t = \frac{\bar{d}}{s/\sqrt{n}} \quad (5)$$

III. RESULTS

Some of the results of text data after processing with and without text preprocessing used in building models are shown in Table IV. The performance results of various experiments without text preprocessing are shown in Table V, where the highest values are printed bold. The fine-tuned DNN architecture with IndoBERT base model to text data of society reports without text preprocessing produced the best accuracy and precision using the CNN algorithm model architecture with a learning rate of 3×10^{-5} and a batch size of 16. The best accuracy and precision obtained were 83.85% and 88.76%, respectively. However, the best result on F1-score and recall was achieved using a learning rate of 5×10^{-5} and a batch size of 16. The best F1-score and recall yielded 85.44% and 83.95%, respectively.

Meanwhile, the performance results of various experiments with text preprocessing are represented in Table VI, where the best values are boldly printed. The fine-tuned deep learning model with text preprocessing obtained the best accuracy, F1-score, and recall using the CNN algorithm with a learning rate of 5×10^{-5} and batch size of 16. The best accuracy, F1-score, and recall yielded 84.47%, 85.92%, and 85.54%, respectively. However, the best precision of 87.37% was produced using a learning rate of 2×10^{-5} and a batch size of 32.

From the two tables, it can be seen that the CNN algorithm produced the best performances compared to other algorithms. CNN even produced better results using text preprocessing. With a learning rate of 5×10^{-5} and a batch size of 16, the

accuracy, F1-score, precision, and recall were improved by 1.45%, 0.48%, 0.06%, and 1.59%, respectively. However, these values indicated that the text preprocessing made minimal performance improvements.

Moreover, in order to make statistical comparisons of performance results of fine-tuned DNN model between with and without text preprocessing, the t-Test was performed. The statistic test can determine whether the differences between two approaches are significant. If the p-value is less than a significant level, the null hypothesis, which states no significant differences between the models, is rejected. The results are shown in Table VII, where p-values less than a significant level of 0.05, which indicated significant differences, are printed bold. It can be seen that text preprocessing had no significant effect on most architectures, such as in CNN, LSTM, and Bi-LSTM. Meanwhile, the text preprocessing significantly affected the performances of GRU as well as the accuracy and the precision of MLP but not the F1-score.

IV. DISCUSSION

The result of insignificant performance differences between DNN architectures with and without text preprocessing is in line with the study conducted by [22]. It performed various experiments with three preprocessing tasks: lowercasing, lemmatizing, and multiword grouping. It concluded that simple tokenization was generally adequate in DNN architectures, particularly CNN. Furthermore, the simple preprocessing worked equally or better than more complex techniques in most cases, except for domain-specific texts, such as in the medical field, where apparent differences were needed to classify cardiovascular disease.

We proved that the study conducted by [20] claimed that removing noises in the text data would significantly improve the accuracy of a pre-trained BERT model could be gone wrong. Instead, a BERT model applied to heavily cleaned text data could make things worse because the contextual information would be lost. This finding is supported by a study conducted by [23] when profiling authors from their writings. When no preprocessing method was used, the study found that BERT best predicted an author's gender. In the best scenario, the model was 86.67% accurate in estimating the writers' gender.

One possible reason for the excellent performance of the model without text preprocessing in this study was the suitable choice of the word embeddings approach. The IndoBERT was trained on an extensive Indonesian text dataset that includes formal and slang language, such as tweets. The results could differ if the pre-trained BERT models were trained using Wikipedia corpus only, like the BERT-Base multilingual pre-trained model [16]. A study conducted in [19] showed that preprocessing steps and further preprocessing processes were needed when using BERT multilingual pre-trained model to improve the classification performance of a DNN. The more data BERT pre-train, the less the negative impact of misspellings and slang words would be because the model has more examples of typos, abbreviated vocabularies, orthographic errors, et cetera.

Furthermore, CNN managed to perform best when utilizing the BERT embeddings compared to the other DNN architec-

TABLE V. PERFORMANCE RESULTS OF MODELS WITHOUT TEXT PREPROCESSING

Architecture	Learning Rate	Batch Size	Accuracy (%)	F1-Score (%)	Precision (%)	Recall (%)
MLP	5x10 ⁻⁵	16	78.26	60.49	66.62	56.87
	3x10 ⁻⁵	16	77.02	60.43	67.04	56.02
	2x10 ⁻⁵	16	76.40	61.24	66.47	57.58
	5x10 ⁻⁵	32	76.81	62.95	65.71	61.08
	3x10 ⁻⁵	32	76.19	58.19	66.86	53.88
	2x10 ⁻⁵	32	73.91	59.56	65.92	54.98
LSTM	5x10 ⁻⁵	16	69.98	54.17	54.93	54.09
	3x10 ⁻⁵	16	72.26	65.14	77.95	61.06
	2x10 ⁻⁵	16	69.36	52.68	57.14	50.20
	5x10 ⁻⁵	32	72.67	55.91	58.63	54.20
	3x10 ⁻⁵	32	72.26	56.38	57.16	55.87
	2x10 ⁻⁵	32	71.01	53.07	55.30	51.40
BiLSTM	5x10 ⁻⁵	16	81.37	79.87	87.92	74.74
	3x10 ⁻⁵	16	79.71	83.19	84.84	82.15
	2x10 ⁻⁵	16	80.54	73.58	84.01	69.85
	5x10 ⁻⁵	32	81.16	79.99	86.28	75.56
	3x10 ⁻⁵	32	80.33	72.34	86.02	67.90
	2x10 ⁻⁵	32	79.50	76.09	82.67	72.10
CNN	5x10 ⁻⁵	16	83.02	85.44	87.20	83.95
	3x10 ⁻⁵	16	83.85	75.56	88.76	70.15
	2x10 ⁻⁵	16	80.12	79.33	86.86	73.99
	5x10 ⁻⁵	32	82.61	80.19	86.65	75.73
	3x10 ⁻⁵	32	79.92	72.41	85.84	66.93
	2x10 ⁻⁵	32	80.54	73.27	87.29	67.17
GRU	5x10 ⁻⁵	16	72.05	65.44	75.55	62.15
	3x10 ⁻⁵	16	74.33	68.36	80.40	64.28
	2x10 ⁻⁵	16	72.26	66.01	79.09	60.98
	5x10 ⁻⁵	32	72.05	67.26	76.99	65.57
	3x10 ⁻⁵	32	74.12	57.74	61.37	54.99
	2x10 ⁻⁵	32	70.81	56.67	60.62	54.36

TABLE VI. PERFORMANCE RESULTS OF MODELS WITH TEXT PREPROCESSING

Architecture	Learning Rate	Batch Size	Accuracy (%)	F1-Score (%)	Precision (%)	Recall (%)
MLP	5x10 ⁻⁵	16	74.74	59.55	63.70	56.61
	3x10 ⁻⁵	16	74.95	60.20	63.39	57.43
	2x10 ⁻⁵	16	73.91	59.27	65.61	54.93
	5x10 ⁻⁵	32	75.36	60.43	63.86	58.34
	3x10 ⁻⁵	32	76.40	59.60	66.27	55.93
	2x10 ⁻⁵	32	73.08	58.44	64.25	54.29
LSTM	5x10 ⁻⁵	16	68.32	51.08	53.48	50.20
	3x10 ⁻⁵	16	73.50	57.67	59.59	56.18
	2x10 ⁻⁵	16	70.19	54.02	57.58	52.07
	5x10 ⁻⁵	32	69.98	61.68	79.68	55.77
	3x10 ⁻⁵	32	71.22	55.08	57.27	54.62
	2x10 ⁻⁵	32	68.32	52.42	54.58	50.74
BiLSTM	5x10 ⁻⁵	16	80.75	79.32	83.81	76.47
	3x10 ⁻⁵	16	79.30	78.14	82.33	75.37
	2x10 ⁻⁵	16	80.33	74	85.77	69.58
	5x10 ⁻⁵	32	79.50	78.70	84.25	75.27
	3x10 ⁻⁵	32	79.50	72.02	83.10	68.04
	2x10 ⁻⁵	32	80.33	78.59	83.12	76.16
CNN	5x10 ⁻⁵	16	84.47	85.92	87.26	85.54
	3x10 ⁻⁵	16	82.61	74.59	85.14	70.83
	2x10 ⁻⁵	16	81.57	80.71	86.60	76.56
	5x10 ⁻⁵	32	83.64	82.40	87.35	79
	3x10 ⁻⁵	32	83.23	65.75	68.06	64.39
	2x10 ⁻⁵	32	80.95	74.43	87.37	68.86
GRU	5x10 ⁻⁵	16	72.67	66.35	78.86	61.16
	3x10 ⁻⁵	16	71.64	56.96	58.05	56
	2x10 ⁻⁵	16	71.43	56.67	59.42	54.64
	5x10 ⁻⁵	32	71.84	57.40	59.34	55.88
	3x10 ⁻⁵	32	70.60	56.60	58.70	55.16
	2x10 ⁻⁵	32	69.15	54.67	57.10	52.87

TABLE VII. P-VALUES OF SIGNIFICANT TEST RESULTS

Architecture	Accuracy	F1-Score	Precision	Recall
MLP	0.0124 (sig.)	0.8727 (not sig.)	0.00519 (sig.)	0.29054 (not sig.)
LSTM	0.10471 (not sig.)	0.31956 (not sig.)	0.48675 (not sig.)	0.16681 (not sig.)
BiLSTM	0.10323 (not sig.)	0.25638 (not sig.)	0.10761 (not sig.)	0.43984 (not sig.)
CNN	0.06955 (not sig.)	0.38748 (not sig.)	0.14476 (not sig.)	0.10301 (not sig.)
GRU	0.04053 (sig.)	0.02643 (sig.)	0.03164 (sig.)	0.02431 (sig.)

tures. It could be because the CNN algorithm might extract local and global features very well from the vectors using the convolutional, the pooling, and the fully connected (dense) layers, which can maintain semantic context meaning on text data. This finding supports studies on sentiment analysis of a commodity review and stance detection for credibility analysis of information on social media conducted by [24], [25]. These studies showed that BERT embeddings and CNN obtained better results than single CNN that ignores relation contextual semantics on text.

BERT's input embeddings are composed of three different embeddings: Token Embeddings, Segment Embeddings, and Position Embeddings. Before being passed to the Token Embeddings layer, the input text is tokenized using a method called WordPiece tokenization. It is a data-driven tokenization strategy that balances vocabulary size and OOV words. Extra tokens are also added to the beginning and the end, namely the classification token ([CLS]) and the NSP token ([SEP]). These tokens have two functions: one serves as a representation input for classification tasks, and the other is to split a pair of input texts. Then, the sentence number is converted into a vector in Segment Embeddings. Meanwhile, the Position Embeddings create a vector for the word's position within the sentence. Finally, the three embeddings are summed up to generate a single shape representation passed to BERT's encoder layer [9]. Our proposed architecture is shown in Fig. 2.

V. CONCLUSION

This study showed that most text preprocessing tasks such as formalizing slang, fixing typos, case-folding, et cetera were not absolute things to do with transfer learning if the word embeddings method and DNN architecture were chosen correctly. There were insignificant differences between models with or without text preprocessing on most DNN architectures such as LSTM, Bi-LSTM, and CNN when utilizing BERT embeddings. Furthermore, combining BERT embeddings and CNN produced the best classification performance. Rather than wasting time preprocessing text data, researchers should focus on finding a suitable word embeddings approach and DNN architecture. Future studies should investigate the significance of each text preprocessing step since there were significant differences in performance results between the model with and without text preprocessing using GRU and MLP.

REFERENCES

[1] A. F. Hidayatullah, S. Cahyaningtyas, and A. M. Hakim, "Sentiment analysis on twitter using neural network: Indonesian presidential election 2019 dataset," *IOP Conference Series: Materials Science and Engineering*, vol. 1077, no. 1, p. 012001, feb 2021, doi: 10.1088/1757-899x/1077/1/012001.

[2] L. P. Manik, H. Febri Mustika, Z. Akbar, Y. A. Kartika, D. Ridwan Saleh, F. A. Setiawan, and I. Atman Satya, "Aspect-based sentiment analysis on candidate character traits in Indonesian presidential election," in

2020 International Conference on Radar, Antenna, Microwave, Electronics, and Telecommunications (ICRAMET), 2020, pp. 224–228, doi: 10.1109/ICRAMET51080.2020.9298595.

[3] E. Haddi, X. Liu, and Y. Shi, "The role of text pre-processing in sentiment analysis," *Procedia Computer Science*, vol. 17, pp. 26–32, 2013, first International Conference on Information Technology and Quantitative Management, doi: 10.1016/j.procs.2013.05.005.

[4] P. P. Adikara, S. Adinugroho, and S. Insani, "Detection of cyber harassment (cyberbullying) on instagram using naïve bayes classifier with bag of words and lexicon based features," in *Proceedings of the 5th International Conference on Sustainable Information Engineering and Technology*, ser. SIET '20. New York, NY, USA: Association for Computing Machinery, 2020, p. 64–68, doi: 10.1145/3427423.3427436.

[5] M. A. Fauzi, "Word2vec model for sentiment analysis of product reviews in Indonesian language," *International Journal of Electrical and Computer Engineering (IJECE)*, vol. 9, no. 1, p. 525, Feb. 2019, doi: 10.11591/ijece.v9i1.pp525-530.

[6] R. P. Nawangsari, R. Kusumaningrum, and A. Wibowo, "Word2vec for Indonesian sentiment analysis towards hotel reviews: An evaluation study," *Procedia Computer Science*, vol. 157, pp. 360–366, 2019, the 4th International Conference on Computer Science and Computational Intelligence (ICCSICI 2019) : Enabling Collaboration to Escalate Impact of Research Results for Society, doi: 10.1016/j.procs.2019.08.178.

[7] L. P. Manik, A. Ferti Syaifandini, H. F. Mustika, A. Fatchuttamam Abka, and Y. Rianto, "Evaluating the morphological and capitalization features for word embedding-based pos tagger in bahasa Indonesia," in *2018 International Conference on Computer, Control, Informatics and its Applications (IC3INA)*, 2018, pp. 49–53, doi: 10.1109/IC3INA.2018.8629519.

[8] J. Abdillah, I. Asror, and Y. F. A. Wibowo, "Emotion classification of song lyrics using bidirectional LSTM method with GloVe word representation weighting," *Jurnal RESTI (Rekayasa Sistem dan Teknologi Informasi)*, vol. 4, no. 4, pp. 723–729, Aug. 2020, doi: 10.29207/resti.v4i4.2156.

[9] J. Devlin, M.-W. Chang, K. Lee, and K. Toutanova, "BERT: Pre-training of deep bidirectional transformers for language understanding," in *Proceedings of the 2019 Conference of the North American Chapter of the Association for Computational Linguistics: Human Language Technologies, Volume 1 (Long and Short Papers)*. Minneapolis, Minnesota: Association for Computational Linguistics, Jun. 2019, pp. 4171–4186, doi: 10.18653/v1/N19-1423.

[10] A. Vaswani, N. Shazeer, N. Parmar, J. Uszkoreit, L. Jones, A. N. Gomez, L. u. Kaiser, and I. Polosukhin, "Attention is all you need," in *Advances in Neural Information Processing Systems*, I. Guyon, U. V. Luxburg, S. Bengio, H. Wallach, R. Fergus, S. Vishwanathan, and R. Garnett, Eds., vol. 30. Curran Associates, Inc., 2017.

[11] H. Tian, K. Yang, D. Liu, and J. Lv, "Anchibert: A pre-trained model for ancient Chinese language understanding and generation," in *2021 International Joint Conference on Neural Networks (IJCNN)*, 2021, pp. 1–8, doi: 10.1109/IJCNN52387.2021.9534342.

[12] D. Q. Nguyen and A. Tuan Nguyen, "PhoBERT: Pre-trained language models for Vietnamese," in *Findings of the Association for Computational Linguistics: EMNLP 2020*. Online: Association for Computational Linguistics, Nov. 2020, pp. 1037–1042, doi: 10.18653/v1/2020.findings-emnlp.92.

[13] B. Wilie, K. Vincentio, G. I. Winata, S. Cahyawijaya, X. Li, Z. Y. Lim, S. Soleman, R. Mahendra, P. Fung, S. Bahar, and A. Purwarianti, "IndoNLU: Benchmark and resources for evaluating Indonesian natural language understanding," in *Proceedings of the 1st Conference of the Asia-Pacific Chapter of the Association for Computational Linguistics and the 10th International Joint Conference on Natural Language Processing*. Suzhou, China: Association for Computational Linguistics, Dec. 2020, pp. 843–857.

- [14] F. Koto, A. Rahimi, J. H. Lau, and T. Baldwin, "IndoLEM and IndoBERT: A benchmark dataset and pre-trained language model for Indonesian NLP," in *Proceedings of the 28th International Conference on Computational Linguistics*. Barcelona, Spain (Online): International Committee on Computational Linguistics, Dec. 2020, pp. 757–770, doi: 10.18653/v1/2020.coling-main.66.
- [15] L. P. Manik, Z. Akbar, H. F. Mustika, A. Indrawati, D. S. Rini, A. D. Fefirenta, and T. Djarwaningsih, "Out-of-scope intent detection on a knowledge-based chatbot," *International Journal of Intelligent Engineering and Systems*, vol. 14, no. 5, pp. 446–457, Oct. 2021, doi: 10.22266/ijies2021.1031.39.
- [16] K. S. Nugroho, A. Y. Sukmadewa, H. Wuswilahaken DW, F. A. Bachtiar, and N. Yudistira, *BERT Fine-Tuning for Sentiment Analysis on Indonesian Mobile Apps Reviews*. New York, NY, USA: Association for Computing Machinery, 2021, p. 258–264, doi: 10.1145/3479645.3479679.
- [17] I. F. Putra and A. Purwarianti, "Improving Indonesian text classification using multilingual language model," in *2020 7th International Conference on Advance Informatics: Concepts, Theory and Applications (ICAICTA)*, 2020, pp. 1–5, doi: 10.1109/ICAICTA49861.2020.9429038.
- [18] J. Fawaid, A. Awalina, R. Y. Krisnabayu, and N. Yudistira, *Indonesia's Fake News Detection Using Transformer Network*. New York, NY, USA: Association for Computing Machinery, 2021, p. 247–251, doi: 10.1145/3479645.3479666.
- [19] M. R. Yanuar and S. Shiramatsu, "Aspect extraction for tourist spot review in Indonesian language using bert," in *2020 International Conference on Artificial Intelligence in Information and Communication (ICAIIIC)*, 2020, pp. 298–302, doi: 10.1109/ICAIIIC48513.2020.9065263.
- [20] W. Maharani, "Sentiment analysis during Jakarta flood for emergency responses and situational awareness in disaster management using bert," in *2020 8th International Conference on Information and Communication Technology (ICoICT)*, 2020, pp. 1–5, doi: 10.1109/ICoICT49345.2020.9166407.
- [21] A. R. Isnain, A. Sihabuddin, and Y. Suyanto, "Bidirectional long short term memory method and word2vec extraction approach for hate speech detection," *IJCCS (Indonesian Journal of Computing and Cybernetics Systems)*, vol. 14, no. 2, p. 169, Apr. 2020, doi: 10.22146/ijccs.51743.
- [22] J. Camacho-Collados and M. T. Pilehvar, "On the role of text preprocessing in neural network architectures: An evaluation study on text categorization and sentiment analysis," in *Proceedings of the 2018 EMNLP Workshop BlackboxNLP: Analyzing and Interpreting Neural Networks for NLP*. Brussels, Belgium: Association for Computational Linguistics, Nov. 2018, pp. 40–46, doi: 10.18653/v1/W18-5406.
- [23] E. Alzahrani and L. Jololian, "How different text-preprocessing techniques using the bert model affect the gender profiling of authors," in *Advances in Machine Learning*. Academy and Industry Research Collaboration Center (AIRCC), Sep. 2021, doi: 10.5121/csit.2021.111501.
- [24] J. Dong, F. He, Y. Guo, and H. Zhang, "A commodity review sentiment analysis based on bert-cnn model," in *2020 5th International Conference on Computer and Communication Systems (ICCCS)*, 2020, pp. 143–147, doi: 10.1109/ICCCS49078.2020.9118434.
- [25] H. Karande, R. Walambe, V. Benjamin, K. Kotecha, and T. Raghu, "Stance detection with BERT embeddings for credibility analysis of information on social media," *PeerJ Computer Science*, vol. 7, p. e467, Apr. 2021, doi: 10.7717/peerj-cs.467.

VIHS with ROTR Technique for Enhanced Light-Weighted Cryptographic System

Sanjeev Kumar A N, Ramesh Naik B
Dept. of Computer Science and Engineering
GITAM School of Technology
GITAM Deemed to be University
Bengaluru, India

Abstract—Developing a bypass parallel processing block is one of the emerging and exciting research areas in the system encrypt/decrypt application areas. A Partial Pseudo-Random-based Hashing VIHS is the most suitable methodology for designing the system to encrypt/decrypt a block in cryptography. For this purpose, various VIHS and register techniques have been developed to process the storage system data. But, it is limited by the problems of reduced efficiency, increased computational complexity, high area consumption, and cost consumption. Thus, this research intends to develop a novel dynamic system register with hashing with optimal Hash Signature design to process the system's encryption /decrypt data. The main intention of this paper is to analyze the transfer characteristics of the current based on the pseudo-differential pair for a proficient system detection. Then, a system window can be created and adjusted to obtain an optimized power flow with less data loss sensitivity. The major stages involved in the proposed block design are register, partition design, and VIHS design. The dynamic system register is designed at first for getting a fast decision and to enable a low input-referred offset value. Then, the partition is formed concerning the output of the register, and the VIHS is used to produce the high proportional logical work. During performance evaluation, various measures have been utilized to analyze the performance of the proposed dynamic system register-based hashing with optimal Hash Signature design. In addition to that, the estimated results are compared with the proposed technique to prove its efficiency.

Keywords—Cryptography – partial pseudo-random based hashing technique; logical to sequential VIHS; system encrypts/decrypt data; dynamic system register; bypass parallel processing

I. INTRODUCTION

Internet of Things (IoT) [1] [2] is one of the most widely used networking paradigms for establishing reliable and secured data transmission, which contains different intelligent devices that help exchange the data across the network in a secure way. Especially in the medical healthcare systems, the patients' information must be protected and secured against unauthenticated access, which guarantees the security and authenticity of the networking system. The Electrocardiogram (ECG) signals [3] [4] are mainly used to monitor the patient's health information, which providing security to this type is also one of the crucial factors. For this purpose, various techniques [5] [6] have been developed to secure the patients' medical healthcare information. Hence, disparate security frameworks and architectures have been deployed in the proposed work. This paper mainly focuses on developing the lightweight data security model for the medical ECG signal transmission system incorporated with the IoT network.

For this purpose, the Viterbi Integrated Hash Signature (VIHS) based architecture of the ECC encryption method is implemented. Here, the random keys have been generated based on the integrated architecture of Hashed signature technique. It is mainly used to reduce the complexity of the model with an enhanced working speed of the algorithm. The reduction of iteration count can reduce the size of architecture, resulting in a lightweight encryption system. Novel lightweight data encryption with an optimal key generation system is proposed for the IoT Network transmission system to overwhelm these problems. This can be achieved by extracting the signal peaks using the Viterbi algorithm to select the best value for random key generation and the fast switching process. This can be processed by referring to the parameters of distance and the phase angle-based reference properties. This will collect information about the pattern of the signature and the size of critical formation in the batch mode of the process to retrieve the topology in parallel [7] [8]. In the encryption process, a light-weighted cryptographic system by using the ROTR Messaging technique. The proposed encryption process reduces the buffer size and reduces the power consumption due to the optimal key size of the cryptographic technique. We developed the VIHS algorithm and integrated it with ROTR in the ECC encryption method. The random critical formation is referred to from the look-up table of the ECC model, and this can generate the public and private keys for the encryption process [9]. The algorithm's implementation is in progress to enhance the performance of the encryption system [10] compared to the other traditional encryption model.

The primary objectives behind this research work are as follows:

- 1) To develop the lightweight security model for processing the medical ECG signals in the IoT framework.
- 2) To ensure the system's increased security and reduced complexity, the Viterbi Integrated Hash Signature (VIHS) verification scheme is utilized.
- 3) The Randomized Off-the Record (ROTR) based messaging technique is employed to reduce the Off-the-Record and power consumption of signal transmission yet.
- 4) To validate the proposed security framework's performance, various evaluation indicators such as error rate, throughput, transmission delay, and key selection time have been used.

The rest of the sections present in the paper are struc-

turalized as follows: Section II discusses some of the existing security techniques used for securing the ECG signals with their advantages and disadvantages. Section III presents a detailed description of the proposed methodology with its flow illustration. The performance and comparative results of both existing and proposed techniques are validated using Section IV's performance measures. Finally, the overall paper is concluded with its future work in Section V.

II. LITERATURE SURVEY

This section presents the literature review of various existing techniques used for ensuring the security of ECG signal processing and transmission systems. Also, it discusses the advantages and disadvantages of each method based on its operating principles.

Wang *et al.* [11] employed a logistic mapping-based encryption model for improving the security of WBAN. The main intention of this paper was to ensure the security and computing ability of biomedical sensors with restricted user access by using the quantized logistic mapping-based encryption technique. Here, the different types of parameters such as Power Spectral Entropy (PSD) and Peak-to-Average Power Ratio (PAPR) have been utilized to evaluate the performance of the suggested mechanism. Moreover, the Lyapunov factor has been considered in this work for analyzing the chaotic characteristics with respect to the random property of the system. In addition to that the normalized spectral entropy was computed based on the parameters of pseudo-random sequence, power spectrum, total power, sequence spectral entropy, and normalization of entropy. At last, binary quantization was also applied for increasing the retention accuracy of the overall security system. The major drawback of this work was, it has an increased complexity in designing algorithms that limits the performance of the entire system. Hameed *et al.* [12] implemented the lossless compression mechanism with Huffman coding scheme for ensuring the security of broadcast transmission in WBAN. It comprises the stages of estimating the buffer blocks, compression, and encryption, which helps to establish the secured transmission in the network. Also, this work intends to obtain the quality control compressed data by employing the cipher block-based chaining encryption algorithm. During the block creation, the QRS complex has been estimated for detecting the peak count of the signal. Consequently, the bandpass filtering technique was applied to eliminate the noisy contents based on the integer coefficients. The advantage of this work was, it efficiently reduced the error rate between the signals by estimating their similarity with high reliability.

Janveja *et al.* [13] designed an efficient AES algorithm for securely transmitting the ECG signals by deploying the modified folded architecture. Here, the key description module has been additionally incorporated with the standard AES technique with reduced functional units. Djelouat *et al.* [14] utilized a lightweight encryption scheme for developing the secured health monitoring architecture. The main considerations of this work were as follows: to obtain the reduced load on data transmission, and to establish the secured data transmission with increased reliability. For this purpose, the Compressing Sensing (CS) platform has been incorporated

with this framework, which helps to perform remote monitoring in a secure way. The benefits of this framework were low transmission power, low coherence, reduced complexity in designing, and simple acquisition. Qiu *et al.* [15] suggested the selective encryption mechanism with the supervised machine learning technique for increasing the security of data privacy and effectiveness in BSNs. Here, the wavelet-based transformation technique has been utilized for compressing the sensor information efficiently. Moreover, the SVM-based machine learning classification technique was employed to classify the disease based on the frequency bands.

Mathivanan *et al.* [16] employed a QR code-based encryption algorithm for processing the ECG signals with increased security. The main factors of this paper were to obtain an increased embedding capacity and ensured security for the complete data retrieval. Moreover, the quick response code has been utilized in this work for storing the hidden information for ensuring data security. The advantages of this paper were better error correction, maximum storage efficiency, and increased data retrieval capacity. Hameed *et al.* [17] recommended an AES-based encryption algorithm for ensuring the properties of authentication, confidentiality, and integrity of the ECG signal transmission system. Here, the encryption and decryption processes were carried out based on the Electronic Code Book (ECB). Yet, the major disadvantages of using AES techniques were increased computational overhead and complexity in handling. Awasarmol *et al.* [18] utilized the DWT technique with the scrambling matrix formation approach for transmitting the ECG signals in a secured way. The main intention of this paper was to extract the secret message with the help of DWT mechanism and to eliminate the noisy contents by using the band pass filtering technique. The stages involved in this work were signal decomposition, de-noising, DWT based feature extraction, scrambling matrix formation, encryption, and decryption. The merits of this work were reduced computational time, complexity and increased accuracy.

Hameed *et al.* [19] utilized a lossless compression mechanism incorporated with the hybrid cryptography technique for securing the ECG signal processing systems. This incorporated the functionalities of Huffman coding scheme with the AES encryption mechanism for enabling a lossless data compression. Also, the Diffie-Hellman based key exchange mechanism was utilized to ensure the increased security of signal transmission. However, it requires more time for signal compression and transmission, which degrades the entire performance of the system. Shaikh *et al.* [20] employed an improved data encryption algorithm for establishing the secured ECG signal transmission. In which, the homomorphic encryption mechanism was utilized to encrypt the ECG signals of patients with ensured reliability and confidentiality. Still, this work limits with the issue of increased information that reduces the performance of this security system. Karthikeyan *et al.* [21] recommended the Secure Force (SF) based cryptographic technique for improving the security of WBANs. Here, the DWT and Daubechies wavelet-based feature extraction techniques have been utilized for signal decomposition and noise removal, because the performance of the signal processing system was highly dependent on the quality of signals. The main factor of this work was to utilize the simple cryptographic technique with reduced complexity, low power consumption, and computational devices.

Premkumar *et al.* [22] recommended an enhanced encryption approach with a scrambling matrix construction technique for hiding the confidential information of patients. Also, the deterministic algorithm named, Pseudo-random binary sequence generation algorithm was employed in this work for ensuring the security of the private healthcare information system. Then, the Elliptic Curve Cryptography (ECC) technique was applied for encrypting and decrypting the user data with ensured confidentiality and reliability. L.Zheng *et al.* [23], a detailed study has been conducted on various data encryption mechanisms used for securing the internet of medical things application system. Here, the performance of standard DES and ECC techniques has been validated based on the terms of accuracy, time consumption, and stability. From this paper, it is studied that the desired properties of security and efficiency could be addressed by the cryptographic techniques for guaranteeing the secured communication of the signal processing system.

Sivasangari *et al.* [24] suggested the lightweight selective encryption mechanism for guaranteeing the confidentiality and authenticity of the users' data. The main consideration of this paper was to minimize the computational overhead of the WBSN by optimizing the energy level of nodes. Also, it aims to improve the security of the system by establishing the three-layered communication in the network. Yet, it has the limitations of requiring more time consumption, and reduced performance outcomes.

From this review, it is observed that the existing security approaches are mainly focusing on establishing reliable signal transmission by incorporating the functions of standard cryptographic mechanisms. However, it faces the major challenges of increased complexity in designing the algorithms, requires more time consumption for transmission, increased loss of information, and reduced accuracy. In order to solve these problems, this research work intends to develop a novel algorithm for securing the ECG signal processing system. The major key points that are observed from these existing methods are to provide a secure data transmission system for the medical ECG signal and its data. For that, these algorithms are consumed more bit size to generate the key-value due to the precision of signal amplitude and its parameters. This leads to an increase in the energy consumption of the overall system and reduces the transmission rate. Further to improve the security service, the key size is increased to the corresponding size of data and its length. This becomes the motivation of the proposed work to implement the lightweight cryptographic system for ECG signals. According to this, the key pattern generation and the encryption model are enhanced for the high precision of amplitude and improve the Quality of Service (QoS).

Security is a core quality of an IoMT system and is linked to certain security aspects frequently required for allowing Trust and Privacy qualities in a system. IoMT Security focuses on securing connected devices and protecting data and networks on the Internet of Medical Things. Further IoMT devices are more prone to attack from the attackers. We proposed a new method of mechanism to protect the data from the IoMT devices.

III. PROPOSED METHOD

This section presents the overall description of the proposed bypass parallel processing optimal Hash Signature-partition design with its clear illustration. The main aim of this work is to develop an optimal Hash Signature VIHS with a new register design for storing data in the system and validate the data with a reduced error rate compared to another application process. In this, the peak value of ECG signal was extracted for the reference to generate the random key value. Here, this implementation reduces the amount of data required to be stored in various stages, and the amount of time essential for processing. According to that, an appropriate low-power hardware architecture has been designed to implement a real-time high performance and low-cost optimal Hash Signature block with the proposed decoder algorithm. This block design is highly more suitable for mobile applications. In which, the distinct data can be simulated based on the random data generation, where the sampling rate of 360Hz is relevant to clock frequency. The overall block representation of the proposed architectural design of VIHS hashing in the cryptography is represented in Fig. 1.

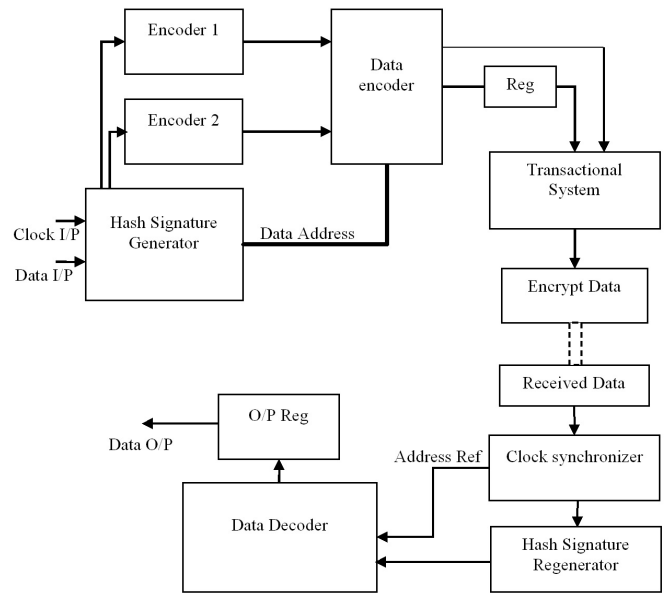


Fig. 1. Block Diagram of Proposed Hashing Technique of ECG Cryptography.

In this figure, the architecture represents the flow architecture of input ECG data and the block design of the encryption and decryption flow line. The block architecture represents the binary transmission of data to the encryption module to retrieve the hash signature and to form the encoded data. Initially, the input data are passed in bit sequence in accordance with the clock pulse that are synchronized with the encoders. Here, the Hash signature generator is to generate the random address and the key patterns based on the VIHS model. This transmit to the encoder block to encode the block that are indexed with the address of data. From that, the data got encoded and passed to the transactional system to transmit data through transmission channel. In the decryption process, the clock synchronizer predicts the data sequence and the

address of it. This provide the reference to Hash Signature Regenerator. The main parameters that are considered for the lightweight architecture of ECG signal secure transmission were the number of bit size, key initialization and the random integer number generation, energy parameter of the overall system, and the Quality of Service (QoS). From this, the data was decoded and reconstructed to the actual ECG signal pattern. The major stages comprise of the proposed register design are as follows:

- 1) VIHS design
- 2) Hashing Model.
- 3) Data Transfer Architecture

A. VIHS Design

The register used in this block design is one of the essential component in electronic block after each Hash Signature connected with the latches. Typically, it is a major building block for most of the applications, in which the logical information has to be recovered from the sequential data specifically in optimal XORs. Moreover, this register is more suitable for the logic blocks, where the latch provides the large and fast output data. Then, its waveform and amplitude are independent of input data. Generally, two types of registers have been used named as static and dynamic, in which each gate output is connected with flags through a decrypt line path by the static registers. Similar to that, the dynamic registers could rely on the temporary storage of data values on the binaries of high sensitive block nodes. Moreover, the static registers are more suitable medium speed applications, and the dynamic registers are more suitable for high sensitive block nodes. But, it is highly sensitive to noise, in which varying sampling rates can be used for different applications.

When compared to the static registers, the dynamic registers gained a significant attraction in medium to high-speed applications. Furthermore, it is energy efficient owing to the non-consumption of static current contrast. Fig.2. shows the schematic representation of the Hash Signature and register allocation flow with corresponding output units. In this, the arrangement of XOR and the Registers was formed to extract the Hash Key pattern. The dotted block indicates the Optimal placement using VIHS for the single-bit pattern. This it will be arranged as the sequential order to construct the 'N' number of bit size for the input signal amplitude. The final output data was arranged in the output register to get the 'OUTr'. It comprises the following stages: pre-amplifier, track and latch, where the pre-amplifier is larger than the input data and is not large sufficient to drive the logical block. Then, a track and latch stages are used to amplify the data to logic with the use of positive feedback loop. The major benefits behind this register design are high input sensitive, no static power consumption, full swing outcome, and fast decision rate.

B. Hashing Model

The proposed hashing with optimal Hash Signature design is fully based on the binary search algorithm, where the partition is a kind of logical controller block that has responsibility to run the binary search procedure. Also, the output of hashing with optimal Hash Signature can be determined with the respect to the register output. So, it has the momentous effect on improving the overall performance of

optimal Hash Signature design. This register contains N bit optimal Hash Signature, which contains three possibilities for each bit that is either 0 or 1. At first, the MSB can be set as 1 and other bits can be reset by 0, and the logical word is converted with respect to the sequential value via the VIHS unit. Then, the output of sequential data can be inserted to the input of register, and is compared with the sampled input. Based on this outcome, the partition controller can estimate the value of MSB, where if the input is higher than the VIHS output the value of MSB can be set as 1; else, set as 0. During the last cycle, the converted logical word is stored, and N+1 clock cycles could be performed for conversion. Moreover, the partition can be designed with the use of register and the controlling block for encoding the Key to cryptography, and the conversion process can be continued only when the Hash Signature input is low.

Fig. 3 shows the schematic representation of the hashing with optimal Hash Signature logic. In that, the (a) shows the block architecture for encryption process and the (b) represents for the decryption flow. The registers and the indexing block are used to find the encoded data samples that are passed through shift registers and count the repeated pattern of data samples. While at the decryption stage, the synchronizer detect the data samples with the clock pulses to reconstruct the data from the decryption block. The major building blocks of this block are dynamic latched register and inverters. The Algorithm I represents the steps for proposed hashing model for random Key generation.

Algorithm 1 VIHS based Data Encryption

Input: Plain text 'M'

Output: Encrypted text 'E'

1: **procedure** ENCRYPTION

2: **Initialize:**

 Elliptical Curve Equation: $y^2 \leftarrow x^3 + ax + c$

 ▷ 'x' and 'y' are the coordinate points of curve.

 ▷ 'a' and 'b' are the constant coefficients.

3: $x \leftarrow 0$

4: Estimate the maximum limit of 'x' value that satisfy the selected curve line equation as 'p'

5: **while** $x < p$ **do**

6: Calculate 'y' value from the selected curve equation for each 'x' value in the loop

7: Estimate modulo division of y with p as Z_p

$Z_p = \text{mod}(y,p)$

8: **if** $Z_p == 0$ **then**

9: $C \leftarrow (x, \sqrt{y}), (x, -\sqrt{y})$.

10: $x = x + 1$

End loop

11: Calculate

$Q_A(x,y) = A * C(x,y)$

$Q_B(x,y) = B * C(x,y)$

 Sender and Receiver respectively.

 ▷ Where,

 ▷ 'A' - Sender

 ▷ 'B' - Receiver

12: Calculate

$R_A(x,y) = A * Q_B(x,y)$

$R_B(x,y) = B * Q_A(x,y)$

 Sender and Receiver respectively to satisfy $R_A = R_B$.

13: Find the median of R_A and R_B to form Secrete key 'S'.

14: Find the median of S and M to get encrypted text 'E'.

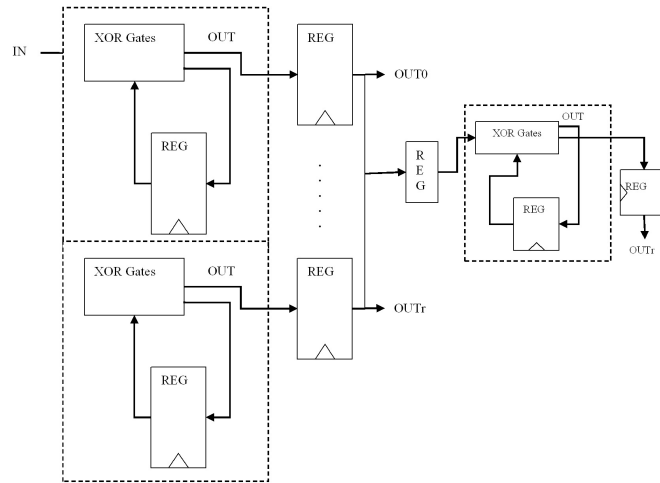


Fig. 2. VIHS Register Allocation Design.

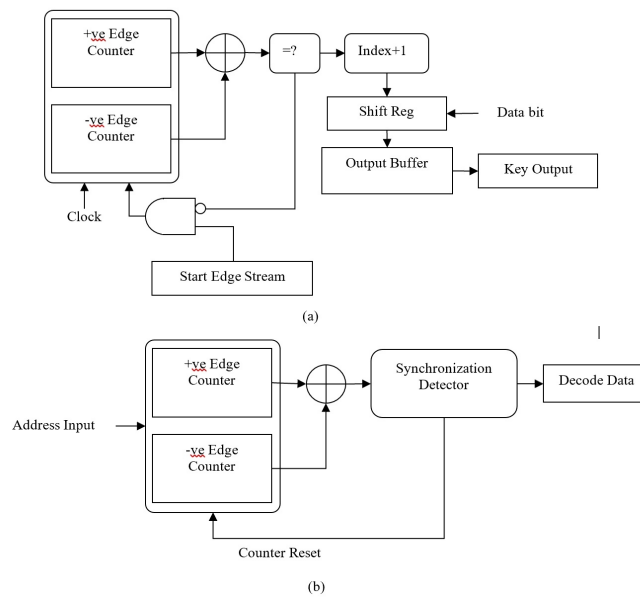


Fig. 3. Block Diagram for Key Passing in Encrypt/Decrypt Process.

Algorithm 2 VIHS based Data Decryption

Input: Encrypted text ‘E’

Output: Decrypted plain text ‘M’

1: **procedure** DECRYPTION

2: Collect Secrete Key ‘S’ generated in encryption stage.

3: Estimate the median of ‘S(x,y)’ and ‘E(x,y)’.

4: Decrypted text

$$M^1(x, y) = C\{2.(E(x)-S(x)), 2.(E(y)-S(y))\}.$$

Let the input binary bits for the system stream can be represent as I_n . For the random Key generation, the Key should be regenerative based on the input matrix. Select a random number between 0 to ‘p’ as ‘A’ from sender and ‘B’ from receiver.

This cross computing generates the random Key for the system storage which can be represent as R_V . The reverse process can regenerate the random Key to encrypt the data from Key location in cryptography.

C. Data Transfer Architecture

Typically, the VIHS is a kind of device that is mainly used to convert the logical input data into an sequential output data. Then, its result is highly proportional to the logical value, in which the conversion tool can be acts as an interface between the logical and sequential blocks. Moreover, it serves a feedback data to correct the errors and estimates the reference data sequence during the process of conversion. During the design of VIHS, the values of supporting blocks should be determined based on the manual estimation process. Then, it can be adjusted further during the time of simulation, where some of the parameters can be considered with respect to the AMS technology. The architecture process can be defined according to the AMS technology as follows:

1. Arrangement of Hash Signature blocks.
2. Combination of Registers and Hash Signature.

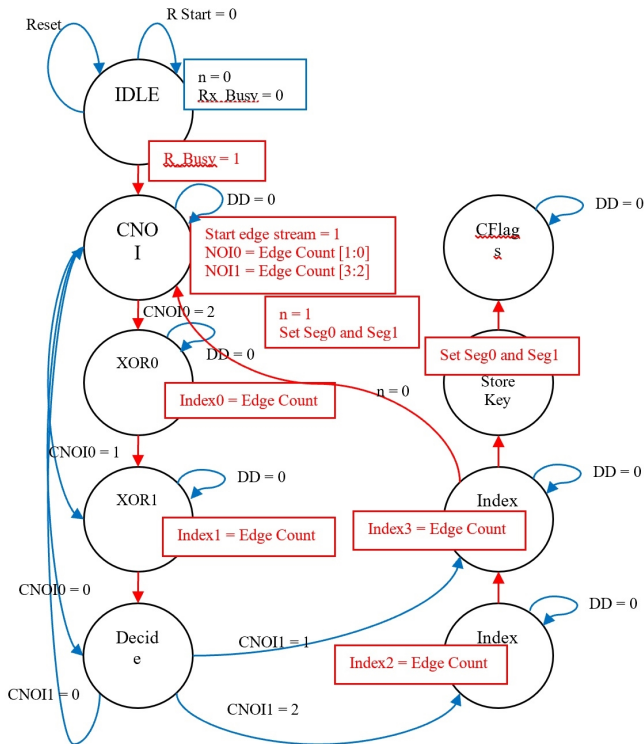


Fig. 4. State Flow for VIHS Generator.

The schematic illustration of VIHS design is depicted in Fig. 4. which comprises three stages. These are all combined with the architecture of XOR and the Register block arrangement. The state flow starts from the idle state of overall design. In this, the CNOI represents the count of number of Instant from the input ECG data samples. This was passed to the XOR combination flow and the flag CNOI are updated each time with respect to the data flow line. The decision was taken that according to the satisfactory level of encryption model and it flow in loop of updating CNOI to make the data pattern in random manner. This was also updated as the edge count that indicates the amount of loop that is running for the data

encryption. Then this was encoded by the indexing method and get the encrypted and encoded data samples.

IV. RESULTS AND DISCUSSION

Since findings suggest that IoT security requires substantial improvement before it is suitable for wide consumer acceptance. There are still many security issues. The most prominent were computation capability, memory, and time issues, and a lack of management mechanisms. Computation capability is critical within the Internet of Medical Things since the devices utilized frequently capture private, sensitive data, such as health information.

The simulation and Key implementation results have been validated for the proposed bypass parallel processing hashing with an optimal Hash Signature model with the output waveforms in the MATLAB 2011b platform. The data samples that are used for the testing of the proposed model was Physionet MITDB database. In that, the ECG signals are pre-processed and saved it in the '.mat' file format. In that file, ECG Data is a structure array with two fields: Data and Labels. Data is a 162x65536 matrix. This indicates there are 162 number of data samples present in the matrix. This time length are represented in terms of time samples with the size of 65536 measured for the length of 1 hour. Moreover, the results are compared with the state-of-the-art models by using the measures of frequency, Gates utilization count, power, area, sampling rate and propagation delay.

TABLE I. BIT SIZE COMPARISON FOR VIHS MODEL

Methods	Message count	Bit size
Mutual authentication	2	1184 bits
Efficient authenticated key for TMIS	2	1184 bits
Enhanced TMIS	2	1344 bits
Burrows-Abadi-Needham logic	3	1600 bits
TMISs	3	1280 bits
MQTT protocol	2	800 bits
Proposed	2	763 bits

Table I evaluates the comparison of the existing random number generation block in the hashing Memory design and proposed technique of VIHS in Cryptography with respect to the measures of components size based on the number of 2-input Hash Signature's, 3-Input Hash Signature's and the number of Flip-Flops that are referred from the paper [25]. For this analysis, some of the existing hashing with optimal Hash Signature designs have been considered. These results stated that the proposed dynamic system register-based hashing with optimal Hash Signature provides the better size in components, when compared to the existing model of VIHS.

TABLE II. COMPARISON OF TIME TAKEN FOR ENCRYPTION AND DECRYPTION (MS)

Methods	Time taken (ms)
Mutual authentication	13.38 ms
Efficient authenticated key for TMIS	13.4 ms
Enhanced TMIS	15.6 ms
Burrows–Abadi–Needham logic	11.17 ms
TMISs	8.9 ms
MQTT protocol	8.9 ms
Proposed	7.4 ms

Table II compares the values of area consumption in the unit of (μm^2) in the existing [25] and proposed hashing with optimal Hash Signature methodologies. For the proposed work, the power consumption is reduced to the range of 25%. From the evaluation, it is evident that the proposed hashing with optimal Hash Signature could efficiently reduce the power and area consumption when compared to the existing technique of the VIHS model. Then, its corresponding graphical illustration of the area consumption is shown in Fig. 6 and Fig. 7 shows the comparison chart of FFs, LUT, and Slices utilization count for the existing [26] and proposed design of the VIHS generator.

TABLE III. COMPARISON TABLE OF MESSAGE COUNT AND BIT SIZE FOR THE VIHS KEY GENERATOR

Methods	Message count	Bit size
Dey and Hossain scheme	5	1312 bits
ECC-CoAP	4	1024 bits
Proposed	4	926 bits

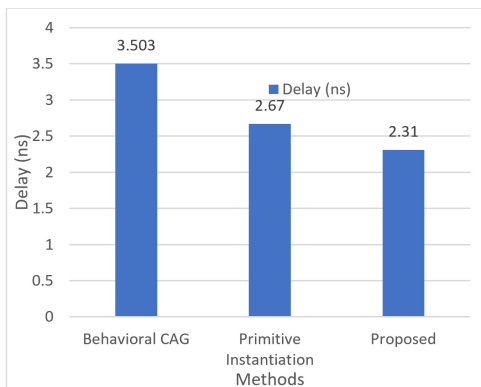


Fig. 5. Delay (ns).

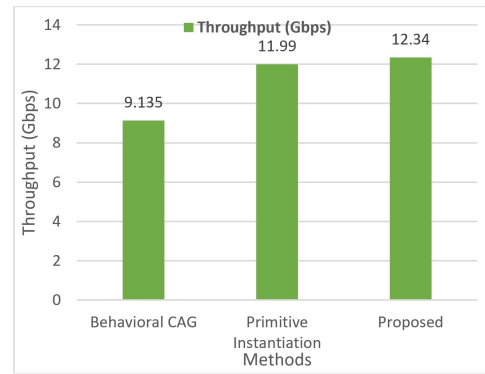


Fig. 6. Throughput (Gbps).

Table III illustrates the utilization count of throughput and delay rate of the existing and proposed VIHS technique. The corresponding graphical illustrations of these measures are represented in Fig. 5 and Fig. 6. From the analysis, it is proved that the proposed hashing with optimal Hash Signature provides better results, when compared to the other register techniques.

TABLE IV. DELAY RATE (NS) AND THROUGHPUT (GBPS) COMPARISON TABLE

Methods	Delay (ns)	Frequency (MHz)	Throughput (Gbps)
Behavioral CAG	3.503	285.47	9.135
Primitive Instantiation	2.67	374.53	11.99
Proposed	2.31	432.9004	12.34

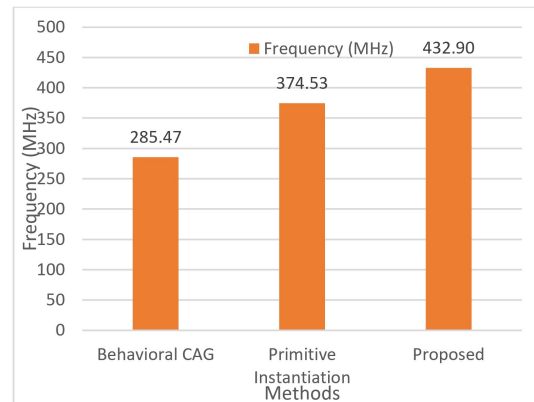


Fig. 7. Frequency (MHz).

Table IV and Fig. 7 shows the delay (ns) along with the frequency (MHz) and the throughput (Gbps) of various existing referred from [26] and the proposed technique of VIHS. In that comparison, the propagation delay is reduced to 2.31 ns by the proposed hashing with optimal Hash Signature design. These results stated that the proposed register could efficiently reduce the delay, when compared to the other techniques. Based on the overall analysis, it is evident that the proposed dynamic system register based hashing with optimal Hash Signature is more suitable and efficient for processing the system encrypt/decrypt applications.

V. CONCLUSION

In this paper, we presented a new register design with hashing with optimal Hash Signature for processing the system encrypt/decrypt data. The main aim behind this work is to encrypt/decrypt data in the system with a reduced amount of error rate. This designing methodology will reduce the amount of data required to be stored in various stages, and the time required for processing the data. Moreover, the proposed dynamic system register adopts the current controller, which generates both the polarity outputs and bypass trigger data during the same conversion. Here, a pseudo-differential pair is constructed to simulate the transfer characteristics. In this design, the charging speed can be adjusted with the process variation, component mismatch, and parasitics along the paths. After that the reference data sequence and binaries data sequences can be modified with respect to the bypass window size. In addition to that the bypass window size and speed of the register have been analyzed for architecture power-saving application area. The hashing with optimal Hash Signature provides low data sequence sensitivity, increased efficiency, and low power consumption. The VIHS could provide a residual data sequence with respect to the linear feedback of the conversion data. During the experimental evaluation, there are metrics have been validated to analyze the performance of the proposed register design. From the results, it is proved that the proposed technique provides better results when compared to the traditional techniques.

Future enhancement, this type of security system for medical applications is integrated with a new register design structure for the logical functionalities to generate the random number formation for a real-time application. This will improve the time complexity and the space complexities of the overall system.

REFERENCES

- [1] M. N. Aman, M. H. Basheer, and B. Sikdar, "Data provenance for iot with light weight authentication and privacy preservation," *IEEE Internet of Things Journal*, vol. 6, no. 6, pp. 10441–10457, 2019.
- [2] —, "A lightweight protocol for secure data provenance in the internet of things using wireless fingerprints," *IEEE Systems Journal*, vol. 15, no. 2, pp. 2948–2958, 2020.
- [3] M. Almulhim and N. Zaman, "Proposing secure and lightweight authentication scheme for iot based e-health applications," pp. 481–487, 2018.
- [4] K. Haseeb, N. Islam, T. Saba, A. Rehman, and Z. Mehmood, "Lsdar: A light-weight structure based data aggregation routing protocol with secure internet of things integrated next-generation sensor networks," *Sustainable Cities and Society*, vol. 54, p. 101995, 2020.
- [5] H. Shin, H. K. Lee, H.-Y. Cha, S. W. Heo, and H. Kim, "Iot security issues and light weight block cipher," pp. 381–384, 2019.
- [6] O. H. Alhazmi and K. S. Aloufi, "Fog-based internet of things: a security scheme," pp. 1–6, 2019.
- [7] S. Suganthi, R. Anitha, V. Sureshkumar, S. Harish, and S. Agalya, "End to end light weight mutual authentication scheme in iot-based healthcare environment," *Journal of Reliable Intelligent Environments*, vol. 6, no. 1, pp. 3–13, 2020.
- [8] W. Haoxiang *et al.*, "Trust management of communication architectures of internet of things," *Journal of trends in Computer Science and Smart technology (TCSST)*, vol. 1, no. 02, pp. 121–130, 2019.
- [9] M. Wazid, A. K. Das, V. Bhat, and A. V. Vasilakos, "Lam-ciot: Lightweight authentication mechanism in cloud-based iot environment," *Journal of Network and Computer Applications*, vol. 150, p. 102496, 2020.
- [10] S. Amanlou, M. K. Hasan, and K. A. A. Bakar, "Lightweight and secure authentication scheme for iot network based on publish–subscribe fog computing model," *Computer Networks*, vol. 199, p. 108465, 2021.
- [11] J. Wang, K. Han, S. Fan, Y. Zhang, H. Tan, G. Jeon, Y. Pang, and J. Lin, "A logistic mapping-based encryption scheme for wireless body area networks," *Future Generation Computer Systems*, vol. 110, pp. 57–67, 2020.
- [12] M. E. Hameed, M. M. Ibrahim, N. Abd Manap, and A. A. Mohammed, "A lossless compression and encryption mechanism for remote monitoring of ecg data using huffman coding and cbc-aes," *Future generation computer systems*, vol. 111, pp. 829–840, 2020.
- [13] M. Janveja, B. Paul, G. Trivedi, G. Vijayakanthi, A. Agrawal, P. Jan, and Z. Nĕmec, "Design of efficient aes architecture for secure ecg signal transmission for low-power iot applications," pp. 1–6, 2020.
- [14] H. Djelouat, A. Amira, F. Bensaali, and I. Boukhenoufa, "Secure compressive sensing for ecg monitoring," *Computers & Security*, vol. 88, p. 101649, 2020.
- [15] H. Qiu, M. Qiu, and Z. Lu, "Selective encryption on ecg data in body sensor network based on supervised machine learning," *Information Fusion*, vol. 55, pp. 59–67, 2020.
- [16] P. Mathivanan, A. B. Ganesh, and R. Venkatesan, "Qr code–based ecg signal encryption/decryption algorithm," *Cryptologia*, vol. 43, no. 3, pp. 233–253, 2019.
- [17] M. E. Hameed, M. M. Ibrahim, N. Abd Manap, and M. L. Attiah, "Comparative study of several operation modes of aes algorithm for encryption ecg biomedical signal," *International Journal of Electrical and Computer Engineering*, vol. 9, no. 6, p. 4850, 2019.
- [18] S. P. Awasarmol, S. Ashtekar, and A. Chintawar, "Securely data hiding and transmission in an ecg signal using dwt," pp. 2850–2854, 2017.
- [19] M. E. Hameed, M. M. Ibrahim, N. A. Manap, and A. A. Mohammed, "An enhanced lossless compression with cryptography hybrid mechanism for ecg biomedical signal monitoring," *International Journal of Electrical & Computer Engineering (2088-8708)*, vol. 10, no. 3, 2020.
- [20] M. U. Shaikh, S. A. Ahmad, and W. A. W. Adnan, "Investigation of data encryption algorithm for secured transmission of electrocardiograph (ecg) signal," pp. 274–278, 2018.
- [21] M. Karthikeyan and J. Manickam, "Ecg-signal based secret key generation (eskg) scheme for wban and hardware implementation," *Wireless Personal Communications*, vol. 106, no. 4, pp. 2037–2052, 2019.
- [22] S. Premkumar and J. Mohana, "A novel ecg based encryption algorithm for securing patient confidential information," *International Journal of Electrical Engineering & Technology (IJEET)*, vol. 2, no. 11, pp. 35–43, 2020.
- [23] L. Zheng, Z. Wang, and S. Tian, "Comparative study on electrocardiogram encryption using elliptic curves cryptography and data encryption standard for applications in internet of medical things," *Concurrency and Computation: Practice and Experience*, p. e5776, 2020.
- [24] A. Sivasangari, S. Bhowal, and R. Subhashini, "Secure encryption in wireless body sensor networks," pp. 679–686, 2019.
- [25] A. Sivasangari, A. Ananthi, D. Deepa, G. Rajesh, and X. M. Raajini, "Security and privacy in wireless body sensor networks using lightweight cryptography scheme," pp. 43–59, 2021.
- [26] L. Xiong, X. Han, C.-N. Yang, and Y.-Q. Shi, "Robust reversible watermarking in encrypted image with secure multi-party based on lightweight cryptography," *IEEE Transactions on Circuits and Systems for Video Technology*, vol. 32, no. 1, pp. 75–91, 2021.

Classification of Palm Trees Diseases using Convolution Neural Network

Marwan Abu-zanona¹, Said Elaiwat², Shayma'a Younis³, Nisreen Innab⁴, M. M. Kamruzzaman⁵

Department of Computer Sciences, College of Shari'a and Islamic Studies in Al Ahsaa,
Al Imam Mohammad IbnSaud Islamic University, Al Ahsaa, Saudi Arabia¹

Department of Computer Science, College of Computer and Information Sciences,
Jouf University, Sakakah, Saudi Arabia^{2,5}

Department Biomedical Informatics engineering,
Yarmouk University, Irbid, Jordan³

Department of Computer Science and Information Systems, College of Applied Sciences,
AlMaarefa University, Riyadh, Saudi Arabia⁴

Abstract—The palm tree is considered one of the most durable trees, and it occupies an advanced position as one of the most famous and most important trees that are planted in different regions around the world, which enter into many uses and have a number of benefits. In the recent years, date palms have been exposed to a large number of diseases. These diseases differ in their symptoms and causes, and sometimes overlap, making the diagnosing process with the naked eye difficult, even by an expert in this field. This paper proposes a CNN-model to detect and classify four common diseases threatening palms today, Bacterial leaf blight, Brown spots, Leaf smut, white scale in addition to healthy leaves. The proposed CNN structure includes four convolutional layers for feature extraction followed by a fully connected layer for classification. For performance evaluation, we investigate the performance of the proposed model and compare to other CNN- structures, VGG-16 and MobileNet, using four evaluation metrics: Accuracy, Precision, Recall and F1 Score. Our proposed model achieves 99.10% accuracy rate while VGG-16 and MobileNet achieve 99.35% and 99.56% accuracy rates, respectively. In general, the performance of our model and other models are very close with a minor advantage to MobileNet over others. In contrast, our model characterized by simplicity and shows low computational training time comparing to others.

Keywords—Palm trees diseases; convolutional neural networks; mobileNet; VGG-16

I. INTRODUCTION

The date palm is considered one of the most important fruit trees in the Arab and Islamic world, as Arab countries account for 71% of its trees in the world, and 81% of the total global production, while this percentage rises to 99% (103.95 million trees) of the number of trees. The world's date palm, amounting to 105 million, when combining the Arab and Islamic worlds, according to the Food and Agriculture Organization of the United Nations. According to the latest statistics adopted in the world, including the statistic conducted by the Egyptian Embassy in Brazil in 1990 as shown in table I, it was found that the palm tree is one of the main agricultural products produced by the Arab countries and is considered a major element in supporting the macro economy in these countries, so it is very important to pay attention to the quality and quantity of production Palm trees, but

unfortunately, the quality, quality and quantity of palm trees are greatly threatened with confinement due to the common palm diseases these days, where in general palm trees are threatened by 4 main types of diseases, which are, Bacterial leaf blight, Brown spots, Leaf smut, white scale, the nature and symptoms of these diseases are different in their form, in the area of their appearance and distribution on palm trees, so it is very important to reveal modern techniques that contribute greatly to discovering them before they cause tremendous pressure on the quality and quantity of palm trees produced.

Symptoms of leaf smut Small irregular brown to black spots occurred on the upper and bottom surfaces of rachis and fronds, ranging in size from 3 to 7 mm [1]. Bacterial Leaf blight symptoms were elongated brown to black patches that grew in size and spread across a considerable region, creating cankers on the midrib [1].

Brown spot disease is characterized by the appearance of non-specific dark spots, and as the infection progresses, the center of the spot turns to a pale color, but the edges remain brown to gray. The spots appear on the leaves, thorns, and the middle vein (the leaves). The size of the spots ranges from one to several centimeters, but their size and color may vary according to the fungus that causes them. Another serious risk is a lethal pest called white scale. White palm Scale is a species of armoured scale insect. This means that they produce a hard outer coating that covers the body, which protects them from pathogens. They're also well protected from topical pesticides. White Scale insects attack palm by sucking the sap through a fine, thin feeding-tubes. Infestations rarely kill plants but can impact vigour [2]. The methods usually used by farmers depend mainly on observing the affected foliage with the naked eye by experts. Unfortunately, this method is not effective because of the distance of the palm tree from the ground and at the same time due to the somewhat similarity between the symptoms of the four palm diseases mentioned previously. In addition to that, the manual examination of palm leaves is time-consuming, especially in the case of large farms. In this paper, a CNN-based model is proposed to detect four of the most frequent palm illnesses is suggested. These illnesses are, Bacterial leaf blight, brown spots, Leaf smut, white scale. The proposed model characterized by simplicity(easy

TABLE I. STATISTICS DONE BY THE EMBASSY OF EGYPT ECONOMIC AND COMMERCIAL OFFICE IN BRAZIL,; MARCH 18, 2019 [1]

Top 10 Largest Date Producers in the World		
Rank	Country	Production (1000 Metric Tons)
1st	Egypt	1,373,57
2nd	Saudi Arabia	1,122,82
3rd	Iran	1,016,61
4th	United Arab Emirates	900,00
5th	Algeria	690,00
6th	Iraq	619,18
7th	Pakistan	557,28
8th	Oman	268,01
9th	Tunisia	180,00
10th	Libya	165,95

to train) and the efficiency comparing to the state of the art techniques. Our model achieves 99.10% average accuracy rate to detect Bacterial leaf blight, brown spots, Leaf smut, white scale diseases and healthy leaves. 56

The remainder of this paper is organized as follows: Section II presents a summary of related work. Section III illustrates System architectures including our proposed model in details. The next section presents the experimental results of our model and compare it with other models. Finally, the conclusion in addition to the feature work are given in Section V.

II. RELATED WORK

This section shows the previous studies that dealt with the problem of palm tree diseases. In [1], The researchers used various classifiers to detect the three most frequent palm illnesses today: leaf spot, blight, and red palm weevil. CNN was used to distinguish between Leaf Spots and Blight Spots illnesses, and SVM was used to distinguish between the Red Palm Weevil pest and the Leaf Spots sickness. The Kaggle dataset (about 90k photos) was utilized as-is, resulting in a 65 percent accuracy for the first CNN model. The data set was split into two parts: 70% for training and 30% for testing. The accuracy ratio success rates for the CNN and SVM algorithms were 97.9% and 92.8%, respectively.

In [3], the illnesses in tomato fruit were detected using multiple classifiers, the first of which was CNN and LVQ. Leaf blight, bacterial spot, late blight, sitoria leaf spot, and yellow curved leaf disease are among the illnesses he classified. The dataset utilized in this experiment was divided into 400 photos to train the model and 100 images to assess the quality and efficiency of the model, which had a size of 512 x 512 and an accuracy of 86%. The only difficulty this study faces is the degree of symptom similarity among the illnesses that affect tomato fruit.

Jiang et al. [4] proposed a system to identify apple leaf illnesses using deep learning algorithms. To identify and categorize alternate leaf spot, brown spot, mosaic, spot Gray, rust, and eventually brown apple leaf disease, the proposed system employed a new CNN based technique called INAR-SSD based on a framework called Caffe on the GPU platform. Set of data The data utilized is made up of 26377 photos that were separated into two groups: one for training the model and the other for verifying the model. The model speed was 23.13 frames per second, and the accuracy of the findings was 78.80 percent mAP.

The proposed work by [5] investigated the ability to identify chimera and anthracnose infections in palm trees. The detection procedure began with the use of a digital camera to capture photographs of the damaged palm trees, which were then subjected to a series of image processing processes following segmentation using the k-mean method. The Gray Correlation Matrix was created by applying the characteristics extraction phase on the segmented pictures using gyro compatibles (GLCM). The accuracy of the findings proved the effectiveness of the support vector machine (SVM) in such circumstances, with Chimera having a 97 percent accuracy and anthracnose having a 95 percent accuracy.

In [6], The authors used a program called Therma CAM Researcher to analyze pictures collected with an uncooled infrared thermal camera linked to a microbolometer sensor in this work. To obtain credible maps of leaf temperature, this software was enhanced with local climatic variables and leaf emission. Each experiment had 4-5 duplicates of control trees and 8-10 replicates of infected trees in each group. The Crop Water Stress Index (CWSI) was produced, and the damaged trees were identified with up to 75% accuracy using this value. In[7], The authors of this article wanted to see if they could tell the difference between healthy palm trees and palm trees afflicted with the red palm weevil by using water stress and temperature rates. Aerial photos were taken using an uncooled infrared thermal camera and a microbolometer connected to begin the procedure. The palm canopy was separated from the soil using a set of image processing techniques, and the watershed method was used to build the palm canopy diagram using the photos. This study yielded no numerical data, however it did show that various palm plants had variable water stress levels.

III. SYSTEM ARCHITECTURE

A. Data Preprocessing

Since the resolution and size of acquired 2D images are usually inconsistent, using them directly as training data is not applicable. In addition, using very high resolution images is time-consuming and may lead to high computational cost. Therefore, all images are resized to 60 x 60 resolution. Furthermore, The correlation between data within the image can slow down the learning process. To address this, we apply image whitening [8] based on Zero Component Analysis (ZCA) to reduce the correlation between data and make key features such as edges and curvatures more prominent, and thus easy to detect by CNN. To achieve that the pixel values in each image is normalized to be between 0 and 1 as the following:

$$\hat{X} = X/255 \quad (1)$$

, where X and \hat{X} are the image before and after normalization, respectively. After that the image is mean normalized by defining the mean value along each feature dimension (pixel position) of training images and then subtracted from the image as the following:

$$\bar{X} = \hat{X} - \mu \quad (2)$$

, where μ represents the mean vector across all the features of \hat{X} while \bar{X} represents the mean normalized image. Finally, the whitened image X_{ZCA} is defined based on Singular Value

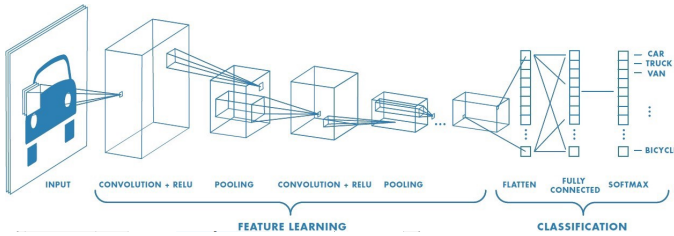


Fig. 1. An Overview of a Convolutional Neural Network (CNN) Architecture [21].

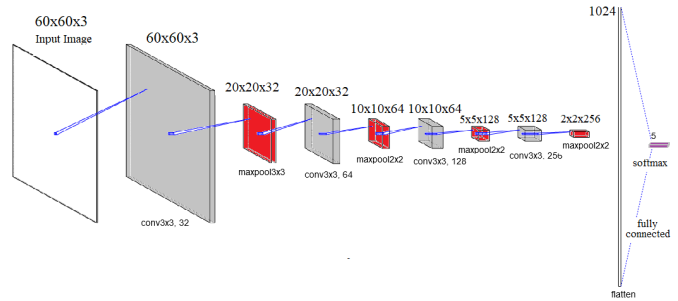


Fig. 2. The Architecture of Proposed CNN.

Decomposition (SVD) of the covariance matrix of \bar{X} as the following

$$X_{ZCA} = U \cdot \text{diag}(1/\sqrt{\text{diag}(S) + \varepsilon}) \cdot U^T \cdot \bar{X} \quad (3)$$

The function $\text{diag}(\cdot)$ returns the diagonal matrix of the input matrix. The variable U and S represent the Eigen vector and Eigen value of the SVD of covariance matrix while the hyper-parameter ε represents whitening coefficient.

B. Convolutional Neural Networks

The Convolutional Neural Network CNN [9], [10] is a deep learning model capable to achieve both feature coding (feature extraction) and classification in a single coherent architecture. In contrast, traditional neural networks are limited for classification task and require well-defined feature (engineered features) to achieve high performance [11], [12]. In general, CNNs are widely applied in many computer vision applications such as face recognition [13], object detection [14], Natural language processing [15], medical image analysis and others [16]. Fig. 1. shows the basic architecture of the CNN which involves three different set of layers, namely, 'Input Layer', 'Feature Learning Layers' and 'Classification Layers'. The first set is a single layer, includes the input image (usually colored image). The second set is a sequence of successive Convolution and Pooling layers which resulting in extracted features. The last set usually involves fully connected layers to achieve classification tasks. The main advantage of CNN is the ability to define local features such as horizontal edges through convolution layers by maintaining the same structure of the input image whilst using a small number of parameters. For example, regardless of the size of the input image, the number of parameters depends on the size and the number of filters (e.g., 10 filters of [3 x 3] size).

In the resents years, numerous attempts have been made to enhance CNN's initial design (by Lecun et al. [9]) in order to achieve better performance. A popular examples of CNN architecture are AlexNet [17], VGG-16 [18], ResNet [19] and MobileNet [20]. In this work, a simple CNN architecture is firstly proposed for the problem of Palm Trees Diseases classification and then the performance of our CNN is compared to two well-known CNN structures: "VGG-16" and "MobileNet".

1) *Proposed CNN*: In this section, we introduce a simple CNN architecture for efficient learning especially with limited training data size. The proposed architecture includes four convolutional layers followed by fully connected layer and softmax as output layer as shown in Fig. 2.

The input layer includes the input image with dimensions [60, 60,3] where the first two represent the width and the height of the image while the last value represents the number of channels (three channels for red, green and blue). The first convolutional layer includes 32 filters of each [3 x 3] size, followed by a maxpool of 3x3. In the next three convolutional layers, 64 filters [3 x 3] are used for the second layer, while 28 and 256 filters are used for the third and forth layers, respectively. Each of these convolutional layers is followed by a maxpool of 2x2. Finally, a flatten process is applied, resulting in a layer with 25600 features, fully connected to a dense layer with activation function "softmax".

2) *VGG-16*: VGG-16 was originally proposed by Simonyan and Zisserman [18] in 2014. The basic idea behind VGG-16 is to increase the depth of the network by adding more convolutional layers while using very small [3 x 3] convolution filters in all layers. Fig. 3 shows the The architecture of VGG-16.

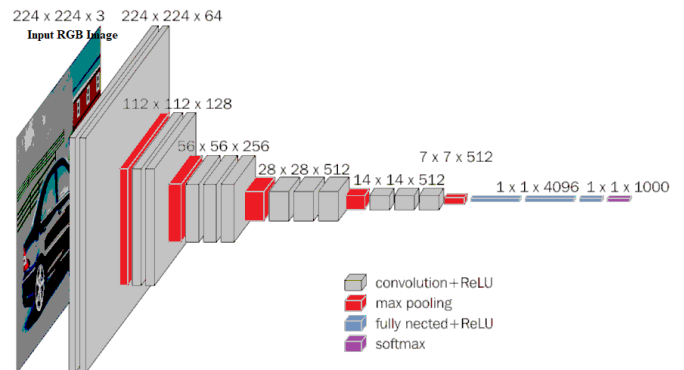


Fig. 3. The Architecture of VGG-16.

During the training phase, the only preprocessing step is to subtract the mean RGB value (calculated over the training set) from each pixel. After that, the image is passed through a set of convolutional layers with small filters ([3 x 3] size). To preserve the spatial resolution the same after the convolution, the stride and the spatial padding are both set to one pixel. Some of the convolutional layers are followed by a max-pooling layer, so a total of five max-pooling layers are applied in the whole network.

3) *MobileNets*: MobileNet is deep learning model, proposed by Howard et al. [20] of Google Research team. This

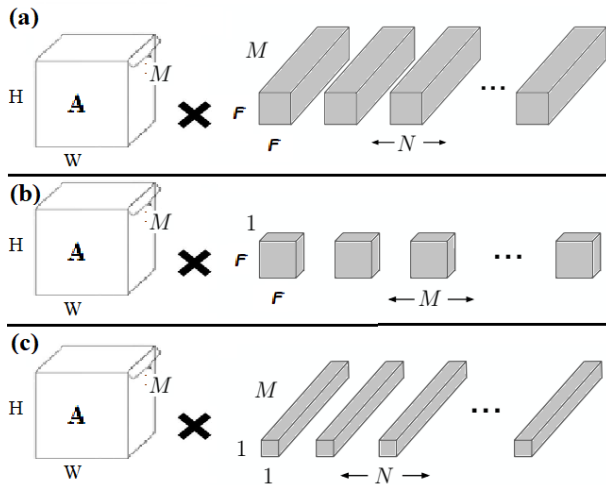


Fig. 4. (a): Standard Convolution Filters. (b): Depthwise Convolutional Filters. (c): Pointwise Convolutional Filters [20].

model was presented to effectively maximize the performance of CNN under limited resources which is ideal for mobile and embedded vision applications. MobileNets is characterized by light weight and hyper-parameters (small number of required wights comparing to other CNN models), which allows to trade-off between latency and accuracy. To achieve that, the standard convolution filters [Fig. 4(a)] replaced by two layers: depthwise convolution [Fig. 4(b)] and and pointwise convolution [Fig. 4(a)].

The computational cost C of the standard convolutional layer can be represented as:

$$C = F \cdot F \cdot M \cdot N \cdot H \cdot W \quad (4)$$

In contrast, MobileNets is capable to reduce the computational cost as:

$$C = F \cdot F \cdot M \cdot H \cdot W + M \cdot N \cdot H \cdot W \quad (5)$$

which includes the cost of the depthwise convolution plus the cost of the pointwise convolution. By comparing the ratio between Eq. 4 and 5 based on [3 x 3] depthwise separable convolutions, MobileNets can achieve 8 to 9 times less computational cost than standard convolutions [20].

IV. EXPERIMENTAL RESULTS

In this section, the performance of the proposed CNN model, in addition to VGG 16 and MobileNet, are evaluated by combining two datasets, ‘Date Palm’ [22] and ‘Leaf_Disease_3’ [23].

A. Dataset

Table II gives a summary of each dataset. In our experiments, Date Palm [22] and Leaf_disease_3 [23] datasets are combined to build a new dataset (DP-disease dataset). In more details, Date Palm dataset includes two types of diseases: Brown Spots with 470 samples and White Scale with 958 samples. In addition to that, the dataset also includes 1013 samples of Healthy leaves. In contrast, Leaf_disease_3 dataset

TABLE II. THE CHARACTERISTIC OF APPLIED DATASETS

Dataset type	Total images	Training images	Testing images
Date Palm	2631	Not partitioned	Not partitioned
Leaf_disease_3	102360	82200	20160
Combined dataset (DP-disease dataset)	4471	4023	448

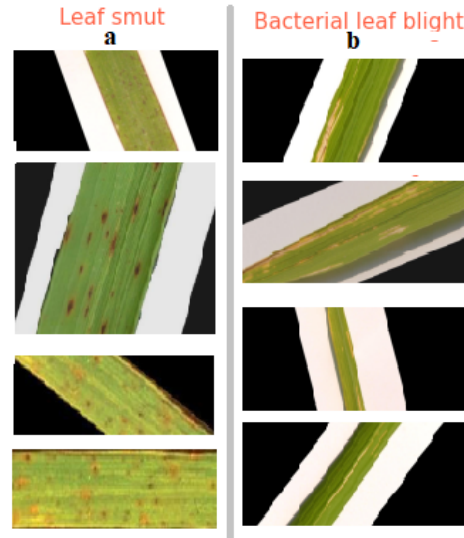


Fig. 5. Samples from: (a) Leaf Smut Disease and (b) Bacterial Leaf Blight Disease.

includes three different types of diseases: Bacterial Leaf Blight, Brown Spot and Leaf Smut. The dataset is partitioned into training and testing sets where 82,200 samples are used for training and 27,360 samples are used for testing. The number of samples for each disease is 27,360 in the training set and 9120 in the testing set. By combining samples from both datasets, it allows use to include more diseases (four different disease) in addition to the healthy case. As a result, the classification task in all experiments embeds five classes: 1) Bacterial Leaf Blight, 2) Leaf Smut, 3) Brown Spots, 4) White Scale and 5) Healthy leaves.

Fig. 5(a) shows samples from Bacterial Leaf Blight disease where 1,013 images with dimension 3081 x 897 are included in our experiments. Fig. 5(b) shows samples from Leaf Smut disease where 827 images with dimension 510 x 383 are included in our experiments.

Samples from Brown Spots disease and White Scale disease are shown in Fig. 6(a) and (b) where 470 images and 958 images are used in our experiments for Brown spots disease and White scale disease, respectively. For the case of healthy leaves, Fig. 6(c) shows sample of Healthy leaves where 1,203 images are included in our experiments.

B. Experiment Configurations

In our experiments, 4023 samples from different type of diseases were used to train each CNN model while 448 samples from different type of diseases were used to test the performance of each CNN model. The size of input images are unified in all experiments to be 60 x 60 x 3, where the first two dimensions represent the width and height while the last

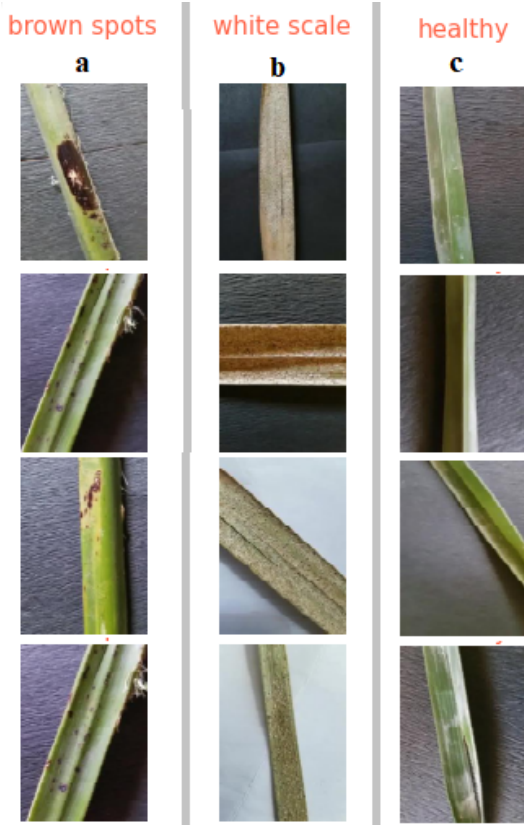


Fig. 6. a)Samples from Brown Spots Disease. b)Samples from White Scale Disease. c) Samples from Healthy Leaves.

TABLE III. THE HYPER-PARAMETERS OF PROPOSED CNN MODE

Hyper Parameters	Proposed CNN Model	
Convolution Layers	4	
Number of neurons for each convolution layer	First Layer	32
	Second Layer	64
	Third Layer	128
	Fourth Layer	256
Max Pooling Layers	4	
Fully Connected Layer	1	
Dropout Layer value	NaN	
Activation function	Relu	Softmax
Train Split	0.8	
Test Split	0.2	
Batch Normalization	4	
Kernal window size	(3,3)	(2,2)
Pool size	(3,3)	(2,2)
Trainable params	395,13	
epochs	25	
Batch size	10	
Optimizer	Adam	

one represent the number of color channels (R G B). During the training phase, Batch Gradient Descent were applied in all experiments. In addition to that, the number of epochs sets to 10 which compromises between sufficient training process and over-fitting. More details about the hyper-parameters of each CNN model are shown in Table III, IV and V.

C. Performance Evaluation

The performance evaluation of each model was analyzed using four known evaluation metrics: Accuracy, Precision,

TABLE IV. THE HYPER-PARAMETERS OF VGG-16 MODE

Hyper Parameters	VGG16 Model	
Convolution Layers	13	
Number of neurons for each convolution layer	First Layer	64
	Second Layer	64
	Third Layer	128
	Fourth Layer	128
	Fifth Layer	256
	Sixth Layer	256
	Seventh Layer	256
	Eighth Layer	512
	ninth Layer	512
	Tenth Layer	512
	eleventh Layer	512
	twelfth Layer	512
	Thirteenth Layer	512
Max Pooling Layers	5	
Fully connected Layer	3	
Dropout Layer value	NaN	
Activation function	Relu	Softmax
Train Split	0.9	
Test Split	0.1	
Kernal window size	(3,3)	
Pool size	(3,3)	
Trainable params	15,245,125	
epochs	25	
Batch size	10	
Optimizer	Adam	

TABLE V. THE HYPER-PARAMETERS OF MOBILENET MODEL

Hyper Parameters	MobileNet Model	
Conv2d Layer	14	
Depthwise Conv2D	13	
Number of neurons for each convolution layer	First Layer	32
	Second Layer	64
	Third Layer	128
	Forth Layer	256
	Fifth Layer	512
	Sixth Layer	1024
Global Average Pooling	1	
Fully connected Layer	2	
Dropout Layer value	1	
Activation function	Relu	Softmax
Train Split	0.9	
Test Split	0.1	
Kernal window size	(3,3)	
Pool size	(7,7)	
Trainable params	5,249,29	
epochs	25	
Batch size	10	
Optimizer	Adam	

Recall and F1 Score. The Accuracy of each CNN model at each type of disease is defined as the following:

$$Accuracy = \frac{TP + TN}{T} \quad (6)$$

, where TP and TN represent number of True Positive and True Negative classifications, respectively, while T represents the total number of samples. Table VI reports the performance of each model based on accuracy. We can notice that MobileNet achieved 99.56% accuracy rate in average which is the best performance. In contrast, our model and VGG16 achieved 99.10% and 99.35% accuracy rate, respectively. It is clear that the performance of the three models are relatively very close with slight variations less than 0.5% .

The Precision of each CNN model at each type of disease is defined as the following:

$$Precision = \frac{TP}{TP + FP} \quad (7)$$

TABLE VI. THE PERFORMANCE OF EACH MODEL BASED ON ACCURACY

Diseases	Our model	MobileNet model	Vgg16 model
Brown Spots	99.55%	100.00%	100.00%
white Scale	99.35%	99.75%	99.35%
Bacterial Leaf Blight	98.79%	98.98%	98.99%
Leaf Smut	99.20%	98.88%	99.5%
Healthy	98.90%	99.90%	98.90%
Average	99.10%	99.56%	99.35%

TABLE VII. THE PERFORMANCE OF EACH MODEL BASED ON RECALL

Diseases	Our model	MobileNet model	Vgg16 model
Brown Spots	100.00%	100.00%	100.00%
white Scale	98.55%	98.55%	99.75%
Bacterial Leaf Blight	96.27%	96.20%	97.27%
Leaf Smut	98.73%	98.73%	98.86%
Healthy	99.15%	99.67%	99.55%
Average	98.54%	98.63%	99.08%

, where TP and FP represent number of True Positive and False Positive classifications, respectively. Table VII reports the performance of each model based on Recall. The highest average precision rate is 99.08% reported by MobileNet, followed by VGG16(98.63%) and our model (98.54%). It is clear that the performance of the three models are relatively very close with slight variations less than 1%.

The performance of each CNN model based Recall and F_1Score are defined as the following:

$$Recall = \frac{TP}{TP+FN}$$

$$F_1Score = 2 \times \frac{Precision \times Recall}{Precision+Recall} \quad (8)$$

, where TP and FN represent number of True Positive and False Negative classifications, respectively. Table VIII and IX report the performance of each model based on precision and F_1Score , receptively. The reported results show that the performance of the three models in both measures are very close with variations less than 1%.

From the previous reported results, the performance of VGG16 and MobileNet in addition to the proposed model very close with a slight advantage to MobileNet over others. We believe that VGG16 can achieve better performance with huge training data. However, in several applications, huge training

TABLE VIII. THE PERFORMANCE OF EACH MODEL BASED ON PRECISION

Diseases	Our model	MobileNet model	Vgg16 model
Brown Spots	100.00%	100.00%	100.00%
white Scale	98.55%	99.75%	98.75%
Bacterial Leaf Blight	99.55%	99.55%	98.93%
Leaf Smut	99.33%	99.33%	99.63%
Healthy	98.73%	97.73%	98.88%
Average	99.23%	99.27%	99.23%

TABLE IX. THE PERFORMANCE OF EACH MODEL BASED ON F1 SCORE

Diseases	Our model	MobileNet model	Vgg16 model
Brown Spots	100.00%	100.00%	100.00%
white Scale	98.55%	98.87%	98.98%
Bacterial Leaf Blight	99.27%	99.27%	99.65%
Leaf Smut	98.94%	98.94%	98.54%
Healthy	99.15%	99.67%	99.65%
Average	99.18%	99.35%	99.36%

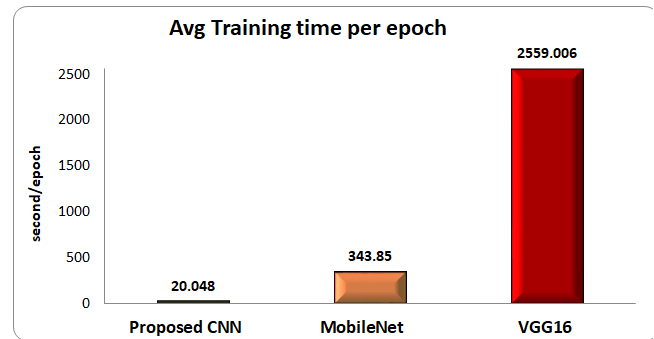


Fig. 7. Avg Training Time per Epoch for each Model.

data is not always available. In contrast, MobileNet and our model showed more capability to deal with limited resources such as training data and training time. Fig. 7 shows the average training time of each model. Note that our model achieved the lowest average training time of 20.048s/epoch while MobileNet achieved 343.85s/epoch average training time followed by VGG16 with a huge rise (2559s/epoch). Thus, the proposed model is capable compromise between the performance (high) and the complexity (simple structure with low training time).

V. CONCLUSION

This paper presented an efficient CNN-model for detecting and classifying palm tree frequent diseases, including Bacterial leaf blight, Brown spots, Leaf smut and white scale. The proposed model consists of three stages. Firstly, data preprocessing was applied on all images by normalizing them using Whitening Transform to reduce the correlation among data within the image. The second stage included four convolutional layers with max pooling to extract distinctive features. Finally, the classification stage was defined using fully connected layer with softmax to detect the type of palm disease. Furthermore, this work investigated the performance of two will-known CNN- models, namely MobileNet and VGG-16, for classifying palm tree diseases. To evaluate the performance of proposed CNN-model and other models, a new dataset (DP-disease dataset) was built by combining data samples from Date Palm and Leaf_disease_3 datasets. This combination allowed us to detect four deferent diseases in addition to healthy cases. A set evaluation metrics was then applied to evaluate the performance of each model including accuracy, Precision, recall and F1 score. Our experimental results showed that the performance of the three models were very close. However, our model characterized by simplicity and low computational training cost (20.048s/epoch) comparing to others (343.85s/epoch and 2559s/epoch for MobileNet and VGG-16, respectively).

Future avenues of work include integrating the proposed model with object segmentation methods such R-CNN for accurately identifying the affected parts of palm trees.

REFERENCES

- [1] H. Alaa, K. Waleed, M. Samir, M. Tarek, H. Sobeah, and M. A. Salam, "An intelligent approach for detecting palm trees diseases using image processing and machine learning," *Int. J. Adv. Comput. Sci. Appl.*, vol. 11, no. 7, pp. 434-441, 2020.

- [2] "White Scale," {<https://candidegardening.com/GB/insects/ace6662f-61ca-4806-99b7-81f4b040faed>}.
- [3] M. Sardogan, A. Tuncer, and Y. Ozen, "Plant leaf disease detection and classification based on cnn with lvq algorithm," in *2018 3rd International Conference on Computer Science and Engineering (UBMK)*. IEEE, 2018, pp. 382–385.
- [4] P. Jiang, Y. Chen, B. Liu, D. He, and C. Liang, "Real-time detection of apple leaf diseases using deep learning approach based on improved convolutional neural networks," *IEEE Access*, vol. 7, pp. 59 069–59 080, 2019.
- [5] M. M. Kamal, A. N. I. Masazhar, and F. A. Rahman, "Classification of leaf disease from image processing technique," *Indonesian Journal of Electrical Engineering and Computer Science*, vol. 10, no. 1, pp. 191–200, 2018.
- [6] O. Golomb, V. Alchanatis, Y. Cohen, N. Levin, Y. Cohen, and V. Soroker, "Detection of red palm weevil infested trees using thermal imaging," in *Precision agriculture'15*. Wageningen Academic Publishers, 2015, pp. 322–37.
- [7] Y. Cohen, V. Alchanatis, A. Prigojin, A. Levi, and V. Soroker, "Use of aerial thermal imaging to estimate water status of palm trees," *Precision Agriculture*, vol. 13, no. 1, pp. 123–140, 2012.
- [8] K. K. Pal and K. S. Sudeep, "Preprocessing for image classification by convolutional neural networks," in *2016 IEEE International Conference on Recent Trends in Electronics, Information Communication Technology (RTEICT)*, 2016, pp. 1778–1781.
- [9] Y. Lecun, L. Bottou, Y. Bengio, and P. Haffner, "Gradient-based learning applied to document recognition," *Proceedings of the IEEE*, vol. 86, no. 11, pp. 2278–2324, 1998.
- [10] S. Dong, P. Wang, and K. Abbas, "A survey on deep learning and its applications," *Computer Science Review*, vol. 40, p. 100379, 2021. [Online]. Available: <https://www.sciencedirect.com/science/article/pii/S1574013721000198>
- [11] S. Elaiwat, M. Bennamoun, F. Boussaïd, and A. A. El-Sallam, "A curvelet-based approach for textured 3d face recognition," *Pattern Recognit.*, vol. 48, pp. 1235–1246, 2015.
- [12] S. Elaiwat, "Holistic word descriptor for lexicon reduction in handwritten arabic documents," *Pattern Recognition*, vol. 119, p. 108072, 2021.
- [13] N. K. Mishra, M. Dutta, and S. K. Singh, "Multiscale parallel deep cnn (mpdcnn) architecture for the real low-resolution face recognition for surveillance," *Image and Vision Computing*, vol. 115, p. 104290, 2021.
- [14] J. Yuan, H.-C. Xiong, Y. Xiao, W. Guan, M. Wang, R. Hong, and Z.-Y. Li, "Gated cnn: Integrating multi-scale feature layers for object detection," *Pattern Recognition*, vol. 105, p. 107131, 2020.
- [15] M. Eltay, A. Zidouri, and I. Ahmad, "Exploring deep learning approaches to recognize handwritten arabic texts," *IEEE Access*, vol. 8, pp. 89 882–89 898, 2020.
- [16] C. Lee, C. Tanikawa, J.-Y. Lim, and T. Yamashiro, "Deep learning based cephalometric landmark identification using landmark-dependent multi-scale patches," 2019.
- [17] A. Krizhevsky, I. Sutskever, and G. E. Hinton, "Imagenet classification with deep convolutional neural networks," *Commun. ACM*, vol. 60, no. 6, p. 84–90, may 2017.
- [18] K. Simonyan and A. Zisserman, "Very deep convolutional networks for large-scale image recognition," 2015.
- [19] K. He, X. Zhang, S. Ren, and J. Sun, "Deep residual learning for image recognition," in *2016 IEEE Conference on Computer Vision and Pattern Recognition (CVPR)*, 2016, pp. 770–778.
- [20] A. G. Howard, M. Zhu, B. Chen, D. Kalenichenko, W. Wang, T. Weyand, M. Andreetto, and H. Adam, "Mobilenets: Efficient convolutional neural networks for mobile vision applications," *arXiv preprint arXiv:1704.04861*, 2017.
- [21] "CNN architecture," <https://towardsdatascience.com/a-comprehensive-guide-to-convolutional-neural-networks-the-eli5-way-3bd2b1164a53>.
- [22] "Date Palm Dataset," {<https://www.kaggle.com/hadjerhamaidi/date-palm-data>}.
- [23] "Leaf Diseases 3 Dataset," {<https://www.kaggle.com/research27/leaf-disease-3>}.

Dynamic Spatial-Temporal Graph Model for Disease Prediction

Ashwin Senthilkumar¹
School of Electronics Engineering
Vellore Institute of Technology
Chennai, 600127

Mihir Gupte²
School of Computer Science
and Engineering
Vellore Institute of Technology
Chennai, 600127

Shridevi S.³
Center for Advanced Data Science
Vellore Institute of Technology
Chennai, 600127

Abstract—Advances in the field of Neural Networks, especially Graph Neural Networks (GNNs) has helped in many fields, mainly in the areas of Chemistry and Biology where recognizing and utilising hidden patterns is of much importance. In Graph Neural Networks, the input graph structures are exploited by using the dependencies formed by the nodes. The data can also be transformed in the form of graphs which can then be used in such models. In this paper, a method is proposed to make appropriate transformations and then to use the structure to predict diseases. Current models in disease prediction do not fully use the temporal features that are associated with diseases, such as the order of the occurrence of symptoms and their significance. In the proposed work, the presented model takes into account the temporal features of a disease and represents it in terms of a graph to fully utilize the power of Graph Neural Networks and Spatial-Temporal models which take into consideration of the underlying structure that change over time. The model can be efficiently used to predict the most likely disease given a set of symptoms as input. The model exhibits the best algorithm based on its accuracy. The accuracy of the algorithm is determined by the performance on the given dataset. The proposed model is compared with the existing baseline models and proves to be outstanding and more promising in the disease prediction.

Keywords—Spatial temporal graph convolution network; disease prediction; graph neural network; graph convolutional network; deep learning; knowledge graph

I. INTRODUCTION

In recent times, Machine Learning has become very popular in the field of Medical Sciences, especially when it comes to detecting patterns that are associated with health and diseases. Disease prediction is one of the most sought after applications here, and the reason for that is the patterns that are associated with each disease, be it physical illness or mental well-being. Diseases are often associated and known for the symptoms that occur when a person is infected, therefore a study of the underlying structure of the symptoms, their behaviour, etc. is important for predicting them. These underlying structures usually have a temporal nature to them as the symptoms don't occur all at once, but they do in more or less sequential order.

It is common to see the use of ML models such as Naive-Bayes, Decision Trees and other classifiers to be used in these scenarios. The most common source for obtaining information about symptoms is by referring to Electronic Health Records (EHRs). Often these are used to extract features for input. In [1], the authors make a heart disease prediction model using ML techniques. They utilize features such as Age, Sex,

Pain levels, etc of patients as input. In [2], it was found that most people tackled this problem using Support Vector Machines (SVM) and Naive-Bayes models. However, this did not prove to be efficient when dealing with huge volumes of Electronic Medical Records (EMRs) data without processing it and simply feeding it to these models, nor can these models take advantage of the temporal structure of the symptoms. To overcome these many researchers have started utilising Deep Learning, as a neural network can detect and represent the hidden and latent features more efficiently. In [3], the authors proposed a graph convolution network with mutual attention networks, to learn from EMR's directly and diagnose the patient. The author obtained an accuracy of 63.46% from the MIMIC-III dataset [4], which was better compared to all the other models in the paper like Convolutional Neural Networks (CNN), Graph Convolutional Network(GCN), etc. The authors in [5] use an Artificial Neural Network (ANN) to develop a model for Parkinson's disease and boast almost perfect accuracy. A method proposed in [6] uses Cascading Neural Networks in order to detect Melanoma, a form of skin cancer. In [7], the authors have developed a model called InceptionGCN for disease prediction and tested it out on various datasets. Thus it can be concluded that neural networks, especially Graph Neural Networks play an important role in the new and upcoming models of disease predictions.

However, most of the above-mentioned papers fail to utilise the temporal features of the symptoms that are associated with the diseases. Some papers [8],[9] make use of GNNs tailored for this specific purpose especially in [9],[10] where the authors use patient data to first construct a dependency of the patient with symptoms on each visit and a final diagnosis and then model a graph from which is fed to the network proposed by them. This model could achieve an accuracy of a little over 85% at the most favourable conditions.

So while the use of spatial-temporal networks is not new to this problem, a new architecture that models symptoms of a patient into a graph is quite novel. This paper proposes a method to model the input data by changing the underlying structure of the graph at each timestep, so as to utilise the temporal features of the input. Knowledge graph for diseases by [11] is utilized for proposed architecture. In this, the authors employ probabilistic models such as logistic regression, naive Bayes classifier, to derive features of various diseases from many EHRs. The authors feature a knowledge graph built on these features and so in the presented work a knowledge graph

based Spatial-Temporal GCN is proposed.

The major contributions of the paper are:

- A temporal approach to predicting diseases in order to make the models more robust and potentially exploiting such dependencies to enhance the quality of the proposed model.
- Graph Convolutional Network(GCN) model is proposed which exploits the spatial dependencies of the input first then uses these to explore the temporal dependencies of the input. This will help to understand how the symptoms relate to each other at each timestep and how that underlying relationship changes. The model will exploit this to predict and classify diseases.
- A graph model of the input data in the form of diseases and the symptoms that occur alongside proposed as well. Each symptom is associated with a probability which indicates how likely the symptom is to occur (as compared to all other symptoms for the same disease). Data is converted into a graph.

II. RELATED WORKS

Disease prediction has been difficult with a lack of patient history and noisy data. The work tries to overcome the difficulties and improve efficiency by using knowledge graphs obtained from medical ontology. Further, mechanism is also discussed to predict diseases using symptoms via a spatial-temporal Graph Convolutional Network.

Xuedong Li et al. [12] takes an innovative approach to overcome the lack of medical history by using medical knowledge. The lack of medical history of patients owing to the nature of rare medical diseases makes it a challenging process even for machine learning approaches to recognize the diseases. They have developed a text classification algorithm to create a bag of knowledge terms from the medical ontology to develop a knowledge graph that can be leveraged for the disease classification task. It works efficiently even if the knowledge graph of medical history is incomplete. The limitation of this approach is that the dataset being used is extremely imbalanced.

Rotmensch, M., Halpern, Y. et al. [9] has directed a review observational investigation utilizing recently gathered information from Electronic Medical Records (EMR) in order to develop a knowledge graph that relates indications to sicknesses and assessed competitor knowledge graphs against physically curated knowledge graph given by (Google well being knowledge graph, or GHKG) and also the expert opinion of physicians. However, the purpose of the knowledge graph was to test how efficiently a given algorithm could recover unknown causal relationships between the diseases and their symptoms. A drawback is that any approach that infers causal relations from observational data has major limitations inherently. The algorithms should be seen as a method of providing casual relations between the entities.

Zhenchao Sun, Hongzhi Yin et al. have introduced an innovative model [13] using GNNs for disease prediction. It uses multiple knowledge bases in order to obtain sufficient

EMR data to learn highly representative node embeddings of medical concepts graph and the patient record graph (which include entities such as, the patients, diseases and symptoms), and are thus constructed from the medical knowledge base and EMRs. This results in accurate disease prediction for new patients under sparse data in an inductive manner.

Li, Y., Qian, B et al. have proposed GNDP, a disease prediction model which is based on a graph convolutional network. It exploits the spatial structure of the EHR data and the temporal dependencies of the entities to predict the patient's future diagnosis which is similar to [8,10]. Sun, Z., Dong, W. et al. propose a Reinforcement Learning mechanism that would take random walks over the knowledge graph with respect to the patient's symptoms and then propose the most likely disease. The authors have manually constructed the knowledge graph using the Mimic-III PLAGH dataset. A single knowledge graph has been made for all diseases. It is limited in terms of accuracy, as accuracy could be improved by using efficient methods. GNN models can be considered as the structure of the data is a graph and the performance can be improved using GNN algorithms.

Yuan, Q., Chen, J., et al. have constructed an elaborate GCN model [3] in which they have extracted symptoms from a given diagnosis in the form of a string. Then they embed the diseases first in the D-D GCN layer and attach symptoms (features) to the diseases in the next D-F GCN layer. Less important features have been pruned from the knowledge graph in this model. Finally, these features are given to a convolutional network modelled using attention, so that the most important disease corresponding to the symptoms is obtained. The accuracy obtained is only 63%. The limitation is that the model is not interpretable and complex to understand. Potential change or simplification of algorithms can lead to better accuracy. It only considers the features extracted from diagnosis and not the temporal relations between the features.

III. METHODOLOGY

In this section, the proposed architecture of spatial-temporal graph convolutional networks(STGCN) is elaborately discussed. STGCN is made up of spatial-temporal convolutional blocks that are arranged in a "sequential" structure with one sequential convolution layer and one spatial graph convolution layer, as shown in Fig. 1. The following sections go over the specifics of each module.

A. Data Collection and Preparation

One authentic medical dataset is experimented on to evaluate the proposed model. knowledge graph from electronic medical records [3], a public accessible benchmark dataset for diseases knowledge graphs with high-quality knowledge bases linking diseases and symptoms derived from the EMRs. These electronic records represent medical concepts collected from over 270,000 patient visits to the Emergency Department at Beth Israel Deaconess Medical Center (BIDMC), thus the knowledge graphs was automatically constructed using maximum likelihood estimation of three probabilistic models.

From the learned parameters, a graph of disease-symptom connections was elicited, and the developed knowledge graphs were assessed and approved, with consent, against Google's

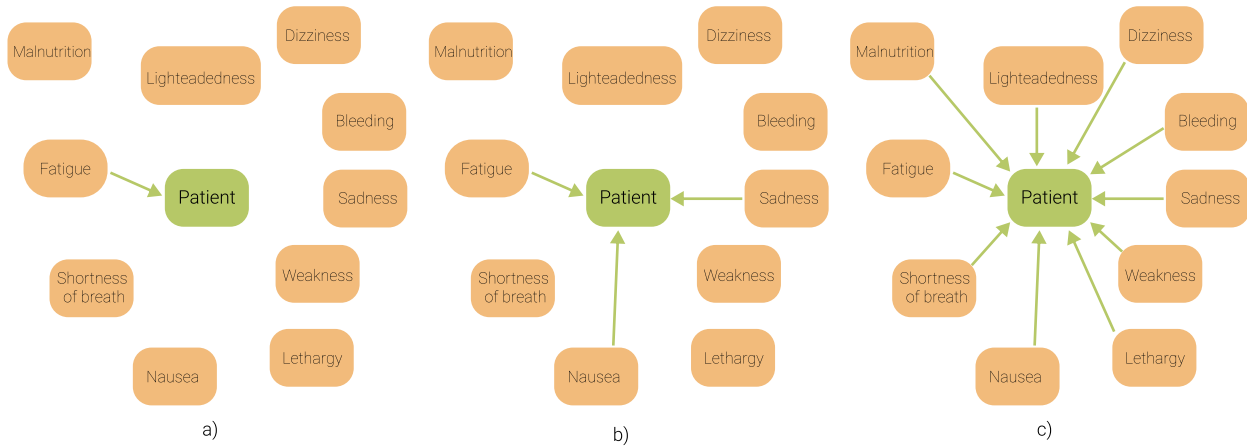


Fig. 1. Example of the Anemia Disease Dynamic Knowledge Graph that Generated in Preprocessing of the Dataset. a) Knowledge Graph at $T = 0$ b) Knowledge Graph at $T = 3$ c) Knowledge Graph at $T = n$, where n is Length of Disease Trajectory

manually built knowledge graph and master doctor suppositions. The graph records all 156 diseases and 491 symptoms, all edges between diseases and symptoms, and the significance scores given to each edge.

Temporal patterns in patient disease trajectories are either disregarded or only taken into account by assessing the temporal directionality of identified co-morbidity pairs [14], [15], [16], Which concludes naturally patients undergo different symptoms at different time instances on disease trajectories (stages of the disease). In this experiment, the temporal pattern for each disease as the preliminary basis of a disease prediction model is utilized.

Provided in Table I are the sample dataset values which includes a given disease and its symptoms along with the probability of a given symptom occurring. In Table II, important statistics of the dataset itself are given.

TABLE I. SAMPLE DATASET

Diseases	Symptoms
abscess	<i>pain</i> (0.318), <i>fever</i> (0.119), ..
anemia	<i>lethargy</i> (0.096), <i>weakness</i> (0.087), ..
common cold	<i>chills</i> (0.083), <i>sorethroat</i> (0.075), ..

Before applying the STGCN model to knowledge graphs extracted from electronic medical records [11], the existing knowledge graph must go through a series of steps to create a dynamic graph structure by leveraging temporal features for each disease knowledge graph.

As the dataset is not available with time element related with disease symptoms, a suitable time feature is created for the knowledge graph collected from electronic medical records [11]. This was done by generating all possible permutations of order symptoms that will occur in the patient’s disease trajectories.

Then using the importance scores associated with each edge of symptoms, the top ten symptoms were selected with the highest probability of occurrence inpatient disease trajectories for all possible permutations. Since the disease prediction

is a multi-class classification task, more than one data point is needed on each class but dataset have only one data point on each class. To overcome this top k permutations were selected with the highest importance scores associated with each edge of symptoms.

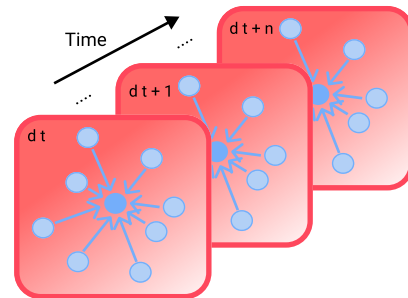


Fig. 2. Graph-Structured Disease Data. Each d_t Indicates a Frame of Current Disease Trajectory at Time Step t , which is Recorded in a Graph Structured Data Matrix.

To generate different graphs for each time instance with available data, by introducing a new initial node with the label as patient and linking new edges between each symptom node and patient node for each disease trajectory growth as shown in the figure.

This results in T unique graphs with the temporal patterns for each disease, where T represents the length of the disease trajectory. Nodal features of each node as initialized with a unique label code of symptoms and each edge weight of each edge assigned based on the importance score of symptoms associated with it.

After preprocessing the knowledge graph extracted from electronic medical records [11], ‘ n ’ disease classes of ‘ k ’ top permutations were generated with the highest importance scores associated with each edge of symptoms and each permutation contains ‘ T ’ unique dynamic graphs with the temporal patterns for each disease. The dimension of each dynamic graph data will be [Number of disease classes ‘ x ’ number to permutations ‘ x ’ length of disease trajectory].

STGCN disease prediction was a spatial-temporal graph

classification task, hence the final dataset will contain, Adjacency matrix with the shape of (length of disease trajectory x number of nodes x number of nodes), Nodal features (length of disease trajectory x number of nodes), graph label (1 x 1).

TABLE II. IMPORTANT STATISTICS OF THE FINAL DATASET

Features	
Size of the Dataset	2000
Unique Diseases	100
Features per Disease	10
Unique Symptoms	308

IV. PROPOSED MODEL

In this section, the proposed architecture of Spatial-Temporal Graph Convolutional Networks (STGCN) is discussed in more detail. STGCN is made up of spatial-temporal convolutional blocks that are arranged in a “sequential” structure with one sequential convolution layer and one spatial graph convolution layer, as illustrated in Fig. 2. Each module’s specifics are as follows.

Fig. 1 depicts an overview of knowledge-based STGCN and Fig. 2 depicts the convolution process. When importing disease data into STGCN in temporal graph format. Two convolution layers comprise the STGCN unit shown below. By broadcasting the features of each node along with the graph edge via the property of graph convolution, the first layer performs spatial graph convolutional operation parallelly on each dynamic graph of a different time instance, then node features vectors containing the aggregation label information of their neighbours can be extracted [17]. The next layer employs the temporal layer to capture the temporal relations of the resultant feature vectors of each entity in the graph.

The entire architecture of the model is depicted via Fig. 3 and Fig. 4. In the former it can be observed how samples of different timestamps are given as input to the network and how they are processed in the spatial layer, while in the latter the input obtained is processed by the temporal layer and the fully connected layer to lastly obtain the output.

A global attention pooling layer [18] is used after the STGCN unit and the output is reshaped in order to achieve proper feature dimension before the output is given to the Fully Connected unit. This unit consists of two linear layers. The first linear layer has an input channel of 55 and an out channel size of 128. The output of the first linear layer was passed through the batch normalization layer, activation function and dropout layer (p=0.3). The following second linear layer has an input channel of 128 and an output channel of n, where n is the number of diseases. Finally, a Softmax layer is applied to predict the final output which is then used for classification. This model is capable of being trained in an end-to-end scenario and the configuration is unified.

A. Spatial Graph Convolution Layer

The spatial graph convolution layer performs the first convolution operation on incoming data. Using the adjacency matrix A and the nodes feature vector F as inputs, the following

function defined by [17] can perform an effective and effective convolution operation. Adjacency matrix A was converted into Edge Index E_i and Edge weight E_w for simplicity.

$$X' = (D'^{-1/2} A' D'^{-1/2}) \cdot X \quad (1)$$

Where $A' = A + I$ denoted the adjacency matrix with inserted self-loop and $D'_{ii} = \sum A'_{ij}$ its diagonal degree matrix. The adjacency matrix can include other values than 1 representing edge weights via optional edge weight E_w tensor.

Its nodes wise formulation is given by:

$$X'_i = \sum_{j \in N(v) \cup i} \left(\frac{e_{i,j}}{\sqrt{d'_j \cdot d'_i}} \cdot X_j \right) \quad (2)$$

with $d'_i = 1 + \sum_{j \in N(i)} e_{i,j}$ denoted the edge weight from the source node j to target node i.

In this experiment, the temporal patterns for each disease knowledge graph simulate changing nodal features and adjacency matrix for each time instance by creating dynamic graph data for each disease. To perform spatial convolution operations for each time instance. The knowledge graph data is passed to T parallel spatial convolution layers, where T represents the length of disease trajectory (the number of time instances recorded in the disease knowledge graph).

A tensor of (Nf, Ei, Ew) can be used to represent the input feature of a spatial graph convolutional layer, where Nf represents node features (symptom labels) of the dynamic disease knowledge graph, Ei represents the edge index of the dynamic graph data, and Ew represents the edge weight of the dynamic graph data. A new tensor with the shape of (output Channel, Number of nodes, dimension of node features) is generated by using the Conv2D layer which is the standard 2D convolution layer. This is implemented using [1,1] kernel size and (4,4) stride as features on the input tensor, which is obtained by multiplying the input matrix with learnable weight matrix W and adding the bias b. The graph convolution is the result of the product of the normalised adjacency matrix A' and the new tensor’s 2^{nd} dimension. Finally, a tensor with the dimensions (output Channel, Number of Nodes, Node Features Dimension) can be created.

$$F_{spatial} = GCN(F_{in}) = A' \times F'_{in} \quad (3)$$

$$F'_{in} = \sum F_{in} \cdot W + b \quad (4)$$

B. Temporal Convolutional Layer

The dynamic disease graph’s temporal aspect is created by stacking the output of the spatial convolutional layer and generating a feature matrix. The temporal axis is well-ordered, with the duration of the disease trajectory limitation, allowing for a straightforward convolutional process to extract temporal information.

The input feature matrix $F_{spatial}$ is implemented as a tensor with the dimensions (T, Number of nodes, spatial Output

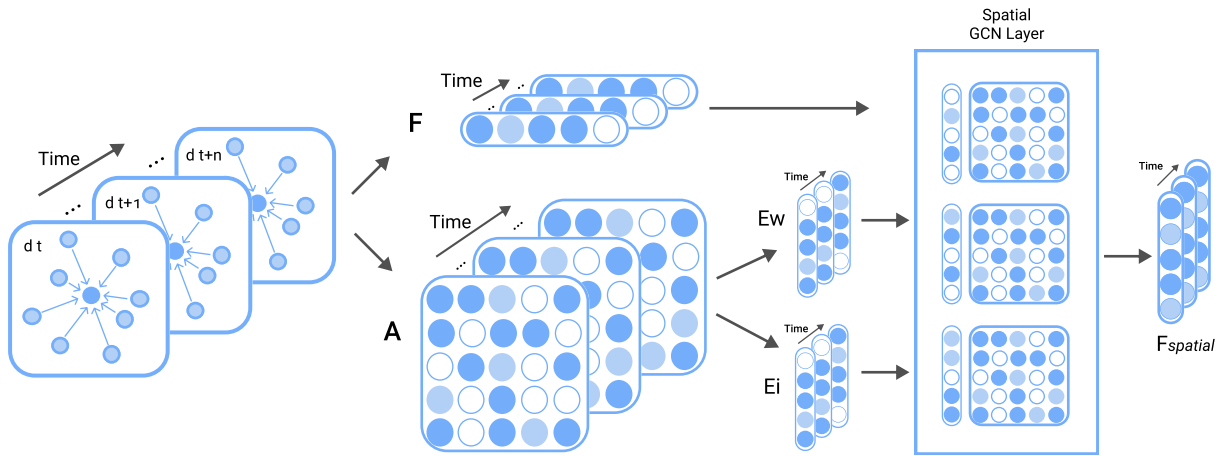


Fig. 3. F Includes the Input Node Feature for given Graph, A Indicates the Adjacency Matrix in Time Order, E_w Means Edge Weight in Time Order, E_i Signifies Edge Index Matrix in Time Order, $F_{spatial}$ is the Final Feature Vector which is Obtained as the Output.

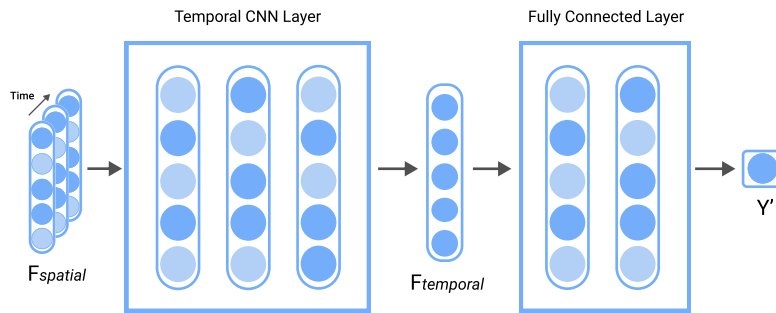


Fig. 4. The $F_{spatial}$ Denotes the Output Features of Spatial Convolutional Layer in Time Order, $F_{temporal}$ Denotes the Output Features of Temporal Convolutional Layer, Y' Denotes the Predicted Disease Class.

channel), where T is the length of the illness trajectory. The temporal kernel size is a parameter that controls how many timestamps are included in the disease graph sequence. The temporal convolutional layer's output channel dimension was determined by parameter γ [19].

$$Output\ channel = (Input\ Channel - \gamma) + 1 \quad (5)$$

Thus, inspired by [20], [21], the temporal convolution operation can be defined as

$$F_{temporal} = TCN(F_{spatial}) = \sum_{i=0}^{\gamma-1} F_{spatial} \cdot W + b \quad (6)$$

V. RESULT

A. Objective Function

Cross-entropy loss is used as the objective function because disease prediction is a multi-class classification task. Using cross-entropy loss, the loss is quantified between the ground truth class d and the model output y' , represented by the following formula:

$$loss(y', d) = \frac{1}{n} \sum d^T \cdot \log(y') + (1 - d)^T \cdot \log(1 - y') \quad (7)$$

where n is the total number of category classes.

B. Implementation Details

All the mentioned approaches are implemented using PyTorch 1.9.0, PyTorch-Geometric, PyTorch Geometric Temporal. All training processes are refined through Nvidia T4 GPU of 8.1 TFLOPS Performance and CUDA 11.1 with Intel(R) Xeon(R) processor. The dataset is then divided into various proportions to assess the performance of the model. It is haphazardly separated into training, validation, testing set in a 0.70 : 0.15 : 0.15.

C. Baseline Methods

A comparison is established with the models given below in Table 3, but since the other models work on different datasets a direct comparison cannot be made. However their performance is highlighted with respect to the proposed model in terms of their accuracy, precision, recall, etc.. These models are:

- Graph Neural Disease Prediction model is proposed in [9] which also implements STGCN blocks on patient data for prediction.

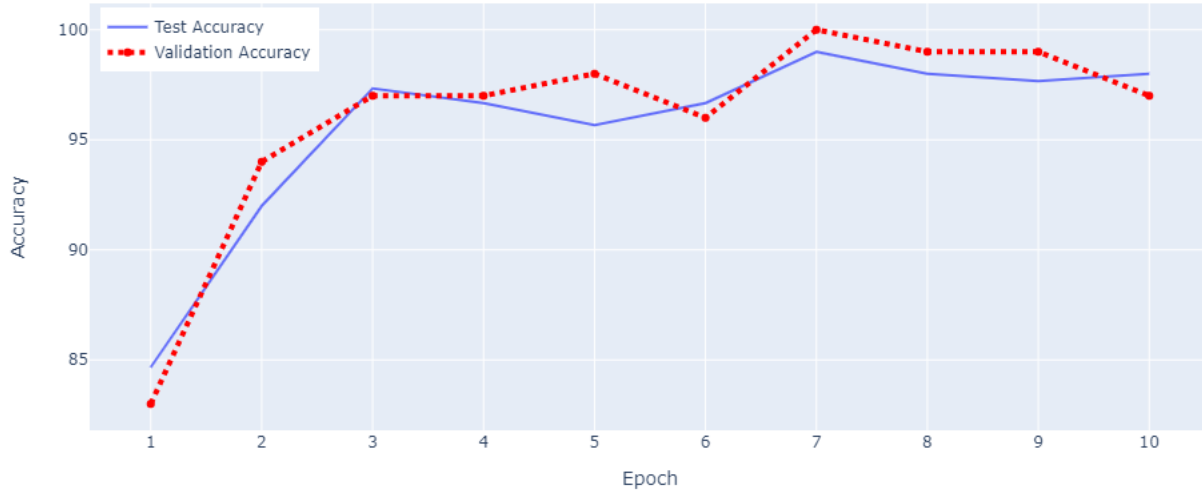


Fig. 5. Validation Accuracy and Test Accuracy Score for each Epoch

TABLE III. COMPARISON WITH OTHER DISEASE PREDICTION MODELS (CONSIDER METRIC AS ACCURACY IF NOT MENTIONED OTHERWISE)

Sr No.	Model	Dataset used	Number of Classes	Performance Metrics
1	Proposed	EMR [11]	100	98.00%
2	DP-GNN [13]	Proprietary EMR	71	Recall - 75.70% Precision - 22.40%
3	Inception GCN [7]	TADPOLE [22]	1	83.40%
2*4	2*RPL [23]	PLAGH [24]	2*65	AUC - 74.30%
		MIMIC [4]		AUC - 63.9%
2*5	2*GNBP [9]	MIMIC [4]	171	86.29%
		EHR Database	154	87.49%
2*6	2*LPNL [25]	TADPOLE [22]	2*1	91.85%
		UKBB		63.91%
7	HRP [26]	NHANES [27]	13	85.50%
8	GMAN [3]	MIMIC [4]	50	Recall - 62.13% Precision - 63.46%

- This is a GNN model for disease prediction proposed in [13] (DP-GNN). The authors map a graph of symptoms linked to the diseases and then use Graph Neural Networks to test their model.
- The model InceptionGCN is proposed in [7]. The author’s utilise GCN layers in their model, however it is used to predict only one class of brain disease.
- The model proposed in [23] utilises Reinforcement Path Learning (RPL) over knowledge graph to predict diseases.
- This model, [25] makes use of simple Multilayer Perceptrons and Latent patient Network (LPNL) in order to predict diseases.
- The model given in [26] describes a method for representing symptoms in the form of knowledge graphs for health risk prediction (HRP).
- Graph Mutual Attention Network (GMAN) - This model [3] makes use of attention layers over graph convolution layers for disease prediction.

D. Evaluation Results

The model is trained to differentiate among 100 unique diseases by using 308 unique symptoms. Using LabelEncoder each disease is given a unique label id from 1-100, similarly the symptoms are labelled. For batching, 10 dynamic knowledge graphs are used per batch, and the $spatial_{\gamma}$ and $temporal_{\gamma}$ is set to 6. Thus, the channel size and the temporal size will be 5.

After preprocessing, the data set is stratified based on diseases label, and then passed to the Spatial layer. The input here is of the size [10x10x11x5] (which is [batchsize x features x nodes x channel size]), the output of which is passed to the Temporal Layer which is of the size [10x10x11x5], where LeakyReLU is used as the threshold function (with a negative slope of 0.01). This is then passed through Global Pooling Layer where the output dimensions are [10x5x11x1] (which is [batch size x temporal size of features x nodes x new aggregated channel size]) and is then concatenated to shape [10x55].

The completely linked layer receives the output from here.

The first layer, which is a Linear layer, has an input of [10x55] and an output of [10x128]. This is normalised using the received output via a BatchNorm1D layer and then ReLU is used as the threshold function. Then a dropout layer is initialised, with a probability of 0.3, before passing it to the final Linear Layer which has an input of [10x128] and output of [10x100]. Then finally, ReLU is used as the threshold function so that whichever node has the highest value will be the predicted label, and hence the predicted disease.

The model was trained for 10 epochs, in which the validation accuracy obtained is 98.00%, and the test accuracy is 98.66% for $\gamma = 6$.

This accuracy indicates that there is a lot of merit in using temporal dependencies for disease prediction, especially by using the proposed method. This model can be also used practically in clinical sciences as a robust healthcare artificial intelligence system.

In Fig. 5, the validation accuracy and the test accuracy is plotted with respect to each epoch. It can be observed that there is an increasing trend and the model achieves high accuracy in a few epochs only.

E. Comparison with Baseline Models

A comparison is established with the given models in Table III, and their features are highlighted, namely the dataset they use, number of classes that were utilised and the accuracy (or the precision, recall, Area Under the Curve [AUC]) of their models.

The GNDP model [9] has been tested on the MIMIC-III dataset [4], so a direct comparison cannot be made, but the paper also makes use of Spatial Temporal Blocks to construct their architecture. In their network, they implement 5 STGCN units, pool the outputs at specific blocks, and then finally pass the output to the fully connected layer. Compared to that, the model only makes use of one STGCN unit before passing the output to the fully connected layer. It is also important to mention here that in GNDP, the input is processed differently from how the model processes the input, and hence the simplicity. GNDP model achieves a maximum accuracy of 86.29% on MIMIC.

VI. CONCLUSION

This paper proposes a novel deep learning framework STGCN for disease prediction, integrating graph convolution through Spatio-temporal convolutional blocks. GNDP solves the constraints of earlier techniques by using GNNs to learn spatial and temporal patterns from patients' sequential graph data, in which medical ontology knowledge and EMR information travel down distinct channels at different levels. The proposed model beats other state-of-the-art methods on datasets, demonstrating that it has a lot of potential in spatial-temporal structures.

These features are quite promising and practical for scholarly development. Moreover, the proposed framework can be applied to more general Spatio-temporal structured sequence prediction scenarios, such as evolving drug linkage, and preference prediction in diagnosis systems, etc.

VII. FUTURE WORK

In this paper, a template and a model is proposed that works well on that template, however the major challenge that was encountered was the absence of medical datasets in the structured format that is proposed. More work can be done to devise a model which converts EMR or EHR reports into a graph structure that [11] utilises and thus the temporal nature associated can be better exploited.

There is also a need of further structured data for disease prediction uses. The model can be better trained and would definitely give us more accuracy if the temporal as well as the sequential dependencies of the symptoms could be better utilised. For example, a fever is associated with a cold, which is associated with cough. These semantics and dependencies give the symptoms a structure which can be then utilised by the STGCN model directly.

Furthermore, methods could be devised to convert popular EMR databases such as [4] can be converted to the format that is proposed in order to establish better comparisons. This is challenging due to varied nature of each database to store information, and the diverse nature of writing reports.

REFERENCES

- [1] S. Mohan, C. Thirumalai, and G. Srivastava, "Effective heart disease prediction using hybrid machine learning techniques," *IEEE access*, vol. 7, pp. 81 542–81 554, 2019.
- [2] S. Uddin, A. Khan, M. E. Hossain, and M. A. Moni, "Comparing different supervised machine learning algorithms for disease prediction," *BMC medical informatics and decision making*, vol. 19, no. 1, pp. 1–16, 2019.
- [3] Q. Yuan, J. Chen, C. Lu, and H. Huang, "The graph-based mutual attentive network for automatic diagnosis." in *IJCAI*, 2020, pp. 3393–3399.
- [4] A. E. Johnson, T. J. Pollard, L. Shen, H. L. Li-Wei, M. Feng, M. Ghassemi, B. Moody, P. Szolovits, L. A. Celi, and R. G. Mark, "Mimic-iii, a freely accessible critical care database," *Scientific data*, vol. 3, no. 1, pp. 1–9, 2016.
- [5] C. Castro, E. Vargas, A. Sánchez, E. Gutierrez Lopez, and D.-L. Flores, *Parkinson's Disease Classification Using Artificial Neural Networks*, 01 2020, pp. 1060–1065.
- [6] T. Vaiyapuri, P. Balaji, S. S. H. Alaskar, and Z. Sbai, "Computational intelligence-based melanoma detection and classification using dermoscopic images," *Computational Intelligence and Neuroscience*, vol. 2022, p. 2370190, May 2022. [Online]. Available: <https://doi.org/10.1155/2022/2370190>
- [7] A. Kazi, S. Shekarforoush, S. A. Krishna, H. Burwinkel, G. Vivar, K. Kortüm, S.-A. Ahmadi, S. Albarqouni, and N. Navab, "Inceptiongen: receptive field aware graph convolutional network for disease prediction," in *International Conference on Information Processing in Medical Imaging*. Springer, 2019, pp. 73–85.
- [8] D. Ahmedt-Aristizabal, A. Armin, S. Denman, C. Fookes, and L. Petersson, "Graph-based deep learning for medical diagnosis and analysis: Past, present and future," *Sensors*, vol. 21, p. 4758, 07 2021.
- [9] Y. Li, B. Qian, X. Zhang, and H. Liu, "Knowledge guided diagnosis prediction via graph spatial-temporal network," in *Proceedings of the 2020 SIAM International Conference on Data Mining*. SIAM, 2020, pp. 19–27.
- [10] T. Vaiyapuri, Liyakathunisa, H. Alaskar, E. Aljohani, S. Shridevi, and A. Hussain, "Red fox optimizer with data-science-enabled microarray gene expression classification model," *Applied Sciences*, vol. 12, no. 9, 2022. [Online]. Available: <https://www.mdpi.com/2076-3417/12/9/4172>
- [11] M. Rotmensch, Y. Halpern, A. Tlimat, S. Horng, and D. Sontag, "Learning a health knowledge graph from electronic medical records," *Scientific reports*, vol. 7, no. 1, pp. 1–11, 2017.

- [12] X. Li, Y. Wang, D. Wang, W. Yuan, D. Peng, and Q. Mei, "Improving rare disease classification using imperfect knowledge graph," *BMC medical informatics and decision making*, vol. 19, no. 5, pp. 1–10, 2019.
- [13] Z. Sun, H. Yin, H. Chen, T. Chen, L. Cui, and F. Yang, "Disease prediction via graph neural networks," *IEEE Journal of Biomedical and Health Informatics*, vol. 25, no. 3, pp. 818–826, 2020.
- [14] A. Giannoula, A. Gutierrez-Sacristán, Á. Bravo, F. Sanz, and L. I. Furlong, "Identifying temporal patterns in patient disease trajectories using dynamic time warping: A population-based study," *Scientific reports*, vol. 8, no. 1, pp. 1–14, 2018.
- [15] A. B. Jensen, P. Moseley, T. Oprea, S. Ellesøe, R. Eriksson, H. Schmock, P. Jensen, L. Jensen, and S. Brunak, "Temporal disease trajectories condensed from population-wide registry data covering 6.2 million patients," *Nature communications*, vol. 5, p. 4022, 06 2014.
- [16] T. Ploner, S. Heß, M. Grum, P. Drewe-Boss, and J. Walker, "Using gradient boosting with stability selection on health insurance claims data to identify disease trajectories in chronic obstructive pulmonary disease," *Statistical Methods in Medical Research*, vol. 29, 07 2020.
- [17] T. N. Kipf and M. Welling, "Semi-supervised classification with graph convolutional networks," *arXiv preprint arXiv:1609.02907*, 2016.
- [18] Y. Li, D. Tarlow, M. Brockschmidt, and R. S. Zemel, "Gated graph sequence neural networks," *CoRR*, vol. abs/1511.05493, 2016.
- [19] B. Yu, H. Yin, and Z. Zhu, "Spatio-temporal graph convolutional networks: A deep learning framework for traffic forecasting," in *IJCAI*, 07 2018, pp. 3634–3640.
- [20] S. Bai, J. Z. Kolter, and V. Koltun, "An empirical evaluation of generic convolutional and recurrent networks for sequence modeling," *arXiv preprint arXiv:1803.01271*, 2018.
- [21] S. Guo, Y. Lin, N. Feng, C. Song, and H. Wan, "Attention based spatial-temporal graph convolutional networks for traffic flow forecasting," *Proceedings of the AAAI Conference on Artificial Intelligence*, vol. 33, pp. 922–929, 07 2019.
- [22] R. V. Marinescu, N. P. Oxtoby, A. L. Young, Bron *et al.*, "Tadpole challenge: Accurate alzheimer's disease prediction through crowdsourced forecasting of future data," in *International Workshop on Predictive Intelligence In Medicine*. Springer, 2019, pp. 1–10.
- [23] Z. Sun, W. Dong, J. Shi, and Z. Huang, "Interpretable disease prediction based on reinforcement path reasoning over knowledge graphs," *arXiv preprint arXiv:2010.08300*, 10 2020.
- [24] P. Li, C. Xie, T. Pollard, Johnson *et al.*, "Promoting secondary analysis of electronic medical records in china: summary of the plagh-mit critical data conference and health datathon," *JMIR medical informatics*, vol. 5, no. 4, p. e43, 2017.
- [25] L. Cosmo, A. Kazi, S.-A. Ahmadi, N. Navab, and M. Bronstein, "Latent patient network learning for automatic diagnosis," *Medical Image Computing and Computer Assisted Intervention – MICCAI 2020*.
- [26] X. Tao, T. Pham, J. Zhang, J. Yong, W. P. Goh, W. Zhang, and Y. Cai, "Mining health knowledge graph for health risk prediction," *World Wide Web*, vol. 23, no. 4, pp. 2341–2362, 2020.
- [27] S. Kranz, L. J. Mahood, and D. A. Wagstaff, "Diagnostic criteria patterns of us children with metabolic syndrome: Nhanes 1999–2002," *Nutrition Journal*, vol. 6, no. 1, pp. 1–9, 2007.

Password Systems: Problems and Solutions

Lanfranco Lopriore
Dipartimento di Ingegneria dell'Informazione
Università di Pisa
via G. Caruso 16, 56126 Pisa, Italy

Abstract—In a security environment featuring subjects and objects, we consider an alternative to the classical password paradigm. In this alternative, a key includes a password, an object identifier, and an authorization. A master password is associated with each object. A key is valid if the password in that key descends from the master password by using a validity relation expressed in terms of a symmetric-key algorithm. We analyse a number of security problems. For each problem, a solution is presented and discussed. In certain cases, extensions to the original key paradigm are introduced. The problems considered include the revocation of access authorizations; bounded keys expressing limitations on the number of iterated utilizations of the same key to access the corresponding object; repositories, which are objects aimed at storing keys, possibly organized into hierarchical structures; and the merging of two keys into a single key featuring a composite authorization that includes the access rights in the two keys.

Keywords—Access authorization; key; password; revocation; security

I. INTRODUCTION

We will refer to the classical security paradigm featuring active entities, called *subjects*, that generate access attempts to passive entities, called *objects* [15], [16], [20], [24], [29]. A subject can be a process, or the activity generated by the occurrence of an event, e.g. a hardware interrupt. Objects are typed. The definition of the type of a given object includes the specification of a set of values, and a set of operations that act on these values. For each operation, the type definition specifies the *access authorization*, i.e. the set of access rights, that is necessary to execute this operation successfully.

In an environment featuring subjects and objects, a basic problem is to allow subjects to certify permission to access objects, i.e. the subject should possess the corresponding access authorization [6]. A classical solution is based on the association of a number of *passwords* with each object, one password for each significant access authorization [4], [13]. In this solution, a subject that holds a password for a given object, and is aimed at executing a given operation on that object, presents the password to the object. If the password is valid, and the access authorization associated with the password includes the required access rights, then the execution of the operation is permitted.

Password proliferation is an inherent problem in password systems. Let us refer to an object type defining four access rights, for instance. In this type, up to fifteen passwords are necessary, if all access right combinations are meaningful. Significant memory requirements follow from the necessity to store these passwords within the internal representation of each object. Alternatively, we can associate a password with each

access right. This solution reduces the memory requirements, but is prone to significant complications of the whole password management process. For instance, a subject that should be granted a full access authorization that includes all the access rights for a given object must possess all the passwords defined for that object. The arguments of an operation requiring several access rights must include as many passwords. A subject that is aimed at passing an access authorization to a recipient must transmit one password for each access right in the authorization.

In a different approach, we associate a *master password* with each object. This password is generated at random when the object is created. Master passwords should be large and sparse, according to the overall security requirements of the system. A subject certifies its own right to access an object whose identifier is *id* by presenting a *key* K referencing this object. The key has the form $K = (psw, id, au)$, where *au* specifies an access authorization, and *psw* is a password. The key is valid if the password is valid, i.e. if $psw = E_{mp}(id || au)$, where the $||$ symbol denotes a concatenation. In this *validity relation*, E denotes a symmetric-key algorithm, the *password cipher*, which is universally known. The password is valid if it is the result of the application of the password cipher to the concatenation of the identifier and the authorization. The encryption key is the master password of the object identified by *id*. If the password is valid, possession of the key grants access to the object, to carry out those operations that are authorized by the access rights in *au*, according to the specification of the object type. The *au* field features one bit for each access right. If a given bit is asserted, the authorization includes the corresponding access right. Thus, for instance, an *au* field of all 1's corresponds to a full access authorization including all the access rights. A subject certifies possession of a full access authorization for the given object by a single key, i.e. key $(psw, id, 11\dots 1)$.

In this approach, a single password, the master password, needs to be stored into the internal representation of each object, and a single key is necessary in each operation to certify possession of the access authorization required by that operation. A subject that holds an access authorization expressed in terms of a given key can transmit this authorization to a recipient by copying the key to the recipient.

The rest of this paper presents the background, first (Section II). Afterwards, with reference to a key-based method of password specification and storage, a collection of significant problems is analysed, which are connected with password utilization and management. The problems considered include the revocation of access authorizations (Section III); bounded keys aimed at forcing upper limits to the number of successful

key utilizations (Section IV); key repositories, which are containers for collections of keys that can be connected to form a hierarchy (Section V); and a mechanism to merge two or more keys into a single key including all the access rights in the respective authorizations (Section VI). For each problem, we present a solution in terms of the corresponding password treatment approach. Extensions to the key format are introduced.

II. BACKGROUND

Password capabilities are a well-known implementation of the password concept, which was introduced in Section I [5], [9], [10], [14], [21]. Several computing systems implementing an object referencing approach based on password capabilities were designed and actually implemented in the past. Examples are Annex [19], Walnut [4], Mungi [9], Opal [5], and the Password Capability System [1]. In a password capability environment, a set of passwords is associated with each given object, one password for each significant access authorization. A password capability is a pair (psw, id) where psw is a password, and id is an object identifier. A subject that possesses a given password capability can access the named object to carry out those operations which are made possible by the access rights in the authorization associated with the password. If passwords are sparse, large, and generated at random, it is virtually impossible for an attacker to generate a valid password capability from scratch. It follows that password capabilities can be freely mixed in memory with ordinary information items. In this respect, password capabilities are an important improvement over the capability concept [12]. In a classical capability environment, the specification of the access authorization is part of the capability [7], [17], [22]. Consequently, capabilities should be segregated, into reserved memory regions [11], or by taking advantage of memory tagging techniques [2], [3], [18], [28].

Password capabilities suffer from the password proliferation problem. For a type defining several access rights, many passwords should be stored into the internal representation of an object of that type, one password for each meaningful access authorization. Negative effects follow in terms of complicated password management and high memory costs for password storage, especially for forms of fine-grained object access security featuring small-sized objects.

Consider a subject that holds a password capability including the password for a given access authorization. The subject may transfer the authorization to a recipient by passing the password capability to the recipient. In turn, the recipient can transmit the authorization further, by new actions of a password capability copy. Now suppose that the original subject is aimed at revoking the grant from the recipients. If the subject owns the object, it can modify the password. This form of revocation extends automatically to all subjects that hold a password capability expressed in terms of that password. However, we cannot reduce the authorization by eliminating a subset of the access rights associated with the password, and we cannot limit the revocation to a specific subset of the subjects.

Of course, after changing a password, the object owner can proceed to a new distribution of password capabilities with the new password to selected recipients. The whole process is

much more complicated than implied by the desired effect. This is especially the case for those subjects that received the password capability through intermediate recipients, which may well be unwilling, or even unable, to cooperate in the new distribution. In fact, one of the main advantage of password capability systems is simplicity in access right transmission between subject. This simplicity should be also preserved for revocation.

No bound exists on the transmission ability of a subject that holds a given password capability. In fact, the subject is free to pass the password capability to an unlimited number of recipients. In turn, each recipient can transmit the password capability further. In the original definition of the password capability concept, no mechanism is provided to limit this form of password capability proliferation.

The password capability format does not include an authorization field. It follows that we cannot argue the authorization granted by a given password capability by inspection of the password capability itself. In fact, in the original password capability paradigm, the association between a password for a given object and the authorization granted by that password is part of the internal representation of the object. An *ad-hoc* operation would be necessary to convert passwords into the corresponding authorizations.

III. REVOCATION

At the security system level, the key-based approach introduced in Section I is supported by a collection of system primitives for object and key management (Fig. 1). A first example is $K \leftarrow \text{new}(T, arg_0, arg_1, \dots)$. In the execution of this primitive, the constructor of type T is used to create a new object of this type, according to the specifications of the type. Arguments arg_0, arg_1, \dots are transmitted to the constructor. The primitive returns a key referencing the new object, with a full access authorization that includes all access rights. Primitive $\text{delete}(K)$ uses the destructor of the type of the object referenced by key K to delete this object. The execution terminates correctly only if K specifies an access authorization that includes access right OWN. Primitive $\text{exec}(K, op, arg_0, arg_1, \dots)$ executes operation op on the object referenced by key K . Arguments arg_0, arg_1, \dots are transmitted to op . The execution terminates correctly only if K specifies an access authorization that includes all the access rights required by op . Finally, let $K_0 = (psw_0, id, au_0)$ be a key, and msk be a mask having the same size as an authorization. Primitive $K_1 \leftarrow \text{reduce}(K_0, msk)$ returns a key $K_1 = (psw_1, id, au_1)$ referencing the same object as key K_0 , with the reduced authorization au_1 that results from relation $au_1 = au_0 \& msk$, i.e. the bitwise AND of authorization au_0 and mask msk . The execution of this primitive uses the validity relation and the master password of the object identified by id to evaluate the new password psw_1 .

One of the main advantages of a password-based environment is simplicity in access right distribution. Consider a subject that holds the password corresponding to a given authorization. The subject can grant this authorization to one or more recipients by simply distributing a copy of the password to these recipients. In turn, each recipient can grant the authorization to additional subjects, by further password copy

$K \leftarrow \text{new}(T, \text{arg}_0, \text{arg}_1, \dots)$
 Uses the constructor of type T to create a new object of this type. Arguments $\text{arg}_0, \text{arg}_1, \dots$ are transmitted to the constructor. Returns a key referencing the new object, with a full access authorization that includes all access rights.

$\text{delete}(K)$
 Uses the destructor of the type of the object referenced by key K to delete this object. K should specify access right OWN.

$\text{exec}(K, \text{op}, \text{arg}_0, \text{arg}_1, \dots)$
 Executes operation op on the object referenced by key K . Arguments $\text{arg}_0, \text{arg}_1, \dots$ are transmitted to op . K should specify all the access rights required by op .

$K_1 \leftarrow \text{reduce}(K_0, \text{msk})$
 Returns a key $K_1 = (\text{psw}_1, \text{id}, \text{au}_1)$ referencing the same object as key $K_0 = (\text{psw}_0, \text{id}, \text{au}_0)$, where $\text{au}_1 = \text{au}_0 \& \text{msk}$, the $\&$ symbol denotes a bitwise AND, and mask msk has the same size as an authorization.

Fig. 1. Primitives for Object and Key Management.

actions. We will now consider the case that the original subject modifies its own intention, and is aimed at revoking the grants from the recipients. Revocation is especially useful to comply with the *principle of least privilege*: at any given time, each subject should possess only those access privileges that are necessary at that time for its legitimate purposes [23], [25]–[27].

Of course, by changing the password associated with a given authorization we obtain a form of revocation that includes only this authorization. The revocation involves all the subjects that received the authorization in the form of that password. Restricting revocation to a subset of these recipient subjects is a problem that is hard to solve. We can modify the password, and then proceed to a distribution of the new password to the desired recipients. However, consider the case of a recipient that was reached by means of two or more distribution steps through intermediate subjects. Collaboration will be necessary in the new distribution, but these intermediate subjects may well be unwilling, or even unable, to cooperate.

In our key-based environment, consider a subject that holds a key for a given object, and distributes a copy of this key to one or more recipients. A form of total revocation that involves all access authorizations can be obtained at little effort by a system primitive having the form $K_1 \leftarrow \text{mpReplace}(K)$. The execution of this primitive modifies the master password of the object referenced by key K , whose authorization should specify all access rights. The primitive returns a key K_1 defined in terms of the new master password and including all access rights. After the execution of this primitive, all keys generated by using the old master password are revoked; it will no longer possible to use these keys for successful object accesses. However, it is impossible to take advantage of an approach of this type to implement forms of revocation that involve only a subset of the recipients, or only a subset of the access rights. We will now introduce more flexible approaches to the solution of the revocation problem.

A. Instances

A first approach is based on a different form of the access authorization field. In au , we associate more than a single bit with each access right. This means that we can have several

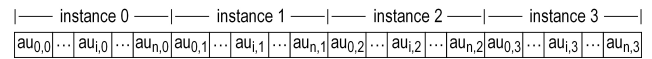


Fig. 2. An Access Authorization Field Featuring Four Instances of n Access Rights.

instances of the same access right. Fig. 2 considers an example of an access authorization field featuring four instances of n access rights. For the i -th access right in the authorization, these instances are named $\text{au}_{i,0}$ to $\text{au}_{i,3}$. If bit $\text{au}_{i,j}$ is asserted, then the access authorization includes instance j of access right i . The internal representation of each object is modified to contain an authorization *mask*, which applies to all keys referencing that object. The structure of the mask is similar to that of an authorization field. If $\text{mask}_{i,j}$ is cleared, then $\text{au}_{i,j}$ is revoked.

When a subject generates an access attempt to a given object, the key presented by the subject is considered to certify the access. The access is permitted if, for each access right required by the access, at least one instance is asserted in the authorization field of the key, and this instance is not revoked by the corresponding mask bits. Conversely, the object access is negated if all instances of one or more of the required access rights are cleared, or are revoked by the mask. Let eff denote the *effective* authorization resulting from the bitwise AND of the authorization field and the mask; thus we have $\text{eff} = \text{au} \& \text{mask}$. The i -th access right is granted by the key if at least one instance of this access right is asserted in eff , that is, for m instances, $\text{eff}_{i,0} \vee \text{eff}_{i,1} \vee \dots \vee \text{eff}_{i,m} = 1$. In the mask, the bits corresponding to instance 0 are always asserted for all access rights. It follows that, in a key, an access right in instance 0 is never revoked.

The primitives to create and access objects, introduced previously and illustrated in Fig. 1, should be modified to deal with effective authorizations. When primitive new is issued to create a new object, the mask of that object is set to all 1's, to validate all access right instances. The key returned by new features an access authorization that includes all access rights in all instances. The execution of primitive $\text{delete}(K)$ terminates successfully only if the effective authorization granted by key K includes access right OWN. In the execution of primitive $\text{exec}(K, \text{op}, \text{arg}_0, \text{arg}_1, \dots)$, the effective authorization should include the access rights required by the operation specified by argument op .

The mask of a given object can be modified by issuing primitive $\text{mask}(K, \text{msk})$. Argument K is a key referencing the object, argument msk is the new mask, which should specify all 1's for instance 0. The execution accesses the internal representation of the object to modify the mask. The operation terminates successfully only if key K specifies all access rights in instance 0.

B. Categories

In a different approach to access right revocation, we extend the key format to include the specification of a *category*. A key assumes the form $K = (\text{psw}, \text{id}, t, \text{au})$, where the t field specifies the category. Each category has a *degree*. The degree of a given category expresses a limitation on the access rights granted by every key in that category.

changeDegree(K, t, d)
Assigns degree d to category t of the object referenced by key K , which should specify category 0.

$K_1 \leftarrow changeCategory(K, t)$
Returns a new key in category t for the object referenced by key K , with the same access authorization. K should specify category 0.

Fig. 3. Primitives for Category Management.

Let us refer to an object type featuring n access rights. As seen in Section I, authorization field au is encoded in n bits, one bit for each access right. If a given bit is asserted, the corresponding access right is part of the authorization. The internal representation of each object is modified to include a *category table* featuring an entry for each category. The entry for a given category contains the degree of that category. A degree is encoded in n bits. For a given key, the *effective* authorization results from the bitwise AND of the au field and the degree of the category specified by the t field. It follows that a degree of all 1's for a given category implies that all the access rights in the authorization of a key in that category are effective. Conversely, a degree of all 0's means that all these access rights are revoked.

In an extended key environment featuring categories, the primitives for object management, introduced previously and illustrated in Fig. 1, should be modified to deal with degrees. Primitive *new* assigns degree 0 to all categories, and returns a key featuring category 0. This category is special in that its degree always is all 1's, and cannot be changed. The execution of primitives *delete* and *exec* considers the effective access authorization granted by key K , as follows from the compound effect of the authorization field and the degree of the category specified by the key.

Category management is supported by two primitives (Fig. 3). Primitive *changeDegree(K, t, d)* makes it possible to modify category degrees. Its execution assigns degree d to category t of the object referenced by key K . The execution is successful only if K specifies category 0. Primitive $K_1 \leftarrow changeCategory(K, t)$ returns a new key in category t for the object referenced by key K , with the same access authorization. The execution is successful only if K specifies category 0.

C. Comparison

Let us refer to the classical properties of an access right revocation system [8]. In the approach based on access right instances, revocation is *partial*, that is, we can revoke any desired subset of the access rights. To this aim, we clear the mask bits corresponding to these access rights in all instances. Revocation is *selective*, that is, we can revoke an access right from a subset of the recipients of that access right. To this aim, we clear the mask bits of the instances specified by the keys held by these recipients. Revocation is *independent*, that is, keys received from different distributors can be revoked independently of each other, if these keys specify different instances of the same access rights. Revocation is *transitive*, that is, it propagates to all copies of the same key, independently of the path followed by the copy to reach its recipient; and in fact, a key copy cannot be distinguished from the original.

Revocation is *temporal*, as it can be reversed through the same mechanism, i.e. the mask, by setting the mask bits that were cleared for revocation.

In the category-based approach, we can obtain a partial revocation by clearing the bits of the degree field corresponding to the access rights to be revoked from the category. Selective revocation is intrinsic in the category model, and will be simply obtained by clearing the degree of selected categories. Independent revocation can be obtained at little effort for keys belonging to different categories, by modifying the degree of only those categories that are involved in the revocation; the other degrees will be left unaltered. Transitive revocation is implicit in the key model. Finally, temporality can be obtained by simply setting the bits of the degree that were cleared for revocation to reverse the effects of the revocation.

Instances imply no modification of the key format. In fact, instances need to be introduced only in those object types for which an option for revocation is necessary. In these types, the access authorization field will be extended to include several bits for each access rights. The size of the extension will be decided on a type basis. In fact, we can have different numbers of instances for different types. Conversely, in the category based approach, the key format should be extended to include the category field. This modification applies to all types. The number of categories is fixed for all types, and is determined by the size of the category field.

The memory costs of instances are connected with mask storage and the size of the access authorization field, which is increased to include several bits for each access rights. For four access rights and four instances of each access right, a two-byte access right field and a two-byte mask will be necessary. These memory costs are to be paid only for those object types for which revocation is necessary. On the other hand, a four-bit category field is sufficient to implement up to 16 categories. The memory costs for storage of the category table in the internal representation of each object are quite limited. Let us refer to an object type defining four access right, for instance. In a situation of this type, for 16 categories, a 64-bit word will be sufficient.

IV. BOUNDED KEYS

The password paradigm, as is implemented by the key construct, implies no limitation on iterated utilizations of the same given key to access the corresponding object. We will now present an extension of the key concept aimed at forcing an upper bound to the number of successful applications of the same key.

We modify the key format by introducing a new field, the *bound field* b . In the new format, a *bounded key* B is a quadruple $B = (psw, id, au, b)$ (Table I). The validity relation is modified to take the bound field into account. The key is valid if $psw = E_{mp}(id || au || b)$, where mp is the master password of the object identified by id , au is the authorization granted by the key, and b identifies the bound. A *bound table* is associated with each object. The bound table features an entry for each bound. The entry for a given bound contains the *extent* of that bound. The extent is the total number of times that bounded keys in that bound can be successfully used to access the object (if the extent is 0, these keys can no longer

TABLE I. BOUNDED KEY FORMAT

$B = (psw, id, au, b)$: bounded key
$psw = E_{mp}(id au b)$: validity relation
psw : password
id : object identifier
au : access authorization
b : bound
E : password cipher
mp : master password

be used). If the bound is 0, then the key is a *primary key* that has no bound, and can be used for an unlimited number of accesses to the object.

The bound table of a given object will be stored as part of the internal representation of the object. The memory requirements for storage of the bound table are determined by the number of bounds and the maximum extent permitted for each bound. For instance, a bound field of three bits allows for up to 7 bounds (bound 0 being reserved to specify a primary key). If an extent is encoded in 16 bits, for each bound we can have up to 65,535 executions of the *exec* primitive using a bounded key in that bound. In a configuration of this type, the whole bound table can be contained in two 64-bit words.

A. Primitives

The primitives for object management, introduced in Section III and illustrated in Fig. 1, should be modified to deal with bounds and extents. Primitive $B \leftarrow new(T, arg_0, arg_1 \dots)$ uses arguments arg_0, arg_1, \dots in the constructor of type T to create a new object of this type, and returns a primary key for that object, which includes all access rights. The extents of the bounds of the object are all equal to 0. This means that the object can only be accessed by using the primary key, until one or more bounds are *recharged* to specify new extents (see below). Primitive *delete*(B) uses the destructor of the type of the object referenced by bounded key B to delete the object. B should be a primary key, and should include an access authorization that specifies access right OWN. Primitive *exec*($B, op, arg_0, arg_1, \dots$) uses arguments arg_0, arg_1, \dots to execute operation op on the object identified by id . The execution is successful if B specifies an access authorization that includes all the access rights required by op . B should be a primary key, or the extent of the bound of B should be greater than 0. If this is the case, the extent is decremented by 1.

The primitives for bound management are summarized in Fig. 4. Primitive $e \leftarrow extent(B, b)$ returns the extent e of the bound b of the object referenced by bounded key B , which should be a primary key. Primitive *recharge*(B, b, e) increments the extent of the bound b of the object referenced by bounded key B by quantity e . B should be a primary key. Primitive $B_1 \leftarrow newBound(B_0, b)$ returns a bounded key B_1 referencing the same object as bounded key B_0 , with the same access authorization and bound b . B_0 should be a primary key.

V. REPOSITORIES

The *Repository* data type allows us to define objects aimed at key storage [15]. A name is associated with each key in a

$e \leftarrow extent(B, b)$ Returns the extent e of the bound b of the object referenced by bounded key B , which should be a primary key.
<i>recharge</i> (B, b, e) Increments the extent of the bound b of the object referenced by bounded key B by quantity e . B should be a primary key.
$B_1 \leftarrow newBound(B_0, b)$ Returns a bounded key B_1 referencing the same object as bounded key B_0 , with the same access authorization and bound b . B_0 should be a primary key.

Fig. 4. Primitives for Bound Management.

TABLE II. ACCESS RIGHTS IN THE *Repository* TYPE.

Access right	Operation
GET	<i>read</i>
PUT	<i>write</i>
INSPECT	<i>list</i>
OWN	<i>delete</i>

repository. The name is unique within the repository, that is, it will never be the case that two keys in a given repository are associated with the same name (on the other hand, the same key name can be freely used in different repositories).

Table II enumerates the access rights that are included in the definition of the *Repository* type. For each access right, the table shows the operation whose execution is made possible by that access right. For a given repository, access right GET makes it possible to read those keys in the repository whose names are known. Access right PUT makes it possible to insert keys into the repository. Access right INSPECT allows us to read the names of the keys in the repository. Access right OWN allows us to delete the repository.

Fig. 5 presents the operations defined by the *Repository* type, and gives short indications of the effects of the execution of each of them. Primitive $K \leftarrow new(Repository)$ uses the constructor of the type to create a new, empty repository, and return a key referencing that repository, with a full access authorization that includes all the access rights. Primitive *delete*(K) uses the destructor to delete the repository referenced by key K . This key should specify access right OWN.

The other operations of the *Repository* type are implemented taking advantage of primitive *exec*. A first example is $K_1 \leftarrow exec(K_0, read, nm)$. The execution of this operation accesses the repository referenced by key K_0 to return the key named nm in that repository. The execution is successful if K_0 specifies access right GET. Operation *exec*($K_0, write, nm, K_1$) adds key K_1 to the repository referenced by key K_0 , and associates name nm to K_1 . K_0 should specify access right PUT. Operation $lst \leftarrow exec(K, list)$ returns a list of the names of the keys contained in the repository referenced by key K . This key should specify access right INSPECT.

A. Hierarchies

The *Repository* object type makes it possible to organize keys into hierarchies. In an organization of this type, each repository can include keys for other repositories at a lower

$K \leftarrow \text{new}(\text{Repository})$
Uses the constructor of the *Repository* type to create a new, empty repository. Returns a key referencing that repository, with an access authorization that includes all access rights.

$\text{delete}(K)$
Uses the destructor of the *Repository* type to delete the repository referenced by key K , which should specify access right OWN

$K_1 \leftarrow \text{exec}(K_0, \text{read}, nm)$
Returns the key named nm taken from the repository referenced by key K_0 , which should specify access right GET.

$\text{exec}(K_0, \text{write}, nm, K_1)$
Adds key K_1 to the repository referenced by key K_0 , and associates name nm to K_1 . K_0 should specify access right PUT.

$lst \leftarrow \text{exec}(K, \text{list})$
Returns a list of the names of the keys stored in the repository referenced by key K , which should specify access right INSPECT.

Fig. 5. Operations of the *Repository* Type.

hierarchical level. Each repository can also include keys for objects of any other type, which represent the leaves of the hierarchy. In a given repository, the name associated with each key identifies the object referenced by that key.

A subject that knows the name of a key in a given repository, and possesses a key for that repository with access right GET, can access the repository to read the key. If the subject does not know the key name, it can use the *list* operation, but an action of this type requires access right INSPECT for the repository.

B. Access Right Amplification

The *read* operation implements a form of access right amplification, whereby a subject that possesses access right GET for a given repository can read the keys in that repository independently of the access rights specified by these keys. For instance, consider the case of a repository R_0 that includes a key K referencing another repository R_1 , and K specifies all access rights. A subject that possesses a key for R_0 featuring a single access right, GET, can read K from R_0 . In this way, the subject acquires a full access authorization for R_1 , which is an amplification of the authorization that the subject holds for R_0 .

VI. MERGING KEYS

Let us refer to a subject S that holds two keys that reference the same object, say $K_0 = (psw_0, id, au_0)$ and $K_1 = (psw_1, id, au_1)$, where id is the object identifier. Let us suppose that the type of the object includes an operation op whose execution requires both the access rights in au_0 and the access rights in au_1 . Primitive $\text{exec}(K, op, arg_0, arg_1, \dots)$ features a single key, whose authorization field should include all the required access rights. It follows that subject S is not in the position to execute op , unless the two keys K_0 and K_1 are merged to form a single key including the union of the access rights in the authorizations. To this aim, primitive $K \leftarrow \text{merge}(K_0, K_1)$ can be provided. The execution of this operation returns a key $K = (psw, id, au)$ for the object identified by id . K features an authorization au that includes the union of the access rights in au_0 and au_1 .

It should be noted that *merge* implement a form of access right amplification. In the example above, by using *merge*, subject S amplifies its own execution ability to include operation op , which would be negated in the absence of *merge*. In fact, the decision to include *merge* in the set of primitives of the security system is a design choice. If this form of access right amplification should be permitted, *merge* will be made available.

In a more flexible approach, an *ad-hoc* access right, the JOIN access right, will be required in all the keys involved in an access right merging activity. In this case, in the example above, a successful execution of primitive *merge* will be possible only if both keys K_0 and K_1 include JOIN in the respective authorizations.

Primitive *merge* also supports a form of cooperation between subjects. Consider two subjects S_0 and S_1 that hold keys K_0 and K_1 , respectively. These subjects cannot execute an operation requiring the union of the access rights in au_0 and au_1 , unless they agree to merge the two keys.

VII. CONCLUSION

With reference to a security system featuring subjects and objects, we have considered a paradigm of object access, which is an alternative to classical password-based environments. Our paradigm takes advantage of keys. In particular:

- The key definition includes a password, an object identifier, and an authorization.
- A master password is associated with each object. A key is valid if the password descends from the master password by using a validity relation expressed in terms of a symmetric-key algorithm.

We analysed a number of security problems, which include:

- The revocation of access authorizations.
- Bounded keys expressing limitations on the number of iterated utilizations of the same key to access the corresponding object.
- Repositories, which are objects aimed at storing keys, possibly organized into hierarchical structures whereby each repository may include keys for other repositories at a lower hierarchical level.
- The merging of two keys into a single key featuring a composite authorization that includes all the access rights in the two authorizations.

For each problem, we have proposed a solution expressed in terms of a key treatment approach. Extensions to the original key format have been introduced and discussed.

ACKNOWLEDGMENT

This work was supported in part by the Italian Ministry of University and Research (MUR) in the framework of the *CrossLab* project (Departments of Excellence).

REFERENCES

- [1] M. Anderson, R. D. Pose, and C. S. Wallace, "A Password-Capability System," *The Computer Journal*, vol. 29, pp. 1–8, February 1986.
- [2] K. M. Bresniker, P. Faraboschi, A. Mendelson, D. Milojicic, T. Roscoe, and R. N. Watson, "Rack-scale capabilities: fine-grained protection for large-scale memories," *Computer*, vol. 52, no. 2, pp. 52–62, 2019.
- [3] J. Brown, J. Grossman, A. Huang, and T. F. Knight Jr, "A capability representation with embedded address and nearly-exact object bounds," tech. rep., Project Aries, ARIES-TM-005, Artificial Intelligence Laboratory, Department of Electrical Engineering and Computer Science, Massachusetts Institute of Technology, Cambridge, MA, USA, 2000.
- [4] M. D. Castro, R. D. Pose, and C. Kopp, "Password-capabilities and the Walnut kernel," *The Computer Journal*, vol. 51, no. 5, pp. 595–607, 2008.
- [5] J. S. Chase, H. M. Levy, E. D. Lazowska, and M. Baker-Harvey, "Lightweight shared objects in a 64-bit operating system," in *Proceedings of the Conference on Object-Oriented Programming Systems, Languages, and Applications*, (Vancouver, British Columbia, Canada), pp. 397–413, ACM, October 1992.
- [6] S. De Capitani di Vimercati, S. Paraboschi, and P. Samarati, "Access control: principles and solutions," *Software – Practice and Experience*, vol. 33, no. 5, pp. 397–421, 2003.
- [7] A. L. Georges, A. Guéneau, T. Van Strydonck, A. Timany, A. Trieu, S. Huyghebaert, D. Devriese, and L. Birkedal, "Efficient and provable local capability revocation using uninitialized capabilities," *Proceedings of the ACM on Programming Languages*, vol. 5, no. POPL, pp. 1–30, 2021.
- [8] V. D. Gligor, "Review and revocation of access privileges distributed through capabilities," *IEEE Transactions on Software Engineering*, vol. SE-5, pp. 575–586, November 1979.
- [9] G. Heiser, K. Elphinstone, J. Vochteloo, S. Russell, and J. Liedtke, "The Mungi single-address-space operating system," *Software – Practice and Experience*, vol. 28, pp. 901–928, July 1998.
- [10] J. King-Lacroix and A. Martin, "BottleCap: a credential manager for capability systems," in *Proceedings of the Seventh ACM Workshop on Scalable Trusted Computing*, (Raleigh, NC, USA), pp. 45–54, ACM, October 2012.
- [11] G. Klein, K. Elphinstone, G. Heiser, J. Andronick, D. Cock, P. Derrin, D. Elkaduwe, K. Engelhardt, R. Kolanski, M. Norrish, T. Sewell, H. Tuch, and S. Winwood, "seL4: formal verification of an OS kernel," in *Proceedings of the 22nd ACM Symposium on Operating Systems Principles*, (Big Sky, MT, USA), pp. 207–220, ACM, October 2009.
- [12] H. M. Levy, *Capability-Based Computer Systems*. Bedford, Mass., USA: Digital Press, 1984.
- [13] L. Lopriore, "Password capabilities revisited," *The Computer Journal*, vol. 58, pp. 782–791, April 2015.
- [14] L. Lopriore, "Access right management by extended password capabilities," *International Journal of Information Security*, vol. 17, pp. 603–612, October 2018.
- [15] L. Lopriore and A. Santone, "Extended pointers for memory protection in single address space systems," *Computers & Electrical Engineering*, vol. 82, pp. 1–14, 2020.
- [16] M. S. Miller and J. S. Shapiro, "Paradigm regained: abstraction mechanisms for access control," in *Proceedings of the 8th Asian Computing Science Conference*, (Mumbai, India), pp. 224–242, Springer, December 2003.
- [17] Y. Nakamura, Y. Zhang, M. Sasabe, and S. Kasahara, "Exploiting smart contracts for capability-based access control in the Internet of Things," *Sensors*, vol. 20, no. 6, p. 1793, 2020.
- [18] P. G. Neumann and R. J. Feiertag, "PSOS revisited," in *Proceedings of the 19th Annual Computer Security Applications Conference*, (Las Vegas, NV, USA), pp. 208–216, IEEE, December 2003.
- [19] T. Newby, D. A. Grove, A. P. Murray, C. A. Owen, J. McCarthy, and C. J. North, "Annex: a middleware for constructing high-assurance software systems," in *Proceedings of the 13th Australasian Information Security Conference*, (Sydney, Australia), pp. 25–34, ACS, January 2015.
- [20] F. Paci, A. Squicciarini, and N. Zannone, "Survey on access control for community-centered collaborative systems," *ACM Computing Surveys*, vol. 51, no. 1, pp. 1–38, 2018.
- [21] R. Pose, "Password-capabilities: their evolution from the Password-Capability System into Walnut and beyond," in *Proceedings of the Sixth Australasian Computer Systems Architecture Conference*, (Gold Coast, Australia), pp. 105–113, IEEE, January 2001.
- [22] A. Randal, "The ideal versus the real: revisiting the history of virtual machines and containers," *ACM Computing Surveys*, vol. 53, no. 1, pp. 1–31, 2020.
- [23] J. H. Saltzer and M. D. Schroeder, "The protection of information in computer systems," *Proceedings of the IEEE*, vol. 63, pp. 1278–1308, September 1975.
- [24] P. Samarati and S. De Capitani Di Vimercati, "Access control: policies, models, and mechanisms," in *Foundations of Security Analysis and Design* (R. Focardi and R. Gorrieri, eds.), pp. 137–196, Berlin, Heidelberg: Springer, 2001.
- [25] M. W. Sanders and C. Yue, "Mining least privilege attribute based access control policies," in *Proceedings of the 35th Annual Computer Security Applications Conference*, (San Juan, Puerto Rico, USA), pp. 404–416, December 2019.
- [26] F. B. Schneider, "Least privilege and more," *IEEE Security & Privacy*, vol. 1, pp. 55–59, September 2003.
- [27] H. Shrobe, D. L. Shrier, and A. Pentland, "Fundamental trustworthiness principles in CHERI," in *New Solutions for Cybersecurity*, pp. 199–236, MIT Press, 2018.
- [28] R. N. Watson, J. Woodruff, P. G. Neumann, S. W. Moore, J. Anderson, D. Chisnall, N. Dave, B. Davis, K. Gudka, B. Laurie, S. Murdoch, R. Norton, M. Roe, S. Son, and V. Munraj, "CHERI: a hybrid capability-system architecture for scalable software compartmentalization," in *Proceedings of the 36th IEEE Symposium on Security and Privacy*, (San Jose, California, USA), May 2015.
- [29] X. Zhang, Y. Li, and D. Nalla, "An attribute-based access matrix model," in *Proceedings of the 2005 ACM Symposium on Applied Computing*, (Santa Fe, New Mexico, USA), pp. 359–363, ACM, March 2005.